20th Balkan Mineral Processing Congress

PROCEEDINGS BOOK

Editors
Esra Baştürkcü
Yusuf Enes Pural
Zeynep Üçerler Çamur

APRIL 9-11
2026

ISTANBUL
TÜRKİYE

20th Balkan Mineral Processing Congress

PROCEEDINGS BOOK

Editors
Esra Baştürkcü
Yusuf Enes Pural
Zeynep Üçerler Çamur

ISBN: 978-975-7946-48-9

Publishing of Proceedings was sponsored by YMGV (Turkish Mining Development Foundation)

All rights reserved. No part of this publication may be reproduced or transmitted in any form or any means, electronic or mechanical, including photocopy, recording or any information storage and retrieval system, without permission in writing from the Turkish Mining Development Foundation.

YMGV
Turkish Mining Development Foundation
(Yurt Madenciliğini Geliştirme Vakfı)

Harbiye, Cumhuriyet Cad. 295/5 Daire:110 Şişli
34367-Istanbul/TÜRKİYE

Web : www.ymgv.org.tr
e-mail : ymgv@ymgv.org.tr

©2026 YMGV

ISBN : 978-975-7946-48-9

Published by
YMGV

This congress is dedicated to the memory of Prof. Dr. Güven ÖNAL.

Prof. Dr. Güven ÖNAL
(1940-2024)

President of Balkan Mineral Processing Scientific Committee
(1995-2024)

President of Balkan Mineral Processing Science Academy
(2001-2024)

Dear Readers,

Putting together the proceedings of a congress is, in many ways, a quieter kind of work. One that happens behind the scenes while everything else is taking shape. As the editorial board of BMPC 2026, we have had the privilege of being close to this process from early on, and this volume is the result of that collective effort.

Of the 139 papers included, 13 are plenary presentations, 86 are oral, and 40 are poster contributions. The most active sessions in terms of submissions were Hydrometallurgy, Pyrometallurgy and Bio-Processing with 22 papers, Flotation and Surface Chemistry Processes with 20, and Material Analysis and Mineral Characterization with 18, together accounting for more than 43% of all contributions. These figures reflect where much of the current research energy in the field is concentrated, though the breadth of topics across all 16 sessions points to a community that remains wide in its interests.

Geographically, Türkiye led with 65 contributions, followed by Albania with 11 and Kosovo with 6. Beyond the immediate region, researchers from Finland, Germany, Norway, Brazil, Algeria, and Australia were also among the contributors, reflecting a community that has quietly but steadily grown in reach over the years.

We would like to thank all authors for their submissions and their patience through the review and editing process. Our gratitude also goes to the reviewers, whose careful evaluations were essential in maintaining the scientific quality of this collection.

We hope this volume serves as a useful reference, and perhaps as a starting point for new collaborations.

Dr. Esra BAŞTÜRKÇÜ Dr. Yusuf Enes PURAL Dr. Zeynep ÜÇERLER ÇAMUR

Editorial Board, BMPC 2026 Proceedings

Since 1973: Advancing Mineral Processing Together

For several decades, a significant number of researchers and specialists in the Balkan region have devoted their efforts to advancing the science and practice of mineral processing. Their work has focused on establishing and improving industrial concentration processes, expanding production capacities, optimizing operational performance, enhancing energy efficiency in processes and equipment, and developing innovative machinery and technologies. Through these sustained efforts, mining and mineral processing activities in the Balkans have achieved steady progress and continue to play an important role in the region today.

This long-standing scientific endeavor has led to the emergence of many distinguished researchers in mineral processing across the Balkan region. In 1973, the first Balkan Mineral Processing Committee (BMPC) was established by its founding members: Prof. Dr. Kiriak Petrov Kovachev (Bulgaria), Prof. Dr. Parachiv Ilie (Romania), Prof. Dr. Dusan Salatic (Serbia), and Prof. Dr. Zeki Doğan (Türkiye).

The Balkan Mineral Processing Congress (BMPC) has been held for more than fifty years. The first Balkan Mineral Processing Conference took place in Varna, Bulgaria, from November 12 to 15, 1973. During the final session of that event, the Balkan Mineral Processing Scientific Committee (BMPSC) for Conferences was formally established. Today BMPSC has 27 active members from Albania (3), Bosnia-Herzegovina (2), Bulgaria (2), Greece (3), Republic of Kosovo (3), Moldova (1), Montenegro (3), North Macedonia (3), Romania (3), Slovenia (1), Turkiye (3), and 12 honorary members from Albania (2), Bulgaria (2), North Macedonia (1), Romania (3), Serbia (1), Türkiye (3).

In early meetings of BMPSC, the Committee decided that a Balkan Mineral Processing Conference would be organized every two years (later changed to three years), each time hosted by a different Balkan country. A major milestone in the development of BMPC occurred during the 9th Balkan Mineral Processing Conference, held in Istanbul (Türkiye) from September 11 to 13, 2001, under the chairmanship of Prof. Dr. Güven Önal. At that time, the event evolved from a “Conference” into a “Congress,” reflecting its growing scientific impact, the increasing number of participants, and the high quality of the papers presented. To date, nineteen (19) conferences/congresses have been successfully organized in various Balkan countries, including Albania (2), Bosnia-Herzegovina (1), Bulgaria (3), Greece (1), Republic of Kosovo (1), Romania (3), North Macedonia (1), Serbia (3), and Türkiye (3).

Following the establishment of the Balkan Mineral Processing Scientific Committee, the Balkan Mineral Processing Science Academy (BMPSA) was founded in 2001. Its founding members included Prof. Dr. Güven Önal (Türkiye), Prof. Dr. Zeki Doğan (Türkiye), Prof. Dr. Gülhan Özbayoğlu (Türkiye), Prof. Dr. Suna Atak (Türkiye), Prof. Dr. Dusan Salatic (Serbia), Prof. Dr. Nadezda Calic (Serbia), and Prof. Dr. Parachiv Ilie (Romania). Today, BMPSA has 43 members, including founding members, full members, and corresponding members; unfortunately, some of these distinguished members have passed away. Prof. Dr. Güven Önal served as the President of both the Balkan Mineral Processing Scientific Committee from 1995 and the Balkan Mineral Processing Science Academy from 2001 until his passing on March 31, 2024. Following his leadership, Prof. Dr. Fatma Arslan has continued this responsibility as President.

Participation in the activities of the Balkan Mineral Processing Scientific Committee has created a strong connection between regional scientific development and global

technological trends. It has also provided valuable opportunities for direct interaction among researchers, designers, equipment manufacturers, and investors from the Balkan region and beyond. Over time, the BMPC has evolved into a well-established international event held every three years, attracting participants not only from the Balkan countries but also from many other parts of the world.

The XXth Balkan Mineral Processing Congress (BMPC 2026) was held in Istanbul, Türkiye, on April 9-11, 2026, for the fourth time in the country. The congress is organized by the Mineral Processing Engineering Department of the Mining Faculty at Istanbul Technical University, in cooperation with the Turkish Mining Development Foundation (YMGV). This congress is the first one after Prof. Güven Önal's loss and is dedicated to the memory of Prof. Dr. Güven Önal.

I would like to express my sincere gratitude to the Head of the Mineral Processing Engineering Department, Prof. Dr. Murat Olgaç Kangal, and to the President of the Turkish Mining Development Foundation, Mr. Ali Türkoğlu, for their leadership in organizing this congress. I also extend my thanks to the secretaries of the organizing committee, Prof. Dr. Feridun Boylu and Prof. Dr. Gülay Bulut (BMPSC Secretary), and to Assoc. Prof. Dr. Genc Demi (BMPSC Vice President), to all members of the Balkan Mineral Processing Scientific Committee, to the members of the organizing committee, and to all participants whose contributions have made this congress both valuable and memorable. Without their dedication and support, this congress would not have been possible.

Finally, I would also like to extend our sincere appreciation to the sponsoring organizations and institutions whose generous support has significantly contributed to the successful organization of BMPC 2026.

Prof. Dr. Fatma ARSLAN

President

Balkan Mineral Processing Scientific Committee

Balkan Mineral Processing Science Academy

Dear Participants,

The Mining Development Foundation of Turkey has, since its establishment, continued its efforts to support the development of mining and mineral processing in Türkiye, to promote the effective utilization of domestic resources, and to contribute to the dissemination of scientific knowledge through congresses, conferences, and publications.

The XXth Balkan Mineral Processing Congress (BMPC 2026), held in Istanbul on April 9–11, 2026, represents a well-established regional platform that enables the exchange of scientific and technical knowledge in the field of mineral processing. Organized in cooperation with the Department of Mineral Processing Engineering of the Faculty of Mines at Istanbul Technical University, the congress continues a long-standing tradition of collaboration and knowledge sharing across the Balkan region and beyond.

Over time, BMPC has evolved into an international platform where researchers, engineers, and industry representatives come together to discuss technological developments, operational challenges, and new approaches. The congress supports not only scientific exchange but also the strengthening of professional networks and the development of regional collaborations.

At a time when our Foundation marks its 40th anniversary, the organization of the Balkan Mineral Processing Congress for the 20th time demonstrates both the continuity of institutional knowledge and its transformation into a scientific platform with international recognition.

This year's congress holds additional significance as it is the first BMPC organized following the passing of the late Prof. Dr. Güven Önal, who made important contributions to the Turkish mining sector and the Balkan mineral processing community. Prof. Dr. Güven Önal, who served for many years as the President of the Mining Development Foundation of Turkey and played a key role in shaping its current institutional structure, also held long-term leadership positions within the Balkan Mineral Processing Scientific Committee (BMPSC) and the Balkan Mineral Processing Science Academy (BMPSA). Through these roles, he guided the institutional and scientific development of BMPC and made pioneering contributions to its establishment as an international platform. We remember him with respect, gratitude, and deep appreciation.

As the Mining Development Foundation of Turkey, we would like to express our sincere thanks to the Ministry of Energy and Natural Resources of the Republic of Türkiye, Istanbul Technical University, the Faculty of Mines, and the Department of Mineral Processing Engineering, as well as to all institutions and organizations that contributed to the organization of the congress. We also extend our gratitude to our sponsors, invited speakers, session chairs, authors, reviewers, members of the organizing and scientific committees, and all participants.

We are pleased to present this proceedings book to the national and international mining and mineral processing community and hope that it will serve as a valuable resource for future studies.

M. Ali TÜRKOĞLU
Chairman of the Board
Mining Development Foundation of Turkey

Dear Colleagues,

It is a great honor and privilege to present the proceedings of the 20th Balkan Mineral Processing Congress (BMPC 2026).

Since its inception in 1973 in Varna, Bulgaria, the Balkan Mineral Processing Congress has evolved into a well-established and respected scientific platform, bringing together researchers, academics, and industry professionals from across the region and beyond. Over the decades, BMPC has played a significant role in promoting knowledge exchange, fostering collaboration, and advancing the field of mineral processing.

The 20th edition of the Congress proudly continues this strong tradition by addressing contemporary challenges and emerging opportunities in mineral processing and extractive metallurgy. Particular emphasis has been placed on innovative and sustainable approaches in mineral beneficiation, recycling of secondary resources, critical raw materials, and environmentally responsible processing technologies.

This volume comprises a total of 139 scientific papers, contributed by researchers from 30 different countries, reflecting the truly international character of the congress. The contributions are organized across 16 thematic sections, covering a broad spectrum of topics and demonstrating the diversity and interdisciplinary nature of current research in mineral processing.

The papers included in this proceedings volume represent a high level of scientific quality and provide valuable insights into current research trends, technological advancements, and industrial applications. We believe that this collection will serve as an important reference for both academic researchers and industry practitioners.

I would like to express my sincere gratitude to all authors for their valuable contributions, to the members of the Scientific and Organizing Committees for their dedicated efforts, and to all reviewers for their careful evaluations, which have ensured the high quality of this publication.

I also extend my appreciation to all participants, sponsors, and supporting institutions whose contributions have made BMPC 2026 a successful and impactful event.

I hope that this volume will inspire further research, strengthen international collaboration, and contribute to innovation in the field of mineral processing.

Yours sincerely,

Prof. Dr. Murat Olgaç KANGAL

Chairman, BMPC 2026

BALKAN MINERAL PROCESSING SCIENTIFIC COMMITTEE MEMBERS

President: Prof. Dr. Fatma ARSLAN, Türkiye

Vice President: Assoc. Prof. Dr. Genc DEMI, Albania

Secretary: Prof. Dr. Gülay BULUT, Türkiye

Members

MSc. Ekita FETAHU TOSKA, Albania

Asst. Prof. Dr. Kimet FETAHU, Albania

Prof. Dr. Ljiljana TANKOSIĆ, Bosnia and Herzegovina

Prof. Dr. Nedzad ALIC, Bosnia and Herzegovina

Prof. Dr. Irena GRIGOROVA, Bulgaria

Prof. Dr. Marinela PANAYOTOVA, Bulgaria

Prof. Dr. Georgios N. ANASTASSAKIS, Greece

Prof. Dr. Maria TAXIARHOU, Greece

Asst. Prof. Dr. Panagiotis ANGELOPOULOS, Greece

Prof. Dr. Igor NICOARA, Moldova

Alen ŠTULIĆ, Montenegro

Boško ŠLJIVANČANIN, Montenegro

Branislav VUKOVIĆ, Montenegro

Prof. Dr. Afrodita ZENDELSKA, North Macedonia

Prof. Dr. Boris KRSTEV, North Macedonia

Mrsc. Davor TONEVSKI, North Macedonia

Dr. Habib BASHOLLI, Republic of Kosovo

Prof. Dr. Naser PECI, Republic of Kosovo

Prof. Dr. Nurten DEVA, Republic of Kosovo

Dr. Alexandru MIHAI, Romania

Dr. Gelu MARACINEANU, Romania

Prof. Dr. Traistă Eugen NICOLAE, Romania

Prof. Dr. Slavomír Hredzák, Slovakia

Prof. Dr. Ayhan Ali SİRKECİ, Türkiye

Honorary Members

Prof. Dr. Vladimir PEZA, Albania

Prof. Dr. Avni KALTANI, Albania

Prof. Dr. Nadezda DAVCHEVA, Bulgaria

Prof. Dr. Ivan NISHKOV, Bulgaria

Prof. Dr. Boris FIDANCHIEV, North Macedonia

Prof. Dr. Sanda KRAUSZ, Romania

Dr. Lilliana CIOBANU, Romania

Dr. Viorica CIOCAN, Romania

Prof. Dr. Nadezda CALIC, Serbia

Prof. Dr. Suna ATAK, Türkiye

Prof. Dr. Gülhan ÖZBAYOĞLU, Türkiye

Prof. Dr. Neşet ACARKAN, Türkiye

XX BALKAN MINERAL PROCESSING CONGRESS ORGANIZING COMMITTEE

President

Ali TÜRKOĞLU, Head of Turkish Mining Development Foundation, Türkiye

Prof. Dr. Murat Olgaç KANGAL, Head of Mineral Processing Eng. Depart., ITU, Türkiye

Secretary

Prof. Dr. Feridun BOYLU, Mineral Processing Eng. Depart., ITU, Türkiye

Prof. Dr. Gülay BULUT, Mineral Processing Eng. Depart. ITU, Türkiye

Members

Prof. Dr. Mustafa KUMRAL, Dean of Faculty of Mines ITU, Türkiye

Ali EMİROĞLU, Vice Head of Turkish Mining Development Foundation, Türkiye

Prof. Dr. Ayhan Ali SİRKECİ, Mineral Processing Eng. Depart., ITU, Türkiye

Prof. Dr. Orhan ÖZDEMİR, Mineral Processing Eng. Depart., ITU, Türkiye

Prof. Dr. Fırat BURAT, Mineral Processing Eng. Depart., ITU, Türkiye

Assoc. Prof. Dr. Birgül BENLİ, Mineral Processing Eng. Depart., ITU, Türkiye

Assoc. Prof. Dr. Hüseyin BAŞTÜRKCÜ, Mineral Processing Eng. Depart., ITU, Türkiye

Assoc. Prof. Dr. Mustafa ÖZER, Mineral Processing Eng. Depart., ITU, Türkiye

Dr. Kudret Tahsin PEREK, Mineral Processing Eng. Depart., ITU, Türkiye

Dr. Şükriye Beste AYDIN, Mineral Processing Eng. Depart., ITU, Türkiye

Dr. Esra BAŞTÜRKCÜ, Mineral Processing Eng. Depart., ITU, Türkiye

Dr. Yusuf Enes PURAL, Mineral Processing Eng. Depart., ITU, Türkiye

Res. Asst. Dr. Zeynep ÜÇERLER ÇAMUR, Mineral Processing Eng. Depart., ITU, Türkiye

Res. Asst. Tülay TÜRK, Mineral Processing Eng. Depart., ITU, Türkiye

Res. Asst. Oğuzhan Mert GÜRKAN, Mineral Processing Eng. Depart., ITU, Türkiye

Res. Asst. Ceyda GÜRKAN, Mineral Processing Eng. Depart., ITU, Türkiye

Res. Asst. Nazlım İlkyaz DİNÇ, Mineral Processing Eng. Depart., ITU, Türkiye

Res. Asst. Yunus Emre ÇAVDAR, Mineral Processing Eng. Depart. ITU, Türkiye

Res. Asst. Gülşah GÜVEN, Mineral Processing Eng. Depart., ITU, Türkiye

Res. Asst. Tülin ULUCAN, Mineral Processing Eng. Depart., ITU, Türkiye

Res. Asst. Ulaş USLU, Mineral Processing Eng. Depart., ITU, Türkiye

Berna BABA, Mineral Processing Eng. Depart., ITU, Türkiye

Eng. Zeynep AKTUNA ÜSTÜNDAĞ, Mineral Processing Eng. Depart., ITU, Türkiye

Gülseren KOÇER, Turkish Mining Development Foundation, Türkiye

Ferah DUKUL, Turkish Mining Development Foundation, Türkiye

XX BMPC SCIENTIFIC COMMITTEE

Assoc. Prof. Dr. Boris ALBIJANIC, Australia

Prof. Dr. N. Emre ALTUN, Türkiye

Prof. Dr. Cüneyt ARSLAN, Türkiye

Prof. Dr. Seher ATA, Australia

Dr. Khandjamts BATJARGAL, Mongolia

Prof. Dr. Oktay BAYAT, Türkiye

Prof. Dr. Zarife Bajraktari GASHI, Kosovo

Prof. Dr. Saeed Chehreh CHELGANI, Sweden

Prof. Dr. Mohamed CHETTIBI, Algeria

Prof. Dr. Mehmet S. ÇELİK, Türkiye

Prof. Dr. Üner ÇOLAK, Türkiye

Prof. Dr. Hao DU, China

Prof. Dr. Hasan ERGİN, Türkiye

Prof. Dr. Lev FILIPPOV, France

Prof. Dr. Helmut FLACHBERGER, Austria

Prof. Dr. Zhiyong GAO, China

Prof. Dr. Ferihan GÖKTEPE, Türkiye

Prof. Dr. Alim GÜL, Türkiye

Prof. Dr. Sebahattin GÜRMEN, Türkiye

Prof. Dr. Anh H. NGUYEN, Australia

Prof. Dr. Stoyan I. KARAKASHEV, Bulgaria

Assoc. Prof. Dr. Jože KORTNIK, Slovenia

Prof. Dr. Przemyslaw B. KOWALCZUK, Norway

Dr. Ozan KÖKKILIÇ, Canada

Prof. Dr. Haldun KURAMA, Türkiye

Prof. Dr. İlgin KURŞUN, Türkiye

Assoc. Prof. Dr. Malibongwe MANONO, South Africa

Prof. Dr. İslam MUSTAFAYEV, Azerbaijan

Prof. Dr. Hasan Can OKUTAN, Türkiye

Prof. Dr. Şafak Gökhan ÖZKAN, Türkiye

Prof. Dr. Marinela PANAYOTOVA, Bulgaria

Dr. Martin RUDOLPH, Germany

Prof. Dr. André Carlos SILVA, Brazil

Prof. Dr. Elenice Maria Schons SILVA, Brazil

Prof. Dr. Ayhan Ali SİRKECİ, Türkiye

Prof. Dr. Hikmet SİS, Türkiye

Prof. Dr. Xuming WANG, USA

Dr. Ünzile YENİAL ARSLAN, Australia

Prof. Dr. A. Ekrem YÜCE, Türkiye

Assoc. Prof. Dr. Jan ZAWALA, Poland

PARTICIPATING COUNTRIES

Albania (11)
Albania-Kosovo (1)
Algeria (5)
Algeria-India (1)
Australia (2)
Austria (1)
Bosnia and Herzegovina (5)
Bosnia and Herzegovina-Montenegro (1)
Brazil (3)
Bulgaria (3)
Canada (1)
Chile-Finland (2)
Finland (3)
Finland-Ghana (1)
Finland-Türkiye (1)
France (1)
Germany (1)
Hungary (1)
Japan (1)
Kosovo (6)
Kosovo-North Macedonia-Türkiye (1)
Mexico-Germany-Finland (1)
North Macedonia (2)
North Macedonia-Albania-Türkiye-Kosovo (1)
Norway (3)
Romania (5)
Serbia-Bosnia and Herzegovina (1)
Slovenia (1)
South Africa (1)
Sweden (1)
Türkiye (65)
Türkiye-Australia (2)
Türkiye-France (1)
Türkiye-Germany (1)
Türkiye-South Africa (1)
USA (1)

Total: 139 ***Türkiye: 65*** ***Other Countries: 74***

TABLE OF CONTENTS

PLENARY PAPERS

REVIEW OF THE CONCEPT AND MEASUREMENT OF HYDROPHOBICITY 1
Cyril T. O'CONNOR

THE USE OF ECO-FRIENDLY COLLECTORS FOR FELDSPAR FLOTATION 11
Lev O. FILIPPOV; Inna V. FILIPPOVA

WASTE FROM SOME NONFERROUS BASE METALS EXTRACTION AS SOURCE OF CRITICAL METALS 22
Marinela PANAYOTOVA; Irena GRIGOROVA; Vladko PANAYOTOV

EXPLOITATION OF NATURAL RESOURCES THE ECONOMIC AND ENVIRONMENTAL IMPACT OF 47
THEIR UTILIZATION
Nurten DEVA

APPLICATION OF AI IN MINERAL PROCESSING: EVOLUTION, INDUSTRIAL UPTAKE, AND CURRENT . 55
USE
Saeed Chehreh CHELGANI

FLOTATION 4.0: GREENER, SMARTER, SUSTAINABLE 66
Przemyslaw B. KOWALCZUK

INTEGRATING ADVANCED SEPARATION TECHNIQUES FOR SUSTAINABLE RECOVERY OF CRITICAL 76
METALS FROM DEEP-SEA FERROMANGANESE CRUSTS
Gjergj DODBIBA; Cheng-En LEE

ORE SILOS AND FLOW PROBLEMS 83
Ayhan Ali SİRKECİ

NIOBIUM AND TANTALUM CONCENTRATION 92
Elenice Maria Schons SILVA; Amanda Paranhos MACEDO; Raydse Linny Silva SOUZA; Jaciany Mayara Batista SOARES; André Carlos SILVA

ELECTROSTATIC SEPARATION AFTER TRIBOELECTRIC CHARGING IN THE PROCESSING OF 106
PRIMARY RAW MATERIALS – STATUS QUO IN RESEARCH AND OUTLOOK FOR POTENTIAL APPLICATIONS
Helmut FLACHBERGER; Dominic PREM

EFFECTS OF ULTRASOUND ON SETTLING BEHAVIOUR OF SOME CRITICAL RAW MATERIALS 116
Şafak Gökhan ÖZKAN

BONDING MECHANISMS IN BRIQUETTING OF RECYCLED WASTE POWDERS – USED COFFEE 135
GROUNDS GRANULATE
Jože KORTNIK; Lara ANŽIČ

EFFECT OF WASTE ROCK DILUTION ON THE FLOTATION OF MAIN CRITICAL RAW MATERIALS . . . 146
(CRM)
Maria SINCHE-GONZALEZ

COAL PROCESSING, AGGLOMERATION AND BRIQUETTING

EVALUATION OF THE WASHABILITY CHARACTERISTICS OF ZONGULDAK COAL SEAMS: THE CASE 154
OF ÇATALAĞZI COAL PREPARATION PLANT
Eljona MUNISHI; Valona PROKSHI; Albina RAMA; Elona IDRIZI; Omer GUCATI; Leutrim BOGIQI; Berat SINANI; Mehmet BİLEN

EXTRACTION OF TAR FROM LOW-RANK TURKISH COALS BY PYROLYSIS FOR CARBON FIBER . . . 164
PRODUCTION
Ensar Eray METE; Hüma VELİDEDEOĞLU; Kerim ÇELİK; Yunus Emre ÇAVDAR; Muhammed Fatih CAN; Alper SARIOĞLAN; Hasan Can OKUTAN; Feridun BOYLU; Mehmet Sabri ÇELİK

MODELING OF COMPOSITE COAL-BASED BRIQUETTES AIMED AT REDUCING SULFUR EMISSIONS 174
INTO THE ATMOSPHERE
Nedžad ALIĆ; Rusmir RAZIĆ

VALUE-ADDED CONVERSION of ZONGULDAK HARD COALS: INTEGRATED APPROACHES FOR 188
INJECTION COAL, ACTIVATED CARBON, and INDUSTRIAL APPLICATIONS
Faik ALP; Serdar YILMAZ; Mehmet BİLEN; İhsan TOROĞLU

SECOND-STAGE SEPARATION DENSITY CONTROL IN A GRAVITY-FED THREE-PRODUCT DENSE MEDIUM CYCLONE . . 198
Yusuf Enes PURAL; Mustafa ÖZER; Fırat BURAT; Feridun BOYLU

COMMINUTION AND CLASSIFICATION

INVESTIGATION OF THE EFFECTS OF ORE ABRASIVITY INDEX ON BALL WEAR IN WET BALL MILLING OPERATIONS WITH LAB SCALE TESTS 203
Yağız Kerem YALÇIN; Ahmet YAKAR; İbrahim GÖKTAŞ

EVALUATION OF COMPUTER APPLICATIONS FOR COMMINUTION CIRCUIT DESIGN 215
Kudret Tahsin PEREK; Jemshit RECEPOV; Ceyda TUNÇOK

CONSERVATION, REHABILITATION AND RECYCLING IN MINERAL PROCESSING

ANALYSIS OF THE REUSE POTENTIAL OF SOLID WASTES AFTER HCL LEACHING FROM A CIRCULAR ECONOMY PERSPECTIVE USING MICROSCOPE IMAGES AND MACHINE LEARNING 223
Tuğba Deniz TOMBAL KARA; Burçin KAYMAKOĞLU; Nevzat Yağız TOMBAL

ENVIRONMENTALLY FRIENDLY LEACHING OF LITHIUM-ION BATTERY WITH FORMIC ACID PROCESS OPTIMIZATION AND KINETIC INSIGHTS 238
Muammer KAYA; Hossein DELAVANDANI

DEWATERING, WASTE WATER TREATMENT

CREATING VALUE FROM WATER IN MINING 246
Riina SALMIMIES; Nina HARJULA; Elsi STRAND

EFFECT OF FLOCCULANT DOSAGE AND WATER TYPE ON THE SEDIMENTATION BEHAVIOR OF SULFIDE IRON ORE TAILING . . 251
Argun ÇIPER; Yunus Emre ÇAVDAR; Orhan ÖZDEMIR

EDUCATION, SUSTAINABILITY IN MINERAL PROCESSING

ALIGNMENT OF ALBANIAN GEO-MINING LEGISLATION WITH THE LEGISLATION OF BALKAN COUNTRIES AND THE EUROPEAN UNION 259
Ekita TOSKA; Kimet FETAHU; Habib BASHOLLI; Lavdie MOISIU

AN OVERVIEW OF MINERAL PROCESSING INNOVATIONS IN BULGARIA 267
Irena GRIGOROVA; Teodora YANKOVA; Mihail PETROV; Nikolay NESTOROV

APPLICATION OF THE CIRCULAR ECONOMY IN THE MINING SECTORS OF BOSNIA AND HERZEGOVINA: FROM A LINEAR TO A SUSTAINABLE CIRCULAR MODEL THROUGH WASTE VALORIZATION 275
Nedžad ALIĆ; Admir SOFTIĆ; Alma NUHANOVIĆ

RECULTIVATION OF ORE FIELDS AFTER EXPLOITATION - METHODOLOGY OF COLLECTION OF FUNDS FOR RECULTIVATION . . . 287
Jahir GASHI; Habib BASHOLLI

FLOTATION AND SURFACE CHEMISTRY PROCESSES

A SUSTAINABLE APPROACH OF FLOTATION-BASED RECYLCING OF VIRGIN AND POST-CONSUMER MULTIPLE PLASTICS WITH DETERMINATION OF THEIR SURFACE CHARACTERISTICS 293
Cemal Cem BAKIR; Murat Olgaç KANGAL; Zeynep ÜÇERLER ÇAMUR; Tülay TÜRK

COMPARATIVE PERFORMANCE OF NaCN and SMBS DEPRESSANTS IN THE FLOTATION OF THE UZBEKISTAN Pb–Zn ORE . . 301
Sinem DOĞAN; Mert SARIKAYA

EFFECT OF PULP AERATION ON LEAD-ZINC FLOTATION PERFORMANCE 307
Irmak DEMIREL; Şükriye Beste AYDIN

EVALUATING CASHEW NUTSHELL LIQUID AS A SUSTAINABLE COLLECTOR FOR COPPER-MOLYBDENUM ORE FLOTATION 315
Justin PARIS; Ebuka CHUKWUMA; Helmi F. KALAHARI; Alex KELISKY; James FINET; Ozan KÖKKILIÇ; Shiva MOHAMMADI-JAM; Kristian E. WATERS

FROM ELECTRICAL SIGNATURES TO FLOTATION: A MULTI-PARAMETER ANALYSIS OF COPPER RECOVERY . . 325
Ünzile YENIAL ARSLAN; Elizaveta FORBES

GAS DISPERSION CHARACTERISTICS OF THE CONCORDE CELL 333
Berivan TUNÇ; Toni MATTSSON; Alejandro YANEZ; Gülay BULUT

GREEN EMULSION STRATEGIES FOR GRAPHITE FLOTATION: BIOSURFACTANT-COLLECTOR INTERACTIONS IN LIB BLACK MASS RECYCLING 341
Chiedza NZUMA; Przemyslaw B. KOWALCZUK

INFLUENCE OF GLYCOL AND ALCOHOL TYPE FROTHER ON CRITICAL COALESCENCE CONCENTRATION AND BUBBLE SIZE 349
Gülşah GÜVEN; Şükriye Beste AYDIN; Ferihan GÖKTEPE; Gülay BULUT

INVESTIGATION ON LEAD DEPRESSION IN ANTIMONY FLOTATION CIRCUIT 356
Begüm YÜCEL; İbrahim GÖKTAŞ

REAGENT OPTIMIZATION IN THE FLOTATION BENEFICIATION OF SILICA SAND USED IN GLASS PRODUCTION . . . 365
Selen ULUSKAN; Gülay BULUT

RECENT ADVANCES IN FLOTATION TECHNOLOGIES FOR COARSE AND FINE PARTICLE RECOVERY 372
Ceyda GÜRKAN; Hüseyin BAŞTÜRKCÜ

SPHALERITE FLOTATION USING A NEW CHELATING COLLECTOR N-HEXYLAMINOETHANETHIOL . . 380
Badr-Elboudour BENAISSA; Mohamed CHETTIBI; Ramanathan NATARAJAN; Salima SALHI

STUDY OF COPPER ORE FLOTATION REAGENTS APPLICATION 386
Vladimir PEZA

SULFIDE GOLD ORE FLOTATION RICH IN FINE PARTICLES 395
Elenice Maria Schons SILVA; Antônio de Pádua Arlindo DANTAS; Jaciany Mayara Batista SOARES; Poliana Felipe PACHECO; Kascielle Braga AMORIM; Luiz Henrique Coelho Pessoa SANTOS; Bruno Gomes da MOTA; Vinicius Curcino de Carvalho VIEIRA; André Carlos SILVA

TESTING THE SELECTIVE SEPARATION OF LIMONITE-BARITE ORE FROM THE 'VIDRENJAK' DEPOSIT 403
Ljiljana TANKOSIĆ; Branka ŠOLAJA

THE CONTRIBUTION OF ROUGHNESS PARAMETER ON COAGULATION AND FLOCCULATION CHARACTERISTICS OF FINE CHROMITE 411
Onur GÜVEN

THE EFFECT OF SODIUM HEXAMETAPHOSPHATE AS A DISPERSANT AND ANIONIC POLYACRYLAMIDE-BASED FLOCCULANT ON THE ZETA POTENTIAL OF NATURAL GOETHITE, QUARTZ, AND CLAY MINERALS 422
Ljiljana TANKOSIĆ; Svjetlana SREDIĆ

THE EFFECT OF WATER TYPE ON FLOTATION PERFORMANCE AND FROTH CHARACTERISTICS IN COPPER SLAG FLOTATION 430
Ulaş USLU; Zeynep ÜÇERLER ÇAMUR; Yunus Emre ÇAVDAR; Şükriye Beste AYDIN; Gülay BULUT

A COMPREHENSIVE PILOT-SCALE STUDY ON PNEUMATIC IMHOFLOT FLOTATION PERFORMANCE AT THE ÇAYELİ BAKIR 437
Atıf DEMİRCAN; Ekin GÜNGÖR; Ahmad HASSANZADEH; Dilay HACIOSMANOĞLU; Aytekin TIRNAKÇIOĞLU

OPTIMIZATION OF APATITE DEPRESSION USING K-NA TARTRATE / AL2(SO4)3 IN PHOSPHATE SLIMES FROM DJEBEL ONK (ALGERIA) . . . 445
Djamel NETTOUR; Yousra BOUKHAMLA; Rachid CHAIB; Mohamed CHETTIBI; Nesrine DERRADIJA

GEOLOGICAL STUDIES

ASSESSMENT AND CALCULATION OF HYDROGEOLOGICAL PARAMETERS OF THE AQUIFER IN THE SOUTHERN PART OF THE KOSOVO COAL BASIN . . . 450
Sabri AVDULLAHI

CHARACTERIZATION AND PROCESSING OF VOLCANIC ROCKS FROM MONTENEGRO FOR USE AS INDUSTRIAL RAW MATERIALS **457**
Ljiljana TANKOSIĆ; Alen ŠTULIĆ

DETECTION OF ORE DEPOSITS USING IMAGE PROCESSING TECHNIQUES, WEST OF ELAZIG̃ (TURKEY) **463**
İmren Sumru TOSUN; Melek URAL; Mustafa EĞRİ

GEOLOGICAL – MINERALOGICAL CHARACTERISTICS OF POLYMETALLIC ORES AND THEIR BENEFICIATION POTENTIAL IN THE MUSHTE – GURTH SPAC – LETITEN REGION, MIRDITA, ALBANIA **469**
Asllan DACI; Agim SINOJMERI; Cem Koray YAGCI; Mehmet YAVUZ; Hasan USTUNDAG

IMAGE PROCESSING STUDIES IN THE AKDAĞ REGION (ELAZIĞ, TURKEY) **482**
Melek URAL; Mustafa EĞRİ

IMAGING ANALYSIS OF ORE OCCURRENCES WITHIN UPPER CRETACEOUS LAVA SEQUENCES (KOÇKALE, ELAZIĞ-TURKEY) **487**
Melek URAL; Mustafa EĞRİ

MINERALOGICAL CONTROLS AND BENEFICIATION ASSESSMENT OF VANADIUM (V) ENRICHED META-GABBROIC ROCKS FROM THE AZITEPE–ALAŞEHİR **493**
N. Merve SÜTÇÜ; Zeynep DÖNER; Mustafa KUMRAL; Tülay TÜRK; Gülşah GÜVEN

HYDROMETALLURGY, PYROMETALLURGY AND BIO-PROCESSING

A BRIEF HISTORICAL DEVELOPMENT OF REFRACTORIES **502**
Arman EHSANI; Ilhan EHSANI

A NEW APPROACH TO STUDYING THE EFFECTS OF CYANIDE DOSAGE ON SILVER METAL THROUGH A QCM SENSOR **512**
Ömer CANIEREN; Cengiz KARAGÜZEL; Oktay ŞAHBAZ

A REVIEW ON FILTRATION PERFORMANCE EVALUATION AND OPERATIONAL OPTIMIZATION IN CCD-MERRILL CROWE PROCESSING **519**
Semih ERZENOĞLU; Hüseyin BAŞTÜRKCÜ

ACID LEACHING OF MECHANICALLY ACTIVATED BENTONITE CLAY FOR ALUMINUM EXTRACTION **525**
Mustafa BİRİNCİ; Kader ŞENTÜRK

DIAGNOSTIC LEACHING OF A DOUBLE REFRACTORY GOLD ORE **531**
Deus Albert MSUMANGE; Hacı DEVECİ; Ersin Yener YAZICI; Oktay CELEP; J. Albert MSUMANGE

ELECTROWINNING OF ZINC FROM AMMONIACAL LEACH SOLUTIONS OBTAINED FROM CARBONATE-CONTAINING SMITHSONITE ORE **539**
Fatih ÇAVUŞLU; Arman EHSANI; Ilhan EHSANI

EVALUATION OF ALTERNATIVE SULFATION AGENTS FOR RARE EARTH ELEMENT PRETREATMENT-A COMPARATIVE STUDY **549**
Esra BAŞTÜRKCÜ

FLASH FURNACE DUST PROCESSING VIA ROASTING AND ACID LEACHING OPERATION **555**
Melikenur AYCAN; Merve DOĞAN; Abdullah Erdem YILDIZHAN; Fatih ÖZEL; İbrahim GÖKTAŞ; Mehmet CANBAZOĞLU

HYDROMETALLURGICAL PROCESSING AND SUSTAINABLE VALORIZATION OF BRUCITIC DOLOMITES FOR HIGH-PURITY MAGNESIUM OXIDE PRODUCTION **561**
Camelia BĂDULESCU; Camelia TRAISTĂ

HYDROMETALLURGICAL RECOVERY OF HIGH-PURITY MANGANESE DIOXIDE AND ASSOCIATED COMPOUNDS FROM SILICO-MANGANESE PRODUCTION DUSTS **570**
Mariana DUMITRACHE; Maria LAZAR; Camelia TRAISTĂ

INVESTIGATION OF THE BENEFICIATION OF MANGANESE ORE IN THE KARABURUN REGION BY LEACHING **580**
Yaşar Hakan GÜRSOY; Koray Emre AKGÖÇMEN

ORP MODULATION IN HCL- AND H2SO4-BASED LEACHING SYSTEMS THROUGH SYNERGISTIC NACL EFFECTS **591**
Kobra REZAEI; Claudio ACUNA

PYROMETALLURGICAL AND HYDROMETALLURGICAL VALORIZATION OF BLAST FURNACE SLUDGE FROM THE MĂLINA SETTLING POND (GALATI, ROMANIA) 602
Camelia TRAISTĂ; Tiberiu RUS; Eugen TRAISTĂ

RECOVERY OF METALLIC VALUES FROM COPPER SLAGS 610
Fatma ARSLAN; Gülay BULUT; Cüneyt ARSLAN

RESEARCH ON FACTORS INFLUENCING HIGH FUEL CONSUMPTION IN ROTARY KILNS 617
Zarife BAJRAKTARI GASHI; Mimoza KOVAÇI AZEMI

SELECTIVE EXTRACTION OF LANTHANUM, NEODYMIUM AND PRASEODYMIUM FROM SYNTHETIC LEACH SOLUTION USING PC-88A-TBP SYSTEM . . . 623
Esra BAŞTÜRKCÜ; Norman KELLY; A. Ekrem YÜCE; Servet İ. TİMUR

SELECTIVE METAL LEACHING FROM SmCo PERMANENT MAGNETS 629
Mert SARIKAYA; Fatma Elif GENCELI GÜNER; Şükriye Beste AYDIN

STRIPPING PRECIPITATION OF CALCIUM VANADATES FROM ORGANIC V(V) EXTRACTS 635
María Guadalupe SÁNCHEZ-LOREDO; Salvador Antonio PALOMARES-SÁNCHEZ; Paul CHEKHONIN; Doreen EBERT; Robert MÖCKEL; Norman KELLY; Ajay Bhagwan PATIL

SUSTAINABLE SYNTHESIS AND CHARACTERIZATION OF NANO ZINC BORATE FROM METALLURGICAL WASTE 643
Gülnihal AYGÜN; Hüseyin BAŞTÜRKCÜ; Bihter ZEYTUNCU GÖKOĞLU

THE POTENTIAL OF MINING AND PROCESSING OF ALBANIAN NICKEL LATERITIC RAW ORES 648
Genc DEMI; Fatos AHMATAJ

SYNTHESIS OF PSEUDOBROOKITE POWDER VIA OXIDATIVE CALCINATION OF ILMENITE FOR PHOTOCATALYTIC APPLICATIONS . . . 657
Yahya SORKHE; Onur OZTÜRK; Pegah BAVAFA; Fatma ARSLAN; Cüneyt ARSLAN

THE LEACHING KINETICS OF HIGH-GRADE ZINC SILICATE ORE IN SULFURIC ACID 672
Moloud NAZERI; Claudio ACUNA; Emad ABKHOSHK; Zahra RAZI

MANAGEMENT OF MINERAL PROCESSING TAILINGS

EVALUATION OF MINERAL PROCESSING AND HYDROMETALLURGICAL PLANT WASTES A COMPREHENSIVE ASSESSMENT WITH CASE STUDIES FROM TURKIYE 680
Gülay BULUT; Nursun ŞİRVANCI; Fatma ARSLAN

EVALUATION OF WASTE AND BY-PRODUCTS FROM THE ZONGULDAK HARD COAL BASIN WITHIN THE FRAMEWORK OF THE ZERO-WASTE APPROACH . . . 688
Mehmet BİLEN; Hayri VELİOĞLU; Haşim DURU; İhsan TOROĞLU

INVESTIGATION OF THE PERMITTING PROCESSES FOR ORE DRESSING AND WASTE STORAGE FACILITIES OF TÜRKİYE . . . 705
Ali Koray ÖZDOĞAN; Hakan AKINCI; Gizem ÖZDOĞAN

MINING WASTE AND CRITICAL RAW MATERIALS RECOVERY POTENTIAL FROM THE KURBNESH COPPER TAILINGS, ALBANIA . . . 712
Shahin BARAMAJ; Kristo RODI; Mimoza SIMIXHIU; Ledi MOISIU; Ana FOCIRO

PRODUCTION OF MAGNETITE CONCENTRATE FROM COPPER CONCENTRATOR PLANT TAILINGS . . . 719
Alperen KÖLE; Ahmet YAKAR; Yağız Kerem YALÇIN; Abdullah Erdem YILDIZHAN; Mustafa ÖZTÜRK; İbrahim GÖKTAŞ

SELECTIVE ACTIVATION OF COAL MINE TAILINGS AS SUPPLEMENTARY CEMENTITIOUS MATERIALS FOR SUSTAINABLE CONSTRUCTION 726
Serkan TUYLU; Deniz ADIGÜZEL; İsmail DEMİR; Mehmet Selçuk AVDAN

SPATIAL DISTRIBUTION OF SELECTED VARIABLES IN ARTANA TAILINGS FOR SUSTAINABLE MANAGEMENT 742
Naser PECI; Kemajl ZEQIRI; Berat SINANI; Nazmije SEJDIU

THE EFFECTS OF THE CHEMICAL STRUCTURE OF FLOCCULANTS ON FLOCCULATION IN MURGUL FLOTATION PLANT TAILINGS 752
Yağız ŞEN; Zafer GÖLLER; Gülay BULUT

BACKFILLING OF UNDERGROUND EXCAVATIONS WITH CEMENTED PASTE IN MODERN UNDERGROUND MINING 758
Sanja BAJIC; Rudolf TOMANEC; Ljiljana TANKOSIĆ; Dragoljub BAJIC; Josip ISEK

MATERIAL ANALYSIS AND MINERAL CHARACTERIZATION

ANALYSIS OF ACCIDENTS IN UNDERGROUND MINES IN ALBANIA **764**
Shahin BARAMAJ; Lavdie MOISIU; Mimoza SIMIXHIU; Dhurim KURTI

ANTHROPOGENIC RAW MATERIALS PROCESSING APPLICATION EXAMPLES FOR THE CONSERVATION OF NATURAL RESOURCES **771**
József FAITLI

BEHAVIOR OF ULTRA-HIGH PERFORMANCE FIBER CONCRETE BASED ON RECYCLED GRANITE WASTE FILLERS . . **778**
Houria HEBHOUB; Said BERDOUDI; Nouha REZAIGUIA; Nedjma MEZIANI; Mohammed I. BENHALILOU; Bilal BOULKENAFET

CEMENT MAKING BY USING THE GEOCEMENTING CONCEPT **784**
Hakan ARDEN KAHRAMAN; Hakan BENZER

CHARACTERIZATION AND PROPOSED MINERALURGICAL PURIFICATION METHODS FOR FELDSPAR FROM AÏN BARBAR, EASTERN ALGERIA **797**
Assia BOUTEMEDJET; Zohir MEKTI; Ghofrane BOUDRAA; Fatima Zohra BOUGHABA

CHARACTERIZATION OF CONSTRUCTION AND DEMOLITION WASTES FOR VALORIZATION AS RAW MATERIALS RESOURCE **802**
Hikmet SİS; Murat ERDEMOĞLU; Tufan KIYAK; M. Kürşat AYDEMİR; Kader ŞENTÜRK; Mustafa BİRİNCİ; İsmail BENTLİ; Didem EREN SARICI; Sema ERDEMOĞLU

CHARACTERIZATION OF MANGANOFERROUS (Fe-Mn) OXIDE ORE FROM TURKIYE-ŞIRNAK REGION **810**
A. Ufuk DENİZ; Arman EHSANI; Fatih ÇAVUŞLU; Ilhan EHSANI

DIRECT RECYCLING OF GRAPHITE LINKING MINERAL PROCESSING WITH NANOSTRUCTURAL RESTORATION . . . **818**
Eray TABAK; Recep BAKAR; Sadullah ÖZTÜRK; Şahika Sena BAYAZİT; Birgül BENLİ

INFLUENCE OF ROCK WEATHERING DEGREE ON PROCESSING EFFICIENCY AND PRODUCT QUALITY IN AGGREGATE QUARRIES **830**
Danciu CIPRIAN; Camelia TRAISTĂ

PROCESS MINERALOGY INSIGHTS INTO BENEFICIATION OF RARE EARTH CARBONATITE ORES . . **838**
Ezgi AKYILDIZ; Camilo M. SILVA; Stefanie LODE; Kornel TOBICZYK; Przemyslaw B. KOWALCZUK

PROFESSIONAL RISK ASSESSMENT IN MINERAL PROCESSING **848**
Marija HADZI-NIKOLOVA; Dejan MIRAKOVSKI; Afrodita ZENDELSKA; Nikolinka DONEVA

SELECTION OF AN APPROPRIATE TECHNOLOGY FOR FLOTATION TAILINGS DISPOSAL USING THE SAW METHOD **854**
Afrodita ZENDELSKA; Nikolinka DONEVA; Marija HADZI-NIKOLOVA; Dejan MIRAKOVSKI; Blagoj GOLOMEOV

SOME CHARACTERISTICS OF CHROMITES IN THE TROPOJE – HAS – GJAKOVE MASSIF AND THEIR FEATURES FOR ENRICHMENT **862**
Ibrahim MILUSHI; Genc DEMI; Edmond PLLANA

STATISTICAL AND GEOSTATISTICAL ANALYSIS OF SELECTED TECHNOLOGY-CRITICAL ELEMENTS IN THE TREPÇA MINE AND THEIR CORRELATION WITH Pb-Zn MINERALIZATION **871**
Berat SINANI; Milazim DEMAKU; Naser PECI; Bahri SINANI; Mehmet BİLEN

STRUCTURAL DATA AND CHROMITE ENRICHMENT CHARACTERISTICS IN THE ULTRABASIC MASSIF OF LUBOTEN, KOSOVO **881**
Edmond PLLANA; Ibrahim MILUSHI; Genc DEMI

TECHNICAL EVALUATION OF AN ADDITIONAL GOLD EXTRACTION TECHNOLOGY **889**
Nikolay NESTOROV; Irena GRIGOROVA; Teodora YANKOVA; Mihail PETROV

THE IMPORTANCE OF ZETA POTENTIAL MEASUREMENT IN THE FLOTATION OF DIASPORA AND CALCIUM MINERALS . . **897**
Yaşar Hakan GÜRSOY; Abdullah FİLAR; Yakup UMUCU

THE PETROGRAPHIC CHARACTERIZATION OF THE URANIUM ORE OF TAHAGGART, EL-HOGGAR, SOUTHEAST OF ALGERIA . . **913**
Zohir MEKTI; Fatima Zohra BELAID; Assia BOUTEMEDJET; Said BERDOUDI

MINING OPERATIONS (OPEN-PIT, UNDERGROUND, SOLUTION MINING) RELATED TO MINERAL PROCESSING

NATURAL SODA ASH PRODUCTION THROUGH IN-SITU LEACHING: OPERATIONAL FRAMEWORK FROM KAZAN SODA PLANT **926**
Erdem KUMRUOĞLU; Engin OCALAN; Barış KANDEMIR

STUDY AND EVALUATION OF CURRENT PILLAR DESIGN USING DIFFERENT APPROACHES –ALGERIA **939**
Said BERDOUDI; Houria HEBHOUB; Nouha REZAIGUIA

MODELING, SIMULATION, CONTROL AND AUTOMATION IN MINERAL PROCESSING

APPLICATION OF DATA ANALYTICS IN MINERAL PROCESSING TOWARDS DIGITAL PERFORMANCE PREDICTION AND PROCESS OPTIMIZATION **949**
Oğuzhan Mert GÜRKAN; Hüseyin BAŞTÜRKCÜ

APPLICATION OF THE RESPONSE SURFACE METHODOLOGY (RSM) TO THE ENRICHMENT OF ESPEY COLEMANITE WASTES BY MICROWAVE **959**
Arzu KAHVECİOĞLU; Kırali MÜRTEZAOĞLU; Zehra ZEYBEK; Ahmet AYDIN

DIGITAL APPROACHES TO SUSTAINABLE MINERAL PROCESSING MATLAB-BASED SIMULATION OF SENSOR-ASSISTED ORE SORTING **969**
Ali Cemal TANRIKULU; Birgül BENLİ

MODELLING OF MULTI GRAVITY SEPARATOR (MGS) FOR FINE LIGNITE CLEANING BY CENTRAL COMPOSITE DESIGN (CCD) METHOD **976**
Derya OZ AKSOY; Sabiha KOCA; Hüseyin KOCA

NUMERICAL PREDICTION OF IMPACT AND SHEAR ENERGY PROFILES ON MILL LIFTERS **983**
Hüseyin Efe SELVI; Tahir Abbas JAUHAR; Yusuf Enes PURAL

PHYSICAL AND PHYSICOCHEMICAL PROCESS SIMULATION AND MODELLING TO BENEFICIATE LITHIUM FROM NEPHELINE SYENITE ROCKS **989**
Zeynep ÜÇERLER ÇAMUR; Ozgul KELES; Murat Olgaç KANGAL; Marie-Véronique DURANCE; Stephane BROCHOT; Manuel GONZALEZ; Lucas REGNAULT

REALISING THE SMART GRINDING MILL OPTIMISING MILL PERFORMANCE THROUGH REAL-TIME LIFTER BAR WEAR MONITORING AND PREDICTIVE MAINTENANCE PLANNING **1000**
Ahmet ALTUNCU; Büşra ÇALIŞKAN; Ufuk KOÇBIYIK; Oğuzhan ÇAKIR; Ayhan YAZGAN; Uğur ŞEVİK; Tolga BERBER; Oğuzhan BAŞER; Ersin Yener YAZICI; Oktay CELEP

TONNEX A CONTRACT-DRIVEN DIGITAL ECOSYSTEM FOR MINERAL PROCESSING OPERATIONS **1007**
Hasan Berke AKKÖSE; Hayri Atalay KUL

TOWARD AUTONOMOUS MINERAL SORTING INTEGRATING MACHINE LEARNING AND ROBOTICS IN ORE PROCESSING **1014**
Alexandru MIHAI; Mihai CULEA; Adriana BURLIBASA; Gabriela IORGA; Victor MIHAI

PHYSICAL CONCENTRATION METHODS

ANALYSIS OF SETTLING MACHINE PERFORMANCE AS A FUNCTION OF PARTICLE SIZE AT RMU “BANOVIĆI” D.D. BANOVIĆI **1028**
Nedžad ALIĆ; Admir SOFTIĆ; Semir MEHIC

BENEFICIATION OF A HIGH-GRADE LATERITIC NICKEL ORE BY PHYSICAL SEPARATION METHODS **1046**
Yunus Emre ÇAVDAR; Hüseyin BAŞTÜRKCÜ

CASSITERITE FINES RECOVERY FROM JIGGING TAILINGS USING SHAKING TABLES **1053**
Cirila Raquel de Araújo Gomes e SILVA; Igo Marinho Serafim BORGES; Jaquelynne Cassia de AMORIM; Wesley Oliveira LEMOS; Luís Felipe Schons SILVA; Elenice Maria Schons SILVA; André Carlos SILVA

COMPARISON OF WET AND DRY MAGNETIC SEPARATION IN THE BENEFICIATION OF QUARTZ ORES **1064**
Arda ARAPOĞLU; Oğuzhan Mert GÜRKAN; Ali Kaan ACAR; Emre UĞURLAR; Hüseyin BAŞTÜRKCÜ

DESCRIPTION AND ANALYSIS OF THE TECHNOLOGICAL PROCESS OF THE KALIMASH IMI CHROMIUM ENRICHMENT PLANT 1071
Ferhat AKINOGLU; Genc DEMI

DRY BENEFICIATION OF MINERAL ORES USING TRIBO-ELECTROSTATIC BELT SEPARATION 1077
Abhishek GUPTA; Tom NEWMAN; Frank HRACH

EFFECT OF GRAVITY CONCENTRATOR PERFORMANCE ON CIL EFFICIENCY AND OVERALL GOLD RECOVERY 1088
Cumhur Erdem KARAHAN; Fehmi Can SUTER; Durmuş Ali KIZILCADAM; Kasım MEYDANAL

EVALUATION FOR THE PROFITABILITY OF A CHROMIUM ENRICHMENT PLANT CONSTRUCTION . . 1094
Genc DEMI; Aida BODE

PROCESS IMPROVEMENT OF A CHROMIUM ENRICHMENT PLANT 1103
Genc DEMI; Safet BOCI

RESEARCH ON THE RECOVERY OF LEAD AND IRON FROM THE SLAG OF A LEAD-ACID BATTERY RECYCLING PLANT USING PHYSICAL METHODS 1111
Tülin ULUCAN; Nazlım İlkyaz DİNÇ; Şevval YILDIRIM; Kerem BÖLÜKBAŞ; Fırat BURAT

UPGRADING OF LOW-GRADE TITANIUM ORES BY HIGH-INTENSITY MAGNETIC SEPARATION: A CASE STUDY FROM ESKİŞEHİR, TÜRKİYE . . 1121
Ulaş USLU; Yusuf Enes PURAL; Mustafa ÖZER

THE ROLE OF TOMRA´S XRT-BASED ORE SORTING IN METALLIC ORE PROCESSING 1129
Carolina VARGAS

PLANT AND PROCESS DESIGN AND OPERATING PRACTICE

APPLICATION OF NEW TECHNOLOGIES - A NECESSITY FOR BENEFICIATION OF ALBANIAN CHROMITE ORES 1130
Kimet FETAHU; Bukurosh KOCI; Ekita TOSKA

BULK SOLIDS HANDLING THE OVERLOOKED DRIVER OF PLANT PERFORMANCE 1136
Enes KAYA

DIGITAL PROTOTYPING AND SEQUENTIAL ASSEMBLY SIMULATION FOR A RAYMOND MILL INSTALLATION 1144
Doğan DEMİROK; Ahmet TANRIKULU

REAGENT OPTIMIZATION FOR COST-EFFECTIVE AND SUSTAINABLE GOLD PROCESSING AT GOLD FIELDS GHANA, TARKWA MINE . . . 1150
Michael Mawuenyega Kwame KUATSIENU; Maria SINCHE-GONZALEZ; Prince Pappoe AWOTWE; Eric ANDERSON

UPGRADING ULTRA-LOW-QUALITY LIGNITE THROUGH WASTE HEAT–DRIVEN FLUIDIZED BED DRYING AND DENSITY-BASED SEGREGATION . . . 1156
Harun BILIRGEN; Fatma BILIRGEN

VALIDATION OF PROCESS SIMULATION THROUGH LOCKED CYCLE TEST AND PILOT FOR NORDIC TALC PLANT DESIGN 1166
Erdem ÖZDEMIR; Erkki KURONEN; Heikki VAUHKONEN; Vesa-Pekka TAKALO; Juha SAARI; Mikko RANTAMAKI

PROCESSING OF INDUSTRIAL MINERALS

A HYBRID MICROWAVE-THERMAL METHOD TO OPTIMIZE THE GRINDING OF MOIST CLAY MINERALS 1175
Doğan DEMİROK

A REVIEW ON THE RECOVERY OF RARE EARTH ELEMENT (REE) RESOURCES OF TURKİYE 1181
İlgin KURŞUN; Mert TERZİ; Can GUNGOREN; İsmail DEMİR; Osman YAVUZ

A STUDY ON UNDERSTANDING OF THE BEHAVIOR OF CALCIUM AND MAGNESIUM IMPURITIES ON THE BORAX PENTAHYDRATE CRYSTALLIZATION . . 1195
Şahan GÜL; Haldun KURAMA

ENRICHED HUNTITE AS A GREEN FLAME RETARDANT THERMAL AND PHYSICAL BEHAVIORS IN POLYURETHANE MATRICES . . 1202
Tülay TÜRK; Birgül BENLİ; Murat Olgaç KANGAL

STRUCTURAL AND MORPHOLOGICAL ROLES OF CLAY-BASED CATALYSTS FOR GREEN HYDROGEN GENERATION **1209**
Helin HAZAR; Zeynep Burçak ŞAHİN; Birgül BENLİ

SOIL REMEDIATION

SOIL CONTAMINATION FROM THE IMPACT OF THE PIM INDUSTRIAL LANDFILL, MITROVICA **1217**
Elona IDRIZI

PLENARY PAPERS

REVIEW OF THE CONCEPT AND MEASUREMENT OF HYDROPHOBICITY

Cyril T. O'CONNOR*

Centre for Minerals Research, Department of Chemical Engineering, University of Cape Town, Cape Town, South Africa
**Corresponding author: Cyril.oconnor@uct.ac.za*

A B S T R A C T

One of the most important of all physiochemical phenomena is the interaction of water with solid surfaces. When the solid favours adsorbing water it is hydrophilic or if it repels water it is hydrophobic. Such interactions constitute the basis of many important processes especially in mineral beneficiation. For example, flotation relies on the extent to which a particle is sufficiently hydrophobic to attach to a bubble and rise to the surface of a flotation cell. This paper reviews the fundamentals defining the hydrophobicity of mineral particles which incorporates the concepts of surface energy, surface tension, roughness, interfacial energy and work of adhesion of water. It discusses the origins of natural hydrophobicity and how reagents such as collectors are able to impart hydrophobicity to a mineral particle. It will present a review of the various methods used to measure and quantify hydrophobicity which includes methods other than contact angle, which is traditionally used for that purpose, such as the use of the heat of immersion and the concept of excess Gibbs energy. Finally, it will address briefly the mechanisms proposed to explain how the hydrophobic particle attaches to a bubble which is ultimately fundamental to the flotation process.

Key words**:** *Hydrophobicity, flotation, surface energy, interfacial energy, contact angle, heat of immersion, excess Gibbs energy*

1. INTRODUCTION

The interaction of water with substances is arguably one of the most important and pervasive of all physicochemical processes. Depending on their propensity to either interact positively or not with water, such substances are generally characterized as being either hydrophilic or hydrophobic. The term hydrophobic comes from a Greek word combining hydro, which means water, and phobic which means fear or repel. Its opposite is hydrophilicity ("water loving"). Another term for hydrophobic is lipophilic which is the propensity of water to absorb in lipids or fats. In liquid phase systems a substance which is hydrophobic will be attracted to the lipid phase rather than remain in the water phase. For example, this is the basis underlying the pharmacological behaviour of drugs in the body. In a solid-liquid-gas system, such as those that occur in the flotation process, solids which are hydrophobic will preferably be attracted to the gas/air phase (the bubble) rather than remain dissolved in water.

Hydrophobicity essentially arises from the disruption of the intermolecular structure of water molecules within a continuous water phase. In the liquid phase water molecules interact through van der Waals forces as well as hydrogen bonding. When specific molecules adsorb on the surface of a substance such as a mineral particle it can cause this disruption of the structure of the water continuum and hence induce hydrophobicity. As is well known flotation is a critically important process in the concentration of minerals and almost 90% of the world's ores are beneficiated using flotation. Flotation is based on the principle whereby a mineral particle is either naturally hydrophobic or is rendered so by adsorption of a reagent such as a collector thus causing the particle-collector aggregate to be repelled from water and consequently attach to an air bubble.

This review will firstly address the origin of natural hydrophobicity of solids and will explain how this is related to solid state characteristics such as surface energy, surface tension and roughness. This will be followed by showing how collectors adsorbed on a mineral result in the mineral becoming hydrophobic. Finally, methods used to quantify hydrophobicity will be reviewed.

2. FUNDAMENTALS: SURFACE ENERGY, SURFACE TENSION, ROUGHNESS, WORK OF ADHESION

Surface energy is variously defined as the energy generated due to the disruption of intermolecular bonds that occur when the surface of a solid material is created. It thus follows that the atoms on the surface of a solid have more energy than the fully bonded atoms in the bulk. The surface energy is thus frequently defined as the excess energy at the surface of a material compared to the bulk where all bonds between atoms are filled. Essentially it is the work required to cleave the bonds of a material in creating a fresh surface. It follows from this that the surface of a material will have different interactions with water molecules or molecules with various molecular structures such as alcohols. One of the most widely used methods of calculating surface energy is the Zisman model. This model assumes that the surface energy of a solid is equal to the maximum surface tension liquid that will give a contact angle (θ) of 0°. This is known as the critical surface tension. (Fox and Zisman, 1950). In this method the contact angle of a mineral particle is determined for a variety of reagents adsorbed on the mineral and a plot is made of the cos θ against the surface tension of the reagent used. The value of the surface tension measured when the plot is extrapolated to cos θ = 1 (θ=0°) is equal to the surface energy of the solid being tested. The extent to which a liquid will bond to a mineral surface will be determined by the relationship between the relative strength of the bonds between the molecules constituting the liquid (which is related to its surface tension) and the bonds between the liquid molecules and the solid surface (which is related to the solid surface energy). Clearly when the former bond strength is stronger than the latter the liquid will adsorb very weakly on the solid surface and vice versa. Hence when a liquid is in contact with a solid surface there will be a competition between cohesive intermolecular forces in the liquid which results in the liquid molecules being preferentially attracted to each other compared to the forces between the liquid molecules and the surface atoms of the solid. In other words there is an interaction between surface tension of the liquid and the surface energy of the solid. If the adhesive forces between the liquid molecules and the surface atoms are greater than the cohesive forces between the liquid molecules then the wettability of the surface will be preferred and vice versa. Thus, in the case of water, which has a relatively high surface tension (72mN/m) meaning that the intermolecular bonds are relatively strong, hydrophobicity will occur when those bonds are stronger than the bonding strength on a surface where the surface energy is relatively weak.

These interactions result in different degrees of hydrophobicity which is frequently indicated by different contact angles. Relatively higher cohesive forces will result in the liquid being pulled into a spherical shape and yield a relatively high contact angle and be termed hydrophobic. The opposite condition is indicated by the particle being termed hydrophilic (Fig. 1).

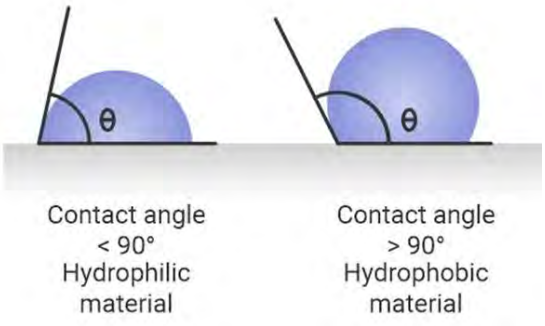

Figure 1. The relationship between contact angle and hydrophobicity/hydrophilicity (https://measurlabs.com/methods/contact-angle-measurement/)

It is thus the balance between these fundamental forces of cohesion and adhesion which underlies the concept of hydrophobicity or hydrophilicity, the former being favoured when the cohesive forces are dominant and vice versa for the latter.

Another attribute of a surface which is important in the context of hydrophobicity is surface roughness. The surface roughness is frequently determined using atomic force microscopy. It has been shown that as roughness increases, the adhesive forces between the liquid and solid decreases and thus the surface becomes more hydrophobic with higher contact angles compared to a smooth surface. Figure 2 illustrates the relationship between surface energy, roughness and contact angle, the latter being an indication of hydrophobicity. It can be seen that surface energy decreases as roughness increases from 0.13 to 3.21 and that this corresponds to an increase in contact angle (from ~93° to ~128°) or greater degree of hydrophobicity.

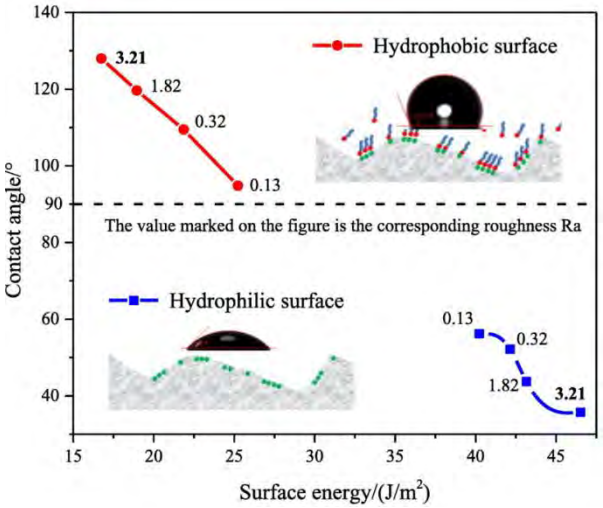

Figure 2. The relationship between surface roughness, surface energy and wettability for the natural hydrophilic mineral surface and hydrophobic surface modified by NaOL(3×10−4 mol/L) (Wang and Zhang, 2020) (Reprinted with permission)

Work of adhesion is the work required to remove water from the solid surface leaving an adsorbed layer of water in equilibrium with a saturated gas (air) phase. Clearly therefore work of adhesion will be low for hydrophobic surfaces meaning that the water is not strongly bound to the surface. Hence if the work of adhesion is low it follows that the solid is essentially hydrophobic and thus will readily attach to a bubble. The extent of the interaction between particles and bubbles immersed in water is known as the interfacial energy ΔG_s . The

thermodynamic criterion for bubble-particle attachment in flotation is given by the Young-Dupre equation:

$$\Delta G_s = \gamma_{sv} - \gamma_{lv} - \gamma_{sl} = \gamma_{lv}(\cos\theta - 1) < 0 \quad (1)$$

where ΔG_s = the interfacial energy (J/m^2); γ = the surface tension (N/m); θ = the contact angle and s,v,l denote the solid, vapour and liquid phases. The criterion for spontaneous bubble-particle attachment is that the interfacial energy is less than zero ($\Delta G < 0$) and hence that $\theta > 0$ ($\cos\theta < 1$). Clearly the more negative the value of ΔG, the greater the probability of bubble-particle attachment and subsequently of flotation occurring.

The VGC model, developed by Van Oss, Chaudhury and Good (1988), has been useful in characterising the surface energetics of solids using the contact angle as an input parameter. This model asserts that the surface tensions of solids and liquids can be categorised into two additive components, viz. Liftshitz-Van der Waals component and the Lewis acid/base components. The major assumptions of the VGC model are that the Liftshitz-Van der Waals forces do not interact with polar forces and acidic forces only interact with basic forces.

Table 1 shows the relationship between the interfacial energy and work adhesion for a range of minerals. Clearly the lower the work of adhesion the lower is the interfacial energy or the more favourable is the probability of particle – bubble attachment all of which is consistent with the concept of hydrophobicity. The magnitude of the interfacial Gibbs energy is a quantitative measure of wettability (hydrophobicity / hydrophilicity) (van Oss and Giese, 1995).

Table 1. Interfacial energy and work of adhesion for the interaction of water with various minerals (Taguta, 2018)

Mineral	Interfacial energy (mJ/m2)	Work of adhesion(mJ/m2)
Talc	-42	194
Realgar	-24	212
Galena	113	347
Albite	198	434
Mica	307	543
Wollastonite	2363	2600

It is important to note that hydrophobicity may naturally arise due to the mineralogical characteristics of the ore. The reason for the natural hydrophobicity and subsequent floatability of sulphide minerals in particular has also been widely researched. It has been reported by Gardner and Woods (1979) that sulphide mineral oxidation leaves a sulphur-rich layer on the mineral surface which is naturally hydrophobic and this is generally accepted as being the reason for the natural hydrophobicity of sulphide minerals.

3.QUANTIFYING HYDROPHOBICITY

3.1. Contact Angle as an Indication of Hydrophobicity

Contact angle measurements have been the traditional method used to determine the hydrophobicity of a solid. Traditionally it is measured using a goniometer which is an instrument using the sessile drop method which is an optical technique to measure liquid-solid wetting by placing a liquid drop on a surface, capturing its profile with a camera, and using software to calculate the contact angle.

Numerous studies have been undertaken on contact angle measurements to predict hydrophobicity and often these are related to the relationship between spreading coefficient

and the interfacial tensions (e.g. Kitchener 1960; Leja and Poling, 1960). Other studies have focused on the relationship between contact angle and flotation recovery and the general area of wetting (Read and Kitchener, 1967; Finch and Smith, 1972; Kelebek et al, 1986). However, as Nagaraj and Ravishanker (2007) have pointed out, contact angles determined on a polished flat surface serve little purpose in predicting flotation recovery of real minerals since such surfaces are hardly representative of real ore samples which are typically highly heterogeneous. Moreover it is worth noting that the Young-Laplace equation is entirely theoretical and cannot be applied to real systems. Leja and Poling (1960) have suggested that the contact angle is simply an indication of the extent to which the given solid-liquid-air system is utilizing the available free energy of interfaces in the bubble deformation process. This limitation, however, does not detract from the general utility of the contact angle as a useful indicator, but not a measure, of the hydrophobic character of solids.

3.2. Heat of Immersion

The enthalpy/heat of immersion can be used to characterise the surface energetics of different minerals. This is because the chemically different sites present in on a mineral surface will interact differently with probe liquids of different polarities. Using the enthalpy of immersion, the application of the Van Oss, Good and Chaudhury (VGC) model, referred to above, then allows the calculation of the surface energetics of the minerals (van Oss et al, 1988).

The heat of immersion is the heat given off when water interacts with a solid surface. It has been established that a theoretical relationship exists between the enthalpy of immersion and contact angle (Melrose, 1965) (Eqn.2) and hence this property should be an indicator of hydrophobicity.

$$\Delta H_{imm} = T\gamma \ (d\ cos\theta)/dT - (\gamma_{lv} - T\ (d\gamma_{lv})/dT) cos\theta \quad (2)$$

where ΔH_{imm} = enthalpy of immersion; T = temperature; γ_{lv} = liquid-vapour surface tension; θ= contact angle. A simplified form of this relationship for low energy (high hydrophobicity) surfaces was developed by Spagnolo et al (1996). This is shown in Eqn 3.

$$cos\theta = (-0.07T + \Delta H_{imm})/\gamma_{lv} \quad (3)$$

Heat of immersion is determined using a microcalorimeter. Figure 3 shows a plot of the measured heats of immersion of immersion for a range of pure minerals as well as for galena samples treated with a xanthate collector (% coverage shown) and a realgar sample with 25% xanthate coverage. The results are correlated with the first order flotation rate constant obtained using a microflotation cell. It is clear that the rate of flotation in the microflotation cell, which as will be shown below is an important indicator of the hydrophobicity of the particles, is strongly related to the heat of immersion. The reaction between water and the surface of the mineral is exothermic which results in a very negative value of $-\Delta H_{imm}$ implying that the surface is very hydrophilic and hence unlikely to report to the concentrate in a microflotation cell. The major advantage of using heat of immersion is that the particles being investigated are real particles typical of those treated on a plant and that $-\Delta H_{imm}$ is a direct measurement of hydrophobicity/hydrophilicity. The results shown in Figure 3 suggest that when heats of immersion are more positive than approximately -200 mJ/m^2 the particle or the collector-treated particle has become sufficiently hydrophobic to report to the concentrate in a microflotation cell.

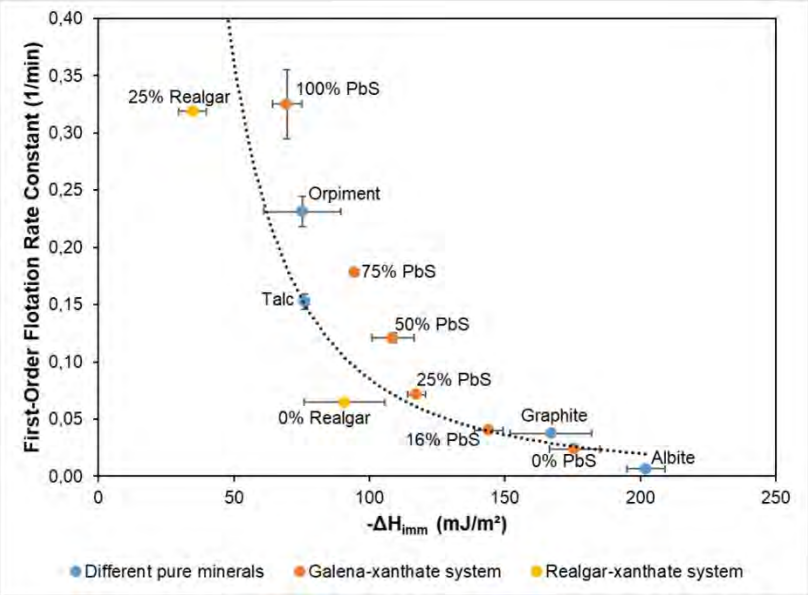

Figure 3. Combined enthalpies of immersion of the model system (galena / amyl xanthate system) and different pure minerals in water – the floatable region (Taguta et al., 2016)

3.3. Washburn Method

The Washburn method dates back to 1921 (Washburn, 1921). It has the advantage of using real powders and is based on the use of capillary pressure to drive a fluid at an observable rate through a packed bed of the powder in a capillary tube. The increase in the mass of the tube, which is suspended from a force sensor, is determined with respect to time during the measurement. The contact angle is then determined using the Washburn equation. This method however has a number of limitations. It is not a fundamental physical quantity since the contact angle is inferred from the surface energies. It is also difficult to obtain reproducible contact angle values or to measure the contact angle for very hydrophobic particles with large contact angles using pure water. Another disadvantage of this method is that the experiments are tedious and time-consuming.

3.4. Determining the Hydrophobicity of Particles Made Hydrophobic by Adsorption of a Collector

Flotation collectors are molecules with a polar and non-polar end. Typically, collectors which used in the flotation of a mineral consist of a polar end which results adsorbs onto the mineral surface via chemical bonding or otherwise following a series of redox reactions. The non-polar end is typically a hydrocarbon species. The reason why collectors impart hydrophobicity is because this hydrocarbon moiety is hydrophobic and its hydrophobicity is based on the thermodynamic concept of excess Gibbs energy. As seen in the Young Dupre equation (Eqn. 1) the interfacial energy is dependent on the interfacial tensions of the solid, liquid and vapour phase and these can be manipulated by the use of collectors. Collector adsorption lowers the surface tension of a given mineral surface, thus increasing the contact angle, i.e. the hydrophobicity, of a mineral surface. This renders the value of interfacial energy more negative and thus promotes bubble-particle attachment. By adsorbing specific collector molecules on the surface of mineral particles a particle can hence be made hydrophobic.

Typically in the case of sulfides, xanthates or their oxidation product, viz.dimers, perform this function. Similarly amines do the same to oxide minerals. Hydrophobicity thus arises when water molecules are prevented from forming hydrogen bonds with the solid. Hence once a collector has adsorbed onto a solid the molecules extending into the water phase are hydrocarbons which do not readily mix well with water. An ideal binary mixture is one in which

each of the two substances continue to behave as if they were on their own. However when the behaviour of the components is such that they do not readily mix this results in the formation of a non-ideal mixture. Mixtures of water and hydrocarbons are typical of such non-ideal mixtures. The extent to which a mixture deviates from ideal behaviour is quantified using the thermodynamic concept of excess Gibbs energy which is related to the activity coefficient as shown in eqn. 4 where the subscript i refers to component i in the mixture, R is the universal gas constant, γi is the activity coefficient of component i, and T and P are the temperature and pressure of the system.

$$\Delta G_i^{ex} = RT \ln \gamma_i (T,P,x) \quad (4)$$

Hence by determining the activity coefficient of the hydrocarbon in the hydrocarbon-water mixture, its non-ideality, viz. its propensity to migrate from the water phase to the gas phase, as given by ΔG_i^{ex} , is determined. This is a direct measure of the hydrophobicity of the solid-collector aggregate. There are various well-known models for calculating activity coefficient the most efficient being the use of the UNIFAC (Uniquac Functional-group Activity Coefficient) method (Fredenslund et al. 1977; Fredenslund et al. 1975).

In the application of this method the alcohol of the hydrocarbon is an adequate proxy for the hydrocarbon moiety of the collector. For example, an isobutyl alcohol-water mixture mimics the interaction of the isobutyl component of the collector isobutylxanthate with the surrounding water. Numerous investigations (O'Connor, 2012) have been carried out to validate this approach by relating the excess Gibbs energy, as obtained from the activity coefficient, to the hydrophobicity as indicated by contact angle. Figure 4(a) shows the relationship between contact angle and excess Gibbs energy for a sylvite – amine system for amines of different carbon chain lengths. Figure 4 (b) shows the relationship between recovery and excess Gibbs energy for a galena – xanthate system for xanthates of different chain lengths.

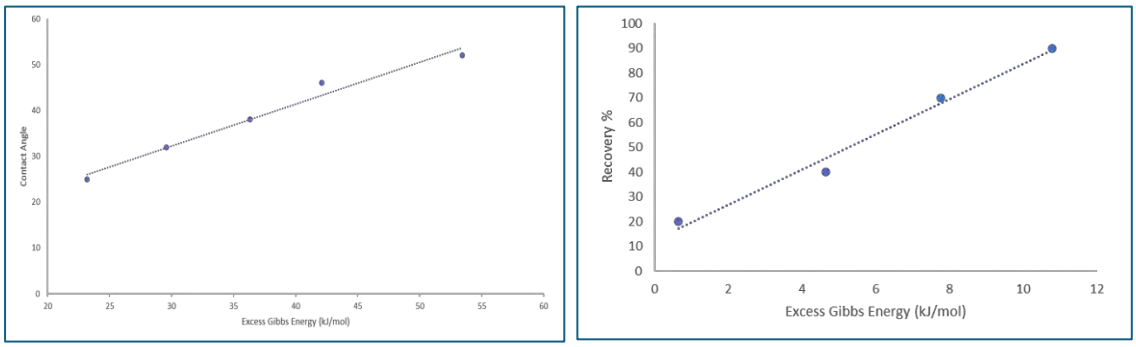

(a) (b)

Figure 4(a): Contact angle vs Partial molar excess Gibbs energy for sylvite- amine system (C8-C18 amines) (Fuerstenau and Fuerstenau, 1956); (b): Relationship between recovery of galena and the partial molar excess Gibbs energy of different xanthates (methyl, ethyl, isopropyl and butyl) (Gaudin, 1928)

It is clear that the use of excess Gibbs energy is a robust indicator of hydrophobicity and hence of recovery in a microflotation cell and has the advantage that it is based on fundamental intermolecular forces.

3.5. Microflotation

The first reports correlating microfloation recovery to contact angle were published in a seminal paper by Gaudin and Fuerstenau (1955) in which they correlated contact angle with microflotation recovery for a quartz-amine system (Figure 5) although Gaudin had already earlier used such a device to examine the recovery of galena for various xanthates (Figure … (b); Gaudin 1928)

In Figure 5 the x-axis represents pH changes. Fundamentally, in a well-controlled microflotation experiment, recovery is a simple indication of the extent to which a particle can adhere to a bubble and report to the concentrate in an essentially quiescent regime. The particles used are greater than about 40μm (to avoid entrainment) and the recovery is directly related to the hydrophobicity of the mineral particle. In this figure the contact angle, surface coverage and recovery increase in a similar manner. Interestingly both the contact angle and zeta potential show a hysteresis behaviour which has been discussed elsewhere at length.

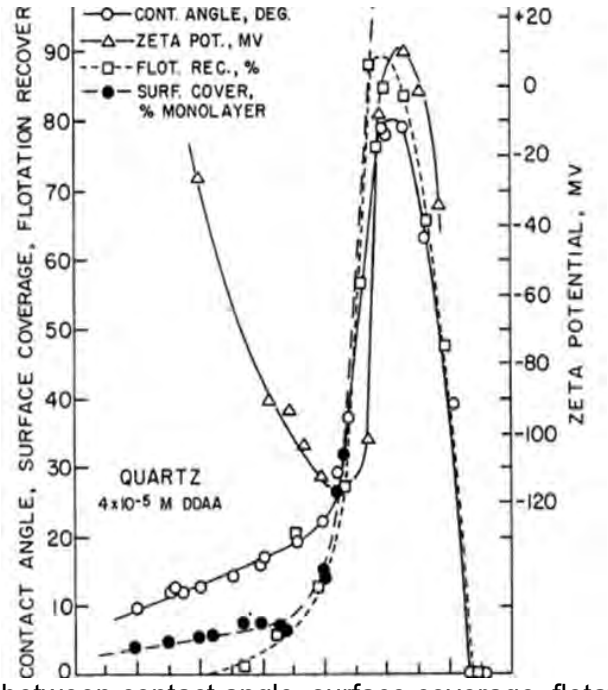

Figure 5. Relationship between contact angle, surface coverage, flotation recovery and zeta potential for a quartz-amine system as a function of pH (Gaudin and Fuerstenau, 1955).

3.6. Other Methods to Determine Hydrophobicity

Various other methods have been proposed for measuring hydrophobicity, One of these uses the concept of inverse gas chromatography. In this method the chromatographic column is composed of the mineral particles. Water vapour is passed through the column and the degree of hydrophobicity of the mineral will determine the extent to which the water molecules are adsorbed or retarded in passing through the column. Hence the retention time of the water vapour in the column is an indicator of the work of adhesion which of course is related to the hydrophobicity since, as shown above, the stronger the work of adhesion the lower the hydrophobicity. This method has also been used to determine surface energy of quartz. (Mohammadi-Jam and Waters, 2014). Other methods include thin layer wicking (TLW) which is really a version of the Washburn Method (Chibowski and González-Caballero , 1993). TOF-SIMS has also been used to determine hydrophobicity. This is not a direct method to determine hydrophobicity but attempts to correlate TOF-SIMS signals with the values of contact angles determined using the Washburn method (Brito de Abreu and Skinner, 2011).

4. ADSORPTION OF HYDROPHOBIC PARTICLES TO A BUBBLE

A review of the mechanism whereby a particle which is hydrophobic adsorbs on a bubble warrants an entire paper. The process of bubble–particle interaction is usually divided into three subprocesses, including collision, adhesion and detachment. The latter two are of specific interest here. The particle-bubble collision in the flotation cell takes place in milliseconds during which the disjoining film separating the particle and bubble must thin and

burst for the particle to adhere to the bubble. The surface forces which influence the stability of thin liquid films between air bubbles and mineral surfaces can be described by extended Derjaguin-Landau-Verwey-Overbeek (DLVO) forces. These are the double-layer electrostatic force, the van der Waals forces and the hydrophobic forces.

Under the conditions employed in flotation both the bubbles and particles are generally negatively charged. Therefore, it is unlikely that electrostatic forces are responsible for the rupture of wetting films. Moreover, Van der Waals dispersion forces in wetting films are repulsive. It is thus speculated that there must be a third force, other than the electrostatic and van der Waals dispersion force, that is responsible for the bubble–particle adhesion. This force is called the “hydrophobic force” which is an attractive force. (Yoon, 2000). The hydrophobic force reduces the energy barrier between the bubble and the particle and dominates the process. It has been proposed that this force may be due to water forming clathrate cages for guest molecules (Eriksson and Yoon, 2007).

5. CONCLUSION

As already indicated the interaction of water with solids is of fundamental importance in many processes such as flotation. This review has shown how hydrophobicity of a solid is related to the concept of surface energy which in turn is related to surface tension as illustrated by the Zisman model. The interaction of water with a solid can also be quantified by determining the interfacial energy and the work of adhesion using the OGC model. The most common method of quantifying hydrophobicity has been the use of contact angle. However it is shown that other more direct measurements of solid-water interactions such as determining the heat of immersion may provide a more fundamental indication of the hydrophobicity of a solid. In a similar manner using the concept of excess Gibbs energy and activity coefficient may provide a more fundamental description of the extent to which collectors render a particle hydrophobic. Finally, since in flotation the ultimate main objective is to achieve particle-bubble attachment, the mechanisms whereby this attachment occurs are briefly alluded to with special reference to the concept of hydrophobic force.

REFERENCES

Brito de Abreu, S., Skinner, W., (2011) “Predicting the surface chemistry contribution to the flotation recovery of chalcopyrite by ToF-SIMS”, Minerals Engineering, 24 (2) 160–168.

Chibowski, E., González-Caballero, F., (1993) “Theory and practice of thin-layer wicking”, Langmuir, 9, 330–340.

Eriksson, J. C., Yoon, R. H., (2007) “The nature of hydrophobic attraction forces”, in: Fuerstenau, M. C., Jameson, G., Yoon, R. H. (Eds.), Froth Flotation: A Century of Innovation, Society for Mining Engineers, Golden, Colorado, 133–178.

Finch, J. A., Smith, G. W., (1972) “Dynamic surface tension of alkaline dodecylamine acetate solutions in oxide flotation”, Transactions of the Institution of Mining and Metallurgy, 81, C213–C218.

Fox, H. W., Zisman, W. A., (1950) “The spreading of liquids on low energy surfaces”, Journal of Colloid Science, 5, 514–531.

Fredenslund, A., Gmehling, J., Rasmussen, P., (1977) “Vapor-liquid equilibria using UNIFAC: A group contribution method”, Elsevier, New York.

Fredenslund, A., Jones, R. L., Prausnitz, J. M., (1975) “Group-contribution estimation of activity coefficients in nonideal liquid mixtures”, AIChE Journal, 21 (6) 1086–1099.

Fuerstenau, D. W., Fuerstenau, M. C., (1956) “Ionic size in flotation collection of alkali halides”, Transactions AIME, 302–330.

Fuerstenau, D. W., Healy, T. W., Somasundaran, P., (1964) “The role of hydrocarbon chain of alkyl collectors in flotation”, Transactions AIME, 229, 321–325.

Gardner, J. R., Woods, R., (1979) “An electrochemical investigation of the natural floatability of chalcopyrite”, International Journal of Mineral Processing, 6 (1) 1–16.

Gaudin, A. M., (1928) “Flotation mechanism: A discussion of the functions of flotation agents”, in: Flotation Practice, AIME, New York, 50.

Gaudin, A. M., Fuerstenau, D. W., (1955) “Quartz flotation with cationic collectors”, Transactions AIME, 202, 66.

Kelebek, S., Finch, J. A., Yoruk, S., Smith, G. W., (1986) “Wettability and floatability of galena–xanthate system as a function of solution surface tension”, Colloids and Surfaces, 20, 89–100.

Kitchener, J. A., (1960) “Gravity, the angle of contact and Young's equation: A critical review”, Proceedings of the Third International Congress of Surface Activity, 2, 426–432.

Leja, J., Poling, G. W., (1960) “On the interpretation of contact angle”, Proceedings of the V International Mineral Processing Congress, London, 325–332.

Melrose, J. C., (1965) “On the thermodynamic relations between immersional and adhesional wetting”, Journal of Colloid Science, 20 (8) 801–821.

Mohammadi-Jam, S., Waters, K. E., (2014) “Inverse gas chromatography applications: A review”, Advances in Colloid and Interface Science, 212, 21–44.

Nagaraj, D. R., Ravishanker, S. A., (2007) “Flotation reagents: A critical overview from an industry perspective”, in: Froth Flotation: A Century of Innovation, SME, 375–.

O’Connor, C. T., (2012) “Investigating the use of excess Gibbs energy to predict the hydrophobicity of a mineral treated with a collector”, Minerals Engineering, 160, 106692.

Read, A. D., Kitchener, J. A., (1967) “The thickness of wetting films”, in: Wetting, Society of Chemical Industry Monograph No. 25, Gordon & Breach, New York, 300–313.

Spagnolo, D. A., Maham, Y., Chuang, K. T., (1996) “Calculation of contact angle for hydrophobic powders using heat of immersion data”, Journal of Physical Chemistry, 100, 6626–6630.

Taguta, J., O’Connor, C. T., McFadzean, B., (2016) “Relating enthalpies of adsorption of thiol collectors and collector mixtures on base metal sulfide minerals to their floatability”, Proceedings of the XXVIII International Mineral Processing Congress.

Taguta, J., (2018) “Using the enthalpy of immersion to characterise mineral surface hydrophobicity”, PhD Thesis, University of Cape Town.

van Oss, C. J., Chaudhury, M. K., Good, R. J., (1988) “Interfacial Lifshitz-van der Waals and polar interactions in macroscopic systems”, Chemical Reviews, 88, 927–941.

van Oss, C., Giese, R. F., (1995) “The hydrophilicity and hydrophobicity of clay minerals”, Clays and Clay Minerals, 43 (4) 474–477.

Wang, X., Zhang, Q., (2020) “Role of surface roughness on the wettability, surface energy and flotation kinetics of calcite”, Powder Technology, 371, 55–63.

Washburn, E. W., (1921) “The dynamics of capillary flow”, Physical Review, 17 (3) 273.

Yoon, R. H., (2000) “The role of hydrodynamic and surface forces in bubble–particle interaction”, International Journal of Mineral Processing, 58, 129–143.

THE USE OF ECO-FRIENDLY COLLECTORS FOR FELDSPAR FLOTATION

Lev O. FILIPPOV*, Inna V. FILIPPOVA

University of Lorraine, CNRS, Georessources, F54000 Nancy, FRANCE
**Corresponding author: lev.filippov@univ-lorraine.fr*

A B S T R A C T

Brines and crystalline rocks, namely pegmatites and greisens enriched in silicate minerals and/or Li phosphates, are the main source of lithium in the world. Granitic pegmatites and rare metals granites (RMG) may be considered as an important Li source as well as the source of many other critical metals, such as Ta, Nb, Sn, Be, Cs, Sc, U, Th and REE in the Europe. This work is aiming at evaluation of the processing routes to unlock the “hard Li” European deposits not only to produce the high-quality Li concentrate (>4.0-4.5 %Li_2O), but also to increase the economic viability of the deposits exploitation by recovering the others critical metals (Ta, Nb, Sn,) and industrial minerals (quartz and feldspar) to reach near zero processing circuit. The flotation was used as the main separation method for recovering Li-bearing minerals. There are some alternative methods such dense media separation, magnetic separation, electrostatic separation and ore sorting for the preconcentration of lithium-containing minerals (spodumene, lepidolite, zinnwaldite) from the pegmatites and greisens. The combination of the gravity concentration to recover the Ta-Nb and Sn bearing heavy minerals and flotation to recover the lithium bearing mica (lepidolite) was used in this work to process the rare metals granites from Beauvoir deposit (Allier, France) while the processing approach based on the optical sorting and electrostatic separation at coarse size followed by flotation was applied to process the pegmatite ores from Gonçalo deposit (Portugal).

Key words: *Energy minerals, lithium, critical metals, flotation, sorting, gravity concentration*

1. INTRODUCTION

Lithium is an essential material for green energy storage technologies and is fast becoming a metal of crucial importance to the world. The growing use of lithium in rechargeable batteries for portable electronic devices (smart electronic gadgets, computers and rechargeable power tools) and hybrid and electric vehicles has significantly increased the demand for lithium. The abundance of lithium in the average continental crust varies from 20 to 70 ppm. It is a low-atomic-weight alkaline metal with a high charge-to-weight ratio. Lithium-ion batteries, which generate ~3 volts/cell, have been one of the main lithium consumers in recent years. By contrast, lead-acid batteries generate 2.1 volts/cell and zinc-carbon batteries 1.5 volts.

Lithium is generally extracted from two economic sources: brines and hard rock ores. Approximately 60% of global production comes from brines, but the concentration of the metal is very low (0.2-0.7 ppm) (Aylmore et al., 2018; Meng et al., 2019; Tadesse et al., 2019. Brines and crystalline rocks, namely granites, pegmatites and greisens enriched in silicate minerals and/or Li phosphates, are the main source of lithium (Gruber et al., 2011; Kesler et al., 2012; Penner, 1978). Both pegmatites and granites contain lithium at different grades and are reported in different parts of the world. Several new projects are therefore being explored and developed to fill the gaps in supply and demand (Kesler et al., 2012; Salakjani et al., 2020).

Ten deposits account for more than 83% of world lithium resources with a domination of the brines deposits. The lithium resources and reserves reported in the literature were estimated by Mohr (2012) at 38.3 Mt and 3.9 Mt respectively in 2012. The resource estimate was increased by 255% in 2023, while the USGS estimated lithium reserves at 4.1 Mt in 2009, and this figure rose to 14 Mt by 2016 (U.S. Geological Survey, 2009, 2016). The current USGS

reserve estimate has been revised upwards to 28 million tonnes in 2023 (USGS, 2024). The recent USGS report shows that identified deposits are increasing rapidly over the years due to ongoing exploration and discovery.

World resources are estimated at 105 million tonnes (USGS, 2024), with larger reserves reported in Bolivia, (23 Mt), Argentina (22 Mt), Chile (11 Mt), Australia (8,. Mt) and China (6.8 Mt). In terms of production, Australia, Chile, China and Argentina are major producers worldwide. In addition, several countries (Austria, Brazil, Canada, China, Congo (Kinshasa), Czech Republic, Finland, Germany, Mali, Namibia, Portugal, Serbia, Spain and Zimbabwe) are also developing mineral-based lithium extractions from different types of mineral deposits (Table 1)

Table 1. Mine production and World resources and reserves of Lithium as estimated by the USGS

Mine production			
Country	**2021**	**2022**	**2023**
Argentina	5,970	6,590	9600
Australia	55,300	74,700	86,000
Brazil	1,700	2,630	4,900
Canada	-	520	3400
Chile	28,300	38,000	44,000
China	14,000	22,600	33,000
Portugal	900	380	380
Zimbabwe	710	1030	34000
World total (rounded)	107,000	146,000	180,000

Source: Adapted from USGS 2023, 2024

Estimated Li resources in hard rock deposits were significantly increased recently due to the advanced exploration and discovery of new deposits and the number of advanced mining projects has increased in several European countries. Granitic pegmatites and rare metals granites (RMG) have been exploited in Europe mainly for the industrial minerals (quartz, feldspar, kaolinite). Granitic pegmatite is an important lithium source and also the source of many other critical metals, such as Ta, Nb, Sn, Be, Cs, Ru, Sc, U, Th and REE. The supply of some of these elements, i.e. Li and Ta are of concern, therefore, it is very important to investigate recovery of such metals from granitic pegmatite. Thus, it is crucial to evaluate the potential and contribution of hard rock Li sources to decrease the supply risks of critical materials for the European economy.

2. HARD ROCK LITHIUM SOURCES

In the Earth's crust, more than 120 lithium minerals have been identified (Christmann et al., 2015; Garrett, 2004). However, only a few of them have commercial/industrial potential (Table

2 such as lepidolite, spodumene, petalite, amblygonite-montebrasite and zinnwaldite (Christmann et al., 2015, Filippov et al., 2019).

Table 2. Main lithium minerals

Mineral	Formula	Content, % Li_2O		SG, g/cm^3	Hardness (Moos)
		Theoretical	Actual		
Spodumene	$LiAlSi_2O_6$	8.03	4.5–8	3.2	6.5–7
Lepidolite	$KLi_{1.5}Al_{1.5}[Si_3AlO_{10}][F,OH]_2$	5.9	1.2–5.9	2.8–2.9	2–3
Petalite	$(Li,Na)AlSi_4O_{11}$	4.89	2–4	2.39–2.46	6–6.5
Amblygonite	$LiAl(PO_4)(F,OH)$ or $Li_2O_3.2LiF.P_2O_5.Li_2O$	10.1	8–9.5	3–3.2	6
Zinnwaldite	$KLiFeAl[Si_3AlO_{10}][F,OH]_2$	4.13	2–3	2.9–3.2	2–3

The most important type of lithium deposit in crystalline rock is pegmatite (Tkachev et al., 2018, Meng et al., 2021). The largest lithium pegmatite resource is the Kings Mountain pegmatite belt in North America with 62.3 Mt at an average grade of 0.67% Li (0.42 Mt lithium). The Australian Greenbushes deposit is Australia's largest lithium deposit, a 31.4 Mt spodumene deposit averaging 1.44% Li_2O (0.45 Mt lithium). The Bikita pegmatite (South Africa), exploited for more than a century, contains 10.8 million tonnes of lithium with an average content of 1.4% (0.15 million tonnes of lithium).

The largest lithium pegmatite in Europe is found in Portugal and adjacent Spain, which contains numerous 0.3% Li aplite pegmatites. Recent exploration has been carried out in Finland (Ullava Länttä), indicating that these are 32 distinct bodies with a composition of 56% feldspar, 25% quartz and 16% spodumene, with a resource of 2.947 Mt containing 0.43% Li (0.013 Mt lithium) (Gruber et al., 2011; Kesler et al., 2012).

The most advanced hard Li project in France is the EMILI project operated by Imerys, which aims to mine the rare-metal granites of Beauvoir. The Beauvoir granite is reported, along with the Colettes granite, in the Echassières granitic complex and more specifically in the Massif Central. The main minerals associated with the Beauvoir granite deposit are quartz, K-feldspar, albite and micas (muscovite and lepidolite). These minerals can be found in different abundances and habitus in the units. In addition, several minor mineral phases (amblygonite, topaz, columbo-tantalite, microlite, cassiterite, zircon, apatite, rutile, sphalerite and phosphates such as herderite) are also found in the same deposit (Cuney et al., 1992; Gourcerol et al., 2019; Harlaux et al., 2017; Demeusy et al., 2023).

Table 3. Advanced European lithium projects

Project name	Company	Deposit/ Li mineral	Comments	Source
Alvarrões-Gonçalo Li project	Felmica	Pegmatite aplite, lepidolite	Mine is operating to produce feldspar product for ceramics. 2.38 Mt @ 2.54% Li_2O,	N/C (author)

			2.64 Mt @ 1.76% Li_2O,	
Keliber Li project	Sibanye-Stillwater	Pegmatite LCT,spodumene	15,000 t/year of battery-grade lithium hydroxide monohydrate over 16 years	*https://thevault.exchange/?get_group_doc=245/1669636132-ssw-presentation-keliber-approval-event-28Nov2022.pdf*
Barroso Project,	Savannah Resources	Pegmatite LCT, spodumene	The deposit could contain 27 million tonnes of lithium ore, including over 285,900 tonnes of lithium oxide.	*https://www.savannahresources.com/project/barroso-lithium-project-portugal/*
EMILI Project,	Imerys	Rare metal granite, lépidolite	34,000 tonnes of lithium hydroxide per year from 2028 over 25 years »	*Personal communication*
Cinovec Project	European Metals Holding	Greisen, zinwaldite	29,386 tonnes of battery-grade lithium hydroxide per year over a 25-year period based on 13.1% of measured (3.8 Mt LCE) or 7.7 % of measured (7.39 Mt LCE at 0.64 % LiO2) resources	*https://www.europeanmet.com/cinovec-project-overview/*
Wolfsberg Project	European Lithium	Pegmatite LCT, spodumene	Measured and indicated resources of 6.3 Mt at 1.17% Li2O. Spodumene concentrate >6% LiO2	*https://europeanlithium.com/wolfsberg-lithium-project/*

In the RMG, lithium is mainly contained in lepidolite ($K(Li,Al)_3(Si,Al)_4O_{10}(F,OH)_2$), which forms a solid solution with other micas, particularly muscovite. Minerals of the columbo-tantalite series ($(Fe,Mn)(Ta,Nb)_2O_6$), which are abundant with niobium and tantalum. These elements are also found in the microlite-pyrochlore series ($(Na,Ca)_2Ta_2O_6(OH,F)$). Tungsten occurs in minor quantities in granite, while tin is found in the form of cassiterite (SnO_2). The mineral of beryllium is not well identified in granite, and the main hosts are probably phosphates such as herderite ($CaBePO_4(F,OH)$). However, it is also found in lepidolite, which may be due to the presence of phosphates (fluorapatite) as inclusions or in the mineral as a secondary substitution. Small amounts of uranium are also found in granite in the columbo-tantalite, microlite and uraninite (UO_2) mineral series.

3. PROCESSING ROUTES FOR THE EXPLOITATION OF HARD ROCK LITHIUM DEPOSIT

3.1. Main Processing Approaches

Several upgrading options have been reported for lithium deposits, including gravity separation (dense media separation; spiral concentrator), flotation, magnetic separation (high-intensity wet magnetic separation) (Bulatovic, 2015; Filippov et al., 2019; Leißner et al., 2016; Moon and Fuerstenau, 2003; Siame and Pascoe, 2011). However, most research and industrial practice is limited to spodumene, petalite and zinnwaldite, which are the main lithium-bearing

minerals (Tadesse et al., 2019). The literature also shows that the processing and mineralogy of lepidolite-rich lithium deposits are not well documented (Korbel et al., 2023).

Flotation is used for most mineral deposits as the main separation method for recovering Li-bearing minerals (Bulatovic, 2015; Filippov et al., 2019; Tadesse et al., 2019). However, as a wet process, flotation enrichment requires fine grinding (<200 µm) while the liberation degree of lepidolite and spodumene in the pegmatite and RMG ores occurs at coarse grinding size of 0.5 to 1.0 mm or more (Souza et al., 2019, 2020; Filippov et al., 2019, 2022; Demeusy et al., 2023).

There are some alternative methods such as magnetic separation, electrostatic separation and ore sorting for dry preconcentration of lithium-containing minerals at coarse size fraction (Brandt and Haus, 2010; Iuga et al., 2004; Leißner et al., 2016). Furthermore, electrostatic separation and mineral sorting are dry separation methods that use both the conductivity and optical properties of particles to separate them from each other. Dense media separation is also used to recover spodumene, whose density (3.0 g/cm3) is slightly different from that of gangue minerals (quartz, feldspars). However, there is no literature on the application of these technologies to the preconcentration of lepidolite-rich ore deposits. Similarly, optical sorting of ores has seen technological advances (Lessard et al., 2014), but there is little information in the literature concerning Li-bearing ores (Sousa et al., 2019; Filippov et al., 2022). Nevertheless, some studies have shown that electrostatic separation may be suitable for mica concentration (Iuga et al., 2004; Lindley and Rowson, 1996; Yuga et al., 1995) but with lower grade compared to the flotation (Filippov et al., 2022). The recent works showed that the decreasing top size of the flotation feed led to the increasing losses of the lepidolite with the hydrocyclone overflow during the desliming stage at 10 µm (Korbel et al., 2025).

It is therefore of interest to understand the challenges related to the flotation of lepidolite from the pegmatite and rare metals granite ore deposits.

3.2. Processing Routes for the Rare Metal Granite from Beauvoir Deposit (Allier, France)

3.2.1. Multiscale liberation: Risk of overgrinding

Flowsheet development should consider the selection of a preconcentration strategy at a coarse size (gravity concentration, sorting, flotation of coarse particles, …other) to limit grinding and avoid overgrinding of the other critical minerals. In this work, the flotation study performed on the two fractions of the rare metal granite samples showed a big difference in the concentrate grade. If the Li grade was high (4.8 to 5.2 LiO_2) for the coarse size fraction (250-500 µm) the Li grade decreased to 3.8-3.92 for the size fraction 90-250 µm. However, the Li recovery in the coarse concentrate was limited to 40-50% only, while the Li recovery for the size fraction 90-250 µm reached 82-90%. The relatively low Li grade for the finer size fraction was attributed to the geochemical variability of the lepidolite and the presence of mineral inclusions in the mica particles, while the low recovery of the coarse particles was related to the hydrodynamics of the flotation process favoring the intensive particle detachment. Thus, the optimization of the degree of liberation and the flotation of the fine and coarse size fractions at optimized hydrodynamic conditions can be considered as promising ways to reach improved metallurgical performance of the flotation of the lepidolite.

3.2.2. Combined flow-sheet for recovering of lithium and by-products

Figure 1 presents the optimized flow-sheet for the processing of Li minerals from rare metals granite from the Beauvoir deposit. Each step of the flow sheet presented in Fig. 1 includes a number of challenges to overcome and issues to solve. Lithium mineral liberation requires a staged comminution approach to avoid overgrinding.

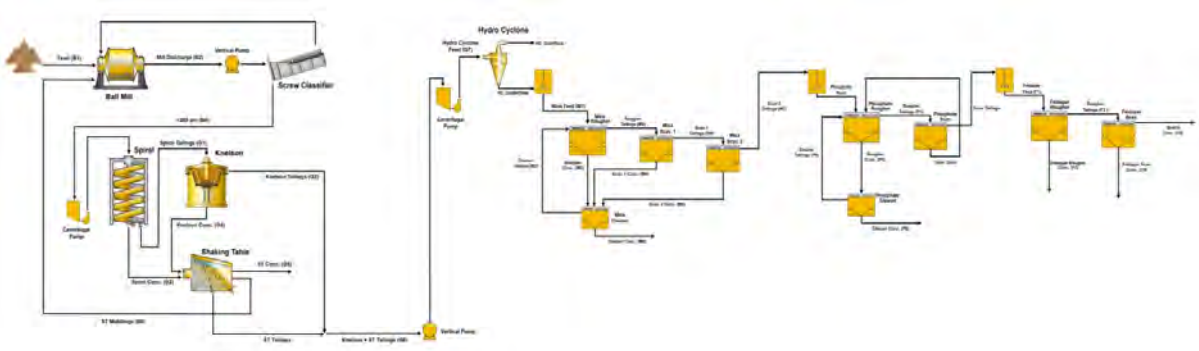

Figure 1. Proposed flowsheet for Li and critical metals recovery from rare metal granite of Beauvoir deposit

The crushed ore is fed in grinding circuits composed of a ball mill working in close loupe with a spiral classifier to reach the lepidolite liberation degree defined previously at d80 = 280 µm (Demeusy et al., 2023; Korbel et al., 2025) which was considered as compromising solution to optimize the grade/recovery.

The first concentration step is the recovery of heavy minerals such as cassiterite and columbo tantalite. It was demonstrated in previous study that the recovery of those metallic by-products should be performed before the Li flotation stage to increase their recovery (Korbel et al., 2025; Demeusy et al., 2026). The concentration is performed through a combination of gravity-based equipment. A spiral is used as a rougher stage to recover as much as possible of the heavy minerals from the ore. The tailings from spiral are sent to a continuous variable discharge Knelson concentrator for scavenging. Both spiral and Knelson concentrates are cleaned on a shaking table whose concentrate is the final Sn/Nb/Ta concentrate. Middlings from the shaking table are sent back to the ball mill for regrinding. Lights from the shaking table are mixed with those from spiral and Knelson and pumped to the hydrocyclone to perform a desliming at 20 µm before Li flotation circuit. After gravity concentration hydrocycloning is performed to increase percentage solid of the ore and remove the –20 µm fraction as it was shown previous study (Korbel et al., 2025).

The second concentration step was the recovery of the Li-rich micas. The lepidolite concentrate is the main product from the deposit, and its recovery is implemented to assess the impact of the whole process on its recovery. Li flotation circuit is composed of a rougher stage followed by two consecutive scavengers. The recovery of phosphates (main Be bearing phase) is achieved using rougher and cleaner stages. The final concentration step is the flotation of feldspars by using HF-free method (Filippov, 2017). The tails of feldspar flotation is the quartz concentrate.

Thus, the optimization of the degree of liberation and the sequential flotation at optimized hydrodynamic conditions can be considered as promising ways to reach the near zero-waste flotation circuit allowing to recover the Li lepidolite concentrate, heavy minerals concentrate including Sn and Ta-Nb minerals, Be-rich phosphate concentrate, as well as the feldspar and quartz concentrates.

In sum, the lithium flotation stage should define the cut size of deslimed materials to achieve the requested Li concentrate grade for future processing. The recovery of heavy minerals is faced with selectivity issues if gravity separation is used. Finally, the tailings of the heavy minerals concentration or/and flotation are used to produce industrial minerals by-products. Non-hydrofluoric acid process (HF-free) was used to perform the quartz-feldspar separation allowing to generate a high qu-lity feldspar concentrate for ceramics and quartz products to be used in the building industry or for other purposes.

3.3. Li Minerals Recovery from Pegmatite Ores

3.3.1. Development of a processing approach for aplitic pegmatite of the Gonçalo deposit (Portugal)

Lepidolite in the granitic pegmatite and RMG is recovered by flotation with a cationic collector at acidic pH close to 2 (Korbel et al., 2023). Development of the lepidolite pegmatite ore processing circuit was carried out on ore samples from the Gonçalo deposit (Portugal) as part of the H2020 "FAME" project funded by the European Commission. Mineralogical study of the lithium-bearing mica-rich pegmatite ore indicated an overall composition of ≈ 10% lepidolite associated with gangue minerals such as quartz (≈ 40%), muscovite (≈ 30%) potassic feldspar (≈ 10%.) %) and albite (≈ 10%).

The strategy for developing the adapted processing circuit included:
- a preparation stage to generate different size fractions;
- a pre-concentration stage using a dry separation process;
- a principal concentration stage by flotation.

The feed size distribution and lithium analysis is shown in Figure 2.

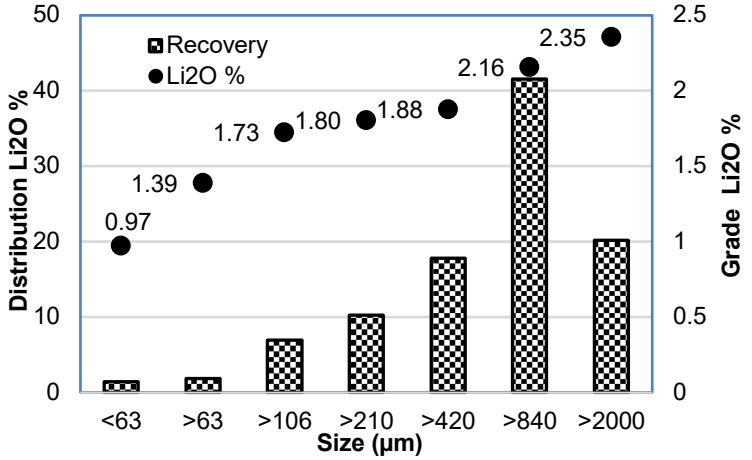

Figure 2. Lithium grade and deportment according to size distribution of crushed and ground sample of Gonçalo pegmatite ore (adapted from Filippov et al., 2022)

The fractions coarser than 840 µm had a higher lithium content than the average feed (2.02% Li), reaching 2.35% Li for the fraction > 2 mm. Lithium content decreased with decreasing particle size, and was found to be <1% Li_2O (0.93%) in the ultrafine fraction (-0.063 mm). Maximum Li_2O distribution occurred in the coarsest particle range. This finding further supports the recovery of lepidolite at coarse liberation sizes as a potentially cost-effective separation method that avoids the use of fine grinding.

These results have led to the consideration of optical sorting as a pre-concentration method at the crushing stage as a promising approach (Souza et al., 2020; Filippov et al., 2022). Furthermore, preconcentration of muscovite-type minerals in pegmatite is achievable using an electrostatic separation method (Yuga et al, 1994; Iuga et al, 2004). Muscovite has stronger insulating properties than quartz and feldspar. Due to the mineralogical similarities between muscovite and lepidolite, it was deduced that both minerals would behave in the same way during electrostatic separation and that this technique could therefore be implemented as a pre-concentration step.
Electrostatic separation was applied to the fraction > 210 µm, as a pre-concentration step prior to the flotation step. Three size fractions were tested: [2-0.84 mm], [0.84-0.42 mm] and [0.42-0.21 mm]. Finally, the <200 mm fraction was processed by flotation at a pH range of 2-5, using

an etheramine reagent as flotation collector. The studies carried out resulted in the proposal of a processing circuit for aplitic pegmatites combining dry preconcentration methods and flotation as the main process for recovering lepidolite from pegmatite (Figure 3).

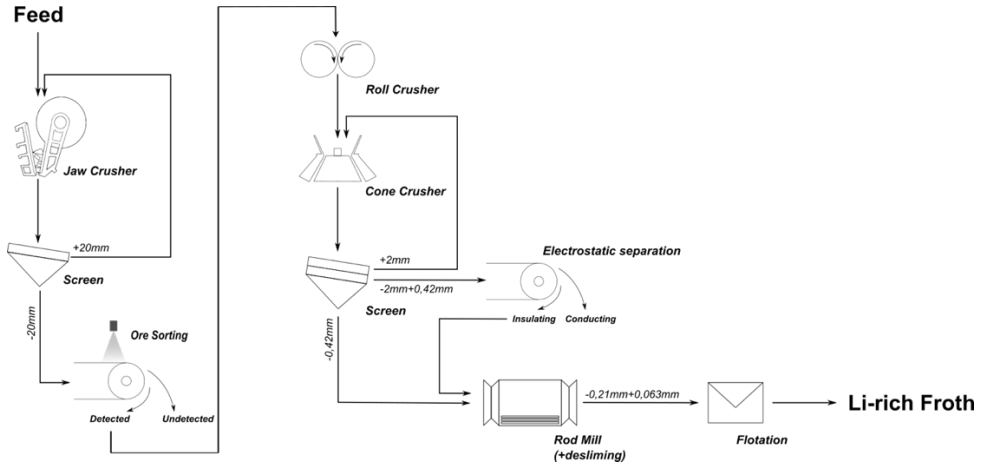

Figure 3. Processing circuit combining dry preconcentration methods and flotation for recovering lepidolite from for aplitic pegmatites (Filippov et al., 2022) Source: Filippov et al., 2022

The flotation separation process yielded very interesting and promising results, both in terms of the quality of the Li concentrate (>4.0%) and the level of recovery, reaching 77%.

3.3.2. Processing challenges for LCT pegmatite ore

3.3.2.1. Activation of spodumene prior to anionic flotation

Spodumene in Lithium-Cerium-Tantalum (LCT is) pegmatite recovered by flotation with anionic collector but it is inefficient (Filippov et al., 2019). Process optimization requires the use of collector blends and preliminary activation with the metallic cations. Literature provides extensive information about the crystal structure of spodumene during grinding. The total broken bond strength per unit cell area varies according to the plans between 4.7 to 9.75 10^{18} valence per m^2 according to the series (Moon and Fuerstenau, 2003):

{ 110 } < { 010 } < { 001}< { 100 }

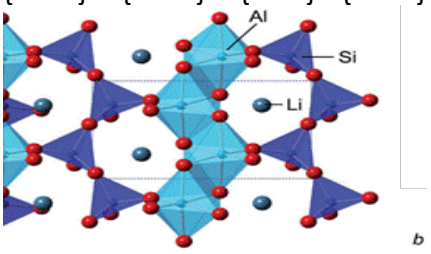

Figure 4. Grinding and surface exposure of spodumene (adapted from Filippov et al., 2019)

The comminution of the LCT pegmatite leads to the exposure of the {110} of spodumene planes where the density of Al sites in the unit cell area is higher except the {001} plane and defines carboxylate collector adsorption and efficient flotation. However, collector adsorption efficiency is not sufficient for efficient flotation with carboxylate collector alone. The flotation process is performed with a preliminary activation by the Ca^{2+} cation (Figure 6).

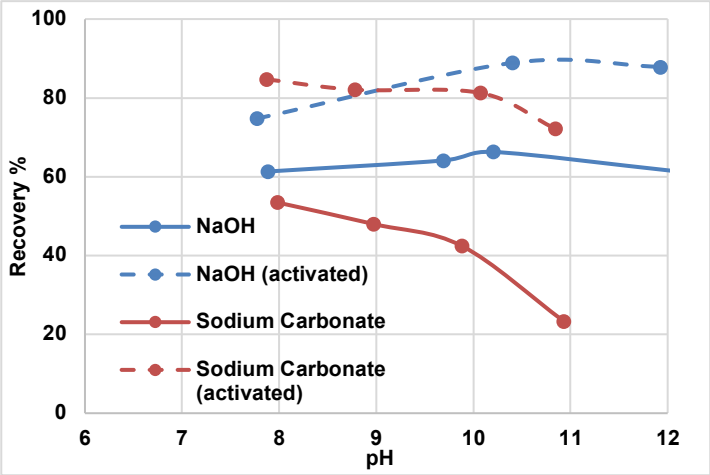

Figure 5. Influence of pH regulators on the flotation of spodumene with a preliminary activation with $CaCl_2$ and flotation with sodium oleate (adapted from Filippov et al., 2019)

It was demonstrated that activated spodumene has a much higher recovery than the non-activated sample when either NaOH or Na_2CO_3 is used. This suggests that $CaCl_2$ has an activating effect on spodumene in flotation, even if a depressant (i.e., Na_2CO_3 in the current case) is present.

3.3.2.2. Mineral/collector interactions depending on the surface properties

The choice of collectors is dependent on the surface properties which is dependent on the degree of mineral alteration and limits Li recovery. The difficulties in flotation of spodumene are linked to the anisotropy of the physicochemical properties according to the planes most exposed during the liberation. The main surfaces exposed during spodumene grinding are the {100}, {010}, {001} planes and the {110} cleavage plane (Moon and Fuerstenau, 2003). From a structural point of view the silicate and the tetrahedral structures must generate a negative charge (hydrolysis $SiOH = SiO^- + H_3O^+$), therefore the interaction with cationic collectors (ammonium salts RNH_3^+) can be promoted. On the other hand, Al of the exposed alumina groups on the {110} have two broken bonds (Moon & Fuerstenau, 2003; Quezada & Toledo, 2020). This leads to positive valences of +1 of aluminous sites (Quezada & Toledo, 2020) allowing interactions with anionic collectors (carboxylate $R\text{-}COO^-$). These phenomena are at the origin of the differential hydration of the different planes and partly explain the poor flotation with cationic and anionic collectors without prior activation (Filippov et al., 2019).

4. CONCLUSION

Estimated “hard Li” resources and reserves were significantly increased recently due to the advanced exploration and discovery of new deposits. The USGS estimates probable European lithium resources at 7% of the world total. The number of lithium mining projects has increased in recent years in several European countries. The mining projects in development could eventually cover 80 % of the European needs for battery Li. The European Commission supported several largescale research and innovation projects involving partners from industry (research (process development) and engineering companies (upscaling and process implementation).

The proposed processing flow-sheet includes sorting, gravity and magnetic separation and flotation to recover Li concentrate to produce battery quality Li hydroxide but also to target by-product recovery such as Ta, Nb, Sn, W, quartz and feldspar products for the ceramic industry.

ACKNOWLEDGEMENT

The author acknowledge the financial support of the Horizon Europe EXCEED project, “Cost-effective, sustainable and responsible extraction routes for recovering distinct critical metals and industrial minerals as by-products from key European hard-rock lithium projects”, Grant Agreement No. 101091543, https://exceed-horizon.eu/consortium/

REFERENCES

Aylmore, M. G., Merigot, K., Rickard, W. D. A., Evans, N. J., McDonald, B. J., Catovic, E., Spitalny, P., (2018) “Assessment of a spodumene ore by advanced analytical and mass spectrometry techniques to determine its amenability to processing for the extraction of lithium”, Minerals Engineering, 11 137– 148.

Brandt, F., Haus, R., (2010) “New concepts for lithium minerals processing”, Minerals Engineering, 23 (8) 659–661.

Bulatovic, S., (2015), Beneficiation of Lithium Ores. Handbook of Flotation Reagents: Chemistry, Theory and Practice.

Christmann, P., Gloaguen, E., Labbé, J.-F., Melleton, J., Piantone, P., (2015) Global Lithium Resources and Sustainability Issues, Lithium Process Chemistry, 1–40.

Cuney, M., Marignac, C., Weisbrod, A., (1992) “The Beauvoir topaz-lepidolite albite granite (Massif Central, France); the disseminated magmatic Sn-Li-Ta-Nb-Be mineralization”, Economic Geology, 87 1766–1794.

Demeusy, B., Arias-Quintero, CA, Butin, G., Lainé, J., Tripathy S.K., Marin, J., Filippov L., (2023) “Characterization and liberation study of the Beauvoir granite for lithium mica recovery”, Minerals, 13 (7) 950.

Demeusy, B., Dehaine, Q., Sanders, E., Filippov, L. O., (2026) “Recovery of tin, niobium, and tantalum as by-products of lithium from rare metal granites using a Falcon concentrator”, Separation and Purification Technology, 384 13626.

Filippov, L. O., Flotation process for recovering feldspar from a feldspar ore US Patent 9,675,980.

Filippov, L., Farrokhpay, S., Lyo, L., Filippova, I., (2019) “Spodumene flotation mechanism”, Minerals, 9 372.

Filippov, L. O., Filippova, I. V., Crumiere, G., Sousa, R., Machado Leite, M., Botelho de Sousa, A., Korbel, C., Tripathy, S. K., (2022) “Separation of lepidolite from hard-rock pegmatite ore via dry processing and flotation”, Minerals Engineering, 187 107768.

Garrett, D. E., (2004), Handbook of Lithium and Natural Calcium Chloride, 483.

Gourcerol, B., Gloaguen, E., Melleton J., Tuduri, Y., Galiègue, X., (2019) “Re-assessing the European lithium resource potential – A review of hard-rock resources and metallogeny”, Ore Geology Review, 109 494-519.

Gruber, P. W., Medina, P. A., Keoleian, G. A., Kesler, S. E., Everson, M. P., Wallington, T. J., (2011) “Global lithium availability a constraint for electric vehicles”, Journal of Industrial Ecology, 15 (5) 760–775.

Harlaux, M., Romer, R. L., Mercadier, J., Morlot, C., Marignac, C., Cuney, M., (2018) “40 Ma of hydrothermal W mineralization during the Variscan orogenic evolution of the French Massif Central revealed by U-Pb dating of wolframite”, Mineralium Deposita, 53 21–51.

Iuga, A., Cuglesan, I., Samuila, A., Blajan, M., Vadan, D., Dascalescu, L., (2004) “Electrostatic separation of muscovite mica from feldspathic pegmatites”, IEEE Transactions on Industry Applications, 40 422–429.

Kesler, Stephen E., Gruber, P. W., Medina, P. A., Keoleian, G. A., Everson, M. P., Wallington, T. J., (2012) “Global lithium resources: Relative importance of pegmatite, brine and other deposits”, Ore Geology Reviews, 48 55–69.

Korbel, C., Filippova, I., Filippov, L. O., (2023) « Froth flotation of lithium micas–A review”, Minerals Engineering, 192 107986.

Korbel, C., Demeusy, B., Kahou, Z.S., Filippova, I. V., Dehaine, D., Filippov, L. O., (2025) “Flowsheet development for the selective flotation of lepidolite from the Beauvoir granite from mineralogical insights”, Minerals Engineering, 225 109207.

Leißner, T., Bachmann, K., Gutzmer, J., Peuker, U., (2016) “MLA-based partition curves for magnetic separation”, Minerals Engineering, 94 94–103.

Lessard, J., de Bakker, J., McHugh, L., (2014) “Development of ore sorting and its impact on mineral processing economics”, Minerals Engineering, 65 88–97.

Lindley, K. S., Rowson, N. A., (1996) “Feed preparation factors affecting the efficiency of electrostatic separation”, Magnetic and Electrical Separation, 8 161–173.

Meng, F., McNeice, J., Zadeh, S. S., Ghahreman, A., (202). “Review of lithium production and recovery from minerals, brines, and lithium-ion batteries”, Mineral Processing and Extractive Metallurgy Review, 42 (2) 123-141.

Moon, K. S., Fuerstenau, D. W., (2003) “Surface crystal chemistry in selective flotation of spodumene (lial[sio3]2) from other aluminosilicates”, International Journal of Mineral Processing, 72 11–24.

Mohr, S. H., (2012) “Lithium resources and production: Critical assessment and global projections”, Minerals, 2 (1) 65–84.

Penner, S. S., (1978), Lithium Needs and Resources. Elsevier.

Salakjani, N. K., Singh, P., Nikoloski, A. N., (2020) “Production of lithium–A literature review part 1: Pretreatment of spodumene”, Mineral Processing and Extractive Metallurgy Review, 41 (5) 335-348.

Siame, E., Pascoe, R. D., (2011) « Extraction of lithium from micaceous waste from China clay production”, Minerals Engineering, 24 1595–1602.

Sousa, R., Futuro, A., Fiúza, A., Leite, M. M., (2020) “Pre-concentration at crushing sizes for low-grade ores processing – Ore macro texture characterization and liberation assessment”, Minerals Engineering, 147 106156.

Tadesse, B., Makuei, F., Albijanic, B., Dyer, L., (2019) “The beneficiation of lithium minerals from hard rock ores: A review”, Minerals Engineering, 131 170–184.

Tkachev, A. V., Rundqvist, D. V., Vishnevskaya, N. A., (2018) “Metallogeny of lithium through geological time”, Russian Journal of Earth Sciences,18 1–13.

U.S. Geological Survey, (2009), Lithium summarises in 2009, (703), 94–95.

U.S. Geological Survey, (2016), Lithium summarises in 2016, (703), 2015–2016.

Yuga, A. I., Dascalescu, L., Morar, R., Samuila, A., Cuglesan, I., (1995) “Electrostatic shape separation of flake mica from pegmatites”, Magnetic and Electrical Separation, 6 135–149.

WASTE FROM SOME NONFERROUS BASE METALS EXTRACTION AS SOURCE OF CRITICAL METALS

Marinela PANAYOTOVA[1,*], Irena GRIGOROVA[1], Vladko PANAYOTOV[1,2]

[1]University of Mining and Geology "St. Ivan Rilski", Mining-Technological Faculty, Mineral Processing and Recycling Department, 1700, Sofia, BULGARIA
[2]Bulgarian Academy of Sciences, Engineering Sciences Unit, 1000 Sofia, BULGARIA
**Corresponding author: marichim@mgu.bg*

A B S T R A C T

Many metals are needed for the sustainable development of our society and for our everyday life. Based on their importance and availability some of them are classified as critical by the EU, the USA, China, etc. Driven by the global green transition and the rapid growth of advanced technologies, the demand for aluminium, antimony, cobalt, lithium, nickel and rare earth elements has significantly increased, creating supply chain risks and emphasizing the need for secondary sources. The paper objective is to emphasize the solid mining waste (including historical one), contemporary beneficiation tailings and metallurgical waste from some nonferrous base metals' extraction as valuable sources of critical metals. Wastewater from these metals' recovery from their single and polymetallic sulfide ores is also highlighted as critical metals source. These technogenic materials are reviewed as alternative resources supporting circular economy principles and reducing dependence on primary mining.

Nowadays available technologies for metals extraction from mentioned waste streams are briefly described, calling attention to the abilities of the mineral processing technologies. An integrated approach combining beneficiation, hydrometallurgical or pyrometallurgical and biotechnological methods is outlined as a sustainable route for critical metals recovery from solid waste. The need of joining different technologies to extract high-tech metals from liquid waste streams is highlighted. Constrains in critical metals recovery from extraction waste and future research and development directions are pointed out. Overall, the paper contribution consists in the accenting the role of mineral processing technologies for recovering metals crucial for our future from technogenic waste. The results underline their importance for achieving resource efficiency, strategic autonomy and the objectives of the EU Critical Raw Materials strategy.

Key words: *Waste from nonferrous base metals extraction, critical metals, mineral processing*

1. INTRODUCTION - THE ROLE OF CRITICAL METALS IN MODERN SOCIETY

Modern society is based on the constant use of metals – from our everyday life to advanced medicine and space technologies. Some metals are of strategic importance for the development of energy and transportation systems, advanced technologies and industrial progress, while their availability is subject to risk due to geological, economic, or geopolitical factors (Montana et al., 2025, Müller et al., 2025). According to the European Commission (2023) and the International Energy Agency (2023), the sustainable economy growth and the development of a low-carbon economy requires a significant increase in the consumption of metals such as aluminum (Al), antimony (Sb), bismuth (Bi), cobalt (Co), copper (Cu), gallium (Ga), germanium (Ge), lithium (Li), nickel (Ni), platinum group metals (PGM), rare earth elements (REEs), etc. For example, aluminium is used in construction, electronics, aircraft, cars, power lines (Sun, 2023). Antimony is very important for the development of nuclear energy, semiconductors, military equipment and fire retardants (Zhao et al., 2023). Bismuth is widely used in pharmaceuticals, metallurgical (malleable cast iron, alloys and steels, nontoxic replacement for lead in brass), semiconductor producing industry and atomic research (USGS, 2025). Gallium is crucial in integrated circuits, optical devices and CIGS solar cells production. The fabrication of optical fibers, infrared optics, satellite solar cells, the development of military

equipment are unthinkable without germanium. Indium (In) is used in alloys, semiconductors and LEDs, production of thermal interface materials and photovoltaic cells (European Commission, 2020). Lithium is indispensable for preparation of Li ion and polymer batteries that are inceasingly employed in all braches of industry (Michaux et al., 2022). Except in litium batteries, Co is used in catalysts, special steel industry, magnets (Savinova et al., 2023). Global electrification and almost all sectors of the economy (advanced electronics, construction, cars, aircraft, medicine) can not be imagined without copper – Cu (Liu et al., 2023). Nickel is utilized in steel industry, catalysts, anticorrosion plating, batteries (Dilshara et al., 2022). The main use of PGM is as catalysts in vehicles and chemical industry (European Commission, 2020). Fabrication of electronics, super magnets, fibre optics, superconductors, radar, high speed computers is impossible without REEs (Dushyantha et al., 2020).

According to the IEA (2023), in the period 2017 – 2022 the need of the energy sector was the main reson for a tripling in overall demand for Li, a 70% increase in demand for Co, and a 40% rise in demand for Ni. The ambition to achieve carbon neutrality lead to an increase of nearly 138% of the Li metal price in first quarter of 2022 (Sun et al., 2024). The demand for Li could increase more than fortyfold by 2040, the demand for Ni and Co may rise by 20 to 25 times and demand for REEs is expected to increase up to seven times (IEA, 2022), if global cimate stabilization and decarbonization goals are achieved. This makes some metals an indispensable factor in the energy transition, yet it also gives rise to significant economic and environmental challenges.

In addition, the access to mentioned metals is becoming increasingly limited due to the depletion of ore deposits, geopolitical dependencies, and environmental and technological constraints. The current production of many metals needed for high technologies development is geographically concentrated – Figure 1.

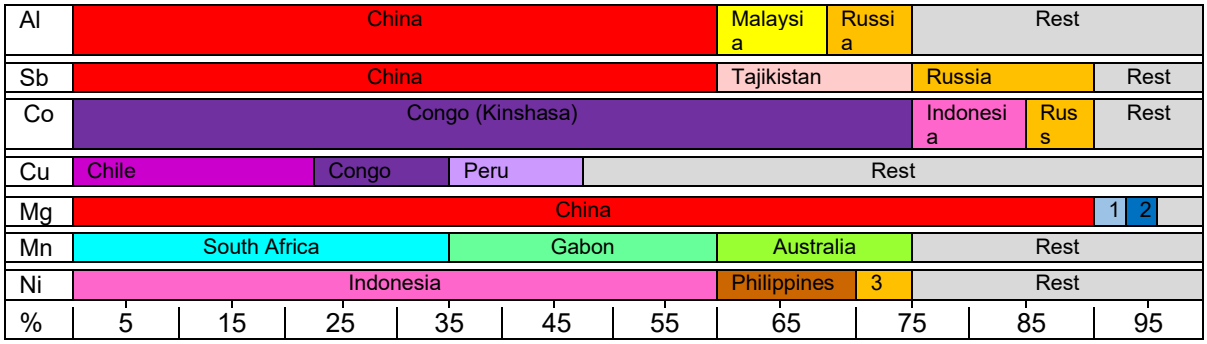

Figure 1. First three worldwide producers of some CRM in 2024: 1 - Kazakhstan, 2 - Brazil, 3 - Russia; Rest – all other worldwide producers of the corresponding metal; Compilled by authors based on data from USGS, 2025

As it can be seen in Figure 1, China is the main producer of many high-tech metals while the Democratic Republic of Congo is illustrated for its dominance in production of Co. In addition, China appears prominently as a major producer of REEs (IEA, 2023). Data in Figure 1 underscore the strategic risks and dependencies inherent in current supply chains.

The European Union economy is highly dependent on imports of some metals. For example, it imports 100% of the needed Sb, Li, PGM and REEs, 98 % of Ga, 89 % of Al, 81 % of Co, 75 % of Ni, 71 % of Bi, etc. China is the major EU sourcing country for Bi, Ga, Ge, and REEs; South Africa is the main supplier of PGM, Guinea - of Al, the Democratic Republic of Congo – of Co, Chile - of Li, and Turkey - of Sb (European Commission, 2023, IEA, 2023). Some of the main EU sourcing countries are politically unstable or are steadily decreasing their export quotas. This creates a strategic vulnerability that underpins the adoption of the Critical raw materials (CRM) lists.

The European Commission (2020, 2023), the United States (USGS, 2022) and China (Andersson, 2020, Ren, 2025) have already identified a number of the above-mentioned raw metals as CRMs. The term "Critical Raw Materials" refers to a group of raw materials that are extremely essential to economics development and security of political entities and are simultaneously exposed to a high risk of disruptions in the supply chain due to geopolitical, market, or technological factors. These materials are crucial for strategic industries such as energy, electronics, transportation, defense and high-tech manufacturing (USGS, 2022, European Commission, 2023). The U.S. list includes 50 minerals and metals, the 2023 EU list includes 34 minerals, metals and specific metals groups (PGM, heavy REE and light REE), while Chinese recent list comprises 32 metals and minerals (REEs are grouped together). Despite some differences in methodologies for CRMs determination, the EU, the U.S., and China share a common view regarding the strategic importance of metals that foster modern technologies and the green transition. It is worth to note that Al, Sb, Co, Li, Ni and REEs are included in the USA, EU and China's lists of CRMs (Ren, 2025).

According to the European Commission (2020), harmonizing international approaches to criticality assessment and establishing transparent supply chains are key to global resource security. In turn, the IEA (2023) warns that without coordinated policies on mining, recycling, and sustainable consumption, shortages of CRM could become a major barrier to the energy transition. Nassar et al. point that critical metals are increasingly central to the geopolitical and economic strategies of leading industrial nations. Their role goes far beyond the traditional economic value of raw materials - they are becoming strategic instruments of global influence and determinants of technological sovereignty (Nassar et al., 2020). For example, the U.S. and the EU remain technologically dependent on China for the production of neodymium and dysprosium magnets, which are critical for electric motors and wind turbines. This underscores the need to diversify supply sources and to increase the share of secondary raw materials.

Figure 2 shows that, while recycling of end of life (EOL) products contributes to the supply of certain metals, its share remains limited - especially for Li, Ge, In where recycled input rates (RIR) are very low. Even more, the reported EOL-RIR for Bi and Ga are zero. This underscores the need to develop and scale up not only recycling of EOL products to obtain CRMs but also reinforces the use of alternative sources- such as mining, mineral processing and metallurgical waste. Lottermoser contended that one of the most promising approaches to ensuring sustainable access to these resources is the utilization of anthropogenic sources - mining and metallurgical wastes, including historical tailings storage facilities and wastewater from mineral processing (Lottermoser, 2010). Ndlovu at al. (2017) confirmed further that beneficiation waste, mine wastewater and waste from base non-ferrous metals production can be a vialable source of critical metals.

Mathieux et al. (2017) pointed the approximate annual quantity of some metals in the EU extractive waste disposed in situ in tailings (i.e. in 'the waste solids or slurries that remain after the treatment of minerals by separation processes, e.g. crushing, grinding, size-sorting, flotation and other physico-chemical techniques to remove the valuable minerals from the less valuable rock'): Co - 200 t, Ga - 95 t, In – 10 t, platinum (Pt) – 0.12 t, palladium (Pd) - 0.12 t. The same authors highlight the evaluated amounts of the 'stock in tailings', i.e. the quantity of the metal disposed in tailings and accumulated over time in EU: Co – 1000 t, Ga - 2000 t, In – 200 t, Pt – 6 t, Pd - 5 t. Europe hosts more than 28000 sites of historical mining waste, many of which contain valuable amounts of Cu, zinc (Zn), lead (Pb), tungsten (W), and REEs (European Commission, 2020).

Similar findings have drawn the attention of the political governing bodies. It is noted that the supply sources diversification has to include a secondary extraction from anthropogenic wastes, and promote innovations in recycling technologies (European Commission, 2020). In response to the growing dependence on external suppliers, the European Union (2024) adopted the Critical Raw Materials Act (CRMA) which pays a special attention to the recovery.

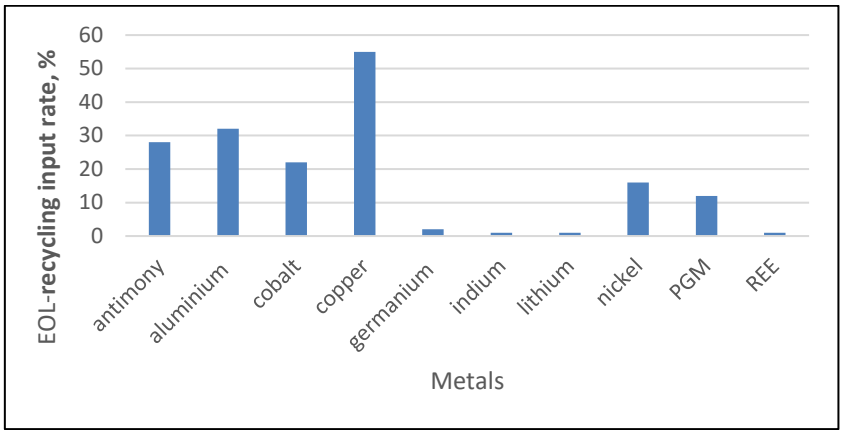

Figure 2. End-of-life recycling input rate (EOL-RIR) for some metals (compiled based on the data from European Commission, 2023): End-of-life recycling input rate (EOL-RIR) is the ‘’Metal produced from EOL feedstock / Total metal production’’of critical raw materials from extractive waste facilities in historical mining regions

The United States, in turn, has pursued a similar course through the Inflation Reduction Act (IRA, 2022) and Defense Production Act (Title III: Expansion of Productive Capacity and Supply**)**, which provide government funding for domestic production of strategic materials. The goal is to reduce dependence on China and establish a domestic industrial base for advanced technologies (DOE, 2023, Neenan, 2023). Therefore, the strategies of the EU, the U.S., and other countries for ensuring strategic autonomy and industrial resilience in modern society include promoting:
- Innovations in technologies for extracting metals from mining waste and industrial tailings by environmentally friendly and sustainable means;
- Investments in sustainable mining practices that minimize social and environmental impacts.

In this context, solid mining waste, contemporary beneficiation tailings, and metallurgical residues represent untapped yet strategically significant secondary sources of critical metals. By focusing on these technogenic resources, the present study addresses both the scarcity of critical metals and the environmental challenges associated with primary extraction waste. The paper contributes to the field by ponting the waste from some nonferrous base metals’ recovery as valuable sources of critical metals, reviewing available extraction technologies, highlighting the potential of mineral processing techniques, and identifying constraints and future research directions for metal recovery. Thus, the study is highly relevant not only for advancing technological solutions in mineral processing and metals recovery but also for supporting strategic autonomy and industrial resilience of EU, as well as the sustainability of global supply chains. By emphasizing the valorization of mining and metallurgical wastes, the research directly contributes to mitigating critical metals dependency, fostering circular economy practices, and reinforcing the broader objectives of the green energy transition.

2. METHODS

Elsevier (Science Direct, Mendeley, Scopus) and Web of Science databases were selected as primary sources due to their extensive coverage of high-impact journals and robust citation tracking capabilities, and Google Scholar - as supplementary discovery. The USGS databases are also searched for. The survey was conducted for the recent 25 years using the relevant keywords. The procedure followed the PRISMA prinsiples (Page et al., 2021). The initial search yelded relevant corresponding papers (totally 1253) and book chapters, and reports (36) that have been further critically reviewed. Refining was done choosing papers/chapers/reports (i) focused on critical metals and presenting data on those metals

concentrations, (ii) devoted on the assessment of eventual amounts available, (iii) where modern analytical methods are applied and (iv) describing contemporary technologies. Reliable data on the recent figures on production, future needs and recycling have been gathered (and crosschecked) for the metals tackled in this paper. The recycling methods have been evaluated from the technological, environmental and sustainability point of view and the soundest ones are briefly presented. Finally, the barriers to metal recycling from technogenic waste are briefly discussed.

3. MINING AND METALLURGICAL WASTE AS SECONDARY SOURCES OF METALS

3.1. Solid Waste

With the increasing global demand for strategic raw materials and the limited potential for discovering new ore deposits, technogenic resources - such as mining waste, processing tailings, metallurgical slags, anode sludges and electrofilter dusts are increasingly considered as secondary sources of critical metals. According to the European Commission (2020, 2023) and the IEA (2023), these resources can significantly contribute to reducing dependence on primary mining and support the transition to a circular economy.

An increasing number of studies have found that mining wastes, including historical tailings and flotation processing residues, contain significant amounts of base and rare metals that were previously not economically feasible to extract. According to Lottermoser (2010), such deposits represent a vast unused potential, containing Co, Cu, molybdenum (Mo), silver (Ag), and even REEs. Reuter et al. (2019) pointed that the design and processing of non-ferrous metals can lead to significant losses of valuable elements, particularly in complex sulfide ores, with up to 30% of the contained metals not recovered. Metallurgical residues, such as Cu and Pb smelting slags and dusts, Zn dusts and sludges, often contain economically relevant concentrations of critical metals including Ni, Co, Ge, In, Pt, Bi, vanadium (V), and titanium (Ti), highlighting the potential for improved circularity through resource-efficient design and recycling strategies (Reuter et al., 2019). In recent years, researchers' attention has shifted to tailings ponds containing residual amounts of metals mined using outdated technologies. Tailings from concentration of nickel sulfide ores, except in Ni, are reach in other critical metals. The following concentrations are presented for such material, in wt. %: Ni – 0,22, Cu – 0,08, Co – 0,03, Mg – 18,72 and As – 0,0256 (Mashingaidze, 2025). Material from Medet flotation tailings dam, Bulgaria bare the following critical metals, in wt. %: Al – 4,59, barium (Ba) – 0,0514, Cu – 0,105, magnesium (Mg) – 1,02, manganese (Mn) – 0,0295, Ni – 0,0012, Ti – 0,21, and vanadium (V) – 0,0186 (Angelov, 2022). A comprehensive study estimated that totally 42 worthies to be considered tailings piles (from mining, mineral processing and metallurgy) of nonferrous metals production from sulfide ores contain different CRM, as follows, in tons: Sb – 15000, Bi - 3100, Cu - 310000, Mo – 55000, W – 3700. In addition, 73 t of gold (Au), 1500 t of Ag, 260 t of In, 5,3 t of rhenium (Re), 620000 t of Pb, and 970000 t of Zn are present. For example, some abandoned Cu flotation tailings contain Cu in the range of 0,17 – 0,40 % and in some piles of slag from Cu smelting the range is 0,27 – 0,70 %. Some old Pb / Zn tailings and waste from Pb / Zn metallurgy hold Bi in the concentration range 0,0055 – 0,0110%. Abandoned tailings damps from Pb / Zn concentration bear W in the range 0,0130-0,0220 % (Šajn, 2022).

It is estimated that in the U.S. in the beginning of this century the sectors producing Cu, Pb, and Zn (mainly from sulfide ores) generated between 23300000 and 24000000 t residue and waste per year (Ally et al., 2001). The U.S. Cu production sector generated 10500000 – 11000000 t per year of residues that are not returned in the process. These residues mainly include fine particles and dust from size reducing operations before flotation, flotation tailings, slag from primary smelting and converters, and gas cleaning sludge. Tailings contain 0,11-0,72 wt % Cu, depending on the technology used. Slag from Cu smelting contains 0,8 -1,1 wt

% Cu. The U.S. Pb producing sector generated 3000000 - 3200000 t per year of waste streams. These process residues included mostly dust and fine particles from size reducing operations before flotation, tailings from flotation, waste slag from the metallurgical stages.The U.S. Zn producing sector generated 9800000 t per year of waste streams. The process residues comprised primarily dust and fine particles from size reducing operations before flotation, flotation tailings, slag, and residues from liquor purification (Ally et al., 2001).

Approximately 50–66 Mt of non-ferrous slag were produced worldwide in 2011 (Piatak et al., 2015). In 2019 these volumes were estimated to over 116.4 Mt worldwide (Walsh, 2019). Producing one ton of Cu from copper concentrate by a typical pyrometallurgical process generates approximately 2 tons of waste Cu slag (Shi et. al., 2008). All above-mentioned figures point that the mining, mineral processing and metallurgical waste is a serious source of metals. A study estimated that if the copper of the final slag produced annually in Finland could be recovered, it would supply 1,2% of the annual Cu production in the country (Kaksonen et al., 2011).

Although not exhaustive, Tables 1-3 provide a clear picture of the presence, type and concentrations of various critical raw materials (according to the EU CRM list, 2023) in waste from the extraction of metals from sulphide ores. As it can be seen the solid waste may contain CRM, sometimes in concentrations higher than in the ores (i.e., primary sources). In addition, it should be noted that the waste from Cu, Pb and Zn production sometimes bears relatively high amounts of Au, Ag, Ge, Ga and PGM (Kaksonen et al., 2011, Guo et al., 2016, Reuter et al., 2019, Lobo, 2022, Huston and Bastrakov, 2024). These are not included in the tables, due to the fact that Au and Ag are not classified as CRM, and the data on PGM, Ga, and Ge are appropriately and very scarce in the literature.

Table 1. Critical and strategic raw materials* in some residues from copper production

Waste	Al	Sb	Ba	Bi	Co	Cu	Mg	Mn	Ni	Ti	Reference
slag[1]	0,46				0,051	0,353		0,042	0,0845	0,122	Kaksonen,2011
slag		0,021		0,020	0,043	1,14	0,288		0,017		Mihailova,2010
slag		0,064		0,007	0,160	5,07			0,036		Mihailova,2010
slag[2]	1,49-9,80	0,0067-0,218	0,024-0,1965	0,0001-0,0056	0,0027-0,4244	0,49-12,2	0,41-3,3	0,075-0,20	0,0008-0,0252	0,09-0,42	Ettler, 2009
slag[3]	3,27		0,223		0,332	2,509	1,074	0,418	0,0071	0,234	Piatak, 2015
slag	2,173						0,72				Kim, 2013
flue dust		3,1		2,8		5,3					Mihailova,2010
flue dust	0,11	9,55		0,12		1,1					Guo, 2016
speiss		8,8		0,003		51,4			8,6		Wikedzi, 2016
anode slimes[4]		0,5-3,4		0,1-0,77		4,8-18,5			0,05-28,1		Khakmardan, 2023
anode slimes[5]		0,5-5,0		0,5-2		20-50			0,5-2,0		Ally, 2001
Cu mining waste	0,7-0,9	0,46-1,03				21-22	0,37-0,41				Wu, 2023
flotat. tailings[6]		15,39		3,9		0,21					Zha,2019

*Data – in wt, %; [1] contains also V - 0,0052 %; [2] contains also Ge – 0,0002 to 0,0123 %; [3] average from 25 slags; [4] based on data from 8 companies; [5] from different companies worldwide; [6] from the copper-anode dressing-metallurgy

Tailings, slags and other residues created by metals production from sulfide ores usually contain pyrite that can dissolve at contacting with water and air thus generating acidity (acid mine drainage - AMD), as presented by the following generalized reaction:

$$FeS_2 + 3{,}75O_2 + 3{,}5H_2O \rightarrow 2SO_4^{2-} + 4H^+ + Fe(OH)_{3(s)}$$

Increased acidity accelerates weathering and leaching reactions, bringing hazardous metals and metalloids (As, Se) to groundwater and nearby soils (Navarro 2008 et al., Lottermoser 2010, Piatak et al., 2015, Minga et al., 2023). The AMD impacts negatively many countries

Table 2. Critical and strategic raw materials* in some residues from lead production

Waste	Al	Sb	Ba	Co	Cu	Mg	Mn	Ni	Ti	V	Reference
slag[1]	2,618		2,063	0,004	0,250	1,002	1,889	0,0097	0,348		Piatak, 2015
slag	1,59-5,02				0,10-0,24	1,20-2,37					Osmani, 2009
slag	1,889	0,0201	0,0169	0,0185	0,0554	3,264	1,11	0,0082	0,15	0,0058	De Andrade, 2011
slag	0,005-1,367	0,0022-0,062	0,44-19,00	0,001-0,0083	0,0045-0,0183	0,62-0,76	0,121-0,995	0,003-0,021	0,036-0,582	0,0051-0,0134	Navarro, 2008
slag		6,5			10,7			2,5			Wikedzi, 2016
hot filter cake				0,5-3,0	0,07-0,08		6-16	0,075-0,085			Ashtari, 2015
matte		0,9			45,3						Minić, 2005
slime[2]		63,6			1,47						Cao, 2010
lead anode slime[3]	0,98	22,70				0,228					Li, 2016
lead smelting flue dust		0,35									Li, 2025
lead softening slag	0,1	17,7			0,1						Ling, 2021

*Data – in wt, %; [1] average from 10 slags (Pb-Ag, Ag-Pb, and Pb-Zn); [2] contains also Bi – 3,31; [3] contains also Bi – 0,86

Table 3. Critical and strategic raw materials* in some residues from zinc production

Waste	Al	Ba	Bi	Co	Cu	Mg	Mn	Ni	Ti	Reference
slag[1]	7,579	0,110		0,0040	0,073	2,412	0,231	0,0047	0,396	Piatak, 2015
slag	2,67				0,90	2,33	0,83			Peng, 2008
slag		0,117		0,0242	0,636			0,0107		Piatak, 2010
ZLR	1,15		0,131		0,91	0,37	1,41	0,0011	0,0566	Li, 2013
ZLR[2]	0,21				0,35					Guo, 2010
hot filter cake				0,5-1,5			3-8	0,04-0,042		Haghighi, 2015

*Data – in wt, %; [1] average from 10 slags (Zn and Zn-Pb); [2]contains In – 0,60 %; ZLR zinc leaching residue

around the world. According to the statistics, about 20000 - 50000 mines are existing in the world, producing AMD, and 19300 km^2 of freshwater and 720 km^2 of lakes and reservoirs have been polluted (Yang et al., 2023). It is found that for many of the minor and trace elements, the concentrations in the leachate generally correlate with their concentrations in the bulk slag sample, when comparing the various slag types. Low concentrations of some elements in the leachates indicate that the elements are hosted by phases that are relatively insoluble under the respective leaching conditions. Soils near to deposed Cu slag are commonly polluted with As, Co, Cr, Cu, Pb, and Zn, and locally – Cd. Elements that usually exceed the environmental levels for soil adjacent to Pb slag are As, Ba, Co, Mn, Pb, and Zn. Elements – pollutants of soil near to Zn slag deposits commonly are As, Cr, Pb, and Zn (Piatak et al., 2015). Recycling of mine tailings will reduce their ability to generate AMD (Park et al., 2019). Thus, recovering CRM from solid waste generated by metals extraction from sulfide ores will not only contribute to ensuring needed commodities but will also contribute to cleaner and safer environment.

3.2. Liquid Waste

Wastewaters generated during mining, mineral beneficiation and metallurgical processes are also considered a potential source of metals. According to an estimation, 10527 Mm^3/year wastewater was generated by mining in years 2008-2018 (Szlachta, 2020). As illustration, approximately 15000 m^3 /day of AMD has been produced by the Liwu mud-retaining dam, China with a yearly averaged discharge per day, as follows, in kg/day: Cu -220,20, Fe - 4967,55, Zn - 1206,15 and Mn - 994,20 (Chen, et. al, 2014). For example, the liquid effluent from ore flotation (a DR Congo Concentrator) contains - 0,38 mg/L Cu, 0,24 mg/L Co and 0,03 mg/L Ni (Lutandula and Mpanga, 2021). AMD holds significant amounts of dissolved critical, strategic and other valuable metals such as Al, Co, Mn, Cu, Ni, Zn, etc. Mine drainage water may contain REEs, for example stream waters draining an old mining area (Fenice Capanne mining, Italy) have REEs contents, reaching 0,928 mg/L as the maximum (on average in the range 0,524 - 0,670 mg/L) at pH around 3,9 (Protano and Riccobono, 2002). The recovery of these valuable metals can contribute to those metals supply besides solving the potential pollution issues. Table 4 presents examples on some critical and strategic metals presence in wastewater generated by metals' recovery from sulfide ores – data are chosen with the aim to illustrate that those valuable metals present in the wastewater from the whole world. For the purpose of the presentation below: mining effluent (ME) is water that is used to crush and size the ore or that is used to process the ore applying beneficiation or hydrometallurgical extraction techniques; Mine drainage (MD) water is surface or ground water that flows from the active or abandoned mine site into surrounding areas; AMD is low pH surface or ground water that is formed from the oxidation of sulfide minerals and flows from the mine site into surrounding areas.

Table 4. Critical and strategic raw materials* in mining effluents (ME), mine drainage water (MD), and acid mine drainage (AMD) due to mining and processing of sulfide ores of nonferrous base metals, mg/L

Conc, mg/L	pH	Al	Li	Co	Cu	Mg	Mn	Ni	V	ΣREE	Refe-rence
China ME	2,5				2670		6590				Song, 2022
Chile ME	2,5	1139			2298		224,5				Yuan, 2022
Russia ME**	2,1	520		4,2	32	420	18	4,8			Bortnikova,2020
Särkiniemi, MD Finland	nn	9	0,04	0,18	0,225	23,3	1,04	2,79		0,0723	Szlachta, 2020
Kotalahti MD Finland,	nn	11,2	0,19	0,45	0,5	185	2,82	16,2		0,2484	Szlachta, 2020
Hammaslahti, MD Finland	nn		0,065	0,68	0,715	365	11,15	0,625		4,484	Szlachta, 2020
Hitura, MD Finland,	nn	114,5	0,03	10,5		1725	6,51	20,1		0,247	Szlachta, 2020
South Africa MD	nn	0,016				860	2,5	0,21			Masindi, 2022
South Africa AMD	2-4	75-500			0,4-10	50-400	10-100	0,21-10			Masindi, 2022
Australia AMD	2,7	2317		5,2	65	4562	245	2,1			Brewster, 2020
Australia AMD	3,74		0,39	4,05	77,26	2265	161,5	1,54			Kaur, 2018
China, AMD[1]	2,4-2,7	533-580			44-48		62-66				Hu, 2022

China, AMD	2,43	63,43	0,08	67,01	14,68		66,28	0,26	0,04		Chen, 2014
S. Korea, AMD	3,14	24,4			4,8	20,5	26,2				Oh, 2016
Chile, AMD	2	382,6		0,38	531,2		72,0				Pino, 2020
AMD, Chile	-	293		2,33	615	436	203				Pino, 2020
Spain AMD	3,1	117		0,901	10	267	19	0,973	0,014		Caraballo 2009
Spain[2], AMD	2,7	128			7	263	18			7,9	Ayora, 2016
Spain[3], AMD	2,6	251			165	1104	467			3,5	Ayora, 2016
Spain[4], AMD	2,7	386		0,0034	64	414	37	0,001	0,065		España, 2008
Slovakia, AMD	3,8	108,38			8,38		35,50				Macingova, 2012
USA, AMD	4,14	314		1,81	62	631	617	1,382			
Canada, AMD	2,75	131,1					36,7				Park, 2019

*According to the EU CRM list (2023); ** - in addition to the presented in the table – Sb 0,18, Bi 1,7 and In 0,054 mg/L; nn nearly neutral; [1] – from a tailing pond, averaged from 6 different samples, [2] - Monte Romero, [3] – Almagrera, [4] - average chemical composition of 62 AMD waters from 25 mines of the Iberian Pyrite Belt

Wastewater from metallurgy of nonferrous metals also contains CRM in elevated concentrations. A typical example is copper metallurgy, and illustative data are presented in Table 5 (Cusano et al., 2017).

Table 5. Some critical and strategic raw materials* in wastewater from copper production

Parameter Industry	Flow, m^3/yr.	H_2SO_4, g/L[1] (pH)	Cu, mg/L,	As, mg/L	Ni, mg/L	Zn**, mg/L
Aurubis Pirdop[2]	950000	60	2100	2200	450	500
Aurubis Hamburg[3]	180000	50	2000	2000	1000	1000
Atlantic Copper[4]		(pH < 1)	2000	10000	4000	5000
Umicore Hoboken - A[5]	-	35 (pH~1)	0,08–2,450	0,9–10,000	0,03–450	0,1–4,400
Umicore Hoboken - B[5]	-	35 (pH~1)	0,1–2,900	0,2–2,600	0,4–270	0,05–1,100
Umicore Hoboken - sewer[5]	-	(pH 9)	0,03–37	0,1–24	0,1–27	0,03–8

*According to the EU CRM list (2023), ** not in the EU CRM list, but present in the USA CRM list (2022); [1] acid concentration is given as an indication of the effluent acidity; [2] The process water treatment at Aurubis Pirdop gathers weak acid from the acid plant, wet scrubber water from the smelter secondary gas cleaning, bleed from the electrolytic refining, and some surface water; [3] The process water treatment in Aurubis Hamburg collects mainly weak acid from the off-gas cleaning of primary and secondary copper smelters, effluents from the precious metals plant, condensates, laboratory waste water; [4] The Atlantic Copper waste water treatment plant gathers effluents primarily from the slag cleaning electric furnace gas scrubber, the concentrates storage area, ion exchange resins regeneration, and the fire refining gas scrubbers' bleed; [5] At Umicore Hoboken (a smelter treating Cu, Pb and primary and secondary raw materials containing precious metals), there are three circuits: A - treating acid process waters with As, B - treating acid process waters without As, and a sewer - rainwater, excess sprinkling water, contact cooling water, some process waters.

4. MODERN TECHNOLOGİES FOR METALS EXTRACTİON FROM INDUSTRİAL AND MİNİNG WASTE SOURCES

4.1. Solid Waste Treatment

Technogenic waste, including mining waste, tailings and metallurgical slags, represent a valuable secondary source of critical metals. Despite its significant potential, the use of mining and mineral processing waste to recover critical metals faces technological challenges, such as (i) heterogeneity of the material composition and problems with representative sampling in big areas where the waste was dumped for long time; (ii) lack of standardized methods for analyzing and assessing metal content; (iii) need of modification of technologies for metals recovery from ores or development of new technologies. The regulatory and environmental constraints are another barrier usually met. In addition, economic factors are very important: (i) generally, the implementation of new technologies needs high capital costs; (ii) sometimes the particular metal production from primary raw material is cheaper than its recycling (Matinde et al., 2018). Advancing technologies for the extraction of metals from solid technogenic sources (mining waste, tailings, slags, and other industrial residues) is vital for ensuring a sustainable supply of essential raw materials and decreasing reliance on primary mining.

Pyrometallurgy and hydrometallurgy are conventional technologies in metals recycling, including for metals recovery from waste from nonferrous metals production. In order to achieve good results, they have to be preceded by a physical-mechanical pre-treatment. New developments of established technologies (such as biometallurgy) and employment of new technologies (electrochemical, supercritical fluid) are being extensively studied with the aim to permanently enter the field of metals recovery.

Physical-mechanical methods involve processes that utilize the mechanical or physical properties of materials without altering their chemical composition. Their primary purpose is the separation, concentration, and preliminary processing of the secondary raw material. Key methods include (Lottermoser, 2010, Reuter et al., 2019):

- Crushing and grinding – reducing the size of the material to fractions suitable for further processing;
- Screening (sieving) – separating materials by size or shape;
- Gravity separation – exploiting differences in mineral density using jigs, sluices, or spiral concentrators;
- Pneumatic separation – separating particles by size, shape, density using air, etc,;
- Magnetic and electrostatic separation – sorting out magnetic or conductive minerals from non-metallic (and/or non-magnetic) components;
- Froth flotation – a physico-chemical method that concentrates minerals based on differences in surface properties.

Physical-mechanical methods are used as a preliminary processing step, concentrating the metals and reducing the material volume for subsequent treatments.

Mainly chemical composition of the materials, as well as volumes to be processed, determine what will be the subsequent treatment - pyro- or hydrometallurgy. According to Reuter, pyrometallurgical methods, which rely on high temperatures to extract metals, play a central role in non-ferrous metal processing. These processes include smelting slags to recover elements such as Cu, Ni, V and W; refining metals through oxidation and reduction; and applying integrated techniques for the recovery of precious metals from complex metallurgical wastes, thereby enhancing resource efficiency (Reuter et al., 2019). Although energy-intensive and needing expensive equipment to meet the environmental requirements, pyrometallurgy remains suitable for high-concentration wastes and slags, where chemical and biotechnological methods are less effective.

Hydrometallurgy is a method of separating looked-for metals from materials by applying suitable solutions (inorganic or organic). The metals are dissolved and then recovered from the pregnant leach solution (PLS). The recovery from PLS involves purification and separation by applying different procedures, such as precipitation / crystallization, ion adsorption or ion exchange, solvent extraction, electrochemical reduction, etc. (Panayotova and Panayotov, 2017). Membrane processes are also attempted (Meschke et al., 2020). Hydrometallurgy advantages in comparison to pyrometallurgy are lower capital costs, possibility of treating smaller volumes of material, fast adaptation to changing composition of the material to be treated, good selectivity to target metals, easy operation and process control, less environment pollution, inherent to the process including the application of low-toxicity solvents. Due to its advantages, it seems more applicable for treating technogenic waste from metals production from sulfide ores. Generation of liquid wastes and sludge that must be handled and sometimes slow leaching kinetic, low leaching rate or low lixiviant stability can be pointed out as drawback of the process (Pozo, 2025).

Bio-metallurgical treatment utilizes microorganisms or biological materials to mobilize and extract metals. Bio-metallurgy comprises two main approaches, bioleaching and biosorption. Bioleaching refers to employing specific microorganisms (bacteria, fungi, algae) or their metabolites to interact with metals and extract them into solution. The method is considered suitable for solubilizing Cu, Mn, Zn, Co from tailings, slag, metallurgical dust (Sethurajan et. al., 2018). Kara and co-authors (2023) exhaustively presented the microbial diversity and specific mechanisms of bioleaching aimed at metal recovery. Bioleaching advantages are process simplicity, selectively, and flexibility, low cost and less environmental pollution. The key disadvantages of the process are low leaching rates and long operation time, limitations in the type and amounts of recycled metal, the possibility for poisoning the used for leaching microorganisms by the toxic elements, presenting in the waste and leached. Biosorption is a metabolism independent physico-chemical process that removes substances from solution by biological materials. Actually, this is a process of extraction from the solution of already leached or dissolved metal. It uses biomass (e.g., algae, fungi, bacteria) to selectively separate Co, Cu, Ni, Mn and Zn (Johnson, 2014). Bio-metallurgical methods are environmentally friendly, consume less energy, and can be applied to low-concentration solid waste as mining / mineral processing tailings or dilute streams, where conventional technologies are economically unfeasible.

Electrochemical technology is promising due to its minimal chemicals' usage. Anodic current can facilitate the solid materials disintegration and leaching. After the leaching, another reactor can be installed where the dissolved metals can be electro-won. In general, this is an environment-friendly technology, but the sludge generated (often classified as hazardous waste) needs further treatment and disposal (Samarjeet et al., 2023). Supercritical fluids technologies, which are able to dissolve materials like a liquid and effuse through solids like a gas, are considered as promising means for the extraction of metals (Lin et al., 2014). However, after applying the supercritical technology, the remaining metals mixture still needs to be further separated through other technologies.

Modern technologies increasingly aim to integrate multiple methods to enhance metal recovery from solid waste and the overall efficiency. The process typically involves physical-mechanical beneficiation to concentrate metals, hydrometallurgical leaching to extract specific metals, a biotechnological stage for further recovery of dissolved metals, and pyrometallurgical treatment to reclaim high-concentration residues (Reuter et al., 2019). For example, Ndlovu et al., (2017) demonstrated that combining flotation and hydrometallurgy can increase the recovery of Co and Ni from tailings, achieving over 80% efficiency. Such a multi-stage approach maximizes extraction efficiency while minimizing environmental impact and reducing losses of valuable and critical metals.

4.2. Liquid Waste Treatment

Methods for treating waste liquid effluents from metal production with the aim to separate and further recycle specific metals can be classified as active and passive. The active treatment is most appropriate to operating mines, mineral beneficiation and metallurgical enterprises or for the closure and post-closure applications typically associated with large flows. The passive treatment is more suitable for the closure and post-closure phases of mines and abandoned mine sites or areas around ancient mineral beneficiation and/or metallurgy. From the other hand the methods can be divided in abiotic and biological treatment. Abiotic methods are generally classified into physical, chemical and physicochemical. Mainly they are applied to recover valuable metals from waste liquid streams generated by metals production.
Physical methods use large shallow sedimentary lakes or tanks allowing suspended solids to settle out of the water. The water stays long enough in order the oxygen dissolved in the water to promote the formation of iron hydroxides that settle also down. Other heavy metals are adsorbed on the hydroxides. This simple but effective process is able to remove a significant portion of pollutants. However, usually it is not enough to achieve the maximum permissible levels for water discharge in natural water bodies or to separate efficiently valuable metals.

The chemical treatment is largely used to remove dissolved metals (Bortnikova, et al. 2020, Meng et al. 2022) from waste liquid streams. The most widely applied process is neutralization, followed by chemical precipitation of heavy metals hydroxides. Lime, limestone, slaked lime, caustic soda, magnesium hydroxide are the reagents often used. In general, the solid phase generated, besides heavy metals hydroxides, contains gypsum and unreacted alkalizing reagent, which facilitate precipitation and counteract eventual acidification and mobilization of the heavy metal ions. However, the precipitate / sludge formed in large volumes usually is classified as hazardous waste that requires drying facilities and further handling. The sludge disposal is the most expensive and the most difficult part of this mode of treatment and it is also a likely permanent environmental hazard. In addition, thus realized treatment generally does not recover valuable metals. In order to recuperate valuable metals from waste liquid streams selective stepwise (at different pH values) (Masindi et al., 2018) and /or sequential precipitation (with specific precipitants, such as sulfides - H_2S, Na_2S and NaHS) (Macingova and Luptakova, 2012, Oh et al., 2016), oxidation followed by several steps fractional precipitation (Chen et al., 2014) or variation of the redox conditions (Christoferson, 2020) are proposed. The treatment approach is applicable both for mine drainage and wastewater from mineral beneficiation and metallurgy (Weijma et al., 2022, Mazur and Penha, 2025).

Physicochemical methods (appropriate to all types of waste effluents from mining, mineral processing and metallurgy), comprise mainly flocculants and coagulants addition followed by precipitation (Cusano et al., 2017, Song et al., 2021), flotation (Deliyanni et al., 2017, Yenial and Bulut, 2017), adsorption (Motsi et al., 2009, Jagadeesh et. al., 2023), methods based on electrochemical reactions (Wu et al., 2019), on use of ion exchange (Felipe et al., 2021), solvent extraction (Pino et al., 2020) and membrane processes. Membrane processes most often proposed include microfiltration, ultrafiltration, nanofiltration and reverse osmosis (Mulopo, 2022, Yang et al., 2023). Chemical coagulation and flocculation, followed by precipitation are widely used processes to eleminate pollutants from mineral-processing wastewater (Park et al., 2018) owed to their simplicity and effectiveness. The processes remove suspended solids and heavy metals from treated water. However, the introduced counter-ions and residual chemicals may interfere with treated water use, for example further in the flotation. In addition, valuable metals are practically lost. Adsorption is considered one of the most effective methods for recovering metals from low-concentration streams. It is a simple process, uses abundant and low-cost adsorbents. Limited adsorption capacity, which leads to poor performance in highly concentrated solutions (such as AMD or in some cases waste liquid streams from metallurgy), some difficulties with adsorbents regeneration and challenges associated with loaded adsorbents disposal can be pointed as drawbacks. Solvent extraction, followed by electrodeposition, is employed to extract metals from waste streams at

high concentrations of those metals. Due to higher costs, the method is mostly suitable for small volumes of water with relatibvely high concentrations of dissolved metal. Recently the electrochemical treatment (electro-reduction, electro-oxidation, electro-adsorption, and electro-coagulation and precipitation) of AMD or process water with the aim to recover metals and/or water reuse, has attracted the attention as controllable and environment-friendly method (Maarof et al., 2017, Yang et al., 2021). The catholyte produced via electrolysis contains a high concentration of hydroxide ions generated by the cathodic reaction. It can be successfully used as a neutralizing agent to change stepwise the pH value of an acidic effluent containing Al, Fe, Cu and Zn and recover selectively those metals (Park, 2015). An electrochemical treatment of the effluent (containing arsenic in high concentrations) from flue gas washing in copper metallurgy is proposed. Recovery of 75-80 % of Cu and 50 % of the As dissolved is achieved - both critical elements were separated in a state suitable for further utilization (Panayotov et al., 2019). Brewster et al. (2020) also used catholyte to neutralize AMD. They found that the electrochemical treatment exhibited the same capacity as $Ca(OH)_2$ addition to neutralise AMD and remove sulfates, and both were much better than NaOH. Furthermore, the electrochemical treatment produced less voluminous and more easily settleable sludge than $Ca(OH)_2$. Chemical's addition is avoided. Furthermore, the staged treatment approach demonstrated the potential to produce metal-rich powdered solids with a targeted composition, including rare earth elements and yttrium (REY). In the dried solids, metals recovered by the chemical neutralization and precipitation were found in lower concentrations compared to metals precipitated electrochemically. When the price for the produced sludge treatment, water savings by eliminating slaking needs and the possibility to selectively recover metals and REY using pH-driven staged precipitation are considered, the costs for electrochemical treatment are even somehow smaller compared to classical reagents precipitation (Brewster, 2020). Very recently the design and demonstration of an electrochemically activated limestone (EAL) system for AMD treatment and valuable metal extraction are reported (Li et al., 2025). The EAL system extracted 82,3-100,0% of Cu, Cd, Zn with high purity (~81,3 wt% of metals) using electro-reduction and local high pH-mediated precipitation when treating a real AMD at energy consumption of 0,006-0,180 kW·h/g metal. The effluent after the EAL treatment contains Ca^{2+} and is high alkaline, thus having CO_2 sequestration potential. This way, the EAL decreases treatment total costs by 17,9% and CO_2 emissions by 60,1% compared to conventional lime dosing treatment.

Membrane technologies are widely investigated with the aim to facilitate the recovering of valuable metals from wastewater from mining, mineral processing and extractive metallurgy. At the same time, they ensure high quality of treated water. However, they are still underused in real mining industry. Membranes are semi-permeable films or structures of materials that permit only certain species or substances to pass and prevent passage of others. Different forces can drive ions / substances through membrane - pressure difference, electric potential difference, chemical potential difference or temperature difference (Song et al., 2018). Mainly pressure driven processes (ultrafiltration - UF, nanofiltration - NF, and reverse osmosis – RO) are applied to treat waste liquid streams from metal production, although the studies on forward osmosis – FO, based on chemical potential difference are advancing (Panayotova and Panayotov, 2021). Results from studies and applications of UF, NF, RO and electrodialysis ED (a membrane process driven by the electric potential difference) for the treatment of AMD and mine influenced water are comprehensively presented and discussed by Mortazavi (2008). Zhong studied commercial polyamide ultra-low-pressure RO and NF membranes for their capability to remove heavy metal ions from AMD. Rejections achieved were 97 % and 95 % respectively pointing at the possibility to recover metals from the concentrate obtained (Zhong, et al., 2007). Samaei and co-workers evaluated the performance of RO as a wastewater post-treatment process in mining operations in Victoria, Australia (Samaei et al., 2020). It is found that the RO treatment significantly improves the quality of the final water to be discharged. The rejection efficiency and correspondingly the concentration of metals for further recovery for 4-years evaluation period was 95 %, 66 %, 82 %, 48 % for antimony, arsenic, nickel, and zinc respectively. Although the RO can treat AMD to reclaim drinking water (Masindi et al., 2019) it

is still not very cheap process mainly due to the energy required to achieve a high pressure needed as a driving force. That is why other lower pressure processes (UF, NF, FO) are extensively considered. Nanofiltration needs lower pressure, compared to RO, does not need addition of surfactants and polymers and is able to preferable concentrate two and higher valency ions, like critical metals Co, Cu, Ni, etc. This is why this process has been widely studied for concentrating metals from liquid streams from mineral processing and metals production enterprises (Rieger et al. 2009, Mullett et al., 2014, Junior et al., 2023). The usability of different RO and NF membranes for treating AMD is studied, including with the aim to check the applicability at a commercial scale (Al-Zoubi et. al., 2010, Pino et al., 2020). The results showed that NF membranes successfully treated AMD, the heavy metals rejection and concentration is over 98% at higher fluxes and at lower pressure (consequently energy consumption) compared to RO. An adsorptive PVC nanofibrous/thiol-functionalized titanate nanotubes composite UF membranes have been prepared and showed removal (concentrating) efficiency of 90% and 86,7%, respectively for Cu(II) and Ni(II) in presence of competing ions (Hezarjaribi et al., 2021). Micellar-enhanced UF membrane process has been developed and successfully used at experimental scale for recovering of Cu, Ni, and Co ions from synthetic mining wastewater. The rejection rates of all three metals exceeded 99% and they were conveniently concentrated for further recovery (Lin et al., 2017). Polymer-enhanced ultrafiltration (PEUF) showed promising results for concentration and recovery of some CRM (Co, Mg, Ni, Zn) and especially Cu from AMD and other process waste liquid streams (Huang and Feng, 2019). The Forward osmosis promotes concentration of water flux from a solution to be concentrated, by contacting it with a solution presenting a higher osmotic potential, referred to as draw solution (DS). Contact of both solutions is mediated by a thin-film composite membrane that enables the permeation of water, but rejects solutes. The application of FO for the treatment of AMD is studied with NaCl as draw solution (Vital et al., 2018). The individual rejections and concentration rates achieved for some CRM are as follows: Al - 99,8%, Co - 99,4%, Cu - 98,9%, Mg - 98,9%, Mn - 99,6%, Si - 97,1%, and Zn - 99,5%. It is reported that FO could effectively reject three REEs (e.g., lanthanum, cerium, and dysprosium) using NaCl as draw solution. The rejection / concentration of these REEs can reach 86–96% at 20 ^{o}C, (Pramanik et al., 2019). Studies have shown that often integrating different membrane processes improved the treatment performance (Thiruvenkatachari et al., 2016, Amaral et al., 2018). The advantages of membrane technologies are high efficiency and high degree of automation, while the drawbacks are easy contamination, poor permeability and acid resistance (Yang, 2023). In addition, the processes are still of relatively high cost that leads to the employment of membrane technologies to recover mainly gold, silver and PGM from those metals mining, processing and metallurgy wastewater (Gebreslassie et al., 2024).

Biological methods for metals recovery from liquid waste streams (mainly MD and AMD) are based on the metal-microbe interactions that allow precipitation, reduction or sorption process that concentrate and separate metals. Bioprecipitation is a biologically caused processes empowering the formation of sulfides, hydrogen sulfide, carbonates, phosphates or hydroxides that can precipitate metals. The most well-known process for the recovery of metals from wastewater streams apply biological sulfate / sulfur reduction by bacteria to precipitate sulfides. The use of biogenic sulfide not only allows the formation of insoluble metal sulfides thus separating metals, even from acidic streams and at low metal concentrations, but it decreases the sulfates concentration. The method is suitable to separate metals with significantly different solubility products of their sulfides, for example Ni and Fe. The treatment method is used to immobilize different CRM (Al, Co, Cu, Li, Mg, Mn, Ni, Zn) from real AMD (Dev et al., 2017, Akinpelu et al., 2021). The process has reached commercial applications for the recovery of Zn and Cu from mine and metallurgical waste streams (Weijma et al., 2022). Bio-reduction is process where metal ions are reduced to metals or to ions that are easily precipitated under the treatment conditions. In both cases ions are immobilized and concentrated in a solid / sludge. Critical metals that could be recovered through bioreduction include Co, Ni, V (Gomez et al., 2025). Biosorption and bioaccumulation are two processes that immobilize ions from a solution using non-living and living biomass, respectively. When extracted ions are bound to

the to a cell's surface the process is named biosorption, and when they are taken and accumulated into a cell, the process is called bioaccumulation. Different biosorption studies have used bacteria, algae, seagrass and crab shells, to extract Co, Ni, W, and V, as well as Re and tin (Sn), from aqueous solutions. Some studies have used bioaccumulation in bacteria and yeast, to recover of Co and Ni from aqueous solutions. Johnson (2014) demonstrated that biotechnological processes, including bioleaching, and biosorption can recover up to 90% of metals, transforming wastewaters into a valuable secondary source of strategic raw materials. However, the studies have been carried out predominately on lab-scale using synthetic solutions (Gomez et al, 2025). In the bioelectrochemical systems (BES) microbes, metal ions and electrodes interact to recover metals. In these systems microorganisms transfer electrons driving the redox reactions. The microorganisms can employ both oxidation and reduction processes and can be attached to one electrode only (bioanode) or to both electrodes (bioanode and biocathode) space (Dominguez-Benetton et al., 2018). A selective metal recovery can be achieved by fine-tuning the potential at which oxidation (or reduction) occurs. In addition, power can be produced when the metal ions have positive standard reduction potentials and the anode has negative standard reduction potentials. The critical metals recovery using BES has been largely studied recently. The CRM extracted through BES include Al, Co, Mg, Mo, Ni, W, V and even REY (Gd, Nd, Y) (Pozo et al., 2017). However, the studies are mainly at lab level, majority are with model solutions. Effect of different factors have to be studied and optimized to upscale these systems for commercial metal recovery.

Finally, it can be summarized that fractional precipitation by addition of alkalizing reagents appears to be the most mature method for CMR separation and recovery, applicable to liquid streams with different concentrations of metal ions. Solvent extraction is most suitable for small volumes of liquid waste that contains metals in relatively high concentrations. Adsorption is proper for immobilizing metal ions from dilute wastewater. Membrane processes exhibit their advantages when the valuable metals have to be concentrated from streams where they present at low concentrations. However, the treatment total costs limit their application mainly to precious metals. Different electrochemically based methods seem to be suitable for a wide range of metal ions concentrations. Bioprecipitation and to a certain extent metal ions immobilization, based on bio-reduction, have achieved maturity, however they are applicable only for specific metals. Although very promising, BES will go long way of optimization before being able to be used in real life. In addition, it has to be stressed that except for some electrochemically based methods (electroreduction with externally applied electricity or by addition of metal with lower potential, i.e., replacement), all mentioned methods immobilize / separate metal ions from the solution as precipitate, concentrate, eluate, raffinate and additional treatment is needed to obtain a metal. In very limited cases the precipitates produced are enough high-quality compounds of the corresponding metals and may be directly used.

4.3. Limitations, Challenges and Future Directions

Above mentioned examples of metals presence in and their extraction from technogenic sources demonstrate that mining and metallurgical solid wastes can be valuable resources rather than merely environmental liabilities. Despite the significant potential of technogenic sources, metals recovery from these materials is associated with a range of challenges. Firstly, metal concentrations are often low, necessitating the processing of large volumes of material with high energy and financial costs. Secondly, the chemical complexity and mineralogical heterogeneity of the wastes complicates use of standard mineral beneficiation and hydrometallurgical methods. Moreover, a report points (European Commission, 2020) that the reprocessing of old tailings can pose environmental risks, including site erosion, groundwater contamination, and the generation of acid drainage. So, while technogenic sources hold considerable potential for supplementing primary metal supplies, realizing this potential requires addressing multiple technological, environmental, and regulatory challenges.

The low metal concentrations, combined wih complex compositions, and the environmental risks associated with reprocessing the solid waste from metals recovery demand continued research, innovative technologies, and the development of efficient, safe and environmentally friendly, as well as cost-effective recovery methods. Future research should focus on the development of flexible, multi-stage, integrated approaches that combine physical, hydro- and/or pyrometallurgical, and biotechnological methods. Technologies combination has to be based on the physical and chemical properties of the materials that will be processed in a given plant and waste volume. Low concentrations of CRM, different and changeable composition, often large but also changeable volume of liquid waste streams hint to the need to develop site specific technology, most often a combination of different treatment approaches, when the aim is to recover metals from liquid waste streams.

Advances in biotechnologies are expected to play a pivotal role in environmentally friendly metal recovery, enabling the selective extraction of metals from low-concentration and complex waste streams (Kara et al., 2023). In addition, progress in nanotechnology, materials science, and process engineering offers new opportunities to enhance recovery efficiency, reduce energy consumption, and minimize environmental impacts. Ndlovu and co-authors (2017) emphasize that the application of digital technologies, artificial intelligence, and sensor-based control can significantly enhance process efficiency. Finally, the future technologies combination for sustainable and environmentally-friendly metals recovery from technogenic waste should be prepared to face commercialization, and suit for small and medium-sized enterprises in terms of investment and equipment.

Future research should be supported by effective policy frameworks and economic incentives that are essential to stimulate investment and foster collaboration between industry, governments, and research institutions. Addressing these limitations is crucial for advancing sustainable approaches to metal recovery from secondary resources. The European Commission (2023) also highlights the lack of sufficient incentives and regulatory frameworks for investing in secondary resource recovery, which requires coordinated efforts among industry, governments, and research organizations. The Commission calls for the establishment of strategic reserves and the promotion of research and development activities to ensure the sustainable management of critical raw materials.

5. CONCLUSION

Mining and metallurgical solid and liquid waste constitute a substantial, yet largely untapped, source of metals essential for the society sustainable development and the green transition. Several directions for future progress can be identified to enhance the sustainable recovery of critical metals from those secondary sources:

- Development and implementation of integrated technologies that combine beneficiation, hydrometallurgical or pyrometallurgical, and biotechnological approaches in order to achieve maximum recovery of critical metals from solid waste; Opting a combination of technologies to recover CRM from liquid waste streams. Key considerations to the selection of appropriate and reliable set of technologies are: proven performance; low reliance on different chemicals; low energy usage, capital, operation and maintenance cost; ease of operations; robust processes able to deal with changeable volums and compositions; small amounts of hazardous (secondary) waste generation and ways of its handling; clean water recovery; environmetal friendliness.
- Advancing the policies that promote secondary raw materials usage by creating and implementing regulatory measures and financial incentives for recycling and application of technogenic waste-derived metals.
- Fostering the research and innovation that enhance process efficiency and reduce the environmental footprint by applying biotechnological approaches, automation, digital

technologies and focusing on direct production of innovative materials based on the CRM recovered from technogenic solid and / or liquid waste.
- Establishing of standardized methodologies for the assessment of anthropogenic sources and quality control of extracted CRMs that are essential to facilitate the recovered metals integration into industrial supply chains.

Critical metals are no longer merely industrial resources but strategic assets that determine technological independence, industrial resilience, and the society future. The integration of research and innovation in different scientific areas with industrial implementations of advanced technologies, underpinned by supportive policies and strategic investments, will ensure a secure and sustainable supply of these resources in the coming decades.

Acknowledgement. This research was funded by the National Science Program “Critical and strategic raw materials for a green transition and sustainable development”, which was approved by the Resolution of the Council of Ministers № 508/18.07.2024 and funded by the Ministry of Education and Science (MES) of Bulgaria.

REFERENCES

Akinpelu, E. A., Ntwampe, S. K. O., Fosso-Kankeu, E., Waanders, F., (2021) ’’Comparative analysis of brewing wastewater and lactate as carbon sources for microbial community treating acid mine drainage in anaerobic MBBR systems’’, Environmental Technology, 42 (25) 3955–3962.

Al-Zoubi, H., Rieger, A., Steinberger, P., Pelz, W., Haseneder, R., Härtel, G., (2010) ’’Optimization Study for Treatment of Acid Mine Drainage Using Membrane Technology’’, Separation Science and Technology, 45 (14) 2004–2016.

Ally, M. R., Berry, J. B., Dole, L. R., Ferrada, J. J., Van Dyke, J. W., (2001), Economical Recovery of By-products in the Mining Industry, Oak Ridge National Laboratory, Oak Ridge, Tennessee.

Amaral, M. C. S., Grossi, L. B., Ramos, R. L., Ricci, B. C., Andrade, L. H., (2018) ’’Integrated UF–NF–RO route for gold mining effluent treatment: From bench-scale to pilot-scale’’, Desalination, 440 111–121.

Andersson, P., (2020) ’’Chinese assessments of “critical” and “strategic” raw materials: Concepts, categories, policies, and implications’’, The Extractive Industries and Society, 7 127–137.

Angelov, T., (2022) ’’Mineralogical and hydraulic characterisation of historic flotation tailings’’, Sustainable extraction and processing of raw materials journal, 3 6-10.

Ashtari, P., Pourghahramani, P., (2015) ’’Selective mechano-chemical alkaline leaching of zinc from zinc plants residue’’, Hydrometallurgy, 156, 165-172.

Ayora, C., Macias, F., Torres, E., Lozano, A., Carrero, S., Nieto, J. M., Perez-Lopez, R., Fernandez-Martinez, A., Castillo-Michel, H., (2016) ’’Recovery of rare earth elements and yttrium from passive-remediation systems of acid mine drainage’’, Environmental Science & Technology, 50 8255–8262.
Bortnikova, S., Gaskova, O., Yurkevich, N., Saeva, O., Abrosimova, N., (2020) ’’Chemical treatment of highly toxic acid mine drainage at a gold mining site in southwestern Siberia, Russia’’, Minerals, 10 867.

Brewster, E. T., Freguia, S., Edraki, M., Berry, L., Ledezma, P., (2020) ’’Staged electrochemical treatment guided by modelling allows for targeted recovery of metals and rare earth elements from acid mine drainage’’, Journal of Environmental Management, 275 111266.

Cao, H., Chen, J., Yuan, H., Zheng, G., (2010) ’’Preparation of pure $SbCl_3$ from lead anode slime bearing high antimony and low silver’’, Transactions of Nonferrous Metals Society of China, 20 2397–2403.

Caraballo, M. A., Rőtting, T. S., Machas, F., Nieto, J. M., Ayora, C. (2009) ''Field multi-step limestone and MgO passive system to treat acid mine drainage with high metal concentrations'', Applied Geochemistry, 24 2301–2311.

Chen, T., Yan, B., Lei, C., Xiao, X. M., (2014) ''Pollution control and metal resource recovery for acid mine drainage'', Hydrometallurgy 147–148 112–119.

Chen, T., Yan, B., Lei, C., Xiao, X. M., (2014) ''Pollution control and metal resource recovery for acid mine drainage'', Hydrometallurgy, 147–148112–119.

Christoferson, R. L., (2020) "Selective Precipitation and Recovery of Rare Earth Elements from Acid Mine Drainage", Graduate Theses, Dissertations, and Problem Reports, 7825.

Cusano, G., Gonzalo, M. R., Farrell, F., Remus, R., Roudier, S., Sancho L. D., (2017), Best Available Techniques (BAT) Reference Document for the main Non-Ferrous Metals Industries, EUR 28648, Luxembourg, Publications Office of the European Union.

De Andrade, L. R. P., Lima, L. R. P., Bernardez, L. A., (2011) ''Characterization of the lead smelter slag in Santo Amaro, Bahia, Brazil'', Journal of Hazardous Materials, 189 (3) 692–699.

Deliyanni, E. A., Kyzas, G. Z., Matis, K. A., (2017) ''Various flotation techniques for metal ions removal'', Journal of Molecular Liquids, 225 260–264,

Dev, S., Roy, S., Bhattacharya, J., (2017) ''Optimization of the operation of packed bed bioreactor to improve the sulfate and metal removal from acid mine drainage'', Journal of Environmental Management, 200135–144.

Dilshara, P., Abeysinghe, B., Premasiri, R., Dushyantha, N., Ratnayake, N., Senarath, S., Wang, X., Wang, A., Zhong, W., Zhu, D., Wang, C., (2022) ''Analysis of international nickel flow based on the industrial chain'', Resources Policy, 77 102729.

DOE – U.S. Department of Energy, (2023), Critical Materials Assessment". Washington, DC.

Dominguez-Benetton, X., Varia, J. C., Pozo, G., Modin, O., Heijne A. T., Fransaer, J., Rabaey, K., (2018) ''Metal recovery by microbial electro-metallurgy'', Progress in Materials Science, 94 435–61.

Dupont, D., Arnout, S., Jones, P.T., Binnemans, K., (2016) ''Antimony recovery from end-of-life products and industrial process residues: A critical review'', Journal of Sustainable Metallurgy, 2 79–103.

Dushyantha, N., Batapola, N., Ilankoon, I.M., Rohitha, S., Premasiri, R., Abeysinghe, B., Ratnayake, N., Dissanayake, K., (2020) ''The story of rare earth elements (REEs): occurrences, global distribution, genesis, geology, mineralogy and global production'', Ore Geology Reviews, 122 103521.

España, J. S., (2008) ''Acid Mine Drainage in the Iberian Pyrite Belt: an Overview with Special Emphasis on Generation Mechanisms, Aqueous Composition and Associated Mineral Phases'', Macla, 10 34-43.
Ettler, V., Johan, Z., Kříbek, B., Šebek, O., Mihaljevič, M., (2009) ''Mineralogy and environmental stability of slags from the Tsumeb smelter, Namibia'', Applied Geochemistry, 24 (1) 1–15.

European Commission, (2020), Study on the EU's list of Critical Raw Materials – Final Report (2020), Luxemburg, Publication Office of the European Union. https://single-market-economy.ec.europa.eu/sectors/raw-materials/areas-specific-interest/critical-raw-materials_en

European Commission, (2023), COM(2023) 160 final 2023/0079(COD) ANNEXES to the Proposal for a Regulation of the European Parliament and of the 625 Council establishing a framework for ensuring a secure and sustainable supply of critical raw materials and amending Regulation European Commission s (EU) 168/2013, (EU) 2018/858, 2018/1724 and (EU) 2019/1020' https://eur-lex.europa.eu/legal-content/EN/TXT/HTML/?uri=CELEX:52023PC0160

European Commission, (2023), Study on the Critical Raw Materials for the EU 2023 – Final report, Luxemburg, Publication Office of the European Union. https://op.europa.eu/en/publication-detail/-/publication/57318397-fdd4-11ed-a05c-01aa75ed71a1

European Commission, (2024), Regulation (EU) 2024/1252 of the European Parliament and of the Council of 11 April 2024 establishing a framework for ensuring a secure and sustainable supply of critical raw materials and amending Regulations (EU) No 168/2013, (EU) 2018/858, (EU) 2018/1724 and (EU) 2019/1020, Official Journal of the European Union - 3.5.2024. http://data.europa.eu/eli/reg/2024/1252/oj

Felipe, E. C. B., Batista, K. A., Ladeira, A. C. Q., (2021). ''Recovery of rare earth elements from acid mine drainage by ion exchange'', Environmental Technology, 42 (17) 2721–2732.

Gammons, C. H., Icopini, G, A., (2020) ''Improvements to the Water Quality of the Acidic Berkeley Pit Lake due to Copper Recovery and Sludge Disposal'', Mine Water and the Environment, 39 427–439.

Gebreslassie, G., Desta, H. G., Dong, Y., Zheng, X., Zhao, M., Lin, B., (2024) ''Advanced membrane-based high-value metal recovery from wastewater'', Water Research, 265 122122.

Gomez, D. V., Whitworth, A. J., Vaughan, J., Sultana, U., Ledezma, P., Parbhakar-Fox, A., (2025) ''Review on Developments in Technologies for Critical Metal Recovery from Mining and Processing Wastes'', Mineral Processing and Extractive Metallurgy Review, 46 (7) 751–770.

Guo, X., Yi, Y., Shi, J., Tian, Q., (2016) ''Leaching behavior of metals from high-arsenic dust by NaOH−Na2S alkaline leaching'', Transactions of Nonferrous Metals Society of China, 26 575–580.

Guo, Z. H., Pan, F. K., Xiao, X. Y., Zhang, L., Jiang K. Q., (2010) ''Optimization of brine leaching of metals from hydrometallurgical residue'', Transactions of Nonferrous Metals Society of China, 20 2000−2005.

Haghighi, K. K., Moradkhani, D., Sardari, M. H., Sedaghat, B., (2015) ''Production of zinc powder from Co-Zn plant rezidue using selective alkaline leachimg by electrowinning'', Physicochemical Problems of Mineral Processing, 51 (2) 411−425.

Hezarjaribi, M., Bakeri, G., Sillanpaa, M., Chaichi, M. J., Akbari, S., Rahimpour, A., (2021) ''Novel adsorptive PVC nanofibrous/thiol-functionalized TNT composite UF membranes for effective dynamic removal of heavy metal ions'', Journal of Environmental Management, 284 111996.

Hu, X., Yang, H., Tan, K. Y., Hou, S. T., Cai, J. Y., Yuan, X., Lan, Q. P., Cao, J. R., Yan, S. M., (2022) ''Treatment and recovery of iron from acid mine drainage: A pilot-scale study'', Journal of Environmental Chemical Engineering, 10 106974.

Huang, Y., Feng, X., (2019) ''Polymer-enhanced ultrafiltration: Fundamentals, applications and recent developments'', Journal of Membrane Science, 586 53–83.

Huston, D. L., Bastrakov, E., (2024) ''Germanium, indium, gallium and cadmium in zinc ores: a mineral system approach'', Australian Journal of Earth Sciences, 71 (8) 1125-1155.
Inflation Reduction Act (IRA), (2022), Public Law No. 117–169. Washington, DC.

International Energy Agency (IEA), (2022), The Role of Critical Minerals in Clean Energy Transitions, IEA Publications, France.

International Energy Agency (IEA), (2023), Critical Minerals Market Review - 2023, IEA Publications, France.

International Energy Agency (IEA), (2024), Recycling of Critical Minerals (Strategies to scale up recycling and urban mining), IEA Publications, France.

Jagadeesh, N., Sundaram, B., (2023) ''Adsorption of pollutants from wastewater by biochar: a review'', Journal of Hazardous Materials Advances, 9 100226.

Johnson, D. B., (2014) "Biomining - biotechnologies for extracting and recovering metals from ores and waste materials", Current Opinion in Biotechnology, 30 24–31.

Junior, A. B. B., Tenório, J. A. S., Espinosa, D. C. R., (2023) ''Separation of Critical Metals by Membrane Technology under a Circular Economy Framework: A Review of the State-of-the-Art'', Processes, 11 1256.

Kaksonen, A. H., Lavonen, L., Kuusenaho, M., Kolli, A., Närhi, H., Vestola, E., Puhakka, J. A., Tuovinen, O. H., (2011) ''Bioleaching and recovery of metals from final slag waste of the copper smelting industry'', Minerals Engineering, 24 (11) 1113–1121.

Kara, T. I., Kremser, K., Wagland, S. T., Coulon, F., (2023) „Bioleaching metal-bearing wastes and by-products for resource recovery: a review“, Environmental Chemistry Letters, 21 3329–3350.

Kaur, G., Couperthwaite, S. J., Hatton-Jones, B. W., Millar, G. J., (2018) ''Alternative neutralisation materials for acid mine drainage treatment'', Journal of Water Process Engineering, 22 46–58.

Khakmardan, S., Rezai, B., Abdollahzadeh, A., Ghorbani, Y., (2023) ''From waste to wealth: Unlocking the value of copper anode slimes through systematic characterization and pretreatment'', Minerals Engineering, 200 108141.

Kim, B. S., Jo, S. K., Shin, D., Lee, J. C., Jeong, S. B., (2013) ''A physico-chemical separation process for upgrading iron from waste copper slag'', International Journal of Mineral Processing, 124 124–127.

Li, M., Peng, B., Min, X. B., Chai, L. Y., Peng, N., Xie, X. D., Yan, H., (2013) ''Technological mineralogy and environmental activity of zinc leaching residue from zinc hydrometallurgical process'', Transactions of Nonferrous Metals Society of China, 23 1480−1488.

Li, W., Liu, W., Jiao, F., Xie, L., Qin, W. (2025) ''Comprehensive recovery of arsenic and valuable metals from lead smelting flue dust: Process optimization and mechanism investigation'', Separation and Purification Technology, 353 128497.

Li, W., Wang, J., Zhan, Z., Luo, J., Zhou, D., Lei, Y., (2025) ''Extraction of valuable metals from acid mine drainage by an electrochemically activated limestone system'', Nature Communications, 16 6719.

Li, Y., Liu, Z., Li, Q., Liu, F., Liu, Z., (2016) ''Alkaline oxidative pressure leaching of arsenic and antimony bearing dusts'', Hydrometallurgy, 166 41–47.

Lin, F., Liu, D., Das, S. M., Prempeh, N., Hua, Y., Lu, J., (2014) ''Recent Progress in Heavy Metal Extraction by Supercritical CO_2'', Industrial & Engineering Chemistry Research, 53 (5) 1866–1877

Lin, W., Jing, L., Zhu, Z., (2017) ''Removal of Heavy Metals from Mining Wastewater by Micellar-Enhanced Ultrafiltration (MEUF): Experimental Investigation and Monte Carlo-Based Artificial Neural Network Modeling'', Water, Air, & Soil Pollution, 228 206.
Ling, H., Blanpain, B., Guo, M., Malfliet, A. (2021) ''Characterization of antimony-containing metallurgical residues for antimony recovery'', Journal of Cleaner Production, 327 129491.

Liu, L., Zhang, L., Jiang, S., Yuan, Z., Chen, J., (2023) ''Global copper cycles in the anthroposphere since the 1960s'', Resources, Conservation and Recycling, 199 107294.

Lobo, L., (2022), Geochemical study of trace and critical elements in chalcopyrite and pyrite from the Assarel Porphyry-Cu-Au deposit, Bulgaria, Department of Earth Sciences, Uppsala University, Uppsala, Sweden.

Lottermoser, B., (2010), Mine Wastes: Characterization, Treatment and Environmental Impacts (3rd ed.), Springer, Berlin, Heidelberg.

Lutandula, M. S., Mpanga, F. I., (2021) ''Review of Wastewater Treatment Technologies in View their Application in the DR Congo Mining Industry'', Global Environment Engineering, 8 14-26.

Maarof, H. I., Daud, W. M. A. W., Aroua, M. K., (2017) ''Recent trends in removal and recovery of heavy metals from wastewater by electrochemical technologies'', Reviews in Chemical Engineering, 33 (4) 359–386.

Macingova, E., Luptakova, A., (2012) ''Recovery of metals from acid mine drainage'', Chemical Engineering Transactions, 28 109–114.

Mashingaidze, M. M., Murova, D. T., Bukasa, P. M., Sigauke. T., (2025) ''Enhanced froth flotation recovery of nickel sulphides from concentrator tailings'', Academia Engineering, 2 7747.

Masindi, V., Foteinis, S., Renforth, P., Ndiritu, J., Maree, J. P., Tekere, M., Chatzisymeon, E., (2022) ''Challenges and avenues for acid mine drainage treatment, beneficiation, and valorisation in circular economy: A review'', Ecological Engineering, 183 106740.

Masindi, V., Ndiritu, J. G., Maree, J. P., (2018) ''Fractional and step-wise recovery of chemical species from acid mine drainage using calcined cryptocrystalline magnesite nano-sheets: an experimental and geochemical modelling approach'', Journal of Environmental Chemical Engineering, 6 1634–1650.

Masindi, V., Osman, M. S., Shingwenyana, R., (2019) ''Valorization of acid mine drainage (AMD): A simplified approach to reclaim drinking water and synthesize valuable minerals – Pilot study'', Journal of Environmental Chemical Engineering, 7 103082.

Mathieux, F., Ardente, F., Bobba, S., Nuss, P., Blengini, G., Alves Dias, P., Blagoeva, D., Torres De Matos, C., Wittmer, D., Pavel, C., Hamor, T., Saveyn, H., Gawlik, B., Orveillon, G., Huygens, D., Garbarino, E., Tzimas, E., Bouraoui, F., Solar, S., (2017), Critical Raw Materials and the Circular Economy – Background report. JRC Science-for-policy report, Publications Office of the European Union, Luxembourg.

Matinde, E., Simate, G. S., Ndlovu, S., (2018) ''Mining and metallurgical wastes: a review of recycling and re-use practices'', The Journal of the Southern African Institute of Mining and Metallurgy, 118 825-844.

Mazur, A., Penha, F. M., (2025) ''Fractional and simultaneous precipitation: recovering critical metals from multicomponent solutions'', Frontiers of Chemical Science and Engineering, 19, 107.

Meng, S., Wen, S., Han, G., Wang, X., Feng, Q., (2022) ''WastewaterTreatment in Mineral Processing of Non-Ferrous Metal Resources: A Review'', Water, 14 726.

Meschke, K., Hofmann, R., Haseneder, R., Repke, J. U., (2020) ''Membrane treatment of leached mining waste – A potential process chain for the separation of the strategic elements germanium and rhenium'', Chemical Engineering Journal, 380 122476.

Michaux, S. P., Vaden, T., Korhonen, J. M., Eronen, J. T., (2022), Assessment of the scope of tasks to completely phase out fossil fuels in Finland, (Report No. 18/2022). Geological Survey of Finland. https://tupa.gtk.fi/raportti/arkisto/18_2022.pdf

Mihailova, I., Mehandjiev, D., (2010) ''Characterization of fayalite from copper slags'', Journal of the University of Chemical Technology and Metallurgy, 45 (3), 317-326.

Minga, J. C., Elorza, F. J., Rodriguez, R., Iglesias, A., Esenarro, D., (2023) ''Assessment of Water Resources Pollution Associated with Mining Activities in the Parac Subbasin of the Rimac River'', Water, 15 965.

Minić, D., Štrbac, N., Mihajlović, I., Živković, Ž. (2005) ''Thermal analysis and kinetics of the copper-lead matte roasting process'', Journal of Thermal Analysis and Calorimetry, 82 383–388.

Montana, F., Cellura, M., Di Silvestre, M. L., Longo, S., Luu, L., Sanseverino, E., Sciumè, G., (2025) „Assessing Critical Raw Materials and Their Supply Risk in Energy Technologies - A Literature Review“, Energies, 18 (1) 86.

Mortazavi, S., (2008), Application of membrane separation technology to mitigation of mine effluente and acidic drainage. Mine Environment Neutral Drainage Program (MEND) Report 3.15.1., MEND and CANMET, Canada.

Motsi, T., Rowson, N. A., Simmons, M. J. H., (2009) ''Adsorption of heavy metals from acid mine drainage by natural zeolite'', International Journal of Mineral Processing, 92 (1-2) 42–48

Mullett, M., Fornarelli, R., Ralph, D., (2014) ''Nanofiltration of mine water: impact of feed pH and membrane charge on resource recovery and water discharge'', Membranes, 4 163-180,

Mulopo, J., (2022) ''Active Physical Remediation of Acid Mine Drainage: Technologies Review and Perspectives'', Journal of Ecological Engineering, 23 (6) 148–163.

Müller, D., Groves, D., Santosh, M., Yang, C., (2025) „Critical metals: Their applications with emphasis on the clean energy transition“, Geosystems and Geoenvironment, 4 (1) 100310.

Nassar, N. T., Brainard, J., Gulley, A., Manley, R., Matos, G., Lederer, G., Bird, L.R., Pineault, D., Alonso, E., Gambogi, J., Fortier, S. M., (2020) “Evaluating the mineral commodity supply risk of the U.S. Manufacturing sector”, Science Advances, 6 (8) 1–11.

Navarro, A., Cardellach, E., Mendoza, J. L., Corbella, M., Domènech, L. M., (2008) ''Metal mobilization from base-metal smelting slag dumps in Sierra Almagrera (Almería, Spain)'', Applied Geochemistry, 23 (4), 895–913.

Ndlovu, S., Simate, G., Matinde, E., (2017), Waste Production and Utilization in the Metal Extraction Industry, Boca Raton : Taylor & Francis, CRC Press.

Neenan, A. G., (2023), The Defense Production Act of 1950: History, Authorities, and Considerations for Congress, Congressional Research Service (CRS), Washington, DC.

Oh, C., Han, Y. S., Park, J. H., Bok, S., Cheong, Y., Yim, G., Ji, S., (2016) ''Field application of selective precipitation for recovering Cu and Zn in drainage discharged from an operating mine'', Science of the Total Environment, 557–558 212–220.

Osmani, A., Rizaj, M., Terziqi, A., Kamberaj, N., (2009) ''Slag valorisation of reductive smelting process by shaft furnace in the lead metallurgy of “Trepça” Complex with economical and environmental effects'', Journal of International Environmental Application and Science, 4 (2) 198-206.

Page, M., McKenzie, J., Bossuyt, P. (2021) “The PRISMA 2020 statement: An updated guideline for reporting systematic reviews,” BMJ, 372 n71.
Panayotov, V., Imhof, R., Panayotova, M., (2019), ''A possibility for purification of industrial effluents from arsenic in high concentrations'', XIII International Mineral Processing and Recycling Conference, 90-97.

Panayotova, M., Panayotov, V., (2017), Chapter 1-Hydrometallurgy: The Basics and Applications to Extract Some Precious, Base, and REE Metals, Hydrometallurgy: Applications, Technology and Research, Ed. Rodrigo Cabrera, Nova Science Publishers Inc., New York, 1-91.

Panayotova, M., Panayotov, V., (2021) ''Application of membrane processes in mining and mineral processing'', E3S Web of Conferences, 280 08016.

Park, I., Tabelin, C. B., Jeon, S., Li, X., Seno, K., Ito, M., (2019) ''A review of recent strategies for acid mine drainage prevention and mine tailings recycling'', Chemosphere, 219 588–606.

Park, J. H., Han, Y. S., Ji, S. W., (2018) ''Investigation of Mineral-Processing Wastewater Recycling Processes: A Pilot Study'', Sustainability, 10 (9) 3069.

Park, S. M., Shin, S. Y., Yang, J. S., Ji, S. W., Baek, K., (2015) ''Selective Recovery of Dissolved Metals from Mine Drainage Using Electrochemical Reactions'', Electrochimica Acta, 181 248–254.

Peng, B., Gao, H. M., Chai, L.Y., Shu, Y. D., (2008) ''Leaching and recycling of zinc from liquid waste sediments'', Transactions of Nonferrous Metals Society of China, 18 1269−1274.

Piatak N. M., Parsons M. B., Seal II R. R., (2015) ''Characteristics and environmental aspects of slag: A review'', Applied Geochemistry, 57 236–266.

Piatak, N. M., Seal, II R. R., (2010) ''Mineralogy and the release of trace elements from slag from the Hegeler Zinc smelter, Illinois (USA)'', Applied Geochemistry, 25 302–320.

Pino, L., Beltran, E., Schwarz, A., Ruiz, M. C., Borquez, R., (2020) ''Optimization of nanofiltration for treatment of acid mine drainage and copper recovery by solvent extraction'', Hydrometallurgy, 195 105361.

Pozo, G., Pongy, S., Keller, J., Ledezma, P., Freguia, S., (2017) ''A novel bioelectrochemical system for chemical-free permanent treatment of acid mine drainage'', Water Research, 126 411–20. doi:10.1016/j.watres.2017.09.058.

Pozo, M. T. P., Fernandez, E. L., Villaseñor, J., Leon-Fernandez, L. F., Fernandez-Morales, F. J., (2025) ''Metal Recovery from Wastes: A Review of Recent Advances in the Use of Bioelectrochemical Systems'', Applied Sciences, 15 1456.

Pramanik, B. K., Shu, L., Jegatheesan, J., Shah, K., Haque, N., Bhuiyan, M. A., (2019) ''Rejection of rare earth elements from a simulated acid mine drainage using forward osmosis: the role of membrane orientation, solution pH, and temperature variation'', Process Safety and Environmental Protection, 126 53–59.

Protano, G., Riccobono, F. (2002) ''High contents of rare earth elements (REEs) in stream waters of a Cu-Pb-Zn mining area'', Environmental Pollution, 117 499–514.

Ren, X., Fan, F., Liu, Q., Lv, Y., (2025) "Evaluation of the importance of critical minerals in China", Frontiers in Earth Science, 13 1491360.

Reuter, M. A., van Schaik, A., Gutzmer, J., Bartie N. Abadías-Llamas, A., (2019) „Challenges of the Circular Economy: A Material, Metallurgical, and Product Design Perspective“, Annual Review of Materials Research, 49 253–274.

Rieger, A., Steinberger, P., Pelz, W., Haseneder, R., Hartel, G., (2009) ''Mine water treatment by membrane filtration processes - Experimental investigations on applicability'', Desalination and Water Treatment, 6 (1-3) 54-60.
Šajn, R., Ristović, I., Čeplak, B., (2022) ''Mining and metallurgical waste as potential secondary sources of metals - A case study for the west balkan region'', Minerals, 12 547.

Samaei, S. M., Trinidad, S. G., Altaee, A., (2020) ''Performance evaluation of reverse osmosis process in the post-treatment of mining wastewaters: Case study of Costerfield mining operations, Victoria, Australia'', Journal of Water Process Engineering, 34 101116.

Savinova, E., Evans, C., Lebre, E., Stringer, M., Azadi, M., Valenta, R. K., (2023) ''Will global cobalt supply meet demand? The geological, mineral processing, production and geographic risk profile of cobalt'', Resources, Conservation and Recycling, 190 106855.

Sethurajan, M., van Hullebusch, E. D., Nancharaiah, Y. V., (2018) ''Biotechnology in the management and resource recovery from metal bearing solid wastes: Recent advances'', Journal of Environmental Management, 211 138-153.

Shi, C., Meyer, C., Behnood, A., (2008) ''Utilization of copper slag in cement and concrete'', Resources, Conservation and Recycling, 52 (10) 1115–1120.

Siwal, S. S., Kaur, H., Deng, R., Zhang, Q., (2023) ''A review on electrochemical techniques for metal recovery from waste resources'', Current Opinion in Green and Sustainable Chemistry, 39 100722.

Song, G. R., Wang, X. C., Romero, C., Chen, H. Z., Yao, Z., Kaziunas, A., Schlake, R., Anand, M., Lowe, T., Driscoll, G., Kreglow, B., Schobert, H., Baltrusaitis, J., (2021) ''Extraction of selected rare earth elements from anthracite acid mine drainage using supercritical CO_2 via coagulation and complexation'',Journal of Rare Earths, 39 (1) 83–89.

Song, J., Huang, T., Qiu, H., Niu, X., Li, X. M., Xie, Y., He, T., (2018) ''A critical review on membrane extraction with improved stability: Potential application for recycling metals from city mine'', Desalination 440 18–38.

Song, Y. W., Guo, Z. H., Wang, R., Yang, L. L., Cao, Y. X., Wang, H. R., (2022) ''A novel approach for treating acid mine drainage by forming schwertmannite driven by a combination of biooxidation and electroreduction before lime neutralization'', Water Research, 221 118748.

Sun, X., Fang, W., Gao, X., An, H., Si, J., Wei, H. (2024) "Dynamic interactions among new energy metals and price adjustment strategies: A cross-industry chain perspective", Energy, 303 131923.

Sun, Y., (2023) ''The use of aluminum alloys in structures: review and outlook'', Structures, 57 105290.

Szlachta, M., (2020) ''Mining water treatment and recovery strategies'', presentation at "Industrial and Mine Wastes as a Source of Technology Critical Elements", Educational Workshop of EIT RM Morecovery project, May, 2020.

Thiruvenkatachari, R., Francis, M., Cunnington, M., Su, S., (2016) ''Application of integrated forward and reverse osmosis for coal mine wastewater desalination'', Separation and Purification Technology, 163 181-188.

USGS, U.S. Geological Survey, (2022) ''Final List of Critical Minerals 2022'', (87 FR 10381). Federal Register/Vol. 87, No. 37/Thursday, February 24, 2022/ 10381-10382. https://www.federalregister.gov/documents/2022/02/24/2022-04027/2022-final-list-of-critical-minerals

USGS, U.S. Geological Survey, (2025), Mineral commodity summaries 2025 (ver. 1.2, March 2025): U.S. Geological Survey, 212 p. https://doi.org/10.3133/mcs2025.

Vital, B., Bartacek, J., Ortega-Bravo, J. C., Jeison, D., (2018) ''Treatment of acid mine drainage by forward osmosis: Heavy metal rejection and reverse flux of draw solution constituents'', Chemical Engineering Journal, 332 85–91.

Vital, B., Bartacek, J., Ortega-Bravo, J. C., Jeison, D., (2018) ''Treatment of acid mine drainage by forward osmosis: heavy metal rejection and reverse flux of draw solution constituents'', Chemical Engineering Journal, 332 85–91.

Walsh, S., (2019), The Future of Non-Ferrous Slag to 2029, Smithers Information Division, United States. https://www.smithers.com/services/market-reports/materials/the-future-of-non-ferrous-slag-to-2029

Weijma, J., Klok, J. B. M., Dijkman, H., Jansen, G., Sànchez-Andrea, I., Buisman, C. J. N., van Hullebusch, E. D., Hennebel, T., du Laing, G., Cruz, H., (2022), Chapter 11 - Established technologies for metal recovery from industrial wastewater streams, Resource Recovery from Water: Principles and Application.

Wikedzi, A., Sandström, Å., Awe, S. A., (2016) ''Recovery of antimony compounds from alkaline sulphide leachates'', International Journal of Mineral Processing, 152 26–35.

Wu, M., Hu, Y., Liu, R., Lin, S., Sun, W., Lu, H., (2019) ''Electrocoagulation method for treatment and reuse of sulphide mineral processing wastewater: Characterization and kinetics'', Science of the Total Environment, 696 134063.

Wu, X. (2023), Process Flowsheet Development for Recovering Antimony from Sb-Bearing Copper Concentrates'', Degree Project in Molecular Science and Engineering; KTH Royal Institute of

Technology: Stockholm, Sweden, Available online: https://kth.diva-portal.org/smash/get/diva2:1811335/FULLTEXT01.pdf (accessed on 25 May 2025).

Yang, L., Hu, W., Chang, Z., Liu, T., Fang, D., Shao, P., Shi, H., Luo, X., (2021) ''Electrochemical recovery and high value-added reutilization of heavy metal ions from wastewater: Recent advances and future trends'', Environment International, 152 106512.

Yang, Y., Li, B., Li, T., Liu, P., Zhang, B., Che, L. (2023) ''A review of treatment technologies for acid mine drainage and sustainability assessment'', Journal of Water Process Engineering, 55 104213.

Yenial, Ü., Bulut, G., (2017) ''Examination of flotation behavior of metal ions for process water remediation'', Journal of Molecular Liquids, 241 130–135.

Yuan, J., Ding, Z., Bi, Y., Li, J., Wen, S., Bai, S., (2022) ''Resource utilization of acid mine drainage (AMD): A review'', Water, 14 2385.

Zha, G., Yang, C., Wang, Y., Guo, X., Jiang, W., Yang, B., (2019) ''New vacuum distillation technology for separating and recovering valuable metals from a high value-added waste'', Separation and Purification Technology, 209 863–869.

Zhao, G., Li, W., Geng, Y., Bleischwitz, R., (2023) ''Uncovering the features of global antimony resource trade network'', Resources Policy. 85, part A 103815.

Zhong, C. M., Xu, Z. L., Fang, X. H., Cheng, L., (2007) ''Treatment of acid mine drainage (AMD) by ultra-low-pressure reverse osmosis and nanofiltration'', Environmental Engineering Science, 24 1297-1306

EXPLOITATION OF NATURAL RESOURCES: THE ECONOMIC AND ENVIRONMENTAL IMPACT OF THEIR UTILIZATION

Nurten DEVA*

University Isa Boletini Mitrovice, Geosciences Faculty Engineering
KOSOVA
**Corresponding author: nurten.deva@umib.net*

A B S T R A C T

This work is based in analyzes of the economic, environmental impacts of natural resources utilizing and to emphasize the importance of their sustainable management in the context of global economic development. The paper examines the contribution of these resources to economic growth, as well as the negative effects that appear through environmental degradation.

The economic evolution of a natural resource origin is strongly linked with the term ore. The sustainable use of these resources can increase social well-being, stimulate the creation of new jobs and ensure long-term economic growth. In many countries around the world, natural resources have been a key factor for industrial development and economic growth, providing raw materials, energy and opportunities for the development of various sectors of the economy.
The assessment of one country's potential natural resources and reserves involves a series of technical and economic activities, based on globally accepted technical standards and regulations, including the legislative framework and international trade conditions in the mining sector, especially base metals.

The use of natural resources in Kosovo is considered as a case study, with the aim of examining its economic benefits and environmental challenges. The assessment of natural resources follows global standards and regulations. Uncontrolled use risks overexploitation, damage to the ecosystem and economic costs.

Key words: *Natural resources*, *impacts, development, environment*

1. INTRODUCTION

The economy aims for maximum growth and profit, while the environment requires the limitation, protection and sustainable use of resources. This conflict of interests makes it necessary to find a balance between economic development and environmental protection. Natural resources constitute the basis of economic development, but they are limited, especially non-renewable resources such as coal, oil, gas and minerals.

The main questions that will be addressed are: How does the exploitation of natural resources affect economic development? and What are the environmental consequences of their use and how can they be minimized?

The study tries to answer the research questions: how does the exploitation of natural resources affect economic development and what are the environmental consequences of their use, contributing to the existing literature through an integrated analysis of economic and environmental dimensions. For this reason, the issue of sustainable management of natural resources has become one of the main priorities of economic and environmental policies at the global level. Growing pressure on ecosystems requires effective policies that balance economic development with environmental protection through efficient and sustainable resource use. In this context, sustainable natural resource management is essential for aligning economic and environmental goals.

The use of natural resources contributes to the growth of gross domestic product, the development of exports and the improvement of the trade balance. It also attracts foreign direct investment and encourages the development of supporting industries (World Commission on Environment and Development, 1987). However, economic growth based solely on the exploitation of resources is often short-term and exposed to market shocks. Economic growth in many countries is directly linked to sectors that exploit natural resources. Energy and the mining industry have the largest contribution to economic output and job creation (World Bank, 2020).

Key policies and measures should be identified to implement reforms, attract investment and protect the environment, while awareness of sustainable development should be prioritized at all levels and integrated into Kosovo's economic and environmental plans.Citizen education and training through social activities and awareness programs are essential for community engagement.

2. MATERIAL AND METHODS

This paper is based on the analysis of scientific literature and a case study of Kosovo in order to examine the relationship between the utilization of natural resources and their impacts on economic development and the environment.

2.1. Literature Review

Literature review refers to the analysis and evaluation of existing scientific studies related to the research topic. Below are some relevant literature sources.

Intensive use of natural resources poses serious environmental challenges. Economic activities are major sources of pollution and greenhouse gas emissions (Sachs et al., 2022), making sustainable resource management a key priority for long-term development and integrated environmental policies (Stiglitz et al., 2023).

Natural resources form the foundation of the global economy and ecology, including minerals, energy, water, forests, and biodiversity. Considered natural capital, they are vital for economic value and social welfare (Dasgupta, 2021) and, alongside physical, human, and technological capital, require efficient management for long-term development and ecological balance (Costanza et al., 2017; Stiglitz et al., 2023).

Natural resources are essential for human survival and development, providing energy, food, and industrial materials (Pearce & Turner, 1990). Historically, societal development has depended on how resources are used.

Natural resources provide materials and energy for economic and social use. They are either renewable, like forests, water, solar energy, wind, and biological resources (Dasgupta, 2021; European Commission, 2023), or non-renewable, such as minerals, oil, natural gas, and coal (World Bank, 2020; OECD, 2022).

A study on natural resources, low-carbon energy, and technological innovation in BRICS countries highlights how technology can reduce the environmental impact of resource use.(BRICS economies T. Jarijari1 · A. Deka2 · B. Cavusoglu).

An article shows that education and financial inclusion influence how natural resources impact the environment, linking economic development to environmental outcomes.Springer Nature Qamruzzama).

A study that analyses the effects of natural resource heterogeneity and environmental sustainability in the most developed countries (G20) after COP28. This literature can be used to inform the global context of the economic and environmental impact of resources and to compare with local situations(Alomair et. al., 2025)

Resource exploitation boosts growth but impacts ecosystems. Regulation fosters innovation (Esty & Porter, 2005), sustainable development protects future needs (Brundtland, 1987), and in Kosovo, uncontrolled mining and deforestation cause environmental harm.

Environmental policies and strong legal standards, to monitor and limit air, water and land pollution, and to promote waste management and recycling (Kosovo Environmental Protection Agency, 2023).

Economic instruments and fiscal incentives to encourage investments in green technologies, low-emission industries and sustainable natural resource projects (OECD, 2022; Stiglitz et al., 2023).

In conclusion, the literature demonstrates that sustainable management of natural resources requires an integrated approach that combines environmental regulation, technological innovation, education, and economic incentives in order to ensure both economic growth and environmental sustainability.

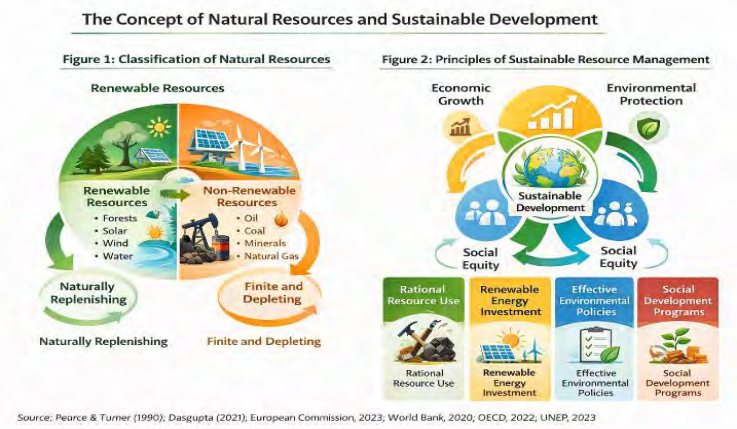

Figure 1. Natural sources - Economic growth and environmental impacts

2.2. Case study - Kosova Utilizing Of Natural Resources - Economic And Environmental Impacts

Natural resources in Kosova, as a case study, highlight both economic benefits and environmental challenges. Their use significantly promotes economic development while generating substantial environmental impacts. Kosovo (10,908 km²) has considerable potential in mineral and energy resources, offering economic gains, but their exploitation also poses environmental risks. Kosovo's key natural resources include minerals, water, renewable energy, agricultural land, forests, and tourism. Efficient use of minerals such as lignite, lead, zinc, and nickel can create jobs, boost exports, and support economic growth, while other resources provide opportunities for sustainable development. Below are maps of Kosovo showing the identified mineral resources (Figure 2).

Assessing these resources requires adherence to global standards and regulations for mineral trade. Effective management of waste from resource use is a critical environmental concern and must be integrated into economic and environmental planning. Sustainable policies and good governance ensure that natural resources support economic growth while

protecting the environment, contributing directly to improved living standards. Some of the important natural resources for Kosovo are shown maps that identified mineral resources.

The wise use of natural and human resources can foster sustainable economic development, ensure continued growth, social well-being and socio-economic, environmental and political stability. The exploitation of natural resources in Kosovo causes significant environmental impacts, affecting the quality of life and ecological capacity. The World Bank (2024) and OECD (2020) recommend that Kosovo diversify its energy sector by using renewable sources such as solar, wind and hydropower to reduce its dependence on coal and greenhouse gas emissions (UN, 2015). The country's economic development depends on policies that transform natural resources into sustainable growth and are carefully managed through clean technologies and strategic investments.

Citizen education and training through social activities and awareness programs are essential for community engagement. Key policies and measures should be identified to implement reforms, attract investment and protect the environment, while awareness of sustainable development should be prioritized at all levels and integrated into Kosovo's economic and environmental plans.

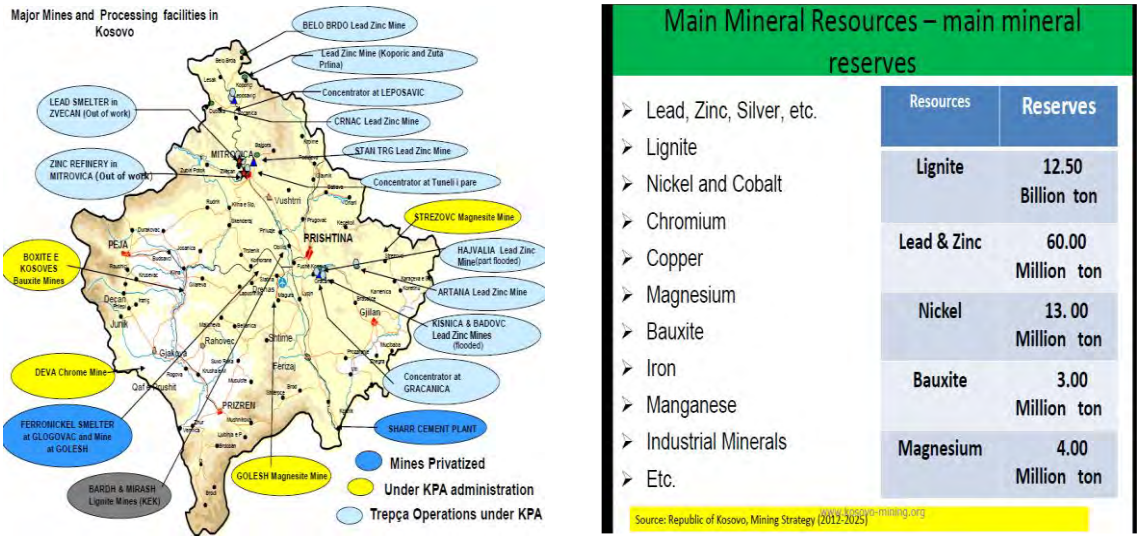

Figure 2. Maps of Kosovo showing the identified mineral resources

3. DISCUSSION

Conceptual model of the natural resource utilizing is presented in Figure 3. There are described independent and depended variable, their impacts in economy and environment.

- Independent variable : Natural resource exploitation
- Dependent variable : Economic and environmental development

Figure 3. Natural resources utilization

Moderating factors:

- Government policies- Institutional management-economic development
- Environmental policies-environmental regulations-Environmental impact
- Technology & innovation
- Domestic & foreign investments

The use of natural resources depends on these factors and directly impacts economic and environmental development, shown Table 1-3.

Table 1. Type of natural resources and economic impacts

Type of resource	**Examples**	**Economic effects**
Mineral resources	Lignite, lead, zinc	Development of the mining industry
Energy resources	Coal, solar energy	Power generation
Water resources	Rivers, lakes	Agriculture and hydropower
Forest resources	Natural forests	Wood industry and tourism

Table 2. Environmental impacts from resource exploitation

Economic activity	**Environmental impact**
Mining	Land degradation
Energy industry	Air pollution
Deforestation	Biodiversity loss
Heavy industry	Water pollution

Table 3. Relationship between economic development and environmental impact

Level of resource utilziation	**Economic growth**	**Environmental impact**
Low	Limited	Minimal
Average	Stable	Moderate
High	Rapid	High

Correspondence between natural resource exploitation and economic growth is shown in Figure 3.

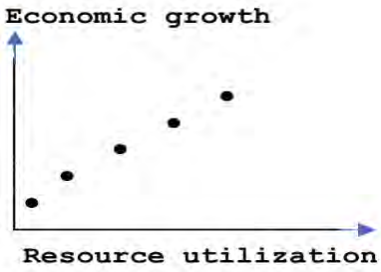

Figure 3. Correspondence between natural resource exploitation and economic growth

Interpretation: The greater the exploitation of natural resources, the greater the increase in economic activity

The relationship between industrial activity and environmental pollution is given in Figure 4.

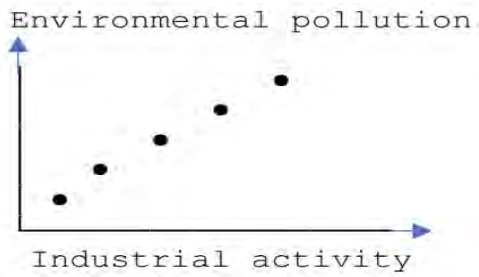

Figure 4. The relationship between industrial activity and environmental pollution

Interpretion:Industrial activity is often accompained by increased environmental pollution

Table 4. Sector Economic contribution

Sector Economic contribution	**(%)**
Energy	35
Mining industry	25
Agriculture	20
Forestry	10
Water resources	10

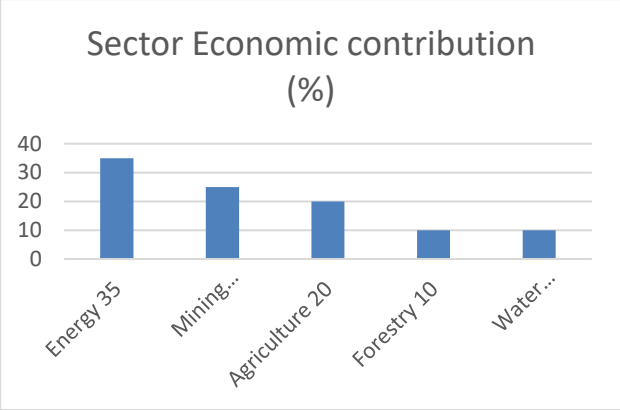

Figure 5. Contribution of natural resource sectors to economic development

Interpretation of the paper: Economic growth in many countries is directly linked to sectors that exploit natural resources. Energy and the mining industry have the largest contribution to economic output and job creation (World Bank, 2020).

Table 5. Impact of natural resource exploitation on the environment

Activity	**Environmental impact level**
Mining industry	Very high
Coal power	High
Intensive agriculture	Medium
Nature tourism	Low

Interpretation: Sectors with intensive exploitation of natural resources usually cause greater environmental impacts, particularly through air pollution, water pollution and land degradation (UNEP, 2023).

The concept of sustainable development is given in Figure 6.

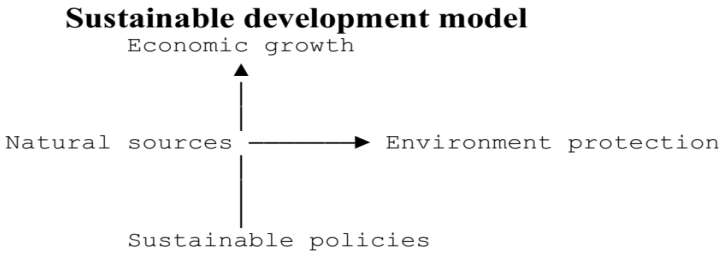

Figure 6. Sustainable development model

Interpretation: Sustainable development requires a balance between the economic use of natural resources and environmental protection.

Table 6. Environmental impacts from natural resource exploitation activities

Type activity	**Air pollution**	**Land degradation**	**Water pollution**
Coal energy	Very high	Medium	High
Mining industry	High	Very high	Medium
Intensive agriculture	Medium	Low	Medium
Forestry	Low	Low	Low

4. CONCLUSION

Natural resources in Kosovo, as a case study, illustrate both economic benefits and environmental challenges. Literature analysis shows that their use significantly promotes economic development while also generating substantial environmental impacts. Kosovo, offers significant natural resource potential, including mineral and energy resources, which provide economic benefits; however, their exploitation also generates notable environmental impacts that cannot be overlooked. When assessing natural resources, it is important to follow global standards and regulations for mineral trade. Using these resources supports sustainable economic growth and has clear social benefits. The management of waste generated from resource exploitation is a critical environmental issue and must be prioritized and integrated into economic and environmental development plans. Sustainable policies and good governance regarding natural resources should promote economic growth while protecting the environment, directly contributing to improved living standards. Sustainable development requires a balance between the economic use of natural resources and environmental protection.

- The use of natural resources has a positive impact on economic growth.
- The intensive use of natural resources increases the level of environmental degradation.
- Sustainable management of natural resources can balance economic development and environmental protection.
- Investments in clean technologies and renewable energy reduce the negative environmental impacts of the use of natural resources.
- For this reason, researchers emphasize the importance of integrating environmental policies into economic development strategies and the efficient use of natural resources (OECD, 2022; European Commission, 2023; Stiglitz et al., 2023).

REFERENCES

Alomair, A., Ibrahim, R. L., Al Naim, A. S., (2025), “Natural resources heterogeneity and environmental sustainability in G20 nations: post-COP28 analysis”, Frontiers in Environmental Science.

Costanza, R., de Groot, R., Sutton, P., van der Ploeg, S., Anderson, S. J., Kubiszewski, I., Farber, S., Turner, R. K., (2017), “Valuing the world’s ecosystem services and natural capital”, Ecological Economics, 101, 29–39.

Dasgupta, P., (2021), “The Economics of Biodiversity: The Dasgupta Review”, Cambridge University Press.

European Commission, (2023), “Circular Economy Action Plan and Sustainable Resource Management”, Brussels.

Esty, D. C., Porter, M. E., (2005), “National environmental performance: an empirical analysis of policy results and determinants”.

Jarijari, T., Deka, A., Cavusoglu, B., (n.d.), “The synergistic role of natural resources, low carbon energy and technological innovation in promoting environmental sustainability: the evidence of BRICS economies”.

Kosovo Environmental Protection Agency, (2023).

OECD, (2022), “Global Material Resources Outlook to 2060: Economic Drivers and Environmental Consequences”, Paris.

Pearce, D., Turner, R. K., (1990), “Economics of Natural Resources and the Environment”, London: Harvester Wheatsheaf.

Qamruzzaman, M., (n.d.), “The effects of natural resources, education, and financial inclusion in achieving environmental sustainability in resource abundance nations”.

Sachs, J., Lafortune, G., Kroll, C., Fuller, G., Woelm, F., (2022), “Sustainable Development Report 2022”, Cambridge University Press.

Stiglitz, J., Fitoussi, J., Durand, M., (2023), “Measuring What Counts for Economic and Social Performance”, OECD Publishing.

United Nations, (2015), “Transforming Our World: The 2030 Agenda for Sustainable Development”, New York: United Nations.

UNEP, (2023), “Global Resources Outlook 2024: Bend the Trend – Pathways to a Liveable Planet”, Nairobi: United Nations Environment Programme.

World Bank, (2020), “World Development Report 2020: Trading for Development in the Age of Global Value Chains”, Washington, DC.

World Bank, (2024), “Kosovo Country Climate and Development Report”.

World Commission on Environment and Development, (1987), “Our Common Future”

APPLICATION OF AI IN MINERAL PROCESSING: EVOLUTION, INDUSTRIAL UPTAKE, AND CURRENT USE

Saeed Chehreh CHELGANI*

Minerals and Metallurgical Engineering, Department of Civil, Environmental and Natural Resources Engineering, Swedish School of Mines, Luleå University of Technology, Luleå, Sweden
**Corresponding author: Saeed.chelgani@ltu.se*

A B S T R A C T

Artificial intelligence (AI) in mineral processing has evolved from early rule-based expert systems to today's data-driven machine learning (ML), deep learning, advanced process control, and hybrid digital-twin platforms. This article reviews this evolution decade by decade, explaining why mineral processing has remained a strong "use case" for AI: relationships are mostly nonlinear, time-varying, disturbance-driven, and only partially observable, while key metallurgical indicators are often delayed or sparsely measured. This work summarizes how progress has been enabled by improved sensing, data historians, connectivity, and computing, shifting AI from offline decision support to online supervision, prediction (soft sensing), and real-time optimization. The review also highlights modern application clusters across comminution, sensor-based sorting and preconcentration, flotation (including froth-image analytics), and plant-wide digital twins, with increasing interest in hybrid modelling and reinforcement learning for control under uncertainty. Finally, we discuss practical data foundations (preprocessing, multicollinearity handling, and multivariate methods such as PCA) that strongly influence whether AI models become reliable operational tools.

Key words: *AI, machine learning, flotation, crushing, grinding*

1. INTRODUCTION

Artificial intelligence (AI) in mineral processing has progressed from knowledge-based "expert systems" (rules capturing operator know-how) to data-driven machine learning (ML), computer vision, and hybrid digital-twin/advanced control platforms. The key driver has been the same throughout: mineral processing circuits are nonlinear, time-varying, and often partially observable, making purely first-principles control difficult. Recent decades have improved AI performance mainly through better instrumentation, computing, data historians, and plant connectivity, enabling AI to move from decision support to real-time supervisory control and optimization. From another perspective, mineral processing plants operate under strong measurement delays and significant disturbances. These conditions motivated early knowledge-based AI (expert systems) that captured operator heuristics, followed by data-driven ML, computer vision, advanced control (e.g., MPC), and, more recently, hybrid digital twins and reinforcement learning concepts. Over the decades, the main improvements have come from (i) better instrumentation and analysers, (ii) plant-wide data historians and connectivity, (iii) higher computing, and (iv) better algorithms and integration with control systems. Therefore, "AI" in mineral processing has evolved through several recognizable waves: rule-based expert systems (classic AI), then data-driven modelling and advanced process control, and more recently, machine learning/deep learning integrated with modern sensing, plant historians, and digital infrastructure (Bearman et al. 1992; Bai et al., 2025; Nobahar et al., 2024; Hasidi et al., 2024).

AI was first used (as explicitly labelled "AI," i.e., expert systems) in mineral processing around 1988-1989. The earliest clearly documented industrial online applications explicitly described as "AI" in mineral processing appear in the late 1980s, mainly as expert systems: 1988 (Polaris Mine): an early and widely cited industrial expert-system application in a mineral processing

context. 1989 (Brenda Mines grinding): a real-time expert system implemented on an industrial grinding circuit; the paper discusses real-time feasibility and performance relative to existing supervisory approaches. ~1989-1990 (Brenda Mines flotation): an expert-system approach to flotation supervisory control is documented in thesis work and later case histories (Harris et al., 1988; Spring 1989; Bearman et al., 1992; Edwards, 1990; Edwards and Mular, 1991).

Based on my assessments and investigations, the earliest clearly evidenced “introducers” (by named, documented industrial/online cases) include Harris & Kosick (Polaris) and Spring (Brenda grinding), with Edwards representing early academic-to-industrial flotation expert-system work. When I say the first, I checked the first concept, the prototype, and the first online industrial deployment. Using documented early industrial expert-system cases and early synthesis literature: Harris & Kosick (Polaris Mine, 1988): early industrial expert-system technology application in a mineral processing environment. R. Spring (Brenda Mines grinding, 1989): documented real-time expert system control on an operating grinding circuit. Edwards (UBC, 1990): thesis documenting expert-system control for a flotation circuit (research-to-plant translation). The early spread and opportunity space across the minerals industry are summarized in a major early-1990s review that captures the state and direction of expert systems at that time (Harris et al., 1988; Spring 1989; Bearman et al., 1992; Edwards, 1990; Edwards and Mular, 1991).

2. HOW AI APPLICATIONS IMPROVED OVER THE DECADES (DECADE-BY-DECADE)

1980s: Expert systems as supervisory “operator-in-a-box”. The typical approach was rule-based knowledge (IF-THEN logic), supervisory recommendations, or setpoint adjustments, rather than conventional control. Over the past decade, it has been demonstrated that symbolic AI can run online and support real-time supervision of grinding/flotation decisions in industrial settings (Harris et al., 1988; Spring 1989; Bearman et al., 1992; Edwards, 1990; Edwards and Mular, 1991).

1990s: Broader deployment + first data-driven learning (early neural nets). Trend: expert systems are broadening across tasks; early neural networks are emerging for prediction/estimation when mechanistic models are difficult. AI modelling throughout this decade has shown that broader adoption across the minerals industry and increasing “online/real-time” ambitions. Early neural-network work on comminution-related predictions (e.g., SAG mill power prediction) signaled a shift from rule-based encoding to learning from data (Bearman et al., 1992; Pu et al., 2020).

2000s: Advanced control (Model Predictive Control “MPC”) becomes more practical in grinding and beyond. The main trend was that multivariable control and constraint handling gained traction; MPC is studied and applied in grinding-circuit contexts. The main improvements were better management of interacting variables and constraints (typical of grinding circuits), compared with simpler single-loop control, and increased computing and data availability, which support more complex optimization/control strategies (Ramasamy et al., 2005).

2010s: During this decade, the main focus was on Hybrid modelling, increased sensor use, and the growth of computer vision in flotation. The trend was to combine mechanistic understanding with data-driven models, with improved simulation/calibration supporting advanced control development. Hybrid simulation and calibration methods for evaluating control strategies in flotation plants were significantly improved during this period. Early deep-learning approaches applied to complex plant datasets (including flotation modeling) improved nonlinear mapping and feature learning compared with manual feature engineering (Putz and Cipriano, 2015; Zheng et al., 2024).

2020s–mid 2020s: ML at scale, deep learning for images, sorting/preconcentration, and digital twins; RL emerges, and all were applied. The main trend was that AI expands across the flowsheet, grinding, sorting, flotation, magnetic separation, roasting, and into plant-wide optimization and digital twins. What improved were broad, structured “AI across unit operations” frameworks emphasizing prediction, intelligent control, recognition/vision, fault diagnosis, and digital-twin visualization (Bai et al., 2025). Sensor-based sorting (often using sensor fusion + ML classifiers) is recognized for enabling earlier waste rejection and downstream stability/efficiency benefits (Peukert et al., 2022; Okada et al., 2024). Digital twin concepts are increasingly tied to real-time prediction and decision support for concentrate quality and recovery (Nobahar et al., 2024; Hasidi et al., 2024). Reinforcement-learning-based flotation control research begins to appear, targeting learned control policies under uncertainty (often carefully constrained or simulation-heavy) (Dai et al., 2025).

Thus, if I want to say that, when industrial applications became more popular, there were two main waves. The first wave: 1990s (expert systems were spreading and maturing), when expert systems were widely applied across the minerals industry and highlighted increasing interest in online/real-time systems, consistent with broader industrial uptake during that period (Bearman et al., 1992. Second wave: 2010s-present (data + sensors + compute + connectivity), when rapid expansion of AI in mineral processing is enabled by digitalization, richer sensors (including imaging), and scalable ML and deep learning methods across multiple unit operations and plant-level decision layers (Nobahar et al., 2024; Hasidi et al., 2024).

3. AI CLASSIFICATION

A clean way to classify AI “like ANN, machine learning, deep learning” is by paradigm (Table 1): Symbolic systems (explicit rules/logic), statistical machine learning (learned patterns from data, often with engineered features), and neural approaches (ANNs). Within neural approaches, deep learning is a subset of ANNs; it refers to larger, multi-layer neural networks (e.g., transformers, deep CNNs). Other major families, such as probabilistic/Bayesian methods, reinforcement learning, and evolutionary optimization, are often used on their own or in combination (e.g., deep RL). This family-based taxonomy is helpful because it explains what assumptions the system makes and what kinds of problems it tends to solve well.

Table 1. Approach-based AI classification.

Family/paradigm	Core idea	Typical methods/models	What it’s good at	Common limits
Rule-based / Symbolic AI	Hand-coded logic and representations	If, then rules, expert systems, ontologies, theorem provers, search/planning (A*)	Clear logic, traceable decisions, well-defined domains	Brittle outside rules; costly to maintain; weak with messy data
Classical Machine Learning (non-neural)	Learn patterns from features you define	Linear/logistic regression, SVM, k-NN, decision trees, random forests, gradient boosting (XGBoost/LightGBM)	Strong on tabular data, efficient training, and good baselines	Needs feature engineering; limited on unstructured data vs deep nets
Artificial Neural Networks (ANNs)	Learn layered functions from data	MLP (feed-forward), RNN/LSTM/GRU, CNN (also overlaps with deep learning when many layers)	Nonlinear modeling: handles complex relationships	Data-hungry; harder to interpret; training can be compute-heavy

Deep Learning (DL) *(subset of ANN)*	Large neural nets learn hierarchical representations	Deep CNNs, Transformers, deep RNNs, autoencoders, diffusion models	Best for unstructured data (text/image/audio), representation learning, scaling	High compute/data; robustness and explainability challenges
Probabilistic / Bayesian AI	Model uncertainty explicitly	Bayesian networks, HMMs, Gaussian processes, Bayesian regression	Uncertainty-aware predictions, principled inference	Can scale poorly; modeling assumptions matter
Reinforcement Learning (RL)	Learn actions by maximizing reward	Q-learning, policy gradients, actor–critic; deep RL combines with DL	Control, games, robotics, sequential decisions	Sample-inefficient; reward design issues; safety/stability concerns
Evolutionary / Swarm / Metaheuristics	Search solutions via population-based optimization	Genetic algorithms, CMA-ES, PSO	Black-box optimization, design/search problems	Can be slow; no guarantee of the best solution
Hybrid / Neuro-symbolic	Combine learning with rules/constraints	Retrieval + rules, constrained decoding, program synthesis + ML	Better control + generalization, improved reasoning/consistency	Engineering complexity; integration is hard

4. DATA MINING IMPORTANCE

Mineral processing data are rarely “AI-ready.” Plants are dynamic systems driven by ore variability, changing operating modes, sensor drift, delays, and intermittent laboratory assays. In this environment, data mining and classical statistical analysis (e.g., data cleaning, visualization, correlation screening, Principal Component Analysis (PCA) and Partial Least Squares (PLS), outlier detection, change-point checks) are not optional preliminaries; they often determine whether an AI model becomes a reliable decision tool or an unstable curve fit. A first reason is the quality and realism of the data. Process historians contain missing values, frozen tags, instrument dropouts, maintenance artifacts, and periods of abnormal operation. A broad review of ML data preprocessing emphasizes that raw data are vulnerable to noise, corruption, missingness, and inconsistency, and that preprocessing (cleaning, integration, transformation, reduction) is essential because poor data can cause false predictions and degrade accuracy (Maharana et al., 2022). Mineral processing amplifies this risk because many key performance indicators (e.g., grade/recovery) are measured infrequently and with uncertainty, while manipulated variables are sampled continuously. Soft-sensor literature highlights this exact challenge: combining real-time plant signals with infrequent or low-quality laboratory measurements, and updating models over time as conditions change (Shardt et al., 2023). If these realities are not surfaced early through basic analytics (missingness maps, tag validation, lag analysis), AI training can “learn” maintenance events, assay timing artifacts, or sampling biases instead of metallurgy.

A second reason is multicollinearity and redundancy, which are endemic in process plants. Many variables move together (e.g., feed rate, power draw, bearing pressure in comminution; air rate, froth depth, mass pull in flotation), and naive AI can become brittle when several correlated inputs are simultaneously used. Correlation analysis (Pearson/Spearman), variance checks, and clustering of correlated tags are practical ways to remove redundancy and reduce model instability. The feature-selection literature is explicit that multicollinearity (strong correlations among features) can make regression-style models unstable and overly complex, motivating feature-selection strategies that reduce redundancy (Wosiak, 2017). In mineral

processing, this is more than a statistical nicety: unstable models lead to oscillatory control suggestions, poor extrapolation during ore changes, and loss of operator trust.

Third, multivariate statistical methods such as PCA provide both dimensionality reduction and process understanding, two things many AI deployments lack if they jump straight to black-box modeling. A classic mineral-processing-specific reference (U.S. Bureau of Mines-related work) describes PCA as a versatile multivariate method applied to mineral processing data for data simplification and pattern recognition, where PCA replaces many measured variables with fewer components and "at the same time removes a significant amount of experimental error," improving usefulness for process control and detection of significant variations via component plots (Stanley et al., 1993). That is exactly the kind of value that "pre-AI" statistical analysis brings: it reveals dominant modes of variation (e.g., throughput-driven vs. grind-quality-driven), exposes sensor groups that move together, and creates low-noise latent variables that can improve downstream modelling.

Fourth, statistical exploration is crucial for time structure and causality-adjacent logic. Mineral processing systems have transport delays, residence time effects, recycle streams, and slow drifts. Simple time-lagged correlations, cross-correlation functions, PCA on appropriately windowed/lagged data, and regime segmentation (startup/steady state/shutdown) often determine whether an AI model generalizes. This becomes even more important in modern computer vision and deep learning applications (e.g., for image analysis). Recent deep learning reviews in flotation explicitly discuss the full pipeline, including data collection, dataset preprocessing, feature extraction, and modeling, because model performance depends strongly on upstream data handling (Chen et al., 2025). In other words, even state-of-the-art AI methods still rely heavily on disciplined preprocessing and exploratory statistics.

Finally, mineral processing is a high-stakes, high-cost decision environment. Operators and metallurgists must understand why a model is recommending a change (air, reagent, water, grind target). PCA loadings, correlation maps, and statistical summaries act as "interpretability scaffolding," linking patterns back to physical mechanisms and allowing plausibility checks. This improves adoption: models that are statistically coherent and physically interpretable are easier to validate, troubleshoot, and maintain over time, especially when ore types, equipment condition, or reagent suites change (Stanley et al., 1993; Shardt et al., 2023).

In practice, the most robust workflows in mineral processing treat statistics as the "first AI": clean → validate → explore → reduce → interpret → model. By first conducting correlation screening, PCA/PLS, outlier/regime detection, and careful preprocessing, AI is far more likely to deliver stable improvements in prediction, monitoring, and control than to become another short-lived pilot.

5. EXPLAINABLE ARTIFICIAL INTELLIGENCE

Mineral processing performance is determined by coupled phenomena of size reduction, sizing/classification, and separation. In practice, operators can adjust only a subset of variables that are routinely monitored (e.g., feed rate, pressure, water addition, reagent dosages, and a few particle-size indicators). Meanwhile, decisive mechanisms such as liberation, bubble-particle attachment, entrainment, and froth stability occur at micro-scales that are rarely measured continuously. The consequence is the remaining gaps between what the plant can observe and what the plant needs to understand to maintain stable product size and grade-recovery targets. One solution for these challenges is to build a plant-scale digital surrogate ("Conscious Lab", CL) directly from industrial databases, then use explainable artificial intelligence (XAI) to translate predictive power into interpretable process knowledge. CL has been applied to various units and has provided reasonable results, which are summarized here.

5.1. Comminution

Comminution commonly dominates circuit energy consumption and strongly conditions downstream separation by setting the liberation and surface area available for reagent adsorption. The CL literature presented here focuses on industrial HPGR and ball mill datasets, in which the targets are either power draw or product-sizing metrics (e.g., P_{80}). A consistent conclusion is that plant-scale responses depend on interacting operating variables, and data-driven multivariable models can reveal which levers matter most under industrial constraints.

5.1.1. HPGR

Tohry et al. (2021) developed a CL for HPGR power consumption using a boosted neural network (BNN) trained on an industrial monitoring dataset. HPGR size reduction is controlled by the compressive bed-breakage created between a fixed and a floating roll; thus, pressure and material properties interact with roll kinematics. The CL approach was used to model two power components (power-float and power-fixed), reflecting the distinct mechanical roles of the floating versus fixed rolls. The multivariable importance analysis ranked roller speed as the dominant driver of power-float, while feed rate was the most influential variable for power-fixed. Importantly, the study emphasized that building the CL from industrial data helps avoid representativeness limitations of lab-scale tests and supports decision-making using the same variable ranges encountered in routine operation.

In a complementary HPGR study, Chelgani et al. (2021) modelled HPGR product particle sizes (notably P_{80}) using XGBoost and SHAP to create an explainable CL for industrial product sizing control. Under steady-state conditions, the working gap emerged as the highest-importance variable for P_{80} prediction, with a positive relationship between working gap and P_{80} (a larger gap tended to produce a coarser product). The authors highlight that HPGR variables are interdependent (e.g., speed-gap interactions), so multivariable explainability is more informative than one-at-a-time linear correlations for setting operating windows. This is particularly relevant for plant control: the working gap is both a constraint (mechanical and safety limits) and a powerful lever for product sizing; SHAP-based models quantify its effect in the context of other measured variables.

5.1.2. Ball mill power draw

For wet tumbling mills, Tohry et al. (2020) used random forest (RF) regression to predict industrial ball mill power draw from routinely measured variables in a plant dataset (Chadormalu tailing recovery plant). The monitored variable set included feed rate, ball charge, F_{80} and P_{80} size indicators, Bond work index, and water/slurry flow variables, capturing both ore grindability and operating state. Reported descriptive statistics indicate a power draw ranging from approximately 1625 to 3153 kW, along with substantial variation in ball charge and work index. A Pearson correlation analysis indicated a strong positive correlation between ball charge and power draw ($r \sim 0.81$), and a moderate positive correlation between work index and power draw ($r \sim 0.52$). From an operational perspective, these findings align with physical intuition: more grinding media increases charge mass and torque demand, while a higher work index indicates harder ore requiring more energy for the same size reduction. The RF model's value lies in its ability to learn nonlinear combinations of these drivers and to predict power draw as a function of controllable variables (e.g., ball charge, feed rate, water addition), while implicitly accounting for ore variability captured by work index and size distributions.

Across the HPGR and ball mill CL studies, three practical points emerge: Use multivariable models to rank true industrial levers. For HPGR, power, speed, and feed rate can dominate different power components, implying that one setpoint change may redistribute load rather than uniformly reduce total power. For HPGR sizing control, the working gap is a high-leverage

parameter for P80, but its effect must be interpreted alongside other variables (e.g., roll speed and throughput) to avoid misleading linear conclusions. For ball milling, the power draw is strongly influenced by ball charge and ore hardness proxies; predictive models can serve as energy KPI forecasters and diagnostic tools when power deviates from expected behaviour under fixed operating conditions.

5.1.3. Hydrocyclone

Classification units shape the particle-size distribution delivered to downstream separation stages and close the mass balance of grinding circuits. Even when the grinding device is stable, classification behaviour can shift product fineness and circulating load, altering both energy use and separation performance. The CL studies provided focus on hydrocyclone overflow sizing (O_{80}) and, as a broader sizing/separation example, dense-medium Tri-Flo separators.

Chelgani et al. (2023) developed an industrial hydrocyclone CL using CatBoost for prediction and SHAP for explanation, targeting hydrocyclone overflow size (O_{80}) and a downstream product size (K_{80}) in a magnetite circuit. The motivation was explicit: hydrocyclone responses often show nonlinear dependence on operating variables and interactions that single-variable correlation tools fail to capture. By ranking variables using SHAP, the authors identified overflow solidity (Xo) as the most effective predictor of O_{80}, with a positive mean contribution (i.e., higher overflow solids are associated with coarser overflow). A key contribution of the work was the discussion of interaction effects: SHAP interaction analysis showed that the combined effect of overflow solidity and working pressure can change sign depending on the operating range, positive in one band and negative outside it, highlighting why fixed linear rules may not generalize across days or ore types. The study also reported a meaningful positive relationship between hydrocyclone overflow size (O_{80}) and downstream magnetic separator product size (K_{80}), reinforcing that classification control directly conditions subsequent separation performance.

5.2. Dense-Medium-Tri-Flo Separation

Although not a flotation unit, dense-medium separation provides a useful contrast because it is a sizing/separation step where operational variables can be interpreted through CL modeling. Alidokht et al. (2021) built a BNN-based CL for an industrial coal Tri-Flo separator, a dense-medium cyclone-type device widely used in coal washeries. The study frames Tri-Flo as an environmentally friendly technique and notes the historical lack of detailed investigation into the effectiveness of its operating variables. In the CL approach, plant data are used to model metallurgical responses and to determine which monitored variables most strongly govern performance under real conditions. While the detailed rankings depend on the site dataset, the broader lesson is transferable: even for mature separation technologies, plant data plus explainable modelling can reveal which setpoints are truly high leverage and where interactions dominate the response. CL showed that treating overflow solidity (and the variables controlling it: water balance, feed dilution) is a primary lever for classification control when O_{80} stability is the goal. If a pressure change unexpectedly makes overflow finer/coarser, SHAP interaction results suggest the effect may depend on the current solids regime rather than indicating instrumentation error. Explicitly link classification KPIs to downstream separation KPIs. The positive O_{80}-K_{80} linkage implies that classification drift can propagate into separation variability even if the separator itself is not malfunctioning.

5.3. Flotation

Froth flotation adds another layer of complexity because the dominant mechanisms involve reagent chemistry, surface properties, hydrodynamics, and froth structure. Chelgani et al. (2021) developed an interpretable CL for an industrial coal column flotation circuit using XGBoost and SHAP. The circuit at the Tabas Parvadeh coal plant includes six columns and treats high-ash feed to produce low-ash concentrate. Process variables were recorded at the shift scale over approximately one year, including solid percentage, frother dosage, collector dosage, airflow, washing water, froth level, and specific gravity. The key extracted result is the SHAP ranking: washing water was identified as the most influential variable for yield prediction, and its relationship with yield was negative (higher washing water tends to reduce yield). For separation efficiency, solid percentage had the greatest positive effect, while collector dosage had the least effect under the observed operating regime. This is operationally valuable because column flotation is often tuned by reagent selection, yet the CL indicates that water management and pulp density may dominate metallurgical responses in practice, particularly through entrainment control and froth washing behaviours.

A more recent and detailed flotation CL study investigated industrial copper flotation at the Delijan plant (Isfahan, Iran), using a dataset of 684 shift-scale records from 2021-03-21 to 2022-02-26 and a flowsheet comprising grinding (two ball mills) followed by rougher, scavenger, and cleaner banks (Chelgani et al., 2025). The reagent scheme included lime and sodium silicate (SS) in grinding; SIPX as initial collector and MIBC as frother in flotation; and a secondary collector substitution from Sodium Ethyl Xanthate (SEX) to Potassium Amyl Xanthate (PAX) implemented on 2021-06-06. The outputs of interest were Cu recovery (%) and Cu grade (%), modelled from ten inputs including size fractions (+149 μm, +74 μm, −74 μm), dosages of SIPX, MIBC, SS, lime, and the relevant secondary collector (SEX or PAX), and ball load. The authors compared several algorithms (CatBoost, XGBoost, random forest, SVR, and CNN) and selected CatBoost for its superior accuracy on both grade and recovery across both collector regimes. Reported R^2 values for CatBoost were approximately 0.90-level under SEX and remained high under PAX (though with a modest decrease), and the maximum absolute difference between actual and CatBoost-predicted responses was reported to be below ~2%. Beyond prediction, the essential CL outcome is interpretability: Pearson correlations showed no strong linear associations ($|r| \leq 0.7$) between any operating variable and the metallurgical responses under steady-state conditions. SHAP, however, revealed meaningful rankings and interaction windows. One of the most consequential findings is that the secondary collector concentration was not the dominant driver; both secondary collectors had negative effects beyond certain dosage ranges, and the authors conclude that the secondary collector was not essential in determining metallurgical responses relative to other interacting variables. Under SEX conditions, the initial collector SIPX had the strongest influence on Cu grade (with a negative average SHAP contribution), and the coarse fraction (+149 μm) was the second most influential variable, acting negatively on grade, consistent with reduced liberation at coarser sizes. Lime showed a positive influence on grade, consistent with pH modification and potential depression of pyrite, improving selectivity but potentially lowering recovery. Under PAX conditions, the variable network shifted: SS became the strongest positive influence on Cu grade, while it also showed a strong negative influence on Cu recovery (reflecting the selectivity-recovery trade-off typical of depressants). The importance of MIBC increased under PAX, with the paper attributing this to PAX effects at the air–liquid interface and bubble stability, which can alter froth structure and thus grade response. The study reports that increasing MIBC above about 125 g/t could enhance grade even at lower SS levels under PAX conditions.

The flotation CL findings translate into several practical recommendations: Treat reagent substitutions as “network” changes, not single-lever changes. After SEX → PAX substitution, variable importance and interactions shifted (SS and MIBC gained importance), and process predictability decreased modestly, implying tighter control is needed to maintain stability.

Under SEX regimes, prioritize SIPX and coarse size control for grade stability, and interpret lime adjustments primarily through selectivity mechanisms. Under PAX regimes, use SS to target grade but monitor recovery penalties; coordinate frother (MIBC) strategy with SS because froth stability effects can dominate grade response. For column circuits, treat washing water as a first-class yield lever and solids percentage as a separation-efficiency lever; do not assume collector dosage is the dominant knob under all regimes.

6. DISCUSSION

Across comminution, classification, and flotation, the CL literature converges on several cross-cutting lessons. First, industrial steady-state operation frequently masks linear relationships. In the copper flotation case, the Pearson correlation showed no strong linear dependencies with a single variable, yet SHAP identified ranked drivers and interaction windows. Similarly, hydrocyclone sizing behaviour exhibited range-dependent interactions between solids and pressure that would be missed in a fixed linear rule. Second, operational regimes matter. The copper study demonstrates that changing a secondary collector can restructure the interaction network and reduce predictability, meaning that control rules calibrated under one regime can become unreliable after a chemical change. Third, explainability is most useful when paired with a high-accuracy model. Both flotation papers emphasize that SHAP explanations are grounded in strong learners (XGBoost or CatBoost), and the comminution studies similarly evaluate predictive models as a foundation before extracting importance rankings. Finally, CL is not limited to ore processing: analogous “conscious lab” approaches have been reported for cement raw ball mill ventilation and cement rotary kiln variables, reinforcing the general principle that plant databases can be converted into interpretable control insight when combined with XAI methods (Fathi et al., 2021 and 2023).

Based on the extracted methods and results, the following implementation pathway is recommended: 1) Define the response and the operating regime(s). Segment datasets when major changes occur (reagent regimes, ore sources, equipment changes), as shown in the SEX vs PAX analysis. 2) Build a robust predictive model and validate it with plant-holdout data. Compare multiple algorithms; CatBoost and XGBoost consistently performed well in the studies. 3) Apply SHAP for global ranking and local troubleshooting. Use global SHAP to identify the small set of high-leverage levers; use local SHAP to explain day-to-day deviations. 4) Convert SHAP results into operating windows and training materials. Interaction plots can be transformed into “safe–effective” ranges (e.g., solids–pressure regimes in cyclones; SS–MIBC coordination under PAX in flotation). 5) Track predictability as a stability KPI. A drop in model predictability after a regime change can act as an early warning that the circuit has become more variable or that a new variable is missing from monitoring.

7. CONCLUSIONS

AI adoption in mineral processing has progressed in recognizable waves: (i) expert systems that encoded operator knowledge for supervisory decision-making, (ii) broader data-driven modelling and multivariable control as instrumentation and computing improved, and (iii) the current era of scalable ML/deep learning, sensor fusion, and digital twins supported by plant connectivity and richer data streams. Across this timeline, the key success factor has been integration, linking algorithms to trustworthy measurements, validated preprocessing, and control-system workflows that operators can interpret and act on.

Looking ahead, the most impactful deployments are likely to be hybrid: physics- and knowledge-guided models combined with data-driven learners, embedded in digital twin environments for monitoring, prediction, and optimization. Reinforcement learning and data-driven MPC methods are promising when they remain constrained, explainable, and validated

in high-fidelity simulation or shadow-mode trials. Ultimately, robust data practices (tag quality assurance, assay alignment, redundancy reduction, and multivariate diagnostics) will remain the difference between impressive demonstrations and sustained industrial value.

REFERENCES

Alidokht, M., Yazdani, S., Hadavandi, E., Chehreh Chelgani, S., (2021), “Modeling metallurgical responses of coal Tri-Flo separators by a novel BNN: a ‘Conscious-Lab’ development”, International Journal of Coal Science & Technology, 8, 1324–1336.

Bai, Z., Gao, P., Chu, M., Han, Y., Yuan, S., Tang, J., Li, Y., Shi, Q., Qiao, J., He, J., (2025), “Artificial intelligence of mineral processing process: A review of research progress”, Journal of Environmental Chemical Engineering, 13 (5), 118313.

Bearman, R. A., Milne, R. W., (1992), “Expert systems: Opportunities in the minerals industry”, Minerals Engineering, 5 (10–12), 1307–1323.

Chen, X., Liu, D., Yu, L., Shao, P., An, M., Wen, S., (2025), “Recent advances in flotation froth image analysis via deep learning”, Engineering Applications of Artificial Intelligence, 147, 110283.

Chehreh Chelgani, S., Homafar, A., Nasiri, H., Rezaei Laksar, M., (2024), “CatBoost–SHAP for modeling industrial operational flotation variables—A ‘conscious lab’ approach”, Minerals Engineering, 213, 108754.

Chehreh Chelgani, S., Nasiri, H., Alidokht, M., (2021), “Interpretable modeling of metallurgical responses for an industrial coal column flotation circuit by XGBoost and SHAP—A ‘conscious-lab’ development”, International Journal of Mining Science and Technology, 31, 1135–1144.

Chehreh Chelgani, S., Nasiri, H., Tohry, A., (2021), “Modeling of particle sizes for industrial HPGR products by a unique explainable AI tool—A ‘Conscious Lab’ development”, Advanced Powder Technology, 32, 4141–4148.

Chehreh Chelgani, S., Nasiri, H., Tohry, A., Heidari, H. R., (2023), “Modeling industrial hydrocyclone operational variables by SHAP–CatBoost—A ‘conscious lab’ approach”, Powder Technology, 420, 118416.

Dai, W., Tian, Q., Yang, Y.-Z., (2025), “Multi-rate data-driven model predictive control for ball mill grinding process”, Minerals Engineering, 232, 109535.

Fatahi, R., Khosravi, R., Siavoshi, H., Yazdani, S., Hadavandi, E., Chehreh Chelgani, S., (2021), “Ventilation prediction for an industrial cement raw ball mill by BNN—A ‘Conscious Lab’ approach”, Materials, 14, 3220.

Fatahi, R., Nasiri, H., Homafar, A., Khosravi, R., Siavoshi, H., Chehreh Chelgani, S., (2023), “Modeling operational cement rotary kiln variables with explainable artificial intelligence methods—A ‘conscious lab’ development”, Particulate Science and Technology.

Hasidi, O., (2024), “Digital twin of minerals processing operations for an advanced monitoring and supervision: froth flotation process case study”, The International Journal of Advanced Manufacturing Technology, 132, 1031–1049.

Katrutsa, A., Strijov, V., (2017), “Comprehensive study of feature selection methods to solve multicollinearity problem according to evaluation criteria”, Expert Systems with Applications, 76, 1–11.
Maharana, K., Mondal, S., Nemade, B., (2022), “A review: Data pre-processing and data augmentation techniques”, Global Transitions Proceedings, 3 (1), 91–99.

Nobahar, P., Xu, C., Dowd, P., Shirani Faradonbeh, R., (2024), “Exploring digital twin systems in mining operations: A review”, Green and Smart Mining Engineering, 1 (4), 474–492.

Okada, N., Nozaki, H., Nakamura, S., Manjate, E. P. A., Gebretsadik, A., Ohtomo, Y., Arima, T., Kawamura, Y., (2024), “Optimizing multi-spectral ore sorting incorporating wavelength selection utilizing neighborhood component analysis for effective arsenic mineral detection”, Scientific Reports, 14 (1).

Peukert, D., Xu, C., Dowd, P., (2022), “A Review of Sensor-Based Sorting in Mineral Processing: The Potential Benefits of Sensor Fusion”, Minerals, 12 (11), 1364.

Pu, Y., Szmigiel, A., Chen, J., Apel, D. B., (2020), “FlotationNet: A hierarchical deep learning network for froth flotation recovery prediction”, Powder Technology, 375, 604–614.

Putz, E., Cipriano, A., (2015), “Hybrid model predictive control for flotation plants”, Minerals Engineering, 70, 26–35.

Ramasamy, M., (2005), “Control of ball mill grinding circuit using model predictive control scheme”, Journal of Process Control, 15, 273–283.

Shardt, Y. A. W., Brooks, K., Yang, X., Kim, S., (2023), “Advanced Soft-Sensor Systems for Process Monitoring, Control, Optimisation, and Fault Diagnosis”, IFAC-PapersOnLine, 56 (2), 11768–11777.

Tohry, A., Chehreh Chelgani, S., Matin, S. S., Noormohammadi, M., (2020), “Power-draw prediction by random forest based on operating parameters for an industrial ball mill”, Advanced Powder Technology, 31, 967–972.

Tohry, A., Yazdani, S., Hadavandi, E., Mahmudzadeh, E., Chehreh Chelgani, S., (2021), “Advanced modeling of HPGR power consumption based on operational parameters by BNN: A ‘Conscious-Lab’ development”, Powder Technology, 381, 280–284.

Zheng, J., Jia, R., Liu, S., He, D., Li, K., Wang, F., (2024), “Sample-efficient reinforcement learning with knowledge-embedded hybrid model for optimal control of mining industry”, Expert Systems with Applications, 254, 124402.

FLOTATION 4.0: GREENER, SMARTER, SUSTAINABLE

Przemyslaw B. KOWALCZUK*

Norwegian University of Science and Technology, Department of Geosciences, S.P. Andersens veg 15, 7031 Trondheim, NORWAY
**Corresponding author: pshem.kowalczuk@ntnu.no*

A B S T R A C T

Mineral processing is undergoing a profound transformation. Declining ore grades, complex mineralogy, and environmental constraints demand a shift from incremental improvements to disruptive innovation. Flotation, the cornerstone of mineral beneficiation, is central to this transition, and is now evolving towards what can be termed 'Flotation 4.0'. The development of flotation can be viewed in stages: Flotation 1.0 established mechanized, industrial-scale flotation; Flotation 2.0 delivered major progress through improved reagents, cell design, and circuit configuration; Flotation 3.0 introduced automation and advanced process control; and now Flotation 4.0 integrates green chemistry, advanced technologies, and digital intelligence into adaptive and sustainable flotation systems. Recent advances in flotation chemistry highlight the promise of biosurfactants, peptides, and biopolymer-based reagents as environmentally friendly alternatives to conventional, petroleum-based chemicals. At the same time, breakthroughs in flotation technology are providing equally transformative advances. Next-generation pneumatic flotation cells, such as the REFLUX Flotation Cell (RFC), Concorde Cell, and micro- to nanobubble flotation devices, offer step-changes in recovery, kinetics, energy efficiency, and fine-particle processing. Combined with digitalization, machine learning, and automated mineralogy, these innovations are turning flotation into an adaptive and intelligent process. Sustainability and circularity provide the guiding framework for these advances. This paper explores their convergence — from green reagents to next-generation flotation cells and digital twins — and highlights their role in shaping a greener, smarter, and more sustainable mineral industry.

Key words: *Flotation, green collectors, machine learning, digital twins, process intensification*

1. INTRODUCTION

The global mineral industry is facing challenges. Declining ore grades, increasing mineralogical complexity, and stricter environmental regulations are placing growing pressure on mineral processing operations to deliver higher efficiency with lower environmental impact (Bontempi and Saccani, 2026). At the same time, the demand for critical (CRM) and strategic (SRM) raw materials — including rare earth elements (REEs) and battery metals — is increasing rapidly due to the global green energy transition (Granvik et al., 2025). These trends require a fundamental rethinking of how mineral resources are processed and utilized.

Flotation remains the most widely applied separation method in mineral processing and is necessary for the beneficiation of both primary and secondary resources. However, conventional flotation practices are often associated with high reagent consumption, limited selectivity, and significant environmental footprints (Pearse, 2005). Incremental improvements to existing technologies are no longer sufficient to meet the combined technical, economic, and sustainability challenges faced by the industry.

Recent years have witnessed rapid advances across multiple fronts. In reagent chemistry, increasing attention is being given to green chemicals such as biosurfactants, peptides, and biopolymer-based depressants, designed to interact selectively with mineral surfaces while minimizing environmental impact (Nagaraj and Farinato, 2016, Chernyshova et al., 2023, Oulkhir et al., 2023, Sahraei et al., 2023, Ku et al., 2024, Chelgani et al., 2024, Bednarek et al., 2025a). In parallel, flotation technology has advanced through the development of

intensified and pneumatic flotation cells, as well as micro- and nanobubble systems capable of improving fine and coarse particle recovery as well as process efficiency (Hassanzadeh et al., 2022a). At the same time, digitalization — real-time sensing, machine learning, and digital twins — is reshaping how flotation processes are designed, monitored, and optimized (Ohenoja et al., 2023, Güner et al., 2024, Szmigiel et al., 2024, Hasidi et al., 2024). These developments are not independent; rather, they are converging toward a new paradigm that can be described as 'Flotation 4.0'. Analogous to the concept of Industry 4.0, Flotation 4.0 represents the integration of chemistry, technology, and data-driven intelligence to create adaptive, efficient, and sustainable flotation systems.

2. FLOTATION 4.0: CONCEPT AND FRAMEWORK

To place Flotation 4.0 in context, flotation development can be summarized in four broad stages (Table 1, Fig. 1). Flotation 1.0 corresponds to mechanization and industrial deployment of mechanically agitated flotation cells. Flotation 2.0 reflects systematic progress in reagent chemistry and equipment design, enabling higher recovery and improved selectivity across a wide range of ores. Flotation 3.0 introduced automation, sensors, and control systems that improved stability and repeatability. Flotation 4.0 builds on these foundations by integrating chemistry, technology, and digital tools into a coordinated, system-level approach that enables adaptive operation and improved resource efficiency. This paradigm is particularly relevant for the processing of complex ores, secondary resources, critical (CRM) and strategic (SRM) raw materials, where traditional approaches often reach their technical and economic limits.

Figure 1. Conceptual evaluation of flotation systems, from Flotation 1.0 to Flotation 4.0

The Flotation 4.0 framework can be described through three interconnected pillars: (i) green reagent chemistry, (ii) advanced flotation technologies, and (iii) digitalization and intelligent process control. The strength of the concept lies not in any single pillar, but in their integration. Figure 2 schematically illustrates the Flotation 4.0 concept and emphasizes the interrelations between pillars. Advances in one pillar influence and reinforce the others; for example, smart reagents require appropriate hydrodynamics to reach their full potential, while digital tools enable real-time optimization of both chemistry and operating conditions. The framework shown is intentionally modular, and additional elements (e.g., automated mineralogy, standardized benchmarking, life-cycle assessment, techno-economic analysis, or reporting/traceability metrics) can be incorporated as the concept evolves.

Table 1. Conceptual evaluation of flotation systems

Dimension	Flotation 1.0	Flotation 2.0	Flotation 3.0	Flotation 4.0
Primary Objective	Industrial mechanization of flotation	Performance optimization	Operational stability and automation	System-level performance optimization
Technological Basis	Mechanically agitated cells	Improved reagents and cell designs	Instrumentation and automated control systems	Advanced cells combined with data-driven control
Reagent Approach	Empirical selection	Chemistry refinement and selectivity improvement	Controlled and optimized dosing	Biobased, selective, and condition-responsive reagents
Cell Technology	Conventional mechanical flotation machines	Optimized mechanical configurations	Automated operation of conventional cells	Pneumatic, intensified, micro-/nanobubble-assisted systems
Process Control	Manual control	Parameter optimization	Feedback-based automation	Predictive and model-assisted control
Data Utilization	Limited process data	Laboratory and periodic analysis	Real-time monitoring	Continuous data integration and modelling
Response to Ore Variability	Reactive	Improved but limited	Stabilized through control systems	Adaptive adjustment supported by modelling tools
Energy & Resource Consideration	Secondary	Efficiency improvement	Variability reduction	Energy-, water-, and reagent-aware optimization
Sustainability Perspective	Not explicitly considered	Efficiency-oriented	Regulatory compliance driven	Embedded in process design and evaluation
Conceptual Framing	Unit operation	Optimized unit operation	Automated unit operation	Data-supported separation platform

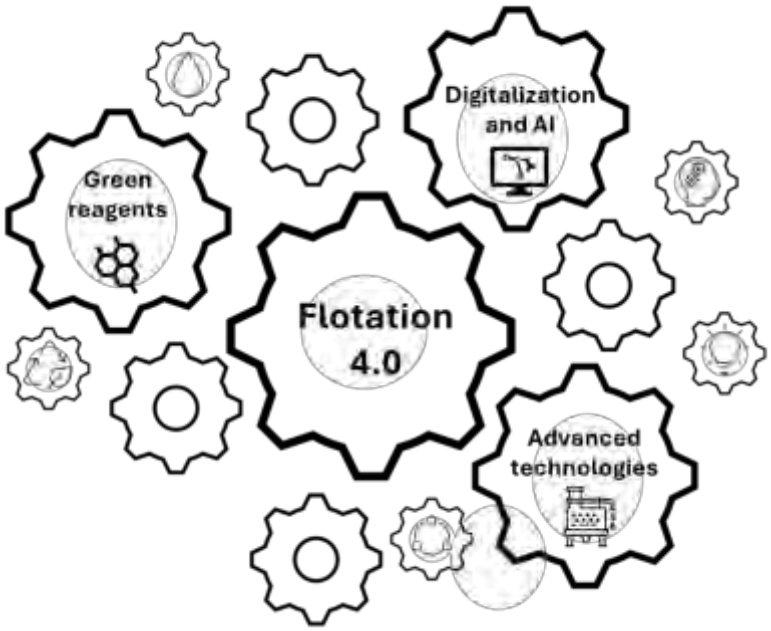

Figure 2. Flotation 4.0 concept

Green reagent chemistry focuses on replacing conventional petroleum-based reagents with environmentally friendly alternatives while enhancing selectivity and performance. Biosurfactants, peptides, and biopolymer-based reagents are designed to interact selectively with mineral surfaces, reduce chemical consumption, and minimize environmental impact. Advanced flotation technologies aim to intensify separation processes through improved hydrodynamics, bubble–particle interactions, and energy efficiency. Next-generation pneumatic flotation cells, such as the REFLUX Flotation Cell and the Concorde Cell, as well as micro- and nanobubble flotation systems, enable improved recovery kinetics and fine particle processing while reducing footprint and energy demand. Digitalization and intelligent processing provide the tools required to connect chemistry and technology into adaptive systems. Automated mineralogy, real-time sensors, machine learning algorithms, and digital twins enable predictive control, continuous optimization, and rapid response to feed variability. These tools transform flotation from a static operation into a dynamic, data-driven process.
A defining feature of Flotation 4.0 is its alignment with sustainability and circular economy principles. By integrating green reagents, energy-efficient technologies, and intelligent control strategies, Flotation 4.0 aims to reduce chemical usage, water consumption, and energy intensity. At the same time, it enables the effective processing of secondary raw materials, tailings, and complex ores that are increasingly important for securing SRM and CRM. Flotation 4.0 therefore, represents not only a technological evolution but also a strategic framework for mineral processing in support of the global green energy transition. The following sections discuss each pillar of Flotation 4.0, beginning with recent advances in green reagent chemistry.

3. GREEN CHEMISTRY IN FLOTATION

Conventional flotation reagents have been developed primarily to maximize recovery and selectivity, often with limited consideration of environmental impact. Many widely used collectors, frothers, and modifiers are derived from petroleum-based feedstocks, exhibit limited biodegradability, and may pose environmental and health risks. Increasing regulatory pressure, together with the need to reduce the environmental footprint of mineral processing, has accelerated the search for greener alternatives.

Biosurfactants represent one of the most promising classes of green flotation reagents. Produced by microorganisms or derived from renewable biological sources, biosurfactants offer several advantages over conventional synthetic surfactants, including low toxicity, high biodegradability, and effectiveness over a wide range of pH and salinity conditions (Chernyshova et al., 2023). In flotation applications, biosurfactants have demonstrated the ability to selectively modify mineral surface hydrophobicity through specific molecular interactions rather than non-specific adsorption. Their complex molecular structures, often containing multiple functional groups, enable stronger and more selective binding to target mineral surfaces. This can lead to improved separation efficiency, particularly in complex and finely disseminated ores. Despite their potential, challenges remain related to large-scale production, cost, and consistency of biosurfactants.

Peptides represent an emerging class of highly selective flotation reagents with the potential to revolutionize surface modification strategies. Designed through molecular modelling or experimental screening, peptides can be tailored to recognize specific mineral surfaces based on crystallographic structure, surface chemistry, or charge distribution (Ku et al., 2024). The key advantage of peptide-based reagents lies in their molecular-level selectivity. Unlike conventional collectors that rely primarily on electrostatic or hydrophobic interactions, peptides can exhibit highly specific binding affinities. This opens new possibilities for separating minerals with very similar surface properties, a common challenge in the beneficiation of complex ores and critical raw materials. Although peptide-based flotation is still at an early stage of development, advances in computational chemistry, high-throughput screening, and bioengineering are rapidly expanding their feasibility. Peptides exemplify the shift toward precision flotation chemistry guided by fundamental surface science and data-driven design.

Biopolymers such as polysaccharides, cellulose and lignin derivatives are increasingly investigated as green depressants and modifiers in flotation systems. These materials are often renewable, biodegradable, and capable of selectively inhibiting the flotation of gangue minerals (Bednarek et al., 2025b). Biopolymer-based depressants can provide improved selectivity by forming structured adsorption layers on mineral surfaces, reducing non-selective entrainment, and improving concentrate quality. Their performance can be further enhanced through chemical modification or combination with other green reagents. Biopolymers are particularly attractive for applications involving water recycling and closed-loop processing, as they tend to be more compatible with complex water chemistries than conventional inorganic depressants.

Reagent chemistry plays a central role in the Flotation 4.0 concept. Green flotation reagents are designed not only to reduce toxicity and improve biodegradability, but also to enhance selectivity and process robustness. In this context, green chemistry extends beyond the substitution of conventional reagents with less harmful alternatives; it encompasses the development of new molecular designs and surface-interaction strategies that enable more controlled and efficient modification of mineral surfaces. By combining environmentally compatible materials with molecular-level selectivity and, in some cases, condition-responsive behavior, such reagents contribute to flotation systems that are both more sustainable and technically robust. At the same time, significant challenges remain, including scalable production, cost competitiveness, performance consistency, and reliable selectivity under complex and recycled water chemistries.

4. ADVANCES IN FLOTATION TECHNOLOGIES

Technological innovation in flotation has been driven by the need to process increasingly complex and finely disseminated ores while reducing energy consumption, water use, and equipment footprint. Conventional mechanical flotation cells, although robust and widely used, often struggle with fine particle recovery, limited mass transfer efficiency, and scale-up

constraints (Hassanzadeh et al., 2022b). These limitations have stimulated the development of intensified and pneumatic flotation technologies (Hassanzadeh et al., 2022b). Advanced flotation cells achieve intensification through improved hydrodynamics, optimized air dispersion, and enhanced mass transfer. These improvements enable faster kinetics, higher recoveries, and reduced reagent consumption. From a sustainability perspective, lower energy demand and reduced water usage are critical advantages, particularly for operations processing low-grade ores or operating in water-scarce regions.

Comparative studies of pneumatic and conventional mechanical flotation cells generally demonstrate improved performance of pneumatic systems in terms of kinetics, energy efficiency, and fine and coarse particle recovery (Cole et al., 2021, Dadzie et al., 2026.). These studies have contributed to a growing acceptance of pneumatic flotation as a viable alternative to mechanically agitated cells. However, although the literature comparing pneumatic and mechanical technologies continues to expand, rigorous cross-comparisons among different pneumatic flotation designs remain limited. Next-generation systems — including the REFLUX Flotation Cell (RFC), the Concorde Cell, HydroFloat, and other intensified configurations — differ substantially in air dispersion mechanisms, hydrodynamic regimes, and residence time characteristics, all of which influence separation performance. In the absence of standardized benchmarking under comparable operating conditions, technology selection is frequently based on case-specific results rather than systematic evaluation across alternative designs.

Micro- and nanobubble flotation has emerged as a promising technology for enhancing fine and ultra-fine particle recovery (Chen et al., 2024). Smaller bubbles increase the probability of collision and attachment with fine particles, addressing one of the fundamental limitations of conventional flotation systems. Nanobubbles, in particular, exhibit unique physicochemical properties, including high stability and large surface area-to-volume ratios. These properties can enhance particle aggregation, modify surface wettability, and improve flotation selectivity. When combined with appropriate reagents, micro- and nanobubbles can significantly improve the recovery of difficult-to-float particles.

Additive manufacturing (3D printing) is emerging as a complementary tool for the design and testing of flotation cell components, including rotor–stator systems and internal flow modifiers (Bednarek et al., 2025). The ability to fabricate complex geometries enables systematic hydrodynamic optimization and rapid prototyping of novel bubble-generation concepts. While still developing at industrial scale, additive manufacturing offers new opportunities for customized cell design and experimental validation of intensified flotation configurations.

In Flotation 4.0, advanced flotation technologies are not deployed in isolation but are integrated with green reagent systems and digital control strategies. Equipment performance is continuously monitored using sensors and process data, enabling real-time optimization of operating conditions such as air flow, pulp density, and reagent dosage. This enables faster response to feed variability and provides a basis for systematic comparison of emerging flotation technologies under industrial conditions. As a result, technological innovation in flotation has become a key enabler of intelligent, efficient, and sustainable mineral processing.

5. DIGITALIZATION AND INTELLIGENT FLOTATION

Digitalization has become an important driver in the modernization of mineral processing. In flotation, the increasing availability of high-frequency process data, advanced sensing technologies, and computational tools is changing how circuits are monitored and controlled. Traditionally, flotation performance relied on periodic sampling and laboratory analysis, which often introduced delays between process disturbance and corrective action. The adoption of real-time data acquisition and analytics reduces this lag and supports more informed operational decisions.

Machine learning (ML) methods are increasingly applied to capture the complex, non-linear relationships between operating variables and performance indicators such as recovery, grade, and reagent consumption. By training models on historical and live process data, it becomes possible to estimate process responses under varying feed and operating conditions. These models can assist operators in adjusting reagent dosage, air flow, and residence time in response to changes in ore characteristics. Compared with conventional rule-based control, data-driven approaches offer greater flexibility, particularly in circuits treating mineralogically complex ores.

Beyond predictive modeling, digital twins extend this capability by providing a continuously updated virtual representation of the flotation process. Such models allow simulation of alternative reagent schemes, cell configurations, and operating strategies before modifications are implemented in the plant. This capability is especially relevant for evaluating emerging technologies, including different pneumatic flotation designs, under comparable and controlled scenarios. In this way, digital twins contribute to more systematic technology assessment and scale-up.

The broader effect of digitalization is a gradual transition from static, parameter-based operation toward adaptive process management. Continuous data analysis supports stabilization of performance targets despite feed variability and process disturbances. In addition to operational benefits, improved control of reagent addition, energy input, and water use contributes to reduced resource consumption. Digital monitoring also facilitates documentation and traceability, which are increasingly required in the context of environmental regulation and supply chain transparency.

In comparison with the automation focus characteristic of Flotation 3.0, the current stage emphasizes predictive modeling and circuit-level optimization informed by integrated datasets. Digitalization, therefore provides the analytical foundation that links reagent design, equipment performance, and sustainability objectives within a common decision-support environment.

6. SUSTAINABILITY AND CIRCULARITY IN FLOTATION 4.0

Sustainability has become a central consideration in mineral processing due to increasing environmental regulation, societal expectations, and the demand for raw materials driven by the global energy transition. Conventional flotation operations are often associated with substantial consumption of chemicals, water, and energy, as well as the generation of large volumes of tailings. These pressures are intensified by declining ore grades and increasing mineralogical complexity, which require more intensive processing to achieve comparable recoveries.

Addressing these challenges requires moving beyond short-term optimization of recovery and grade toward process design that accounts for resource efficiency and environmental performance at the system level. In this context, the developments described under Flotation 4.0 contribute to reduced chemical input, lower specific energy demand, and improved robustness under variable operating conditions.

The adoption of more selective and environmentally compatible reagents can decrease overall reagent consumption while maintaining or improving separation efficiency. Condition-responsive reagent systems further limit over-dosing by adapting to feed variability. In parallel, intensified and pneumatic flotation technologies improve mass transfer and separation kinetics, often enabling shorter residence times and lower specific energy consumption compared with conventional mechanical cells. Micro- and nanobubble approaches support improved recovery of fine particles without proportionally increasing energy demand.

Water management represents another critical constraint. Increasing reliance on recycled process water introduces variability in ionic composition and residual reagents, which can destabilize flotation performance. Reagent systems with improved tolerance to complex water chemistries, combined with real-time monitoring and data-supported control strategies, enhance process stability and facilitate higher rates of water recycling. This contributes directly to reduced freshwater intake and improved operational resilience.

The same technological advances also support circular economy objectives. As attention shifts toward secondary raw materials — including tailings, slags, and industrial residues — flotation remains an essential separation method for recovering valuable components from materials previously considered waste. Improved selectivity and enhanced fine particle recovery expand the technical feasibility of valorizing such resources, thereby reducing reliance on primary extraction.

Demand for critical and strategic raw materials further reinforces the need for efficient and responsible processing technologies. These materials are frequently associated with complex mineral assemblages and unconventional deposits, where precise control of surface chemistry and hydrodynamics becomes essential. Advances in reagent design, intensified cell configurations, and data-informed process control collectively improve the ability to recover these materials while limiting environmental impact.

Sustainability in this context is not treated as a separate objective but emerges from coordinated improvements in chemistry, equipment design, and process control. By embedding resource awareness into circuit design and operational decision-making, the Flotation 4.0 perspective aligns technical performance with environmental and economic considerations.

7. CONCLUSIONS

The challenges facing mineral processing — declining ore grades, increasing mineralogical complexity, and increasing environmental and societal expectations — call for a reconsideration of how flotation systems are designed and operated. Incremental refinement of conventional approaches is unlikely to be sufficient under these conditions. This paper has therefore proposed Flotation 4.0 as a structured framework that brings together developments in reagent chemistry, flotation technology, and digital process control within a coherent system perspective.

Recent advances in biosurfactants, peptides, biopolymer-based reagents, and condition-responsive collectors expand the possibilities for selective and environmentally compatible surface modification. At the same time, intensified and pneumatic flotation technologies, including micro- and nanobubble systems, improve hydrodynamic performance, energy efficiency, and fine particle recovery. Digital tools — automated mineralogy, machine learning, and digital twins — provide the analytical foundation for predictive modeling, technology assessment, and circuit-level optimization.

Future progress will depend on systematic evaluation of emerging technologies and clearer benchmarking methodologies, particularly for pneumatic flotation systems, where direct comparisons remain limited. Data-supported modeling and virtual testing environments offer practical pathways for improving technology selection and scale-up decisions.

The full impact of these developments becomes evident when considered at the circuit and system levels. Reagent selectivity, hydrodynamics, water chemistry, and process control are interdependent variables that influence overall performance. Addressing them collectively

enables improved resource efficiency, reduced environmental footprint, and greater operational resilience.

Within the historical progression from mechanization to automation, Flotation 4.0 can be understood as the stage characterized by coordinated, data-informed optimization across chemical, mechanical, and operational domains. The framework is intentionally adaptable and may incorporate additional elements such as life-cycle assessment, techno-economic analysis, and standardized reporting as industrial and regulatory conditions evolve.

In summary, Flotation 4.0 represents a consolidation of recent advances into a system-oriented approach to flotation design and operation. Continued research, cross-disciplinary collaboration, and industrial validation will determine how effectively this framework can be translated into robust and scalable practice.

REFERENCES

Bednarek, P. S., Zawala, J., Kowalczuk, P. B., (2025a) “Polymer-based collectors in flotation: A review”, Advances in Colloid and Interface Science, 335, 103351.

Bednarek, P. S., Razavi, N., Kowalczuk, P. B., (2025b) “The role of additive manufacturing in mineral and metal extraction”, Proceedings of the XVI International Mineral Processing and Recycling Conference, 320–326.

Bontempi, E., Saccani, N., (2026) “The energy transition paradox: How declining ore grades are undermining the sustainability of primary metal extraction”, Resources, Conservation & Recycling, 226, 108658.

Chelgani, S. C., Neisiani, A. A., Wonyen, D., Zadeh, A. H. M., Saneie, R., (2024) “Green flotation depressants”, Springer Nature Switzerland.

Chen, J., Chen, J., Cheng, Y., (2024) “Current status of research on nanobubbles in particle flotation”, Physicochemical Problems of Mineral Processing, 60 (1) 183613.

Chernyshova, I., Slabov, V., Kota, H. R., (2023) “Emerging application of biosurfactants in metal extraction”, Current Opinion in Colloid & Interface Science, 68, 101763.

Cole, M. J., Galvin, K. P., Dickinson, J. E., (2021) “Maximizing recovery, grade and throughput in a single stage reflux flotation cell”, Minerals Engineering, 163, 106761.

Dadzie, R. A., Zanin, M., Skinner, W., Asamoah, R., Addai-Mensah, J., Abaka-Wood, G. B., (2026) “Enhanced size-by-split flotation of sulphide tailings: Mechanical, HydroFloat, REFLUX flotation benchmarking”, Chemical Engineering Research and Design, 227, 35–45.

Granvik, P., Hanski, J., Lahdesmaki, S., Jokilaakso, A., Huttunen-Saarivirta, E., (2025) “Critical raw materials for green transition: Key parameters and feasibility index for sufficiency”, Resources, Conservation & Recycling, 218, 108197.

Guner, M. K., Akyildiz, O., Basarir, H., Kowalczuk, P., (2024) “Exploring the impact of thiol collectors system on copper sulfide flotation through machine learning-driven modeling”, Physicochemical Problems of Mineral Processing, 60 (4) 191709.

Hasidi, O., Abdelwahed, E. H., El Alaoui-Chrifi, M. A., Qazdar, A., Benzakour, I., Bourzeix, F., Bendaouia, A., (2024) “Digital twin of minerals processing operations for an advanced monitoring and supervision: Froth flotation process case study”, International Journal of Advanced Manufacturing Technology, 132, 1031–1049.

Hassanzadeh, A., Safari, M., Hoang, D. H., Khoshdast, H., Albijanic, B., Kowalczuk, P. B., (2022b) “Technological assessments on recent developments in fine and coarse particle flotation systems”, Minerals Engineering, 180, 107509.

Hassanzadeh, A., Safari, M., Khoshdast, H., Guner, M. K., Hoang, D. H., Sambrook, T., Kowalczuk, P. B., (2022a) “Introducing key advantages of intensified flotation cells over conventionally used mechanical and column cells”, Physicochemical Problems of Mineral Processing, 58 (5) 155101.

Ku, L. I., Forbes, L., Abreu, S. B., (2024) “An efficient peptide screening method for mineral-binding peptides”, Minerals, 14 (2) 207.

Nagaraj, D. R., Farinato, R. S., (2016) “Evolution of flotation chemistry and chemicals: A century of innovations and the lingering challenges”, Minerals Engineering, 96–97, 2–14.

Ohenoja, M., Koistinen, A., Hultgren, M., Remes, A., Kortelainen, J., Kaartinen, J., Peltoniemi, M., Ruusunen, M., (2023) “Continuous adaptation of a digital twin model for a pilot flotation plant”, Minerals Engineering, 198, 108081.

Oulkhir, A., Lyamlouli, K., Danouche, M., Ouazzani, J., Benhida, R., (2023) “A critical review on natural surfactants and their potential for sustainable mineral flotation”, Reviews in Environmental Science and Biotechnology, 22, 105–131.

Pearse, M. J., (2005) “An overview of the use of chemical reagents in mineral processing”, Minerals Engineering, 18 (2) 139–149.

Sahraei, A. A., Bohorquez, B. M., Tremblay, D., Moineau, S., Garnier, A., Larachi, F., Lague, P., (2023) “Insight into binding mechanisms of quartz/selective peptides: Toward greener flotation processes”, ACS Applied Materials & Interfaces, 15, 17922–17937.

Szmigiel, A., Apel, D. B., Skrzypkowski, K., Wojtecki, L., Pu, Y., (2024) “Advancements in machine learning for optimal performance in flotation processes: A review”, Minerals, 14 (4) 331.

INTEGRATING ADVANCED SEPARATION TECHNIQUES FOR SUSTAINABLE RECOVERY OF CRITICAL METALS FROM DEEP-SEA FERROMANGANESE CRUSTS

Gjergj DODBIBA*, Cheng-En LEE

Department of Systems Innovation, Graduate School of Engineering, The University of Tokyo, Tokyo 113-8656, JAPAN
**Corresponding author: dodbiba@g.ecc.u-tokyo.ac.jp*

A B S T R A C T

Recent technological advancements are raising the demand for valuable metals. In a quest to find new sources of valuable metals, ferromanganese cobalt-rich crust is considered a promising alternative, as it contains various metals, including cobalt (Co), nickel (Ni), platinum (Pt), and rare-earth elements (REEs). The aim was to (1) investigate the efficiency of the enhanced gravity separation by the Falcon concentrator, and (3) study the efficiency of reverse flotation. The main finding of this research was that Mn, Co, and Ni could be enriched by combining the enhanced gravity separation with the reverse flotation.

Key words: *Ferromanganese crust, falcon concentrator, reverse flotation*

1. INTRODUCTION

Recent technological advancements are increasing demand for valuable metals, especially cobalt (Co), which is used in the manufacturing of batteries, superalloys, supermagnets, and cell phones (Wang, 2006). Therefore, in a quest to find new resources for valuable metals, ferromanganese cobalt-rich crust is generally considered a new alternative, since it contains various valuable metals, including cobalt (Co), nickel (Ni), platinum (Pt), and rare earth elements (REEs), (Hein et. al., 2013).

Several published papers have suggested different ways of how to recover valuable metals from ferromanganese cobalt-rich crust, including physical methods (such as jigging (Ito et al., 2008) and floatation (Hirt et. al., 1991; Shao et. al., 2006) and chemical methods (such as leaching (Das et. al., 1986; Inoue et. al., 1997; Wang et. al., 2002; Kongolo et. al., 2003, etc.). Although chemical processes can achieve high extraction rates, subsequent solvent treatment is of great concern. Thus, physical separation methods are usually considered environmentally friendly pretreatment techniques. Nevertheless, the reported physical processes did not focus on the simultaneous recovery of manganese, cobalt, and nickel. To address this problem, both enhanced gravity separation using a Falcon concentrator and reverse flotation are employed to recover manganese, cobalt, and nickel from ferromanganese cobalt-rich crust. The aim was to investigate the efficiency of (1) the Falcon concentrator, which adds centrifugal force in gravity separation, and (2) the reverse flotation, which collects the valuable metals as tails instead of froth, as in the case of conventional flotation.

2. MATERIAL AND METHODS

2.1. Method

In this work, the sample was first subject to enhanced gravity separation using a Falcon concentrator and reverse flotation. Enhanced gravity separators (EGSs) were developed to overcome the poor performance of conventional devices (jigs, spirals, tables) at low concentration values and fine sizes by superimposing a centrifugal field many times greater than 1 G. The additional centrifugal force increases the differential settling velocities between high- and low-density particles, enabling viable separation even when the concentration criterion is below about 2.5 or when particle sizes are in the fine-to-ultrafine range (Oruç et al., 2020; Das et al., 2023).

In this work, the Falcon concentrator was employed for enhanced gravity separation. The concentrator consists of a rotating bowl in which a thin, flowing film develops along the wall under high G. As a result, dense particles migrate toward the wall. In contrast, lighter particles remain in the outer layers and are carried to the tailings under the combined action of fluid drag and centrifugal force (Luttrell, G. H., et al., 1995). Kroll-Rabotin et al. (2012) have presented a model of the Falcon UF bowl, describing separation as governed by particle trajectories within the thin film under the combined effects of centrifugal force, drag, and secondary flows.

In addition, reverse flotation, where the valuable mineral is kept in the pulp while the gangue is floated and removed, i.e., the opposite of conventional (direct) flotation, was also employed (Mark M., 2012). This method is widely applied in ore beneficiation, where gangue phases are floated, and valuable minerals are depressed. In other words, in conventional (direct) flotation, collectors selectively adsorb on the valuable mineral, making it hydrophobic so it reports to the froth, while gangue remains hydrophilic in the pulp. In reverse flotation, on the other hand, the reagent scheme is designed so that gangue becomes hydrophobic and floats, whereas the valuable mineral is rendered hydrophilic by depressants and remains in the slurry as concentrate.

During each test, the sample was first subject to grinding and size classification by sieving. Then, the enrichment of valuable metals from ferromanganese cobalt-rich crust is carried out in two stages (Fig. 1) (Dodbiba et. al., 2022). In the first stage, two different size fractions (-74, -100+74, and -250+100 μm) were subject to enhanced gravity separation by using a Falcon concentrator, operating at varying rotation speeds (0-1700 RPM). After the first stage, the recovered underflow fractions were subject to the grinding and sieving to prepare three different size fractions (-20, +20-37, +37-100, and +50-100 μm), which were then enriched by the reverse flotation, using Dodecyl Amino Acetate (DAA) as surfactants (dosage of DAA: 0.12 g/l) at a constant pH 4, (Fig. 1).

2.2. Qualitative Analysis of Sample

An X-ray fluorescence spectrometer (XRF) is used to analyze the elemental chemical composition of the sample, and the results are shown in Table 1. The combined content of manganese and iron exceeds 60 wt.%. The content of other valuable metals, such as nickel and cobalt, is 1.38 wt.% and 1.20 wt.%, respectively.

It is important to note that the ferromanganese cobalt-rich crust is comprised of two layers (Fig. 2), i.e., (1) the layer of cobalt-rich crust and (2) the layer of nuclei rock. Table 1, on the other hand, shows the components of these two layers. It can be seen that the content of Mn, Co, and Ni in the cobalt-rich crust layer is 46.95 wt.%, 1.93 wt.%, and 2.04 wt.%, whereas their contents in the nuclei rock are 2.01 wt.%, 0.03 wt.%, and 0.16 wt.%, respectively. Thus, the immediate conclusion is that, since layers of cobalt-rich

ferromanganese crusts have different compositions, gravity separation would effectively enrich the valuable metals.

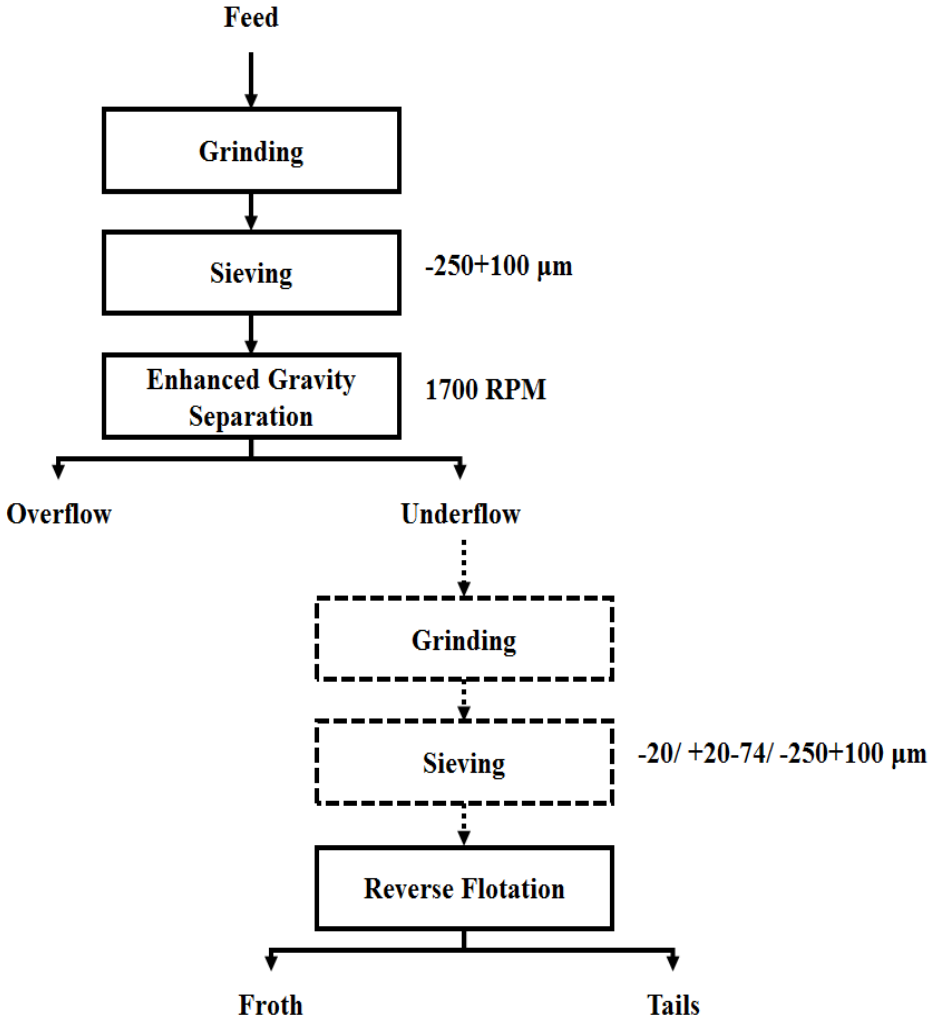

Figure 1. Flowchart

Table 1. Composition of the cobalt-rich ferromanganese crust sample

Components	wt.%	Cobalt-rich crust layer, (wt.%)	Nuclei rock layer (wt. %)
MnO	39.10	50.12	2.01
Fe_2O_3	26.88	16.68	30.16
CaO	11.91	14.71	20.12
SiO_2	6.53	4.11	22.98
NiO	1.38	2.04	0.16
Co_2O_3	1.20	1.93	0.03
others	13.00	-	

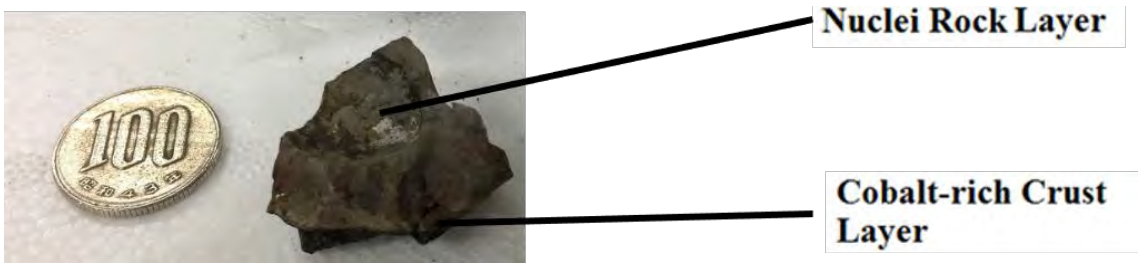

Figure 2. Texture of ferromanganese cobalt-rich crust, which has two different layers

3. RESULTS AND DISCUSSION

3.1. First Stage: Enhanced Gravity Separation

The results of the enrichment by enhanced gravity separation using a Falcon concentrator are plotted in Figure 3, which shows the grades of Mn, Co, and Ni as a function of particle size and rotating speed (0-1700 RPM). It should be noted that Mn, Co, and Ni were collected in the underflow fraction, especially when the rotational speed was kept under 1700 RPM. It was found that the grades of Mn, Co, and Ni in the coarsest size fraction reached 48, 1.7, and 1.5 %, respectively. On the other hand, another important finding is that coarser size fractions (+100-250 μm) performed better than finer size fractions (-74 and +74-100 μm). Thus, if particles are subject to finer grinding, the differences in particle size between the concentrate and the gangue will decrease, worsening the results.

3.2. Second Stage: Reverse Flotation

The results of reverse flotation after the scavenging stage are shown in Figure 4, which shows the grades of Mn, Co, and Ni as a function of particle size fractions at pH 4 and with 0.12 g/L DAA dosage. It was found that reverse flotation can be effective, especially for enriching coarser particles. The reason is that the small particles are sensitive to bubble motion during reverse flotation. Therefore, small particles have a higher possibility of being brought up to the froth layer, no matter the surface charge. Under the best conditions, the Mn, Co, and Ni grades reached 49.62, 1.81, and 1.68%, respectively.

4. CONCLUSION

It is found that Mn, Co, and Ni would be enriched by combining the enhanced gravity separation and the reverse flotation. As a result, the Mn, Co, and Ni grades reached 49.62%, 1.81%, and 1.68%, respectively.

Another important finding of this work is that controlling the size of particles is crucial. Finer particles tend to accumulate together, worsening the separation results. Nevertheless, to achieve the best results, the particle size should be carefully controlled between 100 and 250 μ m. In other words, the over-grinding of the sample should be avoided.

The authors believe that combining the enhanced gravity separation and the reverse flotation to concentrate Co, Ni, and Mn containing particles from the cobalt-rich ferromanganese crust would reduce the cost and the environmental burden of the subsequent leaching process.

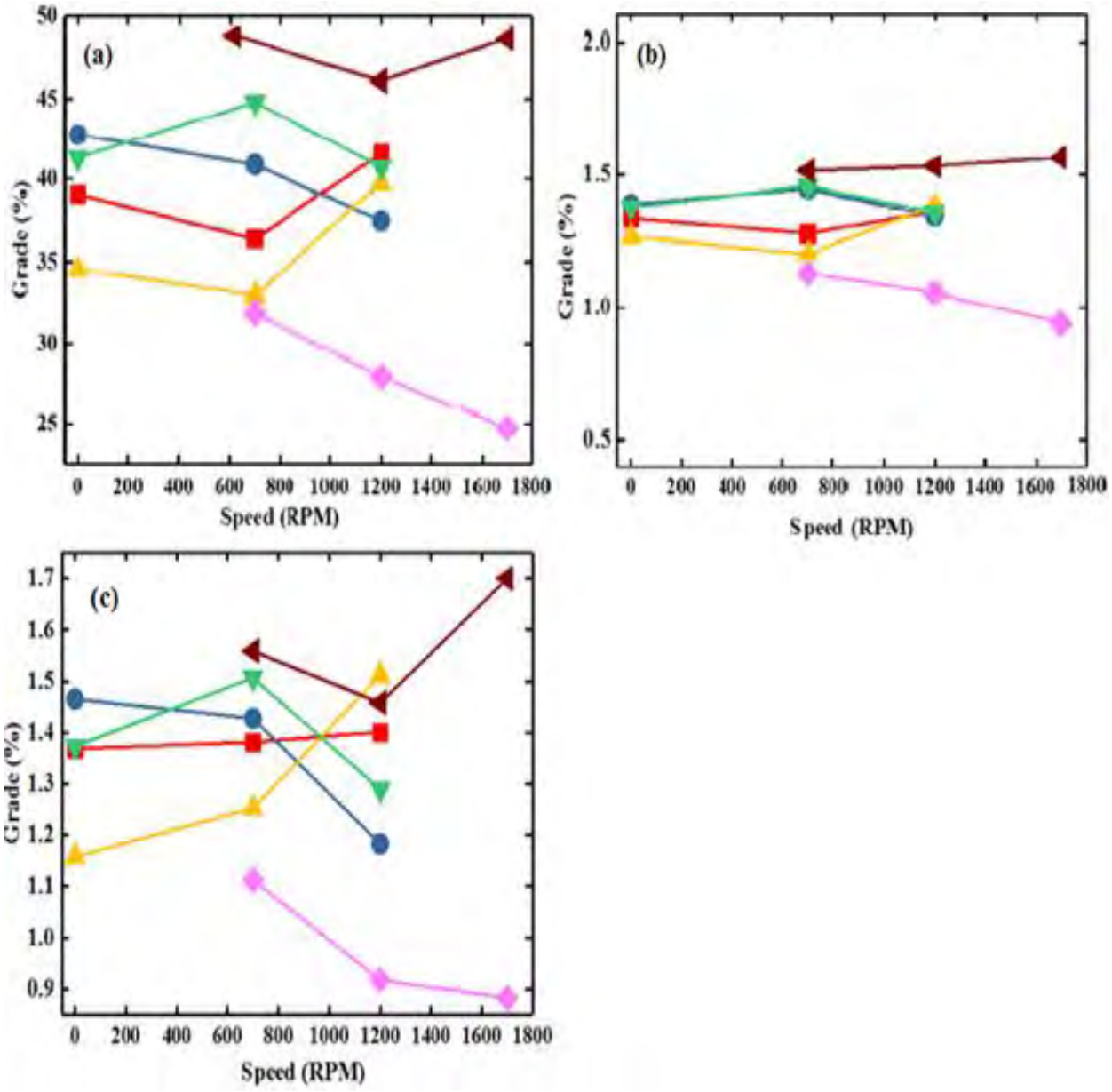

Figure 3. The results of enhanced gravity separation: (a) Mn, (b) Ni, (c) Co

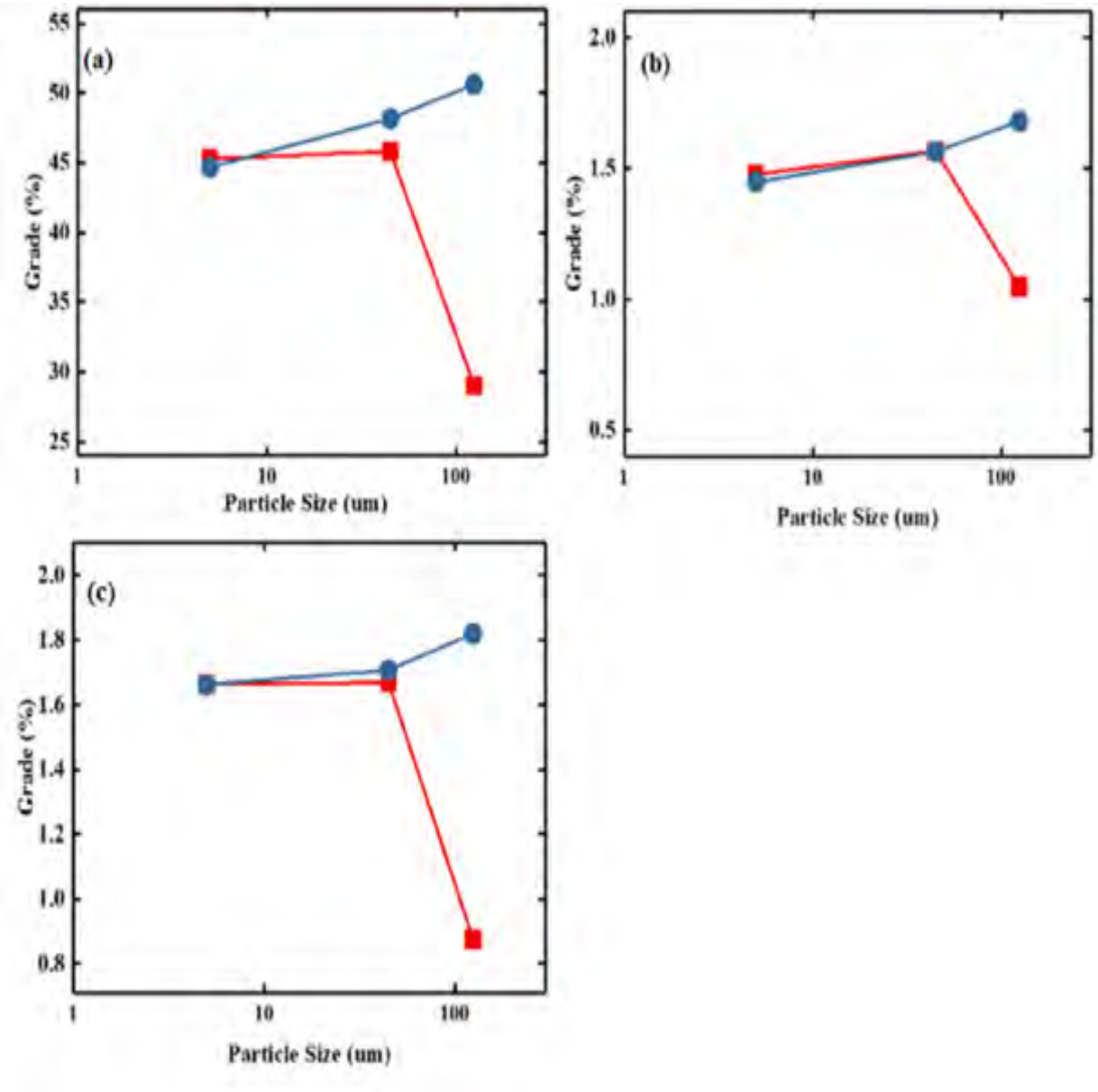

Figure 4. The results of reverse flotation after the enhanced gravity concentration: (a) Mn, (b) Ni, (c) Co

REFERENCES

Das, R. P., Anand, S., Das, S. C., Jena, P. K., (1986), "Leaching of manganese nodules in ammoniacal medium using glucose as reductant". Hydrometallurgy, 16 (3), 335–344.

Das, S. K., Tan, J., Kundu, T., Rath, S. S., Angadi, S. I., (2023), "Performance evaluation of Falcon fluidized bowl and ultrafine (UF) bowl concentrators for the recovery of ultrafine scheelite particles". Advanced Powder Technology, 34 (10), 104193.

Dodbiba, G., Lee, C. E., Kim, Y., Fujita, K., (2022), "Enrichment of Co, Ni, and Mn from Cobalt-rich Ferromanganese Crust by Combining Enhanced Gravity Separation and Reverse Froth Flotation". Int. J. Soc. Mater. Eng. Resour., 25 (1), 129–136.

Hein, J. R., Mizell, K., Koschinsky, A., Conrad, T. A., (2013), "Deep-ocean Mineral Deposits as a Source of Critical Metals for High- and Green-technology Applications: Comparison with Land-based Resources". Ore Geol. Rev., 51, 1–14.

Hirt, W. C., Rice, D. A., Shirts, M. B., (1991), "Flotation of Cobalt-rich Ferromanganese Crust from the Pacific Ocean". Miner. Eng., 4 (5–6), 535–551.

Inoue, A., Kawahara, M., (1997), "Extraction and Separation of Acidity of Valuable obtained from Metals Cobalt in Leaching Crust Solution". Shigen-to-Sozai, 113, 193–197.

Ito, M. et al., (2008), "Estimation of degree of liberation in a coarse crushed product of cobalt-rich ferromanganese crust/nodules and its gravity separation". Int. J. Miner. Process., 87 (3–4), 100–105.

Kongolo, K., Kipoka, M., Minanga, K., Mpoyo, M., (2003), "Improving the efficiency of oxide copper-cobalt ores flotation by a combination of sulphidisers". Miner. Eng., 16 (10), 1023–1026.

Kordloo, M., Khodadadmahmoudi, G., Ebrahimi, E. et al., (2023), "Green hematite depression for reverse selective flotation separation from quartz by locust bean gum". Sci. Rep., 13, 8980.

Kroll-Rabotin, J. S., Bourgeois, F., Climent, E., (2012), "Experimental validation of a fluid dynamics based model of the UF Falcon concentrator in the ultrafine range". Separation and Purification Technology, 92, 129–135.

Luttrell, G. H. et al., (1995), "Enhanced gravity separators: New alternatives for fine coal cleaning". Report Number: CONF-950579, OSTI ID: 81495.

Mark, M., (2012), "Froth Flotation of Iron Ores". International Journal of Mining Engineering and Mineral Processing, 1 (2), 56–61.

Oruç, F., Özgen, S., Sabah, E., (2010), "An enhanced-gravity method to recover ultra-fine coal from tailings: Falcon concentrator". Fuel, 89 (9), 2433–2437.

Shao, G. Q., Wu, P. R., Liu, W. F., Zhang, X. P., Bai, X. M., (2006), "Research on Flotation of Cored and Gravel Cobalt-rich Crust from Pacific Ocean". Nonferrous Met. Mineral Process. Sect., 58, 57–60.

Wang, S., (2006), "Cobalt—Its Recovery, Recycling, and Application". JOM, 58, 47–50.

Wang, S. D., Jiang, X. X., Yin, C. Q., (2002), "Selective Extraction of Copper from the Acid Leaching Solution of Cobalt-rich Crust with LIX84". Nonferrous Met. Extractive Metall., 2, 6–9.

ORE SILOS AND FLOW PROBLEMS

Ayhan Ali SIRKECI*

Istanbul Technical University, Faculty of Mines, Mineral Processing Engineering Department, 34469, Maslak, Istanbul, TÜRKİYE
**Corresponding auhor: sirkecia@itu.edu.tr*

A B S T R A C T

The handling and storage of bulk solids in silos frequently present operational challenges due to complex flow behavior. This study reviews fundamental flow properties of bulk materials and their influence on silo performance. The distinction between mass flow and funnel flow regimes is examined, emphasizing the design conditions required to ensure reliable discharge. Common flow obstructions, including ratholing, cohesive arching, mechanical arching, and time consolidation (caking), are discussed in relation to material properties such as unconfined yield strength, consolidation stress, and wall friction. The role of shear testing, particularly using the Jenike method, in determining flow parameters and designing appropriate hopper geometries is highlighted. The findings underscore the importance of proper flow characterization and design to prevent discharge interruptions and ensure efficient bulk solid handling systems.

Key words: *Bulk solids, silos, ratholing, arching flow parameters*

1. INTRODUCTION

All particulate materials are collectively referred to as **bulk solids**. Bulk solids are materials handled in large quantities without individual counting (Grant A., 13th International Conference on Bulk Materials Storage, Handling and Transportation, 9–11 July 2019, Queensland, Australia). This category includes materials such as granulated sugar, fertilizers, grains, and particulate ores.

Handling bulk solids is a broad engineering field, and numerous storage systems are used depending on capacity requirements, ranging from large stockpiles to silos and bins. Although storage structures can be properly designed from a structural standpoint, including detailed testing to determine flow properties, discharge from silos often becomes problematic if the design does not adequately consider flow behavior.

In principle, two fundamental flow regimes are defined: **mass flow** and **funnel flow**. Mass flow is generally the preferred regime because it ensures consistent discharge; however, funnel flow may be acceptable or even desirable in specific applications.

Reliable storage and discharge are essential for uninterrupted process operations. Unfortunately, flow from silos is frequently unreliable, leading to operational interruptions and additional costs. Common problems encountered in storage bins include arching, piping (ratholing), solids aggregation, erratic feeding, and flooding. Flow-promoting devices are often installed to mitigate blockages. The systematic study of cohesive bulk solid flow began with the pioneering work of Dr. A. W. Jenike.

A silo or bin consists of two main sections: a **vertical section** and a **hopper section**. The vertical section may have a circular, square, or rectangular cross-section that remains constant throughout its height. The hopper is the converging section, where the cross-sectional area decreases toward the outlet. Figure 1 presents typical bin structures.

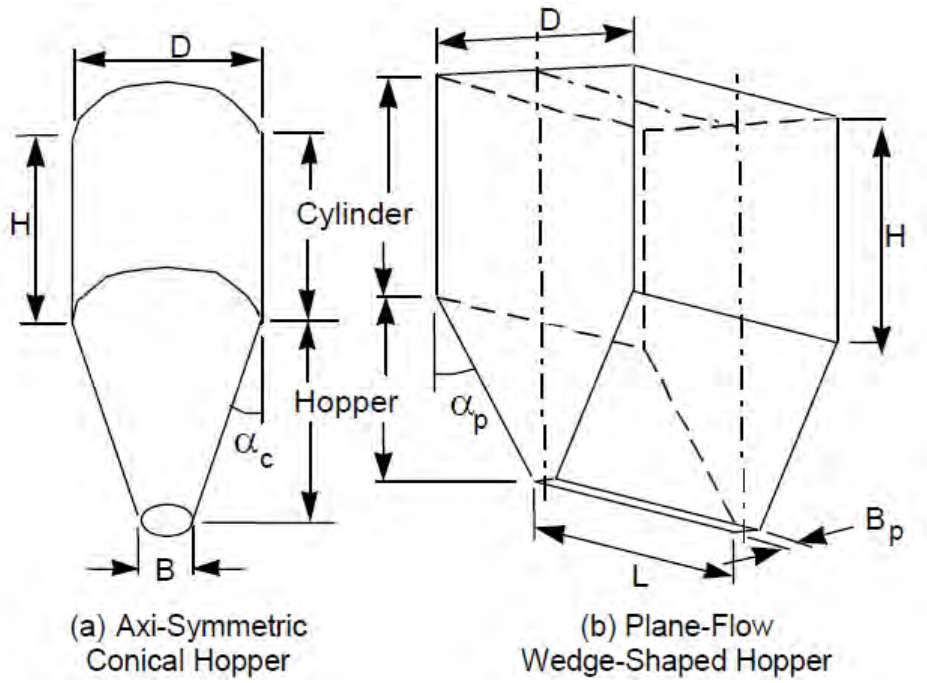

Figure 1. Typical bin structures. (a) cylindrical cross section, (b) rectangular cross section.

2. FLOW PROPERTIES OF BULK SOLIDS

Bulk solids flow under gravity in a manner superficially similar to liquids; however, significant differences exist between the two:

- Under consolidation, many solids retain their shape.
- Shear stresses in bulk solids are largely independent of shear rate but dependent on normal pressure, whereas the opposite is true for Newtonian liquids.
- Under static conditions, bulk solids can transmit shear stresses, while liquids cannot.

Therefore, bulk solids exhibit **plastic behavior** and must be treated differently from liquids. In Figure 2 the depiction of transmitting shearing stresses is seen for liquids and solids.

For example, a container filled with water does not rotate immediately when a stirrer begins to move. In contrast, a container filled with granular solids rotates almost immediately because shear stresses are transmitted through the solid mass.

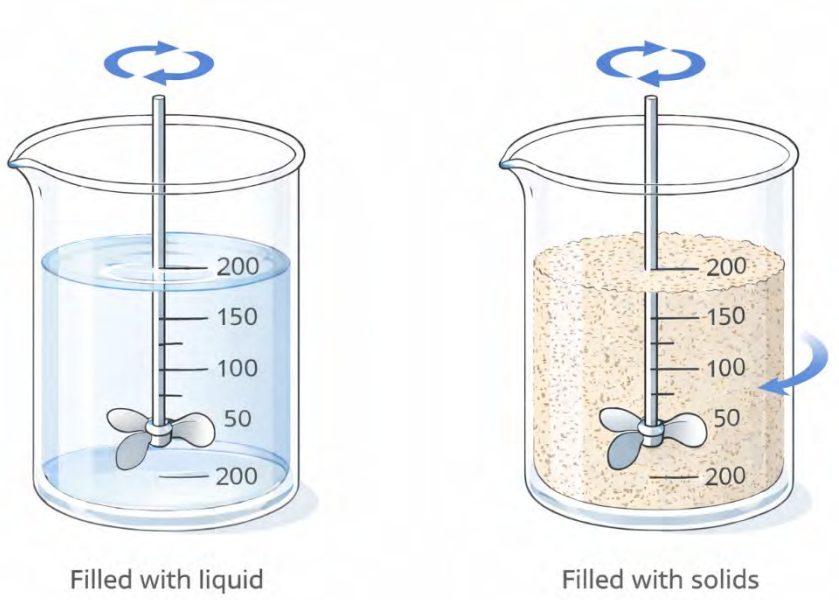

Figure 2. Transmission of shearing stresses in the case of liquids and solids.

3. DETERMINATION OF FLOW PROPERTIES

The **Jenike shear cell (Flow Factor Apparatus)** is widely used to determine the flow properties of bulk solids (Figure 4). During testing, the material is sheared under controlled normal stresses, and the corresponding shear stresses are measured. This procedure produces a series of normal stress versus shear stress loci (Figure 5).
Additional wall friction tests are conducted by sliding the bulk solid against liner materials under known loads. From these experiments, the following parameters are determined:

- Flow factor
- Major consolidation stress, σ_1
- Unconfined yield strength, σ_c
- Kinematic angle of internal friction, φ
- Wall friction angle, φ_w
- Effective angle of internal friction, δ
- Cohesion at zero normal stress, C

From the yield locus, several σ_1-σ_c data pairs are obtained. These data are used to construct the **flow function**, which describes the flowability of the material.

The flow function depends on:
- Consolidation pressure
- Time
- Moisture content
- Temperature

Materials with higher unconfined yield strength at a given consolidation stress exhibit poorer flowability.

Figure 3. Jenike Shear Tester used to determine the flow properties of bulk solids.

The flow properties determined as described above enable the investigator to identify the appropriate flow regime and to design the silo accordingly. As a result of the testing procedures, the corresponding characteristic diagrams are obtained.

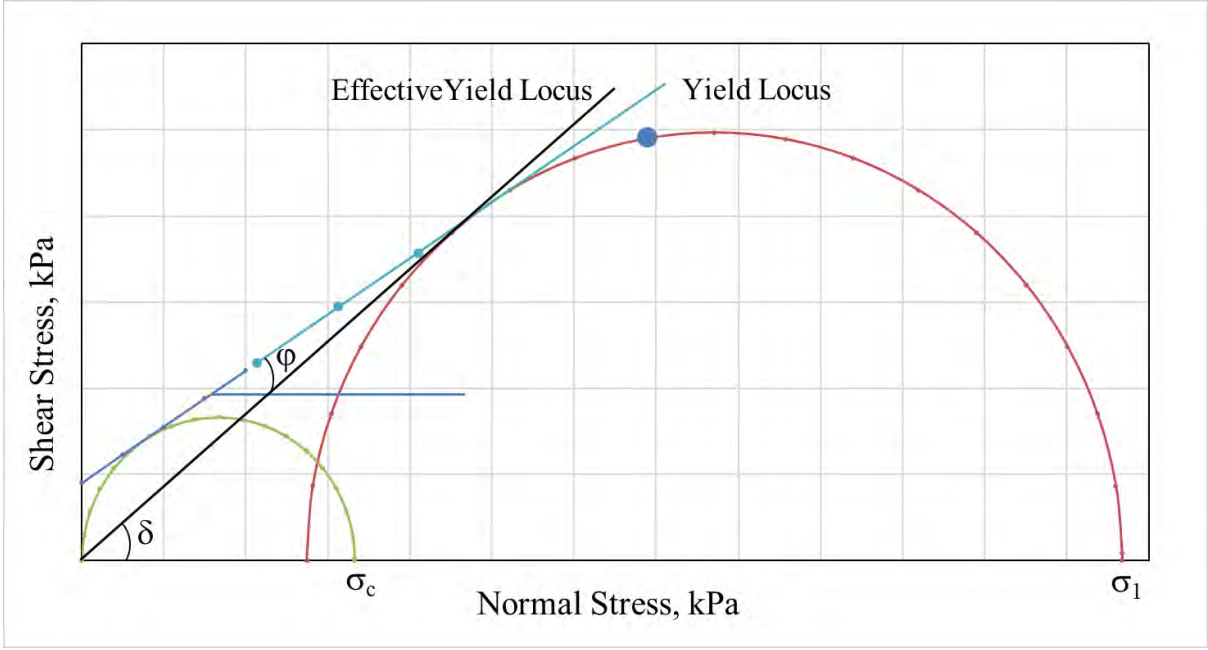

Figure 4. Yield locus drawn by normal stress vs. shear stress test results.

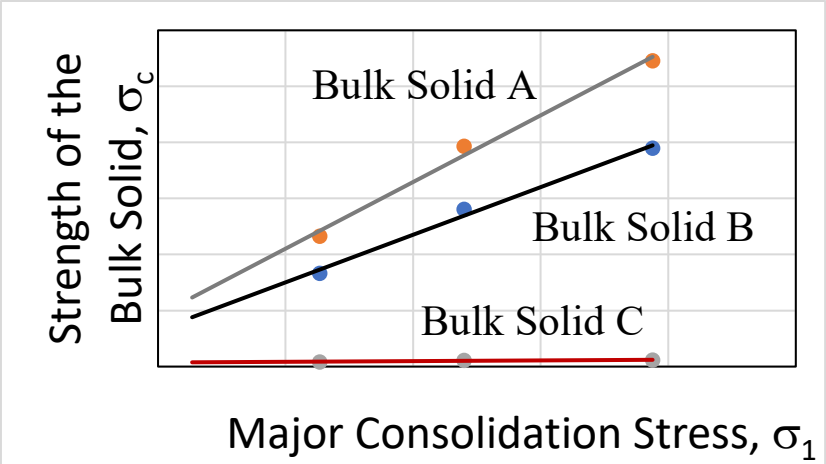

Figure 5. Flow functions of three different bulk solids.

In Figure 5, Bulk Solids A, B, and C exhibit distinct flow behaviors. For a given consolidation stress, Bulk Solid A demonstrates the highest cohesive strength and consequently the poorest flowability. In contrast, Bulk Solid C exhibits negligible cohesive strength over the entire range of consolidation stresses and may therefore be classified as a free-flowing material, similar to dry granular sand. The flow function characterizes the flowability of a bulk solid and reflects its ability to discharge under applied stress conditions. It is influenced by several factors, including consolidation pressure, storage time, moisture content, and temperature.

4. BIN FLOW PATTERNS

Two principal flow patterns are observed during the discharge of bulk solids from a silo: mass flow and funnel flow. In Figure 6, two flow patterns and associated bin types are presented.

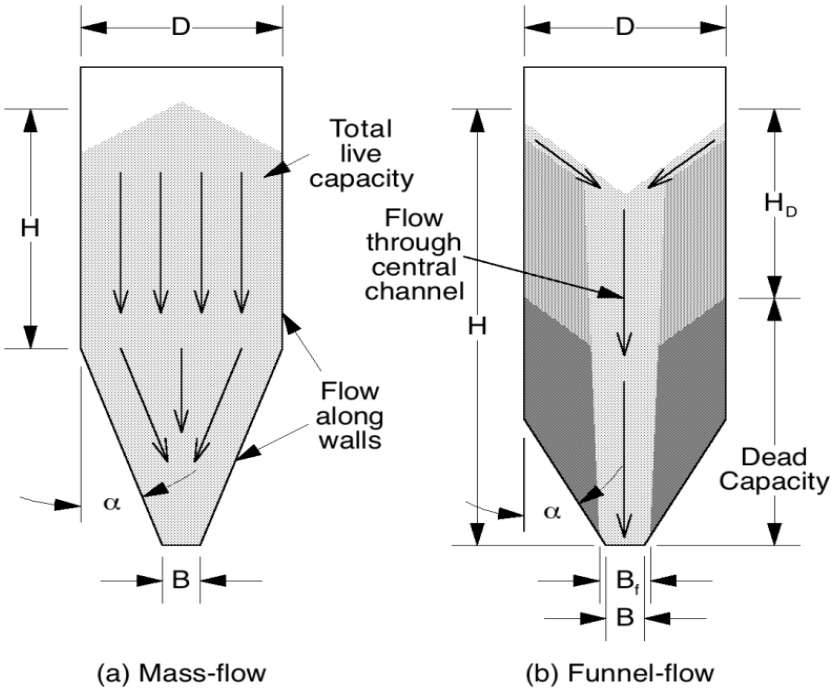

Figure 6. Mass flow and funnel flow patterns

4.1. Mass Flow

In mass flow, all material within the silo is in motion whenever material is withdrawn, although velocities may vary across the cross-section. Mass flow occurs when hopper walls are sufficiently steep and smooth to promote wall slip.
Mass-flow bins are classified by hopper geometry:

- Conical hoppers (axisymmetric flow)
- Wedge-shaped hoppers (plane flow)

In plane-flow hoppers, the required half-angle is typically 8–10° larger than that of conical hoppers. The slot width is approximately half the diameter of an equivalent conical hopper. Although plane-flow bins can offer greater capacity for the same headroom, their elongated outlet may introduce feeding difficulties.
Advantages of mass flow include:

- Absence of hang-ups, surging, and flooding
- Reduced segregation
- Uniform and controlled discharge
- First-in, first-out (FIFO) behavior
- No stagnant zones
- Full utilization of bin capacity

4.2. Funnel Flow

Funnel flow develops when hopper geometry and wall conditions do not promote uniform movement. Only a central flow channel develops, while material near the walls remains stagnant.

Characteristics of funnel flow:

- First-in, last-out discharge
- No remixing of segregated materials
- Erratic flow rates
- Potential aeration and flooding of fine powders
- Reduced effective storage capacity

Funnel flow may function adequately for dry, free-flowing, granular materials
In contrast to the disadvantages outlined above, funnel flow silos may also provide certain advantages. Larger storage capacities can be achieved due to the greater hopper angles employed. In mass flow conditions, the material moves along the hopper walls in continuous frictional contact with the liner surface. Consequently, wall wear is typically reduced in funnel flow silos, as the material primarily discharges through a central vertical channel with limited contact along the walls.

5. COMMON HOPPER PROBLEMS

Regardless of whether the bulk solid discharges under mass-flow or funnel-flow conditions, inadequately designed silos frequently give rise to flow disturbances encountered in practice. Several factors may contribute to the interruption of discharge, and these are outlined below.

5.1. Ratholing (Piping)

Ratholing is a flow channel stability phenomenon that occurs when a central flow channel forms and remains stable while the surrounding material remains stagnant. It is most commonly associated with funnel flow silos. In this regime, only the material directly above the outlet is discharged, whereas material near the walls remains stationary. If the bulk solid possesses sufficient cohesive strength, a stable vertical cavity—referred to as a rathole—may develop above the outlet. Ratholing is particularly likely when cohesive materials are discharged through undersized outlets. When the unconfined yield strength (σ_c) of the material is sufficiently high, the channel walls can sustain the imposed stresses without collapsing, thereby maintaining the stable flow channel. Figure 7 illustrates the formation of a rathole within the silo.

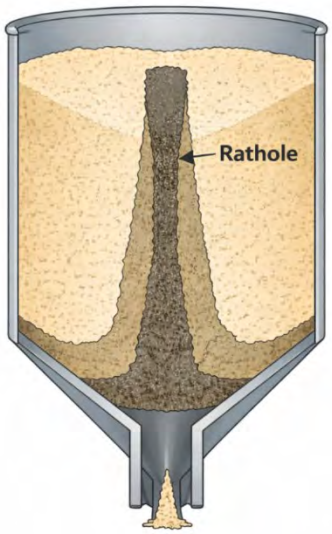

Figure 7. Ratholing or piping formation within the silo.

5.2. Arching (Doming)

Arching occurs when a stable bridge forms across the outlet. Two types exist as seen in Figure 8.

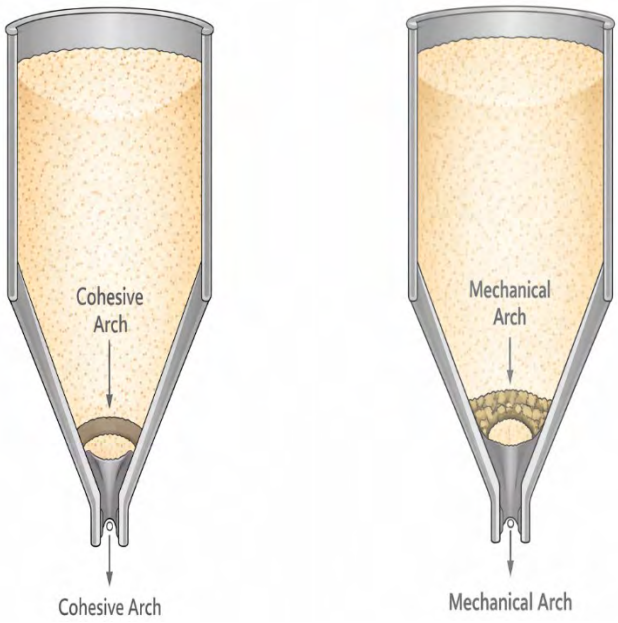

Figure 8. Cohesive and mechanical arching formations within silos.

5.2.1. Cohesive arching

Caused by interparticle attractive forces. The material behaves as a continuum, and the arch acts as a consolidated curved beam spanning the opening. Cohesive arch is a result of the consolidation and strength of the bulk solid

Mechanisms include:

- Van der Waals forces
- Capillary forces due to moisture
- Electrostatic attraction
- Particle bonding
- Time consolidation

5.2.2. Mechanical arching

Occurs when coarse particles interlock geometrically across the outlet. It is governed by particle size, shape, and interlocking rather than cohesion.

Important factors:

- Particle size relative to outlet diameter
- Particle angularity
- Friction coefficient
- Geometric interlocking

5.3. Time consolidation (Caking)

Time consolidation refers to the increase in bulk solid strength while stored under load over time. Caking is the macroscopic manifestation of this phenomenon.

Caking results in:

- Hard lumps
- Agglomerates
- Solidified masses

Consequences include:

- Arching
- Ratholing
- Reduced discharge rates
- Sudden collapse events
- Product degradation

6. ANGLE OF REPOSE

The angle of repose is the maximum angle between the free surface of a bulk solid and the horizontal at which the material remains stable without sliding (Figure 9)
It represents the balance between gravitational forces and frictional/cohesive resistance.

However, the angle of repose is **not sufficient for silo design**. Proper mass flow design requires:

- Shear testing
- Wall friction measurement
- Determination of unconfined yield strength

The angle of repose only reflects surface stability, not internal flow behavior.

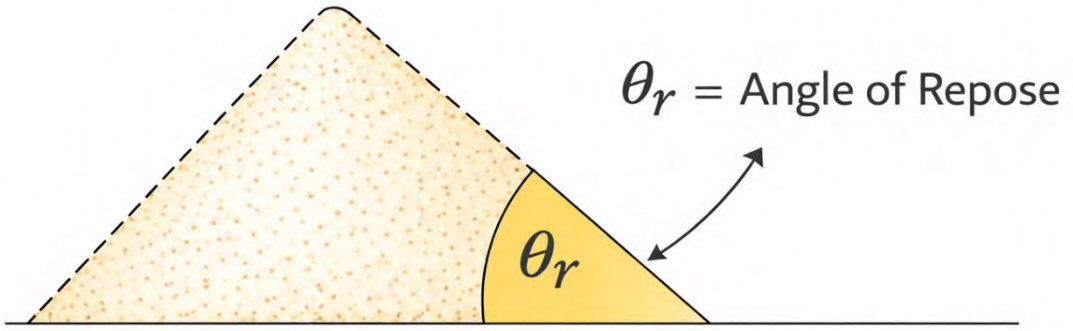

Figure 9. Development of angle of repose alongside the surface of a pile.

7. CONCLUSION

The reliable storage and discharge of bulk solids from silos depend fundamentally on a proper understanding of material flow properties and appropriate hopper design. This study has highlighted the critical differences between mass flow and funnel flow regimes and their impact on operational performance. Common flow obstructions, including ratholing, cohesive and mechanical arching, and time consolidation, were examined in relation to material strength and consolidation behavior. The determination of flow properties through shear testing, particularly using the Jenike method, is essential for predicting flowability and selecting suitable outlet dimensions and hopper geometries. Ultimately, effective silo design requires integrating material characterization with sound engineering principles to minimize flow interruptions and ensure efficient and continuous process operation.

REFERENCES

Lobato, J. C. M., Mascarenhas, F. P., Mesquita, A. L. A., (2016), “Conical Hopper Design For Mass Flow – Case Of Red Mud”, HOLOS, Year 32, Vol. 2, 120-131.

McGlinchey, Don, (2008), “Bulk Solids-Handling Equipment Selection and Operation” Centre for Industrial Bulk Solids Handling, Glasgow Caledonian University, UK, Blackwell Publishing, ISBN: 978-1-4051-5825-1.

Roberts, A.W., (1992), “Basic Principles of Bulk Solids Storage, Flow and Handling”, The University of Newcastle, School of Engineering, Tunra Bulk Solids Research Associate.

Roberts, A.W., (2006), “Bulk Solids Handling – An Historical Overview and Current Developments”, TUNRA Bulk Solids AWR, 1.1-1.49.

Schulze, D., (2007), “Powders and Bulk Solids”, Springer, ISBN 978-3-540-73767-4.

Woodcock, C.R., Mason, J.S., (1987), “Bulk Solids Handling-An Introduction to the Practice and Technology”, Published by Blackie Academic and Professional, ISBN-13: 978-94-010-7689-0.

NIOBIUM AND TANTALUM CONCENTRATION

Elenice Maria Schons SILVA, Amanda Paranhos MACEDO, Raydse Linny Silva SOUZA, Jaciany Mayara Batista SOARES, André Carlos SILVA*

Federal University of Catalão, Mineral Processing Research Center (CPMin), 75705-321, Catalão, Goiás, BRAZIL
**Corresponding author: ancarsil@ufcat.edu.br*

A B S T R A C T

Niobium (Nb) plays a crucial role in the economic and industrial advancement of several nations, being a strategic element of high added value with applications in diverse sectors, ranging from medicinal to aerospace applications. Brazil stands out as one of the world leaders in niobium mineral reserves and plays a significant role in global production. Niobium is used to create HSLA steels to improve strength and corrosion resistance. It is also essential for aerospace superalloys, MRI scanner magnets, and advanced electric vehicle batteries. Tantalum (Ta), on the other hand, is a highly corrosion-resistant, ductile refractory metal, used in electronics, aerospace & defense, medical and chemical industry. Niobium extraction presents a series of complex challenges, from research and identification of deposits to obtaining the final product. This process involves extensive and complex mineral processing, encompassing many stages. Pyrochlore ($(Na,Ca)_2Nb_2O_6(OH,F)$), a complex niobium-rich oxide mineral, is the main Nb ore in Brazil, mined by CBMM and CMOC. However, Nb and Ta can occur associate in manganocolumbite ($(Mn,Fe^{++})(Nb,Ta)_2O_6$), a mineral presented in cassiterite deposits. Flotation tests were carried out with low grade Nb ore samples from a placer deposit located in the Brazilian Amazon region, aiming to develop a route to enrich Nb and Ta in the natural fines. The ore was rich in quartz and topaz, alongside other silicates, with presence of manganocolumbite and cassiterite. The found results indicate that a reverse flotation route could be used in association with the gravity route, such as jigs and spirals, to recover Nb and Ta bearing minerals in the natural fine fraction, resulting in concentrates with reaching Nb_2O_5 of 34.30% and Ta_2O_5 of 4.05%, with yield of 72.45% and Nb recovery of 96.51%.

Key words: *Flotation, niobium, tantalum, pyrochlore, manganocolumbite*

1. INTRODUCTION

Niobium is a chemical element that plays a crucial role in various technological and industrial applications. Its resistance to corrosion, high temperatures, and excellent thermal and electrical conductivity make it a valuable material in sectors such as aerospace, renewable energy, the automotive industry, electronics, and civil construction. Furthermore, niobium is widely used in the production of metal alloys, mainly steel, giving them greater strength, durability, and weldability. Niobium is considered a critical raw material (CRM) for the European Union (EU) since its first list, back in 2011. In its most recent version (Grohol and Veeh, 2023), niobium was evaluated with supply risk (SR) of 4.4, only behind Heavy Rare Earth Elements (HREEs) such as dysprosium (5.6) and some Light Rare Earth Elements (LREE) like neodymium (4.5). Regarding its economic importance (EI), niobium had a score of 6.5 (the maximum score was tungsten with 8.7). Tantalum, is used in capacitors for electronic devices and in super alloys, has SR of 1.3 and EI of 4.8. Figure 1 shows the criticality assessment results in 2023. It is possible to notice the importance of niobium and tantalum for the EU economy.

According to Ni et al. (2012), Nb usually exists as oxide minerals (such as pyrochlore, columbite, fersmite) in the Earth's crust, and they are rare in mass abundance. Obtaining niobium, however, is not a simple task due to its occurrence in complex minerals, such as pyrochlore and other mineral associations. There are approximately 130 different minerals that

contain tantalum and niobium, of which about 80 are Ta/Nb only, and there is little information available on the processing of Ta/Nb containing ores (Bulatovic, 2010).

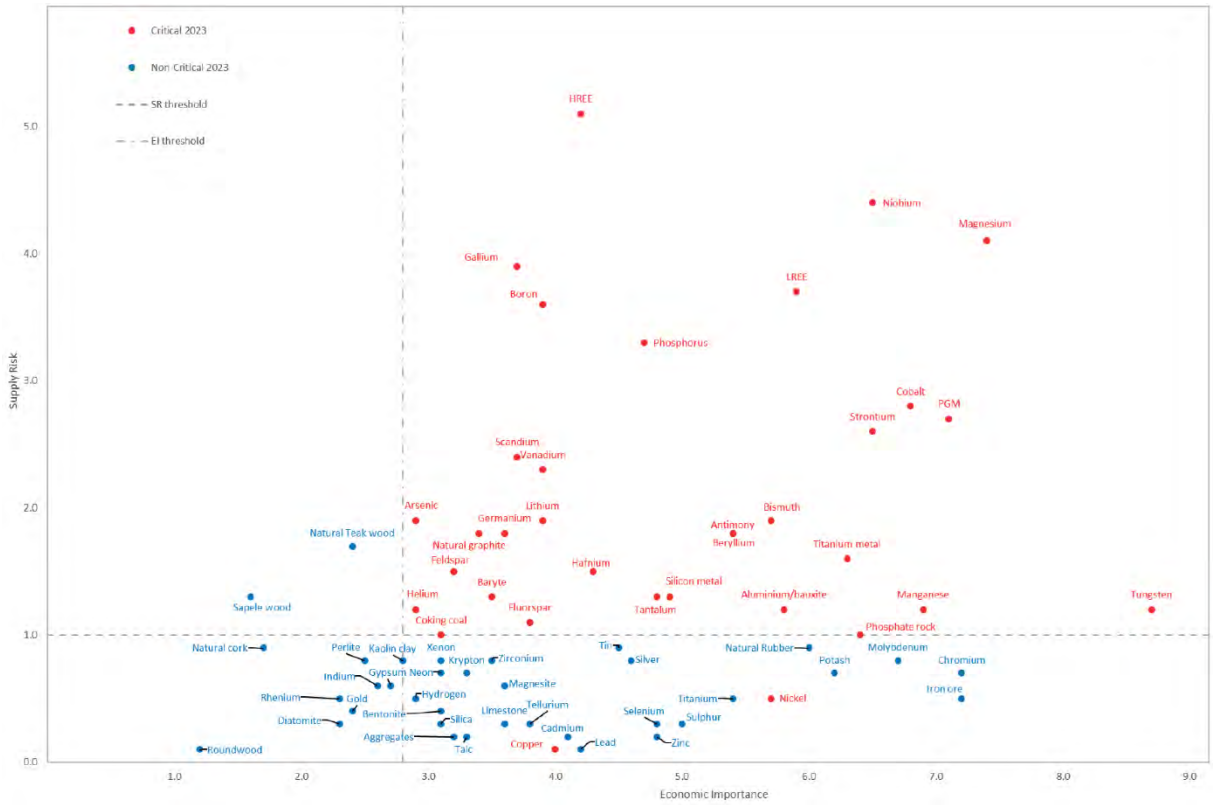

Figure 1. Criticality assessment results (individual materials and groups) in 2023, Source: Grohol and Veeh, 2023

Pyrochlore ($(Na,Ca)_2Nb_2O_6(OH,F)$) is a rare oxide found in specific parageneses and is considered the main niobium ore. The world's largest niobium producers are CBMM, located in Araxá, with 80% of the global market, and China Molybdenum Company Ltd. (10%), or CMOC, in Catalão, followed by Canada (Niobec) and Russia. According to Pinheiro et al. (2016) other Brazilian companies like Mineração Taboca S.A., Metalmig Mineração Indústria e Comércio Ltda., Coop. Mineradora dos Garimpeiros de Ariquemes Ltda, Cooperativa de Garimpeiros Mineralcoop, and Estanho de Rondônia S.A. also produced columbite concentrates. However, it is worth mentioning that these companies focus on tin and tantalum, and Nb is a coproduct. Figure 2 shows the Nb mining production evolution from 1995 to 2025 (adapted from USGS). The world Nb mine production gad an increase above six time fold when compared to 1995, going from 17,784 t to 111,630 t, with a step increase in 2019, just before COVID-19 pandemic. After a brief period of the reduction in production, Nb mine production resume its growth in 2023, remaining stable until 2025. The Brazil's contribution in the Nb production is evident, as shown in Figure 3, ranging from 85.81% in 2021 to 94.81% in 2007.

Currently, the term pyrochlore no longer refers to a specific mineral, but rather to a supergroup of chemically complex cubic oxides containing niobium, tantalum, and titanium. This supergroup is divided into six groups, one of which is the Pyrochlore Group, with the general formula mentioned above. The Pyrochlore Group is composed of 20 different minerals, and there are more than 10 pyrochlore varieties. The precise identification of individual members of the group is only possible through a combination of several analytical methods (Silva, 2018). Nelsonite is the pyrochlore host rock and plays a fundamental role in the primary mineralization of niobium. It is characterized by an abundance of pyrochlore, commonly presenting pockets

of granular calcitic carbonatite, which are rich in apatite, sulfides, as well as the presence of tetraferriflogopite, and magnetite (Palmieri et al., 2009).

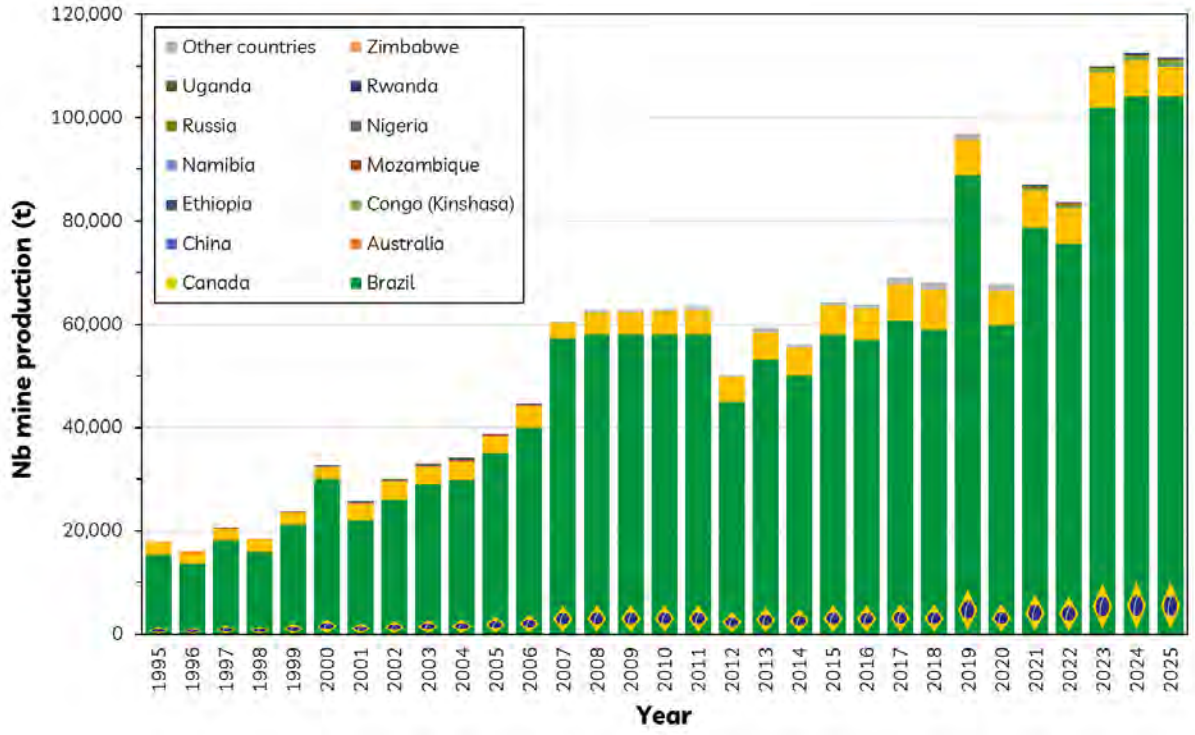

Figure 2. Niobium mining production evolution from 1995 to 2025, Source: adapted from Friedline, 2026

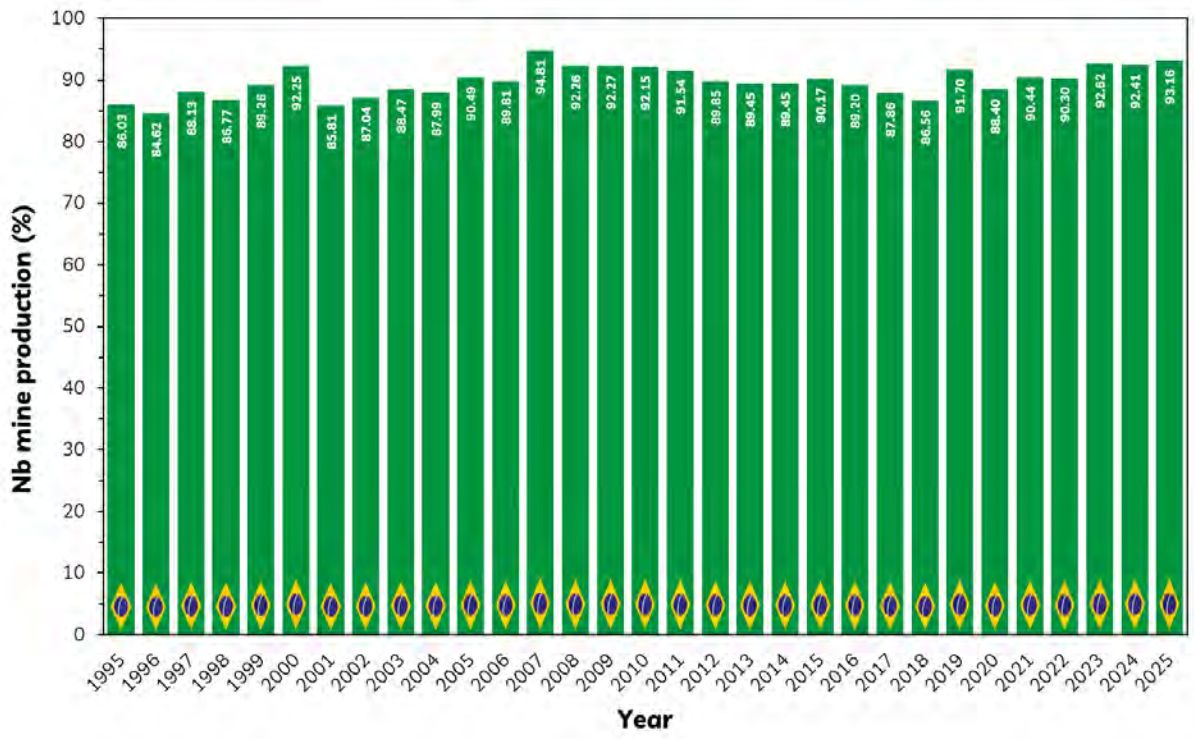

Figure 3. Brazilian contribution to the total Nb mine production, Source: adapted from Friedline, 2026

Pyrochlore processing is complex and involves many steps to produce a final concentrate with Nb_2O_5 content of around 56%, starting with average ROM grades around 0,89% of Nb_2O_5. These steps include comminution (crushing and grinding), classification, magnetic separation, desliming, and flotation. After all these steps, the concentrate is filtered, calcinated, and an aluminothermic process is used to transform the pyrochlore concentrate into NbFe alloy.

According to Ren et al. (2009), flotation is a cost-effective mineral processing method and is widely used to enrich niobium-containing minerals. Pyrochlore flotation is a complex process that requires a series of specialized steps and operations to separate Nb from other minerals and impurities. Operational practice has shown that at least three flotation stages are required to obtain a concentrate with the specifications necessary for the metallurgical process. The first flotation stage aims at the silicates removal by reverse flotation, using amine as collector. According to Ni (2013), pyrochlore isoelectric point (IEP) occurs in pH around 2.6 whereas silicates in approximately 2. Therefore, both mineral phases have similar surface charges, limiting the use of a collector based on physical adsorption. Depressants are used to confer selectivity to the process, in an alkaline pH. The flotation circuit comprises rougher and cleaner stages. A carbonate reverse flotation is the second flotation stage, carried out in rougher, scavenger, and cleaner stages. Fatty acids are used as collector, also in alkaline pH. The concentrate is sent to a WHIMS magnetic separator to remove magnetite. The non-magnetic fraction feeds the pyrochlore direct flotation.

Pyrochlore flotation is carried out in acidic pH, in rougher, scavenger, and cleaner stages, using amine as collector. Since carbonates are dissolved in acidic pH, consuming enormous quantities of acid, they need to be removed before the pyrochlore flotation. If necessary, a final flotation stage is carried out to remove sulfides by reverse flotation using xanthate as collector at alkaline pH. Corn starch is used as depressant in all three flotation stages. The pH is controlled using fluorosilicic acid (H_2SiF_6) and NaOH. Figure 4 summarizes the Nb processing route by CMOC.

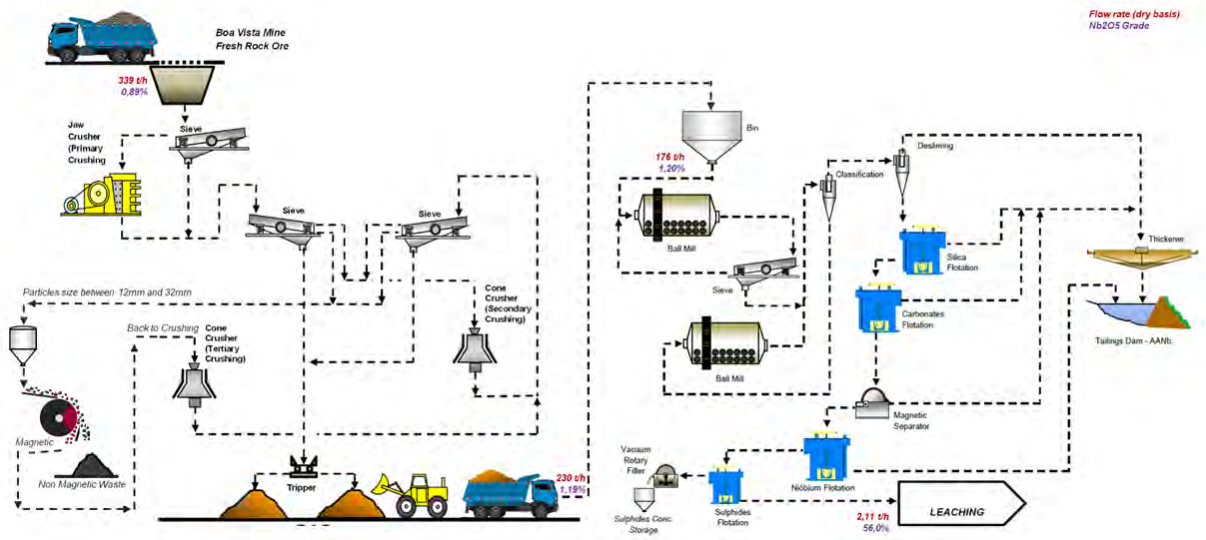

Figure 4. Nb processing route by CMOC, Source: adapted from Moura Jr, 2016

Figure 5 shows Tantalum mining production evolution from 1995 to 2025 (data from USGS. Friedline, 2026). In 2024 the Ta mine production reached its peak, with a global production of 2.485 t, a production around 7 times the 95's mine production. It is possible to notice that the Ta producers have being chance over the years, having a steady participation from Australia, Canada, and African countries. The only country who appeared in all considered period was Brazil, even with mine productions as low as 6.09% of the global production in 2017 (see Figure

6). The Brazilian Ta higher production was in 2009, with 27.07% of the Ta world mine production.

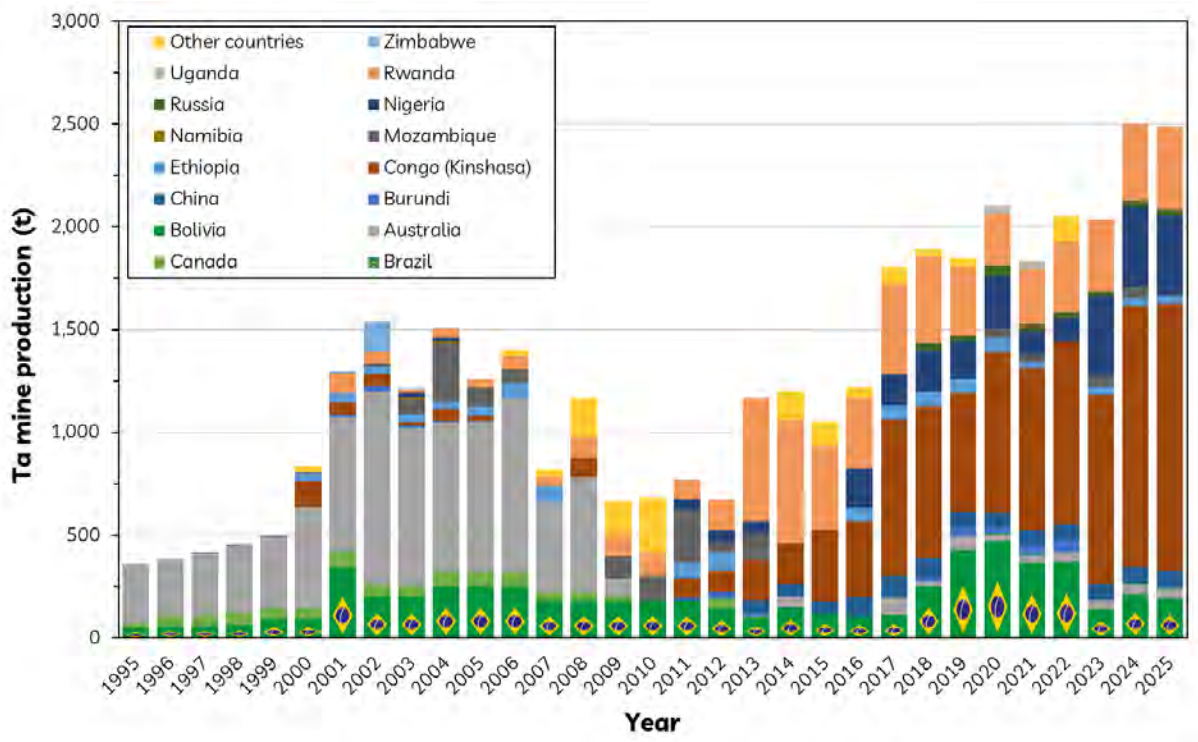

Figure 5. Tantalum mining production evolution from 1995 to 2025, Source: adapted from Friedline, 2026

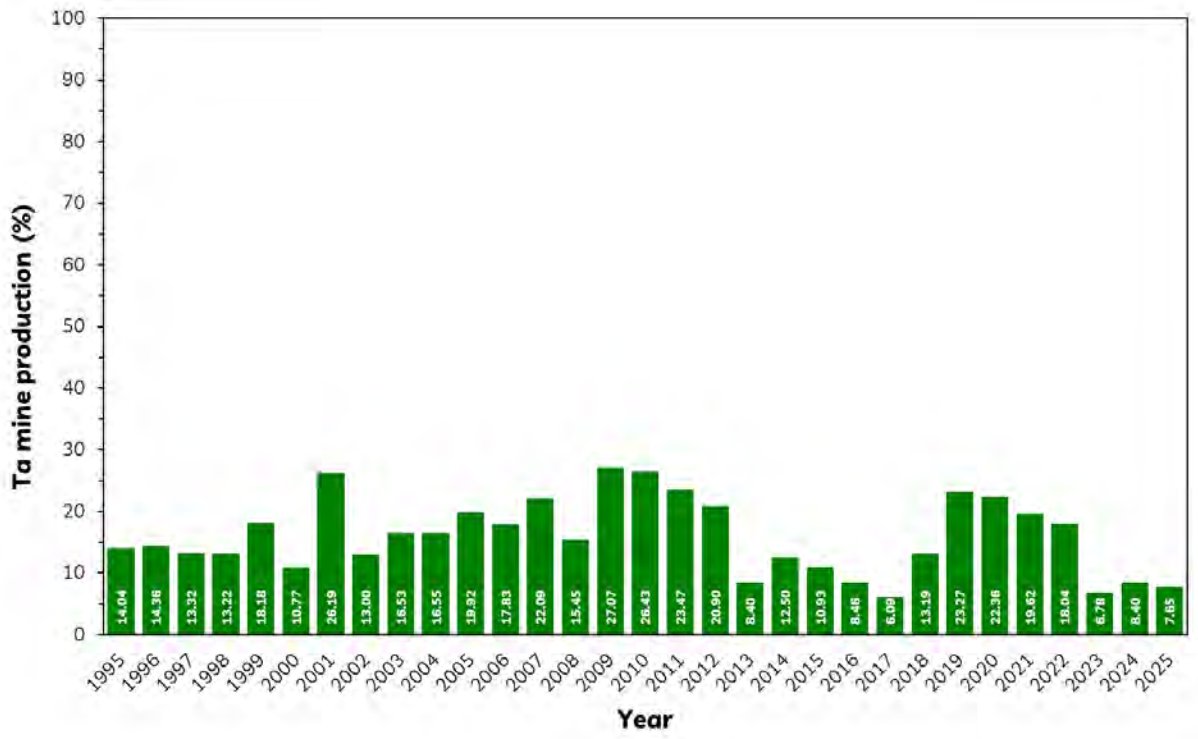

Figure 6. Brazilian contribution to the total Ta mine production, Source: adapted from Friedline, 2026

According to Santos and Ribeiro (2025), mineral exploration has a relevant socioeconomic role in the Amazonian context, but it is also associated with environmental impacts resulting from the inadequate disposal of tailings and the contamination of water bodies. However, the same authors pointed out that the absence of strict technical control in mining operations could lead to the accumulation of heavy metals in the soil and water, requiring regional geochemical investigations to help diagnose and mitigate these impacts. According to Angadi et al. (2015), world's major tin output is from placer deposits that are in Brazil, Thailand, Indonesia, and Malaysia, with numerous types of gravity separators are used in the concentration of tin ores. Units such as jigs, spirals, and tables are used in the primary concentration stage, and the final concentrate can be achieved using enhanced gravity concentrators or flotation cells. Many enhanced gravity concentrators have been developed in the recent past to address the complex issues of beneficiation. This study shows the preliminary results of bench scale flotation tests using low grade Nb ore samples from the Brazilian Amazon region, aiming to develop a new processing route focused on the fine particles, considering that the Brazilian Ta production takes place as Nb and Sn coproducts. Therefore, increase in Nb recovery can directly reflects in Ta increase too. The low-grade cassiterite deposits present in the Western Amazon are characterized by their predominantly secondary nature, resulting from intense chemical weathering processes and residual concentration of heavy minerals from tin-enriched granitic rocks. These processes act over long geological periods, promoting the disaggregation of primary rocks and the selective accumulation of resistant minerals, including cassiterite (SnO_2), the main source of economically exploitable tin (Santos and Ribeiro, 2025).

2. MATERIAL AND METHODS

2.1. Material

A columbite ore representative sample (~ 500 kg) was collected in a mine located in Itapuã do Oeste, Rondonia, Brazil. Figure 7 shows the mine and the sample extraction using a Hyundai digger ROBEX 145LCR-9 with bucket capacity of 14 t.

Figure 7. Nb/Ta ore sampling at the Itapuã do Oeste

A second sample, with similar weight (around 500 kg), was collected from the jig plant concentrate. The plant was composed by two twin cell Pan-American jigs (rougher and cleaner

stages) and one single cell Pan-American jig (recleaner), as seen in Figure 8. The samples were received at the Mineral Processing Research Center (CPMin) of the Federal University of Catalão (UFCAT) where they were oven dried, characterized, and flotated.

Figure 8. Jig plant operating at the Itapuã do Oeste deposit

2.2. Method

An aliquot of the ROM sample was wet sieved using a Brastorno suspended sieve, operating with 16 circular screens (8" in diameter and 2" in height). Sodium metasilicate (Na_2SiO_3) was used as dispersant (3 mL at 10% v/v). The sieving duration was 15 minutes. The chemical composition of the samples was determined by X-ray fluorescence spectrometry (XRF) using an S8 Tiger spectrometer (Bruker), operating with a 4 kW X-ray generator, rhodium (Rh) tube, and WDS detector for quantitative determination by the fused pellet method using lithium tetraborate. The determination of loss (or gain) on ignition (LOI) was performed at 1200 °C using a Precisa prepASH 340 thermogravimetric analyzer, model 212, and lithium tetraborate as a flux.

The major mineralogical composition of the sample was determined by X-ray diffraction (XRD) using a D8 Discover diffractometer (Bruker). The analyses were performed by the powder method, in high resolution, in the θ–2θ Bragg–Brentano configuration, with Cu $K\alpha_1$ monochromatic radiation and a LinxEye one-dimensional linear detector. The scan was conducted in the range of 10° to 90° (2θ), with an angular step of 0.02° and a counting time of 2 s per step. The XRD and XRF analyses were performed at the Regional Center for Technological Development and Innovation (CRTI) of the Federal University of Goiás (UFG).
Although some studies used sodium oleate as tantalite and columbite collectors (Polkin and Glatkin,1963; Polkin et al., 1987), previous tests with this collector carried out at the CPMin with dosages ranging from 400 to 600 g/t at alkali pH did not produce any results recovering columbite. Therefore, reverse flotation tests in a mechanical bench cell were performed in a CDC CFB 1666 EEPN model with 2 L cell. The fraction -150 µm was used in the tests to avoid any milling. Initially, the ore sample was pulped with water in a 2 L tank and conditioned for three minutes with the collector (CADM 25-167 from Clariant) in four dosages (300, 450, 600, and 750 g/t). According to Gibson et al. (2017), one challenge identified in the flotation of Nb bearing minerals with hydroxamates, such as benzohydroxamic acid (BHA), is the recovery of gangue minerals which can result in concentrate grade dilution. This phenomenon is especially

important when ilmenite is present in the ore, and that is the case with the ore studied in the present work.

The depressant used was the starch Penetrose 80 (1,000 g/t), a modified corn starch, usually dextrinized, known for its high water solubility and lower viscosity, supplied by Corn Product Brasil Ingredientes Industriais. Flotanol M 28 was used as frother in three dosages (25, 50, and 100 g/t). The condition times were five minutes for the collector and depressant and one minute for the frother. The flotation was carried out until full extinction of the froth (around 10 minutes). All test were carried out in two stages (rougher and cleaner) at pH 10. Table 1 presents the mechanical bench scale cell flotation tests planning. The flotation products were sent to chemical analysis by XRF.

Table 2. Mechanical bench scale cell flotation tests planning.

Test	Collector dosage (g/t)	Frother dosage (g/t)
3	600	50
5	300	50
7	750	50
1	450	100
2	450	50
4	450	25

3. RESULTS AND DISCUSSION

Figure 9 shows the ROM and jig concentrates particle size distribution (PSD). It is possible to notice that the ROM d_{80} was approximately 3,700 µm and d_{20} around 600 µm. The jig concentrate, on the other hand, had d_{80} around 780 µm and d_{20} around 250 µm. Therefore, it is possible to notice that the jigs are desliming the ore and acting as a classification stage, completely changing the PSD of the concentrate. The granulochemical analysis of the Nb, Ta, and Sn in the ROM can be seen in Figure 10. More than 70% of the three oxides are below 2 mm. However, the jigs had a small efficiency recovering the fine fractions (-200 µm).
Figure 11 shows the diffractogram of the ROM fraction -150+106 µm, one of the richest fractions in Nb. The sample was composed of quartz (SiO_2, 90.09%), kaolinite (22.22%), topaz (9.03%), tridymite (8.89%), and anorthite (7.57%). Comparable results were obtained for the other fractions. In contrast, Figure 12 presents the diffractogram of the jig concentrated fraction -300+150 µm. The sample was composed of topaz (42.12%), rhodonite (14.23%), manganocolumbite (12.44%), quartz (10.11%), anorthite (7.90%), palygorskite (5.34%), anorthite (2.74%), antigorite (2.70%), ferrocolumbite (1.61%), and cassiterite (0.81%). This result clearly expresses the change in mineralogy from the feed to the jig concentrate. Even more, the Nb and Ta bearing minerals were manganocolumbite ((Mn, Fe)$(Nb,Ta)_2O_6$) and ferrocolumbite. According to Santos and Ribeiro (2025), pointed out that the mineralogy associated with the cassiterite deposits of the Western Amazon is diversified and includes accessory minerals of high economic importance, such as ilmenite ($FeTiO_3$), wolframite ($(Fe,Mn)WO_4$), columbite-tantalite ((Fe,Mn) $(Nb,Ta)_2O_6$) and zircon ($ZrSiO_4$).

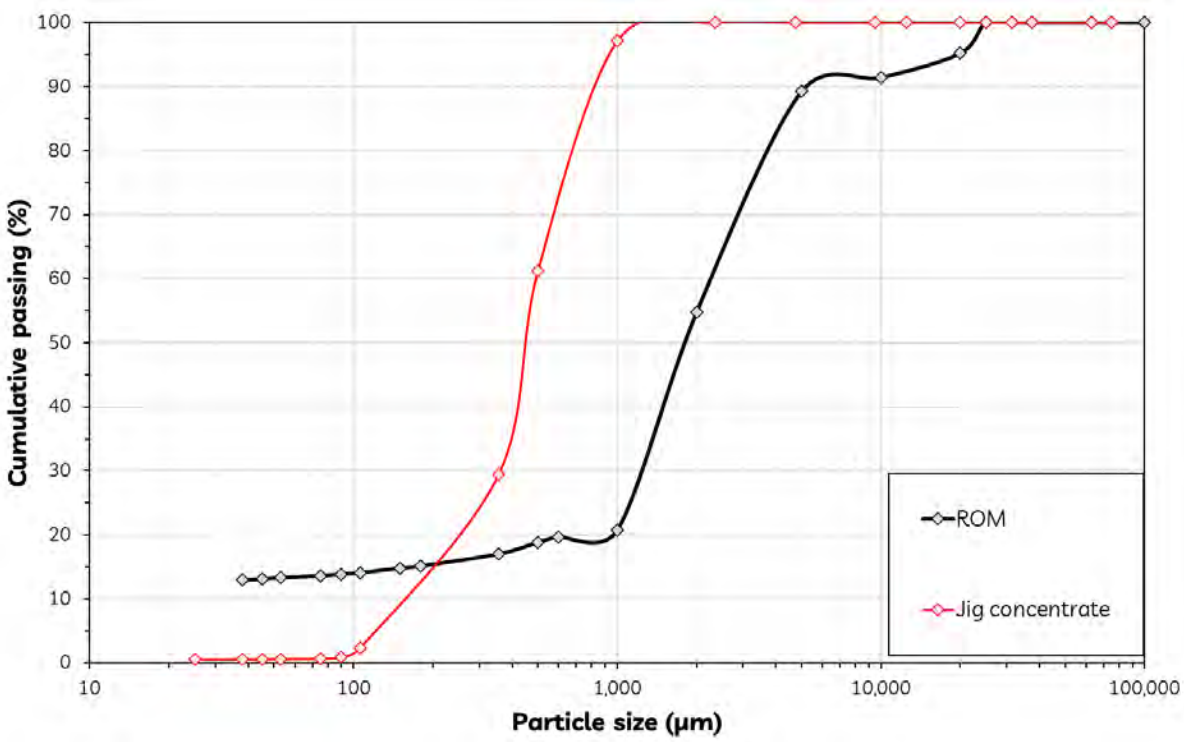

Figure 9. ROM and jig concentrate particle size distribution

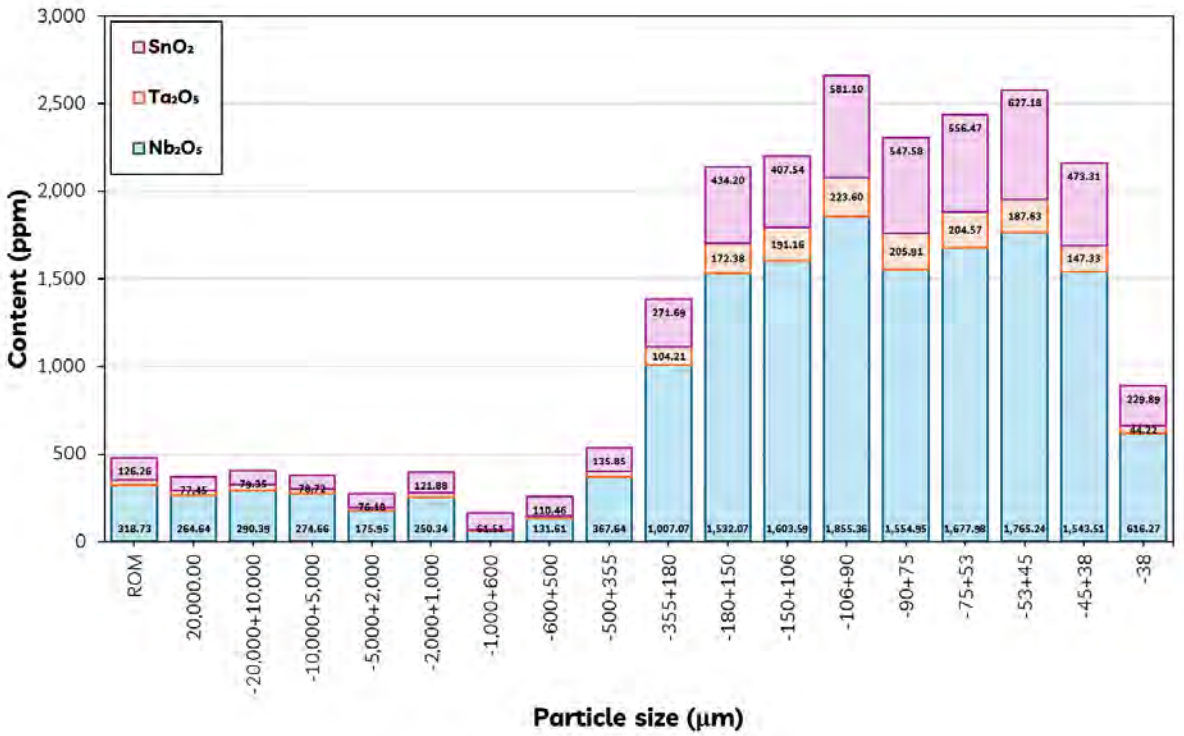

Figure 10. Granulochemical analysis of the Nb, Ta, and Sn in the ROM

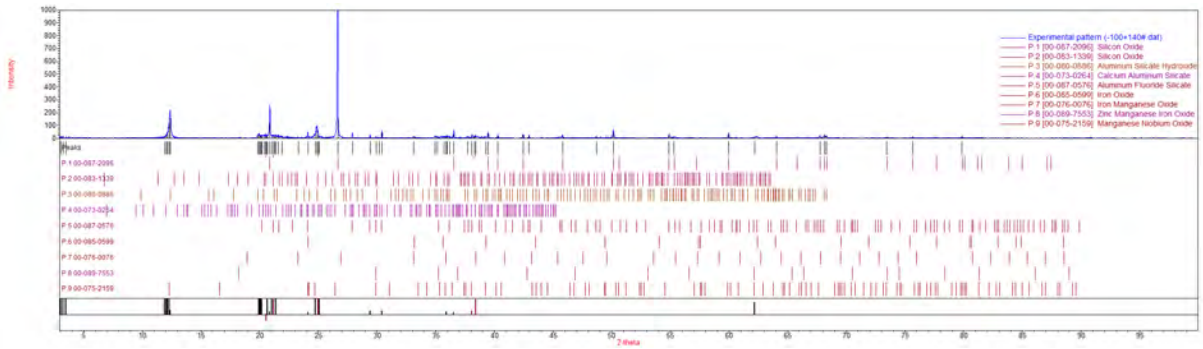

Figure 11. Diffractogram of the ROM fraction -150+106 µm

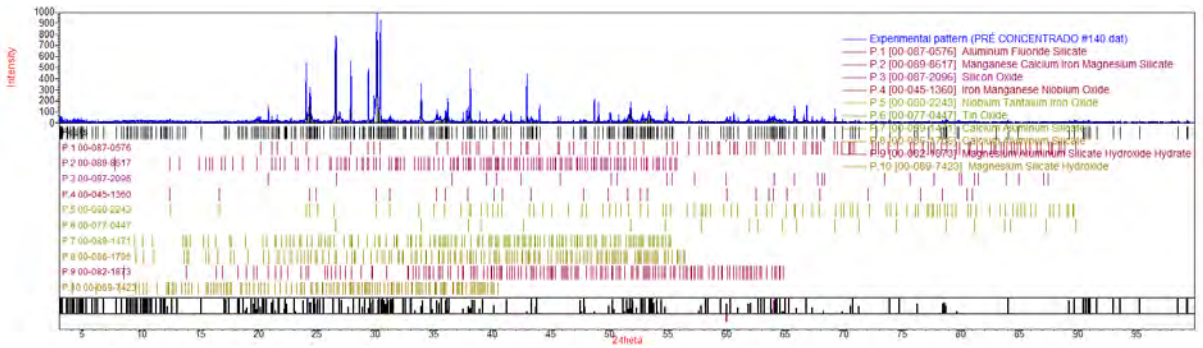

Figure 12. Diffractogram of the jig concentrated fraction -300+150 µm

The flotation tests feed chemical composition, which was the fraction -106µm of the jig concentrate can be seen in Figure 13. It is possible to notice that the samples Nb content Nb_2O_5 were near 25%, indicating that the jigs produced an Nb enrichment around 135, an outstanding result. However, the overall jig yield was below 10%, with Nb recovery equally small. According to Bulatovic (2010), there are several large deposits that contain Ta/Nb minerals associated with zircon in a complex gangue matrix, such as the ones in the Middle East (Arabia), Africa (Malawi), and Brazil. That is exactly the case of the Itapuã do Oeste deposits, rich in ZrO_2.

Figures 14 and 15 presents the non-floated (depressed) flow chemical composition for the rougher and cleaner stages, respectively. It is possible to notice the SiO_2 reduction from the feed to the flotation non-floated products. That was expected, since the CADM 25-167 collector is a silicate collector. On the other hand, the Nb_2O_5 content increased, reaching 34.30% in the Test 1, with yield of 72.45% and recovery of 96.51%. For this test, the Ta_2O_5 content was 4.05%, also the higher content obtained. It was observed an increase in the SnO_2 content in all flotation tests.

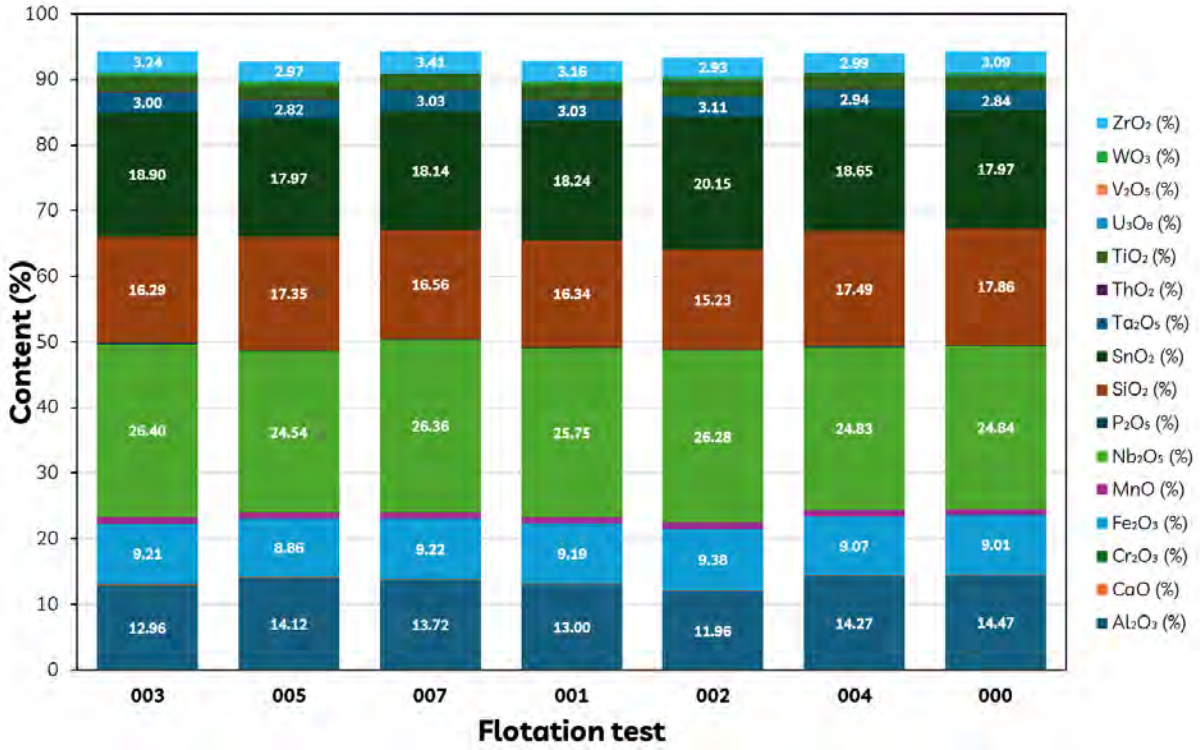

Figure 13. Chemical composition of the flotation tests (fraction -106µm of the jig concentrate)

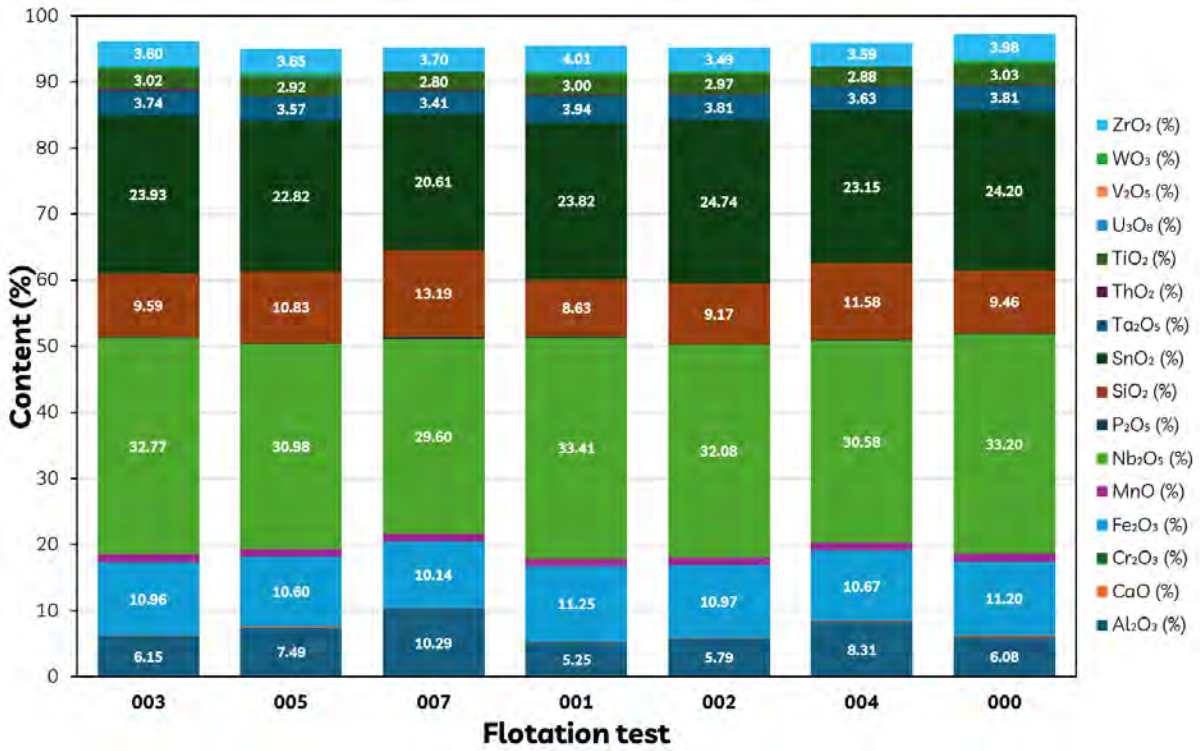

Figure 14. Chemical composition of the rougher non-floated (depressed)

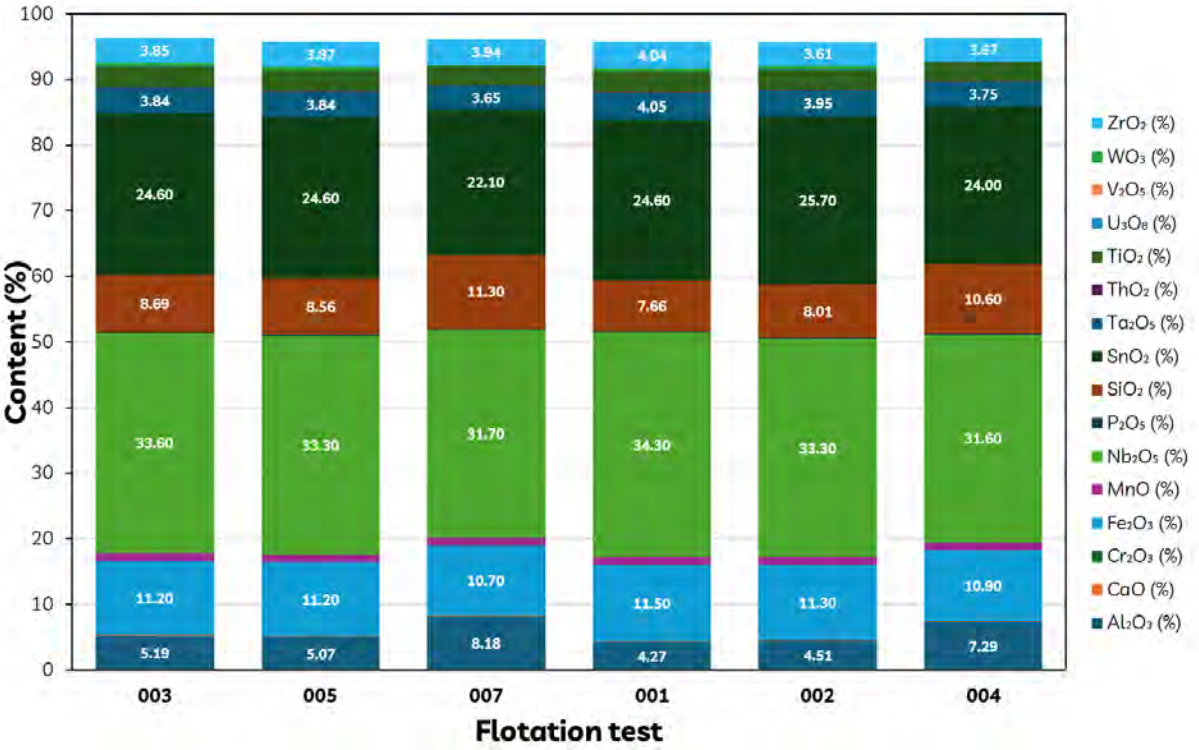

Figure 15. Chemical composition of the cleaner non-floated (depressed)

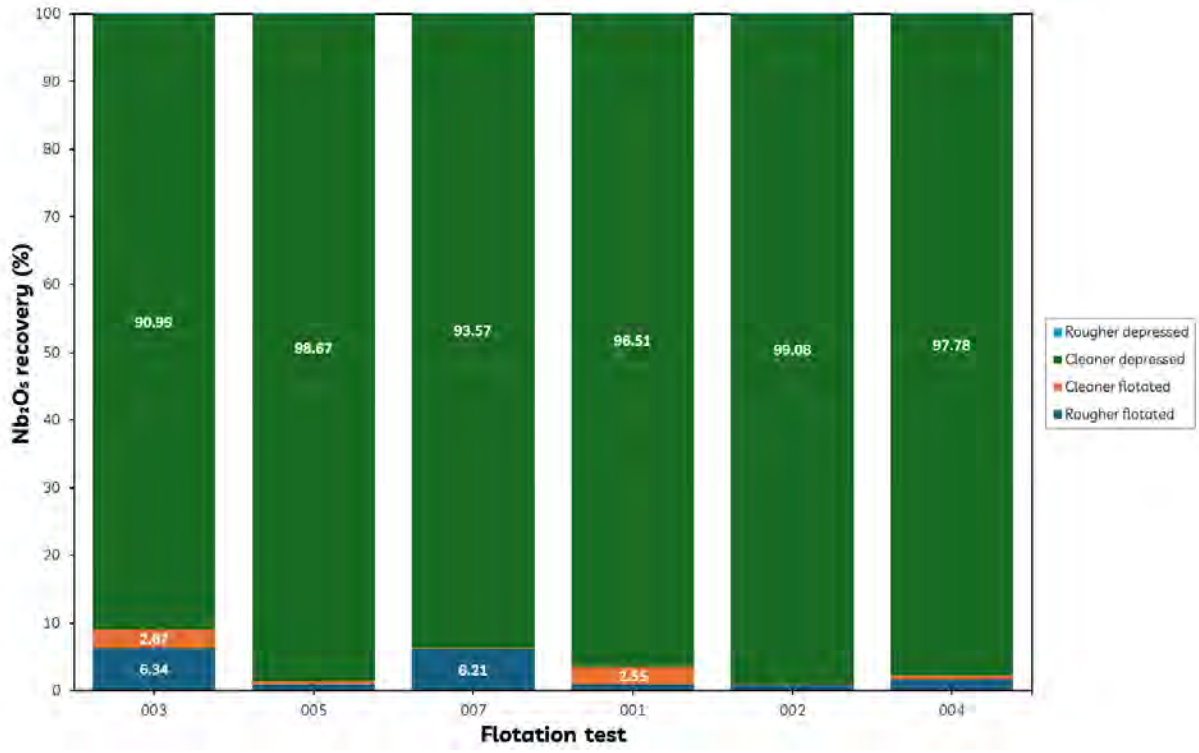

Figure 16. Nb_2O_5 recovery over the flotation tests

4. CONCLUSION

Brazil holds most of the Nb concentrate and Nb alloys market, with major deposits in three areas around the country, a CRM of great relevance for the entire world. Pyrochlore is the most important Nb ore, but it normally does not have Ta associations. The columbite family, on the

other hand, has the potential to supply both elements. With occurrences in the Brazilian Amazon, these deposits present themselves as a new niobium and tantalum sources.
Gravity concentrators can be used to recover the coarse with high efficiency, with emphasis on jigs, spirals, and shaking tables. The fine particles, on the other hand, need to the processed using different methods and more research. Flotation tests were performed aiming to float the silicates present in the samples. Although the Nb recovery was above 90%, the enrichment was low, with Nb_2O_5 content of 34.30% and Ta_2O_5 of 4.05%. Therefore, more tests are needed to develop a flotation route to reach the commercial grades (above 50%).

ACKNOWLEDGMENTS

The authors would like to thank the Federal University of Catalão, the Multi-user High Resolution Microscopy Laboratory (LabMic) and the Regional Center for Technological Development and Innovation (CRTI) at the Federal University of Goiás for conducting the analyses, and the funding agencies FAPEG, FUNAPE, CAPES, and CNPq for the financial support granted to CPMin researchers.

REFERENCES

Angadi, S. I., Sreenivas, T., Jeon, H. S., Baek, S. H., Mishra, B. K., (2015) “A review of cassiterite beneficiation fundamentals and plant practices”, Minerals Engineering, 70 178-200.

Bulatovic, S. M., (2010), Chapter 23-Flotation of Tantalum/Niobium Ores, Handbook of Flotation Reagents: Chemistry, Theory and Practice, 127-149.

Friedline, C., (2026), USGS: Niobium and Tantalum Statistics and Information, Available at https://www.usgs.gov/centers/national-minerals-information-center/niobium-and-tantalum-statistics-and-information

Gibson, C. E., Hansuld, R., Kelebek, S., Aghamirian, M., (2017) “Behaviour of ilmenite as a gangue mineral in the benzohydroxamic flotation of a complex pyrochlore-bearing ore”, Minerals Engineering, 109 98-108.

Grohol, M., Veeh, C., (2023), European Commission, Study on the Critical Raw Materials for the EU 2023, Final Report, Luxembourg, Publications Office of the European Union,158.

Moura Jr, L. F., (2016) “O Processo de Beneficiamento e metalurgia do nióbio e seu potencial para produção de Terras Raras”, Workshop Goiano de Terras Raras, 17.

Ni, X., (2013) “Direct flotation of niobium oxide minerals from carbonatite niobium ores”, Thesis Doctoral Dissertation, Materials Engineering, University of Alberta, Edmonton.

Ni, X., Parrent, M., Cao, M., Huang, L., Bouajila, A., Liu, Q., (2012) “Developing flotation reagents for niobium oxide recovery from carbonatite Nb ores”, Minerals Engineering, 36-38 111-118.

Palmieri, M., Silva, S. E., Brod, J. A., Ferrari, A. J. D., Barbosa, P. A. B, Jácomo, M. H., Junqueira-Brod, T. C., Cordeiro, P. F. O., (2009) “A mineralização de nióbio do Alvo Morro do Padre, Catalão II”, XI Simpósio de Geologia do Centro Oeste, 32-32.

Pinheiro, W. F., Ferreira Filho, O. B., Neves, C. A. R., (2016) “Anuário Mineral Brasileiro: Principais Substâncias Metálicas”, Brasília, Departamento Nacional de Produção Mineral, 31.

Polkin, C. I., (1987), Concentration of Rare Earth Ores from Sedimentary Deposits, Izdatelstvo Nedra Moskva, 268-275.

Polkin, C. I., Glatkin, U. F., (1963) “Concentration of tantalum niobium Ores”, M. Gosgortexizdat, 160-85.

Santos, J. C., Ribeiro, S. B., (2025) “Chemical characterization and determination of contaminant elements in low-grade cassiterite from the bom futuro mine (RO), western amazon”, Revista de Geopolítica, 16 (5) e793.

Silva, A. S., (2018) “Uso potencial das terras no município de Catalão (GO)”, Master's Thesis, Geography, Federal University of Uberlândia, 140.

ELECTROSTATIC SEPARATION AFTER TRIBOELECTRIC CHARGING IN THE PROCESSING OF PRIMARY RAW MATERIALS – STATUS QUO IN RESEARCH AND OUTLOOK FOR POTENTIAL APPLICATIONS

Helmut FLACHBERGER*, Dominic PREM

Montanuniversität Leoben, Department Mineral Resources Engineering, Chair of Mineral Processing, 8700 Leoben, AUSTRIA
**Corresponding author: helmut.flachberger@unileoben.ac.at*

A B S T R A C T

Many established treatment processes are currently still operated wet. The emphasis is on “still,” because the signs of increasing restrictions on access to water and greater public awareness of the need to use this resource, which is already limited in many regions, can no longer be overlooked. The raw materials extraction and processing industry is responding to this on the one hand by stepping up its efforts to ensure strict recycling and post-treatment of process water and comprehensive process control, and on the other hand by considering the increased use of dry processing methods. Sensor-based sorting processes and developments in electrostatic separation offer particularly good prospects for achieving the latter objective in a wide range of applications. (Flachberger and Böhm, 2015)

The Chair of Mineral Processing at the Montanuniversität Leoben has been dedicated to electrostatic separation for 20 years now, focusing on expanding applications in the mineral raw materials industry, fine and ultra-fine grain sorting in the grain size range < 100 µm, and improving understanding of the controlled charging of grain surfaces.

Key words: *Electrostatic separation, dry separation process, industrial minerals processing*

1. INTRODUCTION

For several years now, electrostatic separation has been a research focus of the Chair of Mineral Processing at the Montanuniversität Leoben as a dry and largely reagent-free sorting process. The diverse research work carried out by the research group “Let´s try it dry” is impressive testimony to this. Several dissertations (especially those of Mangelberger, 2007, Oberrauner, 2012, Mirkowska, 2016, Lämmerer, 2018, Gehringer 2021, and Luckeneder, 2023) and a large number of master's theses dealt with research-related topics concerning electrostatic separation.

Furthermore, the raw materials processing industries have also recognized the importance of electrostatic separation and carefully examined its potential applications. This applies not only to secondary raw material processing, where metal/plastic and plastic/plastic mixtures are separated electrostatically in many recycling plants, but also to mineral raw material processing, where there is currently increased research activity into the implementation of electrostatic separators in existing processing plants.

Electrostatic separation, just as flotation, is a surface-controlled sorting process. It exploits differences in surface conductivity or surface charges in terms of magnitude and polarity. The actual separation takes place in electrostatic or electrodynamic fields, predominantly according to the principle of deflection sorting.

2. BRIEF HISTORICAL OVERVIEW OF THE DEVELOPMENT OF ELECTROSTATIC SEPARATION

The first attempts to use electrostatic separation to separate mixtures of materials can be traced back to the beginning of the last century. While flotation started at around the same time and quickly proved successful in its application, the beginnings of electrostatic separation were quite bumpy. For several decades, electrostatic separation led a niche existence. The reasons for this included the requirement for dry or hot feed material, which was difficult to meet at the high throughput rates demanded at the time, but technical reasons can also be cited, such as the lack of suitable, simple units for high-voltage generation (generators and high-voltage transformers), high-voltage-resistant cable insulation, and components. (Flachberger and Köhnlechner, 2009)

The industrial use of electrostatic separation for the processing of raw potash salts since the 1970s marked a breakthrough that was based on intensive research activities, primarily in Germany, since the 1950s. Introduced as the ESTA process and operated with great success ever since, this method makes particular use of selective charge exchange through triboelectric charging at certain relative humidity levels. (Flachberger and Mangelberger, 2009)

Since the 1990s, electrostatic separation has been used for new tasks in the field of secondary raw material processing. A whole range of material mixtures that cannot be separated using conventional methods can be processed using electrostatic separation. The main areas of application include the processing of fine fractions of metal/plastic mixtures, as well as the separation of plastic/plastic mixtures, where insufficient or even non-existent differences in “conventional” characteristics – such as density, magnetizability, etc. – often make further processing impossible. Without claiming to be exhaustive, examples of metal/plastic mixtures include copper/plastic separation in the recycling of old cables, metal separation from electronic scrap, and the separation of aluminum/plastic mixtures in the recycling of bottle caps. Examples of plastic/plastic mixtures include the separation of PE/PP, PVC/rubber, PET/PVC, or PS/ABS. (Flachberger and Köhnlechner, 2009)

It can be assumed that electrostatic separation will also be used increasingly in mineral processing as a dry and largely reagent-free process. In addition to the aforementioned large-scale industrial use of electrostatic separation in the processing of raw potash salts, electrostatic separation has so far been found mainly in niche applications, such as the processing of heavy mineral sands – cassiterite/rutile or ilmenite/rutile separation – or tantalite/columbite preconcentrates. However, successes in quartz/feldspar separation, (Niermöller, 1988), in the depletion of interfering accompanying minerals from carbonate fillers (Mangelberger, 2007), (Eichas, 1993), and in the separation of unburned carbon from fly ash (Bittner and Gasiorowski, 2001) point to a significantly broader range of applications.

3. RAW MATERIAL PROPERTIES AND SEPARATION CHARACTERISTICS

The classification of materials into conductors, semiconductors, and non-conductors commonly used in physics - i.e., based on differences in electrical properties—is only of limited use in raw material processing. Surface impurities, complex intergrowth, misalignments in the crystal lattice, adhesions, etc., as well as process-relevant parameters such as air humidity, ambient temperature, and raw material moisture, are reasons for difficulties in clear classification.

From a processing technology perspective, classification according to the available separation features has therefore proven successful. This results in the following classification option based on the separation features in Table 1.

Table 1: Separation feature and assigned separation process

Separation Feature	Separation Process
Surface Conductivity	Conductor/Non-conductor Separation
Electron Work Function	Non-conductor/Non-conductor Separation

As Table 1 shows, differences in electrical conductivity are used for conductor/non-conductor separation, and differences in electron work function are used for non-conductor/non-conductor separation. Both separation principles are increasingly used in mineral processing, but differ significantly in terms of their physical principles, equipment design, and possible applications and limitations.
However, this article does not focus on a detailed physical description of the separation and charging mechanisms (for this, see Mirkowska et al., 2016, for example), but rather on a systematic approach to the experimental design, implementation, and evaluation of electrostatic sorting tests in the laboratory. The aim is to present a practical best-practice approach that specifically aligns the knowledge gained with the respective requirements for the enrichment and yield of the valuable (mineral) phases.

4. SPECIAL FEATURES OF ELECTROSTATIC SEPARATION

It has already been mentioned that electrostatic separation is carried out in dry mode. In particular for electrostatic separation after triboelectric charging, the hydration shells around the particles and grains must be completely removed in order to enable charge transfer. Environment plays a decisive role and highly influences separation performance. Controlling environmental conditions is particularly important in all research activities involving electrostatic separation after triboelectric charging. Those who cannot control and influence these conditions will fail. The Chair of Mineral Processing therefore has an air-conditioned lab room where temperature and humidity can be set and kept constant.

Since the field forces are limited due to the dielectric breakdown strength as well as the forces acting - e.g., the Coulomb force - are relatively weak, the grain size ranges that can be processed are limited to the lower millimeter range. Based on the research group's experience, these can be defined as follows:

< 1.2 (max 2) mm in mineral processing
< 8.0 (max 10) mm in secondary raw material processing

It is pleasing to note that electrostatic separation is comparatively inexpensive in terms of purchase, operation, and maintenance. Less pleasing is the fact that the achievable throughput rates are comparatively low. This makes it unattractive for processing tasks where very high throughput rates are required. This led to the working group's decision to focus its research on the field of industrial mineral processing.

5. PROCEDURE FOR ELABORATING RESEARCH REQUESTS ON ELECTROSTATIC SEPARATION

5.1. General Specifications

In the industrial minerals sector in particular, electrostatic separation trials are often requested by small to medium-sized companies that themselves have only limited experience with these sorting methods and their process-specific characteristics. Experience in recent years has clearly shown that dry electrostatic separation is often considered a potential alternative to separation processes that have previously been carried out using wet methods, such as flotation.

Due to the many process parameters that influence the separation result, a structured and comprehensible approach to planning and conducting laboratory tests is crucial in order to find optimized process conditions and derive reliable conclusions about the fundamental technical suitability of electrostatic separation. In addition to the necessary infrastructure on a laboratory or pilot scale, this usually requires a methodologically sound design of the tests and corresponding experience in interpreting the test results.

Before starting the tests, an initial coordination meeting with the client to figure out the samples, their mineralogical composition, relevant grain size ranges, and necessary preparatory work is of importance. On this basis, the electrostatic separation units suitable for the respective grain size ranges are selected. In addition, the client's target priorities, the boundary conditions of the subsequent application, the intended scope of the investigations, and the analytical methods to be used to assess the success of the processing are agreed upon. Depending on the objectives and the mineral phases contained, these can be simple physical parameters such as the determination of specific density or whiteness, as well as more advanced chemical and mineralogical analyses.

The coordination meeting is followed by a research and design phase, during which available literature data and the results of comparable previous studies are evaluated. In particular, known charge differences between the relevant mineral phases, for example based on the triboelectric series, are taken into account in order to assess the expected charge behavior of the mineral phases involved. On this basis, the test parameters relevant for successful implementation are identified and their meaningful variation ranges are defined. The test series are preferably based on a statistical design of experiments (DoE) in order to systematically and efficiently investigate the influence of several parameters. Depending on the number of parameters considered, full factorial or fractional factorial designs, for example 2^k or $2^{(k-1)}$ designs, are applied, in which the respective parameters are investigated at two defined setting levels (e.g., high and low values). This design of experiments approach enables a structured recording of the main effects and relevant interactions while keeping the experimental effort manageable.

A finer differentiation of the parameters and their optimization is only planned for a subsequent series of tests and is based on the results of the preliminary tests.

Parallel to this research and design phase, the client provides sufficient quantities of fresh and representative sample material for the investigations. Aging effects can lead to large deviations, especially in surface-sensitive electrostatic separation. Insufficiently representative samples and any associated differences in mineral phase association and intergrowth conditions generally have a significant effect on sorting behavior in electrostatic separation.

Once the test strategy has been determined, the samples are delivered to the laboratory. Depending on the initial condition of the material, preparatory steps such as drying, comminution, and classification are carried out to ensure defined, reproducible, and suitable starting conditions for electrostatic separation.

5.2. Test procedure and Analysis

Once sample preparation is complete, electrostatic separation is conducted in accordance with the defined test procedure, either jointly with the client or independently by the laboratory staff. The tests are performed under defined boundary conditions, whereby only the specified test parameters are varied. Relevant operating and environmental variables, in particular air temperature and relative humidity, are continuously recorded and documented. Relative humidity is particularly important here, as it can significantly influence the charging behavior of the particles and thus the results of electrostatic separation tests. It has proven useful to carry

out the tests under controlled environmental conditions, for example in a climate-controlled room with adjustable temperature and humidity.

After each electrostatic separation test, the product fractions are collected and weighed. The units are cleaned between individual test runs to prevent cross-contamination. The packaged product fractions are then either examined directly in the laboratory or sent to external facilities for further analysis in accordance with the previously agreed analysis methods.

5.3. Data Evaluation and Logic of Decision-Making

Once the analytical results are available, metallurgical accounting with a focus on balance sheets serves as the central tool for data evaluation. For a consistent assessment, the product analyses are either used to back-calculate the feed characteristics or – if the feed has been analytically characterized – balanced using a Gaussian adjustment. Based on the established mass balances, it is subsequently assessed whether individual tests already show a recognizable enrichment or desired change in the relevant evaluation parameters, or whether no significant separation effect has been achieved.

This initial evaluation forms the basis for further decision-making:

- If a separation effect is evident, the balance sheets are evaluated in greater depth, for example with respect to the influence of individual process parameters and potential trade-offs between grade and valuable mineral recovery.

- If no or only insufficient separation is observed, it is examined whether clearly defined adjustments to the test parameters, boundary conditions, or feed characteristics - such as a modification of the feed particle size distribution or the relative humidity - can be expected to lead to an improvement.

At this stage, the fundamental decision is made as to whether electrostatic separation should be further pursued for the given task or discontinued.

If satisfactory results are obtained, it is subsequently evaluated whether an extended test phase is justified. This may include, for example, a second test series with an expanded parameter variation, multi-stage test configurations, or the execution of locked-cycle tests in order to assess the separation performance under process conditions closer to industrial reality. Depending on the results achieved, scale-up to pilot scale may be considered.

Only on this basis are the laboratory results classified with regard to potential industrial implementation. It must be taken into account that industrial electrostatic separation units, due to longer residence times, higher throughputs, and the possibility of multi-stage operation, may in many cases achieve improved separation performance compared to laboratory or semi-technical trials.

6. CASE STUDY: TESTS ON THE ENRICHMENT OF TALC

The procedure described above is exemplified below using a case study from the field of industrial mineral processing, which was carried out in the form of a master's thesis (Zöhrer, 2025). The subject of the study was talc-containing preconcentrates, which still contained chlorite as an associated mineral phase. The aim of the investigations was to evaluate the basic suitability of electrostatic separation for the removal of chlorite. No specific target grade was specified; rather, the aim was to investigate the extent to which a reduction in chlorite is achievable under laboratory conditions.

6.1. Experimental Setup

The investigations were carried out on three defined grain size fractions produced during the existing processing: 500/300 µm, 300/100 µm, and 100/0 µm. Adapted to the respective grain size range, two different separation units were used for electrostatic separation. For the two coarser fractions, the EMS 500 electrostatic pilot free-fall separator from hamos GmbH Recycling- und Separationstechnik, based in Penzberg, Germany, was used, while the finest fraction was examined using an electrostatic laboratory belt separator from ST Equipment & Technology LLC, based in Needham, USA. Both units are installed in the laboratory climate chamber of the Chair of Mineral Processing.

6.2. Investigation with the Free-fall Separator

In order to reduce the machine and process parameters that were to be varied in the further course of the investigation, a series of preliminary tests were carried out at the beginning of the study. In a first step, the material of the preceding charging unit was determined, since this unit has a significant effect on the triboelectric particle charging and thus on the resulting separation behavior. Based on the observed charging and separation behavior, an aluminum charging unit was selected. Building on this, the evaluation of further preliminary tests showed that the 500/300 µm particle size fraction proved slightly more favorable for operation on the free-fall separator compared to the 300/100 µm fraction. This was reflected in a more stable mass distribution of the generated product fractions and lower material losses during sorting. Based on these results, the grain size range 500/300 µm was defined as the preferred working range for the subsequent parameter study. For the evaluation of the preliminary tests, simple and rapidly available key performance indicators were initially used, in particular the loss on ignition (LOI), which allowed a first assessment of the separation effect with comparatively low analytical effort. In this context, a lower LOI was interpreted as an indicator of a higher talc grade.

Within the subsequent parameter study, the analytical program was expanded. In addition to physical parameters, chemical analyses using X-ray fluorescence (XRF) were conducted to quantitatively determine the elemental distribution. Based on the preliminary tests, a full factorial parameter study was carried out on the free-fall separator.

Each parameter was examined at two defined levels (shown in Table 2), resulting in the 2^3 full factorial design presented in Table 3.

Table 2. Parameter levels applied in the full factorial design for the free-fall separator

Parameter	**Label**	**-**	**+**
Feed rate	A	20%	60%
Charging intensity	B	20%	60%
Feed temperature	C	Room temperature	100°C

Table 3. Full factorial design matrix for the free-fall separator

Test Number	**A**	**B**	**C**
1	+	+	+
2	+	+	-
3	+	-	+
4	+	-	-
5	-	-	-
6	-	-	+
7	-	+	-
8	-	+	+

For evaluation purposes, the balance sheet of a selected experiment (Table 4) is examined. It shows an enrichment of the talc grade in the feed from 35.5% to 68.4% in the talc concentrate, with a talc recovery of 31.8%. This clearly illustrates the fundamental enrichment potential of electrostatic separation in the grain size range under consideration, but at the same time shows the losses of talc associated with the separation.

Table 4. Balance sheet of a sorting test of a talc sample on the free-fall separator

Product	Mass yield	Talc grade	Talc recovery
	r_m	g_{ij}	r_{ij}
	%	%	%
Concentrate	16.5	68.4	31.8
Tailings	83.5	29.0	68.2
Feed	100.0	35.5	100.0

The evaluation of the main effects of the parameter study shown in Figure 1 indicates that a low feed rate and an increased feed temperature are associated with higher talc grades in the concentrate. The influence of the charging intensity on the talc grade is low within the investigated parameter range.

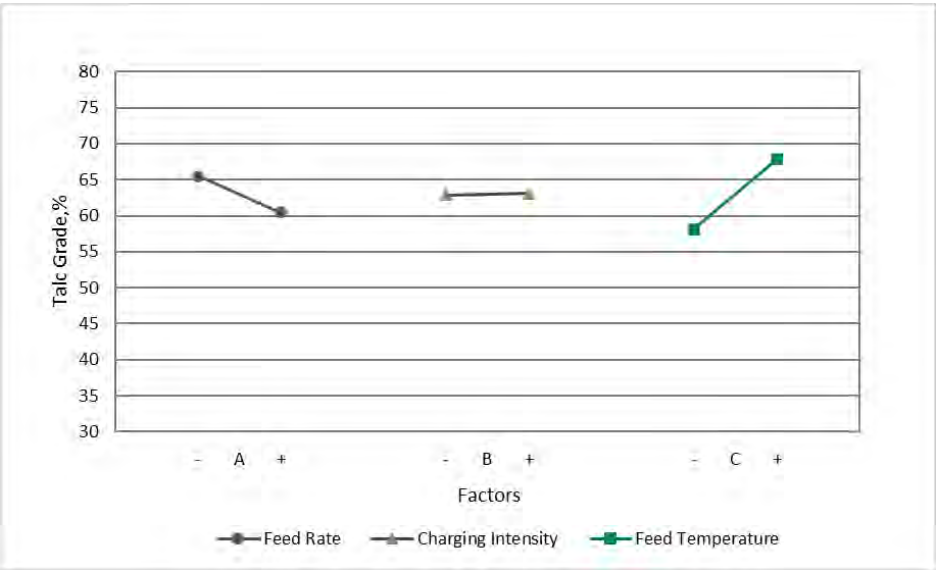

Figure 1. Main effects of selected parameter levels on the talc grade in the concentrate (free-fall separator)

6.3. Investigations with the Belt Separator

For the investigations on the belt separator with the finest fraction (100/0 µm), prior experience from previous experiments, including polarization settings, was available. Therefore a 2^{4-1} fractional factorial design (Table 5) with the parameter levels shown in Table 6 was implemented directly without preliminary tests. The talc grade of the feed was higher in the belt separator tests than in those on the free-fall separator, which is related to the lower crushing resistance of talc and thus its preferential enrichment in the finer grain size fraction.

Table 5. Fractional factorial design for the belt separator

Test Number	A	B	C	D
1	+	+	+	+
2	-	+	+	-
3	+	-	+	-
4	-	-	+	+

5	+	+	-	-
6	-	+	-	+
7	+	-	-	+
8	-	-	-	-

Table 6. Parameter levels applied in the fractional factorial design for the belt separator

Parameter	**Label**	**-**	**+**
Feed rate	A	5	10
Feed temperature	B	Room temperature	60°C
Relative humidity	C	< 30%	> 30%
Belt speed	D	18 fps	36 fps

The tests on the belt separator were evaluated using the same method as applied for the free-fall separator. The results shown in Table 7 indicate an enrichment of the talc grade from 45.4% in the feed to 77.6% in the concentrate, with a talc recovery of 58.2%. This confirms that electrostatic belt separation also has fundamental enrichment potential in the fine grain size range.

Table 7. Balance sheet of a sorting test of a talc sample on the belt separator

Product	**Mass yield**	**Talc grade**	**Talc recovery**
	r_m	g_{ij}	r_{ij}
	%	%	%
Concentrate	34.0	77.6	58.2
Tailings	66.0	28.8	41.8
Feed	100.0	45.4	100.0

The evaluation of the main effects of the parameter study (Figure 2) indicates that feed rate, belt speed, and relative humidity in particular have a measurable influence on the talc grade in the concentrate, while feed temperature within the investigated parameter range tends to result in lower talc grades.

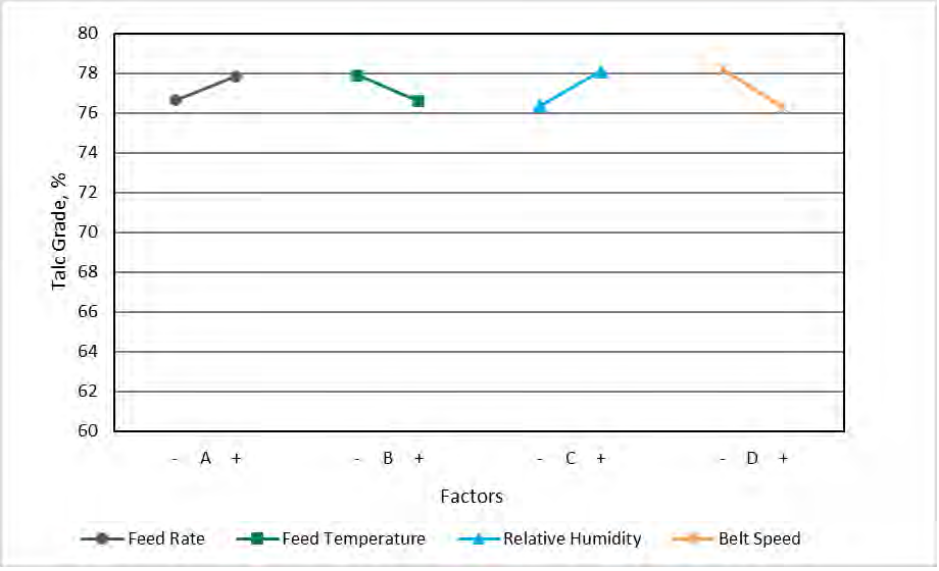

Figure 2. Main effects of selected parameter levels on the talc grade in the concentrate (belt separator)

6.4. Case-Scientific Findings

The results of the laboratory and pilot scale tests show a relevant enrichment potential for the talc fractions investigated, both for the free-fall separator and for the belt separator. This confirms the basic suitability of electrostatic separation for the task at hand. The focus was on achieving the highest possible talc grade in the concentrate.

In accordance with the decision-making logic described above, electrostatic separation was not rejected, but evaluated as an option to be pursued further. In such cases, the next step in the project sequence is usually to consult with equipment manufacturers and conduct pilot or industrial-scale tests to verify the transferability of the laboratory results. The final evaluation of the process control takes into account possible marketing options for both the concentrate and the separated by-products. No further laboratory test series were conducted in this case, as the results provided a sufficient basis for subsequent project decisions.

7. CONCLUSIONS

The consumption of water resources is steadily increasing, partly due to a growing population and increasing industrialization. It can therefore be assumed that dry processing methods in general, and electrostatic separation in particular, will become increasingly important. This applies especially to mineral processing, where large amounts of water are currently used.
The currently used and established equipment operates in a grain size range of less than approximately 2 mm for mineral processing and less than approximately 10 mm for secondary raw material processing.

Electrostatic separation can be used for a wide range of sorting tasks. Its potential for use is particularly great in industrial mineral processing. While the separation of conductor/non-conductor mixtures is also highly successful in more complex material systems, the separation of non-conductor/non-conductor mixtures-i.e., sorting processes based on triboelectric charging-has so far been mainly focused on the separation of binary material systems. It can be assumed that controlled triboelectric charging will also enable the separation of multiphase mixtures.

The advantages of electrostatic separation lie in a high degree of automation, low-maintenance operation, a wide range of process parameters for finding optimized operating conditions, and low operating costs. Disadvantages include the sometimes lower specific throughput rate compared to other sorting methods and the sometimes energy-intensive drying of raw materials for material flow preparation.

REFERENCES

Bittner, J. D., Gasiorowski, S. A., (2001) “Commercial beneficiation of high LOI fly ash: 1 million tons of process ash delivered”, Proceedings of the 14th International Symposium on Management and Use of Coal Combustion Products, 17-1–17-8.

Bulatovic, S. M., (2015) “Beneficiation of feldspar ore”, in: Handbook of Flotation Reagents: Chemistry, Theory and Practice, Elsevier, 107–119.

Eichas, K., (1993) “Triboelektrische Sortierung im Feinstkornbereich”, Dissertation, Technische Universität Clausthal.

Flachberger, H., Böhm, A., (2015) “Entwicklungstendenzen im Fachgebiet Aufbereitung und Veredlung”, Berg- und Hüttenmännische Monatshefte, 160, 465–474.

Flachberger, H., Köhnlechner, R., (2009) “Unter Hochspannung sauber trennen”, Müllmagazin, 1, 36–41.

Flachberger, H., Mangelberger, T., (2009) “Trennmechanismen in elektrischen Feldern – eine Bestandsaufnahme”, Berg- und Hüttenmännische Monatshefte, 154, 129–135.

Gehringer, S., (2021) “Zu Fragen einer kontrollierten Aufladung von Mineraloberflächen für eine erfolgreiche Trennung im elektrostatischen Feld”, Dissertation, Montanuniversität Leoben.

Lämmerer, W., (2018) “Zu Fragen der Charakterisierung, Aufbereitung und Veredlung von natürlichen Graphiten”, Dissertation, Montanuniversität Leoben.

Liu, Y., Gong, Y., (1985) “A new flotation technique for feldspar–quartz separation”, Proceedings of the XXIII International Mineral Processing Congress, 4, 857–862.

Luckeneder, C., (2023) “The processing of talc-rich run-of-mine for obtaining a high-grade and high-quality talc concentrate by utilization of electrostatic separation with triboelectric charging”, Dissertation, Montanuniversität Leoben.

Mangelberger, T., (2007) “Grenzen und Optimierungsmöglichkeiten der Aufbereitung von Calciumcarbonat für den Einsatz in der Füllstoffindustrie”, Dissertation, Montanuniversität Leoben.

Mirkowska, M., (2016) “Triboelectric charge behavior of minerals at microscale for understanding the triboelectrostatic separation process”, Dissertation, Montanuniversität Leoben.

Mirkowska, M., Kratzer, M., Teichert, C., Flachberger, H., (2016) “Principal factors of contact charging of minerals for a successful triboelectrostatic separation process – a review”, Berg- und Hüttenmännische Monatshefte, 161, 359–382.

Niermöller, F., (1988) “Ladungsverteilung in Mineralgemischen und elektrostatische Sortierung nach Triboaufladung”, Dissertation, Technische Universität Clausthal.

Oberrauner, A., (2012) “Nutzung der Elektroscheidung zur trockenen Aufbereitung von fein- und feinstdispersen Körnerschwämmen”, Dissertation, Montanuniversität Leoben.

Sekulić, Ž., Canić, N., Bartulović, Z., Daković, A., (2004) “Application of different collectors in the flotation concentration of feldspar, mica and quartz sand”, Minerals Engineering, 17 (1) 77–80.

Zöhrer, A., (2025) “Evaluierung des Potentials der Elektroscheidung nach Triboaufladung zur Anreicherung von Talk aus Fraktionen des Mahlwerkes Oberfeistritz der Firma Imerys Talc Austria GmbH”, Master’s Thesis, Montanuniversität Leoben.

EFFECTS OF ULTRASOUND ON SETTLING BEHAVIOUR OF SOME CRITICAL RAW MATERIALS

Şafak Gökhan ÖZKAN*

Turkish-German University, The Institute of the Graduate Studies in Science and Engineering, Department of Robotics and Intelligent Systems, 34820, Beykoz, Istanbul, TÜRKİYE
**Corresponding author: safak.ozkan@tau.edu.tr*

A B S T R A C T

The efficient management of critical raw materials (CRMs) requires not only effective recovery processes but also sustainable waste handling strategies. One of the main challenges in processing CRM ores and tailings lies in their fine particle size, which leads to slow sedimentation, poor thickening, and high water demand. Ultrasound has been proposed as an innovative method to modify particle-fluid interactions through cavitation, microstreaming, and shear forces. This study investigates the effects of ultrasound on the settling behavior of selected critical raw materials, highlighting its dual role in promoting dispersion or flocculation depending on operating conditions. Experimental observations and literature analysis suggest that moderate ultrasound power enhances flocculant adsorption and accelerates clarification, whereas excessive energy disrupts flocs and stabilizes suspensions. The findings indicate potential applications of ultrasound in tailings thickening and water recovery circuits in CRM processing. The growing global demand for critical raw materials (CRMs) such as rare earth elements, lithium, cobalt, and high-purity industrial minerals has intensified research into efficient and sustainable mineral processing methods. One of the persistent challenges in treating finely ground ores and tailings associated with these resources is their slow sedimentation and poor dewatering performance, largely due to ultrafine particle size, high surface area, and strong colloidal stability. Conventional flocculation and thickening methods often prove insufficient, leading to high water consumption, large tailings storage requirements, and increased environmental risks.

Key words: *Mineral processing, settling behavior, sedimentation, ultrasound, critical raw materials*

1. INTRODUCTION

1.1. Critical Raw Materials

In the contemporary global economy, the demand for raw materials is projected to triple by 2030 as the world transitions toward renewable energy systems and a net-zero carbon future. This paradigm shift has redefined traditional mining concepts, transitioning from a focus on high-grade primary ore deposits to the “valorization of mine waste” and the recovery of “Critical Raw Materials (CRMs)”. CRMs are defined by their high economic importance and significant supply risk, often due to geographical concentration or technical complexities in extraction. Table 1 aims to consolidate the classification of natural resources, strategic metals, and waste streams, integrated with the technical stages of ore processing and metallurgical recovery (Whitworth et al., 2022, Anon., 2023, Kinnaird and Nex, 2024).

Table 1. Classification of resources in terms of different origins and recovery steps

Resource Origin	Material Category	Strategic Status	Life Cycle Stage	Technical Operations	Key Examples
Primary (Natural) Sources	Critical & Strategic Metals	High (Supply Risk & Impact	Mining (Exploitation	Open-pit/Underground mining, Drilling, Blasting, Loading	Rare Earth Elements (REEs) (Nd, Dy, Tb), Lithium, Cobalt, Niobium

	Metallic Ores (Base/Precious)	Variable	Beneficiation (Mineral Processing)	Physical: Crushing, Grinding (Milling), Flotation, Magnetic/Electrostatic Separation	Iron (Magnetite, Hematite), Copper (Chalcopyrite), Gold (Native), Nickel
	Industrial & Energy Minerals	Essential for Infrastructure	Refining (Metallurgical Extraction)	Chemical/Thermal: Smelting, Roasting, Leaching, Solvent Extraction, Electrowinning	Borates, Potash, Silicon Metal, Coking Coal, Magnesite
Secondary (Technogenic) Sources	Mineral Processing Tailings	Increasing (Recovery Potential)	Waste Reprocessing (Valorization)	Reprocessing of tailings using Advanced Hydrometallurgy, Bioleaching, and Molecular Recognition Tech (MRT).	Sulfide Tailings** (Manganese, Indium), **Coal Gangue** (Al, Li, Ga), **Acid Mine Drainage (AMD)** (REEs)
	Manufacturing & Post-Consumer Scrap	Strategic (Resource Security)	Recycling	Collection, Sorting, Pyrolysis, Remelting (Refiners/Remelters)	Aluminum Scrap (95% energy saving), E-waste (PGMs, Gold), PGM recovery from Catalysts

In Table 1, while unit operations in mineral processing and beneficiation cover physical stages like crushing and classification that do not change the mineral's chemical nature but increase the metal content (Concentrate), metallurgical extraction involves chemical or electrochemical transformations, such as leaching (dissolving metals in solvents like sulfuric acid) and electrowinning (plating metal onto a cathode).

Primary raw materials are unprocessed materials extracted directly from the Earth. A subset of these, “Critical Raw Materials”, is currently dominated by global supply from a few countries, with “China” providing a substantial share (e.g., 95% of REEs, 87% of Antimony). The strategic importance of these materials is linked to their use in clean technologies such as wind turbines, electric vehicles, and PV panels.

Mine tailings represent one of the largest waste streams globally, but contain significant unrecovered metals. Modern “Life Cycle Sustainability Assessments (LCSA)” and “Circular Economy” principles prioritize the recovery of secondary raw materials from these sources. For example, coal gangue might be important for Lithium, Gallium, and Alumina recovery.
Acid Mine Drainage (AMD) is also crucial for environmental liability and a promising source for “Rare Earth Element (REE)” recovery via selective precipitation. Technogenic Resources term defined the tailings from older mines, often containing grades comparable to primary deposits due to previously inefficient processing technologies.

The integration of primary and secondary resource management is essential for long-term economic and ecological resilience. While primary mining remains the backbone of supply, the recovery of critical metals from tailings and industrial waste offers a dual benefit: mitigating environmental risks like groundwater contamination and securing the raw materials necessary for the global green transition (Moro et al., 2025).

The growing global demand for critical raw materials (CRMs) such as rare earth elements, lithium, cobalt, and high-purity industrial minerals has intensified research into efficient and

sustainable mineral processing methods. One of the persistent challenges in treating finely ground ores and tailings associated with these resources is their slow sedimentation and poor dewatering performance, largely due to ultrafine particle size, high surface area, and strong colloidal stability. Conventional flocculation and thickening methods often prove insufficient, leading to high water consumption, large tailings storage requirements, and increased environmental risks.

1.2. Effect of Ultrasound on Settling or Sedimentation Behavior of Slurries

In 2025, the global demand for critical raw materials (CRMs) such as lithium, cobalt, and rare earth elements has intensified the need for efficient sedimentation processes to reclaim process water and ensure tailings dam safety. Fine particles exhibit slow sedimentation rates and high colloidal stability which standard chemical flocculation often fails to overcome.
The management of ultrafine particles (minus 20 microns), commonly referred to as "slimes," remains a significant challenge in mineral processing and tailings management due to their low settling velocities and high water retention. Settling or sedimentation behaviour of slurries can be investigated using beaker tests shown in Figure 1 and can be mathematically categorized into three distinct zones: constant rate sedimentation, variable rate (hindered) sedimentation, and sediment compaction.

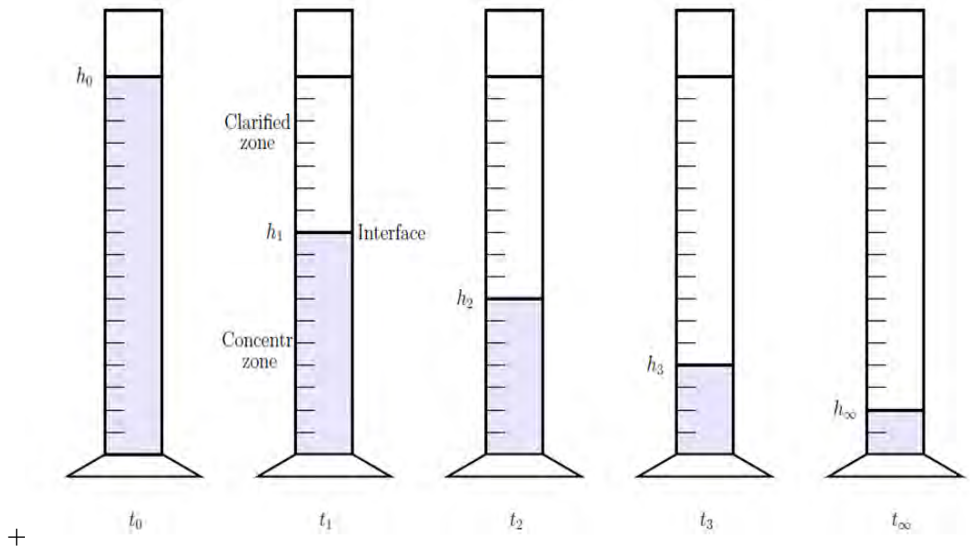

Figure 1. Beaker or jar test for sedimentation or settling (Moura et al., 2023)

This study evaluates the dynamics of solid-liquid separation in beaker systems by integrating the fundamental principles of Stokes' Law and Newton's Law.

$$v_T = \frac{g(\rho_S - \rho_F)d^2}{18\mu} \quad \text{for viscous resistance (Stokes' Law)}$$

$$v_T = \sqrt{\frac{4g(\rho_S - \rho_F)d}{3C_D\rho_F}} \quad \text{for turbulent resistance (Newton's Law)}$$

where d = particle diameter,
ρ_S, ρ_F = density of solid and fluid respectively,
C_D = the drag coefficient,
μ = fluid viscosity and
g = gravitational acceleration.

In dilute suspensions where particles do not interact, "free settling" occurs. For laminar flow conditions (Reynolds number, $Re<1$), the terminal settling velocity (V_T) of a spherical particle is governed by Stokes' Law. This equation demonstrates that velocity is proportional to the square of the radius, explaining why ultrafine slimes settle so slowly. In this stage, velocity is proportional to the square root of the particle diameter, typically observed in coarser mineral fractions. As particle size increases or flow becomes turbulent, the settling behavior transitions to the Newton Regime, where the resistance is dominated by inertial forces rather than viscosity.

Ultrasound (US) has emerged as a promising tool to address the limitations of recovery and recycling of primary and secondary mineral resources, including tailings and wastes of critical raw materials. Its application in mineral suspensions induces acoustic cavitation, microstreaming, and localized shear fields, which can alter particle-particle and particle-fluid interactions. Depending on the operational conditions, ultrasound may either promote deagglomeration and dispersion (reducing settling rates) or enhance flocculation and consolidation (improving settling rates and bed density). The dual nature of these effects makes ultrasound particularly attractive for tailoring the settling behavior of critical raw material suspensions, where both efficient recovery and environmentally responsible waste management are essential (Zhang et al., 2024, Shi et al., 2025, Zhou et al., 2025).

Recent studies have reported that moderate-intensity ultrasound can increase collision frequency and promote polymer flocculant adsorption, accelerating clarification, whereas high-intensity or prolonged ultrasound exposure can disrupt floc structures and re-stabilize suspensions. Despite growing interest, the systematic application of ultrasound in the context of critical raw materials remains underexplored. A better understanding of its mechanisms and process variables (particle type, size distribution, slurry chemistry, ultrasound frequency and power, and the presence of additives) is crucial for evaluating its potential integration into industrial thickening and tailings management circuits (Önal et al., 2003, Silva et al., 2025, Güngören et al., 2025).

This study investigates the effects of ultrasound on the settling behavior of selected critical raw materials; to clarify its potential role in enhancing dewatering efficiency and supporting sustainable processing strategies.

2. MATERIALS AND METHODS

2.1. Mineralogical and Chemical Characterization

2.1.1. Colemanite

The previously archived representative colemanite samples from the Hisarcik mine in Türkiye was firstly checked against aging, damage, corrosion, or oxidation before using the proper sample preparation method for mineralogical and chemical identification analyses, such as X-ray diffraction and mineral liberation (MLA). A mortar type grinder was used to obtain proper size fraction (d_{80}: minus 100 microns) for the further characterization before sedimentation tests (Özkan and Rudolph, 2025).

After obtaining properly prepared representative samples, the investigation continued by using PANalytical Empyrean model X-ray diffraction analysis device according to phase identification (qualitative XRD) based on the ICDD PDF-4+2020 database. PANalytical HighScore 3.0.4 program (semi-) quantitative phase identification and Profex 3.10.2 software (using Rietveld refinement) were also used with PIXcel3D-Medipix3 1x1 detector. Figure 2 shows the XRD analyses results.

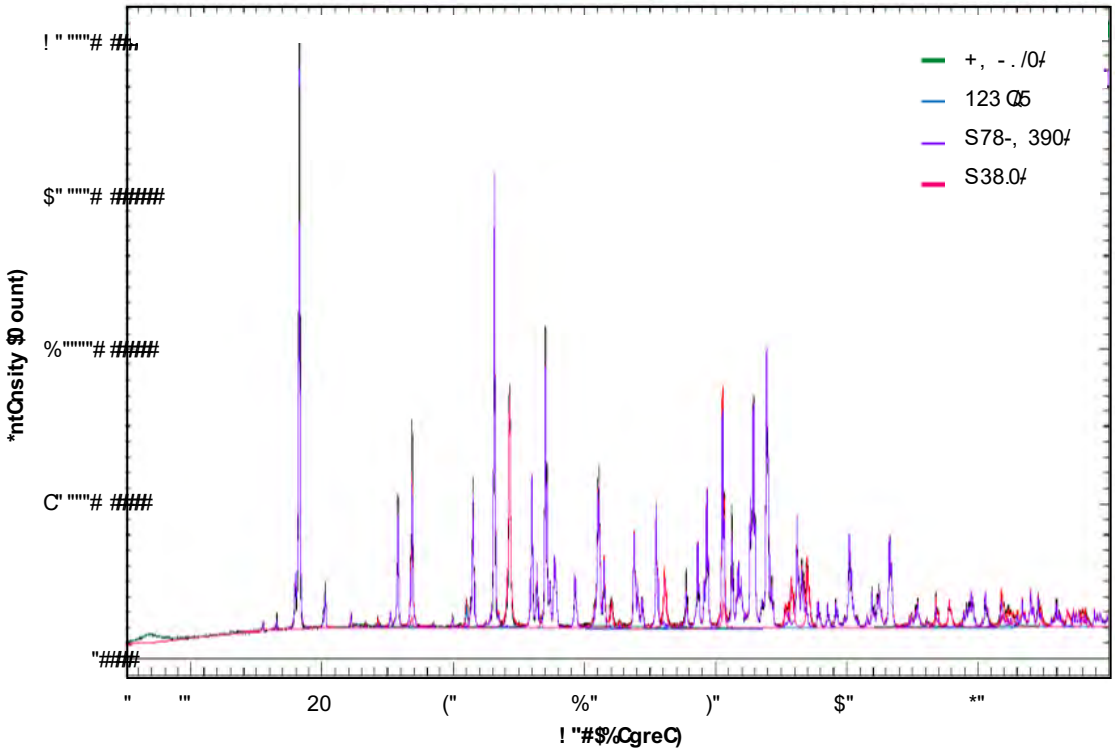

Figure 2. The current XRD patterns of the colemanite sample

The XRD analyses showed colemanite peaks together with colemanite, calcite, quartz, and smectite peaks. Afterwards, Mineral Liberation Analyses (MLA) were also conducted to reveal different mineral associations and their relations inside current colemanite crystals. The device model is FEI Quanta 650 MLA-FEG with Bruker Quantax X-Flash 5030 EDS-Detectors using MLA-Suite software. Figure 3 shows the processed SEM images (a), modal mineralogy (b), mineral locking for colemanite (c), the particle size of the sample, (d) particle size distribution of main minerals, and (e) data from the MLA measurements.

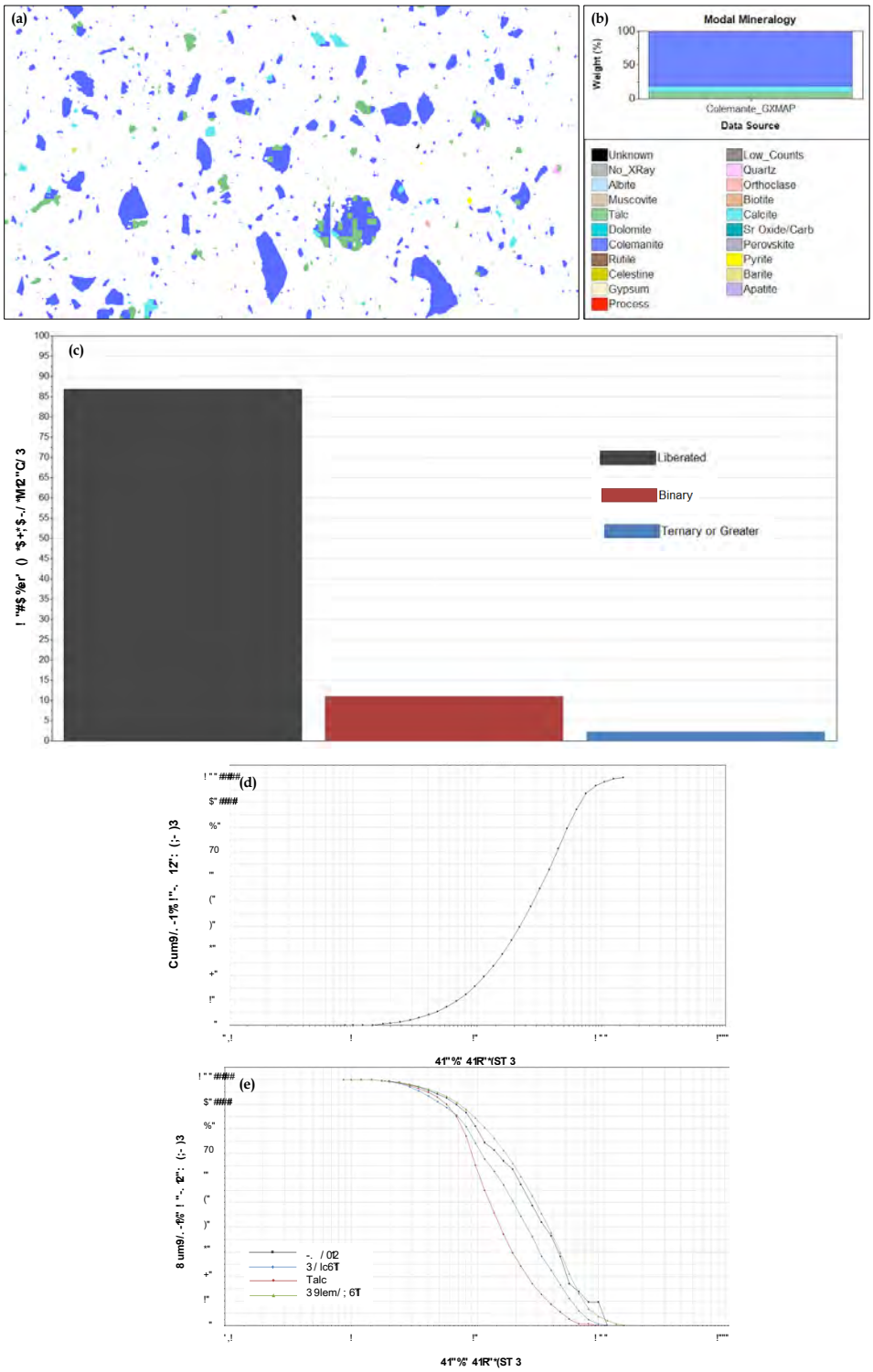

Figure 3. The MLA analysis results (a) processed SEM image of the feed by MLA (b) estimated modal mineralogy by MLA (c) mineral locking for colemanite mineral by MLA (d) particle size distribution of main minerals by MLA, and (e) particle size distribution of the current colemanite sample by MLA

The MLA analysis results in parallel to the current XRD analysis data showed that the sample contained significant amount of colemanite, calcite, talc, and quartz minerals, and their mineral particle size distributions differ from each other as seen in Figure 3.

Table 2 presents the calculated assay of the current colemanite sample according to the MLA method.

Table 2. The calculated assay of the Colemanite sample according to the MLA

Element	Weight (%)	Element	Weight (%)
Al	0.03995	Mg	1.72658
B	12.71762	Na	0.00237
Ba	0.01189	O	59.65479
C	1.09283	P	0.00093
Ca	19.33916	S	0.04690
Cl	0.00012	Si	3.03219
F	0.00423	Sr	0.08205
Fe	0.03566	Ti	0.02328
H	2.02380	Unknown	0.11176
K	0.05325	Total	99.99937

2.1.2. Ancient metal mine tailings

The ancient metal mine tailings sample was supplied in big bags from the dumps of an ancient metal mine in a central European country by a private company. After splitting the samples and classified for the further characterization, identification and sedimentation tests, a mortar type grinder was used to obtain a size fraction (d_{80}: minus 100 microns).

According to the XRD patterns from previous research studies, the sample mainly contains quartz, chlorite, muscovite, plagioclase, calcite and pyrite minerals in certain weight percentages as shown in Figure 4.

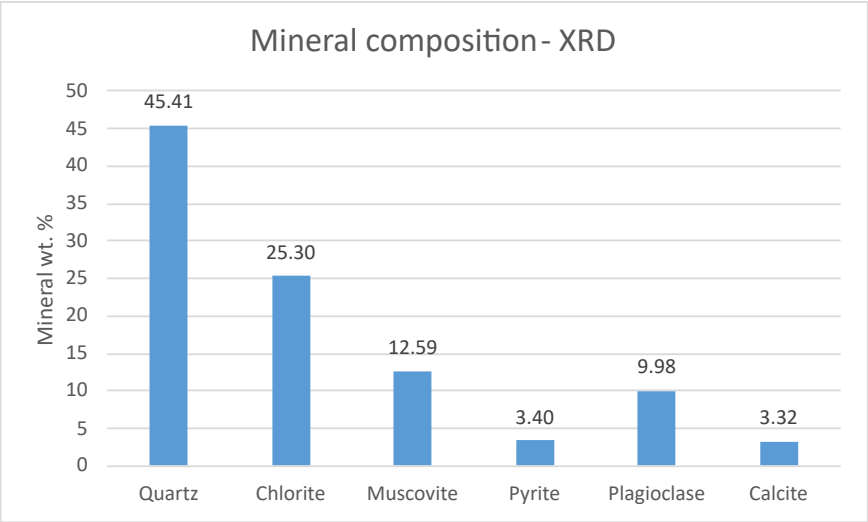

Figure 4. The rough mineral composition of the ancient metal mine tailings sample

In order to determine the chemical composition of the tailings sample, a portable XRF (pXRF, S1 TITAN, Bruker Nano GmbH Berlin, Germany) was used for the elemental composition with three repetitions. Figure 5 shows the accessories of the pXRF analyzer, including a USB cable, AC adapter, and an interlocked Benchtop stand, which directly measures the bags, and pellets. The interlocked Benchtop stand provides the XRF analyzer to analyze the horizontal sample and can connect to the extension pole. Moreover, the analyzer is a transportable and great choice for analyzing heavier elements beginning with sulfur.

Figure 5. Portable XRF device

In Table 3, chemical composition of the ancient metal mine tailings is shown in detail.

Table 3. The results of the XRF analyses of the ancient metal mine tailings

Component	(%)	Component	(%)
Al_2O_3	6.7435	Fe_2O_3	8.5873
SiO_2	34.0348	S	1.1912
K_2O	1.8966	Cu	0.0581
CaO	1.2476	Zn	0.2396
TiO_2	0.3699	As	0.0030
MnO	0.1961	Rb	0.0207

2.1.3. Graphite and recycled black mass from used batteries

Li Ion Batteries (LiBs) with the unique features of excellent energy density, high charging efficiency, and reasonable cycle performance, are widely applied in electronic devices including electrical vehicles, laptops, mobile phones, power banks, watches, and lawnmowers etc. Sharp development of advanced technologies has led to a massive increase in using LiBs and consequently resulted in an increasing amount of spent LiBs reaching end-of-life. Since these batteries contain precious metals such as Li, Co, Cu, Mn, and Ni, their recyclability and recoverability of these metallic elements are extremely crucial from economic and environmental perspectives (Nazari et al, 2024).

The spent LiBs are composed of the anode, cathode, electrolyte, separator, and shell (Table 4). Cathodes are mainly composed of aluminum foil and cathode materials, i.e. $LiCoO_2$, $LiMn_2O_4$, and $LiFePO_4$, as well as other lithium metal oxides, while anode contains copper foil and graphite. Cathodes containing high-value metal materials are the most attractive components of the spent LiBs. Therefore, it is a significant process for the disposal of spent LiBs from the viewpoint of recourse recycling and environmental protection. In the context of LiBs recycling, froth flotation can be used to separate valuable cathode materials (such as LCO, NMC, NCMA, and LMO) from other cathode materials, as well as to separate graphite from other anode materials.

Table 2. Material recovery and resource conservation through froth flotation in LiBs recycling (Nazari et al, 2024)

Component	Materials	Froth flotation	Significance
Cathode	Lithium cobalt oxide (LCO), lithium nickel-manganese-cobalt oxide (NMC), lithium iron phosphate (LFP), lithium nickel-cobalt-aluminum oxide (NCMA), lithium manganese oxide (LMO) [Active material and polymer binder, which are loaded on an aluminum foil; Active material includes lithium transition metal oxides ($LiCoO_2$, $LiNiO_2$, $LiMn_2O_4$, $LiNi_xCo_yMn_zO_2$ (LNCM)), phosphates, silicates, borates, and sulfates]	Can be used to separate valuable metals such as cobalt, nickel, and lithium from other cathode materials	Valuable cathode materials can be recovered and reused, reducing the need for mining and processing new materials, and conserving resources.
Anode	Graphite, silicon [Active material and polymer binder, which are coated on a copper foil; Graphite is basically used as the anode material for commercial LiBs, while the binder is typically polyvinylidene fluoride (PVDF)]	Can be used to separate graphite from other anode materials	Graphite can be recovered and reused, reducing the need for mining and processing new materials and conserving resources.
Electrolyte	Lithium salt dissolved in a Solvent [Organic solutions, such as lithium hexafluorophosphate (LiPF6), diethyl carbonate (DEC), ethylene carbonate (EC), dimethyl carbonate (DMC), and methyl ethyl carbonate (EMC)]	Can be used to separate the electrolyte from other battery components	The electrolyte can be treated and reused, reducing the need for disposing of waste electrolyte and protecting the environment.
Separator	Polymer film	Can be used to separate the separator from other battery components	The separator can be recycled into new products, such as plastic bags and films, reducing waste and conserving resources.

Figure 6 shows the most common design of a LIB, its basic components and the schematic design of single battery cell. A single cell consists of two electrodes, a separator (S) made of polyolefin membrane, an electrolyte made of lithium salt in organic solvents and a casing (C) made of steel or plastic. The positive electrode (P), called cathode is made of lithium metal oxide coated onto an aluminum foil. The negative electrode (N), called anode is made of graphite coated onto a high purity copper foil.

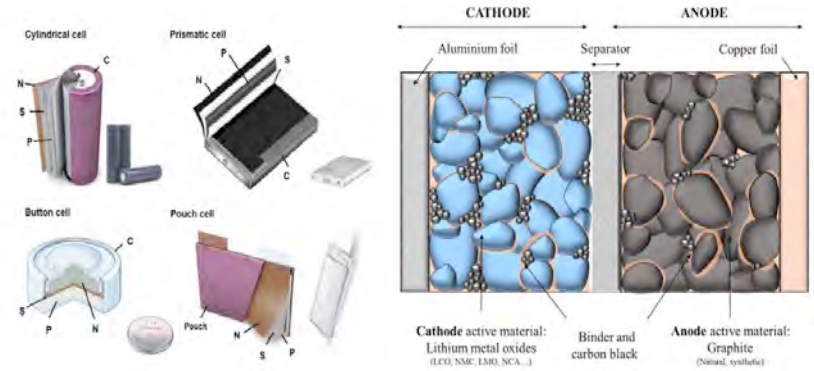

Figure 6. The most common cell type of LIBs and their components, and schematic design of single battery cell (Salcez et al., 2021)

In recent studies (Salces et al., 2022, Vanderbruggen et al, 2022), froth flotation has been proposed to treat the fine fraction of black mass (minus 100 microns) as a method to separate anodic graphite particles from cathodic lithium metal oxides (LMOs). So far, pyrolysis has been considered as an effective treatment to remove organic binders in the black mass in preparation for flotation separation. In their work, the flotation performance of a pyrolyzed black mass obtained from an industrial recycling plant was improved by adding a pre-treatment step consisting of mechanical attrition with and without kerosene addition. The LMO recovery in the underflow product increased from 70% to 85% and the graphite recovery remained similar, around 86% recovery in the overflow product. To understand the flotation behaviour, the spent black mass from pyrolyzed LIBs was compared to a model black mass, comprising fully liberated LMOs and graphite particles. In addition, ultrafine hydrophilic particles were added to the flotation feed as an entrainment tracer, showing that the LMO recovery in overflow products is a combination of entrainment and true flotation mechanisms. Their study also highlighted that adding kerosene during attrition enhances the emulsification of kerosene, simultaneously increasing its (partial) spread on the LMOs, graphite, and residual binder, with a subsequent reduction in selectivity. Their study summarized the possible effects of attrition pre-treatment, shown in Figure 7. They explained that attrition pre-treatment removes a part of the residual binder, reducing the true flotation of the spent LMOs (Figure 7, on the right). In addition, one hypothesis is the disaggregation and full wetting of the particles during attrition (Figure 7, on the left), which would explain the decrease in LMO recovery for the model black mass.

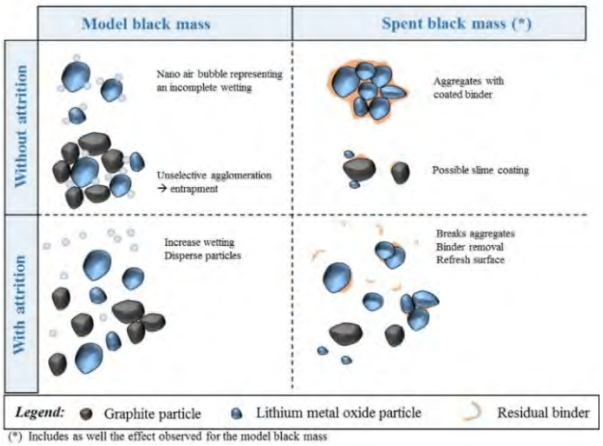

Figure 7: The potential effects of attrition on the black mass (Vanderbruggen et al., 2021, 2022).

2.2. Particle Size Analyses

Particle size distribution analysis of very finely sized feed, concentrate and tailings part of the current flotation tests was conducted by using HELOS laser diffraction device from Sympatec GmbH, Germany.

Using compressed air and particle acceleration of up to 100 m/s, RODOS dry dispersion achieves a unique dispersion performance of powders and granules in the size range from under 0.1 to 4000 microns. The compressed air pressure is maintained at 3 bar. To minimize cross-contamination, the disperser is cleaned after each measurement. To ensure the reproducibility of the results, three repetitions are considered. For dry dispersion tests, the smallest range R1: 0-35 microns is used for all the samples. The HELOS device consists of a vibratory channel on which small amount of sample in powdered form is placed and the experiment is run. The device then automatically generates particle size distribution curves.

The CUVETTE is a wet dispersion system designed for use with HELOS and has been specifically developed for the particle size analysis of suspensions and emulsions, requiring

small sample volumes of less than 50 ml. The cuvette is made of high-quality optical glass and are sintered. For wet dispersion tests, three mixtures are considered with an ethanol-to-DI water ratio of 0, 1:2 and 1:1 respectively. A concentrated solution of 1 g/l of particles in the mixtures is prepared. A suspension is prepared by adding some of the concentrated dispersion is added to the 50 ml cuvette. A magnetic stirrer is placed in the suspension and the cuvette is positioned in the path of the laser beam within the wet dispersion unit. As the laser beam passes through the cuvette, it scatters upon hitting the particles. The scattered light is then detected and analyzed to determine the particle size distribution based on the scattering pattern. With a rotation rate between 1000 – 1800 rpm, a proper volume is ensured to keep the optical concentration below 25 %. At high concentrations, particles can scatter light multiple times before it reaches the detector which can distort the scattering pattern, leading to inaccurate size measurements. At lower concentrations, it is easier to maintain a homogeneous suspension of particles within the cuvette. By keeping the concentration low, the likelihood of multiple scattering events is reduced, ensuring that the detected light is primarily from single scattering events, which are more straightforward to interpret. The test is then run and in case of any irregular particle size curves, the measurement range is either lowered or raised. Figure 8 shows the laser particle size measurement device setup and its schematic diagram.

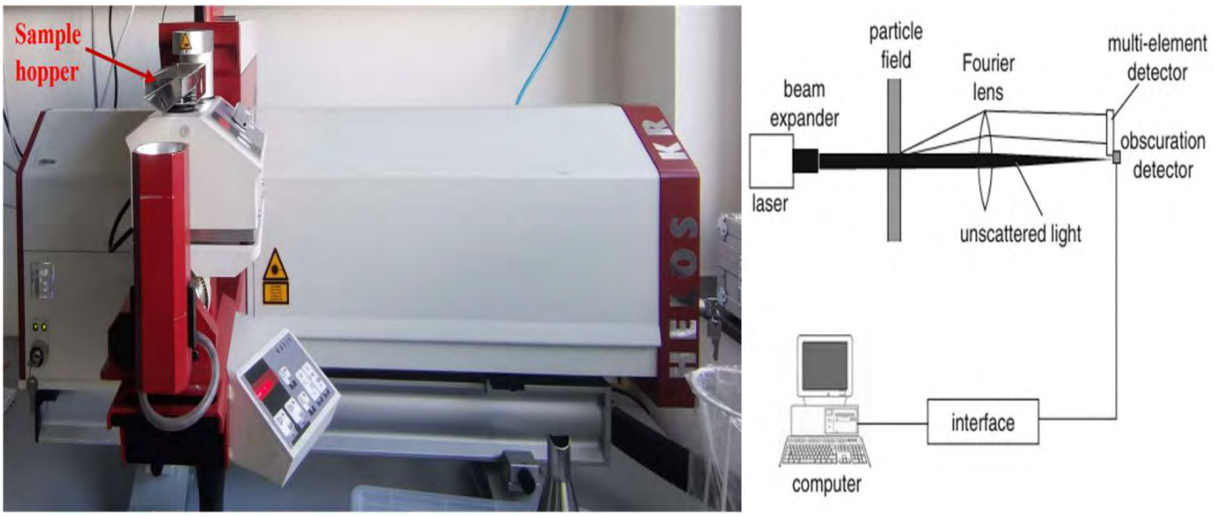

Figure 8. The laser particle size measurement device and its schematic diagram

2.3. Ultrasonic Treatment for Settling Tests

While ultrasound can be used for recovery of fine and ultrafine particles by froth flotation, simultaneously or as a pre-treatment, it can also be effective for settling or sedimentation of very finely sized products in pulp form. In a recent research, use of ultrasound in physical and chemical mineral processing operations was reviewed in detail (Güngören et al., 2024) and it was stated that ultrasound is applied with two common devices in practice; ultrasonic baths and ultrasonic probes (horns) (Figure 9). In ultrasonic baths, an ultrasonic transducer is attached to the outer surface of a liquid container. Meanwhile, in ultrasonic probes, an ultrasonic wave is radiated from a tip (immersed in a liquid) that is much smaller than the acoustic wavelength. Both devices have some advantages and disadvantages that need to be considered for experimental studies.

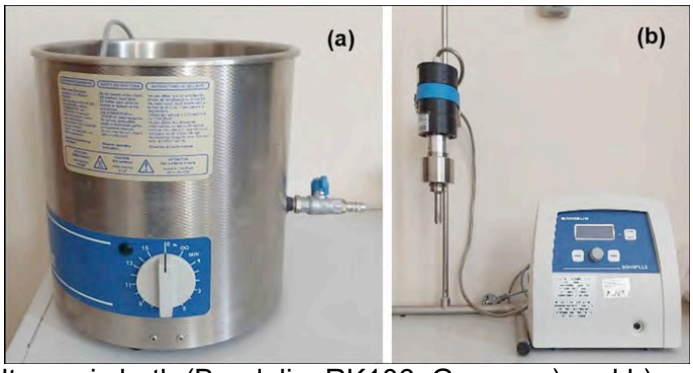

Figure 9. a) An ultrasonic bath (Bandelin, RK106, Germany) and b) an ultrasonic probe (Bandelin, HD3200, Germany) (Güngören et al., 2024)

Ultrasonic baths have low purchase and operational costs. They are more silent than probes. They usually do not require any additional equipment and are easy to use. Because of these advantages, they are more preferred in the studies. However, they have several disadvantages that affect the reproducibility of the experiments. Since they need additional water to transmit ultrasonic waves to the sample, and the sample should be in another container in most cases, there are high energy losses in addition to the lack of a uniform distribution of the ultrasound. Furthermore, although they have a time adjustment knob in most cases, the power or amplitude cannot be controlled by ultrasonic baths. Ultrasonic probes, on the other hand, focus the energy to a point, providing more effective cavitation. The power and amplitude can be adjusted. However, they are pricey, and different kinds of probe extensions may be required according to the used sample container. They create more noise, and operators may need ear protectors in prolonged applications.

In the current sedimentation study, a Bandelin HD2200 Sonopuls model ultrasonic generator, transducer and probe combination was used. The HF generator transforms the mains energy input (mains frequency 50 or 60 Hz) into high-frequency energy (200 W) with a frequency of 20 kHz. The device's weight is 2.5 kg and its dimensions are 257x180x115 mm. Thanks to the ultrasonic transducer that is connected to the HF generator, the high-frequency energy of the HF generator is converted into ultrasound and thus into mechanical energy. This takes place with an efficient and robust PZT ultrasonic oscillating system. Thus, mechanical deflections with the same frequency of 20 kHz are generated on the tip of the probe and transferred into the sonication medium as ultrasound waves with a high power intensity. The amplitude is held constant by the ultrasonic transducer (AMPLICHRON® system), independently of the applied load, using a signal feedback as long as the maximum power allowed is not exceeded. Thanks to these measures, the reproducibility of the process parameters is guaranteed, and validation of the process is supported. Standard and/or booster horns with probes (micro tips, tapered tips or titanium plates) are mounted on the ultrasonic transducer. These work as mechanical transformers and enable a multiple mechanical amplification of the ultrasound amplitude at the tip (Bandelin, 2024).

Sedimentation tests using variable mixing conditions was also performed at 10 % pulp ratio in order to deslime roughly a couple of micron size slimes to calculate decantation time and cycle before flotation. Variation of the particle size distribution for variable mixing condiditons was also discussed. Interface height, settling velocity and particle size of settled particles can be calculated using Stoke's law as described in the previous section (Drzymala, 2007).

Before starting conditioning, sedimentation, and flotation tests with solid sample addition, this equipment was checked by a digital power meter to calibrate power and temperature data according to scalable power level by just using tap water at ambient conditions. The ultrasound related experimetal setup is seen as a photo in Figure 10 in detail.

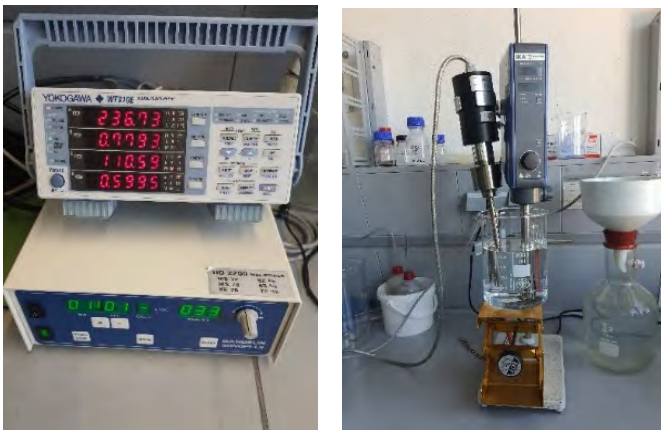

Figure 10. A photo of ultrasonic equipment and power&temperature control during ultrasonication

In order to determine the settling behaviour of very finely sized solid samples, the standard jar test procedure was used according to ASTM D2035. This procedure was designed to optimize sedimentation parameters. The test began with a rapid mix phase at 100–120 RPM with a mechanical stirrer for approximately 5 minutes to ensure the solid particles at roughly 10% suspension with distilled water are evenly dispersed in a beaker as shown in Figure 10 firstly without ultrasonication, and then transferred into a measured cylindirical beaker to determine the interface height of the settled solid particles versus increasing time as illustrated in Figure 1. Finally, the similar procedure was also applied for the samples with 5 minutes of power ultrasound at 20 kHz frequency and roughly 100 W power input, then all necessary parameters and results were recorded for graphical comparison.

3. RESULTS

3.1. Effect of Ultrasound on Colemanite Sedimentation

In order to understand the settling behavior of very finely sized colemanite as a single mineral, for which its characterization test results were given in the previous section, the jar test procedure with and without ultrasonic treatment was applied. Figure 11 shows the photo of the settled colemanite particles.

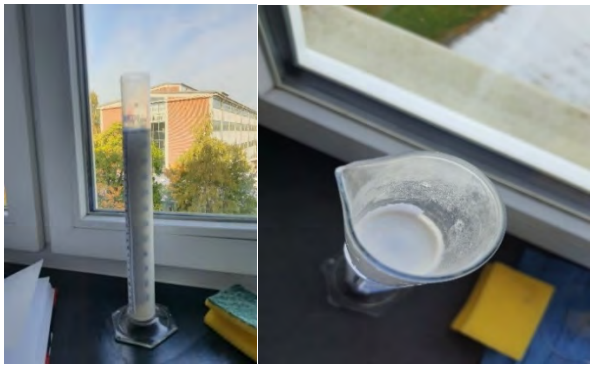

Figure 11. Colemanite settling tests

Figure 12 illustrates the effect of power ultrasound as a pre-treatment on settling test results of colemanite mineral together with the particle size distribution as separate graphs.

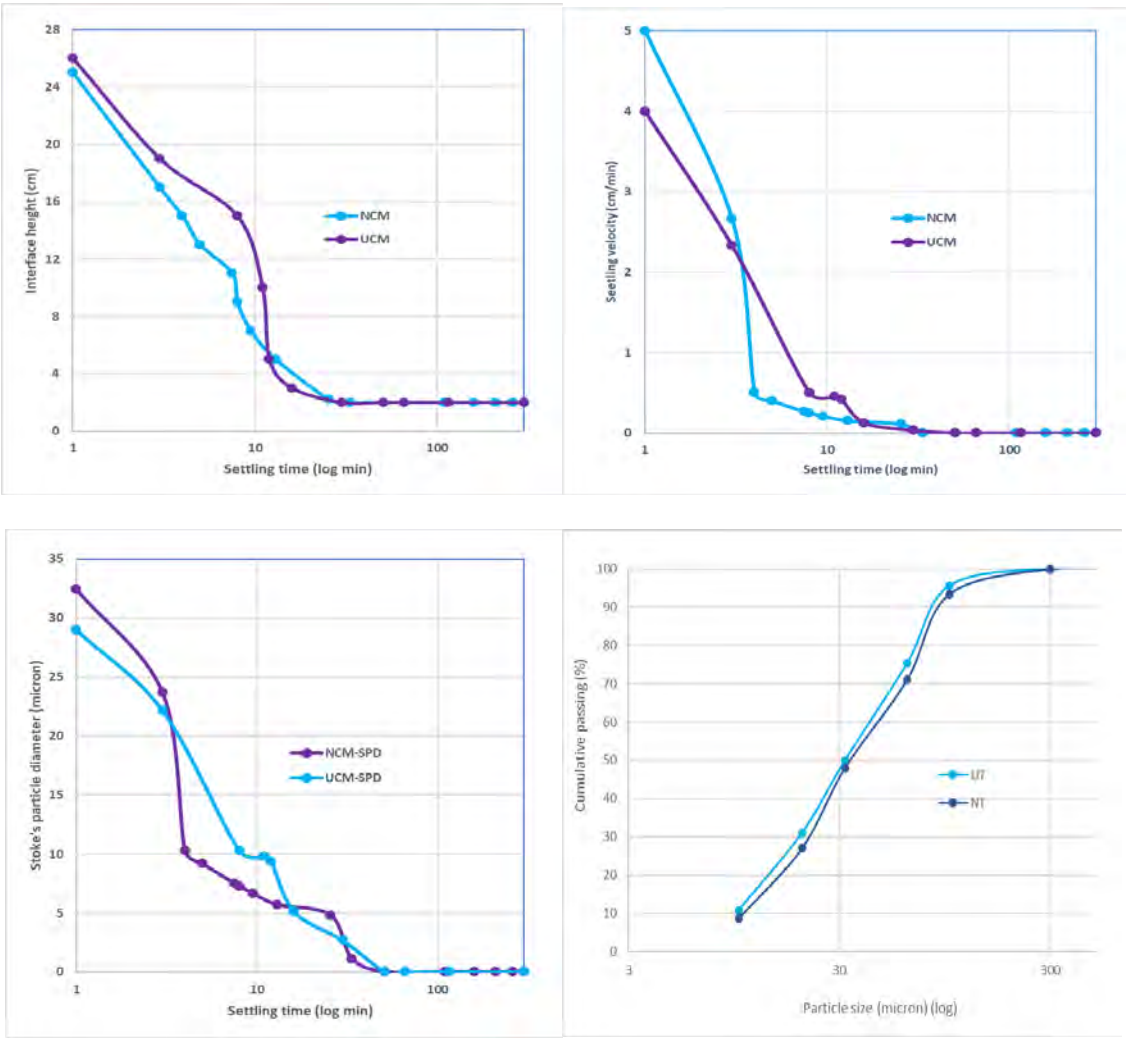

Figure 12. Effect of ultrasonic pre-treatment on settling behaviour of colemanite (NCM: non-treated, UCM: ultrasonically pre-treated)

3.2. Effect of Ultrasound on Sedimentation of Ancient Metal Mine Tailings

In order to understand the settling behavior of very finely sized, oxidized and corroded ancient metal mine tailings as a sulfide type example of which its characterization test results were given in previous section, the jar test procedure with and without ultrasonic treatment was applied. Figure 13 shows the photo of the settled tailing particles.

Figure 13. Settling tests of the ancient metal mine tailings

Figure 14 illustrates the effect of power ultrasound as a pre-treatment on settling test results of the tailings from an ancient metal mine together with the particle size distribution as separate graphs.

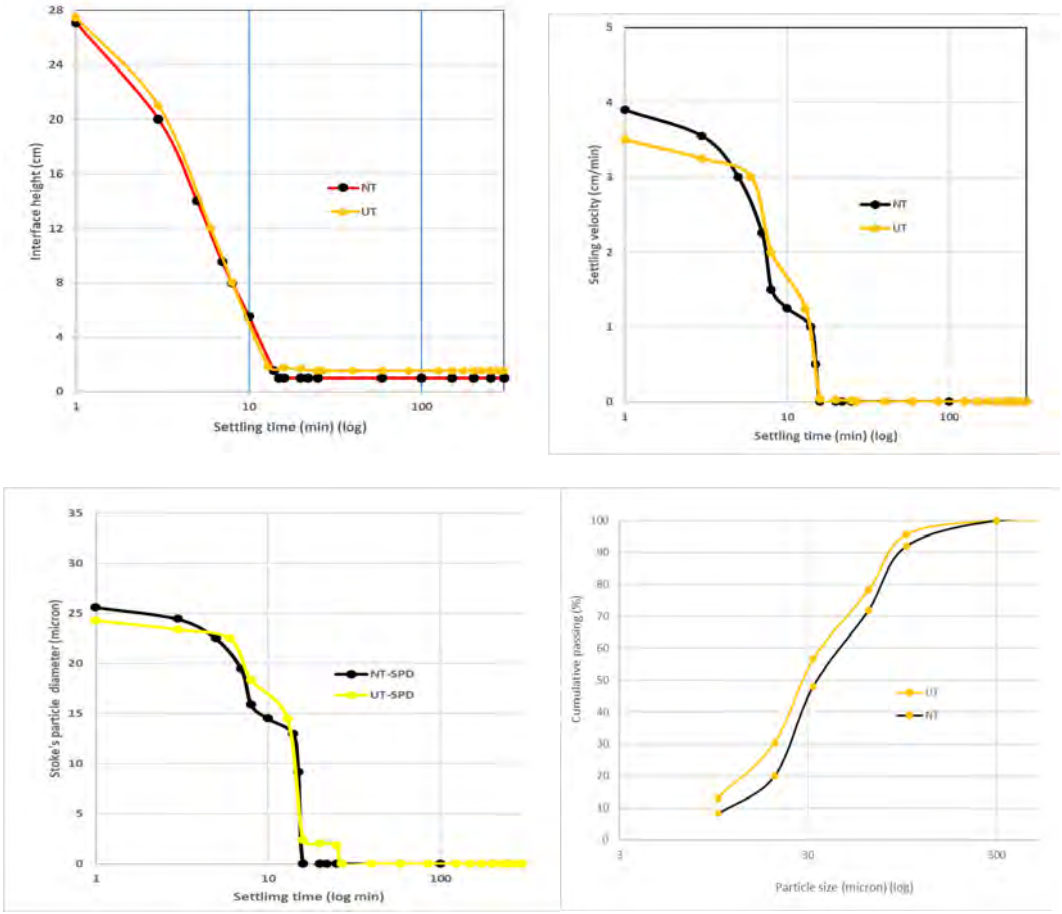

Figure 14. Effect of ultrasonic pre-treatment on settling behaviour of ancient metal mine tailings (NT: non-treated, UT: ultrasonically pre-treated)

3.3. Effect of Ultrasound on Sedimentation of Graphite and Recycled Blackmass from Used Batteries (NMC and LFP types)

In order to understand the settling behaviour of graphite and recycled blackmass from used batteries (NMC and LFP types) which their characterization test results were given in previous section, the jar test procedure with and without ultrasonic treatment was applied. Figure 15 shows the photo of the settled tailing particles.

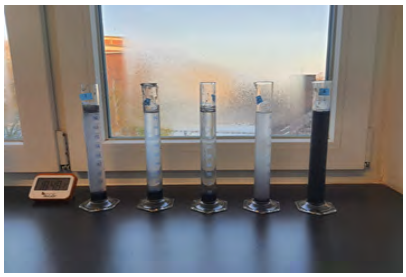

Figure 15. Settling tests of graphite and recycled blackmass from used batteries (NMC and LFP types)

Figure 16 illustrates the effect of power ultrasound as a pre-treatment on settling test results of graphite and recycled blackmass from used batteries (NMC and LFP types) together with the particle size distribution as separate graphs.

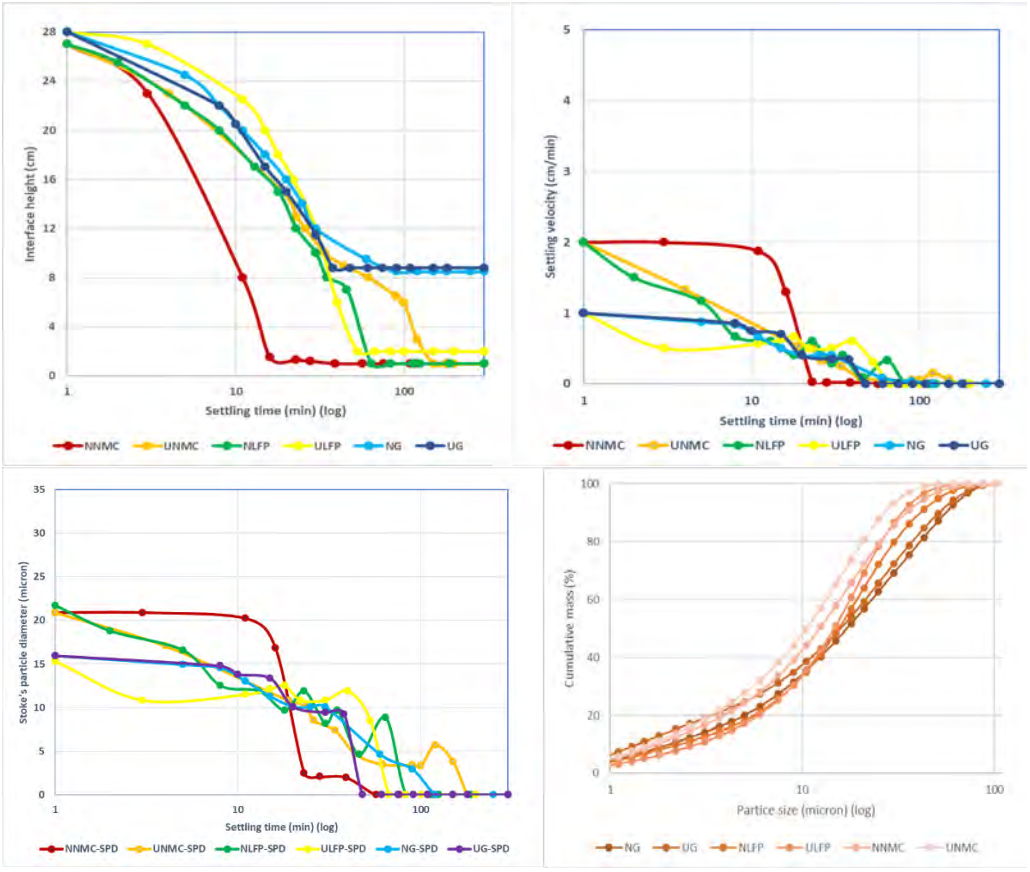

Figure 16. Effect of ultrasonic pre-treatment on settling behaviour of graphite and recycled blackmass from used batteries (NNMC: non-treated NMC type, UNMC: ultrasonically pre-treated NMC type, NLFP: non-treated LFP type, ULFP: ultrasonically pre-treated LFP type, NG: non-treated graphite, UG: ultrasonically pre-treated graphite)

4. CONCLUSION

With the depletion of high-grade deposits in ore processing plants, finer grinding of the ore has become necessary to ensure the release of economically viable minerals. This has led to an increase in the amount of ultra-fine-grained tailings and "slimes" (typically minus 20 microns) with very poor sedimentation and dewatering properties in the plants. Traditional gravity sedimentation and chemical flocculation methods are insufficient to overcome the colloidal stability created by these fine particles, resulting in low downstream densities and high water loss. Ultrasonic technology stands out as an environmentally friendly and innovative alternative that transforms these processes at the microscopic level by utilizing acoustic cavitation, micro-flow, and radiation forces.

It is seen from the current sedimentation test results of three different critical raw materials, colemanite, ancient metal mine tailings and recycled graphite-black mass samples; sedimentation velocities of ultrasonically pre-treated solid particles were lowered as well as the particle sizes, and interface heights were higher when ultrasound was applied.

The effect mechanism of ultrasound during sedimentation and settling behavior of solid particles in a liquid system and controllable parameters during the whole process, can be simulated from previous research (Özkan and Kuyumcu, 2006) shown as a three-phase system (Solid-Liquid-Gas) in Figure 17.

Of course, the main focus here in this figure should be directed towards solid-liquid interactions except gas. However there might be some common parameters, such as cavitation created by power ultrasound that may affect the surfaces of the settled particles, and this may cause corrosion and size reduction, accordingly sedimentation is influenced.

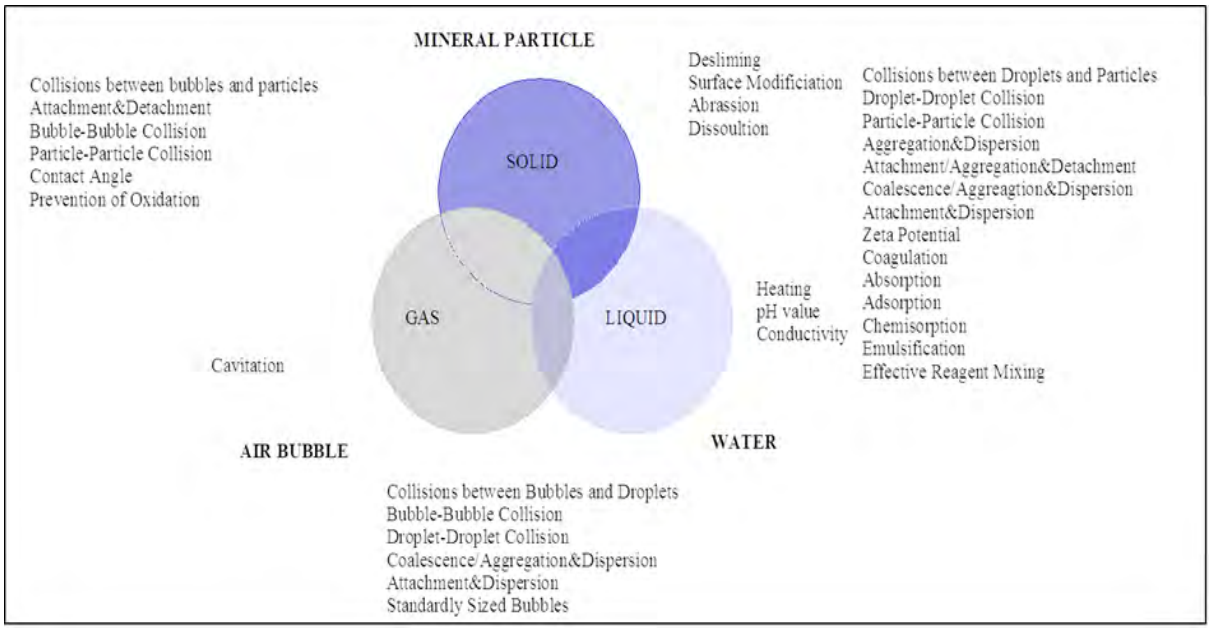

Figure 17. Effects of ultrasound on flotation phases (Özkan and Kuyumcu, 2006)

This structure summarizes the independent effects of ultrasonic energy on each phase and the complex physicochemical processes at the interface (intersection) where the two phases meet.

1. Solid Phase (Effects on Mineral Particles): Changes related only to the physical integrity and surface condition of the mineral, for example;

Desliming: Cavitation shock waves remove thin layers of slime coating from the mineral surface.

Surface Modification: Creates micro-cracks and roughness on the particle surface, increasing the area where reactants can adhere.

Abrasion: Mechanical removal of oxidation films and impurities on the surface.

Dissolution: Triggering the passage of ions from the mineral surface into the liquid.

2. Liquid Phase (Effects on Water and Reagents, if present): Changes in the thermodynamic and chemical equilibrium of the liquid medium such as;

Heating: Local increases in ambient temperature due to the absorption of acoustic energy.

pH Value: Shift in acidity/basicity balance due to the ionization of water molecules (formation of H+ and OH-).

Conductivity: Increased electrical conductivity due to increased free ion concentration.

Radical Formation: Free radicals produced by the breakdown of water during cavitation trigger oxidation.

3. Solid-Liquid Interface and Interactions: Processes that directly affect mineral processing (flotation/sedimentation) at the point where two phases meet, such as;

Aggregation and Dispersion: Aggregation or homogeneous distribution of fine particles by acoustic radiation forces (Bjerknes forces).

Zeta Potential Modulation: Facilitating coagulation by balancing the particle surface charge.

Adsorption and Chemical Binding (Chemisorption): Stronger and faster adhesion of reactants to the mineral surface. Entry of ions in the liquid into the mineral pores.
Emulsification: Excellent dispersion of oily collectors in water by breaking them down into micro-droplets.
Effective Reagent Mixing: Accelerating the transport of chemicals to the particle surface through acoustic streaming.

ACKNOWLEDGEMENT

This research was supported by the Tübitak, BİDEB 2219 Post-doctoral fellowship program. I would like to thank the authorities of the Tübitak and the Helmholtz Institute Freiberg for Resource Technology (HIF)-HZDR, especially Dr. Martin Rudolph and other colleagues in the FWGP research group.

REFERENCES

Anon., (2023) Study on the critical raw materials for the EU, European Union Report, Brussels, 152

Drzymala, J., (2007), Mineral Processing, Foundations of Theory and Practice of Minerallurgy, 381-382.

Güngören, C., Özdemir, O., Özkan, S. G., (2025) “Surface properties and beneficiation of quartz with flotation”, Minerals, 15 (8) 846.

Güngören, C., Özkan, S. G., Özdemir, O., (2024), Use of Ultrasound in Physical and Chemical Mineral Processing Operations, Advances in Minerals Research, 25-54.

Güngören, C., Vay, M. M., Demir, İ., Terzi, M., Kurşun Ünver, İ., Özdemir, O., (2025) “Ultrasound-assisted shear flocculation of quartz tailings with dodecylamine hydrochloride (DAH)”, Physicochemical Problems of Mineral Processing, 61 (5) 211353.

Kinnaird, J., Nex, P., (2024) “Critical raw materials, a global perspective”, The 19th Freiberg Short Course in Economical Geology.

Moro, K., Hoth, N., Roscher, M., Kaulfuss, F., Vianney, J. M., Drebenstedt, C., (2025) “Characterization of historical tailings dam materials for li-sn recovery and potential use in silicate products-a case study of the Bielatal tailings dam, Eastern Erzgebirge, Saxony, Germany”, Sustainability, 17 (10) 4469.

Moura, M. J., Vertis, C. S., Redondo, V., Oliveira, N. M., Duarte, B. P., (2023) “Modeling the batch sedimentation of calcium carbonate particles in laboratory experiments—A systematic approach”, Materials, 16 (13) 4822.

Nazari, S., Vakylabad, A. B., Asgari, K., Li, J., Khoshdast, H., He, Y., Hassanzadeh, A., (2024) “Bubbles to batteries: A review of froth flotation for sustainably recycling spent lithium-ion batteries”, Journal of Energy Storage, 84 110702.

Önal, G., Özer, M., Arslan, F., (2003) “Sedimentation of clay in ultrasonic medium”, Minerals Engineering, 16 (2) 129-134.

Özkan, S. G., Kuyumcu, H. Z., (2006) “Zum Einfluss von Ultraschall auf die Steinkohleflotation”, Aufbereitungs Technik, 47 (1-2) 23-33.

Özkan, Ş. G., Rudolph, M., (2025) “Assessment of the batch flotation results of finely sized colemanite in terms of gangue minerals and the importance of desliming”, Physicochemical Problems of Mineral Processing, 61 (2).

Salces, A. M., Bremerstein, I., Rudolph, M., Vanderbruggen, A., (2022) “Joint recovery of graphite and lithium metal oxides from spent lithium-ion batteries using froth flotation and investigation on process water re-use”, Minerals Engineering, 184 107670.

Shi, Y., Zheng, B., Lai, W., Sheng, J., Peng, L., Qi, H., Zhou, J., (2025) “Ultrasonic-enhanced flocculation and sedimentation of lead-zinc tailings: mechanisms and efficiency improvements”, Ultrasonics, 107751.

Silva, L. A., Prates, L. M., Pereira, A. M., Correia, J. C. G., Marques, M. L. S., Filippova, I. V., Filippov, L. O., (2025) “Ultrasonic dispersion for ıron recovery from slime tailings: Microprocesses unveiled through molecular dynamics simulations”, Langmuir, 41 (11) 7235-7250.

Vanderbruggen, A., Hayagan, N., Bachmann, K., Ferreira, A., Werner, D., Horn, D., Peuker, U., Serna-Guerrero, R., Rudolph, M., (2022) “Lithium-ion battery recycling-influence of recycling processes on component liberation and flotation separation efficiency”, ACS ES&T Engineering, 2 (11) 2130-2141.

Vanderbruggen, A., Salces, A., Ferreira, A., Rudolph, M., Serna-Guerrero, R., (2022) “Improving separation efficiency in end-of-life lithium-ion batteries flotation using attrition pre-treatment”, Minerals, 12 (1) 72.

Vanderbruggen, A., Sygusch, J., Rudolph, M., Serna-Guerrero, R., (2021) “A contribution to understanding the flotation behavior of lithium metal oxides and spheroidized graphite for lithium-ion battery recycling”, Colloids and Surfaces A: Physicochemical and Engineering Aspects, 626 127111.

Whitworth, A. J., Forbes, E., Verster, I., Jokovic, V., Awatey, B., Parbhakar-Fox, A., (2022) “Review on advances in mineral processing technologies suitable for critical metal recovery from mining and processing wastes”, Cleaner Engineering and Technology, 100451.

Zhang, X., Cheng, H., Xu, K., Ding, D., Wang, X., Wang, B., Ma, Z., (2024) “Ultrasonic enhancement for mineral flotation: Technology, device, and engineering applications”, Minerals, 14 (10) 986.

Zhou, W., Cao, W., Wei, H., Shi, S., Li, C., Dong, L., (2025) “Sonication-assisted surface erosion and ıts ımpact on the flotation of ultrafine smithsonite”, Metals, 15 (7) 731.

BONDING MECHANISMS IN BRIQUETTING OF RECYCLED WASTE POWDERS– USED COFFEE GROUNDS GRANULATE

Jože KORTNIK[1,*], Lara ANŽIČ[1]

[1]*University of Ljubljana, Faculty of Natural Sciences and Engineering, Department of Geotechnology, Mining and Environment, Ljubljana, Slovenia*
[*]*Corresponding author: joze.kortnik@guest.arnes.si*

A B S T R A C T

In the environment in which we live, more and more waste is generated, the majority of which still ends up in the environment or is still disposed of in non-hazardous waste landfills. Used coffee grounds (UCG) in Slovenia represent a smaller share of waste in the total waste stream, around 1.5%, which means that over 30 tons of UCG granulate are generated every day (according to statistics, each Slovenian consumes around 5.8 kg of coffee per year), which could be used for energy instead of composting or disposing of it in municipal solid waste landfills, as it has a comparable or even higher calorific value than wood and brown coal, over 20 MJ/kg. The great added value of this alternative source is also that it is suitable for wider consumption in households and not only for industrial use, since, when incinerated, we also do not need additional treatment plants that would capture and purify hazardous flue gases. The paper presents the process of making briquettes with an emphasis on the use of UCG as recycled waste powder.

***Key words**: Briquetting, fuel from waste, used coffee grounds granulate (UCG), urban mining*

1. INTRODUCTION

Many recycled waste materials are in the form of powders or granulate due to technological recycling processes. This often causes problems in transport, packaging, and storage; especially when they are in the form of powders, due to their low bulk density and dustiness. The solution is provided by various surface reduction or agglomeration processes. Agglomeration is the process of combining small particles into larger aggregates, so-called agglomerates, such as pellets, briquettes, tablets, and sintered agglomerates, which must have certain strength properties (Kortnik, 2011).

Surface reduction or agglomeration processes must meet several requirements, especially in the case of the necessary addition of binders to form agglomerates, no components that negatively affect the quality of the final product must enter the production process - nor must they increase the production of gaseous pollutants, especially organic compounds such as polychlorinated biphenyls-PCB and dioxins-PCDD/PCDF or polycyclic aromatic hydrocarbons-PAH (Spence and Shi, 2005; Valls and Vàzquez, 2000). After binding the recycled granulate, the agglomerate must remain solid and meet the requirements for mechanical properties. Binders can be in solid or liquid form, organic (bitumen, tar, resin, starch, or molasses) or inorganic (lime, cement, water glass, or clays). Molasses and other common binders are not suitable for briquetting fine-grained metallurgical waste due to their phosphorus and sulfur content. In contrast, resins are suitable – e.g. acrylic, formaldehyde or phenolic resins (Spence and Shi, 2005; Valls and Vàzquez, 2000). The choice of binder should also depend on its impact on chemical reactions in the aggregate, especially on the reduction of iron oxide Drobikova et al., 2016). In addition, the formation of unwanted gaseous by-products with a potential negative impact on the environment should be limited during heat treatment (Wang et al., 2018).

In practice, the most commonly used method for producing solid briquettes from recycled granulates is the briquetting/tabletting. Briquetting/tabletting is a process in which the material is compressed under pressure in a forming channel.

The most appropriate moisture content generally varies and depends on the physical properties of the granulate material; the usual content is between 8÷12 wt.%. The maximum permissible moisture content in mechanical piston presses is around 15 wt.%, while in hydraulic presses, the moisture content is up to 30 wt.%. When the moisture content is >15 wt.%, there is a risk of steam explosion due to the increase in pressure and temperature in the compression process (Anžič, 2024). Furthermore, the particle size of the recycled granulate is important in the production of briquettes. The particle size should generally not exceed 25% of the diameter of the final product/briquette to ensure proper strength. At this stage, superheated steam can be added to the recycled granulate, making it softer and enabling better bonding. The briquetting process follows by establishing a compressive force on the granulate particles in the forming channel.

The quality of briquettes is assessed by their compressive strength, and in the case of coals, also by their moisture resistance. In doing so, we follow the standard for permissible moisture and ash content in solid biofuels SIST EN ISO 17225-7, which prescribes the maximum permissible moisture content in solid biofuels of 15 wt.% and the ash content for wood briquettes below 3 wt.%, and for non-wood briquettes <10 wt.% (Anžič, 2024).

The strength of the briquette depends on both the pressure applied and the granulation composition and particle size of the granulate being briquetted. The main purpose of briquetting is to reduce the volume and increase the density of the solid. When densification occurs, two quality aspects must be considered. First, the briquette must remain compact until it fulfills its purpose, and second, it must achieve an adequate calorific value as a solid fuel (Kortnik, 2011; Briquette Solution, 2020).

2. BASIC BRIQUETTING MECHANISMS

The basic mechanisms of agglomeration are shown in Figure 1. and it can proceed in three ways (Kortnik, 2011):

- by adhesive bonding of granulate (pelleting) - the snowball principle (see Figure 1a),
- by pressing the granulate in a forming channel (briquetting or tabletting) (see Figure 1b) and
- by bonding bridges with the application of heat (sintering) (see Figure 1c).

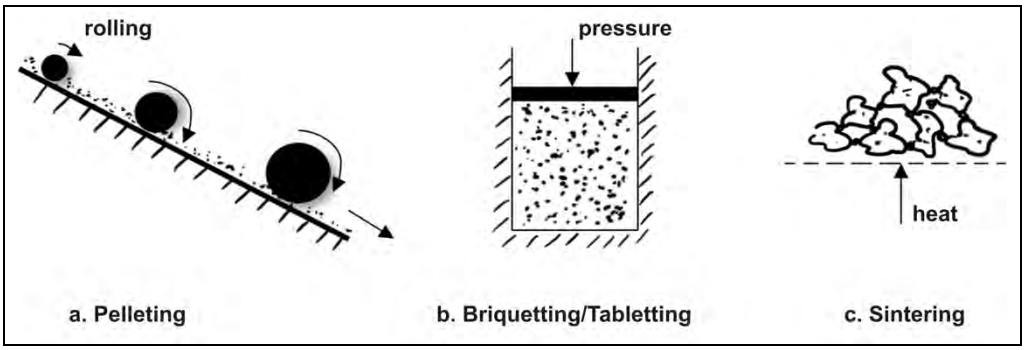

Figure 1. Basic mechanisms of agglomeration a. Pelleting, b. Briquetting/Tabletting, c. Sintering (Kortnik, 2011)

Successful briquetting depends on many different factors, such as moisture content, particle size, particle shape, presence of impurities, etc. There are several different theories that attempt to explain the mechanism of the briquetting process, but none of them

comprehensively presents the actual mechanism of briquetting. Theories are divided into two basic groups: without the use of binders and with the use of binders (Zhang et al., 2018).

In briquetting, we use compressive force, or we are talking about the compression process due to the compression of the granulate between two surfaces (Spence and Shi, 2005), as shown in Figure 2. Since we have brought the particles very close to each other, on the one hand, the distance between them decreases, on the other hand, the number of contact points increases and with appropriate humidity, we get more liquid bridges due to the reduction of porosity and thus greater capillary forces. In the final stage of compression, elastic or plastic deformation of the particle surface also occurs, and due to local heat concentration, the surface of the solid particles fuses together, or sintering.

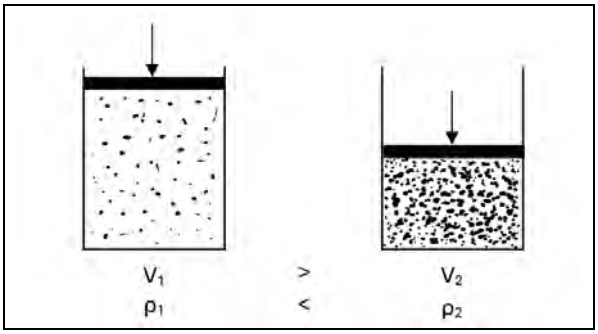

Figure 2. Briquetting principle (V - volume, ρ - density) (Anžič, 2024; Kornik and Anžič, 2025)

Theories of briquetting without the use of binders are mainly divided according to the different properties of the granulate for briquetting into (Zhang et al., 2018):

- lignin briquetting theory,
- capillary briquetting theory,
- colloidal briquetting theory and
- adhesive briquetting theory.

The theory of lignin briquetting involves the use of lignin as a natural binder, which is already present in the granulate. The binder has physicochemical properties that help to bind the particles into solid, compact briquettes. Lignin is an organic binder in wood that softens and becomes a plastic substance at elevated temperatures. In the case of recycled UCG granulate, the lignin in the coffee grounds acts as a natural binder, which, under the influence of external/compressive force and temperature due to friction, binds the recycled particles into a solid briquette, as shown in Figure 3.

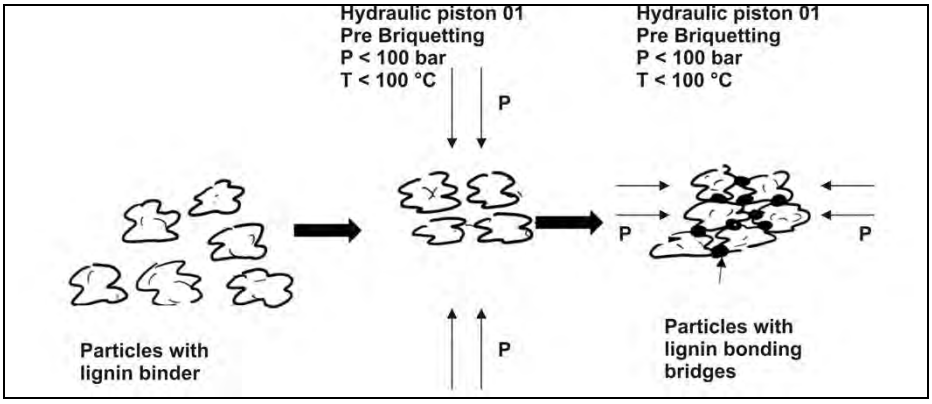

Figure 3. The principle of binding recycled particles in the briquetting process (P - pressure, T - temperature) (Anžič, 2024; Kornik and Anžič, 2025)

The capillary theory of briquetting assumes that there is a large amount of water-saturated capillaries in the recyclate particles. During briquetting, under the influence of an external

force, the capillaries are crushed, water is squeezed out of them, which covers the surface of the particles and forms a water film. The water film then fills the spaces between the particles and becomes an interaction/binding force. When the pressure is released, the capillaries expand slightly, some water re-enters the capillary, and some remains on the surface of the particles, where a meniscus (concave or convex) is formed due to the effect of surface tension. The recyclate particles are connected mainly due to capillary forces into a solid briquette.

The colloidal theory of briquetting assumes that the lignin present in the recyclate consists of solid and liquid colloidal material. The solid material consists of tiny granules of humic substance. These combine under the influence of external force and form gelatinous colloidal particles due to intermolecular cohesion in solution. The particles of the recyclate are connected to each other by means of Van der Waals forces or molecular forces under pressure. The smaller the particles, the greater their specific surface area and binding force.

The adhesive theory of briquetting assumes that the bonding of particles is a result of the pressure of water from the primary capillary pores. The water present in the spaces between the recyclate particles causes surface tension and thus the formation of a secondary capillary adsorption force. The recyclate particles are interconnected due to Van der Waals and capillary forces. When the recyclate particles come close enough to each other, a molecular bonding force is created that connects the particle surfaces.

The binder has a dual function, first as a lubricant, which enables the redistribution of the recyclate particles during briquetting, and at the same time it binds the recyclate particles into a solid briquette. A suitable binder must enable strong bonding, be environmentally acceptable, and be economically affordable. Theories of briquetting using binders are divided according to the type of binder into (Zhang et al., 2018):

- inorganic binders,
- organic binders,
- combined binders.

Inorganic binders have advantages over organic binders, mainly due to their lower cost, higher heat resistance, and water resistance or hydrophilicity. The main disadvantage of using inorganic binders is the higher ash content. The most commonly used inorganic binders for briquetting are clay, lime, gypsum, cement and sodium silicate (Karlhager, 2008).
Organic binders not only have good properties for binding granulate particles, but briquettes generally achieve high compressive strength, high mechanical resistance, and lower ash content. The main disadvantage is the price and the risk of briquettes disintegrating at high temperatures due to the low mechanical strength and poor thermal stability of the binder. Organic binders can be divided into biomass binders (cellulose and starch binders), tar pitch and petroleum bitumen, lignosulfonate and polymer binders (Zhang et al., 2018). Lignin is a cellulose binder that is naturally present in woody biomass. Lignin is a complex organic compound with the chemical formula: $C_9H_{10}O_2$, $C_{10}H_{12}O_3$, $C_{11}H_{14}O_4$, and the second most common organic material on Earth after cellulose, and together they are an important component of the cell walls of woody plants. It is a polymer that plays a role in ensuring the structural strength and resistance of plant tissues, especially in perennial plants such as trees. Lignin helps plants become more rigid and resistant to mechanical stress, drought, and bacteria. Lignin is mainly used in industry as a binder, e.g., for particle boards and similar laminated or composite wood products. Lignin can also be leached, either in powder form or liquefied, as it has very good binding properties and is often used as a binder additive in briquetting.

Combined binders are a combination of organic and inorganic binders, which utilize the good properties of both binders.

3. PRINCIPLES OF BRIQUETTING MACHINES

Depending on the operating mode and briquetting pressure, we know the following briquetting machines:

- Screw briquetting machines,
- Piston briquetting machines,
- Roller briquetting machines and
- Hydraulic briquetting machines.

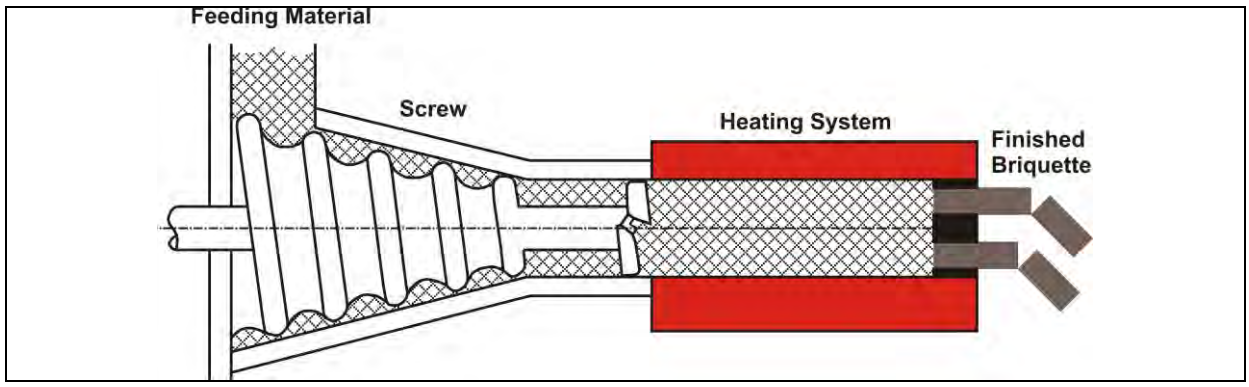

Figure 4. The working principle of a screw briquetting machine (Briquette Solution, 2020)

The screw briquetting machine, Figure 4, uses a dosing screw to transfer the compressive force to the recycled granulate, and can be additionally equipped with a heating system for the purpose of drying the input material. The granulate is dosed into a storage tank, from where the dosing screw, which also provides the appropriate briquetting pressure, transports it to the forming channel and briquetting. Depending on the shape of the forming channel, the granulate can be compressed into any shape (square, round, etc.). Since the roller briquetting machine does not operate with high pressure, it is necessary to add binders to form a solid briquette.

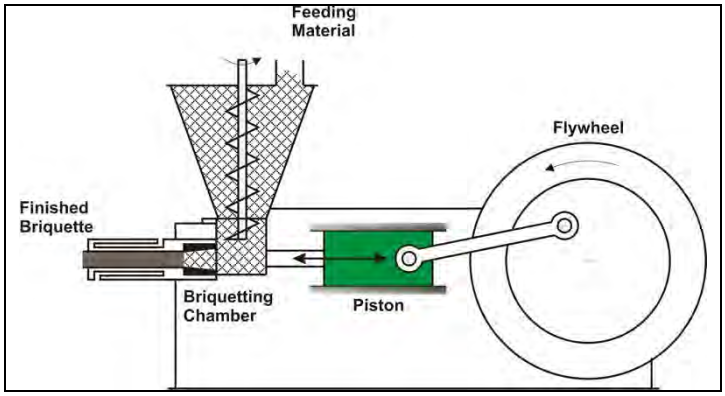

Figure 5. The working principle of a piston briquetting machine (Briquette Solution, 2020)

The piston briquetting machine, Figure 5, uses a piston driven by a flywheel to compress the granulate. The piston in the forming channel applies a compressive force to the granulate, and the friction causes the temperature to increase, which activates the binders and thus the bonding of the briquette particles.

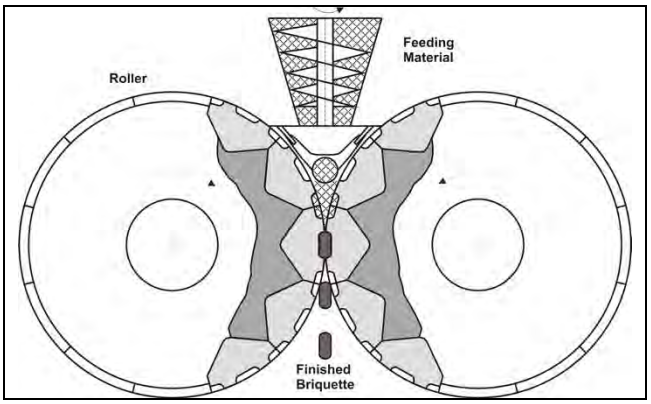

Figure 6. The working principle of a roller briquetting machine (Briquette Solution, 2020)

A roller briquetting machine, Figure 6, uses two oppositely rotating rollers at the same speed to compress the material (Briquette Solution, 2020). The rollers have openings on their surfaces; as they move, two identical openings or molds are caught in the middle, where the material is compressed into the desired shape.

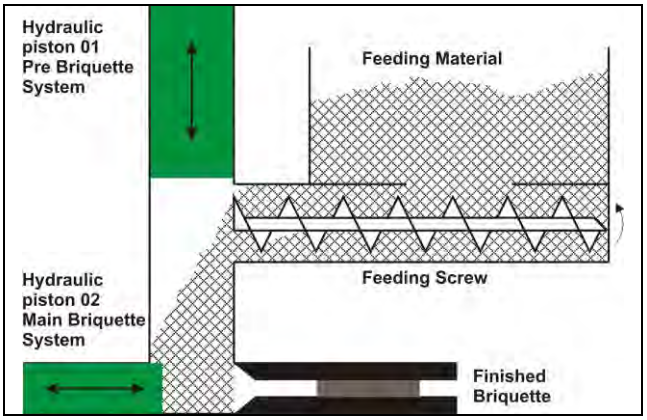

Figure 7. The working principle of a hydraulic briquetting machine (Briquette Solution, 2020)

The hydraulic briquetting machine, Figure 7, operates with the two hydraulic pistons, which allows high pressures to be achieved in the forming channel on the granulate, which enables the briquetting of practically all recycled materials of various materials, including metal powders. The working process begins with the feeding of powder particles/material into the hopper, from where the dosing screw transfers the material to the forming channel of the first hydraulic piston. Here, the material is compacted in one direction, and then the dosing screw transfers it to the second hydraulic piston, where the briquette is compacted in the other direction. The briquetting machine establishes pressure on the surface of the briquette, which causes deformation of the surface of the material particles and thus their bonding. During the briquetting process, the temperature in the forming channel increases due to friction, thus activating the binder, which allows better bonding of the particles into a solid briquette (Figure 3). A purpose-built hydraulic briquetting machine from the Hungarian manufacturer Mekom MiniBrik-30 was used to produce briquettes from recycled UCG granulate. Compared to other types of briquetting machines, the MiniBrik-30 briquetting machine enables high-pressure briquetting up to 180 bar. The briquetting machine has a welded steel frame, and the consumable parts of the briquetting machine are made of hardened steel. In the hopper, which has a special trapezoidal shape for easier entry of the granulate into the dosing screw, we can insert approx. 0.5 m^3 of recycled granulate, which is then transferred by the dosing screw into the forming channel. In the forming channel, first the first hydraulic piston briquetting the granulate in the longitudinal direction, then the second hydraulic piston briquetting the granulate in the transverse direction, and we obtain a solid briquette (Figure 7).

4. EXAMPLE OF BRIQUETTING RECYCLED UCG GRANULATE

The process of making briquettes first involves reducing the moisture content of the UCG. Excessive moisture can cause a lot of problems during storage, as it leads to the development of mold, shown in Figure 8, which is even more intense in the summer months (Anžič, 2024).

Figure 8. Mold and fungus growth on damp UCG granulate (Anžič, 2024; Kornik and Anžič, 2025)

Before briquetting the recycled UCG granulate, we first had to reduce the moisture content, usually by about 70 wt.%, using a laboratory dryer with a power of 6.6 kW at a temperature of 105 ± 2 ˚C to a constant mass for approximately 12÷14 hours. Drying was also carried out with a fan dryer with a power of 0.22 kW at a temperature of 32 ± 2 ˚C to a constant mass for 3 - 5 days. The advantage of the fan dryer was mainly in the 4 times lower electricity consumption for the same amount of recycled material, but the disadvantage was the up to 8 times longer drying time. Drying also represents the highest cost in the production of briquettes. Before briquetting began, the moisture content had to be <10 wt.% (Kornik and Anžič, 2025). The moisture content was determined gravimetrically and with a manual Bosch Universal-Humid moisture meter.

To achieve the strength and mechanical durability of the briquettes, it is important that the recycled granulate has an appropriate particle size. The particle size must not exceed 25% of the final diameter of the briquette (Kortnik, 2011). For this purpose, we performed granulation analysis with a Fritsch Analysette 22 NanoTec laser particle size analyzer. The analysis used samples of granulates of recycled UCG granulate Barcaffe brand, Franck brand, and Escobar brand, as well as samples of cellulose and starch binder. The results of the granulation analysis, which comply with the requirement, are shown in Table 1.

Table 1. Results of granulation analysis of recycled UCG of Barcaffe brand, Franck brand and Escobar brand.

Recycled UCG granulate	**Max. particle size (µm)**	**Average particle size d_{50} (µm)**
Barcaffe brand	1209	275
Franck brand	1321	336
Escobar brand	1116	237
Cellulose binder CB (spruce sawdust)	1475	585
Starch binder SB (flour type 500)	221	61

Figure 9. MiniBrik-30 hydraulic briquetting machine used for briquetting recycled UCG (Anžič, 2024; Kornik and Anžič, 2025)

Briquetting of recycled UCG granulate was carried out using a Mekom MiniBrik-30 hydraulic briquetting machine and is shown in Figure 9. The briquetting machine performs briquetting using two hydraulic cylinders that move in sync with calibrated PLC controllers for pressure control. Briquetting took place at a pressure between 100 and 120 bar. The hydraulic briquetting machine is manufactured in accordance with the regulations, Directive 89/392/EEC and amendments to Directives 73/23/EEC and 89/336/EEC.

Figure 10. Device for determining mechanical durability of briquettes (Anžič, 2024; Kornik and Anžič, 2025)

The mechanical durability (compactness) of briquettes made from recycled UCG granulate was determined in accordance with the standard SIST EN 15210-1:2010 – Solid biofuels – Methods for determining the mechanical durability of pellets and briquettes – Part 1: Pellets. Since the standardized procedure is intended only for wood pellets, the procedure was appropriately adapted for the case of briquettes on the device shown in Figure 10.

Table 2. Results of the analysis of mechanical durability of UCG briquettes made from recycled UCG Franck brand.

Sample	Volume [cm^3]	Density ρ [kg/m^3]	Mass - beginning [g]	Mass – end [g]	Mechanical durability [%]	Moisture-average [mas. %]
A1	109.9	726.8	79.9	78.2	97.9	7.8
A2	98.5	798.1	78.6	76.3	97.1	8.4
A3	109.9	796.0	87.5	84.8	96.9	8.4
A4	98.5	852.0	83.9	82.6	98.5	8.2
		793.2			97.6	8.2

In accordance with the SIST EN 15210-2:2011 standard, the briquettes were subjected to 500 rotations at a rotation speed of 1 revolution per minute and then the proportion of waste material from the briquette was calculated. The results of the mechanical durability of the A1-A4 briquettes are in accordance with the standard, which is shown in Table 2. The average density of the Franck coffee residue recycled briquettes is 811.0 and the average moisture content is 8.4 wt. %.

5. ANALYSIS OF BRIQUETTING RESULTS AND DISCUSSION

To check the suitability of the briquettes, we had to define a suitable and an unsuitable briquette. A suitable briquette must be compact, i.e., it must achieve a mechanical durability of > 95 wt.% according to the pellet standard SIST EN 15210-2:2011. It must also comply with the standard for moisture and ash content in solid biofuels SIST EN ISO 17225-7. Figure 11 shows unsuitable briquettes (left) and suitable briquettes (right), which must, in addition to the requirements of both standards, have a length of at least 50 mm and a diameter of 50 mm.

Figure 11. Final briquettes, appropriate briquettes (left) and inappropriate briquettes (right) (Anžič, 2024; Kornik and Anžič, 2025)

Suitable briquettes made from recycled UCG granulate are characterized by a moisture content of <9 wt.% and an ash content of <2 wt.%, which is why they are classified as non-wood briquettes according to the SIST EN ISO 17225-7 standard (moisture content < 12 wt.%, ash content <6 wt.%).

During briquetting, we encountered a certain small proportion of unsuitable briquettes, which we managed to rehabilitate into suitable briquettes by adding 5 – 10 wt.% cellulose binder. We attributed the reason to the excessive moisture content in the recycled UCG granulate before briquetting. When making briquettes from recycled UCG granulate, we used the organic cellulose binder lignin, which is naturally present in UCG. When optimizing the strength of the briquettes, we also used the organic starch binder, wheat starch.

6. CONCLUSION

In the total mass flow of waste generated in Slovenia, UCG represents a smaller share of waste, which is around 1.5% or >11,000 t annually. Taking into account the average weight of a UCG briquette of 120 g, over 250,000 UCG briquettes could be produced daily with an average upper calorific value of 20.5 MJ/kg. Taking into account the maximum upper calorific value of 21.5 MJ/kg, around 72 GWh of energy could be produced annually, which is the energy consumed by around 18,000 households annually. We assume that UCG briquettes could be used primarily for heating households. The added value of coffee briquettes compared to classic fuels from waste lies primarily in the fact that, due to their composition, they are also suitable for individual combustion chambers in households and not only for industrial combustion chambers, like conventional RDF&SRF fuels made from waste. Laboratory results of briquettes made from recycled UCG granulate have shown that UCG represents a suitable raw material for the production of waste fuels, which is comparable or even higher quality than conventional wood briquettes. Compared to wood briquettes, coffee briquettes have a slightly higher ash content but also a slightly higher upper calorific value.

For briquetting recycled UCG granulate, the hydraulic briquetting machine from the Hungarian manufacturer Mekom MiniBrik-30 proved to be the most suitable.

The potential of UCG has already been recognized worldwide, both in terms of organic composting, energy generation, production of new products (e.g., for skin care), and production of fuels (biodiesel, pellets/briquettes for heating). The problem of reusing UCG lies primarily in the costs of preparing the raw material on an industrial scale and the organization/logistics of collection itself. Of key importance in establishing a UCG collection system is also the necessary cooperation of households. UCG are residues that are generated during the brewing/preparation process of coffee. The relatively large amount of UCG generated in Slovenia would therefore require a nationally developed UCG Management Plan that would be in line with applicable national regulations.

REFERENCES

Anžič, L., (2024) “Use of coffee briquettes as fuel from waste in households“, Master's Thesis, UL-Faculty of Natural Sciences and Engineering.

Briquettesolution.com. (2020) “How does a briquette machine work - types and making“, Accessed on: [online] <https://briquettesolution.com/how-does-a-briquette-machine-work-types-and-making-process/> [accessed 15 Mar 2025].

Drobikova, K., Placha, D., Motyka, O., Gabor, R., Kutláková, K. M., Vallová, S., Seidlerová, J., (2016) “Recycling of blast furnace sludge by briquetting with starch binder: Waste gas from thermal treatment utilizable as a fuel“, Waste Management, 48 471-477.

Karlhager, J., (2008), Institutionen för skogens produkter: The Swedish market for wood briquettes - Production and market development. Accessed on: [online] <https://core.ac.uk/download/pdf/211579807.pdf> [31 Feb. ?? 2025].

Kortnik, J., (2011), Mechanical process engineering II. [electronic script] Ljubljana, Faculty of Natural Sciences and Engineering, 47.

Kortnik, J., Anžič, L., (2025) “Bonding mechanisms in in briquetting of powder recycles“, Proceedings of 16th conference with international participation, 49. Jump obver the leather skin, 92-102.

Spence, D. R., Shi, C., (2005), Stabilization and Solidification of Hazardous, Radioactive, and Mixed Waste, 365.

Valls, S., Vàzquez, E., (2000) “Stabilization and solidification of sewage sludges with Portland cement“, Cement and Concrete Research, 30 1671-1678.

Zhang, G., Sun, Y., Xu, Y., (2018) “Review of briquette binders and briquetting mechanism“, Renewable and sustainable energy reviews, 82, 477–487.

Wang, T., Xiao, F., Zhu, X., Huang, B., Wang, J., Amirkhanian, S., (2018) “Energy consumption and environmental impact of rubberized asphalt pavement“, Journal of Cleaner Production, 180 139-158.

EFFECT OF WASTE ROCK DILUTION ON THE FLOTATION OF MAIN CRITICAL RAW MATERIALS (CRM)

Maria SINCHE GONZALEZ*

University of Oulu, Oulu Mining School, P.O. Box 3000, 90570, OULU, FINLAND
**Corresponding author: maria.sinchegonzalez@oulu.fi*

A B S T R A C T

The effect of waste rock minerals introduced by dilution on the flotation of valuable minerals is a critical factor that negatively impacts the efficiency and economics of the flotation process. Although this is recognized, dilution is more tackled from the point of view of mining extraction and not from the effect caused during the separation processes of minerals.

The objective of this paper is to present a review of the influence of waste dilution in the flotation of CRM, possible mitigation measures, and an example of the effects on spodumene flotation. It looks at how Mg-bearing minerals added into the flotation system of a Lithium mineral through waste rock dilution affect flotation recovery and grades. Gangue minerals, particularly Mg-bearing minerals introduced by waste rock dilution, float into the concentrate because of their comparable surface characteristics to spodumene.

Key words: *Dilution, spodumene, flotation, waste rock, Mg-bearing minerals*

1. INTRODUCTION

In the modern mining landscape, the focus has shifted toward Critical Raw Materials (CRMs) elements like lithium, cobalt, and rare earth elements that are essential for the green energy transition. However, extracting these materials is rarely straightforward. One of the most significant technical and economic hurdles in mineral processing is waste rock dilution (Santhiya and Ting, 2005). Dilution affects the plant design and economics of an operation.
Waste rock dilution can be defined as the contamination of the ore with sterile material (low grade, below the cut-off grade) that has not been separated from the ore during the ore extraction, and then it is sent into the beneficiation process.

Waste rocks contain gangue minerals outside of the actual planned ore body, which can affect the mineral separation process in several negative ways (plant design, separation process and economics of an operation).

1.1.Understanding Waste Rock Dilution

Dilution occurs when non-ore material (waste rock) is inadvertently extracted alongside the valuable ore during the mining process. This effectively "waters down" the grade of the material sent to the processing plant (Mining Doc, 2025).
There are two primary types of dilution, as it is shown in Figure 1 (Ebrahimi, 2013):

Planned (Internal dilution): Contamination from low-grade material located within the designated ore body that is impossible to separate during blasting

Unplanned (External dilution): Material from the hanging wall or footwall that falls into the ore stream during excavation. Contamination from barren rock outside the ore block, often due to over-breaking or sloughing of walls.

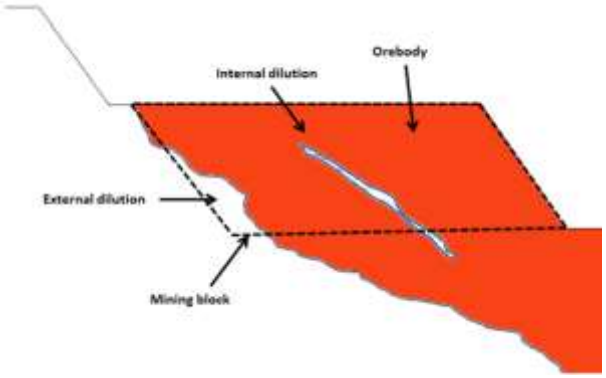

Figure 1. Different types of dilution (Ebrahimi, 2013)

The eq. 1 to 6 show the planned, unplanned, and total dilution, demonstrating that dilution is the ratio of sterile material to the amount of mineral fed to the plant.

$$Planned\ dilution\ (\%) = \frac{Planned\ Waste, Wp}{Mining\ resserves\ , Tm} x100 \quad eq.1$$

$$Unplanned\ dilution\ (\%) = \frac{Unplanned\ Waste, Wu}{Run\ of\ mine\ ore, Tf} x100 \quad eq.2$$

$$Final\ dilution\ (\%) = \frac{Total\ Waste, Tw}{Ore + waste\ tons} x100 \quad eq.3$$

$$Final\ dilution\ (\%) = \frac{Wp + Wu}{Tg + Wp + Wu} x100 \quad eq.4$$

$$Final\ dilution\ (\%) = \frac{Tw}{Tf} x100 \quad eq.5$$

$$Final\ dilution\ (\%) = \frac{Tw}{To} x100 \quad eq.6$$

Where:
T_w is the amount of the total waste rock
T_f is run of mine or the amount of mill feed
T_o is the amount of ore
W_p is the planned waste
W_u is the unplanned waste

Figure 2 shows various types of waste, reserves, and dilution for a simple stope:

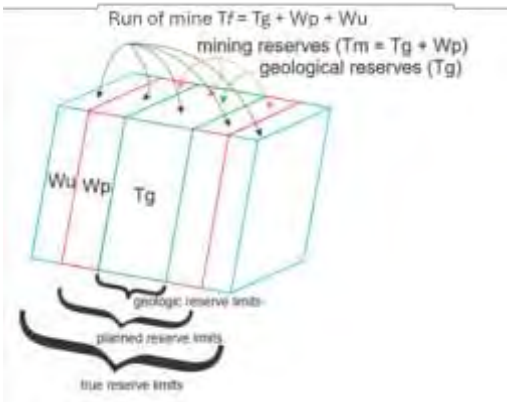

Figure 2. Planned and unplanned dilution (DeSouza, 2010) cited by (911Metallurgist, n.d.)

1.2.Consequences for CRM Recovery

The recovery of CRMs is particularly sensitive to dilution because these materials often exist in much lower concentrations than traditional base metals like iron or copper (Nordic Council of Ministers, n.d.).

1.2.1. Reduced feed grade and plant efficiency

The primary effect of dilution is the lowering of the feed grade. For example, if a lithium deposit is diluted by 20% with barren waste rock, the processing plant must handle 20% more mass to retrieve the same amount of lithium. This forces the plant to operate beyond its design capacity or slows down the overall throughput.

1.2.2. Increased reagent consumption

CRM recovery often relies on complex chemical processes, such as froth flotation or hydrometallurgical leaching. Waste rock often contains "gangue" minerals that react with expensive reagents (Kitchener, 1984; Okon Recycling, n.d.; Yang and Wang, 2024).

- **Acid Consumption:** In cobalt or nickel leaching, carbonate-rich waste rock can neutralize the acid, significantly increasing costs.
-
- **Froth Interference:** Silicates in waste rock can interfere with the chemistry of flotation cells, reducing the selectivity of the CRM.
  - For example: Gangue can compete for reagent absorption, leading to increased reagent consumption. This, in turn, causes gangue activation and flotation, contaminating the concentrate, resulting in poor selectivity and a decline in the final concentrate grade.

1.3. Complexity in Mineralogy

Dilution doesn't just add mass; it adds complexity. Waste rock may introduce "penalty elements"—impurities that are difficult to separate from the CRM. For example, in Rare Earth Element (REE) processing, the introduction of excess calcium or phosphorus from surrounding rock can complicate the separation stages, leading to lower final product purity.

2.THE ECONOMIC RIPPLE EFFECT

The "hidden cost" of dilution is often the most damaging. It creates a feedback loop that affects the entire mining value chain:

Table 1. The hidden cost of dilution

Factor	Impact of High Dilution
Energy	Higher energy required for crushing and grinding "dead" weight.
Tailings	Increased volume of waste material requiring storage and environmental management.
Recovery Rate	Lower grades often lead to lower recovery percentages (R), as defined by: $$R = \frac{c(f-t)}{f(c-t)}\ x\ 100$$ where f is feed grade, c is concentrate grade, and t is tailings grade. As f drops due to dilution, R typically follows.

3. MITIGATION STRATEGIES

To mitigate these effects, plants often require increased cleaning stages, adjusted reagents, and improved ore sorting to manage the increased volume of waste material entering the circuit.

To maximize CRM recovery, mining operations are increasingly turning to advanced technology:

- **Sensor-Based Ore Sorting (SBS):** Using X-ray transmission or infrared sensors to identify and eject waste rock at coarse size before it enters the energy-intensive grinding circuit.
-
- **Precision Blasting:** Using GPS-guided drilling and electronic detonators to minimize "overbreak" into waste zones
- .
- **Real-time Grade Control:** Utilizing automated scanners on conveyor belts to monitor the CRM grade in real-time.
-
- **Magnetic Separation:** Implementing a wet low-intensity magnetic separation (LIMS) stage before flotation can remove ferromagnetic minerals introduced by waste rock dilution.
-
- **Selective Modifiers:** Adding specific chemicals like $Na2CO_3$ or starch can help depress unwanted gangue minerals and improve the selectivity of the flotation process.
-
- **Cleaning Stages:** Increasing the number of cleaning flotation stages can help achieve target grades despite high dilution (Kinnunen et al., 2021; Tanhua et al., 2020).

4. CASE STUDY OF DILUTION EFFECT ON SPODUMENE FLOTATION

Spodumene is a type of monoclinic pyroxene mineral with a single-chain structure and chemical formula of $LiAlSi_2O_6$ that is most found in granitic pegmatite rocks (Moon, K. S., Fuerstenau 2003).

Typical gangue minerals of spodumene and lithium ores are oxides and silicates, and they are the most diverse group of minerals when it comes to flotation.

Laboratory flotation tests were conducted with modifications to the standard procedure and new conditions in the feed. A blended sample was prepared mixing a regular crushed Finico ore (-3.35 mm) and 12 % of waste rock crushed to -3.35 mm, the sample was homogenized and the blend was divided into 1 kg (bags) for flotation tests.

Typical minerals associated with spodumene (Finico ore): plagioclase ($NaAlSi_3O_8$ – $CaAl_2Si_2O_8$), quartz (SiO_2), microcline ($KAlSi_3O_8$), different kinds of mica like biotite ($K(Mg,Fe)_3(AlSi_3O_{10})(F,OH)_2$) and muscovite ($KAl_2(AlSi_3O_{10})(F,OH)_2$).

Mineral liberation analysis (MLA) and Table 2 showed that biotite contains most of the Mg (80-90 %), other minerals are apatite, amphiboles (mainly Edenite and Hornblende), and in less extent chlorite and clays. Biotite and amphiboles end up in the final concentrate mostly fully liberated, while apatite is mostly coarse mixed grains.

Table 2. Calculated biotite compositions (EPMA and EMC).

Mineral	Si%	Ti%	Al%	Fe%	Mn%	Mg%	Ca %	Na%	K %	O %
Biotite	17.5	1.32	10.10	13.64	0,21	6.92	0.01	0.01	7.32	42.99

Mg, Al, K, and Si are the major elements in the composition of Biotite. Mg content is 6.92% and is assumed to have a negative effect on the flotation of Spodumene.

Table 3 shows that the waste rock contains 24.20% of biotite, and the regular ore only has 0.05%. Additional gangue minerals are introduced in higher percentages than in the average ore (chlorite, clays, and 1.99% amphiboles).Different types of mica, such as biotite ($K(Mg,Fe)_3(AlSi_3O_{10})(F,OH)_2$) and muscovite, are also present.

Table 3. Qualitative and quantitative mineralogy of Finico ore (ROM) and waste rock determined by MLA

Mineral	Average ore Wt%	Waste rock Wt%
Quartz	27.21	23.53
Plagioclase	33.37	30.03
Microcline	16.76	1.56
Spodumene	13.19	0.02
Cookeite	0.28	0.02
Muscovite	7.61	7.69
Biotite	0.05	24.20
Chlorite	0.08	2.05
Clay	0.26	1.21
Montmorillonite	0.02	0.55
Garnet	0.31	0.01
Tourmaline	0.21	2.52
Epidote	0.00	1.76
Titanite	0.00	0.45
Forsterite	0.00	0.07
Amphibole	0.00	1.99
Zircon	0.00	0.01
Apatite	0.21	0.65
Sicklerite	0.19	0.00
Calcite	0.03	0.46
Pyrrhotite	0.00	0.68
Pyrite	0.03	0.04
Arsenopyrite	0.01	0.09
Process Metal	0.04	0.02
Unknown	0.13	0.36
Total	100.00	100.00
Nr of measured particles	20258	20186

The target grade and recovery of Li_2O for the selected ore were established at 4.5 % and 84.18 % (standard test).

5.RESULTS AND DISCUSSION

Differently to the standard test with five cleaner stages, when the ore was diluted with waste rock for achieving comparable grade and recovery, seven cleaning stages were required.

Mg-bearing minerals float into the concentrate because of similar surface properties with spodumene.

Mg-distribution (Figure 3) in the samples was determined based on the MLA results. The Mg-content of amphiboles, chlorite and clay minerals was determined from semi-quantitative EDS - spectrums gained from the SEM analyses. Other minerals were determined by stoichiometric Mg-content, these results could present some inaccuracy. Amphiboles could not be determined with certainty but those seem to be Edenite and Hornblende

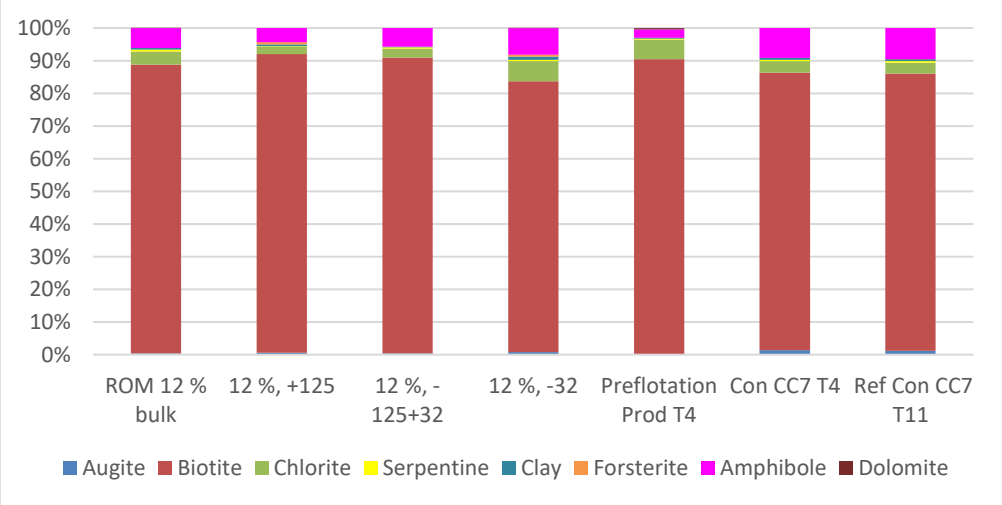

Figure 3. Mg distribution in the tested samples

Introducing minerals with similar surface properties to the target mineral, such as **biotite** and **amphiboles** in spodumene flotation, leads to these gangue minerals floating into the final concentrate, lowering its purity.

The flotation test using Na_2CO_3 as a modifier (Figure 4) showed the most promising Li_2O grade recovery results, achieving the target grade of 4.5% Li_2O with 85.29% recovery as early as cleaning step 5 and ending with a final concentrate of 4.9% grade and 82.13% recovery. Flotation test using starch as a modifier) with a final concentrate of 4.73% grade and 83.38% recovery.

The association between lithium and magnesium oxide recovery and spodumene and biotite recovery (Figures 4) was evaluated in each test to see if any of these results showed similarities and/or selectivity between spodumene and biotite.
All Li_2O and MgO recoveries showed a decreasing trend, with MgO recovery decreasing at a slightly faster rate than Li_2O. However, no significant selectivity was observed in any of the tests.

The calculated spodumene and biotite recoveries varied somewhat more depending on the test. Overall, spodumene recoveries followed Li_2O recoveries. Changes in biotite recovery appear to follow spodumene on average in cleaner concentrates 2 and 5 (CC2-CC5), with a slight increase in selectivity in CC6-CC7 (tests 4 and 6). Negative selectivity is observed from coarser flotation down to CC1, and spodumene recovery decreases faster than biotite recovery. Alternatively, biotite recovery may increase compared to spodumene recovery.

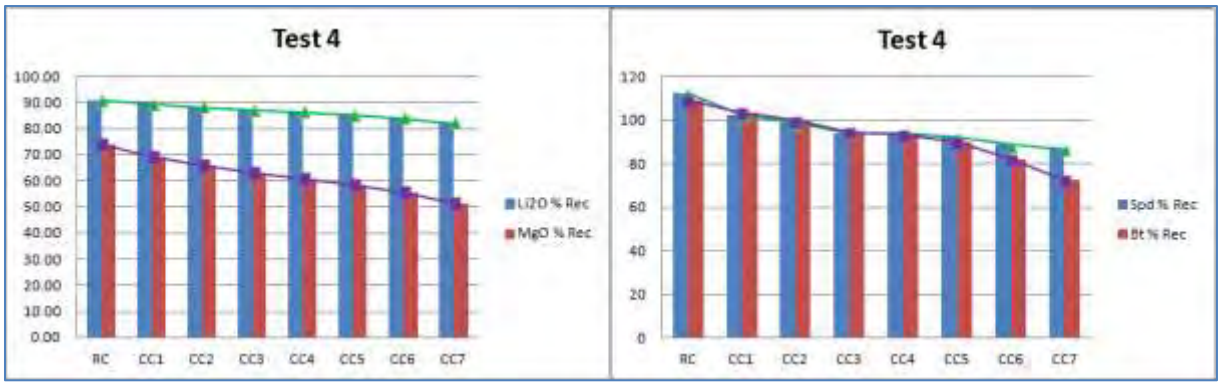

Figure 4. Flotation test 4 with Na_2CO_3 modifier

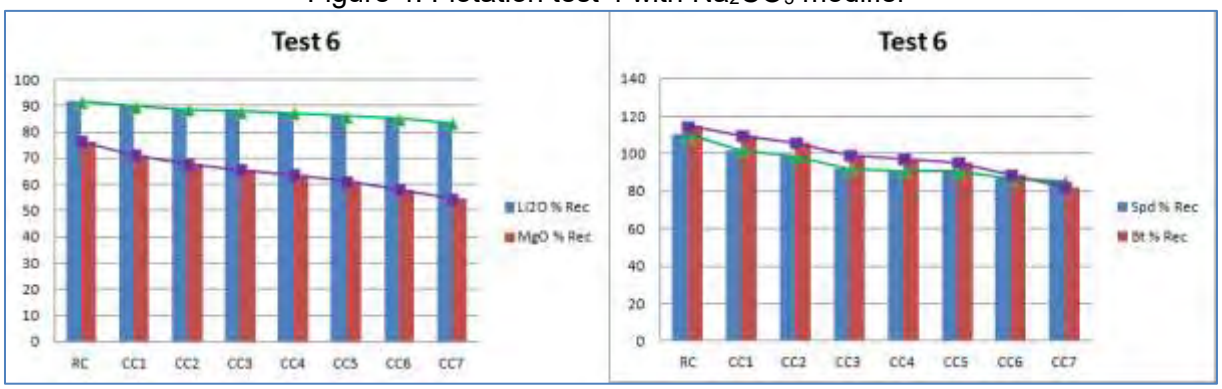

Figure 5. Flotation test 6 with Starch modifier

6.CONCLUSION

Waste rock dilution is more than just a logistical nuisance; it is a direct threat to the economic viability of CRM projects. As we pursue a more sustainable future, minimizing dilution will be key to ensuring that we can extract the materials we need without unnecessary energy waste or environmental impact.

In the case study dilution introduces unwanted minerals specifically Mg-bearing minerals like biotite and amphiboles in spodumene ores that increase slurry viscosity, interfere with reagent selectivity, and lower the grade of final concentrates

- The flotation procedure showed suboptimal results when waste rock dilution is introduced to the system.

- MLA results show that biotite contains a high percentage of Mg between the minerals (80-90 %). Also, Mg-bearing minerals are amphiboles.

- Mineral containing Mg, like biotite and amphiboles, float in the final concentrate because of the same kind of Al-O sites on the mineral surfaces. Al-O sites act as active sites for collector attachment and float in the same way as spodumene.

- Biotite is one of the most unwanted impurities to end up in the final concentrate. Apatite contains most of the phosphorus in the deposit, and is also one of the more deleterious impurities to end up in the final concentrate. Apatite is readily digestible in the same conditions as beta spodumene and is the main cause of P-impurities in the final lithium carbonate product.

- In the downstream metallurgical process, biotite can cause partial melting of the concentrate during high temperature treatment (for converting alpha spodumene to beta spodumene). The formation of the partial melt can result in agglomeration during the lithium digestion method, reducing lithium recovery and making the process more complex to operate.

ACKNOWLEDGMENT

Recognition to the consortium of EMJM-PROMISE and organizers of the XX Balkan Mineral Processing Congress.

REFERENCES

911Metallurgist, (n.d.) “Ore dilution & recovery in mining”, Available at: https://www.911metallurgist.com/blog/ore-dilution-recovery-mining/

Ebrahimi, A., (2013) “The importance of dilution factor for open pit mining projects”.

Kinnunen, P., Obenaus-Emler, R., Raatikainen, J., Guignot, S., Guimerà, J., Ciroth, A., Heiskanen, K., (2021) “Review of closed water loops with ore sorting and tailings valorisation for a more sustainable mining industry”, Journal of Cleaner Production, 278, 123237.

Kitchener, J. A., (1984) “The froth flotation process: Past, present and future – in brief”, in: Ives, K. J. (Ed.), The Scientific Basis of Flotation, NATO Advanced Study Institute, Cambridge, 3–51.

Mining Doc, (2025) “What is mining dilution?”, Available at: https://www.miningdoc.tech/question/what-is-mining-dilution/

Nordic Council of Ministers, (n.d.) “Evaluation of potential measures to reach the recycling benchmarks of the Critical Raw Materials Act”, Available at: https://pub.norden.org/temanord2025-505/2-waste-streams-with-crm-recycling-potential.html

Okon Recycling, (n.d.) “Froth flotation: Process, components, and key operational considerations in mineral separation”, Available at: https://www.okonrecycling.com/industrial-scrap-metal-recycling/copper-recovery/froth-flotation-work/

Santhiya, D., Ting, Y.-P., (2005) “Bioleaching of spent refinery processing catalyst using Aspergillus niger with high-yield oxalic acid”, Journal of Biotechnology, 116, 171–184.

Tanhua, A., Sinche-Gonzalez, M., Kalapudas, R., Tanskanen, P., Lamberg, P., (2020) “Effect of waste rock dilution on spodumene flotation”, Minerals Engineering, 150, 106282.

Yang, A., Wang, L., (2024) “A fundamental study of flotation separation of mineral particles using ultrasound-induced bubbles”, Minerals Engineering, 207, 108573.

COAL PROCESSING, AGGLOMERATION AND BRIQUETTING

EVALUATION OF THE WASHABILITY CHARACTERISTICS OF ZONGULDAK COAL SEAMS: THE CASE OF ÇATALAĞZI COAL PREPARATION PLANT

Eljona MUNISHI[1], Valona PROKSHi[1], Albina RAMA[1], Elona IDRIZI[1], Omer GUCATI[1], Leutrim BOGIQI[1], Berat SINANI[2], Mehmet BILEN[3,*]

[1]Faculty of Geosciences, University "Isa Boletini" 40 000, Mitrovicë, Kosovë
[2]Department of Petrology, Mineralogy and Geochemistry, Faculty of Natural and Technical Science, University "Goce Delchev", Shtip, 2000, North Macedonia
[3]Zonguldak Bülent Ecevit University, Engineering Faculty, Department of Mining Engineering, İncivez, 67100, Zonguldak, Turkiye
**Corresponding author: mehmetubilen@yandex.com*

A B S T R A C T

This study evaluates the washability characteristics of coal seams from the Kilimli and Gelik regions of the Karadon Hard Coal Enterprise, operated by the Turkish Hard Coal Authority (TTK), and to assess their beneficiation potential for efficient use in coal preparation processes. Laboratory-scale float-sink tests were conducted on run-of-mine coals supplied to the Çatalağzı Coal Preparation Plant and on seam samples collected from the Kilimli (-460/-360, -360/-260) and Gelik (-360/-260, -260/-160) levels. Analyses performed on different size fractions determined ash content distributions by density and overall washability performance. Results showed significant variability among seams. The Kilimli Taban Acılık seam reduced ash from about 34–36% to below 10% at 1.60 g/cm³ with over 60% clean coal yield, while the Gelik Sulu seam achieved over 65% clean coal with ash under 9%. In contrast, seams such as Kilimli Unudulmuş and Nasifoğlu showed poor separation due to high middling ratios and low density contrast. The findings demonstrate that certain seams are well-suited for gravity-based beneficiation, while others require alternative processing. Image analysis results for the Çatalağzı Coal Preparation Plant samples indicate relatively low brightness values (V ≈ 39–58) and limited saturation variability (S ≈ 3–22), supporting the moderate-to-good washability characteristics of Zonguldak hard coals. These findings are consistent with stable ash–yield behavior and relatively low near-gravity material influence, confirming favorable separation performance under appropriate operating conditions. This study contributes to mineral processing by providing seam-specific data to optimize plant feed strategies, improve process design, and enhance resource utilization efficiency.

Key words: *Coal washability, sink–float analysis, coal preparation plant, Zonguldak, image analysis, Çatalağzı coal preparation plant*

1. INTRODUCTION

Coal washability constitutes one of the most critical parameters governing the technical feasibility, economic performance, and operational stability of coal preparation plants. Fundamentally, washability reflects the density-based distribution of organic matter and mineral impurities within coal particles and is strongly influenced by coal rank, maceral composition, mineral matter association, and the degree of liberation across particle size classes. Consequently, accurate washability characterization forms the backbone of separation strategy selection, cut-density optimization, and overall process design in coal cleaning operations.

Traditionally, coal washability assessment has relied on standardized laboratory-scale sink–float (float–sink) tests combined with size analysis to determine theoretical yield–ash relationships and separation efficiencies. Despite their widespread acceptance, research specifically addressing the prediction of floating and sinking fractions in raw coal remains relatively limited compared with studies devoted to washability curve modeling. Moreover, most existing online prediction approaches are largely based on historical float–sink data and

statistical techniques, yet their predictive capability has frequently been reported as inadequate. In addition, methods that estimate float and sink ratios solely from raw coal ash content often exhibit substantial deviations between predicted and actual values, highlighting the need for more robust and responsive modeling frameworks (Wang et al., 2012).

Although conventional sink–float methods remain indispensable due to their direct physical basis and regulatory acceptance, their practical application in modern coal preparation plants is increasingly constrained by labor-intensive procedures, extended turnaround times, and the mismatch between controlled laboratory conditions and continuously evolving industrial feed characteristics. As a result, washability information derived exclusively from laboratory testing may not fully capture the dynamic behavior of full-scale separation systems operating under variable process conditions, thereby limiting its effectiveness for real-time decision-making and process optimization.

To address these limitations, numerous quantitative indices have been proposed to describe washability behavior in a more systematic and comparable manner. These indices typically integrate density distribution characteristics, near-gravity material proportions, and separation difficulty parameters derived from float–sink data. Recent research has demonstrated that washability cannot be sufficiently described using a single indicator and that multi-criteria evaluation approaches are required to capture the complexity of coal separation behavior. In this context, Sokolović et al. (2025) emphasized the importance of evaluating multiple washability indices simultaneously and demonstrated that their relative significance varies depending on coal rank, separation objective, and decision criteria. Their findings underline the necessity of decision-oriented frameworks that move beyond isolated indices toward integrated assessment strategies.

Recent advancements in coal preparation research have increasingly emphasized the development of rapid and intelligent characterization techniques to support real-time or near-real-time decision-making. Among these approaches, machine vision has emerged as an effective non-destructive tool for analyzing coal particle properties based on geometric, textural, and color-related features. Early studies primarily utilized monocular vision systems, where two-dimensional (2D) image data were employed to estimate particle geometry and indirectly derive volumetric characteristics. For example, Zhang et al. (2012) applied multiple linear regression to predict particle thickness from 2D geometric parameters, while Wang and Huang (2019) introduced volume estimation methods based on gray-weighted super-pixels and equivalent ellipse representations. These approaches were further extended by Huang et al. (2023), who transformed 2D image data into approximate three-dimensional (3D) representations.

Despite these developments, monocular systems inherently lack direct depth information, resulting in uncertainties in volumetric estimation and limiting their applicability for density-based washability prediction. To overcome this limitation, binocular vision systems have been increasingly investigated, as they enable direct depth acquisition through stereo reconstruction. Such systems have been successfully applied in coal-related studies for underground distance measurement and spatial positioning (Zhang et al., 2024; Cheng et al., 2024), demonstrating the importance of depth information for accurate 3D characterization, although their direct application to washability modeling remains limited.

More recently, binocular vision techniques have been extended to coal volume estimation in stockpile and conveyor environments, often combined with deep learning and sensor fusion methods (Mo et al., 2024; Li et al., 2024; Wen et al., 2024). However, challenges such as particle overlap, stacking effects, and the limited visibility of lower particle layers restrict their effectiveness at the individual particle scale, thereby limiting their direct applicability in density-based separation analysis.

Beyond geometric reconstruction, identifying representative feature parameters and developing robust predictive models remain key challenges in intelligent coal characterization. Zhang et al. (2014) extracted extensive color and texture features and optimized feature selection using genetic algorithms, while Zhang et al. (2022) integrated monocular and binocular features through correlation-based methods. In parallel, machine learning-based approaches have been widely explored for density prediction, with Zhang and Yang (2015, 2016) reporting classification accuracies exceeding 80% using support vector machine (SVM) models. Nevertheless, these approaches typically require large datasets and extensive calibration, which may limit their generalizability and industrial applicability.

To improve model robustness and interpretability, hybrid optimization-based frameworks have also been proposed. Qi and Dou (2022) demonstrated that image-derived density features could be extended to sulfur content prediction by integrating grasshopper optimization algorithms with GWO-SVM (Mirjalili et al., 2014), while Zhang et al. (2024) applied XGBoost combined with SHAP-based feature importance analysis to identify optimal descriptors. Despite these advancements, most existing studies remain limited to laboratory-scale datasets or specific coal types and rarely incorporate long-term industrial plant data, which restricts their direct application in real coal preparation systems (Chen et al., 2025).

In contrast to these data-intensive and model-driven approaches, the present study focuses on a conventional yet robust evaluation framework based on washability characteristics and actual plant performance data. By integrating laboratory-derived washability curves with operational results from the coal preparation plant, this study aims to provide a realistic assessment of separation efficiency and process performance under industrial conditions, without relying on complex modeling or image-based prediction techniques.

In this context, the present study focuses on the evaluation of washability characteristics of coals processed at the Çatalağzı Coal Preparation Plant by integrating conventional sink–float analysis with image-based color characterization. Unlike model-driven or data-intensive approaches, the study emphasizes direct experimental observations derived from both laboratory tests and image analysis of representative samples. A total of 10 coal samples from the Çatalağzı plant were analyzed in detail to investigate their RGB and HSV properties alongside washability behavior. By combining density-based separation data with visual characteristics of coal particles, this study aims to provide a more comprehensive understanding of coal heterogeneity and its influence on beneficiation performance under real plant conditions.

2. MATERIAL AND METHOD

2.1. Study Area and Sampling Strategy

A total of 10 samples were collected from the coal preparation plants in Catalagzı. Samples collected from “Catalagzı”, correspond to hardcoal samples obtained from Zonguldak hardcoal basin. Collected coal samples have coarse size distribution in the beginning and they were about 20 kg initially. The representative samples were taken from the collected samples after size reduction was realized.

2.1.1. Catalagzı coal preparation plant

The Çatalağzı Coal Preparation Plant is one of the key coal processing facilities serving the Zonguldak Coal Basin, a region with a long-standing history of underground coal mining in Türkiye. The plant is designed to treat run-of-mine coal extracted from nearby production areas and to upgrade its quality to meet the requirements of thermal power generation and industrial consumers. Given the heterogeneous nature of the feed coal, characterized by variable ash

content and mineral matter distribution, the facility plays a crucial role in improving product consistency and overall coal utilization efficiency.

The preparation plant operates through a combination of size classification, gravity-based separation, and dewatering circuits, enabling the effective removal of high-density mineral impurities from the coal matrix. Coarse and fine coal fractions are treated separately using appropriate separation technologies to optimize recovery and product quality. The process flow is structured to maximize combustible recovery while maintaining target ash specifications, thereby supporting stable plant performance under fluctuating feed conditions.

Beyond its technical function, the Çatalağzı Coal Preparation Plant holds strategic importance for regional energy supply and operational sustainability. By enhancing coal quality prior to combustion, the plant contributes to improved boiler performance, reduced ash disposal requirements, and lower environmental impacts associated with coal utilization.

2.2. Image Analysis

Prior to image analysis, the coal samples were dried in an oven at 105 °C and subsequently ground to meet the preparation requirements of the procedure. To ensure a well-defined and uniform particle size distribution, the samples were sieved to obtain a narrow fraction of −106 + 90 µm, thereby improving homogeneity for image analysis. The prepared samples were then transferred into aluminum containers, as illustrated in Figure 1, with approximately 15 g of material placed in each container.

Figure 1. Sample preparation, imaging setup, and image analysis workflow, including sample placement and leveling, microscope-based image acquisition under controlled conditions, and representative output of RGB and HSV color analysis (adapted from Cevik, 2019)

Subsequently, the sample containers were placed beneath a microscope-mounted camera system (Figure 1). To ensure consistent positioning for all samples, a custom-designed sample holder was used. In addition, a closed imaging chamber was constructed to provide a controlled environment by eliminating external light interference. Once the samples were placed inside the chamber, only the microscope's own illumination was used during image acquisition. Following the completion of all preparation steps, images of the samples were captured under identical and controlled conditions. The experimental setup was carefully designed to eliminate any external environmental influences, ensuring that variations in the

results were solely attributable to differences in sample characteristics. For image processing, an open-source online tool known as Image Color Summarizer, developed by Martin Krzywinski, was utilized. This tool analyzes the acquired images and generates output data in both RGB and HSV color spaces, including minimum, maximum, and average values for each parameter (Figure 1).

3. RESULTS AND DISCUSSION

3.1. Çatalağzı Coal Preparation Plant - Coal Washability Results

The Zonguldak Coal Basin represents the most significant hard coal production region in Türkiye and has played a strategic role for decades in supplying coal for both industrial applications and energy generation. In this context, a comprehensive understanding of the washability characteristics of coals from this basin is of critical importance, not only for improving product quality but also for optimizing the operational efficiency and separation performance of coal preparation plants.

The present study focuses on the washability behavior of run-of-mine (ROM) coal processed at the Çatalağzı Coal Preparation Plant, which is widely regarded as representative of the Zonguldak Basin. The findings are evaluated in conjunction with plant performance indicators to provide a more integrated assessment of coal cleaning efficiency under industrial operating conditions. The Çatalağzı Coal Preparation Plant is a key facility in the region, designed to upgrade ROM coal extracted from underground mines to meet the quality requirements of thermal power plants and industrial users. Due to the inherently heterogeneous nature of the feed coal, characterized by variable ash content, particle size distribution, and mineral matter association, the plant plays a crucial role in ensuring product consistency and enhancing overall coal utilization efficiency.

The plant operates through a combination of size classification, density-based separation, and dewatering processes. Coarse and fine coal fractions are treated separately using appropriate gravity separation techniques, allowing for the efficient removal of high-density mineral impurities. The process is designed to maximize combustible recovery while maintaining target ash levels, thereby ensuring stable and efficient plant operation despite fluctuations in feed characteristics. In addition to its technical role, the facility has strategic importance in supporting regional energy supply, reducing ash-related handling and disposal requirements, and minimizing environmental impacts associated with coal combustion.

Coals processed at the Çatalağzı plant are generally characterized by medium to high ash contents and exhibit washability properties suitable for gravity-based separation. However, due to the complex mineralogical structure and varying degrees of liberation, the washability behavior differs significantly across density fractions. To quantify this behavior, sink–float (washability) analyses were conducted under controlled density conditions. These tests enabled the determination of ash distribution, cumulative float and sink yields, and theoretical separation limits, providing a robust basis for evaluating coal cleaning potential.

The washability curves presented in Figure 2 clearly illustrate the relationship between ash content, yield, and separation density. At lower density fractions, the cumulative float curve indicates relatively high yields associated with low ash content, reflecting the effective recovery of clean coal. This suggests that a significant portion of the combustible material is well liberated and can be efficiently separated at lower cut densities. As the separation density increases, a noticeable rise in ash content is observed, as reflected by the fractional ash curve, indicating the increasing presence of mineral matter in the product.

The washability results further indicate that Çatalağzı coals exhibit better cleaning performance in the fine and intermediate particle size fractions, where the degree of liberation between coal and

mineral matter is relatively high. Improved liberation in these size ranges enhances the efficiency of density-based separation and contributes to higher combustible recovery at acceptable ash levels. In contrast, very fine fractions tend to show a slight reduction in separation efficiency due to the presence of clay minerals and ultra-fine inorganic matter adhering to coal particle surfaces. This phenomenon highlights the importance of appropriate fine coal handling strategies, including effective desliming, flocculation, and dewatering operations within the plant flowsheet.

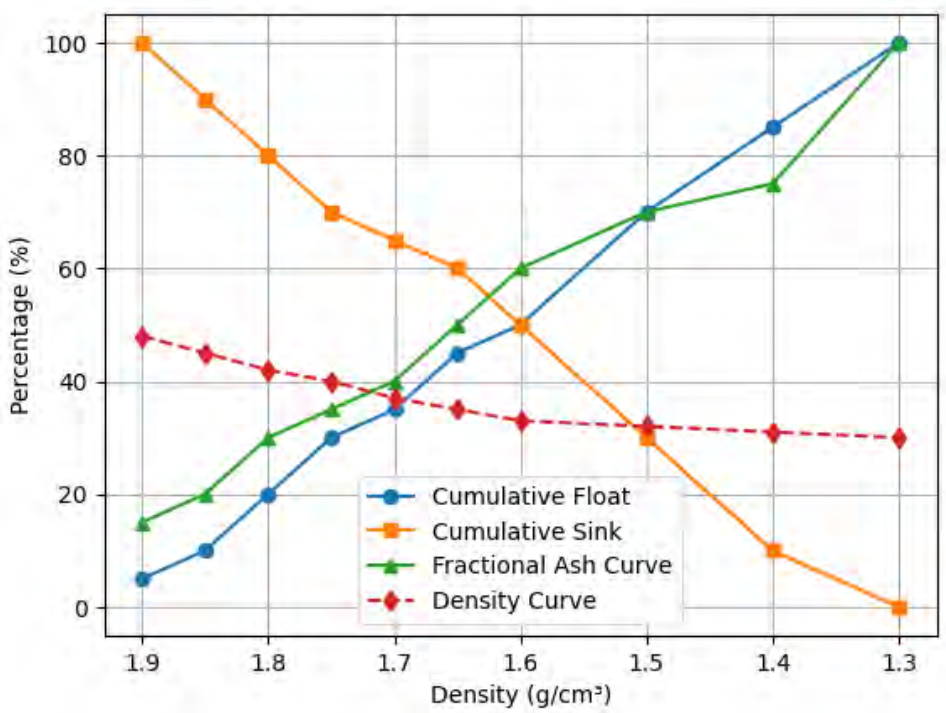

Figure 2. Washability curves of the Çatalağzı feed coal, including cumulative float, cumulative sink, fractional ash, and density distribution as a function of density (g/cm³)

The distribution of ash content across different density fractions is presented in Figure 1. A pronounced and systematic increase in ash content is observed particularly within the 1.40–1.60 g/cm³ density interval, identifying this range as a critical separation zone for Çatalağzı coals. The steep ash gradient within this density window clearly indicates the presence of a significant proportion of near-density (near-gravity) material. This fraction is well known to limit the efficiency of density-based separation processes, as small variations in cut density can lead to substantial changes in both product quality and recovery. Therefore, this behavior highlights the sensitivity of the separation process and underscores the necessity for precise control of operating parameters in industrial applications.

The shape and slope of the ash distribution curve further suggest that while low-density fractions consist predominantly of well-liberated, low-ash coal particles, the intermediate density range contains a mixture of partially liberated coal and mineral matter. This heterogeneity significantly increases the difficulty of achieving sharp separation and results in increased misplacement of both combustible material and high-ash particles. In practical terms, this implies that maintaining a stable cut density in this critical interval is essential for minimizing efficiency losses and ensuring consistent product specifications.

The performance of the Çatalağzı Coal Preparation Plant was evaluated by comparing theoretical washability data obtained from laboratory-scale sink–float tests with actual plant operating results. This comparison provides a clear assessment of how closely the plant approaches its theoretical separation limits under industrial conditions. The results show strong agreement at lower

separation densities, indicating high separation efficiency when treating well-liberated coal fractions.

However, within the 1.40–1.60 g/cm³ density range, a sharp increase in ash content is observed. This behavior reflects a high concentration of near-gravity material (NGM) and demonstrates the strong sensitivity of separation efficiency to small variations in cut density. As widely reported in the literature, such intermediate density zones increase the likelihood of misplacement and represent a key limitation to separation performance. Sokolović et al. (2025) highlighted that NGM is a critical factor controlling separation difficulty, particularly in hard coals, where minor operational deviations can significantly affect product quality. The present findings support this interpretation and emphasize the need for dynamic optimization of cut density under varying operating conditions.

Despite these constraints, the overall performance of the Çatalağzı Coal Preparation Plant can be considered satisfactory, given the complex geological structure and variable feed characteristics of the Zonguldak Coal Basin. Although perfect separation is limited by the presence of near-density material, the plant operates within acceptable efficiency ranges and maintains effective coal upgrading performance.

From a washability perspective, Zonguldak hard coals exhibit favorable separation characteristics, with high combustible recovery and relatively low ash content achieved at lower densities. This indicates effective mineral matter liberation and aligns with classical washability theory, where higher-rank coals show clearer density differentiation and lower NGM proportions.

Deviations between theoretical and actual performance become more pronounced at intermediate densities, where combustible losses and ash misplacement increase. These differences are consistent with previous studies and are generally attributed to operational factors such as feed variability, incomplete liberation, and equipment limitations. Wang et al. (2012) similarly noted that laboratory-based washability models may overestimate plant performance due to their inability to reflect real-time process conditions. Therefore, incorporating plant data into the evaluation framework is essential to ensure realistic and applicable performance assessments.

Size-dependent analysis further shows that separation efficiency improves in intermediate size fractions, where coal–mineral liberation is more favorable. In contrast, fine fractions exhibit reduced efficiency due to slime coating and clay-related effects, which hinder gravity-based separation. These findings are consistent with previous studies and highlight the importance of appropriate fine coal treatment strategies.

3.2. Image Analysis Results

In this study, RGB and HSV color space parameters were analyzed to characterize the visual properties of coal samples through image-based evaluation. The analysis focuses on identifying differences in color intensity and distribution across the samples. The image analysis results obtained from 10 hard coal samples collected from the Çatalağzı Coal Preparation Plant are presented in Table 1. The findings indicate that RGB values are generally distributed within mid-range intensity levels, whereas HSV parameters exhibit a wider variability, particularly in saturation (S) and brightness (V). This variability reflects the heterogeneous nature of Zonguldak hard coals, which is associated with differences in the distribution of organic matter and mineral content. In particular, samples with lower brightness and saturation values may correspond to higher mineral matter content, while higher V values are likely indicative of regions richer in organic material.

Table 1. Image analysis results for Çatalağzı hard coal samples (average RGB and HSV values)

Sample No	Average R	Average G	Average B	Average H	Average S	Average V	Image-Based Washability Indicator
1	124	123	123	345	3	49	Moderate–Good
2	130	136	148	222	12	58	Moderate
3	97	111	119	201	19	47	Difficult
4	104	112	115	193	10	45	Moderate–Difficult
5	95	98	100	201	5	39	Good
6	118	124	134	219	12	53	Moderate
7	105	122	133	204	22	52	Difficult
8	133	134	149	236	11	58	Moderate
9	124	123	123	345	3	49	Moderate–Good
10	130	136	148	222	12	58	Moderate

Overall, the results presented in Table 1 demonstrate a noticeable variation in both RGB and HSV parameters among the analyzed samples. While RGB values remain relatively clustered within a moderate intensity range, the broader spread observed in saturation (S) and brightness (V) suggests significant differences in surface composition and optical properties. Samples exhibiting lower V and S values tend to indicate darker and less reflective regions, which may be associated with higher mineral matter presence, whereas higher brightness values point to comparatively cleaner, organic-rich zones. This variation confirms that image-derived color parameters can effectively capture the inherent heterogeneity of Çatalağzı hard coal samples.

The observed variability in HSV parameters, particularly in brightness (V) and saturation (S), is consistent with previous studies emphasizing the capability of image-based methods to capture compositional differences in coal (Zhang et al., 2014; Zhang et al., 2022). While RGB values remain relatively stable, the wider spread in HSV parameters suggests that these descriptors are more sensitive to variations in mineral matter distribution and organic content, supporting their use in coal characterization.

The relationship between lower brightness values and increased mineral matter presence aligns with findings reported by Zhang and Yang (2015, 2016), who demonstrated that image-derived features can be effectively linked to density and ash-related properties. In this context, the darker and less saturated regions identified in the present study may correspond to higher-density fractions, which are typically associated with elevated ash content in washability analysis. Similarly, higher brightness values can be interpreted as indicative of organic-rich, low-density coal fractions that are preferentially recovered during separation.

Moreover, the heterogeneity reflected in the HSV distribution is consistent with the known complexity of coal structure and the presence of partially liberated particles, which play a critical role in separation efficiency (Sokolović et al., 2025). Such intermediate characteristics are particularly important in near-gravity material zones, where small variations in composition significantly affect washability behavior.

Overall, these findings support the growing body of research suggesting that image analysis can serve as a rapid and non-destructive complementary tool for coal quality assessment. Although it cannot replace conventional sink–float analysis, its integration into coal preparation

studies offers valuable potential for supporting real-time monitoring and improving process understanding under variable operating conditions (Wang et al., 2012).

4. CONCLUSIONS

This study provides a comprehensive evaluation of the washability characteristics of Zonguldak coals and the operational performance of the Çatalağzı Coal Preparation Plant by integrating laboratory-based sink–float data with actual plant performance. The findings demonstrate that the plant operates close to its theoretical separation limits, particularly at lower density ranges where coal–mineral liberation is more effective and separation efficiency is high.

A key finding of the study is the identification of the 1.40–1.60 g/cm³ density interval as a critical separation zone dominated by near-gravity material (NGM), which significantly limits separation efficiency and increases the sensitivity of the process to minor cut-density fluctuations, thereby elevating the risks of combustible loss and ash misplacement. Complementing conventional washability evaluation, the analysis of RGB and HSV color parameters reveals notable optical heterogeneity among coal samples, with variations in brightness and saturation reflecting differences in organic matter distribution and mineral content. These results indicate that image-based characterization can serve as a rapid, non-destructive supportive tool for coal quality assessment and process monitoring. The findings emphasize the necessity of integrating laboratory-derived theoretical data with long-term plant performance observations to achieve realistic evaluations of separation efficiency, while the discrepancies observed at intermediate densities highlight the importance of dynamic process optimization — particularly precise cut-density control and effective feed homogenization — for improving beneficiation performance in geologically complex coal basins such as Zonguldak.

Overall, this study contributes to the advancement of coal preparation practice by providing seam-representative washability insights and demonstrating the value of combining conventional experimental methods with emerging characterization approaches. The outcomes support more informed decision-making in plant feed management, process parameter optimization, and resource utilization strategies. Future research should focus on integrating real-time sensing technologies, intelligent control systems, and predictive modeling tools with conventional washability frameworks in order to enhance separation selectivity, reduce operational uncertainty, and promote more sustainable and efficient utilization of hard coal resources.

REFERENCES

Chen, C., Dou, D., Wei, J., (2025) “Predicting density and particle size distribution of coal based on binocular vision and gray wolf optimization-support vector machine”, Powder Technology, 121993.

Cheng, J. M., Jiang, H., Wang, D. J., Zheng, W., Shen, Y., Wu, M., (2024) “Analysis of position measurement accuracy of boom-type roadheader based on binocular vision”, IEEE Transactions on Instrumentation and Measurement, 73.

Çevik, R., (2019) “Kömür kalori değerlerinin renk uzayı (RGB ve HSV) ölçüm değerleriyle ilişkilendirilmesi”, Yüksek lisans tezi, Fen Bilimleri Enstitüsü, Zonguldak Bülent Ecevit Üniversitesi.

Huang, H. X., Dou, D. Y., Liu, G. Y., (2023) “Modeling of coal and gangue volume based on shape clustering and image analysis”, International Journal of Coal Preparation and Utilization, 43 (2) 329–345.

Li, J. W., Dou, D. Y., Huang, G. D., (2024) “Load prediction of bucket elevator for jigging sorting based on binocular vision and global filter networks”, International Journal of Coal Preparation and Utilization.

Mirjalili, S., Mirjalili, S. M., Lewis, A., (2014) “Grey wolf optimizer”, Advances in Engineering Software, 69 46–61.

Mo, J. T., Dou, D. Y., Chen, C. H., Liu, J., (2024) ”Research on alarm of coal content in gangue based on binocular vision and YOLACT segmentation network”, International Journal of Coal Preparation and Utilization.

Qi, Z. Y., Dou, D. Y., (2022) “Prediction of density and sulfur content level of high-sulfur coal based on image processing”, Powder Technology, 407 117669.

Sokolović, J., Stanujkić, D., Štirbanović, Z., Ilić, I., (2025) “Comparative analysis on washability indices of anthracite coal by using MCDM methods”, Physicochemical Problems of Mineral Processing, 61 (1).

Wang, G., Kuang, Y., Wang, Z., Ji, L., Wang, Y., (2012) “Rapid prediction of floating and sinking components of raw coal”, International Journal of Mining Science and Technology, 22 (5) 735-738.

Wen, L., Liang, B., Zhang, L. Y., HAo, H., Yang, Z., (2024) “Research on coal volume detection and energy-saving optimization intelligent control method of belt conveyor based on laser and binocular visual fusion”, IEEE Access, 12 75238–75248.

Zhang, C. L., Dou, D. Y., Sun, F. J., Huang, Z., (2022) “Detecting coal content in gangue via machine vision and genetic algorithm–backpropagation neural network”, Measurement, 201 111739.

Zhang, J. J., Li, J. C., Liu, H. T., Wang, H., yi, D., Li, Q., (2024). “Robust distance measurement using illumination map estimation and MAHNet in underground coal mines” Measurement Science and Technology, 35 (8).

Zhang, Z. L., Yang, J. G., (2016). “Narrow density fraction prediction of coarse coal by image analysis and MIV-SVM”, International Journal of Oil, Gas and Coal Technology, 11 (3) 279–289.

Zhang, Z. L., Yang, J. G., Ding, L. H., Zhao, Y., (2012) “An improved estimation of coal particle mass using image analysis”, Powder Technology, 229 178–184.

Zhang, Z. L., Yang, J. G., Wang, Y. L., Dou, D., Xia, W., (2014). “Ash content prediction of coarse coal by image analysis and GA-SVM”, Powder Technology, 268 429–435.

Zhang, Z., Yang, J., (2015) “The density fraction estimation of coarse coal by use of the kernel method and machine vision”, Energy Sources, Part A: Recovery, Utilization, and Environmental Effects, 37 (2) 181–191.

EXTRACTION OF TAR FROM LOW-RANK TURKISH COALS BY PYROLYSIS FOR CARBON FIBER PRODUCTION

Ensar Eray METE[1], Hüma VELIDEDEOĞLU[1], Kerim ÇELIK[1], Yunus Emre ÇAVDAR[1], Muhammed Fatih CAN[2],Alper SARIOĞLAN[3], Hasan Can OKUTAN[3], Feridun BOYLU[1], Mehmet Sabri ÇELİK[1,*]

[1]:Istanbul Technical University, Mineral Processing Engineering Dept., Istanbul, Türkiye
[2]:Afyon Kocatepe University, Mining Engineering Dept., Afyon, Türkiye
[3]:Istanbul Technical University, Chemical Engineering Dept., Istanbul, Türkiye
**Corresponding author: mcelik@itu.edu.tr*

A B S T R A C T

Carbon fiber with its unique physical, chemical and biological properties, is a versatile material composed of carbon atoms arranged in a hexagonal structure. Carbon fibers with high performance are critically important materials for various industries. PAN (polyacrylonitrile) based carbon fiber is generally used worldwide for carbon fiber production. Despite a smaller 10% market share of coal-based isotropic and mesophase pitchs, they can be alternative to produce carbon fiber with cheaper and higher efficiency particularly for premium markets such as aviation and defense industry where extraordinary properties are required. Pitch-based carbon fiber production is a complicated process including raw material pretreatment, pitch preparation, melt-spinning, stabilization, carbonization, and graphitization. Each step has a significant influence on the properties and performance of the final carbon fiber product, and thus should be controlled effectively for preparing carbon fiber with desirable performance.

In this study, a pyrolysis study has been undertaken for eight Turkish coals of different ranks from lignite to bituminous coals. All coals sizing -3.36-0.42 mm and ash contents varying from 7.25 to 49.20 % have been subjected to pyrolysis at 850 ºC for two hours under nitrogen atmosphere in the absence of oxygen during which the emission of released gases of H_2, CO_2, CO and CH_4 have been in situ measured. The amounts of char, tar and gas have been recorded for each coal. The results based on tar recoveries are evaluated for a suitable coal precursor to be used in carbon fiber production.

Key words: *Carbon fiber, coal, tar, pyrolysis*

1. INTRODUCTION

Carbon fiber (fiber) is a next-generation fibrous material containing at least 92% carbon in its structure, possessing low density, biocompatibility, superior mechanical properties, and thermal and electrical conductivity. Fibers containing more than 99% carbon are called graphitized fiber or graphite fiber. Carbon fibers, consisting of carbon atoms arranged in a hexagonal structure, are produced by the thermal and chemical decomposition of various organic fiber precursors.

The bonding strength of carbon atoms provides high tensile strength to the fiber (Keboletse, et al., 2021. Moreover, due to its compositional advantage, it is even lighter than aluminum. Although carbon fiber has only 20% of the density of steel, it has a tensile strength 10 times higher than steel. For this reason, it is a preferred material in sports equipment, the automobile industry, wind turbines, medical devices, and especially aerospace and aviation, which require high mechanical strength and lightness. A chronological summary of carbon fiber research is presented in Figure 1 (Choi et al., 2019).

Due to its high strength, lightness, and ergonomics, the global carbon fiber market has exceeded 150,000 tons, and this amount is expected to triple in the next 10 years. Among the most popular precursor materials, polyacrylonitrile (PAN) fibers account for 90% of the carbon

fiber market. In recent years, the share and importance of coal/petroleum-based mesophase pitch is increasing; fossil-based carbon fibers due to the lower production cost and superior electrical and thermal properties compared to polymeric PAN-based ones, their use in more technological fields such as the defense industry has given serious momentum to coal-based carbon fiber production.

Figure 1. A chronological summary of carbon fiber research (Choi et al., 2019)

Petroleum and coal-based mesophase are prepared by catalytic thermal or direct thermal (non-catalytic) methods. Thermal catalytic methods are not preferred due to many disadvantages (Shi and Ma, 2019). Direct thermal methods have continued to be used since the late 1990s. The formation of a carbonaceous mesophase ideally consists of PAHs with a molecular weight between 300 and 1200 Daltons (AMU). Numerous studies show that free radical reactions in coal pitch can change the content of macromolecules, the size of PAHs, the content of aliphatic or heteroatom-containing functional groups, and the stacking degrees of condensed PAHs in the mesophase (Apicella, et al., 2017; Cho et al., 2021; Kim, et al., 2016; Niu et al., 2021; Yang et al., 2016).

Currently, coal tar (CT) or coal tar pitch (CTP) are mainly produced as a byproduct of the metallurgical coking process; however, this process remains limited by stricter environmental regulations due to the cost of high-quality coals and shrinking market demand. In this case, relatively abundant low-rank coals could be a cheaper source to reduce the production cost of CT/CTP. However, due to the chemical nature of low-rank coal tar, CT/CTP produced by pyrolysis, gasification, or metallurgical coking processes needs further refining as it cannot meet mesophase (MP) criteria. Especially since general properties such as low tar yield (about 5-10% by weight) and lower carbon content, higher ash and oxygen content are not suitable for mesophase pitch feedstock, methods of liquefying coal with a solvent or carbon dioxide under temperature and pressure to convert coal into liquid fuel are receiving more interest instead (Wang et al. 2023). In this way, the organic part of the coal can be separated from inorganic ash-forming substances. Subsequent liquefaction reactions trigger hydrogenation reactions by adjusting the temperature (250–450 ºC) and pressure (up to 300 bar), facilitating the production of desired chemical products by converting approximately 40-95% of the raw coal by weight (Hutchenson, et al., 1991.

The relative molecular weight of currently widely used mesophase pitch varies between 370-2000 AMU; this is approximately 3.5 times that of a typical isotropic pitch, with a volatile content of 15-20%, a density of 1.4-1.6 g/cm³ and a hydrogen/carbon atom ratio between 0.35-0.5. While solution spinning technique is normally used in carbon fiber production processes where PAN polymer is used, melt spinning fiber production technique is generally preferred in coal-based mesophase pitch processes. After the fiber is drawn, it is oxidized a to make it thermoset polymer under air at low pressure and 200-300 ºC temperature to ensure the alignment of the molecules of the precursor fiber. The resulting relatively stable fiber is finally carbonized at approximately 1500 ºC in an inert environment to obtain the final carbon fiber.

In this study, pyrolysis of eight different types of Turkish coals, from lignite to hard coal, were carried out at 850 ºC under nitrogen atmosphere, and the emissions of H_2, CO_2, CO and CH_4 gases formed were measured in-situ.

2. EXPERIMENTAL

Seven coal samples and one asphaltite sample of different characters and coalification degrees from various regions of Türkiye were prepared for analysis upon reducing their size with sample reduction methods. The proximate coal analysis results on a dry basis for these samples are given in Table 1.

Table 1. Proximate analysis results of coal and asphaltite samples used in experimental studies on a dry basis

	COAL	ASH, %	VOLATILE MATTER, %	FIXED C, %	S, %	CALORIFIC VALUE, kcal/kg
DRY BASIS	Kozlu	12.38	25.55	62.07	0.21	7305
	Kısrakdere	7.25	44.88	47.87	2.23	6321
	Çan	21.61	41.07	37.32	7.68	5192
	Tunçbilek	45.41	32.85	21.74	3.81	3406
	Keles	22.10	48.03	29.87	3.22	4602
	İmbat	40.78	39.20	20.02	0.73	3127
	Beypazarı	41.77	39.39	18.84	3.19	3562
	Silopi	49.22	32.76	18.02	5.34	3616

As can be observed from Table 1; the % ash content of these samples varied between 7-49, and their calorific values varied in the range of 3600-7300 Kcal/kg. While preparing samples for pyrolysis experiments, the samples were prepared as much as possible free from very fine sizes (-3.36+0.42 mm) in order to increase the reaction rate with small size but also to prevent the entrainment of powders due to the nitrogen gas given to the reactor. In order not to deviate from the original coal sample due to sample losses, size reduction processes were carried out with sieve control. The samples were dried in an oven at 105 ºC to remove the moisture of about 10%.

Pyrolysis experiments were carried out on eight Turkish coals at 850 ºC to treat them at the same reference state, despite rank differences can cause on tar production. In order to prevent undesired oxidation reactions during the experiments, nitrogen gas was fed to the reactor at a flow rate of 1 L/min throughout the pyrolysis. The nitrogen gas flow rate also determines the residence time of the formed pyrolysis vapors in the reactor. Similarly, for effective heat transfer, based on experience gained from previous experimental studies, the reactor rotation speed was selected as 5 Hz, corresponding to 3 rpm.

Each experiment was carried out for approximately 3 hours until the pyrolysis gas exit from the reactor ceased. Solid and liquid pyrolysis product yields were determined by weighing the solid residue (char) remaining in the reactor at the end of the experiment and the liquid pyrolysis products collected in the liquid traps at the reactor exit. The gas product yield was calculated by subtracting the amount of collected solid and liquid products from the amount of coal initially loaded into the reactor. The composition of the pyrolysis gas was followed by taking instantaneous gas measurements throughout the pyrolysis reaction.

All of the experimental studies were carried out in the existing semi-pilot scale batch pyrolysis system at the ITU Synthetic Fuels and Chemicals Technology Center, Pyrolysis Technologies Laboratory. The block diagram of the pyrolysis unit is shown in Figure 2. Approximately 1 kg lignite samples were used in pyrolysis experiments. The coal content loaded into the cylindrical flanged tube reactor is continuously stirred by blades built on a rotating shaft. The rotation speed of the shaft set to 5 rpm was adjusted remotely with a control program. Continuous nitrogen/water vapor/carbon dioxide gas feed line to the reactor allows the pyrolysis reaction

to take place under inert or reactive gas atmospheres. The temperature of the reactor is controlled by thermocouples from inside the furnace but from the outer surface of the reactor.

The system includes a wax/oil catcher, a cooling column, and an open spray-type washing column. After the pyrolysis gas is freed from pyrolysis oil and wax compounds, it is sampled online by the syngas analyzer (MRU SWG 200) connected to the gas line of the pyrolysis unit. All gas products are safely discharged to the atmosphere by burning in an afterburner. At the end of the tests, the reactor is cooled to ambient temperature in a nitrogen gas atmosphere. Then, solid carbon residue (char) is taken from the reactor and weighed for mass balance calculations. Wax, pyrolysis oil, and aqueous products are collected in traps and containers under the cooler and washing columns, respectively. Gas yield is calculated by subtracting the collected char and wax/liquid products from the weight of the raw material pyrolyzed for that particular experiment.

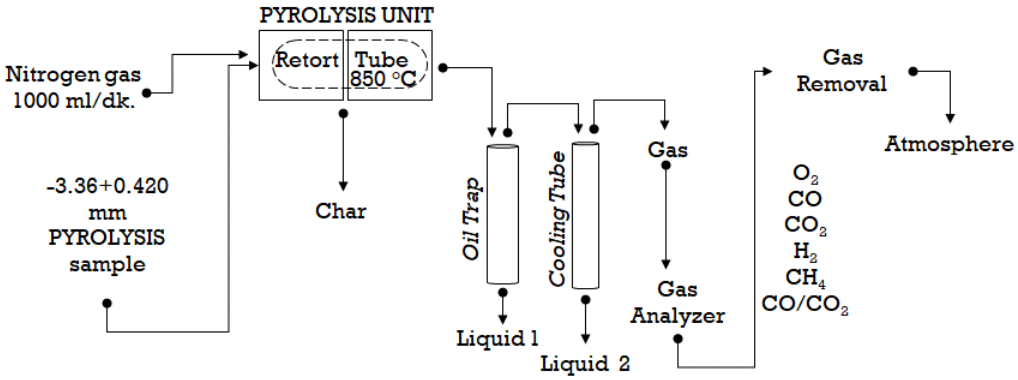

Figure 2. Block diagram of the batch pyrolysis experimental unit

3. RESULTS AND DISCUSSION

The experimental conditions and experimental results of the high-temperature pyrolysis study carried out for eight different Turkish coals are given separately below in the form of Tables and Figures. H_2, CH_4, CO_2, and CO gas emissions observed as a function of time during the pyrolysis process are given in Figures 3-6, respectively. As seen from Table 2, as a result of the pyrolysis of Çan lignite, 59.7% char, 20.2% pyrolysis oil, and 20.1% pyrolysis gas were obtained. The high char yield is evaluated to be a result of the high ash content of Çan coal which contains approximately 20.61% ash on a dry basis.

Table 2. Comparative pyrolysis products of various coals

Product	Coal sample pyrolyzed at (850 ºC)							
	Çan	Kozlu	Silopi	Keles	Kısrakdere	Beypazarı	Tunçbilek	İmbat
Char	59.7	73.7	69.6	41.4	59.0	55.2	71.5	65.8
Tar	20.2	5.9	5.2	36.2	17.6	20.7	13.3	12.3
Gas	20.1	20.4	25.2	22.5	23.4	24.1	15.3	21.9
Hydrogen Amount*, m^3	0.215	0.360	0.055	0.209	0.287	0.139	0.155	0.050

*Amount of released hydrogen gas.

In high-temperature pyrolysis of Çan lignite, carbon dioxide, methane, and carbon monoxide are formed first. With the progress of pyrolysis, hydrogen gas (Fig. 3) is released with a maximum production rate. Along with hydrogen, the carbon monoxide concentration also increases. Lignite pyrolysis can be evaluated in three stages; in the first stage, free and

chemically bound water loss occurs. In this stage, volatile organic compounds also thermally decompose with the dehydration of organic components partially. As a result of dehydration, decarboxylation, and decarbonylation reactions, a pyrolysis gas rich in H_2O, CO_2, and CO is formed initially. In this way, a significant part of the oxygen content of the lignite passes into the gas phase.

CO/CO_2 formation continues through the rearrangement or cleavage of acetyl ($CH_3CO–$), ether (C–O–C), and/or ester (–COOR) bonds found in the coal structure. Due to the exothermic nature of decarboxylation reactions, CO_2 formation occurs at lower temperatures compared to decarbonylation reactions, which are endothermic and give CO. For this reason, it is expected that the CO_2 concentration is higher than the CO concentration in the initial stage of the reaction.

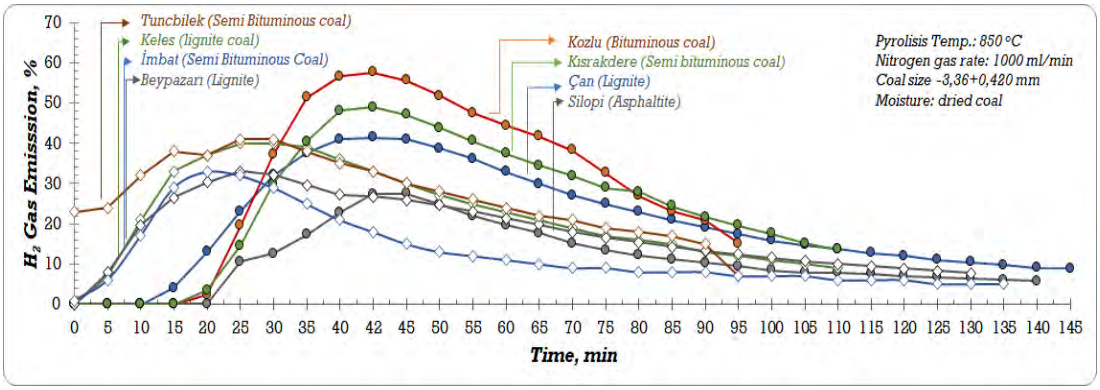

Figure 3: H_2 gas emissions released in pyrolysis processes carried out on different coals (scaled on total gas amount basis)

Methane formation in Fig. 4 is associated with the breakdown of methoxyl ($–O–CH_3$), methyl ($–CH_3$), and methylene ($–CH_2–$) groups. It is evaluated that the presence of these structures in the structure of coal can increase methane formation. In addition, methane and hydrogen formation is expected to increase with the thermal breakdown of condensable organic vapors formed during pyrolysis. The high hydrogen concentration observed in the later stage of pyrolysis is evaluated to be a result of this situation. Hydrogen and carbon monoxide formation is also a result of other secondary reactions taking place in the gas phase and under the catalytic effect of char. For example, hydrogen and carbon monoxide are formed as a result of the reaction of char with water vapor, and methane is formed as a result of dealkylation of tar with water vapor (Ahamed, et al., 2019).

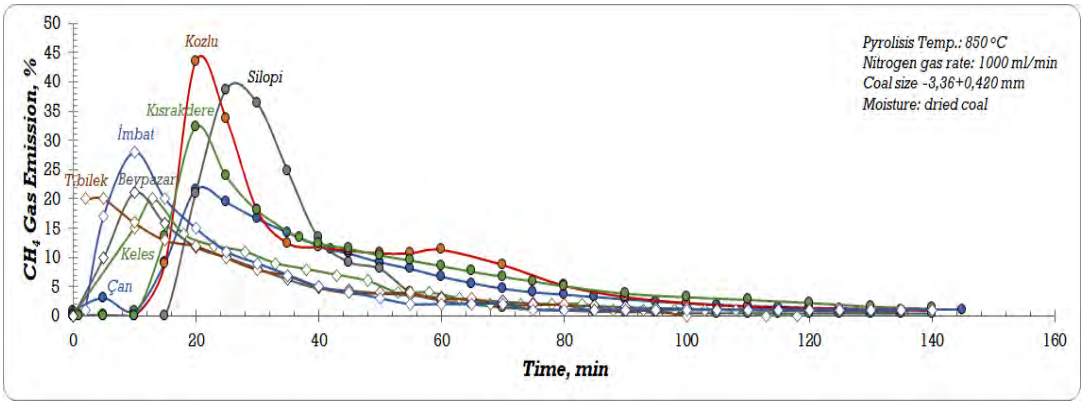

Figure 4: CH_4 gas emissions released in pyrolysis processes carried out on different coals (scaled on total gas amount basis)

Gas emissions in the pyrolysis process carried out on Kozlu coal was observed as a function of time. Pyrolysis process carried out on Kozlu coal is given in Figures 3 to 6. When the

pyrolysis results of Kozlu coal are examined, it is seen that the pyrolysis tar product yield is 5.9%. The char yield was observed as 73.74% and the gas product yield as 20.4% (Table 2). When the gas analysis trends were examined, it was observed that carbon dioxide formation in Fig. 5 was also very limited. This behavior was evaluated to be a result of the low pyrolysis reactivity of Kozlu coal composed of a bituminous structure. The char formed under the effect of high heat gasifies and turns into carbon monoxide and hydrogen. Dehydration, decarbonylation, and decarboxylation reactions taking place was limited during pyrolysis, and as a result, liquid product formation was also at a minimum level.

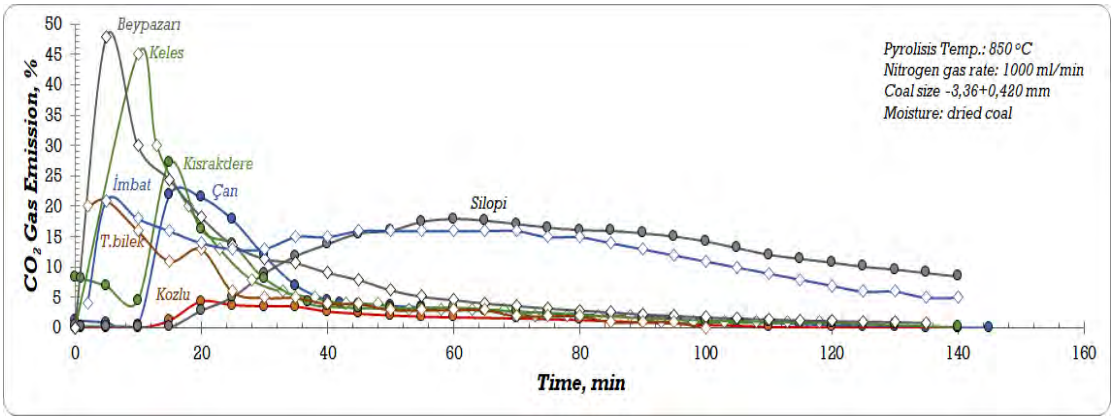

Figure 5. CO_2 gas emissions released in pyrolysis processes carried out on different coals (scaled on total gas amount basis)

Gas emissions in the pyrolysis process carried out on Silopi Asphaltite was observed as a function of time. The results on Silopi Asphaltite are given in Table 2; the pyrolysis product yield of Silopi coal shows similarity with Kozlu coal. As a result of Silopi coal pyrolysis, 69.60% char, 5.20% pyrolysis oil, and 25.20% gas product yield were obtained. Although a similar product yield profile to Kozlu coal was obtained, it exhibited a different behavior compared to Kozlu coal when the gas composition was examined. High methane formation draws attention as a result of the pyrolysis of Silopi coal; this result may occur as a result of the bond breaking of the polymeric tar content and/or methoxyl (–O–CH_3), methyl (–CH_3), and methylene (–CH_2–) groups of Silopi coal. It is envisaged that Kozlu and Silopi coals could give different product distributions if the pyrolysis temperature is lowered.

A quite high tar product yield of 36.2% (Table 2) was obtained on pyrolysis of Keles coal at a temperature like 850 ºC. The gas product yield is 22.5%, and it has been determined that it shows similar behaviors with other coal samples tested. A liquid product with a low H/C ratio in a more aromatic structure may have been obtained at a high carbonization degree at 850 ºC. Hydrogenation reactions may be decisive on the characteristic of the pyrolysis liquid hydrogen formed as a result of secondary pyrolysis reactions. Furthermore, more aromatic formation can be expected through the reaction of furanic compounds with light olefins via Diels-Alder and subsequent dehydration reactions. These reactions offer clues that can help predict the liquid product characteristic of the pyrolysis gas composition. Methane and hydrogen formation trends as a result of Keles pyrolysis point to the presence of similar reactions.

The pyrolysis process carried out on Kısrakdere Coal gas emissions were observed as a function of time as given in Table 2. The pyrolysis product yield of Kısrakdere coal show 59.0% char, 17.6% pyrolysis oil, and 23.4% pyrolysis gas. Gas composition trends and concentration changes are quite similar to the results obtained with Keles coal. However, 50% less pyrolysis oil yield was obtained compared to Keles coal which may be a result of Kısrakdere coal having a similar pyrolysis reactivity to Keles coal but having less volatile matter content.

Beypazarı Coal gas emissions followed as a function of time during the Pyrolysis process carried out on Beypazarı Coal are given in Table 2. It is seen that the pyrolysis results of Beypazarı coal and Kısrakdere coal are quite similar to each other. While 55.2% char, 20.7% pyrolysis oil, and 24.1% pyrolysis gas yield were obtained with Beypazarı coal, these values were recorded as 59%, 17.6%, and 23.4% respectively with Kısrakdere coal. The observation of a quite severe carbon dioxide peak in the first stage of pyrolysis with Beypazarı coal points to the presence of carboxylic groups of Beypazarı coal. An increase in the carboxylic group concentration of coal is a measure of the coal being more reactive pyrolytically. Since decarboxylation reactions are exothermic, a spontaneous temperature increase in the reactor is expected due to the exothermic reaction heat. This situation acts positively in terms of pyrolysis kinetics. Thus, Beypazarı coal can be pyrolyzed at a lower temperature with a higher yield compared to Kısrakdere coal.

Gas emissions observed as a function of time for the Pyrolysis of Tunçbilek Coal are given in Figure 3-6. A very high char yield of 71.5% char, 13.3% pyrolysis oil, and 15.3% pyrolysis gas were observed as a result of pyrolysis at 850 ºC. When the pyrolysis gas formation trend was examined, a carbon dioxide peak was not observed, and a formation trend with a quite wide and low percentage concentration was obtained for carbon dioxide. Low carbon dioxide formation shows that the pyrolysis reactivity of Tunçbilek coal is low. Hydrogen, carbon monoxide, and methane formation as an indicator of the char gasification reaction draws attention. The ash of Tunçbilek coal is around 40-45% on a dry basis, and thus high char yield originates from the high ash content of Tunçbilek coal. Pyrolysis oil yield also remained low as a result of the 28-30% volatile matter content of Tunçbilek coal on a dry basis.

Gas emissions observed as a function of time during the pyrolysis process on İmbat Coal are given in Table 2. The pyrolysis of İmbat coal yields 65.8% char, 12.3% pyrolysis oil, and 21.9%. High amount of carbon monoxide formation (Fig. 6) draws attention in İmbat coal. Carbon monoxide is formed as a result of endothermic carbonylation and secondary pyrolysis reactions. Decarbonylation reaction is a primary pyrolysis reaction and is also a measure of the oxygen content of coal. As the oxygen content of coal increases, pyrolysis oil with a high oxygen content, which oligomerizes more easily, is obtained. In addition, the presence of organic acids makes the pyrolysis oil quite corrosive; the oxygen content of the pyrolysis oil of İmbat pyrolysis will be high.

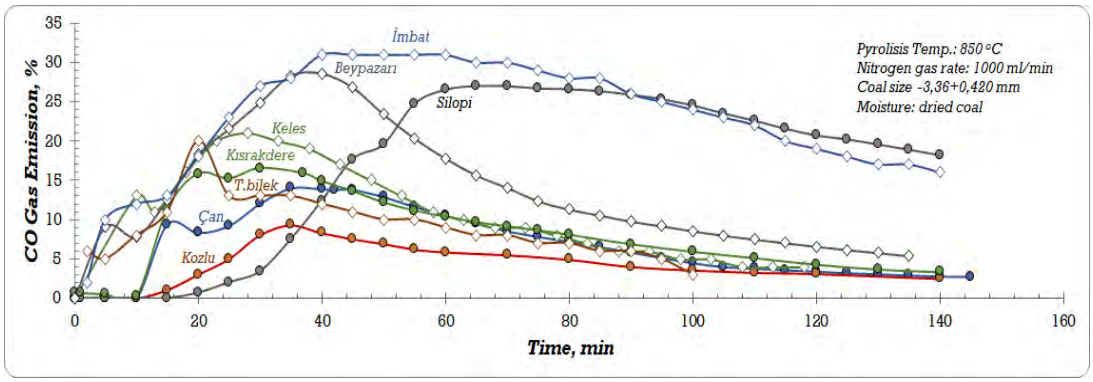

Figure 6. CO gas emissions released in pyrolysis processes carried out on different coals (scaled on total gas amount basis)

When hydrogen gas formation trends are compared (Fig. 3); it is seen that the highest hydrogen concentration was reached with Kozlu coal. Hydrogen formation trends obtained for Kozlu, Kısrakdere, Çan coals, and Silopi asphaltite are quite similar to each other, and maximum hydrogen concentrations are 58%, 49%, 42%, and 28%, respectively. Pyrolysis oil yields for these coals were recorded as 5.9%, 17.6%, 20.2%, and 5.2%, respectively. A change was observed in this ranking only for Silopi asphaltite. Differently, very high methane

concentration was obtained in the Silopi sample. This situation occurred because Silopi asphaltite has a different structure from the other three coals.

When methane formation trends are examined (Fig. 4), the highest methane concentrations were obtained for Kozlu, Silopi, Kısrakdere, and İmbat coals. Methane concentrations of 44%, 39%, 33%, and 28% were reached for these coals, respectively. While methane formation was observed in the first stage of pyrolysis for İmbat, Beypazarı, Keles, and Tunçbilek coals, methane formation increased in the later stage of pyrolysis for other coals. 12.3%, 20.7%, 36.2%, and 13.3% pyrolysis oil were obtained for İmbat, Beypazarı, Keles, and Tunçbilek coals. It seems that there is no direct relationship between methane formation and pyrolysis oil yield.

When carbon dioxide concentrations (Fig. 5) are examined, it is seen that the initial carbon dioxide formations of Beypazarı and Keles coals are the highest. Around 45-50% carbon dioxide formation was observed initially for both coals, and it is evaluated that these coals are quite reactive. Pyrolysis oil yields obtained with Beypazarı and Keles coals are 20.7% and 36.2%, and there seems to be a decisive factor between coal reactivity and pyrolysis oil yield.

When carbon monoxide formation trends are examined (Fig. 6); it is seen that the highest concentrations lie between 25-30% for İmbat, Silopi, and Beypazarı coals. The lowest carbon dioxide and carbon monoxide concentrations were obtained with Kozlu coal. This situation indicates that the reactivity of Kozlu coal is extremely low. An extremely low pyrolysis oil yield of 5.9% was obtained with Kozlu coal. The low pyrolysis yield observed for Kozlu coal may have originated from the insufficiency of the concentration of carboxyl and carbonyl surface groups.

Because the ash contents of the coal and asphaltite samples (Apak et al., 2002) used in pyrolysis studies are different from each other, in order to better understand the effect of changes occurring only from the organic structure on pyrolysis products and especially gas emission concentrations, pyrolysis products distributions were recalculated on a dry ash-free basis and given in Table 2.

Table 2. Pyrolysis product distributions obtained as a result of pyrolysis processes (dry ash-free basis)

Moisture –ash free basis	COAL	Ash %	Char %	Tar %	Gas %
	Kozlu	12.38	69.98	6.73	23.28
	Silopi	49.22	40.13	10.24	49.63
	Kısrakdere	7.25	55.80	18.98	25.23
	İmbat	40.78	42.25	20.77	36.98
	Tunçbilek	45.41	47.61	24.36	28.03
	Çan	21.61	48.59	25.77	25.64
	Beypazarı	41.77	23.06	35.55	41.39
	Keles	22.1	24.65	46.47	28.88

Table 2 shows that the highest liquid yields were obtained in the pyrolysis of Keles (46.47%) and Beypazarı (35.55%) coals.

4. CONCLUSIONS

Pyrolysis studies indicated that the initial composition of the coal determines the pyrolysis reactivity of the coal. The oxygen content of the coal originates from carboxyl and carbonyl

groups. As the concentration of these groups increases, the pyrolysis kinetics of the coal increases, and the pyrolysis oil yield improves at this rate.

In this framework, the highest pyrolysis oil yield was obtained with Keles coal which could positively affect the process efficiency for carbon fiber production. However, the pyrolysis oil yield increases with the concentration of oxygenated surface functional groups, and a pyrolysis oil with a higher oxygen content is obtained. Successive hydrogenation processes are needed to reduce the oxygen content of pyrolysis oil. On the other hand, although an extremely low pyrolysis oil yield was obtained for Kozlu and Silopi, it is possible to obtain a pyrolysis oil with a higher degree of carbonization and lower oxygen content. It is envisaged that carbon fiber production efficiency could be negatively affected due to low pyrolysis oil yields. However, obtaining a pyrolysis oil with high carbon content and low oxygen content appears interesting for carbon fiber production despite low pyrolysis oil yields. In summary, it is of importance to design the sequential processes to be applied for carbon fiber production by characterizing the pyrolysis oils separately.

ACKNOWLEDGEMENT

The financial support of Turkish Coal Enterprise is greatly acknowledged.

REFERENCES

Ahamed, M. A. A., Perera, M. S. A., Matthai, S. K., Ranjith, P. G., Dong-yin, L., (2019) “Coal composition and structural variation with rank and its influence on the coal-moisture interactions under coal seam temperature conditions – A review”, Journal of Petroleum Science and Engineering, 180, 901–917.

Apak, E., Yardim, M. F., Ekinci, E., (2002) “Preparation of carbon fibre precursors from the pyrolysis and copyrolysis of Avgamasya asphaltite and Göynük oil shale: Vacuum distillation and hexane extraction”, Carbon, 40 (8) 1331–1337.

Apicella, B., Tregrossi, A., Stanzione, F., Ciajolo, A., Russo, C., (2017) “Analysis of petroleum and coal tar pitches as large PAH”, Chemical Engineering Transactions, 57, 1–6.

Cho, J. H., Kim, M., Sun, J., (2021) “Study of the molecular-weight distribution of binder pitches for carbon blocks”, ACS Omega, 6, 10180–10186.

Choi, D., Kil, H. S., Lee, S., (2019) “Fabrication of low-cost carbon fibers using economical precursors and advanced processing technologies”, Carbon, 142, 610–649.

Hutchenson, K. W., Roebers, J. R., Thies, M. C., (1991) “Fractionation of petroleum pitch by supercritical fluid extraction”, Carbon, 29 (2) 215–223.

Keboletse, K. P., Ntuli, F., Oladijo, O. P., (2021) “Influence of coal properties on coal conversion processes – coal carbonization, carbon fiber production, gasification and liquefaction technologies: A review”, International Journal of Coal Science & Technology, 1–27.

Kim, J., Im, U., Lee, B., Peck, D., Yoon, S., Jung, D., (2016) “Pitch-based carbon fibers from coal tar or petroleum residue under the same processing condition”, Carbon Letters, 19, 72–78.

Niu, H., Zuo, P., Shen, W., Qu, S., (2021) “A comprehensive investigation on the chemical structure character of spinnable pitch for improving and optimizing the oxidative stabilization of coal tar pitch-based fiber”, Polymer, 224, 123737.

Shi, J. L., Ma, C., (2019) “Preparation and characterization of spinnable mesophase pitches: A review”, New Carbon Materials, 34, 211–219.

Wang, W., Nelson, M. G., Jolley, K., Preciado, I., Eddings, E., (2023) “Efficient mesophase pitch precursor production from low-rank Utah Sufco coal via mild solvolysis liquefaction”, SSRN.

Yang, J., Nakabayashi, K., Miyawaki, J., Yoon, S. H., (2016) “Preparation of pitch based carbon fibers using hyper-coal as a raw material”, Carbon, 106, 28–36.

MODELING OF COMPOSITE COAL-BASED BRIQUETTES AIMED AT REDUCING SULFUR EMISSIONS INTO THE ATMOSPHERE

Nedžad ALIĆ[1,*], Rusmir RAZIĆ[2]

[1]*University of Tuzla, Faculty of Mining, Geology and Civil Engineering in Tuzla, B&H*
[2]*Coal Mine „Gračanica“ Gornji Vakuf – Uskoplje, B&H*
[*]*Corresponding author: nedzad.alic@untz.ba*

A B S T R A C T

The tendency to phase out heat production from coal in order to reduce atmospheric pollution has led to the closure of coal deposits. An alternative source of heat, particularly in the category of heating smaller residential buildings, is wood pellets. Although environmentally acceptable from a certain perspective, this option also has its drawbacks when considering the scale of the required energy quantities and the role of forests in air purification.

Both woody biomass and coal, as primary energy carriers, contain hydrocarbon compounds. Thus, in both cases, gaseous combustion products include COx and NOx emissions. The difference lies in their relative proportions. In contrast to woody biomass, coal combustion also generates sulfur compounds, which makes coal an environmentally unacceptable fuel.

In this study, the addition of a specific proportion of woody biomass and an additive—pyrophyllite shale—to coal was investigated in order to assess its influence on the energy and environmental aspects of heat release from such a composite fuel mixture. The environmental aspect was emphasized through the reduction of sulfur release from coal during combustion.

The prepared mixture was subjected to a briquetting process, and the obtained samples were tested for relevant parameters, primarily the lower heating value (LHV) and the sulfur (SOx) content in the resulting products. The obtained results are highly encouraging with respect to both of the aforementioned parameters and may serve as a guideline for further research based on the proposed concept.

Key words: *Coal, wood sawdust, briquette, heating value, sulfur, environmental protection*

1. INTRODUCTION

The core research problem is reflected in the following question: does the cessation (or prohibition) of coal use within a specific group of consumers fully resolve the problem of air pollution at the local and global levels? Coal, as an energy source, is used for multiple purposes and, among other applications, a significant amount is utilized in less developed countries for heating small residential units. On the other hand, there is a strong tendency to phase out heat production from coal in order to reduce atmospheric pollution, which consequently leads to the closure of coal deposits.

An alternative for heat generation, particularly in the category of heating smaller residential buildings, is the use of wood pellets. Although environmentally acceptable from a certain perspective, this option also has its drawbacks when considering the scale of the required energy demand and the role of forests in air purification.

The most commonly proposed substitute for coal in the aforementioned category is biomass, primarily wood or wood pellets as a processed energy product. Although this type of fuel significantly reduces the emission of primary gases affecting air pollution during combustion, it is important to consider that such primary improvements may, in the long term, result in different overall consequences. Excessive exploitation of woody biomass reduces the total

forest resources, which represent a natural “air filter”; forests are often referred to as the “lungs of the Earth.” Therefore, the hypothesis of replacing one type of energy source with another does not guarantee a definitive positive outcome in terms of pollution reduction and its broader impact on general climatic conditions.

2. RESEARCH OBJECTIVES

The relevance of the research problem lies in examining one of the possible approaches to utilizing coal as an energy source with reduced environmental risk (impact on the environment). The objectives of the research presented in this dissertation are as follows:

- To obtain a composite coal pellet with reduced emission of atmospheric pollutants;
- To reduce the consumption of woody biomass for heating purposes among small-scale consumers;
- To enable the continued exploitation of coal in accordance with acceptable environmental standards.

By modulating the content and type of additives introduced into coal during the briquetting process, it is possible to significantly influence the reduction of gaseous emissions released into the atmosphere during combustion.

3. FUNDAMENTALS, METHODS, AND MATERIALS

The basic postulates of the proposed hypothesis relate to two processes: the combustion of solid fuels and the preparation, i.e., the physical form, of the combustible material.
The equipment used for all procedures during the research, as well as the applied standards, are listed below:

- Preparation of input components and briquette production: material size reduction using laboratory jaw and hammer crushers; analytical balance with an accuracy of 0.01 g; drying oven; laboratory sieve shaker equipped with a series of square-aperture sieves (mm); laboratory homogenizer; and a laboratory extruder press for briquette production.
- Measurement procedures and devices for determining the parameters of the obtained experimental briquettes: Elemental analysis of the input components and experimental briquettes was performed using an EA3000 elemental analyzer. The heating value was determined using a C 5000 calorimetric system. The applied standards are listed in Tables 2, 3, 4, and 5 below.

Coal sample: The coal sample was collected from the Kotezi coal deposit, located in the northwestern part of the Bugojno coal basin, in a total quantity of 60 kg. The sample was taken in situ from a surface layer of the deposit and subsequently subjected to size reduction, with simultaneous determination of particle size reduction parameters using laboratory equipment, down to a grain size of 1 mm.

Sawdust sample: A 20 kg sample of pine sawdust was collected from the Bunta Sawmill in Bugojno.
Pyrophyllite sample: For testing purposes, a 5000 g ground sample of a purple variety of pyrophyllite shale originating from Parsovići was used.
The binder suspension used for the preparation of all experimental briquette types in this study consisted of a 10% starch solution (type H), produced by Helios Domžale, dissolved in water.

3.1. Research Methods

The research methodology, i.e., the research model, was structured according to the following principles:

- Identification of characteristic or representative (key) indicators relevant to the study;
- Determination of sample processing methods, including:

a) the procedure for preparing samples for testing;
b) the selection of appropriate laboratory testing methods;

- Interpretation and processing of the research results;
- Formulation of the research conclusions.

3.1.1. Representative research indicators

The representative research indicators are the lower heating value of the briquettes on a moisture-free basis, and the contents of total sulfur, combustible sulfur, and sulfur in the ash.

3.1.2. Testing procedure

For the materials described above, the composition of individual briquettes and the procedure for their production under laboratory conditions were established. In accordance with the research objectives, it was decided to produce five briquettes with different compositions, emphasizing the variable content of additives while keeping the quantities of the combustible constituents constant. Accordingly, the following compositions were formulated, with their corresponding designations:

- **Briquette A1:** 100% coal, total mass 2000 g;
- **Briquette A2:** 1400 g coal + 600 g wood sawdust;
- **Briquette A3:** 1400 g coal + 600 g wood sawdust + 40 g pyrophyllite;
- **Briquette A4:** 1400 g coal + 600 g wood sawdust + 120 g pyrophyllite;
- **Briquette A5:** 1400 g coal + 600 g wood sawdust + 200 g pyrophyllite.

The coal sample used for producing these briquettes was labeled as **A0**. The total mass composition of the individual components in each briquette is presented in Table 1.

Table 1. Mass composition of individual components in the total sample of each briquette

No.	Type of input component	Mass, g				
		A1	A2	A3	A4	A5
1.	sawdust	0	600	600	600	600
2.	coal	2000	1400	1400	1400	1400
3.	pyrophyllite	0	0	40	120	200
4.	starch	1,89	1,28	1,49	1,57	1,65
Total		2001,89	2001,28	2201,65	2121,57	2201,65

The mixture for the extruder press was prepared using a specially designed laboratory feeder, which consisted of three separate hoppers: one for coal powder, a second for wood sawdust, and a third for ground pyrophyllite shale. These hoppers were arranged in series, one after the other, with different discharge heights. All discharge hoppers fed a straight metal dosing ramp, 10 cm in width.

Each hopper and the metal dosing ramp were mounted on a common vibrating device, which provided the same frequency for all hoppers and the ramp. The quantity of each component discharged from the hoppers was controlled by the size of the openings at the hopper outlets. In this way, a thin layer of coal powder, 10 cm wide, was deposited from the first hopper, followed by a slightly thinner layer of wood sawdust of the same width from the second hopper, and finally a significantly thinner layer of pyrophyllite shale from the third hopper. This procedure produced a well-homogenized layered mixture of the three materials.
The resulting mixture was then introduced via the flat metal dosing ramp into a cylindrical-jacketed mixer, where water was added in very fine droplets (similar to the principle used in

conical pelletizers). This ensured maximum homogenization of the mixture while simultaneously achieving sufficient moisture content for briquetting[2].
The added amount of binder suspension enabled the next phase: briquetting using an extruder press with a die opening of 6 mm in diameter. The resulting green briquettes were air-dried, thus completing the laboratory procedure for briquette production. The external appearance as well as the cross-section of the pellets reflects the characteristics of the components from which they were made.

Briquettes made entirely from coal exhibit a finer, smoother structure on the outer surface of the cylinder and are more homogeneous, as can be generally observed in Figure 1. When examining the cross-section of the various briquette mixtures, also shown in Figure 1, the structural characterization clearly reveals the individual components of the different materials forming the composite.

From a general physical perspective, the produced briquettes possess satisfactory mechanical strength, sufficient to withstand all handling operations during their use. It is also evident that the briquettes are highly hygroscopic, and their mechanical properties deteriorate significantly with increased moisture, eventually leading to complete disintegration.

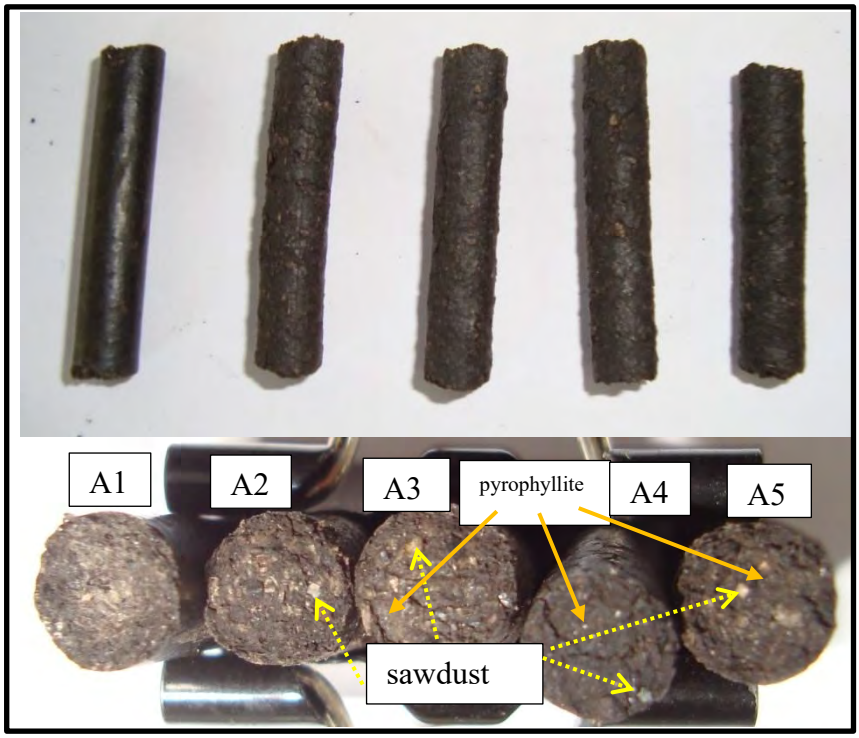

Figure 1. Structural appearance of the briquette and its cross-section

4. RESEARCH RESULTS

Table 2 presents the summarized results of the elemental and technical analysis of coal and pine sawdust, used as a supplement to coal in the briquette production for this study.

Table 2. Results of the technical and chemical analysis of coal (sample A0) and pine sawdust used in briquette production and tested at RGH Kakanj [3], on a moisture-free basis

Type of analysis	Units	Method	Moisture-free	
			COAL, A0	SAWDUST
Ash	%m/m	BAS ISO 1171:2012	29,56	8,04
Combustible	%m/m	INS 80625200:2019	70,44	91,96

matter				
Volatile matter	%m/m	BAS ISO 5071-1:2014 ; BAS ISO 562:2012	44,87	78,99
Coke	%m/m	INS 80625201:2019	55,13	21,01
Cfl_x	%m/m	INS 80625201:2019	25,56	12,95
Total carbon	%m/m	BAS ASTM D 5373:2016	46,17	48,96
Hydrogen	%m/m	BAS ASTM D 5373:2016	2,92	7,2
Nitrogen	%m/m	BAS ASTM D 5373:2016	0,8	0,15
Oxygen	%m/m	ASTM D 3176:2015	18,91	35,62
HHV	kJ/kg	BAS ISO 1928:2010	17402	18588
LHV	kJ/kg	BAS ISO 1928:2010	16800	17473
Total sulfur	%m/m	BAS ISO 334:2015	3,06	0,02
Sulfur in ash	%m/m	ASTM D 1757:1996	1,42	0
Combustible sulfur	%m/m	INS 80625211:2019	1,64	0,02

The values of the characteristic parameters of the solid residue (ash) from the combustion of coal and wood sawdust, tested at the RGH Kakanj laboratory, as well as the silicate analysis of pyrophyllite shale [1], are presented in Table 3.

Table 3. Results of the chemical analysis of pyrophyllite shale and the ash of coal and wood sawdust

Type of analysis	Method	Unit	Coal A0	Sawdust	Pyrophyllite shale
SiO_2 content	BAS 1009:2003	%m/m	36,58	55,88	65,10
Fe_2O_3 content	BAS 1011:2003	%m/m	16,5	2,69	1,65
Al_2O_3 content	BAS 1013:2003	%m/m	11,64	8,61	18,38
CaO content	BAS 1014:2003	%m/m	12,54	13,89	2,70
MgO content	BAS 1015:2003	%m/m	5,34	8,44	1,49
SO_3 content	BAS 1018:2003	%m/m	15,60	1,14	0,58
TiO_2 content	BAS 1012:2003	%m/m	0,22	0,16	0,08
Na_2O content	ASTM D 6349:2013	%m/m	0,29	5,11	0,23
K_2O content	ASTM D 6349:2013	%m/m	1,29	4,09	1,77
MnO content	-	-	-	-	0,02
P_2O_5 content	-	-	-	-	0,06
CO_2 content	-	-	-	-	4,04
KH_2O content	-	-	-	-	3,90
		Total	100,0	100,0	100,0

For all produced briquettes, prepared according to the described procedures and formulations, measurements of the elemental and proximate analysis indicators were performed. Both analyses were conducted on three separately taken samples from each briquette type or formulation, including samples with raw moisture, moisture in the analytical sample, and moisture-free samples. The results are presented in Table 4.

Table 5 presents the results of the silicate analysis of the briquette ash.

Table 4. Results of the technical and chemical analysis of experimental briquettes, on a moisture-free basis

Type of analysis	Unit	Method	Briquette samples (moisture-free)												
			A1	A2-1	A2-2	A2-3	A3-1	A3-2	A3-3	A4-1	A4-2	A4-3	A5-1	A5-2	A5-3
Ash	%m/m	BAS ISO 1171:2012	25,36	20,73	20,63	20,77	21,25	21,24	20,94	24,89	24,62	24,95	25,92	25,58	25,86
Combustible matter	%m/m	INS 80625200:2019	74,64	79,27	79,37	79,23	78,75	78,76	79,06	75,11	75,38	75,05	74,08	74,42	74,14
Volatile matter	%m/m	BAS ISO 5071-1:2014 ; BAS ISO 562:2012	45,28	54,3	54,17	54,42	54,39	54,41	54,23	53,1	53,1	53,12	51,37	51,94	51,74
Coke	%m/m	INS 80625201:2019	54,72	45,7	45,83	45,58	45,61	45,59	45,77	46,9	46,9	46,88	48,63	48,06	48,26
Cfl_x	%m/m	INS 80625201:2019	29,36	24,96	25,21	24,81	24,36	24,35	24,83	22,01	22,28	21,93	22,7	22,48	22,4
Total carbon	%m/m	BAS ASTM D 5373:2016	49,1	50,89	50,93	50,79	50,31	50,31	50,48	47,99	48,14	47,95	49,76	49,95	49,61
Hydrogen	%m/m	BAS ASTM D 5373:2016	3,13	3,31	3,32	3,32	3,29	3,3	3,31	3,13	3,16	3,13	3,11	3,12	3,1
Nitrogen	%m/m	BAS ASTM D 5373:2016	0,87	0,92	0,92	0,92	0,93	0,93	0,93	0,87	0,88	0,87	0,87	0,87	0,88
Oxygen	%m/m	ASTM D 3176:2015	19,73	22,61	22,66	22,57	22,53	22,55	22,61	21,54	21,59	21,55	19,22	19,34	19,38
HHV	kJ/kg	BAS ISO 1928:2010	18605	18958	18978	18945	18769	18776	18851	17884	17967	17861	18803	18868	18704
LHV	kJ/kg	BAS ISO 1928:2010	17961	18276	18295	18261	18091	18097	18169	17239	17316	17216	18163	18226	18065
Total sulfur	%m/m	BAS ISO 334:2015	3,29	2,2	2,21	2,29	2,49	2,48	2,53	2,71	2,77	2,69	2,53	2,55	2,57
Sulfur in ash	%m/m	ASTM D 1757:1996	1,47	0,66	0,67	0,67	0,81	0,8	0,8	1,14	1,15	1,14	1,41	1,4	1,4
Combustible sulfur	%m/m	INS 80625211:2019	1,82	1,54	1,54	1,62	1,68	1,68	1,73	1,57	1,62	1,55	1,12	1,15	1,17

Table 5. Results of the chemical analysis of briquettes

Type of analysis	Method	Unit	Chemical analysis of briquette ash samples												
			A1	A2-1	A2-2	A2-3	A3-1	A3-2	A3-3	A4-1	A4-2	A4-3	A5-1	A5-2	A5-3
SiO2 content	BAS 1009:2003	% m/m	37,64	49,43	49,59	49,37	41,85	41,51	41,65	47,07	47,16	46,88	38,59	38,22	38,47
Fe2O3 content	BAS 1011:2003	% m/m	13,57	16,37	15,97	15,97	15,57	15,78	15,57	13,17	13,38	13,13	15,77	15,58	15,57
Al2O3 content	BAS 1013:2003	% m/m	14,34	10,84	11,16	10,84	11,48	11,79	11,79	9,56	9,88	9,88	14,03	13,38	13,7
CaO content	BAS 1014:2003	% m/m	13,4	10,25	10,2	10,3	12,1	12,05	12,05	11,6	11,4	11,65	12,2	12,55	12,4
MgO content	BAS 1015:2003	% m/m	4,3	2,95	2,9	3	6,8	6,9	6,7	3,6	3,7	3,6	3,05	3,25	3,1
SO3 content	BAS 1018:2003	% m/m	14,72	8,22	8,31	8,18	9,68	9,79	9,74	11,73	11,66	11,7	13,94	14,03	13,86
TiO2 content	BAS 1012:2003	% m/m	0,25	0,3	0,27	0,28	0,21	0,23	0,21	0,25	0,23	0,25	0,21	0,24	0,22
Na2O content	ASTM D 6349:2013	% m/m	0,331	0,281	0,266	0,271	0,255	0,261	0,249	0,364	0,333	0,341	0,247	0,259	0,239
K2O content	ASTM D 6349:2013	% m/m	1,291	1,279	1,265	1,277	1,207	1,211	1,205	1,305	1,297	1,242	1,202	1,218	1,199

5. DISCUSSION OF THE OBTAINED RESULTS

The analysis of the results obtained in this study must take into account the expected deviations between calculated and experimentally measured values of the relevant research indicators. Two main factors significantly influence the sampling and final form of the briquettes in the different experimental variants:

- First, the standardized methods for determining the parameters of representative quantities of the materials composing the target composite. For example, from the total amount of homogenized material, the heating value in the calorimeter (as well as all other indicators) is determined on a 1-gram sample, while the materials used are inherently highly heterogeneous.
- Second, although precisely measured amounts of constituents (coal, wood sawdust, and pyrophyllite) are incorporated into the final briquette form, it is nearly impossible to distribute these components evenly throughout each part of the resulting briquette and across all produced briquettes, regardless of the dosing and mixing methods used.

The problem becomes particularly relevant when attempting to define parameter values using analytical instruments, which generally require minimal sample masses. This minimal amount is obtained according to laboratory procedures for establishing a representative sample. Due to the physical characteristics of the briquettes (shape, size, and other factors), obtaining a truly representative sample is very challenging.

These considerations motivated us to first perform a theoretical analysis of the indicators of the products of the agglomeration process, incorporating the experimentally determined values of the parameters of the input components into the analysis.

5.1. Analysis of Sample Composition in Measurement Procedures

The previously mentioned observation regarding the quantities of materials present in the sample taken for instrumental analysis cannot be determined with absolute accuracy by either analytical or instrumental methods. For this reason, a model was applied in this study that provides unquestionable accuracy in determining the proportion of individual materials in a 1-gram measurement sample. Deviations from the exact ratios in this model are not relevant for significantly altering the assessment of their influence on the relevant research indicators. The calculation model is based on the following conditions: the samples were taken from individual experiments in which the masses of coal and sawdust were kept constant while the mass of pyrophyllite was varied, and ultimately, these samples belong to a precisely defined set of briquettes. On this basis, an analysis of the composition of the samples subjected to testing was conducted.

Initially, the elemental composition of the produced briquettes was calculated based on the formulations and the characteristics of the input components used in the briquettes. In the same way, all other parameters of the briquettes were calculated considering the total mass of the added components.

The calculation model is the same for all indicators. The general principle of this model for determining the values of briquette parameters is illustrated below using the example of ash content:

$$P_B = \frac{(P_u \cdot m_u) + (P_D \cdot m_D) + (P_p \cdot m_p)}{m_u + m_D + m_p};\ \% \qquad \text{(Eq. 1)}$$

where:

- P_p- ash content of pyrophyllite, %
- m_p – mass of pyrophyllite in the mixture, g
- P_u – ash content of coal in the briquette, %
- P_D – ash content of wood sawdust, %
- m_u – total mass of coal in mixture A2, g
- m_D – total mass of wood sawdust in mixture A2, g

It is clear that the total combustible mass in the briquette consists of the combustible components of coal and wood, since pyrophyllite contains no combustible elements in its composition [1]. From this fact, the proportion of combustible matter from coal and sawdust in the briquette, based on the total mass introduced into the mixture, can be calculated using the following relationship:

$$S_{mb} = \frac{m_{Smu} + m_{Smd}}{m_{Smb}}; \% \text{ odnosno, } S_{mb} = \frac{m_{Smu}}{m_{Smb}} + \frac{m_{Smd}}{m_{Smd}}; \ \% \quad \text{(Eq.2)}$$

Thus, in the briquette, the total amount of combustible matter, expressed in relative terms, consists of the combustible components from coal and sawdust, whose sum equals 100%, as represented in the following formula [4][5].

$$S'_{mu} + S'_{md} = 100\%$$

Accordingly, by considering the previous relationships, i.e., the relative proportions of coal and sawdust in the combustible mass, and the determined value of the briquette's combustible matter, we can calculate the contribution of each component to the total combustible matter using the following relationship [5]:

$$S'_{mu} = \left(\frac{m_{Smu}}{m_{Smb}}\right) \cdot 100; \% \ \text{ i } \ S'_{md} = \left(\frac{m_{Smd}}{m_{Smb}}\right) \cdot 100; \ \% \quad \text{(Eq.3)}$$

Absolute participation of the individual components can then be obtained by multiplying this relative participation by the value of combustible materials in each of the briquette samples:

$$S_{mu} = S'_{mu} \cdot \left(\frac{S_{mb}}{100}\right); \text{ odnosno, } S_{md} = S'_{md} \cdot \left(\frac{S_{mb}}{100}\right); \ \% \quad \text{(Eq.4)}$$

where:

- m_{Smu}- mass of combustible matter from coal in the briquette, g,
- m_{Smd}- mass of combustible matter from sawdust in the briquette, g,
- m_{Smb}- mass of combustible matter in the briquette, g,
- Sm_b- share of combustible mass in the briquette, %,
- Sm_u- share of coal combustible mass in the briquette, %,
- Sm_{ud}- share of wood combustible mass in the briquette, %,
- $S'm_u$- relative share of coal combustible mass in the briquette, %,
- $S'm_{ud}$- relative share of wood combustible mass in the briquette, %.

Under this condition, the content of combustible matter from coal in each measured briquette sample can be determined using the following formula:

$$SM_U = \left(\frac{S_{UKB}}{S_{UKU}}\right) \cdot SM_B, \ \% \quad \text{(Eq.5)}$$

where:

- SM_U - combustible matter of coal in the i-th briquette sample, %
- SM_B – combustible matter of the i-th briquette, %

- $S_{UK\,B}$- total sulfur in the i-th briquette, %
- $S_{UK\,U}$- total sulfur from coal in the i-th briquette, %

By obtaining the value of coal combustible matter, it is easy to calculate the combustible matter of sawdust as the difference between this value and the total for each sample. This model, illustrated through the calculation of the combustible matter content of coal and sawdust and, based on that, the determination of the contribution of these two materials using a compilation of theoretically and experimentally obtained parameters, is presented for briquette A4 (i.e., A4-1, A4-2, and A4-3) in Table 6 [1].

Table 6. Analysis of briquette content based on combustible materials

Briquette		SM	Suku	Spu	Sgu	Coal	Sawdust
Analytical	A4	75,65	2,18	0,97	1,21	49,51	26,14
Experimental	A4-3	75,05	2,69	1,14	1,55	61,00	14,05
Experimental	A4-1	75,11	2,71	1,14	1,57	61,46	13,65
Experimental	A4-2	75,38	2,77	1,15	1,62	62,82	12,56

Further analysis of the content of these samples taken from the briquettes according to the model we present was carried out using ash, again approximating with the results obtained from the analytical model [3], and the results of this analysis for sample A4 are presented in Table 7.

The individual amounts of ash were obtained using the following formulas:

$$P_U = \left(\frac{P_{Bt}}{P_{Be}}\right)\cdot P_{Ut},\ P_D = \left(\frac{P_{Bt}}{P_{Be}}\right)\cdot P_{Dt},\ P_p = \left(\frac{P_{Bt}}{P_{Be}}\right)\cdot P_{pt},\ \% \quad \text{(Eq.6)}$$

where:

- P_U - ash from coal in the i-th briquette, %
- P_{Bt} - ash content in the analytical sample of the i-th pellet, %
- P_{Be} - ash content in the measured sample of the i-th pellet, %
- P_{Ut} - ash content in the theoretical (analytical) coal sample in the i-th pellet, %
- P_U - ash from coal in the i-th briquette, %

Table 7. Analysis of briquette content based on ash in the measurement sample

Briquette	P	Coal	Sawdust	Pyrophillite
A4	24,35	16,82	2,29	5,25
A4-3	24,95	17,23	2,34	5,38
A4-1	24,89	17,19	2,34	5,36
A4-2	24,62	17,01	2,31	5,30

In the same way, the remaining samples from the conducted experiments were determined, and by summing the combustible matter and ash from coal, wood sawdust, and pyrophyllite shale, we obtained the actual ratios of these materials, which were then used in the analysis, i.e., introduced into the instrument (e.g., for calorific value measurement in a 1 g calorimeter). The analysis for sulfur was carried out in the same manner, and the results are presented in Table 8.

5.2. Effect of Pyrophyllite on the Reduction of Sulfur Gas Emissions in Composite Briquettes

It is clear that the addition of materials with significantly lower sulfur content, such as wood

sawdust and pyrophyllite, reduces the total sulfur content in the briquette. According to the investigation of the main components, as emphasized earlier, coal contains both forms of sulfur, whereas sawdust and pyrophyllite contain only one form of sulfur. Based on this, the reduction of sulfur in the briquette results from the mass distribution of the briquette constituents. This mass distribution must be proportional to the total input values of the briquette constituents and the values determined through instrument measurements, and it applies to all types of sulfur (total, combustible, and in ash).

Another factor or mechanism that can influence the behavior of this type of sulfur is related to the content of pyrophyllite shale. The carbonates present in this shale convert into Ca and Mg oxides during coal combustion, which possess significant reactivity toward sulfur. In essence, this process mirrors the desulfurization with quicklime in coal-fired power plants. During this chemical reaction, gypsum is formed, which is incorporated into the ash. The presence of a higher amount of sulfur in the ash than predicted by the mass distribution supports the idea of combustible sulfur being converted into sulfur in the ash. This observation is also evident in TG (thermogravimetric) analysis, where a mass loss at temperatures around 850 °C corresponds to the release of CO_2 from the carbonates (Ca and Mg).

This finding highlights part of the mechanism of pyrophyllite action in the briquette during combustion, affecting the behavior of sulfur from coal. Sulfur released from coal, along with calcium and magnesium oxides from the carbonates, is reactive, and their reaction produces gypsum. As a result, in addition to the sulfur in the briquette ash derived from the non-combustible coal compounds, sulfur released during combustion is also captured. This mechanism is reflected in the research results through an increased amount of sulfur in the ash and a decreased amount of combustible sulfur, i.e., sulfur released into the atmosphere during combustion.

One should also consider the release of crystalline water from the pyrophyllite shale minerals and the potential molecular-level reactions that may occur. Additionally, the structure of pyrophyllite, with its fine, open porosity, enables adsorption of certain values, further contributing to the reduction of sulfur emissions.

Thus, the indicators of atmospheric impact for such a briquette mixture are the mass reduction of sulfur in the fuel and the relative ratio of sulfur released after briquette combustion.

Based on the experimental results presented in the table, the following table calculates the total sulfur reduction compared to a briquette made solely of coal.

Table 8. Total sulfur reduction relative to the coal-only briquette

Briquette	Coal	Sawdust	Pyrophillite	LHV, kJ/kg	Suk %	Sp %	Sg %	Reduction Suk, %
A1	*100*	*0*	*0*	*17961*	*3,29*	*1,747*	*1,82*	-
A2-3	73,06	18,8	8,14	18163	2,53	1,41	1,12	30,04
A2-2	73,94	17,95	8,12	17065	2,57	1,4	1,17	28,02
A2-1	73,31	18,66	8,03	18226	2,55	1,4	1,15	29,02
A4-3	75,05	19,57	5,38	17239	2,71	1,14	1,57	21,40
A4-2	75,11	19,53	5,36	17316	2,77	1,15	1,62	18,77
A4-1	75,38	19,32	5,3	16271	2,72	1,58	1,14	20,96
A3-3	73,6	24,62	1,78	18091	2,49	0,81	1,68	32,13
A3-1	73,36	24,86	1,78	18097	2,48	0,8	1,68	32,66
A3-2	74,25	23,99	1,76	18169	2,53	0,8	1,73	30,04
A5-3	68,27	31,73	0	18295	2,21	0,67	1,54	48,87
A5-2	70,21	29,79	0	18261	2,29	0,67	1,62	43,67
A5-1	72,25	27,75	0	16448	2,23	0,67	1,56	47,53

Let us examine the effects of individual briquette constituents on total sulfur, combustible sulfur, and sulfur in ash. In Figure 2, this dependence is shown for coal, in Figure 3 for sawdust, and in Figure 4 for pyrophyllite.

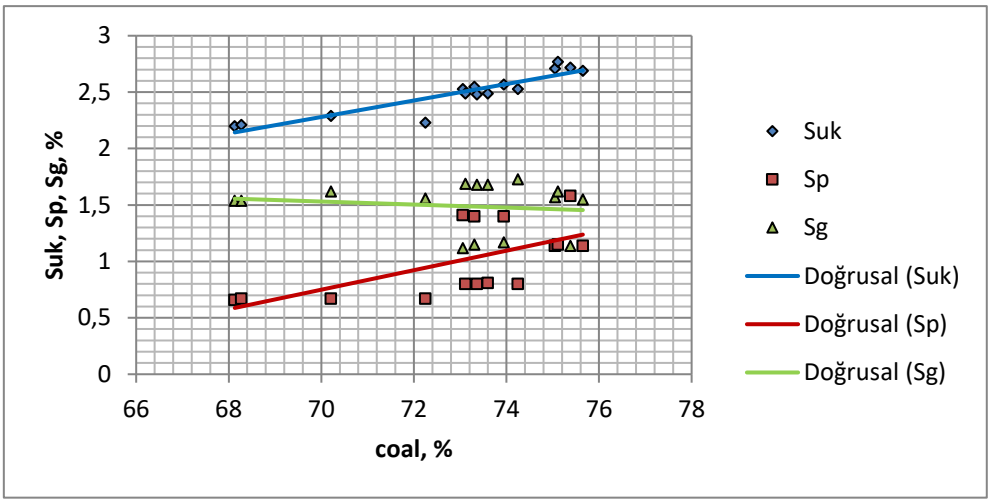

Figure 2. Effect of coal in the briquette on sulfur

According to this figure, coal affects total sulfur such that increasing its proportion in the mixed briquette raises both total sulfur and sulfur in ash, while the combustible sulfur decreases only slightly.

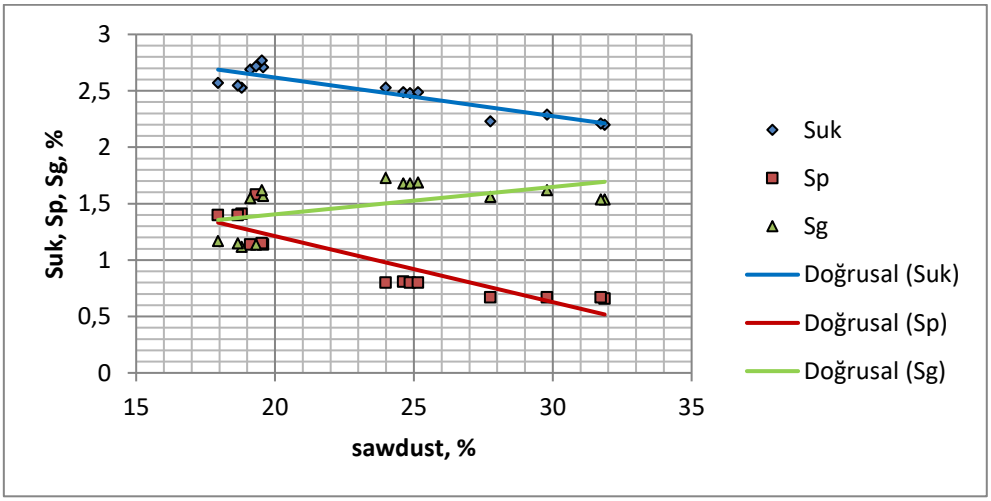

Figure 3. Effect of sawdust in the briquette on sulfur

From this relationship, it is evident that as the proportion of sawdust in the briquette increases, the total sulfur and sulfur in ash decrease, while the amount of combustible sulfur increases.

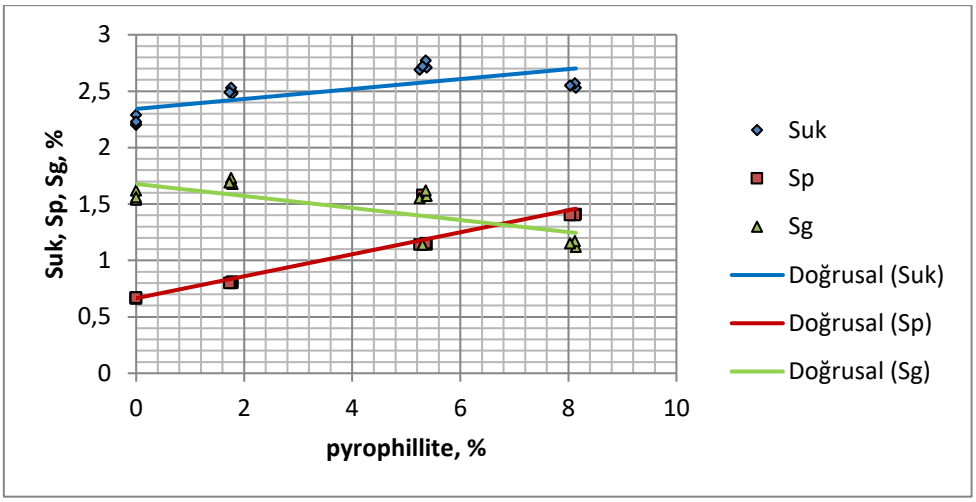

Figure 4. Effect of pyrophyllite in the briquette on sulfur

Increasing the content of pyrophyllite shale in the briquette leads to a slight increase in total sulfur, but a significant rise in sulfur in ash and a considerable decrease in combustible sulfur.

The reduction of total sulfur and the individual amounts of combustible sulfur and sulfur in ash is also related to the "dilution" effect through the addition of wood sawdust and pyrophyllite, which contain significantly lower sulfur content. This mass-based dilution of sulfur has been calculated and is presented in Table 9, along with the measured values of the same indicators obtained from experimental samples for comparison.

Table 9. The measured values of the same indicators obtained from experimental samples for comparison

			due to dilution			*Experimental*		
Briquette	Average Coal in Briquette, %	Pyrophillite shale, %	Sukt	Sp	Sg	*Suk*	*Sp*	*Sg*
A1	100,00	0,00	3,29	1,470	1,820	*3,290*	*1,470*	*1,820*
A2	70,24	0,00	2,31	1,033	1,278	*2,243*	*0,670*	*1,573*
A3	73,74	1,77	2,43	1,084	1,342	*2,513*	*1,003*	*1,510*
A4	75,18	5,35	2,47	1,105	1,368	*2,563*	*1,063*	*1,500*
A5	73,44	8,10	2,42	1,080	1,337	*2,550*	*1,403*	*1,147*

The relationship of the reduction of all forms of sulfur in the briquette due to mass dilution by the addition of wood sawdust and pyrophyllite is shown in the diagrams: Figure 5 for total sulfur, Figure 6 for combustible sulfur, and Figure 7 for sulfur in ash.

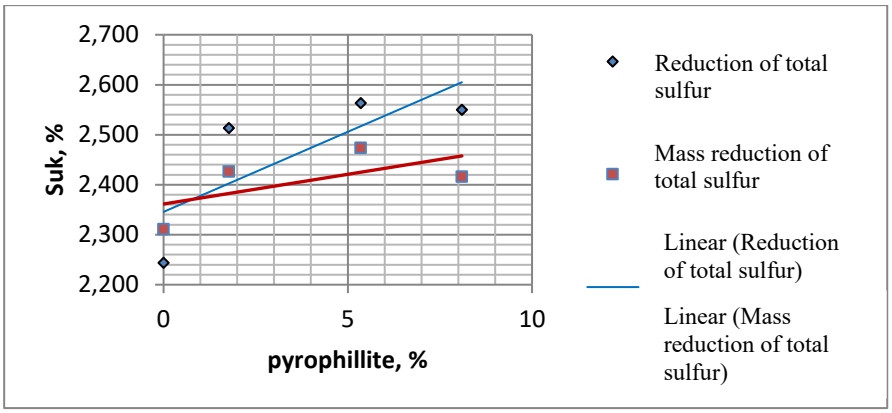

Figure 5. Relationship between mass-based and experimentally determined total sulfur versus the amount of pyrophyllite shale in the briquette

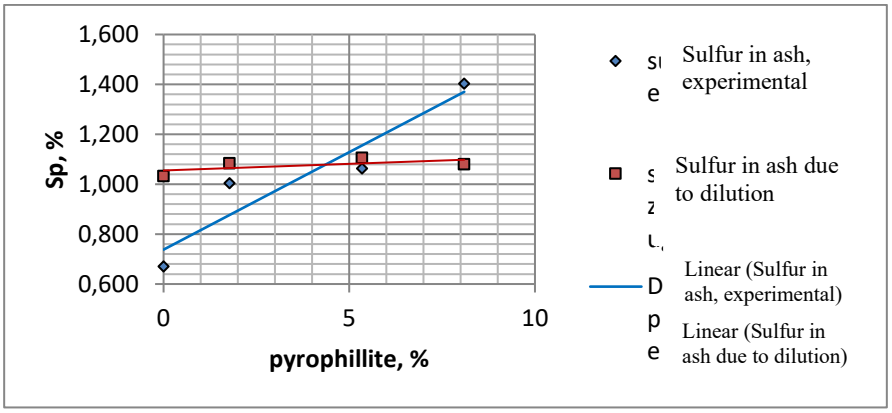

Figure 6. Relationship between mass-based and experimentally determined sulfur in ash versus the amount of pyrophyllite shale in the briquette

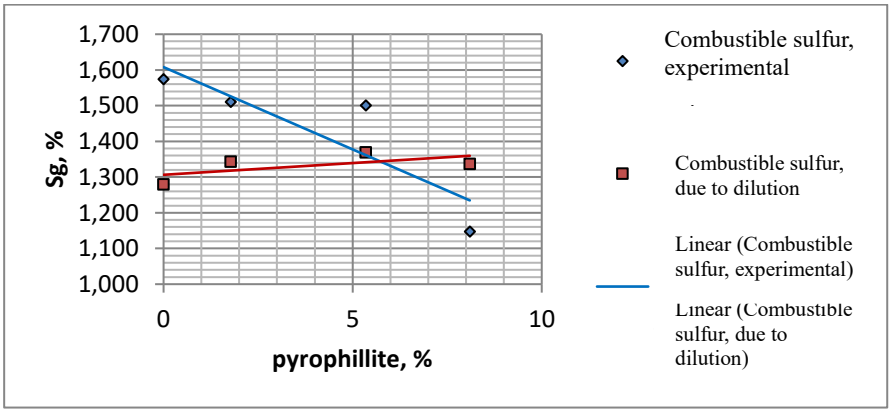

Figure 7. Relationship between mass-based and experimentally determined combustible sulfur versus the amount of pyrophyllite shale in the briquette

6. CONCLUSION

The basis of the hypothesis is the environmental impact of coal combustion, primarily on the atmosphere. For this reason, the majority of the research focused on the emissions released during this process, with sulfur highlighted as the primary ecological concern during coal combustion and investigated in detail. The experimental briquette samples were formulated so

that the combustible materials—coal and pine wood sawdust—always maintained the same mass proportion, while pyrophyllite was added in varying amounts across different briquettes. A total of five different combinations of this mixture were prepared in individual quantities of approximately 2.00 kg. The initial experimental sample consisted of a briquette with 100% coal content, while the remaining four contained a constant 1400 g of coal, 600 g of wood sawdust, and 40, 120, and 200 g of pyrophyllite shale. The briquettes were prepared under laboratory conditions.

The analysis therefore required two interdependent steps. In the first step, the analysis of the obtained indicators had a dual purpose: an analytical calculation of the relevant research indicators based on the prescribed recipe and the properties of the input components, and an analytical calculation of the content of the samples subjected to measurements.

The key indicator of the study, and the answer to the hypothesis, is reflected in the analysis of sulfur gases during the combustion of the experimental briquettes. In this case, inhomogeneities are observable, as noted in the previously described conclusions. These inhomogeneities can be approximated by observing the trends of the established dependencies in both the analytical and instrumental measurements of the experimental briquettes.

As expected, the analytical results show a reduction in all forms of sulfur due to the “dilution” of the coal material (the main carrier of sulfur) with sawdust and pyrophyllite shale. From this perspective, the results show certain deviations, but the trend for total sulfur is similar between analytically calculated values and those obtained through instrumental measurements. However, the distribution of total sulfur between combustible sulfur and sulfur in ash, in the context of mass reduction of coal in the briquette, differs significantly between the analytical model and the experimental results.

In Figure 6, the trend of a slight increase with changing pyrophyllite content is visible for the analytical model, alongside a sharp increase in sulfur in ash. Conversely, Figure 7 shows that while the trend is similar in the analytical model, it is completely opposite in the experimental model.

These diagrams provide clear evidence supporting the working hypothesis: the addition of pyrophyllite shale to the coal mass reduces the impact of sulfur gases released from the combustion of this mixture on the atmosphere.

REFERENCES

Alić N., (2020), Studija : “Istraživanje mogućnosti koncentracije pirofilita, iz ljubičastog varijiteta škriljca, ležišta Parsovići“, RGGF Tuzla.

Alić N., (2020), Mogućnost alternativne primjene ugljeva krekanskog bazena, Glasnik RGGF Tuzla.

Delić, I., Alić, N., Osmić, M., Stuhli, V., (2023), Energija iz uglja, stanje i perspektive, OFF set, Tuzla.

Razić, R., (2024), Modeliranje kompozitnog briketa na bazi uglja u cilju smanjenja emisije produkata sagorijevanja u atmosferu, Doktorski rad, RGGF Tuzla.

Tomanec, R. A., (2000), Metode ispitivanja mineralnih sirovina u pripremi mineralnih sirovina, Rudarsko Geološki fakultet u Beogradu.

VALUE-ADDED CONVERSION OF ZONGULDAK HARD COALS: INTEGRATED APPROACHES FOR INJECTION COAL, ACTIVATED CARBON, AND INDUSTRIAL APPLICATIONS

Faik ALP[1,*], Serdar YILMAZ[2], Mehmet BİLEN[2], İhsan TOROĞLU[2]

[1]Türkiye Taşkömürü Kurumu, 67100, Zonguldak, Turkiye
[2]Zonguldak Bülent Ecevit University, Engineering Faculty, Department of Mining Engineering, İncivez, 67100, Zonguldak, Turkiye
**Corresponding author: faikerim@hotmail.com*

A B S T R A C T

The Zonguldak Hard Coal Basin is the only region in Türkiye that encompasses the country's entire hard coal potential, offering coal with varying coking properties. This study presents the outcomes of three major projects focused on converting coking and semi-coking coals from Armutçuk and its vicinity into high value-added industrial products beyond their conventional use as power plant fuel. First, it was demonstrated that coal with high ash content—due to outdated washing systems—can be upgraded using modern washing technologies to produce pulverized coal injection (PCI) coal, foundry sand additives, barbecue/hookah charcoal, and raw material for activated carbon. Second, a novel prototype furnace system operating on the physical activation principle was developed to produce high-surface-area activated carbon from coking coal. Third, a comprehensive set of accredited analyses was conducted to assess the suitability of Zonguldak coals for various industrial applications (e.g., metallurgy, environmental technologies, foundry, and water treatment). The study proposes a strategic transformation model for the sustainable utilization of Zonguldak coals and supports innovative, local solutions to reduce import dependency.

Key words: *Zonguldak hard coal, injection coal, activated carbon, carbonization, foundry additive, value-added product*

1. INTRODUCTION

Located in northwestern Türkiye, the Zonguldak Coal Basin is the country's sole hard coal basin, characterized by high-volatile bituminous coals with strong coking potential (FSI: 7–9), although pronounced lateral and vertical quality variations arise from complex depositional and tectonic conditions. While non-coking coals (FSI: 0–1) occur in the Amasra sub-basin, the Armutçuk region is dominated by weakly coking coals (FSI: 2–4; LC: 8–12), which directly influence their technological behavior and utilization potential. In this context, the present study evaluates the suitability of Armutçuk (TTK) coals for high value-added applications beyond conventional combustion, employing an integrated framework of physicochemical, petrographic, and technological analyses to identify alternative utilization pathways and promote more sustainable and efficient resource use.

2. ZONGULDAK COAL BASIN

The Zonguldak Coal Basin is Türkiye's only hard coal region and the principal source of bituminous reserves, including both coking and non-coking coals. High-quality metallurgical coals are mainly found in Kozlu, Üzülmez, and Karadon, while Armutçuk and Amasra coals are suitable for blending. The basin extends from the Upper Carboniferous Alacaağzı to the Karadon Formation and contains 46 seams, 18 of which are economically viable. Total reserves are about 1.514 billion tons (48% proven), with seam thicknesses typically between 0.8 and 3.5 m. Mining has reached depths of up to −630 m, and operations are constrained by

complex geological conditions. Coking coals account for around 57% of reserves, underlining the basin's strategic importance.

Table 1. Information on operating collieries in the basin (Öztürk, 2014)

Colliery	Reserve (10^6 ton)	Production (10^3 ton/year)	Number of Employees	Average Production Depth (m)
Armutçuk	37		1,120	550
Amasra	618	250	720	236
Karadon	405	806	2,948	373
Kozlu	154	647	1,824	630
Üzülmez	300	486	1,598	200
Total	1,514	2,441	9,074	

Table 2. World coal trade (million tons)

Type	Exp. 2023	Exp. 2024	Imp. 2023	Imp. 2024
Thermal & Lignite	1,151	1,178	1,157	1,178
Coking Coal	351	369	352	368
Total	1,502	1,547	1,510	1,546

3. TTK ARMUTÇUK HARD COAL ENTERPRISE

Hard coal mining in Türkiye began with the discovery by Uzun Mehmet in 1829 in the Karadeniz Ereğli region, followed by the initiation of systematic production in the Zonguldak Coal Basin in 1848, which established the foundation of sustained underground mining. Within this basin, the TTK Armutçuk Enterprise, located approximately 35 km west of Zonguldak, spans nearly 100 km² and hosts about 38 million tons of reserves, predominantly concentrated in the Büyük seam. This principal production horizon, situated between the Kozlu and Alacaağzı formations, exhibits thicknesses ranging from 3 to 25 m (averaging ~6 m) (TTK 2021, Didari et al. 2015).

3.1. Armutçuk Coal Preparation Plant

The Armutçuk Coal Preparation Plant, commissioned in 1960 by McNally with a capacity of 210 t/h, treats ROM coal from the TTK Armutçuk Enterprise. Originally incorporating a Baum jig, shaking tables, and flotation units, the flowsheet was later simplified by removing fine coal cleaning circuits. This modification significantly reduced separation efficiency—particularly in the 0–10 mm size fraction—and led to increased ash content in the clean coal, as reflected in December 2024 supply data (Table 3).

Table 3. December 2024 TTK Armutçuk coal supply

Date	TTK Loading Amount (Ton)	Ash (%)	Moisture (%)	ERDEMİR Discharge Amount (Ton)	Ash (%)	Moisture (%)	Payable (Average of TTK & ERDEMİR) Loading Amount (Ton)	Ash (%)	Moisture (%)	Ash Diff	Moisture Diff
3.12.2024	113,320	21,00	8,60	112,96	19,92	8,59	113,320	20,46	8,60	1,08	0,01
4.12.2024	113,780	20,30	8,90	113,50	21,28	8,64	113,780	20,30	8,90	-0,98	0,26
5.12.2024	56,500	20,80	9,70	56,12	23,56	9,62	56,500	22,18	9,70	-2,76	0,08
6.12.2024	85,000	21,50	8,40	84,68	22,17	9,53	85,000	21,50	8,97	-0,67	-1,13
11.12.2024	56,440	19,00	8,30	56,36	20,94	8,67	56,440	19,97	8,30	-1,94	-0,37
12.12.2024	113,900	20,30	8,80	113,44	21,91	10,23	113,900	21,11	9,52	-1,61	-1,43
13.12.2024	85,300	20,50	8,90	84,88	21,92	9,54	85,300	21,21	8,90	-1,42	-0,64
16.12.2024	84,420	15,40	9,20	84,22	19,05	9,90	84,420	17,23	9,20	-3,65	-0,70
17.12.2024	84,380	18,10	7,60	84,92	19,40	9,23	84,380	18,75	8,42	-1,30	-1,63
18.12.2024	113,620	14,30	7,30	113,26							

As shown in Table 3, ash often exceeds 20%, with loading–discharge differences indicating variable quality; although moisture is acceptable, high ash reduces performance, a trend also seen in November 2024 (Table 4).

Table 4. November 2024 TTK Armutçuk coal supply

Date	TTK Loading Amount (Ton)	Ash (%)	Moisture (%)	ERDEMİR Discharge Amount (Ton)	Ash (%)	Moisture (%)	Payable (Average of TTK & ERDEMİR) Loading Amount (Ton)	Ash (%)	Moisture (%)	Ash Diff	Moisture Diff
1.11.2024	56,880	16,40	7,00	56,74	18,60	8,67	56,880	17,50	7,84	-2,20	-1,67
4.11.2024	56,660	16,50	6,60	56,54	19,38	7,50	56,660	17,94	6,60	-2,88	-0,90
6.11.2024	113,800	15,80	7,10	113,50	19,38	7,50	113,800	17,59	7,10	-3,58	-0,40
7.11.2024	111,820	16,90	9,00	111,60	19,74	10,25	111,820	18,32	9,63	-2,84	-1,25
18.11.2024	113,320	20,36	9,72	112,90	23,86	11,38	113,320	22,11	10,55	-3,50	-1,66
19.11.2024	113,760	20,55	8,80	113,30	26,77	10,39	113,760	23,66	9,60	-6,22	-1,59
20.11.2024	56,580	20,76	9,04	56,46	25,92	10,20	56,580	23,34	9,62	-5,16	-1,16
21.11.2024	85,220	19,45	8,86	84,98	18,54	10,59	85,220	19,45	9,73	0,91	-1,73
22.11.2024	85,240	21,60	9,40	84,80	17,89	10,31	85,240	19,75	9,40	3,71	-0,91
25.11.2024	84,920	20,70	7,60	84,32	19,59	7,80	84,920	20,15	7,60	1,11	-0,20
26.11.2024	56,640	19,80	7,30	56,52	20,66	23,11	56,640	19,80	15,21	-0,86	-15,81
TOTAL / AVG	934,840	18,99	8,36	931,660	21,10	10,40	934,840	20,06	9,28	-21,51	-27,28

Table 4 shows ~20% ash, with some batches >22–23%, indicating poor control from lack of fine coal cleaning, also seen in October 2024 (Table 5).

Table 5. October 2024 TTK Armutçuk coal supply

Date	TTK Loading Amount (Ton)	Ash (%)	Moisture (%)	ERDEMİR Discharge Amount (Ton)	Ash (%)	Moisture (%)	Payable (Average of TTK & ERDEMİR) Loading Amount (Ton)	Ash (%)	Moisture (%)	Ash Diff	Moisture Diff
1.10.2024	56,560	15,50	9,20	56,70	18,49	10,50	56,560	17,00	9,85	-2,99	-1,30
3.10.2024	84,780	19,80	9,00	84,60	20,32	9,34	84,780	19,80	9,00	-0,52	-0,34
9.10.2024	113,780	19,00	9,60	113,40	15,49	10,20	113,780	17,25	9,60	3,51	-0,60
10.10.2024	113,140	17,20	8,80	112,80	21,17	9,14	113,140	19,19	8,80	-3,97	-0,34
11.10.2024	85,220	18,90	8,90	85,00	20,34	9,61	85,220	19,62	8,90	-1,44	-0,71
14.10.2024	84,540	18,60	9,00	84,30	20,75	9,59	84,540	19,68	9,00	-2,15	-0,59
15.10.2024	85,880	16,10	7,50	84,40	14,90	9,26	85,880	15,50	8,38	1,20	-1,76
16.10.2024	56,620	17,20	7,40	56,40	22,38	8,15	56,620	19,79	7,40	-5,18	-0,75
17.10.2024	85,080	16,30	7,80	85,10	18,46	9,82	85,080	17,38	8,81	-2,16	-2,02
22.10.2024	85,000	17,50	9,90	84,70	24,02	10,82	85,000	20,76	9,90	-6,52	-0,92
24.10.2024	85,240	19,30	8,70	85,00	15,47	10,32	85,240	17,39	9,51	3,83	-1,62
25.10.2024	84,980	20,30	8,30	84,54	18,92	10,08	84,980	19,61	9,19	1,38	-1,78
30.10.2024	56,820	21,40	8,80	56,74	17,05	9,33	56,820	19,23	8,80	4,35	-0,53
TOTAL / AVG	1.077,640	18,25	8,73	1.073,680	19,00	9,73	1.077,640	18,60	9,05	-16,39	-10,95

October shows slightly lower ash than November–December, but still above optimal PCI limits. Variability indicates inconsistent quality. September data are in Table 6.

Table 6. September 2024 TTK Armutçuk coal supply

Date	TTK Loading Amount (Ton)	Ash (%)	Moisture (%)	ERDEMİR Discharge Amount (Ton)	Ash (%)	Moisture (%)	Payable (Average of TTK & ERDEMİR) Loading Amount (Ton)	Ash (%)	Moisture (%)	Ash Diff	Moisture Diff
2.09.2024	113,100	14,80	6,20	112,98	16,83	5,91	113,100	15,82	6,20	-2,03	0,29
9.09.2024	84,760	14,60	7,10	84,58	14,84	9,44	84,760	14,60	8,27	-0,24	-2,34
10.09.2024	113,100	13,40	8,60	112,76	16,94	8,13	113,100	15,17	8,60	-3,54	0,47
11.09.2024	85,280	14,20	8,20	84,94	16,85	8,34	85,280	15,53	8,20	-2,65	-0,14
12.09.2024	56,360	13,50	7,40	56,18	15,68	8,21	56,360	14,59	7,40	-2,18	-0,81
16.09.2024	84,480	13,40	7,80	84,34	15,95	7,84	84,480	14,68	7,80	-2,55	-0,04
17.09.2024	84,700	13,70	7,60	84,46	13,99	12,70	84,700	13,70	10,15	-0,29	-5,10
18.09.2024	85,200	15,90	8,50	84,68	18,91	8,23	85,200	17,41	8,50	-3,01	0,27
19.09.2024	56,840	16,30	7,90	56,58	19,47	8,78	56,840	17,89	7,90	-3,17	-0,88
24.09.2024	84,740	15,80	7,90	84,60	19,77	8,71	84,740	17,79	7,90	-3,97	-0,81
25.09.2024	56,720	14,70	8,30	56,62	20,01	8,36	56,720	17,36	8,30	-5,31	-0,06
26.09.2024	56,640	15,20	8,80	56,44	19,64	7,69	56,640	17,42	8,25	-4,44	1,11
27.09.2024	85,240	14,80	9,30	85,08	16,48	9,86	85,240	15,64	9,30	-1,68	-0,56
TOTAL / AVG	1.047,160	14,58	7,93	1.044,240	17,17	8,58	1.047,160	15,85	8,20	-28,94	-9,15

Table 6 shows lower ash (~15–16%), but rising values from October to December indicate declining performance and the need for modernization, continuing into January 2025 (Table 7).

Table 7. January 2025 TTK Armutçuk coal supply

Date	TTK Loading Quantity (t)	Ash (%)	Moisture (%)	ERDEMİR Discharge Quantity (t)	Ash (%)	Moisture (%)	Payable Quantity (t)	Ash (%)	Moisture (%)	Difference Ash	Difference Moisture
14.01.2025	112.58	21.20	10.60	112.26	18.76	10.38	112.58	19.98	10.60	2.44	0.22
15.01.2025	84.72	16.40	9.10	84.40	12.95	8.97	84.72	14.68	9.10	3.45	0.13
20.01.2025	84.56	12.20	10.50	83.74	15.69	13.88	84.56	13.95	12.19	-3.49	-3.38
21.01.2025	28.32	11.70	9.40	28.12	15.35	9.44	28.32	13.53	9.40	-3.65	-0.04
22.01.2025	56.72	18.80	11.70	56.10	19.67	13.76	56.72	18.80	12.73	-0.87	-2.06
23.01.2025	113.00	20.10	11.10	111.98	19.17	11.48	113.00	20.10	11.10	0.93	-0.38
27.01.2025	84.48	21.00	7.70	83.88	19.89	8.04	84.48	20.45	7.70	1.11	-0.34
28.01.2025	56.86	19.60	7.10	56.42	22.71	9.13	56.86	21.16	8.12	-3.11	-2.03
29.01.2025	83.86	20.70	9.10	83.44	22.36	8.48	83.86	21.53	9.10	-1.66	0.62
30.01.2025	56.72	21.80	8.50	56.36	21.18	9.39	56.72	21.80	8.50	0.62	-0.89
TOTAL / AVG	761.820	18.82	9.63	756.700	18.77	10.35	761.820	18.86	9.97	-4.23	-8.15

Table 7 shows payable ash remains near 19% while moisture meets limits, indicating the main issue is insufficient ash reduction. Financial impacts are summarized in Tables 8 and 9.

Table 8: TTK customer premium-penalty table (2024, Excl. VAT)

Customer	Quantity (ton)	Amount (TL)	Ash/Calorific Bonus (TL)	Ash/Calorific Deduction (TL)	Moisture Bonus (TL)	Moisture Deduction (TL)	Net Premium Compensation (TL)	Total Amount (TL)	Avg. Sales Price (TL/ton)
ÇATES Electricity Generation Inc.	490,202.460	468,820,448.22	0	0	0	0	0	468,820,448.22	956
Other Industry	2,000.655	13,689,483.86	0	0	0	0	0	13,689,483.86	6,842.50
ERDEMİR	17,186.701	89,023,547.39	262,281.77	3,054,550.59	1,075,603.90	51,813.16	-1,768,478.08	87,255,069.31	5,076.89
Internal Consumption	9,369.093	49,130,943.14	0	0	0	0	0	49,130,943.14	5,243.94
KARDEMİR	197,465.623	1,208,386,900.24	5,608,545.96	21,436,398.28	30,095,628.39	1,076,960.52	13,190,815.55	1,221,577,715.79	6,186.28
TESHİN	6,073.420	47,263,292.49	0	0	0	0	0	47,263,292.49	7,781.99
TOTAL	722,297.952	1,876,314,615.34	5,870,827.73	24,490,948.87	31,171,232.29	1,128,773.68	11,422,337.47	1,888,100,902.57	2,614.02

Table 9: Summary premium-penalty table

Customer	Quantity (ton)	Amount (TL)	Premium (TL)	Compensation (TL)	Net Premium Compensation (TL)	Total Amount (TL)	Avg. Sales Price (TL/ton)
ÇATES Electricity Generation Inc.	490,202.460	468,820,448.22	0	0	0	468,820,448.22	956
Other Industry	2,000.655	13,689,483.86	0	0	0	13,689,483.86	6,842.50
ERDEMİR	17,186.701	89,023,547.39	1,337,885.67	3,106,363.75	-1,768,478.08	87,255,069.31	5,076.89
Internal Consumption	9,369.093	49,130,943.14	0	0	0	49,130,943.14	5,243.94
KARDEMİR	197,465.623	1,208,386,900.24	35,704,174.35	22,513,358.80	13,190,815.55	1,221,577,715.79	6,186.28
TESHİN	6,073.420	47,263,292.49	0	0	0	47,263,292.49	7,781.99
TOTAL	722,297.952	1,876,314,615.34	37,042,060.02	25,619,722.55	11,422,337.47	1,888,100,902.57	2,614.02

Tables 8–9 show ash penalties exceed bonuses for ERDEMİR, causing net losses; overall (Tables 3–9), the plant has reached its limits, and high ash in the 0–10 mm fraction necessitates a modern facility.

4. UTILIZATION OF ARMUTÇUK COAL

Armutçuk coal is a semi-coking, high-volatile bituminous coal characterized by high lustrous carbon, which enhances its reactivity in metallurgical processes. Although the ROM coal

contains 45–50% ash, efficient washing can reduce this to 5–10%, significantly improving quality and value. Such coals are relatively rare, increasing their strategic importance.

Thanks to these properties, Armutçuk coal is suitable for high value-added uses such as PCI in blast furnaces, carbon additives in foundries, activated carbon production, barbecue and hookah charcoal, and as a carbon and energy source in EAF steelmaking, making it a versatile industrial resource.

4.1. Use as a Carbon Additive in Foundry Sand

Mold quality in casting depends on the binding system. Molding sands are mainly clay-bonded (greensand) or chemically bonded. Greensand typically contains silica sand (85–95%), bentonite (4–10%), carbon additives (2–10%), and minor components, and is widely used due to its low cost, recyclability, and stable performance (Figure 1).

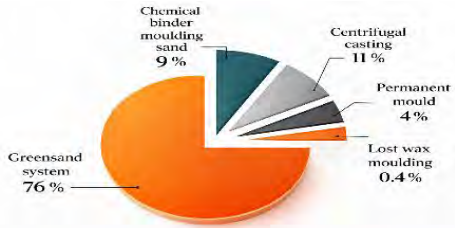

Figure 1: Share of the Greensand System molding method (Kwaśniewska and Holtzer 2013)

Figure 2: Greensand casting advantages

Figure 3: Greensand casting

As shown in Figure 1, greensand dominates casting due to its flexibility and compatibility with carbon additives. In these systems, low-ash coal with high lustrous carbon improves surface quality, reduces defects, and limits oxidation; key properties such as ash, VM, S, N, and an FSI of 2–4 must be controlled.

Despite being more environmentally acceptable than chemical systems, some organic additives release harmful emissions (VOC, PAH, BTEX) and are generally avoided. Greensand casting is widely used across industries including automotive, machinery, mining, and steel production (Figure 2).

Figures 2 and 3 illustrate advantages of greensand molding, practice and casting quality, showing mold structure and improved surface finish with proper carbon additives. In Türkiye, the foundry sector includes about 1,040 enterprises and holds strong global significance, with greensand systems widely used. However, only limited coal resources meet the required properties for such applications.

Armutçuk coal satisfies these criteria, with suitable volatile matter, 10–12% lustrous carbon, low sulfur, and appropriate grindability. Although ROM coal contains high ash, washing reduces it to 5–10%, producing a high-quality coal suitable for foundry use.

4.2. Use of Pulverized Coal Injection (PCI) in Blast Furnaces

Pulverized Coal Injection (PCI) is used in blast furnaces to reduce coke consumption, improve efficiency, and lower costs by injecting fine coal through tuyeres. Its performance depends on coal properties such as rank, ash, volatile matter, moisture, sulfur, maceral composition, and particle size, which affect combustion behavior (Dike 2008).

The industrial use of PCI began in the early 1980s in Europe and Japan, mainly driven by the need to reduce reliance on expensive coke. Its importance increased after the 1979 oil crisis,

when coal injection replaced fuel oil systems, demonstrating strong economic benefits; approximately 0.9 tons of injected coal can substitute about 1.4 tons of coking coal.

In Türkiye, the only coal source meeting PCI quality requirements is the Armutçuk coal field. When run-of-mine coal from this region is beneficiated to reduce ash content below 10%, it becomes suitable for high injection rates without negatively affecting combustion or slag chemistry. Under the agreement between Erdemir and TTK, this coal is supplied for PCI applications, priced at 127 USD per ton (for 10% moisture and 12% ash), and ground below 75–85 microns before injection. Although Erdemir and İsdemir consume around 1,000,000 tons of PCI coal annually, only a small fraction is supplied domestically, with the majority being imported at approximately 250 USD per ton. Türkiye's total PCI demand is about 1.6 million tons per year, while Armutçuk holds around 35 million tons of geological reserves. Increasing local production and improving coal preparation infrastructure would significantly reduce import dependency.

Globally, coal remains essential in steel production, with about 14% of hard coal used in the iron and steel industry and nearly 70% of crude steel still produced via coal-based routes. PCI coal, in particular, has gained importance in international trade due to its cost advantage and its role in reducing blast furnace operating costs, leading to a steady increase in global demand.

Table 10. Countries Using PCI Coal Worldwide (thousand tons)

Country	2015	2016	2017	Country	2015	2016	2017	Country	2015	2016	2017
Japan	14,005	14,043	14,376	Netherlands	1,496	1,459	1,641	Sweden	313	441	406
Korea	9,592	8,266	8,539	United Kingdom	1,544	1,364	1,301	Czechia	300	319	278
Russia	5,080	6,264	6,376	Belgium	1,253	1,495	1,495	Finland	53	304	333
Germany	4,881	4,841	4,933	Italy	672	855	483	Poland	270	283	366
India	3,390	3,461	3,696	Spain	879	819	909	Serbia	56	74	82
France	2,421	2,359	2,873	Austria	764	806	838	Australia	60	73	73
Taiwan	2,161	2,066	1,815	Türkiye	690	660	1,394	Norway	74	55	101
USA	870	1,462	1,376	Slovakia	608	586	668	World Total	51,419	52,355	54,351

Table 10 shows PCI use rose to 54.351 Mt (2015–2017), led by Japan, Korea, Russia, Germany, and India (~70%); Türkiye also increased, confirming PCI's growing role in cost-efficient ironmaking.

4.3. Blast Furnace Process

Steel production mainly follows two routes: the blast furnace–basic oxygen furnace (BF–BOF) and the electric arc furnace (EAF). These differ in raw materials, process chemistry, and energy use. BF–BOF is generally used for flat products, while EAF is more common for long products, although modern EAFs can also produce flat steel. Despite this, the BF–BOF route remains dominant, and the overall process flow is illustrated in Figure 4 and Figure 5.

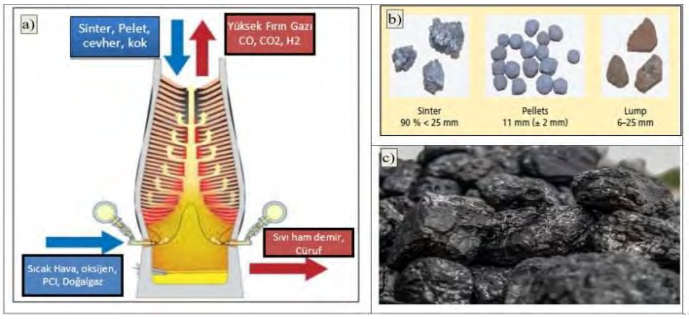

Figure 4 a) Blast furnace inputs/outputs, b) iron-bearing burden materials, c) metallurgical coking coal (Geerdes et al., 2015; Chaigneau and Wise 2009)

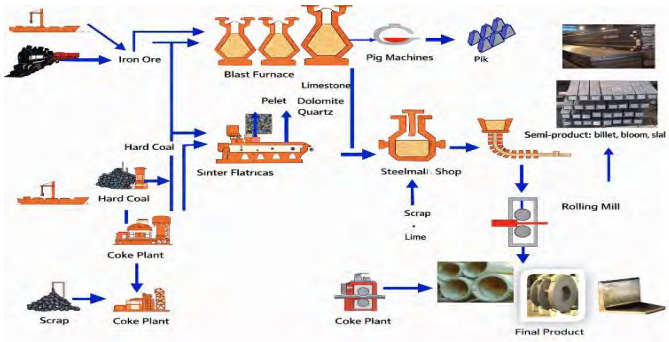

Figure 5. Blast furnace inputs, outputs, and final products

As shown in Figure 4 and Figure 5, blast furnace ironmaking involves iron-bearing materials, coke, and auxiliary fuels within an integrated production system. Unlike the EAF route (Maki et al., 1996), this process relies on chemical reduction using coke and PCI; the system configuration is illustrated in Figure 6–Figure 8.

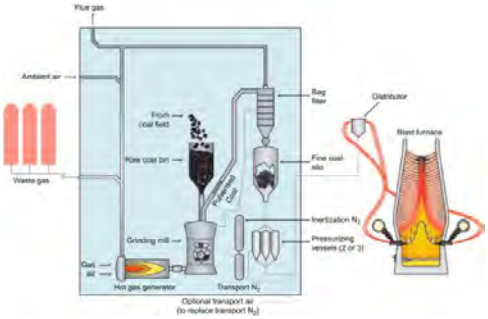

Figure 6. Blast furnace

Figure 7. PCI coal grinding unit and ground PCI coal (<80 microns).

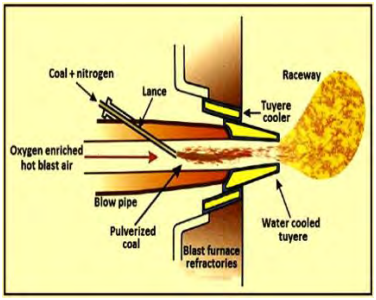

Figure 8. Schematic view of pulverized coal injection in blast furnace.

Figures 6–8 show PCI-assisted blast furnace operation, including furnace structure, fine coal grinding, and tuyere injection, while Figure 9 highlights coal's role as fuel and reducing agent. Coke undergoes drying, limited reaction, and structural support as it descends, ensuring permeability in the cohesive zone. At higher temperatures, it interacts with molten phases and moves toward the raceway, where combustion processes are illustrated in Figure 9 and Figure 10.

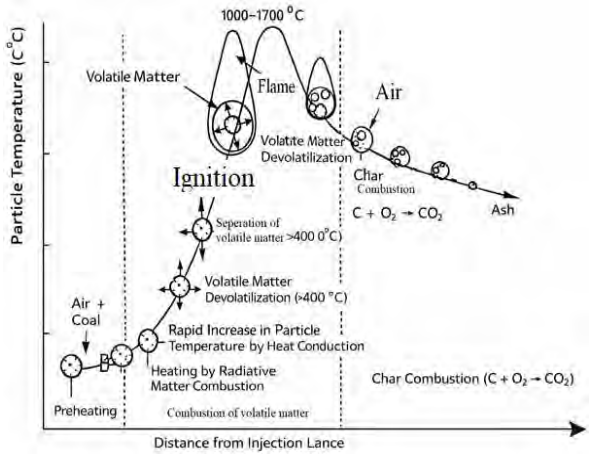

Figure 9. Pulverized coal combustion process

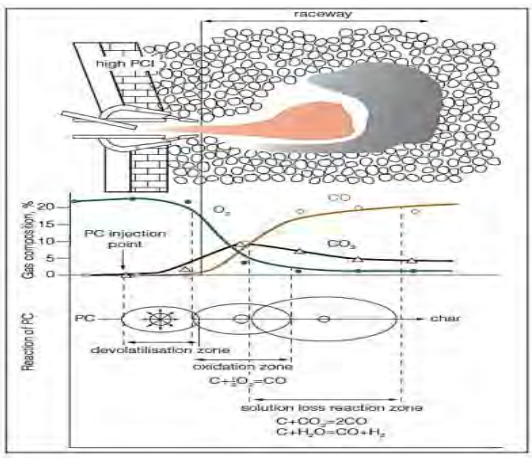

Figure 10. Schematic representation of raceway reactions (Mousa 2019).

As shown in Figure 9 and Figure 10, injected pulverized coal rapidly devolatilizes and reacts within the raceway through oxidation and gasification mechanisms. Most coke is consumed in this zone, while a small portion reaches the hearth and dissolves slowly in molten iron (Baran 2019). Overall, the PCI-supported blast furnace remains the dominant route for large-scale ironmaking, as illustrated by the figures.

5. THE EFFECT OF PCI COAL ON COSTS

Increasing PCI rates reduces coke consumption while improving combustion intensity, furnace efficiency, and productivity. It also lowers energy costs since coal is cheaper than coke and reduces the load on coke ovens. Industrial applications confirm significant economic gains, highlighting PCI's importance in cost-effective ironmaking. However, maintaining performance at high injection rates requires strict control of coal quality.

Table 11. Specifications of Pulverized Coal Used at ERDEMİR–İSDEMİR Inc.

Property	Value (%)	Applicable Standards
Moisture	8% max	ASTM D2961–93
Ash	11% max	ASTM D3174–93
Fixed Carbon	53% min	ASTM D3172–89 (1993)
Volatile Matter	30–36%	ASTM D3175–89a (1993)
Sulfur	0.50% max	ASTM D4239–94
K_2O in Ash	1.40% max	ASTM D4326–94
Na_2O in Ash	0.40% max	ASTM D4326–94
Total Alkali in Ash	1.8% max	ASTM D4326–94
Al_2O_3 in Ash	27% max	ASTM D4326–94
P in Ash	0.40% max	ASTM D4326–94
O_2 Amount	10% max	ASTM D3176–89
Light Transmittance (applied to bituminous coals)	90% min	ASTM D5263–92

As shown in Table 11, moisture and ash are limited, while fixed carbon, volatile matter, sulfur, and alkalis are controlled to ensure stable operation and prevent slag and refractory issues. These criteria indicate that PCI coal selection depends on strict technical requirements as well as cost.

6. ACTIVATED CARBON PRODUCTION

Activated carbon is a carbon-rich material with a highly developed porous structure and large internal surface area, which governs its strong adsorption capacity. It is widely used for removing contaminants from gas and liquid phases. According to IUPAC classification, pores are divided into micropores (<2 nm), mesopores (2–50 nm), and macropores (>50 nm), with micropores contributing approximately 95% of the total surface area and playing a dominant role in adsorption. It can be produced from various low-cost carbonaceous precursors such as wood, coal, peat, coconut shells, and agricultural wastes. The properties of the raw material—including carbon content, mineral matter, and structural characteristics—significantly influence the pore structure and adsorption performance of the final product. Among these, coal is commonly preferred due to its availability and mechanical strength, and its use in activated carbon production has gained importance as an alternative to direct combustion under increasing environmental constraints (Döngel 1997, Demir and Elbinsoy (2019)). Activated carbon is commercially produced in several forms, including lump, pelletized, granular, and powdered types, as shown in Figure 11 and Figure 12.

Figure 11 Lump, pellet, and powdered activated carbon.

Figure 12 Coal-based activated carbon used in toxic gas filters.

As shown in Figure 11, particle morphology and size distribution vary with production method and application, while Figure 12 highlights the critical role of coal-based activated carbon in gas masks and industrial filters for effective removal of toxic gases via its well-developed microporous structure. PAC is typically used in batch processes, whereas GAC is preferred in fixed-bed systems due to its mechanical strength. Production involves preparation, granulation, carbonization (500–600 °C), and activation (900–950 °C), where pore structure and surface area are progressively developed.

The global activated carbon market is valued at approximately 4.7 billion USD, with Türkiye consuming around 6,000 tons annually, predominantly in water treatment. Limited domestic production indicates strong potential for coal-based alternatives to reduce imports and support exports. Key quality parameters include surface area, iodine number, ash, moisture, and particle size. In this study, high-quality GAC (iodine number ≥900 mg/g; surface area 1000–1600 m²/g) is targeted, and results demonstrate that beneficiated TTK Armutçuk coal can achieve BET surface areas of 1250–2500 m²/g, indicating high adsorption performance.

7. BARBECUE CHARCOAL PRODUCTION

Wood exhibits favorable combustion characteristics compared to conventional solid fuels, including rapid ignition, lower air requirement (7–9 m³/kg versus 15–17 m³/kg for coal), and relatively low ash content (~5%). Its calorific value depends on factors such as moisture, density, and extractive content, with higher moisture reducing heating efficiency. Oven-dry forest residues typically range between 3000–4500 kcal/kg.

Carbonized materials such as coal and biomass residues can be densified through briquetting into various shapes using binders and controlled moisture (8–25%). The process involves crushing, mixing, compaction, and drying, with binder type and moisture content critically affecting product quality and combustion performance.

Armutçuk coal, when beneficiated to reduce ash below 9–10%, shows strong potential for smokeless barbecue charcoal production. It can be co-briquetted with carbonized biomass (e.g., hazelnut shells, olive and apricot pits), as illustrated in Figure 13.

Figure 13. Coal-based smokeless barbecue charcoal.

8. CONCLUSIONS

Armutçuk coals represent a rare domestic resource in Türkiye with properties suitable for high value-added applications such as PCI, foundry additives, activated carbon, and smokeless charcoal. While their use in PCI and foundry processes is established, their potential in activated carbon and charcoal production remains underutilized. Efficient evaluation of this potential requires modernization of the existing preparation plant, which has exceeded its service life.

Given their limited global availability, Armutçuk coals should be considered strategic industrial raw materials rather than solely energy resources. In PCI applications, they enable partial substitution of costly coke, with injection rates up to 115 kg/thm achievable under controlled conditions. Key operational challenges—such as ash, sulfur, and combustion efficiency—can be mitigated through process optimization, ensuring stable furnace performance and improved metallurgical efficiency.

REFERENCES

Baran, F., (2022), "Dökümhanelerde kullanılan kalıp ve maça kumları kaynaklı döküm hataları ve önlenmesi". Yüksek Lisans Tezi, Sakarya Üniversitesi, Fen Bilimleri Enstitüsü, 79 s.

Chaigneau, T. V. R., Wise, J., (2009), "Modern Blast Furnace Ironmaking".

Demir, U., Elbinsoy, S., (2019), "Investigation of the Usability of High Sulfur Coal in Activated Carbon".

Didari, V., Oskan, M., Barış, K., (2015), "TTK Armutçuk Müessesesi Büyük damar gaz içeriğinin doğrudan ölçme yöntemiyle belirlenmesi". Bilimsel Madencilik Dergisi, 54 (2), 3–12.

Dike, Ö. S., (2008), "Pulverize kömür enjeksiyonu kullanımının yüksek fırın çalışmasına etkileri". Yüksek Lisans Tezi, Çukurova Üniversitesi, Fen Bilimleri Enstitüsü, 74 s., Adana.

Döngel, B., (1997), "Zonguldak kömürlerinden aktif karbon üretimi". Yüksek Lisans Tezi, Zonguldak Karaelmas Üniversitesi, Fen Bilimleri Enstitüsü, 76 s., Zonguldak.

Geerdes, M., Chaigneau, R., Kurunov, I., (2015), "Modern Blast Furnace Ironmaking: An Introduction" (Third Edition). IOS Press.

Kwaśniewska-Królikowska, D., Holtzer, M., (2013), "Selection criteria of lustrous carbon carriers in the aspect of properties of greensand system". Metalurgija, 52 (1), 62–64.

Maki, A., Sakai, A., Takagaki, N., Mori, K., Ariyama, T., Sato, M., Murai, R., (1996), "High rate coal injection of 218 kg/t at Fukuyama No. 4 blast furnace". ISIJ International, 36 (6), 650–657.

Mousa, E., (2019), "Modern blast furnace ironmaking technology: potentials to meet the demand of high hot metal production and lower energy consumption". Metallurgical and Materials Engineering, 25 (2), 69–104.

Öztürk, M., (2014), "Taşkömürü Havzası Damar Gaz İçerikleri Tespit Çalışmaları". Türkiye Taşkömürü Kurumu İş Sağlığı Güvenliği ve Eğitim Daire Başkanlığı, Zonguldak, 71 s.
TTK, (2021), "Türkiye Taşkömürü Kurumu 2021 yılı Faaliyet Raporu".

SECOND-STAGE SEPARATION DENSITY CONTROL IN A GRAVITY-FED THREE-PRODUCT DENSE MEDIUM CYCLONE

Yusuf Enes PURAL*, Mustafa ÖZER, Fırat BURAT, Feridun BOYLU

Istanbul Technical University, Faculty of Mines, Mineral Processing Engineering Department, 34469, Maslak, Istanbul, TÜRKİYE
**Corresponding author: pural@itu.edu.tr*

A B S T R A C T

Three-product dense medium cyclones (TPDMCs) generate clean coal, middlings, and reject from a single medium circuit. While the operator sets one circulating medium density, a higher cut-point develops autonomously in the second stage due to magnetite segregation in the primary unit. This spontaneous and uncontrollable secondary density has long been regarded as a fundamental limitation of TPDMC technology. In this study, a Box–Behnken response surface experiment was conducted on a gravity-fed pilot TPDMC to determine whether this secondary cut-point can be brought under deliberate control. Five variables were investigated across 18 experimental conditions, and performance was quantified through density tracer-based Tromp curves. Second-order quadratic models achieved R^2 > 70% for all key secondary-unit responses, demonstrating that the secondary separation density is primarily governed by the LARCODEM feed-pipe immersion depth, with DMC vortex-finder depth and feed pressure as secondary levers.

Key words: *Three-product dense medium cyclone, second-stage separation density, Box–Behnken design, response surface methodology, density tracer*

1. INTRODUCTION

Dense medium cyclones (DMCs) are the established technology for coarse and intermediate coal washing, valued for their high centrifugal forces and sharp density-based separation. Performance is characterised by the Tromp partition curve, from which the cut-point density (d_{50}) and the probable error (Ep) are derived; lower Ep indicates fewer misplaced particles (He & Laskowski, 1995).

Three-product dense medium cyclones (TPDMCs) replace sequential washing circuits by coupling a cylindrical primary separator (LARCODEM-type) with a conventional conical DMC connected to the primary underflow. A single circulating medium density yields three products - clean coal, middlings, and reject - with capital cost reductions exceeding 20% compared to conventional two-stage flowsheets (Pural et al., 2023). The fundamental operating characteristic of the TPDMC is the spontaneous density elevation in the secondary stage: the LARCODEM's centrifugal field preferentially directs coarser magnetite to the primary underflow and finer magnetite to the overflow, so the medium delivered to the DMC inlet carries a higher apparent density than the circulating feed. A second, higher cut-point therefore develops without operator intervention (Shah, 1992). Simulation work by Pural et al. (2023) showed that standard DMC models can predict TPDMC product yields, but secondary density control was not addressed.

Several authors have qualitatively noted that secondary density could theoretically be adjusted through orifice geometry (Jacobs & de Korte, 2013), yet no prior study has employed a factorial design to quantify the contribution of individual parameters. Medium stability - expressed as the density difference between DMC underflow and overflow - must remain within 0.1-0.4 g/cm³; values outside this range promote particle retention and surging, distorting partition curves (Luttrell et al., 2005). The present study fills this gap by providing the first statistically

validated evidence that the secondary cut-point in a gravity-fed TPDMC can be deliberately controlled.

2. MATERIAL AND METHODS

2.1. Pilot Unit and Medium Preparation

Experiments were conducted on a gravity-fed TPDMC modified by KARBOMET Ltd. (Turkey), comprising a LARCODEM primary separator (length 93 cm, diameter 21 cm) and a conical DMC secondary separator (length 48 cm, diameter 23 cm). The circulating medium was prepared by blending magnetite powder (45% passing 45 µm) with water; density was verified gravimetrically. Medium samples were drawn from four stream points - LARCODEM overflow, DMC feed, DMC overflow (middlings), and DMC underflow (reject) - to determine stream densities and derive stability and split values.

2.2. Density Tracer Protocol and Partition Analysis

Partition curves were determined using plastic density tracer cubes (Partition Enterprises, Australia). Three tracer sizes were used: 16, 8, and 4 mm, covering the density range 1.30–2.00 g/cm³ with 20 tracers per density class per experiment. After steady-state operation was confirmed, all tracers were introduced at the feed inlet, collected from drain-and-rinse screens after 5 minutes, and counted per product stream. Tracers retained due to surging were excluded from partition calculations (Luttrell et al., 2005).

Measured data were fitted to the standard logistic partition function to extract d_{50} and Ep. Medium stability and split were calculated as:

$$Stability = \rho_{muf} - \rho_{mof}, \qquad \varphi = \frac{\rho_{muf} - \rho_{mf}}{\rho_{muf} - \rho_{mof}}$$

where ρ_{mf}, ρ_{mof}, and ρ_{muf} are feed, overflow, and underflow medium densities respectively. Density shift was defined as $\Delta d_{50} = d_{50} - \rho_{mf}$.

2.3 Experimental Design and Modelling

A Box–Behnken response surface design in five factors was constructed in Minitab 21, yielding 18 experimental conditions (Table 1). Magnetite particle size was held constant throughout. Second-order quadratic models were fitted by least squares; terms with $p > 0.15$ were removed sequentially. Response variables included: LARCODEM and DMC separation densities, DMC density shift, DMC medium stability ($Stability_2$), and DMC *E*p at all three tracer sizes.

Table 1. Independent variables and coded levels

Symbol	Variable	Low (−1)	Centre (0)	High (+1)
X_1	LARCODEM vortex-finder depth (cm)	8	11	14
X_2	LARCODEM feed-pipe depth (cm)	11	14	17
X_3	DMC vortex-finder depth (cm)	5	10	15
X_4	Feed pressure (inlet head)	6.0	6.5	7.0
X_5	Medium density (g/cm³)	1.40	—	1.50

3. RESULTS AND DISCUSSION

3.1. Overall Performance

LARCODEM probable errors were consistently low (Ep ≤ 0.050) across all tracer sizes throughout the experimental range, confirming stable primary-stage separation. DMC Ep values were more variable (0.003–0.151 at 4 mm), reflecting sensitivity to operating conditions and the occurrence of retention and surging at certain parameter combinations. Medium stability $Stability_2$ ranged from 0.095 to 0.427 g/cm³, with most runs within the recommended 0.10–0.40 g/cm³ window. Medium split to overflow (φ) ranged from 0.391 to 0.965; the majority of runs exceeded the minimum recommended value of 0.66 (He & Laskowski, 1995). The runs where $Stability_2$ exceeded 0.40 (Runs 2, 3, 8) coincided with the highest DMC Ep values and observable surging, consistent with the established link between medium instability, particle retention, and degraded separation efficiency (Luttrell et al., 2005).

3.2. Primary Stage (LARCODEM) Models

Response surface models for LARCODEM separation density achieved R² values of 94.6%, 89.2%, and 93.8% at 16, 8, and 4 mm tracer sizes respectively. Three consistent trends emerged. LARCODEM vortex-finder depth (X_1) had a negative effect on d_{50}: increasing depth reduces the effective overflow collection zone and lowers the cut-point. LARCODEM feed-pipe depth (X_2) had a positive effect: deeper immersion extends the separation zone and raises the cut-point. Feed pressure (X_4) reduced the primary d_{50}, consistent with enhanced magnetite transport to the primary overflow at higher rotational energies. These trends align with the density-shift observations reported at industrial scale by Pural et al. (2023), where the primary cut-point was found to deviate systematically from the set medium density under varying operating conditions.

3.3. Secondary Stage: Density Shift and Separation Density

DMC density shift models achieved R² values of 82.3%, 78.1%, and 73.2% for 16, 8, and 4 mm tracers respectively. DMC separation density models attained 68.0%, 61.4%, and 61.1%. The fitted equations for DMC d_{50} are:

Size	Equation
16 mm	$d_{50} = 17.28 + 0.952^{*}X_2 - 0.224^{*}X_4 - 0.021X_2^2 + 0.001X_4^2 - 0.009X_2X_3 + 0.001X_3X_4$
8 mm	$d_{50} = 8.50 + 1.125^{*}X_2 - 0.149X_4 - 0.022X_2^2 - 0.010X_1X_2 - 0.009X_2X_3$
4 mm	$d_{50} = 10.23 + 1.094^{*}X_2 - 0.155X_4 - 0.020X_2^2 - 0.010X_1X_2 - 0.007X_2X_3$

(*statistically significant at $p < 0.10$)

The LARCODEM feed-pipe immersion depth (X_2) is the dominant positive predictor of secondary d_{50} across all tracer sizes. Mechanistically, deeper feed-pipe immersion delivers medium to a higher-velocity zone within the LARCODEM cylinder, intensifying centrifugal separation of magnetite and directing proportionally more coarse magnetite to the primary underflow. The DMC inlet consequently receives medium enriched in fine magnetite at higher apparent density, establishing a higher secondary cut-point. This is consistent with secondary density increases of 0.15–0.25 g/cm³ above the circulating density reported by Pural et al. (2023) at plant scale.

Feed pressure (X_4) appeared with a negative coefficient in all secondary d_{50} models: higher pressure distributes magnetite more uniformly across both stages simultaneously, attenuating the density elevation in the DMC feed. DMC vortex-finder depth (X_3) exerted a secondary negative effect on density shift at the 16 mm level, indicating that a deeper vortex finder

constricts the secondary overflow and retains more fine magnetite in the secondary underflow, marginally raising the cut-point.

3.4. Medium Stability and Separation Efficiency

The DMC Stability$_2$ model achieved the highest fit quality among all responses (R^2 = 92.6%, predicted R^2 = 82.0%), with LARCODEM feed-pipe depth (X_2), DMC vortex-finder depth (X_3), and feed pressure (X_4) all statistically significant. The DMC Ep model at 16 mm reached R^2 = 82.3%, with X_2 and X_4 as principal predictors. The Ep degradation at smaller tracer sizes is consistent with breakaway-size theory: separation efficiency falls sharply below a critical particle size for a given cyclone diameter, and medium instability amplifies this effect (He & Laskowski, 1995). At the 4 mm tracer size, Ep reached 0.151 under elevated stability conditions (Stability$_2$ = 0.300), reinforcing the need to maintain Stability$_2$ below 0.40 g/cm³.

In practical terms, the contour plots derived from the fitted models (omitted here for brevity; available in the full manuscript) show that near-zero density shift — the most controllable operating condition — is attained at feed pressure above 6.5 head combined with LARCODEM feed-pipe depth in the lower-to-middle range (11–13 cm) and DMC vortex-finder depth of 8–12 cm.

4. CONCLUSION

This study has provided the first statistically validated evidence that the spontaneous secondary separation density in a gravity-fed TPDMC can be deliberately adjusted through accessible geometric and operating parameters. Key findings are:

1. Second-order response surface models relating TPDMC geometry and operating conditions to secondary DMC separation density achieved R^2 > 70% across all tracer sizes, confirming meaningful controllability.
2. The LARCODEM feed-pipe immersion depth is the dominant lever: increasing it raises the secondary cut-point by enriching the DMC feed in fine magnetite; decreasing it moves the secondary cut-point toward the set circulating density.
3. Feed pressure and DMC vortex-finder depth are secondary but significant controls; moderate pressure levels and intermediate vortex-finder depths represent the practical optimum for simultaneous density control and stability.
4. LARCODEM primary-stage separation was robust throughout (Ep ≤ 0.050), while DMC secondary-stage Ep deteriorated at finer tracer sizes and elevated medium stability, consistent with breakaway-size and surging mechanisms

ACKNOWLEDGEMENTS

This work was supported by Istanbul Technical University Scientific Research Projects Coordination Unit (ITU-BAP, Project No. MGA-2019-41890). The authors thank KARBOMET Ltd. for the pilot unit.

REFERENCES

He, Y. B., Laskowski, J. S., (1995), “Dense medium cyclone separation of fine particles”, Coal Preparation, 16 (1–2), 1–49.

Jacobs, J., de Korte, G. J., (2013), “The three-product cyclone: Adding value to South African coal processing”, Journal of the Southern African Institute of Mining and Metallurgy, 113 (11), 859–863.

Luttrell, G. H., Barbee, C. J., Bethell, P. J., Wood, C. J., (2005), “Dense medium cyclone optimization”, Final Technical Report, US Department of Energy.

Pural, Y. E., Sirkeci, A. A., Boylu, F., (2023), “Simulation and performance evaluation of three product dense medium cyclone”, International Journal of Coal Preparation and Utilization, 43 (8), 1299–1312.

Shah, C. L., (1992), “LARCODEM separator — Development of three-product unit”, in Innovations in Physical Separation Technologies, 263–274, Springer Netherlands.

COMMINUTION AND CLASSIFICATION

INVESTIGATION OF THE EFFECTS OF ORE ABRASIVITY INDEX ON BALL WEAR IN WET BALL MILLING OPERATIONS WITH LAB SCALE TESTS

Yağız Kerem YALÇIN*, Ahmet YAKAR, İbrahim GÖKTAŞ

ETİ Bakır C.O R&D Center, 55300, Tekkeköy,Samsun,TÜRKİYE
**Corresponding author: kerem.yalcin@etibakir.com.tr*

A B S T R A C T

The operational costs of a mineral processing plant are largely dominated by energy consumption and the use of consumable materials during the grinding operations. Mills come in various types and sizes, with grinding media such as balls and rods that differ in hardness and properties. Ore characteristics, such as hardness and abrasiveness, influence the wear of these consumables. The selection of appropriate grinding media based on ore abrasivity is therefore critical. This study investigates the wear of grinding media during wet grinding in ball mills made from cast iron at ETİ Bakır C.O's Samsun plant. A laboratory-scale ball mill and the LCPC abrasivity test were used to assess grinding media wear. Samples from various ores were collected from the company's mines. The relationship between media wear and ore characteristics was analyzed using the LCPC and Bond Wi tests. The study evaluated the effects of different ore types on grinding media wear and determined the relationship between ore abrasiveness and ball wear. A ball wear index model was developed to relate ore characterization parameters to grinding media wear under controlled laboratory conditions.

Key words: *Grinding, abrasivity, lab scale ball mill, LCPC abrasivity test*

1. INTRODUCTION

In mineral processing plants, grinding operations account for some of the highest operating costs. In these operations, grinding media consumption accounts for a large portion of operating expenditure (Bond, 1961). Ball wear is a complex phenomenon resulting from the interaction between the mineralogical and physical properties of the ore, ball metallurgy, and operational parameters (Radziszewski, 2002). According to Jankovic (2003), the combined effects of parameters in the grinding environment, such as abrasion, impact, and corrosion, must be better understood to predict grinding media wear accurately.

To characterize ball wear in the mill, it is necessary to have information on the ore's abrasiveness and grindability. The Bond abrasion index has been used for many years to measure ore abrasiveness. Parameters such as the amount and size of material introduced, as measured by the Bond abrasion index, make the test difficult to apply. As highlighted by Peres et al. (2018), the LCPC (LAC, g/t) test emerges as a significant alternative to the Bond abrasion index, requiring less material and finer particle size. In their study of copper sulfide ores, the LCPC index was shown to be effective in determining abrasiveness and to correlate strongly with the Bond AI. These advantages make the LCPC test a promising tool for rapid ore characterization. This approach supports the development of the ball wear index model, which is the objective of this study.

Studies investigating wear mechanisms in grinding operations have mainly relied on data from the Bond Abrasion Index or field observations (Bond, 1961; Radziszewski, 2002). The applicability of these valuable studies is generally limited by difficulties such as particle size and test procedures. Studies have shown that the LCPC abrasion index test correlates strongly with traditional abrasion indices and offers advantages, including requiring fewer samples and working with finer particle sizes, making it a reliable alternative for ore characterization (Thuro, 2006; Peres, 2018). However, studies integrating LCPC abrasivity data directly with laboratory-

scale grinding media wear measurements remain limited. For these reasons, a laboratory study integrating LCPC test data with wear behaviour observed in the grinding environments highlights a gap in the mineral processing literature.

To address the gap identified in the literature, this study investigated the relationship between ore characterization and wear in grinding environments using laboratory-scale experiments. The study focused on integrating controlled ball wear data from marked ball wear tests with data obtained from LCPC abrasiveness index tests. A ball wear index has been proposed to evaluate and compare ball wear under different conditions.

The main contribution of this study is to establish a quantitative relationship between the LCPC abrasiveness index test and ball wear in a laboratory environment. Unlike the traditional Bond abrasion index approach, the proposed model aims to quickly and practically pre-evaluate ore abrasiveness. By correlating the indices obtained from the LCPC test with experimentally observed ball wear, an alternative screening methodology is presented that supports grinding medium selection and wear risk assessment prior to grinding operations.

The Bond Abrasion Index (Ai) and other empirical approaches provide estimations for the wear rate of grinding media and the abrasiveness of the ore being processed; however, these traditional wear prediction methods rely on the collection of large quantities of samples and/or extensive testing time. Alternatively, LCPC abrasivity testing necessitates smaller sample sizes and shorter testing durations. Thus, the proposed ball wear index model serves as a rapid laboratory assessment of ore abrasiveness and likely grinding media wear, which can then be used as a screening technique.

Therefore, the main objective of this study is to investigate the relationship between ore abrasivity determined by the LCPC test and grinding media wear measured by marked ball wear tests conducted in a laboratory-scale ball mill. In addition, a predictive ball wear index model is proposed to evaluate the influence of ore characteristics on grinding media wear.

2. MATERIAL AND METHODS

2.1. Material

Grinding balls used in this study were sourced from ETİ Bakır C.O ball production plant located at the Samsun facility. Steel balls with diameters of 20, 25, 30, and 40 mm were used in the experiments. Chemical compositions of steel balls are shown in Table 1, and microscope images are shown in Figure 1.

Table 1. Chemical compositions of steel balls

Ball Diameter	%C		%Mn		%Si		%Cr		%Cu
	Min.	Max.	Min.	Max.	Min.	Max.	Min.	Max.	Maximum
20	0,55	0,65	0,55	0,75	0,15	0,25	0,05	0,20	0,20
25	0,55	0,65	0,55	0,75	0,15	0,25	0,05	0,20	0,20
30	0,55	0,65	0,55	0,75	0,15	0,25	0,05	0,20	0,20
40	0,60	0,70	0,65	0,85	0,15	0,30	0,30	0,40	0,40

(a) (b) (c)

Figure 1. Microscope images of steel balls with different diameters: (a) 20 mm ball, (b) 30 mm ball, (c) 40 mm ball

Ore samples were also taken from various ETİ Bakır C.O. plants in Adıyaman and Samsun, from plant feed ores, and from the Artvin/Murgul silica ore to simulate different ore types in grinding operations. Chemical composition of ores is given in Table 2.

Table 2. Chemical compositions of ores

Ore	%SiO2	%Cu	%Fe	%S	%Zn
Adıyaman	12,68	3,41	30,14	29,20	0,95
Samsun	35,19	1,55	37,10	0,59	3,69
Artvin/Murgul	83,36	0,57	2,82	2,78	0,08

2.2. Method

2.2.1 Marked ball wear test

At marked ball wear tests (MBWT), a laboratory-scale ball mill with an internal diameter of 178 mm and a length of 356 mm was used. The ball charge was kept constant at 40%, and pulp density was maintained 66% solids by weight during the grinding tests. Of the total 15.85 kg of balls loaded, 25% by weight of each size fraction was marked. A total of 40 marked balls were used in the tests. Of these, 8 balls each of 20.25 and 30 mm, and 16 balls of 40 mm were marked.MBWT was planned for 100 hours of total grinding time. The balls were weighed before the test began. The marked balls were weighed at regular time intervals, and the cumulative weight loss was determined (Çolak, 2018).

Table 3. Grinding media charge and marked ball distribution used in MBWT

Ball diameter (mm)	Number	Marked number
40	31	8
30	31	8
25	32	8
20	64	16

2.2.2 LCPC abrasiveness index test

LCPC abrasiveness index (LAC, g/t) tests were conducted in accordance with the AFNOR P18-579 standard. Each test was performed under controlled laboratory conditions, and careful weighing procedures were applied to minimize experimental error.50x25x5 mm metal plates with a Rockwell B hardness of 60-75 were used in the LCPC tests. 500-gram samples were ground for 5 minutes at each test. Metal plates were weighed before and after the tests. Weight loss from metal plates is noted, and the abrasiveness index of ores is calculated in

terms of g/t. After the test, the ground ore was screened to 1.6 mm, and the breakability coefficient (LBC, %) was calculated (Thuro et al., 2006).

2.2.3 Bond work index test

As part of the Bond Work Index analysis conducted to determine the grindability characteristics of the ore, according to the standard Bond procedure, a sample of 3.35 mm was crushed and subjected to a closed-loop grinding test in a Bond mill (305x305 mm). The net product quantity per revolution and size data obtained at equilibrium were used to determine the grinding resistance and the unit energy requirement (kWh/t) of the ore based on the calculated index value.

2.2.4 Statistical evaluations

Statistical analyses were performed to develop a predictive model for ball wear based on laboratory test data. A ball wear index model was presented using multiple linear regression based on ANOVA. The coefficients of the independent variables were estimated using ordinary least squares (OLS) to minimize the sum of squared residuals. Model reliability has been verified using methods such as residual plots, line fit plots, and normal probability plots.

2.2.5 Test repeatability and measurement accuracy

To ensure the reliability of the experimental results, LCPC abrasivity tests were repeated under identical operating conditions for each ore sample. The marked ball wear tests were carried out with the same ball charge, pulp density, and mill operating conditions throughout the experiments to minimize operational variability. All weight measurements of grinding balls and LCPC metal plates were performed using a precision laboratory balance. These precautions ensured acceptable repeatability and measurement accuracy for the data used in the regression analysis.

3. RESULTS AND DISCUSSION

3.1 LCPC and Bond Work Index Results

As a result of the conducted tests, a linear relationship was observed between the LCPC abrasiveness index and ball wear. The highest LCPC abrasiveness index was obtained at Samsun ore, whereas the highest ball wear was observed for the Artvin/Murgul silica ore. Although the Samsun ore exhibited higher LAC values, the elevated wear associated with the Artvin/Murgul ore is attributed to its high silica content and mineralogical characteristics. The LCPC test results and Bond Work Index results are shown in Table 4.

Table 4. LCPC abrasivity index and Bond work index results

Ore	LAC (g/t)	LBC (%)	Wi (kWh/t)
Adıyaman	280	67,16	12,80
Samsun	1940	42,70	15,00
Artvin/Murgul	1080	24,23	20,00

3.2 MBWT Results

As a result of MBWT, ball diameter is an effective parameter for ball wear. The wear rate of 40 mm balls differed from that of 20 mm balls depending on the surface area/volume ratio. MBWT results are shown in Table 5.

Table 5. MBWT results

Ore	Time (h)	Feed (t)	Mass loss (g/t) 40Ø	Mass loss (g/t) 30Ø	Mass loss (g/t) 25Ø	Mass loss (g/t) 20Ø
Adıyaman	100	0,40	16,83	9,62	6,28	4,43
Samsun	100	0,38	10,64	6,85	3,97	2,93
Artvin/Murgul	100	0,29	26,76	15,38	9,86	6,40

3.3 Regression Analysis Results

In the first stage of ball wear index studies, LAC (g/t), Wi (kWh/t), and ball diameters, obtained from the tests, were kept as independent variables. The resulting regression model yielded a correlation coefficient (R^2) of 0.9932. Since Murgul silica ore recorded the highest wear in the tests, the highest wear was taken as the reference point. To create a scale for the ball wear index, the data were normalized using wear data obtained from 40 mm diameter Murgul silica ore. Regression analysis parameters are shown below.

Table 6. First regression analysis results

R^2	Adjusted R^2	Significance F	Intercept Coefficient	LAC Exponent	Wi Exponent	Diameter Exponent
0,9932	0,9905	$5{,}36 \times 10^{-9}$	2,6819	0,8830	-4,7717	1,9884

The proposed ball wear index formula, with the Bond Work Index, is represented in equation 1.

$$\boldsymbol{BWI = 0,546.\frac{d^{1,9884}.LAC^{0,8830}}{Wi^{4,7717}}} \quad (1)$$

Where:

- *BWI: Ball Wear Index*
- *d: Ball diameter*
- *LAC: Abrasivity index (g/t)*
- *Wi: Bond work index*

According to the line fit plot from the regression based on the bond index, there is a strong correlation in the data. The estimated values of the independent variables are nearly perfectly consistent. Line fit plots are shown below in Figure 2.

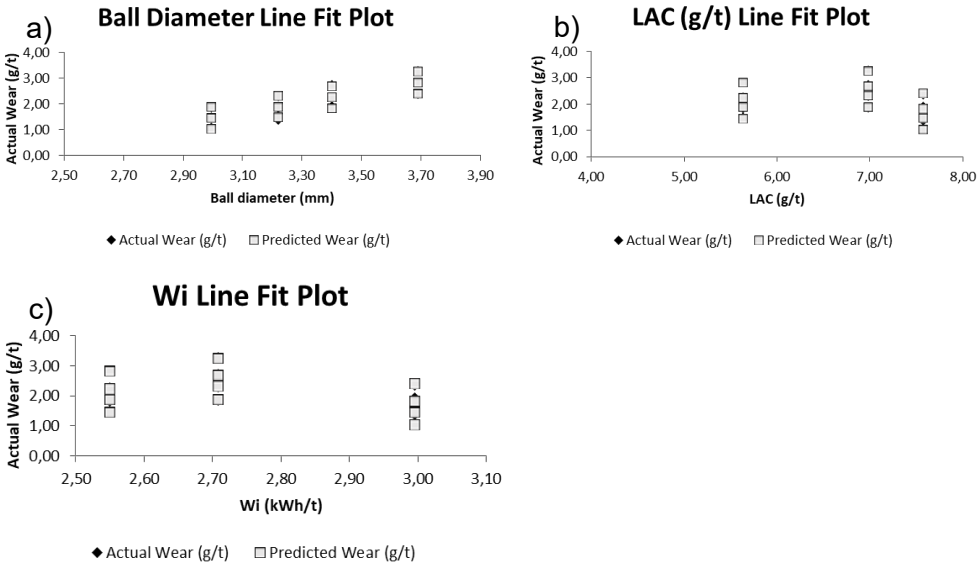

Figure 2. Line fit plots showing the relationship between ball wear and independent variables: (a) ball diameter, (b) LCPC abrasivity index (LAC), and (c) Bond work index (Wi)

Residual plot analysis was used to examine the prediction errors of the Bond work index-based regression. Upon examining the graph, it was evident that the residuals were distributed around the origin on the x-axis. The fact that all data remained within the range of plus or minus 0,1 proves the reliability of the regression. The residual plots of the independent variables are shown in Figure 3.

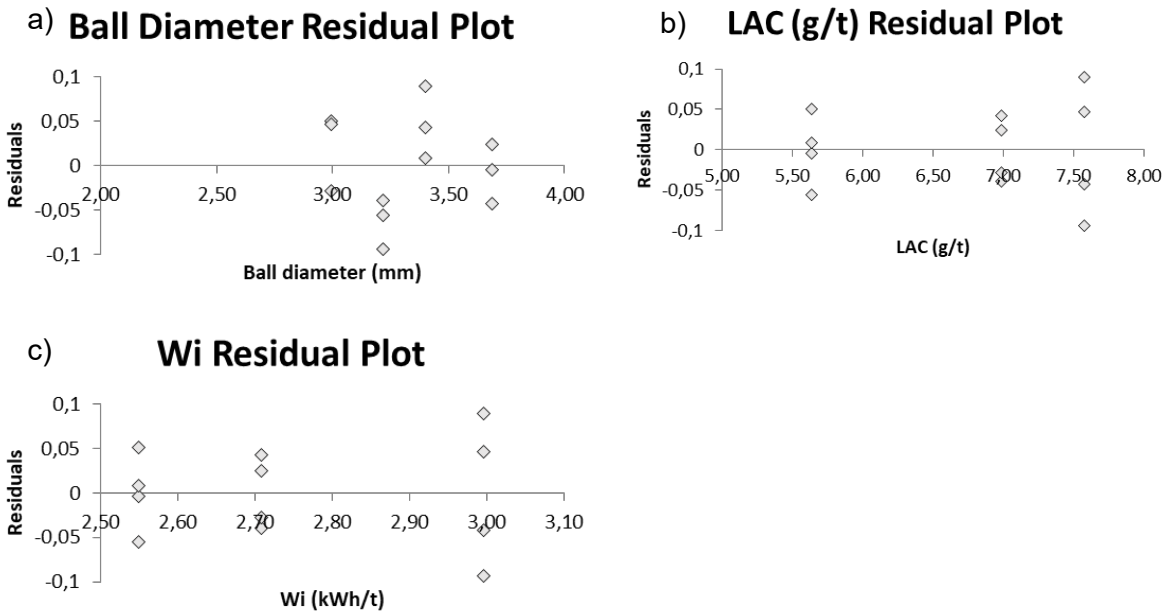

Figure 3. Residual plots showing the distribution of prediction errors for the independent variables used in the regression analysis: (a) Ball diameter (mm), (b) LBC (%), and (c) Wi (kWh/t)

The data distribution was evaluated using a normal probability graph and bond-based regression analysis. Upon examination of the graph, the data points show a linear trend. This

slope indicates that the residuals are normally distributed and that extreme values did not drive the R2 value for the study. The normal probability plot is shown in Figure 4.

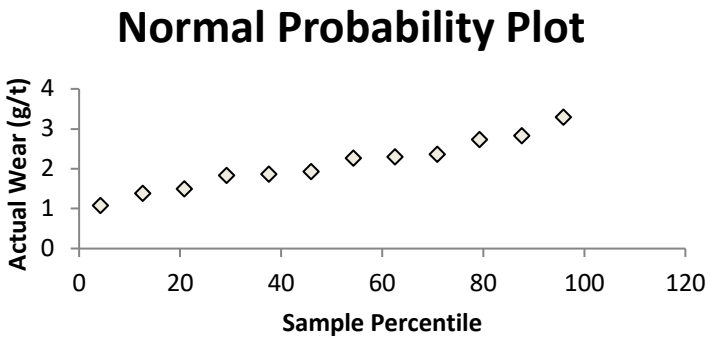

Figure 4. Normal probability plot

The linear extension of the data along the correlation line between the actual and predicted wear graphs shown in Figure 5 demonstrates the model's high predictive power. The results obtained show that, in terms of sensitivity, the proposed LAC-based BWI yields performance comparable to that of a similar grinding-behavior parameter, without using the Bond work index.

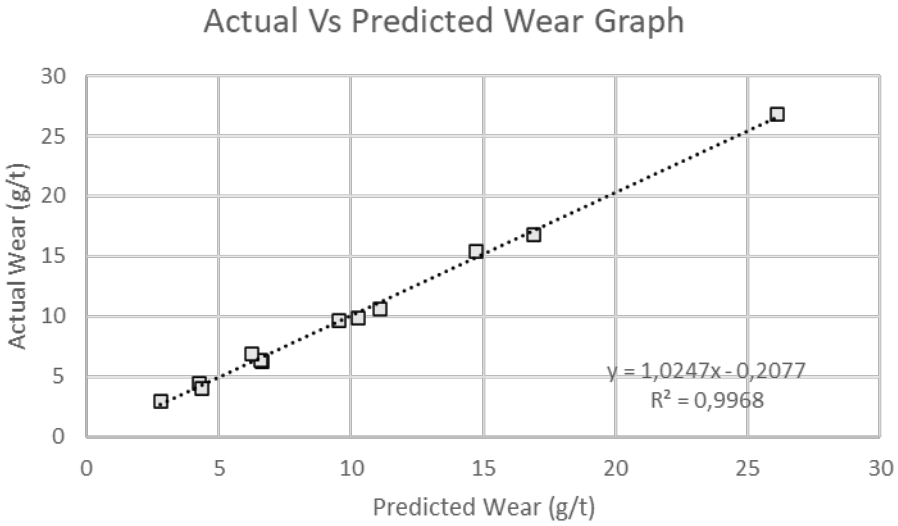

Figure 5. Comparison between experimentally measured wear values and predicted wear values obtained from the regression model 1

In the second phase of the study, it was planned to evaluate the ore's grinding characterization in the model using a single test. For this reason, the LAC and LBC values obtained from the LCPC test, and the ball sizes were kept as independent variables, and a second regression analysis was performed. This regression analysis, performed with the same correlation coefficient of 0.9932, strengthened the relationship between wear and LCPC data. Since Murgul silica ore recorded the highest wear in the tests, the highest wear was taken as the reference point. To create a scale for the ball wear index, the data were normalized using wear data obtained from 40 mm diameter Murgul silica ore. Regression analysis parameters are shown below.

Table 7. Second regression analysis results

R^2	Adjusted R^2	Significance F	Intercept Coefficient	LAC Exponent	LBC Exponent	Diameter Exponent
0,9932	0,9905	$5{,}36 \times 10^{-9}$	2,4352	-0,4593	-1,0350	1,9883

The proposed ball wear index formula with breakability coefficient is represented in equation 2.

$$BWI = 0{,}4267.\left(\frac{d^{1{,}9883}}{LAC^{0{,}4593}.LBC^{1{,}0350}}\right) \quad (2)$$

Where:

- *BWI: Ball Wear Index*
- *d: Ball diameter*
- *LAC: Abrasivity index (g/t)*
- *LBC: Breakability coefficient (%)*

When examining the line fit plots shown in Figure 6, the effect of each independent variable analyzed on ball wear is evident. The close match between the model-predicted values and the experimental data indicates that the model accurately explains the relationship between the variable parameters and the wear results. This fit also confirms the R^2 value obtained from the ANOVA analysis.

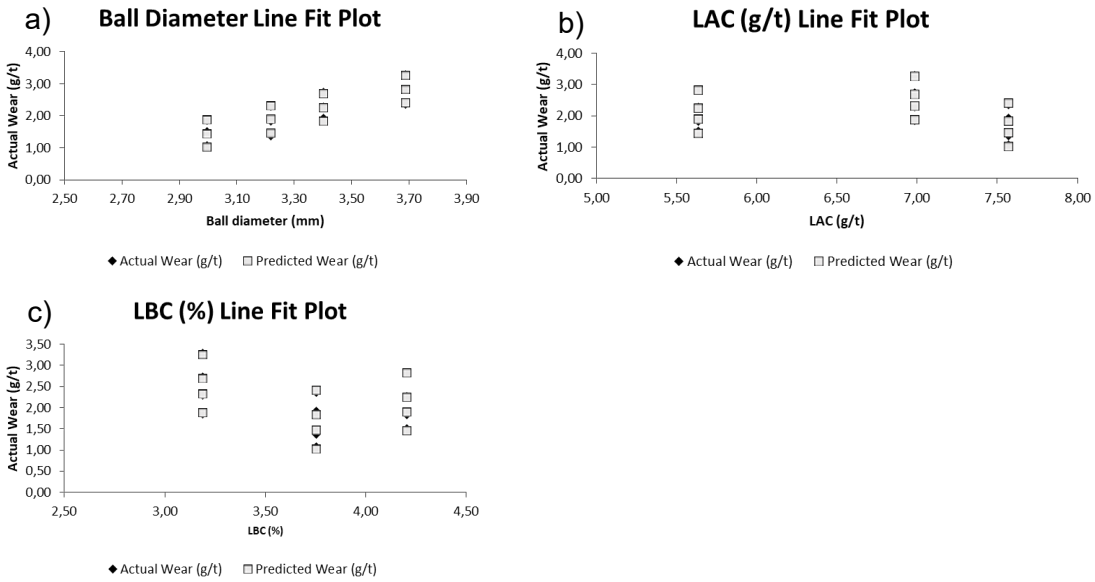

Figure 6. Line fit plots showing the relationship between ball wear and independent variables: (a) ball diameter, (b) LCPC abrasivity index (LAC), and (c) Breakability coefficient (LBC)

Residual plots were created to define the regression analysis performed. Upon examining the residual plot, it was evident that the residuals were randomly distributed along the horizontal axis and showed no systematic deviation. The margin of error remained within the range of plus or minus 0,1. The graphs validate the accuracy of the BWI formula. Residual plots are shown in Figure 7.

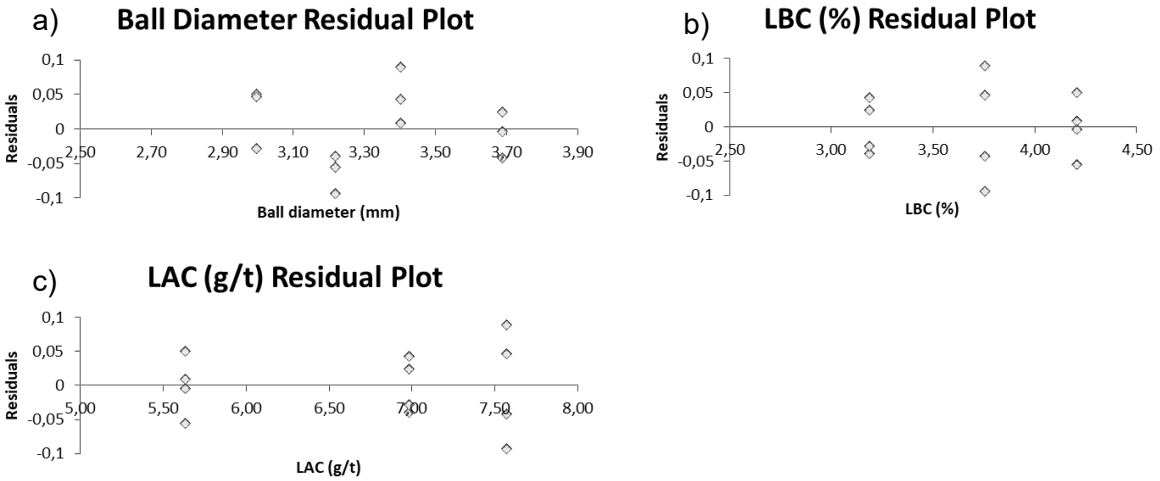

Figure 7. Residual plots showing the distribution of prediction errors for the independent variables used in the regression analysis: (a) Ball diameter (mm), (b) LBC (%), and (c) LAC (g/t)

A normal probability plot, shown in Figure 8, was used to assess the statistical assumptions of the multiple linear regression analysis. The data points on the plot progress along a diagonal line with a clear linear slope. This consistency indicates that the correlation coefficients were not obtained from random outliers.

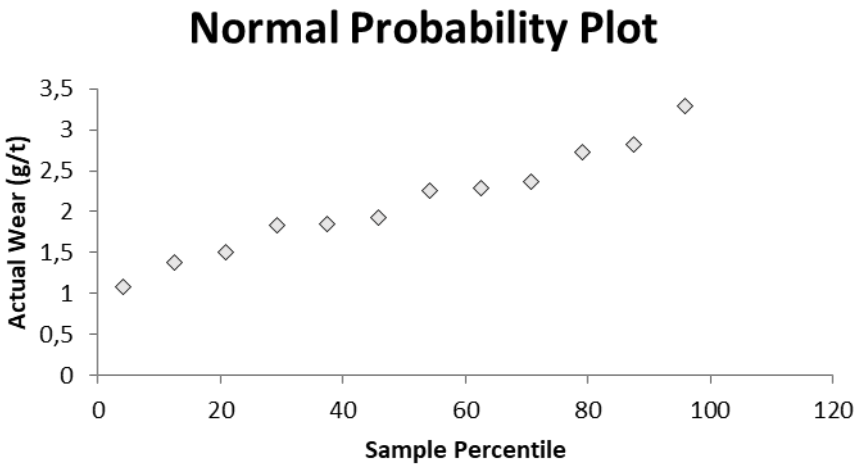

Figure 8. Comparison between experimentally measured wear values and predicted wear values obtained from the regression model 2

An actual vs. predicted wear graph in Figure 9 was created to summarize the model's performance. This graph obtained a correlation coefficient higher than that of the regression analysis, with an R2 value of 0,9968.

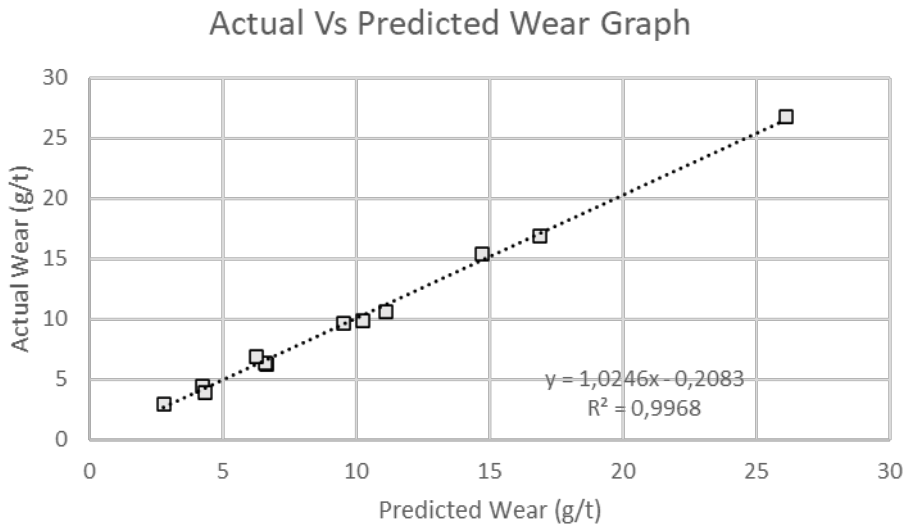

Figure 9. Actual vs predicted wear graph

A standard classification scale, shown in Table 8, has been defined to evaluate the performance of grinding media balls. Using this scale, BWI results can be evaluated in four different categories ranging from 0,00 to 1,00.

Table 8. Wear classes

BWİ	**Wear Class**
0,00-0,20	Low
0,20-0,40	Low-Medium
0,40-0,70	Medium
0,70-1,00	High

The experimental results obtained suggest a consistent relationship between LCPC test results and ball wear observed in the laboratory environment. The regression-based modeling study highlights the combined effect of ball size and ore properties. The findings, together with the LCPC test data, provide useful inputs for evaluating grinding media wear under test conditions. To better understand the underlying reasons for this observed relationship, the physical mechanisms governing abrasivity and grinding media wear are discussed below.

The relationship between LCPC abrasion indices and grinding media wear at the laboratory scale can be physically interpreted in terms of the dominant wear mechanisms in both environments. LCPC tests, under controlled impact and shear conditions, can be thought of as increasing micro-shearing and sliding mechanisms, analogous to ball-ore contacts in ball mills, where the same physical mechanisms are expected to occur through repeated particle-surface interactions. Grinding media wear generally results from abrasive interactions between hard, angular mineral phases and balls. Although stress states and contact geometries differ between the LCPC device and grinding conditions, properties such as hardness, angularity, and roughness exhibit similar mechanisms of action in both systems. Consequently, the LCPC index does not directly represent an abrasion value. However, it can be used as an effective indicator because it captures the relative abrasiveness tendencies that influence the grinding medium's abrasion behavior under laboratory conditions.

4. CONCLUSION

A ball wear index (BWI) model was developed based on laboratory-scale grinding experiments and ore characterization data. The proposed model was calibrated and validated based on

balls in the 20 to 40 mm range, LAC values in the 280 to 1940 g/t range, and LBC values in the 24 to 67% range. A successful fit between the experimental data and the predicted wear index was obtained, with R2=0.9931 from multiple linear regression analysis. The model's reliability is also supported by normal probability and residual plots. The results have been integrated into a proposed wear-class table (ranging from 0.00 to 1.00) to facilitate estimation of grinding media wear. Although the developed model demonstrates strong predictive capability, the limited dataset limits its direct generalization to industry. Therefore, the study should be considered a pilot model. Future research should include different ore types and metallurgical structures to strengthen the model's industrial reliability and universal applicability. The proposed Ball Wear Index (BWI) model demonstrates high statistical reliability for the ores examined; however, the dataset is currently limited to three ore types. Future research will focus on expanding the dataset with different mineralogical compositions to enhance the model's predictive power. Furthermore, applying these laboratory-scale findings to industrial-scale mills (scaling up) will require integrating operational factors, including mill diameter, liner profiles, and pulp density.

The ball wear index proposed in this study offers a practical and decision-oriented tool for mineral processing applications, in addition to its academic contribution. Integrating the results of the LCPC abrasiveness index test currently used in industry with laboratory-scale grinding media wear tests enables early-stage ore characterization. In this context, it enables the rapid prediction of grinding media wear, serving as an alternative to the time-consuming and material-intensive Bond wear index. As a result, the model can be used as an effective screening tool to classify ore abrasiveness, support grinding media selection, and inform wear-related operational decisions in a controlled laboratory environment prior to plant-scale use.

REFERENCES

Albertin, E., Sinatora, A., Tavares, L. M., Silva, M. A., (2001) “A methodology for ball wear testing in the laboratory”, Wear, 250 (1–12) 121–129.

Archard, J. F., (1953) “Contact and rubbing of flat surfaces”, Journal of Applied Physics, 24 (8) 981–988.

Austin, L. G., (1981) “An analysis of fine dry grinding in ball mills”, Powder Technology, 28 (1) 83–90.

Bond, F. C., (1961) “The third theory of comminution”, AIME Transactions, 220 403–411.

Cleary, P. W., (1998) “Predicting charge motion, power draw, segregation, and wear in ball mills using discrete element methods”, Minerals Engineering, 11 (11) 1061–1080.

Çolak, S. S., (2018), Investigating the effects of the ball and material properties on media wear results for cement grinding applications, Master’s Thesis, Hacettepe Üniversitesi.

Iwasaki, I., Riemer, S. C., Orlich, J. N., Natarajan, K. A., (1985) “Corrosive and abrasive wear in ore grinding”, Wear, 103 (3) 253-267.

Jankovic, S., (2003) “Variables affecting the fine grinding of minerals using stirred mills”, Minerals Engineering, 16 (4) 337–345.

Matsanga, N., Nheta, W., Chimwani, N., (2023) “A review of the grinding media in ball mills for mineral processing”, Minerals, 13 (10) 1373.

Misra, A., Finnie, I., (1981) “On the size effect in abrasive and erosive wear”, Wear, 65 (3) 359–373.

Peres, L. M., Massola, C. P., Bergerman, M. G., (2018) “Abrasiveness evaluation of pre-concentration of copper sulfide ore products through the LCPC test”, Tecnologia em Metalurgia, Materiais e Mineração, 15 (2) 91–95.

Powell, M. S., Weerasekara, N. S., Cole, S., LaRoche, R. D., Favier, J., (2011) “DEM modelling of liner evolution and its influence on grinding rate in ball mills”, Minerals Engineering, 24 (3-4) 341–351.

Radziszewski, P., (2002) “Exploring total media wear”, Minerals Engineering, 15 (12) 1073–1087.

Thuro, K., Singer, J., Käsling, H., Bauer, M., (2006) “Determining abrasivity with the LCPC test”, Felsbau, 24 (6) 37–45.

Marked Ball Wear Test - 911Metallurgist https://www.911metallurgist.com/blog/marked-ball-wear-test

EVALUATION OF COMPUTER APPLICATIONS FOR COMMINUTION CIRCUIT DESIGN

K.Tahsin PEREK*, Jemshit REJEPOV, Ceyda TUNÇOK

Istanbul Technical University, Faculty of Mines, Mineral Processing Engineering Department, 34469, Maslak, Istanbul, TÜRKİYE
**Corresponding author: perek@itu.edu.tr*

A B S T R A C T

Comminution represents one of the most energy-intensive stages in mineral processing plants and plays a critical role in determining plant efficiency and operational costs. Consequently, the design of crushing circuits requires detailed analysis and accurate estimation of particle size distributions. Computer-based simulation tools provide engineers with the ability to evaluate alternative circuit configurations prior to plant construction or modification. Detailed analysis and optimization are critical, making modern computer-aided modeling and simulation tools indispensable for facility planning and operation.

This study presents the development, validation, and extended evaluation of an application designed for the design of comminution circuits. The initial version of the program was implemented as a desktop application written in the C programming language. The software allowed engineers to estimate particle size distributions, perform basic mass balance calculations and generate simplified crushing circuit configurations. There is another application is a modern, visually enhanced web-based platform built with ASP.NET Core MVC and Microsoft SQL Server. It concentrates on crushing and screening circuits, offering extensive catalogs for equipment and automated flow diagram generation, aiming for enhanced user-friendliness and sustainability. Both studies successfully validated their computational models against established methods, demonstrating the ability to efficiently design and simulate multi-stage comminution circuits under specified conditions. This study showcases the evolution of software tools, from foundational C-based programs to dynamic web applications, providing plant engineers with vital tools for optimized plant design and process control.

Key words: *Comminution, crushing circuit design, process simulation, mineral processing software*

1. INTRODUCTION

Comminution is widely recognized as the most energy-intensive operation in mineral processing plants and may account for nearly half of the total energy consumption in concentrators (Wills & Finch, 2016). Crushing and grinding circuits therefore play a critical role in determining the economic performance of mineral processing operations. Efficient design of comminution circuits requires detailed understanding of particle size distributions, reduction ratios and equipment performance.

Traditionally, the design of comminution circuits has been based on empirical methodologies supported by accumulated engineering experience. While such approaches have proven useful, they are inherently limited in their ability to evaluate complex process interactions and alternative configurations. The advancement of computational modeling techniques has fundamentally transformed this landscape, enabling the use of simulation tools that provide predictive insights into circuit behavior under diverse operational scenarios. These tools are grounded in mathematical representations of particle breakage kinetics, size distribution evolution, and mass balance relationships (King, 2001).

A number of specialized software platforms have been developed to support comminution circuit modeling. Among these, JKSimMet is widely recognized for its ability to incorporate breakage test data into circuit simulations (Morrison & Richardson, 2002). Similarly,

PlantDesigner and Bruno software are frequently employed for equipment selection and process design (Hedvall & Nordin, 2002; Kaja, 2002). USIM PAC offers an integrated simulation environment covering a wide range of mineral processing operations (Brochot et al., 2002). In addition, advanced numerical techniques such as Discrete Element Modeling (DEM) and Computational Fluid Dynamics (CFD) provide high-resolution insights into particle-scale interactions and flow dynamics (Herbst & Nordell, 2002).

BKDT V0.1 is another circuit design application which is developed by Saltuklaroğlu and has written for the design of size reduction process in mineral processing. The application helps the engineer to design the size reduction circuit in the direction of the given information using the database it incorporates. The application is capable of designing communition circuit for size ranges between 1500 and 0.038 mm (Saltuklaroğlu, 2003).

Empirical particle size distribution models have also been widely used in comminution research. Among these models, the Gaudin–Schuhmann distribution has been widely applied to represent cumulative undersize particle distributions obtained from sieve analysis (Wills & Finch, 2016). Other empirical models such as the Rosin–Rammler and Gaudin–Meloy distributions are also frequently used to describe particle size distributions in mineral processing operations.

The aim of this study is to develop a computer-aided application capable of automatically generating crushing circuit flowsheets and estimating particle size distribution parameters. The study also aims to demonstrate the transition from traditional desktop-based implementations to modern web-based systems that offer improved usability and scalability.

2. THE APPLICATION ARCHITECTURE AND IMPLEMENTATION

Particle size distribution plays an important role in the design and analysis of comminution circuits. Empirical models are commonly employed to represent cumulative particle size distributions derived from sieve analysis data. Among these models, the Gaudin–Schuhmann relationship remains one of the most widely applied:

$$P(d) = (d/d_0)^{\alpha}$$

n this formulation, P(d) denotes the cumulative passing fraction, d represents particle size, d_0 corresponds to the maximum particle size, and α is the distribution coefficient. This coefficient is directly related to the slope of the particle size distribution curve on a logarithmic scale and provides important information about breakage characteristics of the material (Wills, & Finch, 2016). As illustrated in Figure 1, the slope parameter can be derived from sieve analysis data plotted on log–log axes. This parameter plays a crucial role in predicting product size distributions and evaluating comminution performance. The developed application automates this calculation, thereby reducing reliance on manual analysis and improving computational efficiency.

2.1. Application Development for Designing Circuit

The application, named C&G Circuit Designer, was initially developed using the C programming language. The application adopts a structured workflow that guides users through the sequential definition of key process parameters, including ore characteristics, comminution type, feed and product size specifications, and the number of processing stages.

One of the distinguishing features of the system is its ability to automatically generate process flowsheets. Traditionally, flowsheet development requires manual drafting and iterative calculations, which can be both time-consuming and prone to error. By contrast, the developed application streamlines this process through algorithmic generation of circuit configurations.

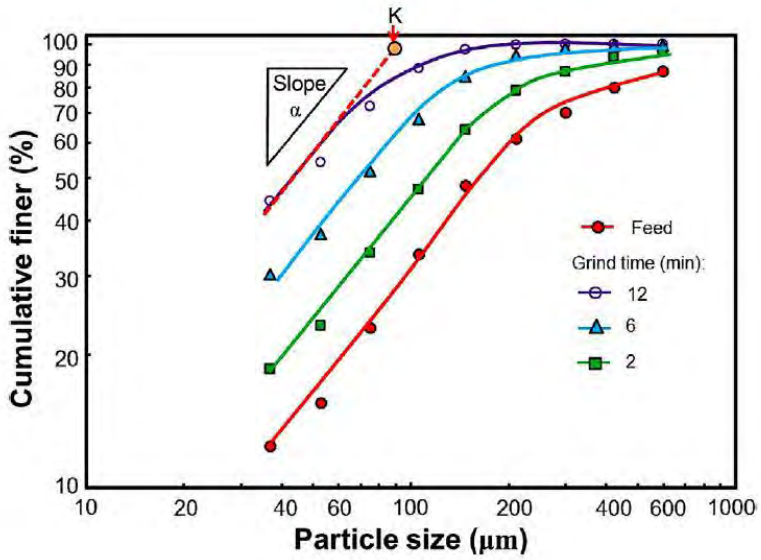

Figure 1. Gaudin–Schuhmann Distribution representation (Wills, & Finch, 2016, p. 96)

In addition to flowsheet generation, the software estimates equipment capacities, evaluates power consumption, and enables simulation-based analysis of existing circuits. The overall system workflow, including stage determination and simulation steps, is depicted in Figure 2 (Rejepov, 2019).

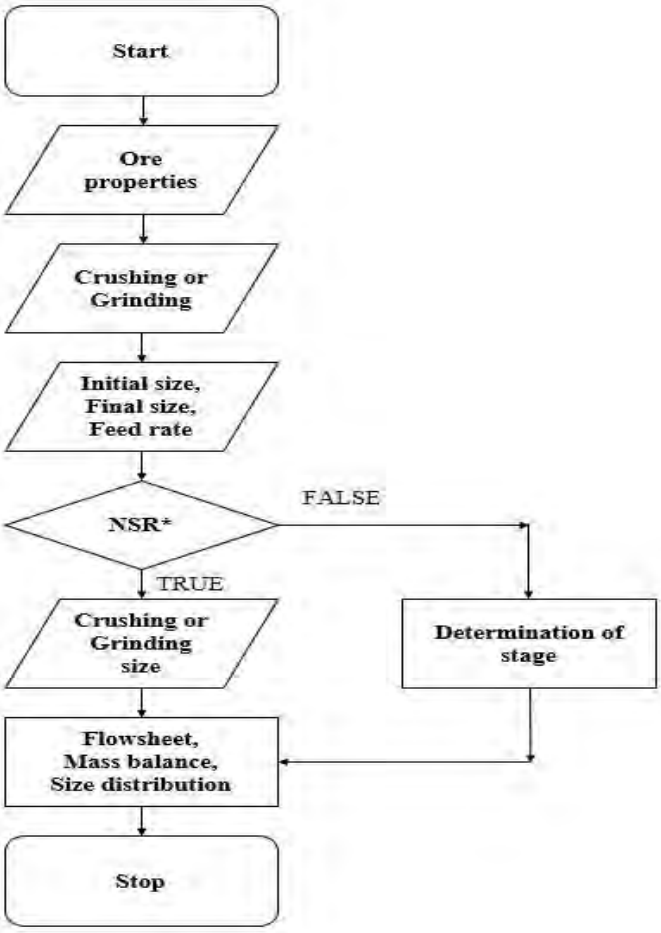

Figure-2. Overview of the design and simulation of circuit application.
(NSR: Number of stage required for crushing or grinding)* (Rejepov, 2019)

3. RESULTS AND DISCUSSION

The development of the proposed system was carried out in two main stages. The first stage focused on developing a desktop-based application coded in the C programming language. The second stage involved extending the system to a web-based platform using ASP.NET Core MVC architecture.

Desktop Application : The first version of the system was developed as an executable desktop application using the C programming language. The software allows users to design and simulate comminution circuits consisting of crushing and wet grinding stages. The program performs mass balance calculations and particle size distribution analysis based on user-defined input parameters. The distribution coefficient of ore particles can also be determined using sieve analysis data entered by the user. The main menu from C&G Circuit Designer is shown in Figure 3. (Rejepov, 2019

Web-Based Extension : In order to improve accessibility and visualization capabilities, the application was later extended to a web-based platform developed using ASP.NET Core MVC architecture. The web application integrates Microsoft SQL Server for data storage and management. The system includes equipment catalogs such as crushers and screens, allows users to generate process flowsheets automatically, and provides a more intuitive graphical interface for circuit design and simulation (Tunçok, 2023).

```
************************** C&G Circuit Designer ************************************************

C&G Circuit Designer is a process design and simulation program for
crushing circuit and wet grinding circuit in a mineral processing plant.

The program is created based on literature and works accordingly.

In this program, maximum stage of crushing circuit is 3.
Also, maximum stage of grinding circuit is 2.

The stage of communition process with proper reduction ratios and distribution coefficient of ore
in log-log graph can be determined if they are unknown.

In NOTIFICATIONS option, some notifications are collected to inform a user.

In PARAMETERS option, there are initial values for each definition used to design and
simulate the circuit in an optimum way. They can be changed by user.

In 4.option, user can determine the distribution coefficient of a specific sample
from the results of sieve analysis.

*******************************************************************************************************

Start                                  : [1]
Notifications                          : [2]
Parameters                             : [3]
Determination of distribution coefficient : [4]
The last saved communition process     : [5]

Enter your choice                      : _
```

Figure 3. Main menu from the C&G Circuit Designer application (Rejepov, 2019)

When compared to established commercial simulation platforms such as JKSimMet and USIM PAC, the developed application exhibits a different positioning in terms of functionality and complexity. While commercial tools offer highly detailed and data-intensive modeling capabilities, they often require extensive calibration data and specialized expertise (Morrison & Richardson, 2002; Brochot et al., 2002). In contrast, the present system prioritizes

accessibility and computational efficiency, making it particularly suitable for preliminary design studies and educational applications. This trade-off between model complexity and usability reflects a broader challenge in engineering software development.

3.1. Design of Crushing Circuit

The application requires several input parameters including clay content of the ore, distribution coefficient, work index, feed size, product size, and number of circuit stages. If the number of stages is known, the system performs simulation of the predefined circuit configuration. If the stage number is unknown, the software can estimate an optimum circuit configuration automatically. After determining the circuit structure, the program performs mass balance calculations and particle size distribution analysis for each stage of the comminution process.

The performance of the developed application was evaluated using case studies derived from previously published plant design data (Koyuncu, 2017). For testing the Application, the screen efficiencies are chosen 90%, 95%, and 87% for each stage respectively, then the number of crushing stage, crusher types and crushing size for each stage, And also the feed and final crushing sizes entered to be same as the actual circuit (Figure 4).

```
************ For CRUSHING CIRCUIT ************************************************************************

Maximum size of run of mine ore before crushing circuit (mm)                    (Min. 30 mm) : 600

Final crushing size of ore (mm)                                                  (Min. 5 mm) : 10

Feed rate (t/h)                                                               (Max. 1000 t/h) : 200

Enter the number of crushing stage                                 (Enter 0 for determination) : 3

-------------------------------------------------------------------------
[1] Cone Crusher / [2] Jaw Crusher / [3] Impact Crusher / [4] Roll Crusher

Enter your choice for crusher type

First crusher                                                      : 2

Second crusher                                                     : 2

Third crusher                                                      : 1

Crushing size at first stage (mm)                                  : 150

Crushing size at second stage (mm)                                 : 30

Crushing size at third stage (mm)                                  : 10.00
```

Figure 4.Given sizes and crusher types for designing of crushing circuit by C&G Circuit Designer (Rejepov, 2019)

In design mode, the software successfully determined the number of comminution stages, appropriate crusher or mill types, and overall circuit configuration based on feed characteristics and target product size. Stage-wise mass balances were calculated consistently for all evaluated scenarios. The flowsheets generated by the software exhibit strong agreement with manually developed circuits, as illustrated in Figure 5 (Rejepov, 2019).

Furthermore, the mass balance outputs for each stage, presented in Figure 6, confirm the internal consistency of the simulation results.

When compared to established commercial simulation platforms such as JKSimMet and USIM PAC, the developed application exhibits a different positioning in terms of functionality and

complexity. While commercial tools offer highly detailed and data-intensive modeling capabilities, they often require extensive calibration data and specialized expertise (Morrison & Richardson, 2002; Brochot et al., 2002). In contrast, the present system prioritizes accessibility and computational efficiency, making it particularly suitable for preliminary design studies and educational applications. This trade-off between model complexity and usability reflects a broader challenge in engineering software development.

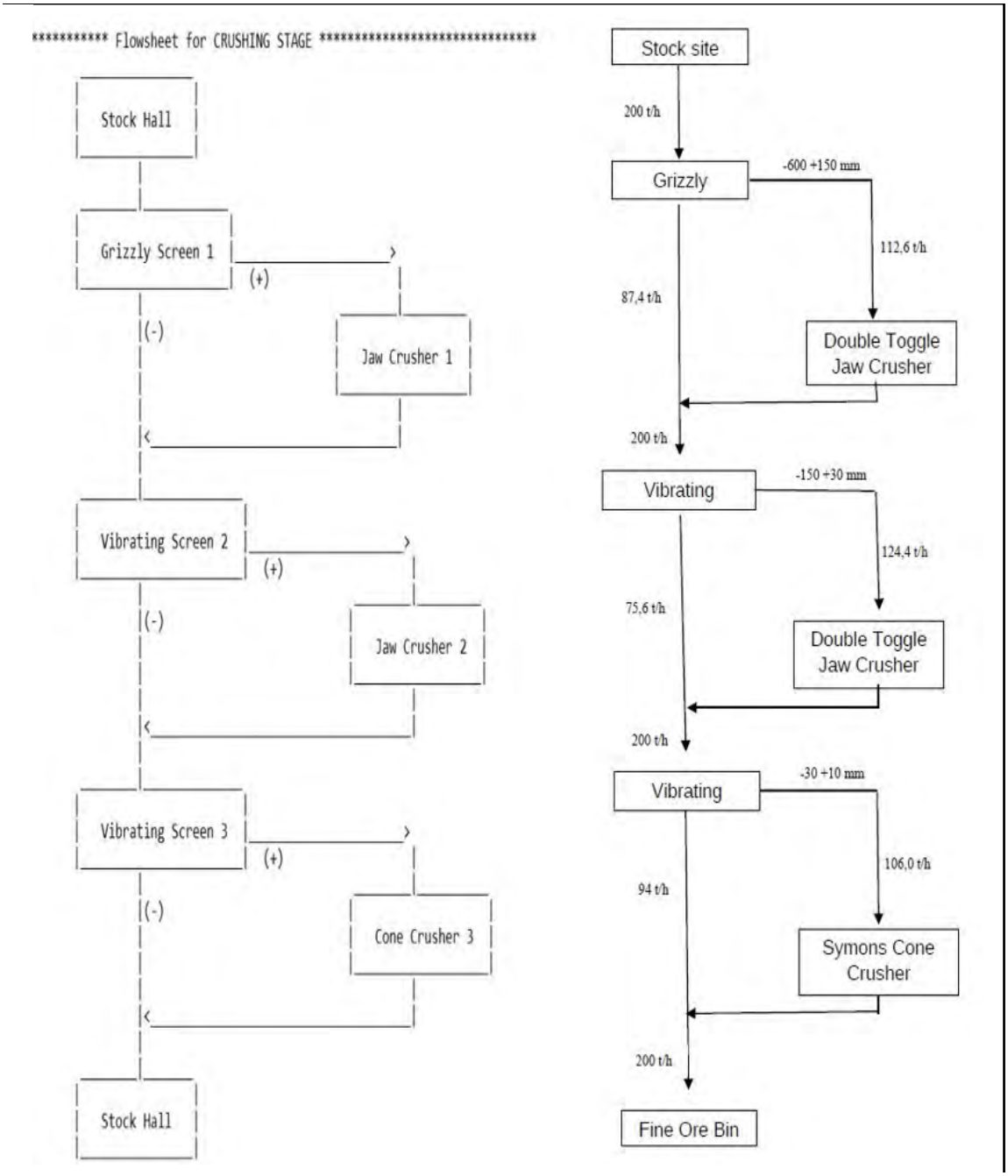

Figure 5. Flowsheet of crushing circuit created by C&G Circuit Designer (left) desktop version and (right) manually created actual circuit. (Rejepov, 2019)

********** Mass Balance for 1st CRUSHING STAGE **********

For Grizzly Screen 1

	d100 (mm)	Solid (t/h)
Feed	600.00	200.00
Oversize	600.00	111.61
Undersize	150.00	88.39

For Jaw Crusher 1

	d100 (mm)	Solid (t/h)
Feed	600.00	111.61
Product	150.00	111.61

********** Mass Balance for 3rd CRUSHING STAGE **********

For Vibrating Screen 3

	d100 (mm)	Solid (t/h)
Feed	30.00	200.00
Oversize	30.00	105.12
Undersize	10.00	94.88

For Cone Crusher 3

	d100 (mm)	Solid (t/h)
Feed	30.00	105.12
Product	10.00	105.12

********** Mass Balance for 3rd CRUSHING STAGE **********

For Vibrating Screen 3

	d100 (mm)	Solid (t/h)
Feed	30.00	200.00
Oversize	30.00	105.12
Undersize	10.00	94.88

For Cone Crusher 3

	d100 (mm)	Solid (t/h)
Feed	30.00	105.12
Product	10.00	105.12

Figure 6. Mass balance for each stage of simulated circuit created by C&G Circuit Designer.

Overall, the results of this study demonstrate that the developed application provides a practical and efficient tool for comminution circuit design. Its ability to combine ease of use with essential modeling functionality makes it particularly valuable for early-stage design, sensitivity analysis, and educational purposes. However, the integration of more advanced modeling techniques and expanded validation remains necessary to fully establish its applicability in industrial contexts.

4. CONCLUSION

This study presents the development of a computer-aided application for designing comminution circuits in mineral processing plants. The system evolved from a desktop-based application developed using the C programming language into a web-based platform implemented using ASP.NET Core MVC architecture. The developed application enables engineers to simulate crushing circuits, calculate mass balance, and determine particle size distributions efficiently.

The results indicate that the developed tool is particularly suitable for preliminary design studies, scenario analysis, and educational purposes. Although further development is required to extend applicability toward detailed industrial design, the current version provides a transparent and efficient alternative to conventional manual design methods.

Future research will focus on expanding the functionality of the software by integrating additional equipment models, incorporating grinding circuit optimization algorithms, and applying artificial intelligence techniques for automated plant design. The integration of machine learning models may also allow the system to predict circuit performance under varying operational conditions.

REFERENCES

Brochot, S., Villeneuve, J., Guillaneau, J. C., Durance, M., Bourgeois, F., (2002), “Mineral processing plant/circuit simulators: An overview”, in Mineral Processing Plant Design, Practice and Control, SME.

Hedvall, P., Nordin, M., (2002), “Mineral processing plant/circuit simulators: An overview”, in Mular, A. L., Haibe, D. N., Barrett, D. J. (Eds.), Mineral Processing Plant Design, Practice, and Control, 421–441, SME, Colorado.

Herbst, J. A., Nordell, L. K., (2002), “Mineral processing plant/circuit simulators: An overview”, in Mular, A. L., Haibe, D. N., Barrett, D. J. (Eds.), Mineral Processing Plant Design, Practice, and Control, 495–506, SME, Colorado.

Kaja, D. M., (2002), “Mineral processing plant/circuit simulators: An overview”, in Mular, A. L., Haibe, D. N., Barrett, D. J. (Eds.), Mineral Processing Plant Design, Practice, and Control, 404–407, SME, Colorado.

King, R. P., (2001), “Modeling and Simulation of Mineral Processing Systems”, Butterworth-Heinemann, Oxford.

Koyuncu, E., (2017), “Plant design of a copper–zinc processing plant”, Unpublished B.Sc. Thesis, Istanbul Technical University, Istanbul, Turkey.

Morrison, R. D., Richardson, J. M., (2002), “Mineral processing plant/circuit simulators: An overview”, in Mular, A. L., Haibe, D. N., Barrett, D. J. (Eds.), Mineral Processing Plant Design, Practice, and Control, 442–460, SME, Colorado.

Rejepov, J., (2019), “Developing of a computer application for comminution circuits design”, Unpublished B.Sc. Thesis, Istanbul Technical University, Istanbul, Turkey.

Saltuklaroğlu, L., (2003), “Computer aided design of size reduction circuits”, Unpublished B.Sc. Thesis, Istanbul Technical University, Istanbul, Turkey.

Tunçok, C., (2023), “Computer aided plant design application”, Unpublished B.Sc. Thesis, Istanbul Technical University, Istanbul, Turkey.

Wills, B. A., Finch, J., (2016), “Wills' Mineral Processing Technology: An Introduction to the Practical Aspects of Ore Treatment and Mineral Recovery”, 8th ed., Elsevier.

CONSERVATION, REHABILITATION AND RECYCLING IN MINERAL PROCESSING

ANALYSIS OF THE REUSE POTENTIAL OF SOLID WASTES AFTER HCl LEACHING FROM A CIRCULAR ECONOMY PERSPECTIVE USING MICROSCOPE IMAGES AND MACHINE LEARNING

Tuğba Deniz TOMBAL KARA[1,*], Burçin KAYMAKOĞLU[2], Nevzat Yağız TOMBAL[3]

[1]Adana Alparslan Turkes Science and Technology University, Faculty of Engineering, Mining Engineering Department, 01250, ADANA-TÜRKİYE
[2]Adana Alparslan Turkes Science and Technology University, Faculty of Engineering, Materials Science and Engineering Department, 01250, ADANA-TÜRKİYE
[3]Istanbul Gelisim University, Faculty of Engineering and Architecture, Electrical and Electronics Engineering Department, 34310, ISTANBUL-TÜRKİYE
**Corresponding author: ttombal@atu.edu.tr*

A B S T R A C T

In recent years, the growing commitment to circular economy principles has encouraged the transformation of wastes into secondary raw materials instead of consigning them to disposal. Among these, Pb-Zn tailings stand out for their high contents of carbonates, silicates, and minor sulfides. When properly treated and stabilized, these materials can offer useful physical and chemical properties for construction or ceramic industries. Hydrochloric acid (HCL) leaching is a common method to extract valuable metals from tailings. Nevertheless, any materials remaining after leaching are hardly examined for their potential for reuse. Traditional analytical tools like XRF, XRD, and ICP-MS are proficient in compositional analysis but provide insufficient information regarding microstructural characteristics such as porosity, particle size, or surface texture-elements crucial for evaluating the safe and effective reuse of materials. This study examines the residues left behind after HCL leaching of Pb-Zn flotation tailings and explores how these materials might be given a second life instead of being discarded. Using a combination of microscopic imaging and machine learning, it seeks to uncover the microstructural features that determine whether the residues can be safely and effectively reused. Ultimately, this approach supports a more sustainable form of resource management, where the by-products of mineral processing are reimagined as valuable components within a circular economy.

Key words: *Pb-Zn tailings, circular economy, image analysis, machine learning, reusability potential*

1. INTRODUCTION

Lead-zinc (Pb-Zn) flotation tailings are a significant type of waste generated globally from mining processes, including Turkey. The production of Pb-Zn ores typically results in significant amounts of flotation tailings containing residual metals at high concentrations. Globally, mining activities are increasingly burdened by waste management issues, and the need for efficient use of these waste materials is being emphasised. Recent studies indicate that flotation tailings may constitute a significant portion of the mining waste disposed of in countries such as Serbia. Estimates suggest that this proportion could be as high as 95% (Vujović et al., 2025). Furthermore, the potential economic gains from reprocessing waste demonstrate its usability as a secondary resource (Lemos et al., 2021). Significant amounts of Pb-Zn waste are produced in Turkey, requiring innovative recycling and reuse strategies to comply with circular economy principles.

Traditional storage methods for mining and metallurgical waste cause severe environmental problems, such as soil and water pollution from heavy metals leaching from the waste. Lead, zinc, and arsenic are heavy metals proven to contaminate nearby ecosystems and can therefore be harmful to both humans and animals (Han et al., 2023). The economic impacts of permanent storage are significant. Mining companies are often required to pay long-term

liability costs because they are obliged to clean up and comply with regulations (Folens et al., 2021). Traditional approaches mostly focus on protection. There is insufficient focus on recovery or reuse. This leads to more waste accumulation rather than providing real economic benefits (Külekçi, 2021). The transition to circular economy models aims to address these challenges by promoting waste as a resource. It thus aims to reduce the ecological footprint and create new job opportunities by adding value to waste (Makhathini et al., 2023).

Within the circular economy framework, secondary resources are increasingly understood not as discarded materials, but as potential inputs for new value-adding processes. This shift in perspective is especially relevant for mining wastes such as flotation tailings. Although these materials are often classified as hazardous, they frequently contain appreciable amounts of metals that can be recovered using appropriate technologies. Recent studies have demonstrated that a wide range of metals can be successfully extracted from mining wastes, highlighting their potential as alternative raw material sources (Lemos et al., 2023). At the same time, considerable research efforts are focused on developing advanced recovery techniques that both minimize environmental risks and maximize the efficient extraction of valuable elements (Álvarez et al., 2022). In line with circular economy principles, the utilization of mining waste as a source of secondary raw materials supports resource conservation and long-term sustainability. Current innovations extend beyond metal recovery and include the reuse of processed tailings as construction aggregates or functional materials, thereby broadening their application potential. Such integrated approaches not only reduce the volume of waste requiring disposal but also create additional economic value, reinforcing the role of mining waste reprocessing as a key strategy in sustainable resource management (Tileuberdi et al., 2024).

The leaching of Pb-Zn flotation tailings using hydrochloric acid (HCL) has been explored as an effective method for metal recovery. Studies indicate that HCL can selectively dissolve lead (Pb) and zinc (Zn) from various types of tailings, creating a pathway for their recovery instead of traditional disposal. Silwamba et al. highlight that using a concurrent dissolution-cementation process facilitates the extraction of metals like Pb and Zn from leach residues, achieving significant recovery rates while minimizing the environmental footprint (Silwamba et al., 2020). Furthermore, the research conducted by Turan et al. on zinc plant residues demonstrates that a combination of roasting and acid leaching can yield recoveries of substantial lead and zinc from similar matrices, although exact recovery rates vary according to specific methods used (Turan et al., 2004). The addition of sodium chloride during the leaching process has enabled improved metal recovery, underscoring the chemical versatility of HCL in extracting valuable metals from complex ore types (Silwamba et al., 2020).

Despite successful studies on the recovery of metals from flotation tailings using HCL leaching, there is limited research on the solid residues produced after leaching. However, these residues may still contain valuable materials and can cause environmental damage if not managed appropriately. The research by Ristović and colleagues highlights the importance of addressing the residual materials left after the leaching process. They suggest that these residues can be reprocessed to extract additional metals or stabilized to reduce environmental risks (Ristović et al., 2022). Schueler et al. propose conversion processes for effective reuse and emphasize the need to optimize leaching conditions (Schueler et al., 2025). More comprehensive research on these post-leaching residues could significantly contribute to waste minimization strategies in the mining sector.

Microscopic images are extremely important for identifying and separating components in waste management operations. Microscopic analysis facilitates the evaluation of material homogeneity, phase distribution, and potential contaminants in waste samples (Ghisellini et al., 2016).

Recent advances in image analysis techniques, such as digital imaging and machine learning (ML), have also made it possible to classify materials in new ways. Efficient algorithms can be used to analyse high-resolution images. This enables automatic sorting systems to distinguish between different types of waste based on their shapes (Nnamoko et al., 2022). The integration of these technologies can significantly improve the decision-making process in waste management. This leads to the optimal recovery and utilization of materials.

Digital image analysis combined with machine learning is transforming waste assessment methods by providing rapid and accurate classifications that surpass traditional methodologies. For example, convolutional neural networks (CNNs) are frequently employed to classify waste types from visual data effectively. Nnamoko et al. demonstrated the efficacy of CNNs in sorted waste using a comprehensive dataset, achieving notable accuracy in differentiating between organic and recyclable materials (Nnamoko et al., 2022). Hyperspectral imaging has been used in recent studies to separate waste materials based on their spectral behavior. The main advantage of this method is that it provides information that cannot be obtained from standard optical images. Wu et al. examined its application for the identification of organic waste and reported that it can distinguish materials that are usually difficult to classify, including textiles and polymer-based wastes (Wu et al., 2023). This suggests that hyperspectral imaging can be useful in practical recycling applications. Better separation of waste streams improves recovery efficiency and reduces contamination, which is an important issue in circular economy-based waste management.

Traditional chemical analyses are reliable for determining the elemental composition and contaminant levels in waste materials. However, they are often time-consuming and face limitations in terms of adaptability. These methods typically require extensive sample preparation, laboratory equipment, and technical expertise. This can hinder the rapid assessment of waste materials (Lau et al., 2020). In contrast, data-driven approaches using machine learning and digital image analysis facilitate the rapid and non-destructive evaluation of waste materials. These methods enable real-time evaluation without the need for labour-intensive chemical processes. This increases efficiency and reduces operating costs (Alonso et al., 2021). Furthermore, the integration of machine learning with imaging technology can reveal complex relationships in waste data that may not be apparent using traditional methods. This feature facilitates the identification of recycling potentials. It also allows for a more detailed understanding of waste material properties (Xia et al., 2021; Qin et al., 2021).

The innovative aspect of this study is its adoption of an integrated and process-oriented approach to evaluate the reuse potential of solid wastes generated after the leaching of Pb-Zn flotation wastes with HCL. The microstructural transformation of the solid residues produced after leaching was systematically analyzed and quantified using microscopic images. The features obtained from these images were directly linked to process-related reuse scenarios through a machine learning framework. Machine learning was used not as an independent prediction tool, but as a decision support methodology that bridges microstructural characteristics with engineering-based reuse criteria. By placing this approach within a circular economy perspective, the study offers a structured pathway to transform leaching residues from a disposal burden into a secondary resource with defined application potential.

The main objective of this study is to assess the reuse potential of solid residues obtained after HCL leaching of Pb-Zn flotation tailings by adopting a process-oriented, image-based machine learning approach within the framework of the circular economy. For this purpose, microscopic images of the leached residues were acquired and analyzed to extract quantitative features that reflect material characteristics relevant to process behavior and potential reuse. These image-derived features were then used as inputs for machine learning models to determine the reuse potential of the residues based on process-related criteria, rather than relying solely on statistical pattern recognition. Based on the clustering outcomes, the study further aimed to

propose realistic reuse and valorization routes for the leached solid residues, taking into account engineering feasibility as well as environmental and sustainability considerations.

2. MATERIAL AND METHODS

2.1. Material

The foundation of the research is the lead-zinc ore from Balya, located in Balıkesir province. Balıkesir province is notably abundant in base metal mineralizations due to its geological composition. The Balya lead-zinc deposit is the most prominent, having been intermittently exploited since antiquity. The Balya lead-zinc deposit encompasses an area of approximately 8 km^2, including the town center of Balya and its vicinity. Proven reserves of 3,260,000 tones were identified in the deposit, with concentrations of 7.2% Zn, 2.7% Pb, and 0.3% Cu (MTA, 2019).

The material characterization of the Pb-Zn flotation tailings revealed that the sample did not contain high moisture content physically, had a bulk density of 3.089 g/cm^3, and exhibited a fine-grained structure with $d_{50} \approx 25$ µm. Chemical analysis results showed that the material has a carbonate-silica matrix mainly composed of CaO-SiO_2-CO_2, along with significant levels of Pb (≈1329 ppm) and Zn (≈1335 ppm) and environmentally critical As and Cd content. Mineralogical investigations using XRD, SEM-EDS and polished section studies revealed that the main phases are carbonates such as calcite and dolomite, and quartz; valuable metal-bearing minerals are mostly galena (PbS) and sphalerite ((Zn,Fe)S), with pyrite and chalcopyrite occasionally present. These findings reveal that the sample has a heterogeneous and multi-phase structure with both re-enrichment and metal recovery potential, as well as environmental risks due to the presence of As and Cd.

Leaching experiments with HCL were carried out to recover valuable metals from the sample. The leaching experiments focused on recovering Ce, Nd, La, Ni and Co. In leaching experiments, it was observed that REE dissolution rates were higher, particularly at low solid ratios, and that dissolution efficiencies began to be limited as the solid ratio increased due to a decrease in the acid/solid ratio. Increasing the acid dosage generally resulted in a significant increase in dissolution efficiencies. Reaction rates and dissolution amounts increased at high concentrations. Dissolution efficiencies increased for most elements as the leaching time was extended. The increase in temperature provided significant gains for Ce-Nd-La and Ni, while Co, which already had a high dissolution yield, showed relatively lower sensitivity to temperature. The reduction in particle size significantly increased dissolution for all elements. Maximum recoveries were achieved, particularly in the 38 µm fraction. Optimum leaching conditions and maximum recoveries of REE, Ni and Co in HCL medium was shown in Table 1.

Table 1. Optimum leaching conditions and maximum recoveries of REE, Ni and Co in HCL medium

Element	Optimum Solid Ratio (%)	Optimum HCL Dosage	Optimum Leaching Time (min)	Optimum Temperature (°C)	Optimum Particle Size (µm)	Maximum Recovery (%)
Ce	10	2-5M	90	50-70	38	50.53
La	10	2-5M	90	50-70	38	67.00
Nd	10	2-5M	90	50-70	38	60.47
Ni	15	2-5M	60-90	50-70	38	58.94
Co	15	2-5M	≥ 90	50-70	38	89.28

2.2. Method

Microscopic imaging, quantitative image analysis, and machine learning were integrated to assess both the process behavior and reuse potential of leached solid residues. To address sample heterogeneity caused by HCL leaching, microscopic images were captured from multiple randomly selected regions of each sample. All images were acquired under standardized conditions and categorized according to leaching parameters, ensuring a consistent and comparable dataset for analysis. The images were analyzed to extract quantitative descriptors directly related to processing behavior and reuse potential. Prior to feature extraction, all images were pre-processed in ImageJ under standardized conditions, including noise reduction, contrast enhancement, and grayscale conversion to improve particle–pore distinction. Particle segmentation was then applied to isolate individual grains and voids, enabling objective and reproducible measurements across different samples and leaching conditions. The selected image-derived parameters were chosen for their direct relevance to reuse-oriented process performance. Aspect ratio quantified particle shape anisotropy, which influences compaction efficiency and mechanical interlocking in stabilized or load-bearing applications. Circularity measured particle roundness and flowability, impacting granulation behavior and binder distribution in cementitious or geopolymer systems. Porosity-including both surface roughness and leaching-induced internal voids-was quantified as a critical factor governing material reactivity, binder interaction, and stabilization efficiency. Additionally, solidity and roundness were included to capture surface degradation and edge alterations resulting from leaching, aspects not fully represented by global shape metrics. Solidity reflects surface integrity and the development of concavities associated with chemical etching and binder anchoring, while roundness characterizes edge angularity, which affects packing behavior and mechanical response. Collectively, these parameters establish a process-oriented link between microstructural changes and engineering performance. When integrated into the machine learning–based decision-support framework, they enable systematic and quantitative classification of reuse potential.

In this study, unsupervised machine learning methods were used to comprehensively evaluate the microstructural properties of solid residues obtained after HCL leaching and to objectively group materials with similar properties. An unsupervised learning approach was preferred because there was no predefined class label in the study, and the aim was to reveal the natural structure and internal distinctions of the data set. In the machine learning analyses, the circularity, solidity, roundness, aspect ratio, and porosity values obtained from the microscope images using ImageJ software were used. A total of 122 different microscope photographs, comprising a dataset of five quantitative microstructure parameters, were analyzed. All parameters were standardized (mean = 0, standard deviation = 1) to prevent scale differences from affecting the analysis.

To examine the relationships between parameters in the multidimensional dataset and represent the dataset in a lower-dimensional space, Principal Component Analysis (PCA) was applied. PCA is a statistical reduction method that aims to produce new components that best explain the variance while minimizing information loss in high-dimensional data. PCA was used to reveal correlations between parameters, identify dominant microstructure features, and determine the appropriate number of components for clustering analyses. Cumulative explained variance and the elbow approach were evaluated together. The Mann-Whitney U test was applied to test whether the clusters obtained through machine learning were statistically significant, not just visually or algorithmically. The Mann-Whitney U test is a non-parametric statistical test that evaluates whether two independent groups come from the same distribution. The reasons for choosing this test are that the groups obtained as a result of clustering do not need to meet the assumption of normal distribution, the sample sizes do not need to be equal between clusters, and the distributions of the analyzed parameters have the potential to be asymmetric. The Mann-Whitney U test was applied separately for each microstructure parameter to assess whether the difference between the two clusters was

statistically significant. The Mann-Whitney U statistic for two independent samples is defined as follows:

$$U_1 = n_1\, n_2 + \frac{n_1(n_1+1)}{2} - R_1 \quad \text{(Eq. 1)}$$

$$U_2 = n_1 n_2 \frac{n_2(n_2+1)}{2} - R_2 \quad \text{(Eq. 2)}$$

where:
n_1 and n_2: the number of samples in the first and second sets
R_1 and R_2: the total ranking values of the ordered data belonging to the first and second sets, respectively.

The test statistic was calculated using U=min (U_1, U_2). The calculated p-value represents the probability of the observed difference occurring under the null hypothesis (the assumption that the two groups come from the same distribution). In this study, $p<0.05$ was considered statistically significant, and $p<0.01$ was considered a strong statistical significance criterion.

3. RESULTS AND DISCUSSION

3.1. Quantitative Microstructural Results of Images and General Microstructural Relationships with Leaching Conditions

All optical microscope images were evaluated as a single dataset using ImageJ, and the overall effects of the leaching process on microstructure were quantitatively assessed. After image processing, circularity, solidity, aspect ratio, and roundness were calculated for each particle, and area-based porosity was also determined. The results indicate that leaching did not completely disrupt particle geometry but primarily modified surface characteristics. Although circularity and roundness showed a broad distribution, most particles fell within the medium-to-high roundness range, suggesting that dissolution occurred mainly at corners and edges. The consistently high solidity values demonstrate that excessive boundary irregularity or internal void development did not occur, and the mechanical integrity of the microstructure was largely preserved. Figure 1 presents representative microscope images of the sample at 200× magnification.

When examining the aspect ratio distributions, it was observed that the vast majority of particles exhibited moderately elongated geometries and that excessively oriented or fibrous structures were not dominant. This indicated that the leaching conditions did not deform the particle morphology in a specific direction and that shape changes occurred more at the micro scale. Although a small number of particles had high aspect ratio values, this did not determine the overall distribution character. Porosity values were concentrated at medium levels and varied within a limited range when all samples were considered. This result indicated that micro voids and roughness developed on the particle surface during the leaching process, but excessive porosity or particle fragmentation did not occur at the macro scale. The observed increase in porosity contributed to an increase in reactive surface area, while the preservation of particle integrity demonstrated that microstructural stability was maintained.
When the entire dataset was evaluated together, it was clear that the microstructure parameters derived from ImageJ were sensitive to leaching conditions. An increase in porosity values was observed under conditions of increased leaching intensity, indicating the development of micro voids on the particle surface due to dissolution. Parallel to this, an increase in circularity and roundness values occurred in some samples, which was associated with corner rounding due to surface abrasion. In contrast, the high solidity values indicated that the leaching process did not completely weaken the microstructure and that dissolution occurred through a more surface-controlled mechanism. The fact that the overall distribution of aspect ratios has been largely preserved indicates that the leaching conditions did not directionally distort the particle geometry and that shape changes were limited. When these findings were evaluated together, it could be said that the leaching process created a controlled

transformation in the microstructure. The preservation of particle integrity while increasing the reactive surface area and porosity indicated a microstructural equilibrium that was advantageous in terms of increasing dissolution efficiency.

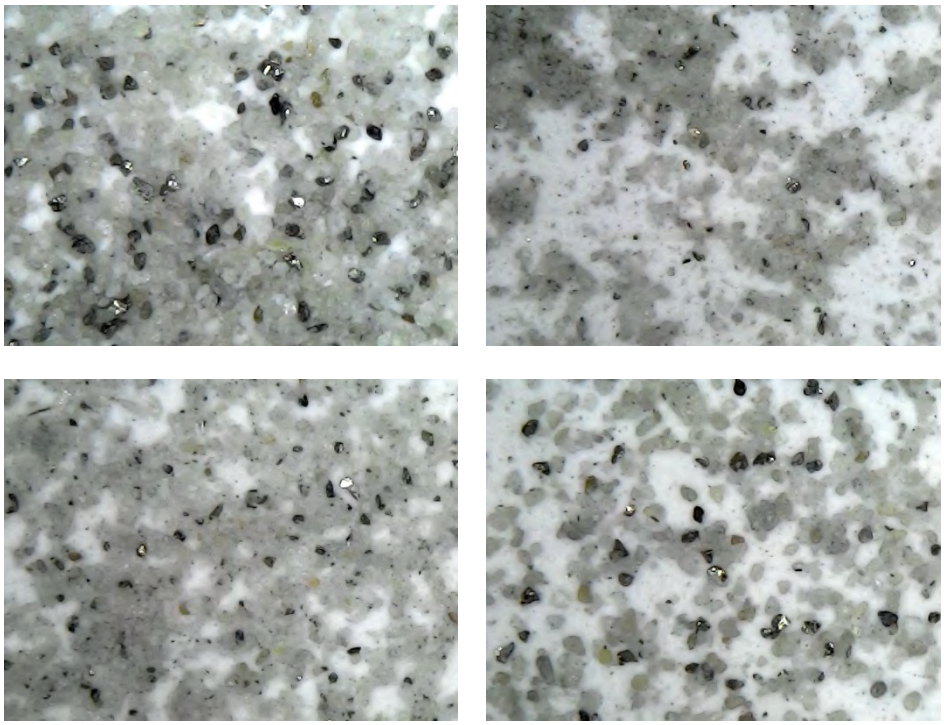

Figure 1. Representative microscope photographs of the sample

Table 2 provides the average circularity, roundness, solidity, aspect ratio and porosity values obtained from 122 photographs.

Table 2. Image-Based Shape Parameter Averages (n = 122)

Parameter	Mean
Circularity	0.66
Aspect Ratio	1.75
Roundness	0.57
Solidity	0.84
Porosity	0.43

3.2. Unsupervised Machine Learning Approach for Microstructure-Based Evaluation

To evaluate the intrinsic structure of the image-derived microstructural dataset and to identify natural groupings among the leached solid residues, an unsupervised machine learning approach was applied. The analysis was performed using principal component analysis (PCA) followed by K-means clustering, supported by statistical validation.

3.2.1. Dimensionality reduction by principal component analysis

The dataset consists of 122 separate material samples defined by five microstructural parameters (circularity, solidity, roundness, aspect ratio, and porosity) obtained from microscope images. The multivariate nature of the dataset was taken into account. Therefore, the dimensions were first reduced using PCA, and the dominant features determining the variability were identified (Table 3).

Table 3. The main dataset

	PC1	PC2	PC3	….	PC15	PC16	PC17
circularity_avg	0.348837	0.023375	-0.035870	…	0.482839	-0.327048	-0.562197
circularity_std	0.290233	-0.132710	0.144053	…	-0.296762	-0.198465	-0.018128
circularity_min	0.054337	0.054973	-0.513700	…	0.037179	-0.054379	-0.019971
circularity_max	0.336316	-0.098304	0.047209	…	0.165533	0.384373	0.046134
solidity_avg	0.336716	0.041914	-0.174230	…	0.004971	0.564670	0.307008
solidity_std	-0.078921	-0.292785	0.519190	…	0.240972	0.109595	0.076850
solidity_min	0.143351	0.269120	-0.426751	…	0.140597	0.000948	0.002717
solidity_max	0.310202	-0.108239	0.063438	…	-0.293178	-0.274722	-0.006640
aspect_ratio_avg	-0.281039	-0.217259	-0.138346	…	0.228695	-0.287230	0.393459
aspect_ratio_std	-0.109190	-0.430054	-0.323925	…	-0.438212	0.068816	-0.256907
aspect_ratio_min	-0.266407	0.210968	-0.050485	…	-0.158579	0.118582	-0.100000
aspect_ratio_max	-0.074781	-0.424837	-0.270525	…	0.306188	0.012709	0.087133
roundness_avg	0.336418	0.055729	-0.034580	…	-0.056896	-0.417448	0.574592
roundness_std	0.208118	-0.312561	-0.016536	…	0.216876	0.125176	-0.021012
roundness_min	0.116186	0.436104	0.150843	…	0.019573	0.049780	-0.006659
roundness_max	0.296876	-0.178249	0.040215	…	-0.267334	0.048781	-0.106303
porosity	-0.126650	0.132792	-0.012295	…	0.029136	-0.019130	0.022826

The cumulative explained variance curve is shown in Figure 2. It can be seen that the first two principal components account for approximately 73% of the total variance. This indicates that the data set can be effectively represented in a two-dimensional feature space without significant loss of information. The elbow point observed after the second component further supports the selection of two principal components as the optimal representation of the dataset.

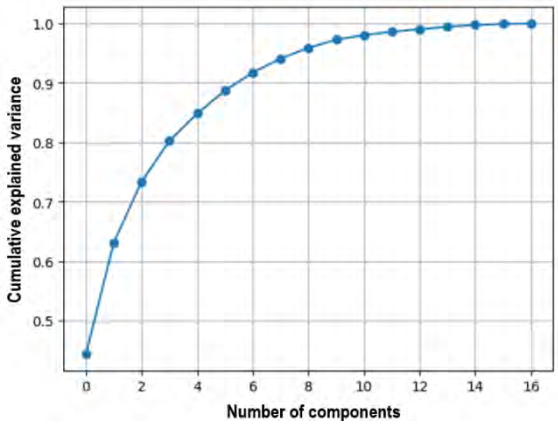

Figure 2. Cumulative explained variance as a function of the number of principal components

An examination of the PCA loading values presented in Table 3.2 highlights a clear separation of microstructural features across the two principal components. The first principal component (PC1) is largely controlled by circularity, solidity, and roundness, suggesting that it mainly captures variations in particle compactness and geometric regularity. In contrast, the second principal component (PC2) is dominated by aspect ratio and porosity, indicating that this component reflects differences in particle elongation as well as the development of internal or surface voids.

3.2.2. Visualization of microstructural distribution

Projecting all samples onto the PC1-PC2 plane provides a clear visual overview of the underlying structure of the dataset (Figure 3). The distribution of the data points reveals two dominant and well-separated groups, mainly differentiated along the PC1 axis. This pattern

suggests that variations in particle compactness-related features play a more influential role in distinguishing the samples than porosity-related characteristics alone.

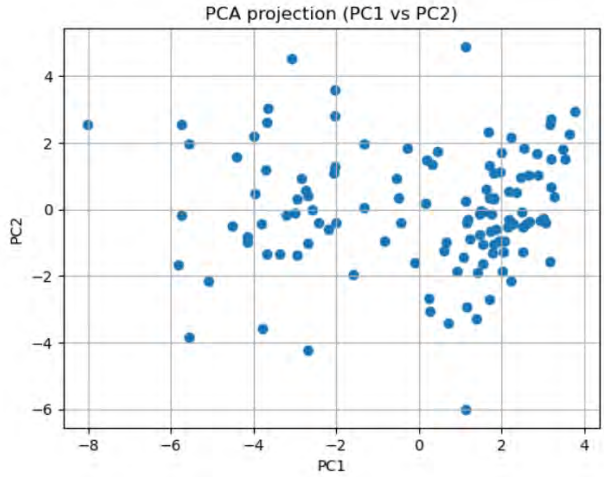

Figure 3. Projection of samples in the PC1-PC2 feature space

3.2.3. Clustering results and cluster characteristics

Based on the PCA results and the observed data structure, K-means clustering was performed with k=2. The clustering outcome mapped onto the PCA space (Figure 4) confirms the visual interpretation of the PCA distribution, with samples clearly grouped into two distinct clusters.

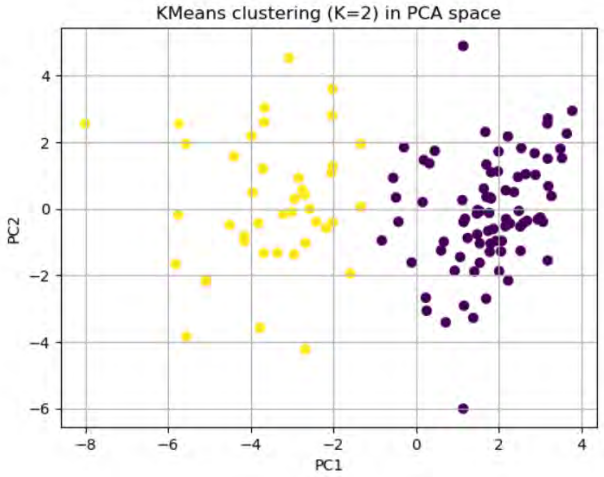

Figure 4. K-means clustering results (k=2) projected onto the PCA space

The average of the original microstructural parameters based on clusters is given in Table 4. As can be seen from the values, Cluster 0 is characterized by higher circularity, solidity, and roundness values. This indicates compact, regular, and mechanically stable particle morphologies. In contrast, Cluster 1 exhibits higher aspect ratio and porosity values associated with longer and more porous microstructures.

Table 4. Average microstructural parameter values for each cluster

cluster	circularity_avg	solidity_avg	aspect_ratio_avg	roundness_avg	porosity_avg
0	0.736790	0.874975	1.686370	0.596679	0.404753
1	0.465098	0.769341	1.865049	0.489098	0.469537

Box plots created to better illustrate the cluster separation among individual parameters are shown in Figure 5. These plots reinforce the robustness of the clustering result by showing consistent and systematic differences between clusters, particularly in terms of circularity, solidity, roundness, aspect ratio, and porosity.

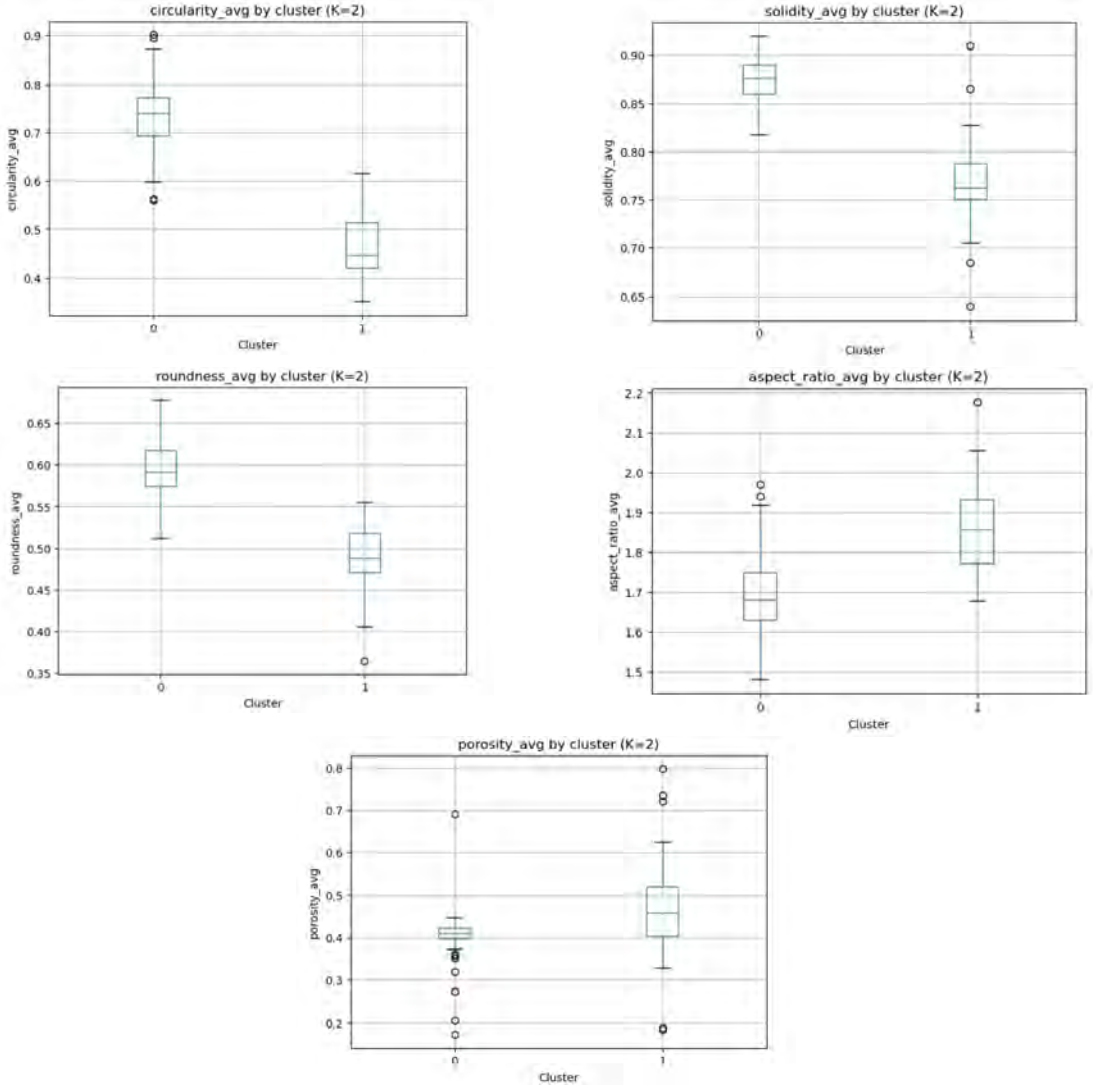

Figure 5. Boxplots of selected microstructural parameters for Cluster 0 and Cluster 1

Figure 6 provides a consolidated visual summary of the unsupervised learning results, illustrating the separation of clusters in PCA space and the corresponding differences in compactness-related and porosity-related microstructural parameters.

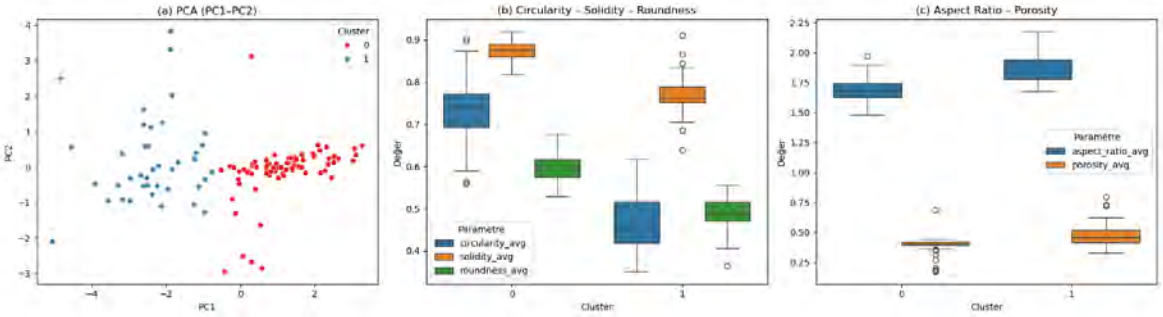

Figure 6. Summary visualization of unsupervised machine learning results, including PCA projection and cluster-wise distribution of key microstructural parameters

3.2.4. Statistical validation of cluster separation

To statistically verify whether the two clusters originate from distinct distributions, the Mann-Whitney U test was applied to each microstructural parameter. The resulting p-values (Table 5) indicate that differences between clusters are statistically significant for circularity, solidity, aspect ratio, roundness, and porosity. The extremely low p-values obtained ($p < 0.01$) confirm that the observed cluster separation is not a consequence of random variation but reflects meaningful and systematic microstructural differences among the leached solid residues.

Table 5. Mann-Whitney U test results for microstructural parameters between clusters

Parameter	p-value
circularity_avg	4,26E-13
solidity_avg	3,75E-11
aspect_ratio_avg	5,58E-06
roundness_avg	3,28E-12
porosity_avg	1,78E+01

3.4. Linking Microstructure to Reuse-Oriented Process Behavior

The unsupervised machine learning analysis identified two dominant microstructural groups within the leached solid residues. Porosity-related characteristics (aspect ratio and porosity) and particle compactness-related features (circularity, solidity, and roundness) are the primary distinguishing factors between these categories. These microstructural distinctions are important since they clearly affect how well the residues will work and how reactive they will be in possible reuse situations.

Materials classified within Cluster 0 exhibit higher circularity, solidity, and roundness values, indicating more compact and geometrically regular particle morphologies. These characteristics are commonly associated with improved mechanical stability, enhanced packing behaviour, and a lower susceptibility to particle breakage. As a result, Cluster 0 materials are particularly well suited for direct reuse applications, such as filling or construction-related uses, where load-bearing capacity and dimensional stability are critical requirements.

Cluster 1, in contrast, is characterized by higher aspect ratio and porosity values, indicating more elongated particles with a more developed pore structure. Increased porosity and surface irregularity generally lead to a higher specific surface area and enhanced particle–binder interactions, which can be advantageous in binder-assisted systems such as cementitious or geopolymer composites. At the same time, pronounced porosity and anisotropic particle morphologies may reduce mechanical strength. Consequently, materials in this cluster are more suitable for controlled reuse pathways involving stabilisation, agglomeration, or binder addition rather than direct application.

The separation of the two clusters represents a progression from compact and mechanically stable particles to fractions that have become more reactive and structurally altered after leaching. This result shows that post-leaching residues cannot be regarded as a single uniform material, but instead consist of microstructurally different fractions. Relating image-derived parameters directly to mechanical and reactive behavior allows reuse potential to be evaluated in a way that is both physically based and relevant to processing conditions.

3.5. Contribution of Machine Learning to Process Decision-Making

In this study, machine learning has been used as a decision support methodology designed to structure and interpret complex microstructural data. The fundamental contribution of the applied unsupervised learning framework is to objectively reveal natural groupings within heterogeneous waste materials. This supports process-oriented decision making. While

traditional evaluation approaches for filtered solid residues provide valuable information, they often fail to capture the combined effects of particle morphology on process performance. As demonstrated in this study, materials with similar chemical compositions can exhibit distinctly different microstructural properties. This can lead to significantly different mechanical or reactive behaviors during reuse.

By integrating PCA and clustering analysis, the proposed machine learning framework enables the simultaneous evaluation of multiple microstructural parameters. This identifies the dominant features that determine material behavior. This multivariate perspective enables the early identification of reuse pathways. Consequently, it reduces dependence on trial-and-error testing and extensive experimental work. Furthermore, the statistical validation of clustering results ensures that the defined groups are not arbitrary but represent meaningful and reproducible distinctions within the dataset.

Compared to traditional classification methods, the machine learning-based approach offers better interpretability and flexibility. It provides a scalable framework that can be extended to larger data sets or different waste streams. Most importantly, it bridges the gap between microscopic observations and engineering-level decisions. This facilitates the selection of appropriate reuse strategies based on measurable and physically interpretable microstructural criteria. In this study, the contribution of machine learning is to improve process understanding. This approach supports more conscious, efficient, and sustainable decision-making for the reuse of leached solid residues within the circular economy framework.

3.6. Circular Economy Implications

The results show that the solid residues obtained after HCL leaching of Pb-Zn flotation tailings should not be considered only as materials for disposal. Rather, they can be treated as potential secondary raw materials, whose reuse options can be evaluated in a systematic way based on their microstructural characteristics. By bringing together image-based microstructural analysis and unsupervised machine learning, this study presents a practical approach for identifying residue fractions with real reuse potential within a circular economy framework.

The unsupervised clustering results revealed that post-leaching residues are inherently heterogeneous, consisting of fractions with markedly different mechanical stability and reactivity. This heterogeneity is a critical factor in circular economy implementation, as it implies that a single, uniform reuse strategy is unlikely to be effective. Instead, selective valorization pathways tailored to microstructural characteristics are required. Fractions exhibiting compact and mechanically stable microstructures may be redirected toward direct reuse applications, while more porous and reactive fractions can be integrated into binder-assisted or stabilized systems. Such differentiation supports the core circular economy principle of maximizing material value while minimizing additional processing and environmental burden.

From an industrial perspective, the proposed approach offers a practical decision-support tool for Pb-Zn processing plants. In conventional operations, leaching residues are generally handled through long-term storage or disposal, which leads to ongoing environmental liabilities and additional costs. The framework proposed in this study allows residues to be screened at an early stage, immediately after leaching, enabling operators to identify fractions with reuse potential without the need for extensive secondary testing. By focusing on microstructural indicators rather than relying only on bulk chemical composition, the approach captures process-relevant characteristics that have a direct impact on reuse performance.

A plausible implementation scenario for industrial Pb-Zn facilities involves integrating microscopic imaging and machine learning analysis as a downstream assessment step

following hydrometallurgical processing. Solid residues could be routinely sampled, imaged, and analyzed to determine their placement within predefined reuse-oriented categories. Based on this classification, residues could be directed to appropriate valorization routes, such as direct reuse as construction-related materials, incorporation into cementitious or geopolymer products, or stabilization and conditioning prior to reuse. This adaptive strategy reduces reliance on landfill disposal and aligns waste management practices with circular economy objectives.

4. CONCLUSION

This study demonstrates that the solid residues resulting from the leaching of Pb-Zn flotation tailings with HCL have concrete potential for reuse. Microscopic image analysis revealed significant microstructural heterogeneity in the residues produced after leaching. It emphasizes the need for a differentiated and process-oriented assessment rather than a uniform disposal approach. The results show that a significant portion of the residues exhibit microstructural properties compatible with reuse scenarios, provided that their mechanical stability and reactivity are appropriately matched with suitable applications.

Unsupervised machine learning effectively supported the process by structuring complex microstructural information and identifying natural groupings within the residue material. By using principal component analysis and clustering methods along with statistical checks, the study showed that important microstructural features, especially those related to how compact and porous the particles are, help distinguish material fractions that can be reused. Machine learning was used not as a black-box model that makes predictions, but as an interpretable framework that helps people understand processes and make decisions based on engineering.

From a circular economy perspective, the proposed approach contributes to the transformation of leaching residues from a waste management liability into a potential secondary raw material. The ability to screen and classify residues based on microstructure-informed criteria enables more targeted valorization pathways, reduces reliance on landfill disposal, and supports resource efficiency in Pb-Zn processing operations. The framework aligns with circular economy principles by promoting material loop closure while minimizing additional processing and environmental burden.

Despite its promising outcomes, this study has certain limitations. The size of the dataset indicates the breadth of the material under investigation, and the analysis was based on image-derived parameters acquired under carefully monitored laboratory conditions. Future research should focus on expanding the dataset to include residues from different ore types, leaching agents, and operational conditions. Also, combining the study of small structures with tests on how materials perform, their environmental impact, and cost-effectiveness would make the suggested decision-support system even more useful. Such developments would enhance the robustness and industrial relevance of image-based machine learning approaches for sustainable waste valorization in the mining and metallurgical sectors.

REFERENCES

Alonso, S., Forradellas, R., Morell, O., Jorge-Vázquez, J., (2021) “Digitalization, circular economy and environmental sustainability: The application of artificial intelligence in the efficient self-management of waste”, Sustainability, 13 (4) 2092.

Álvarez, M., Gascó, G., Rodíguez-Pacheco, R., Paz-Ferreiro, J., Méndez, A., (2022) “Recovery of metals from mine wastes: The effect of biochar–Fe composites in the immobilization of arsenic”, Journal of Sustainable Metallurgy, 8 (1) 419-429.

Folens, K., Williamson, A., Damme, K., Ostermeyer, P., García-Timermans, C., Laing, G., Hennebel, T., (2021) “Citrate-mediated hydrometallurgical lead extraction and integrated electrochemical recovery from zinc leaching residue”, Acs Sustainable Chemistry & Engineering, 9 (28) 9282-9288.

General Directorate of Mineral Research and Exploration (MTA), (2019), Turkey's metallic minerals inventory. Ankara: MTA Publications.

Ghisellini, P., Cialani, C., Ulgiati, S., (2016) “A review on circular economy: the expected transition to a balanced interplay of environmental and economic systems”, Journal of Cleaner Production, 114 11-32.

Han, W., Zhao, R., Liu, W., Wang, Y., Zhang, S., Zhao, K., Nie, J., (2023) “Environmental contamination characteristics of heavy metals from abandoned lead–zinc mine tailings in China”, Frontiers in Earth Science, 11.

Külekçi, G., (2021) “The effect of pozzolans and mineral wastes on alkali-silica reaction in recycled aggregated mortar”, Periodica Polytechnica Civil Engineering.

Lau, W., Shiran, Y., Bailey, R., Cook, E., Stuchtey, M., Koskella, J., Palardy, J., (2020) “Evaluating scenarios toward zero plastic pollution”, Science, 369 (6510) 1455-1461.

Lemos, M., Valente, T., Reis, A., Fonsceca, R., Dumont, J., Ferreira, G., Delbem, I., (2021) “Geoenvironmental study of gold mining tailings in a circular economy context: Santa Barbara, Minas Gerais, Brazil”, Mine Water and the Environment, 40 (1) 257-269.

Lemos, M., Valente, T., Reis, A., Fonseca, R., Pantaleão, J., Guabiroba, F., Delbem, I., (2023) “Geochemistry and mineralogy of auriferous tailings deposits and their potential for reuse in Nova Lima Region, Brazil”, Scientific Reports, 13 (1).

Makhathini, T., Bwapwa, J., Mtsweni, S., (2023) “Various options for mining and metallurgical waste in the circular economy: A review”, Sustainability, 15 (3) 2518.

Nnamoko, N., Barrowclough, J., Procter, J., (2022) “Solid waste image classification using deep convolutional neural network”, Infrastructures, 7 (4) 47.

Qin, L., Ahmad, M., Ali, I., Mumtaz, R., Zaidi, S., Alshamrani, S., Tahir, M., (2021) “Precision measurement for industry 4.0 standards towards solid waste classification through enhanced imaging sensors and deep learning model”, Wireless Communications and Mobile Computing, 2021 (1).

Ristović, I., Štyriaková, D., Štyriaková, I., Šuba, J., Širadović, E., (2022) “Bioleaching process for copper extraction from waste in alkaline and acid medium”, Minerals, 12 (1) 100.

Schueler, T., Mettke, L., Crutziger, F., Rasenack, K., Yagmurlu, B., Goldmann, D., (2025) “Leaching of mine tailings flotation fractions using inorganic and organic acids for metals extraction”, Journal of Sustainable Metallurgy, 11 (3) 3014-3030.

Silwamba, M., Ito, M., Hiroyoshi, N., Tabelin, C., Hashizume, R., Fukushima, T., Ishizuka, M., (2020) “Recovery of lead and zinc from zinc plant leach residues by concurrent dissolution-cementation using zero-valent aluminum in chloride medium”, Metals, 10 (4) 531.

Tileuberdi, A., Zhaksylyk, A., Pazylova, D., Sagyndykova, N., Tleuov, A., Tleuova, S., (2024) “Mathematical approach to solving the problem of waste-free processing of metallurgical wastes”, Polish Journal of Environmental Studies, 33 (5) 5887-5892.

Turan, M., Altundoğan, H., Tümen, F., (2004) “Recovery of zinc and lead from zinc plant residue”, Hydrometallurgy, 75 (1-4) 169-176.

Vujović, N., Alivojvodić, V., Radovanović, D., Štulović, M., Sokić, M., Kokalj, F., (2025) “Towards circularity in Serbian mining: Unlocking the potential of flotation tailings and fly ash”, Minerals, 15 (3), 254.

Wu, T., He, P., Lan, D., Lü, F., Long, J., Zhang, H., (2023) “Application of XGBoost for fast identification of typical industrial organic waste samples with near-infrared hyperspectral imaging”, Acs Es&t Engineering, 3 (6) 841-850.

Xia, W., Jiang, Y., Chen, X., Zhao, R., (2021) “Application of machine learning algorithms in municipal solid waste management: A mini review”, Waste Management & Research the Journal for a Sustainable Circular Economy, 40 (6), 609-624.

ENVIRONMENTALLY FRIENDLY LEACHING OF LITHIUM-ION BATTERY WITH FORMIC ACID: PROCESS OPTIMIZATION AND KINETIC INSIGHTS

Muammer KAYA*, Hossein DELAVANDANI*

Mining Engineering Department, Eskisehir Osmangazi University, 26040 Eskisehir, Turkey;
**Corresponding author: mkaya@ogu.edu.tr , hossein.delavandani@gmail.com*

A B S T R A C T

The rapid growth of modern technologies has made electronic devices such as mobile phones, laptops, and electric vehicles indispensable in daily life. These devices rely on lithium-ion batteries (LIBs), creating a rising demand for critical elements such as cobalt (Co), lithium (Li), nickel (Ni), and manganese (Mn). Recycling spent LIBs has become essential not only to conserve valuable resources but also to reduce the environmental and economic impacts of raw materials.

This study aims to develop an environmentally friendly and cost-effective method for recovering critical metals from LIBs to establish a closed-loop recycling process with high efficiency and minimal environmental impact. Formic acid (HCOOH), a low-impact organic acid, was used as a leaching agent. The recovery of Co, Li, Ni, and Mn from the black mass (BM) was investigated using response surface methodology (RSM) to optimize leaching parameters, including acid concentration (0.5–3 mol/L), H_2O_2 concentration (1–4 vol%) as a reducing agent, solid-to-liquid ratio (10–50 g/L), temperature (20–80 °C), and time (1–6 h). Sodium metabisulfite ($Na_2S_2O_5$) was also tested as an alternative reducing agent.

Analysis of variance (ANOVA) showed that acid and reducing agent concentrations were the most significant parameters. Under optimized conditions, recovery efficiencies reached 98% for Co, 93% for Li, 81% for Ni, and 88% for Mn. Kinetic analysis using the shrinking-core model indicated chemically controlled dissolution for Co, Li, and Ni, and diffusion-controlled dissolution for Mn. These findings highlight the potential of organic acids for sustainable hydrometallurgical recovery of critical metals from LIBs.

Key words: *Lithium-ion batteries (LIBs), leaching, organic acid, formic acid, lithium, cobalt, recovery, critical metals*

1. INTRODUCTION

The growth of portable electronics and especially the rapid growth of electric vehicles has significantly increased the demand for lithium-ion batteries (LIBs) and their critical metals (Co, Ni, Li, and Mn). The limited mineral resources and the high environmental cost of their extraction highlight the necessity of sustainable recycling of these metals (Kaya and Delavandani, 2025). Among the recycling technologies, hydrometallurgical methods are considered more efficient and flexible due to their operation at lower temperatures, higher selectivity, reduced energy consumption, and higher recovery rates compared to other methods (Rezaei et al., 2025). However, conventional leaching usually relies on strong mineral acids, which cause corrosion and produce hazardous effluents, ultimately raising environmental concerns (Li et al., 2025, Güloğlu and Orhan, 2026, Kaya, 2025, Kaya and Delavandani, 2025).

Recently, organic acids have been considered as alternatives to previous chemicals due to their lower toxicity, biodegradability, and milder operating conditions (Geng et al., 2026). Formic acid (HCOOH) has attracted special attention due to its moderate acidity, low corrosiveness, availability, and dual function as an acid and a mild reducing agent. Studies show that combining organic acids with appropriate reducing agents can increase the

extraction efficiency while minimizing secondary pollutants. Optimization tools such as response surface methodology (RSM) effectively determine the optimal conditions with fewer experiments, while kinetic modeling helps to elucidate the dissolution mechanisms (Abbas and Jung, 2026).

Despite the progress, many hydrometallurgical processes still face challenges such as long leaching time, high reagent consumption, and operational complexity, which limit industrial application. Therefore, the development of efficient and environmentally friendly alternatives remains essential. In this study, formic acid was investigated as a green leaching agent for the recovery of Co, Li, Ni, and Mn from spent LIB (S-LIB) black mass. The effects of key parameters were optimized using RSM, reducing agents were compared, and kinetics were analyzed using a core shrinkage model to identify the controlling mechanisms. The overall goal is to develop a sustainable and scalable process for closed-loop recovery of critical metals.

2. MATERIAL AND METHODS

2.1. Material

Spent lithium-ion batteries from iPhone devices were used as raw material. After complete discharge for safety, batteries were mechanically crushed, followed by magnetic separation and sieving to remove metallic fractions (Al, Cu, Fe). The remaining fraction, defined as black mass (BM), mainly contained cathode materials, graphite, and minor components, and was obtained at an industrial scale from the Exitcom company. The homogenized BM was sieved to <212 µm and stored in sealed containers. Its main metals were Co, Li, Ni, and Mn. Formic acid (98–100%) was used as the leaching agent due to its low toxicity and biodegradability. Hydrogen peroxide (30%) served as the primary reducing agent, while sodium metabisulfite was evaluated as an alternative. All solutions were prepared with deionized water, and analytical-grade reagents were used. As shown in Figure 1, ICP-AES analysis of the black mass sample determined the composition and percentage of the critical elements present.

Element	% Elements
C	55-65
Co	17-27
Ni	3.5-6
Mn	2-4
Fe	0.3-0.6
Cu	0.4-0.6
Al	0.2-2
Li	2.5-3.5

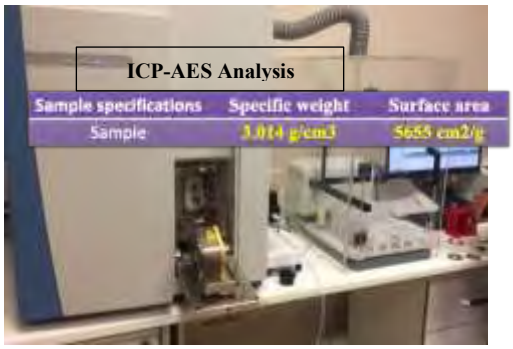

Figure 1. Analysis of the black mass used in this study and determination of the percentage of critical elements present

2.2. Experimental Procedure

Leaching tests were carried out in temperature-controlled glass reactors with 2 g BM and specified acid concentrations according to the design of the experiment (DoE). Temperature (20–80 °C), reducing agent dosage, reaction time (1–6 h), and solid–liquid ratio was varied systematically. Samples were periodically withdrawn, diluted, centrifuged (5000 rpm, 10 min), filtered (0.45 µm), and analyzed for Co, Li, Ni, and Mn concentrations. All experiments were performed in triplicate. Glassware was acid-washed to avoid contamination, and fresh solutions were prepared for each test.

2.3. Kinetic Analysis

Leaching kinetics were interpreted using the shrinking-core model to determine rate-controlling mechanisms. Experimental data were fitted to equations representing chemical reaction control and product-layer diffusion control. The mechanism with the highest correlation coefficient was considered dominant. Temperature-dependent rate constants were analyzed using the Arrhenius equation to calculate activation energies, enabling differentiation between diffusion-controlled and reaction-controlled processes. This kinetic evaluation provided insight into dissolution behavior and supports process optimization and scale-up.

3. RESULTS AND DISCUSSION

3.1. Feed Characterization and Acid Screening

The results of the characterization analyses of the black mass used in this study showed that this material contains a mixture of different active cathodic phases, confirming the presence of compounds such as LFP, LMO, and NCA. This indicates that the sample under study was obtained from a mixture of several types of LIBs, which is very common in the industry and is considered a good representative of real battery waste. The data from the ICP tests also confirmed the presence of the critical elements such as Co, Li, Ni, and Mn in significant amounts, indicating the high recycling value of this feed (Figure 1). In order to select the appropriate leaching agent, a series of preliminary screening experiments was conducted using different organic acids under the same operating conditions to compare the solubility of critical metals. The results showed that the type of acid plays a decisive role in the metal extraction efficiency, and a significant difference was observed between the performances of different acids. Among the acids studied, formic acid showed the highest simultaneous dissolution efficiency of Co, Li, Ni, and Mn metals. Accordingly, formic acid was selected as the main leaching agent, and all subsequent experiments were conducted based on this acid to optimize the operating conditions and analyze the kinetics of the process.

3.2. Statistical Modeling and Analysis of Variance (ANOVA)

To quantitatively evaluate the effect of operational variables on the recovery of valuable metals from battery BM, Response surface methodology based on multivariate experimental design was used. A quadratic model was developed to describe the relationship between independent variables, including formic acid concentration, H_2O_2 concentration, solid-to-liquid ratio, temperature, and time, with the extraction responses of Co, Li, Ni, and Mn metals using Minitab software. Table 1 shows the coded parameter levels and values used in the experimental design.

Table 1. The coded parameter levels and values used in the experimental design

Parameter	Units	Symbols	Coded variables and levels		
			-1	0	1
Formic acid concentration	$molL^{-1}$	X_1	0,5	1,75	3
H_2O_2 concentration	Vol%	X_2	1	2,5	4
Solid-to-liquid ratio	–	X_3	10	30	50
Leaching temperature	°C	X_4	20	50	80
Leaching time	h	X_5	1	3,5	6

A series of experiments was conducted using the experimental design proposed by the software, and the results of the analyses were entered into the constructed model. (Table 2) The adequacy of the models was assessed using analysis of variance (ANOVA), determination coefficients, and diagnostic tests.

Table 2. The layout of the experimental design and the central composite response table for the leaching of Co, Li, Mn, and Ni

Std Order	Run Order	Acid concentration	H_2O_2 concentration	Solid-to-liquid ratio	Temp.	Time	Co recovery (%)	Li recovery (%)	Ni recovery (%)	Mn recovery (%)
16	1	3	4	50	80	6	96	90	77	88
25	2	1,75	2,5	30	50	1	95	91	80	86
3	3	0,5	4	10	20	1	65	66	59	62
14	4	3	1	50	80	1	90	85	67	70
31	5	1,75	2,5	30	50	3,5	95	91	80	86
18	6	3	2,5	30	50	3,5	94	82	69	78
9	7	0,5	1	10	80	1	57	55	55	60
5	8	0,5	1	50	20	1	59	57	58	58
17	9	0,5	2,5	30	50	3,5	65	60	56	66
20	10	1,75	4	30	50	3,5	97	93	83	89
11	11	0,5	4	10	80	6	64	68	58	61
26	12	1,75	2,5	30	50	6	95	91	80	86
2	13	3	1	10	20	1	80	75	67	74
21	14	1,75	2,5	10	50	3,5	90	88	75	75
8	15	3	4	50	20	1	92	88	78	85
28	16	1,75	2,5	30	50	3,5	95	91	80	86
4	17	3	4	10	20	6	94	89	76	84
12	18	3	4	10	80	1	93	90	75	85
10	19	3	1	10	80	6	85	91	70	75
6	20	3	1	50	20	6	87	79	69	74
13	21	0,5	1	50	80	6	60	59	53	56
19	22	1,75	1	30	50	3,5	80	81	75	77
22	23	1,75	2,5	50	50	3,5	93	92	80	79
24	24	1,75	2,5	30	80	3,5	93	90	81	75
30	25	1,75	2,5	30	50	3,5	95	91	80	86
29	26	1,75	2,5	30	50	3,5	95	91	80	86
27	27	1,75	2,5	30	50	3,5	95	91	80	86
7	28	0,5	4	50	20	6	68	71	56	59
23	29	1,75	2,5	30	20	3,5	89	88	77	72
15	30	0,5	4	50	80	1	69	55	54	57
1	31	0,5	1	10	20	6	57	55	50	55
32	32	1,75	2,5	30	50	3,5	95	91	80	86

The analysis of variance (ANOVA) was used to assess the importance of the individual factors and their interactions by comparing their response variables at the different levels (Montgomery, 2017). The ANOVA results showed that the developed models were statistically significant for all metals ($P < 0.001$), indicating the model's ability to describe the dissolution behavior of metals in the studied system. The linear effects analysis showed that the acid

concentration and the reducing agent concentration were the most important parameters affecting the metal extraction. physical parameters such as solid-to-liquid ratio, temperature, and time did not show a significant linear effect in most cases. This suggests that the dominant mechanism of metal dissolution is mainly controlled by the chemical conditions of the reaction medium rather than mass transfer factors or physical parameters.

The study of the interaction effects of parameters showed that some interactions, especially between acid concentration and reducing agent, play an important role in controlling the dissolution of metals. The significance of this interaction indicates that the oxidation-reduction conditions of the solution have a direct effect on the dissolution mechanism of metals. Overall, the statistical modeling results showed that the developed quadratic models are able to describe the metal extraction behavior with high accuracy and can be used to predict responses and determine optimal operating conditions. Therefore, these models provide a reliable basis for the multi-response optimization stage. The RSM combined with CCD facilitated the establishment of a statistical relationship between the leaching parameters and percent recoveries, represented by four polynomial quadratic equations for Co (Eq. (1)), Li (Eq (2)), Ni (Eq. (3)), and Mn (Eq. (4)). The model equation illustrates the influence of the linear, two-way, and square interactions between the process conditions and responses. Using these empirical equations, it is feasible to forecast the leaching recoveries for any desired parameter level and ascertain the relative influence of the factors based on their coefficients. The summary analysis of variances for each response in this study is displayed in Table 3.

$$Co\ recovery\ (\%) = 21.0+39.1x_1+13.2x_2+0.3x_3+0.2x_4-2.0x_5-8.4x_1^2-1.8x_2^2+0.4x_5^2+0.2x_1x_5 \quad (1)$$

$$Li\ recovery\ (\%) = 22.2+48.3x_1+10.2x_2+0.6x_3+0.1x_4-2.1x_5-11.5x_1^2-0.9x_2^2+0.3x_5^2-0.2x_1x_2+0.1x_1x_4-0.2x_1x_5+0.1x_2x_5 \quad (2)$$

$$Ni\ recovery\ (\%) = 36.9+39.6x_1+0.5x_2+0.3x_3-3.1x_5-10.4x_1^2+0.1x_2^2+0.2x_5^2+0.7x_1x_2+0.3x_1x_5+0.1x_2x_5 \quad (3)$$

$$Mn\ recovery\ (\%) = 40.0+23.8x_1-4.2x_2+0.6x_3+0.8x_4-7.1x_5-5.9x_1^2+0.8x_2^2+0.8x5_2+1.3x_1x_2+0.3x_1x_5+0.1x_2x_5 \quad (4)$$

Table 3. The summary of ANOVA tables for the regression models.

Response	F-value	p-value	R^2	Adjusted R^2
Co recovery (%)	56,60	< 0,0001	0,9904	0,9729
Li recovery (%)	67,97	< 0,0001	0,9920	0,9774
Ni recovery (%)	52,61	< 0,0001	0,9897	0,9708
Mn recovery (%)	14,26	< 0,0001	0,9629	0,8954

3.3. Effect of Process Parameters on Metal Extraction

To investigate the effect of operational variables on the recovery of valuable metals, the effect of five main parameters, including acid concentration, reducing agent concentration, solid to liquid ratio, temperature, and time, on the extraction of Co, Li, Ni, and Mn was analyzed.

- **Effect of Acid Concentration:** Acid concentration was identified as the most important parameter controlling extraction for all metals. ANOVA results showed that this parameter had the lowest P-value for all four metals and contributed the most to the response changes. However, excessive increase in acid concentration led to a decrease in extraction efficiency, which was probably due to the change in chemical equilibria, the increase in the formation of stable complexes, or the limitations of mass transfer at high concentrations.

- **Effect of Reducing Agent Concentration:** H_2O_2 concentration played an important role in increasing the extraction of metals, especially Co, Ni, and Mn. Increasing the reducing agent concentration facilitated the reduction reactions of the oxide phases of the metals and their conversion to the soluble state.

- Effect of solid-to-liquid ratio: The results showed that the solid-to-liquid ratio did not have a significant direct effect on most metals, but in some cases, significant interactions with temperature or reducing agent concentration were observed.

- Effect of temperature: Temperature showed a different effect on different metals. For some metals, such as Ni and Li, increasing the temperature improved the recovery, indicating the kinetic control of their dissolution reaction. In contrast, for Mn, the effect of temperature was less, and the presence of a significant quadratic term indicated that there was an optimum temperature for Mn dissolution.

- Effect of Time: The leaching time showed a limited effect on the recovery of most metals, indicating that the dissolution reactions were carried out rapidly in the early stages of the process.

The Pareto chart for the standardized effects as presented in Fig. 2 (a), (b), (c), and (d) for cobalt, lithium, nickel, and manganese, respectively, shows in descending order: the level of importance for the effects of various factors as well as their interactions. Notably, it provides standardized effects beyond 95 % confidence level (beyond the line at 2.20). The distinct response patterns observed for each metal confirm that their dissolution behaviors are governed by different controlling mechanisms.

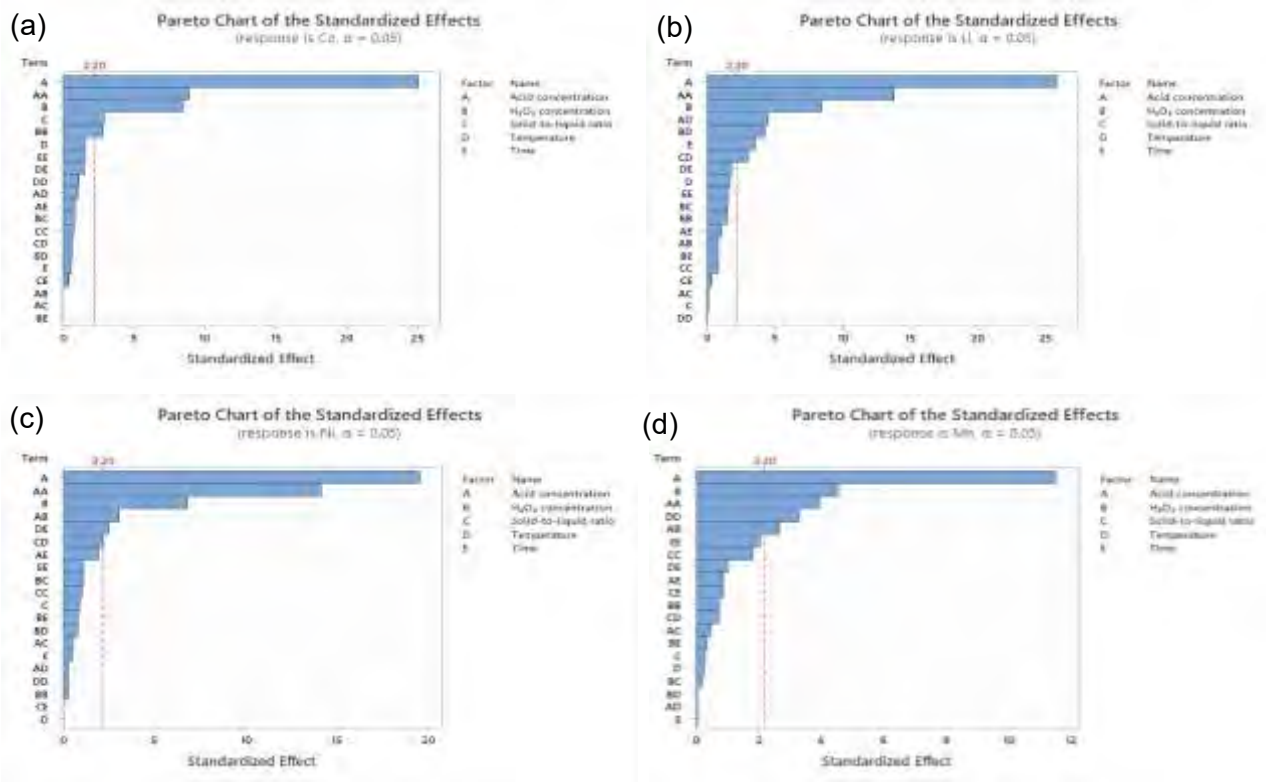

Figure 2. The Pareto Chart of the standardized effects for (a) Co; (b) Li (c) Ni; (d) Mn

3.4. Kinetic Analysis

In order to determine the mechanism controlling the dissolution of metals from the black mass, the kinetic data were analyzed using the Shrinking Core Model (SCM). The results showed that the best fit for different metals was different, indicating the difference in their dissolution path. For Co, the kinetic analysis showed that the Co extraction data showed the best fit to the chemical reaction-controlling model. For Li, this result indicates that the dissolution of Li from the cathode structure is mainly dependent on the chemical reactions of the solution. In Ni, the kinetic behavior of Ni showed that the dissolution of this metal follows a mixed mechanism. And in Mn, unlike other metals, the kinetic data of Mn showed the best fit to the diffusion-controlled model from the product layer. These differences indicate that the crystal structure, oxidation state of the metal, and the type of mineral phase play a decisive role in the dissolution kinetic behavior. Therefore, the selection of optimal operating conditions should be done in such a way that the kinetic limitations of each metal are simultaneously reduced. A comparison of the kinetic results shows in Table 4 that the mechanism controlling the dissolution of metals is as follows:

Table 4. A comparison of the kinetic results

Metal	Controlling Mechanism
Co	Chemical reaction control
Li	Chemical reaction control
Ni	Mixed control
Mn	Diffusion control

3.5. Optimization of Leaching Conditions

To identify the parameter ranges suitable for the optimal recovery of the valuable minerals, the response optimizer function of Minitab software was employed for each response. The optimization studies were based on the analyzed experimental data. The goal was to maximize the leaching recoveries by varying the process parameters to a set desirability. The software was accordingly generated for each critical element and also for all of them in response to high desirability (Table 5). In all, the validation studies demonstrated that the RSM models could be utilized for the efficient recovery of valuable contents via leaching. Under these conditions, the predicted metal recovery values are respectively: 98% for Co, 93% for Li, 81% for Ni, and 88% for Mn.

Table 5. The solutions obtained for the numerical optimization of Co, Li, Ni, and Mn.

Run	Acid concentration ($molL^{-1}$)	H_2O_2 concentration (Vol%)	Solid-to-liquid ratio	Leaching temperature (°C)	Leaching time (h)
Co	2,39	3,21	46,36	70	1
Li	2,24	2,64	10	80	6
Ni	2,17	4	21,31	80	6
Mn	2,65	4	32,22	52	7
All of the Elements	2,14	3,64	44,4	43	6

4. CONCLUSION

In this study, a green hydrometallurgical process was successfully developed for the recovery of critical metals from lithium-ion battery black mass using formic acid as an environmentally benign leaching agent. The results demonstrated that organic acids can serve as efficient and

sustainable alternatives to conventional inorganic acids, with formic acid exhibiting superior leaching performance and therefore being selected as the primary lixiviant for detailed investigation. To systematically evaluate the influence of operational parameters, key factors including acid concentration, hydrogen peroxide dosage, solid-to-liquid ratio, temperature, and reaction time were analyzed using response surface methodology (RSM) based on a central composite design (CCD). Statistical modeling and ANOVA confirmed that acid concentration and reducing agent concentration were the most significant variables affecting metal recovery, while other parameters showed element-specific effects. Under optimized conditions, the predicted recoveries reached 98% for Co, 93% for Li, 81% for Ni, and 88% for Mn, indicating excellent model reliability and process efficiency.

Kinetic analysis based on the shrinking core model revealed that the leaching mechanism varies among metals: Co and Li dissolution were primarily governed by surface chemical reaction, Mn by diffusion control, and Ni by a mixed mechanism. Activation energy evaluation further supported these mechanistic differences, highlighting the importance of understanding dissolution kinetics for process design and scale-up. Overall, the findings demonstrate that formic acid–assisted leaching provides an efficient, scalable, and environmentally sustainable strategy for recovering valuable metals from spent lithium-ion batteries. The combination of high extraction efficiency, mild operating conditions, and reduced environmental impact makes the proposed method a promising candidate for future industrial implementation and supports the advancement of circular economy approaches in battery recycling.

ACKNOWLEDGEMENT:

This project was supported by Eskisehir Osmangazi University (ESOGU) Scientific Research Projects (BAP) Department (FDK-2024-3025).

REFERENCES

Abbas, Z., Jung, S. M., (2026) “Efficient recovery of critical metals from spent NMC811 (LiNi0.8Mn0.1Co0.1O2) cathodes in lithium-ion batteries via tandem leaching and selective separation”, Resources, Conservation and Recycling, 229, 108854.

Geng, L., Deng, P., Li, H., Meng, W., Liu, X., Wei, X., (2026) “Reaction mechanism of binary organic acid leaching of cathode materials from spent lithium-ion batteries”, Journal of Power Sources, 667, 239244.

Güloğlu, E., Orhan, G., (2026) “Sustainable recycling of spent mixed LIB cathodes via organic acid-based DES: NMC532 regeneration and electrochemical performance”, Separation and Purification Technology, 382 (Part 2) 135817.

Kaya, M., Recovery of lithium from secondary sources; Recycling technologies of spent lithium-ion batteries, (2025) CRC Press, Taylor and Francis Group, Fl. USA.

Kaya, M., Delavandani, H., (2025) “State-of-the-art lithium-ion battery pretreatment methods for the recovery of critical metals”, Minerals, 15 (5) 546.

Li, X. L., Zhu, X. N., Li, X. G., Zhao, X. T., Wei, G. L., Gao, W. H., Nie, C. C., Yan, S., Ge, L. H., Wang, Z. Y., (2025) “Recent advances in the extraction of critical metals from spent lithium-ion batteries: Challenges and solutions — a review”, Separation and Purification Technology, 376 (Part 3) 134070.

Montgomery, D. C., (2017) Design and analysis of experiments, John Wiley & Sons.
Rezaei, M., Nekahi, A., Kumar, A. K. M. R., Nizami, A., Li, X., Deng, S., Nanda, J., Zaghib, K., (2025) “A review of lithium-ion battery recycling for enabling a circular economy”, Journal of Power Sources, 630, 236157.

DEWATERING, WASTE WATER TREATMENT

CREATING VALUE FROM WATER IN MINING

Riina SALMIMIES*, Nina HARJULA, Elsi STRAND

Sofi Filtration Oy, Tillinmäentie 3 B FI-02330 Espoo, Finland
**Corresponding author: riina@sofifiltration.com*

A B S T R A C T

Water is essential in mining operations, but we have yet been unable to truly maximize the hidden value in water. This talk emphasizes three use cases where value in water can be maximized by introducing advanced yet simple particle filtration technology: 1) recovery of (ultra)fine mineral concentrate from process waters of a flotation-based concentrator, 2) removal of unwanted fines to maximize water reuse and 3) removal of impurities to maximize product quality. Due to the physical nature of particle filtration, the solution is not limited by chemistry and is applicable to a wide range of different ores. For a mining company, the benefits include higher revenue and profit or decrease in costs of processing in addition to access to cleaner water and a boost in water stewardship. If you are responsible for operations or a mineral concentrator and are interested in increasing reliability and efficiency, do not miss out on this talk.

Key words: *Filtration, water, mineral processing*

1. INTRODUCTION

Water is the common denominator for a number of concerns in mining operations. Firstly, mineral processing plants commonly operate at 80-99 % recovery, meaning that up to 20 % of valuable minerals are lost in the mineral processing plant alone ending up in various water streams. Secondly, most mineral processing is reliant on the use of water and various aqueous solutions ultimately resulting in discharge waters. Both recovery of minerals and water use are affected by the steady decline in particle sizes we have seen in the past decades in mineral processing. This decline is due to declining ore grades and increasing complexity of ore bodies that subsequently result in the need to grind finer to liberate valuable particles.

Clarification is used to separate particulate matter to create a clear liquid. Clarification can be achieved by a number of different means, also including the use of chemicals for flocculation and coagulation. Filtration is also used to achieve clarification. This is when we speak of clarification filtration, or sometimes polishing filtration. Commonly used polishing filters include different media filters, cartridge and bag filters and membrane filters. All these technologies come with disadvantages including the use of chemicals, large footprints, low unit capacities and the need to replace the filter medium thus leading to generation of waste. Furthermore, and often most importantly, operator hours are tied to maintaining filters, which rarely is core to a plant operator.

Self-cleaning filters, or screen filters, offer multiple benefits in polishing filtration. They are commonly fully automated, do not require replacement of the medium as the medium is commonly made of stainless steel and filtration capacity is restored through the self-cleaning action of the filter. However, not all self-cleaning filters are the same. They rely on different kinds of self-cleaning mechanisms and thus cater to different kinds of needs. Many of the self-cleaning filters in the market are effective only down to a screen rating of 10 µm.

The Sofi Filter® is a patented self-cleaning filtration solution for the separation of

(ultra)fine particles from water. This paper investigates the performance of the Sofi Filter® in value creation in mining, in particular in recovery of fine mineral concentrate in a flotation-based flowsheet, in water reuse and in removal of impurities from an aqueous product solution.

2. MATERIALS AND METHODS

In all our experimentation we used the Sofi Filter® SF200, which is a compact self-cleaning microfiltration solution for (ultra)fine particles. The filter is made out of stainless steel with a stainless steel wire mesh as the filter medium, it is fully automated and runs on unique ultrasonically assisted self-cleaning to ensure capacity restoration after each filtration cycle.

Figure 1. Sofi Filter SF200

The Sofi Filter® SF200 filtration system, as shown in Figure 1, consists of an SF200 filter, a control unit, a feed pump and a feed tank. Pressure and flow data are recorded by a computer. The filter is equipped with an ultrasonic rod and employs patented cross-flow technology. All the functions e.g. pump speed, valve openings and back washing parameters can be managed from the control unit. The filter can be operated in either dead-end or cross-flow mode. The flow arrangements for these vary. In dead-end all feed is driven through the filter element and separates into two streams: filtrate and reject. In cross-flow, the feed flows over the filter medium tangentially. In cross-flow, the feed separates into three streams: filtrate, concentrate and reject. The selection of the filter element is key for separation. Both the pore size of the filter element as well as the micro geometry of the filter medium varies. Different geometries are good for different types of solids and the pore size (i.e. micron rating) is indicative of the size of the solids separated from the feed. Our filter elements vary from 0.3 up to 500µm nominal.

The solids concentration of the various waters was analyzed according to the SFS-EN 872:2005 standard, where the measurement uncertainty is 10%. Metal analyses were conducted by a third-party laboratory, where necessary.

The Sofi Filter® SF200 is not commonly used for mining applications, where volumetric flowrates can be high. The SF1000, which is our larger industrial filter, is often the tool of choice for mining applications. The filtration chamber of the SF1000 is shown in Figure 2 (Left). The technology is modular, as shown in Figure 2 (Right), and target capacity is reached by multiplying the number of filtration units to manufacture a full turn-key skid.

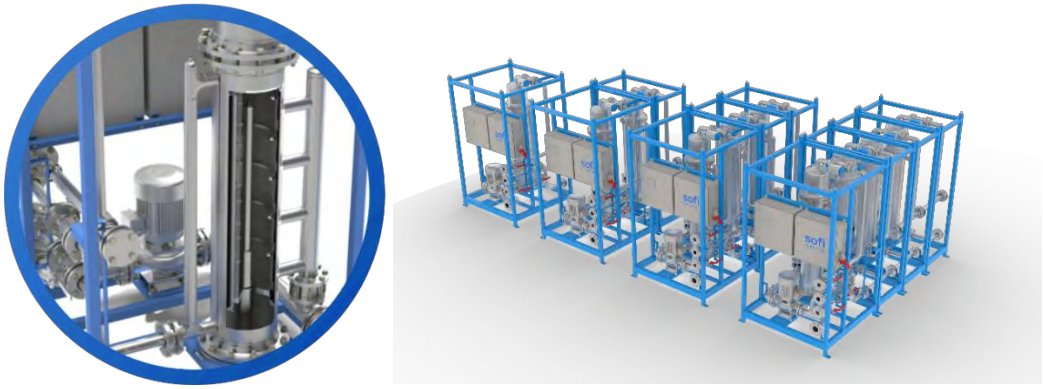

Figure 2. (Left) Sofi Filter® SF1000 and (Right) modular units of SF1000

There are several ways to create value from water in mining using the Sofi Filter® and we will be highlighting a few ways in this paper: 1) recovery of (ultra)fine mineral concentrate from process waters of a flotation-based concentrator, 2) removal of unwanted fines to maximize water reuse and 3) removal of impurities to maximize product quality.

Our recovery solution, **Sofi Alchemist**, is a water treatment solution for recovering (ultra)fine mineral concentrate from process waters. As a result, overall recovery can be boosted and more concentrate is produced for the benefit of the process owner. The guiding principle of Sofi Alchemist is shown in Figure 3.

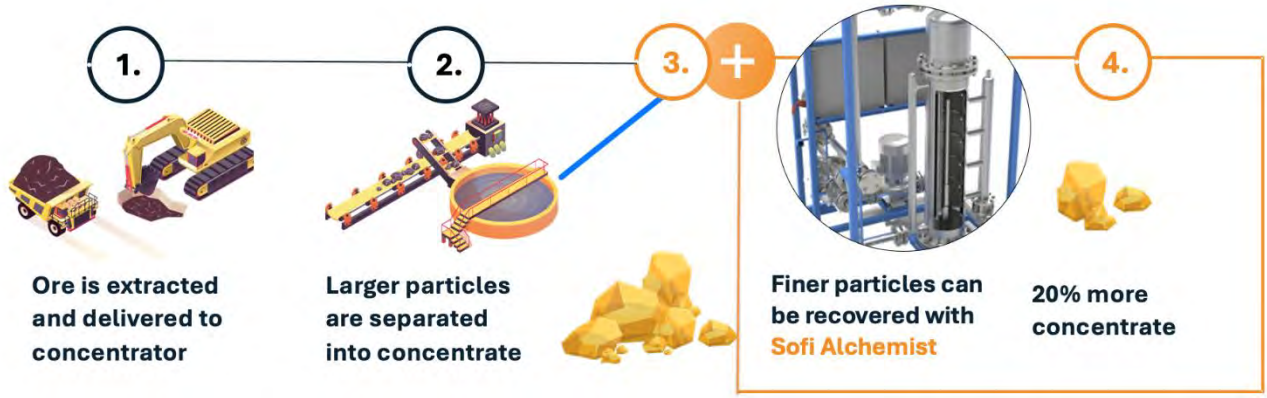

Figure 3. Recovery of fine mineral concentrate by Sofi Alchemist

Our water treatment solution, **Sofi Prima**, is our original approach to creating value from water for process owners. Sofi Prima allows for the removal of unwanted solids from water and various aqueous streams to improve product quality or enable water reuse without concerns over fine particles causing disruptions or increasing processing costs.

3.RESULTS AND DISCUSSIONS

In this section, we summarize some of the key findings of our test work in treating process waters from the mining industry. Firstly, we will address the recovery of fine mineral concentrate. Secondly, we will report on the results of treating dam water for recirculation. Thirdly, we will look into the removal of impurities from a product solution.

Recovery of fine mineral concentrate

The solid concentration of process water varies from site to site and periodically within mineral processing plants. Table 1 highlights some of the concentrations we have

observed during testing our technology. As can be seen from the table, initially the solid concentrations might feel low to an engineer, an operator or a manager, who are used to operating at the solids concentrations typically present in mineral processing. This may easily lead to quick conclusions of poor economic viability.

Table 1. Solid concentration of some waters from various mineral processing plants

Mineral	Solid concentration, mg/L	Recovery, %
Gold	3,986	99
Gold	160	100
Copper	18,850	100
Nickel	555	100

As can be seen from Table 1, close to ideal recovery of fine concentrate can be achieved with our Sofi Filter®. As our standardized analytics for solids concentration is limited down to 2 mg/L, concentration below that cannot be detected in the filtrate and thus **recoveries of fine mineral concentrate, otherwise lost in mineral processing, reach 100 %**.

Removal of unwanted solids to reuse process water

In recirculating process water from a storage dam, it is important that the water is free from fine solids. Table 2 summarizes our testing results for when we treated dam water to remove fine solids to enable the recirculation of that water into froth flotation. The customer is particularly concerned over **increased fines and the subsequent chemical consumption** in flotation.

Table 2. Performance of the Sofi Filter® against dam water for recirculation

Pore size, µm	Filtration mode	TSS, mg/L		Flux, $m^3/h/m^2$
		Feed	Filtrate	
1 (wire mesh)	Dead-end	8.8	10.8	12.4
0.5 (wire mesh)	Dead-end	10.4	1.2	12.3
0.5 (powder sintered)	Dead-end	10.2	2.6	4.8

As can be seen from Table 2, significant reduction in solids concentration can be achieved even in very low solid concentrations. The lower the solids concentration, the more important the screening effect becomes in filtration. When solid concentrations are this low, it is important to employ a very fine mesh to achieve a high degree of separation.

Removal of impurities from a product solution

Sometimes product quality suffers from fine impurities in low concentrations. We recently tested for a mining customer, who has attempted to address the problem of impurities using media filters. Those were unsuccessful. Our trials were limited by the low concentration of the impurities as we could not use our standardized analytics to determine the solids concentration of the feed or the filtrate. To overcome this problem, we used visual inspection of filter papers, as seen in Figure 4, and image analysis to calculate an approximate number of particles.

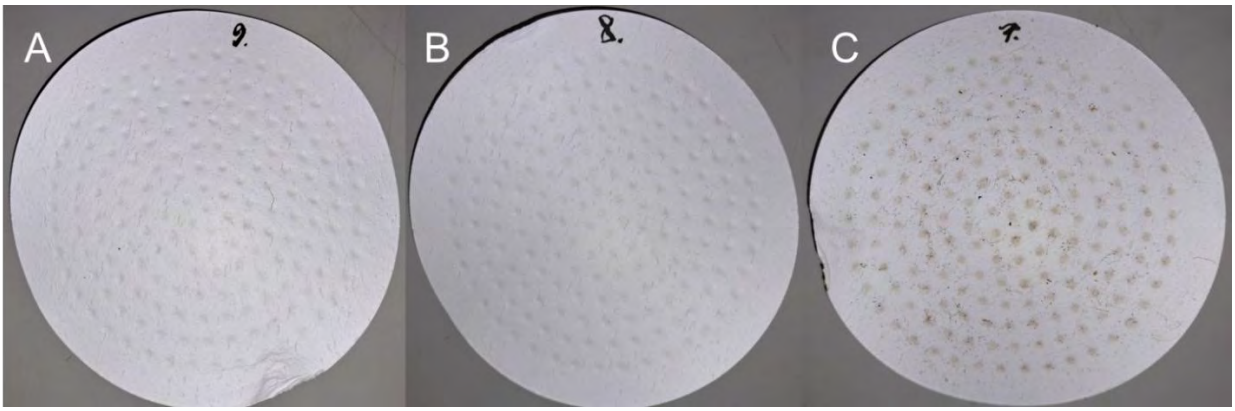

Figure 4. Filter papers of (A) feed, (B) filtrate and (C) reject. Despite it being impossible to visually differentiate between the feed and the filtrate, the reject clearly shows the accumulation of impurities.

As can be seen in Figure 4, the reject sample (C) clearly showed the impurities despite them being difficult to observe visually on the feed side (A). Overall, a capacity of approximately 100 m^3/h can be treated with 4xSF1000 filters. As a result, **product quality is improved and ensures that the operator can deliver sufficiently high quality product to their customers**.

4. CONCLUSION

As new technologies emerge, efficiency of mineral processing can be further increased. This can be achieved by more effective recovery of fine mineral particles and by removal of unwanted solids, whether from process water or leach solutions.

We have demonstrated through practice that our science-based advanced filtration technology can effectively recover fine mineral particles that are commonly lost in mineral processing. This increases production and promotes responsible mining as virgin resources are recovered to their allowed maximum using the latest in technology in mining operations.

Furthermore, we have demonstrated that unwanted fine particles can be effectively removed from process water to enable water recirculation. Removing fines from process water that is to be recirculated into milling or flotation promotes improved operation of the concentrator. Reuse of process water in turn promotes water stewardship and ensures responsible operation in mining.

Efficient extraction, elimination of waste and water efficiency all promote social acceptability of mining. This is critical as mining operations are not separate from communities and societies.

Adopting new technologies and capitalizing on their benefits can, however, only be achieved in close collaboration between operators and technology companies.

EFFECT OF FLOCCULANT DOSAGE AND WATER TYPE ON THE SEDIMENTATION BEHAVIOR OF SULFIDE IRON ORE TAILINGS

Argun ÇIPER[1,2], Yunus Emre ÇAVDAR[1], Orhan ÖZDEMIR[1,*]

[1]Istanbul Technical University, Faculty of Mines, Department of Mineral Processing Engineering, Istanbul-TÜRKİYE
[2]YÖN Proses Filtrasyon Teknoloji Makina Müh. San. Ve Tic. Ltd. Şti. Sakarya-TÜRKİYE
**Corresponding author: orhanozdemir@itu.edu.tr*

A B S T R A C T

Efficient dewatering of mineral processing tailings is essential for improving water recovery and reducing the environmental footprint of mining operations. In this study, the effects of flocculant dosage and water type on the sedimentation behaviour of sulfide iron ore tailings were investigated. Sedimentation experiments were performed using an anionic commercial polymer at different dosages (15, 30, 60, and 120 g/t) in both pure water and process water media. Settling performance was evaluated by monitoring the interface height and supernatant turbidity over time. The results showed that flocculant addition significantly enhanced settling performance compared to the flocculant-free condition. Among the tested dosages, 30 g/t provided the most favourable balance between settling rate and supernatant clarity. While pure water generally resulted in faster interface descent, process water consistently produced lower turbidity values, indicating improved clarification. This behaviour was attributed to the presence of dissolved multivalent cations in the process water, which enhanced flocculation through combined coagulation-flocculation mechanisms. At excessive dosages (60-120 g/t), the formation of bulky and loosely packed flocs led to increased bed heights and partial restabilisation of fine particles due to steric stabilisation. The findings highlight the importance of optimising flocculant dosage and considering water chemistry in the design and operation of tailings dewatering systems.

Key words: *Flocculation, flocculant dosage, solid-liquid separation, dewatering*

1. INTRODUCTION

Mineral processing operations are predominantly conducted using wet methods, in which large quantities of water are consumed during grinding, classification, separation, and slurry transportation processes (Chaves, 2013; Ossa-Moreno et al., 2018). As a result, significant volumes of mine tailings with high moisture content are generated. Currently, more than 10 billion tons of mine tailings are produced annually worldwide, and this amount is expected to increase substantially in the coming decades (Araya et al., 2021). Under increasing global water shortage conditions, efficient tailings dewatering and water recovery have become essential for sustainable mining operations.

Dewatering of mineral tailings is commonly achieved using mechanical separation technologies such as thickeners, centrifuges, vacuum filters, and pressure filter presses (Dias et al., 2003; Hakkinen and Ekberg, 2009). Among these methods, filtration using filter presses has been shown to provide high water recovery and a significant reduction in tailings disposal volumes (Dias et al., 2003). However, filtration performance is strongly influenced by slurry conditioning through chemical additives, particularly flocculants, surfactants, and coagulants (Qi et al., 2011). These reagents modify slurry properties by affecting zeta potential, surface chemistry, floc formation, and rheological behaviour, thereby influencing filtration kinetics and cake characteristics (Amarante et al., 2002; McGuire et al., 2006).

Fine particle suspensions in mineral processing tailings generally show high stability due to electrochemical interactions in aqueous environments, which prevent natural aggregation. (Li

et al., 2013). To overcome this stability, coagulation and flocculation are commonly applied as destabilization techniques. While coagulation reduces electrostatic repulsion through oppositely charged ions (Palomino et al., 2012), flocculation promotes particle aggregation via polymer bridging mechanisms using long-chain flocculants (Gregory and Barany, 2011). The efficiency of flocculation depends on flocculant properties and slurry characteristics, including molecular weight, charge density, particle size, pH, ionic strength, and hydrodynamic conditions. (Sworska et al., 2000a; Sworska et al., 2000b; Zhu et al., 2009).

Flocculation performance is also strongly affected by operational parameters such as solids concentration, mixing intensity, and conditioning time, which determine floc size, structure, and mechanical strength (Johnson et al., 2000; Jarvis et al., 2005). Strong and high-density flocs are generally preferred for filtration processes, as they enhance cake permeability and dewatering efficiency. However, excessive flocculant addition may significantly increase operating costs, highlighting the importance of determining optimum conditioning conditions (Alam et al., 2011). Accordingly, the present study focuses on evaluating settling performance under different flocculant dosages using both process water and pure water in order to support the optimization of industrial tailings dewatering systems.

2. MATERIAL AND METHODS

2.1. Material

A representative sulfide iron ore tailings sample was obtained from an operating concentrator plant in Türkiye. The particle size distribution of the sample was determined using a laser diffraction particle size analyzer (Malvern Mastersizer2000). According to the particle size analysis, the d_{90}, d_{50}, and d_{10} values of the sample were obtained as ~63 µm, ~17 µm, and ~2.5 µm, respectively.

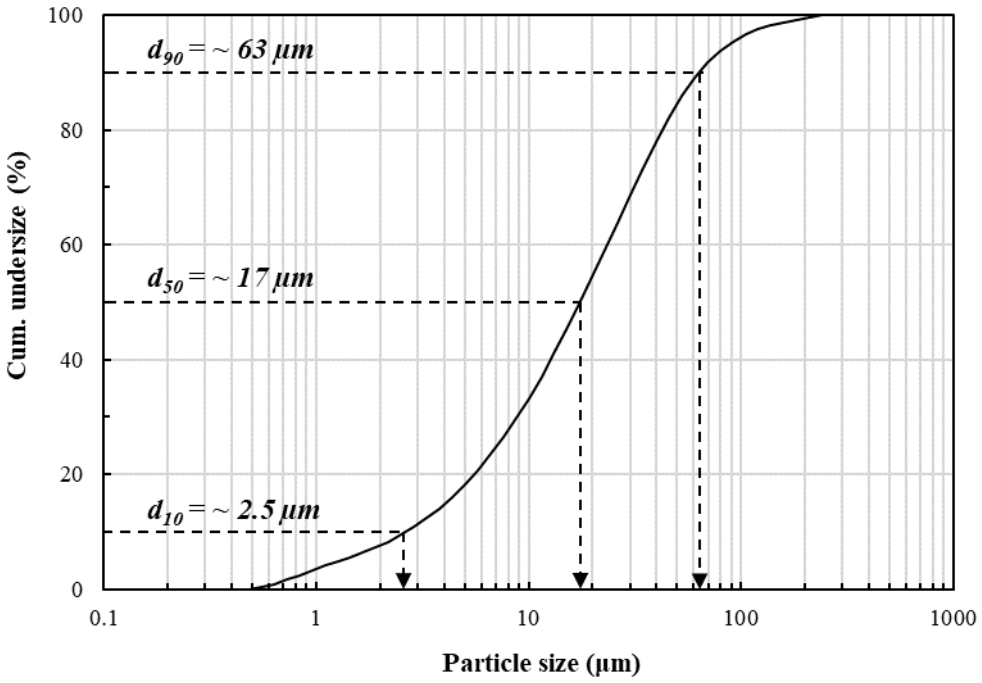

Figure 1. Particle size distribution of representative ore sample

2.2. Method

Flocculation-assisted sedimentation tests were performed to evaluate the settling behavior of sulfide iron ore tailings under different flocculant dosages and water types. A commercial anionic polymer was used as a flocculant for the flocculation experiments. A 0.1 wt.% flocculant stock solution was prepared using pure water and allowed sufficient time for complete dissolution. The experiments were carried out in pure and process water. The sedimentation tests were conducted without flocculant and with flocculant dosages of 15 g/t, 30 g/t, 60 g/t, and 120 g/t.

The suspension was prepared at 30% solids by pulp. The mixture was stirred using a mechanical overhead stirrer for 5 minutes to ensure adequate dispersion. For each condition, a predetermined volume of tailings slurry was transferred into graduated cylinders. The required amount of flocculant was added, and the slurry was mixed for a fixed conditioning period to ensure proper polymer dispersion. After conditioning, the slurry was allowed to settle without further mixing. The interface height between the clarified supernatant and the settled solids was recorded at regular time intervals to determine settling rates. Supernatant clarity was quantitatively measured using a turbidity meter (WTW Turb 430).

3. RESULTS AND DISCUSSION

The sedimentation tests showed that flocculant dosage has a strong effect on the settling behavior of sulfide iron ore tailings in both pure water and process water. In the absence of flocculant, low settling rates and high turbidity values were observed, indicating the stable suspension of fine particles.

With the addition of 15 g/t flocculant, settling performance improved due to particle aggregation. A more significant improvement was observed at 30 g/t. At this dosage, a faster decrease in bed height and lower turbidity values were obtained in both water types, indicating more effective floc formation and particle aggregation.

Comparative results showed that pure water generally provided faster interface descent than process water. In contrast, process water produced improved supernatant clarity. At 30 g/t, the turbidity after 30 minu was 20.50 NTU in process water and 35.83 NTU in pure water, suggesting a combined coagulation-flocculation effect in the presence of dissolved ions.

The significant improvement in settling performance observed at 30 g/t aligns with the bridging flocculation mechanism described by Gregory and Barany (2011), where polymer chains adsorb onto multiple particle surfaces, forming floc structures with enhanced settling velocity. At low dosages (15 g/t), insufficient polymer amount limits effective bridging, resulting in only partial aggregation, as also reported by Sworska et al. (2000a) for fine tailings systems. Further increases in flocculant dosage to 60 g/t and 120 g/t did not result in similar improvements in settling performance. While 60 g/t provided relatively low turbidity values, a noticeable increase in turbidity was observed at 120 g/t in both water types, indicating partial restabilization of fine particles. In addition, higher dosages led to increased final bed heights, suggesting the formation of large but loosely packed flocs due to excessive polymer adsorption. These bulky floc structures limited sediment consolidation and reduced dewatering efficiency. The effects of flocculant dosage and water type on bed height and turbidity are illustrated in Figures 2 and 3 for pure water and process water, respectively.

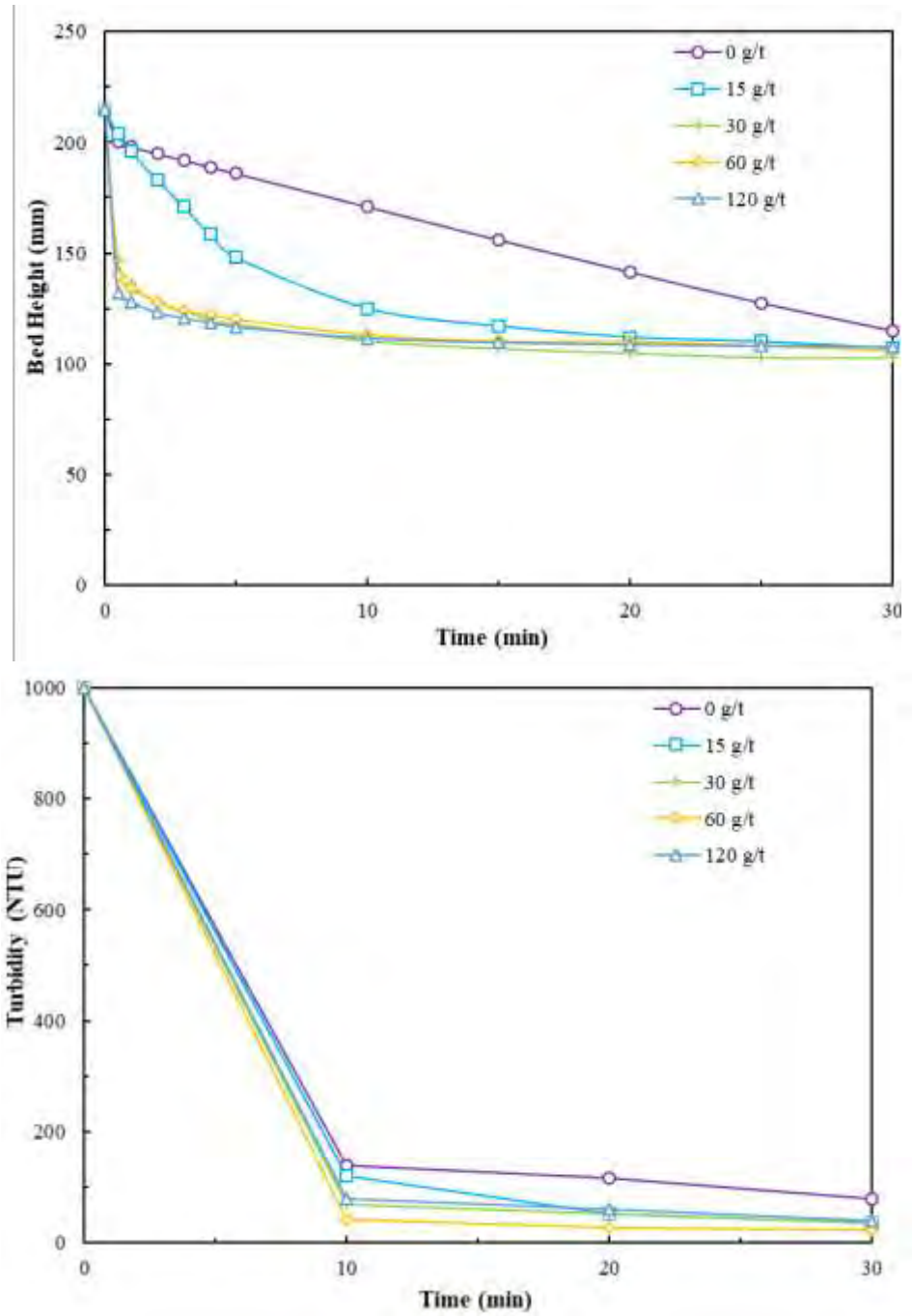

Figure 2. Effect of flocculant dosage on settling behavior and supernatant turbidity in pure water.

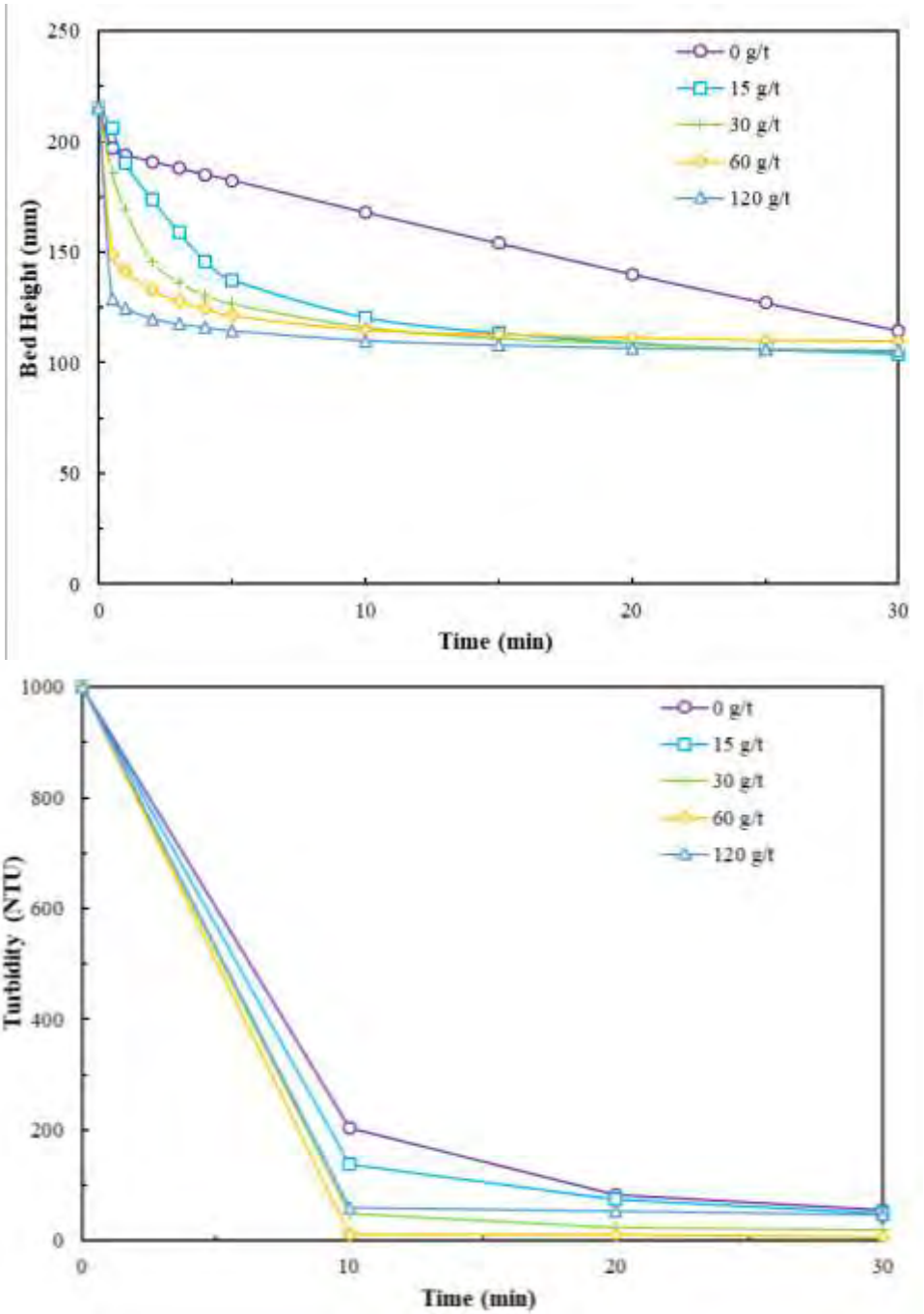

Figure 3. Effect of flocculant dosage on settling behavior and supernatant turbidity in process water

The decline in settling performance observed at excessive flocculant dosages (60-120 g/t) can be explained by steric stabilisation. When polymer adsorption on particle surfaces exceeds the saturation level, repulsive interactions between fully coated particles prevent effective aggregation, resulting in the restabilisation of the suspension (Zhu et al., 2009; Alam et al., 2011). This behaviour is consistent with the higher turbidity values measured at a dosage of 120 g/t. These findings highlight the importance of maintaining an optimum flocculant dosage, as overdosing not only reduces settling efficiency but also leads to unnecessary reagent consumption.

The contrasting behavior observed between pure water and process water deserves particular attention. Although pure water resulted in faster interface descent, process water consistently produced lower turbidity values, indicating better supernatant clarity. This behavior can be

attributed to the presence of dissolved multivalent cations (e.g., Ca^{2+} and Mg^{2+}) in process water, which act as bridging agents between negatively charged particle surfaces and the anionic flocculant, thereby improving flocculation efficiency (Sworska et al., 2000a; Palomino et al., 2012). This combined coagulation-flocculation effect likely promotes the formation of denser floc structures with greater resistance to settling, explaining the slower yet clearer settling compared with pure water. Since a dosage of 30 g/t provided the most favorable balance between settling behavior and sediment consolidation, a detailed comparison between pure water and process water at this dosage is presented in Figure 4.

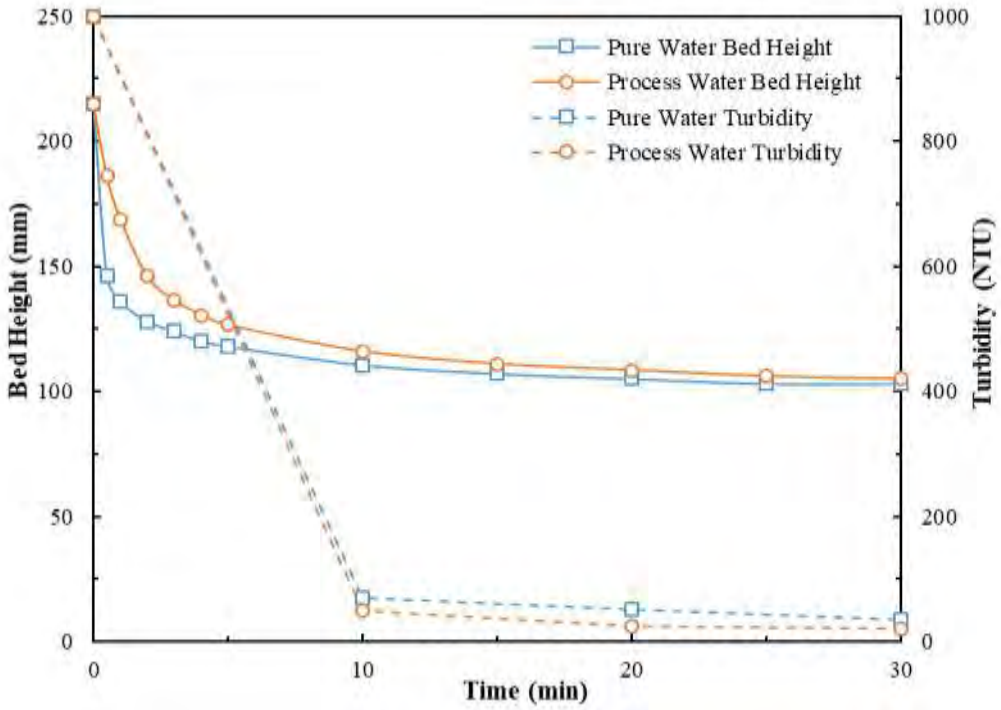

Figure 4. Effect of water type on sedimentation behavior at a flocculant dosage of 30 g/t

From a practical standpoint, these findings have direct implications for the design and optimisation of industrial tailings dewatering circuits. The use of process water—which is commonly recycled in concentrator plants to reduce freshwater consumption—does not appear to compromise, and in some respects improves, clarification performance relative to pure water. This is an encouraging finding given the increasing emphasis on water recycling in sustainable mining operations (Ossa-Moreno et al., 2018). Nevertheless, the sensitivity of flocculation performance to dissolved ion concentration suggests that careful monitoring of process water chemistry is necessary to maintain consistent dewatering efficiency, particularly as water chemistry may evolve with seasonal changes or variations in ore feed composition.

4. CONCLUSION

In this study, the effects of flocculation on the sedimentation behavior of sulfide iron ore tailings were investigated using different flocculant dosages and water types. The experimental results showed that, across all investigated dosages, pure water generally promoted faster bed height reduction, and process water consistently provided superior supernatant clarity. This indicates that water chemistry has a systematic influence on flocculation behavior.

Increasing the flocculant dosage from 15 g/t to 30 g/t resulted in a marked improvement in settling performance and clarity. The 30 g/t dosage provided the most favorable balance

between settling behavior and sediment consolidation, with the comparative trends between pure water and process water consistent across all investigated conditions

.

At higher dosages (60-120 g/t), loose and bulky floc structures were formed, leading to increased final bed heights and reduced sediment consolidation. In addition, an increase in turbidity was observed at 120 g/t, indicating partial restabilization of fine particles due to excessive polymer adsorption. Based on these results, 30 g/t was identified as the optimum flocculant dosage under the investigated conditions. The findings highlight the importance of optimizing flocculant dosage and considering water chemistry for efficient tailings sedimentatin

REFERENCES

Alam, N., Ozdemir, O., Hampton, M. A., Nguyen, A. V., (2011) “Dewatering of coal plant tailings: Flocculation followed by filtration”, Fuel, 90, 26–35.

Amarante, S. C., Araujo, A. C., Valadão, G. E. S., Peres, A. E. C., (2002) “Cake dewatering of some iron ore industrial products”, Minerals and Metallurgical Processing, 19 (3) 161–164.

Araya, N., Ramirez, Y., Kraslawski, A., Cisternas, L. A., (2021) “Feasibility of re-processing mine tailings to obtain critical raw materials using real options analysis”, Journal of Environmental Management, 284, 112060.

Chaves, A. P., (2013) “Teoria e prática do tratamento de minérios: Desaguamento, espessamento e filtragem”, Oficina de Textos, São Paulo.

Dias, C. L. P., Valadão, G. E. S., Araujo, A. C., Peres, A. E. C., Amarante, S. C., (2003) “The effect of reagents on ultrafine iron ore vacuum filtration”, Filtration & Separation, 40 (5) 36–39.

Gregory, J., Barany, S., (2011) “Adsorption and flocculation by polymers and polymer mixtures”, Advances in Colloid and Interface Science, 169 (1) 1–12.

Hakkinen, A., Ekberg, B., (2009) “Dewatering of iron ore slurry by a ceramic vacuum disc filter”, Chemical Engineering Transactions, 17, 1431–1436.

Jarvis, P., Jefferson, B., Gregory, J., Parsons, S. A., (2005) “A review of floc strength and breakage”, Water Research, 39, 3121–3137.

Johnson, S. B., Franks, G. V., Scales, P. J., Boger, D. V., Healy, T. W., (2000) “Surface chemistry-rheology relationships in concentrated mineral suspensions”, International Journal of Mineral Processing, 58, 267–304.

Li, J., Jiao, S., Zhong, L., Pan, J., Ma, Q., (2013) “Optimizing coagulation and flocculation process for kaolinite suspension with chitosan”, Colloids and Surfaces A, 428, 100–110.

McGuire, M. J., Addai-Mensah, J., Bremmell, K. E., (2006) “The effect of polymer structure type, pH and shear on the interfacial chemistry, rheology and dewaterability of model iron oxide dispersions”, Colloids and Surfaces A, 275, 153–160.

Ossa-Moreno, J., McIntyre, N., Ali, S., Smart, J. C. R., Rivera, D., Lall, U., Keir, G., (2018) “The hydro-economics of mining”, Ecological Economics, 145, 368–379.

Palomino, D., Hunkeler, D., Stoll, S., (2012) “Salt concentration influence on the efficiency of two cationic polymeric flocculants”, Colloid and Polymer Science, 290 (13) 1301–1308.

Qi, Y., Thapa, K. B., Hoadley, A. F., (2011) “Application of filtration aids for improving sludge dewatering properties – A review”, Chemical Engineering Journal, 171 (2) 373–384.

Sworska, A., Laskowski, J. S., Cymerman, G., (2000a) “Flocculation of the syncrude fine tailings. Part I. Effect of pH, polymer dosage and Mg^{2+} and Ca^{2+} cations”, International Journal of Mineral Processing, 60, 143–152.

Sworska, A., Laskowski, J. S., Cymerman, G., (2000b) “Flocculation of the syncrude fine tailings. Part II. Effect of hydrodynamic conditions”, International Journal of Mineral Processing, 60, 153–161.

Zhu, Z., Li, T., Lu, J., Wang, D., Yao, C., (2009) “Characterization of kaoline flocs by polyacrylamide as flocculation aids”, International Journal of Mineral Processing, 91, 94–99.

EDUCATION, SUSTAINABILITY IN MINERAL PROCESSING

ALIGNMENT OF ALBANIAN GEO-MINING LEGISLATION WITH THE LEGISLATION OF BALKAN COUNTRIES AND THE EUROPEAN UNION

Ekita TOSKA[1,*], Kimet FETAHU[2], Habib BASHOLLI[3], Lavdie MOISIU[4]

[1]*National Agency of Natural Resources (AKBN), Tirana, ALBANIA*
[2]*Geology and Mining Faculty, Polytechnic University of Tirana, Elbasani Street, Tirana, Albania.*
[3]*Independent Mining Commission (IMC), Prishtina, KOSOVO*
[4]*EIT Raw Materials Regional Centre, Elbasan, ALBANIA*
**Corresponding author: Ekita.Toska@akbn.gov.al*

A B S T R A C T

The economic transformations after 1990 brought about a profound reconfiguration of Albania's geo-mining industry, from an integrated state model to a fragmented model largely based on permits and concession arrangements. These developments affected the structure of investments, the technologies used for extraction and beneficiation, and the management of mining waste (tailings and waste rock). In the context of the European integration process, alignment with the European Union (EU) acquis requires not only formal harmonization of rules, but also operational adaptation of approaches to technical oversight, environmental safety and the circular economy.

This paper analyses Albania's legal and institutional framework for the mining sector (Law No. 10304/2010 and the relevant secondary legislation) and links it to the technical realities of geological exploration, mining, beneficiation and waste management. The paper includes a comparison with representative practices in the region (Turkey, Bulgaria, North Macedonia and Kosovo), as well as with key EU requirements on the management of waste from extractive industries and BAT/BREF standards for tailings facilities. Based on a comparative methodology and a combined legal-technical analysis, the paper proposes a package of legal and institutional interventions aimed at: national planning of geological exploration; periodic auditing of reserves; standardization of reporting on beneficiation performance; integrating recycling into licensing; and strengthening safety requirements and closure obligations for disposal facilities. The objective is to develop an alignment model that increases economic efficiency and reduces environmental risk, positioning Albania's sector in line with European and regional practice.

Key words: *Legal approximation, geological exploration, mining, beneficiation, mining waste, recycling, European Union, Balkans Countries*

1. INTRODUCTION

The mining industry in Albania remains one of the sectors with a significant impact on regional development, employment and the trade balance. The country's mining tradition (chromium, copper, iron-nickel, industrial minerals) has created a broad base of geological data, but part of this potential remains unused due to a lack of sustained investment in exploration and technological modernization.

After 1990, the sector's development was characterized by privatization and decentralization of activities, and by an orientation towards rapid exploitation of deposits with known reserves. This shifted the focus from long-term development (exploration, innovation, advanced processing) towards short production cycles and export of raw materials, limiting domestic value creation. In parallel, rising environmental standards and social expectations have made a structured approach to impact management essential, particularly regarding water pollution, dust, land degradation and the safety of tailings dams.

Within the framework of European integration, alignment with EU instruments directly related to the extractive sector and waste management - including Directive 2006/21/EC and the Waste Framework Directive 2008/98/EC - requires improvements not only at the normative level, but also in implementation, control and monitoring capacity. Accordingly, this paper seeks to identify the key areas where the Albanian framework can be improved, drawing lessons from analogous Balkan practices and adapting them to the country's technical and institutional realities.

1.1. Purpose, Research Questions and Contribution

The purpose of this paper is to propose a practical model for aligning Albanian geo-mining legislation with EU requirements and with the most common practices in the region, focusing on the main links of the mining value chain: exploration, extraction, beneficiation, and the management/recycling of mining waste.

The main research questions are:

1. Which elements of the Albanian legal framework create practical gaps in technical and environmental control and in performance reporting in the mining sector?
2. How do selected Balkan jurisdictions address licensing, technical reporting and mining waste management, and which mechanisms are transferable to Albania?
3. Which legal and institutional changes would improve compliance with the EU acquis and increase extraction efficiency through the circular economy?

The contribution of this paper lies in linking legal requirements with the technical parameters of mineral beneficiation and in formulating recommendations that can be operationalized in licensees, periodic reports and inspection protocols. Since a significant part of 'legal risk' in the mining sector stems from technical failures and insufficient verification, this paper treats alignment as an engineering-institutional process, not only a textual one.

2. METHODOLOGY AND CONCEPTUAL BASIS

2.1. Methodological Approach

The paper combines legal analysis with technical analysis of the mining value chain and a comparative method. Sources include Albanian legislation and secondary acts, EU instruments, and regional regulatory practice. The analysis is conducted by link in the chain (exploration - extraction - beneficiation - waste - closure) to identify where regulation must intervene to deliver outcomes in practice.

2.2. Conceptual Framework: the Value Chain and Integrated Risk

In the mining management literature, the difference between a deposit with value and a deposit with risk is the quality of data management and process control. This translates into three core concepts:

(I) Standardization of data (reserves, mass balance, performance);
(II) Risk-based control (disposal facilities); and
(III) Circular economy (recovery/recycling as part of the business model).

2.3. Limitations and Scope

This paper focuses on the metal minerals sector and on beneficiation waste, without addressing in depth other issues such as mining taxation or land ownership. Regional practices are presented as functional models rather than exhaustive descriptions of each regime. The

summaries are sufficient for the purpose of a conference article, where the objective is to evidence the transferability of mechanisms rather than a doctrinal analysis of every provision.

3. LEGAL AND INSTITUTIONAL FRAMEWORK OF THE MINING SECTOR IN ALBANIA

3.1. Licensing and Reporting: the Formal Framework

Law No. 10304/2010 and secondary legislation set out permit procedures, time limits and the operator's basic obligations. At a formal level, licensing architecture exists that foresees technical requirements and work plans. However, a typical gap in transition countries is that reporting, monitoring and auditing are not always standardized and comparable, making it difficult to track performance over time.

3.2. Institutions, Inspection and Coordination

AKBN, inspections and environmental permits create a system with several decision-making nodes. If these nodes do not share the same 'technical language' (e.g., performance indicators, risk classification), implementation becomes fragmented. A practical issue arises when waste management is treated as a separate environmental document, while the mining license does not incorporate it as a mandatory condition.

3.3. Operational Risk as Legal Risk

In the mining sector, legal risk typically materializes in two forms:

(I) Environmental incidents and liabilities; and

(II) Failure to meet extraction/processing objectives, leading to economic underperformance and non-compliance with permit conditions. For this reason, alignment should create direct links between legal rules and the technical indicators of implementation.

- Non-unified technical reporting, not always linked to performance indicators (recovery, losses, energy/water consumption).
- Limited periodic auditing of reserves and of the mass balance across the 'mine - plant - waste' chain.
- Waste management often treated as a parallel requirement (environmental permit), rather than as an integral element of the mining license.
- Lack of detailed standards on tailings dam safety and on financial guarantees for closure.

4. THE EU FRAMEWORK FOR THE EXTRACTIVE SECTOR: TECHNICALLY GROUNDED LEGAL REQUIREMENTS

4.1. Directive 2006/21/EC: the Logic of the Waste Management Plan

Directive 2006/21/EC requires the operator to prepare and implement a waste management plan covering minimization, treatment, recovery and safe disposal. Beyond the document itself, the core is the control system: facility classification, monitoring requirements, and responsibility for closure. In implementation, the most important requirement is that a tailings facility is treated as part of mining operations, not as a peripheral asset.

4.2. Directive 2008/98/EC: the Waste Hierarchy and Recovery

The Waste Framework Directive prioritizes prevention and recovery. In a mining context, this provides a basis for policies that set recycling and metallurgical recovery objectives. A practical

approach is to integrate recovery targets into license conditions and periodic reporting, making technical efficiency an element that the authority can verify.

4.3. BAT/BREF: Standards for Technical “Best” Practice

BAT/BREF supports the definition of minimum technical and emission standards. For international mineral processing ores, this is where science and public policy intersect: BAT standards create incentives for technological optimization, loss reduction and increased recovery, while simultaneously delivering environmental benefits.

4.4. EIA, Permits and Responsibility For Monitoring

Under the EU approach, environmental impact assessment (EIA) is not merely a procedural step, but an instrument to set measurable parameters and to monitor them over time. If an EIA remains formal and post-approval monitoring is absent, the likelihood of deviations in beneficiation and tailings management increases. For Albania, it is recommended to link monitoring results to the operator’s periodic reports and to decision-making on permit extension/amendment.

4.5. Regulation (EU) 2024/1252: The Strategic Dimension of Secondary Resources

The Critical Raw Materials Regulation strengthens the argument that mining waste should be treated as a potential reserve. It encourages the development of processing and recycling capacity and creates measurable objectives at EU level. This is relevant for Albania not only from an integration perspective, but also as an economic opportunity for projects recovering value from historic waste with reduced environmental risk.

5. ANALOGOUS BALKAN PRACTICES: RESULTS OF THE COMPARATIVE ANALYSIS

5.1. Turkey

Turkey represents a regime where operator discipline is achieved through capacity criteria and rehabilitation obligations. Practice indicates that financial guarantees and closure-planning requirements reduce the risk of abandoned facilities.

5.2. Bulgaria

Bulgaria, as an EU Member State, has integrated the requirements of Directive 2006/21/EC into its procedures. The key lesson is the strong link between the mining permit and the waste management plan, with clear control of disposal facilities.

5.3. North Macedonia

North Macedonia demonstrates the importance of gradual standardization and minimum reporting indicators, providing the administration with tools to assess performance without excessive bureaucratic burden.

5.4. Kosovo

Kosovo highlights a risk-based inspection approach, where resources focus on facilities and processes with a higher probability of harm.

5.5 Comparative matrix

Table 1. Summaries the main elements of comparison and their transferability to Albania

Element	**Albania (typical situation)**	**Turkey**	**Bulgaria**	**North Macedonia/Kosovo**
Geological exploration planning	No mandatory national plan; fragmented investments	More structured framework; capacity criteria	Planning linked to EU policies	Partial requirements; focus on priorities
Reserve reporting/auditing	Periodic auditing not unified	More standardized reporting in some segments	More integrated reporting and verification	Different practices; scope for standardization
Management of tailings and dams	Often parallel to environmental permits; uneven control	Stronger emphasis on guarantees/rehabilitation	Implementation of Directive 2006/21/EC and waste plans	Risk prioritization; reporting requirements
Recycling/recovery from waste	Not systematically linked to licensing	Growing potential for historic waste	Incentives for the circular economy	Partial initiatives; high potential

5.6. Most Transferable Elements

- Based on the comparative analysis, the elements most transferable to Albania are:
- Minimum requirements for performance indicators (recovery, losses, energy/water consumption) as the basis for periodic reporting.
- Classification of disposal facilities by risk and differentiated inspection protocols.
- Financial guarantees for closure and rehabilitation, linked to actual risk and updated periodically.
- Unified registers of permits and technical reports that increase transparency and facilitate oversight.

6. THEMATIC PILLARS OF REFORM

6.1. Geological Exploration and Reserve Auditing

A National Geological Exploration Plan would direct investment towards priority areas and prevent project overlap. Periodic auditing of reserves and standardization of classification increase data reliability and reduce disputes over deposit valuation.

6.2. Mining and Beneficiation: Performance as a Licensing Condition

Licensing should be accompanied by measurable indicators and a ‘mandatory improvement’ mechanism were performance falls below certain thresholds. This creates incentives for technological modernization and reduces losses into waste.

6.3. Mining Waste and the Circular Economy

Integrating a Recycling and Recovery Plan into licensing is a direct way to implement the waste hierarchy. In practical terms, this implies measurable objectives and reporting on their achievement.

6.4. Safety of Tailings Dams

Tailings dams are high-risk facilities. EU compliance requires design standards, geotechnical monitoring and continuous reporting. Such a regime should be proportional to risk and link continued operation to monitoring results.

6.5. Closure, Rehabilitation and Financial Guarantees

Closure should be planned from the early stages and funded through genuine guarantees. Periodic updating of guarantees and transparency about them are critical to reduce public risk.

6.6. Transparency and Social Acceptability

Publication of key indicators and summary reports increases accountability and provides a basis for dialogue with communities. This makes the sector more acceptable and reduces conflicts that often delay projects.

6.7. Proposed Integrated Licensing Model

The proposed integrated licensing model provides that key documents are treated as a single package:
1. The extraction and beneficiation plan with a mass balance;
2. The waste management plan;
3. The closure and rehabilitation plan; and
4. The set of periodic reporting indicators.
This package should be verified in a differentiated manner according to risk and updated in regular cycles. In this way, the permit becomes a dynamic governance tool, not only a formal authorization.

7. CONCRETE PROPOSALS AND IMPLEMENTATION ROADMAP

7.1. Legal Interventions

The recommended legal interventions are:
1. National Geological Exploration Plan and methodological standardization.
2. Periodic auditing of reserves and verification of the mass balance.
3. Mandatory performance indicators in periodic reporting for beneficiation.
4. Waste Management Plan as an integral part of the license.
5. Detailed rules on tailings dam safety and monitoring.
6. Financial guarantees for closure and rehabilitation with periodic updates.
7. An authorization scheme for recovery from historic waste.

7.2. Institutional Measures

- A unified digital register of permits, reports and indicators.
- Risk-based inspections and standardized protocols.
- Training for geotechnical monitoring and assessment of waste plans.
- Formalized inter-institutional coordination (mining/environment).

- Pilot projects with universities for recovery from waste rock/sterile material.

7.3. Phased Roadmap

Table 2. Presents a suggested phased implementation plan.

Phase	Timeframe	Key priorities	Expected outcome
Phase I	0-12 months	Minimum reporting standardization; Risk-based inspection protocols; Updating requirements for waste plans	Improved operational control and transparency
Phase II	12-24 months	Reserve auditing; Unified register of permits/indicators; Training of specialists	Comparable data and reduced uncertainty
Phase III	24-36 months	Recovery scheme for historic waste; Full financial guarantees; Deeper integration of BAT	Reduced environmental risk and increased value added

8. DISCUSSION: COSTS, TRADE-OFFS AND IMPACT OF REFORM

The proposed reforms entail the following initial costs:
- increased reporting requirements,
- a need for inspection capacity, and
- investment in monitoring.

However, these costs are justified by long-term benefits such as:
- fewer incidents,
- increased recovery, and
- reduced environmental liabilities.

At policy level, the main trade-off is between flexibility for investors and discipline to ensure minimum standards. The most effective approach is proportionality:
- stricter requirements for high-risk facilities; and
- a simplified regime for low-risk activities.

In the context of international experience, this model is increasingly regarded as ‘good governance’ for the extractive sector. It is also suitable for countries seeking EU integration, because it makes implementation more credible and measurable.

9. CONCLUSIONS

Aligning Albanian geo-mining legislation with the EU framework and Balkan practice requires a shift from a formal approach to an operational one. Success is measured by data standardization, risk-based control and integration of the circular economy into licensing. The paper’s recommendations aim to create a system in which economic value and environmental protection reinforce each other.

REFERENCES

Directive 2006/21/EC of the European Parliament and of the Council of 15 March 2006 on the management of waste from extractive industries and amending Directive 2004/35/EC. EUR-Lex.

Directive 2008/98/EC of the European Parliament and of the Council of 19 November 2008 on waste and repealing certain Directives. EUR-Lex.

Law No. 10304, dated 15.07.2010, 'On the mining sector in the Republic of Albania', and the relevant secondary legislation.

Mining laws and the relevant acts of Turkey, Bulgaria, North Macedonia and Kosovo.

Regulation (EU) 2024/1252 of the European Parliament and of the Council of 11 April 2024 establishing a framework for ensuring a secure and sustainable supply of critical raw materials. EUR-Lex.

AN OVERVIEW OF MINERAL PROCESSING INNOVATIONS IN BULGARIA

Irena GRIGOROVA*, Teodora YANKOVA, Mihail PETROV, Nikolay NESTOROV

University of Mining and Geology "St. Ivan Rilski", Faculty of Mining technology, Mineral Processing and Recycling Department, 1700 Sofia, BULGARIA
**Corresponding author: irena.grigorova@mgu.bg*

A B S T R A C T

The mineral resources sector is of strategic importance to the Bulgarian economy, supplying essential raw materials for energy, construction, mechanical engineering, and high-technology industries. In recent years, the sector has undergone a dynamic transformation driven by the increasing requirements for sustainable development, digitalization, and technological modernization aimed at improving efficiency and reducing environmental impact. Bulgaria possesses significant deposits of metallic ores, coal, industrial minerals, and construction materials, which provide a solid basis for continuous industrial development and the implementation of advanced mineral processing technologies.

The aim of this paper is to present an overview of recent technological advancements and innovation trends in mineral processing in Bulgaria, with a particular focus on automation, digital transformation, and sustainable resource management. The study is based on a synthesis of industrial case studies, academic research, and national and European strategic documents, allowing the identification of key drivers, challenges, and opportunities for future sector development. The analysis demonstrates an increasing implementation of automated and digitalized process control systems, improved operational safety, enhanced energy efficiency, and the gradual integration of circular economy principles, including water reuse and mine waste valorization. At the same time, the sector continues to face challenges related to limited investment in research and development, the processing of low-grade and complex ores, and the need to align economic performance with stringent environmental and regulatory requirements. The presented review highlights the significant potential of technological innovation and digitalization as key enablers for the sustainable and competitive development of mineral processing in Bulgaria.

Key words: *Mineral processing, innovation, automation, sustainability, Bulgaria, circular economy*

1. INTRODUCTION

Bulgaria has a long-standing tradition and well-established expertise in the exploration, extraction, and processing of mineral resources, occupying a strategic position in the supply of copper, lead, zinc, and gold to the European market. Copper ore extraction is carried out by open-pit mining at the Asarel-Medet AD and Elatsite-Med AD complexes, while underground mining of copper-gold ores is conducted at DPM Chelopech EAD.

The porphyry copper deposits of Elatsite and Asarel represent major raw material bases, with gold recovered as an accompanying component of copper production. A substantial share of the country's gold output is derived from the processing of copper and gold-bearing ores from the Chelopech, Elatsite, and Asarel deposits, while additional gold-bearing mineralization is reported at the Khan Krum, Chala, and other deposits (Milev et al., 2007). Lead–zinc ore deposits are predominantly concentrated in the Eastern Rhodopes region (Laki, Rudozem, Zlatograd, Erma Reka), where extraction is mainly performed by underground mining in accordance with the geological characteristics of the deposits (Dimitrov et al., 1988).

In addition to metallic ores, Bulgaria possesses significant deposits of non-metallic mineral resources, including gypsum, limestone, bentonite, kaolin, quartz sands, clays, and marble. Extensive quartz-kaolin sand deposits are located in Northeastern Bulgaria and are processed

at the beneficiation plants of Kaolin AD, the largest producer of industrial minerals in the country and a subsidiary of Quarzwerke GmbH.

The mineral processing infrastructure for copper, copper-gold, and polymetallic ores is concentrated in several high-capacity beneficiation plants located in close proximity to the major deposits. These facilities predominantly employ flotation-based technologies, adapted to the mineralogical characteristics of the processed ores and oriented toward the production of copper, copper-gold, and lead-zinc concentrates with valuable by-products. Porphyry copper ores are processed at the Asarel and Elatsite-Med concentrators using conventional flotation flowsheets, while the Chelopech concentrator applies fine grinding and selective flotation to treat gold-copper-pyrite ores. Polymetallic lead–zinc ores from the Eastern Rhodopes are processed through crushing, grinding, and selective flotation circuits, producing lead and zinc concentrates containing silver and other accompanying elements.

In recent years, Bulgarian beneficiation plants have undergone intensive modernization, encompassing automation of production operations, digitalization of process control, and the implementation of sustainable resource management practices (Lottermoser, 2010). These developments are closely aligned with European policies on the green transition, the circular economy, and the reduction of industrial carbon footprints (European Commission, 2019). Under increasingly stringent environmental regulations and the global shift toward sustainable development, traditional processing flowsheets are being progressively upgraded through targeted optimization solutions.

Within the framework of the European Union Critical Raw Materials Act, mineral processing plays a pivotal role in enhancing the recovery of critical and strategic raw materials, particularly copper and associated by-products such as gold and silver. The optimization of beneficiation technologies and the valorization of secondary resources contribute directly to strengthening the resilience and sustainability of European raw material supply chains. Rather than providing an exhaustive inventory of all processing facilities, this paper adopts a review-based approach, highlighting representative industrial case studies that illustrate key technological trends and innovation pathways in the Bulgarian mineral processing sector.

2. AUTOMATION AND DIGITIZATION

The mineral raw materials sector in Bulgaria is well established and primarily focused on the beneficiation of copper, lead-zinc, and gold-bearing ores, as well as a wide range of industrial minerals (Kostov-Kytin, 2023). Within this framework, preliminary research activities constitute a fundamental component of the mineral extraction and processing chain. The systematic integration of geological and geophysical data significantly enhances the reliability of technological decision-making while contributing to operational cost optimization. Data obtained from borehole investigations, in situ measurements, and structural imaging techniques, such as electrical resistivity tomography, have proven particularly effective for improving resource characterization, process planning, and overall production efficiency (Grigorova, 2020).

In recent years, the Bulgarian mineral processing sector has been undergoing a gradual yet systematic technological transformation, driven by the need to increase process efficiency, reduce operating costs, and comply with increasingly stringent environmental regulations. In line with global trends, modernization efforts in beneficiation plants are primarily focused on three interrelated directions: automation and advanced process control, digital monitoring and data-driven optimization, and process innovation through technological flowsheet modernization. These developments represent the sector’s response to the challenges associated with declining ore grades, increasing mineralogical complexity, and the transition

2.1. Automation and Process Control

Automation is a key driver for improving the operational efficiency, stability, and safety of mineral processing plants. The implementation of modern automated control systems enables continuous monitoring and regulation of critical technological parameters, including throughput, particle size distribution, reagent consumption, and energy use. Beyond productivity gains, automation contributes significantly to improved occupational safety by reducing the need for direct human intervention in hazardous areas and enabling remote operation of equipment. As such, automation forms the technological backbone upon which further digitalization and process optimization initiatives can be built.

In Bulgarian beneficiation plants, automation increasingly relies on programmable logic controllers (PLCs), supervisory control and data acquisition (SCADA) systems, and integrated process control platforms, which together support centralized supervision and real-time operational decision-making. A representative example of this trend is the modernization of the automated control systems in the crushing and grinding departments of the Elatsite-Med concentrator, where advanced Siemens-based solutions, including PCS7 and TIA Portal environments, have been implemented. These systems enhance process visualization, enable improved fault detection, and allow more precise control of critical operations, resulting in higher process reliability and a reduction in unplanned downtime (McKee, 2018).

In addition to productivity and recovery improvements, automation and digital process optimization contribute significantly to energy-efficient comminution and overall decarbonization of mineral processing operations. Advanced process control, real-time monitoring, and optimized grinding strategies reduce specific energy consumption, minimize process variability, and consequently lower indirect CO_2 emissions. Furthermore, the increasing electrification of mining and processing equipment, combined with smart energy management systems, enables more efficient use of electrical energy and supports alignment with European climate and sustainability objectives.

2.2. Digital Monitoring and Data-Driven Optimization

The ongoing evolution of mineral processing technologies increasingly emphasizes the integration of advanced digital monitoring systems and data-driven optimization strategies. Recent developments in sensor technologies, online analytical instruments, and industrial communication networks enable the continuous acquisition of high-resolution, real-time process data, providing a foundation for sophisticated control algorithms, predictive analytics, and performance optimization. A prominent example of this trend is the implementation of real-time particle size analyzers, such as the PSI® 300i system at the Elatsite-Med Concentrator, which exemplifies the digitalization of the comminution stage. Continuous measurement of particle size distribution facilitates dynamic adjustment of milling parameters, thereby enhancing downstream flotation efficiency and reducing energy consumption. Analogous digital solutions are increasingly deployed to monitor flotation performance, optimize reagent dosing, and maintain water balance across processing circuits.

The proliferation of large-scale process datasets creates new opportunities for the application of advanced data-driven methodologies, including multivariate statistical analysis, machine learning, and digital twin technologies. Although the adoption of such approaches in Bulgaria is currently in its nascent stages, preliminary results demonstrate substantial potential for predictive process control, early fault detection, and long-term operational optimization. This paradigm shift - from reactive to proactive process management - promises significant improvements in both economic performance and environmental sustainability. Future developments are expected to increasingly leverage artificial intelligence-based process optimization, predictive maintenance, and fully integrated digital twins, supporting enhanced metal recovery, energy efficiency, and operational stability across the sector.

2.3. Process Innovation and Flowsheet Optimization

In parallel with automation and digitalization, significant research and industrial efforts are devoted to the optimization of mineral processing flowsheets and the introduction of novel processing solutions. These innovations are particularly critical in the context of declining ore grades and increasing mineralogical complexity, which demand more flexible, efficient, and resource-conscious processing strategies.

Recent studies and industrial implementations demonstrate that targeted modifications to existing flowsheets, such as optimization of comminution stages, enhanced classification efficiency, and integration of gravity concentration or alternative separation methods can substantially improve metal recovery and energy efficiency. For example, at the lead-zinc sulfide concentrator in Zlatograd (Erma Reka), the transition from a three-stage to a two-stage crushing system, including a Nordberg C 116 jaw crusher, a Nordberg GP 220 cone crusher, and a Nordberg TS 4.2 double-deck vibrating screen, increased crushing efficiency by approximately 40% while reducing electricity consumption by 37.2% (Petrov, 2025). The finer particle size distribution achieved enhanced the performance of subsequent grinding and flotation stages, illustrating the critical role of process integration and collaboration between industry and the scientific community for the development of innovative solutions.

At the Chelopech Concentrator (DPM Metals), optimization research focused on enhancing gold recovery from copper-gold ores. The processing sequence includes single-stage primary crushing underground, semi-autogenous milling, and three-stage flotation (bulk, copper, and pyrite sections) producing copper-gold and pyrite concentrates. Semi-industrial gravity concentration tests, using a Knelson KC-CD12 concentrator, pilot hydrocyclones, and combined configurations, were conducted to assess potential recovery improvements. While gravity concentration of bulk flotation tailings increased gold grades, overall recovery decreased, whereas pre-concentration with hydrocyclones showed minimal effect. Redirecting approximately 30% of the cleaner flotation feed directly to the final concentrate improved both copper and gold recoveries without compromising concentrate quality. These results highlight the value of experimental validation and data-driven optimization for refining flowsheets under complex ore conditions (Sabeva-Domuschieva et al., 2025).

Technological innovations at DPM Metals also include the integration of a SMART Center, enabling real-time monitoring, process modeling, and operational planning across both the mine and concentrator. This system enhances process transparency, traceability, and efficiency, supporting informed decision-making and resource optimization. Similarly, at the Vetovo Concentrator (Kaolin AD), the implementation of wet ball milling for quartz sand processing achieved higher kaolin recovery while maintaining low mill recirculating loads and reduced energy consumption compared to conventional methods (Annual Bulletin of the BMGC, 2025).

The global trend toward processing low-grade ores is increasingly evident, driven by depletion of high-grade deposits and rising demand for critical metals such as copper, fueled by electrification, renewable energy, and electric vehicle technologies. Modern processing techniques now enable economically viable extraction from ores with copper concentrations as low as 0.2-0.5%. The Assarel-Medet AD concentrator exemplifies high-tech management of low-grade ore, sustainably processing ores with only 0.27% copper content per ton. Extensive modernization, including upgrades to the Siemens PCS7 control system, has enabled fully automated operation of milling, grinding, flotation, and material handling processes. The integrated system allows real-time monitoring and active management of all critical variables, optimizing both efficiency and product quality.

The advancement of digital technologies, coupled with the availability of large datasets (Big Data), provides unprecedented opportunities to predict process behavior, optimize

performance, and reduce operational costs (Umucua et al., 2024). Although digitalization in Bulgaria is still in a gradual implementation phase, current developments demonstrate significant potential for enhancing process efficiency, recovery rates, and sustainability across the mineral processing sector.

3. SUSTAINABLE RESOURCE MANAGEMENT AND CIRCULAR ECONOMY

Sustainable management of mineral resources constitutes a cornerstone of contemporary mineral processing practices. The adoption of circular economy principles promotes the reuse and valorization of process waste, while minimizing the volumes of materials directed to landfills (United Nations, 2018). In Bulgaria, these principles are increasingly realized through the implementation of closed-loop water systems, energy-efficient equipment, and emission-reduction technologies in compliance with European environmental standards (ICMM, 2021).

In recent years, the Bulgarian mineral processing industry has progressively incorporated innovative technological solutions aimed at enhancing process sustainability and reducing environmental impacts. A prominent example is the development and deployment of Integrated Mine Waste Facilities (IMWFs), designed for the safe disposal of mine waste and dewatered flotation tailings (Dimitrov et al., 2023). IMWFs represent a major innovation in mine waste and water management, offering multiple advantages over conventional tailings storage facilities. These include improved geotechnical stability, reduced risks of soil and water contamination, optimized land utilization, and lower long-term monitoring and maintenance costs. Consequently, IMWFs serve as an effective tool for operationalizing sustainable resource management and circular economy principles within the mineral processing sector.

A key feature of IMWF technology is the dewatering of flotation tailings to a paste-like consistency, with the recovered water being recycled back into the processing circuit. This approach significantly reduces freshwater consumption - a critical consideration in regions facing stringent environmental regulations, while enhancing overall resource efficiency and minimizing the water footprint of concentrator operations. Structurally, IMWFs differ substantially from conventional tailings storage sites. They are typically constructed on a main platform composed entirely of mining waste, with an integrated drainage system and sequentially developed terraces of predefined height. Terraces are formed by compacted embankment walls, behind which a controlled mixture of dewatered flotation tailings and rock material is deposited. The integrated drainage network ensures efficient removal of water released during tailings consolidation, thereby reinforcing both the stability and long-term safety of the facility.

A notable implementation of IMWF technology in Bulgaria is the integrated mine waste disposal facility constructed by DPM Metals Krumovgrad EAD - the first and currently only facility of its kind in the country. Using the upstream stacking method, the facility accommodates dewatered flotation tailings from the Ada Tepe gold ore deposit within specially designed cells built from mining waste. This exemplifies the integrated, resource-efficient nature of the technology and its alignment with circular economy objectives.

Beyond IMWFs, other approaches to sustainable resource utilization are also being applied in Bulgaria. At the Chelopech underground mine (DPM Chelopech EAD), a backfill system is employed in mined-out areas. This involves the placement of paste backfill or cemented paste backfill (CPB), composed of flotation tailings mixed with water and cement. The CPB provides structural support to underground walls and ceilings, mitigating deformation risks while simultaneously enabling efficient waste utilization and significantly reducing surface tailings disposal (NI 43-101, 2022).

Overall, these examples demonstrate the growing integration of circular economy principles into Bulgarian mineral processing practices. By combining advanced mine waste management, process water recycling, and environmental impact mitigation, such technologies constitute essential components for the sustainable development and long-term competitiveness of the sector.

4. CHALLENGES AND PROSPECTS

Within the framework of the EU Critical Raw Materials Act, mineral processing assumes a pivotal role in enhancing the recovery of critical and strategic raw materials, including copper and associated by-products, thereby contributing to the resilience and security of European supply chains.

The mineral processing sector in Bulgaria faces a complex and interrelated set of challenges, spanning technological, economic, and human resource dimensions. A primary constraint is the insufficient level of investment in research and development, which limits the deployment of advanced processing technologies. Additionally, the sector is affected by a shortage of highly qualified specialists, particularly in areas such as mineral processing, automation, and process control. The integration of new, often capital-intensive technologies into existing production facilities - originally designed under different technological and regulatory frameworks - further complicates modernization efforts (Pavloudakis et al., 2024).

Addressing these challenges necessitates a comprehensive, systemic approach that combines technological advancement, human capital development, and targeted investment instruments. Stimulating research and development through increased public and private investment, coupled with strengthened collaboration between academic institutions and industry, is essential for facilitating knowledge transfer and accelerating the adoption of innovative technologies.

Mitigating the shortage of skilled personnel requires modernization of educational programs and enhanced cooperation between universities and industry. The development of interdisciplinary competencies in automation, digitalization, and sustainable resource management is critical for cultivating specialists capable of meeting contemporary sector demands. Continuing education and workforce retraining programs further support rapid adaptation to emerging technological approaches.

Technological challenges can be addressed through the deployment of pilot plants, digital twins, and phased automation strategies, which allow for gradual implementation while minimizing financial and operational risks associated with facility modernization.

The adoption of circular economy principles significantly reinforces the sustainable development of the sector. Initiatives such as process water recycling, mine waste valorization, and integrated resource management systems not only reduce environmental impact but also enhance overall resource efficiency and economic viability. National and European funding programs, targeting resource-efficient technologies, decarbonization, and industrial transformation, provide additional opportunities for accelerating mineral processing modernization. Effective utilization of these instruments, combined with a long-term strategic vision, can support the transition toward a more competitive, technologically advanced, and sustainably developed mineral processing industry in Bulgaria.

5. CONCLUSION

The mineral raw materials sector in Bulgaria is currently undergoing a significant transformation, driven by the growing demand for enhanced resource efficiency, sustainable processing practices, and increased competitiveness within the context of the global energy transition and European environmental policies. This review demonstrates that substantial technological progress has been achieved in the Bulgarian mineral processing industry through the modernization of conventional flotation circuits, the implementation of automated and digital process control systems, and the adoption of innovative approaches for sustainable water and material flow management.

The presented industrial case studies indicate that Bulgarian processing plants are successfully adapting modern technologies for the treatment of low-grade and complex ores, achieving improved recovery rates, reduced energy consumption, and enhanced operational stability. Automation, real-time monitoring, and data-driven optimization have proven to be key factors for increasing both economic efficiency and process reliability, while simultaneously improving occupational safety and environmental performance. These developments highlight the critical role of innovation in extending the life cycle of mineral deposits and ensuring the efficient utilization of mineral resources.

Particular emphasis is placed on the application of circular economy principles, especially through advanced solutions for mine waste and tailings management, such as integrated mine waste facilities (IMWFs) and paste backfill technologies. These approaches enable the reuse of process water, the reduction of surface waste disposal, and improved long-term geotechnical stability, thereby significantly reducing the environmental footprint of mineral processing operations. The successful implementation of such technologies in Bulgarian practice demonstrates their potential as effective tools for achieving sustainable development objectives.

Despite these positive developments, the sector continues to face challenges related to insufficient investment in research and development, a shortage of highly qualified specialists, and the complexity of integrating new technologies into existing production infrastructures. Addressing these challenges requires a long-term strategic vision, strengthened collaboration between industry, academia, and research institutions, and the effective utilization of national and European funding mechanisms supporting innovation, digital transformation, and sustainable industrial development.

In conclusion, the Bulgarian mineral processing industry possesses substantial potential for future growth based on technological innovation, automation, digitalization, and the implementation of circular economy principles. The continued advancement and integration of these approaches will be essential for positioning the sector as a competitive, resilient, and environmentally responsible component of the European raw materials and industrial system.

REFERENCES

Annual Bulletin of the Bulgarian Mining and Geological Chamber (BMGC): The Mineral Resources Industry of Bulgaria, 2025.

Dimitrov, L., Grigorova, I., Yankova, T., (2023) “Possibilities to Construct Combined Mine Waste Dump Facility with Better Operational Sequence”, The Eurasia Proceedings of Science, Technology, Engineering & Mathematics, (23) 42-49.

European Commission, (2019), The European Green Deal.

European Commission, (2020), Action Plan for the Circular Economy.

United Nations, (2018) “Sustainable Consumption and Production – Goal 12”. [Online]. Available: https://www.un.org/sustainable-development/sustainable-consumption-production/

International Council on Mining and Metals (ICMM), (2021) “Innovation and Sustainability in Mining”, London: ICMM.

Kostov-Kytin, V., (2023) “Encyclopedia "Minerals in Bulgaria", Sofia, Academic Publishing House “Prof. Marin Drinov”, ISBN 978-619-245-365-7.

Grigorova, M., (2020) “Geophysical and mining technologies for increasing efficiency in “Han krum” open pit mine”, Proceedings of the XX International Multidisciplinary Scientific Conference, 111–118.

Lottermoser, B., (2010), Sustainable Mining Practices, Springer.

McKee, D., (2018), Automation in Mining, Springer.

Napier-Munn, T., (2015), Minerals Engineering, Elsevier.

NI 43-101 Technical report, (2022) “Mineral Resource and Mineral Reserve Update, Chelopech Mine”, Chelopech, Bulgaria.

Pavloudakis, F., Roumpos, Ch., Spanidis, P. M., (2024) “Sustainable Mining and Processing of Mineral Resources”, Sustainability, 16 (19) 8393.

Petrov, M., (2025) “Alternative approaches for optimizing technological parameters in the processing of lead-zinc ores”, Doctoral dissertation, Department of Mineral Processing and Recycling, University of Mining and Geology “St. Ivan Rilskii”.

Sabeva-Domuschieva, D., Madanski, D., Dzhamyarov, S., (2025), “Technological solutions for increasing gold recovery in copper-gold ore processing in Dundee Precious Metals Chelopech”, Annual of the University of Mining and Geology “St. Ivan Rilski”, 68 184–189.

Umucu, Y., Deniz, V., Gürsoya, Y. H., (2024) “Artificial ıntelligence in mineral processing: transforming mining operations through smart technology”, Bilimssel Madencilik Dergisi, 63 (2) 67-85.

APPLICATION OF THE CIRCULAR ECONOMY IN THE MINING SECTORS OF BOSNIA AND HERZEGOVINA: FROM A LINEAR TO A SUSTAINABLE CIRCULAR MODEL THROUGH WASTE VALORIZATION

Nedžad ALIĆ[1,*], Admir SOFTIĆ[2], Alma NUHANOVIĆ[3]

[1]University of Tuzla, Faculty of Mining, Geology and Civil Engineering in Tuzla, BH
[2]Ministry of Foreign Trade and Economic Relations of Bosnia and Herzegovina, BH
[3]University of Tuzla, Faculty of Mining, Geology and Civil Engineering in Tuzla, BH
**Corresponding author: nedzad.alic@untz.ba*

A B S T R A C T

Barite ($BaSO_4$) is a strategic industrial mineral widely used in petroleum drilling, chemical manufacturing, and radiation shielding. With increasing global demand for critical raw materials driven by the energy transition, the circular economy (CE) provides a framework for valorizing secondary mineral resources derived from mining waste. This study evaluates the potential for barite recovery from polymetallic flotation tailings in Bosnia and Herzegovina, focusing on the Vareš mining area as a representative case. The analysis is based on literature review, examination of technical documentation prepared according to the NI 43-101 standard (SRK Consulting, 2025), and conceptual evaluation of gravity concentration methods. Technical data confirm significant barite content (>60% $BaSO_4$) in ore samples from the Vareš deposit, supporting the premise that barite may be present in flotation tailings as a non-target mineral phase.

This conceptual study explores whether gravity separation could enable barite recovery based on density differences between barite ($\rho \approx 4.5$ g/cm³) and gangue minerals, subject to adequate particle liberation. The approach aligns with circular economy principles by treating tailings as potential secondary resources rather than waste, potentially reducing environmental liabilities associated with legacy tailings facilities while decreasing reliance on primary barite extraction.

The findings provide a preliminary framework for future experimental investigation of barite recovery from BiH tailings, contributing to discussions on resource efficiency and circular economy implementation in the mining sector of Bosnia and Herzegovina.

***Key words**: Barite, flotation tailings, circular economy, gravity concentration, Bosnia and Herzegovina*

1. INTRODUCTION

The European Union has redefined its approach to raw materials through climate transition policies, industrial strategy, and the Critical Raw Materials Act (CRMA), which establishes quantified targets for domestic extraction, processing, and recycling by 2030 (European Commission, 2023; Council of the European Union, 2024). The CRMA designates strategic raw materials-including barite, lithium, nickel, cobalt, and rare earth elements-as essential for green and digital transitions, while the European Green Deal and Fit for 55 package align investments with decarbonization objectives (European Commission, 2020).

Circular economy (CE) principles, centered on 'reduce-reuse-recycle' strategies, provide an alternative to the linear 'extract-use-dispose' model by maximizing resource utilization and minimizing waste generation (Green Economy Council of Bosnia and Herzegovina, 2022; Young et al., 2022). In the mining sector, CE implementation includes valorization of tailings, industrial by-products, and end-of-life technologies (e.g., batteries, electronic waste) as secondary sources of critical minerals (United Nations Economic Commission for Europe, 2024).

Western Balkan countries, including Bosnia and Herzegovina (BiH), possess significant mining heritage and accumulated tailings from historical operations. Through the Energy Community Treaty, Paris Agreement, and Sofia Declaration on the Green Agenda for the Western Balkans, BiH has committed to emission reduction targets aligned with European climate neutrality goals by 2050 (United Nations Framework Convention on Climate Change, 2015; European Commission, 2020). Within this policy context, the reprocessing of mining waste offers dual benefits: mitigation of environmental risks associated with legacy tailings facilities and contribution to sustainable resource supply chains (Regional Cooperation Council, 2024).

The traditional mining model, based on a linear logic of primary resource extraction and waste disposal, has resulted in the generation of large volumes of tailings in which associated minerals and fine fractions remained unutilized. Such an approach has led to the loss of potentially valuable mineral resources that were not considered technological or economic priorities at the time of exploitation.

In this context, the circular economy in mining represents an operational framework that enables the redefinition of mining waste—particularly tailings—from being viewed solely as an environmental burden to being recognized as a potential source of secondary mineral raw materials. Unlike the linear approach, the circular model aims to extend the life cycle of mineral resources through reprocessing and reintegration into production streams, thereby reducing the need for primary extraction.

The application of circular economy principles is particularly relevant for stable mineral raw materials that can be recovered using conventional mineral processing techniques. Such minerals are often present in tailings as liberated or partially liberated particles, allowing for secondary valorization without the need for complex or energy-intensive processes.

The importance of the circular economy in mining is especially pronounced in countries with a long mining tradition and significant volumes of legacy mining waste, where tailings valorization can contribute to reducing environmental risks and improving resource efficiency. The analysis of secondary barite recovery from tailings presented in this study illustrates the application of these principles to a specific mining context in Bosnia and Herzegovina, with a focus on technical feasibility.

Despite extensive mining history, the potential for critical mineral recovery from tailings in BiH remains largely unexplored. Existing tailings facilities from polymetallic ore processing (e.g., Pb-Zn operations in Vareš, Srebrenica) contain non-target minerals that were not economically viable during initial processing but may represent secondary resources under current market and regulatory conditions (Mining Institute Tuzla, 2025).

This paper presents a conceptual analysis of barite recovery potential from flotation tailings in the Vareš mining area of Bosnia and Herzegovina. The analysis examines whether gravity concentration methods could enable selective barite separation based on published ore characterization data and established mineral processing principles. This case study serves as an illustrative example of CE thinking applied to BiH mining sector challenges, with implications for tailings management, resource efficiency, and alignment with European sustainability frameworks.

2. BARITE AS A CRITICAL MINERAL AND THE CIRCULAR ECONOMY FRAMEWORK

Barite ($BaSO_4$, barium sulfate) is characterized by high specific gravity (4.3–4.6 g/cm³), chemical inertness, and low solubility, making it suitable for specialized industrial applications. Approximately 75–80% of global barite consumption is in oil and gas drilling fluids, where its density and rheological properties are essential for wellbore pressure control. Additional

applications include fillers in paints and plastics, radiation shielding (medical and nuclear facilities), and chemical feedstock for barium compounds. The European Union classifies barite as a strategic raw material within the CRMA framework due to supply concentration risks and anticipated demand growth (European Commission, 2023; Council of the European Union, 2024).

Traditional mining operations generate substantial volumes of tailings- fine-grained residues from mineral processing-that are stored in tailings facilities and often represent long-term environmental liabilities. Circular economy approaches reframe tailings as potential secondary resources, particularly where non-target minerals with current economic value were discarded during historical operations (Green Economy Council of Bosnia and Herzegovina, 2022; Young et al., 2022).

Reprocessing tailings offers multiple advantages: (i) access to mineralized material without new land disturbance, (ii) avoidance of primary extraction impacts (energy, water, reagents, waste rock generation), (iii) reduction of tailings facility footprints and associated risks (acid mine drainage, physical stability, dust), and (iv) contribution to local and regional supply chains for critical and strategic (UNECE, 2024; Young et al., 2022).

The technical feasibility of tailings reprocessing depends on: mineralogical composition, particle size distribution, degree of mineral liberation, and availability of cost-effective separation methods. Gravity concentration, flotation, and magnetic/electrostatic separation are commonly employed techniques, with method selection determined by mineralogical characteristics and target mineral properties (Young et al., 2022).

Bosnia and Herzegovina has a long mining tradition, with significant historical production of lead, zinc, bauxite, iron ore, and magnesite. Many former mining sites retain tailings facilities from flotation or other beneficiation processes. Potential sites for secondary resource evaluation include:

- Srebrenica (Pb-Zn-Ag tailings)
- Vareš (polymetallic Pb-Zn tailings)
- Zvornik and Mostar (bauxite processing residues)
- Thermal power plant ash deposits (Tuzla, Ugljevik, Gacko, Kakanj)

While preliminary assessments suggest these sites may contain recoverable materials, systematic characterization studies are lacking. The following sections examine the Vareš case as an illustrative example of how CE principles could be applied to evaluate barite recovery potential from polymetallic tailings. Figure 1 shows map of critical raw material occurrences in Bosnia and Herzegovina, numbers 1–14 denote the main tectonostratigraphic units of Bosnia and Herzegovina, as listed in the legend. The map symbols represent different types of critical mineral raw material deposits. The map provides a regional overview and is intended to illustrate the spatial distribution of critical mineral raw materials.

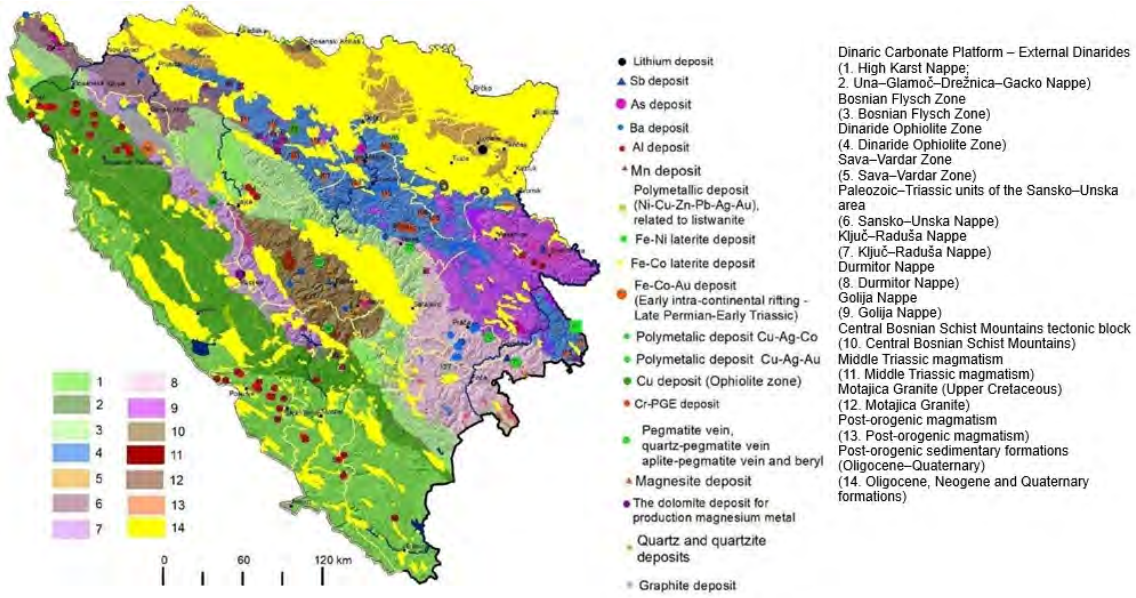

Figure 1. Map of critical raw material occurrences in Bosnia and Herzegovina (Source: Adapted from Mining Institute Tuzla)

3. METHODOLOGY

This study employs an analytical-conceptual approach to evaluate the potential for barite recovery from flotation tailings in Bosnia and Herzegovina, specifically examining the Vareš mining area as a case study. Due to access limitations and the preliminary nature of this investigation, the analysis is based on secondary data sources rather than primary experimental work.

Methodological components include:

1. Literature Review: Systematic examination of scientific publications, technical reports, and policy documents related to barite processing, tailings valorization, circular economy in mining, and critical mineral supply chains.
2. Technical Documentation Analysis: Review of the NI 43-101 technical report on the Vareš Mine, with focus on mineralogical data, ore characterization results (QEMSCAN analysis, chemical assays), and implications for flotation tailings composition.
3. Conceptual Process Evaluation: Assessment of gravity concentration methods for barite separation based on established mineral processing principles, considering physical property differences (density, particle size) and liberation requirements.
4. Policy and Regulatory Context: Examination of European Union frameworks (CRMA, Green Deal) and BiH commitments (Energy Community Treaty, Sofia Declaration) relevant to critical minerals and circular economy.

This research is constrained by the absence of primary experimental data on Vareš tailings composition, particle size distribution, mineral liberation characteristics, or gravity separation test results. Conclusions regarding technical feasibility are therefore hypothetical and require validation through laboratory or pilot-scale testing. Economic viability, environmental impacts, and quantitative emission reduction potential are beyond the scope of this conceptual study.

3.1. Case Study: Barite Potential in Vareš Flotation Tailings

The Vareš mining area in central Bosnia and Herzegovina has a long history of polymetallic (Pb-Zn-Ag) ore extraction and processing. Mineralization is associated with hydrothermal

processes, with ore assemblages including galena (PbS), sphalerite (ZnS), pyrite (FeS_2), and gangue minerals including barite ($BaSO_4$), quartz (SiO_2), and carbonates (SRK Consulting, 2025, Mining Institute Tuzla, 2025). Flotation plants historically focused on lead, zinc, and silver recovery, with non-sulfide minerals such as barite reporting to tailings streams.
NI 43-101 is a Canadian regulatory standard for mineral project disclosure, requiring specific technical reporting formats and qualified person certification. The SRK Consulting technical report on Vareš, prepared in compliance with this standard, presents mineralogical and chemical characterization data from ore samples used in metallurgical testwork.
Mineralogical analysis using QEMSCAN (quantitative evaluation of minerals by scanning electron microscopy) identified barite as a significant non-metallic mineral phase in ore samples. Chemical assays of testwork head samples (Table 1) report $BaSO_4$ content exceeding 60%, with some samples reaching >80% $BaSO_4$. These data confirm that barite is a major component of the ore mineralogy entering flotation circuits.

Table 1. Barite ($BaSO_4$) content in ore samples from Vareš deposit based on NI 43-101 technical report

Parameter	Value
Sample Type	Ore feed samples for metallurgical testing
Analytical Method	Chemical assay (DFS testwork head assays)
$BaSO_4$ Content Range	60–80%
Reporting Standard	NI 43-101 (Canadian mineral project disclosure standard)
Data Source	SRK Consulting (UK) Limited, 2025 [6]

Note: Data represent ore samples, not flotation tailings. Barite presence in tailings is inferred from flotation process selectivity for sulfide minerals.

Chemical assays of ore samples from the Vareš deposit, as reported in the NI 43-101 technical report, indicate substantial barite content. Table 1 summarizes the range of $BaSO_4$ concentrations measured in metallurgical testwork head samples.
The NI 43-101 report characterizes ore feed samples, not flotation tailings. Since flotation circuits were optimized for sulfide mineral recovery (Pb-Zn), barite-with its non-sulfide mineralogy and high density-would not be selectively floated and is expected to report predominantly to tailings. However, direct analytical data on tailings composition, particle size distribution, and barite liberation are not available in the reviewed documentation. The premise that significant barite remains in tailings is therefore a reasonable inference based on process mineralogy, but requires empirical verification through tailings sampling and analysis.
Tailings facilities at Vareš, like many legacy sites, represent both environmental liabilities (potential for acid mine drainage from sulfide oxidation, physical stability concerns, land use constraints) and potential secondary resources (Mining Institute Tuzla, 2025). Reprocessing tailings to recover barite could:

- Reduce tailings volume and facility footprint
- Mitigate long-term environmental risks
- Generate revenue to offset remediation costs
- Provide domestic barite supply, reducing import dependence.

These benefits are contingent on technical and economic feasibility, which cannot be determined without site-specific testing.
In order to conceptually assess the technical potential of barite recovery from flotation tailings, standard mineral processing performance indicators were considered. These include mineral recovery, concentrate grade, and enrichment ratio, which are commonly used in flotation and gravity separation evaluation. Recovery (R) and enrichment ratio (ER) were determined using

conventional mass balance relationships widely adopted in mineral processing and flotation performance evaluation (Wills and Finch, 2016).

Mineral Recovery (R)

Mineral recovery represents the proportion of valuable mineral recovered into the concentrate relative to its amount in the feed material:

$$R = \frac{\mathrm{C} * \mathrm{c}}{\mathrm{F} * \mathrm{f}} * 100$$

Where:

- C – mass of concentrate (t)
- c – grade of concentrate (% $BaSO_4$)
- F – mass of feed material (tailings) (t)
- f – grade of feed material (% $BaSO_4$)

This expression is a standard mass-balance relation applied in mineral processing performance evaluation (Young et al., 2022).
For illustration purposes only, if 100 t of tailings containing 25% $BaSO_4$ produce 20 t of concentrate grading 95% $BaSO_4$, the recovery would be:

$$R = \frac{20 * 95}{100 * 25} * 100 = 76\%$$

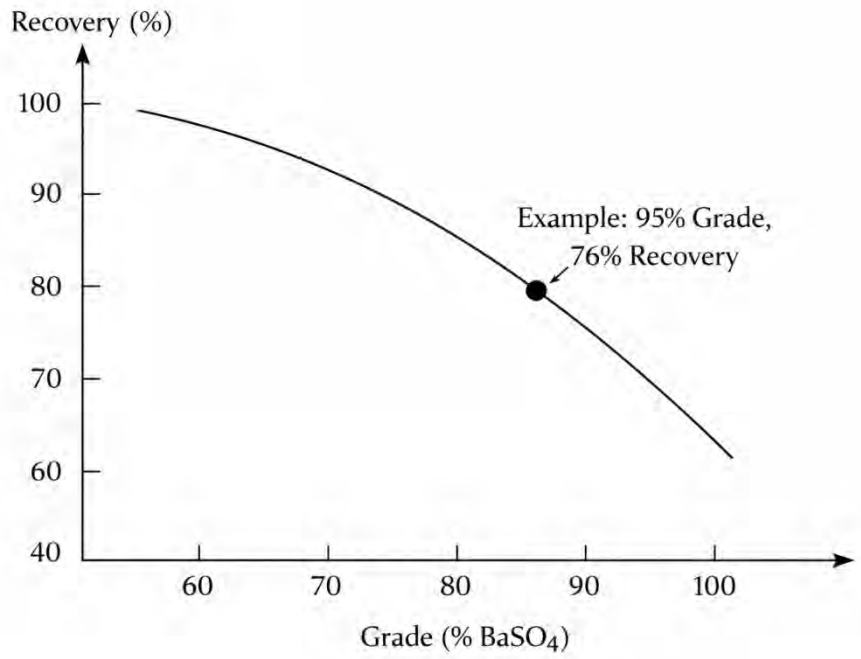

Figure 2. Illustrative grade–recovery curve for barite flotation

The curve demonstrates the trade-off between concentrate grade (% $BaSO_4$) and recovery (%). The marked point (95% Grade, 76% Recovery) represents a theoretical example based on conceptual mass balance calculations.
This example is theoretical and does not represent measured data from the Vareš tailings.

Enrichment Ratio (ER)

The enrichment ratio expresses the upgrading efficiency of the process:

$$ER = \frac{\mathrm{c}}{\mathrm{f}}$$

In the above example:

$$ER = \frac{95}{25} = 3.8$$

This indicator reflects the degree of concentration achieved relative to the feed grade.

Conceptual Mass Estimation of Barite in Tailings

For preliminary estimation of contained barite mass within a tailings facility, the following relation may be used. Contained mass estimation follows conventional volumetric resource estimation principles, where tonnage is calculated as the product of volume, bulk density, and grade proportion.
$m = V * \rho * \mathrm{p}$
Where:

- m – mass of contained barite (t)
- V – volume of tailings (m^3)
- ρ – bulk density of tailings (t/m^3)
- p – proportion of $BaSO_4$ (decimal fraction)

Barite density in massive zones is typically 4.2–4.6 g/cm^3 (SRK, 2025; NI 43-101 Technical Report on Vareš).
This calculation provides only a volumetric approximation and requires site-specific density and grade data for reliable estimation.
These quantitative indicators are presented solely as conceptual tools for evaluating potential process performance. No experimental testwork on Vareš tailings has been conducted within this study; therefore, actual recovery, concentrate grade, and economic feasibility remain to be verified through laboratory and pilot-scale testing.

4. DISCUSSION

Gravity concentration exploits density differences between minerals to achieve separation. Barite (ρ = 4.3–4.6 g/cm^3) has significantly higher specific gravity than typical gangue minerals in polymetallic tailings:

- Quartz (SiO_2): ρ ≈ 2.65 g/cm^3
- Calcite ($CaCO_3$): ρ ≈ 2.71 g/cm^3
- Dolomite: ρ ≈ 2.85 g/cm^3

This density contrast (concentration criterion Cc = ρ_heavy / ρ_light ≈ 1.7–1.9) suggests gravity methods could theoretically separate barite from silicate/carbonate gangue (Young et al., 2022). However, successful separation depends on three critical factors:

1. Mineral Liberation: Barite must be present as free particles, not locked in composite grains with sulfides or gangue. Liberation is a function of ore texture and particle size; insufficient grinding results in composite particles that behave according to average density rather than pure mineral density.
2. Particle Size Distribution: Gravity separators have optimal size ranges. Excessive fines (<20 μm) are difficult to recover due to high surface area-to-mass ratios and fluid drag effects, while oversized particles may contain unliberated composites.
3. Process Selectivity: Equipment selection (shaking tables, spirals, centrifugal concentrators, dense media separation) must match particle characteristics and throughput requirements.

A generalized process for evaluating barite recovery from Vareš tailings would involve the following sequential stages:

1. Tailings Characterization: Representative sampling, mineralogical analysis (XRD, automated mineralogy), particle size distribution, and liberation studies to establish barite content, deportment, and liberation characteristics.
2. Feasibility Assessment: Evaluation of characterization results against minimum criteria for gravity separation (e.g., barite content >10%, liberation at achievable grind sizes, acceptable particle size distribution).
3. Size Reduction (if required): Controlled grinding to enhance mineral liberation while minimizing ultra-fine particle generation. Classification to remove pre-existing fines before grinding may improve efficiency.
4. Classification: Screening or hydrocyclone separation to produce size fractions optimal for gravity concentration (typically 75 μm to 2 mm) and remove excessive fines (<20 μm) that reduce separator efficiency.
5. Gravity Concentration: Primary separation using equipment selected based on particle characteristics:
6. -Shaking tables (intermediate to fine particles, high selectivity)
   -Spiral concentrators (fine to medium particles, high throughput)
   -Centrifugal concentrators (fine particles, high G-force separation)
   -Dense media separation (coarse particles, if applicable)
7. Product Streams:
8. -Barite concentrate: High-grade product for market
   -Middlings: Intermediate-grade material recirculated to cleaning stage
   -Final tailings: Depleted material with reduced volume compared to original facility
9. Cleaning Stage: Re-processing of middlings through secondary gravity separation to maximize barite recovery and concentrate grade.
10. Dewatering and Product Handling: Thickening, filtration, and potentially drying to meet market specifications. Quality control testing for $BaSO_4$ grade, impurities, particle size, and application-specific requirements (e.g., drilling-grade specifications).
11. Tailings Management: Disposal or stabilization of final tailings; potential for co-management with environmental remediation objectives (volume reduction, revegetation).

This framework is conceptual and illustrative. Actual process design requires systematic test work (batch tests, locked-cycle tests, pilot trials) to determine achievable performance, optimize operating parameters, and generate engineering design data.

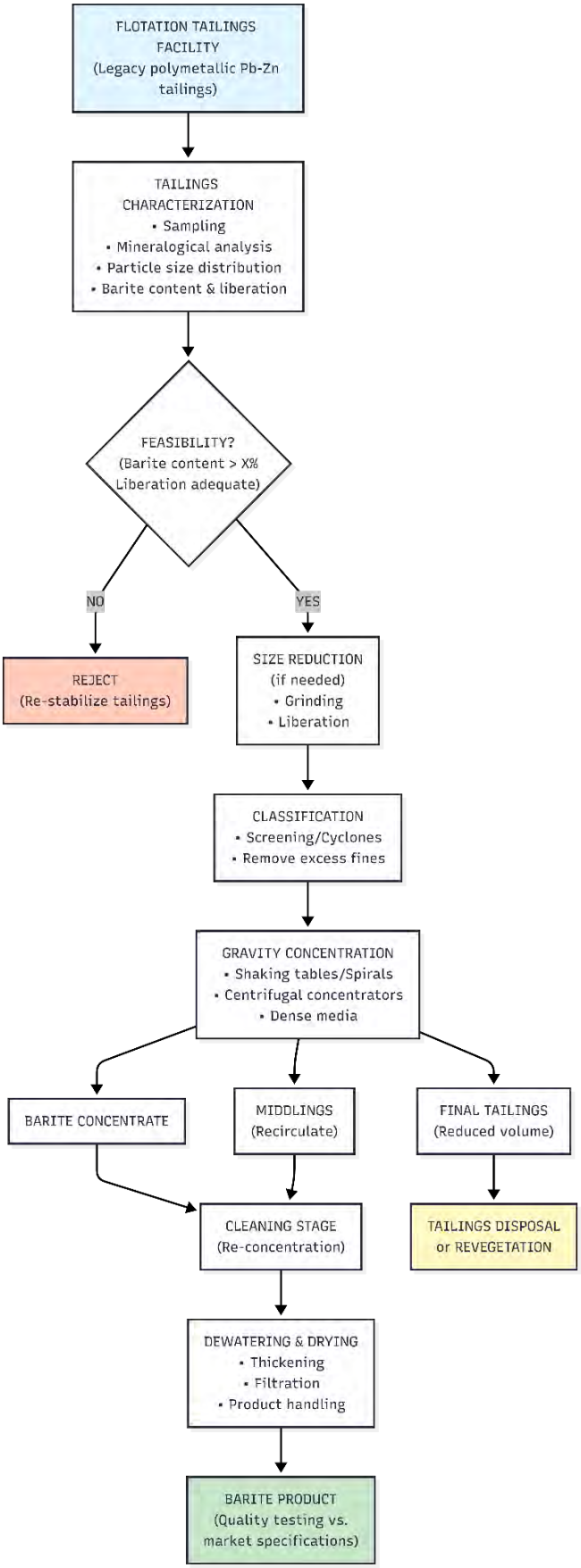

Figure 3. Conceptual process framework for barite recovery from flotation tailings. This simplified flowsheet illustrates potential process stages; actual design requires site-specific test work and optimization

Several factors could limit technical or economic feasibility:

- Heterogeneity: Tailings composition may vary spatially (depth, location) within the facility, complicating resource estimation and process consistency.
- Intergrowth Textures: If barite occurs predominantly as fine intergrowths with sulfides or gangue, liberation may require grinding to impractically fine sizes, increasing losses and processing costs.
- Sulfide Oxidation: Aged tailings may contain oxidized sulfides, producing acidic drainage that complicates water management and reagent consumption.
- Market Requirements: Barite product specifications (grade, whiteness, particle size) vary by application; drilling-grade barite requires >95% $BaSO_4$ and <250 mg/kg soluble alkaline salts, which may necessitate additional upgrading steps.

From a CE perspective, barite recovery from tailings exemplifies the 'waste-to-resource' principle. Rather than constructing new mines with associated land disturbance, energy consumption, and waste generation, reprocessing leverages materials already extracted and partially processed. Potential CE benefits include:
- Reduction in primary mining demand (if recovered barite displaces new extraction)
- Tailings volume reduction, lowering facility management costs and environmental risks
- Extension of value from historical mining investments
- Contribution to regional supply chain resilience.

However, these benefits are hypothetical until demonstrated through feasibility studies that include life cycle assessment (LCA), techno-economic analysis (TEA), and comparison with primary barite production pathways.

5. CONCLUSION

This study provides a preliminary conceptual analysis of barite recovery potential from polymetallic flotation tailings in Bosnia and Herzegovina, using the Vareš mining area as a case study. Based on examination of technical documentation prepared according to NI 43-101 standards (SRK Consulting, 2025) and mineral processing principles, the following conclusions are drawn:

Technical Findings:

1. Barite Presence Confirmed in Ore: Chemical and mineralogical analyses of Vareš ore samples indicate significant barite ($BaSO_4$) content, with concentrations ranging from 60% to >80% in test work feed materials. As flotation circuits were designed for sulfide mineral recovery, barite is expected to report predominantly to tailings streams, though direct tailings composition data are not available in reviewed sources.
2. Conceptual Feasibility of Gravity Separation: The substantial density difference between barite ($\rho \approx 4.5$ g/cm³) and common gangue minerals ($\rho \approx 2.6–2.9$ g/cm³) provides a physical basis for gravity concentration. However, process viability depends on particle liberation, size distribution, and equipment performance characteristics that cannot be predicted without experimental testing.
3. Data Gaps Require Empirical Validation: Critical information needed to assess technical and economic feasibility includes: (i) representative tailings sampling and analysis, (ii) mineralogical characterization and liberation studies, (iii) particle size distribution, (iv) batch and locked-cycle gravity separation tests, (v) product quality evaluation against market specifications, and (vi) techno-economic and environmental assessment.

Tailings reprocessing aligns with circular economy principles by treating waste materials as potential resources, offering pathways to reduce primary extraction, mitigate environmental

liabilities associated with legacy facilities, and enhance regional supply chain resilience. The Vareš case illustrates how CE thinking can be applied in BiH mining sector planning, particularly for sites with diverse mineralogy and non-target minerals that have gained strategic importance under current EU critical minerals frameworks (European Commission, 2023; Council of the European Union, 2024).

To advance from conceptual analysis to feasibility determination, the following research steps are recommended:

1. Tailings Characterization Program: Systematic sampling (accounting for spatial variability), chemical assays, quantitative mineralogical analysis (QEMSCAN or MLA), and liberation studies.
2. Laboratory Testwork: Gravity separation tests (shaking table, spiral, centrifugal concentrator) across multiple size fractions, optimization of grind size for liberation vs. fines generation trade-offs, and evaluation of concentrate grade and recovery.
3. Pilot-Scale Demonstration: If laboratory results are favorable, pilot testing using representative tailings tonnages to validate flowsheet, generate design data, and produce product samples for market evaluation.
4. Integrated Assessment: Life cycle assessment (LCA) comparing tailings reprocessing to primary barite production, techno-economic analysis including capital and operating costs, and evaluation of environmental co-benefits (tailings volume reduction, acid mine drainage mitigation).

While this study identifies barite recovery from Vareš tailings as a plausible opportunity warranting further investigation, conclusions remain preliminary pending empirical validation. The application of circular economy principles to mining waste in Bosnia and Herzegovina requires site-specific technical studies, stakeholder engagement, and alignment with European policy frameworks to transition from conceptual potential to operational reality.

REFERENCES

Council of the European Union, (2024), Critical raw materials, https://www.consilium.europa.eu/hr/infographics/critical-raw-materials/

Drzymała, J., (2007), Mineral Processing: Foundations of Theory and Practice of Minerallurgy.

European Commission, (2020), Sofia declaration on the green agenda for the Western Balkans, https://neighbourhood-enlargement.ec.europa.eu/sofia-declaration-green-agenda-western-balkans_en

European Commission, (2023), Study on the review of the list of critical raw materials, https://hytechcycling.eu/wp-content/uploads/Study-on-the-review-of-the-list-of-Critical-Raw-Materials.pdf

International Council on Mining and Metals (ICMM), (2023), Circular Economy Indicators for the Mining and Metals Industry, London.

International Energy Agency, (2021), The role of critical minerals in clean energy transitions, https://www.iea.org/reports/the-role-of-critical-minerals-in-clean-energy-transitions

Mining Institute Tuzla, (2025), Mogućnosti i potencijal kritičnih sirovina Bosne i Hercegovine – Trenutni resursi kritičnih sirovina.

Muroni, L., (2022) “Critical raw materials and sustainable development”, Master’s Thesis, https://www.ie-ei.eu/Ressources/FCK/image/Theses/2022/EUDIPLO_Muroni_Thesis.pdf

Regional Cooperation Council, (2024), Green agenda for the Western Balkans, Revised action plan 2025–2030 (Circular economy pillar).

Rossi, M. E., Deutsch, C. V., (2014), Mineral Resource Estimation, Springer.

SRK Consulting (UK) Limited, (2025), NI 43-101 technical report on the Vareš mine, Bosnia and Herzegovina, https://minedocs.com/29/Vares-TR-04012025.pdf

United Nations Economic Commission for Europe, (2024), Critical minerals for sustainable energy transition – A guidebook to support intergenerational action, https://unece.org/sites/default/files/2024-04/RMYMG-Critical-Minerals-for-Sustainable-Energy-Transition.pdf

United Nations Framework Convention on Climate Change, (2015), Paris agreement, United Nations, https://unfccc.int/process-and-meetings/the-paris-agreement/the-paris-agreement

White paper on circular economy and sustainable resource management, (2022). https://zelenaekonomija.komorabih.ba/wp-content/uploads/2023/10/White_Paper_Publication_28042022.pdf

Wills, B. A.,Finch, J. A., (2015), Wills' Mineral Processing Technology: An Introduction to the Practical Aspects of Ore Treatment and Mineral Recovery.

Young, R., Barreto, L., Chovan, M., (2022), Towards a circular economy approach to mining operations. Materials Efficiency Research Group. https://circulareconomyleaders.ca/wp-content/uploads/2024/04/Towards-a-Circular-Economy-Approach-to-Mining-Operations.pdf

RECULTIVATION OF ORE FIELDS AFTER EXPLOITATION - METHODOLOGY OF COLLECTION OF FUNDS FOR RECULTIVATION

Jahir GASHI, Habib BASHOLLI*

Independent Commission for Mines and Minerals, Republic of Kosova, Prishtina
**Corresponding author: habib.basholli@gmail.com*

A B S T R A C T

Mining exploitation and recultivation mining fields is one of the challenges facing the mining sector. The methodology of collecting financial resources during the exploitation phase will be considered the best method for the effective conditioning of mining companies for mine recultivation. This method of collecting funds collected during mine exploitation is presented as effective because the mine is developed in accordance with the stipulated norms. Legal norms, method the “bank guarantee” or recultiavtion bond method, do not provide a guarantee that a mining company that is in the development phase and that has somehow lost the criteria for maintaining a license or is in the final phase, will resolve the situation.

For this reason, this methodology, which can be used as a prerequisite, has clarified the methodology by which it is intended that financial resources during the mine development phase can be collected as accumulated revenues that are facilitated by companies and at the same time create incentives for the recultivation phase from institutional and companies by returning the accumulated amount - collected as a process after standard recultivation with accepted reclcultivation criteria.

Key words: *Collection, bonds, re-cultivation, deposited money*

1. INTRODUCTION

Surface mines, which carry out their activities according to the method of exploitation in many methods, but those that have been applied to the exploitation of the mineral so far in our country are:

• Excavation,
• Cutting and
• Mining activities.

It is necessary that mining activities be developed, always respecting environmental norms and be as rational and economically viable as possible. The economization of each phase of the development of the mine from the beginning of mining activities is of great importance. This means not only economizing the method of carrying out mining activities, but also the most economical way to close and re-cultivate the mine.
During mining activities, a different terrain is created than before, as well as spaces that are visible, which will later be areas where even after filling, they will present a landscape with a changed appearance. This phenomenon of quarry development is known as a damage to the image and a threat to the environment, but since the market demands such a resource, it must be utilized, which increases vigilance on the part of both institutions and businesses to exercise this control carefully and within the permitted parameters.

In order to have certainty that the enterprise is operating in accordance with the project and that the post-mining condition is acceptable according to the Mining Legislation of the Republic of Kosovo, mechanisms have been created to guarantee that the re-cultivation of these quarries - mines is safe and accepted.

Based on the practice so far in some cases this mechanism has not shown its effect and that in two cases:

First, when the criterion of maintaining the license has been lost (as a result of bankruptcy or non-compliance with the qualifying criteria by other institutions or even by the ICMM itself).

Second, when the criterion of the final phase of the license is in an unacceptable state and there is no financial cost to guarantee that these means can re-cultivate that quarry area.

The Law on Mines and Minerals [3] respectively the Administrative Instruction of the ICMM No. 002/2014 has created two possibilities for creating accumulated funds as assets - bank guarantee, i.e. in advance, the enterprise, before withdrawing the license, must deposit an amount of financial assets in one of the banks operating in the Republic of Kosovo and those assets serve as a financial guarantee for re-cultivation in the event of failures as mentioned above.

The bank guarantee according to Article 5 of AI No. 002/2014 [2] provides that each mining activity must deposit a financial amount of 5000 (€/ha) in case the activity is carried out with mining or 12000 (€/ha) in case the activity is carried out without mining.

The deposited funds present difficulties for businesses because these funds will also be subject to interest for holding as funds deposited in banks and what is most important is that these funds often do not guarantee that the license owner has an interest in recultivating it depending on his status. ICMM has already encountered these difficulties because in most cases the deposited funds do not provide encouragement for any third party enterprise to rehabilitate or recultivate the quarry-mine.

For these reasons, through this work, a model of collecting financial resources has been created and no longer from the financial sources of depositing funds in the Bank, but a study has been made on how accumulated funds can be created that would not be burdensome for the business from the beginning and that gradually by developing the mine, the enterprise's own fund will be created.

The own fund created by the enterprise itself that operates with mining activity will be done by adding an additional financial cost within the framework of the mining royalty. The additional cost of the collected funds will be done in harmony with the amount-volume paid of the mining royalty. The logic is more than understood that the development of mining activity also implies the degree of degradation for the environment but at the same time the determination of the financial value of the deposits. The greater the development of mining activity, the greater the environmental damage will be, but the deposited funds may also be greater and vice versa.

Such a procedure should be analyzed in three cases: when the activity is in clay and the mining rent is very low, when we are dealing with cutting decorative stones and the activity is in hard rocks and explosives must be used.

2. REALIZATION OF THE POSSIBILITY OF COLLECTING FINANCIAL FOUNDS IN COMPLIANCE WITH THE REALZIATION OF MINING ACTIVITY

An area that has the coverage of the geodetic situation has been taken for analysis and an artificial surface of 3 (ha) has been created.

The exploitation system of this mine is with mining and is realized from the quota of +705 m to the quota of +675 m and from the parameters of the working steps, the final square between

the final steps has been created with a distance of 4 (m), which is more than necessary for the re-cultivation of this area after the mining activity.

During the exploitation system, it begins to be exploited with a top-down system and figure 1 presents the initial state of the mine development [4].

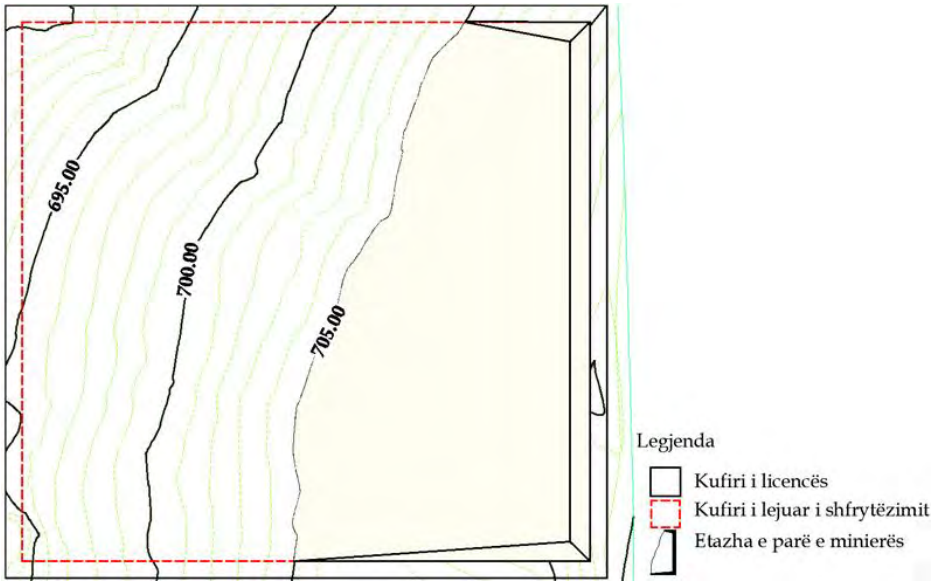

Figure 1. Exploitation system - first phase

In the following, we will present the tabular situation in which each situation is presented with the necessary data, but first we will present the situation of how much a meter of drilling-mining costs to calculate the cost of the volume for 1 (m3) of mined mass.

Table 1 presents the situation with which it results that how much 1 (m3) will cost including all parameters from labor, energy used for drilling, the amount of explosives and other consumables. The table does not present the cost of loading the mined material and transportation, but this expense will be covered by the right to sell-commercialize this mass, excluding the payment for the mining royalty of the mined material.

Table 1. Calculated cost parameters 1(m^3) with drilling and mining costs

Nr.	Title	Geometry a x b	Unit	Cost [€/unit], without tax	Cost [€/unit], me with tax
1	Miming service	2.5 m x2.5 m	m^3	€ 2.20	€ 2.60
2	Miming service	2.6 m x2.6 m	m^3	€ 2.10	€ 2.48
3	Miming service	2.7m x 2.7 m	m^3	€ 2.00	€ 2.36
4	Miming service	2.8 m x2.8 m	m^3	€ 1.91	€ 2.25
5	Miming service	2.9 m x2.9 m	m^3	€ 1.80	€ 2.12
6	Miming service	3.0 m x3.0 m	m3	€ 1.69	€ 1.99
7	Miming service	3.2 m x3.2 m	m^3	€ 1.48	€ 1.74
8	Miming service	3.5 m x3.5 m	m^3	€ 1.33	€ 1.57
9	Miming service	3.7 m x3.7 m	m^3	€ 1.18	€ 1.39
10	Miming service	4.0 m x 4.0 m	m^3	€ 1.05	€ 1.24

The most approximate value in most cases will be taken within the parameters of rows 3 to 6 of this table (1) and the high average unit price value of 2.25 (€/m^3) will be taken into

account. For accuracy of calculation, taking into account the possible change in market prices, we will consider the value of 2.3 (€/m^3)

Table 2. Calculation of the value for collection of funds and the calculated value for recultivation

Atitude	**Utilized volume m^3**	**Storage capacity (m^3/yeasr)**	**Mining rent (€)**	**Collection for re-cultivati (€)**	**Time of use (year)**	**Volume during re-cultivation (m^3)**	**Cost (€/m^3)**	**Re-cultivation rent (€)**	**Amount for re-coltivatin (€)**
+705 m	38782.2	50000	19391.1	3878.2	1,2	1591.3	2.3	795.6	2864.2
+695 m	128508.2	50000	64254.2	12850.8	2,5	4680.2	2.3	2340.1	8424.4
+685 m	169599.4	50000	84799.7	16959.9	4	6155.9	2.3	3077.9	11080.6
+675 m	94285.7	50000	47142.8	9428.5	4,5	10651	2.3	5325.5	19172.0
Total	431175.9	50000	215587.9	**43117.5**	**12 vite**	23079		11539.2	**41541.3**

.

From table 2 it can be seen that the mine for an area of S= 30000 (m^2) or expressed in hectares S= 3 (ha) as an example planned to exploit 4 levels with a depth of h=10 (m) at each level and the maximum designed depth is 40 (m) [4]. The total amount of exploitable reserves of the mineral resource is 431175 (m^3). The production capacity is taken as a mine with an average exploitation capacity of 50000 (m^3/year). The mining royalty is taken for hard stone from the mining royalty list 0.5 (€/m^3) [5]. The exploitation time is divided into years depending on the exploitation level and the resource capacities that that level has [4]. The section (volume during recultivation) analyzes the amount that can be created if the enterprise fails to practice recultivation and that the creation of a scale to remediate the situation creates a volume with a value that is presented in table [4]. The rent for recultivation is presented as a calculated value that the contractor who is charged with recultivation must pay to the institution [5], while the section (amount for recultivation) presents the cost that is incurred in the event of drilling and mining.

3. MEHTOD OF CALCULATING COLLECTION AND INSTITUTIONAL AND BUSINESS BENEFITS.

How this will be benefited from can be explained analytically.

The enterprise must first, before starting work, take care to leave a space around the license boundary with a distance of 5 (m). The reason is practical because if the enterprise fails to execute the height of the scale in function of the safety factor, then the license activity, namely the mining activity, must be suspended and it is obliged to create the boundary of this safety area of 5 (m) as a safety measure to regulate the mine space.

Each phase of development must obtain approval from the institution that it will start the exploitation system at a level lower than the completed one and only then should the work be started and again to ensure that the newly created and cultivated scale does not pose a risk for re-cultivation. All completed stairs must receive approval until the mine is completed.

Table 3. Comparison between the means of recultivation according to U.A. No. 002/2014 and the model for change with the method of collection

Surface (ha)	**Bank guarantee cost (€/ha)**	**Bank guarantee until the license expires (€)**	**Collection in re-cultivation (€)**	**Re-cultivation cost**			
				Volume (m^3)	**Cost (€/m^3)**	**Re-cultivation rent (€)**	**Amount (€)**
3	5000	15000	3878.2	1591.25	2.3	795.625	2864.25
			12850.8	4680.23	2.3	2340.115	8424.414
			16959.9	6155.91	2.3	3077.955	11080.64
			9428.5	10651.15	2.3	5325.575	19172.07
			43117.5	23078.54	2.3	11539.27	**41541.37**
Bank guarantee for re-cultivation from the beginning to the end of the licence year		**15000**	**43117.5**				

From Table 2 and Table 3 it can be concluded that the collection of funds will be done by collecting the tax from the Renta. Mining rent has a tax of 0.5 (€/ m^3) [5], while the collection for funds accumulated in the function of exploitation is in the amount of 0.1 (€/ m^3). From Table 3 it can be seen that the funds deposited according to U.A. No. 002/2014 [2] is not a value that can encourage the legal entity to carry out re-cultivation, while the funds collected according to this model amount to 43117.5 (€) which is almost three times the funds deposited as a bank guarantee [2].

Table 4. SWOT Analysis regarding the model of collection of funds for recultivation

Strength	**Weaknesses**
Will not deposit money in the Bank from the strat of the business Will not pay for maintenance or credit for money deposited int he Bank; Secure way of collection; The more we use, the more we degarde, but the more we collect financial resources; Ways to encourage license holders to deposit funds for withdrawl at the end of the licence; The funds used from the new culltivation process can serve as a means to cover some of the expenses for opening a new business in this sector; Encouragement of the license to implement the project safaty; Easy way to control and remediate from the start;	A special program or software must be created to control and monitor this process; Other possibilities for other resouces should also be analyzes because it is nor practiacal to change a process based on this analysis alone; Control over the development of the mine should always be controlled at the levels are created. The new cultivation method will be more costly;
Oportunitis	**Dangers**
Models should also be created for other resouces since this form has chosen only one of the methods of exploitation and only of the resource where the mineral is extracted by mining; Relevan models can also be created partial asset recovery for mining with large areas; The possibility of cellecting funds can also be created with flexible options in accordance with levels, years or production capacities;	The method of calculating expenses generated by the cost of drilling and mining may change; The state may experience inflation and the value of collected funds may decline; Bureucracy that can influence inter-institutional relations that will accept re-cultivation without completing partial re-cultivation works according to plan ; What will be done in cases where the enterise loses the criteria for a licence and the procedures are legal for decision-making and the funds cannot be returned to the third party holer for re-cultivation?;

4. CONCLUSIONS AND RECOMANDATIONS

To draw a comparison of the procedures practiced so far and that such a model can give the best results is to conduct a SWOT analysis. The main and most important action of conducting a SWOT analysis is the identification and evaluation of factors.

It is recommended to also work on collecting other resources and to conduct an analysis and propose changes in the method of collecting funds for the purposes of new mining cultivation

REFERENCES

Brahimaj, F., (n.d.) “Tabela e llogaritjes së shpim-plasjes sipas ndërmarrjes afariste”.

KPMM, (2014) “Udhëzimi Administrativ Nr. 002/2014 për garancionet bankare dhe sigurimet ‘për të gjitha rreziqet ndaj palëve të treta’”.

“Ligji për minierat dhe mineralet Nr. 03/L-163”, (2010).

“Ligji Nr. 04/L-158 për ndryshimin dhe plotësimin e ligjit Nr. 03/L-163 për minierat dhe mineralet”, (2013).

Ministry of Economy (Kosovo), (n.d.) “Lista e rentës minerare”, Available at: https://me.rksgov.net/repository/docs/Vendimi__Lista_e_Rentes_Minerare.pdf

“Projektimi nga autorët i një miniere model në programin AutoCAD Civil 3D-2018”, (2018).

FLOTATION AND SURFACE CHEMISTRY PROCESSES

A SUSTAINABLE APPROACH OF FLOTATION-BASED RECYLCING OF VIRGIN AND POST-CONSUMER MULTIPLE PLASTICS WITH DETERMINATION OF THEIR SURFACE CHARACTERISTICS

Cemal Cem BAKIR*, M. Olgaç KANGAL, Zeynep ÜÇERLER ÇAMUR, Tülay TÜRK

Istanbul Technical University, Faculty of Mines, Mineral Processing Engineering Department, 34469, Maslak, Istanbul, TÜRKİYE
**Corresponding author: bakir19@itu.edu.tr*

A B S T R A C T

Plastics are widely used materials whose global production has increased dramatically, reaching 413.8 million tones and is projected to triple by 2060. This growth has led to a significant rise in plastic waste, posing serious environmental and sustainability challenges. Conventional disposal methods such as landfilling and incineration are not environmentally friendly, as they may cause ecosystem damage and toxic gas emissions. Therefore, plastic recycling has become a crucial option from both waste management and production perspectives.

Plastic recycling generally involves collection, separation, size reduction, washing, and reprocessing stages, all of which strongly influence final product quality. Effective recycling requires accurate separation of plastics according to polymer type. Although manual and density-based separation methods are commonly used, they are insufficient for systems with similar densities, such as HDPE–LDPE or PVC–PET–POM mixtures. In such cases, flotation, a physicochemical separation method, offers an effective alternative. Flotation exploits differences in surface chemical properties and wettability, enabling selective separation through surface modification using appropriate reagents. The efficiency of flotation is influenced not only by surface chemistry but also by the density, size, and shape of plastic particles.

In this study, the selective separation of mixed plastic systems consisting of HDPE, and PP was investigated using flotation-based techniques. Surface physicochemical properties of the plastics and reagents were systematically characterized using surface tension measurements, contact angle measurements and zeta potential analysis to evaluate their wettability and surface charge behavior. The effects of surface conditioning and flotation parameters on separation efficiency were examined, and the relationship between surface characteristics and flotation response was discussed in detail.

Key words: *Plastic, flotation, surface chemistry, recycling*

1. INTRODUCTION

Plastics utilize hydrocarbons sourced from natural resources such as petroleum and natural gas. Technically speaking, plastics are created by polymerizing monomers via chemical bonding. There are various categories and names connected with polymers. Plastics are divided into two groups according to their behavior in heat environments: thermoplastics and thermosets. Thermoplastic polymers may be classified into two subclasses: amorphous and semi-crystalline. When heated, thermoplastic polymer-based products may change shape or form. Thermosets, on the other hand, cannot alter their form by heating; once the original components react, they suffer an irreversible chemical change (Mills et al., 2020).

Various plastics are used in various applications, from toys and electrical gadgets to medical equipment, packaging, and even space flight. Plastics significantly impact the way we shape our lives. Their durability, safety, lightweight nature, capacity to adopt many shapes, and cost advantages give unique solutions in many domains. When examined across their entire lives, they contribute to resource savings. Additives added into plastics impart varying qualities

based on the intended purpose. These additives include fillers and reinforcements, stabilizers, antioxidants, plasticizers, flame retardants, colorants, lubricants, slide agents, catalysts, antistatic agents, and foaming agents (Alp, 2003).

Since the early 20th century, the plastics sector has steadily developed, finding uses in several industries. Today, plastics have replaced numerous natural materials such as wood, paper, metal, glass, cotton, wool, silk, and rubber, becoming an integral element of contemporary life. In addition to their adaptability in processing, the economic benefits of plastics have made them crucial in numerous technological breakthroughs (Alp, 2003).

When abandoned, plastics survive in the environment for lengthy years without deteriorating, rusting, dissolving, or undergoing biological deterioration. Some polymers may endure for up to 700 years in nature. They contribute to soil and water contamination, impair aquatic life, and even cause mortality among marine species (Sevencan and Vaizoğlu, 2007).

Plastics are used predominantly in packaging, construction, automotive, electrical–electronic, and household applications. Globally, packaging accounts for approximately 40% of total plastic consumption, making it the largest application area. Construction follows with a share of nearly 20%, driven by the use of plastics in pipes, insulation materials, profiles, and coatings. The automotive sector represents around 10% of total plastic usage, where plastics contribute significantly to vehicle weight reduction and fuel efficiency. Electrical and electronic applications account for approximately 6–7%, while the remaining share is distributed among household goods, agriculture, and medical applications (Plastics Europe, 2023).

The plastic sector in Turkey is highly concentrated geographically and industrially. Approximately 70% of plastic processing enterprises are located in and around Istanbul. Domestic manufacturers supply nearly 80–90% of the processing machinery used in the sector, indicating a strong local production capability. Turkey's plastic processing industry is largely oriented toward packaging, construction materials, and household products. Despite high production capacity, recycling activities remain limited, and recycled plastics account for only a small fraction of total plastic consumption. Existing recycling operations are mainly focused on widely used polymers such as polyethylene and polypropylene, while engineering plastics are recycled at much lower rates (PAGEV, 2022).

Global plastic production has increased rapidly over the last decades, reaching approximately 413.8 million tons annually. Polyolefins dominate global production, with polyethylene and polypropylene together accounting for more than 50% of total plastic output. Other major polymers include polyvinyl chloride, polyethylene terephthalate, and polystyrene. Despite increasing awareness, only about 9–10% of global plastic waste is currently recycled, while the majority is disposed of through landfilling or incineration. This imbalance between production and recycling highlights the growing environmental burden associated with plastic materials (Plastics Europe, 2023). World plastic production and world plastic production by plastic type are given in Figure 1 and Figure 2 respectively.

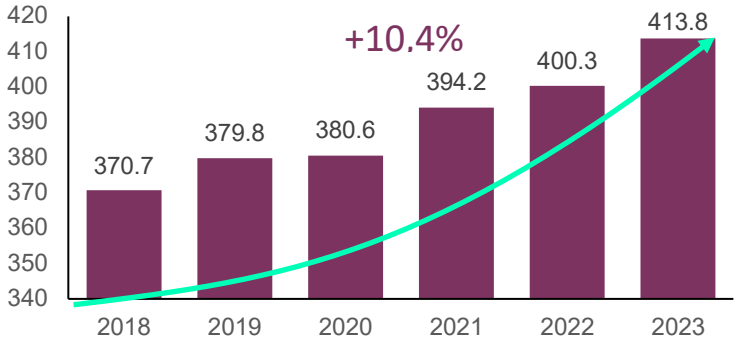

Figure 1. World plastic production

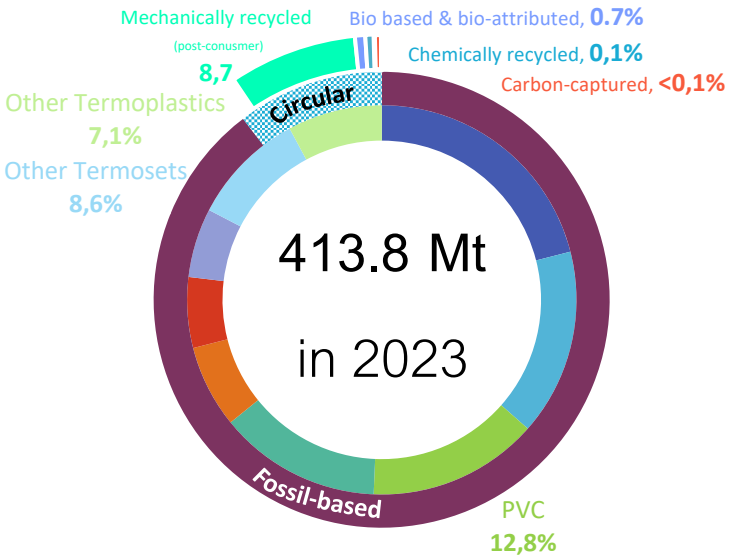

Figure 2. World plastic production by plastic type

Future projections indicate a significant increase in plastic production and consumption. According to international outlooks, global plastic production is expected to nearly triple by 2060 if current trends continue. By this time, annual consumption of polypropylene is projected to reach approximately 195 million tons, while high-density polyethylene consumption is expected to increase to around 165 million tons. Engineering plastics such as acrylonitrile–butadiene–styrene is projected to reach consumption levels of approximately 10 million tons. Without substantial improvements in recycling technologies and circular economy practices, global plastic waste generation is expected to increase proportionally, intensifying environmental pressures worldwide (OECD, 2022). Figure 3 shows baseline scenario of plastic use by polymer and application.

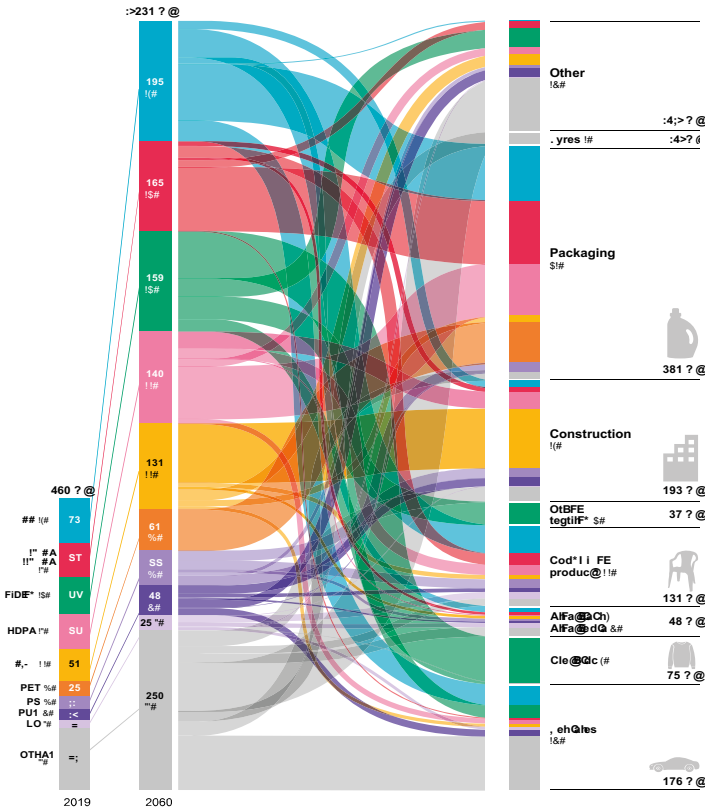

Figure 3. Baseline scenario of plastic use by polymer and application

Plastic waste recycling consists of a sequence of interconnected stages in which each step directly influences the overall efficiency and final product quality. The recycling chain typically includes collection, sorting, size reduction, washing, separation, and reprocessing stages, and the effectiveness of sorting operations depends strongly on the composition and characteristics of the collected plastic waste stream (Serrantini and Bonifazi, 2019).

Collection strategies vary according to waste sources and may involve source-separated plastic waste or mixed municipal solid waste streams. Depending on the collection method, plastic waste can be classified as mono-material or multi-material, which significantly affects subsequent sorting requirements. Sorting operations are generally categorized as sorting at the source, sorting during collection, and sorting at centralized facilities, where a combination of manual, mechanical, and automated techniques may be employed to reduce contamination levels (Serrantini and Bonifazi, 2019).

Following initial sorting, screening operations are applied to remove fine particles such as glass fragments and stones, while size reduction is commonly performed by cutting or shredding plastics into flakes with sizes typically ranging between 5 and 10 mm. Material and polymer sorting stages aim to remove non-plastic contaminants and separate different polymer types based on their physical and physicochemical properties, including size, shape, density, color, and chemical composition (Serrantini and Bonifazi, 2019).

Several separation technologies are applied in plastic waste processing. Dry gravity separation methods, such as air classifiers and ballistic separators, exploit differences in particle mass, shape, and aerodynamic behavior. Wet gravity separation techniques, including sink–float separation, jigging, and hydrocycloning, utilize density differences between polymers; however, their effectiveness is limited when polymers have similar density values or when additives and surface contamination alter apparent density. Electrostatic separation is based on triboelectric charging behavior of polymers, while magnetic density separation enables the separation of plastics with very close density values by using magnetic fluids. Sensor-based sorting systems rely on optical or spectroscopic identification of materials and are mainly effective for large, well-defined plastic products or color-based separation of mono-material streams (Serrantini and Bonifazi, 2019).

Materials' various surface wettability characteristics serve as the foundation for flotation operations. In theory, flotation functions very similarly to a sink and float procedure, in which the basis of the separation is the density characteristics of the materials relative to the medium in which they are deposited. A centrifugal field is sometimes used to improve separation. In contrast, flotation involves the introduction of air bubbles as a "carrier" in a liquid media, often water, which causes hydrophobic particles to float and stick to the bubbles while hydrophilic ones sink. Theoretically, this method may be used to sort waste polymers commercially based on surface plastic properties. Using suitable collectors, conditioners, and flotation cell operating parameters (such as air flow rate and agitation) may improve or decrease plastic surfaces' hydrophobic or hydrophilic properties. Plastic flotation often occurs in alkaline environments. Hydrophilic polymers sink to the bottom of the cell, whereas hydrophobic polymers are retrieved after flotation. Even though this method is well-known and, in theory, very effective, it is not commonly used for three main reasons: (1) it is a wet method, meaning that water must be recovered and processed before being used again because of the presence of contaminants and reagents; (2) the surface status of the polymer (i.e., the presence of contaminants or dirtiness and/or physical or chemical alteration) can significantly affect floatability; and (3) there is a significant variation in the composition of waste plastics feed. Mixed polyolefins (MPO), PS, PVC, PET, and PC may all be separated using flotation (Serrantini and Bonifazi, 2019, p.21).

2. MATERIAL AND METHODS

2.1. Material

Arçelik A.Ş. provided virgin Polypropylene (PP), high density polyethylene (HDPE) and acrylonitrile butadiene styrene (ABS) granules with particle sizes of 3.36 mm and 2 mm, respectively. Despite being white, the two polyolefins have different hues. Compared to HDPE, PP is much more translucent. Additionally, the cylindrical shape of HDPE granules and the spherical shape of PP granules make it easier to visually identify the experimental products. ABS, compared to HDPE and PP, has a more yellowish colour and can be visually distinguished from them.

Sodium hydroxide as a wetting agent, NaOH and HCl as pH modifiers, MIBC (Dow Chemical Company, USA) as a frother, Triton X-100 (Dow Chemical Company, USA), diethylene glycol dibenzoate (DIB) (from Sigma Aldrich Corp., USA), sodium dodecyl sulfate (SDS) (from Sigma Aldrich Corp., USA), lignin alkaline (LA) (from Sigma Aldrich Corp., USA), and calcium lignosulfonate (CaLS) (from Sigma Aldrich Corp., USA) as plasticizers. All of the trials were conducted using distilled water.

2.2. Method

Prior to the flotation experiments conducted to investigate the interactions between the plastics and reagents mentioned in the Materials section, a series of surface chemistry studies were carried out. These studies included measurements of the surface tension of the reagents, determination of the zeta potential values of pure plastics, and contact angle measurements between the reagents and pure plastic plates with identical surface characteristics.

In the surface tension studies were performed Krüss K-8 model with Ring Method and surface tension values of each reagent were measured at pH values of 4, 6, 8, and 10 over a concentration range from 10^{-7} to 10^{0} M, and the corresponding critical micelle concentration values were determined. Based on the surface tension results, zeta potential measurements of pre-ground pure plastics in the presence of the reagents were subsequently performed at five different pH values (2, 4, 6, 8, and 10).

In the subsequent micro-flotation studies, an alkaline treatment was applied to 1 g of pure plastic using 20 cc of NaOH solution corresponding to a 5% pulp solid ratio prior to micro-flotation. After the alkaline treatment, micro-flotation experiments were carried out to determine the separation efficiency of the reagents for the plastics.

3. RESULTS AND DISCUSSION

In this study, micro-flotation experiments were conducted to investigate the interactions between plastics and the selected reagents/plasticizers as a function of molarity. The experimental conditions employed in the micro-flotation tests are presented in Table 1. The results obtained for two of the reagents used in this study, DIB and LA, are illustrated in Figure 4 and Figure 5, respectively.

Table 1. Micro-flotation conditions

DIB	LA
Alkaline Treatment: 5 min with NaOH	Alkaline Treatment: 5 min with NaOH
Conditioning Time: 3 min	Conditioning Time: 3 min
Flotation Time: 3 min	Flotation Time: 3 min
NaOH Treatment: 5 min for conditioning	NaOH Treatment: 5 min for conditioning
pH: 4	pH: 8

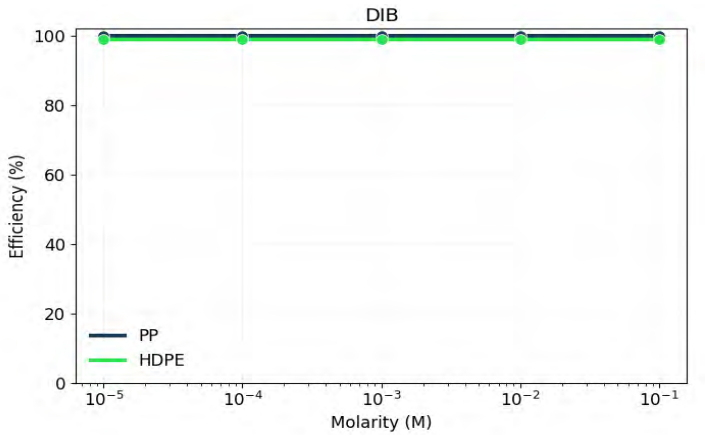

Figure 4. Micro-Flotation test results for DIB

The figure illustrates the effect of DIB concentration on the flotation efficiency of PP and HDPE plastics. As observed in the graph, the flotation efficiencies of both PP and HDPE remain approximately 100% within the molarity range of 10^{-5}–10^{-1} M. This indicates that, within the investigated concentration range, DIB does not exhibit a significant selective or depressant effect on the surfaces of the plastics.

Despite the increase in DIB concentration, no noticeable decrease or increase in flotation efficiency is observed, suggesting that the reagent does not establish a strong chemical interaction with the plastic surfaces. In other words, the adsorption of DIB molecules onto the surfaces of PP and HDPE appears to be limited or insufficient to induce a surface modification that could alter their flotation behavior. Therefore, it can be concluded that within the studied molarity range, DIB does not cause any significant change in the surface properties of the plastics.

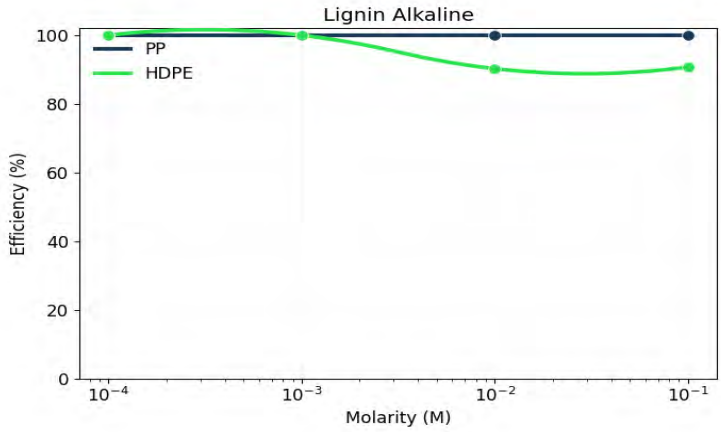

Figure 5. Micro-flotation test results for LA

The figure shows the effect of Lignin Alkaline concentration on the flotation efficiency of PP and HDPE plastics. As observed in the graph, at low molarity values (10^{-4}–10^{-3} M), the flotation efficiencies of both PP and HDPE remain approximately 100%. This indicates that at low lignin concentrations, the reagent does not exert a significant influence on the plastic surfaces.

However, when the lignin alkaline concentration reaches 10^{-2} M, a noticeable decrease in the flotation efficiency of HDPE is observed. While the flotation efficiency of HDPE decreases to approximately 90%, the flotation efficiency of PP remains nearly constant at around 100% across the entire molarity range. This suggests that lignin alkaline interacts more strongly with the HDPE surface. Nevertheless, these results also indicate that the desired separation could not be achieved as effectively as in the case of DIB.

According to a study by Kangal and Üçerler (2018), selective flotation separation of PP and HDPE was achieved by modifying the polymers' surfaces with calcium lignosulfonate (CaLS) as a wetting agent. When CaLS was applied at 500 g/t under alkaline conditions, HDPE showed a stronger tendency toward surface wetting than PP, resulting in a more hydrophilic surface. This behavior caused HDPE particles to remain in the flotation pulp, while PP particles preferentially attached to air bubbles and reported to the froth phase.

The separation selectivity was further enhanced by alkaline conditioning with sodium hydroxide prior to flotation. Conditioning with 50 kg/t NaOH for 5 minutes at room temperature effectively altered the surface properties of HDPE without significantly affecting PP. Flotation experiments carried out at pH 9 and using 500 g/t methyl isobutyl carbinol (MIBC) as a frother resulted in an efficient separation, where PP was recovered as the floated product and HDPE as the sunken product. Under these optimized conditions, both polymers were obtained with high purities (98.2%) and recovery rates (99.8%), demonstrating the effectiveness of CaLS-assisted selective flotation for PP–HDPE systems (2018).

4. CONCLUSION

In this study, the interactions between plastics and selected reagents were investigated through micro-flotation experiments in order to evaluate their potential for selective plastic separation. The results indicated that DIB did not produce any noticeable effect on the flotation behavior of PP and HDPE. Both polymers-maintained flotation efficiencies close to 100% throughout the investigated molarity range, suggesting that DIB does not significantly alter the surface properties of these plastics under the tested conditions.

Similarly, lignin alkaline (LA) showed only a limited influence on the flotation responses of the plastics. Although a slight decrease in the flotation efficiency of HDPE was observed at higher molarity values, the overall flotation behavior of both PP and HDPE remained largely unchanged. This indicates that LA does not provide sufficient selectivity to achieve an effective separation between these two polymers under the studied conditions.

Previous studies have reported that more effective selective separation between PP and HDPE can be achieved using calcium lignosulfonate (CaLS), which modifies the surface wettability of the polymers and enhances flotation selectivity. Therefore, the findings of this study highlight the importance of reagent selection in flotation-based plastic recycling systems and suggest that further research should focus on identifying reagents capable of producing stronger surface modification and higher separation selectivity.

REFERENCES

Alp, K., (2003), Plastik malzemeler ve uygulamaları, Teknik Yayıncılık.

Kangal, M. O., Üçerler, Z., (2018) “Recycling of virgin and post-consumer polypropylene and high-density polyethylene”, International Polymer Processing, 33 (2) 268-275.

Mills, N. J., Gilchrist, A., Jenkins, M., (2020), Plastics, Microstructure, Properties and Applications. Elsevier.

OECD, (2022), Global plastics outlook: Economic drivers, environmental impacts and policy options. OECD Publishing. https://doi.org/10.1787/de747aef-en

PAGEV, (2022), Türk plastik sanayi sektör raporu, Turkish Plastics Industry Foundation.

Plastics Europe, (2023), Plastics – the facts 2023. Plastics Europe Association.

Serrantini, M., Bonifazi, G., (2019), Recycling of Plastic Waste, Separation Technologies and Strategies, Springer.

Sevencan, F., Vaizoğlu, S., (2007) “Çevresel açıdan plastik atıklar ve insan sağlığı”, Toplum ve Hekim, 22 (4) 287–292.

COMPARATIVE PERFORMANCE OF NaCN AND SMBS DEPRESSANTS IN THE FLOTATION OF THE UZBEKISTAN Pb–Zn ORE

Sinem DOGAN[1,*], Mert SARIKAYA[1,2]

[1]*Esan Eczacıbaşı Industrial Raw Materials Co., R&D Center, Maltepe, Istanbul, Turkey*
[2]*Istanbul Technical University, Chemical and Metallurgical Engineering Faculty, Chemical Engineering Department, 34469, Maslak, Istanbul, TÜRKİYE*
**Corresponding author: sinem.dogan@esan.com.tr*

A B S T R A C T

In the Pb–Zn ore from Uzbekistan, elevated Zn reporting to the Pb circuit (pre-activation) and fines entrainment reduce Pb–Zn selectivity, making depressant choice critical. This study compares two depressant strategies via locked-cycle tests (LCT): $ZnSO_4$+SMBS (cyanide-free) and $ZnSO_4$+NaCN. Both were evaluated at a primary grind of P80≈75 µm, with pH≈9–9.5 in the Pb circuit and pH≈11–11.5 in the Zn circuit; in LCT-1, the Zn rougher concentrate was reground to P80≈10 µm and cleaned in three stages, while in LCT-2, recycling Pb Cleaner-1 tails back to the Pb rougher improved circuit stability. LCT results show that the NaCN route achieved 60.5% Pb at 91.5% recovery with Zn→Pb transfer reduced to 14.9%, whereas the SMBS route yielded 50.5% Pb at 83.0% recovery with Zn→Pb at 20.5%. In both routes, the Zn concentrate grade target (>45% Zn) was satisfied, with NaCN providing higher Zn recovery (73.8%) relative to SMBS (69.9%). Overall, $ZnSO_4$+NaCN demonstrated superior selectivity and circuit stability, while SMBS, despite being cyanide-free, required more stringent dosage control and stability management to reach comparable metallurgical performance.

Key words: *Pb–Zn flotation, pre-activation, entrainment, NaCN, SMBS, locked-cycle test, selectivity*

1. INTRODUCTION

Lead–zinc sulphide ores typically require sequential flotation to produce saleable galena and sphalerite rich concentrates, with process selectivity governed by mineral liberation, pulp chemistry, and the effectiveness of depressant/activator schemes. In carbonate hosted systems, fines generation and fines entrainment can further compromise separation efficiency, elevating the transfer of Zn into the Pb circuit and Pb into the Zn circuit. These factors make depressant selection and circuit configuration decisive for achieving concentrate quality at acceptable recoveries.

Among the reagents employed to improve flotation selectivity, sodium metabisulfite (SMBS) has received considerable attention as a depressant for pyrite and sphalerite, acting primarily by modifying mineral surface chemistry through redox reactions under mildly acidic to neutral pH conditions. In the case of pyrite, SMBS facilitates the conversion of surface ferrous iron to ferric species, leading to the formation of hydrophilic iron hydroxide layers that inhibit collector adsorption (Corona-Arroyo et al., 2024). Karimi et al. (2026) investigated the effects of treated wastewater on Pb-Zn sulfide flotation, reporting that microorganisms in treated wastewater biodegraded the SEX collector and reduced galena recovery significantly, while SMBS was employed alongside $ZnSO_4$ as a sphalerite and pyrite depressant. Gomes et al. (2025) compared SMBS and quebracho as pyrite depressants in Pb-Zn sulfide flotation, demonstrating that SMBS at 200 g/t achieved 91.73% Zn recovery while significantly reducing galena carryover into the zinc circuit, with Pb recovery in the sphalerite stage declining from 8.79% to 1.33%, confirming SMBS's effectiveness in Pb-Zn selectivity. Namgar et al. (2025) demonstrated that SMBS at its optimal dosage of 400 g/t achieved a lead recovery of 59.5%, approximately 2.8% higher than cyanide, yet proved less effective in depressing iron and zinc at this level, with higher dosages of 1000 g/t significantly depressing both unwanted minerals

at the expense of lead recovery, highlighting a trade-off between selectivity and metallurgical efficiency. More recently, Zhang et al. (2025) introduced an alkali-free zinc beneficiation technology combining the novel collector MPECT with NaMBS as a pyrite depressant under neutral pH conditions, where NaMBS effectively depressed pyrite while leaving sphalerite recovery unaffected above 90%, and the technology was successfully industrialized at the Huangshaping Lead-Zinc Concentrator, improving Zn recovery from 93.03% to 93.54% while reducing reagent costs by 208,000 USD annually.

The present study focuses on a Pb–Zn ore from Uzbekistan, where test work consistently indicated elevated Zn reporting to the Pb rougher (pre-activation) alongside entrainment effects that reduce Pb–Zn selectivity. To address this, two depressant strategies were benchmarked across a comprehensive program of rougher/cleaner tests and locked cycle tests (LCT): a cyanide-free $ZnSO_4$+SMBS route and a $ZnSO_4$+NaCN route. Both routes were investigated at a primary grind of P80 ≈ 75 µm, with pH ≈ 9–9.5 in the Pb circuit and pH ≈ 11–11.5 in the Zn circuit; the SMBS route incorporated regrinding of the Zn rougher concentrate to P80 ≈ 10 µm, whereas the NaCN route implemented Pb Cleaner 1 tails recycle to the Pb rougher to enhance circuit stability. Locked cycle testing was selected to approximate steady-state plant behaviour, allowing a realistic assessment of metal deportment, cross-contamination between circuits, and reagent strategy robustness under recycle conditions. Within this framework, the study quantifies comparative impacts on Pb grade/recovery, Zn grade/recovery, and cross-transfer metrics (Zn→Pb and Pb→Zn), and distils practical guidance on flowsheet configuration for a cyanide-free option versus a conventional cyanide-bearing option.

2. MATERIAL AND METHODS

2.1. Materials

Flotation Tests

Batch flotation tests were conducted using a Denver flotation machine equipped with a 4.5 L cell and tap water. Chalcopyrite and sphalerite were floated separately at approximately 30% solids, with an impeller speed of 1000 rpm and an air flow rate of 4 dm³/min. The pulp pH was adjusted to 11.5 using lime and monitored with a WTW pH meter (Model 7310). Flotation recovery (R) was calculated using the standard equation based on feed (f), concentrate (c), and tailings (t) grades, providing an accurate measure of flotation efficiency.

$$R = 100 * \frac{c(f-t)}{f(c-t)} \qquad \textbf{(Eq.1)}$$

Bond Ball Work Index (BBWi) testing classified the ore as soft with 7.2 kWh/t, implying low energy demand to reach target sizes. Grind calibration indicated P80 ≈ 75 µm as a suitable primary grind for both routes. In the SMBS route, the Zn rougher concentrate was reground to P80 ≈ 10 µm before cleaning to improve liberation and reduce Zn losses. The Pb circuit was operated at pH ≈ 9–9.5, while the Zn circuit was maintained at pH ≈ 11–11.5 using lime. Aerophine 3418A was used as collector in the Pb circuit, and xanthate-type collectors (SEX/SIPX/PEX) were employed in the Zn circuit, with MIBC used as frother throughout.

2.2. Method

Two depressant routes were evaluated in parallel. In the first route ($ZnSO_4$+SMBS), $ZnSO_4$ at 1500 g/t was added to depress sphalerite in the Pb stage, and SMBS was escalated from 500

to 3750 g/t across the Pb cleaners to curb Zn carryover into the Pb concentrate. The performance of SMBS at varying dosages was evaluated and compared against NaCN at 50 g/t as the reference depressant to minimize sphalerite activation and reduce Zn reporting to the Pb concentrate. Na_2S at 100 g/t was subsequently added to sulphidise mineral surfaces, with a conditioning time of 5 minutes applied for each reagent. PAX at 50 g/t and MIBC at 10 g/t were then added as collector and frother, respectively, and three-stage flotation was performed at pH 9 to obtain the Pb concentrate. In this route, the Zn rougher concentrate was reground to P80 ≈ 10 µm prior to three-stage Zn cleaning.

In the second route ($ZnSO_4$+NaCN), NaCN and $ZnSO_4$ were applied in the Pb cleaners as a cyanide-bearing depressant strategy, with Pb Cleaner-1 tails recycled to the Pb rougher feed to enhance circuit stability and selectivity.

In the Zn circuit, the pulp pH was raised to 11.5 using lime, after which $CuSO_4$ at 1500 g/t was added to activate sphalerite, followed by sodium silicate at 500 g/t to depress silicate minerals, with a conditioning time of 5 minutes applied for each reagent. PEX at 50 g/t and MIBC at 10 g/t were then added as collector and frother, respectively, and three-stage flotation was carried out to recover the Zn concentrate.

Batch rougher/cleaner tests established kinetics, reagent windows, and cleaner configurations per route, while open-circuit tests (OCT) refined regrind sizes and cleaner dosages. These operating envelopes fed directly into the locked cycle test (LCT) design. Seven-cycle LCTs were executed per route, with recycle streams and process water carried forward between cycles. Mass and elemental closure stabilised by approximately cycle 3, with cycles 5–6 used for final, wet-chemistry-confirmed reporting. LCTs quantified Pb grade/recovery, Zn grade/recovery, and cross-contamination metrics (Zn→Pb and Pb→Zn) under realistic recycle conditions, enabling a robust side-by-side comparison of the cyanide-free and cyanide-bearing depressant routes.

3. RESULTS AND DISCUSSION

Mineral Characterization

The composite Pb–Zn ore from Uzbekistan was characterized by triplicate ICP/AA head assays and C–S speciation (Table 1). The feed averaged 3.98% Pb, 4.18% Zn, and a carbonate-rich gangue (Ba, Ca, Mg), with ~99.8% of S as sulphide and ~99.7% of C as carbonate, indicating a dolomitic host and negligible organic carbon interference in flotation.

QEMSCAN/polished sections identified galena (PbS) and sphalerite (ZnS) as the main valuables with barite/dolomite-dominant gangue. Galena showed moderate good liberation in −75 + 20 µm, while sphalerite liberated better at <20 µm; barite displayed ~78% free/liberated particles trends consistent with observed size-by-assay behavior (finer Pb deportment; Zn broadly distributed by size).

Table 1. Head assay and speciation

Metric	Value
Pb (%)	3.98
Zn (%)	4.18
Ag (g/t)	10.7
Fe (%)	1.15
Ba (%)	11.8
Ca (%)	15.77

Mg (%)	7.34
C (total / carbonate / organic) (%)	7.64 / 7.61 / 0.03
S (total / sulphide / sulphate) (%)	5.52 / 5.51 / 0.01

Effect of depressant type on Pb circuit performance

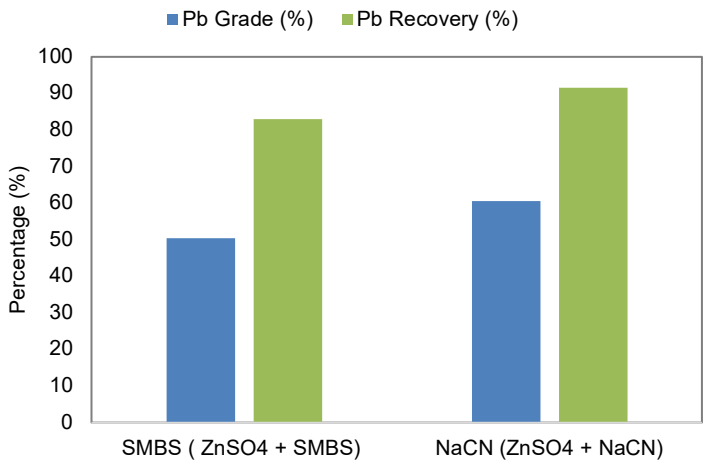

Figure 1. Pb Performance (grade / recovery)

The $ZnSO_4$+NaCN route achieved a Pb grade of approximately 60.5% and a Pb recovery of approximately 91.5%, outperforming the $ZnSO_4$+SMBS route which yielded a Pb grade of approximately 51% and a Pb recovery of approximately 85% (Fig 1.). Although NaCN demonstrated superior selectivity in the Pb circuit, its well-known environmental and safety concerns make it a less desirable option in modern flotation practice. The SMBS route, while falling short of the NaCN benchmark in terms of both grade and recovery, nonetheless demonstrated a meaningful depressant effect on sphalerite, indicating its potential as a cyanide-free alternative. These results suggest that with further optimization of SMBS dosage and circuit configuration, the performance gap between the two routes may be narrowed.

Effect of depressant type on Zn circuit performance

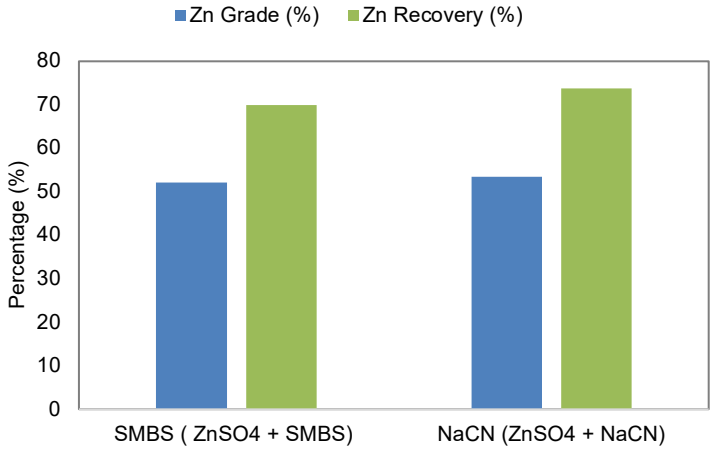

Figure 2. Zn Performance (grade / recovery)

The Zn grade/recovery comparison shows that both routes met the target Zn concentrate grade of above 45%, with the $ZnSO_4$+SMBS route achieving approximately 52% Zn grade and 70% Zn recovery, and the $ZnSO_4$+NaCN route yielding approximately 54% Zn grade and 74% Zn recovery (Fig 2.). Although the difference in Zn grade between the two routes is relatively modest, the NaCN route delivered a notably higher Zn recovery of 73.8% alongside lower Pb contamination in the Zn concentrate (Pb→Zn = 4.4%), reflecting a cleaner Zn circuit feed and more effective Pb depression downstream. The slightly lower Zn recovery in the SMBS route may be attributed to greater cross-contamination and less selective depression in the Pb circuit, which in turn affects the quality of the feed entering the Zn circuit. Nevertheless, the fact that both routes achieved the Zn grade target underlines the viability of the cyanide-free SMBS route, particularly when concentrate grade is the primary criterion.

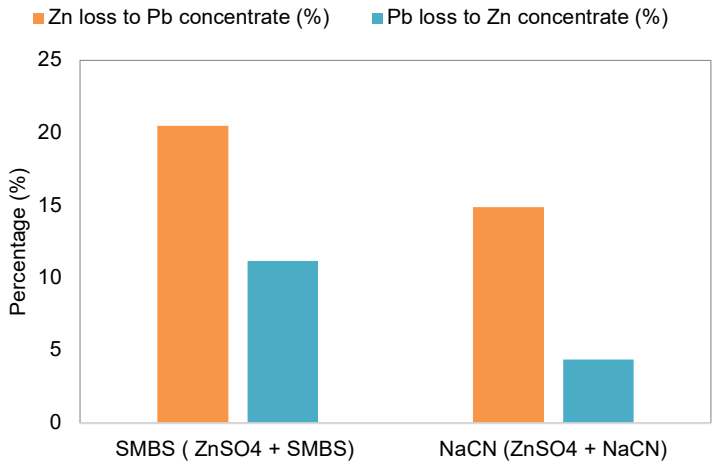

Figure 3. Cross-Contamination (Zn→Pb, Pb→Zn)

The cross-contamination results clearly demonstrate the superior selectivity of the NaCN route over the SMBS route under recycle conditions. The $ZnSO_4$+NaCN route yielded significantly lower Zn loss to the Pb concentrate (Zn→Pb = 14.9%) and Pb loss to the Zn concentrate (Pb→Zn = 4.4%), whereas the $ZnSO_4$+SMBS route exhibited notably higher cross-transfer in both directions, with Zn→Pb reaching 20.5% and Pb→Zn at 11.2% (Fig 3.). The particularly large difference in Pb→Zn contamination between the two routes suggests that the SMBS route was less effective in preventing galena from reporting to the Zn circuit, which directly contributed to the lower Pb grade observed in the Pb concentrate. While the NaCN route controls cross-migration more effectively, the SMBS route still presents a workable level of selectivity, and the elevated cross-contamination values may be addressable through further optimization of depressant dosage, regrind targets, and cleaner configurations in future test work.

4. CONCLUSION

This study evaluates the depressant performance and flotation response of a Pb–Zn ore from Uzbekistan under two alternative flowsheets: $ZnSO_4$+SMBS (cyanide-free) and $ZnSO_4$+NaCN.

Mineralogical characterization indicates that galena shows moderate–good liberation in the −75 + 20 µm fraction, while sphalerite liberates predominantly at finer sizes (<20 µm), with fines entrainment and pre-activation contributing to Zn reporting to the Pb circuit. These mineralogical characteristics underline the importance of depressant selection and regrind strategy in achieving acceptable circuit selectivity.

Flotation tests carried out under the $ZnSO_4$+SMBS route produced a Pb concentrate grading 50.5% Pb at 83.0% recovery, while the Zn concentrate reached 52.1% Zn with 69.9% recovery. Under the $ZnSO_4$+NaCN route, improved selectivity was achieved, yielding a Pb concentrate containing 60.5% Pb at 91.5% recovery, and a Zn concentrate with 53.4% Zn at 73.8% recovery. Cross-contamination between circuits was significantly reduced in the NaCN flowsheet (Zn→Pb = 14.9%, Pb→Zn = 4.4%) compared with the SMBS flowsheet (Zn→Pb = 20.5%, Pb→Zn = 11.2%), confirming stronger and more stable depression in the Pb cleaners.

While the $ZnSO_4$+NaCN route demonstrated superior metallurgical performance across all key metrics, its environmental and safety implications associated with cyanide use remain a significant concern for industrial application. In contrast, the $ZnSO_4$+SMBS route, despite delivering comparatively lower Pb grade and recovery, presents a more environmentally responsible alternative with no toxic reagent handling requirements. Importantly, both routes met the Zn concentrate grade target of above 45%, demonstrating the fundamental viability of the cyanide-free approach. The performance gap observed between the two routes is considered addressable through further optimisation of SMBS dosage escalation across cleaners, regrind configuration, and cleaner circuit design. Overall, the results position the $ZnSO_4$+SMBS route as a promising cyanide-free alternative for this ore type, warranting continued development towards pilot-scale validation.

REFERENCES

Corona-Arroyo, M. A., López-Frías, K., Solorzano, K., Echeveste, C., Salazar-Hernandez, M. M., Pineda-Urbina, K., Yang, B., (2024) “Pyrite depression by sodium metabisulfite and dextrin with xanthates: contact angle, floatability, zeta potential and IR spectroscopy studies”, Physicochemical Problems of Mineral Processing, 60 (6) 1–13.

Da Costa Gomes, P. V., Nogueira, S. D. C. S., Fonseca, M. E. R., Cipriano, P. P. G., Pereira, C. A., Nogueira, F. C., (2025) “Influence of pyrite depressant reagents on the flotation efficiency of lead and zinc sulfides”, Tecnologia em Metalurgia, Materiais e Mineração, 22.

Karimi, M., Zarei, M., Faramarzpour, A., Chelgani, S. C., (2026) “The impacts of treated wastewater on Pb-Zn sulfide flotation performance and potential improvement”, Water Resources and Industry 100349.

Namgar, S. M., Foroutan, A., Abdollahzadeh, A. A., Zinjanab, M. T., (2025) “Eco-friendly alternatives to cyanide in the flotation of lead and zinc ore”, Canadian Metallurgical Quarterly, 1-17.

Zhang, H., Sun, W., Wang, F., Xie, Z., Zeng, J., Hu, Z., Lin, S., (2025) “Application of a new reagent O-(2-methylpropyl) N-prop-2-enylcarbamothioate in industrial purification of zinc sulfides: Practice study”, Minerals Engineering, 232 109482.

EFFECT OF PULP AERATION ON LEAD-ZINC FLOTATION PERFORMANCE

Irmak DEMIREL*, Şükriye Beste AYDIN

Istanbul Technical University, Mining Faculty, Mineral Processing Engineering Department, 34469, Maslak, Istanbul, TÜRKİYE
**Corresponding author: demireli19@itu.edu.tr*

A B S T R A C T

Lead and zinc are important base metals with extensive industrial applications and strategic importance, particularly for the metallurgy, chemical, energy, and manufacturing sectors. Therefore, the economic evaluation of lead–zinc ores is a significant area of study in mineral processing and beneficiation. Flotation is the most widely used method for the beneficiation of sulfide lead and zinc minerals due to its high selectivity and efficiency. However, flotation performance is influenced by several factors, including the mineralogical structure of the ore, surface oxidation, reagents, and operating conditions. This study investigates the effects of pulp aeration and depressant amount on the flotation behavior of a complex lead–zinc ore obtained from the Esan Balya region. Within the scope of the study, the influence of the amount of $ZnSO_4$ (300 and 450 g/t), used as a sphalerite depressant, on lead and zinc recoveries was comparatively evaluated under aerated and non-aerated conditions. The results showed that increasing the amount of $ZnSO_4$ enhanced sphalerite depression and improved the selectivity of Pb–Zn separation. Pulp aeration exhibited a limited influence on Pb recovery, showing a slight increase at lower $ZnSO_4$ amounts but a decrease at higher amounts. Similarly, Zn recovery slightly decreased under aerated conditions. These findings indicate that flotation performance is primarily controlled by the amount of depressant, while pulp aeration may modify flotation behavior through changes in pulp chemistry and mineral surface conditions.

Key words: *Lead–Zinc, flotation, pulp aeration*

1. INTRODUCTION

Sulphide lead–zinc ores are among the most common and economically important types of metallic ores found in the Earth's crust. Lead and zinc are important base metals widely used in many industrial applications such as battery production, galvanization, alloy manufacturing, and construction materials. Due to the growing global demand for these metals, the efficient processing of lead–zinc ores have become increasingly important. These ores are generally located in vein-type or massive sulfide deposits formed as a result of hydrothermal processes. Their primary minerals are galena (PbS) and sphalerite (ZnS), and they may also occur together with associated minerals such as pyrite (FeS_2), chalcopyrite ($CuFeS_2$), and marcasite. These ores are separated and upgraded using physicochemical beneficiation techniques such as flotation, after which they are converted into their metallic forms. In the flotation process, sulfide minerals are concentrated by attaching to air bubbles and collecting in the froth based on their surface properties, while the remaining gangue minerals are separated as tailings (Wills and Finch, 2016). Additionally, sulfide lead–zinc ores are of strategic importance because they may also contain valuable metals such as gold and silver.

During flotation, galena is typically floated easily using xanthate-type collectors within a pH range of 8–9. Although zinc should not generally float with xanthate-type collectors, dissolved ions in the pulp (such as Pb++, Cu++) can activate and cause it to float. To depress zinc, zinc sulfate $ZnSO_4$ is commonly utilized. Furthermore, sodium metabisulfite can be used in conjunction with zinc sulfate to ensure the depression of both zinc and pyrite minerals. Following the depression of sphalerite and pyrite, collectors such as ethyl xanthate (KEX) is employed in galena flotation (Wills, and Finch, 2016; Atak, 2017).

Sphalerite is generally floated in the pH range of 10–11 after being activated with copper sulfate $CuSO_4$ (Fuerstenau, 2007). Since copper sulfate also activates pyrite, it is beneficial to maintain a very high alkalinity (pH 10–12). The adsorption of Cu^{2+} ions onto the sphalerite surface forms a CuS layer, which reacts with xanthate to render the surface active. The activation process required for sphalerite flotation begins with the adsorption of copper ions onto the surface, making it hydrophobic and accessible for interaction with collectors. As the activation of zinc is a relatively slow reaction, a conditioning time of 5–30 minutes is provided (Bulatovic, 2007; Atak, 2017). During this process, pH control is of paramount importance; high pH values aid in the depression of other minerals like galena while optimizing the activation of sphalerite. Additionally, the ionic composition of the flotation environment, the quality of the process water, and the surface conditions of the minerals resulting from prior treatments can directly influence flotation efficiency (Liu et al., 2013). Therefore, when performing galena-sphalerite separation, experimental conditions must be carefully adjusted, and process parameters must be precisely optimized.

In the study conducted by Ağaçayak et al. (2021), the effect of $ZnSO_4$ addition to the grinding circuit on sphalerite depression was evaluated in terms of lead (Pb) and zinc (Zn) recoveries. Within the scope of the study, the use of the $ZnSO_4$ reagent in different circuits was investigated in order to improve flotation performance. Accordingly, 1000 g/t $ZnSO_4$ was added to both the grinding circuit and the Pb flotation circuit. According to the obtained results, under these conditions a Pb concentrate containing 40.18% Pb with a recovery of 66.40% was achieved. Based on these findings, the amount of 1000 g/t $ZnSO_4$ used in both the grinding circuit and the Pb flotation circuit was determined to provide the optimum conditions for the system.

Pulp aeration is commonly used in flotation systems to increase the dissolved oxygen concentration and regulate the redox conditions of the pulp. The introduction of air into the pulp promotes oxidation reactions at mineral surfaces, which can influence the flotation behavior of sulfide minerals. In some cases, controlled aeration can enhance the recovery of target minerals, while excessive oxidation may lead to surface passivation and reduced flotation efficiency. Although chemical oxidation is a viable method for enhancing the efficiency of reagents, its application is limited by high operational costs and environmental drawbacks. In contrast, pulp aeration has been preferred as a low-cost, controllable, and eco-friendly alternative.

Wang et al. (2023) reported that the traditional high alkaline process (HAP) encounters significant challenges in the beneficiation of pyrrhotite-rich copper sulfide ores, particularly due to the slow flotation rate and limited copper recovery. To overcome this issue, the process was optimized through pulp aeration and lime-assisted grinding. The results demonstrated that pulp aeration increased the dissolved oxygen concentration in the pulp, accelerated chalcopyrite flotation, and improved the Cu recovery from 74.6% to 90.0%. Industrial tests further confirmed that the optimized method was suitable for pyrrhotite-rich ores and increased Cu recovery from 79.8% to 87.7%.

In lead–zinc flotation systems, pulp aeration can influence the selective flotation of galena and sphalerite as well as the depression of unwanted sulfide minerals such as pyrite. Therefore, understanding the role of aeration in controlling pulp chemistry is essential for optimizing flotation performance. The aim of this study is to investigate the effect of pulp aeration on the flotation performance of lead–zinc sulfide minerals.

2. MATERIAL AND METHODS

2.1.Materials

In this study, a sample was obtained from the Esan Balya Lead–Zinc Plant. The obtained sample was sequentially comminuted using jaw, cone, and roll crushers, and the entire material was reduced to −2 mm. After crushing, it was ground at 60% PKO for 5 minutes to reduce it to -0.212 mm using a ball mill for flotation tests. The particle size distribution of the grounded sample was determined using a Malvern Mastersizer 2000 particle size analyzer. As shown in Figure 1, the results indicated a d_{10} value of 2.89 µm, representing the finer fraction of the particle population. In addition, the d_{50} and d_{90} values were measured as 22.15 µm and 84.07 µm, respectively. These results indicate that the sample exhibits a relatively fine particle size distribution, which is considered suitable for subsequent flotation processes. Chemical analysis of the prepared sample was also carried out to determine its elemental composition. The results indicated that the ore contains 4.41% Pb and 4.93% Zn as the main valuable components. The detailed chemical composition of the ore is presented in Table 1**.**

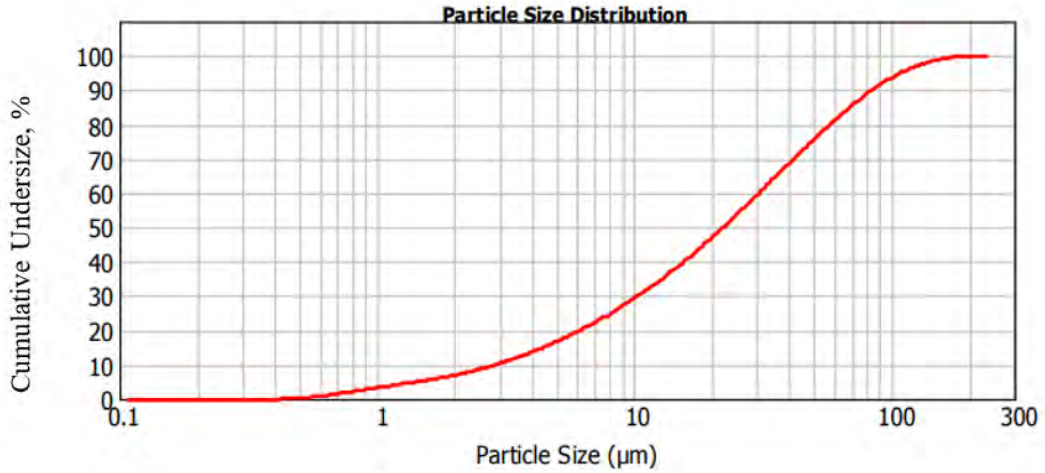

Figure 1. Malvern particle size distribution

Table 1. Chemical composition of the sample

Elements	Pb, %	Zn, %	Cu, %	Fe, %	S, %	As, %	Ag, ppm	Au, ppm
Content	4.41	4.93	0.25	8.11	13.84	0.12	86.0	0.15

2.2.Method

The types and number of depressants, activators, and collectors used in the flotation tests are the same as the test conditions applied in the Esan Lead-Zinc Enrichment Circuit. The tests were conducted using 200 g of the ground sample. A Denver D12 model flotation machine was used with a 1 L flotation cell at 1200 rpm. $ZnSO_4$ as the zinc depressant, Na_2SiO_3 as the silicate depressant, $FeSO_4$ as the pyrite depressant, and $CuSO_4$ as the zinc activator were used in the experiments. KEX (Galen Flotation) and KAX (Zinc Flotation) were added as collectors. MIBC was used in Pb-Zn circuit as frother. Depressants and activators were prepared at 10%, while collectors and frothers were prepared at 1%. The lead flotation stage was carried out at pH 10, whereas the zinc flotation stage was performed at pH 12. Lime was used as a pH adjuster.

The flotation test was conducted as a single-stage process. First, during lead flotation, $ZnSO_4$, Na_2SiO_3, and $FeSO_4$ were added sequentially, with a conditioning time of 5 minutes between each addition. Then KEX was added, followed by an additional 3 minutes of conditioning. Finally, MIBC was added, and froth was collected for 3 minutes.

In the zinc circuit, $CuSO_4$ and Na_2SiO_3 were added sequentially, with a 5-minute conditioning period between additions. Then, KAX was added and conditioned for 3 minutes, followed by the addition of MIBC, and the froth was collected for 3 minutes.

3. RESULTS AND DISCUSSION

3.1.Optimization of $ZnSO_4$ Depressant Amount

The aim of this study is to investigate the effects of controlled oxidation created by pulp aeration on the flotation performance of sulfide lead–zinc ores. To evaluate the effect of pulp aeration on flotation efficiency, preliminary experiments were conducted without aeration using different $ZnSO_4$ amounts (300 g/t, 450 g/t, and 600 g/t). The purpose of these tests was not to determine the optimum depressant amount, but rather to establish a reference flotation condition so that the effect of aeration could be more clearly observed. Therefore, the influence of different $ZnSO_4$ amounts on flotation performance was comparatively examined, and the results are presented in Table 2**.**

Table 2. The flotation results of different amounts of $ZnSO_4$

$ZnSO_4$ Amount, g/t	Products	Weight, %	Pb, %		Zn, %	
			C	R	C	R
300	Pb Concentrate	29.3	12.29	83.7	8.68	58.0
	Zn Concentrate	12.1	3.87	10.9	13.91	38.4
	Tailing	58.5	0.40	5.4	0.27	3.6
	Total	100.0	4.31	100.0	4.39	100.0
450	Pb Concentrate	21.4	15.72	76.4	4.46	19.4
	Zn Concentrate	18.8	4.11	17.5	19.96	76.0
	Tailing	59.8	0.45	6.1	0.38	4.6
	Total	100.0	4.41	100.0	4.93	100.0
600	Pb Concentrate	22.7	17.02	87.5	2.11	9.7
	Zn Concentrate	21.3	1.82	8.8	20.57	89.0
	Tailing	56.0	0.29	3.7	0.11	1.2
	Total	100.0	4.41	100.0	4.93	100.0

C: Content, R: Recovery

At a $ZnSO_4$ amount of 300 g/t, the Pb concentrate constituted 29.3 wt.% of the total product, with a Pb content of 12.29% and a Pb recovery of 83.7%. However, a considerable amount of zinc was also recovered in the Pb concentrate, with a Zn recovery of 58.0%, indicating insufficient depression of sphalerite during the lead flotation stage. Consequently, the Zn concentrate exhibited a Zn content of 13.91% with a Zn recovery of 38.4%, suggesting that a significant portion of sphalerite floated together with galena in the lead circuit.
When the $ZnSO_4$ amount was increased to 450 g/t, the separation selectivity between lead and zinc minerals improved significantly. The Pb content increased to 15.72%, while the Pb recovery decreased to 76.4%, indicating the formation of a cleaner lead concentrate. At the same time, the Zn recovery in the Pb concentrate decreased markedly to 19.4%, demonstrating more effective sphalerite depression. As a result, zinc minerals were more efficiently recovered in the zinc flotation stage, producing a Zn concentrate with a Zn content of 19.96% and a Zn recovery of 76.0%.

Further increasing the $ZnSO_4$ amount to 600 g/t resulted in stronger depression of sphalerite during the lead flotation stage. Under these conditions, the Pb content increased to 17.02%,

while the Pb recovery reached 87.5%. In addition, the Zn recovery in the Pb concentrate decreased significantly to 9.7%, indicating a highly selective Pb–Zn separation. Consequently, the Zn concentrate achieved the highest Zn recovery of 89.0% with a Zn content of 20.57%, confirming that a larger proportion of zinc minerals was effectively transferred to the zinc flotation stage.

3.2.Effect of Aeration

In the experiments, the effect of pulp aeration on flotation recovery was investigated. In the Denver D-12 flotation machine, air was supplied to the pulp for 3 minutes by opening the air valve. The aeration valve was then closed, and the pulp remained without aeration for 5 minutes. This 8-minute procedure was defined as one aeration cycle (Grano, 2009). pH adjustment was not performed during the pulp aeration stage. After six aeration cycles, the pulp pH was adjusted to 10 prior to the lead flotation stage, and the flotation tests were subsequently carried out under these conditions. Table 3 shows the flotation results after six aeration cycles were applied to the sample. In the aeration experiments, $ZnSO_4$ amounts of 300 g/t and 450 g/t were used. In contrast, the 600 g/t $ZnSO_4$ amount was not selected for the aerated tests because it already provided a highly selective separation between lead and zinc minerals. Therefore, to more clearly reveal the effect of pulp aeration on flotation performance, this amount was not included in the aeration experiments. A comparison of the results obtained with different amounts of $ZnSO_4$ is presented in Table 3.

Table 3. The effect of aeration at different $ZnSO_4$ amounts.

$ZnSO_4$ Amount, g/t	**Products**	**Weight %**	**Pb, %**		**Zn, %**	
			C	**R**	**C**	**R**
300	Pb Concentrate	34.3	10.80	84.1	8.49	59.2
	Zn Concentrate	19.8	2.38	10.7	9.47	38.0
	Tailing	45.8	0.50	5.2	0.30	2.8
	Total	100.0	4.41	100.0	4.93	100.0
450	Pb Concentrate	17.9	17.10	69.6	6.55	23.8
	Zn Concentrate	15.7	6.46	23.1	22.58	72.1
	Tailing	66.3	0.49	7.4	0.30	4.0
	Total	100.0	4.41	100.0	4.93	100.0

C: Content, R: Recovery

Under aerated conditions with 300 g/t $ZnSO_4$**,** the Pb concentrate represented 34.3 wt.% of the total product, with a Pb content of 10.80% and a Pb recovery of 84.1%**.** However, a considerable amount of zinc was also recovered in the Pb concentrate, with a Zn content of 8.49% and a Zn recovery of 59.2%**.** These results indicate that, under aerated conditions, the relatively low amount of $ZnSO_4$ was insufficient to effectively depress sphalerite, resulting in the flotation of a significant portion of zinc minerals along with galena in the lead circuit. Consequently, the Zn concentrate exhibited relatively poor performance, with a Zn content of 9.47% and a Zn recovery of 38.0%**.**

In contrast, under aerated conditions with 450 g/t $ZnSO_4$, the weight of the Pb concentrate decreased to 17.9 wt.%, while the Pb content increased to 17.10% and the Pb recovery was 69.6%. The most notable observation is the substantial reduction in the amount of zinc reporting to the Pb concentrate, with the Zn recovery decreasing to 23.8%. This behavior can be attributed to the combined effect of the increased $ZnSO_4$ amount enhancing sphalerite depression and the aeration conditions modifying pulp chemistry, thereby influencing separation selectivity. Consequently, the Zn concentrate exhibited a Zn content of 22.58% and

a Zn recovery of 72.1%, indicating that zinc minerals were more effectively recovered in the zinc circuit.

In order to evaluate the effect of pulp aeration on flotation performance, comparative experiments were conducted under aerated and non-aerated conditions at different $ZnSO_4$ amounts the influence of aeration on both Pb and Zn recoveries was investigated to determine its impact on the selectivity of the Pb–Zn flotation process. The results obtained for the Pb and Zn circuits are presented in Figures 4 and 5.

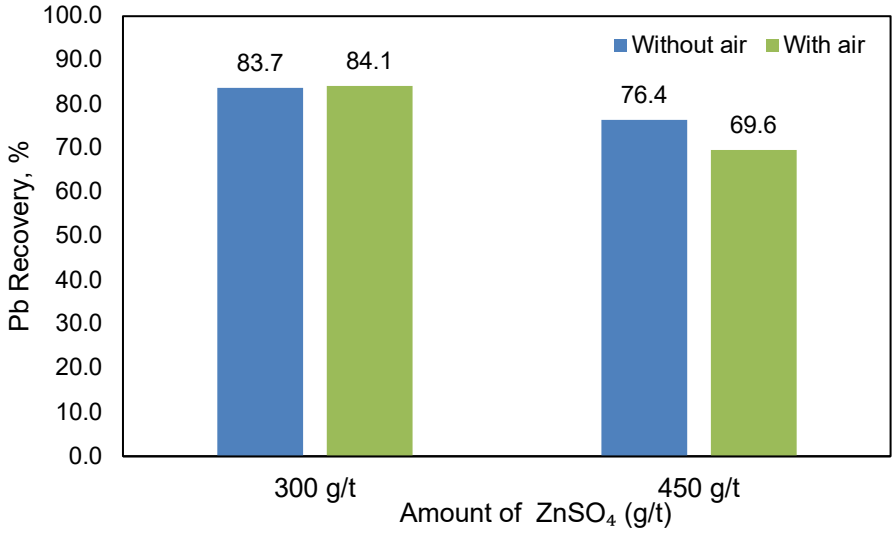

Figure 2. The effect of pulp aeration on the Pb circuit

According to Figure 4, the effect of pulp aeration on lead recovery varies depending on the $ZnSO_4$ amount. At 300 g/t $ZnSO_4$, aeration does not show a significant influence on Pb recovery. In the non-aerated test, Pb recovery was 83.7%, whereas it was obtained as 84.1% under aerated conditions. These values are very close to each other, indicating that pulp aeration does not cause a notable change in galena flotation at lower $ZnSO_4$ amounts. In contrast, at 450 g/t $ZnSO_4$, aeration leads to a slight decrease in Pb recovery. While Pb recovery was 76.4% without aeration, it decreased to 69.6% with aeration. This reduction may be associated with changes in pulp chemistry induced by aeration, which can cause partial oxidation of the galena surface and consequently reduce collector adsorption. Overall, the results indicate that the effect of pulp aeration on Pb recovery is limited at lower $ZnSO_4$ amounts, while a slight decrease in recovery is observed at higher $ZnSO_4$ amounts. This suggests that the influence of aeration in the Pb circuit is more related to flotation selectivity rather than recovery.

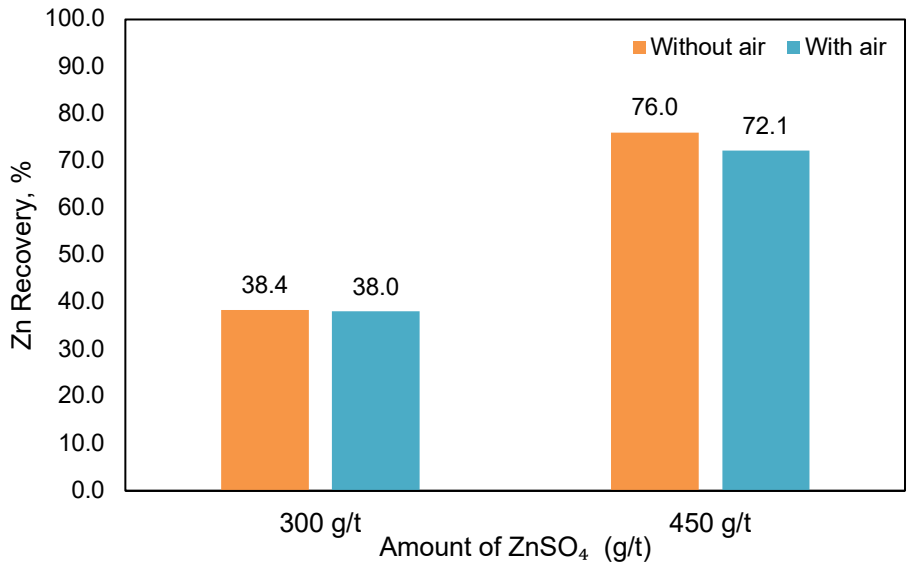

Figure 3. The effect of pulp aeration on the Zn circuit

According to Figure 5, the variation in Zn recovery under aerated and non-aerated conditions depends on the $ZnSO_4$ amount. At 300 g/t $ZnSO_4$, the Zn recovery values obtained with and without aeration are very similar. Zn recovery was 38.4% under non-aerated conditions and 38.0% under aerated conditions. This negligible difference indicates that pulp aeration does not significantly influence sphalerite recovery at lower $ZnSO_4$ amounts. At 450 g/t $ZnSO_4$, a slightly different behavior is observed. Zn recovery reached 76.0% without aeration, whereas it decreased to 72.1% under aerated conditions. The reduction in Zn recovery may be related to aeration-induced changes in pulp chemistry, which can alter mineral surface oxidation states and consequently influence collector adsorption and flotation performance. The results suggest that pulp aeration has a limited influence on Zn recovery at lower $ZnSO_4$ amounts, while a moderate decrease in recovery is observed at higher $ZnSO_4$ amounts. This behavior indicates that aeration can influence sphalerite flotation by altering pulp chemistry and mineral surface conditions.

The results indicate that flotation performance is influenced by both the amount of $ZnSO_4$ and the use of pulp aeration. Increasing the amount of $ZnSO_4$ enhances sphalerite depression and improves the selectivity of separation between lead and zinc minerals. In contrast, pulp aeration slightly reduced Pb and Zn recoveries under certain conditions, suggesting that aeration may have a partial negative effect on flotation performance. This behavior can be associated with aeration-induced changes in pulp chemistry and mineral surface oxidation.

4. CONCLUSION

In the study, the effect of pulp aeration on the flotation recoveries of both lead and zinc minerals was investigated. The comparison of aerated and non-aerated experiments indicates that pulp aeration did not improve flotation performance under the conditions applied in this study. In particular, slight decreases in both Pb and Zn recoveries were observed in the aerated tests, and sphalerite depression was less effective at lower $ZnSO_4$ amounts. This behavior may be attributed to the relatively high number of aeration cycles, which could have exposed the pulp to excessive oxygen and promoted surface oxidation of minerals, thereby adversely affecting flotation performance. These results suggest that pulp aeration may have a limited and partially negative influence on flotation performance under the investigated conditions. Therefore, in future work, additional experiments with fewer aeration cycles and more controlled oxygen exposure will be conducted in order to determine more suitable operating conditions.

ACKNOWLEDGEMENTS

This study was supported by Project (MYLB-2026-48096) funded by the BAP (Scientific Research Projects) Department of Istanbul Technical University.

REFERENCES

Ağaçayak, T., Yılmaz, N. B., (2021) “Niğde (Ulukışla) kompleks Pb-Zn cevherinin optimum flotasyon şartlarının belirlenmesi”, Pamukkale Üniversitesi Mühendislik Bilimleri Dergisi, 27 (7) 856-862.

Atak, S., (2017), Flotasyon Cevher Hazırlamada 100 Yıl.

Bulatovic, S. M., (2007), Handbook of Flotation Reagents, Chemistry, Theory and Practice.

Fuerstenau, M. C., Jameson, G. J., Yoon, R. H. (Eds.), (2007), Froth Flotation, A Century of Innovation. SME.

Grano, S., (2009) “The critical importance of the grinding environment on fine particle recovery in flotation”, Minerals engineering, 22 (4) 386-394.

Liu, W., Moran, C. J., Vink, S., (2013) “A review of the effect of water quality on flotation”, Minerals Engineering, 53 91-100.

Wang, C., Liu, R., Zhai, Q., Xie, Z., Sun, W., Li, P., Wang, Z., (2023) “Exploring the effect of pulp aeration and lime-aid grinding on pyrrhotite-rich type copper sulfide ore flotation separation”, Separation and Purification Technology, 311 123268.

Wills, B. A., Finch, J. A., (2016). Wills' Mineral Processing Technology, An Introduction to the Practical Aspects of Ore Treatment and Mineral Recovery (8th ed.), Elsevier.

EVALUATING CASHEW NUTSHELL LIQUID AS A SUSTAINABLE COLLECTOR FOR COPPER-MOLYBDENUM ORE FLOTATION

Justin PARIS, Ebuka E. CHUKWUMA, Helmi F. KALAHARI, Alex KELISKY, James FINET, Ozan KÖKKILIÇ, Shiva MOHAMMADI-JAM, Kristian E. WATERS*

McGill University, Department of Mining and Materials, H3A 0C5, Montreal, QC, CANADA
**Corresponding author: kristian.waters@mcgill.ca*

A B S T R A C T

Flotation schemes for processing sulphide ores typically rely on xanthates as collectors, despite their well-documented environmental and health risks due to toxicity and instability. This work explores the potential of cashew nutshell liquid (CNSL) as an environmentally sustainable alternative for copper-molybdenum sulphide flotation. CNSL is an inexpensive, widely available agro-industrial byproduct of cashew production. It is composed primarily of the phenolic compounds cardanol and cardol. These molecules feature a polar hydroxyl or carboxyl head and a long hydrophobic alkyl tail, like surfactants commonly used as collectors in flotation. Bench-scale flotation tests were conducted on Cu-Mo ore from Pinto Valley Mine, yielding a bulk sulphide concentrate. To further understand the flotation behaviour, zeta potential and microflotation experiments were performed on monomineralic samples of the main target minerals (chalcopyrite and molybdenite) and gangue minerals (pyrite and quartz). The zeta potential and FTIR measurements indicate strong interactions of CNSL with chalcopyrite, molybdenite, and pyrite, but negligible interaction with quartz. Correspondingly, low quartz recovery in microflotation tests confirm CNSL's weaker affinity for silicate minerals. The results demonstrate CNSL's potential as a viable, eco-friendly collector for Cu-Mo flotation.

Key words: *Cu-Mo sulphide ore, cashew nutshell liquid, flotation, surface chemistry*

1. INTRODUCTION

Copper–molybdenum flotation is a key separation process in the beneficiation of porphyry copper ores, where molybdenum commonly occurs as molybdenite (MoS_2) associated with copper sulphide minerals such as chalcopyrite ($CuFeS_2$) and sulphide gangue such as pyrite (FeS_2) and pyrrhotite ($Fe_{1-x}S$). Froth flotation is widely applied due to its efficiency and selectivity for sulphide mineral recovery.

In most Cu-Mo operations, xanthate is used as the primary collector. A variety of secondary collectors are also used including dithiophosphates, xanthogen formates, thionocarbamates, xanthic esters and mercaptobenzothiazole (Bulatovic, 2007). In a conventional Cu-Mo flotation circuit, the rougher flotation stage produces a bulk copper sulphide and molybdenite concentrate where pyrite is depressed. Subsequent cleaning stages focus on the selective flotation of molybdenite by its natural hydrophobicity coupled with the depression of copper minerals, or by flotation of the copper minerals with depression of molybdenite (Castro et al., 2016). Xanthate and other thiol collectors are generally non-selective and have been shown to decompose relatively quickly and form carbon disulphide in acidic conditions. Therefore, there is increasing research interest in developing more selective and sustainable reagents (Elizondo-Álvarez et al., 2021).

Cashew nutshell liquid (CNSL) could have potential as a possible alternative. CNSL is an agro-industrial waste product resulting from the cultivation and processing of cashews. Cashews are sourced from the cashew tree (*Anacardium occidentale*), from which cashew nuts grow as single seeds at the bottom of cashew apples. The edible kernels contained in the nuts are surrounded by natural CNSL, which is dermally toxic. The nuts are subjected to roasting to aid

in removing the outer shell, after which the liquid is removed and discarded (Lomonaco et al., 2017). The natural CNSL prior to roasting is primarily composed of anacardic acid (60 – 70 %), with minor amounts of cardol (10 – 20 %), cardanol (< 10 %) and 2-methyl cardol (< 5 %) (Lomonaco et al., 2017; Veeramanoharan & Kim, 2024). During the roasting process, the anacardic acid undergoes decarboxylation to become cardanol. The cardanol-rich liquid is referred to as technical CNSL, and has the general composition of 70 – 80 % cardanol and 10 – 20 % cardol (Veeramanoharan & Kim, 2024).

Owing to its phenolic group, long alkyl chain, and sustainable origin, the application of cardanol from CNSL has attracted growing interest in various domains of chemical synthesis (Caillol, 2023). Cardanol can be converted into a wide range of high-value products, including resins, surfactants, lubricants, and plasticizers, and its structure allows for versatile chemical functionalization. In particular, a wide range of cationic, anionic, and non-ionic surfactants have been developed that implement cardanol as the base component (Veeramanoharan & Kim, 2024) and have good biodegradability (Tyman & Bruce, 2004). Seeing as flotation collectors are surfactants used for modifying surface hydrophobicity of minerals, there may be potential for cardanol-derived surfactants to act as sustainable flotation collectors.

However, little research has considered CNSL in the context of flotation. So far, two mineral systems have been considered. Perera et al. (2024b) found that chalcopyrite could be selectively floated from a synthetic chalcopyrite/pyrite mixture using an acyl thiourea collector synthesized from cardanol with two coordinating groups of C=O and –NH-C(=S)-N. The separation was further improved by using reversible addition−fragmentation chain transfer polymerization to incorporate *O*-ethyl acetylcarbamothioate (R−O−C(=S)−NH−C(=O)−CH_3) functionality for selective binding and cardanyl acrylate moiety as a hydrophobic component (Perera et al., 2024a). In coal flotation, cardanol polyoxyethylene ether has been found to act as a good emulsifier to form stable microemulsions for the recovery of coal slime (He et al., 2025; Li et al., 2026).

Despite the successful application of CNSL derivatives for the flotation of chalcopyrite and coal slime, to date there has been no evaluation of the potential for technical CNSL without chemical modification to act as a flotation reagent. Additionally, no work has considered its application to the flotation of an ore, which is likely to exhibit more complex flotation behaviour due to variable mineralogy and pulp chemistry. This study investigates the feasibility of using unmodified technical CNSL as a collector for Cu-Mo ore flotation.

2. MATERIALS AND METHODS

2.1. Materials

Monomineralic samples of chalcopyrite, molybdenite, pyrite, and quartz were sourced from Ward's Science. The as-received samples were stage ground dry using a Pulverisette 6 planetary monomill (Fritsch, Germany) with agate grinding media and sieved to produce samples in the size range of −106+38 µm for microflotation experiments. The fine −38 µm fractions produced during stage grinding were used for additional surface chemistry measurements.

Ore flotation was conducted on ball mill feed samples collected from the Pinto Valley Mine in Arizona, USA containing 0.35 % Cu and 0.01 % Mo. The ore samples were ground wet at 60 $\%_{w/w}$ solids using a laboratory ball mill for 30 min to produce a particle size distribution with a P_{80} of 80 µm. Calcium oxide (CaO) [Fisher Scientific, USA] was mixed with water to form a lime slurry for pH adjustment. Methyl isobutyl carbinol (MIBC) [Sigma-Aldrich, Canada] was added as frother.

Technical grade cashew nutshell liquid was obtained from Palmer International (USA). The highly viscous, dark brown oil had a nutty aroma and was immiscible in water. Well-dispersed emulsions of CNSL in de-ionized water were made using a high intensity static mixer operating at 8000 rpm.

Potassium chloride (KCl) [Fisher Scientific, USA] was used as a background electrolyte for zeta potential measurements. Hydrochloric acid (HCl) and sodium hydroxide (NaOH) used for pH adjustment in the surface chemistry analyses and microflotation experiments were purchased from Sigma-Aldrich (Canada).

2.2. Methods

2.2.1.Zeta potential measurements

Zeta potential measurements were conducted using a NanoBrook ZetaPlus electrophoretic analyser (Brookhaven Instruments, USA). The monomineralic samples were suspended in 200 mL of 10^{-3} mol/L KCl solution at a solids concentration of 0.04 wt.%. The suspensions were subjected to 30 seconds of ultrasonic dispersion using a UP400S processor (Hielscher, USA), followed by continuous stirring with a magnetic stirrer to maintain a uniform particle distribution during measurements. The samples were conditioned for 30 min after collector addition at a dosage of 100 kg/t, and were allowed to equilibrate for 5 min at each pH prior to taking a measurement. Measurements were taken in steps of 1 pH units in the range of pH 3 to 10, within the instrument's operational limits. Fresh suspensions were prepared for acidic and basic zeta potential measurements to avoid zeta potential hysteresis.

2.2.2 .Microflotation experiments

Prior to microflotation, one gram of mineral sample was placed in a beaker and conditioned for 5 min in 30 mL of pH adjusted collector solution. After conditioning with collector, 1 mL of 2.4 g/L MIBC frother solution was added to the suspension. After conditioning, the suspension was transferred to a modified Hallimond tube and filled to a volume of approximately 170 mL with pH adjusted reverse osmosis water. Air was then introduced to the cell at a rate of 36 mL/min and flotation was conducted for 1 min. The floated and non-floated material were dried and weighed to calculate recovery.

2.2.3.Fourier-transform infrared spectroscopy

Fourier-transform infrared spectroscopy (FTIR) measurements were carried out using a Vertex 70 spectrometer (Bruker, USA). Each spectrum represents the average of 64 scans collected at a resolution of 4 cm^{-1} across the 4000–400 cm^{-1} range. Approximately 1 g of the sample was mixed with 100 mL of a reagent solution containing CNSL at a dosage of 100 kg/t. The suspension was dispersed using a UP400S ultrasonic processor (Hielscher, Germany) for 30 seconds. The pH was adjusted using dilute HCl and NaOH at pH 9, followed by 15 min of conditioning. The suspension was then filtered, and the solids were rinsed three times with pH-adjusted reverse osmosis water to remove excess reagent. Samples were air-dried for 24 hours, further dried in a vacuum oven for 8 hours, and stored in a desiccator until analysis.

2.2.4. Ore flotation experiments

Ore flotation was carried out on 500 g ore samples in a 1.3 L Denver D12 flotation cell operating at an impellor speed of 1200 rpm. In each experiment, a fresh batch of ore was mixed with tap water in the flotation cell, with the water level adjusted to a set height. The pH was adjusted using lime. CNSL was added as collector at a dosage of 40 g/t, followed by 15 ppm of MIBC as frother. The ore was conditioned for 3 min after collector and frother addition. Following the conditioning step, the air was turned on at a flow rate of 3 L/min and froth was collected after

0.5, 1, 3, 10 and 16 min to produce five concentrates. After each concentrate, the pH was readjusted to the desired value and the water level was readjusted to the set height. In all cases flotation experiments were performed in triplicate.

2.2.5. X-ray fluorescence (XRF)

X-ray Fluorescence (XRF) was used to determine the chemical composition of the ore sample and bench scale flotation products. Solid glass beads were fluxed with 49.75 % lithium tetraborate ($Li_2B_4O_7$), 49.75 % lithium metaborate ($LiBO_2$), and 0.5 % lithium bromide (LiBr) [Katanax, Canada]. The beads were analyzed by Energy Dispersive XRF (ED-XRF) under 75 kPa He purge using an Epsilon 4 XRF spectrometer (Malvern Panalytical, The Netherlands) coupled with the Omnian application.

3. RESULTS AND DISCUSSION

3.1 Monomineralic microflotation and surface chemistry

3.1.1 Zeta potential measurements

Figure 1 shows the zeta potential measurements for the four single minerals. In the presence and absence of CNSL, all four minerals had a negative zeta potential that decreased with increasing pH for the pH range considered.

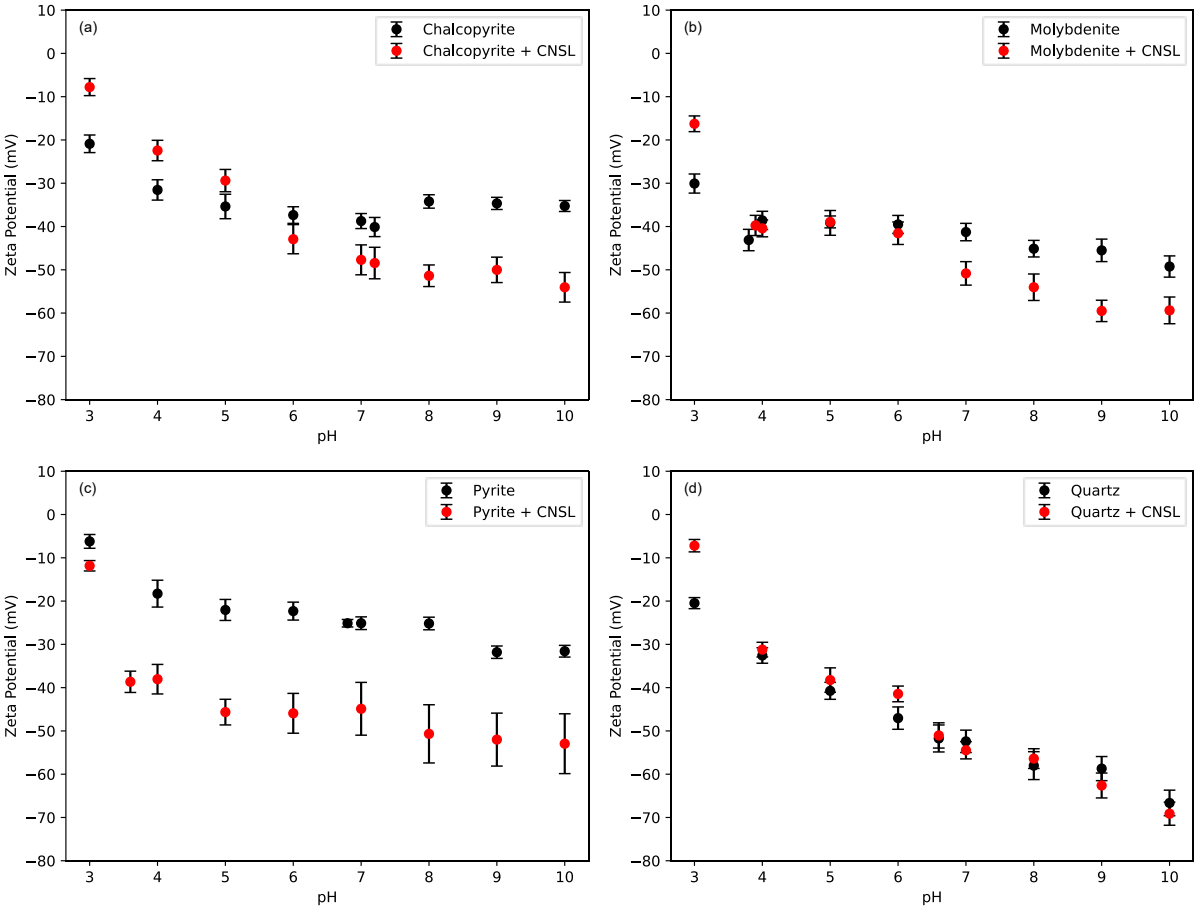

Figure 1. Zeta potential trends of (a) chalcopyrite, (b) molybdenite, (c) pyrite, and (d) quartz in the presence and absence of cashew nutshell liquid at a dosage of 100 kg/t. Error bars indicate 95 % confidence intervals.

The zeta potential of chalcopyrite and molybdenite exhibited a slight negative shift at pH > 6, suggesting physisorption of the CNSL compounds at alkaline pH. The zeta potential for pyrite displayed a more significant negative shift in the range of pH 4–10, likely indicating chemisorption of the CNSL compounds. In contrast, the zeta potential trends for quartz with and without CNSL had minimal variation, indicating little to no interaction with CNSL.

3.1.2 FTIR results

Figure 3 presents the FTIR spectrum of chalcopyrite and molybdenite, before and after conditioning with CNSL, highlighting the presence of various functional groups characteristic of its major peaks. In the spectrum of CNSL, the broad absorption band at 3357 cm^{-1} is attributed to polymeric O–H stretching, indicating the presence of phenolic hydroxyl groups (Kyei et al., 2019). A band at 3078 cm^{-1} corresponds to aromatic C–H stretching, while the peak at 3008 cm^{-1} is assigned to aliphatic C–H stretching, likely arising from unsaturated hydrocarbon chains (alkene groups) (Kyei et al., 2019; Rahmawati et al., 2019). The intense bands at 2925 cm^{-1} and 2852 cm^{-1} are associated with asymmetric and symmetric C–H stretching vibrations of the alkyl side chains, respectively (Eke et al., 2021; Kyei et al., 2019). A strong absorption at 1592 cm^{-1} is indicative of aromatic C=C stretching, likely originating from benzene rings (Eke et al., 2021; Kyei et al., 2019). A similar vibrational mode is observed at 1456 cm^{-1}, further supporting the aromatic nature of the CNSL components (Kyei et al., 2019). The 1265 cm^{-1} peak is attributed to C–O stretching vibrations of ester groups, whereas the 1153 cm^{-1} peak is also consistent with C–O stretching, possibly from phenolic structures (Eke et al., 2021). The band at 1072 cm^{-1} is characteristic of C–O vibrations specifically associated with cardanol (Rahmawati et al., 2019). At lower wavenumbers, distinct bands at 995 cm^{-1} and 910 cm^{-1} correspond to C–H out-of-plane bending vibrations, attributed to conjugated cis–trans double bonds and terminal vinyl groups present in polycardanol, respectively (Eke et al., 2021; Kyei et al., 2019). The band at 779 cm^{-1} reflects C–H deformation (out-of-plane), while the peak at 694 cm^{-1} is also assigned to C–H out-of-plane bending, commonly observed in aromatic ring substitutions (Rahmawati et al., 2019).

No significant differences were observed in the FTIR spectra of chalcopyrite before and after treatment with CNSL (Figure 2a), suggesting that CNSL exhibits only weak, non-specific interactions characteristic of physical adsorption on the chalcopyrite surface.

In terms of molybdenite (Figure 2b), several new peaks appeared after treatment with CNSL, indicating the adsorption of CNSL onto the mineral surface. The bands observed at 690, 777, 907, and 991 cm^{-1} correspond to C–H vibrations. The peaks at 1151 and 1263 cm^{-1} are attributed to C–O stretching and vibration, respectively, while the bands at 1452 and 1587 cm^{-1} are associated with C=C stretching. However, these peaks appear at lower wavenumbers and are not distinct, which is more characteristic of physisorption rather than strong chemical adsorption.

The FTIR spectrum of untreated pyrite (Figure 2c) shows no distinct absorption bands in the mid-infrared region, consistent with its metallic character and weak IR activity. Several new absorption bands appear in the spectrum for pyrite treated with CNSL, specifically at 2915 cm^{-1} and 2848 cm^{-1}, corresponding to the asymmetric and symmetric stretching vibrations of aliphatic C–H groups from the long hydrocarbon chains of CNSL. In addition, the emergence of a band at 1591 cm^{-1} is attributed to aromatic C=C stretching vibrations, while the peak at 1153 cm^{-1} is assigned to C–O stretching vibrations associated with phenolic or ether functional groups. The appearance of these CNSL-related bands confirms adsorption of CNSL onto the pyrite surface. However, the relatively low intensity of these peaks and the absence of significant shifts relative to pure CNSL suggest that the interaction is dominated by physical adsorption, likely driven by hydrophobic interactions rather than by strong chemical bonding to surface Fe sites.

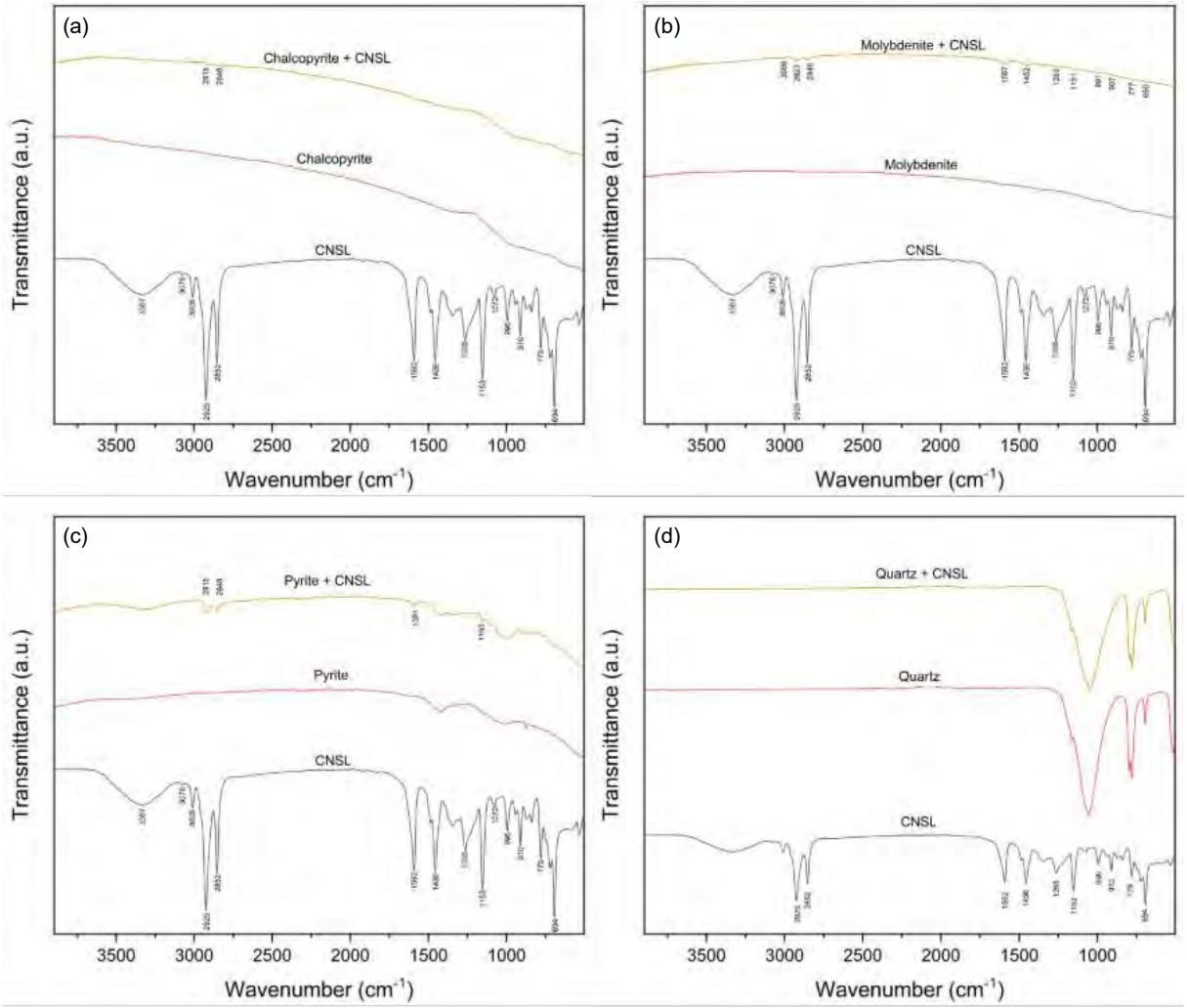

Figure 2. FT-IR spectra of (a) chalcopyrite, (b) molybdenite, (c) pyrite, and (d) quartz in the presence and absence of CNSL, with the spectrum of CNSL for reference

The FTIR spectrum of quartz (Figure 2d) is dominated by the characteristic Si–O–Si stretching vibrations in the 1000–1100 cm^{-1} region. Comparison of the spectra before and after CNSL treatment shows no new absorption bands attributable to CNSL, and no noticeable shifts in the quartz vibrational features. This indicates that CNSL does not adsorb appreciably onto the quartz surface under the studied conditions. The absence of CNSL-related peaks suggests minimal interaction between CNSL and quartz, consistent with the highly hydrophilic nature of the quartz surface and its low affinity for hydrophobic organic molecules.

3.1.3. Microflotation results

A summary of the microflotation results is shown in Figure 3. The recovery of each mineral was considered at pH 5, 7, 9, and 11. CNSL was added at a high dosage (10 kg/t) to ensure that there was sufficient reagent available for the larger proportion of mineral surfaces in contrast to what their deportment would be in an ore. The three sulphide minerals, chalopyrite, molybdenite, and pyrite, all had recoveries greater than 80 % for the pH values considered. Quartz had much lower recoveries (< 40 %).

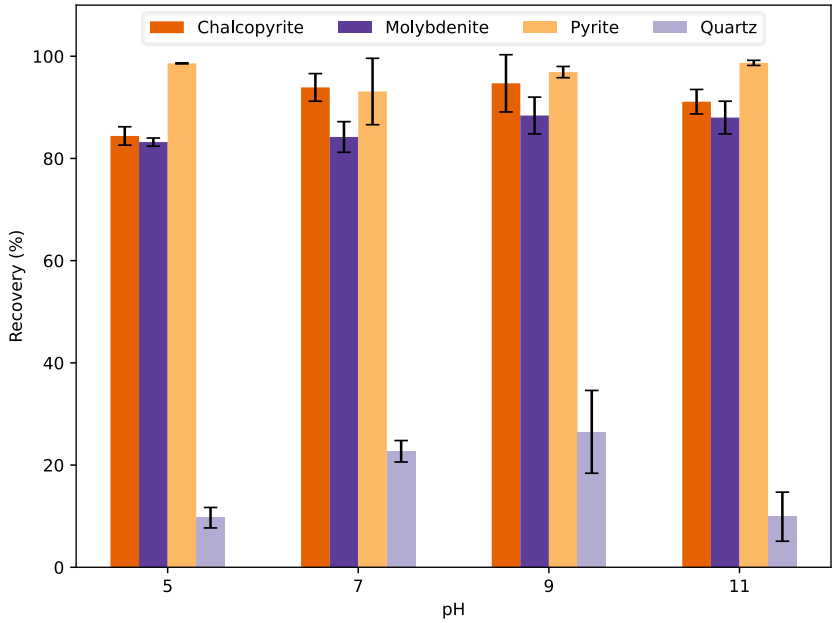

Figure 3. Microflotation results of chalcopyrite, molybdenite, pyrite and quartz using 10 kg/t cashew nutshell liquid. Error bars indicate 95 % confidence intervals

3.2 Ore Flotation Results

The applied ore flotation scheme was chosen to approximate a practical flotation flowsheet rather than to reproduce the single-collector environments used in the single-mineral studies. The initial ore flotation experiments were conducted at pH 11.5 with lime as a pH modifier. This was done primarily for frother stabilization and depression of pyrite, consistent with previously reported flotation schemes for beneficiation of the Pinto Valley Mine deposit (Bulatovic, 2007; Craig et al., 2021). It has also been proposed in the most recent NI 43-101 report that reducing the rougher flotation pH to less than 10 during the copper flotation stage should be considered as it will likely improve the recovery of locked pyrite/chalcopyrite particles (Craig et al., 2021). For this reason, additional flotation experiments were conducted at pH 9.

3.2.1. Effect of CNSL collector and pH on recovery

Figure 4 shows the cumulative copper and molybdenum recoveries as a function of flotation time at pH 9 and 11.5 using CNSL as collector at a dosage of 40 g/t. For both minerals, recovery increased rapidly during the initial stages of flotation followed by a gradual approach to a plateau, indicating fast initial kinetics under both pH conditions. For copper, marginally higher recoveries were achieved at pH 11.5 compared to pH 9. At pH 11.5, copper recovery increased rapidly within the first 1 - 2 minutes, reaching approximately 90 %, and reaching a final recovery of about 95 – 97 % after 16 minutes. In contrast, flotation at pH 9 resulted in slower kinetics and lower maximum copper recovery, plateauing at approximately 85 – 88 %. A similar trend was observed for molybdenum recovery, although overall recoveries were lower than those of copper. At pH 11.5, molybdenum recovery rapidly increased to approximately 80–85% within the first few minutes and remained relatively consistent throughout the flotation time. At pH 9, molybdenum recovery was consistently lower, reaching only about 70 – 75 % after 16 minutes.

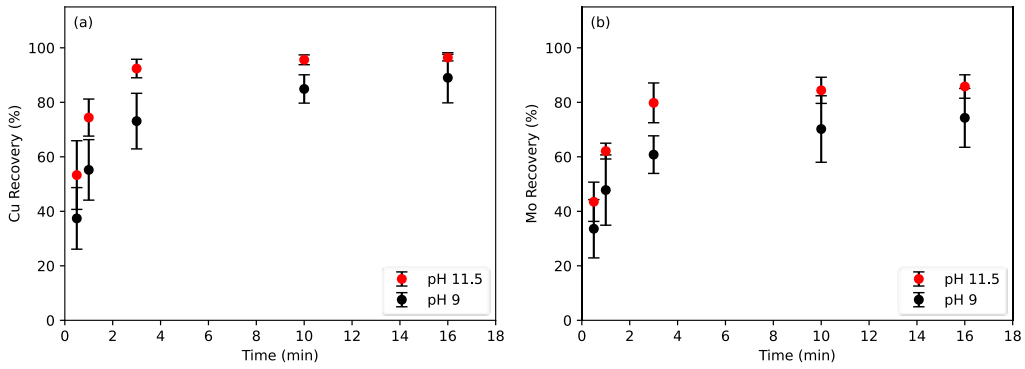

Figure 4. Cumulative recovery of (a) copper and (b) molybdenum with flotation time at pH 9 and 11.5 using cashew nutshell liquid at a dosage of 40 g/t

The improved copper recovery at higher pH suggests enhanced collector ionization and stronger collector–mineral interactions, leading to more efficient bubble–particle attachment. The reduced molybdenum recovery at lower pH may be attributed to weaker collector adsorption on molybdenite surfaces and increased competition from other sulphide or gangue species, including non-depressed pyrite. Overall, these results demonstrate that higher alkaline conditions (pH 11.5) significantly enhance both copper and molybdenum recovery in Cu–Mo bulk flotation when using CNSL as a collector.

3.2.2. Effect of CNSL collector and pH on grade-recovery relationship

Figure 5 illustrates the relationship between concentrate grade and recovery for copper and molybdenum obtained during the ore flotation at pH 9 and pH 11.5. For copper, flotation at pH 11.5 produced consistently high recoveries (>90%) at relatively low concentrate grades (~2 – 4 % Cu). The steep, near-vertical nature of the grade–recovery curve at pH 11.5 indicates rapid mass pull and limited upgrading, suggesting a more non-selective flotation regime where a larger proportion of material is recovered early. In contrast, flotation at pH 9 exhibited a more gradual grade–recovery trend, achieving higher copper grades (up to ~7 – 20 % Cu) at the expense of reduced recovery. This behaviour indicates improved selectivity at pH 9, likely due to the recovery of fully liberated copper-bearing mineral or a higher-grade mineral. A similar trend was observed for molybdenum. At pH 11.5, molybdenum recovery remained relatively high (~80–85%) over a narrow range of low concentrate grades (~0.02 – 0.06 % Mo), reflecting fast flotation kinetics and minimal upgrading. Conversely, flotation at pH 9 resulted in a broader grade–recovery curve, with molybdenum grades increasing to approximately 0.4 % Mo while recovery progressively declined to ~35 – 40 %. This suggests that lower pH conditions favor selective enrichment of molybdenum at the cost of recovery.

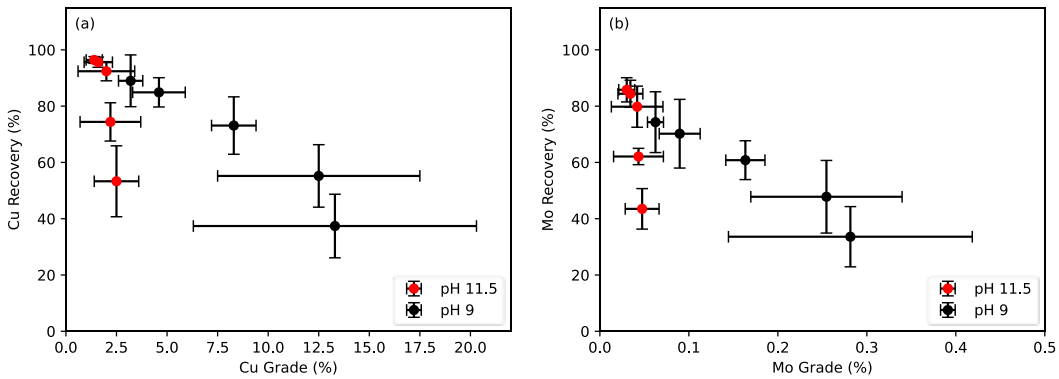

Figure 5. Cumulative grade and recovery of (a) copper and (b) molybdenum at pH 9 and 11.5 using cashew nutshell liquid at a dosage of 40 g/t.

Overall, the grade–recovery analysis indicates that pH 11.5 promotes high recovery but poor selectivity, whereas pH 9 enhances concentrate grade through more selective flotation. These results are consistent with the recovery trends observed earlier and suggest that operating at higher pH may be advantageous for maximizing bulk recovery, while lower pH conditions may be better suited for applications where concentrate upgrading is prioritized.

4. CONCLUSION

This work investigated the application of unmodified technical CNSL as a collector for the separation of a Cu-Mo ore sourced from Pinto Valley Mine. The investigation included zeta-potential and FT-IR measurements to understand the reagent interactions with chalcopyrite, molybdenite, pyrite and quartz. Microflotation experiments were done to evaluate the flotation response for each individual mineral with CNSL. Bench scale flotation experiments were conducted on the ore at pH 9 and 11.5 to evaluate Cu and Mo grade and recovery. The conclusions are as follows:

1. The zeta potential and FTIR measurements suggest that technical CNSL adsorbs by physisorption onto chalcopyrite and molybdenite, chemisorption onto pyrite, and has negligible interaction with quartz.

2. Microflotation of the minerals in the presence of CNSL resulted in > 80 % recovery for the three sulphide minerals and < 40 % recovery for quartz across pH 5 – 11.

3. The ore flotation experiments achieved high recoveries of Cu (95 – 97 %) and Mo (85 – 88 %), with faster kinetics and greater recovery at pH 11.5.

4. The grade-recovery curves generated from the ore flotation data showed that flotation at pH 9 led to improved selectivity for copper and molybdenum.

5. Technical CNSL has the potential to be used as a sustainable flotation collector to produce an initial bulk chalcopyrite and molybdenite concentrate at pH 11.5, which can then be upgraded at lower pH conditions

REFERENCES

Bulatovic, S. M., (2007) “Flotation of copper sulfide ores”, Handbook of Flotation Reagents, Elsevier, 235–293.

Caillol, S., (2023) “The future of cardanol as small giant for biobased aromatic polymers and additives”, European Polymer Journal, 193, 112096.

Castro, S., Lopez-Valdivieso, A., Laskowski, J. S., (2016) “Review of the flotation of molybdenite. Part I: Surface properties and floatability”, International Journal of Mineral Processing, 148, 48–58.

Craig, C., Freiman, T. J., Harvey, J. T., Kirkham, G., Roche, C., Triebel, K., Wellman, E. C., (2021) “NI 43-101 Technical Report on the Pinto Valley Mine, Arizona, USA”, Capstone Mining Corp.

Eke, W. I., Kyei, S. K., Ajienka, J., Akaranta, O., (2021) “Effect of bio-based flow improver on the microscopic and low-temperature flow properties of waxy crude oil”, Journal of Petroleum Exploration and Production Technology, 11 (2) 711–724.

Elizondo-Álvarez, M. A., Uribe-Salas, A., Bello-Teodoro, S., (2021) “Chemical stability of xanthates, dithiophosphinates and hydroxamic acids in aqueous solutions and their environmental implications”, Ecotoxicology and Environmental Safety, 207, 111509.

He, M., Wang, J., Yang, S., Wang, F., Yan, X., Sun, L., You, X., Li, L., Wang, Q., (2025) “Preparation of bio-based microemulsion collector and its flotation performance for coal slime”, Separation and Purification Technology, 354, 128855.

Kyei, S. K., Akaranta, O., Darko, G., Chukwu, U. J., (2019) “Extraction, characterization and application of cashew nut shell liquid from cashew nut shells”, Chemical Science International Journal, 28 (3) 1–10.

Li, L., Wang, J., Hou, Y., Zhang, H., Yan, X., He, M., You, X., (2026) “Study on the effect of cashew phenol-based surfactants on the wettability of coal surface using molecular dynamics simulation”, Applied Surface Science, 715, 164557.

Lomonaco, D., Mele, G., Mazzetto, S. E., (2017) “Cashew nutshell liquid (CNSL): From an agro-industrial waste to a sustainable alternative to petrochemical resources”, Cashew Nut Shell Liquid: A Goldfield for Functional Materials, Springer International Publishing, 19–38.

Perera, T. D. S., Fan, B., Hsia, T., Ritchie, C., Thang, S. H., (2024a) “Polymers with biobased hydrophobic cardanyl acrylate and O-ethyl acetylcarbamothioate functionality for chalcopyrite selective flotation”, ACS Applied Polymer Materials, 6 (20) 12719–12733.

Perera, T. D. S., Hsia, T., Ritchie, C., Thang, S. H., (2024b) “Flotation efficiency and surface adsorption mechanism on chalcopyrite and pyrite by a novel cardanol derivative 3-pentadecylphenyl 4-(3,3-diethylthiouredo-4-oxobutanoate)”, Minerals Engineering, 207, 108566.

Rahmawati, P., Ramelan, A. H., Marliyana, S. D., Suharty, N. S., Wahyuningsih, S., (2019) “Synthesis of cardanol-based novolac resin from cashew nut shell liquid”, Journal of Engineering Science, 15 (1) 23–33.

Tyman, J. H. P., Bruce, I. E., (2004) “Surfactant properties and biodegradation of polyethoxylates from phenolic lipids”, Journal of Surfactants and Detergents, 7 (2) 169–173.

Veeramanoharan, A., Kim, S.-C., (2024) “A comprehensive review on sustainable surfactants from CNSL: chemistry, key applications and research perspectives”, RSC Advances, 14 (35) 25429–25471.

FROM ELECTRICAL SIGNATURES TO FLOTATION: A MULTI-PARAMETER ANALYSIS OF COPPER RECOVERY

Ünzile YENIAL ARSLAN[1,2,*], Elizaveta FORBES[1,2]

[1]Julius Kruttschnitt Mineral Research Centre, Sustainable Minerals Institute, University of Queensland, QLD 4068 Australia
[2]ARC Centre of Excellence on Eco-Efficient Beneficiation of Minerals, University of Newcastle, Callaghan, Australia
**Corresponding author: u.yenialarslan@uq.edu.au*

A B S T R A C T

The induced polarisation (IP) technique is a geophysical method used to visualise chargeability and resistivity, providing crucial insights into subsurface geological structures. Traditionally, IP measurements have been instrumental in exploring disseminated sulphide deposits, leveraging the strong polarisation response of metallic particles. Researchers can extract valuable information about rock mineralisation, matrix composition, and formation polarizability by analysing electrical parameters.

In our study, we conducted IP tests, mineralogy analyses, and flotation tests on copper sulphide rock samples. We examined the samples' electrical properties and mineral characteristics using a standard core-induced polarisation (SCIP) tester and Mineralogy Liberation Analyser (MLA).

Higher chargeability values, typically associated with greater sulphide mineral content, are associated with enhanced copper recovery. This relationship suggests that IP parameters can serve as predictive indicators. By linking electrical signatures to metallurgical outcomes, this study demonstrates the potential for using IP-based assessments to support more effective mine planning strategies.

Key words: *Resistivity, chargeability, flotation, copper*

1. INTRODUCTION

Induced polarisation (IP) is a geophysical technique that measures the ability of subsurface materials to store and release electrical charge when subjected to a low-frequency electrical field. First explored in early resistivity work by Schlumberger and later formalised through foundational studies (Marshall & Madden, 1959). IP has become indispensable for detecting and delineating disseminated metallic ore bodies—including pyrite, chalcopyrite, magnetite, and other sulphides—whose polarisation behaviour differs significantly from that of the surrounding rock matrix. In mineral exploration, The IP signal strength is primarily controlled by the abundance, size distribution, surface area and connectivity of the sulphidic or metallic particles in the rock, and the conductivity is a function of touching conductive particles (Gurin et al., 2013; Pelton et al., 1978; Revil et al., 2022). These attributes allow IP to outperform traditional resistivity imaging when targeting disseminated ores that may not significantly alter bulk conductivity.

IP data could help with mine-to-mill integration by enabling more accurate feed forecasting, optimising flotation and comminution processing strategies, and identifying zones that may present metallurgical challenges, such as clay-rich or graphitic materials. As a result, IP contributes to more efficient resource evaluation and improved processing outcomes. Figure 1 shows the IP values (in terms of mV/V) for several mineralised rocks and common rocks. Note that the IP effect due to sulphide mineralisation (the electrode polarisation effect) is much larger than that due to clay minerals (membrane polarisation) in sandstone and siltstones (Loke, 2004). Another study evaluates the effectiveness of Spectral Induced Polarisation (SIP) for

detecting conductive mineral phases in sand–pyrite mixtures. The results demonstrate that SIP is highly sensitive to conductive mineral fractions and has strong potential as a rapid, non-invasive tool for characterising metallic inclusions in porous geological materials(Mandloi et al., 2025)

IP observations are directly relevant to mineral processing, particularly froth flotation. Many minerals that display strong IP responses—such as sulphides—also possess high electrical conductivity, distinct surface charge distributions, and electrochemical interface behaviour that governs flotation efficiency. In this context, IP-derived insights into grain-scale polarisation mechanisms, electron–hole dynamics, and surface charge accumulation (Abdulsamad et al., 2017; Wong, 1979) help clarify why certain sulphide assemblages exhibit characteristic flotation responses. For example, pyrite-rich zones mapped by IP often correspond to flotation-active ore where mineral liberation and sulphide surface chemistry are critical in optimising collector adsorption and bubble attachment. Thus, IP not only supports exploration targeting but also provides complementary information about ore mineralogy relevant to downstream beneficiation.

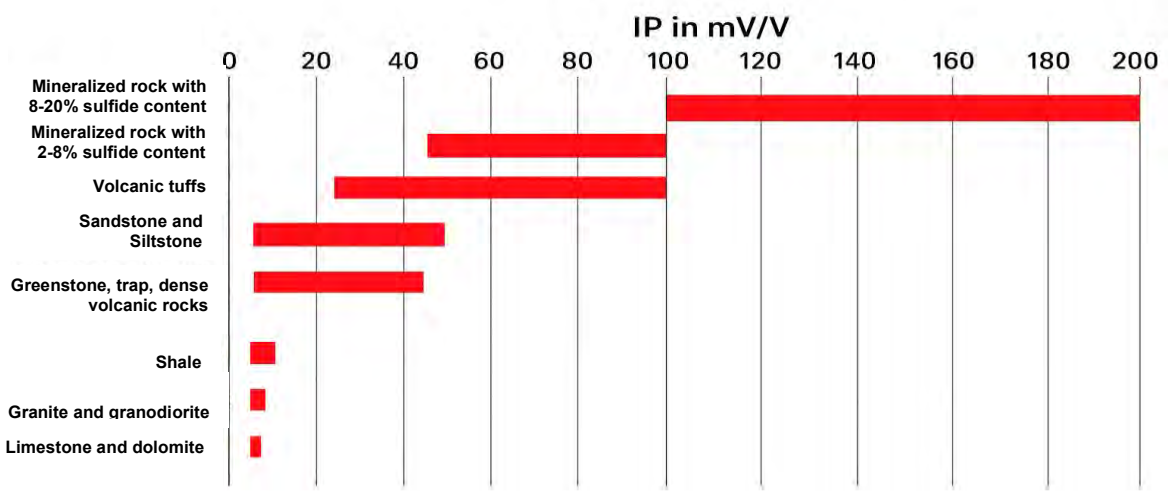

Figure 1. IP Response of the rocks (Loke, 2004)

Collectively, these developments show that induced polarisation is far more than an exploration tool. It bridges mineral discovery, ore beneficiation, and environmental stewardship by providing a unified framework for interpreting subsurface electrical responses driven by mineralogical, electrochemical, and hydrological processes. In mineral systems, IP highlights charge-accumulating metallic grains that are both exploration targets and flotation-responsive minerals. In environmental systems, IP reveals contamination pathways, redox interfaces, and zones of active fluid–mineral interaction. This versatility underscores the method's growing importance in sustainable resource development and integrated subsurface characterisation.
This study aims to evaluate how induced polarisation (IP) parameters—chargeability and conductivity—relate to the mineralogical characteristics and metallurgical performance of copper sulphide ores. By integrating IP measurements with mineralogical analyses and flotation testing, the research aims to determine whether electrical signatures can serve as predictive indicators of flotation recovery. The overarching goal is to establish IP as a practical geometallurgical tool that links subsurface electrical behaviour to ore processing outcomes, thereby supporting improved mine planning and resource characterisation.

2. MATERIALS AND METHODS

2.1. Samples

The samples were obtained from Glencore's Mount Isa Copper deposit. The modal mineralogy of the materials used in this study is summarised in Table 1. The studied ore samples of this work were received from leached and unleached areas in the deposit. The rock types for sampled orebodies are crystalline dolomite, irregularly brecciated shale, recrystallised shales, and sheared shales, and crystalline dolomite is the dominant host to economic copper mineralisation. Sulphide mineralisation is predominantly chalcopyrite, with nodular and euhedral pyrite, subhedral pyrrhotite and minor arsenopyrite. In addition, massive coarse-grained pyrite and pyrrhotite occur in the Domain 1- lode, often with chalcopyrite (Perkins, 1984). The samples originated from two ore domains characterised by similar pyrite textures. Domain-1 can be broken into leached and primary ore zones, with the southern portions experiencing deep leaching associated with transverse faulting (Mathias & Clark, 1975). Domain-2 has been the main ore-producing orebody for over 30 years with the classic Mount Isa halo structure. CGP refers to coarse-grained pyrite, whereas FGP denotes fine-grained pyrite. The leached samples experienced carbonate dissolution due to acidic conditions within the deposit; consequently, they contain substantially higher proportions of silicate minerals. In addition, the samples exhibit a wide range of pyrite-to-chalcopyrite ratios.
Prior to testing, the bulk materials were crushed to 3.35 mm, split into 200 g sub-samples, and stored in a freezer. Further details regarding the sample selection, sample preparation, sample origin and characteristics are available in the literature(Yenial-Arslan et al., 2023).

Table 1. Mineralogy of the ore samples

Mineral Grouping	Wt % Composition				
	D1- CGP	D1- FGP	D1- Leached	D2-CGP	D2-FGP
Chalcopyrite	8.41	4.56	7.54	11.67	4.02
Silicates	28.06	34.82	70.40	33.64	30.03
Calcium Carbonates	55.45	33.32	1.72	39.57	27.39
Pyrite	4.30	22.23	11.69	11.56	34.60
Pyrrhotite	0.13	0.14	0.12	1.32	0.49
Other Sulphides	0.01	0.03	0.24	0.01	0.01
Phyllosilicates	1.66	3.31	3.65	1.56	2.64
Cobaltite	0.00	0.07	0.02	0.00	0.01
Galena	0.00	0.02	0.00	0.00	0.01
Other	1.97	1.51	4.59	0.66	0.81
Deleterious	0.02	0.02	0.02	0.01	0.01

2.2. IP Measurement Cell

The design of the cell is adapted from the literature (Hupfer et al., 2016), and built in JKMRC labs. This cell is divided into three parts: a central main part where the material is located, and the two outer parts. The outer parts contain distance pieces filled with conductive water (0.001 M) and copper electrodes connected to the current electrode C1, and C2 taps at the outside. The four potential taps (two pairs, P1-P2 and P3-P4 of taps at the opposite sides) are arranged at the main part in the middle. During the measurements, only P1-P2 taps were used. This section is enclosed with porous sponges that prevent the sample from entering other compartments. The sample core IP tester (SCIP) machine, manufactured by Instrumentation GDD, helps evaluate the resistance and IP response of core samples. Instead of using core samples, the designed cell was used to measure crushed samples. The SCIP machine and measurement cell are shown in Figure 2.

2.3. IP Measurements

The IP measurements were performed in a 0.001 M NaCl conductive solution and recorded for 3.0 hrs. Each test condition was replicated three times, and their averages are shown here with error margins. The last recordings at the end of 2 hours were used for the correlation analysis.

2.4. Flotation Tests

The flotation tests aimed to estimate the natural floatability of pyrite and chalcopyrite and to provide a benchmark for comparing the ore domains. In each flotation test, 1.6 kg of freshly crushed ore was wet-ground in a stainless-steel rod mill at a 60 % solids ratio, followed by flotation in a 3 L bottom-driven Denver cell at 1200 rpm. The concentration of methyl isobutyl carbinol (MIBC) was kept at 20 ppm during the tests. The air was turned on one minute after the MIBC addition, and the concentrate was collected for 3 min by scraping every 10 s. The mineral floatability was also evaluated for entrainment due very small particle size. Further details about the process water, test measurements and flotation test results can be found in our previously published papers (Forbes et al., 2024; Yenial-Arslan et al., 2023).

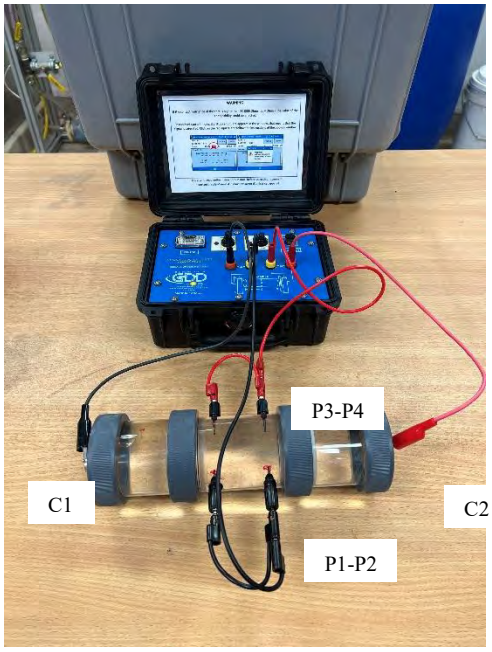

Figure 2. The SCIP machine and measurement cell

2.5. Statistical Analysis

A series of statistical analyses were conducted as follows:

- Error Bars

All error bars displayed in this work represent the 95% confidence limit of the mean values calculated based on test replicates.

- Correlation significance

The correlations between data sets (e.g., flotation data vs. geological data) were evaluated using the standard correlation coefficient (R). The significance of the correlation coefficient was determined by calculating the probability value (*p*) associated with the Student's t distribution of the correlation coefficient. The t value was calculated using Equation (1), where n is the number of data points (Napier-Munn, 2014).

$$t = \frac{R \cdot \sqrt{n-2}}{\sqrt{1-R^2}} \quad (1)$$

The correlation was deemed significant if the probability exceeded 90%.

3. RESULTS AND DISCUSSIONS

3.1. Flotation Test Results

The flotation responses of chalcopyrite and pyrite across all ore domains are presented in Figures 3 and 4, respectively. The flotation data show mineral recovery in terms of prefloat (PF), true flotation (TF), and entrainment (ENT). The purpose of these tests is not to maximise the recovery, but to get comparable flotation recovery in the presence of a low dosage of collector and frother. The highest chalcopyrite recovery (93.2%) occurred in the D1-CGP sample, followed by 70% in D1-Leached. For the remaining ore samples, chalcopyrite recoveries were 60 to 8%. The natural flotability of chalcopyrite was only minor (less than 4%).

Overall, pyrite recovery was found to be lower than chalcopyrite recovery. The highest pyrite recovery is obtained with the D1-leached sample (48%), followed by the 34% D1 CGP sample. The natural floatability of pyrite was considerably higher than that of chalcopyrite. Approximately 13% pyrite recovery was obtained from the FGP samples of both domains (D1 and D2), and around 10% from the leached sample. In contrast, only about 5% pyrite recovery was recorded for the CGP ore samples from both domains.

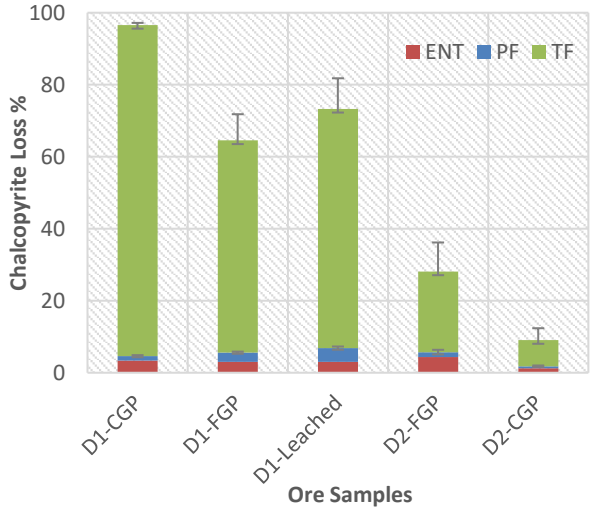

Figure 3. Chalcopyrite recovery

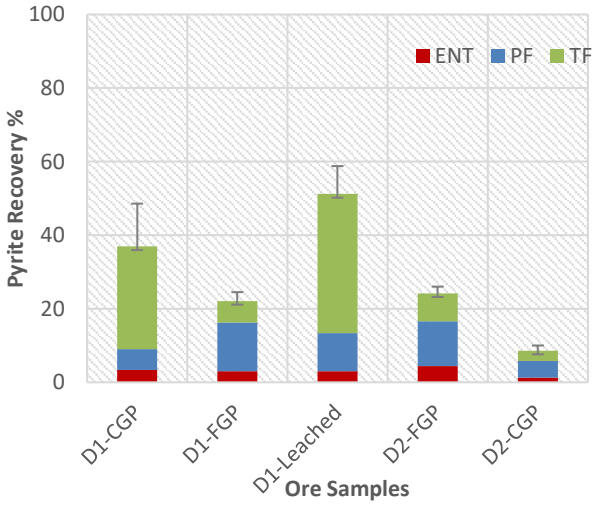

Figure 4. Pyrite recovery

3.2. IP Measurements

Figures 5 and 6 show the conductivity and the chargeability of the samples. Across the test period, the D1-Leached sample shows a much higher conductivity (≈0.15–0.26 S/m) than all CGP and FGP materials, which mostly remain below ~10 S/m. The dissolution of carbonates in the leached ore promotes the release of soluble ionic species from the silicate-rich gangue and altered surfaces, thereby producing a more conductive pulp. In contrast, the CGP and FGP samples retain more intact carbonate and sulphide assemblages, limiting ion release to solution.

The time trend also shows that conductivity increases rapidly over the first 60 minutes and then levels off. This behaviour suggests an initial fast dissolution/ion-transfer stage from fresh mineral surfaces, followed by a slower kinetic stage to reach equilibrium. The plateau is strongest for the leached sample, indicating its oxidised nature and its presence of mobile ions. A slight decline in conductivity after ~100 min is observed in the leached sample, suggesting re-adsorption or precipitation of dissolved ionic species as the system approaches chemical equilibrium. In oxidised or previously leached materials, these back-reactions can be stronger because many reactive species are already present in solution and can readily recombine or form surface coatings.

The chargeability of the minerals is almost the inverse of the conductivity; instead of releasing ions into solution, it reflects the amount of polarisable minerals present, their distribution, and their surface area. The FGP samples displayed stronger chargeability than others due to their fine-grained pyrite texture, which increased their surface area and promoted polarisation.
The leached sample showed the lowest chargeability among all the samples. The leaching caused alterations and partial oxidation of the sulphide minerals, thereby reducing the amount of polarisable material.
Variations between ore domains likely reflect the differences in sulphide content and pyrite/chalcopyrite ratios.

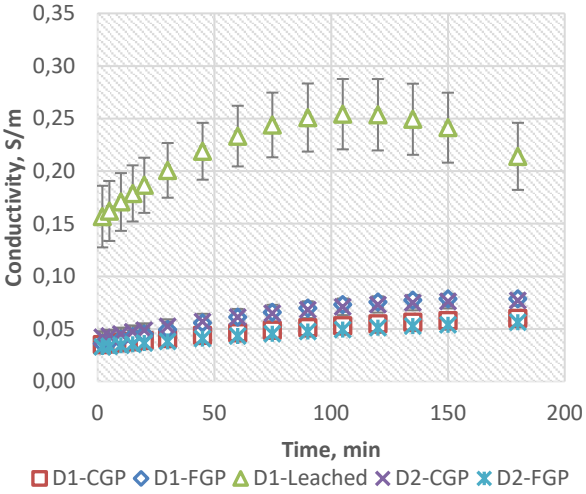

Figure 5. Conductivity measurements

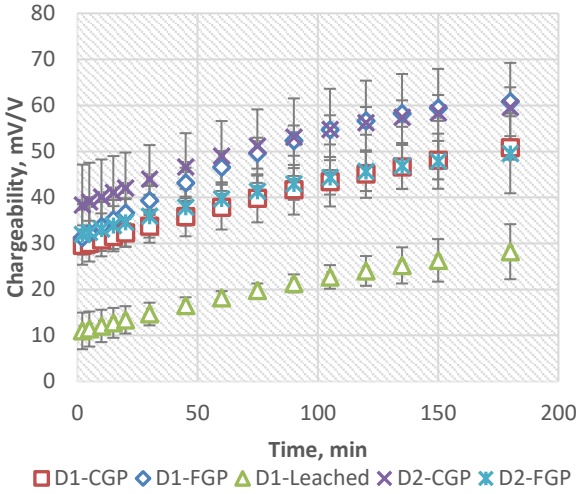

Figure 6. Chargeability measurements of the samples

3.3. Statistical Correlations Between IP and Flotation Data

Statistical correlation coefficients were calculated between sets of flotation and IP data. The probability of significance was then calculated, and only *p*-values above 90% were considered statistically significant. Their trend was plotted on a linear scale and is shown here. For flotation data, the flotation results were considered:

- Overall chalcopyrite loss and pyrite recovery;
- True flotation of chalcopyrite loss and pyrite recovery;
- Entrainment in chalcopyrite loss and pyrite recovery.

Figure 7 shows the relationship between conductivity and pre-float chalcopyrite recovery. Conductivity displays a strong positive correlation with chalcopyrite pre-float recovery (R^2=0.79; P=96%), indicating that more conductive samples tend to exhibit higher natural recoveries. This relationship suggests that conductivity may serve as a proxy for ore characteristics that favour natural flotability of chalcopyrite under the tested conditions.

In contrast, chargeability shows a negative correlation of recovered chalcopyrite/pyrite ratio in the prefloat concentrate (R^2=0.72; P=93%) as shown in Figure 8. This relationship indicates that samples with higher IP responses—reflecting higher pyrite content—tend to produce concentrates increasingly dominated by pyrite, with a corresponding decrease in chalcopyrite selectivity. Ores that generate stronger chargeability signals are more likely to result in flotation products where pyrite preferentially reports to the pre-float concentrate, highlighting the direct impact of pyrite abundance on flotation selectivity. Consequently, ore domains characterised by higher conductivity, but lower chargeability, are expected to produce chalcopyrite-rich, selective pre-float concentrates.

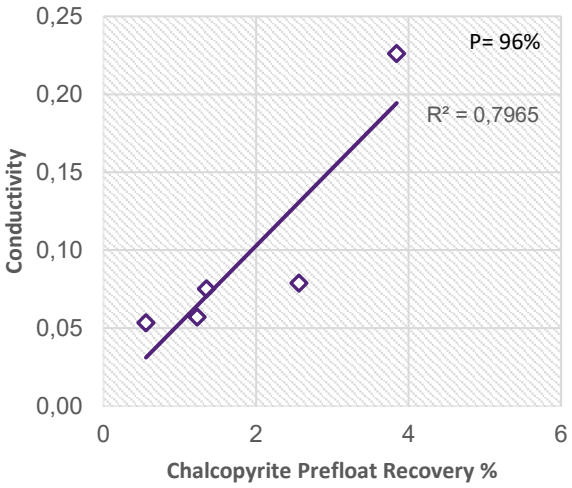

Figure 7. Conductivity and chalcopyrite prefloat recovery correlation

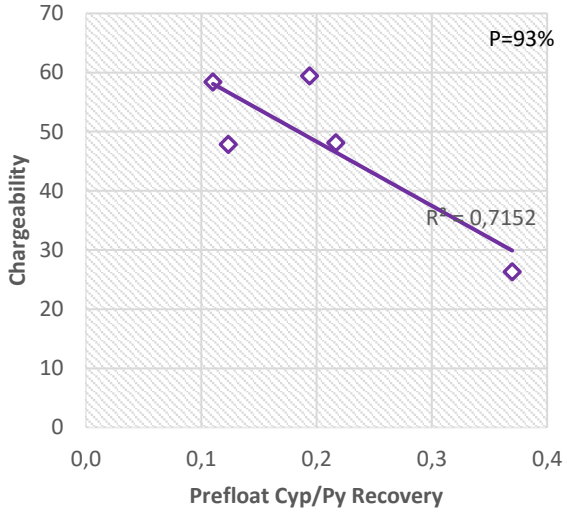

Figure 8. Chargeability and true flotation of pyrite recovery correlation

4. CONCLUSION

This study demonstrates that induced polarisation (IP) measurements provide valuable insights into metallurgical behaviour in copper sulphide ores. By integrating IP parameters with mineralogical and flotation assessments, distinct relationships were observed: conductivity correlated positively with chalcopyrite recovery under frother-only conditions, reflecting conductive domains that favour bubble–particle attachment, whereas chargeability showed an inverse trend, with highly polarisable or fine-grained components reducing flotation selectivity. Under collector-induced conditions, reagent effects can partially mask these inherent mineralogical controls, complicating direct interpretation of IP responses.

Pyrite's electrochemical reactivity, hydrolysis, and grain-size distribution strongly influence both chargeability and flotation selectivity, highlighting the dependence of IP interpretation on ore type. These findings are most applicable to sulphide systems with similar mineral textures and surface chemistry, and broader validation is needed for generalisation. Conductivity and chargeability capture complementary aspects of ore texture, mineral distribution, and surface reactivity, showing statistically significant correlations with flotation outcomes. Consequently, IP measurements hold potential as rapid indicators of ore variability, supporting

geometallurgical characterisation, flotation forecasting, and process design, though their application remains prospective and further studies with larger sample sets are recommended.

FUNDING

The authors acknowledge the support by the Australian Research Council under the ARC Centre of Excellence for Enabling Eco-Efficient Beneficiation of Minerals [CE200100009] and the Queensland Government and Glencore through the Advance Queensland Industrial Research Fellowship scheme (AQIRF112-2019RD2).

REFERENCES

Abdulsamad, F., Florsch, N., & Camerlynck, C. (2017). Spectral induced polarization in a sandy medium containing semiconductor materials: Experimental results and numerical modelling of the polarization mechanism. *Near Surface Geophysics*, *15*(6), 669-683. https://doi.org/10.3997/1873-0604.2017052

Forbes, E., Jefferson, M., Yenial-Arslan, U., Curtis-Morar, C., & O'Donnell, R. (2024). Solving the mystery of natural pyrite flotation – A mineralogy-based approach. *Minerals Engineering*, *207*, 108544. https://doi.org/https://doi.org/10.1016/j.mineng.2023.108544

Gurin, G., Tarasov, A., Ilyin, Y., & Titov, K. (2013). Time domain spectral induced polarization of disseminated electronic conductors: Laboratory data analysis through the Debye decomposition approach. *Journal of Applied Geophysics*, *98*, 44-53. https://doi.org/10.1016/j.jappgeo.2013.07.008

Hupfer, S., Martin, T., Weller, A., Günther, T., Kuhn, K., Ngninjio, V. D. N., & Noell, U. (2016). Polarization effects of unconsolidated sulphide-sand-mixtures. *Journal of Applied Geophysics*, *135*, 456-465.

Loke, M. H. (2004). Tutorial: 2-D and 3-D electrical imaging surveys.

Mandloi, P., Coles, H., Sufian, A., Edraki, M., & Bore, T. (2025). Characterisation of metal particles in porous sand using spectral induced polarisation. EPJ Web of Conferences

Marshall, D. J., & Madden, T. R. (1959). Induced polarization, a study of its causes. *Geophysics*, *24*(4), 790-816.

Mathias, B., & Clark, G. (1975). Mount Isa copper and silver-lead-zinc orebodies—Isa and Hilton mines. *Economic Geology of Australia and Papua New Guinea*, *1*, 351-372.

Napier-Munn, T. (2014). Statistical methods for mineral engineers-How to design experiments and analyse data.

Pelton, W. H., Ward, S. H., Hallof, P. G., Sill, W. R., & Nelson, P. H. (1978). Mineral discrimination and removal of inductive coupling with multifrequency IP. *Geophysics*, *43*(3), 588-609. https://doi.org/10.1190/1.1440839

Perkins, W. (1984). Mount Isa silica dolomite and copper orebodies; the result of a syntectonic hydrothermal alteration system. *Economic Geology*, *79*(4), 601-637.

Revil, A., Vaudelet, P., Su, Z., & Chen, R. (2022). Induced polarization as a tool to assess mineral deposits: A review. *Minerals*, *12*(5), 571.

Wong, J. (1979). An electrochemical model of the induced-polarization phenomenon in disseminated sulfide ores. *Geophysics*, *44*(7), 1245-1265. https://doi.org/10.1190/1.1440995

Yenial-Arslan, U., Jefferson, M., Curtis-Morar, C., & Forbes, E. (2023). Pathway to prediction of pyrite floatability from copper ore geological domain data. *Minerals*, *13*(6), 801.

GAS DISPERSION CHARACTERISTICS OF THE CONCORDE CELL™

Berivan TUNÇ[1,*], Toni MATTSSON[1], Alejandro YÁÑEZ[1], Gülay BULUT[2]

[1]Metso Finland, Rauhalanpuisto 9, 02230 ESPOO, FINLAND
[2]Istanbul Technical University, Mining Faculty, Mineral Processing Engineering Department, 34469, ISTANBUL-TÜRKİYE
**Corresponding author: berivan.tunc@metso.com*

A B S T R A C T

The flotation of fine and ultrafine particles has become increasingly important as ore grades decline and more complex deposits are processed. On one hand, these small particles present inherent challenges due to their high surface area, low mass, and elevated surface energy, which contribute to rapid oxidation, reduced attachment energy, greater reagent demand, and increased entrainment. The bubble–particle capture process depends on collision, attachment, and stability, and for fine particles, improving collision efficiency is critical. Smaller bubbles enhance collision probability and provide greater surface area, making gas dispersion a key factor in flotation performance. Important gas dispersion parameters include bubble size, superficial gas velocity, gas hold-up, and bubble surface area flux, which is closely linked to flotation kinetics. On the other hand, the Concorde Cell™ is a high-intensity pneumatic flotation cell that relies on high-shearing and fine bubbles to improve the probability of collision with particles and enhance the recovery of fines and ultrafines.

This study investigates the gas dispersion behaviour of the Concorde Cell at laboratory,pilot and industrial scales under various operating conditions. Measurements in a two-phase air–water system provide insight into how hydrodynamics influence bubble generation, with implications for fine particle recovery.

Key words: *Concorde Cell, fine – ultrafine flotation, gas dispersion, sauter mean diameter*

1. INTRODUCTION

The flotation performance is governed by the interaction of three key parameters: chemistry, ore, and machine (Klimpel, 1984). In recent years, the demand for extracting mineral resources has increased significantly (Calvo & Valero, 2022), leading to the processing of more complex ore bodies with lower head grades. Consequently, the need to effectively treat fine and ultrafine particles has become increasingly important. These particles present several inherent challenges due to their natural physical and chemical properties, such as high surface area, low momentum, small mass, and elevated surface energy. As a result, they tend to exhibit rapid oxidation, reduced energy for bubble attachment, higher reagent consumption, and increased entrainment (Farrokhpay et al., 2021; Pease et al., 2006).

The successful bubble–particle capture process is controlled by the efficiency of collision, attachment, and stability (Dai et al., 1999). For fine particles, once attachment occurs, detachment is unlikely because the adhesive forces associated with surface tension dominate over centrifugal forces, which decrease more rapidly with particle size (Jameson, 2010). Thus, improving collision efficiency becomes a primary focus when aiming to enhance the flotation rate of fine and ultrafine particles (Schubert, 2008). Collision efficiency is strongly influenced by particle size and bubble size, varying as the square of the particle size and inversely as the square of bubble size (Yoon & Luttrell, 1989). This relationship supports observations that smaller bubbles, including micro- and nanobubbles, can significantly improve the recovery of fine particles (Ahmadi et al., 2014).

Bubble size reduction can be achieved through mechanical or physicochemical means (Miettinen et al., 2010). Among mechanical approaches, cell design and hydrodynamic conditions—such as flow regime, mixing intensity, solids suspension, gas dispersion, and bubble–particle interaction—play a critical role (Finch et al., 2000). Gas dispersion, in particular, is a key parameter for characterizing flotation hydrodynamics and encompasses bubble size (d32), superficial gas velocity (Jg), gas hold-up (εg), and the derived bubble surface area flux (Sb = 6Jg / d32) (Grau & Heiskanen, 2003). Of these, Sb has received increasing attention due to its strong correlation with flotation kinetics (Gorain et al., 1997).

In this context, the Concorde Cell™—a high-intensity pneumatic flotation cell—utilizes high shear and fine bubbles to enhance the probability of collision, particularly for fine and ultrafine particles. This study investigates the gas dispersion behavior of the Concorde Cell at industrial, pilot and laboratory scales under various conditions. Measurements conducted in a two-phase air–water system provide insight into how hydrodynamics influence bubble generation.

2. MATERIAL AND METHODS

2.1. Material

The main focus of this paper is establishing gas dispersion characteristics of the Concorde Cell™ under different operating conditions at three different scales.

The experimental work was conducted in a Concorde Cell Lab, Pilot and Industrial Unit as shown in
Figure 1.

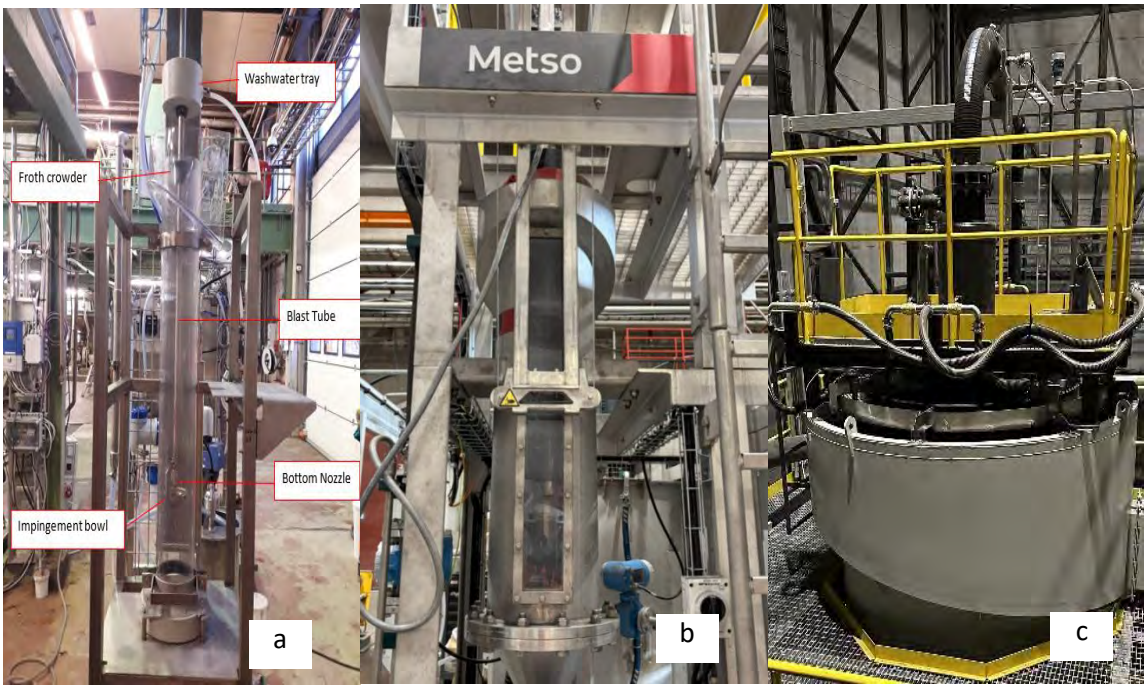

Figure 1. Concorde Cell Lab (a), Pilot (b) and Industrial Unit (c)

In Lab scale, two-phase measurements were carried out with a Pixact bubble sizer (1(a)) that measures the bubble size, superficial gas velocity and gas hold-up (Pixact, 2023). In Pilot and Industrial scale, two phase measurements were carried out with a McGill bubble sizer (1(b)) that measures the bubble size and superficial gas velocity. Gas hold up was measured using a separate dedicated device.

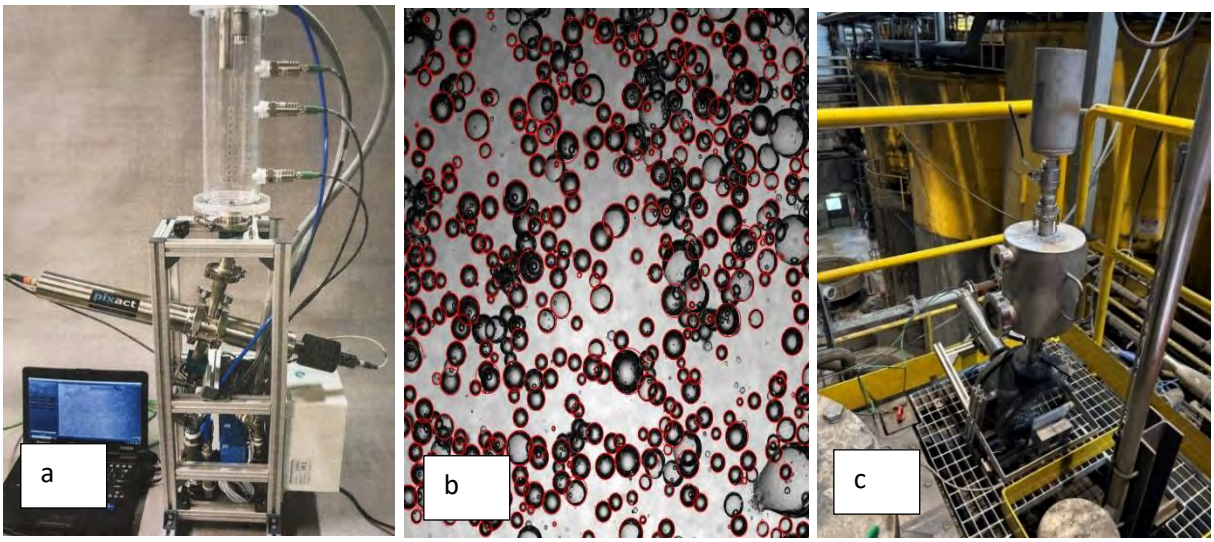

Figure 2. Pixact bubble sizer (a) and detected bubble boundaries (b) Mcgill bubble sizer (c)

Bubble sizer comprises a water tank, a camera, a sampling tube and two pressure transducers. The 5-megapixel CMOS (complementary metal-oxide semiconductor) camera unit was manufactured with IP67 protection with a bi-telecentric 0.24x macro-objective and can produce an image scale of 14.2 um per pixel. In Pixact bubble sizer, the water tank has three level sensors for J_g measurement.

The sampling-tube tip was positioned 70 cm, 86 cm, and 150 cm below the cell launder lip—directly beneath the froth interface—for the laboratory, pilot, and industrial units, respectively. All measurements were taken from the same relative location within each unit.

A glycol-ether-based frother was used for the measurements and the amount was adjusted to be above critical coalescence concentration (CCC).

2.2. Method

Measurements were conducted in fully automated Concorde Cell units at three different scales: laboratory, pilot, and industrial. During the operation, pressures as well as air and feed flow rates were monitored and recorded.

Tap water was used for the measurements in the laboratory and pilot units, whereas process water was used in the industrial unit. First, water was fed into the Concorde Blast Tube using a centrifugal pump until the water level reached the lip of the cell. A water-soluble frother was then added stepwise. Air was introduced and bubble size measurements were conducted. After each frother addition, bubble size measurements were repeated to ensure that the bubble size had reached a threshold point at which no further changes were observed. Additionally, the water passed through the bubble viewer and the tank above was adjusted to the same concentration to avoid diluting the overall concentration in the system.

In the industrial unit, the overflow from the cell could not be recirculated due to constraints in the setup. However, in the pilot and laboratory units, the measurements were conducted with recirculated overflow, which helped maintain a consistent frother concentration from start to finish.

Gas hold up measurements repeated three times and average was taken.

3. RESULTS AND DISCUSSION

This study investigates the impact of superficial gas velocity, jet velocity and scale of Concorde Cell to gas dispersion characteristics.

The jet velocity through the top nozzle was adjusted using two different approaches. First, the flow rate through the Blast Tube was varied while keeping the nozzle size fixed. Second, the nozzle sizes were changed while maintaining a constant flow rate. In Figure 3, The Sauter mean diameter was presented as a function of superficial gas velocity at flow rates of 3.5 m³/h and 4 m³/h, separately, using different nozzles as described in the second approach. It is clearly observed that the sauter mean diameter increases with increasing superficial velocity, regardless of the Blast-Tube flow rate. The jet velocities are governed by the selected nozzle sizes; smaller nozzles produce higher jet velocities. In this regard, operating with higher jet velocities results in slightly larger sauter mean diameters. This effect becomes more pronounced at the higher superficial gas velocities tested.

The Sauter mean diameter ranged between 0.4 mm and 1.2 mm across the tested superficial gas velocities.

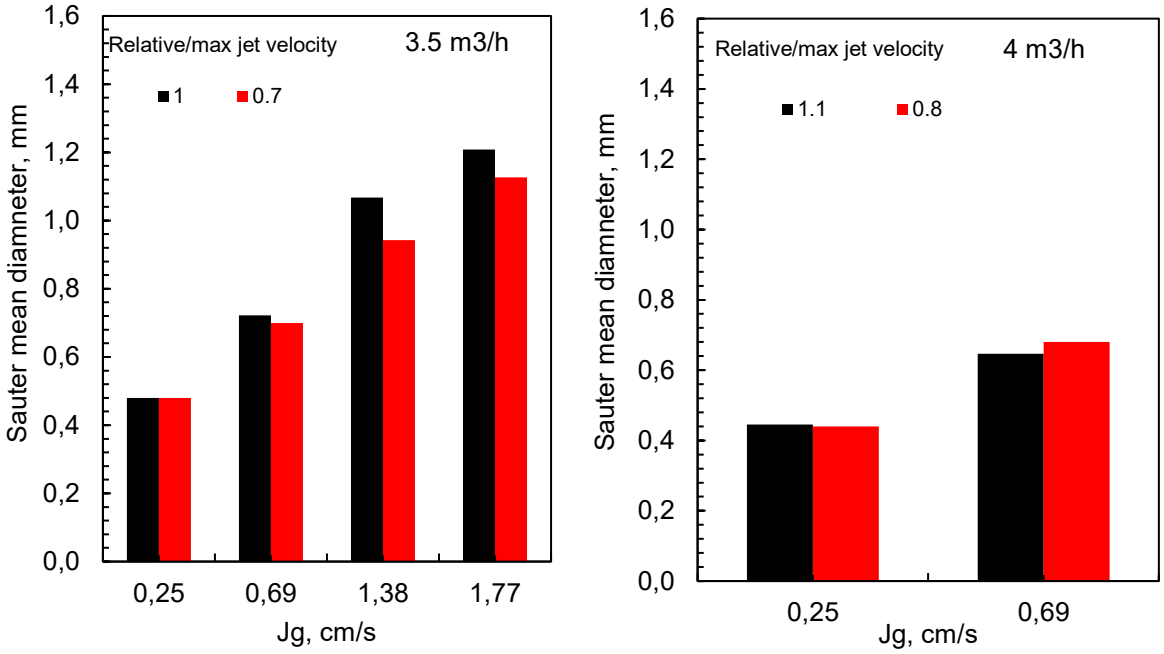

Figure 3. Sauter mean diameter as a function of superficial velocity – pilot scale unit

In following Figure 4, the results from the second approach are presented, in which the Blast Tube flowrate was changed. Similar to the observations described in the previous section, the superficial gas velocity consistently remained the dominant factor influencing bubble size, exerting a much stronger effect than the jet velocity. While jet velocity was intentionally manipulated through changes in nozzle diameter, its contribution to bubble size variation was relatively minor in comparison. This indicates that the hydrodynamic conditions associated with gas introduction play a far more substantial role in determining bubble characteristics than the momentum of the liquid jet.

In contrast to the trend shown in the earlier figure, the results from this dataset exhibit slightly larger bubbles at lower superficial gas velocities. Although this reversal appears noteworthy at first glance, the magnitude of the difference is very small and does not constitute a meaningful deviation in practical terms. The bubble sizes measured across the various jet velocities remain within a narrow range, and the observed differences are well within the expected experimental

variability. Furthermore, the relationship between bubble size and jet velocity follows a comparable pattern for both the smaller and larger nozzles, reinforcing the conclusion that nozzle-induced changes in jet velocity do not substantially modify bubble formation under these conditions.

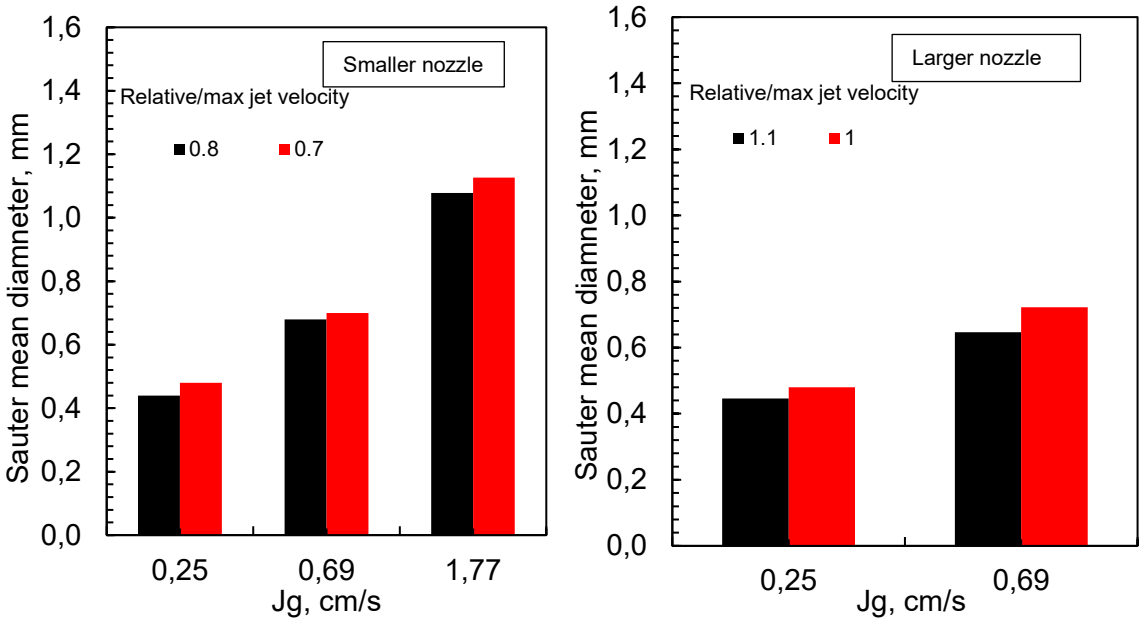

Figure 4. Sauter mean diameter as a function of superficial velocity – pilot scale unit

In order to see the bigger image, data complied into one figure as shown in Figure 5. Overall, when considering both figures together, it becomes evident that the influence of jet velocity is negligible at low superficial gas velocities. The superficial gas velocity dictates bubble size, while the effect of jet velocity—regardless of whether it is altered through flow-rate adjustments or nozzle-size modifications—remains comparatively insignificant. This insight highlights the primary role of gas-phase hydrodynamics in controlling bubble behaviour, particularly in operational regimes where superficial gas velocity is low.

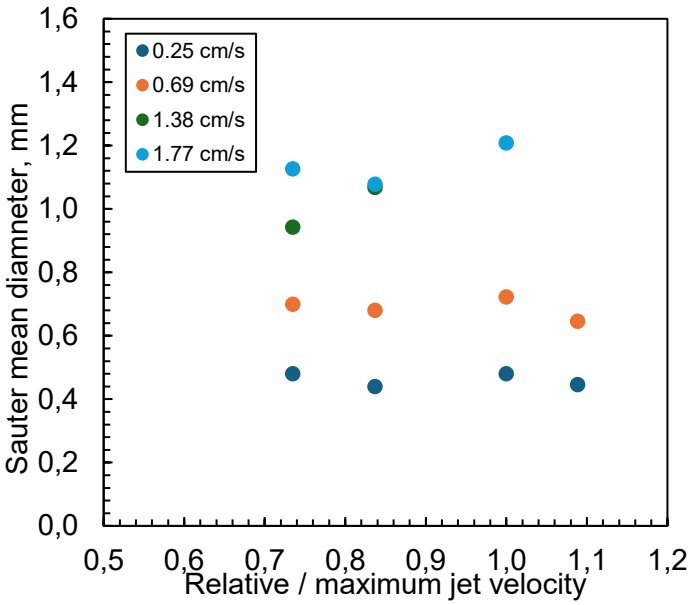

Figure 5. Sauter mean diameter variation as a function of superficial gas velocity - pilot scale unit

Following the same methodology as in the previous analysis, the same operating conditions were applied to the industrial-scale unit. However, in this case the nozzle configuration was kept constant, meaning that only the flow rate was varied to adjust the jet velocity. This approach allowed the assessment of flow-rate-driven jet velocity effects under industrial conditions without introducing additional variability associated with changes in nozzle size. Results are shown in Figure 6.

In this series of tests, the superficial gas velocity was increased up to a maximum of 2.5 cm/s. Under these conditions, the local gas hold-up was observed to vary between approximately 6.5 % and 35 %, while the sauter mean diameter ranged from 0.6 mm to 1.4 mm. These findings indicate a broad but consistent response of the two phase system to changes in gas velocity.

Similar conclusions can also be drawn for the industrial-scale unit. Even though larger equipment inherently introduces additional hydrodynamic complexity, the influence of jet velocity remained insignificant. The bubble size distribution and gas hold-up were predominantly governed by the superficial gas velocity rather than by variations in jet velocity generated through changes in liquid flow rate. This reinforces the overall conclusion that, in both laboratory and industrial scales, jet velocity plays only a minor role compared with the dominant effect of superficial gas velocity.

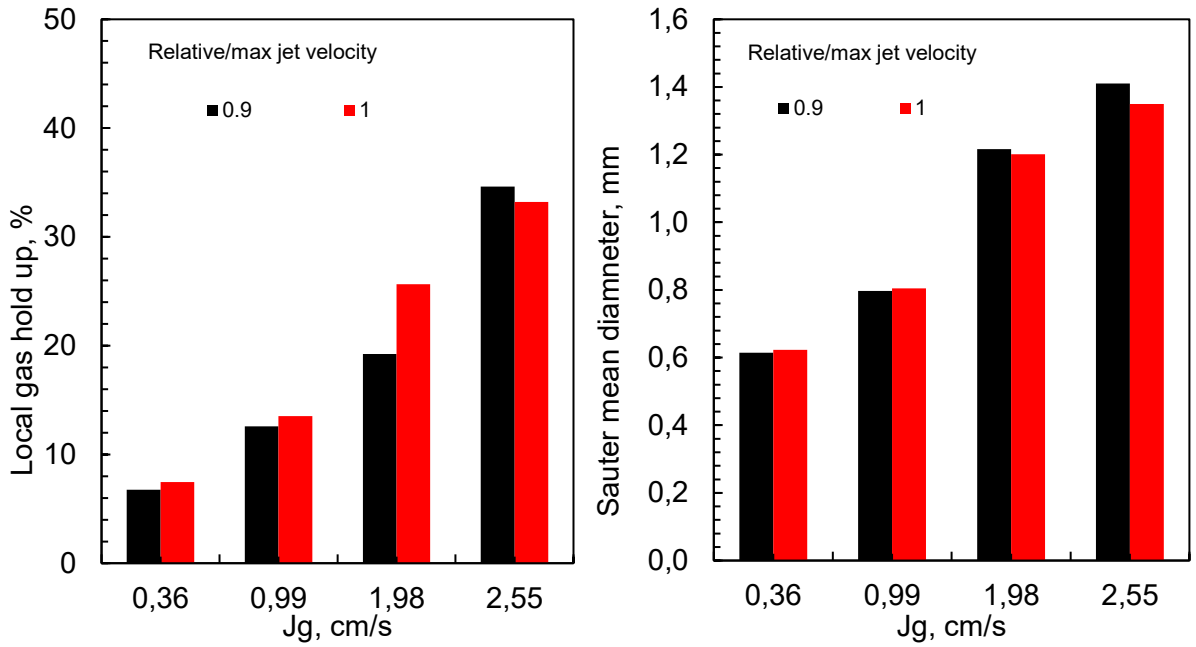

Figure 6. Sauter mean diameter and gas hold up as a function of superficial gas velocity - industrial scale

After an extensive investigation of the parameters influencing the Sauter mean diameter at different scales, Figure 7 compares all Concorde Cell units across laboratory, pilot, and industrial scales to evaluate potential scale-related effects. The industrial and pilot-scale units clearly follow the same trend line, indicating consistent hydrodynamic behaviour at larger scales. The laboratory-scale data, produced in Metso Research Center as part of research and development study, show slightly larger bubble sizes compared with the larger units. This deviation is likely attributable to the use of a different commercial frother brand in the laboratory measurements, which can influence bubble coalescence dynamics and consequently affect the resulting bubble size distribution.”

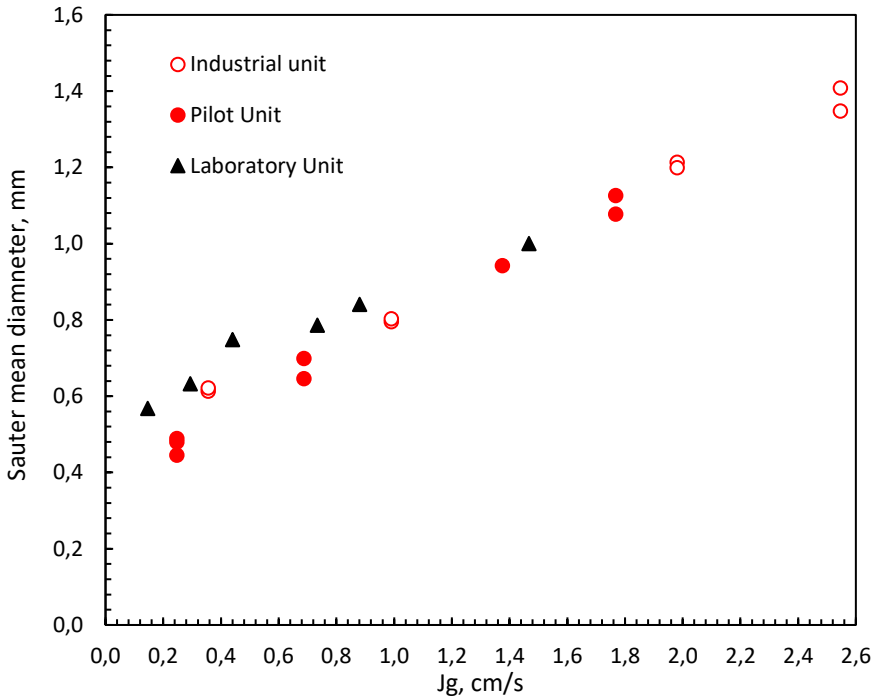

Figure 7. Sauter mean diameter as a function of superficial gas velocity at lab, pilot and industrial scale Concorde Cell

4. CONCLUSION

The results of this work demonstrate that air flowrate or superficial gas velocity is the primary factor governing bubble size and gas–liquid dispersion behavior in the Concorde Cell across all tested scales. Variations in jet velocity, whether created by adjusting the Concorde Blast Tube flow rate or by modifying nozzle size, produced only minor changes in bubble characteristics. These effects were consistent in both the pilot and industrial units and remained negligible, particularly at low superficial gas velocities.

The comparison between laboratory, pilot, and industrial data further supports this outcome. Despite differences in equipment size and operating environment, the pilot and industrial units exhibited nearly identical trends, indicating reliable scale-up behavior. The slightly larger bubble sizes observed in the laboratory unit can be attributed to differences in the commercial frother brand used during testing rather than to scale-related hydrodynamics.

REFERENCES

Ahmadi, R., Khodadadi, D. A., Abdollahy, M., Fan, M., (2014), “Nano-microbubble flotation of fine and ultrafine chalcopyrite particles”, International Journal of Mining Science and Technology, 24 (4), 559–566.

Calvo, G., Valero, A., (2022), “Strategic mineral resources: Availability and future estimations for the renewable energy sector”, Environmental Development, 41, 100640. https://doi.org/10.1016/j.envdev.2021.100640

Dai, Z., Fornasiero, D., Ralston, J., (1999), “Particle–bubble attachment in mineral flotation”, Journal of Colloid and Interface Science, 217 (1), 70–76.

Farrokhpay, S., Filippov, L., Fornasiero, D., (2021), “Flotation of fine particles: A review”, Mineral Processing and Extractive Metallurgy Review, 42 (7), 473–483.

Jameson, G. J., (2010), “Advances in fine and coarse particle flotation”, Canadian Metallurgical Quarterly, 49 (4), 325–330.

Klimpel, R., (1984), “Use of chemical reagents in flotation”, Chemical Engineering (New York, NY), 91 (18), 75–79.

Pease, J., Curry, D., Young, M., (2006), “Designing flotation circuits for high fines recovery”, Minerals Engineering, 19 (6–8), 831–840.

Schubert, H., (2008), “On the optimization of hydrodynamics in fine particle flotation”, Minerals Engineering, 21 (12–14), 930–936.

Yoon, R. H., Luttrell, G. H., (1989), “The effect of bubble size on fine particle flotation”, Mineral Processing and Extractive Metallurgy Review, 5 (1–4), 101–122. https://doi.org/10.1080/08827508908952646

GREEN EMULSION STRATEGIES FOR GRAPHITE FLOTATION: BIOSURFACTANT-COLLECTOR INTERACTIONS IN LIB BLACK MASS RECYCLING

Chiedza NZUMA*, Przemyslaw B. KOWALCZUK

Norwegian University of Science and Technology (NTNU), Department of Geosciences, S.P. Andersens veg 15,7031 Trondheim, Norway.
**Corresponding author: chiedza.t.nzuma@ntnu.no*

A B S T R A C T

The growing need for sustainable recycling of lithium-ion battery (LIB) black mass has intensified research on efficient graphite recovery with reduced dependence on non-renewable flotation reagents. Conventional petroleum-based collectors, such as kerosene and n-dodecane, are effective but contribute to high reagent consumption, and environmental impact. This study investigates the emulsification of these collectors with biosurfactants to enhance dispersion and reduce dosage without compromising flotation performance. Stable oil-in-water emulsions were prepared using xylolipid biosurfactants. The emulsions were subsequently evaluated for interfacial behavior and flotation efficiency.

A synthetic black mass composed of spheroidized graphite and $LiNi_{0.33}Mn_{0.33}Co_{0.33}O_2$ (NMC-111) enabled controlled analysis of collector–biosurfactant interactions. Interfacial tension measurements showed that biosurfactant emulsification reduced oil–water interfacial tension from 52-55 mN/m to below 10 mN/m, significantly improving collector dispersion and emulsion stability. As a result, n-dodecane dosage was reduced from 150 to 50 g/t without loss in graphite grade or recovery.

The findings demonstrate that biosurfactant-assisted emulsification enhances petroleum collector utilization through synergistic effects of improved dispersion and weak collector action. Overall, biosurfactant-emulsified collectors present a sustainable route to lower hydrocarbon usage and environmental impact in graphite flotation, supporting greener, low-reagent-intensity recycling processes for LIB black mass.

***Key words**: Flotation, battery recycling, green reagents*

1. INTRODUCTION

End-of-life lithium-ion battery (LIB) recycling generates a fine “black mass” powder composed primarily of graphite anode material and lithium metal oxide cathodes (e.g., NMC) (Anticoi et al., 2025). Froth flotation has emerged as an effective short-loop recycling route to separate graphite from this black mass by exploiting differences in surface wettability: graphite is inherently hydrophobic, whereas transition metal oxides are comparatively hydrophilic (Rieger et al., 2020). Conventional flotation of LIB black mass typically employs petroleum-derived collectors such as kerosene, diesel, or n-dodecane to selectively render graphite floatable (Arshad et al., 2020; Nazari et al., 2024). For instance, kerosene or diesel used in conjunction with frothers such as methyl isobutyl carbinol (MIBC) or pine oil can achieve graphite recoveries on the order of 85–90% from spent LIB materials (Nazari et al., 2024). However, these reagents present environmental and operational drawbacks. Their poor dispersion in water often requires high dosages, increasing costs, emissions, and process complexity (Cebeci, 2002; Maiyoh et al., 2015).

This motivates development of eco-friendly reagent strategies. Biosurfactants, including glycolipids and lipopeptides produced via microbial fermentation, have attracted increasing

interest as green substitutes for petrochemical surfactants (Chernyshova et al., 2023). They are typically biodegradable, renewable, exhibit low toxicity, and efficiently reduce surface and interfacial tension (Drakontis and Amin, 2020). Previous studies have demonstrated that enhancing the dispersion of oily collectors through emulsification can markedly improve flotation performance while lowering the required oil dosage. In graphite flotation, improved stability of diesel-in-water emulsions has been linked to enhanced graphite recovery (Shi et al., 2015). Similarly, Gao et al., (2022) reported that a β-cyclodextrin–stabilized emulsion of kerosene serves as an efficient graphite collector, achieving higher recovery than pure kerosene.

Building on this concept, the present work investigates a biosurfactant-emulsified collector system for environmentally benign graphite flotation. A naturally derived xylolipid biosurfactant was employed to emulsify n-dodecane, forming a stable oil in water emulsion suitable for addition to flotation pulps. Xylolipids, a class of glycolipids with xylose headgroups, were selected due to their pronounced surface activity; and ability to reduce the surface tension of water from 72 to approximately 36 mN/m at a concentration of 1 mg/L (Navare et al., 2014). We hypothesize that such a biosurfactant-emulsified oil will disperse more effectively and interact more selectively with graphite than conventional, non-emulsified oil, thereby enhancing graphite recovery and concentrate grade at reduced collector dosages.

2. MATERIAL AND METHODS

2.1. Materials

For this study, two different electrode powder materials for LIB manufacturing were used. For the cathode electrode, $LiNi_{0.33}Mn_{0.33}Co_{0.33}O_2$ (NMC-111) from MSE supplies (Product No. PO0126) and for the anode electrode, natural spheroidized graphite was obtained from ProGraphite GmbH (Product No. 1112–1). A model black mass was prepared by mixing Nickel-Manganese-Cobalt oxides (NMC) and graphite at a ratio of 67:33 based on compositions found in previous characterization of industrial black mass. N-dodecane (CAS. 112-40-3) was used as a promoter/collector. Methyl isobutyl carbinol (MIBC) supplied by Sigma Aldrich (99% $C_6H_{14}O$, Product No. 108-11-2) was used as a frother with a concentration of 7 ppm. Xylolipids supplied by Glycosurf were used as a biosurfactant. A fresh xylolipid stock solution (1%) was prepared weekly, using 1 g xylolipid and 100 mL of demineralised water. The xylolipid stock solution was stored at 4°C before use. For comparison, flotation with pure n-dodecane was conducted at 150 g/t, while the xylolipid-emulsified system was tested at a reduced collector dosage of 50 g/t.

2.2. Emulsion Preparation

To investigate the effect of oil–water emulsions on flotation behaviour, two different oil-in-water emulsions were prepared and characterized. A control emulsion was prepared by dispersing 2.5 mL of n-dodecane into 97.5 mL of deionized water without the addition of any biosurfactant. Emulsification was carried out using a high-shear homogenizer (Ultra-Turrax T25, IKA, Germany) operated at 11 000 min^{-1} for 60 s. This control system was used to assess the intrinsic stability and dispersion characteristics of oil droplets in the absence of surface-active compounds.

For the preparation of xylolipid-stabilized emulsions, a 1 wt% xylolipid stock solution was first prepared by dissolving the required amount of xylolipid in deionized water under magnetic stirring for 30 min. This stock solution was subsequently diluted to obtain a working concentration of 20 ppm. The required volume of the diluted xylolipid solution was then mixed with deionized water to yield a total aqueous volume of 97.5 mL, into which 2.5 mL of n-dodecane was added dropwise under continuous stirring. All emulsions were subjected to high-

shear mixing under identical conditions (11 000 min^{-1}, 60 s) to ensure comparable droplet size distributions.

2.3. Interfacial Tension Tests

Interfacial tension (IFT) measurements were carried out using the pendant drop method with a Krüss DSA100 drop shape analyzer (KRÜSS GmbH, Germany). In all experiments, deionized water or aqueous xylolipid solution was used as the heavier phase and introduced into a stainless-steel needle with an outer diameter of 2 mm. N-dodecane was used as the surrounding lighter phase and placed in an 80 mL glass cuvette.

Prior to each measurement, both liquid phases were equilibrated to room temperature (22 ± 1 °C). The shape of the pendant drop was recorded using a high-resolution CCD camera and analyzed using the Young–Laplace equation implemented in the instrument software. The B-factor, which relates the gravitational forces to surface forces and determines the quality of the curve fitting, was optimized in the range of 0.5–0.6 for all measurements to ensure accurate drop shape analysis.

For pure water–n-dodecane measurements, a water droplet volume of 31 µL was generated. For measurements involving biosurfactant, the 1 wt% xylolipid stock solution was diluted with deionized water to a final concentration of 20 ppm. A droplet volume of 12 µL was used for the xylolipid solution to avoid gravitational deformation and detachment. The reported IFT values were obtained by averaging four independent measurements to ensure reproducibility.

2.4. Flotation Setup

Flotation was conducted in a laboratory-scale mechanically stirred cell (XFD) using a 1.5 L capacity cell. The flotation experiments were performed with fixed parameters including impeller speed of 1200 rpm, air flowrate of 2.5 L/min. After each flotation experiment, the mass of collected froth was measured before and after drying in an oven under natural convection for 12 h at 50 °C to determine mass and water pull. Finally, representative samples of the froth phase product were analyzed by X-Ray Fluorescence (XRF) (Niton™ XL3t 980 from Thermo Scientific).

3. RESULTS AND DISCUSSION

The aim of the present work is to evaluate the effectiveness of a green emulsion flotation strategy for the separation of graphite from a synthetic LIB black mass. Accordingly, systematic investigations were conducted to: (i) examine the influence of the biosurfactant on oil–water interfacial tension and emulsion droplet size, (ii) assess the impact of reduced oil dosage on graphite flotation kinetics and overall recovery, and (iii) determine the selectivity of the process in producing a high-purity graphite concentrate while minimizing the use of petroleum-based reagents. The outcomes of this study aim to demonstrate the potential of this approach for developing more sustainable lithium-ion battery recycling flowsheets.

3.1. Emulsions

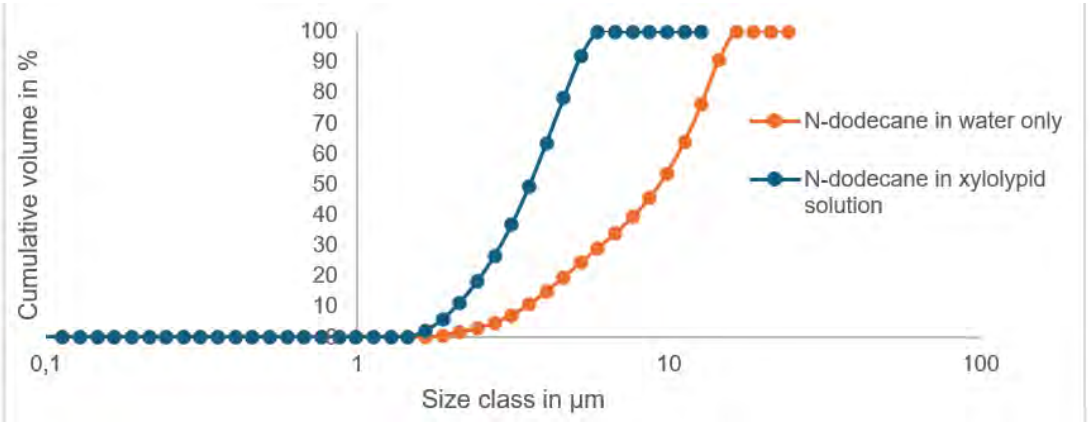

Figure 1. Oil droplet sizes in water and xylolipid solution emulsions

The oil droplet size distribution results indicate that n-dodecane forms considerably coarser and less stable emulsions in water alone compared with a 20 ppm xylolipid solution. In the water-only system, the d_{50} was 10 µm, whereas in the 20 ppm xylolipid solution it decreased to 4.5 µm (Figure 1). This indicates poor dispersion and rapid coalescence due to high oil–water interfacial tension, in the absence of xylolipids, (Cao et al., 2021; Pekdemir et al., 2005). Such coarse emulsions in flotation reduce collector efficiency because of lower surface area and reduced probability of droplet–particle interactions (Peng et al., 2017).

3.2. Interfacial Tension Tests

The IFT of the n-dodecane–deionized water system measured in the absence of surfactant was 52.83 ± 0.52 mN/m, as shown in appendix. This value agrees with literature data for the water–n-dodecane interface at ambient temperature, which typically range between 51 and 53 mN/m.

Addition of 20 ppm xylolipid, the IFT decreased to 9.97 ± 0.37 mN/m, corresponding to an approximately 81% reduction relative to the surfactant-free system. The pronounced reduction in interfacial tension from ~53 mN/m to ~10 mN/m in the presence of xylolipid has direct implications for both emulsion formation and flotation behaviour. Lower interfacial tension reduces the energy required to generate and disperse oil droplets, promoting the formation of finer and more stable oil-in-water emulsions and increasing the available interfacial area for particle–oil interactions (Cao et al., 2021; Zeppieri et al., 2001). In flotation systems, enhanced oil dispersion facilitates hydrophobic bridging and spreading mechanisms, thereby increasing the effective hydrophobicity of particles and improving particle–bubble attachment, particularly for fine or weakly hydrophobic particles. Reduced interfacial tension may also contribute to smaller bubble sizes and increased froth stability, further influencing particle recovery (Nguyen et al., 1998; Peng et al., 2017; Song et al., 1999).

3.3. Flotation Experiments

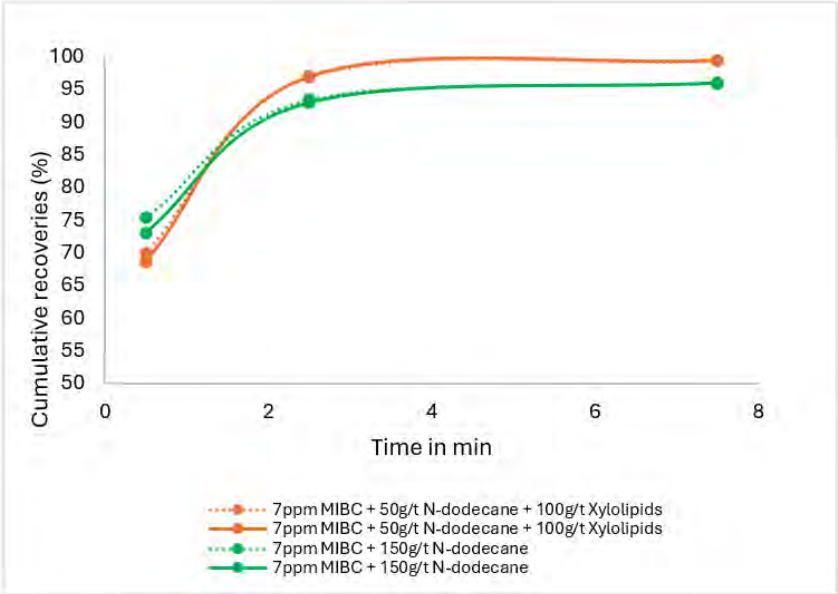

Figure 2. Time vs Graphite cumulative recoveries

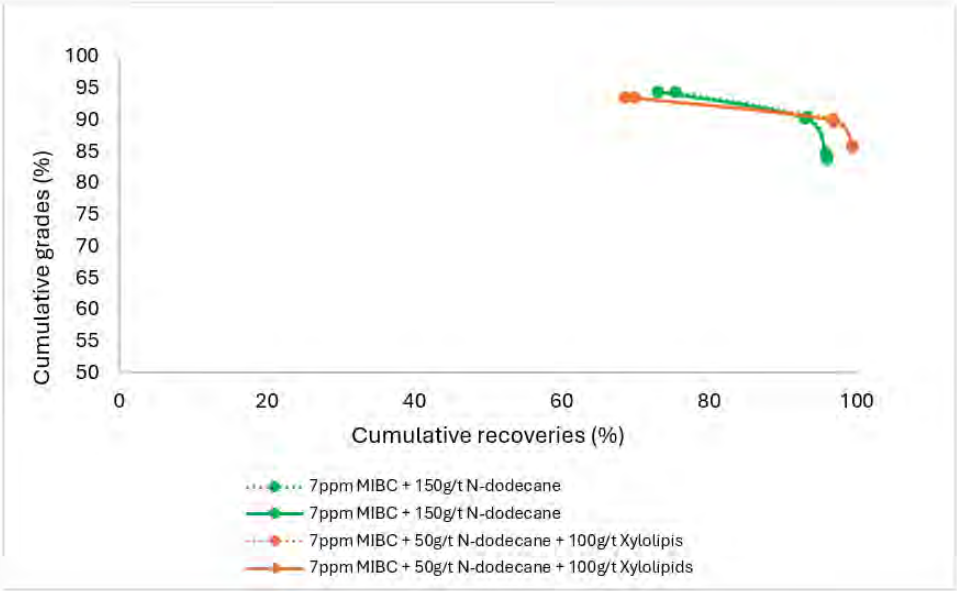

Figure 3. Graphite grade vs recovery curve

The graphite flotation results exhibit typical time-dependent behavior, characterized by rapid recovery of highly hydrophobic particles followed by slower recovery of less floatable material. At 0.5 min, both reagent schemes produced very high graphite grades (>93%) as shown in Figure 2, indicating that the initial concentrates consisted predominantly of well-liberated graphite.

At C2 (2.5 min), the xylolipid-containing system achieved a higher recovery (99%) compared with the n-dodecane-only system (96%) at comparable grades, demonstrating faster flotation kinetics. This improvement can be attributed to enhanced collector dispersion and adsorption in the presence of the biosurfactant, which promotes more efficient graphite hydrophobization and particle–bubble attachment. Cumulative recoveries reached 99% and 96% for the xylolipid and n-dodecane only systems, respectively. The corresponding cumulative grades were

similar, at 85% and 84% (Figure 3), indicating that the biosurfactant-emulsified collector improved recovery without compromising concentrate quality, with a reduction in N-dodecane dosage from 150 to 50g/t. Overall, the results confirm that xylolipid addition enhances flotation kinetics and collector efficiency.

4. CONCLUSION

This study demonstrates that biosurfactant-assisted emulsification provides an effective and more sustainable strategy for graphite flotation from lithium-ion battery black mass. Xylolipid-stabilized n-dodecane emulsions significantly reduced oil–water interfacial tension and produced finer, more stable collector dispersions, enabling a threefold reduction in collector dosage without compromising graphite grade or recovery. The improved dispersion enhanced flotation kinetics and collector utilization, while the biosurfactant also contributed to froth stabilization. These findings highlight the potential of biosurfactant–collector systems to decrease petroleum reagent consumption and environmental impact in LIB recycling. Overall, green emulsion flotation using renewable biosurfactants represents a promising pathway toward low-reagent-intensity and environmentally responsible graphite recovery processes.

REFERENCES

Anticoi, H., Garcia, L., Dan, G., Sola, P., Dorado, A. D., (2025) “Methodology for evaluation of lithium-ion black-mass battery recycling”, Journal of Material Cycles and Waste Management, 27 (2) 1019–1033.

Arshad, F., Li, L., Amin, K., Fan, E., Manurkar, N., Ahmad, A., Yang, J., Wu, F., Chen, R., (2020) “A comprehensive review of the advancement in recycling the anode and electrolyte from spent lithium ion batteries”, ACS Sustainable Chemistry & Engineering.

Cao, L., Chen, X., Peng, Y., (2021) “The formation and stabilization of oily collector emulsions – A critical review”, Mineral Processing and Extractive Metallurgy Review, 42 (6) 388–405.

Cebeci, Y., (2002) “The investigation of the floatability improvement of Yozgat Ayrıdam lignite using various collectors”, Fuel, 81 (3) 281–289.

Chernyshova, I., Slabov, V., Kota, H. R., (2023) “Emerging application of biosurfactants in metal extraction”, Current Opinion in Colloid & Interface Science, 68, 101763.

Drakontis, C. E., Amin, S., (2020) “Biosurfactants: Formulations, properties, and applications”, Current Opinion in Colloid & Interface Science, 48, 77–90.

Gao, J., Bu, X., Zhou, S., Wang, X., Alheshibri, M., Peng, Y., Xie, G., (2022) “Graphite flotation by β-cyclodextrin/kerosene Pickering emulsion as a novel collector”, Minerals Engineering, 178, 107412.

Joshi Navare, K., Singh, P., Prabhune, A., (2014) “New yeast isolate Pichia caribbica synthesizes xylolipid biosurfactant with enhanced functionality”, European Journal of Lipid Science and Technology, 116.

Maiyoh, G. K., Njoroge, R. W., Tuei, V. C., (2015) “Effects and mechanisms of kerosene use-related toxicity”, Environmental Toxicology and Pharmacology, 40 (1) 57–70.

Nazari, S., Vakylabad, A. B., Asgari, K., Li, J., Khoshdast, H., He, Y., Hassanzadeh, A., (2024) “Bubbles to batteries: A review of froth flotation for sustainably recycling spent lithium-ion batteries”, Journal of Energy Storage, 84, 110702.

Nguyen, A. V., Ralston, J., Schulze, H. J., (1998) “On modelling of bubble-particle attachment probability in flotation”, International Journal of Mineral Processing, 53, 225–249.

Pekdemir, T., Çopur, M., Urum, K., (2005) “Emulsification of crude oil–water systems using biosurfactants”, Process Safety and Environmental Protection, 83 (1) 38–46.

Peng, W., Wang, C., Hu, Y., Song, S., (2017) “Effect of droplet size of the emulsified kerosene on the floatation of amorphous graphite”, Journal of Dispersion Science and Technology, 38 (6) 889–894.

Rieger, J., Stuhr, S., Rutrecht, B., Morgenbesser, S., Nigl, T., Arnberger, A., Kunanz, H., Lesiak, S., (2020) “Graphite separation from lithium-ion battery black mass using froth flotation and quality evaluation for reuse as a secondary raw material including non-battery applications”, Energy & Fuels, 4, 5387–5416.

Shi, Q., Liang, X., Feng, Q., Chen, Y., Wu, B., (2015) “The relationship between the stability of emulsified diesel and flotation of graphite”, Minerals Engineering, 78, 89–92.

Song, S., Lopez-Valdivieso, A., Ding, Y., (1999) “Effects of nonpolar oil on hydrophobic flocculation of hematite and rhodochrosite fines”, Powder Technology, 101, 73–80.

Zeppieri, S., Rodríguez, J., López de Ramos, A. L., (2001) “Interfacial tension of alkane + water systems”, Journal of Chemical & Engineering Data, 46 (5) 1086–1088.

APPENDIX

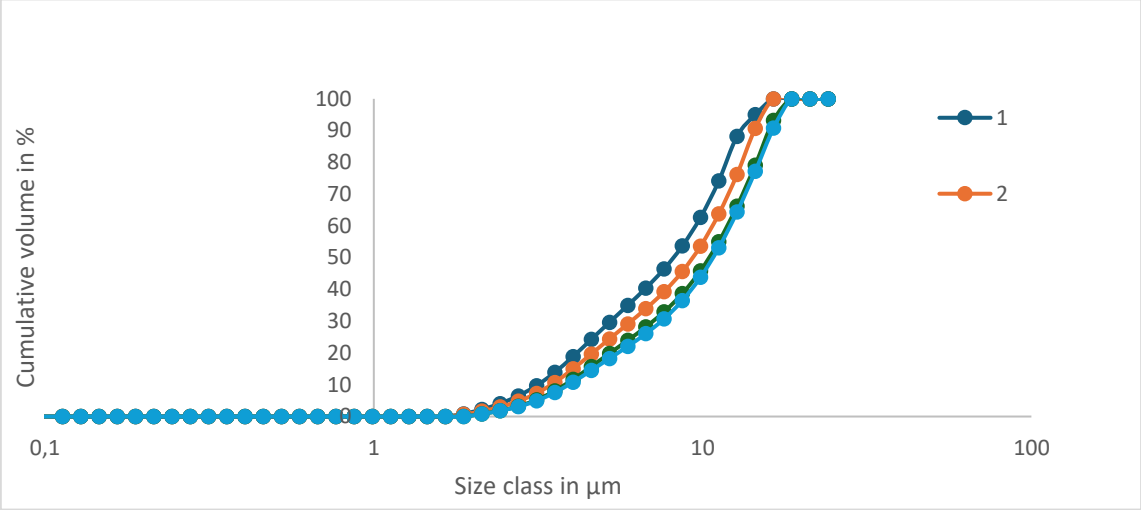

Figure 4. Repetitions for oil droplet sizes in water only

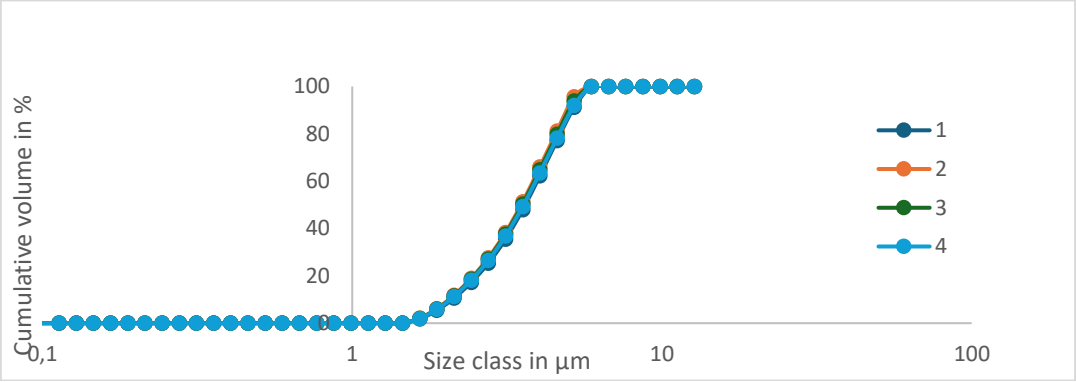

Figure 5. Repetitions for oil in xylolipid solution emulsions

Table 1. IFT measurements for N-dodecane-deionised water system

Test	Bubble volume	B factor	IFT mN/m
1	31	0,503	53,08
2	30,9	0,504	52,77
3	30,9	0,501	53,43
4	31	0,507	52,03
Average			52,82
SD			0,516

Table 2. IFT measurements for N-dodecane-20 ppm xylolipid system

Test	Bubble volume	B factor	IFT mN/m
1	12,1	0,642	10,33
2	11,9	0,649	9,82
3	11,9	0,643	10,2
4	12,1	0,655	9,52
Average			9,96
SD			0,319

INFLUENCE OF GLYCOL AND ALCOHOL TYPE FROTHER ON CRITICAL COALESCENCE CONCENTRATION AND BUBBLE SIZE

Gülşah GÜVEN[1,*], Şükriye Beste AYDIN[1], Ferihan GÖKTEPE[2], Gülay BULUT[2]

[1]*Istanbul Technical University, Faculty of Mines, Mineral Processing Engineering Department, 34469, Maslak, Istanbul, TÜRKİYE*
[2]*Balıkesir University, Balıkesir Technical College, Mining Department, 10145, Balıkesir, TÜRKİYE*
**Corresponding author: guveng15@itu.edu.tr*

A B S T R A C T

Flotation is a widely applied mineral beneficiation method that separates minerals based on their physicochemical surface properties using specific reagents. Depending on the objective, valuable minerals can be collected in the froth (direct flotation) or removed with the gangue (reverse flotation). This study investigates the effects of frother mixtures on flotation performance by analyzing their physicochemical behaviors through various measurements.

Methyl isobutyl carbinol (MIBC) and Butyl Glycol were used as frothers, both individually and in binary combinations. Parameters such as critical coalescence concentration (CCC), Sauter mean diameter, and froth thickness were measured under controlled conditions using a microflotation cell. Among the single frothers, MIBC exhibited a higher CCC value at 10.9 ppm, showing lower efficiency in preventing bubble coalescence compared to the blended systems. Conversely, the binary mixture of Butyl Glycol and MIBC demonstrated superior performance, achieving the lowest CCC at 7.8 ppm. The study concludes that the use of frother mixtures produces smaller and more stable bubbles through synergistic interactions between the reagents. These results indicate that strategic frother blending can significantly enhance flotation performance compared to the use of single frothers.

Key words: *Flotation, frother, Sauter diameter, froth thickness*

1. INTRODUCTION

The efficiency of flotation relies on the principle that mineral particles are selectively rendered hydrophobic, allowing them to attach to air bubbles and be transported to the pulp surface, where a froth layer is formed. However, when the particle size decreases below 10 μm, both floatability and selectivity are significantly reduced. To overcome these challenges, optimizing hydrodynamic conditions and reagent chemistry becomes critically important (Gaudin et al., 1931, Rulyov, 2001).

In addition to collectors and modifiers, frothers active at the air–water interface play a critical role in the success of flotation. Frothers are heteropolar surface-active compounds consisting of a hydrophilic (polar) group and a hydrophobic (apolar) hydrocarbon chain. These molecules align at the air–water interface, with their polar groups facing the water phase and their hydrophobic chains facing the air phase, thereby reducing the surface tension of water (Wills and Finch, 2015).

The main functions of frothers are to promote the formation of small bubbles, to create a protective film that prevents bubble coalescence, and to control the bubble rise velocity, thereby increasing their residence time within the pulp.

In evaluating frother performance, the Critical Coalescence Concentration (CCC) is considered one of the most important parameters. The CCC represents the minimum frother concentration required to prevent bubble coalescence, beyond which bubble size becomes independent of

further increases in concentration. The literature emphasizes that a reduction in bubble size enhances gas hold-up capacity, thereby improving the probability of mineral–bubble collisions. The molecular characteristics of different frothers, such as their HLB (hydrophile–lipophile balance) values and molecular weight, directly influence CCC values and bubble morphology (Drzymala and Kowalzcuk, 2018).

Increasing the concentration of a frother leads to a reduction in the Sauter mean bubble size until it hits the CCC, at which stage bubbles no longer merge. Although this trend is consistent for all frothers, the exact concentration required to reach the CCC varies depending on the type of frother used (Güven et al., 2020; Karakashev et al., 2021; Kowalczuk, 2013).

In recent years, the use of frother blends has become increasingly common in order to overcome the limitations associated with single reagent applications. Frother mixtures can enhance flotation performance by allowing independent control of bubble size and froth stability. Alcohol-type frothers (such as Methyl Isobutyl Carbinol (MIBC)) promote bubble size reduction and are particularly effective for the recovery of fine particles, whereas polyglycol-type frothers produce more persistent and viscous froths, providing advantages in the recovery of coarse particles. Accordingly, this study aims to systematically investigate the effects of single and binary combinations of Methyl Isobutyl Carbinol (MIBC) and Butyl Glycol, on bubble diameter (Sauter mean diameter), in a two-phase (air–water) system (An et al., 2018, Cappuccitti and Finch, 2008, Güven et al., 2020, Laskowski et al., 2003, Sam and Khoshdast, 2011, Tan et al., 2004).

2. MATERIAL AND METHODS

2.1. Material

Bubble size measurements were conducted using a micro flotation cell with an internal diameter of 30 mm, a height of 220 mm, and a total volume of 170 mL. Nitrogen gas was introduced into the system through a 15 μm pore diameter frit located at the cell's base, while the flow rate was maintained at a constant superficial gas velocity of 0.23 cm/s using a Dwyer flow meter.

Visual data of the bubbles were captured from the froth zone using a computer-interfaced digital USB microscope (BushmanCMOS 8 Led) with 1000× magnification. The experiments involved both individual frothers and dual frother blends across a concentration range of 1×10^{-6} to 50×10^{-6}. The detailed experimental setup and procedure are illustrated in Figure 1. For each condition, the diameters of approximately 50 to 200 bubbles per image were precisely analyzed using ImageJ software (version 1.8.0).

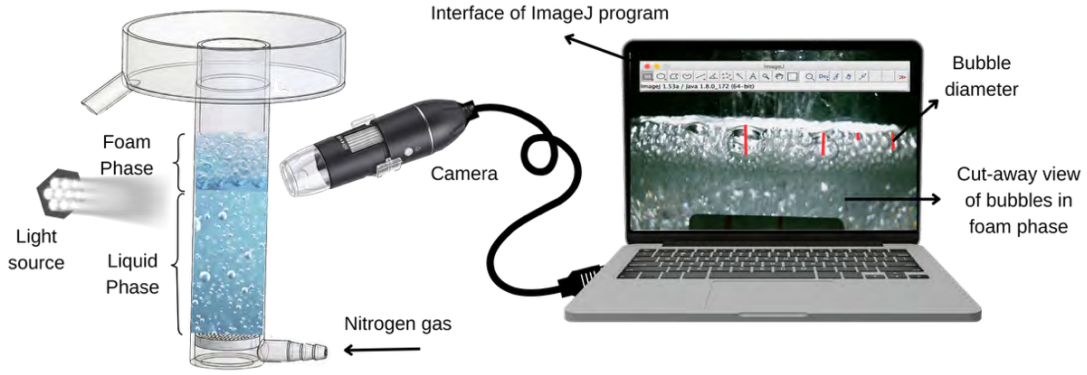

Figure 1. Experimental setup for the measurements

2.2. Method

Several operating conditions were kept constant throughout the tests. Frothers and their blends were introduced into the microflotation cell at concentrations of 1, 3, 5, 8, 10, 15, 20, 25, 30, 40, and 50 ppm in a total volume of 100 mL. The blend was prepared by mixing the two frothers in a 50:50 ratio. The information regarding the frothers used in this study is presented in Table 1.

Table 1. Chemical classification and physicochemical characteristics of selected flotation frothers

Frothers	Chemical Formula	Chemical Class	Molecular Weight (g/mol)	HLB
Butyl Glycol	$HOCH_2CH_2O(CH_2)_3CH_3$	Glycol Ether (Solvent-type)	118.17	-
MIBC	$(CH_3)_2CHCH_2CH(OH)CH_3$	Aliphatic Alcohol	102	6.1

MIBC used in the study is a low-molecular-weight aliphatic alcohol commonly preferred in the flotation industry. On the other hand, Butyl Glycol belongs to the glycol ether group and has a different molecular structure and foam stability potential compared to MIBC. These two frothers were selected to compare their ability to control bubble size in flotation systems and to represent different chemical groups.

Microflotation

Flotation is a relatively complex process involving many variables, including pH, collector type and concentration, frother type and concentration, temperature, and air flow rate. In order to better understand and control the parameters affecting flotation performance, microflotation is commonly used as a laboratory-scale preliminary technique. Microflotation tests are generally conducted on pure minerals as well as ores, and when pure minerals are studied, the technique is particularly useful for investigating the interactions between gangue or valuable minerals and flotation reagents. Microflotation is not only practical but also advantageous because it requires only small amounts of material. As a potential solution to the challenges associated with fine particle flotation, a technique referred to as microflotation has been applied, involving the use of relatively small amounts of microbubbles together with coarse air bubbles (Rulyov et al., 2020). Microflotation cells have been widely used to evaluate the suitability of flotation reagents and pulp chemistry conditions. Compared to other flotation devices, such as mechanical cells, the microflotation cell provides a low-turbulence environment due to the absence of an impeller and offers a high level of repeatability (Zhou et al., 2019). Typically made of glass and resembling a miniature column flotation unit, the microflotation cell consists of a gas inlet at the bottom, a body containing the pulp and a micro-porous material that disperses the gas into fine bubbles, an overflow section for the floated material, and an outlet for product collection.

Bubble Size and Froth Thickness Measurements

The Sauter Mean Diameter, defined as the ratio of volume to surface area, is a standard metric for characterizing gas/liquid or liquid/liquid dispersions. As the concentration of the frother increases, the Sauter mean diameter progressively declines until it reaches the Critical Coalescence Concentration (CCC)—the specific point at which bubble coalescence is effectively eliminated.

Different effects were observed for each frother and their respective mixtures used in the study. After frother additions at predetermined intervals, all froth images were recorded and analyzed using the ImageJ software to determine bubble diameter. Bubble diameters were calculated from camera-captured images for each frother and concentration. For each ppm level, approximately 50 to 100 bubbles were measured, and the average Feret diameter was

determined. The Sauter mean diameter (d_{32}) values were then calculated using the average Feret diameters obtained for each concentration.

Froth thickness measurements were also performed using the ImageJ program. A 1 cm reference line scale was used during the measurements.

Figure 2 shows the ImageJ program interface during measurements.

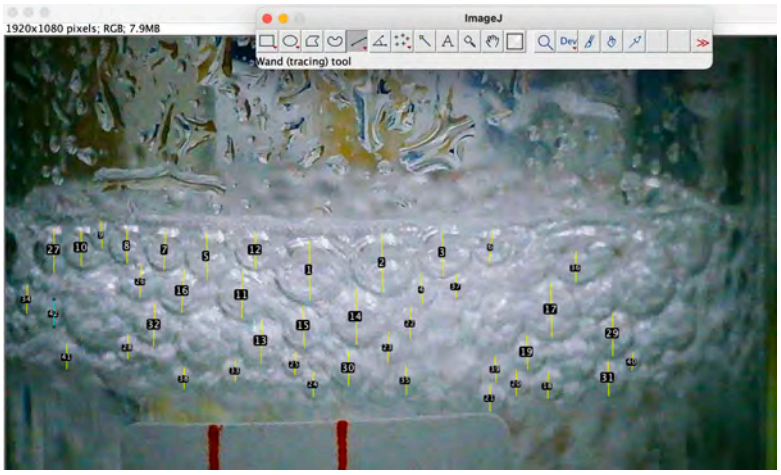

Figure 2. Interface of ImageJ program

The formulation (Equation (1)) used to calculate the Sauter mean diameter based on the average Feret diameter is provided below.

$$d_{32} = 6 * \frac{\left(\frac{4}{3}\right)*\pi*r^3}{4*\pi*r^2} \quad \text{(Eq.1)}$$

In the given formula:
d_{32}: Sauter mean diameter
r: Bubble radius (cm).

3. RESULTS AND DISCUSSION

3.1. Bubble Size

The variation in bubble size as a function of frother concentration was investigated for each frother used in the experiments. The results show that bubble size decreases with increasing frother concentration until it reaches the critical coalescence concentration (CCC), consistent with the behavior reported in the literature. Beyond the CCC value, no significant change in bubble diameter was observed, and the bubble size remained relatively stable. In Figure 3, the sample images of Butyl Glycol and MIBC at 50 ppm concentration are given.

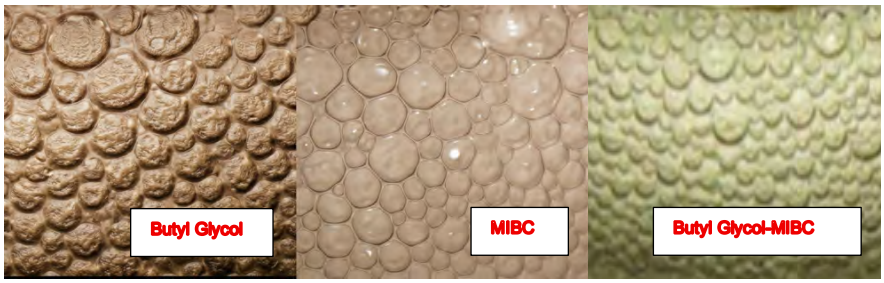

Figure 3. The images of Butyl Glycol, MIBC, and blends at 50 ppm concentration

The data presented in Figure 4 show that the Sauter mean diameter (d32) of the frothers studied decreased with increasing concentration until it stabilized at the CCC.

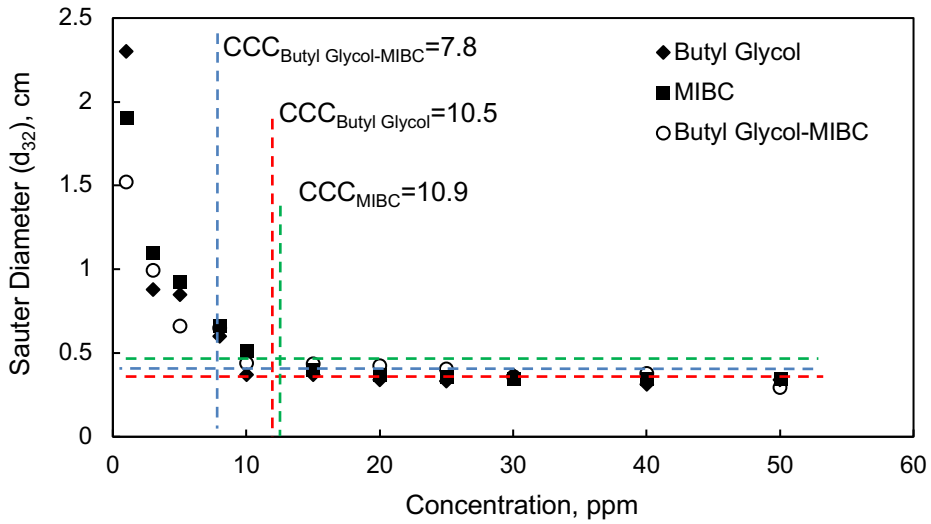

Figure 4. Sauter mean diameter depending on concentration of frother and frother blend

When the effects of the Butyl Glycol–MIBC mixture and the individual frothers on the Sauter mean diameter are compared, it is observed that the mixture exhibits a lower critical coalescence concentration (CCC) than the frothers used individually. For instance, when MIBC is used alone, the CCC value is 10.9, whereas when it is used in combination with Butyl Glycol, the CCC value decreases to 7.8. At the CCC point, Butyl Glycol produced the smallest Sauter mean bubble diameter among the tested frother systems. MIBC and the Butyl Glycol–MIBC mixture exhibited relatively similar bubble diameters, both being larger than that obtained with Butyl Glycol alone.

According to Güven et al. (2024), increasing the frother concentration quickly decreases the Sauter mean diameter up to a certain point where the bubble size stabilizes. It was reported that the CCC value of 10.9 ppm for MIBC can be improved to more efficient levels through the use of suitable mixtures.

3.2. Froth Thickness

To evaluate the effect of frother type and concentration on froth characteristics, the froth thickness was investigated. Figure 5 presents the effect of each frother used in the experiments on the froth phase thickness. According to the obtained results, Butyl Glycol produced the highest froth formation among the tested frothers. In general, the frothers reached their maximum froth thickness at concentrations between 30 and 40 ppm. Beyond this concentration range, the froth thickness remained mostly constant or exhibited only slight increases.

These results indicate that frother mixtures can reach the optimum operating conditions at lower reagent dosages compared to single frother systems, suggesting a potential advantage in terms of reagent consumption and process efficiency.

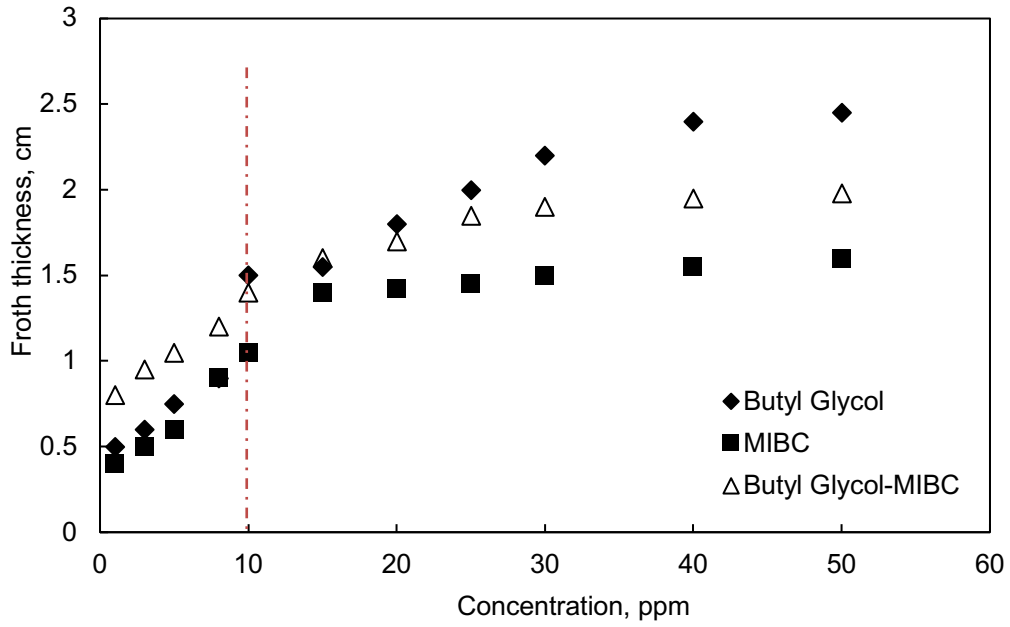

Figure 5. Effect of frothers on foam thickness

In flotation applications, frother concentrations lower than 10 ppm are typically used to determine froth thickness (Cappucitti and Finch, 2008). In the present study, at a 10 ppm frother concentration, Butyl Glycol was observed to produce a higher froth zone thickness (~1.5 cm) than MIBC (~1 cm). However, when the frothers were used as a mixture, the froth thickness was intermediate between those obtained with the individual frothers. Generally, smaller bubble sizes (lower Sauter diameters) increase specific surface area and liquid film volume, thereby enhancing water retention and froth stability and leading to increased roth thickness. The froth thickness observed with Butyl Glycol relative to MIBC is consistent with this principle, as Butyl Glycol stabilizes the froth more effectively by producing finer bubbles.

4. CONCLUSION

In this study, the behavior of frothers and their blends was investigated in terms of critical coalescence concentration (CCC), bubble size, and froth thickness. The experiments were conducted in a microflotation cell under constant conditions, using MIBC and Butyl Glycol at increasing concentrations, both individually and as mixtures. In all bubble size measurement tests, the frothers exhibxited a similar behavior; the bubble diameters decreased rapidly at first and then remained almost constant after reaching a specific concentration, showing no further effect from the frother concentration. Among the single frothers, MIBC had the highest CCC value at 10.9 ppm. In the tests with mixtures, the Butyl Glycol-MIBC blend reached a CCC point of 7.8 ppm. At the CCC point, the smallest Sauter mean bubble diameter was obtained with Butyl Glycol, whereas MIBC and the Butyl Glycol–MIBC mixture showed comparable but relatively larger bubble sizes.

Froth thickness increased with increasing frother concentration for all frother systems and approached a plateau at higher concentrations. Among the tested frothers, Butyl Glycol produced the highest froth thickness, indicating stronger froth stabilization compared to MIBC. The frother mixture exhibited intermediate behavior between the two individual frothers, suggesting that the combined use of the frothers modifies the froth structure without exceeding the stabilization effect of Butyl Glycol alone. In conclusion, using frother blends in flotation provided better results than using them individually. However, to better understand the effects

of these frothers and their blends, it is suggested that further studies should be conducted on pure minerals.

REFERENCES

An, M., Liao, Y., Zhao, Y., Li, X., Lai, Q., Liu, Z., He, Y., (2018) “Effect of frothers on removal of unburned carbon from coal-fired power plant fly ash by froth flotation”, Separation Science and Technology, 53 (3) 535-543.

Cappuccitti, F., Finch, J., (2008) “Development of new frothers through hydrodynamic characterization”, Mineral Engineering, 21 944-945.

Drzymala, J., Kowalczuk, P. B., (2018) “Classification and flotation frothers” Minerals, 8 (2) 53 1-24.

Gaudin, A. M., Groh, J. O., Henderson, H. B., (1931) “AIME”, Tech. Publ. No.414

Güven, G., Tunç, B., Aydin, Ş. B., Bulut, G., (2024) “Effects of frothers on bubbles size and flotation performance of hydrophobic minerals”, Journal of Central South University, 31 (7) 2280-2299.

Karakashev, S. I., Grozev, N. A., Ozdemır, O., (2021) “On the frother’s strength and its performance”, Minerals Engineering, 171 107093.

Kowalczuk P. B., (2013) “Determination of critical coalescence concentration and bubble size for surfactants used as flotation frothers”, Industrial & Engineering Chemistry Research, 52 (33) 11752−11757.

Laskowski, J., Tlhone, T., Williams, P., Ding, K., (2003) “Fundamental properties of the polyoxypropylene alkyl ether flotation frothers”, International Journal of Mineral Processing, 72 289-299.

Rulyov, N. N., (2001) “Turbulent microflotation: theory and experiment”, Colloids and Surfaces A: Physicochemical Engineering Aspects, 192 (1-3) 73-91.

Sam, A., Khoshdast, H., (2011) “Flotation Frothers: Review of Their Classifications, Properties and Preparation”, The Open Mineral Processing Journal, 26-35.

Tan, S. N., Fornasiero, D., Sedev, R., Ralston, J., (2004) “The interfacial conformation of polypropylene glycols and foam behaviour”, Colloids and Surfaces A: Physicochemical and Engineering Aspects, 250 (1-3) 307-315.

Wills, B. A., Finch, J. A., (2015), Froth Flotation, Wills’ Mineral Processing Technology: An Introduction to the Practical Aspects of Ore Treatment and Mineral Recovery, 8 265–380.

Zhou, Y., Albijanic, B., Tadesse, B., Wang, Y., Yang, J., Zhu, X., (2019) “Flotation behavior of pyrite in sub-bituminous and meta-bituminous coals with starch depressant in a microflotation cell”, Fuel Processing Technology, 187 1-15.

INVESTIGATION ON LEAD DEPRESSION IN ANTIMONY FLOTATION CIRCUIT

Begüm YÜCEL*, İbrahim GÖKTAŞ

ETİ BAKIR CO., Research and Development Center, 55300, Tekkeköy, Samsun, Türkiye
**Corresponding author: begum.ozdur@etibakir.com.tr*

A B S T R A C T

Antimony is a strategic metal defined as a critical raw material by the European Union. One of the key factors determining the quality of antimony concentrates is the level of impurities, with lead (Pb) content playing a particularly restrictive role in terms of both marketability and metallurgical performance. In the literature, various reagents such as sodium metabisulfite, polysaccharides, and dichromates have been tested for Pb depression in different ore types, and their influence on selectivity has been reported. At the Eti Bakır Halıköy Plant, periodic increases in Pb grade have been observed to negatively affect concentrate quality, leading to laboratory and plant-scale flotation experiments aimed at addressing this issue. The results demonstrated that among the reagents tested, sodium metabisulfite was the most effective compound for Pb depression. Plant-scale trials similarly showed that the Pb content of the concentrate decreased by nearly half. These findings reveal that sodium metabisulfite is an effective reagent for Pb depression in antimony flotation circuits, consistent with literature reports, while its industrial application improves concentrate quality.

Key words: *Antimony, lead, flotation, raw material, depression*

1. INTRODUCTION

Antimony (Sb) is a critical metalloid widely used in many strategic applications such as flame retardants, alloys, electronic components, and energy storage systems (USGS, 2024), and it is defined as a critical raw material by the European Union due to limited global supply and geographically concentrated production (European Commission, 2020). Froth flotation is widely applied in the beneficiation of sulfidic antimony ores; however, antimony flotation involves significant selectivity problems because sulfide impurity minerals associated with stibnite (Sb_2S_3) exhibit similar surface properties, and the flotation of Pb-bearing minerals (e.g., galena and Pb-bearing sulfosalts) together with stibnite can increase Pb contamination in antimony concentrates (Özer, 2022; Segura-Salazar & Brito-Parada, 2021). The presence of high Pb impurities in antimony concentrates increases slag formation (i.e., slagging/refining load) during pyrometallurgical processing and may lead to additional Sb losses to slag; therefore, Pb depression has emerged as one of the fundamental process challenges, especially given that some smelters impose strict Pb limits for stibnite concentrates (Segura-Salazar & Brito-Parada, 2021; Moosavi-Khoonsari et al., 2022; Anderson, 2012). In the literature, various approaches for Pb depression have been reported, including the use of strong oxidizing depressants such as dichromates, polysaccharide-based reagents, sulfidizing and reducing reagents, as well as optimization strategies based on pH and particle size (Bulatovic, 2007; Nyakubaya et al., 2016).

In this study, depressant and activator reagents were evaluated in laboratory flotation tests to control Pb impurities in the antimony flotation circuit of the Eti Bakır Halıköy Plant. The most effective depressant was then tested at plant scale to validate the laboratory findings and support process optimization for reducing Pb impurities in antimony flotation circuits.

2. MATERIAL AND METHODS

2.1. Sample and Ore Characterization

This study was carried out on an antimony ore sample obtained from the Eti Bakır Halıköy Plant located in the Beydağ district of İzmir, Türkiye. The flotation feed sample used in the experiments was selected to represent operating periods during which Pb impurities adversely affected concentrate quality at the plant. The chemical composition of the ore sample was determined by ICP-OES following appropriate sample digestion for As, Sb, Pb, and Fe, while S was analyzed by combustion at 950 °C. The analytical results are presented in Table 1.

Table 1. Chemical analysis of feed ore

Element	Sb	Pb	As	S	Fe
%	4,17	0,18	0,25	4,4	2,72

Mineralogical characterization studies were carried out using scanning electron microscopy equipped with a Mineral Liberation Analyzer (SEM–MLA) system to determine the distribution of antimony and gangue minerals in the flotation feed. Modal mineralogy was quantified for the −212+150, −150+106, −106+75, −75+53, −53+38, and −38+20 µm size fractions, and the results are summarized in Table 2. Quartz is the dominant mineral in all fractions (>70%). Antimony occurs almost entirely as stibnite, accounting for ~5–14% across the size range. Sulfides are mainly pyrite with minor arsenopyrite and generally remain below 10%. Pb-bearing minerals are present in minor amounts, dominated by oxidized/secondary phases (predominantly wulfenite) with subordinate anglesite and clausthalite–galena. Minor jacobsite–magnetite is observed in all fractions, while dolomite–ankerite and clay/silicate gangue (muscovite, illite, smectite) become relatively more abundant in the finer fractions.

Table 2. Modal mineralogy analysis results of sample

	Modal Mineralogy					
Mineral, Mass (%)	**-212+150 µm**	**-150+106 µm**	**-106+75 µm**	**-75+53 µm**	**-53+38 µm**	**-38+20 µm**
Stibnite	13,91	8,70	8,15	6,09	5,10	6,40
Quartz	67,74	76,28	75,29	75,20	76,23	69,51
Pyrite	8,27	6,18	6,14	5,32	5,38	7,05
Muscovite	1,96	2,43	3,96	6,72	6,18	9,07
Jacobsite-Magnetite	1,90	1,51	1,17	1,43	1,64	2,10
Arsenopyrite	0,30	0,15	0,04	0,15	0,13	0,21
Dolomite-Ankerite	0,43	0,62	0,63	0,65	0,94	1,04
Illite	0,71	0,64	0,63	0,56	0,52	0,40
Smectite	0,94	0,87	0,92	0,91	0,95	0,86
Anglesite	0,37	0,09	0,18	0,07	0,09	0,08
Wulfenite	0,10	0,09	0,07	0,05	0,05	0,05
Clausthalite-Galena	0,11	0,03	0,06	0,03	0,04	0,08
Others	3,26	2,41	2,76	2,82	2,74	3,15
Total	100,00	100,00	100,00	100,00	100,00	100,00

The distribution of lead-bearing mineral phases identified in the flotation feed is presented in Table 3. According to the results, lead occurs predominantly in the form of wulfenite, accounting for 60,61% of the total Pb-bearing phases. Anglesite is identified as the second most abundant Pb mineral with a proportion of 19,59%, followed by mathewrogersite at 10,43%. Lead is also present at lower proportions as clausthalite–galena 7,04% and elemental lead 2,33%. The predominance of oxidized and secondary lead minerals indicates that Pb in the ore is primarily associated with secondary mineral phases rather than sulfide phases, which is a critical factor influencing Pb flotation behavior and the selection of appropriate depression strategies.

Table 3. Distribution of Pb-bearing mineral phases identified in the flotation feed based on mineralogical analysis.

Pb-Bearing Minerals (%)				
Anglesite	**Clausthalite-Galena**	**Lead**	**Mathewrogersite**	**Wulfenite**
19,59	7,04	2,33	10,43	60,61

2.2. Method

Flotation experiments were conducted using a Denver-type laboratory flotation machine to simulate the rougher and cleaner flotation stages applied in the plant. The tests were performed under plant-representative conditions, using a particle size of 130 µm and a pulp pH of 6.0–6.5. Rougher flotation tests were carried out at a slurry solids concentration of 30–35%, whereas cleaner flotation tests were conducted at approximately 20% solids. Copper sulfate was used as the activator to reduce the Pb grade in the antimony concentrate, while starch, potassium dichromate, and sodium metabisulfite were evaluated as depressants at different dosage levels.

Table 4. The all flotation parameters in the experiments

Parameter	**Value**
Flotation machine	Denver
Grind size	130 µm
Rougher solids	30–35%
Cleaner solids	20%
pH range	6-6.5
Collector	Aero 3477
Activators	$Pb(NO_3)_2$, $CuSO_4$
Depressants	Starch, $K_2Cr_2O_7$, SMBS

3. RESULTS AND DISCUSSION

3.1. Effect of Copper Sulfate

As the reference flotation condition, the reagent scheme applied in the plant operation, consisting of 110 g/t Aero 3477 collector and 90 g/t lead nitrate ($Pb(NO_3)_2$) as activator, was used. The results obtained under these conditions indicated that Pb-bearing mineral phases were also activated and subsequently recovered into the concentrate. Considering that lead nitrate may activate not only stibnite but also Pb-bearing mineral phases, copper sulfate ($CuSO_4$) was evaluated as an alternative activator. Copper sulfate was tested at a dosage of 500 g/t under the same flotation conditions with a conditioning time of 10 minutes applied prior to flotation.

Table 5. Effect of activator type on Sb and Pb grades and recoveries in antimony flotation

Activators	**Grade (%)**		**Recovery (%)**	
	Sb	**Pb**	**Sb**	**Pb**
$Pb(NO_3)_2$	61,31	2,20	27,18	25,58
$CuSO_4$	59,17	2,00	39,58	33,25

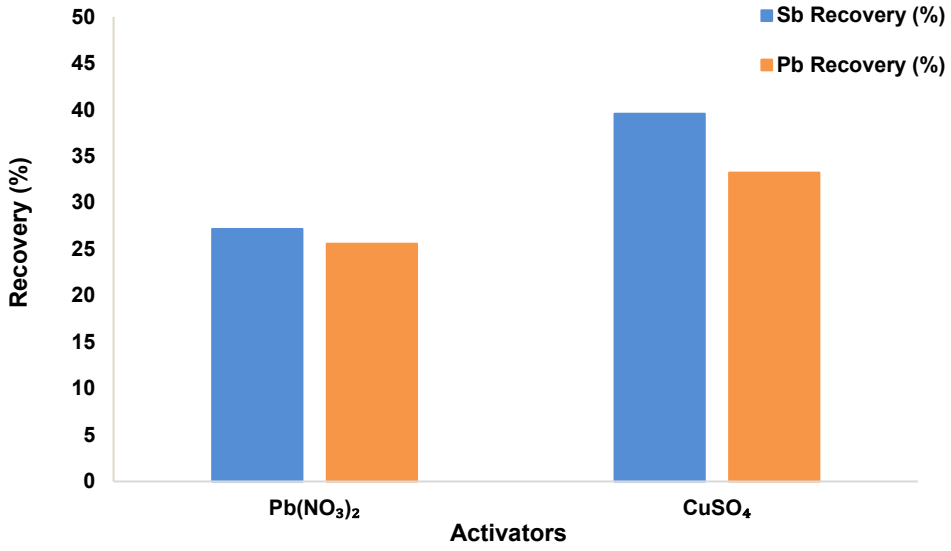

Figure 2. Relationship between Sb recovery and Pb recovery obtained using different activators in antimony flotation.

Table 5 and Figure 2 comparatively illustrate the effects of $Pb(NO_3)_2$ and $CuSO_4$ activators on Sb and Pb recovery behavior in antimony flotation. $Pb(NO_3)_2$ produced a higher Sb grade, but Sb recovery remained limited and Pb recovery was relatively low. In contrast, $CuSO_4$ significantly increased Sb recovery; however, this improvement was accompanied by a simultaneous increase in Pb recovery, indicating a stronger but less selective activation response. Overall, $CuSO_4$ is an effective activator for antimony flotation, but when used alone, it does not provide sufficient selectivity for Pb depression.

3.2. Effect of Potassium Dichromate

In order to evaluate the effect of potassium dichromate on Pb depression behavior, flotation tests were conducted by adding potassium dichromate to the plant reference reagent scheme consisting of 110 g/t Aero 3477 collector and 90 g/t lead nitrate $Pb(NO_3)_2$ activator. Potassium dichromate was applied at dosages of 500, 1000, and 2000 g/t, and a conditioning time of 10 minutes was used prior to flotation. The resulting flotation performance was comparatively assessed in terms of Sb recovery and Pb transport to the concentrate.

Table 6. Effect of potassium dichromate dosage on Sb–Pb grade and recovery selectivity in antimony flotation

Potassium Dichromate ($K_2Cr_2O_7$)	**Grade (%)**		**Recovery (%)**	
	Sb	**Pb**	**Sb**	**Pb**
0 (Base)	61,31	2,20	27,18	25,58
500	36,94	1,20	5,57	4,09
1000	31,56	1,03	10,20	5,97
2000	31,37	1,24	4,29	4,02

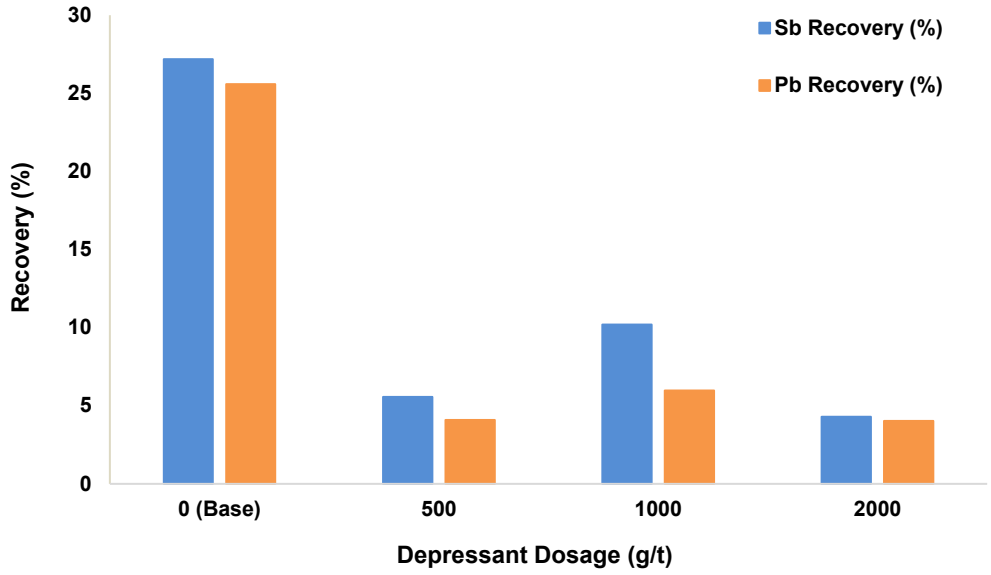

Figure 3. Relationship between Sb recovery and Pb recovery at different potassium dichromate ($K_2Cr_2O_7$) dosages

Table 6 and Figure 3 evaluate the effect of potassium dichromate on Pb depression in terms of Sb–Pb selectivity, based on both grade and recovery data. The addition of potassium dichromate resulted in a pronounced decrease in Pb recovery, indicating that dichromate effectively suppresses the flotation behavior of Pb-bearing mineral phases by altering their surface properties. However, the addition of potassium dichromate also adversely affected Sb recovery, and at higher dosages the system was observed to enter an over-depression regime. This observation suggests that potassium dichromate exerts a depressing effect not only on Pb-bearing minerals but also on stibnite surfaces. According to the experimental results, a potassium dichromate dosage of 1000 g/t provides the most favorable condition for Pb depression; nevertheless, even at this dosage, noticeable reductions in stibnite grade and recovery were observed, leading to a decrease in overall concentrate efficiency.

3.3. Effect of Starch

Starch is a polysaccharide-based depressant that is widely used to suppress the flotation behavior of Pb-bearing mineral phases. In this study, the effect of starch on the control of Pb impurity in antimony flotation was investigated through flotation tests conducted by adding starch at different dosages to the base flotation condition. Starch was applied at dosages of 500, 1000, and 1500 g/t, with the pulp conditioned for 10 minutes prior to flotation, and the resulting flotation performance was comparatively evaluated in terms of Sb recovery and Pb transport to the concentrate.

Table 7. Effect of starch dosage on Sb and Pb grade and recovery

Starch	Grade (%)		Recovery (%)	
	Sb	Pb	Sb	Pb
0 (Base)	61,31	2,20	27,18	25,58
500	55,26	2,61	64,43	67,06
1000	59,55	1,92	23,02	17,52
1500	57,09	2,43	54,60	53,89

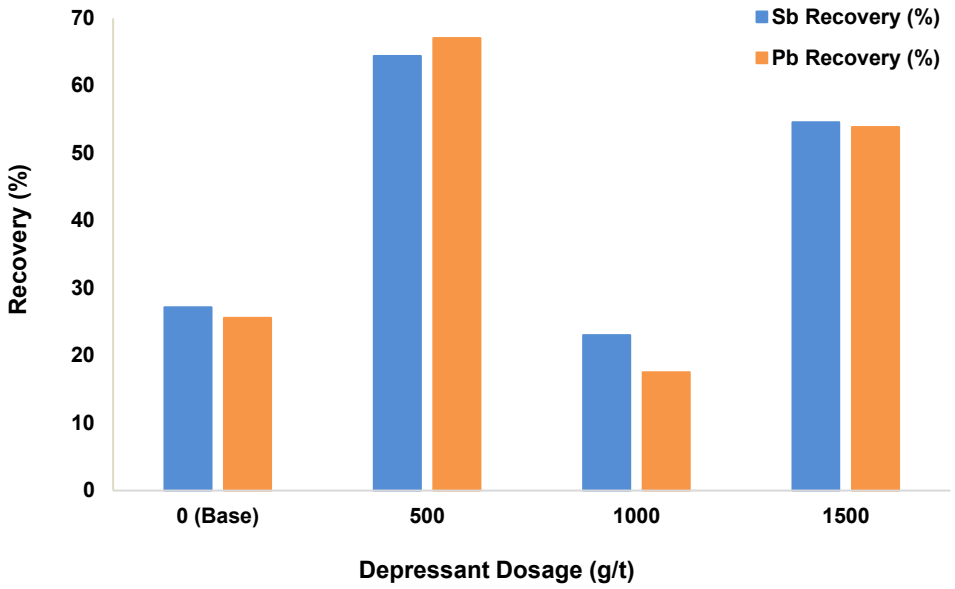

Figure 4. Relationship between Sb recovery and Pb recovery at different starch dosages

Table 7 and Figure 4 evaluate the effect of starch dosage on Sb–Pb selectivity based on Sb and Pb recovery data. At a starch dosage of 500 g/t, a marked increase in both Sb and Pb recoveries was observed; however, the parallel increase in Pb recovery relative to Sb recovery indicates that starch did not provide sufficient selectivity for Pb depression at this dosage. A similar trend was observed at a starch dosage of 1500 g/t, where simultaneous increases in Sb and Pb recoveries suggested continued Pb carryover to the concentrate. In contrast, at a starch dosage of 1000 g/t, a pronounced decrease in Pb recovery was achieved while Sb recovery was maintained at an acceptable level. These results indicate that starch has the potential to depress Pb-bearing mineral phases in antimony flotation; however, this effect is accompanied by partial losses in stibnite grade and recovery.

3.4. Effect of Sodium Metabisulfite

Sodium metabisulfite (SMBS) is a reducing reagent widely used in sulfide flotation systems to control mineral surface oxidation and, in particular, to suppress the floatability of Pb-bearing phases. In this study, the effect of SMBS on the control of Pb impurity in antimony flotation was evaluated through flotation tests conducted by adding SMBS to the base flotation condition at dosages of 1500 and 2000 g/t.

Table 8. Effect of sodium metabisulfite dosage on Sb and Pb grade and recovery

Sodium Metabisulfite	Grade (%)		Recovery (%)	
	Sb	Pb	Sb	Pb
0 (Base)	61,31	2,20	27,18	25,58
1500	60,29	0,58	20,63	4,42
2000	65,46	1,35	20,55	7,74

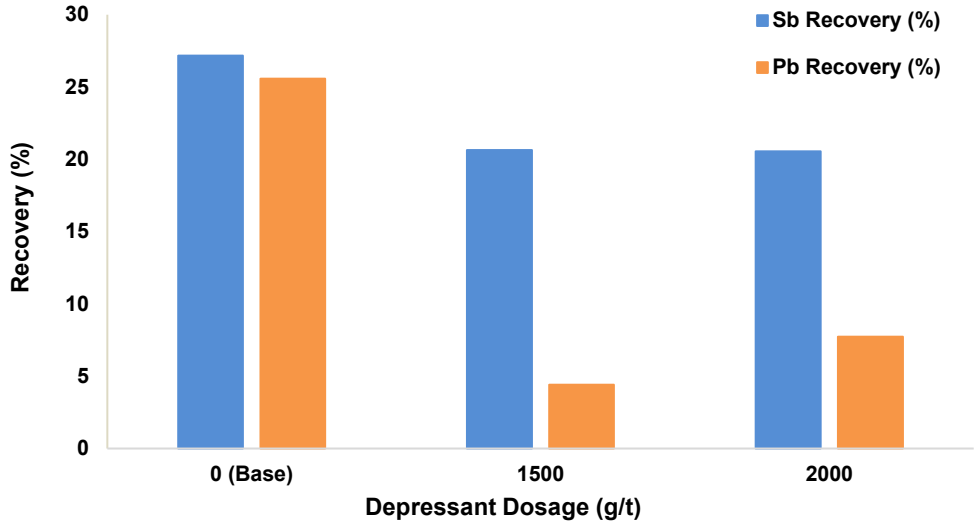

Figure 5. Relationship between Sb recovery and Pb recovery at different sodium metabisulfite dosages.

Table 8 and Figure 5 evaluate the effect of sodium metabisulfite (SMBS) addition on Sb–Pb selectivity based on Sb and Pb recovery data. A pronounced decrease in Pb recovery was observed with the addition of SMBS, indicating that SMBS effectively suppresses the flotation behavior of Pb-bearing mineral phases by passivating their surfaces under reducing conditions.

At an SMBS dosage of 1500 g/t, Pb recovery decreased to a minimum level while Sb recovery was largely preserved, demonstrating a high degree of selectivity under these conditions. These findings indicate that an SMBS dosage of 1500 g/t provides the most favorable balance between effective Pb depression and Sb recovery and confirm that SMBS is a highly effective and selective depressant for controlling Pb impurity in antimony flotation.

3.5. Plant Trial Results

Sodium metabisulfite (SMBS), which yielded the most effective Pb depression performance in laboratory-scale flotation tests, was subsequently applied at industrial scale under plant operating conditions. In the plant trial, SMBS was added to the grinding circuit at a dosage of 1500 g/t to provide preconditioning prior to flotation, and the application was maintained for one week under normal operating conditions. Plant performance was evaluated based on weekly average analytical results obtained before and after the SMBS application period. Since the SMBS application was implemented as a process control measure during operating periods characterized by elevated feed Pb grade (%), plant performance was not assessed using overall weekly averages. Instead, the evaluation focused on the relationship between Pb feed and concentrate grades, allowing a more representative assessment of the Pb depression effectiveness of SMBS under high Pb feed regimes.

Table 9. Plant-scale comparison of feed and concentrate Pb grades and enrichment ratios under baseline and SMBS application condition

Condition	Feed		Concentrate		Enrichment Ratio (ER)	
	Pb, %	Sb, %	Pb, %	Sb, %	Pb	Sb
Baseline	0,17	2,89	3,58	68,53	21,06	23,71
SMBS (1500 g/t, 1 week)	0,27	2,88	1,45	69,01	5,37	23,96

According to the plant-scale results presented in Table 9, under the base operating conditions without SMBS addition, the Pb grade of the feed was 0.17%, while the Pb grade in the concentrate was determined to be 3.58%. In contrast, during the application week in which SMBS was added to the grinding circuit at a dosage of 1500 g/t, a pronounced decrease in concentrate Pb grade was observed, declining to 1.45%, despite an increase in the feed Pb grade to 0.27%. The reduction in concentrate Pb grade under elevated feed Pb conditions clearly demonstrates the effectiveness of SMBS in suppressing the flotation behavior of Pb-bearing mineral phases. The marked decrease in the enrichment ratio further supports that the floatability of Pb was significantly restricted within the flotation circuit. This behavior suggests that SMBS alters the surface chemistry of Pb-bearing mineral phases through its reducing properties, thereby limiting collector adsorption. At the same time, the Sb grade of the concentrate remained stable and exhibited a slight increase during SMBS application, indicating that stibnite flotation was not adversely affected and that the overall flotation performance was not disrupted. The plant-scale findings are consistent with the Pb depression mechanism identified in laboratory-scale flotation experiments and confirm that SMBS is an effective and industrially applicable process control reagent for controlling Pb impurity in antimony flotation circuits.

4. CONCLUSION

In this study, laboratory- and plant-scale flotation investigations were conducted to suppress lead (Pb), a key impurity limiting concentrate quality in an antimony flotation circuit. The effects of depressant and activator reagents on Pb depression were evaluated using grade–recovery data and Sb–Pb recovery comparisons.

Among the tested reagents, potassium dichromate provided effective Pb depression but also depressed stibnite, causing marked losses in Sb grade and recovery. In addition, the toxicity and environmental risks of dichromate compounds limit their suitability for industrial application; therefore, potassium dichromate was not considered for plant use.
Starch partially reduced Pb transfer at certain dosages, but its negative impact on Sb recovery and the narrow optimum window resulted in limited selectivity. In contrast, sodium metabisulfite (SMBS) selectively suppressed Pb-bearing phases while largely preserving Sb recovery. In laboratory tests, SMBS reduced the Pb grade in the antimony concentrate from 2.20% to 0.58% and decreased Pb recovery from 25.58% to 4.42%.
Plant trials confirmed these findings, particularly under elevated Pb feed grades. SMBS preconditioning in the grinding circuit reduced Pb floatability and lowered the average concentrate Pb grade from 3.58% to 1.45%, while slightly improving Sb grade from 68.53% to 69.01%.

Overall, the combined laboratory and plant results indicate that SMBS is the most suitable option for Pb control in antimony flotation from technical, operational, and environmental perspectives, offering lower risk and better acceptability than chromate-based depressants.

REFERENCES

Anderson, C. G., (2012) “The metallurgy of antimony”, Chemie der Erde – Geochemistry, 72 (S4) 3–8.
Bulatovic, S. M., (2007) “Handbook of flotation reagents”, Elsevier.

European Commission, (2020) “Critical raw materials resilience: Charting a path towards greater security and sustainability”, European Commission.

Moosavi-Khoonsari, E., Mostaghel, S., Siegmund, A., Cloutier, J.-P., (2022) “A review on pyrometallurgical extraction of antimony from primary resources: Current practices and evolving processes”, Processes, 10 (8) 1590.

Nyakubaya, K., Muleya, E., Mutatu, W., (2016) “Selective froth flotation concentration of antimonite ore from a mixture of antimony, lead and arsenic ores”, International Journal of Engineering and Applied Sciences, 3 (5) 25–29.

Özer, M., (2022) “Flotation of antimony ores with high arsenic content”, Physicochemical Problems of Mineral Processing, 58 (5).

Segura-Salazar, J., Brito-Parada, P. R., (2021) “Stibnite froth flotation: A critical review”, Minerals Engineering, 163, 106713.

USGS, (2024) “Mineral commodity summaries: Antimony”, United States Geological Survey.

REAGENT OPTIMIZATION IN THE FLOTATION BENEFICIATION OF SILICA SAND USED IN GLASS PRODUCTION

Selen ULUSKAN*, Gülay BULUT

Istanbul Technical University, Faculty of Mines, Mineral Processing Engineering Department, 34469, Maslak, Istanbul, TÜRKİYE
**Corresponding author: uluskan19@itu.edu.tr*

A B S T R A C T

Silica sand is one of the main raw materials of the glass industry and requires beneficiation processes due to its high purity requirements. Flotation stands out as an effective method among the beneficiation processes applied for this purpose. The reverse flotation method applied to silica sand is mainly used to remove undesirable impurities, particularly iron-bearing minerals. In this study, the effect of reagent dosage on flotation processes was investigated, and laboratory-industrial scale results were comparatively evaluated. In the experiments, a flotation feed silica sand sample containing 0.033% Fe_2O_3, obtained from the Camiş Mining Yalıköy Sand Preparation Plant, was used. As a result of the industrial scale flotation, an Fe_2O_3 value of 0.017% was achieved. In the laboratory scale experiments, the lowest Fe_2O_3 value obtained at higher reagent dosages compared to industrial conditions was determined to be 0.023%. The data obtained from this study enable a comparison between laboratory-industrial scale results and reveal the effect of reagent dosage on flotation efficiency.

Key words: *Silica sand, enrichment, flotation, reagent, glass production.*

1. INTRODUCTION

Silicon is the second most abundant element in the Earth's crust after oxygen, constituting approximately 27.2%. Silicon (Si) does not occur in nature in its free form; instead, it forms silicates by combining with oxygen and other elements (Götze, 2009). Quartz is also a type of silicate. It is one of the most abundant minerals in the Earth’s crust and is considered the most important silica mineral. Quartz commonly occurs worldwide in three different forms: Quartz mineral, quartzite, and quartz/silica sand (Arıkan, 2023). The term silica/quartz sand refers to sand composed of the mineral quartz. It can also be obtained by crushing and grinding hard quartz sandstones or quartzites (Ketner, 1973). Silica sand, consisting of quartz particles smaller than 2 mm, is generally colorless or light white. Undesirable impurities in silica sand include clay, feldspar, carbonate compounds, and iron and titanium oxides. The main application of silica sand is glass production (Hacıfazlıoğlu et al., 2016).

Depending on the mineral types present in the ore, silica sands can be efficiently beneficiated by selecting appropriate methods. Some of these methods are based on physical separation, while others rely on physicochemical and chemical (leaching) processes. Physical beneficiation methods include scrubbing and classification, gravity separation, magnetic separation, and electrostatic separation. Scrubbing is used to remove clay from particle surfaces, hydrocyclones are employed for the removal and classification of fine particles, and magnetic separators are used for the separation of iron-bearing minerals (Hacıfazlıoğlu et al., 2016). In flotation, which is a physicochemical method, separation is achieved with the aid of various reagents. Most minerals are hydrophilic and must be rendered hydrophobic by adding selected surface-active chemicals known as collectors. The classification of flotation reagents is based on their function; accordingly, they are divided into collectors, frothers, and modifiers (Fuerstenau and Han, 2003).

There are several main raw materials used in glass production, including silica sand, dolomite, limestone, soda, and feldspar. Among these, silica sand is the most widely used raw material in the glass batch in terms of proportion. In glass sand production, the contents of Fe_2O_3, TiO_2, and heavy minerals must be reduced to very low levels; therefore, it is often not possible to remove these impurities solely by physical methods. For this reason, flotation plays an important role in the beneficiation of silica sands. The method applied is generally reverse flotation. In reverse flotation of silica sand, quartz particles are depressed while other minerals are floated. Various collectors are used to float impurities present in the sand. The most commonly used collectors are fatty acids, soaps, sulfonates, and amine-type collectors. Fatty acids and soaps are anionic collectors belonging to the carboxyl group. Oleic acid and synthetic fatty acids constitute the fatty acids used in iron flotation (Köse and Türeli, 1986).
In this study, the effect of reagent dosage on flotation experiments carried out to obtain silica sand of suitable quality for glass production was investigated. For this purpose, laboratory scale flotation experiments were conducted using one collector and one frother reagent. The results obtained were comparatively evaluated with the industrial flotation results obtained from the Yalıköy Sand Preparation Plant, where the same sample and reagents were used.

2. MATERIAL AND METHODS

2.1. Material

The representative sample used in the flotation experiments was obtained from the flotation feed of the Şişecam Camiş Mining Yalıköy Sand Preparation Plant. In this facility, the run-of-mine material is subjected to crushing, screening, grinding, and washing (hydrocyclone) processes prior to being fed to the flotation unit. The sample collected from the flotation feed was dried, and all analyses were conducted on the dry material.

Sieve analysis was performed to determine the particle size distribution of the sample, with the results presented in Figure 1. Based on the obtained undersize curve, 0.37% of the sample was found to be larger than 0.500 mm, while 52.63% was smaller than 0.106 mm. Accordingly, the d_{50} value was determined as 0.100 mm, and the d_{80} value as 0.180 mm.

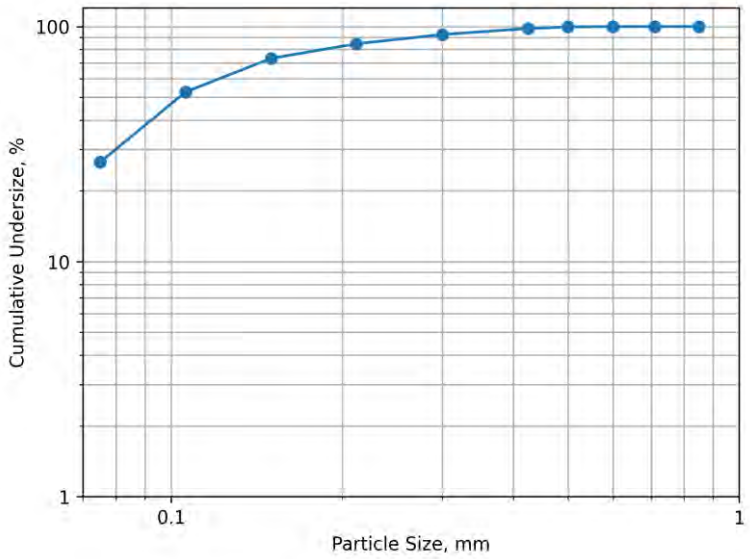

Figure 1. Particle size distribution of the sample

The chemical composition of the sample was determined by X-ray Fluorescence (XRF) Spectroscopy analysis, and the results are presented in Table 1. The sample was found to contain 0.033% Fe_2O_3.

Table 1. Chemical analysis of the sample

Chemical Analysis (%)	SiO_2	Al_2O_3	Fe_2O_3	TiO_2	CaO	MgO	Na_2O	K_2O
Sample	99,52	0,29	**0,033**	0,091	0,01	0,00	0,00	0,06

The results of the X-ray Diffraction (XRD) analysis, conducted to determine the mineral phases of the sample, are presented in Figure 2. According to the XRD analysis, quartz is the dominant phase in the sample. The presence of several low-intensity peaks in the diffractogram indicates that minor amounts of other mineral phases may also be present.

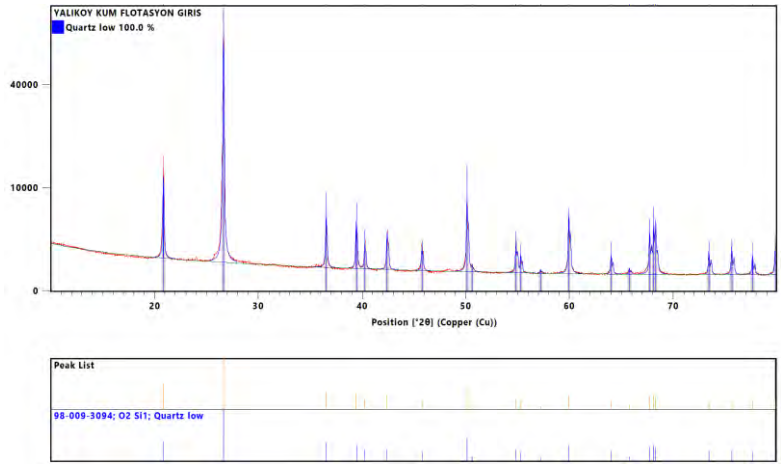

Figure 2. XRD analysis of the sample

Figures 3 and 4 present the results of the Fourier Transform Infrared (FTIR) Spectroscopy analyses performed on the collector and frother reagents used in the flotation experiments. When the structure of the collector whose spectrum is presented in Figure 3 is examined, the peak at 1710 cm^{-1} can be attributed to the C=O stretching vibration. This peak corresponds to the carbonyl group commonly observed in organic fatty acids. The bands around 2900 cm^{-1} indicate the aliphatic C–H stretching vibrations of a long-chain fatty acid. A low-intensity peak is observed in the 3300–3600 cm^{-1} wavenumber range; however, it remains at the noise level. Based on these findings, the structure is considered to be a salt of oleic acid.

In the frother spectrum shown in Figure 4, unlike the collector, a broad band is observed in the 3200–3600 cm^{-1} region, indicating the presence of an O–H group. These results suggest an acidic structure.

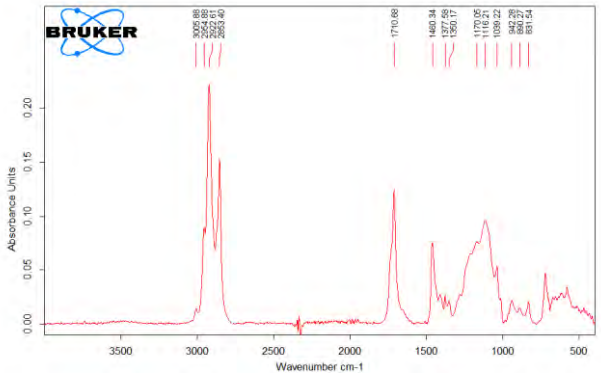

Figure 3. FTIR analysis of the collector

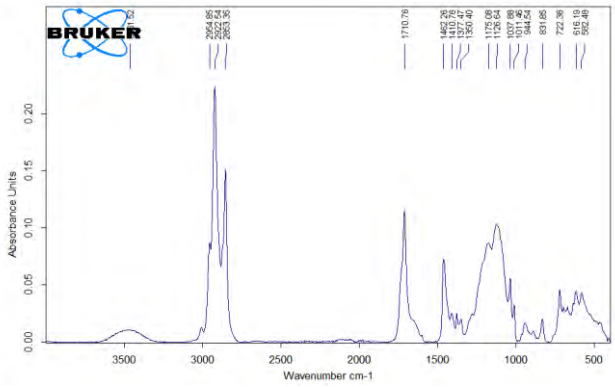

Figure 4. FTIR analysis of the frother

2.2. Method

In order to obtain silica sand of a quality suitable for glass production, the removal of iron oxides by flotation was targeted. One collector and one frother reagent were used in the flotation experiments. The tests were conducted in a Denver D-12 flotation machine with a 1.5 L cell volume, operated at 1000 rpm, using tap water and at neutral pH. A pulp containing 28% solids was prepared using 300 g of sample. After the machine was started and thorough mixing of the sample and water was achieved, the collector and frother reagents, prepared at a concentration of 2%, were added simultaneously. Following a conditioning period of 5 minutes, air was introduced to initiate flotation. Froth was collected for 2 minutes. The iron oxide–rich fraction recovered in the froth was discarded as tailings, while the sink fraction was taken as the product. Flotation experiments were conducted by varying reagent dosages. The obtained products were analyzed by XRF analysis, and iron removal efficiencies were calculated. XRF analysis with a Rigaku Primus II, XRD analysis with a Panalytical Empyrean, and FTIR analysis with a Bruker instrument were carried out.

3. RESULTS AND DISCUSSION

Laboratory tests were conducted at different reagent dosages. The results and those obtained using the current plant dosage are presented in Table 2 for comparison.

The Fe_2O_3 content of the flotation feed sample was determined to be 0.033%. In the plant scale flotation, 300 g/t collector and 100 g/t frother were used. As a result, the iron content decreased to 0.017%, and an iron removal efficiency of 48.48% was achieved. In the laboratory scale experiment conducted using the same reagent dosages, the iron content decreased to 0.026%, and an iron removal efficiency of 21.21% was achieved. The reagent dosage used under laboratory conditions was found to be insufficient to achieve the plant scale results.

In industrial systems, flotation is carried out under continuous flow conditions. In continuous systems, the probability of contact between mineral particles and air bubbles is higher, which may increase flotation efficiency. In addition, the larger volume of flotation cells is an important factor affecting separation efficiency. The process water used also has a significant effect. The recycled process water used in the plant may contain a certain amount of residual reagents remaining from previous flotation stages. This may create an additional reagent effect in the flotation environment and positively influence flotation performance.

Table 2. Flotation tests and plant result

Experiment	Collector (g/t)	Frother (g/t)	Chemical Analysis - Oxides (%)				Iron Removal Efficiency (%)
			SiO_2	Al_2O_3	Fe_2O_3	TiO_2	
Flotation Feed Sample			99.51	0.29	**0.033**	0.091	-
Plant-Scale Flotation Product	**300**	**100**	99.72	0.18	**0.017**	0.038	48.48
Laboratory-Scale Flotation Products	**300**	**0**	99.55	0.26	**0.027**	0.081	18.18
	300	**50**	99.56	0.26	**0.027**	0.078	18.18
	600	**50**	99.56	0.26	**0.026**	0.075	21.21
	300	**100**	99.56	0.26	**0.026**	0.075	21.21
	350	**100**	99.55	0.26	**0.026**	0.089	21.21
	400	**100**	99.55	0.26	**0.025**	0.085	24.24
	500	**100**	99.57	0.25	**0.025**	0.079	24.24
	600	**100**	99.58	0.25	**0.024**	0.071	27.27
	400	**150**	99.61	0.23	**0.023**	0.069	30.30
	500	**150**	99.60	0.24	**0.024**	0.065	27.27
	600	**150**	99.60	0.24	**0.024**	0.064	27.27

Figure 5 shows how the collector dosage affects the iron content in the obtained glass sand. A limited decrease in iron content was observed with increasing collector dosage. While the Fe_2O_3 content was 0.026% at a collector dosage of 300 g/t, it decreased to 0.025% when the dosage was increased to 400 g/t. No significant change in iron content was observed at a dosage of 500 g/t. At a collector dosage of 600 g/t, the Fe_2O_3 content further decreased to 0.024%.

These results indicate that increasing the collector dosage beyond a certain level does not lead to a significant improvement in flotation efficiency. This suggests that mineral surfaces reach a saturation point after a certain stage and that the additional collector contributes only limited benefits to the system. Furthermore, excessive collector usage may reduce selectivity in the flotation environment and may also lead to the transfer of siliceous minerals into the froth phase.

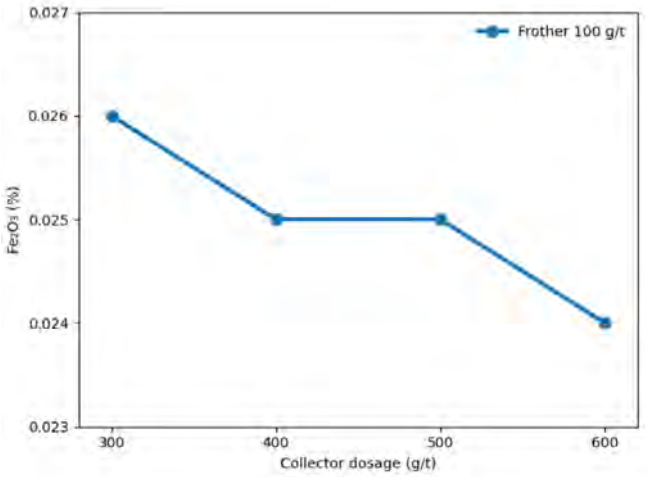

Figure 5. Effect of collector dosage

Figure 6 shows the effect of collector and frother dosage variations on iron oxide content in glass sand.

The effect of frother dosage was evaluated, and it was observed that the use of 150 g/t frother resulted in lower iron content. While the Fe_2O_3 values ranged between 0.024–0.025% at a frother dosage of 100 g/t, these values were in the range of 0.023–0.024% when the frother dosage was increased to 150 g/t. These results indicate that increasing the frother dosage leads to a limited decrease in iron content and suggest that an optimum frother dosage may exist in the system.

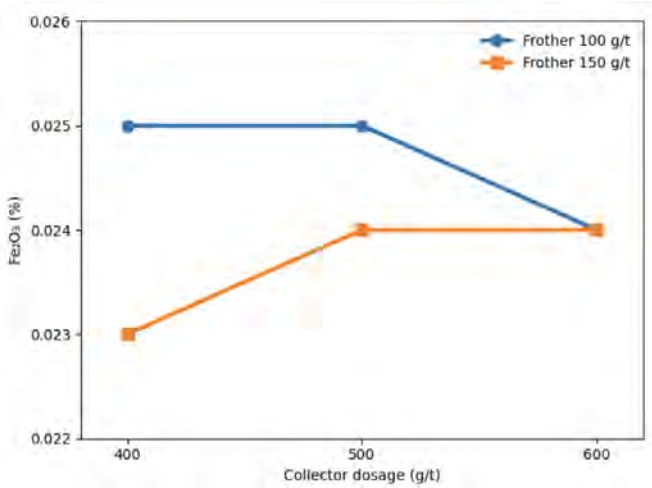

Figure 6. Effect of frother and collector dosages

Overall, the Fe_2O_3 value of 0.017% achieved under plant conditions is considered suitable for glass production, particularly for glassware applications where very low iron content is required. While the Fe_2O_3 values obtained under laboratory scale conditions range between 0.023% and 0.026%, these values remain slightly above the specifications required for glassware production. Nevertheless, these values fall within the acceptable quality range for other glass manufacturing sectors such as flat glass and glass packaging. These results demonstrate that silica sand can be beneficiated through flotation to meet the quality requirements of different glass production fields depending on the level of iron removal achieved.

4. CONCLUSION

In this study, the reverse flotation method applied to obtain silica sand suitable for glass production was found to be effective in removing iron oxide-bearing minerals. The comparison of laboratory and plant scale flotation results revealed that lower iron contents can be achieved in industrial systems. Under the same reagent dosage conditions, the iron removal efficiency was 48.48% at the plant scale, while it was 21.21% at the laboratory scale. In addition, laboratory scale experiments indicated that variations in reagent dosage influence flotation performance and suggest the presence of an optimum reagent dosage range within the system. These results demonstrate that flotation performance can be further improved through the optimization of reagent conditions. It is considered that flotation performance could be further improved by increasing the reagent dosage or by evaluating different types of reagents under laboratory conditions.

REFERENCES

Arıkan, F., (2023) “Dünyada ve Türkiye’de Kuvars, Kuvarsit ve Kuvars Kumu”, Maden Tetkik ve Arama Genel Müdürlüğü.

Fuerstenau, M. C., & Han, K. N. (Eds.)., (2003) “Principles of Mineral Processing”, Society for Mining, Metallurgy, and Exploration, Inc.

Götze, J., (2009) “Chemistry, textures and physical properties of quartz – geological interpretation and technical application”, Mineralogical Magazine, 73(4) 645–671.

Hacıfazlıoğlu, H., Terzi, M., Tombal, T. D., Kurşun, İ., (2016) “Silis kumunun liç yöntemi ile saflaştırılmasında organik ve inorganik asitlerin verimliliğinin araştırılması”, Adıyaman Üniversitesi Mühendislik Bilimleri Dergisi, 4 11–18.

Ketner, K. B., (1973) “Silica Sand”, United States Mineral Resources, Geological Survey Professional Paper 820, 577-580.

Köse, M., Türeli, T. K., (1986) “Cam Üretiminde Kullanılan Kuvars Kumlarında Aranan Özellikler-Zenginleştirme Yöntemleri ve Yozgat Sarıkaya Kuvarsitlerinin Bu Açıdan İncelenmesi”, Madencilik, 25 (4).

RECENT ADVANCES IN FLOTATION TECHNOLOGIES FOR COARSE AND FINE PARTICLE RECOVERY

Ceyda GÜRKAN*, Hüseyin BAŞTÜRKCÜ

Istanbul Technical University, Faculty of Mines, Mineral Processing Engineering Department, 34469, Maslak, Istanbul, TÜRKİYE
**Corresponding author: savran15@itu.edu.tr*

A B S T R A C T

While the need for coarse particle flotation arises from the desire to reduce the increasing energy costs associated with grinding and to recover valuable minerals lost in coarse fractions, the progressive depletion of mineral reserves has also created a demand for fine particle flotation due to the decreasing liberation sizes of ores. However, fine particles present challenges such as low particle–bubble collision efficiency, whereas coarse particles suffer from high detachment rates. To overcome these challenges, research has shifted from conventional flotation techniques toward innovative equipment designs. Examples include the Jameson cell, Concorde cell, Imhoflot G-Cell, StackCell, and Reflux flotation cell for fine particles, and the HydroFloat and Imhoflot V-Cell for coarse particles. These systems improve flotation performance by enhancing particle–bubble interactions and optimizing hydrodynamics. This review aims to summarize these technological advancements and evaluate their implications for future flotation practice. The analysis concludes that overcoming the inherent limitations of the "elephant curve" requires a strategic shift toward integrated, size-specific flotation circuits where specialized technologies are paired to maximize global recovery and reduce comminution energy by up to 50%.

Key words**:** *Flotation technology, coarse particle flotation, fine particle flotation, Jameson cell, HydroFloat, StackCell, Imhoflot, Reflux flotation cell, hydrodynamics, energy efficiency*

1. INTRODUCTION

Froth flotation has been the cornerstone of mineral processing for over a century, enabling the selective separation of valuable minerals from gangue. Conventional mechanical flotation cells typically achieve optimal performance within an intermediate particle size range, generally between 20-150 μm (Hassanzadeh et al., 2022; Jameson, 2010). The relationship between particle size and flotation recovery is well-documented, a concept sometimes referred to in the literature as the "elephant curve" (Kohmuench et al., 2018). However, both ends of this size spectrum present significant challenges: ultrafine particles (< 20 μm) exhibit poor recovery mainly related to a low frequency of collision with air bubbles, while coarse particles (> 150 μm) suffer from low particle-bubble aggregation buoyancy and high detachment rates due to turbulence within the cell (Hassanzadeh et al., 2022; Jameson, 2010). Recent studies confirm that this poor recovery of coarse particles is strictly related to these adverse hydrodynamic conditions in the cell, rather than a lack of mineral liberation (Jameson, 2012). The declining ore grades worldwide and progressive depletion of high-quality mineral deposits have intensified the need to process lower-grade, more complex ores (Hassanzadeh et al., 2022; Yianatos & Vallejos, 2024). This reality has dramatically increased energy consumption in comminution stages, which already accounts for 2-4% of global electricity usage and can increase by 50-100% as feed grades decline (Hassanzadeh et al., 2022; Jameson, 2010; Yianatos & Vallejos, 2024). Consequently, technologies enabling the flotation of coarser particles can raise the upper grinding size limit, potentially reducing overall grinding energy by up to 50%, thereby yielding substantial economic and environmental benefits (Hassanzadeh et al., 2022; Jameson, 2010). This review examines recent technological advances in flotation

equipment, with an emphasis on innovative cells that modify traditional hydrodynamic principles to extend the effective flotation size range.

2. FUNDAMENTAL CHALLENGES IN SIZE-SPECIFIC FLOTATION

2.1. Fine Particle Flotation

Fine and ultrafine particles present unique challenges stemming from fundamental physical principles due to their small size and mass. In conventional flows, the primary issue is that these low-inertia particles tend to follow fluid streamlines rather than colliding with bubbles (Yáñez et al., 2024). Although the collision rate between fine particles and bubbles can be sufficiently high in highly turbulent environments, the main problem is that their attachment efficiency remains quite low; this is because fine particles lack the sufficient push force required to rupture the thin liquid film between them and the bubble to form a three-phase contact line (TPCL) (Karakashev et al., 2022). Once fine particles do attach to a bubble, the particle-bubble bond is actually strong, and the detachment probability is low; however, the excessive entrainment of hydrophilic gangue minerals into the froth compromises both concentrate grade and selectivity (Yáñez et al., 2024). To overcome these physical limitations, recent technological innovations focus on modifying the hydrodynamic environment (Xu et al., 2024; Yáñez et al., 2024). These specialized designs generate fine or micro bubbles, which improve the attachment probability by increasing capillary pressure (Karakashev et al., 2022; Yáñez et al., 2024), create high-shear and high-turbulence mixing zones to enhance particle-bubble interaction, and incorporate froth washing along with weakly turbulent separation zones to reduce gangue entrainment (Xu et al., 2024; Yáñez et al., 2024).

2.2. Coarse Particle Flotation

Coarse particle flotation faces fundamentally different challenges. The primary obstacle is high probability of bubble-particle detachment due to turbulence. In conventional mechanical flotation cells, turbulent energy dissipation creates centrifugal forces that exceed the attachment force for coarse particles. Particles larger than approximately 150 μm for sulfides and 250-500 μm for coal experience rapid detachment rates that severely limit recovery. Additionally, coarse particles require greater buoyancy force to penetrate and traverse the froth layer. These fundamental challenges have driven development of specialized flotation technologies that minimize turbulence, provide enhanced buoyancy, and eliminate or minimize the froth phase (Anzoom et al., 2024; Kohmuench et al., 2018).

3. TECHNOLOGIES FOR FINE PARTICLE RECOVERY

3.1. Jameson Cell

The Jameson Cell is a high-intensity flotation device developed jointly by Mount Isa Mines and Prof. G.J. Jameson of the University of Newcastle in 1986, and has since been installed in over 225 applications worldwide treating coal, copper, lead, zinc, and nickel sulphides (Harbort et al., 2003). The cell operates through a vertical downcomer in which a pressurised slurry jet naturally aspirates air under vacuum, generating fine bubbles and achieving rapid bubble-particle contact without mechanical agitation; as You et al. (2017) describe, *"due to high mixing velocity and large interfacial area, the contact and collection of particles are rapid."* This mechanism produces extraordinarily short downcomer residence times — as low as 4.5 seconds — while achieving recoveries comparable to mechanical flotation cells requiring 8 minutes or more (Harbort et al., 2003). Kinetic modelling of the downcomer demonstrates that the flotation rate constant follows a non-monotonic relationship with particle size, peaking at intermediate sizes where collision and stability efficiencies are jointly optimised, with fine

particle recovery being collision-limited and coarse particle recovery being stability-limited (You et al., 2017). From a design perspective, successive innovations including the high-density alumina orifice plate, the Slurry Lens, the Mark 3 downcomer, and the AISE valve have collectively extended wear life, improved air entrainment, and enhanced operational stability, contributing to a 15% increase in effective downcomer length and measurable gains in recovery at industrial installations such as the Riverside and Hail Creek coal mines (Cowburn et al., 2005; Harbort et al., 1994).

3.2. Concorde Cell

The Concorde Cell™ is a high-intensity pneumatic flotation technology developed by Professor Graeme Jameson and commercialized by Metso, designed to improve recovery of fine and ultrafine particles lost in conventional flotation (Yáñez et al., 2024). The cell accelerates feed slurry mixed with pressurized air to sonic velocity, generating shockwaves that produce fine bubbles at energy dissipation rates of ~100 kW/m³ — far exceeding conventional mechanical cells (Yáñez et al., 2024). At industrial scale, it has demonstrated superior metallurgical performance over both mechanical and self-aspirated pneumatic cells across copper, nickel, gold and metallurgical coal applications, with improvements most pronounced in the finest particle fractions (Dube et al., 2025).

3.3. Imhoflot G-Cell

The Imhoflot™ G-Cell is a pneumatic flotation technology developed by Dr. Rainer Imhof and commercialized by Maelgwyn Mineral Services Ltd., in which feed slurry is aerated externally via a high-shear venturi aerator and introduced tangentially into a cylindro-conical separator, generating centrifugal forces that reduce residence time to approximately 30 seconds (Imhof et al., 2007; Mohanty et al., 2005). This design produces fine bubbles that enhance particle-bubble collision efficiency, making the technology particularly effective for fine and ultrafine particle recovery across a wide range of commodities including gold, copper, zinc, nickel, and coal (Hoang et al., 2022; Hassanzadeh et al., 2023). Industrial trials demonstrated that a single H-16 cell achieved 89% copper recovery with an enrichment ratio of 4.84 in pre-rougher duty, matching or exceeding the performance of four conventional 50 m³ mechanical cells in the cleaning stage (Hassanzadeh et al., 2024), while pilot-scale gold recovery tests achieved concentrate grades of ~20 g/t Au with recoveries of 65–68% for the sub-20 µm fraction (Hoang et al., 2022).

3.4. StackCell Technology

The StackCell, developed by Eriez Flotation Division, decouples bubble-particle contacting from phase separation by subjecting feed slurry to intense shear within a compact contacting chamber, where turbulent dissipation rates reach up to 150 W/kg — nearly five times higher than conventional rotor/stator mechanisms (Dohm et al., 2022). This accelerates flotation kinetics significantly, enabling comparable copper recoveries to conventional cells in one-sixth to one-ninth of the residence time (Mankosa et al., 2018), and yielding up to 28% higher fine particle recovery compared to conventional mechanical cells (Xu et al., 2024). These metallurgical advantages are accompanied by reductions of 40–50% in capital cost, 40–60% in power consumption, and over 50% in plant footprint (Mankosa et al., 2018; Kohmuench et al., 2010).

3.5. Reflux Flotation Cell

The REFLUX™ Flotation Cell (RFC), developed at the University of Newcastle and commercialized by FLSmidth, consists of a high-shear downcomer, a reverse fluidized bed, and inclined channels that work together to exploit the Boycott effect. This design breaks the ~1 cm/s feed flux barrier of conventional cells — single-stage tests have shown stable

operation at feed fluxes up to 7.2 cm/s without any meaningful loss in combustible recovery (Cole et al., 2021; Chen et al., 2022). Full-scale trials have confirmed similar gains, achieving roughly twice the conventional flux limit while keeping cleaning efficiency high (Iveson et al., 2022). Applying a downward liquid bias flux through the bubbly bed keeps fine gangue out of the product, bringing ash content down to as low as 6.7% — close to what Coal Grain Analysis identifies as the theoretical limit for the feed (Cole et al., 2020; Chen et al., 2022; Iveson et al., 2022). RTD measurements add another layer to this picture, showing that flow inside the cell behaves more like plug flow than perfect mixing, with residence times under 60 seconds and no dead zones detected (Guner et al., 2023).

4. TECHNOLOGIES FOR COARSE PARTICLE RECOVERY

4.1. HydroFloat Technology

The HydroFloat, developed by Eriez Flotation Division in the late 1990s, represents a paradigm shift in coarse particle flotation through a fluidized bed mechanism (Ozsoy et al., 2025). The unit creates hindered settling conditions by introducing fine air bubbles and up-current water at the base of the vessel, suspending coarse particles in a relatively quiescent environment within an upper separation chamber, while a lower dewatering cone handles tailings discharge (Fosu et al., 2015). The absence of mechanical agitation eliminates turbulence-induced detachment, and even a single bubble attachment provides sufficient buoyancy to prevent particle penetration through the fluidized bed, effectively extending residence time for attachment (Kohmuench et al., 2018). These advantages are particularly pronounced for poorly liberated particles; complex locking texture particle recovery improved from 38% in conventional mechanical cells to 87% in the HydroFloat under comparable conditions (Fosu et al., 2015). Recent parametric studies on a newly developed 82-mm laboratory-scale unit confirmed that fluidization water flow rate, collector dosage, and conditioning time are the dominant operational parameters, with optimized conditions achieving up to 75–80% copper recovery using only 1.5–2 kg of feed per test (Ozsoy et al., 2025). At BHP's Carrapateena copper mine, commissioned in 2025, the HydroFloat installation has increased ore throughput to approximately 20,000 tonnes per day, with economic analyses suggesting grinding energy savings of 30–50% through coarser mill product (Concha et al., 2023).

4.2. Imhoflot V-Cell

The ImhoflotTM V-cell is a pneumatic flotation cell operating on self-aspirating multi-jet venturi aerators, generating finely dispersed bubbles with a mean bubble size of approximately 1.1 mm and a Sauter mean diameter of 1.5 mm at gauge pressures of 1.5–2.5 bar (Ayoglu et al., 2025). Unlike conventional mechanical cells, it directly injects air into the pulp through an external aerator, eliminating the need for mechanical agitation and providing more effective particle-bubble collision, particularly for fine and ultrafine particles (Ayoglu et al., 2025; Hassanzadeh et al., 2024). The V-cell is primarily designed for intermediate to coarse particle recovery (50–400 μm) with a residence time of 3–4 minutes (Ayoglu et al., 2025). Laboratory-scale (V-018, 8 dm^3) and mini-pilot scale (VM-04, 42.1 L) versions have been developed and tested under varying hydrodynamic conditions, with the VM-04 cell achieving 94% copper recovery compared to 74% obtained by a mechanical cell under identical reagent regimes (Hassanzadeh et al., 2024; Hassanzadeh et al., 2023). At industrial scale, a single H-16 ImhoflotTM cell operated as flash flotation at the Acacia copper plant achieved an enrichment ratio of 4.84 and 89% copper recovery, while at the cleaner stage, one H-16 cell matched the performance of four conventional mechanical cells (50 m^3 each) in series, yielding 64% recovery compared to 60% (Hassanzadeh et al., 2024).

5. HYDRODYNAMIC AND ENERGY CONSIDERATIONS

The technologies reviewed in Sections 3 and 4 represent two broadly opposing hydrodynamic design philosophies, each targeting a different failure mode of conventional flotation. Fine particle technologies — the Jameson Cell, Concorde Cell, Imhoflot G-Cell, StackCell, and RFC — generate intense contacting environments or fine bubble populations to overcome the low collision and attachment efficiencies that limit recovery at small particle sizes (Karakashev et al., 2022; Yáñez et al., 2024). Coarse particle technologies, by contrast, deliberately minimise turbulence: the HydroFloat operates as a fluidized bed to eliminate detachment forces entirely, while the Imhoflot V-Cell — designed for the intermediate-to-coarse range (50–400 μm) — uses external pneumatic aeration to avoid the high-shear conditions of mechanical agitation (Kohmuench et al., 2018; Ayoglu et al., 2025). A key insight is that these are not mutually exclusive strategies: several technologies, including the StackCell and Jameson Cell, achieve both high contacting intensity and a quiescent separation zone by physically decoupling the two stages, suggesting that spatial separation of sub-processes is a unifying design principle across size classes (Dohm et al., 2022; Hassanzadeh et al., 2022).

From an energy standpoint, the reviewed technologies offer advantages along two distinct pathways. Pneumatic cells such as the Concorde Cell and Imhoflot G-Cell eliminate the mechanical rotor–stator assembly entirely, reducing cell-level power draw relative to conventional mechanical flotation. Compact high-intensity designs such as the StackCell achieve comparable metallurgical performance in a fraction of the residence time and plant footprint, translating to lower capital and operating costs (Mankosa et al., 2018). At the circuit level, the ability of the HydroFloat to process coarser mill products reduces the comminution burden upstream, with grinding energy savings of 30–50% reported at industrial scale (Concha et al., 2023). These gains are complementary and reinforce the case for integrated circuit configurations that pair technologies from both size categories.

6. FUTURE DIRECTIONS

The concept of the “elephant curve” makes clear that no single cell design achieves optimal recovery across the full particle size range (Kohmuench et al., 2018). A central future priority is therefore the development of integrated, size-classified circuits that route different particle size fractions to the most appropriate technology — pairing coarse-particle devices such as the HydroFloat with fine-particle units such as the Concorde Cell or RFC (Hassanzadeh et al., 2022). The processing of ultrafine particles below 10 μm remains a further open challenge, where low collision efficiencies severely limit conventional flotation; strategies including selective flocculation, carrier flotation, and high-intensity pneumatic contacting continue to be investigated to bridge this gap (Karakashev et al., 2022; Yáñez et al., 2024).

Advances in process monitoring and CFD modelling will also be critical to the next generation of flotation design. The complex, nonlinear interactions between air flow rate, froth depth, and reagent dosage are difficult to optimize manually, and data-driven control strategies informed by real-time hydrodynamic measurements could substantially improve recovery and selectivity under varying feed conditions (Yianatos & Vallejos, 2024). CFD has already demonstrated value in characterizing flow patterns within novel cell geometries (Dohm et al., 2022), and its integration with population balance models is expected to accelerate the rational design of future flotation equipment.

Finally, translating laboratory and pilot-scale results to full industrial implementation remains a key challenge. Scale-up of flotation kinetics and froth transport behaviour is non-trivial, as hydrodynamic conditions and residence time distributions change substantially with cell volume (Yianatos & Vallejos, 2024). Reliable scale-up methodologies, supported by systematic industrial trials such as those conducted for the RFC (Iveson et al., 2022) and HydroFloat

(Concha et al., 2023), will be essential to building confidence in next-generation flotation technologies across a wider range of ore types and operating conditions.

An emerging research direction is the development of energy-efficient flotation cells that maintain or improve metallurgical performance while significantly reducing power consumption. As the mining industry faces increasing pressure to reduce operating costs and carbon footprint, innovations in flotation cell design focused on energy efficiency represent a critical pathway toward more sustainable mineral processing.

7. CONCLUSIONS

This review has examined recent advances in flotation technology for fine and coarse particle recovery. The performance limitations of conventional mechanical cells at both extremes of the particle size range are fundamentally rooted in adverse hydrodynamic conditions (Jameson, 2010; Jameson, 2012; Hassanzadeh et al., 2022). The technologies discussed demonstrate that these limitations can be overcome through purpose-built designs: the Jameson Cell and Concorde Cell generate intense fine-bubble contacting for fine and ultrafine particles (Yáñez et al., 2024); the RFC achieves high throughput fluxes with low gangue entrainment (Cole et al., 2021; Iveson et al., 2022); the StackCell maximizes flotation kinetics while reducing power draw by 40–60% (Mankosa et al., 2018); and the HydroFloat extends efficient flotation to coarse composites, with recovery improving from 38% to 87% compared to conventional cells under comparable conditions (Fosu et al., 2015).

Collectively, these developments confirm a paradigm shift toward size-specific flotation strategies aimed at extending the efficient flotation size range (Kohmuench et al., 2018). Their implications for future practice are significant: deploying these technologies in integrated, size-classified circuits can recover valuable minerals across a broader size range while reducing comminution energy by 30–50% (Concha et al., 2023), offering direct benefits in terms of energy efficiency, resource recovery, and environmental footprint. As ore grades continue to decline worldwide, the adoption of such strategies will become not merely advantageous but necessary for economically and environmentally sustainable mineral processing.

REFERENCES

Anzoom, S. J., Bournival, G., Ata, S., (2024) "Coarse particle flotation: A review", Minerals Engineering, 206, 108499.

Ayoglu, O., Hoang, D. H., Sinche-Gonzalez, M., Hassanzadeh, A., Rudolph, M., (2025) "Investigating hydrodynamics of a laboratory-scale ImhoflotTM V-cell in recovering ultrafine magnesite from a dolomite-rich tailing", Minerals Engineering, 232, 109548.

Chen, J., Chimonyo, W., Peng, Y., (2022) "Flotation behaviour in reflux flotation cell—A critical review", Minerals Engineering, 181, 107519.

Cole, M. J., Dickinson, J. E., Galvin, K. P., (2020) "Recovery and cleaning of fine hydrophobic particles using the Reflux™ Flotation Cell", Separation and Purification Technology, 240, 116641.

Cole, M. J., Galvin, K. P., Dickinson, J. E., (2021) "Maximizing recovery, grade and throughput in a single stage Reflux Flotation Cell", Minerals Engineering, 163, 106761.

Concha, J., Hobert, D., Lempens, P., Zhmarin, E., Wasmund, E., (2023) "The role of coarse particle flotation in the development of more efficient concentrator plants", Proceedings of the 62nd Conference of Metallurgists, COM 2023, Springer, Cham.

Cowburn, J., Stone, R., Bourke, S., Hill, B., (2005) "Design developments of the Jameson Cell", Centenary of Flotation Symposium, Brisbane, 5–9 June 2005.

Dohm, E., Fayed, H., Wagoner, R. V., (2022) "Metallurgical testing and CFD simulation of StackCell® SC-50 high-intensity flotation machine", Minerals Engineering, 184, 107632.

Dube, R., Kupka, N., Yáñez, A., Rinne, A., (2025) "Metallurgical performance of industrial scale Concorde Cell™ in improving fines recovery", 12th International Copper Conference, 1349–1352.

Fosu, S., Awatey, B., Skinner, W., Zanin, M., (2015) "Flotation of coarse composite particles in mechanical cell vs. the fluidised-bed separator (The HydroFloat™)", Minerals Engineering, 77, 137–149.

Guner, M. K., Hassanzadeh, A., Vinnett, L., Yianatos, J., Kowalczuk, P. B., (2023) "Effects of operating parameters on residence time distribution in a REFLUX flotation cell", Minerals Engineering, 204, 108439.

Harbort, G. J., Jackson, B. R., Manlapig, E. V., (1994) "Recent advances in Jameson Flotation Cell technology", Minerals Engineering, 7 (2/3), 319–332.

Harbort, G., De Bono, S., Carr, D., Lawson, V., (2003) "Jameson Cell fundamentals — A revised perspective", Minerals Engineering, 16 (10), 1091–1101.

Hassanzadeh, A., Safari, M., Hoang, D. H., Khoshdast, H., Albijanic, B., Kowalczuk, P. B., (2022) "Technological assessments on recent developments in fine and coarse particle flotation systems", Minerals Engineering, 180.

Hassanzadeh, A., Gungor, E., Samet, E., Durunesil, D., Hoang, D. H., Köse, B., (2023) "A comparative study between Imhoflot™ and mechanical flotation cells", Proceedings of MEI Flotation Conference, Cape Town, South Africa, 4–7 November 2023.

Hassanzadeh, A., Gungor, E., Samet, E., Durunesil, D., Hoang, D. H., Vinnett, L., (2024) "ImhoflotTM flotation cell performance in mini-pilot and industrial scales on the Acacia copper ore", Minerals, 14 (6), 590.

Hoang, D. H., Imhof, R., Sambrook, T., Bakulin, A. E., Murzabekov, K. M., Abubakirov, B. A., Baygunakov, R. K., Rudolph, M., (2022) "Recovery of fine gold loss to tailings using advanced reactor pneumatic flotation ImhoflotTM", Minerals Engineering, 184, 107649.

Imhof, R., Fletcher, M., Vathavooran, A., Singh, A., (2007) "Application of Imhoflot G-Cell centrifugal flotation technology", Journal of the Southern African Institute of Mining and Metallurgy, 107, 623–631.

Iveson, S. M., Sutherland, J. L., Cole, M. J., Borrow, D. J., Zhou, J., Galvin, K. P., (2022) "Full-scale trial of the REFLUX flotation cell", Minerals Engineering, 177, 107385.

Jameson, G. J., (2010) "New directions in flotation machine design", Minerals Engineering, 23 (11–13), 835–841.
Jameson, G. J., (2012) "The effect of surface liberation and particle size on flotation rate constants", Minerals Engineering, 36–38, 132–137.

Karakashev, S. I., Grozev, N. A., Ozdemir, O., Guven, O., Ata, S., Bournival, G., Batjargal, K., Boylu, F., Hristova, S., Çelik, M. S., (2022) "Physical restrictions of the flotation of fine particles and ways to overcome them", Physicochemical Problems of Mineral Processing, 58 (5).

Kohmuench, J. N., Mankosa, M. J., Yan, E. S., (2010) "Evaluation of the StackCell technology for coal applications", International Journal of Coal Preparation and Utilization, 30 (2–5), 189–203.

Kohmuench, J. N., Mankosa, M. J., Thanasekaran, H., Hobert, A., (2018) "Improving coarse particle flotation using the HydroFloat (raising the trunk of the elephant curve)", Minerals Engineering, 121, 137–145.

Mankosa, M. J., Kohmuench, J. N., Christodoulou, L., Yan, E., (2018) "Improving fine particle flotation using the StackCell (raising the tail of the elephant curve)", Minerals Engineering, 121, 83–89.

Mohanty, M. K., Huang, Z., Gupta, V., Biswal, S. K., (2005) "Performance optimisation of the Imhoflot G-Cell for fine coal cleaning", Proceedings of the Centenary of Flotation Symposium, Brisbane, Australia, 6–9 June 2005.

Ozsoy, Y., Honaker, R. Q., Mankosa, M., Hobert, A., Bhambhani, T., Lycans, S. J., (2025) "Revolutionizing coarse particle flotation Part I – A comprehensive exploration method for the HydroFloat™ technology", Minerals Engineering, 231, 109453.

Xu, Q., Hu, W., Zhang, M., (2024) "High-turbulence fine particle flotation cell optimization and verification", Scientific Reports, 14, 23124.

Yáñez, A., Kupka, N., Tunç, B., Suhonen, J., Rinne, A., (2024) "Fine and ultrafine flotation with the Concorde Cell™—A journey", Minerals Engineering, 206, 108538.

Yianatos, J., Vallejos, P., (2024) "Challenges in flotation scale-up: The impact of flotation kinetics and froth transport", Minerals Engineering, 207, 108541.

You, X., Li, L., Liu, J., Wu, L., He, M., Lyu, X., (2017) "Investigation of particle collection and flotation kinetics within the Jameson Cell downcomer", Powder Technology, 310, 221–227.

SPHALERITE FLOTATION USING A NEW CHELATING COLLECTOR N-HEXYLAMINOETHANETHIOL

Badr-Elboudour BENAISSA[1], Mohamed CHETTIBI[1,*], Ramanathan NATARAJAN[2], Salima SALHI[1]

Laboratory of mineral processing and environment "LAVAMINE", Badji Mokhtar-Annaba University, P.O. Box12, 23000 Annaba-Algeria
Saranathan College of Engineering, Tiruchirappalli 620 012, Tamil Nadu, India
**Corresponding author: mohamed.chettibi@univ-annaba.dz*

A B S T R A C T

Selective or differential flotation sphalerite from pyrite, galena and dolomite gangue becomes difficult with the depletion of high-grade ores. The conventional xanthate reagent scheme using reagent such as copper sulfate as activator is one of the major environmental concerns.

The objective of this work is to investigate the use of an alternative collector for the pre-concentration of sphalerite without preliminary activation. N-hexylaminoethanethiol, a N-S type chelating collector was synthesized and evaluated for an Algerian ore, Chaâbet El Hamra deposit of sphalerite. Micro-flotation tests were carried out using a custom designed flotation cell.

N-hexylaminoethanethiol, the new chelating collector exhibits selectivity for Zn mineral rather than other minerals. Thus, using the new collector leads to the best sphalerite recovery which is about 60% (grade 39.53%) in reagent condition of 2 g collector/1kg of ore at pH 9.

Key words: *Chaâbet El Hamra deposit, sphalerite, flotation, aminothiol, activation, chelating collector*

1. INTRODUCTION

The main key to efficient minerals separation by froth flotation is to selectively induce hydrophobicity on a desired mineral surface to be recovered, while avoiding the hydrophilicity of the undesirable mineral as far as possible. Collectors play a decisive role in froth flotation, they selectively decrease the mineral surface free energy, that means they render the mineral surface more hydrophobic. The modern flotation began in the 1920s with the large-scale application of xanthates as mineral collectors. Owing to the wide applications of xanthate (Bag et al., 2011, Chen et al., 2014, Deng et al., 2015, Sarvaramini et al., 2016, Weng et al., 2019). Xanthate is commonly used in the mineral processing industry to float sulphide minerals. In the sphalerite flotation, this collector usually combined with copper sulphate ($CuSO_4$) as activator, to improve the xanthate adsorption mechanism (Hamilton, 2009).

The separation of sphalerite by using activation process, became problematic when pyrite was activated together with sphalerite, because pyrite (FeS_2) is a mineral that responds to copper activation and can be floated with sphalerite (Chandra et al., 2009. In this case, the pyrite usually remains in the concentrates, reducing their grade and economic value.(Zhang et al., 2020)

Since copper sulphate is a highly corrosive chemical, it can reduce the equipment life. The factories that treat zinc ores not only spend a lot of money on copper sulfate, the most expensive auxiliary chemical in the flotation circuit, but they also produce toxic wastes.

However, the conventional collectors suffer from practical disadvantages due to the lack of selectivity and specificity, many research groups made efforts to improve conventional

collectors and develop new ones (Yekeler et al., 2005). For instance, several studies on collectors type chelating to remove copper sulphate from the sphalerite flotation process were realized. (Natarajan et al., 1997, Natarajan et al., 2002, Natarajan et al., 2003, Natarajan et al., 2006, Hamilton et al., 2009).

Several chelating reagents were found to be good flotation collectors and classified as chelating collectors. These latter are therefore, organic compounds that form water insoluble chelate on the surface or the mineral by chelation. Chelating reagents are a specific type of complexing reagents composed of an organic molecule that can form one or more bands when they interact to the metal ion through two or more functional groups.

The main purpose of the present study consists in the improvement of the sphalerite flotation from pyrite, galena and the gangue by using a new chelating collector n-hexylaminoethanethiol N-S type in order to avoid the conventional activation technique with copper sulphate in the flotation process. Consequently, by one hand we can increase the ZnS contents in the concentrate and preserve flotation cells and environment by the other hand.

Chaâbet El Hamra is the most important zinc deposit in Algeria. It is located in Ain Azel, Sétif province, Algeria, which produces 70000 tonne per year and ZnS content of the ores is about 6 % (Chettibi et al., 2002). The recovery of zinc concentrate of Chaâbet El Hamra ore is carried out using ethyl xanthate (EX) as collector with activation by copper sulphate ($CuSO_4$) and pine oil as a frother.

The present work is an exploration of the potential of a chelating collector in the flotation of the Algerian sphalerite ore without ZnS activation. The microflotation was realized by mean of Halimond apparatuse.

2. MATERIALS AND METHODS

2.1. Materials

- The ore samples used in this study is from Chaâbet El Hamra deposit. The samples were crushed with a jaw crusher, and grinded with a ceramic ball mill in the laboratory of higher school of technology and engineering, Annaba. The final samples pass through 75 µm sieve (-75 µm) and the mineralogical and chemical analyses were carried out on the passing fraction (< 75µm) using X-ray diffraction (XRD) and X-ray fluorescence (XRF), respectively.

- Synthesis process ofcollector: The collector N-hexylaminoethanethiol was synthesized in laboratory conditions. Hexylamine in toluene was taken in a round-bottomed flask and heated under reflux. Ethylene sulphide in toluene was added slowly through a separating funnel over a period of one hour. The reaction mixture was then refluxed for twenty hours. The solution was cooled and the toluene with any unreacted ethylene sulphide was removed by boiling under reduced pressure using a flash evaporator. The resultant product was cleaned by passing through a short column of silica gel.

2.2. Methods

Micro flotation experiments were performed in pneumatic Hallimond tube at two pH values namely pH 7 and pH 9. Usually, pure minerals are used in the micro-flotation tests. However, in the present study instead of pure minerals, sphalerite ore was used for the micro-flotation test. The ore was ground and sieved through 100 µm sieve. After liberating fresh solid surface by attrition in a mortar and pestle, 5 g of ore with an aliquot of collector solution taken in the micro-flotation cell see figure 1. In each test, pH of the solution was adjusted using decinormal NaOH/HCl solution and was conditioned for 20 min by continuous stirring using a magnetic

stirrer. Afterwards, the distilled water at the same pH as conditioning was added to the pulp to perform the experiments with one drop frother (soap oil) and 1L/min air was passed. Following each micro-flotation experiment, the concentrates was filtered, dried and weighed, respectively. The recovery of Zn was calculated using Equation (1) (Zhang et al., 2021)

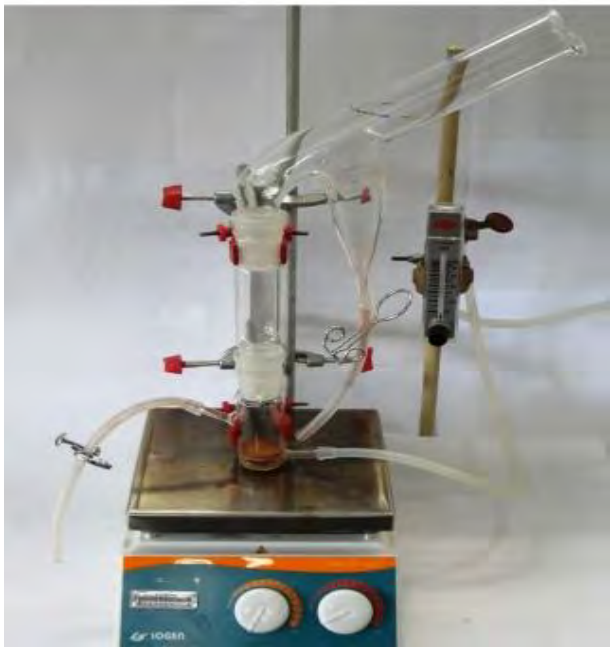

Figure 1. Micro-flotation cel

$$\varepsilon=(C\times c)/(A\times a)\times 100\ (\%) \quad \text{..... (1)}$$

Where,
- C, A: are the weights of concentrate and feed, respectively.
- c, a: are the grade of concentrates and feed respectively.

3. RESULTS AND DISCUSSION

The results of X-ray analysis on the ore are presented in Table 1 and a typical XRD spectrum showed that, the main mineral phase observed is dolomite (Ca Mg $(CO_3)_2$), indicating that the Chaabat El Hamra deposit is essentially composed of carbonate dolomite. The XRF results recapitulated in Table 1, showed that the contents of Zn and Fe particularly similar they are about 18.17 % and 17.51%, respectively.

Table 1. Results of XRF analysis

	Element content (%)					
	Zn	S	Fe	Pb	Mg	Ca
Ore	18.17	07.18	17.51	0.89	7.09	49.17

3.1. Effect of Collector Concentration on Sphalerite Recovery

A blank test was performed at two pH values (7 and 9); all chemicals except the collector were added, and air was passed. Practically no solid was floated in the bank test. As a result, after adding the collector, the floats obtained were only due to the collector's hydrophobicity on the

minerals. The theory of flotation showed that no matter the surface mineral is naturally hydrophobic, the presence of the collector has a primary importance in flotation kinetic process, bubbles interaction with mineral surface, important role of physical sorption in increasing the surface hydrophobicity, etc. (Chettibi et al., 2014).

The effect of collector concentration was studied by using three different dosages of collector from (1, 2 and 2,5) g/kg (g of collector/1kg of ore) in the tests in order to test the floatability of the ore.

The results of mass recovery at whether pH 7 or pH 9 shows that increasing the collector dosage does not mean increase the mass recovery. The highest mass recovery of float concentrates is at collector dosage of 2g/kg of the ore. That can be explained by the following; in fact, the collector role is rending the mineral surface hydrophobic, that doesn't mean more increasing the collector concentration more the surface becomes hydrophobic, there is an optimal concentration value of the collector that we never exceed, over that value the particle density increased and their transport to the pulp surface becomes difficult for the bubbles. And lower that concentration, the particle surface couldn't have enough coverage to be hydrophobic (Nettour et al., 2018).

3.2. Effect of pH on Minerals Recovery

The major minerals in the ore and float are sphalerite, galena, dolomite and pyrite; the float concentrate at using 2g/kg of ore at pH 7 and pH 9 was analyzed. The results are recapitulated in Table 2.

Table 2. Mineral composition of the float concentrate using 2g of collector/kg of the ore

Mineral	**Composition (%)**	
	pH 7	pH 9
Zn mineral (sphalerite)	40.10	39.53
Pb mineral (galena)	5.11	4.18
Ca & Mg mineral (dolomite)	24.61	43.14
Fe mineral (pyrite)	8.01	3.33

The micro-flotation experiments were performed to float Zn mineral (Sphalerite) without activation by copper sulphate. Hence, Zn mineral had a good floatability in the absence of activator $CuSO_4$ at both value of pH. By comparing the results of mineral recoveries at pH 7 and pH 9 clearly; higher sphalerite recovery at pH 9, increased from 21.7% at pH 7 to 59.7% at pH 9. Though the recovery of sphalerite had increased the Sphalerite grade of the concentrate is only 39.5%. This is because of the increased flotation of carbonate minerals (dolomite) that are naturally hydrophobic and float in higher amount at higher pH. Moreover, the carbonate slimes could have covered the valuable mineral and made the flotation of sphalerite complicated. (D. Li et al., 2017) It may be noted that other than the collector and frother no chemical was added either to suppress the carbonate gangue or to activate the flotation of valuable sphalerite. Hence, the results using the new collector is very encouraging. Another very important observation is the pyrite floated is not in ratio with the sphalerite. There is no significant increase in the flotation of pyrite. That confirmed in his work (Chettibi et al., 2015) where it was determined that the optimal condition of pyrite flotation is both type of collector adsorptions physical and chemical should be insured otherwise the pyrite flotation never be realized. Comparing the composition of pyrite in the ore whereas the pyrite grade in the float at pH 7 is 8% while the pyrite grade of float at pH 9 is 3.3%. This is a very significant advantage of using the new collector. The new aminothiol collector preferably adsorb on sphalerite and this results in differential flotation of sphalerite rejecting pyrite. As discussed above flotation of dolomite is due to its natural hydrophobicity. It may be suppressed using a depressant such as carboxymethyl cellulose (CMC).

4. CONCLUSION

In the current study, a new collector was synthesized and classified as chelating collector N-S type. The flotation separation of sphalerite using the common xanthate reagent scheme with $CuSO_4$ activation and CaO as pH modifier was improved using a new flotation reagent system of N-hexylaminoethanethiol as a collector with NaOH as pH modifier and no activator. The most signification of this work were:

The chelating collector was able to float sphalerite without activation process by copper sulfate. Therefore, the activation mechanism is not necessary to form a soluble complex on sphalerite surface while using the N-hexylaminoethanethiol collector. The micro-flotation results showed that the collector N-hexylaminoethanethiol has proven its capacity of selectivity towards sphalerite.

The pH value ensuring maximum surface hydrophobicity and flotation of sphalerite was defined about 9. and the new aminothiol collector performed better at pH 9 comparing to pH 7.
The influence of the collector dosage change on the flotation of sphalerite at both value of pH; the best flotation recovery of 59.74 % for sphalerite was achieved with a collector dosage 2 g/ kg of the ore at pH 9.

The use of the new collector has a signification advantage as the pyrite floating is not in the same ratio as sphalerite, because of the absence of the optimal conditions of its flotation. However, the flotation of dolomite gangue, due to its natural hydrophobicity, can be suppressed by adding a depressant such as carboxymethyl cellulose.

REFERENCES

Bag, B., Das, B., Mishra, B. K., (2011) “Geometrical optimization of xanthate collectors with copper ions and their response to flotation”, Minerals Engineering, 24 (8) 760–765.

Chandra, A. P., Gerson, A. R., (2009) “A review of the fundamental studies of the copper activation mechanisms for selective flotation of the sulfide minerals, sphalerite and pyrite”, Advances in Colloid and Interface Science, 145 (1–2) 97–110.

Chen, J.-H., Li, Y.-Q., Lan, L.-H., Guo, J., (2014) “Interactions of xanthate with pyrite and galena surfaces in the presence and absence of oxygen”, Journal of Industrial and Engineering Chemistry, 20 (1) 268–273.

Chen, Y., Liu, X., Chen, J., (2021) “Steric hindrance effect on adsorption of xanthate on sphalerite surface: A DFT study”, Minerals Engineering, 165, 106834.

Chettibi, M., (2002) “Optimisation of sulfur mineral flotation (ZnS, PbS, FeS_2)”, Moscow Mining State University.

Chettibi, M., Abramov, A. A., Boutrid, A., (2014) “Physicochemical modeling of galena flotation system”, Journal of Mining Science, 50 (6) 1069–1078.

Chettibi, M., Boutrid, A., Laraba, A., Abramov, A. A., (2015) “Optimization of physicochemical parameters of pyrite flotation”, Journal of Mining Science, 51 (6) 1262–1270.

Deng, J., Lei, Y., Wen, S., Chen, Z., (2015) “Modeling interactions between ethyl xanthate and Cu/Fe ions using DFT/B3LYP approach”, International Journal of Mineral Processing, 140, 43–49.

Hamilton, D., (2009) “Reducing the environmental impact of the flotation of sphalerite: An alternative reagent scheme”, Thesis.

Hamilton, D., Natarajan, R., Nirdosh, I., (2009) “Sphalerite flotation using an arylhydroxamic acid collector: Improving grade while using a reduced amount of copper sulfate for activation”, Industrial & Engineering Chemistry Research, 48 (12) 5584–5589.

Li, D., Yin, W., Xue, J., Yao, J., Fu, Y., Liu, Q., (2017) “Solution chemistry of carbonate minerals and its effects on the flotation of hematite with sodium oleate”, International Journal of Minerals, Metallurgy and Materials, 24 (7) 736–744.

Li, Y., Liu, Y., Chen, J., Zhao, C., (2020) “Structure–activity of chelating collectors for flotation: A DFT study”, Minerals Engineering, 146, 106133.

Marabini, A. M., Ciriachi, M., Plescia, P., Barbaro, M., (2007) “Chelating reagents for flotation”, Minerals Engineering, 20 (10) 1014–1025.

Natarajan, R., Nirdosh, I., (2003) “Application of topochemical, topostructural, physicochemical and geometrical parameters to model the flotation efficiencies of N-arylhydroxamic acids”, International Journal of Mineral Processing, 71 (1–4) 113–129.

Natarajan, R., Nirdosh, I., (2006) “New collectors for sphalerite flotation”, International Journal of Mineral Processing, 79 (3) 141–148.

Natarajan, R., Nirdosh, I., Basak, S. C., Mills, D. R., (2002) “QSAR modeling of flotation collectors using principal components extracted from topological indices”, Journal of Chemical Information and Computer Sciences, 42 (6) 1425–1430.

Natarajan, R., Nirdosh, I., Muthuswami, S. V., (1997) “Flotation of a copper–zinc ore using p-nonylcupferron as collector”, Developments in Chemical Engineering and Mineral Processing, 5 (3–4) 183–193.

Nettour, D., Chettibi, M., Bouhedja, A., Bulut, G., (2018) “Determination of physicochemical parameters of Djebel Onk phosphate flotation (Algeria)”, Naukovyi Visnyk Natsionalnoho Hirnychoho Universytetu, 4, 43–49.

Sarvaramini, A., Larachi, F., Hart, B., (2016) “Ethyl xanthate collector interaction with precipitated iron and copper hydroxides – Experiments and DFT simulations”, Computational Materials Science, 120, 108–116.

Uysal, T., Guven, O., Ozdemir, O., Karaagaclioglu, İ. E., Tunç, B., Çelik, M. S., (2021) “Contribution of particle morphology on flotation and aggregation of sphalerite particles”, Minerals Engineering, 165, 106860.

Yang, B., Tong, X., Lan, Z., Cui, Y., Xie, X., (2018) “Influence of the interaction between sphalerite and pyrite on the copper activation of sphalerite”, Minerals, 8 (1) 16.

Yekeler, M., Yekeler, H., (2005) “Molecular modeling study on the relative stabilities of the flotation products for arsenic-containing minerals: Dixanthogens and arsenic(III) xanthates”, Journal of Colloid and Interface Science, 284 (2) 694–697.

Zeng, Y., Liu, J., Ru, S., Wen, S., Wang, Y., (2019) “DFT study of the adsorption of ethyl xanthate on the S-site of Cu-activated sphalerite (110) surface in the presence of water molecule”, Results in Physics, 13, 102271.

Zhang, L., Gao, J., Khoso, S. A., Wang, L., Liu, Y., Ge, P., Tian, M., Sun, W., (2021) “A reagent scheme for galena/sphalerite flotation separation: Insights from first-principles calculations”, Minerals Engineering, 167, 106885.

Zhang, W., Feng, Z., Mulenga, H., Sun, W., Cao, J., Gao, Z., (2020) “Synthesis of a novel collector based on selective nitrogen coordination for improved separation of galena and sphalerite against pyrite”, Chemical Engineering Science, 226, 115860.

STUDY OF COPPER ORE FLOTATION REAGENTS APPLICATION

Vladimir PEZA*

Polytechnic University of Tirana, Faculty of Geology and Mines, Mine Deposit Engineering Department, Rruga e Elbasanit, Tirana, Albania
**Corresponding author: vladimirpeza@gmail.com*

A B S T R A C T

Most of the copper ores in Albania have been exploited from low grade porphyry deposits and some deposits are still being exploited. Of particular importance in their enrichment is the choice of the group of reagents for flotation, which depends greatly on the type and quantity of the various minerals present. The choice of reagents is related to the main and secondary copper minerals, iron sulfide, contained in the ores, as well as the tendency to float, such as chalcopyrite, pyrite, pyrrhotite, marcasite, etc. Therefore, the material composition of the constituent minerals has been studied, including oxidized minerals, the presence of arsenic and bismuth minerals, the presence of silver and gold, as well as silicates, clay minerals and talc. The influence of the natural pH of the ore after grinding and the rate of liberation of various valuable minerals and sterile minerals has also been examined. Based on the composition of the raw material, flotation experiments were carried out on a laboratory scale. As a result of the experiments, the type and regime of reagents that should be used for the flotation of copper ores was found.

Key words: *Flotation, reagents, grinding, release rate, sterile minerals*

1. INTRODUCTION

Many reagents are in use in the floatation treatment of sulfide and metallic ores containing such metals as copper, zinc, lead, iron, precious metals Au, Ag and such penalty elements as As, Te, Bi, Se etc.

The principals factors affecting the choice of collectors are the mineral forms (sulphide, oxidized and/ or metallic species) and their associations with each other and gangue minerals.

Recent trends in floatation practice have shown that in many cases, a combination of two or more different reagent collectors provides better metallurgy than a single collectors. This is not surprising when one considers that, even in such a simple case as copper ores, there may be a variety of Copper minerals present (for eg. chalcopyrite, chalcocite, covellite, bornite, native copper, tetrahedrite and oxidized or tarnished copper minerals) each of which responds differently to different collector chemistries.

Obviously, this aspect is even more important when making a bulky float of minerals of two metals. For many decades, the most commonly used collectors combinations were those of xanthate and dithiophosphate or xanthate and dialkyl thionocarbamate. However in the past 19- 15 year, a large number of new collector chemistries has been developed. Whilst increasing the complexity of the reagent testing process, this has undoubtedly greatly expanded the opportunity of establishing the optimum reagent combination for any specific ore.

2. GEOLOGY OF COPPER ORE IN ALBANIA

In the Ophiolites of Albania up to now have been discovered over 40 Copper Ore Deposits, totaling about 100 million factice industrial reserves and about 400 million tons are reported as prognostic ores (Milushi etc. Geoscience Institute, 2022). Annual production of Copper ore has been during last 10 year about 1, 25 million ton/ year with average 0,7 -1,4 % Cu (Bakallbashi, Mati, F.Gj.M, 2022). The Jurassic Ophiolites in Albania, named The MIRDITA OPHIOLITIC BELT (MORB) in a part of the Mesosoic Tethyan Ophiolitic Belt. They occupy about 5000 km² or nearly on seventh of Albanian territory. Copper Sulphide Mineralization are localized in different levels of Ophiolite rocks formation. Complex, porphyry, veins-volcanogenic- sedimentary formation developed in periphery of Ophiolites rocks.

There are distinguished four tipes of Copper deposits: 1. Hydrothermal Metasomatic Deposits. [Munella, Qaf Bari, Lajthize, Lak Rroshi, Gurth Spaç, Spaç, Reps, Kaçinar, Perlat etc.]. 2. Volcanogeneo -hydrothermal veins deposits. [Tuç, Derven, Kulme, Mashterkor, Maje e madhe, Gjazuj, Thirre ecc]. 3. Porphyry- volcanogenic Sedimentary. [Gjegjan, Pala, Rubik ecc]. veins Massive Metasomatic of quartz sulphide deposits [Kurbnesh, Rehove, Urake, Deje, Golaj, Gdheshte, Shenmri, Nikoliq ecc]. The volcanic sequence of Ophiolites in Copper Ore comprises from sheeted dyce complex the flow and massive lamas, followed by tuff aglomerated volcanic glass and quartz keratophyre extrusion bodies. Mineralization has characterized from Fe sulphide, Cu sulphide and Cu oxide, Fe-Cu, Zn-Cu etc., both the ore assembled and the hydrothermal metamorphic ore zoned. High precious metals Au and Ag, Bi, Se, As etc. contents are related to the agglomerate and accident glasses appear to be proportional to the increase in Cu and Zn contents.

3. FLOTATION PRACTICE FOR COPPER ORE

Copper ore today are mined from porphyry deposits, though a few vein- type deposits are still being exploited. Nevertheless the choice of reagent suite for flotation of these ores dependents more on the type and amount of the various minerals present than in the origin of the ore. The major considerations include: 1. The ration of CaFeS2 to secondary minerals. 2. Tendency to float of the iron sulphide. 3. Copper mineral are tarnished or oxidized. 4. Minerals containing penalty elements such as As, Bi, Te 5.The ore contains recoverable amount of gold and silver associated. 6. The ore contains significant of primary slimes such as clay and talc silicate minerals 7. The natural pH of the ore pulp after grinding and sliming. 8. The degree of liberation of the various valuable and gangue minerals.

3.1. Parameters of Flotation, pH Range

The use of a lime circuits in practically universal in the floatation of copper Sulphide ore. Lime alkalinity is generally maintained in the pH of 9.5 to 11.5 in the rougher circuit and as high as 12 in the cleaner circuits. The higher pH serves to depress the iron sulfide gangue minerals which are commonly present. The pH can also influence the froth structure and floatability of the copper minerals.

These characteristics are adversely affected below some minimum pH value which varies from ore to ore, especially when xanthates and dithiophospates are used. Some of the new chemistries such as the collector Series 5000 Cytex may allow for operation at considerably lower pH value (pH 8-10, for example).

It free gold is present, the use of lime should be carefully controlled since excessive lime concentrations have been reported to have a depressing effect on the gold. If lime depression of gold becomes a problem, soda ash can be used in place of lime. In a limited

number of operations, flotation is carried out at natural pH without any pH regulating agents, or in acid circuits.

3.2. Sulfide Collectors (Promoters) And Combination Of Reagents For Spaçi Copper Ore

The choice of collectors can be made on the basis of the mineralogy of the ore and the operating conditions. In the existing plants the choice of collectors is influenced by the pH of the operating circuits and whether or not the pH can be changed.

Statistical methods can be used to optimize operating conditions.

Plant experience in the past 10 years has established Series Collectors Cytec' 5000 and formulations containing these can offer a wide range of benefits such as:
1. Very high selectively against pyrite etc. in mildly alkaline circuits.
2. Selectively arsenic, tellur, bismuth minerals.
3. Significant reduction in lime usage.
4. Rapid flotation kinetics especially of coarse middling resulting in improved copper recovery.
5. Better copper separation compared to xanthate.
6. Les sensitive to pulp potential changes than xanthate.

The 5000 Series collectors can sometimes be used with xanthate to meet a specific industrial objective.

In the case of slightly oxidized or easily tarnished copper ores AERO 404, 407 and 412 primoters are in commercial use in conjunction with the 5000 Series collectors and xanthate. Best industry is usually obtained when the former collectors are added to the grinding mill or lengthy conditioning stage, in amounts from 5 to 30 g/ t. In acid circuits excellent performance has been observed with AERO6697 promoter and the 400 Series prometer.

Copper Sulfide in massive iron sulfide host are usually finely disseminated with pyrite and pyrrhotite (Spaç cooper ore). The intimate mineral associations may require very fine grinding for adequate liberation of the copper minerals. Preference should be given to selective flotation rather than bulk flotation of the sulfides, the rougher concentrate may still require regrinding to achieve satisfactory liberation and concentrate grades. The choice of collectors is similar to that for porphyry copper ore, except that the most selective collectors are utilized. These include AEROPHINE collectors, series AERO 5000- 7000. All these collectors can be used alone or conjunction with dithiophospates such sodium AEROFLOAT promotors. The optimum collectors chemistry should be established by a systematic laboratory study. If necessarily, small amounts of rthyl or isopropyl xanthate can be used as an auxiliary collectors. Stage- additions of collectors may be desirable to enhance selectivity.

For ores with high pyrite/ pyrrhotite, increased selectivity is sometimes achieved by the ise of sulfur dioxide or alkaline sulfides. Recently, several synthetic polymer depressants have been developed (reagent S).

For copper ore that contain Au, Ag, the collector selection should include AERO prometers in addition to the 5000 Series prompters mentioned above. AEROFLOAT 208 promoter is also well recognized as a good promoter for native gold.
In any of the copper flotation circuits discussed above, it "slimes " pose a problem by reducing recovery or grade the use of a slimes dispersant or depressants is highly recommended. Examples include the reagent S-7260 series and CYQUEST3223 dispersant, either alone or a combination with sodium silicate or soda ash, modifying agents.

4.OXIDE COPPER ORE of GJEGJAN DEPOSIT

Oxide copper ore is a general term used to describe non sulfide copper minerals found in oxidised zones of copper deposits. These non sulfide cooper minerals include malachite, azurite, chrysocollite, cuprite, native copper etc.
All of these minrals are referred to in this article as" well oxide copper minerals".
Oxide copper minerals generally do not respond well to traditional methods of concentration using known sulfide copper collectors. Their recovery in a froth flotation circuit requires special treatment

The traditional methods involves sulfidisation (at 500 -600 mV a combination Sulfide Ion Electrode) using sodium sulfide Na2S, or NaHS, or ammonium sulfide followed by flotation using xanthate or other sulfide collectors. Sulfidising agents are usually stage-aded for both efficacy and controll. The use of NaHS with reduce excessive alkalinity with Na2S can cause. A pH greater than 10,5 can adversely affect copper oxide mineral recovery. Sulfidisation in best conducted using a ionelectrode or a noble metal; the former is strongly recommended. Oxide copper minerals will float withing certain limits of pulp redox potential. These limits may mat be be broad or narrow and sightly different for each oxide minerals. For an ore containing several oxide copper minerals, it is common to have varying froth mineralisation in different sections of the flotation circuits as the pulp potential changes.
Crysocolla is generally found to respond poorly sulfidisatin-flotation. Many of the collectors used for copper sulfide flotation are also applicable for the floatation of sulfidised copper oxide minerals.

Some collectors have been found to be particularly effective for sulfidised oxides. Exemple of these include AERO3300.../or412 promoters, often in combination with a small amount of xanthate.

In principle the sulfidisation flotation method is quite attractive , but in prctice it suthers fom two major disadvantages: (a) it is difficult to control the dosage of the sulfidised agent, an excess causes depression of both sulfide and oxide .minerals, and an insufficient amount produces poor recoveries , and (b) the diferent oxide minerals respond differently sulfidisation (Laskowski 1973) and frequently sulfidisation simple fails to provide acceptable oxide copper recovery.

The decission to recover oxide copper minerals from an ore depends on whether the ore contains sufficent oxide copper to be economically viable and whether such oxide copper is in a form that is amenable to flotation. It is often assumed that sulfidisation- flotation is the preferred methods for oxide copper recovery but this is not necessarily valid until other options have been evaluated.

A wide variety of collectors has been tested in the laboratory for oxide copper flotation without sulfidisation. Those were include include a large number of organic completing agents, fatty acids, fatty amines and petroleum sulfonates (Deng 1991). Expect for a very limited use of tatty acids none of the proposed reagent has been used in an operating plant because of high cost, consumption and inadequate performance. Alkyl hydroxamates AERO 6493 prometer, however, are among the very few collectors that have shown significant promise. Extensive laboratory studies and plant experience on a wide variety of oxide abd mixed sulfide-oxide ore from arround the world have shown that well defined oxide copper minerals such as malachite, cuprite, tenerite, etc. are floated by AERO 6493 promoter. Experience has shown that any lack of performance with AERO 6493 promoter is usually attributed to mineralogy constraints in the ore.

AERO 6493 promotor should be added "neat ar "as it". At temperatures below 20°C this collector may beg to soliddity and it may be necessary to warm it slightly. For laboratory tests AERO 6493 promote can be added to the flotation cells either in the rougher stage along with the sulfide collectors and/ or frother, or to the scavenger stage. The recommended conditioning time is 1- 3 min. For plant evaluation, reagent can be added wither to the mill discharge _cyclone overflow or to the scavenger circuit. The appropriate addition necessary point will have to be determined in the individual plants. The frother dosage and from depth may need adjustments because AERO 6493 promoyter may have a tendency to enhance frothing on certain ore tipes. Addition of AERO 6493 promoter to the grinding mill is generally not recommended in view of the fact that there is an iron- rich environment in the mill which may cause loss of hydroxantates via complexities with iron minerals.

Gangue species that readily generates slimes, for example clay and silikates, sericite, limonite etc. may interfere with oxide copper flotation with hydroxamates and cause exssive frothing. One obvious solution would be to include a desliming step. If this is not feasible then a dispersant such as sodium silicate or CYQUEST 3223 antiprecipitant may be necessary. These can be added either to the mill or to the flotation bank. They can also be stage added. Typically dosages are 200- 500 g/ t for sodium silcate and 25- 50 g/ t for CYQUEST 3223 dispersant. Dispersant dosage must be selected carefully. because an excess of dispersant may hunder or even depress oxide copper flotation. Soda ash can be used as a dispersant and pH modifier in non lime circuits. It is important to note, however, that oxide copper minerals slime easily and, therefore, any desliming step may result in copper losses in the slimes fractiin.

If the ore contains large amounts of pyrite and pyrrhotite they may be depressed using sodium cyanide, sodium metabisulfide, SO2 or a combination of these. These depressants should should be added prior to hydroxamate addition. Again the dossages of these depressants mist be evaluated carefully because they can hinder oxide copper flotation. The froth character associated with the use of AERO6493 promoter is very important. An excessive froth is indicative of one or more of the following, dosage of the hydroxamate is too high, ore has problem gangue minerals, ore has activated pyrite and pyrrhotite, ore has large amounts of goethite. If the froth has a tendency to fllatten and additional frother does not help, it may be indicative of a more fundamental problem related to the absorption of hydroxamates on undesired minerals.

Optimum pH range for oxide minerals flotation with AREO6493 promoter is 8, 5 - 10. Minor pH adjustment in the scavenger circuit may be possible, but pyrite flotation may be enhanced at lower pH value if xanthate is the collector. Alternatively, the entire circuits can be run at a lower pH be using a selective sulfide collector such as the 5000 series and related collectors. The will not only be beneficial to the performance of hydroxamates, but also result in saving in lime cost. An alternative to sulfidisation- flotation and alkyl hydroxamates flotation for oxide minerals recovery in the LPF (leach precipitation flotation) process The ore is leached with sulfuric acid and the copper in solution is precipitated on to iron powder. The precipitated copper minerals is then floated in acid circuits. Prrhaps the best collecttors for this application are AERO6697 promoter and AERO5698 promoter which have been used in commercial operations. Metallic copper native present in the ore, responds readly to flotation, preferably in a low pH circuits. The most effective collector for recovery of metallic copper is Reagent S-7151 promoter, AERO404 and AERO406promoter have aso been used commercially with success.

5. COPPER - ZINC ORE of MUNELLA DEPOSIT

The separation of copper sulfides from sfalerite or marmatite, particularly in the presence of iron sulfide, requires careful selection of collectors, pH regulators and depressants. The

following general procedures and reagents have been found to give good separations on many copper-zinc ores.

To minimise activation of the zinc minerals by any dissolved salts in the grinding circuit, alkalinity is maintained at pH 8 to 10 by the addition of lime and/ ore soda ash. If the floatation feed contains liberated precious metal values soda ash is preferred as the principal alkalinity regulator. To further aid selectivity against iron and zinc sulfides in the copper flotation step, sodium sulfide or bi- sulfide, or zinc sulfate and cyanide, an added to the grinding circuits or the conditioners ahead of copper flotation. Sulfur dioxide may also be used, added yo the conditioners ahead of copper flotation.

During the copper flotation step dithiophospates such as AEROFLOAT 208 or 238 promoter and AERO 3501 or 3477 promoter have traditionaly been used. However for increased copper- zinc selectivity, collectors such as AEROPHINE promoter are now recommended.
The use of an alcohol- type frother is preferred to assist selectivity. After flotation of the copper minerals the zinc minerals are activated and float as previously described under zinc ores.

The most common oxidized zinc minerals are smithsonite, hydrozincite, hemimorphite and willemite, often in association with carbonate and siliceous gangue. Usually these oxide zinc minerals occur with the copper oxide and sulfide minerals as well as the zinc sulfide minerals. The most widely accepted technique for the flotation of oxide minerals has b in use at zinc operations in the Mediterranean area for a number of years. By the use of the sodium sulfide and an amine, both carbonate and silicate zinc minerals are recovered. The amines which should be investigated are AERO8625promoter. Recent studies indicate promising results with the used of AERO 6493 promoter without sulfidisation.
As most oxide zinc and copper minerals occur in mixed sulfide-oxide ore of zinc and copper, the procedure consists of floating the copper and zinc sulfides then the copper oxide and finally the oxide zinc minerals.

The feed to the oxide zinc flotation circuit requires careful desliming prior to flotations and in then floated with a relatively large amount of sulfidising agents and a cationic collectors, such as AERO 8625 and 8651 promoter, with frother added as required. Investigators originally reported best results at pH levels between 10,5 and 11, although some of ores responder well to the process at lower pH levels. Reagent consumption are usually of 1000 to 5000 g/t sodium dulfide and 50 to 300 g/t cations collector. Soda ash and sodium silcate can be used to improve flotation.
Less common is a process which utilities large amounts of amylxanthate, in conjunction with sodium sulfide. In this process desliming prior to z oxide flotation is also necessary.

Consideration should be given in thid latter process to evaluating the more powerful alkyl dithiophospates in particular AERO 3477 and3501 promoter, as well as the Series promoters. Depression of copper minerals are more.

Although not commonly practiced, when there is less than two parts of zink or lead to one part of copper in bulk concentrates it may be preferable to depress the copper minerals un order to make theirs sparation from the zink minerals. For the depression of copper minerals, cyanide or the cyanide - zinc complex are used. In ghis process short conditioning with cyanide is proffered and the stage addition of cyanide can be advantageous.The zinc concentrate is usually cleaned at least once with small amounts of cyanide. Control of pH in the range 7,5 to9 is desirable and in determined experimentally.
When using a straight cyanide separation, losses of precious metal and secondary copper minerals may occur through dissolution. These losses are largely eliminated when using the zinc- cyanide complex. This complex can be prepared on site by mixing the following

ingredients in a tank with 100% freetboard: .100 kg of technical grade zink-sulfate contained 36% Zn or 45 kg pure oxide zinc..55 kg sodium cyanide.600- 650 kg (liters) cool water.

6.GOLD - SILVER - COPPER ORE of GJAZUJ DEPOSIT

Treatment methods for the recovery of gold from gold-bearing ores depends on various factors, such as: (a) the mode of ocurrence of the gold and associated minerals and (b) the the grade of gold in the ore.

Ore in which the gold is associated with mostly non-sulfide gangue minerals, and is readily recoverable by gravity methods, flotation or cyanidation, are generally referred to as "free-milling" ore.
The choice of treatment methods for such ore depends upon (a) the grade of the gold in the ore, (b) the recovery obtained by each method, (c) possible environmental constraints, and (d) overall process economics. It flotation is used to upgrade such ore prior to cyanidation, the common collectors used are xanthate such as AERO343 or 317. The use of a secondary collectors such as AEROFLOAT...promoters can often improve recoveries. If the gold is tarnished and slow-floating the use of 400 Series collector such as AERO 3418A promoter can often improve recoveries. If the gold is tarnished and slow-floating, the use of 400 Series collector such as AERO 407 or 412 promoter is often helpful. By carefully designed flotation test work, Cytec has the ability to design a custom collector formulations for specific ores and process conditions.

It is interesting to note that Nagaraj (1992) have reported that 100% pure metallic gold does not readily absorb any known sulfide collectors. However, if the gold is allowed with even a small amount of siver or copper, absorption is significantly enhanced. Fortunately, almost all naturally-occurring, gold does contain silver, usually in the range of 2 to 12 %; this is sufficient for good collector absorption and flotation (uncless the gold suface is heavily tarnished). Other elements such as copper and tellurium are also frequently found in native gold.

Gold is commonly found in deposits which contain significant amounts of sulfide copper minerals. The treatments methods for these so called "refractory " gold ore depends upon whether or not significant amount of the gold are associated by intimate physical locking with, or in solid-solution in, the iron sulfide minerals.

Ores in which little of the gold is associated with sulfide minerals can often be treated by direct cyanidation of the whole ore. In many cases, however, results are unsatisfactory due to the adverse effect of the sulfides minerals on both cyanide consumption and gold recovery. In this case, the gold is separated from the sulfides minerals by flotation snd the concentrate treated by cyanidation. The gold collectors mentioned above are suitable, but addition of lime to pH 11 or higher is often necessary to prevent the sulfides minerals from floating. An alternative method for these ore types is the use of AERO6697 promoter it pH 8 to9 to float the free gold away from the sulfides.

For ores in which a significant amount of the gold is intimately locked with, or in solid solution in, the iron sulfide minerals, these sulfides must be floated together with any free gold, prior to further treatment of the flotation concentrate. The flotation is usually conducted at natural pH with a combination of a strong sulfides collector such as AERO317 or 350 xanthate. In many cases the use of a secondary collectors for thr free gold is benefical. Such collectors would include AEROFLOAT....promoters. For tarnished ores and for ore containing significant quantities of arsenopyrite, the use of copper dulfste to activate the sulfides should be investigated. The fl concentrate is then generally subjected to oxidation.

Finally, it dhold be noted that much of the current global production of gold comes from ores which contains their major value as minerals of base metals, particularly copper. These ore are usually referred to as base-metak ores, but msy contain sufficient amounts of gold to influence the selection of the optimum flotation reagent. The treatment of thrse ore types is discussed.

Most of the silver recovered commercially is associated with the base metal sulfide ore of copper and coper-zinc ore in Albania. Silver occurrence ranges from a minor to a major constituent in these ore tipes. Of major importance in the floatation of these silver bearing ores is the choice of collectors, regulating agents and depressants.

The generak, the silver tends to concentrate with ghe copper and xinc sulfides in these types of ores. AEROFLOAT 242 promoter and AEROPHINE 3418A promoter are strongly preferred as collectors. AERO7518 and AERO7640 promoters have demonstrated good recovery of silver associated with copper sulfides. They may also be used as auxiliary collectors for silver in the flotation of argentiferrous sulfides. Silver also occurs in association with sphallerite, arsenophyrite and even with pyrite. In the later case, depending of the silver content of the pyrite, a pyrite concentrate may be produced from the base metal circuit tailing which can be treated by roasting and cyanidation for silver recovery. If cyanide must be used in the base metal flotation circiuts, is it recommended that the zinc cyanide complex be used to reduce the dissolution of the silver

When the silver ore contains only minor amounts of base metal sulfides, bulk flotation of all sulfides is usually the best practice for maximum silver recovery. It silver- bearing zinc sulfides, pyrite, are present, copper sulfate with usually be required to activate these minerals prior to collectors addition. If, on the other hand, these sulfide minerals do not contain silver, then careful use of lime may be required to prevent concentrate dilution.
The u of the dithiophospates, AEROFLOAT promoters with small amounts of a lower xanthate, such as isopropyl xanthate are recommended for these ore type.

With partially oxidized silver-bearing ores, cyanidation of flotation tailing for silver and gold recovery may be economically justified. In addition, sulfidisation prior to flotation is commonly practiced when the silver values are associated with oxide minerals such as malachite, cuprite ect. When sulfidisation is practiced the use to AERO promoters are recommended.

7.CONCLUSION

Many collectors and frothers are in use in the flotation treatment of sulfide and metallic ores containing such metals as copper, zinc, gold, silver and such penalty elements as arsenic, bismuth, tellur etc. The principal factors affecting the choice of collectors are the mineral forms (sulfide, oxidized and /or metallic species) and their associations with each other and the gangue minerals.

Recent trends in flotation practice have shown that, in many cases, and combination of two or more different collectors provides better technological figures than a single collector. This is not surprising when considering that, even in such a simple case as copper ore, there may be a variety of copper minerals present each of which responds differently to different collector chemistries. Obviously, this aspect is even more important when making a bulk float of minerals of two different metals (for example zinc and copper). For many decades the most commonly used collectors combinations were those of xanthate and dithiophosphate, or of xanthate and dialkyl thionocarbamate.

However, in the past 10- 15 years, a large numbers of new collectors has been developed and introduced by Cytec's. Whilst increasing the complexity of the reagent testing process, this

has undoubtedly greatly expanded the opportunity of establishing the optimum reagent combination for any specific ore.

REFERENCES

Basilio, C., et al. (1988). “Flotation and adsorption studies”. *Proceedings of the Annual Meeting*, Phoenix.

Iwasaki, I. (1988). “Flotation behaviour of sulfide–oxide mineral systems”.

Nagaraj, D. R., et al. (1990). “Electrochemical and spectroscopic studies of flotation systems”. University of Florida.

Nagaraj, D. R., et al. (1993). “*Copper mineral system”s*. CRC Press.

Taggart, A. F. (1980). “*Handbook of mineral dressing”*. McGraw-Hill, New York.

Young, C. A., Luttrell, G. H., & Anderson, C. G. (1999). “*Advances in flotation technology”*. Society for Mining, Metallurgy and Exploration, Littleton, Colorado.

SULFIDE GOLD ORE FLOTATION RICH IN FINE PARTICLES

Elenice Maria Schons SILVA*, Antônio de Pádua Arlindo DANTAS, Jaciany Mayara Batista SOARES, Poliana Felipe PACHECO, Kascielle Braga AMORIM, Luiz Henrique Coelho Pessoa SANTOS, Bruno Gomes da MOTA, Vinicius Curcino de Carvalho VIEIRA, André Carlos SILVA

Federal University of Catalão, Mineral Processing Research Center (CPMin), 75705-321, Catalão, Goiás, BRAZIL
**Corresponding author: eschons@ufcat.edu.br*

A B S T R A C T

Gold ore processing presents specific characteristics that differentiate it from other mineral commodities. Sulfide gold ore processing routes may involve, in addition to comminution, concentration steps that exploit differentiating physical and physicochemical properties, such as the difference in specific gravity and hydrophobicity (natural or induced) between the gold-bearing minerals and the gangue minerals. The physical and surface properties of fine particles impose a series of limitations on flotation performance, especially when they coexist with coarse particles. The present work evaluated the influence of fine and ultrafine particles (also known as slime) in the flotation of a sulfide gold ore from the Nova Xavantina Mine, located in the state of Mato Grosso, assessing recovery and gold content in the generated concentrate. The methodology comprised the sampling at the ERO Brasil Nova Xavantina mineral processing plant, carried out by company employees, followed by preparation, chemical characterization (XRF and Fire Assay), granulometric analysis (wet sieving), and mineralogical analysis (XRD). The ore sample was classified by hydrocycloning to generate three samples with different granulometric distributions, which were subjected to flotation tests in a bench-scale mechanical cell, in rougher stage, varying the percentage of solids and pH. The sample tested was mainly composed of quartz and pyrite, which explains its high Si and Fe contents. Granulometric analysis indicated a large presence of fine particles (92.53% -25 µm). Flotation tests indicate that the slime significantly influences the Au content and recovery, thus affecting the selectivity of flotation. The best results were obtained for hydrocyclone overflow samples with 10% solids.

Key words: *Flotation, gold ore, sulfides, fine particles, slimes*

1. INTRODUCTION

Gold mining is surrounded by precautions, especially in relation to fine gold. The recovery of these fines is an essential yet challenging process, due to the complex mineralogy of gold ores, their low grade, and the imperfections of traditional methods. This recovery process involves the separation of exceedingly small gold particles, which, due to their size, are lost in conventional concentration processes. Innovative techniques have been employed to minimize the loss of this precious metal. Gravimetric recovery methods, widely used today , perform this separation based on the specific mass of the minerals present, i.e., between the particles of gangue minerals and the particles of free gold, also known as gravity-recoverable gold (GRG) (Fullam et al., 2016). However, other methods can be used to recover fine gold particles, with flotation being a method that has been gaining prominence in the processing of sulfide gold ores. Unlike gravity methods, flotation performs this separation by adhering air bubbles to the surface of the gold-bearing mineral. Chemical reagents must act on the surface of the gold ore, making it hydrophobic, for the flotation to occur. This reagent is called a collector, and collectors from the xanthate family are most used in the flotation of sulfides.

The effects of the presence of fine and ultrafine particles (also known as slimes) in mineral concentration processes, especially in flotation, have been widely discussed in technical literature due to the operational, economic, and environmental impacts associated with these

particle size fractions. The growing need to exploit increasingly complex and poor ores has intensified the generation of slime in the comminution stages, making this topic particularly relevant for the processing of sulfide gold ores. According to Baltar (2010), the physical and surface properties of fine particles impose several limitations on flotation performance, especially when they coexist with coarser particles. Among the main effects observed are increased foam stability, increased pulp viscosity, interference in bubble-particle contact, and the covering of coarser particles by ultrafine particles, a phenomenon known as slime coating. Slime coating consists of the adhesion of ultrafine particles to the surface of coarser particles through intermolecular forces like those involved in the interaction between mineral particles and air bubbles. According to Cruz (2010), this phenomenon can negatively affect flotation when fine gangue particles adhere to the particles of the mineral of interest, thus hindering effective contact with the bubbles and significantly reducing Au recovery. In addition, the high specific surface area of the slimes intensifies the interaction with the reagents, resulting in higher consumption and, often, lower selectivity of the process.

In situations where the slime is dragged into the concentrate (a phenomenon known as hydraulic entrainment), depletion of the concentrate is also observed. High reagent consumption in pulps with substantial amounts of fine particles is associated with the considerable number of active sites available on the surface of these particles. Baltar (2010) points out that the high surface energy of slimes, resulting from the abundance of edges, corners, and crystallographic defects, favors the non-selective adsorption of collectors, altering the electrochemical characteristics of mineral surfaces and compromising the efficiency of bubble-particle interactions.

Although there is no single granulometric definition for fine particles, it is common to associate the concept of slimes with the fraction of ore that exhibits critical behavior in flotation processes. According to Peres & Araujo (2006), there is an attempt to quantify the concept of slimes. According to the authors, particles -100+10 μm are designated as fine particles, -10+1 μm would be ultrafine particles, and particles -1 μm would be called colloidal particles. The particle size range of ultrafine and colloidal particles constitutes slimes. Based on this criterion, the present study considers particles with a particle size of less than 10 μm present in the flotation feed to be slimes.

The presence of slimes also influences important operating parameters, such as the loading rate, defined by Martínez-Gómez, Pérez-Garibay, and Rubio (2013) as the maximum flow of solids per unit area of the cross-section of the flotation column, and lip loading, a concept presented by Amelunxen and Amelunxen (2013) and defined as the maximum mass flow rate of pulp recovered in the concentrate per linear meter of overflow edge. The same authors observed values as high as 20 t.h-1.m-1for large-scale commercial columns. The covering of bubbles by ultrafine particles, characterized by low mass and high surface area, limits these rates and restricts the operational capacity of the flotation circuit.

Given this scenario, this study aimed to evaluate the influence of the presence of slime on the flotation of gold ore from the Nova Xavantina Mine, located in the state of Mato Grosso, assessing the impacts on yield, Au recovery, and grade in the flotation concentrate.

2. MATERIAL AND METHODS

2.1. Material

A representative sample of sulfide gold ore was collected from the hydrocyclone overflow at the Ero Brasil Nova Xavantina Unit plant during a sampling campaign carried out in May 2025. The sampling point (hydrocyclone overflow) is indicated as a red circle in Figure 1. The samples were received at the Mineral Processing Research Center (CPMin) of the Federal

University of Catalão (UFCAT) in the form of pulp, packed in four 50 L bottles. Additionally, a 20 L bottle containing process water from the company was received. The cylinders containing the ore sample were subjected to siphoning after precipitation of the solids, with the siphoned liquid being stored in a separate cylinder for use in flotation tests. After this procedure, the samples were combined in a single cylinder to promote the ore homogenization.

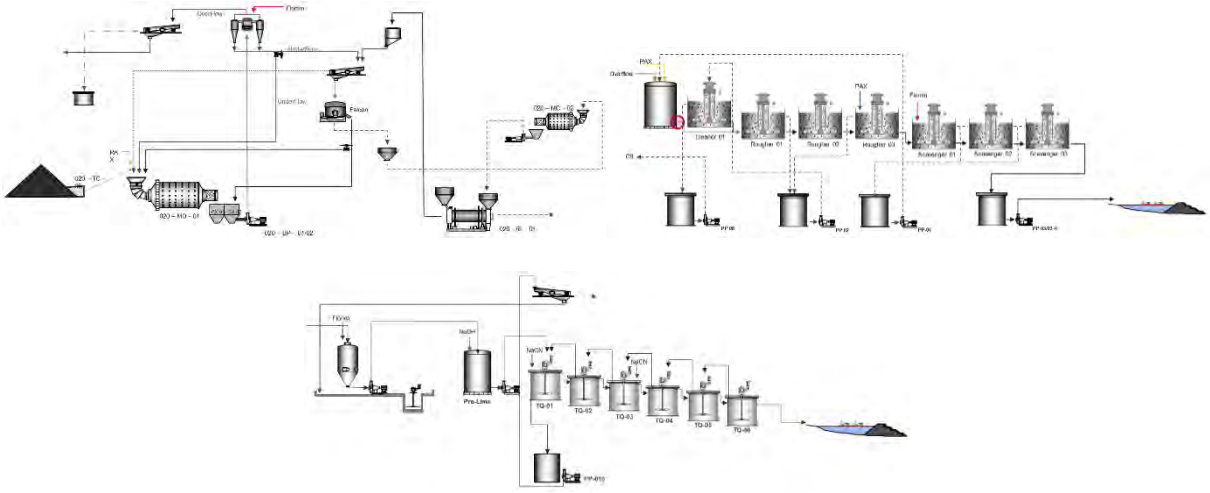

Figure 1. Flowchart of the Ero Brasil Nova Xavantina mineral processing plant. The sampling point is represented by the red circle.

2.2. Method

An aliquot of the sample was collected and used for ore characterization. Wet sieving was performed using a Brastorno suspended screen, operating with 10 circular screens 8" in diameter and 2" in height. Masses of 300 g of sample were pulped with 500 mL of water. Sodium metasilicate (Na_2SiO_3) was used as a dispersant (3 mL at 10% v/v). The screening time adopted was 15 minutes. The chemical composition of the sulfide gold ore sample was determined by X-ray fluorescence spectrometry (XRF) using an S8 Tiger spectrometer (Bruker), operating with a 4 kW X-ray generator, rhodium (Rh) tube, and WDS detector for quantitative determination by the fused pellet method using lithium tetraborate. The determination of loss (or gain) on ignition (LOI) was performed at 1200 °C using a Precisa prepASH 340 thermogravimetric analyzer, model 212, and lithium tetraborate as a flux.

The major mineralogical composition of the sample was determined by X-ray diffraction (XRD) using a D8 Discover diffractometer (Bruker). The analyses were performed by the powder method, in high resolution, in the θ–2θ Bragg–Brentano configuration, with Cu $K\alpha_1$ monochromatic radiation and a LinxEye one-dimensional linear detector. The scan was conducted in the range of 10° to 90° (2θ), with an angular step of 0.02° and a counting time of 2 s per step. The XRD and XRF analyses were performed at the Regional Center for Technological Development and Innovation (CRTI) of the Federal University of Goiás (UFG).
The remaining ore mass was cut (classified) in two by hydrocycloning, using an 80 mm diameter hydrocyclone, operating at 40% solid, feed pressure of 17.24 kPa (2.5 PSI), and feed flow rate of 4 L/min. The products obtained (overflow and underflow) were collected, dried, weighed, and used in subsequent steps. Three samples were prepared for flotation tests in a bench-scale mechanical cell, one consisting only of the hydrocyclone underflow, one consisting only of the hydrocyclone overflow, and one consisting of 65% hydrocyclone overflow and 35% hydrocyclone underflow (denoted 65% O + 35% U). After composing the three samples with different particle size distributions, they were quartered using a Jones quartering machine to generate 200 g aliquots for the flotation tests.

The flotation tests in a mechanical bench cell were performed in a CDC CFB 1666 EEPN model cell, with 1 L and 2 L tanks. Initially, the ore sample was pulped with process water in a 2 L tank and conditioned for 3 minutes with potassium amyl xanthate collector (PAX, reference 1207 supplied by Marquimm) at a dosage of 147 g/t. This was followed by conditioning with Marquimm's Flomin 102 frother (40 g/t) for 1 minute. The flotation time was 5 minutes (rougher stage). Flotation was performed at 1,400 RPM rotor rotation and with 4 L/min of atmospheric air flow injected into the cell at a pressure of 27.6 kPa (4.0 PSI). The methodology employed was analogous to that used at Ero Brasil's Nova Xavantina Unit. Eighteen tests were performed, varying the percentage of solids (10 and 20%), the pH of the pulp (6 and 8), and the percentage of fines present in the sample. The flotation products (floated and sunk) were sent for analysis via Fire Assay at the company. The planning of the flotation tests in a mechanical bench cell can be seen in Table 1.

Table 1. Mechanical bench scale cell flotation tests planning.

Flotation assays	Sample	pH	Solids %
1, 2, and 3	*Underflow*	8	20
4, 5, and 6	*Underflow*	8	10
7, 8, and 9	65% O + 35% U	6	20
10, 11, and 12	65% O + 35% U	6	10
13, 14, and 15	*Overflow*	6	20
16, 17, and 18	*Overflow*	6	10

3. RESULTS AND DISCUSSION

Figure 2 shows four representative samples from the Ero Brasil Nova Xavantina gold deposit, one of which has a grain size of +20 mm and a sulfide content of > 50%, one with a grain size of -10+5 mm and a sulfide content of > 50%, and one with a sulfide content of < 50% and one with a grain size of -20+10 mm composed mainly by graphite.

Figure 3a shows the diffractogram of the flotation feed sample from Ero Brasil's Nova Xavantina Unit before particle size reduction (as-received sample). The sample was composed of quartz (SiO_2, 90.09%) and pyrite (FeS_2, 9.76%). Sphalerite (ZnS, 0.13%) and ferric sphalerite (ZnFeS, 0.02%) were identified as secondary minerals. Costa (2016) obtained comparable results for the sulfide gold ore from the Morro do Ouro mine, located in the municipality of Paracatu/MG, which accounted for 29% of national gold production in 2012.

Figure 3b shows the predominant oxides determined by XRF in the feed, concentrate (after three rougher stages and one cleaner stage), and flotation tailings samples from Ero Brasil's Nova Xavantina Unit. The samples referring to the flotation products were collected in the same campaign. It can be observed that the flotation feed consisted of SiO_2 (76.25%), Fe_2O_3 (5.00%), and Al_2O_3 (4.67%), results similar to those obtained for the flotation tailings. The flotation concentrate was composed of SiO_2 (24.86%), Fe_2O_3 (11.35%), PbO (9.57%), ZnO (7.78%), and Al_2O_3 (7.82%). The Au content for the feed, concentrate, and tailings samples was 3.89 g/t, 75.79 g/t, and 0.71 g/t, respectively. It should be noted that, for this sampling campaign, the yield was 4.24%, the Au recovery was 82.65%, and the enrichment was 19.48.

Figure 4 shows the particle size analysis of the sample before and after the hydrocyclone classification. It can be seen that 92.53% of the sample mass before classification was -25 µm, which characterizes the material as too fine for flotation. It is believed that this excessive amount of fine particles (also called slime) may be associated with low grinding efficiency of this ore, which is probably causing it to be overground. However, it is possible to find studies in literature reporting flotation tests of sulfide gold ore with a large amount of fine particles.

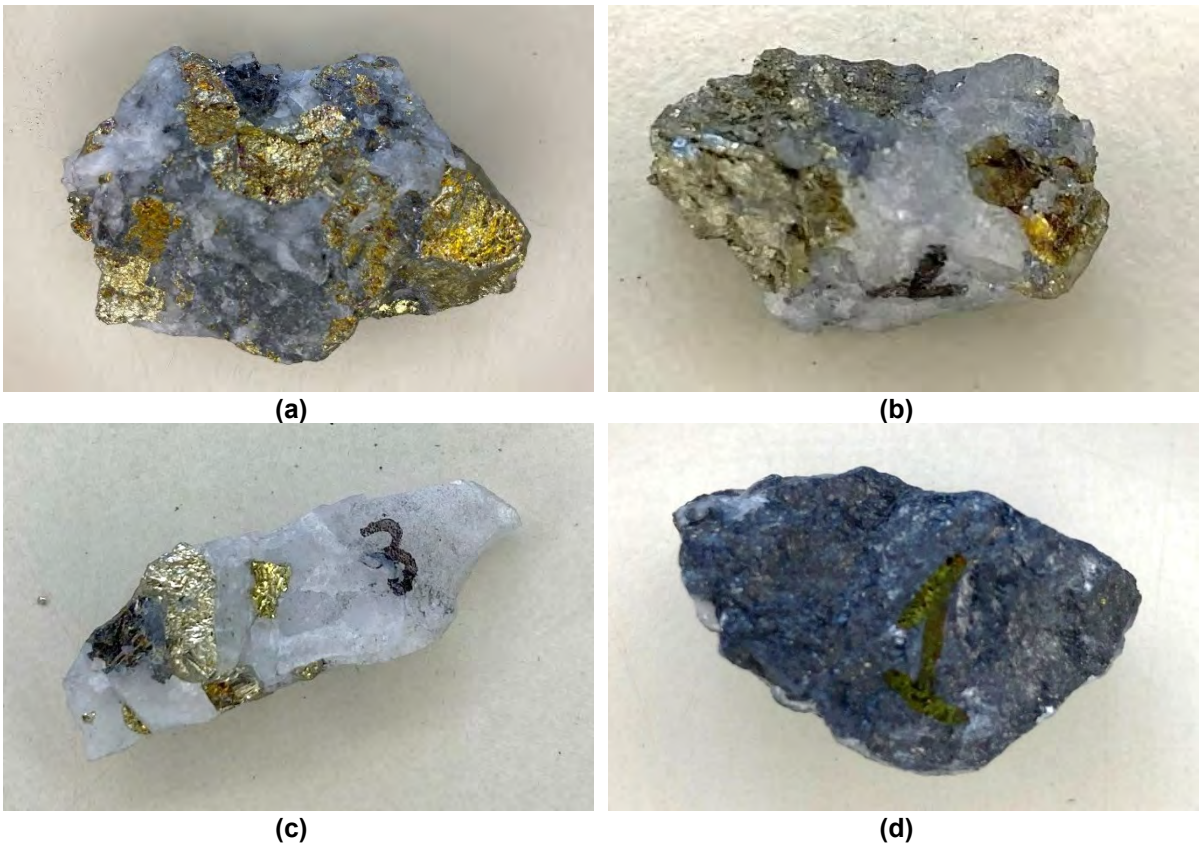

(a) (b) (c) (d)

Figure 2. Representative samples from the Ero Brasil Nova Xavantina gold deposit.

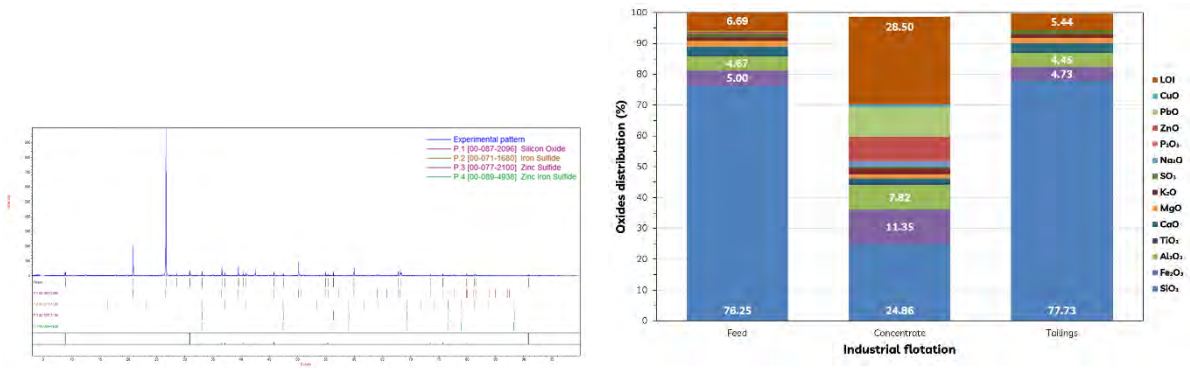

(a) (b)

Figure 3. (a) flotation feed sample before comminution (as it is) diffractogram and (b) major oxides present in the feed, concentrate, and flotation tailings.

Reis, Cunha, and Magalhães (2015) obtained the best results for both gold and sulfide recovery by floating samples with 90% passing through a 53 µm mesh and an average feed grade of 5.28 g/t Au. However, the authors obtained a lower degree of selectivity at this particle size. After particle size cut, the hydrocyclone underflow d_{80} of the ore was approximately 50 µm, with a reduction of -25 µm particles to 36.69% (60.35% reduction). Finally, the sample composed of 65% overflow and 35% underflow had a d_{80} equal to 40 µm.

Figure 4 shows the Au grades in the feed and rougher concentrate from the bench-scale flotation tests. The average Au grade calculated in the feed of the flotation tests was 3.87 ± 0.61%, remarkably close to the grade measured for the sample without size reduction (3.89 g/t). It can be noted that the Au content in the rougher concentrate underwent a noticeable reduction with the increase in fines in the sample. Furthermore, the decrease in the percentage

of solids from 20% to 10% promoted an increase in the average Au content in the rougher concentrate for the three samples tested, ranging from 20.06 ± 5.97% to 23.58 ± 7.63% for the samples composed of the hydrocyclone underflow, from 9.99 ± 0.42% to 17.27 ± 1.30% for the composite samples (65% O + 35% U), and from 7.21 ± 0.20% to 11.21 ± 1.13% for the hydrocyclone overflow samples. Thus, similar behavior can be seen in the Au enrichment (Figure 5), with the highest average enrichment obtained for the hydrocyclone underflow samples floated with 10% solids (6.83 ± 1.87%). The lowest average enrichment was obtained for hydrocyclone overflow samples floated with 20% solids (1.61 ± 0.09%).

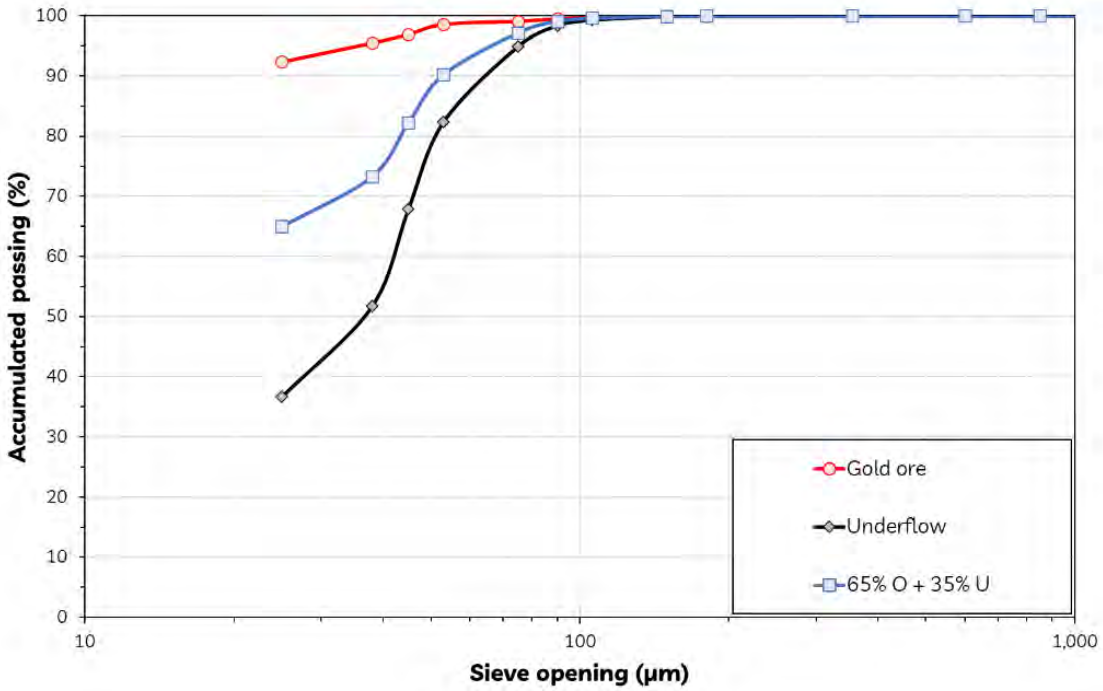

Figure 4. Particle size distribution of the sample before hydrocycloning (gold ore), underflow, and sample composed of 65% overflow plus 35% underflow.

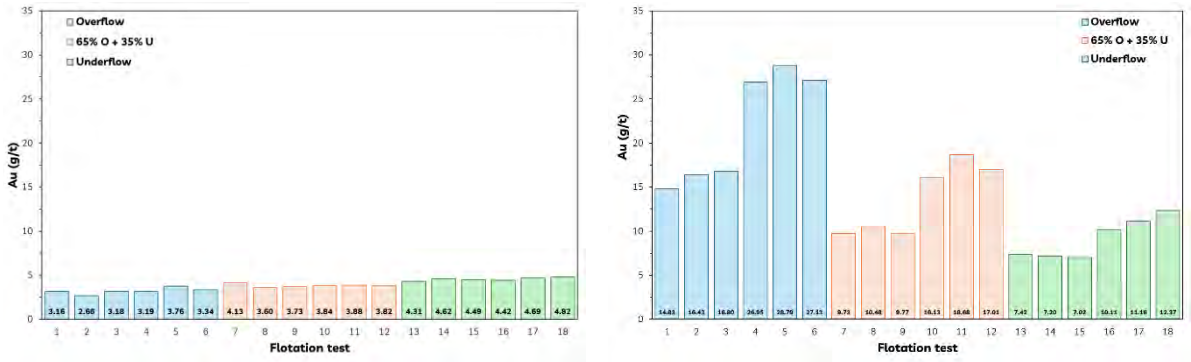

(a) (b)

Figure 5. Gold content in (a) flotation feed and (b) concentrate.

Figure 7 shows the yield and Au recovery for the rougher stage of bench-scale flotation. It should be noted that a low yield is a positive result, given the low grade of the element of interest. The yield varied directly with the amount of fines present in the sample and inversely with the percentage of solids. The lowest average yield (13.24 ± 6.19%) was obtained for the samples with the highest average Au content (hydrocyclone underflow floated with 10% solids). Recovery followed an inverse trend to grade and enrichment, as expected. Thus, increasing the concentrate grade reduced the Au recovery. The highest average Au recovery (90.71 ± 4.28%) was obtained for hydrocyclone underflow samples with 20% solids. For

hydrocyclone underflow samples floated with 10% solids (highest average Au grade), the average Au recovery was 82.88 ± 13.17%. Thus, it can be concluded that the best conditions for the rougher flotation stage were for coarse particles (hydrocyclone underflow) with 20% solids and at pH 8.

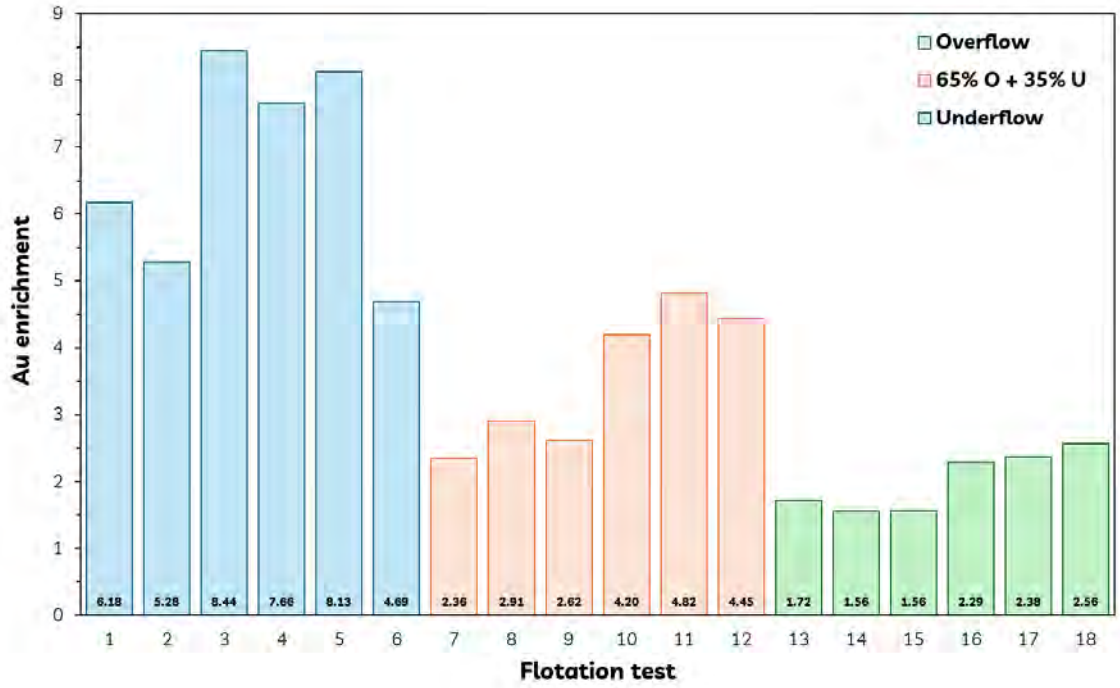

Figure 6. Au enrichment.

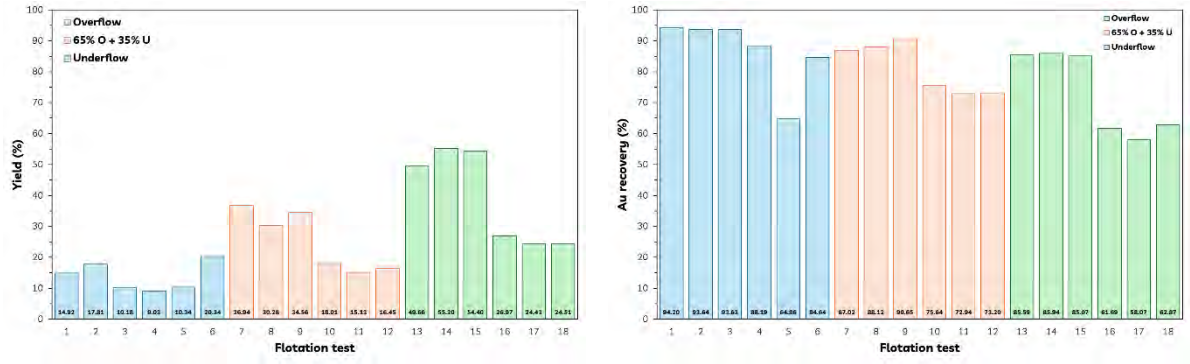

(a) **(b)**

Figure 7. Flotation tests results: (a) yield and (b) Au recovery.

4. CONCLUSION

The processing of gold-bearing ores tends to be extraordinarily complex, often due to the low grade of the ore, the fine particle size of the element of interest (or the minerals that carry it), and the wide variability in grades. In this context, e y flotation plays a fundamental role in the recovery of gold associated with the fine fractions of the ore, making it essential to understand the effects of slimes on the performance of this process. Thus, the results obtained in this study contribute to the improvement of gold ore processing practices, especially sulfide ores, providing technical support for decision-making in industrial plants that face challenges related to the strong presence of fine and ultrafine particles in the flotation feed.

It should also be noted that overgrinding should be thoroughly investigated, as this may be the root cause of the problem of high fines in the flotation feed. Hydrocyclones are typically used to close grinding circuits in sulfide gold ore processing plants. If fine particles of sulfide minerals are being sent to the underflow when they should be sent to the overflow (a phenomenon known as fines bypass), they may be overground. Therefore, an in-depth study of the grinding process should be conducted with a view to optimizing it.

ACKNOWLEDGMENTS

The authors would like to thank the Specialization Course in Mineral Processing at the Federal University of Catalão for the knowledge imparted, Ero Brasil Unidade Nova Xavantina for conducting this study, the Multi-user High Resolution Microscopy Laboratory (LabMic) and the Regional Center for Technological Development and Innovation (CRTI) at the Federal University of Goiás for conducting the analyses, and the funding agencies FAPEG, FUNAPE, CAPES, and CNPq for the financial support granted to CPMin researchers.

REFERENCES

Amelunxen, P. A., Amelunxen, R. L., (2013), “Aminpro’s methodology for applying current flotation modeling starting from batch kinetics (part 2 of 2)”, In Proceedings of XXV Encontro Nacional de Tratamento de Minérios e Metalurgia Extrativa & VIII Meeting of the Southern Hemisphere on Mineral Technology, Goiânia – GO, 35–45.

Baltar, C. A. M., (2010), Flotação no Tratamento de Minérios, 2ª Ed., Editora da UFPE.

Costa, F. R., (2016), “Caracterização tecnológica do minério de ouro da Mina Morro do Ouro – Paracatu, MG”, Master Thesis, Universidade de São Paulo. https://doi.org/10.11606/D.3.2016.tde-22062016-144932

Cruz, M. R., (2010), “Flotação fracionada: Aumento do rendimento da flotação através da divisão da alimentação em duas frações granulométricas”, Master Thesis, Universidade Federal de Minas Gerais. https://hdl.handle.net/1843/BUOS-8DBK9G

Fullam, M., Watson, B., Laplante, A., Gray, S., (2016), “Advances in gravity gold technology”, In: Adams, M. D. (Ed.), Gold Ore Processing, Elsevier B.V., 280–307. https://doi.org/10.1016/B978-0-444-63658-4.00019-0

Martínez-Gómez, V., Pérez-Garibay, R., Rubio, J., (2013), “Factors involving the solids-carrying flotation capacity of microbubbles”, Minerals Engineering, 53, 160–166. https://doi.org/10.1016/j.mineng.2013.07.016

Mota, B. G., Santos, L. H. C. P., Vieira, V. C. C., Amorim, K. B., Americo, R. C. B., Silva, E. M. S., Silva, A. C., (2025), “Testes em escala laboratorial com um concentrador centrífugo Falcon L40 para a recuperação de ouro livre”, Revista Delos, 18 (64), 1–19. https://doi.org/10.55905/rdelosv18.n64-087

Peres, A. E. C., Araujo, A. C., (2006), “A flotação como operação unitária no tratamento de minérios”, In: Teoria e Prática do Tratamento de Minérios: Flotação – O estado da arte no Brasil, Editora Signus, 1–29.

Reis, A. C. F., Cunha, A. A., Magalhães, D. G., (2015), “Flotação de minério sulfetado de ouro com diferentes faixas granulométricas”, In Proceedings of 70th ABM Annual Congress, 70, 721–728. https://doi.org/10.5151/1516-392X-26417

TESTING THE SELECTIVE SEPARATION OF LIMONITE-BARITE ORE FROM THE 'VIDRENJAK' DEPOSIT

Ljiljana TANKOSIĆ[1,*], Branka ŠOLAJA[2]

[1]University of Banja Luka, Faculty of Mining Prijedo, Aleja Kozarskog odreda No1 79101 Prijedor, Bosnia and Herzegovina
[2]ArcelorMittal Prijedor d.o.o. Prijedor, Akademika Jovana Raškovića 1., 79 101 Prijedor, Bosnia and Herzegovina
**Corresponding author: ljiljana.tankosic@rf.unibl.org*

A B S T R A C T

The limonite-barite ore from the Vidrenjak deposit contains barite ($BaSO_4$) impurities that are closely associated with limonite. Due to this composition, the ore is not suitable for processing at the existing iron ore plant in Omarska. The high barite content, which introduces sulfur, makes the ore unsuitable for blast furnace operations because of the emission of harmful gases.This study investigates the potential application of selective flocculation to separate barite from limonite and thus obtain a usable mineral raw material suitable for blast furnace use. The flocculation process was performed using both anionic and cationic flocculants under varying pH conditions.

Chemical analysis of the processed samples showed no significant differences between the overflow and sediment compositions. Therefore, under the applied experimental conditions, the effectiveness of selective flocculation could not be confirmed. Nonetheless, the findings highlight the need for further investigation and process optimization.

***Key words**: Limonite-barite ore, selective flocculation, goethite, barite, surface charge, pH conditions, mineral processing*

1. INTRODUCTION

The “Vidrenjak” deposit is part of the Ljubija metallogenetic region, situated in the western sector of Republika Srpska. Limonite ore from this deposit contains barite ($BaSO_4$) admixtures in varying proportions depending on ore type, with barite being closely associated with limonite. Owing to its complex mineralogical composition, exploitation has not yet been undertaken. Although extensive investigations have been carried out over the years, the technology for separating barite from limonite remains undefined.

Selective flocculation is one of the promising methods for the utilization of fine-grained iron ores, which has been the subject of research for the last decades in the process of processing iron minerals (Tammishetti, 2017, Sarma, 2022, Alvim, 2023). The main goal of this research is to examine the possibility of applying selective flocculation to separate iron minerals from other impurities.

2. MATERIALS AND METHODS

2.1. Materials

For research purposes, a sample of limonite–barite ore from the Vidrenjak deposit was collected. The laboratory testing sample was obtained using the chessboard field method, followed by sample reduction through quartering. In the Quality Control Laboratory of the

Omarska Mine, the sample was prepared for chemical and granulometric analyses, including washing, sieving, drying, and grinding.

2.2. Methods

Selective flocculation is based on the separation of a specific type of mineral from a complex mixture, with the success of the process being conditioned by high particle dispersion and the selective adsorption of the flocculant.

When particles are in suspension, they collide due to Brownian motion and/or external induced agitation, magnetic fields, etc. The probability of aggregation in such collisions is determined by the nature of the interactions between particles. Attractive forces arise as a result of Van der Waals-type forces, while repulsive interactions are mainly due to electrostatic forces (Stechemesser, 2005; Healy, 1962; Ćalić, 2012, Tankosić Lj., 2022.).

2.2.1. Sample characterization

The granulometric and chemical composition of the raw sample was determined in the Quality Control Laboratory of the Omarska Mine in accordance with standards.

The mineralogical composition of the limonite–barite ore from the Vidrenjak deposit is described in the Report on exploration, interpretation, reserve calculation, and iron ore quality at the Vidrenjak deposit. For the purposes of determination, microscopic examinations, chemical analyses, differential thermal analyses, thermogravimetric analyses, and X-ray diffraction analyses were employed.

2.2.2. Sedimentation and flocculation experiments

Experiments on natural sedimentation, flocculation, and selective flocculation were conducted using 10% solids pulp. Sedimentation tests in 100 mL cylinders employed anionic and cationic flocculants (250 g/t, 100 g/t, 20 ppm) at pH 4, 6.7–6.8, and 10.5, with 80 g/t NHMF as a dispersant. Samples were mixed with 100 mL distilled water, conditioned on a magnetic stirrer (2–5 min), then transferred to cylinders for 1–10 min sedimentation. The supernatant and sediment were separated, dried, and weighed (Tankosić, 2022).

2.2.3. Reagents

The study used anionic (SUPERFLOC, Kemira) and cationic (AQUAFLOK 3040, Hemija Patenting) flocculants, sodium hexametaphosphate ($Na_6P_6O_{18}$) as a dispersant, and NaOH and HCl as pH regulators. Flocculants and dispersant were dissolved in distilled water at 0.1% and 1% concentrations, while pH regulators were 0.1 mol/dm³ solutions, prepared and applied as needed (Cytec Industries Inc., 1976–2002).

3. RESULTS AND DISCUSSION

3.1. Chemical Composition of the Sample

The limonite–barite ore from the Vidrenjak deposit was analyzed for chemical composition in the –0.025 mm fraction, suitable for selective flocculation (Table 1). The sample contained 35.75% Fe, 1.93% $BaSO_4$, and minor gangue components. Density was 3.44 g/cm³.

Table 1. Chemical composition of sample

Sample	Chemical Composition						
	Fe %	Mn %	SiO2 %	Al_2O_3%	BaSO4 %	Ba %	S %
	35,75	2,56	20,12	7,11	1,93	1,13	0,26

Chemical composition by particle size (Table 2) shows decreasing Fe content and increasing gangue in finer fractions, except barite, which peaks in –30+20 mm and –20+8 mm fractions. This indicates that additional grinding may improve liberation of barite from limonite.

Table 2. Chemical composition of sample by size class

Granulation, mm	Fe %		Mn %		SiO2 %		Al_2O_3%		BaSO4 %		Ba %		S %	
	Input	by Classes	Input	by Classes	Input	by Classes	Input	by Classes	Input	by Classes	Input	by Classes	Input	by Classes
+40		47,60		2,27		9,56		2,85		2,71		1,60		0,37
-40+30		46,67		2,62		10,40		3,25		1,88		1,11		0,26
-30+20		42,68		2,05		11,16		3,50		4,98		2,93		0,68
-20+8		41,14		2,75		12,90		4,05		3,79		2,23		0,52
-8+5		39,83		4,04		12,18		3,60		1,99		1,17		0,27
-5+1,6	35,75	44,42	2,56	3,52	20,12	9,54	7,11	2,62	1,93	1,86	1,13	1,10	0,26	0,25
-1,6+1		44,90		3,69		8,90		2,63		1,88		1,11		0,26
-1+0,5		43,59		4,13		9,88		2,88		1,80		1,06		0,25
-0,5+0,3		41,54		4,73		13,00		3,13		2,20		1,30		0,30
-0,3+0,025		34,75		4,10		25,94		3,25		2,28		1,34		0,31
-0,025+0		26,17		1,74		30,96		12,50		0,55		0,32		0,08

3.2. Granulometric Composition

Granulometric analysis (Table 3, Figure 1) revealed that the –0.025 mm fraction constituted 41.1% of the total sample, highlighting the prevalence of fine particles in the ore.

Table 3.Particle size distribution of sample

Actual Fraction (mm)	% Weight	% OS Cum.	% US Cum.
1	2	3	4
+40	5,2	5,2	100
-40+30	4,1	9,3	94,8
-30+20	6,1	15,4	90,7
-20+8	17,4	32,8	84,6
-8+5	3,2	36,0	67,2
-5+1,6	9,5	45,5	64,0
-1,6+1	2,8	48,3	54,5
-1+0,5	3,2	51,5	51,7
-0,5+0,3	1,8	53,3	48,5
-0,3+0,025	5,6	58,9	46,7
-0,025+0	41,1	100,0	41,1

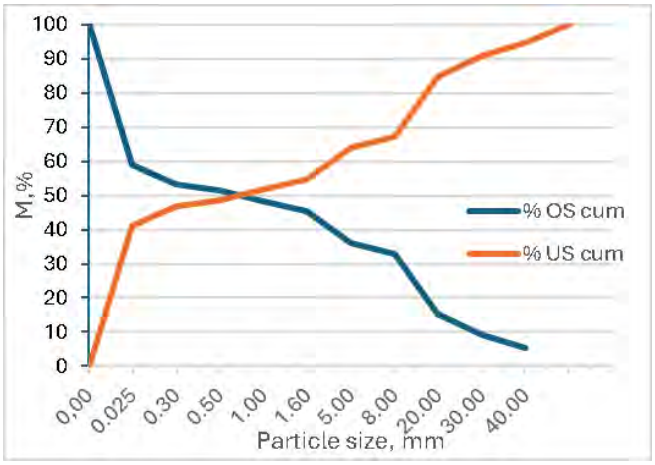

Figure 1. Granulometric curve of sample

3.3. Mineralogical Composition of the Samples

Based on microscopic examinations, chemical, differential thermal, thermogravimetric, and X-ray diffraction analyses, the qualitative mineralogical composition of the ore and gangue components was determined. The identified minerals include limonite, barite, quartz, and silicates (chlorite and illite), with minor amounts of sulfides (pyrite and marcasite).

Within the limonite, two types of iron hydroxides were distinguished: lighter porous fine-grained aggregates and darker compact coarse-grained granules of limonite (RŽR Ljubija, 1974).

3.4. Sedimentation and Flocculation

3.4.1. Natural sedimentation

Natural sedimentation was conducted at pH 4, 6.8, and 10.5. The sedimentation curves as a function of time are presented in Figure 2. Chemical analysis (Table 4) shows partial purification: harmful components decreased in the overflow.

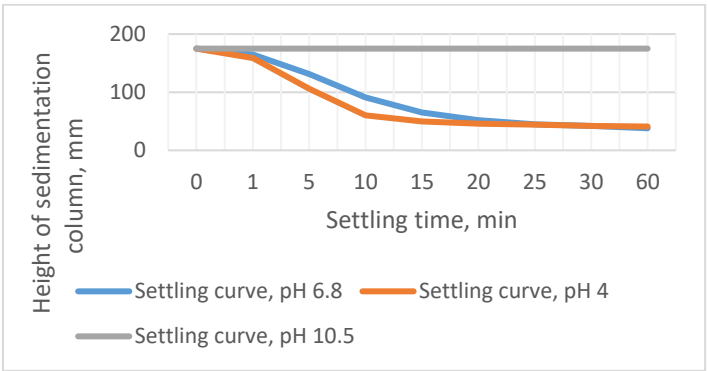

Figure 2. Natural sedimentation curves of limonite–barite ore at pH 4 and 6.8

The fastest sedimentation occurred at pH 4, while no sedimentation was observed at pH 10.5. Table 4 provides the chemical analyses of the overflow and sediment obtained from natural sedimentation. The results indicate a reduction of harmful components in the overflow, demonstrating partial purification during the natural settling process.

3.4.2. Sedimentation with flocculation

Sedimentation using the anionic flocculant A100 (1% solution, 250 g/t and 100 g/t) and AQUAFLOC 3040 (0.1%, 20 ppm) was tested at pH 4, 6.8, and 10.5 (Figures 3–5).

- **pH 6.8** consistently provided the fastest settling.
- At pH 4, Fe content increased in the sediment, while harmful components decreased in the overflow.
- At pH 6.8, enrichment of Fe occurred in the overflow.
- At pH 10.5, no significant changes were observed.

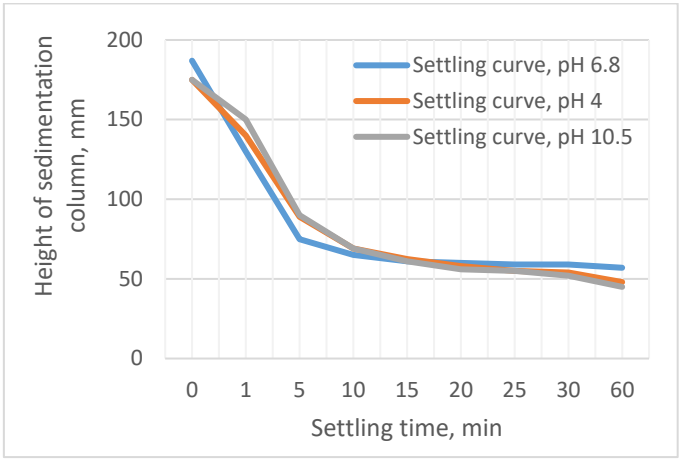

Figure 3. Sedimentation curves under varying flocculant types, dosages, and pH values (AQUAFLOC 3040, Dosage of 20 ppm)

Chemical analysis confirms that pH 6.8 is optimal for settling kinetics and partial enrichment of the useful component (Table 4).

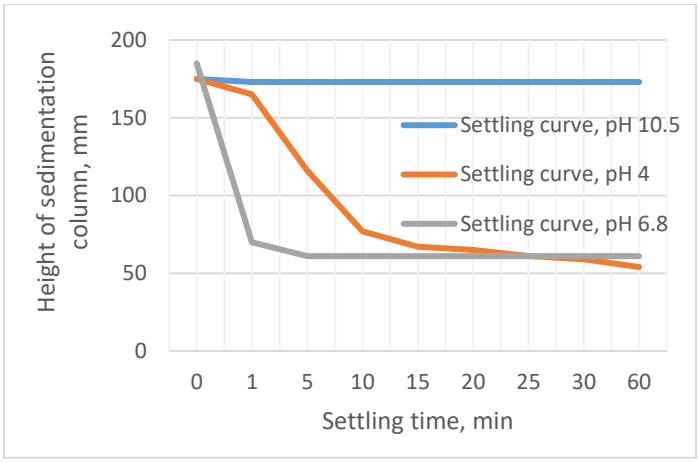

Figure 4. Sedimentation curves under varying flocculant types, dosages, and pH values (A100, Dosage of 250 g/t)

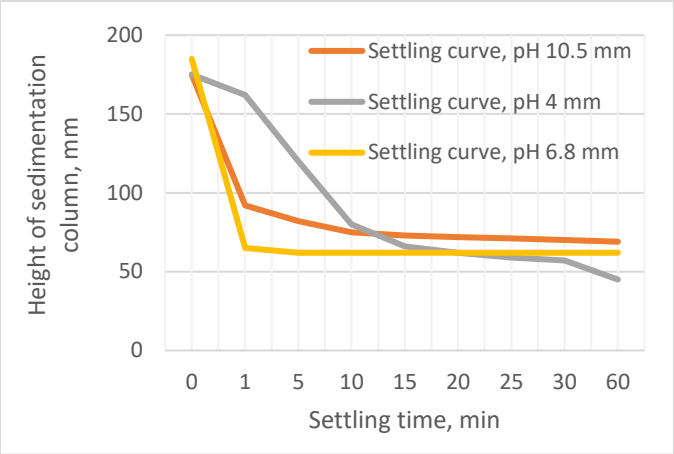

Figures 5. Sedimentation curves under varying flocculant types, dosages, and pH values (A100, Dosage of 100 g/t

3.4.3. Selective flocculation

Selective flocculation tests were conducted with:

- Anionic flocculants: 250 g/t and 100 g/t
- Cationic flocculant: 100 g/t
- Dispersant NHMF: 80 g/t

At all pH values, anionic flocculants increased Fe content in the overflow and reduced gangue components. Cationic flocculants at 20 ppm gave comparable results.
The results of selective flocculation are presented in Table 4.

Table 4. Summary of natural sedimentation, flocculation, and selective flocculation outcomes

			Settled Material							Floated Material						
pH	**Floc. dosage**	**Disp.**	**Settled Weight (%)**	**Fe (%)**	**Mn (%)**	**SiO2 (%)**	**BaSO4 (%)**	**Ba (%)**	**S (%)**	**Float Weight (%)**	**Fe (%)**	**Mn (%)**	**SiO2 (%)**	**BaSO4 (%)**	**Ba (%)**	**S (%)**
4	No	No		26,92	1,83	32,02	0,81	0,477	3,84		26,74	1,78	32,50	0,75	0,442	3,71
6,8	No	No		26,88	1,86	32,60	0,72	0,424	2,06		28,87	1,81	33,28	0,73	0,430	2,61
10,5	No	No		29,76	2,09	31,52	0,76	0,448	3,98		27,01	1,83	32,20	0,75	0,442	3,57
	250 g/t		26	26,63	1,96	27,94	1,87	1,10		74	26,11	1,64	28,18	1,99	1,172	0,005
4	100 g/t	No	19	26,86	1,79	29,34	4,37	2,57	0,022	81	26,00	1,69	29,50	2,64	1,555	0,016
	20ppm		38	27,26	1,81	29,02	0,92	0,54	0,03	62	26,93	1,77	29,10	0,82	0,483	0,026
	250 g/t		80	26,32	1,86	27,64	2,37	1,40	0,007	20	26,52	1,76	28,84	1,04	0,613	
6,8	100 g/t	No	83	26,52	1,84	27,94	0,71	0,42	0,018	17	26,46	1,76	29,48			
	20ppm		20	27,55	1,82	28,00				80	27,95	1,82	28,24	0,88	0,518	0,023
	250 g/t		1	26,88	1,74	27,74				99	26,46	1,74	27,64	0,66	0,389	0,040
10,5	100 g/t	No	66	27,48	1,82	28,18	0,63	0,37	0,018	34	26,84	1,87	27,46	0,75	0,442	0,029
	20ppm		19	27,52	1,84	28,28				81	27,30	1,72	28,00	0,90	0,530	0,015
	250 g/t		35	26,54	1,82	27,54	0,83	0,489	0,015	65	25,95	1,66	27,26	0,75	0,442	0,010
4	100 g/t	Yes	85	26,95	1,79	27,84	0,67	0,395	0,023	15	26,53	1,82	27,72	0,43	0,253	0,002
	20ppm		35	27,63	1,88	27,58	1,07	0,630	0,004	65	27,78	1,71	27,92	1,00	0,589	0,021
	250 g/t		85	26,86	1,74	29,26	2,18	1,284	0,014	15	27,13	1,76	29,42			
6,8	100 g/t	Yes	85	27,71	1,89	27,84	0,73	0,430	0,023	15	27,83	1,82	26,94			
	20ppm		19	28,00	1,79	28,60	0,90	0,530		81	28,21	1,81	28,82	0,69	0,406	0,005
	250 g/t		30	26,39	1,84	29,54	3,31	1,950		70	26,49	1,79	29,20	1,51	0,889	0,010
10,5	100 g/t	Yes	25	27,83	1,92	27,50				75	28,07	1,82	27,50	0,59	0,348	0,005
	20ppm		27	27,85	1,94	28,32	1,05	0,618		73	28,32	1,78	28,50	0,80		0,008

4. CONCLUSION

This study investigated the applicability of selective flocculation for the separation of barite from limonite in limonite–barite ore from the “Vidrenjak” deposit, with the aim of obtaining a mineral raw material suitable for blast furnace processing. The research focused on fine-grained ore fractions and examined the effects of different pH conditions, as well as anionic and cationic flocculants, on sedimentation and separation behavior.

The experimental results showed that pH value, flocculant type, and flocculant dosage significantly influenced the sedimentation kinetics of the ore pulp. However, chemical analyses of the obtained sediment and overflow fractions did not reveal significant differences in composition that would indicate effective selective separation of barite from limonite. Under the applied experimental conditions, the selective adsorption of flocculants and preferential aggregation of limonite could not be clearly achieved.

Consequently, the effectiveness of selective flocculation for the beneficiation of limonite–barite ore from the “Vidrenjak” deposit could not be confirmed in this study. Nevertheless, the results provide useful insight into the flocculation behavior of this complex ore system and indicate the need for further research focused on process optimization, improved mineral liberation, and refinement of reagent regimes. Such investigations may contribute to the development of an efficient technological solution for the utilization of this currently unexploited iron ore resource. The findings can inform further pilot-scale testing to optimize selective flocculation of similar ores.

REFERENCES

Alvim, E. S., Fernandes Lima, R. M., (2023), “Selective Flocculation/Magnetic Separation of Ultrafine Iron Ore Particles with Corn Starch and Polyacrylamides: A Comparative Study”, Miner. Process. Extr. Metall. Rev., 45, 606–615.

Cytec Industries Inc., (1976, 1989, 2002), Cytec Mining Chemicals Handbook, pp. 187–202.

Ćalić, N., (2012), Priprema mineralnih sirovina [Preparation of Mineral Raw Materials], RF Prijedor.

Ćalić, N., Glušac, M., Ignjatović, M., (2009), “Limonite concentration from mud”, Annals of the University of Petrosani, Mining Engineering, 10, 165–172.

Healy, L. W., La Mer, V. K., (1962), “The adsorption flocculation reactions of a polymer with an aqueous colloidal dispersion”, Journal of Physical Chemistry, 66.

RŽR Ljubija, (1974), “Elaborate on Exploration, Interpretation, Calculation of Reserves and Ore Quality of the Vidrenjak Iron Ore Deposit”, Internal Technical Report.

Sarma, J., Rajkhowa, S., Mahiuddin, S., (2022), “Upgradation of Iron Ore Fines and Slime by Selective Flocculation Using Surface-Active Agents, Settling Study, and Characterization of the Beneficiation Waste for Value Addition”, Journal of Chemistry, 2022, 6451187.

Stechemesser, H., Dobias, B. (Eds.), (2005), Coagulation and Flocculation, Surfactant Science Series, Vol. 126.

Tankosić, Lj., (2022), Doctoral Thesis, University of Banja Luka, Faculty of Mining.

THE CONTRIBUTION OF ROUGHNESS PARAMETER ON COAGULATION AND FLOCCULATION CHARACTERISTICS OF FINE CHROMITE

Onur GÜVEN*

Adana Alparslan Türkeş Science and Technology University, Faculty of Engineering, Mining Engineering Department, 01250, Sarıçam, Adana, TÜRKİYE
**Corresponding author: oguven@atu.edu.tr*

A B S T R A C T

In this study, the coagulation and flocculation characteristics of chromite are shown as a function of the roughness parameter formed on their surfaces by grinding under different conditions. The contributions of especially roughness values were investigated by adapting both experimental and theoretical calculations. In the experimental sections, after the samples were ground in ball and rod mills, their roughness levels were determined using optical profilometry and atomic force microscopy (AFM). Coagulation tests of the particles were performed using sedimentation tests in the presence of NaCl and $CaCl_2$ coagulants while flocculation recoveries were then determined using the same experimental procedure using anionic and cationic flocculants. Zeta potential analyses were performed to determine changes in surface charge values of particles under the same conditions of coagulation and flocculation tests. Consequently, experimental studies conducted with samples of varying roughness values showed the impact of particle roughness on coagulation and flocculation processes which are important for storage and transportation of very fine sized samples in mineral processing plants.

Key words: *Roughness, coagulation, flocculation, AFM*

1. INTRODUCTION

Coagulation and flocculation processes are important processes, especially in mineral processing to make aggregates of fine-sized particles based on particle-particle interactions (Ozun and Ulus, 2019; Guven et al., 2026). During these processes, apart from physical properties of particles like size, shape, density difference, or the charge of the particles (Ersoy, 2005), the contribution of coagulants with different valences or flocculants with different types and molarities are role changing parameters to gather bridges between fine-sized particles via particle-particle interactions (Suresh et al., 1996). As mentioned above, studies in the literature address numerous parameters related to these processes, including the type or the concentration of the coagulant or flocculant, and the pH of the medium (A. Ozkan, 2003; Amuda et al., 2007; Önen et al., 2018). However, in literature, the effect of morphology is generally conducted for its role on flotation of particles (Ulusoy et al., 2003; Yekeler et al., 2004; Verelli et al., 2014; Guven et al., 2015; Guven et al., 2020; Guven et al., 2022). Considering that, only a few studies have been conducted to systematically address the contribution of that parameter during coagulation and flocculation processes. In this manner, Rahimi et al. in 2012, showed that in flotation experiments conducted with quartz ground in ball and rod mills, flotation efficiencies increased in parallel with increasing particle roughness and aspect ratio. Similarly, in another study with quartz (Güven et al., 2016), it was shown that flotation efficiency could be increased in parallel with increasing roughness and angularity values. In another study published in 2016, Karakaş and Hassas determined that as particles roughness increases, the effective force between glass spheres becomes more attractive which can be ascribed to higher efficiencies of interactions. But different from those dependencies, little et al., 2015, suggested that flotation rates decreased as the sphericity of the particles increased in very fine sized chromite flotation.

Thus, these results are quite important in terms of quantitatively demonstrating the role of the roughness parameter in particle-bubble interactions. For example, Zhu et al. 2020 showed that quartz particles with high roughness values provided higher flotation kinetics values. In a recent review study published in 2023, Ulusoy presented examples showing that particle morphology is an important parameter that should be evaluated as much as particle size in mining, construction, and other engineering fields, as well as in many other areas. In this context, understanding particle morphology enables the optimization of the type and dosage of coagulants and flocculants, thereby increasing efficiency. For example, Zhang et al. (2024) investigated the effect of the roughness parameter of Haynes 230 powder, an industrial product, on the fluidity of the particles.

Based on the results obtained from experimental studies, they concluded that as the roughness of the medium increases, the surface energy of the particles increases, and consequently, their fluidity decreases. In another study examining the roughness parameter in particle-to-particle interactions, it was determined that particle-particle interaction increases in parallel with increasing particle roughness (Zhang et al., 2025).

As stated in many studies in literature, the interaction between particles is first determined by assessing the coagulation and flocculation efficiencies of the particles in the presence of coagulants or flocculants (Gungoren et al., 2020), and then these results are correlated with the zeta potential values measured under the same conditions (Megersa et al., 2019). However, as mentioned above, studies on particle morphology have generally focused on their effects in flotation processes, and there is no systematic study in the literature on how different grinding media affect particle morphology, especially in very fine particles, and consequently, to what extent this affects the coagulation and flocculation parameters of the resulting particles. Considering that lack of knowledge in literature, the aim of this study is to present the effects of roughness values for both coagulation and flocculation processes of fine chromite particles.

2. MATERIAL AND METHODS

2.1. Material

2.1.1. Preparation of samples for coagulation and flocculation tests

The chromite samples were obtained from the Eti Krom facilities in Elazığ. The chemical composition of the sample was determined using a "Rikagu" XRF (X-Ray Fluorescence) and the crystallographic structures of the samples were determined using a Rikagu Mini-Flex brand XRD (X-Ray Diffraction) device. The size distributions of the samples from the facilities were determined using a Retsch brand AS200 model automatic sieve with standard screen apertures as (0.500 mm; 0.212 mm; 0.150 mm; 0.106 mm; 0.075 mm and 0.045 mm).

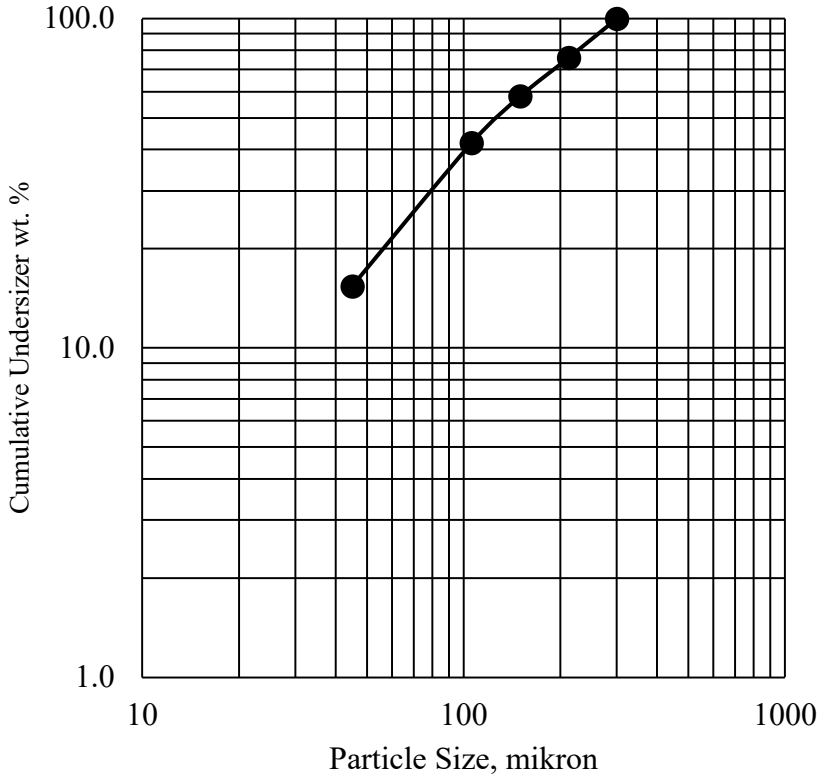

Figure 1. Particle size distribution of representative ore sample

The composition of the samples used in the experimental studies was determined by X-ray Diffraction (XRD) and X-ray Fluorescence (XRF) methods, and the values for these analyses are shown in Table 1, Figure 2, respectively.

Table 1. X-ray Fluorescence (XRF) analysis results of samples used in experimental studies

Compound	**Content %**
Al_2O_3	8,0
SiO_2	8,2
CaO	0,51
TiO_2	0,24
Cr_2O_3	54,57
MnO	1,17
Fe_2O_3	26,5
Other	0,81

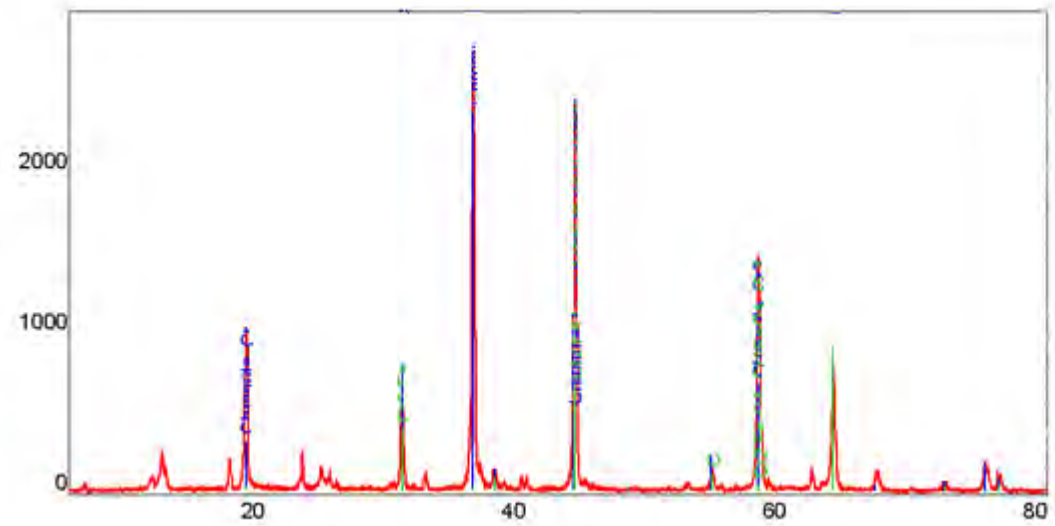

Figure 2. XRD analysis of the chromite sample

As mentioned above, different grinding conditions in terms of grinding media were chosen to investigate the variation of roughness value. During these tests, a laboratory type ball mill and rod mills with steel balls 30, 25 and 20 mm in diameter and steel rods with diameters of 31.7, 24.6, 15.9 and 9.8 mm were used as grinding media. The sizes of these mills were (5224 cm^3 volume (D=19.5 cm, H=17.5 cm)), (7850 cm^3 (D=20 cm, H=25 cm)) for ball and rod mills respectively.

The samples were ground in the mills for varying durations ranging from 20 to 25 minutes, then wet sieving was used to reduce the entire sample size to below 0.038 mm. Afterwards, size analysis of the ground samples was performed using the “Malvern Particle Sizer 3000”.

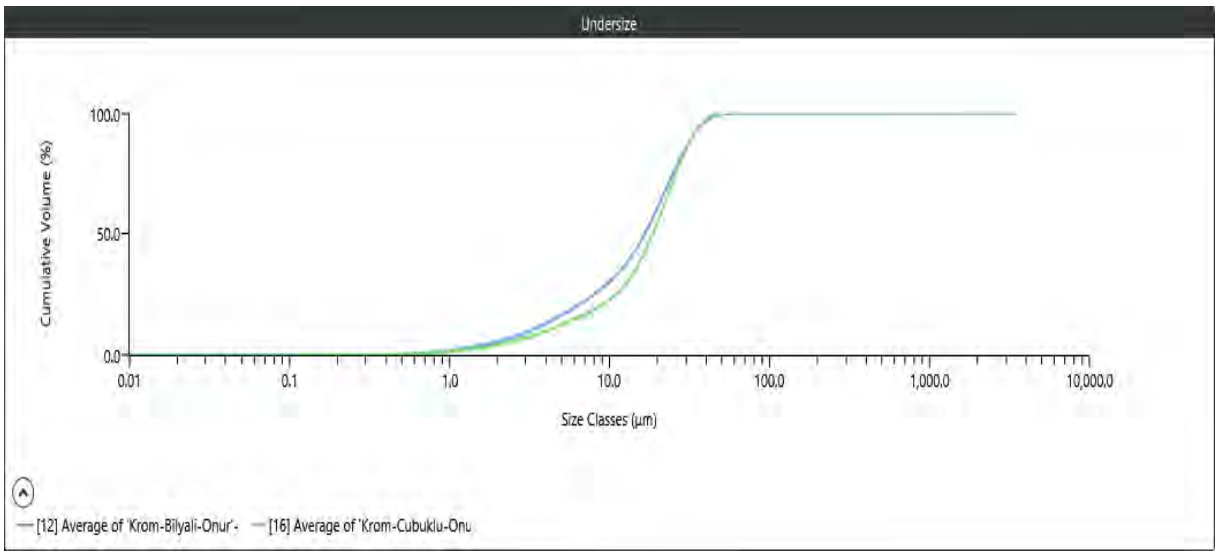

Figure 3. Size analysis of chromite samples after grinding a. Ball mill, b. Rod mill products

As can be seen in Figures 3, the size distributions of the samples ground in different grinding environments are quite similar, and as stated above the effect that may arise due to size distribution in flocculation and coagulation experiments has been minimized. Indeed, if we give numerical values for the size distributions of each sample, the average d_{80} size of the chromite sample ground with a ball mill is 27.0 microns, while the average d_{80} size of the chromite sample ground with a rod mill is 27.9 microns.

2.1.2. Particle roughness analyses of samples after grinding

Following the grinding process, to determine the roughness values of chromite particles, two instrumental analyses such as AFM (Atomic force microscopy) and optical profilometer were used. For AFM analysis, NX100 model Atomic Force Microscope from Park System was used with a 10x10 micron scanning area in tapping mode. The average roughness (Ra) value was used. The results of these analyses were shown in Figures 4 and 5.

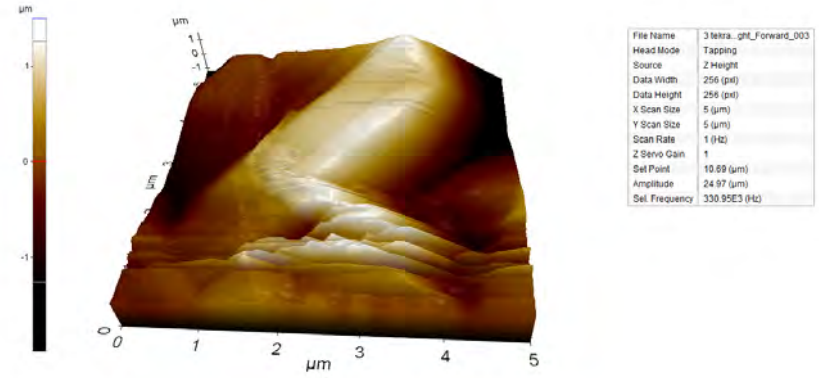

Figure 4. The AFM picture of chromite (Ball mill) (Ra: 437 nm)

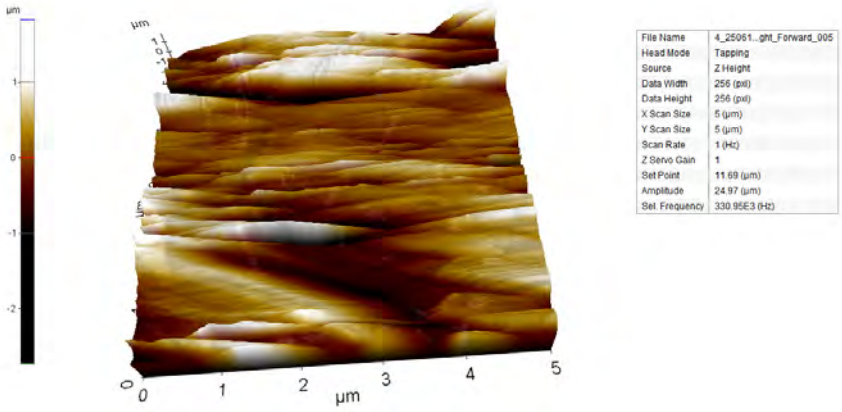

Figure 5. The AFM picture of chromite (Rod mill) (Ra:165 nm)

As mentioned above, the roughness values of particles were also determined with Filmmetrics Profilm 3D model optical profilometer, located in the Central Laboratory of Çukurova University, which can take measurements over a larger surface area. Measurement images for each sample are shown in Figure 6 and the average roughness values measured with both devices are shown in Table 2.

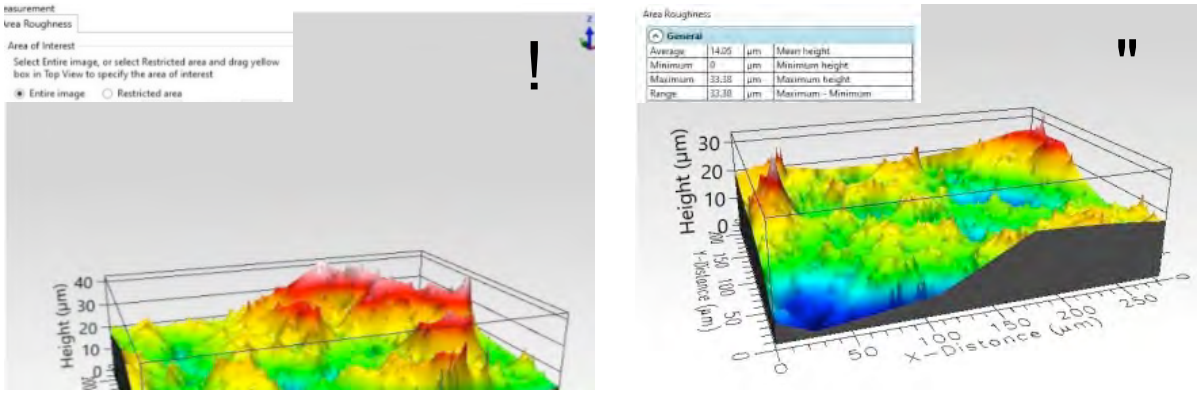

Figure 6. The optic profilometer pictures of chromite (A: Ball mill) (B: Rod mill)

Table 2. Roughness results of samples used in experimental studies measured with an optic profilometer and AFM

Roughness Analysis	**Ball Mill**	**Rod Mill**
Profilometer	21.23 µm	14.05 µm
Atomic Force Microscopy	437 nm	165 nm

As can be seen from the values shown in Table 2, although average roughness with different units were obtained from different units, the trends between these values are almost the same regarding the efficient measurement area limitations for each unit. A similar dependency was also reported in a previous study (Mei and Guan, 2023). In that study, it was also mentioned that roughness values obtained with AFM were more accurate than those obtained with a profilometer. Taking these results into account, it is possible to evaluate the effects of different grinding conditions on particle size and surface area, as well as particle roughness, from a different perspective.

2.2. Methods

2.2.1. Coagulation and flocculation experiments

The coagulation and flocculation properties of samples with different characteristics were determined by measuring cylinder tests (or settling tests). During these tests, a 250 ml measuring cylinder was used and considering previous studies in the literature (Guven et al., 2025), experiments were conducted at a 3% solids concentration. The suspensions prepared at a specific solids concentration that were mixed in the measuring cylinder with an appropriately sized magnetic stirrer at 360 rpm for 5 minutes, after which the time-dependent settling characteristics were recorded. During this process, the height of the clarified portion was recorded at each time point, and the settling velocity (cm/s) was calculated from the slope of the curves obtained at the end of the process. Although the literature indicates that a linear precipitation trend is expected at solids concentrations below 5%, in this study, where the type of salt and specifically its valence value are examined in relation to coagulation characteristics. Therefore, all experimental studies were carried out at a solid concentration of 3%. Subsequently, the effectiveness of salts with different valencies during the coagulation of samples at the same solids' concentration was determined with NaCl and $CaCl_2$.

2.2.2. Zeta potential measurements

When a solid substance is placed in water, even if no other ions are present in the environment, the surface of the solid substance acquires a positive or negative electric charge due to ions passing from the solid substance into the water and the H^+ and OH^- ions in the water. The movements of an electrically charged surface and the surrounding solution containing various ions relative to each other create electrokinetic phenomena. Surface and zeta potentials,

electrical double layers, Stern plane, diffuse and double layers are fundamental elements of electrokinetic. Each particle has an electric charge in the liquid due to potential-determining ions (pdi). In this way, the particles repel or attract each other. For example, a negatively charged particle attracts positive ions in the liquid, while cations and anions are generally in equilibrium. Cations are most densely located on the grain surface. The layer one molecule thick from the grain surface is called the "Stern layer"; The layer extending from this point to the distance where anions and cations reach equilibrium is called the "diffuse layer"; the system where both are present together is called the "electrical double layer". Measurements were performed using a microelectrophoresis method with microprocessor-equipped Zeta Plus (Brookhaven, NY, USA) device. The device can automatically calculate the zeta potential value by considering voltage and particle velocity. The sample chamber of the device is made of plexiglass. In the measurement processes, the voltage was adjusted according to conductivity. Zeta potential measurements could not be performed at pH values lower than 2.5 and higher than 11.5 because conductivity is high. During zeta potential measurements, the movement of the particles was monitored on the screen by attaching the wires to the anode and cathode terminals in reverse according to their colors. An average of 10 measurements were taken with samples taken from suspensions prepared with a 1% solids ratio in the pulp, and the obtained zeta potential values were calculated by the device. The determined mean and standard deviation were recorded.

3. RESULTS AND DISCUSSION

3.1. Coagulation and Flocculation Experiments

When examining the coagulation results of chromite ground in different grinding media, the sedimentation rate of chromite in pure water was measured as an average of 0.1150 cm/s, while this value showed a relative increase with increasing NaCl concentrations, to 0.1161 cm/s. In experimental studies conducted with another type of salt, $CaCl_2$, an increase in sedimentation rate was measured up to 0.1172 cm/s, parallel to the increasing concentration. The results were shown in Figure 7.

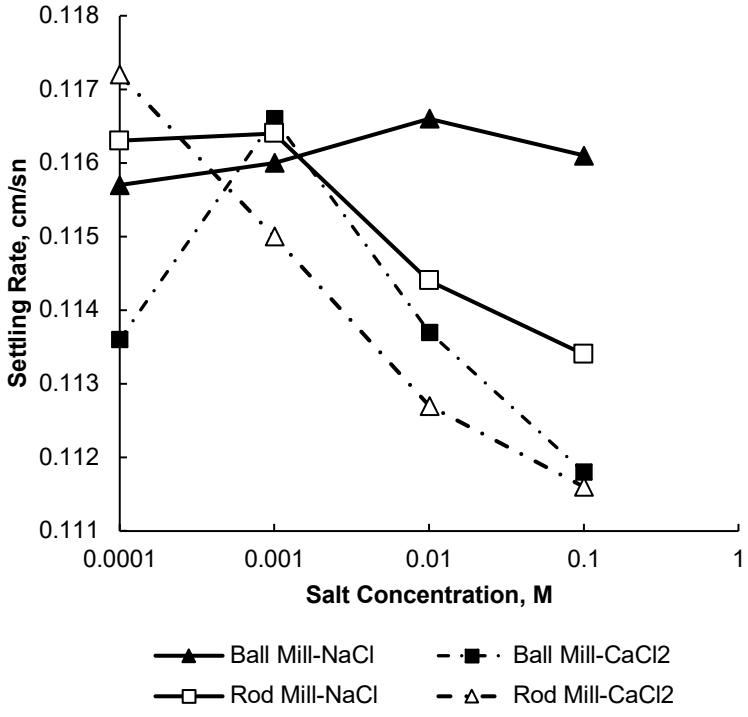

Figure 7. The coagulation results of chromite particles as a function of NaCl and $CaCl_2$ concentration

As shown in Figure, when the effect of particle roughness values was examined, the settling velocity values of particles with a roughness of 21.23 µm obtained with ball mills were determined as 0.1131, 0.1160 and 0.1166 cm/s for pure water, NaCl and $CaCl_2$ salts, respectively, while the settling velocity values of particles with a roughness of 14.05 µm obtained with rod mills under the same conditions were determined as 0.1161, 0.1164 and 0.1150. These results are quite important for a more comprehensive evaluation of the results obtained in processes related to the processing of fine particles such as coagulation, as well as considering particle roughness in addition to salt type and concentration.

3.2. Flocculation Experiments

In this study, the effects of different concentrations (5, 10 and 15 g/t) of anionic and cationic flocculants on the flocculation characteristics of particles with different roughness values were determined according to the settling velocity ratios, as in coagulation tests. The results were shown in Figure 8.

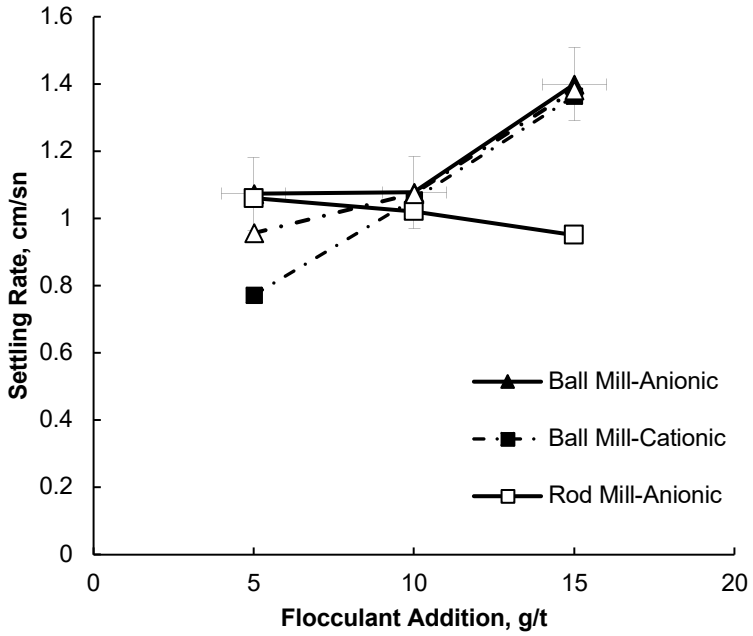

Figure 8. The flocculation results of chromite particles as a function of flocculant addition, g/t

When the results of experimental studies conducted with another mineral, chromite, were examined (Figure 8), it was observed that anionic flocculants had higher sedimentation rate values compared to cationic flocculants in experiments conducted at natural ph. This is an expected result considering the surface properties of chromite, and when evaluated in terms of different grinding systems, it was determined that particles with less roughness flocculated relatively faster.

3.3. Zeta Potential Analysis

Similarly, in Table 3, when the changes in chromite zeta potential values at a salt concentration of 10^{-3} M are examined, the zeta potential value, which was 0.72 mV when NaCl was added to the medium, increased to 4.83 mV, while after the addition of $CaCl_2$, this value increased to 19.9 mV. When this situation is evaluated in terms of zeta potential, it can be concluded that dispersion of the particles is expected; however, since maintaining the pH of the medium at the natural pH after the addition of salt prevents the active role of Ca ions, the difference in coagulation characteristics can be explained by the change in debye length. In zeta potential measurements using different flocculant types, the zeta potential value, which was -4.72 mV

after the addition of 5 g/t anionic flocculant, decreased to -22.09 mV with increasing concentrations, while the zeta potential value, which was -4.69 mV after the addition of 5 g/t cationic flocculant, it decreased to -25.36 mV.

Table 3. Zeta potential analysis of chromite in the presence of coagulants (10^{-3} M conc.) and flocculants at different dosages

Zeta Potential Values, mV				
Coagulation		**Flocculation**		
Coagulant Type		**Flocculant Dos., g/t**	**Anionic**	**Cationic**
Distilled Water	0,72	5	-4,72	-4,69
NaCl	4,85	10	-8,64	-25,36
CaC_{l2}	19,9	15	-22,09	6,16

4. CONCLUSIONS

As mentioned in the objective of paper, the main objective of this study is to determine how grinding conditions affect the roughness of very fine particles, and to reveal the role of particle roughness in coagulation and flocculation processes through experimental studies. To this end, the following results were obtained using chromite.

1. -1 mm sized samples were ground in ball and rod mill environments, and -38 µm sized samples, corresponding to the resulting coagulation and flocculation sizes, were separated. Roughness analyses performed on these samples showed that rougher grains were obtained in the ball mill compared to rod mill products.
2. In coagulation experiments conducted with different coagulants (NaCl and $CaCl_2$) but at the same concentrations, it was determined that samples with lower roughness showed higher settling velocity values. This was also observed in flocculation experiments with the same samples that higher settling velocity values were obtained in samples with lower roughness
3. Based on these results obtained for samples of different morphology, it is necessary to consider particle morphology as well as liberation in the design of grinding systems to increase coagulation and flocculation efficiencies on an industrial scale. Considering the morphological aspect as well as the size of the samples released after certain processes can be an important parameter in controlling the efficiency of fine-sized processing.

ACKNOWLEDGMENTS

This study is supported by The Scientific and Technological Research Council of Turkey (TUBITAK) with Project Number 124M905.

REFERENCES

Amuda, O. S., Amoo, I. A., (2007) “Coagulation/flocculation process and sludge conditioning in beverage industrial wastewater treatment”, Journal of Hazardous Materials, 141 (3) 778-783.

Ersoy, B., (2005) “Effect of pH and polymer charge density on settling rate and turbidity of natural stone suspensions”, International Journal of Mineral Processing, 75 207-216.

Gungoren C, Guven O, Cinar M, Ozdemir, O., (2020) “An investigation of the effect of clay type on coal flotation along with DLVO theoretical analyses”, International Journal of Coal Preparation and Utilization, 40 (3) 210-222.

Guven O, Celik M. S., (2016) “Interplay of particle shape and surface roughness to reach maximum flotation efficiencies depending on collector concentration", Mineral Processing and Extractive Metallurgy Review, 37 (6) 412-417.

Guven O, Kaymakoğlu B, Ehsani A, Hassanzadeh, A., Sivrikaya, O., (2022) “Effects of grinding time on morphology and collectorless flotation of coal particles”, Powder Technology, 399 117010.

Guven, O., Kayabaşı, H., Daday, M., Birinci, M., Ozdemir, O., (2026) “Effect of chloride salts on coagulation behaviour of chromite particles having different roughness produced by rod and ball mills”, Canadian Metallurgical Quarterly, 1-10.

Guven, O., Kayabaşı, H. R., Ehsani, A., Kaymakoğlu, B., Kara, T. D. T., (2025) “The effect of grinding type on roughness and coagulation of magnesite particles”, Physicochemical Problems of Mineral Processing, 61 (3) 203708

Guven, O., Ozdemir, O., Karaagaclioglu, E., Celik M. S., (2015) “Surface morphologies and floatability of sand-blasted quartz particles”, Minerals Engineering, 70 1–7.

Guven, O., Serdengeçti M. T., Tunç, B., Özdemir, O., Karaağaçlıoğlu, İ. E., Çelik, M. S., (2020), “Effect of particle shape properties on selective separation of chromite from serpentine by flotation”, Physicochemical Problems of Mineral Processing, 56 (5) 818-828.

Karakas F, Vaziri Hassas B., (2016) “Effect of surface roughness on interaction of particles in flotation”, Physicochemical Problems of Mineral Processing, 52 (1) 18–34.

Megersa, M., Gach, W., Beyene, A., Ambelu, A., Triest, L., (2019) “Effect of salt solutions on coagulation performance of Moringa stenopetala and Maerua subcordata for turbid water treatment”, Separation and Purification Technology, 221 319-324.

Mei, L., Guan, G., (2023) “Profilometry and atomic force microscopy for surface characterization”, Nano Transmed, 2 (1) e9130017.

Ozkan, A., (2003) “Coagulation and flocculation characteristics of talc by different flocculants in the presence of cations”, Minerals Engineering, 16 (1) 59-61.

Ozun, S., Ulus, D. A., (2019) “Coagulation and flocculation behavior of fines in foid-bearing rock processing plant (FRPP) wastewater at alkaline environment”, Powder Technology, 344 335-342.

Önen, V., Göçer, M., Taner, H. A., (2018) “Effect of coagulants and flocculants on dewatering of kaolin suspensions”, Omer Halisdemir University Journal of Engineering Sciences, 7 (1) 297-305.

Rahimi, M., Dehghani, F., Rezai, B., Aslani, M. R., (2012) “Influence of the roughness and shape of quartz particles on their flotation kinetics”, International Journal of Minerals, Metallurgy, and Materials, 19 284-289.

Suresh, L., Walz, J. Y., (1996) “Effect of surface roughness on the interaction energy between a colloidal sphere and a flat plate”, Journal of Colloid and Interface Science, 183 199-213.

Ulusoy, U., (2023) “A review of particle shape effects on material properties for various engineering applications: From Macro to Nanoscale”, Minerals, 13 (1) 91.

Ulusoy, U., Yekeler, M., Hiçyilmaz, C., (2003) “Determination of the shape, morphological and wettability properties of quartz and their correlations”, Minerals Engineering, 16(10) 951–964.

Verrelli, D. I., Bruckard, W. J. , Koh, P. T. L., (2014) “Particle shape effects in flotation. Part 1: Microscale experimental observations”, Minerals Engineering, 58 80–89.

Yekeler, M., Ulusoy, U., Hiçyilmaz, C., (2004) “Effect of particle shape and roughness of talc mineral ground by different mills on the wettability and floatability”, Powder Technology, 140 (1–2) 68–78.

Zhang, Z., Wan, L., Meng, X., Xie, Y., Tian, H., Mao, D., Dong, W., Sun, X., Ma, X., Huang, Y., (2024) “Robotic wire-based friction stir additive manufacturing”, Additive Manufacturing, 88 104261

Zhang, Z., Wan, L., Wen, Q., Shi, Y., Feng, Z., (2025) “Wire-based friction stir additive manufacturing of TiC reinforced Al-Cu-Mg composite: Particle refinement and dispersion”, Composites Part A: Applied Science and Manufacturing, 196 109009.

Zhu, Z., Yin, W., Wang, D., Sun, H., (2020) “The role of surface roughness in the wettability and floatability of quartz particles”, Applied Surface Science, 527 146799.

THE EFFECT OF SODIUM HEXAMETAPHOSPHATE AS A DISPERSANT AND ANIONIC POLYACRYLAMIDE-BASED FLOCCULANT ON THE ZETA POTENTIAL OF NATURAL GOETHITE, QUARTZ, AND CLAY MINERALS

Ljiljana TANKOSIĆ*, Svjetlana SREDIĆ

University of Banja Luka, Faculty of Mining Prijedor, *Aleja Kozarskog odreda No1 79101 Prijedor, Bosnia and Herzegovina*
**Corresponding author: ljiljana.tankosic@rf.unibl.org*

A B S T R A C T

The aim of this study was to investigate the electrochemical properties of natural goethite, quartz, and clay minerals and to evaluate the effects of the inorganic dispersant sodium hexametaphosphate (SHMP) and an anionic polyacrylamide-based flocculant (PAM) on their surface charge behavior. All experiments were conducted using natural mineral samples collected from the Omarska iron ore mine (Bosnia and Herzegovina). The zeta potential of goethite, quartz, and clay was determined as a function of pH in the absence and presence of SHMP and PAM.

The results showed that increasing suspension pH led to an increase in negative surface charge for all investigated minerals. Clay exhibited no isoelectric point (IEP) within the studied pH range, while quartz and goethite showed IEPs at approximately pH 2.6 and 6.7, respectively. The addition of SHMP significantly increased the negative zeta potential, resulting in highly stable dispersions and the absence of detectable IEPs over the pH range 2–12. In contrast, the combined presence of SHMP and PAM reduced the magnitude of the negative zeta potential, indicating favorable conditions for flocculation. Based on surface charge behavior, optimal flocculation conditions were identified at pH 9 in the presence of all reagents.

Key words: *Zeta potential, selective flocculation, goethite, quartz, clay, polyacrylamide, sodium hexametaphosphate, pH, mineral processing*

1. INTRODUCTION

Surface electrochemical properties of minerals are essential in mineral processing operations such as flotation, flocculation, selective dispersion, and other concentration methods. Among these, zeta potential is a key parameter for understanding particle–particle and particle–reagent interactions in aqueous suspensions, and its determination is crucial for optimal reagent selection and process efficiency.

In natural mineral lattices, deviations from stoichiometry create structural defects that influence surface charge. Electropositive defects attract anions, while electronegative defects favor cation adsorption, directly affecting mineral reactivity. Ion exchange at the mineral surface leads to the formation of an electrical double layer (EDL), which governs electrostatic interactions and determines suspension stability (Ćalić, 1990). Particles with high absolute zeta potential are electrostatically stabilized, whereas low zeta potential favors coagulation or flocculation. The isoelectric point (IEP), where zeta potential is zero, indicates the pH at which particle aggregation occurs (Ćalić, 2017; Milošević, 1997).

Understanding the effects of chemical reagents, such as inorganic dispersants and polymeric flocculants, on mineral surface charge is of both scientific and practical interest. Goethite, quartz, and clay frequently coexist in iron ore deposits and strongly influence separation efficiency due to contrasting surface properties. This study investigates their electrochemical behavior and the influence of sodium hexametaphosphate (SHMP) and anionic polyacrylamide

(PAM) on zeta potential, providing insights for selective flocculation and mineral processing applications.

2. MATERIALS AND METHODS

2.1. Materials

Experimental investigations were carried out on samples of goethite, quartz, and clay ("pure" minerals), hand-picked from the open pit "Buvač"at the 'Omarska' mine (Bosnia and Heryegovina).

The following reagents were used in the experiments: sodium hexametaphosphate, (as dispersants) manufactured by Lach-Ner, s.r.o. (Czech Republic), SHMP; polyacrylamide designated Superfloc A100 (as flocculants), manufactured by Kemira, PAM, and pH regulators (hydrochloric acid and sodium hydroxide).

2.2. Methods

In order to define and address the problems in this article, testing methods were applied, including:

- Methods for testing the samples,
- Methods for testing reagent adsorption on the mineral particle surfaces (mineral surface charging measurements).

2.2.1. Sample preparation and testing methods

Sample preparation involved drying, crushing, grinding, classification, and homogenization of monomineralic fractions. Goethite, clay, and quartz samples were crushed using a RETSCH BB200 laboratory crusher and ground in a ROCKLAB SRM ring mill. Homogenization was performed in a BENCH TOP RSD-ROCKLABS homogenizer (5 kg capacity, 0–1.5 kg/min).

Prepared samples underwent:

- Particle size distribution determination,
- Moisture content and density measurement,
- Chemical and mineralogical composition analysis.

To obtain –25 μm fractions, each sample was ground using a disc mill, sieved to –53+25 μm, and further reduced to –25 μm. Particle size distribution was measured with a MALVERN MASTERSIZER 2000 (dry and wet).

Samples were dried in a drying oven FD 240 ERIEL at 105 °C until constant weight. Density was measured with a MICROMERITICS ACCUPYS II 1340 gas pycnometer. Chemical composition analyses were performed at ArcelorMittal's Quality Control Laboratory (Omarska), ArcelorMittal Research Center "Maizières-lès-Metz," and control laboratories in Ireland.

2.2.2. Determination of mineralogical composition of samples

To accurately determine the mineral phases present and their chemical compositions, detailed mineralogical characterization of all samples was performed using powder X-ray diffraction (XRPD), and scanning electron microscopy with energy-dispersive X-ray spectroscopy (SEM-EDS). XRD and SEM-EDS analyses were carried out at the Global Research and Development Laboratory, Mining and Mineral Processing, Maizières-lès-Metz, France.

2.2.3. Zeta potential measurements

Surface properties of goethite, quartz, and clay in aqueous suspensions were investigated by measuring their electrokinetic (zeta) potential under varying conditions (pH 2–12), both in the absence and presence of dispersants and flocculants. Measurements were performed at different laboratories using a ZM3-D-G Zeta Meter system 3.0+ (Universidade Federal de Minas Gerais, Brazil.

Mineral samples were ground to 10 µm and conditioned in two stages: first, the pH regulator and dispersant were added, followed by the flocculant. Zeta potential measurements were conducted on 0.010 g of sample in 100 ml solution at 20 °C. Suspensions were homogenized, pH-adjusted, and allowed to equilibrate for two hours prior to analysis, ensuring reliable determination of surface charge behavior (Ćalić N., 1990; Ljiljana Tankosić et al., 2018).

3. RESULTS

3.1. Particle Size Distribution

Figure 1 show the particle size distribution of goethite, clay, and quartz after one and two grindings in a disc mill, aimed at achieving uniform particle size for all samples, specifically below 25 µm.

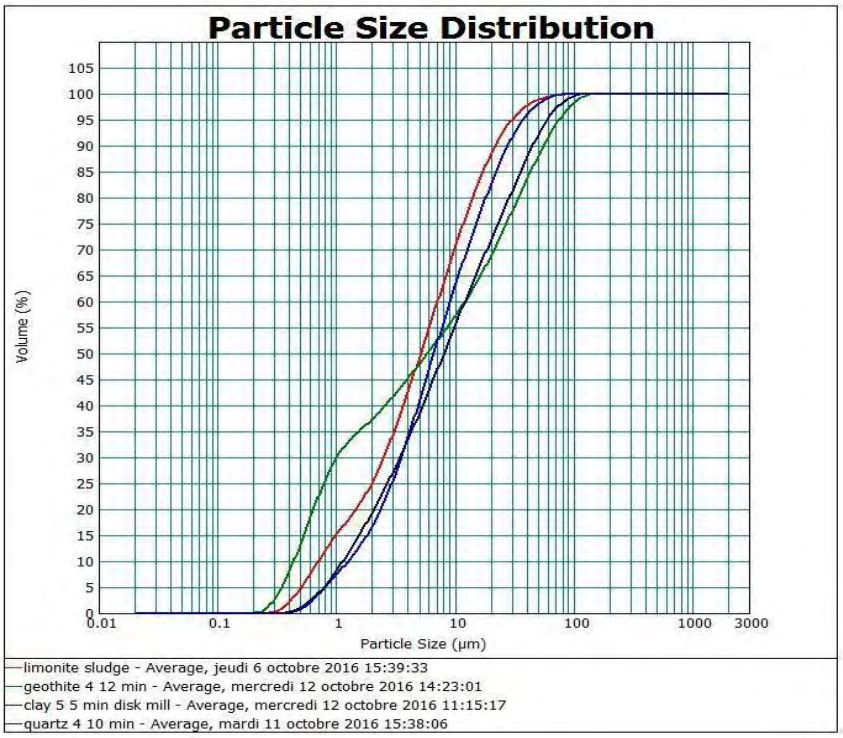

Figure 1. Particle size distribution of goethite, clay, and quartz

The values of characteristic particle sizes were determined directly from Figure 1. The d50 values range approximately from 8 to 12 µm, depending on the sample, while the d80 values are in the range of approximately 20 to 35 µm. Detailed particle size analysis of goethite, quartz, clay, and especially limonite sludge samples was conducted due to the significant influence of particle size on reagent adsorption, flocculation rate, floc size, and sedimentation rate of flocs. According to the literature (Tankosic, 2022.), the most suitable particles for

flocculation are in the range of 60–270 nm, and the tendency for flocculation decreases with increasing particle size, i.e., smaller particles flocculate more rapidly.

3.2. Moisture and Density

The moisture content of the samples is presented in Table 1.

Table 1. The moisture content of the samples

Sample	The moisture content %
Goethite	10,08
Quartz	8,53
Clay	16,14

The density of the samples is presented in Table 2.

Table 2. The density of the samples

Sample	Density, g/cm^3
Goethite	3,940
Quartz	2,663
Clay	2,734

3.3. Chemical and mineralogical composition

Table 3 presents the chemical analysis of goethite, quartz and clay samples. The chemical analysis was performed at the ArcelorMittal Research Center in Maizières-lès-Metz and at the control laboratory in Ireland. Table 4 presents the quantitative mineralogical analysis of goethite, quartz, and clay samples.

Table 3. Chemical analysis of goethite, quartz and clay

Sample	Fe, total. (%)	SiO_2 (%)	Al_2O_3 (%)	CaO (%)	MgO (%)	TiO_2 (%)	P (%)	Mn (%)	S (%)	Na_2O (%)	K_2O (%)	LOI. (%)
Goethite	57.16	4.44	0.59	0.03	0.22	<0.01	0.078	1.18	0.007	0.009	0.033	10.86
Quartz	0.74	92.90	3.28	0.06	0.14	0.22	0.005	0.00	0.404	0.079	0.506	1.62
Clay	4.48	69.90	14.50	0.26	0.58	0.86	0.023	0.07	0.148	0.356	2.420	4.80

Table 4. Mineralogical analysis of goethite, quartz, and clay samples

Goethite		Quartz		Clay	
Mineral	% Content	Mineral	% Content	Mineral	% Content
Goethite	86.28	Quartz	93.61	Quartz	49.71
Quartz	3.56	Muscovite	5.97	Muscovite	30.94
Hematite	10.16	Hematite	0.42	Chlorite	2.87
				Kaolinite	10.07
				Goethite	4.19
				Chloritoid	1.85
				Hematite	0.36

3.4. Effect of pH on Zeta Potential of Goethite, Quartz, and Clay

The mechanism of double electric layer formation on mineral particles is crucial in flocculation, as it determines how reagents interact with particle surfaces. The zeta potential, measured as a function of pH, indicates surface charge: in acidic conditions, H^+ ions dominate, giving positive charge, while in basic conditions, OH^- ions dominate, giving negative charge. The isoelectric point (IEP) is the pH at which the zeta potential is zero and the particle surface is electrically neutral. At the IEP, electrostatic repulsion disappears, enabling coagulation,

flocculation, and sedimentation. Mineral solubility and adsorption of dissolved ions can modify these behaviors (Tankosić Lj, 2022).

3.4.1. Zeta potential of goethite, quartz, and clay samples as a function of pH

The zeta potential of goethite, quartz, and clay samples was measured as a function of pH to evaluate their surface charge behavior under different pH levels (Figure 2).

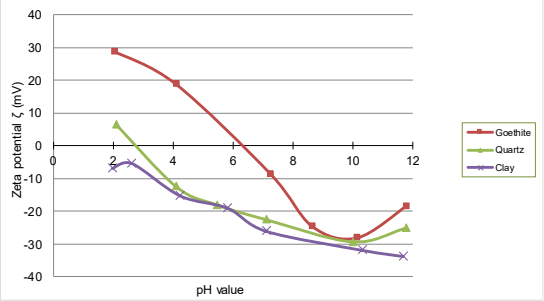

Figure 2. Zeta potential of goethite, quartz, and clay as a function of pH

The zeta potential of goethite shows an isoelectric point (IEP) at pH 6.7. Above this pH, the surface becomes negatively charged due to OH^- adsorption, while below it, positive charges increase due to H^+ adsorption. This suggests that selective flocculation of goethite can be achieved using anionic flocculants below the IEP, whereas cationic flocculants are more effective under alkaline conditions.

Quartz and clay exhibit consistently negative zeta potentials across the tested pH range, with quartz IEP around pH 2.5 and no IEP observed for clay. Based on flocculation theory, selective sedimentation of goethite near pH 6.5 is possible, leaving quartz and clay dispersed even without flocculants. The zeta potential trends are consistent with literature data (Somasundaran, P.et al,2000., Tankosić Lj. et al, 2018, Rodrigues O.M.S at all, 2010., Rath, R K et al, 2011., Yukselen**,** Y.et al, 2003.).

3.5. Influence of Sodium Hexametaphosphate (SHMP)

SHMP showed a strong dispersing effect on goethite, quartz, and clay across a wide pH range, significantly increasing their negative zeta potential. For goethite, SHMP caused the most pronounced changes in electrokinetic potential, particularly under acidic and neutral conditions, indicating strong and specific adsorption of phosphate anions even above its isoelectric point (Somasundaran, 2000; Weissenborn, et al., 1998; Iwasaki, 1981; Tankosić, et al., 2018).

In quartz, SHMP increased negative surface charge throughout the tested pH range, with no isoelectric point observed, confirming effective dispersion and stabilization. Clay exhibited consistently strong negative zeta potential when treated with SHMP, showing the highest increase among the minerals and activating its surface for further interaction with anionic reagents (Tankosić Lj. et al., 2018; Somasundaran, P. et al., 2000; Dohlanova, Ž. et al., 2008).

Overall, SHMP proved the most effective dispersant among those tested, providing stable dispersion of all three minerals through specific phosphate adsorption, which is crucial for controlling selective flocculation in complex mineral systems.

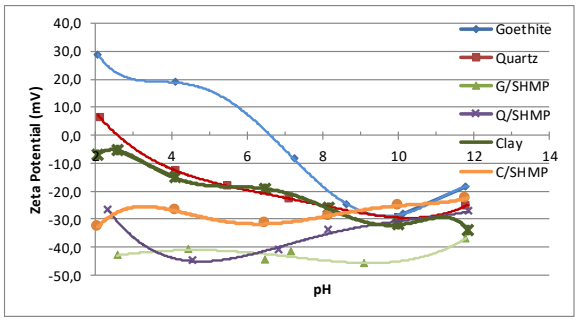

Figure 3. Zeta potential of goethite, quartz, and clay in the presence/absence of SHMP

3.6. Combined Effect of SHMP and PAM

For the investigation of the zeta potential of minerals in the presence of dispersant and flocculant, SHMP was used as the dispersant, while PAM was used as a flocculant.

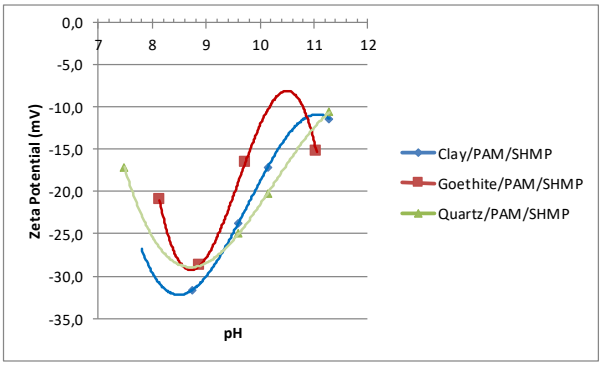

Figure 4. Zeta potential of goethite, quartz, and clay in the presence of PAM and SHMP

The electrokinetic behavior of goethite, quartz, and clay was investigated in the pH range 2–12 in the presence of SHMP and PAM. SHMP enhanced dispersion of all three minerals by increasing the negative surface charge, while PAM modulated surface interactions and promoted flocculation depending on pH.

With SHMP and PAM, goethite remained negatively charged above pH 5, showing stable dispersion in acidic conditions and flocculation primarily at pH 4–6 and around pH 9. Quartz stayed negatively charged throughout the pH range; PAM reduced the negative zeta potential in alkaline conditions, while the combination of SHMP and PAM favored flocculation under acidic conditions. Clay exhibited consistently negative zeta potential, with flocculation most likely near pH 6.

These results indicate that the combined application of SHMP and PAM enables effective control of dispersion and flocculation of goethite, quartz, and clay through electrokinetic interactions.

4. CONCLUSION

The study demonstrates the significant influence of SHMP as a dispersant and PAM as a flocculant on the electrokinetic properties of natural goethite, quartz, and clay minerals. Zeta potential measurements revealed that all three minerals exhibit increased negative surface charge with increasing pH, with goethite and quartz showing isoelectric points at pH ~6.7 and ~2.6, respectively, while clay remained negatively charged across the entire pH range. The addition of SHMP effectively enhanced the negative surface charge, stabilizing the

suspensions and promoting dispersion of all tested minerals. Conversely, the combined application of SHMP and PAM decreased the magnitude of the zeta potential in specific pH ranges, creating favorable conditions for selective flocculation.

For goethite, flocculation is expected in acidic to neutral conditions (pH 4–6) and around pH 9, while quartz remained largely dispersed, especially in alkaline media. Clay exhibited potential for flocculation around pH 6 in the presence of PAM. The results of the zeta potential behavior of the individual samples indicate the possibility of applying selective flocculation at controlled pH values in the presence of SHMP and PAM. These findings highlight the importance of controlling pH and reagent dosage to achieve desired dispersion or flocculation behavior, in line with classical DLVO theory and double-layer interactions.

From an industrial perspective, the results provide practical insights for mineral processing applications, including selective flocculation and sedimentation in iron ore treatment, fine particle recovery from mining sludge, and stabilization of mineral suspensions. The effective combination of SHMP and PAM enables targeted control of particle interactions, which can improve separation efficiency, reduce reagent consumption, and optimize water management in mineral processing plants. Additionally, these findings can be applied to tailings management and the recovery of fine valuable minerals, supporting sustainable practices and circular economy initiatives in the mining sector.

REFERENCES

Ćalić, N., (1990), Theoretical Foundations of Mineral Raw Material Preparation, Faculty of Mining and Geology, Belgrade.

Ćalić, N., (2017), “Application of flocculation in processing of mineral sludge”, XVII BMPC Antalya, 51–59.

Dohlanova, Ž., Svoboda, L., Šulcova, P., (2008), “Characterization of kaolin dispersion using acoustic and electroacoustic spectroscopy”, Journal of Mining and Metallurgy, 44B, 63–72.

Iwasaki, I., Paul, St., Minn., (1981), “Selective flocculation, magnetic separation, and flotation of ores”, United States Patent 4,298,169.

Milošević, S., (1997), “Suspensions: Aspects of selective concentration of the solid phase and separation of solid and liquid phases”, in Multiphase Dispersed Systems, ITNMS Book 4, Belgrade, 47–117.

Rath, R. K., Kar, A. K., Mohanta, M. K., Singh, R., Kumar, A., (2011), “Surface chemical and settling studies on hematite, quartz, and kaolinite in the presence of organic reagents”, Proceedings of the International Conference on Mineral Processing Technology (MPT 2011), Udaipur, 20–22 Oct.

Rodrigues, O. M. S., et al., (2010), “Kaolinite microflotation and zeta potential measurements in the presence of ammonium quaternary salts”, Revista de la Facultad de Ingeniería, 24, 40–44.

Somasundaran, P., Runkana, V., (2000), “Selective flocculation of fines”, Transactions, Columbia University, Langmuir Center for Colloids and Interfaces, Vol. 10, Special Issue, New York, USA.

Somasundaran, P., Runkana, V., (2000), “Selective flocculation of fines”, Transactions of Nonferrous Metals Society of China, 10.

Tankosić, Lj., Tančić, P., Sredić, S., Nedić, Z., (2018), “Comparative study of the mineral composition and its connection with some properties important for the sludge flocculation process – examples from Omarska Mine”, Minerals.

Tankosić, Lj., (2022), Doctoral Thesis, University of Banja Luka, Faculty of Mining.

Yukselen, Y., Kaya, A., (2003), “Zeta potential of kaolinite in the presence of alkali, alkaline earth, and hydrolyzable metal ions”, Water, Air & Soil Pollution, 145, 155–168.

Weissenborn, P. K., Warren, L. J., Dunn, J. G., (1995), “Selective flocculation of ultrafine iron ore. Part 2: Mechanism of selective flocculation”, Colloids and Surfaces A: Physicochemical and Engineering Aspects, 99, 29–43.

THE EFFECT OF WATER TYPE ON FLOTATION PERFORMANCE AND FROTH CHARACTERISTICS IN COPPER SLAG FLOTATION

Ulaş USLU*, Zeynep ÜÇERLER ÇAMUR, Yunus Emre ÇAVDAR, Şükriye Beste AYDIN, Gülay BULUT

Istanbul Technical University, Faculty of Mines, Mineral Processing Engineering Department, 34469, Maslak, Istanbul, TÜRKİYE
**Corresponding author: usluu19@itu.edu.tr*

A B S T R A C T

Copper slag, a metallurgical byproduct, is a valuable secondary resource whose reprocessing via flotation is critical for sustainability. Driven by fresh water scarcity, this study investigates the viability of using seawater as an alternative process water for copper recovery from slag sourced from the Eti Bakır A.Ş. Samsun Plant. Comparative laboratory-scale flotation tests were performed using Sodium Isopropyl Xanthate (SIPX) as collector and Methyl Isobutyl Carbinol (MIBC) as frother. The obtained results indicated that flotation performance can be significantly improved depending on the type of water used. While tap water resulted in a high-grade concentrate (32.52% Cu) with 70.0% recovery, seawater achieved a significantly higher recovery of 80.1% at a lower grade of 20.62% Cu. Dynamic Foam Analysis (DFA) linked the enhanced recovery in seawater to its more stable foam structure. These findings confirm that seawater is a viable alternative for copper slag flotation, especially when maximizing metal recovery is the primary objective. This presents significant economic and environmental opportunities for mineral processing plants in coastal regions or those facing water scarcity, highlighting a key process choice between maximizing concentrate grade and overall metal recovery.

Key words: *Copper slag, flotation, water types, Dynamic Foam Analysis*

1. INTRODUCTION

The escalating global demand for copper, driven by the rapid expansion of renewable energy infrastructure and electrification, has led to a critical structural deficit as high-grade primary sulfide ores become increasingly depleted (El-Bacha et al., 2025). Consequently, the metallurgical sector is pivoting toward the comprehensive reprocessing of secondary resources. Copper smelting slag, generated at a staggering rate of over 39 million tonnes annually worldwide, is no longer viewed merely as an environmental liability but as a highly valuable, polymetallic "artificial ore". The mineralogical matrix of this slag is predominantly composed of fayalite (Fe_2SiO_4) and magnetite, with residual copper entrenched as entrained matte droplets, metallic copper, and various sulfide phases such as chalcopyrite and chalcocite (Chen & Zhang, 2025). Given that the residual copper concentration in these dumps frequently exceeds the cut-off grades of primary natural ores, froth flotation remains the most robust and economically viable method for bulk processing and resource recovery (Kierczak et al., 2013).

However, froth flotation is an inherently water-intensive physico-chemical separation process. As global freshwater scarcity evolves into an existential operational risk for the mining industry, there is an urgent mandate to transition toward alternative fluid media, primarily raw seawater and extreme closed-loop recycled process water (Jeldres et al., 2016). Seawater, constituting approximately 97.5% of Earth's water inventory, presents a complex hypersaline environment with high concentrations of primary electrolytes (Na^+, Cl^-) and secondary multivalent cations (Mg^{2+}, Ca^{2+}). The influx of these inorganic electrolytes severely compresses the electrical double layer (EDL) surrounding both the solid mineral particles and ascending air bubbles (Romero et al., 2018). This EDL compression not only enhances particle-bubble attachment

kinetics but also severely inhibits bubble coalescence, generating a dense swarm of micro-bubbles that drastically improves the total interfacial surface area flux within the cell (Castro et al., 2013).

Despite these hydrodynamic advantages, the complex chemistry of seawater introduces profound challenges. At natural or slightly alkaline pH levels, multivalent ions—specifically magnesium—hydrolyze and precipitate as fine colloidal $Mg(OH)_2$ films. These hydrophilic precipitates possess a strong affinity for copper active sites, effectively shielding the valuable minerals from thiol collector adsorption and severely depressing recovery (Li et al., 2019; Yu et al., 2024a). Recent mechanistic studies utilizing Density Functional Theory (DFT) and micro-flotation emphasize that these complex chemical interactions fundamentally alter the surface thermodynamics of the slag particles (Yu et al., 2024b). To counteract these inhibitory mechanisms, contemporary research is actively exploring the integration of novel modifier interactions, ester-based co-collectors, and targeted sulfidization techniques to restore surface hydrophobicity in hypersaline media (Chen and Zhang, 2025).

Simultaneously, the alternative strategy of utilizing completely closed-loop process water introduces entirely different, organic-driven toxicity. Continuous recirculation saturates the process water with unconsumed residual flotation reagents—such as excess xanthates and frothers alongside dissolved transition metal ions (Cu^{2+}, Fe^{3+}) generated during intense mechanical comminution. These dissolved heavy metals act as unintended activators, precipitating onto the negatively charged surfaces of the hydrophilic fayalite and silica gangue. Once artificially coated, residual xanthates bind to these gangue particles, rendering vast swathes of the iron-silicate matrix pseudo-hydrophobic and leading to catastrophic non-selective mass pull. To navigate this, the industry is increasingly adopting machine learning (ML) algorithms to dynamically predict and optimize the blending ratios of fresh, process, and seawater to mitigate real-time fluctuations in water toxicity (El-Bacha et al., 2025).

This study empirically investigates the effect of standard tap water, recycled process water, and saline seawater on the flotation of copper slag. This research provides the actionable intelligence required to engineer resilient, zero-freshwater mineral processing circuits.

2. MATERIAL AND METHODS

2.1. Material

The copper slag sample used in the experiments was a flotation feed sample (approximately -2 mm particle size) from the Eti Bakır A.Ş. Samsun Flotation Plant. The plant processes a highly complex blended feed consisting of flash furnace residues (containing 1.5% to 4.0% Cu) and converter furnace residues (containing 5.0% to 10.0% Cu), which are homogenized prior to beneficiation. The chemical composition of the copper slag sample is % 1.58 Cu, % 37.42 Fe, % 3.79 Zn and % 34.28 SiO_2.

To achieve the necessary liberation of the locked copper sulfide and metallic phases from the hard fayalite matrix, the slag sample was subjected to a wet grinding. A 500 g sample was milled in a laboratory-scale steel ball mill for 50 minutes at a pulp density of 60% solids by weight. Particle size analysis conducted with Malvern laser diffraction particle size analyzer, confirmed a highly fine particle distribution essential for slag liberation. The d_{50} of the ground product was established at 19.41 µm, with a d_{90} of 58.00 µm, ensuring that the vast majority of the feed material met the optimal liberation criteria for sulfide flotation. The particle size distribution after wet grinding is shown in Figure 1.

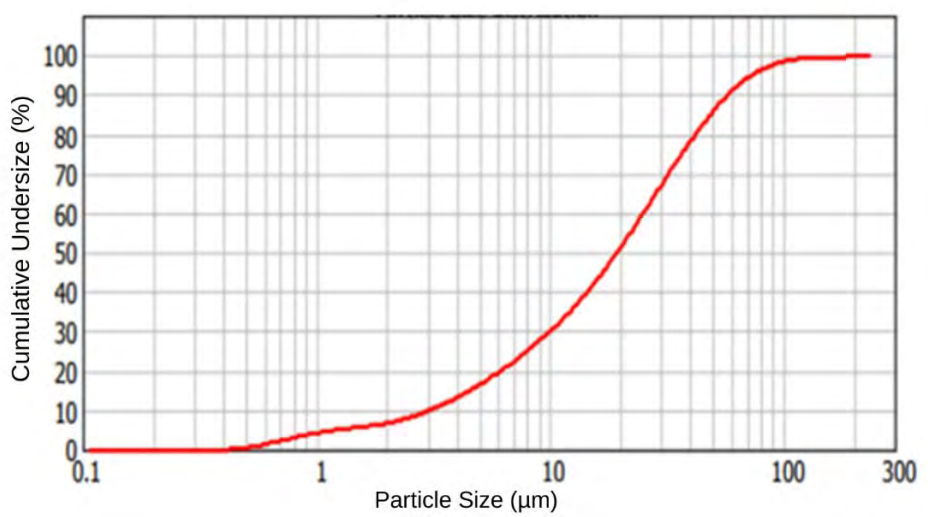

Figure 1. Particle size distribution of slag sample after grinding

Seawater taken from the Black Sea, and process water taken from the Eti Bakır A.Ş. Samsun Facility were used in the experiments. The tap water used in the laboratory was sourced from the Sarıyer district of Istanbul. The chemical analyses of the water types used in the experiments are shown in Table 1.

Table 1. Chemical content of different water types

Water Type	Ca (ppm)	Mg (ppm)	Na (ppm)	SO_4 (%)	Cl (ppm)
Tap Water	60.978	11.219	29.925	0.0065	<1.0
Seawater	250.500	693.424	3452.16	0.132	<1.0
Process Water	90.800	12.788	5.833	0.0151	<1.0

2.2. Method

Flotation tests were executed utilizing a laboratory-scale Denver D-12 flotation machine. The impeller speed was maintained at a constant 1200 rpm. Flotation processes were carried out in a single stage. The pulp solids concentration was kept at 18 wt.% in flotation.

The operation was conducted at the natural pH of the slag pulp (ranging from 7.7 to 8.31). The conditioning was performed as an initial 5-minute conditioning phase following the dosing of 250 g/t SIPX (sodium isopropyl xanthate) as collector, followed by a 1-minute conditioning phase of 50 g/t MIBC (methyl isobuthyl carbinol) as frother. The froth collection time was 3 minutes. The concentrates and tailings were dried at 100°C, and subjected to ICP-OES analysis to definitively obtain grade and calculate total recovery.

Froth diameter measurements were performed with the ImageJ software. During flotation, high-resolution photos were captured at the apex of the flotation cell exactly one minute after the initiation of the air valve. The images were calibrated against a physical scale and processed utilizing the ImageJ software, calculating the maximum Feret diameter of discrete froths across the surface plane to establish a statistically robust mean diameter.

The dynamic foam formation and stability were measured using a Krüss Dynamic Foam Analyzer (DFA-100). The DFA-100 utilizes a vertical cell equipped with optical sensors to continuously monitor the vertical expansion and subsequent temporal decay of a foam column over a 60-second window. Measurements were carried out under two conditions: (i) reagent-

only solutions (SIPX + MIBC in the respective water types without solids) and (ii) suspensions containing reagents and fine slag particles, in order to evaluate the effect of particles on foam stability. For suspension measurements, the slag sample was ground to below 0.038 mm using a ring mill. The measurements were performed using the −0.038 + 0.020 mm particle size fraction.

3. RESULTS AND DISCUSSION

3.1. Effect of Water Type on Flotation Performance and Froth Diameter

This study summarizes the results of investigations conducted to examine the effect of different water types used in copper slag flotation and compares them in terms of product grade, flotation recovery and froth size and froth stability. As presented in Table 1, the chemical analyses of the three different water types indicate that ion concentrations are lowest in tap water and progressively increase toward seawater, while process water exhibits intermediate values between these two water types. The results regarding the effects of different water types on flotation performance and froth diameter are presented in Table 2.

Table 2. The effects of different water types on flotation performance and froth diameter

Water Type	Products	Amount (%)	Cu (%)		Mean Froth Diameter (cm)
			Content	Recovery	
Tap Water	Concentrate	3.3	32.52	70.0	0.80
	Tailings	96.7	0.47	30.0	
	Total Feed	100.0	1.52	100.0	
Process Water	Concentrate	9.1	14.41	75.4	0.32
	Tailings	90.9	0.47	24.6	
	Total Feed	100.0	1.74	100.0	
Seawater	Concentrate	6.3	20.62	80.1	0.39
	Tailings	93.8	0.34	19.9	
	Total Feed	100.0	1.61	100.0	

As shown in Table 2, in the experiment conducted with seawater, the copper content was 20.60%, while the recovery rate was 80%. With tap water, a very clean concentrate with a content of 32.52% was obtained with a lower recovery rate. The lowest copper grade was obtained with process water. It is thought that this is due to the negative effect of certain reactants remaining in the water returned to the plant at the end of the flotation process.

Table 2 shows that the froth diameter in tap water is larger than that in seawater and process water. Consequently, the copper recovery from tap water remains low. Although the froth diameters of process water and seawater are similar, the efficiency is lower for process water due to its contamination with reactants. Froth images obtained for different water types are presented in Figure 2.

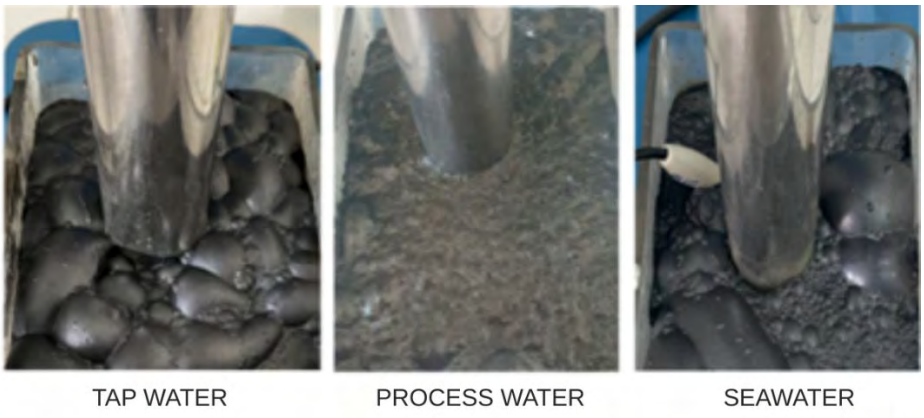

Figure 2. Froth images corresponding to different water types

3.2. Effect of DFA Measurements on Froth Stability

Froth stability measurements conducted using only reagents (250 g/t SIPX and 50 g/t MIBC) and with the addition of copper slag particles are presented in Figures 3 and 4, respectively.

The DFA data empirically corroborates the visual froth diameter observations. As shown in Figure 3, when tested with reagents alone (in the complete absence of solid particles), tap water produced a highly unstable froth. Conversely, both seawater and process water generated more stable and persistent foam columns that remained intact throughout the 60-second test period.

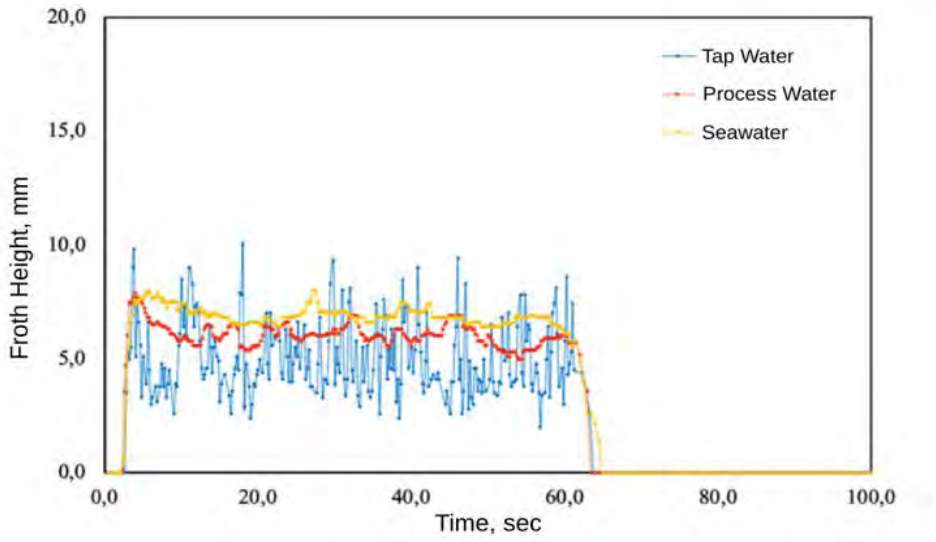

Figure 3. Dynamic Foam Analysis (DFA) results without solid addition

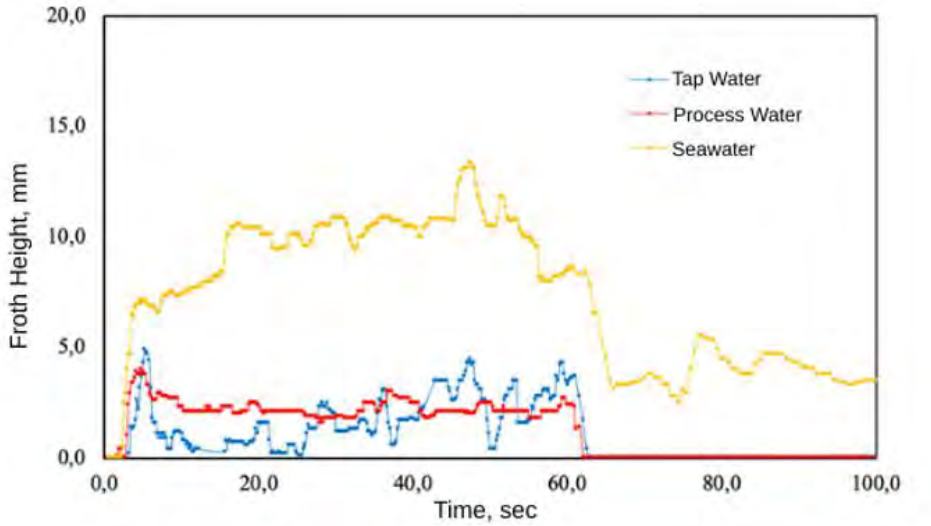

Figure 4. Dynamic Foam Analysis (DFA) results with solid addition

The DFA results obtained with the addition of solid particles in Figure 4 show a trend consistent with the froth diameter and flotation performance results. Seawater produced the highest and most stable froth column, reaching approximately 10–13 mm throughout the test period. In contrast, tap water exhibited a lower and more fluctuating froth height, generally ranging between 1–4 mm, while process water showed moderate froth stability with froth heights around 2–3 mm. Overall, the smaller froth diameter and higher froth stability observed in seawater improved the transport of copper particles within the froth phase, resulting in the highest copper recovery. In contrast, the larger froth size and lower froth stability in tap water limited the particle carrying capacity, leading to lower recovery.

4. CONCLUSION

This study investigated the effect of different water types on the flotation performance and froth characteristics of copper slag. The experimental results demonstrated that water type significantly influences both flotation performance and froth behavior. In the tests performed with seawater, a copper grade of 20.60% was obtained with the highest recovery of 80%. In contrast, tap water produced a cleaner concentrate with a copper grade of 32.52%, although the recovery remained lower. The poorest concentrate grade (14.4%) was obtained in experiments conducted with process water, which may be attributed to the negative effects of residual flotation reagents present in the recycled plant water.

In terms of recovery, seawater yielded the highest copper recovery, followed by process water, while tap water showed the lowest recovery values. Analysis of froth characteristics revealed that the largest froth diameters were observed in tap water, whereas smaller froth sizes were obtained in seawater and process water. Furthermore, the highest froth height and stability were observed in seawater. Overall, these results indicate that seawater enhances froth stability and particle transport within the froth phase, thereby improving copper recovery.

REFERENCES

Beşe, A. V., (2017) “Bakır curuflarından metallerin kazanılması”, Sinop Üniversitesi Fen Bilimleri Dergisi, 2(1), 140-149.

Bulatovic, S. M., (2007) “Handbook of Flotation Reagents: Chemistry, Theory and Practice”, Elsevier.

Castro, S., Miranda, C., Toledo, P., & Laskowski, J., (2013) “Effect of frothers on bubble coalescence and foaming in electrolyte solutions and seawater”, International Journal of Mineral Processing, 124, 8-14.

Chen, Y., Zhang, W., (2025) “Reprocessing of copper by flotation via mineralogical characteristics from a copper slag case study”, RSC Advances, 15, 34138-34148.

Cruz, C., Herrera-León, S., Calisaya-Azpilcueta, D., Salazar, R., Cisternas, L. A., Kraslawski, A., (2022) “Using waste brine from desalination plant as a source of industrial water in copper mining industry”, Minerals, 12(9), 1162.

El-Bacha, R., Salhi, A., Abderrafia, H., Rabi, S., (2025) “Optimising water use in copper flotation with the design of experiments and machine learning”, South African Journal of Science, 121(3/4).

Jeldres, R. I., Forbes, L., Cisternas, L. A., (2016) “Effect of seawater on sulfide ore flotation: A review”, Mineral Processing and Extractive Metallurgy Review, 37(6), 369-384.

Kierczak, J., Potysz, A., Pietranik, A., Tyszka, R., Modelska, M., Néel, C., Ettler, V., Mihaljevič, M., (2013) “Environmental impact of the historical Cu smelting in the Rudawy Janowickie Mountains (south-western Poland)”, Journal of Geochemical Exploration, 124, 183–194.

Laskowski, J. S., Castro, S., Gutierrez, L., (2018) “Flotation in seawater”, Mining, Metallurgy & Exploration, 35, 1-13.

Li, W., Li, Y., Xie, S., Duan, W., Chen, W., (2022) “Roles and influences of kerosene on chalcopyrite flotation in MgCl2 solution: EDLVO and DFT approaches”, Minerals, 12(1), 48.

Li, Y., Zhu, H., Li, W., Zhu, Y., (2019) “A fundamental study of chalcopyrite flotation in sea water using sodium silicate”, Minerals Engineering, 134, 105862.

Romero, C. P., Jeldres, R. I., Quezada, G. R., Concha, F., Toledo, P. G., (2018) “Zeta potential and viscosity of colloidal silica suspensions: Effect of seawater salts, pH, flocculant, and shear rate”, Colloids and Surfaces A: Physicochemical and Engineering Aspects, 538, 210-218.

Yu, X. C., Yu, B., Wang, H., Shen, P. L., Liu, D. W., (2024a) “Evolution of sulfur species on malachite surfaces in the presence of calcium and magnesium ions and implications for xanthate flotation”, Advanced Powder Technology, 35(7), 104538.

Yu, X. C., Yin, Z. D., Chen, Y., Shen, P. L., Wang, H., Mao, Y. Q., Liu, D. W., (2024b) “Experimental and DFT study of modified malachite with 2.5-dimercap-to-1.3,4-thiadiazole and its response to sulfidization-xanthate behavior”, Colloids and Surfaces A: Physicochemical and Engineering Aspects, 693, 134057.

A COMPREHENSIVE PILOT-SCALE STUDY ON PNEUMATIC IMHOFLOT FLOTATION PERFORMANCE AT THE ÇAYELİ BAKIR

Atıf DEMIRCAN[1,*], Ekin GÜNGÖR[2], Ahmad HASSANZADEH[2] Dilay HACIOSMANOĞLU[1], Aytekin TIRNAKÇIOĞLU[1]

[1]Çayeli Bakır, Çayeli-Rize, Türkiye
[2]Maelgwyn Mineral Services, South Africa
**Corresponding author: atif.demircan@fqml.com*

A B S T R A C T

This study presents the results of a comprehensive pilot-scale flotation campaign conducted at the processing plant of Çayeli Bakır. The pilot circuit comprised two conditioning tanks and two pneumatic flotation stages. The operating pressure for both cells was maintained between 1.5 and 2.2 bar. Tests were performed over a wide range of pulp solids content, from 7% to 17%, which reflects the variable nature of the feed material.

The feed consisted of samples from the newly discovered “South Orebody,” representing two distinct mineralogical types:
1. Chalcopyrite-rich and sphalerite-poor ore.
2. Secondary copper minerals-rich (bornite, covellite, chalcocite) associated with sphalerite.

Feed copper grades varied between 1% and 10% Cu, while zinc content in some tests reached up to 4%. The pilot plant was operated at a feed rate of 15–20 m³/h, using material sourced from column flotation tailings and scavenger concentrate streams. Test work was performed under three reagent regimes: (i) no collector addition, (ii) dosing MIBC as frother, and (iii) dosing a combination of MIBC as frother and SIPX as collector.

The addition of MIBC frother led to an increase in copper recovery particularly at higher feed grades. For example, no frother condition, the recovery was only 54.7% at a feed grade of 11.1% Cu. When frother was added to a similar high feed grade (10.1% Cu), the recovery sharply increased to 95.1%. Even at lower feed grades (4.5% Cu), the use of frother resulted in a high recovery of 95.5%. These findings emphasize the critical role of frother addition in improving the flotation kinetics and overall copper recovery performance of the pilot scale pneumatic flotation system.

The results demonstrated the capability of the pneumatic flotation system to produce saleable copper concentrate with a minimum grade of 22.0% Cu and overall copper recoveries up to 95%, depending on ore type and operating conditions.

This work provides valuable insights into the application of pneumatic flotation technology in complex polymetallic ore processing, particularly for ores with variable mineralogy and grades. The findings have significant implications for improving copper recovery and optimizing the circuit performance.

***Key words**: Çayeli, pilot plant trial, pneumatic cells, chalcopyrite flotation, copper recovery*

1. INTRODUCTION

Generally speaking, flotation, as a downstream separation process, accounts for 4-10% of a mine's total energy consumption. Since its invention in the 1900s (Almond, 2000), flotation has played a significant role in effectively separating metallic and industrial valuable minerals despite its complexity and environmental challenges. These days, due to the sharp reduction in ore grades and electrification and modernization, the mining industry and concentration plants have to increase throughput to make the entire process economically viable, leading to an increase in flotation cell volumes. However, this leads to a rise in carbon footprint and, in

turn, massive energy and water consumption. One way to mitigate this is to integrate reactor-separator flotation cells, also known as pneumatic or intensified flotation cells, which have relatively lower capital and operating costs compared to conventionally used mechanical and column cells (Hassanzadeh et al., 2022). Imhoflot™ cells are one of the oldest pneumatic cells invented at TU Clausthal (Germany) in the 1970s and later developed further (Imhof, 1988), and so far, more than 144 of them are installed worldwide. A short mean retention time of 2-3 min per cell, together with the capability to recirculate tailings back to the feed, allows this technology to recover even slow-floating particles, thereby reducing the total required retention time by a factor of 3-5 compared to conventional cells. By this, the requirement for a lower number of cells that have no moving parts and are self-aspirated theoretically, it is feasible to diminish the CAPEX and OPEX of flotation plants, and for some commodities significantly. Table 1 briefly summarizes several pilot trials and their characteristics using 1-3 pilot-scale Imhoflot™ cells in series.

Table 1. List of some pilot plants and their properties

Target element	d_{80} (µm)	Duty(ies)	Cell size(s)	Flow rate (m^3/h)	Country	Reference
Au	20	Pre-rougher	2xG-14	30-40	Kazakhstan	Hoang et al. 2022
Au	140	Rougher scalper and cleaner	UN	UN	Russia	Pyle et al., 2022
Ni	11	Scavenger tailings	3xG-12	20-35	Spain	Battersby et al., 2011
Cu	25	Pre-rougher flotation, rougher concentrate, cleaner-scavenger tailing, and first-cleaning concentrate	1xH-16	30-40	Türkiye	Hassanzadeh et al., 2023
Cu	75, 82, and 38	Scavenger feed, final tailings, and cleaner	1xG-14	15-35	Poland	Hoang et al., (2023)

The ÇBI ore processing facility was commissioned in August 1994, with the first concentrate production occurring in November 1994.

The facility has been in continuous operation for over thirty years, treating ore from the Main Orebody. Ore throughput rates have varied over the years, with a peak rate of 1.34 Mtpa reached in 2014.

Discovery of the South Orebody will lead to a currently planned mine life extending to 2036, treating a mix of Main and South Orebody feed from 2025, and South Orebody ores exclusively from 2028.
The current study presents the performance of a pilot plant (VM-12 followed by G-12), examined on Cayeli Bakır concentration plant, as pre-rougher/scalper, cleaner, and rougher-scavenger tailings duties.

2. MATERIALS AND METHODS

The process flowsheet of the Çayeli Bakır copper–zinc processing plant consists of comminution, flotation, concentrate handling, and tailings management stages. Shown in Figure 1.

Run-of-mine ore is crushed through a jaw and cone crusher circuit following screening and stored in a fine ore bin prior to grinding. Size reduction is achieved in a two-stage ball milling circuit (primary and secondary mills), producing a flotation feed with a target size of 75% passing 36 µm.

The flotation circuit comprises sequential copper and zinc recovery stages. Copper is recovered via rougher–scavenger flotation followed by cleaner and column flotation, producing a high-grade concentrate. The copper concentrate is subsequently thickened and filtered, while processing water is recycled.

The remaining slurry is processed in the zinc circuit, where zinc is recovered through rougher and column flotation stages. The final zinc concentrate is thickened, filtered, and prepared for shipment.

Final tailings are thickened, with underflow directed either to a paste fill plant or discharged via a pipeline system, including deep see storage. Thickener overflow and underground drainage waters are recovered and reused within the process.

The circuit design allows operational flexibility through optional bypassing of selected units depending on ore characteristics and production requirements.

Çayeli Copper Mine applies a systematic ore blending strategy to manage variability arising from distinct ore types within the deposit. This approach is particularly critical for maintaining stable plant performance and achieving target concentrate specifications.

In the South Ore Body, two primary operational campaigns are defined based on ore characteristics:

Specification (Spec) Campaign: This campaign processes footwall yellow ore (SYO),

Non-Spec Campaign: This campaign focuses on black ore (SBO), which exhibits greater variability and requires controlled blending. The SBO feed is composed of a balanced mixture of approximately 50% high-zinc ore and 50% low-zinc ore. The distinction between these campaigns enables the plant to optimize metallurgical performance by adapting operating conditions to ore type, while ensuring consistent concentrate quality and minimizing process disturbances.

The pilot plant was designed with a two-stage conditioning system followed by a two-stage pneumatic flotation circuit. Conditioning was carried out in two sequential conditioning tanks to ensure adequate reagent dispersion and particle–bubble interaction prior to flotation.
The flotation circuit consisted of two pneumatic cells arranged in series. The first stage was implemented using a Maelgwyn V-Cell, which primarily functioned as a rougher unit, while the second stage employed a Maelgwyn G-Cell, operating as an upgrading (cleaner) stage. This configuration enabled both effective recovery and grade improvement within a compact circuit design.

To ensure stable and controlled operation, the pilot plant was equipped with flowmeters and manometers installed at critical points throughout the system. These instruments continuously monitored key process parameters such as slurry flow rate and air pressure. The collected data were transmitted to an automation system, allowing real-time monitoring and control of operating conditions. This instrumentation framework enabled precise adjustment of process variables, contributing to improved process stability, repeatability, and overall metallurgical performance.

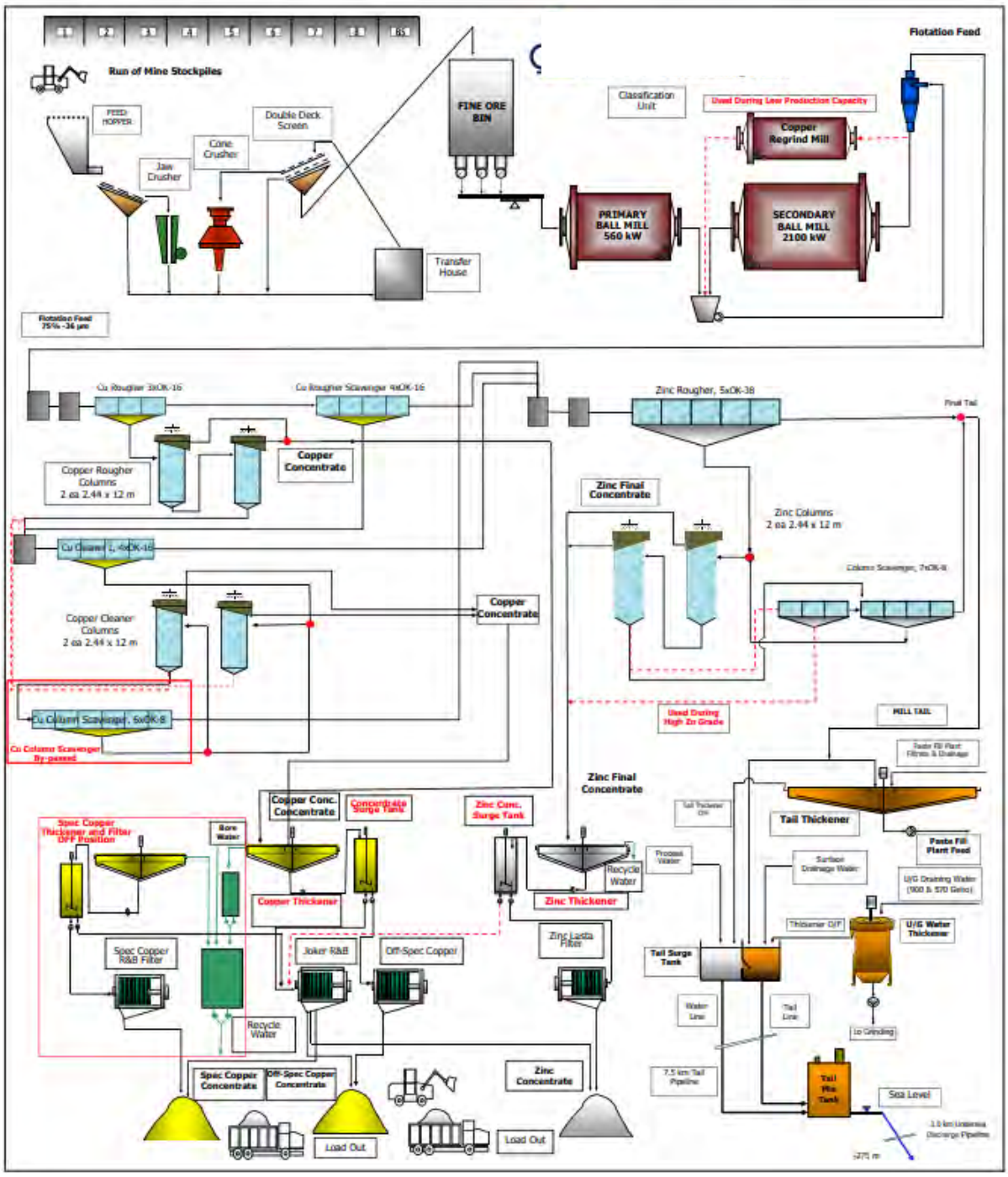

Figure 1. Flowsheet

The experimental study was conducted through two separate campaigns, referred to as SYO and SBO, in order to evaluate the performance of the pneumatic flotation system under varying operating conditions. The test work was performed on three different process streams: cleaner feed, rougher feed, and rougher tail.

Within each campaign, experiments were carried out at different feed grades, and the effects of frother and collector addition on flotation performance were systematically investigated.
All experimental work was conducted under the operating conditions summarized below, where the effects of feed type, reagent regime, and operating pressure on flotation performance were systematically evaluated.

Cleaner Feed Stream Tests

Cleaner feed tests were conducted under both SYO and SBO campaigns at similar operating pressures. The V-Cell feed pressure was maintained in the range of approximately 2.0–2.5 bar, while the G-Cell feed pressure varied between 1.0 and 1.6 bar.
In the SYO campaign, two sets of tests were performed:

- without reagent addition, and
- with frother addition at a dosage of 30 g/t, without collector.

In the SBO campaign, tests were conducted using a frother dosage of 30 g/t without collector addition.

Rougher Feed Stream Tests

Rougher feed experiments were carried out within the SYO campaign. The operating pressures were consistent with the cleaner feed tests, with V-Cell pressures of 2.0–2.5 bar and G-Cell pressures of 1.0–1.6 bar.

In these tests, both frother and collector were applied at dosages of 30 g/t each, allowing evaluation of combined reagent effects on flotation performance.

Rougher Tail Stream Tests

Rougher tail tests were also conducted under the SYO campaign at the same pressure ranges (V-Cell: 2.0–2.5 bar; G-Cell: 1.0–1.6 bar).

Higher reagent dosages were employed in this stream, with frother added at 60 g/t and collector at 45 g/t, in order to assess the recovery potential of low-grade tailings material.

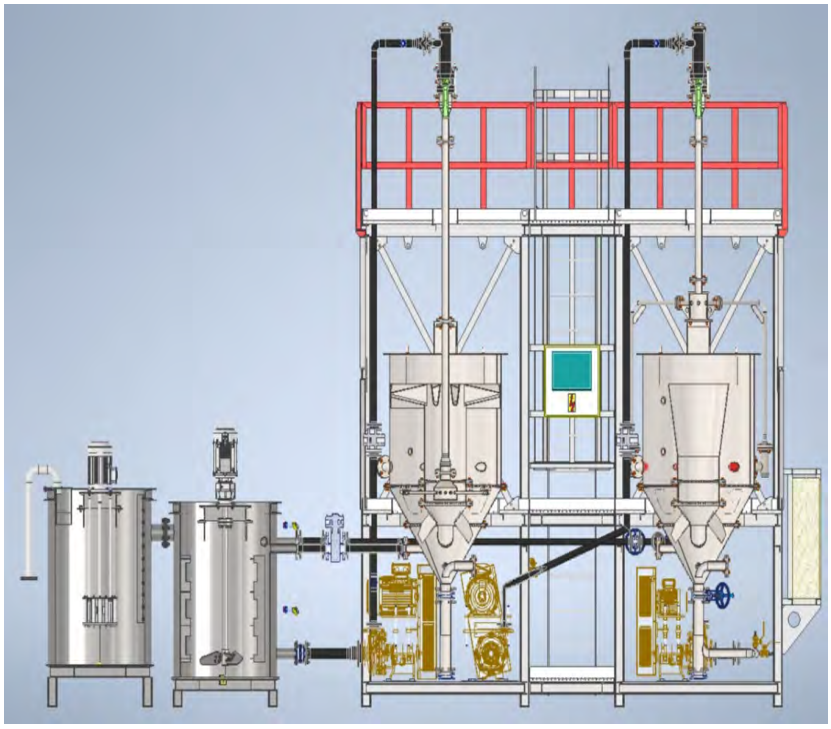

Figure 2. Pilot plant

3. RESULTS AND DISCUSSIONS

The experimental results presented in Table 2 demonstrate the influence of feed type, reagent regime, and solids concentration on the performance of the pneumatic flotation system.

Table 2. Summary of experimental conditions and metallurgical performance

Campaign	Stream	V-Cell Pressure (bar)	G-Cell Pressure (bar)	Frother (g/t)	Collector (g/t)	Solids (%)	Recovery (%)	Remarks
SYO	Cleaner Feed	2.0 – 2.5	1.0 – 1.6	0	0	12	72	No reagent condition
SYO	Cleaner Feed	2.0 – 2.5	1.0 – 1.6	30	0	10.6	76	Frother effect evaluated
SBO	Cleaner Feed	2.0 – 2.5	1.0 – 1.6	30	0	13	87	Frother-only condition
SYO	Rougher Feed	2.0 – 2.5	1.0 – 1.6	30	30	30	86	Combined reagent condition
SYO	Rougher Tail	2.0 – 2.5	1.0 – 1.6	60	45	25	81	High reagent dosage for low-grade feed

The experimental results presented in Table 2 demonstrate the influence of feed type, reagent regime, and solids concentration on the performance of the pneumatic flotation system.

Effect of Reagent Addition

A clear improvement in flotation performance was observed with the addition of frother. In the cleaner feed tests under the SYO campaign, recovery increased from 72% (no reagent) to 76% with the addition of 30 g/t frother, despite a slight decrease in solids content (from 12.0% to 10.6%). A more pronounced improvement was achieved in the SBO campaign, where recovery reached 87% at 13% solids under frother-only conditions. This indicates that frother plays a critical role in enhancing bubble formation and stability in pneumatic flotation systems, thereby significantly improving recovery.

The combined use of frother and collector in the rougher feed tests (30 g/t each) resulted in a recovery of 86% at a substantially higher solids concentration of 30%. This suggests that the addition of collector further improves particle hydrophobicity and attachment efficiency, particularly under high pulp density conditions.

Effect of Solids Concentration

The results indicate that solids concentration has a notable impact on flotation performance. While cleaner feed tests were conducted at relatively low solids content (10.6–13%), the rougher feed and rougher tail tests were performed at higher solids levels (25–30%). Despite the increased pulp density, high recoveries (81–86%) were achieved, demonstrating the robustness of the pneumatic flotation system under elevated solids conditions.

However, a slight decrease in recovery was observed in the rougher tail test (81% at 25% solids) compared to the rougher feed test (86% at 30% solids). This can be attributed to the lower feed grade and reduced floatability of tailings material, despite higher reagent dosages (60 g/t frother and 45 g/t collector).

Effect of Feed Type

Feed characteristics were found to be a key factor influencing flotation performance. Cleaner feed streams, which are relatively higher in grade and already partially upgraded, showed moderate to high recoveries (72–87%) depending on reagent conditions. In contrast, rougher feed exhibited high recovery (86%) when both frother and collector were applied, highlighting the effectiveness of the pneumatic system in treating primary flotation feeds.

The rougher tail stream, representing low-grade material, required significantly higher reagent dosages to achieve a recovery of 81%. This indicates that while the system is capable of recovering valuable minerals from tailings, the efficiency is inherently limited by mineral liberation and particle surface characteristics.

Overall System Performance

Overall, the results confirm that the pneumatic flotation system (V-Cell and G-Cell configuration) is capable of achieving high recoveries across a range of operating conditions. The system demonstrated strong sensitivity to reagent regime, particularly frother addition, and maintained stable performance even at elevated solids concentrations. The findings also highlight the importance of feed characteristics, with higher-grade feeds yielding superior metallurgical performance.

4. CONCLUSIONS

This study evaluated the performance of a pilot-scale pneumatic flotation system, consisting of a two-stage conditioning unit followed by sequential Maelgwyn V-Cell and G-Cell flotation stages, under different operating conditions and feed characteristics.

The results demonstrate that the pneumatic flotation system is capable of achieving high copper recoveries across a wide range of operating conditions. Frother addition was identified as a critical parameter, significantly enhancing flotation performance, with recovery improvements observed from 72% to as high as 87% under optimized conditions. The combined use of frother and collector further improved recovery, particularly in rougher feed applications.

The system exhibited strong operational robustness at elevated solids concentrations (up to 30%), maintaining high recovery levels (up to 86%). This highlights the suitability of pneumatic flotation technology for high-throughput applications where conventional systems may face limitations due to pulp density constraints.

Feed characteristics were also found to have a substantial impact on performance. Higher-grade feeds responded more favorably, while lower-grade rougher tail streams required increased reagent dosages to achieve acceptable recovery levels. Despite this, the system demonstrated the capability to recover valuable minerals even from low-grade streams.

REFERENCES

Almond, J. K., (2000) “The Elmore brothers and the flotation process for separating minerals”, Historical Metallurgy, 34 (1) 31-46.

Battersby, M., Battersby, R. M., Flatman, S., Imhof, R., Sprenger, H., Bragado, T., (2011) ,Recovery of ultrafine using Imhoflot pneumatic flotation–Two pilot plant case studies recovering nickel and zinc from tailings streams, https://www.maelgwyn.com/wp-content/uploads/2016/04/Recovery_of_Ultra_fines.pdf

Hassanzadeh, A., Cinar, Y. A., Gungor, E., Hoang, D. H., (2023) “Application of a self-aspirated Imhoflot™ H-16-Cell in a copper flotation circuit: A pilot-scale study”, IMCET Antalya, 1133-1141.

Hassanzadeh, A., Safari, M., Khoshdast, H., Güner, M. K., Hoang, D. H., Sambrook, T., Kowalczuk, P. B., (2022) “Introducing key advantages of intensified flotation cells over conventionally used mechanical and column cells”. Physicochemical Problems of Mineral Processing, 58.

Hoang, D. H., Imhof, R., Sambrook, T., Bakulin, A. E., Murzabekov, K. M., Abubakirov, B. A., Baygunakov, R. K., Rudolph, M., (2022) “Recovery of fine gold loss to tailings using advanced reactor pneumatic flotation Imhoflot™”, Minerals Engineering, 184 107649.

Hoang, D. H., Kurzydło, P., Kwiatkowski, P., Imhof, R., Hassanzadeh, A., Pereira, L., Rudolph, M., (2023) “Application of pneumatic Imhoflot™ G-Cell in recovering fine particles: A case study of KGHM copper ore”, Proceedings of the Flotation 23, MEi Conferences.

Imhof, R., (1988) “Pneumatic flotation–a modern alternative”, Aufbereitungs Technik, 29 451–458.

Pyle, L., Tabosa, E., Vianna, S., Sinclair, S., Valery, W., (2022) “Future (and present) trends in circuit design”, IMPC Asia-Pacific, 1068-1083.

OPTIMIZATION OF APATITE DEPRESSION USING K–NA TARTRATE / $Al_2(SO_4)_3$ IN PHOSPHATE SLUDGES FROM DJEBEL ONK (ALGERIA)

Yousra BOUKHAMLA[1,*], Djamel NETTOUR[1], Mohamed CHETTIBI[2], Nesrine DERRARDJIA[1], Rachid CHAIB[3]

[1]National Higher School of Technology and Engineering, Mining, Metallurgy and Materials (L3M) Laboratory, 23005, Annaba, Algeria
[2]Laboratory of Mineral processing and Environment (LAVAMINE), Badji Mokhtar - Annaba University, P.O.Box 12, 23000 Annaba, Algeria
[3]Laboratory of Transports and Environment Engineering, Department of Transport Engineering, Mentouri Brothers University Constantine 1, Constantine 25000, Algeria.
**Corresponding author: y.boukhamla@etu.ensti-annaba.dz*

A B S T R A C T

The valorization of sludges generated during the processing of phosphate ore from Djebel Onk (Algeria) is investigated to reconcile metallurgical performance with environmental constraints. Multi-technique analyses (laser particle size, XRF, XRD,) confirm a matrix dominated by apatite, associated with calcite, dolomite, and quartz, while trace elements (heavy metals) remain below international limits. Selective desliming significantly reduces the clay–siliceous fraction and enriches the phosphatic phase. In reverse flotation, the use of sulfuric acid as a depressant, leads to poor selectivity due to Ca^{2+} release and the formation of surface $CaHPO_4$, which inhibits collector adsorption on apatite. Conversely, the combination of K–Na tartrate and aluminum sulfate, acting through cation complexation and pulp chemistry control, achieves a concentrate with 28.67% P_2O_5, and MgO and SiO_2 contents compliant with industrial specifications. These findings open the way for pilot-scale optimization and process water recycling.

Key words: *Phosphate sludge, reverse flotation, apatite; K–Na tartrate, mineral valorization*

1. INTRODUCTION

Phosphate ore is a vital non-renewable and non-recyclable natural resource widely used as a raw material in the production of phosphoric acid and fertilizers (Sis et al., 2003). It predominantly occurs in sedimentary deposits distributed across several countries, including Morocco, the United States, Algeria, Tunisia, and China. The quality of phosphate ore is strongly influenced by the presence of gangue minerals, which play a key role in determining its grade, commonly expressed as P_2O_5 content (Dong et al., 2021). In phosphoric acid production, high levels of dolomite negatively impact ore quality and result in increased reagent consumption (Ge et al., 2023). Similarly, in the fertilizer industry, market requirements typically demand phosphate concentrates with P_2O_5 content exceeding 30%, a CaO/P_2O_5 ratio lower than 1.6, and MgO content below 1% (Ruan et al., 2019).

Algeria is recognized as one of the major producers of high-grade phosphate ore, with an annual production of approximately 1,200 million tons. However, phosphate mining and processing operations, whether through dry or wet methods, generate considerable amounts of solid and liquid waste. It is estimated that nearly 20% of the daily production is discharged into nearby watercourses (Oued) in the form of sludge (Tahri et al., 2023). This not only represents a loss of valuable resources but also poses potential environmental challenges. Therefore, the present study aims to carry out a comprehensive characterization of phosphate sludge and to evaluate its valorization through flotation, with the objective of identifying optimal conditions for improving phosphate recovery from the sludge generated at the Djebel Onk processing plant.

2. MATERIAL AND METHODS

2.1. Material

For this study, approximately 150 L of phosphate sludge was collected from the desliming outlet. The collected sample was subsequently subjected to desliming at 38 µm to remove fine particles, followed by drying prior to flotation experiments.

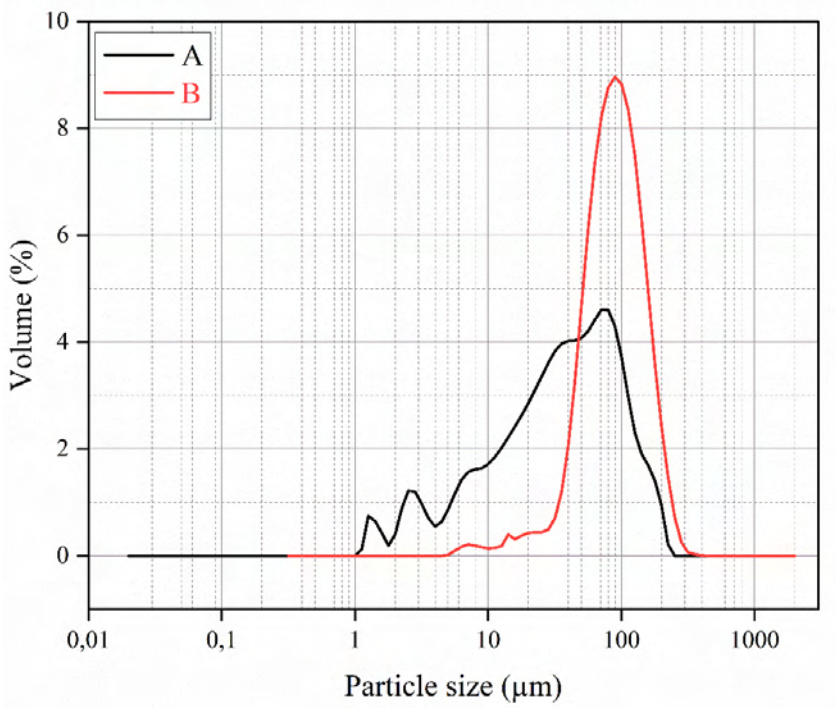

Figure 1. Particle size distribution of the raw and deslimed sample

2.2. Method

Following desliming, the samples were characterized in terms of particle size distribution using laser diffraction techniques. Mineralogical analysis was conducted by X-ray diffraction (XRD), while the chemical composition was determined using standard analytical methods. Thereafter, flotation tests were carried out under specific operating conditions, which are detailed in Table 1.

Table 1. Flotation conditions for phosphate sludge

N°	Experiment conditions			Chemical reagents (g/t)		
	% wt. solids	pH	flotation time (min)	Collectors	Depressants	Frother
01	21.4	4.5	3	Potassium oleate (1000)	Sulfuric acid (1000)	MIBC (10)
02	21.4	6.97	3	Potassium oleate (1000)	-	MIBC (10)
03	21.4	7.16	3	Na-K tartrate (1000) + Aluminum sulfate (500)	Potassium oleate (1000)	MIBC (10)

3. RESULTS AND DISCUSSION

3.1. X-ray Diffraction

The diffraction pattern is dominated by characteristic peaks of apatite (figure 2), mainly present as carbonate hydroxyapatite [$Ca_{10}(PO_4)_3(CO_3)_3(OH)_2$], indicating that it is the principal mineral phase. In addition, the presence of gangue minerals, including dolomite ($CaMg(CO_3)_2$) and quartz (SiO_2), is confirmed by their respective diffraction peaks. The relative intensities of these peaks suggest a significant proportion of carbonate minerals, which may adversely affect the efficiency of subsequent flotation processes.

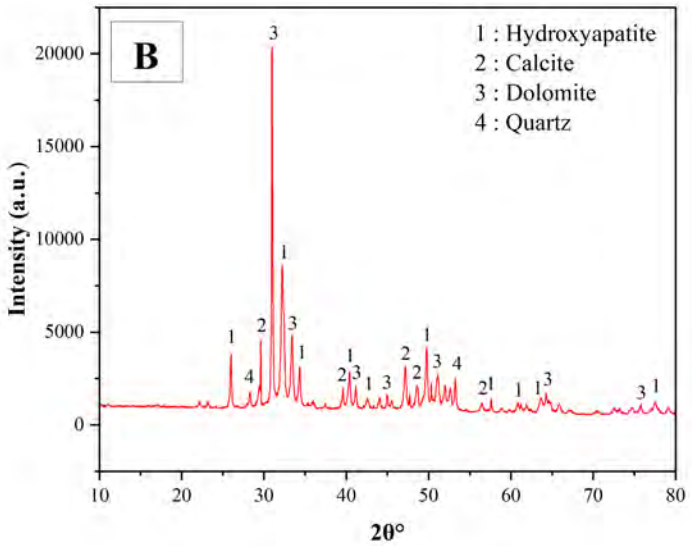

Figure 2. Results of X-ray diffraction analysis of deslimed sample

3.2. Chemical Analysis

Table 2 summarizes the chemical composition of the major oxides and selected heavy metals in both the raw sample and the deslimed sample. The results indicate that the P_2O_5 content, representing the valuable component, increased from 23.59% in the raw sample to 27.01% after desliming. In contrast, the contents of gangue-related oxides decreased significantly, with SiO_2 dropping from 10.95% to 2.30% and MgO from 3.05% to 2.85%.

These findings demonstrate that the removal of fine particles prior to flotation leads to a noticeable improvement in sample quality by enriching the valuable phosphate fraction. This pre-treatment step not only enhances the efficiency of subsequent beneficiation processes but also contributes to lowering operational costs and reducing the consumption of chemical reagents.

Table 2. Chemical analysis results of the raw and deslimed sample

E	P_2O_5 %	CaO %	MgO %	SiO_2 %	H_2O %	Fe_2O_3 %	Na_2O %
RS	23.59	38.92	3.05	10.95	1.95	0.61	1.08
DS	27.01	44.56	2.85	2.30	1.42	0.22	1.20
E	**K_2O %**	**LOI %**	**Cd $mg.kg^{-1}$**	**Zn $mg.kg^{-1}$**	**Cu $mg.kg^{-1}$**	**Pb $mg.kg^{-1}$**	**As $mg.kg^{-1}$**
RS	0.12	14.80	33	220	8	5	6
DS	0.08	14.30	25	180	6	4	5.5

**RS: Raw Sample, *DS: Deslimed Sample, E*: element*

3.3. Flotation Results

In the first experiment, sulfuric acid was used as a depressant for apatite; however, the results were unsatisfactory. The P_2O_5 grade in the concentrate decreased from 27.01% to 26.69%, while the tailings showed a higher content (27.47%), indicating poor selectivity. This behavior can be attributed to the partial dissolution of apatite, leading to the release of Ca^{2+} ions and the formation of $CaHPO_4$ layers on the surface$_4$ (Mohammadkhani et al., 2011), which alter its flotation behavior and may even enhance its floatability (El-Mofty et al., 2018).

In the second test, potassium oleate was applied as a collector for carbonates, followed by a cleaning stage. This approach improved the concentrate grade to 29.66%, although the recovery remained moderate (65.84%), likely due to fine particle entrainment and suboptimal pH conditions affecting selectivity.

In the third test, a mixture of sodium and potassium tartrate was used as a depressant, combined with aluminum sulfate as a pH regulator. This system yielded the best performance, achieving a concentrate grade of 28.67% and a high recovery of 97.80%. The improved efficiency is attributed to enhanced apatite depression and favorable pulp chemistry, resulting in effective separation and high selectivity.

Table 3. Flotation experiment results

Experiment	Type	P_2O_5 content (%)	P_2O_5 recovery (%)	MgO content (%)	MgO recovery (%)	SiO_2 content (%)	SiO_2 recovery (%)
01	F	27.47	73.89	2.45	82.19	1.97	33.82
	S	26.69	26.11	1.46	17.81	10.60	66.18
02	F_1	14.21	2.83	4.21	11.40	2.07	3.44
	F_2	26.25	31.33	2.85	46.30	2.19	21.83
	S	29.66	65.84	1.40	42.30	3.22	74.73
03	F	12.34	2.20	4.30	9.92	3.22	6.50
	S	28.67	97.80	2.04	90.80	2.42	93.50

4. CONCLUSION

This study investigated the characteristics and flotation behavior of phosphate sludge from ore processing. XRD and chemical analyses were applied to both raw and deslimed samples, providing detailed information on major and trace elements. Initial flotation tests using sulfuric acid as an apatite depressant were ineffective due to the interference of Ca^{2+} ions. Replacing sulfuric acid with a K-Na tartrate mixture combined with aluminum sulfate significantly improved apatite depression and selectivity demonstrating that the optimized flotation strategy enhances phosphate recovery while minimizing gangue contamination.

REFERENCES

Dong, L., Wei, Q., Jiao, F., Qin, W., (2021) “Utilization of polyepoxysuccinic acid as the green selective depressant for the clean flotation of phosphate ores”, Journal of Cleaner Production, 282 124532.

El-Mofty, S. E., El-Midany, A. A., (2018) “Role of calcium ions and their interaction with depressants in phosphate flotation” Chemical Papers, 72 (10) 2641-2646.

Ge, R., Yang, B., Martin, R., Luo, H., He, D., Arroyo, M. A. C., (2023) “The application of poly (sodium 4-styrene sulfonate) as an efficient dolomite depressant in the direct flotation of apatite from dolomite”, Powder Technology, 425 118583.

Mohammadkhani, M., Noaparast, M., Shafaei, S. Z., Amini, A., Amini, E., Abdollahi, H., (2011) “Double reverse flotation of a very low-grade sedimentary phosphate rock, rich in carbonate and silicate” International Journal of Mineral Processing, 100 (3-4) 157-165.

Ruan, Y., He, D., Chi, R., (2019) “Review on beneficiation techniques and reagents used for phosphate ores”, Minerals, 9 (4) 253.

Sis, H., Chander, S., (2003) “Reagents used in the flotation of phosphate ores: A critical review”, Minerals Engineering, 16 (7) 577-585.

Tahri, T., Narsis, S., Bezzi, N., Grairia, A., Benghadab, K. M., Benselhoub, A., (2023) “Environmental polluting effects of liquid wastes and phosphate sludge generated by the Djebel Onk mining complex” Journal of Geology, Geography and Geoecology, 32 (1) 178-184.

GEOLOGICAL STUDIES

ASSESSMENT AND CALCULATION OF HYDROGEOLOGICAL PARAMETERS OF THE AQUIFER IN THE SOUTHERN PART OF THE KOSOVO COAL BASIN

Sabri AVDULLAHI*

Faculty of Geosciences, University Isa Boletini in Mitrovica, Republic of Kosovo
**Corresponding author: sabri.avdullahi@umib.net*

A B S T R A C T

This study deals with the analysis of hydrogeological parameters of the aquifer in the southern area of the Kosovo Basin, with the aim of assessing the potential of groundwater resources and the possibilities of their sustainable use. The study was conducted in the southern area by combining geological, hydrogeological and experimental research methods through drilling and testing of wells. As part of the research, six test drillings were carried out, where the lithological conditions and hydraulic characteristics of the aquifers were analyzed. Through pumping tests and piezometric measurements, the main hydrogeological parameters such as transmissivity (T) and, hydraulic conductivity (K) were determined.

The results show that the aquifer of the study area has limited hydraulic permeability and moderated water reserves, which depend on the thickness of the alluvial layers and their lithological composition. The presence of low-permeability clays and the influence of tectonic formations make the groundwater circulation relatively slow.

In conclusion, the study provides a complete overview of the hydrogeological conditions of the Kosovo Basin and emphasizes the importance of continuous monitoring for water resources management, especially in the context of industrial developments and environmental impacts related to the exploitation of coalmines in this region.

Key words: *Hydrogeological parameters, aquifer, alluvial, drillings, testing*

1. INTRODUCTION

Numerous studies have shown that the accurate calculation of hydrogeological parameters is essential for the assessment and sustainable management of groundwater resources. Pumping tests remain the most widely used method for determining the transmissivity (T), hydraulic conductivity (K) particularly in unconfined and confined aquifers. Application of variable-rate pumping tests to estimate aquifer and storage conductivity and coefficients, demonstrating that this approach improves the accuracy of aquifer parameter estimation (Li et al., 2023).

The calculation of hydrogeological parameters constitutes the scientific basis for the assessment and management of groundwater resources. Pumping tests are the primary method for determining transmissivity and hydraulic conductivity (Freeze and Cherry, 1979). Other researchers also emphasize the importance of understanding flow in porous media for the correct interpretation of these parameters (Bear, 1979).

Analytical methods for pumping test analysis, such as the Theis and Cooper-Jacob methods, provide reliable results when the aquifer boundary conditions are properly defined (Kruseman and de Ridder, 1990), Test duration and consistent pumping rates are key factors in reducing uncertainty in estimating hydrogeological parameters (Fetter, 2001, Todd and Mays, 2005). The reliability of hydrogeological parameter calculations depends on the quality of pumping data, test duration, and boundary conditions, all of which directly influence the final results. In

alluvial and sedimentary aquifers, the influence of lithology has been emphasized by various authors, who demonstrated that layers with high clay content significantly reduce hydraulic conductivity (Domenico and Schwartz, 1998). Zhang et al. (2019) reinforced this conclusion by demonstrating that increasing clay content induces non-linear flow behavior and a reduction in transmissivity. Several studies have calculated hydrogeological parameters of shallow aquifers and confirmed the effectiveness of traditional pumping tests. The influence of stress and compression on the hydraulic conductivity of sedimentary materials, emphasizing the spatial variability of the parameters, was analyzed by Kaczmarek et al. (2023). Uncertainty analysis in the estimation of hydrogeological parameters which showed that errors in pumping test data directly affect the results was also addressed by Bashandy et al. (2024). Finally, emphasized the influence of lithology and well performance on the accurate evaluation of hydrogeological parameters (Sobri et al., 2021).

2. STUDY AREA

The study area is located within the coal basin of the Kosovo Plain, specifically within the territory of the municipalities of Fushe Kosove and Obiliq. It extends over a predominantly flat terrain, with an average elevation ranging from approximately 530 to 670 m above sea level, and includes areas such as Lismir, Sibovc, Hade, and Shipitull (Figure 1). The area is characterized by the presence of a surface hydrological network, particularly the Sitnica River and the Drenica River, which play an important role in the recharge and circulation of groundwater in this region (Avdullahi et al., 2008).

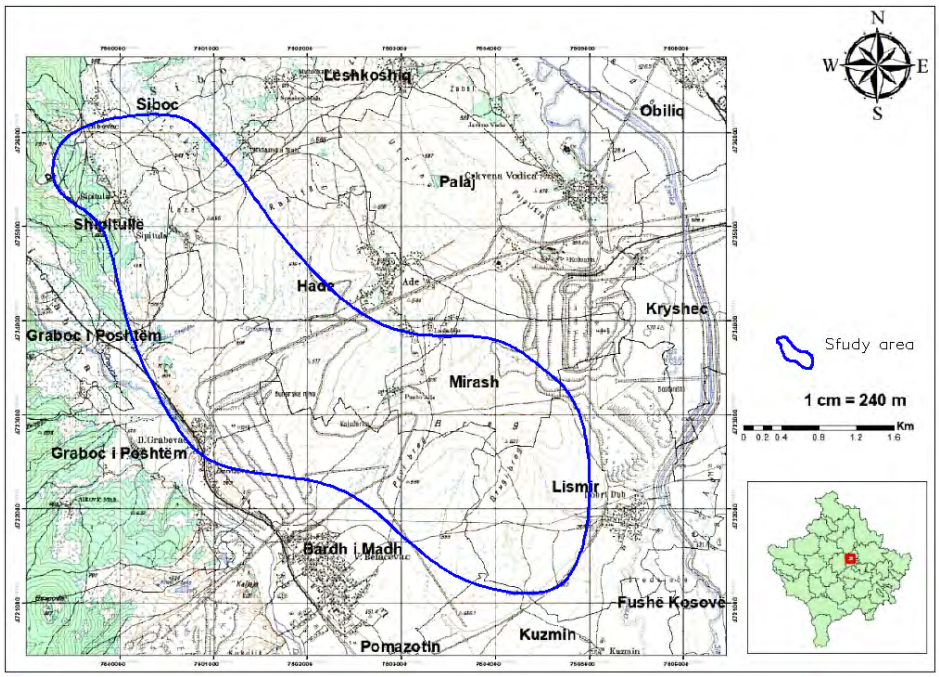

Figure 1. Topographic map of the study area

The study area is part of the coal basin of the Kosovo Plain, which represents a tectonic structure formed during the Oligocene and infilled predominantly with sedimentary deposits during the Pliocene. From a structural perspective, the basin belongs to the Dinaride-Albanide-Hellenide tectonic belt, specifically the Vardar Zone, and is characterized by a complex geological framework involving formations of Paleozoic, Mesozoic, and Cenozoic age (Figure 2).

The oldest formations are represented by Paleozoic metamorphic rocks, which occur mainly in the mountainous areas surrounding the basin and act as the structural basement. These are

overlain by Mesozoic formations composed of volcanogenic–sedimentary sequences, ultrabasic massifs, and Cretaceous carbonate deposits, which appear as erosional windows along the margins and within the interior of the basin (Ymeri, 2003). Cenozoic sediments, particularly those of Neogene age, constitute the main infill of the basin and include lacustrine clayey, sandy, and marly deposits, above which Quaternary alluvial, proluvial, and terrace deposits have developed (Huertas et al., 2012).

From a hydrogeological perspective, the area is characterized by complex groundwater circulation conditions influenced by lithology, tectonics, and the presence of surface waters. The main aquifers are associated with alluvial and proluvial deposits composed of sands and gravels, which exhibit relatively good permeability and are recharged primarily by atmospheric precipitation and surrounding rivers, particularly the Sitnica and Drenica rivers. In contrast, clayey formations and compact rocks act as hydrogeological aquitards, limiting vertical groundwater flow (Peci et al., 2012).

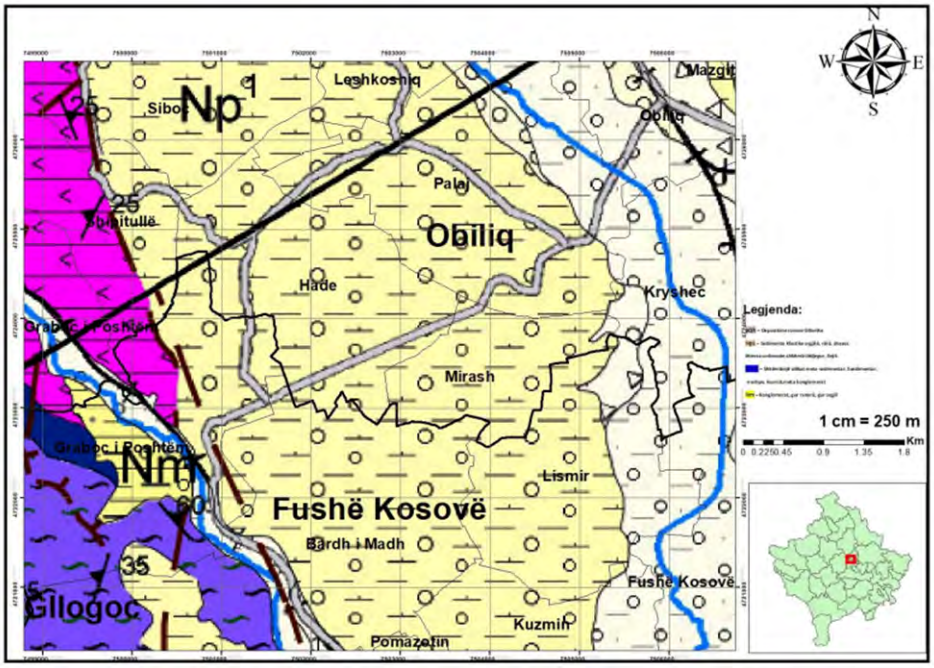

Figure 2. Geological map of study area

The interaction of groundwater with active tectonic structures and the surface hydrological network is of particular importance for mining activities in the area, as it directly affects the amount of water infiltrating the coal deposit and the need for controlled water management during exploitation.

3. MATERIAL AND METHODS

In the initial phase, data from previous investigations were analyzed, including geological and hydrogeological maps, technical reports, and documentation from existing boreholes, which served as the basis for planning fieldwork and interpreting the results. Field investigations included the drilling of six exploratory hydrogeological boreholes, which were advanced down to the roof contact of the coal-bearing strata (Figure 3).

As part of the experimental investigations, well tests were conducted using pumping methods, including measurements of static and dynamic groundwater levels, as well as monitoring water-level recovery after pumping cessation. Water-level meters, controlled-capacity pumps, and auxiliary equipment for hydraulic data recording were used for these measurements.

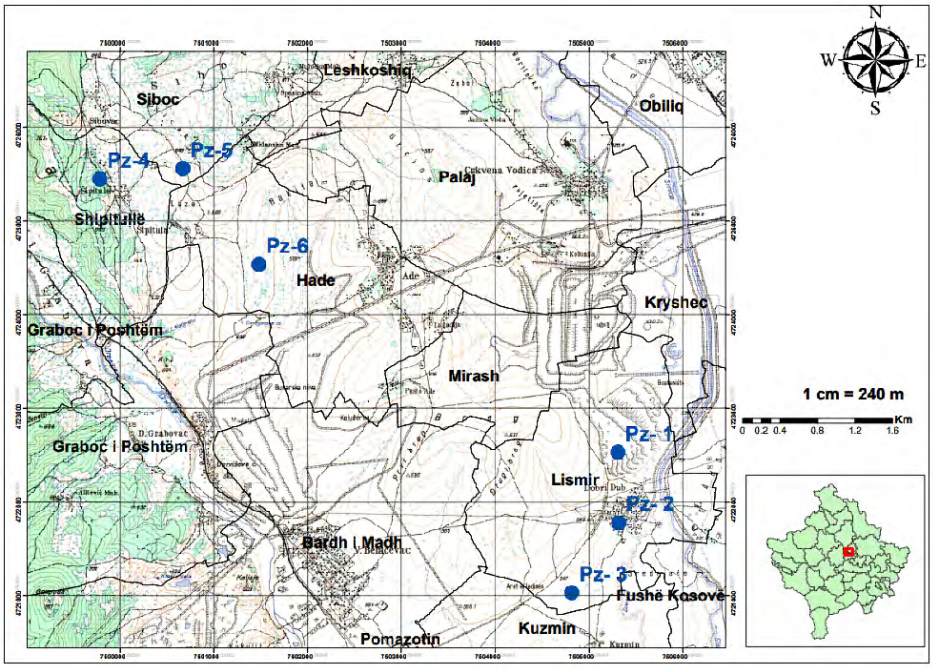

Figure 3 The map of the drilling locations

The calculation of aquifer hydraulic parameters has a very important role in the sustainability and management of groundwater (Sethi, 2011). The application of pumping tests is an effective method for assessing the hydraulic parameters of aquifers and wells, including transmissivity , hydraulic conductivity (Li et al., 2021; Alqarawy, 2023).

The measurements of T can be carried out according to (Jacob, 1950; Kruseman and de Ridder, 1990). The pumping test data applied to the study area were interpreted using the testing software and calculations were performed using Equations 1 and 2:

$$T = 2.3\ Q/4\pi\ \Delta s \qquad \text{(Eq.1)}$$

$$K = T/B \qquad \text{(Eq. 2)}$$

where:

Q - is the discharge rate (m^3),
T - is the aquifer transmittance (m^2/day),
Δs - is the slope of a straight line per logarithmic cycle of a single logarithmic graph,
B - is the aquifer thickness (m).

4. RESULTS AND DISCUSSION

In this study, a total of six (6) exploratory wells, designated as Pz-1, Pz-2, Pz-3, Pz-4, Pz-5, and Pz-6, were analyzed. These wells are distributed across the study area according to the geological and hydrogeological conditions of the terrain. For each well, the results of experimental pumping tests were evaluated, including static and dynamic groundwater levels as well as drawdown during pumping.

Based on these data, the main hydrogeological parameters were calculated and interpreted, specifically the transmissivity (T), hydraulic conductivity (K), which are used to assess the water-bearing capacity and hydraulic behavior of the aquifers in the study area.

Table 1. Calculation of hydraulic parameters

Wells	T (m²/day)	K (m/s)
Pz-1	0.30	2.40×10^{-6}
Pz-2	5.75	1.10×10^{-5}
Pz-3	18.30	4.23×10^{-5}
Pz-4	4.37	8.40×10^{-7}
Pz-5	3.36	2.30×10^{-6}
Pz-6	4.05	2.10×10^{-6}

The table 1 presents the transmissivity (T) and hydraulic conductivity (K) values for the six exploratory wells (Pz-1 to Pz-6). The data indicate a clear variability in hydrogeological properties across the study area. Well Pz-3 exhibits the highest transmissivity (18.30 m²/day) and hydraulic conductivity (4.23×10^{-5} m/s), reflecting a highly permeable aquifer section likely composed of coarse sandy-gravelly materials, making it the most suitable for water supply. Wells Pz-2 and Pz-4 also show relatively high values (T = 5.75 m²/day and 4.37 m²/day; K = 1.1×10^{-5} m/s and 8.4×10^{-7} m/s), though Pz-4 has notably lower K, indicating reduced permeability despite moderate transmissivity.

The remaining wells (Pz-1, Pz-5, and Pz-6) have lower transmissivity and hydraulic conductivity (T = 0.30–4.05 m²/day; K = 2.1×10^{-6}–2.4×10^{-6} m/s), suggesting the dominance of less permeable layers, likely with higher clay content. Overall, these results highlight the hydrogeological heterogeneity of the area, with implications for groundwater flow, aquifer recharge, and water supply potential, indicating that careful selection of well locations is critical for efficient water extraction.

In contrast, wells Pz-1, Pz-4, Pz-5, and Pz-6 are characterized by lower filtration coefficient values, indicating the dominance of clay-rich layers with limited permeability. In these areas, groundwater circulation is slower and water-yielding capacity is lower, causing these layers to act partially as hydrogeological aquitards. The analysis of static and dynamic groundwater levels shows that pumping causes significant drawdown, particularly in wells with lower permeability, where water-level recovery is slower. This behavior confirms the direct influence of lithological properties on the aquifer's response to pumping.

Overall, the results of well testing and groundwater-level measurements provide a solid basis for evaluating the hydrogeological conditions of the area and for planning groundwater management measures during mining activities. The integration of these data is essential for minimizing technical risks and ensuring the sustainable use of water resources in the study area.

5. CONCLUSION

The results of the exploratory boreholes (Pz-1 to Pz-6) show significant variability in depth, thickness, and lithological composition. Wells Pz-3 and Pz-2 represent areas with higher hydraulic permeability (K up to 4.23×10^{-5} m/s), making them suitable for water supply. In contrast, Pz-4 and Pz-1 exhibit lower values, characterizing them as aquifers with limited transmissivity.

Analyses of piezometric levels revealed pronounced seasonal variations. Groundwater levels rise during the warmer seasons (spring–summer) and decline in winter, reflecting an open hydrogeological system with natural recharge dependent on precipitation and surface infiltration. The hydraulic coefficients (K and T) indicate significant horizontal and vertical heterogeneity within the aquifer. This heterogeneity results from lithological variability and the tectonic structure of the area, which influences the water-bearing capacity of the layers. The

results indicate that the aquifer in the Lismir-Sibovc-Hade area has a mixed character - partially phreatic in shallow layers and partially confined at greater depths - with considerable potential for local use, particularly for technological needs and agricultural irrigation.

REFERENCES

Alqarawy, A., (2023) “Characterization of groundwater in Quaternary aquifer of the Yanbu Al-Nakhl Basin, Al-Madinah Al-Munawarah Province using pumping tests and hydrochemical techniques”, Arabian Journal of Chemistry, 16 105327

Avdullahi, S., Fejza, I., Syla, A., (2008) “Water resources in Kosova”, Journal of International Environmental Applica-tion & Science (JIEAS), 3 (6) 51-56.

Bashandy, A. M., Bekhit, H. M., Radwan, H. G., (2024) “Uncertainty assessment of aquifer hydraulic parameters from pumping test data”, Applied Water Science, 14 84.

Bear, J., (1979), Hydraulics of groundwater, McGraw-Hill series in water resources and environmental engineering. McGraw-Hill, New York.

Domenico, P. A., Schwartz, F. W., (1998), Physical and Chemical Hydrogeology (2nd ed.). New York: John Wiley & Sons, Inc.

Fetter, C. W., (2001), Applied Hydrogeology. 4th Edition, Prentice Hall, Upper Saddle River.

Freeze, R. A., Cherry, J. A., (1979), Groundwater. Prentice-Hall Inc., Englewood Cliffs, Vol. 7632 604.

Huertas, J. I., Camacho, D. A., Huertas, M. E., (2012) “Standardized emissions inventory methodology for open-pit mining areas”, Environmental Science and Pollution Research, 19 2784–2794

Jacob, C. E., (1950), Flow of groundwater in engineering hydraulic. John Wiley and Sons, New York, 321–386.

Kaczmarek, Ł., Grodzka-Łukaszewska, M., Sinicyn, G., Grygoruk, M., Jastrzębska, M., Szatyłowicz, J., (2023) “Hydraulic Conductivity Tests in the Triaxial Stress State: Is Peat an Aquitard or an Aquifer? Water, 15 (6) 1064.

Kruseman, G. P., De Ridder, N. A., (1990), Analysis and evaluation of pumping test data, 2nd edn. Inter. Instit. For Land Recl. Improv (ILRI), Netherlands, 377.

Li, Y. H., Shao, J., Zhan, G., Zhou, R., (2023) “The Impact of Enterprise Digital Transformation on Financial Performance-Evidence from Mainland China Manufacturing Firms”, Managerial and Decision Economics, 44 2110-2124.

Li, Y., Zhou, Z., Zhuang, Ch., Dou, Z., (2021) “Estimating Hydraulic Parameters of Aquifers Using Type Curve Analysis of Pumping Tests with Piecewise-Constant Rates”, Water, 15 1661.

Peci, N., Shala, B., Hajra, H., Baruti, B., (2012) “Spatial analysis of the Drenica coal basin – field Skenderaj, Kosovo”, 12th GeoConference SGEM, Bulgaria.

Sethi, R., (2011) “A dual-well step drawdown method for the estimation of linear and non-linear flow parameters and wellbore skin factor in confined aquifer systems”, Journal of Hydrology, 400 187–194.

Sobri, M. S., Abd Malik, A. K., Md Dan, M. F., Hussin, H., Alshameri, B., (2021) “Assessment of Tube Well Pumping Test Performance on Different Geological Formation”, Journal Sustainable Underground Exploration, 1 (1) 25-31.

Todd, D., Mays, L. (2005), Groundwater Hydrology. 3rd Edition, John Wiley and Sons, Inc., Hoboken, 652.

Ymeri, A., (2003) “Stratigraphy of Neocene deposits and the tectonic characteristics of Kosova cool bearing Basin”, 20 (2) 5-16.

Zhang, X., Zhang, Y., Ijiri, D., Kanda, R., Ohtsuka, A., (2019) “Effect of feeding a dry-heat-processed sweet potato waste on the growth performance and meat quality of broilers”, Nihon Danchi Chikusan Gakkaiho, 62 (2) 107-114

CHARACTERIZATION AND PROCESSING OF VOLCANIC ROCKS FROM MONTENEGRO FOR USE AS INDUSTRIAL RAW MATERIALS

Ljiljana TANKOSIĆ[1,*], Alen ŠTULIĆ[2]

[1]University of Banja Luka, Faculty of Mining Prijedor, Aleja Kozarskog odreda No 1 ,79101 Prijedor, Bosnia and Herzegovina
[2]D.O.O. Muriz Bar, Mila Boškovića No 18, 85000 Bar, Montenegro
**Corresponding author: ljiljana.tankosic@rf.unibl.org*

A B S T R A C T

Volcanic rocks from several locations in southern Montenegro (Brčelice, Crni Krš, Bukovik, Kufi, and Đurmani) were studied within the framework of a regional geological project, with the aim of evaluating their petrographic, chemical, and physical-mechanical properties in the context of their potential application in industrial mineral processing. Special emphasis was placed on their suitability for comminution, separation, and further processing into technical stone and industrial aggregates.

Based on petrographic and chemical analyses, the rocks were classified as andesites and dacites. The chemical composition shows SiO_2 contents ranging from 55.7% to 69.6%, while the sum of $Na_2O + K_2O$ ranges from 6.1% to 10.4%, confirming their classification as intermediate to acidic volcanic rocks.

Testing of the physical-mechanical properties revealed low porosity (0.78–0.83%), high bulk density (approximately 2720 kg/m³), and excellent resistance to frost, abrasion, and dynamic impact. Compressive strength, flexural strength, and impact resistance indicate a high degree of durability, making these rocks suitable for mechanical processing—crushing, screening, and use in various aggregate fractions.

The results suggest that these volcanic rocks are highly suitable for use as raw material in the production of graded aggregate for roads, hydraulic structures, cement concrete, and other construction and industrial applications. As such, they represent a valuable local resource for the future development of the mineral processing industry in the region.

***Key words**: Crushing, processing, mineral raw materials, volcanic rocks, particle size reduction, mineral preparation, construction materials, mineral beneficiation*

1. INTRODUCTION

Volcanic rocks, such as andesite and dacite, are widely used as industrial raw materials due to their favorable mineralogical, physical, and chemical properties. They are commonly applied in construction aggregates, technical stone, road materials, and industrial fillers, with performance in crushing, screening, and classification suitable for large-scale industrial use.

Increasing demand for high-quality construction materials highlights the importance of characterizing local resources, which supports economic efficiency and sustainable development by reducing transport and environmental impacts. Volcanic rocks in southern Montenegro represent a significant but underexplored resource for mineral processing.

Their industrial suitability depends on mineralogical composition, silica and alkali content, porosity, density, strength, and resistance to frost and abrasion, which affect comminution behavior and end-use performance. Comprehensive laboratory testing is therefore essential to evaluate processing behavior and potential applications.

This study systematically investigates volcanic rocks from Brčelice, Crni Krš, Bukovik, Kufi, and Đurmani within a regional geological project. Special focus was given to mineral processing characteristics, including particle size reduction, separation, and production of graded aggregates.

The main objective is to assess the applicability of Montenegrin andesitic and dacitic rocks for construction and industrial use, evaluating their mechanical processing behavior and potential as a reliable local resource for regional mineral processing development (Korać, M. et al., 2018.)

2. GEOLOGICAL SETTING AND OCCURRENCE OF VOLCANIC ROCKS IN MONTENEGRO

Volcanic rocks in Montenegro are mainly found in the northern and northeastern regions (Bjelasica, Visitor, Sjekirica, Ljubišnja, Krnja Jela) with smaller occurrences in central (Nikšić Župa, Piva) and southern Montenegro (Crmnica, Sozina, Rumija slopes). These formations include andesites, dacites, diabases, spilites, rhyolites, and occasionally serpentinites, along with pyroclastic equivalents such as tuff, ash, volcanic bombs, and agglomerates. Mineralogically, they consist of quartz, feldspars, and mafic minerals, which determine their physical-mechanical properties and industrial potential.

Despite wide distribution, volcanic rocks in Montenegro have been poorly studied regarding their use as architectural or construction stone. Currently, no magmatic stone deposits are commercially exploited for architectural purposes, as existing architectural stone is carbonate-based. Regional studies suggest that certain volcanic rocks could serve as high-quality technical and architectural construction materials. Potential reserves are substantial but underexplored in terms of processing and industrial applicability.

At present, only one producer of volcanic-origin technical construction stone operates near Okrugličkі krš–Štitarica (Mojkovac). With growing demand for high-performance volcanic aggregates, particularly for roads and railways, exploiting these resources could reduce dependence on imported silicate aggregates, support domestic mineral processing, and provide feedstock for value-added applications (Korać, M. et al., 2018.).

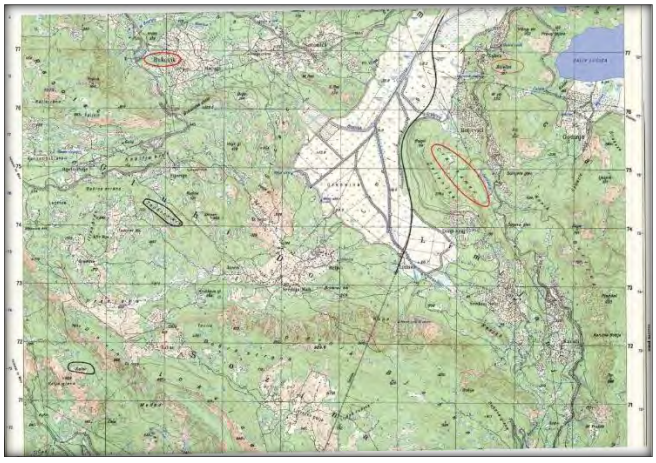

Figure 1. Sampling sites of volcanic rocks in southern Montenegro with potential for industrial aggregate production (Virpazar sheet, scale 1:250,000) (Mirković, M. et al, 1978)

3. MATERIALS AND METHODS

3.1. Studied Locations and Sampling

Within the framework of a regional geological project, volcanic rocks from several locations in southern Montenegro were investigated. Detailed sampling for petrographic, chemical, and physical-mechanical testing was conducted at the Bukovik, Crni Krš, Brčelice and Kalac sites. Additional petrographic analyses were performed on samples collected from the Kufin and Đurmani areas.

Representative block samples and cubic specimens (Picture 2) were collected for comprehensive laboratory testing, including petrographic characterization, chemical analysis, and determination of physical-mechanical properties relevant to mineral processing and construction applications.

Figure 2. Andesite sample from the Kalac locality near Bar, Montenegro (photo: Alen Štulić)

3.2. Pterographic and Chemical Characterization

Petrographic investigations were performed using standard optical microscopy on thin sections, enabling mineral identification, textural analysis, and assessment of alteration processes. Chemical composition was determined using standard analytical procedures, with particular attention paid to SiO_2 content and total alkali content ($Na_2O + K_2O$), which are critical for volcanic rock classification and assessment of industrial suitability.

Based on combined petrographic and chemical criteria, the investigated rocks were classified as andesites and dacites, corresponding to intermediate to acidic volcanic rocks (Manojlović, M.2001.), .

4. RESULTS AND DISCUSSION

4.1. Petrographic Characteristics of Selected Localities

Brčelice

The volcanic rocks from the Brčelice locality are compact, grey-green to dark-green rocks with porphyritic structure and massive texture. They consist of plagioclase and pyroxene phenocrysts embedded in a holocrystalline porphyritic groundmass with fluidal microtexture. Plagioclases are commonly altered and display lamellar twinning, while pyroxenes are largely transformed into secondary minerals. Based on petrographic observations and chemical composition (SiO_2 = 55.71%, $Na_2O + K_2O$ = 6.15%), these rocks were classified as andesites.

Table 1. Chemical composition of Brčelice volcanic rock samples, relevant for classification and processing as industrial aggregate

	SiO_2 (%)	Al_2O_3 (%)	Fe_2O_3 (%)	MgO (%)	CaO (%)	Na_2O (%)	K_2O (%)	TiO_2 (%)	P_2O_5 (%)
BR/22	55,71	17,36	8,01	1.66	3,87	2,94	3,75	0,81	0,17

Bukovik

Rocks from the Bukovik area are light-grey, porphyritic, and locally hydrothermally altered. They contain plagioclase phenocrysts, rare amphiboles and biotite, and a microcrystalline groundmass enriched with quartz and chalcedony filling vesicles. Chemical analysis indicates a high SiO_2 content (69.60%) and elevated alkali content ($Na_2O + K_2O$ = 10.42%), consistent with dacitic composition. Increased silica and alkali contents are attributed to secondary silicification and alteration processes.

Table 2. Chemical composition of Bukovik volcanic rock samples, relevant for classification and processing as industrial aggregate

	SiO_2 (%)	Al_2O_3 (%)	Fe_2O_3 (%)	MgO (%)	CaO (%)	Na_2O (%)	K_2O (%)	TiO_2 (%)	P_2O_5 (%)
BU/22	69,60	14,80	1,93	0,17	0,15	0,58	9,84	0,13	0,04

Crni Krš.

Volcanic rocks from the Crni Krš locality are dark grey-green, porphyritic, and partially altered. They are composed of plagioclase and mafic phenocrysts within a micro- to cryptocrystalline groundmass. Chemical analysis (SiO_2 = 61.58%, $Na_2O + K_2O$ = 6.56%) confirms classification as andesite.

Table 3. Chemical composition of Crni Krš volcanic rock samples, relevant for classification and processing as industrial aggregate.

	SiO_2 (%)	Al_2O_3 (%)	Fe_2O_3 (%)	MgO (%)	CaO (%)	Na_2O (%)	K_2O (%)	TiO_2 (%)	P_2O_5 (%)
CK/22	61,58	16,69	5,65	1,23	2,93	4,03	2,53	0,64	0,21

4.2. Physical-Mehanical Properties

Laboratory testing revealed highly favorable physical-mechanical characteristics of the investigated volcanic rocks. Bulk density values ranged from 2715 to 2722 kg/m³, while particle density values ranged from 2727 to 2739 kg/m³, indicating a compact and dense material. The coefficient of compactness ranged from 0.994 to 0.996, and absolute porosity was very low, averaging between 0.78% and 0.83%.

Water absorption values were low (0.26–0.33%), consistent with the low porosity and high compactness of the rock. All samples exhibited excellent resistance to frost action, showing no visible damage after freeze–thaw cycles and sodium sulfate testing.

Abrasion resistance determined by the Böhme method yielded favorable values (13.2–14.5 cm³/50 cm²). Mechanical strength tests demonstrated satisfactory compressive strength under

dry, saturated, and freeze–thaw conditions, as well as adequate flexural strength (10.1–11.3 MPa). Impact resistance (Treton method) and Los Angeles abrasion values (16.9–17.7) further confirm the suitability of these rocks for aggregate production and intensive mechanical processing (Manojlović, 2001).

5. INDUSTRIAL APPLICATION POTENTIAL

Based on laboratory test results and compliance with relevant technical standards, the investigated volcanic rocks are suitable for use as technical construction stone for the production of both graded and ungraded aggregates. Potential applications include mechanically stabilized base layers, bituminous mixtures, cement concrete, hydraulic engineering structures, and masonry in both low-rise and high-rise construction.

In addition, favorable chemical and petrographic characteristics indicate potential applicability in other industrial sectors. The large, yet underexplored, reserves of volcanic rocks in Montenegro represent an important opportunity for sustainable development of domestic mineral resources and reduction of reliance on imported raw materials.

5.1. Mineral Processing Aspects and Processing Scheme Considerations

The investigated volcanic rocks are well suited for processing using standard mineral processing technologies applied in aggregate production. Due to their high mechanical strength and abrasion resistance, primary crushing using jaw or gyratory crushers can be applied efficiently, followed by secondary and tertiary crushing in cone or impact crushers, depending on the required final particle size distribution.

Screening operations enable the production of both ungraded and graded aggregate fractions suitable for road construction, concrete production, and hydraulic engineering applications. The favorable Los Angeles abrasion values indicate good resistance to degradation during handling and transport, which is critical for maintaining aggregate quality throughout the processing chain.

Given the low water absorption and compact structure of the rocks, washing and classification processes can be applied where necessary, without significant material losses. Furthermore, the chemical stability and low sulfate content allow the use of these aggregates in cement-based materials without risk of harmful chemical reactions.

The results suggest that future research should focus on optimizing comminution parameters, evaluating energy consumption during crushing, and assessing the long-term performance of aggregates produced from these volcanic rocks under real service conditions.

6. CONCLUSIONS

Based on the comprehensive petrographic, chemical, and physical-mechanical characterization of volcanic rocks from southern Montenegro, it can be concluded that these materials possess highly favorable properties for use as industrial mineral raw materials. The investigated rocks, classified as andesites and dacites, exhibit high compactness, low porosity, low water absorption, and excellent resistance to frost, abrasion, and dynamic loading.

The obtained results indicate that the volcanic rocks demonstrate very good behavior during mechanical processing operations. High resistance to crushing and abrasion, as confirmed by Los Angeles and Böhme test results, suggests their suitability for intensive comminution

processes without excessive generation of fines. This makes them particularly appropriate for the production of graded aggregates with stable granulometric composition.

From a mineral processing perspective, the physical-mechanical properties of the investigated rocks enable efficient processing through conventional crushing and screening circuits. The low porosity and high density contribute to predictable fragmentation behavior, reduced energy losses during particle size reduction, and consistent aggregate quality. These characteristics are especially important for applications requiring high-performance aggregates, such as heavily loaded road pavements, hydraulic engineering structures, and railway infrastructure.

In addition to their technical suitability, the investigated volcanic rocks represent a significant local resource with considerable economic and strategic importance. The exploitation and processing of these materials could reduce dependence on imported silicate aggregates, support the development of the domestic mineral processing industry, and contribute to sustainable use of mineral resources in Montenegro.

Overall, the results of this study confirm that volcanic rocks from southern Montenegro have strong potential for wide industrial application and justify further detailed investigations focused on optimization of processing flowsheets and large-scale production conditions.
Future work should focus on pilot-scale crushing and screening trials, evaluation of energy consumption, and performance testing of aggregates under real-life loading conditions.

REFERENCES

Korać, M., Milić, V., Lacman, R., Pajović, M., Radusinović, S., Božović, D., (2018), Državni plan eksploatacije mineralnih sirovina za period 2019–2029 godine, Ministry of Economy, Directorate for Mining and Geological Research, Podgorica, Montenegro.

Manojlović, M., (2001), Izvještaj o rezultatima prospekcije tehničko-građevinskog kamena (vulkanita) u južnom dijelu Republike Crne Gore, Geological Survey of Montenegro, Podgorica.

Mirković, M., Kalezić, M., Pajović, M., Živaljević, M., Škuletić, D., (1978), Basic Geological Map of SFR Yugoslavia, Sheet Bar and Ulcinj, Scale 1:100,000 (K 34-63 and K 34-75), Federal Geological Survey, Belgrade.

DETECTION OF ORE DEPOSITS USING IMAGE PROCESSING TECHNIQUES, WEST OF ELAZIĞ (TURKEY)

İmren Sumru TOSUN[1], Melek URAL[1,*], Mustafa EĞRİ[2]

[1]Firat University, Faculty of Engineering, Department of Geological Engineering, 23119, Elazığ,TURKEY
[2]Pamukkale University, Faculty of Engineering, Geological Department, 20020, Denizli,TURKEY
**Corresponding author: melekural@firat.edu.tr*

A B S T R A C T

The study area is located in the eastern part of Keban District, in the west of Elazığ Province. In the studied area, the presence of various types of mineralization is known, including contact metamorphic, hydrothermal, and disseminated types. Metamorphic units cut by intrusive rocks have led to the formation of mineralized zones through contact metamorphic effects in the contact zones. The ore bearing zones have developed primarily in magmatic contacts. The mineralized zones in the study area were analyzed using the minimum noise fraction method. The detection of mning areas were made to discover by collecting data in the visible to near and shortwave infrared wavelength regions. All of the analyses were performed by the Aster band images. The SWIR 1, 2, 3, 4, 5, 6, 7, 8, and 9 bands and the VNIR 1, 2, and 3 bands were analyzed using the minimum noise fraction method. As a result, in this area, it was observed that a correlation of over 70% was achieved by combining processed satellite data with validated ground-truth data. It was determined that the images obtained by combining (SWIR Band 5 / VNIR Band 3) + (VNIR Band 1 / VNIR Band 2) with the method of minimum noise fraction (MNF) provided the best representation for identifying Ore Deposits in the region.

Key words: *Elazığ, ore deposits, image processing, band combination*

1. INTRODUCTION

Remote sensing images are used for mineral exploration in two applications: (1) map geology and the faults and fractures that localize ore deposits; (2) recognize hydrothermally altered rocks by their spectral signatures (Sabins, 1999). Remote sensing technology is a greatly applicable tool for regional geological mapping and ore mineral exploration at a low cost (Pour et al., 2023). There are numerous deposits and occurrences of metallic minerals in Elazığ Province and its immediate vicinity. In the vicinity of northwest of Elazığ, deposits of galena (lead sulfide) are found, while in the vicinity of Keban (Figure 1), an iron mine was once in operation. It is important to explore and exploit all these mineral deposits using both conventional and technological methods; in recent years, significant progress has been made in exploration through the use of remote sensing and image processing techniques. For this purpose, to identify the most characteristic iron occurrences in the region, image enhancement studies were performed on the VNIR and SWIR bands of ASTER satellite images, and composite images were created. In this context, the iron indices and band algorithms mentioned in the literature on remote sensing were applied sequentially.

Figure 1. The location of the study area on Google Maps (URL-1)

2. MATERIAL AND METHODS

2.1. Material

The area around Keban district in the northwestern part of Elazığ Province has been designated as the target area (Figure 2). The ASTER (AST_L1T_00303052001083742_20150501094600_59519) image (URL-2; Figure 1) was cropped to match this study area, and the entire study was conducted using this dataset. The dataset used is a daytime image product from the ASTER image with a timestamp of March 5, 2001, at 08:37:42, featuring less than 10% cloud cover (URL-2; Figure 1). The image was selected as a two tile to cover the study area (Figure 2).

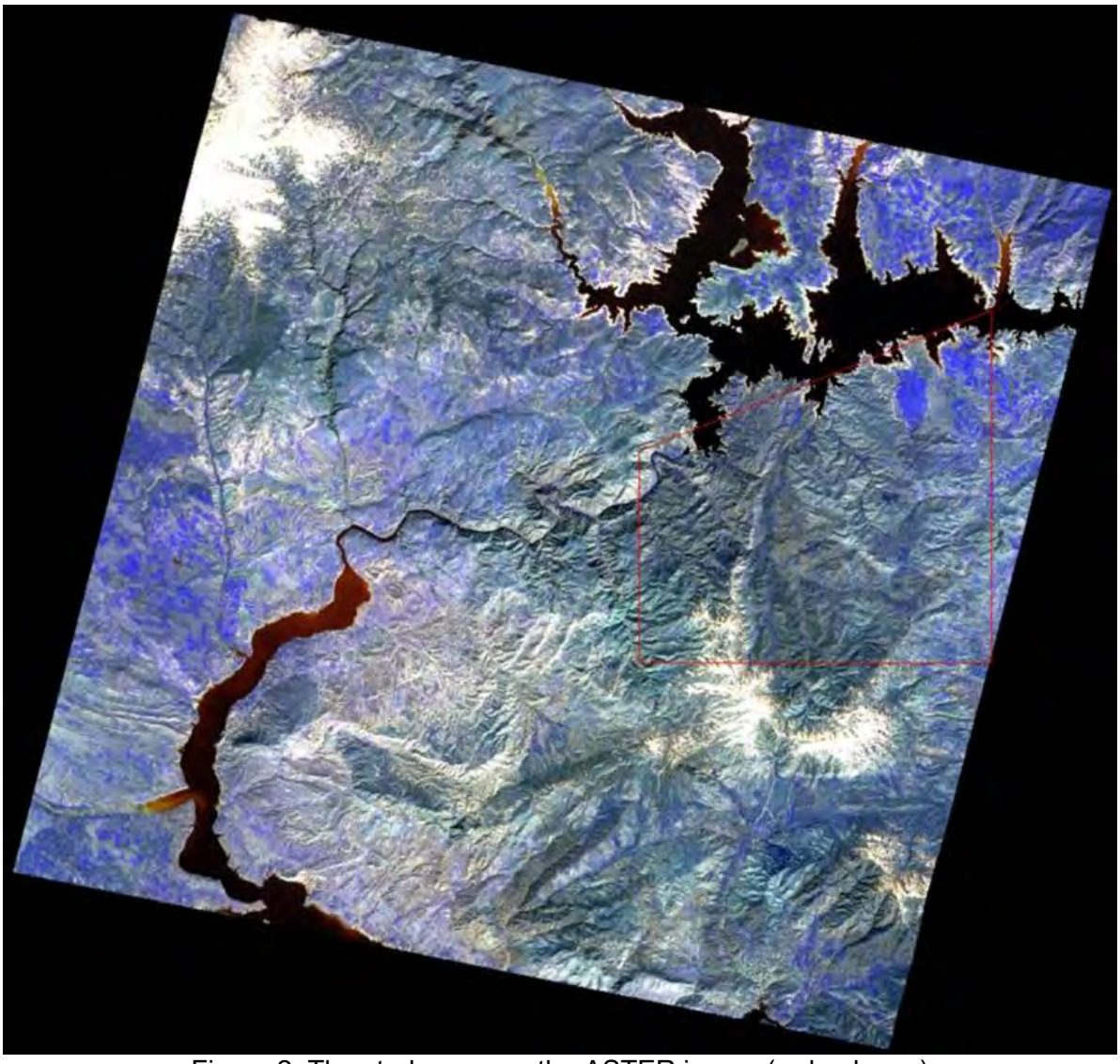

Figure 2. The study area on the ASTER image (red polygon)

2.2. Method

The detection of Ore Deposits were made to discover by collecting data in the visible to near and shortwave infrared (VNIR-SWIR) wavelength regions. All of the analyses were performed by the ASTER band images (Figure 3). The SWIR 1, 2, 3, 4, 5, 6, 7, 8, and 9 bands and the VNIR 1, 2, and 3 bands were analyzed using the minimum noise fraction method. Radiometric and Atmospheric corrections were applied to the dataset, and spectral anomalies were minimized to segregate noise from data (Figure 4).

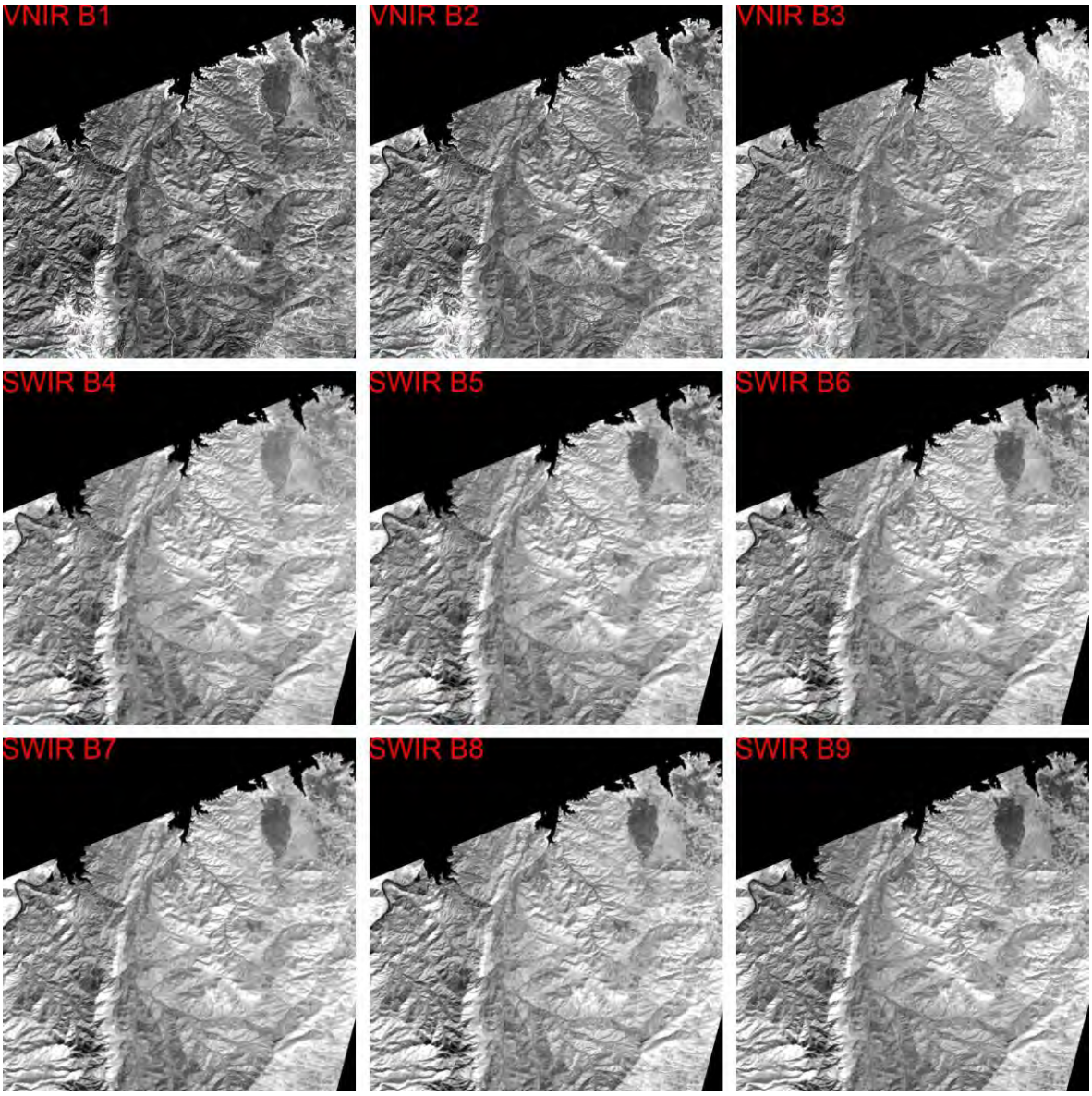

Figure 3. The VNIR and SWIR bands in the ASTER dataset, cropped according to the study area

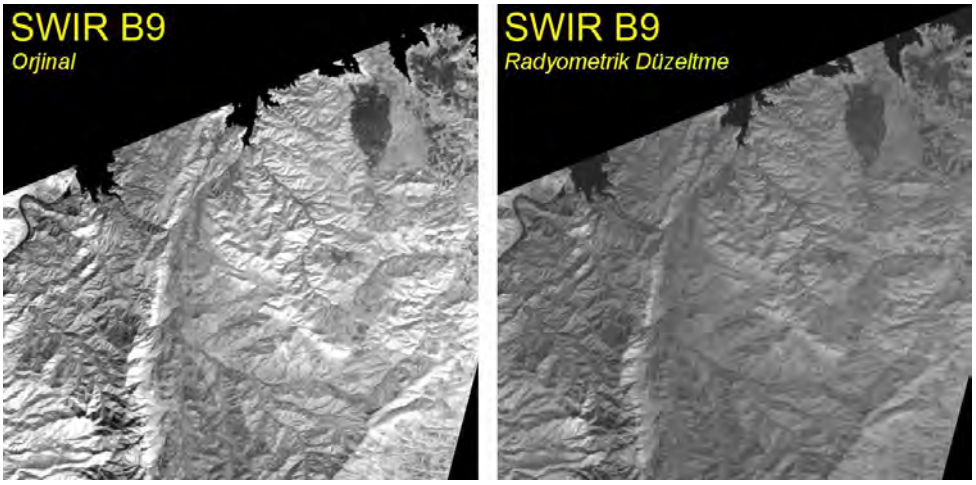

Figure 4. The corrections applied to the datasets

3. RESULTS AND DISCUSSION

In the study, combinations of VNIR bands 1 and 3 with SWIR bands 5, 6, 7, 8, and 9 were tested. The band algorithms used are as follows: VNIR Band 2 / VNIR Band 1, SWIR Band 4 / VNIR Band 2, SWIR Band 4 / VNIR Band 3, SWIR Band 4 / SWIR Band 5, (SWIR Band 5 / VNIR Band 3) + (VNIR Band 1 / VNIR Band 2), SWIR Band 5 / SWIR Band 4. The applied band algorithms and the images they represent are shown in Figure 5.

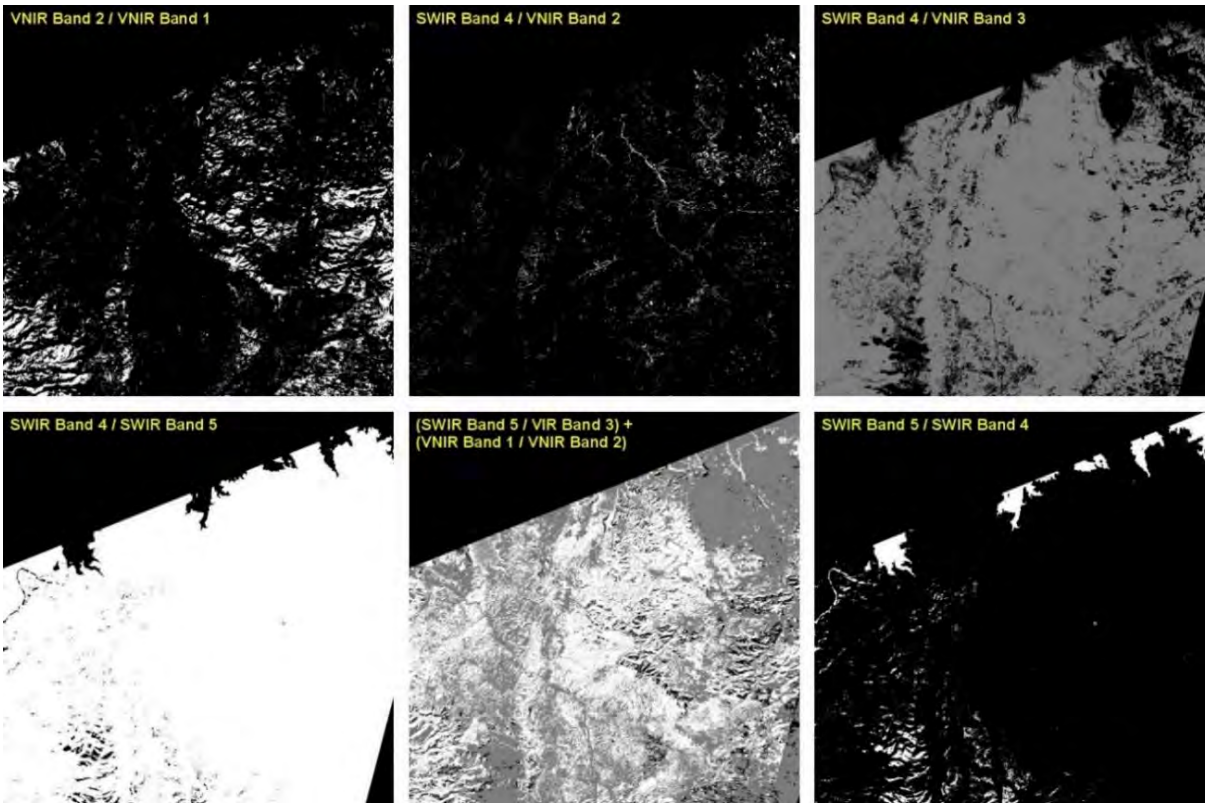

Figure 5. The applied banding algorithms and representative images

4. CONCLUSION

In this area, it was observed that a correlation of over 70% was achieved by combining processed satellite data with validated ground-truth data (Figure 5). It was determined that the images obtained by combining (SWIR Band 5 / VNIR Band 3) + (VNIR Band 1 / VNIR Band 2) with the method of minimum noise fraction provided the best representation for identifying Ore Deposits.

ACKNOWLEDGMENT

This study was supported by the Scientific Research Coordination Unit of Fırat University under project number FÜBAP-MF.25.08

REFERENCES

Pour, A. B., Ranjbar, H., Sekandari, M., Abd El-Wahed, M., Hossain, M. S., Hashim, M., Yousefi, M., Zoheir, B., Takodjou Wambo J. D., Muslim, A. M., (2023) “Remote sensing for mineral exploration”, In Geospatial analysis applied to mineral exploration, 17-149.

Sabins, F. F., (1999) “Remote sensing for mineral exploration”, Ore geology reviews, 14 (3-4) 157-183.

URL-1: https://maps.google.com

URL-2: https://terra.nasa.gov/data

GEOLOGICAL – MINERALOGICAL CHARACTERISTICS OF POLYMETALLIC ORES AND THEIR BENEFICIATION POTENTIAL IN THE MUSHTE – GURTH SPAC – LETITEN REGION, MIRDITA, ALBANIA

Asllan DACI[1,*], Agim SINOJMERI[2], Cem Koray YAGCI[1], Mehmet YAVUZ[1], Hasan USTUNDAG[1]

[1]Tete Albania Tunnel & Mining" Sh.A. Company, Mirdite, Albania
[2]Polytechnic University of Tirana, Faculty of Geology-Mining, Albania
**Corresponding author: asllandaci@gmail.com*

A B S T R A C T

The "Mushte - Gurth Spac - Letiten" region is part of the main belt of polymetallic copper sulfide mineralization in Albania. In this region, several important copper deposits have been discovered, with massive concentrations of pyrite-chalcopyrite-sphalerite, localized in the upper and middle parts of the basaltic-dacitic volcanogenic formacoin. This article discusses the geological-mineralogical characteristics of the rich polymetallic ores Py, Cp, Sph, and gold-bearing deposits of this region, based on the latest data from geological exploration works.

Microscopic study of several ore samples, not only reveals the mineral-forming composition, but also confirms important data on the formation and genesis of polymetallic sulfide mineralizations in this region. Furthermore, the mineralogical characteristics of these ores, play a crucial role in determining the efficiency of the enrichment process.

The rate of mineral release, the textural relationships between pyrite, chalcopyrite, and sphalerite, as well as the presence of microinclusions and intermixtures, directly affect the selectivity and recovery rates during flotation. Therefore, a detailed mineralogical analysis is essential to optimize enrichment parameters and achieve higher concentrate quality and metal recovery.

Key words: *Pyrite, chalcopyrite, sphalerite, volcanogenic formation, flotation*

1. INTRODUCTION

The "Mushte - Gurth Spac - Letiten" region, represents the southernmost part of the Qafe Mali - Reps copper sulfide mineralization belt, one of the most important in Albania for its copper-bearing potential. In this belt, for more than 60 years, several polymetallic copper deposits have been discovered, such as; Paluca, Lak Roshi, Tuçi, Qafe Bari, Munella, Gurth Spac, Spac, Letitena and in the southernmost extreme, the Perlati deposit. The polymetallic sulfide mineralization of these deposits are located in the basalt-dacitic sequence, part of the eastern belt of Albanian ophiolites. The textures revealed by microscopic studies suggest their formation from the hydrothermal activity at the sea-bottom, similar to those discovered at the ***black smoker*** sites.

2. GEOLOGICAL - STRUCTURAL CONSTRUCTION OF THE MUSHTE – GURTH SPAC LETITEN REGION

2.1. Geological Composition of the Region

The "Mushte - Gurth Spac - Letiten" region, is located within volcanic rocks of the eastern ophiolites of Albania. The eastern-type ophiolites, in this region are represented by the gabbro-plagiogranitic plutonic sequence, the sheeted dyke complex and the basalt-dacitic

volcanogenic formation that constitutes about 60% of the rocks of the region. Limited outcrops of ophiolitic melange are discovered close to the mineral deposits while Cretaceous limestones emerging at the North-East constitute the crown of the Munella Mountain (Figure 1).

The plutonic sequence, is represented by a small outcrop of gabbroic rocks composed of gabbro-diabase, dolerite, and microgabbro, elongated in a meridional direction and traceable on the surface for about 2 km, from Southern Gurth to Mesul (Daci A. et al., 2003; Deda T., 2004). Further east, appears intrusive bodies of quartz diorites and plagiogranites, with a north–south extension and intrusive contacts with gabbros and volcanogenic rocks (Figure 1).

The sheeted dykes complex, is well developed in this region and is represented by diabase, quartz gabbro-diabase, microdiorites, boninites, rarely pyroxenites, and dacite–rhyolite. Within the complex of sheeted dikes, there is developed a sulfide mineralization of pyrite, more rarely of chalcopyrite and magnetite of stockwerk type, which apparently represents the roots of the sulfide mineralization and which is assumed to have formed under the seafloor as a result of hydrothermal circulation and metasomatic alteration.

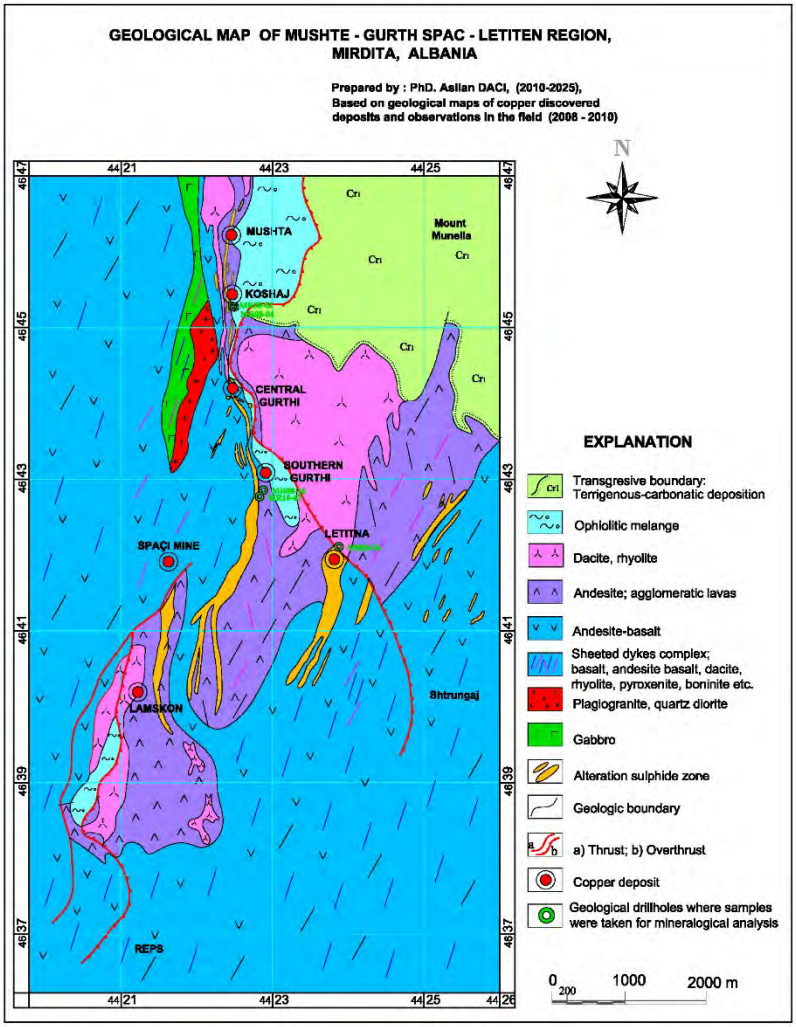

Figure 1. Geological map of Mushte - Gurth Spac - Letiten Region, Mirdita, Albania

The basalt–andesite–dacite formation, is represented by volcanites, mainly pillow lavas, agglomerates, and rarely massive flows, with compositions ranging from basic, intermediate-basic, intermediate, and intermediate-acid to acid. This formation is associated with copper sulfide mineralizations, which account for about 90% of the region. The volcanites of this formation are divided into two main units, succeeding one another in near conformity but also

with local unconformities (Shallo M. et al., 1996; Zaçaj M. et al. 2001; Daci A. et al., 2003; Deda T., 2004). These are designated as: the lower basaltic sequence, consisting of intersertal basalts, mainly basaltic pillow lavas and massive flows; and the upper andesitic sequence, composed of glassy agglomerates and rhyodacites.

The lower basaltic sequence in the sectors, of this region constitutes about 60% of the volcanogenic rocks and has a thickness of 300–1000 m. It is mainly characterized by basaltic pillow lavas and massive flows, while in their upper part there is a gradual transition into basaltic–andesites and andesites.

The upper sequence, is composed of andesitic–basaltic agglomerates, andesites, dacites, and rhyolites, accompanied by volcanic glass that is mainly distributed in the central sectors of the region, and overlies the lower basaltic volcanic sequence. The thickness of the dacite–rhyolites reaches 200–400 m, and they are clearly distinguished in the higher relief areas (such as in Koshaj and Southern Gurth). They are partially mineralized, especially near andesite-basalts.

The heterogeneous colored ophiolitic melange, of J3-Cr1, with a thickness of 200-350 m, is located over the radiolaritic siliciclastic rocks that close the volcanic activity. This formation is represented by shales, sandstones, conglomerates, siliciclastic blocks, limestone blocks, volcanic and plutonic rocks blocks, with discordant placement on different types of volcanics (underwater washes), but in many cases, it is also placed in compliance with the volcanogenic rocks through a belt of radiolaritic siliciclastics that constitute the ceiling of the volcanics (Daci A. et al. (2003).

The terrigenous–carbonate deposits of the Lower Cretaceous (Cr1, Baremian–Aptian)
They are exposed in the northeastern part of the region, above Mushta and in Guri i Vashes–Livadhet e Buta. They are represented by terrigenous–carbonate formations of the Lower Cretaceous Cr1 (Baremian–Aptian), according to Marku D. (2000), with a thickness of 300–1700 m, emplaced unconformably and transgressively over the volcanic formations and the heterogeneous ophiolitic mélange.

2.2. Tectonic Structure Of The Region

The “Mushte-Gurth Spac – Letiten” region and beyond, from a tectonic perspective, has not been stable. According to the majority of geologists, an early non-intensive folding tectonics is recognized, whereas the overthrust, is strongly expressed and exhibits a regional character (Kolndreu D. et. al. 1984., Zaçaj M. Et.al. 2001, Daci A. et.al. 2003; Deda T., 2004).

Folding tectonics in the Gurth - Spaç region, is poorly defined and should be developed before the sulfide mineralization and the formation of subvolcanic dikes. It is relatively weak because the dikes, subvolcanic formations, and sulfide mineralization (as documented by geological and mining works) are not folded. The dikes dip steeply to the east, at 70–85°, and only rarely are slightly curved.

The thrust tectonics (overthrust), occurring after the mélange (J3) and before the Cretaceous (Barremian), belongs to the Jurassic–Cretaceous tectonogenesis. In this region, the thrust tectonics is represented by the main Mushta - Gurth Spaç - Letiten overthrust, and further south in Shtrungaj (Figure 1). It has a displacement amplitude of more than 250 - 300 m, with a meridional extension and an eastern dipping angle of 30–50°, placing the terrigenous–carbonate formations of the Cretaceous in contact with the ophiolitic mélange. Further, from central Gurth to Letiten over thrust puts on the rhyodacitic massif with the ophiolitic mélange (as confirmed by exploration drillings), whereas to the southeast towards Shtrungaj, this thrust tectonics places the andesites and basalts in contact with the ophiolitic mélange. Another thrust fault, nearly parallel to the one above, is also observed in the

southwest of the Gurthi region, which brings into contact the subvolcanic rhyodacitic bodies with the ophiolitic mélange (Figure 1).

3. SULFIDE MINERALIZATION OF THE MUSHTE – GURTH SPAC – LETITEN REGION

Historical geological works carried out in the Mushte - Gurth Spac - Letiten region, since 1975 onwards, as well as those conducted by Tirex Explorations Sh.p.k. (2007–2011) and Tete Albania Tunnel & Mining Sh. A. (2014–2025), have revealed several ore bodies of copper, zinc, and pyrite with their associates. These ore bodies follow one another along a main axis of the ore structure, with a near-meridional strike, extending from Mushta and Koshaj in the north to the southernmost part of this region in Letiten (Daci A. & Tirex Group 2011).

The copper sulfide mineralization, is developed within a zone of meridional to sub-meridional extension for 3 km, with a thickness of 8–10 m at the surface and reaching 150–200 m at the depth. This mineralization is mainly located at the contact between andesites and basalts, as observed in the Central and Southern Gurth Spac and in Letiten, as well as in the upper sequence of glassy agglomeratic andesite–rhyodacite at the Mushta deposit.

The massive ore bodies, present lenticular shape to pseudo-layered appearance, with wavy and irregular boundaries in the upper part, and measure 150 to 300 m in length, 100 to 120 m in depth and a thickness that varies from 1 to 12 m.

The mineral composition of the ore bodies, is heterogeneous and includes: sphalerite, chalcopyrite, pyrite (marcasite) and second-hand; minerals phalerite (tennantite), galena, bornite, rarely native gold, in the associations pyrite (marcasite)-chalcopyrite, pyrite-chalcopyrite-sphalerite, sphalerite-chalcopyrite-phalerite-barite-galena, sphalerite-chalcopyrite-pyrite.

The chemical composition of the sulfide ores is as follows: Cu 0.5–4.5%; Zn 0.7–26%. In some parts of the massive ore bodies, the Au content ranges from 3 to 13.7 g/t while the Ag content varies from 5 to 25 g/t, although it occasionally reaches 50 or 120 g/t. The most important associated elements are: Pb in general under 0.1%, rarely 0.17–0.46%; As in general under 0.1%, rarely up to 0.34–0.82%; Sb up to 0.1%; Cd occasionally up to 0.16%; In under 0.01%; Bi sporadically up to 0.03%; Ga under 0.01%; Ge under 0.01%; Mo under 0.001%; Sn sporadically attempt 0.007%; Mn under 0.03%; Co under 0.01%; Ba rarely up to 0.5–0.84% (sample with $BaSO_4$ 2–3%). (Zaçaj M. et.al. 2001; Daci A. & Tirex Group 2011).

4. MINERALOGICAL COMPOSITION AND ORE TEXTURES

Mineralogical composition of orebodies is rather complex. The principal minerals found in the mineralised ores are pyrite, chalcopyrite, sphalerite while little presence of galenite, tennantite, marcasite, bornite and rare native gold are detected.

Mineralized orebodies at Central and Southern Gurthi area are almost of massive sulphide mineralization, while the mineralization at Mushta – Koshaj area are almost of disseminated mineralization. The mineralization at Letiten area is represented by sulphide veins and veinlets, mainly of pyritic composition.

4.1. Gurthi Mineralization

Pyrite is the principal mineral composing up to 90% of the orebodies but an inconspicuous zonation can be detected from lower to upper parts of mineralized orebodies. Occasionally this zonation is clearly evidenced as in drilling 3, where samples of massive mineralization (only 5% of gangue minerals) from 139.2 m deep, 129.8 m deep and 126.75 m deep reveal respective content of pyrite 85%, 40% and 10%, while chalcopyrite content vary from 10% to 55-90%.

Pyrite forms in general, irregular massive formations, but also cockade texture and singular cubic idiomorphic crystals are observed. Cockade textures of pyrite are observed mainly at brecciated mineralization similar to the model proposed by Tosun (2024) and present frequently marcasite formations at the bordures (**Error! Reference source not found.**/a) suggesting the pH of hydrothermal fluids moves to less than 5 at the end of mineral-forming process (Georgieva et al. 2021).

Chalcopyrite, in general present irregular and colloform formation associated to small pyritic crystals (**Error! Reference source not found.**/b) but some chalcopyrite of trigonal shape indicating the presence of idiomorphic tetrahedral crystals are also found at the contact with gangue minerals. Very fine formations of chalcopyrite penetrating the pyrite crystals and also fine inclusions of chalcopyrite within pyrite are found. Besides chalcopyrite, at the central parts of the deposit, traces of sphalerite are detected, while tennantite is observed only associated to chalcopyrite rich ores.

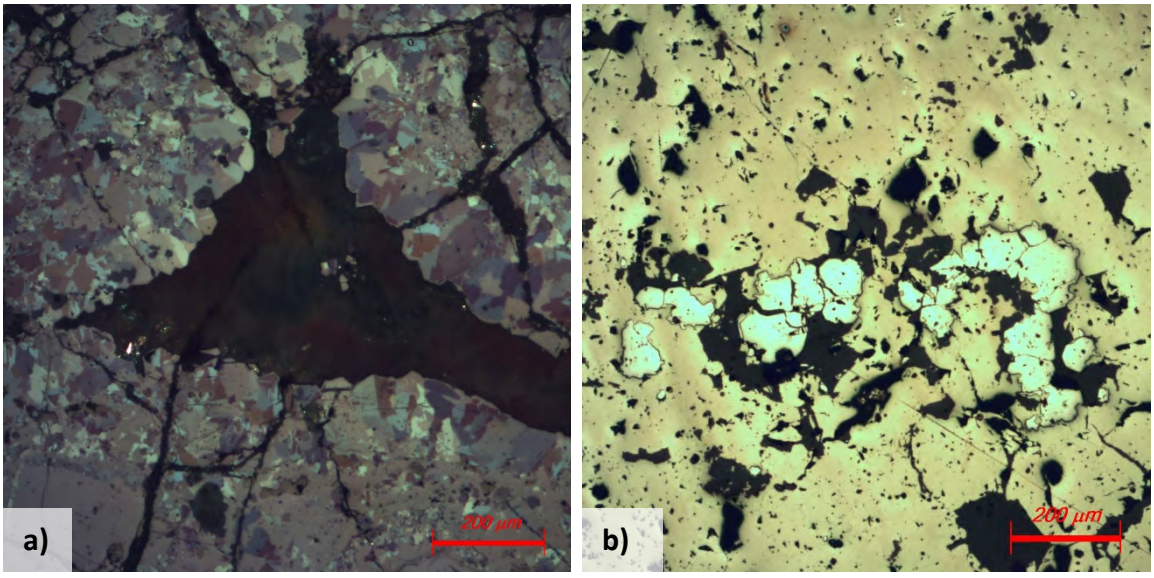

Figure 2. Microscopic images from massive ore of central Gurth. a) marcasite formation at the bordure of pyrite-marcasite cockade texture, reflected, cross polarized light; b) chalcopyrite massive formation, associated to fine pyrite crystals, reflected, plane polarized light

4.2. Koshaj-Mushta Mineralization

At the north of Gurthi area, about 400 m from, are developed Zn-rich, almost disseminated orebodies. The sulphide minerals, generally compose up to 30% of ore samples, where gangue minerals compose the rests. But massive ores (up to 80% of sulphides) with a predominance of galenite and sphalerite are also found. The predomination of sphalerite and galenite between other sulphide minerals is frequent and gives these mineralizations a polymetallic character.

Among these mineralizations, very interesting textures, reminiscent of the wildlife living near black smokers are observed (Figure 2). These kinds of organisms are frequently detected at active and fossil hydrothermal deep-sea vents (Sinojmeri A. 1990, 1994; Symes et al. 2011; Lines et al. 2019; Georgieva et al. 2021). The main ore minerals at this area are sphalerite, pyrite, galena and chalcopyrite.

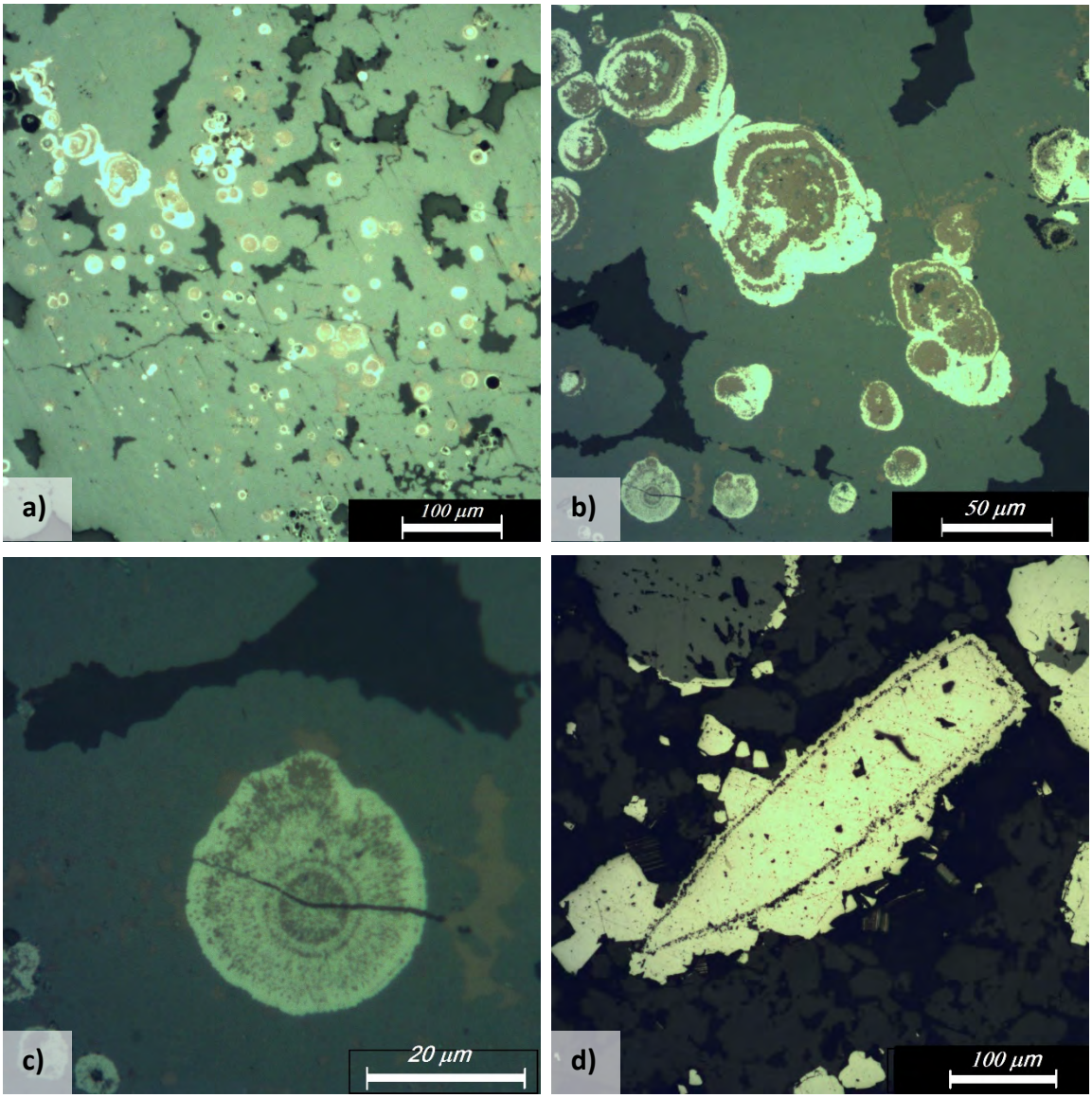

Figure 2. Pseudomorphosis of sulphide minerals by microfauna living at the sea bottom. Images under reflected plane polarised light. a) tiny pyrite-bornite-chalcopyrite formations included within sphalerite; b) detail from photo a, the shape of rounded pyrite-bornite formations suggests pseudomorphs of living organisms, c) detail from photo b, pyrite-bornite-chalcopyrite formations of gastropod-like shape, d) bullet shape of pyrite that evoke the exoskeleton of any microbelemnites

Sphalerite constitutes in general, formation of irregular shape or colloform textures, frequently embedding fine concentric formations of pyrite-tenantite-bornite-covellite and occasionally galena, all of some microns in diameter. Colloform sphalerite presents a clear zonation putted in evidence by fine exsolutions of tennantite (Figure 3/a) and also by the variations of reflectance. Tennantite inclusions delineate two generations of sphalerite, the inner one darker and the outer one lighter.

Fine galena inclusions are found also at the centre of the colloform formations, but is clear the majority of Pb crystalizes at the end of the hydrothermal sequence. These last formations of galena of irregular shape surround also fine idiomorphic crystals of sphalerite (Figure 3/b and c).

Native gold inclusions are detected within sphalerite of second generation, at the lateral parts of colloform formations (Figure 3/d). These inclusions, up to 20μm in length and only e few microns thick, indicate the enrichment of solutions with Au at the end of hydrothermal activity. The reflectance of sphalerite at the central area of colloform formations vary between 17.5% and 17.8%, while the reflectance at the lateral parts attempts values as low as 16.6%.

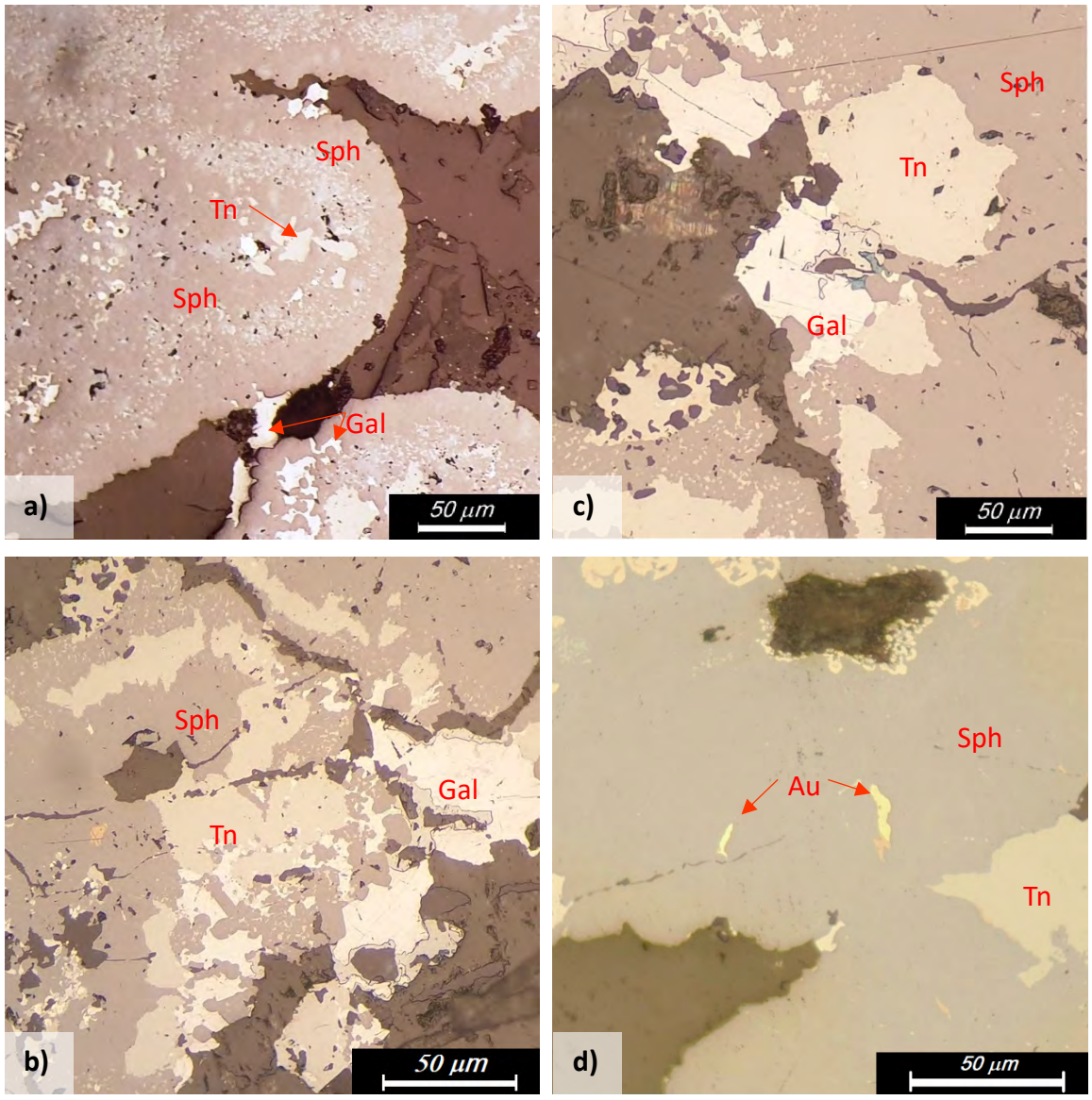

Figure 3. Textures of sphalerite-rich colloform mineralization. Images under reflected plane polarized light. a) zonation of sphalerite with tennantite inclusions; b) galena and tennantite between sphalerite and gangue minerals; c) galena surrounding fine automorphic crystals of sphalerite; d) gold formation at the lateral parts of colloform formations

The large presence of tennantite inclusions suggests an influence of reflectance by the Cu content (Wiggins and Craig 1980; Kim et al. 2024) but the influence of Fe content cannot be excluded. In similar colloform mineralization of sphalerite at the same belt area in Albania, other isomorphic substitutions at Zn sites, as In, Ga, As and Sb are observed, besides Cd and Fe (Sinojmeri, 1994). At the border of colloform sphalerite, important inclusions of tennantite

are developed, whereas galena is developed at the contact between sphalerite and gangue minerals.

5. BENEFICIATION POTENTIAL AND FLOTATION BEHAVIOUR

At present, the ores from which copper, zinc, and lead are produced generally contain substantial amounts of pyrite together with copper-, zinc-, and lead-bearing minerals within a complex mineralogical assemblage. At first glance, this situation may appear to increase the nominal value of the ore. However, although modern mineral processing technology is not yet capable of economically recovering all metals contained in such complex ores, intensive research carried out over approximately the last three decades has transformed a significant portion of these ores from potential reserves into economically exploitable resources in many countries. Japan, Canada, and Australia are representative examples of countries that have been mining and processing such complex ores for nearly thirty years (Hendriks and Ounpuu, 1985; Boman et al, 1985; Wakamatsu and Shibata, 1989).

Many of the characteristics of complex ores represent serious challenges for mineral processing engineers. For instance, the heterogeneous distribution of minerals and grades within an ore deposit raises, at an early stage, the question of how representative and reliable laboratory-scale test results actually are. For this reason, in complex Cu–Zn–Pb or Cu–Zn deposits, it is essential to work on multiple composite samples with different characteristics, each representing specific zones of the deposit, rather than relying on a single composite sample. Such an approach is necessary both to design a flexible processing flowsheet and to avoid unpleasant and costly surprises during plant operation. This is because, regardless of how well the mine production plan is designed, the ore fed to the plant will inevitably originate from specific sections of the deposit. Unless a substantial investment is made in effective ore blending facilities, daily, weekly, and monthly variations in the characteristics of the plant feed are unavoidable (Bayraktar İ. & Altım Y., 1996).

5.1. Mineralogical Structure, Grade and Impurities

The potential benefits of ore microscopy in the evaluation of complex ores are briefly illustrated below.

5.1.1. Liberation grain size

The upper and lower limits of the grinding fineness required to produce selective concentrates can be determined rapidly and effectively. For example, for the ore shown in Figure 1, it appears quite difficult to achieve successful selective flotation without grinding finer than 38 µm (400 mesh). On the other hand, in some complex ores, complete liberation of certain minerals may not be possible. A typical example is *chalcopyrite disease* in sphalerite (Gray P.M.J., 1984), which leads to either increased zinc content in the copper concentrate or increased copper content in the zinc concentrate. If the presence and extent of this phenomenon in the ore are identified, the impurity levels of the selective copper and zinc concentrates can be reasonably predicted (Bayraktar İ. & Altım Y., 1996).

5.1.2. Minerals hosting impurities

The identification of minerals such as tetrahedrite and tennantite allows a qualitative prediction that impurities subject to penalty, such as antimony, arsenic, and mercury, will inevitably report to the copper concentrate. The flotation behavior of tetrahedrite differs from that of chalcopyrite and, in some cases, resembles that of stibnite and galena. For instance, similar to galena, tetrahedrite cannot be effectively depressed using cyanide (Bayraktar İ. & Altım Y., 1996).

5.1.3. Degree of ore oxidation

Oxidation may occur both in drill core samples and when the ore is stored in stockpiles for a certain period of time. As the degree of oxidation increases, the efficiency of selective flotation decreases accordingly.

5.2. Clay and Primary Slime Content

In complex ores formed by relatively young volcanic activity and not affected by metamorphism, problems related to clay and primary slime content are frequently encountered. Primary slimes can be defined as naturally occurring very fine ore and/or gangue particles, as well as fine material generated during mining operations. In contrast, slimes generated during grinding are referred to as secondary slimes.

During ore formation, alteration of structures such as dykes within the ore body may lead to the formation of flotation-detrimental clay and primary slime minerals such as kaolinite and sericite. If the ore contains significant amounts of clay and primary slimes, it is essential that these materials be washed and removed from the ore during the crushing stage. Otherwise, the processing plant is likely to encounter serious operational problems, first in flotation and subsequently in thickeners and filters (Bayraktar İ. & Altım Y., 1996).

5.3. Ore Description of the Region and Processing Plant Operations

The beneficiation of the polymetallic sulphide ores from the Gurth Spaç–Spaç–Letiten region requires a highly selective flotation process due to the complex mineralogical associations present in these deposits. The coexistence of pyrite, chalcopyrite, sphalerite, and locally gold-bearing sulphides affects the efficiency of separation, particularly in ore types where the degree of mineral liberation remains limited. In the plant, the target grind size is d80:38 μm, which improves liberation yet cannot fully eliminate fine intergrowths that restrict flotation selectivity (Figure 3).

Operations at the plant are carried out through a single copper flotation circuit. Selective flotation is performed under high alkaline conditions (pH 11.5–12), where sphalerite and gangue minerals are depressed using $ZnSO_4$ (30–40 g/t) and Na_2SiO_3 (45–50 g/t) (Bayraktar İ. & Altım Y., 1996). Collector reagents include Aerophine 3418A (25–27 g/t), PEX (18–23 g/t) and PAX (7–10 g/t), while MIBC (20–25 g/t) is applied as the frother. This reagent suite enhances chalcopyrite activation while effectively depressing sphalerite and pyrite, thus improving the selectivity of copper flotation. In addition, sodium metabisulfite ($Na_2S_2O_5$, 10–12 g/t) is added in the final cleaning stage to enhance pyrite depression.

Plant performance varies depending on ore type; however, typical results yield 18–19% Cu concentrate grades with 85–92% Cu recovery. Gold, which occurs at low levels in the feed (0.2–0.4 ppm), is predominantly hosted within sphalerite, and less frequently within pyrite (Figure 4). Therefore, Au has limited response in the Cu circuit unless sphalerite activation occurs. Since gold is not strongly associated with chalcopyrite, its flotation response is limited, and gold recovery in the copper circuit ranges between 45–60%. When increased gold recovery is targeted, operational adjustments are made by increasing $ZnSO_4$ dosage and collector additions, which enhances sphalerite activation and gold reporting to the final concentrate. Under these conditions, gold grades in the copper concentrate increase to 2–5 ppm, improving the overall economic performance.

5.3.1. Process flowsheet of the plant

The Tete Albania flotation plant operates a closed-circuit grinding system followed by closed-circuit grinding followed by conventional Cu flotation (rougher–scavenger–cleaner stages. The simplified process flowsheet (Figure 5) is summarized below:

1. Stockpile: Ore is homogenized prior to feeding.
2. Crushing and screening: The crushed ore is reduced to approximately d80:9 mm, suitable for the grinding circuit.
3. Primary ball mill: The first stage of grinding is carried out here.
4. Hydrocyclone classifier: Primary mill discharge is classified; fines proceed forward, while coarse material returns for further grinding.
5. Secondary ball mill – closed circuit: Hydrocyclone underflow is fed to the secondary mill, forming a closed grinding loop. The objective is to achieve a flotation feed size of d80:38 µm.
6. Conditioners: The ground pulp is conditioned with Aerophine 3418A, PEX, PAX, Na_2SiO_3, and lime. The pH is maintained at ~11.5, and MIBC is introduced as the frother.
7. Cu Rougher flotation: The primary copper recovery is achieved in the rougher cells.
8. Cu Scavenger flotation: Additional recovery of copper from rougher tailings is achieved in the scavenger stage. Aerophine 3418A, PEX, and MIBC are also applied here.
9. Cleaning stages: Rougher and scavenger concentrates are upgraded through a multi-stage cleaning circuit (Rougher Cleaner, Scavenger Cleaner, Final Cleaner, and Re-Cleaner). Prior to the final cleaner, additional lime is added to increase pH to ~12.2 and $Na_2S_2O_5$, (10–12 g/t) is added to improve concentrate grade.
10. Final copper concentrate: The multi-stage cleaning process produces a final concentrate grading 18–19% Cu.
11. Tailings and water recycling: Final flotation tailings are sent to the tailings storage facility. Clarified water from the facility is helping to reduce freshwater consumption and stabilize process water chemistry.

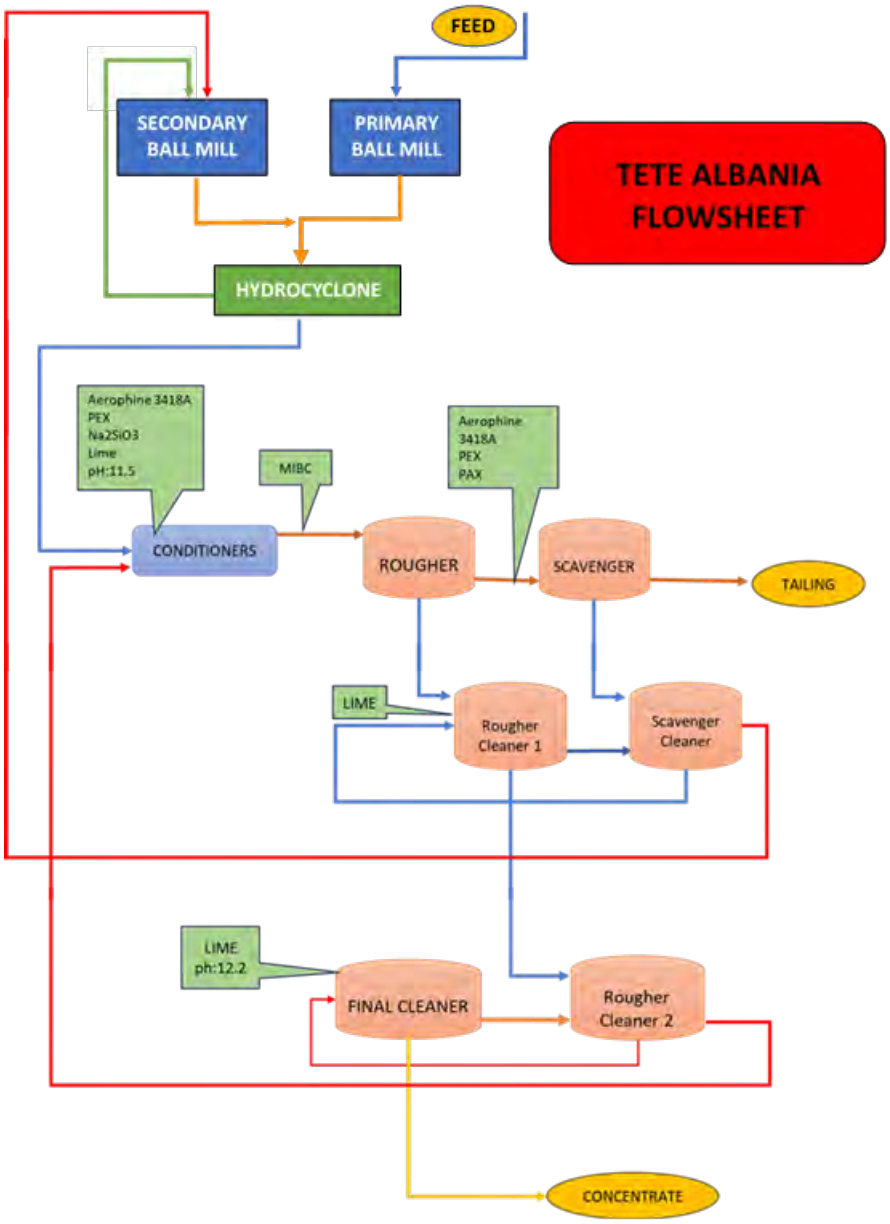

Figure 4. Schematic presentation of beneficiation process at TETE ALBANIA

This flowsheet, designed for fine-grained polymetallic sulphide ores, relies on closed-circuit grinding, high-pH selective flotation, effective depressant control, and multi-stage cleaning to maximize copper recovery and concentrate quality.

6. CONCLUSIONS

1. The Mushta – Gurth Spaç – Letiten region, represents the southernmost segment of the Qafë Mali – Reps polymetallic sulfide copper mineralization belt in Albania.
2. In this region, several important copper deposits have been discovered, with massive concentrations of pyrite, chalcopyrite, and sphalerite, such as Gurth Spaç, Koshaj, Southern Gurth Letiten, and Mushta, located in the upper and middle parts of the basalt–dacite volcanogenic formation.

3. The region is characterized by the development of early, non-intensive folding tectonics, while the overthrust fault tectonics are strongly expressed and have a regional character.
4. Sulfide mineralization occurs within the volcanogenic rocks of the basalt–dacite formation, encompassing the entire volcanic sequence: from basalts in the deepest parts to andesites and rhyodacites in the uppermost sections.
5. Data from historical works (since 1975) and recent explorations by various companies have revealed several ore bodies of copper, zinc, and pyrite, accompanied by other elements (Au, Ag). These ore bodies follow one another along a main axis of the ore-bearing structure with a near-meridional strike, extending from Mushta and Koshaj in the north to Letiten and Lamskon in the south.
6. The main polymetallic sulphide mineralization of this region, is represented by an altered sulphide zone with a meridional - near-meridional extension with a length of about 3 km and an eastern dip. This mineralization, in the Central, Southern Gurth and Letiten deposits, is mainly located at the contact between two volcanic sequences; andesites with basalts, while in the upper sequence of andesite-rhyodacites the Mushta target is located.
7. Massive ore bodies have a lenticular shape, sometimes appearing pseudo-layered, with undulating and irregular boundaries in the upper part. Their dimensions are: 150–300 m in strike length, 100–120 m in dip, and thickness varying from 1–12 m.
8. The beneficiation performance of the Gurth Spaç–Spaç–Letiten ores indicates that effective copper recovery can be achieved through a single high-pH flotation circuit. A grind size of –38 μm provides sufficient liberation for chalcopyrite, though fine intergrowths with pyrite and sphalerite continue to constrain selectivity.
9. The applied reagent scheme—$ZnSO_4$ and Na_2SiO_3 as depressants and a mixed collector system (Aerophine 3418A, KEX, KAX)—ensures stable metallurgical results, yielding 18–19% Cu concentrate grades with 85–92% recovery. Gold recovery remains moderate due to its association with sphalerite but improves when $ZnSO_4$ dosage and collector addition is increased.
10. Overall, the current flowsheet demonstrates technical suitability for these polymetallic sulphide ores, and further optimization should focus on improving mineral liberation and refining depressant–collector balance to enhance copper and gold recovery.

REFERENCES

Bayraktar, İ., Altım, Y., (1996), “Characteristics, economic evaluation and processing of complex copper–zinc–lead ores”, The Journal of the Chamber of Mining Engineers, Ankara, Turkey.

Daci, A., Tirex Group, (2011), “Summary report of geological–exploration works carried out in the Qafë Mali–Perlat region by Tirex Explorations Ltd. during 2007–2011”, Archive of Tirex Explorations Ltd., Tirana.

Daci, A., et al., (2003), “The perspective of copper mineralizations and their associates (Au, Zn, S) outside the contour of discovered deposits in the Mirdita zone (Qafë Mali–Munella region)”, Study Report, Central Archive of the Albanian Geological Survey, Tirana.

Deda, T., (2004), Metallogenic analysis of sulfide mineralizations of the Qafë Mali–Munella–Reps belt, PhD Thesis, Faculty of Geology and Mining, Tirana.

Gaudin, A. M., (1957), Flotation, 2nd ed., McGraw-Hill, New York.

Gray, P. M. J., (1984), “Metallurgy of the complex sulphide ores”, Mining Magazine, October, 315–321.

Fuerstenau, D. W. (ed.), (1962), Froth flotation, Society of Mining Engineers, New York.

King, R. P., (1982), “Flotation of fine particles”, in: Principles of Flotation, South African Institute of Mining and Metallurgy, Johannesburg, pp. 215–225.

Kolndreu, D., (1984), Geological report on the calculation of reserves of the Spaç deposit (01.01.1984), Central Archive of AGS.

Marku, D., (2000), “On the Baremian transgression in the Munellë region (Central Mirdita) and changes in stratigraphic scheme”, Proceedings of the 8th National Congress of Geosciences.

Zaçaj, M., et al., (2001), Monographic study: “Geology and metallogeny of copper sulfide mineralizations of Albania”, Central Archive of the Albanian Geological Survey, Tirana.

Georgieva, M. N., Crispin, T. S. L., Maslennikov, V. V., Glover, A. G., Ayupova, N. R., Herrington, R. J., (2021), “The history of life at hydrothermal vents”, Earth-Science Reviews, 217, 103602.

Kim, H., Shin, D., Im, H., Yu, B., Choi, S. K., (2024), “Distribution of indium and gallium in sphalerite from skarn and hydrothermal vein deposits in the Hwanggangri district, South Korea”, Journal of Geochemical Exploration. https://doi.org/10.1016/j.gexplo.2024.107418

Lines, K., Roterman, C. N., Chen, C., (2019), “A new vent limpet in the genus Lepetodrilus from Southern Ocean hydrothermal vent fields”, Frontiers in Marine Science, 6, 381. https://doi.org/10.3389/fmars.2019.00381

Sinojmeri, A., (1990), Minéralogie et paragenèses du gisement volcanogène à Cu, Zn, Pb, Au de Munellës, PhD Thesis, Orléans, France.

Sinojmeri, A., (1994), “Sea-floor sulfide mineralization of Munella deposits, Central Mirdita, Albania”, Bulletin of the Geological Society of Greece, 30(3), 265–274.

Symes, M., (2011), Hydrothermal vents: Ephemeral underwater oases of the ocean depths, Science XRay-MAG.

Tosun, L., (2024), Formation mechanisms of cockade texture in breccias and their relation to hydrothermal mineral textures, PhD Thesis, Cardiff University, UK.

Wiggins, B., Craig, J. R., (1980), “Reconnaissance of the Cu–Fe–Zn–S system: Sphalerite phase relationships”, Economic Geology, 75, 742–751.

IMAGE PROCESSING STUDIES IN THE AKDAĞ REGION (ELAZIĞ, TURKEY)

Melek URAL[1,*], Mustafa EĞRİ[2]

[1]Firat University, Faculty of Engineering, Department of Geological Engineering, 23119, Elazığ,TURKEY
[2]Pamukkale University, Faculty of Engineering, Geological Department, 20020, Denizli,TURKEY
**Corresponding author: melekural@firat.edu.tr*

A B S T R A C T

In this study, alteration analyses were conducted on the geological units exposed along the route between Erimli, Palu, Beyhan, and Şenova. The image processing tecniques were conducted to identify zones containing iron oxide (FeOx) in the region around the Akdağ Mountains (Elazığ, Eastern Turkey), covering the area from north of Erimli to the Murat River. All studies were conducted on ASTER images by enhancing and combining SWIR and VNIR images to create composite images. The AST_L1A_00406082003082039_20250310152007 image representing the region was selected. After examining the different band ratios applied, it was determined that the best result was obtained with the iron oxide index (SWIR Band 4 / VNIR Band 3). In the controls performed with the most suitable band ratios for this index, a significant correlation was found at the observation points.

Key words: *Akdağ, alteration, image processing, band combination*

1. INTRODUCTION

The rectangular area of 416 km² bounded by Erimli to the south, Palu to the west, Beyhan to the northeast, and Şenova to the north has been designated as the target area (URL-1, Figure 1). The ASTER image (AST_L1A_00406082003082039_20250310152007) (URL-2, Figure 2) was first reprojected and cropped according to the study area to make it suitable for the study. Iron-bearing alterations in the region were attempted to be detected by applying ASTER image enhancement methods.

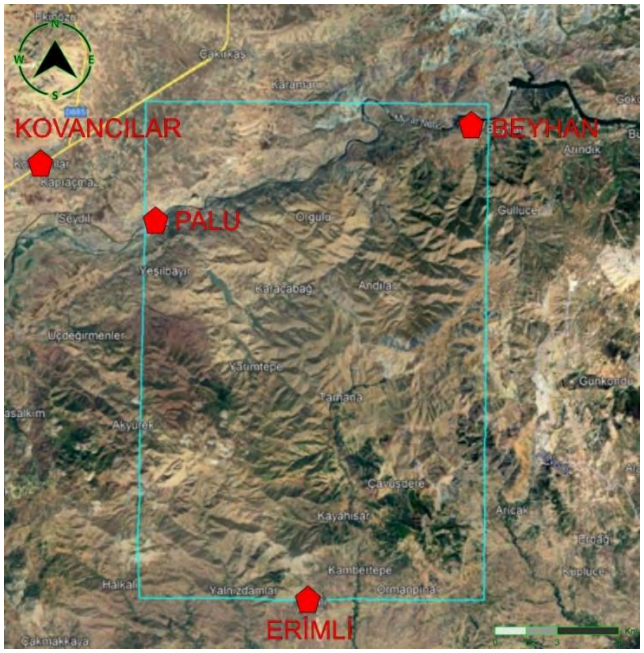

Figure 1. Location of the study area on Google Earth (URL-1).

2. MATERIAL AND METHODS

The dataset used is a daytime image product from the ASTER image with a timestamp of 2006.08.20 08:20:39 and less than 10% cloud cover (Figure 2). The image was selected to cover the target area in a single piece (Figure 2). The image set was cropped (subset) according to the study area, and the area to be studied was limited (Figure 2).

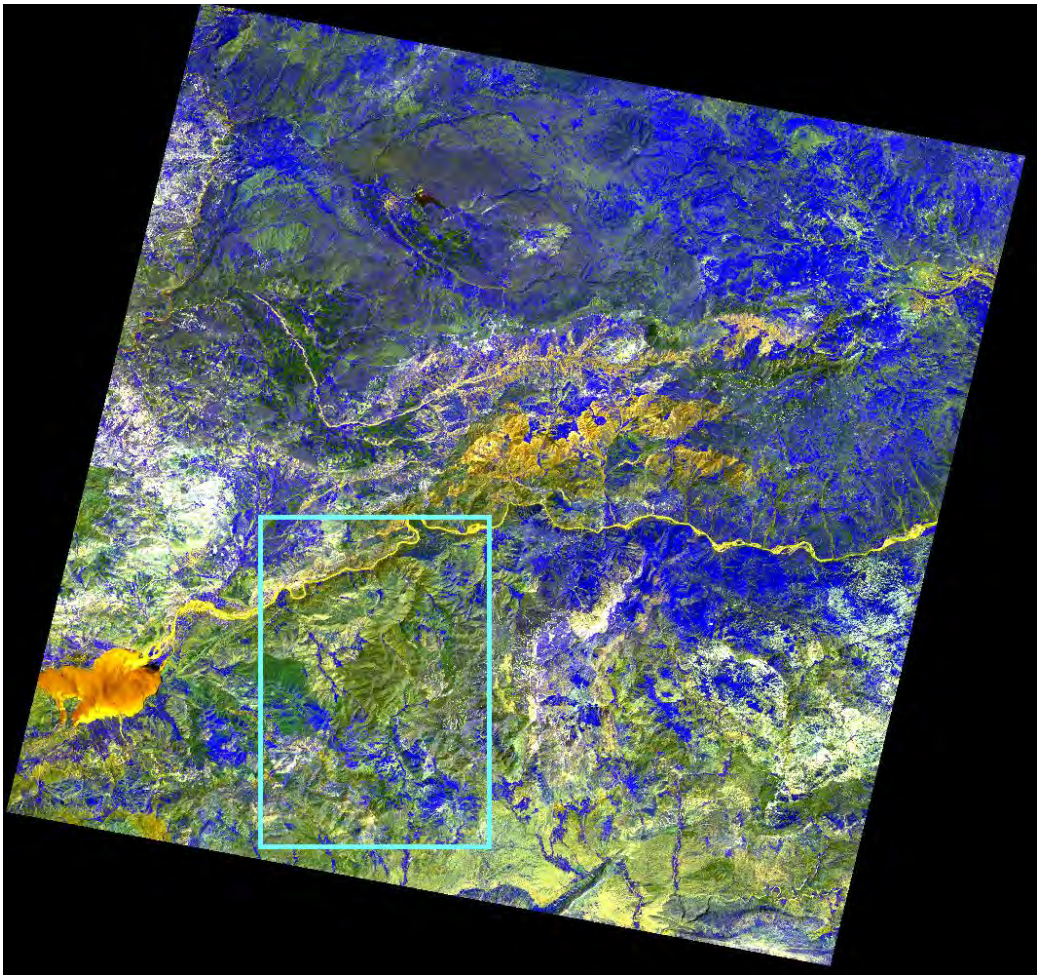

Figure 2. Study area (turquoise polygon) on the ASTER image (URL-2)

All studies were performed using only the VNIR and SWIR bands of the ASTER image (Figure 3). Radiometric corrections were made on the relevant data set, and spectral anomalies were minimized (Figure 4).

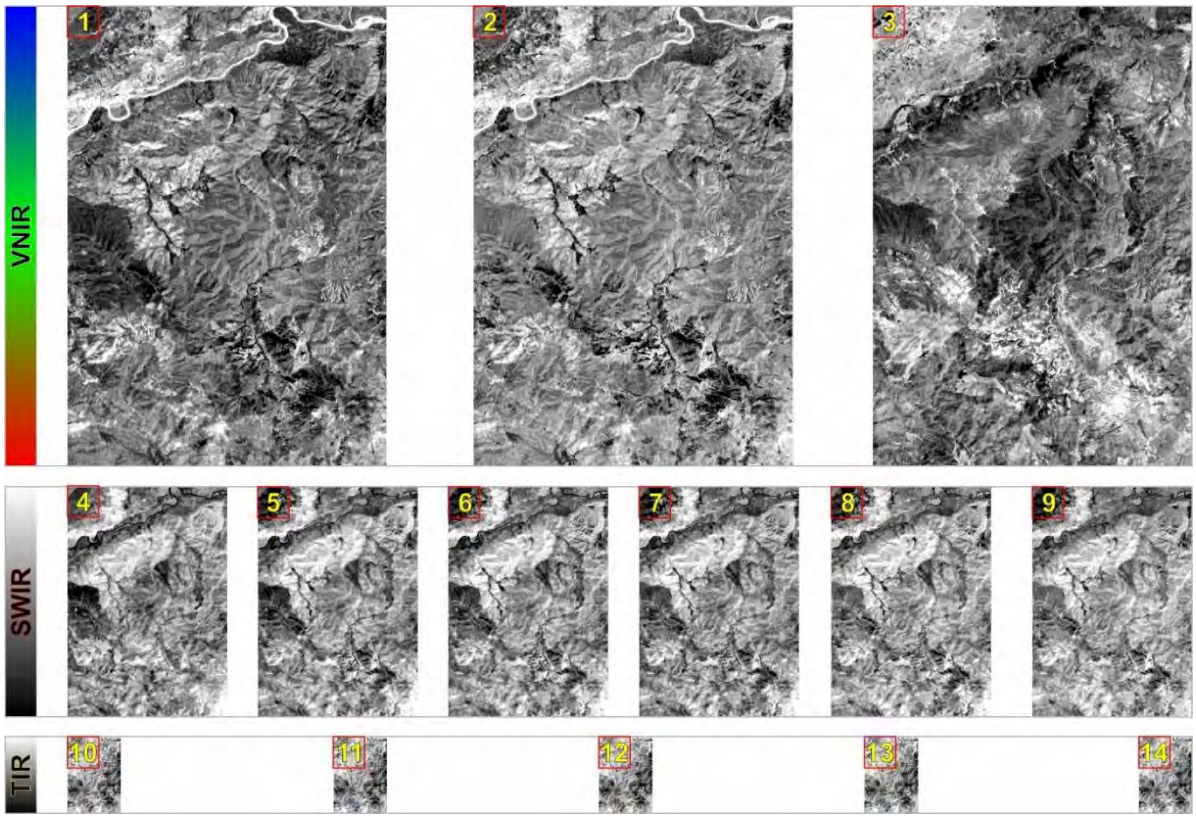

Figure 3. The cropped state of the VNIR, SWIR, and TIR bands in the ASTER dataset according to the study area

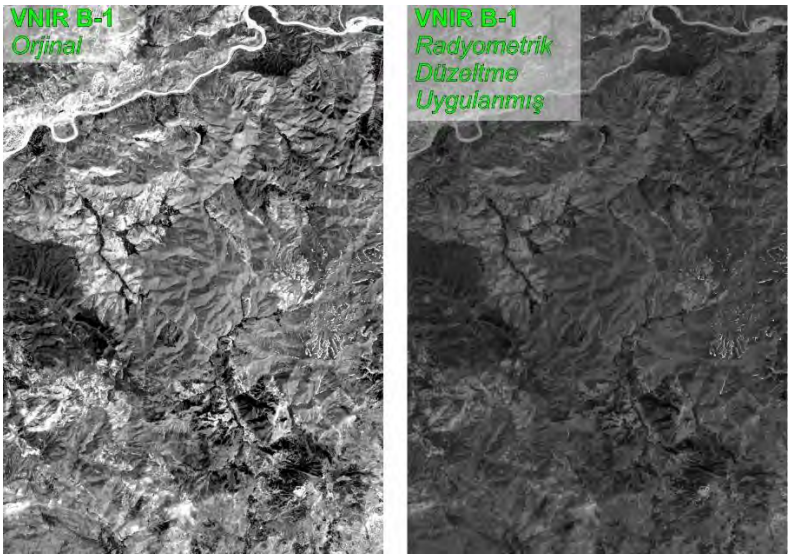

Figure 4. Images with radiometric correction applied and noise minimized.

3. RESULTS AND DISCUSSION

In this study, the VNIR spectral bands of the Aster satellite, which have a 15-meter ground resolution, were downsampled to 30 meters and balanced with SWIR spectral bands. Although there are many sources in the literature on finding iron formations with ASTER images, these methods are not equally sensitive to all terrain and ore types, and combined methods should be tried and tested. In this context, iron indices used in remote sensing in the literature have been applied individually to the relevant images (Figure 5).

4. CONCLUSION

By comparing with known ground control points; different band ratios were examined, and it was determined that the best result was obtained using the “Ferric Oxides Index” (SWIR Band 4 / VNIR Band 3). The checks revealed a significant correlation at the observation points (Figure 6).

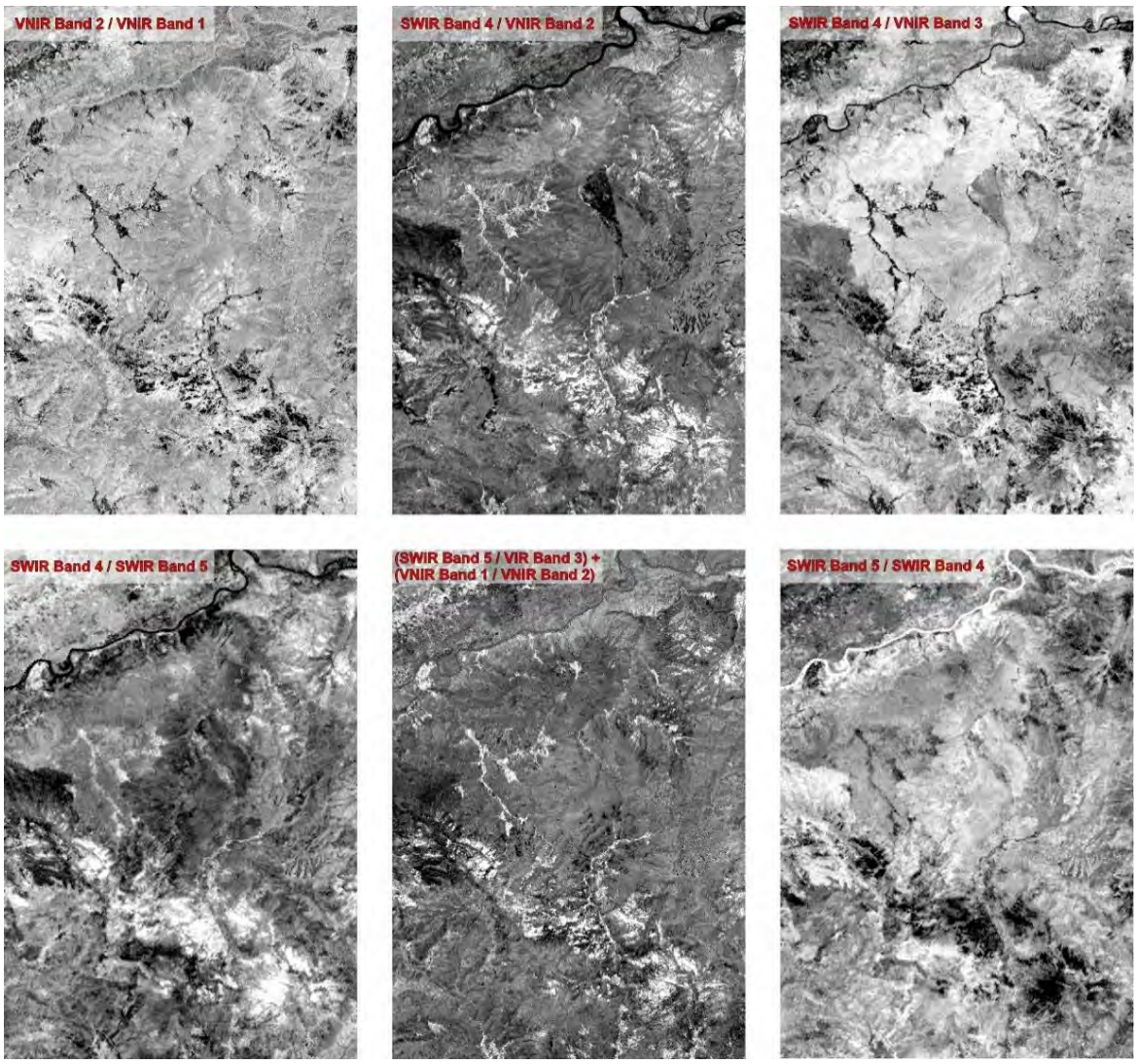

Figure 5. Band algorithms that are applied and represent images

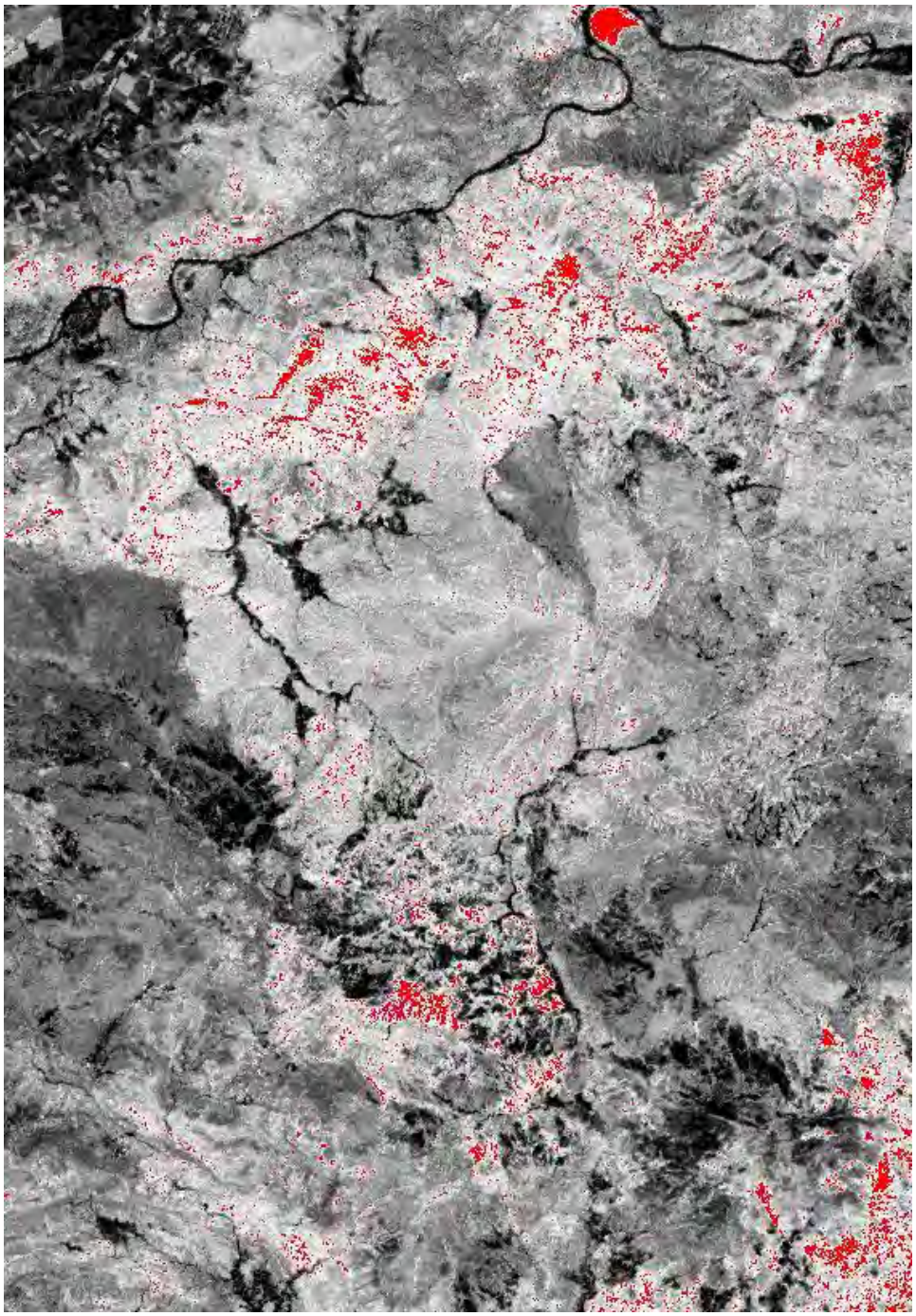

Figure 6. In the method using the Ferric Oxides Index, it was determined that the brightest pixels indicate high FeOx (iron oxide) alteration.

ACKNOWLEDGMENT

This study was supported by the Firat University Scientific Research Projects Coordination Unit with Project Number FÜBAP-MF.24.79.

REFERENCES

URL-1: https://earth.google.com
URL-2: https://terra.nasa.gov/data

IMAGING ANALYSIS OF ORE OCCURRENCES WITHIN UPPER CRETACEOUS LAVA SEQUENCES (KOÇKALE, ELAZIĞ-TÜRKİYE)

Melek URAL[1,*], Mustafa EĞRİ[2]

[1]*Firat University, Faculty of Engineering, Department of Geological Engineering, 23119, Elazığ,TURKEY*
[2]*Pamukkale University, Faculty of Engineering, Geological Department, 20020, Denizli,TURKEY*
**Corresponding author: melekural@firat.edu.tr*

A B S T R A C T

Iron-manganese-rich ore occurrences in the Koçkale area (Elazığ) and its surroundings have been identified within the Maden Complex Unit in studies conducted in recent years. Indeed, previous studies have emphasized that these formations likely developed within the Maden Complex unit, including both syngenetic deposits associated with volcanosedimentary mudstones and epigenetic formations potentially located within the fracture zones of hydrothermal mineralizations. In this study, detailed map combinations based on data from current maps, primarily MTA maps, have shown that these formations developed within the Yüksekova Complex in association with an Upper Cretaceous-aged volcanosedimentary lava series. The location of the ore-bearing formations on the geological map, along with the locations of previously mined and potential ore veins in the reserve area, were created by modifying the MTA 1:500,000-scale map. The resulting map was overlaid onto previously created geological maps and satellite imagery, and its accuracy was verified through the necessary checks. As a result, this image processing and multispectral image analysis study revealed that the outcrop mineral occurrences in the Koçkale region of Elazığ Province are located within Upper Cretaceous lava series.

Key words: *Koçkale, upper cretaceous, volcanic-sedimentary lavas, ore-bearing deposits*

1. INTRODUCTION

The study area is located approximately 30 km southeast of Elazığ Province, which lies along the Southeast Anatolian Fault Zone (Figure 1). This area encompasses the village of Koçkale, which is under the jurisdiction of the provincial center, and has been designated as the study area. Other villages within the target area include Yenikapı, Gölardı, Dereboğazı, Elmapınarı, Korucu, and Aluskomu (Figure 1). In the study area, where volcanic-sedimentary units (Figure 2) are primarily exposed, ore occurrences associated with these volcanic-sedimentary formations are present. The mineralizations near Koçkale Village have been previously discussed as a mining area that was operated for a period in the past (Altunbey and Sağıroğlu, 1995).

2. MATERIAL AND METHODS

2.1. Material

The ASTER satellite image, which covers a large area, was cropped to the target area and then projected to UTM-WGS84 Zone 37. ASTER images with different spatial resolutions (VNIR=15m, SWIR=30m, TIR=90m) were upscaled or downscaled to ensure all images were consistent at a 30-meter resolution (Figures 3, 4).

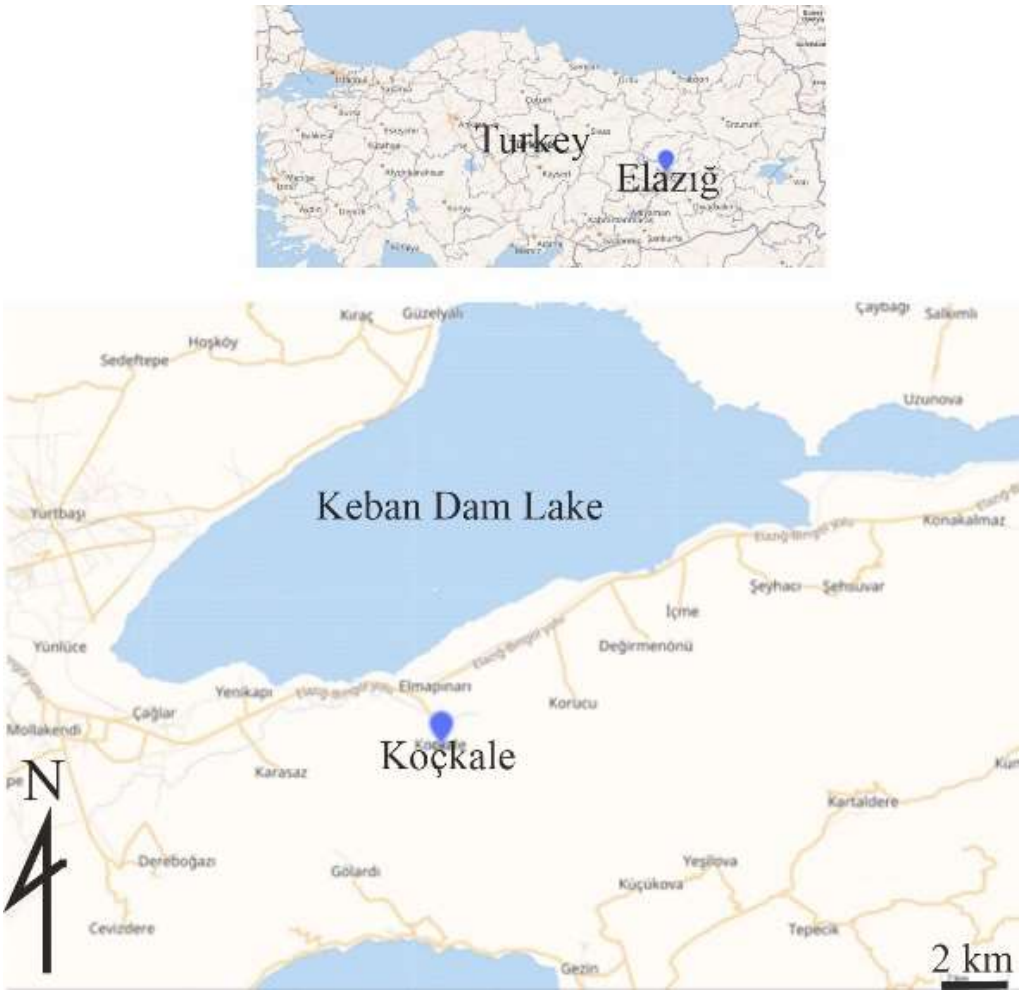

Figure 1. The map showing the location of the study area.

Figure 2. a, b) Volcanosedimentary sequences, including ore deposits

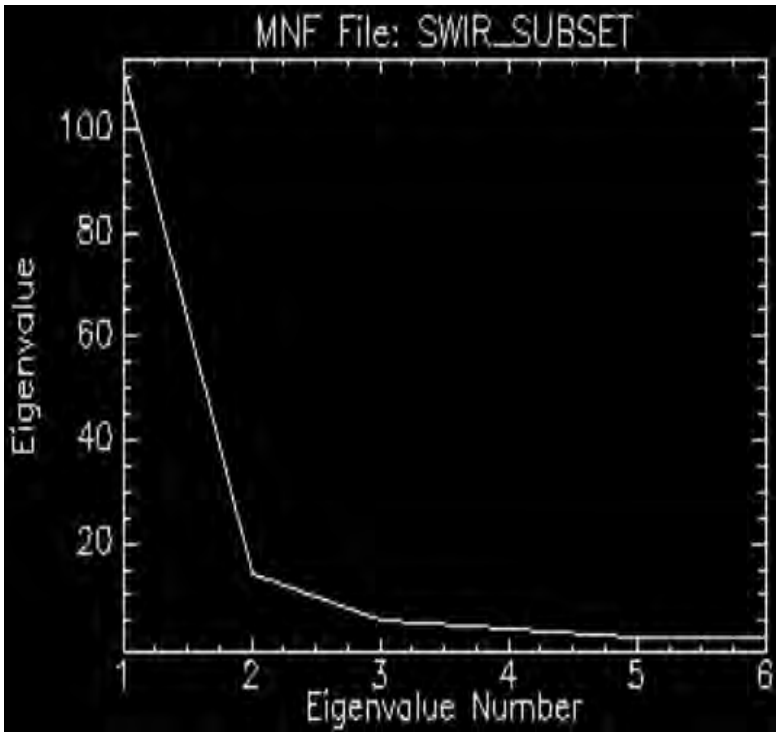

Figure 3. Subset-eigenvalue plot of the obtained images

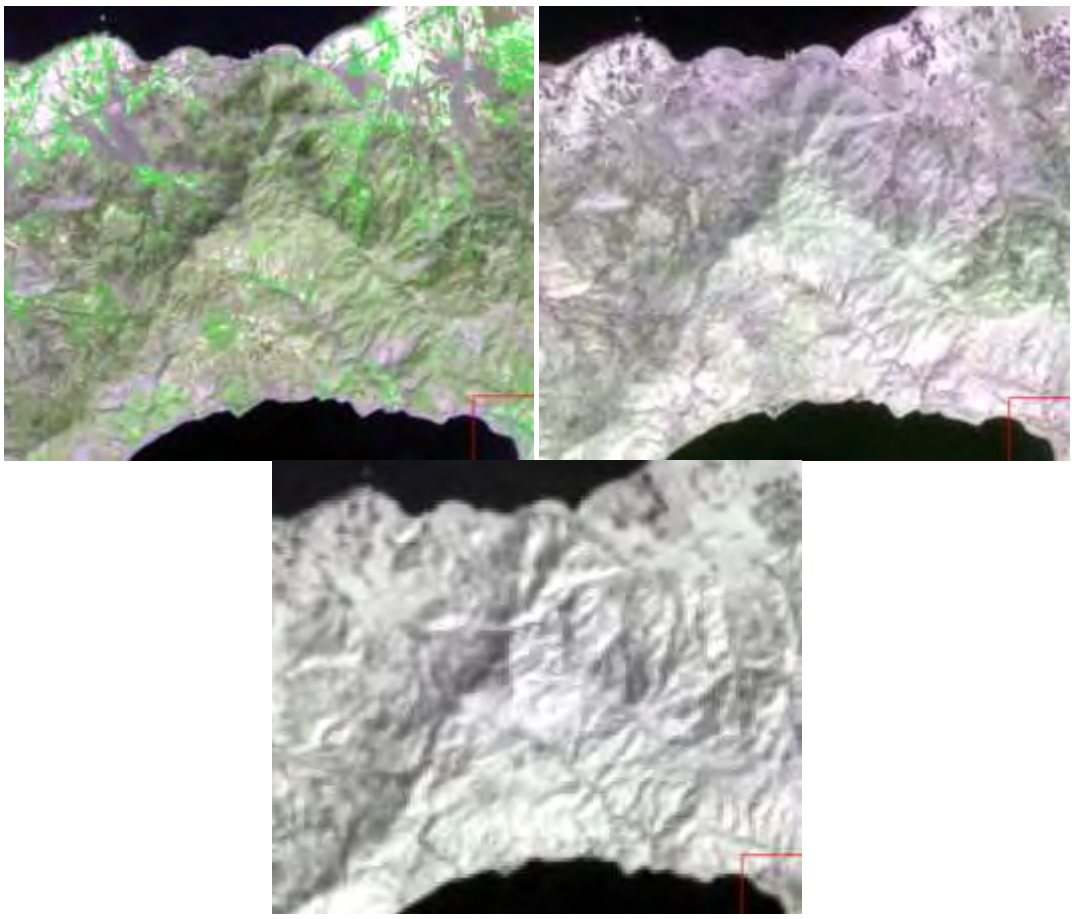

Figure 4. ASTER images with different spatial resolutions (VNIR=15 m, SWIR=30 m, TIR=90 m) (a: VNIR=1/2/3N, b: SWIR=4/5/6, c: TIR=10/11/12)

3. RESULTS AND DISCUSSION

As a result, using image processing and multispectral imagery, the mineralized hydrothermal veins and mining areas (indicated by red circles) in the Koçkale region of Elazığ Province were successfully mapped onto the geological maps (Figures 5, 6). The generated map was first overlaid onto the geological map and the Aster satellite image, and its accuracy was verified through the necessary checks (Figures 5, 6). This image processing and multispectral image analysis revealed that the ore occurrences exposed in the Koçkale region of Elazığ Province are located within Upper Cretaceous lava series.

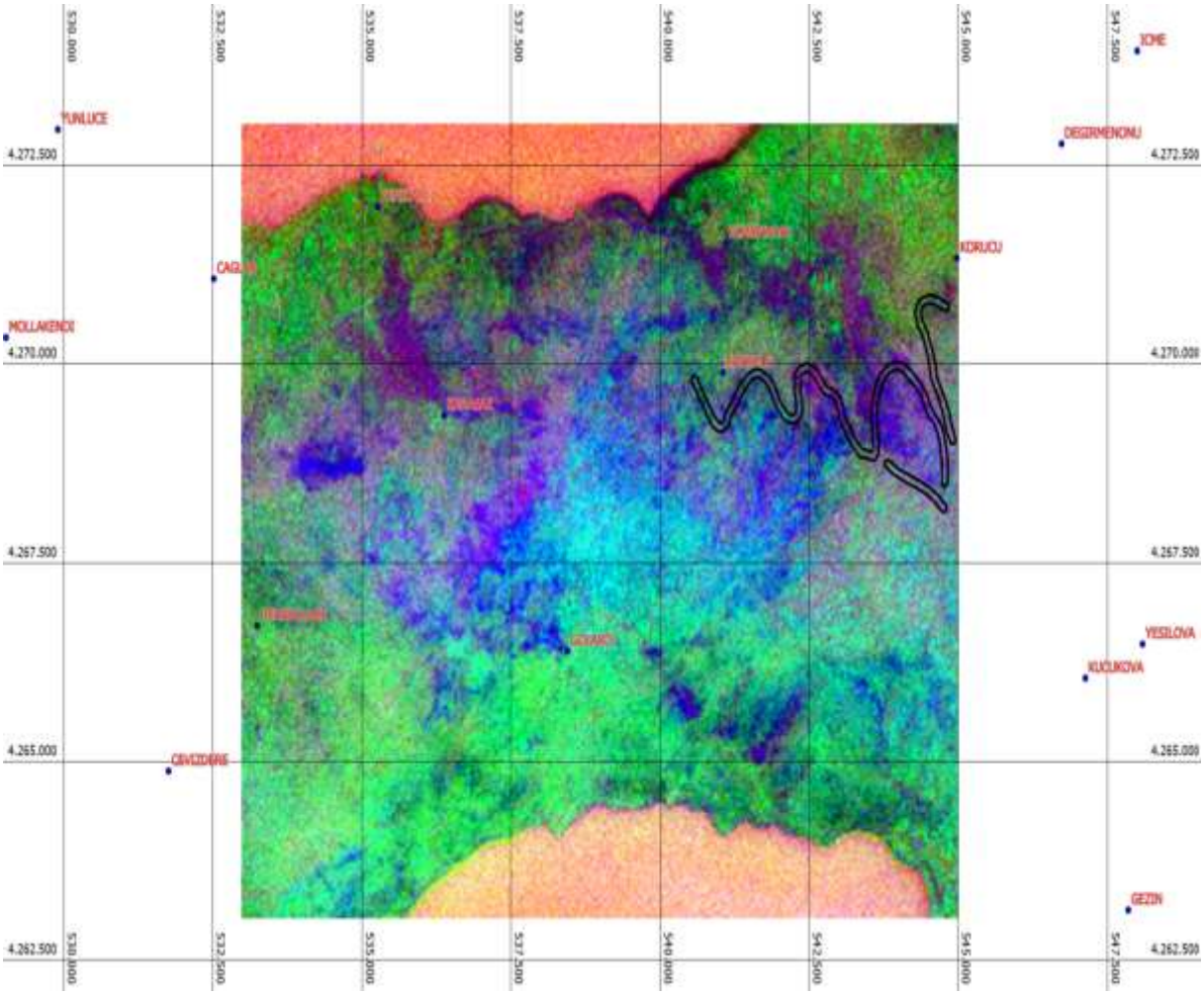

Figure 5. The location of ore-bearing formations in the region on the composite map (revised from Sertdemir et al., 2024)

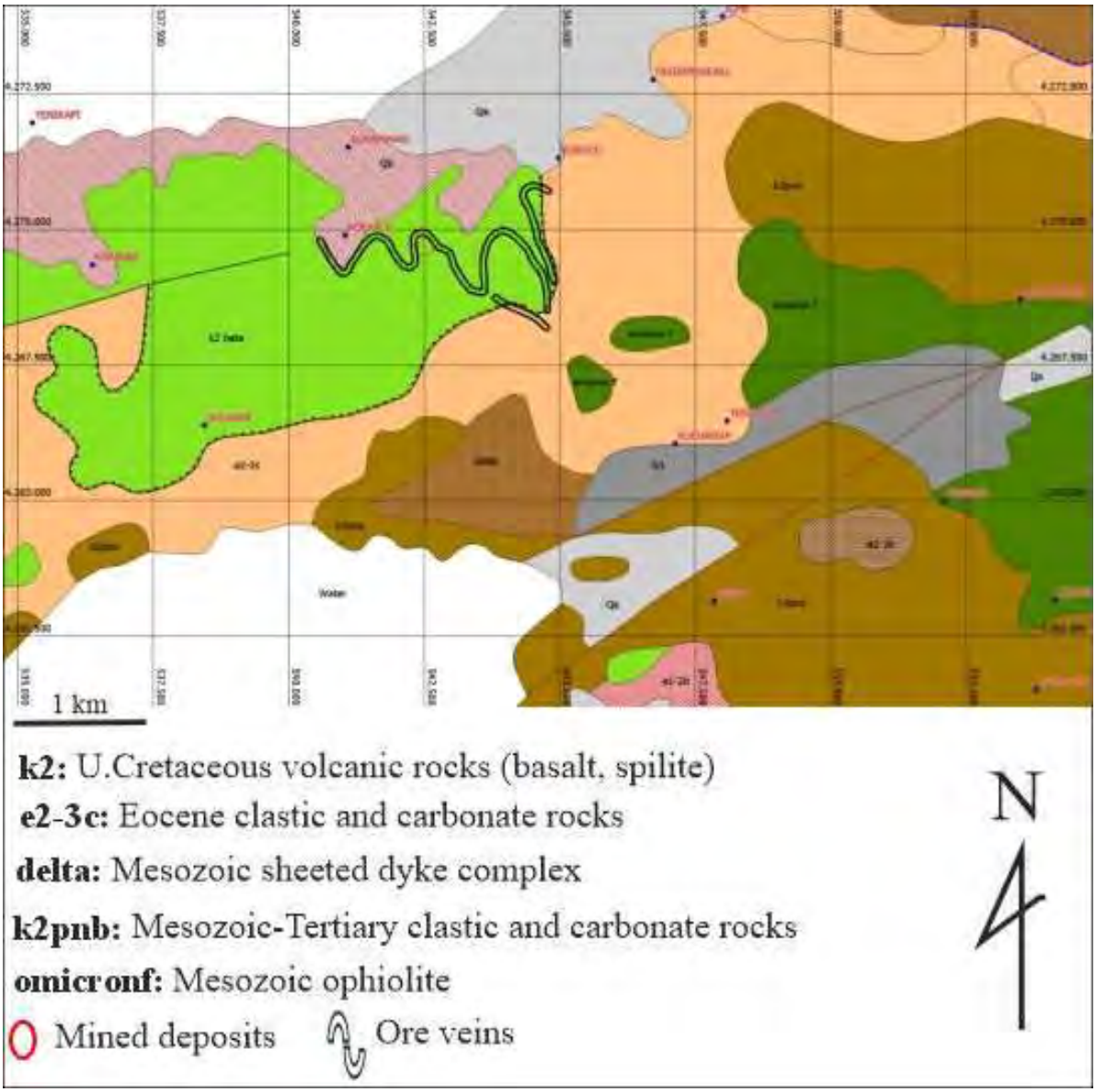

Figure 6. The location of ore-bearing formations on the geological map. Location of ore veins in previously mined areas and potential reserve areas (adapted from the MTA 1:500,000 scale map; revised from Altunbey and Sağıroğlu, 1995)

4. CONCLUSION

As a result, the volcanosedimentary units (purple-colored areas) in the Koçkale region of eastern Elazığ Province have been lithologically distinguished through image processing and multispectral image analysis. These maps, created by overlaying the data onto a geological map and the Aster satellite imagery and subjecting them to the necessary checks, have been validated with over 80% accuracy (Figure 7).

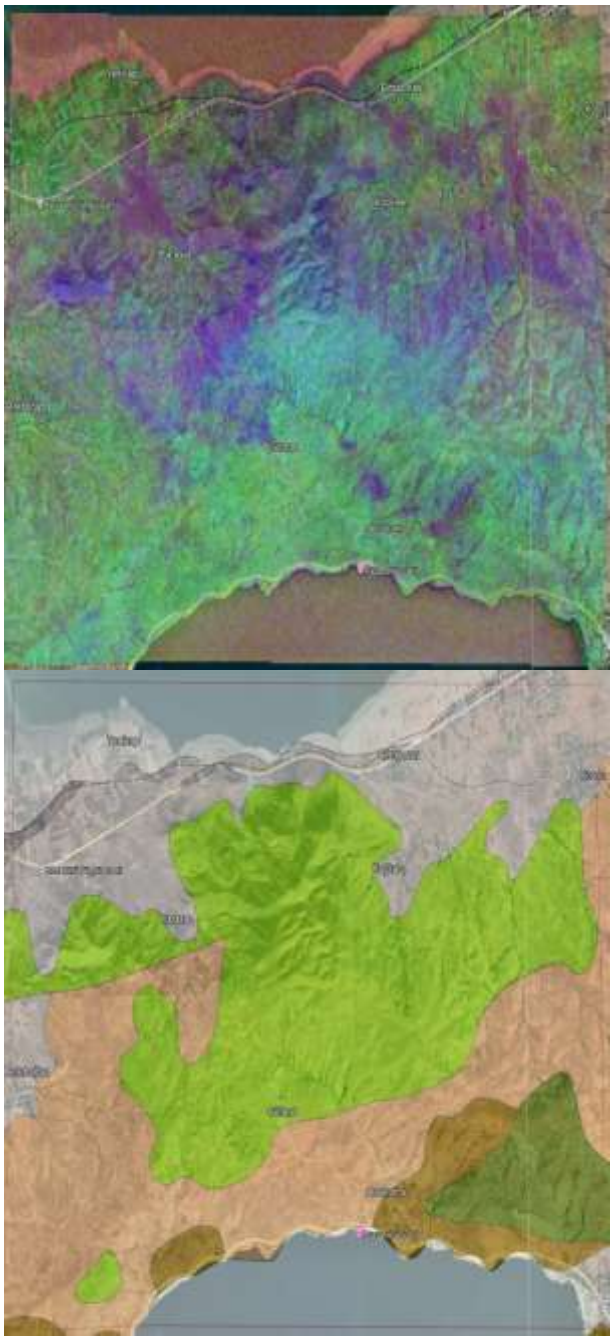

Figure 7. Maps verified by overlaying them onto a geological map and the Aster satellite imagery and performing the necessary checks. The light green areas represent Upper Cretaceous volcanosedimentary sequences.

REFERENCES

Altunbey, M., Sağıroğlu, A., (1995) “Characteristics and origin of the Koçkale-Elazığ manganese deposits”, Journal of Mineral Exploration and Research, 117 139-148.

MTA (2002), “1:500,000 Scale Geological Map of Turkey”, General Directorate of Mineral Research and Exploration, Ankara.

Sertdemir, Ç., Ural, M., Eğri, M., (2024), “Detection of Koçkale (Elazığ) Manganese Mineralizations by Satellite Images”, 9th Symposium on Remote Sensing and Geographic Information Systems (UZAL-CBS 2024), Proceedings, October 17–19, Aksaray.

MINERALOGICAL CONTROLS AND BENEFICIATION ASSESSMENT OF VANADIUM (V) ENRICHED META-GABBROIC ROCKS FROM THE AZITEPE–ALAŞEHİR (MANİSA, TÜRKIYE) AREA

N. Merve SÜTÇÜ[1,*], Zeynep DÖNER[1], Mustafa KUMRAL[1], Tülay TÜRK[2], Gülşah GÜVEN[2]

[1]*Istanbul Technical University, Faculty of Mines, Geological Engineering Department, 34469, Maslak, Istanbul, TÜRKİYE*
[2]*Istanbul Technical University, Faculty of Mines, Mineral Processing Engineering Department, 34469, Maslak, Istanbul, TÜRKİYE*
**Corresponding author: sutcun@itu.edu.tr*

A B S T R A C T

V is a critical metal vital for renewable energy technologies and high-performance alloys. This study examines Late-Neoproterozoic meta-gabbroic rocks from the Azıtepe-Alaşehir (Manisa, Türkiye) area to evaluate the mineralogical controls, liberation behavior, and recoverability of V through mineral processing experiments. The intrusion comprises a relatively well-preserved magmatic core (meta-gabbro) and progressively metamorphosed marginal amphibolites. Petrographic and ore microscopy observations reveal abundant Fe–Ti–(V) oxides (5–25 vol%), mainly Ti-magnetite, magnetite, and ilmenite. EPMA analyses of Fe–Ti–(V) oxides indicate that V is primarily incorporated into magnetite (up to 0.60 wt.% V_2O_3). V substitution can also be in silicate minerals, confirming partial redistribution during metamorphism. These microanalytical results are consistent with the beneficiation data, which show that a significant proportion of V remains in nonmagnetic silicate-rich fractions. Dry-disc high magnetic separation tests revealed that V is hosted in magnetite and partially distributed in silicate phases. Dry disc magnetic separation results demonstrate progressive V enrichment with decreasing particle size, reaching up to 776 ppm in -212 + 106 µm size fraction. This study suggests that under optimized grinding conditions, subsequent wet high-intensity magnetic treatment and gravity separations can provide more efficient recovery of Fe–Ti–(V) oxides compared to dry-disc magnetic separation for finer size fractions.

Key words: *Dry-disc magnetic separation, Fe–Ti–V, meta-gabbro, Menderes Massif, magnetite*

1. INTRODUCTION

The rising importance of critical elements is driven by rapid technological transformation and shifts in the global economy, which have elevated certain minerals to strategic status. Their high demand and limited supply create geopolitical vulnerabilities, as supply disruptions or price volatility can threaten economic stability and industrial continuity. Although national definitions of critical minerals vary according to economic and technological priorities, several elements consistently emerge as globally significant, and the critical mineral strategies implemented by major economies and political unions (e.g., the United States, the European Union, Japan, the United Kingdom, and Australia) play a decisive role in shaping short- and medium-term natural resource policies (e.g., BEIS, 2022; DISR, 2023; European Commission, 2023; USDOE, 2023). Among these, vanadium (V) has recently gained increasing attention and has been included in the current critical raw materials lists of both the European Union and the USGS, with respect to high supply risk and high economic importance (European Commission, 2023; U.S. Geological Survey, 2024). V is widely used in high-strength low-alloy (HSLA) steels and titanium alloys, where it improves mechanical strength, durability, and high-temperature performance, and it is also extensively applied in aerospace components such as gas turbines and airframes due to its favorable strength-to-weight ratio (Kelley et al., 2017; Polyak, 2012); moreover, in the energy sector, vanadium redox batteries (VRBs) are increasingly recognized as a key large-scale storage technology owing to their long service life, high operational safety, and lower carbon footprint compared to lithium-ion systems.

Vanadiferous titanomagnetite (VTM) deposits represent the most economically significant source of V and are commonly linked to mafic–ultramafic intrusions, where V is incorporated into Fe–Ti oxides such as Ti-magnetite, magnetite, and ilmenite. The genesis of Fe–Ti-(V) oxide deposits is typically associated with several magmatic processes, such as fractional crystallization accompanied by crystal settling and sorting, liquid immiscibility, magma addition and mixing, and fluctuations in oxygen fugacity and pressure (e.g., Cawthorn and McCarthy, 1980; Klemm et al., 1985; Lee et al., 2022; Namur et al., 2010; Reynolds, 1985; Wager and Brown, 1968; Zhou et al., 2005).

In this scope, the Late Neoproterozoic Azıtepe–Alaşehir (Manisa) gabbroic intrusion, located within the central Menderes Massif, has been proposed as a potentially V-bearing titanomagnetite system (Figure 1a; Sutcun et al., 2025). Similar late Neoproterozoic gabbroic intrusions occur in the central Menderes Massif (Candan et al., 2016), including Azıtepe, and were subjected to polyphase metamorphic evolution. These bodies are currently represented by meta-gabbro, garnet amphibolite, and amphibolite (Gürsu et al., 2023, and references therein). Previous investigations in the region have focused primarily on regional geological evolution, petrographic characteristics of the gabbroic units, and Ti enrichment (Kun et al., 1988; Candan, 1994, 1996; Candan et al., 1998, 2001; Sümer et al., 2002; Sümer, 2005). This study aims to investigate the mineralogical controls on V–Ti enrichment and to assess the beneficiation potential of V–Ti-bearing meta-gabbroic rocks from the Azıtepe area. In this context, the distribution, textural characteristics, and mineral-chemical behavior of Fe–Ti–(V) oxide phases are examined, and their response to physical separation methods is evaluated to determine the factors governing V concentration and recovery efficiency.

2. GEOLOGICAL BACKGROUND

The Menderes Massif (MM), covering approximately 60,000 km², represents the largest metamorphic core complex within the Anatolide–Tauride block of southwestern Türkiye. The Menderes Massif (MM) consists of two principal units. The first is the Late Neoproterozoic Pan-African basement, also referred to as the core series, which is predominantly composed of meta-clastic sediments represented by paragneiss and schists. This basement sequence is intruded by granitoid rocks (orthogneisses) and gabbroic rocks (meta-gabbro/norite, eclogite, and amphibolite) (Dora et al., 2001). Zircon U–Pb crystallization ages of these gabbroic rocks indicate values of 563 ± 1 Ma (Candan et al., 2016) and 554–537 Ma (Gürsu, 2023). This basement is unconformably overlain by a Paleozoic to Early Tertiary cover series (e.g., Candan et al., 2001; Catlos and Çemen, 2005; Candan et al., 2011). The Paleozoic units mainly consist of quartzite, marble, and phyllite (Dora et al., 2001) and are locally cut by Triassic leucocratic metagranites. The Mesozoic cover units comprise platform-type marbles of Triassic to Upper Cretaceous age, Upper Campanian–Upper Maastrichtian pelagic carbonates, and an overlying Middle Paleocene–Eocene flysch-type blocky unit (Candan et al., 2011, references therein).

The Azıtepe gabbroic intrusion is emplaced within high-grade Pan-African metamorphic rocks—such as augen gneisses, marbles, and migmatites—of the Ödemiş–Kiraz (Central) MM sub-massif (Figure 1b; Gökalp and Ünal, n.d.). The meta-gabbro and the surrounding Pan-African units are unconformably overlain by Paleozoic formations (Figure 1b). This entire metamorphic assemblage is subsequently covered by Neogene to Quaternary lacustrine sediments, while Lower Miocene lacustrine epiclastic deposits are intruded by Middle Miocene andesitic rocks (Figure 1b).

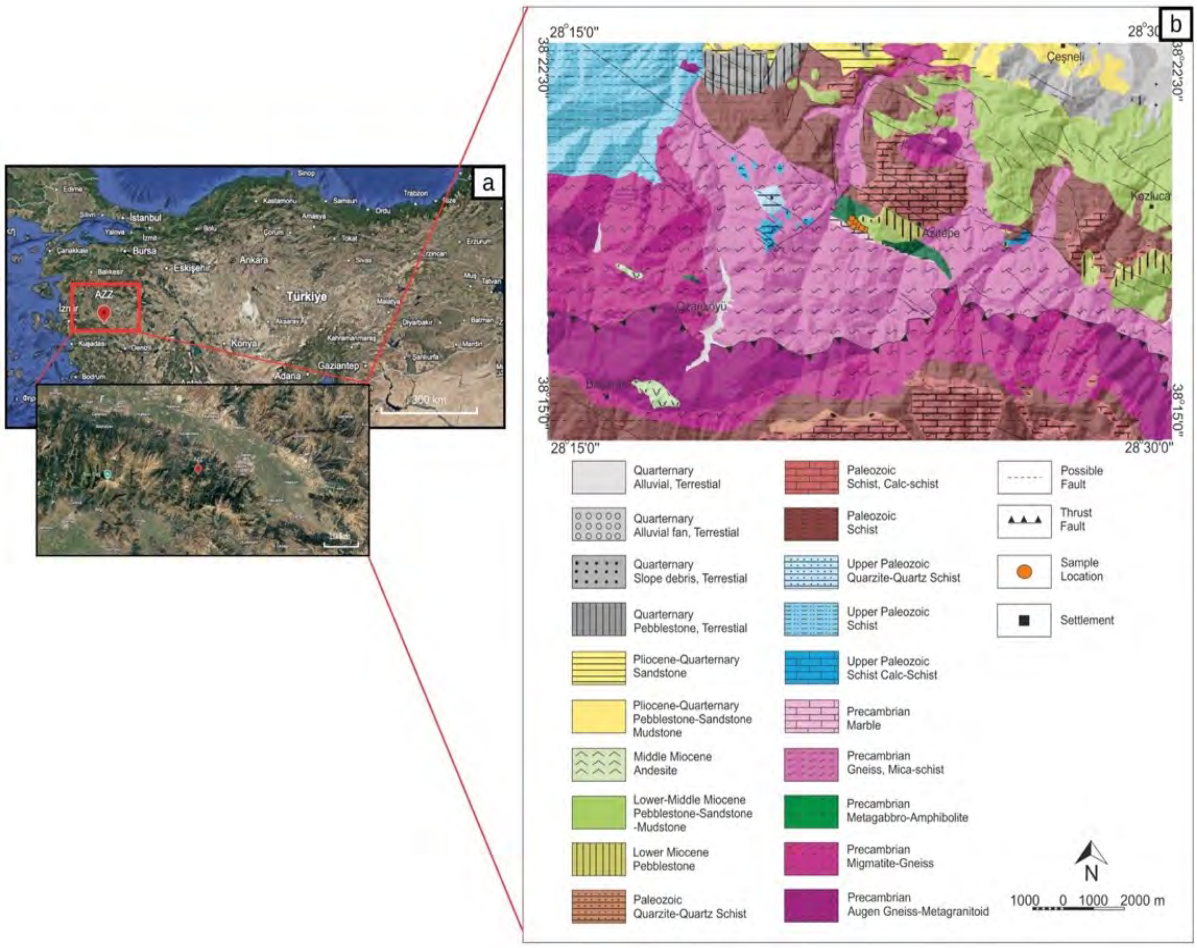

Figure 1. (a) Location of the study area (b) Geological map of the study area (modified from Gökalp and Ünal, n.d.)

The meta-gabbroic body forms an elliptical intrusion characterized by a comparatively well-preserved central core retaining primary gabbroic textures, whereas its marginal zones are dominated by strongly metamorphosed amphibolitic rocks (Sümer, 2005). The core lithologies are largely undeformed and only minimally altered, preserving their primary igneous textures and mineral assemblages, which allows them to be readily distinguished from the surrounding amphibolites. In the coarse-grained varieties, relict pyroxene and plagioclase crystals are commonly preserved. In contrast, some of the amphibolite rocks display a yellowish-brown coloration and have undergone intense weathering; their fine-grained and altered nature makes macroscopic identification of constituent minerals difficult.

3. MATERIAL AND METHODS

3.1. Material

Samples from the V-enriched Azıtepe metagabbroic rocks were thoroughly mixed to obtain a homogeneous representative sample. The particle size distribution is is shown in Figure 2. Cumulative undersize curve of the crushed sample plotted on log–log axes, showing the fitted power-law regression line (R^2 = 0.9887). Based on the cumulative undersize data, the characteristic particle sizes were calculated as d_{50}= 0.85, and d_{80}= 1.65 mm.

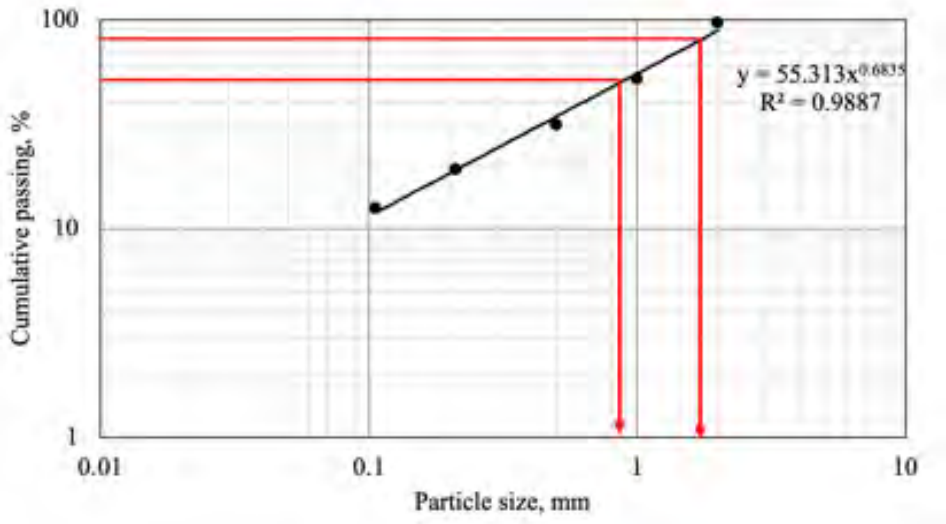

Figure 2. Particle size distribution of the representative ore sample

Whole-rock geochemical analysis was conducted at the Geochemistry Research Laboratories, Istanbul Technical University (ITU/JAL). Whole-rock major and trace element measurements were conducted with a Bruker S8 TIGER wavelength-dispersive X-ray fluorescence (WDXRF) spectrometer, running in a 0.01–12 nm wavelength range with an analytical uncertainty of less than 5%. The analysis was completed on finely powdered samples homogenized and mixed with chemical binders in appropriate ratios, pressed with a HERZOG pellet press. The detection limit was 0.01 wt.% for major oxides and 1 ppm for trace elements. Loss on ignition was estimated prior to XRF analysis to quantify volatile contents. A portion of about 1.5–2 g of the powdered samples heated in the oven was transferred to pre-heated porcelain porcelain crucibles and ignited at 1050 °C for 1.5 hours in a muffle furnace. After cooling in a desiccator, the weight loss was taken and reported as LOI (%). The analytical precision was tested with certified reference materials (CRM) treated in identical ways. The run-of-mine material contains approximately 493 ppm V, 18.4 wt.% Fe_2O_3, 4.47 wt.% TiO_2, and 38.7 wt.% SiO_2 (Table 1).

Table 1. Chemical composition of the representative sample (in wt. %, ppm)

Oxides	**SiO_2**	**Al_2O_3**	**Fe_2O_3**	**MgO**	**CaO**	**Na_2O**	**K_2O**	**TiO_2**	**P_2O_5**	**MnO**
Content, %	38.7	11.2	18.4	8.51	9.76	1.21	1.32	4.47	0.34	0.23
Element	**V**	**Ni**	**Cu**	**Zn**	**Rb**	**Sr**	**Zr**	**Nb**	**Ba**	**Pb**
Content, ppm	493	127	57	301	20	417	157	28	167	50

3.2. Method

The run-of-mine sample was classified into six particle-size fractions. The +2 mm and −0.106 mm fractions were excluded from magnetic separation due to their coarse and ultra-fine characteristics, respectively. The remaining four size fractions (−2+1 mm, −1+0.5 mm, −0.5+0.212 mm, and −0.212+0.106 mm) were subjected to dry magnetic separation using a laboratory-scale, dry disc magnetic separator capable of generating high magnetic field strengths of up to 10500 Gauss. All of the four size fractions, identical same operating conditions were applied to ensure consistency and comparability of the separation results. The experimental flowchart using dry disc magnetic separation procedure is illustrated in Figure 4. The magnetic separation experiments were conducted at the Department of Mineral Processing Engineering at Istanbul Technical University.

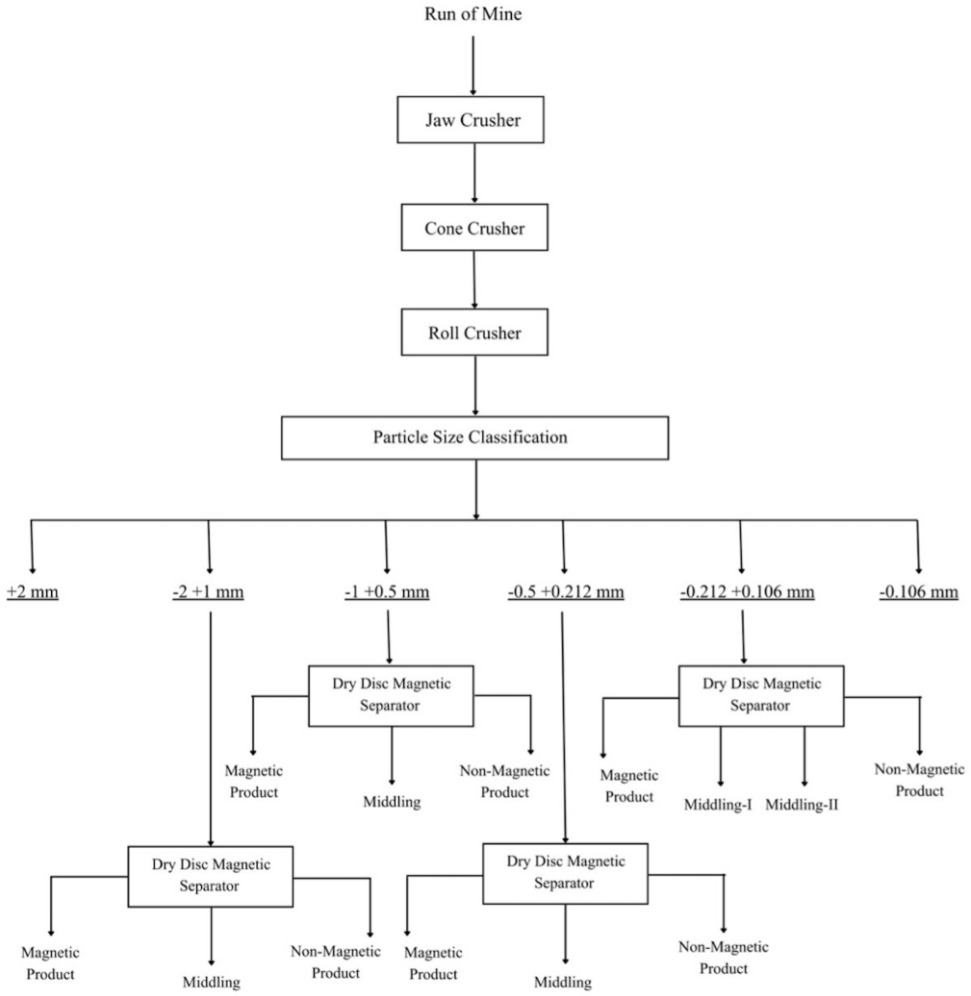

Figure 3. Flowchart of the magnetic separation experiments.

For each particle-size interval, the separator produced three distinct products based on magnetic susceptibility: a magnetic fraction containing strongly magnetic minerals, middlings fraction composed of weakly magnetic or partially liberated grains, and a non-magnetic fraction dominated by silicate minerals. In the −0.212+0.106 mm size range, the middlings were further subdivided into two products (middlings-I and middlings-II) to allow a more detailed evaluation of mineral partitioning.

4. RESULTS AND DISCUSSION

4.1. Mineralogical and Petrographical Examinations

The Azıtepe intrusion comprises a relatively well-preserved magmatic core and progressively metamorphosed marginal zones, defining two principal lithologies: meta-gabbro and amphibolite (Figures 4a, b, d, e). The meta-gabbros preserve primary igneous assemblages composed of clinopyroxene, orthopyroxene, plagioclase, amphibole, clinozoisite, and abundant opaque phases (Figure 4c). In contrast, the amphibolites are dominated by amphibole and plagioclase, with subordinate clinozoisite, biotite, chlorite, rutile, garnet, and opaque minerals (Figure 4f).

In addition, meta-gabbros contain 15–25 vol% opaque minerals, predominantly Ti-magnetite, magnetite, and ilmenite, with minor hematite, goethite, and sulfides (Figure 4g-i). Amphibolites exhibit comparable overall opaque proportions (5–25 vol%), but these are generally finer-

grained, with relatively lower magnetite and higher ilmenite contents (Figure 4j-k). In meta-gabbros, magnetite typically occurs as subhedral to anhedral grains and commonly displays trellis-type ilmenite exsolution lamellae oriented subparallel to the (111) plane of magnetite (Figure 4g). These microtextures indicate subsolidus high-temperature oxidation and exsolution of the ulvöspinel component within Ti-magnetite (Buddington and Lindsley, 1964; Taner et al., 1998).

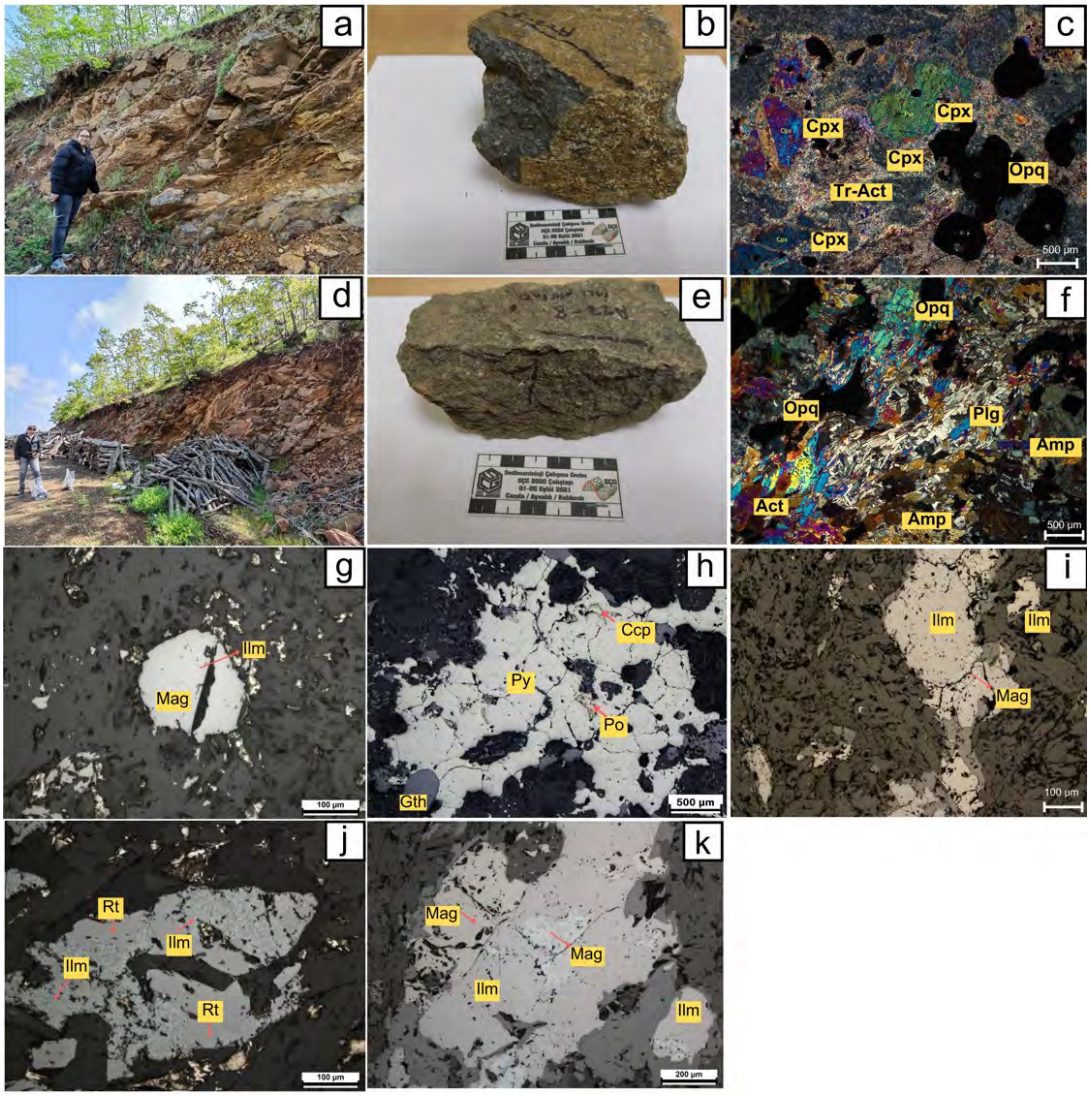

Figure 4. General view of the study area (a,d), hand specimens (b,e), and [thin (c, f) and polished (g-k) sections] of Azıtepe samples.

The investigated meta-gabbroic rocks are enriched in Fe, Ti, Ni, Cr, and V, with V concentrations ranging from 355–473 ppm in meta-gabbros and 217–628 ppm in amphibolites, and EPMA analyses of possible V-bearing oxides (magnetite, ilmenite, and rutile) indicate preferential partitioning of V into magnetite, where it reaches 0.22–0.70 wt.% (Sutcu et al., 2025).

4.2. Mineral Beneficiation Experiments

The beneficiation experiments in this study were focused to Fe–Ti–(V) oxide–bearing meta-gabbroic rocks from the Azıtepe intrusion, where V is mainly concentrated in magnetite and titanomagnetite. In this context, the method chosen was dry disc magnetic separation. In

addition, the chemical compositions of the magnetic, middling, and non-magnetic products obtained for each particle size fraction are presented, respectively (Table 2).

Table 2. Results of dry disc magnetic separator test.

Size fractions, mm	Product	Amount, %	V		TiO_2		SiO_2		Fe_2O_3	
			C, ppm	R, %	C, ppm	R, %	C, ppm	R, %	C, ppm	R, %
+2		100.0	487.0	100.0	4.30	100.0	38.6	100.0	18.6	100.0
-2+1	Magnetic	8.9	565.0	10.7	4.37	8.6	35.3	8.44	16.3	7.99
	Middling	1.2	507.0	1.3	5.83	1.6	38.4	1.28	17.9	1.22
	Nonmagnetic	89.9	461.0	88.0	4.52	89.8	37.4	90.3	18.4	90.8
	Total	100.0	470.8	100.0	4.52	100.0	37.2	100.0	18.2	100.0
-1+0,5	Magnetic	16.8	596.0	20.5	6.98	25.1	38.3	16.4	20.8	19.6
	Middling	2.6	501.0	2.7	8.19	4.6	37.9	2.54	18.4	2.72
	Nonmagnetic	80.6	463.0	76.8	4.06	70.3	39.3	81.0	17.1	77.7
	Total	100.0	486.3	100.0	4.66	100.0	39.1	100.0	17.7	100.0
-0,5+0,212	Magnetic	12.4	619.0	16.4	9.79	26.5	32.4	10.6	28.3	17.8
	Middling	21.6	474.0	21.9	6.02	28.4	35.0	19.9	24.3	26.8
	Nonmagnetic	66.0	436.0	61.7	3.13	45.1	39.8	69.5	16.5	55.4
	Total	100.0	466.9	100.0	4.58	100.0	37.9	100.0	19.6	100.0
-0,212+0,106	Magnetic	8.2	776.0	13.4	14.0	24.8	28.9	6.47	31.3	11.4
	Middling-I	25.1	490.0	25.9	5.38	29.2	35.7	24.4	24.2	26.9
	Middling-II	35.2	459.0	33.9	2.40	18.2	38.0	36.4	22.8	35.5
	Nonmagnetic	31.5	404.0	26.7	4.07	27.7	38.2	32.8	18.7	26.1
	Total	100.0	475.6	100.0	4.63	100.0	36.7	100.0	22.6	100.0
-0,106		100.0	485.0	100.0	4.22	100.0	38.9	100.0	19.6	100.0
TOTAL		100.0	476.1	100.0	4.52	100.0	37.9	100.0	24.3	100.0

C:Content, R:Recovery

When the results are evaluated, it is observed that finer particle size is accompanied by an increase in V content, together with corresponding increases in Ti and Fe contents, whereas Si content shows a slight decreasing trend. In particular, as particle size decreases, a greater proportion of material is recovered in the magnetic fraction, and the associated V content reaches up to 776 ppm. This behavior suggests that V content increases with the finer particle sizes and/or is partly locked within composite grains that require further size reduction for effective liberation. The test results indicate that complete mineral liberation was not achieved within the investigated particle size fractions. Consequently, these observations demonstrate the limitations of dry magnetic separation for fine and insufficient liberated particles and therefore require the application of wet high intensity magnetic separation (WHIMS), which is more effective for processing finer size fractions.

4. CONCLUSION

In conclusion, dry disc magnetic separation results demonstrate progressive V enrichment with decreasing particle size, reaching up to 776 ppm in the finest fraction. However, incomplete liberation limits separation efficiency. These findings indicate that V enrichment is controlled primarily by Fe–Ti oxide minerals and partially distributed in silicate phases. that high-intensity magnetic separation methods (e.g., WHIMS) are required for improved recovery. Also, gravity separation can be employed according to the mineralogical analysis of the sample which consist of minerals with high specific gravity such as magnetite, Ti-magnetite and minerals with low specific gravity such as silicate minerals.

REFERENCES

BEIS (2022) ‘‘Resilience for the future: The United Kingdom’s critical minerals strategy’’, Department for Business, Energy & Industrial Strategy.

Buddington, A.F., and Lindsley, D.H. (1964) ‘‘Iron–titanium oxide minerals and synthetic equivalents’’, Journal of Petrology, 5, 310–357.

Candan, O. (1994) ‘‘Alaşehir kuzeyinde (Menderes Masifi, Demirci–Gördes Asmasifi) gözlenen metagabroların petrografisi ve metamorfizması’’, Türkiye Jeoloji Bülteni, 37 (1), 29–40.

Candan, O., (1996) ‘‘Kiraz-Birgi gevresindeki (Menderes Masifi / Ödemiş-Kiraz Asmasifi) metagabrolann petrografisi ve metamorfizması’’, Yerbilimleri, 18, 1-25.

Candan, O., Dora, O.Ö., Oberhansli, R., Çetinkaplan, M., Oelsner, F., Dürr, S., (1998) ‘‘Menderes Masifi’nde iki farklı yüksek basınç metamorfizması’’, 51. Türkiye Jeoloji Kurultayı 52.

Candan, O., Dora, O.Ö., Oberhänsli, R., Çetinkaplan, M., Partzsch, J.H., Warkus, F.C., and Dürr, S. (2001) ‘‘Pan-African high-pressure metamorphism in the Precambrian basement of the Menderes Massif, western Anatolia, Turkey’’, International Journal of Earth Sciences, 89, 793–811.

Candan, O., Koralay, O., Topuz, G., Oberhänsli, R., Fritz, H., Collins, A., and Chen, F. (2016) ‘‘Late Neoproterozoic gabbro emplacement followed by early Cambrian eclogite-facies metamorphism in the Menderes Massif (W Turkey): Implications for the final assembly of Gondwana’’. Gondwana Research, 34, 158–173.

Candan, O., Oberhänslı, R., Dora, O. Ö., Çetinkaplan, M., Koralay, E., Rımmelé, G., ... & Akal, C. (2011) ‘‘Polymetamorphic evolution of the Pan-African Basement and Palaeozoic–Early Tertiary cover series of the Menderes Massif’’, Bulletin of the Mineral Research and Exploration, 142(142), 121-163.

Catlos, E.J., and Çemen, I. (2005) ‘‘Monazite ages and the evolution of the Menderes Massif, western Turkey’’, International Journal of Earth Sciences, 94, 204–217.

Cawthorn, R.G., and McCarthy, T. (1980) ‘‘Variations in Cr content of magnetite from the Upper Zone of the Bushveld Complex—Evidence for heterogeneity and convection currents in magma chambers’’, Earth and Planetary Science Letters, 46, 335–343.

DISR. (2023) ‘‘Australia Critical Minerals Strategy’’, 2023–2030. Department of Industry, Science and Resources.

Dora, O.Ö., Candan, O., Kaya, O., Koralay, E., and Dürr, S. (2001) ‘‘Revision of “leptite gneisses” in the Menderes Massif: A supracrustal metasedimentary origin’’, International Journal of Earth Sciences, 89, 836–851.

European Commission (2023) ‘‘Study on the critical raw materials for the EU 2023 – Final report’’, Brussels: European Commission.

Gökalp, E., and Ünal, D. (n.d.) 1/25.000 ölçekli sayısal jeoloji haritası, İzmir L20-b3 Paftası. Maden Tetkik ve Arama Genel Müdürlüğü, Ankara.

Gürsu, S., Möller, A., Inglis, J.D., Göncüoğlu, M.C., Hefferan, K., Toksoy-Köksal, F., Küçük, A., and Köksal, S. (2023) ‘‘Tracing the protoliths of the garnet amphibolitic and retrogressed eclogitic slices of the Central Menderes Massif, Turkey’’. Bulletin, 135, 2486–2509.

Kelley, K.D., Scott, C.T., Polyak, D.E., and Kimball, B.E. (2017) Vanadium. In K.J. Schulz, J.H. DeYoung Jr., R.R. Seal, II, and D.C. Bradley, Eds., Critical Mineral Resources of the United States—Economic and Environmental Geology and Prospects for Future Supply, Professional Paper 1802, U1–U36. U.S. Geological Survey.

Klemm, D., Henckel, J., Dehm, R., and von Gruenewaldt, G. (1985) ‘‘The geochemistry of titanomagnetite in magnetite layers and their host rocks of the eastern Bushveld Complex’’ Economic Geology, 80, 1075–1088.

Kun, N., Candan, O., and Dora, O.Ö. (1988) ‘‘Kiraz–Birgi yöresinde (Ödemiş Menderes Asmasifi) metavolkanitlerin (leptitlerin) varlığı’’, Türkiye Jeoloji Bülteni, 31 (2), 21–28.

Lee, J., Yang, S., White, N.C., Shin, D., and Kim, E. (2022) ‘‘Whole-rock geochemistry and mineral compositions of gabbroic rocks and the associated Fe–Ti (–V) oxide deposit in the Gonamsan intrusion’’, South Korea. Ore Geology Reviews, 148, 105054.

Namur, O., Charlier, B., Toplis, M.J., Higgins, M.D., Liégeois, J.-P., and Vander Auwera, J. (2010) ‘‘Crystallization sequence and magma chamber processes in the ferrobasaltic Sept Îles layered intrusion’’, Canada. Journal of Petrology, 51, 1203–1236.

Polyak, D.E. (2012) Vanadium. In Metals and minerals: U.S. Geological Survey Minerals Yearbook 2011 (Vol. I, pp. 80.1–80.9). U.S. Geological Survey.

Reynolds, I.M. (1985). ‘‘Contrasted mineralogy and textural relationships in the uppermost titaniferous magnetite layers of the Bushveld Complex in the Bierkraal area north of Rustenburg’’, Economic Geology, 80, 1027–1048.

Sutcu, N.M., Doner, Z., Kumral, M., Unluer, A.T., and Ciftci, E. (2025) ‘‘Origin and evolution of vanadium (V) enrichment in Azıtepe (Alaşehir-Manisa) meta-gabbroic rocks in Menderes massif (Western Turkiye)’’. Geochemistry, 85 (3), 126321

Sümer, E.Ö. (2005) Petrologic and metallogenic features of gabbro and metagabbro in the Menderes Metamorphites (Southwest Manisa-Alaşehir) (PhD Thesis). Hacettepe University, Ankara, Türkiye.

Sümer, E.Ö., Koruyucu, M., Kırkoğlu, M., Ağrılı, H., Kayakıran, S., Çokyaman, S., Demirhan, M., and Minareci, F. (2002) ‘‘Menderes Masifi, Manisa-Alaşehir Güneyinde Yeralan Azıtepe Metagabrosundaki Titanyum Cevher Oluşumunun Jeolojik Özellikleri’’, 55. Türkiye Jeoloji Kurultayı Bildiri Özleri, 259–260.

Taner, M.F., Ercit, T.S., and Gault, R.A. (1998) ‘‘Vanadium-bearing magnetite from the Matagami and Chibougamau mining districts, Abitibi, Quebec, Canada’’, Exploration and Mining Geology, 7, 299–311.

U.S. Department of Energy (USDOE) (2023) ‘‘Notice of Final Determination on the 2023 DOE Critical Materials List’’, U.S. Department of Energy, Washington, DC.

U.S. Geological Survey (2024). ‘‘Mineral Commodity Summaries 2024’’, U.S. Geological Survey, 212.
Wager, L.R., and Brown, G.M. (1968) Layered igneous rocks. Edinburgh: Oliver and Boyd.

Zhou, M., Robinson, P.T., Lesher, C.M., Keays, R.R., Zhang, C.-J., and Malpas, J. (2005) ‘‘Geochemistry, petrogenesis and metallogenesis of the Panzhihua gabbroic layered intrusion and associated Fe–Ti–V oxide deposits, Sichuan Province, SW China’’, Journal of Petrology, 46, 2253–2280.

HYDROMETALLURGY, PYROMETALLURGY AND BIO-PROCESSING

A BRIEF HISTORICAL DEVELOPMENT OF REFRACTORIES

Arman EHSANI[1,*], Ilhan EHSANI[2]

[1]Adana Alparslan Türkeş Science and Technology University, Faculty of Engineering, Mining Engineering Department, 34469, Sarıçam, Adana, TÜRKİYE
[2]Şırnak University, Engineering Faculty, Mining Engineering Department, Şırnak-TÜRKİYE
**Corresponding author: aehsani@atu.edu.tr*

A B S T R A C T

Refractory materials can withstand high temperatures and the physical and chemical interactions of substances at these temperatures. In the classification of materials, refractory materials are categorized as non-metallics, which are often referred to as industrial ceramics, and play a crucial role in mineral processing/mining and the pyrometallurgical industry.

From the perspective of historical development, the technological evolution of refractory materials started with the discovery of fire. Thus, all the technological and scientific developments we experience today have been made possible by the discovery and development of refractory materials. Refractory materials have been fundamental to the development of high-temperature technologies since the earliest stages of human civilization.

This extended review presents a brief chronologically structured expression of the historical evolution of refractory materials from prehistoric times to the present day, divided into two eras, i.e., the ancient (from the beginning to the 15th century) and the modern (from the 15th century). Particular emphasis is placed on the transition from natural clay-based refractories to engineered alumina-, magnesia-, carbon-, and zirconia-based systems, as well as recent trends toward recycling and sustainability. This study aims to draw attention to the refractory technology that has evolved over the centuries and the reasons behind this technology in a concise manner.

Key words: *Refractories, industrial ceramics, pyrometallurgy, raw materials, historical development, metallurgy, ceramics, industrial furnaces, sustainability*

1. INTRODUCTION

Refractory materials are defined as materials capable of tolerating high temperatures and resisting the physical and chemical interactions of gases, liquids, and solids under extreme thermal conditions. Etymologically derived from the Latin term refractarius, meaning resistant or persistent, refractories constitute a fundamental class of industrial ceramic materials. They are typically characterized by high melting points, chemical stability, heterogeneous microstructures, and relatively high porosity (Norton, 1968; DPT, 2001; Garbers-Craig, 2008).

Their capability to preserve dimensional stability and functional performance under such extreme service conditions enables the safe and efficient operation of industrial units. In other words, refractory materials are indispensable components of all high-temperature industrial systems, including metallurgy, glass production, ceramics, and energy generation. Defined as materials capable of maintaining structural integrity and chemical stability under extreme thermal, mechanical, and chemical conditions, refractories represent a technological bridge between raw materials and industrial transformation processes (Norton, 1968; Surendranathan, 2015).

Refractory materials are indispensable components of furnaces, kilns, reactors, and other high-temperature systems used in metallurgy, ceramics, glass production, and energy-intensive industries. While modern refractory systems are the result of advanced ceramic

engineering, their conceptual foundations extend back to early human efforts to confine and control high-temperature reactions. Initial refractory applications developed through experimentation with fire, leading to the selection of clay-rich materials capable of enduring repeated heating cycles (Kingery et al., 1976; Wildgoose, 2004).

The historical development of refractories closely parallels the evolution of pyrotechnology. As early societies learned to control fire for metal extraction, pottery firing, and construction, the need for heat-resistant materials emerged naturally. Over time, empirical knowledge gradually transformed into scientifically designed refractory systems, particularly after the Industrial Revolution and the emergence of materials science as a discipline. Consequently, the evolution of civilization, metallurgy, and industrial technology has proceeded in parallel with the development of refractory materials (Kingery et al., 1976; Refractories Institute, 1987, Lee and Moore, 1998).

Previous studies have often addressed specific periods or technological developments in isolation. This review differs by presenting a continuous, chronologically integrated narrative that links early clay-based refractories to contemporary high-performance and sustainable refractory systems. This study presents a fully chronological review of refractory material development, beginning with prehistoric applications and progressing through ancient, medieval, and modern technological stages, based exclusively on historical, mineralogical, and technological information documented in the literature. The historical development of refractory materials (both ancient and modern times) will be briefly discussed in this study.

2. HISTORICAL DEVELOPMENT OF REFRACTORIES

2.1. Ancient Era (from the beginning to the 15th century)

The earliest archaeological evidence of heat-resistant materials dates back approximately 30,000 years, identified in primitive baking ovens discovered in China. These early structures represent humanity’s first attempts to control thermal environments for food preparation and material transformation (Refractories Institute, 1987).

By around 24,000–10,000 B.C., primitive clay ovens had become widespread in the Middle East, indicating a growing understanding of the thermal behavior of natural clays. Archaeological findings show that by 7000–6000 B.C., lime mortar was being used in shelter construction, marking one of the earliest applications of thermally processed mineral binders. During the same period, evidence of plaster and gypsum usage suggests increasingly sophisticated thermal processing techniques (Garbers-Craig, 2008; Sugita, 2008). In Mesopotamia, particularly during the Sumerian period, arsenical copper and early tin bronze metallurgy required clay-based furnace linings with enhanced thermal resistance (Chen, 2021).

The earliest refractory materials were derived almost exclusively from naturally occurring clays and aluminosilicate-rich soils. Archaeological studies indicate that Neolithic communities utilized clay-lined hearths and simple pit furnaces for pottery and early metalworking (Nicholson and Shaw, 2000; Tite, 2008). Between 6500 and 6000 B.C., pottery kilns constructed from clay materials were widely used in West Asia and Anatolia. These installations required controlled heating cycles and represented the first intentional use of refractory-like materials. In Anatolia, particularly in the Çayönü and Ergani regions, archaeological evidence reveals early copper pyrometallurgical operations dating between 6500 and 4000 B.C., further demonstrating the necessity of thermally stable furnace linings (Ehsani and Yazıcı, 2016; Garbers-Craig, 2008).

By approximately 4000–4500 B.C., ceramic firing ovens constructed from natural silicate stones and clay minerals were discovered in the Tepe Gawra region of Iraq. These furnaces achieved temperatures approaching 1100 °C, requiring improved resistance against thermal degradation. The increasing demand for higher temperatures led to progressive improvements in furnace lining materials (Sugita, 2008). In Ancient Egypt, refractory-like materials were applied in copper smelting furnaces as early as the third millennium B.C. These furnaces typically employed Nile silt mixed with sand and organic temper to enhance thermal resistance and mechanical stability (Nicholson and Shaw, 2000). Similarly, in this period, practices are documented in Anatolia, where early copper mining and smelting activities required furnace linings capable of withstanding high-temperatures (Ehsani and Yazıcı, 2016). Ceramic production technologies played a decisive role in early refractory development. According to Tite (2008), the control of firing temperature and kiln atmosphere represented a crucial step toward intentional material design, even if the underlying mechanisms were not scientifically understood.

The emergence of the Iron Age around 2000 B.C. represented a critical turning point in refractory development. Iron smelting demanded significantly higher temperatures and imposed severe mechanical, chemical, and abrasive conditions on furnace linings. Consequently, refractory concepts such as thermal insulation, chemical resistance, and wear resistance became essential functional requirements for furnace design (Garbers-Craig, 2008). During this period, refractory materials were primarily composed of silica-rich rocks, fireclays (Al_2O_3–SiO_2), and mixtures of charcoal and clay. These materials were used extensively in Europe, China, and Japan. Although empirically developed, these early refractories formed the conceptual foundation of modern refractory technology (Sugita, 2008).

In classical antiquity, Greek and Roman civilizations advanced furnace construction techniques through the systematic use of lime-based mortars. These binders improved the structural stability and thermal endurance of kilns and metallurgical furnaces. During the Classical Greek and Roman periods, refractory materials became increasingly sophisticated. Roman engineering achievements, particularly in large-scale construction and metallurgy, demanded more reliable heat-resistant materials (Oleson, 2008). Roman lime kilns, glass furnaces, and metalworking installations utilized refractory bricks produced from selected clays with controlled particle size distributions. The development of concrete vaulted structures further required kiln technologies capable of producing consistent high-temperature materials (Lancaster, 2005). Although refractories were still produced empirically, systematic craftsmanship and accumulated experience resulted in improved durability and thermal performance. These advances laid the foundation for later medieval furnace technologies.

The emergence of proto-porcelain in China during the Shang and Zhou periods involved high-fired ceramic bodies that required refractory kiln environments, reflecting early mastery of controlled high-temperature processes (Yin et al., 2011). By approximately 600 A.D., porcelain production in China was achieved in kilns operating at temperatures approaching 1350 °C, representing one of the most advanced thermal technologies of the ancient world (Garbers-Craig, 2008).

The medieval era (especially the late medieval period) marked a significant expansion in metallurgical activity, particularly iron production in bloomery and early blast furnaces. Around 1400 A.D., the first European blast furnaces capable of operating near 1500 °C were introduced for iron production. These furnaces were fueled by charcoal, and their linings during this period relied primarily on silica- and alumina-rich clays and chamotte-type fireclays, often locally sourced and adapted through trial and error (Norton, 1968; Yılmaz and Kurnaz, 2001; Sugita, 2008). Also, throughout the Middle Ages, the widespread use of brick and clay products led to gradual improvements in kiln technology. Fireclay-based bricks became common in glass and ceramic industries, although production remained localized and empirical in nature (Hockensmith, 2002). A landmark contribution to metallurgical knowledge is Georgius

Agricola's De Re Metallica, first published in 1556. Agricola (1950/1556) provided detailed descriptions of furnace construction, refractory stone selection, and maintenance practices, representing one of the earliest systematic technical documentations of refractory usage. These developments demonstrate a transition from purely empirical methods toward semi-systematic engineering approaches, although scientific material characterization had not yet emerged. In other words, despite the absence of mineralogical or thermodynamic understanding, this period established continuity in refractory practice and preserved high-temperature knowledge across centuries. Moreover, the growing scale of metallurgical operations during this era significantly increased the demand for more durable and chemically resistant refractory materials, setting the stage for the technological transitions of the modern period.

The historical/technological evolution of refractory materials is briefly illustrated in Table 1 (Kingery et al., 1976; Garbes-Craige, 2008; Sugita, 2008; Tite, 2008; Ehsani and Yazıcı, 2016).

Table 1. Brief historical development of refractory materials in the Ancient Era

Period	Technological Development
~28.000-10.000 B.C.	First usage of refractory materials. First usage of baking ovens in the Middle East. Evidence of the first burnt clay artifacts (23.000 B.C.- Dolni Figurines- Czech Republic)
10.000-6000 B.C.	First controlled firing, primitive kilns in Neolithic societies. Usage of Clay, mud, and straw-reinforced earth. Ancient Egyptians used molds of Steatite to pour or press glass (7000 B.C.).
~7000-4500 B.C.	First usage of lime mortar in construction. Pottery and clay cooking ovens were discovered in West Asia and Türkiye. The first pyro-metallurgical processes of Cu were discovered in Anatolia.
~6000-3000 B.C.	Usage of Brick kilns, early ceramics in Mesopotamia, Fireclay-type alumina-silicate clays.
~4500- 2000 B.C.	Ceramic baking ovens from natural silicate stones and clay minerals discovered in Iraq. Drying ovens are made up of aggregate and clay materials.
3000-2000 B.C.	Glass melting furnaces in Ancient Egypt. The usage of alumina silicate materials. Usage of clay and silica-rich materials in copper smelting furnaces in Anatolia.
2000-1200 B.C.	Iron Age (2000-1000 B.C.); iron-containing materials were produced by reducing iron ore in a furnace using charcoal; Hittite Civilization in Anatolia; Usage of iron oxide-bearing clays in iron smelting. Glass and porcelain glazing and coating processes were first realized in China (1750-1150 BC).
1200-300 B.C.	Usage of kaolinite, silica-rich clays in Ancient China (1200-500 B.C.) High temperature porcelain Klins; Usage of siliceous clays, lime mortars in Metallurgical furnaces in Ancient Greece (800-300 B.C.).
1-600 A.D.	Greeks and Romans used lime mortar in furnace constructions (1-400 A.D.). Usage of brick and pozzolanic materials in the Roman Empire. Porcelain production began in China with furnaces reaching 1350 °C.
500-1000 A.D.	Usage of Aluminosilicate refractories in Advanced glass and ceramic production in İslamic World.
1000-1400 A.D.	Medieval Europe; First production of iron in a blast furnace (1500 °C); Charcoal was used as fuel; Rocks and chamotte clay (based on Al_2O_3 and SiO_2) were used as refractory materials.

2.2. Modern Era (From 15th Century)

In this section, we will focus on the historical development of Si-, Si-O-Al-O, MgO-C, CrO-MgO composite, and modern refractories. To better understand the historical development of refractory materials in the modern era, we divide this era into four distinct periods. The first period covers the transition to industrial refractory materials, the development of refractories during the early Industrial period, and spans from the 15th to the 19th century. The second period, named the Industrial Revolution and scientific refractory engineering era, spans from the 19th century to the 1950s. This era contains the development of refractories during the Industrial Revolution. The third part of this era spans from the 1950s until the 2000s, during which advances in modern refractory systems, such as the development of monolithic and Zr-based refractories, occurred. The last part of this era, from the 2000s to the present, focuses on emerging trends in refractories and environmental sustainability in the production process of these materials.

In the first period, i.e., from the 15th to the 19th century, as mentioned before, Agricola's De Re Metallica represents a milestone in documenting furnace construction and refractory usage, bridging empirical practice and early scientific understanding (Agricola, 1556/1950). From the 15th century onward, metallurgical demand increased due to weapon manufacturing, mining expansion, and early industrialization. The Industrial Revolution fundamentally transformed refractory technology. Rapid growth in iron production and the development of continuously operating blast furnaces imposed unprecedented thermal and chemical demands on furnace linings (Habashi, 2012). Furnace sizes grew, operating temperatures increased, and refractory failure became a major economic concern. During this period, silica and fireclay refractories became dominant materials, particularly in ironmaking operations. Improved quarrying and material selection practices contributed to more reliable furnace performance (Norton, 1968).

During the second period, the Industrial Revolution fundamentally transformed refractory technology. Large blast furnaces, coke-based ironmaking, and continuous production demanded materials with consistent chemical composition and predictable thermal behavior (Geerdes et al., 2009). By the late nineteenth century, refractory materials began to be classified according to their chemical behavior under high-temperature conditions. The concepts of acidic, basic, and neutral refractories were established, particularly in response to slag–refractory interactions in steelmaking processes (Chesters, 1973). This classification system marked a critical step toward scientific refractory engineering and enabled more rational material selection in metallurgical furnaces (Norton, 1968). Silica bricks were first invented in England in 1820 and commercially produced in South Wales by 1842. These materials exhibited excellent high-temperature strength and abrasion resistance but suffered from low thermal shock resistance due to polymorphic phase transformations of quartz (Norton, 1968; Garbers-Craig, 2008). By 1858, lime-bonded silica bricks were patented in England, and shortly thereafter, similar developments occurred in the United States. Silica refractories dominated steel furnace applications until the mid-20th century, when basic refractories capable of withstanding higher operating temperatures became increasingly important (Sugita, 2008). Moreover, Carbon and graphite-based refractories represent another critical technological milestone. Graphite exhibits extremely high refractoriness, sublimating at approximately 3600 °C, and demonstrates excellent thermal and electrical conductivity. The first graphite crucibles were produced in 1834, followed by graphite blocks in 1863 (Garbers-Craig, 2008). Silicon carbide, first produced commercially in 1891, offered high thermal conductivity and abrasion resistance, making it suitable for advanced furnace systems (Geçkinli, 1991; Garbers-Craig, 2008).

The growing complexity of metallurgical systems during this era created the conditions necessary for the later scientific investigation of refractory behavior. By the late 19th and early 20th centuries, refractories began to be classified according to chemical composition, such as acidic, basic, and neutral materials. The introduction of magnesia and dolomite refractories

significantly improved steelmaking efficiency (Norton, 1968; Refractories Institute, 1987). This period also marked the emergence of refractory manufacturing as an industrial sector rather than a craft-based activity.

The first half of the 20th century represents the most transformative era in refractory technology. Advances in ceramic science enabled the systematic design of materials based on phase equilibria, microstructure control, and thermomechanical properties. In other words, this period witnessed the application of ceramic science principles to refractory materials. Fundamental studies on bonding mechanisms, sintering behavior, and phase equilibria significantly advanced refractory design (Kingery, 1950; Kingery et al., 1976). The publication of phase diagrams in the 1920s marked a scientific breakthrough that enabled the systematic design of alumina–silicate refractories. In 1926, mullite bricks were produced in the United States, followed by sintered corundum bricks in Germany in 1931 and fused-cast alumina bricks in 1936 (Garbers-Craig, 2008). Lee and Moore (1998) documented the evolution of in situ refractories, highlighting innovations such as monolithic refractories, castables, and gunning materials. These developments reduced installation time and improved furnace availability. The use of chromite as a refractory raw material expanded significantly due to its high refractoriness and corrosion resistance in metallurgical environments (McEwan et al., 2011). Simultaneously, global steel industry growth accelerated refractory research and standardization (Sugita, 2008). Another major transformation in refractory technology occurred with the development of unshaped or monolithic refractories. First introduced in the United States in 1914, these materials included castable, ramming mixes, and gunning materials. The discovery of calcium aluminate cement as a refractory binder in France in 1918 enabled the production of commercial castable. By the 1930s, pneumatic installation methods were introduced, allowing rapid furnace construction and repair. Although monolithic refractories accounted for only 2–3% of the market in the 1940s, their share increased dramatically, reaching nearly 44% by 2016 (Garbers-Craig, 2008; Reis, 2015). Monolithic refractories offer advantages such as lower installation cost, superior thermal shock resistance, and improved maintenance efficiency, making them indispensable in modern high-temperature industries.

In the post-1950 period, i.e., the third period, refractories evolved into highly engineered materials. High-purity alumina, zirconia, silicon carbide, and carbon-based refractories became essential for modern steel, non-ferrous metallurgy, and glass industries (Schacht, 2004; Surendranathan, 2015). From the 1970s onward, carbon-containing refractories—particularly magnesia–carbon bricks—revolutionized steelmaking technology. Their exceptional thermal shock resistance and reduced slag wettability significantly extended lining service life (Ewais, 2004). These materials became integral components of modern steel furnaces and remain among the most influential refractory developments of the twentieth century (Engel, 2013).

The development of the Bayer process for alumina production further accelerated refractory innovation. Calcined and tabular alumina became key raw materials, particularly after tabular alumina was first produced commercially in 1960. These materials provided superior purity, thermal stability, and corrosion resistance for high-performance applications. In addition, the rapid growth of steelmaking technologies led to an increasing demand for basic refractories. Magnesite-based refractories (MgO) became widely used due to their high melting point (~2800 °C) and excellent resistance to iron-rich slags (Garbers-Craig, 2008). Dolomite and magnesia–dolomite refractories gained importance with the introduction of basic oxygen furnaces (BOF) in the 1950s. However, the hydration sensitivity of CaO-containing refractories posed limitations, which were addressed through tempering and improved processing methods (Sugita, 2008). During the 1960s and 1970s, magnesia–carbon (MgO–C) refractories were developed, particularly in Japan, and became widely adopted in electric arc furnaces. These materials significantly extended refractory service life and remain essential components of modern steelmaking systems. Additionally, until the 1970s, carbon refractories were primarily used with pitch or tar binders. The introduction of resin-based binders in the early 1970s

substantially improved mechanical strength and oxidation resistance. Specialized refractories such as zircon ($ZrSiO_4$), zirconia (ZrO_2), and silicon carbide (SiC) were developed for severe service environments. Zircon refractories were first used in 1933 in the United States, while zirconia gained widespread application after the 1960s due to its exceptional chemical stability (Geçkinli, 1991; Garbers-Craig, 2008). Likewise, calcium zirconate ($CaZrO_3$), a high-performance ceramic material characterized by its high melting point, low thermal expansion, and excellent chemical and thermal stability, is also used in refractory applications, particularly in the form of MgO–$CaZrO_3$ composites exhibiting superior thermal shock and corrosion resistance in cement clinker production and high-temperature metallurgical environments (Krasny et al., 2024).

From 1990 until 2010, the influence of refractories on steel cleanliness and product quality received increased attention (Poirier, 2015). Simultaneously, environmental concerns related to chromium-containing refractories encouraged the exploration of alternative raw materials (McEwan et al., 2011). Monolithic refractories, including low- and ultra-low-cement castables, experienced widespread adoption due to their installation flexibility and improved thermo-mechanical performance (Lee and Moore, 1998). In this period, the global refractory industry has evolved into a technologically intensive sector. Market analyses indicate increasing demand for high-performance and environmentally sustainable materials (Deneen and Gross, 2010; Reis, 2015). Also, nanotechnology constitutes the latest phase in the historical development of refractory materials, reflecting a shift from traditional composition-based design toward microstructure-controlled systems. The introduction of nanoparticles such as nanosilica and nano-alumina has enabled improved densification, enhanced mechanical strength, and greater thermal shock resistance in castable refractories. This evolution represents a significant milestone in modern refractory technology, driven by the need for higher performance under increasingly severe industrial conditions (Sarkar, 2018; Roy et al., 2019). Additionally, global refractory producers have increasingly aligned product development with environmental regulations and digitalized industrial systems (Prietl, 2010). To last but not least, academic and industrial education programs continue to play a key role in transferring refractory knowledge to future engineers (Yılmaz et al., 2015; Geçkinli, 1991).

The historical/technological development of refractory materials is briefly illustrated in Table 2 (Norton, 1968; Chesters, 1973; Garbes-Craige, 2008; Sugita, 2008).

Table 2. Brief historical development of refractory materials in Modern Era

Period	Technological Development
1400-1800	Usage of fireclay bricks in iron production (15-16th century; continuous high furnaces). Usage of silica refractories in glass production (17th century). First usage of silicate rock, i.e., mica schist, (1645) and chamotte clay, chamotte brick, (1793) in the USA.
1800-1850	Invention of silica brick (1820) and first production (1842) in England. Mass industrialization and standardilization production of refractories (massive usage of fireclay and silica).
1850-1900	The invention of lime-bonded (CaO) silicate bricks was patented in England by Thomas James (1858). The first silicate brick patent (1858) and first production (1866) in the USA by J.P. Alexander in the state of Ohio. The first bauxite deposit in the USA was discovered in 1888. First usage of chromite ore (Cr_2O_3) as a refractory material in France (1879). First usage of chromite bricks in the USA (1896). Usage of Basic refractories (dolomite, magnesite). Application of basic refractories containing pitch in basic Bessemer furnaces (late 1800s).
1900-1950	Development of alumina-silicate refractory bricks in 1920's. High-purity alumina refractories and improved steel quality. First production of alumina silica (mullite) refractory in the USA (1926). In 1931, the development of sintered corundum brick in Germany (1931). First production of fused cast alumina brick in the USA (1936).

	Development of carbon refractories; Innovation of thermal shock resistance materials. (1930-1950s).
1950-2000	Development of basic refractory bricks (1950s). Application of Mg refractories in Siemens-Martin furnaces (1950-1960s). Development of refractory concretes and castable refractories (late 1970s and early 1980s). development of Monolithic refractories (1950s-1970s), caused in reducing downtime. Production of tabular alumina (1960s). Introduction of pitch-bonded dolomite, dolomite-magnesite, Mg-dolomite and magnesite bricks (late 1950s/early 1960s). Developing high-strength sintered MgO bricks (late 1960s). The development of Magnesite carbon (MgO-C) bricks in the USA (mid-1960s), all enhanced corrosion resistance. Application of MgO-C bricks in water-cooled electric arc furnaces in Japan (late 1970s). In recent years, due to the impact of climate change, the development of green, eco-friendly, computer-aided design of refractories has also taken place. The development of Zirconia-based refractories (1980s-2000s), caused specialized applications.
2000-2010	The development of low-cement castables, and focused on energy efficiency.
2010-2020	Chromite refractories affect the production cost-performance balance of materials. Development of nano-structured refractories caused in microstructural control of refractories. Nano-Modified Castables; Incorporation of nanosilica and nano-alumina into refractory matrices.
2020-present	Integration of nanotechnology with sustainability and performance optimization. Focuses on extended service life, reduced energy consumption, and next-generation refractory design strategies. Recycling and circular economy; sustainability in production processes.

4. CONCLUSIONS

The historical development of refractory materials reflects the technological evolution of human civilization itself. From primitive clay ovens to advanced oxide-carbon composite systems, refractories have continuously adapted to increasing temperature demands, aggressive chemical environments, and industrial efficiency requirements. Throughout history, advances in metallurgy, ceramics, and materials science have directly influenced refractory innovation. Modern refractory technology—characterized by engineered microstructures, high-purity raw materials, and optimized installation methods—represents the culmination of thousands of years of empirical knowledge and scientific progress. It took approximately 28.000 years for humankind to develop refractory materials to reach the required temperatures around 1600°C (i.e., iron production temperature) from the temperature of the flame.

The historical evolution of refractory materials demonstrates a continuous response to increasing thermal demands and industrial complexity. From primitive clay linings to engineered, sustainable refractory systems, each technological leap has enabled advances in metallurgy, ceramics, and energy production. Understanding this historical trajectory is essential for guiding future developments, particularly in the context of sustainability and advanced materials engineering. Based exclusively on the referenced literature, the historical evolution of refractory materials can be characterized as a progressive transformation:

- from empirical clay-based furnace linings in early metallurgy,
- to industrialized refractory production during the Industrial Revolution,
- followed by scientific material engineering in the twentieth century,
- and ultimately toward high-performance, sustainable, and nanostructured refractory systems in the modern era.

This chronological development reflects the close interdependence between refractory technology and the advancement of metallurgical, ceramic, and industrial engineering systems.

In closing, understanding the chronological evolution of refractory materials is essential not only for appreciating their technological significance but also for guiding future developments in sustainable and high-performance refractory systems.

REFERENCES

Agricola, G., (1950), De re metallica (H. C. Hoover and L. H. Hoover, Trans.), Dover Publications. (Original work published 1556).

Chen, L. B., (2021) “Sumerian arsenic copper and tin bronze metallurgy (5300-1500 BC): The archaeological and cuneiform textual evidence”, Archaeological Discovery, 09 (03) 185–197.

Chesters, J. H., (1973), Refractories: Production and properties, The Iron and Steel Institute.

Deneen, M. A., Gross, A. C., (2010) “Refractory materials: The global market, the global industry”, Business Economics, 45 (4) 288–295.

Devlet Planlama Teşkilatı (DPT), (2001), Taş ve toprağa dayalı ürünler sanayii özel ihtisas komisyonu raporu (Refrakter), OİK Report No: 567, Ankara.

Ehsani, A., Yazıcı, E. Y., (2016) “A brief history of copper mining and use in Anatolia”, Madencilik Türkiye Bilimsel, 5 (9), 43–48.

Engel, R., (2013), Magnesia-Carbon Brick: A Retrospective: The Refractories Engineer, 20–23.

Ewais, E. M. M., (2004) “Carbon based refractories”, Journal of Ceramic Society of Japan, 112 (10), 517–532.

Garbers-Craig, A. M., (2008) “How cool are refractory materials?”, Journal of the Southern African Institute of Mining and Metallurgy, 108 (9) 491–506.

Geçkinli, A. E., (1991), “İleri teknoloji malzemeleri”, İstanbul Teknik Üniversitesi Kimya-Metalurji Fakültesi.

Geerdes, M., Chaigneau, R., Lingiardi, O., (2020), Modern Blast Furnace Ironmaking (Fourth Edition), IOS Press under the imprint Delft University Press.

Habashi, F., (2012) “Refractories and the industrial revolution”, Interceraam Refractories, 2012 (1) 14–18.

Hockensmith, C. D., (2002) “A brief history of the brick and clay products industries in Kentucky: 1788-2002”, Ohio Valley Historical Archaeology, 17 73–90.

Kingery W. D. (1950) “Fundamental study of phosphate bonding in refractories: I, literature review”, Journal of the American Ceramic Society, 33 (8) 239–241.

Kingery, W. D., Bowen, H. K., Uhlmann, D. R. (1976), Introduction to Ceramics (Second Edition), John Wiley & Sons.

Krasny, B. L., Makarov, N. A., Ikonnikov, K. I., Lemeshev, D. O., Bernt, D. D., Galganova, A. L., Sizova, A. S. Rodimov, O. I., (2024) “Calcium zirconate: Methods of synthesis and applications of ceramic and refractory materials based thereon—A review: Part 2, Applications of ceramic and refractory materials based on calcium zirconate”, Glass and Ceramics, 81 (1) 73-77.

Lancaster, L., (2005), Concrete vaulted construction in imperial Rome, Cambridge University Press.

Lee, W. E., Moore, R. E., (1998) “Evolution of in situ refractories in the 20th century”, Journal of the American Ceramic Society, 81 (6) 1385–1410.

McEwan, N., Courtney, T., Parry, R. A., Knupfer, P., (2011) “Chromite—A cost-effective refractory raw material for metallurgical applications”, Southern African Pyrometallurgy, 359–372.

Nicholson, P. T., Shaw, I., (2000), Ancient Egyptian materials and technology, Cambridge University Press.

Norton, F. H., (1968), Refractories, 4th ed., McGraw-Hill.

Oleson, J. P., (2008), The Oxford Handbook of Engineering and Technology in The Classical World, Oxford University Press.

Poirier, J., (2015) “A review: Influence of refractories on steel quality”, Metallurgical Research & Technology, 112 (4), 410.

Prietl, T., (2010) “The World of Refractories and RHI AG as a Global Player and Reliable Partner”, The Southern African Institute of Mining and Metallurgy Refractories 2010 Conference, 9–22.

Refractories Institute, (1987), Refractories handbook, The Refractories Institute.

Reis, O. L., (2015) “Global refractories market overview”, Magmin Conference Proceedings.

Roy, J., Chandra, S., Maitra, S. (2019) “Nanotechnology in castable refractory, Ceramics International”, 45(1), 19–29.

Sarkar, R., (2018) “Nanotechnology in refractory castables—An overview, Interceram - International ceramic review”, 67(S1) 22–31.

Schacht, C. A., (2004), Refractories handbook, Marcel Dekker.

Sugita, K., (2008) “Historical overview of refractory technology in the steel industry”, Nippon Steel Technical Report, 98 1–10.

Surendranathan, A. O., (2015), An introduction to ceramics and refractories, CRC Press.

Tite, M. S., (2008) “Ceramic production, provenance and use-A review”, Archaeometry, 50 (2) 216–231.

Wildgoose, D. G., Johnson, A., Winstanley, R. B., (2004) “Glass/ceramic/refractory techniques, their development and introduction into dentistry: A historical literature review”, The Journal of Prosthetic Dentistry, 91 (2) 136–143.

Yin, M., Rehren, T., Zheng, J., (2011) “The earliest high-fired glazed ceramics in China: The composition of the proto-porcelain from Zhejiang during the Shang and Zhou periods (c. 1700–221 BC)”, Journal of Archaeological Science, 38 (9) 2352–2365.

Yılmaz, Ş., Kurnaz, C., (2001) “Metalurjik süreçler ve arkeometalurji”, Sakarya Üniversitesi Fen Bilimleri Enstitüsü Dergisi, 5 (1), 45–49.

Yılmaz, Ş., Toplan, Ö., Demirkıran, Ş., (2015) “Ceramic materials lecture notes: Refractory materials”, Sakarya University.

A NEW APPROACH TO STUDYING THE EFFECTS OF CYANIDE DOSAGE ON SILVER METAL THROUGH A QCM SENSOR

Ömer CANIEREN*, Cengiz KARAGÜZEL, Oktay ŞAHBAZ

Kütahya Dumlupınar University, Faculty of Engineering, Mining Engineering Department, 43270, Kütahya, TÜRKİYE
**Corresponding author: omer.canieren@dpu.edu.tr*

A B S T R A C T

This study investigates the usability of a QCM sensor-based system in the field of hydrometallurgy, extending its applications beyond those currently documented in the existing literature. The experimental set comprising a silver sensor, oscillator, and frequency counter was utilised in the system. Different amounts of NaCN solution were delivered to the sensor, whose sensing element is coated with silver, and the changes in the oscillation frequency of the QCM sensor were measured using the system. According to the obtained results, it was observed that the silver sensor placed in the oscillator circuit produced higher oscillations upon an increase in the amount of cyanide delivered to its surface due to higher mass loss. The changes in mass loss (Δm) corresponding to different NaCN concentrations, such as 0.5 g/L, 1 g/L, and 2 g/L, were calculated as 70,145.1 ng, 198,133.8 ng, and 231,179.7 ng, respectively, using the Sauerbrey equation. This method can help to shorter analyze the solubility of a silver metal like by a chemical solvent, and give useful information to accurate determine of reactive solvent dosage.

Key words: *Silver metal, sodium cyanide, hydrometallurgy, quartz crystal microbalance, Sauerbrey equation*

1. INTRODUCTION

Today, new recognition elements and their combinations are being studied due to the need for improvement in detection properties such as fast identification, selectivity, stability and cost-effectiveness. In recent years, quartz crystal microbalance (QCM) based biosensors have become a new technology in scientific studies due to their simplicity in concept, ease of use, low cost, shorter analysis times, and suitability for label-free quantification. As an analytical tool, QCM sensors are used as a mass-sensitive detector. QCM sensors, whose surface image is shown in Figure 1, are used in various specific areas, including the detergent, cosmetics, pharmaceutical, paint, food, and agriculture industries.

Figure 1. Image of the QCM sensor surface (Kadirsoy, 2021)

The operating principle of a QCM sensor is based on the piezoelectric effect that occurs in quartz materials. A type of mass-based sensor, a QCM measures activity by detecting mass differences on its surface. When an electric charge is applied to the electrodes on the quartz crystal in the QCM sensor, mechanical power is generated due to the piezoelectric effect, and the quartz crystal produces resonance at its natural frequency through an oscillator. Depending on the mass change in the sensor surface area, its oscillation also alters (Aydemir and Ebeoğlu, 2017; Yuwono and Lammers, 2004). By looking at the this change in the oscillation

frequency and mass loss, the relationship between a reactive solvent and an analyte is interpreted. Figure 2 shows the structural diagram of the QCM sensor.

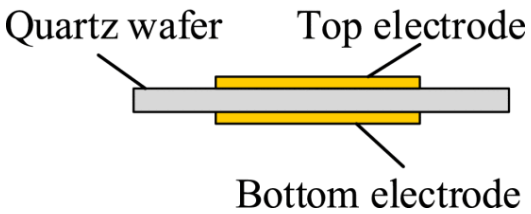

Figure 2. Structural diagram of QCM sensors (Hu and Huang, 2018)

QCM sensor applications available in the literature in recent years are summarised below:
Gupta et al. (2015) conducted a study oriented towards the agrochemical industry. In this study, for the first time, a gold QCM sensor surface was coated with atrazine-printed p(HEMA-phenol) film, an herbicide. This QCM sensor was used for the identification of trace amounts of ATR (atrazine) in wastewater. The researchers determined the linear range of the sensor to be 0.08-1.5 nM and calculated the detection limit of the prepared material to be 0.028 nM. As a result, they successfully applied the developed QCM sensor to the analysis of wastewater samples.

In their study, Liu et al. (2025) used a specially designed QCM sensor to detect linalool with high sensitivity and specificity in sweet potatoes infected with Ceratocystis fimbriata disease. Experimental results showed that the (QCM) gas sensor developed by surface coating with a gel exhibits high sensitivity (0.873 Hz/ppm), a low detection limit (0.237 ppm), a slight standard deviation (0.83%), good reproducibility, and outstanding selectivity. The researchers demonstrated that this application of QCM sensors could be an effective method for rapid and early diagnosis of black rot disease in sweet potatoes.

In their study, Kundu et al. (2025) developed a QCM sensor, MIP-QCM@CT, coated with MIP (Molecularly Imprinted Polymer) to classify various essential oils based on citral concentrations. The developed sensor was correlated with gas chromatography analysis to determine its efficiency and accuracy. As a result, they found that the proposed sensor exhibited linear operation between 10 and 600 ppm, with a sensitivity of 0.172 Hz/ppm. At the same time, tests conducted on the same samples showed a significant correlation between the performance of the QCM sensor and gas chromatography analysis.
Yağmurluoğlu and Diltemiz (2020) developed a Quartz Crystal Microbalance (QCM) sensor that selectively recognises the organophosphoric compound Paraoxon molecule. For this purpose, the QCM electrode surface was coated with a nanofibre immobilised with acetylcholinesterase (AChE) enzyme. As a result of the experimental studies, it was emphasised that the developed QCM sensor can be used for detecting these compounds, which are absorbed through the skin and are highly detrimental to human health, and that its performance is excellent.

In their study, Das et al. (2025) investigated the use of a QCM sensor integrated with tungsten trioxide for detecting volatile organic substances, such as Benzene, Toluene, and Xylene, abbreviated as BTX. As a result of the research, it was revealed that BTX vapour, which poses carcinogenic health risks in certain workplaces, can be detected with high sensitivity and a fast response time at room temperature using this tungsten trioxide-coated QCM sensor.
Golshadi et al. (2025) highlighted the use of QCM-D sensors in preventing environmental pollution. They emphasised that Quartz Crystal Microbalance (QCM) sensors are a promising solution for highly sensitive, fast, and convenient detection of these contaminants. They suggested that, by combining multiple QCM sensors with different characteristics, it is possible to simultaneously detect various types of pollutants, including heavy metals, organic pollutants, and those in air and water.

In the literature, QCM sensor applications include sensitive applications where the fundamental interactions of tiny molecules are analysed. It is worth noting that QCM sensors are widely used in various applications, including monitoring biomolecules, pesticide development, disease detection in the agricultural sector, identifying compounds harmful to human health, such as Paraoxon in medicine, classifying essential oils, and detecting volatile substances and pollutants. QCM sensor applications in the literature are elaborated in Table 1.

Table 1. A short list of available QCM based studies and their usage areas in the literature

Coating Type	Area of utilization	References
HEMA-phenol	Agrochemical	Gupta et. al., 2015
Chemical gel	Agriculture	Liu et al. (2025)
Molecularly Imprinted Polymer (MIP)	Environment	Kundu et al. (2025)
Acetylcholinesterase (AChE) enzyme	Chemistry	Yağmurluoğlu and Diltemiz (2020)
Tungsten trioxide	Chemistry	Das et al. (2025)
HKUST-1/MWCNT-gel (MIP)	Environment	Golshadi et al. (2025)
Phthalocyanines (Toluene; chloroform; and carbon tetrachloride)	Environment	Aydemir and Ebeoğlu., (2017)
Protein fibronectin (FBN); nucleic acid (DNA); proteinase-K and bovine serum albumin (BSA)	Biomedical/medicine	Mohammed and Ebeoğlu., (2022)

As can be seen in Table 1, the usage of QCM sensors are mostly concentrated in the fields of chemistry, agriculture, environment and medicine. There is no a QCM sensor-based an application in the field of hydrometallurgy of mineral processing. Considering the microbalance features, the practicality and wide range of usage potential of QCM sensors, their use in the field of hydrometallurgy may be possible.

Hydrometallurgy is based on the selective dissolution of valuable minerals in ores or concentrates using a suitable reactive solvent in an aqueous medium, followed by the subsequent extraction of pure metals through various refining and recovery techniques. At the same time, the conventional leaching technique is based on the enrichment of metal ores by mixing them in a tank for a long time. An investigation on solvent dosage and type through this method results in longer leaching times, higher solvent consumption and a greater quantity of release of some harmful gases, such as hydrogen cyanide gas (HCN) and chloride gas (Cl_2) into the atmosphere, especially for scientific studies in the laboratory.

This study aims to adapt a QCM sensor-based system for use in the hydrometallurgical field and apply it as an innovative to conventional leaching tests. In the designed experimental setup, the effect of a cyanide solution on the silver QCM sensor was investigated by applying different amounts of the solution to the sensor surface. The solubility relation between a precious metal of silver, and as a reactive solvent of sodium cyanide is also interpreted with the help of the Sauerbrey equation.

2. MATERIAL AND METHODS

2.1. Materials

An AT-cut QCM crystal with a resonant frequency of 5 MHz was used in the experiments conducted with the QCM sensor set. In the experiments, the QCM device designed by Aydemir and Ebeoğlu (2017) was employed to detect the frequency differences of the sensors. NaCN solution was used as the analyte in the study, and a silver QCM sensor was used to analyse the changes in the analyte. The block diagram of the oscillator circuit used in the study is presented in Figure 3.

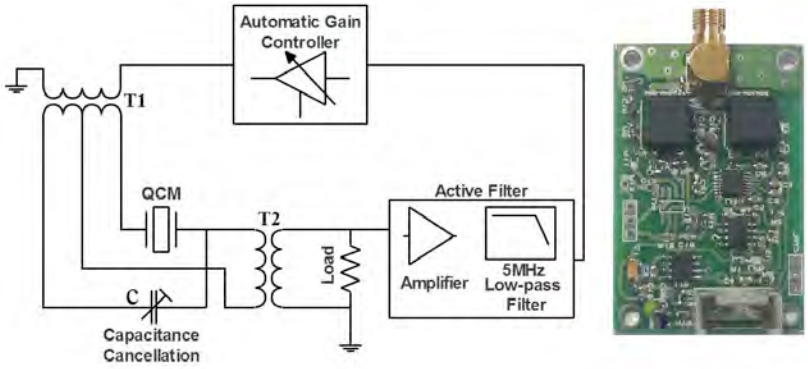

Figure 3. Block diagram of the oscillator circuit (Aydemir and Ebeoğlu, 2017)

2.2. Method

The QCM set shown in Figure 4, consisting of a quartz electrode coated with silver metal, an oscillator, and a frequency counter, was used in the study. In the prepared experimental set, the silver sensor was first placed in the oscillator cell, as shown in Figure 5. Pure water was then added to the silver sensor surface for calibration, and a resonance frequency of approximately 5 MHz was obtained for 15 minutes. After calibration, the frequency changes were measured against three different concentrations of the analyte (0.5 g/L, 1 g/L, and 2 g/L NaCN) using three different silver sensors and recorded on a laptop computer. As a result of the contact between the QCM sensor, which is a mass-based sensor type, and cyanide, there was a loss of mass on the sensor surface. Accordingly, resonance frequencies were obtained.

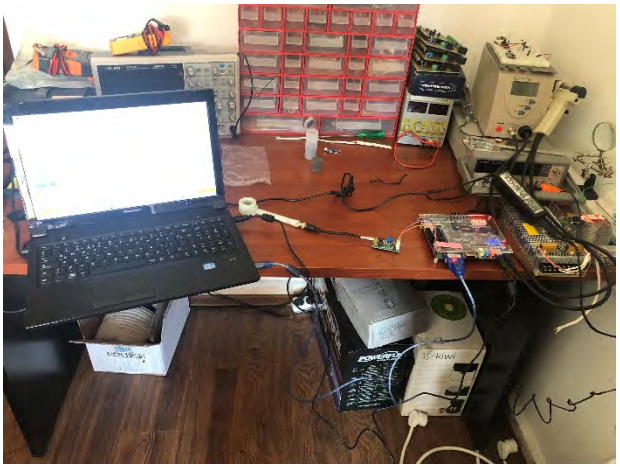

Figure 4. QCM experiment set

Figure 5. Image of the oscillator cell used in the experiments

3. RESULTS AND DISCUSSION

During the QCM sensor tests, measurements were taken with the sample liquid containing three different dosages of cyanide solution. Before each sample, the fundamental frequency was re-measured using pure water, and the difference between this fundamental frequency and the operating frequency in the sample liquid was evaluated as the sensor response. The frequency responses obtained for different samples are shown in Figure 6.

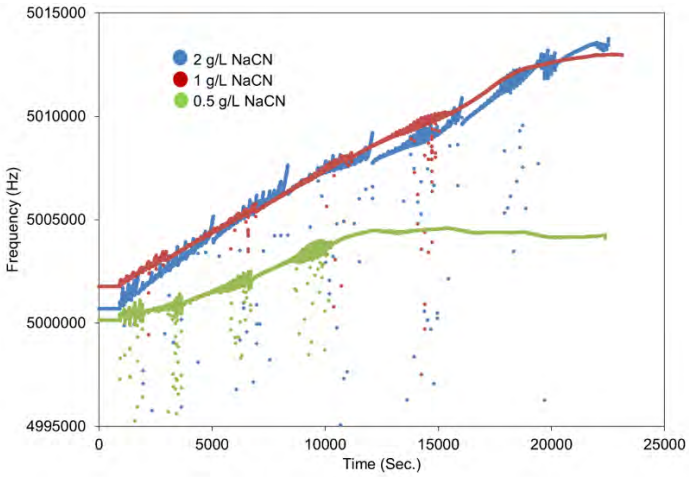

Figure 6. Response of the silver sensor to cyanide at different dosages

It can be seen in Figure 6, as the cyanide dosage increased from 0.5 g/L to 2 g/L, the corresponding frequencies from the sensors increased. At the end of the tests, the silver sensor frequencies of 5004113 Hz, 5012966 Hz and 5013755 Hz were measured, in response to 0.5-1-2 g/L NaCN concentration, respectively. This is due to the increase in solubility depending on the solvent concentration, causing more silver particles to extract from the surface. Analytical chemistry explains this situation with the principle that solubility increases as the dosage of solvent increases (Skoog et al., 1996). As a result, it is thought that increasing the NaCN dosage caused more silver particles to be extracted from the surface, which in turn increases the oscillation frequencies.

The change in analyte dosage or mass in a QCM system can be calculated using the Sauerbrey equation (Eq.1) (Sauerbrey, 1959; Mohammed and Ebeoglu, 2022).

$$\Delta m = -C_{QCM} \times \Delta f \quad \text{(Eq.1)}$$

In the equation, Δm represents the mass change, and Δf represents the frequency change. C_{QCM} is the mass sensitivity constant for 5 MHz AT-cut QCMs with a value of 17.7 ng cm^2 Hz^{-1}. QCM-based electronic-nose (e-nose) and electronic-tongue systems were developed based on this. In current studies, the Sauerbrey equation is used with the e-nose system to monitor changes in gaseous media and the e-tonque system to monitor mass changes in liquid media (Bai and Huang, 2017; Mohammed and Ebeoğlu, 2022).

When the measurement results obtained were analysed, it was observed that the frequency change increased as the cyanide concentration increased, and the Δf frequency difference rose compared to the reference frequency. The pure water frequency of the QCM sensor, as well as the frequency changes corresponding to cyanide concentrations (Δf) and mass losses calculated according to Equation 1 (Δm), are given in Table 2.

Table 2. Table of silver sensor frequency, frequency, and mass loss differences

NaCN concentration (g/L)	Distilled water (Hz)	Silver sensor response (Hz)	Frequency differences Δf (Hz)	Mass loss Δm (ng)
0.5	5000150	5004113	3963	70145.1
1	5001772	5012966	11194	198133.8
2	5000694	5013755	13061	231179.7

When the mass losses at different concentrations, as given in Table 2, are analysed, it is observed that a high cyanide concentration applied to the silver sensor results in more mass loss. According to Equation 1, the changes in mass loss (Δm) corresponding to NaCN concentrations of 0.5 g/L, 1 g/L, and 2 g/L were calculated as 70145.1 ng, 198133.8 ng, and 231179.7 ng, respectively. Post-test images of the silver sensors treated with cyanide solution in the QCM set are given in Figure 7.

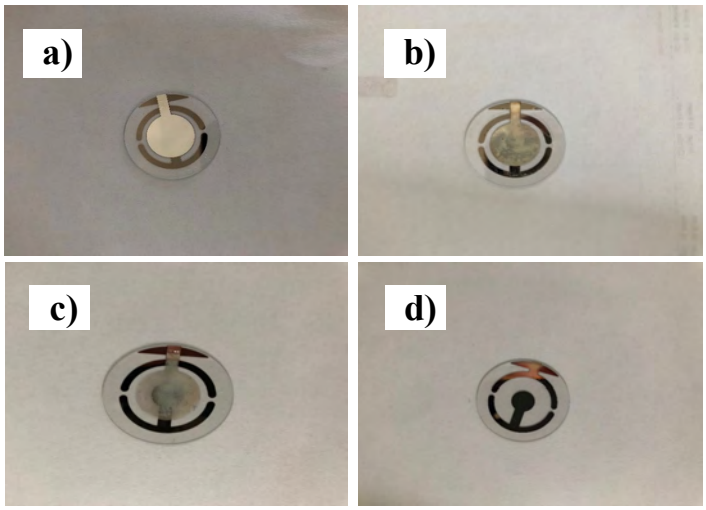

Figure 7. Images of silver sensors before and after cyanide treatment (a) Original state before cyanide treatment; b) treatment of 0.5 g/L NaCN; c) treatment of 1 g/L NaCN; d) treatment of 2 g/L NaCN)

The QCM sensor images obtained after the test demonstrate that the abrasions and mass losses on the sensor surface area vary depending on the cyanide concentration, resulting from the contact between the QCM sensor, a mass-based sensor type, and cyanide.

4. CONCLUSION

This study investigates the applicability of a QCM sensor-based system across various fields, including agriculture, medicine, chemistry, and biomedicine, with particular emphasis on hydrometallurgy. Cyanide leaching is commonly used in the hydrometallurgical enrichment of ores containing precious metals. This study can be considered an alternative way to conventional leaching method, which is particularly preferred for the extraction of base and precious metals. In the study, silver-coated QCM sensors were first obtained. The oscillator circuit was then used to oscillate the QCM sensor in cyanide solution. Data for different cyanide concentrations were obtained using a microthermia-based measurement system. The data obtained showed that the silver sensor reacts to cyanide, and high-frequency variations and high mass losses occur at high cyanide concentrations. In particular, the changes in mass loss (Δm) corresponding to NaCN concentrations of 0.5 g/L, 1 g/L, and 2 g/L were calculated using Sauerbrey's equation as 70145.1 ng, 198133.8 ng, and 231179.7 ng, respectively. As a result, a system was obtained that can measure the solubility of silver metal on the surface, depending on the amount of cyanide, using a QCM sensor whose surface is coated with silver metal.

REFERENCES

Aydemir, F., Ebeoğlu, M. A., (2017) “A QCM sensor array-based electronic tongue with the optimised oscillator circuit using FPGA”, IEEE Transactions on Instrumentation and Measurement, 67 (2), 431-438.

Bai, Q., Huang, X., (2017) “Effective mass layer of a single drop of liquid located on a quartz crystal microbalance”, Sensors and Materials, 29 (5), 539.

Battal, D., Akgönüllü, S., Yalcin, M. S., Yavuz, H., Denizli, A., (2018) “Molecularly imprinted polymer based quartz crystal microbalance sensor system for sensitive and label-free detection of synthetic cannabinoids in urine”, Biosensors and Bioelectronics, 111, 10-17.

Das, A., Manjunatha, R., Kumar, K. N., De, D., Bandyopadhyay, R., (2025) “Fabrication of surface functionalized QCM sensor for BTX detection at ambient conditions”, Talanta, 283, 127081.

Golshadi, Z., Dinari, M., Knebel, A., Lützenkirchen, J., Monjezi, B. H., (2024) “Metal organic and covalent organic framework-based QCM sensors for environmental pollutant detection and beyond”, Coordination Chemistry Reviews, 521, 216163.

Gupta, V. K., Yola, M. L., Eren, T., Atar, N., (2015) “Selective QCM sensor based on atrazine imprinted polymer: its application to wastewater sample”, Sensors and Actuators B: Chemical, 218, 215-221.

Hu, J., Huang, X., (2018) “QCM mass sensitivity analysis based on finite element method”, IEEE Transactions on Applied Superconductivity, 29 (2), 1-4.

Kadirsoy, S., (2021) “Preparation of novel molecular imprinted QCM sensors for the determination of chlorpyrifos”, Master’s Thesis, Applied Sciences, Iskenderun Technical University.

Kourdi, A., (2021) “The direct detection of Escherichia coli ATCC 25922 strain in saliva based on quartz crystal microbalance (QCM) sensor”, Master’s Thesis, Applied Sciences, Erciyes University.

A REVIEW ON FILTRATION PERFORMANCE EVALUATION AND OPERATIONAL OPTIMIZATION IN CCD-MERRILL CROWE PROCESSING

Semih ERZENOĞLU, Hüseyin BAŞTÜRKCÜ*

Istanbul Technical University, Faculty of Mines, Mineral Processing Engineering Department, 34469, Maslak, Istanbul, TÜRKİYE
**Corresponding author: basturkcu@itu.edu.tr*

A B S T R A C T

Counter-current decantation (CCD) followed by Merrill Crowe precipitation is among the most widely adopted hydrometallurgical routes for the recovery of gold and silver from cyanide leach solutions. A critical but frequently underappreciated unit operation within this circuit is solid-liquid separation, particularly the pressure or vacuum filtration stage that precedes zinc cementation. The quality and clarity of the clarified solution fed to the precipitation step exerts a direct influence on product purity, zinc consumption and downstream refining burden. Filter aids derived from siliceous minerals - principally diatomaceous earth (diatomite) and expanded perlite - are routinely employed to improve cake permeability and solution clarity. However, both materials exhibit operational limitations, the most consequential of which is the tendency to form a gelatinous phase when exposed to the acidic conditions encountered during refinery-grade sulfuric acid washing of the zinc precipitate (Merrill Crowe mud). This review synthesizes current understanding of CCD-Merrill Crowe integration, the role of siliceous filter aids, and the operational parameters governing filtration performance, with emphasis on the gelation phenomenon and strategies for its mitigation.

Key words: *Merrill Crowe, CCD, diatomite, perlite, filtration aid, gold recovery, gelation, sulfuric acid, operational optimization*

1. INTRODUCTION

The hydrometallurgical treatment of gold and silver ores via alkaline cyanidation followed by zinc cementation - the Merrill Crowe process - has been in commercial use since the late nineteenth century and continues to represent the dominant recovery pathway for high-grade heap-leach and vat-leach operations worldwide (Marsden and House, 2006). The preceding solid–liquid separation circuit, typically configured as a counter-current decantation (CCD) thickener train, is tasked with washing pregnant liquor from the leached pulp and delivering a clarified, particle-free solution to the precipitation section. The efficiency of this separation fundamentally determines downstream process economics: suspended solids in the pregnant solution increase zinc consumption, contaminate the precipitate and complicate smelting (Adams, 2016).

Filtration, whether by pressure-leaf, horizontal-belt or drum filter, forms the final polishing step in the clarification circuit. To achieve acceptable flow rates and solution clarity simultaneously, plant operators universally apply precoat and/or body-feed quantities of filter aids. Diatomaceous earth (diatomite, DE) and thermally expanded perlite are the two mineral classes most frequently specified for this duty (Purchas and Sutherland, 2002). Both materials owe their utility to a highly porous, rigid skeletal structure that builds a permeable cake whilst retaining fine mineral particles and precipitate fines.

Despite their long service history, siliceous filter aids present a specific chemical vulnerability: in the presence of strong acids - notably the sulfuric acid routinely used to dissolve the zinc precipitate prior to smelt or to wash filter cloths - amorphous silica undergoes dissolution and subsequent re-precipitation as a colloidal gel. This gelation phenomenon clogs filter media,

raises differential pressure, reduces throughput and, in severe cases, renders a filter circuit inoperable (Iler, 1979). The present paper reviews the technical basis of these phenomena, surveys global operational experience, and identifies the parameter space available to plant metallurgists for optimization.

2. THE MERRILL CROWE PROCESS: PRINCIPLES AND GLOBAL APPLICATIONS

2.1. Process Chemistry

The Merrill Crowe process exploits the electrochemical displacement of gold and silver from their cyanide complexes by zinc metal. The overall cementation reaction for gold may be written as:

$$2Au(CN)_2^- + Zn^0 \rightarrow 2Au^0 + Zn(CN)_4^{2-}$$

For efficient cementation, the pregnant solution must be de-aerated (dissolved oxygen < 0.5 mg/L) and clarified (suspended solids < 1 mg/L) before contact with zinc dust. De-aeration is accomplished through vacuum towers or degassing columns, while clarification is achieved by the combination of CCD thickening and filtration (Marsden and House, 2006; Adams, 2016). Lead nitrate addition activates the zinc surface and is standard practice in most operations.

2.2. CCD Circuit Configuration

A CCD train typically comprises three to six thickeners arranged in series with countercurrent wash liquor flow. Leached slurry enters the first thickener and progressively washes; barren slurry exits the final unit, whilst the pregnant overflow advances to the clarification circuit. Underflow densities of 55-70 wt% solids are targeted to minimize wash liquor dilution and gold losses in the barren tailings stream (Adams, 2016). Flocculant addition (synthetic polyacrylamide, 10-50 g/t) is required to promote settling at typical cyanide pulp densities. Overflow turbidity from CCD thickeners typically ranges from 50 to 500 NTU, necessitating filtration before Merrill Crowe precipitation (Svarovsky, 2000).

2.3. Global Operational Footprint

Merrill Crowe circuits are standard in operations processing free-milling, oxide and transitional ores where solution grades exceed approximately 1-2 g/t Au. Major applications include heap-leach facilities in Nevada (USA), northern Mexico, northern Chile and Western Australia, as well as vat-leach plants in West Africa and Central Asia. Notable installations include Barrick's Goldstrike autoclave complex (Nevada), Newmont's Yanacocha operation (Peru), Kinross Fort Knox (Alaska) and numerous junior and mid-tier producers in the Tethyan belt (World Gold Council, 2023). In Türkiye, the Merrill Crowe route has been employed at several oxide gold projects in the Aegean and Pontid metallogenic belts, where the combination of free-milling ore mineralogy and relatively simple gangue chemistry favors this approach over carbon-in-pulp (CIP) or resin-based alternatives.

3. SILICEOUS FILTER AIDS: DIATOMITE AND PERLITE

3.1. Mineralogy and Physical Characteristics

Diatomaceous earth consists of the fossilized opaline silica ($SiO_2 \cdot nH_2O$) frustules of unicellular algae (diatoms). Commercial grades are calcined and/or flux-calcined to adjust particle size distribution, color and flow resistance. Particle sizes range from 5 to 100 μm, with specific

surface areas of 1-20 m²/g and permeabilities characterized by Darcian resistance values in the range of 10^{-13} to 10^{-11} m² (Purchas and Sutherland, 2002). The amorphous silica content of filter-grade DE is typically 85-95 wt%, with minor aluminum, iron and calcium impurities.

Perlite filter aid is produced by rapid thermal expansion (870-1100 °C) of glassy volcanic rhyolite (perlite ore), which causes the occluded water to vaporize and expand the particle to a foam-like structure. The resulting material has densities of 60–120 kg/m³ and a highly irregular, conchoidal surface morphology that promotes mechanical entrapment of fine particles. Perlite filter aids typically contain 70–76 wt% SiO_2, 12–15 wt% Al_2O_3, with the balance comprising alkali and alkaline earth oxides (Perlite Institute, 2019).

3.2. Role and Benefits in Merrill Crowe Filtration

Filter aids are applied in two modes: (i) precoat, in which a suspension of filter aid is deposited on the filter medium prior to process filtration to form a thin, permeable barrier that protects the cloth and provides the initial filtration surface; and (ii) body-feed, in which filter aid is continuously dosed into the process stream to maintain cake permeability as fine solids accumulate (Purchas and Sutherland, 2002). Typical precoat loadings are 0.5-1.0 kg/m² of filter area, and body-feed dosages in Merrill Crowe service commonly range from 100 to 400 g per cubic meter of solution processed.

The principal technical benefits conferred by siliceous filter aids in this application are: improvement in filtrate clarity (turbidity reduction from hundreds of NTU to < 1 NTU), increased filter throughput by maintaining cake permeability through bridging of fine solids, extended filter-run duration before blinding, and protection of the filter cloth from abrasive wear. Clean filtrate clarity is critical because residual suspended solids in the pregnant solution coat zinc dust particles during cementation, inhibit metal contact, and contaminate the precipitate with gangue minerals that increase acid consumption and smelting slag volumes (Adams, 2016; Svarovsky, 2000).

3.3. Comparative Performance: Diatomite versus Perlite

Both materials are broadly interchangeable for Merrill Crowe service but exhibit performance differences that influence selection. Diatomite generally provides superior particle retention efficiency at equivalent addition rates, owing to its higher surface area and regular frustule geometry. Perlite offers lower bulk density, facilitating suspension handling, and is often preferred where silica contamination of the precipitate is a secondary concern. Cost and local availability are frequently the dominant selection criteria; perlite is produced domestically in Türkiye - which holds the world’s largest confirmed reserves - offering a significant supply-chain advantage for Turkish operations (Perlite Institute, 2019).

4. GELATION OF SILICEOUS FILTER AIDS UNDER ACIDIC CONDITIONS

4.1. Mechanism of Silica Gelation

Amorphous silica exhibits pH-dependent solubility governed by the dissociation of surface silanol groups (Si-OH). In the circumneutral to alkaline pH range typical of cyanide leach solutions (pH 10-11), silica solubility is moderate (5-10 mg/L as SiO_2) and surface charge is negative, imparting colloidal stability to dispersed particles. Upon acidification with sulfuric acid - routinely applied during filter-cloth washing or zinc precipitate dissolution - the pH drops below 3, dramatically increasing silica solubility and promoting dissolution of the amorphous silica framework of the filter aid (Iler, 1979).

As the acid solution becomes silica-saturated and is subsequently neutralized - intentionally or through contact with downstream reagents - supersaturation drives polymerization of silicic acid monomers ($Si(OH)_4$) via condensation reactions, forming siloxane (Si-O-Si) oligomers that progressively aggregate into a three-dimensional gel network. This gel is characterized by a high-water content (typically 95-98 wt%), very low permeability, and strong adhesion to filter media surfaces. The kinetics of gelation are strongly temperature-dependent (accelerated above 40 °C) and catalyzed by elevated ionic strength and the presence of multivalent cations (Fe^{3+}, Al^{3+}) (Iler, 1979; Bergna and Roberts, 2006).

4.2. Operational Consequences

The formation of silica gel within a Merrill Crowe filter circuit produces a cascade of adverse effects. Filter cloths become uniformly blinded with a gel film that is resistant to conventional backwash or air-bump procedures, as the gel collapses rather than fracturing. Differential pressure across the filter rises rapidly, triggering premature cycle termination and reducing effective filtering area per unit time. In severe cases, gel formation within the pressure vessel internals can require extended manual cleaning with hot caustic (NaOH at pH > 12) or hydrofluoric acid solutions, both of which present significant occupational health risks and generate hazardous waste streams requiring treatment (Bergna and Roberts, 2006). Throughput reductions of 30-60% have been reported at operations experiencing chronic gelation problems, with associated increases in unit operating cost and metal inventory locked in the offline filter circuit.

4.3. Mitigation Strategies

Mitigation of silica gelation in Merrill Crowe filtration requires an integrated approach addressing both the chemical and operational drivers of the phenomenon. Primary preventive strategies include: substitution of acid washing with alkaline (NaOH or lime) washing procedures where precipitate composition permits; reduction of acid contact time with filter media by sequential water rinsing before and after acid washing; maintenance of wash solution pH above 4 to limit silica dissolution; and control of wash solution temperature to below 30 °C. Where acid washing cannot be avoided - as in operations processing high-sulfide precipitates - replacement of siliceous filter aids with alternative materials such as cellulose fiber aids or synthetic polymer pre-coats (e.g., polypropylene fiber) offers a gel-resistant option, albeit at higher cost and with some sacrifice of filtration efficiency (Purchas and Sutherland, 2002). Operational parameters such as precoat thickness, body-feed rate and filtration pressure are also subject to optimization to reduce the silica loading presented to the acid wash stage.

5. OPERATIONAL PARAMETER OPTIMISATION FOR CCD–MERRILL CROWE FILTRATION

Achieving optimal filtration performance in an integrated CCD-Merrill Crowe circuit requires systematic evaluation and control of a defined set of interacting parameters spanning both the upstream decantation and downstream filtration stages.

Pregnant solution turbidity entering the filter circuit is the primary determinant of filter-aid demand. CCD thickener performance is therefore directly linked to filtration operating cost: improvements in flocculant type and dosage, underflow density control and overflow laundering that reduce turbidity from 300 NTU to 100 NTU can halve body-feed requirements and double filter-run duration (Svarovsky, 2000; Adams, 2016). Automation of thickener underflow density via on-line density measurement and flocculant dosage control provides the most direct lever for reducing filtration burden.

Filter-aid addition rate must be matched to the actual solids loading of the incoming solution. Under-dosing results in rapid cake compressibility and declining flux; over-dosing increases reagent cost and raises the volume of filter aid-contaminated zinc precipitate reporting to the retort, increasing silica content in bullion and raising refining penalties. In practice, optimal body-feed rates are determined by pilot-scale filtration tests using actual plant solution and locally available filter-aid grades, targeting a specific filtration resistance (SFR) in the range of 1-5 × 10^{10} m/kg (Purchas and Sutherland, 2002).

Operating pressure is a critical variable for compressible filter cakes typical of Merrill Crowe service. Pressure-leaf filters operating at 300-500 kPa (3-5 bar) generally provide the best combination of flow rate, cake moisture and cycle time. Excessively high pressures compact the cake, increasing resistance and potentially fracturing the precoat layer, allowing solids breakthrough. Pulse-jet or mechanical cake discharge systems preserve precoat integrity better than manual techniques and allow shorter, more frequent cycles that maintain consistent filtrate quality (Svarovsky, 2000).

Solution pH management during filter operation warrants particular attention. Pregnant solution in cyanide circuits is maintained at pH 10-11 to prevent HCN volatilization; however, if localized pH excursions occur - for example, through inadvertent CO_2 absorption or inadequate lime dosing upstream - the solubility of zinc cyanide complexes decreases and precipitate can form within the filter circuit, contributing to premature blinding. Continuous pH monitoring at the filter feed is therefore a minimum instrumentation requirement (Marsden and House, 2006; Nicol et al., 1987).

Zinc precipitate moisture content exiting the filter directly affects retort capacity and fuel consumption. Higher filtration efficiency (lower cake moisture) reduces the thermal load in the retort drying stage. Target moisture contents of 30-45 wt% are typical for pressure-leaf filtered Merrill Crowe precipitates; values above 55 wt% indicate sub-optimal cake washing or excessive compressibility and warrant investigation (Adams, 2016; Botz, 2001).

6. CONCLUSIONS

The integration of CCD and Merrill Crowe processing represents a technically mature but operationally nuanced hydrometallurgical circuit in which filtration performance exerts disproportionate influence on overall process efficiency and product quality. Siliceous filter aids - diatomite and expanded perlite - deliver well-established benefits in terms of solution clarity and filter throughput, but their inherent susceptibility to gelation under acidic conditions constitutes a significant operational risk that must be managed through careful reagent selection, pH control and procedural discipline.

The gelation mechanism is chemically well understood: dissolution of amorphous silica at low pH followed by polymerization upon neutralization produces an impermeable gel that resists conventional cleaning methods and can cause extended filter downtime. Mitigation requires either avoidance of acidic conditions in the filter environment or substitution of gel-resistant alternative filter aids. Broader optimization of the CCD-filtration circuit, encompassing thickener flocculant performance, filtration pressure, body-feed dosage and solution chemistry management, provides the operational framework within which sustainable, low-cost precious metals recovery can be maintained.

Further pilot-scale and plant-scale investigations are warranted to quantify the performance benefits of emerging synthetic and natural-fiber filter aid alternatives under realistic Merrill Crowe conditions, particularly for operations in silica-rich geological environments such as the

Turkish Tethyan belt, where perlite is abundantly available as a locally sourced alternative to imported diatomaceous earth.

REFERENCES

Adams, M. D., (2016) “Gold Ore Processing: Project Development and Operations”, Elsevier, Amsterdam.

Bergna, H. E., Roberts, W. O., (2006) “Colloidal Silica: Fundamentals and Applications”, CRC Press / Taylor & Francis, Boca Raton.

Botz, M. M., (2001) “Overview of cyanide treatment methods”, Mining Environmental Management, 9 (5) 28–30.

Iler, R. K., (1979) “The Chemistry of Silica: Solubility, Polymerization, Colloid and Surface Properties, and Biochemistry”, Wiley-Interscience, New York.

Marsden, J. O., House, C. I., (2006) “The Chemistry of Gold Extraction”, Society for Mining, Metallurgy and Exploration (SME), Littleton, Colorado.

Nicol, M., Fleming, C., Paul, R., (1987) “The chemistry of the extraction of gold”, The Extractive Metallurgy of Gold in South Africa, South African Institute of Mining and Metallurgy, Johannesburg.

Perlite Institute, (2019) “Perlite: The Mineral and Its Applications”, Perlite Institute, Harleysville, Pennsylvania.

Purchas, D. B., Sutherland, K., (2002) “Handbook of Filter Media”, Elsevier Advanced Technology, Oxford.

Svarovsky, L., (2000) “Solid-Liquid Separation”, Butterworth-Heinemann, Oxford.

World Gold Council, (2023) “Gold Demand Trends Full Year 2022”, World Gold Council, Londo

ACID LEACHING OF MECHANICALLY ACTIVATED BENTONITE CLAY FOR ALUMINUM EXTRACTION

Mustafa BİRİNCİ*, Kader ŞENTÜRK

İnönü University, Faculty of Engineering, Mining Engineering Department, 44280 Battalgazı, Malatya, TÜRKİYE
**Corresponding author: Mustafa.birinci@inonu.edu.tr*

A B S T R A C T

Nowadays, there is an increasing focus on the alumina production from non-bauxite sources. Besides, the decreasing of bauxite reserves or the presence of low-grade bauxite in some countries has increased the significance of aluminosilicate sources such as clay minerals and fly ash. Bentonite is a clay mineral of the montmorillonite group with a high aluminum content. The overall process for obtaining alumina from clay minerals generally begins with acid leaching. However, activation of the clay, often through pre-treatments like mechanical activation, is usually required prior to the leaching step. In this study, the mechanical activation and acid leaching behavior of bentonite clay obtained from the Ünye (Ordu/Türkiye) region were investigated for its potential use in alumina production. The clay was subjected to intensive milling using a planetary mill to achieve mechanical activation. Batch leaching tests were then performed with hydrochloric acid solutions. The experimental results indicated that mechanical activation significantly increased the dissolution kinetic of aluminum. Consequently, aluminum recovery was able to be increased up to 80%.

Key words: *Bentonite, aluminum, alumina, intensive milling, mechanical activation, acidic leaching*

1. INTRODUCTION

Aluminum oxide or alumina (Al_2O_3) and its primary refined product aluminum (Al) are materials of paramount importance to modern industrial society, touching nearly every sector from aerospace to consumer goods. Their widespread utility stems from an exceptional combination of physical and chemical properties that are unmatched by many other materials. (Ashkenazi, 2019). Also, Alumina (Al_2O_3), the most common Al-containing compound, is widely used in ceramics, abrasives, refractories, and cement industries due to its desirable physical and chemical properties. It is also used in the production of aluminum metal through the Hall-H´eroult process, following the Bayer process (Habashi, 1997). However, bauxite-based alumina production faces significant technological and environmental challenges. These include insufficient bauxite reserves in certain countries, depletion of existing reserves, reactive silica issues, high energy consumption, CO_2 emissions, and challenges in red mud storage and management. Rapid technological advancements have led to an increase in the global consumption of aluminum, with a decrease in high-grade bauxite reserves, thus spurring research efforts toward the utilization of non-bauxite ores as a secondary source such as kaolinite (Bazin et al., 2007) sericite (Kumar et al., 2020), pyrophyllite (Erdemoğlu et al., 2018) nepheline syenite (Akhmadiyeva et al., 2024), alunite (Shabab et al., 2016), anorthite, and coal shales and fly ash (Ding et al., 2016).

Bentonite is a kind of clay mineral consisting essentially of montmorillonite, which is generally classified into sodium (Na) or calcium (Ca) types depending on dominant exchangeable ion. Bentonite is highly valued by its sorption properties, which stem from its high surface area, swelling capacity and cation exchange capacity (CEC). Bentonitic clays, currently in use in over a hundred areas, are among the most important industrial raw materials. Principal clay minerals of bentonites are smectites such as montmorillonite, beidellite, saponite, nontronite, hectorite, and laponite. Bentonites are predominantly consists of montmorillonite rather than

other smectites (Bayram et al., 2010). Bentonite is a multi-layered clay mineral formed through the geological devitrification and hydrothermal alteration of volcanic ash. It is characterized by significant water absorption and swelling capacities. Owing to its unique physicochemical attributes - including a high specific surface area, substantial cation exchange capacity (CEC), and distinct colloidal properties - bentonite finds extensive application across diverse industrial sectors, ranging from foundry sand binders and drilling fluids to waterproofing membranes and heterogeneous catalysis. Recent investigations highlight the potential of aluminum-rich bentonite clays, as well as various chemically modified bentonite derivatives, to serve as viable precursors or auxiliary agents for the extraction of aluminum compounds, specifically alumina and aluminum salts.

Extraction of Al_2O_3 from clay minerals is a complex process that involves several steps, including: (i) pre-treatment, (ii) acid leaching, (iii) solution purification (iv) aluminum precipitation (v) roasting at high temperatures to convert it into alumina (Al2O3). The purity of the alumina obtained from this process depends on the purity of the starting clay mineral and the efficiency of the various steps in the process. Various studies exist on obtaining alumina from aluminum-containing minerals using the acid leaching method (Ding et al., 2017).

A pre-treatment stage is required to activate clays and improve their solubility in acid solutions. Thermal activation through calcination is most frequently employed; however, this method is characterized by intensive energy demands and environmental concerns. As a result, the refinement of thermal activation processes for kaolinitic minerals continues to be a focal point of contemporary research (Al-Ajeel, 2006; Bazin, 2007). It is very well-known that mechanical activation is defined as a process that enhances the reactivity of a solid without altering its chemical composition. In this process, the mineral is intensively milled to fine sizes, reducing the particle size. Depending on the intensity of the applied mechanical energy during the milling, deformation occurs in the crystal structure of the mineral, leading to the formation of an amorphous structure. Simultaneously, new surfaces that have not undergone any chemical reaction are exposed. This structure becomes more active during metallurgical processes like calcination or leaching, resulting in a decrease in reaction temperature or an increase in process rate (Petrov and Milošević, 1999; Baláž, 2008).

This study investigated the potential use of a montmorillonite-rich clay ore, containing cristobalite and anorthite, for alumina production. The primary objective was to evaluate the impact of mechanical activation on the ore's clay minerals to enhance aluminum recovery during the subsequent leaching process.

2. MATERIAL AND METHODS

2.1. Material

A representative sample was obtained from Ünye (Ordu/Türkiye) region. The sample was crushed to -4.75 mm in size by jaw crusher and then was completely ground to -1 mm using a laboratory porcelain ball mill. The ground ore was divided into small lots (approx. 50 g) using rotary sample divider, which were dried at 105 °C for 60 min prior to experiments. As analyzed by X-ray diffractometer (Figure 1), the ore contains mainly montmorillonite (85.57%) cristobalite (6.63%), magnetite (3.31%) and anorthite (1.27%), and has 16.51% Al_2O_3 grade as determined by XRF spectrometer (Table 1).

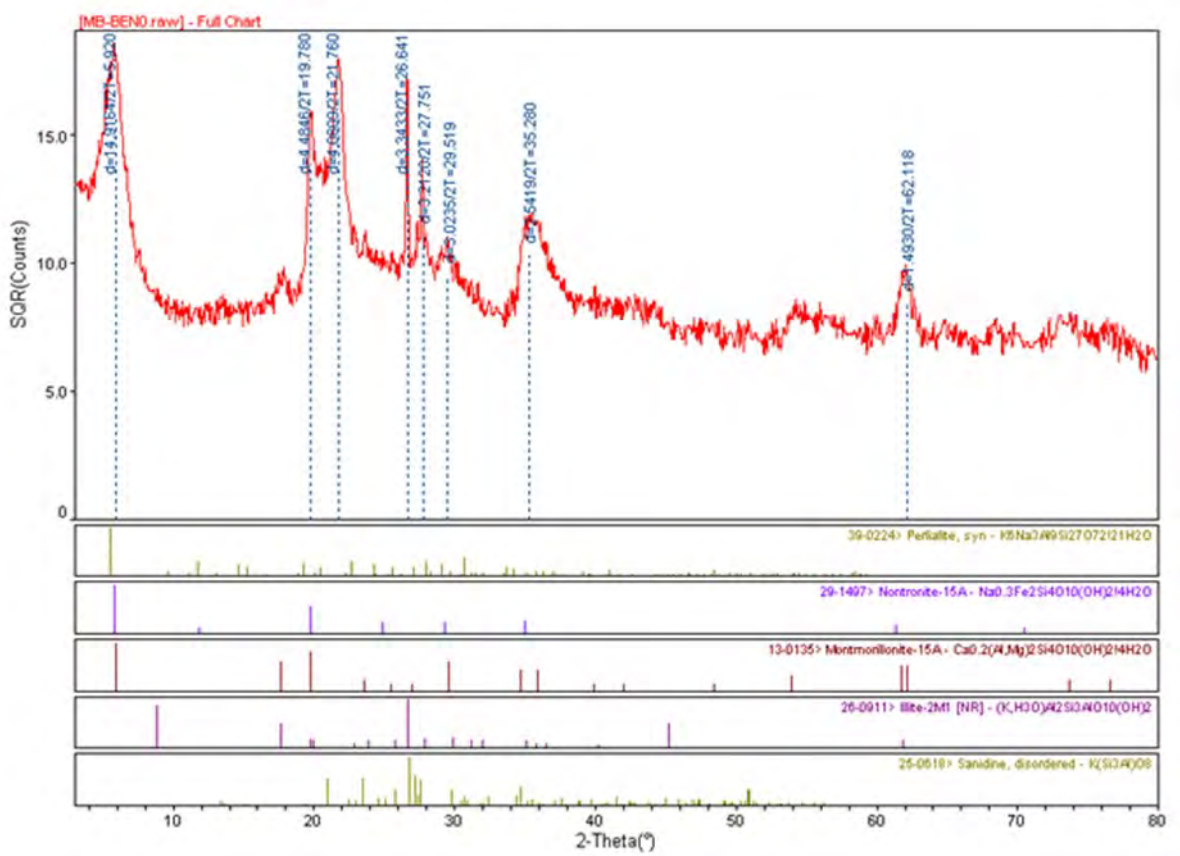

Figure 1. XRD result of representative ore sample (raw bentonite)

Table 1. Chemical compositions of the raw bentonite

Main oxide	SiO_2	Al_2O_3	Fe_2O_3	CaO	MgO	Na_2O	K_2O	TiO_2	LOI*
%	64.25	16.51	1.58	2.13	2.47	0.40	0.37	0.34	11.93

*Loss on ignition at 1000 °C

2.2. Method

Intensive milling: To achieve mechanical activation, a Fritsch Pulverisette 6 mono mill (Idar-Oberstein, Germany) was used. Approximately 20 g of the bentonite ore was fed to 250 cm^3 milling chamber made from tungsten carbide (WC) using 50 pieces of 10 mm in diameter WC balls. Therefore, ball-to-ore ratio was 20 by weight and it was kept constant. The ore was drymilled for 20 min. Rotational speed of the mill was kept constant at 500 rpm. The milling experiments were kept on for 10 min at 10-min intervals to prevent temperature rise in the mill. The milling tests were carried out in air atmosphere and at room temperature.

Acid leaching: For determining the effects of mechanical activation on dissolution of aluminum, unmilled and milled ore samples were separately subjected to batch-leaching experiment using HCl solution. For both experiments,10 g of sample was leached in 200 cm^3 of 4 M HCl solution 500 cm^3 four-necked borosilicate glass reactor equipped with a thermocouple and a water-cooled condenser, placed in a MTOPS model stirring heater mantle, was used as leaching medium. Temperature of the reactor was controlled by a programmable controller of the mantle. Magnetic stirring was used to mix the slurry, where the stirring speed was kept constant at 600 rev/min. By the end of leaching, the slurry was vacuum-filtered to separate pregnant solution from undissolved material and it was then washed three times with diluted HCl acid solution. The filtrate and washings were composed to have a constant volume of 250 cm^3 in a volumetric flask to obtain stock pregnant solution to be used for aluminum analysis. Aluminum

analysis was carried out by FAAS (Flame Atomic Absorption Spectroscopy) method. Aluminum recovery is calculated by proportioning the amount of aluminum determined in the pregnant solution with the amount of aluminum in the ore added to the leaching medium.

3. RESULTS AND DISCUSSION

The XRD pattern of the activated bentonite sample is shown in Figure 2 and the crystallographic parameters are evaluated by measuring the (001) and (080) peaks. The peaks marked as montmorillonite are indicative of 2:1 swelling clay and confirm the characteristics of the montmorillonite type clay. The other peaks are impurities corresponding to cristobalite. Montmorillonite exhibits a diffraction peak of the (001) plane at 2θ = 19.733, which corresponds to its basal spacing of 4.99 Å. The (080) reflection at 2θ = 62.118 indicates that montmorillonite has a dioctahedral structure.

When XRD pattern of the milled sample was examined, it was observed that the peak intensities of all minerals are typically declined and the peaks belonging to bentonite minerals are entirely lost. The remaining XRD peaks observed in the patterns after mechanical activation was attributed to cristobalite and quartz. The most intense peak associated with quartz, appearing at 26.56° 2θ (CuKα), shows a slight decrease in intensity. This suggests that the crystal structure of quartz within the ore is also distorted to some extent due to intensive milling. Petrov and Milošević (1999) explain that varying resistances to mechanical activation are due to the different crystal lattice types.

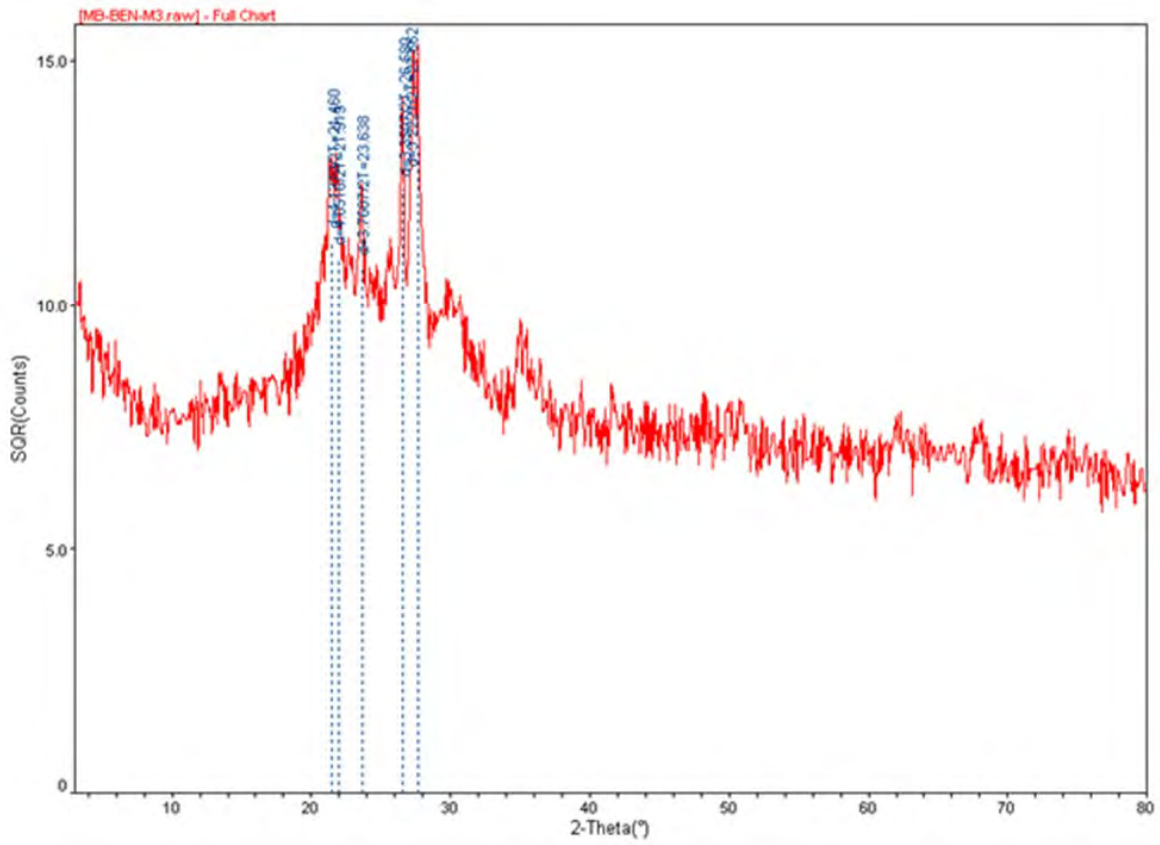

Figure 2. XRD pattern of the activated bentonite sample

Table 2 shows data on the amorphization degrees and particle size parameters for both activated and inactivated samples. This table clearly demonstrates the effects of the intensive milling process on the structural properties of the materials. Raw bentonite with its original form, particle size d90, d50, and d10 values are 905.30, 415.41, and 12.85 µm, respectively.

For bentonite ore activated by intensive millling, these values were 27.41, 0.35, and 0.09 μm, respectively. Additionally, mechanical activation led to twenty times increase in the specific surface area from 2.75 to 55.16 m^2/g. The degree of amorphization clearly reveals the change in mineral crystal structural characteristics. Table 2 shows degree of amorphization of montmorillonite and cristobalite, being the major minerals in the ore. These minerals in the ore are subjected to XRD amorphization by milling just for 20 min. For cristobalite, the amorphization degree is about 12.95% at the end of 20 min of milling, while it is 100% for montmorillonite, respectively.

Table 2. Particle size and amorphization parameters of raw and activated bentonite samples

Bentonite ore	Particle size parameter, μm			S_{BET}, m^2/g	Degree of amorphization, %	
					Montmorillonite	Cristobalite
	d_{10}	d_{50}	d_{90}			
Raw	12.85	415.41	905.30	2.75	0	0
Activated	0.09	0.35	27.41	55.16	100	12.95

The condition that will entirely reveal whether a mineral is mechanically activated is prevalence of an increase in the reactivity of it in the last step in which it is processed. Based on this fact, an experimental study was designed to reveal the extents of aluminum recovery either from unmilled or milled ore by leaching in acidic solutions. For determining the maximum amount of aluminum which can be leached from the unmilled bentonite ore in the acidic solutions, a series of batch-leaching tests were carried out by taking into account to aluminum recovery as dependent variable. Leaching conditions determined for the unmilled ore were as follows: HCl concentration, 4 M; leaching temperature, boiling point of the pulp (105 °C); leaching time, 24 hour; liquid -to- solid ratio, 250/20 mL/g. The particle size used in the batchleaching test of the unmilled ore was - 1 mm, whereas the particle size of the feed in the batch leaching of the milled ore samples was the particle size that was achieved at the end of the intensive milling. According to the data in Table 3, mechanical activation with intensive milling has a profound impact on the extraction efficiency of aluminum. While the unmilled bentonite ore yielded a maximum aluminum recovery of only 53.15%, mechanical activation significantly enhanced these results. When bentonite ore was activated by the intensive milling method, a high aluminum recovery efficiency of 80% was achieved.

Table 3. Al recovery of the raw and activated bentonite samples

Mechanical activation by intensive milling			Leaching efficiency
Mill speed, rpm	Milling time, min	Ball-to-ore ratio	Al recovery, %
500	20	20	79.77
Raw ore (i.e. inactivated ore/untreated ore)			53.15

4. CONCLUSION

According to the results obtained from studies, the following conclusions can be drawn:
1) Mechanical activation significantly enhances the reactivity of bentonite by reducing particle size and distorting its crystal structure into an amorphous state.
2) Intensive milling for 20 minutes achieves 100% amorphization of montmorillonite, the primary clay mineral in the ore.
3) The intensive milling process dramatically increases the specific surface area of the clay, increasing from 2.75 m^2/g to 55.16 m^2/g after activation.
4) Mechanical activation effectively increases aluminum recovery during acid leaching with HCl. While raw (unmilled) bentonite yielded a recovery of 53.15%, the activated sample achieved a recovery of approximately 80%.

ACKNOWLEDGEMENTS

This study is financially supported by the İnönü University Scientific Research Projects Coordination Unit (Project Number: FDK-2024-3710).

REFERENCES

Akhmadiyeva, N.; Abdulvaliyev, R., Gladyshev, S., Kassymzhanova, A. (2024), “Hydrochemical Method for the Production of Alumina from Nepheline Using Effective Calcium Reagents”, Processes, 12 (7), 1355.

Al-Ajeel A.W.A., Al-Sindy S.I., (2006), “Alumina recovery from Iraqi kaolinitic clay by hydrochloric acid route”, Iraqi Bull Geol Min, 2 (1) 67-76.

Ashkenazi, D., (2019), “How Aluminum Changed the World: A Metallurgical Revolution Through Technological and Cultural Perspectives”, Technological Forecasting and Social Change,143 101-103.

Baláž, P., (2008), Mechanochemistry in Nanoscience and Minerals Engineering. Berlin Heidelberg: Springer.

Bayram H., Önal M., Yılmaz, H., Sarıkaya, Y., (2010), “Thermal analysis of a white calcium bentonite”, Journal of Thermal Analysis and Calorimetry, 101, 873-879.

Bazin, C., El-Ouassiti, K., Ouellet, V., (2007), “Sequential leaching for the recovery of alumina from a Canadian clay”, Hydrometallurgy, 88, 196-201.

Ding, J., Ma, S., Shen, S., Xie, Z., Zheng, S., Zhang, Y., (2017), “Research and industrialization progress of recovery alumina from fly ash: a concise review”, Waste Management, 60, 375-387.

Ding, J., Ma, S., Zheng, S., Zhang, Y., Xie, Z., Shen, S., Liu, Z., (2016), “Study of extracting alumina from high-alumina PC fly ash by a hydro-chemical process”, Hydrometallurgy, 161, 58-64.

Erdemoğlu, M., Birinci, M., Uysal, T., Porgalı, E., Barry, T.S., (2018), “Acid leaching performance of mechanically activated pyrophyllite ore for Al_2O_3 extraction”, Journal of Materials Science, 53, 13801-13812

Habashi, F., (1997), Handbook of Extractive Metallurgy, 2nd ed. New York: Wiley-VCH.

Kumar, A., Agrawal, S., Dhawan, N., (2020), “Hydrometallurgical investigation of sericite clay for extraction of alumina and potash under controlled conditions”, Mining, Metallurgy & Exploration, 37 (3) 911-921.

Petrov, M., Milošević, S., (1999), Physical Properties of Mechanically Activated Grains. In: Advanced Science and Technology of Sintering. Monograph, Springer, p.193.

Shabab, A., Mohammad Mehdi, S., Aghajani, A., (2016), “Alunite processing method selection using the AHP and TOPSIS approaches under fuzzy environment”, International Journal of Mining Science and Technology, 26 (6) 1017-1023.

DIAGNOSTIC LEACHING OF A DOUBLE REFRACTORY GOLD ORE

Deus Albert MSUMANGE[1,2], Hacı DEVECİ[1], Ersin Yener YAZICI[1,*], Oktay CELEP[1], J. Albert MSUMANGE[1]

[1]Hydromet B&PM Research Group, Division of Mineral &Coal Processing, Department of Mining Engineering, Karadeniz Technical University (KTU), 61080, Trabzon, TÜRKİYE
[2]Centre for Advanced Materials and Industrial Chemistry (CAMIC), School of Science, RMIT University, Melbourne, VIC 3000, AUSTRALIA
** Corresponding author: eyazici@ktu.edu.tr*

A B S T R A C T

This study investigates the refractory behaviour of gold ore sourced from the Mastra (Gümüşhane, Türkiye) sulphide zone through diagnostic leaching tests. Conventional cyanide leaching of the ore yielded an Au extraction of only ~18.4%, indicative of the refractory nature of the ore. Sequential acid treatments employing HCl and HNO_3 significantly enhanced gold extraction to 88.6%, with the remaining unexposed gold associated with quartz, highlighting that acid treatments are effective in rendering previously refractory gold accessible. The refractory nature is attributed to the fine dissemination and association of gold with soluble phases such as carbonates, silicates, oxides, and sulphides, in these acids. In this context, about 47.6% of the refractory gold was associated with sulphide minerals. Moreover, silver extraction also showed a marked improvement from 26.9% to 90.9% following the same acid treatments, suggesting similar refractory characteristics. The study highlights the need for appropriate pretreatment methods to address the challenges posed by the refractory nature of the Mastra ore in the sulphide zone.

Key words: *Diagnostic leaching, cyanidation, acid treatment, refractory gold, extraction methods*

1. INTRODUCTION

Gold ores are commonly classified as either free-milling or refractory, based on their response to conventional cyanidation (Celep et al., 2008; La Brooy et al., 1994; Marsden and House, 2006; Msumange et al., 2020). Free-milling ores typically achieve gold recoveries exceeding 90% by cyanidation. In contrast, refractory ores generally yield less than 80% owing to their complex mineralogy and the encapsulation of gold within sulphide or silicate matrices (Msumange et al., 2021; Navas Jaramillo and Gonzalez Zuñiga, 2025; Shafiei et al., 2025;). Specifically, sulphide encapsulation, the presence of carbonaceous matter with preg-robbing characteristics, and phases that consume excessive reagents like cyanide and oxygen, such as reactive copper minerals and pyrrhotite are the most common reasons for refractory behaviour (Celep and Serbest, 2015; Msumange et al., 2022; Msumange et al., 2023). Refractory gold ores, which include carbonaceous, telluride, and sulphide types, pose significant challenges for gold recovery, necessitating advanced analytical techniques such as diagnostic leaching (Li et al., 2023). Understanding the nature and occurrence of refractory gold ore is crucial for optimising gold extraction (Quaicoe et al., 2023). The deportment of gold within an ore can be determined using diagnostic leaching, an analytical technique developed by Anglo American Research Laboratories (AARL) in the mid-1980s (Lorenzen, 1995; Lorenzen and Tumilty, 1992; Tumilty et al., 1987). Diagnostic leaching involves the sequential, selective oxidative leaching/destruction of the least stable minerals associated with gold, followed by cyanidation of liberated gold at each stage (Celep et al., 2008; Lorenzen, 1995; Tumilty et al., 1987). While diagnostic leaching is a powerful tool, it has limitations. The drawback of this method is that the pretreatment leach stages of diagnostic leaching sometimes dissolve multiple minerals and are therefore not selective for any one mineral

(Henley et al., 2001). Additionally, the destruction of target minerals may not be complete (Lorenzen, 1995).

Table 1 illustrates the different pretreatment stages and the minerals expected to be dissolved during diagnostic leaching. The leaching sequence can be tailored based on the sample's specific mineralogical characteristics, allowing for the omission of certain steps as per guidelines (Celep et al., 2008; Celep et al., 2009; Guner et al., 2023; Lorenzen, 1995). The future of diagnostic leaching lies in refining the technique to improve its selectivity and broaden its applicability to a broader range of ores. Advances in automated mineralogy and analytical methods will play a crucial role in improving the accuracy and efficiency of diagnostic leaching (Guner et al., 2023). Additionally, integrating diagnostic leaching with other advanced ore characterisation methods can provide a more comprehensive understanding of ore mineralogy, leading to more effective gold recovery strategies. The decomposition of various mineral phases during different acid leaching stages can be represented by the following reactions (Lorenzen and Tumilty, 1992).

$$CaCO_3 + 2HCl \rightarrow CaCl_2 + H_2O + CO_2 \quad (1)$$

$$MS + H_2SO_4 \rightarrow MSO_4 + H_2S \text{ [M: Metals like Cu, Zn, Pb etc.]} \quad (2)$$

$$2FeS_2 + 10HNO_3 \rightarrow 2Fe^{3+} + 2H^+ + 4SO_4^{2-} + 10NO + 4H_2O \quad (3)$$

$$SiO_2 + 6HF \rightarrow H_2SiF_6 + 2H_2O \quad (4)$$

Table 1. Selective pretreatment leach stages and the targeted minerals to be destroyed (Henley et al., 2001; Lorenzen, 1995; Lorenzen and Van Deventer, 1993)

Pretreatment stages		**Minerals targeted to be destroyed**
1	NaCN washes	Precipitated gold
2	NaCN	Gold
3	Na_2CO_3	Gypsum and arsenates
4	HCl	Pyrrhotite, galena, calcite, dolomite, geothite, calcium carbonate
5	$HCl/SnCl_2$	Calcine, ferrites, hematite
6	H_2SO_4	Uraninite, labile copper sulphides, sohalerite, labile base metal sulphides, labile pyrite
7	$FeCl_3$	Sphalerite, labile sulphides, galena, tetrahedrite, sulphide concentrates
8	HNO_3	Pyrite, marcasite, arsenopyrite
9	Oxalic acid washes	Oxide coatings
10	HF	Silicates
11	Acetonitrile elution	Gold adsorbed on carbon, kerogen, coal

Lorenzen and Van Deventer (1993) employed diagnostic leaching to explore the refractory nature of a gold ore. They discovered that less than 2% of the gold present in the ore could be recovered through direct cyanidation. The remaining gold (>95%) required the breakdown of gold-bearing phases with HNO_3 and H_2SO_4 to make the associated gold available for cyanide leaching. Similarly, Celep et al. (2008) investigated the refractory behaviour of the Kaletaş ore using a diagnostic leaching approach. They reported that 72% of the gold could be recovered from the untreated ore by direct cyanidation, whereas successive acid treatments (HCl, H_2SO_4, HNO_3 and HF) increased gold recovery to 100%. These results indicated that approximately 28% of the gold was initially inaccessible, most likely due to encapsulation within various gold-bearing mineral phases. The recovery of Au from an ore containing 0.9% pyrite, 5.9% pyrrhotite, and 1.3% arsenopyrite was investigated using flotation, with diagnostic leaching employed to determine the distribution of gold among the host minerals. The results showed that a significant proportion of the Au was locked within pyrite (around 20%) and pyrrhotite (approximately 10%). Based on these findings, an effective flotation strategy was developed to maximise Au recovery (Teague et al., 1998). Another study characterised a refractory

arsenical silver ore using mineral liberation analysis (MLA) together with diagnostic leaching. The results demonstrated that using diagnostic leaching alongside MLA is an effective approach for identifying and characterising the refractory nature of highly complex silver ores (Celep et al., 2019). Henley et al. (2001) examined the cyanide leaching of native gold and gold-silver tellurides from a flotation concentrate containing approximately 37 ppm Au and 47 ppm Te. They tested a diagnostic leach procedure to quantify gold in native gold and in gold-silver tellurides. Their findings indicated that gold is present as native gold (approximately 77%), calaverite (approximately 23%), and gold-bearing hessite and petzite (less than 1%).

Preliminary studies have confirmed that the ore from the sulphide zones of the Mastra deposit is highly refractory, as cyanide leaching, with and without pretreatments, was ineffective in achieving acceptable gold extractions. Intensive cyanidation (1-8 g/L NaCN), physical pretreatment (ultrafine grinding to d_{80}: 8-73 µm), and acid pretreatment (1M H_2SO_4) failed to improve gold extraction to acceptable levels during cyanide leaching, with both approaches yielding less than 80% gold extraction (Msumange, 2019; Msumange et al., 2020). Msumange et al. (2023) demonstrated that the roasted sample had high concentrations of gold and copper, with 78 g/t Au and 1.38% Cu, respectively, along with 6.8 g/t Ag and 3.09% Fe. XRD analysis revealed that the ore's primary phase after roasting was quartz. Therefore, this study was undertaken to explore the refractory nature of the Mastra ore from the sulphide zone using a diagnostic leaching procedure.

2. EXPERIMENTAL

2.1. Materials

A representative sample of sulphidic Mastra ore (108 g/t Au, 9.3 g/t Ag, 1.6% Cu), composed predominantly of quartz and pyrite, was obtained from the Mastra Mine (Gümüşhane, Türkiye). Whole-rock and trace-element compositions were determined by X-ray fluorescence (XRF) and inductively coupled plasma mass spectrometry (ICP-MS), respectively, at an accredited analytical laboratory (ARGETEST, Ankara/Türkiye). Figure 1 presents the XRD pattern of the ore sample. The ore sample was initially crushed to -4 mm and subsequently ground for 30 minutes in a laboratory rod mill to achieve a particle size of -73 µm (d_{80}). The ground ore was then subdivided by riffle splitting and further processed using a rotary sample divider (Fritsch Laborette 27) to obtain representative sub-samples for characterisation and leaching tests. The chemical composition of the ore sample is presented in Table 2.

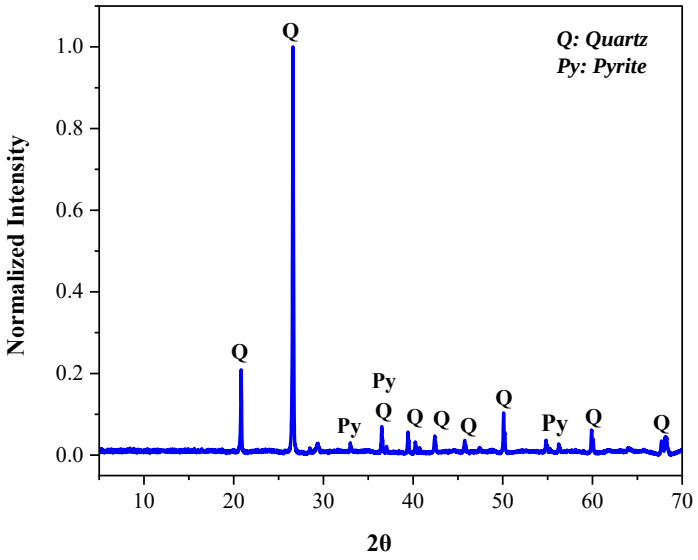

Figure 1. XRD profile of the ore sample (Msumange et al., 2020)

Table 2. Chemical composition of the ore sample (Msumange et al., 2020)

Element/Compound	Content (%)	Element	Content (g/t)
SiO_2	67.3	Au	107.7
Al_2O_3	11.51	Cu	15960
Fe_2O_3	6.06	Al	3900
MgO	0.45	Ni	604.5
CaO	0.46	Zn	926.1
Na_2O	0.06	Pb	838.1
K_2O	2.58	As	225
TiO_2	0.02	Ba	1211
P_2O_5	0.19	Ag	9.3
MnO	0.18	Sb	93.21
Cr_2O_3	0.015	Mo	24.64
Fe	4.02	Cd	10.7
S	3.46	La	1.64
K	0.21	Na	270
Ca	0.22	Mg	710
P	<0.001	Ti	23
LOI	6.03	Ga	<5
Total C	0.15	Bi	<5
Total S	4.56	Hg	<5
Sum	95.31	Be	<1

2.2. Cyanide Leaching Tests

Cyanide leaching tests were conducted in 1000-mL Pyrex beakers over a 24-hour period. The beakers were agitated at a constant stirring speed of 650 rpm using mechanical stirrers fitted with four-blade, PTFE-coated stainless-steel impellers with a 45° pitch and a blade diameter of 6.4 cm. The experimental setup is shown in Figure 2. Leach solutions were prepared using sodium cyanide (NaCN; ≥95%, Merck) at a concentration of 1.5 g/L. A pulp density of 25% (w/w), corresponding to 120 g of ore and 360 mL of cyanide solution, was maintained throughout the leaching tests. Continuous aeration was provided at a flow rate of 1.5 L/min using an air pump. Samples were withdrawn at predetermined intervals and centrifuged to obtain clear supernatants for the determination of Cu, Au, Ag, Fe and Zn concentrations by atomic absorption spectrometry (AAS). The pH of the leach solutions was adjusted to 10.5-11 using lime if it deviated. Free cyanide concentration in the tests was monitored by titration with 0.02 M silver nitrate ($AgNO_3$) using p-dimethylaminobenzylidene rhodanine as the indicator, allowing cyanide consumption to be determined. The NaCN concentration was maintained at 1.5 g/L by the addition of cyanide from a stock solution when the free cyanide level fell below this set value. It should be noted that the silver nitrate titration method may overestimate free cyanide concentrations, as a fraction of cyanide can be released from copper-cyanide complexes present in solution. Following the 24 h leaching period, the residues were filtered, dried at 105 °C, and digested in hot aqua regia prior to metal analysis. Metal extraction during leaching was calculated based on the analytical results obtained from the residues.

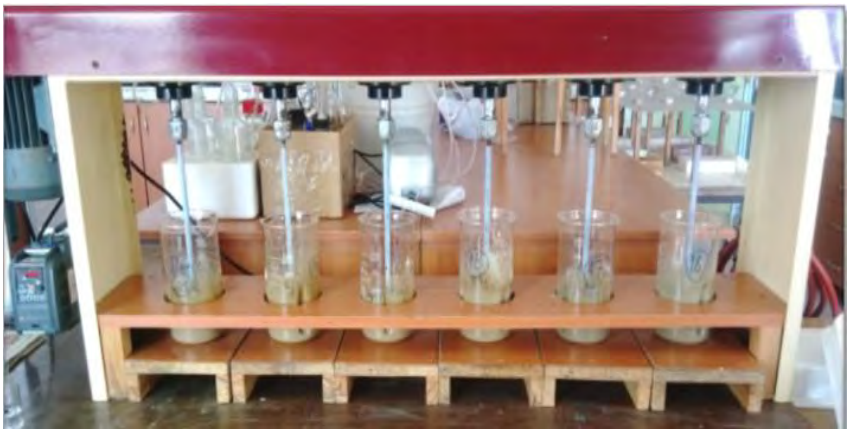

Figure 2. Multi mechanical stirrer set-up used in leaching tests

2.3. Diagnostic Leaching Tests

Diagnostic leaching tests comprised a sequence of acid leaching stages designed to decompose specific mineral phases, followed by cyanidation of the residue from each stage. Table 3 presents the diagnostic stages, operating conditions, and target mineral phases. The solid residues obtained after each leaching step were digested in hot aqua regia and analysed for metal content by atomic absorption spectrometry (AAS). Metal recoveries were calculated based on both solution and residue assays.

Table 3. Conditions of diagnostic leaching tests

Treatment step	Lixiviant	Leaching parameters	Concentration	Minerals likely to be destroyed
Cyanide leaching	NaCN	Time:24h, pH: 10.5, pulp ratio: 25% w/w	1.5 g/L	Gold
Acid leaching	HCl	S/L=1:2, Temperature: 60℃, Time: 8 h	12% (v/v)	Calcite, Galena, Dolomite,Pyrhotite, Hematite
Cyanide leaching	NaCN	Time:24h, pH: 10.5, pulp ratio: 25% w/w	1.5 g/L	Gold
Acid leaching	HNO_3	S/L=1:2, Temperature: 60℃, Time: 6 h	33% (v/v)	Arsenopyrite, marcasite, pyrite
Cyanide leaching	NaCN	Time:24h, pH: 10.5, pulp ratio: 25% w/w	1.5 g/L	Gold

3. RESULTS AND DISCUSSION

Direct cyanide leaching of the ore at a NaCN concentration of 1.5 g/L, without any pretreatment (i.e., acid leaching or roasting), resulted in limited gold and silver extractions of 18.4% and 26.9%, respectively, after 24-hour leaching (Figure 3). These data indicate that the ore exhibits a strongly refractory behaviour. The total cyanide consumption during the test was approximately 6.75 kg/t. This elevated cyanide demand suggests significant consumption by copper and other cyanide-reactive species, which likely hinder precious metal dissolution and increase overall reagent consumption.

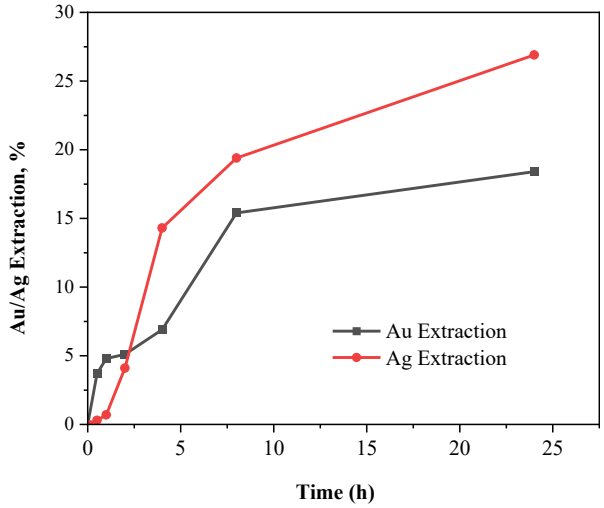

Figure 3. Extraction of gold and silver in direct cyanide leaching tests (1.5 g/L NaCN, 25% w/w solids ratio, Air flow rate: 1.5 L/min, pH 10.5-11)

Figure 4a illustrates the results of the diagnostic leaching test, which comprised conventional cyanide leaching following each acid treatment stage. Initial cyanide leaching of the as-received ore resulted in a gold extraction of 18.4% (Figure 4a), representing the fraction of gold amenable to direct cyanidation. The remaining 81.6% of the gold can therefore be considered refractory, most likely due to physical encapsulation or limited permeability of the ore matrix, which restricts access of the cyanide solution to the gold particles. Successive acid treatments with HCl and HNO_3 substantially improved gold recovery, increasing extraction to 88.6%, approximately four-fold the recovery in direct cyanidation.

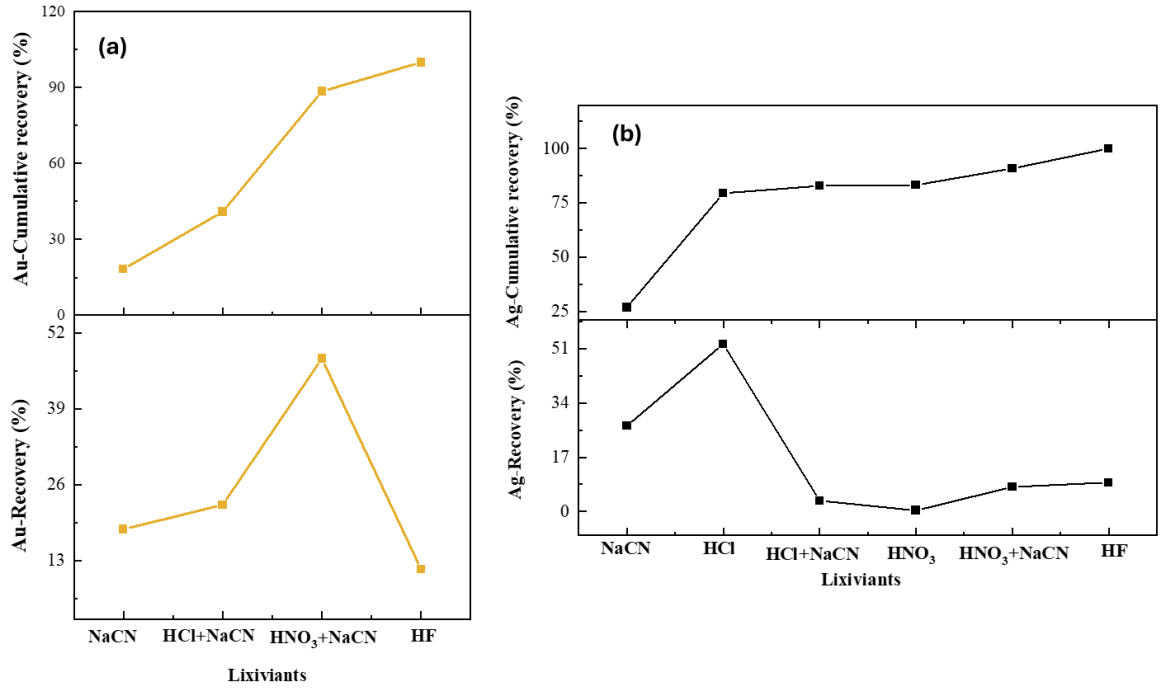

Figure 4. Deportment of gold (a) and silver (b) in the Mastra ore sample following successive diagnostic leaching stages.

Based on the diagnostic leaching results and the chemical composition presented in Table 2, the refractory nature of the ore is likely attributable to the fine dissemination of gold and its association with carbonate, oxide, silicate and sulphide phases. This interpretation is further supported by the bulk composition of the ore, which is dominated by quartz (67.3% SiO_2).

Additional evidence is provided by calcination studies reported by Msumange et al. (2023) in which the XRD pattern of the calcined material exhibited only quartz reflections, thereby confirming the refractory character of the ore. Approximately 47.6% of the gold extracted during the HNO_3 + CN stage indicates that nearly half of the refractory gold is associated with sulphide minerals. Following successive treatments with HCl and HNO_3, gold extraction increased to 88.6%, while the remaining 11.4% is likely attributable to gold encapsulated within silicate phases, which may require further treatment, such as hydrofluoric acid (HF) leaching, for complete liberation. Figure 4b presents the results of silver extraction obtained by conventional cyanide leaching following each diagnostic leaching stage. Similar to gold, silver recovery increased from 26.9% in direct cyanidation to 90.9% after sequential acid treatments with HCl and HNO_3, corresponding to an approximately 2.4-fold improvement.

4. CONCLUSION

Diagnostic leaching of the Mastra sulphide zone gold ore confirmed its strongly refractory nature, with direct cyanidation yielding only 18.4% gold extraction. Sequential acid treatments with HCl and HNO_3 substantially enhanced gold recovery to 88.6%, demonstrating the effectiveness of these treatments in rendering previously inaccessible gold amenable to cyanidation. Silver exhibited a similar response, with extraction increasing from 26.9% to 90.9% following acid pretreatment. The refractory behaviour of the ore is attributed to the fine dissemination of gold and its association with oxide, carbonate, silicate, and sulphide phases. Approximately 47.6% of the refractory gold was associated with sulphide minerals, while the residual 11.4% was likely encapsulated within silicate phases, particularly quartz. These results emphasise the importance of tailored pretreatment strategies to improve precious metal recovery from complex refractory ores, such as those from the Mastra sulphide zone.

ACKNOWLEDGMENTS

The authors gratefully acknowledge Mastra Gold Mine for providing the ore sample used in this study. They also thank Dr Fatih Özkalaycı (Department of Metallurgical and Materials Engineering, Karadeniz Technical University) for conducting the XRD analyses. Financial support from the Scientific Research Committee of Karadeniz Technical University (KTU BAP) under the research project FBA-2018-7399 is also gratefully acknowledged.

REFERENCES

Celep, O., Alp, I., Deveci, H., (2008), “Application of diagnostic leaching technique for refractory gold ores”, Dumlupınar Üniversitesi Fen Bilimleri Enstitüsü Dergisi, 16, 81–90.

Celep, O., Alp, İ., Deveci, H., Vicil, M., (2009), “Characterization of refractory behaviour of complex gold/silver ore by diagnostic leaching”, Transactions of Nonferrous Metals Society of China, 19 (3), 707–713.

Celep, O., Serbest, V., (2015), “Characterization of an iron oxy/hydroxide (gossan type) bearing refractory gold and silver ore by diagnostic leaching”, Transactions of Nonferrous Metals Society of China, 25 (4), 1286–1297.

Celep, O., Yazici, E. Y., Altinkaya, P., Deveci, H., (2019), “Characterization of a refractory arsenical silver ore by mineral liberation analysis (MLA) and diagnostic leaching”, Hydrometallurgy, 189, 105106.

Guner, M. K., Bulut, G., Hassanzadeh, A., Lode, S., Aasly, K., (2023), “Automated Mineralogy and Diagnostic Leaching Studies on Bulk Sulfide Flotation Concentrate of a Refractory Gold Ore”, Minerals, 13 (10), 1243.

Henley, K. J., Clarke, N. C., Sauter, P., (2001), “Evaluation of a diagnostic leaching technique for gold in native gold and gold ± silver tellurides”, Minerals Engineering, 14 (1), 1–12.

La Brooy, S. R., Linge, H. G., Walker, G. S., (1994), “Review of gold extraction from ores”, Minerals Engineering, 7 (10), 1213–1241.

Li, J., Yang, H., Zhao, R., Tong, L., Chen, Q., (2023), “Mineralogical characteristics and recovery process optimization analysis of a refractory gold ore with gold particles mainly encapsulated in pyrite and arsenopyrite”, Geochemistry, 83 (1), 125941.

Lorenzen, L., (1995), “Some guidelines to the design of a diagnostic leaching experiment”, Minerals Engineering, 8 (3), 247–256.

Lorenzen, L., Tumilty, J. A., (1992), “Diagnostic leaching as an analytical tool for evaluating the effect of reagents on the performance of a gold plant”, Minerals Engineering, 5 (3), 503–512.

Lorenzen, L., Van Deventer, J. S. J., (1993), “The identification of refractoriness in gold ores by the selective destruction of minerals”, Minerals Engineering, 6 (8), 1013–1023.

Marsden, J., House, I., (2006), The Chemistry of Gold Extraction, SME.

Msumange, D., (2019), “Recovery of gold from copper-rich ores using ion exchange resins”, MSc Thesis, Karadeniz Technical University, Department of Mining Engineering, Trabzon, 108 pp.

Msumange, D. A., Celep, O., Deveci, H., (2020), “Investigation of the amenability of a copper-rich refractory gold ore to cyanide leaching”, Bilimsel Madencilik Dergisi, 59 (4), 225–234.

Msumange, D. A., Celep, O., Deveci, H., (2021), “The effectiveness of adsorbents for selective recovery of gold from copper-bearing cyanide leach solutions”, Bilimsel Madencilik Dergisi, 60 (1), 21–30.

Msumange, D. A., Celep, O., Deveci, H., (2022), “A comparison of ion-exchange resins and activated carbon in recovering gold from cyanide leach solutions with low levels of copper”, Bulletin of the Mineral Research and Exploration, 168, 35–41.

Msumange, D. A., Yazici, E. Y., Celep, O., Deveci, H., Kritskii, A., Karimov, K., (2023), “Recovery of Au and Ag from the roasted calcine of a copper-rich pyritic refractory gold ore using ion exchange resins”, Minerals Engineering, 195, 108017.

Navas Jaramillo, S. J., Gonzalez Zuñiga, R. E., (2025), “Characteristics of mineralization of refractory gold and its influence on cyanide gold leaching rates: A case study in Pituca II, Zamora Chinchipe, Ecuador”, Minerals, 15 (5), 523.

Quaicoe, I., Beyuo, M., Quaicoe, S., Lasidzi, N., (2023), “Diagnostic gold deportment studies and leaching behaviour of small-scale gold mining tailings from Eastern Region, Ghana”, Journal of Sustainable Mining, 22, 81–88.

Shafiei, M., Hosseini, M. R., Azimi, E., Farnaud, S., (2025), “Responses of the refractory and free-milling gold ores to chloride leaching as an eco-friendly alternative to the cyanidation method”, Inorganic Chemistry Communications, 180, 115104.

Teague, A. J., Swaminathan, C., Van Deventer, J. S. J., (1998), “The behaviour of gold bearing minerals during froth flotation as determined by diagnostic leaching”, Minerals Engineering, 11 (6), 523–533.

Tumilty, J. A., Sweeney, A. G., Lorenzen, L., (1987), “Diagnostic leaching in the development of flowsheets for new ore deposits”, Proceedings of the Metallurgical Society of the Canadian Institute of Mining and Metallurgy, Pergamon, Oxford, 157–167.

ELECTROWINNING OF ZINC FROM AMMONIACAL LEACH SOLUTIONS OBTAINED FROM CARBONATE-CONTAINING SMITHSONITE ORE

Fatih ÇAVUŞLU[1,*], Arman EHSANİ[2], İlhan EHSANİ[3]

[1]*Adana Alparslan Türkeş Science and Technoloy University, Department of Materials Science and Engineering, Faculty of Engineering, 01250, Sarıçam, Adana, TÜRKİYE*
[2]*Adana Alparslan Türkeş Science and Technoloy University, Department of Mining Engineering, Faculty of Engineering, 01250, Sarıçam, Adana, TÜRKİYE*
[3]*Şırnak University, Department of Mining Engineering, Faculty of Engineering, Şırnak, TÜRKİYE*
**Corresponding author: fcavuslul@atu.edu.tr*

A B S T R A C T

In this study, zinc was selectively leached from a carbonate-containing smithsonite ore using aqueous ammonia (NH_3) solution as an environmentally friendly solvent. Leaching was performed under predetermined conditions (leaching time: 120 minutes; stirring rate: 600 rpm; NH3 concentration 6 M; ambient temperature). The resulting pregnant leach solution was then subjected to electrowinning for 60 minutes. Current densities ranged from 100 to 1000 A/m² to recover metallic zinc. At high current densities, dendritic zinc deposits formed along the edge of the cathode. Biodegradable and non-toxic organic additives, such as thiourea and polyethylene glycol (PEG-2000), were added to mitigate dendrite formation and enhance deposit morphology. Without additives, current efficiency increased with current density up to about 400 A/m². It then decreased at higher densities. Dendritic growth began at approximately 100 A/m², especially at the cathode edges. The use of organic additives alone was insufficient to fully inhibit dendritic growth, particularly at elevated current densities. However, the synergistic use of thiourea and PEG 2000 effectively suppressed dendritic growth and produced compact, uniform zinc deposits. The highest performance was obtained at 100 A/m² with 1 g/L PEG 2000 + 100 ppm thiourea, yielding a current efficiency of approximately 95% and a minimum energy consumption of about 4.98 kWh·kg^{-1} Zn, while completely suppressing dendritic growth. X-ray diffraction (XRD) and scanning electron microscopy (SEM) analyses confirmed the recovery of metallic zinc (Zn) and the formation of zinc oxide (ZnO). Using ammonia-based leaching and organic additive-assisted electrowinning provides a more sustainable and environmentally friendly route for zinc recovery from low-grade ores. This supports the shift toward lower-impact hydrometallurgical processes.

Key words: *Zinc electrowinning, smithsonite, organic solvents, current efficiency*

1. INTRODUCTION

Zinc is the third-most-important non-ferrous metal in terms of usage, after aluminum and copper. According to the International Lead and Zinc Study Group (ILZSG, 2024), more than 13 million tonnes of refined zinc are produced annually from ores, concentrates, and recycled materials. The primary application of zinc is galvanizing, which protects steel by enhancing the durability and service life of construction, transportation, and consumer products. In addition, zinc is widely used in copper alloying to produce brass, in aluminum-zinc die-casting alloys, in the production of rolled zinc sheets, and as a chemical component in rubber, fertilizer, and personal care products (Van Genderen et al., 2016).

There are two main zinc resources for the industry: zinc sulfide ores, which are easily separated from gangue minerals by flotation but are becoming depleted, and low-grade, non-sulfide zinc oxide ores. Sulfuric acid leaching can extract zinc from oxide ores, but it requires high acid consumption and complex purification. Recently, alkaline solutions, especially sodium hydroxide and ammonia, have proven efficient for leaching zinc oxide ores (Ehsani et al., 2019; Ehsani et al., 2021; Zhang et al., 2014).

Non-sulfide zinc ores are primarily composed of economically significant minerals, including smithsonite, hemimorphite, hydrozincite, willemite, and sauconite. However, the generally low grades and complex mineralogical structures of these ores hinder efficient utilization. As a result, leaching has been adopted as a practical method for zinc extraction (Ehsani et al., 2021). Traditionally, extraction methods have employed acidic leaching systems. More recently, though, research has investigated various alkaline leaching systems, such as those utilizing sodium hydroxide (Ehsani et al., 2019) and ammonia solutions (Ehsani et al., 2021), for the dissolution of zinc from smithsonite ores. Notably, alkaline leaching systems have demonstrated greater selectivity for smithsonite ores than acidic alternatives. Additionally, energy consumption during electrowinning from sodium hydroxide solutions is lower than that associated with acidic systems (Ehsani et al., 2019).

Electrowinning is the most important method for zinc production, accounting for approximately 80% of global zinc output. The majority of industrial operations use the acidic sulfate process, which has been extensively studied. However, the zinc industry continues to investigate new technologies to reduce capital investment and increase energy efficiency. Among the potential alternative technologies, the electrowinning of metallic zinc from alkaline solutions has attracted significant attention (St-Pierre and Piron, 1986).

In studies on the electrowinning of metallic zinc from alkaline solutions, the effects of various parameters—including solution concentration, current density, temperature, cathode material, and impurities—on current efficiency and cell voltage have been investigated in order to minimize energy consumption (St-Pierre and Piron, 1986). Furthermore, alongside research on zinc electrowinning from inorganic minerals, the literature reports studies examining the effects of free sulfuric acid concentration and current density in synthetic and high-purity zinc-containing solutions on the current efficiency and morphology of electrodeposited zinc (Saba and Elsherief, 2000; Zhao et al., 2021; Viswanath and George, 2011; Gu et al., 2018; Jiang et al., 2022; Afifi et al., 1991). Additives in the electrowinning of zinc are primarily used to improve the physical properties of the deposits (such as smoothness, brightness, and grain size) and to enhance operating performance by increasing cathodic current efficiency (CE) and decreasing energy consumption (EC). They generally function as crystal growth modifiers and hydrogen inhibitors by adsorbing onto the cathode surface (Sorour et al., 2017).

In this study, zinc was leached from smithsonite ore using alkaline leaching, and metallic zinc was recovered from the resulting solution by electrowinning. The study aims to determine optimum parameters, including additive concentration and current density, to maximize current efficiency and enhance surface morphology during the electrowinning process.

2. MATERIAL AND METHODS

2.1. Material

In this study, zinc-containing carbonate (i.e., smithsonite) ore from Yahyalı, Kayseri, Türkiye, was used. The ore was crushed to −3.36 mm using a jaw crusher, ground in a ball mill, and sieved to obtain particles smaller than 355 µm. A representative sample was then selected from the prepared material for further analysis. Table 1 presents the chemical composition of the ore sample determined by the XRF method. The ore sample also contains significant concentrations of iron, lead, and cadmium.

Table 1. The chemical composition of the ore sample

Compound	ZnO	Fe_2O_3	SiO_2	Al_2O_3	PbO	Cd
%	21,2	11,7	18,2	9,87	0,51	0,07

2.2. Method

A preliminary leaching study was carried out on the smithsonite ore using distilled water and an ammoniacal (NH_3) solution, which selectively dissolves zinc. The experimental methods described by Ehsani et al. (2021) were generally followed. Leaching was performed at room temperature in 400 mL of 6 M NH_3 with constant stirring at 600 rpm for 120 minutes. This concentration was selected because higher NH_3 levels significantly decreased zinc dissolution rates, making 6 M NH_3 optimal for balancing ammonia consumption and zinc recovery.

Zinc electrowinning was carried out from a pregnant leach solution obtained from a smithsonite ore sample at current densities ranging from 100 to 1000 A/m² for 1 hour. The electrowinning experiments were performed both with the additive-free pregnant leach solution and with the addition of organic additives. In this context, thiourea was added at a concentration of 100 ppm, while PEG 2000 was added to the pregnant leach solution at 0.5–2 g/L to obtain metallic zinc electrolytically. In addition, electrowinning experiments were conducted by adding organic additive mixtures containing 100 ppm thiourea and 1 g/L PEG 2000 to the pregnant leach solution, with electrolysis durations of 1, 2, and 4 hours.

Electrowinning was performed using an adjustable DC power supply capable of 30 V and 5 A (model: UNI-T UTP3315TFL-II). All experiments were carried out in an electrowinning cell containing 200 mL of pregnant leach solution, with stainless steel as the working electrode (cathode) and a mixed-metal oxide coated electrode as the counter electrode (anode). Prior to the electrowinning experiments, the stainless-steel electrodes were successively polished using SiC abrasive papers with grit sizes of 120, 240, 400, 800, and 1200. The electrodes were then cleaned with distilled water and acetone. After electrowinning, the obtained metallic zinc deposits were rinsed with distilled water without stripping from the substrate and subsequently dried in an oven at 60 °C. The experimental (ΔW) and theoretical (Wt) amounts of zinc recovered after electrowinning, as well as the current efficiency (CE) and energy consumption (EC), were calculated using the following equations:

$$\Delta W = W_f - W_i \quad (1)$$

$$W_t = (I * t * M) / (n * F) \quad (2)$$

$$CE = \Delta W / Wt * 100 \quad (3)$$

$$EC = (V * I * t) / \Delta W \quad (4)$$

where ΔW is the experimentally measured mass of zinc deposited (g), W_f and W_i are the final and initial cathode masses (g), respectively, W_t is the theoretical mass of zinc deposited (g), I is the applied current (A), t is the electrowinning time (s), M is the molar mass of zinc (65 g·mol⁻¹), n is the number of electrons transferred per zinc ion (n = 2 for Zn^{2+}), F is Faraday's constant (96,500 C·mol⁻¹), V is the cell voltage (V), and EC is expressed as energy consumption per unit mass of zinc deposited.

Phase analyses of the smithsonite ore and the metallic coatings deposited on the stainless-steel substrates after electrowinning were performed using X-ray diffraction (XRD) in the 2θ range of 20°–90° at a scanning rate of 2°/min. The XRD analyses were carried out using a Rigaku MiniFlex 600 diffractometer. The surface morphology of the zinc coatings was examined using a FEI Quanta 650 Field Emission Scanning Electron Microscope (SEM).

3. RESULTS AND DISCUSSION

3.1. X-Ray Diffraction (XRD) Pattern and Surface Morphologies of Additive-Free Zinc Electrowinning

The surface XRD patterns of the zinc deposit obtained by electrowinning at a current density of 100 A/m² for 1 h without additives are shown in Figure 1. XRD analysis indicates that the deposit consists of zinc (Zn) and zinc oxide (ZnO) phases. The occurrence of ZnO indicates that partial oxidation of the zinc deposit may have taken place, either during the electrowinning process or upon exposure to air after deposition.

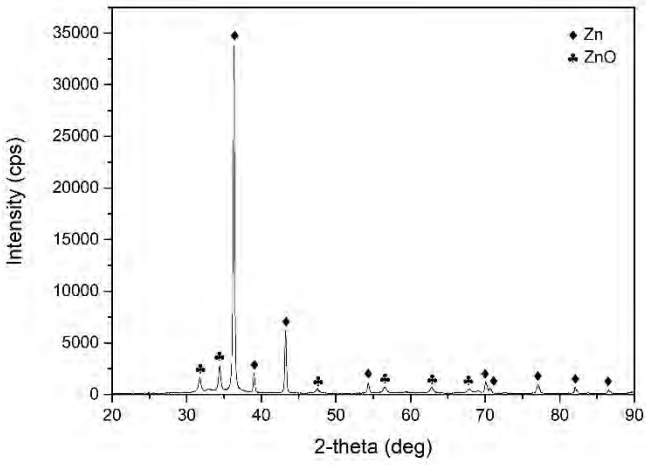

Figure 1. of the zinc deposit obtained by electrowinning at a current density of 100 A/m² for 1 hour without additives

Figure 2 illustrates the variation of current efficiency and specific energy consumption as a function of current density for zinc electrowinning from a pregnant leach solution in the absence of additives. The surface morphologies of electrowinning zinc obtained at 100 A/m² and 400 A/m² current densities are also presented in Figure 3. At a relatively low current density of 100 A/m², the process exhibits a moderate current efficiency (~80%) and low energy consumption.

The corresponding SEM image reveals a relatively uniform, compact morphology composed of fine, plate-like crystals distributed homogeneously over the cathode surface (Figure 3a). Increasing the current density to 400 A/m² results in a maximum current efficiency (~86%), indicating more effective utilization of the applied current for zinc electrowinning. However, the SEM image at this current density shows a significant coarsening of the surface morphology, with larger plate-like grains and increased surface roughness (Figure 3b). At higher current densities beyond 400 A/m² (800–1000 A/m²), the electrochemical performance deteriorates sharply, as evidenced by a pronounced drop in current efficiency and a steep increase in energy consumption. While relatively compact and uniform deposits are obtained at lower current densities, dendritic growth begins during electrowinning and becomes increasingly evident at higher current densities, particularly near the edges of the stainless-steel cathode. This behavior is attributed to edge effects, where geometric discontinuities enhance the local electric field and generate locally amplified current densities relative to the nominal applied value (Youcai et al., 2013).

At current densities approaching 1000 A/m², extensive dendritic deposition develops preferentially at the cathode edges, significantly degrading deposit compactness and mechanical stability. The rapid propagation of dendritic protrusions can cause electrical short-circuiting and poor cathode adhesion, thereby shorten the effective electrowinning duration and limiting the practical applicability of very high current densities in additive-free zinc electrowinning systems (Jiang et al., 2022).

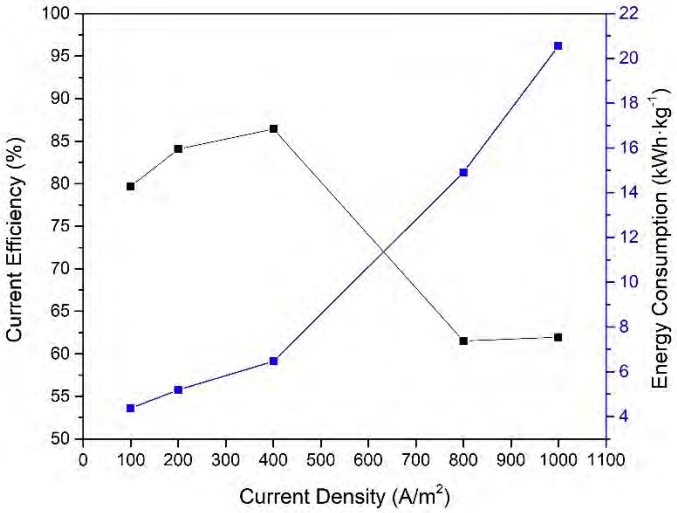

Figure 2. Current efficiency and specific energy consumption as a function of current density for additive-free zinc electrowinning

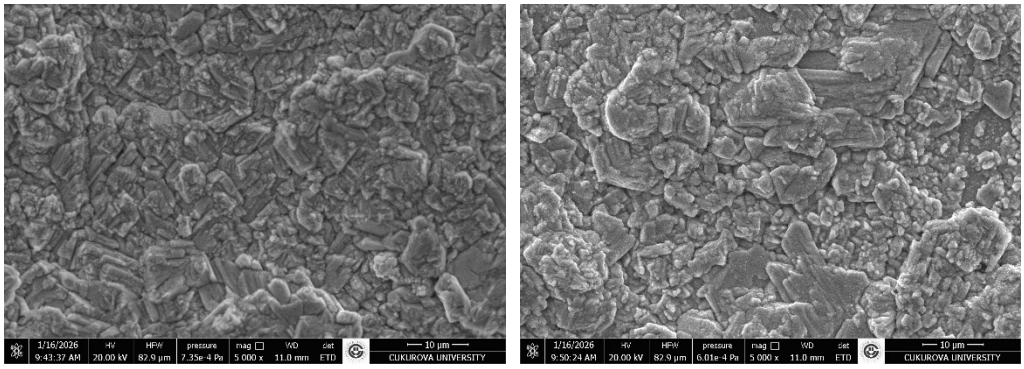

a) b)

Figure 3. SEM images of zinc deposits obtained by additive-free electrowinning at current densities of (a) 100 A/m² and (b) 400 A/m², each at ×5000 magnification

3.2. Effect of the Addition of Organic Additives on The Morphology of The Electrowinning Zinc

In order to investigate the effect of the addition of organic additives on the morphology of the deposited zinc, firstly thiourea was added to the pregnant leach solution. Figure 4 illustrates the variation of current efficiency and specific energy consumption with current density for zinc electrowinning in the presence of 100 ppm thiourea, together with representative SEM images of zinc deposits obtained at 100 and 400 A/m² current densities (Figure 5). It is observed that adding thiourea to the pregnant leach solution acts as a stabilizing agent for zinc deposition over a wide current density range. At 100 A/m², the electrowinning process exhibits a high current efficiency (~89%) and relatively low energy consumption with a compact and comparatively fine-grained surface morphology, composed of plate-like crystallites with reduced roughness relative to the additive-free electrolyte (Figure 5a). When the current density is increased to 400 A/m², the system reaches a maximum current efficiency (~94%), while energy consumption increases moderately due to the higher applied current. The SEM image at this condition shows a more homogeneous and refined deposit compared to the additive-free case at the same current density (Figure 5b). At higher current densities (800–1000 A/m²), the current efficiency decreases sharply, accompanied by a significant increase in energy consumption.

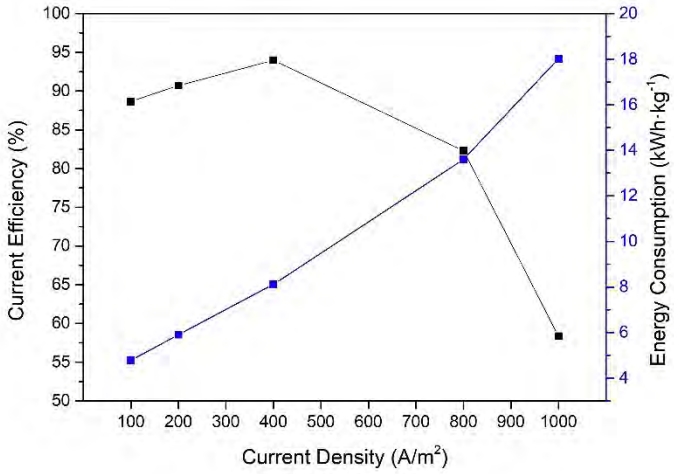

Figure 4. Effect of current density on current efficiency and specific energy consumption during zinc electrowinning with the addition of 100 ppm thiourea

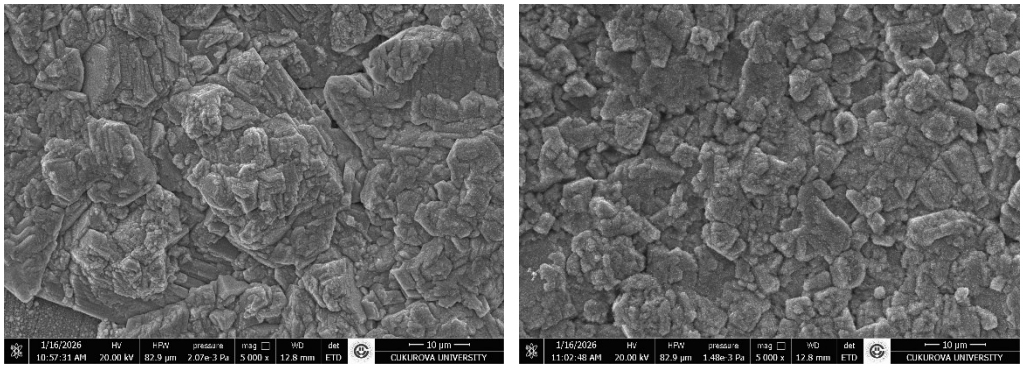

a) b)

Figure 5. SEM images of zinc deposits obtained by electrowinning with the addition of 100 ppm thiourea at current densities of (a) 100 A/m² and (b) 400 A/m², each at ×5000 magnification

Secondly, PEG 2000 is added to the pregnant leach solution with different concentrations. Figure 6 presents the variation of current efficiency and specific energy consumption with current density for zinc electrowinning in the presence of PEG 2000 at concentrations of 0.5, 1, and 2 g/L. The surface morphologies of zinc deposits obtained at 200 A/m^2 current density is also shown in Figure 6. At a PEG 2000 concentration of 0.5 g/L, the current efficiency increases initially with current density, reaching relatively high values at low to intermediate current densities, but decreases markedly at higher current densities. The zinc deposit exhibits a rough and heterogeneous surface morphology, characterized by irregular plate-like crystallites and localized agglomeration (Figure 6a). Pronounced agglomeration and non-uniform grain growth indicate that the additive concentration is insufficient to provide uniform surface coverage. Increasing the PEG 2000 concentration to 1 g/L, the current efficiency remains comparatively high over a broader current density range, while the increase in energy consumption with current density is more gradual. SEM image shows a compact, fine-grained, and homogeneous zinc deposit, with significantly reduced surface roughness and porosity (Figure 6b). The zinc deposit becomes more homogeneous, with a noticeable reduction in grain size. At a higher PEG 2000 concentration of 2 g/L, the current efficiency decreases more rapidly with increasing current density, despite the continued rise in energy consumption. The surface morphology changes noticeably, showing the formation of larger clustered structures composed of fine plate-like grains (Figure 6c). Although grain refinement is still apparent, the deposit becomes less uniform compared to that obtained at 1 g/L. This behavior suggests

over-adsorption of PEG 2000, which can hinder zinc ion transport and locally suppress deposition, leading to uneven growth and agglomeration.

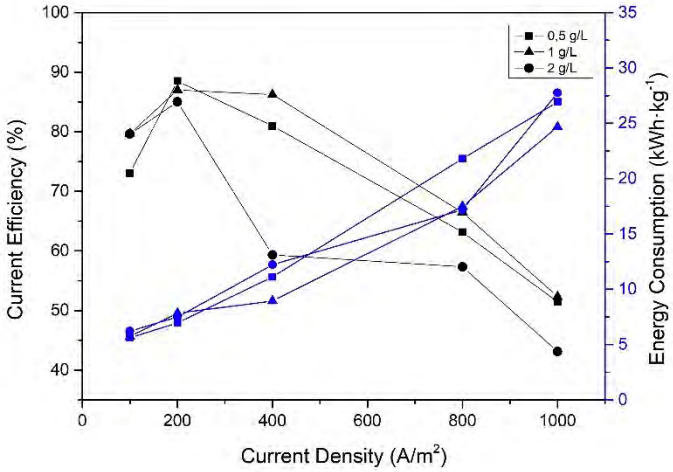

Figure 5. Effect of PEG 2000 concentration (0.5, 1, and 2 g/L) on current efficiency and specific energy consumption as a function of current density during zinc electrowinning

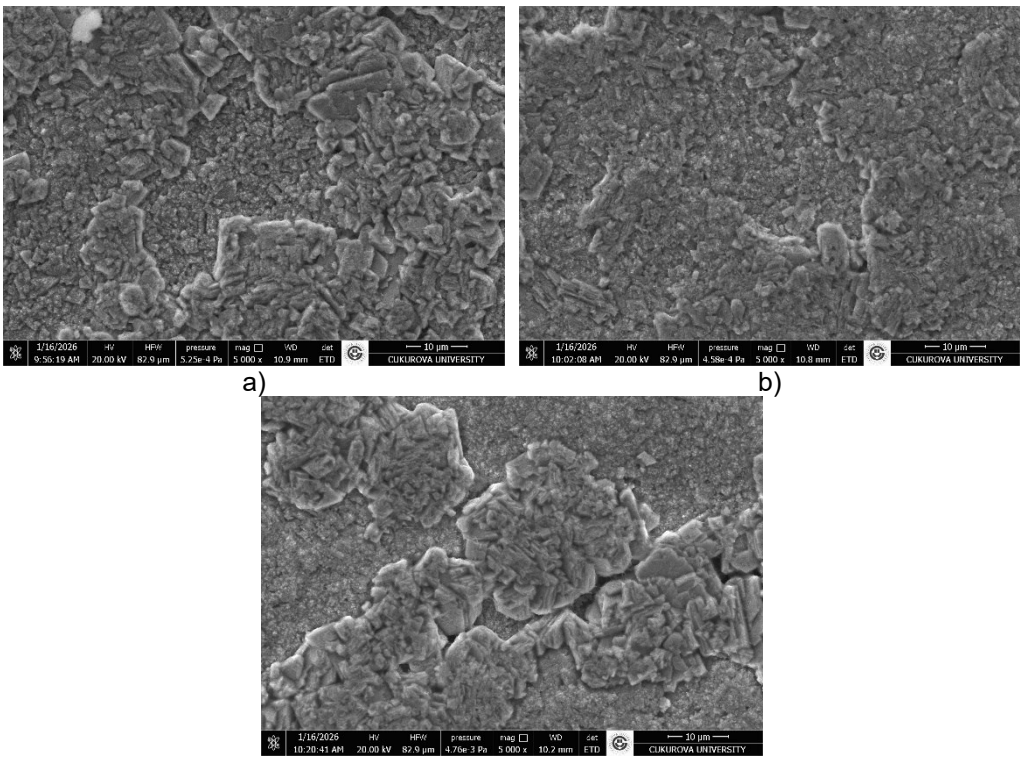

Figure 6. SEM images of zinc deposits obtained by electrowinning at a current density of 200 A/m² in the presence of PEG 2000 at concentrations of (a) 0.5 g/L, (b) 1 g/L, and (c) 2 g/L, all images taken at ×5000 magnification

Finally, in addition to thiourea and PEG 2000 additves, both 100 ppm thiourea and 1 g/L PEG 2000 additives are added together to the pregnant leach solution to take advantage of the synergistic effect of both additives. Figure 7 illustrates the variation of current efficiency and specific energy consumption as a function of electrowinning time. Figure 8 presents surface morphology of zinc deposits obtained from the pregnant leach solution containing 100 ppm thiourea and 1 g/L PEG 2000 for 2 hours.

During the initial electrowinning stage (1 h), the system exhibits moderate current efficiency (~80%) and slightly elevated energy consumption, corresponding to the formation of an initial compact nucleation layer. As electrowinning proceeds to 2 h, the current efficiency reaches a maximum value of approximately 95%, while the energy consumption decreases to its minimum. This optimum performance coincides with the development of the most compact and homogeneous zinc deposit, as confirmed by SEM analysis. The zinc deposit exhibits a highly compact and uniform surface morphology, with the near-complete suppression of large plate-like crystallites typically observed in additive-free or single-additive systems (Figure 8a). The surface is dominated by fine, densely packed grains, indicating effective control of zinc electrocrystallization over the entire cathode surface. This morphology reflects the complementary action of PEG 2000 and thiourea: PEG 2000 acts as a leveling agent that moderates overall crystal growth, while thiourea selectively adsorbs at high-energy sites and inhibits anisotropic growth. At high magnification, the zinc deposit shows a fine nodular structure consisting of densely packed, nearly spherical grains, indicating enhanced nucleation and effective suppression of anisotropic crystal growth (Figure 8b). Compared to deposits obtained with PEG 2000 alone, the synergistic system exhibits a significantly finer grain structure, while also avoiding the excessive inhibition and clustering observed at high PEG concentrations. At extended electrowinning times (4 h), a slight decrease in current efficiency is observed, accompanied by a moderate increase in energy consumption. This behavior can be attributed to gradual thickening of the zinc deposit, which increases electrical resistance and limits ion transport through the deposit layer. Nevertheless, the current efficiency remains above 90%, demonstrating that the synergistic additive system maintains deposition stability over prolonged operation, unlike additive-free or single-additive systems where efficiency deteriorates rapidly due to dendritic growth and hydrogen evolution.

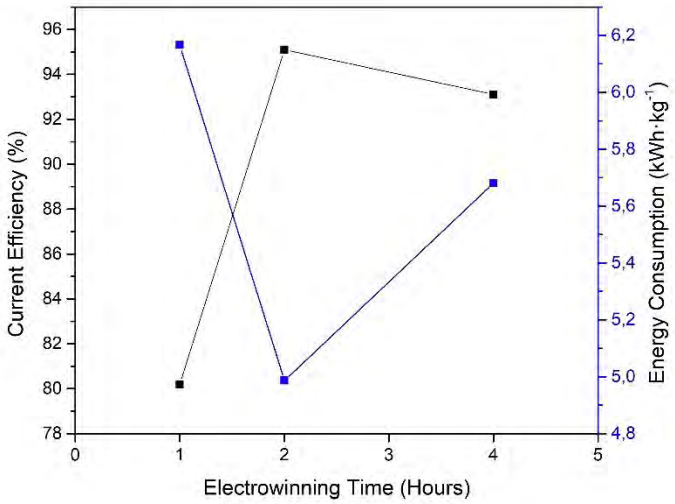

Figure 7. Current efficiency and specific energy consumption as a function of electrowinning time at a current density of 100 A/m² over 2 h in the presence of 100 ppm thiourea and 1 g/L PEG 2000, added simultaneously

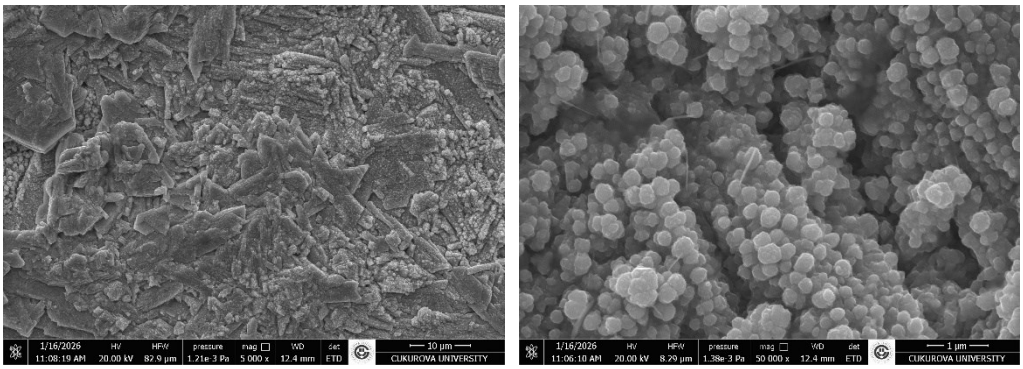

a) b)

Figure 8. SEM images of zinc deposits obtained by electrowinning at a current density of 100 A/m² in the presence of 100 ppm thiourea and 1 g/L PEG 2000 after 2 h, taken at (a) ×5000 and (b) ×50,000 magnifications

Based on the combined evaluation of current efficiency (CE), specific energy consumption (EC), and deposit morphology, the optimum zinc electrowinning conditions were achieved at a current density of 100 A/m² for 2 hours using the synergistic addition of 1 g/L PEG 2000 and 100 ppm thiourea. Under these conditions, the current efficiency reached approximately 94–96%, while the specific energy consumption was minimized to about 4.98 kWh·kg^{-1} Zn, as shown in Figure 7. In comparison, additive-free electrowinning and systems containing single additives exhibited lower current efficiencies (<88%) and higher energy consumption, particularly at elevated current densities, due to dendritic growth and increased hydrogen evolution. Therefore, the combined use of PEG 2000 and thiourea effectively maximizes current utilization while minimizing energy demand, providing a stable and energy-efficient operating window for zinc electrowinning from ammoniacal leach solutions.

4. CONCLUSION

In this work, electrowinning of zinc from pregnant leach solution obtained by alkaline leaching of the smithsonite ore is studied. Electrowinning of zinc is employed by additive-free, thiourea, PEG 2000, and the combination of thiourea with PEG 2000. Without additives, electrowinning zinc surface results in coarse, dendritic deposits, lower current efficiency, and higher energy consumption. The addition of PEG 2000 enhances surface uniformity by promoting wetting, thereby increasing efficiency within a limited current-density range. Thiourea suppresses anisotropic growth and dendrite formation more effectively, thereby sustaining higher current efficiency at elevated current densities. The synergistic addition of PEG 2000 and thiourea resulted in a current efficiency of approximately 95% and a specific energy consumption of ~5.0 kWh·kg^{-1} Zn, while completely suppressing dendritic growth. The synergistic effect of thiourea and PEG 2000 yields the most compact, fine-grained deposit. In this system, PEG 2000 provides uniform surface coverage, while thiourea selectively inhibits high-energy growth sites, leading to reduced hydrogen evolution and lower energy consumption.

ACKNOWLEGEMENTS

This research was supported by the Scientific Research Projects Coordination Unit of Adana Alparslan Türkeş Science and Technology University (Project No. 23103005). The authors would also like to express their sincere thanks to Mr. Oktay Akat (Akat Engineering Co.) for kindly providing the mixed-metal oxide-coated anode.

REFERENCES

Afifi, S., Ebaid, A., Hegazy, M., Donya, K., (1991), “On the electrowinning of zinc from alkaline zincate solutions”, Journal of The Electrochemical Society, 138(7), 1929–1933.

Ehsani, A., Ehsani, I., Obut, A., (2021), “Preparation of different zinc compounds from a smithsonite ore through ammonia leaching and subsequent heat treatment”, Physicochemical Problems of Mineral Processing, 57(4), 96–106.

Ehsani, I., Ucyildiz, A., Obut, A., (2019), “Leaching behaviour of zinc from a smithsonite ore in sodium hydroxide solutions”, Physicochemical Problems of Mineral Processing, 55(2), 407–416.

Gu, W., Liu, C., Tang, J., Liu, R., Yang, H., Hu, J., (2018), “Improving zinc electrodeposition in ammoniacal electrolytes with the saturated dissolved methyltrioctylammonium chloride”, Hydrometallurgy, 175, 43–51.

International Lead and Zinc Study Group (ILZSG), (2024), The World Zinc Factbook 2024.

Jiang, C., Huang, H., Ji, Q., Li, J., Chen, B., He, Y., Guo, Z., (2022), “Investigation of high current density on zinc electrodeposition and anodic corrosion in zinc electrowinning”, Journal of Solid-State Electrochemistry, 26(6), 1455–1467.

Saba, A. E., Elsherief, A. E., (2000), “Continuous electrowinning of zinc”, Hydrometallurgy, 54(2–3), 91–106.

Sorour, N., Zhang, W., Ghali, E., Houlachi, G., (2017), “A review of organic additives in zinc electrodeposition process (performance and evaluation)”, Hydrometallurgy, 171, 320–332.

St-Pierre, J., Piron, D. L., (1986), “Electrowinning of zinc from alkaline solutions”, Journal of Applied Electrochemistry, 16(3), 447–456.

Van Genderen, E., Wildnauer, M., Santero, N., Sidi, N., (2016), “A global life cycle assessment for primary zinc production”, The International Journal of Life Cycle Assessment, 21(11), 1580–1593.

Viswanath, S. G., George, S., (2011), “Electrowinning of zinc from ammonia and glycerol bath and study of the morphology of zinc deposit”, Association of Metallurgical Engineers of Serbia, 17(2), 57–69.

Youcai, Z., Qiang, L., Chenglong, Z., Jiachao, J., (2013), “Production of ultrafine zinc powder from wastes containing zinc by electrowinning in alkaline solution”, Brazilian Journal of Chemical Engineering, 30(4), 857–864.

Zhang, Y., Deng, J., Chen, J., Yu, R., Xing, X., (2014), “The electrowinning of zinc from sodium hydroxide solutions”, Hydrometallurgy, 146, 59–63.

Zhao, D., Yang, S., Chen, Y., Jie, Y., He, J., Tang, C., (2021), “Effects of gelatin and polyoxyethylene ether on zinc electrowinning in a Zn(II)-NH_4Cl-H_2O system”, Hydrometallurgy, 201, 105567.

EVALUATION OF ALTERNATIVE SULFATION AGENTS FOR RARE EARTH ELEMENT PRETREATMENT: A COMPARATIVE STUDY

Esra BAŞTÜRKCÜ*

Department of Mineral Processing Engineering, Faculty of Mines, Istanbul Technical University, 34467, Istanbul, Türkiye
**Corresponding author: tanisali@itu.edu.tr*

A B S T R A C T

Bisulfate-based sulfation has emerged as a promising alternative to conventional acid baking in the pretreatment of rare earth element (REE)–bearing materials. This study systematically evaluates the sulfation roasting efficiency of sodium bisulfate ($NaHSO_4$), potassium bisulfate ($KHSO_4$), and ammonium sulfate ($(NH_4)_2SO_4$) in comparison to sulfuric acid (H_2SO_4) roasting (reference) for the recovery of La, Ce, Nd, Pr, and Th from an Eskişehir-Beylikova bastnäsite pre-concentrate. Roasting temperatures were selected based on reported literature optimum for each reagent. Experiments were conducted at reagent-to-sample ratios of 1:1, 2:1, and 3:1 (wt/wt), followed by water leaching under identical conditions (20°C, L/S = 4:1, 400 rpm). Among the alternative reagents, $(NH_4)_2SO_4$ delivered the highest recovery, reaching 77.7% for Ce and 65.8% for Th at the 3:1 ratio, attributed to its gas-phase decomposition mechanism that promotes efficient mass transfer to REE mineral surfaces. $NaHSO_4$ yielded moderate recoveries (28.6-49.8% for Ce), while $KHSO_4$ was the least effective reagent tested (10–22% across all elements). H_2SO_4 roasting achieved the highest overall recovery (up to 93.9% for Th), confirming its benchmark status. The findings highlight $(NH_4)_2SO_4$ as an environmentally preferable and operationally simpler alternative to H_2SO_4 baking for REE pretreatment.

Key words: *Rare earth elements, sulfation roasting, $NaHSO_4$, $KHSO_4$, ammonium sulfate, bisulfate*

1.INTRODUCTION

Rare earth elements (REEs) are critical materials for modern technologies including permanent magnets, catalysts, phosphors, and defense systems (Balaram, 2019; Binnemans et al., 2013). Global REE production is dominated by bastnäsite ($REFCO_3$), monazite ($REPO_4$), and xenotime (YPO_4) deposits. An efficient decomposition pretreatment is required to convert refractory REE minerals into water-soluble forms prior to hydrometallurgical recovery (Sadri et al., 2017).

Several pretreatment routes have been proposed, including alkaline roasting, chlorination roasting, and sulfation roasting. Sulfation roasting with H_2SO_4 is the most industrially established approach, converting REE minerals directly into water-soluble sulfates that can be recovered by mild water leaching, eliminating concentrated acid in the leaching circuit (Borra et al., 2016; Sadri et al., 2017). However, the use of concentrated H_2SO_4 at elevated temperatures presents operational challenges such as corrosive fume generation and stringent equipment requirements, motivating research into solid-state alternative sulfating agents (Baştürkcü et al., 2022).

Sodium bisulfate ($NaHSO_4$), potassium bisulfate ($KHSO_4$), and ammonium sulfate ($(NH_4)_2SO_4$) all release reactive SO_3 upon thermal decomposition and have been explored in the processing of various metal-bearing materials (Liu et al., 2021; Mulwanda et al., 2023; Junior and Afonso, 2010). $(NH_4)_2SO_4$ roasting has attracted particular interest for REE recovery from NdFeB magnet scrap due to its gas-phase decomposition mechanism, which selectively converts REE oxides to water-soluble sulfates while leaving iron as an insoluble

oxide (Shi et al., 2025; Liu et al., 2021). To the best of the authors' knowledge, $NaHSO_4$ and $KHSO_4$ have not previously been evaluated as sulfation roasting agents for REE-bearing mineral concentrates. The present study therefore addresses this gap by providing a direct comparative assessment of these reagents alongside $(NH_4)_2SO_4$ and H_2SO_4 under controlled conditions. In addition, a systematic comparison of $NaHSO_4$, $KHSO_4$, and $(NH_4)_2SO_4$ applied to a primary REE ore concentrate under identical conditions has not been reported. In the present study, these three reagents were evaluated against H_2SO_4 roasting, using an REE pre-concentrate from the Eskişehir-Beylikova deposit, Türkiye.

2. MATERIALS AND METHODS

2.1. Materials

The sample used was a pre-concentrate prepared from bastnäsite-bearing ore from the Eskişehir-Beylikova deposit, Türkiye, following the procedure of Baştürkcü et al. (2022), at a particle size of -38 µm. The ICP-OES analysis of the pre-concentrate is given in Table 1. La and Ce are the dominant REEs, each exceeding 36,000 ppm, consistent with the bastnäsite mineralogy of the deposit.

Table 1. Light REE and Th content of the pre-concentrate (ICP-OES)

Sample	La (ppm)	Ce (ppm)	Nd (ppm)	Pr (ppm)	Th (ppm)
Pre-concentrate	36.812	36.406	5637	2557	1483

2.2. Experimental Procedure

Sulfation roasting experiments were performed using $NaHSO_4$, $KHSO_4$, $(NH_4)_2SO_4$, and H_2SO_4 at reagent-to-sample ratios of 1:1, 2:1, and 3:1 (wt/wt). Roasting temperatures were selected based on reported literature optimum data for each reagent: 300°C for $NaHSO_4$ (Mulwanda et al., 2023), 300°C for $KHSO_4$ (Junior and Afonso, 2010), 500°C for $(NH_4)_2SO_4$ (Liu et al., 2021; Shi et al., 2025), and 250°C for H_2SO_4 (Demol et al., 2018). Roasting duration was fixed at 2 h for all experiments. After roasting, the roasted product was leached with water under identical conditions for all experiments. The complete set of experimental parameters is summarised in Table 2. Leaching residues (cakes) were filtered, dried, and analysed by ICP-OES. Element recoveries were calculated from the mass and composition of the cake relative to the feed.

Table 2. Experimental parameters for sulfation roasting and water leaching

ROASTING CONDITIONS				
Parameter	**$NaHSO_4$**	**$KHSO_4$**	**$(NH_4)_2SO_4$**	**H_2SO_4**
Temperature (°C)	300	300	400	250
Roasting time (h)	2	2	2	2
Reagent:sample ratio (wt/wt)	1:1, 2:1, 3:1	1:1, 2:1, 3:1	1:1, 2:1, 3:1	1:1, 2:1, 3:1
Particle size (µm)	-38	-38	-38	-38
LEACHING CONDITIONS				
Leachant	Water			
Temperature (°C)	20			
L/S ratio (mL/g)	4:1			
Stirring speed (rpm)	400			

3. RESULTS AND DISCUSSION

3.1. Effect of $NaHSO_4$

Recovery efficiencies with $NaHSO_4$ are presented in Figure 1. At the 1:1 ratio, recoveries were: La 39.2%, Ce 48.6%, Nd 38.6%, Pr 36.8%, and Th 41.6%. Values decreased at 2:1 (Ce: 44.3%, La: 28.6%) before partially recovering at 3:1 (Ce: 49.8%, La: 34.5%). Ce consistently showed the highest recovery across all ratios. The reduced recovery at higher $NaHSO_4$ dosages may be attributed to the in-situ formation of poorly water-soluble $NaRE(SO_4)_2$ double sulfate phases during roasting. The low water solubility of these phases particularly for light REEs (La, Ce, Pr, Nd) is well established in the literature (Kul et al., 2008) and their formation would directly limit REE transfer to solution during the subsequent water leaching step.

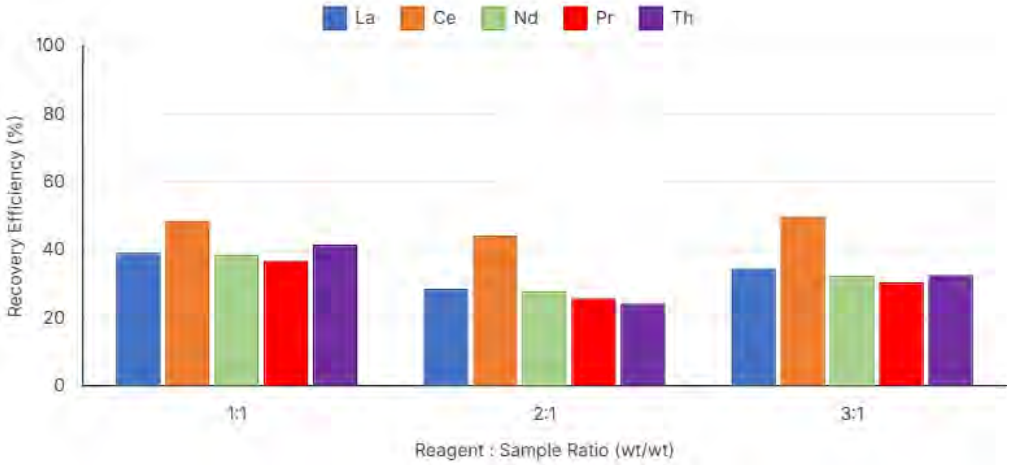

Figure 1. REE recovery efficiency as a function of $NaHSO_4$:sample ratio

3.2. Effect of $KHSO_4$

$KHSO_4$ yielded the lowest recoveries of all reagents tested (Figure 2): La 16.7%, Ce 22.0%, Nd 18.4%, Pr 15.8%, Th 14.3% at 1:1, with near-identical values at 2:1 and 3:1. The insensitivity to reagent dosage indicates kinetic limitation under the applied conditions. The formation of water-insoluble $KRE(SO_4)_2$ double sulfate phases, analogous to those reported by Junior and Afonso, (2010) for platinum-group metal catalyst processing with $KHSO_4$, likely traps REEs in an insoluble form during water leaching. These results suggest $KHSO_4$ is not an effective sulfation agent for bastnäsite-type concentrates under the conditions tested.

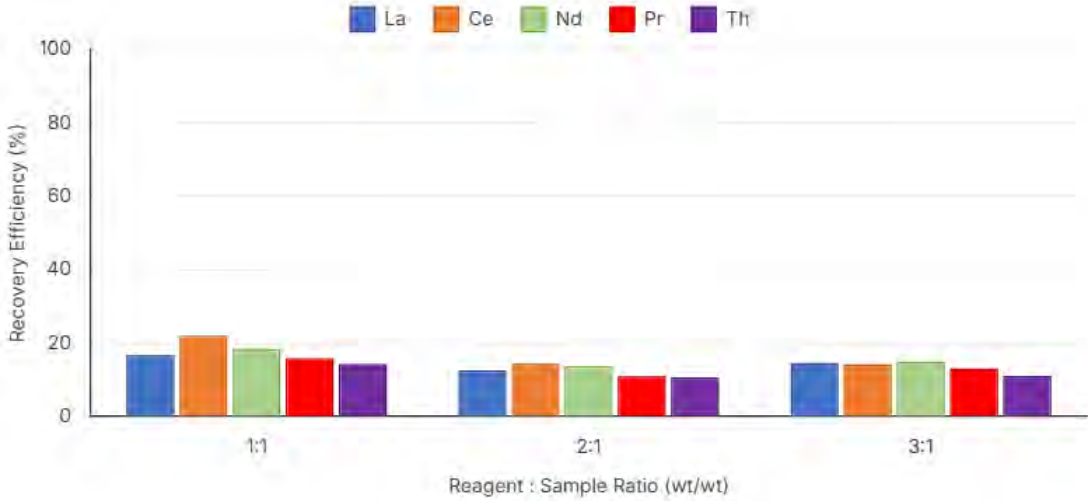

Figure 2. REE recovery efficiency as a function of $KHSO_4$:sample ratio.

3.3. Effect of $(NH_4)_2SO_4$

$(NH_4)_2SO_4$ delivered the highest recoveries among the alternative reagents (Figure 3): La 54.4%, Ce 70.8%, Nd 49.9%, Pr 48.6%, Th 64.9% at 1:1. Ce showed a progressive increase with dosage reaching 77.7% at 3:1, while Th remained stable at ~65% across all ratios. The superior performance is attributed to the gas-phase decomposition of $(NH_4)_2SO_4$ above 280°C, generating NH_3(g), SO_3(g), and H_2SO_4(g) that penetrate the ore matrix and enable efficient solid-gas sulfation a mechanism fundamentally distinct from the solid-solid contact of $NaHSO_4$ and $KHSO_4$ (Shi et al., 2025; Liu et al., 2021). Liu et al. (2021) reported ~80% REE recovery from NdFeB scrap at 400°C using $(NH_4)_2SO_4$, with selectivity over iron owing to the insolubility of iron oxides in water leaching. The moderate recovery values in the present work (49–78%) compared to NdFeB scrap processing reflect the greater mineralogical complexity and refractory character of the bastnäsite-bearing concentrate.

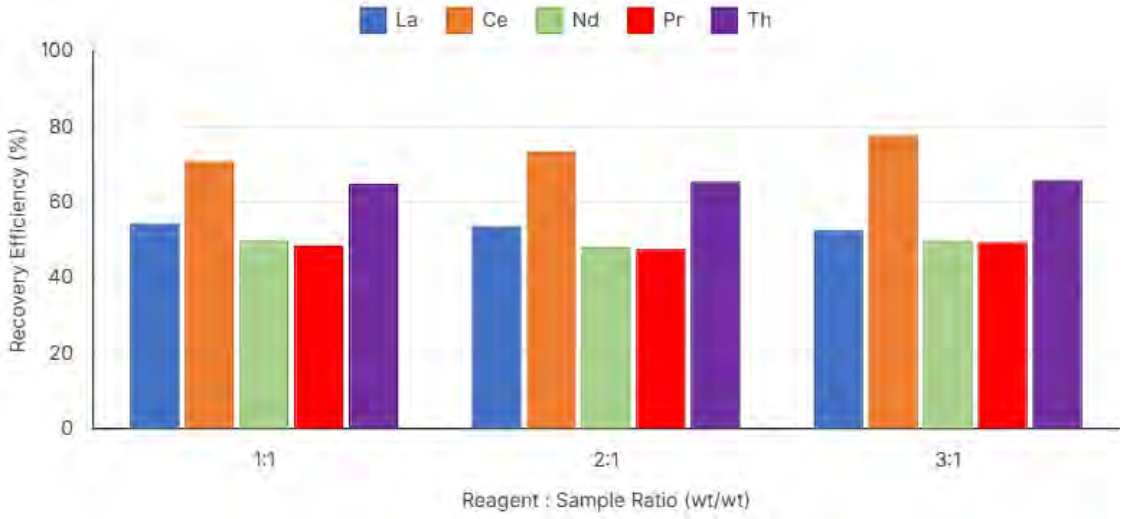

Figure 3. REE recovery efficiency as a function of $(NH_4)_2SO_4$:sample ratio

3.4. Effect of H_2SO_4

H_2SO_4 roasting achieved the highest recoveries across all conditions (Figure 4), reaching La 90.5%, Ce 91.6%, Nd 89.1%, Pr 90.5%, and Th 93.9% at 3:1. Recovery increased systematically with acid dosage for all elements, consistent with progressive conversion of residual mineral phases at higher acid loadings (Borra et al., 2016). The very high Th recovery (up to 93.9%) aligns with the thermodynamic favourability of $ThSO_4$ formation at 250°C (Demol et al., 2018), before the onset of insoluble thorium pyrophosphate phases reported above 300°C for phosphate-bearing matrices. These benchmark values confirm H_2SO_4 as the most effective reagent, while underscoring the operational motivation for pursuing solid-state alternatives such as $(NH_4)_2SO_4$.

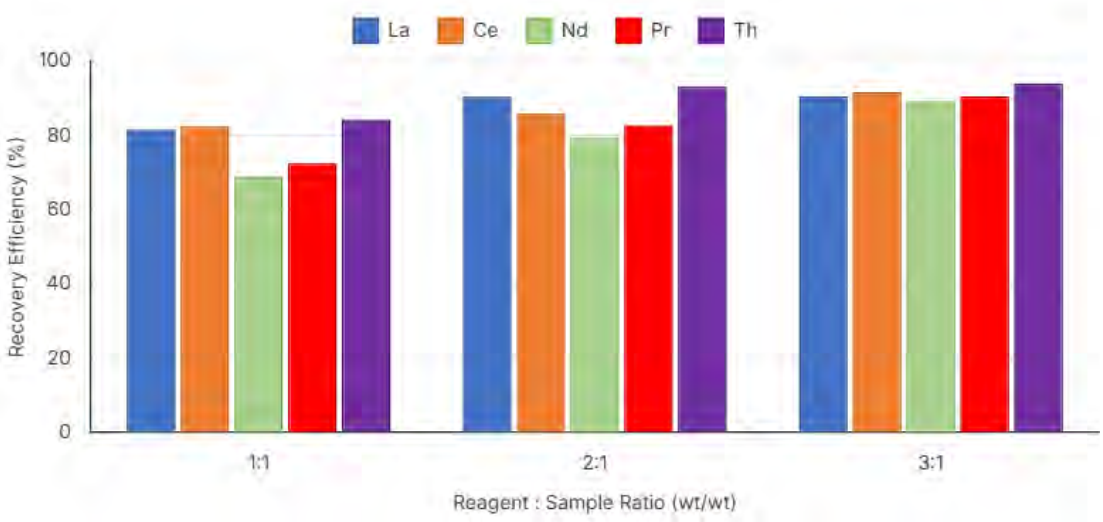

Figure 4. REE recovery efficiency as a function of H_2SO_4:sample ratio

4. CONCLUSION

The sulfation roasting performance of $NaHSO_4$, $KHSO_4$, $(NH_4)_2SO_4$, and H_2SO_4 was comparatively evaluated for REE recovery from a bastnäsite pre-concentrate. The key findings are:

- $(NH_4)_2SO_4$ was the most effective alternative reagent, achieving up to 77.7% Ce and 65.8% Th recovery at 3:1 (wt/wt), owing to its gas-phase sulfation mechanism. The reagent:sample ratio had minimal effect on La, Nd, and Pr but progressively improved Ce recovery.
- $NaHSO_4$ delivered moderate and non-monotonic recoveries (28–50%), suggesting competitive formation of $NaRE(SO_4)_2$ double salt phases at higher reagent dosages.
- $KHSO_4$ was ineffective (10–22%), showing no improvement with increasing dosage and underperforming direct dissolution, likely due to insoluble $KRE(SO_4)_2$ phase formation.
- H_2SO_4 roasting (reference) achieved the highest recoveries (up to 93.9% for Th), confirming the benchmark role of acid baking, while the results for $(NH_4)_2SO_4$ demonstrate meaningful recovery without handling concentrated liquid acid.

Future work should focus on optimisation of $(NH_4)_2SO_4$ roasting temperature and duration, XRD/SEM-EDS characterisation of roasting cake phases, and process scale-up assessment including NH_3/SO_2 gas recovery and recycling.

REFERENCES

Balaram, V., (2019) “Rare earth elements: A review of applications, occurrence, exploration, analysis, recycling, and environmental impact”, Geoscience Frontiers, 10 (4) 1285–1303.

Bastürkcü, E., Şavran, C., Yüce, A. E., Timur, S. I., (2022) “Revealing the effects of mechanical attrition applied on Eskişehir-Beylikova REE ore utilizing MLA”, Minerals Engineering, 186, 107733.

Binnemans, K., Jones, P. T., Blanpain, B., Van Gerven, T., Yang, Y., Walton, A., Buchert, M., (2013) “Recycling of rare earths: A critical review”, Journal of Cleaner Production, 51, 1–22.

Borra, C. R., Mermans, J., Blanpain, B., Pontikes, Y., Binnemans, K., Van Gerven, T., (2016) “Selective recovery of rare earths from bauxite residue by combination of sulfation, roasting and leaching”, Minerals Engineering, 92, 151–159.

Demol, J., Ho, E., Senanayake, G., (2018) “Sulfuric acid baking and leaching of rare earth elements, thorium and phosphate from a monazite concentrate: Effect of bake temperature from 200 to 800 °C”, Hydrometallurgy, 179, 254–267.

Liu, F., Chen, F., Wang, L., Ma, S., Wan, X., Wang, J., (2021) “Selective separation of rare earths from spent Nd–Fe–B magnets using two-stage ammonium sulfate roasting followed by water leaching”, Hydrometallurgy, 203, 105626.

Kul, M., Topkaya, Y., Karakaya, İ., (2008) “Rare earth double sulfates from pre-concentrated bastnasite”, Hydrometallurgy, 93 (3–4) 129–135.

Mulwanda, J., Senanayake, G., Oskierski, H. C., Altarawneh, M., Dlugogorski, B. Z., (2023) “Extraction of lithium from lepidolite by sodium bisulphate roasting, water leaching and precipitation as lithium phosphate from purified leach liquors”, Hydrometallurgy, 222, 106139.

Batista Júnior, S. G., Afonso, J. C., (2010) “Processing of spent platinum-based catalysts via fusion with potassium hydrogenosulfate”, Journal of Hazardous Materials, 184, 717–723.

Sadri, F., Nazari, A. M., Ghahreman, A., (2017) “A review on the cracking, baking and leaching processes of rare earth element concentrates”, Journal of Rare Earths, 35 (8) 739–752.

Shi, J., Chen, D., Chen, M., Qiu, Y., Dong, J., Hou, C., Zhang, F., Li, J., (2025) “Sulfation roasting for rare earth recovery from NdFeB scrap: Kinetics, thermodynamics, and phase transformation”, Process Safety and Environmental Protection, 195, 106804.

FLASH FURNACE DUST PROCESSING VIA ROASTING AND ACID LEACHING OPERATION

Melikenur AYCAN*, Merve DOĞAN, A. Erdem YILDIZHAN, Fatih ÖZEL, İbrahim GÖKTAŞ, Mehmet CANBAZOĞLU

ETİ BAKIR CO., Research and Development Center, 55300, Tekkeköy, Samsun, Türkiye
**Corresponding author: melike.aycan@etibakir.com.tr*

A B S T R A C T

In a smelting plant, enrichment experiments involving roasting and acid leaching were conducted to recover copper and zinc from cyclone, boiler, and electrostatic precipitator (ESP) dusts, which accumulate in recycling loops and cannot be reintegrated into the mainstream process. In acid leaching tests performed without prior roasting at 90 °C, zinc recovery rates for cyclone, boiler, and ESP dusts were determined as 40.4%, 44.4%, and 51.6%, respectively; while copper recovery rates were found to be 70.7%, 73.0%, and 73.4%, respectively. These low recovery efficiencies indicate that sufficient oxidation could not be achieved during the eight-hour leaching period due to the chemical composition of the feed material, which directly restricted metal solubility.

To improve leaching performance, composite dust samples were treated by roasting at temperatures between 600 °C and 900 °C. However, thermal sintering occurred at elevated temperatures, causing the particles to agglomerate.

The highest metal recoveries were obtained at 600 °C, with copper and zinc recovery rates determined as 93.1% and 88.7%, respectively. These results demonstrate that the integration of roasting and acid leaching significantly enhances process efficiency and highlights the high potential for industrial feasibility of the method.

Key words: *Acid Leaching, roasting, smelting dust, ESP*

1. INTRODUCTION

Dusts generated as by-products in copper smelting processes contain significant amounts of copper and zinc; however, they also incorporate critical impurities such as arsenic, bismuth, antimony, and iron. Directly recirculating these materials into the flash smelting furnace without any pretreatment increases the impurity concentration in the feed, leading to a reduction in furnace capacity. These elements, which form a cyclic accumulation within the system, cause technical complications during the electrolytic refining of copper and directly degrade the final cathode quality. Furthermore, volatile arsenic compounds carried by furnace gases lead to the poisoning of vanadium-based catalysts in acid plants, thereby shortening their service life. To minimize such environmental and metallurgical risks, isolating these dusts from the main production line, selectively recovering high-value metals, and discharging harmful components in compliance with ecological standards constitutes a sustainable production model (Tan et al., 2012; Xu et al., 2010).

High temperatures and the presence of oxygen during smelting processes prevent dust particles from forming a regular crystal lattice structure, leading to the development of amorphous phases; this phenomenon significantly complicates the mineralogical characterization of the material. According to the mineralogical analysis of Bottom Blown Bath Smelting (BBS) and Flash Smelting (FS) (the two primary copper smelting technologies in China) magnetite ($Fe3O4$) and copper sulfate ($CuSO4$) are the dominant crystalline phases in FS dusts, whereas magnetite, lead sulfate ($PbSO4$) and copper-iron oxide ($CuFe5O8$)

structures are prominent in BBS dusts. Examination of the amorphous phases revealed multi-component amorphous Cu-Zn-FeOx phases in FS samples, while amorphous Cu-Zn-S structures and complex copper-zinc-sulfur melts were detected in BBS samples; furthermore, arsenic, a critical impurity for copper smelting, was found to exist predominantly in amorphous form in both processes (Chen et al., 2020). Electric Arc Furnace (EAF) dusts are selected as model materials for investigating zinc phases because they form under high-temperature and oxidative conditions similar to copper smelting processes and contain high concentrations of zinc. In a study on EAF dust characterization, the primary zinc phase was identified as franklinite ($ZnFe2O4$), which forms through the contact of zinc vaporized at high temperatures with iron particles in an oxidizing atmosphere, while the secondary zinc phase was determined to be zincite (ZnO) (Machado et al., 2006).

The leaching methods applied based on the mineralogical complexity of smelting dusts and the target metal yield directly influence process efficiency. Atmospheric sulfuric acid leaching performed at temperatures of 60-95 °C is a common method for dissolving copper oxides and sulfates; however, pressure (autoclave) leaching conducted under oxygen pressure provides higher yields, particularly in the dissolution of sulfidic structures. As an alternative strategy, water leaching applied to selectively recover soluble sulfates not only reduces acid consumption by providing mass loss but also assists in impurity control. Additionally, caustic (alkaline) leaching, which aims to selectively extract arsenic into the liquid phase while preventing copper dissolution, is among the options evaluated depending on the mineralogical structure. In this study, direct leaching processes were applied to dust samples obtained from the smelting unit, and the effect of the increase in oxygen partial pressure within the furnace on recovery efficiency was investigated. To optimize the process, a roasting step as a thermal pretreatment was integrated into the system, and metal recovery yields were evaluated comparatively. The analyses revealed that the variation in oxidation potential within the furnace atmosphere and the roasting process made the mineralogical structure more suitable for leaching, thereby enabling high recovery yields.

2. MATERIAL AND METHODS

2.1. Material

The cyclone, boiler, and electrostatic precipitator (ESP) dusts collected from various units of the smelting plant were subjected to leaching tests both individually and as composite samples prepared through homogeneous blending. The coarse fraction exceeding 500 µm was crushed in a cone crusher, then recombined and homogenized with the remaining material before being divided into representative equal portions for analysis. The results of the sieve analysis, performed to determine the particle size distribution of the prepared samples, are presented in Figure 1.

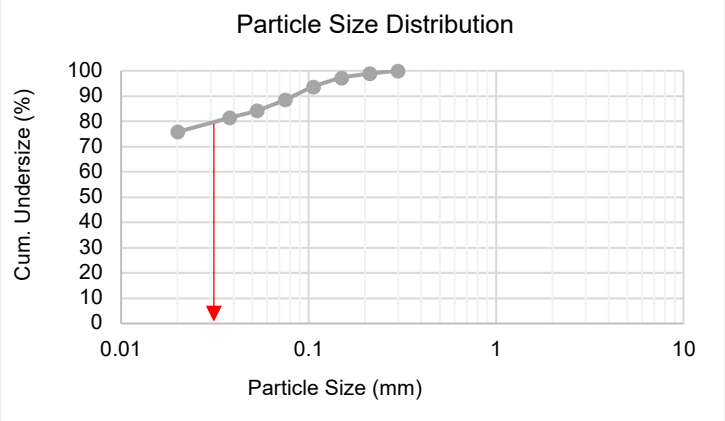

Figure 1. Particle size distribution of the representative sample (P80 = 33.5 µm)

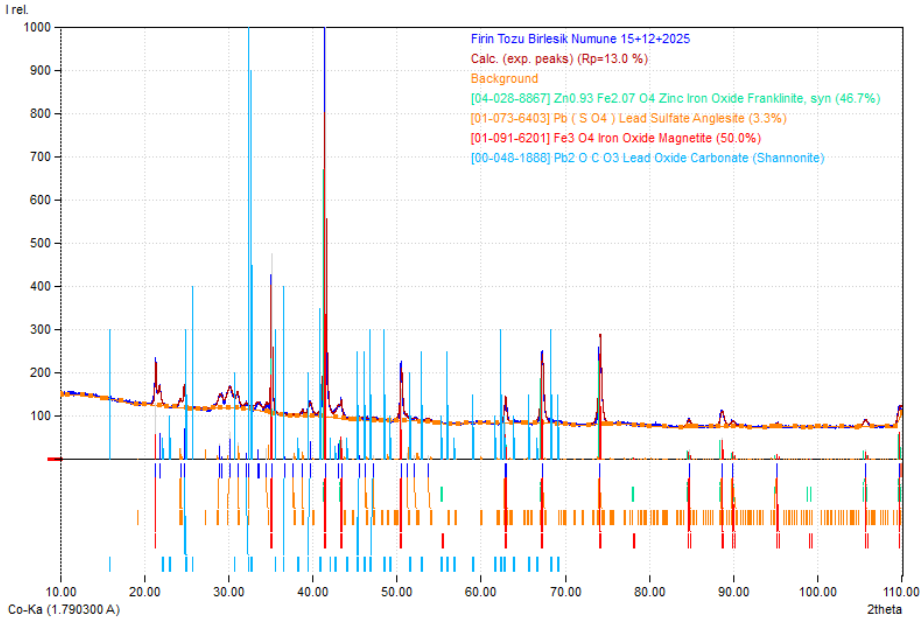

Figure 2. X-ray diffraction analysis of blended furnace dust sample

According to the XRD (X-Ray Diffraction) analysis results of the combined furnace, boiler, and cyclone dust samples, although the amorphous nature of the material complicates the precise identification of mineral phases and their percentage ratios, zinc-iron oxide (franklinite) and various iron oxide structures were identified as the predominant mineral phases.

2.2. Method

In the experimental design, while the raw cyclone, boiler, and ESP dusts were leached individually as non-roasted samples, these dusts were homogenized and subjected to thermal treatment during the roasting stage. The roasting step, acting as a thermal pretreatment, was performed in a laboratory-scale rotary kiln at temperatures ranging from 600 to 900 °C with 50 °C increments, under a 220 L/min oxygen flow rate and a 3 rpm rotation speed for 8 hours. After roasting, the samples were split into equal portions to prepare them for subsequent leaching. To overcome the mineralogical refractory nature of the non-roasted samples, aggressive leaching conditions were employed at 90 °C with a 1.0 M sulfuric acid (H2SO4) concentration and a 1/8 solid-to-liquid ratio for a constant duration of 8 hours. For the roasted samples, comparative tests were conducted for the same 8-hour period at both ambient temperature with 0.15 M H2SO4 and at 90 °C with 1.0 M H2SO4, while maintaining the same solid-to-liquid ratio. Following the leaching processes, the leach solutions were filtered for solid-liquid separation, and metal concentrations were determined using the ICP-OES technique.

3. RESULTS AND DISCUSSION

Table 1. 90 °C temperature, 1.0 M sulfuric acid (H_2SO_4)

Recovery	Cyclone	Boiler	ESP
%Bi	55.4	62.2	31.9
%Cd	83.3	86.2	84.2
%Cu	70.7	73.3	73.4
%Fe	17.7	21.3	15.0

%Zn	40.3	44.5	51.6
%As	90.7	82.6	37.4
%Sb	22.6	16.0	3.7

Following the increase in the oxygen partial pressure within the furnace regime, sulfuric acid leaching was performed on the dust samples collected from the cyclone, boiler, and electrostatic precipitator (ESP) units; the resulting metal recovery efficiencies are presented in Table 1. To enhance the dissolution yield of the dust samples, the materials collected from different units were homogenized and underwent roasting preceding the leaching process.

Table 2. Chemical analyses and density results after roasting

Roaster Temperature	%Bi	%Cd	%Cu	%Fe	%Zn	%As	%S	Density (g/cm³)	Weight Loss (%)
600 °C	0.1	1.1	15.0	26.9	8.0	2.3	5.9	6.2	8.0
650 °C	0.1	1.2	15.4	27.4	8.2	2.3	5.7	6.6	9.7
700 °C	0.1	1.3	16.6	30.2	8.7	2.4	3.9	5.8	18.7
750 °C	0.1	1.3	17.1	30.3	8.4	2.4	2.1	5.2	20.5
800 °C	0.1	1.3	17.8	31.2	8.1	2.7	1.9	4.9	21.1
850 °C	0.1	1.4	17.8	31.0	7.8	2.8	1.0	4.8	22.3
900 °C	0.1	1.4	17.4	30.9	8.4	4.4	1.2	4.8	23.2

LECO analysis of the samples revealed that they contained no carbon. During the roasting process, a significant decrease in both sulfur content and sample density was observed with increasing temperatures. SEM (Scanning Electron Microscopy) imaging was performed to examine the microstructural changes post-roasting, and sieve analyses were conducted to determine the particle size distribution. The combined evaluation of SEM images and sieve analysis data indicates that as the roasting temperature increased, the interaction between particles strengthened, leading to an increase in particle size due to sintering (agglomeration).

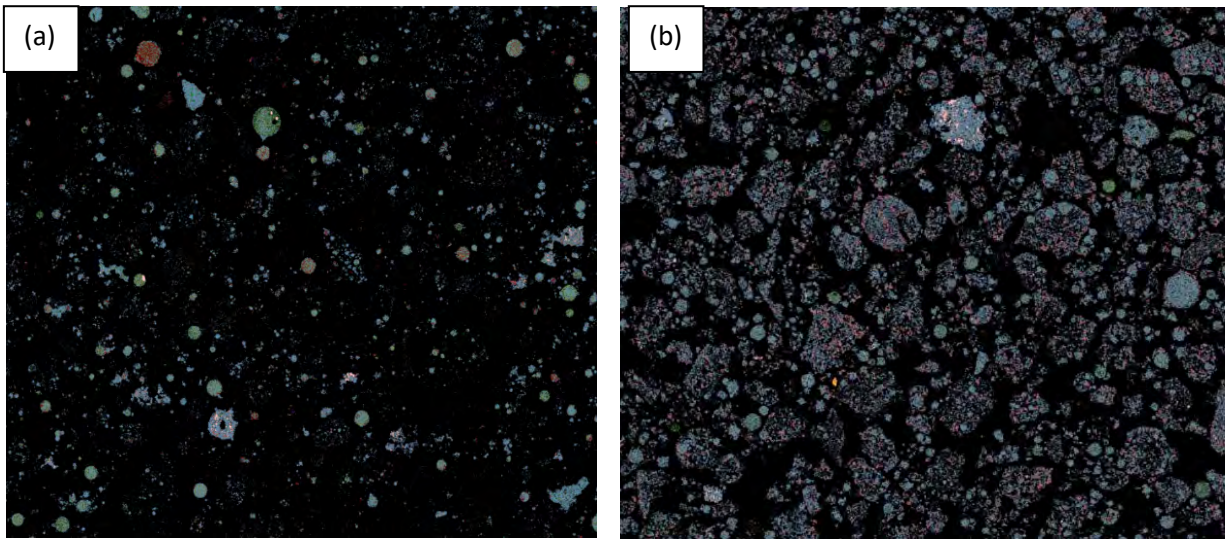

Figure 3. SEM images of roasted dust (a) 600 °C; (b) 900 °C.

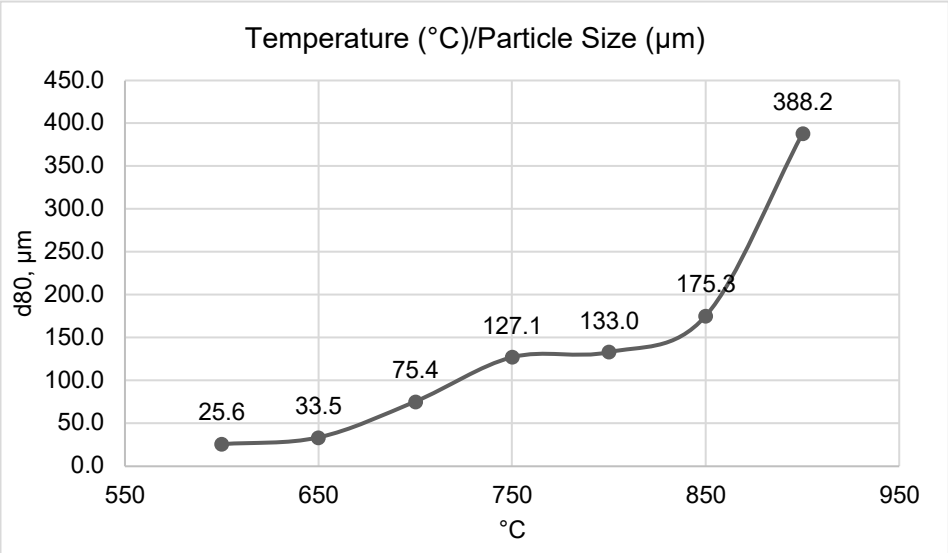

Figure 4. Sieve analyses of blended furnace dust sample

The experimental results indicated that metal dissolution yields exhibited a downward trend in parallel with the increase in roasting temperature. This phenomenon is attributed to the fact that grain coarsening caused by sintering at high temperatures reduces the particle surface area, thereby adversely affecting the leaching kinetics. The optimum roasting temperature, where copper and zinc recovery efficiencies peaked under both leaching conditions, was determined to be 600 °C. Furthermore, it was found that increasing the leaching temperature and acid concentration accelerated the reaction kinetics, exerting a positive impact on total metal recovery yields.

Table 3. Results of 0.15 M sulfuric acid leaching under ambient conditions (25 °C)

Recovery	600°C	650°C	700°C	750°C
%Bi	32.4	32.1	26.9	29.1
%Cd	89.3	91.0	91.1	89.7
%Cu	57.3	58.9	49.4	21.1
%Fe	5.3	5.7	10.1	2.1
%Zn	54.5	54.1	52.2	34.4
%As	51.6	88.6	81.9	91.6
%Sb	2.3	0.3	0.8	0.0

Table 4. Results of 90 °C, 1 M sulfuric acid leaching

Recovery	600°C	650°C	700°C	750°C	800°C	850°C	900°C
%Bi	79.2	85.2	78.5	79.8	79.2	73.3	72.5
%Cd	98.1	98.2	94.4	95.5	94.4	95.4	91.3
%Cu	93.1	92.3	74.8	77.1	71.6	73.7	68.5
%Fe	63.3	60.1	44.5	56.1	47.9	51.8	38.6
%Zn	88.7	87.9	70.8	70.8	57.5	55.9	54.8
%As	98.6	98.7	97.6	98.3	97.9	98.0	98.0
%Sb	64.2	62.3	43.2	61.4	53.4	53.5	41.5
%Ag	96.4	97.1	91.5	95.5	97.0	97.9	97.7
%Au	29.0	30.2	37.6	48.4	27.7	24.5	28.7

4.CONCLUSION

This study demonstrates the effects of roasting as a thermal pretreatment for the recovery of copper and zinc from flash smelting furnace dusts. The research findings indicate that under direct leaching conditions, zinc recovery rates for cyclone, boiler, and ESP dusts were determined as 40.3%, 44.4%, and 51.6%, respectively, while copper recovery rates were found to be 70.7%, 73.0%, and 73.4%, respectively. However, the application of a roasting pretreatment at 600 °C on the composite mixture of cyclone, boiler, and ESP dusts proves to maximize process efficiency by increasing these yields to 93.1% Cu and 88.7% Zn. Characterization studies revealed that acid-resistant amorphous phases, such as franklinite ($ZnFe2O4$), restricted metal recovery, whereas thermal treatment improved leaching kinetics by breaking down these mineralogical barriers. Conversely, sintering and subsequent grain coarsening at temperatures above 600 °C reduced the particle surface area, leading to a gradual decline in dissolution yields. Consequently, 600 °C was determined as the optimum roasting temperature for a high-efficiency hydrometallurgical recovery cycle; furthermore, it was found that increases in leaching temperature and acid concentration play a critical role in the transfer of metallic values into the sulfuric acid medium.

REFERENCES

Chen, Y., Zhao, Z., Taskinen, P., Liang, Y., Ouyang, H., Peng, B., Jokilaakso, A., Zhou, S., Chen, T., Peng, N., Liu, H., (2020) “Characterization of copper smelting flue dusts from a bottom-blowing bath smelting furnace and a flash smelting furnace”, Metallurgical and Materials Transactions B, 51 (6) 2596-2608

Machado, J. G. M. S., Brehm, F. A., Moraes, C. A. M., dos Santos, C. A., Vilela, A. C. F., da Cunha, J. B. M., (2006) “Chemical, physical, structural and morphological characterization of the electric arc furnace dust”, Journal of Hazardous Materials, 136 (3) 953-960.

Tan, C., Li, L., Zhong, D., (2012) “Recovery of copper and zinc from copper smelting flue dusts by a hydrometallurgical process”, Journal of Metallurgy, 1-7.

Xu, B., Li, Z., He, J., (2010) “Characterization and treatment of copper smelting flue dusts. Modern copper smelting”, Science Press, Beijing, 23-45.

HYDROMETALLURGICAL PROCESSING AND SUSTAINABLE VALORIZATION OF BRUCITIC DOLOMITES FOR HIGH-PURITY MAGNESIUM OXIDE PRODUCTION

Camelia BĂDULESCU*, Camelia TRAISTĂ

University of Petroșani, Mining Faculty, Environmental Engineering and Geology Department, 332006 Petroșani, Romania
**Corresponding author: badulescu_c@yahoo.com*

A B S T R A C T

Brucitic dolomites represent an important secondary source of magnesium, offering significant potential for the sustainable production of high-purity magnesium oxide (MgO). Due to their complex mineralogical composition—typically a mixture of brucite, dolomite, and calcite with an average MgO content of 22–25%—conventional beneficiation methods often prove inefficient. Experimental studies have shown that two-stage grinding followed by pneumatic concentration can produce a brucitic concentrate containing 35–40% MgO. Controlled calcination at 500–600°C leads to the decomposition of brucite into reactive magnesia, suitable for subsequent carbonation or hydrometallurgical treatment. The technological flow involves the solubilization of calcined concentrate in carbon dioxide under moderate pressure (2–5 atm), followed by precipitation of high-purity magnesium carbonate and recovery of magnesia with a purity of approximately 98%. This process ensures a global efficiency above 85%, low energy consumption, and total valorization of the raw material without generating tailings. The study emphasizes the potential of integrating extraction, calcination, and carbonation operations into a circular and low-carbon technological system. The proposed approach supports the development of eco-efficient magnesia production technologies and highlights the strategic importance of brucitic dolomites in sustainable mineral resource management.

Key words: *Brucitic dolomites, magnesium oxide (MgO), calcination, hydrometallurgical processing, sustainable resource management*

1. INTRODUCTION

Magnesium oxide (MgO) is a high-performance material widely applied in refractory linings, steel production, environmental remediation systems, catalysts, fertilizers, pharmaceuticals and advanced ceramics (Kirk-Othmer, 2014). The global demand for high-purity MgO continues to grow, driven by expansion in infrastructure, environmental regulation and high-temperature industrial processes.

The dominant industrial production route remains magnesite calcination:

$$\mathrm{Mg(HCO_3)_2 \rightarrow MgO + 2CO_2 + H_2O}$$

This reaction requires temperatures exceeding 800–1000°C (Habashi, 1997) and generates significant CO_2 emissions from both mineral decomposition and fuel combustion (International Energy Agency, 2022). Even with kiln efficiency improvements, the inherent decarbonation step limits deep decarbonization.

In response to global carbon mitigation policies and circular economy strategies (United States Geological Survey, 2023), alternative magnesium sources and lower-temperature processing routes have gained attention. Brucitic dolomites constitute one such alternative. Their mineralogical association includes brucite ($Mg(OH)_2$), which dehydroxylates at approximately

420°C (INCDMRR, 2007), significantly below carbonate decomposition temperature (~800–880°C).

This thermal gap creates an opportunity for selective activation of magnesium without full decarbonation, fundamentally differentiating brucitic dolomites from magnesite.

The Budureasa deposit represents the only economically relevant brucitic dolomite resource in Romania. This study develops a thermodynamically guided hydrometallurgical route for high-purity MgO production from this resource and critically evaluates its technical and environmental implications.

2. TECHNOLOGICAL VALORIZATION ROUTES

2.1. Conventional MgO Production Technologies

Magnesite calcination remains the benchmark technology (Habashi, 1997). Typical energy consumption ranges from 4–6 GJ/t MgO, depending on kiln type and heat recovery systems (International Energy Agency, 2022). CO_2 emissions originate both from fuel combustion and mineral decomposition.

Seawater-based processes involve precipitation of $Mg(OH)_2$ via lime addition, followed by calcination (Harben, 2016). Although industrially established, they require substantial reagent input and generate calcium-rich residues.
Both routes share common limitations: high energy demand and incomplete carbon mitigation.

2.2. Carbonation-Based Hydrometallurgical Systems

Hydrometallurgical systems utilize aqueous equilibria to control phase separation. The Mg–Ca–CO_2–H_2O system has been extensively modeled in aquatic chemistry literature.
The selective precipitation principle relies on the significant difference between:

$$K_{sp}(CaCO_3) \approx 10^{-8}$$
$$K_{sp}(MgCO_3) \approx 10^{-5}$$

This three-order-of-magnitude difference permits selective Ca removal under appropriate pH–CO_2 conditions.

Mineral carbonation research has primarily focused on CO_2 sequestration (O'Connor et al., 2005), yet the integration of carbonation into magnesium recovery circuits remains underdeveloped.

3. MATERIALS AND METHODS

3.1. Mineralogical and Chemical Characterization

Mineralogical investigations performed on the brucitic dolomites from the Budureasa deposit reveal a complex but structurally coherent mineral assemblage. The rock is characterized by the coexistence of three major phases: brucite (≈23.2%), calcite (≈42.7%) and dolomite as the dominant carbonate matrix (INCDMRR, 2007). Rather than occurring as isolated grains, these phases are intimately intergrown at fine scale, generating a compact Ca–Mg carbonate framework in which brucite is disseminated as micro-aggregates and locally as pseudomorphic replacements.

The relatively high proportion of calcite, combined with the dolomitic matrix, explains the limited efficiency of purely physical beneficiation routes, as the separation of Mg-bearing phases from Ca-rich carbonates is hindered by textural interlocking. This mineralogical configuration underscores the necessity of a selective thermally assisted approach rather than conventional mechanical upgrading.

Bulk chemical analysis confirms the mineralogical observations. The average MgO content is approximately 23.18% (INCDMRR, 2007), consistent with the quantified brucite and dolomite fractions. The CaO content reflects the substantial presence of calcite and dolomite, while impurity levels remain comparatively low, indicating favorable raw material quality for high-purity MgO production.

Thermal analysis (DTA–TG) provides decisive insight into the reactivity of the mineral system. Two clearly separated endothermic events are observed (INCDMRR, 2007). The first, occurring at approximately 420°C, corresponds to the dehydroxylation of brucite:

$$Mg(OH)_2 \rightarrow MgO + H_2O$$

This reaction results in the formation of highly reactive MgO while preserving the integrity of the carbonate framework. The second thermal event, occurring between 800 and 880°C, is associated with the decomposition of carbonate phases. The substantial temperature gap—exceeding 350°C—between these two transformations constitutes the thermodynamic foundation of the selective calcination strategy.

In essence, the mineralogical and thermal characteristics of the Budureasa dolomite demonstrate that magnesium activation can be achieved independently of full carbonate decarbonation. This intrinsic property of the deposit enables the development of a low-temperature hydrometallurgical route fundamentally distinct from conventional magnesite processing.

3.2. Selective Calcination

Selective calcination underpins the proposed separation strategy by exploiting the thermal stability gap between brucite and carbonate phases. DTA–TG analysis shows complete brucite dehydroxylation at ~420°C, whereas carbonate decomposition begins at 800–880°C (INCDMRR, 2007). Operating at 500–650°C therefore ensures full conversion of brucite to reactive MgO while preserving calcite and dolomite.

This controlled temperature range prevents CaO formation and maintains downstream selectivity. Moreover, MgO produced at moderate temperatures exhibits enhanced reactivity due to increased surface area and porosity, favoring subsequent carbonation. The maximum temperature of 650°C is more than 200°C lower than that required for magnesite decarbonation (>850°C) (Habashi, 1997), reducing energy demand and improving process integration.

Thus, selective calcination constitutes the thermodynamic foundation of efficient Mg–Ca separation and the energy advantage of the proposed route.

3.3. Controlled Carbonation and Filtrate Characterization

Following selective calcination, the reactive MgO phase was subjected to controlled carbonation in an aqueous medium. Carbonation was performed at a CO_2 partial pressure of 2–5 atm using sub-stoichiometric dosing (approximately 0.8 equivalents relative to theoretical

MgO conversion) (INCDMRR, 2008). The choice of these operating parameters was deliberate and directly linked to the thermodynamic behavior of the Mg–Ca–CO_2–H_2O system.

The applied CO_2 pressure range ensures sufficient dissolution of carbon dioxide into the aqueous phase according to Henry's law, thereby promoting the formation of carbonic acid and subsequent carbonate and bicarbonate species. However, the use of sub-stoichiometric CO_2 dosing is critical. Supplying the full stoichiometric amount of CO_2 would increase carbonate ion concentration excessively, potentially destabilizing the selective equilibrium window and promoting unwanted dissolution or re-precipitation phenomena involving calcium. By limiting CO_2 input to approximately 0.8 equivalents, the process maintains a controlled carbonate activity that favors magnesium stabilization while minimizing calcium solubilization. Under these controlled conditions, MgO reacts to form soluble magnesium bicarbonate species:

$$MgO + 2CO_2 + H_2O \rightarrow Mg(HCO_3)_2$$

Feasibility data indicate that the resulting filtrate contains a magnesium ion concentration of approximately:

$$[Mg^{2+}] \approx 0.50M$$

This relatively high concentration reflects both the efficiency of selective activation during calcination and the favorable dissolution kinetics of reactive MgO in the carbonated aqueous environment. However, such elevated magnesium concentration has important thermodynamic implications. The precipitation condition for carbonate phases is governed by:

$$[M^{2+}][CO_3^{2-}] \geq K_{sp}$$

At $[Mg^{2+}] \approx 0.50$ M, even small variations in carbonate ion concentration can shift the ionic product toward the solubility limit of $MgCO_3$. Because carbonate concentration is strongly dependent on pH (approximately proportional to $1/[H^+]^2$), minor pH fluctuations may significantly affect system stability. Consequently, the selective operational window becomes relatively narrow at high magnesium concentrations.

This requirement for tight equilibrium control arises from two coupled effects:

1. **Risk of premature $MgCO_3$ precipitation.**
   Elevated magnesium concentration increases the ionic product $[Mg^{2+}][CO_3^{2-}]$. If pH increases slightly, carbonate ion concentration rises exponentially, potentially exceeding the solubility product of $MgCO_3$ and leading to co-precipitation with calcium carbonate.
2. **Calcium breakthrough sensitivity.**
   Although $CaCO_3$ has a much lower solubility product, excessive CO_2 dosing or pH deviations may destabilize the selective domain, allowing calcium to remain partially dissolved and compromising product purity.

Therefore, maintaining equilibrium parameters—specifically pH and CO_2 partial pressure—within a well-defined domain is essential to preserve selective separation. In practical terms, this implies continuous monitoring of pH, controlled CO_2 injection rates, and optimized residence time within the carbonation reactor. The characterization of the filtrate confirms that the process operates within the intended selective regime. The high magnesium concentration, combined with limited calcium solubility, demonstrates that carbonation proceeds under conditions that favor magnesium stabilization as bicarbonate while promoting preferential precipitation of calcium as $CaCO_3$.

In summary, controlled carbonation is not merely a dissolution step but a finely tuned equilibrium operation. The combination of moderate CO_2 pressure, sub-stoichiometric dosing, and reactive MgO ensures efficient magnesium transfer into solution while preserving the thermodynamic conditions required for selective Ca–Mg separation.

3.4. Thermodynamic Modeling and Sensitivity Analysis

Selective Mg–Ca separation during carbonation is governed by the thermodynamic behavior of the Mg–Ca–CO_2–H_2O system. Carbonate speciation depends on coupled equilibria involving CO_2 dissolution and carbonic acid dissociation:

$$CO_2(g) \leftrightarrow CO_2(aq)$$
$$CO_2(aq) + H_2O \leftrightarrow HCO_3^- + H^+$$
$$HCO_3^- \leftrightarrow CO_3^{2-} + H^+$$

Carbonate concentration is strongly dependent on both pCO_2 and pH and can be

$$[CO_3^{2-}] \propto \frac{pCO_2}{[H^+]^2}$$

The quadratic dependence on pH implies that small pH variations produce exponential changes in carbonate activity.

Precipitation occurs when:

$$[M^{2+}][CO_3^{2-}] \geq K_{sp}$$

Because (difference ≈ three orders of magnitude (INCDMRR, 2008)), selective $CaCO_3$ precipitation is thermodynamically feasible. Using calibrated parameters and the measured magnesium concentration ($[Mg^{2+}]$ ≈ 0.50 M), the selective window is defined at:

- pH 6.2–6.8
- pCO_2 2–5 atm

Within this domain, $CaCO_3$ becomes supersaturated while Mg remains stabilized in solution.

Sensitivity Analysis

At elevated magnesium concentrations, the system approaches the $MgCO_3$ saturation boundary. Since carbonate concentration increases with $1/[H^+]^2$, a pH rise of more than ~0.3 units may induce $MgCO_3$ supersaturation, narrowing the selective window. Similarly, increasing pCO_2 enhances dissolved inorganic carbon. While moderate CO_2 stabilizes magnesium as bicarbonate, excessive dosing may destabilize calcium precipitation equilibria and reduce selectivity. Thus, the selective domain is dynamic rather than fixed, shifting with composition and operating conditions. At high Mg loadings, the permissible operating range may contract to ±0.3 pH units.

Industrial Implications

The process requires dynamic control rather than simple batch operation. Continuous pH monitoring, controlled CO_2 injection, optimized residence time, and efficient mixing are essential to prevent co-precipitation and maintain selectivity. Thermodynamic modeling therefore defines not only feasibility but also the operational constraints necessary for stable industrial implementation.

4. RESULTS AND DISCUSSION

4.1. Experimental Results

The following section presents the experimental results obtained under controlled laboratory conditions, aimed at evaluating the efficiency, selectivity, and operational sensitivity of the proposed hydrometallurgical route.

Table 1. Evolution of MgO/CaO ratio as a function of MgO extraction

MgO Extraction [%]	MgO/CaO Ratio
10	2.70
24	3.45
35	4.80

The progressive increase in the MgO/CaO ratio confirms the preferential dissolution of magnesium relative to calcium. As Mg extraction increases, the liquid phase becomes increasingly enriched in magnesium, demonstrating improved selectivity.

Table 2. Influence of dilution on MgO recovery

Dilution Ratio	MgO Recovery [%]
2.5 : 1	45.0
5 : 1	52.5
7.5 : 1	58.5
10 : 1	61.5
12.5 : 1	62.8
15 : 1	63.5

Recovery increases significantly up to dilution ratios of 8–10:1, after which the curve approaches a plateau, indicating that magnesium bicarbonate solubility becomes the limiting factor.

Table 3. Influence of agitation speed on MgO recovery

Agitation Speed [rpm]	MgO Recovery [%]
300	38.5
400	45.8
500	54.8
600	61.8
700	62.2
800	62.5

A significant increase in recovery is observed between 300–600 rpm, indicating mass transfer control. Above 600 rpm, the system approaches kinetic saturation, suggesting transition toward equilibrium limitation.

Table 4. Influence of temperature and time on MgO recovery

Time [h]	15°C [%]	20°C [%]	25°C [%]	30°C [%]	40°C [%]
2	14.0	12.0	9.0	15.0	13.5
6	20.0	18.0	14.5	19.0	17.5
10	24.5	22.5	18.5	27.5	24.0
15	36.0	33.0	29.0	34.5	28.0
20	44.5	41.0	35.0	37.5	30.0
25	49.5	45.5	39.0	38.5	33.0
30	56.5	47.5	42.0	40.5	34.5
35	59.0	54.0	53.0	41.0	35.5
38–40	63.0	59.0	55.0	42.5	36.0

4.2. Observations and Discussion

1. Lower temperatures (15–20°C) lead to the highest final recoveries (≈59–63%).
2. Increasing the temperature above 25°C results in a systematic decrease in recovery.
3. At 30–40°C, premature plateauing of the recovery curve is observed, confirming the limitation imposed by CO_2 solubility.
4. The differences become more pronounced after 15–20 hours, when the system transitions from a kinetically controlled regime to an equilibrium-controlled regime.

These results support the thermodynamic model: the decrease in CO_2 solubility with increasing temperature limits the formation of $Mg(HCO_3)_2$ and consequently reduces overall magnesium recovery.

Final Recovery at Different Temperatures (≈ 38–40 h)

Table 5. Influence of T-temperature and time on MgO recovery

Temperature [°C]	Final Recovery [%]
15	63
20	59
25	55
30	42
40	36

Recovery decreases with increasing temperature, confirming that CO_2 solubility governs the dissolution mechanism. Lower temperatures favor magnesium bicarbonate stabilization and higher extraction efficiency.

4.3. Precipitation of Magnesium Carbonate and the Necessity of Recarbonation

Magnesium Carbonate Precipitation Mechanism.

Following controlled carbonation, magnesium is stabilized in solution primarily as magnesium bicarbonate:

$$Mg(HCO_3)_2(aq)$$

This species is stable only under elevated CO_2 partial pressure and moderately acidic conditions. When pCO_2 decreases, pH increases, or temperature rises, the equilibrium shifts toward carbonate formation:

$$Mg(HCO_3)_2 \rightarrow MgCO_3(s) + CO_2(g) + H_2O$$

The reduction in dissolved CO_2 increases carbonate ion concentration, raising the ionic product $[Mg^{2+}][CO_3^{2-}]$ and inducing precipitation once the solubility limit is exceeded.

Necessity of Recarbonation.

During initial carbonation, $CaCO_3$ precipitates preferentially due to its much lower solubility product. However, the resulting solid phase may contain mixed Ca–Mg carbonates, basic magnesium carbonates, or incompletely carbonated hydroxides.

Recarbonation under controlled CO_2 atmosphere serves two essential purposes:

1. **Phase Stabilization:** It promotes dissolution–reprecipitation processes, converts residual hydroxides to bicarbonate, and improves phase homogeneity.

2. **Selectivity Enhancement:** Incomplete initial carbonation may cause partial Mg co-precipitation with Ca. Recarbonation preferentially redissolves magnesium as $Mg(HCO_3)_2$, while $CaCO_3$ remains largely insoluble, thereby improving the Mg/Ca ratio in solution.

Thus, recarbonation functions as a thermodynamic re-equilibration step that increases magnesium recovery, enhances selectivity, and stabilizes the carbonate phases prior to downstream processing.

5. CONCLUSIONS

This study demonstrates that brucitic dolomites can serve as a viable alternative magnesium source when processed through a thermodynamically guided hydrometallurgical route.

Selective calcination at 500–650°C activates magnesium without full decarbonation. Controlled carbonation within pH 6.2–6.8 under moderate CO_2 pressure enables selective Ca removal and Mg stabilization. Thermal destabilization yields MgO with 98–99% purity and recovery above 85%.

Beyond technical performance, the process embodies a transition from energy-intensive decarbonation to equilibrium-controlled mineral processing, consistent with low-carbon industrial strategies.

REFERENCES

Habashi, F., Principles of Extractive Metallurgy, Vols. 1–2. Gordon and Breach Science Publishers, New York, 1997. ISBN: 978-2881240122.

Harben, P.W., The Industrial Minerals HandyBook. Industrial Minerals Information Ltd., London, 2016. ISBN: 978-1908976153.

INCDMRR, DTA–TG characterization study of brucitic dolomites from the Budureasa deposit. Internal mineralogical laboratory report (material1_eugen), National Research and Development Institute for Metals and Radioactive Resources, Bucharest, Romania, 2007.

INCDMRR, Solubilization and technological validation report for brucitic dolomites (material2_eugen). Technical report, National Research and Development Institute for Metals and Radioactive Resources, Bucharest, Romania, 2008.

International Energy Agency (IEA), Industrial Heat Decarbonisation – Technology Report. IEA Publications, Paris, 2022. Available at: https://www.iea.org/reports/industrial-heat-decarbonisation

Kirk-Othmer Encyclopedia of Chemical Technology, Magnesium Compounds. John Wiley & Sons, New York, 2014. DOI: 10.1002/0471238961.magnesium

Kung, H.H., Processing of dolomitic ores for magnesium recovery. Minerals Engineering 14 (2001) 1241–1250. https://doi.org/10.1016/S0892-6875(01)00124-6

O'Connor, W.K., Dahlin, D.C., Rush, G.E., Gerdemann, S.J., Penner, L.R., Nilsen, D.N., Carbon dioxide sequestration by direct mineral carbonation with carbonic acid. Minerals Engineering 18 (2005) 1157–1162. https://doi.org/10.1016/j.mineng.2005.01.018

Pourbaix, M., Atlas of Electrochemical Equilibria in Aqueous Solutions, 2nd ed. NACE International, Houston, TX, 1974. ISBN: 978-0915567986.

Stumm, W., Morgan, J.J., Aquatic Chemistry: Chemical Equilibria and Rates in Natural Waters, 3rd ed. John Wiley & Sons, New York, 1996. ISBN: 978-0471511850.

United States Geological Survey (USGS), Mineral Commodity Summaries 2023: Magnesium. U.S. Geological Survey, Reston, VA, 2023. DOI: 10.3133/mcs2023

HYDROMETALLURGICAL RECOVERY OF HIGH-PURITY MANGANESE DIOXIDE AND ASSOCIATED COMPOUNDS FROM SILICO-MANGANESE PRODUCTION DUSTS

Mariana DUMITRACHE*, Maria LAZĂR, Camelia TRAISTĂ

Petroșani University, Mining Faculty, Environmental Engineering and Geology Department, 332006, PETROȘANI-ROMANIA
**Corresponding author: mariana.ionela.dumitrache@gmail.com*

A B S T R A C T

Dusts generated during silico-manganese production constitute a valuable yet technologically challenging secondary raw material, in which manganese is intimately associated with silico-aluminosilicate matrices. Preliminary beneficiation by granulometric and magnetic separation proved inherently ineffective, as X-ray diffraction (XRD) revealed highly heterogeneous and structurally stable mineral assemblages that fundamentally limit physical separation. Under these conditions, hydrometallurgical processing was not merely evaluated as an alternative, but as a necessary recovery route.

Leaching experiments using sulphuric and hydrochloric acids enabled the selective dissolution of manganese and associated elements, leading to high recovery yields. The study focused on the production of high-purity manganese dioxide (MnO_2) suitable for battery applications, alongside the recovery of iron and aluminium oxides and potassium salts as potential by-products. Although chemical leaching involves higher operational costs, the generation of marketable, high-value compounds provides a realistic basis for economic and environmental feasibility.

The results demonstrate that, for complex and historically deposited silico-manganese dusts, controlled hydrometallurgical treatment represents the most effective strategy for comprehensive valorisation, contributing to resource efficiency and waste minimisation within the ferroalloy industry.

Key words: *Silico-manganese dusts, hydrometallurgical processing, leaching, manganese dioxide (MnO_2), sustainable development*

1. INTRODUCTION

Silicomanganese is a ferroalloy widely used in the steel industry, mainly as a deoxidising and alloying agent in steel production (Olsen et al., 2007). It is produced in submerged arc electric furnaces by reducing manganese and silicon oxides in oxide raw materials using carbon (Gasik, 2013; Subramanyam, 2010).

In addition to liquid metal and slag, this process generates significant amounts of fine powders and slurries, which are discharged together with process gases and collected in purification systems (Rankin et al., 2011). These result from the partial volatilisation of manganese at high temperatures, the mechanical entrainment of fine particles and the secondary oxidation of metal vapours (Henao et al., 2011; Tangstad, 2015).

In terms of composition, silicomanganese slurries contain manganese oxides, silicon dioxide, iron and aluminium oxides, as well as variable amounts of unreacted carbon (Zhang et al., 2004).

This paper aims to evaluate the possibilities of recovering manganese from silicomanganese slimes by physical and hydrometallurgical methods, with a focus on the limitations of physical separation and the potential of acid leaching to obtain value-added manganese products.

In the case of silicomanganese slimes from historical deposits, the intimate association of manganese with the silicon matrix and stable oxide phases generates structural limitations of classical physical separation methods, which requires the evaluation of hydrometallurgical recovery as the main technological route, not just a complementary one.

2. EXISTING RESEARCH ON THE RECOVERY OF SILICOMANGANESE SLURRIES

Over the last two decades, the recovery of slimes resulting from the production of manganese ferroalloys has been a topic of interest, with the objectives of recovering manganese and reducing the environmental impact associated with storage (Shen et al., 2005; Shen et al., 2010; Liu et al., 2025). The reported approaches can be grouped into two main directions: pyrometallurgical recycling and hydrometallurgical recovery.

Pyrometallurgical recycling involves drying and agglomerating the fine material, followed by reintroducing it into the furnace. Although it allows for partial recovery of manganese, numerous studies highlight limitations related to the accumulation of volatile elements and operational instabilities, which restrict the industrial application of this solution (Shen et al., 2010; Gaal et al., 2010).

At the same time, the literature indicates a growing interest in hydrometallurgical recovery, based on leaching manganese from oxide phases in acidic environments, frequently sulphuric or hydrochloric (Ghafarizadeh et al., 2011; Önal et al., 2021). This approach allows the production of manganese products with high added value and superior technological flexibility, being compatible with current environmental requirements and BAT/BREF documents (European Commission, 2019).

3. MATERIAL AND METHODS

3.1. Materials

The material investigated consists of silicomanganese sludge from an industrial deposit resulting from the historical accumulation of slag and dust generated in the silicomanganese production process. The deposit is heterogeneous, with alternating areas enriched in manganese and predominantly siliceous areas, corresponding to technological variations in the production process.

To ensure the representativeness of the samples, 35 individual samples were taken from different points of the deposit, distributed uniformly over its surface. The sampling was carried out manually, aiming to include fine material and fragments characteristic of the different types of sludge identified visually. The samples were dried, homogenised and combined by weighted mixing to obtain a composite sample, which was used in all physical-chemical and technological tests.

3.2. Methods

The composite sample was dried at 105 °C to constant weight, mechanically homogenised and divided on a laboratory scale to obtain the subsamples used in the physical-chemical analyses and technological tests. The chemical composition of the material was determined by X-ray fluorescence (XRF) using a Rigaku Supermini 200 WDXRF spectrometer, with the identification of major oxides and minor elements based on certified reference materials and matrix corrections.

Mineralogical characterisation was performed by X-ray diffraction (XRD) on powders, using Cu Kα radiation in Bragg–Brentano geometry, with crystalline phases identified by comparing diffractograms with standard databases. The particle size distribution was determined by dry mechanical sieving, with the results expressed as mass percentage per size class.

Physical separation tests included weak field magnetic separation to obtain magnetic and non-magnetic fractions, as well as densimetric separation in bromoform ($\rho \approx 2.89$ g/cm³) to obtain heavy (sink) and light (float) fractions. The resulting fractions were weighed and chemically analysed to evaluate the distribution of manganese and calculate mass balances.

The hydrometallurgical behaviour of the material was investigated by discontinuous acid leaching tests, using hydrochloric acid in different concentrations and temperature conditions. After the reaction, the solutions were separated by centrifugation, and the concentration of dissolved manganese was determined by atomic absorption spectrometry (AAS).

4. RESULTS AND DISCUSSION

4.1. Chemical Composition

Chemical analysis performed by XRF on the 35 individual samples taken from the heap shows significant variability in composition, characteristic of materials deposited under variable technological conditions and with alternating manganese-siliceous stratification.

The ranges of variation of the major and minor elements are presented in Table 4.1.

Table 1. Variation limits of element concentrations in the 35 samples analysed

Component	UM	Min	Max	Average
Mn	%	3.64	20.47	15.50
SiO	%	18.88	83.54	35.57
Al_2O_3	%	0.39	1.77	0.86
S	%	0.42	1.17	0.77
P	%	0.023	0.051	0.034
Fe	%	2.06	6.04	3.31

The wide range of variation for Mn (3.64–20.47%) confirms the heterogeneous nature of the deposit, with alternating manganese-rich and silica-rich areas, while the variations in SiO_2 (18.88–83.54%) reflect the presence of siliceous layers with a dominant silica content. In contrast, sulphur and phosphorus show relatively small variations, suggesting a more uniform distribution throughout the deposit. Given this heterogeneity, an average (composite) sample, obtained by weighted mixing of the 35 samples, was used for mineralogical analyses and subsequent technological tests (magnetic, densimetric and leaching separation) to ensure the representativeness of the results and the comparability of the mass balances.

4.2. Mineralogical Analysis

XRD analysis revealed the presence of manganese oxide and silico-oxide phases, with direct implications for physical separation and leaching. Birnessite, a weakly crystallised oxide with a high specific surface area, exhibits good reactivity in an acidic environment, but is non-magnetic or very weakly paramagnetic (Zhang, et al. 2004, Cornell, R. et al. 2003). Hausmannite, a mixed oxide with a spinel structure, may contribute partially to the magnetic fraction, but its dissolution requires more severe conditions compared to birnessite (Fuerstenau, M. et al. 2002, Deer, W. et al. 1992). Braunite, a stable silico-oxide, is non-magnetic and relatively refractory, limiting the efficiency of physical methods and conventional leaching (Gaspar, J. C. 2011, O'Neill, and Navrotsky, 1983). The presence of jacobsite (Mn–Fe spinel) explains the appearance of a ferrimagnetic component, but the dissolution of

manganese from this phase may be accompanied by the co-dissolution of iron, requiring purification (Zakeri and Larachi, 2016, Shen, Y., et al 2007). Overall, the intimate association of manganese with the silicon matrix justifies the use of an integrated scheme, in which physical separations play a preconditioning role and the main recovery is achieved hydrometallurgically.

4.3. Results of Granulometric Analysis

The granulometric analysis performed by dry mechanical sieving on the 35 individual samples showed a relatively stable distribution of the dominant granulometric fractions, with moderate variations between samples, reflecting the heterogeneous nature of the deposited material. The average distribution of granulometric classes and variation limits are presented in Table 4.2.

Table 2. Variation limits of the granulometric distribution for the 35 samples

Grain size class (mm)	Minimum (%)	Maximum (%)	Average (%)
>10	~0,3	~0,7	0,50
10–6,3	~1,6	~2,3	2,00
6,3–3,15	~6,0	~7,0	6,53
3,15–2,5	~8,5	~9,5	9,03
2,5–1,25	~27,0	~29,0	28,16
1,25–0,5	~23,5	~25,5	24,34
<0,5	~28,0	~31,0	29,46

The results indicate a predominance of fine and medium fractions, with fractions below 1.25 mm accounting for approximately 54% of the total mass. Coarse fractions (>6.3 mm) account for less than 3%, suggesting an advanced degree of fragmentation of the material during the formation, transport and storage processes.

For subsequent technological tests (magnetic separation, densimetric separation and leaching), the average (composite) sample was used, obtained by weighting the 35 individual samples. The particle size distribution of this sample is shown in Table 4.3, which is considered representative of the overall behaviour of the investigated material and allows direct correlation with the results of chemical analyses and the performance of separation methods.

Table 3. Granulometric composition of the average sample used in subsequent tests

Grain size class (mm)	Content (%)
>10	0,52
10–6,3	1,98
6,3–3,15	6,55
3,15–2,5	9,05
2,5–1,25	28,10
1,25–0,5	24,30
<0,5	29,50
Total	**100,00**

4.4. Chemical Analysis Of Particle Size Fractions

In order to evaluate the distribution of manganese and the main constituents according to particle size, the granulometric fractions obtained by sieving were chemically analysed by X-ray fluorescence (XRF), using the composite sample. The average chemical composition of the granulometric fractions is presented in Table 4.4.

Table 4. Average chemical composition of particle size fractions (composite sample)

Particle size class (mm)	Mn (%)	SiO_2 (%)	Al_2O_3 (%)	S (%)	P (%)	Fe (%)
>10	11,47	~48	0,80	0,70	0,035	3,0
10–6,3	12,91	~45	0,85	0,72	0,035	3,1
6,3–3,15	13,86	~40	0,85	0,74	0,034	3,2
3,15–2,5	14,82	~36	0,86	0,75	0,034	3,3
2,5–1,25	15,10	~34	0,86	0,77	0,034	3,3

1,25–0,5	15,48	~33	0,87	0,78	0,034	3,4
<0,5	16,73	~31	0,90	0,80	0,033	3,5

The results show a clear trend of increasing manganese content with decreasing particle size. The fine fraction (<0.5 mm) has the highest Mn content (≈16.7%), while the coarse fractions (>10 mm) contain approximately 11–12% Mn. At the same time, there is a progressive decrease in SiO_2 content towards the fine fractions, indicating a relative concentration of manganese-bearing phases in these grain size classes.

However, the differences in manganese content between fractions are moderate (≈5 percentage points between extreme values), indicating that manganese is not concentrated exclusively in a single granulometric class, but is distributed across the entire dimensional spectrum, being partially associated with the slag-silicate matrix.

The mass balance shows that the fine and intermediate fractions contribute most to the total amount of manganese relative to the mass of the material, while the coarse fractions, although poorer in Mn, still contain technologically relevant amounts. This distribution limits the efficiency of a recovery strategy based exclusively on granulometric classification and justifies the need to integrate it with other separation methods or hydrometallurgical processes.

4.5. Densimetric Analysis

Densimetric separation of the composite sample of silico-manganese slime was performed in bromoform ($\rho \approx 2.89$ g/cm³), resulting in two distinct fractions: the heavy fraction (sink) and the light fraction (float). The results of the densimetric separation, expressed in terms of mass yields and the chemical composition of the fractions obtained, are presented in Table 4.5.

Table 4.5. Results of densimetric separation (composite sample)

Parameter	UM	Heavy fraction	Light fraction
Mass fraction	%	17.73	82.27
Mn	%	25.43	14.08
SiO_2	%	13.31	50.08
Al_2O_3	%	0.68	2.35
S	%	0.44	0.61
P	%	0.05	0.05
Fe	%	3.28	4.70
Extraction degree Mn	%	24.41	–

The heavy fraction represents 17.73% of the total mass of the sample, but has a high manganese content (25.43%), significantly higher than that of the initial material (18.47%). At the same time, the light fraction, which is dominant in terms of mass (82.27%), contains 14.08% Mn, a value that remains relevant from a technological point of view.

The significant reduction in SiO_2 content in the heavy fraction (13.31%), compared to the light fraction (50.08%), confirms the preferential separation of low-density silicon components from the denser manganese-bearing phases. The higher Fe concentration in the light fraction suggests the presence of ferric oxide or silicate phases with an apparent density below the heavy liquid threshold.

The manganese extraction rate in the heavy fraction is 24.41%, indicating that approximately one quarter of the total manganese in the sample is concentrated in this fraction. However, over 75% of the manganese remains distributed in the light fraction due to its high mass fraction. This distribution highlights the fact that, although densimetric separation leads to a manganese concentrate with an enrichment factor of approximately 1.38, the overall recovery efficiency is limited.

The results obtained indicate a distribution of manganese both in dense phases, probably represented by compact oxides and Mn–Fe spinels, and in phases with lower density, associated with the slag-silicate matrix. Consequently, densimetric separation can be considered an effective preconcentration method, useful for reducing the SiO_2 content and increasing the manganese content in the heavy fraction, but insufficient as a sole recovery method.

Density tests were performed on the average (composite) sample, considered representative of the entire investigated material, with the results obtained reflecting the overall behaviour of the silicomanganese slurry and allowing a realistic assessment of the potential for manganese recovery by physical methods.

4.6. Magnetic Concentration

Magnetic separation is a physical method frequently used in the treatment of metallurgical waste, based on the differences in magnetic susceptibility of the constituent phases. In the case of silicomanganese slurries, this method was analysed to assess the possibility of concentrating manganese and iron, given that SiO_2, the major component of the solid matrix, is non-magnetic.

According to the literature (Shen, Y., et al. 2007), manganese in silico-manganese slurries is predominantly present in the form of weakly paramagnetic oxides, finely dispersed and intimately associated with the silicon matrix, which limits the efficiency of separation in low-intensity magnetic fields. This characteristic is an essential element for interpreting the experimental results obtained.

Magnetic separation was applied to the previously obtained particle size fractions (<0.075 mm; 0.075–1 mm; 1–3.15 mm; >3.15 mm) using a weak magnetic field generated by a permanent ferrite magnet. For each particle size class, the mass weights and chemical compositions of the magnetic and non-magnetic fractions were determined. The results are summarised in Table 4.6.

Table 4.6. Summary of the results of magnetic separation by particle size classes

Grain size class (mm)	Magnetic fraction weight (%)	MnO magnetic fraction (%)	MnO non-magnetic fraction (%)	MnO initial material (%)	Mn extraction rate (%)	Overall Mn recovery (%)
>3,15	13,04	27,11	23,25	23,63	14,96	6,11
3,15–1	23,08	27,11	23,25	23,96	26,11	7,24
1–0,075	21,20	27,11	23,25	24,05	23,90	5,93
<0,075	46,24	27,11	23,25	24,98	50,17	3,32

The results indicate a modest enrichment in MnO in the magnetic fraction, with the content increasing by approximately 2–4 percentage points compared to the initial material. The coarse fraction (>3.15 mm) has the lowest separation efficiency, both in terms of the weight of the magnetic fraction and the overall manganese recovery.

The very fine fraction (<0.075 mm) is characterised by the highest proportion of the magnetic fraction (46.24%) and the highest degree of manganese extraction (50.17%). However, the overall recovery relative to the initial material remains low (3.32%) due to the limited mass contribution of this fraction, which explains the apparent paradox between the extraction rate and the actual recovery.

The maintenance of a high SiO_2 content in both fractions confirms the close association of manganese with the siliceous matrix, limiting selective separation by simple magnetic methods. In the absence of pre-treatments that modify the magnetic properties of manganese (e.g. reductive roasting), magnetic separation in a weak field leads only to limited enrichment.

In conclusion, magnetic separation applied independently does not allow for the efficient recovery of manganese from the analysed silico-manganese slurries. The method can only be used as a preliminary pre-concentration step in the hydrometallurgical process, without ensuring the production of a concentrate with technological parameters suitable for direct recovery. The results obtained justify directing research towards combined methods or hydrometallurgical processes.

4.7. Hydrometallurgical Recovery Of Manganese

Given the limited efficiency of physical separation methods (granulometric classification, magnetic separation and densimetric separation), the possibility of recovering manganese by hydrometallurgical methods based on the selective dissolution of manganese-bearing phases in an acidic environment was investigated. The literature indicates that the phases identified by mineralogical analysis (birnessite, hausmannite and braunite) have high solubility in hydrochloric acid, especially at elevated temperatures and high acid concentrations.

In this context, leaching tests were carried out using hydrochloric acid (HCl) in different concentrations, as well as aqua regia (HNO_3 : 3HCl), in two operating modes: at atmospheric pressure (25 °C and 80 °C) and at high pressure in laboratory autoclaves (130 °C). The liquid/solid ratio was kept constant at 1 : 16.5, and the duration of each test was 2 hours. After the reaction, the liquid phase was separated by centrifugation, and the concentration of dissolved manganese was determined by atomic absorption spectrometry (AAS). In the tests performed with concentrated HCl and aqua regia, chlorine gas was observed to be released, indicating redox reactions associated with the dissolution of the manganese-bearing phases.

Values slightly above 100% are attributed to the analytical uncertainty associated with AAS determination, cumulative mass balance errors, and rounding effects that occurred when calculating dissolved manganese relative to the initial average Mn content of the composite sample. The experimental results obtained are summarised in Table 4.7.

Table 4.7. Results of leaching tests with acid solutions

No.	HCl (ml)	Water (ml)	Temperature (°C)	Mn dissolved (%)
1	8.25	8.25	25	85.2
2	8.25	8.25	80	87.0
3	16.5	0	25	75.4
4	16.5	0	80	100.4
5	Aqua regia	–	25	101.0
6	Aqua regia	–	80	98.4
7	1	15.5	25	30.2
8	1	15.5	80	76.9
9	2	14.5	25	51.6
10	2	14.5	80	84.7
11	4	12.5	25	81.9
12	4	12.5	80	83.8
13	0.5	16	130	17.6
14	1	15.5	130	28.2
15	1.5	15	130	55.6
16	2	14.5	130	57.8

The results highlight a major influence of both acid concentration and temperature on the degree of manganese dissolution. At ambient temperature (25 °C), low HCl concentrations lead to low dissolution (≈30–50%), while increasing the concentration to 4 ml HCl results in dissolution of over 80%. The use of concentrated HCl at 80 °C leads to almost complete dissolution of manganese (~100%).

Increasing the temperature from 25 °C to 80 °C causes a significant increase in the degree of dissolution for all concentrations investigated, confirming the dominant role of temperature on

the kinetics of manganese oxide dissolution reactions. For example, for 1 ml of HCl, manganese dissolution increases from 30.2% to 76.9%, and for 2 ml of HCl from 51.6% to 84.7%.

Tests performed under high pressure (130 °C) show that dissolution efficiency is mainly controlled by acid concentration, not pressure. At very low HCl concentrations, manganese recovery remains limited (17–28%), increasing to approximately 58% for 2 ml HCl. Compared to tests at 80 °C and high acid concentrations, autoclaving does not lead to significant improvements under dilute acid conditions.

The use of aqua regia led to complete dissolution of manganese (~100%), confirming the susceptibility of the material to total dissolution in strongly oxidising environments. Compared to the physical methods investigated previously, hydrometallurgical recovery shows significantly superior performance, with maximum recoveries of less than 10% for magnetic separation, approximately 24% for densimetric separation, and up to 100% for acid leaching.

Overall, the results show that manganese in silico-manganese slurries is mostly soluble in hydrochloric acid, especially at high temperatures and adequate acid concentrations. Hydrometallurgical recovery is thus the most efficient and promising method for recovering manganese from the investigated material, justifying the focus of research on optimising leaching parameters and developing an integrated technological flow.

Compared to pyrometallurgical routes or the physical methods investigated, acid leaching offers superior control over process parameters and allows the technological scheme to be adapted to the composition of the material. This aspect is essential in the case of heterogeneous deposits, characteristic of historical silico-manganese slimes.

5. CONCLUSIONS

The study conducted on silico-manganese slimes from silicomanganese production allowed for a detailed characterisation of the material from a chemical, mineralogical and technological point of view, as well as a comparative evaluation of the possibilities for manganese recovery by physical and hydrometallurgical methods.

Chemical analysis of the 35 samples revealed a pronounced heterogeneity of the deposit, with an average Mn content of 15-18% and wide variations in SiO_2 content. The particle size distribution is dominated by fine fractions (<1.25 mm), which account for over 50% of the total mass. XRD analysis confirmed the presence of manganese oxide phases (birnessite, hausmannite, braunite), closely associated with silicate phases and an amorphous slag matrix, explaining the complex technological behaviour of the material.

Manganese is distributed across the entire grain size spectrum, with no clearly sterile fraction, and moderate differences in content between fractions limit the efficiency of concentration by size classification. Weak field magnetic separation led to modest enrichment and low overall recovery (below 10%) due to the presence of manganese in weakly paramagnetic forms or associated with the siliceous matrix. Densimetric separation allowed the obtaining of a heavy fraction enriched in manganese (≈25% Mn), but the overall recovery was limited to approximately 24%, with a majority of the manganese remaining in the light fraction.

In contrast, leaching tests with hydrochloric acid demonstrated a high capacity for manganese dissolution, especially at high acid concentrations and temperatures of 80 °C, where recoveries of over 85% and, under certain conditions, almost complete dissolution were achieved. Compared to the physical methods investigated, hydrometallurgical recovery proves to be clearly superior in terms of efficiency.

Overall, the results indicate that manganese in silico-manganese slimes is predominantly associated with finely dispersed oxide phases and the siliceous matrix, which limits the applicability of simple physical methods. Physical methods can only be used as preliminary steps in an integrated technological flow, while hydrometallurgical recovery through controlled acid leaching is the optimal direction for the efficient recovery of this type of material.

The results obtained indicate that, for silico-manganese slimes with complex mineralogy and heterogeneous manganese distribution, hydrometallurgical recovery through controlled acid leaching should be considered the main technological route for recovery, while physical methods can only play a preliminary role in an integrated flow.

REFERENCES

Barcza, N. A., (1999), “Gas-phase reactions and dust formation in electric arc furnaces”, Ironmaking & Steelmaking, 26, 45–52.

Brække, E., et al., (2018), “Airborne emissions from Mn ferroalloy production”, JOM.

Cornell, R. M., Schwertmann, U., (2003), The Iron Oxides: Structure, Properties, Reactions, Occurrences and Uses, Wiley-VCH.

Deer, W. A., Howie, R. A., Zussman, J., (1992), An Introduction to the Rock-Forming Minerals, Longman, London.

Dumitrache, M., Traistă, C., Lang, M., (2024), “Preliminary Studies on the Utilization of Silicomanganese Slurry”, Mining Revue, 30(s1), 152–157.

Eric, R. H., Burucu, E., (2008), “Reduction mechanisms in silicomanganese smelting”, Minerals Engineering, 21, 203–212.

European Commission, Joint Research Centre, (2017/2019), Best Available Techniques (BAT) Reference Document for the Non-Ferrous Metals Industries (NFM BREF).

Fuerstenau, M. C., Han, K. N., (2002), “Leaching of manganese oxides”, Minerals & Metallurgical Processing, 19, 106–113.

Gaal, S., et al., (2010), “Recycling of waste materials from the production of ferromanganese and silicomanganese”, Proceedings of INFACON XII.

Gasik, M., (2013), Handbook of Ferroalloys: Theory and Technology, Butterworth-Heinemann, Oxford.

Gaspar, J. C., (2011), “Refractory behavior of silicate-bound manganese phases”, Minerals Engineering, 24, 115–123.

Ghafarizadeh, B., Rashchi, F., Vahidi, E., (2011), “Recovery of manganese from electric arc furnace dust of ferromanganese production units by reductive leaching”, Minerals Engineering, 24(2), 174–176.

Henao, H., Olsen, S. E., (2001), “Thermodynamics of manganese volatilization in submerged arc furnaces”, Metallurgical and Materials Transactions B, 32, 701–709.

Liu, X., et al., (2025), “Kinetics of isothermal reduction of carbon-containing silicomanganese dust”, International Journal of Minerals, Metallurgy and Materials.

Nkosi, S., et al., (2011), “Hydrometallurgical process for the recovery of manganese from pelletized silicomanganese submerged arc furnace dust”, Proceedings of the Fray International Symposium, Cancun, Mexico, 4–7.

O'Neill, H. St. C., Navrotsky, A., (1983), "Cation distributions and thermodynamic properties of spinel solid solutions", American Mineralogist, 68, 181–194.

Olsen, S. E., Tangstad, M., (2002), "Process control in silicomanganese production", Scandinavian Journal of Metallurgy, 31, 227–236.

Olsen, S. E., Tangstad, M., Lindstad, T., (2007), Production of Manganese Ferroalloys, SINTEF and Tapir Academic Press, Trondheim.

Önal, M. A. R., Panda, L., Kopparthi, P., Singh, V., Venkatesan, P., Borra, C. R., (2021), "Hydrometallurgical Production of Electrolytic Manganese Dioxide (EMD) from Furnace Fines", Minerals, 11, 712.

Rankin, W. J., (2011), Minerals, Metals and Sustainability, CSIRO Publishing, Melbourne.

Shen, R., Zhang, G., Dell'Amico, M., Brown, P., Ostrovski, O., (2005), "Characterisation of manganese furnace dust and zinc balance in production of manganese alloys", ISIJ International, 45(9), 1248–1254.

Shen, R., Zhang, G., Dell'Amico, M., Brown, P., Ostrovski, O., (2010), "A feasibility study of recycling of manganese furnace dust", Proceedings of INFACON XI, 507–519.

Shen, Y., et al., (2007), "A feasibility study of recycling of manganese furnace dust", Proceedings of INFACON XI, 507–516.

Subramanyam, D. K., (2010), "Silicomanganese production processes", Journal of Minerals and Materials Characterization and Engineering, 9(4), 325–337.

Tangstad, M., (2015), "Fume formation mechanisms in ferroalloy production", INFACON Proceedings, Cape Town.

Zakeri, A., Larachi, F., (2016), "Acid leaching behavior of ferrimagnetic manganese oxides", Hydrometallurgy, 162, 41–49.

Zhang, L., Jahanshahi, S., (2004), "Characterization of silicomanganese furnace dust", ISIJ International, 44, 1669–1676.

Zhang, W., Cheng, C. Y., (2007), "Manganese metallurgy review. Part I: Leaching of ores/secondary materials", Hydrometallurgy, 89, 137–159.

INVESTIGATION OF THE BENEFICIATION OF MANGANESE ORE IN THE KARABURUN REGION BY LEACHING

Yaşar Hakan GÜRSOY*, Koray Emre AKGÖÇMEN

Eskişehir Osmangazi University, Faculty of Engineering and Arcitecture,
Mining Engineering Department, 26040, Odunpazarı, Eskişehir, TÜRKİYE
**Corresponding author: hgursoy@ogu.edu.tr*

A B S T R A C T

Manganese, widely used in the iron and steel industry, the chemical industry, and especially in energy storage systems and batteries recently, is one of the important metals needed for various industries. Many regions in our country have low-grade manganese ores, and it is important to utilize these deposits and bring them into the economy. With the depletion of high-grade ores worldwide, the need to obtain manganese from low-grade ores is increasing.

This study aims to investigate the enrichment of low-grade manganese ore obtained from the Karaburun District of İzmir Province through leaching. Mineralogical investigations of the ore were carried out, and the manganese content of the ore, which contains a high percentage of pyrolusite, was determined to be 16.55%. Microscopic examinations, XRD and XRF analyses, wet and dry sieve analysis, and density determination were performed on the ore with a particle size of -1150 microns as part of the mineralogical studies.

Based on the data obtained, the ore was beneficiation using a high-field wet magnetic separator by reducing the particle size to -150 microns due to its low liberation size. Wet magnetic separation yielded a manganese content of 31.24% with a yield of 49.63%. To achieve higher manganese content values, a leaching process was applied to the ore. The experimental design was created by analyzing the samples prepared for leaching using Mastersizer and XRF. The results of the leaching experiments were obtained by AAS analysis. Sulfuric acid was used as the solvent and hydrogen peroxide as the reducing agent in the experiments. It was determined that a 95.86% Mn recovery yield could be obtained from the concentrate obtained after high-field wet magnetic separation, using a 1/10 solids ratio, a stirring speed of 400 rpm, an acid concentration of 2.97 M, and a reducing agent concentration of 2 M, at 32.12°C, and a leaching time of 30 minutes.

Key words: *Manganese ore, magnetic beneficiation, manganese leaching.*

1. INTRODUCTION

The enrichment of manganese ores by leaching is considered one of the important applications of hydrometallurgical processes and plays a critical role, especially in the evaluation of ores with low grade or complex mineralogical structures. Currently, a significant portion of the world's manganese reserves are not high-grade, and in many deposits, manganese minerals are found together with iron oxides, silica minerals, or clay phases. This fact limits the effectiveness of traditional physical enrichment methods. Since methods such as gravity separation, magnetic separation, or flotation generally operate depending on the degree of liberation and grain size of the mineral, it becomes difficult to achieve sufficient separation with these methods if manganese minerals are bound to gangue minerals in a fine-grained or complex manner (Gürsoy, 2021; İnce, 2014; Özgen et al., 2020). At this point, the leaching method, based on chemical dissolution, becomes an important alternative because the leaching process focuses on dissolving the target metal in solution through chemical reactions rather than physically separating the mineral (Sinha and Purcell, 2019).

The fundamental principle of manganese ore enrichment by leaching is the conversion of manganese into a solution-soluble ionic form. In pyrolusite, one of the most common manganese oxide minerals, manganese is usually found in its tetravalent form (Mn^{4+}). This form doesn't dissolve easily in acidic environments, so most leaching processes need a reducing medium. With the help of reducing agents, Mn^{4+} ions are reduced to the Mn^{2+} form, which becomes readily soluble in acidic solutions. This transformation allows manganese to exist in solutions in the form of sulfate or chloride, enabling its subsequent recovery by hydrometallurgical methods such as precipitation, solvent extraction, or electrolysis. Leaching is a crucial initial step, particularly in processes requiring high purity, such as the electrolytic production of manganese metal or electrolytic manganese dioxide (Akgöçmen, 2021; Zhang, 2007; Bahçeli, 2011; Nayl et al., 2011).

Another reason for the importance of leaching is that it allows for the economic utilization of low-grade ores. A large portion of the global demand for manganese is met by the steel industry, where manganese is used as an alloying element in steel production. In addition, manganese is increasingly used in modern battery technologies. Some cathode materials used in lithium-ion batteries contain manganese, leading to a growing demand for it. This increased demand has necessitated the utilization of low-grade manganese ores, previously considered uneconomical. Leaching provides an economic recovery opportunity by selectively dissolving manganese in such ores (Hariprasad et al., 2013).

The leaching of manganese ores also allows for the processing of complex or refractory ores. Refractory ores are difficult to separate using conventional enrichment methods because manganese is found within silicate structures or in combination with iron oxides. Since direct separation of manganese minerals is not possible in such ores, methods based on chemical reactions are preferred. During the leaching process, the structure of the manganese mineral is broken down, manganese ions pass into the solution, and a large portion of the gangue minerals remain undissolved in the solid phase. Thus, manganese and gangue minerals are chemically separated (Lasheen, 2009; Momade el al., 1999; Moro et al., 2021; Sahoo et al., 2001; Su et al., 2008; Tian et al., 2010).

Another important advantage of the leaching method is its applicability under relatively low temperature and pressure conditions. Pyrometallurgical processes require high-temperature smelting operations for manganese production, leading to very high energy consumption Eroğlu and Şahiner, 2020). Hydrometallurgical leaching processes, on the other hand, can generally be carried out under atmospheric pressure and medium temperature conditions. This contributes to a reduction in energy consumption. Furthermore, in some cases, leaching can be carried out in a more environmentally friendly way using biological or organic acids. Bioleaching methods, in particular, are based on the principle of dissolving manganese minerals with organic acids produced by microorganisms, and these methods have become an important research area in terms of reducing environmental impacts (Goswami, 2021).

Another important aspect of manganese leaching is that it allows for the utilization of waste and secondary resources. Today, not only natural ores but also secondary sources containing manganese, such as metallurgical slags, industrial waste, and used batteries, represent significant potential. Leaching methods enable the dissolution of manganese found in such materials, making its recovery possible. This process contributes both to the conservation of natural resources and the reduction of environmental waste (Baba et al., 2014).

In conclusion, manganese enrichment through leaching is a technology that enables the utilization of low-grade and complex manganese ores, allows to produce high-purity manganese, and constitutes an important part of modern hydrometallurgical processes. The increasing demand for manganese, particularly in the region, is driving the need for more efficient extraction methods. The increasing demand for manganese, and especially

advancements in battery technologies, are making this method increasingly important in both academic research and industrial applications.

In the first stage of this study, methods used in the enrichment of manganese minerals were examined, and the parameters considered in these methods were investigated. In the next stage, the aim was to bring the ore grade of manganese ore obtained from the Karaburun District of İzmir Province to suitable conditions according to industrial needs through pre-enrichment and leaching processes. Since high-purity manganese ore could not be obtained in the pre-enrichment processes, the coarsely crushed ore was ground below 150 microns. To increase the grade of the ore to be fed into the leaching processes, wet magnetic enrichment was carried out without detailed processing. Then, during the leaching process, sulfuric acid (H_2SO_4) was used as the acid and hydrogen peroxide (H_2O_2) as the reducing agent, considering cost, to achieve maximum efficiency in the leaching process.

2. MATERIAL AND METHODS

2.1. Material

During ore enrichment processes, considering that the raw material from the mine would be fed into the facility without prolonged storage, the goal was to maintain the integrity of the ore's raw structure; therefore, the ore was preserved under suitable conditions and prepared for leaching experiments. In the preliminary stage of ore enrichment, to observe the effect of manganese on leaching processes, a high-field intensity wet magnetic enrichment process was carried out, taking advantage of the difference in magnetic susceptibility, with the aim of adding the process to existing facilities in Turkey. This concentrated ore was then extracted into a solution using the leaching process, a hydrometallurgical enrichment method.

In the leaching process, a low particle size of the fed ore is required to increase the surface area of the particles and thus the reaction rate and to increase the liberation rate. Furthermore, it is evident that having the ore below the liberation particle size will lead to higher efficiency for magnetic separation. For these reasons, it was determined that the crushed ore reached a particle size below 150 µm in 30 minutes with a 40% charge rate in the ball mill. The particle size analysis of the ore, which underwent high-field wet magnetic enrichment after grinding, was determined using a Malvern Mastersizer S2000 laser-type instrument. The fine particle size analysis results for the leaching feed are given in Figure 1. The analyses were performed in triplicate, and the figure was created using the averages of the analysis results.

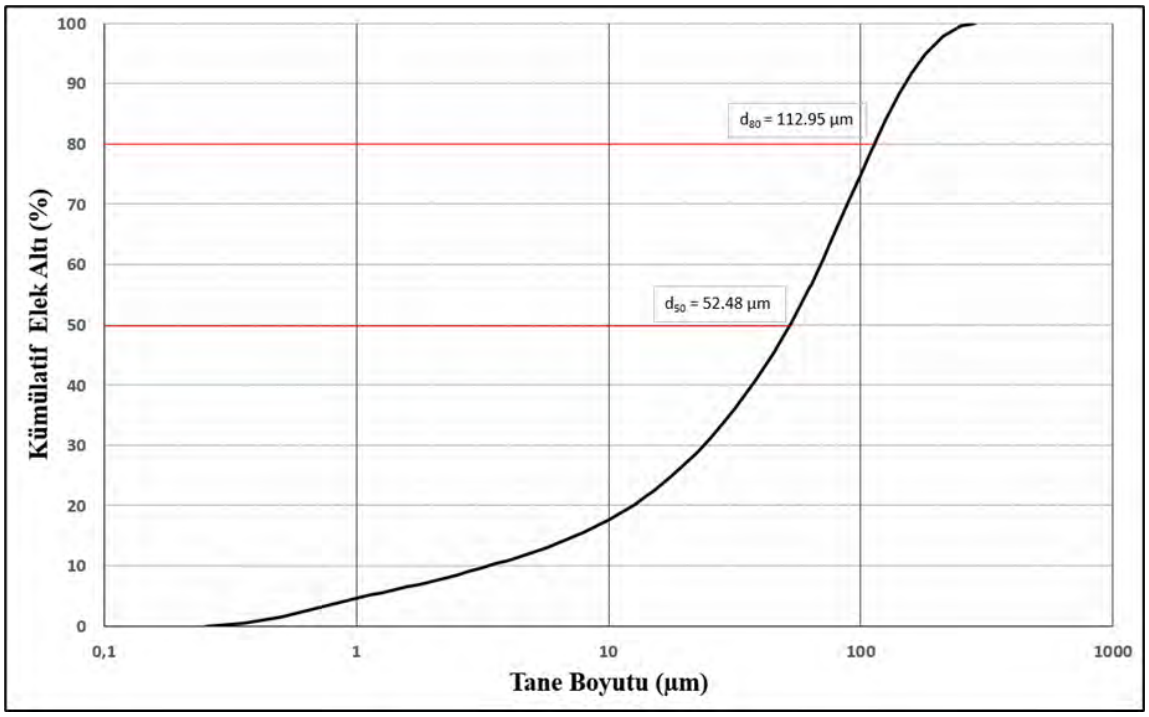

Figure 1. Particle size analysis of the ground ore

XRF analysis of the sample was performed at Eskişehir Osmangazi University ARUM. XRF results according to different particle size ranges are given in Table 1. The table indicates the percentage values of the specific particle size ranges present in the ore according to the sieve analysis performed. The presence of volatile gases in the sample results in a noticeable loss at ignition (LOI). In addition to what is indicated in the table, trace amounts of Ce, P, Ni, Co, Zn, V, Cu, Cl, Na, S, and as were detected in each experiment, varying in each analysis. However, the total presence of all these elements ranged from 0.02% to 1.30% in each analysis.

Table 1. XRF result of the leaching feed sample

Elements	Contents (%)	Elements	Contents (%)
Si	25.18	Na	0.30
Mn	31.24	P	0.03
Fe	2.39	Ni	0.04
Ca	0.74	Co	0.03
Mg	0.99	Zn	0.02
Al	0.85	V	0.04
Ba	1.30	Cl	0.03
K	0.72	S	0.02
Sr	0.90	LOI	35.18

2.2. Method

The study consists of two stages. In the first stage, a pre-enrichment process was carried out in a high-field wet magnetic separator, considering the magnetic enrichment process applied in Turkey and worldwide. The concentrate obtained from this process is suitable for feeding direct to the leaching process. The reason for performing this process can be considered as adapting to the existing process, which aims to improve efficiency and optimize the recovery

of valuable minerals during the subsequent leaching stage. These steps are presented sequentially.

2.2.1. Beneficiation with wet magnetic separator

Due to the difficulties encountered in enriching small-sized ore particles using dry magnetic separation, wet magnetic separation was applied to the ore. For particles smaller than 150 microns, separation efficiency is low in dry methods due to static attraction between particles and the shielding of particles on the conveyor belt. Therefore, after reducing the ore to the liberation particle size, magnetic separation was applied to the entire ore using a wire matrix with a 10% solids content at 30 amperes, 200 volts, and approximately 12,000 gauss intensity. Figure 2 shows a photograph of a Master Magnets Limited separator used in high-field wet magnetic beneficiation.

Figure 2. Master Magnets Limited brand separator used in high field intensity wet magnetic enrichment

The chemical analysis of the concentrate fed into the wet magnetic separator within the scope of the study is given in Table 2.

Table 2. Chemical analysis of the concentrate fed into the wet magnetic separator

Products	Si	Mn	Fe	Ca	Mg	Al	Ba	K	Sr	LOI
Feed	27,63	19,22	1,78	1,30	0,88	0,74	0,80	0,43	0,50	40.13
Concentrate	25.18	31.24	2.39	0.74	0.99	0.85	1.30	0.72	0.90	35.18

2.2.2. Beneficiation by leaching

Since a concentrate with a high Mn content could not be obtained by magnetic enrichment, leaching enrichment studies were carried out as the next stage, guided by literature research for the enrichment of the ore (Figure 3). After the grinding process, 25-gram samples were prepared from the magnetic products obtained by passing the ore through a high-field wet magnetic separator, using a sample splitter and then the grid method.

Figure 3. Leaching experimental setup

To optimize the leaching process, acid concentration, reduction agent concentration, temperature, and time were selected as variables in the experiments. In all experiments, the solid ratio was chosen as 1/10, and the stirrer speed was kept constant at 400 rpm.
The parameter ranges for the leaching experiments are as follows:

Acid concentration: 0.5 – 1 – 2 – 4 M
Reducing agent concentration: 0.5 – 1 – 1.5 – 2 M
Temperature: 20 – 40 – 60 – 80°C
Leaching time: 30 – 60 – 120 – 180 minutes

In experiments conducted at low pH values, a digital leaching experimental setup was used to minimize evaporation losses and to more accurately measure the solution temperature (Figure 3). Although time was added as a variable in the experimental process, instead of planning separate experiments for each time variable, three milliliters of solution were drawn from the leaching solution at specific time intervals in all experiments and analyzed. This increased the amount of data that could be obtained from the experiments and also increased the probability of detecting any experimental errors.

After the experiment, the leaching solutions were filtered, the remaining solid amounts were weighed and stored, and the leaching solutions were analyzed in the AAS instrument as described in the previous section, and the results were calculated using Equation 1. Photographs of the experiments are shown in Figure 4.

Equation 1. Yield calculation based on AAS result;

$$\boldsymbol{Metal\ Recovery\ Yield}\ (\%) = \frac{\boldsymbol{AAS\ Result}\ (\boldsymbol{ppm}) * \boldsymbol{Volume}\ (\boldsymbol{ml}) * \boldsymbol{Dilution\ Factor}\ (\mathbf{10^4})}{\boldsymbol{Material\ Amount}\ (\boldsymbol{g}) * \boldsymbol{Material\ Grade}\ (\%)}$$

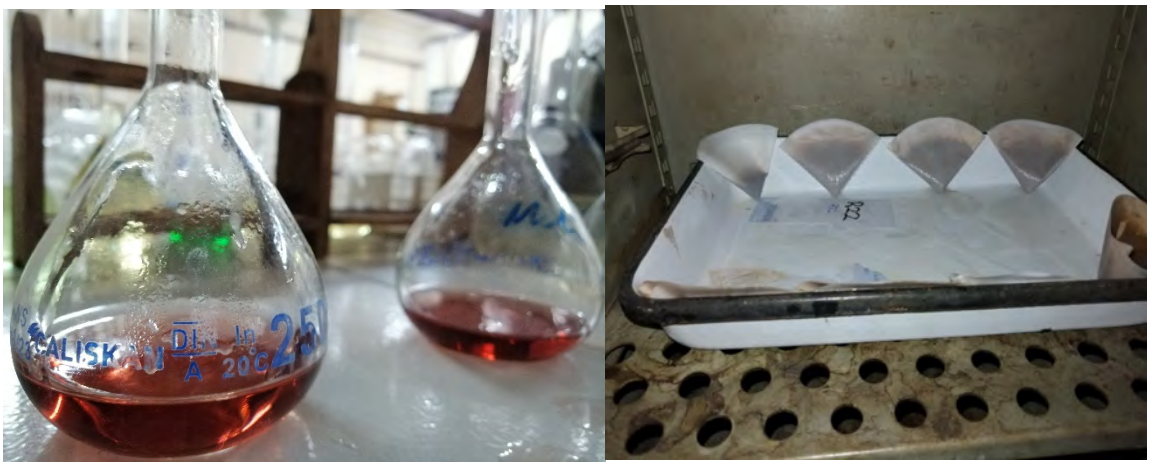

Figure 4. (a) Solution after filtration, (b) Drying of leaching precipitate in an oven.

3. RESULTS AND DISCUSSION

Since the ore concentrate with 31.24% Mn content obtained from wet magnetic separation could not be used as a raw material in the metallurgy, battery, and chemical industries, enrichment by leaching was applied to the ore after this stage. This stage highlights the importance of this process, as the manganese ore used in the studies could not achieve sufficient level of content with magnetic enrichment alone, and using ore that had not undergone magnetic enrichment for leaching would not yield sufficient manganese recovery performance. The results of the leaching experiments were analyzed using Atomic Absorption Spectrometry (AAS). Using the results obtained from the AAS instrument, the manganese recovery efficiencies obtained from different leaching parameters were calculated.

The results of the experiments are only indicative for manganese. Since the results obtained from the AAS instrument are obtained using lamps corresponding to the mineral being sought in the solution, the results directly provide data related to the relevant element. Results and relationships of leaching experiments in which acid and reducing agent concentrations, temperature, and time were determined as variable parameters are presented in Figures 5-6-7.

High temperatures are generated during the leaching process due to chemical reactions occurring at very low pH values. Even in experiments conducted at room temperature without the use of any heating device, it was determined that the solution temperature was in the range of 60-70°C at the beginning of the experiment and maintained at these temperatures for approximately half an hour to an hour. Afterwards, the solution reaches saturation, and the redox reaction reverses, during which a slight decrease in solution temperature is observed. The restoration of ion saturation in the solution varies depending on other parameters and continues for approximately 1 to 1.5 hours. Subsequently, the chemical reaction resumes its rightward shift, increasing manganese recovery in the solution again.

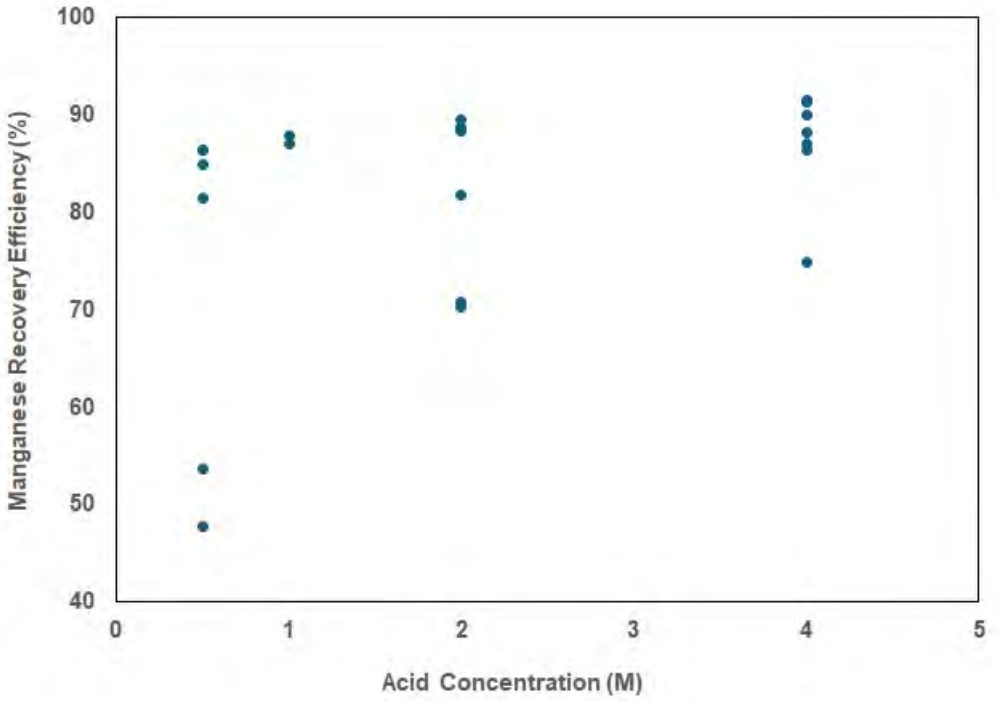

Figure 5. Mn Recovery Efficiency (%) Depending on Experimental Acid Concentration

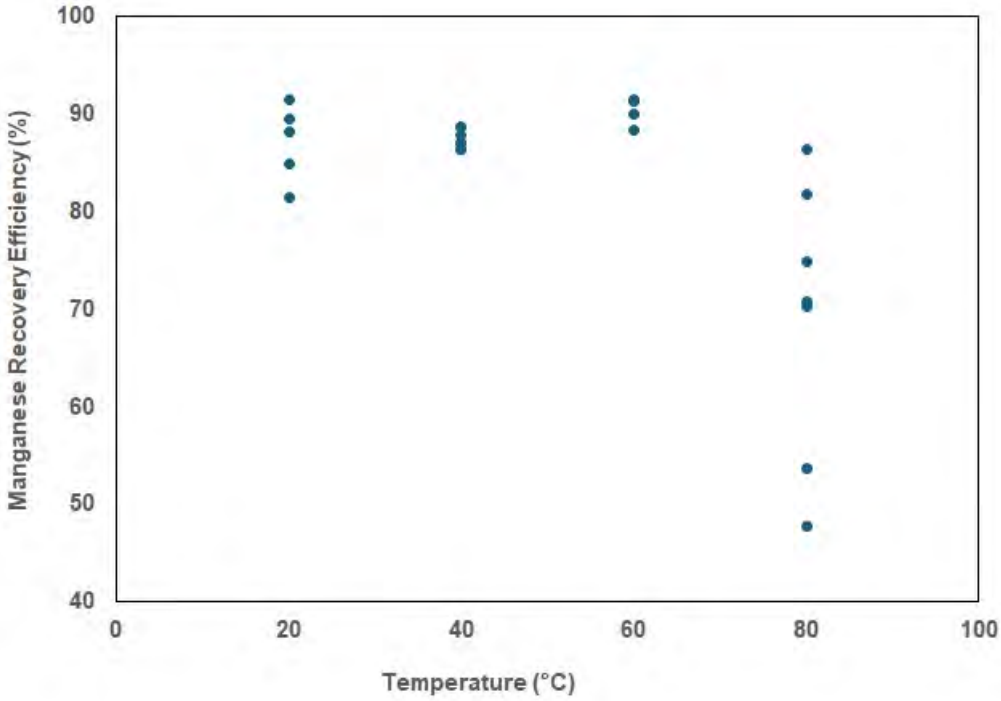

Figure 6. Mn Recovery Efficiency (%) Depending on Experimental temperature

Although temperature, one of the experimental parameters, was selected at values of 20, 40, 60, and 80°C, the temperature spontaneously reaches 60-65°C during the leaching process, which is an exothermic reaction. Therefore, in the first three parameters, only the initial temperatures change; the final temperature values remain approximately the same. In this experimental setup, a linear relationship between leaching efficiency and temperature cannot be established; efficiency increases up to 50-55°C with increasing temperature, after which a rapid decrease occurs. This decrease can be explained by the fact that the high amount of

silica present in the solid begins to dissolve (Equation 3). The dissolving silica releases water into the solution, reducing the ion concentration.
Equation 3. Dissolution of silica during leaching

$$2H_2SO_{4(aq)} + SiO_{2(k)} = 2H_2O_{(s)} + Si(SO_4)_{2(aq)}$$
$$\mathrm{H} + H_2O_{(aq)} = OH + H_2$$

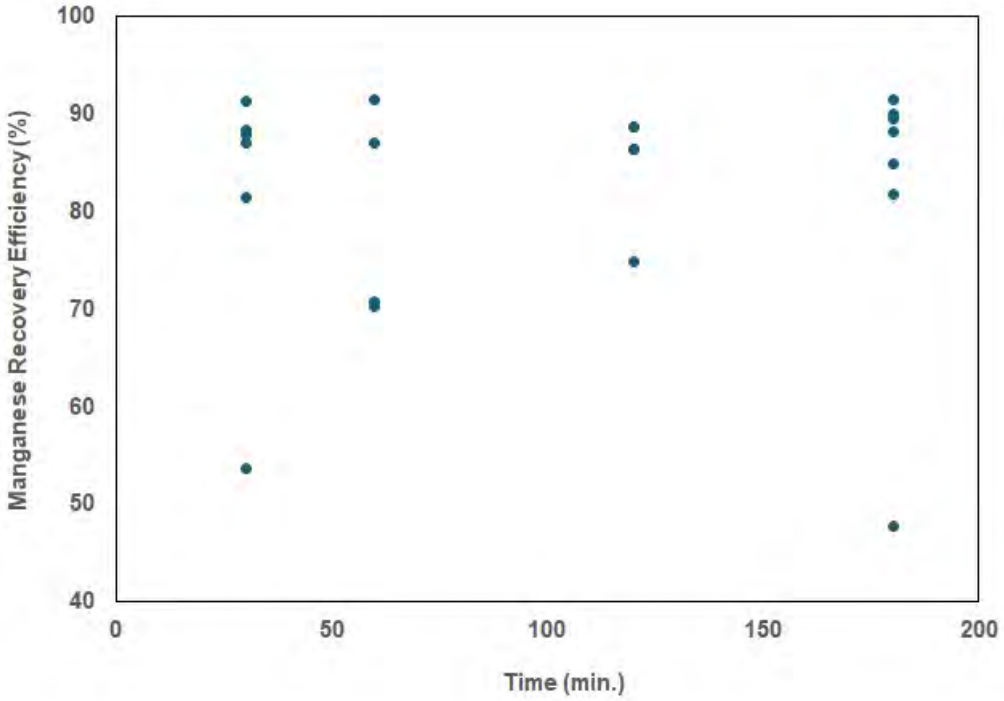

Figure 6. Figure 7. Mn Recovery Efficiency (%) Depending on Experimental temperature

4. CONCLUSION

This study investigated the beneficiation of manganese ore obtained from the Karaburun District of İzmir Province, and leaching experiments were conducted to increase ore grade and enrichment efficiency. The manganese grade in the ore, which is predominantly pyrolusite, was determined to be 16.55%.

In today's world, where high-grade ores are increasingly scarce and research into the enrichment of lower-grade ores is accelerating, studies aimed at bringing low-grade manganese ores into industrial use have gained importance. Although Turkey's manganese production has increased significantly in recent years, it cannot meet the needs of the industry; a large portion of the produced ore is used domestically or sold abroad, and high-value products suitable for these needs are imported.

The ore with a particle size of -150 microns was pre-enriched using a high-field wet magnetic separator. Following an enrichment process carried out in accordance with industrial practices, a magnetic product with a Mn content of 31.24% was obtained with a yield of 49.63%. For this purpose, the magnetic enrichment process was applied, taking into account the integration of the leaching process in accordance with the flowchart of a manganese enrichment plant.

To obtain higher-grade products after magnetic enrichment, hydrometallurgical methods were investigated. Considering easy and inexpensive accessibility, an experimental design was created using sulfuric acid as the solvent and hydrogen peroxide as the reducing agent, based on temperature and leaching time.

The best result in the leaching studies was obtained with 4 M acid, 2 M reducing agent, 60°C temperature, and 180 minutes of leaching; the Mn recovery yield was analyzed as 91.55%. Experiments with similar Mn recovery yields using smaller amounts of chemical reagents exist. Based on the experiments conducted within the scope of this study, considering the experiment that yielded the maximum content, for leaching 1 ton of ore in 10 tons of solution, 1.68 kg/t of acid is required for 95% pure H_2SO_4 at a 2 M acid concentration, and 1.22 kg/t of reducing agent is required for 50% pure H_2O_2 at a 1 M concentration.

REFERENCES

Akgöçmen, K. E., (2023) “Karaburun Bölgesi Mangan Cevherinin Liç ile Zenginleştirilmesinin Araştırılması”, Master's Thesis, Eskişehir Osmangazi University, Institute of Science.

Baba, A., Ibrahim, L., Adekola, F., Bale, R., Ghosh, M., Sheik, A., Pradhan, S., Ayanda, O., Folorunsho, I., (2014) “Hydrometallurgical processing of manganese ores: A review”, Journal of Minerals and Materials Characterization and Engineering, 2 230-247.

Bahçeli, A., (2011) “İspendere (Malatya) Bölgesi Manganez Cevherleşmelerinin Jeolojik ve Madencilik Açısından İncelenmesi”, Master's Thesis, Çukurova University, Institute of Science.

Eroğlu, G., Şahiner, M., (2020) “Üretimden ticarete manganez”, MTA Doğal Kaynaklar ve Ekonomi Bülteni, 30:99-109, 2020, https://www.mta.gov.tr/v3.0/sayfalar/hizmetler/kutuphane/ekonomibultenleri/2020_30/8.pdf, Access date: 27 December 2022.

Goswami, B., (2021) “Studies on mineral resources of manganese”, SunText Review of Material Science, 02.

Gürsoy, Y. H., (2021) “Düşük tenörlü mangan cevherinin kuru manyetik ayırma yöntemi ile zenginleştirilmesinde tane boyutunun etkisi”, Eskişehir Osmangazi University, Journal of the Faculty of Engineering and Architecture, 29 (3) 337-345.

Hariprasad, D, Mohapatra, M., Anand, S., (2013) “Sulphuric acid leaching of low/medium grade managanese ores using a novel nitrogeneous reductant-NH3NH2HSO4”, Journal of Mining and Metallurgy, Section B: Metallurgy, 49 97-106.

İnce, E., (2014) “Düşük tenörlü mangan cevherlerinin zenginleştirilmesinin araştırılması”, Master's Thesis, Çukurova University, Institute of Science.

Lasheen, T. A., El Hazek, M. N., Helal, A. S., (2009) “Kinetics of reductive leaching of manganese oxide ore with molasses in nitric acid solution”, Hydrometallurgy, 98 314-317.

Momade, F. W. Y., Momade, Z. G., (1999) “Reductive leaching of manganese oxide ore in aqueous methanol-sulpuric acid medium”, Hydrometallurgy, 51 103-113.

Moro, K., Haubrich, F., Martin, M., (2021) “Preliminary study on the reductive leaching of manganese ores using feso4/iron powder as reducing agents under room temperature”, European Journal of Engineering and Technology Research, 6 14-18.

Nayl, A. A., Ismail, I. M., Aly, H. F., (2011) “Recovery of pure $MnSO_4.H_2O$ by reductive leaching of manganese from pyrolusite ore by sulfuric acid and hydrogen peroxide”, International Journal of Mineral Processing, 100 116-123.

Özgen, S., Arsoy, Z., Ersoy, B., (2020) “Yüksek alan şiddetli manyetik ayırıcı ile manganez cevherinin zenginleştirilmesi”, El-Cezeri Journal of Science and Engineering.

Sahoo, R. N., Naik, P. K., Das, S. C., (2001) “Leaching of manganese from low-grade manganese ore using oxalic acid as reductant in sulphuric acid solution”, Hydrometallurgy, 62 157-163.

Sinha, M., Purcell, W., (2019) “Reducing agents in the leaching of manganese ores: A comprehensive review”, Hydrometallurgy, 187 168-186.

Su, H., Wen, Y., Wang, F., Sun, Y., Tong, Z., (2008) “Reductive leaching of manganese from low-grade manganese ore in h2so4 using cane molasses as reductant”, Hydrometallurgy, 93 136-139.

Tian, X., Wen, X., Yang, C., Liang, Y., Pi, Z., Wang, Y., (2010) “Reductive leaching of manganese from low-grade manganese dioxide ores using corncob as reductant in sulfuric acid solution”, Hydrometallurgy, 100 157-160.

Zhang, W., Cheng, C., (2007) “Manganese metallurgy review. Part I: Leaching of ores/secondary materials and recovery of electrolytic/chemical manganese dioxide”, Hydrometallurgy, 89 137-159.

ORP MODULATION IN HCl- AND H_2SO_4-BASED LEACHING SYSTEMS THROUGH SYNERGISTIC NACL EFFECTS

Kobra REZAEI[1,*], Claudio ACUNA[2]

[1]*University of Oulu, Faculty of Technology, Oulu Mining School, Oulu, FINLAND*
[2]*Universidad Técnica Federico Santa María, Chemical and Environmental Engineering Department, Valparaiso, CHILE*
**Corresponding author: kobrarezaei1997@gmail.com*

A B S T R A C T

The positive effect of sodium chloride (NaCl) in the acidic leaching of sulfide minerals is widely reported. The influence of this common and cheap salt is mostly interpreted through surface-related mechanisms, while its effect on the redox potential (ORP) of environment as an important factor in stability of solution and leachability of metal remains insufficiently quantified.

This research investigates the role of NaCl in acidic leaching systems by focusing on its effect on redox potential in the initial leaching solutions. The analysis considers both the individual and combined contributions of NaCl and $FeCl_3$ to the redox behavior of the solution and evaluates how different NaCl concentrations modify key electrochemical parameters in acid-based environments. The results demonstrate that NaCl can significantly elevate ORP in acidic solutions and the mechanism of enhancement strongly dependent on type of the acid medium. In NaCl–HCl solutions, redox potentials can reach close to 900 mV through shifting the redox regime toward chlorine-based couples, and in NaCl–H_2SO_4 solutions, ORP stabilize near 600 mV by enhancing oxygen-dominated redox equilibria in sulfate media. In such acidic system, the comparable buffered ORP plateaus of NaCl to the oxidative strength of 0.1 M FeCl3 indicates that NaCl acts as a conditional redox modulator rather than a consumable oxidant.

Overall, the findings demonstrate that NaCl's positive role in leaching extends beyond surface chemistry. In acidified systems, it can modify the bulk redox environment and change the thermodynamic conditions which governing stability and metal solubility in leaching systems. The resulting dataset supports ORP modeling for NaCl–HCl and NaCl–H_2SO_4 systems using neural-network-based tools, providing a quantitative framework for enhancing leaching performance through deliberate redox control.

Key words: *Acidic leaching, sodium chloride (NaCl), redox potential (ORP)*

1. INTRODUCTION

Hydrometallurgy as a metal-extraction technique relies on aqueous solutions to dissolve and recover metals. In leaching systems, efficiency and selectivity of metal dissolution are controlled by many physiochemical and electrochemical parameters like acid type and concentration, oxidation–reduction potential (ORP) of the solution, ionic strength and composition of the leachate (Winand, 1991; Bhargava, 2017). Sodium chloride (NaCl) is a prevalent additive used to enhance leaching performance, particularly for sulfide minerals like chalcopyrite (Carneiro and Leão, 2007; Jumbo et al., 2023). In the same context, seawater use is increasingly common in metal processing which has been reported to benefit chalcopyrite leaching due to its chloride content (Torres et al., 2015).

Literature primarily attributes the positive effects of NaCl to surface-related mechanisms and thermodynamic shifts (Zhong and Li, 2019; Liang et al., 2012). Key interpretations for predominantly chalcopyrite systems include:

- Increasing surface area and transformation of surface properties from amorphous to crystalline (Liang et al., 2012; Mustafa et al., 2017; Carneiro and Leão, 2007).
- Reduction of activation energy for chalcopyrite leaching (Kinnunen and Puhakka, 2004; Liang et al., 2012).
- Formation of Cu(I)/Cu(II) chloro-complexes and stabilization of chloro cuprate(I) ions (Ping et al., 2009; Torres et al., 2015; Hernández et al., 2015).

The commonly cited explanations for NaCl-enhanced leaching are largely framed in terms of surface chemistry; however, chloride ions sourced from this salt can also modify the electrochemical environment of the solution and cause the contribution of chloride to the bulk redox potential (Suslow, 2004, Winand, 1991, Senanayake, 2009, Seisko et al., 2020). ORP—together with pH—defines the thermodynamic stability of aqueous redox species and therefore influences whether metals remain in the dissolved form or not (Pourbaix 1966). Electrochemical studies on sulfide dissolution demonstrate that leaching performance is strongly potential-dependent: maintaining the solution within an optimal ORP window promotes chalcopyrite dissolution and prevents passivation (Córdoba et al., 2008; Velásquez-Yévenes et al., 2010). Chloride-containing systems show that the solution redox potential depends on its chemical composition and can correlate with dissolution behavior, which means that chloride can influences the bulk electrochemical environment (Seisko et al., 2020). Moreover, under anodic/electrochemical conditions, chloride can participate in oxidant-generating pathways (e.g., chlorine/oxychlorine chemistry), reinforcing the need to quantify ORP responses in chloride–acid matrices (Ping et al., 2009).

Selecting the leaching medium is a fundamental step in hydrometallurgical design. While sulfate media remain at the industrial standard due to lower capital costs and established solvent extraction processes, chloride-based systems offer superior metal solubility and faster kinetics (Watling, 2013; Watling, 2014). Comparative studies indicate that copper dissolution increases significantly when NaCl is added to ferric sulfate compared to ferric chloride systems (Sepúlveda et al., 2023; Carneiro and Leão, 2007). One highlighted point in such studies is that they focus more on surface interactions and the presence of NaCl, without fully addressing the influence of the type of pH-adjusted medium. Hence, the benefit of NaCl cannot be considered a generic chloride effect but is contingent upon the acid medium.

There is a distinct gap in understanding how NaCl assists leaching through ORP modulation across different acid matrices. Respecting the importance of leachate composition, the present research is conducted to systematically map ORP as a function of composition in NaCl–HCl and NaCl–H_2SO_4 systems. By aligning with the observed behavior where NaCl acts as a conditional redox modulator, this study utilizes the resulting dataset to develop neural-network-based ORP models. This provides a quantitative framework for designing leaching conditions through deliberate redox control.

2. MATERIAL AND METHODS

2.1. Material

Synthetic aqueous solutions were prepared using distilled water, ferric chloride (97% purity, 2.80 g/cm³), and commercial salt (Na content: 39 g per 100 g) for sodium chloride. Medium characterization relied on mass fraction and density (Table 1) to ensure internal consistency and eliminate volume-based concentration ambiguities. This approach accounts for non-ideal behavior where ionic strength and volume changes in high-concentration systems are often neglected in standard molarity-based reporting (Thomsen, 2009).

Table 1. Characteristics of prepared stock solutions

Solution	Sodium chloride	Ferric chloride	Sulfuric acid	Hydrochloric acid
Mass fraction (%)	25	26	98	35
Density (g/mL)	1.18	1.20	1.84	1.18

2.2. Experimental design

To quantify the influence of NaCl on the redox potential in two H_2SO_4 and HCl systems, 3 sets of experiments are designed;

(i) Baseline profiling: Individual reagents (H_2SO_4, HCl, and NaCl) were incrementally added to 200 mL of distilled water to assess their independent effects on redox potential.
(ii) Oxidant comparison: Ferric chloride was introduced under similar conditions to compare its oxidation performance with NaCl.
(iii) Chloride addition strategies: The impact of NaCl in acidic systems was evaluated using two protocols:

- Fixed-acid background: NaCl was gradually added to pre-prepared acidic solutions (0.5 M and 2 M H_2SO_4 or HCl), resulting in gradual dilution of the acid concentration.
- Acid-compensated addition: NaCl and acid were co-added, with back-calculated corrections to maintain a background medium with constant acid or salinity mass fraction and to minimize dilution effects.

2.3. Measurement methodology

Continuous magnetic stirring ensures solution to homogeneity. Redox potential (ORP) was measured using a platinum electrode with an Ag/AgCl reference system, while pH was recorded via a dedicated probe to avoid the inaccuracies inherent in dual-function sensors.

Following the report by (Suslow, 2004) and our observations during the experiments, ORP was interpreted as an operational window. To account for inherent sensor fluctuations (±10 mV), a standardized and uniform measurement protocol was followed. Also, all measurements were recorded only after a 5-to-10-minute stabilization period following reagent addition. This standardized procedure ensured data reproducibility and minimized transient instabilities.

3. RESULTS AND DISCUSSION

The results from baseline ORP behaviour of individual solution components and the interaction of NaCl in H_2SO_4 and HCl systems will be discussed to evaluate the potential of NaCl in modulating the oxidative environment of acidic solutions.

3.1. Baseline ORP behavior incremental addition of NaCl, HCl and H_2SO_4

Data collected from distilled water-based media is demonstrated schematically in Figure 1, where both H_2SO_4 and HCl in lower concentrations quickly shift the system toward an oxidative regime by the introduction of H^+ ions in the half-reaction, which can be explained by the Nernst equation (Eq. 1) for oxygen reduction. However, despite the H_2SO_4 with a steady oxidative effect, the ORP performance of HCl, declines gradually with further acidification. It might be due to high ionic strength at near-saturation where activity coefficients (γ) of H^+ is much less than 1 and ions in solution have strong non-ideal behavior (Schneider et al. 2004). In addition, possible adsorption of chloride ions onto pt electrodes can lower measured Eh (Priyantha and Malavipathirana, 1996). The performance of NaCl alone, as a source of Cl^- ions tend to reduce

ORP and the Pt ORP electrode typically reports a mixed potential that is strongly influenced by the dissolved oxygen system.

$$E = E° - \frac{RT}{nF} \ln\left(\frac{\text{Reductant}}{\text{Oxidant}}\right) \quad \text{Equation 1}$$

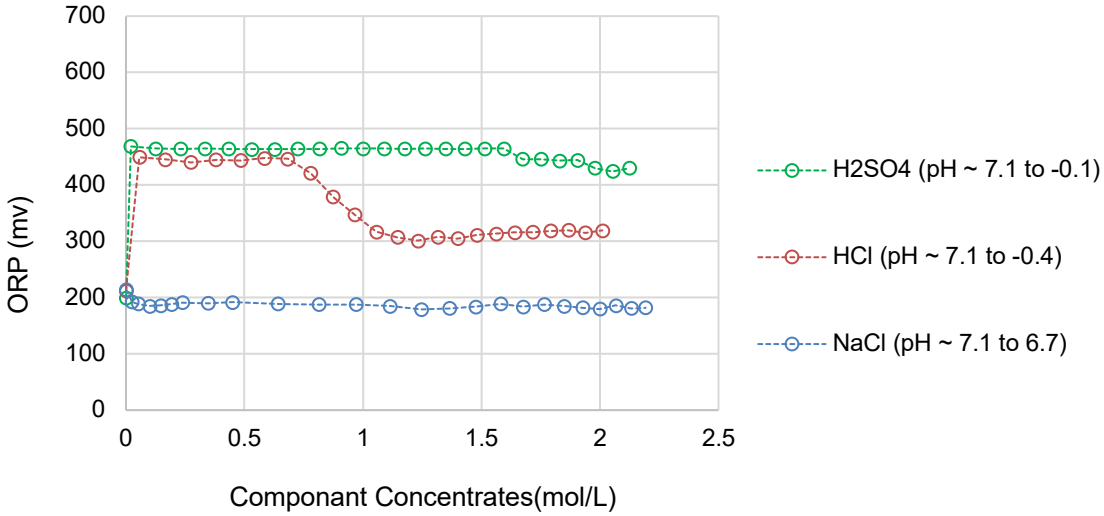

Figure 1. ORP variation to NaCl, HCl and H_2SO_4 in distilled water

3.2. ORP modulation in NaCl–HCl systems

The interaction between NaCl and HCl on solution redox potential was quantified across three experimental conditions. As illustrated in Figure 2, the incremental NaCl addition systematically elevated ORP despite the concurrent dilution of the HCl background. This trend confirms that redox enhancement is not governed by proton activity alone. The asymptotic behavior observed at high salinity is attributed to ionic strength saturation and suppressed activity coefficients. To ensure data integrity, measurements were recorded following a 10-minute stabilization period, accounting for an identified ±10 mV operational uncertainty.

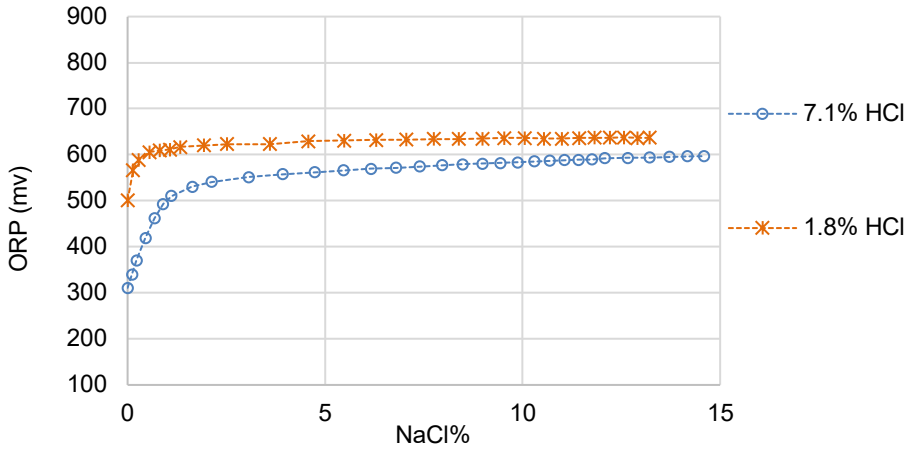

Figure 2. ORP response to NaCl in HCl background

Synergistic interactions between NaCl and HCl indicate that NaCl functions as an active redox modulator rather than a passive electrolyte. To mitigate dilution bias and isolate component-specific effects observed in initial tests, a secondary dataset was generated using compensated acid addition. This protocol maintained a constant HCl mass fraction, providing

a controlled environment to quantify the independent impact of NaCl concentration on solution oxidation-reduction potential.

Figure 3 presents the ORP response to NaCl concentration at fixed HCl levels (0.5 M and 2 M) relative to a ferric chloride benchmark. In highly acidic media (7 wt.% HCl, pH < 0), NaCl additions exceeding 10 wt.% trigger a potential escalation to approximately 900 mV. This behavior is attributed to the transition from oxygen-dominated to chlorine-dominated redox equilibria, facilitating Cl_2–HOCl speciation (Eq. 2). The observed values characterize a mixed potential, remaining below the E° = 1.36 V standard potential for the Cl_2/Cl^- couple (Nimmo, 2021; Eq. 3). Under non-ideal conditions, high chloride activity shifts the Nernstian potential into the 0.80–0.95 V range, exhibiting oxidative strength comparable to alkaline $HOCl/ClO^-$ systems (Bard et al., 2017; Eq. 5). Further test results at higher concentrations, up to 20% NaCl, show a similar plateau around 900 mV. This provides corroborating evidence that ORP stabilizes in high-chloride matrices once free chlorine exceeds 25 ppm, effectively creating a redox-buffered environment (Suslow, 2004).

$$Cl^- + H^+ + HClO \leftrightarrow Cl_2 + H_2O \quad \text{Equation 1}$$

$$\mathbf{Cl_2(g) + 2e^- \leftrightarrow 2Cl^-, \quad E° = 1.36\ (v)} \quad \text{Equation 3}$$

$$\mathbf{E = E° - \frac{RT}{2F} ln\left(\frac{a_{Cl^-}^2}{a_{Cl_2}}\right)} \quad \text{Equation 4}$$

$$\mathbf{ClO^- + H_2O + 2e^- \leftrightarrow Cl^- + 2OH^-, \quad E° = 0.89\ (v)\ in\ NaOH} \quad \text{Equation 5}$$

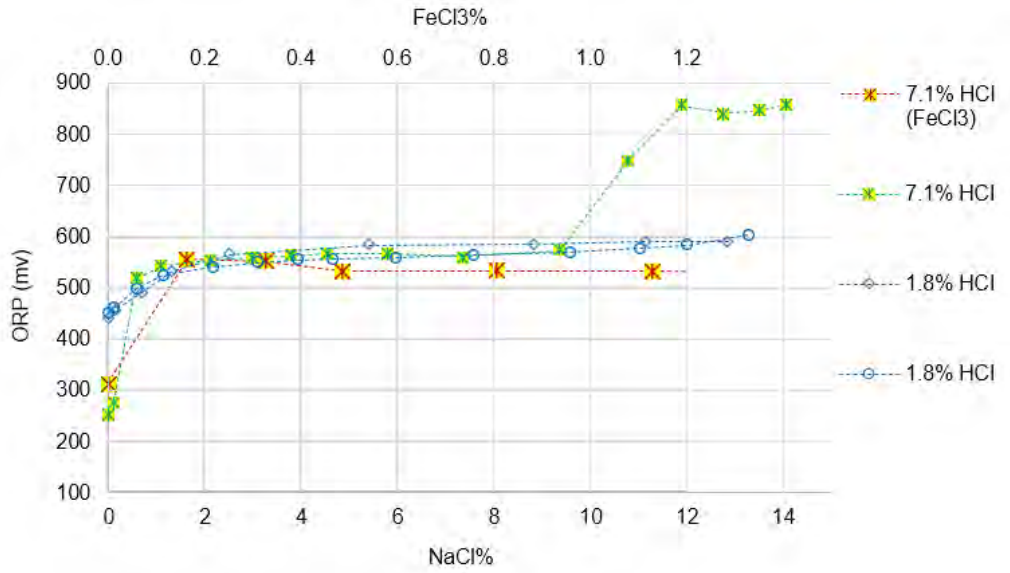

Figure 3. ORP response to NaCl at two concentrations of HCl and $FeCl_3$ as a reference

Complementary tests evaluating reagent addition sequence confirm that the ORP response is independent of the acidification path (Figure 4). The consistent nonlinear escalation and subsequent plateauing behavior across different addition orders indicate that the final electrolyte composition, rather than the reaction sequence, governs the redox equilibrium. Comparative benchmarking against $FeCl_3$ (Figures 3 and 4) demonstrates that NaCl-HCl systems generate active chlorine species with oxidizing potentials comparable to, and under certain conditions exceeding the Fe^{3+}/Fe^{2+} couple (E° = 0.771 V). While NaCl does not function as a primary consumable oxidant, it acts as a redox modulator by stabilizing high-potential Cl_2/Cl^- and $HOCl/Cl^-$ couples within the acidic matrix. In contrast, increasing HCl concentrations in $FeCl_3$ systems results in a discernible ORP decrease. This attenuation is attributed to Fe(III) speciation shifts, specifically chloride complexation and hydrolysis effects,

which diminish the activity of the free Fe^{3+} oxidant (Persson, 2018; Stefansson et al., 2019; Irto et al., 2023).

$$Fe^{3+} + 4Cl^{-} \leftrightarrow [FeCl_4]^{-} \quad \text{Equation 6}$$

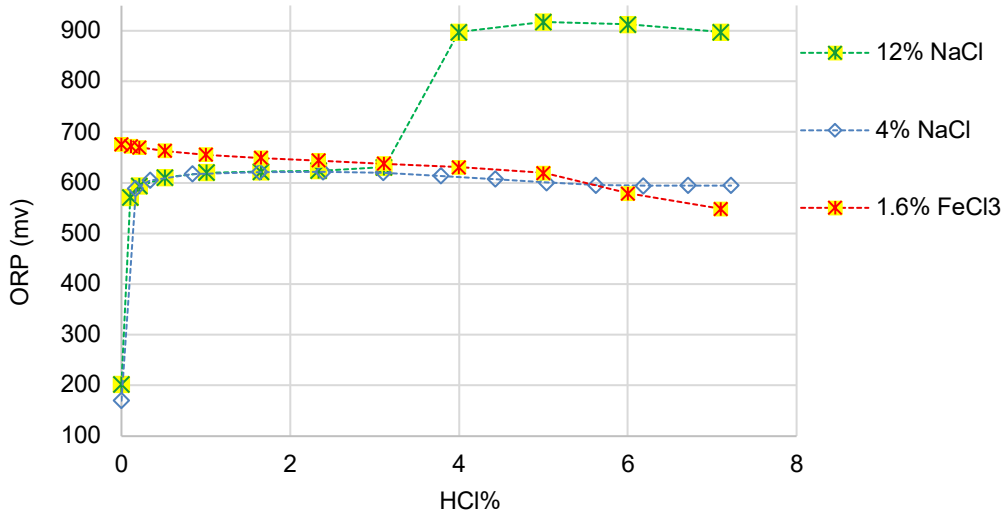

Figure 4. ORP response to HCl addition with NaCl background and ferric ($FeCl_3$)

3.3. ORP modulation in NaCl–H_2SO_4 systems

Electrochemical monitoring of NaCl-H_2SO_4 systems was conducted to evaluate the interactive effects of electrolyte concentration on redox potential. Figure 5 illustrates ORP response during incremental NaCl addition to 0.5 M and 2 M H_2SO_4 backgrounds. Initial baselines align with the 450-mV range shown in Figure 1, while NaCl addition in the absence of acid yielded no systematic ORP increase, stabilizing near 200 mV. NaCl addition enhanced ORP until reaching critical concentrations of 1.15 wt.% for the 2 M H_2SO_4 system and 0.55 wt.% for the 0.5 M H_2SO_4 system. This enhancement is attributed to the combined influence of proton activity and ionic strength on the mixed potential at the platinum electrode (Nimmo, 2021). Unlike NaCl-HCl systems, the ORP in NaCl-H_2SO_4 media is not governed by chlorine-based redox equilibria but likely by oxygen-proton mixed potentials.

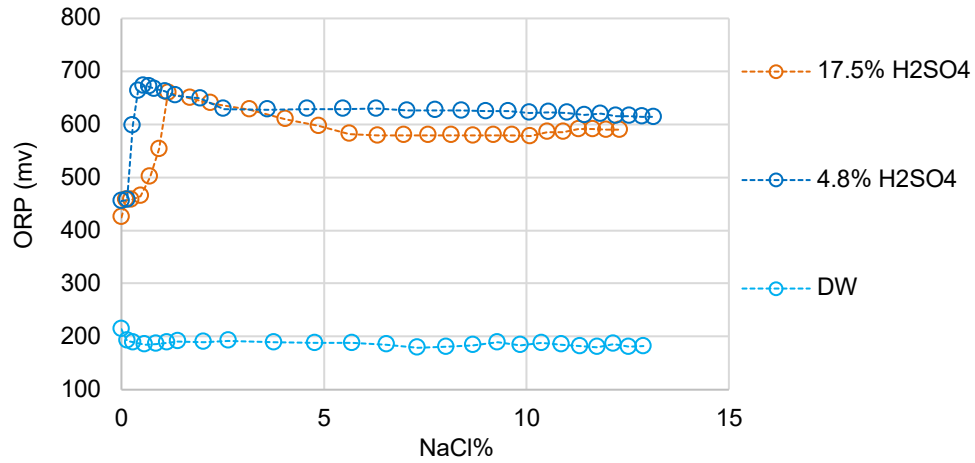

Figure 5. ORP response to NaCl in H_2SO_4 (0, 0.5M, 2M) with concurrent dilution effect

In Figure 5, excess NaCl addition resulted in ORP reduction and a plateau near 600 mV. This non-ideal electrochemical behavior stems from the concurrent dilution of sulfuric acid, which reduces proton activity, and the reduction of activity coefficients due to high ionic strength. These factors collectively limit oxidative responses in high-salinity regimes.

To minimize the effect of dilution and better isolate the role of NaCl in H_2SO_4 media, a second experimental dataset was collected under a constant mass fraction of acidity background during NaCl addition. The dataset resulting from this approach in Figure 6, shows that in the high-acidity system (≈17.5 wt.% H_2SO_4), high proton activity promotes a rapid increase in ORP at low NaCl additions. However, in the lower acidity system (≈4.9 wt.% H_2SO_4), a higher chloride concentration is required to achieve comparable ORP levels, which might be due to the reduced contribution of proton-coupled redox reactions. The saturation of both systems at higher salt concentrations clarifies that ORP plateau in sulfate media is not caused by acid dilution alone. It is likely ORP is controlled by oxygen-related redox equilibria, mixed-potential behavior at the platinum electrode, and chloride role as an ionic-strength modifier rather than an active redox participant.

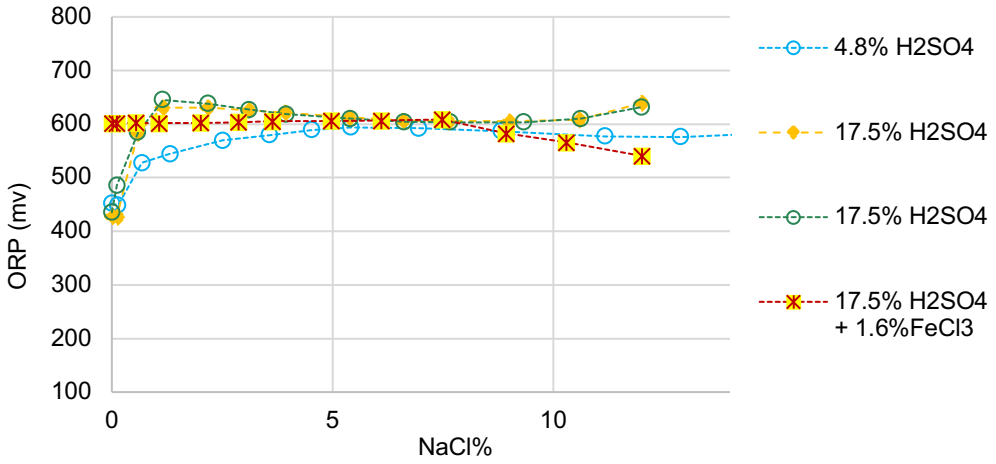

Figure 6. ORP response to NaCl in H_2SO_4 - $FeCl_3$ without concurrent dilution effect

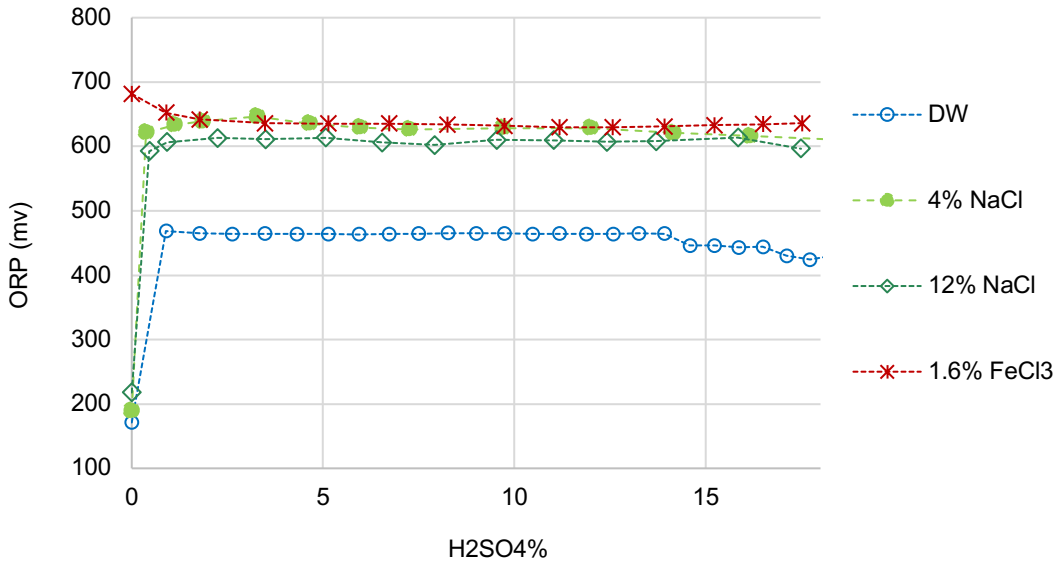

Figure 7. ORP response to H_2SO_4 addition in solutions of NaCl and $FeCl_3$

Figure 6 illustrates that ferric chloride ORP in acidic sulfate media remains largely independent of NaCl concentration, bounded by the Fe^{3+}/Fe^{2+} redox regime (E° approximately +0.77 V)

(Seisko et al., 2020). Minor ORP decreases at high chloride concentrations are attributed to ferric-chloride complexation and the consequent reduction in Fe^{3+} activity (Persson, 2018; Stefansson et al., 2019; Cigala et al., 2023).

Comparative data in Figure 7 evaluate acidification effects and reagent sequencing under constant NaCl or $FeCl_3$ backgrounds. Consistent with Figure 1, H_2SO_4 addition to distilled water increases ORP via H+ activity, stabilizing the electrochemical environment at approximately 450 mV. In NaCl backgrounds (4 wt.% and 12 wt.%), acidification elevates ORP to approximately 620 mV, likely activating oxygen-related redox reactions and mixed-potential behavior at the platinum electrode. Validation datasets for $FeCl_3$ backgrounds show an initial high ORP (approximately 680 mV), confirming that the Fe^{3+}/Fe^{2+} couple governs oxidative capacity independently of reagent order or pH below 1. Notably, despite an adiabatic temperature rise of 10-15 °C during H_2SO_4 addition, ORP trends exhibit no significant thermal correlation, indicating robust potential stabilization.

Standardized ORP measurement protocols involved a 5-minute homogenization period followed by 3 to 5 minutes of electrode stabilization prior to data acquisition. Continuous monitoring at 0.5-minute intervals revealed transient ORP spikes during the acidification of high-salinity NaCl-H_2SO_4 media, consistent with previously reported anomalous values in similar systems (Cubarol, 2024). Scaling tests in 40 ml and 400 ml volumes demonstrated that increasing acidity to approximately 2 M H_2SO_4 in 12 wt.% NaCl solutions triggered momentary potential jumps to 900-970 mV.

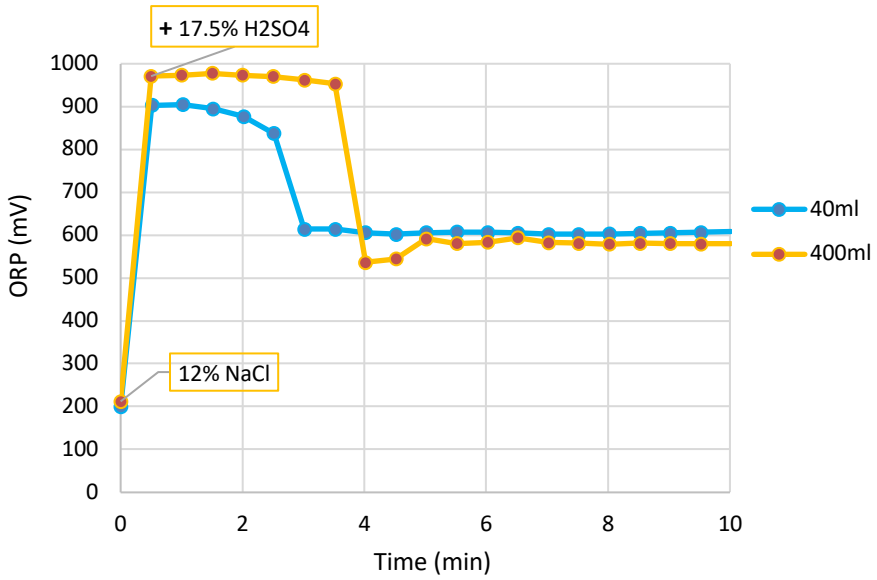

Figure 8. Dynamic ORP response to H_2SO_4 in 12 wt.% NaCl salinity background media

As illustrated in Figure 8, these spikes occurred within the first minute of reagent addition, followed by rapid decay to a steady-state potential between 580 and 610 mV. These transients reflect non-equilibrium conditions at the sensor-electrolyte interface rather than the bulk thermodynamic redox state (Rabenhorst, Hively et al., 2009). In accordance with fundamental electrochemical principles, measured potentials are representative of the steady-state environment only after solution homogenization and the equilibration of the diffusion layers at the platinum electrode (Suslow, 2004). Consequently, all reported data were recorded only after sufficient polarization and stabilization to ensure analytical validity.

3.4. Neural network-based prediction of redox potentials in saline acidic media

Feedforward neural network models were developed for NaCl-H_2SO_4 and NaCl-HCl systems to predict redox potential under the following parameters (Input variables): NaCl% (wt.%), HCl% (wt.%), H_2SO_4 (wt.%), $FeCl_3$% (wt.%), DW/TW (binary 0/1), T.C (degrees C), Conductivity (mS/cm), [H+] (mol/L), Total-Ions (wt.%), Ionic Strength. Datasets were normalized to the [0, 1] range via Min-Max scaling to ensure numerical stability. The architecture, implemented using the MATLAB fitnet function, consisted of two hidden layers (10 and 5 neurons) trained with the Levenberg-Marquardt backpropagation algorithm. Data were partitioned into training (80%) and validation (20%) subsets using the partition function.

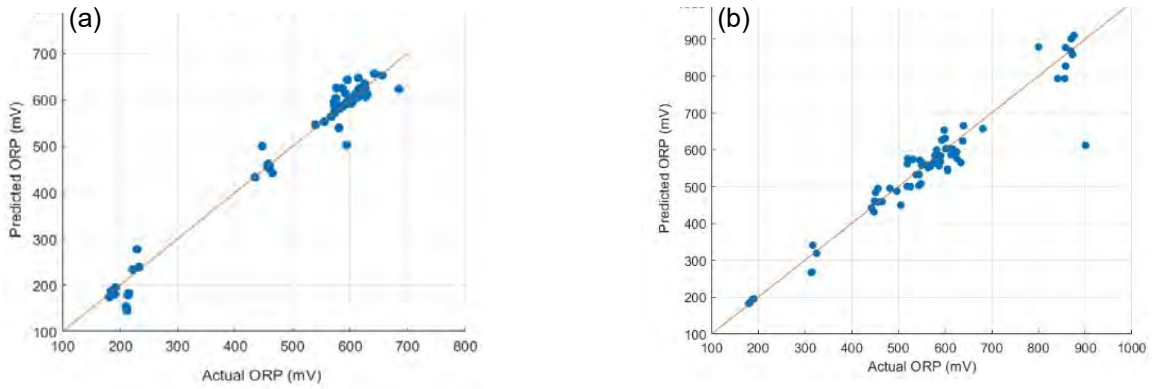

Figure 9. Scatter plot comparing actual and predicted ORP values for (a): NaCl–HCl and (b): NaCl–H_2SO_4 systems using the neural network model

Model performance was evaluated using the metrics in Table 2 and the regression analysis presented in Figure 9. Given the complexities of mixed-potential effects, non-ideal electrochemical behavior, and measurement noise, an average prediction error of +/-30 mV and a residual variance of approximately 1.6 are considered acceptable for regression-based ORP estimation in complex aqueous systems.

Table 2. Performance metrics of neural network models for ORP prediction

System	MAE (Mean Absolute Error)	RMSE (Root Mean Squared Error)	R^2	RMSE/MAE
NaCl–HCl	28.45	46.80	92.08	1.64
NaCl–H_2SO_4	14.66	25.52	97.68	1.74

4. CONCLUSION

This study elucidates the role of NaCl as a redox modulator in acidic media, moving beyond traditional interpretations centered solely on surface passivation. Results demonstrate that NaCl modifies the bulk solution redox environment via mechanisms highly dependent on the acid matrix. In NaCl-HCl systems, high chloride activity and acidity shift the dominant redox control from oxygen-based equilibria toward chlorine-based regimes (Cl_2/Cl^- and $HOCl/Cl^-$), stabilizing ORP near 900 mV. Conversely, in NaCl-H_2SO_4 media, ORP is limited to approximately 600 mV, governed by oxygen-related couples (O_2/H_2O) and proton activity rather than chlorine formation. While high salinity cannot substitute for primary oxidants like Fe^{3+}, it significantly enhances oxidant efficiency by modifying ionic strength and mixed-potential behavior.

Time-dependent profiles identified transient ORP spikes during acidification, underscoring the necessity of rigorous stabilization protocols to distinguish non-equilibrium sensor responses from true thermodynamic states. When translating these findings from synthetic solutions to mineral-rich environments, the presence of sulfide minerals will likely act as a redox sink, where the NaCl-enhanced potential facilitates faster electron transfer at the mineral-electrolyte interface. In industrial mining applications, integrating chloride into sulfate-based leaching circuits provides a strategic pathway to increase oxidative capacity and reduce ferric consumption. Ultimately, NaCl acts as a chemical lever to optimize the solution redox landscape, facilitating the oxidative dissolution of refractory sulfides through improved electrochemical stability.

REFERENCES

Bard, A. J., R. Parsons, Jordan J., (2017), Standard potentials in aqueous solution, Routledge.

Bhargava, S. K., Pownceby, M. I., Ram R., (2017) “Hydrometallurgy”, Metals, 6 (5), 17-19.

Carneiro M. F. C., Leão V. A., (2007) "The role of sodium chloride on surface properties of chalcopyrite leached with ferric sulphate", Hydrometallurgy, 87 (3-4).

Cubarol, R. J., (2024) “Experimental evaluation and modeling of leaching kinetics and fine particle challenges in sodium chloride and sulfuric acid solutions for lithium-ion battery recycling plant design”, Master’s Thesis, Universidad Técnica Federico Santa María.

Córdoba, E. M., Muñoz, J. A., Blázquez, M. L., González, F., Ballester A., (2008) "Leaching of chalcopyrite with ferric ion. Part II: Effect of redox potential", Hydrometallurgy, 93 (3-4).

Hernández, P. C., Taboada, M. E., Herreros, O. O., Torres, C. M., Ghorbani Y., (2015) "Chalcopyrite dissolution using seawater-based acidic media in the presence of oxidants", Hydrometallurgy, 157.

Irto, A., Cigala, R. M., De Stefano, C., Crea F., (2023) "Advances in iron(III) hydrolysis studies. Effect of the metal concentration, ionic medium and ionic strength", Journal of Molecular Liquids, 391 123361.

Jumbo-Pacheco, P., Townley, B., Kelm, U., Vargas, T., (2023) "Chloride leaching of copper ores: influence of NaCl on gangue dissolution and its effect on copper leaching kinetics", Minerals Engineering, 233.

Kinnunen, P., Puhakka J. A., (2004) "Chloride-promoted leaching of chalcopyrite concentrate by biologically-produced ferric sulfate", Journal of Chemical Technology & Biotechnology, 79 (8).

Chang-Li, L., Jin-Lan, X., ZhenYuan, N., Yi, Y., Chen-Yan, M., (2012) "Effect of sodium chloride on sulfur speciation of chalcopyrite bioleached by the extreme thermophile Acidianus manzaensis", Bioresource Technology, 110 462-467.

Mustafa, J., Karimi, G., Ahmadi, R., (2017) "Improvement of chalcopyrite atmospheric leaching using controlled slurry potential and additive treatments", Physicochemical Problems of Mineral Processing 53 1228-1240.

Nimmo, T., (2021) "The role of water in the electrochemical response of platinum”, Doctoral Dissertation, University of Southampton.

Persson, I., (2018) "Ferric chloride complexes in aqueous solution: an EXAFS study", Journal of solution Chemistry, 47 (5) 797-805.

Ping, Z., ZeYun, F., Jie, L., Qiang, L., GuangRen, Q., Ming, Z., (2009) “Enhancement of leaching copper by electro-oxidation from metal powders of waste printed circuit board”, Journal of Hazardous Materials, 166 (2-3) 746-750.

Pourbaix, M., (1966), Atlas of electrochemical equilibria in aqueous solutions, NACE.

Priyantha, N., Malavipathirana S., (1996) "Effect of chloride irons on the electrochemical behaviour of platinum surfaces", Journal of the National Science Foundation of Sri Lanka, 24 (3).

Rabenhorst, M. C., Hively, W. D., James, B. R., (2009) "Measurements of soil redox potential", Soil Science Society of America Journal, 73 (2) 668-674.

Schneider, A. C., Pasel, C., Luckas, M., Schmidt, K. G., Herbell, J. D., (2004) "Determination of hydrogen single ion activity coefficients in aqueous HCl solutions at 25 C", Journal of solution chemistry, 33 (3) 257-273.

Seisko, S., Aromaa J., Lundström, M., (2020) "Effect of redox potential and OCP in ferric and cupric chloride leaching of gold", Hydrometallurgy, 195 105374.

Senanayake, G., (2009) "A review of chloride assisted copper sulfide leaching by oxygenated sulfuric acid and mechanistic considerations", Hydrometallurgy, 98 (1-2) 21-32.

Sepúlveda, R., Martínez, M., Hernández, P., Guzmán, A., Castillo, J., Sepúlveda, R., Martínez, M., Hernández, P., Guzmán, A., Castillo, J., (2023) "Effect of chloride and ferrous ions on improving copper leaching from black copper ores", Processes, 12 (1) 13.

Stefánsson, A., Lemke, K. H., Seward, T. M. (2019) "Iron(III) chloride complexation in hydrothermal solutions: A combined spectrophotometric and density functional theory study", Chemical Geology, 524 77-87.

Suslow, T. V., (2004), Oxidation-Reduction Potential (ORP) for Water Disinfection Monitoring, Control, and Documentation."

Thomsen, K., (2009), Electrolyte Solutions: Thermodynamics, Crystallization, Separation Methods, 38-40.

Torres, C. M., Taboada, M.E., Graber, T. A., Herreros, O. O., Ghorbani, Y., Watling, H. R., (2015) "The effect of seawater-based media on copper dissolution from low-grade copper ore", Minerals Engineering 71 139-145.

Velásquez-Yévenes, L., Nicol, M., Miki, H., (2010) "The dissolution of chalcopyrite in chloride solutions: Part 1. The effect of solution potential", Hydrometallurgy 103 (1-4).

Watling, H. R., (2013) "Chalcopyrite hydrometallurgy at atmospheric pressure: 1. Review of acidic sulfate, sulfate–chloride and sulfate–nitrate process options", Hydrometallurgy, 140 163–180.

Watling, H. R., (2014) "Chalcopyrite hydrometallurgy at atmospheric pressure: 2. Review of acidic chloride process options", Hydrometallurgy, 146 96–110.

Winand, R., (1991) "Chloride hydrometallurgy", Hydrometallurgy, 27 (3).

Zhong, S., Li, Y., (2019) "An improved understanding of chalcopyrite leaching kinetics and mechanisms in the presence of NaCl", Journal of Materials Research and Technology, 8 (4) 3487-3494.

PYROMETALLURGICAL AND HYDROMETALLURGICAL VALORIZATION OF BLAST FURNACE SLUDGE FROM THE MĂLINA SETTLING POND (GALATI, ROMANIA)

Camelia TRAISTĂ[1], Tiberiu RUS[1], Eugen TRAISTĂ[2,*]

[1]Technical University of Cluj-Napoca, Romania
[2]University of Petrosani
**Corresponding author: eugen_traista@yahoo.com*

A B S T R A C T

Blast furnace sludge (BFS) generated in the Romanian steel industry, particularly at the Galați steel plant, represents a significant environmental and technological challenge due to its high content of fine particles enriched in zinc, iron, and carbon. The presence of zinc severely limits the direct recycling of iron-bearing fractions into the blast furnace, as zinc volatilizes at operating temperatures, leading to accretions, refractory damage, and process instability. This paper presents a comprehensive study on the characterization and treatment of BFS from the Mălina settling pond. Hydrometallurgical routes (acid, alkaline and CO_2 leaching) and pyrometallurgical pilot-scale tests were investigated for zinc removal and iron recovery. The results demonstrate that hydrometallurgical methods are constrained by the refractory nature of zinc ferrite, whereas pyrometallurgical processing enables efficient zinc volatilization and the production of zinc-depleted, iron-rich products suitable for metallurgical reuse. The study supports the implementation of combined thermal and pyrometallurgical technologies as a viable and sustainable route for BFS valorization in Romania.

Key words: *Blast furnace sludge, zinc removal, pyrometallurgy, hydrometallurgy, waste valorization, blast furnace sludge, zinc removal, hydrometallurgy, waste valorization*

1. INTRODUCTION

The continuous development of the iron and steel industry has led to the generation of increasing quantities of metallurgical wastes. Among these, blast furnace sludge (BFS) is considered one of the most problematic residues due to its fine particle size and high content of potentially hazardous elements such as zinc and lead (Mansfeldt & Dohrmann, 2004; Das et al., 2007). BFS is generated during the wet cleaning of blast furnace gases and is typically stored in settling ponds, posing long-term environmental risks through metal leaching into soil and groundwater.

Zinc is particularly problematic in blast furnace operation (Van Herck et al., 2000; United States Steel Corporation, 1985). At high temperatures, zinc evaporates and subsequently condenses in cooler furnace zones, forming crusts that hinder burden descent and disrupt thermal balance. For this reason, the zinc input to a blast furnace is typically limited to approximately 120 g Zn per ton of hot metal. Consequently, BFS with zinc contents of 1–3% cannot be directly recycled without prior treatment.

This paper is based on the final study carried out at Galați and aims to present an integrated evaluation of BFS from the Mălina settling pond, including chemical characterization, assessment of reuse potential, and analysis of different zinc removal technologies.

2. MATERIALS AND METHODS

2.1. Sampling and Preparation

A total of 29 representative samples were collected from the entire surface of the Mălina settling pond. The samples were dried, homogenized, and prepared for chemical analysis. This sampling strategy ensured reliable assessment of both average composition and spatial variability.

2.2. Chemical Characterization

Chemical composition was determined by X-ray fluorescence (XRF) analysis. The average elemental composition shows a high Fe2O3 content (~66%), significant CaO (~16%), and ZnO contents averaging 0.68%, with local values reaching up to 1.59%. Loss on ignition values around 13% indicate the presence of carbonaceous material and hydrated phases.

Table 1. Average chemical composition of blast furnace sludge from the Mălina settling pond (significant components)

Component	Content (%)
Fe_2O_3	65.95
CaO	16.37
MnO	1.24
ZnO	0.68
PbO	0.12
PC (LOI)	13.07

3. RESULTS AND DISCUSSION

3.1. Variability of Sludge Composition

The results indicate considerable heterogeneity in the sludge composition. Fe2O3 content ranged from 45.9% to 86.1%, while ZnO varied between 0.29% and 1.59%. Approximately 41% of samples failed to meet the minimum commercial requirement of 62% Fe2O3 for recycling. Moreover, only about 10% of samples complied with the zinc limit of 0.5% ZnO.

Table 2. Range of variation for significant components in blast furnace sludge

Component	Minimum [%]	Maximum [%]
Fe_2O_3	45.88	86.11
CaO	7.39	25.70
MnO	0.85	1.61
ZnO	0.29	1.59
PbO	0.00	0.30
PC (LOI)	0.17	26.33

These findings suggest that complete valorization of BFS is possible only through appropriate management, including blending low-iron with high-iron fractions and implementing zinc reduction treatments.

3.2. Mineralogical Considerations

Zinc in BFS occurs predominantly as zinc ferrite (ZnFe2O4, franklinite), a highly stable and refractory phase, and to a lesser extent as zinc oxide (ZnO). Iron is mainly present as

magnetite (Fe3O4) and hematite (Fe2O3). The presence of zinc ferrite explains the limited efficiency of conventional leaching processes (Kelebek et al., 2004; Van Herck et al., 2000).

4. HYDROMETALLURGICAL TREATMENT

4.1. Acid Leaching

Sulphuric acid leaching tests showed zinc removal efficiencies of up to 56%. Acid leaching effectively dissolves ZnO and partially decomposes zinc ferrite; however, it also leads to partial dissolution of iron, increasing solution purification requirements. Despite its efficiency, acid leaching raises environmental and economic concerns due to acid consumption and secondary effluents (Das et al., 2007).

Table 3. Zinc removal efficiency for different leaching methods (three independent tests)

Leaching method	Test	ZnO after treatment [%]	Zinc removal [%]
Acid leaching (H_2SO_4)	Test 1	0.72	54.8
	Test 2	0.69	56.4
	Test 3	0.71	55.2
CO_2 leaching	Test 1	1.10	30.9
	Test 2	1.08	32.0
	Test 3	1.05	34.0
Alkaline leaching (NaOH)	Test 1	1.58	2.0
	Test 2	1.56	2.2
	Test 3	1.54	3.1

Leaching method	ZnO after treatment [%]	Zinc removal [%]
Acid leaching (H2SO4)	0.69	56.41
CO2 leaching	1.08	31.97
Alkaline leaching (NaOH)	1.56	2.24

4.2. Alkaline Leaching

Alkaline leaching using NaOH proved highly selective towards zinc over iron. Zinc and lead oxides dissolve readily, while iron remains largely in the residue. However, zinc ferrite shows limited solubility, restricting overall zinc recovery. High NaOH concentrations (6–10 M) and elevated temperatures (80–95 °C) are required to achieve zinc recoveries of 65–85%, as reported in both literature and experimental results filecite turnfile .

4.3. CO_2 Leaching

Leaching with carbon dioxide solutions resulted in moderate zinc removal (32–58%), particularly when applied to thermally treated material. Although environmentally attractive, this method requires large volumes of water due to the low solubility of zinc carbonate, limiting its industrial applicability.

5. EFFECT OF THERMAL PRETREATMENT

Thermal treatment at approximately 400 °C significantly increased zinc leachability by altering mineral phases and weakening the zinc ferrite structure. Experimental results showed an increase in zinc removal from 2–3% to over 40% after calcination followed by alkaline leaching. These findings confirm the importance of combined thermal–hydrometallurgical routes (Cantarino et al., 2018; Hamann et al., 2021).

6. PYROMETALLURGICAL VALORIZATION

The pilot-scale experiments for zinc removal from blast furnace sludge were carried out at the Teliuc industrial platform using a rotary kiln installation designed for thermal treatment of fine metallurgical residues. The rotary kiln had a length of 8 m, an internal diameter of 0.8 m, and was equipped with temperature monitoring along multiple zones, adjustable rotational speed (0.5–2 rpm), and controlled air supply to regulate the oxidation-reduction atmosphere.

Raw Material Preparation. Prior to thermal treatment, the blast furnace sludge underwent:

- mechanical homogenization,
- partial drying (moisture reduction below 10%),
- removal of oversized agglomerates.

The average chemical composition of the feed material showed significant iron content (mainly as Fe_2O_3 and Fe_3O_4), zinc present predominantly as ZnO and zinc ferrite ($ZnFe_2O_4$), along with carbonaceous matter acting as an internal reducing agent.
The presence of carbon in the sludge played a key role in the reduction mechanism, contributing to the carbothermic reduction of zinc compounds.

Reaction Mechanism. At temperatures above 900 °C, zinc oxide and zinc ferrite undergo reduction reactions such as:

$$ZnO + C \rightarrow Zn(g) + CO(g)$$
$$ZnFe_2O_4 + 2C \rightarrow Zn(g) + 2FeO + 2CO(g)$$

Due to the relatively low boiling point of zinc (907 °C), metallic zinc volatilizes and exits the solid matrix as vapor. Upon contact with secondary air in the cooler zones or in the gas treatment system, zinc vapor re-oxidizes to ZnO and is captured in the dust collection unit (cyclones and bag filters).

This mechanism enables selective zinc removal while retaining iron oxides in the solid residue (Wei et al., 2023).

Operational Parameters. The pilot tests were conducted at temperatures between 900 and 1200 °C, with optimal zinc volatilization observed in the range of 1000–1100 °C. Key operational parameters included:

- Residence time: 30–60 minutes
- Controlled excess air coefficient: 1.05–1.15
- Kiln inclination: 2–3%
- Feed rate adjusted to maintain thermal stability

Zinc removal efficiencies exceeded 70% under optimized conditions, with some tests approaching 75–80% depending on initial zinc content and thermal regime stability.

It should be noted that although the monitored bulk operating temperature was maintained within the specified range, local temperature peaks may occur inside the rotary kiln. These localized overheating zones can be generated by uneven material distribution, variable feed composition, fluctuations in air supply, or localized exothermic reactions associated with carbon oxidation. As a result, even when the average kiln temperature remains below 1300–1400 °C, certain areas of the charge may temporarily experience significantly higher temperatures.

Such local thermal spikes can promote partial melting of iron-bearing phases and early slag formation, favoring material agglomeration and the development of rings along the kiln lining. Therefore, careful control of feed uniformity, rotational speed, and combustion parameters is essential to minimize the risk of localized overheating and ensure stable operation.

Technological Observations and Constraints. It was observed that:

- Temperatures exceeding 1300–1400 °C led to incipient melting of iron-bearing phases.
- Above 1500 °C, partial slag formation occurred, causing material agglomeration and ring formation inside the kiln.
- Excessive air input resulted in over-oxidation, reducing the effectiveness of zinc volatilization and increasing fuel consumption.
- Refractory lining degradation accelerated significantly at excessive temperatures due to localized overheating.

Maintaining a stable thermal gradient along the kiln length proved essential for avoiding accretions and ensuring continuous operation.

Characteristics of the Treated Residue. The solid residue after treatment exhibited:

- Significantly reduced zinc content,
- Increased relative iron concentration,
- Improved suitability for reintegration into the sintering or blast furnace feed,
- Stable granulometric behavior without excessive fine generation.

The treated material maintained mechanical integrity and did not show vitrification when
The Teliuc pilot tests confirmed the technical feasibility of rotary kiln pyrometallurgical treatment as a scalable solution for zinc removal from blast furnace sludge. The process allows:

Recovery of a zinc-rich dust fraction,

- Production of an iron-rich recyclable residue,
- Reduction of hazardous waste accumulation,
- Improved circularity within the steel production cycle.

From a technological standpoint, rotary kiln treatment provides a controlled and relatively energy-efficient method compared to alternative high-temperature shaft or cupola furnaces, especially for fine-grained sludge materials.

Table 5. Pilot-scale rotary kiln tests – zinc removal performance

Test location	Temperature range [°C]	Fe content [%]	Zn content [%]	Zn removal [%]
Teliuc – Test 1	900–1000	50.85	4.33	79.9
Teliuc – Test 2	950–1050	41.93	3.83	82.2
Teliuc – Test 3	1000–1100	52.88	5.14	76.2

Subsequent trials in cupola furnaces operating above 1250 °C confirmed that zinc can be almost completely eliminated through volatilization, while iron is reduced and recovered either as sponge iron or pig iron.

Laboratory-scale experiments were performed in order to simulate the high-temperature behavior of blast furnace sludge under controlled reducing conditions and to evaluate zinc removal efficiency as a function of thermal regime and degree of reduction. The tests were conducted in an induction furnace using graphite crucibles, where graphite fulfilled a dual role: refractory containment material and reducing medium supporting carbothermic reactions.

Charge Preparation. Prior to testing, the blast furnace sludge was:

- dried to remove residual moisture and stabilize heating behavior,
- homogenized to ensure compositional uniformity,
- either pelletized (for reduced pellet tests) or compacted as loose charge, depending on the experimental configuration.

In selected experiments, additional carbon (fine coke or graphite) was introduced to control the reduction potential and ensure sufficient reducing atmosphere for iron oxides and zinc compounds (ZnO, $ZnFe_2O_4$).

Experimental Procedure and Thermal Regimes. The prepared charge was placed inside graphite crucibles and heated by induction to the target temperatures. A controlled holding time was applied at each temperature level to allow reduction reactions and phase transformations to proceed.
Three main temperature regimes were investigated:

1. **1250 °C – Reduced Pellets**

At this temperature, partial reduction of iron oxides occurred, accompanied by significant zinc volatilization. The product maintained a predominantly solid structure without complete melting.

- Typical composition: Fe ~60.27%, Zn ~0.27%.

2. **1350 °C – Iron Sponge**

Increasing the temperature enhanced the reduction of iron oxides toward metallic iron, resulting in a porous, sponge-like metallic structure. Zinc removal efficiency improved considerably due to intensified volatilization.

- Typical composition: Fe ~75.64%, Zn ~0.06%.

3. **>1400 °C – Pig Iron (Test 1 and Test 2)**

At temperatures exceeding 1400 °C, melting and metal–slag separation occurred. A metallic phase (pig iron) formed, clearly separated from the slag. Due to zinc's high volatility at elevated temperatures, it was almost entirely removed from the metallic phase.

- Typical composition: Fe ~93.3–93.37%, Zn <0.01%.

Product Separation and Characterization. After the thermal treatment and controlled cooling, the products were separated:

- reduced solid phase (pellets or sponge iron), or
- metallic pig iron and associated slag (for high-temperature tests).

Chemical analyses confirmed a clear trend: increasing temperature led to enhanced iron reduction and progressively lower zinc content, reaching values below 0.01% in the pig iron samples.

These laboratory results demonstrate that high-temperature induction furnace treatment in graphite crucibles provides efficient zinc removal and enables the production of iron-rich products with progressively higher metallization degrees, supporting the feasibility of scaling the process toward industrial applications.

Table 6. Cupola furnace tests – iron recovery and residual zinc

Product type	Temperature [°C]	Fe content [%]	Zn content [%]
Reduced pellets	1250	60.27	0.27
Iron sponge	1350	75.64	0.06
Pig iron – Test 1	>1400	93.37	<0.01
Pig iron – Test 2	>1400	93.30	<0.01

Based on pilot test results, a combined technological route is proposed, consisting of a rotary kiln for drying, partial reduction, and initial zinc removal, followed by a cupola furnace for final zinc volatilization and iron melting. This integrated approach ensures compliance with metallurgical quality requirements and minimizes environmental impact.

7. ENVIRONMENTAL AND TECHNOLOGICAL ASSESSMENT

The environmental implications associated with long-term storage of blast furnace sludge in settling ponds are significant, particularly due to the potential mobility of zinc and lead under changing geochemical conditions. Numerous studies have demonstrated that fine-grained metallurgical residues may release heavy metals through leaching, especially under acidic or carbonate-rich groundwater regimes (Mansfeldt & Dohrmann, 2004). In the case of the Mălina settling pond, the heterogeneous composition and high loss on ignition values further increase the risk of contaminant release as a result of oxidation of carbonaceous phases and subsequent pH variations.

From a regulatory perspective, current European environmental policies increasingly discourage indefinite storage of industrial residues and promote waste minimization, recycling, and recovery of secondary raw materials. Consequently, the continued disposal of blast furnace sludge without valorization is not compatible with long-term compliance strategies. The transformation of BFS into reusable metallurgical products directly supports the objectives of circular economy frameworks by reintegrating iron units into the production cycle and reducing the demand for primary raw materials.

Technologically, the comparison between hydrometallurgical and pyrometallurgical routes highlights fundamental differences in robustness and industrial readiness. Hydrometallurgical treatments are sensitive to mineralogical composition and require careful control of reagent consumption, effluent treatment, and solid–liquid separation. While suitable for selected low-zinc fractions, their application as a stand-alone solution for the entire sludge inventory remains limited.

Pyrometallurgical processing, although more energy-intensive, provides a stable and scalable solution capable of handling compositional variability (Hamann et al., 2021; Wei et al., 2023). The pilot-scale results demonstrate that controlled thermal treatment effectively decouples zinc from iron-bearing phases, producing a zinc-rich off-gas dust and an iron-rich product suitable for metallurgical reuse. When integrated with appropriate gas cleaning and heat recovery systems, the overall environmental footprint of the process can be substantially reduced.

In practical terms, the proposed integrated route combining rotary kiln pre-treatment with cupola furnace melting offers operational flexibility and compatibility with existing metallurgical infrastructure. Such an approach allows gradual implementation, starting with pilot or semi-industrial units, and provides a clear pathway toward full-scale deployment.

8. CONCLUSIONS

The comprehensive investigation of blast furnace sludge from the Mălina settling pond confirms that this residue should be regarded as a valuable secondary resource rather than a material destined for long-term disposal. The high iron content, combined with significant but manageable zinc concentrations, positions BFS as a candidate for recovery-based treatment strategies provided that appropriate technologies are applied.

Hydrometallurgical routes offer partial solutions for zinc removal, particularly for zinc present in more reactive oxide forms. However, the dominance of zinc ferrite significantly constrains overall extraction efficiency and leads to increased reagent consumption and secondary waste generation. These limitations restrict the applicability of purely hydrometallurgical approaches when dealing with large volumes of heterogeneous blast furnace sludge.

Pyrometallurgical valorization demonstrates clear advantages in terms of zinc removal efficiency and process reliability. Pilot-scale experiments in rotary kilns and cupola furnaces confirm that zinc can be effectively volatilized at elevated temperatures, while iron is simultaneously upgraded and recovered either as sponge iron or as pig iron with negligible

residual zinc. The ability to produce pig iron that meets metallurgical quality requirements represents a critical advantage, enabling direct reintegration into ironmaking operations without operational risk.

The combination of rotary kiln and cupola furnace processing emerges as a technically sound and industrially viable route for full-scale implementation. This staged configuration accommodates feed variability, minimizes operational disturbances, and creates an additional zinc-rich by-product stream with potential economic value. Moreover, the proposed route significantly reduces the environmental risks associated with sludge storage and aligns with modern sustainability and circular economy principles.
Future research should address detailed process optimization, including energy efficiency improvements, off-gas treatment and dust capture, and comprehensive techno-economic assessment under Romanian industrial conditions. Such efforts will support the transition from pilot-scale validation to industrial deployment and contribute to the sustainable management of metallurgical residues in the iron and steel industry.

REFERENCES

Andersson, A., Gullberg, A., Kullerstedt, A., Ahmed, H., Sundqvist-Ökvist, L., Samuelsson, C., (2019), “Upgrading of blast furnace sludge and recycling of the low-zinc fraction via cold-bonded briquettes”, Journal of Sustainable Metallurgy, 5, 350–361. https://doi.org/10.1007/s40831-019-00225-x

Das, B., Prakash, S., Reddy, P. S. R., Misra, V. N., (2007), “An overview of utilization of slag and sludge from steel industries”, Resources, Conservation and Recycling, 50 (1), 40–57.

Hamann, C., Spanka, M., Stolle, D., Auer, G., Weingart, E., Al-Sabbagh, D., Ostermann, M., Adam, C., (2021), “Recycling of blast-furnace sludge by thermochemical treatment with spent iron(II) chloride solution from steel pickling”, Journal of Hazardous Materials, 402, 123511. https://doi.org/10.1016/j.jhazmat.2020.123511

Kelebek, S., Yörük, S., Davis, B., (2004), “Characterization of basic oxygen furnace dust and zinc removal by acid leaching”, Minerals Engineering, 17 (2), 285–291. https://doi.org/10.1016/j.mineng.2003.10.030

Mansfeldt, T., Dohrmann, R., (2004), “Chemical and mineralogical characterization of blast-furnace sludge from an abandoned landfill”, Environmental Science & Technology, 38 (22), 5977–5984. https://doi.org/10.1021/es040002

United States Steel Corporation, (1985), “The Making, Shaping, and Treating of Steel”, 10th ed., Association of Iron and Steel Engineers (AISE).

Van Herck, P., Vandecasteele, C., Swennen, R., Mortier, R., (2000), “Zinc and lead removal from blast furnace sludge with a hydrometallurgical process”, Environmental Science & Technology, 34 (17), 3802–3808. https://doi.org/10.1021/es991033

Wei, R., Zhang, F., Wang, X., Meng, D., Meng, K., Long, H., (2023), “A novel approach for the resource utilization of zinc-bearing dust and sludge via the blast furnace main trough”, Waste Management, 172, 127–139. https://doi.org/10.1016/j.wasman.2023.10.014

van Herck, P., (2000), “Zinc behavior in blast furnaces”, Ironmaking & Steelmaking.

Dvorak, P., (2002), “Characterization of blast furnace sludge”, Waste Management.

RECOVERY OF METALLIC VALUES FROM COPPER SLAGS

Fatma ARSLAN[1,*], Gülay BULUT[1], Cüneyt ARSLAN[2]

[1]Istanbul Technical University, Faculty of Mines, Mineral Processing Engineering Department, 34469, Maslak, Istanbul, TÜRKİYE
[2]Istanbul Technical University, Faculty of Chemistry and Metallurgy, Metalurgy and Materials Engineering Department, 34469, Maslak, Istanbul, TÜRKİYE
**Corresponding author: arslanf@itu.edu.tr*

A B S T R A C T

During the pyrometallurgical production of metallic copper from copper concentrates, various by-products are generated. Among these, copper slags represent a major waste material, typically containing iron oxide, silica, calcium oxide, alumina, and residual copper. Although often stockpiled or used in landfill applications, slags still contain significant amounts of valuable metals in entrained metallic, sulphide, or oxidized forms. To recover these metal values, a range of processes, including mineral processing, pyro-, hydro-, and pyro-hydrometallurgical techniques, are employed. Flotation, in particular, plays a key role in the beneficiation of copper slags and is widely applied in many smelting operations. This paper discusses the properties of smelting, converting, refining, and ancient copper slags produced during pyrometallurgical copper processing and reviews methods developed for metal recovery from these materials. Our laboratory studies related to metal recoveries from different types of copper slags supplied from industrial plants (Turkey) are summarized.

Key words: *Copper slags, flotation, pyrometallurgy, hydrometallurgy*

1. INTRODUCTION

Various slags are generated as by products of metallurgical processes and, depending on their origin and characteristics, are commonly classified into three main categories: ferrous slags, non-ferrous slags, and incineration slags (Shen and Forssberg, 2003). Large quantities of slag are produced annually, and some slags contain significant amounts of hazardous or heavy metals. The release of these metals poses potential environmental risks. Conventional slag disposal methods primarily involve landfilling; however, the increasing accumulation of slag not only occupies vast areas of land but also represents a loss of valuable resources and poses risks of environmental contamination, particularly water pollution. Consequently, the recovery of metals from slags and the valorization of these materials are essential for both resource conservation and environmental protection.

During the pyrometallurgical production of metallic copper from concentrates, various by-products, including slags, dusts, and fumes, are generated, many of which contain considerable amounts of valuable metals in addition to copper. Flash smelting, which has largely replaced reverberatory furnaces in modern copper production, has been widely adopted for this purpose. However, due to substantial copper lock-up in flash furnace slags, downstream processing units, such as electric furnace slag-cleaning, converting, and fire-refining stages, are typically required. In some operations, copper converter slag is recycled back into the flash furnace, resulting in increased matte grade (Antonioni et al., 1982). In other plants, flash furnace slags containing 1.6-2% Cu and converter slags with 5-7% Cu are treated in electric arc furnaces using coke as a reductant, reducing the residual copper content to 0.5-0.8% (Kim, 1982; Suzuki et al., 1982). The Ausmelt top-entry submerged lance technology has also been employed to recover Cu, Ni, and Co from copper slags (Hughes, 2000; Vernon and Burks, 1997).

In copper production, concentrates obtained after flotation undergo smelting, converting, and fire refining to produce anode plates. Throughout these stages, substantial amounts of copper slag are generated, representing one of the most significant challenges faced by the copper industry. Figure 1 illustrates the formation of copper slags at various stages of pyrometallurgical copper production. These slags often contain considerable quantities of valuable metals and can therefore be regarded as secondary metal resources. Through the application of mineral processing techniques, such as crushing, grinding, magnetic separation, eddy current separation, and flotation, as well as pyro-, hydro-, and pyrometallurgical processes, metals including Fe, Cr, Cu, Al, Pb, Zn, Co, Ni, Nb, Ta, Au, and Ag can be recovered from slags.

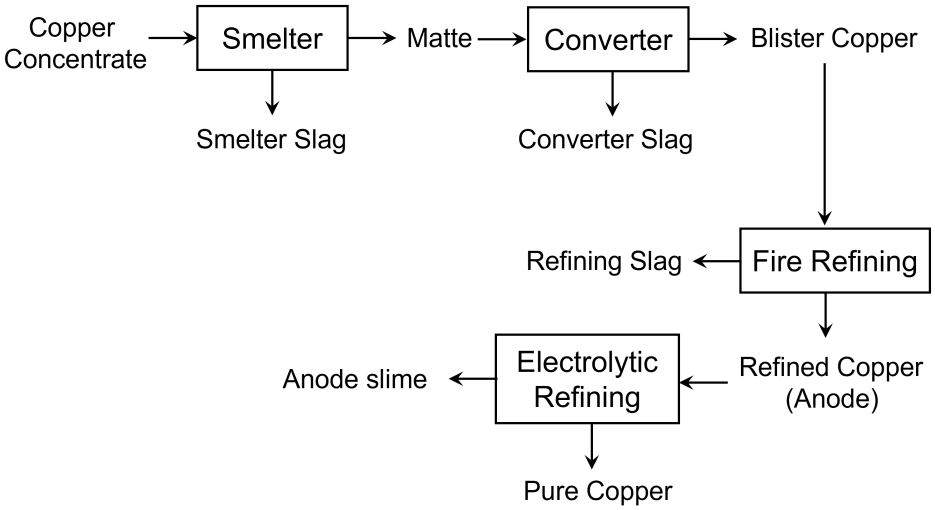

Figure 1. Slags produced during the various stages of pyrometallurgical copper production

2. ANCIENT COPPER SLAGS

Copper was the first metal smelted by humans, approximately seven thousand years ago in the ancient Near East. For most pre-industrial periods, knowledge of copper metallurgy relies largely on the study of metallurgical waste, particularly copper slags recovered from archaeological ites. These slags typically comprise oxide phases (e.g., iron and manganese oxides), fayalitic olivine, and/or pyroxenes embedded in a partially glassy polymetallic matrix, reflecting both the charge materials and operating conditions of ancient furnaces (Bourgarit, 2019).

Potysz et al. (2016) demonstrated that ancient copper slags, formed under poorly controlled smelting conditions, are mineralogically heterogeneous and exhibit enhanced metal release during pH-dependent leaching, causing them to behave as complex anthropogenic ores. In contrast, modern slags are characterized by uniform fayalite–spinel assemblages, lower metal mobility, and greater environmental stability, reflecting improved metallurgical control.

By contrast, international studies confirm that ancient copper slags can be treated as viable secondary resources. Potysz (2019) showed that Polish historical slags are amenable to acid and bioleaching, while Dzinomwa et al. (2023) and Ettlinger (2020) demonstrated the economic feasibility of reprocessing ancient slag deposits in Namibia and Sweden, respectively. Amorphous slags, in particular, exhibit the highest dissolution efficiencies and recovery potential (Potysz and Kierczak, 2019). In this context, Küre slags represent the only extensively studied reprocessing-focused example in Türkiye.

The ancient copper slags of the Küre region are among the most characteristic fayalitic smelting residues, containing significant amounts of Cu, Co, Fe, and minor metals entrapped within olivine-rich matrices and spinel phases (Bulut, 2006). Owing to their metal content and large accumulated volumes, these slags have been investigated for secondary metal recovery for over three decades.

Topkaya (1990) first demonstrated the feasibility of carbothermic reduction, achieving recoveries of 97.7% Co and 86.7% Cu at 1400°C. Subsequent studies employed submerged electric arc and DC arc furnaces to produce metal-rich alloys, followed by sulfuric acid leaching and selective recovery of copper, cobalt, and iron products (Açma et al., 1992; Sesigür et al., 1995; Açma et al., 1997). Closed DC arc systems further improved recoveries to 95.7% Co and 90% Cu (Yücel et al., 1999), while integrated flowsheets incorporating reduction, leaching, recipitation, and sulfidation roasting were later developed (Derin et al., 2003).

More recent work has shifted toward combined pyro-hydrometallurgical and flotation-based approaches. Bulut et al. (2007) achieved 77% Cu recovery and 87% Co dissolution using pyrite roasting and flotation, while Tegin and Ziyadanoğulları (2018) reported Cu recoveries exceeding 98% using H_2S-assisted sulfidizing flotation. The most advanced hydrometallurgical study to date employed oxidative pressure leaching, achieving over 92% recovery of Cu, Co, and Zn with minimal Fe dissolution (Seyrankaya and Canbazoglu, 2021).

Overall, research on Küre ancient slags has evolved from early reduction studies to advanced integrated reprocessing routes. The increasing emphasis on mineralogical control, environmental compatibility, and product diversification highlights the strong potential of Küre slags as anthropogenic ores and supports their near zero-waste valorization.

3. COPPER SMELTING SLAGS

Metal contents of smelter and converter slags produced in copper smelting plants are typically very high and should be recovered for economic reasons. Numerous studies have been conducted on this subject. Arslan and Arslan (2002) investigated the recovery of Cu, Co, and Zn from slag through a pyro-hydrometallurgical route as an alternative to flotation. A mixture of flash smelting and converter slags supplied by the Black Sea Copper Works, Türkiye, was subjected to acid roasting followed by either direct hot water leaching or thermal decomposition combined with hot water leaching. The chemical composition of the slag sample was 2.64% Cu, 0.095% Co, 0.67% Zn, 47.2% Fe, 0.13% Pb, 0.004% Cd, 0.065% Ni, 8.5% Si, and 1.3% S. Microscopic and XRD analyses indicated that copper existed as bornite, ferrites, and minor metallic Cu, whereas zinc, cobalt, and nickel occurred as silicates and ferrites; iron was present in a fayalite-type matrix. Roasting the slag mixture with sulfuric acid resulted in sulfation of slag constituents, consistent with theoretical expectations. Roasting followed by hot water leaching showed that the highest metal recoveries occurred at 150°C, whereas increasing the roasting temperature decreased sulfation of Co and Zn. After 2 h of roasting at 150°C and a 3:1 acid/slag ratio, recoveries were 88% Cu, 87% Co, 93% Zn, and 83% Fe. Extending roasting to 4 h increased Cu extraction to 95%. Higher roasting temperatures favored Cu sulfate formation, and 100% Cu dissolution was achieved by roasting at 250°C for 3 h at a 3:1 acid/slag ratio. Applying thermal decomposition after acid roasting lowered metal dissolution. However, Fe dissolution decreased to nearly zero after 2 h of thermal decomposition at 650°C having an advantage for downstream solution purification. Ultimately, 79% Cu, 66% Co, and 41% Zn were dissolved under these conditions.

Akhmedov (2024) examined the dissolution behavior of Cu, Fe, and Zn from copper slags in sulfuric acid under controlled conditions. Optimal parameters were 2.5 M H_2SO_4, 90°C, and 120 min, yielding up to 95% Cu and ~90% Fe recovery. Higher acid concentration, elevated

temperature, and reducing particle size below 100 μm significantly enhanced metal dissolution. In a similar study, Başkurt et al. (2022) applied flotation to a slag containing 0.9% Cu and achieved a concentrate grade of 22.7% Cu with ~40% recovery. Direct H_2SO_4 leaching caused gel formation, so HCl was used instead. With 25 g/L H_2O_2, 20-25% solids, and 300 g/L HCl, Cu and Ce extractions reached 70 to 80% in 2 h. Silica gel commonly forms during sulfuric acid leaching because of the amorphous nature of slags, hindering filtration and causing crud formation in solvent extraction. This problem was mitigated by adding hydrogen peroxide (Banza et al., 2002). Their peroxide assisted H_2SO_4 leaching of a slag (<100 μm) from Lubumbashi (DRC) containing 1.4% Cu, 0.7% Co, 8.9% Zn, and 20.9% Fe(II) produced gel free solutions. Copper was extracted using LIX 984 in Shellsol D70, followed by collective extraction of Co and Zn with D2EHPA and selective scrubbing. Overall recoveries reached 80% Cu, 90% Co, and 90% Zn in separated solutions which could be further treated by electrowinning or salt precipitation.

Wang et al. (2024) proposed a novel two stage (evaporation + water washing) method for selective Fe and Zn recovery from copper slag. Under optimal conditions (evaporation: 3 M H_2SO_4, 60 min, 120°C, liquid/solid ratio 4; water washing: liquid/solid ratio 5), leaching efficiencies were 99.94% Fe, 97.40% Zn, and only 0.15% Si. Silica gel aggregated into amorphous silica, inhibiting Si dissolution. The process transformed slag into iron red, electrolytic zinc, and geopolymers.

Yang et al. (2010) developed a selective atmospheric pressure hydrometallurgical method using sulfuric acid and sodium chlorate oxidant, followed by $Ca(OH)_2$ neutralization for faster filtration of the precipitate. Recoveries were 98% Co, 97% Zn, and 89% Cu, while only 3.2% Si and 0.02% Fe dissolved. The simplicity and economy of this process make it industrially attractive.

Alam et al. (2025) investigated sodium sulfate assisted structural decomposition of complex copper slag compounds. Using 20% Na_2SO_4 yielded an 89% decomposition rate. Optimal fayalite decomposition occurred at 900°C with a reaction time of 90 min. Subsequent H_2SO_4 leaching achieved 97% Cu, 96% Fe, and 93% Zn recoveries. Untreated samples showed much lower recoveries (61% Cu, 59% Fe, 65% Zn). The method also prevented silica gel formation.

A novel aluminothermic smelting reduction (ASR) process was investigated for treating waste Phiri et al. (2025) investigated the low temperature carbothermic reduction of copper slag using charcoal and borax, followed by sulfuric acid leaching. Mineralogical analysis showed that the slag was mainly composed of fayalite and magnetite. Magnetite reduced stepwise ($Fe_3O_4 \rightarrow FeO \rightarrow Fe$), while fayalite was catalyzed at 300 °C and reduced to metal at 545 °C. Optimal extraction conditions were 20% borax and 10% charcoal, with 90 min reduction at 850 °C, followed by 90 min leaching in 2 M H_2SO_4. Under these conditions, Cu, Co, and Fe extractions reached 77.33%, 83.35%, and 86.53%, respectively, demonstrating that carbothermic reduction is a key step enabling efficient downstream metal recovery.

4. COPPER CONVERTER SLAGS

In a study aimed at developing a pressure-leaching process for converter slag using dilute sulfuric acid, where iron contamination could be minimized by oxidation and hydrolysis, Anand et al. (1983) examined various parameters including leaching time, pulp density, particle size, acid concentration, and oxygen partial pressure. Under optimized conditions, approximately 90% of copper and more than 95% of both nickel and cobalt were extracted, while iron dissolution was limited to only 0.8%.

Altundoğan et al. (2004) investigated the extraction characteristics of Cu, Co, Zn, and Fe from copper converter slag using an oxidative lixiviant containing potassium dichromate and sulfuric

acid. The results showed that dichromate had a significant effect on metal extraction. Copper recovery was notably high with this lixiviant, largely due to high Cu dissolution coupled with low Fe concentration in solution. Increasing dichromate concentration enhanced Cu extraction but markedly decreased the dissolution of Co, Zn, and Fe.

Beşe (2007) studied the dissolution behavior of copper from converter slag in sulfuric acid–ferric sulfate mixtures, both with and without ultrasound. Parameters investigated included reaction temperature, acid concentration, ferric sulfate concentration, and reaction time. The optimum conditions for maximum copper dissolution were: 65°C reaction temperature, 0.2 M acid concentration, 0.15 M ferric sulfate concentration, and 180 min reaction time. Under these conditions and with ultrasound, extraction efficiencies for copper, zinc, cobalt, and iron were 89.28%, 51.32%, 69.87%, and 13.73%, respectively. In the absence of ultrasound, the corresponding values were 80.41%, 48.28%, 64.52%, and 12.16%. These results clearly demonstrate that ultrasound enhances dissolution of Cu, Zn, Co, and Fe from slag.

A study on the recovery of copper, cobalt, nickel, and zinc from copper converter slag by roasting with ferric sulfate was reported by Altundoğan and Tümen (1997). Converter slag was roasted with ferric sulfate and subsequently leached with water to dissolve the metal values. At 500°C, 120 min roasting time, and a ferric sulfate/slag ratio of 1, recoveries were approximately 93% Cu, 38% Co, 13% Ni, and 59% Zn. Higher ferric sulfate/slag ratios improved Cu and Zn extraction, whereas Co and Ni could not be recovered at acceptable levels. Using H_2SO_4 in the leaching step significantly improved metal recoveries.

Khalid et al. (2019) investigated a hydrometallurgical method for recovering copper from copper-rich converter slag. The primary copper-bearing phases identified were cuprite, delafossite, and metallic copper. The effects of particle size, temperature, acid concentration, agitation, and leaching time under oxidizing conditions were evaluated. Under optimum conditions: 40°C, 2 M H_2SO_4, 60 min leaching time, 0.26 kW/m^3 mixing power, and 2000 mL/min oxygen flow, approximately 100% of the copper was extracted. XRD analysis confirmed the absence of Cu-containing phases in the leach residue. The results also indicated that temperatures ≤40°C had a strong influence on Cu and Fe extraction, while temperatures >40°C favored Ni and Zn dissolution. Acid consumption under optimized conditions was 23.7 mol H_2SO_4 per kg Cu.

5. COPPER REFINNING SLAGS

A significant amount of copper is lost during the refining process, and slags produced in copper refining furnaces may contain as much as 1-13% Cu if process parameters and other factors influencing copper losses are not optimized (Soroush, 1992). In an earlier study, Soroush (1992) conducted a series of experiments on the recovery of copper from Sarkuysan fire-refining slags. The results were analyzed to determine the optimum conditions for controlling factors responsible for copper losses and for identifying processing conditions that minimize copper retention in slags.

Another study investigated the recovery of copper from the same Sarkuysan refining slags using a pyro-hydrometallurgical method involving sodium sulfate roasting followed by sulfuric acid leaching; however, only 65% Cu recovery was achieved (Yıldız et al., 2000). In a subsequent investigation using the same slags, Arslan et al. (2002) conducted size reduction, flotation, and leaching tests to improve the recoveries of Cu and Sn. Chemical analysis showed that the slag contained approximately 22% Cu and 2.3% Sn. Microscopic examinations revealed that some heavy metals (Pb, Sn, Bi, Sb, As) were encapsulated within metallic copper, particularly in acidic slags, while others were incorporated into the silicate matrix. Size reduction, classification, and flotation produced a concentrate containing 49.67% Cu and

1.69% Sn, with recovery efficiencies of 81.12% for Cu and 27% for Sn. This concentrate could be recycled in copper production. All remaining Cu and Sn in the flotation tailings were leached with HCl. Overall, the study demonstrated that both Cu and Sn in copper refining slags can be efficiently recovered, marking a successful recycling approach.

6. CONCLUSION

This review summarizes and critically evaluates the properties of copper slags generated during smelting, converting, refining, and ancient metallurgical activities, together with the processes developed for the recovery of valuable metals from these materials. Emphasis is placed on the influence of slag composition, mineralogy, and formation conditions on process selection and metal recovery efficiency. The reviewed studies collectively illustrate the evolution of slag-treatment strategies, from early pyrometallurgical approaches to increasingly integrated, selective, and environmentally conscious recovery flowsheets. Furthermore, by compiling and discussing studies conducted on copper slags originating from industrial operations and historical deposits in Türkiye, this paper highlights the significant potential of these materials as secondary metal resources. Overall, the reviewed literature demonstrates that copper slags can play an important role in sustainable metallurgy and circular-economy frameworks when appropriately characterized and processed, and it underscores the need for further integration of resource efficiency and environmental considerations in future slag valorization strategies.

REFERENCES

Açma, E., Sesigür, H., Addemir, O., Tekin, A., (1997) “Processing of Küre (Turkey) copper slag for the recovery of copper and cobalt and the production of γ Fe_2O_3”, Transactions of the Indian İnstitute of Metals, 2-3 147-151.

Açma, E., Toy, Ç., Addemir, O., Tekin, A., (1992) “Beneficiation of copper slag for the production of magnetic oxide”, Conference Recycling Metals; Düsseldorf/Neuss, Germany.

Akhmedov, M., (2024) “Research on the extraction of copper and other metals from copper slags using sulfuric acid leaching”, Acta of Turin Polytechnic University in Tashkent, 14 (2) 7–12.

Alam, S., Tolibov, B., Akhmedov, M., Khujamov, U., Yarlakabov, S., (2025) “Enhanced extraction of valuable metals from copper slags by disrupting fayalite and spinel structures using sodium sulfate”, Minerals, 15 (8) 771.

Altundoğan, H. S., Tümen, F., (1997) “Metal recovery from copper converter slag by roasting with ferric sulfate”, Hydrometallurgy, 44 (1) 261-267.

Altundogan, H. S., Boyrazli, M., Tumen, F., (2004) “A study on the sulphuric acid leaching of copper converter slag in the presence of dichromate”, Minerals Engineering, 17 465–467.

Anand, S., Rao, K. S., Jena, P. K., (1983) “Pressure leaching of copper converter slag using dilute sulphuric acid for the extraction of cobalt, nickel and copper values”, Hydrometallurgy, 10 (3) 305-312.

Arslan, C., Arslan, F., (2002) “Recovery of copper, cobalt, and zinc from copper smelter and converter slags”, Hydrometallurgy, 67 (1-3) 1-7.

Arslan, F., Giray K., Onal G., Gürkan V., (2002) “Development of a flowsheet for recovering Copper and Tin from copper refining slags”, The Europan Journal of Mineral Processing and Environmental Protection, 2 94-102.

Banza, A. N., Gock, E., Kongolo, K., (2002) “Base metals recovery from copper smelter slag by oxidising leaching and solvent extraction”, Hydrometallurgy, 67 (1-3) 63-69.

Beşe, A. V., (2007) “Effect of ultrasound on the dissolution of copper from copper converter slag by acid leaching”, Ultrasonics Sonochemistry, 14 790–796.

Bourgarit, D., (2019), Mineralogy of Slags: A Key Approach for our Understanding of Ancient Copper Smelting Processes: The Contribution of Mineralogy to Cultural Heritage.

Bulut, G., (2006) “Recovery of copper and cobalt from ancient slag”, Waste Management & Research, 24 118-124.

Bulut, G., Perek, K. T., Gül, A., Arslan, F., Önal, G., (2007) “Recovery of metallic values from copper slags by flotation and roasting with pyrite”, Mining, Metallurgy and Exploration, 24 (1) 13-18.

Dzinomwa, G., Mapani, B., Manyepa, K., Nyaoro, T., Kakulu, J. T., Andreasen, M., Chingwaru, K., (2023). “Mineralogical characterization of historic copper slag to guide the recovery of valuable metals: A Namibian case study”, Materials, 16 (18) 6126.

Ettlinger, V., (2020) “Cost–benefit analysis of historical copper slags and tailings: A case study from Boliden Rönnskär Smelter in Skelleftehamn”, Master’s Thesis, Department of Economics, Swedish University of Agricultural Sciences.

Phiri, T. C., Singh, P., Hara, Y. S., Siame, J., Nikoloski, A. N., (2025) “Carbothermic reduction of copper slag in the presence of borax”, Mineral Processing and Extractive Metallurgy Review, 46(2) 165-176.

Potysz, A., Kierczak, J., (2019) “Prospective (bio)leaching of historical copper slags as an alternative to their disposal”, Minerals, 9 (9) 542.

Potysz, A., Kierczak, J., Fuchs, Y., Grybos, M., Gilles Guibaud, G., Lens, P. N. L., (2016) “Characterization and pH-dependent leaching behaviour of historical and modern copper slags”, Journal of Geochemical Exploration, 160 1-15.

Sesigür, H., Açma, E., Addemir, O., Tekin, A., Ekinci, E., (1995) “Utilisation of copper slags for chemicals production, cleaner technologies and cleaner products for sustainable development”, NATO ASI Series, 2 351–357.

Seyrankaya, A., Canbazoğlu, M., (2021) “Recovery of cobalt, copper and zinc from kure-kastamonu historical copper slag by high pressure oxidative acid leaching”, Russian Journal Of Non-Ferrous Metals, 62 (4) 390-402.
Shen, H., Forssberg, E., (2003) “An overview of recovery of metals from slags”, Waste Management, 23 (10) 933-949..

Soroush, S., (1992) “Recovery of copper from fire refining slags”, Master’s Thesis, Metallurgical Engineering, Graduate School of Natural and Applied Sciences, Middle East Technical University.

Tegin, İ., Ziyadanoğulları, R., (2018) “Recovery of copper and cobalt from converter slag with a new flotation method using H_2S”, Journal of Environmental Science and Engineering A, 7 69-75.

Topkaya, Y. A., (1990) “Extraction of Co and Cu from historical slags of Küre”, ATB Metall, 30(1 2) (23) 8.

Wang, L., Xu, Y., Tian, L., Chen, Y., Yang, A., Gan, G., Ma, Y., Du, Y., (2024) “Two-stage method recovery of metals from copper slag: Realize the resource utilization of all components”, Minerals Engineering, 206 108503.

Yang, Z., Rui-lin, M., Wang-dong, N., Hui, W., (2010) “Selective leaching of base metals from copper smelter slag”, Hydrometallurgy, 103 (1-4) 25-29.

Yücel, O., Addemir, O., Tekin, A., Nizamoglu, S., (1992) “Recovery of cobalt from copper slags”, Mineral Processing and Extractive Metallurgy Review, 10 (1) 99–107.

Yıldız K., Alp A., Aydın A. O., (2000) “Utilization of copper refining slags by a pyro-hydrometallurgical method”, 10th International Metallurgy and Material Congress, 127-132.

RESEARCH ON FACTORS INFLUENCING HIGH FUEL CONSUMPTION IN ROTARY KILNS

Zarife BAJRAKTARI GASHI, Mimoza KOVAÇI AZEMI*

University ''Isa Boletini'' Mitrovica, Faculty of Geoscience, Department Materials and Metallurgy, St.Ukshin Kovaçica 40 000, Mitrovica, Republic of KOSOVO
**Corresponding author: mimoza.kovaci@umib.net*

A B S T R A C T

This study examines fuel consumption during the preparation of calcines in rotary kilns used for ferronickel production. Due to the low nickel content of the processed ore, a high energy input is required, which is supplied through a combination of fuels, including lignite, coal, petroleum coke, biomass, coal-derived steam, and heavy fuel oil. The diversity of fuel sources reflects the effort to meet the thermal demands of calcination and pre-reduction under varying operational conditions.

An analysis of operational data collected between 2010 and 2019 reveals significant discrepancies between planned and actual fuel consumption. While planned fuel usage was approximately 4%, actual consumption frequently exceeded 13%. In addition, the target temperatures required for effective calcination and pre-reduction were often not reached, indicating notable process inefficiencies. These deviations point to limitations in energy utilization and highlight challenges in maintaining stable thermal conditions within the rotary kilns.

The study identifies several key factors influencing kiln temperature, pre-reduction efficiency, and overall fuel consumption, including fuel quality, ore moisture content, and operational practices. Variations in these parameters have a pronounced impact on energy demand and the consistency of calcine quality. The findings emphasize the necessity for process optimization through improved control strategies and the implementation of more efficient combustion technologies. Addressing these inefficiencies can lead to reduced fuel consumption, lower operational costs, and decreased environmental impacts, thereby enhancing the sustainability and economic performance of rotary kiln operations in ferronickel production.

Key words: *Calcine, rotary kilns, fuel*

Graphical abstract

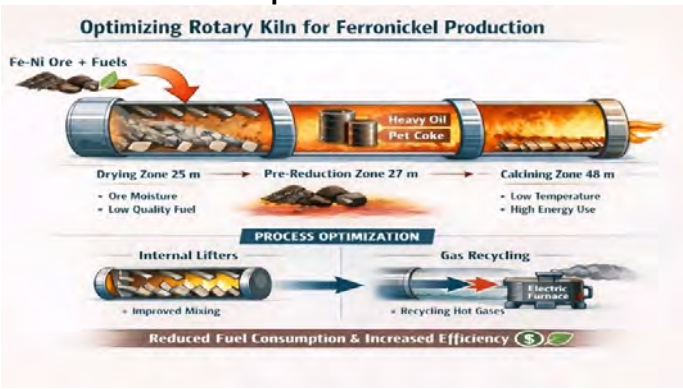

1.INTRODUCTION

The Ferronikeli smelter in Drenas is located near the “Old Çikatove” source, approximately 37 km northwest of Prishtina. Metallurgical production in the Republic of Kosovo has historically been oriented toward the processing of locally mined lateritic ores from Golesh and Çikatove, while since 2007 the production has been supplemented with imported ores from Indonesia,

the Philippines, Guatemala, Albania, North Macedonia, and Turkey (Bajraktari-Gashi, 2012; Official Documentation, 2009–2019; Bajraktari-Gashi, 2022).

Ore processing is carried out through an electro-reduction route, with ferronickel (FeNi) as the final product, following technological schemes developed and optimized through extensive industrial and experimental research (Gashi et al., 2011; Bajraktari-Gashi, 2012). The core technological units of the smelter consist of two rotary kilns manufactured by Schmid (Copenhagen), two electric furnaces supplied by Elkem (Oslo), and two LD converters produced by Krupp (Düsseldorf), forming an integrated production line for ferronickel manufacturing (Bajraktari-Gashi and Halilaj, 2018).

Within this production route, the rotary kilns play a critical role in ore drying, calcination, and pre-reduction, directly influencing energy efficiency and downstream smelting performance (Gashi et al., 2011; Gashi and Gashi, 2013). This study focuses on fuel consumption during the preparation of calcines in the rotary kilns. The relatively low nickel content of the processed ores necessitates high thermal energy input, which is supplied through a diverse fuel mix including lignite, coal, petroleum coke, biomass, coal-derived steam, and heavy fuel oil (Bajraktari-Gashi et al., 2015; Bajraktari-Gashi and Zabeli, 2018).

Analysis of operational data from 2010 to 2019 reveals significant discrepancies between planned fuel consumption, estimated at approximately 4%, and actual fuel consumption, which frequently exceeded 13% (Official Documentation, 2009–2019; Bajraktari-Gashi, 2022). Moreover, the target temperatures required for effective calcination and pre-reduction were often not achieved, indicating notable process inefficiencies. Key factors affecting kiln temperature stability and pre-reduction efficiency include fuel quality, ore moisture content, and operational practices, as previously demonstrated through experimental, modeling, and industrial-scale investigations (Gashi et al., 2013; Bajraktari-Gashi and Zabeli, 2017).

Variations in these parameters strongly influence both energy consumption and the uniformity of calcine quality. The findings underline the necessity for process optimization through improved control strategies and the application of more efficient combustion technologies, which can reduce fuel consumption, lower operational costs, and mitigate environmental impacts associated with excessive fuel usage (Bajraktari-Gashi et al., 2018; Rong et al., 2017). By systematically addressing these inefficiencies, the present study provides practical insights for enhancing the sustainability and economic performance of rotary kiln operations in ferronickel production (Rong et al., 2017).

2. MATERIAL AND METHODS

2.1. Material

This study is based on industrial and experimental investigations conducted at the Ferronickel production plant in Drenas, Republic of Kosovo, focusing on fuel consumption and thermal efficiency during the preparation of calcines in rotary kilns. Lateritic nickel ores with relatively low nickel content were processed, requiring high energy input to achieve effective calcination and pre-reduction, as previously reported by Bajraktari-Gashi (2012). The nickel ores were supplied in a wet condition, with variable moisture content depending on ore origin and operational conditions. Elevated moisture levels increased the thermal demand of the process and strongly influenced kiln temperature profiles and pre-reduction efficiency, in agreement with earlier experimental findings (Gashi et al., 2014). Thermal energy was supplied using a multi-fuel system, including lignite, coal, petroleum coke (pet coke), biomass, coal-derived steam, and heavy fuel oil. The influence of fuel type and calorific value on kiln performance and fuel substitution strategies has been extensively analyzed in previous studies conducted at the same facility (Bajraktari Gashi et al., 2015).

The graphical representation indicates that during the period 2010–2019, the consumption of fuels in the ferronickel calcine (firing) production process in rotary kilns remained relatively stable (Fig.1) In the years 2010–2011, fuel utilization shows an almost constant level, while a decrease in fuel consumption is observed during 2014–2015. In 2016, an increase in fuel usage is recorded, followed by a continuous decline throughout 2017–2018. In 2019, fuel consumption exhibits a slight increase again (Bajraktari Gashi, 2023).

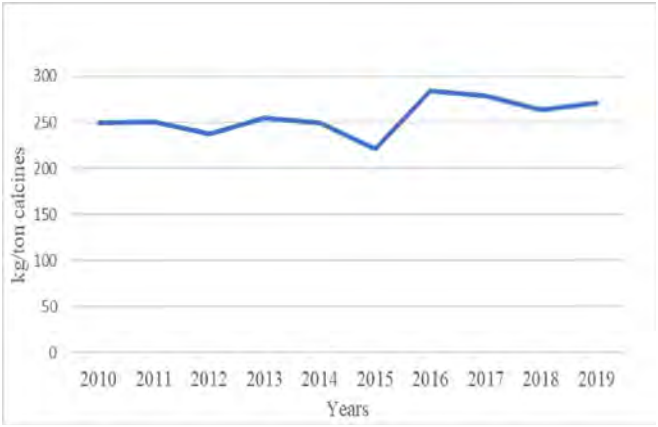

Figure 1. Average Fuel Consumption in Rotary Kilns during 2010–2019

Figure 2 presents the amount of iron–nickel ore consumed in rotary kilns during the analyzed period (2010–2019). The results reveal pronounced annual fluctuations, with higher consumption levels recorded in the early years and in 2015, while substantial decreases are observed in 2016 and 2018, mainly due to production interruptions and operational inefficiencies in the rotary kiln process (Bajraktari-Gashi, 2023).”

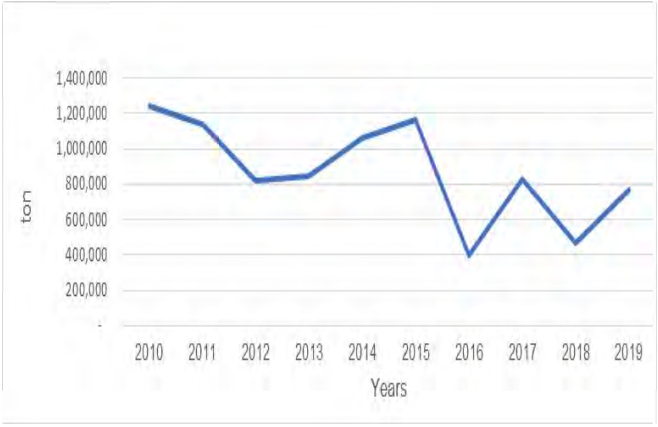

Figure 2. The industrial data on ore consumption in the rotary furnace process over the analyzed years

The average annual fergese production from the two rotary kilns is about 620 thousand tons, showing considerable year-to-year variability. These fluctuations are mainly associated with production interruptions and operational inefficiencies, with the most pronounced reductions observed in 2016 and 2018.

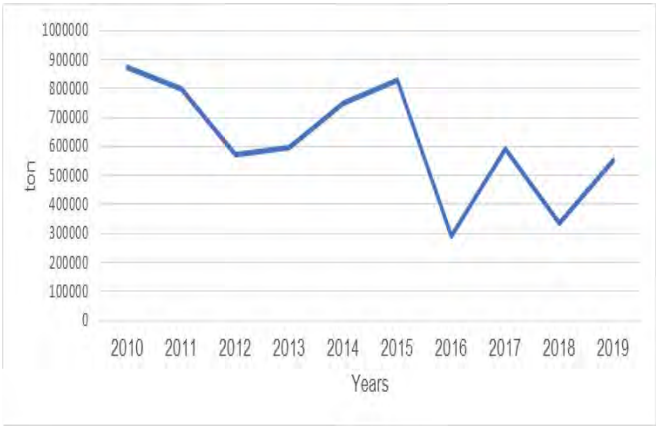

Figure 3. The average production of the calcine during the analyzed years

3.RESULTS AND DISCUSSION

Frequent production interruptions caused by technological and operational problems in the processing line, as observed during the analyzed period (Fig. 1 and Fig. 2), particularly in 2012, 2016, and 2018, had a significant negative impact on the performance of the rotary kilns. During these years, the kilns were out of operation for several months due to plant-related issues. Such operational inefficiencies resulted in unstable kiln operation and led to increased specific fuel consumption per ton of calcine produced. Based on the graphical analysis of iron–nickel ore characteristics, calcine production, and fuel consumption during the period 2010–2019, several key observations can be made. The high moisture content of the ore, frequently reaching approximately 28%, substantially increases the energy demand required for drying and pre-treatment stages.

As a consequence, higher amounts of fuel are required to achieve and maintain the necessary process temperatures inside the rotary kilns. In addition, the relatively low nickel content of certain Fe–Ni ores, particularly those originating from Kosovo (1.05% Ni) and Albania (0.99% Ni), results in lower metal recovery rates and necessitates the processing of larger ore quantities to achieve the desired ferronickel output. Combined with frequent production interruptions caused by ore quality variability and operational inefficiencies, this leads to non-continuous kiln operation and a further increase in specific fuel consumption per ton of calcine. Moreover, insufficient temperature attainment within the rotary kilns, mainly due to the high moisture content of the feed material, requires the introduction of excessive amounts of fuel. This excessive fuel input not only increases overall energy consumption but also negatively affects the quality of the calcine, which in turn impacts the metallurgical quality and yield of ferronickel. Therefore, process optimization measures, particularly focused on ore pre-drying, moisture control, and stabilization of kiln operation, are essential to reduce fuel consumption, improve calcine quality, and enhance the overall efficiency of the ferronickel production process.

The analysis (Fig.3) of industrial data for the period 2010–2019 reveals a strong correlation between iron–nickel ore consumption and calcine production in rotary kilns. Variations in ore input are directly reflected in calcine output, confirming the dependence of production performance on raw material throughput. Significant reductions in both ore consumption and calcine production are observed in 2012, 2016, and 2018, corresponding to periods of operational interruptions and reduced kiln stability (Bajraktari Gashi and Kovaçi Azemi, 2025). Despite the lower production levels recorded in these years, the specific fuel consumption per ton of calcine increased markedly, reaching its highest values in 2016 and remaining elevated thereafter. This trend indicates inefficient energy utilization under unstable operating conditions. The increase in specific fuel consumption is primarily associated with non-

continuous kiln operation, high moisture content of the ore, and difficulties in maintaining optimal thermal regimes within the rotary kilns. Overall, the results demonstrate that increased fuel consumption is not linked to higher production rates, but rather to process instability and unfavorable raw material characteristics. These findings highlight the critical impact of operational continuity and feed quality on energy efficiency and calcine yield in ferronickel production.

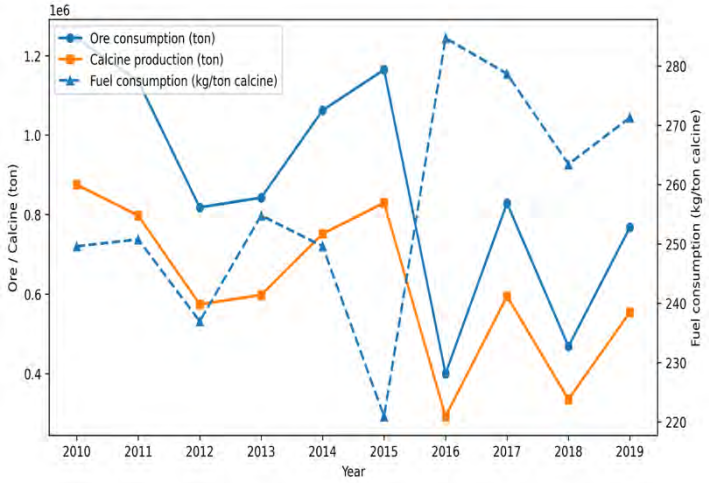

Figure 4. Comparative trends of ore consumption, calcine production, and specific fuel consumption in rotary kilns over the period 2010–2019

4.CONCLUSION

The analysis confirms that improving energy efficiency in rotary kilns is primarily dependent on targeted process optimization rather than increased fuel input. Pre-drying of the Fe–Ni ore is essential to reduce the high moisture content of the feed, thereby lowering the energy demand for drying inside the kiln and stabilizing the thermal regime. In parallel, the optimized installation of internal lifters (blades) within the rotary kilns can significantly enhance heat transfer and material–gas contact, ensuring more uniform heating and improved calcine quality.
Furthermore, the recovery and recirculation of off-gases from the electric furnace to the rotary kilns represents an effective measure for utilizing waste heat, reducing overall fuel consumption, and improving process sustainability. The combined implementation of ore drying, improved kiln internals, and gas recirculation can substantially decrease specific fuel consumption, enhance operational stability, and increase the overall efficiency of the ferronickel production process.

REFERENCES

Bajraktari-Gashi, Z., (2012) “Theoretical and experimental research in order to reach optimum technical, technological and productive parameters during qualitative reduction of Ni ore in Fe–Ni foundry in Drenas”, PhD Dissertation, University ‘’Isa Boletini’’ Mitrovica, Republic of Kosovo.

Bajraktari-Gashi, Z., (2023), Nickel and ferronickel production in Drenas: University textbook, Mitrovica.

Bajraktari-Gashi, Z., Halilaj, B., (2018) “Material balance of the technological process in the new foundry of New Ferronikel in Drenas during 2017”, Journal of Technology and Exploitation in Mechanical Engineering, 4 (1) 29–35.

Bajraktari-Gashi, Z., Kovaçi Azemi, M., (2025) “Environmental and health impacts of lignite dust pollution: a case study of heavy metal emissions in Kosovo”. Revue Roumaine de Chimie, 70 (3–4) 197–204.

Bajraktari-Gashi, Z., Maksuti, R., Murati, N., (2015) “The usage of pet-coke as a possibility of reducing the amount of heavy oil in rotary kilns in the new foundry of Ferronikel in Drenas”, Applied Mechanics and Materials, 749 111–115.

Bajraktari-Gashi, Z., Zabeli, M., (2017) “Factors affecting the increase in the pre-reduction scale of Fe–Ni ore in rotary kilns”, Journal of International Environmental Science, 12 52–58.

Bajraktari-Gashi, Z., Zabeli, M., Halilaj, B., (2018) “The impact of pet-coke on the technological process of Fe–Ni production in the new Ferronikel foundry in Drenas”, Journal of International Environmental Science, 13.

Gashi, Z., Gashi, I., Rama, M., (2013) “Mathematical modeling of nickel ore pre-reduction simulations in a laboratory rotary kiln (Linder)”, International Journal of General Engineering and Technology, 2 (3) 17–28.

Gashi, Z., Imeri, Sh., Lohja, N., Zabeli, M., Tahiraj, N., Murati, N., (2011) “Experimental research on pre-reduction of nickel silicate ore in the New Ferronikel Factory in Drenas”, Proceedings of the WSEAS and NAUN Conferences, 306–311.

Gashi, Z., Imeri, Sh., Tahiraj, N., (2011) “Kosovo dry lignite treatment in the process of ore frying in the smelter of New Co Ferronikel in Drenas” Proceedings of the 11th International Multidisciplinary Scientific GeoConference (SGEM 2011), 1125–1129.

Official documentation of the melting complex of New Ferronikeli Complex L.L.C., Gllogoc, operational data for the period 2009–2019.

Rong, W., Li, B., Liu, P., Qi, F., (2017) “Exergy assessment of a rotary kiln–electric furnace smelting process for ferronickel alloy”, Energy, 138 942–953.

SELECTIVE EXTRACTION OF LANTHANUM, NEODYMIUM AND PRASEODYMIUM FROM SYNTHETIC LEACH SOLUTION USING PC-88A/TBP SYSTEM

Esra BAŞTÜRKCÜ*, Norman KELLY, A. Ekrem YÜCE, Servet İ. TİMUR

[1]Istanbul Technical University, Mining Faculty, Mineral Processing Engineering Department, 34463, ISTANBUL-TURKIYE
[2]Helmholtz-Zentrum Dresden-Rossendorf, Helmholtz Institute Freiberg for Resource Technology, Chemnitzer Strasse 40, 09599 FREIBERG, GERMANY
[3]Istanbul Technical University, Chemistry-Metallurgy Faculty, Material and Metallurgical Engineering Department, 34467, ISTANBUL-TURKIYE
**Corresponding author: tanisali@itu.edu.tr*

A B S T R A C T

The mutual separation of lanthanum (La), neodymium (Nd), and praseodymium (Pr) by solvent extraction is inherently challenging due to their nearly identical ionic radii and similar chemical properties. The use of phase modifiers such as tributyl phosphate (TBP) in combination with cationic extractants has been widely adopted to improve phase disengagement, increase metal loading capacity, and enhance separation selectivity in rare earth element (REE) processing. This study investigated the solvent extraction behavior of La, Nd, and Pr from synthetic aqueous solutions using a PC-88A/TBP (2-ethylhexyl phosphoric acid / tributyl phosphate) binary extractant system in kerosene. The effects of initial pH, total extractant concentration, and PC-88A:TBP molar ratio on extraction efficiency were systematically evaluated. Results demonstrated that Nd and Pr are selectively extracted over La under all tested conditions. Increasing pH from 1 to 3 and total extractant concentration from 10% to 30% (v/v) significantly enhanced Nd and Pr extraction efficiencies, reaching approximately 62% and 54%, respectively, while La extraction remained below 9% across all conditions. Furthermore, increasing the proportion of TBP relative to PC-88A was found to suppress overall extraction efficiencies for all three elements, with loading yields declining progressively as the TBP content increased. This behavior suggests that TBP, while improving phase characteristics, competes with or dilutes the active PC-88A sites responsible for metal complexation, thereby reducing the net extraction capacity of the organic phase.

Key words: *Solvent extraction, PC-88A, TBP, rare earth elements, lanthanum, neodymium, praseodymium, selective separation*

1. INTRODUCTION

Rare earth elements (REEs) are a group of 17 chemically similar metals that are indispensable in a wide range of modern technologies, including permanent magnets, electric vehicle motors, wind turbines, and various electronic devices. Among these, neodymium (Nd) and praseodymium (Pr) are of particular industrial significance due to their critical role in the production of NdFeB permanent magnets, while lanthanum (La) finds applications in catalysts and optical glasses. The global demand for these elements continues to grow, driven by the accelerating transition toward clean energy technologies.(Binnemans et al., 2013; Balaram, 2019).

The mutual separation of La, Nd, and Pr by hydrometallurgical methods is inherently difficult due to their nearly identical ionic radii and chemical behavior arising from the lanthanide contraction (Xie et al., 2014). Among the available separation techniques, solvent extraction has long been established as the most scalable and commercially viable method for the processing of REE-bearing leach solutions (Hidayah and Abidin, 2018). A typical solvent extraction system comprises three main components: an extractant responsible for selective

metal complexation, a diluent that dissolves the extractant and controls phase viscosity, and a modifier that improves phase disengagement and prevents the formation of a third phase (Xie et al., 2014). Among extractant classes, acidic organophosphorus compounds have been most widely employed for REE separation due to their high selectivity, chemical stability, and compatibility with industrial-scale processes (Hidayah and Abidin, 2018). PC-88A (2-ethylhexylphosphonic acid mono-2-ethylhexyl ester, also known as EHEHPA or P-507) is one of the most important representatives of this group for REE applications. Compared to the closely related D2EHPA, PC-88A offers a higher selectivity between adjacent lanthanides and allows stripping of loaded metals at lower acid concentrations, making it particularly advantageous for industrial rare earth separation circuits (Xie et al., 2014; Lee et al., 2005).

PC-88A operates via a cation-exchange mechanism in which protons are released from the dimeric extractant upon complexation with trivalent REE ions. Several studies have employed PC-88A or its structural analogue EHEHPA for the separation of light REEs including La, Nd, and Pr. Lee et al. investigated the extraction of Nd(III) from hydrochloric acid solutions using PC-88A and saponified PC-88A, demonstrating that pH and saponification degree strongly influence both extraction efficiency and stripping behavior (Lee et al., 2005). Agarwal et al. studied the co-extraction of La, Ce, Nd, and Pr from monazite leach solutions using PC-88A and reported high inter-element separation factors, with βNd/La and βPr/La values reaching up to 72 and 98, respectively, at pH 3.5 (Agarwal et al., 2018). Tributyl phosphate (TBP) is a neutral organophosphorus modifier widely employed in REE solvent extraction systems to suppress third-phase formation, reduce organic phase viscosity, and improve phase separation kinetics; in some systems, TBP also participates directly in the solvation of the extracted complex (Dashti et al., 2021; Swain et al., 2015).

Dzulqornain et al. compared several binary extractant systems including PC-88A/TBP for the selective isolation of light REEs (La, Ce, Nd, Pr, Sm) from chloride solutions, showing that TBP addition to PC-88A improved phase disengagement and modified the extraction order among lanthanides (Dzulqornain et al., 2025).

However, to the best of the authors' knowledge, the systematic influence of the PC-88A:TBP molar ratio on extraction efficiency and selectivity for the La/Nd/Pr ternary system in sulfate medium has not been previously reported. The present study addresses this gap by evaluating the effects of initial pH, total extractant concentration, and PC-88A:TBP molar ratio on extraction efficiency and selectivity for La, Nd, and Pr from a synthetic sulfate leach solution.

2. MATERIALS AND METHODS

2.1. Reagents and Solutions

Synthetic aqueous feed solutions were prepared by dissolving analytical-grade La_2O_3, Nd_2O_3, and Pr_6O_{11} in dilute sulfuric acid (H_2SO_4), yielding a mixed REE sulfate solution. The initial metal concentrations in the feed solution were approximately 6380 mg/L La, 1400 mg/L Nd, and 800 mg/L Pr, representing a simplified synthetic pregnant leach solution (PLS). Solution pH was adjusted to the desired values using dilute H_2SO_4 and sodium hydroxide (NaOH) solutions

PC-88A and tributyl phosphate were used as received. Kerosene (technical grade) was used as the organic diluent. Extractant solutions were prepared at total concentrations of 10%, 20%, and 30% (v/v) in kerosene, with PC-88A:TBP molar ratios of 1:1, 2:1, 3:1, and 4:1.

2.2. Extraction Experiments

Batch extraction experiments were conducted by contacting equal volumes of aqueous and organic phases (O:A = 1:1, v/v) in 50 mL polypropylene centrifuge tubes. Mixtures were agitated at 300 rpm on a mechanical shaker for 10 minutes at 20 ± 1°C, a contact time previously confirmed to be sufficient for equilibrium. Following phase separation by centrifugation (3000 rpm, 5 min), both phases were collected and analyzed. Initial and equilibrium pH values were measured using a calibrated pH meter.

Metal concentrations in the aqueous phases before and after extraction were determined by inductively coupled plasma optical emission spectrometry (ICP-OES; [Instrument Model]). Organic phase metal concentrations were calculated by mass balance. All experiments were performed in duplicate, and the mean values are reported. The extraction efficiency (E, %), distribution coefficient (D), and separation factor (β) were calculated as follows (equation 1,2,3):

$$E\ (\%) = ([M]i - [M]eq) / [M]i \times 100 \quad (1)$$

$$D = [M]org / [M]aq = (E/100) / (1 - E/100) \quad (2)$$

$$\beta A/B = DA / DB \quad (3)$$

where [M]i and [M]eq are the initial and equilibrium metal concentrations in the aqueous phase, respectively, and DA and DB are the distribution coefficients of metals A and B.

The effects of three independent parameters were systematically investigated: initial solution pH (1, 2, 3, and 4), total extractant concentration (10%, 20%, and 30% v/v), and PC-88A:TBP molar ratio (1:1, 2:1, 3:1, and 4:1). Each parameter series was evaluated while keeping the remaining variables constant.

3. RESULTS AND DISCUSSION

3.1. Effect of Initial pH

The influence of initial pH on the extraction efficiency of La, Nd, and Pr is presented in Figure 1. Extraction efficiencies for all three elements increased monotonically with increasing pH over the range 1–4. At pH 1, extraction efficiencies were very low for all elements (La: 0.31%, Nd: 2.86%, Pr: 9.75%), consistent with the cation-exchange mechanism of PC-88A, in which higher proton concentrations suppress metal-extractant complex formation. As pH increased to 3, Nd and Pr extraction rose markedly to 35.4% and 31.5%, respectively, while La remained below 4%. Beyond pH 3, all extraction curves exhibited a plateau behavior, with only marginal improvement observed at pH 4 (Nd: 37.8%, Pr: 33.6%), suggesting that the system approaches equilibrium saturation under these conditions. pH 3 was therefore selected as the optimum initial pH for subsequent experiments, balancing extraction efficiency with operational practicality.

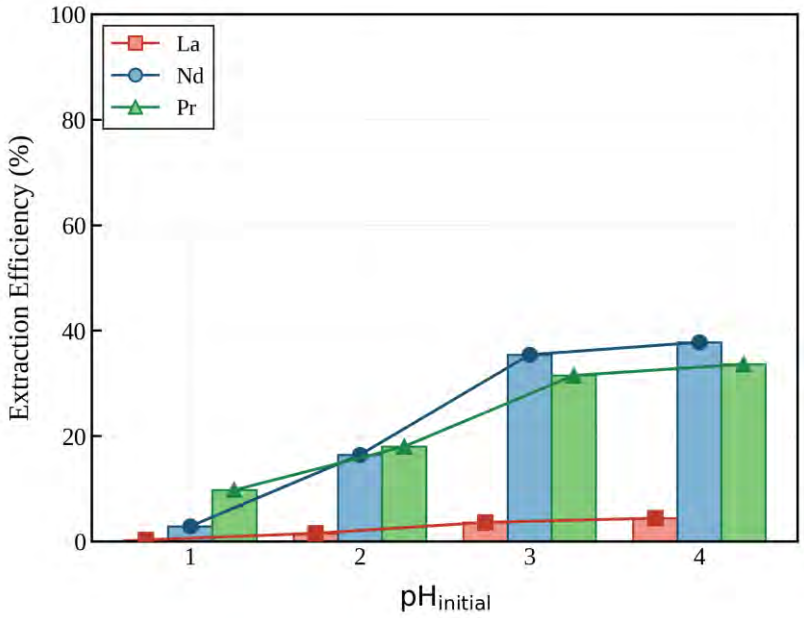

Figure 1. Effect of initial pH on extraction efficiency of La, Nd, and Pr. Conditions: [Ext.] = 10% (v/v), PC-88A:TBP = 2:1, O:A = 1:1, t = 30 min, T = 25°C.

3.2. Effect of Total Extractant Concentration

The effect of total extractant concentration (10–30%, v/v) on extraction efficiency at pH 3 and a PC-88A:TBP ratio of 2:1 is shown in Figure 2. Increasing the total extractant concentration from 10% to 30% resulted in substantial improvements in Nd and Pr extraction, from 36.9% to 58.2% and from 32.3% to 50.5%, respectively. In contrast, La extraction showed minimal response to concentration variation, remaining below 5% across the entire range. This differential response further reinforces the inherent selectivity of the PC-88A/TBP system for the heavier light REEs (Nd, Pr) over La.

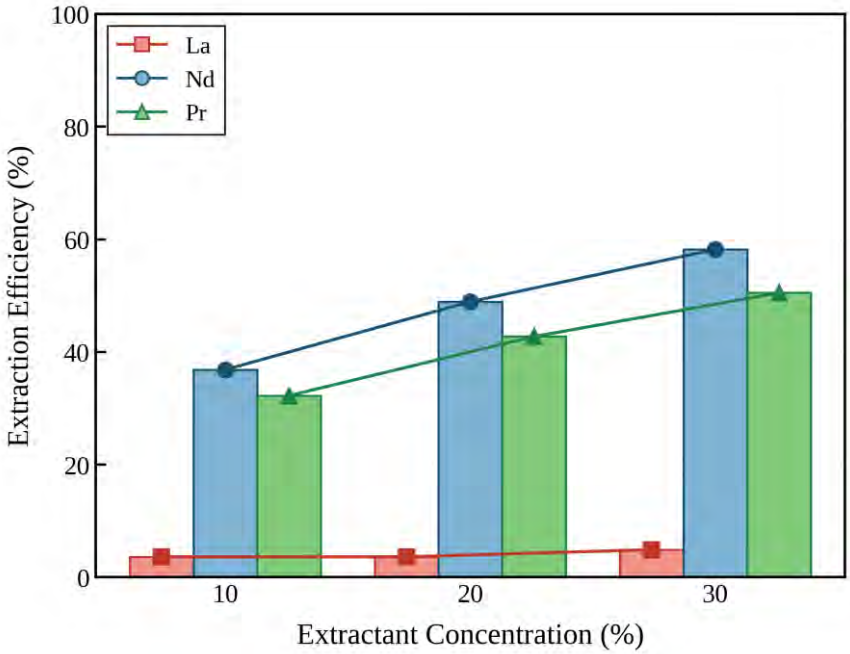

Figure 2. Effect of total extractant concentration on extraction efficiency of La, Nd, and Pr. Conditions: pH = 3, PC-88A:TBP = 2:1, O:A = 1:1, t = 30 min, T = 25°C.

3.3. Effect of PC-88A:TBP Molar Ratio

The influence of PC-88A:TBP molar ratio (1:1 to 4:1) on extraction efficiency at pH 3 and 30% total extractant concentration is illustrated in Figure 3. Increasing the PC-88A proportion consistently increased extraction efficiencies for all three elements. At a 1:1 ratio, Nd and Pr extraction reached 51.1% and 44.5%, respectively, which increased to 62.0% and 54.1% at a 4:1 ratio. La extraction also increased from 2.7% to 8.2% across the same range, though it remained substantially lower than the other two elements.

While higher PC-88A ratios improve overall extraction, a critical trade-off with selectivity was observed. The separation factor βNd/La decreased systematically from 37.9 at 1:1 to 18.2 at 4:1, and βPr/La decreased from 29.1 to 13.2 over the same range. This inverse relationship between extraction efficiency and selectivity is a well-known phenomenon in cation-exchange systems and arises because increasing the relative concentration of the cationic exchanger (PC-88A) raises the extraction of all metal ions, including the less-extractable La. Conversely, a higher TBP proportion (lower PC-88A:TBP ratio) appears to moderate the extraction of all elements but disproportionately suppresses La extraction, thereby enhancing selectivity. The 1:1 and 2:1 ratios therefore represent the most favorable conditions for achieving high La/Nd and La/Pr separation factors in this system.

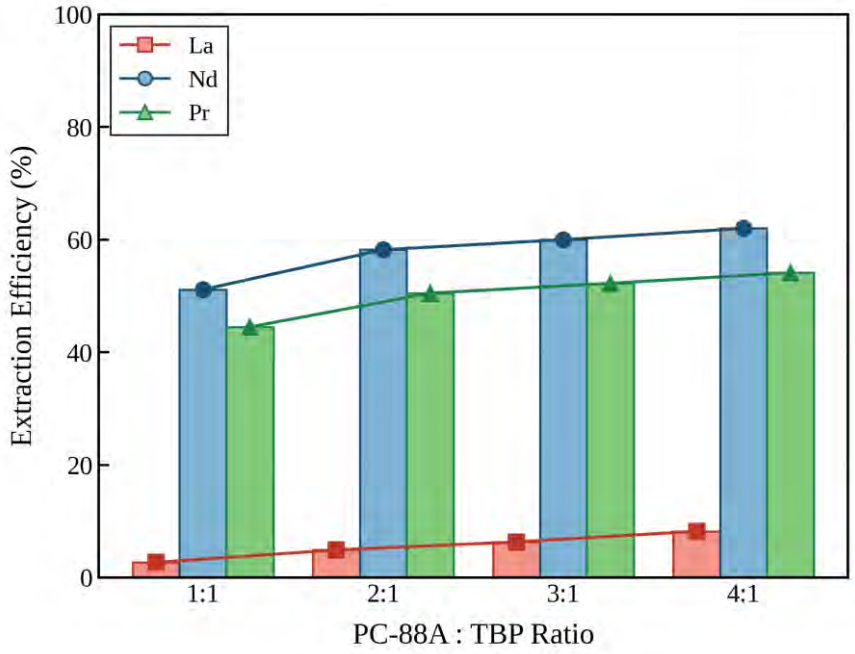

Figure 3. Effect of PC-88A:TBP molar ratio on extraction efficiency of La, Nd, and Pr. Conditions: pH = 3, [Ext.] = 30% (v/v), O:A = 1:1, t = 30 min, T = 25°C.

4. CONCLUSIONS

The extraction behavior of La, Nd, and Pr from synthetic leach solutions using the PC-88A/TBP binary extractant system in kerosene was systematically investigated as a function of initial pH, total extractant concentration, and PC-88A:TBP molar ratio. The following principal conclusions are drawn:

(1) The PC-88A/TBP system exhibits strong inherent selectivity for Nd and Pr over La under all tested conditions. La extraction remained consistently below 9%, while Nd and Pr extraction reached up to 62% and 54%, respectively, under optimized conditions.

(2) Increasing initial pH from 1 to 3 significantly enhanced Nd and Pr extraction, consistent with the cation-exchange mechanism of PC-88A. A plateau in extraction efficiency was observed above pH 3, establishing this as the optimal initial pH.

(3) Increasing total extractant concentration from 10% to 30% (v/v) substantially improved Nd and Pr extraction, whereas La showed minimal response, thereby improving overall selectivity at higher concentrations.

Future work will focus on stripping condition optimization, multistage extraction design via McCabe-Thiele analysis, and validation using real industrial PLS matrices toward a complete La/Nd/Pr separation flowsheet.

REFERENCES

Agarwal, V., Safarzadeh, M. S., Galvin, J., (2018) “Solvent extraction of La, Ce, Pr and Nd from monazite leach solutions using PC-88A”, Minerals Engineering, 126, 87–95.

Balaram, V., (2019) “Rare earth elements: A review of applications, occurrence, exploration, analysis, recycling, and environmental impact”, Geoscience Frontiers, 10 (4) 1285–1303.

Binnemans, K., Jones, P. T., Blanpain, B., Van Gerven, T., Yang, Y., Walton, A., Buchert, M., (2013) “Recycling of rare earths: A critical review”, Journal of Cleaner Production, 51, 1–22.

Dashti, A., Ahmadi Azqhandi, M. H., Foroughi, M. M., (2021) “Synergistic effect between Cyanex 572 and tributyl phosphate (TBP) in separating various light and heavy REEs”, Separation and Purification Technology, 276, 119366.

Dzulqornain, M. I., Mohamad Zin, N. H., Norlizah, I., Ab Aziz, N. A., (2025) “Solvent extraction systems for selective isolation of light rare earth elements with high selectivity for Sm and La”, Rare Metals, 44, 2345–2360.

Hidayah, N. N., Abidin, S. Z., (2018) “The evolution of mineral processing in extraction of rare earth elements using liquid–liquid extraction: A review”, Minerals Engineering, 121, 146–157.

Lee, M. S., Lee, J. Y., Kim, J. S., Lee, G. S., (2005) “Solvent extraction of neodymium ions from hydrochloric acid solution using PC88A and saponified PC88A”, Separation and Purification Technology, 46 (1–2) 72–78.

Swain, B., Otu, E. O., Lee, C. G., (2015) “Acidic organophosphorus extractants for REE solvent extraction: Classification, mechanisms and applications”, Hydrometallurgy, 156, 220–240.

Xie, F., Zhang, T. A., Dreisinger, D., Doyle, F., (2014) “A critical review on solvent extraction of rare earths from aqueous solutions”, Minerals Engineering, 56, 10–28.

SELECTIVE METAL LEACHING FROM SmCo PERMANENT MAGNETS

Mert SARIKAYA[1,*], Fatma Elif GENCELI GÜNER[2], Şükriye Beste AYDIN[1]

[1]Istanbul Technical University, Mining Faculty, Mineral Processing Engineering Department, 34469, Maslak, Istanbul, TÜRKİYE
[2]Istanbul Technical University, Chemical and Metallurgical Engineering Faculty, Chemical Engineering Department, 34469, Maslak, Istanbul, TÜRKİYE
Corresponding author: sarikayam19@itu.edu.tr*

A B S T R A C T

Samarium–cobalt (SmCo) magnets are high-performance rare-earth permanent magnets widely used in aerospace, high-temperature motors, sensors, and advanced magnetic systems due to their superior thermal stability and corrosion resistance. Owing to their high samarium and cobalt content, these materials also represent strategically important secondary resources. This study investigates the dissolution behavior of SmCo magnets in H_2SO_4, HNO_3, and HCl, with particular emphasis on selective SmCo recovery and the influence of temperature. Among the investigated acids, HNO_3 enabled nearly complete dissolution of Sm and Co but exhibited poor selectivity due to extensive co-dissolution of impurity elements. In contrast, H_2SO_4 provided a more selective dissolution environment, particularly limiting Sr dissolution due to sulfate-related precipitation effects. Temperature significantly enhanced the leaching of Co, Fe, and Zr in sulfuric acid, indicating kinetically controlled behavior; although Cu dissolution increased at elevated temperatures, the relative increase remained lower than that observed for Co, Fe, and Zr. Overall, sulfuric acid emerges as a promising leaching agent for selective Sm–Co recovery, provided that process parameters are optimized to balance recovery efficiency and impurity control. These findings contribute to the development of more efficient and sustainable hydrometallurgical recycling strategies for SmCo magnets.

Key words: *SmCo magnets, critical metals, hydrometallurgy, acid leaching*

1. INTRODUCTION

Rare earth elements (REEs) and cobalt (Co) are classified as critical raw materials due to their high economic importance and substantial supply risks within the global industrial landscape. As emphasized by Koen Binnemans et al. (2013), the limited primary reserves of these elements and the geographical concentration of their production in a small number of countries significantly increase supply vulnerability, thereby rendering the recycling of secondary resources progressively more strategic. In this context, the development of efficient and sustainable recovery technologies is essential to ensure long-term supply security and to facilitate the transition toward a circular economy.

Among rare-earth-based permanent magnets, SmCo alloys, particularly $SmCo_5$ and Sm_2Co_{17}, are distinguished by their superior magnetic performance, high coercivity, and exceptional thermal stability (Duerrschnabel et al., 2017). These intrinsic properties make SmCo magnets indispensable for high-performance applications, including aerospace systems, defense technologies, and electric vehicle powertrains, where alternative magnets such as NdFeB may exhibit performance limitations due to lower temperature resistance (Mengesha and Nagessar, 2025). The expanding utilization of SmCo magnets has consequently led to an increasing volume of end-of-life waste, presenting both environmental concerns and significant opportunities for resource recovery.

Hydrometallurgical methods are currently the most widely adopted approaches for recovering valuable metals from SmCo magnet waste. These processes generally involve an initial acid

leaching step followed by selective separation and purification stages. Strong inorganic acids such as HCl, H_2SO_4, and HNO_3 are commonly used as lixiviants; however, their leaching efficiencies depend strongly on alloy composition and process parameters. Papakci et al. (2024) implemented a sulfation–selective oxidation strategy for SmCo magnets, followed by water leaching, achieving 65% Sm dissolution while the leaching efficiencies of Fe, Co, and Cu remained negligible. Sinha et al. (2017) subjected SmCo magnets to roasting at 850 °C and subsequently performed leaching in 4 M HCl at 95 °C for 180 min with a pulp density of 100 g/L, resulting in complete metal dissolution. Emil-Kaya et al. (2024) applied oxidative leaching using 3 M HNO_3 at a solid–liquid ratio of 1:10 and 60 °C for 1 h, obtaining leaching efficiencies of 99% for Sm and Co while suppressing Fe dissolution (0%). Wang et al. (2023) investigated organic acid systems employing citric and malic acids; under optimized conditions, citric acid achieved leaching efficiencies of 87.62%, 93.82%, 97.10%, and 92.84% for Sm, Co, Fe, and Cu, respectively, whereas malic acid resulted in efficiencies of 75.18%, 74.58%, 82.42%, and 1.35% for the same elements.

In this context, the present study aims to establish an optimized recovery framework for SmCo magnet scrap through sulfuric acid leaching. The influence of key operational parameters, particularly acid selection and reaction temperature, will be systematically examined to elucidate their effects on metal dissolution efficiency and process selectivity. By integrating process optimization with sustainability considerations, this study proposes a technically robust and economically viable recovery strategy that improves metal recovery performance and promotes the circular utilization of critical rare-earth materials.

2. MATERIAL AND METHODS

2.1. Materials

The SmCo magnet samples were collected from MAGNETEKSAN A.Ş., a magnet-producing company located in Turkey. The samples were in powder form, so they did not require any demagnetization and size reduction processes. The particle size distribution of SmCo magnet powders was determined using a Malvern Mastersizer 3000. The particle size distribution of the magnet powders D_{10}, D_{50}, and D_{90} values were found to be 11.5, 27.0, and 57.1 μm, respectively, indicating a particle size distribution suitable for the leaching process. To determine the chemical composition of the magnet, the samples were subjected to a four-acid digestion method and subsequently analyzed by ICP. The results are presented in Table 1.

Table 1. Chemical composition of the SmCo magnet sample

Elements	Co	Fe	Sm	Cu	Zr	Sr	Ba	Total
wt%	44.92	29.08	17.35	4.22	2.41	1.82	0.19	100.00

2.2. Method

Leaching experiments were conducted in a 600 mL glass beaker containing 300 mL of a diluted acid solution under mechanical stirring with a temperature-controlled magnetic stirrer to dissolve the magnet powder. During leaching, sulfuric acid (H_2SO_4, 95–97% purity), nitric acid (HNO_3, 65% purity), and hydrochloric acid (HCl, 37% purity) were obtained from Merck (Darmstadt, Germany). At the end of the leaching process, solid–liquid separation was achieved by vacuum filtration, and the solid residue was thoroughly washed with deionized water to remove soluble salts, then dried at 90 °C for 2 h. De-ionized water (by Milli-Q brand) was used in different stages. All chemicals used in this study were of analytical grade.

The leaching efficiency of each metal was calculated using Eq. (1), where R_c and R_m represent the metal content in the residue and the mass of the residue, respectively, while M_c and M_m

denote the metal content and total metal mass in the feed material. To ensure data reliability and account for experimental variability, all experiments were conducted in duplicate.

$$\text{(Leaching efficiency) } L\ (\%) = \frac{R_c * R_m}{M_c * M_m} x100 \qquad (1)$$

To calculate the leaching efficiencies, the solid residues were subjected to a four-acid digestion method, and the resulting solutions were analyzed by inductively coupled plasma mass spectrometry (ICP-MS) using an Agilent 7800.

3. RESULTS AND DISCUSSION

3.1. Effect of Acid Type

The primary objective of this study was to evaluate the effect of acid type on the selective dissolution behavior of Sm and Co from SmCo permanent magnets. Leaching experiments were conducted using 1 M H_2SO_4, HNO_3, and HCl solutions under identical conditions (25 °C, solid-to-liquid ratio of 1:40, 2 h reaction time, and 250 rpm stirring). The obtained results are presented in Fig. 1. The findings demonstrate that the type of mineral acid significantly influences both dissolution efficiency and selectivity. In the H_2SO_4 medium, leaching efficiencies were determined as 99.17%, 52.52%, 27.51%, 26.53%, 0.10%, and 7.35% for Sm, Fe, Co, Zr, Cu, and Sr, respectively. The high dissolution efficiency of Sm, combined with the limited dissolution of Co, Cu, and Sr, indicates a relatively selective dissolution behavior toward Sm. The low dissolution of Sr in sulfuric acid is consistent with literature findings. Longbutsri et al. (2026) reported that during H_2SO_4 leaching of strontium ferrite magnet sludge ($SrFe_{12}O_{19}$), Sr dissolution remained limited and Sr ultimately precipitated as $SrSO_4$. This behavior can be attributed to the low solubility of $SrSO_4$ in sulfate media, which may also explain the limited Sr dissolution observed in the present study. However, although sulfuric acid exhibits promising selectivity characteristics, the moderate Co dissolution suggests that further optimization of process parameters may be required to achieve simultaneous high recovery of both target metals.

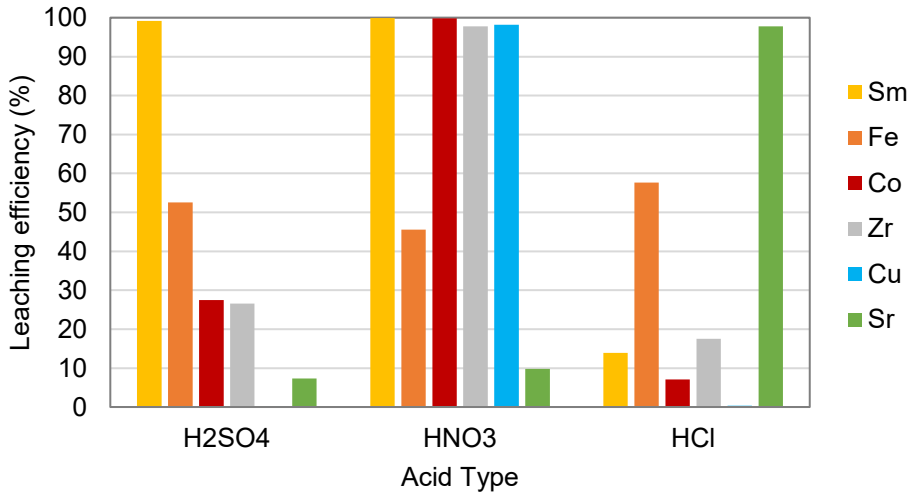

Figure 1. Leaching efficiencies of metals with different mineral acids

In the HNO_3 medium, leaching efficiencies reached 99.89% for Sm and 99.86% for Co. Similar high dissolution efficiencies were reported by Uysal et al. (2024), who achieved approximately 99% dissolution of Sm and Co during HNO_3 leaching of SmCo magnets under comparable conditions. While nitric acid ensures nearly complete dissolution of the target elements, the present results show that Zr and Cu were also extensively dissolved (>97%), indicating a

substantial loss of selectivity. This non-selective behavior can be attributed to the strong oxidative nature of nitric acid, which facilitates the oxidation and dissolution of multiple metallic phases within the alloy matrix. Conversely, the HCl system resulted in relatively low dissolution efficiencies for Sm (13.92%) and Co (7.08%), demonstrating insufficient leaching performance under the investigated conditions. Although Fe and Sr exhibited comparatively higher dissolution in hydrochloric acid, the recovery of the primary target elements remained limited. Overall, the results indicate that HNO_3 provides maximum dissolution efficiency for both Sm and Co but lacks selectivity, whereas H_2SO_4 offers a more selective dissolution environment, particularly for Sm, due in part to sulfate-mediated precipitation phenomena and limited co-dissolution of impurity elements. From a process perspective, sulfuric acid appears to be a promising candidate for selective SmCo recovery, provided that operational parameters such as temperature, acid concentration, or multi-stage leaching strategies are further optimized.

3.2. Effect of Reaction Temperature

After selecting sulfuric acid as the most promising leaching agent, the effect of reaction temperature on metal dissolution was systematically investigated. The experiments were conducted using 1 M H_2SO_4 at a solid-to-liquid ratio of 1:40 for 2 h under 250 rpm stirring, while the reaction temperature was varied between 25 and 90 °C. The results are presented in Fig. 2. A clear positive correlation was observed between reaction temperature and the leaching efficiencies of Sm, Fe, Co, and Zr. As the temperature increased from 25 to 90 °C, Sm dissolution slightly increased from 99.17% to 99.997%, indicating that Sm dissolution is already highly favorable even at room temperature. In contrast, Co leaching efficiency increased significantly from 27.51% to 95.97%, while Fe and Zr increased from 52.53% to 98.98% and from 26.53% to 90.73%, respectively. The pronounced temperature dependence of Co and Zr dissolution suggests that their leaching behavior is kinetically controlled, with increasing temperature enhancing reaction rates by accelerating surface reactions and mass transfer. The dissolution of Sr showed only a marginal increase from 7.35% to 9.35% over the investigated temperature range. This limited temperature dependency can be attributed to the low solubility product of $SrSO_4$ in sulfate media, indicating that Sr dissolution is likely governed by solubility equilibrium rather than reaction kinetics. From a process perspective, this behavior is advantageous, as the limited co-dissolution of Sr may reduce the complexity of downstream purification steps. Interestingly, Cu exhibited negligible dissolution at lower temperatures (0.10% at 25 °C), followed by a sharp increase to 15.03% at 90 °C. This behavior may be associated with enhanced redox interactions at elevated temperatures. The increased oxidation of Fe^{2+} to Fe^{3+} under higher temperature conditions can promote the oxidation of metallic Cu^0 to soluble Cu^{2+} species, thereby increasing its dissolution.

Overall, increasing temperature significantly improves the dissolution of Co and Zr while maintaining limited Sr dissolution. Although higher temperatures enhance the simultaneous recovery of Sm and Co, the increased dissolution of impurity elements such as Fe and Cu at elevated temperatures indicates a trade-off between recovery efficiency and selectivity. Therefore, an optimal temperature should be determined by balancing high SmCo recovery with acceptable impurity dissolution levels.

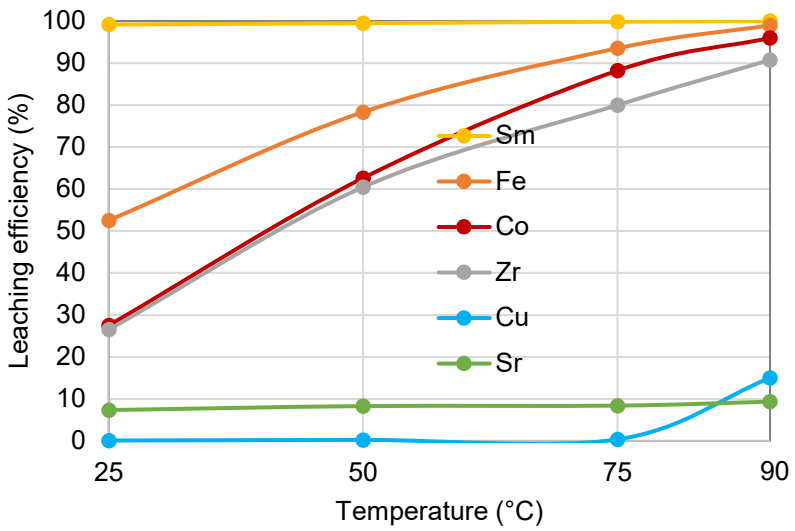

Figure 2. Leaching efficiencies of metals with different reaction temperatures.

4. CONCLUSION

This study demonstrated that acid type and reaction temperature play decisive roles in the selective dissolution of Sm and Co from SmCo permanent magnets. Among the investigated mineral acids, HNO_3 provided nearly complete dissolution of both target metals; however, its non-selective nature resulted in extensive co-dissolution of impurity elements. In contrast, H_2SO_4 exhibited a more selective dissolution behavior, particularly toward Sm, while limiting the dissolution of Sr due to sulfate-induced precipitation effects. Temperature significantly enhanced Co, Fe, and Zr dissolution in sulfuric acid, indicating kinetically controlled leaching behavior. Although increasing temperature improved simultaneous SmCo recovery, it also promoted the dissolution of impurity elements such as Fe and Cu, the latter showing a sharp increase at elevated temperatures likely due to enhanced redox and surface reaction kinetics. Overall, sulfuric acid emerges as a promising leaching agent for selective SmCo recovery, provided that process parameters are carefully optimized to balance high recovery efficiency with controlled impurity dissolution.

ACKNOWLEDGEMENTS

This study was supported by Project (MYL-2025-47248) funded by the BAP (Scientific Research Projects) Department of Istanbul Technical University.

REFERENCES

Binnemans, K., Jones, P. T., Blanpain, B., Van Gerven, T., Yang, Y., Walton, A., Buchert, M., (2013) “Recycling of rare earths: A critical review”, Journal of Cleaner Production, 51, 1–22.

Binnemans, K., Pontikes, Y., Jones, P. T., Van Gerven, T., Blanpain, B., Malfliet, A., Guo, M., (2013) “Recovery of rare earths from industrial waste residues: A concise review”, Proceedings of the 3rd International Slag Valorisation Symposium: The Transition to Sustainable Materials Management, 191–205.

Duerrschnabel, M., Yi, M., Üstüner, K., Liesegang, M., Katter, M., Kleebe, H. J., Molina-Luna, L., (2017) “Atomic structure and domain wall pinning in samarium-cobalt-based permanent magnets”, Nature Communications, 8 (1) 54.

Emil-Kaya, E., Papakci, M., Friedrich, B., (2024) “Recycling of SmCo magnets by removal of iron via oxidative leaching”, Mining, Metallurgy & Exploration, 41 (2) 479–486.

Longbutsri, C., Yingnakorn, T., Kansomket, C., Chandakhiaw, T., Somla, S., Ma-Ud, N., Khumkoa, S., (2026) “Hydrometallurgical valorization of strontium ferrite magnet sludge for the selective production of high-purity hematite (α-Fe_2O_3) and strontium carbonate ($SrCO_3$)”, Current Research in Green and Sustainable Chemistry, 100507.

Mengesha, W. G., Nagessar, K., (2025) “Advanced thermal and magnetic materials for high-power and high-temperature applications: A comprehensive review”, Discover Materials, 5 (1) 180.

Papakci, M., Emil-Kaya, E., Stopic, S., Gurmen, S., Friedrich, B., (2024) “Recovery of valuable metals from SmCo magnets through sulfation, selective oxidation, and water leaching”, Separation Science and Technology, 59 (10–14) 1241–1254.

Sinha, M. K., Pramanik, S., Kumari, A., Sahu, S. K., Prasad, L. B., Jha, M. K., Pandey, B. D., (2017) “Recovery of value added products of Sm and Co from waste SmCo magnet by hydrometallurgical route”, Separation and Purification Technology, 179, 1–12.

Uysal, E., Emil-Kaya, E., Dursun, H. N., Papakci, M., Gürmen, S., Friedrich, B., (2024) “Recovery of samarium from waste SmCo magnets via selective precipitation with ammonium bicarbonate: Optimization of process efficiency”, Metals, 14 (12) 1363.

Wang, J. Z., Tang, Y. C., Shen, Y. H., (2023) “Leaching of Sm, Co, Fe, and Cu from spent SmCo magnets using organic acid”, Metals, 13 (2) 233.

STRIPPING PRECIPITATION OF CALCIUM VANADATES FROM ORGANIC V(V) EXTRACTS

María Guadalupe SÁNCHEZ-LOREDO[1,2], Salvador Antonio PALOMARES-SÁNCHEZ[3], Paul CHEKHONIN[4], Doreen EBERT[1], Robert MÖCKEL[1], Norman KELLY[1], Ajay Bhagwan PATIL[1,5]

[1]Helmholtz-Zentrum Dresden-Rossendorf, Helmholtz-Institut Freiberg für Ressourcentechnologie, FREIBERG, GERMANY
[2]Instituto de Metalurgia/Facultad de Ingeniería, Universidad Autónoma de San Luis Potosí, SAN LUIS POTOSÍ, MEXICO
[3]Facultad de Ciencias, Universidad Autónoma de San Luis Potosí, SAN LUIS POTOSÍ, MEXICO
[4]Helmholtz-Zentrum Dresden-Rossendorf, Institut für Ressourcenökologie, DRESDEN, GERMANY
[5]The University of Jyväskylä, Faculty of Science and Mathematics, Department of Chemistry, JYVASKYLA, FINLAND
**Corresponding authors: msanchez@uaslp.mx, n.kelly@hzdr.de*

A B S T R A C T

In this work, a modified solvent extraction process with a crystallization operation of low-soluble calcium vanadates is presented. The vanadium(V) loading was carried out using Aliquat®336 as extractant, and the precipitation stripping was performed using alkaline aqueous $Ca(NO_3)_2$ solutions. For some tests, polyvinylpyrrolidone (PVP) was dissolved in the aqueous stripping phase, in order to study the influence of the polymer on the morphology and chemical structure of the solid phases.

The presence of PVP leads to a significant change in the characteristics of the calcium vanadate nanostructures, where a material composed of flake-like particles with 2D morphology, changes to sheaf-shaped structures under the influence of the polymer. The results pointed out the advantages of combining the selectivity of the solvent extraction process with the possibility of direct fabrication of high-value nanoproducts with the desired characteristics. PVP as a template, acts as regulator and growth controller.

Key words: *Solvent extraction, precipitation stripping, calcium vanadates, nanostructures*

1. INTRODUCTION

Metal vanadates have shown potential applications as sensors, photocatalysts, and, due to their high theoretical capacity, safety, easy preparation, and low cost, also as electrode materials for primary and rechargeable batteries (Mahmoud et al., 2019). Layered and hydrated vanadium oxides with open-framework structures, where metal ions are bonded to oxygen atoms acting as pillars between V_2O_5 layers, are capable of expanding the interlayer spacing to promote fast and effective intercalation and removal of metal ions, thus improving rate performance and capacity through multiple oxidation states of vanadium (Ahmad et al., 2023). Particularly alkaline and earth-alkaline ions, acting as pillar cations, are capable of increasing the interlayer distance and of stabilizing the crystal structure against the changes due to multiple charging/discharging cycles (Vujković et al., 2022). Morphology and particle size determine the overall current densities of these materials.

For these reasons, plenty of research work has been done on the synthesis and electrochemical studies of various metallic vanadates, that are normally synthesized by hydrothermal methods, requiring high temperatures and pressures. This makes the synthesis expensive, and the control of the microstructure and composition difficult to achieve (Ni et al., 2010; Yu et al., 2022). Particularly, the complex chemistry of the vanadium leads to the

formation of secondary phases of VO_2, V_2O_5, etc., under the chemical and thermal treatment conditions (Sharma et al., 2018).

Hydrometallurgical operations include, after leaching, a step for the separation and purification of valuable metallic species. Solvent extraction is a separation process that consists of extraction of target metal ions from an aqueous feed, scrubbing of impurities and stripping from the loaded organic phase. After the last step, the re-extracted solute is recovered, for instance using electrowinning. A promising modification of the conventional stripping step is the addition of a crystallization operation directly from the organic phase, where theoretically any kind of low-solubility metal salts, for example oxides or sulfides, can be precipitated (precipitation stripping). Recently, we have established and reported extraction processes with the addition of a crystallization operation, where low-solubility metal vanadates are precipitated (Sánchez-Loredo et al., 2023; Sánchez-Loredo et al., 2024). Studies were conducted in which V(V) was extracted using solutions of Aliquat®336 in a mixture of *n*-octanol and kerosene. After extraction, solutions containing different metallic ions in highly concentrated chloride solutions were used to precipitate the corresponding vanadates. The effect of the addition time of the stripping agent determined composition, size and morphology of zinc(II), cobalt(II), manganese(II) and nickel(II) vanadates (Sánchez-Loredo et al., 2024). Experimental parameters deeply affected the recovery of V(V) as Volborthite, a basic hydrated copper(II) vanadate (Sánchez-Loredo et al., 2023).

In the present work, we conducted experiments where the V(V) organic extracts were used for the preparation of calcium vanadates, where the hydroxyl ions act as the stripping agent, and Ca(II) as the precipitating ion. The addition of the polymer polyvinylpyrrolidone (PVP) in the aqueous stripping phase, and its influence on the structural characteristics of the vanadate solid phases containing calcium(II) ions, is discussed. It is a known fact that organic compounds can be used as templates in hydrothermal methods for the preparation of layered calcium vanadates (Kong et al., 2004), where single-crystal $CaV_6O_{16}.3H_2O$ nanoribbons were grown under hydrothermal process in the presence of dodecyl sulfate (SDS).

2. MATERIAL AND METHODS

2.1. Material

All chemicals were reagent grade. Aliquat®336 (methyltri-*n*-alkylammonium chloride), is a liquid anion exchanger based on short-chain quaternary ammonium cations and an effective phase transfer catalyst and well-known metal extraction reagent.

2.2. Methods

The V(V) loading was carried out by ion exchange using a Aliquat®336 solution (20% (v/v)) in *n*-octanol (10% v/v)/kerosene as organic phase, and vanadium pentoxide dissolved in 0.1 M NaOH (2 g/L V(V)) as aqueous feed solution. Contact time was 1 h, and the A/O for the extraction and stripping steps was kept 1:1. The V(V) contents in the aqueous phase before and after extraction were measured by ICP-OES analysis (Analytik Jena PlasmaQuant PQ9000), and the extraction rate was calculated from the mass balance.
Precipitation stripping was carried out with the loaded organic phase. For the preparation of the calcium vanadates, $Ca(NO_3)_2$ dissolved in alkaline solutions was used and for selected experiments PVP was dissolved in the aqueous stripping phase. After adding the strip solution, the stirring was continued for 1 hour. The precipitates were collected by centrifugation and washed with deionized water, water/ethanol mixtures (1:1), ethanol, acetone for 3 times each, iso-propanol, and water.

The solids were recovered after vacuum-drying for 72 h, and characterized by X-ray diffraction by means of a PANalytical Empyrean diffractometer (Almelo, Netherlands), at scan range between 5 - 80 with a step size of 0.0131 and an overall measurement time of 10 h. Phase analysis and quantifications were implemented by the Rietveld refinement method (full profile fitting) using the software Material Analysis Using Diffraction (MAUD, Lutterotti et al., 1999), leading to a reasonable goodness of fit. The scanning electron microscopy characterization was carried out using an EVO 50 SEM, Zeiss, with a tungsten filament and operated at 15 kV acceleration voltage. Finally, infrared spectroscopy measurements were performed using a Cary 630 FTIR spectrometer (Agilent).

3. RESULTS AND DISCUSSION

A vanadium extraction yield of around 76% was obtained with the organic system consisting of Aliquat®336 20%(v/v)/1-octanol 10%(v/v)/kerosene, corresponding to an organic phase loaded with 1.52 g/L V(V), which was separated by centrifugation from the raffinate phase. During stripping, the loaded organic solution was equilibrated with the alkaline calcium(II) nitrate solutions. Table 1 shows a summary of the different phases identified using the X-ray diffraction pattern and the software MAUD, as well as the composition and some structure parameters. The refined diffractograms are shown in Figure 1. The refinement of a sample synthesized in the absence of PVP, and 0.05 M Ca^{2+} and 0.025 N OH^-, indicates that the solid contained a higher proportion of the divanadate $Ca_2V_2O_7{\cdot}2H_2O$ (triclinic, space group *P-1,* Card no. 159-1949, Konnert and Evans Jr., 1975), and also $Ca_2V_2O_7$ (triclinic and space group *P-1,* JCPDS-ICDD, #72-2312, calculated by Pekov et al., 2023). The structure of the pyrovanadate $Ca_2V_2O_7{\cdot}2H_2O$ contains layers of packed $V_2O_7^{4-}$ groups and H_2O molecules, interleaved with Ca^{2+} ions. In an extensive piece of work, to be submitted, we found that higher Ca^{2+} and OH^- concentration in the stripping solution lead to mixtures of vanadates with different stoichiometries. On the contrary, at low concentrations of precursors, both divanadates are present, and sometimes some large calcium carbonate particles appear, presumably from a rapid carbonation process. These particles could theoretically be removed by size exclusion. For this work, we used conditions that could allow us to obtain pure phases with less impurities. Another complication during the refining of the structure is the nature of the particles, the broad peaks in the diffraction patterns and the results obtained for the crystallite size indicate that they are nanometrical in size, or possess amorphous character.

If PVP is present in the stripping phase (20 g/L), the chemical phases seem to remain the same, but the anhydrous vanadate appears to be the predominant chemical compound. Interestingly, whereas the anhydrous phase has a nanometrical crystallite size, the crystallite size for the dihydrated compound is micrometrical, showing the important role of the polymer PVP in controlling growth. The goodness of fit of the refinement result is not as good as for the sample without PVP, as PVP could contribute to the diffraction pattern.

Table 1. Different phases for the vanadate samples identified from the XRD patterns using the software MAUD

Sample	Ca^{2+}, mol/L	OH^-, mol/L	Chemical formula	Symmetry	Crystallite size (nm)	Wt. (%)
CaV	0.05	0.025	$Ca_2V_2O_7$	Triclinic (*P-1*)	90	37.78
			$Ca_2V_2O_7{\times}2H_2O$	Triclinic (*P-1*)	65	62.21
CaV-PVP	0.05	0.025	$Ca_2V_2O_7$	Triclinic (*P-1*)	84	62.4
			$Ca_2V_2O_7{\times}2H_2O$	Triclinic (*P-1*)	4188	37.6

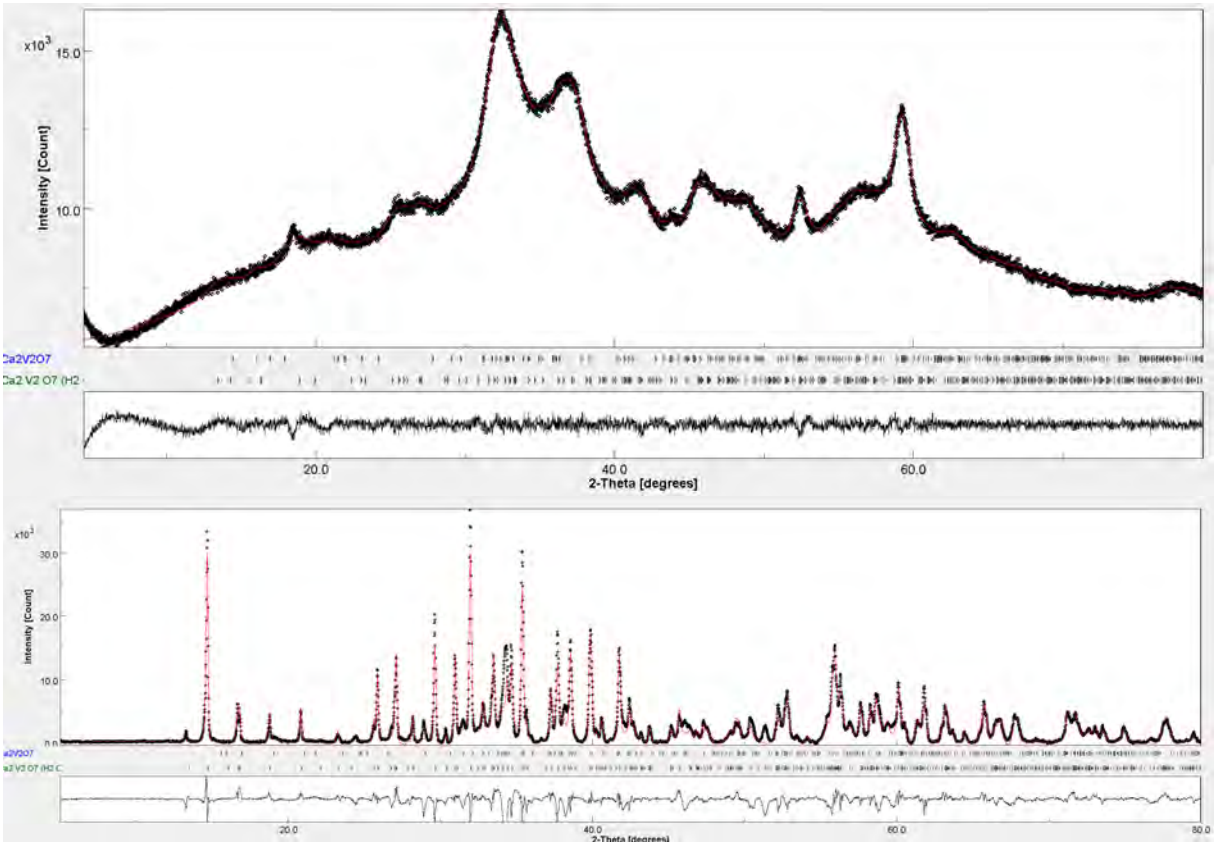

Figure 1. Observed (red) and calculated (black) X-ray diffractograms of samples (up) CaV and (down) CaV-PVP. The vertical bars indicate the angular positions of the allowed Bragg reflections where (blue) corresponds to $Ca_2V_2O_7$, space group *P-1* and (green) corresponds to $Ca_2V_2O_7 \cdot 2H_2O$, also space group *P-1*. Stripping solution: Ca^{2+} 0.05 mol/L, OH^- 0.025 mol/L

According to the SEM observations, in absence of PVP (CaV), precipitates appear to be composed of self-assembled ultra-thin sheets of nanopetals (Figure 2). PVP leads to a significant change in the characteristics of the calcium vanadate nanostructures. Images of the sample CaV-PVP show bigger particles, some of them possess a sheaf-shaped structure. Nanorod bundles, with sheaves of about 3 m in length, have been synthesized by a hydrothermal method by Pei et al. (2012) at 180 C for 24 h. According to these authors, sheaf-shaped structures are formed by a crystal splitting mechanism, associated with fast crystal growth. An individual crystal splits, and forms a number of sub-individuals with sheaf-shaped structure. This mechanism is also present in some minerals, but is rare to find this kind of structures in nature. Depending mainly on the crystal structure, different materials possess specific ‘‘splitting ability’’. With other experimental conditions being the same, crystal growth depends strongly on the solution oversaturation, which should exceed a certain critical level, specific for each kind of material and the conditions used during synthesis (Pei et al., 2012).

The formation of calcium vanadate nanorods with sheaf-shaped morphology gives a hint about the crystal splitting ability of the calcium(II) vanadates prepared by precipitation stripping in the present of the polymer PVP as surfactant. In a former work of us (Sánchez-Loredo et al., 2023), the presence of PVP during the synthesis of a copper(II) vanadate, results only in smaller particle sizes, and more rounded edges, but such a change in morphology does not take place. In the work mentioned above, related to the synthesis of Volborthite in experiments carried out varying different stripping parameters, the results showed that the presence of PVP also provides higher recoveries of V(V) as a solid, presumably because the aqueous phase becomes less polar. A study about this effect on the calcium(II) vanadate system was beyond the scope of this work.

According to Tang and Alivisatos (2006), an interesting feature of the mechanism of crystal splitting is that during the process, new surfaces result each time the crystal splits. In the presence of an effective surface stabilizer (in our study, the polymer PVP), crystal splitting is favored, and at equilibrium the balance of bulk and surface energies determines the crystal size. As normally at lower temperatures fewer nuclei are formed, and fast growth can lead to metastability, the particles grow beyond this size. In this situation, due to the strong adhesion of the surfactant to the newly created surface, it can be thermodynamically favorable for the system to undergo splitting of large crystals.

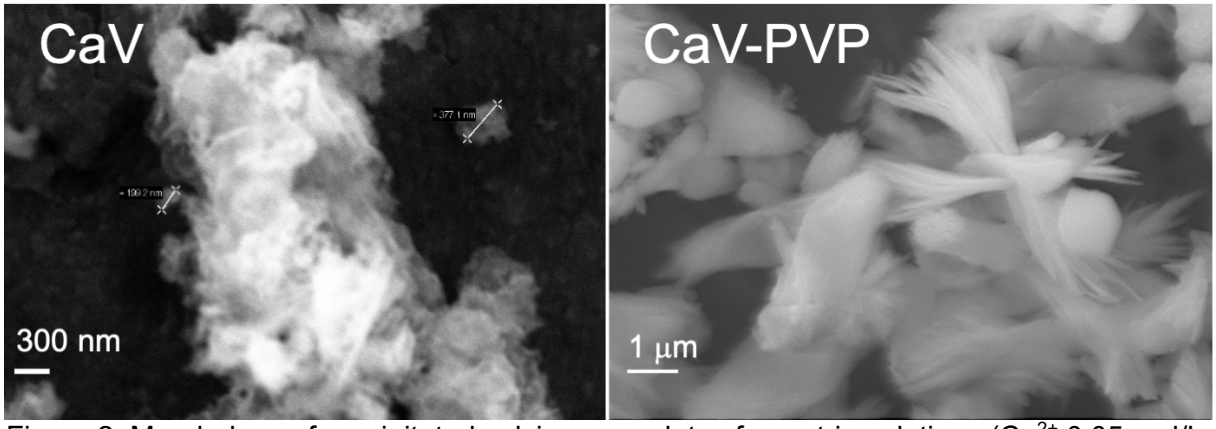

Figure 2. Morphology of precipitated calcium vanadates from strip solutions (Ca^{2+} 0.05 mol/L, OH^- 0.025 mol/L, CaV-PVP 20 g/L PVP in the stripping aqueous phase)

In order to find out if the extractant or the polymer remain attached at the surface of the particles, FTIR measurements were carried out at the solid samples (Figure 3), and the spectra were compared to the ones of Aliquat®336 and PVP (Sánchez-Loredo et al., 2023). Two strong bands are featured in the Aliquat®336 spectrum, at 2852 cm^{-1} and 2921 cm^{-1} (corresponding to symmetric and asymmetric sp^3 C-H stretching), and also a band at 1465 cm^{-1} (CH_2-bending) (Naz et al., 2016). In our study, a band is found at 2929 cm^{-1} in the spectrum of the metal vanadate CaV, but the characteristic absorption bands at 1377 cm^{-1} (CH_3 bending), 722 cm^{-1} (corresponding to the in-plane rocking mode of the methylene $(-CH_2-)_n$ chain), and the band at 1465 cm^{-1} (belonging to $(CH_3)-N^+$, Lee et al., 2019; Nguyen et al., 2020), are absent. Aliquat®336 is soluble in ethanol and can be removed easily if is not strongly adsorbed on the particles surface.

On the other hand, signals corresponding to the polymer PVP could be detected in sample CaV-PVP. Main IR vibrational assignments of PVP are the -OH asymmetric stretching at 3264 cm^{-1}, the C=O stretching vibration at 1635 cm^{-1}, CH_2-bending at 1464 cm^{-1}, and finally, C-N stretching at 1294 cm^{-1} (Mireles et al., 2020). According to the literature, the nucleophilic enol form of PVP donates the lone pair electron from the O-atom of the hydroxyl group, forming a weak polymer-metal coordinated complex (Ram and Fecht, 2011, Triphaty et al., 2009). Behera and Ram (2014) attributed the stability of Au colloids to the electrosteric effect of PVP.

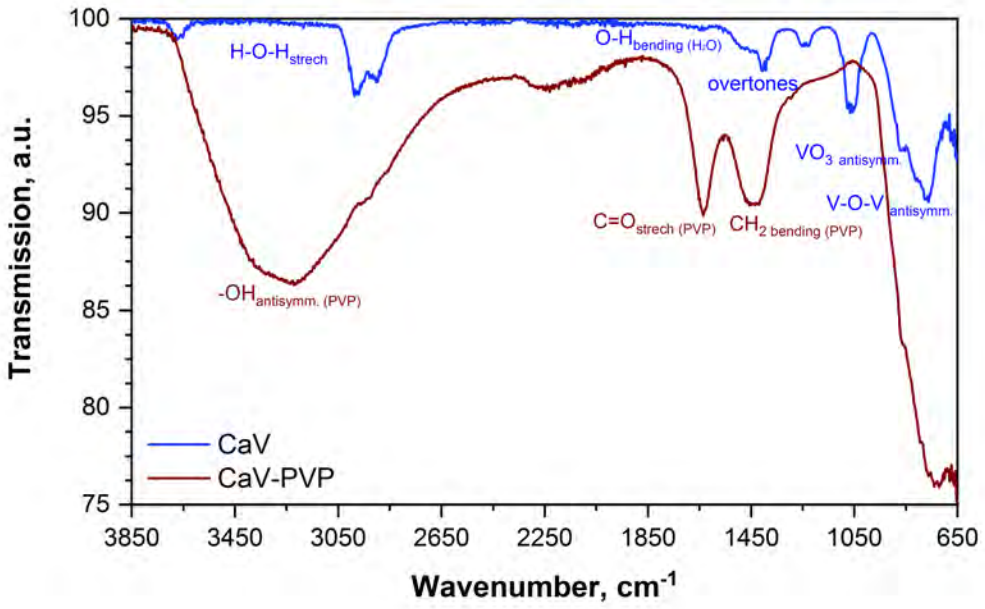

Figure 3. Infrared spectra of selected calcium vanadates

A surfactant such as PVP is used in materials synthesis to guide the growth of 2D materials. However, the removal is time consuming and sometimes not completely successful, an important fact if the vanadates are aimed at catalytic applications.

Sharma et al. (2018) reported stretching vibrations of metal-oxygen bonds and bending vibrations of VO_4^{3-} groups in triclinic structured $A_2V_2O_7$ pyrovanadates: $_1$ (950-900 cm^{-1}), $_2$ (830-810 cm^{-1}), $_3$ (750-700 cm^{-1}), and $_4$ (650-700 cm^{-1}). $_4$ and $_3$ result from V-O-V bridge vibrations and asymmetric stretching of longer V-O bond. The rest, $_1$ and $_2$, are ascribed to symmetric stretching of the other shorter V-O bonds. Bayat et al. (2018) reported characteristic absorption peaks for colloidal Volborthite, $Cu_3V_2O_7(OH)_2{\cdot}(H_2O)_2$, where the bands at 841 cm^{-1} and 1018 cm^{-1} are assigned to V-O-V and V-O vibrations. The spectra in Figure 3 confirm the existence of the pyrovanadates. The band at 1066 cm^{-1} in the spectrum of CaV could correspond to the C-O stretching of carbonates. The absence of this band in the spectrum of CaV-PVP gives a hint about the protective effect of the polymer, avoiding carbonation.

These results indicate that these precipitates are composed of the same V(V) chemical phases as the ones prepared in absence of PVP, indicating that the organic molecule does not influence the crystal composition, but only the morphology, crystallite size, and proportion of the anhydrous and the dihydrated phases.

4. CONCLUSION

The results of this study pointed out the advantages of combining the selectivity of the solvent extraction process with the possibility of direct fabrication of high-value nano-products by precipitation stripping. Also, the synthesis of a variety of types of nanoparticles and nanostructures is feasible utilizing organic compounds, i.e. PVP, as templates, acting as regulators and growth controllers, as demonstrated during the precipitation step. SEM observations show that the products change from 2D materials to rod-shaped nanostructures, resembling a wheat sheaf, in the presence of PVP.

ACKNOWLEDGEMENTS

M.G. Sánchez-Loredo thanks the German Academic Exchange Service and the Helmholtz Institute Freiberg for Resource Technology for financial support. This project received funding from the European Union's Horizon 2020 Research and Innovation program under Grant Agreement no 730471. The authors thank the German Federal Ministry of Research, Technology and Space for the financial support within the program WIR! (LiDoVa - Project No. 03WIR1915A).

REFERENCES

Ahmad, M. I., Bahtiyar, D., Khan, H. W., Shah, M. U. H., Kiran, L., Aydinol, M. K., Yusuf, M., Kamyab, H., Rezania, S., (2023) "Ionic liquids-assisted electrolytes in aqueous zinc ion batteries", Journal of Energy Storage 72 108765.

Bayat, A., Mahjoub, A. R., Amini, M. M., (2018) "Facile hydrothermal synthesis of the colloidal hierarchical Volborthite ($Cu_3V_2O_7(OH)_2 \cdot 2H_2O$) hollow sphere phosphors", Journal of Luminescence, 204 382–385.

Behera, M., Ram, S., (2014) "Inquiring the mechanism of formation, encapsulation, and stabilization of gold nanoparticles by poly(vinyl pyrrolidone) molecules in 1-butanol", Applied Nanoscience 4 247-254.

Khachani, M., El Hamidi, A., Halim, M., Arsalane, S., (2014) "Non-isothermal kinetic and thermodynamic studies of the dehydroxylation process of synthetic calcium hydroxide $Ca(OH)_2$", Journal of Materials and Environmental Science 5 615–624.

Kong, L., Shao, M. W., Xie, Q., Liu, J., Qian, Y., (2004) "Hydrothemal growth of single crystal $CaV_6O_{16} \bullet 3H_2O$ nanoribbons", Journal of Crystal Growth 260 435-439.

Konnert, J. A., Evans Jr., H. T., (1975) "Calcium Divanadate Dihydrate", Acta Crystallographica B31 2688-2690.

Le, M. N., Son, S. H., Lee, M. S., (2019) "Extraction behavior of hydrogen ion by an ionic liquid mixture of Aliquat 336 and Cyanex 272 in chloride solution", Korean Journal of Metals and Materials, 57 162–169.

Lutterotti, L., Matthies, S., Wenk, H.-R. "MAUD: A friendly Java program for Material Analysis Using Diffraction". Newsletter CPD 1999, 21 14–15.

Mahmoud, S. A., Bendary, S. H., Salem, A. A., Fouad, O. A., (2019) "Facile synthesis of high yield two-dimensional zinc vanadate nanoflakes", SN Applied Sciences, 1(497).

Mireles, L. K., Wu, M.-R.; Saadeh, N.; Yahia, L. H.; Sacher, E., (2020) "Physicochemical characterization of polyvinyl pyrrolidone: A tale of two polyvinyl pyrrolidones", ACS Omega, 5 30461–30467.

Naz, G., Othaman, Z., Shamsuddin, M., Krishna Ghoshal, S., (2016) "Aliquat 336 stabilized multi-faceted gold nanoparticles with minimal ligand density", Applied Surface Science, 363 74–82.

Nguyen, V. N. H., Le, M. N., Lee, M. S., (2020) "Comparison of extraction ability between a mixture of Alamine 336/Aliquat 336 and D2EHPA and ionic liquid ALi-D2 from weak hydrochloric acid solution", Metals, 10 1678.

Ni, Sh., Wang, X., Zhou, G., Yang, F., Wang, J., He, D., (2010) "Hydrothermal synthesis and magnetic property of $Cu_3(OH)_2V_2O_7 \cdot nH_2O$", Materials Letters 64 516–519.

Pei L.Z., Pei, Y.Q., Xie, Y.K., Yuan, C.Z., Li, D.K., Zhang, Q.-F., (2012) "Growth of calcium vanadate nanorods", CrystEngComm, 14 4262-4265.

Pekov, I. V., Agakhanov, A. A., Koshlyakova, N. N., Zubkova, N. V., Yapaskurt, V. O., Britvin, S. N., Vigasina, M. F., Turchkova, A. G., Nazarova, M. A., (2023) "Bakakinite, $Ca^2V_2O_7$, a new mineral from

fumarolic exhalations of the Tolbachik volcano, Kamchatka, Russia", Mineralogical Magazine, 87 695–701.

Ram, S., Fecht, H.-J., (2011) "Modulating up-energy transfer and violet-blue light emission in gold nanoparticles with surface adsorption of poly(vinyl pyrrolidone) molecules", The Journal of Physical Chemistry C, 115 (16) 7817–7828.

Sánchez-Loredo, M. G., Palomares-Sánchez, S. A., Labrada-Delgado, G. J., Helbig, T., Chekhonin, P., Ebert, D., Möckel, R., Owusu Afriyie, J., Kelly, N., (2023) "Preparation of volborthite by a facile synthetic chemical solvent extraction method, Nanomaterials 13 (13) 1977.

Sánchez-Loredo, M. G., Chekhonin, P., Ebert, D., Fischer, U., Liu, X., Möckel, R., Labrada-Delgado, G. J., Passerini, S., Kelly, N., (2024) "Precipitation stripping of V(V) as a novel approach for the preparation of two-dimensional transition metal vanadates", Nanomaterials, 14 38.

Sharma A., Varschney, M., Chae, K.-H., Won, S. O., (2018) "Electronic structure and luminescence assets in white-light emitting $Ca_2V_2O_7$, $Sr_2V_2O_7$ and $Ba_2V_2O_7$ pyro-vanadates: X-ray absorption spectroscopy investigations", RSC Advances, 8 26423-26431.

Tang, J., Alivisatos, A. P., (2006) "Crystal splitting in the growth of Bi_2S_3", Nanoletters, 6 (12) 2701-2706.

Tripathy, P., Mishra, A., Ram, S., Fecht, H.-J., Bansmann, J., Behm, R. J., (2009) "X-ray photoelectron spectrum in surface interfacing of gold nanoparticles with polymer molecules in a hybrid nanocomposite structure", Nanotechnology, 20 075701–075709.

Vujković, M. J., Mladenović, D., Milović, M., Petrović, T., Bajuk-Bogdanović, D., Šljukić Paunković, B., Mentus, S., (2022) "Sodium-pillared vanadium oxides as next-gen materials: Does co-inserted water control the cyclic stability of vanadates in an aqueous electrolyte?", Electrochimica Acta, 425 140603.

Yu, X., Hu, F., Guo, Z., Liu, L., Song, G., & Zhu, K., (2022), "High-performance Cu0.95V2O5 nanoflowers as cathode materials for aqueous zinc-ion batteries", Rare Metals ,41 (1) 29–36.

SUSTAINABLE SYNTHESIS AND CHARACTERIZATION OF NANO ZINC BORATE FROM METALLURGICAL WASTE

Gülnihal AYGÜN[1,*], Hüseyin BAŞTÜRKCÜ[2], Bihter ZEYTUNCU GÖKOĞLU[1,3]

[1]Istanbul Technical University, Graduate School, Nanoscience and Nanoengineering Department, 34469, Maslak, Istanbul, TÜRKİYE
[2]Istanbul Technical University, Faculty of Mines, Mineral Processing Engineering Department, 34469, Maslak, Istanbul, TÜRKİYE
[3]Istanbul Technical University, Faculty of Chemistry-Metallurgy, Department of Metallurgical and Materials Engineering, 34469, Maslak, Istanbul, TÜRKİYE
**Corresponding author: aygung19@itu.edu.tr*

A B S T R A C T

Zinc ash, a solid waste generated during the hot-dip galvanizing process, contains 55–85% Zn by weight, which is significantly higher than the Zn grade of primary ores (1–10%). Given that primary zinc reserves are estimated to last only 17–25 years and that secondary zinc production emits 76% less CO_2 compared to primary production, the valorization of zinc ash represents both an environmental and economic opportunity within the framework of the circular economy. In this study, zinc ash with a Zn content of 61.55% was subjected to leaching with 200 g/L sulfuric acid at room temperature to obtain a $ZnSO_4$ solution. A layered zinc hydroxide structure, $Zn_4(SO_4)(OH)_6 \cdot 0.5H_2O$, was then precipitated by dropwise addition of Na_2CO_3, followed by calcination at 800°C for 1 hour to produce nano ZnO particles. The resulting nano ZnO was reacted with boric acid (H_3BO_3) at defined molar ratios under optimized synthesis conditions to produce nano zinc borate particles. XRD analysis confirmed the crystal structure as $2ZnO \cdot 3B_2O_3 \cdot 3H_2O$ (JCPDS No. 32-1464) with a phase purity of 99.1%, as determined by the reference intensity ratio (RIR) method. Minor impurities of metaboric acid (0.8%) and zincite (0.1%) were identified and considered acceptable. SEM characterization revealed a characteristic plate-like crystal morphology with sub-micron particle size distribution and consistent with the XRD results. These findings demonstrate that zinc ash can serve as a sustainable and cost-effective secondary raw material for the synthesis of high-purity nano zinc borate and with promising potential for functional applications including use as a lubricant additive.

Key words: *Zinc ash, nano zinc borate, hydrometallurgy, ZnO, secondary raw material*

1. INTRODUCTION

Zinc ash, a byproduct of the galvanizing process applied for corrosion resistance in the iron and steel industry, has a higher Zn content compared to primary sources. Galvanizing is one of the main industrial methods that protects steel surfaces against corrosion by dipping them into molten zinc bath or through electrolytic coating, and this process inevitably produces various zinc-containing byproducts and wastes. In primary sources, the Zn grade ranges between 1% and 10% (Van Rythoven, 2023). One quarter of the one ton of zinc entering a galvanizing plant leaves the system as waste. Zinc ash, which is one of these wastes, contains 55–85% Zn (Kania ve Saternus, 2023). This ratio is well above the Zn grade of primary ore, which places zinc ash in the position of a highly valuable secondary raw material in terms of recovery. According to the data, the fact that the lifespan of primary sources is between 17 and 25 years makes it necessary to prefer secondary sources in Zn production. In addition, producing Zn from secondary sources during production emits 76% less CO_2 compared to production from primary sources, while significantly reducing energy consumption (Ma, et al. 2020). When all these data are evaluated together, it becomes clear that zinc ash should be considered not only as an industrial waste, but as a strategic resource from which value can be created within the framework of the circular economy.

Zinc can be involved in the synthesis of many compounds thanks to its reactive structure. While compounds such as ZnO, $ZnCl_2$, $ZnSO_4$, and $Zn_3(PO_4)_2$ are used in industry, zinc borates can be used in a much more comprehensive and diverse way. Among these compounds, zinc sulfate ($ZnSO_4$) is widely used in the agriculture and textile sectors, zinc chloride ($ZnCl_2$) in wood preservation and soldering applications, and zinc phosphate ($Zn_3(PO_4)_2$) as a corrosion-inhibiting coating pigment on metal surfaces. Zinc borates, which are used as flame retardants, corrosion inhibitors, and lubricant additives, can be synthesized at different ZnO/B_2O_3 ratios and by different methods, and their morphological structures can be controlled (Baltacı, 2020). Zinc borate particles reduced to the nano scale show significantly superior performance in these application areas compared to bulk material, thanks to increased surface area and reactivity. Some studies on nano zinc borate in recent years have also presented important findings on synthesis methods. For example, in one study, nano zinc borate was synthesized by the reaction of zinc nitrate and borax under low temperature and low concentration conditions, and it was shown that template agents such as Span 60 and PEG 4000 affect the particle morphology. The size of the amorphous particles obtained was determined to be approximately 40–80 nm (Savrık, et al. 2011). In the study conducted by Baltacı, nano zinc borate was synthesized by the sol-gel method, and the effect of different Zn/B ratios and pH conditions on the morphology and structure of the product was examined. It was reported that the product was amorphous in XRD analyses, and particles in the size range of 50–200 nm were obtained in SEM images. Although the study mainly focused on flame retardant additives in polymers, it was emphasized that the more homogeneous dispersion and surface interaction provided by the nano size increases the additive performance (2022). On the other hand, in another study, hydrophobic zinc borate nanoplatelets were synthesized in a single step using oleic acid by the in-situ method. The polycrystalline structure in the form of $Zn_2B_6O_{11}\cdot 3H_2O$ was confirmed by XRD analyses, and nanoplatelets with a diameter of 100–500 nm and a thickness of 30 ± 5 nm were obtained according to SEM/TEM results. Due to the oleic acid modification, the surface of the particles became hydrophobic and the contact angle rose up to 132°. This feature greatly increases the dispersion stability of zinc borate particles in oil when used as a lubricant additive, and increases the effectiveness of the additive (Tian, et al. 2006). All these studies show that the synthesis conditions of zinc borate have a decisive role on the structure and morphology of the obtained phase; therefore, careful optimization of raw material selection and process parameters is of critical importance.

2. MATERIAL AND METHODS

2.1. Material

The primary raw material used in this study is waste zinc ash obtained from hot-dip galvanizing processes, with a zinc content of 61.55% by weight. Sulfuric acid (H_2SO_4, 95-97%) was used at a concentration of 200 g/L for the leaching step and obtained from Merck. Sodium carbonate (Na_2CO_3) served as the precipitation agent for layered zinc hydroxide sulfate (LZH) formation, and boric acid (H_3BO_3) was used as the boron source for nano zinc borate synthesis and obtained from Merc. All chemicals were of analytical grade and deionized water was used throughout all experimental stages.

2.2. Method

Leaching of zinc ash was performed using a 200 g/L H_2SO_4 solution at a solid-to-liquid ratio of 100 g/L for 1 hour at room temperature under continuous mechanical stirring. After the reaction, the suspension was filtered to separate the leach residue from the pregnant leach solution, and the resulting $ZnSO_4$ solution was collected for subsequent processing steps. The leach residue was washed with deionized water to remove soluble salts, and subsequently dissolved by four-acid digestion to determine the Zn leaching efficiency. The Zn extraction yield was calculated to be approximately 95%. Na_2CO_3 solution was added dropwise into the $ZnSO_4$

solution under stirring to precipitate $Zn_4(SO_4)(OH)_6 \cdot 0.5H_2O$. The precipitate was filtered, washed, and dried at 50°C. Phase purity was confirmed by XRD. The dried LZH intermediate was calcined at 800°C for 1 hour in a muffle furnace (NUVE MF 306), yielding nano ZnO particles, which were subsequently characterized by SEM and XRD. Nano ZnO was reacted with boric acid solution at various molar ratios and synthesis conditions to produce $2ZnO \cdot 3B_2O_3 \cdot 3H_2O$. The optimum conditions were determined and the final product was characterized by SEM (Thermo Fisher Scientific Quattro Sem-Esem) and XRD (Perkin-Elmer). The complete production flow is shown in Figure 1.

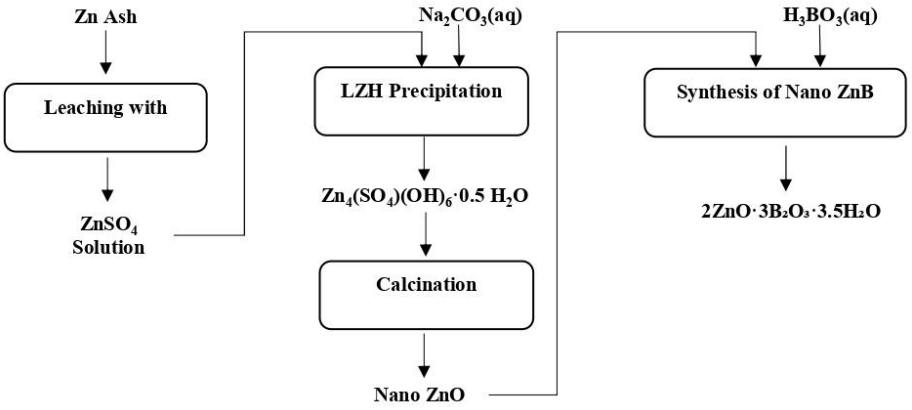

Figure 1. Flowchart of the nano zinc borate production

3. RESULTS AND DISCUSSION

The crystal structure of the synthesized nano zinc borate particles was confirmed as $2ZnO \cdot 3B_2O_3 \cdot 3H_2O$ by XRD analysis. Peaks were observed at 18.06, 20.56, 21.72, 23.70, 25.78, 28.72, 30.17, 36.70, and 42.97° (2θ). The main diffraction peaks are consistent with the $2ZnO \cdot 3B_2O_3 \cdot 3H_2O$ phase (JCPDS No. 32-1464), and a product with 99.1% purity was obtained [3]. The remaining impurities were identified as metaboric acid (0.8%) and zincite (0.1%), and were considered acceptable at this stage. Phase quantification was carried out using the reference intensity ratio (RIR) method. The XRD pattern is given in Figure 2.

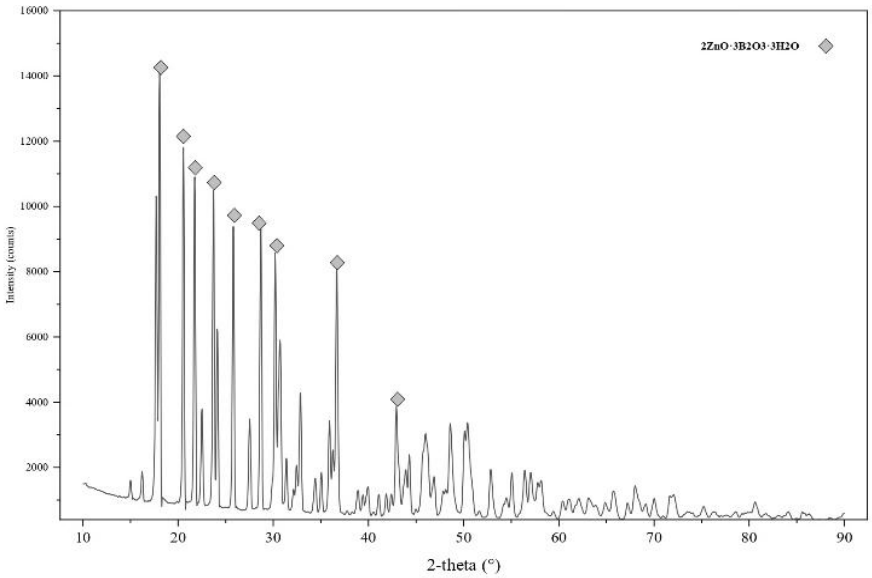

Figure 2. XRD analaysis of synthesized nano zinc borate

The SEM image shown in Figure 3 presents the morphological properties of the synthesized zinc borate sample. When the image is examined, it was determined that the sample has a characteristic plate-like crystal morphology and that the particle sizes show a sub-micron level distribution. The fact that the crystal structure has clear and sharp edges proves that a product with high purity and crystallinity was obtained, which is consistent with the XRD analysis results. The agglomeration observed between the particles is an expected situation in nano-scale synthesis processes. These morphological findings reveal that the structural integrity of the nano zinc borate produced from the waste-derived zinc source is preserved, and that a product suitable for use in various functional applications, particularly as a lubricant additive, has been obtained in further studies.

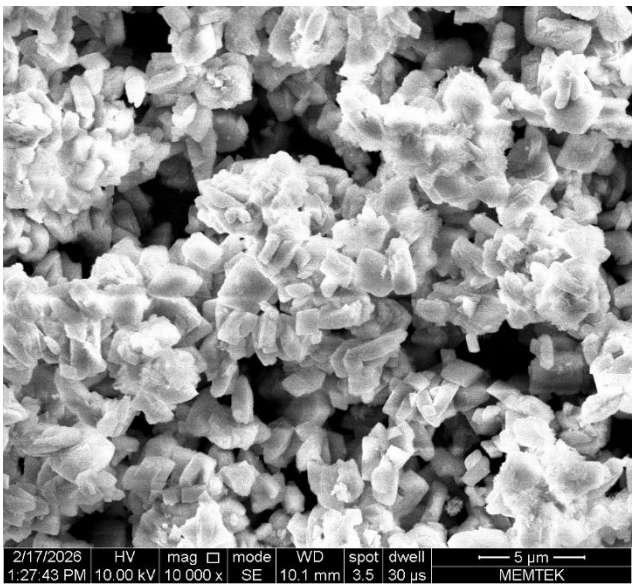

Figure 3. SEM image of synthesized nano zinc borate

4. CONCLUSION

In this study, nano zinc borate ($2ZnO{\cdot}3B_2O_3{\cdot}3H_2O$) was successfully synthesized from zinc ash, an industrial waste generated during the galvanizing process. The hydrometallurgical route followed leaching, precipitation of layered zinc hydroxide, calcination to nano ZnO, and subsequent reaction with boric acid proved to be an effective approach for producing high-purity nano zinc borate from a secondary raw material. XRD analysis confirmed the crystal structure with 99.1% phase purity (JCPDS No. 32-1464), and SEM characterization revealed a characteristic plate-like morphology with sub-micron particle size distribution. These results demonstrate that zinc ash can serve as a viable and sustainable zinc source for the synthesis of value-added nanomaterials. The produced nano zinc borate shows promising potential for functional applications, particularly as a lubricant additive, and future work will focus on evaluating its tribological performance.

REFERENCES

Baltacı, B. (2010). Synthesis and characterization of nano zinc borate and its usage as a flame retardant for polymers, M.S. thesis, Department of Chemical Engineering, Istanbul Technical University, Istanbul, Turkey.

Kania, H. and Saternus, M. (2023). Evaluation and Current State of Primary and Secondary Zinc Production—A Review, Applied Sciences, 13(3), 2003.

Ma, X., Hou, J., Zhao, B. and Chen, Y. (2020). Critical review on secondary zinc resources and their recycling technologies, Resources, Conservation and Recycling, 154, 104560.

Savrık, S. A., Balköse, D. and Ülkü, S. 2011. Synthesis of zinc borate by inverse emulsion technique for lubrication, Journal of Thermal Analysis and Calorimetry, 104(2), 605-612.

Tian, Y., Guo, Y., Jiang, M., Sheng, Y., Hari, B., Zhang, G., Jiang, Y., Zhou, B., Zhu, Y. and Wang, Z. (2006). Synthesis of hydrophobic zinc borate nanodiscs for lubrication, Materials Letters, 60(20), 2511-2515.

Van Rythoven, A. (2023). Critical Mineral: Zinc, Montana Bureau of Mines and Geology, Butte, MT, USA, Fact Sheet 8.

THE POTENTIAL OF MINING AND PROCESSING OF ALBANIAN NICKEL LATERITIC RAW ORES

Genc DEMI[1,*], Fatos AHMATAJ[2]

[1]Polytechnic University of Tirana, Faculty of Geology and Mines, Mine Deposit Engineering Department, Rruga e Elbasanit, Tirana-ALBANIA
[2]Alflexim Company, Rruga Myslym Shyri, Tirana-ALBANIA
**Corresponding author: genc.demi.al@gmail.com*

A B S T R A C T

The quantity of nickel metal in our reserves at about 3.0 million tons ranked Albania among 10 countries with nickel laterite reserves in the world. The main components of laterite raw ores are: Nickel, Cobalt, Iron, Chromium, Magnesium oxide, Aluminum oxide and some other rare elements. The reserves are about 312 million ton with average content of Ni 1.06 % and Co 0.057 %. It is shown the location of nickel lateritic deposits in the map of Albania, the exploitation conditions, as well as mineralogical composition in different deposits. Also it is presented the history of exploitation and processing of nickel lateritic ores in the past and actually in nowadays. In the year 1981 a Caron Plant was commissioned for processing of lateritic ores from underground mining. By the end of 1989 a new electro-winning section was commissioned for production of refined electrolytic Nickel with 99% Ni content and Cobalt by-product at about 2.8-2.9%, both designated for export. In 1995 due to dropping down of nickel prices in the world market below 9,000 $US/ton, it was decided to close Nickel-Cobalt Plant.

The aim of the paper is to promote processing of considerable nickel lateritic reserves in Albania between studies and projects to implement new technologies in this field. It is concluded that application of processing of nickel lateritic ores in Albania will be of great interest for possible investors and giving a great benefit as well for the Albanian economy.

Key words: *Nickel, cobalt, reserves, laterite*

1. INTRODUCTION

One of the biggest mineral resources in Albania are lateritic raw ores which have the greatest potential in terms of reserves and high variety of valuable components. Actually laterites, Nickel-Cobalt raw ores in Albania, represent the largest lateritic reserves in both Europe and Continental Asia. On the other hand, Albania's laterite reserves globally comprise about 3% of the world lateritic reserves. The quantity of nickel metal in our reserves at about 3.0 Million tons ranked Albania among 10 countries with the highest nickel reserves in the world. This indicator is more than enough to understand why the mining and processing of these minerals are of a great importance.

Lateritic ores in Albania are limonite, yellow and red and saprolite ores. The spread of these ores in earth is limited. They are located mainly in Indonesia, Philippines, New Caledonia, Caribbean Islands, Australia, Africa, Central and South America. About 4% of world reserves are located in Continental Europe and Continental Asia, of which about 2/3 of them are in Albanian territory.

2. MAIN DEPOSITS, THEIR LOCATION AND RESERVES (Goskolli, 2025)

Lateritic raw ores of Albania are found in two types of mineralization; limonite (yellow and red), and saprolite. This types of mineralization are found either in separate deposits or even within

the same deposit. The main components of laterite minerals are: Nickel, Cobalt, Iron, Chromium, Magnesium oxide, Aluminum oxide and some other rare elements. The mineral content of main elements is depending on the genesis of the rock formation.

Table 1. Raw ore reserves in different regions

No	Region	Reserves in thousand tons	Content, %	
			Ni	Co
1	Kukës			
	Saprolite	29,221	1.06	0.053
	Laterite	65,504	1.03	0.055
2	Librazhd- Pogradec			
	Laterite	105,592	1.00	0.069
3	Devolli			
	Saprolite	52,179	1.20	0.04
	Laterite	59,193	1.07	0.056
4	Total saprolite	81,400	1.15	0.045
	Total laterite	230,289	1.03	0.062
5	Laterite/Saprolite	311,689	1.06	0.057

The above table showing raw ore deposits and the content of main components: nickel and cobalt. While the map below showing the location of laterite resources throughout the country.

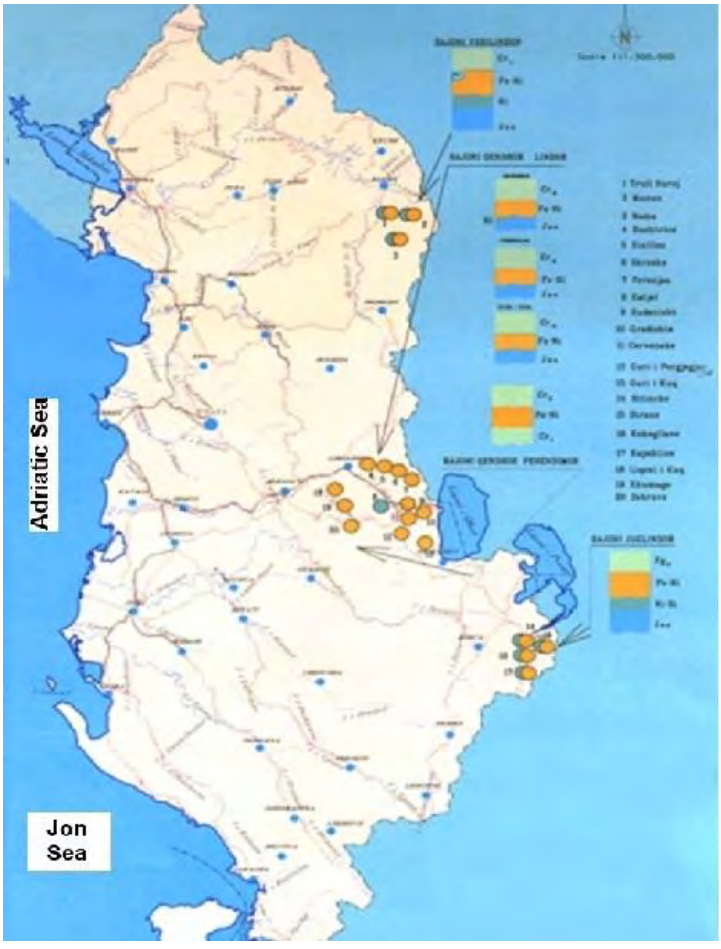

Figure 1. Nickel laterite and saprolite deposits in Albania

Laterite reserves in Albania are at about 310 million tons, from which 230 million tons of Red and Yellow Limonite and 80 million tons in Saprolites. The nickel content ranging from 0.9% to 1.3% and cobalt content ranging from 0.04% to 0.08%. These ores could be classified in the group of medium rich ores of Nickel and Cobalt.

3. A BRIEF HISTORY OF MINING AND PROCESSING

Laterite reserves in Albania are at about 310 million tons, from which 230 million tons of Red and Yellow Limonite and 80 million tons in Saprolites. The nickel content ranging from 0.9% to 1.3% and cobalt content ranging from 0.04% to 0.08%. These ores could be classified in the group of medium rich ores of Nickel and Cobalt. (Shouldice, 2010)

The first mining exploitation of Iron-Nickel dated in the year 1957 in Pishkashi open pit mine. Some years later new mines were opened in Përrenjas, Guri i Kuq, Cervenakë and Bitinckë.

Before the start of the operation of plant 12 in Elbasan in 1981, the entire amount of FeNi ore was exported, mainly to the former Czechoslovakia, where a processing plant was built, which applied the basic refining process of nickel ore, the so-called Caron process (CARON process is a combined pyrometallurgical and hydrometallurgical method used to extract nickel and cobalt from limonite type nickel laterite ores), while NiSi minerals were not extracted due to the lack of processing and export opportunities. Production of NiSi minerals resumed after 2006.

Based on the large deposits of iron-nickel ores located in the Librazhd-Guri Kuq area (estimated at approximately 260 million tons), with a Fe content of 40-45% and Ni 1.0%, the Elbasan Metallurgical Plant was studied in China and then designed and construction began. In the year 1981 the Caron HPAL plant 12 in Elbasani (HPAL High-Pressure Acid Leaching, is a hydrometallurgical process used to extract mainly nickel and cobalt from laterite ores), was commissioned in Albania for processing of lateritic ores from underground mining of Guri i Kuq mine near Pogradeci.

FeNi ores, after preliminary processing, were subjected to the “Caron” process (a hydrometallurgical process of ammoniacal leaching, with preliminary reduction of the mineral), where Ni and Co were separated in solution form, which were subjected to further processing to obtain metallic Ni and Co in salt form. The Fe concentrate was further subjected to the pyrometallurgical process for the production of cast iron and steel.

In the plant 12 in Elbasan, for the period of time from 1981 to 1990, a total of about 34 thousand tons of basic nickel carbonate (NiCO3xH2O with about 50.0% Ni) were produced, and since 1989, when the complex for smelting basic nickel carbonate and electrolytic refining of nickel anodes began operating, a total of about 3523 tons of electrolytic nickel have been produced.

The final products of plant 12 were the concentrate of nickel-cobalt hydroxide containing about 42% Nickel and 2.8% Cobalt and iron concentrate containing about 61% Fe2O3. The iron concentrate was designed for the production of Cast-iron and Steel, after reduction of Sulphur and Chromium.

Processing capacity of this plant was about 1 million tons/year raw ore and production of 400k tons/year of cast-iron and steel.

However, a part of raw ore from other mines was still exported in the former Czechoslovakia to Nova Huta Plant (now in Slovak Republic) which was designed for processing of Albanian Laterites raw ore by using the Caron HPAL process.

In 1995 due to dropping down of nickel prices in the world market below 9,000 $US/ton, Albanian Government decided to close Nickel-Cobalt Plant. After this decision, the plant was demolished in 2002.

For the period after 1994, nickel ore was mainly destined for export to supply the ferronickel production plants in North Macedonia and Kosovo. In these circumstances, the nickel ore export market can be considered saturated without the possibility of further expansion and development. Actually, the lateritic ore production is very low, at a maximum of 600 thousand tons/year. The raw ore designated for export in Kosovo and North Macedonia is using as a mixture with imported mineral coming from Guatemala for their ferronickel production to pyro metallurgical smelter plants.

4. STUDIES CONDUCTED ON THE POSSIBILITY OF TREATING LATERITE NICKEL ORES

Continuous efforts have been made to bring into economic circulation the considerable reserves of laterite nickel minerals, from laboratory and pilot tests to industrial scale tests, both domestically and abroad. Two of the studies carried out are briefly presented:

4.1. Technical And Economic Assessment for The Nickel Silicate Industry In Our Country (Lleshi, 2018)

Based on the world experience in processing nickel silicate ores using the pyro metallurgical method, during 1994-1995 a study was undertaken on the possibility of processing laterite Ni ores in the reconstructed metallurgical complex in Elbasan.

The investment cost would become possible after a full realization of the project feasibility, basing this on an experimentation in a pilot plant specialized for this purpose. The pilot plant ELKEM, Research Kristiansend, Norway was chosen as the best option.

The mineral was taken from Albania, the Bitincka deposit. The mineral that was chosen as a representative sample of the deposit, i.e. a mixed NiSi and FeNi minerals, while the lignite was taken from the Valias and Mborje Drenova deposits in Albania, in a ratio of 50% to 50%. The amount of mineral was 37 tons, while the lignite was 4.5 tons.

The RKEF Scheme (the Rotary Kiln-Electric Furnace is the pyrometallurgical method for extracting nickel from laterite ores, producing ferronickel alloy) for the processing of mixed nickel silicate and nickel iron ore was reviewed because extracting nickel silicate ore separately from nickel iron is a difficult and costly process, also for the reason that the separation between them in the ore is not clear.

The results of the pilot test were Nickel in FeNi was at the rate of 15%, while the recovery reached about 90%.

From world experience it results that the construction of a metallurgical complex for the processing of about 2.0 million tons of lateritic nickel silicate ore per year, with the RKEF process would cost a total of 629.0 million US$, including the capital cost of the mine, the total cost goes to about 1,235.0 million US$.

The most likely mixed ore to be produced in total is a total of 2.825 million tons per year, in the ratio: NiSi : FeNi = 1.38

Making the assessment, the most suitable technological process to be applied for the processing of mixed ore is the mixed Caron process (pyro and hydro metallurgy) and the RKEF process.

Based on more than 10 years of experience in implementing the CARON process for the processing of laterite minerals in the former Elbasan Metallurgical Plant, which resulted in relatively low Ni and Co recovery, very high processing costs, significant environmental pollution, and the iron concentrate produced is not suitable for use in the production of cast iron, as it results in a high Cr content, for the removal of which an additional process is required. Based on the above and the experience gained during the technological test on a pilot scale at ELKEM, using a mineral similar to that resulting from the study (mixed mineral), it results that the most suitable and economical process for the metallurgical processing of our laterites is the RKEF process.

An economic evaluation of FeNi production was made based on some data and definitions. Based on the above data, a CASH FLOW was drawn up for the FeNi production process, for a 10-year period, including the construction time of the facility, which results in NPV = $420.65 million and IRR = 22%. (NPV, Net Present Value or Discounted Cash Flow, Present Worth measures the money value added by a project, calculated as the sum of present values of cash inflows minus outflows). (IRR, Internal Rate of Return or Economic Rate of Return, Discounted Cash Flow Rate of Return is the percentage rate at which the project's NPV equals zero.)

4.2. Pre-Feasibility and Sustainable Study for Hydrometallurgical Processing of Nickel Laterite Ores in Albania (Ahmataj, 2015).

This study was conducted to examine the possibility of applying of hydrometallurgical methods that in recent years have taken the advantage, due to low cost of overall investments of the plant, highest metal recovery and lower operation cost.

However to determine the most appropriate method a certain number of factors should consider which determines the method and the technology selection, which must be done by a deep and professional mineralogical and chemical study of the raw ore. World experience arguing that selection of the process flow sheet of laterites is very complex. A careful study in specialized institutions and pilot plants is the key factor for choosing the final flow sheet.

Like as an example: a high efficient pilot plant developed in Australia can process both types of laterite ores in one single hydrometallurgical flow sheet, which calls “Direct Nickel”. This solution may result in low capital investments and low operation cost as well.

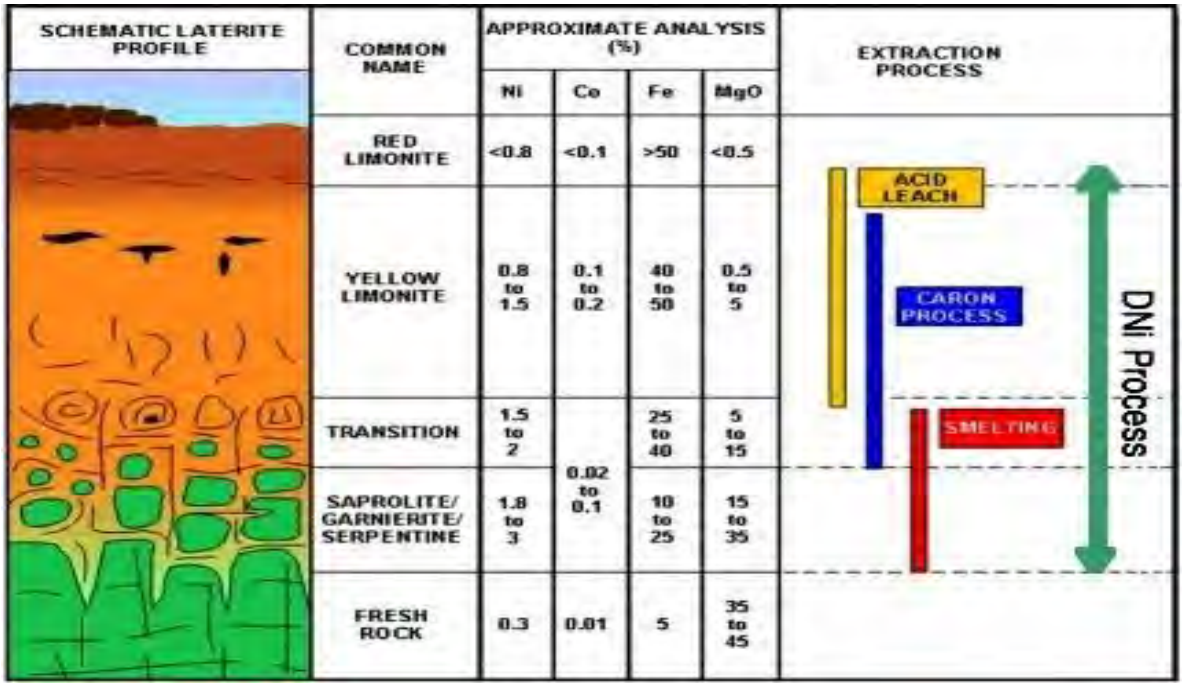

Figure 2. Schema of different methods used in laterite ore treatment

Table 2. Advantages of DNi process

DNi	HPAL	Ferronickel
Lower Capex	Very High Capex	High Capex
Utilise full profile	Mostly uses limonite	Only uses saprolite
Low Opex	Mod to High Opex	Mod Opex
Simple atmospheric technology	High pressure and temperature operation	High temperature technology
High recoveries of Ni and Co	High recoveries of Ni and Co	High recoveries of Ni, Co not paid
Low scale-up thresholds	High scale-up threshold	Mod scale-up threshold
Possible by-products – Hematite, MgO	Possible by-products – Ammonium Sulphate	Fe units paid

The scheme in Fig. 2 and the table 2 show the advantages of DNi process ((Direct Nickel Process is a hydrometallurgical method for extracting nickel and cobalt from all laterite types limonite and saprolite using nitric acid) comparing with other methods. (McCarthy, 2014, 2018). PT Nickel Halmahera Timur Indonesia and Teck's Araguaia Brazil are examples, where the first one provides a return on investment at the level of 37.5 % per annum. (Ahmataj, 2019).

In regard to the above arguments, we think that the construction of the hydrometallurgical plant for laterites (including both types of Iron-Nickel ore Nickel-Silicate ores) would create a secure future for a range of investments in other areas.

Let take an example: currently the copper flotation plant in Fush Arez is not producing pyrite concentrate and store it as slurries in tailing pond. The demand for sulfuric acid, or other acids like nitric or hydrochloric in the process of acid leaching in the hydrometallurgical plant of Nickel

and Cobalt would open the possibility of sulfuric acid production as the basis for other acids, which will affect developing other sulphide ore basins of Mirdita and Puka as well as respective industries for acid production.

The building of hydrometallurgical plant will immediately increase the demand for raw laterite ores. This will result in developing mining areas in Librazhd, Pogradec and Devoll. In the future the experience from this area will be transferred in the region of Kukes-Krumë area, where there are significant reserves of Nickel and Cobalt ores.

In order to succeed the above plan should be submitted to an Institute and Pilot Plant with experience in this field a representative sample in the quantity required and to be sent in the destination after reaching in an agreement for this purpose.

The starting point for this would be the possibility to carry out a technological study for processing and developing of the projects for construction of a hydrometallurgical plant to process both types of ores in the country: Iron-Nickel and Nickel-Silicate.

The research and development of technological projects for investment calculation based on the proposal of the above-mentioned points will require a period of around nine months from the time when the parties reach an agreement and make a decision about the realization of the project. The preliminary cost and income evaluation is shown in Table 3.

Table 3. Hydrometallurgical processing of Nickel ores in Albania

Key - Facts		
Estimated reserve in Albania		310.000.000 t
Present mining activity		8,00%
Running Grade	Nickel (Ni)	1,00%
Running Grade	Iron (Fe)	43,00%
Current processing plant		not existing
Yearly production	Nickel (Ni)	13.500 t
Yearly production	Cobalt	900 t
By-Products	Magnesium	
	Chrome Ore	
	Iron Ore	

Cost & income evaluation			
Study & Design Work			$ 3.000.000,00
Total project cost			$ 500.000.000,00
payback period		7 years	
Yearly income from Nickel sales	12.000 $ per t	13.500 t	$ 162.000.000,00
Yearly income from Cobalt sales	31.000 $ per t	900 t	$ 27.900.000,00
Yearly running cost for processing incl. salaries	5.000 $ per t	14.400 t	$ 72.000.000,00
Estimated yearly profit			**$ 117.900.000,00**

Time-Frame	
Feasibility-Study & Design work;	12 - 18 month
Plant setup & installation	30 month
Total time unitl first full production	42 - 48 month

5. CONCLUSION

The geological reserves of laterite nickel ores with a Ni content of about 1.05 % and Co of about 0.06% are in the amount of about 310 million tons in Albania. It is recommended that a reassessment of the reserves be made initially.

From the studies carried out and from the experience in the country and in the world, it results that there is the possibility of their exploitation and processing with economic benefit, but for this, full feasibility studies are needed, as well as projects of factories that will process them.

From the studies carried out, it results that mixed iron nickel and nickel silicate ores can be exploited and processed in the amount of 2 to 4 million tons per year, with positive technical and economic indicators.

There are two possible processing schemes, the RKEF and DNi.

The RKEF process has been experimented in a pilot plant for laterite ores, with a sample where Ni-Si predominated with good recovery in value 90 %, but the final product Fe-Ni contained 15 % Ni. It is necessary to continue testing obtaining Ni content in vale 25 % in Fe-Ni.

The DNi process should be experimented, since according to tests carried out in a pilot plant in Australia and two plants in industrial scale with laterite raw materials of Fe-Ni and Ni-Si has resulted with good technical and economic indicators, making complex use of all constituent minerals of Ni, Co, Fe, Mg and Cr.

REFERENCES

Ahmataj, F., Demi, G., Goskolli, E., Swanepoel, R., Wilson, H., (2015), “Pre-Feasibility and Sustainable Study for Hydrometallurgical Processing of Nickel Laterite Ores in Albania”, Proposal to the Ministry of Energy, Albania.

Ahmataj, F., Demi, G., (2019), “Proceedings of XVIII Balkan Mineral Processing Congress”, 333–339.

Goskolli, E., (2025), “Nickel in Albania”, Paper presented at the Conference for CRM/SRM organized by Regional Innovation Centre in Albania.

Lleshi, Z., Demi, G., Fetahu, K., Lohja, N., (2018), “Technical and Economic Assessment for the Nickel Silicate Industry in Albania”, Study for the Ministry of Economy, Albania.

McCarthy, F., Brock, G., (2014), “Direct Nickel Projects Pty Limited”.

McCarthy, F., Gower, C., (2018), “Direct Nickel Process – Breakthrough Technology”.

Shouldice, T., Folinsbee, J. G., (2010), “Mineralogical Assessment of a Nickel Iron Ore Sample, Skroska Mine – Albania”, T Metallurgical Services Ltd., Canada.

SYNTHESIS OF PSEUDOBROOKITE POWDER VIA OXIDATIVE CALCINATION OF ILMENITE FOR PHOTOCATALYTIC APPLICATIONS

Yahya SORKHE[1,*], Onur OZTÜRK[2], Pegah BAVAFA[1], Fatma ARSLAN[3], Cüneyt ARSLAN[1]

[1]Metallurgical and Materials Engineering Department, Istanbul Technical University, Istanbul, Türkiye
[2]ONATUS Öngörü Teknolojileri, Türkiye
[3]Mineral Processing Engineering Department, Istanbul Technical University, Istanbul, Türkiye
**Corresponding author: sorkhe20@itu.edu.tr*

A B S T R A C T

Pseudobrookite is an iron–titanium oxide whose phase formation and defect chemistry are governed by composition, oxygen activity, and impurity content. Here, pseudobrookite is synthesized directly from natural ilmenite concentrate using a combined CALPHAD-based thermodynamic and experimental approach. Single-step oxidative calcination under ambient atmosphere enables direct conversion without acid leaching, solvent-based processing, or precursor purification. Thermodynamic calculations show a broad stability window for pseudobrookite under oxidizing conditions and reveal the influence of mineral-derived impurities on phase equilibria and defect formation. These findings are supported experimentally, with X-ray diffraction confirming pseudobrookite formation after calcination at 1200 °C and electron microscopy revealing a mesoporous microstructure. X-ray photoelectron spectroscopy indicates mixed Fe^{2+}/Fe^{3+} states and oxygen vacancies, while UV–Vis diffuse reflectance spectroscopy shows strong visible-light absorption with direct band gaps of 2.1–2.2 eV. As functional validation, the material exhibits visible-light-driven methylene blue degradation, achieving ~39% removal after 240 min.

Key words: *Pseudobrookite, ilmenite, oxidation calcination, CalPhad, photocatalysis*

1. INTRODUCTION

Pseudobrookite (Fe_2TiO_5) is an iron–titanium oxide with an orthorhombic crystal structure that has attracted increasing attention owing to its high thermal stability, structural flexibility, and tunable electronic properties. The pseudobrookite lattice consists of a close-packed oxygen framework with Fe and Ti cations occupying octahedral sites, allowing a wide range of cation distributions and oxidation states. Owing to this structural adaptability, pseudobrookite has been explored in various functional applications, including photocatalysis (Anh et al., 2022; Melo et al., 2020), photoelectrochemical water splitting (Bassi et al., 2014; Centurion et al., 2023), gas sensing (Nikolić et al., 2018; IEEE, 2016), and magnetic or semiconducting devices (Pakizeh and Mohammadi, 2021; Haerani et al., 2023). In addition, its high refractive index, strong visible-light absorption, and resistance to thermal degradation make pseudobrookite relevant for high-temperature ceramic applications such as pigments and protective coatings (Dondi et al., 2007).

From a materials processing perspective, pseudobrookite is conventionally synthesized via solid-state reactions between TiO_2 and Fe_2O_3 at elevated temperatures, typically above 1300 °C, to obtain phase-pure products (Hirota and Bradt, 1991; Dondi et al., 2007). Although effective, these routes are energy-intensive and rely on high-purity oxide precursors. Alternative wet-chemical approaches, including sol–gel, co-precipitation, and polymer-assisted synthesis, offer improved compositional homogeneity and particle size control but introduce additional processing steps, organic additives, and post-synthesis heat treatments (Ramezani et al., 2015; Vinogradov et al., 2012). These complexities increase production costs and limit scalability, particularly for large-volume ceramic applications. Consequently, increasing attention has been directed toward the use of natural mineral resources as alternative precursors for pseudobrookite synthesis.

Natural ilmenite ($FeTiO_3$) represents an abundant and low-cost feedstock for Fe–Ti oxide ceramics. Several studies have reported the formation of ilmenite-derived pseudobrookite through routes involving acid leaching, selective dissolution, or chemical adjustment of the Fe/Ti ratio prior to calcination (Mahmoud et al., 2018; Chen et al., 2010). While these approaches can improve phase purity, they introduce additional chemical consumption, generate waste streams, and complicate environmental management. Furthermore, low-temperature sol–gel and nanoparticle-based strategies, although valuable for fundamental studies, are less compatible with scalable ceramic processing and industrial deployment (Vinogradov et al., 2012; Gao et al., 2015).

Despite extensive experimental work on pseudobrookite synthesized from synthetic precursors, the direct formation of pseudobrookite from natural ilmenite concentrates via simple thermal processing remains insufficiently explored. In particular, the role of mineral-derived impurity elements in governing phase stability, solid-solution behavior, and defect chemistry has not been systematically addressed. Ilmenite concentrates commonly contain Mg, Mn, Al, Si, and Ca as accessory components, which can alter phase equilibria, influence cation distribution, and promote defect formation during high-temperature oxidation (Guo et al., 1999; Xirouchakis et al., 2002). These impurity effects are often treated as undesirable or eliminated through chemical processing, rather than being examined as intrinsic thermodynamic variables in mineral-based synthesis routes.

Thermodynamic analysis provides a powerful framework for understanding phase formation and stability in multicomponent oxide systems. CALPHAD-based approaches enable quantitative prediction of phase equilibria, solid-solution limits, and impurity partitioning as functions of temperature, composition, and oxygen activity. Although CALPHAD methods have been widely applied to Fe–Ti–O systems in metallurgical and geochemical contexts (Eriksson et al., 1996; den Hoed and Luckos, 2011), their application to guiding the synthesis of functional Fe–Ti oxide ceramics directly from natural mineral sources remains limited.

In this work, these gaps are addressed through a combined experimental and thermodynamic investigation of pseudobrookite formation directly from natural ilmenite concentrate. A single-step oxidative calcination under ambient atmosphere is employed to convert ilmenite to pseudobrookite without acid leaching or solvent-based processing. CALPHAD-based thermodynamic analysis is used to elucidate phase stability, impurity solubility, and defect-related nonstoichiometry under the selected processing conditions. The resulting materials are systematically characterized to correlate thermodynamically predicted impurity behavior with experimentally observed phase assemblages, defect chemistry, and optical properties. This integrated approach establishes a thermodynamic basis for impurity-tolerant, scalable synthesis of pseudobrookite from natural resources and provides insight into the defect-mediated properties of mineral-derived Fe–Ti oxide ceramics.

2. MATERIAL AND METHODS

2.1. Material

In this study, ilmenite concentrate obtained from Kahnuj, Iran, with the chemical composition listed in Table 1, was used as the primary precursor for pseudobrookite synthesis. The ilmenite powder (particle size < 30 mesh) was pre-ground using a vibratory disk mill to ensure homogeneity. For comparison, a reference sample was prepared by mixing commercial TiO_2 and Fe_2O_3 powders in a 1:1 molar ratio. The TiO_2 powder had a purity of 97% and an average particle size below 0.2 μm, while the hematite powder had a purity of 98% and a particle size below 45 μm. The reference sample provides a thermodynamically simplified Fe–Ti–O system for comparison with the impurity-containing ilmenite-derived material.

Table 1. Composition of the ilmenite concentrate

Component	TiO_2	Fe_2O_3 [t]	SiO_2	Al_2O_3	MgO	MnO	CaO	FeO	P_2O_5
Wt.%	44.74	48.59	4.65	0.97	1.31	0.8	1.81	35.5	0.1

2.2. Method

For pseudobrookite synthesis, both the ilmenite-derived and reference powder mixtures were calcined in a tube furnace at 1200 °C for 2 h under ambient atmosphere. The morphology and elemental distribution of the synthesized powders were examined using scanning electron microscopy (SEM) coupled with elemental mapping, employing a TESCAN field-emission scanning electron microscope (FESEM, MIRA3). Phase composition was analyzed by X-ray diffraction (XRD) using a PANalytical AERIS diffractometer with Co Kα radiation (λ = 1.79 Å). The collected diffraction patterns were converted to Cu Kα format using HighScore Plus software for phase identification and comparison. The specific surface area and pore characteristics were determined by N_2 adsorption–desorption measurements using a Chem BET-3000 analyzer. Particle size distribution was measured by dynamic light scattering (DLS) using a 3-MPT instrument. X-ray photoelectron spectroscopy (XPS) was performed using a SPECS XPS system to analyze surface chemical states.

Thermodynamic calculations were conducted using the CALPHAD approach with Thermo-Calc software (version 2023a) to investigate phase stability and equilibrium behavior during the calcination of ilmenite and TiO_2–Fe_2O_3 mixtures. The stability regions of pseudobrookite and associated phases were evaluated using the TCOX v12 thermodynamic database. The solubility behavior of common ilmenite-derived impurities (MgO, MnO, Al_2O_3, CaO, and SiO_2) within the pseudobrookite structure was also assessed. All calculations were performed at a total pressure of 1 atm with a system size of 1 mol. Phase stability diagrams were additionally visualized using HSC Chemistry (version 9), and the TiO_2–Fe_2O_3 binary phase diagram was examined using the online FactSage database. All thermodynamic calculations assume local equilibrium conditions during high-temperature calcination, which is justified by the prolonged dwell time (2 h) at 1200 °C and the enhanced cation mobility under oxidizing conditions. The calculations therefore represent equilibrium phase relations approached during synthesis rather than transient kinetic states.

3. RESULTS AND DISCUSSION

3.1. Computational Thermodynamic Analysis

The binary TiO_2–FeO phase diagram (Figure 1) indicates that pseudobrookite is thermodynamically stable at elevated temperatures, typically above ~800 °C, within the TiO_2-rich region of the system (approximately 0.52–1.0 TiO_2 mole fraction). Under these conditions, pseudobrookite forms through solid-state reactions between ilmenite and rutile and remains stable up to the liquidus region at approximately 1500–1550 °C. This wide stability window and compositional tolerance make pseudobrookite suitable for high-temperature ceramic applications and enable flexibility in the Fe/Ti ratio (Chen et al., 2010). With increasing temperature, phase evolution proceeds from rutile and ilmenite toward pseudobrookite, followed by partial melting and the formation of a pseudobrookite–liquid region (den Hoed and Luckos, 2011). While the binary phase diagram provides a useful first approximation, it does not fully capture the complexity of practical systems derived from natural minerals. A more realistic description is provided by the ternary Fe_2O_3–FeO–TiO_2 phase diagram, in which pseudobrookite coexists in equilibrium with hematite (Fe_2O_3) and rutile (TiO_2) over a broad compositional range (Eriksson et al., 1996). This framework more accurately reflects the phase relations expected during ilmenite calcination under oxidizing conditions.

Although thermodynamic calculations predict decomposition of pseudobrookite at lower temperatures, its persistence at room temperature can be explained by kinetic stabilization. The transformation of pseudobrookite into TiO_2 and Fe_2O_3 (or ilmenite) requires overcoming high activation energy barriers, which suppress spontaneous decomposition (Gao et al., 2015). In addition, the orthorhombic crystal structure accommodates Fe^{3+} and Ti^{4+} cations over multiple octahedral sites, providing structural tolerance to compositional variation. Naturally occurring impurities or dopants may further stabilize the lattice through substitutional incorporation or local defect formation (Berry et al., 1997). This intrinsic flexibility enables the formation of solid solutions between Fe_2TiO_5 and $FeTi_2O_5$, allowing control over iron oxidation state and associated electronic and optical properties (Guo et al., 1999; Pakizeh and Mohammadi, 2021).

The phase stability diagram of the Fe–O–Ti system at 1200 °C (Figure 2) shows that phase equilibria are governed by the chemical potential of TiO_2 and the oxygen partial pressure. At high oxygen activity and elevated TiO_2 chemical potential, Ti-rich pseudobrookite ($FeTi_2O_5$) is stabilized, whereas lower Ti chemical potential and reduced oxygen activity favor Fe-rich pseudobrookite (Fe_2TiO_5). The formation of pseudobrookite during calcination in air indicates that the ilmenite precursor composition and oxidizing atmosphere promote Fe^{2+} oxidation to Fe^{3+}, thereby stabilizing the ferric pseudobrookite phase under the selected processing conditions (Son et al., 2019).

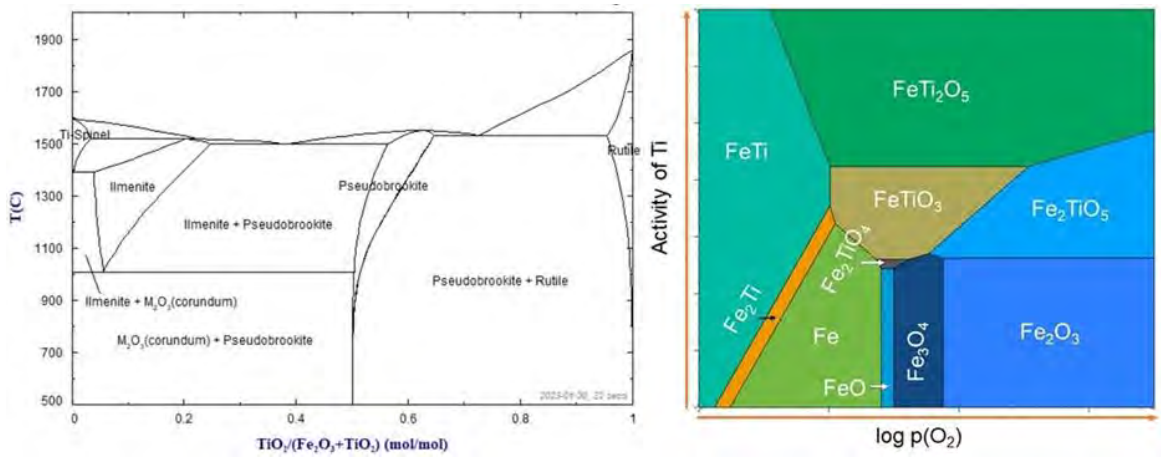

Figure 1. Binary phase diagram of Fe_2O_3-TiO_2 (a) and phase stability diagram of Fe-Ti-O at the temperature of 1200°C

The crystal structures of ferrous $FeTi_2O_5$ and ferric Fe_2TiO_5 pseudobrookite, illustrated in Figure 2(a), are based on a common orthorhombic lattice consisting of a close-packed oxygen framework with cations occupying octahedral sites. In $FeTi_2O_5$, Fe^{2+} and Ti^{4+} cations are preferentially ordered in alternating layers along the b-axis, resulting in a partially ordered structure. In contrast, Fe_2TiO_5 exhibits a higher degree of cation disorder, with Fe^{3+} and Ti^{4+} distributed over multiple octahedral sites within the Cmcm space group. This disordered arrangement arises from the similar ionic radii and comparable charges of Fe^{3+} and Ti^{4+}, allowing both cations to occupy equivalent crystallographic positions with minimal energetic penalty (Guo et al., 1999). Iron cations preferentially occupy the 4c sites at lower Fe contents but increasingly populate the 8f sites as the Fe/Ti ratio increases, reflecting the compositional flexibility of the pseudobrookite structure.

Impurity incorporation within the pseudobrookite lattice is governed primarily by ionic size, charge compatibility, and associated lattice strain. Cations with ionic radii and charges comparable to Fe^{3+} or Ti^{4+}, such as Mn^{2+}, Mn^{3+}, and Al^{3+}, can partially substitute into the Fe_2TiO_5 structure within defined solubility limits (Wu et al., 2012; Siegel and Müller, 1979). In contrast, larger cations such as Ca^{2+} and Mg^{2+} exhibit limited solubility due to significant size

mismatch with the available octahedral sites, leading to the formation of secondary oxide or silicate phases rather than lattice incorporation (Balcells et al., 2006; Xirouchakis et al., 2002). Similar impurity behavior is expected for Ti-rich pseudobrookite ($FeTi_2O_5$).

Figure 2(b) presents the calculated phase evolution during ilmenite calcination as a function of temperature. Pseudobrookite is the dominant solid phase over a wide temperature range between 500 and 1200 °C, confirming its thermodynamic stability under typical calcination conditions. At temperatures above approximately 1270 °C, the fraction of pseudobrookite decreases sharply with the onset of liquid-phase formation. Minor phases such as spinel, olivine, halite, and melilite are thermodynamically unstable at elevated temperatures. The presence of Ca and Si impurities promotes the formation of calcium silicate phases such as $CaSiO_3$, while limited formation of $CaSiTiO_4$ may occur through reactions involving Ti extracted from the pseudobrookite lattice (Mostafa et al., 2022; CrystEngComm, 2020).

The temperature-dependent solubility of impurity oxides within pseudobrookite is shown in Figure 2(c). The decreasing solubility of SiO_2 and MgO with increasing temperature reflects their poor structural compatibility with the host lattice and may result in impurity exsolution or silicate phase formation during cooling (Kim et al., 2012; Mohassab-Ahmed et al., 2014). In contrast, MnO and Al_2O_3 exhibit increasing solubility at elevated temperatures, consistent with their favorable ionic radii and substitutional behavior within the pseudobrookite structure (Woo et al., 2010; Liu et al., 2017). The calculated increase in Ti content within pseudobrookite at higher temperatures suggests a compositional shift toward Ti-rich end-members approaching $FeTi_2O_5$, while the Fe content remains relatively stable, reflecting the strong preference of Fe^{3+} for octahedral coordination in the pseudobrookite lattice (Eriksson et al., 1996).

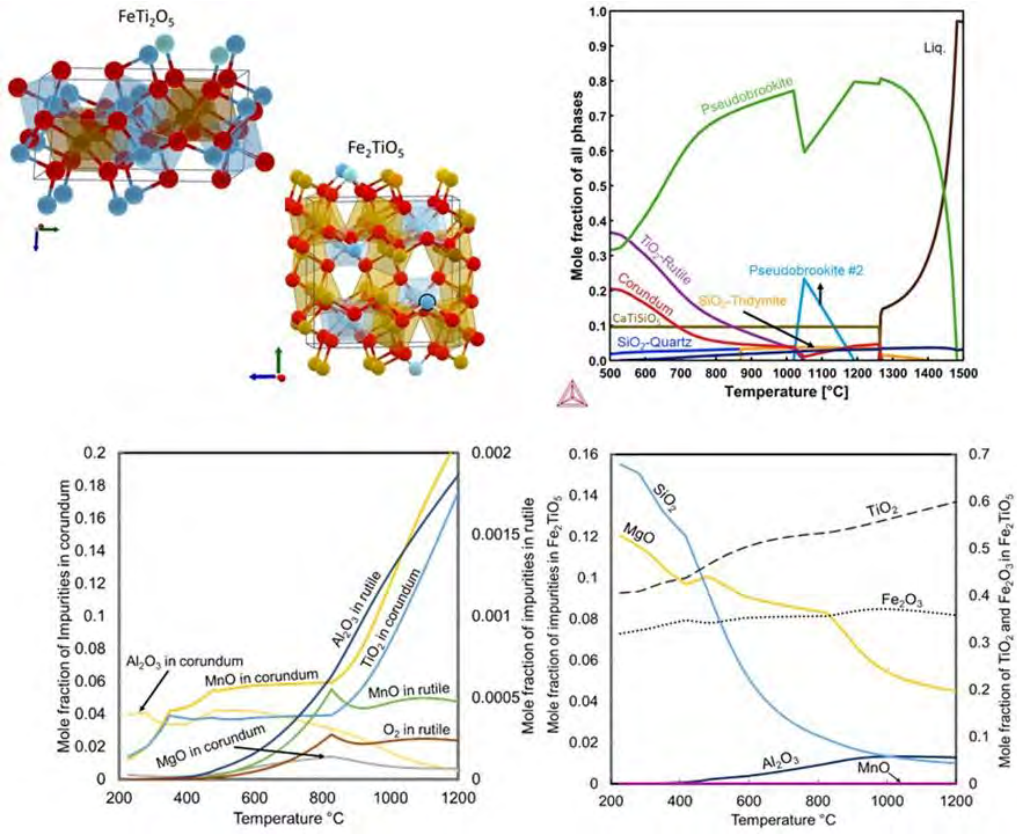

Figure 2. Crystal structure of ferric and ferrous pseudobrookite obtained from the Materials project website (a), mass fraction of all phases during calcination of Ilmenite (b), mole fraction of TiO_2, Fe_2O_3, and impurities in the Pseudobrookite phase (c) and mole fraction of impurities in rutile and corundum phases (d)

The calculated solubility behavior of impurity elements in coexisting phases is summarized in Figure 2(d). Magnesium predominantly forms MgO-rich phases with only limited incorporation into pseudobrookite over a narrow temperature interval, while MnO and Al_2O_3 dissolve preferentially in hematite and rutile. Excess Fe_2O_3 and TiO_2 contribute to solid-solution formation in pseudobrookite or doping of rutile and corundum phases, further highlighting the impurity-tolerant nature of the Fe–Ti–O system during ilmenite calcination (Xirouchakis et al., 2002; Carmichael and Ghiorso, 2018).

3.2. Phase Analysis

Figure 4(a) presents the XRD patterns of the raw ilmenite concentrate and the calcined samples PB1 and PB2. The diffraction pattern of the untreated ilmenite exhibits intense reflections at $2\theta \approx 32°$ and 35°, which are characteristic of $FeTiO_3$, confirming ilmenite as the dominant crystalline phase (Dewan et al., 2010; Minerals, 2021). Additional weak reflections are attributed to minor accessory phases associated with the impurity components listed in Table 1. After calcination at 1200 °C, pronounced changes in the diffraction patterns are observed, indicating successful phase transformation to pseudobrookite.

Sample PB1 shows sharp and well-defined diffraction peaks that can be indexed exclusively to Fe_2TiO_5 (PDF 96-101-1343), demonstrating the formation of a highly crystalline and phase-pure pseudobrookite structure (Chen et al., 2010). This behavior is consistent with previous studies reporting that high-temperature solid-state synthesis enhances crystallinity and phase purity in pseudobrookite ceramics (Hirota and Bradt, 1991; RSC Advances, 2021). In contrast, PB2 exhibits pseudobrookite as the dominant phase but with broader and lower-intensity reflections. As highlighted in the enlarged view of the main pseudobrookite peak at $2\theta \approx 25.5°$ in Figure 4(b), PB1 displays significantly narrower peak widths than PB2. The peak broadening observed for PB2 is attributed to lattice distortion and compositional disorder arising from the incorporation of naturally occurring impurities present in the ilmenite precursor. Such impurity-induced lattice distortion is thermodynamically expected in multicomponent Fe–Ti–O systems and reflects substitutional solid-solution formation within the pseudobrookite stability domain (Guo et al., 1999; Xirouchakis et al., 2002).

Raman spectra of the ilmenite precursor and calcined samples are shown in Figure 4(c), together with reference spectra for rutile TiO_2, Fe_2TiO_5, and Fe_2O_3. The Raman spectrum of PB1 is characterized by sharp and well-resolved bands, particularly in the 200–300 cm^{-1} region corresponding to Fe–O–Ti lattice vibrations, and in the 650–700 cm^{-1} range associated with symmetric stretching of FeO_6 and TiO_6 octahedra (Mullen and McCallum, 2013; Naveed-Ul-Haq et al., 2023). The well-defined nature of these modes reflects the high crystallinity and structural ordering of PB1. In contrast, PB2 exhibits broader Raman features, indicative of increased structural disorder. The disappearance of ilmenite-related modes and the emergence of characteristic pseudobrookite bands confirm complete phase transformation. Broad spectral features observed in the 400–600 cm^{-1} range suggest mixed Fe^{3+}–Ti^{4+} interactions and are indicative of Fe^{2+} oxidation to Fe^{3+} during high-temperature calcination (ISIJ International, 2015).

FTIR spectra of the raw ilmenite and synthesized pseudobrookite samples are presented in Figure 4(d). The ilmenite spectrum exhibits a broad absorption band in the 3400–3600 cm^{-1} region, attributed to O–H stretching vibrations arising from adsorbed moisture or hydroxyl groups, along with distinct metal–oxygen vibrational modes in the 1000–500 cm^{-1} range corresponding to Fe–O and Ti–O bonds (Schwertmann et al., 1995). Following calcination, the pseudobrookite samples display pronounced changes in the fingerprint region. The emergence of multiple absorption bands between 700 and 500 cm^{-1} is characteristic of Fe–O–Ti bridging vibrations and Fe–O stretching modes within the Fe_2TiO_5 structure (Inorganic Chemistry, 2016). The increased intensity and sharpening of these bands reflect the formation of a robust

oxide framework, consistent with the enhanced thermal and structural stability of pseudobrookite (Dondi et al., 2007). Moreover, the reduced intensity of the O–H stretching band indicates diminished surface-adsorbed species, which may facilitate improved surface reactivity during photocatalytic processes (Chen et al., 2015).

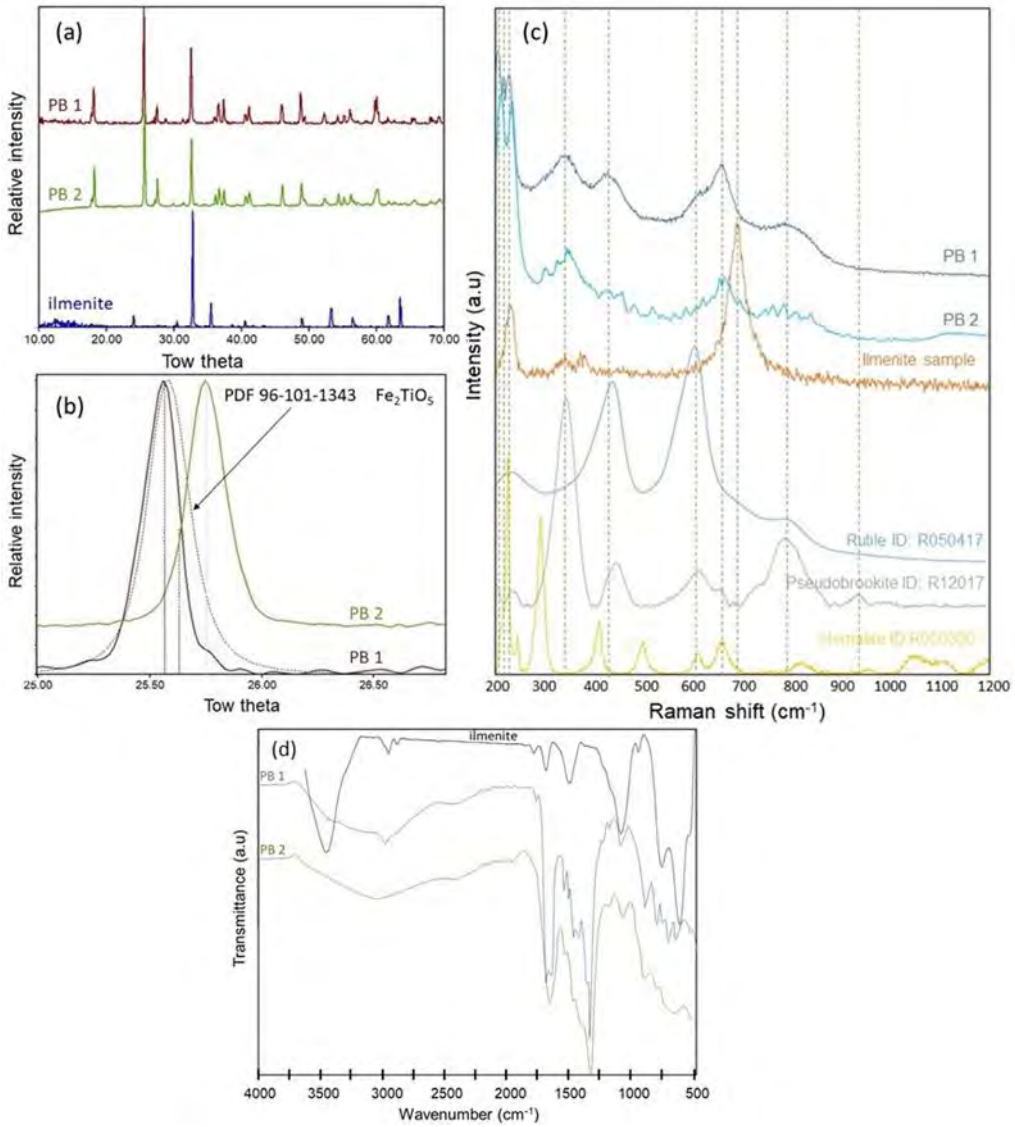

Figure 4. XRD analysis of the raw ilmenite and synthesized samples (a), main peaks shift in synthesized pseudobrookite (b), Raman spectra (c), and FTIR spectra of ilmenite and synthesized samples

3.3. Morphological Characterization

Figure 5 presents the SEM image and corresponding elemental mapping (EDS) analysis of the PB2 sample. The Fe and Ti elemental maps reveal a relatively homogeneous distribution across the particles, consistent with the formation of a pseudobrookite matrix with uniform Fe–Ti composition. This observation supports the XRD and Raman results, which identified pseudobrookite as the dominant crystalline phase after calcination (Chen et al., 2010; Guo et al., 1999). In contrast, the elemental maps of Si, Al, Ca, Mg, and Mn exhibit localized enrichment and depletion in specific regions, indicating non-uniform incorporation of impurity elements. Such behavior suggests the presence of impurity-rich domains or secondary phases located within or at the boundaries of the pseudobrookite matrix. Among these elements, Si displays particularly low solubility in the pseudobrookite structure due to its strong tendency to form silicate compounds rather than substitute into octahedral Fe or Ti sites (Xirouchakis et

al., 2002). Accordingly, the Si-rich regions observed in the EDS maps are most likely associated with silica-based or calcium silicate phases, such as SiO_2, $CaSiO_3$, $CaSiTiO_5$, or Al–Ca silicates, depending on local chemical availability (Balcells et al., 2006; Mostafa et al., 2022).

The heterogeneous spatial distribution of Al, Ca, Mg, and Mn can be attributed to their limited and temperature-dependent solubility within the pseudobrookite lattice. These elements may partially dissolve into the structure or segregate to form secondary oxide or silicate phases depending on ionic radius, charge compatibility, and local thermodynamic driving forces (Guo et al., 1999; Xirouchakis et al., 2002). Such non-uniform impurity distributions are commonly observed in mineral-derived ceramic oxides and can arise from limited solid-state diffusion, impurity rejection during lattice growth, or segregation during high-temperature oxidation, consistent with thermodynamically constrained substitutional solubility (Carmichael and Ghiorso, 2018).

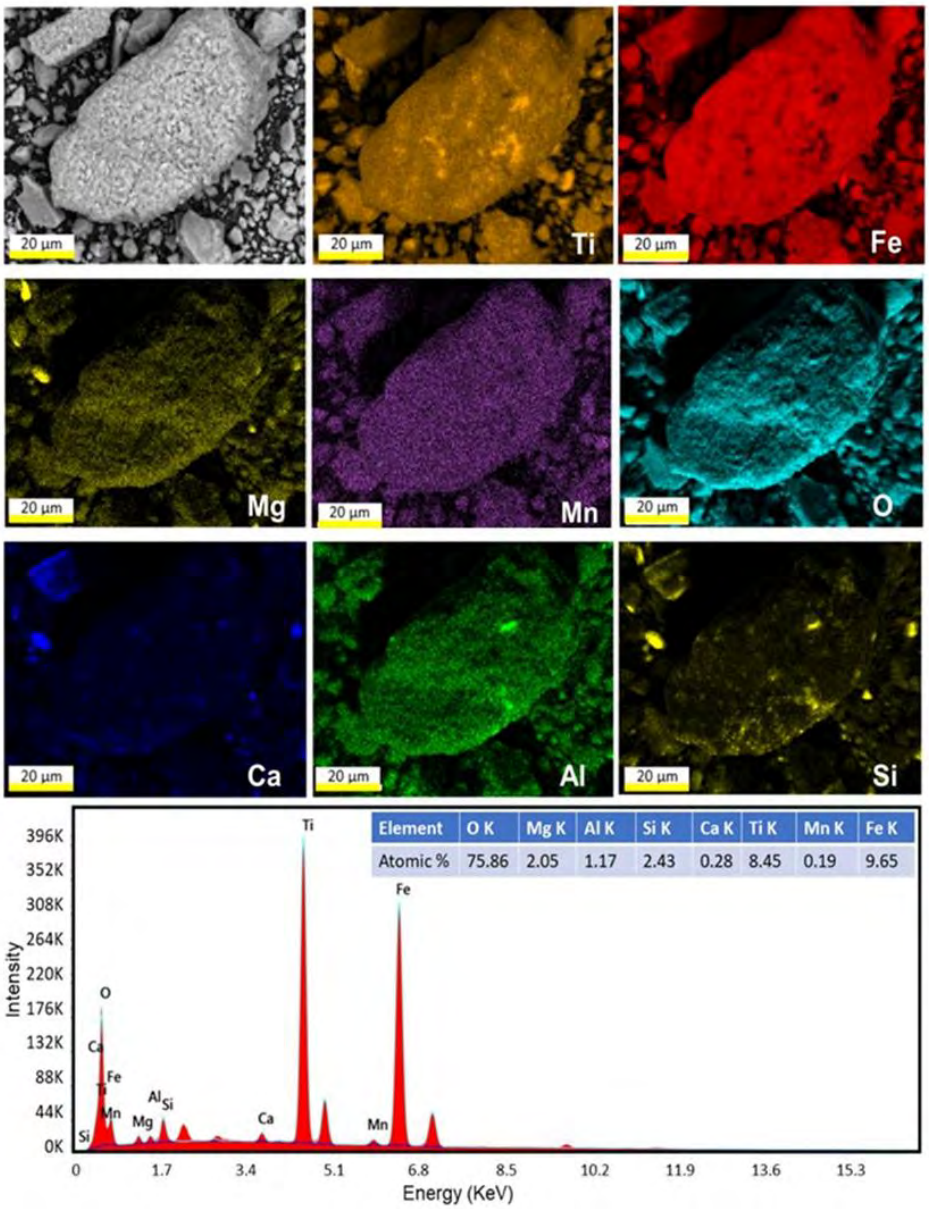

Figure 5. SEM, EDS and MAP analysis of produced PB2 sample

Figure 6(a) shows the morphology of the raw ilmenite concentrate, which consists of large, angular particles with characteristic sizes in the hundreds of micrometers. Following high-temperature calcination and subsequent mechanical milling, a pronounced morphological

transformation is observed, as shown in Figures 6(b) and 6(c). The processed material exhibits significantly reduced particle size and a markedly increased surface roughness relative to the raw ilmenite. The higher-magnification image in Figure 6(c) reveals irregularly shaped particles with jagged edges and a highly textured surface morphology.
This morphological evolution can be attributed to the combined effects of thermal oxidation and mechanical fragmentation. High-temperature calcination induces atomic rearrangement within the ilmenite structure, promoting defect formation, including oxygen vacancies. These defects act as nucleation sites for pore development, while enhanced atomic mobility at elevated temperatures facilitates defect coalescence into mesopores through mechanisms such as surface diffusion and the Kirkendall effect (Chun et al., 2013). Subsequent mechanical milling further fragments the calcined material, exposing defect-rich surfaces and contributing to the development of a rough and porous morphology. Such defect-mediated microstructural evolution is consistent with thermodynamic stabilization of vacancy-rich pseudobrookite under oxidizing conditions (Xirouchakis et al., 2002; Vinogradov et al., 2012).

Quantitative particle size distribution (PSD) analysis, shown in Figure 6(d), corroborates the SEM observations. The majority of particles fall within the 2–8 μm size range, with a peak centered at approximately 5–6 μm, indicating effective size reduction and a relatively narrow distribution. A minor fraction of larger particles (>8 μm) remains, which may be advantageous for solid–liquid separation and handling without significantly compromising accessible surface area (Horváth et al., 2014).

The textural properties of the synthesized pseudobrookite were further evaluated by nitrogen adsorption–desorption measurements. The isotherm shown in Figure 6(e) exhibits a Type IV profile with a pronounced hysteresis loop, characteristic of mesoporous materials (Yu et al., 2007). The corresponding pore size distribution in Figure 6(f) confirms the presence of mesopores predominantly in the 2–20 nm range. This mesoporous architecture promotes efficient mass transport, enhances adsorption of methylene blue molecules, and provides confined environments that facilitate photocatalytic reactions, consistent with defect-assisted mesopore formation in multicomponent Fe–Ti–O systems (Jiao et al., 2008; Dong et al., 2011).

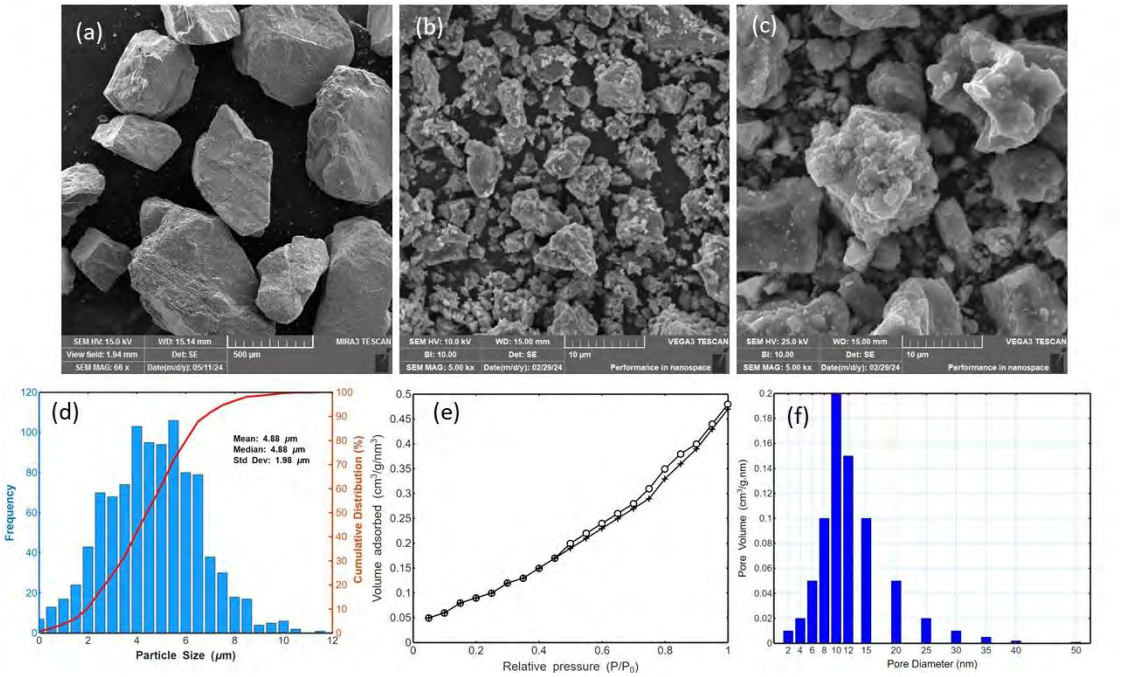

Figure 6. SEM image of raw ilmenite (a), pseudobrookite sample PB2 (b), higher magnification of sample PB2 (c), PSD analysis of synthesized PB2 sample (d), BET analysis of PB2 sample (e), and relative pore diameter (f)

3.4. XPS Analysis

Figure 7(a) presents the survey XPS spectrum of the synthesized pseudobrookite sample, confirming the presence of Fe, Ti, and O as the main constituent elements, together with minor signals arising from impurity elements inherited from the ilmenite precursor. The absence of extraneous peaks indicates effective removal of volatile species during high-temperature calcination and the formation of a chemically stable oxide surface.
The high-resolution Ti 2p spectrum shown in Figure 7(b) exhibits two dominant peaks at binding energies of approximately 458.7 eV and 464.4 eV, corresponding to the Ti $2p_3/_2$ and Ti $2p_1/_2$ spin–orbit components, respectively. These binding energies are characteristic of Ti^{4+} species in octahedrally coordinated TiO_6 environments (Oku et al., 1999; AIP, 2018). A slight asymmetry toward lower binding energies suggests the presence of a minor fraction of reduced Ti^{3+} species, which is commonly associated with oxygen vacancy formation and nonstoichiometric oxide structures generated during high-temperature processing (Chen et al., 2015; Wu et al., 2012).

The Fe 2p spectrum (Figure 7(c)) displays Fe $2p_3/_2$ and Fe $2p_1/_2$ peaks centered at approximately 710.5 eV and 724.1 eV, respectively, accompanied by characteristic satellite features. These spectral characteristics indicate the coexistence of Fe^{3+} and Fe^{2+} oxidation states within the pseudobrookite lattice (Surface Science Spectra, 2000; AIP, 2023). Deconvolution of the Fe $2p_3/_2$ peak reveals a dominant Fe^{3+} contribution with a measurable Fe^{2+} fraction, reflecting partial reduction and charge compensation associated with oxygen deficiency. Such mixed-valence behavior is thermodynamically favored in Fe–Ti–O systems subjected to high-temperature oxidation followed by cooling under ambient atmosphere (Carmichael and Ghiorso, 2018).

The O 1s spectrum shown in Figure 7(d) can be deconvoluted into two primary components. The lower binding energy peak at approximately 530.1 eV corresponds to lattice oxygen (O^{2-}) in the pseudobrookite framework, while the higher binding energy component at around 531.3 eV is attributed to oxygen-deficient environments, surface hydroxyl groups, or defect-related oxygen species (Wang et al., 2016; ZnO Defects, 2019). The relatively high contribution of the defect-related O 1s component (approximately 16% of the total oxygen signal) indicates a substantial concentration of oxygen vacancies within the synthesized pseudobrookite. These oxygen vacancies, together with mixed Fe^{2+}/Fe^{3+} and Ti^{3+}/Ti^{4+} states, reflect defect-mediated charge compensation mechanisms that are thermodynamically stabilized under the applied calcination conditions (Berry et al., 1997; Guo et al., 1999).

Overall, the XPS results confirm that the ilmenite-derived pseudobrookite exhibits significant defect-related nonstoichiometry, characterized by oxygen vacancies and mixed metal oxidation states. These electronic defects play a crucial role in modifying the surface chemistry and electronic structure of pseudobrookite, directly influencing its optical absorption behavior and photocatalytic performance discussed in subsequent sections (Anh et al., 2022; Centurion et al., 2023).

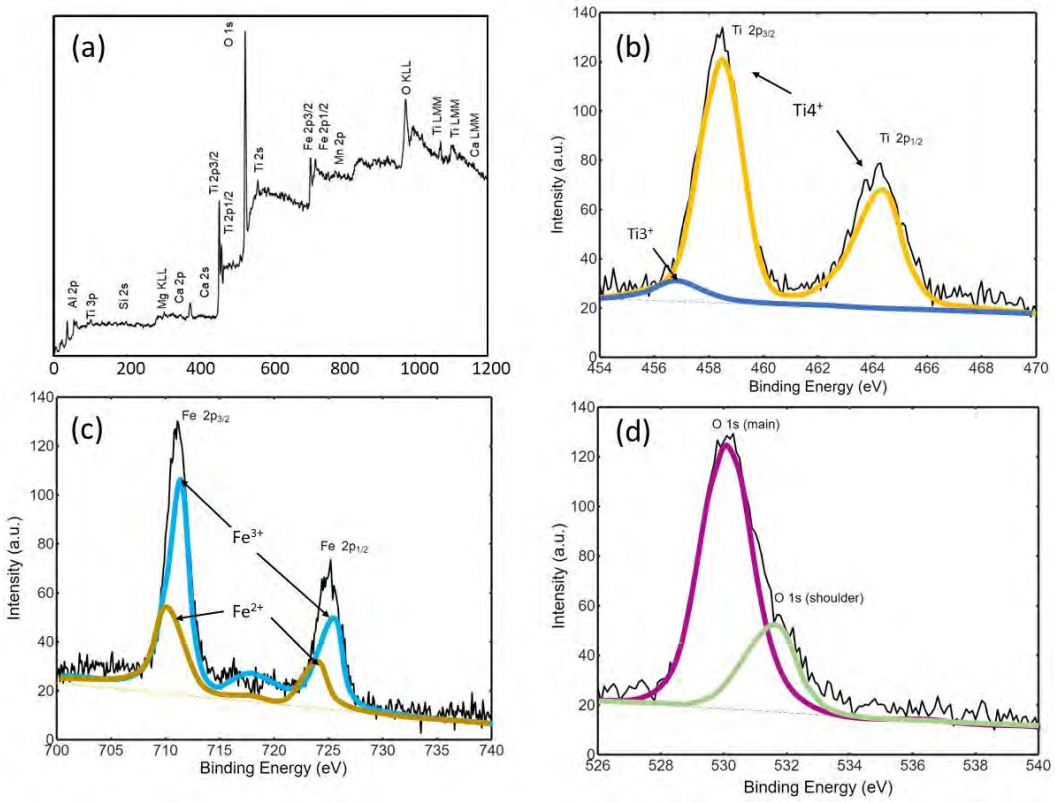

Figure 7. XPS analysis of produced pseudobrookite sample PB2. Wide scan spectrum (a), high resolution spectra of Ti2p (b), Fe2p (c) and O1s (d)

3.5. UV–Vis Spectra Analysis

The optical properties of PB1 and PB2 were investigated using UV–Vis diffuse reflectance spectroscopy (DRS) to evaluate electronic structure modifications arising from defect chemistry and nonstoichiometry. The UV–Vis spectra of the pseudobrookite samples are shown in Figure 8(a). Both PB1 and PB2 exhibit strong absorption in the ultraviolet and visible regions, which is characteristic of Fe-containing oxide materials (Guo et al., 2020). The absorption intensity gradually decreases with increasing wavelength and extends into the visible region up to approximately 650–700 nm, reflecting the presence of Fe-related electronic states within the band structure.

Compared to PB1, sample PB2 exhibits enhanced absorption intensity in the 400–600 nm range. This behavior is attributed to differences in defect concentration and cation distribution within the pseudobrookite lattice, which modify the electronic density of states and light–matter interaction. The enhanced visible-light absorption observed for PB2 is consistent with its lighter brown coloration and reflects increased electronic disorder induced by impurity incorporation and oxidation-state heterogeneity (Pakizeh and Mohammadi, 2021). The broad absorption features observed for both samples arise from overlapping ligand-to-metal charge transfer transitions together with Fe-related d–d electronic transitions in octahedrally coordinated environments (Wongrawang et al., 2016; Wongrawang et al., 2016). Such transitions are commonly observed in mixed-valence transition metal oxides and are strongly influenced by defect chemistry and local coordination symmetry (Predicting Band Structure, 2008).

Optical band gap energies were estimated using Tauc plots, as shown in Figure 8(b), assuming direct allowed electronic transitions. The calculated band gap values are approximately 2.12 eV for PB1 and 2.22 eV for PB2. The slightly larger band gap observed for PB2 is attributed to variations in electronic structure associated with defect chemistry, including differences in

oxygen vacancy concentration and Fe^{2+}/Fe^{3+} valence distribution, as supported by XPS analysis. Changes in oxygen vacancy density are known to induce band-gap modulation by altering the conduction band edge and introducing localized defect states (Kong et al., 2013; Wang et al., 2013). Overall, the UV–Vis results demonstrate that impurity-assisted defect formation and charge compensation mechanisms significantly influence the optical properties of ilmenite-derived pseudobrookite. The resulting visible-light absorption and tunable band gap values in the range of 2.1–2.2 eV provide a thermodynamic basis for the observed photocatalytic behavior discussed in the following section (Anh et al., 2022; Centurion et al., 2023).

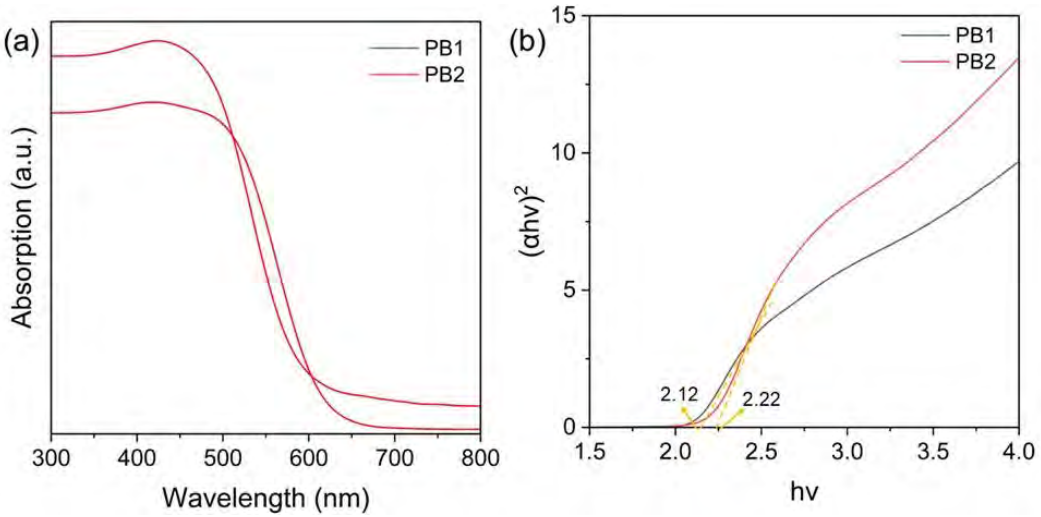

Figure 8. UV-visible spectra of pseudobrookite samples (a), calculated Tauc plot for direct band gap (b)

3.6. Methylene Blue Degradation

The photocatalytic performance of the synthesized pseudobrookite samples was evaluated through methylene blue (MB) degradation under visible-light irradiation as a functional probe of defect-mediated electronic structure. As shown in Figure 9(a), both PB1 and PB2 exhibit measurable photocatalytic activity despite their relatively large particle sizes (2–12 μm). Similar behavior has been reported for micron-sized TiO_2 powders, where photocatalytic efficiency is governed not solely by particle size but also by defect chemistry, surface structure, and electronic properties (Chuan et al., 2008; de Lima et al., 2020). These results indicate that microstructured oxide materials can sustain photoinduced charge transfer when appropriate defect-related electronic states are present.

The observed MB degradation can be rationalized by considering the combined effects of oxygen vacancies, mixed metal oxidation states, and defect-modified optical absorption. XPS analysis confirms a substantial concentration of oxygen vacancies, which act as electron trapping centers and suppress rapid electron–hole recombination, thereby prolonging charge carrier lifetimes (Wang et al., 2023; Patnaik et al., 2018). In addition, the coexistence of Fe^{2+}/Fe^{3+} and Ti^{3+}/Ti^{4+} redox couples enhance internal charge transfer and facilitates the generation of reactive oxygen species under visible-light irradiation (Melo and Gonçalves, 2022; Wongrawang et al., 2016). Upon photoexcitation, Ti^{4+} ions can capture photogenerated electrons to form Ti^{3+} species (Eq. 1), which subsequently transfer electrons to adsorbed oxygen molecules, generating superoxide radicals ($\bullet O_2^-$) (Eq. 2). These radicals play a dominant role in the oxidative degradation of MB molecules (Chen et al., 2010; Vadivel et al., 2016):

$$Ti^{4+} + e^- \rightarrow Ti^{3+} \quad \text{(Eq. 1)}$$

$$Ti^{3+} + O_2 \rightarrow Ti^{4+} + \bullet O_2^- \quad \text{(Eq. 2)}$$

Simultaneously, Fe^{2+} ions can function as hole traps, oxidizing to Fe^{3+} (Eq. 3) and promoting the generation of hydroxyl radicals (•OH) through reactions with water or surface hydroxyl groups (Eq. 4). Hydroxyl radicals are highly reactive oxidizing species capable of attacking and decomposing MB molecules (Xian et al., 2013; Alhashmialameer et al., 2024):

$$Fe^{2+} + h^+ \rightarrow Fe^{3+} \quad \text{(Eq. 3)}$$

$$Fe^{3+} + H_2O \rightarrow Fe^{2+} + \bullet OH + H^+ \quad \text{(Eq. 4)}$$

Previous studies have demonstrated that superoxide radicals play a dominant role in MB degradation under visible-light photocatalysis, particularly in iron- and titanium-based oxide systems (Thin Films ACS Omega, 2022; Vadivel et al., 2016). The interconnected FeO_6 and TiO_6 octahedra within the pseudobrookite crystal structure facilitate efficient charge transport between metal cations and oxygen vacancies, further promoting charge separation and suppressing recombination (Melo et al., 2020; Anh et al., 2022). In addition, the mesoporous morphology observed in PB2 provides accessible surface area and diffusion pathways that compensate for the relatively large particle size, enabling effective interaction between reactive species and MB molecules (Yu et al., 2007; Dong et al., 2011).

Figure 9(b) illustrates the effect of irradiation time on MB removal efficiency. For both samples, degradation efficiency increases steadily with irradiation time. After 240 min of visible-light exposure, PB2 achieves an MB removal efficiency of approximately 39%, whereas PB1 reaches approximately 16.5%. The higher degradation performance of PB2 is attributed to its increased concentration of oxygen vacancies and enhanced defect-mediated electronic disorder, which collectively promote visible-light absorption and reactive species generation (Kong et al., 2013; Anh et al., 2022).

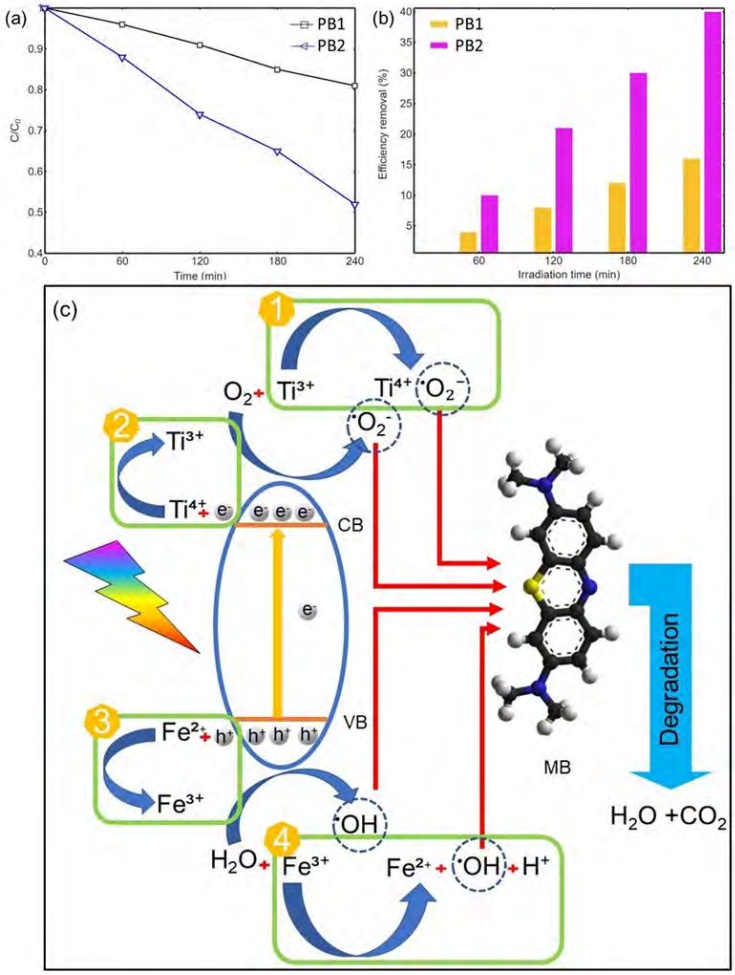

Figure 9. MB degradation with produced PB1 and PB2 psuedobrookite samples (a) and the effect of irradiation time on removing efficiency (b)

4. CONCLUSION

This work investigates the formation of pseudobrookite (Fe_2TiO_5) from natural ilmenite through a combined CALPHAD-based thermodynamic and experimental approach. Emphasis is placed on phase stability, impurity effects, and defect chemistry under high-temperature oxidative conditions, with functional behavior employed solely as validation of thermodynamically predicted features.

i. Thermodynamic calculations confirm that pseudobrookite is stable over a wide temperature range under oxidizing conditions, allowing its direct formation from ilmenite without chemical pre-treatment.
ii. Mineral-derived impurities exhibit limited solubility in pseudobrookite, promoting substitutional disorder, charge compensation, and defect formation consistent with multicomponent Fe–Ti–O equilibria.
iii. Structural and spectroscopic analyses verify pseudobrookite as the dominant phase, with impurity segregation and mesoporosity reflecting thermodynamically constrained solubility and phase evolution.
iv. Mixed Fe^{2+}/Fe^{3+} and Ti^{3+}/Ti^{4+} states together with oxygen vacancies modify the electronic structure, resulting in strong visible-light absorption and direct band gaps of 2.1–2.2 eV consistent with defect-mediated electronic disorder.
v. Visible-light-driven methylene blue degradation provides functional confirmation of the defect chemistry predicted by thermodynamic analysis.

ACKNOWLEDGMENT

Financial support from the Scientific Research Projects Coordination Unit of Istanbul Technical University (BAP), Project No. 45611, is gratefully acknowledged.

REFERENCES

Alhashmialameer, D., Shariq, M., Althikrallah, H. A., Al-Amari, M. M., BaQais, A., Alayyafi, A. A., Assran, A. S., (2024) “Hydrothermally synthesized Nb-doped TiO_2 nanosheets for efficient removal of methylene blue dye on photocatalytic performance”, Physica Scripta, 99 (8) 085915.

Anh, H. C., Anh, N. P., Tri, N., Cuong, H. T., Van, N. T. T., Loc, L. C., (2022) “Small band gap ferric pseudobrookite as a new photo-Fenton catalyst for degradation of phenolic acid”, Journal of Science: Advanced Materials and Devices, 7 (3) 100453.

Balcells, L., et al., (2006) “Absence of ferromagnetism in Fe-doped TiO_2 nanoparticles”, Applied Physics Letters, 89 122501.

Bassi, P. S., Chiam, S. Y., Gurudayal, Barber, J., Wong, L. H., (2014) “Hydrothermal grown nanoporous iron-based titanate (Fe_2TiO_5) for light-driven water splitting”, ACS Applied Materials & Interfaces, 6 (24) 22490–22495.

Berry, F. J., Greaves, C., McManus, J. G., Mortimer, M., Oates, G., (1997) “Structural characterization of tin- and titanium-doped α-Fe_2O_3”, Journal of Solid-State Chemistry, 130 (2) 272–276.

Carmichael, I. S. E., Ghiorso, M. S., (2018), The Effect of Oxygen Fugacity on The Redox State of Natural Liquids, Modern Methods of Igneous Petrology, 191–212.

Centurion, H. A., et al., (2023) “Emerging trends of pseudobrookite Fe_2TiO_5 photocatalyst”, Journal of Alloys and Compounds, 933 167710.

Chen, C.-C., Hu, S.-H., Fu, Y.-P., (2015) “Effects of surface hydroxyl group density on photocatalytic activity of Fe^{3+}-doped TiO_2”, Journal of Alloys and Compounds, 632 326–334.

Chen, X., Deng, J., Yu, R., Chen, J., Hu, P., Xing, X., (2010) “A simple oxidation route to prepare pseudobrookite from raw ilmenite”, Journal of the American Ceramic Society, 93 3296–3300.

Chuan, X.-Y., Lu, A. H., Chen, J., Li, N., Guo, Y. J., (2008) “Photocatalytic activity of natural rutile”, Mineralogy and Petrology, 93 143–152.

Chun, S. R., Sasangka, W. A., Ng, M. Z., Liu, Q., Du, A., Zhu, J., Gan, C. L., (2013) « Joining copper oxide nanotube arrays driven by the Kirkendall effect”, Small, 9 400–406.

den Hoed, P., Luckos, A., (2011) “Oxidation and reduction of iron–titanium oxides”, Oil & Gas Science and Technology, 66 (2).

Dewan, M. A. R., Zhang, G., Ostrovski, O., (2010) “Phase development in carbothermal reduction of ilmenite”, ISIJ International, 50 (5) 647–653.

Dondi, M., Matteucci, F., Cruciani, G., Gasparotto, G., Tobaldi, D. M., (2007) “Pseudobrookite ceramic pigments”, Solid State Sciences, 9 362–369.

Dong, Y., Lu, B., Zang, S., Zhao, J., Wang, X., Cai, Q., (2011) “Removal of methylene blue by adsorption onto SBA-15”, Journal of Chemical Technology & Biotechnology, 86 616–619.
Eriksson, G., et al., (1996) “Phase equilibria in the Fe–Ti–O system”, Berichte der Bunsengesellschaft, 100 1650–1657.

Gao, X. M., Li, M. W., Hou, Y. L., Wang, C. Y., (2015) “Characterization of Fe_2TiO_5 nanocrystallites”, Materials Research Innovations, 19 1–6.

Guo, W. Q., Malus, S., Ryan, D. H., Altounian, Z., (1999) “Crystal structure of $FeTi_2O_5$–Fe_2TiO_5 solid solutions”, Journal of Physics: Condensed Matter, 11 6337.

Horváth, K., Lukács, D., Sepsey, A., Felinger, A., (2014) “Effect of particle size distribution on separation efficiency”, Journal of Chromatography A, 1361 203–208.

Melo, M. A., Centurion, H. A., Lucas, T. T., Muche, D. N., Souza, F. L., Gonçalves, R. V., (2020) “Pseudobrookite Fe_2TiO_5 nanoparticles for photocatalytic O_2 evolution”, ACS Applied Nano Materials, 3 9303–9317.

Mostafa, M., Alrowaili, Z. A., Al Shehri, M. M., Mobarak, M., Abbas, A. M., (2022) “Structural and optical properties of calcium titanate”, Journal of Nanotechnology, 2022 (1) 6020378.

Pakizeh, E., Mohammadi, M., (2021) “Electronic and thermoelectric properties of $Fe_{2-x}Ti_{1+x}O_5$”, Journal of Physical Chemistry of Solids, 149 109802.

Patnaik, S., Swain, G., Parida, K. M., (2018) “Efficient charge transfer in photocatalysts”. Nanoscale, 10 5950–5964.

Vadivel, S., et al., (2016) “Visible-light degradation of methylene blue”, Journal of Colloid and Interface Science, 480 126–136.

Xirouchakis, D., Smirnov, A., Woody, K., Lindsley, D. H., Andersen, D. J., (2002) “Thermodynamics and stability of pseudobrookite-type $MgTi_2O_5$”, American Mineralogist, 87 658–667.

Yu, J., Zhang, L., Cheng, B., Su, Y., (2007) “Hierarchically mesoporous titania”, Journal of Physical Chemistry C, 111 10582–10589.

THE LEACHING KINETICS OF HIGH-GRADE ZINC SILICATE ORE IN SULFURIC ACID

Moloud NAZERI[1,*], Claudio ACUNA[2], Emad ABKHOSHK[1], Zahra RAZI[1]

[1]University of Oulu, Oulu Mining School, P.O. Box 3000, 90570, OULU, FINLAND
[2]Department of Chemical Engineering, Universidad Técnica Federico Santa María, Valparaíso, Chile
**Corresponding author: Moloud.Nazeri@student.oulu.fi*

A B S T R A C T

This study examines the dissolution behavior of a high-grade zinc silicate ore (willemite) in sulfuric acid to improve the efficiency of hydrometallurgical zinc recovery. The limited understanding of kinetic parameters in silicate leaching restricts process optimization in industrial operations. To address this, batch leaching experiments were conducted varying temperature, acid concentration, particle size, solid–liquid ratio, and stirring speed. Higher temperature and acid concentration, smaller particle size, and lower solid loading enhanced zinc extraction, with the best performance at 0.96 M H_2SO_4, 45 °C, and 63–105 µm particle size, achieving 95% zinc extraction within 50 minutes. Applying the shrinking-core model revealed that diffusion through the product layer governs the leaching rate, with an apparent activation energy of 5.02 kJ/mol. These findings clarify the kinetics of zinc silicate dissolution and support more efficient design and control of industrial leaching processes.

Key words: *Zinc silicate ore, willemite, sulfuric acid leaching, leaching kinetics*

1. INTRODUCTION

Zinc is one of the most important non-ferrous metals, widely used in galvanizing, corrosion protection, alloy production, batteries, and various chemical applications. Traditionally, zinc production has relied predominantly on sulfide ores, which can be efficiently beneficiated by flotation and processed through the conventional roast–leach–electrowinning (RLE) route. However, the continuous depletion of high-grade sulfide zinc deposits and the increasing global demand for zinc have shifted attention toward alternative zinc resources, particularly non-sulfide (oxidized) zinc ores (Abkhoshk et al., 2014; Zhou et al., 2020)

Non-sulfide zinc ores occur mainly in silicate and carbonate forms, including minerals such as willemite (Zn_2SiO_4), hemimorphite ($Zn_4Si_2O_7(OH)_2{\cdot}H_2O$), smithsonite ($ZnCO_3$), and hydrozincite. These ores represent a significant portion of the world's undeveloped zinc resources and are increasingly considered strategic feedstocks for future zinc production (Gilg et al., 2008; Hitzman and Reynolds, 2019). Despite their abundance, the processing of oxidized zinc ores remains challenging due to their complex mineralogy, high gangue content, and the presence of reactive silica phases.

Among the available hydrometallurgical routes, sulfuric acid leaching is the most widely applied and industrially established method for zinc extraction from high-grade oxidized zinc ores and concentrates. This process is compatible with existing electrolytic zinc plants and offers high zinc recoveries under controlled conditions (Moradi and Monhemius, 2011; Abdel-Aal and Rashad, 2018). Nevertheless, acid leaching of zinc silicate ores is often accompanied by several drawbacks, including excessive acid consumption, dissolution of impurity elements, and the formation of polymerized silica species that may hinder mass transfer and solid–liquid separation (Li et al., 2023; Zhang et alb., 2024).

To overcome these challenges, alternative leaching systems such as ammoniacal solutions and alkaline media (e.g., NaOH) have been extensively investigated, showing improved

selectivity toward zinc and reduced dissolution of gangue minerals (Ding et al., 2011; Santos et al., 2010; Zhou et al., 2020; Nazeri et al.,2025). Despite these advantages, alkaline leaching routes may suffer from higher reagent costs, solution regeneration issues, and, in some cases, slower reaction kinetics (Abkhoshk et al.,2014).

Compared with zinc sulfide and zinc carbonate ores, the dissolution kinetics of zinc silicate minerals have been far less investigated (Abdel-Aal, 2000; Souza et al., 2007; Abdel-Aal and Rashad, 2018). Moreover, limited kinetic data are available for high-grade zinc silicate ores of Iranian origin. Therefore, the objective of the present study is to investigate the dissolution kinetics of a high-grade zinc silicate ore in sulfuric acid solution. The effects of temperature, acid concentration, particle size, solid-to-liquid ratio, and stirring speed on the zinc leaching rate are systematically examined. In addition, the kinetic data are analyzed using the shrinking core model (SCM) to determine the rate-controlling mechanism, considering both surface chemical reaction and diffusion through the product layer.

2. MATERIAL AND METHODS

2.1. Material

A high-grade zinc silicate ore sample was obtained from the Bagherabad mine located in central Iran. The chemical composition of the ore was determined by X-ray fluorescence (XRF) analysis, and the results are presented in Table 1. The analysis confirmed a high zinc content, mainly in the form of zinc oxide (ZnO), along with silica and minor amounts of lead and iron oxides.

The mineralogical composition of the sample was investigated using X-ray diffraction (XRD). The XRD pattern of the zinc silicate ore is shown in Figure 1. The diffraction peaks indicate that willemite (Zn_2SiO_4) is the dominant zinc-bearing mineral, accompanied by minor phases such as smithsonite, galena, sphalerite, and iron oxides. The dominance of willemite confirms that the studied sample is representative of a high-grade zinc silicate ore, making it suitable for investigating the dissolution kinetics of zinc silicate minerals.

Table 1. Chemical composition of the zinc silicate ore (wt.%)

ZnO	**PbO**	**SiO_2**	**Fe_2O_3**	**CaO**	**MgO**	**Al_2O_3**
66.2	3.64	19.24	3.44	0.46	0.04	2.92
MnO	**Na_2O**	**K_2O**	**TiO_2**	**P_2O_5**	**SO_3**	**LOI**
0.023	0.05	0.16	0.074	0.003	0.45	2.99

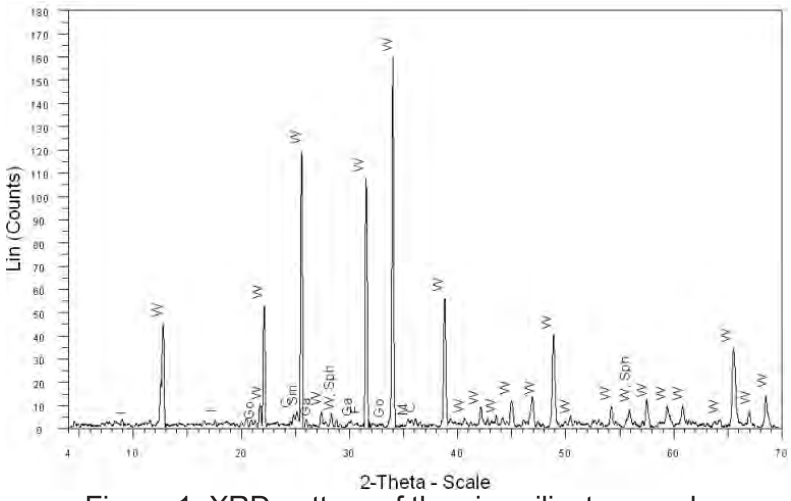

Figure 1. XRD pattern of the zinc silicate sample
(W: Willemite, I: Illite, Go: Goethite, Sm: Smithsonite, Ga: Galena, Sph: Sphalerite)

2.2. Method

Leaching experiments were conducted under atmospheric pressure in a 500 mL glass reactor equipped with an overhead mechanical stirrer fitted with a two-blade impeller (6 cm diameter) and a temperature control system. Sulfuric acid solutions were prepared using analytical-grade reagents and distilled water. In each experiment, the leaching solution was heated to the desired temperature before adding the zinc silicate ore sample.
Batch leaching tests were performed to investigate the effects of temperature (30–75 °C), sulfuric acid concentration (0.86–1.16 M), particle size (−63 to 212 µm), solid-to-liquid ratio (1:6–1:10 g/mL), and stirring speed (0–600 rpm) on zinc extraction. During leaching, slurry samples were withdrawn at predetermined time intervals, filtered, and analyzed for zinc concentration using atomic absorption spectrometry (AAS). The zinc extraction was calculated by considering the solution volume change resulting from sampling.

3. RESULTS AND DISCUSSION

Reaction between willemite and sulfuric acid can be written as follows:

$$Zn_2SiO_4 + 2H_2SO_4 \rightarrow 2ZnSO_4 + Si(OH)_4 \quad (1)$$

During leaching, zinc is selectively transferred into the solution, while silica remains on the particle surface as a hydrated silica layer. The formation of this product layer may hinder mass transfer between the unreacted core and the leaching solution, particularly at advanced reaction stages. Consequently, the development of a silica-rich layer plays an important role in controlling the dissolution behavior of willemite and provides a mechanistic basis for interpreting the kinetic results and diffusion-controlled leaching behavior discussed in the following sections (Abdel-Al and Rashid 2018; Bodas et al., 1996; Espiari et al., 2006; Soza et al.,2007)

3.1. Effect of Key Leaching Parameters

The effects of temperature, sulfuric acid concentration, and particle size on zinc dissolution from the zinc silicate ore were investigated. These parameters were selected due to their direct influence on reaction kinetics, mass transfer, and availability of the leaching agent.

The influence of temperature on the zinc extraction, under following conditions: leaching time 50 min, 0.96 M H_2SO_4, stirring speed 400 rpm, particle size 63-105 µm and S/L ratio of 1:8 g/mL is shown in Fig. 2(A). Temperature exhibited a pronounced effect on the rate of zinc dissolution. As shown in Figure 2(A), increasing the leaching temperature significantly enhanced zinc extraction, particularly during the early stages of leaching. Higher temperatures accelerate ion diffusion and reaction rates, resulting in faster zinc dissolution. However, the overall shape of the extraction curves remained similar across the studied temperature range, suggesting that temperature mainly influences the reaction rate rather than altering the dissolution mechanism.

The influence of sulfuric acid concentration on zinc extraction was studied by varying the initial concentration of H_2SO_4 from 0.86 to 1.16 M while keeping leaching time, temperature, stirring speed, particle size and S/L ratio constant at 50 min, 45 °C, 400 rpm, 63-105 µm and 1:8 g/mL, respectively. Based on Fig. 2(B), increasing acid concentration increased zinc dissolution by enhancing the availability of hydrogen ions required for the dissolution of willemite. The experimental results show that 0.96 M sulfuric acid was sufficient to extract about 95% Zn, and at acid concentration higher than 0.96 M, the increase in Zn extraction is not significant after 50 min.

A low recovery at low acid concentration (0.86 M) could be due to the availability of acid less than the stoichiometric requirement due to the consumption of H^+ in the reaction.

Fig. 2(C), shows the effect of the feed particle size on zinc extraction. Four different particles sizes -63, 63-105, 105-150 and 150-212 µm were examined while keeping the leaching time, temperature, H2SO4 concentration, stirring speed and S/L ratio constant at 50 min, 45 °C, 0.96M, 400 rpm and 1:8 g/ml, respectively. Smaller particle sizes resulted in higher zinc extraction due to increased surface area available for reaction. After 5 min of leaching time, 68–79% of zinc was extracted and after 50 min it rose to 84 and 96.5%, for particle size of 150-212 and −63 µm respectively. Similar trends were observed for various particle sizes. The zinc extraction was achieved with particle sizes −63 µm was about 12% higher than that was achieved with particle sizes in the range of 150-212 µm.

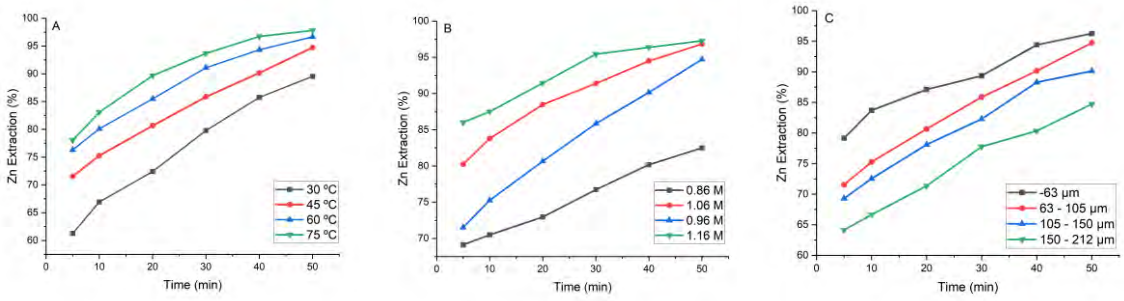

Figure 2. Effect of key leaching parameters on zinc extraction: (A) Temperature (30–75 °C), (B) sulfuric acid concentration (0.86–1.16 M H_2SO_4), and (C) particle size (−63 to 150–212 µm). Unless otherwise specified, the leaching conditions were: 50 min leaching time, 0.96 M H_2SO_4, 45 °C, 400 rpm stirring speed, particle size 63–105 µm, and S/L ratio of 1:8 g/mL

3.2. Effect Of Secondary Leaching Parameters

The effects of leaching time, stirring speed, and solid-to-liquid (S/L) ratio on zinc extraction were investigated to evaluate their influence on the leaching behavior of the zinc silicate ore (Fig.3).

Leaching time had a significant effect on zinc extraction during the early stages of the process. Under standard leaching conditions (0.96 M H_2SO_4, 45 °C, particle size of 63–105 µm, S/L ratio of 1:8 g/mL, and stirring speed of 400 rpm), approximately 82% of zinc was extracted within the first 20 minutes, while zinc recovery increased to about 95% after 50 minutes (Fig. 3(A)). Increasing the leaching time beyond 50 minutes resulted in negligible improvement in zinc extraction, indicating that the reaction rate decreased substantially at advanced stages of leaching.

To investigate the effect of stirring speed on the zinc extraction, experiments were carried out using seven different stirring speeds in the range of 0–600 rpm. Other leaching variables held constant at a leaching temperature of 45 ºC, leaching time of 50 min, acid concentration of 0.96 M, S/L ratio of 1:8 g/mL and particle size of 63-105 µm. Based on Fig. 3(B), in the absence of stirring, zinc extraction after 50 minutes was limited to approximately 39%, whereas increasing the stirring speed to 50 rpm increased the recovery to about 72%. Further increases in stirring speed to 200 and 300 rpm enhanced zinc extraction to approximately 88% and 90%, respectively. At stirring speeds of 400 rpm and higher, zinc extraction approached 95%, and no significant improvement was observed with further increases in agitation rate. This behavior suggests that external mass transfer resistance was effectively eliminated at stirring speeds above 400 rpm.

The influence of solid to liquid ratio on the zinc extraction was examined for three different ratios (1:6, 1:8, 1:10 g/mL) with the other leaching variables held at a leaching time of 50 min, temperature of 45 ºC, acid concentration of 0.96 mol/L, a particle size of 63-105 µm and stirring speed of 400 rpm. Results given in Fig. 3(C) show that the solid-to-liquid ratio also affected zinc dissolution. Zinc extraction after 50 minutes increased from approximately 77% at S/L ratio of 1:6 g/mL to about 95% at an S/L ratio of 1:8 g/mL. Further decreases in the S/L ratio produced only minor improvements in zinc recovery, indicating that sufficient leaching solution was available at this ratio to sustain the dissolution process.

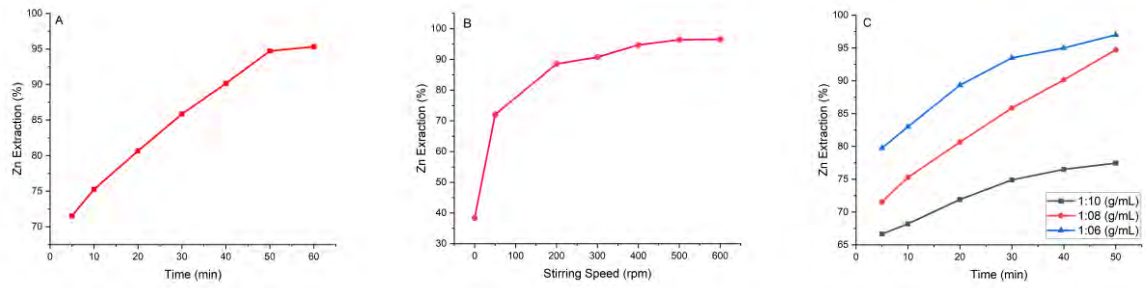

Figure 3. Effect of secondary leaching parameters on zinc extraction: (A) leaching time, (B) stirring speed (0–600 rpm), and (C) solid-to-liquid (S/L) ratio (1:6–1:10 g/mL). Unless otherwise specified, the leaching conditions were: 0.96 M H_2SO_4, 45 °C, particle size 63–105 µm, 400 rpm stirring speed, S/L ratio of 1:8 g/mL, and leaching time of 50 min

3.3. Kinetic Modeling and Activation Energy

To identify the rate-controlling mechanism of zinc dissolution from the zinc silicate ore, the experimental leaching data were analyzed using the shrinking core model (SCM). In fluid–solid reaction systems, the overall leaching rate may be controlled by diffusion through the liquid film, diffusion through the product (ash) layer, or the surface chemical reaction at the unreacted core.

The experimental data obtained at different temperatures were fitted to the SCM equations corresponding to the various controlling mechanisms. Among the tested models, the diffusion through the product (ash) layer model showed the best agreement with the experimental data

over the entire range of leaching conditions. The fitting results for different temperatures are presented in Fig. 4.

The linearity of the plots and the high correlation coefficients indicate that zinc dissolution is predominantly controlled by diffusion through the silica-rich product layer formed on the particle surface during leaching. This observation is consistent with the limited influence of stirring speed at higher agitation rates and the rapid initial dissolution followed by a slower reaction stage discussed in previous sections.

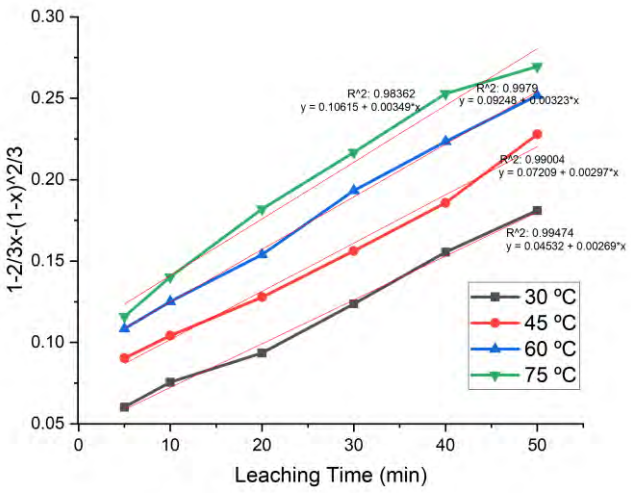

Figure 4. The variation of 1-(2/3)x-(1-x)$^{2/3}$ with time at various temperatures

The apparent activation energy of the leaching process was determined using the Arrhenius equation by plotting the natural logarithm of the rate constant obtained from the ash layer diffusion model against the reciprocal of absolute temperature. The resulting Arrhenius plot is shown in Figure 5.

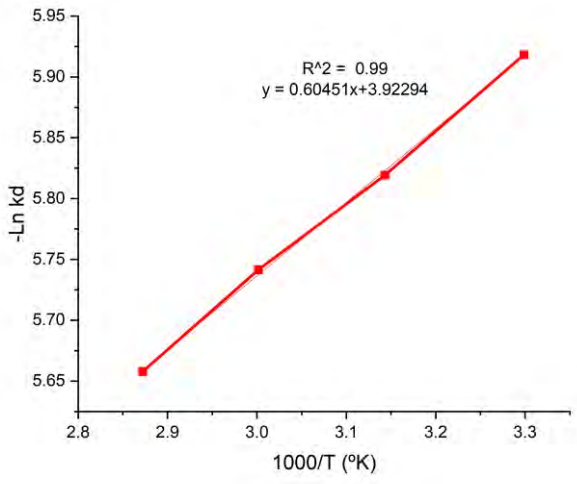

Figure 5. Arrhenius plot for the dissolution process

From the slope of the Arrhenius plot, an activation energy of 5.02 kJ/mol was calculated. This relatively low activation energy value is characteristic of diffusion-controlled processes and further confirms that the dissolution of zinc from willemite in sulfuric acid is governed by diffusion through the product layer rather than by surface chemical reaction.

The morphology of high-grade zinc silicate ore before and after 30 and 50 min of leaching under the optimum condition was examined by SEM and presented in Fig. 6. The particles of the zinc silicate ore before the leaching process present a clear surface and have approximately the same form and size (Fig. 5 (A,B)). After the leaching progress, the morphology of the leach residues show increase in roughness and porosity of the solid and also an increase in the amount of product layer covering the particle surfaces (Fig. 6 (C-F)).

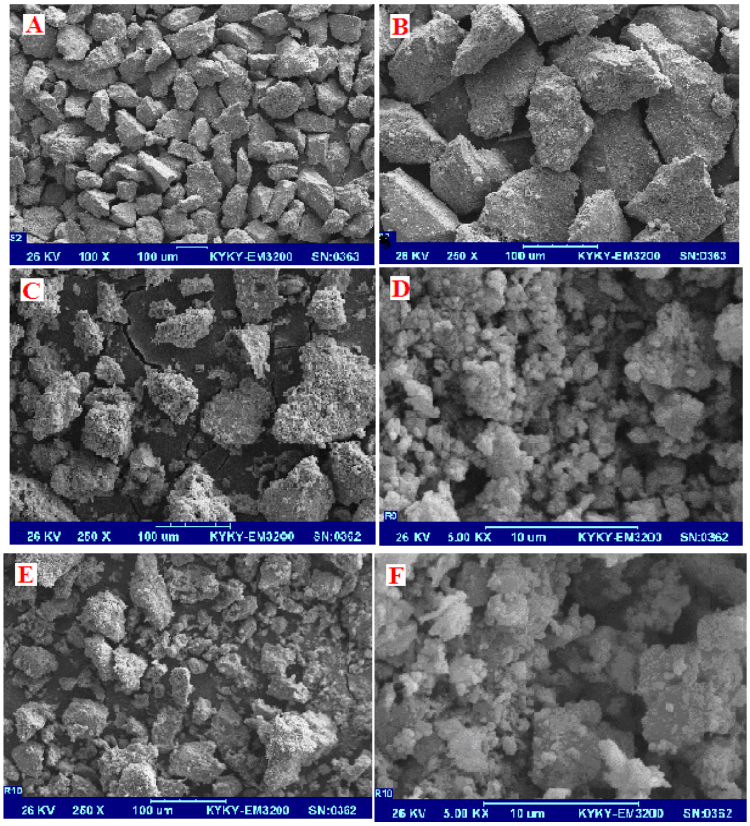

Figure 6. (A, B) Particles of zinc silicate ore before leaching; (C, D) after 30 min leaching; and (E, F) after 50 min leaching

4. CONCLUSION

The sulfuric acid leaching behavior of a high-grade zinc silicate ore dominated by willemite was investigated under atmospheric conditions. The results showed that zinc extraction increased with increasing temperature and acid concentration and decreasing particle size. Under optimum conditions (0.96 M H_2SO_4, 45 °C, particle size of 63–105 µm, solid-to-liquid ratio of 1:8 g/mL, and stirring speed of 400 rpm), approximately 95% zinc extraction was achieved within 50 minutes.

Secondary parameters such as stirring speed and extended leaching time had a limited effect once sufficient mixing was ensured. Kinetic analysis based on the shrinking core model indicated that zinc dissolution is controlled by diffusion through the silica-rich product layer, with an apparent activation energy of 5.02 kJ/mol. These findings provide useful kinetic insight for optimizing sulfuric acid leaching of high-grade zinc silicate ores.

ACKNOWLEDGMENT

I would like to sincerely acknowledge the Erasmus Mundus PROMISE Consortium for their support, which greatly facilitated the preparation and publication of this paper. Their support and commitment to academic excellence are deeply appreciated.

REFERENCES

Abdel-Aal, E. A., (2000), “Kinetics of sulfuric acid leaching of low-grade zinc silicate ore”, Hydrometallurgy, 55, 247–254.

Abdel-Aal, E. A., Rashad, M. M., (2018), “Leaching behavior and kinetics of zinc silicate ores in sulfuric acid solutions”, Hydrometallurgy, 178, 44–52.

Abkhoshk, E., Jorjani, E., Al-Harahsheh, M. S., Rashchi, F., Nazeri, M., (2014), “Review of the hydrometallurgical processing of non-sulfide zinc ores”, Hydrometallurgy, 149, 153–167.

Bodas, M. G., (1996), “Hydrometallurgical treatment of zinc silicate ore from Thailand”, Hydrometallurgy, 40, 37–49.

Ding, Z., Yin, Z., Wu, X., Hu, H., Chen, Q., (2011), “Leaching kinetics of willemite in ammonia–ammonium chloride solution”, Metallurgical and Materials Transactions B, 42B, 633–640.

Espiari, S., Rashchi, F., Sadrnezhaad, S. K., (2006), “Hydrometallurgical treatment of tailings with high zinc content”, Hydrometallurgy, 82, 54–62.

Gilg, H. A., Boni, M., Cook, N. J., (2008), “A special issue devoted to nonsulfide Zn–Pb deposits – Editorial”, Ore Geology Reviews, 33, 115–116.

Hitzman, M. W., Reynolds, N. A., (2019), “Non-sulfide zinc deposits: Geology, processing and future trends”, Ore Geology Reviews, 112, 103033.

Li, H., Wang, J., Zhao, Z., (2023), “Kinetic modeling and silica behavior during acid leaching of zinc silicate ores”, Hydrometallurgy, 216, 106027.

Moradi, S., Monhemius, A. J., (2011), “Mixed sulfide lead and zinc ores: Problems and solutions”, Minerals Engineering, 24, 1062–1076.

Nazeri, M., Sinche-Gonzalez, M., Abkhoshk, E., (2025), “Dissolution kinetics of low-grade zinc silicate ore in hydroxide solution”. XVI International Mineral Processing and Recycling Conference, Belgrade, Serbia.

Santos, F. M., Peina, P. S., Porcaro, A., Oliveira, V. A., Silva, C. A., Leão, V. A., (2010), “The kinetics of zinc silicate leaching in sodium hydroxide”, Hydrometallurgy, 102, 43–49.

Souza, A. D., Peina, P. S., Lima, E. V. O., da Silva, C. A., Leão, V. A., (2007), “Kinetics of sulphuric acid leaching of a zinc silicate calcine”, Hydrometallurgy, 89, 337–345.

Zhang, X., Liu, Z., Wei, C., (2024), “Process optimization and kinetic evaluation of zinc extraction from oxidized zinc ores”, Journal of Sustainable Metallurgy, 10, 245–258.

Zhou, X., Wei, C., Deng, Z., (2020), “Advances in hydrometallurgy of oxidized zinc ores”, Minerals Engineering, 155, 10642.

MANAGEMENT OF MINERAL PROCESSING TAILINGS

EVALUATION OF MINERAL PROCESSING AND HYDROMETALLURGICAL PLANT WASTES: A COMPREHENSIVE ASSESSMENT WITH CASE STUDIES FROM TÜRKIYE

Gülay BULUT[1], Nursun ŞİRVANCI[2,*], Fatma ARSLAN[1]

[1]Istanbul Technical University, Faculty of Mines, Mineral Processing Engineering Department, 34469, Maslak, Istanbul, TÜRKİYE
[2]Zenit Madencilik Co. Sanayi ve Ticaret A.Ş., Balıkesir, Türkiye
**Corresponding author: n.sirvanci@zenitmadencilik.com*

A B S T R A C T

Mineral processing and metallurgical plant wastes contain considerable amounts of base, rare, and precious metals which can be recovered and resulted in environmental and economical benefits. Physical and chemical beneficiation processes create mineral processing wastes (tailings) to separate valuable minerals from the ore. Additionally, mining companies that produce metals such as copper, gold, and silver from low grade ores also leave wastes after leaching operations with acid or cyanide. In this study, the evaluation of wastes from plants will include beneficiation methods such as gravity and flotation, as well as hydrometallurgical processes. This study presents some examples of laboratory scale case studies, such as evaluation of lead-zinc plant tailings, iron ore concentration plant tailings, gold-silver cyanide leaching plant residues, feldspar concentration plant tailings and ilmenite bearing tailings.

Key words: *Plant tailings, leaching residues, lead-zinc, gold-silver, iron, titanium*

1. INTRODUCTION

The mineral processing and metallurgical plants generate substantial quantities of waste containing various amounts of valuable metals. The conventional method for the disposal and storage of waste is usually dumping. The other methods are reuse of mining by-products in other industries and reprocessing of mine wastes to recover valuable metals such as copper, iron, gold, rare earth elements, or strategic metals. Thus mineral processing, pyrometallurgical, hydrometallurgical, pyro-hydrometallurgical, and electrometallurgical methods are applied.

Türkiye produces 26 million tons of tailings annually after mineral processing works. Extensive researches have been conducted on the evaluation of these tailings, but the lack of serious investment in this area is due to the continuing extraction of valuable metals from the potentially available reserves. In the future, beneficiation of these tailings will be inevitable. This study provides examples of studies conducted on the evaluation of industrial plant wastes from some mineral processing and metallurgical plants in Türkiye. This paper discusses tailings from lead-zinc flotation, iron concentration, gold-silver cyanide leaching, and feldspar concentration plants, and it also emphasizes the importance of evaluating these wastes from economic and environmental perspectives.

2. EXAMPLES FROM THE EVALUATION OF PLANT WASTES

2.1. Lead-Zinc Flotation Tailings

The lead-zinc ore deposits located near Balya (Balıkesir, Türkiye) were extensively exploited by French mining enterprises between 1880 and 1935, primarily for the extraction of lead and silver. During this period, they used pyrometallurgical processing methods to recover metallic

lead and silver from the produced concentrates. Following a progressive decline in ore grades and metal recoveries, mining operations were eventually terminated. As a consequence of the technological limitations and low processing efficiencies characteristic of that era, approximately one million tonnes of gravity and flotation tailings, along with metallurgical slags, were generated and accumulated in the vicinity of the site, containing significant residual concentrations of lead and zinc (Bulut et al., 1994; Göktepe et al., 2000).

Numerous studies have been carried out to evaluate and recover valuable components from these tailings and slags (Bulut, 1991; Atak, et al.,1990; Bulut et al., 1994; Güven et al., 2010). In a study (Güven et al., 2010), the evaluation of tailings generated from mineral processing plants remains a critical aspect of sustainable resource management. In this study, lead–zinc tailings containing 3.12% Zn, 3.43% Pb, 0.71 g/t Au, and 74 g/t Ag were investigated with the aim of developing an efficient recovery strategy. Laboratory-scale flotation experiments were conducted to establish an appropriate flowsheet for the reprocessing of these tailings. Selective sulfide flotation experiments failed to produce satisfactory results, particularly for lead, due to the extensive oxidation of galena surfaces. Therefore, a concentrate was produced using a bulk sulfide flotation method. Furthermore, it was observed that increasing the number of rougher and cleaner stages significantly improved the metal grades of the obtained concentrates. Through sulfide flotation, a bulk lead-zinc concentrate assaying 43.02% Zn and 12.23% Pb was produced. In contrast, the maximum lead grade achieved through oxide flotation reached 22.7% Pb. Overall, the findings suggest that a marketable bulk concentrate containing 55.52% Pb–Zn, along with 430 g/t Ag and 1.8 g/t Au, can be obtained, corresponding to 60% zinc and 40% lead recoveries from the investigated tailings. Based on the results of the flotation experiments conducted under various operating conditions, a conceptual flowsheet for the processing of these tailings has been proposed, as illustrated in Figure 1.

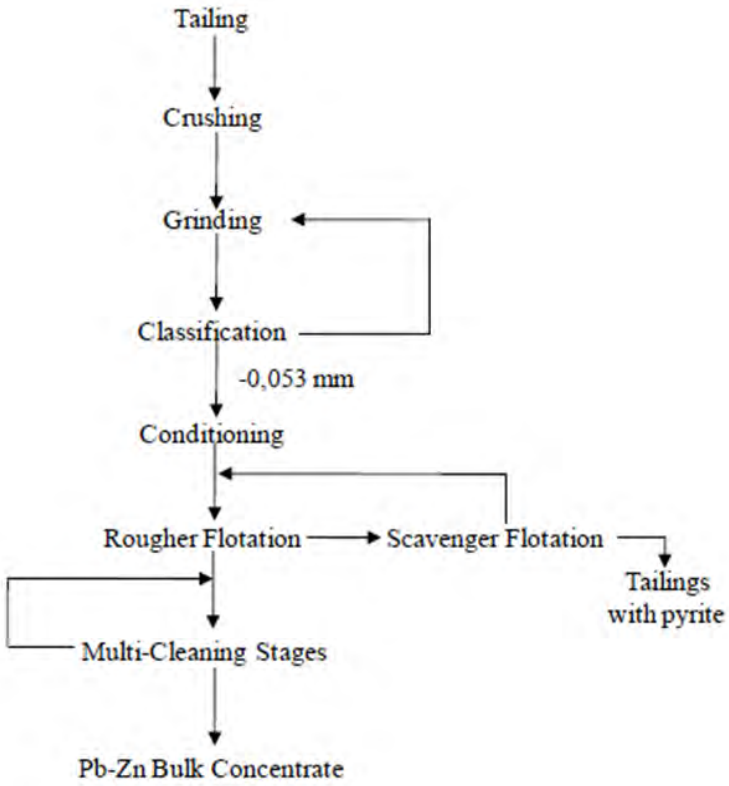

Figure 1. Proposed flowsheet for the beneficiation of Pb-Zn flotation tailings (Güven et al., 2010)

Reprocessing old flotation and jig tailings gave favorable results, but the slag samples did not produce similar success. However, because of their relatively high metal contents (approximately 13% Zn and 3.40% Pb), the suggestion is to blend these slags with the flotation concentrates periodically produced in the region and subsequently remove them through processing. In this way, the acid mine drainage (AMD) potential of such waste materials can be mitigated while simultaneously recovering additional economic value from the waste (Bulut et al., 1994).

Arslan et al. (2006) also studied Aladağ (Kayseri-Türkiye) lead-zinc sulfide-oxide ores containing 10.17% Pb, 10.98 %Zn, 164 g/t Cd and 57 g/t Ag. During the laboratory scale flotation tests of these ores, it was found that almost all zinc was remained in the tailings that contain 12.31% Zn, 1.35%Pb, 198.3 g/t Cd, and 22.3%Fe. Three different methods were studied such as basic (NaOH) leaching, roasting followed by acidic (H_2SO_4) leaching, and direct acidic (H_2SO_4) leaching for recovering metals in that tailings. In the direct acidic leaching studies, which gave the best results, dissolution efficiencies of 91.5% zinc, 78.2% cadmium, and 14.3% iron were achieved under optimum leaching conditions while Pb remained in the leach residues and the acid consumption was 422.3 kg/t of tailings. As a result, this project led to the construction of a flotation plant in Aladağ-Kayseri, but there is no work on flotation tailings.

2.2. Iron Ore Concentration Plant Tailings

Divriği Iron Ore Concentrator (Türkiye) was designed to process 670 t/h magnetite ore containing 53-55% Fe and to produce 310 t/h of coarse concentrate assaying 63-65% Fe and 210 t/h of pellet concentrate of 67-68% Fe. About 1 million t of fine size tailings until today have been discarded into the tailing ponds. The plant dumps roughly 600 000 t of fresh tailings into the ponds annually. Concentrator tailings contain some valuable metals, such as cobalt, nickel, and copper, in addition to Fe. Divriği Iron Concentrator tailings contain various amounts of FeS_2 (pyrite), FeS (pyrrhotite), SiO_2 (quartz), $(FeNi)_9S_8$ (pentlandite), (Ni, Fe)S_2 (bravoite), (Co, Fe)AsS (cobaltite), Cu_2S (chalcosite), CuS (Covellite), $CuFeS_2$ (chalcopyrite), ZnS (sphalerite), Fe_2O_3 (hematite), Fe_3O_4 (magnetite), Al_2O_3 (korundum), FeAsS (arsenopyrite), and $CaCO_3$ (calcite), depending on the location (Gürkan, Acarkan, Önal, 1993).

The presence of Co, Ni, and Cu in the Divriği Iron Ore Concentrator tailings makes the beneficiation of those tailings attractive. In the experimental work, sulphide concentrates were produced from these two types of tailings by flotation (Sirkeci et al., 2006). Under optimum flotation conditions, a bulk sulphide concentrate assaying 0.376% Co, 0.721% Ni, and 0.403% Cu was obtained with 83.1% Co, 57.7% Ni, and 59.0% Cu recoveries from the old tailings. On the other hand, another concentrate containing 0.384% Co, 0.687% Ni, and 0.393% Cu was produced from the new process tailings under the same flotation conditions with 94.7% Co, 84.6% Ni, and 76.8% Cu flotation recoveries.

A roasting-leaching-H_2S precipitation procedure was used to treat this flotation concentrate (Açma et al., 1993). Sulfatizing roasting was carried out at 690°C and roasted product was leached with 10g/L H_2SO_4 at 70°C and 30% pulp density. For the precipitation of desired metal, H_2S is bubbled through the concentrated solution of repeated leaching, under controlled temperature and pH. Final metal recoveries of 91% Cu, 91% Co, 50% Ni, and 92 % Zn are attained. Roasting gases with 13% SO_2 content was produced suitable for H_2SO_4 production and the leach residues can be integrated with the iron ore processing plant as they contain 57.4% Fe and minor amount of nonferrous metals. As a result of these researches, a general flowsheet was proposed given in Figure 2. According to this flowsheet, the general process includes flotation after grinding of tailings, sulphatizing roasting of coarse concentrate, leaching of calcine with sulphuric acid, and the recovery of Co, Ni and Cu from solution with H_2S precipitation. Iron concentrate was also produced from coarse flotation tailings with magnetic

separation. With application this flowsheet, it is possible to produce CoS, NiS, and CuS precipitates along with iron concentrate from the iron tailings.

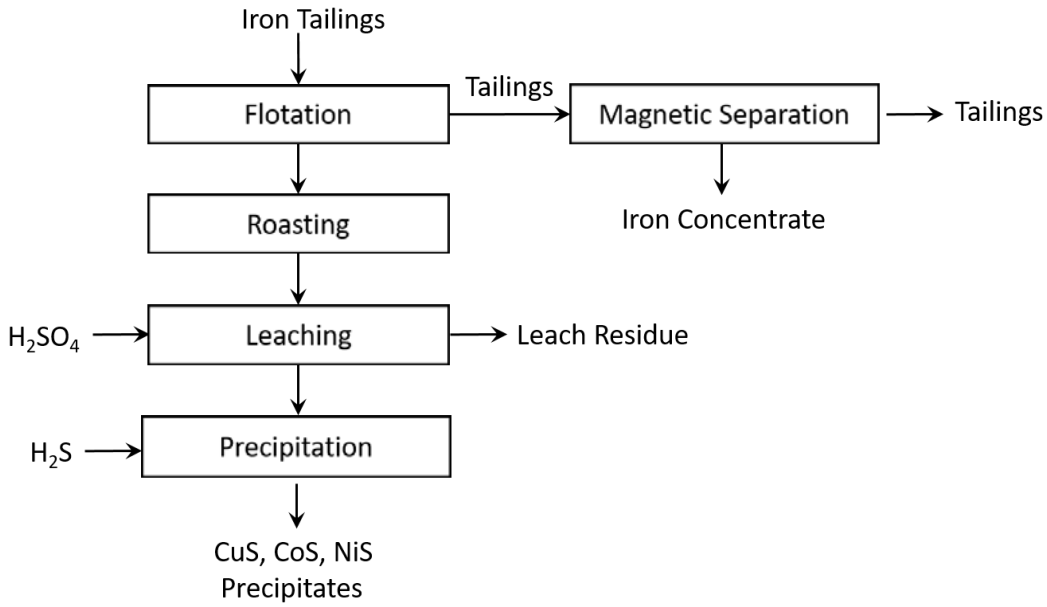

Figure 2. Proposed flowsheet for the beneficiation of Divriği iron ore concentration plant tailings (produced from Açma et al., 1993)

2.3. Gold-Silver Cyanide Leaching Plant Residues

Dinçer (1997) studied the recovery of silver from the tailings taken from the 100. Yıl Gümüşköy Plant (Silver Cyanidation Plant) that processed poly metallic refractory silver ores. Since these types of refractory ores contain metals like Cu, Zn, Fe inside silver minerals, recovery of silver is not high and remains in the tailings, resulting in high cyanide consumption. The study aimed at recovering silver in the plant tailings and, in the meantime, increase the plant efficiency.

Chemical analysis of the tailings taken from the plant tailing pond contained 100 g/L Ag and 14.6% $BaSO_4$. Therefore, Dinçer, Önal, and Arslan (1998) also recovered barite together with silver. Additionally, tailings also include 4.93% Fe_2O_3, 2.2% Pb, 1.4% Zn, 2.05% As, 0.91% Sb, 5.54% Al_2O_3, 1.34% K_2O, and 50.2% SiO_2 (Dinçer, 1997). Mineralogical analysis showed the Ag minerals as native silver, pyrargyrite, silver-bearing tetrahedrite, argentite, and proustite along with sulfide and clayey minerals. Most of the silver minerals was below 40 μm in size and coated with other minerals, which is the reason for Ag loss into tailings.

The plant silver recovery was about 60% which is low because of sulfide and clayey type minerals. Acarkan et al (1992) studied a blend sample composed of five different type silver ores from Gümüşköy mine site. Their studies include removal of clay and sulfide flotation followed by cyanide leaching. As a result, they could increase the silver recovery to 73%. Arslan et al (1995) studied thiourea leaching of silicious tuff ores from the same site, and they could leach 48% of Ag in 8 hours and even to 85 % in 48 hours. Acarkan, Gurkan, and Arslan (1994) also studied, the effect of protective alkali on the extraction of silver from refractory ores, taken from the same mine site in order to investigate the possibility of Ag recovery. High concentrations of protective alkali found to be beneficial in the cyanidation of these ores, in contrast to gold cyanidation where they prohibit gold dissolution. Calcium ions are advantageous in the cyanidation of sulphidic silver ores since they prevent the detrimental effects of S ions which hinder silver dissolution and consume CN^- ions. Using high concentrations of protective alkali decreases the cyanide consumption. Açma et al (1995) also studied mining waste ore, which is the richest one among the five types of ore from the same

region using pressure leaching followed by thiourea leaching. They were able leach almost all silver out (98%). Four studies mentioned here show the unconventional types of processes can increase the silver recovery. But still, there are piles of old tailings with high silver content accumulated over the years that need to be treated.

Peroxide assisted cyanide leaching of gold-silver ore, obtained from Artvin, Cerattepe region of Turkey, was investigated (Müdüroğlu 1997; Arslan, Ozdamar, Müdüroğlu, 2003). Almost all gold and 71% of Ag were extracted with the addition of 15g/L H_2O_2 during the cyanidation carried out for 48 hours. The study proved that adding H_2O_2 as an oxidant during cyanide leaching increased the leaching recoveries of Au and Ag and decreased the leaching period. From that point, peroxide addition on cyanide leaching of Gümüşköy plant tailings were also studied (Dinçer 1997; Müdüroğlu 1997; Dinçer, Önal, Arslan, 1998). In an earlier study, Alp (1992) found 20-30% Ag recovery by using cyanide leaching of tailings from Gümüşköy. In the experiments by Dinçer (1997), effects of cyanide concentration, H_2O_2 concentration, $Ca(OH)_2$ concentration, particle size, pulp density, and leaching time were investigated. 45% Ag recovery was reached at the optimum leaching conditions, which over than earlier study findings (Alp 1992, Dinçer 1997). To investigate how H_2O_2 affected the surface properties, the researchers treated the tailing sample with peroxide. The measurements show that surface area of the particles increased almost 35% while porosity of sample increased 19%. This explains the dissolution of silver from tailings. With this, plant recovery can go up from 60 to 80%.

In the same studies with these tailings to recover barite, shaking table, flotation, and MGS were utilized (Alp 1992, Dinçer 1997). In shaking table experiments (within particle size range of -74+37 microns), 78.43% $BaSO_4$ containing concentrate with 48.26% recovery, in the flotation experiments (particle size range of under 37 microns), 51.33% $BaSO_4$ containing concentrate with 48.26% recovery were produced (Alp, 1992). By applying MGS to the original sample, a concentrate with 65% $BaSO_4$ content was accomplished by 48.26% recovery while with the sample under 37 microns, a concentrate with 81.42% $BaSO_4$ content was produced by 22.85% recovery. All these concentrates produced as a result of physical concentration tests, found not suitable enough for chemical and drilling industries.

2.4. Feldspar Concentration Plant and Ilmenite-Bearing Tailings

Titanium dioxide is a strategic industrial raw material widely used in pigment, metallurgical, ceramic and advanced material applications. Rutile (TiO_2) is the most valuable titanium mineral due to its high grade and favorable physical and chemical properties. Increasing interest in secondary resources such as tailings has emerged due to sustainability and resource efficiency concerns. In the feldspar enrichment process, titanium minerals are rejected to tailings to meet feldspar quality requirements, creating potential for by-product recovery.

ESAN Milas Feldspar Concentrator in Milas in Muğla (Türkiye) produce flotation tailings which contains rutile with the TiO_2 grade between 2.70% and 3.45%. Mineralogical investigations and chemical analyses carried out on representative samples taken from the flotation tailings indicated that the sample mainly consists of albite, quartz, rutile, zircon, mica and apatite. According to the chemical analysis results, it was found that the tailings contained 0.15% Fe_2O_3, 3.06% TiO_2, 17.95% Al_2O_3, 8.08% Na_2O and 0.51% K_2O. Sieve analyses showed that 95-98% of the sample is below 0.5 mm and 31-37% is below 0.038 mm (Sirvanci, 1993).

Although rutile has low electrical conductivity and shows only a slight increase at elevated temperatures, electrostatic separation tests at room temperature and 55-60°C were unsuccessful due to insufficient liberation and low selectivity Magnetic separation tests with high-intensity dry and wet separators (Frantz and Capco Amax) failed to produce an economical TiO_2 grade for separating feldspar and mica from rutile; likewise, combined

electrostatic and magnetic tests on the representative tailings were unsuccessful due to the fine liberation size of rutile such as −0.074 mm (Sirvanci, 1993).

In gravity based tests, the sample was processed using laboratory scale Wilfley shaking tables and Mozley tables. However, effective separation could not be achieved in either the shaking table or the Mozley table tests because the particle surfaces in the flotation tailings were coated with reagents (olive pomace oil), which caused the particles to attach to air bubbles and thus behave as if they had a much lower specific gravity than their true values. When the representative sample was washed with NaOH to remove oil and treated on a shaking table, 4.2% of the feed was recovered as a concentrate containing 20.60% TiO_2 with a recovery of 32%. For the deslimed sample ground to below 0.074 mm and treated on a Mozley table, a concentrate grade of 28.27% TiO_2 was obtained with a low recovery of 10% (Sirvanci, 1993).

In order to produce a rutile concentrate with high TiO_2 content and with optimum recovery, flotation method was applied. For this purpose, flotation tests were carried out on samples ground to different size ranges and deslimed. The flowsheet of the flotation tests was presented in the Figure 3.

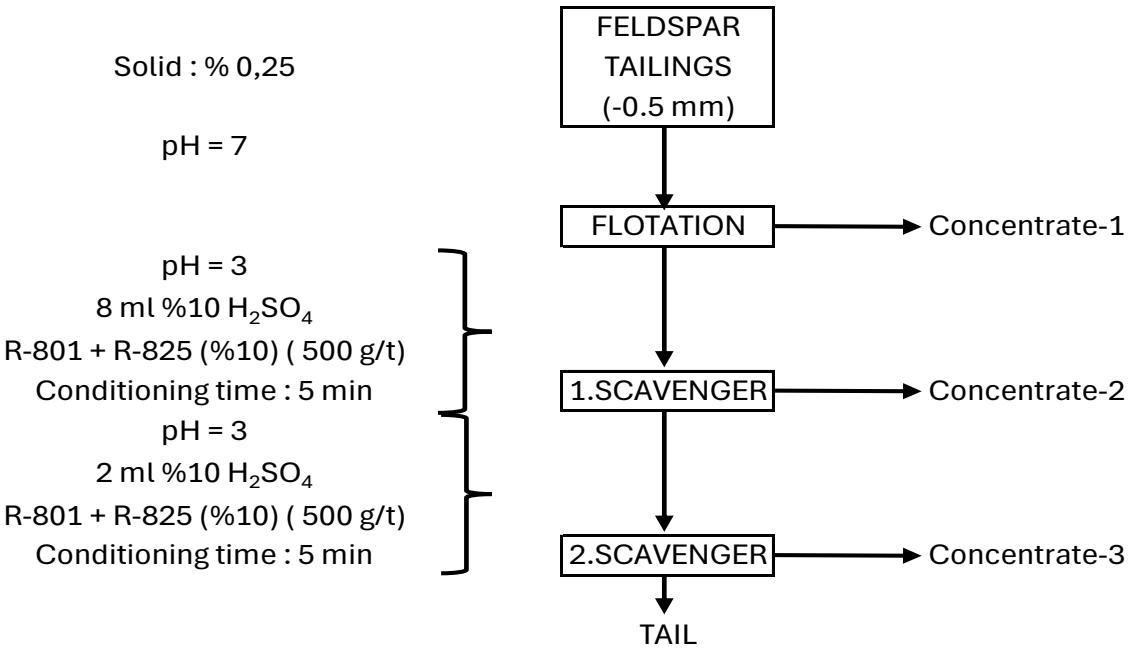

Figure 3. Flowsheet of flotation tests for beneficiation of feldspar tailings under 0.5 mm

The flotation tests showed that a large portion of rutile floated without using collector at the size fraction of -0.100+0.038 mm. In this flotation test, 17% of the mass recovered at the concentrate grade of 13.42% TiO_2 with a recovery of 74.5%. In order to minimize TiO_2 losses in the tailings and to obtain a high grade of rutile concentrate, a rougher flotation was conducted on a sample at the size fraction of -0.300+0.038 mm (Sirvanci, 1993). Scavenger flotation was performed using sulfonate type collectors at pH 3 and oleic acid at pH 8-9, resulting in 3-12% of the mass recovery at the concentrate grade of 8-12% TiO_2. Based on all physical and surface chemistry analyses carried out on the flotation tailings from the ESAN Milas Feldspar Concentrator, flotation was the most effective enrichment method for recovering of titanium. A concentrate with grade of 13.42% TiO_2 was produced with 74.5% recovery in the size fraction of -0.100 +0.038 mm.

Tailings coming from beach sands mineral slimes dams of KwaZulu-Natal coast of South Africa were also subjected to beneficiation studies by Mulaba-Bafubiandi et al. (2002). In the tests

screening, spiral concentration, flotation, and magnetic separation, applied separately and in combination in order to recover ilmenite from that tailings containing 42% ilmenite, 6% rutile, 6% iron oxides and zircon. Flotation of the spiral concentrate yielded 61% ilmenite recovery while 62% of the hematite reported in the flotation tailings. The combined process produced a concentrate containing up to 71% ilmenite and 19% hematite and a high-grade natural ilmenite product with 87% ilmenite and 13% hematite contents was obtained from the spiral sink fraction treated by flotation. A subsequent magnetic separation further increased the hematite content.

3. CONCLUSIONS

The results from the experimental studies of the lead-zinc plant tailings, iron ore concentration plant tailings, gold-silver cyanide leaching plant residues, and feldspar concentration plant tailings from Türkiye were summarized as follows;

- A marketable bulk concentrate containing 55.52% Pb-Zn, along with 430 g/t Ag and 1.8 g/t Au, was obtained with a zinc recovery of 60% and a lead recovery of 40% as a result of flotation of Pb-Zn flotation tailings.
- The direct acid leaching of Aladağ (Kayseri-Turkey) Pb-Zn sulfide-oxide tailings resulted in leaching 91.5% of Zn, 78.2% of Cd, and 14.3% of Fe, while leaving Pb in the tailings.
- The Divriği Iron Ore Concentrator tailings containing Co, Ni, and Cu was retreated through a series of mineral processing and hydrometallurgical methods and the final metal recoveries of 91% Cu, 91% Co, 50% Ni, and 92 % Zn are attained.
- The 100. Yıl Gümüşköy Silver Cyanidation Plant the tailings were treated with H_2O_2 assisted cyanide leaching, Ag leaching efficiency increased from 60% to 80% with the addition of an oxidant such as H_2O_2. The barit content of the tailings from Silver Cyanidation Plant was 14.6% $BaSO_4$ and the concentrate produced was not suitable for chemical and drilling industries.
- Studies on the flotation tailings from the ESAN Milas Feldspar Concentrator showed that flotation was the most effective enrichment method for recovering titanium and the concentrate grading 13.42% TiO_2 was recovered with 74.5% efficiency in the size fraction of -0.100 +0.038 mm.

REFERENCES

Acarkan, N., Gurkan, V., Arslan, F., The role of protective alkalinity and Ca^{2+} ions in the cyanidation of refractory silver ores. Hydrometallurgy, 1994, 36, 361-367.

Acarkan et al., 1992, Investigation of increasing possibilities of silver recovery from Kütahya Gümüşköy Ores, Istanbul Technical University Research Project (in Turkish).

Açma E., Arslan F., Wuth W., Recovery of silver from a refractory type ore by thiourea leaching, Hydrometallurgy, 34, 1993, pp. 263-274.

Açma, E., Oktaybaş, C., Arslan, F., Addemir, O., Acarkan, N., and Önal, G. (1993) Recovery Of Copper, Cobalt And Nickel From Divrigi Sulfide Concentrates. In: Reddy R. G. & R. Weizenbach, N. (Eds): The Paul E. Queneau International Symposium Extractive Metallurgy of Copper, Nickel and Cobalt, Vol. I: Fundamental Aspects, Reno, NV, USA, TMS, pp. 1269-295.

Alp I, 1992, recovery of silver and barite from kütahya gümüşköy plant tailings, MSc Thesis, Anadolu University, Faculty of Science and Letters (in Turkish).

Arslan, F., Ozdamar, D., Müdüroğlu, M., 2003, Cyanidation of Turkish gold-silver ore and the use of hydrogen peroxide, The European Journal of Mineral Processing and Environmental Protection, No.3, 1303-0868, pp. 309-315.

Arslan F., Aykaç Y., Perek K.T., Önal G., Evaluation of lead-zinc flotation tailings, Proceedings of 2006 TMS Fall Extraction and Processing Division: Sohn International Symposium, San Diego, CA, USA, 27-30 Aug 2006, pp 387-395.

Atak, S., Acarkan, N., Gürkan, V., Bulut, G., Güney, A., 1990. Evaluation of Balya lead-zinc tailings and slags, In: III. International Mineral Processing Symposium, September 11-13, Istanbul, pp. 118-129) (In Turkish).

Bulut, G., 1991. Evaluation of Balıkesir Balya region lead-zinc plant tailings, MSc. Thesis, Istanbul Technical University, Science and Letters Faculty, Istanbul (in Turkish).

Bulut, G., Arslan, F., Gül, A., Kaytaz, Y., Atak, S., 1994. recovery of metalic values from the acient lead zinc wastes", 16 th World Mining Congress, The Mining Industry on the Threshold of XXI Century 1, 12-16 September, Sofia, Bulgaria, pp.520-529.

Bulut, G., Aslan, F., Gül, A., Kaytaz, Y., Atak, S., 1994. Recovery of metals from old lead–zinc waste, 16. World Mining Congress, Bulgaria, pp. 520-529.

Dinçer H., Evluation of Gümüşköy tailings and increasing plant silver recovery, 1997, Doctoral Dissertation, Istanbul Technical University, Faculty of Science and Letters (in Turkish).

Dinçer H., Evluation of Gümüşköy Tailings and Increasing Plant Silver Recovery, 1997, Doctoral Dissertation, Istanbul Technical University, Faculty of Science and Letters (in Turkish).

Dincer, H., Onal, G., Arslan, F., The recovery of silver and barite from cyanidation plant tailings. 4th International Symposium on Environmental Geotechnology and Global Sustainable Development, Boston-USA, August 9-13, 1998.

Göktepe, F., Pooley, F.D. and Williams, K.P., 2000 Characterisation and beneficiation studies for Balya lead–zinc mine wastes, In: Proceedings of the Eighth International Mineral Processing Symposium, pp. 683-687.

Gürkan, V., Acarkan, N., Önal, G. (1993) Valuable metals and their distributions in the Divrigi Iron Ore Concentrator tailings. Journal of Mining Science & Technology, Cumhuriyet University, Faculty of Engineering 1, pp.157-165 (in Turkish).

Güven, O., Burat, F., Bulut, G., G. Önal, G., 2010. evaluation of lead-zinc ore tailings by flotation, Proceedings of XIIth International Mineral Processing Symposium, 6-8 October, Cappadocia, Nevşehir, Turkey, pp. 415-420.

Mulaba-Bafubiandi, A.F., Mukendi-Ngalula, D., Wanders, F.B., 2002. Ilmenite Mineral's Recovery from Beach Sand, Hyperfine Interact. 139/140, 485–494, Kluwer Academic Publishers.

Müdüroğlu M., 1997, Effect of peroxide addition on cyanide leaching of Artvin-Cerattepe gold-silver Ores, Graduation Thesis, Istanbul Technical University, Mining Faculty, Mining Engineering Department, Istanbul (In Turkish).

Sirvanci, N., 1993, Beneficiation of Rutil from the Feldspar flotation tailings, Graduation Thesis, Istanbul Technical University, Mining Faculty, Mining Engineering Department, Istanbul (In Turkish).

Sirkeci, A. A., Gül, A., Bulut, G, Arslan, F., Önal, G., Yüce, A.E. (2006) Recovery of Co, Ni, and Cu from the tailings of Divriği iron ore concentrator. Mineral Processing and Extractive Metallurgy Review: An International Journal, 27, 131-141.

Uçurum, M., Ulu, E.,1987. investigation of flotation possibilities of the jig and first flotation tailings of the balikesir-balya lead mine's old processing, Madencilik Dergisi (Mining Journal), Vol. 26 No. 3 pp. 5- 13.

EVALUATION OF WASTE AND BY-PRODUCTS FROM THE ZONGULDAK HARD COAL BASIN WITHIN THE FRAMEWORK OF THE ZERO-WASTE APPROACH

Mehmet BİLEN[1], Hayri VELİOĞLU[2], Haşim DURU[1], İhsan TOROĞLU[1,*]

[1]Zonguldak Bülent Ecevit University, Engineering Faculty, Department of Mining Engineering, İncivez, 67100, Zonguldak, Turkiye
[2]Zonguldak Maden İşletmeleri Enerji Madencilik San. Tic. A.Ş. Zonguldak, Turkiye
**Corresponding author: itoroglu@hotmail.com*

A B S T R A C T

The Zonguldak Basin has a 200-year history of coal mining, during which numerous mines of various scales have been operated, resulting in the accumulation of millions of tons of coal spoil and washing residues. Although some of these waste piles have been rehabilitated, an estimated 20–25 million tons of spoil heaps of different sizes remain scattered throughout the basin, causing both environmental and visual pollution. In addition, coal washing plants (lavoirs) generate shale-type residues that further contribute to the growing waste problem. The recycling and reuse of these spoil and residue materials are therefore crucial for minimizing environmental impacts and creating economic value. Utilizing advanced technologies such as air jigs, air shaking tables, and optical and X-ray sorting systems enhances separation efficiency, reduces costs, and allows waste materials to be reintroduced into production processes. Studies have shown that these materials are largely inert, with calorific values between 500 and 1500 kcal/kg. In the present study, samples collected from spoil and residue sites were processed using these technologies to separate the organic (coal) fraction from the inert inorganic components (shale, limestone, sandstone, etc.). The results show that the recovered coal fraction can serve as power plant fuel, shale and limestone as raw materials in cement and ceramics, limestone and sandstone as crushed stone, and fine-grained materials as filling material. Overall, the findings indicate that spoil and waste in the Zonguldak Basin can be efficiently utilized within a zero-waste framework, supporting sustainability and the circular economy.

Key words: *Zonguldak, coal, spoil, residue, coal washing plant, air jig, air shaking table, air-based separators, optical and X-ray sorters, recycling/reuse, zero waste*

1. INTRODUCTION

Mining activities, particularly in energy-producing sectors such as coal mining, leave lasting environmental footprints that can significantly impact the surrounding ecosystem. The Zonguldak Basin, which has been a central hub for coal mining for over 200 years, stands as a testament to the long-term effects of mining on both the environment and local communities. Throughout this period, various mines of varying scales have been operational, leading to the accumulation of millions of tons of coal spoil and washing residues. While some of these waste piles have been rehabilitated, an estimated 20 to 25 million tons of spoil heaps of different sizes remain scattered across the basin, contributing not only to environmental pollution but also to visual degradation of the landscape. In addition to the spoil heaps, coal washing plants (lavoirs) generate shale-type residues, further exacerbating the growing waste issue. These residues, characterized by their toxic and hazardous components, pose significant risks to environmental and human health. Therefore, the management, recycling, and reuse of these mining by-products have become an urgent necessity to mitigate their environmental impact and to promote sustainability in the coal mining industry (Yıldız, 2020; Yıldız, 2024b).

Mining activities, while essential for economic development and industrial progress, are widely recognized as major contributors to land degradation at a global scale. In particular, open-pit mining imposes intense pressure on natural ecosystems, leading to widespread deforestation, compaction of soil layers, depletion of nutrients, and significant disruption of soil structure due to the stripping of topsoil and the formation of large excavation voids (Shrestha & Lal, 2011; Frouz et al., 2015; Gu et al., 2019). The initial removal of vegetation interrupts key ecological functions, and subsequent operations involving heavy machinery and the accumulation of waste materials further exacerbate environmental instability, often resulting in persistent ecological disturbances. In addition, the reduction of soil organic matter and the loss of critical nutrients—particularly nitrogen—further degrade soil quality, thereby limiting the potential for natural ecosystem recovery (Asensio et al., 2013; Rodríguez-Vila et al., 2016). Consequently, without targeted reclamation efforts, post-mining landscapes are commonly left in a degraded, unproductive, and ecologically vulnerable state.

Globally, a considerable proportion of mineral resources is located within forested regions (Burton & Macdonald, 2011). The extraction of these resources not only removes vegetation cover but also induces substantial changes in the physicochemical and biological properties of soils, ultimately weakening ecosystem stability and resilience (Ahirwal & Maiti, 2016). For this reason, the restoration of abandoned mining areas has become a critical priority in environmental management practices (Frouz et al., 2015). Among the available rehabilitation strategies, revegetation—especially through afforestation—has been identified as one of the most effective approaches. However, the success of such restoration efforts largely depends on the careful selection of plant species, as different species vary in their ability to stabilize soils, increase organic matter content, and promote nutrient cycling processes (Mukhopadhyay et al., 2013). As illustrated in Figure 1, open-pit mining significantly transforms landforms, vegetation structure, and soil properties, resulting in degraded landscapes that require comprehensive and systematic ecological restoration.

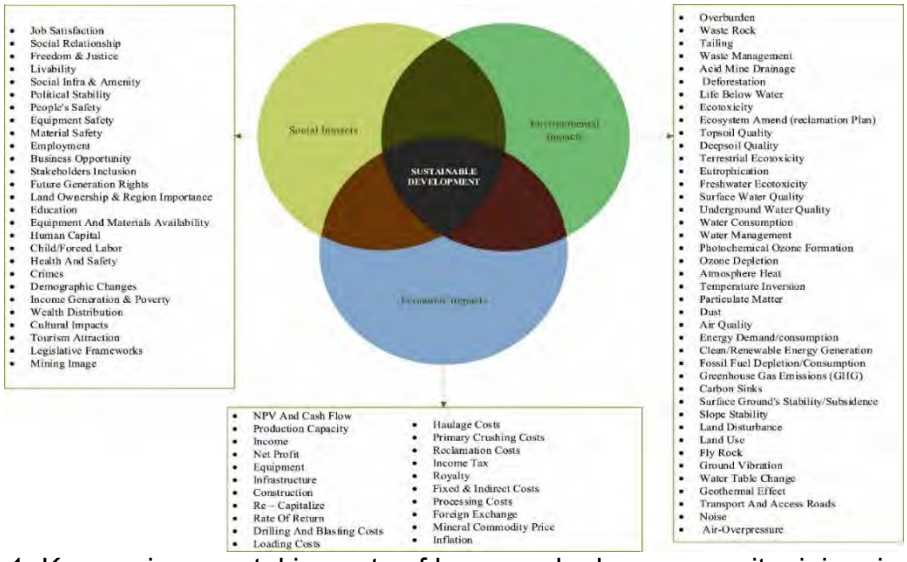

Figure 1. Key environmental impacts of large-scale deep open-pit mining, including deforestation, soil compaction, topsoil loss, and persistent ecological degradation (adapted from Heydari and Osanloo, 2024)

Waste management and recycling are increasingly recognized as critical concerns worldwide, especially in the context of industries that generate large volumes of by-products. In the case of coal mining, the environmental impacts of waste disposal and the potential for resource recovery have led to a surge in research focused on innovative strategies for transforming these waste materials into valuable commodities. Advanced technologies such as air jigs, air shaking tables, and optical and X-ray sorting systems have emerged as effective tools to enhance separation efficiency, reduce processing costs, and enable the reintegration of waste

materials into productive cycles. These technologies not only improve the separation of coal from inert inorganic components but also facilitate the extraction of valuable resources from what would otherwise be considered waste.

The coal waste in the Zonguldak Basin, despite being largely inert, contains calorific values ranging from 500 to 1500 kcal/kg, making it a viable candidate for energy production. The current study focuses on the processing of coal spoil and residue samples collected from various sites across the basin. The separation process, which utilizes advanced separation technologies, effectively isolates the organic coal fraction from the inert inorganic components such as shale, limestone, and sandstone. The recovered coal can be utilized as fuel in power plants, while the shale and limestone can serve as raw materials for the cement and ceramics industries. Furthermore, the limestone and sandstone can be processed into crushed stone, and the fine-grained materials can be repurposed as filling material for construction projects. These findings underscore the potential of coal waste and by-products in the Zonguldak Basin to be efficiently repurposed within a zero-waste framework, aligning with principles of sustainability and the circular economy. The results demonstrate that coal spoil and residues, often perceived as a burden on the environment, can be transformed into valuable resources that contribute to both economic growth and environmental preservation. This study aims to showcase how the Zonguldak Basin's coal waste can be managed sustainably, offering a model for similar mining regions worldwide.

The research presented here highlights the importance of integrating waste management and recycling strategies into the coal mining industry, not only to minimize environmental damage but also to create opportunities for resource recovery and economic development. By adopting a zero-waste approach, mining operations can reduce their ecological footprint, contribute to the circular economy, and promote the long-term sustainability of the industry. This paper seeks to explore how the coal waste in the Zonguldak Basin can be evaluated, processed, and reused in a manner that minimizes environmental impacts while maximizing economic value, paving the way for more sustainable mining practices globally.

The potential applications of the materials recovered from coal waste are broad and impactful. The extracted coal can be utilized as fuel in power plants, while the inert components, such as shale and limestone, can be repurposed for use in the cement and ceramics industries. Additionally, sandstone can be processed into crushed stone, and fine-grained materials can be applied as filling material in various construction projects. This multi-faceted approach not only reduces the environmental impacts associated with coal mining waste but also facilitates the creation of a circular economy, where waste materials are reincorporated into productive industries. By employing advanced sorting technologies, this research explores the viability of turning coal spoil and washing residues from the Zonguldak Basin into valuable commodities, offering a practical pathway toward a zero-waste mining solution.

This study emphasizes the crucial role of integrating effective waste management and recycling strategies within the coal mining industry. By adopting a zero-waste approach, mining operations can significantly reduce their environmental footprint while simultaneously fostering resource recovery and contributing to economic development. Such an approach not only minimizes the harmful effects of waste accumulation but also promotes the transition toward a circular economy. Through the efficient evaluation, processing, and reuse of coal waste in the Zonguldak Basin, this research aims to demonstrate how these materials can be transformed into valuable resources, thus enhancing both the sustainability and economic viability of coal mining operations. The study seeks to establish a model for sustainable mining practices that can be replicated in other regions facing similar waste management challenges.

2. MINING WASTE

Mining waste refers to the by-products generated during the extraction and processing of minerals. These wastes are materials that must be carefully managed due to their environmental impacts and the challenges associated with their disposal. The management of mining waste plays a crucial role in promoting sustainable practices and minimizing environmental harm. Proper management strategies and innovative disposal methods are critical in reducing the negative impacts of the mining industry on the environment. Mining wastes are generally classified into two main categories: a) materials extracted from open-pit and underground mines, and b) materials generated during mineral processing(Yıldız et al., 2024a; Vural et al., 2024).

2.1. Types of Mining Waste

Open-Pit and Quarry Mining Wastes

- Soil and Rocks: Large volumes of soil and rock fragments are produced during the mining extraction process.
- Low-Grade Ore: Ore that contains a low concentration of metals, making it economically unfeasible for extraction.

Mineral Processing Wastes

- Waste Rock (Gangue): Non-economic minerals separated from the ore during the processing stage.
- Tailings: Fine-grained residues left after mineral processing. These tailings often contain chemical substances.
- Flotation Wastes: Wastes resulting from the flotation method used to separate minerals.
- Filter Press Wastes: Tailings that are separated from water through filtration processes.

2.2. Environmental Impacts of Mining Waste

Mining waste can have significant environmental effects, such as:

- Soil and Water Pollution: The chemical substances or heavy metals in mining waste can seep into soil and water sources, leading to contamination.
- Erosion and Habitat Destruction: Improper waste management can lead to erosion and the destruction of natural habitats.

2.3. Management and Disposal Methods for Mining Waste

- Storage: Safe storage of mining waste requires creating proper disposal areas.
- Recycling and Reuse: Some mining wastes can be reused in construction, road-building, and other industrial applications.

2.4. Recycling and Reuse of Mining Waste

The recycling and reuse of mining waste are essential for reducing environmental impacts and generating economic value. These practices help recover valuable metals and contribute to the sustainable use of resources (Table 1).

Table 1. Some of the recoverable products resulting from recycling mining and aggregate plant waste

Construction and Road Construction	Metal Recycling	Ceramic and Glass Production	Cement Production
Crushed Stone and Aggregate	Metal Content	Raw Material	Cement Additive
Mining waste can be used in road and infrastructure projects as construction material. This reduces the consumption of natural resources.	Metal ores can be extracted through recycling. Mining waste can be used for recovering metals and materials like gold, silver, and precious metals.	Mining waste, ceramics, and cement production can be used as raw material. This includes silica-containing materials used in glass production.	Mining waste, cement production waste, and alternative fuels can be used in cement factories, reducing energy costs and carbon emissions.
Reuse	Reuse	Reuse	Reuse
Landscaping and Recreational Areas	Industrial and Manufacturing	Water Treatment	Agricultural Use
Reclamation	Soil Improvement	Chemical Production	Filter Materials
Mining areas can be converted to recreational areas like parks, golf courses, or agricultural fields.	Mining waste can be used in soil restoration projects, providing additional soil improvement.	Some mining waste can be reused as raw materials in the chemical industry.	Some mining waste can be used in water treatment as filter material, improving water cleaning processes.

Methods and Benefits of Recycling Mining Waste

Different techniques are applied to recycle mining waste, such as:

- Use in Construction: Aggregates from mining waste can be used as construction materials, such as in road-building and building construction.
- Chemical Treatment: Harmful chemicals in mining waste can be neutralized through chemical processes.
- Biological Treatment: Microorganisms are used to treat biological mining waste, providing an eco-friendly disposal option.

The benefits of recycling mining waste include reduced resource consumption, lower energy usage, and decreased carbon footprint. Additionally, it can help create new job opportunities in industries such as construction, recycling, and energy production. Recycling also promotes environmental sustainability and contributes to broader economic growth.

Social and Economic Benefits of Recycling Mining Waste

Recycling mining waste not only contributes to environmental sustainability but also promotes social and economic development. Government initiatives, such as tax incentives and subsidies for recycling projects, encourage the participation of companies in recycling and reuse activities. Investments in recycling technologies can lead to more efficient mining waste management, reduce costs, and increase profitability. By reducing the environmental impact and ensuring the sustainability of mining practices, these efforts support long-term development goals.

Governments and organizations focused on sustainable development can benefit from enhanced public awareness and increased support for these projects. In addition, the proper management of mining waste creates new industries and business opportunities, fostering overall economic growth. Finally, by minimizing the environmental and economic impacts of mining waste, recycling contributes directly to achieving global sustainability targets.

3. CRITERIA FOR THE USE OF MINING WASTES IN LAND RECLAMATION

When using mining wastes for land reclamation, several criteria and factors need to be considered. These criteria are essential for improving soil quality, minimizing environmental impacts, and supporting plant growth.

3.1. Physical Criteria

- Particle Size: The particle size of the waste affects soil structure and its ability to retain water. Fine-grained wastes may improve soil permeability and water retention capacity.
- Bulk Density: The bulk density of the waste impacts soil porosity and root development. Lightweight and porous materials enhance soil aeration.
- Adhesiveness and Plasticity: The adhesive and plastic properties of the waste influence the soil's workability and stability. Excessively sticky materials may reduce the soil's permeability.

3.2. Chemical Criteria

- pH Level: The pH level of the waste affects the soil's acidity or alkalinity, directly influencing the availability of nutrients for plants.
- Nutrient Content: Waste containing nutrients such as nitrogen, phosphorus, and potassium can enhance soil fertility. However, excessive amounts of nutrients may be harmful.
- Heavy Metals and Toxic Substances: Waste containing heavy metals and toxic substances can damage soil and plant growth. The levels of such substances must remain within acceptable limits.
- Organic Matter Content: Organic material in the waste can improve soil fertility and support microbial activity, enhancing soil health.

3.3. Biological Criteria

- Microbial Activity: The impact of mining waste on soil microbial activity should be evaluated. Microorganisms are critical for maintaining soil ecosystem balance.
- Effect on Plant Growth: It is necessary to observe how the waste affects plant growth. Some wastes promote root development, while others may inhibit it.

3.4. Environmental and Legal Criteria

- Environmental Impact Assessment: The environmental impacts of the waste, such as contamination, must be carefully assessed. Environmental risks should be minimized.
- Legal Regulations: The use of mining wastes should comply with local environmental regulations. This ensures that the waste is used sustainably and safely.
- Amount and Proportion of Use: The amount and proportion of waste used in reclamation must be carefully determined. Excessive use may negatively impact soil health.

3.5. Practical Application Criteria

- Mixing and Application Techniques: It is important to mix mining waste with appropriate materials. Suitable techniques for applying the waste should be employed to ensure its effective placement in the soil.
- Storage and Transport: The storage and transportation of mining waste should minimize environmental risks. Proper planning for storage areas and transport routes is necessary to prevent erosion and pollution.

3.6. Legal Framework and Regulations Related to the Use of Mining Waste in Land Reclamation

In land reclamation projects, the environmental impact of the materials to be used must be assessed. These projects must be proven to be safe for both the environment and public health. The following steps should be taken:

- The mining wastes must undergo chemical and physical analyses to ensure they do not contain harmful levels of heavy metals or other contaminants.
- Land reclamation projects must obtain necessary approvals from local authorities and environmental protection agencies.
- Projects should be monitored and reported regularly to ensure they meet environmental standards.

Legal frameworks and regulations regarding the use of mining waste in land reclamation are crucial for environmental protection and public health. These regulations set specific criteria and standards for the safe and sustainable use of mining waste. Projects must adhere to local and international legal requirements, including compliance with environmental protection and public health standards. Regulations may vary depending on the country or region, but they typically address soil quality, waste management, and the protection of the environment. In Turkey, related regulations are summarized in Table 2, while European Union regulations and other international standards are presented in Table 3.

Table 2: Legal Regulations Regarding the Use of Mining Waste in Land Reclamation in Turkiye

Waste Management Regulations	EIA Regulations	Regulations on Soil Pollution Control and Point Source Contaminated Areas	Regulations on Agricultural Land Protection, Use, and Planning
General principles related to waste management and disposal are outlined.	Mining activities and their environmental impacts are evaluated in EIA.	Soil pollution control and prevention measures are specified.	Regulations related to the protection and sustainable use of agricultural lands.
Mining waste used for land reclamation must meet specific conditions and standards.	Land reclamation projects may require an EIA.	Emphasizes that materials used in reclamation must not negatively affect soil quality.	Specifies that materials used in agricultural land reclamation must not harm its productive capacity.
Limits for heavy metals and other toxic substances are set.			

Table 3. Relevant regulations and other international standards in the European Union

EU Waste Framework Directive (2008/98/EC)	EU Soil Protection Strategy	FAO (Food and Agriculture Organization) Guidelines
Defines the principles of waste management and recycling.	Sets strategic goals related to soil protection and sustainable use.	Encourages the use of environmentally friendly and sustainable methods in agriculture and soil restoration projects.
Regulates the reuse of waste to improve soil quality and minimize health risks.	Includes guidelines for sustainable soil use and improving soil quality.	Specifies environmental and health criteria for materials used in soil restoration projects.

4. ZONGULDAK COAL BASIN

The Zonguldak Coal Basin constitutes the only hard coal–bearing region of Türkiye and represents the strategic core of the country's bituminous coal resources. Coals produced within the basin are broadly classified into two principal quality categories: coking and non-coking coals. Metallurgical-grade reserves suitable for direct coke production are concentrated in the operational fields of Kozlu, Üzülmez, and Karadon collieries, whereas the Armutçuk coals exhibit semi-coking characteristics and the Amasra coals are classified as partially or non-coking depending on blending behavior [1]. This quality differentiation is closely associated with variations in maceral composition, rank distribution, and depositional conditions across the basin.

Stratigraphically, coal-bearing sequences commence with the Alacaağzı Formation of Upper Carboniferous (Namurian) age and continue upward through the Lower Westphalian A Kılıç Formation, the Upper Westphalian A Kozlu Formation, and finally the Westphalian B–C–D aged Karadon Formation. Within this Carboniferous succession, a total of 46 coal seams with varying structural and technological properties have been identified, of which 18 are currently mined under economically viable conditions. Production is predominantly concentrated in the highly productive seams of the Kozlu Formation, reflecting both favorable thickness and quality parameters.

The geological reserve of the basin, calculated down to a depth of −1200 m, is approximately 1.514 billion tons, nearly 48% of which is categorized as proven reserve. Seam dips range between 0° and 90°, while seam thickness generally varies from 0.8 to 3.5 m; however, exceptional thicknesses up to 25 m are observed in the Büyük seam of the Armutçuk Colliery. The predominance of steep and near-vertical seam geometries has led to rapid deepening of underground operations, with an average annual increase in production depth of approximately 12 m. Currently, production and development activities continue at depths of −540 m in Karadon and −630 m in Kozlu, and infrastructure preparations for deep mining operations extending to −1000 m are ongoing [1]. Comprehensive information regarding reserve distribution, annual production, workforce capacity, and average operating depths of active collieries is presented in Table 1, which clearly demonstrates the relative dominance of Karadon, Kozlu, and Üzülmez in terms of production volume and employment, while highlighting the substantial reserve potential of Amasra and Armutçuk.

Mining methods are selected according to seam inclination and geotechnical conditions. In seams dipping between 0° and 45°, advancing longwall with caving is commonly applied, whereas retreat longwall with caving is preferred in fire-prone seams, particularly in Armutçuk and Kozlu. Semi-mechanized methods are implemented in steep seams exceeding 45°. The abundance of faults, intense folding, and local compressional structures significantly restrict the applicability of fully mechanized systems, thereby maintaining a relatively labor-intensive production structure.

From a global perspective, reserve definitions emphasize economically recoverable quantities under existing technological and market conditions. In order to enhance reserve reliability and explore new resource potential, extensive geophysical surveys covering approximately 40 km and totaling 6,144.80 m of drilling were conducted by the General Directorate of Mineral Research and Exploration (MTA), primarily in the Armutçuk and Kozlu regions. As a result of drilling activities within the Armutçuk TIM area, an additional 5,090,262 tons of reserves were delineated in Blocks I and II.

In this context, the operational and structural characteristics summarized in Table 4 should be evaluated together with the international coal market dynamics presented in Table 5, which indicate a sustained increase in global trade volumes for both thermal and coking coal between 2023 and 2024. The upward trend in global coking coal exports and imports (Table 5)

underscores the strategic importance of optimizing the utilization of domestic coking and semi-coking reserves within the Zonguldak Coal Basin, particularly in light of increasing global demand for metallurgical coal.

Table 4. Information on operating collieries in the basin

Colliery	Reserve (10^6 ton)	Production (10^3 ton/year)	Number of Employees	Average Production Depth (m)
General Directorate				860
Armutçuk	37		1,120	550
Amasra	618	250	720	236
Karadon	405	806	2,948	373
Kozlu	154	647	1,824	630
Üzülmez	300	486	1,598	200
Total	1,514	2,441	9,074	

Table 5. World Coal Trade (Million Tons)

World Coal Trade	2023	2024
Exports		
Thermal Coal and Lignite	1,151	1,178
Coking Coal	351	369
Imports		
Thermal Coal and Lignite	1,157	1,178
Coking Coal	352	368
Total Exports	1,502	1,547
Total Imports	1,510	1,546

5. MATERIAL and METHOD

The materials and methods applied in this study focus on processing the coal spoil and residue materials sourced from the Zonguldak Basin. A systematic evaluation of these materials was conducted with the goal of separating valuable organic (coal) components from inert inorganic materials (shale, limestone, sandstone, etc.), employing advanced separation technologies.

The spoil material excavated from the spoil stock area by means of an excavator is transported to the spoil blending and feeding unit. From there, the homogenized material is conveyed to the spoil evaluation unit. Within this unit, the spoil is processed and transformed into two distinct marketable products: (i) power plant coal (coal intermediate product, low-calorific coal) and (ii) fill/brick/cement and other construction raw materials.

The process flow diagram illustrating the evaluation of coal spoil is presented in Figure 2. Both product streams are designed to be marketed to different sectors according to prevailing market conditions and material characteristics. The spoil evaluation project has been developed based on a zero-waste approach, aiming to convert mining waste into economically valuable and sustainable products.

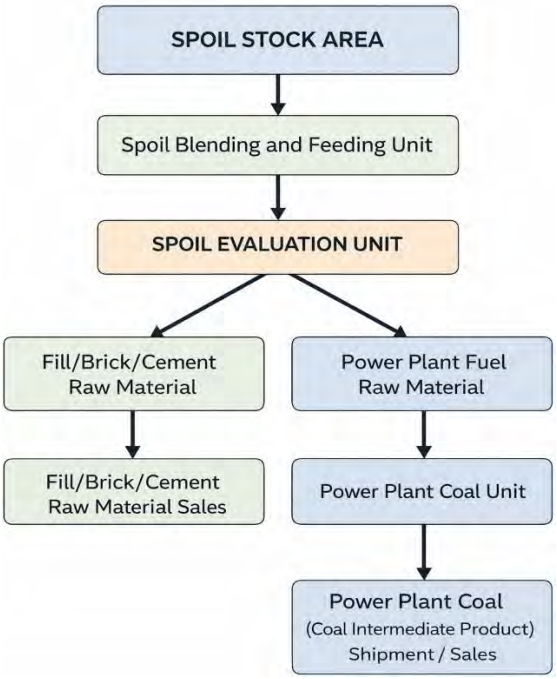

Figure 2. Schematic representation of the coal spoil evaluation process

Material from the spoil stock area is transferred to the blending and feeding unit, followed by processing in the spoil evaluation unit. The evaluated material is separated into two main streams: (i) mineral-based fractions for fill, brick, and cement raw material applications, and (ii) coal-based fractions directed to the power plant coal unit for fuel production and subsequent shipment/sales.

Figure 2 illustrates the operational workflow developed for the evaluation and utilization of coal spoil materials. The process begins at the spoil stock area, where accumulated spoil is excavated and transferred to the spoil blending and feeding unit. In this unit, the material is homogenized to ensure consistent feed characteristics before being conveyed to the spoil evaluation unit.

Within the spoil evaluation unit, the material undergoes classification and separation processes to distinguish combustible coal fractions from inert mineral components. Following evaluation, the material is divided into two principal product streams. The first stream consists of mineral-based fractions suitable for use as fill material and as raw materials in brick, cement, and other construction-related industries. These materials are prepared for direct sales to relevant sectors.

The second stream comprises coal-rich fractions that are directed to the power plant coal unit. After necessary processing, this fraction is converted into a coal intermediate product suitable for use as power plant fuel. The final product is then dispatched for shipment and commercial sale.

Overall, the process flow presented in Figure 2 demonstrates a zero-waste-oriented approach, in which coal spoil is systematically transformed into value-added products for both the energy and construction sectors.

5.1. Sample Collection

Samples were collected from multiple spoil heaps and coal washing residue sites across the Zonguldak Basin, where waste and by-products from over 200 years of coal mining operations have accumulated. The material samples include a mixture of various coal types, spoil, and washing residues, all of which vary in their chemical and physical properties.

5.2. Advanced Separation Technologies

To optimize the recovery of coal from the spoil and residue materials, several separation technologies were employed:

1. Air Jigs: These were used to separate materials based on their density, allowing for the efficient separation of coal particles from inert materials like shale and limestone.
2. Air Shaking Tables: This technology further refines the separation process by utilizing shaking tables to increase the accuracy and efficiency of material sorting.
3. Optical and X-ray Sorting Systems: These technologies were employed for the final refinement of materials, ensuring that the separation between organic and inorganic materials was as precise as possible, based on their distinct properties.

5.3. Particle Size Distribution and Analysis

A crucial component of the material evaluation was the sieve analysis of the spoil and residue samples. The materials were sorted into different size fractions, as shown in Figures 1 and 2 of the report. The samples were categorized by particle sizes, which provided insight into their composition and potential for further separation. The sieve analysis provided the following distribution for coal spoil particles:

- Particles larger than 150 mm were analyzed for ash content, and a significant amount of coal was observed.
- The 0-150 mm fraction showed distinct proportions of coal, shale, and limestone, offering insight into the composition of waste.
- Fine fractions (0-15 mm) were further analyzed for their coal content and were found to contain substantial coal recovery potential, even when subjected to flotation processes.

5.4. Flotation and Settling Test

For smaller fractions of the spoil, particularly those in the -15+1 mm size range, flotation tests using $ZnCl_2$ solutions were conducted to separate organic coal from inert components. The flotation test revealed that a substantial proportion of the coal could be separated effectively, leaving behind shale and limestone. The results indicated that the extracted coal could serve as fuel, while the non-coal components could be utilized in construction and industrial applications.

Flotation tests, could have a clue for having higher calorific values, making them suitable for energy production. Meanwhile, the sinking materials, primarily composed of inorganic elements, were identified as valuable materials for cement, ceramic, and construction industries.

5.5. Calorific Value Analysis

The calorific value of the processed materials was also a key focus of the study. The samples exhibited calorific values ranging between 500 and 1500 kcal/kg. This broad range indicates the variability in the energy potential of the coal spoil, with higher calorific values aligning with

the organic (coal) fractions that were successfully separated. The extracted coal, therefore, holds considerable potential as a power plant fuel.

5.6. Material Recovery and Utilization

Based on the analyses, the recovered materials from the Zonguldak coal spoil can be repurposed as follows:

- Coal fraction**:** The extracted coal can be utilized as fuel for power plants, contributing to energy generation.
- Shale and Limestone**:** These inert components are valuable as raw materials for cement production, ceramics, and construction projects.
- Sandstone**:** Can be processed into crushed stone for use in construction and infrastructure development.
- Fine-grained materials**:** These materials can be employed as filling material in various construction projects, offering an additional avenue for their reuse.

The results from the various separation methods confirm the feasibility of utilizing waste from the Zonguldak Basin within a zero-waste framework, enhancing the sustainability of coal mining practices in the region. This approach not only mitigates environmental pollution caused by waste accumulation but also contributes to the circular economy by transforming waste into valuable resources.

6. RESULTS and DISCUSSION

The waste and by-product materials collected from various sites across the Zonguldak Basin were processed using advanced separation technologies, including air jigs, air shaking tables, and optical and X-ray sorters. These methods aimed at effectively separating the coal fraction from the inert inorganic components such as shale, limestone, and sandstone, ensuring optimal recycling and reuse of materials.

The spoil and residue samples were categorized based on particle sizes, with key data from the sieve and washing analyses provided in the following tables.

The sieve analysis for coal spoil particles larger than 150 mm and within the 0-150 mm size range revealed significant quantities of coal particles, as indicated in Table 6**.** The distribution of coal and other components such as shale and limestone in various size fractions provides insight into the composition of the waste and its potential for separation. The results for each size fraction are as follows:

Table 6. Sieve Analysis for 0-150 mm coal spoil particles

Size Fraction (mm)	Amount (%)	Ash (%)
-150+50	10.0	88.0
-50+15	50.0	85.0
-15+1	25.0	80.0
Total	100.0	75.0

Further analysis of the smaller 0-15 mm particles is shown in Table 7**.** This size fraction revealed a substantial proportion of coal, with varying ash content and other components, supporting the viability of separating reusable coal from waste for energy production. The data shows the distribution of materials in the 0-15 mm size range, with the majority of the particles being inert.

Table 7. Sieve Analysis for 0-15 mm coal spoil particles

Size Fraction (mm)	Amount (%)	Ash (k) (%)
-15+1	60.0	80.0
+1+0.3	20.0	76.0
-0.3+0.150	15.0	74.0
Total	100.0	75.0

Further tests were conducted on the -15+1 mm fraction to determine its behavior when subjected to flotation and settling processes using ZnCl2 solutions, as seen in Table 8. The flotation results reveal the potential for separating organic and inorganic components in the sample, showing that the recovered coal can be utilized as fuel, while the remaining shale and limestone can be repurposed for construction or industrial applications.

Table 8. Batting Test results for -15+1 mm coal spoil with $ZnCl_2$ solution

Product	Amount (%)	Ash (M) (%)	M (%)	Sum (%)
Floating (1.90)	28.00	204.4	28.00	204.4
Sinking (+1.90)	72.00	92.8	72.00	92.8
Total	100.00	83.78	83.78	83.78

The results indicate that by employing advanced separation technologies, a substantial proportion of coal can be extracted from the waste spoil and residue materials in the Zonguldak Basin. The sieve and flotation analyses suggest that the recovered coal fraction can be effectively used as fuel in power plants, contributing to energy production. The non-coal materials, such as shale and limestone, hold significant value as raw materials for cement and ceramics production, and as crushed stone for construction purposes.

The findings align with previous studies that indicated the inert nature of coal washing residues, with calorific values ranging between 500 and 1500 kcal/kg. These results further confirm that the materials from the Zonguldak Basin, which were previously considered waste, have the potential to be repurposed into valuable resources. The efficient separation of coal and inert components can reduce environmental pollution, mitigate the risks associated with waste accumulation, and contribute to the circular economy by recycling these materials for various industrial uses.

Overall, the use of air-based separators, shaking tables, and flotation methods has proven effective in recovering valuable coal while minimizing waste. The results demonstrate the feasibility of implementing a zero-waste strategy in the Zonguldak Basin, where coal spoil and washing residues can be efficiently reused, supporting sustainable practices and contributing to the local economy.

7. CONCLUSIONS

In conclusion, the findings of this study clearly demonstrate that the long-accumulated spoil heaps and coal washing residues in the Zonguldak Coal Basin represent not merely an environmental liability but a substantial secondary resource potential within a zero-waste framework. For over two centuries, intensive underground coal mining has generated millions of tons of waste materials, much of which has remained unmanaged or underutilized. Through systematic sampling, particle size distribution analysis, flotation tests, and advanced air-based separation techniques, this research has proven that a considerable portion of these materials still contains recoverable organic fractions with meaningful calorific value. The recovery of coal fractions within the 500–1500 kcal/kg range confirms that these wastes can be re-integrated

into the energy production chain, thereby reducing raw coal demand while simultaneously mitigating the environmental footprint of legacy spoil accumulations.

The technological approach adopted in this study—integrating air jigs, air shaking tables, and optical/X-ray sorting systems—has demonstrated high efficiency in distinguishing combustible coal particles from inert mineral components such as shale, limestone, and sandstone. The separation results obtained from both coarse and fine fractions indicate that even materials previously regarded as low-grade or uneconomic possess recoverable value when processed using appropriate modern technologies. Particularly in the -15+1 mm fraction, flotation experiments revealed a significant separation capability between floating coal-rich fractions and sinking mineral-rich fractions, highlighting the feasibility of multi-stage beneficiation. This technological validation confirms that the transformation of mining waste into marketable products is not only technically achievable but also operationally adaptable to existing industrial infrastructures in the basin.

Beyond energy recovery, the study underscores the multi-sectoral reuse potential of the separated inorganic fractions. Shale and limestone components can be redirected to cement and ceramic industries as alternative raw materials, sandstone can be processed as crushed aggregate for construction, and fine-grained fractions may be utilized as filling or reclamation material. Such diversified utilization pathways directly support circular economy principles by minimizing landfill requirements, reducing natural aggregate extraction, and lowering carbon emissions associated with primary raw material production. Furthermore, compliance with national regulations in Türkiye and alignment with European waste management directives reinforce the environmental legitimacy and regulatory feasibility of implementing these recovery strategies at industrial scale. The integration of environmental, technical, and legal criteria ensures that waste valorization does not compromise soil quality, water resources, or public health.

Ultimately, this research establishes a comprehensive model for sustainable spoil management in mature coal basins. By shifting the perception of mining waste from an environmental burden to a recoverable asset, the proposed zero-waste-oriented processing framework contributes simultaneously to environmental remediation, resource efficiency, and regional economic development. The approach presented for the Zonguldak Basin may serve as a replicable model for other long-established coal-producing regions worldwide facing similar legacy waste challenges. In this respect, the study not only provides practical technical solutions but also advances the broader strategic objective of transitioning the coal mining sector toward more sustainable and circular production paradigms.

REFERENCES

Ahirwal, J. & Maiti, S. K. (2016). Assessment of soil properties of different land uses generated due to surface coal mining activities in tropical Sal (Shorea robusta) forest, India. Catena, 140, 155–163. doi:10.1016/j.catena.2016.01.028.

Asensio, V., Vega, F. A., Andrade, M. L. & Covelo, E. F. (2013). Tree vegetation and waste amendments to improve the physical condition of copper mine soils. Chemosphere, 90(2), 603-610. doi:10.1016/j.chemosphere.2012.08.050.

Bulut, M., & Yıldız, T. D. (2023). Agrega tesislerinde bulunan filtre pres ünitelerindeki atık çamurlarının değerlendirilmesi. II. Uluslararası Avrasya Zirvesi & Bilimsel Araştırmalar ve Güncel Gelişmeler Kongresi, 22–23 Haziran 2023, Göreme, Nevşehir. ISBN: 978-625-367-182-2, 29–31.

Burton, P. J. & Macdonald, S. E. (2011). The restorative imperative: Challenges, objectives and approaches to restoring naturalness in forests. Silva Fennica, 45, 843–863. doi: 10.7939/R34746R3T.

Demir-Şahin, D., Kumaş, C., & Eker, H. (2022). Research of the use of mine tailings in agriculture. Journal of Current Research in Engineering, 8(2), 71–84. https://doi.org/10.26579/jocrest.8.2.6

Eker, H. (2023). Investigation of the usability of industrial mining wastes in agriculture. Frontiers in Environmental Science, 11, 1248188. https://doi.org/10.3389/fenvs.2023.1248188

Frouz, J., Vobořilová, V., Janoušová, I., Kadochová, Š. & Matějíček, L. (2015). Spontaneous establishment of late successional tree species English oak (Quercus robur) and European beech (Fagus sylvatica) at reclaimed alder plantation and unreclaimed post mining sites. Ecological Engineering, 77, 1-8. Doi: 10.1016/j.ecoleng.2015.01.001.

Heydari, M., & Osanloo, M. (2024). Untangling the complex web of environmental, social, and economic impacts in deep and large-scale open-pit mining projects using a dynamic modeling framework. Resources Policy, 90, 104690.

Gu, L. P., Kong, J. J., Chen, K. & Guo, Y. Q. (2019). Monitoring soil biological properties during the restoration of a phosphate mine under different tree species and plantation types. Ecotoxicology and Environmental Safety, 180(1), 130-138. doi:10.1016/j.ecoenv.2019.05.001.

Güven, O., Burat, F., Kangal, O., Acarkan, N., & Önal, G. (2012). Beneficiation of antimony tailings. In XIII International Mineral Processing Symposium, Bodrum, Türkiye.

Pehlivan, H., & Aytekin, M. (2017). Geri kazanılmış agrega kullanımının sürdürülebilir kalkınma üzerine etkilerinin araştırılması. Beton İstanbul 2017 Hazır Beton Kongresi, Türkiye Hazır Beton Birliği (THBB), İstanbul, 1–8.

Mukhopadhyay, S. & Maiti, S. K. (2011). Trace metal accumulation and natural mycorrhizal colonisation in an afforested coalmine overburden dump—a case study from India. International Journal of Mining Reclamation and Environment, 25(2), 187–207. doi: 10.1080/17480930.2010.548663.

Resmi Gazete. (2010). Evsel ve kentsel arıtma çamurlarının toprakta kullanılmasına dair yönetmelik (Sayı: 27661, 03 Ağustos 2010). T.C. Resmi Gazete.

Rodríguez-Vila, A., Asensio, V., Forján, R. & Covelo E. F. (2016). Carbon fractionation in a mine soil amended with compost and biochar and vegetated with Brassica juncea L. Journal of Geochemical Exploration, 169, 137-143. doi: 10.1016/j.gexplo.2016.07.021.

Tuğrul, A., & Yılmaz, M. (2017). Megakentler için agrega kaynak planlamasının önemi: İstanbul örneği. *4. Uluslararası Taş Kongresi Bildiriler Kitabı* (20–25 Mart 2017), İzmir, 501–506. ISBN: 978-605-01-1133-0.

Shrestha, R. K. & Lal, R. (2011). Changes in physical and chemical properties of soil after surface mining and reclamation. Geoderma, 161(3-4), 168-176. doi: 10.1016/j.geoderma.2010.12.015.

Uliasz-Bochenczyk, A., Mazurkiewicz, M., & Mokrzycki, E. (2015). Fly ash from energy production – a waste, byproduct and raw material. *Gospodarka Surowcami Mineralnymi – Mineral Resources Management*, 31(4), 139–149. https://doi.org/10.1515/gospo-2015-0042

Uz, B., Yıldız, T. D., Gültekin, A. H., Esenli, F., Özdamar, Ş., & Kural, O. (2017). Bir kalker sahasında yapılacak patlatmanın arkeolojik yapılara ve SIT alanlarına etkisi. *IV. Uluslararası Delme-Patlatma Sempozyumu* (1–2 Aralık 2017), Ankara, 27–38. ISBN: 978-605-01-1107-1.

Vural, N., Yılmaz, M., Onat, B., Tuğrul, A., & Uzun-Ayvaz, B. (2024). Agrega madenciliğinde çevresel etkilerin yaşam döngüsü yaklaşımı ile değerlendirilmesi: Cebeci agrega ocakları örneği. *Jeoloji Mühendisliği Dergisi*, 48(2), 123–138. https://doi.org/10.24232/jmd.1548854

Yıldız, T. D. (2020). Waste management costs (WMC) of mining companies in Turkey: Can waste recovery help meeting these costs? *Resources Policy*, 68, 101706. https://doi.org/10.1016/j.resourpol.2020.101706

Yıldız, T. D. (2021). Possible effects of mining zone regulation on mining companies in Turkey & evaluation of mining companies. *Resources Policy*, 71, 102011. https://doi.org/10.1016/j.resourpol.2021.102011

Yıldız, T. D. (2024a). Opportunities for the recovery of rare earth elements from mining tailings and urban mining. In P. Singh & A. Borthakur (Eds.), *Trash or Treasure: Entrepreneurial Opportunities in Waste Management* (pp. 183–205). Springer, Cham. ISBN: 978-3-031-55130-7; 978-3-031-55131-4.

Yıldız, T. D. (2024b). Considering the development levels of countries, contributions of mineral recovery from mining tailings and urban mining wastes to sustainability criteria – A review. *Resources Policy*, 99, 105399. https://doi.org/10.1016/j.resourpol.2024.105399

Yıldız, T. D. (2024c). Developing industrial and mining heritage sites: Lavrion Technology and Cultural Park, Greece. Taylor & Francis Group, Routledge (1st ed.). ISBN: 9781003408437. https://doi.org/10.4324/9781003408437

Yıldız, T. D. (2025a). Rehabilitation costs paid by mining enterprises in Turkey: Comparison of rehabilitation costs with their shares in mining operation costs and other environmental costs. *Resources Policy*, 104, 105593. https://doi.org/10.1016/j.resourpol.2025.105593

Yıldız, T. D. (2025b). Sustainable contributions of the use of phosphorus, potassium, coal and natural stone mine wastes in soil improvement and agriculture – A review. *Resources Policy*, 102, 105506. https://doi.org/10.1016/j.resourpol.2025.105506

Yıldız, T. D. (2026). A review of the sustainable contributions of the use of some mine wastes in soil improvement and as fertilizer in agriculture. *Gospodarka Surowcami Mineralnymi – Mineral Resources Management*. (Unpublished manuscript).

Yıldız, T. D. (2025c). Beton ve yol malzemesi üretimlerinde agrega atıklarının ve diğer sektör atıklarının sürdürülebilir katkıları. *Agrega Dergisi*, 36, 24–31.

Yıldız, T. D., & Tombal-Kara, T. D. (2024). Challenges and recovery opportunities in waste management during the mining and enrichment processes of uranium and thorium containing ores – A review. *Gospodarka Surowcami Mineralnymi – Mineral Resources Management*, 40(1), 25–62. https://doi.org/10.24425/gsm.2024.149305

Yıldız, T. D., & Bulut, M. (2025). Use of waste sludge from filter press units in aggregate facilities in agriculture. In P. Singh & A. Borthakur (Eds.), *Circular Economy and Green Transition in the Global South: Perspectives and Prospects*. Springer, Cham. (Accepted).

Yıldız, T. D., Samsunlu, A., & Kural, O. (2016). Urban development and mining in Istanbul – Cebeci field and its rehabilitation. *SWEMP 2016* (5–7 October 2016), Istanbul, 1–11. ISBN: 978-605-66638-1-9.

Yıldız, T. D., Güner, M. O., & Kural, O. (2017). Türkiye'de Maden Atıkları Yönetmeliği'nin madencilik sektörüne etkileri. *25. Uluslararası Madencilik Kongresi ve Sergisi* (11–14 Nisan 2017), Antalya, 457–472. ISBN: 978-605-01-1008-1.

Yıldız, T. D., Güner, M. O., & Kural, O. (2024a). Effects of EU-compliant mining waste regulation on Turkish mining sector: A review of characterization, classification, storage, management, recovery of mineral wastes. *Resources Policy*, 90, 104836. https://doi.org/10.1016/j.resourpol.2024.104836

Yıldız, T. D., Tombal-Kara, T. D., & Kurşun-Ünver, İ. (2024b). Challenges and recovery opportunities in waste management during the mining and enrichment processes of rare earth elements containing ores. In P. Singh & A. Borthakur (Eds.), *Trash or Treasure: Entrepreneurial Opportunities in Waste Management* (pp. 277–306). Springer, Cham. ISBN: 978-3-031-55130-7. https://doi.org/10.1007/978-3-031-55131-4_11

Yıldız, T. D., Uz, B., Coşkun, N. D., & Uz, V. (2025). Geological, mineralogical, petrographic, hydrogeological, and environmental evaluation of a marble site: Can the site damage water protection zone? *SSRN Journal*. (Unpublished manuscript).

INVESTIGATION OF THE PERMITTING PROCESSES FOR ORE DRESSING AND WASTE STORAGE FACILITIES OF TÜRKİYE

Ali Koray ÖZDOĞAN[1,*], Hakan AKINCI[2], Gizem ÖZDOĞAN[3]

[1]Mining Engineer M.Sc., PhD. Student, 06560, Ankara-TÜRKİYE
[2]Irmak Engineering Consultancy Ltd. Co.,06500, Ankara-TÜRKİYE
[3]Türkiye Coal Enterprises, Garp Lignites Enterprise, 43900, Kütahya-TÜRKİYE
**Corresponding author: akozdogan@gmail.com*

A B S T R A C T

Anatolia has been an important centre for mining activities (production and processing) throughout history and has earned the title of cradle of mining in addition to its status as the zero point of history. Anatolia is also considered the geographical location where the first mining licence was granted, as evidenced by a 2,800-year-old inscription found at the foot of the Bolkar Mountains. From ancient times to the present day, mines have continued to operate according to certain criteria. In addition, legal regulations concerning the processing of minerals have been in force from past periods to the present day. Essentially, the Maadin Nizamnamesi (Mining Regulations), considered the first comprehensive regulation on mining activities, also included ore dressing plants in the legal permit process. Today, it is believed that a comprehensive examination of the permits or institutional opinions required for ore dressing and waste storage facilities, which are of particular importance within the scope of environmental legislation, will contribute to sectoral awareness. It is important for sustainable mining that these permits are not seen as a necessity by enterprises in terms of mining in the activities to be carried out. This study will outline the historical development process of permits obtained for ore dressing and waste storage facilities and comprehensively explain the various mandatory permits or opinions that must be obtained, ranging from the current Environmental Impact Assessment Decision to property permits, wastewater discharge permits, and waste storage facility approval certificates.

Key words: *Mineral processing, waste storage, licence*

1. INTRODUCTION

The mining sector is a dynamic industry characterised by high investment costs and long payback periods. Ore dressing plants are located at the stage where the extracted raw ore is processed to achieve economic value. Ore dressing plants, which constitute the most critical and technological stage of the mining industry, convert ore into value-added products, and it is mandatory that operations are carried out in accordance with legal requirements. In Türkiye, ore dressing plants (flotation, heap leaching, gravity, magnetic separation, etc.) require over 30 permits or institutional opinions throughout the legal process, from the project stage to the operation and closure processes. It is anticipated that a comprehensive explanation in light of Mining Law No. 3213, Environmental Law No. 2872, and related regulations will significantly contribute to the research of industry stakeholders. Furthermore, it is important to view the permit processes not merely as bureaucratic procedures but as engineering processes that guarantee sustainable and efficient working conditions.

This study aims to clarify the legal basis for these permits and to outline the legal framework governing ore dressing plants. By classifying the permits according to their chronological and technical dependencies, explaining why each permit is necessary, what technical parameters it is based on, and detailing the process (e.g., emphasising the relationship between the waste storage approval and soil mechanics, the impact of legislation on engineering practice), the study aims to increase sectoral awareness.

2. MATERIAL AND METHODS

2.1. Material

The primary material of this research consists of a detailed explanation of the permits that must be obtained from the planning stage to the operational stage of the project, the relevant institutions, and the circumstances under which these permits are required (e.g., 'acquisition of pasture-qualified parcels'). This study provides detailed explanations of all permits required by all facilities (depending on ownership status, etc.), rather than just the permits obtained by a single example facility.

2.2. Method

As a research method, the permit items on the list in question have been explained in light of the technical information contained in the current mining and environmental legislation of the Republic of Türkiye (Resmi Gazete, Regulations, Circulars) and classified into four stages according to the necessity of the permit list. Legal requirements (e.g., 'Heap Leach Plant Implementation Project') have been matched with the relevant laws and regulations (Mining Waste Regulation, etc.). Not only the administrative aspects of the permits but also the required engineering work (geotechnical studies, hydrological modelling, etc.) have been explained.

3. RESULTS AND DISCUSSION

3.1. Planning and Environmental Impact Assessment (EIA)

Prior to the design of ore dressing plants, the fact that technical feasibility takes a back seat and environmental feasibility is the primary research topic should be considered the first condition for the project's feasibility and sustainability. The EIA Decision is the backbone of the project. Following its publication in the Official Gazette on June 26, 2025, the decision attained legal force. Article 3 of the Regulation Amending the Environmental Impact Assessment Regulation states: 'c) Facilities performing at least one of the following processes: crushing, screening, washing, drying, and ore dressing at a rate of 400,000 tonnes/year or more.' It has been announced that this has been added to Article 25 of Annex 1 of the EIA Regulation. For these facilities, it is mandatory to prepare a detailed EIA Report, hold a public participation meeting, and complete the Review and Evaluation Commission (REC) process at the Ministry. On the other hand, facilities that perform at least one of the processes of crushing, screening, washing, drying, and ore dressing but remain below the specified capacity threshold are subject to the EIA process as listed in Annex 2 of the EIA Regulation (Güngör & Özdoğan, 2025).

The most important point at this stage is that the EIA process is not merely a process in which environmental impacts (dust, noise) are declared, but also the stage at which the location of the facility is finalised and all processes are evaluated in detail. The scope of the project is determined by the commitments made in the EIA report. An error made in the EIA process can lead to irreversible consequences in the later stages of the project. In this context, it is important for the EIA process to be carried out with the collective wisdom of experts and experienced individuals, ensuring that knowledge is transferred correctly for sustainable memory.

3.2. Land Ownership and Usage Permits

As an ore dressing plant is a fixed, permanent and large-scale industrial structure, unlike a mine, the location and ownership status of the land must be prioritised as one of the most

important aspects in the project design. This process is shaped according to the characteristics of the plot where the plant will be established.

3.2.1. Forest permits

Some of the mining areas in Türkiye are located on forest lands. Pursuant to Article 16 of the Forest Law, definitive permission must be obtained from the General Directorate of Forests for comprehensive facilities such as dressing plants and waste dams. This permission process requires a decision on 'public benefit' and the payment of forest rehabilitation/reforestation fees (Resmi Gazete, 2024).

3.2.2. Permits required for agricultural and pasture areas

If the facility area corresponds to agricultural land, a 'Permit for Non-Agricultural Use' must be obtained in accordance with the Soil Protection and Land Use Law No. 5403, with the decision of the Soil Protection Board and the approval of the Ministry of Agriculture and Forestry (Resmi Gazete, 2017). Similarly, for pasture areas, a 'Change of Allocation Purpose' must be made under the Pasture Law No. 4342 (Resmi Gazete, 1998).

Property permits are required to commence construction of the facility; a GSM licence or construction permit cannot be issued for an area without a property permit. Other matters related to property permits include, for example, the acquisition of title deeds in the case of private property, leasing, or the acquisition of 2B-qualified parcels in the case of expropriation. Careful examination of the property status of the land on which the facility will be established is an important factor in the initial investment cost.

3.3. Permits Required for Critical Infrastructure and Relocation Works

Ore dressing plants are generally established in rural and undeveloped areas, but sometimes existing infrastructure lines (roads, water, electricity) may remain within the project site. The physical removal of these structures within the plant area provides an opportunity to prevent potential negative situations in the future. These permits are, in short, the Water Pipeline Relocation Project suitability; the permit required to change the route of existing water pipelines passing through the plant area so that they are not affected by plant operations. The PTL Relocation Project is defined as the permit required to relocate high-voltage power lines so that they do not remain under the plant buildings or the waste dam reservoir. The Village Road Relocation Project suitability is known as the permit required to move existing roads outside the site for the safety of the facility site and the public (Volkan Pusa Personal Interview, 2025). The two issues on which the DSI has provided an opinion are of particular importance. Stream Relocation Project; if the waste dam or leach field, considered one of the most critical items, coincides with the stream bed, the stream bed must be altered. The Circumferential Channels Planning Report outlines a drainage system designed to divert surface runoff away from the facility, thereby preventing site contamination(ÇŞİDB, 2017). These two aspects are particularly vital for sustainable environmental management. The principle of 'preventing clean water from mixing with polluted water' is one of the cornerstones of environmental management. It is important to examine these two processes specifically (TOB, 2023).

3.4. Specific Permits for Heap Leaching and Waste Storage Facilities

Ore dressing plants are established based on different processing techniques according to different conditions. Today, particularly with regard to facilities that require special consideration in terms of the area they cover or issues related to waste storage processes, studies should be evaluated in a holistic manner.

3.4.1. Approval of the heap leaching plant implementation project

The heap leaching method, widely used in gold, silver and copper mining, is one of the processes requiring high precision. As the highest level technical document required from the Ministry of Environment, Urbanisation and Climate Change for the construction of the facility, the documents that must absolutely be included in the submitted project are, in short: impermeability system (design of clay and geomembrane layers to be laid on the base of the leach pad, stability analyses (analysis of the slope stability of the heap under static and dynamic earthquake conditions, etc. conditions), drainage system (piping system laid to collect the enriched solution), and hydrological calculations (risk assessment based on rainfall transport capacities) (ÇŞİDB, 2018).

The construction process after approval is also supervised by companies authorised by the Ministry.

3.4.2. Waste storage facility approval certificate

The establishment of a mining waste storage facility for the waste generated after the dressing process is mandatory. The regulation classifies waste as ‘inert’, ‘non-hazardous’ and ‘hazardous’. Dressing waste is generally classified as hazardous or non-hazardous and requires a Category A storage facility. The dam project is prepared according to the waste characterisation determined during the EIA phase (ABA tests, seepage water analyses). Without this document, waste cannot be fed into the facility (Özdoğan, Özdoğan & Akbulut, 2025).

Permission is also required for the storage of tailings that do not contain ore but are extracted during excavation. If the tailings contain sulphur and have the potential to create Acid Mine Drainage (AMD), it is also mandatory to make these areas impermeable (Güngör & Özdoğan, 2025).

3.5. Operational Readiness and Environmental Permitting

Once the physical construction of the facility is complete, the process of transitioning to ‘legal operation’ status begins. This phase is the period during which the facility's compliance with environmental regulations is tested.

3.5.1. Regulatory compliance: temporary operation certificate (gfb - geçici faaliyet belgesi) and environmental licensing

Temporary Activity Certificate(GFB); once the facility construction is complete and the machinery installations are finished, it is obtained by applying to the Provincial Environment Directorate. The GFB permits the facility to operate for a period of one year.

Emission and Discharge Measurements: During the GFB period, while the facility is operating at full capacity, dust and gases emitted from chimneys (emission measurements) and discharged water are measured by accredited laboratories.

Environmental Permit and Licence Certificate; if the measurement results comply with the regulations, the facility is granted an Environmental Permit and Licence valid for 5 years. For dressing facilities, this licence is generally an integrated permit covering ‘Air Emissions’, ‘Wastewater Discharge’ and ‘Mining Waste Processing’ (Resmi Gazete, 2014).

3.5.2. Workplace opening and operating license(gsm)

The Business Opening and Operating License represents the official commercial and legal authorization of a facility. Ore dressing plants are classified under 1st Class Non-Sanitary Enterprise (NSE) regulations due to their environmental and health implications (Resmi Gazete, 2005). As a comprehensive 'umbrella' permit, the GSM license requires all other approvals—such as EIA, Fire Department clearance, Building Occupancy, and Environmental Permits—to be finalized. In its absence, the facility cannot even qualify for industrial electricity tariffs.

3.6. Water Management

Dressing plants (particularly flotation and leaching) are known to be processes with high water and energy requirements.

Water Supply - YAS Certificate: If process water is supplied from underground wells, a ‘YAS (Groundwater) Exploration and Use Certificate’ must be obtained from the State Hydraulic Works (DSI) in accordance with Law No. 167. Unauthorised use of wells results in heavy administrative fines and the closure of wells (Resmi Gazete, 1972).

A Wastewater Treatment Project Approval must be obtained for the discharge of the water used (process water or domestic wastewater). Although the ‘Zero Discharge’ principle is generally targeted in dressing plants, a treatment plant and project approval are required for emergencies or domestic water (ÇŞİDB, 2025).

In water usage, it is mandatory to open one observation well at the head of the waste dam and two observation wells at the tail, and to report these observation wells to the DSI.

3.7. Hazardous Materials and Waste Management

Measures must be taken to prevent potential risks that may arise due to the chemicals used in ore dressing plants. In this context, there are mandatory documents required for chemicals classified as hazardous substances by legal regulations, and the waste management plan must be prepared in accordance with these processes.

Dangerous Goods Activity Certificate (TMFB): This certificate, obtained from the Ministry of Transport and Infrastructure, regulates the logistics and stock management of hazardous materials entering the plant (UAB, 2019).

Waste Management Plan: This plan outlines how hazardous waste (waste oils, contaminated packaging) and non-hazardous waste generated by the facility will be disposed of. At the beginning of each year, waste declarations for the previous year are made within the framework of this plan (Resmi Gazete, 2015).

4. CONCLUSION

This study clearly demonstrates that the legal processes of ore dressing plants have a complex structure. The permits that must be obtained are not a mere requirement but form the basis of the principle of sustainability in terms of health, safety and the environment. A sustainable ore dressing project is not only possible by having a high-grade ore deposit or an efficient flotation circuit; it is also possible by having the ability to manage this complex permit process in a predictable and transparent manner.

Recent changes in Türkiye's mining and environmental legislation enable investors to operate correctly without compromising environmental standards. In this context, technical designs must be properly integrated into the regulatory processes.

In the coming period, in line with the European Green Deal and sustainability principles, the concepts of ‘Zero Waste’ and ‘Circular Economy’ will be more strongly embedded at the heart of the permitting processes. It is anticipated that the proper management of past knowledge and experience will play a key role in establishing the technical and legal infrastructure for this transformation and in the sector's adaptation to these new ‘green’ permit standards.

REFERENCES

ÇŞİDB, (2017), “Çevre ve Şehircilik Bakanlığının ÇED Alanında Kapasitesinin Güçlendirilmesi için Teknik Yardım Projesi: Çevresel Etkiler ve Alınacak Önlemler Kılavuzu – Madencilik Projeleri”, https://share.google/c8kn7DiA3xxbSYeIX (Accessed on: 21 December 2025).

ÇŞİDB, (2018), “Maden Atıkları Yönetmeliğinin Uygulanmasına İlişkin Açıklamalar”, https://webdosya.csb.gov.tr/db/cygm/duyurular/may-ac-klama201805-20180601164229.pdf (Accessed on: 21 December 2025).

ÇŞİDB, (2025), “2025/5 Genelge Atıksu Arıtma Tesisi Proje Onayı”, https://webdosya.csb.gov.tr/db/cygm/icerikler/2025-5-sayili-genelge-20250930103540.pdf (Accessed on: 21 December 2025).

Güngör, N., Özdoğan, A. K., (2025), “Place and Importance of Metallic Mines in EIA Regulations”, KETBTD, 2, 33–43.

Özdoğan, A. K., Özdoğan, G., Akbulut, A., (2025), “Roadmap and Disaster/Emergency Awareness in Waste Management for Safe Mining from EU Perspective”, International Symposium on Occupational Health and Safety in Mining 2025 Proceedings Book, 316–332.

Pusa, V., (2025), Personal communication, November 8.

Resmi Gazete, (1972), “DSİ Yeraltısuları Teknik Yönetmeliği”, https://www.mevzuat.gov.tr/anasayfa/MevzuatFihristDetayIframe?MevzuatTur=7&MevzuatNo=13933&MevzuatTertip=5 (Accessed on: 21 December 2025).

Resmi Gazete, (1998), “Mera Yönetmeliği”, https://resmigazete.gov.tr/eskiler/2017/12/20171209-3.htm (Accessed on: 21 December 2025).

Resmi Gazete, (2005), “İşyeri Açma ve Çalışma Ruhsatlarına İlişkin Yönetmelik”, https://www.mevzuat.gov.tr/mevzuat?MevzuatNo=20059207&MevzuatTur=21&MevzuatTertip=5 (Accessed on: 21 December 2025).

Resmi Gazete, (2014), “Çevre İzin ve Lisans Yönetmeliği”, https://www.resmigazete.gov.tr/eskiler/2024/09/20240924-2.htm (Accessed on: 21 December 2025).

Resmi Gazete, (2015), “Atık Yönetimi Yönetmeliği”, https://www.mevzuat.gov.tr/mevzuat?MevzuatNo=20644&MevzuatTur=7&MevzuatTertip=5 (Accessed on: 21 December 2025).

Resmi Gazete, (2017), “Tarım Arazilerinin Korunması, Kullanılması ve Planlanmasına Dair Yönetmelik”, https://resmigazete.gov.tr/eskiler/2017/12/20171209-3.htm (Accessed on: 21 December 2025).
Resmi Gazete, (2024), “Orman Kanununun 16ncı Maddesinin Uygulanması Hakkında Yönetmelik”, https://www.resmigazete.gov.tr/eskiler/2024/09/20240924-2.htm (Accessed on: 21 December 2025).

TOB, (2023), “Su Verimliliği Rehber Dokümanları Serisi: Diğer Demir Dışı Metal Cevherleri Madenciliği”, https://cdniys.tarimorman.gov.tr/api/File/GetGaleriFile/502/DosyaGaleri/8390/02.pdf (Accessed on: 21 December 2025).

UAB, (2019), “Tehlikeli Madde Faaliyet Belgesi Düzenlenmesine İlişkin Usul ve Esaslar Hakkında Yönerge”, https://uhdgm.uab.gov.tr/uploads/pages/yonergeler/tehlikeli-madde-faaliyet-belgesi-duzenlenmesine-iliskin-usul-ve-esaslar-hakkinda-yonerge-5de8fa8d53a40-6320770ee12cc.pdf (Accessed on: 21 December 2025).

MINING WASTE AND CRITICAL RAW MATERIALS RECOVERY POTENTIAL FROM THE KURBNESH COPPER TAILINGS, ALBANIA

Shahin BARAMAJ*, Kristo RODI, Mimoza SIMIXHIU, Ledi MOISIU, Ana FOCIRO

EIT Raw Materials, Regional Innovation Centre
**Corresponding author: inibaramaj@gmail.com*

A B S T R A C T

Albania, like other countries in the region, has inherited large volumes of mine waste generated from copper ore beneficiation, and Kurbnesh represents the largest copper tailings dam in the country, with nearly 40 years of operational legacy. The Kurbnesh copper tailings dams, containing ~1.78 Mt of historical mine waste derived from the processing of 3.8 Mt of ore, represent both an environmental hotspot and a strategic secondary source of Critical Raw Materials (CRM) in Albania. Based on the latest geochemical analyses, the tailings contain significant concentrations of Cu, Cr, Ni, and Zn, while persistent acid mine drainage (pH ≈ 3) continues to mobilize metals into the Uraka River system. Within the OSF-WB project “Enhancement of Regional Collaboration in CRM and Circular Economy in the Balkans”, Kurbnesh serves as one of the pilot sites for a prefeasibility study assessing the technical and economic potential of CRM recovery from mining waste in Albania, Kosovo, and North Macedonia. The objective is twofold: (1) evaluate metal re-processing options through mineralogical–geochemical characterization and process simulation, and (2) provide decision-support data for policy, investment, and youth involvement in the raw-materials innovation chain. Preliminary results suggest feasible re-processing scenarios that could reduce environmental risk while contributing to the EU CRM Act targets on secondary supply.

Keywords: *Tailings, circular economy, CRM recovery, Balkans, prefeasibility study*

1. INTRODUCTION

The transition toward a resource-efficient and low-carbon economy has significantly increased the strategic importance of Critical Raw Materials (CRMs), which are essential for renewable energy technologies, electrification, digitalisation, and advanced manufacturing. At the same time, the European Union faces strong dependency on external suppliers for many of these materials, prompting renewed interest in alternative and secondary raw material sources. In this context, mining and metallurgical waste generated from historical exploitation activities is increasingly recognised as a potential resource rather than solely an environmental liability.

Across the Western Balkans, decades of mining activity have resulted in large volumes of tailings and industrial residues containing economically relevant concentrations of metals such as copper, chromium, nickel, zinc, and associated elements. Many of these sites remain insufficiently characterised, posing ongoing environmental risks to soil, water, and nearby communities, while their potential contribution to CRM supply chains remains largely unexplored. The lack of harmonised data, systematic sampling, and integrated technical assessments has limited the incorporation of such secondary resources into circular-economy strategies at national and regional levels.

In Albania, legacy mining areas represent a particularly pressing challenge. The Kurbnesh copper tailings site is one of the most significant historical mining residues in the country, long identified as an environmental hotspot. Despite its scale and strategic location, comprehensive evaluations addressing both environmental impact and resource recovery potential have been scarce. This gap hinders informed decision-making regarding remediation priorities, potential reprocessing, and alignment with European raw-materials and sustainability policies.

This paper presents the results of a targeted assessment of mining waste valorisation potential, with a specific focus on the Kurbnesh copper tailings area (Bortolotti, V.,1996, Gawlick H.J., 2008), within a broader Western Balkan framework (Figure 1). The study integrates geological and geochemical investigations, including systematic sampling and laboratory analyses using ICP-OES and AAS techniques, with a preliminary evaluation of CRM recovery feasibility. Beyond the technical dimension, the work contributes to regional knowledge exchange and supports evidence-based approaches to sustainable raw-materials management.

The main objectives of this research are to:

- characterize the geochemical composition of selected mining and metallurgical waste deposits with respect to CRM content;
- assess environmental conditions and potential risks associated with legacy tailings;
- evaluate the feasibility of resource recovery and valorisation within a circular-economy framework; and
- provide a scientific basis to support policy development and future investment decisions in the Western Balkans.

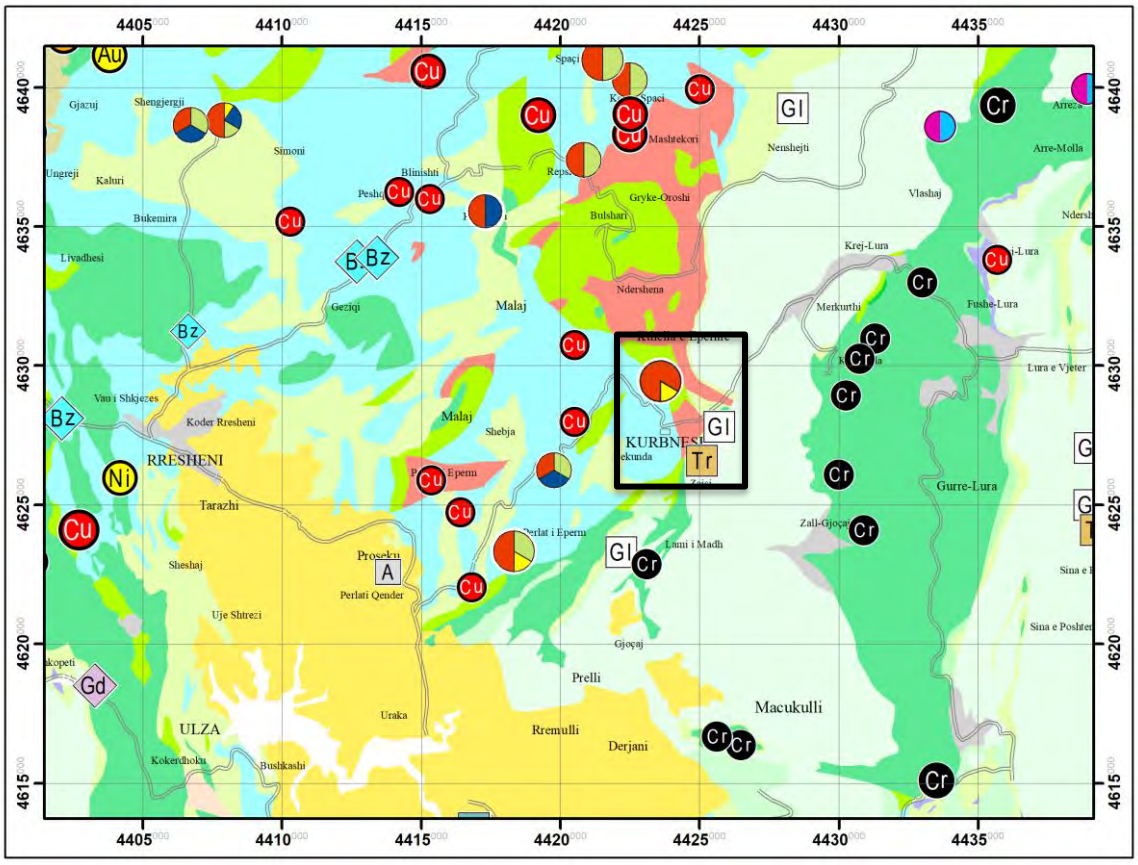

Figure 1. Geological position and related ore deposits in the study area (black rectangle)

2. MATERIAL AND METHODS

2.1. Methodological Approach

The study followed an integrated methodological approach combining desk-based data collection, field investigations, systematic sampling, and laboratory-based geochemical analyses. The methodology was designed to support both environmental assessment and the evaluation of Critical Raw Materials (CRM) potential in legacy mining waste, with a specific

focus on the Kurbnesh copper tailings site in Albania. Prior to field activities, existing geological, environmental, and historical mining and production data related to the Kurbnesh area were collected and reviewed (Hoxha L., 2005, Hoxha L., 2008; Hoxha L., 2015). This preliminary analysis supported the definition of sampling locations and ensured consistency with regional assessment methodologies applied across the Western Balkans.

2.2. Field Investigation and Sampling

Fieldwork was conducted at the Kurbnesh copper tailings site, where detailed site observations and mapping were performed across the tailings' dams and adjacent impact zones. A systematic sampling grid was implemented to capture spatial variability within the deposited tailings material. Sampling followed established field protocols to ensure representativeness and minimise contamination. All samples were clearly labelled, documented, and prepared for laboratory analysis (Figure 2).

Figure 2. Close-up view of the subsidence features and corresponding sampling locations

2.3. Sample Preparation and Laboratory Analysis

Collected samples were processed and analysed at laboratories of the Albanian Geological Survey. Laboratory preparation included drying, homogenisation, and preparation of representative sub-samples suitable for chemical analysis.

Geochemical analyses were performed using:

- Inductively Coupled Plasma–Optical Emission Spectrometry (ICP-OES), and
- Atomic Absorption Spectroscopy (AAS).

These analytical techniques were used to determine concentrations of key elements relevant to both CRM potential and environmental assessment, including copper (Cu), cobalt (Co), indium (In), gold (Au), and silver (Ag). The combination of ICP-OES and AAS ensured reliable quantification across a range of concentration levels.

2.4. Data Integration and Evaluation

Analytical results were integrated with field observations and geological information to support a pre-feasibility evaluation of recovery and valorization options for the Kurbnesh pilot area. Element concentrations were assessed in relation to their potential economic relevance as secondary raw materials, as well as their environmental implications.

The methodological framework enabled the generation of site-specific, evidence-based data suitable for supporting decision-making related to legacy mining waste management, CRM recovery potential, and future remediation or reprocessing strategies.

3. RESULTS AND DISCUSSION

3.1. Sampling Plan and Field Work

A systematic sampling program was implemented across the Kurbnesh copper tailings deposit, covering different spatial scales and geomorphological zones. The primary objective was to obtain representative material from surface, intermediate, and deeper horizons in order to evaluate grain-size distribution, geochemical composition, and potential environmental impacts.

Sampling was conducted using hand shovel excavation, depending on material compactness and accessibility. Surface samples were collected from depths of 0–20 cm at regular intervals to capture spatial variability across the tailings plateau, erosion scarps, and footslope accumulation zones. For deeper materials, sampling pits were opened at depths of 30–50 cm and 70–100 cm, except in areas where strong compaction or water saturation prevented further penetration.

In total, 15 samples were collected, proportionally distributed across the main morphological units of the tailings deposit:

1. Upper plateau and flat surfaces, representing consolidated tailings;
2. Central eroded zones, exposing older depositional layers;
3. Steep scarps and collapse areas, characterised by unstable and freshly exposed material;
4. Peripheral accumulation zones, consisting of reworked tailings transported downslope.

Each sampling location was georeferenced using a handheld GPS, and geographic coordinates were recorded for all points. Sampling spacing was designed to ensure that all major geomorphological features and textural transitions within the deposit were represented.

All samples were collected using clean tools and stored in labelled bags prior to transport to the laboratory.

3.2. Granulometric Characteristics

Granulometric analysis reveals a strong dominance of fine material within the tailings. The finest fraction (45 µm) accounts for 65.3% of the total sample mass, followed by 18.8% at 71 µm**,** 6.4% at 160 µm, 5.3% at 250 µm, and only 4.2% at 315 µm. The cumulative values sum to 100%, confirming negligible material loss during the procedure.

The grain-size data were processed using GRADISTAT software (Blott S. A 2020), applying the Folk and Ward (1957) statistical method. Although the software issued an automated warning indicating that the sample is “not unimodal,” this message reflects algorithmic sensitivity to the dominance of a single fine fraction rather than true bimodality. Visual inspection of the cumulative distribution curve confirms a smooth, continuous, unimodal distribution without secondary peaks.

The sediment is characterized by poor sorting, strong positive (fine) skewness, and a leptokurtic distribution. The mean grain size falls within the fine sand to coarse silt range, indicating a depositional environment favoring accumulation of fine particles. These results suggest that the ore processed at the Kurbnesh flotation plant was not ground to the required fineness, as the material does not meet the criterion of 80% passing below 0.071 mm.

3.3. XRF Analysis

XRF analysis indicates that the tailings material is dominated by silicate and iron-rich components. Silica (SiO_2) constitutes 55.14%, reflecting the prevalence of quartz and silicate minerals derived from the host rocks. Iron oxides (Fe_2O_3) account for 21.06%, indicating abundant primary iron minerals and secondary oxidation products formed during long-term weathering
.
Calcium oxide (CaO) is present at 4.40%, suggesting carbonate or Ca-rich alteration phases, while TiO_2 (0.52%) and K_2O (0.19%) occur in minor amounts.

The XRF results also reveal enrichment in several metals of economic and environmental relevance, including Cu (1,165 g/t), Cr (499 g/t), Ni (183 g/t), and Zn (406 g/t). Lead is detected at 95 g/t, while silver is below 1 g/t. These results confirm that a significant proportion of metal content remains in the tailings, highlighting both secondary resource potential and environmental risk.

3.4. ICP-OES and AAS Results

ICP-OES and AAS analyses confirm elevated copper concentrations, with maximum values reaching 3114 ppm, indicating substantial unrecovered copper from historical processing. This confirms the low efficiency of older flotation technologies and positions the tailings as a significant secondary copper resource.

Cobalt and indium were detected at 679.1 ppm and 5.8 ppm, respectively. Although present at relatively low concentrations, both elements are listed as EU Critical Raw Materials, increasing the strategic relevance of the deposit. Gold and silver occur at low levels (Au_max = 0.36 ppm; Ag_max = 4.08 ppm), confirming negligible precious-metal recovery potential.

Cu–Co plots show strong spatial variability in copper concentrations, while cobalt remains consistently low across samples. Au–Ag plots confirm uniformly low gold values and modest

silver variability, reinforcing the conclusion that copper is the dominant recoverable metal (Demi G., 2000).

3.5. Interpretation in the Context of EU Critical and Strategic Raw Materials

The combined XRF, ICP-OES, and AAS results demonstrate that the Kurbnesh tailings contain elevated concentrations of Cu, Ni, Cr, Zn, and Pb, reflecting incomplete metal recovery during historical operations. While copper is classified as a Strategic Raw Material under the EU Critical Raw Materials Act (2023), nickel also holds strategic importance due to its role in battery and energy technologies.

Although zinc and chromium are not listed as critical, their industrial relevance supports the concept of multi-metal recovery. Lead, despite its environmental hazards, highlights the importance of controlled management and potential selective extraction.

The metal assemblage identified in the tailings highlights a dual significance:
(1) Resource potential, as a secondary source of strategic and industrial metals supporting EU circular-economy objectives; and
(2) Environmental risk, due to the potential for metal leaching, acid mine drainage, and long-term contamination.

These findings align closely with the objectives of the EU Critical Raw Materials Act (2023), which promotes recovery of strategic materials from mining waste while mitigating environmental impacts.

4. CONCLUSION

This study provides a comprehensive mineralogical and geochemical characterization of the Kurbnesh copper tailings deposit, combining systematic field sampling, granulometric analysis, and multi-method geochemical investigation (XRF, ICP-OES, and AAS). The results confirm that the tailings represent both an environmental concern and a potentially valuable secondary raw-material resource.

Granulometric analysis demonstrates a strong dominance of fine material, with more than 65% of the sediment retained in the <45 μm fraction. This fine-grained, poorly sorted nature reflects insufficient grinding during historical ore processing and has important implications for both metal recovery efficiency and environmental behaviour. The predominance of fine particles enhances metal retention but also increases the risk of metal mobility through weathering and leaching processes.

Geochemical analyses reveal significant residual metal concentrations, particularly copper, which reaches values exceeding 3000 ppm in several samples. This clearly indicates that a substantial proportion of copper remained unrecovered during past flotation operations. In addition, measurable concentrations of nickel, chromium, zinc, cobalt, and indium were detected, confirming the polymetallic character of the tailings. While gold and silver occur only at low levels and do not present meaningful recovery potential, their presence contributes to a more complete geochemical understanding of the deposit.

From a resource perspective, the elevated copper content positions the Kurbnesh tailings as a promising secondary source of a Strategic Raw Material under the EU Critical Raw Materials Act (2023). The presence of nickel further enhances the strategic relevance of the deposit, given its importance for battery technologies and the energy transition. Although cobalt and indium occur at modest concentrations, their classification as Critical Raw Materials increases the overall significance of the site within a circular-economy framework.

At the same time, the enrichment of copper, lead, zinc, nickel, and chromium highlights the long-term environmental risks associated with unmanaged tailings, including acid mine drainage and metal leaching. These findings underline the necessity of integrated approaches that combine resource recovery with environmental risk mitigation.

The results demonstrate that the Kurbnesh tailings should not be regarded solely as legacy waste, but rather as a secondary resource with strategic importance and environmental urgency. The study provides a robust scientific basis for further techno-economic assessments and supports EU policy objectives aimed at recovering strategic raw materials from mining waste while reducing environmental impacts.

REFERENCES

Blott, S. A., (2020), "Grain Size Distribution and Statistics Package for the Analysis of Unconsolidated Sediments by Sieving or Laser Granulometer".

Bortolotti, V., Kodra, A., Marroni, M., Mustafa, F., Polfi, L., Principi, G., Saccani, E., (1996), "Geology and Petrology of ophiolite sequences in the Mirdita region (Northern Albania)". Ofioliti, 21 (1), 3–20.

Demi, G., (2000), "Waste Assessment of Copper Mines and Plants in Albania and Their Impact in Surrounding Areas".

Gawlick, H. J., Frisch, W., Hoxha, L., Dumitrica, P., Krystyn, L., Lein, R., Missoni, S., Schlagintweit, F., (2008), "Mirdita Zone ophiolites and associated sediments in Albania reveal Neotethys Ocean origin". Int. J. Earth Sci., 97, 865–881. https://doi.org/10.1007/s00531-007-0193-z

Hoxha, L., Gawlick, H-J., (2008), "The eroded Late Jurassic Kurbnesh carbonate platform in the Mirdita Ophiolite Zone of Albania and its bearing on the Jurassic orogeny of the Neotethys realm". Swiss Journal of Geosciences. https://doi.org/10.1007/S00015-008-1254-4

Hoxha, L., Gawlick, H-J., Schlagintweit, F., (2012), "Onset of an Aptian carbonate platform overlying a Middle-Late Jurassic radiolaritic-ophiolithic mélange in the Mirdita Zone of Albania". Geologia Croatica. https://doi.org/10.4154/GC.2012.02

Hoxha, L., Scott, P. W., Eyre, J. M., (2005), "The geological setting of volcanogenic sulphide orebodies in Albanian ophiolites". Applied Earth Science. https://doi.org/10.1179_037174505X45487

PRODUCTION OF MAGNETITE CONCENTRATE FROM COPPER CONCENTRATOR PLANT TAILINGS

Alperen KÖLE*, Ahmet YAKAR, Yağız Kerem YALÇIN, Abdullah Erdem YILDIZHAN, Mustafa ÖZTÜRK, İbrahim GÖKTAŞ

ETİ Bakır CO, Research and Development Center, 55300, TEKKEKOY-SAMSUN
**Corresponding author: alperen.kole@etibakir.com.tr*

A B S T R A C T

Waste management is one of the most critical issues in ore preparation plants. Enriching valuable minerals found in plant waste to make them saleable not only contributes to waste manipulation operations but also increases the plant's economic input. Following the detection of magnetite mineral in the waste of the ETİ Bakır Siirt Copper Concentrator Plant, the aim was to enrich the magnetite and contribute to the economy.

This study includes low-field high-intensity wet magnetic separation and flotation tests performed on waste from the Siirt concentrator plant. A three-stage magnetic separation process was applied to samples taken from the plant waste. Flotation tests were conducted under different conditions on the concentrate obtained from magnetic separation, ensuring the removal of sulfide minerals. As a result of the studies, a concentrate containing 77.50% magnetite was obtained from the waste sample containing 3.44% magnetite, with 52% recovery. Final iron concentrate contains 63.68% Fe, 0.02% Cu, and 0.25% S.

Key words: *Magnetite, magnetic separation, flotation, tailings management*

1. INTRODUCTION

The rapid depletion of high-grade primary ore deposits and the escalating global demand for industrial raw materials have necessitated the transition toward secondary resource recovery from mining wastes. Copper processing plants generate significant volumes of flotation tailings, which are increasingly recognized as "anthropogenic ores" due to their substantial magnetite (Fe_3O_4) and sulfide mineral content (Lottermoser, 2010). The valorization of these tailings not only aligns with circular economy principles but also mitigates the environmental liabilities associated with conventional tailings storage facilities, such as acid mine drainage and land degradation (Kinnunen et al., 2018).

Magnetite recovery from copper tailings is often favored due to the mineral's high magnetic susceptibility, allowing for cost-effective separation using Low-Intensity Magnetic Separation (LIMS). However, the presence of associated sulfide minerals, particularly pyrite (Fe_3O_4), poses a significant challenge for the iron and steel industry, which requires sulfur concentrations in iron concentrates to be below 0.1–0.2% to prevent detrimental effects on steel quality (Rao and Leja, 2004). Consequently, a single-stage separation often fails to meet industrial specifications, necessitating hybrid processing circuits.

This study investigates a dual-stage enrichment strategy designed to produce high-grade, low-sulfur magnetite concentrate. The proposed methodology involves a preliminary concentration via LIMS to isolate the magnetic fraction, followed by reverse sulfide flotation to selectively remove residual sulfur-bearing minerals. The following sections detail the optimization of magnetic field intensities and flotation reagents, evaluating the impact of these parameters on the final iron grade and sulfur rejection efficiency.

2. MATERIAL AND METHODS

2.1. Material

The tailings samples used in this study were obtained from ETİ Bakır CO Siirt Madenköy copper concentrator plant processing massive sulfide copper ore. The primary copper mineral in the deposit is chalcopyrite ($CuFeS_2$), which is recovered via conventional froth flotation. The discharge from the copper flotation circuit, traditionally considered waste, serves as the feed material for this study. Preliminary mineralogical investigations indicate that the tailings consist of significant amounts of magnetite (Fe_3O_4) and residual pyrite (FeS_2), along with silicate gangue minerals. The chemical analysis and density determination of the sample used in the experiments are shown in Table 1.

Table 1. Chemical analysis and density determination results of sample

Cu, %	Fe, %	Zn, %	S, %	Magnetite, %	Density, g/cm^3
0,13	33,25	0,34	25,64	3,43	3,80

Cu and Zn analyses were performed using ICP-OES device, Fe analysis using titration method, S analysis using LECO carbon-sulfur analyzer, and magnetite analysis using SATMAGAN device.

As a result of the sieve analysis, the particle size (d_{80}) of the sample used in the experiments was calculated as 68.41 microns. The sieve analysis results are shown in Table 2.

Table 2. The sieve analysis results of feed sample

Screen Size,µm	**Mass, g**	**Mass, %**	**ΣOS, %**	**ΣUS, %**
212,00	0	0,00	0,00	100,00
150,00	7,03	7,03	7,03	92,97
106,00	5,10	5,10	12,13	87,87
75,00	4,35	4,35	16,48	83,52
53,00	11,75	11,75	28,23	71,77
38,00	11,24	11,24	39,47	60,53
20,00	15,23	15,23	54,70	45,30
-20,00	45,30	45,30	100,00	0,00
Total	100,00	100,00	**d80, µm**	**68,41**

2.2. Method

The pre-concentration of magnetite was conducted using a Low-Intensity Magnetic Separator (LIMS). The operation was performed at a constant magnetic field intensity of 800 Gauss. This stage aimed to separate the ferromagnetic magnetite fraction from the non-magnetic silicate matrix and a portion of the sulfide minerals. The resulting magnetic concentrate was collected as the feed for the subsequent cleaning stage. The parameters for the magnetic separation experiments are presented in Table 3.

Table 3. Magnetic separation test parameters

Drum Speed, rpm	Feed Size (d80), microns	Solid Ratio, %	Magnetic Field, Gauss	Drum Dimensions, mm
30	68,41	28-30	800	200x300Ø

In the reverse sulfide flotation stage, process parameters were meticulously optimized to ensure the selective removal of residual pyrite from the LIMS concentrate. The pulp pH was maintained at 11.0 to ensure full compatibility with the existing operational conditions of the copper concentrator plant, thereby facilitating seamless industrial integration and eliminating the need for additional pH modification reagents. Within this highly alkaline environment, the

amine-based cationic collector Green Chemicals Mine-Treat 3452-1 was employed to selectively float the sulfide minerals away from the magnetite surfaces. Following the principles of reverse flotation, pyrite and other sulfur-bearing minerals were recovered in the froth fraction, while the sink product characterized by minimized sulfur content and enriched iron grade constituted the final magnetite concentrate of the study. The information about sulfur flotation is given in Table 4.

Table 4. Sulfur flotation test parameters

Collector (3452-1), g/t	Frother (MIBC), g/t	Solid, g	Cell Volume, cc	Solid Ratio, %	pH	Flotation Time, min
50	50	500	1200	31,88	11	5

3. RESULTS AND DISCUSSION

Since the total iron (Fe) content in massive sulfide ore structures encompasses iron derived from both magnetite and pyrite, the enrichment performance in this study was evaluated based specifically on the magnetite content to ensure metallurgical accuracy. According to the data presented in Figure 1 and Table 1, the three-stage LIMS circuit operating at 800 Gauss exhibited high selectivity toward magnetite minerals. The magnetite content, which was initially only 3.43% in the feed, increased systematically to 64.18% in the final magnetic concentrate, aided by the disruption of magnetic flocs via inter-stage demagnetization. These results indicate that the magnetic separation circuit achieved a significant enrichment ratio of approximately 18.7 for the targeted magnetite mineral.

The magnetite recovery reached a high level of 79.38% after the three stages of separation. The concurrent reduction in impurities, such as sulfur (from 27.79% to 7.43%) and copper (from 0.14% to 0.06%), confirms the successful rejection of the pyrite-associated iron fraction and the enrichment of the product in terms of magnetite. However, the residual sulfur content of 7.43% in the final magnetic concentrate suggests that certain pyrite particles remain either mineralogically interlocked with magnetite or were subject to residual magnetic entrainment. Notably, the overall iron recovery (Fe Rec.) remained as low as 7.90%, which serves as a concrete technical indicator that the non-magnetic iron within the pyrite structure was successfully diverted to the tailings, thereby validating the process's focus on selective magnetite recovery. The current diagram and metallurgical balance tables for the three-stage magnetic separation test are shown in Figure 1.

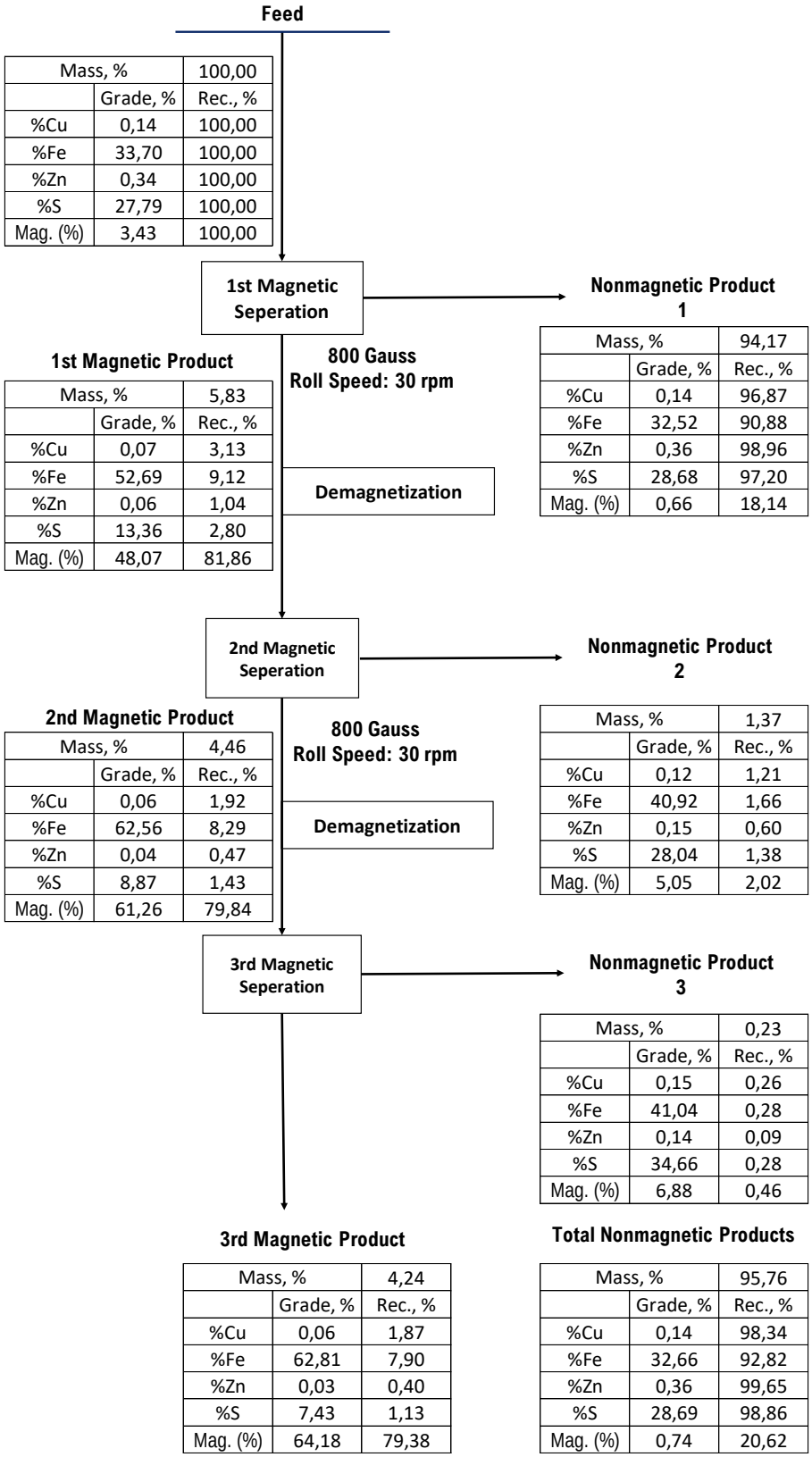

Mass, %		100,00
	Grade, %	Rec., %
%Cu	0,14	100,00
%Fe	33,70	100,00
%Zn	0,34	100,00
%S	27,79	100,00
Mag. (%)	3,43	100,00

Mass, %		94,17
	Grade, %	Rec., %
%Cu	0,14	96,87
%Fe	32,52	90,88
%Zn	0,36	98,96
%S	28,68	97,20
Mag. (%)	0,66	18,14

Mass, %		5,83
	Grade, %	Rec., %
%Cu	0,07	3,13
%Fe	52,69	9,12
%Zn	0,06	1,04
%S	13,36	2,80
Mag. (%)	48,07	81,86

Mass, %		1,37
	Grade, %	Rec., %
%Cu	0,12	1,21
%Fe	40,92	1,66
%Zn	0,15	0,60
%S	28,04	1,38
Mag. (%)	5,05	2,02

Mass, %		4,46
	Grade, %	Rec., %
%Cu	0,06	1,92
%Fe	62,56	8,29
%Zn	0,04	0,47
%S	8,87	1,43
Mag. (%)	61,26	79,84

Mass, %		0,23
	Grade, %	Rec., %
%Cu	0,15	0,26
%Fe	41,04	0,28
%Zn	0,14	0,09
%S	34,66	0,28
Mag. (%)	6,88	0,46

Mass, %		4,24
	Grade, %	Rec., %
%Cu	0,06	1,87
%Fe	62,81	7,90
%Zn	0,03	0,40
%S	7,43	1,13
Mag. (%)	64,18	79,38

Mass, %		95,76
	Grade, %	Rec., %
%Cu	0,14	98,34
%Fe	32,66	92,82
%Zn	0,36	99,65
%S	28,69	98,86
Mag. (%)	0,74	20,62

Figure 1. Flowsheet and metal balance tables for magnetic separation tests

The residual sulfur content (7.43% S) and magnetite grade (64.18% Man.) in the third-stage magnetic concentrate necessitated a final purification step through reverse sulfide flotation. By utilizing an amine-based collector (Green Chemicals 3452-1) at a dosage of 50 g/t and a highly

alkaline environment (pH 11), a selective separation between magnetite and pyrite was achieved. This stage successfully removed the bulk of the remaining sulfide minerals into the froth product, which contained 15.94% S.

The sink product, which represents the final magnetite concentrate, showed a dramatic improvement in quality. The sulfur content was sharply reduced from 7.43% down to 0.25% S, meeting industrial requirements for iron ore concentrates. More importantly, the magnetite grade was enriched from 64.18% to 77.50%, with a partial magnetite recovery of 65.48% in this stage. The decrease in copper (from 0.05% to 0.02%) and zinc (from 0.03% to 0.03%) further validates the effectiveness of the reverse flotation in rejecting non-ferrous sulfide impurities. These results demonstrate that while LIMS is effective for primary concentration, the integration of reverse flotation is mandatory to achieve high-grade magnetite purity from complex massive sulfide tailings. The results of sulfur flotation test are presented in Table 5.

Table 5. Sulfur flotation test results

Products	Mass, g	Mass, %	Grade, %					Recovery, %				
			Cu	Fe	Zn	S	Mag.	Cu	Fe	Zn	S	Mag.
Sulfur Concentrate	228,50	45,77	0,10	61,78	0,04	15,94	48,40	82,51	45,02	54,57	98,18	34,52
Sink Product	270,71	54,23	0,02	63,68	0,03	0,25	77,50	17,49	54,98	45,43	1,82	65,48
Total*	499,21	100,00	0,05	62,81	0,03	7,43	64,18	100,00	100,00	100,00	100,00	100,00

* Calculated values

4. CONCLUSION

The present study demonstrates the technical feasibility of recovering high-quality magnetite concentrate from complex massive sulfide tailings through an integrated beneficiation circuit. The multi-stage Low-Intensity Magnetic Separation (LIMS) circuit proved highly effective for primary concentration, upgrading the magnetite content from an initial 3.43% in the feed to 64.18% in the final magnetic product. A critical component of this success was the implementation of demagnetization between LIMS stages, which prevented magnetic flocculation and significantly reduced the mechanical entrainment of pyrite and silicate gangue minerals. Despite the high degree of enrichment achieved through magnetic forces, the residual sulfur content of 7.43% necessitated a final purification step.

The application of reverse sulfide flotation at pH 11.0 using the MineTreat 3452-1 collector effectively addressed this challenge, selectively removing the remaining sulfides and reducing the sulfur content to a remarkable 0.25% S. Consequently, the integrated process yielded a final magnetite concentrate with a purity of 77.50% and minimal impurities, achieving an overall magnetite recovery of 51.98%. These results confirm that the combination of LIMS, inter-stage demagnetization, and reverse flotation provides a robust pathway for the valorization of low-grade sulfide tailings into industrial-grade feedstock. The general flow diagram and metal balance tables of the study are shown in Figure 2.

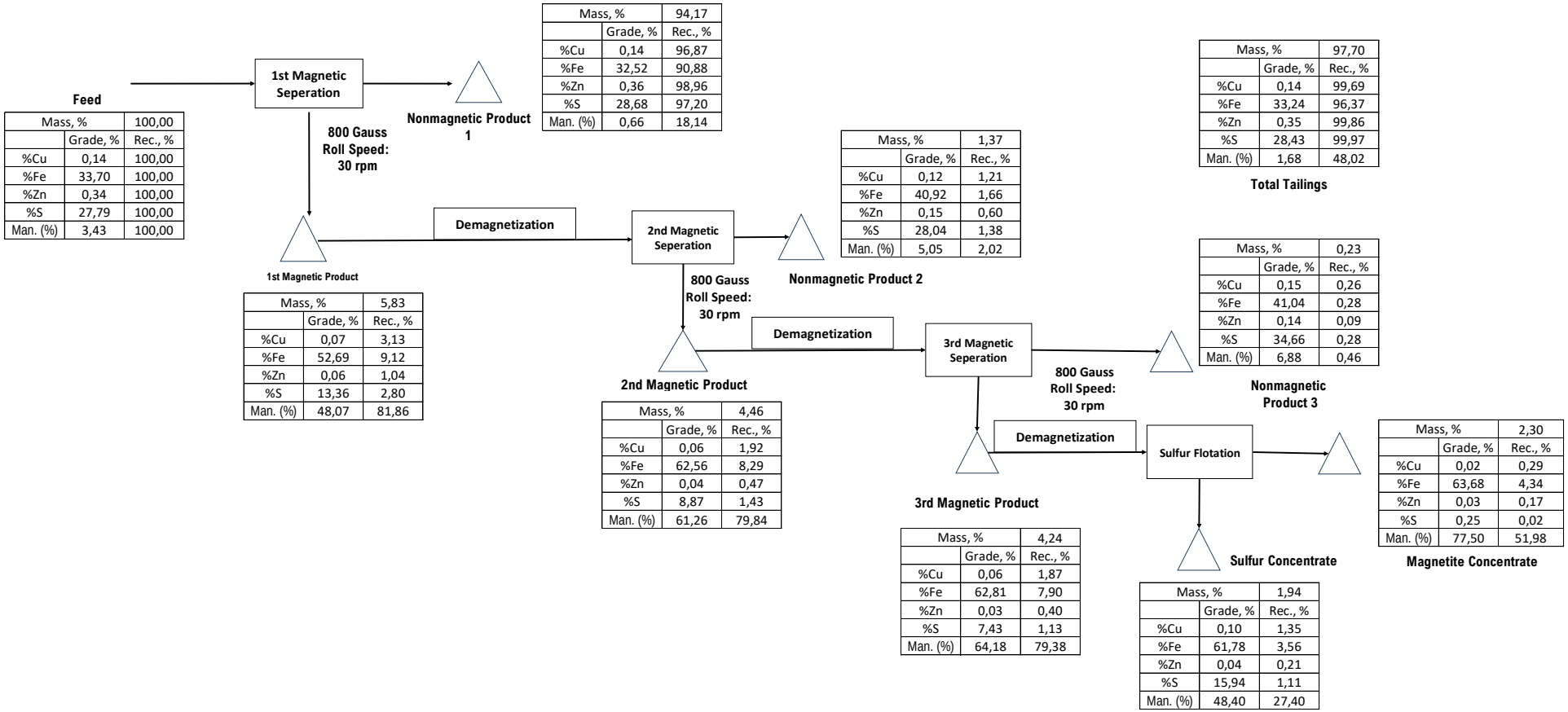

Mass, %		100,00
	Grade, %	Rec., %
%Cu	0,14	100,00
%Fe	33,70	100,00
%Zn	0,34	100,00
%S	27,79	100,00
Man. (%)	3,43	100,00

Mass, %		94,17
	Grade, %	Rec., %
%Cu	0,14	96,87
%Fe	32,52	90,88
%Zn	0,36	98,96
%S	28,68	97,20
Man. (%)	0,66	18,14

Mass, %		5,83
	Grade, %	Rec., %
%Cu	0,07	3,13
%Fe	52,69	9,12
%Zn	0,06	1,04
%S	13,36	2,80
Man. (%)	48,07	81,86

Mass, %		1,37
	Grade, %	Rec., %
%Cu	0,12	1,21
%Fe	40,92	1,66
%Zn	0,15	0,60
%S	28,04	1,38
Man. (%)	5,05	2,02

Mass, %		4,46
	Grade, %	Rec., %
%Cu	0,06	1,92
%Fe	62,56	8,29
%Zn	0,04	0,47
%S	8,87	1,43
Man. (%)	61,26	79,84

Mass, %		4,24
	Grade, %	Rec., %
%Cu	0,06	1,87
%Fe	62,81	7,90
%Zn	0,03	0,40
%S	7,43	1,13
Man. (%)	64,18	79,38

Mass, %		97,70
	Grade, %	Rec., %
%Cu	0,14	99,69
%Fe	33,24	96,37
%Zn	0,35	99,86
%S	28,43	99,97
Man. (%)	1,68	48,02

Mass, %		0,23
	Grade, %	Rec., %
%Cu	0,15	0,26
%Fe	41,04	0,28
%Zn	0,14	0,09
%S	34,66	0,28
Man. (%)	6,88	0,46

Mass, %		1,94
	Grade, %	Rec., %
%Cu	0,10	1,35
%Fe	61,78	3,56
%Zn	0,04	0,21
%S	15,94	1,11
Man. (%)	48,40	27,40

Mass, %		2,30
	Grade, %	Rec., %
%Cu	0,02	0,29
%Fe	63,68	4,34
%Zn	0,03	0,17
%S	0,25	0,02
Man. (%)	77,50	51,98

Figure 1. General flowsheet and metal balance tables of magnetite circuit

REFERENCES

Kinnunen, P. H., Kaksonen, A. H., (2018) “Towards circular economy in mining: Opportunities and challenges for recycling and recovering metals from industrial wastes”, Journal of Cleaner Production.

Lottermoser, B. G., (2010) “Mine Wastes: Characterization, Treatment and Environmental Impacts”, Springer Science & Business Media.

Rao, S. R., Leja, J., (2004) “Surface Chemistry of Froth Flotation”, Kluwer Academic/Plenum Publishers.
Yao, G., et al., (2020) “Recovery of iron from copper tailings by magnetic separation and reduction roasting”.

SELECTIVE ACTIVATION OF COAL MINE TAILINGS AS SUPPLEMENTARY CEMENTITIOUS MATERIALS FOR SUSTAINABLE CONSTRUCTION

Serkan TUYLU[1], Deniz ADIGUZEL[1], İsmail DEMİR[2,*], Mehmet Selçuk AVDAN[3]

[1]Istanbul University - Cerrahpaşa, Engineering Faculty, Mining Engineering Department, Mining Division, 34500, Istanbul, TÜRKİYE
[2]Istanbul University - Cerrahpaşa, Engineering Faculty, Mining Engineering Department, Mineral Processing Division, 34500, Istanbul, TÜRKİYE
[3]Istanbul University - Cerrahpaşa, Engineering Faculty, Mining Engineering Department, Mining Mechanization and Technology Division, 34500, Istanbul, TÜRKİYE
**Corresponding author: dismail@iuc.edu.tr*

A B S T R A C T

The reuse of coal processing wastes as supplementary cementitious materials offers significant environmental and technical benefits for sustainable construction. This study investigates the selective activation of coal mine tailings (CMT) obtained from a coal washing plant through mechanical grinding, pozzolan-assisted blending, and thermal activation in order to enhance their reactivity and strength contribution in cementitious systems. Mortars were prepared by replacing 5-20 wt.% of Portland cement with CMT in accordance with EN 196-1; for each mixture, three specimens were tested, and compressive strength values represent the average results obtained at 28 and 90 days.

The results indicate that mechanical activation by grinding effectively reduced particle size but did not improve compressive strength, as mortars containing untreated CMT consistently outperformed mechanically activated counterparts at all replacement levels. In contrast, pozzolan-assisted blending improved strength development, particularly at later ages, with mixtures incorporating natural pozzolan (trass) exhibiting clear synergistic effects and superior long-term performance compared to fly ash. Among the investigated activation routes, thermal activation proved to be the most effective. Calcination at 600 °C provided a balanced enhancement at both early and later ages, while activation at 800 °C yielded the highest long-term strength, reaching approximately 50 MPa at a 10% replacement level after 90 days and surpassing the control mixture.

Overall, the findings demonstrate that coal mine tailings can be transformed from a largely inert waste into a reactive pozzolanic material through appropriate selective activation strategies. When optimally activated and used at moderate replacement levels, CMT can serve as a viable partial cement replacement, contributing to improved mechanical performance while supporting waste valorization and sustainability in mineral processing and construction industries. However, since thermal activation involves additional energy input, the sustainability of this approach should be assessed by considering the performance-energy trade-off, particularly for large-scale applications.

Key words: *Selective activation, coal mine tailings, supplementary cementitious materials*

1. INTRODUCTION

Coal mining and coal preparation plants play a critical role in ensuring energy supply security; however, they also generate large volumes of fine-grained waste materials. Coal mine tailings (CMT) produced during beneficiation processes pose significant environmental challenges due to their high storage requirements, potential for acid mine drainage, heavy metal leaching, and dust emissions, positioning coal-derived wastes as a major concern within sustainable mining and circular economy frameworks (Adiguzel et al., 2022; Acordi et al., 2023). At the same time, considering the substantial contribution of cement production to global CO_2 emissions and natural resource consumption, the valorization of such wastes in cementitious binder systems emerges as a strategic opportunity for both waste management and carbon footprint reduction

in the construction sector, while also supporting energy and resource efficient decision-making in coal processing systems (Zhang and Ling, 2020; Demir et al., 2024; Xu et al., 2025).

Coal-derived wastes constitute a heterogeneous group, including fly ash, coal gangue, slags, and washing tailings, with diverse mineralogical and chemical characteristics. Numerous studies have demonstrated that coal gangue and fly ash can be effectively utilized as supplementary cementitious materials (SCMs) or as precursors in alkali-activated binders (Wang et al., 2024; Zhang et al., 2025). Nevertheless, most coal-origin wastes exhibit low initial pozzolanic activity and relatively inert crystalline structures, limiting their direct use as reactive binders. Consequently, activation processes that modify the physical and/or chemical structure of the waste are essential to unlock their binding potential.

Recent research highlights the effectiveness of mechanical, chemical (particularly alkali activation), thermal, and hybrid activation methods in enhancing the performance of coal-derived wastes in cementitious systems. Mechanical activation primarily acts by refining particle size and increasing specific surface area, which can promote pozzolanic reactivity and early-age strength development (Korkmaz and Kayıran, 2022; Bakil and Gábor, 2024; Hu et al., 2024). However, its effectiveness is highly dependent on waste-specific parameters, and excessive grinding may lead to increased energy consumption without proportional performance gains (Wang et al., 2024; Xu et al., 2025).

Chemical activation studies have shown that the use of alkaline activators such as NaOH, sodium silicate, lime, or MgO promotes the formation of C-(A)-S-H and N-A-S-H type gels in coal gangue-slag-fly ash systems, leading to dense microstructures and compressive strengths exceeding 50-60 MPa at 28 days under optimized conditions (Guo et al., 2024; Kong et al., 2024; Xu et al., 2024). However, excessive alkali dosages may adversely affect hydration kinetics, reduce workability, and compromise long-term durability, underscoring the need for careful mixture design (Adesanya et al., 2021; Kumar et al., 2023).

Thermal activation, particularly in the temperature range of 600-800 °C, is widely reported as an effective approach for coal wastes containing kaolinite, illite, or smectite. Calcination within this range induces dehydroxylation and partial amorphization of crystalline phases, significantly enhancing pozzolanic reactivity and long-term mechanical performance (Zhang and Ling, 2020; Zhang et al., 2022; Zou et al., 2024). In contrast, temperatures above approximately 850 °C may lead to recrystallization and vitrification, resulting in reduced reactivity and strength loss (Kong et al., 2024).

Hybrid activation strategies, combining mechanical, thermal, and chemical processes either sequentially or simultaneously, have recently gained attention due to their synergistic effects on hydration kinetics and microstructural development. Studies report that composite activation can yield activity indices exceeding 100% and outperform single activation methods in terms of strength and durability (Zhang et al., 2024; Li et al., 2025). Despite these promising findings, existing studies indicate that the binder performance of coal-derived wastes is highly sensitive to activation type and process parameters. Moreover, critical knowledge gaps remain regarding energy consumption, cost efficiency, environmental impacts, and long-term durability.

In particular, the literature reveals that: (i) systematic comparisons of different activation methods applied to the same coal waste source are limited; (ii) experimental studies focusing specifically on coal washing tailings are fewer than those on coal gangue or fly ash; (iii) synergistic effects arising from the combined use of activated coal wastes with other SCMs, such as fly ash or natural pozzolans, remain insufficiently explored; and (iv) standardized protocols addressing long-term durability, leaching behavior, and life-cycle performance are still lacking.

Motivated by these gaps, the present study aims to evaluate the potential of fine-grained coal washing tailings obtained from a single preparation plant as a supplementary cementitious material through selective activation approaches. The coal waste was subjected to (i) mechanical activation, (ii) pozzolanic-additive-assisted activation, and (iii) thermal activation. Cement mortars were prepared in accordance with EN 196-1 using 5-20 wt.% CMT replacement, and their compressive strength performance was assessed at 28 and 90 days. Additionally, selected mixtures incorporating fly ash and natural pozzolan were investigated to examine potential synergistic effects on early-age strength development. Through this approach, the study seeks to identify optimal activation-replacement combinations and to provide practical guidance for the design of sustainable, low-carbon cementitious binders based on coal washing tailings.

2. MATERIAL AND METHODS

2.1. Material

2.1.1. Physical and chemical characteristics of CMTs

Helium pycnometry and BET analyses revealed that the CMTs exhibit a true density of approximately 2.25 g/cm³, a specific surface area of 23.6 m²/g, and a pore structure dominated by micro- and mesopores, indicating favorable physical characteristics for enhanced reactivity and binding performance. Particle size distribution analysis showed a fine-grained and broadly distributed material, with approximately 10% of the particles below ~2 µm, 50% (D_{50}) within the range of ~10-12 µm, and 90% (D_{90}) below ~90-100 µm. This distribution confirms that a significant portion of the material lies within the micrometer scale, contributing to an increased specific surface area and, consequently, improved chemical reactivity. The coexistence of fine and medium-sized particles also promotes improved particle packing and mixture homogeneity, which is advantageous for both workability and mechanical strength development in binder systems. To further elucidate the chemical characteristics of the CMTs, the mineralogical composition was first investigated, and the corresponding X-ray diffraction (XRD) pattern is presented in Figure 1.

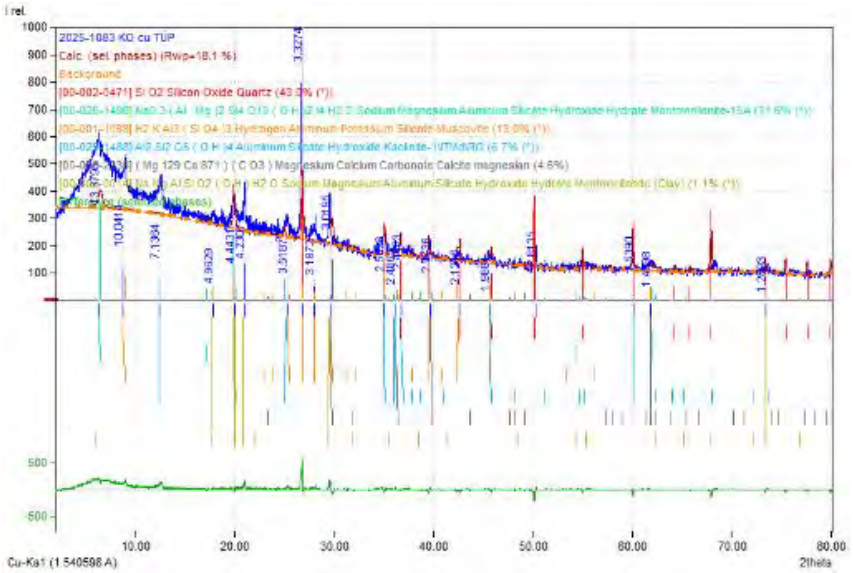

Figure 1. XRD pattern of the CMT sample obtained using Cu-Kα radiation and the results of the Rietveld phase analysis

According to the XRD pattern and quantitative phase analysis presented in Figure 1, the raw coal mine waste is composed predominantly of quartz (SiO_2, ~43%), smectite/montmorillonite

(Na-Mg-Al silicate, ~31.6%), muscovite (~13%), kaolinite (~6.7%), and magnesian calcite (Mg-Ca carbonate, ~4.6%), with a minor secondary montmorillonite phase (~1.1%). The high quartz content indicates a largely crystalline and inert component that contributes mainly as a filler and skeletal framework rather than participating directly in pozzolanic reactions. In contrast, the combined clay and aluminosilicate phases exceed 50%, dominated by montmorillonite, kaolinite, and muscovite, which are rich in reactive Al-Si species and can be transformed into pozzolanic or alkali-activated phases through appropriate activation. The basal reflections at approximately 13.9 Å, 10 Å, and 7.1 Å correspond to smectite, mica, and kaolinite minerals, respectively, confirming the clay-rich nature of the coal waste. The presence of magnesian calcite in the range of ~4-5% suggests that thermal activation at 600-800 °C is expected to induce carbonate decomposition, yielding CaO and CO_2; the resulting CaO may contribute to C-S-H and C-A-S-H gel formation, albeit accompanied by CO_2 release. Overall, the XRD results indicate a material with a high crystalline fraction and a limited amorphous phase, implying low pozzolanic activity in its raw state. Nevertheless, the abundance of Al-Si rich clay minerals highlights the strong potential of the material to be converted into a highly reactive binder precursor through selective activation. To further clarify the chemical composition underlying these phase distributions, XRF analysis was conducted using a Rigaku ZSX Primus II spectrometer, and the results are summarized in Table 1.

Table 1. Major oxide composition of CMT determined by XRF analysis (wt.%)

Major oxides	CO_2	SiO_2	Al_2O_3	Fe_2O_3	CaO	MgO	K_2O	Na_2O	TiO_2	SO_3
Content (%)	35.93%	33.89%	13.41%	5.56%	3.46%	3.31%	1.76%	0.92%	0.49%	0.29%

The XRF results indicate that the coal waste is characterized by a high aluminosilicate content and a low calcium level, after excluding CO_2 and normalizing the remaining oxides. Under CO_2-free normalization, the composition is dominated by SiO_2 (~53%), Al_2O_3 (~21%), and Fe_2O_3 (~9%), yielding a combined (SiO_2 + Al_2O_3 + Fe_2O_3) content of approximately 82-83%, while CaO remains below 10% (~5.5%) and MgO contributes ~5.1%. The total alkali content (Na_2O + K_2O) is around 4.2%. These values are further supported by simple compositional indices, including a silica modulus (SM) of ~1.8, an alumina modulus (AM) of ~2.0, and a low basicity ratio ((CaO + MgO)/(SiO_2 + Al_2O_3)) of ~0.14, confirming a strongly acidic, Al-Si rich system. Chemically, this composition closely resembles a low-calcium ASTM C618 Class F fly ash or calcined clay-type material, which is not directly hydraulic but highly suitable for pozzolanic and alkali-activated binder systems. The presence of moderate CaO and MgO (~10-11% combined) suggests favorable conditions for hybrid binding mechanisms involving both N-A-S-H and C-(A)-S-H gel formation. The exceptionally high CO_2 content is consistent with the presence of magnesian calcite and residual organic matter identified by XRD, indicating that thermal treatment is expected to induce significant mass loss and porosity development, thereby enhancing reactivity. Overall, the XRF-XRD compositional characteristics demonstrate that the raw CMT_0 sample represents a Ca-poor, aluminosilicate-rich waste material with high potential for selective thermal and mechanical activation, pozzolanic use, alkali-activated/geopolymer binders, and paste backfill or geotechnical improvement applications. In this context, the TGA-DSC curves of the raw CMT_0 sample are presented in Figure 2 to elucidate the temperature-dependent decomposition and transformation mechanisms.

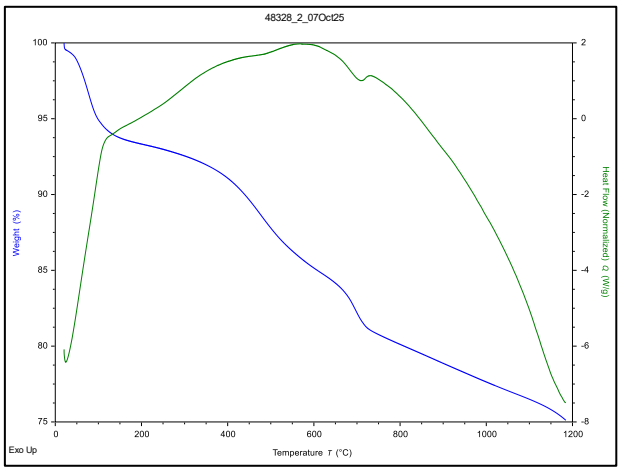

Figure 2. Thermogravimetric (TGA) and differential scanning calorimetry (DSC) results of the raw CMT sample

Figure 2 illustrates the TGA-DSC thermal behavior of the raw CMT sample under an inert atmosphere. The initial mass loss observed between 25 and 150 °C is attributed to the removal of free and physically adsorbed water, accompanied by a weak endothermic effect on the DSC curve, indicating moisture evaporation. This behavior confirms the presence of clay minerals with high water-retention capacity, such as smectite/montmorillonite. In the temperature range of 150-350 °C, a gradual increase in mass loss is detected, which is associated with the release of weakly bound interlayer water and the pyrolysis of residual organic matter inherent to coal waste. The absence of oxidative reactions under nitrogen atmosphere supports this interpretation. The most critical transformation occurs between 350 and 650 °C, where a pronounced mass loss and a broad endothermic region are observed, corresponding to the dehydroxylation of clay minerals, including montmorillonite, kaolinite, and muscovite. This process leads to the formation of amorphous and highly reactive aluminosilicate phases, explaining the enhanced pozzolanic activity achieved through thermal activation at approximately 600 °C. A sharp mass loss in the 650-900 °C interval, together with a strong endothermic peak centered around 750-800 °C, is attributed to the decomposition of carbonate phases ($CaCO_3$ and $MgCO_3$) identified by XRF analysis, resulting in the release of CO_2 and the formation of CaO and MgO. This transformation accounts for the reduced CO_2 content in thermally treated samples (e.g., CMT_800T) and contributes to the development of a more reactive oxide-rich matrix suitable for alkali activation. At temperatures above 900 °C, mass loss becomes negligible, and the DSC signal exhibits broad fluctuations associated with structural rearrangement and the onset of sintering, indicating that further temperature increase may reduce reactivity due to crystallization and vitrification effects.

Thermal analysis provides insight into the temperature-dependent phase transformations and mass-loss mechanisms of the raw CMT sample; however, the microstructural characteristics governing its reactivity cannot be fully assessed solely through bulk thermal behavior. Therefore, scanning electron microscopy (SEM) was employed to examine the morphology, particle size distribution, and textural features of the untreated CMT_0 sample. The SEM observations aim to complement the TGA-DSC findings by revealing the physical structure of clay-rich agglomerates, particle packing, and surface characteristics that influence water retention, thermal decomposition, and subsequent activation behavior (Figure 3).

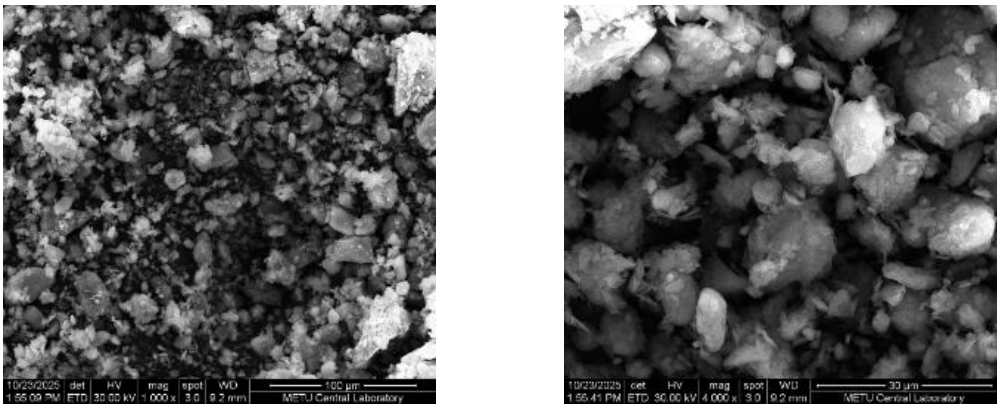

Figure 3. SEM micrographs of the raw CMT_0 sample at different magnifications: (left) 100 µm and (right) 30 µm

Figure 3 presents SEM micrographs of the raw CMT_0 sample at 100 µm and 30 µm magnifications, revealing a heterogeneous and weakly bonded microstructure characteristic of untreated coal waste. At the 100 µm scale, the morphology is dominated by irregular, angular, and fractured particles, with a wide particle size distribution comprising coarse fragments (~20-60 µm) and finer fractions below 10 µm. This bimodal texture is consistent with the unground nature of the material and its composite origin, consisting of clay, silt, organic carbon, and carbonate phases. The prevalence of sharp-edged particles reflects mechanical breakage during coal preparation processes, a feature typically preserved in non-thermally treated materials. Several particles exhibit dull, rough, and darkened surface textures, indicating the presence of organic carbon residues, in agreement with the elevated carbon content detected by EDS (~23%). Interparticle spaces are partially filled by a soft, fine-grained matrix attributed to clay–silt phases, representing the typical morphology of kaolinite- and montmorillonite-rich assemblages prior to thermal activation. At the higher magnification (30 µm), angular particles in the 20-40 µm range remain prominent, while the surrounding amorphous-looking matrix appears loosely packed and non-compact, confirming the absence of dehydroxylation and structural reorganization at this stage. Minor microcracks observed between particles are attributed to mechanical fragmentation rather than thermal stress. Overall, the observed microstructure indicates a low-cohesion and weakly reactive raw material, suggesting that significant morphological transformation and enhanced reactivity are expected following thermal activation in the 600-800 °C range.

2.1.2. Mixing materials

In this study, CEN standard reference sand, CEM I 42.5R Portland cement, fly ash (FA), trass, and mixing water were used as constituent materials in accordance with EN 196-1. The CEN reference sand is a rounded natural siliceous sand with a SiO_2 content exceeding 98% and a moisture content below 0.2%. The sand was supplied in pre-packed bags of (1350 ± 5) g with a standardized particle size distribution compliant with the relevant standards.

The performance of cement in mortar and concrete systems is governed not only by its chemical composition but also by its physical and mechanical properties. Therefore, the physical characteristics of the CEM I 42.5R cement used in this study were determined in accordance with EN 196, and the results are presented in Table 2. The chemical compositions of the cement as well as those of the fly ash and trass used as cement replacement materials are summarized in Table 3. As observed from the chemical analysis, both trass and fly ash are rich in SiO_2, Al_2O_3, and Fe_2O_3, indicating pronounced pozzolanic characteristics, while their CaO contents are considerably lower than that of Portland cement. This compositional feature suggests that these materials can contribute to strength development in cementitious systems through secondary hydration reactions.

Table 2. Physical properties of the CEM I 42.5R cement used in this study

Cement type	CEM I 42,5R
Specific gravity (g/cm³)	3.12
Blaine specific surface area (cm²/g)	350
Residue on 200 µm sieve (%)	0
Residue on 90 µm sieve (%)	2.5

Note: The physical properties were determined in accordance with EN 196 standards.

Table 3. Chemical compositions of cement, fly ash (FA), and trass (wt.%)

Component	**SiO_2**	**Fe_2O_3**	**Al_2O_3**	**K_2O**	**Na_2O**	**CaO**	**MgO**	**Cl^-**	**SO_3**	***LOI**
Trass	56.28	7.90	16.08	1.21	2.03	6.03	3.79	0.0399	0.1	5.72
Fly ash	54.57	8.38	23.51	1.57	1.19	3.26	1.90	0.0191	0.72	2.5
Cement	19.22	3.49	4.59	0.85	0.28	63.63	0.92	-	3.21	-

*LOI: loss on ignition

A comparison of the particle size distributions of cement, trass, fly ash, and coal mine tailings is presented in Figure 4. Particle size distribution is a key parameter directly influencing specific surface area, water demand, reaction kinetics, and the workability and mechanical performance of the hardened product. Fine-grained materials, owing to their higher specific surface area, are generally more reactive and can enhance binding properties; however, excessive fineness may increase water demand and adversely affect workability. Coarser particles, on the other hand, contribute to the formation of a skeletal structure, playing a decisive role in strength development and pore structure. Therefore, the appropriate combination of materials with different particle size ranges is critical for achieving optimal packing density, mechanical performance, and workability. Mixing water conforming to EN 196-1, with a pH value between 6 and 8 and low chloride and sulfate contents, was used throughout the experimental program. The water quality was considered suitable and not detrimental to cement setting or strength development.

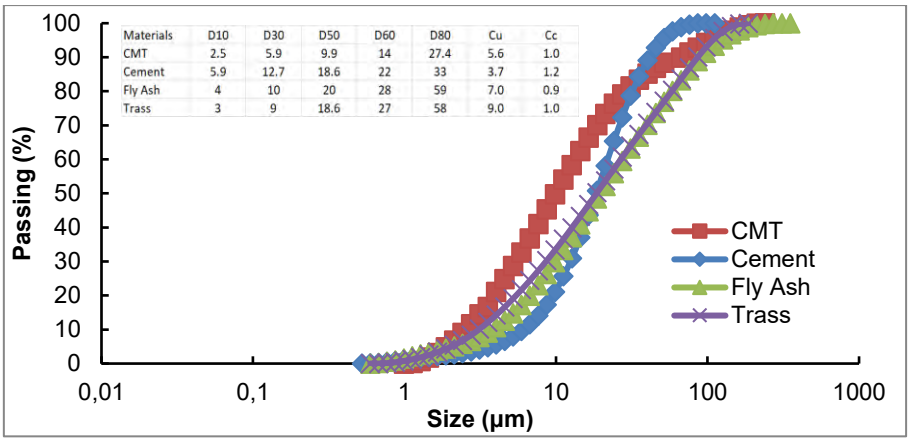

Figure 4. Cumulative particle size distribution curves of CMT, trass, cement, and fly ash (FA)

The pozzolanic activity values of fly ash and trass are presented in Table 4. The higher activity index and KP (k_p) value of trass compared to fly ash indicate that trass can provide a greater contribution to binder performance when used as a cement replacement material. The KP factor represents the degree to which a pozzolan can deliver mechanical performance equivalent to that of cement at a given replacement level and is commonly evaluated based on compressive strength results. In addition, the significantly higher reactive silica content of trass further supports its superior pozzolanic reactivity, explaining the enhanced strength development observed in trass-containing mixtures.

Table 4. Pozzolanic activity values of fly ash and trass

Type of pozzolan	Activity values (MPa)	*KP (k_p)	Reactive silica (%)
Trass	8.46	6.0	25.25
Fly ash	6.05	4.8	0.3

*KP (k_p): pozzolanic activity coefficient based on compressive strength.

2.2. Methodology

In this study, an experimental methodology was adopted to enhance the binding performance of coal mine tailings (CMT), based on similar investigations reported in the literature (Figure 5). The experimental program consisted of four main stages: (i) preparation of reference materials, (ii) activation processes, (iii) mortar preparation, and (iv) evaluation of mechanical performance. All mortar preparation, curing, and mechanical testing procedures were conducted in accordance with EN 196-1.

Figure 5. Flowchart of the experimental methodology adopted in this study

2.2.1. Activation methods

Mechanical Activation

For mechanical activation, CMT samples were ground in batches of 500 g using a planetary ball mill. Grinding durations of 30, 60, 120, 150, and 180 min were applied. The grinding process was carried out in a planetary ball mill with a 20 cm diameter grinding bowl, operating at a rotational speed of 60 rpm. A mixture of grinding balls with four different diameters was used, occupying approximately one-third of the mill volume.
After grinding, particle size distributions were determined using a Malvern Mastersizer 3000 laser diffraction analyzer with a dry dispersion unit. The obtained distributions were evaluated using the coefficient of uniformity (Cu) and coefficient of curvature (Cc), as defined in ASTM D2487, and samples exhibiting optimal liberation characteristics were selected for mortar production.

Pozzolan-Assisted Chemical Activation

In the pozzolan-assisted activation stage, fly ash (FA) and trass were incorporated to enhance the binding performance of CMT. Pozzolans were evaluated in binary and ternary combinations together with CMT as partial cement replacement materials.

Replacement ratios were determined based on the compressive strength results obtained at 28 and 90 days for reference mixtures, and the total replacement level was fixed at 5 wt.% for both curing ages. Accordingly, mortar mixtures containing 2.5% CMT + 2.5% trass, 2.5% CMT + 2.5% FA, and 2.5% CMT + 1.25% trass + 1.25% FA were prepared and subjected to mechanical testing.

Thermal Activation

Thermal activation was performed in a metallurgical muffle furnace at target temperatures of 600 °C and 800 °C, with a heating rate of 10 °C/min and a holding time of 1 h for each condition. The calcination process was carried out under ambient air atmosphere. After thermal treatment, the samples were allowed to cool naturally inside the furnace to room temperature (furnace cooling) to avoid thermal shock and ensure phase stability. The thermally activated samples were then used for mortar preparation and casting. The effect of thermal activation was evaluated based on compressive strength results obtained after 28 and 90 days of curing.

2.2.2. Mortar preparation and curing

Prior to use, CMT samples were oven-dried at 105 °C for 24 h and sieved through a 1 mm mesh. Mortar mixtures were prepared with cement replacement levels of 5%, 10%, 15%, and 20% by mass.

For each mixture, 1350 g of CEN standard sand, 220.5 g of mixing water, and 4.5 g of superplasticizer were used. Mortars were mixed in accordance with the mixing procedure specified in EN 196-1, using low- and high-speed mixing stages, and cast into 40 × 40 × 160 mm prismatic molds.

After casting, the specimens were stored in molds for 24 h at 20 ± 2 °C and 90% relative humidity. The demolded specimens were then cured in a water curing tank for 28 and 90 days. At the end of the curing periods, uniaxial compressive strength tests were performed on the specimens. For each mixture, three prismatic specimens were prepared and tested, and the reported compressive strength values represent the average of three measurements. The variability of the results was evaluated using standard deviation.

3. RESULTS AND DISCUSSION

This compressive strength results obtained under three different activation approaches; mechanical activation, pozzolan-assisted chemical activation, and thermal activation. These are presented and discussed in this section.

3.1. Effect of Mechanical Activation

The reactivity of pozzolanic materials in cementitious systems, and consequently strength development, is closely related to particle fineness, as finer particles provide a larger specific surface area that can accelerate pozzolanic reactions. Following mechanical grinding of coal mine tailings (CMT), the particle size characteristics and distribution curve classifications determined according to ASTM D2487 are summarized in Table 5.

Table 5. Percent finer than 150 µm and coefficients of curvature (Cc) and uniformity (Cu)

-150µm	D_{10}	D_{30}	D_{50}	D_{60}	D_{80}	Cu	Cc	Distribution curve
0 min.	2.7	5.3	9.8	12.7	30	4.7	0.82	Even graded
30 min.	2.13	4.5	8.7	12.7	42	4.7	0.76	Even graded
60 min.	2.13	4.5	8.7	12.7	42	6	0.76	Medium graded
90 min.	2.1	4	6.7	8.7	17	6	0.92	Medium graded
120 min.	2	4.3	8.7	12.7	24	6.35	0.73	Medium graded
150 min.	2	3.7	6	8.5	18.7	4.25	0.8	Even graded
180 min.	2	3.7	6	9	24.3	4.5	0.76	Even graded

As shown in Table 5, a systematic reduction in characteristic particle sizes (D_{10}, D_{30}, D_{50}, D_{60}, and D_{80}) is observed with increasing grinding time up to 90 min, indicating significant particle refinement and a decrease in the proportion of coarse fractions. In particular, the reduction of D_{50} to 6.7 µm and D_{80} to 17 µm confirms that approximately 80% of the material reached substantially finer sizes after 90 min of grinding. However, further grinding beyond 90 min (120-180 min) did not result in a notable additional fineness gain, and minor fluctuations in particle size parameters were observed.

This behavior can be attributed to the dominance of ultra-fine particles at prolonged grinding durations, which promotes particle agglomeration driven by van der Waals forces and electrostatic interactions. Although excessive grinding increases the nominal specific surface area, the formation of agglomerates limits the accessibility of reactive surfaces and reduces the effective fineness of the material. Moreover, ultra-fine and agglomerated particles significantly increase water demand, as additional mixing water is required to wet the enlarged surface area and disperse particle clusters. This increased water demand reduces the availability of free water for cement hydration, thereby impairing hydration efficiency and potentially limiting strength development.

Accordingly, a grinding duration of 90 min was selected as an optimal balance between particle refinement and energy efficiency, as it maximizes fineness development while avoiding the adverse effects associated with excessive fineness, particle agglomeration, and inefficient water utilization.

Mechanically activated CMT ground for 90 min (CMT_MA) was subsequently incorporated into mortar mixtures as a partial cement replacement at levels of 5%, 10%, 15%, and 20%. The uniaxial compressive strength (UCS) results obtained after 28 and 90 days of curing are presented in Figure 6, together with the corresponding results of untreated CMT (CMT_0).

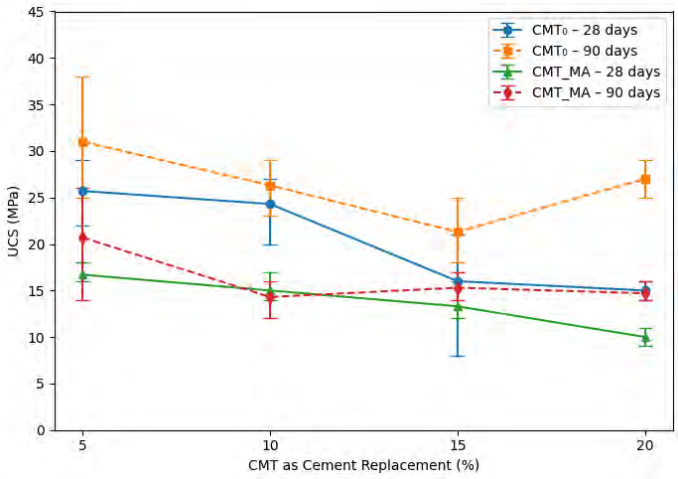

Figure 6. Compressive strength results of mechanically activated CMT (CMT_MA, 90 min grinding) and untreated CMT (CMT_0) after 28 and 90 days of curing

As illustrated in Figure 6, mechanical activation did not lead to an improvement in compressive strength at either early or later curing ages. On the contrary, mortars incorporating untreated CMT (CMT_0) consistently exhibited higher UCS values than those containing mechanically activated CMT (CMT_MA) across all replacement ratios and curing durations. At 28 days, the mixture with 5% CMT_0 achieved a UCS of approximately 26 MPa, whereas the corresponding CMT_MA mixture reached only about 16-17 MPa, corresponding to a strength reduction of nearly 35% due to mechanical activation. A similar trend was observed at 10% replacement, where UCS values decreased from approximately 23 MPa (CMT_0) to 15 MPa (CMT_MA).

At 90 days of curing, although all mixtures exhibited higher strength compared to their 28-day counterparts, untreated CMT mixtures maintained a clear strength advantage. In particular, at 5% replacement, the UCS of the CMT_0 mixture increased to approximately 31 MPa, while the CMT_MA mixture reached only about 21 MPa. Even at higher replacement levels (15-20%), CMT_0 mixtures consistently outperformed mechanically activated counterparts, confirming that mechanical grinding did not provide any measurable benefit in terms of long-term strength development.

This behavior can be attributed to excessive fineness and particle agglomeration induced by mechanical grinding, which likely increased water demand and restricted effective hydration, thereby offsetting the potential benefits of increased surface area. Similar findings have been reported in the literature, where excessive mechanical activation of coal-derived wastes was shown to limit strength development due to agglomeration effects and unfavorable water-binder interactions (Zhang and Ling, 2020, Bakil and Gábor, 2024).

With increasing cement replacement from 5% to 20%, a gradual decrease in compressive strength was observed for both CMT_0 and CMT_MA mixtures. For instance, the UCS of CMT_0 mixtures decreased from approximately 26–31 MPa at 5% replacement to around 15-27 MPa at 20% replacement, depending on curing age. This trend can be explained by the dilution effect associated with the reduction in the amount of active cement in the binder system. At higher replacement levels (15-20%), disruption of paste continuity and weakening of the load-bearing skeleton further contributed to strength loss.

Overall, the results presented in Figure 6 demonstrate that although coal mine tailings can be utilized as a partial cement replacement, the mechanical activation approach adopted in this study did not enhance binder performance. From a performance-sustainability perspective, the use of untreated CMT at replacement levels of 5-10% appears to provide a more effective and energy-efficient solution than mechanically activated CMT under the investigated conditions.

3.2. Effect of Pozzolan-Assisted Chemical Activation

The compressive strength results of mortar mixtures prepared using untreated coal mine tailings (CMT_0) in combination with natural and artificial pozzolanic materials are presented in Figure 7 for curing ages of 28 and 90 days.

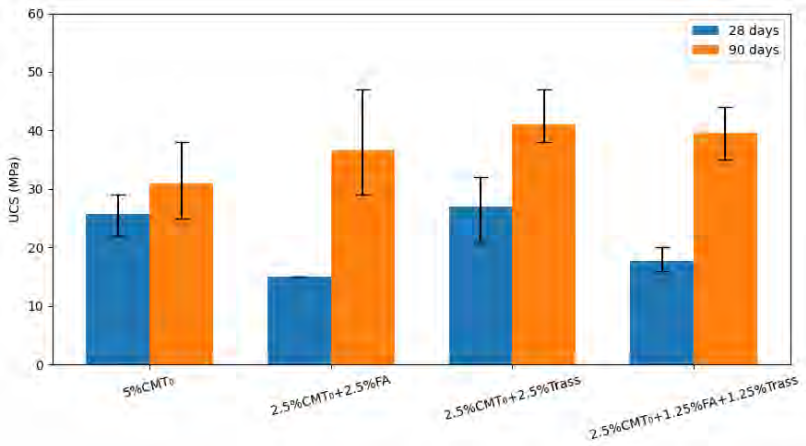

Figure 7. Compressive strength results of mortars incorporating untreated CMT (CMT_0) and pozzolanic materials at 28 and 90 days of curing

Figure 7 illustrates the UCS results of mortars containing untreated coal mine tailings (CMT_0) either alone or in binary and ternary combinations with fly ash (FA) and trass at curing ages of 28 and 90 days. At 28 days, the mixture incorporating 5% CMT_0 achieved a UCS of approximately 26 MPa, which was higher than those of the binary and ternary mixtures containing pozzolanic additives. Specifically, the UCS values of the mixtures containing 2.5% CMT_0 + 2.5% FA and 2.5% CMT_0 + 1.25% FA + 1.25% trass were approximately 18 MPa, indicating that the incorporation of pozzolans did not enhance early-age strength under the investigated conditions. Among the pozzolan-containing mixtures, the binary blend consisting of 2.5% CMT_0 + 2.5% trass exhibited the highest 28-day UCS, reaching approximately 27 MPa, demonstrating that trass contributed more effectively to early-age reactions than fly ash.

After 90 days of curing, a pronounced increase in compressive strength was observed for all mixtures, reflecting the continued progression of cement hydration and secondary pozzolanic reactions. Notably, mixtures incorporating pozzolanic additives outperformed the mixture containing only untreated coal mine tailings (CMT_0) at the same total replacement level. While the UCS of the 5% CMT_0 mixture increased to approximately 31 MPa, the binary mixture containing 2.5% CMT_0 + 2.5% trass achieved the highest UCS value of about 41 MPa, corresponding to an increase of nearly 32% compared to the CMT_0 only mixture. This superior performance can be attributed to the higher content of reactive amorphous silica in trass, which actively participates in sustained secondary pozzolanic reactions with calcium hydroxide released during cement hydration, promoting the formation of additional C-(A)-S-H gel and a denser microstructure.

The ternary blend (2.5% CMT_0 + 1.25% fly ash + 1.25% trass) followed closely, achieving a UCS of approximately 39–40 MPa, indicating a synergistic contribution of the two pozzolanic materials. In contrast, the mixture containing 2.5% CMT_0 + 2.5% fly ash reached a UCS of around 36 MPa, reflecting the comparatively lower long-term contribution of fly ash under the applied curing conditions. This behavior is associated with the delayed pozzolanic reactivity of fly ash and its reduced availability of reactive silica at later ages, resulting in a less pronounced formation of secondary hydration products compared to trass.

The superior performance of trass containing mixtures can be attributed to the higher pozzolanic activity and reactive silica content of trass, which promote sustained secondary hydration reactions and contribute to the formation of strength-giving C-(A)-S-H type gels. Similar trends have been reported in the literature, where natural pozzolans rich in reactive silica were shown to significantly enhance late-age strength in blended cementitious systems (Zhang and Ling, 2020; Kong et al., 2024).

Overall, the results presented in Figure 7 demonstrate that untreated CMT_0 can be used as a partial cement replacement without compromising early-age strength at low replacement levels. However, its combined use with natural pozzolans particularly trass leads to substantially superior mechanical performance at later curing ages. In this context, binary and ternary pozzolanic blends represent a viable and sustainable strategy for reducing cement consumption while maintaining or enhancing mechanical performance.

3.3. Effect of Thermal Activation

The compressive strength results of mortar specimens prepared using untreated coal mine tailings (CMT_0) and thermally activated CMT at 600 °C and 800 °C are presented in Figure 8 for curing ages of 28 and 90 days.

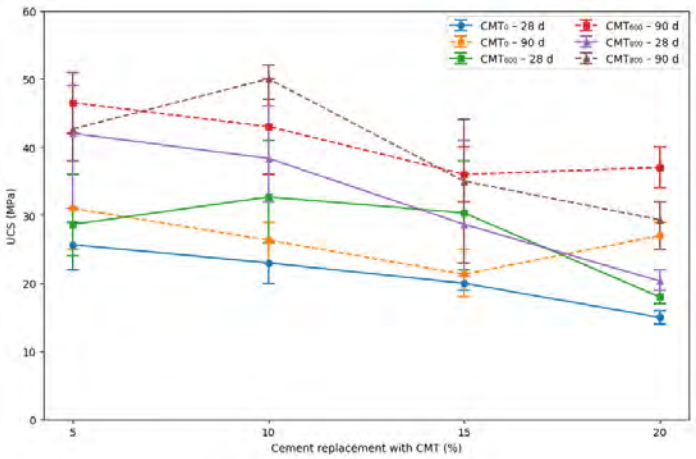

Figure 8. Effect of thermal activation temperature (600 °C and 800 °C) on the compressive strength of mortars containing CMT as a cement replacement

Figure 8 compares the UCS values of mortars incorporating CMT_0 and thermally activated CMT at 600 °C and 800 °C for curing ages of 28 and 90 days. Overall, thermal activation markedly influenced the binding performance of CMT, with its effectiveness strongly dependent on both activation temperature and curing duration.

At 28 days, CMT activated at 600 °C exhibited higher UCS values than untreated CMT_0 at low to moderate replacement ratios. Specifically, at 5% replacement, the UCS of the CMT_600T mixture reached approximately 33 MPa, compared to about 26 MPa for the untreated CMT_0 mixture. A similar enhancement was observed at 10% replacement, where CMT_600T achieved around 32 MPa, while CMT_0 remained close to 23 MPa. In contrast, CMT activated at 800 °C showed a decreasing strength trend with increasing replacement level; UCS values declined from approximately 26 MPa at 5% to about 20 MPa at 20% replacement, indicating that high-temperature activation may adversely affect early-age reactivity, likely due to excessive sintering and partial recrystallization reducing the availability of reactive amorphous phases.

At 90 days of curing, the beneficial effect of thermal activation became more pronounced, particularly for mixtures incorporating thermally treated coal mine tailings. CMT activated at 800 °C achieved the highest UCS value at a 10% replacement level, reaching approximately 50 MPa, which corresponds to an increase of nearly 40% compared to the untreated CMT_0 mixture at the same replacement ratio (~36 MPa). This pronounced long-term strength gain is directly associated with the thermal transformations identified by TGA–DSC and XRD analyses. The TGA–DSC results indicate significant dehydroxylation of clay-bearing phases at elevated temperatures, leading to the breakdown of hydroxyl-containing crystalline structures. Consistently, XRD patterns reveal a reduction in crystalline peak intensities and

partial amorphization, confirming the formation of highly reactive amorphous aluminosilicate phases.

These thermally induced structural changes enhance the pozzolanic reactivity of CMT by increasing the availability of reactive silica and alumina, thereby promoting sustained secondary pozzolanic reactions and prolonged C-(A)-S-H gel formation during extended curing periods. Consequently, the cementitious matrix becomes progressively densified, resulting in superior long-term strength development for CMT activated at 800 °C. In comparison, CMT activated at 600 °C exhibited a more balanced strength evolution, providing consistently higher UCS values than untreated CMT_0 at both curing ages. For example, at a 20% replacement level, the UCS of CMT_600T reached approximately 37 MPa, compared to about 27 MPa for CMT_0, indicating that moderate thermal activation effectively enhances reactivity while limiting excessive phase transformation.

Untreated CMT_0 specimens exhibited lower compressive strength values than thermally activated counterparts at both curing ages, confirming that thermal activation significantly improves the suitability of CMT as a cement replacement material. Nevertheless, a general reduction in UCS was observed for all mixtures at the 20% replacement level, highlighting the dominance of the dilution effect at high substitution ratios and indicating that the optimal replacement level should be limited.
These findings are consistent with previous studies reporting that thermal activation in the range of 600–800 °C enhances the pozzolanic reactivity of clay-rich coal wastes through dehydroxylation and partial amorphization, while excessively high temperatures may induce recrystallization and compromise early-age performance (Zhang and Ling, 2020; Zou et al., 2024). Overall, the results presented in Figure 8 demonstrate that thermal activation substantially improves the mechanical performance of CMT; however, its effectiveness strongly depends on both the activation temperature and the replacement level.
From a sustainability perspective, it is important to consider the energy demand associated with high-temperature activation, particularly at 800 °C. Although activation at 800 °C provides the highest long-term compressive strength due to enhanced amorphization and sustained secondary pozzolanic reactions, it is also considerably more energy-intensive. Therefore, its application is best justified in performance-critical scenarios where long-term strength and durability requirements outweigh energy-related concerns. In contrast, activation at 600 °C offers a more favorable performance–energy trade-off, delivering substantial improvements in both early- and late-age strength with lower energy consumption. Accordingly, thermal activation at 600 °C combined with moderate replacement levels (5–10%) emerges as a more practical and sustainable option for large-scale applications, while 800 °C activation should be selectively employed when enhanced long-term strength is a primary design objective.

4. CONCLUSION

This study evaluated the feasibility of utilizing coal mine tailings (CMT) as a supplementary cementitious material through selective activation strategies, including mechanical grinding, pozzolan-assisted blending, and thermal activation. The findings demonstrate that the effectiveness of CMT is strongly governed by the activation method, curing age, and replacement level, highlighting the importance of a tailored activation–replacement strategy for performance optimization.

Mechanical activation through grinding successfully refined particle size but did not translate into improved mechanical performance. Mortars containing untreated CMT consistently outperformed those incorporating mechanically activated CMT, indicating that excessive fineness led to particle agglomeration and increased water demand, which limited effective hydration and strength development. Accordingly, mechanical activation under the applied conditions cannot be considered a viable route for enhancing CMT performance.

In contrast, pozzolan-assisted blending proved to be an effective strategy, particularly at later curing ages. Binary and ternary mixtures incorporating trass and fly ash exhibited clear synergistic effects, with trass playing a dominant role in long-term strength development due to its higher pozzolanic reactivity. These results confirm that combining CMT with suitable natural or industrial pozzolans can significantly enhance its contribution as a cement replacement material.

Among the investigated approaches, thermal activation yielded the most pronounced improvement in performance. Activation at 600 °C provided a balanced enhancement of both early- and late-age strength at low to moderate replacement levels, whereas activation at 800 °C was more effective in promoting long-term strength development through increased amorphization and sustained pozzolanic reactivity. However, strength reductions observed at higher replacement levels across all mixtures emphasize the dominance of dilution effects and indicate that excessive substitution should be avoided.

From a practical and sustainability perspective, the results suggest that thermal activation at 600 °C combined with moderate replacement ratios (5–10%) offers a favorable balance between mechanical performance, energy demand, and industrial feasibility, making it a promising option for large-scale implementation. While activation at 800 °C may be justified in performance-critical applications requiring enhanced long-term strength, its higher energy intensity necessitates careful consideration within a broader sustainability framework.

Overall, this study demonstrates that coal washing tailings can be effectively valorized as a partial cement replacement when appropriate activation and blending strategies are employed. Future research should extend beyond strength-based assessment to include durability performance, leaching behavior, and comprehensive energy and CO_2 footprint analyses to support environmentally responsible and industrially viable utilization of CMT in cementitious systems.

REFERENCES

Acordi, J., Simão, L., Faraco, M.N.S., Borgert, C. H., Olivo, E., Montedo, ORK, Raupp-Pereira, F., (2023) “Waste valorization of coal mining waste from a circular economy perspective: A Brazilian case study based on environmental and physicochemical features”, Resources Policy, 80 103243.

Adesanya, E., Perumal, P., Luukkonen, T., Yliniemi, J., Ohenoja, K., Kinnunen, P., Illikainen, M., (2021) “Opportunities to improve sustainability of alkali-activated materials: A review of side-stream based activators”, Journal of Cleaner Production, 286 125558.

Adiguzel, D., Tuylu, S., Eker, H., (2022) “Utilization of tailings in concrete products: A review”, Construction and Building Materials, 360 29574.

Bakil, S. N. A., Gábor, M., (2024) “Investigation mechanical activation coal gangue for geopolymer”, fib Symposium, 833–840.

Demir, I., Adiguzel, D., Tuylu, S., Ozkan, S. G., (2024) “Investigation of the effects of coal properties, environmental conditions, and costs on coal drying method selection using multicriteria decision-making method (AHP)”, Physicochemical Problems of Mineral Processing, 60 (5) 193741.

Guo, L., Liu, J., Zhou, M., An, S., (2024) “Effect of an alkali activators on the compressive strength and reaction mechanism of coal gangue-slag-fly ash geopolymer grouting materials”, Construction and Building Materials, 426 136012.

Hu, K., Chen, X., Li, T., Zhang, J., Gao, X., Yang, T., (2024) “Effect of mechanical activation on early-age performance of sodium carbonate-activated gbfs binders”, Bulletin of the Chinese Ceramic Society, 43 (7) 2577-2583.

Kong, D., Wang, T., Zhang, J., Li, T., Liu, T., (2024) “Improvement of strength and microstructure of low-carbon cementitious materials with high volume of calcined coal gangue”, Construction and Building Materials, 444 137916.

Korkmaz, A. V., Kayıran, H. F., (2022) “Investigation of mechanical activation effect on high-volume natural pozzolanic cements”, Open Chemistry, 20 1029-1044.

Kumar, S. S., Rithuparna, R., Senthilkumar, R., Bahurudeen, A., (2023) “Cleaner production of waste-derived alkali activators from industrial and agricultural by-products for sustainable alkali activated binders”, Construction and Building Materials, 391 121824.

Li, F., Yang, H., Wang, L., Yang, T., Li, J., (2025) “Enhancement of the aging resistance performance of asphalt binder using activated coal gangue waste and determination of the ınfluence mechanism based on ınterfacial ınteraction ability”, Journal of Materials in Civil Engineering, 37 (8) 20149.

Wang, C.-Q., Duan, D.-Y., Li, X., Bai, D.-S., (2024) “Safe and environmentally friendly use of coal gangue in C30 concrete”, Sustainable Chemistry and Pharmacy, 38 101502.

Xu, H., Yin, H., Ge, P., (2024) “Design and microstructural analysis of the mixture proportion of alkali-activated fly ash-slag composite cementitious material”, Materials Research Express, 11 (11) 115303,

Xu, D., Sun, Q., Xu, R., Chu, L., Xie, W., (2025) “Study on microstructure change of coal slag and mechanism of pozzolanic activity enhancement under composite activation”, Materials Today Communications, 46 112862.

Zhang, Y., Ling, T.-C., (2020) “Reactivity activation of waste coal gangue and its impact on the properties of cement-based materials – A review”, Construction and Building Materials, 234 117424.

Zhang, X., Feng, X., Wang, Z., Jian, J., Chen, S., Luo, W., Zhang, C., (2022). “Experimental study on the physico-mechanical properties and microstructure of foam concrete mixed with coal gangue”, Construction and Building Materials.

Zhang, W., Long, H., Zhu, D., Pan, J., Li, S., Guo, Z., (2024) "Preparation of high-activity mineral powder from coal gangue through thermal and chemical activation" International Journal of Chemical Reactor Engineering, 22 (12) 1423-1432.

Zhang, L., Zhu, D., Marani, A., Nehdi, M. L., Wang, L., Yang, G., Zhang, J., (2025) “Toward sustainable construction: Comprehensive utilization of coal gangue in building materials”, Case Studies in Construction Materials, 23 e04930.

Zou, Y., Song, Q., Zhang, P., Xu. S., Bao, J., Xue, S., Qin, L., Wang, H., Lin, L., Liu, C., (2024) “Research status of building materials utilization and CO_2 curing technology on typical coal-based solid waste: A critical review”, Journal of CO_2 Utilization, 84 102860.

SPATIAL DISTRIBUTION OF SELECTED VARIABLES IN ARTANA TAILINGS FOR SUSTAINABLE MANAGEMENT

Naser PECI[1,*], Kemajl ZEQIRI[1], Berat SINANI[2], Nazmije SEJDIU[3]

[1]University "Isa Boletini" of Mitrovica, Faculty of Geosciences, 40000 Mitrovicë-Kosova
[2]Geological Survey of Kosovo, 10000 Prishtinë-Kosova, PhD Candidate
[3]Independent Researcher, MSc
[*]Corresponding author: naser.peci@umib.net

A B S T R A C T

The sustainable management of tailings requires detailed characterization of their mineral/chemical content and spatial distribution. The Artana tailings were selected for the study by focusing on selected elements of environmental and economic importance, including silver (Ag), arsenic (As), cadmium (Cd), copper (Cu), manganese (Mn), nickel (Ni), lead (Pb), and zinc (Zn) in order to ensure efficient and sustainable management.

Exploration of tailings formed by mining and metallurgical activities from the perspective of mineral resources and environmental issues involves understanding the dual potential that these tailings represent: they can be a valuable secondary resource and a significant environmental concern. This requires attention, especially in recent times, related to the issue of critical minerals, which has become one of the main priorities of economic, technological and geopolitical development at the global level.

The paper includes the methodology and interpretation of geostatistical analyses including database creation, univariate statistical analyses for each selected variable through descriptive statistics, coefficient of variation and distribution; multivariate statistical analysis through correlation analysis as well as spatial geostatistical analysis for each variable (Ag, As, Cd, Cu, Mn, Ni, Pb and Zn) by constructing post maps, contour maps and 3D surface maps.

These visualizations provide a clear representation of element distribution patterns across the tailing facility. The findings reveal both zones of elevated metal concentrations and areas with potential environmental risk, offering valuable insights for sustainable tailings management.

Key words: Artana tailing, geostatistical analysis, spatial distribution, sustainable management

1. INTRODUCTION

The exploration of mining tailings from the perspectives of mineral resource potential and environmental impact requires an understanding of their dual nature, as they may represent both a valuable secondary resource and a significant source of environmental risk.
In recent years, mining tailings have attracted increasing attention not only as sources of environmental risk but also as potential secondary resources of critical and strategic minerals. Tailings are finely ground residues generated during ore processing and are typically stored in surface impoundments or tailings dams.

The industrial dumps of the Trepça Complex are the result of long-term processing of Pb–Zn ores using flotation techniques (Kosovo Environmental Protection Agency (KEPA), 2011).

Beyond the environmental benefits associated with the removal or stabilization of harmful components, tailings reprocessing may also offer additional economic advantages through the recovery and reuse of valuable materials. As suggested by Struthers (1999), under certain technical and economic conditions, the reprocessing of tailings can be both feasible and economically viable. For these reasons, the detailed study of tailings deposits is essential to

ensure their efficient and sustainable management. Accurate knowledge of the geometry, structure, and spatial extent of tailings, combined with an understanding of their geological and geochemical characteristics, provides a solid foundation for effective mine planning, environmental assessment, and remediation strategies (Louwrens E.L., 2015).

The acquisition of reliable information through systematic exploration of tailings forms the basis of a comprehensive database for further analysis. Over recent decades, geostatistical methods have been widely applied to evaluate the spatial distribution of contaminants in soils, sediments, and mine wastes, offering a robust framework for spatial modeling and uncertainty assessment.

Laboratory analytical data obtained from the Artana tailings deposit were used for geostatistical processing. Sampling was conducted within the tailings material to depths of up to 60 cm. Based on these results, a geochemical database was developed to analyze the spatial distribution of selected elements: silver (Ag), arsenic (As), cadmium (Cd), copper (Cu), manganese (Mn), nickel (Ni), lead (Pb), and zinc (Zn) using geostatistical techniques (Sejdiu N, 2024; UNEP, 2024).

The objective of this study is to analyze the spatial distribution of selected elements (Ag, As, Cd, Cu, Mn, Ni, Pb, and Zn) in the Artana tailings using geostatistical methods. By characterizing spatial patterns, identifying contamination hotspots, and evaluating spatial continuity, this research aims to provide a scientific basis for sustainable tailings management, environmental risk assessment, and future remediation planning in the Artana mining area.

2. MATERIAL AND METHODS

2.1. Material

Quantitative methods for the analysis of geological data have become widely used in the field of Earth sciences. To maximize their utility, available data must be processed and organized to allow accurate assessment of the relevant parameters.

The study was conducted on the Artana tailings deposit, a legacy mining site formed from historical processing of Pb–Zn ores via flotation. Sampling was carried out to a depth of 60 cm, collecting samples across the deposit to capture spatial variability (fig.1). The focus was on eight elements with both environmental and economic relevance: Ag, As, Cd, Cu, Mn, Ni, Pb, and Zn (Sejdiu N., 2024; Peci et al., 2016).

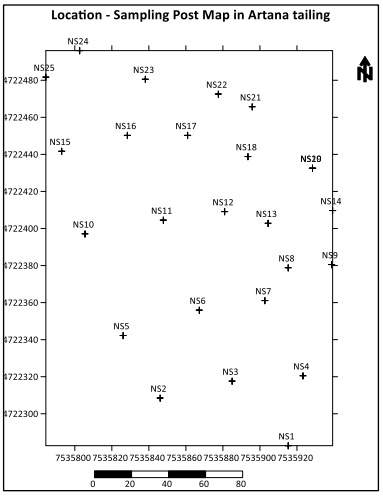

Figure 1. Sampling map in Artana tailing

2.2. Method

The processing of experimental results begins with statistical analysis, which examines the dataset or population and its underlying statistical structure (Kelmendi Sh., 2012).

Univariate statistical methods, which involve the analysis of a single variable at a time, can be applied to organize and extract information for each individual element. The initial step consists of calculating descriptive statistics for each variable, followed by the analysis of the frequency distribution of the dataset. This can be visualized using frequency histograms, probability plots, or cumulative frequency plots (Clemens et al., 2008, Peci et al., 2014; Microsoft Corporation (2019).

Geospatial data are generally multivariate, meaning that each sample often contains multiple variables, such as concentrations of several elements in a single tailings sample. A variety of multivariate statistical methods can be applied to assess relationships within such multi-element datasets. These methods typically include correlation matrices, which use linear regression to evaluate correlations between pairs of elements [Hair et al., 2014; Clemens et al., 2008; Peci et al., 2015,).

The main goal of the spatial analysis for this tailing is to characterize the distribution of selected elements within the tailings deposit. This study aims to achieve numerical characterization of the selected elements: Ag, As, Cd, Cu, Mn, Ni, Pb, and Zn based on the compiled geochemical database. After pre-processing, the raw data were represented as a combination of maps and visualizations, including a post (location map), contour map, and 3D surface map (Surfer Golden Software, 2024).

Spatial analysis, or spatial statistics, comprises a set of techniques for examining the distribution and relationships of variables in space. The software used for this analysis requires access to both the location of each sample and its associated attributes. In this study, SURFER Golden Software was employed to enable geostatistical analysis. Grid files were generated to produce various maps illustrating the spatial distribution of the selected elements [Peci et al, 2016, 2015, 2014).

3. RESULTS AND DISCUSSION

3.1. Summary Statistics and Variability

The summary statistics of the analyzed elements (Ag, As, Cd, Cu, Mn, Ni, Pb, and Zn) indicate substantial geochemical heterogeneity within the Artana tailings (table 1).

Table.1. Summary statistics and coefficient of variation of selected variables

Statistical parameter/ Variable	*Ag [ppm]*	*As [ppm]*	*Cd [ppm}*	*Cu [ppm]*	*Mn [ppm]*	*Ni [ppm]*	*Pb [ppm]*	*Zn [ppm]*
Mean	23.18	3712.63	46.07	365.00	1072.84	30.45	4935.33	3158.49
Standard Error	2.29	387.44	9.29	88.44	453.19	3.29	616.75	997.00
Median	20.94	3109.02	25.59	114.68	171.55	29.77	3734.37	676.55
Mode	#N/A	#N/A	#N/A	#N/A	#N/A	10.00	#N/A	#N/A
Standard Deviation	11.47	1937.19	46.43	442.18	2265.93	16.46	3083.76	4985.02
Sample Variance	131.47	3752721.73	2155.56	195524.84	5134420.95	270.96	9509572.47	24850445.26
Kurtosis	8.42	0.32	5.26	1.44	14.35	-0.91	7.04	5.14
Skewness	2.63	0.92	2.31	1.57	3.61	0.17	2.59	2.35
Range	54.52	6902.61	190.57	1427.72	10654.42	56.29	13491.18	18752.15
Minimum	12.18	1279.12	7.02	41.88	33.22	5.37	2579.32	164.21
Maximum	66.71	8181.73	197.60	1469.60	10687.64	61.67	16070.50	18916.37
Sum	579.52	92815.73	1151.67	9124.94	26821.02	761.34	123383.25	78962.35
Count	25	25	25	25	25	25	25	25
Coefficient of variation [%]	**49.46**	**52.18**	**100.78**	**121.15**	**211.21**	**54.05**	**62.48**	**157.83**

The arithmetic mean concentrations indicate values exceeding 1000 ppm for Pb (4935.33 ppm), As (3,712.18 ppm), Zn (3,158.49 ppm), and Mn (1,072.84 ppm). The average concentration of Ag is 23.18 ppm.

Based on the coefficient of skewness (Cs), the distributions are positively skewed, indicating right-tailed asymmetry. The degree of asymmetry follows the decreasing order: Mn > Ag > Pb > Zn > Cd > Cu > As.

In the Artana tailings, high coefficient of variation (Cv) values observed for elements such as Cd, Cu, Zn, and Mn indicate strong spatial heterogeneity and the presence of localized enrichment zones. This behavior is characteristic of elements associated with discrete sulfide mineral phases and uneven deposition during ore processing.

Frequency histograms highlight skewed distributions for most elements, with several outliers corresponding to high-concentration hotspots. Almost all histograms of the studied elements exhibit a lognormal distribution with positive (right-tailed) skewness. Samples with higher concentrations, representing extreme values (outliers), are observed for Mn, Ag, Pb, Cd, and Zn, and to a lesser extent for Cu and As.

3.2. Correlation Analysis

The Pearson correlation coefficient matrix was used to distinguish the relationships between the studied variables as presented in Table 3.

Table 3. Correlation matrix between variables

	Ag [ppm]	*As [ppm]*	*Cd [ppm}*	*Cu [ppm]*	*Mn [ppm]*	*Ni [ppm]*	*Pb [ppm]*	*Zn [ppm]*
Ag [ppm]	1,00							
As [ppm]	-0,20	1,00						
Cd [ppm}	-0,05	0,36	1,00					
Cu [ppm]	0,23	0,64	0,57	1,00				
Mn [ppm]	0,26	0,12	**0,83**	0,66	1,00			
Ni [ppm]	-0,09	0,18	-0,15	0,12	-0,03	1,00		
Pb [ppm]	**0,95**	-0,14	0,07	0,30	0,39	0,00	1,00	
Zn [ppm]	0,08	0,04	0,49	0,44	0,60	0,10	0,19	1,00

Correlation matrices revealed significant relationships among several elements, reflecting their common mineralogical hosts:

- A very strong positive correlation was observed between Ag and Pb (r = 0.95) and between Cd and Mn (r = 0.83), suggesting that these elements are likely associated with the same mineral phases in the ore. This implies that during flotation, these elements tend to be recovered together, and their concentrations in the industrial waste are closely related.
- Cd showed a moderate correlation with Zn, reflecting its substitution within sphalerite lattices.

These correlations provide valuable insight for both environmental risk assessment and potential selective recovery strategies for economically important metals.

3.3. Spatial Distribution

Ordinary kriging was applied to interpolate element concentrations across the tailings deposit. The resulting post, contour, and 3D surface maps reveal to identify locations with the highest concentrations, visualize the spatial distribution of element values across the tailing, and assess how concentrations change throughout the study area. In this paper, contour (isoline) maps were used to visualize spatial distribution (Figures 3–10).

This provides insight into the spatial structure and topography of element content levels:

- Hotspots of potentially toxic elements (As, Cd, Pb) concentrated in the northern and central parts of the deposit. The spatial distribution maps for As (Fig.3) show three zones of elevated concentrations located in the eastern and southeastern parts of the landfill, with the maximum value occurring in the southeastern sector. The Cd variable (Fig. 4) exhibits a spatial pattern characterized by three main peaks in the central part of the tailing. The spatial maps for Pb indicate extreme values located in the central part of the tailing (Fig.5), with a maximum concentration of 16,070.5 ppm, representing a pronounced anomaly relative to the remaining values.

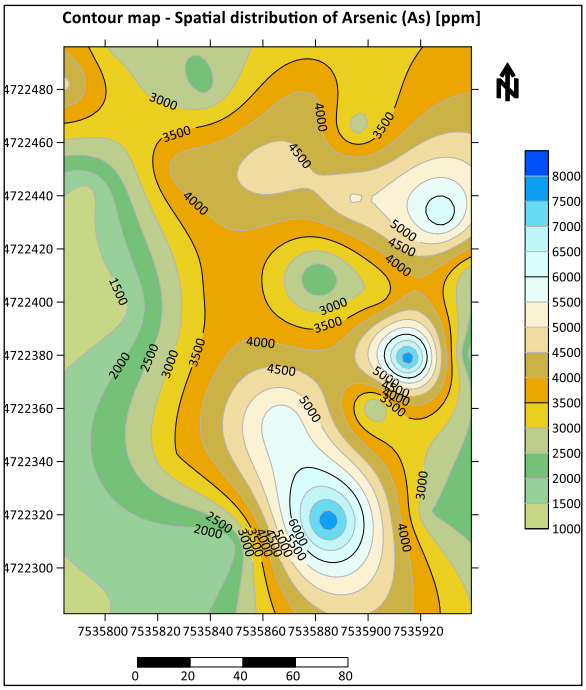

Figure 3. Contour map – Spatial distribution for Arsenic (As) (ppm)

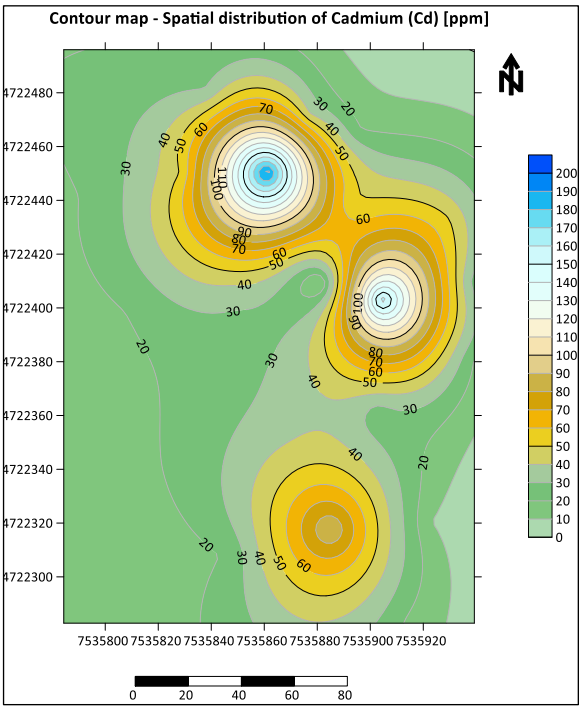

Figure 4. Contour map – Spatial distribution for Cadmium (Cd) (ppm)

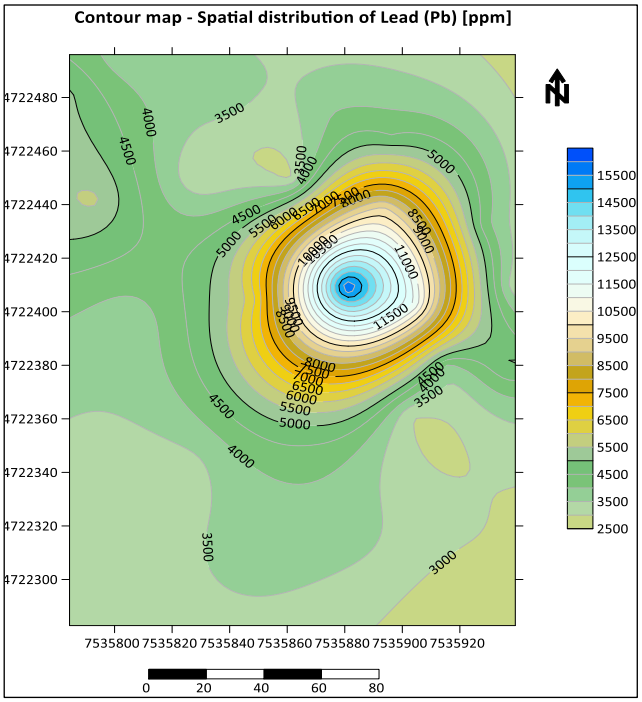

Figure 5. Contour map – Spatial distribution for Lead (Pb) (ppm)

- Zones of higher economic potential, where Cu, Ag, and Zn reach elevated concentrations, suggesting possible targets for secondary resource recovery. The spatial distribution of Cu shows the highest values (>1,000 ppm) in the eastern and southeastern parts of the tailing (Fig.6). The spatial distribution of Ag (Fig. 7) indicates elevated values throughout the tailing, with the maximum concentration located in the central part. A characteristic feature of the Zn distribution is that the highest concentrations (extreme values) occur in the central western part (18,916.4 ppm) and in the eastern part of the tailing (16,784.4 ppm) (Fig.8). The third highest Zn value is located in the southeastern part of the tailing (9,603.44 ppm).

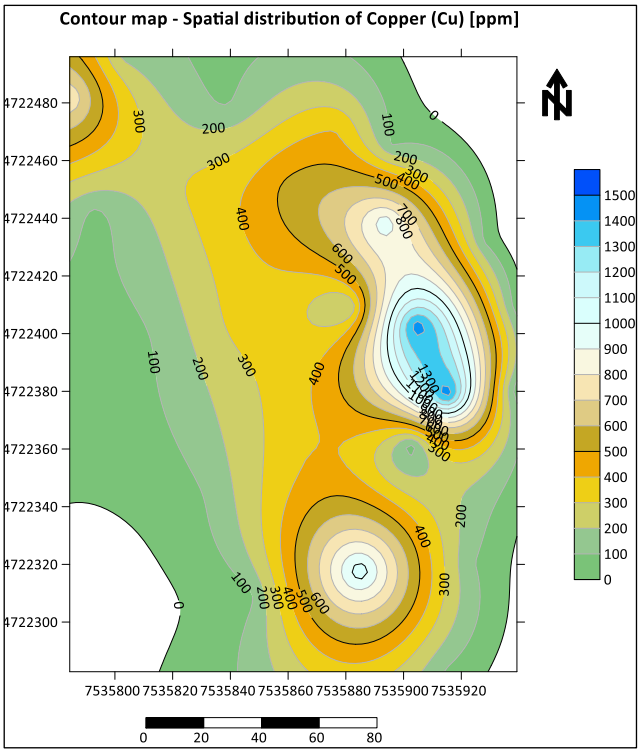

Figure 6. Contour map – Spatial distribution for Copper (Cu) (ppm)

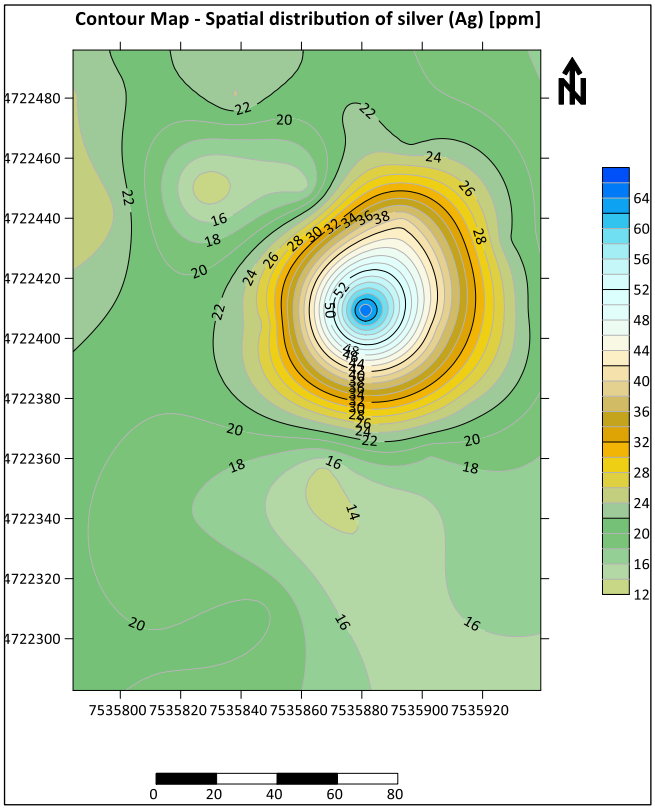

Figure 7. Contour map – Spatial distribution for Silver (Ag) (ppm)

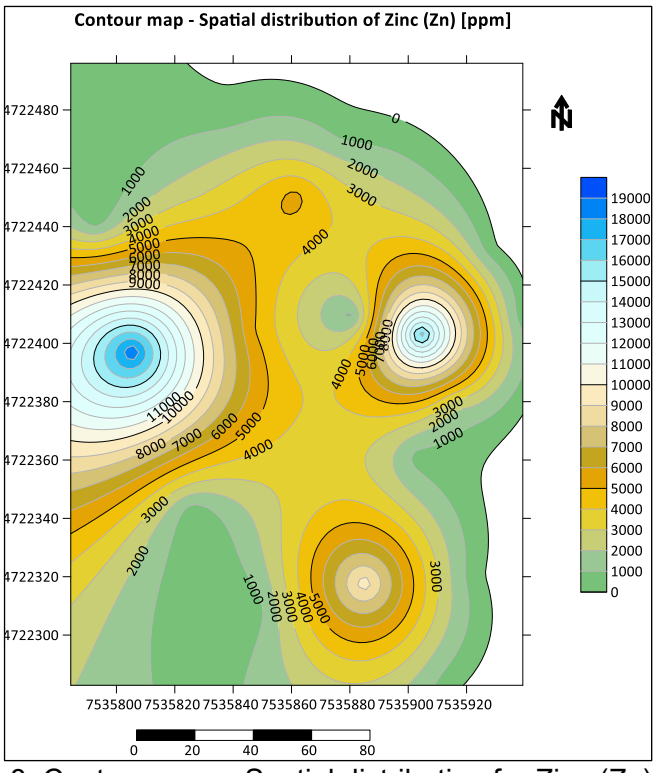

Figure 8. Contour map – Spatial distribution for Zinc (Zn) (ppm)

- More uniform distributions for Mn (Fig.9) and Ni (Fig.10), reflecting greater geochemical stability and lower environmental risk in those areas.

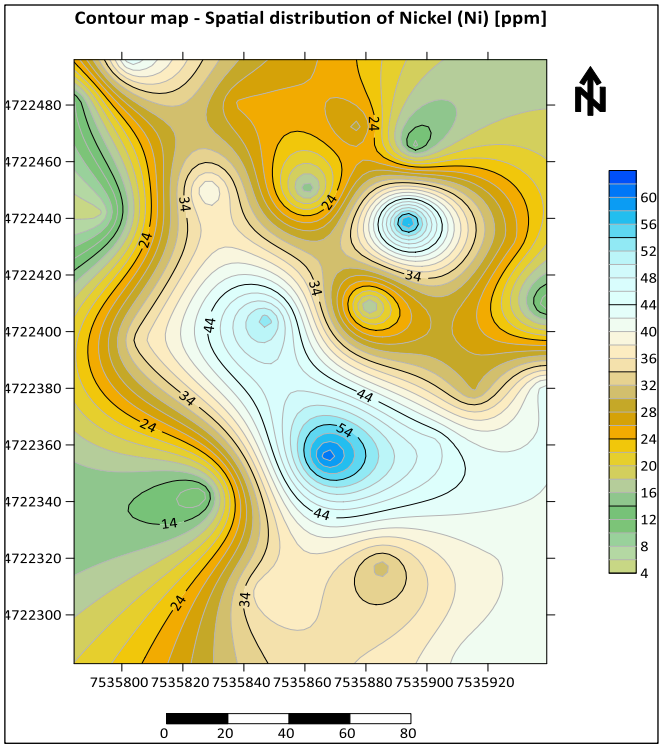

Figure 9. Contour map – Spatial distribution for Nickel (Ni) (ppm)

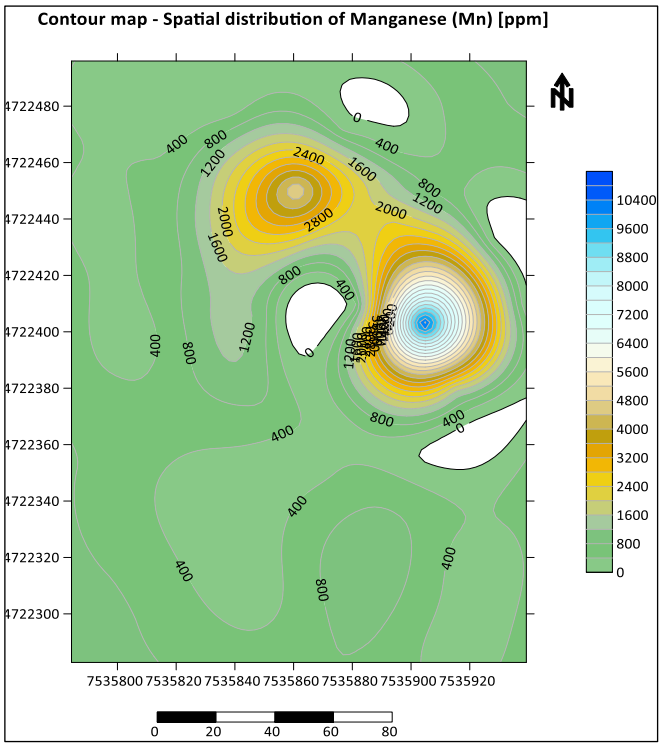

Figure10. Contour map – Spatial distribution for Manganese (Mn) (ppm)

3.4. Implications for Sustainable Management

The spatial patterns observed provide a scientific basis for risk assessment and sustainable management:

Environmental risk: Areas with elevated As, Cd, and Pb require monitoring, containment, or remediation to prevent leaching into surrounding soils and water (Table 4).

Table 4.Variable values in the Artana tailing compared to limit values for sutface waters and soil polution

Variable [ppm]	Minimum	Average	Maximum	Variable [mg/l] - average	Surface waters [mg/l]	Soil pollution [mg/kg]
Ag	12.18	23.18	66.71	**23.15**	**0.10**	
As	1,279.12	3,712.63	8,181.73	**3,708.39**	**0.10**	**80.00**
Cd	7.02	46.07	197.60	**46.02**	**0.01**	**25.00**
Cu	41.88	365.00	1,469.60	**364.58**	**0.50**	**500.00**
Mn	33.22	1,072.84	10,687.64	**1,071.62**	**2.00**	
Ni	5.37	30.45	61.67	**30.42**	**0.50**	**800.00**
Pb	2,579.32	4,935.33	16,070.50	**4,929.70**	**0.50**	**600.00**
Zn	164.21	3,158.49	18,916.37	**3,154.89**	**2.00**	**1,000.00**

Resource recovery: Zones enriched in Ag, Cu, and Zn could be considered for selective reprocessing, providing economic benefits while reducing environmental hazards.

Polymetallic tailings often contain significant concentrations of metals that are now classified as critical or near-critical due to changing technological and geopolitical conditions.

Sampling and monitoring optimization: The identified spatial structures allow the design of targeted monitoring networks, reducing costs while ensuring accurate environmental assessment.

Overall, the geostatistical analysis demonstrates the dual nature of tailings as both an environmental concern and a potential secondary resource. This underscores the importance of integrated spatial analysis in supporting sustainable tailings management strategies.

4. CONCLUSION

The study of Pb–Zn tailings highlights their dual character as both a potential secondary resource and a source of environmental risk. The Artana tailings deposit, part of the Trepça Complex, contains element concentrations that exceed permissible limits for soil and surface water, emphasizing the need for effective management strategies.

Geostatistical analysis proved to be a robust tool for characterizing the spatial distribution of selected elements, supporting the identification of contamination hotspots and zones with resource recovery potential. The results demonstrate that tailings should be considered complex anthropogenic deposits rather than waste alone.

Integrated approaches combining geostatistics, geochemistry, and environmental assessment provide a scientific basis for sustainable tailings management, enabling both risk mitigation and recovery of critical metals. Further investigations, including drilling across the full tailings depth, are recommended to improve resource evaluation and support long-term management decisions.

REFERENCES

Agency of Kosovo Environmental Protection (KEPA), (2011) Environmental Hotspots in Kosovo, Ministry of Environment and Spatial Planning, Prishtinë, Kosova.

Hair, J. F., Black, W. C., Babin, B. J., Anderson, R. E., (2014), Multivariate data analysis (7th ed.). Pearson.

Louwrens, E. L. (2015) “A novel geometallurgical approach to tailings storage facility characterisation and evaluation”, Doctoral Dissertation, Sustainable Minerals Institute, Julius Kruttschnitt Mineral Research Centre, The University of Queensland.

Microsoft Corporation (2019): Microsoft Excel Office – Data analysis tools.

Peci, N., Elezaj, Z., Krasniqi, R., Sinani, B., Berisha, S., (2014) “Trace metals in stream sediment of Kosova based on statistical analysis of lead, zinc, copper, nickel, chromium and cobalt”, 14th International Multidisciplinary Scientific GeoConference SGEM 2014, 383-390.

Peci, N., Shala, B., Sheremeti, F. K., (2015) “Spatial analysis of coal seam in Sibovc south west coal deposit”, AKTET – Journal of Institute Alb-Shkenca.

Peci, N., Shala, B., Sheremeti, F., (2016) “Geochemical background heavy metals and spatial distribution of stream sediments in Dukagjini basin”, International Journal of Ecosystems and Ecology Sciences, 6 (3) 395-400.

Reimann, C., Filzmoser, P., Garret, R., Dutter R., (2008), Statistical Data Analysis Exploined – Applied Environmental Statistics with R, Wiley, England.

Sejdiu, N., (2024) “Geostatistical analysis of selected variables from the exploration results of the Artana tailing”, Master’s Thesis, Faculty of Geoscience, Department of Geology, Mineral Deposits Program, University “Isa Boletini’ of Mitrovicë.

Shyqri, K., Izet, Z., (2012), Hyrje në Gjeostatistikë – Aplikimet në Miniera, Mitrovicë. Universiteti Prishtinës – Fakulteti Gjeoshkencave dhe Teknologjisë. Mitrovicë.

Surfer Golden Software (2024): Contouring and 3D surface mapping for Scientifics and Engineers. www.goldensoftware.com

UNEP (2024): Mining and environment in the Westen Ballkans. ENV-SEC

THE EFFECTS OF THE CHEMICAL STRUCTURE OF FLOCCULANTS ON FLOCCULATION IN MURGUL FLOTATION PLANT TAILINGS

Yağız ŞEN[1,*], Zafer GÖLLER[2], Gülay BULUT[3]

[1]ETI Bakır Inc. -Samsun Operation, Tekkeköy, Samsun, TÜRKIYE
[2]ETI Bakır Inc. -Murgul Operation, Damar 08510, Murgul, Artvin, TÜRKİYE
[3]Istanbul Technical University, Mining Faculty, Mineral Processing Engineering Department, 34463, ISTANBUL-TÜRKİYE
**Corresponding author: yagizsen@etibakir.com*

A B S T R A C T

Effective management of flotation tailings is critical in mining operations to prevent environmental pollution and ensure sustainable resource use. This study investigates the sedimentation behavior of flotation tailings derived from chalcopyrite ore processed at the Artvin Murgul Çakmakkaya and Cerattepe operations.

Chemical analysis of the tailings indicated 0.08% Cu, 0.05% Zn, 8.24% Fe, 69.14% SiO_2, and 7.90% S, 14% solids content, and a pH of 7.8. The particle size distribution analysis revealed a d_{80} value of 88 µm. Sedimentation experiments were performed using ten different flocculants with varying charge types, molecular weights, and densities at four dosage levels.

The clarity of supernatant water was evaluated by turbidity measurements under standard conditions. Among the tested reagents, the cationic, high-charge-density, and high–molecular-weight flocculant Mine-Treat 6070 exhibited the best performance in enhancing sedimentation and water recovery. These findings highlight the potential of optimized flocculation techniques for effective tailings disposal and reduced environmental impact, contributing to more sustainable mining practices.

Key words: *Flocculans, sedimentation, tailings management*

1. INTRODUCTION

Efficient management of mineral processing tailings is a paramount concern for the global mining industry due to environmental regulations and the necessity for water recycling (Wills & Finch, 2015). Sedimentation, enhanced by polymeric flocculants, is the most widely adopted method for solid-liquid separation (Gregory & Barany, 2011).

Flocculation is the process where destabilized colloidal particles are induced to gather into larger aggregates, known as flocs, through the addition of high-molecular-weight polymers or flocculants (Bratby, 2016). Unlike coagulation, which relies on neutralizing surface charges to reduce repulsive forces flocculation primarily functions through a bridging mechanism (Gregory & Barany, 2011). In this mechanism, the long chains of the polymer attach to multiple particles simultaneously, tethering them together into a macro-structure that settles rapidly under gravity (Wills & Finch, 2015). Figure 1 illustrates the principal mechanisms involved in the aggregation of colloidal particles, including charge neutralization, sweep coagulation, polymer bridging, and patch flocculation. In charge neutralization, oppositely charged ions reduce the electrostatic repulsion between particles, allowing aggregation.

Sweep coagulation occurs when particles are enmeshed within precipitating coagulant hydroxides. In the bridging mechanism, high-molecular-weight polymer chains adsorb onto multiple particle surfaces simultaneously, forming interparticle links and producing large, dense flocs. Patch flocculation involves localized adsorption of polymers, creating regions of opposite charge that promote particle attraction and aggregation. Among these mechanisms, polymer

bridging is the dominant process in flocculation using polymeric flocculants and plays a critical role in enhancing particle settling and solid–liquid separation efficiency.

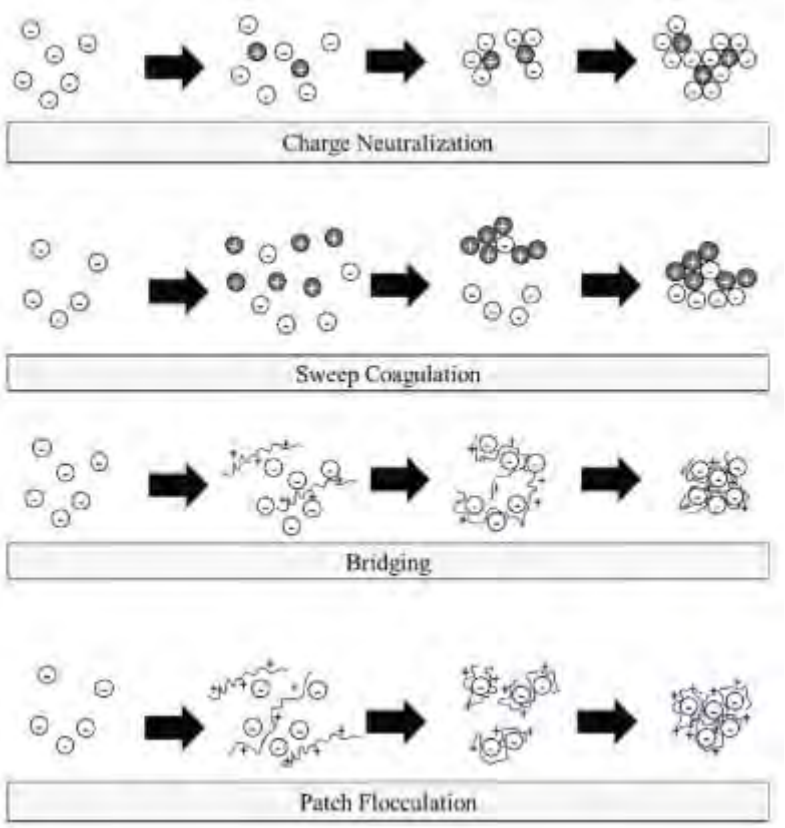

Figure 1. Mechanism of flocculation and coagulation (Kurniawan et al., *2020)*

The effectiveness of this process is dictated by the chemical structure of the polymers, including charge type and molecular weight (Sabah & Erkan, 2006). These parameters determine the prevailing mechanism, such as charge neutralization or bridging (Bolto & Gregory, 2007).

While anionic flocculants are common, their performance is often limited on specific mineral surfaces requiring specialized ionic interactions (Pearse, 2003). Murgul Plant tailings, with over 69.14% SiO_2, present challenges that necessitate a specialized chemical approach based on the ionic character of the polymers (Şen, 2025).

2. MATERIALS AND METHODS

2.1. Material Characterization

The facility incorporates two distinct flotation circuits. The first circuit is dedicated to the grinding and flotation of chalcopyrite ore sourced from the co-located Çakmakkaya underground mine, characterized by a copper (Cu) content ranging between 0.5% and 0.8%. The second circuit involves the grinding and flotation processes of another chalcopyrite ore originating from the Cerattepe underground mine in Artvin province, which features a higher copper grade varying between 2.0% and 2.5%. The flotation plant generates 4,000 tonnes of tailings per day as a result of concentrate production. A general view of the tailings pond from the flotation plant is shown in Figure 2. Tailings from Eti Bakır A.Ş. Murgul Plant were used in this study. The chemical composition determined by X-ray fluorescence (XRF) analysis revealed a high silica content (SiO_2 of 69.14%), as presented in Table 1. Particle size

distribution analysis was carried out with Ro-Tap Sieve Shaker, Retsch AS 200 Basic, showed that the material has a d_{80} size of 88 µm, illustrated in Table 2. All tests utilized plant process water to simulate real conditions.

Figure 2. Murgul concentrator tailing dam

Table 1. Chemical composition of the Murgul flotation tailings

Element	Assays, %
Cu	0,08
Fe	8,24
Zn	0,05
SiO_2	69,14
S	7,90
Al	0,65
Ba	1,00
Ca	0,46
Mn	0,02
Na	0,42
K	0,21
Mg	0,50
Density, gr/cm³	2,84

Table 2. Particle size distribution of the tailings sample

Screen Size, µm	Mass, %	∑ OS, %	∑ US, %
106	14,42	14,42	85,58
75	10,02	24,44	75,56
53	13,39	37,83	62,18
38	8,74	46,57	53,43
20	12,14	58,71	41,29
-20	41,29	100,0	0,0
Toplam	100,0	**d_{80}**	**88,74**

2.2. Flocculants

Five commercial polymers were used in this study. These included anionic polyelectrolytes for bridging and cationic polyelectrolytes selected to interact with negative silicate surfaces. The detailed properties of these reagents are summarized in Table 3.

Table 3. Flocculants and chemical structure

Flocculants	Charge Type	Charge Density	Molecular Weight
Zetag 8127	Cationic	Low	High
Mine-Treat 6070	Cationic	Medium	Medium
Mine-Treat 6020	Anionic	Medium	Medium
Nalco 9901	Anionic	Medium	Low

2.3. Experimental Procedure

Sedimentation tests were conducted in 1000 mL cylinders at 14% solids by weight. Flocculant dosages ranged from 20 to 50 g/t. After adding the reagent, cylinders were inverted ten times for mixing. After 3 minutes of settling, supernatant turbidity was measured in NTU (Nephelometric Turbidity Unit) at a natural pH of 7.8 (Şen, 2025). The NTU (Nephelometric Turbidity Unit) value serves as a fundamental indicator of water quality by providing a quantitative measure of suspended particulate matter, such as clay, silt, and microscopic organisms, which contribute to the physical cloudiness of a liquid. Technically, this value represents the degree to which light is scattered and absorbed by these particles rather than being transmitted in a straight line through the sample. In the context of public health and water treatment, elevated turbidity levels are critical as they can shield pathogenic microorganisms from disinfection processes, thereby compromising filtration efficacy and increasing microbiological risks. Furthermore, high NTU levels in natural water bodies inhibit light penetration, which subsequently disrupts photosynthetic activity and can lead to adverse ecological consequences by reducing dissolved oxygen levels in aquatic habitats (Metcalf & Eddy, Inc., 2014). Turbidity measurements were performed using a Hach 2100Q portable turbidimeter. The procedure of the experiments is illustrated in Figure 3.

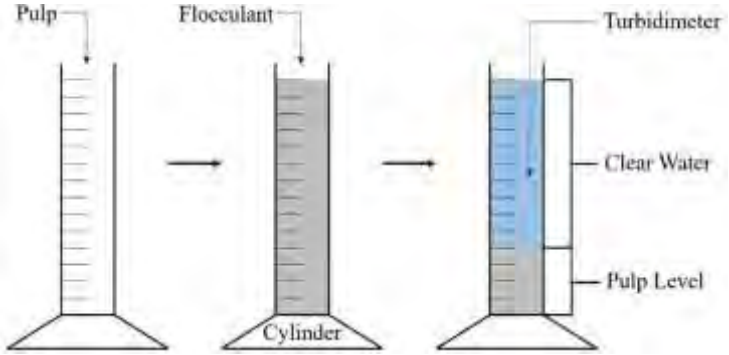

Figure 3. Flocculation tests procedure

3. RESULTS AND DISCUSSION

Evaluation of Flocculant Type on Settling Velocity

Figure 4 presents the settling levels of the material observed at the end of the measurement durations as a function of different flocculant dosages. Among the tested flocculants, Mine-Treat 6070 exhibited the lowest sedimentation levels (24.0–24.6 cm), indicating faster settling behavior compared to the others. In contrast, Zetag 8127 and Nalco 9901 showed higher final sedimentation levels (up to 27.7 cm), suggesting relatively slower settling performance. The

lower settling efficiency of anionic flocculants can be attributed to electrostatic repulsion between the negatively charged silicate surfaces and anionic polymer chains (Sabah & Erkan, 2006). Conversely, cationic flocculants achieved improved settling performance due to stronger adsorption onto negatively charged particle surfaces. Mine-Treat 6070, in particular, demonstrated the most effective sedimentation behavior, which can be attributed to its high molecular weight, promoting the formation of larger and denser flocs through charge neutralization and polymer bridging mechanisms (Bolto & Gregory, 2007).

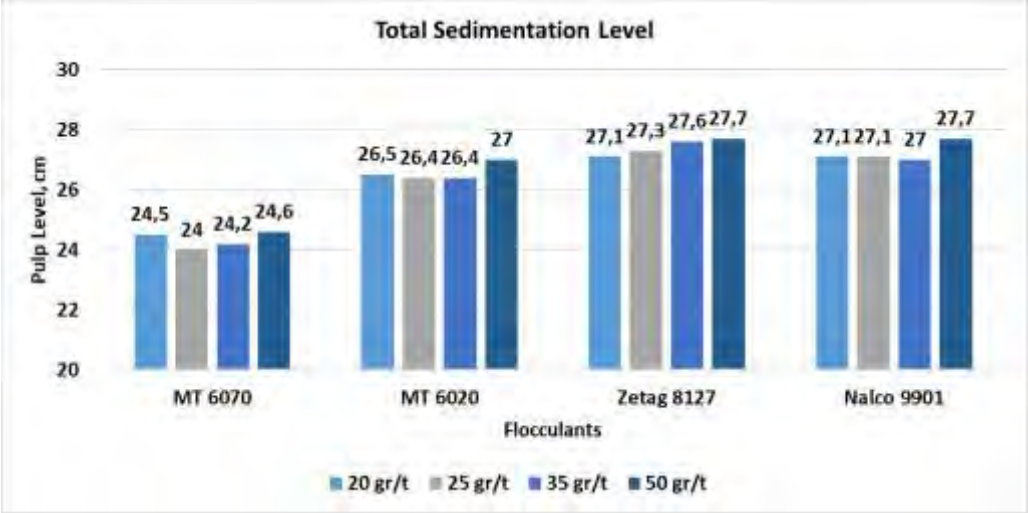

Figure 4. Sedimentation level

Supernatant Turbidity and Overflow Clarity

Cationic flocculants produced significantly clearer overflow compared to the other flocculants, as illustrated in Figure 5. Among the tested reagents, Mine-Treat 6070 achieved the lowest turbidity value of 12.8 NTU at a dosage of 50 g/t, indicating the most efficient removal of ultrafine particles. Similarly, Nalco 9901 and Zetag 8127 also showed substantial turbidity reductions at higher dosages, reaching 18.3 NTU and 27.9 NTU, respectively. The improved clarification performance of cationic flocculants can be attributed to their strong electrostatic attraction to negatively charged silicate particles present in the Murgul tailings, promoting effective aggregation and settling. This behavior suggests that charge neutralization and polymer bridging are the dominant mechanisms for capturing ultrafine particles, which is consistent with the findings of Gregory and Barany (2011), who emphasized the effectiveness of cationic polyelectrolytes in destabilizing negatively charged mineral suspensions.

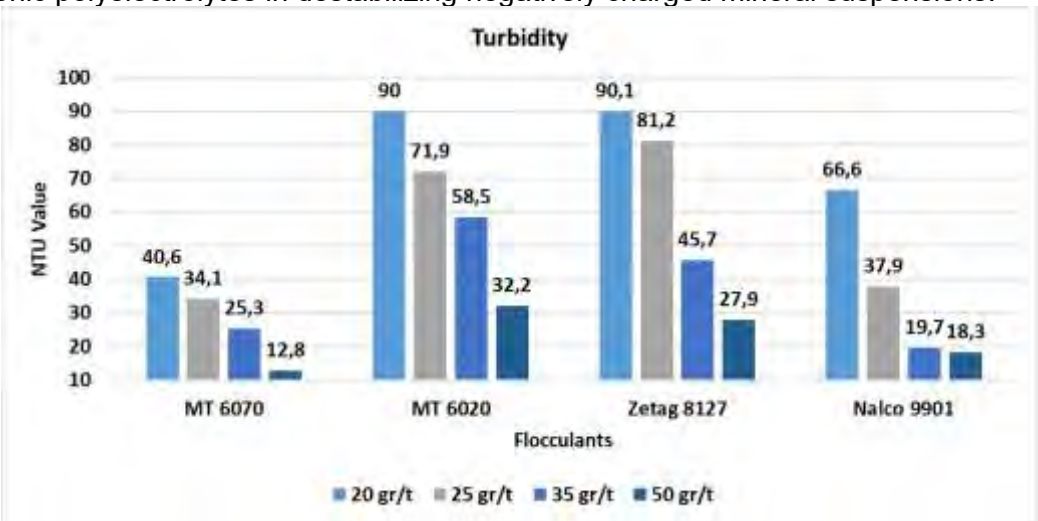

Figure 5. Turbidity results of flocculant dosage

4. CONCLUSION

According to recent findings, ionic charge and density have been identified as the most critical factors governing the settling behavior of Murgul tailings. Comparative analysis (as illustrated in Figures 4 and 5) demonstrates that the cationic structure of Mine-Treat 6070 outperformed other reagents, achieving both rapid sedimentation and high overflow clarity simultaneously. In contrast, anionic flocculants exhibited limited effectiveness regarding clarity, likely due to electrostatic repulsion with the negatively charged silicate surfaces present in the tailings.
The superior performance of the cationic Mine-Treat 6070 is attributed to a dual mechanism involving charge neutralization and bridging. Consequently, a cationic system is highly recommended for the Murgul Plant to optimize water recovery and ensure superior overflow quality.

REFERENCES

Bolto, B., Gregory, J., (2007) “Organic polyelectrolytes in water treatment”, Water Research, 41 (11) 2301–2324.

Bratby, J., (2016) “Coagulation and flocculation in water and wastewater treatment”, IWA Publishing.
Gregory, J., Barany, S., (2011) “Adsorption and flocculation by polymers and surfactants”, Advances in Colloid and Interface Science, 169 (1) 1–12.

Kurniawan, S., Abdullah, S., Imron, M., Said, N., Ismail, N., Hasan, H., Othman, A., Purwanti, I., (2020) “Challenges and opportunities of biocoagulant/bioflocculant application for drinking water and wastewater treatment and its potential for sludge recovery”, International Journal of Environmental Research and Public Health, 17 (24) 9312.

Metcalf & Eddy, Inc., Aecom, Abu-Orf, M., Bowden, G., Burton, F. L., Pfrang, W., Stensel, H. D., Tsuchihashi, R., Tchobanoglous, G., (2014) “Wastewater engineering: Treatment and resource recovery”, McGraw-Hill Education.

Pearse, M. J., (2003) “Historical review of polyelectrolytes applied to flocculation in the mining industry”, Minerals Engineering, 16 (2) 103–108.

Sabah, E., Erkan, Z. E., (2006) “Interaction mechanisms of flocculants with coal waste slurry”, Fuel, 85 (3) 350–359.

Şen, Y., (2025) “The effects of the chemical structure of flocculants on flocculation in Murgul plant flotation tails”, M.Sc. Thesis, Istanbul Technical University, Graduate School.

Wills, B. A., Finch, J., (2015) “Wills' Mineral Processing Technology: An Introduction to the Practical Aspects of Ore Treatment and Mineral Recovery”, Butterworth-Heinemann.

BACKFILLING OF UNDERGROUND EXCAVATIONS WITH CEMENTED PASTE IN MODERN UNDERGROUND MINING

Bajić SANJA[1,*], Tomanec RUDOLF[1], Tankosić LJILJANA[2], Bajić DRAGOLJUB[1,2], Išek JOSIP[3]

[1]University of Belgrade, Faculty of Mining and Geology, Belgrade, Republic of Serbia
[2]University of Banja Luka, Faculty of Mining, Banja Luka, Republic of Srpska, Bosnia and Herzegovina
[3]Mining Insitute Ltd. Belgrade, Belgrade, Republic of Serbia
**Corresponding author: sanja.bajic@rgf.bg.ac.rs*

A B S T R A C T

Backfilling of underground excavations is a critical technological and geotechnical operation in modern underground mining, with significant economic, safety, and environmental implications. Cemented paste backfill (CPB), composed of mine tailings, binder, and water, enables hydraulic transport and controlled placement within mined-out voids, providing effective tailings management, improving the stability of underground openings, and reducing environmental impacts. This study is based on the hypothesis that optimized CPB mixtures derived from mine tailings, with controlled rheological and mechanical properties, can enhance the stability of chambers and pillars, reduce ore losses, and mitigate subsidence risk. Particular emphasis is placed on the interaction between CPB and surrounding geological and hydrogeological conditions, including groundwater presence, pore pressure variations, and dewatering regimes, which significantly influence backfill behavior and geotechnical safety. The research methodology combines “in situ” monitoring under underground mining conditions with laboratory testing of CPB rheological and mechanical properties. The results are analyzed using applied mathematical methods to develop predictive models for backfill strength development and its contribution to the stability of underground excavations under different operational scenarios. The results demonstrate the potential to establish robust correlations between CPB rheology, strength evolution, and geotechnical stability. These correlations support the definition of reference design criteria and enable optimization of cement consumption while maintaining required performance. The scientific contribution lies in the integration of experimental, geotechnical, and mathematical approaches to CPB design, while the engineering contribution is reflected in improved ore recovery, enhanced operational safety, and support for the sustainable development of underground mining under variable hydrogeological and climatic conditions.

Key words: *Cemented paste backfill, underground backfilling, mine tailings, rheology, groundwater, geotechnical stability, underground mining, applied mathematics in mining, sustainable development*

1. INTRODUCTION

Mineral processing operations generate large quantities of flotation tailings as a by-product of ore beneficiation.Traditional disposal of tailings in surface landfill occupies extensive areas and represents a potential source of soil and groundwater contamination, as well as a long-term geotechnical risk. Increasingly stringent environmental regulations and sustainable development principles necessitate an integrated approach to mine waste management.

Backfilling of underground excavations represents one of the key operations in modern underground mining, with significant economic, safety, and environmental implications. The use of cemented paste backfill (CPB) technology allows the return of thickened tailings into mined-out voids after ore extraction, simultaneously reducing the load on tailings storage facilities and enhancing the stability of underground chambers and pillars. In this way, a functional link is established between mineral processing and underground mining, while also applying the principles of circular economy.

The performance of a CPB system depends on the tailings' particle size distribution, the proportion of fine fractions, and the degree of thickening prior to paste preparation. These parameters influence the mixture's rheological behavior, resistance to segregation, and the development of mechanical properties during curing. Their optimization represents a crucial step toward achieving technological efficiency and long-term geotechnical reliability (Đurđevac Ignjatović L. et al. 2023).

In recent decades, the backfilling of underground voids has gained increasing importance from both economic and environmental perspectives, further stimulated by rapid technological development and the growing number of scientific studies in this field. The application of CPB reduces the surface area required for tailings disposal, thereby mitigating the negative environmental impact of mining activities (Yilmaz and Fall, 2017). At the same time, it reduces the risk of long-term environmental incidents (Chongchong Qi and A. Fourie 2019). Additionally, backfilling contributes to a higher degree of ore recovery, reduced ore losses, and improved occupational safety by enhancing the stability of underground workings (Grice 1998; Belem et al. 2002; Deb et al. 2017; Edraki et al. 2014).

The aim of this study is to establish functional correlations between the rheological properties of the mixture (flow limit, viscosity), the dynamics of uniaxial compressive strength (UCS) development, hydrogeological conditions in the deposit, and the overall geotechnical stability of underground excavations.

Strength development of the cemented paste is a key factor in ensuring the stability of underground workings, with mathematical modeling providing the capability to predict backfill behavior under various operational conditions.

2. METHODOLOGY

The methodological approach is based on a combination of field and laboratory investigations supported by mathematical analysis. The field component includes "*in situ"* monitoring of backfilled chambers, observation of deformation behavior, stress variations, and overall system performance under conditions of groundwater presence. Particular attention is given to the analysis of pore pressure influence and drainage conditions on the hardening process of the backfill.

Laboratory investigations include:

- determination of the rheological parameters of the fresh paste mixture,
- testing of uniaxial compressive strength at different curing stages,
- analysis of the influence of binder content on mechanical properties,
- evaluation of material deformability and stiffness.

The obtained results are analyzed using regression and correlation analysis in order to define mathematical models describing strength development and its relationship with the input parameters of the mixture.

The phased optimization of cemented paste backfill (CPB) is based on the definition of target criteria and the consideration of alternative variables that enable achieving an optimal balance between technological and geotechnical requirements. The proposed approach includes three optimization phases: process, mechanical, and geotechnical. For each phase, specific criteria and possible alternatives are defined. An overview of the defined criteria and alternatives is presented in Table 1.

Table 1. Criteria and alternative phase optimizations of the CPB system

Phase	Criteria	Alternatives
Process	Maximization of CPB mixture homogeneity Viscosity Segregation resistance	Particle size distribution of tailings (fine-to-coarse ratio) Degree of thickening Water-to-solid ratio
Mechanical	Maximization of compressive strength (UCS ≥ UCS_min) Minimization of cement/binder consumption	Binder content Water-to-binder ratio Setting accelerator
Geotechnical	Maintenance of the safety factor (FS ≥ FS_min) Control of deformations of underground pillars and chambers Stability under variable pore pressure conditions (hydrogeological conditions)	Paste transport strategies (pipeline length, flow velocity) Periodic monitoring of water saturation Potential integration of mechanical and hydrogeological monitoring

Within the framework of CPB system optimization, each phase is defined by objective functions that reflect the balance between technological performance and geotechnical reliability. Criteria serve as indicators of goal attainment, while alternatives define the variables that can be adjusted during the optimization process. For instance, in the processing phase, particle size distribution and the degree of thickening control the rheological properties of the mixture, whereas in the mechanical phase, binder content and the water-to-binder ratio determine strength development and the system's cost-effectiveness. The geotechnical phase integrates these results into the context of the underground excavation, taking into account safety factors and interactions with hydrogeological conditions (Fall Benzaazoua and Saa, 2008).

The proposed approach enables continuous feedback between phases: results from each phase are used to adjust the input parameters of the subsequent phase, thereby achieving a systemic optimization of the CPB system.

To formalize the optimization process, the backfilling system can be represented as a multi-objective optimization problem, in which the objective function is minimized or maximized depending on the design requirements.

The general form of the optimization problem can be expressed as:

$$F(x) = w_1 f_r(x) + w_2 f_m(x) + w_3 f_g(x) \quad \text{(Eq. 1)}$$

where are:

- $f_r(x)$– function representing the rheological performance of the mixture (viscosity, yield stress),
- $f_m(x)$– function describing the mechanical properties (development of compressive strength),
- $f_g(x)$– function representing the geotechnical stability of the system,
- w_1, w_2, w_3– weighting coefficients representing the relative importance of individual criteria.

The variable vector $x$includes the technological parameters of the system, such as the granulometric composition of tailings, the degree of thickening, the water-to-solid ratio, and the

binder content. The optimization is performed under constraints that ensure the minimum stability and performance requirements of the system:

$$UCS(x) \geq UCS_{min}$$
$$FS(x) \geq FS_{min}$$

where:

- UCS– uniaxial compressive strength of the backfill,
- FS– safety factor of the underground excavation. (Yanjun Xu et al. 2022).

3. EXPECTED RESULTS AND PROPOSED RESEARCH FLOW

The analysis of the proposed conceptual model indicates the potential to establish reliable correlations between the rheological properties of the CPB mixture, the development of uniaxial compressive strength (UCS), and the geotechnical stability of underground excavations. Such correlations could enable the definition of reference design criteria and the optimization of cement consumption while maintaining the required system performance, as also evidenced by previous studies on the design of cemented backfills in mining operations (Yilmaz and Fall, 2017).

Control of the tailings particle size distribution and the degree of thickening is expected to be a key parameter in the optimization process. The particle size distribution directly affects the mixture's rheological structure, the homogeneity of the backfill, and its resistance to segregation. An increased proportion of fine particles is expected to enhance mixture homogeneity and reduce segregation, but it may also increase viscosity and yield stress, requiring careful balancing of the solid-to-water ratio.

The degree of thickening is anticipated to be one of the dominant technological parameters affecting the efficiency of the backfilling system. Higher solid content could lead to reduced water and binder consumption while maintaining or improving the mechanical performance of the hardened backfill. However, exceeding the optimal range may reduce pumpability and complicate the transport of the paste through pipelines.

The strength development of the cemented backfill is expected to be a critical factor in assessing the long-term stability of underground excavations. An increase in CPB compressive strength could contribute to stress redistribution in the surrounding rock mass and reduce deformations of chambers and pillars. Strength development is anticipated to depend on the type and quantity of binder, as well as the microstructure formed during the hydration process.

Hydrogeological conditions, particularly variations in pore pressure and the presence of groundwater, are expected to significantly influence the long-term reliability of the backfilling system. Groundwater could affect hydration processes and alter the hydro-mechanical properties of the cemented backfill, as confirmed by studies on CPB system–site hydrogeology interactions.

Within the framework of the proposed conceptual optimization model, these parameters are integrated through the system of criteria and alternatives defined in Table 1. This approach is expected to enable the identification of an optimal mixture composition and transport parameters, depending on geotechnical requirements and site-specific hydrogeological conditions.

The proposed model illustrates the interdependence between the tailings particle size distribution, solid content, mixture rheology, and mechanical property development, as well as their influence on underground excavation stability. In this way, the approach provides a foundation for the further development of mathematical and optimization models that allow a

quantitative analysis of CPB system performance under various mining and hydrogeological conditions.

4. CONCLUSION

The proposed approach demonstrates that it is possible to establish a conceptual framework for the optimization of cemented paste backfill by integrating process-related, rheological, and geotechnical parameters.

By defining key criteria such as the rheological properties of the mixture, the development of compressive strength, and the geotechnical stability of underground openings, a foundation is created for the development of mathematical models that enable the optimization of CPB composition and system performance.

In this context, the presented approach can be considered a methodological example for the development of quantitative optimization models in the design of backfill systems in underground mining. Future research should include more detailed mathematical modeling and model validation based on experimental and in-situ field data.

ACKNOWLEDGMENTS

This research has been supported by the Ministry of Science, Technological Development and Innovation of the Republic of Serbia.

FUNDING

The authors would like to thank the Ministry of Science, Technological Development and Innovation of the Republic of Serbia, Contract on realization and financing of the scientific research work of the Faculty of Mining and Geology in 2026. (451-03-33/2026-03/200126)

REFERENCES

Benzaazoua, M., Fall, M., Belem, T., (2004) “A contribution to understanding the hardening process of cemented pastefill”, Minerals Engineering, 17 (2) 141–152.

Belem, T., Benzaazoua, M., Bussière, B., Dagenais, A., (2002) “Effects of settlement and drainage on strength development in mine paste backfill”, Proceedings of 9th International Conference, Tailings and Mine Waste, 139-148

Cui, L., Fall, M., (2018) “Mathematical modeling and analysis of in-situ strength development in cemented paste backfill structure”, Proceedings of GeoEdmonton 2018 Conference.

Đurđevac Ignjatović, L., Krstić, V., Radonjanin, V., Jovanović, V., Malešev, M., Ignjatović, D., Đurđevac, V., (2023), Application of Cement Paste in Mining Works, Environmental Protection, and the Sustainable Development Goals in the Mining Industry, Sustainability.

Deb, D., Sreenivas, T., Dey, G. K., Panchal, S., (2017) “Paste backfill technology: Essential characteristics and assessment of its application for mill rejects of uranium ores”, Transactions of the Indian Institue of Metals, 70 487–495.

Edraki, M., et al., (2014), Environmental impacts of mine tailings and paste backfill, Resources Policy, 14–23.

Edraki, M., Baumgartl, T., Manlapig ,E., Bradshaw, D., Franks, D. M., Moran, C. J., (2014), Designing Mine Tailings for Better Environmental, Social and Economic Outcomes, A Review of Alternative Approaches, 411–420.

Fall, M., Benzaazoua, M., Saa, E., (2008) “Mix proportioning of underground cemented tailings backfill”, Tunnelling and Underground Space Technology, 23 (1) 80–90.

Grice, A., (1998), Underground Mining With Backfill, The 2th Annual Summit – Mine Taillings Disposal Systems, Brisbane.

Qi, C., Fourie, A., (2019) “Cemented paste backfill for mineral tailings management”, Journal of Rock Mechanics and Geotechnical Engineering, 11 (4) 739–757.

Xu, W., Cao, P., Tian, M., (2018) “Strength development and microstructure evolution of cemented tailings backfill containing different binder types and contents”, Minerals, 8(4) 167.

He, Y., Cheng, Y., Ma, M., Li, F., Song, Y., Liu, L., Wang, X., Huang, J., (2022) “A novel design concept of cemented paste backfill (CPB) materials: Biobjective optimization approach by applying an evolved random forest model”, Materials, 15 (23) 8298.

Yilmaz, E., Fall, M., (2017), Paste Tailings Management, Springer.

Yilmaz, E., Benzaazoua, M., Belem, T., Bussière, B., (2009) “Effect of curing under pressure on compressive strength development of cemented paste backfill”, Minerals Engineering, 22 (9-10) 772-785.

MATERIAL ANALYSIS AND MINERAL CHARACTERIZATION

ANALYSIS OF ACCIDENTS IN UNDERGROUND MINES IN ALBANIA

Shahin BARAMAJ[1,*], Lavdie MOISIU[1], Mimoza SIMIXHIU[1], Dhurim KURTI[2]

[1]EIT RawMaterials, Regional Innovation Centre, Albania.
[2]National Authority for Mine Safety and Emergencies.
**Corresponding author: shahin.baramaj@fgjm.edu.al*

A B S T R A C T

The Albanian mining sector possesses an extensive and multifaceted operational history,fundamentally rooted in the early-stage exploitation of chromoim (Cr) deposits in Bulqize and the subsequent extraction of copper (Cu), iron-nickel (Fe-Ni),and coal resources throughout the 20th century. While underground mining has been a major contributor to the national economy, it remains one of the most hazardous working environments. Despite structural reforms and privatization efforts after the 1990s, accident rates in both metallic and non-metallic mines remain significantly high.

This study analyzes the occurrence, distribution, and trends of occupational accidents in Albanian underground mines over the past two decades. The analysis is based on official data from the National Agency of Natural Resources (AKBN), the State Labor Inspectorate and Occupational Health (ISHPSHSH), and the National Authority for Mine Safety and Emergencies (AKSEM). The research also reviews the existing legal and institutional framework, including the Mining Law and related by-laws, to assess their alignment with European Union standards.

Findings indicate that the frequency of fatal and non-fatal accidents remains above European averages, with a strong spatial concentration in Bulqizë and Pogradec. The paper concludes with practical recommendations to enhance safety performance, institutional oversight, and compliance with EU directives.

Key words: *Underground mining, occupational safety, accident analysis, mining legislation*

1. INTRODUCTION

The mining industry has always played a significant role in the economy of Albania. Prior to the 1990s, the state centrally managed mineral exploitation, establishing an extensive network of both underground and surface mines, particularly for chromium and copper. Following the economic changes after 1990, a marked decline in mining activity occurred; several mines were closed and infrastructure was gradually degraded. The process of privatization and the granting of mining licenses, which began in the late 1990s, gradually redirected attention to the sector, with particular emphasis on chromium exploitation (Bater after 1999 and Bulqizë after 2008), the reopening of copper mines, and the development of quarries for construction materials. This post-privatization increase in activity was accompanied by a rise in the number of employees and an intensification of operations, which consequently led to increased exposure to workplace hazards. In this context, the statistical analysis of accidents assumes particular importance, as it contributes to assessing safety levels and guiding preventive measures for the future (ICMM,2015).

2. MATERIAL AND METHODS

2.1. Material

This study is based on the examination of all accidents recorded in the mining industry during the period 2015–2025. The information was obtained primarily from official documentation

administered by AKSEM, data from the electronic e-Inspektime platform, as well as statistics provided by the Tax Directorate regarding the average annual number of employees in this sector. During the analysis, it was taken into account that approximately 10% of employees constitute administrative staff, who are not directly exposed to operational workplace hazards. For this reason, accident rate calculations were performed using only 90% of the total workforce. Furthermore, in accordance with the realities of the mining industry, a methodological assumption was applied whereby approximately 80% of operational workers are engaged in underground activities, while 20% are involved in surface operations. (Eurostat,n.d.)

Table 1. Permits and types of permits

NR	Permits and types of permits	TOTAL	AKTIVE	PEZULLUAR
1	Mining permit	597	407	190
2	Underground mining permit	199	141	58
3	Surface minig permit	398	266	132
4	Exploration and prospecting permit	13	10	3
5	Permit with subcontracting authotization	41	30	11
6	Chrome	262	151	111
7	Copper	21	12	9
8	Iron Nickel	30	0	30
9	Marble/Sandstone/Decorative stone	61	44	17
10	Clay/kaolin/Gypsum/Alabaster	22	20	2
11	Quarries/Basalt/Others	200	180	20
12	Mineral processing plant	16		
13	Specialized entities licensed for explosives	19		
14	HPP	3		
15	Roads/tunnels/civil works	2		

2.2. Historical trend of accidents (2015-2025)

Table 2. Permits and types of permits

Viti	Accidents with injuries	Fatal accidents	Injured persons	Fatalities
2015	8	10	11	10
2016	7	1	7	1
2017	13	4	15	6
2018	19	7	23	7
2019	16	2	19	2
2020	14	3	15	5
2021	15	5	15	5
2022	15	3	15	3
2023	21	1	23	1
2024	19	3	19	3
2025	18	8	18	8

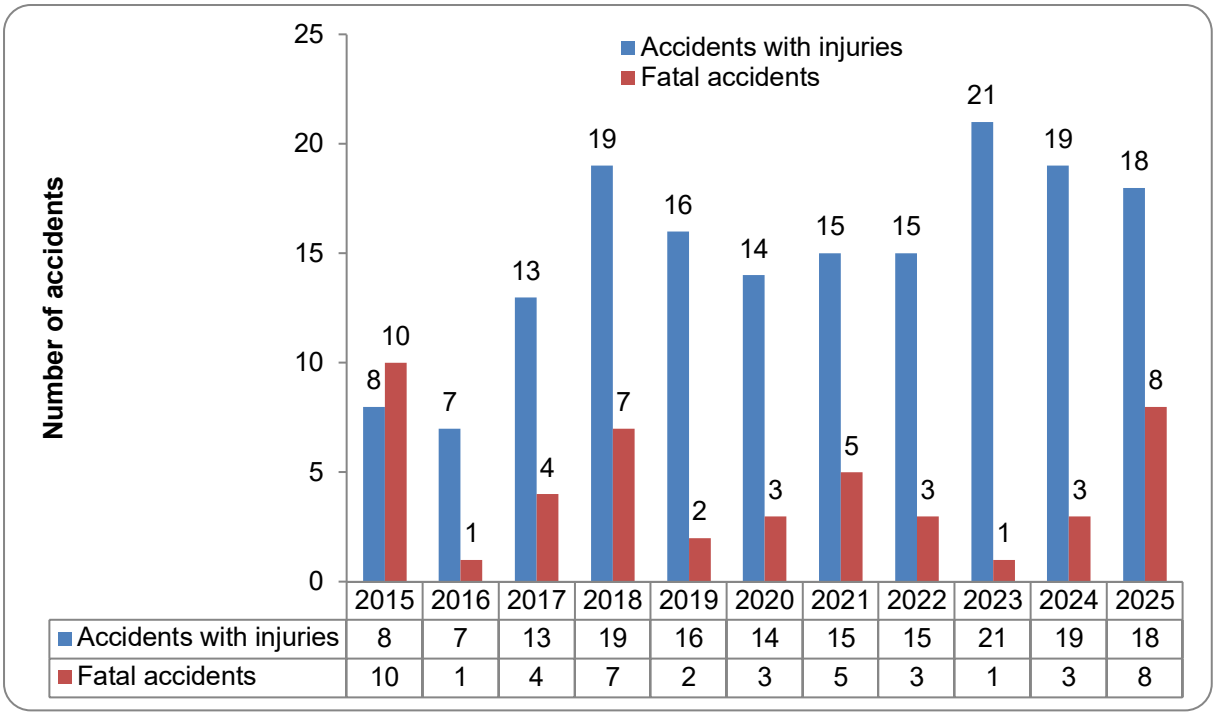

	2015	2016	2017	2018	2019	2020	2021	2022	2023	2024	2025
Accidents with injuries	8	7	13	19	16	14	15	15	21	19	18
Fatal accidents	10	1	4	7	2	3	5	3	1	3	8

Figure 1. Accidents with injuries vs fatal accidents

The years 2018 and 2023 emerge as periods with the highest number of accidents of this type. After 2020, no clear downward trend can be identified; only a slight decline is observed after 2021, indicating that preventive measures have failed to achieve a consistent and long-term improvement in worker safety.When examining the dynamics of injury-related accidents, it is evident that 2018 and 2023 are particularly prominent, as they record the highest levels of such incidents. Following 2020, there are no clear signals of a sustained reduction, suggesting that preventive measures have not resulted in a strong or durable improvement over time. This highlights the need to reassess and strengthen occupational safety strategies, particularly within the mining sector. In contrast, fatal accidents exhibit greater variability and are more difficult to predict. The years 2016 and 2023 are characterized by a marked decrease in fatalities, whereas 2025 shows an alarming increase, identifying it as a critical point requiring special attention and more detailed analysis. This irregular pattern suggests that fatal accidents are more closely associated with isolated high-risk events rather than with overall work volumes.

2.3. Accident Rate per 1000 Exposed Workers

In the statistical analysis, the annual average number of employees in the mining industry was taken into account. Since approximately 10% of this total corresponds to administrative personnel, who are not directly exposed to occupational hazards, the calculation of accident rates was based on 90% of the workforce, considered as exposed workers. For illustrative purposes, if 18 accidents were recorded in 2015 with 15,315 employees, and 21 accidents in 2024 with 19,743 employees, the absolute number of accidents appears to have increased. However, when normalized to the number of exposed workers, the individual risk per worker has actually decreased.

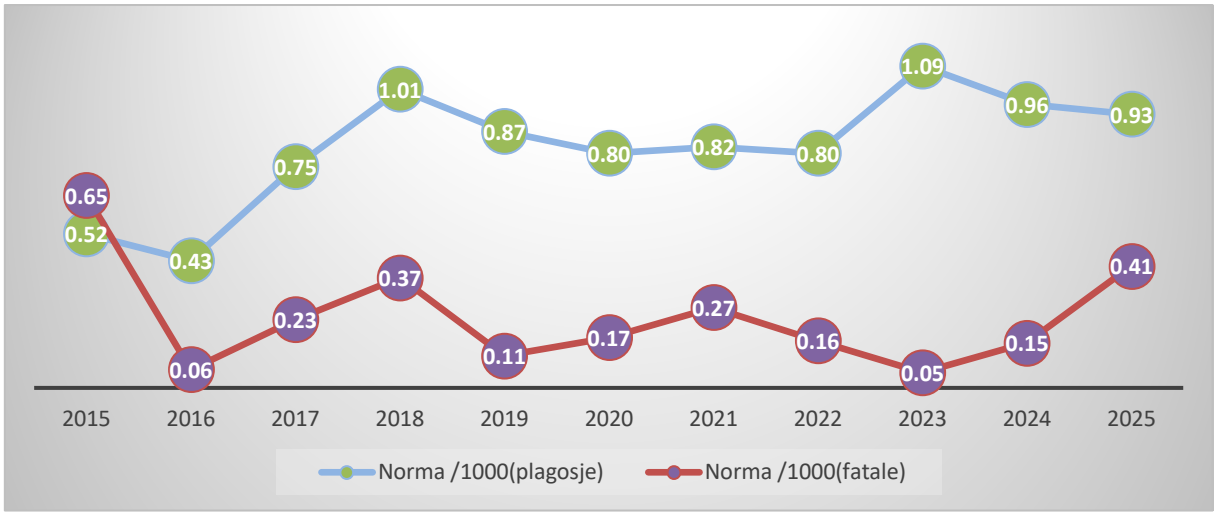

Figure 2. Injury accident rate vs. fatal rate

This analytical approach enhances the robustness and reliability of the study, as it does not rely solely on absolute accident counts, but enables comparative assessments across different time periods. This strengthens the arguments for the development of new safety policies and supports institutions in making well-informed decisions. Furthermore, it introduces the accident rate calculated per 1,000 exposed workers, providing a more accurate representation of the actual occupational risk.

2.4. Accident Rates by Day of the Week

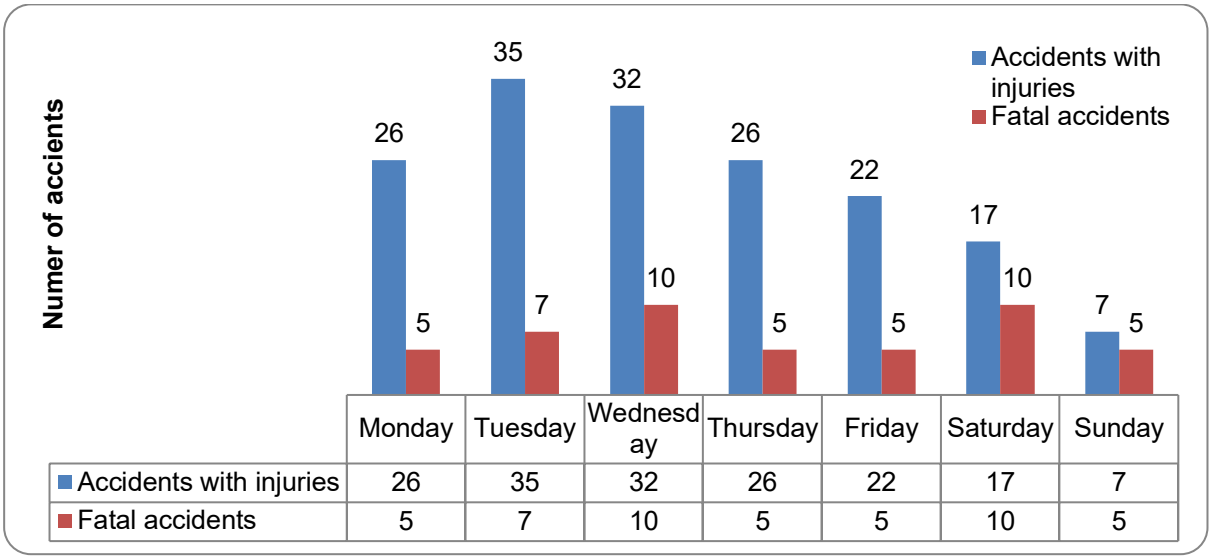

Figure 3. Accident rates by day of the week

The analysis indicates that the majority of injury-related accidents occur on regular working days, when workload and operational pace are higher. In contrast, fatal accidents are more frequent during weekends, particularly on Saturdays. This pattern is often associated with reduced technical supervision, the execution of non-routine tasks, and accumulated worker fatigue (Brogmus,2007). These findings highlight that organizational factors play a significant role in workplace safety and underscore the need to implement targeted control measures, especially during weekends when risk levels increase.

3. DITRIBUTION OF ACCIDENTS BY MAIN CAUSES (2015-2025)

3.1. Methodological approach for cause categorization

In this analysis, a simplified methodological approach was applied by grouping accident causes into five main categories, which realistically reflect the types of hazards, are closely linked to work processes, and facilitate the formulation of clear conclusions and recommendations.

Group I – Rock falls. This is the most frequent accident category, occurring primarily in underground workings, but occasionally also at surface operations. The analysis indicates that the dominant risk in chromium mines is of a geomechanical nature, and that delays in ground support installation significantly affect safety conditions (ICMM, 2015).

Group II – Machinery and equipment. This category includes accidents occurring both at surface and underground operations, mainly related to the use of machinery, mechanical equipment, and electrical installations (Bajpayee, 2004).

Group III – Slips and falls from height. This category comprises accidents resulting from slipping or falling from height, often due to loss of balance during work activities.

Group IV – Explosives. Accidents in this group occur during blasting operations, including drilling and blasting activities, or as a result of non-compliance with safety procedures.

Group V – Gases, explosions, and fires. Although less frequent, accidents involving gases, explosions, or underground fires are extremely hazardous and often result in fatal outcomes (Citizens.al, 2023).

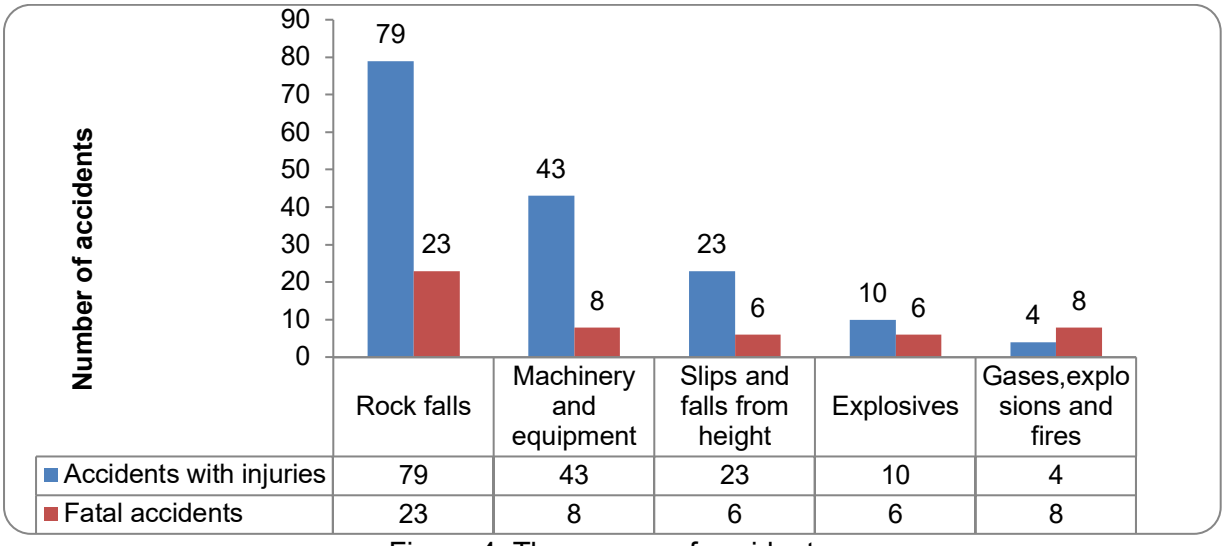

Figure 4. The causes of accidents

4. RECOMMENDATIONS

Technical measures

To reduce accidents caused by rock falls, it is essential that modern ground support techniques, including shotcrete application, rock bolting, and protective mesh, be mandatory implemented before workers enter high-risk areas. This strategy acts as a protective barrier that safeguards miners' lives. In the chromium mining sector, a national plan should be

developed and implemented to replace manual labor with small-scale mechanized equipment, particularly in narrow galleries where risk levels are high. This approach not only reduces worker fatigue and direct exposure, but also improves operational efficiency.

To achieve better control of hazardous gases, the installation of fixed real-time gas sensors with alarm systems (for gases such as CH_4 and CO) is recommended, instead of relying solely on periodic manual measurements. This enables rapid response and helps prevent hazardous situations (Chilton, 2008; Kozielski et al,. 2021).

Organizational measures

Based on the observed increase in fatal accidents during weekends, particularly on Saturdays, it is recommended that high-risk operations be suspended during weekends, except when they are directly supervised by the technical manager and safety inspector. This measure enhances discipline and fosters trust between workers and management.

To prevent excessive fatigue and fatigue-related accidents, regulations should be adopted to limit overtime hours, especially in underground operations.

In addition, the inventory of machinery and equipment should be regularly updated, and the use of improvised or inadequately protected equipment should be strictly prohibited, in order to reduce risks associated with technical failures and human error. (Brogmus,2007)

Regulatory and training measures

Following the ban on detonating fuses in 2019, stricter standards are required for worker training related to modern initiation systems and explosives management, particularly in areas with low geomechanical stability. This will enhance both operational safety and institutional accountability. Therefore, further interventions—possibly comprehensive revisions—are needed, particularly concerning: Regulation No. 533, dated 08.07.2005, on safety techniques for the civil use of explosives in the Republic of Albania, as well as Decision of the Council of Ministers (DCM) No. 294, dated 10.05.2019.

Institutions should adopt the accident rate per 1,000 exposed workers as a key performance indicator for safety assessment, allowing for a realistic identification of shortcomings and achievements, in line with international standards.

Mandatory practical training programs should be organized for miners, focusing on the identification of loose rock fragments, ground securing techniques, and response to unexpected situations, reinforcing the importance of professional competence in occupational safety. These recommendations aim to strengthen mine safety by combining practical experience with systematic risk management. Their effective implementation requires commitment, discipline, and coordinated engagement from all stakeholders. (European Union, 1992; EU-OSHA, 2024)

Placing the study results in a European context

The mining sector is among the highest-risk sectors in the labor market, not only in Albania but across Europe. To assess the findings of this study within a broader European framework, the latest Eurostat data for 2023 were analyzed. Eurostat data indicate that mining and quarrying activities in the European Union exhibit the highest fatal accident rates compared to other economic sectors, with an average of approximately 10.8 fatal accidents per 100,000 workers. Unlike other sectors where a decline has been observed, EU mining activities recorded an increase of approximately 5.9% in fatal accidents in 2023 compared to the previous year. Regarding non-fatal accidents (involving more than three days of absence from work), the EU

average is approximately 1,400 cases per 100,000 workers. Significant differences exist among countries: Germany and Austria report higher rates, largely due to advanced reporting systems, while some Eastern European countries show lower rates, which experts suggest may indicate underreporting. The accident rates calculated for Albania in this study were standardized using the same measurement unit (per 100,000 workers) to enable comparison with EU data. The results indicate that Albania exceeds the EU average for fatal accidents relative to the number of exposed workers, while non-fatal accident rates are lower. (Eurostat, 2025).

REFERENCES

Bajpayee, T. S., (2004) “Blasting injuries in surface mining with emphasis on blasting fatalities”, NIOSH Information Circular, IC 9452, National Institute for Occupational Safety and Health, Pittsburgh, USA.

Brogmus, G. E., (2007) “Day of the week lost time occupational injury trends in the United States”, Applied Ergonomics, 38 (6), 749–754.

Chilton, J. E., (2008) “Use of infrared sensors for monitoring methane in underground mines”, NIOSH Report of Investigations, RI 9673, National Institute for Occupational Safety and Health, USA.

Citizens.al, (2023) “Bulqizë: Gas explosion injures three miners”, Citizens Channel, 14 August 2023, available at: https://citizens.al (accessed 2025).

Citizens.al, (2025) “Workers injured in two mining accidents in Bulqizë and Martanesh”, Citizens Channel, 30 May 2025, available at: https://citizens.al (accessed 2025).

Eurostat, (2025) “Accidents at work claimed 3 298 lives in the EU in 2023”, Eurostat News, European Commission, Luxembourg.

Eurostat, (n.d.) “Accidents at work – statistics by economic activity”, Statistics Explained, European Commission, Luxembourg.

European Union, (1992) “Council Directive 92/104/EEC on minimum requirements for improving the safety and health protection of workers in surface and underground mineral-extracting industries”, Official Journal of the European Communities, L 404, 10–15.

EU-OSHA, (2024) “Safety and health in mineral-extracting industries”, European Agency for Safety and Health at Work, Bilbao, Spain.

ICMM, (2015) “Critical control management: Good practice guide”, International Council on Mining and Metals, London, UK.

Kozielski, M., Wrona, P., Brodny, J., (2021) “Data on methane concentration collected by underground mine monitoring system”, Data in Brief, 38 107384.

Tutak, M., Brodny, J., Siwiec, D., (2024) “Predicting methane concentrations in underground coal mines using machine learning methods”, Sustainability, 16 (19) 8388.

VNA – Albanian Telegraphic Agency, (2025) “Miner dies in Bulqizë; technical staff arrested for safety violations”, VNA News, Tirana.

ANTHROPOGENIC RAW MATERIALS PROCESSING APPLICATION EXAMPLES FOR THE CONSERVATION OF NATURAL RESOURCES

József FAITLI*

University of Miskolc, Institute of Raw Materials Processing and Environmental Technologies
3515 Miskolc-Egyetemváros, Hungary
**Corresponding author: jozsef.faitli@uni-miskolc.hu*

A B S T R A C T

Modern lifestyle requires enormous amount of materials and energy. Still the main resource is the earth crust, but the so called anthropogenic raw materials, - materials that have already been mined - are becoming increasingly important. According to Ambros (2023) “there will be more copper, iron, and zinc (and other metals) in the cities than in the earth’s crust after 2050 (considering current known reserves)”. Another worldwide issue that the grade of newly discovered mineral deposits is decreasing, so the resource requirements, - including energy - for their processing are increasing exponentially. Therefore, the current task is to transfer the known technologies of mining and mineral processing to the field of urban mining. In this paper two urban mining application examples are shown and the focus materials are the municipal solid wastes (MSW). MSW can be called as “flow type of anthropogenic raw materials”. The first case is the development of a new EPR (extended producer responsibility) and DRS (deposit refund scheme) related MSW sampling methodology on the basis of known mineral sampling principles. The other application example is the development of the so called “combined air flow, magnetic and electric separator”, which was named the "MULTI SCREEN Separator” when it was launched on the market. Development started by testing of simple air flow and eddy-current separator models and then by combining them into many combined trial machines, and finally the industrial prototype was made. The upgraded prototype is now working daily in the 20 t/h throughput Zalaegerszeg, Hungary residual municipal solid waste processing plant.

Key words: *Circular economy, urban mining, waste processing, residual municipal solid waste processing plant, combined air flow, magnetic and electric separator*

1. INTRODUCTION

Mineral resources are the foundation of every economy. Global Resources Outlook 2024 indicates that since 1970 global consumption of the Earth’s natural resources has increased from 30 to 106 billion metric tons yearly, and which is an equivalent of 23–39 kg/person/day. Moreover, by 2060 the quantity of globally extracted raw materials is expected to grow by 60% (Wirth and Ka’mierczak, 2026). On the other hand, according to Ambros (2023) “the miners of the present will gradually become recyclers in the future since there will be more copper, iron, and zinc (and other metals) in the cities than in the earth’s crust after 2050 (considering current known reserves)”. Another worldwide issue that the grade of newly discovered mineral deposits is decreasing, so the resource requirements, - including energy - for their processing are increasing exponentially. It is evident that if anthropogenic resources are used for some given tasks that helps preserve natural resources and this is the central element of the so called circular economy. Figure 1 shows the circulation of materials in earth. Let’s note the place where the residues and wastes originate: during and after the minerals extraction and processing and during and after the production and consumption. These continuously generated materials are called “flow type of anthropogenic raw materials”. Of these in this paper the municipal solid wastes (MSW) are in focus. The stored and deposited wastes and residues and all the materials in the still used infrastructure (roads, buildings, bridges) are called “stock type of anthropogenic materials” (Faitli et. al., 2025). Urban mining deals with the exploration, extraction and processing of anthropogenic resources and therefore it is the most

important element of the circular economy. Since urban mining is a relatively new field, therefore, the current task is to transfer the known technologies and experiences of mining and mineral processing to the field of urban mining.

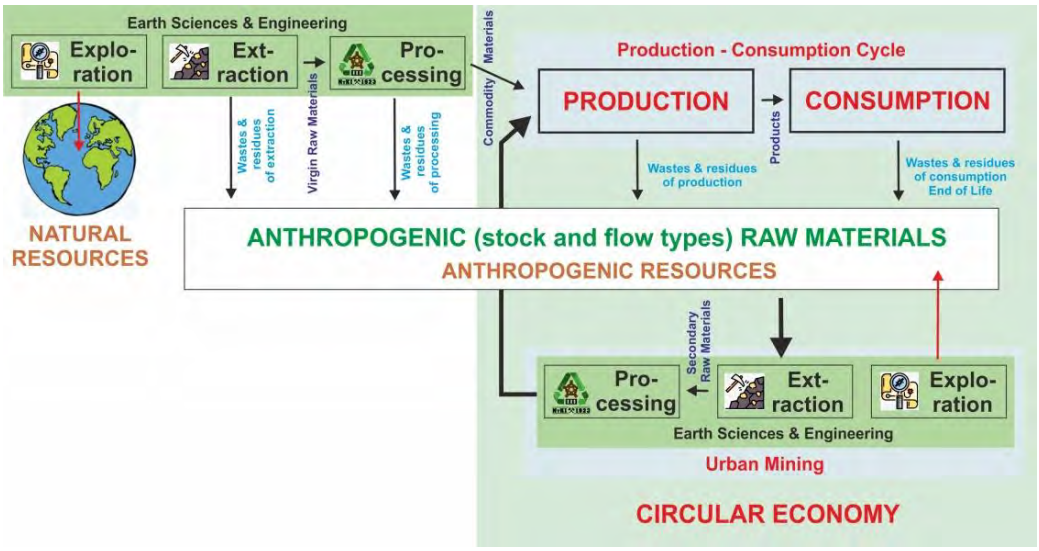

Figure 1. The circulation of the materials in earth

In this paper two application examples are shown for this task. Sampling of mineral bulks before designing a processing technology, checking products quality of a plant and even the complete sampling of an operating processing plant is really important. Sampling is also really important for the flow type of anthropogenic raw materials, namely for municipal solid wastes (MSW). The so called EPR (extended producer responsibility) MSW sampling methodology was developed in 2022 in Hungary and since then, two four-season national level sampling campaigns have been done. This sampling methodology was developed using engineering knowledge gained from mineral sampling. MSW compositional results have been and are used for designing waste processing plants, for the introduction and operation of the national EPR and DRS (deposit refund scheme) systems, reporting data to the EU and different authorities and for many other purposes.

The other application example is the development of the so called “combined air flow, magnetic and electric separator”, which was named the "MULTI SCREEN Separator” when it was launched on the market. Development started by testing of simple air flow and eddy-current separator models and then by combining them into a combined trial machine, then the 400 mm, 1200 mm wide and finally the industrial prototype was made. The upgraded prototype is now working daily in the Zalaegerszeg (Hungary) residual municipal solid waste processing plant.

2. SAMPLING METHODOLOGY DEVELOPMENT

General principles of minerals sampling can be applied in urban mining. In a given task the population, - namely the examined material bulk - and the examined feature, - namely the random variable - are given. The population can be huge or heterogeneous in time or in space, therefore sampling processes always occur on a sub-population (stratum or lot) and it is called stratified sampling. Figure 2 shows the 3+1 fundamental cases of sampling of a given stratum. In the first case the average value of the population (population mean) is the question. The sample average gives a good estimation. In the second case the heterogeneity is the question, the standard deviation is the theoretical statistical metric and the sample corrected standard deviation gives undistorted estimation for smaller number of samples. In engineering the number of samples is always small, because the aim of sampling is to give the possible best

estimation at the lowest price. In Figure 2 a schematic diagram of a typical pill production technology is shown for the 2nd case. The last unit operations are the fine grinding of the active pharmaceutical ingredient (API) and the inert materials, then mixing and tabletting. In this case the random variable is the API concentration in a pill. If there is no API in a pill, that is a placebo, but if there are more than required, that can be poisonous.

1st case	2nd case	3rd case	+1 case
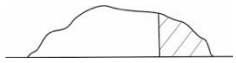	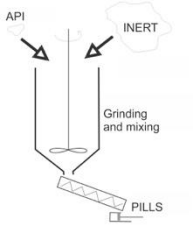	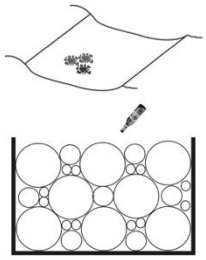	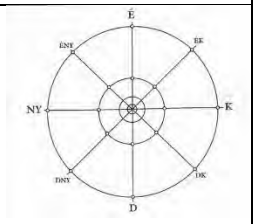
M(x) ← $\bar{x}$	D(x) ← S_n^*	F(x) ← F_n(x) f(x) ← f_n(x)	point samples

Figure 2. The 3+1 fundamental cases of sampling

In the third case the random variable composition of the stratum is the question. The schematic drawing in Figure 2 illustrates the well-known and so called Fuller particle size – distribution function which results good space filling. The empirical random variable – distribution function [F_n(X)] gives a good estimation to the random variable – distribution function [F(X)]. There is a special sampling case for the remediation of contaminated areas. If the question is “what is the quantity of the contaminant in a given area?” that is the first sampling case. But if the question is “where does the contamination go?” that is the +1 case. As a consequence the so called single samples and point samples must be distinguished! In sampling cases no. 1-3, the so called single samples – averaged sample concept must be applied. In mineral sampling the total volume of a stratum has to be subdivided into about typically 200 virtual volume elements and a single sample (increment) has to be taken from each. The averaged sample is made by mixing of these single samples. In the +1 sampling case, the point samples must be processed and analysed individually. These are well known rules of mineral sampling; now let’s apply them for municipal solid wastes (MSW) sampling.

The EU introduced the concept of Extended Producer Responsibility (EPR) in the early 1990s. Extended Producer Responsibility (EPR) is a policy tool that extends the producer’s financial and/or operational responsibility for a product to include the management of the post-consumer stage, in order to help meet national or EU recycling and recovery targets. The Deposit Refund Schemes (DRS) charge users an extra fee when they buy a product, which is refunded if the product packaging is returned for recycling or reuse. Both the EPR and DRS systems are very important tools of the circular economy and urban mining, because these promote the circulation of materials. In accordance with all this the Institute of Raw Materials Preparation and Environmental Technologies of the University of Miskolc was commissioned to develop a new MSW sampling methodology which is suitable for the EPR and DRS related characterisation of the waste in 2022. Waste compositional data were necessary for the introduction of the EPR and DRS systems in Hungary. Finally the Hungarian EPR system (80/2023 Government Decree) was introduced in 14th March 2023 and the so called RePont system (DRS) was introduced in July 2024. Our measured waste compositional data were used for the design and now they are being used for the operation, control and financial accounting.

In Hungary the MSZ 21420 Parts: 28 and 29 MSW sampling standards are in force. These standards were based on the French MODECOM methodology on the basis of Pierre Gy’s sampling theory and were introduced in 2005 (Faitli and Romenda, 2019). In accordance with

the challenges presented by the introduction of the new EPR and DRS systems, it was a main aspect that the results according to the new EPR sampling method should be comparable with the two decades-old results of standard analysis. Therefore many features, such as the organisation of the campaign, the selection of waste collecting vehicles, taking of the average samples were kept identical. These are based on the described principles of mineral sampling. The necessary minimal mass of the averaged samples of different MSW streams was a question. The Pierre Gy sampling nomogram (Figure 3) was used for the design of the new protocol. Principal of the processing of the average sample, - namely primary sorting (>100mm), splitting, secondary sorting (20-100m), splitting, tertiary sorting (8-20mm) - was also kept as well as the main 13 waste categories. However, after the primary and secondary sorting a repeated EPR sub sorting has to be done. This really increases sorting accuracy. Figure 4 shows the flowsheet of the new EPR MSW analytical methodology for processing an average sample.

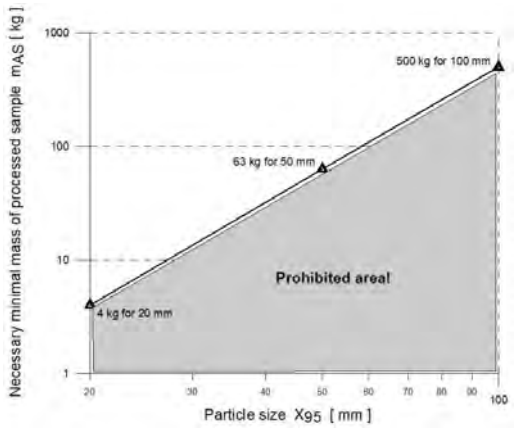

Figure 3. The Pierre Gy sampling nomogram applied for MSW

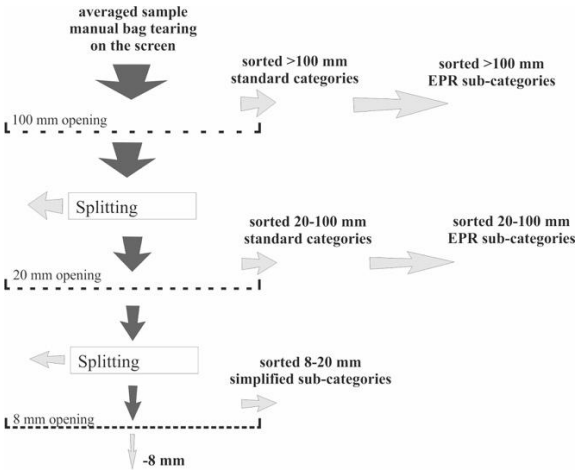

Figure 4. EPR related sample processing of a given averaged sample

This protocol with slight practical modification (sometimes sorting can be more efficient on the ground, individual big particles are taken, etc.) can be applied for all the MSW streams (residual MSW, single and multi-material components selective MSW, bulky, public cleaning, illegally deposited, non-comminuted RDF (refuse derived fuel), etc.). During the analysis on the 100mm and for the 20mm aperture size screens the standard waste categories: 2. Papers, 3. Cardboards, 4. Composites, 5. Textiles, 8. Combustibles, 9. Glasses and 10. Metals are manually sorted onto 120 litres waste bins. These are not the standard names of these waste categories; instead these common words are well understood by sorting workers. These waste categories have to be poured onto a flat surface again for the repeated EPR subcategorization. It is practical to sort many EPR subcategories at first also. These are the 1.1. Food waste, 1.2. Green waste, 1.3. Cooking oil, 6.1. SUP cloth, 7.1. 2D packaging plastics, 7.2. 2D non-packaging plastics, 7.3. DRS drinking packaging plastics, 7.4. non-DRS drinking packaging plastics, 7.5. 3D packaging plastics, 7.6. 3D non-packaging plastics and 11.1. Inert wastes (stone). Since the development and introduction of the new EPR MSW sampling methodology 8 national level seasonal MSW campaigns have been done in Hungary. These resulted in many thousands of compositional tables which have been used by authorities and waste managing companies alike. For reasons of space, these cannot be discussed here, but Figure 6 shows a noticeable good result. In Hungary the yearly quantity of the residual MSW is still about 2.6 million tonnes, and about 54 % of it is still landfilled. Figure 5 shows the mass concentration of the DRS plastics (plastic packaging materials for non-dairy beverages) in the residual MSW as function of time and NUTS2 region of Hungary. It is clearly visible how much the DRS plastics concentration has decreased after the introduction of the RePont (DRS) system in July 2024 in the country.

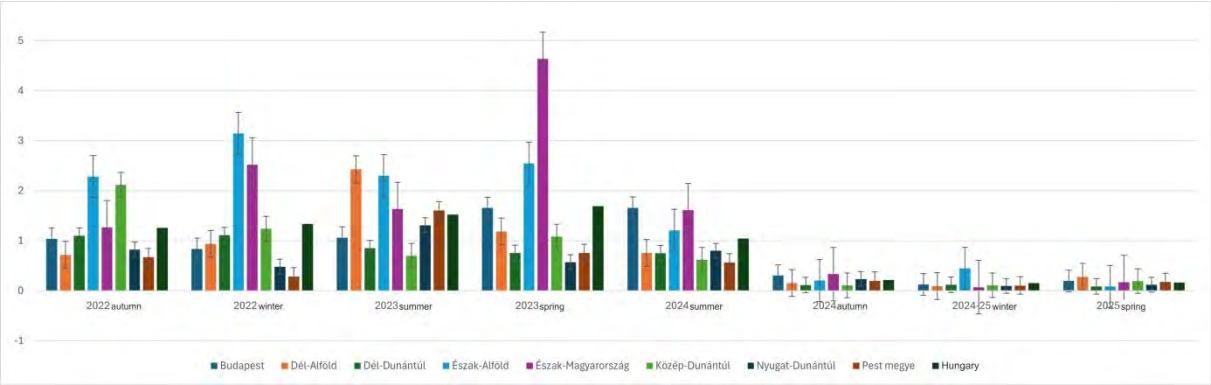

Figure 5. The mass concentration of DRS plastics in the residual municipal solid wastes as function of season and NUTS2 region [unit: %]

3. DEVELOPMENT OF A COMBINED SEPARATOR

If there is MSW compositional data, it enables technological planning. The second urban mining application example is about an MSW separation (upgrading) technological and equipment development. The idea of combining four separators into one unit was born a long time ago and the development work also lasted for a decade, which ultimately led to the development of the MULTI SCREEN separator. A consortium formed from a machine and technology producer (3B Hungary Ltd.) and its scientific partner (Institute of Raw Materials Preparation and Environmental Technologies of the University of Miskolc) was the inventor and developer. To the best of our knowledge, the MULTI SCREEN separator is the only machine in the world that combines four separators in one unit without intermediate conveyors and bins. The advantage is that space and energy requirements are smaller, but to ensure beneficial common operation was a challenge. The development work was started by making single air flow and eddy-current model separators and then a concept combined machine (Figure 6) was made. After numerous tests the 400 mm wide machine (Figure 7) and the first 1200 mm wide prototype separator was produced.

Figure 7. First concept machine of the MULTI SCREEN separator

Figure 8. The 400 mm wide concept machine of the MULTI SCREEN separator

In the first design the separation of the 2D product (mainly flat-shape foil and paper particles) was solved with a rotating cage under vacuum. Unfortunately clogging caused serious problems; therefore a second design with nailed roller was made and tested without full success. Finally the third design with a so called Coanda roller has proven to be good but needed a downstream 2D particles separation unit. This first prototype machine is now working daily in the 20 t/h capacity residual MSW processing plant in Zalaegerszeg, Hungary. The Coanda effect is well known in the literature. In 1910, the Romanian engineer Coanda observed that airflows near surfaces would bend because of the fluid dynamics influence of the surfaces. Figure 9 shows the schematics and the operating principle of the developed MULTI SCREEN separator with a Coanda roller.

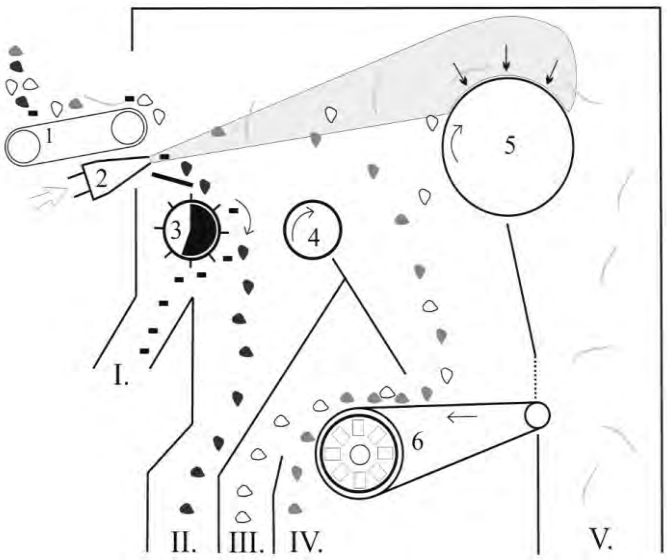

Main technological units:

1. Belt conveyor feeder
2. Air nozzle
3. Magnetic drum
4. Rotated auxiliary cylinder
5. Coanda roller
6. Eddy current separator

Numbers and short names of products:

I.	Magnetic
II.	Inert
III.	Al
IV.	3D
V.	2D

Figure 9. Schematic of the combined MULTI SCREEN separator

The feed of the combined separator is the coarse size fraction of the upstream drum screen with 60 mm aperture size. The feeding is done with a short conveyor belt. An air nozzle is located under the feeding roller of the conveyor belt. Heavy particles fell through the air beam onto the magnetic drum. Magnetic particles are dragged into the Fe product (output I), while heavy inert particles (rocks, bricks and so on, as well as wet and therefore heavy books; shoes, etc.) fell into the inert product (output II). Light particles are blown and transported by the air beam. When a particle falls into the air beam, the initial acceleration part of particle settling is dominant, but afterwards, when the particle is being transported by the air beam, the particle settles in it and has sufficient time to settle; therefore the terminal settling velocity is dominant. Another point is that the density of the particle (body density) and not the material density determine both the initial and terminal particle settlings. The material density of the aluminium cans and the PET bottles is significantly different; however, their particle densities might be similar depending on how they had been compressed previously. Therefore the light particles both in 2D shape (foils and papers) and in 3D shape (aluminium, plastics) are also blown by the air beam. The 3D plastics and aluminium particles settle out from the beam and then an eddy-current separator separates them into two products. The 3D shape aluminium particles go to the Al (III) and the plastic particles go to the 3D (IV) products. If the air nozzle operation is sufficient the air coming out from the nozzle with the retracted air (the air beam blown by the nozzle drags lots of auxiliary air from the open parts of the machine body) together will flow above the Coanda roller into output V. If this flow pattern is fulfilled the evolved Coanda effect helps effective 2D separation, because 2D shaped particles are sucked onto the drum surface by the Coanda effect and the rotating drum transports them to output V. Lately the MULTI

SCREEN separator has been even further developed. Figure 10 shows the inner structure and photo of the market ready combined separator. The 2D separation has been further developed with the shown gravity powder chamber above a belt conveyor.

Figure 10. The patented MULTI SCREEN Separator. Inventors: Z. Nagy, ifj. Z. Nagy, B. Csőke, J. Faitli (2015, 2022)

4. CONCLUSION

I think that urban mining is the tool that significantly helps the conservation of natural resources and therefore it needs special attention. Mining as well as mineral processing is as old as mankind itself, wide knowledge base had been evolved and now it is time to use these in urban mining. The “flow type of anthropogenic raw material” the municipal solid wastes might sound weird for mineral processing people, but in this paper two application examples demonstrate how the known principles can be used for waste sampling and upgrading.

ACKNOWLEDGEMENTS

Recent research was supported by the Hungarian Ministry of Energy under the contracts No. KGVHF/239/2024-EM_SZERZ and KGVHF/239/2024-EM_SZERZ.

REFERENCES

Ambros, W. M., (2023) “Gravity concentration in urban mining applications – A review”, Recycling, 8 85.

Faitli, J., Miaa, J., Gombkötő, I., Repo, E., (2025) “Urban mining comminution technological applications as the most important part of circular economy, A review”. Geosciences and Engineering: A Publication of the University of Miskolc, (13) 1 73-91.

Faitli, J., Romenda, R., (2019) “Detailed sampling protocol for the analysis of residual municipal solid wastes”, Proceedings of the 7th International Conference on Sustainable Solid Waste Management, 1-10.

Nagy, Z., ifj., Nagy, Z., Németh, S. Z., Csőke, B., Faitli J., Gombkötő, I., (2015) “Kombinált légáramú mágneses és elektromos (KLME) szeparátor (Combined airflow, magnetic and electric separator)” Patent number: P1500597, Granted Hungarian patent.

Nagy, Z., ifj. Nagy, Z., Csőke, B., Faitli, J., (2022) “Kompakt szilárdhulladék szeparátor. (Compact solid waste separator)” Patent number: P2200446, Granted Hungarian patent.

Wirth, H., Ka’mierczak, U., (2026) “Role of circular economy in increasing raw material supply by modern mining industry in lower Silesia, Poland”, Sustainability, 18 816.

BEHAVIOR OF ULTRA-HIGH PERFORMANCE FIBER CONCRETE BASED ON RECYCLED GRANITE WASTE FILLERS

Houria HEBHOUB[1,*], Said BERDOUDI[2], Nouha REZAIGUIA[1], Nedjma MEZIANI[3], Mohammed I. BENHALILOU[4], Bilal BOULKENAFET[1]

[1]Department of Civil Engineering, Faculty of technologie, 20 August 1955 University, LMGHU Laboratory, Skikda, ALGERIA
[2]LAVAMINE Laboratory, Department of mining engineering, faculty of earth sciences, Badji Mokhtar University, Annaba, ALGERIA
[3]Department of Hydraulic and Civil Engineering, Faculty of Applied Sciences, University Kasdi Merbah, EVRNZA Laboratory, Ouargla, ALGERIA
[4]TCT, University Batna 2, ALGERIA,
**Corresponding author: hebhoubhouria@yahoo.fr*

A B S T R A C T

The main objective of this study is to enhance the valorization of granite waste by using it as a partial mineral additive to replace silica fume in the formulation of ultra-high performance fiber concrete. This approach aims to reduce the overall production cost of this type of concrete while contributing to environmental preservation through the reuse of industrial by-products and the reduction of the ecological footprint associated with conventional cementitious materials. In this study, 20% of recycled granite waste fillers were incorporated as a partial replacement for silica fume in the formulation of ultra-high performance fiber concrete. The main objective was to evaluate the influence of this substitution on the concrete's properties in both the fresh and hardened states.

In the fresh state, the investigated parameters included density, workability, and entrained air content, in order to assess the effect of granite fillers on the mixture's density and consistency. In the hardened state, mechanical performance was evaluated through compressive and flexural tensile strength tests conducted at 28 days.

The experimental results revealed a slight decrease in density and workability, which can be attributed to the granular nature and morphology of the granite particles. However, the mechanical strengths obtained remained satisfactory and within the acceptable range for ultra-high performance fiber concrete, demonstrating that granite waste can effectively be used as a partial substitute for silica fume without significantly compromising the overall performance of the material.

Key words: *Ultra-high performance fiber concrete, silica fume, recycled fillers, properties, mechanical strengths*

1. INTRODUCTION

Ultra-high performance fiber concrete is one of the materials expected to be most widely used in the future due to its outstanding physical, mechanical, and durability properties. Its use, particularly in the form of prefabricated elements, helps to minimize the impact of civil engineering construction works on traffic. In addition, it provides an extended service life for structures while contributing to reduced maintenance costs (Doiron, 2009).

Their formulation is based on the use of specific materials, such as metallic or organic fibers, superplasticizing admixtures, as well as particular granular compositions consisting of ultrafine particles, fillers, and carefully selected sands, which make it possible to achieve maximum material compactness (Guiraud, 2018).

The partial or total replacement of ultrafine materials with other additives, particularly recycled additions, makes the formulations more cost-effective and environmentally friendly while reducing the use of silica fume. These additives act through a filler effect, filling the voids between cement grains, fibers, and sand; they improve the mixture's rheology and, finally, contribute to the formation of hydration products through their pozzolanic effect (Amanjean, 2015).

Thus, the objective is to partially replace the silica fume in the Ultra-high performance fiber concrete formulation with recycled granite waste additives at a rate of 20%, aiming on one hand to reduce the cost of this type of concrete and on the other hand to preserve the environment.

2. MATERIAL AND EXPERIMENTAL PROGRAM

2.1. Material

The materials used in this study consist of: a CEM II/A-L 52.5N cement supplied by the LAFARGE cement plant in M'sila (Algeria); dune sand (DS) from Oued Zhor, Skikda (Algeria); silica fume (SF) of the TEKNA CHEM type; polypropylene fibers (PF) of the Sika® Fibre 12-34 type, with a length of 12 mm and a diameter of 34 µm; a superplasticizer (SP) of the Master Glenium 26 type; mixing water (W); as well as granite waste fillers (GF) obtained by crushing and grinding granite offcuts from coating activities.

Table 1. Properties of silica fume and recycled granite waste fillers

Designations	**Silica fume SF**	**Granite fillers GF**
Absolute density (g/cm^3)	2.220	2.562
Specific surface (cm^2/g)	220000	6000
Absorption (%)	--	6.20
CaO (%)	0.8	1.10
SiO_2 (%)	95.00	72.3
$Al2O_3$ (%)	0.5	14.50
Fe_2O_3 (%)	1.02	1.04
MgO (%)	1.03	0.58
K_2O (%)	0.5	3.82
Na_2O (%)	--	6.22
Cl (%)	--	0.00
SO_3 (%)	--	0.04

The absolute density of the recycled granite waste fillers is higher than that of silica fume. In contrast, silica fume is characterized by a significantly higher specific surface area compared to the recycled granite fillers. Furthermore, the granite fillers exhibit a substantially higher alumina content.

2.2. Experimental Program

Within the experimental program, 20% of the silica fume in the ultra-high performance fiber concrete was volumetric replaced with recycled granite waste fillers. The reference ultra-high performance fiber concrete mix was prepared in accordance with the principles of standard P 18-470 (2016) and the recommendations of the AFGC (2013), also drawing on certain industrial reference formulations, such as those used on the Ormont-Dessus site (Antilles, 2012), Ductal® (Guiraud, 2018), and BSI® developed by Eiffage (Eiffage, 2016) (Table 2). The experimental tests carried out on the different mixes focused, in the fresh state, on

measuring density measurement by using an 8-litre container, workability measurement by cone spread, and entrained air content measured by a concrete aerometer. In the hardened state, the mechanical performance was evaluated through compressive strength and flexural tensile strength tests at 28 days. Flexural tensile strength was evaluated on specimens measuring 4 × 4 × 16 cm³ using a 250 kN testing machine. Compressive strength was measured on the halves of the prisms resulting from the flexural failure, using a 2000 kN testing machine. The specimens were cured for 28 days in water at 20 °C, in accordance with standards NF EN 12390-5 and EN 12390-3:2012.

Table 2. Mix proportions

Type of concrete	**0%**	**20%GF**
DS (kg)	990	990
CEMII (kg)	920	920
SF (kg)	225	180
GF (kg)	00	52.6
PF (kg)	10	10
SP (kg)	177	177
W (kg)	64	64

3. RESULTS AND DISCUSSION

3.1. Density

The partial replacement of silica fume with 20% recycled fillers (Figure 1) decreases the density of the control concrete, making it lighter. This reduction is mainly due to the lower fineness of the recycled fillers, which makes the mix structure slightly more porous, and to the decreased porosity in the transition zone between the matrix and aggregates in the control ultra-high performance fiber concrete (Amouri, 2009).

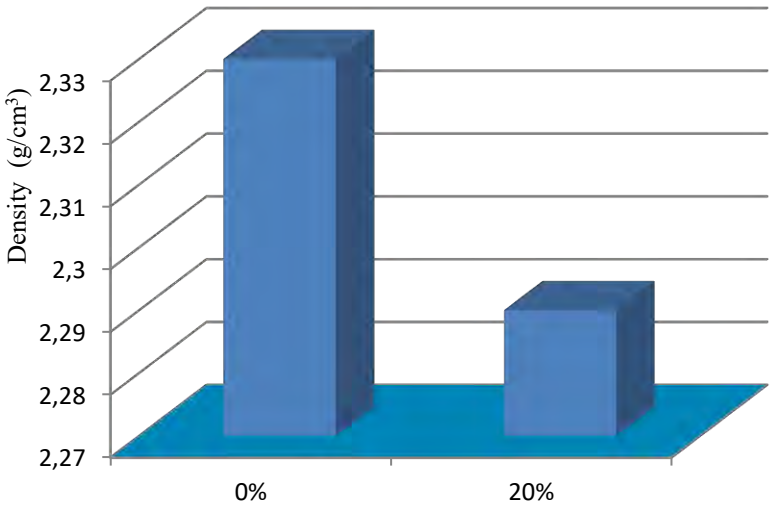

Figure 1. Variation of density as a function of the recycled fillers content

3.2. Workability

The addition of recycled granite fillers (Figure 2) as a partial replacement for silica fume in the ultra-high performance fiber concrete formulation results in reduced workability of the mixes. This reduction is primarily due to the fine particle size and high absorption capacity of the recycled granite fillers (Li et al., 2022).

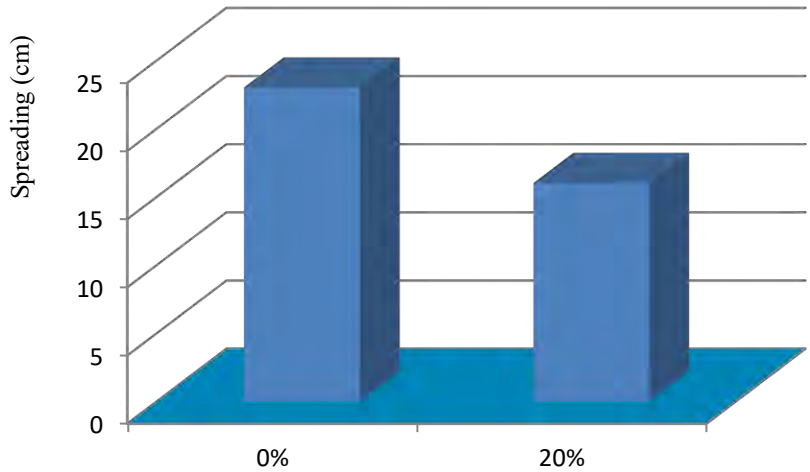

Figure 2. Variation of workability as a function of the recycled fillers content

3.3. Air Content

Concrete incorporating silica fume releases less air than concretes containing recycled waste fillers (Figure 3). The particle size of silica fume is much smaller than that of the recycled fillers, which allows it to fill the concrete pores and consequently reduce the amount of air bubbles (Henan Superior Abrasives, 2022).

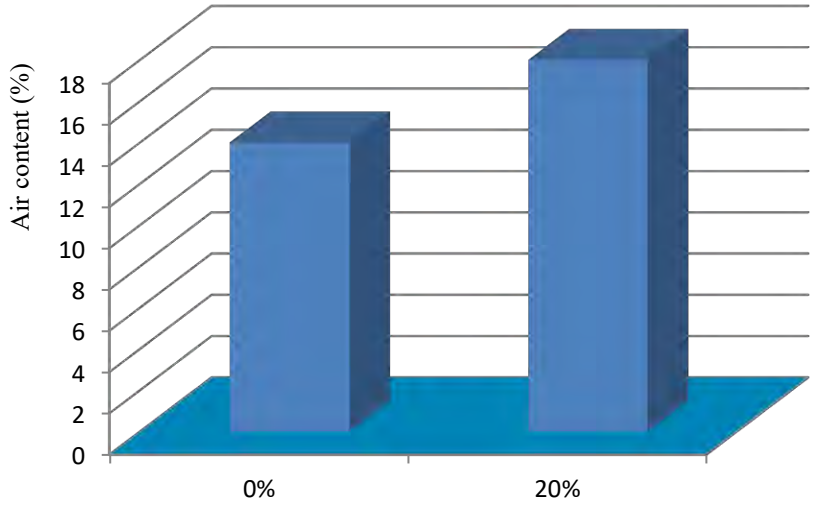

Figure 3. Variation of air content as a function of the recycled fillers content

3.4. Compressive Strength

One can observe in Figure 4 a slight decrease in compressive strength when silica fume is partially replaced by fillers derived from granite waste, compared with the control concrete, which is consistent with the results reported by Shwetha et al. (2022). Nevertheless, the obtained compressive strength remains high, reaching approximately 140.07 MPa. This value exceeds the minimum threshold recommended by AFGC (2013) and falls within the compressive strength range of ultra-high performance fiber concrete, between 120 MPa and 180 MPa, as reported by Droll (2004) and Deaux (2018).

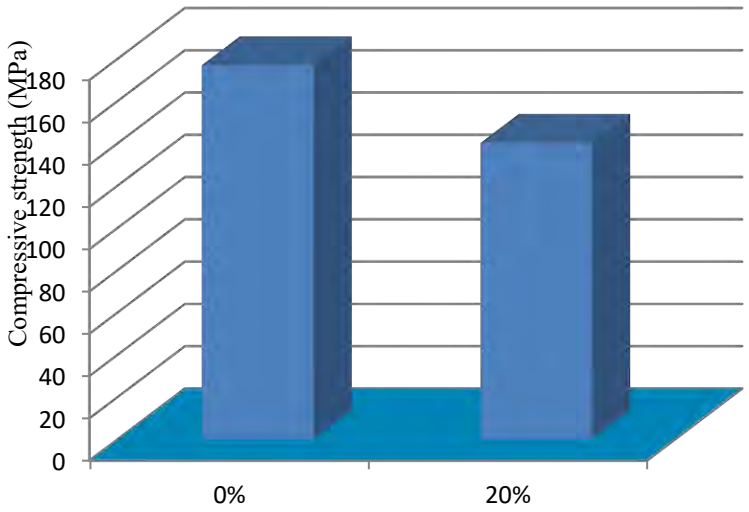

Figure 4. Compressive strength as a function of the recycled fillers content

3.5. Flexural Tensile Strength

Ultra-high performance fiber concrete formulated with silica fume exhibits the best flexural tensile performance (Figure 5) compared with concrete incorporating 20% fillers derived from granite waste. However, the concrete containing 20% granite waste fillers develops a flexural tensile strength of approximately 18 MPa at 28 days. This value is significantly higher than the minimum threshold of 6 MPa recommended by AFGC (2013) and falls within, or even above, the range of 7 to 15 MPa reported by Deaux (2018).

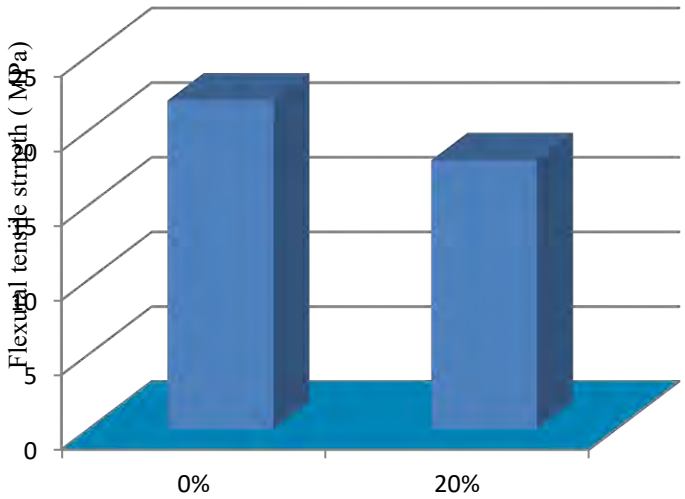

Figure 5. Flexural tensile strength as a function of the recycled fillers content

4. CONCLUSION

The incorporation of recycled fillers at a rate of 20% as a replacement for silica fume results in a lighter ultra-high performance fiber concrete, with reduced workability and a higher air content. This substitution leads to a decrease in both compressive strength and flexural tensile strength; however, the obtained values remain compliant with the requirements and performance ranges of ultra-high performance fiber concrete.

REFERENCES

Abrasifs Supérieurs Henan, (2022), “Fumée de silice pour béton ultra-haute performance (BUHP)”, https://hsamaterial.com

AFGC, (2013), “Bétons fibrés à ultra-hautes performances”, https://www.afgc.asso.fr

Amanjean, E. N. P., (2015), “Développement de bétons fibrés ultra performants pour la réalisation d’éléments de structure préfabriqués”, Thèse de doctorat, Université Toulouse 3 Paul Sabatier.

Amouri, C., (2009), “Contribution à l’étude de l’influence des différents ajouts sur les propriétés des matrices cimentaires: caractérisation, performances, durabilité”, Thèse de doctorat, Université de Constantine, Algérie.

Antille, F., (2012), “Le BFUP – Béton Fibré Ultra Performant”, TECHNI.CH, http://www.techni.ch

Eiffage, (2016), “Le BSI®, béton fibré à ultra-hautes performances développé par Eiffage”, https://www.eiffage.com

Deaux, O., (2018), “Optimisation de bétons fibrés à ultra-hautes performances et caractérisation de leurs propriétés en contexte industriel”, Mémoire de maîtrise, École Polytechnique de Montréal.

Doiron, G., (2009), “Béton fibré à ultra-hautes performances (BFUP) et les ouvrages d’art en Amérique du Nord”, Lafarge Canada Inc. – Ductal.

Droll, K., (2004), “Influence of additions on ultra high performance concretes – grain size optimisation”, Proceedings of the International Symposium on Ultra-High Performance Concrete, Kassel, Allemagne.

Guiraud, P., (2018), “BFUP (Bétons Fibrés à Ultra hautes Performances)”, Infociments, https://www.infociments.fr

NF P 18-470, (2016), “Bétons - Bétons fibrés à ultra hautes performances - Spécifications, performance, production et conformité”.

NF EN 12390-5, (2012), “Essais pour béton durci - Partie 5: résistance à la flexion des éprouvettes”.

NF EN 12390-3, (2012), “Essais pour béton durci - Partie 3: résistance à la compression des éprouvettes”.

Li, Z., Lao, J., Wang, L., Lim, N. S., Tan, K. H., Qian, S., (2022), “A review on substitution of natural sand with granite fines in sustainable concrete”, Construction and Building Materials, 365, 128417.

Shwetha, K. G., Mahesh Kumar, C. L., Dalawai, V. N., Anadinni, S. B., Sowjanya, G. V., (2022), “Comparative study on strengthening of concrete using granite waste”, Materials Today: Proceedings, 62(8), 5317–5322.

Sekulić, Ž., Canić, N., Bartulović, Z., Daković, A., (2004), “Application of different collectors in the flotation concentration of feldspar, mica and quartz sand”, Minerals Engineering, 17(1), 77–80.

CEMENT MAKING BY USING THE GEOCEMENTING CONCEPT

Hakan ARDEN KAHRAMAN[1,*], Hakan BENZER[2]

[1]DMT Türkiye, TR 34742, Istanbul, TÜRKIYE
[2]Hacettepe University, Mining Engineering Department, Ankara, TÜRKIYE
**Corresponding author: Hakan.Arden@dmt-group.com*

A B S T R A C T

This current paper aims to provide detailed information on the "geo-cementing" concept, emphasising that the geology and mineralogy of the raw materials used in cement production directly impact the chemical composition, which in turn influences the quality of the cement produced. This paper formalises the concept of “geo-cementing” as a mineralogy-domain-based framework that integrates geological characterisation, mineralogical quantification, geochemical modelling, quarry extraction strategy, process optimisation, environmental performance, and resource governance into a single predictive system. While the traditional approach to cement production has mainly relied on chemical principles to understand and control the properties of the final product, employing a mineralogical approach could yield more benefits. This approach can be linked to the original depositional conditions of the limestone. It can facilitate better resource management by establishing a strong geological model that incorporates existing geological and mineralogical conditions to control the quality of the final product. This approach not only aligns with modern industry standards but also provides a competitive edge in the market. The framework supports improved clinker phase control, energy efficiency, emission reduction, and long-term quarry life optimisation, while strengthening alignment with international mineral reporting standards such as those developed under CRIRSCO and anticipated ESG integration within the revised JORC Code. In essence, geo-cementing plays a vital role in ensuring the sustainable and efficient extraction of mineral resources, meeting the growing demand for cement while minimising environmental impacts. By re-centring cement production around geological domain variability, geo-cementing establishes a defensible, resource-based governance model for modern cement manufacturing.

Key words: *Geocementing, geology, quarry design, cement making, CRIRSCO, resource and reserves*

1. INTRODUCTION

The dominant paradigm in cement production has historically prioritised chemical homogeneity. Operational stability has been pursued through control of bulk oxide ratios, lime saturation factor (LSF), silica modulus (SM), and alumina modulus (AM), under the assumption that chemical balance alone ensures predictable clinker formation. While this approach has achieved industrial success, it implicitly treats chemistry as the primary control variable and geology as a background supplier of feedstock.

However, chemistry in cement production is not an independent variable; it is the macroscopic expression of mineralogical assemblage and geological history. Two raw material blends exhibiting identical CaO, SiO_2, Al_2O_3, and Fe_2O_3 concentrations may display fundamentally different kiln behaviours if one is derived from recrystallised calcitic limestone and the other from partially dolomitized, silicified, or clay-interbedded facies. Burnability, grindability, coating formation, alkali cycling, and energy demand are governed not solely by oxide percentages but by mineralogical phase identity, grain boundary relationships, crystallinity, porosity, and textural maturity.

This paper argues that a mineralogy-domain philosophy, rather than bulk chemical homogenisation, should form the foundation of raw material management in the cement industry. The proposed geo-cementing framework formalises this shift.

2. GEO-CEMENTING CONCEPT

Geo-cementing adapts the systems integration principles of geo-metallurgy, which is widely applied in metalliferous mining, to industrial mineral deposits used in cement production (Kahraman & Benzer, 2024, 2025; Kahraman, 2025). Geo-metallurgy is an interdisciplinary field designed for metalliferous mines, integrating geological, mining, metallurgical, and environmental information to optimise resource extraction and processing. It focuses on understanding ore body variability and its impact on processing performance. Analogously, geo-cementing integrates geological variability with clinker behaviour and process efficiency (Kahraman & Benzer, 2025). This process encompasses the characterisation, extraction, and optimisation of these materials to enhance the efficiency, quality, and sustainability of cement manufacturing (Figure 1). It connects geological materials directly to the cement industry, making the concept more relevant and relatable for industry professionals.

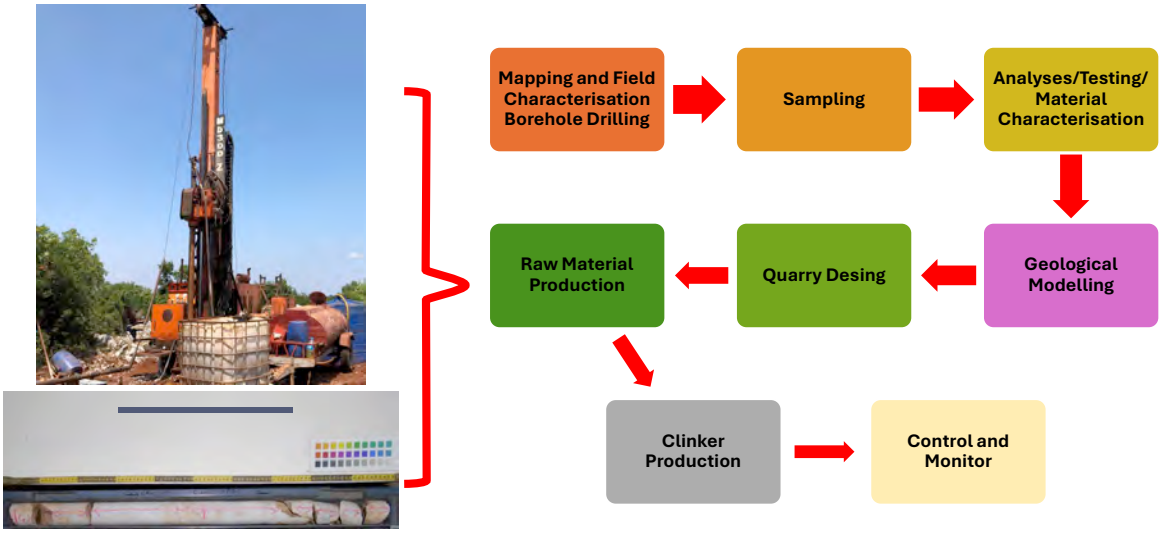

Figure 1. Conceptual approach in geocementing

Ore characterisation involves identifying minerals, assessing their spatial distribution, determining liberation efficiency, and analysing particle size distribution to enhance processing, whilst process selection includes choosing effective methods for crushing, grinding, and concentration, along with appropriate extraction techniques (e.g., smelting, leaching) based on ore characteristics. The main idea is that cement raw material deposits are complex geological systems with varied mineral characteristics locally. These regions, which have different mineralogical, geochemical, physical, and structural features, significantly influence the process.

The entire process begins by analysing the geological features of raw materials. This includes creating 3D geological models, planning quarry operations, and improving the production steps for high-quality cement. Key points in geo-cementing are understanding the raw materials, selecting the right cement-making process, optimising that process, and using predictive modelling.

To characterise raw materials, mineral studies are performed to identify the minerals present in deposits; therefore, the texture of the lithological units is assessed to understand the relationship and distribution of different minerals. This information helps determine how easily valuable minerals can be separated from waste materials. Additionally, analysing particle size distribution reveals how the size of ore particles influences processing efficiency.

When selecting the comminution process, it is essential to choose the best methods for crushing, grinding, and concentrating raw materials, which helps identify the most suitable

extraction techniques based on mineral characteristics. This approach enhances economic viability and profitability in mineral extraction, helping to improve energy efficiency and minimise environmental impact. Predictive modelling through computer simulations forecasts ore behaviour during processing, enabling the identification of optimal operating conditions to maximise efficiency and profitability.

Domain definition serves not only as a geological classification exercise but also as a process-behaviour modelling tool. The necessary steps for a general framework for geo-cementing are outlined below.

1. Geological Characterisation of Raw Material
2. Model Creation
3. Quarry Development/Extraction Strategy
4. Quality Optimisation and Process Efficiency
5. Managing Environmental Impacts
6. Managing Resources and Reserves

3. GEOLOGICAL CHARACTERISATION AS A PREDICTIVE FRAMEWORK

In cement manufacturing, the primary raw materials are mainly limestone, clay, and gypsum. The quality of these raw materials directly affects the quality and consistency of the final product, as well as the efficiency of the production process. Given that limestone is the major component in cement production, the following aspects should be considered for limestone quarry development, extraction, and subsequent processing strategies.

The deposits serving the cement industry are often stratified with layers of limestone alternating with other sedimentary rocks, like shales or clays (Figure 2). The continuity of these layers can vary, which helps geologists correlate layers across a quarry and predict where high-quality limestone may be found. Lateral shifts in the sedimentary environment can lead to facies changes within the limestone deposits. For instance, a limestone facies rich in shell fragments might transition into a micritic limestone facies with different properties. Recognising these changes is essential for maintaining consistency in the raw material. The vertical continuity of limestone deposits can also vary with depth. In some cases, limestone quality is homogeneous, making management easier. In others, alternating bands of pure and impure limestone can complicate mining and processing.

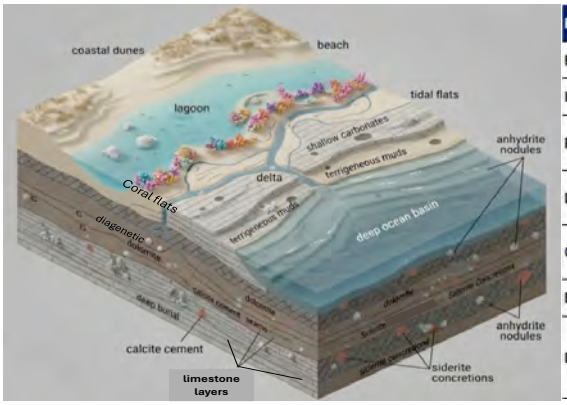

Environment	Primary Sedimentary Mineral(s)	Associated Minerals (Including Diagenetic)
Beach/Tidal Flat	**Calcite** (skeletal fragments, ooids)	**Dolomite** (early replacement of aragonite/calcite in supratidal/sabkha settings)
Lagoon/Sabkha	**Calcite** (mud), **Aragonite** (ooids)	**Dolomite** (early diagenesis in evaporitic settings), **Gypsum**, **Anhydrite** (evaporitic minerals)
Reef/Carbonate Shelf	**Calcite** (skeletal fragments from corals, algae, foraminifera)	**High-Mg Calcite** (initial precipitate), **Dolomite** (later burial), **Chert** (diagenetic replacement of siliceous sponges/radiolarites)
Delta/Shelf Margin	**Calcite** (bioclasts), **Clay Minerals** (terrigenous influx)	**Kaolinite** (close to river source), **Illite**, **Montmorillonite** (mixed further out)
Outer Shelf/Slope	**Calcite** (foraminiferal oozes, calcareous nannofossils)	**Glauconite** (authigenic mineral in low-oxygen/slow deposition areas)
Basin/Deep Ocean (Above CCD)	**Calcite** (pelagic oozes)	**Chert** (formed from dissolution and reprecipitation of biogenic **silica** from radiolaria/diatoms)
Deep Burial (General Diagenesis)	**Calcite** (as cement and recrystallized grains)	**Dolomite** (later burial phase, often coarse-crystalline), **Siderite** (iron-carbonate, forms in anoxic, iron-rich conditions), **Silica** (as quartz cement and chert nodules)

Figure 2. Limestone deposits and expected minerals in these geological settings

Processes like dolomitization and recrystallisation can occur in specific horizons within limestone deposits. These changes can alter the chemical composition and reduce quality continuity, requiring detailed geological modelling to manage variability. Even seemingly homogeneous limestone deposits can contain subtle variations in texture, colour, and

impurities. For example, layers of calcite-rich and clay-rich limestone can affect chemical composition, impacting clinker formation and cement quality (Figure 2).

Figure 3. Lithological variation in a limestone deposit within metres

Finally, geological structures such as faults and fractures, as well as weathering process can also influence mineral distribution within a deposit. For example, a fault may introduce secondary minerals that alter local composition. Understanding these structures and identifying the weathering zones are crucial for optimising extraction and blending strategies, as they can affect cement quality.

The geological characterisation involves collecting data, mapping the mineralogical and chemical composition of the raw materials, understanding their spatial distribution, and identifying zones of high or low quality within the deposit by drilling the strata to the targeted depths (Figure 4).

Undertaking a detailed field mapping to document observable lithological differences at the surface, such as variations in colour, texture, bedding, and any structural features present, even in massive deposits, can often reveal subtle changes.

A detailed core logging in borehole drilling is essential to capture subtle variations in mineralogy, texture, and structure. This allows geologists to identify features not visible at the surface that are critical for defining lithological domains, as well as identifying mineralogical changes that contribute to chemical changes.

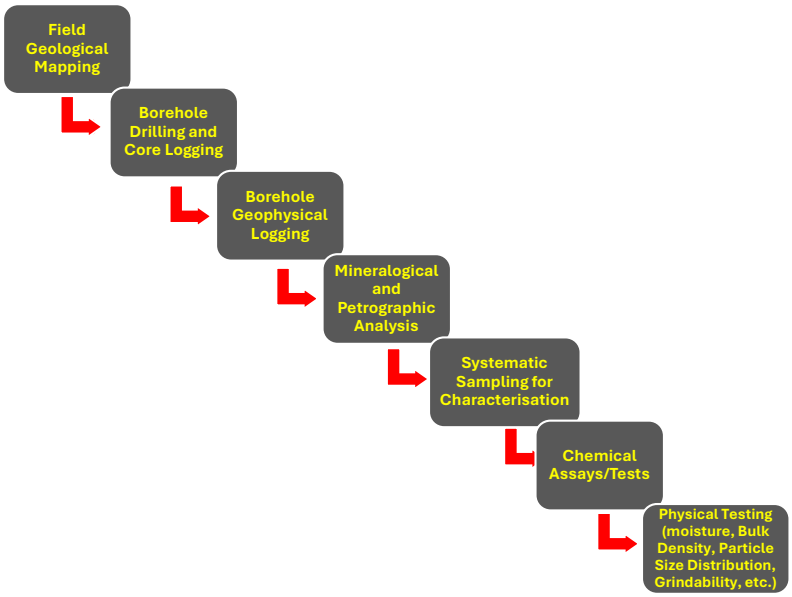

Figure 4. Geological characterisation of the raw material in limestone deposits

The assay results from analytical tests conducted on the samples from core drilling from various locations within the quarry can establish the distribution of $CaCO_3$, MgO, SiO_2, Al_2O_3, and S, coupled with the lithological changes. This data also provides insight into the distribution of high-purity limestone within the deposit. For example, if the limestone has a low $CaCO_3$ content, the addition of corrective materials like bauxite or iron ore may be necessary to adjust the composition, which can increase production costs and complexity. While some MgO is acceptable in cement, high levels can lead to the formation of periclase, resulting in expansion and cracking in the hardened cement.

Limestone is the primary source of calcium oxide (CaO) in cement production, mainly composed of calcite but also containing other minerals that can affect its chemical properties and cement quality. High-purity limestones, known as "high-calcium limestone," contain over 95% calcium carbonate ($CaCO_3$).

Calcite is the most desirable mineral for cement making. High calcite content leads to greater CaO levels in clinker, essential for forming key compounds like alite and belite. Calcite-rich limestone is easier to grind and process, requiring less energy and contributing to efficient kiln operations. However, variations in calcite concentration can lead to inconsistencies in the final product.

Mineral dolomite ($CaMg(CO_3)_2$) adds both calcium and magnesium to the mix, but excessive magnesium can cause expansion issues in cement. Dolomite requires higher kiln temperatures for decomposition, increasing energy use and wear on grinding equipment. Careful management is essential to ensure that dolomite levels do not exceed acceptable limits.

Impurities like silica (SiO_2), alumina (Al_2O_3), and iron oxides (Fe_2O_3) can lower calcium content and impact cement quality. Dolomitic limestones, which contain magnesium carbonate ($MgCO_3$), can be problematic when MgO levels are high, as they may cause expansion and cracking in concrete during clinker production.

Clay minerals in limestone (kaolinite, illite, montmorillonite) introduce silica, alumina, and iron oxide, which are necessary for clinker formation. However, excessive clay can disrupt the raw mix and complicate grinding, resulting in operational inefficiencies and lower cement quality.
Gypsum is a common mineral found in extensive evaporite beds associated with sedimentary rocks. It forms from lake and seawater, hot springs, volcanic vapours, and sulphate solutions. In cement production, gypsum ($CaSO_4 \cdot 2H_2O$) acts as a setting retarder, improving workability before hardening. Its quantity is carefully controlled; too much can slow setting excessively, while too little can cause rapid setting and poor workability. Gypsum also provides sulphur, aiding in clinker formation, and its quality is determined by purity and solubility in water.

Iron minerals are not a primary component like limestone or clay, but they can often be used as a minor addition in cement production. Iron oxide from hematite (Fe_2O_3) or magnetite (Fe_3O_4) can enhance strength and durability, and can adjust colour for aesthetic purposes. It supports the formation of certain clinker phases, improving early strength. However, too much iron oxide can lead to increased shrinkage and sulphate susceptibility, so its use is limited.

Supplementary cementitious materials (SCMs), such as blast-furnace slag, fly ash, and silica fume, can enhance cement properties, reduce carbon footprint, and improve sustainability. Their use varies by local regulations and desired cement characteristics. Careful selection and blending of these materials are crucial for producing high-quality cement.

In geological characterisation, data collection in the field should also focus on clay zones to assess SiO_2 and Al_2O_3 contents. This data is integrated into the geological model to identify clay-rich zones with optimal SiO_2 and Al_2O_3 levels. Moreover, the data collection should

consider zones contributing sulphur, as sulphur, often present as gypsum ($CaSO_4$) or pyrite (FeS_2), is needed in controlled amounts for the formation of ettringite, which regulates the setting time of cement. However, excessive sulphur can lead to issues such as clinker ball formation in the kiln. Furthermore, the alkali content (Na_2O and K_2O) in limestone and clay samples within the deposit needs to be checked, as it can react with reactive silica in aggregates to form alkali-silica gel, which leads to expansion and cracking in concrete structures. The spatial distribution of alkalis should be mapped to manage their input into the kiln.

Borehole drilling to define lithological boundaries in the limestone deposits should be supplemented with a borehole geophysical survey, which should include at least gamma-ray, density, sonic, electrical resistivity, and conductivity logs to delineate the subtle lithological changes in the strata. For example, the gamma tool detects variations in the natural radioactivity of the rock, with higher readings often indicating the presence of clay-rich zones, while lower readings suggest purer limestone. Density and sonic logs measure the density and acoustic properties of the rock, respectively, helping to identify zones with different lithological properties (e.g., denser dolomite versus less dense calcite). They can also assist in predicting the geomechanical behaviour of the strata in quarry design. Electrical resistivity and conductivity measurements can distinguish between different lithologies based on their ability to conduct electricity, which varies with mineral content and porosity.

In sampling highly homogeneous limestone deposits, the core sampling interval can range from 1.5 to 3 meters, and may even extend to 5 or 10 meters, depending on the characteristics of the deposit. To capture variability in material composition, the drilling pattern should encompass all areas of the quarry. In deposits with greater variability or where specific lithological boundaries are of interest, a shorter interval of 1 meter may be necessary for detailed assessment. Borehole core diameters for samples typically range from HQ (63.5 mm) to NQ (47.6 mm). The choice of diameter depends on the degree of heterogeneity, with larger cores (HQ) providing more material for analysis and being preferable in variable deposits. Each sample should weigh around 1 to 2 kilograms, depending on the density of the limestone, which is generally sufficient for chemical and mineralogical analysis. If CRIRSCO (Committee for Mineral Reserves International Reporting Standards)-compliant resource and reserve estimations are considered, all Quality Assurance and Quality Control (QA-QC) procedures required by the CRIRSCO Codes must be followed to ensure unbiased reporting.

High-resolution geochemical profiling for major and trace elements is utilised for systematic geochemical sampling from cores. This method identifies subtle geochemical signatures corresponding to different lithologies. For instance, variations in magnesium (Mg), iron (Fe), or trace elements like strontium (Sr) or manganese (Mn) can indicate changes in mineralogy, such as transitions from calcite-rich to dolomite-rich zones. Other parameters investigated include Loss on Ignition (LOI), which measures the amount of volatile matter (e.g., water, organic matter) lost when the sample is heated, providing insights into the purity of the raw material. pH is measured to determine the acidity or alkalinity of the materials, assessing their reactivity and the overall process chemistry. Portable XRF analysers can also provide rapid, in-situ geochemical analyses. This tool can be used both in the field and on core samples to quickly map chemical variations across the deposit, despite its limitations in the resource estimation process under the CRIRSCO codes.

Other analytical techniques can also be employed to characterise raw materials. These techniques include thin section analysis, X-Ray Diffraction (XRD), and Scanning Electron Microscopy (SEM). Thin sections from drill core samples can be prepared and analysed under a microscope to identify differences in mineral composition, grain size, and texture. This method is particularly effective for detecting subtle lithological variations that may not be visible in hand samples. XRD helps quantify the mineralogical composition of different zones within the deposit, revealing variations in the proportions of calcite, dolomite, clay minerals, and other

constituents, even when these differences are not visually apparent. SEM, combined with energy-dispersive X-ray spectroscopy (EDX), provides detailed images and chemical analyses at a microscopic level, helping to distinguish fine-grained minerals and textures.

Physical tests could also shed light on the characterisation process. They include moisture content, bulk density, specific surface area, and grindability index. Determining moisture content reveals the amount of water in the raw materials and helps control moisture levels during the clinkering process. Bulk density measures the mass of a unit volume of the raw material, facilitating calculations of material quantities and optimising storage and transportation. The particle size distribution test assesses the distribution of particle sizes in raw materials, aiding in understanding grindability and optimising the milling process. The specific surface area test measures the total surface area of particles per unit mass, which is crucial for evaluating the reactivity of raw materials during the clinker formation process. The grindability index test assesses how easily a material can be ground to a specific particle size, informing the selection of appropriate milling equipment and optimising energy consumption.

4. MODEL CREATION BY GEO-CEMENTING CONCEPT

Developing geo-cementing involves the integration of geological, mineralogical, and processing data. The goal is to create a model that maps the variability within the quarry, highlighting areas with different material quality by identifying possible domains by conducting many modelling tasks (Figure 5).

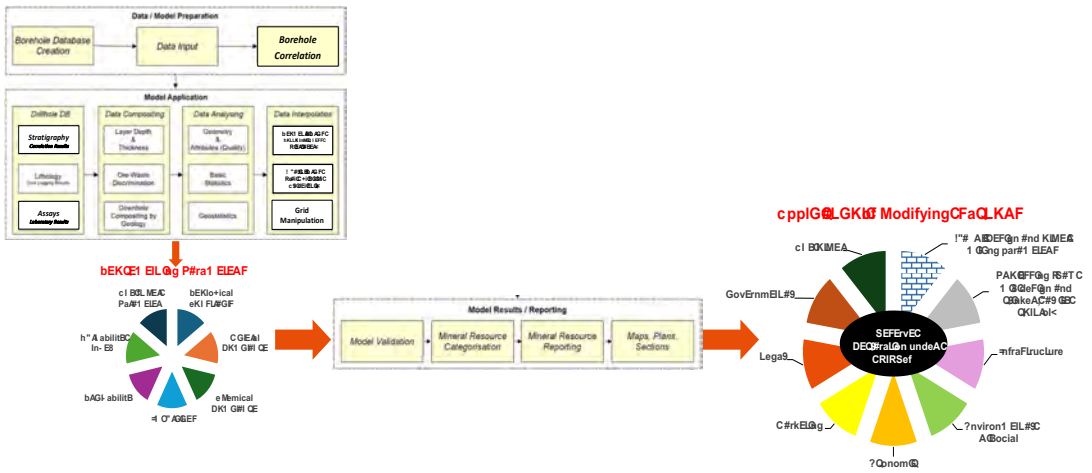

Figure 5. Conceptual modelling workflow with milestones and larger work packages under CRIRSCO

Each domain represents a region within the deposit with relatively homogeneous properties, such as similar mineral composition, chemical characteristics, or physical attributes.
Several parameters can be used to establish domains within a cement raw material deposit:

Domains based on the mineralogical composition can be created based on the concentration and distribution of primary minerals like calcite, dolomite, and clay minerals (such as kaolinite, illite, and montmorillonite). The presence of secondary minerals and impurities, such as pyrite (FeS_2) or gypsum ($CaSO_4$), which contribute sulphur or other undesirable elements, can also define domains that need different treatment during extraction or processing. Some typical domains include:

Calcite-Rich Domains: These zones are characterised by a high concentration of calcite ($CaCO_3$), yielding high CaO and low MgO content, making them suitable for producing high-quality clinker with strong early strength. These areas require minimal corrective materials for

clinker formation. However, the exact CaO yield will depend on the purity of the calcite and the presence of associated minerals like quartz (SiO_2) or clays. Monitoring of trace elements (e.g., Sr, Mn) is important as they can affect clinker properties.

Dolomite-Rich Domains: These domains feature a prevalent presence of dolomite ($CaMg(CO_3)_2$) with elevated levels of MgO alongside CaO. It is essential to monitor the MgO content to avoid the formation of periclase (MgO) in clinker, which can lead to delayed expansion. While these areas may pose challenges due to the introduction of MgO affecting clinker quality, they can be strategically blended with calcite-rich materials to maintain an optimal chemical balance.

Clay-Rich Domains: These areas contain a significant amount of clay minerals (e.g., kaolinite, illite) and typically exhibit high SiO_2, Al_2O_3, and Fe_2O_3 content. The specific ratios depend on the clay mineralogy (e.g., kaolinite-rich clays provide a balanced SiO_2/Al_2O_3 ratio). These domains are crucial for supplying the necessary silica and alumina for clinker formation, but careful management is required to control impurities (e.g., Na_2O, K_2O from illite).

Impurity-Rich Domains: These domains have higher concentrations of undesirable minerals (e.g., pyrite, gypsum, or alkali-bearing minerals) and should be managed carefully to minimise their impact on cement quality.

The mineralogical approach can be used to analyse the phase composition of clinker, identifying key minerals formed during the firing process, such as alite, belite, tricalcium aluminate, and tricalcium silicate. Techniques like scanning electron microscopy (SEM) help examine the microstructure of clinker, revealing the distribution and morphology of these minerals.

This approach also identifies hydration products formed when cement mixes with water, including calcium silicate hydrates (C-S-H), calcium hydroxide (CH), and calcium aluminate hydrates (AFm phase). Understanding these products aids in examining hydration kinetics, providing insights into how different minerals react and contribute to cement strength and durability.

Moreover, the mineralogical approach assesses cement durability by analysing harmful phases, such as sulphate attack products, and evaluating the stability of hydration products over time. This can lead to the development of new cement formulations with improved properties, reduced environmental impact, or specialised applications.

Domains based on the chemical composition can be defined based on the concentration of CaO from calcite. Areas with high CaO content could be prioritised for extraction to ensure a consistent feed for clinker production. MgO levels are critical, as elevated concentrations can negatively impact cement quality. Domains with high MgO can be identified and managed accordingly. Additionally, silica (SiO_2) and alumina (Al_2O_3) are essential for clinker formation; thus, domains with optimal levels of these compounds can be identified for desired clinker properties, while areas with excessive or deficient levels may require different management strategies. High alkali content (Na_2O, K_2O) can cause problems such as alkali-silica reaction (ASR) in concrete, necessitating the isolation or blending of high-alkali domains with lower-alkali materials.

Domains based on the physical properties can also be classified based on the hardness of the material (e.g., soft calcite-rich zones versus hard dolomite-rich zones), which affects grinding energy requirements and equipment wear. Domains may also be based on porosity and moisture content, influencing the material's handling properties and processing behaviour, such as drying or grinding efficiency.

Furthermore, domains based on the geological structure and continuity can be defined by structural features that affect the continuity and accessibility of the material. For example, fault zones may represent domains that require different extraction methods or pose a higher risk of material variability.

By carefully analysing these factors, the extraction and processing of cement raw materials can be optimised to ensure high-quality output.

5. APPLICATION OF GEO-CEMENTING IN EXTRACTION STRATEGIES

Geo-cementing enhances extraction strategies by optimising resource use. It allows for strategic planning of raw material extraction to improve feedstock quality and consistency. For example, targeting calcite-rich areas provides a consistent high-CaO feedstock, while blending materials from different zones can create a balanced raw mix tailored for clinker formation. Extracting from areas that require minimal corrective adjustments helps to reduce operational costs. Avoiding high-MgO domains limits the need for expensive kiln adjustments, and domaining helps identify areas with impurities that can lead to increased waste, allowing for targeted processing.

Real-time data from the geological model can streamline blending during extraction, ensuring a consistent feed to the kiln. Continuously updating the 3D model allows for dynamic adjustments in response to material variability. If certain areas yield suboptimal materials, strategies can be modified accordingly.

From an environmental perspective, geo-cementing and domaining support long-term planning by ensuring efficient use of high-quality material while managing low-quality resources. Understanding the distribution of sulphur-bearing minerals and high-alkali zones aids in establishing emission zones and improving extraction strategies, enabling simulations to assess the impact of material blends on processing efficiency and product quality.

6. QUALITY OPTIMISATION AND PROCESS EFFICIENCY

The traditional method of cement production mainly relies on chemical analysis to control the properties of the final product. However, adopting a mineralogical and geological approach offers additional benefits by linking to the original depositional conditions of materials. This approach enhances resource management by creating a robust geological model that improves quality control. It also supports better reporting practices, utilising CRIRSCO templates for resources and reserves (Kahraman 2024), which is essential for the industry's success amid increasing scrutiny from regulators and investors.

The chemical approach focuses on the elemental composition of materials. Techniques such as X-ray fluorescence (XRF) and inductively coupled plasma mass spectrometry (ICP-MS) help identify the proportions of various elements and impurities affecting cement quality. The control process involves blend optimisation to ensure the desired chemical composition for clinker, which is crucial in cement production.

The mineralogical approach focuses on identifying and characterising specific minerals within materials. A combination of comprehensive field and laboratory techniques, including detailed geological mapping, borehole logging, geophysical logging, X-ray fluorescence (XRF) assays, as well as X-ray diffraction (XRD) and scanning electron microscopy (SEM), provides valuable insights into the microstructure, texture, and behaviour of minerals such as calcite and iron oxides. This information is essential for understanding how these minerals contribute to clinker formation and their reactivity.

This approach also examines hydration products formed when cement reacts with water, including calcium silicate hydrates (C-S-H) and calcium hydroxide (CH). Understanding hydration kinetics helps assess the strength and durability of cement. Additionally, the mineralogical approach can evaluate cement durability by identifying harmful phases that may develop and can also inform the creation of new cement formulations with enhanced properties or lower environmental impact.

In addition, some minerals may require higher kiln temperatures to form clinker or can affect grindability. Knowing this in advance enables optimisation of the kiln and grinding processes, ensuring energy is used efficiently while maintaining clinker quality.

Furthermore, geo-cementing data can predict equipment wear and tear. For instance, harder or more abrasive materials may cause increased wear on grinding equipment, necessitating more frequent maintenance or adjustments to the process.

Using statistical methods, like cluster analysis, can effectively categorise different lithologies, especially in large deposits where visual classification is difficult. Additionally, adopting machine learning models using the collected data to predict lithological variations in areas with sparse data can enhance the geological model and improve the accuracy of lithological domains.

Implementing in-situ monitoring techniques, such as near-infrared (NIR) spectroscopy during drilling or blasting, provides immediate feedback on lithological variations, allowing for real-time adjustments. With a thorough understanding of the raw material properties, kiln operations can be fine-tuned. For example, knowing the exact mineralogical composition allows operators to optimise the temperature profile within the kiln by using sensors to monitor temperatures and adjusting them based on the mineralogy of the feed (Figure 6). This ensures optimal clinker formation and energy efficiency, which can lead to improved formation of clinker phases, reduced energy consumption, and lower CO_2 emissions.

The data from processing can be fed back into the geo-cementing model to refine it further. This continuous feedback loop aids in adjusting quarry development plans and processing strategies, ensuring a dynamic optimisation process, while implementing strict quality control measures to predict and control the quality of the final product. This minimises variability, ensuring that the cement consistently meets the required specifications.

Figure 6. Quality optimisation and process efficiency with the geocementing concept

7. MANAGING ENVIRONMENTAL IMPACTS

Cement production is a major contributor to greenhouse gas emissions and environmental degradation due to quarrying activities (Kahraman, 2023). Geo-cementing can play a crucial role in mitigating these impacts by optimising the use of raw materials, thereby reducing the waste generated during quarrying and processing. This includes minimising the volume of overburden, fines, and other by-products that may otherwise be discarded.

Lower emissions can be achieved by optimising the kiln and grinding processes based on a detailed understanding of the raw materials, leading to more efficient fuel use and reduced CO_2 emissions. Additionally, optimising the raw material blend can decrease the need for corrective additives, further minimising emissions.

Finally, geo-cementing data can facilitate more sustainable quarry management practices by mapping high-quality reserves. Companies can strategically plan their extraction activities to minimise environmental impacts, such as reducing the footprint of active quarry areas or prioritising the use of lower-impact extraction methods.

8. RESOURCE MANAGEMENT IN THE CEMENT INDUSTRY

Effective resource management stands as a cornerstone in the cement industry, especially in an era where high-quality raw materials are dwindling (Kahraman, 2024). Geo-cementing emerges as a powerful ally, offering an array of innovative tools and techniques that enable precise resource estimation and strategic management. By harnessing geo-cementing models, companies unveil a detailed panorama of the quantity and quality of their available resources. This in-depth understanding allows for more accurate predictions regarding a quarry's lifespan and facilitates meticulous planning for future resource needs.

The cement industry's readiness to adopt CRIRSCO templates varies widely (CRIRSCO, 2026). Major global firms like LafargeHolcim (2026), HeidelbergCement (2026), and Cemex (2026) have already integrated these standards into their reporting, recognising their importance for sustainable long-term planning. Conversely, smaller companies, especially in emerging markets, often struggle with the technical and financial demands of compliance.

Transitioning to CRIRSCO-compliant reporting requires significant investment in data collection, geological modelling, and expertise. Companies hesitant to make this shift risk competitive disadvantages as investors and regulators increasingly prioritise transparency.

Financial institutions are also pivotal in promoting CRIRSCO standards by incorporating Environmental, Social, and Governance (ESG) criteria into their decision-making. They are more likely to support companies with CRIRSCO-compliant reporting, which aligns with the growing focus on responsible investment. The adoption of the "***Equator Principles***" by 128 institutions around the world offers a framework for managing environmental and social risks in financing projects, further encouraging compliance among companies (Equator Principles, 2026).

Similarly, the International Finance Corporation (IFC) under the World Bank seeks similar assurances for mining and infrastructure projects. The Environmental Health and Safety (EHS) Guidelines for mining or extractive industries apply to underground and open-pit mining, alluvial mining, solution mining, and marine dredging (IFC, 2007). Extraction of raw materials for construction products is addressed in the EHS Guidelines for Construction Materials Extraction, whilst the similar EHS Guidelines are also applicable to the Cement and Lime Manufacturing (IFC, 2022).

Adhering to CRIRSCO standards and the Equator Principles or IFC Guidelines can lead to more favourable financing terms, including lower interest rates and better loan conditions. As regulators insist on greater disclosure of environmental and social impacts, non-compliant firms may find it difficult to secure financing.

Accurate resource and reserve estimations are also crucial in mergers and acquisitions (M&A) within the cement industry. CRIRSCO-compliant companies present lower risks, making them more attractive acquisition targets, while those with less transparent reporting may struggle to negotiate favourable terms after the Due Diligence process. Due diligence in M&A transactions involves thoroughly examining the target company's resources, operational practices, financial health, legal standing, and environmental impact to ensure a clear understanding of value and risks. Implementing the principles of geocementing can significantly assist in the due diligence process since every aspect in the target company's resource and reserve estimates and operational practices can be traced back to the original geological concepts.

Moreover, possessing intricate insights into the quality and spatial distribution of raw materials empowers cement producers to craft long-term strategic extraction plans that unlock the full value of their resources. This strategy might include a thoughtful sequencing of extraction zones, ensuring a steady flow of raw materials that align with production demands and maintain operational efficiency.

As the cement industry increasingly embraces established frameworks like the CRIRSCO templates for resource and reserve reporting, geo-cementing plays a pivotal role in steering companies toward compliance with these rigorous standards (Kahraman, 2024). By providing solid, data-driven insights into both the quality and quantity of raw materials, companies can create reports that are not only transparent but also reliable. Such reporting is crucial for various stakeholders, including investors and regulators, who seek assurance in their dealings.

In today’s climate, financial institutions and investors are gravitating towards companies that uphold CRIRSCO-compliant reporting, reflecting a broader commitment to sustainable and responsible investment practices. This alignment with ethical and sustainable principles not only enhances corporate reputation but also solidifies trust among stakeholders.

9. CONCLUSION

Geo-cementing formalises a mineralogy-domain philosophy in which geology is not a passive supplier of raw materials but an active determinant of process behaviour, energy efficiency, environmental performance, and financial credibility. In summary, geo-cementing can deliver improved efficiency in extraction and processing by guiding exploration efforts to discover high-grade areas.

By integrating geological variability, mineralogical quantification, domain modelling, process simulation, and reporting standards, the framework repositions cement production as a geological systems management discipline, which offers significant advantages in optimising raw material quality and more consistent product quality, enhancing process efficiency, reducing environmental impact, and improving resource management. These benefits align with broader industry trends towards sustainability, operational efficiency, and compliance with global reporting standards, making geo-cementing a valuable tool for modern cement producers and providing a competitive advantage in the market.

This can lead to optimised processes, which can lower production costs by refining quarry design and ensuring cost-effective processing plant operations based on raw material characteristics while maintaining consistent product quality.

Furthermore, geo-cementing minimises the environmental impact of quarrying and comminution processes by reducing waste generation and maximising resource recovery and resource conservation by understanding material characteristics.

This paradigm shift from chemical correction to mineralogical prediction offers measurable improvements in clinker stability, operational efficiency, emission control, and long-term resource governance. In an industry facing escalating demands for sustainability and transparency, geo-cementing offers a scientifically grounded, academically robust, and strategically aligned methodology for modern cement manufacturing.

REFERENCES

CEMEX, (2026) “CEMEX annual report 2024”, CEMEX.

Committee for Mineral Reserves International Reporting Standards (CRIRSCO), (2026) “Promoting international best practice in the reporting of mineral exploration, mineral resources and mineral reserves”, CRIRSCO.

Equator Principles, (2026) “Equator Principles: Signatories and EPFI reporting”, Equator Principles.

Heidelberg Materials, (2026) “Annual sustainability report 2024”, Heidelberg Materials.

Holcim, (2026) “Holcim MCS booklet 2025”, Holcim.

IFC. 2007. Environmental, Health, and Safety Guidelines: MINING.

IFC. 2022. Environmental, Health, and Safety Guidelines Cement and Lime Manufacturing. 2022. https://www.ifc.org/content/dam/ifc/doc/2022/2022-cement-lime-manufacturing-ehs-guidelines-en.pdf. Accessed on 12 March 2026.

Kahraman Arden, H., (2023) “Balancing act for the developing countries between the use of thermal coal and the Paris Agreement”, Proceedings of the 40th Annual International Pittsburgh Coal Conference, Istanbul, Türkiye, 4–6 October 2023, 70–82.

Kahraman Arden, H., (2024a) “The cement industry's preparedness for resource and reserve estimation: Implications for mergers, acquisitions, financing, and the Paris Agreement”, CemenTürk Magazine, September–October issue, 66–70.

Kahraman Arden, H., (2025) “Geocementing: Impact of geology and mineralogy on quarry planning and cement production”, CUSCIT Cement Olympics, Antalya, Türkiye, 4–8 November 2025.

Kahraman Arden, H., Benzer, H., (2024b) “Geo-cementing concept in the cement industry”, CemenTürk Magazine, January–February issue, 60–68.

Kahraman Arden, H., Benzer, H., (2024c) “Geo-cementing: Influence of raw material mineralogy and geology on cement quality”, CemenTürk Magazine, November–December issue, 50–56.

CHARACTERIZATION AND PROPOSED MINERALURGICAL PURIFICATION METHODS FOR FELDSPAR FROM AÏN BARBAR, EASTERN ALGERIA

Assia BOUTEMEDJET*, Zohir MEKTI, Ghofrane BOUDRAA, Fatima Zohra BOUGHABA

Laboratory of Mineral Resources Valorization and Environment, Badji Mokhtar - Annaba University, 12, P.O.Box. 23000 Annaba. Algeria
**Corresponding Author: assia.boutemedjet@univ-annaba.dz*

A B S T R A C T

Feldspars are a group of minerals widely used in various industries, including ceramics, glass, and construction materials. However, extracted feldspars often contain impurities such as quartz, mica, iron oxides, and other accessory minerals, which can affect the quality of the final products. To meet the purity requirements demanded by user industries, feldspars must be purified. This purification is generally carried out using mineral processing techniques, which consist of a series of physical and physico-chemical operations aimed at separating unwanted minerals from the feldspar.

To achieve our objective, several steps were carried out, including sampling, physicochemical characterization followed by particle size analysis to determine the distribution of minerals. Then, an observation of the different samples was conducted using an optical microscope, and finally, a particle-size chemical analysis using XRF was performed to identify the fraction containing the impurities. The results obtained indicate an excess of iron oxides ranging from 2.28% to 3.03%. A proposal of various purification methods using mineral processing techniques such as flotation and leaching is presented.

Key words: *Feldspar, Ain Barbar, iron oxide, particle-size chemical characterization, flotation, leaching*

1. INTRODUCTION

Feldspars are essential raw materials in several strategic industries, particularly glass and ceramics, due to their favorable physical and chemical properties. However, their industrial use is highly dependent on their purity, especially their iron oxide (Fe_2O_3) content. High levels of iron oxide can lead to undesirable discoloration of the final product and a decrease in its quality, negatively impacting the ore's commercial value. In this context, this study aims to evaluate the characteristics of a feldspar ore using a combined particle size analysis and chemical analysis approach. X-ray fluorescence (XRF) granulochemical analysis was performed in the SOTRAMA company laboratories, which is essential for characterizing the mineralogical and chemical composition of the ore based on its particle size distribution. The results obtained indicate an iron oxide (Fe_2O_3) content between 2.28% and 3.03%, a relatively high value compared to the standards required in industrial applications demanding high-purity raw materials. Therefore, reducing this iron oxide (Fe_2O_3) content is a major challenge for improving ore quality and expanding its exploitation potential.

In the absence of experimental treatments for removing these impurities, we conducted a review of the scientific and technical literature, focusing on previous studies and tests applied to similar ores. The main treatment techniques identified are: electromagnetic separation, flotation, and chemical leaching. To achieve the objectives of this study, four chapters are presented as follows: In the first chapter, we determined the history and generalities, A description of the feldspar production unit in the Ain Barbar region is described in the second chapter, The experimental part in the third chapter aims to determine the different methods of purification of the feldspars from Ain Barbar, We conclude in the last chapter with a study of the impact on the environment.

2. METHODOLOGY

2.1. XRF Analyses

This method is widely used in geology, metallurgy, chemistry, environmental science, and industrial quality control, particularly for analyzing rocks, ores, metals, and glass. It is highly accurate for elements with atomic numbers greater than 11, but less effective for lighter elements. XRD analysis requires precise calibration and can be influenced by the physical state of the sample. The results are shown in the following table.

Elements	SiO_2	Al_2O_3	Fe_2O_3	CaO	MgO	K_2O	Na_2O	Cl	SO_3
%	79.3	12.4	2.28	0.70	0.49	12.06	0.28	0.009	0.05

2.2. Physical Separation

Physical separation is a set of crucial techniques that allow valuable minerals to be separated from waste rock without altering their chemical composition.

These methods exploit differences in the physical properties of minerals, such as their density (for gravimetric separation), their size (screening, classification), their magnetic properties (magnetic separation), their surface properties (flotation), or their electrical conductivity (electrostatic separation). The goal is to pre-concentrate the ore and produce richer concentrates, thereby reducing the costs of subsequent processing steps and maximizing resource recovery. Amidst the technological advancements, we see today, the mining industry has also experienced significant development. Advanced physical separations are cutting-edge technologies, often grouped under the term sensor-based sorting, that go beyond traditional methods. They use sophisticated sensors to analyze each ore particle individually and sort it according to very specific physical properties. These techniques include:

- Optical sorting: to distinguish minerals by their color or brightness.
- X-ray sorting (XRT and XRF): to separate according to atomic density or elemental composition. • Inductive sorting: to identify conductive minerals.
- Laser or spectroscopic sorting (NIR, LIBS): to analyze the surface or fine chemical composition.

These methods allow for very early pre-concentration of the ore, drastically reducing the amount of material to be processed by more methods that are expensive. They thus improve mining efficiency, reduce water and energy consumption, and extend mine life by making lower-grade ores viable.

2.3. Mechanical Separation

The first stage involves primary crushing using jaw or impact crushers. The next stage is gravel production (secondary crushing) using gyratory or vertical shaft impact crushers. These crushing operations are combined with screening to ensure the correct particle size distribution of the crushed product. Gravel between 5 and 10 mm can be sold directly to tile manufacturers, who perform the final grinding after mixing it with clay. The sands (0, 1-1 mm) obtained by screening can be used directly in the ceramic and glass industries. Grinding combined with classification is often the final stage of fragmentation. This is carried out in ball mills. Classification is achieved using sieves, static or dynamic air separators, or cyclones. The

sanitary ware, tableware, enamels and frit industries require products ground to 60 or 80 µm. Ultrafine grinding, or micronization, is intended to obtain powders smaller than 25 µm, intended for mineral fillers.

2.4. Electromagnetic Separation

Electromagnetic separation involves subjecting samples to an electromagnetic field, thereby creating fractions that depend on the varying magnetic permeability of the minerals. These fractions are separated using electromagnets with variable fields. The magnetic properties of minerals depend, in particular, on their chemical composition and primarily on the presence of elements, whose ions possess uncoupled electrons in their surface layers.
Magnetic properties are influenced by the chemical relationship between the ions and by their position within the crystal structure.

2.5. Flotation Separation

Flotation is based on the hydrophobic and hydrophilic properties of solid surfaces. These properties can be natural or stimulated using appropriate reagents added to the water/solid particle mixture to be treated. When air is introduced in the form of small bubbles into such a medium, a selective transport of hydrophobic particles occurs. Particles with hydrophobic surfaces attach to the air bubbles upon collision. This phenomenon is due to the high affinity of hydrophobic surfaces for air, which is non-polar. The air bubbles carry these particles to the surface of the pulp, where they form a foam laden with floating particles. Conversely, particles with hydrophilic surfaces do not bind to the air bubbles and remain suspended in the pulp. When the minerals to be concentrated are hydrophobic, we use direct flotation; otherwise, we use reverse flotation. The pulp must be prepared appropriately depending on the substances to be concentrated, primarily through the addition of various agents: foaming agents, collectors, depressants, and activators are flotation reagents. Foam stability is ensured by the foaming agents. Collectors adhere to surfaces, making them hydrophobic, while depressants make surfaces hydrophilic. Activators alter the surface of particles to make them more receptive to the action of a collector. The activity of most of these reagents depends on the pH of the medium; therefore, it is important to adjust the pH value according to the reagents used.

2.6. Separation by Leaching

Leaching is a technique used to extract metals from ores. This process relies on the specific dissolution of a metal or mineral using a solvent, usually a chemical, which allows the metal to be separated from the remaining undissolved solid matter, known as gangue. This solvent, whether acidic, basic, or neutral, dissolves the precious or industrial metals present in the raw mineral, while impurities remain. For example, in oxidized copper ores, sulfuric acid is often used to dissolve the copper, while insoluble minerals such as silica or iron oxides remain unchanged. This dissolution allows the copper to be recovered in its liquid form, which can then be precipitated or extracted using chemical or electrolytic methods.

The objective of leaching is the transfer of a metal from a solid phase to an aqueous solution using a suitable solvent. Optimizing a leaching process involves defining the conditions that allow for maximum yield in a short time and at a minimum cost. The speed and yield of leaching depend on a large number of highly independent variables:

- Concentration of the agent (solvent)
- Particle size of the ore
- Liquid/solid ratio
- Temperature

- Leaching time
- Agitation.

3. CONCLUSION

Through this extended abstract, we have undertaken a comprehensive theoretical study of feldspar from the Aïn Barbar deposit, addressing both its mineralogical characteristics and aspects related to its extraction and valorization. The theoretical analysis of feldspars has allowed us to understand their composition, crystalline structure, and the most common impurities, thus laying the essential foundations for any processing approach. The experimental approach has enabled us to identify and determine the impurities that compromise the quality of Algerian feldspars and to present the most suitable purification techniques, particularly magnetic separation and flotation, to improve the quality of the finished product and meet industrial standards. These results offer concrete perspectives for optimizing the processes applied to Aïn Barbar feldspar.

REFERENCES

Abdessemed Chem's Eddine, M., Maifia, N., (2021) "Essais d'enrichissement de feldspath de la mine d'Aïn Barbar", Mémoire de projet de fin d'étude, École Nationale Polytechnique.

Akkali, R., (2005–2006) "Étude comparative des procédés minéralurgiques appliqués à la valorisation des feldspaths", Mémoire de Magister, École Nationale Polytechnique.

Belaidi, H., Kitouni, S., Chellat, S., (2024) "Evaluation of some granitic rocks of the Algerian coast as a source of feldspar raw material", Periodico di Mineralogia, 93 (1).

Cosmetics Europe, (2023) "Cosmetics Europe launches COSMILE Europe, a European ingredient database for information on 30,000 ingredients in 14 languages", Cosmetics Europe.

Dondi, M., Conte, S., Molinari, C., Zanelli, C., (2025) "Mineral resources for the ceramic industry: Survey of feldspathic raw materials in Italy", Minerals, 15 (1) 87.

Fuerstenau, D. W., Pradip., (2004) "Zeta potentials in the flotation of oxide and silicate minerals", Advances in Colloid and Interface Science.

Gougazeh, M., (2022) "Beneficiation and upgrading of low-grade feldspar ore in Medina, Saudi Arabia", Journal of Ecological Engineering, 23 (6) 271–277.

Habashi, F., (1997) "Electrochemistry: Past, present, and future", Aqueous Electrotechnologies: Progress in Theory and Practice, 351–366.

Han, F., Pardo, A., Ellis, R. A., (2020) "Students' self-report and observed learning orientations in blended university course design".
Horimek, M., (2002) "Contribution à la valorisation de la felsite d'Aïn-Barbar et de la pegmatite d'Aboudabouada par le procédé de séparation magnétique, flottation et lixiviation", École Nationale Polytechnique.

Ibrahim, S., Darwish, H., (2015) "Effect of SiO_2/B_2O_3 replacements on the structure, physicochemical and electrical properties of Bi_2O_3-containing glasses".

Imerys, (n.d.) "Feldspath", https://www.imerys.com/fr/mineraux/feldspath.

Kim, H.-K., Lee, H.-K., (2020) "Characteristics of CO_2 and energy-saving concrete with porous feldspar", Materials, 13 (18) 4204.

Maryem, E., (2021) “Evaluation de l’impact de l’exploitation minière sur l’environnement au niveau du bassin hydraulique de Sebou: Cas de la mine du Haut Beht (Maroc central)”.

Messaoudi, F., (2023) “Vers l’exploitation de la mine de feldspath de Tizi-Ouzou”, Energy Magazine DZ.

Odent, B. E., (1994) “Mémento roches et minéraux industriels: Feldspath et roches feldspathoïdes”, BRGM.

Paya, C. V., Smith, T. F., Razonable, R. R., et al., (2002) “Role of the laboratory in diagnosis and management of cytomegalovirus infection in hematopoietic stem cell and solid-organ transplant recipients”, Journal of Clinical Microbiology.

Singh, A. N., Raghubanshi, A. S., Singh, J. S., (2002) “Plantations as a tool for mine spoil restoration”, Current Science, 82 (12) 1436–1441.

Tucker, M. E., (2001) “Sedimentary petrology: An introduction to the origin of sedimentary rocks”, Blackwell Science.

Wills, B. A., Finch, J. A., (2016) “Wills’ Mineral Processing Technology: An Introduction to the Practical Aspects of Ore Treatment and Mineral Recovery”, Butterworth-Heinemann.

Winter, J. D., (2010) “Principles of igneous and metamorphic petrology”, Pearson Education.

Yardley, B. W. D., (1989) “An introduction to metamorphic petrology”, Longman.

Young, A. S., Veras, M. M., Neto, D., Petter, C. O., Sampaio, C. H., (2017) “Applications of automatic sensor-based sorting to mining ores”, Society for Mining, Metallurgy & Exploration.

Zahradník, J., Jirásek, J., Starý, J., Sivek, M., (2020) “Production, reserves, and processing of feldspar and feldspathoid rocks in the Czech Republic from 2005 to 2019—An overview”, Minerals, 10 (8) 722.

CHARACTERIZATION OF CONSTRUCTION AND DEMOLITION WASTES FOR VALORIZATION AS RAW MATERIALS RESOURCE

Hikmet SİS[1,*], Murat ERDEMOĞLU[1], Tufan KIYAK[1], M. Kürşat AYDEMİR[1], Kader ŞENTÜRK[1], Mustafa BİRİNCİ[1], İsmail BENTLİ[1], Didem EREN SARICI[1], Sema ERDEMOĞLU[2]

[1]İnönü University, Faculty of Engineering, Mining Engineering Department, Malatya, TÜRKİYE
[2]İnönü University, Faculty of Science and Arts, Chemistry Department, Malatya, TÜRKİYE
**Corresponding author: hikmet.sis@inonu.edu.tr*

A B S T R A C T

Construction and Demolition Waste (C&DW) contain a wide variety of materials, such as concrete, brick, marble, tile, asphalt, mortar, and plaster. Concrete is the most abundant man-made material in the world, and the cement production is one of the most CO_2 gas emitting industry that threatens human health and the planet. Therefore, recycling of C&DW as secondary materials in various industries is very important for the circular economy and preservation of natural resources. Currently, C&DW are mostly utilized in various applications such as coarse aggregate, fine aggregate, road base, and soling materials. Sequestering CO_2 into C&DW to produce recycled carbonated aggregate (RCA) is also gaining importance. Recent developments in recycling technologies enable recycling and valorization of various waste materials. But a comprehensive chemical and mineralogical characterization is required to assess their valorization potential. In this study, the characterization of C&DW, obtained from the earthquake waste disposal area in Malatya (Turkey), was studied for their valorization as a raw material resource. A range of tests, including elemental, XRD, XRF, ICP, Mineral Liberation Analysis (MLA), and TGA/DTA, were carried out for characterization. The results showed that C&DW have very complex composition and contains calcium carbonate as the main constituent. It also contains a notable amount of valuable materials, such as silicon (Si) and aluminum (Al). It was finally concluded that some valuable constituents can be extracted efficiently through a metallurgical route.

Key words: *Construction and demolition waste, characterization, mineral liberation analysis, concrete*

1. INTRODUCTION

C&DW is usually defined as the waste materials from operations of construction, reconstruction, alteration, extension, maintenance, and demolition of buildings and other infrastructure. More than 3.57 billion tons of C&DW are produced annually worldwide, and it accounts for more than a third of all solid waste generated (Patil et al., 2024). This enormous volume of waste addresses major environmental concerns, such as increased landfilling and leaching of harmful substances into soil and water systems. Increasing demand for concrete raises concerns over increasing C&DW volume, depletion of natural resources, and environmental degradation. Cement and natural aggregate are two essential materials for making concrete. Both are mineral-based materials, and their production also comes with several challenges.

Cement production generates large amounts of CO_2 and particulate emissions that also threaten climate, air quality, public health, and high energy consumption. Aggregates make up about 60-80 % of concrete volume, and their production accompanies with soil and biological degradation, noise and dust pollution, and additional waste generation. Increasing demand for natural aggregate (NA) raised concerns over the depletion of natural resources, as global aggregate demand is estimated to surpass 50 billion tons by 2025 (Patil et al., 2024). Therefore, recycling of C&DW presents a significant opportunity for environmental protection

as well as sustainable construction practices and the circular economy (Bianchini et al., 2005; Moschen-Schimek et al., 2023).

Mineral-based materials (e.g., concrete, brick, marble, tile, roof tile) constitute the primary component of C&DW, and there is a potential for them to be reused or recycled at a higher value. Their technical and economical recycling is challenging due to mixing with several organic, hazardous, or non-inert materials during demolishment, transportation, or dumping in landfills. But, the development and implementation of innovative approaches, which can properly process the waste to meet the standard of usage area, can foster sustainable recycling. Material characterization is one of the most important steps to understand whether their key properties are suitable for the task. A straightforward or a single analytical method cannot be enough for suitable characterization of such a complex structure, but it requires a combination of multiple characterization techniques.

Even though significant recycling studies were performed in the last decades, most of them lack a comprehensive characterization of C&DW (Bianchini et al., 2005; Bianchini et al., 2020). This study aims to determine the chemical and mineralogical properties of C&DW from the Malatya (Türkiye) region by performing multiple characterization techniques. The content and key properties of C&DW material were determined, and these properties were correlated with their possible valorization area. Limiting the usage of natural mineral resources can be beneficial for the sustainable development of the construction industry and the circular economy.

2. MATERIAL AND METHODS

2.1. Material

The samples were collected from the C&DW landfill site in Malatya (Türkiye) region. The collection of a representative sample is critical because of the vast volume of waste covering a very large area. Prior to sampling, the entire site was surveyed, visually examined, and 20 locations were marked to take representative samples. Metals, plastics, wood, and packaging materials are excluded as they already have well-established secondary markets and are not predominantly disposed of in landfills (HaitherAli and Anjali, 2024). Organic as well as of inorganic and organic mixtures materials (e.g., textile and asphalt) were also excluded.

The collected samples were transported to the mineral processing laboratories and laid out for drying for three days. The dried samples were weighted, and a total of 2216.17 kg of minerals was recorded. Then, all of the collected samples were mixed together and prepared for detailed characterization techniques. As seen in Fig. 1, as a simplified flowsheet, the dried samples were first crushed below 500 µm size by using jaw, roll, and hammer crushers, successively. Later, the crushed samples were classified by a 38 µm laboratory sieve to avoid over-grinding, and the coarser fraction was carefully ground below 38 µm size by a rod mill.
The ground ore was divided into 500-g representative samples by a rotary sample divider and stored in sealed plastic bags until the characterization test. The comminution and sieving processes were made dry to avoid the binding of particles together by the reaction of cement-containing fractions with water.

2.2. Method

The carried-out sample characterization tests includes elemental, mineral liberation analysis (MLA), X-ray diffraction (XRD), X-ray fluorescence (XRF), thermogravimetric/differential thermal (TGA/DTA), and inductively coupled plasma (ICP) analyses. For the elemental analysis, the Leco CHNS-932 (LECO Corporation, MI, USA) instrument at the Central Research Laboratory of İnönü University was used for the determination of C, H, N, and S

elements. Mineralogical and petrographic analyses were undertaken to identify the minerals or phases in the sample by utilizing MLA and XRD instruments at the Rare Earth Elements Application and Research Center of Munzur University (MUNTEAM). For analysis, a −106+75 µm size sample was prepared to obtain a narrow size range distribution as required by the ThermoFisher Scientific Scios 2 MLA instrument. Rigaku Miniflex 600 model XRD instrument, coupled with monochromatic Cu-Kα radiation (λ = 1.5405 Å), was utilized for XRD tests.

Chemical analysis was conducted by an XRF instrument (Malvern-Pananalytical, Epsilon 4) at the Mining Engineering Department of İnönü University and by ICP-OES instrument at Central Laboratories of Middle East Technical University, to determine the major oxides and elements in the samples, respectively. TGA/DTA analyses were performed to determine the thermal behavior of the sample by utilizing a Shimadzu TGA/DTA 50 instrument at the chemistry laboratories of İnönü University. The measurements were performed on 0.5 g samples in N_2 gas atmosphere between room temperature and 900 °C with a heating rate of 10 °C/min.

Particle size distributions of the ground samples were determined by the Malvern Mastersizer 2000 Particle Size Analyzer (Malvern Instruments Ltd., UK), which utilizes a laser diffraction technique. The results showed that the size distribution was unimodal and the D10, D50, and D80 sizes of the sample were 2.05 µm, 12.94 µm, and 48.96 µm, respectively.

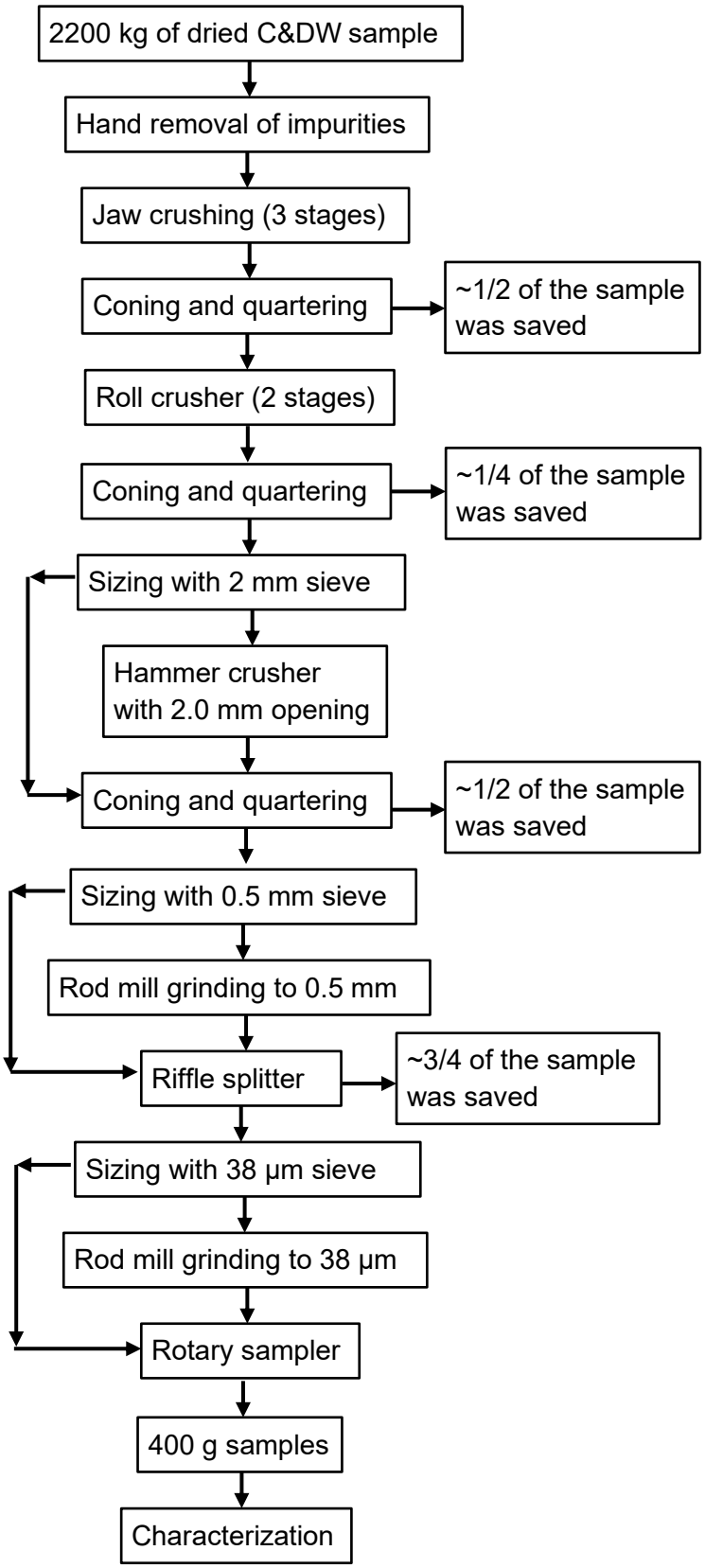

Figure 1. Simplified sample preparation flowsheet for characterization

3. RESULTS AND DISCUSSION

The XRD analysis allows the identification of crystalline phases. The results, given in Fig. 3, showed that the sample is mainly composed of calcite and quartz minerals. Some unidentified minor peaks such as, 2θ = 11.2°, 18.01°, 27.9°, and 31.0°, are also noticeable on the diffractogram. These peaks may belong to certain sintering products, such as larnite (Ca_2SiO_4), wollastonite ($CaSiO_3$), or mullite ($3Al_2O_3•2SiO_2$) in the sample, as they can form during the manufacturing of cement, ceramics, bricks, tiles, or porcelain, contained in the sample. Phase analysis Instrument's software may not match these phases categorically due to polycrystalinity or imperfect crystal structures. Relatively low concentrations of these phases also cause suppression of their peaks.

Elemental analysis of two ground samples showed that the sample contains 0.21 % S, 7.27 % C and 0.32 % H, on average, but no N element was detected. Results depict that the sample is rich in carbonate, which is in line with XRD results. The sulfur in the sample must originate from gypsum ($CaSO_4·2H_2O$), contained in wall plaster and cement.

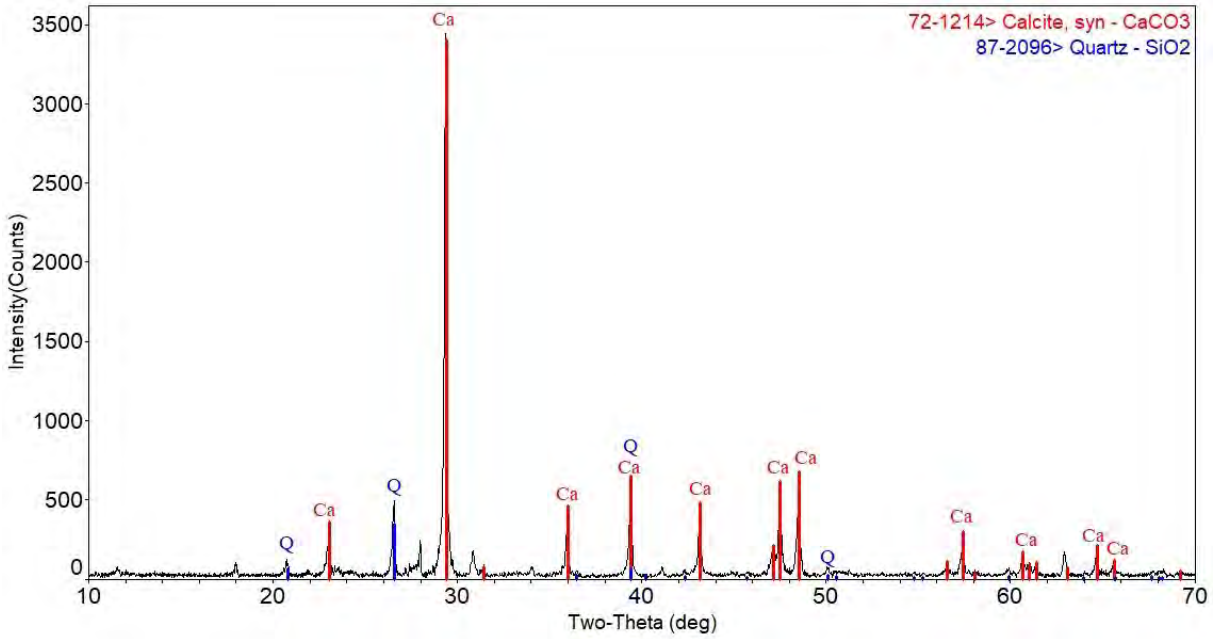

Figure 2. XRD analysis of the sample

XRF analysis of three samples was carried out and the average results are presented in Table 1, which indicates the presence significant amount of calcium carbonate (37.5 % CaO) and hence volatile material (29.39 % LOI) in the sample. The carbonate content of C&DW is expected to be high because of the utilization of calcium carbonate in cement and natural aggregates in concrete manufacturing. The results also revealed the presence of considerable amounts of Si (17.19 % SiO_2) and Al (4.05 % Al_2O_3), as well as some amount of Fe (2.35 % Fe2O3) and Mg (1.99 % MgO). The content of other components remained below 1 %. The presence 0.88 % SO_3 refers to the utilization of gypsum in cement production and wall plasters.

Table 1. XRF analysis of the samples

Component	Content, %
Al_2O_3	4.05
Fe_2O_3	2.35
SiO_2	17.19
CaO	37.55
TiO_2	0.29
MgO	1.99

SO_3	0.88
K_2O	0.54
CuO	0.14
ZnO	0.11
Others	5.53
LOI	29.39

TGA/DTA analysis was performed on the sample to correlate the mass loss at increased temperature, and the results are given in Figure 3. It is seen that a total of 30.79 % mass loss occurred in the temperature range of 25-1000 °C. The mass loss of 1.25 % in the temperature range of 45-150 °C and 1.44 % in the temperature range of 218-486 °C was attributed to the release of moisture and decomposition of hydrated components like gypsum, respectively. A sharp mass loss started at 650 °C and continued to about 800 °C indicated the decomposition of carbonates (mainly calcium carbonate) by the release of CO_2. The presence of a significant amount of carbonate materials was also proved by XRD (Figure 2) and XRF (Table 1) analyses. The DTA behavior shows that the reactions are endothermic, suggesting the absence of carbon-rich organic combustible materials.

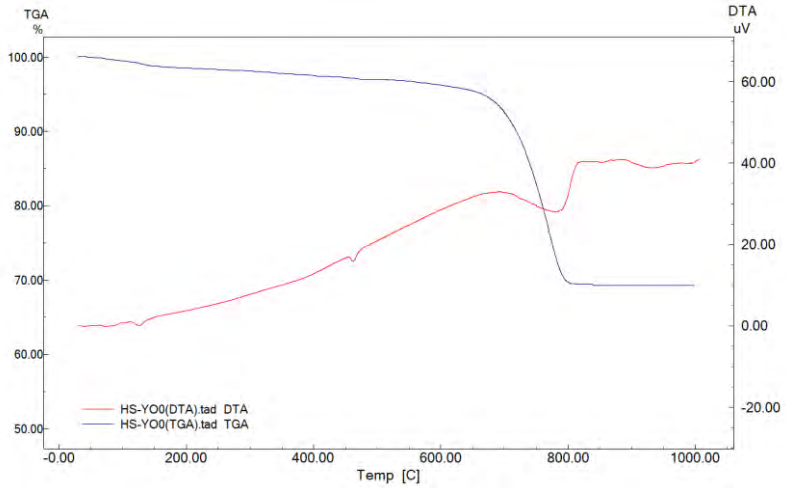

Figure 3. TGA/DTA analysis of the samples

The ICP-OES results of two samples and the average values are presented in Table 2, which indicates a high content of Ca (27 %), resulting from calcite mineral. The Si and Al contents were found to be significant, as 7.3 % and 2.3 %, respectively. The sample also contains 1.52 % Fe, 1.36 % Mg, 0.56 % Na, and 0.15 % Ti elements. Concentrations of Ni, Cu, Pb, and P elements remained below the detection limit of the instrument. The results obtained from the two different techniques (i.e XRF and ICP-OES) are largely consistent, with some deviations. The 0.965 % S achieved with ICP-OES seems to be significantly higher than Elemental (0.21 % S) and XRF (0.88 % SO_3) analysis. Considering that the ICP-OES analysis did not provide very reliable results for sulfur analysis and that high amounts of sulfur is not expected in these samples, XRF results should be more accurate.

Table 2. ICP-OES analysis of waste samples

Element	Sample 1	Sample 2	Average, %
Ca, %	27	27	27
Si, %	7.3	7.4	7.35
Al, %	2.3	2.3	2.3
Fe, %	1.52	1.53	1.525
Mg, %	1.36	1.38	1.37
S, %	0.95	0.98	0.965
Na, %	0.56	0.55	0.555

K, %	0.48	0.48	0.48
Ti, %	0.15	0.15	0.15
Zn, ppm	746	763	754.5
Ba, ppm	503	514	508.5
Mn, ppm	342	347	344.5
Cr, ppm	283	302	292.5
Ni, ppm	-	-	-
Cu, ppm	-	-	-
Pb, ppm		-	-
P, ppm	-	-	-

The MLA instrument provides quantitative mineral analysis and can create digital images of particles. The colored image of particles provided in Figure 4 clearly shows the complexity of the sample, as each particle consists of multiple phases and did not have a characteristic shape. All of the supplied images were carefully inspected, but no liberated particle was encountered. The instrument was able to classify (identify) calcite, dolomite, quartz, albite, zincite, lime, and wollastonite phases, but some phases remained unclassified. It is safe to state that the exposure of constituting raw materials to high temperature and extreme processing conditions caused distortion of original structures and also led to the formation of new and complex phases that might not be categorically identifiable by the software. Among the classified phases, calcite dominated the largest area with 88.6 %, and quartz held the second largest area with 8.77 %. No quantitative data on liberation were provided by the software because of insufficient classification and extreme complexity of the phases. But, it was generally inferred that MLA data markedly overlapped with XRD and XRF data.

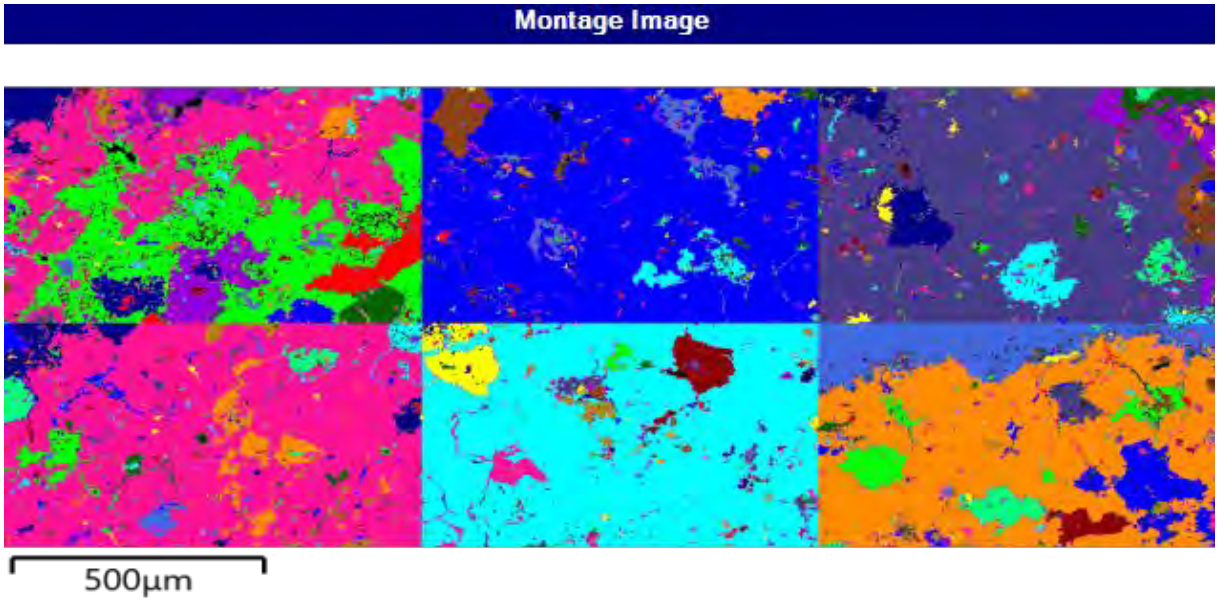

Figure 4. MLA analysis of the sample

4. CONCLUSIONS

In this study, C&DW materials obtained from the earthquake waste disposal area in Malatya (Turkey) were subjected to comprehensive chemical and mineralogical characterization tests. All of the utilized techniques, namely, XRD, XRF, ICP, elemental, mineral liberation analysis (MLA), and TGA/DTA, were found to be very useful for identifying the sample well. Despite some discrepancies, the data obtained by different techniques were very complementary. The MLA technique has been confirmed to be a reliable tool for the identification of most of the mineralogical phases to recognize the composition. It revealed that the sample was very

complicated, and the phase liberation level was quite low. Carbonates, explicitly calcium carbonate, are the most predominant material in the sample that also contains 17.19 % SiO_2 and 4.05 % Al_2O_3, as valuable materials. Beneficiation of constituents, such as carbonates, silicon, and aluminum, may be possible by hydrometallurgical processing techniques after fine grinding for proper liberation.

ACKNOWLEDGEMENT

We acknowledge the financial support of The Scientific and Technological Research Council of Türkiye (TÜBİTAK) through project number 214M294 and The Scientific Research Coordination Unit of İnönü University (Malatya) through project number FBG-2025-3887.

REFERENCES

Bianchini, G., Marrocchino, E., Tassinari, R., Vaccaro, C., (2005) “Recycling of construction and demolition waste materials: a chemical–mineralogical appraisal”, Waste Management, 25 (2) 149-159.

Bianchini, G., Ristovski, I., Milcov, I., Zupac, A., Natali, C., Salani, G. M., Marchina, C., Brombin, V., Ferraboschi, A., (2020) “Chemical characterisation of construction and demolition waste in skopje city and its surroundings (Republic of Macedonia)”, Sustainability, 12 (5) 2055.

HaitherAli, H., Anjali, G., (2024) “Sustainable urban development: Evaluating the potential of mineral-based construction and demolition waste recycling in emerging economies”, Sustainable Futures, 7 100179.

Moschen-Schimek, J., Kasper, T, Huber-Humer, M., (2023) “Critical review of the recovery rates of construction and demolition waste in the European Union – An analysis of influencing factors in selected EU countries”, Waste Management, 167 150-164.

Patil, Y. R., Dakwale, V. A., Ralegaonkar, R. V., (2024) “Recycling construction and demolition waste in the sector of construction”, Advances in Civil Engineering, 6234010.

CHARACTERIZATION OF MANGANOFERROUS (Fe-Mn) OXIDE ORE FROM TÜRKİYE-ŞIRNAK REGION

A. Ufuk DENİZ[1], Arman EHSANI[1,*], Fatih ÇAVUŞLU[2], Ilhan EHSANI[3]

[1]Adana Alparslan Türkeş Science and Technology University, Mining Engineering Department, Adana, TÜRKİYE
[2]Adana Alparslan Türkeş Science and Technology University, Materials Science and Engineering Department, Adana, TÜRKİYE
[3]Şırnak University, Mining Engineering Department, Şırnak, TÜRKİYE
**Corresponding author: aehsani@atu.edu.tr*

A B S T R A C T

This study aims to investigate the mineralogical and chemical characteristics of Fe-Mn ore obtained from Şırnak region (southeast of Türkiye). Analytical methods, including X-ray diffraction (XRD), X-ray fluorescence (XRF), scanning electron microscopy-energy dispersive spectroscopy (SEM-EDS), and mapping analysis, were applied to the sample. XRF results revealed the presence of iron and manganese oxides along with silicate gangue minerals in varying proportions. XRD analysis identified bixbyite, quartz, and goethite as the main mineral phases. SEM-EDS and mapping analyses were conducted to examine the microscopic distribution and coexistence of the minerals; manganese was mainly observed in oxide form, while iron appeared in both oxide and hydroxide phases. Overall, the findings indicate that the ore sample exhibits considerable mineralogical uniqueness and has a notable academic research and economic potential.

Key words: *Iron-manganese ore, manganese, bixbyite, characterization*

1. INTRODUCTION

Manganese (Mn), with atomic number 25 and atomic mass 54.94 g/mol, is a critical transition metal extensively used in steel production due to its deoxidizing, desulfurizing, and alloying properties. Approximately 90–95% of global manganese consumption is associated with the steel industry, where it enhances alloys, removes oxygen, and binds sulfur effectively (U.S. Geological Survey, 2021; Yi et al., 2017). Additionally, manganese has gained increasing importance in recent years with the rise of lithium-ion battery technologies, where it serves as a key component in cathode materials (Li et al., 2021).

Iron (Fe), with atomic number 26, is another essential industrial element and is commonly found alongside manganese in ore deposits. However, the coexistence of Mn and Fe minerals presents a challenge for beneficiation, as they often share similar physical and chemical properties (Ringdalen et al., 2021). Manganese ores are generally classified based on their Mn content. High-grade ores contain more than 44% Mn, medium-grade ores range between 35% and 44%, while low-grade ores contain less than 35% Mn. This classification is widely accepted in metallurgical studies and is used as a reference point for ore processing strategies (Gao et al., 2012). Also, in other words, according to the U.S. Bureau of Mines, ores containing at least 35% manganese are defined as manganese ore. Those containing between 10% and 35% manganese are classified as ferruginous manganese ore, while ores with manganese content between 5% and 10% are referred to as manganiferous iron ore. In modern industrial practices, even manganiferous iron ores with manganese grades as low as 2% are utilized (DPT, 2001).

Manganese deposits occur through a variety of geological processes and are commonly classified into three principal types: sedimentary, hydrothermal, and lateritic (Li and Xu, 2024).

The ferromanganese (Mn–Fe) ores in the Elazığ–Malatya region, in eastern Türkiye, occur at eight different localities, with the thickness of the mineralized levels ranging from 0.3 m to 10 m. Braunite, bixbyite, jacobsite, pyrolusite, manganite, and psilomelane are the main manganese oxide minerals. Hematite, barite, and pyrite are also found in variable amounts in the ferromanganese ores (Şaşmaz et al., 2014). Also, in the İspendere (Malatya) region, manganese minerals such as psilomelane, pyrolusite, and manganite occur as interlayers within clayey and siliceous sedimentary sequences (Yapıcı and Bahçeli, 2012). Additionally, in southeastern Türkiye, including the province of Şırnak, a variety of mineral deposits have formed as a result of long-term sedimentary and metamorphic geological processes. These processes have led to the remobilization and enrichment of certain pre-existing low-grade ores (containing Cu, Zn,Pb, Fe, Mn, Cr, P, and clay minerals). During these geological processes, Apatite-bearing magnetite mineralization is predominantly distributed across three main regions: Bitlis, Bingöl, and Adıyaman (Imamoğlu, 2005).

This study focuses on the mineralogical and chemical characterization of a manganese-bearing ore sample obtained from the Şırnak region in southeastern Türkiye. Prior to analysis, the collected ore sample was subjected to standard comminution processes, including crushing and grinding, in order to reduce particle size and ensure sample homogeneity. To evaluate the mineralogical composition, elemental content, and microstructural features of the ore, a combination of analytical techniques was employed, including X-ray diffraction (XRD), X-ray fluorescence (XRF), scanning electron microscopy (SEM-EDS), and mapping.

The findings aim to provide insight into the ore's composition and industrial potential, as well as to contribute to the broader understanding of Fe-Mn ore characterization in this geologically complex region. In other words, the findings aim to provide insight into the ore's composition and industrial potential, as well as to contribute to a broader understanding of Fe–Mn ore characterization in this geologically complex region, thereby laying a foundation for future research on cost-effective and environmentally sustainable extraction techniques.

2. MATERIAL AND METHODS

2.1. Material

Approximately 30 kilograms of raw ore samples were collected from the Şırnak region, located in southeastern Türkiye (Figure 1). The sample represents a localized occurrence and does not aim to statistically represent the entire mineral deposit. Upon arrival at the laboratory, the bulk sample was carefully laid out on clean trays and allowed to equilibrate with ambient laboratory humidity conditions for a period of ten days. This conditioning step was implemented to minimize moisture-related variability and to ensure consistency in subsequent analytical procedures.

Figure 1. The region where the ore is supplied (Şırnak Province in Southeastern Türkiye)

2.2. Method

After the humidity stabilization phase, the sample underwent size reduction using a jaw crusher (Baz Makina, Türkiye), reducing the material to a particle size of approximately 3.36 cm (mesh#6). The crushed sample was subsequently ground using a laboratory-scale ball mill (Yağmur Makina, Türkiye) for 30 minutes, and an agate mortar to achieve a final particle size of - 500 microns. After grinding, the sample was thoroughly homogenized through manual mixing, and representative subsamples were obtained using the coning and quartering method.

In order to prepare samples for XRF, XRD, and SEM analyses, the representative ground samples (obtained by sampling methods: coning and quartering method, grid base sampling), were further finely ground using an agate mortar grinder (Retsch RM200- Germany) for 15 minutes. This procedure ensured that the particle size and sample uniformity were appropriate for accurate instrumental analysis. Following this fine grinding step, a grid-based sampling method was applied to ensure representative sample selection for XRD, XRF, SEM-EDS, and analysis. The powdered sample was evenly spread on a clean flat surface, and equal-sized amounts were systematically collected from across a marked grid. This method ensured a representative cross-section of the entire sample.

The selected portions were recombined and homogenized, then divided into three separate subsamples for X-ray fluorescence (XRF), X-ray diffraction (XRD), scanning electron microscopy-Energy Dispersive Spectroscopy (SEM-EDS), and mapping analyses. They were stored in labeled, airtight polyethylene containers under stable laboratory conditions.

The particle size distribution of the crushed and ground ore sample was determined using a standard sieve analysis in accordance with ASTM standards. The procedure was conducted using stainless steel test sieves produced by Retsch, and the AS 200 model sieve shaker, also manufactured by Retsch, was employed to ensure uniform vibration and accurate particle separation.

X-ray diffraction (XRD) analysis was conducted to identify the crystalline phases (i.e., minerals) present in the ore samples. The analysis was performed using a Rigaku MiniFlex 600 diffractometer (Japan), equipped with Cu-Kα radiation (λ = 1.5406 Å) operating at a tube voltage of 40 kV and a current of 15 mA. Measurements were carried out in θ/2θ mode under the following conditions: scan range: 5°–65° (2θ); scan speed: 2°/min, and step size: 0.02° (default of instrument).

The chemical composition of the powdered ore samples was determined using a Rigaku ZSX Primus II wavelength-dispersive X-ray fluorescence (WDXRF) spectrometer (Japan). The analysis was conducted on pressed powder samples without a binder. The instrument was calibrated using certified reference materials (CRM), and measurements were carried out under vacuum conditions. The analysis quantified major oxides such as MnO, Fe_2O_3, SiO_2, Al_2O_3, CaO, and MgO, along with selected trace elements.

Scanning Electron Microscopy (SEM) analysis was performed using an FEI Quanta FEG 650 (USA) microscope at the Central Laboratory of Çukurova University. The instrument is equipped with EDS and mapping capabilities, allowing for microstructural and elemental characterization of the samples. Prior to analysis, samples were gold-coated to ensure conductivity. SEM-EDS was used to observe grain boundaries, mineral associations, and elemental distributions.

3. RESULTS AND DISCUSSION

Sieve analysis is a widely used method to determine the particle size distribution of a given sample. In mineral processing, it provides essential data regarding the proportion of coarse and fine particles, helping to evaluate the efficiency of comminution processes and the suitability of materials for subsequent beneficiation operations. The analysis involves passing a dried sample through a stack of sieves with progressively smaller mesh sizes, measuring the retained mass on each sieve, and constructing a cumulative distribution curve.

The particle size distribution of the ore sample (Figure 2) shows a relatively wide particle size distribution, with the values of $d_{25} \approx 92$ µm, $d_{50} \approx 141$ µm, and $d_{80} \approx 341$ µm, which all the curves indicate a uniform and well-distributed particle size profile of the ore sample after size reduction processes.

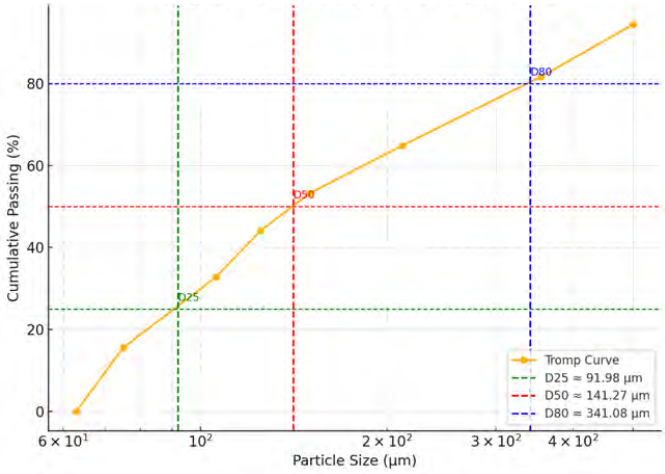

Figure 2. Particle size distribution graphs of the ore sample

X-ray diffraction (XRD) analysis was conducted to identify the crystalline phases present in the ore sample (Figure 3). The measurement was carried out over a 2θ range between 5° and 65° using Cu Kα radiation at 40 kV and 15 mA. The resulting diffraction pattern displayed several distinct peaks, notably at 26.68°, 33.14°, 36.63°, 50.20°, and 60.05°. Table 4 shows the identified phases and corresponding peaks of XRD analysis for the ore sample. These phases were determined through qualitative matching of the peak positions with standard reference patterns.

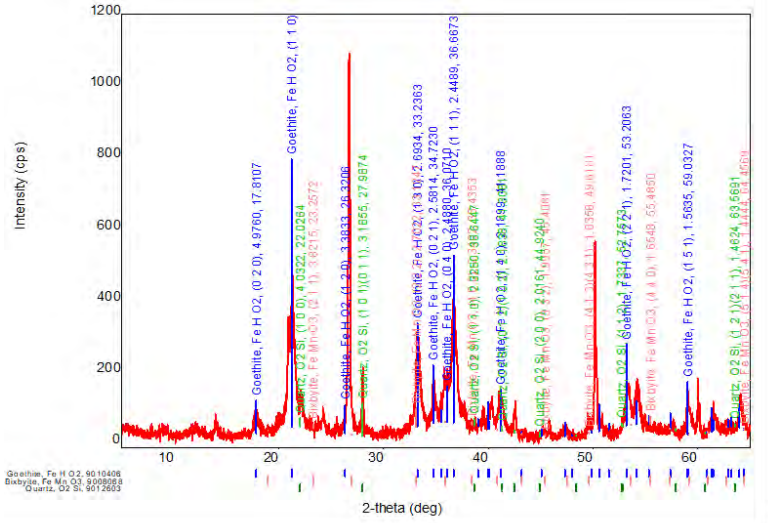

Figure 3. XRD pattern of the ore sample.

The most intense peak at 26.69° is characteristic of quartz (SiO_2), which is commonly found in siliceous matrices. The peak observed at 50.20° is associated with bixbyite $(Fe\text{-}Mn)_2O_3$, a manganese-iron oxide, indicating the presence of manganese-bearing phases. The peak near 36.63° is attributed to goethite (FeO-OH), reflecting the iron content of the sample (Figure 6).

The diffraction data suggest that the ore sample consists of a mixed silicate and oxide composition, dominated by quartz (SiO_2), goethite (FeO-OH), and bixbyite $(Fe\text{-}Mn)_2O_3$. The presence of bixbyite is particularly significant as it indicates the existence of Fe-Mn oxide phases with potential metallurgical importance. The simultaneous identification of quartz implies a siliceous gangue component within the mineral matrix.

The chemical composition of the ore was determined by X-ray fluorescence (XRF) analysis, which revealed that the sample is dominated by iron and manganese oxides, accompanied by a moderate amount of silicate gangue (Table 1). Elemental results show that Fe and Mn are present at 29.7% and 9.77%, respectively, while oxide data reports 49.3% Fe_2O_3 and 14.6% MnO.

Table 1. XRF analysis (major phase and elements) of the ore sample

Component	Fe_2O_3	MnO	SiO_2	Al_2O_3	CaO
Content (%)	49.3	14.6	18.6	4.14	0.769
Element	Fe	Mn	Si	Al	Na_2O
Content (%)	29.7	9.77	7.91	2.00	0.544

The sample also contains SiO_2 at 18.6% and Al_2O_3 at 4.14%, along with minor oxides such as K_2O, Na_2O, MgO, and CaO, suggesting a silicate-alumina gangue structure. Trace elements like Ti, P, S, Zn, and Pb are present in low concentrations and are not expected to significantly impact beneficiation.

Overall, the chemical composition of the manganoferrous ore sample indicates a relatively manganese-enriched iron ore with reasonable gangue content. As mentioned in the introduction section, despite its low grade (i.e., below %30 Mn), the ore contains bixbyite $(Fe\text{-}Mn)_2O_3$ which has unique academic and scientific research potential and also enrichment potential compared to even lower-grade ores (i.e., ores lower than 9% Mn).

SEM images of the ore sample were captured at various magnifications. The sample displays coarser, angular, and fractured particles with porous textures. At lower magnifications (i.e., 100×–500×), larger grains are clearly visible, while at higher magnifications (10,000×–40,000×), some particles appear to have fine-grained secondary phases attached (Figures 4). In short, SEM analysis results of the sample are in agreement with the sieve analysis results in terms of particle size, especially at low magnifications (100×–500×).

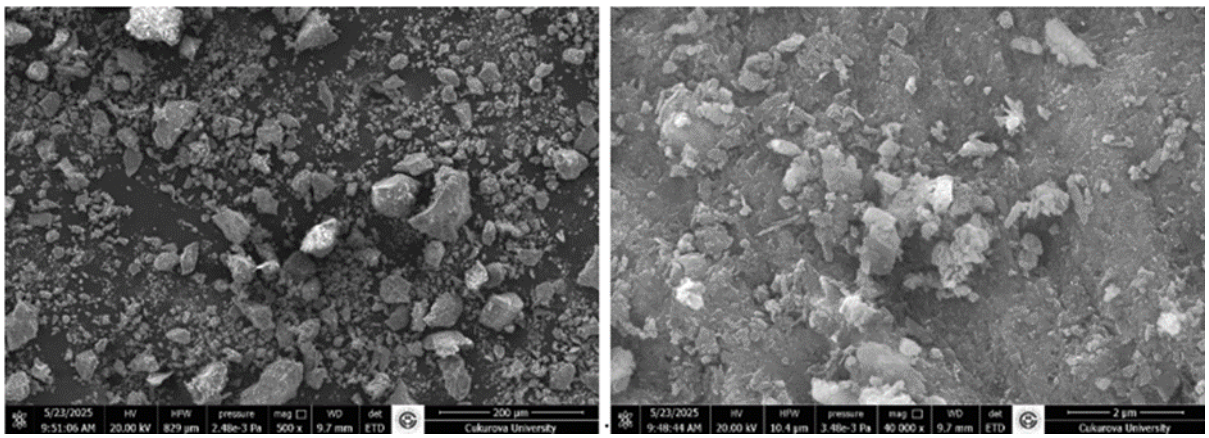

Figure 4. SEM analysis of the ore sample (Left: Mag 500; Right: Mag 40000)

EDS analysis was conducted to identify the elemental composition of selected areas of the sample's surfaces. The results provided qualitative and semi-quantitative information regarding the elements present within the scanned regions. In the ore sample, elements such as oxygen, silicon, aluminum, iron, and manganese were detected. The relative intensities and elemental types in the sample reflect differences in surface chemistry. These results complement the SEM observations by offering insight into the surface-level elemental distribution (Figure 5).

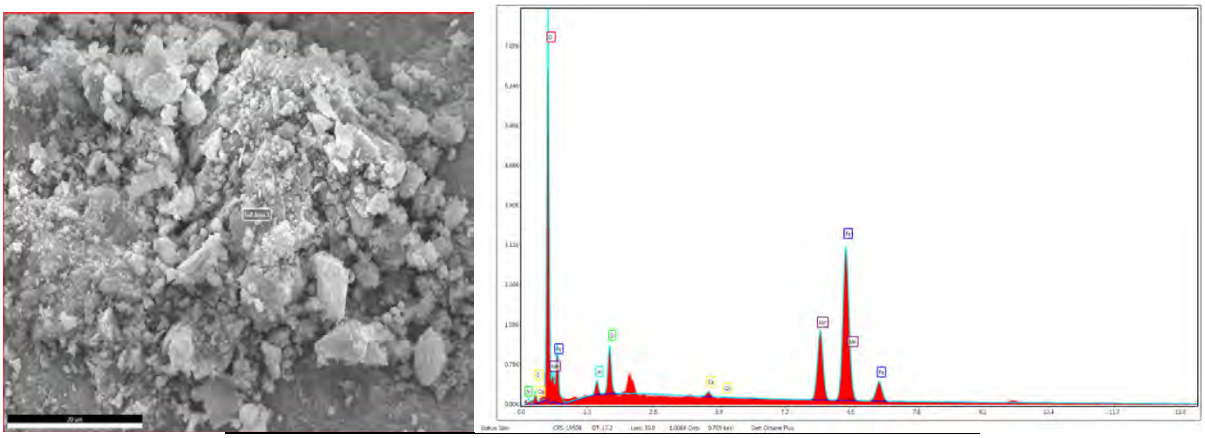

eZAF Smart Quant Results

Element	Weight %	Atomic %	Net Int.
C K	3.51	7.77	70.59
O K	36.84	61.25	2914.45
FeL	35.77	17.04	423.53
AlK	1.17	1.15	125.63
SiK	3.64	3.45	496.06
CaK	0.55	0.36	67.98
MnK	18.52	8.97	1236.75

Figure 5. EDX analysis of the ore sample (Fe, O, Mn, and Si are the main detected elements)

Elemental mapping analyses illustrate the surface distribution of major elements in the samples. In the ore sample, iron, manganese, and oxygen signals are more intense and widely spread. This distribution may indicate a surface dominated by Fe- and Mn-bearing oxide phases. The overlapping presence of these elements could also suggest the occurrence of mineral phases containing both iron and manganese (Figure 6). In other words, the strong association between Fe, Mn, and oxygen suggests the presence of mixed iron–manganese oxide minerals, most likely bixbyite ($(Fe,Mn)_2O_3$), which is consistent with the XRD results.

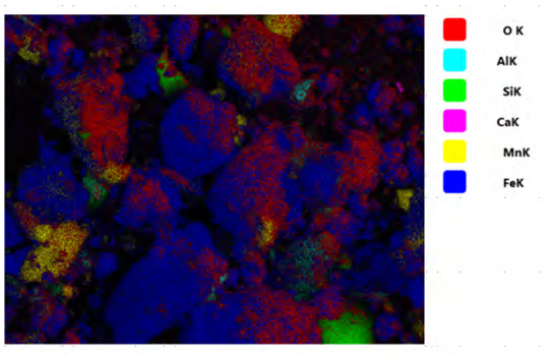

Figure 6. Mapping pattern of the ore sample (Fe and Mn bearing oxide phases are the most intense phases).

4. CONCLUSION

In this study, the mineralogical, chemical, and microstructural characteristics of a Fe-Mn ore sample from Şırnak region were investigated using XRD, XRF, SEM-EDS, and mapping techniques. The aim was to determine their compositional differences and assess their potential for academic research. The findings apply only to the investigated sample and should be interpreted as preliminary and site-specific.

The XRD results revealed that the ore sample mainly consists of goethite (FeO-OH), bixbyite (Fe-Mn oxide), and quartz (SiO_2), indicating a significant Fe-Mn oxide mineralization with silicious gangue content. XRF analyses confirmed these findings by showing that the ore sample contains ~14.6% MnO and ~49.3% Fe_2O_3. These values clearly show that the ore sample is a manganoferrous ore (with a grade of %9 Mn (below %30)) and silicious gauge minerals (18.6% SiO_2). SEM and EDS observations supported the above results by showing that the ore sample has a relatively compact and homogenous grain structure, with Fe and Mn-rich areas. Mapping analysis further illustrated that Fe and Mn are spatially associated in the ore, implying mineral coexistence within bixbyite ($(Fe\text{-}Mn)_2O_3$).

Moreover, to understand the complex mineral associations and phase distributions, additional analyses such as Mineral Liberation analyses (MLA) and Fourier Transformed Infrared Spectroscopy (FT-IR) are planned to be conducted on the Fe-Mn ore.

In conclusion, the manganoferrous ore sample shows notable scientific/academic research due to the existence of bixbyite mineral, as a unique mineral, and its relatively high metal content (Mn: 10%), low gangue, and mineralogical coherence. Therefore, the manganoferrous ore sample with notable content of Mn (10% Mn) can be evaluated in academic research studies, due to the uniqueness of Fe-Mn bearing mineral, and the economic resource of Mn, after applying appropriate ore beneficiation methods.

REFERENCES

Devlet Planlama Teşkilatı (DPT)., (2001) “Madencilik özel ihtisas komisyonu raporu”, ÖİK Report No: 640, Ankara (in Turkish).

Gao, Y., Olivas-Martinez, M., Sohn, H. Y., Kim, H. G., Kim, C. W., (2012) “Upgrading of low-grade manganese ore by selective reduction of iron oxide and magnetic separation”, Metallurgical and Materials Transactions B, 43 (6) 1465–1475.

Imamoğlu, M. Ş. (2005) “Güneydoğu Anadolu bölgesi ve yakın yöresinin maden yatakları yönünden değerlendirilmesi“, Doğu ve Güneydoğu Anadolu Maden Kaynaklarının Değerlendirilmesi Sempozyumu Bildiriler Kitabı, 87–92.

Li, H., Xu, W., (2024) “Geological and economic assessment of manganese deposits”, International Journal of Ecology and Environmental Sciences, 6 (2) 28–31.

Li, H., Zhang, W., Sun, K., Guo, J., Yuan, K., Fu, J., Zhang, T., Zhang, X., Long, H., Zhang, Z., Lai, Y., Sun, H., (2021) “Manganese-based materials for rechargeable batteries beyond lithium-ion”, Advanced Energy Materials”, 11 (25) 2100867.

Ringdalen, E., Gjøvik, J. E., Larssen, T. A., Tangstad, M., (2021) “Pretreatment of manganese ores in different gas-atmospheres- a method to reduce energy consumption and co_2 emissions in mn-alloy production”, Proceedings of the 16th International Ferro-Alloys Congress (INFACON XVI), 1–12.

Şaşmaz, A., Türkyilmaz, B., Öztürk, N., Yavuz, F., Kumral, M., (2014) “Geology and geochemistry of Middle Eocene Maden complex ferromanganese deposits from the Elazığ–Malatya region, eastern Turkey”, Ore Geology Reviews, 56 352–372.

U.S. Geological Survey. (2021) “Mineral Commodity Summaries”, U.S. Geological Survey.

Yapıcı, N., Bahçeli, A., (2012) “Battalgazi (Malatya) bölgesi manganez cevherleşmelerinin mineralojik, jeokimyasal özellikleri ve zenginleştirilebilirliliğinin araştırılması”, Çukurova University Journal of the Faculty of Engineering and Architecture, 27 (2) 61–71.

Yi, L., Huang, Z., Jiang, T., Zhao, P., Zhong, R., Liang, Z., (2017) “Carbothermic reduction of ferruginous manganese ore for mn/fe beneficiation: morphology evolution and separation characteristic”, Minerals, 7 (9) 167.

DIRECT RECYCLING OF GRAPHITE: LINKING MINERAL PROCESSING WITH NANOSTRUCTURAL RESTORATION

Eray TABAK[1,2,*], Recep BAKAR[3], Sadullah ÖZTÜRK[2], Şahika Sena BAYAZİT[2], Birgül BENLİ[1,4]

[1]Istanbul Technical University, Graduate School, Nano Science and Nano Engineering Programme, 34469, Istanbul, Türkiye
[2]Istanbul University-Cerrahpasa, Institute of Nanotechnology and Biotechnology, 34500, Istanbul, Türkiye
[3]Energy Storage & Charging Department, Togg, Gebze, Kocaeli 41400, Türkiye
[4]Istanbul Technical University, Faculty of Mines, Dept. of Mineral Processing Eng., 34469, Istanbul, Türkiye
**Corresponding author: benli@itu.edu.tr*

A B S T R A C T

The direct recycling of graphite, the anode material in lithium-ion batteries, is comprehensively examined in this study. The research integrates mineral processing techniques with a nanostructural regeneration approach. Graphite is a vital component of modern battery technologies due to its high electrical conductivity, chemical stability, and capacity for lithium intercalation. However, traditional pyrometallurgical and hydrometallurgical recycling methods primarily focus on recovering valuable metals, while degrading the graphite structure, which subsequently requires energy-intensive synthesis processes for reuse. The direct recycling approach aims to restore the performance of electrode materials by preserving their crystal structure and morphology. While graphite can be recovered from black mass with over 90% efficiency via flotation following mechanical pre-treatment, preserving its structural integrity, the process remains inherently complex due to surface impurities, heterogeneous phase composition, limitations in particle liberation and selectivity, and the requirement for precise reagent optimization. Furthermore, the study evaluates relithiation methods for cathodes and purification techniques for graphite anodes, including thermal, chemical, electrochemical, and hybrid approaches. The findings indicate that direct recycling significantly reduces energy consumption and lowers global warming potential by 70–96%, while generating high economic added value. In addition, Türkiye's graphite resources are recognised as a strategic raw material for battery production and recycling. In conclusion, the direct recycling approach offers a strong alternative for sustainable battery technologies from environmental, economic and technological perspectives.

Key words: *Direct recycling, graphite, battery technology, physical separation*

1. INTRODUCTION

Graphite is recognized as a strategic resource supporting 21st-century high technologies due to its unique physical and chemical properties. Its combination of metallic properties (such as electrical and thermal conductivity) and non-metallic properties (including high thermal resistance, chemical inertness and lubricity) makes it indispensable to modern industry. Classified as a “Critical Raw Material” by the European Union, graphite is a key component in essential sectors such as lithium-ion batteries, nuclear reactors, aerospace, and steel production (Kaya et al., 2009; Tian et al., 2024). Figure 1 shows various applications of graphite in the energy sector.

Figure 1. Schematic illustration of graphite applications in energy storage systems

Graphite is a layered allotrope of carbon with a hexagonal crystal structure formed by sp^2 hybridisation. These layers are bonded internally by strong covalent bonds and stacked together by weak van der Waals forces. This crystal architecture provides graphite with high electrical conductivity, chemical stability, and excellent intercalation capacity. Due to these properties, graphite is the most widely used anode material, particularly in lithium-ion batteries (LIBs). (Chung, 2002; Zhang, 2011). Consequently, the recovery and regeneration of graphite from spent lithium-ion batteries have attracted significant attention, prompting the development of various recycling strategies.

Spent battery recycling strategies are generally classified into three main categories: pyrometallurgical, hydrometallurgical and direct recycling approaches (Y. Bai et al., 2020; Yu, Bai, Polzin, et al., 2024). These methods employ various physical, chemical, and electrochemical techniques to recover valuable components from complex electrode materials. For example, commonly reported techniques in lithium-ion battery recycling, including acid leaching (Nitta et al., 2015; Yu et al., 2023), direct delamination (Guo et al., 2023), solvent extraction (Kang et al., 2010), hydrothermal treatment (Gao et al., 2023), membrane separation (Wagh et al., 2023), and electrochemical processes (Kim et al., 2021). Pyrometallurgical and hydrometallurgical methods primarly focus recovering valuable elements through thermal or chemical decomposition. In contrast, direct recycling aims to preserve and restore the original structure and functionality of electrode materials without breaking them down into their elemental constituents. This approach offers several advantages, including lower energy consumption, reduced chemical usage, and preservation of the microstructure, physicochemical and surface chemistry of active materials. As a result, direct recycling has emerged as a promising and sustainable strategy, particularly for structurally sensitive materials such as graphite, whose electrochemical performance strongly depends on crystallographic integrity, defect structure, and surface properties (Yu, Bai, & Belharouak, 2024).

Another important step is the pre-treatment process, which involves discharging the battery to eliminate residual charge, followed by the removal of external components such as frames, cables, and electronic circuits. Subsequently, individual materials, including plastics, metals, electrolytes, and electrodes are separated to obtain the black mass containing the active electrode materials (Figure 2) (Barbosa de Mattos et al., 2025).

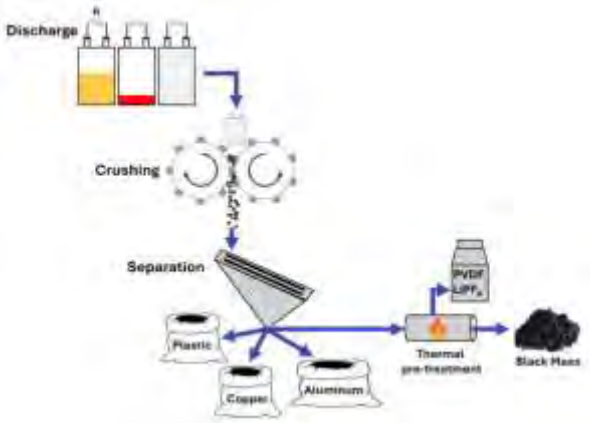

Figure 2. Illustration of mechanical and separation processes used to recover black mass (Barbosa de Mattos et al., 2025)

Figure 3 presents the flowchart illustrating the details of the direct recycling process. From a mineral processing perspective, graphite recovery from spent batteries relies primarily on physical separation techniques. Graphite exhibits natural hydrophobicity, which enables its efficient separation using froth flotation. During flotation, graphite selectively attaches to air bubbles and separates from hydrophilic cathode materials, such as lithium metal oxides. Recovery efficiencies exceeding 90% have been reported under optimized flotation conditions. Flotation is a key mineral processing technique that enables the selective separation of graphite from cathode materials after pre-treatment, allowing its recovery without structural degradation and facilitating its direct recycling (Bhar et al., 2023).

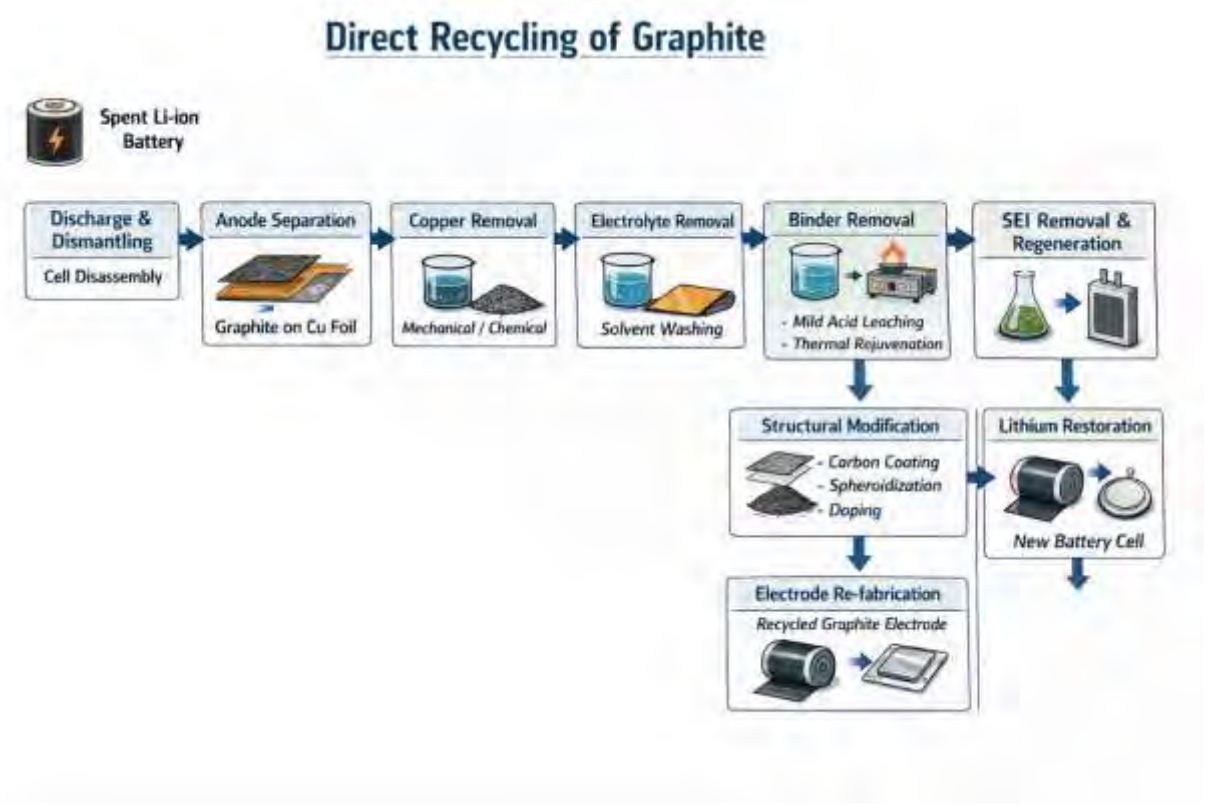

Figure 3. Flowsheet of the direct recycling process

2. TYPES OF GRAPHITE

Graphite can be broadly divided into two principal categories (natural graphite and synthetic graphite) based on its origin and formation mechanism. Natural graphite is formed through geological processes over geological timescales, whereas synthetic graphite is produced through the controlled graphitization of carbon-rich precursor materials at elevated temperatures, typically between 2,300 and 3,000 °C. Conventional synthetic graphite is primarily derived from petroleum coke and coal tar pitch, which enable precise control over purity, crystallinity, and particle morphology. In addition to fossil-based precursors, increasing attention has been directed toward sustainable sources such as biomass-derived carbon, including lignin, cellulose, and agricultural waste. These renewable precursors offer environmentally friendly alternatives for producing synthetic graphite with tunable microstructure, defect density, and nanoscale properties, enhanced ion transport pathways, and potential quantum confinement effects at reduced crystallite sizes.

Natural graphite is primarily classified into three main types based on its geological formation and physical structure: microcrystalline (amorphous), vein (lump), and crystalline flake graphite (Simandl et al., 2015). he morphology and size characteristics of different natural graphite types are shown in Figure 4.

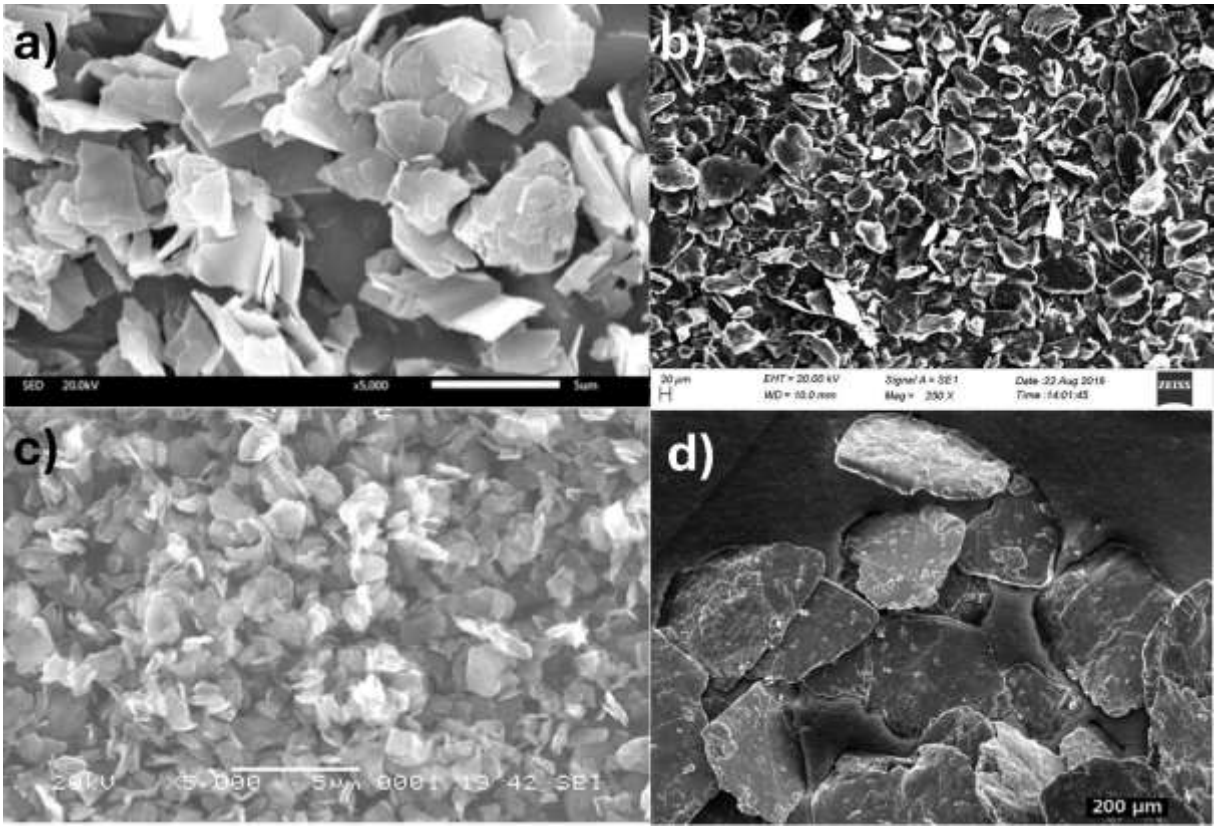

Figure 4. SEM images illustrating the size and morphology of different graphite types: (a) amorphous graphite (Wang et al., 2017), (b) vein graphite (Somaweera et al., 2022), and (c-d) flake graphite (Lai et al., 2012; Meyer-Plath et al., 2015)

2.1. Flake Graphite

Flake graphite occurs as flat, sheet-like particles within metamorphic rocks such as schist, marble, and gneiss. It exhibits a layered, anisotropic structure, with high electrical and thermal conductivity parallel to the basal planes, while conductivity perpendicular to these planes is significantly lower. Flake graphite demonstrates high reversible capacity and high initial Coulombic efficiency (ICE), making it highly suitable for electrochemical energy storage

applications. Its carbon purity typically ranges from 85% to 97% although higher purities exceeding 99% can be achieved through beneficiation and purification processes (*What Role Does the Flake Graphite Play in Our Lives?*, n.d.), which makes it the most critical graphite type for advanced technological applications. Due to its high crystallinity and structural stability, it is the most important graphite type for advanced technological applications. Through mechanical processing, flake graphite can be transformed Physically rolling it into "spherical graphite", which is particularly suitable for use as an anode material in lithium-ion batteries. In addition to battery applications, flake graphite is widely used in refractory materials and lubricants due to its excellent thermal stability and lubricating properties (Dehaine et al., 2020; Kalyoncu et al., 2014; Simandl et al., 2015).

2.2. Vein or Lump Graphite

Vein graphite is found in rock fractures within host rocks, typically forming vein-like or pipe-like structures. It is generally considered to be of hydrothermal origin. This graphite type has a massive structure and is among the purest naturally occurring forms of graphite, with carbon contents ranging from 90% to 99%. The world's most significant deposits are located in Sri Lanka. Due to its high purity and excellent electrical conductivity, vein graphite is commonly used in specialised carbon products and electrical components such as motor brushes. Although it was historically used extensively in refractory applications, it has largely been replaced by flake graphite in this sector (Dehaine et al., 2020; Kalyoncu et al., 2014).

2.3. Microcrystalline (Amorphous) Graphite

Microcrystalline graphite forms through the metamorphism of coal deposits. The term 'amorphous' (meaning 'shapeless') is a commercial designation, as this material consists of very small crystallites with low crystallinity rather than a truly amorphous structure. It typically contains higher percentage of ash and mineral impurities, which can be difficult to remove using conventional beneficiation processes. It exhibits relatively isotropic properties at the macroscopic scale and demonstrates good cycle stability due to its lower volumetric expansion during electrochemical cycling. Microcrystalline graphite is commonly used as a carbon additive in steel production, foundry coatings, lubricants, and pencil manufacturing (Beyssac & Rumble, 2014; Kalyoncu et al., 2014; Simandl et al., 2015).

2.4. Synthetic Graphite

In addition to natural graphite, synthetic graphite is produced through the high-temperature graphitization of carbon-rich precursor materials such as petroleum coke and coal tar pitch. This process typically occurs at temperatures between 2,300 and 3,000 °C, resulting in highly ordered graphite structures. Synthetic graphite generally exhibits higher purity, improved structural uniformity, and longer cycle life compared to natural graphite. However, its production is energy-intensive and associated with significantly higher costs (Dehaine et al., 2020).

2.5. Expanded Graphite and Graphene

Graphite also serves as a precursor material for advanced carbon materials such as expanded graphite and graphene. Expanded graphite is produced by chemically treating flake graphite followed by rapid thermal expansion, which causes separation and expansion of the layered structure. It is widely used in sealing products, thermal management systems, and conductive foils. Graphene, a single atomic layer of graphite, possesses exceptional electrical, thermal, and mechanical properties. Often referred to as a 'miracle material', graphene has significant potential in advanced applications, including energy storage, sensors, electronics, biomedical devices, and additive manufacturing technologies.

2.6. Graphite Resources in Türkiye

Türkiye possesses significant graphite resources, primarily in the form of amorphous and crystalline flake graphite deposits. The total graphite reserve in Türkiye is estimated to be approximately 90 million tons, making it one of the countries with substantial graphite potential globally (Kaya et al., 2009; Tian et al., 2024).

The most important amorphous graphite deposits are in the Kütahya–Oysu region, which represents the only currently active graphite mining area in Türkiye. These deposits typically exhibit moderate carbon grades and are mainly used in industrial applications such as refractories, foundry coatings, and carbon additives. High-quality coarse crystalline graphite has been reported in the Balıkesir (Susurluk) region, while additional prospective graphite-bearing areas have been identified in Adıyaman (Sincik), Konya (Derbent), and Kastamonu. Most graphite occurrences in Türkiye are characterized by microcrystalline graphite disseminated within metamorphic host rocks, which are generally classified as amorphous graphite according to global graphite classification systems. In contrast, graphite-bearing formations in regions such as Kütahya, Bandırma, Konya, Kastamonu, and Muğla commonly exhibit transitional characteristics between semi-graphite and meta-anthracite, reflecting intermediate degrees of metamorphic transformation. Other carbonaceous occurrences found throughout Türkiye are generally associated with meta-anthracite and represent organic matter that has undergone relatively lower degrees of graphitization (*Grafit – İstanbul Maden İhracatçıları Birliği*, n.d.). Flake graphite deposits are particularly important due to their higher crystallinity and suitability for high-value applications such as lithium-ion battery anode materials. With the increasing demand for graphite in energy storage technologies, these domestic resources represent a strategically important raw material for future battery production and recycling initiatives.

3. IMPORTANCE OF DIRECT RECYCLING FOR BATTERY TECHNOLOGIES

Graphite plays a critical role as the primary anode material in modern battery technologies, particularly in lithium-ion batteries (LIBs). Its widely use is primarily attributed to its low lithium intercalation/extraction potential and excellent electrical conductivity. During battery operation, lithium ions intercalate between graphite layers to form the LiC_6, which provides a theoretical specific capacity of 372 mAh/g and a volumetric capacity of approximately 840 mAh/cm³ (Dusastre, 2001). Graphite maintains its structural stability during repeated charge and discharge cycles, enabling efficient Lithium-ion diffusion and long cycle life.

Natural flake graphite is commonly processed into spherical graphite to improve packing density, electrode uniformity, and electrochemical performance. In terms of market share, synthetic graphite accounts of 58% of battery-grade graphite production, while natural graphite represents approximately 39% (Zhao et al., 2022). Natural graphite is preferred due to its low production cost, superior processability, and smaller environmental footprint compared to synthetic graphite. While flake graphite offers high capacity, microcrystalline graphite improved rate capability under certain conditions. Synthetic graphite, offering higher purity and longer cycle life, is associated with higher energy consumption and production costs (Wu et al., 2002; Yazici et al., 2005).

To be used as an anode material in lithium-ion batteries, natural graphite must be converted into spherical graphite through a series of physical and chemical processes. This involves transforming crystalline flake graphite into high-purity, spherical particles suitable for electrochemical applications (Huang et al., 2001). Crystalline flake graphite concentrate is typically used as the primary raw material for producing spherical graphite, with an initial carbon content of approximately 95% (L. Z. Bai et al., 2013; Huang et al., 2001). The flakes are mechanically reduced in size and reshaped into rounded particles resembling 'potatoes',

rather than retaining their original flake morphology. The flexible layered structure of graphite enables these particles to be transformed into spherical shapes. For efficient battery performance, graphite must possess very high purity. Therefore, the mechanically shaped graphite undergoes chemical purification processes to increase its carbon content to approximately 99.9%. In the final stage, surface coating treatments are applied to enhance the electrochemical performance and cycle life of the spheroidised and purified graphite. Spherical graphite is a critical material in lithium-ion technology due to its superior performance as an anode material, and its demand rapidly increasing due to the growth of electric vehicle market (Luo et al., 2022; Tian et al., 2024; Zhao et al., 2022).

The recycling of lithium-ion batteries has become increasingly important, and the methods developed for this purpose are generally classified into three main categories: pyrometallurgical, hydrometallurgical and direct recycling (Xu et al., 2023). Pyrometallurgical recycling is a well-established approach with a high processing capacity, involving the melting of batteries in furnaces at temperatures of approximately 1400 °C (Abdollahifar et al., 2023; Chernyaev et al., 2024). In hydrometallurgical recycling, batteries are processed to obtain 'black mass', and valuable metals are dissolved into a liquid phase using strong acids such as sulphuric acid (Abdollahifar et al., 2023; Tokoro et al., 2025). Metal salts (such as lithium carbonate, nickel sulphate) are then recovered through processes including filtration, precipitation, and solvent extraction. Although hydrometallurgical methods can recover lithium more effectively than pyrometallurgical methods, they have disadvantages such as high chemical consumption, complex wastewater treatment requirements, and the need for material resynthesis (Xu et al., 2023).

Direct recycling of lithium-ion battery components, including natural and synthetic graphite, is an economical and environmentally friendly method that aims to restore spent electrode materials to their original performance without completely breaking down their structure, thereby preserving their morphology and crystal structure (He et al., 2025). This approach enables the reuse of spent battery materials in new battery production, preserving their structural integrity and renewing their performance through physical and/or chemical treatments rather than decomposing them into their elemental forms. These methods generally involve recovering lithium (relithiation) for cathode materials and purifying/improving anode (graphite) materials (Barre et al., 2025).

3.1. Renewal of Cathode Materials (Relithiation Methods)

The main cause of capacity loss in cathode materials is lithium depletion during repeated charge-discharge cycles. Several techniques have been developed to restore lithium content such as hydrothermal/solution-based relithization, eutectic molten salt, ionic liquid and electrochemical relithization. Solid-state sintering involves mixing spent cathode materials with solid lithium sources such as Li_2CO_3 or LiOH, followed by high-temperature heat treatment. In hydrothermal/solution-based relithiation, cathode materials are saturated with lithium ions in aqueous lithium solutions under controlled temperature and pressure conditions. The eutectic molten salt method uses lithium salt mixtures with low melting points (e.g. $LiOH/LiNO_3$) to provide a stable relithiation environment. Ion thermal relithiation employs thermally stable ionic liquids as reaction media. Electrochemical relithiation involves using the spent cathode as an electrode in an electrochemical cell to reinsert lithium ions into the crystal structure (Xu et al., 2023).

3.2. Anode (Graphite) Recycling Methods

Graphite recovery primarily focuses on removing binders and the solid electrolyte interface (SEI) layer. Washing processes involve treating graphite powders with various solvents such as dimethyl carbonate (DMC), N-methyl-2-pyrrolidone (NMP) or water to remove binders (such as PVDF or CMC/SBR) and electrolyte residues. Thermal treatment and pyrolysis involve

heating materials in an inert atmosphere (usually argon) at temperatures ranging from 600°C to 1000°C, or higher (sometimes up to 2900°C) to vaporize organic binders and restore graphite crystallinity (Abdollahifar et al., 2023; Xu et al., 2023; Zheng et al., 2024). Rapid thermal shock treatment involves removing impurities and creating an amorphous carbon layer on the surface to improve performance by heating the graphite to very high temperatures (1000–2500 °C) within seconds and then cooling it rapidly. Hybrid methods combining chemical and thermal treatments typically involve cleaning metal impurities with a mild acid leach (usually a mixture of H_2SO_4 and H_2O_2), followed by thermal restoration. Electrochemical methods (electrolysis) involve electrolysis to separate graphite from copper current foil while simultaneously recovering lithium into solution (Abdollahifar et al., 2023; Martin et al., 2026; Muguruza-Sánchez et al., 2025).

3.3. Advanced Separation and Improvement Techniques

Electrical Pulsed Discharge (EPD) is the physical separation method that uses high-voltage pulses to detach active materials (graphite or cathode materials) from current collector foils (Cu or Al) without the use of heat or chemicals. Surface coating and upcycling techniques involve modifying spent graphite with functional coatings such as calcium silicate (C-S-H), to improve electrochemical performance, particularly fast-charging capabilities. Boron doping involves treating graphite with boron-containing compounds to enhance its electrochemical capacity and conductivity. The indirect recycling approach combines conventional chemical recovery processes with remanufacturing techniques. In this method, the battery components are decomposed into their elemental or precursor forms, which then used directly in the production of new cathode active materials (CAMs). This approach transforms traditional 'recycling' into a closed-loop material regeneration process (Barbosa de Mattos et al., 2025). The advantages and disadvantages of different direct recycling methods are listed in Table 1 (Barbosa de Mattos et al., 2025)

Table 1.: Advantages and disadvantages of different direct recycling methods (Barbosa de Mattos et al., 2025)

Method	Advantages	Disadvantages
Thermal (solid-state)	• Simple • Few steps • Minimized chemical consumption	• Secondary pollution by toxic gas exhaust • Non-uniform Li distribution • Non-uniform crystallinity and morphology • Low scalability
Molten salt	• Simple • Few steps • Higher scalability • Uniform Li distribution • Uniform crystallinity and morphology	• Low technology readiness • $LiNO_3$ is oxidative need for an extra reducing agent • Still needs thermal treatment
Hydrothermal	• High scalability • Uniform Li distribution • Uniform crystallinity and morphology	• Industrial drive towards dry methods • Risk of HF formation • High chemical consumption • Still needs thermal treatment
Chemical	• Mild conditions—green chemistry • Low energy consumption • Simple • Potential high atom economy • Scalability and applicability	• Performance issues for the regenerated CAM—heat treatment may be needed • High chemical consumption • Possibly toxic reagents needed risk for secondary pollution

Method	Advantages	Disadvantages
Electrochemical	• Mild conditions • Low energy consumption • Reduced chemical usage • Minimal secondary pollution • Minimal waste generation	• Relies on providing a source of active Li^+, such as metallic Li or fresh LFP • Low economic incentive • Performance issues for the regenerated materials
Indirect	• Fits existing LIB treatment infrastructure • Possibly applicable to the black mass directly • High performance of products	• Many steps • Higher complexity of the processes • High operational costs

Direct recycling of lithium-ion battery components is an economically and environmentally advantageous approach that aims to directly regenerate spent electrodes materials while preserving their crystal structure and morphology, rather than separating them into their elemental components. This process reduces global warming potential by 70–96% compared to conventional recycling methods and significantly lowers energy consumption by preserving the embodied energy of the original materials. In addition, this approach offers high economic feasibility, with a high Net Present Value (NPV) and short payback periods of approximately 0.5 years, as it produces high-value electrode materials without the need for complete re-synthesis. Furthermore, it reduces dependency on external raw material sources by enabling the local recovery of critical raw materials such as graphite and lithium, thereby forming the development of a closed-loop circular economy for batteries technologies.

4. CONCLUSION

In this study, the critical role of graphite in lithium-ion batteries, the properties of natural and synthetic graphite types, and the importance of direct recycling in sustainable battery technologies have been comprehensively evaluated. From a mineral processing perspective, the natural hydrophobicity of graphite enables its efficient recovery from black mass using flotation techniques while preserving its structural integrity. This represents a significant advantage over conventional recycling methods, which often involve the complete decomposition of materials into their elemental forms.

Various thermal, chemical, electrochemical, and hybrid methods used for cathode relithiation and graphite anode purification offer distinct advantages and limitations. However, direct recycling approach stands out as a superior approach due to its lower energy consumption, reduced chemical usage, and significantly smaller carbon footprint. By preserving the embodied energy of materials, this method minimizes environmental impact while eliminating the need for energy-intensive material re-synthesis, thereby creating substantial economic value.

The high Net Present Value and short investment payback period demonstrate the strong industrial applicability of direct recycling. Moreover, the local recovery of critical raw materials such as graphite and lithium offers strategic advantages in terms of supply security and supports the establishment of a closed-loop battery production. Türkiye's existing graphite resources also represent a strategically important opportunity in this context. These assessments demonstrate that direct recycling is not merely a recovery method but an advanced remanufacturing strategy that forms the fundamental pillar of sustainable, circular, and resource-efficient battery production.

REFERENCES

Abdollahifar, M., Doose, S., Cavers, H., & Kwade, A. (2023). Graphite Recycling from End-of-Life Lithium-Ion Batteries: Processes and Applications. *Advanced Materials Technologies*, *8*(2), 2200368. https://doi.org/10.1002/admt.202200368

Bai, L. Z., Zhao, D. L., Zhang, T. M., Xie, W. G., Zhang, J. M., & Shen, Z. M. (2013). A comparative study of electrochemical performance of graphene sheets, expanded graphite and natural graphite as anode materials for lithium-ion batteries. *Electrochimica Acta*, *107*(5), 555–561. https://doi.org/10.1016/j.electacta.2013.06.032

Bai, Y., Muralidharan, N., Sun, Y. K., Passerini, S., Stanley Whittingham, M., & Belharouak, I. (2020). Energy and environmental aspects in recycling lithium-ion batteries: Concept of Battery Identity Global Passport. *Materials Today*, *41*(24), 304–315. https://doi.org/10.1016/j.mattod.2020.09.001

Barbosa de Mattos, D. F., Duda, S., & Petranikova, M. (2025). Recycling of Lithium Iron Phosphate (LiFePO4) Batteries from the End Product Quality Perspective. *Batteries 2025, Vol. 11, Page 33*, *11*(1), 33. https://doi.org/10.3390/batteries11010033

Barre, F. I., Billy, R. G., Lopez, F. A., & Müller, D. B. (2025). Natural, synthetic, or recycled? A life cycle and techno-economic analysis of battery-grade graphite production. *Journal of Environmental Management*, *395*, 127747. https://doi.org/10.1016/j.resconrec.2024.107709

Beyssac, O., & Rumble, D. (2014). Graphitic Carbon: A Ubiquitous, Diverse, and Useful Geomaterial. *Elements*, *10*(6), 415–420. https://doi.org/10.2113/gselements.10.6.415

Bhar, M., Ghosh, S., Krishnamurthy, S., Kaliprasad, Y., & Martha, S. K. (2023). A review on spent lithium-ion battery recycling: from collection to black mass recovery. *RSC Sustainability*, *1*(5), 1150–1167.

Chernyaev, A., Kobets, A., Liivand, K., Tesfaye, F., Hannula, P. M., Kallio, T., Hupa, L., & Lundström, M. (2024). Graphite recovery from waste Li-ion battery black mass for direct re-use. *Minerals Engineering*, *208*(8), 108587. https://doi.org/10.1016/j.mineng.2024.108587

Dehaine, Q., Michaux, S. P., Pokki, J., Kivinen, M., & Butcher, A. R. (2020). Battery minerals from Finland: Improving the supply chain for the EU battery industry using a geometallurgical approach. *European Geologist Journal*, *49*, 5–11.

Dusastre, V. (2001). Nature insight. *Nature*, *414*(6861), 331. https://doi.org/10.1038/35104596

Gao, H., Yan, Q., Tran, D., Yu, X., Liu, H., Li, M., Li, W., Wu, J., Tang, W., Gupta, V., Luo, J., & Chen, Z. (2023). Upcycling of Spent LiNi0.33Co0.33Mn0.33O2 to Single-Crystal Ni-Rich Cathodes Using Lean Precursors. *ACS Energy Letters*, *8*(10), 4136–4144. https://doi.org/10.1021/acsenergylett.3c01454

Grafit – İstanbul Maden İhracatçıları Birliği. (n.d.). Retrieved February 26, 2026, from https://imib.org.tr/maden/grafit/

Guo, Y., Guo, C., Huang, P., Han, Q., Wang, F., Zhang, H., Liu, H., Cao, Y. C., Yao, Y., & Huang, Y. (2023). Rejuvenating LiNi0.5Co0.2Mn0.3O2 cathode directly from battery scraps. *EScience*, *3*(2), 100091. https://doi.org/10.1016/j.esci.2023.100091

He, Q., Guo, C., Han, K., Liu, F., Feng, Y., Wang, X., Qian, X., & Meng, J. (2025). Direct recycling of spent graphite anode via calcium silicate coating for high-capacity and fast lithium storage. *Carbon*, *244*(1), 120727. https://doi.org/10.1016/j.carbon.2025.120727

Huang, H., Kelder, E. M., & Schoonman, J. (2001). Graphite–metal oxide composites as anode for Li-ion batteries. *Journal of Power Sources*, *97–98*, 114–117. https://doi.org/10.1016/S0378-7753(01)00597-3

Kalyoncu, R. S., Taylor, H. A., & Staff, U. by. (2014). Natural Graphite. *Kirk-Othmer Encyclopedia of Chemical Technology*, 1–21. https://doi.org/10.1002/0471238961.1401202120012512.a01.pub3

Kang, J., Senanayake, G., Sohn, J., & Shin, S. M. (2010). Recovery of cobalt sulfate from spent lithium ion batteries by reductive leaching and solvent extraction with Cyanex 272. *Hydrometallurgy*, *100*(3–4), 168–171. https://doi.org/10.1016/j.hydromet.2009.10.010

Kaya, Ö., Canbazog, M., & Lu. (2009). Chemical demineralization of three different graphite ores from Turkey. *Mining, Metallurgy & Exploration 2009 26:3*, *26*(3), 158–162. https://doi.org/10.1007/bf03402229

Kim, K., Raymond, D., Candeago, R., & Su, X. (2021). Selective cobalt and nickel electrodeposition for lithium-ion battery recycling through integrated electrolyte and interface control. *Nature Communications 2021 12:1*, *12*(1), 6554-. https://doi.org/10.1038/s41467-021-26814-7

Lai, J., Guo, H., Wang, Z., Li, X., Zhang, X., Wu, F., & Yue, P. (2012). Preparation and characterization of flake graphite/silicon/carbon spherical composite as anode materials for lithium-ion batteries. *Journal of Alloys and Compounds*, *530*(9), 30–35. https://doi.org/10.1016/j.jallcom.2012.03.096

Luo, P., Zheng, C., He, J., Tu, X., Sun, W., Pan, H., Zhou, Y., Rui, X., Zhang, B., & Huang, K. (2022). Structural Engineering in Graphite-Based Metal-Ion Batteries. *Advanced Functional Materials*, *32*(9), 2107277. https://doi.org/10.1002/adfm.202107277

Martin, J. P., Oneli, M. F., Axmann, P., Wohlfahrt-Mehrens, M., & Mancini, M. (2026). Battery-grade graphite from direct recycling: effect of the thermal treatment on the properties of the regenerated anode material. *Journal of Power Sources Advances*, *38*(11), 100204. https://doi.org/10.1016/j.powera.2026.100204

Meyer-Plath, A., Beckert, F., Tölle, F. J., Sturm, H., & Mülhaupt, R. (2015). Stable aqueous dispersions of functionalized multi-layer graphene by pulsed underwater plasma exfoliation of graphite. *Journal of Physics D: Applied Physics*, *49*(4), 045301. https://doi.org/10.1088/0022-3727/49/4/045301

Muguruza-Sánchez, A., Sananes-Israel, S., Moliner, E., Contreras, E., Landa-Medrano, I., Palomares, V., & de Meatza, I. (2025). Direct recycling of graphite from spent batteries and production scraps for the development of a circular and sustainable economy. *Journal of Power Sources Advances*, *36*(3), 100191. https://doi.org/10.1016/j.powera.2025.100191

Nitta, N., Wu, F., Lee, J. T., & Yushin, G. (2015). Novel approach to recover cobalt and lithium from spent lithium-ion battery using oxalic acid. *Journal of Hazardous Materials*, *295*(5), 112–118. https://doi.org/10.1016/j.mattod.2014.10.040

Simandl, G. J., Paradis, S., & Akam, C. (2015). Graphite deposit types, their origin, and economic significance. *British Columbia Ministry of Energy and Mines & British Columbia Geological Survey*, *3*, 163–171.

Somaweera, D., Abeygunawardane, G. A., Weragoda, S., & Ranatunga, S. (2022). Effect of vein graphite powder on mechanical, curing, and thermal properties of solid tire vulcanizate. *Materials Today: Proceedings*, *59*, 316–323. https://doi.org/10.1016/j.matpr.2021.11.181

Tian, H., Graczyk-Zajac, M., Kessler, A., Weidenkaff, A., & Riedel, R. (2024). Recycling and Reusing of Graphite from Retired Lithium-ion Batteries: A Review. *Advanced Materials*, *36*(13), 2308494. https://doi.org/10.1002/adma.202308494

Tokoro, C., Horiuchi, M., Narita, A., Kubota, A., & Takaya, Y. (2025). Optimization of graphite anode delamination and contaminant separation via electrical pulsed discharge for direct recycling. *Advanced Powder Technology*, *36*(11), 105066. https://doi.org/10.1016/j.apt.2025.105066

Wagh, P., Islam, S. Z., Lamichhane, T. N., Bhave, R. R., & Paranthaman, M. P. (2023). Separation of Lithium from Aluminum-Containing Clay Mineral Leachate Solution Using Energy-Efficient Membrane Solvent Extraction. *ACS Omega*, *8*(49), 46523–46527. https://doi.org/10.1021/acsomega.3c05009

Wang, F. Y., Wang, H., & Ma, J. W. (2017). Adsorption of Cd(II) at the Interface of water and graphene oxide prepared from flaky graphite and amorphous graphite. *Journal of Environmental Chemical Engineering*, *5*(4), 4157–4164. https://doi.org/10.1016/j.jhazmat.2009.12.032

What Role Does the Flake Graphite Play in Our Lives? (n.d.). Retrieved February 26, 2026, from https://www.samaterials.com/content/what-role-does-the-flake-graphite-play-in-our-lives.html

Wu, Y. P., Jiang, C., Wan, C., & Holze, R. (2002). Modified natural graphite as anode material for lithium ion batteries. *Journal of Power Sources*, *111*(2), 329–334. https://doi.org/10.1016/S0378-7753(02)00349-X

Xu, P., Tan, D. H. S., Jiao, B., Gao, H., Yu, X., & Chen, Z. (2023). A Materials Perspective on Direct Recycling of Lithium-Ion Batteries: Principles, Challenges and Opportunities. *Advanced Functional Materials*, *33*(14), 2213168. https://doi.org/10.1002/adfm.202213168

Yazici, M. S., Krassowski, D., & Prakash, J. (2005). Flexible graphite as battery anode and current collector. *Journal of Power Sources*, *141*(1), 171–176. https://doi.org/10.1016/j.jpowsour.2004.09.009

Yu, L., Bai, Y., & Belharouak, I. (2024). Recycling of Lithium-Ion Batteries via Electrochemical Recovery: A Mini-Review. *Batteries 2024, Vol. 10, Page 337*, *10*(10), 337. https://doi.org/10.3390/batteries10100337

Yu, L., Bai, Y., Essehli, R., Bisht, A., & Belharouak, I. (2023). Efficient separation and coprecipitation for simplified cathode recycling. *Energy Storage Materials*, *63*(11), 103025. https://doi.org/10.1016/j.ensm.2023.103025

Yu, L., Bai, Y., Polzin, B., & Belharouak, I. (2024). Unlocking the value of recycling scrap from Li-ion battery manufacturing: Challenges and outlook. *Journal of Power Sources*, *593*(7781), 233955. https://doi.org/10.1016/j.jpowsour.2023.233955

Zhao, L., Ding, B., Qin, X. Y., Wang, Z., Lv, W., He, Y. B., Yang, Q. H., & Kang, F. (2022). Revisiting the Roles of Natural Graphite in Ongoing Lithium-Ion Batteries. *Advanced Materials*, *34*(18), 2106704. https://doi.org/10.1002/adma.202106704

Zheng, S.-H., Wang, X.-T., Gu, Z.-Y., Lü, H.-Y., Li, S., Zhang, X.-Y., Cao, J.-M., Guo, J.-Z., & Wu, X.-L. (2024). Direct and rapid thermal shock for recycling spent graphite in lithium-ion batteries. *Journal of Colloid and Interface Science*, *667*, 111–118.

INFLUENCE OF ROCK WEATHERING DEGREE ON PROCESSING EFFICIENCY AND PRODUCT QUALITY IN AGGREGATE QUARRIES

Danciu CIPRIAN*, Camelia TRAISTĂ

Petroșani University, Mining Faculty, Department of Mining Engineering, Topography, and Construction, 332006, PETROȘANI-ROMANIA
**Corresponding author: cipriandanciu@upet.ro*

A B S T R A C T

The degree of rock weathering is a key factor influencing both the efficiency of technological processes in aggregate quarries and the quality of the resulting mineral products. Physical-chemical disaggregation, oxidation, and mineralogical transformation processes directly affect the mechanical, granulometric, and petrographic properties of the extracted material. This study investigates the correlation between the degree of weathering—evaluated through petrographic, geotechnical, and wear resistance analyses—and the material's behavior during crushing, screening, and washing operations. The results indicate that a high degree of alteration significantly reduces impact and compressive strength, leading to increased generation of fine fractions and mineral dust, which negatively affect the quality of construction aggregates. Additionally, weathering promotes the detachment of clay films and iron oxides, altering aggregate adhesion in concrete and asphalt mixtures. The paper proposes an integrated assessment model for rock weathering and a corresponding adjustment of the processing flow according to the petro-mineralogical characteristics of the raw material. The objective is to optimize energy consumption, reduce losses, and ensure consistent product quality. The results support the implementation of differentiated exploitation and processing strategies based on the principles of sustainable development and circular economy.

Key words: *Rock weathering, aggregate quarries, processing efficiency, product quality, sustainable development*

1. INTRODUCTION

The extraction and processing of mineral aggregates are essential activities in the construction materials industry, providing key resources for infrastructure, civil engineering, and transportation. The performance of an aggregate quarry depends not only on the geological characteristics of the deposit but also on the physical, mechanical, and petrographic properties of the rock. Among the factors influencing these properties, the degree of rock weathering is particularly significant (Dearman, 1974; Price, 1995).

Rock weathering involves physical disintegration, chemical reactions, and mineralogical transformations caused by water, oxygen, carbon dioxide, and temperature variations (Ollier, 1984). In volcanic rocks commonly used as aggregates, such as andesites and basalts, weathering alters primary minerals: feldspars undergo sericitization and kaolinization, ferromagnesian minerals oxidize, and the rock structure develops microcracks and secondary porosity (Irfan & Dearman, 1978; Fookes et al., 1988).

These changes reduce intergranular cohesion, modify density and porosity, and consequently decrease mechanical strength. Increased porosity facilitates water penetration and accelerates structural degradation, while the formation of clay minerals weakens stress transmission within the rock mass (Tugrul & Zarif, 1999).

Several classification systems have been proposed to describe the degree of weathering. One of the earliest engineering schemes was introduced by Dearman and later standardized by the

International Society for Rock Mechanics (ISRM), which defines weathering states from W0 (fresh rock) to W5 (residual soil) based on macroscopic observations and laboratory tests (Dearman, 1974; ISRM, 1981; ISRM, 2007). Gupta and Rao (2001) further demonstrated that compressive strength may decrease by more than 70% between fresh and intensely weathered rock.

From a geotechnical perspective, weathering reduces abrasion and impact resistance, increases susceptibility to freeze–thaw cycles, and lowers material durability (Fookes et al., 1988). Parameters such as the slake durability index, total porosity, and water absorption are commonly used as indirect indicators of structural degradation (ISRM, 2007; Ollier, 1984).

In comminution theory, energy–size relationships are typically described by models such as Bond's law (Napier-Munn et al., 1996), which often assume rock homogeneity and do not account for microstructural changes induced by weathering. However, studies show that altered rocks have lower fracture toughness and require less specific energy for fragmentation (Bearman & Briggs, 1998). Consequently, crushing generates larger amounts of fine fractions and mineral dust, reducing the yield of commercial aggregate sizes.

Additionally, clay minerals and iron oxide films formed during alteration can reduce the adhesion of aggregates in concrete and asphalt mixtures, affecting the durability of construction materials (Neville, 2011). Therefore, aggregate cleanliness becomes a critical quality parameter.

In the context of sustainable development and the circular economy, optimizing processing technologies according to the petro-mineralogical characteristics of raw materials is increasingly important (European Commission, 2020). Adjusting processing flows to the degree of rock alteration can reduce material losses, lower energy consumption, and improve product quality.

Despite these advances, relatively few studies integrate petrographic alteration with technological performance in aggregate quarries. Most research addresses geological and processing aspects separately.

This study aims to bridge this gap by analyzing the relationship between rock alteration and processing efficiency, as well as the quality of the resulting products. The degree of alteration is evaluated through petrographic analyses, geotechnical tests, and wear resistance determinations, while technological behavior is assessed through granulometric distribution, fine fraction generation, and energy consumption. The correlation of these parameters allows the development of an integrated assessment framework applicable to mining planning and technological flow optimization.

2. MATERIAL AND METHODS

2.1. Material

To evaluate the influence of the degree of alteration on the geomechanical properties of Neogene andesites, representative samples were selected from volcanic areas in the Southern Apuseni Mountains (Valea Căpitanului – Certej, Dealul Motor – Deva, Crișcior, Săcărâmb, Albini–Hanes, and Roșia Poieni). The selection aimed to obtain a comparative series that would include all stages of hydrothermal and meteoric alteration.

The classification into alteration classes was based on:

- macroscopic examination (color, cohesion, disintegration);
- mineralogical analysis in thin sections (according to STAS 6200/4-81);

- the proportion of secondary minerals (sericite, kaolinite, limonite);
- degree of microfracturing.

Four classes were established (Table 1):

Table 1. Alteration classes

Degree	Petro-mineralogical characterization	Structural state
I	Fresh andesite, intact primary minerals	Compact
II	Incipient alteration, weak sericitization	Slightly microfractured
III	Moderate alteration, secondary clay development	Increased porosity
IV	Advanced alteration, extensive transformations	Reduced cohesion

2.2. Method

Monolithic samples were collected in accordance with STAS 6200/3-74. Cylindrical and cubic test specimens were made from each block in accordance with ISRM tolerances (Table 2).

Table 2. Test specimen geometry

Test	Shape	Dimensions (mm)	Applied standard
Monoaxial compression	Cylinder	d=50; h=100	STAS 6200/5-91
Tension (Brazilian)	Cylinder	d=50; h=50	STAS 6200/6-71
Shear	Cylinder	d=42; h=42	STAS 6200/7-71
Elastic modulus	Cylinder	d=42; h=84	STAS 6200/14-74
Density	Cube	50x50x50	STAS 6200/10-73
Water absorption	Cube	50x50x50	STAS 6200/12-73

The loading surfaces were ground to a flatness deviation of ≤ 0.02 mm.

Table 3. Average physical properties

Degree of alteration	Apparent ρ (kg/m³)	Porosity n (%)	Absorption Wa (%)	Saturation coefficient (%)
I	2685	3.8	0.9	85
II	2590	6.5	1.8	88
III	2460	11.2	3.6	92
IV	2280	18.7	6.2	95

There is a directly proportional relationship between the degree of alteration and the hydro-physical parameters (Table 3).

2.2.1. Determination of the degree of rock alteration – chemical method

The degree of rock alteration is a key parameter in engineering geology, geotechnics, and applied petrology, as it strongly influences the physical and mechanical properties, stress behavior, and durability of rocks under natural or anthropogenic conditions (Bell, 2007; Wyllie & Mah, 2004). Weathering results from the interaction between the original geological material and environmental physical, chemical, and biological agents, producing progressive mineralogical, structural, and textural changes (Ollier, 1984).

In practice, alteration is commonly evaluated using qualitative or semi-quantitative methods based on visual and petrographic observations, which classify materials from fresh rock (W1) to completely altered rock or residual soil (W5) (ISRM, 2007). However, these approaches are inherently subjective and dependent on the evaluator’s experience, making comparisons between studies difficult (Fookes et al., 1988).

Therefore, quantitative indicators of alteration are increasingly used. These include geochemical indices such as CIA (Chemical Index of Alteration), CIW (Chemical Index of Weathering), and PIA (Plagioclase Index of Alteration), which quantify chemical changes during weathering (Nesbitt & Young, 1982; Harnois, 1988). In addition, variations in physical properties (density, porosity, ultrasonic wave velocity) and mass loss during controlled degradation tests are frequently correlated with alteration intensity (Tugrul & Zarif, 1999; EN 1367-1, 2007).

Among these methods, the diluted hydrochloric acid (HCl) attack test, particularly at a 10% concentration, represents a simple and reproducible procedure that provides an indirect measure of the chemical and mineralogical alteration of rocks (Irfan & Dearman, 1978).

2.2.2. Chemical alteration of silicate rocks

Chemical alteration of rocks is mainly controlled by dissolution, hydrolysis, oxidation–reduction, and hydration reactions affecting minerals unstable under surface conditions (Ollier, 1984; Blatt et al., 2006). In igneous and metamorphic rocks, the most susceptible minerals are feldspars, plagioclases, ferromagnesian minerals (biotite, amphiboles, pyroxenes), and vitric or microcrystalline phases (Deer et al., 2013).

Common alteration processes include kaolinization and sericitization of feldspars, saussuritization of plagioclases, chloritization and oxidation of mafic minerals, and the formation of clays, iron oxides, hydroxides, and siliceous gels (Blatt et al., 2006; Klein & Dutrow, 2007). As alteration progresses, the primary crystal structure is progressively destroyed and secondary products become more abundant and chemically reactive (Drever, 1997).

Hydrochloric acid at moderate concentrations (5–10%) can dissolve iron and aluminum oxides and hydroxides, destabilize weakly crystallized clays, disintegrate clay aggregates, and extract mobile cations (Ca^{2+}, Mg^{2+}, Na^{+}, K^{+}) from altered minerals (Drever, 1997; White & Brantley, 2003). When no carbonate effervescence occurs, the mass loss after HCl attack mainly results from dissolution of secondary phases, dispersion of fine particles, and weakening of grain cohesion (Irfan & Dearman, 1978; White & Brantley, 2003). Consequently, mass loss provides an indirect indicator of chemical and mineralogical alteration.

The 10% HCl attack method compares the dry mass of a sample before and after controlled exposure to hydrochloric acid for 24–48 hours, following procedures similar to chemical resistance tests for aggregates (EN 1367-1, 2007). The HCl alteration index (IHCl) is calculated from the difference between the initial dry mass (m_0) and the mass after acid treatment, washing, neutralization, and drying (m_1). Expressed as a percentage, IHCl quantifies the amount of dissolved or dispersed material and serves as a measure of alteration (Nesbitt & Young, 1982; Irfan & Dearman, 1978).

The method is mainly applicable to silicate rocks (magmatic, metamorphic, and some siliciclastic sedimentary rocks), natural aggregates without significant carbonate content, and materials where chemical weathering plays an important role in degradation.

3. RESULTS AND DISCUSSION

In order to assess the influence of the degree of alteration on the physical-mechanical properties and chemical behavior of the analyzed andesites, the experimental results obtained through geotechnical and physical determinations and controlled chemical attack tests with 10% HCl solution were synthesized. The comparative analysis of the samples highlights the

relationships between structural and mechanical parameters and alteration indicators for a wide range from fresh rock (W0–W1) to advanced stages of alteration (W4–W5).

Samples 1–6 come from representative areas of the investigated deposits and predominantly characterize slightly to moderately altered states. To complete the evolutionary spectrum of alteration and to allow a systematic comparative analysis of the behavior of the material under conditions of severe degradation, samples 7–10 were selected from intensely altered areas of the same deposits studied, without specifying their exact location. These samples reflect higher stages of mineralogical and structural transformation, corresponding to classes W3–W5.

The parameters analyzed include volumetric density (ρv), total porosity (n), water absorption (Wa), uniaxial compressive strength (σc), static modulus of elasticity (Es), structural continuity index (Ic), fracture degree (Δf), and chemical attack behavior (qualitative reaction to HCl and IHCl alteration index).

For samples 7–10, originating from altered areas of the deposits, a marked decrease in density and compressive strength is observed, accompanied by a significant increase in porosity and cracking index. IHCl values increase progressively from stage W3 to W5, indicating increased chemical susceptibility associated with the dissolution of secondary phases and the dispersion of the fine fraction. These results confirm the direct correlation between chemical alteration, structural degradation, and reduced mechanical performance.

The following table summarizes the experimental results obtained for the ten samples analyzed, highlighting the distribution of parameters according to the alteration class and behavior under chemical attack (Table 4.).

Table 4. Results of mechanical and chemical tests

No	Sample	Alteration class	ρv (g/cm³)	n	Wa (%)	σc (MPa)	Es (GPa)	Ic (%)	Δf	IHCl
1	Albini-Haneș	W0–W1	2.60–2.65	1.2–1.3	1	>110	>40	82.09	0.045	0
2	Motor Hill	W1	2.50–2.65	3	1	100–120	30	77.37	0.308	0
3	Captain's Valley	W1	2.668	3.7	1.62	110.2	35–45	71	0.25	0
4	Crișcior	W1–W2	2.45–2.60	1	1.4	90	25	67.35	0.029	0
5	Săcărâmb	W2	2.45	3.51	3.49	80–100	20	65.38	0.516	0
6	Roșia Poieni	W2	2.45	1.0	1.0	80–100	20	67.11	0.168	0.8
7	Andesite 1	W3	2.32	11.8	6.4	42	14	63	0.62	0.4
8	Andesite 2	W3	2.28	13.5	7.9	34	11	58	0.74	0.9
9	Andesite 3	W4	2.05	21.6	12.3	18	6	47	0.91	2
10	Andesite 4	W5	1.82	31.4	18.7	3	1.5	-	-	3.5

The distribution of parameters confirms the systematic nature of the structural and mineralogical degradation of the investigated andesites, across the entire range from fresh (W0–W1) to intensely altered (W4–W5) stages.

Evolution of physical parameters: Samples 1–3 (W0–W1) show high volumetric densities (2.60–2.67 g/cm³), low porosity, and low water absorption, indicating a compact crystalline structure with minimal microcracking and strong intergranular cohesion. At this stage, alteration is limited and does not significantly affect structural integrity.

With the transition to class W2, porosity and water absorption increase moderately, while density slightly decreases. These changes reflect the onset of chemical alteration processes, particularly feldspar transformation and mafic mineral oxidation, which promote secondary porosity and weaken intercrystalline contacts.

For samples 7–10, representing more altered zones, degradation becomes pronounced. Porosity exceeds 10% in W3 and reaches over 30% in W5, while density decreases to about 1.82 g/cm³. This trend indicates progressive destruction of the primary crystal lattice and accumulation of weakly consolidated secondary phases; in class W5 the material approaches the behavior of an incoherent material.

Mechanical behavior: Uniaxial compressive strength decreases markedly with increasing alteration. Slightly altered samples exceed 110 MPa, typical of competent andesite, whereas strength drops to about 18 MPa in W4 and to only 3 MPa in W5. The modulus of elasticity follows the same trend, indicating a loss of structural rigidity. Decreasing structural continuity (Ic) and increasing cracking degree (Δf) further confirm progressive fragmentation of the rock mass.

Behavior under chemical attack: The 10% HCl test highlights differences between alteration stages. Samples in classes W0–W2 show negligible reactions and very low IHCl values, indicating mineralogical stability. In contrast, IHCl increases progressively from W3 to W5, demonstrating higher chemical susceptibility and confirming that chemical alteration and mechanical degradation act simultaneously on the rock structure.

Technological implications: The results indicate significant differences in processing behavior. Weakly altered rocks generate stable coarse fractions and high yields of commercial aggregates, whereas strongly altered material produces larger amounts of fines and mineral dust, reducing crushing and classification efficiency.

Table 5 summarizes the physical, mechanical, and chemical parameters of the ten analyzed andesite samples, including density (ρv), porosity (n), water absorption (Wa), compressive strength (σc), modulus of elasticity (Es), structural continuity (Ic), cracking degree (Δf), and the IHCl alteration index. Samples 1–6 represent materials currently exploited in industrial installations, while samples 7–10 originate from altered zones and were analyzed under laboratory conditions to cover the higher alteration stages.

Table 5. Structure by grade (%)

Sample no.	Alteration class	0–4 mm	4–8 mm	8–16 mm	16–32.4 mm
1	W0–W1	20.8	18.6	29.7	30.9
2	W0–W1	23.4	17.2	27.9	31.5
3	W0–W1	21.9	19.4	26.8	31.9
4	W2	28.7	21.1	27.6	22.6
5	W2	31.3	18.9	26.4	23.4
6	W2	29.8	22.3	25.7	22.2
7	W3	40.6	23.1	22.4	13.9
8	W3	43.2	20.8	21.6	14.4
9	W4	54.7	19.6	17.8	7.9
10	W5	69.3	15.7	9.8	5.2

For samples 1–3 (W0–W1), the structure by size is dominated by coarse fractions, especially the 16–32.4 mm range, which represents about one-third of the resulting material. The 8–16 mm fraction also has a high proportion, and the proportion of fine material (0–4 mm) remains relatively low. This distribution indicates controlled fragmentation, with the predominant generation of stable and well-defined granules.

In samples 4–6 (W2), the size distribution begins to change noticeably. The proportion of the 0–4 mm fraction increases, and the proportion of the 16–32.4 mm fraction decreases accordingly. The intermediate fractions (4–8 mm and 8–16 mm) remain relatively stable, but

the distribution becomes more balanced between the fine and coarse components. Thus, there is a tendency towards increased secondary fragmentation.

For samples 7–8 (W3), the change is more pronounced. The 0–4 mm fraction becomes dominant, exceeding 40% of the total mass, while the 16–32.4 mm fraction decreases to below 15%. The intermediate fractions gradually decrease, indicating more intense fragmentation and increased generation of fine material.

In the case of sample 9 (W4), the structure by size is characterized by a clear predominance of the fine fraction (over 50%), and the coarse fraction 16–32.4 mm represents a small proportion of the total. The granulometric distribution shifts significantly towards the fine range, reflecting a reduced ability to retain large fragments during crushing.

For sample 10 (W5), the structure is almost entirely dominated by the 0–4 mm fraction, which represents approximately 70% of the material. The 8–16 mm and 16–32.4 mm fractions become minor. This distribution indicates marked fragmentation and a tendency to disintegrate into fine particles. As the degree of alteration increases, the particle size distribution resulting from crushing

The HCl attack method, used in addition to physical-mechanical determinations, provides an additional tool for quantifying chemical alteration and differentiating intermediate stages, contributing to an integrated assessment of the material's behavior under operating conditions.

4. CONCLUSION

This study analyzed the influence of the degree of alteration on the physical, geomechanical, and technological properties of Neogene andesites from the Southern Apuseni Mountains, including their behavior under controlled chemical attack with a 10% HCl solution. The results confirm that alteration strongly controls both the mechanical performance and technological behavior of the material.

Mechanical parameters, particularly uniaxial compressive strength and modulus of elasticity, decrease progressively with increasing alteration. Andesites in classes W0–W2 retain adequate mechanical properties, whereas from W3 onward strength decreases significantly, and in class W5 the material almost completely loses competent rock behavior.

The 10% HCl attack test proved effective in distinguishing alteration stages. While weakly altered samples show negligible mass loss, the IHCl index increases progressively from W3 to W5, indicating increasing chemical susceptibility.

Alteration also affects fragmentation behavior. Fresh samples mainly generate coarse fractions (16–32.4 mm), whereas highly altered rocks produce predominantly fine fractions (0–4 mm), reflecting the influence of structural degradation on crushing processes.

These results highlight the need for differentiated exploitation and processing strategies depending on the degree of alteration. The study demonstrates a clear correlation between chemical–mineralogical alteration, physical–mechanical degradation, and fragmentation behavior, and shows that integrating the IHCl method into geomechanical analysis can support technological decision-making in aggregate quarries.

REFERENCES

Bearman, R. A., Briggs, C. A., (1998), “The effect of rock properties on comminution performance”, Minerals Engineering, 11 (7), 651–666.

Bell, F. G., (2007), Engineering Geology, Butterworth-Heinemann, Oxford.

Blatt, H., Tracy, R. J., Owens, B. E., (2006), Petrology: Igneous, Sedimentary, and Metamorphic, W.H. Freeman.

Dearman, W. R., (1974), “Weathering classification in the characterization of rock for engineering purposes”, Geological Society Engineering Geology Special Publication.

Deer, W. A., Howie, R. A., Zussman, J., (2013), An Introduction to the Rock-Forming Minerals, Mineralogical Society.

Drever, J. I., (1997), The Geochemistry of Natural Waters, Prentice Hall.

EN 1367-1, (2007), “Tests for thermal and weathering properties of aggregates – Determination of resistance to freezing and thawing”.

European Commission, (2020), Circular Economy Action Plan for a Cleaner and More Competitive Europe, Brussels.

Fookes, P. G., Gourley, C. S., Ohikere, C., (1988), “Rock weathering in engineering time”, Quarterly Journal of Engineering Geology, 21, 33–57.

Gupta, V., Rao, K. S., (2001), “Weathering indices and their applicability for rock engineering”, Bulletin of Engineering Geology and the Environment, 60, 201–221.

Harnois, L., (1988), “The CIW index: A new chemical index of weathering”, Sedimentary Geology, 55, 319–322.

Irfan, T. Y., Dearman, W. R., (1978), “Engineering classification and index properties of weathered rocks”, Bulletin of the International Association of Engineering Geology, 17, 79–90.

ISRM, (2007), The Complete ISRM Suggested Methods for Rock Characterization, Testing and Monitoring.

Klein, C., Dutrow, B., (2007), Manual of Mineral Science, Wiley.

Napier-Munn, T., Morrell, S., Morrison, R., Kojovic, T., (1996), Mineral Comminution Circuits: Their Operation and Optimization, JKMRC Monograph Series.

Nesbitt, H. W., Young, G. M., (1982), “Early Proterozoic climates and plate motions inferred from major element chemistry of lutites”, Nature, 299, 715–717.

Neville, A. M., (2011), Properties of Concrete, Pearson Education Limited.

Ollier, C. D., (1984), Weathering, Longman, London.

Price, D. G., (1995), “Weathering and weathering processes”, Quarterly Journal of Engineering Geology.

Tugrul, A., Zarif, I. H., (1999), “Correlation of mineralogical and textural characteristics with engineering properties of selected granitic rocks”, Engineering Geology, 51, 303–317.

White, A. F., Brantley, S. L., (2003), “The effect of time on the weathering of silicate minerals”, Chemical Geology, 202, 479–506.

Wyllie, D. C., Mah, C. W., (2004), Rock Slope Engineering, Spon Press.

PROCESS MINERALOGY INSIGHTS INTO BENEFICIATION OF RARE EARTH CARBONATITE ORES

Ezgi AKYILDIZ[1,*], Camilo M. SILVA[1], Stefanie LODE[1,2], Kornel TOBICZYK, Przemyslaw B. KOWALCZUK[1,*]

[1]Norwegian University of Science and Technology (NTNU), Department of Geosciences, S.P. Andersens vei 15a, 7031, Trondheim, Norway
[2]The Geological Survey of Norway, Leiv Eirikssons vei 39, 7040 Trondheim, Norway
**Corresponding authors: ezgi.akyildiz@ntnu.no, pshem.kowalczuk@ntnu.no*

A B S T R A C T

Rare earth elements (REEs) are crucial for clean energy, electronics, defense, and advanced manufacturing. However, their extraction is often constrained by complex mineralogy and variable ore grades. Economically important rare earth minerals (REMs) such as bastnäsite, monazite, and xenotime typically occur in fine-grained, heterogeneous assemblages with carbonate and silicate gangue. Understanding these mineralogical complexities is critical for designing efficient beneficiation strategies. Process mineralogy offers a quantitative framework to assess mineral abundances, liberation, and associations, thereby supporting robust flowsheet design and minimizing reliance on extensive bench-scale testing. Variations in modal mineralogy, elemental deportment, and liberation along a drill core can affect beneficiation performance by influencing grade distribution, reagent requirements, and recovery efficiency. Linking mineralogical variability to beneficiation outcomes allows for the identification of optimal concentration techniques, including gravity, magnetic, electrostatic, and froth flotation methods. This study investigates mineralogical data from low-, medium-, and high-grade intervals of a rare earth carbonatite drill core to identify the most effective beneficiation processes and develop targeted strategies to enhance rare earth recovery.

Key words: *Rare earth elements, process mineralogy, beneficiation methods*

1.INTRODUCTION

Process mineralogy addresses this inherent complexity by supplying quantitative information on modal mineralogy, liberation behavior, and inter-mineral relationships. These data underpin assessments of ore variability, support the design of resilient processing flowsheets, reduce dependence on extensive laboratory-scale testing, and function as diagnostic tools for interpreting beneficiation performance (Grammatikopoulos and Downing, 2020; Aasly, 2024). Separation techniques, including gravity, magnetic, electrostatic, and froth flotation methods, exploit contrasts in physical and surface properties; however, their success is largely controlled by mineral associations and the degree of liberation achieved (Drzymała, 2007; Wills and Finch, 2016; Al-Ali et al., 2020). Establishing mineralogical trends at an early stage therefore enhances predictions of metallurgical behavior, strengthens resource evaluation, and facilitates a smoother progression from exploration to production (Lotter et al., 2018).

Automated mineralogy has emerged as an essential tool for detailed characterization of both primary and secondary resources and is widely applied as a diagnostic method in mineral processing studies (Gu et al., 2014; Bagger et al., 2025). By providing quantitative information on mineral composition, textural features, and elemental distribution, it plays a critical role in process development, plant optimization, and techno-economic assessments. Detailed evaluation of modal mineralogy, mineral associations, and liberation behavior enables automated mineralogy to inform decision-making throughout the mining value chain, from early resource assessment to the design and refinement of beneficiation flowsheets (Gu et al., 2014; Becker, 2023).

Economically significant REMs, such as bastnäsite ((Ce,La,Nd,Y)(CO_3)F), monazite ((Nd,La,Ce)PO_4), and xenotime (YPO_4), are typically found in finely disseminated and mineralogically complex ores, commonly associated with a wide range of gangue minerals including carbonates and silicates (Balaram, 2019; Drobniak and Mastalerz, 2022). As a result, comprehensive mineralogical characterization is a prerequisite for the development of effective and selective beneficiation routes for these types of complex ores (Jordens et al., 2013; Bradshaw, 2014; Petruk, 2000). Mineral investigation techniques aim to identify mineral phases and characterize their textural, chemical, and compositional features. The outcomes of these studies are frequently applied to estimate deposit distribution, evaluate the recoverability of valuable components, and predict ore response during downstream processing (Petruk, 2000).

Research on the Fen Complex has historically concentrated on geological aspects such as its formation, mineralization processes, and paragenetic relationships, with comparatively little emphasis on mineral processing considerations (Brøgger, 1921; Andersen, 1984; Kresten and Morogan, 1986; Andersen, 1986, 1987, 1988; Lie and Østergaard, 2011; Boesche et al., 2016; Elliott et al., 2018; Marien et al., 2018; Dahlgren, 2019; Cagno et al., 2020). Only a small number of investigations have explored the beneficiation of REMs or the recovery of REEs from Fen-derived materials (Davris et al., 2018; Silva et al., 2023; Gajendra et al., 2025; Akyildiz et al., 2026).

In the present work, low-, medium-, and high-grade samples from a carbonatite-hosted rare earth deposit were characterized chemically and mineralogically using inductively coupled plasma mass spectrometry (ICP-MS) and scanning electron microscopy-based automated mineralogy (SEM-AM). The study aimed to assess the suitability and performance of gravity separation, magnetic separation, and froth flotation for each grade, based on elemental concentrations, modal mineralogy, mineral liberation at the chosen grind size, and mineral association data. Each sample grade was evaluated separately to reflect variability in processing behavior and to accommodate grade-dependent differences in separation response.

2.MATERIALS AND METHODS

2.1.Sample Preparation

The different samples namely, low-, medium-, and high-grade were milled to <150 µm using a high-pressure grinding roll (HPGR) and then split into representative subsamples for further characterization and beneficiation studies.

2.2.Chemical Analysis

The samples were analyzed via ICP-MS using a PerkinElmer SCIEX-ELAN DRC-II spectrometer featuring axial field technology. Approximately, a 0.4 g of material from each sample was digested in a 65% concentrated HNO3 solution at 85 °C for 20 hours. TREO, defined as La_2O_3 + CeO_2 + Pr_6O_{11} + Nd_2O_3, were used to report the ICP-MS results, consistent with conventional REEs concentrate reporting practices (Geoscience Australia, 2023; Nkiawete and Wal, 2025). TREO values were calculated using established stoichiometric conversion factors for each oxide (James Cook University, n.d.). (Total REEs (TREE) = La + Ce + Pr + Nd).

2.3.Mineralogical Analysis

SEM-AM analysis was performed at the Department of Geosciences of NTNU (IGV). The analyses were performed acquired using a ZEISS Sigma 300VP field emission SEM equipped

with two Bruker X-flash 6|60, 129 eV energy dispersive spectroscopy (EDS) detectors and ZEISS Mineralogic Software v.1.08.02, Mining plug-in. The following microscope settings were used: 8.5 mm working distance (WD), 20kV acceleration voltage, and an aperture of 120 µm. The step size was set to 2 µm due to fine intergrowths of various minerals. Mineral associations, indicating which mineral grains share grain boundaries within the particles, are automatically obtained through analysis using ZEISS Mineralogic software, which identifies mineral phases and maps their spatial relationships by calculating the partial perimeter at the extent of contact between minerals phases based on shared grain boundaries. The grains with exposed perimeter more than 90% were classified as 'liberated', between 90% - 30% as 'composites' and with lower than 30% as 'locked'. Mineral association analysis was done for the most abundant mineral subtypes (parisite-Ce, parisite-Ce-La, bastnäsite-Ce-La, monazite-Ce and synchysite-Ce) as well as magnetite, a potential by-product.

3.RESULTS

3.1.Chemical Analysis

Elemental concentration of the sample grades obtained from ICP-MS analyses are given in Table 1. Ce is the dominant REE in all sample grades, followed by La, Nd, and Pr. The TREO contents of the low-, medium-, and high-grade samples are 0.33, 1.12, and 2.18 wt.%, respectively.

Table 1. Elemental concentration of the sample grades based on ICP-MS analyses

Sample grade	**Low**	**Medium**	**High**
Element	**wt.%**	**wt.%**	**wt.%**
Y	0.00	0.00	0.00
La	0.08	0.31	0.65
Ce	0.14	0.46	1.01
Pr	0.01	0.04	0.07
Nd	0.04	0.13	0.09
Sm	0.01	0.02	0.02
Gd	0.01	0.02	0.02
Ho	<LOD	0.00	0.00
Er	<LOD	0.00	0.00
Tm	<LOD	<LOD	<LOD
Yb	<LOD	0.00	<LOD
Lu	<LOD	<LOD	<LOD
Th	0.02	0.05	0.02
Fe	5.30	5.96	8.06
TREE	0.28	0.94	1.82
TREO	0.33	1.12	2.18

*LOD: Limit of detection.

3.2.Mineralogical Analysis

3.2.1.Modal mineralogy

Table 2 presents the quantitative modal mineralogy of the samples. The low-grade material is characterized by monazite (0.43 wt.%) and parisite (0.39 wt.%) as the major REMs, with minor contributions from bastnäsite (0.08 wt.%) and synchysite (0.04 wt.%). Parisite dominates the REM assemblage in the medium-grade sample (1.49 wt.%), whereas bastnäsite is the predominant REM in the high-grade sample (1.59 wt.%).

Table 2. Quantitative modal mineralogy (wt.%) of the samples analyzed – sorted starting from the main gangue minerals. 'Others' refers to minerals present at <0.1 wt.%

Mineral	Chemical formula	Density (g/cm^3)
Parisite	$Ca(Ce,La,Nd)_2(CO3)3F_2$	4.20 – 4.50
Monazite	$(Nd,La,Ce)PO_4$	4.98 – 5.43
Bastnäsite	$(Ce,La,Nd,Y)(CO_3)F$	3.90 – 5.20
Synchysite	$Ca(Ce,La, Nd)(CO_3)_2F$	3.90 – 4.14
Ferroan dolomite	$Ca(Mg,Fe)(CO_3)_2$	2.80 – 2.90
Ankerite	$Ca(Fe,Mg,Mn)(CO3)_2$	2.93 – 3.10
Calcite	$Ca(CO_3)$	2.71
Dolomite	$CaMg(CO3)_2$	2.84
Apatite	$Ca_5(PO_4)_3(Cl,F,OH)$	3.19
Magnetite	Fe_3O_4	5.15
Pyrite	FeS_2	5.01
Barite	$BaSO_4$	4.48
Chlorite	$(Fe,Mg,Al)_{4\text{-}6}(Si, Al)_4O_{10}(OH,O)_8$	2.60 – 3.30

3.2.2.Elemental deportment

Elemental deportment results indicate that, in the low-grade sample, Ce, Nd, and La are partitioned primarily between monazite and parisite, with monazite acting as the principal carrier phase (Fig. 1). In the medium-grade sample, REEs are predominantly hosted by parisite, while monazite represents the second most significant REM phase. For the high-grade sample, Ce and La are largely associated with bastnäsite, whereas Nd is shared among bastnäsite, parisite, and monazite. Synchysite hosts 6%, 4% and 5% of Nd in the low-, medium-, and high-grade sample respectively. Praseodymium (Pr) was excluded from the REMs distribution analysis as its concentration was below the EDS detection limit.

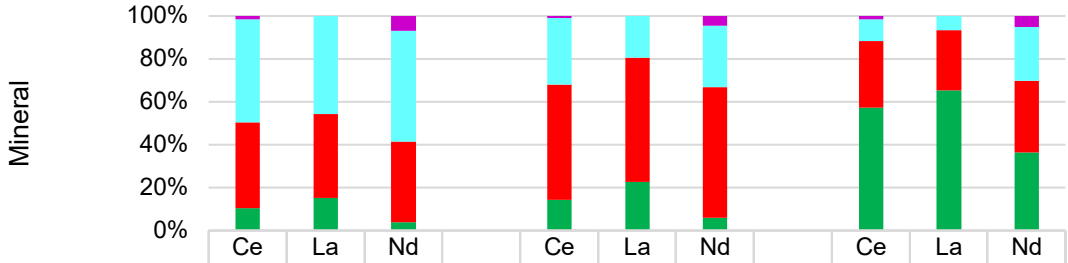

	Low-grade			Medium-grade			High-grade		
	Ce	La	Nd	Ce	La	Nd	Ce	La	Nd
Synchysite	1.4	0.0	6.2	0.9	0.0	4.3	1.4	0.0	4.6
Monazite	47.1	44.7	45.9	29.8	19.1	26.1	10.0	6.4	21.8
Parisite	39.4	38.0	33.4	51.7	57.6	56.0	30.5	27.6	29.4
Bastnäsite	10.2	14.9	3.4	13.8	22.3	5.5	56.3	64.3	31.8

Figure 1. Elemental deportment of Ce, La and Nd by mineral in different sample grades

3.2.3.Liberation

In the high-grade sample, more than 70% of the grains are categorized as locked, with this proportion decreasing to 63% in the medium-grade sample. For the low-grade material, locked and composite parisite grains occur in nearly equal proportions at approximately 50% each, whereas liberated grains represent only about 1% of the population. In both the medium- and high-grade samples, liberated grains account for approximately 0.8%. Bastnäsite in the low-grade sample is predominantly locked, comprising close to 90% of the grains, while liberated particles constitute roughly 1%. In contrast, the medium- and high-grade samples contain

around 30% locked bastnäsite grains, accompanied by similar proportions of composite grains. Among all samples, the high-grade material exhibits the greatest proportion of liberated bastnäsite, reaching 2.7%.

The medium-grade sample exhibits the largest fraction of locked monazite grains (44%), compared with 27% in the low-grade sample and 24% in the high-grade sample. Composite monazite grains constitute 53% of the medium-grade material, whereas both the low- and high-grade samples contain approximately 60%. The highest proportion of liberated monazite is observed in the high-grade sample (14%), followed by the low-grade (8%) and medium-grade samples (2%). In the low-grade sample, 48% of synchysite grains display less than 10% exposed partial perimeter, while fully locked grains account for 54% of the synchysite population. For the medium- and high-grade samples, the fraction of grains with less than 10% exposed perimeter increases to 70% and 64%, respectively. Correspondingly, the overall proportion of locked synchysite grains rises to 91% in the medium-grade sample and 85% in the high-grade sample.

Fully liberated magnetite particles are most prevalent in the medium-grade sample (14%), followed by the high-grade (10%), with the lowest abundance observed in the low-grade sample (5%). A similar pattern is evident for locked magnetite grains, which account for 22% in the medium-grade sample, 20% in the high-grade sample, and 12% in the low-grade sample. These observations highlight the importance of considering mineral association and liberation characteristics when assessing the potential effectiveness of magnetic separation.

3.2.4.Mineral associations

Mineral association data were evaluated for magnetite and the principal REM sub-types, with parisite-Ce, parisite-Ce-La, bastnäsite-Ce-La, monazite-Ce, and synchysite-Ce grouped as TREM. Parisite-Ce exhibits the greatest free surface exposure in the low-grade sample, with progressively lower values in the medium- and high-grade samples (Fig. 2). Its associations with other REMs remain broadly consistent across grades, while carbonate associations show grade-dependent trends. In particular, associations with ferroan dolomite and ankerite increase markedly in the high-grade sample, whereas calcite associations are strongest in the low-grade material. Minor but notable associations with magnetite and chlorite are most pronounced in the medium-grade sample.

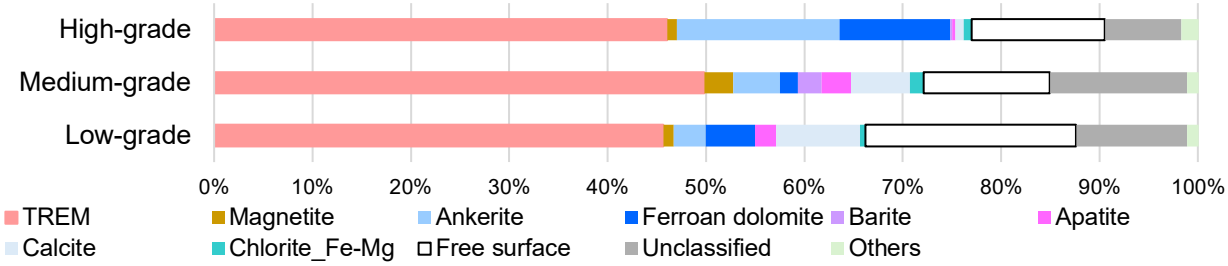

Figure 2. Mineral associations for parisite-Ce grains in low-, medium- and high-grade samples

Parisite-Ce-La displays its highest degree of liberation in the medium-grade sample and is likewise primarily associated with other REMs across all grades. Carbonate associations, especially with ankerite and ferroan dolomite, are most significant in the high-grade sample, while interactions with calcite are more prominent in the low- and medium-grade materials. Associations with magnetite remain generally low, peaking in the medium-grade sample.

Bastnäsite-Ce-La shows the highest free surface exposure in the high-grade sample, reflecting improved liberation relative to the lower-grade materials. As with other REM sub-types, it is chiefly associated with other REMs, although this association weakens with increasing grade.

Carbonate associations follow trends similar to parisite-Ce-La, with stronger links to ankerite and ferroan dolomite in the high-grade sample, and limited interaction in the lower-grade materials. Magnetite associations are minor and most evident in the medium-grade sample. Monazite-Ce demonstrates contrasting association patterns across grades. High free surface exposure is observed in both low- and high-grade samples, whereas the medium-grade sample exhibits significantly lower liberation. In the low- and medium-grade samples, monazite-Ce is predominantly associated with apatite and calcite, while in the high-grade material it shows stronger associations with other REMs and Fe-bearing carbonates. Associations with magnetite decrease systematically from low- to high-grade samples (Fig. 3).

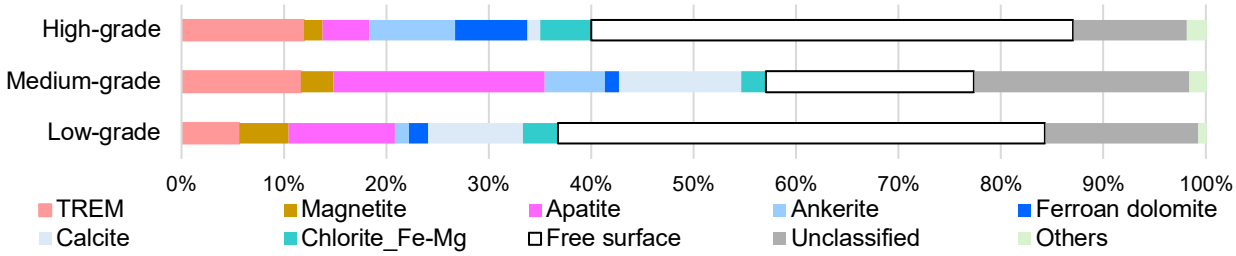

Figure 3. Mineral associations for monazite-Ce grains in low-, medium- and high-grade samples

Overall, these mineral association trends highlight grade-dependent differences in REM liberation and gangue attachment, underscoring the importance of mineralogical context when assessing the suitability of physical separation methods such as flotation and magnetic separation.

4.DISCUSSION

Calcite is the primary gangue mineral in the low- and medium-grade samples, and its low density (2.7 g/cm³) makes these materials more amenable to gravity separation compared to the high-grade sample. The higher monazite content in these samples further enhances density contrast, improving separation efficiency. All rare earth minerals (REMs) are paramagnetic, necessitating high-intensity magnetic separation (HIMS) to both concentrate REMs and remove magnetite, which occurs at ~2.2 wt.% in the low- and medium-grade samples and ~3.2 wt.% in the high-grade sample. While low-intensity magnetic separation (LIMS) can reduce magnetite content and reagent consumption, it also incurs TREM losses of approximately 2 wt.% in the low- and high-grade samples and ~6 wt.% in the medium-grade sample. Actual losses may be higher due to incomplete separation, highlighting the need to interpret these results in the context of mineral associations and liberation data.

Gangue mineralogy varies with grade: ankerite dominates in the medium- and high-grade samples, whereas ferroan dolomite is more abundant in the low-grade material. These carbonates expose different surface ions (Ca, Mg, Fe, Mn), affecting ion release, surface charge, and flotation behavior. Understanding these surface properties is therefore essential for selecting effective collectors in REM beneficiation. Flotation occurs via two mechanisms: physisorption, driven by electrostatic attraction, and chemisorption, which forms covalent or coordinate bonds with surface species (Leja, 1982). Because REMs and their carbonate gangue often carry similar positive surface charges, collectors relying predominantly on physisorption are generally ineffective (Marion et al., 2020).

Hydroxamates and carboxylates, particularly hydroxamates, are the most widely used REM collectors due to their superior selectivity (Gajendra et al., 2025). Hydroxamates form more stable complexes with transition metal cations (Fe^{3+}, Al^{3+}, Cu^{2+}, Pb^{2+}) compared to Ca^{2+}, Mg^{2+}, and Ba^{2+}, which exhibit weaker complexation (Liu et al., 2023; Marion et al., 2020). Rare earth

cations have intermediate complex stability, and even Fe^{2+} forms stronger complexes than Ca^{2+}, which enhances selectivity when stability constants differ significantly. Microflotation studies by Azizi and Larachi (2018) using an alkyl hydroxamate (Aero 6493) and sodium silicate (SS) showed that ankerite floats more readily than calcite or dolomite due to the presence of Fe and Mn, which form stable hydroxamate complexes (Jordens et al., 2014; Nduwa Mushidi & Anderson, 2017).

In the high-grade sample, the abundance of ankerite and ferroan dolomite (~80 wt.% combined) increases hydroxamate adsorption onto gangue, potentially elevating unwanted recovery. This can be mitigated by depressants such as sodium silicate, widely applied in REM flotation (e.g., Bayan Obo) (Kim et al., 2025). SS adsorbs onto hydroxylated Ca and Ba sites on minerals like fluorite, barite, and calcite, producing hydrophilic surfaces and inhibiting flotation. It also scavenges dissolved Ca^{2+} and Mg^{2+}, reducing collector consumption (Liu et al., 2023). The high-grade sample's elevated barite content (5 wt.%) further underscores the relevance of SS for selective depression.

Apatite is most abundant in the medium-grade sample. Nduwa Mushidi and Anderson (2017) demonstrated that octanohydroxamic acid (OHA) chemisorbs onto both monazite and apatite, with adsorption increasing ~3.5 times on monazite between 25 and 80 °C, and a similar trend for apatite. Microflotation tests showed monazite flotation is optimal at pH 7.5–10, while apatite floatability increases with pH, peaking at 12.6. These findings indicate that higher flotation temperatures are required for monazite in low-grade ores, increasing processing costs, and careful pH control is needed in low- and medium-grade samples, which have apatite/TREM ratios of 2.5 and 2.

Mineral association data reveal that in the low- and medium-grade samples, parisite-Ce and parisite-Ce-La exhibit over 60% co-occurrence with other REM sub-types, suggesting relatively straightforward separation. Bastnäsite-Ce-La shows the highest association with other REMs in the low-grade sample (>80%), decreasing to below 50% in the high-grade sample. Despite high locking (~90%) in the low-grade sample, its strong associations indicate that recovery remains feasible. In the high-grade sample, association and liberation data align: 32% of bastnäsite-Ce-La surfaces are exposed, and ~65% of grains have >30% perimeter exposure.

Monazite-Ce consistently exhibits the lowest association with other REMs and the highest with apatite, a commonly observed pairing, along with the largest free surface exposure, reflecting favorable liberation. The pronounced apatite–monazite association in the medium-grade sample may influence monazite flotation but could also enable simultaneous apatite recovery during concentration.

5.CONCLUSIONS

Chemical and mineralogical characterization of three carbonatite sample grades showed major differences in element distribution and mineralogy. Based on assays, modal mineralogy, liberation, and mineral association data, the suitability of various physical separation methods was evaluated. Each sample presents different beneficiation challenges: the low-grade sample contains fewer REMs overall but has enough monazite (the main Nd host) to potentially justify processing, while the medium- and high-grade samples may be harder to float due to their higher apatite and barite contents. Liberation and association data indicate that REMs have sufficient surface exposure for effective flotation at the current grind size.

Overall, the mineralogical variations highlight the need for grade-specific beneficiation strategies tailored to dominant REM and gangue minerals to ensure selective and efficient recovery.

REFERENCES

Akyildiz, E., Silva, C.M., Tobiczyk, K., Lode, S., Aasly, K., Kowalczuk, P. B., (2026) “Flotation response of parisite, monazite, bastnäsite and synchysite from a carbonatite deposit”, Powder Technology, 471 122112.

Al-ali, S., Wall, F., Fitzpatrick, R., Broom-fendley, S., Rollinson, G., Brady, A. E., Pickles, J. R., Williams, A., Dawes, W., (2020) “Key process mineralogy parameters for rare earth fluorcarbonate-bearing carbonatite deposits: The example of Songwe Hill, Malawi”, Minerals Engineering, 159 106617.

Andersen, T., (1984) “Secondary processes in carbonatites: Petrology of “rødberg” (hematite–calcite–dolomite carbonatite) in the Fen central complex, Telemark (South Norway)”, Lithos, 17 227–245.

Andersen, T., (1986) “Compositional variation of some rare earth minerals from the Fen complex (Telemark, SE Norway): Implications for the mobility of rare earths in a carbonatite system”, Mineralogical Magazine, 50 503–509.

Andersen, T., (1987) “A model for the evolution of hematite carbonatite, based on whole-rock major and trace element data from the Fen complex, southeast Norway”, Applied Geochemistry, 2 163–180.

Andersen, T., (1989) “Evolution of peralkaline calcite carbonatite magma in the Fen complex, southeast Norway”, Lithos, 22 99–112.

Azizi, D., Larachi, F., (2018) “Surface interactions and flotation behavior of calcite, dolomite and ankerite with alkyl hydroxamic acid bearing collector and sodium silicate”, Colloids and Surfaces A, 537 126–138.

Bagger, A.T., Kirkelund, G., Lode, S., Jensen, P., Kunther, W., (2025) “Dissolution behavior and mineralogical changes of mine tailings subjected to NaOH solution”, Construction and Building Materials, 493 143075.

Balaram, V., (2019) “Rare earth elements: A review of applications, occurrence, exploration, analysis, recycling, and environmental impact”, Geoscience Frontiers, 10 (4) 1285–1303.

Becker, M., (2023) “The contribution of applied mineralogy to sustainability in the mine life cycle”, Minerals Engineering, 199 108121.

Boesche, N. K., Rogass, C., Mielke, C., Herrmann, S., Körting, F., Papenfuss, A., Lubitz, C., Brell, M., Tonn, S., Altenberger, U., (2016), Hyperspectral Rare Earth Element Mapping of Three Outcrops at the Fen Complex, Norway: Calcitic, Dolomitic, and Ankeritic Carbonatites, Rare Earths Industry, Elsevier, pp. 235–265.

Bradshaw, D., (2014) “The role of process mineralogy in improving the process performance of complex sulphide ores”, Keynote Paper 932, IMPC, Santiago, Chile.

Brøgger, W. C., (1921), Die eruptivgesteine des Kristianiagebietes. 4. Das Fengebiet in Telemark, Norwegen. Videnskaps-Selskapets Skrifter 9, 1–402. Academy of Science, Oslo.

Cagno, S., Lind, O. C., Popic, J. M., Skipperud, L., De Nolf, W., Nuyts, G., Vanmeert, F., Jaroszewicz, J., Janssens, K., Salbu, B., (2020) ”Micro-analytical characterization of thorium-rich aggregates from Norwegian NORM sites (Fen Complex, Telemark)”, Journal of Environmental Radioactivity, 219 106273.

Dahlgren, S., (2019) “REE mineralization in the Fen carbonatite complex, Telemark, Norway – A world-class exploration target for the hi-tech and green-shift” industry””, Report for the Geological Advisor, 1–86.

Davris, P., Marinos, D., Balomenos, E., Alexandri, A., Gregou, M., Panias, D., Paspaliaris, I., (2018) “Leaching of rare earth elements from “Rödberg” ore of Fen carbonatite complex deposit using the ionic liquid HbetTf_2N”, Hydrometallurgy, 175 20–27.

Drobnlak, A., Mastalerz, M., (2022) ”Rare earth elements: A brief overview”, Indiana Journal of Earth Sciences, 4.

Drzymala, J., (2007), Mineral Processing, Foundations of Theory and Practice of Minerallurgy, Oficyna Wydawnicza PWr.

Elliot, H. A. L., Wall, F., Chakhmouradian, A. R., Siegfried, P. R., Dahlgren, S., Weatherley, S., Finch, A. A., Marks, M. A. W., Dowman, E., Deady, E., (2018) “Fenites associated with carbonatite complexes: A review”, Ore Geology Reviews, 93 38–59.

European Commission, (2023), Study on the critical raw materials for the EU 2023: Final report. Publications Office of the European Union.

Geoscience Australia, (2023), Rare earth elements. Geoscience Australia. Available at: webmineral.com (Accessed: 19.12.2023).

Grammatikopoulos, T., Downing, S., (2020) “The disruptive role of process mineralogy in geology and mineral processing industry”, Aspects in Mining & Mineral Science, 5 (2).

Gu, Y., Schouwstra, R. P., Rule, C., (2014) “The value of automated mineralogy”, Minerals Engineering, 58 100–103.

James Cook University, n.d. Element-to-stoichiometric oxide conversion factors. James Cook University.

Jordens, A., Cheng, Y. P., Waters, K. E., (2013) “A review of the beneficiation of rare earth element bearing minerals”, Minerals Engineering, 41 97–114.

Jordens, A., Marion, C., Kuzmina, O., Waters, K. E., (2014) “Surface chemistry considerations in the flotation of bastnäsite”, Minerals Engineering, 66–68 119–129.

Kim, J., Choi, J., Lee, S., (2025), “A review of rare earth elements recovery from bastnäsite ore: From beneficiation to metallurgical processing”, Journal of Sustainable Metallurgy, 11 773–798.

Kresten, P., Morogan, V., (1986) “Fenitization at the Fen complex, southern Norway”, Lithos, 19 27–42.

Leboutillier, N., Shail, R., (2000), The cassiterite–anatase–ilmenite–monazite–sulphide–chlorite assemblage of North Tincroft Lode. Annual Conference of the Ussher Society.

Leja, J., (1982), Surface chemistry of froth flotation, Plenum Press, New York.

Lie, A., Østergaard, C., (2011), The Fen carbonatite complex, Ulefoss, South Norway. Summary of historic work and data. 21st NORTH, Norway.

Liu, C., Xu, L., Deng, J., Tian, J., Wang, D., Xue, K., Zhang, X., Wang, Y., Fang, J., Liu, J., (2023) “A review of flotation reagents for bastnäsite-(Ce) rare earth ore”, Advances in Colloid and Interface Science, 321 103029.

Lotter, N., Baum, W., Reeves, S., Arrué, C., Bradshaw, D., (2018) “The business value of best practice process mineralogy”, Minerals Engineering, 116 226–238.

Marion, C., Li, R., Waters, K. E., (2020) “A review of reagents applied to rare-earth mineral flotation”, Advances in Colloid and Interface Science, 279 102142.

Marien, C., Dijkstra, A.H., Wilkins, C., (2018) “The hydrothermal alteration of carbonatite in the Fen Complex, Norway: Mineralogy, geochemistry, and implications for rare-earth element resource formation”, Mineralogical Magazine, 82(S1) S115–S131.

Nduwa-mushidi, J., Anderson, C. G., (2017) “Surface chemistry and flotation behaviors of monazite–apatite–ilmenite–quartz–rutile–zircon with octanohydroxamic acid”, Journal of Sustainable Metallurgy, 3 62–72.

Nkiawete, M. M., Wal, R. L. V., (2025) “Rare earth elements: Sector allocations and supply chain considerations”, Journal of Rare Earths, 43 1–8.

Petruk, W., (2000), Applied Mineralogy in the Mining Industry, Elsevier, The Netherlands.

Silva, C., Lode, S., Aasly, K., Kowalczuk, P., (2023) “Early-stage application of process mineralogy methodologies for mineral tracking in flotation of rare earth elements (REE)-bearing minerals from a deposit in Norway”, Minerals Engineering, 202 108268.

Wills, B., Finch, J., (2016), Wills’ mineral processing technology, Elsevier.

PROFESSIONAL RISK ASSESSMENT IN MINERAL PROCESSING

Marija HADZI-NIKOLOVA*, Dejan MIRAKOVSKI, Afrodita ZENDELSKA, Nikolinka DONEVA

Faculty of Natural and Technical Sciences, Goce Delcev University, Stip, North Macedonia
**Corresponding author: marija.hadzi-nikolova@ugd.edu.mk*

A B S T R A C T

Risk assessment constitutes a fundamental element in establishing a safe and healthy working environment. The responsibility for conducting the risk assessment process lies with employees, as their active involvement promotes workplace safety, motivation, and organizational trust. Furthermore, risk assessment serves as an indicator of a company's sustainability trajectory by contributing to enhanced capacity development, productivity, and profitability.

In the mineral processing industry, workers are routinely exposed to a wide range of occupational hazards and harmful substances. Accordingly, a qualitative/semi-quantitative risk assessment was conducted using the 5×5 risk assessment matrix across four workstations within a mineral processing plant: flotation operator, filter press operator, mill operator, and flotation shift engineer. The findings indicated that all four positions were classified as high-risk workplaces, leading to the proposal of appropriate control measures aimed at hazard elimination and risk reduction.

Key words: *Flotation, hazards, workplace, safety*

1. INTRODUCTION

The rapid development of technology, accompanied by a constant increase in the power and productivity of machines, contributes to changing working conditions in workplaces in industrial enterprises. Therefore, ensuring safe and hygienic working conditions in production is a serious scientific problem that engineers of literally all specialties have to face, especially at mining (Nuruldaeva et al., 2025). Mining and mineral processing, are with the highest rate of occupational diseases and accidents (Parker at al., 2017), where workers are exposed to the worst and most dangerous working conditions (Marimuthu at al., 2023). Mining can be singled out as an industry with high occupational risk indicators, many works (Gyekye, 2003, Milošević at al., 2025) have singled them out as the most dangerous production environments due to the large number of injuries that occur in them.

Mining has always constituted one of the most dangerous industries. This is confirmed by data published in Eurostat, OECD, or by national organizations, such as, in Poland, the State Mining Authority. The reports presented by these organizations indicate the main risk groups and the effects of their occurrence in mining plants. Prepared reports on accidents in mining indicate their causes and circumstances of occurrence (Tubis at al., 2020).

Many processes in the mining are characterized by specific working conditions, and high occupational health risks for workers. Mining have the highest levels of occupational morbidity - up to 24.3 per 10 thousand workers (Preobrazhenskaya at al., 2016). Increased occupational risk has a negative impact on the health of workers, worsens the indicators of general and occupational morbidity, increases mortality from chronic non-infectious diseases (Mandal at al., 2022; Freeh and Iles, 1985; Chebotarev and Sementsova, 2021; Kiryakov and Sukhova, 2015).

Mineral processing plants are an important element of the overall process of extraction and processing of mineral raw materials. They combine different technologies, various types of

production equipment, operate with high capacities and generally observe a rather complex technological process (Kostadinova and Vladkova, 2025).

Technological processes of mineral processing can be conditionally divided into three main stages: operations of preparation for enrichment - crushing, screening and transportation of raw materials, enrichment processes and operations to obtain concentrates (drying, packaging, loading).

The key occupational hazards associated with mineral processing plants are dust, noise, vibration and mechanical injuries (Nuruldaeva at al., 2025).

Risk assessment is a proven technique for improving the quality of input to safety management, aiming to prevent accidents by “debugging” designs and operating methods etc. before accidents occur, rather than responding to accidents which have happened and aiming to prevent recurrence (Guide to Reviewing a Mine Risk Assessment of mine equipment and operations, 1997).

2. MATERIAL AND METHODS

Risk is defined as hazard or danger having adverse consequences for individuals. The U.S. Atomic Energy Commission in 1975 has identified risk as 'the probability of occurrence of particular consequences over a specific period of time' (Risk assessment and its management in mining industry, 2012). Risk assessment is process for estimate of the likelihood of getting injury or adverse health condition.

The structured process associated with risk assessment helps to characterize the major hazards and evaluate engineering, management and work process factors that impact how a mine mitigates its highest risk.

Although there is a spread range of approaches and risk assessment techniques, in essence, they all contain the same fundamental steps (Risk assessment and its management in mining industry, 2012). These are:

- Identify hazards–something with the potential to cause harm;
- Assess the likelihood, or probability, of harm arising from the hazard;
- Assess the severity of harm resulting from realization of the hazard;
- Combine assessments of likelihood and severity to produce an assessment of risk;
- Use the assessment of risk as an aid to decision making.

A 5x5 matrix to risk assessment of four workplaces (flotation operator, filter press operator, mill operator, and flotation shift engineer) in the mineral processing have been used (Table 1).

Table 1. Particle size distribution of representative ore sample

		Consequence				
		1	2	3	4	5
Likelihood		Minor	Low	Medium	High	Major
Almost certain	5	2	3	4	4	4
Likely	4	2	3	3	4	4
Possible	3	1	2	3	3	4
Unlikely	2	1	2	2	3	4
Rare	1	1	1	1	2	3

Some risks may be higher but will be well managed and therefore acceptable. An example of the actions taken based on the risk rating is shown in Table 2.

Table 2. Risk measures (Risk assessment education resource, Mining Safety and Health Advisory Committee, 2023)

Risk level	Risk measures
4– Major	Immediate action required Identify and implement controls to manage risks Highest level of management needs to be involved
3 – Significant	Immediate action required Identify and implement controls to manage risks Senior site management needs to be involved
2 – Medium	Implement control to manage risks Responsibility must be defined
1– Low	Implement controls as required Manage by routine processes

Risk assessment of four workplaces (flotation operator, filter press operator, mill operator, and flotation shift engineer) in the mineral processing is given in Table 3.

3. RESULTS AND DISCUSSION

Professional risk assessment in mineral processing plant on four workplaces have been conducted based on the findings of more researches study, as well as routine measurements of physical and chemical occupational hazards conducted by the accredited AMBICON Laboratory within the Faculty of Natural and Technical Sciences across numerous mines in North Macedonia. It was determined that operators in mineral processing plant are exposed to a complex combination of adverse working environment and labor process factors. These include industrial noise and vibration, unfavorable microclimatic conditions, elevated airborne dust concentrations in the working zone—predominantly consisting of aerosols with fibro genic effects, as well as increased physical workload and work intensity.

Occupational exposure assessments indicate that noise levels at crushing, grinding, and ore transportation workstations range between 85 and 100 dB, exceeding the maximum permissible limits in nearly 85–90% of the studies reviewed, with some reports documenting exceedances in all observed cases. Airborne dust concentrations at these workplaces vary depending on the type of mineral raw material processed and the effectiveness of ventilation systems, ranging from 3.8 to 5.8 mg/m³ and containing more than 10% free silicon dioxide. Another consistently present occupational hazard is whole-body vibration. The reviewed literature demonstrates that vibration levels in both coarse and fine crushing facilities surpass the maximum permissible values by more than 50%.

Consequently, varying intensities of production-related factors result in different levels of risk for the development of occupational pathologies among workers. Occupational diseases most commonly arise in employees exposed to multiple harmful factors simultaneously. Risk assessment findings and the reviewed literature indicate that dust-related diseases, such as pneumoconiosis, are prevalent among crusher operators. Furthermore, prolonged exposure to whole-body vibration is associated with musculoskeletal disorders, including pain in the lower back, limbs, and joints, while sustained exposure to noise levels exceeding maximum permissible limits is a well-established cause of occupational hearing loss.

Although all four positions in mineral processing plant (flotation operator, filter press operator, mill operator, and flotation shift engineer) were classified as high-risk, the role of the mill

operator was identified as the most hazardous due to additional occupational exposures encountered during routine tasks, including work in confined space and the operation of cranes and elevators.

4. CONCLUSION

The synthesized findings demonstrate a high prevalence of occupational hazards in mineral processing plant, with a strong association between multifactorial exposures and the development of chronic health conditions. These results emphasize the need for integrated protective strategies and further targeted research.

Nevertheless, despite the research conducted to date, numerous unresolved issues and challenges remain regarding the occupational health and safety of workers in mineral processing plants. Evolving working conditions and the introduction of new technologies necessitate continuous monitoring and ongoing adaptation of occupational health and safety management systems.

Future research outcomes may contribute to the enhancement of existing safety practices, including the formulation of policy recommendations, the implementation of innovative technologies, and the development of improved risk assessment tools. Ultimately, ensuring safe and healthy working conditions requires the continuous updating of knowledge and the systematic refinement of occupational health and safety management frameworks.

Table 3. Professional risk assessment in mineral processing plant (MPP). L is Likelihood, C is Consequence and R is Risk

Danger or harmful	Shift engineer in MPP			Floater			Filter press operator			Mill opertaor		
	L	C	R	L	C	R	L	C	R	L	C	R
Insufficient safety due to rotating and moving parts	2	3	2	3	3	3	3	3	3	3	3	3
Internal transport and movement of working machines or vehicles	3	4	3	2	4	3	2	4	3	2	4	3
Exposure to mechanical blow	2	3	2	3	3	3	3	3	3	3	3	3
Hand tools				3	3	3	3	3	3	3	3	3
Crane and elevators	2	3	2							3	4	3
Possibility of slipping, falling (wet or slippery surfaces)	2	3	3	3	3	3	2	3	3	3	3	3
Working at height	2	4	3	3	4	3	2	4	3	3	4	3
Confined space										3	4	3
Electrical hazards	2	4	3	2	4	3	2	4	3	2	4	3
Dust (inhalation, skin absorption)	3	2	2	3	2	2	4	2	3	4	2	3
Hazardous chemical substances (inhalation)	2	4	3	3	4	3	2	4	3	3	4	3
Noise	3	2	2	3	2	2	3	2	2	3	2	2
Vibration	3	2	2	3	2	2	3	2	2	3	2	2
Unfavourable microclimatic conditions (low temperature, humidity, air flow speed)	2	3	3	3	3	3	3	3	3	3	3	3
Harmfuls arising from mental and psychophysiological efforts												
Strains when performing certain tasks that cause psychological strain - stress	4	2	3	3	2	2	3	2	2	3	2	2
Non-physiological body position: prolonged standing, bending.	4	2	3	4	2	3	4	2	3	4	2	3
Need for decision-making	4	1	2									
Using appropriate knowledge and skills	4	1	2	4	1	2	4	1	2	4	1	2
Responsibility in the conducting rules	4	1	2	4	1	2	4	1	2	4	1	2
Conflict situations	3	2	2	3	2	2	3	2	2	3	2	2
Harmfuls related to the organization of work												
Shift working	4	2	3	4	2	3	4	2	3	4	2	3
Night working	4	2	3	4	2	3	4	2	3	4	2	3

REFERENCES

Chebotarev, A. G., Sementsova, D. D., (2021), “Comprehensive assessment of working conditions and occupational disease rates at mining and metallurgical enterprises”, Russian Mining Industry, (1), 114–119. https://doi.org/10.30686/1609-9192-2021-1-114-119

Freeh, E. J., Iles, C. D., (1985), “Experience with operating and controlling an in-pit portable crushing and conveying system”, IFAC Proceedings, 18(6), 153–158. https://doi.org/10.1016/S1474-6670(17)60502-0

Gyekye, S. A., (2003), “Causal attributions of Ghanaian industrial workers for accident occurrence: Miners and non-miners perspective”, Journal of Safety Research, 34(5), 533–538. https://doi.org/10.1016/j.jsr.2003.03.002

Mude, M. A., (2016), “Guide to reviewing a mine risk assessment: Comparison of SAW and TOPSIS methods in the case of MSMEs”, Ilk. J. Ilm. https://doi.org/10.33096/ilkom.v8i2.49.76-81

Foster, P. J., Rose, H. J. M., Talbot, C. F., (1998), “Risk assessment: An opportunity to change health and safety performance”, The Journal of the South African Institute of Mining and Metallurgy.

Marimuthu, R., Sankaranarayanan, B., Karuppia, K., (2023), “Prioritizing the factors affecting the occupational health and safety of workers in the mining industry using the SWARA technique”, Journal of Current Science and Technology, 13(1), 59–73. https://doi.org/10.14456/jcst.2023.6

Milošević, I., Stojanović, A., Nikolić, Đ., Mihajlović, I., Brkić, A., Perišić, M., Spasojević-Brkić, V., (2025), “Occupational health and safety performance in a changing mining environment: Identification of critical factors”, Safety Science, 184, 106745. https://doi.org/10.1016/j.ssci.2024.106745

Mandal, B. B., Bhattacharya, S., Munawar, V. D., Hussain, S. A., (2022), “Health risk of exposure to noise in coal preparation and mineral processing plants”, in: Moitra, A. K., Kayal, J. R., Mukherjee, B., Bhattacharya, J., Das, A. K. (eds.), Innovative Exploration Methods for Minerals, Oil, Gas, and Groundwater for Sustainable Development, Elsevier, pp. 139–157. https://doi.org/10.1016/B978-0-12-823998-8.00062-4

Nuruldaeva, G., Isakhanova, A., Kumar, D., Kumar, B., (2025), “Occupational hazards in mineral ore crushing and grinding: A literature review”, International Journal of Safety and Security Engineering, 15(3), 415–426. http://iieta.org/journals/ijsse

Parker, A. W., Tones, M. J., Ritchie, G. E., (2017), “Development of a multilevel health and safety climate survey tool within a mining setting”, Journal of Safety Research, 62, 173–180. https://doi.org/10.1016/j.jsr.2017.06.007

Preobrazhenskaya, E. A., Sukhova, A. V., Zorkina, L. A., Bondareva, M. V., (2016), “Hygienic assessment of working conditions and health of the workers of mining and processing enterprises”, Hygiene and Sanitation, 95(11), 1065–1070. https://doi.org/10.18821/0016-9900-2016-95-11-1065-107

Tubis, A., Werbinska-Wojciechowska, S., Wroblewski, A., (2020), “Risk assessment methods in mining industry — a systematic review”, Applied Sciences, 10, 5172.

SELECTION OF AN APPROPRIATE TECHNOLOGY FOR FLOTATION TAILINGS DISPOSAL USING THE SAW METHOD

Afrodita ZENDELSKA*, Nikolinka DONEVA, Marija HADZI-NIKOLOVA, Dejan MIRAKOVSKI, Blagoj GOLOMEOV

Faculty of Natural and Technical Sciences, Goce Delcev University, Stip, North Macedonia
**Corresponding author: afrodita.zendelska@ugd.edu.mk*

A B S T R A C T

A global trend is the development of sustainable mining practices to minimize environmental impact. Following these trends, the lead and zinc mine with underground exploitation from North Macedonia applies three variants for the disposal of flotation tailings, including disposal in a tailings dam, dry stacking, and the backfill method. The flotation tailings used for the backfill method account for about 42% of the total amount, about 30% is used for dry stacking, while the remaining part (about 28%) is deposited in a tailings dam. Based on the presented disposal technology for all three variants, a multi-criteria analysis was performed to determine which of these technologies is most appropriate for achieving the goals of sustainable mining and environmental protection. The Simple Additive Weights method was applied, and decision-making criteria were established based on scientific and expert knowledge in this field. The results show that the most appropriate method that will contribute to the development of sustainable mining and environmental protection is the backfill method.

Key words: *Simple additive weights, backfill, dry disposal, tailing dam*

1. INTRODUCTION

The global mining industry is increasingly oriented towards the development and implementation of sustainable practices aimed at minimizing adverse environmental impacts. This transformation reflects the growing recognition of the need to balance mineral resource exploitation with environmental protection, economic efficiency, and social responsibility. As global demand for mineral resources continues to rise, the pressure on mining companies to adopt environmentally responsible and socially acceptable practices has intensified (PWC 2023; UNCCD 2021). In particular, sustainability in mining has evolved from a voluntary commitment to an operational necessity, driven by stricter environmental regulations, international sustainability frameworks, and community expectations (IISD, 2024).

Conventional mining operations, particularly those involving the disposal of flotation tailings, have historically been associated with significant ecological challenges, including soil degradation (Koucham et al., 2025; Barbosa et al., 2025), water contamination (Mahmood & Elektorowicz, 2015), and long-term landscape alteration (UNEP, 2020). The fine-grained nature and chemical composition of tailings often lead to the release of heavy metals and sulfide minerals, which can oxidize and produce acid mine drainage, thereby contaminating surrounding soils and water bodies (Lindsay et al., 2015, Manaviparast et al., 2024). Furthermore, the physical instability of tailings dams poses additional risks of catastrophic failure, resulting in severe and long-lasting environmental damage. These issues underscore the urgent need for improved tailings management technologies that ensure both environmental safety and operational efficiency.

Consequently, the adoption of sustainable tailings management strategies has become an essential component of modern mining operations. Sustainable approaches focus on reducing the generation of tailings at the source, promoting their reuse and recycling, and implementing disposal methods that minimize ecological footprints. Technologies such as dry stacking (Lupo

& Hall), paste backfilling (Tikou and Benzaazoua, 2007), and integrated waste management systems (Koucham et al., 2025) have gained increasing attention for their potential to enhance mine safety, reduce water consumption, and facilitate post-mining land rehabilitation. Moreover, the integration of multi-criteria decision-making methods enables the evaluation of tailings management options based on environmental, technical, and socio-economic indicators, providing a structured framework for selecting the most sustainable solutions (Štilić, and Puška, 2023).

In alignment with these international trends, a lead and zinc mine with underground exploitation in North Macedonia has introduced several alternative approaches for the disposal of flotation tailings. The mine employs three distinct disposal variants: deposition in a tailings dam, dry stacking, and the backfill method. Each of these technologies presents specific technical, environmental, and economic characteristics that influence their suitability within a framework of sustainable mining. To identify the most appropriate disposal method, a comprehensive multi-criteria analysis was conducted using the Simple Additive Weights (SAW) method. The decision-making criteria were established based on relevant scientific findings and expert evaluations. The purpose of this study is to assess and compare the three disposal technologies to determine the most sustainable and environmentally responsible solution for the management of flotation tailings in the context of underground mining operations in North Macedonia.

2. MATERIAL AND METHODS

In order to develop a sustainable mining practice to minimize environmental impact, an underground mine in North Macedonia has introduced several alternative approaches for the disposal of flotation tailings, such as:
- disposal in a tailings dam;
- backfill method;
- dry stacking.

To determine which of these technologies is most appropriate for achieving the goals of sustainable mining and environmental protection, a multi-criteria analysis, such as the Simple Additive Weights method, was performed.

2.1. Flotation Tailings Disposal Methods

Disposal in a tailings dam

Approximately 28% of the flotation tailings generated in the flotation process are gravitationally conveyed to the tailings dam via a pulp pipeline and partially dewatered using hydrocyclones, so that the liquid phase is deposited in the settling pond, and the material from the solid phase is used to build the downstream dam. A settling pond is formed in the rear part of the tailings dam accumulation area, farthest from the dam crest. In order to reduce water consumption in the flotation process, the mine has introduced a system for recirculating part of the clarified water from the settling pond and returning it to the flotation process through installed pumps and a return line for the gravitationally settled wastewater of the settling pond.

a) b)

Figure 1. Flotation tailing dam, a) Dam, b) Settling Pond

Backfill method

The filling of the excavated areas is carried out with backfill material - paste, which consists of: flotation tailings, cement, fly ash and water. The paste is prepared in the Paste plant.
In order to cover all zones of the mine where the Backfill method is applied, about 7.5 km of pipeline have been installed and 1 km of boreholes have been drilled.
Preparatory work for the application of the Backfill method is fastening the backfill pipes, making a barricade, installing pipes for draining the backfill, etc.
After completing these activities, the installation of the paste begins. The length of the block to be filled is 150 m. Three pipelines are installed in the crown of the drift, the first of which is 150 m long, the second 100 m and the third 50 m.

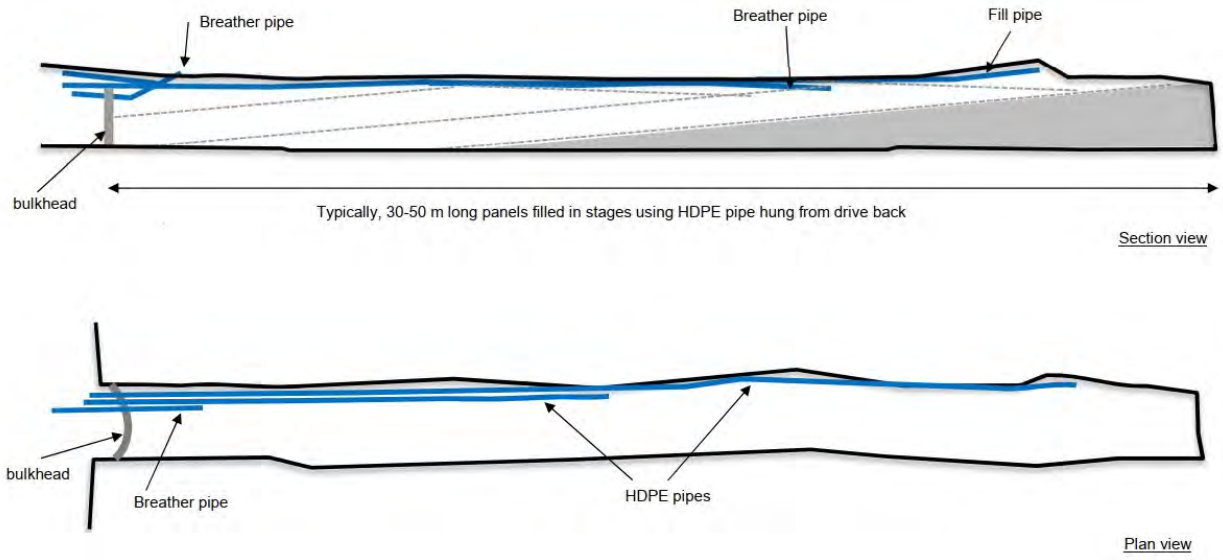

Figure 2. Illustration of the principle of backfill method

The delivery of backfill from the Paste Plant to the excavations is regulated by an automatic regulation system – SCADA system.

Dry stacking

To apply the dry stacking method, it is necessary to have two main parts: Dry Stacking Plant and Dry Stacking Installation (previously suitably prepared space).
As input material to the Dry Stacking Plant, partially dewatered hydro tailings from a thickener with 65% solids are used.

Further dewatering is carried out in a filter press, after which a filter cake with 11.5% moisture is obtained. This material is transported via two conveyor belts to a temporary storage warehouse. It is then transported to the dry disposal installation by conveyor belts or trucks. Approximately 30% of the flotation tailings are stored using this method.

2.2. The Simple Additive Weighting (SAW) Method

The Simple Additive Weighting (SAW) Method is often known as the weighted addition method. The basic concept of the SAW method is to find a weighted sum of the performance ratings for each alternative on all criteria. The SAW method requires a decision matrix normalization process (X) to a scale that can be compared with all existing alternative ratings (Iqbal Panjaitan, (2019) (Mude, 2016).

This SAW method requires the decision-maker to determine the weight for each criterion. The total score for the alternatives is obtained by adding up all the multiplication results between the rating (which can be compared across criteria) and the weight of each criterion. The rating of each criterion must be dimension-free in the sense that it has passed the previous matrix normalization process (Helilintar, 2016).

The rating of each attribute must be dimension-free in the sense that it has passed the previous matrix normalization process.

The quantification of qualitative criteria in the simple additive weights (SAW) method is made according to Table 1 (Despodov, 2002).

Table 1. Quantification of qualitative criteria in the Simple Additive Weight (SAW) method

Type of criteria	Goal	bad	good	average	very good	excellent
C_{max}	Max	1	3	5	7	9
C_{min}	Min	9	7	5	3	1

The formula for carrying out the normalization (Eq. 1) is as follows (Christioko et al., 2017);

$$R_{ij} = \begin{cases} \frac{X_{ij}}{maxX_{ij}}, & for\ C_i \rightarrow max \\ \frac{minX_{ij}}{X_{ij}}, & for\ C_i \rightarrow min \end{cases} \quad \text{(Eq. 1)}$$

Where:

R_{ij} is a normalized performance rating; X_{ij} is the attribute value of each criterion;
Max X_{ij} is the greatest value of each criterion; Min X_{ij} is the smallest value of each criterion;
R_{ij} is the normalized performance rating of the alternatives Ai on criteria Cj;
i = 1,2,…, m and j = 1,2,…, n.
The preference value for each alternative (V_i) is given as:

$$V_i = \sum_{j=1}^{n} W_j \cdot R_{ij} \quad (2)$$

Where V_i is the ranking for each alternative, W_j is the weighted value of each criterion. A larger V_i value indicates that the alternative A_i is preferred.

3. RESULTS AND DISCUSSION

Based on a comprehensive analysis of the three tailings disposal alternatives, it was determined that the most relevant criteria for their evaluation include: geological, hydrogeological, and geotechnical conditions; environmental protection; hazard risk;

sustainability; capital investment costs; operating costs; return on investment; safety and social aspects; and regulatory requirements.

Table 2 provides a descriptive presentation of the selected criteria for all considered alternatives, whereas Table 3 defines the objectives for each criterion and presents the evaluation of the alternatives using the Simple Additive Weighting (SAW) method.

Table 2. Description of the criteria for each alternative

Alternatives / Criteries	Tailing dam	Backfill method	Dry stacking
Geological, Hydrogeological and Geotechnical conditions	Construction of a tailings dam requires impermeable and sterile rocks	The orebody must be suitable for the application of a backfill method	The construction of a dry tailings storage facility requires sufficient available area with impermeable and sterile rocks
Environmental protection	Low level of protection of water, air, and soil	No adverse impact on the environment	Medium level of protection of water, air, and soil
Hazard risk	Risk of dam failure and contamination of water, air, and soil	No significant hazard risk	Risk of air (dust) pollution
Sustainability	Limited disposal capacity	Depends on the operating conditions for applying this method	Limited disposal capacity
Investigation costs	Costs related to the construction and closure of the tailings dam	Costs for construction of the paste backfill plant	Costs for construction of the dry tailings processing plant and for construction and closure of the dry stacking facility
Operation costs	Low operating costs (gravity-driven transport of tailings slurry)	Relatively high operating costs due to electricity consumption, construction of bulkheads, and cement usage	Moderately high operating costs for electricity consumption and dry tailings transport
Return on investment	No direct return on investment	By applying this method, the amount of mined ore reserves increases from 80% to 100%	No direct return on investment
Safety and Social conditions	Risk of dam failure and potential dissatisfaction of the local population	Mandatory implementation of occupational health and safety measures	Mandatory compliance with the designed geometry of the disposal facility
Regulatives	Higher requirements for monitoring and permits	Low requirements for monitoring and permits	Lower requirements for monitoring and permits

Table 3. Evaluation of the criteria for each alternative

Criteries	Tag	Goal	Alternatives		
			Tailing dam	Backfill method	Dry stacking
Geological, Hydrogeological and Geotechnical conditions	C_1	Max	3	9	5
Environmental protection	C_2	Max	1	9	3
Hazard risk	C_3	Min	7	1	3
Sustainability	C_4	Max	3	7	3

Investigation costs	C_5	Min	9	5	7
Operation costs	C_6	Min	3	7	5
Return on investment	C_7	Max	1	9	1
Safety and Social conditions	C_8	Max	3	9	7
Regulatives	C_9	Max	3	9	7

Table 4. Selection of the most acceptable alternative for tailings disposal

Criteria C_j	Goal	Criterion Weight W_j	Alternatives - A_i					
			Tailing dam – A_1		Backfill method – A_2		Dry stacking – A_3	
			Normalized performance rating - R_{ij}	Ranking V_1	Normalized performance rating - Rij	Ranking V_2	Normalized performance rating - Rij	Ranking V_3
C_1	Max	0.15	0.3333	0.0500	1.0000	0.1500	0.5556	0.0833
C_2	Max	0.2	0.1111	0.0222	1.0000	0.2000	0.3333	0.0667
C_3	Min	0.15	0.1429	0.0214	1.0000	0.1500	0.3333	0.0500
C_4	Max	0.05	0.4286	0.0214	1.0000	0.0500	0.4286	0.0214
C_5	Min	0.05	0.5556	0.0278	1.0000	0.0500	0.7143	0.0357
C_6	Min	0.1	1.0000	0.1000	0.4286	0.0429	0.6000	0.0600
C_7	Max	0.1	0.1111	0.0111	1.0000	0.1000	0.1111	0.0111
C_8	Max	0.1	0.3333	0.0333	1.0000	0.1000	0.7778	0.0778
C_9	Max	0.1	0.3333	0.0333	1.0000	0.1000	0.7778	0.0778
Total Ranking				**0.3206**		**0.9429**		**0.4838**

The selection of the most acceptable alternative for tailings disposal was performed using the Simple Additive Weighting (SAW) method and is presented in Table 4.

Considering global trends toward increasingly stringent environmental protection, the highest weights were assigned to the criteria of geological, hydrogeological, and geotechnical conditions; environmental protection; and hazard risk. In the cost analysis, greater weight was assigned to operating costs, as capital investment costs represent one-time expenditures. The scores for each criterion and alternative were assigned in accordance with the descriptions provided in Table 2.

Among the evaluated alternatives, the backfill method achieved the highest overall ranking, primarily due to its minimal environmental impact, elimination of surface tailings disposal, and increased ore recovery rate. In contrast, the tailings dam alternative ranked lowest, mainly as a result of its higher environmental risks, potential for structural failure, and greater regulatory and social concerns. Dry stacking represents an intermediate solution, offering improved environmental performance compared to conventional tailings dams, but with limitations related to operational complexity and storage capacity.

4. CONCLUSION

This study presents a comparative evaluation of three tailings disposal alternatives—tailings dam, backfill method, and dry stacking—using a multi-criteria decision-making approach based on the Simple Additive Weighting (SAW) method. The assessment was conducted by applying

a set of technical, environmental, economic, safety, and regulatory criteria, selected on the basis of a comprehensive analysis of the relevant geological and operational conditions.
The results indicate that environmental protection and hazard-related criteria play a decisive role in the selection process, reflecting current global trends toward more sustainable and environmentally responsible mining practices. By assigning higher weights to geological, hydrogeological, and geotechnical conditions, environmental protection, and hazard risk, the analysis emphasizes the importance of long-term stability and risk reduction in tailings management.

Based on the obtained results, it can be concluded that the backfill method represents the most suitable and sustainable tailings disposal option under the analyzed conditions. The applied methodology has proven to be an effective decision-support tool and can be successfully used for evaluating tailings management alternatives in similar mining projects.

REFERENCES

Barbosa, M., Figueiredo, J. C. G., Negreiros, D., Maia, R., Oki, Y., Rodriques de souza, L., dos Santos, M.P., Ferreira-Reis, R., Ferreira Rocha, Q. E., Ferreira Nunes, Y. R., das Dores Magalhaes Veloso, M., Fernandes, G. W., (2025) “Impact of mining tailings on soil decomposition and carbon stabilisation in a riparian atlantic forest”, Discover Environment, 3 152.

Despodov, Z., (2002) “Determination of optimal parameters of belt conveyors for their application in mining for metallic minerals with underground exploitation in the Republic of Macedonia”, Doctoral Dissertation (unpublished), Faculty of Mining and Geology, University "Cyril and Methodius" Skopje.

Helilintar, R., (2016), Application of saw and fuzzy methods in scholarship acceptance decision support system in decision support system scholarship, Citec J.

International Institute for Sustainable Development, (2024), Navigating global sustainability standards in the mining sector. https://www.iisd.org/system/files/2024-11/global-sustainability-standards-mining.pdf

I. P., Muhammad, (2019), Simple Additive Weighting (SAW) method in Determining Beneficiaries of Foundation Benefits: Jurnal Teknologi Komputer, 19-25.

Koucham, M., Khalil, A., Mouhagir, L., Zouhri, L., El Adnani, M., (2025) “Comprehensive assessment of environmental behavior of mine tailings for sustainable waste management and mitigation of pollution risks”, Water 17 (1) 43.

Lindsay, M. B. J., Moncur, M. C., Bain, J. G., Jambor, J. L., Ptacek, C. J., Blowes, D. W., (2015) “Geochemical and mineralogical aspects of sulfide mine tailings”, Applied Geochemistry, 57 157-177.

Lupo, J., Hall, J., Dry Stack Tailings – Design Considerations, AMEC Earth & Environmental, Englewood, CO, USA. Available at: https://www.iqpc.com/media/6139/588.pdf?utm_source=chatgpt.com

Manaviparast, H. R., Miranda, T., Pereira, E., Cristelo, N., (2024) “A comprehensive review on mine tailings as a raw material in the alkali activation process”, Applied Sciences, 14 (12) 5127.

Mahmood, A. A., Elektorowicz, M., (2015) “A review of sustainable management of mine tailings”, Applied Mechanics and Materials, 773 1256-1260.

Mude, M. A., (2016) “Comparison of SAW and TOPSIS methods in the case of MSMEs”, ILKOM Jurnal Ilmiah.

PWC (2023), Mine 2023: The era of reinvention. PwC. Available at: https://www.pwc.com/id/en/pwc-publications/industries-publications/energy--utilities---mining-publications/mine-2023.html?utm_source=chatgpt.com

Štilić, A., Puška, A., (2023) “Integrating multi-criteria decision-making methods with sustainable engineering: A comprehensive review of current practices”. Engineering, 4 1536-1549.

Tikou, B., Benzaazoua, M., (2007) “Design and application of underground mine paste backfill technology”, Geotechnical and Geological Engineering, 26 147-174.

United Nations Convention to Combat Desertification (UNCCD), (2021), Mineral resource governance. Available at: https://catalogue.unccd.int/1431_extractive_industries.pdf?utm_source=chatgpt.com

United Nations Environment Programme (UNEP), (2020, August), Global Industry Standard on Tailings Management. https://wedocs.unep.org/bitstream/handle/20.500.11822/36139/GISTM_En.pdf

SOME CHARACTERISTICS OF CHROMITES IN THE TROPOJE – HAS – GJAKOVE MASSIF AND THEIR FEATURES FOR ENRICHMENT.

Ibrahim MILUSH[1,*], Genc DEMI[2], Edmond PLLANA[2]

[1]*Institute of Geosciences, Polytechnic University of Tirana, Albania*
[2]*Faculty of Geology and Mine, Polytechnic University of Tirana, Albania*
**Corresponding author: ibrahimmilushi@yahoo.com*

A B S T R A C T

The Tropoje – Has – Gjakove ultramaphic massif constitutes the northeastern extreme of the Albanian ophiolites, precisely where the two belts of ultrabasic (the western lherzolitic belt and the eastern hartzburgitic one) converge. This massif, which spreads both in Albania and Kosovo, is of the harzburgitic type and occupy an area of about 540 km^2. The massif is of industrial importance because it has a high saturation with chromium mineralization and hundreds of outcrops of the metallurgical type have been identified. The aim of the study has been to significantly increase the amount of reserves, making it possible to reduce the condition of exploitation of ores with low chromium content from 18% Cr2O3 that was before 1990 to 7-8% Cr2O3. For this, samples have been taken from different chromium outcrops, which have been tested in heavy liquids and it has been concluded that it is possible to achieve the technological figures required by consumers, the quality of the concentrate and the recovery of Cr_2O_3 in the concentrate. The paper presents the results of the conducted studies, where it is proven that different chromite outcrops belonging to different levels of ultrabasic section show different enrichment characteristics.

Key words: *Chromium, outcrops, enrichment, heavy liquids*

1. INTRODUCTION

The Tropojë–Has–Gjakovë ophiolitic massif forms the northeastern margin of the Albanide ophiolites and extends across Albania and Kosovo, with about 88% located in Albania and 12% in Kosovo (Figures 1, 2). It belongs to the eastern belt of the Albanide ophiolites and represents the convergence between the lherzolitic ophiolite type of the western belt and the harzburgitic type of the eastern belt. The ultrabasic section of the massif is characterized by high chromite mineralization. Approximately 530 chromite occurrences have been identified, including 328 in Albania and 202 in Kosovo, all documented with coordinates, dimensions, geological characteristics, and chemical analyses.

The massif covers an area of about 900 km², while the mantle ultrabasic rocks occupy roughly 540 km². Geological exploration began in the early 20th century and intensified after World War II. Geological mapping has been conducted on both sides of the border at scales ranging from 1:50,000 to 1:2,000, accompanied by geophysical and geochemical studies. Detailed mapping of chromite occurrences was generally carried out at a scale of 1:2,000 in Albania and 1:2,500 in Kosovo.

Exploration activities included extensive trenches, galleries, drillings, and surface openings, with tens of thousands of drillings performed. Mining operations have extracted more than 3.5 million tons of chromite from the Albanian part of the massif and over 500,000 tons from the Kosovo sector. In Kosovo, a beneficiation plant was constructed at Deve about 70 years ago to process low-grade ore from deposits on both sides of the border. Additional processing plants were later built in Bogovë and another near the city of Gjakovë, the latter currently in the testing phase.

Extensive geological documentation is preserved in Albania (Central Geological Archive, Tirana; National Agency of Natural Resources; Institute of Geosciences; Geological Archive, Rubik), in Kosovo (Archive of the Independent Commission for Mines and Minerals – ICMM), and in Belgrade (Geozavod Archive).

2. REGIONAL FRAMEWORK

The Tropojë–Has–Gjakovë ophiolitic massif represents the northeastern margin of the Albanide ophiolites (Jurassic Mirdita ophiolite), with which it is integrated without a clear boundary. These ophiolites form part of the Dinaride–Albanide–Hellenide ophiolitic belt (Figure 1), characterized by significant petrological, geochemical, and metallogenic diversity. The Jurassic Mirdita ophiolite occupies about 4,000 km² in Albania, reaching approximately 7,500 km² when areas covered by post-ophiolitic sediments are included. It continues into Kosovo through the Gjakovë massif and represents an important segment of the Tethyan ophiolites within the Mediterranean Alpine belt.

The Albanian (Mirdita) ophiolite consists of two ultramafic belts: the western lherzolitic belt and the eastern harzburgitic belt. Between them lies a heterogeneous oceanic crust sequence composed of gabbros, sheeted dyke complexes, extrusives, and late intrusions (lherzolites, wehrlite, plagiogranite, quartz diorites, etc.). Both mantle and crustal formations show notable lateral variations.

This heterogeneity has generated significant debate regarding the origin and tectonic setting of these ophiolites, leading to different interpretations (Tashko, 1996; Kodra et al., 2000; Gjata et al., 1995; Nicolas et al., 1999; Beccaluva et al., 1994; Robertson & Shallo., 2000; Dilek et al., 2007; Bortolotti et al., 1996; Vergely et al., 1997; Dimo A., 1997).

3. GEOLOGY OF THE OPHIOLITIC MASSIF

The Tropojë–Has–Gjakovë massif preserves a complete sequence of mantle and oceanic crust. The mantle section occupies the central–northern part of the massif and consists mainly of harzburgites with small dunite lenses, which gradually pass into dunite–harzburgite sequences and massive dunites. Fresh harzburgites and dunites are widely present in the northwestern, central, and eastern areas.

The gabbroic and pyroxenite dyke series is strongly developed, especially in the upper part near the contact with the oceanic crust formations. Another characteristic feature is the wide distribution of pyroxenites in the upper parts of the mantle section, where, in contact with dunites, PGE (Platinum Group Elements) mineralizations occur.

Toward the south and east, the oceanic crust sequence appears, represented by gabbros, sheeted dyke complexes, and extrusive rocks ranging from basalts and andesites to rhyodacites. Plagiogranite and quartz diorite intrusions occur mainly in the southern zone of the massif. Harzburgites generally exhibit a banded texture with well-developed foliation.

The ultramafic section covers about 540 km², including 460 km² in Albania and around 80 km² in Kosovo (Mekshiqi et al., 2007). Petrographic and structural features indicate transitions from fresh and serpentinized harzburgites to harzburgite–dunite sequences in the middle parts and dunite-dominated sequences in the upper levels. The mantle section is relatively homogeneous in petrological characteristics. Based on erosional sections and drilling data, the thickness of this sequence ranges from 3 to 7 km, while geophysical data indicate continuity to depths of about 14 km (Langora et al., 1993).

Figure 1. Main location of ophiolites in the Balkan region (compiled from Jankovic, 1996; Economou et al., 1996; Cina et al., 1996; modified from Milushi, 2015)

4. CHROMITES OF THE TROPOJË–HAS–GJAKOVË ULTRABASIC MASSIF

The ultramafic sequence of the Albanide ophiolites is characterized by high chromite potential (Çina et al., 1986, 1995; Mekshiqi et al., 2007; Meshi et al., 2005; ISPGJ-IGJN, 1983; ISPGJ-IGJN, 1989). The Tropojë–Has–Gjakovë massif contains approximately 530 chromite occurrences, including 328 in Albania and 202 in Kosovo.

Chromite mineralization occurs throughout the ultrabasic sequence, from deep mantle levels to the cumulate zone, though the distribution is uneven. The majority of mineralizations occur in the transition zone and upper mantle, while deep mantle and cumulate chromites represent about one-third of the occurrences.

The Kam–Kepenek–Zogaj sector hosts the densest concentration of ore bodies, including the Vlahën chromite deposit with about 2.5 million tons of reserves. The Tpla–Degë–Dushaj sector contains fewer occurrences, with the Tpla deposit reaching approximately 100,000 tons of

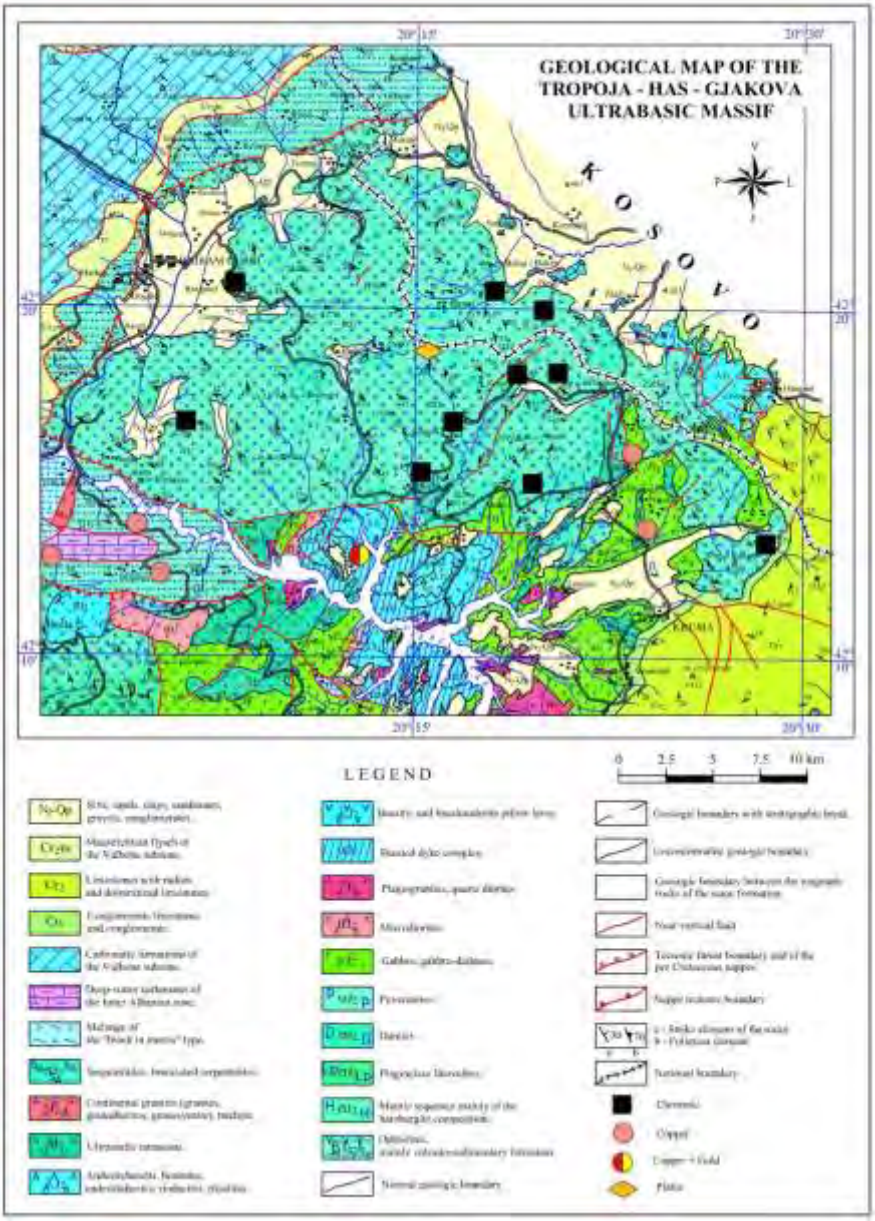

Figure 2: Harta gjeologjike e masivit te Tropoje – Has – Gjakove (Xhomo, et.al., 2002, modified from Milushi

chromite ore. The Lugu i Zi–Mejdan–Rragam sector shows intermediate development, with the Rragami deposit containing about 750,000 tons of discovered reserves. Ore bodies are mainly located within the mantle sequence, roughly 500 m below the contact with oceanic crust formations.

The most economically significant mineralizations occur in the transition zone and are typically concordant within large dunite bodies. Sub-concordant deposits also occur in smaller dunite lenses such as Rragam-2, Tpla, and Pac. Chromite chemistry varies with depth: deep mantle chromites are richer in Al and Mg, whereas upper mantle and transition zone chromites show increased Cr and Fe with decreasing Al. Cumulate chromites are characterized by lower Cr and higher Fe content. Total chromite reserves in the massif exceed 10 million tons, with an average grade of about 18.3% Cr_2O_3. The massif also hosts platinum group element (PGE) mineralization, which can be grouped into four types: associated with deep mantle chromites, upper mantle chromites, base-metal sulfides in transition zone dunites, and chromiferous

pyroxenitic dunites of this zone. The fourth type is the most economically significant, with average PGE contents reaching about 1 g/t.

Chromite bodies display diverse morphologies (tabular, lenticular, tubular, pencil-like) and textures including banded, schlieren, nodular, antinodular, and orbicular types. Grain size varies from fine-grained chromites typical of upper mantle levels to medium and coarse-grained varieties characteristic of mantle deposits.

5. PRELIMINARY TESTING FOR ENRICHMENT OF SOME CHROMIUM OUTCROPS OF TROPOJE – HAS – GJAKOVE MASSIF

The chromium resources of this massif are mainly represented by low-grade chromite ores, with Cr_2O_3 contents ranging from 7% to 20%, which require beneficiation to produce marketable chromium concentrates.

Currently, three beneficiation plants operate in the area, applying gravity separation techniques and processing ore from nearby deposits.

To assess the beneficiation potential of several chromite occurrences under the existing technological conditions, experimental tests were conducted on representative samples from three chromite outcrops and one chromite deposit.

Mineralogical studies indicate that the ores consist predominantly of chromite as the economic mineral and serpentine as the principal gangue mineral, with minor amounts of olivine. Most chromite and serpentine grains are liberated at particle sizes below 1 mm, while complete liberation is generally achieved at sizes finer than 0.3 mm (Mati, 2014).

Chromite ores containing significant gangue minerals, particularly olivine, are currently not processed in these plants due to the unsatisfactory technological figures.

6. MATERIAL & METHOD

Representative samples were collected from the Vllahna chromium deposit and three chromium outcrops: Bashkimi 22, Cahan, and Llagore. The samples were crushed and ground to <1 mm, following the grinding practice used in existing processing plants, and reduced to 100 g each. The <0.1 mm fraction was removed by wet screening, then weighed and analyzed for Cr_2O_3 content.

The −1 mm +0.1 mm fractions were subjected to heavy-liquid separation. As this study represents a preliminary evaluation of the potential for chromite ore beneficiation by gravity methods in existing processing plants, only two heavy liquids were used. Tetrabromoethane (TBE) with a density of 2.89 g/cm³ and methylene iodide with a density of 3.22 g/cm³ were applied. Density control was performed by weighing 100 ml of the heavy liquid prior to each test. The separations were conducted in a separatory funnel. The obtained products were weighed and analyzed for Cr_2O_3 content. Each test was repeated twice, yielding negligible differences in results. To our knowledge, these heavy-liquid separation tests are reported here for the first time for these chromium ores.

7. RESULTS AND DISCUSSION

The results of testing in heavy liquid of chromium ore of “Vllahna” deposit are shown in Table 1.

Table 1. The specific gravity analysis of “Vllahna” chromium outcrop

Fractions	Weight, %	Cr_2O_3 %	Cr_2O_3 Distribution, %
Fraction +2.89 g/cm3	13.21	51.28	70.24
Fraction -2.89 g/cm3	57.18	0.80	4.73
Fraction -0.1 mm	29.61	8.15	25.03
Sample	**100.00**	**9.64**	**100.00**

The results presented in Table 1 indicate that the liberation of the two main minerals, chromite and serpentine, is essentially complete after grinding below 1 mm. Based on these results, the ore was subsequently processed in existing plants using spiral separators and shaking tables, yielding satisfactory beneficiation indicators (Fig. 3). Further studies may focus on increasing the grain size of the material entering the beneficiation process after crushing and/or grinding.

The results of heavy-liquid separation tests for the ore from the “Bashkimi 22” outcrop are presented in Table 2.

Table 2. The specific gravity analysis of “Bashkimi 22” chromium outcrop

Fractions	Weight, %	Cr_2O_3 %	Cr_2O_3 Distribution, %
Fraction +3.22 g/cm3	22.97	43.37	65.88
Fraction -3.22+2.89 g/cm3	21.10	10.20	14.24
Fraction -2.89 g/cm3	32.00	1.81	3.82
Fraction -0.1 mm	23.93	10.14	16.06
Sample	**100.00**	**15.11**	**100.00**

The data in Table 2 indicate that, after grinding under 1 mm, a small proportion of the composite particles remains unliberated, mainly within the density fraction −3.22 + 2.89 g/cm³ and partly in the +3.22 g/cm³ fraction. For this ore, comprehensive beneficiation tests are recommended. Initially, pilot or industrial-scale tests could be conducted in one of the existing chromite processing plants. The middlings obtained from spiral separators and concentration tables should be reground to below 0.3 mm and reprocessed using shaking tables suitable for fine particles.
The results of heavy-liquid separation tests for the ore from the “Cahan” outcrop are presented in Table 3.

Table 3. The specific gravity analysis of “Cahan” chromium outcrop

Fractions	Weight, %	Cr_2O_3 %	Cr_2O_3 Distribution, %
Fraction +3.22 g/cm3	36.29	46.00	78.82
Fraction -3.22+2.89 g/cm3	10.70	12.10	5.80
Fraction -2.89 g/cm3	29.66	2.51	3.36
Fraction -0.1 mm	23.35	15.30	16.02
Sample	**100.00**	**22.31**	**100.00**

According to the results in Table 3, grinding below 1 mm still leaves a small proportion of composite particles unliberated, mainly in the density fraction −3.22 + 2.89 g/cm³ and, to a lesser extent, in the +3.22 g/cm³ fraction. Beneficiation of this ore may produce concentrates with a grade of 48–50% Cr_2O_3. However, it will be necessary to regrind the middlings from spiral separators and concentration tables, followed by further upgrading.

The results of the “Llagore” outcrop are shown in Table 4.

Table 4. The specific gravity analysis of “Llagore” chromium outcrop

Fractions	Weight, %	Cr_2O_3 %	Cr_2O_3 Distribution, %
Fraction +3.22 g/cm3	28.60	41.65	64.81
Fraction -3.22+2.89 g/cm3	28.20	9.87	15.14
Fraction -2.89 g/cm3	14.42	1.95	1.53
Fraction -0.1 mm	28.78	11.83	18.52
Sample	**100.00**	**18.38**	**100.00**

Compared with the other ores mentioned above, this material contains a higher proportion of unliberated particles, as well as a larger fraction of −0.1 mm material. A comprehensive beneficiation study is therefore required to evaluate the possibility of producing concentrates with a grade of 48–50% Cr_2O_3.

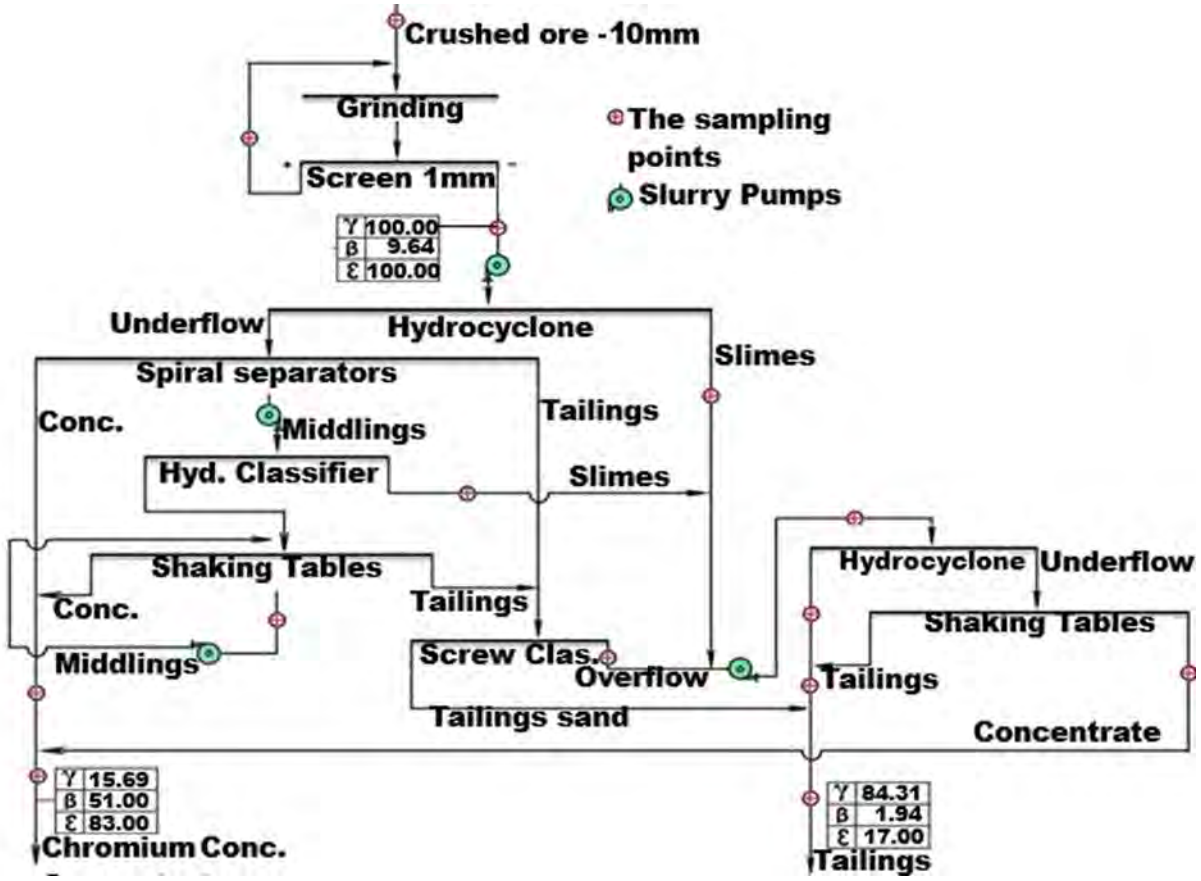

Figure 3. Simplified scheme of existing chromium enrichment plant.

Based on the present tests, it is not yet possible to assess the practical implications of lowering the economic cut-off grade, and full technological beneficiation studies are required. However, based on the beneficiation of ore from the Vllahna chromium deposit in an existing processing plant, and considering current operating costs and chromite concentrate prices, it was estimated that the net profit reaches 155.8 $/t of concentrate when the raw ore contains 9.64% Cr_2O_3. When the Cr_2O_3 content decreases to 6%, the net profit is reduced to approximately $60/t of concentrate, mainly because nearly twice the amount of raw ore must be processed to produce one ton of concentrate (Demi, 2022).

8. CONCLUSIONS

The Tropojë–Has–Gjakovë ophiolitic massif represents the convergence zone between the western lherzolitic and the eastern harzburgitic ophiolitic belts of the Albanides. The massif covers an area of approximately 900 km², of which about 540 km² correspond to the ultramafic sequence. This sequence is characterized by a high concentration of chromite mineralization, with nearly 530 chromite occurrences identified. More than ten million tonnes of chromite reserves have been discovered, the majority of which consist of low-grade ores requiring beneficiation.

Chromite bodies display a wide range of morphologies, including stratiform, lenticular, flattened tubular, and pencil-like forms, occasionally approaching isometric shapes. Their structural and textural characteristics are equally diverse, which necessitates detailed mineralogical and technological investigations in order to achieve efficient recovery during beneficiation. In many deposits, chromite mineralization is hosted by dunites and harzburgites that are weakly serpentinized or fresh, a factor that negatively influences beneficiation performance.

Preliminary beneficiation tests were conducted on samples from a deposit and several chromite outcrops within the massif in order to evaluate their potential processing in the existing chromite enrichment plants operating in the region. The results indicate that ores containing serpentine as the dominant gangue mineral show acceptable technological indicators in heavy liquid separation tests, suggesting the potential applicability of gravimetric beneficiation methods.

Further investigations are recommended, including industrial-scale testing using spiral separators and shaking tables, with regrinding of middlings in existing beneficiation plants. Should the future development of a dedicated chromite beneficiation plant in this massif be considered, comprehensive technological studies and detailed project design will be required, preceded by a feasibility study.

REFERENCES

Beccaluva, L., Coltorti, M., Premti, I., Saccani, E., Siena, F., Zeda, O., (1994) “Mid-ocean ridge and supra-subduction affinities in ophiolitic belts of Albania”, Ofioliti, 19 (1) 77–96.

Bortolotti, V., Kodra, A., Marroni, M., Mustafa, F., Pandolfi, C., Principi, G., Saccani, E., (1996) “Geology and petrology of ophiolitic sequences in the Mirdita region”, Ofioliti, 21 (1) 3–20.

Cina, A., Caslli, H., Goci, L., (1986) “Chromites in the ophiolites of Albania”, Chromites (UNESCO IGCP-197 Project Metallogeny of Ophiolites), Theophrastus Publications S.A.

Çina, A., Neziraj, A., Karaj, N., Ostrosi, B., Boshnjaku, B., (1995) “PGE mineralization related to the Tropoja and Bulqiza massifs, Albanian ophiolitic complex”, Documents du BRGM, 244, 47–61.

Demi, G., (2022) “Project of reconstruction of enrichment chromium plant in Gjakova, Kosovo”.

Demi, G., Milushi, I., (2022) “Report for enrichment possibility of some chromium deposits of Tropoja-Has-Gjakova massif”, Archive of National Agency of Natural Resources, Tirana.

Dilek, Y., Furnes, H., Shallo, M., (2007) “Suprasubduction zone ophiolite formation along the periphery of Mesozoic Gondwana”, Gondwana Research, 11 (4) 453–475.

Dimo, A., (1997) “Le mécanisme de mise en place des ophiolites d’Albanie”, Doctoral Thesis, Université Paris XI, Orsay.

Economou, M., (1986) “Chromite deposits of Greece”, Chromites (UNESCO IGCP-197 Project Metallogeny of Ophiolites), Theophrastus Publications S.A.

Gjata, K., Beccaluva, L., Premti, I., Coltorti, M., Milushi, I., Saccani, E., Siena, F., Zeda, D., (1995) “Petrologjia e ofioliteve të Mirditës qendrore dhe të brezit ofiolitik lindor të Shqipërisë”.

ISPGJ-IGJN, (1983) “Geological map of Albania (scale 1:200,000)”, Tirana.

ISPGJ-IGJN, (1989) “Metallogenic map of Albania (scale 1:200,000)”, Tirana.

Jankovic, S., (1986) “General features of chromite deposits and major ore districts in Yugoslavia”, Chromites (UNESCO IGCP-197 Project Metallogeny of Ophiolites), Theophrastus Publications S.A., 67–89.

Kodra, A., Gjata, K., Xhomo, A., (2000) “Tectonic history of Mirdita oceanic basin (Albania)”, Buletini i Shkencave Gjeologjike, 1/2000, 5–26.

Langore, Ll., Bushati, S., Lika, N., (1983) “Disa mendime për trajtën e përhapjes së shkëmbinjve ofiolitikë në vendin tonë”, Buletini i Shkencave Gjeologjike, 3/1983, 49–63.

Mati, S., (2014) “Technological project of Deva enrichment chromium plant”.

Mekshiqi, N., Gjoni, V., Karaj, N., Hakorja, A., Karanxha, Z., Zhubi, S., Dogjani, H., Shabani, S., Vata, B., Hamzallari, A., (2007) “Rivlerësime dhe rekomandime për krom-bajtjen e masiveve të Shqipërisë”, Arkivi Qendror i Shërbimit Gjeologjik Shqiptar.

Meshi, A., Hoxha, I., Milushi, I., (2005) “Chromitites in the Mirdita ophiolite (Albania): Structure and genetic implications”, Journal of Alpine Geology, 47, 103–118.

Milushi, I., (2015) “An overview of the Albanian ophiolite and related ore minerals”, Acta Geologica Sinica, 89, 61.

Nicolas, A., Boudier, F., Meshi, A., (1999) “Slow spreading accretion and mantle denudation in the Mirdita ophiolite (Albania)”, Journal of Geophysical Research, 104 (7) 15155–15167.

Robertson, A., Shallo, M., (2000) “Mesozoic–Tertiary tectonic evolution of Albania in its regional Eastern Mediterranean context”, Tectonophysics, 316 (3–4) 197–254.

Tashko, A., (1996) “Diversités géochimiques, pétrologiques et structurales des ophiolites des Albanides”, Bulletin de la Société Géologique de France, 167 (3) 335–343.

Vasha, G., Goskolli, E., (1998) “Technical economical evaluation of chromium deposits situated in east-north of Albania, Kukes-Has-Tropoje”, Archive of National Agency of Natural Resources, Tirana.

Vergely, P., Dimo, A., Monié, P., (1997) “Datation des semelles métamorphiques ophiolitiques d’Albanie par la méthode Ar40/Ar39: Conséquences sur le mécanisme d’obduction”, Comptes Rendus de l’Académie des Sciences de Paris, 326, 717–723.

Xhomo, A., Kodra, A., Xhafa, Z., Shallo, M., (2002) “Geological map of Albania (scale 1:200,000)”, AGS, Tirana.

STATISTICAL AND GEOSTATISTICAL ANALYSIS OF SELECTED TECHNOLOGY-CRITICAL ELEMENTS IN THE TREPÇA MINE AND THEIR CORRELATION WITH Pb-Zn MINERALIZATION

Berat SINANI[1,*], Milazim DEMAKU[1], Naser PECI[5], Bahri SINANI[2,3], Mehmet BILEN[4]

[1]Geological Survey of Kosovo, Ministry of Economy, Prishtinë, Republic of Kosova
[2]Department of Chemistry, Faculty of Natural Sciences and Mathematics, University of Tetova, Tetovo, North Macedonia
[3]NanoAlb, Albanian Unit of Nanoscience and Nanotechnology, Academy of Sciences of Albania, Fan Noli Square, 1000 Tirana, Albania.
[4]Department of Mining Engineering, Faculty of Engineering, Zonguldak Bülent Ecevit University, 67100, Zonguldak, Turkey
[5]Faculty of Geo-Science, University of Mitrovica, Mitrovicë, Republic of Kosova
**Corresponding author: mehmetubilen@yandex.com*

A B S T R A C T

Polymetallic deposits, especially hydrothermal Pb-Zn deposits worldwide, have been the focus of recent studies and researchers in recent decades for the research of technology-critical elements, these elements due to the high demand for use. The Trepça mine as a polymetallic mine characterized by large Pb-Zn reserves is the focus of this study. The study included all active horizons in the Trepça mine and all ore bodies of these horizons were sampled. In this paper, Bi, Co, Ge, V, W, Li, Ga, In, Te, Nb, Y, Zr, Mo, Sn, Sb and the correlation of the distribution of these elements with the distribution of Pb-Zn in these ore bodies were studied. The correlation analysis and the PCA clearly show a division into two geogenetic groups where the first group is Pb, Zn, Co, Li, Bi and Te which indicates a hydrothermal and alteration system and this is also confirmed by the PCA, but Pb and Zn also have a distinction between themselves, but they always have concentration and this indicates two mineralogical phases within the hydrothermal system. While the second group consists of V, W, Ge, Ga and Nb which express positive correlations between themselves. While, In is positioned in a special way, suggesting a formation in completely different mineralogical phases. Therefore, based on this result the complexity of the polymetallic and polyphase mineralogical deposit of the Trepça deposit.

Key words: *Technology-critical elements, Trepça, mine, distribution, statistics*

1.INTRODUCTION

The rapid advancement of modern technology has increased attention toward Technology-Critical Elements (TCEs), which are essential for technological development but considered critical due to potential supply risks (Zendehbad et al., 2021). Recent European Commission assessments identify nearly thirty such elements and minerals, including rare earth elements, platinum group elements, and metals such as Te, Ge, Ga, In, Nb, and Ta (Dang et al., 2021; Ebeling et al., 2022). Although the Trepça mining district has been extensively studied for over a century, research has mainly focused on Pb–Zn–Ag mineralization, while the occurrence and distribution of TCEs have remained largely unexplored.

Motivated by recent findings from numerous Pb–Zn hydrothermal deposits worldwide — such as Nanmushu (Wu et al., 2023), Hehuashan (Liu et al., 2024), Chipu (Tan et al., 2021), Zhugongtang (Song et al., 2023), Yangtze (Dao et al., 2023), Guangxi (Yu et al., 2023), Aerhada (Li et al., 2023c), and Qingchengzi deposits (Duan et al., 2024) — this study investigates the distribution, concentration variability, and statistical relationships of TCEs with Pb and Zn in active horizons (VIII–XI) of the Trepça mine. Through correlation analysis and PCA-based grouping, the research aims to provide a comprehensive understanding of TCE occurrence and spatial patterns, thereby expanding the resource perspective of Trepça

beyond traditional Pb–Zn–Ag exploitation toward the growing technological demand for critical elements.

2.MATERIAL and METHOD

2.1. Sampling Methodology and Analyzing

Sampling in the Trepça mine was carried out across all active horizons and ore bodies, with three samples collected from each unit. The samples were dried at 105 °C for 24 h (Sinani et al., 2023), sequentially ground in primary and secondary mills, digested using hydrofluoric acid, and analyzed by ICP-MS (PerkinElmer NexION 300D), a highly sensitive technique for rapid and accurate trace-element determination. Laboratory results were compiled into a Microsoft Excel database, where descriptive statistics, correlation analysis, and Principal Component Analysis (PCA) were applied to evaluate concentration trends, inter-element relationships, and grouping patterns. These combined statistical approaches enabled a comprehensive assessment of the distribution, variability, and spatial concentration of technology-critical elements in the active horizons of the Trepça mine while reducing data complexity with minimal information loss (Taşan et al., 2022; Schiavo et al., 2024; Xiao et al., 2022).

2.2.Study Area

The Trepça deposit is an underground mining system developed in vertically spaced horizons at 60 m intervals. To date, twelve horizons have been opened, with horizons I–VII largely depleted, horizons VIII–XI currently under active exploitation (study area), and horizon XII only partially developed without production. Since antiquity, metals have been widely used for various purposes (Paçarizi et al., 2024), and Trepça has historically focused on large-scale Pb–Zn–Ag extraction exceeding one million tons annually (Falagaan, 2017). The principal deposits include Belo Bërdo, Cërnac, Drazhnje, Stan Tërg, Artana, Hajvalia, and Kizhnica (Mederski, 2021), where dominant mineral phases such as sphalerite, galena, pyrite, pyrrhotite, and arsenopyrite occur. Among these, sphalerite is particularly recognized for its potential to host Technology-Critical Elements (Mederski, 2024), highlighting the relevance of investigating their distribution in the Trepça mining area (Figure 1).

Although numerous studies have been carried out in the Trepça mine over the past decade, research has mainly focused on the distribution of Pb–Zn–Ag and, to a lesser extent, Au and Bi, while Technology-Critical Elements have received limited attention due to their relatively recent technological importance (Sinani et al., 2023). The Trepça mining district is located in the Shala e Bajgora area, about 10 km from Mitrovica, within a geologically complex segment of the Serbo-Kosovo-Macedonian metallogenic belt (Elezaj and Kodra, 2007; Zeqiri et al., 2022; Kelmendi et al., 2024; Peci et al., 2014), and represents one of the largest Pb–Zn deposits in the Balkans with a long mining history dating back to the Middle Ages (Kołodziejczyk, 2016; Hyseni et al., 2010). Historical industrial development accelerated after the establishment of “Trepça Mines Limited” in 1927 (Nikolic et al., 2017). Given the oxidation sensitivity of sulfide minerals and the favorable hydrothermal conditions for element mobilization, the currently active horizons (VIII–XI) and associated ore bodies provide significant potential for investigating the occurrence and distribution of Technology-Critical Elements such as Bi, Co, Ge, V, W, Li, Ga, In, Te, and Nb.

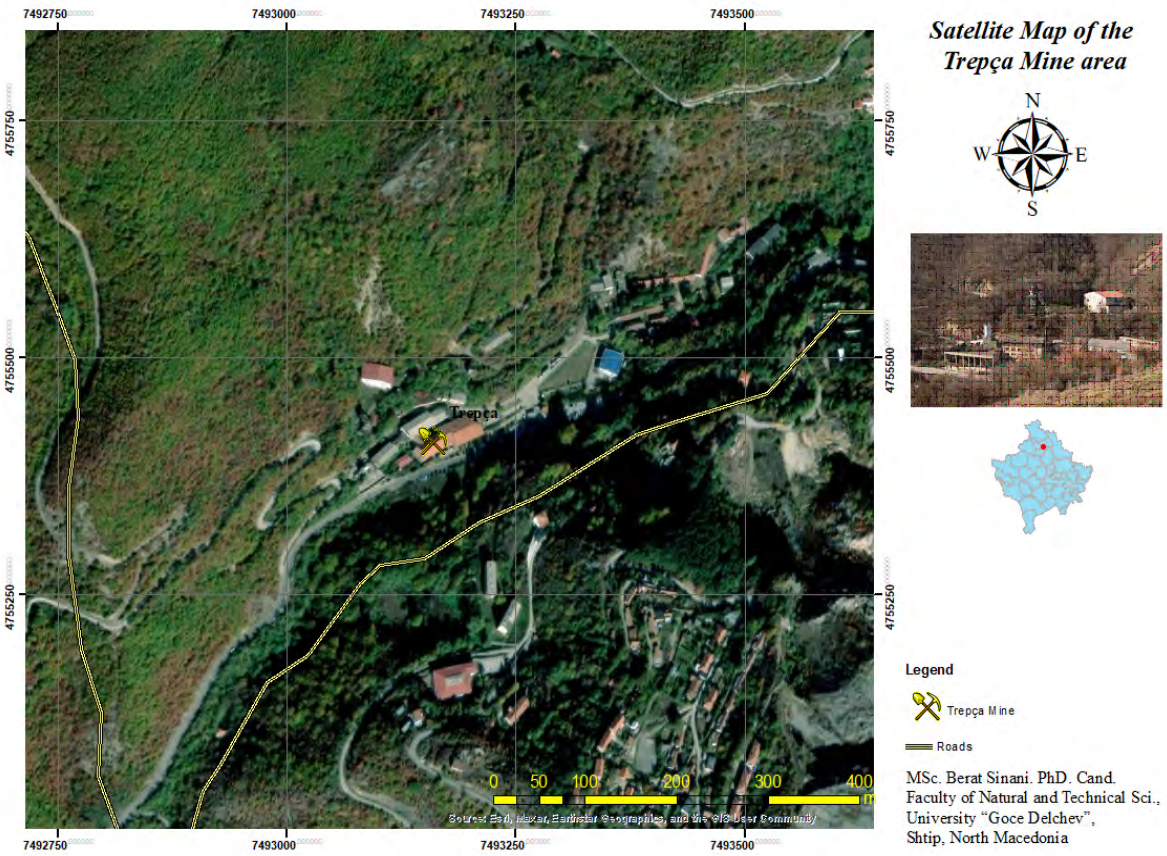

Figure 1. Satellite map of the study area

2.3.Geology Characteristics of the Study Area

The Mitrovica region is characterized by a geological complexity, due to the fact that it consists of different geological and geochemical formations. The Trepça belt, which has a VVW-JJL extension, of the Vardar area includes a length of up to 80km and this belt is one of the most important metallogenic structures of this region. The Trepça belt is characterized by a rather complex geological structure which can be seen in the geological map of the study area in Figure 2.

Deposits of Pb-Zn-Ag in the Trepça region is of Oligocene-Miocene age with hydrothermal origin and which is closely related to post-collisional magmatic activity, a process which has had a key role in the creation of metal-bearing fluids and the construction of mineralization in this area, an area which also has very large premises for the presence of technology-critical elements. The ore bodies are formed with a dip at an angle of 45°. While the formation of the ore field belongs to the Vardar zone with a fracture of 340-35° and the Dinaric zone with a direction of 290-319°.

The structures in the geology of Trepça are mainly volcanic and sedimentary which have contributed to the greatest extent in the formation of mineralizations formed as a mainly metasomatic process between limestone and breccia and limestone and schist. Tectonic fractures and fractures have served as channels for the circulation of mineral deposits, which has created ore bodies. Therefore, all mineralizations in this deposit are of the vein type. Mineralizations in this area have been formed mainly in two different phases:

- Mesozoic phase when skarns were formed and
- Tertiary phase when hydrothermals were formed.
- In general, this type of deposit includes Pb-Zn deposits formed in three main phases, which are:

- Skarn
- Skarn-hydrothermal and
- Hydrothermal.

Where, in this process, it has enabled the creation of mineralizations which are also predisposed to the presence of technology-critical elements.

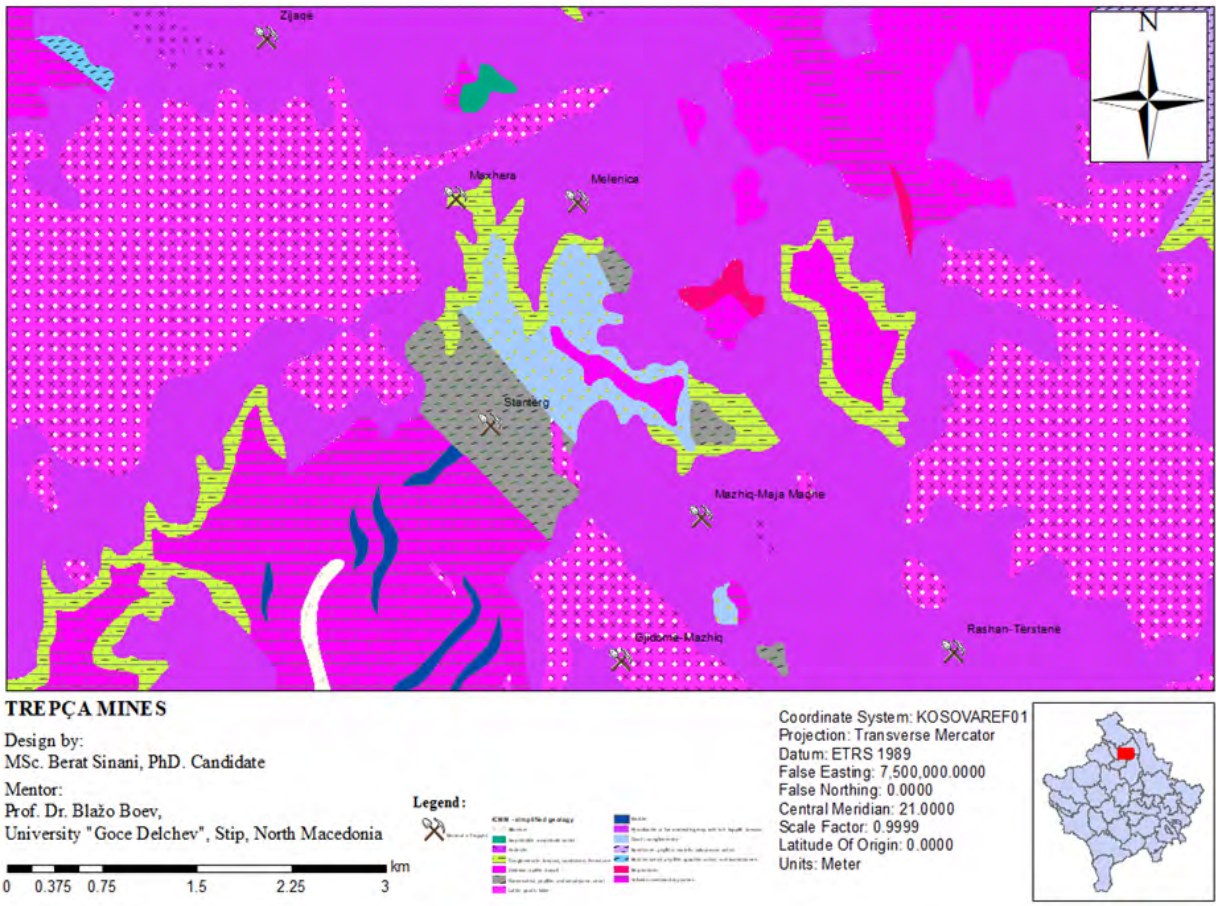

Figure 2. Geological map of the study area

3.RESULTS AND DISCUSSION

After obtaining the laboratory results, descriptive statistics of the selected elements were calculated and are presented in Table 1.

Table 1. Descriptive statistics for the selected elements

	Co	Ge	V	W	Li	Ga
Mean	28.47	0.32	14.74	28.68	2.67	2.18
Median	22.02	0.22	13.29	14.80	0.65	1.47
Std. Dev.	21.12	0.25	8.82	66.56	5.38	2.06
Variance	446.05	0.06	77.82	4430.36	28.90	4.25
CV	0.74	0.78	0.60	2.32	2.01	0.95
Min	8.50	0.01	5.59	2.08	0.27	0.17
Max	81.64	0.96	39.20	308.82	21.12	6.94
Range	73.14	0.95	33.62	306.75	20.85	6.77
IQR	23.33	0.32	7.13	14.72	0.54	2.89
Skewness	1.45	1.01	1.76	4.34	2.89	1.00
Kurtosis	1.28	0.76	3.04	19.14	8.04	-0.08

	In	Te	Nb	Pb	Zn
Mean	2.38	2.68	0.41	69774.93	50478.05
Median	1.16	0.25	0.41	21328.72	24294.20
Std. Dev.	3.46	9.28	0.25	111079.06	65325.13
Variance	11.95	86.03	0.06	12338558234.38	4267373093.44
CV	1.46	3.46	0.61	1.59	1.29
Min	0.10	0.02	0.07	4040.44	596.89
Max	12.08	41.80	0.93	429809.13	262028.25
Range	11.98	41.78	0.87	425768.69	261431.36
IQR	1.39	0.28	0.36	57490.95	48005.93
Skewness	2.34	4.37	0.64	2.41	2.26
Kurtosis	4.77	19.32	-0.30	5.66	5.49

Pb and Zn exhibit distinctly different distributions and coefficients of variation compared to the other elements, indicating different formation processes. Co, Ge, V, Ga, and Nb show relatively low variability and more symmetric distributions, whereas W, Te, Li, and In display higher skewness and anomalous behavior similar to Pb. Overall, Pb and Zn are mainly distinguished by their distribution patterns rather than their absolute values, reflecting two separate groupings. To further evaluate these relationships, radar diagrams were used (Figure 3) to compare the elemental distributions across samples and to assess their association with Pb and Zn mineralizations.

Figure 3 illustrates the elemental distributions and reveals two dominant groups associated with Pb–Zn mineralization. Pb is characterized by high variability and pronounced anomalies, whereas Zn exhibits a more homogeneous and stable distribution. Based on these patterns, the elements can be classified into three groups: (i) Co, Ge, In, and Ga, which follow the Pb-type distribution with high variability and extreme values; (ii) Li, V, and Nb, which resemble Zn with low variability and stable concentrations; and (iii) W, Ga, and Ge, which display intermediate behavior with relatively uniform distributions but occasional anomalies.

Overall, the results indicate two principal distribution trends—a heterogeneous, anomaly-rich group and a homogeneous, stable group—along with a transitional (meso) group exhibiting mixed characteristics. To further assess inter-element relationships, Pearson correlation analysis is presented in Table 2.

Table 2. Pearson correlation analysis

	Pb	Zn	Bi	Co	Ge	V	W	Li	Ga	In	Te	Nb
Pb	1.00	0.06	0.17	0.33	0.22	0.03	0.15	0.37	-0.11	-0.21	0.05	0.22
Zn	0.06	1.00	0.05	-0.03	-0.27	0.38	0.14	0.11	-0.26	0.23	0.26	-0.08
Bi	0.17	0.05	1.00	0.39	0.08	0.39	0.42	0.03	-0.23	-0.10	-0.30	-0.12
Co	0.33	-0.03	0.39	1.00	-0.16	0.36	0.26	0.22	-0.20	-0.05	-0.45	0.01
Ge	0.22	-0.27	0.08	-0.16	1.00	-0.53	-0.44	0.06	0.07	-0.17	0.22	0.42
V	0.03	0.38	0.39	0.36	-0.53	1.00	0.80	0.33	-0.01	0.26	-0.43	-0.66
W	0.15	0.14	0.42	0.26	-0.44	0.80	1.00	0.17	-0.07	-0.11	-0.46	-0.72
Li	0.37	0.11	0.03	0.22	0.06	0.33	0.17	1.00	0.28	0.08	-0.16	0.24
Ga	-0.11	-0.26	-0.23	-0.20	0.07	-0.01	-0.07	0.28	1.00	0.00	-0.15	0.09
In	-0.21	0.23	-0.10	-0.05	-0.17	0.26	-0.11	0.08	0.00	1.00	0.18	-0.04
Te	0.05	0.26	-0.30	-0.45	0.22	-0.43	-0.46	-0.16	-0.15	0.18	1.00	0.27
Nb	0.22	-0.08	-0.12	0.01	0.42	-0.66	-0.72	0.24	0.09	-0.04	0.27	1.00

Pearson correlation analysis supports the radar diagram results, confirming the distinct geochemical behavior of Pb and Zn despite their high concentrations. Pb shows moderate positive correlations with Li (r = 0.37), Co (0.33), Ge (0.22), Nb (0.22), Bi (0.17), and W (0.15),

whereas its negligible correlation with Zn (r = 0.06) indicates separate formation processes. In contrast, Zn is positively correlated with V (0.38), In (0.23), and Te (0.26), suggesting a different geochemical association. W, Ga, and Ge exhibit intermediate relationships, linking both groups.

To further validate these groupings, Principal Component Analysis (PCA) was applied. The eigenvalues and explained variances are presented in Table 3, indicating that the first three components account for 61.17% of the total variance.

Table 3. Eigenvalues and explained variance

PC	Eigenvalue	Percent_variance	Cumulative_percent
PC1	3.27	29.73	29.73
PC2	1.89	17.19	46.91
PC3	1.57	14.26	61.17
PC4	1.33	12.08	73.25
PC5	0.95	8.64	81.90
PC6	0.66	5.99	87.89
PC7	0.50	4.51	92.40
PC8	0.38	3.46	95.86
PC9	0.28	2.54	98.40
PC10	0.13	1.16	99.56
PC11	0.05	0.44	100.00

The PCA loadings (Table 4) further clarify the grouping of elements, highlighting distinct associations consistent with correlation results.

Table 4. PCA loadings for selected elements

Variable	Dim.1	Dim.2	Dim.3	Dim.4	Dim.5
Co	0.431	0.557	0.100	-0.277	-0.546
Ge	-0.652	0.347	-0.035	-0.044	0.180
V	0.942	-0.011	0.166	0.174	0.031
W	0.886	0.078	-0.108	-0.103	0.312
Li	0.203	0.627	0.359	0.521	0.114
Ga	-0.087	0.188	-0.363	0.793	0.205
In	0.102	-0.392	0.445	0.468	-0.447
Te	-0.563	-0.380	0.512	-0.056	0.287
Nb	-0.729	0.402	0.280	0.118	-0.265
Pb	0.021	0.695	0.402	-0.270	0.286
Zn	0.277	-0.286	0.747	-0.022	0.180

Overall, PCA confirms the presence of two main geochemical groups along with an intermediate group, clearly illustrating the distribution and association patterns of the studied elements (See Figure 4).

Principal Component Analysis (PCA) indicates that the first four components explain approximately 73% of the total variance, while PC1 and PC2 alone account for 47%, representing the dominant geochemical structure. PC1 is primarily associated with Zn-related elements, showing strong positive loadings for V (0.94) and W (0.89), and negative loadings for Nb (−0.73), Ge (−0.65), and Te (−0.56). In contrast, PC2 (17.2%) reflects the Pb-related group, dominated by Li (0.63) and Co (0.56).

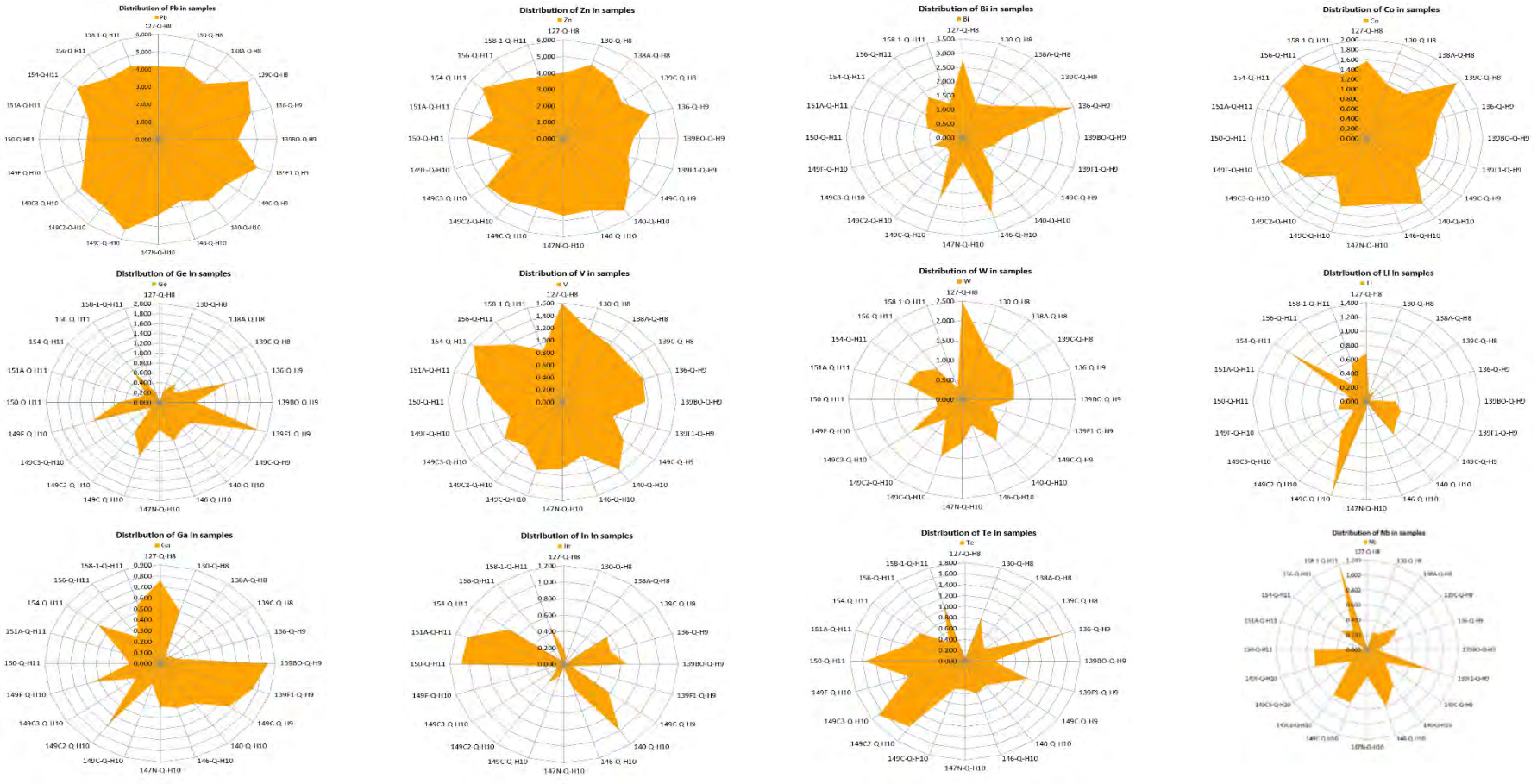

Figure 3. Graphical distribution through radar diagrams for selected elements

These results are consistent with the radar and correlation analyses, confirming two principal geochemical groups: (i) a Pb-associated group (including Li and Co) characterized by heterogeneous distributions and weak correlations with Zn-related elements, and (ii) a Zn-associated group (including V, In, W, and Te) exhibiting more homogeneous and stable distributions. Overall, the agreement among radar diagrams, correlation analysis, and PCA demonstrates a coherent geochemical framework and clearly defines the grouping and formation processes of the studied elements.

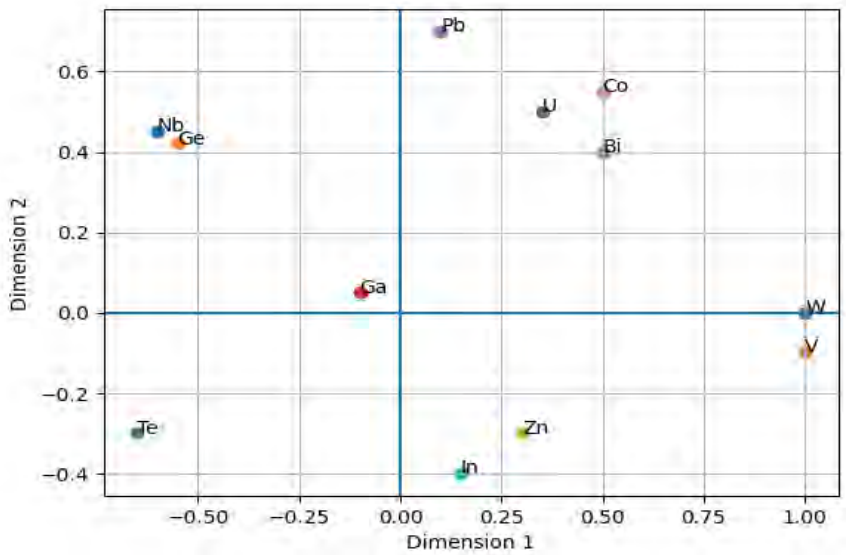

Figure 4. PCA Plot for selected elements

4.CONCLUSIONS

This research provides a detailed statistical and geochemical analysis of the distribution of technologically critical elements (TCE) in the active horizons of the Trepça mine, also examining their relationship with Pb–Zn mineralization. Findings based on descriptive analyses, Pearson correlations and principal component analysis (PCA) clearly highlight the complex geochemical nature and the polyphase mineralogical character of this polymetallic deposit. Descriptive analyses reveal that Pb and Zn are clearly distinguished from the other elements, not only due to their high levels, but especially due to the way of statistical distribution. Lead (Pb) presents pronounced heterogeneity, large positive asymmetry and the presence of isolated anomalies, which indicates a strong influence from hydrothermal processes and certain mineral phases. In contrast, zinc (Zn) presents a more uniform and stable distribution, signaling a broader control by lithology and a more even distribution within the mineralization system.

Correlation analysis supports this conceptual differentiation, showing that Pb is positively correlated only with a few specific elements (such as Co and Li), while with most TCEs and with Zn it presents weak or negative relationships. In contrast, elements such as V, W, Ge and Nb form a group with strong correlations among themselves, reflecting a more stable geochemical behavior and less dependent on localized anomalies. This separation between Pb-type and Zn-type elements reflects different mechanisms of concentration and deposition within the Trepça hydrothermal system.

The PCA analysis summarizes and structures these results, distinguishing two main geochemical trajectories: (i) a lithogenic–structural trend, dominated by the elements V, W, Ge and Nb, and (ii) a heterogeneous Pb-type trend, defined by Pb, Li and Co, which is associated with local enrichments and late stages of hydrothermal processes. The peripheral location of

elements such as In, Ga and Te indicate that they are associated with accessory mineral phases and specialized mineralogical processes, reflecting the polyphase character of the deposit. Overall, the results indicate that the Trepça deposit should not be viewed simply as a common Pb–Zn system, but as a complex polymetallic deposit with significant potential for technologically critical elements. This assessment places Trepça in line with modern directions of mineral geology, where the strategic importance of a deposit is no longer determined only by traditional metals, but also by its capacity to supply TCE.

REFERENCES

Abdou, M., Cobelo-Garcia, A., Santos-Echeandia, J., Schafer, J., (2023), Technology-Critical Elements, Contaminants of Emerging Concern in the Marine Environment, 401-438.

Brahimaj, F., Zeqiri, R., Gashi, J., Haliti, B., (2022) “Comparability of microclimate in the horizons of the Trepça mine in Stantërg”, Rudarsko-Geološko-Naftni Zbornik, 37 (4), 1-8.

Dang, D. H., Filella, M., Omanović, D., (2021) “Technology-critical elements: An emerging and vital resource that requires more in-depth investigation”, Archives of Environmental Contamination and Toxicology, 81 517–520.

Hauser-Davis, R. A., (2023) “This seems fishy: Technology-critical elements as a growing concern to aquatic biota and elasmobranchs in particular”, Frontiers in Ocean Sustainability, 1 1281484.

Haziri, M., (2018) “The first investigations of Britains in Trepça’s Mine in Stan Terg”, Acta Universitatis Danubius: Relationes Internationales, 11 (2) 219–225.

Hetemi, M., Kastrati, S. H., (2008), “Lead-zinc resources in Kosovo”, Mining Magazine.
Huston, D. L., Bastrakov, E., (2024) “Germanium, indium, gallium and cadmium in zinc ores: A mineral system approach”, Australian Journal of Earth Sciences, 71 (8) 1125-1155.

Hyseni, S., Durmishaj, B., (2014) “TREPÇA Ore Belt and Lead and Zinc Distribution in Badovc Mineral Deposit, Kosovo”, SE Europe Article.

Hyseni, S., Durmishaj, B., Fetahaj, B., Shala, F., Berisha, A., Large, D., (2010) “Trepça Ore Belt and Stan Terg mine - Geological overview and interpretation, Kosovo (SE Europe)”, Geologija, 53 (1), 87–92.

Kadriu, S., Sadiku, M., Kelmendi, M., Sadriu, E., (2020) “Studying the heavy metals concentration in discharged water from the Trepça Mine and flotation, Kosovo”, Mining of Mineral Deposits, 14 (4), 47-52.

Kerolli-Mustafa, M., Lajqi Makolli, V., Mustafa, V., (2013) “Environmental Impact Assessment of Metallurgical Waste: Trepça case study in Kosovo”, Conference Paper.

Kołodziejczyk, J., Pršek, J., Voudouris, P., Melfos, V., Asllani, B., (2016) “Sn-bearing minerals and associated sphalerite from lead-zinc deposits, Kosovo: An electron microprobe and LA-ICP-MS study”, Minerals, 6 (2), 40.

Liu, W., Mei, Y., Etschmann, B., Glen, M., MacRae, C. M., Spinks, S. C., Ryan, C. G., Brugger, J., Paterson, D., (2023) “Germanium speciation in experimental and natural sphalerite: Implications for critical metal enrichment in hydrothermal Zn–Pb ores”, Geochimica et Cosmochimica Acta, 342 198-214.

Mederski, S., Pršek, J., Dimitrova, D., (2024) “Distribution of In, Sn, Ga, Ge, and other critical metals in sulfide ores from epithermal listvenite-associated Badovc Pb–Zn–Sb–Ni deposit (Kosovo): Insights from mineralogy and geochemistry”, Ore Geology Reviews, 134 104128.

Mederski, S., Pršek, J., Dimitrova, D., Hyseni, B., (2021) “A combined EPMA and LA-ICP-MS investigation on Bi-Cu-Au mineralization from the Kizhnica ore field (Vardar Zone, Kosovo)”, Minerals, 10 (2) 131.

Mykhailov, V. A., Hrinchenko, O. V., Malyuk, B. I., (2022) “Exploration and mining perspectives of the critical elements for green technologies in Ukraine”, Geological Society, London, Special Publications, 526 1–19.

Paçarizi, M., Qeriqi, E., Sinani, B., Tašev, K., Reka, A., Stafilov, T., (2024) “Geochemistry and mineralogy of lead-zinc mine tailings from the Artana landfill in the Republic of Kosovo”, Geologica Macedonica, 38 (1), 53–64.

Sinani, B., Boev, B., Reka, A. A., Sinani, B., Boev, I., (2025) “Distribution of naturally occurring asbestos in the Mitrovica region: Geochemical and mineralogical characterization”, Geosciences, 15 (9) 335.

Sinani, B., Peci, N., Elezaj, Z., Sinani, B., (2018) “Statistical analysis of distribution of Ag, Au, Pb and Zn in Trepça mine”, International Multidisciplinary Scientific GeoConference: SGEM.

Sinani, B., Qeriqi, E., Sahiti, F., Shala, I., Musa, I., (2018) “Geological sampling with GSKSoft 1.0”, International Multidisciplinary Scientific GeoConference: SGEM.

Sinani, B., Boev, B., Reka, A., Boev, I., Sinani, B., Lecaj, E., (2024) “Statistical and chemical analysis of soil pollution from koshtova landfill Mitrovice—Kosovo”, International Multidiscipliner Scientific GeoConference SGEM 2024, 329–336.

Sinani, B., Elezaj, Z., Peci, N., Sinani, B., (2025), “Engineering geological studies on zhur dam”, International Multidiscipliner Scientific GeoConference SGEM 2015, 299–305.

Sinani., B, Boev., B, Reka., A. A, Sinani., B, Boev, I., Distribution of Naturally Occurring Asbestos in the Mitrovica Region: Geochemical and Mineralogical Characterization.

Tan, T., Peng, H., Qin, E., Wang, Z., Mao, X., (2025) “Study on the occurrence states and enrichment mechanisms of the dispersed elements Ga, Ge, and In in the Chipu Pb-Zn deposit, Sichuan Province, China”, Minerals, 15 (4) 341.

Taşan, M., Demir, Y., Taşan, S., (2022) “Groundwater quality assessment using principal component analysis and hierarchical cluster analysis in Alacam, Turkey”, Water Supply, 22 (3) 3431-3446.

Tmava, A., (2003) “Structural–Metallogenic Features of the Trepça–Stan Tërg Polymetallic Mineralization and Further Research Prospects”, Doctoral Dissertation, Polytechnic University of Tirana, Tirana, Albania.

Trimmel, S., Spörl, P., Haluza, D., Lashin, N., Meisel, T. C., Pitha, U., Prohaska, T., Puschenreiter, M., Rückert, E., Spangl, B., Wiedenhofer, D., Irrgeher, J., (2024) “Green and blue infrastructure as model system for emissions of technology-critical elements”, Science of the Total Environment, 934 173364.

Wei, C., Frenzel, M., Ye, L., Huang, Z., Danyushevsky, L., (2024) “Germanium distribution in Mississippi Valley-Type systems from sulfide deposition to oxidative weathering: A perspective from the Fule Pb–Zn(–Ge) deposit, South China”, American Mineralogist, 109 (9) 1481-1498.

Wippermann, D., Zonderman, A., Zimmermann, T., Pröfrock, D., (2023) “Determination of technology-critical elements in seafood reference materials by inductively coupled plasma-tandem mass spectrometry”, Analytical and Bioanalytical Chemistry, 415 12345–12357.

Wu, J., Dai, H., Cheng, Y., Xu, S., Nie, Q., Wen, Y., Lu, P., (2023) “LA-ICP-MS trace element geochemistry of sphalerite and metallogenic constraints: A case study from Nanmushu Zn–Pb deposit in the Mayuan District, Shaanxi Province, China”, Minerals, 13 (6) 793.

Zawadzki, J., (2024), “Cont-emporary applications of geostatistics to soil studies”, Soil Systems, 8(3) 70 1–16.

STRUCTURAL DATA AND CHROMITE ENRICHMENT CHARACTERISTICS IN THE ULTRABASIC MASSIF OF LUBOTEN, KOSOVO

Edmond PLLANA[1,*], Ibrahim MILUSHI[1], Genc DEMI[2]

[1]Institute of Geosciences, Polytechnic University of Tirana, Albania
[2]Faculty of Geology and Mine, Polytechnic University of Tirana, Albania
**Corresponding author: ep.geology@gmail.com*

A B S T R A C T

The ultrabasic massif of Luboten covers an area of about 70 km^2 and lies in the southeast of Kosovo but its main continuity is in North Macedonia. The massif is of hartzburgitic type and is built in the lower part of the section by hartzburgite with few dunite intercalations and in the upper part by dunite with few hartzburgite intercalations. The part built of dunites with few hartzburgite intercalations is characterized by a high saturation with chromite mineralization. Dozens of chromite occurrences with mainly lens-like morphology are encountered with gradual pass into chromite dunite, which occupy very large areas. Otherwise, in the hartzburgitic area with small dunite lenses intercalations, chromite ore bodies are of limited size and with almost sharp contacts with the host dunite. The chromite in both cases is of metallurgical type. From the beginning of the 19th century until 1973, intensive prospecting-exploration and exploitation works have been carried out, which have resumed again after 2012. In the past, but especially during the last years, numerous tests of chromite ore have been carried out regarding the enrichment characteristics and in general it results that the chromite in the Luboten massif have very good enrichment characteristics.

Key words: *Ultrabasic massif, hartzburgite, dunite, chromite, enrichment characteristics*

1. INTRODUCTION

The ultrabasic massif of Luboten area was, for a period of about 83 years, the main area of exploitation and production of chromite in former Yugoslavia. During the years 1890–1973, around 2.5 million tons of chromite reserves were exploited. Only in the period 1890–1945, about 1.5 million tons of chromite were extracted (Tierre Auge, 2017). The highest intensity of exploitation was reached before World War II and after the construction of the Chemico Electrometallurgical Combine “Jugohrom” in 1957.

To treat the low grade ore, it was built a factory in Radusha, which processed chromites from the entire Luboten massif. Detailed data on the year of construction, capacity, and period of operation are preserved in the archive of the “Jugohrom” company.

The chromite ore was processed with standard enrichment techniques, such as crushing, grinding, and gravity separation (spirals, tables), to concentrate the chromite.

In 2020, an enrichment plant was built in Goranxe to process chromite ore in the part of the ultrabasic massif of Luboten that lies within the territory of Kosovo.

During the period 1890–1973, intensive exploration and exploitation works were carried out throughout the ultrabasic massif of Luboten and in the years 2009–2025, in the part of the massif located in Kosovo. Detailed geological mapping, complex geological-geophysical studies (Sajković I., 1973/74), the opening of hundreds of exploitation and exploitation galleries, numerous drillings, as well as excavations in over 100 chromitic occurrences were realized.

Around 25 deposits were exploited with underground and/or surface works, while in more than 75 occurrences, exploitation excavations were carried out and small amounts of chromite were extracted. Documentation of the works was rigorously maintained, including maps, plans, cross-sections, longitudinal sections, and various sketches. These data provide important information on the morphology and structural features of the deposits. For all deposits, numerous chemical analyses were performed, allowing clear classification of the ore types of chromite.

Extensive information on exploration and exploitation works is found in North Macedonia, in the Archive of the Geological Institute in Skopje, the Archive for Geological Research in Mines in Skopje, and the archive of the “Jugohrom” company in Jegunovce; in the archive of professional documents of Geozavod, Belgrade; as well as in Pristina, in the archive of KPMM. Regarding the scientific treatment of the Luboten massif, there exists a number of scientific articles and reports (Hiessleitner G., 1951/52; Grafenauer S., 1957; 1958, 1975, 1977; Grčev K., 1962, Kolotilov L.I., 1966; Sajković I., 1973; Jankovic S., 1986; Geozavod, 1988 etc).

2. REGIONAL GEOLOGICAL FRAMEWORK

The ultrabasic massif of Luboten is located in the southeastern part of Kosovo and extends over an area of about 70 km² (Figures 1, 2, 4).

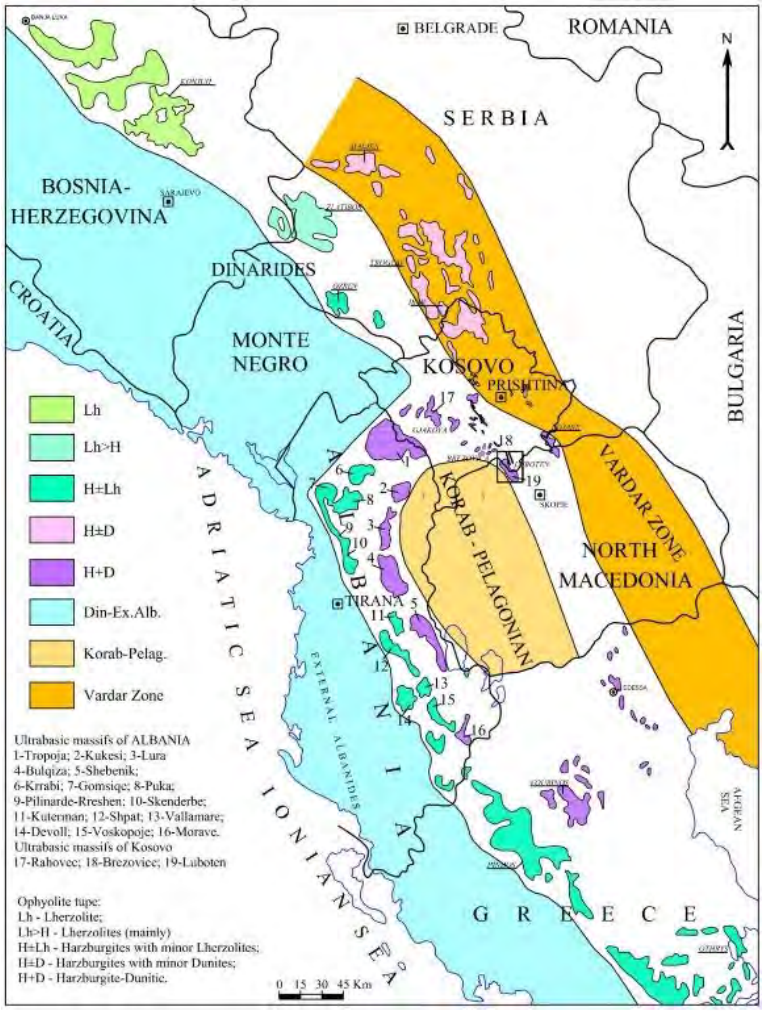

Figure 1. The main ultrabasic massifs of ophiolites in the Balkan region (compiled from Jankovic, 1996; Economou et al., 1996; Cina et al., 1996; modified from Milushi, 2015)

This massif is divided between the territory of the Republic of Kosovo (approximately 17.5 km², or about one quarter of the area) and North Macedonia (approximately 52.5 km², or about three quarters of the area).

From a structural point of view, the massif represents a tectonic nappe situated between the Sharr Metamorphic Complex to the west and the Kačanik metamorphic unit to the east. It is characterized by a high concentration of metallurgical-type chromite mineralization.

In the eastern part, the massif is overlain by carbonate deposits represented by Cretaceous limestones. Beneath these deposits, a weathering crust is often found, enriched with iron–nickel mineralizations, which constitutes an important geological and mineralogical element of the area.

3. GEOLOGY OF THE LUBOTEN OPHIOLITES

The Luboten ophiolite represents a remnant of the oceanic lithosphere and is composed of rocks belonging to the mantle sequence and the oceanic crust (Figure 2). The mantle sequence consists mainly of harzburgite, harzburgite–dunite interlayers, dunite–harzburgite interlayers, orthopyroxene dunite, massive dunite, and pyroxenite (Figure 4). Meanwhile, the oceanic crust sequence is built of basalts and rodingite gabbros (Figure 2). The mantle sequence is widely distributed in the ophiolitic nappe region, whereas the oceanic crust rocks have a very limited distribution.

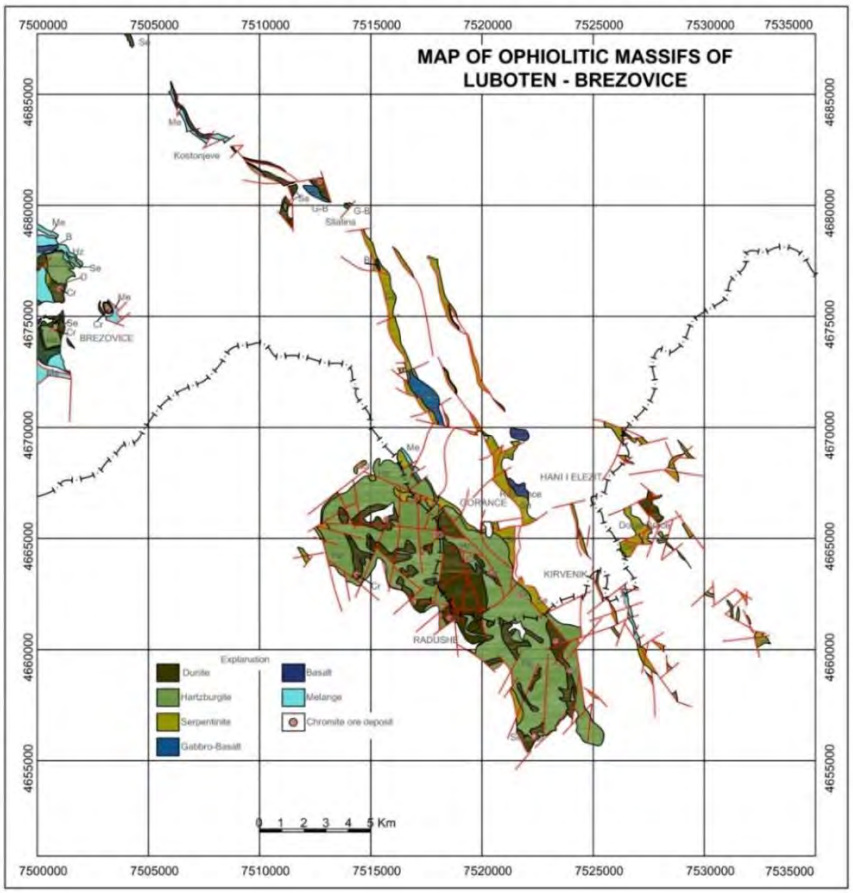

Figure 2. Geological map of the ultrabasic massif of Luboten (Petovski P., Popovski S., Karovik J., 1984). Coordinates in KosovRef system

The dyke series, represented by gabbro and pyroxenite, is relatively well developed, particularly in the “Kafe Oxhak” deposit area. A characteristic phenomenon is the presence of high-quality magnesites, which in some cases reach considerable thicknesses (Figure 3).

The massif is composed of harzburgites with interlayered lenses, mostly small dunite bodies, as well as dunite massifs with relatively small harzburgite lenses. In the Goranxe area, a dunite massif extends over about 6 km². Most of the massif, around 61% of the surface, is built of harzburgites with very rare small dunite lenses. Dunite with small hartzburgite lenses intercalations constitute about 39 % of the Luboten ultrabasic massif. The harzburgites display a clear banded structure, which in some cases is very well expressed (Figure 3).

The most detailed data on the structure of the ultramafic massif and the chromite occurrences within it were provided by Hiessleitner G. (1951), while the most important information was offered by Grafenauer S. (1957, 1975, 1977), Grčev K. and Milenković P. (1962), as well as by Geozavod (1988). However, the most complete documentation is preserved in the Geological Institute Fund in Skopje, the Geological Research Fund in Skopje, and in the mining company “Jugohrom” archive in Jegunovce.

Overall, the massif is serpentinizated to an intensive degree, with a level of serpentinization reaching up to 60%. Nevertheless, relatively fresh dunite zones are also encountered. In the peripheral parts of the massif, serpentinites appear with widths reaching tens of meters. In some areas, particularly in Krivenik, different serpentinization systems occur, creating a characteristic scaly structure (Figure 3).

Fracture tectonics is intensively developed, often in the form of relatively thick tectonic zones, where calcite veins and lenses, as well as magnesite, are prominent (Figure 3).

Figure 3. 1 – Banded harztburgite; 2 – Cavernous serpentinite; 3 – Magnesite; 4 – Tectonic zone with magnesite and calcite.

4. CHROMITE MINERALIZATION IN THE LUBOTEN MASSIF

The ultramafic massif of Luboten has relatively small dimensions, with a length of about 17 km and a width of up to 4 km, covering an area of approximately 70 km² (Figures 2, 4). Nevertheless, it is characterized by a very high saturation with chromite mineralization. In this massif, around 300 chromite occurrences have been identified, of which about 25 represent deposits where considerable chromite reserves have been exploited.
In the geological report of Geozavod (1988), entitled “Report about the basic geological research on the Ljuboten massive during 1987”, a cadastral list of 119 chromitic occurrences located in the territory of Kosovo is presented. This register contains the occurrence number, location, coordinates, type of mineralization, and the formation in which each occurrence is found. In addition, the report includes the results of chemical analyses for the most important occurrences, providing a broad database for the characterization of chromite mineralization in the massif.

5. CHROMITE DEPOSITS IN THE LUBOTEN MASSIF

The deposits where considerable chromite reserves have been exploited, ranked by size, are as follows (Figure 4): Nada, Orašje, Čašak, Gračane, Gorance, Stankovac, Kafe Odžak, Jāžince, Raduška Reka I, II and III, Mala Kula, Golemi Padži, Šopov Prisoj, Nada Raskopi, Sulari–Kisela Voda, Stareoselska Trla, Gornje Orašje, and Debelo Brdo. In addition to these, there is a series of chromite occurrences where surface or shallow mines have been opened, such as Golarnica, Čikin Brdo, Kosmatica, Gornja Voda, Paskurice, Lokve, etc. Furthermore, about one hundred chromite occurrences have been identified where exploitation excavations were carried out, but without significant exploitation, except for ore extraction during the exploration phase.

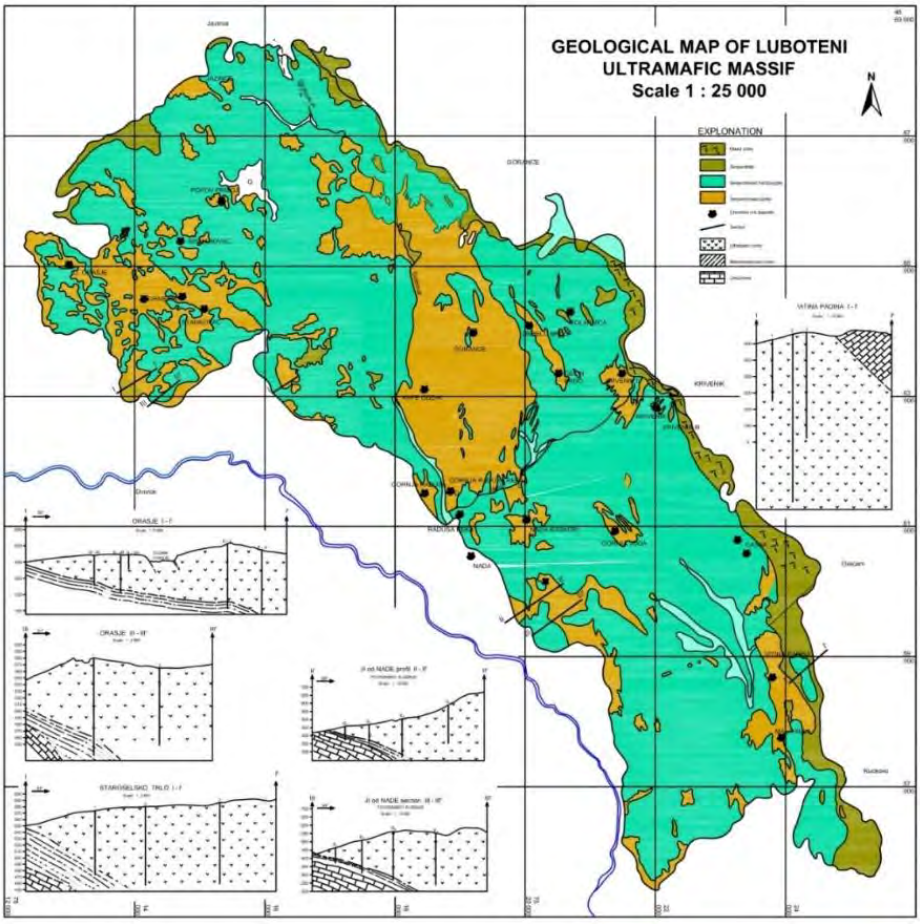

Figure 4. Lithological map of the ultramafic massif of Luboten, at a scale of 1:25,000 (Geozavod, Belgrade, 1988). The original documentation is preserved in the Geozavod Archive in the Serbian.

Of all the mentioned occurrences, the majority and most important ones are located in the territory of North Macedonia. In Kosovo, there are only two large mines, Kafe Odžak and Gorance, with discovered reserves of approximately 200,000 and 250,000 tons, respectively, as well as four “small mines” (Krivenik I, II, and III, and Debelo Brdo) and two important chromite occurrences (Golarnica and Čikin Brdo). However, the territory of Kosovo contains strong chromitic dunite zones and low grade chromitic zones with Cr_2O_3 content between 6–10%, where more than 2 million tons of such reserves can be estimated.

It should be emphasized that throughout the distribution of ultrabasic rocks of the Luboten massif, detailed and complex geological, geochemical, and geophysical mapping and works have been carried out. In the geological report of Geozavod (1988), abundant graphical material is found related to geological-lithological, geochemical, and geophysical mapping, as well as the anomalies identified for the latter two.

6. MORPHOLOGICAL CHARACTERISTICS OF CHROMITE BODIES

The main deposits of the Luboten massif are characterized by a morphology showing very strong plastic deformation, reflected in linear structures. Numerous structural measurements, particularly those of lineation, clearly confirm this phenomenon. In Figure 5a, at the Kafe Oxhak deposit, strong deformation in olivine antinodules is reflected, indicating the direction of lineation, as well as a clearly expressed “pull-apart” structure perpendicular to the lineation. The deformation ratio reaches up to 10–15:1. A similar situation is presented in Figure 5b, at the Čikin Brdo occurrence, where deformation reaches a ratio of 6–7:1.

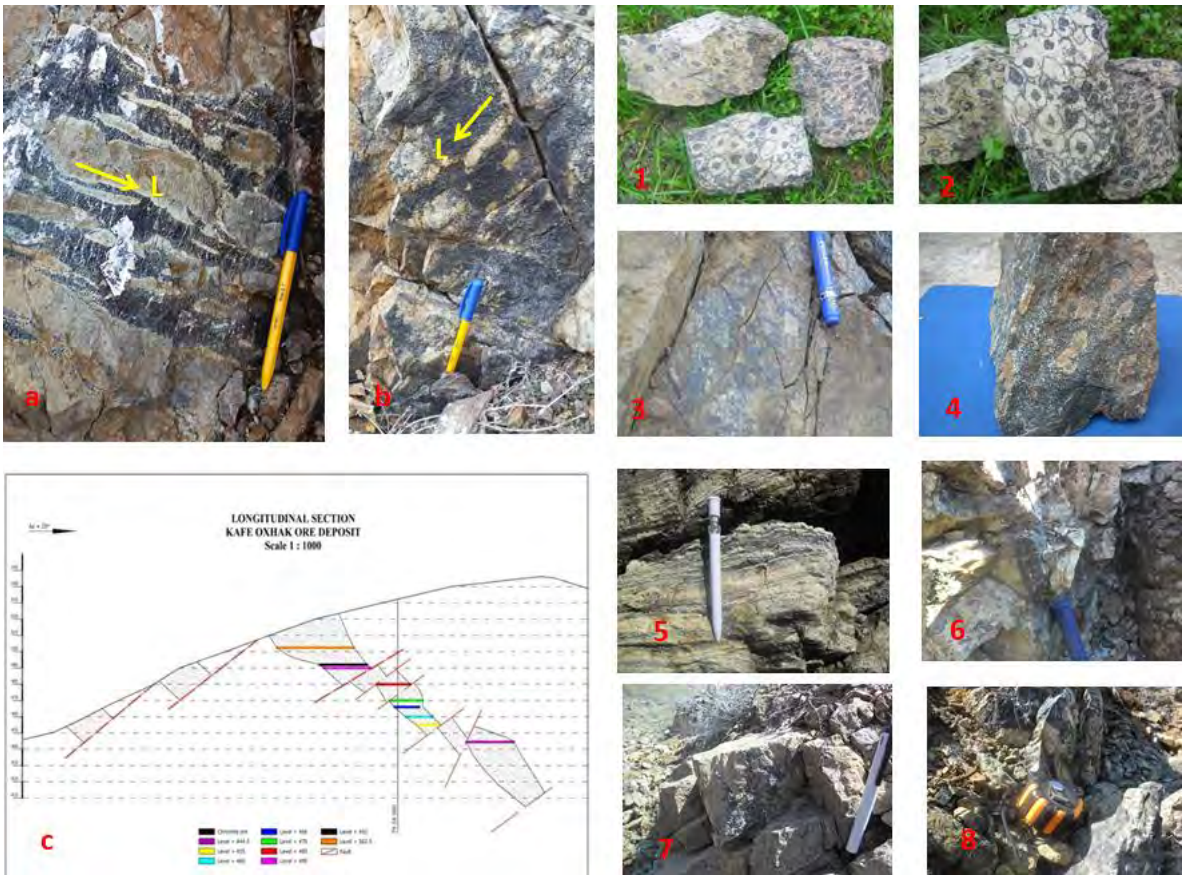

Figure 5: Strong linear plastic deformation and clearly developed “pull-apart” structure and some examples of chromite structures and textrures in the Luboten area.
a.Kafe Oxhak deposit; b. Čikin Brdo occurrence; c. Longitudinal section of the Kafe Oxhak pencil-like ore deposit(Grafenauer S., 1958), modified; 1 & 2. Orbicular and planetary textures in the Kafe Oxhak deposit; 3. Angular antinodules in the Kafe Oxhak deposit; 4. Antinodular texture east of the Kafe Oxhak deposit; 5. Banding–schlieren texture in the Nada Raskopi deposit; 6. Folded ore body at Gornja Voda showing; 7.Coarse graind chromite at Gjarperi showing; 8. Irregular ore body at Jetoni showing

The deposits generally have a tube-shaped compressed morphology and, in some cases, a pencil-like shape (Figure 5c). Lenticular morphology, up to cases of isomorphic lenses, is also characteristic. This morphology makes the exploration of deposits extremely difficult and requires specialized structural studies. The design of exploration works likewise requires special care and a well-studied determination of the exploration grid. For the Kafe Oxhak deposit, complete documentation of the exploitation levels exists, highlighting the tubular form of the chromite body (Figure 5).

Important information regarding the chromite deposits in the Luboten massif can be found in scientific literature and numerous reports, among which stand out: Grafenauer S. (1957, 1958, 1975 1977), Grčev K. and Milenković P. (1962), Hiessleitner G. (1951/52), Karamata S. (1973), Karamata S. and Stepanović I. (1973), Kolotilov L.I. (1966), as well as dozens of reports from the “Jugohrom” company in Skopje, Geozavod in Belgrade, and KPMM in Pristina.

7. TEXTURES IN THE LUBOTEN MASSIF

A wide variety of textures are encountered in the Luboten massif, among which the antinodular texture is particularly notable (Figure 5). In some cases, very characteristic antinodules with rectangular shapes appear. Overall, the textures present include spotted textures, ranging from rare disseminatons to dense disseminations, banded textures, nodular, antinodular, blotchy, and planar textures. The planar texture represents a unique case, which has not been previously reported (Figure 5).

The banded–schlieren texture is quite widespread and often occurs in areas where thin and sparse chromite bands extend within chromitic dunite fields. This textural diversity reflects the complexity of geological processes that influenced the formation of chromite bodies in the massif. A similar morphological diversity has also been described in chromite deposits in Albania (Meshi et al., 2005), indicating geological affinity and common features in the Balkan region.

8. SOME FEATURES OF THE CHROMITES OF THE LUBOTEN ULTRAMAFIC MASSIF

Chromium mineralization in the Luboten massif presents several distinctive features. First of all, it is a typical metallurgical-type mineralization. Another important characteristic is the very high Cr/Fe ratio, which reaches values above 3. In this respect, the Luboten mineralization can be compared with that of Bulqiza in Albania and Brezovica in Kosovo, while it differs significantly from the chromites of the Gjakova massif, where the Cr/Fe ratio ranges between 2.3–2.5. In the chromites of Radusha, the presence of platinum group minerals (PGE) has also been evidenced (Augé et al., 2017), which adds further scientific and economic interest to these mineralizations.

9. CONCLUSIONS

The ultrabasic massif of Luboten extends across the territories of Kosovo and North Macedonia. It is mainly composed of harzburgites with small dunite interlayers, which make up about 61% of the massif, and dunites with small harzburgite interlayers, which account for about 39%. Due to the high percentage of dunites, this massif is unique compared to other massifs in Kosovo, North Macedonia, and the entire Dinarid–Albanid–Hellenid belt.

Although relatively small in size, about 70 km², the massif is characterized by a high saturation with chromite mineralization. Around 300 chromite occurrences have been identified, of which about 25 have developed into deposits where more than 2.5 million tons of chromite ore have been exploited from 1890 to the present. The Luboten chromite is of metallurgical type, with a Cr/Fe ratio greater than 3 and Al_2O_3 content lower than 16%. Studies have also evidenced the presence of platinum group element (PGE) mineralizations, which further increases the interest in these chromites.

In the past, an enrichment plant operated in Radusha with very good recovery indicators, which was mainly based on the chromites of this massif, the Chemico Electrometallurgical

Combine “Jugohrom” was built in Tetovo, which played an important role in the chromium industry of the region.

REFERENCES

Augé, T., Morin, G., Bailly, L., Serafimovsky, T., (2017), “Platinum-group minerals and their host chromitites in Macedonian ophiolites”, European Journal of Mineralogy, 29 (4), 585–596. https://doi.org/10.1127/ejm/2017/0029-2624

Cina, A., Caslli, H., Goci, L., (1986), “Chromites in the ophiolites of Albania”, In Chromites (UNESCO’s IGCP-197 Project Metallogeny of Ophiolites), Theophrastus Publications S.A.
Economou, M., (1986), “Chromite deposits of Greece”, In Chromites (UNESCO’s IGCP-197 Project Metallogeny of Ophiolites), Theophrastus Publications S.A.

Geozavod Belgrade., (1988), “Report about the basic geological research on the Ljuboten massive during 1987”, Geozavod Archive, Belgrade.

Grafenauer, S., (1957), “Geology and origin of chromite ore deposits of Yugoslavia”, Proceedings of the 2nd Congress of Yugoslav Geologists, Sarajevo, 246–250.

Grafenauer, S., (1958), “Chromite deposits of the Ljuboten serpentinite massif”, Proceedings of the Geological Institute of the Republic of Macedonia, T.2, Skopje.

Grafenauer, S., (1975), “Ore petrology of ultramafic associations in Yugoslavia”, Acad. Sci., Cl. IV, 22, Ljubljana.

Grafenauer, S., (1977), “Genesis of chromite in Yugoslavian peridotite”, In D. D. Klemm, H. J. Schneider (Eds.), Time and Strata-Bound Ore Deposits, Springer, 275–284. https://doi.org/10.1007/978-3-642-66806-7_22

Grčev, K., Milenković, P., (1962), “Development of the roof of the Ljuboten part of the Ljuboten serpentinite massif”, Proceedings of the 5th Congress of Yugoslav Geologists, Vol. 2, Belgrade, 275–284.

Grčev, K., (1962), “Prospecting for chromite ores in the Ljuboten serpentinite massif”, Papers of the Conference of the Geological Society of the FNRJ, T.1, Belgrade.

Hiessleitner, G., (1951–1952), “Serpentin- und Chromerzgeologie der Balkanhalbinsel und eines Teiles von Kleinasien”, Jahrbuch der Geologischen Bundesanstalt, Wien.

Jankovic, S., (1986), “General features of chromite deposits and major ore districts in Yugoslavia”, In Chromites (UNESCO’s IGCP-197 Project Metallogeny of Ophiolites), Theophrastus Publications S.A., 67–89.

Karamata, S., (1973), “Synthesis of the documentation of the ore-bearing Ljuboten serpentinite massif”, Part I: Geology of the Beograd massif, FSD of the Raduša Mine.

Karamata, S., Stepanović, I., (1973), “Synthesis of documentation of the ore-bearing Ljuboten serpentinite massif”, Part II: Presentation of individual deposits and occurrence of chromite, Belgrade, FSD of the Raduša Mine.

Kolotilov, L. I., (1966), “Report on the investigation of chromitonosity of Ljubotenskogo and other ultrabasite massifs in the activity zone of the mining basin Raduša”, Skopje, SFRY, Belgrade.

Meshi, A., Hoxha, I., Milushi, I., (2005), “Chromitites in the Mirdita ophiolite (Albania): Structure and genetic implications”, Journal of Alpine Geology, 47, 103–118.

Milushi, I., (2015), “An overview of the Albanian ophiolite and related ore minerals”, Acta Geologica Sinica (English Edition), 89, 61. https://doi.org/10.1111/1755-6724.12308_39

Petovski, P., Popovski, S., Karovik, J., (1984), “Map sheet number K34-67 Kačanik, scale 1:100000”, Skopje, Belgrade, 1977–1983.

Sajković, I., (1973), “Contribution to solving the shape and location of the Ljuboten serpentinite massif based on geophysical tests”, Journal of the Geological and Geophysical Researches, Series C, Vol. XIV/XV, Belgrade.

TECHNICAL EVALUATION OF AN ADDITIONAL GOLD EXTRACTION TECHNOLOGY

Nikolay NESTOROV*, Irena GRIGOROVA, Teodora YANKOVA, Mihail PETROV

University of Mining and Geology "St. Ivan Rilski", Faculty of Mining technology, Mineral Processing and Recycling Department, 1700 Sofia, BULGARIA
**Corresponding author: n.nestorov@mgu.bg*

A B S T R A C T

Improving the efficiency of mineral processing technologies is essential for maximizing metal recovery and optimizing resource utilization, particularly for porphyry copper-molybdenum-gold (Cu-Mo-Au) ores characterized by complex mineralogy. This study presents a technical evaluation of integrating an additional gravity gold recovery stage into an operating flotation circuit. Four one-week in situ pilot-scale campaigns were conducted using a semi-industrial Knelson KC 7.5 MD centrifugal concentrator, supported by laboratory investigations.

Gold-bearing phases were characterized by optical microscopy, SEM-EDX, fire assay, atomic absorption spectroscopy, and gravity recoverable gold (GRG) testing. Gold was found predominantly as free or partially liberated grains with sizes between 100 and 1000 μm, commonly exhibiting surface coatings and inclusions of quartz and sulfide minerals. The GRG results indicate a high potential for gravity concentration, and the obtained concentrates showed elevated gold grades. The results confirm the technical feasibility and economic relevance of introducing an additional gravity concentration stage to improve gold recovery and reduce losses to tailings in porphyry Cu-Mo-Au ore processing.

Key words: *Porphyry Cu-Mo-Au ores, gravity concentration, GRG, Knelson concentrator gold recovery*

1. INTRODUCTION

Porphyry copper deposits represent the dominant global source of copper and are also an important source of gold as a by-product (Effah et al., 2025; Grigorova, 2020). Although gold grades in porphyry Cu-Mo-Au ores are typically low (0.2-1.0 g/t), the large tonnages processed make gold recovery economically significant. However, efficient gold extraction is often hindered by complex mineralogical characteristics and variable gold deportment (Wu et al., 2022).

Over the past decade, global demand and consumption of gold have increased steadily, accompanied by a significant rise in gold prices. As a result, improving the efficiency of gold extraction technologies and minimizing metal losses during mineral processing have become critical objectives for the mining industry. Gold-bearing ores are commonly processed using flotation, gravity concentration, cyanide leaching (Oraby et al., 2020; Qin et al., 2021; Zhang et al., 2022; Piervandi, 2023; Shi, 2024; Han et al., 2024; Liu et al., 2024) or combinations thereof (Gul et al., 2012).

Flotation is effective for fine gold, whereas gravity concentration is particularly suitable for coarse free gold due to its high density. In conventional porphyry ore processing flowsheets, gravity concentration is often omitted, leading to losses of coarse free gold to flotation tailings.

Gravity concentration is an environmentally benign and cost-effective method that enables early recovery of coarse gold without the use of chemical reagents (Surimbayev et al., 2020; Surimbayev et al., 2025). Its effectiveness depends on gold particle size, morphology, and

liberation. In ores containing both coarse and fine gold, gravity concentration is most effective when applied prior to flotation.

The present study aims to assess the technical feasibility of integrating an additional gravity concentration stage into an industrial flotation circuit processing porphyry Cu-Mo-Au ores. The study focuses on gravity recoverable gold potential, pilot-scale performance under industrial conditions, and mineralogical characteristics of gravity concentrates.

2. MATERIAL AND METHODS

2.1. Material

The investigated ore is a gold-bearing copper-molybdenum sulfide ore from a porphyry Cu-Mo-Au deposit, processed in an industrial concentrator using a conventional flotation flowsheet. Gold is recovered as a by-product in copper concentrates during subsequent metallurgical processing. The average gold grade of the run-of-mine ore is approximately 0.25 g/t, while the final flotation tailings contain around 0.14 g/t Au.

Pilot-scale and laboratory investigations were conducted to determine the distribution and behavior of gold within the processing circuit and to evaluate the potential for improving gold recovery through additional gravity concentration. Laboratory-scale gravity tests were initially performed using a Knelson KC 3 MD centrifugal concentrator. Subsequently, pilot-scale tests were carried out using a semi-industrial Knelson KC 7.5 MD centrifugal concentrator installed in situ in the operating plant.

2.2. Gravity Recoverable Gold (GRG) Testing

The gravity recoverable gold (GRG) content of the ore was determined using a standard three-stage GRG test procedure. The test involves progressive grinding of the ore to decreasing particle sizes, followed by gravity concentration at each stage to recover liberated gold particles. Gold grades and recoveries are determined for both concentrates and tailings, allowing the calculation of cumulative gravity-recoverable gold as a function of particle size.

In this study, the GRG test was conducted using a Knelson KC 3 MD concentrator. The ore sample was ground sequentially to P_{80} sizes of 1102 µm, 239 µm, and 73 µm, with gravity concentration performed after each grinding stage. Gold content in all products was determined by fire assay and atomic absorption spectroscopy.

2.3. Pilot-Scale Gravity Concentration

Pilot-scale gravity concentration tests were performed using a Knelson KC 7.5 MD centrifugal concentrator operating in continuous mode. The concentrator was installed in the grinding circuit to treat the hydrocyclone underflow prior to flotation. Test campaigns were conducted over periods of one to two weeks under industrial operating conditions. In addition, gravity concentration tests were performed on final flotation tailings to evaluate the feasibility of gold recovery from this stream. Sampling was carried out at regular intervals, and all products - including feed, gravity concentrate, intermediate products, and tailings - were analyzed for gold content.

2.4. Mineralogical and Analytical Methods

Gravity concentrates were examined using binocular stereomicroscopy to identify visible gold particles. Detailed morphological and chemical analyses were performed using scanning electron microscopy with energy-dispersive X-ray spectroscopy (SEM-EDX). Gold grades of

concentrates were determined by fire assay and atomic absorption spectroscopy. Grain size distribution analyses were also conducted to assess the size-dependent distribution of gold. A schematic flowsheet of the gravity concentration tests conducted in the grinding circuit and on the final flotation tailings is presented in Figure 1.

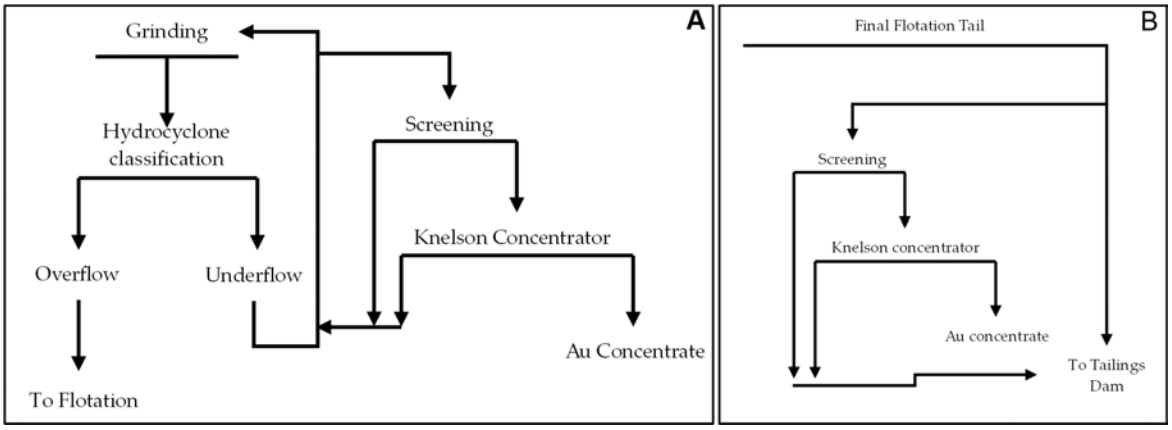

Figure 1. Flowsheet of the investigations carried out for gravity concentration using a Knelson KS 7.5 MD gravity concentrator in the grinding circuit (A) and on the final flotation tailings (B)

3. RESULTS AND DISCUSSION

3.1. Gravity Recoverable Gold (GRG)

The GRG test results indicate that gold recovery during the first grinding stage (P_{80} = 1102 µm) reached 6.9%. Additional recoveries of 10.4% and 9.7% were achieved at P_{80} sizes of 239 µm and 73 µm, respectively. The cumulative GRG value of the ore was calculated at 26.2%, indicating a significant proportion of coarse, gravity-recoverable gold (Fig. 2). For a low-grade porphyry ore, this GRG value is considered relatively high and suggests strong potential for gravity pre-concentration. A scheme of the GRG test performed is shown in Fig. 3 and the test results are presented in Table 1.

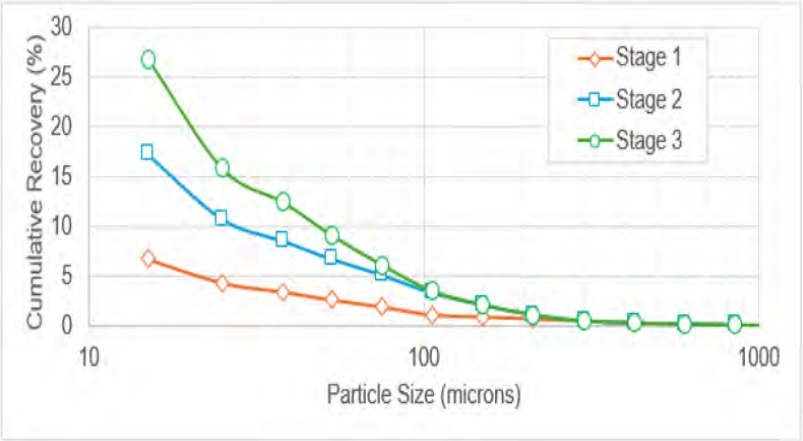

Figure 2. Cumulative gold recovery vs. particle size

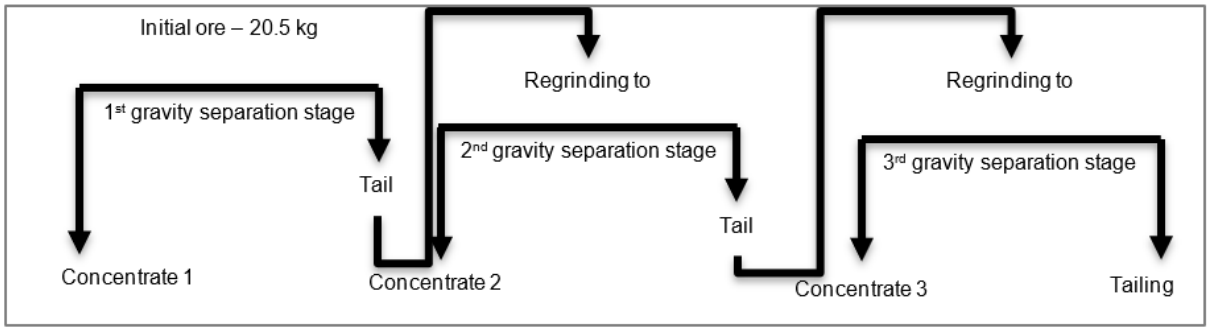

Figure 3. GRG test design

Table 1. GRG test results

Grind Size	Product	Yield		Content Au (g/t)	Distribution (%)
		(g)	(%)		
P_{80} = 1102 µm	Stage 1 Conc.	89.3	0.4	2.1	6.8
	Sampled Tails	174.2	0.8	0.1	0.6
P_{80} = 239 µm	Stage 2 Conc.	89.7	0.4	3.2	10.4
(-75 µm) = 42.3 %	Sampled Tails	169.8	0.8	0.1	0.6
P_{80} = 73 µm	Stage 3 Conc.	79.1	0.4	3.3	9.5
	Final Tails	19 898	97.1	0.1	72.1
Total (Head)		20500	100	0.13	100.0
Knelson Conc.		257.9	1.3	2.8	**26.2**
GRG Value = 26.2					

In Figure 4 the calculated GRG value for the processed Cu-Mo porphyry ore is compared with the literature data for GRG values determined with a Knelson concentrator for ores with different, including very high, gold contents.

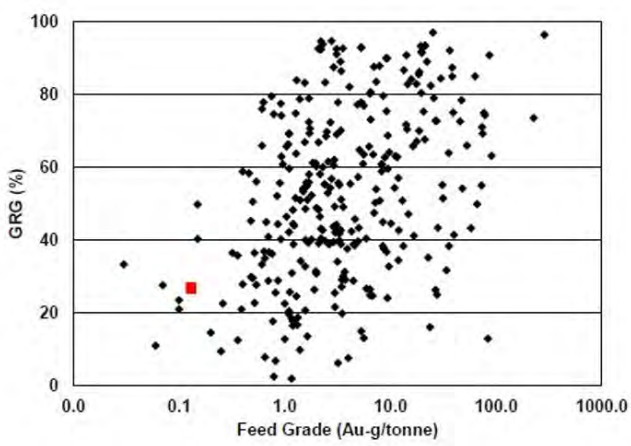

Figure 4. GRG values vs. Au content in the ore processing

3.2. Particle Size Distribution and Gold Deportment

Grain size analysis of the gravity concentrator feed revealed that approximately 38-39% of the gold occurs in the fine fraction below 80 µm. Around 34% of the gold is contained within the intermediate size range of 0.50-0.125 mm, while coarse gold particles larger than 1 mm account for a relatively small proportion. This distribution confirms the coexistence of both coarse free gold and fine gold, requiring a combined processing approach.

Table 2. Particle size distribution and gold content in the process feed entering the Knelson gravity concentrator

Class (mm)	Yield (%)	Content Au (g/t)	Distribution Au (%)
> 2.00	0.41	0.16	0.29
2.00 – 1.00	6.32	0.16	4.50
1.00 – 0.50	16.90	0.13	9.79
0.50 – 0.25	32.08	0.13	18.57
0.25 – 0.125	18.14	0.20	16.16
0.125 – 0.08	6.31	0.42	11.80
< 0.08	19.84	0.44	38.88
Average	100.00	0.22	100.00

3.3. Gravity Concentration in the Grinding Circuit

Pilot-scale gravity concentration tests conducted in the grinding circuit demonstrated stable and reproducible performance. During the two-week continuous operation period, an average gold recovery of 25.55% was achieved, with gravity concentrate grades reaching approximately 161 g/t Au. These results closely correspond to the GRG test outcomes, confirming the effectiveness of gravity concentration for early recovery of coarse gold prior to flotation. The results of the analyses are shown in Table 3.

Table 3. Gold content in the feed to the Knelson KS 7.5 MD, the gravity concentrate, the intermediate product, and the tailings

№	Contents of Au (g/t)			
	Feed	Concentrate	Intermediate	Tailing
1	0.21	368.81	13.60	0.18
2	0.18	919.93	23.38	0.16
3	0.19	792.35	29.70	0.16
4	0.20	1485.92	38.60	0.17
5	0.27	1815.93	74.93	0.24
6	0.33	5653.70	85.83	0.25
7	0.28	3949.37	92.13	0.25
8	0.26	2782.35	77.00	0.21
9	0.23	1658.77	46.15	0.18
10	0.20	3092.43	67.13	0.18
11	0.26	4094.17	78.15	0.23
12	0.24	8579.30	176.95	0.20
13	0.22	4357.20	125.38	0.18
14	0.19	3322.88	67.74	0.17
15	0.23	2136.30	56.25	0.15
16	0.16	2114.28	81.15	0.13
17	0.13	979.58	23.43	0.10
18	0.17	1252.40	36.15	0.15

For the purpose of modeling the gravity concentration process in the grinding circuit, the process balance from the conducted tests was calculated (Table 4) based on the gold content in the individual products and their quantities.

Table 4. Process balance of Au in gravity concentration in the grinding circuit

Test №	Feed ore	Concentrate			Intermediate product			Tailing		
	Content Au (g/t)	Yield (%)	Content Au (g/t)	Distrib. Au (%)	Yield (%)	Content Au (g/t)	Distrib. Au (%)	Yield (%)	Content Au (g/t)	Distrib. Au (%)
1	0.15	0.004	368.81	9.71	0.053	13.60	4.75	99.943	0.13	85.54
2	0.17	0.001	919.93	5.52	0.032	23.38	4.49	99.967	0.15	89.99
3	0.15	0.001	792.35	5.29	0.040	29.70	7.93	99.959	0.13	86.78
4	0.14	0.001	1485.92	10.74	0.035	38.60	9.77	99.964	0.11	79.49
5	0.25	0.001	1815.93	7.32	0.040	74.93	12.08	99.959	0.20	80.60
6	0.25	0.001	5653.70	22.26	0.032	85.83	10.82	99.967	0.17	66.92
7	0.22	0.001	3949.37	17.82	0.035	92.13	14.55	99.964	0.15	67.64
8	0.26	0.001	2782.35	10.60	0.032	77.00	9.39	99.967	0.21	80.01
9	0.19	0.002	1658.77	17.44	0.037	46.15	8.98	99.961	0.14	73.58
10	0.21	0.001	3092.43	14.98	0.038	67.13	12.36	99.961	0.15	72.65
11	0.21	0.001	4094.17	19.31	0.027	78.15	9.95	99.973	0.15	70.74
12	0.20	0.001	8579.30	43.14	0.030	176.95	26.69	99.969	0.06	30.16
13	0.20	0.001	4357.20	21.94	0.020	125.38	12.63	99.980	0.13	65.44
14	0.17	0.001	3322.88	19.94	0.020	67.40	8.09	99.979	0.12	71.98
15	0.16	0.001	2136.30	13.75	0.025	56.25	9.05	99.974	0.12	77.20
16	0.13	0.001	2114.28	16.19	0.024	81.15	14.91	99.975	0.09	68.90
17	0.12	0.001	979.58	7.86	0.021	23.43	3.95	99.978	0.11	88.20
18	0.14	0.001	1252.40	8.89	0.023	36.15	5.90	99.976	0.12	85.20
Avr.	0.19	0.001	2748.89	**14.62**	0.031	66.29	**10.93**	99.968	0.14	74.45

Gold grades in the gravity concentrator feed varied between 0.13 and 0.33 g/t Au, reflecting natural variability in ore composition. Despite these fluctuations, the gravity concentrator consistently produced high-grade concentrates, demonstrating robustness under industrial conditions.

3.4. Gravity Concentration of Final Flotation Tailings

Pilot tests on final flotation tailings were conducted over a seven-day period. During this time, the processed ore exhibited relatively low gold grades (0.14-0.17 g/t Au), resulting in very low gold concentrations in the tailings (0.05-0.06 g/t Au). Under such conditions, gravity concentration of tailings was found to be economically unjustified. These results indicate that tailings treatment should be considered only during periods of elevated gold head grades.

3.5. Mineralogical Characteristics of Gravity Concentrates

Mineralogical examination of gravity concentrates identified 521 visible free gold particles. Most gold grains range in size from 150 to 400 μm, with occasional particles exceeding 1 mm (fig. 5). Fine gold particles smaller than 80 μm were also observed. Gold grains exhibit diverse morphologies, including irregular, isometric, elongated, platy, dendrite-like, and deformed forms. Many particles show rough or matte surfaces and coatings of iron oxides and hydroxides, as well as inclusions of quartz and sulfide minerals.

SEM–EDX analyses indicate the presence of high-purity gold with low silver content, as well as electrum. Silver contents in gold grains range from 2 to 22 wt.%, reflecting compositional variability of gold within the deposit (Fig. 6, Fig. 7).

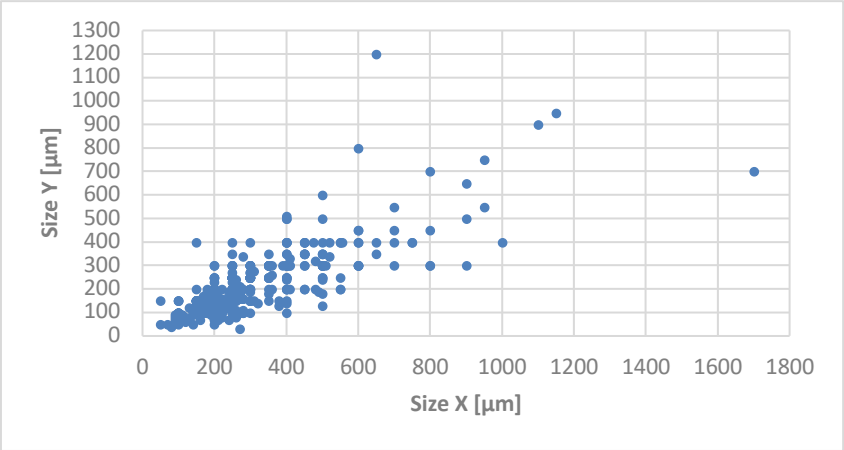

Figure 5. Size-dependent quantitative distribution of coarse gold grains in the gravity concentrates (µm)

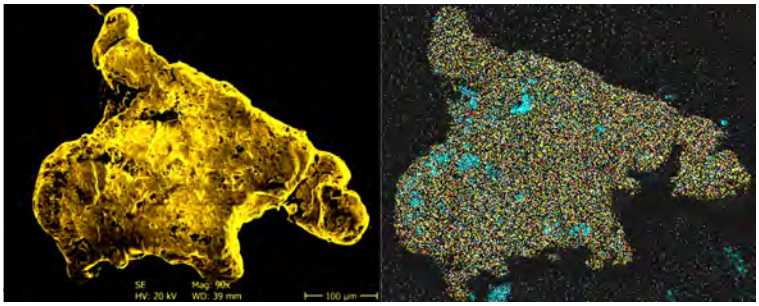

Figure 6. Irregular form of electrum with quartz in micropores, SEM X 90

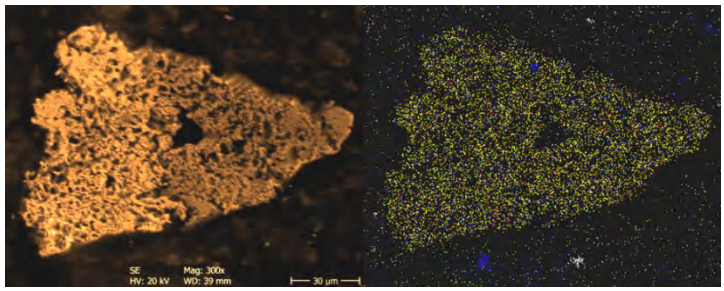

Figure 7. Dendrite-like form of microporous gold, SEM, X 300

4. CONCLUSION

The gravity recoverable gold content of the investigated porphyry Cu–Mo–Au ore was determined to be 26.2%, indicating a substantial proportion of coarse, gravity-recoverable gold. Pilot-scale in situ testing demonstrated that the integration of a centrifugal gravity concentrator into the grinding circuit prior to flotation can recover up to 25.6% of the gold, producing high-grade concentrates exceeding 160 g/t Au.

The results confirm that flotation alone is insufficient for efficient recovery of coarse free gold in this ore type. Early-stage gravity concentration enables effective recovery of coarse gold particles, reduces losses to final tailings, and improves overall gold recovery. The gravity concentration stage represents a low-cost, environmentally favorable modification requiring minimal changes to the existing processing flowsheet.

Gravity treatment of final flotation tailings is economically viable only during periods of elevated gold head grades, highlighting the importance of adaptive process strategies based on ore

variability. Overall, the proposed gravity-flotation flowsheet offers a technically robust and industrially applicable solution for improving gold recovery from porphyry Cu-Mo-Au ores.

ACKNOWLEDGEMENTS

This research is in performance of Project BG05SFPR001-3.004-0002-C01 "Development and improvement of professional and interdisciplinary education in technical and economic sciences and enhancement of the research capacity of the extractive industry through project-based doctoral studies", funded by Programme "Education", co-funded by the European Union.

REFERENCES

Effah, B. B., Djanetey, G. E., Whajah, J., (2025) “Gold (Au) as a by-product of porphyry copper deposit mining”, World Journal of Advanced Research and Reviews, 28 (2) 1559-1566.

Gül, A., Kangal, O., Sirkeci, A. A., Önal, G., (2012) “Beneficiation of the gold bearing ore by gravity and flotation”, International Journal of Minerals, Metallurgy and Materials, 19 (2) 106-110.

Grigorova, M., (2020) “Geophysical and mining technologies for increasing efficiency in “Han krum” open pit mine”, Proceeding of the XX IMSC (1.2) 111–118.

Han, J., Dai, S., Deng, J., Que, S., Zhou, Y., (2024) “Technology for Aiding the Cyanide Leaching of Gold Ores”, Separations, 11 (228) 1-12.

Liu, Z. W., Guo, X. Y., Tian, Q H., Zhang, L., (2022) “A systematic review of gold extraction: Fundamentals, advancements, and challenges toward alternative lixiviants”, Journal of Hazardous Materials, 440 4-16.

Liu, Y., Li, K., Yin, Z., Dong, J., Xu, L., Ma, R., Li, S., (2024) “Pretreatment of refractory gold ore by curing with concentrated sulfuric acid”, Mining, Metallurgy & Exploration, 41 1079-1087.

Oraby, E. A., Eksteen, J. J., Ó. Connor, G. M., (2020) “Gold leaching from oxide ores in alkaline glycine solutions in the presence of permanganate”, Hydrometallurgy, 198 105527.

Piervandi, Z., (2023) “Pretreatment of refractory gold minerals by ozonation before the cyanidation process: A review”, Journal of Environmental Chemical Engineering, 11 (1) 109013.

Qin, H., Guo, X., Tian, Q., Yu, D., Zhang, L., (2021) “Recovery of gold from sulfide refractory gold ore: Oxidation roasting pretreatment and gold extraction”, Minerals Engineering, 164 106822.

Shi, A., (2024) “Review of gold cyanide leaching and the main factors affecting gold dissolution rate”, Naturalis Scientias, 1 (1) 4 56-60.

Surimbayev, B. N., Kanaly, E. S., Bolotova, L. S., Shalgymbayev, S. T., (2020) “Assessment of gravity dressability of gold ore – GRG test”, Mining Science and Technology (Russia), 5 (2) 92-103.

Surimbayev, B., Bolotova, L., Akcil, A., Yessengarayev, Y., Khumarbekuly, Y., Kanaly, Y., Akzharkenov, M., (2025) “Gravity concentration of gold-bearing ores and processing of concentrates: A review”, Mineral Processing and Extractive Metallurgy Review, 46 (7) 726-750.

Wu, J., Ahn, J., Lee, J., (2022) “Characterization of gold deportment and thiosulfate extraction for a copper-gold concentrate treated by pressure oxidation”, Hydrometallurgy, 207 105771.

Zhang, Y., Cui, M., Wang, J., Liu, X., Lyu, X., (2022) “A review of gold extraction using alternatives to cyanide: Focus on current status and future prospects of the novel eco-friendly synthetic gold lixiviants”, Minerals Engineering, 176 107336.

THE IMPORTANCE OF ZETA POTENTIAL MEASUREMENT IN THE FLOTATION OF DIASPORA AND CALCIUM MINERALS

Y. Hakan GÜRSOY, Abdullah FİLAR, Yakup UMUCU*

Eskişehir Osmangazi University, Faculty of Engineering and Arcitecture, Mining Engineering Department, 26040, Odunpazarı, Eskişehir, TÜRKİYE
**Corresponding author: yakup.umucu@ogu.edu.tr*

A B S T R A C T

The combined consideration of particle size and the collector effect is crucial for understanding the flotation mechanism. In fine particles, an increase in surface area can increase collector adsorption, leading to larger changes in zeta potential. However, in very fine particles, surface hydration and electrostatic repulsion forces can increase, making bubble-particle binding more difficult. In larger particles, the surface area decreases, limiting collector adsorption and resulting in smaller changes in zeta potential. Therefore, both surface charge differences and collector adsorption become more pronounced within the optimum particle size range.

The variation of zeta potential depending on particle size and collector type is a significant indicator of flotation selectivity in the removal of calcium-based minerals from bauxite. Anionic collectors have stronger adsorption, especially on carbonate minerals, which makes the zeta potential more negative. Cationic collectors, on the other hand, can change the surface charge of minerals in the opposite direction. As particle size decreases, the increase in surface area makes these effects more pronounced. Therefore, zeta potential data is used as an important evaluation criterion for optimizing flotation conditions and selecting the appropriate collector type in bauxite ores (Somasundaran, 1975; Fuerstenau, 2005).

The removal of calcium-origin minerals (primarily calcite and dolomite) from diasporic bauxite ores represents a significant challenge in the alumina industry, particularly for the Bayer process where calcium impurities cause substantial operational difficulties. This comprehensive review examines the pivotal role of zeta potential measurements in understanding and optimizing the flotation separation of these mineral systems. The electrokinetic properties of diaspora [AlO(OH)] and associated calcium minerals govern collector adsorption mechanisms, selectivity, and overall flotation performance. Through critical analysis of recent literature and fundamental surface chemistry principles, this paper demonstrates that zeta potential serves as an indispensable tool for reagent selection, pH optimization, and process control. The distinct isoelectric points of diaspora (pH 5.0–7.5) and calcium minerals (pH 7.0–8.5) provide the theoretical basis for selective separation, while zeta potential measurements enable quantitative verification of surface interactions.

This review presents the electrokinetic principles, collector-mineral interactions, depressant mineral mechanisms, and the effects of grain size on zeta potential, offering a framework for future research directions in this critical field.

Key words: *Aluminum, calcium, flotation, zeta potential, collector*

1. INTRODUCTION

Flotation is an enrichment method that utilizes differences in the surface properties of minerals. In this process, the electrical properties of mineral surfaces directly affect the adsorption mechanism of collectors and other flotation reagents. One of the most important parameters determining the electrical behavior of mineral surfaces is the zeta potential. The zeta potential represents the potential difference at the shear plane within the electrical double layer between the solid particle and the solution and is accepted as an indicator of mineral surface charge (Somasundaran, 1975).

In flotation research, zeta potential measurements are of great importance for determining mineral surface charge, identifying the isoelectric point (IEP), understanding reagent adsorption mechanisms, and examining the effects of ions present in the solution on surface chemistry. Zeta potential analyses are typically used in conjunction with micro-flotation tests, FTIR spectroscopy, and XPS analyses to contribute to the explanation of flotation mechanisms (Fuerstenau, 2005).

Additionally, the dispersion or flocculation behavior of mineral particles within a suspension is dependent on surface potential. Since the electrical properties of the mineral surface determine the electrostatic repulsive force between particles, they have an indirect but significant effect on flotation performance.

Diaspora [AlO(OH)] is one of the main aluminum minerals found particularly in diasporic bauxite deposits. In such ores, diaspora is typically found together with silicate minerals such as kaolinite, illite, pyrophyllite, and chlorite, as well as calcium-origin minerals. Therefore, it is necessary to have a good understanding of mineral surface properties during the flotation enrichment of diaspora.

Zeta potential studies have indicated that there are significant surface chemistry differences between diaspora and gangue minerals. Electrokinetic studies in the literature indicate that the isoelectric point of diaspora is approximately in the pH 6–7 range. The changing electrical behavior of mineral surfaces with pH directly affects the adsorption of flotation reagents, which is crucial for optimizing flotation processes in mineral separation (Yu et al., 2016; Deng et al., 2015; Jiang et al., 2010).

In flotation studies aimed at removing calcium-based minerals from bauxite ores, zeta potential measurements are an important tool for understanding the surface charge of minerals and the collector adsorption mechanism. Zeta potential is not only dependent on pH; it is also strongly influenced by factors such as particle size, surface area, and the type of collector used. Therefore, when interpreting the flotation separation between diaspore and calcium-based minerals, particularly calcite and dolomite, found in bauxite ores, the variation of zeta potential with particle size and collector type must be carefully evaluated.

As particle size decreases, the mineral surface area increases significantly, increasing the number of active centers on the surface and altering electrokinetic behavior. Fine particles generally exhibit a higher surface charge because there are more broken bonds and reactive surface regions on the surface. Therefore, the absolute value of the zeta potential is often measured higher at very fine particle sizes. This effect has an important consequence for flotation: fine particles can exhibit stronger electrostatic interactions, and collector adsorption can become more pronounced. However, at extremely fine particle sizes, the emergence of colloidal behavior and increased surface hydration can reduce flotation selectivity, leading to challenges in separating valuable minerals from gangue materials during the flotation process. In bauxite flotation, surface charge differences are more pronounced in the medium particle size ranges, especially for minerals such as diaspore and calcite. Therefore, evaluating zeta potential curves depending on particle size contributes to determining the optimum flotation particle size (Massola et al., 2009).

Understanding mineral surface chemistry is of great importance during the flotation enrichment of diaspora and calcium minerals. Studies in the literature indicate that zeta potential measurements play a critical role in determining mineral surface charge, isoelectric point, reagent adsorption, and the effect of ions in solutions. Therefore, zeta potential analyses are widely used in explaining flotation mechanisms in research directed at the flotation of diasporic bauxites and calcium-containing minerals. Within the scope of this study, zeta potentials were determined at different particle sizes to establish suitable flotation conditions for the removal of calcium-origin minerals from diaspora ore, which cause problems in the BAYER process.

Additionally, reactions were measured using different types of cationic collectors (oleic acid, SLS, SDS, DAH, and 811 M). In light of the data obtained, ideas that will guide the removal of calcium-origin minerals from diaspora through flotation enrichment were discussed.

2. MATERIAL AND METHODS

2.1. Material

Within the scope of this investigation, low-grade diasporic bauxite ore sourced from the Morçukur (Mor Pit) locality in the Seydişehir district, operated by ETİ Aluminum Inc., was employed as the feed material. The run-of-mine ore was subsequently classified into narrow particle size fractions, namely -0.212+0.106 mm, -0.106+0.075 mm, -0.075+0.053 mm, -0.053+0.038 mm, -0.053 mm, and -0.038 mm, utilizing standard sieve series in accordance with ASTM E11 specifications.

Comprehensive Mineral Liberation Analysis (MLA) was performed on each size fraction to quantify mineralogical attributes. MLA constitutes an advanced automated process mineralogy platform that integrates scanning electron microscopy (SEM) with energy-dispersive X-ray spectroscopy (EDS) and backscattered electron (BSE) imaging modalities. This integrated analytical approach enables rapid, statistically robust determination of mineralogical composition, particle size distribution, liberation characteristics, and textural properties of complex ore assemblages.

Table 1. MLA analytical data for brecciated bauxite ore from the Morçukur deposit across specified particle size fractions

Particle Size (mm)	**Boehmite AlO(OH)**	**Diasporite AlO(OH)**	**Gibbsite $Al(OH)_3$**	**Kaolinite $Al_2Si_2O_5(OH)_4$**	**Tridymite SiO_2**	**Quartz SiO_2**
-0.212+0.106	5.17	15.63	1.53	1.67	0.57	0.34
-0.106+0.075	4.71	21.43	0.58	2.85	0.64	0.21
-0.075+0.053	1.50	12.16	1.78	2.38	1.56	0.44
-0.053+0.038	2.39	16.46	1.67	2.87	0.94	0.07
-0.038	4.17	13.53	1.10	2.09	0.85	0.35
Particle Size (mm)	**Hematite Fe_2O_3**	**Goetite FeO(OH)**	**Rutile TiO_2**	**Anatase TiO_2**	**Calcite $CaCO_3$**	
-0.212+0.106	5.89	1.24	0.17	0.41	58.05	
-0.106+0.075	7.64	1.27	0.32	0.45	51.68	
-0.075+0.053	10.37	1.36	0.23	0.79	67.32	
-0.053+0.038	8.47	0.76	0.34	0.42	56.93	
-0.038	7.74	1.27	0.17	0.56	58.30	

Upon examination of Table 1, it is evident that diaspora constitutes the predominant mineral phase across all particle size fractions. Furthermore, the ore exhibits elevated calcite content as the primary gangue mineral constituent.

2.2. Method

Zeta potential represents the electrical potential arising from the surface charge of a particle and its associated counter-ions in the electrical double layer. The determination of this parameter provides detailed information regarding dispersion, aggregation, and flocculation mechanisms, which are crucial for understanding the stability and behavior of colloidal systems

in various applications such as pharmaceuticals, food technology, and environmental science. The zeta potential value indicates the potential stability of a colloidal system. If all particles in a suspension possess high positive or negative zeta potentials, mutual electrostatic repulsion occurs. Conversely, at low zeta potential, no sufficient repulsive force exists to prevent particle collision and agglomeration. The boundary between stable and unstable suspensions is generally accepted to lie between -30 mV and +30 mV (Somasundaran, 1975).

Zeta potential is typically measured by observing the motion of a particle in an applied electric field. In this process, the particle velocity serves as a measure of electrophoretic mobility. Zeta potential measurements are fundamentally conducted by determining the velocity of charged particles moving in an electric field, utilizing either Electrophoretic Light Scattering (ELS) or Laser Doppler Electrophoresis (LDE) techniques. This methodology enables the quantification of particle electrophoretic mobility, which is subsequently converted to zeta potential values (in mV) through the application of the Smoluchowski or Henry equations.

Within the scope of this investigation, zeta potential measurements were performed using a Malvern Panalytical Zetasizer Ultra instrument (Figure 1). Measurements were conducted for each sample under both alkaline and acidic conditions.

Figure 1. Malvern Panalytical Zetasizer Ultra instrument utilized for zeta potential measurements

3. RESULTS AND DISCUSSION

In bauxite flotation, anionic collectors (fatty acids, oleate derivatives) are commonly employed. Although alumina minerals carry a slightly negative charge under pH 9–10 conditions, collector adsorption still occurs. This phenomenon is attributed to the fact that adsorption involves not only electrostatic interactions but also chemical (specific) adsorption mechanisms. Zeta potential measurements demonstrate the occurrence of adsorption by revealing changes in surface charge following collector addition (Fuerstenau, 2005; Laitinen et al., 2016).

In the flotation of aluminum ores, common depressants include starch, sodium silicate, and CMC (carboxymethyl cellulose). These reagents function by rendering the zeta potential of gangue minerals more negative, thereby inhibiting collector adsorption and enhancing

selectivity. Bauxite ores are typically fine-grained and clay-rich, wherein zeta potential serves as a critical parameter in determining the flocculation or dispersion tendency of fine particles. Through optimization of pH and reagent conditions, slime coating effects can be mitigated (Yu et al., 2016).

The isoelectric point (IEP) of bauxite minerals is generally situated around pH 8–9, whereas gangue minerals typically exhibit lower IEP values. Consequently, zeta potential constitutes a fundamental parameter governing collector adsorption, pH selection, depressant efficacy, and flotation selectivity (Deng et al., 2015; Jiang et al., 2010).

Within the framework of this investigation, pH-dependent zeta potential measurements were initially conducted for CBF-Alumina (Al_2O_3), Moist Hydrate [$Al(OH)_3$], and Red Mud obtained from the processing plant, with results presented in Figures 2, 3, and 4, respectively.

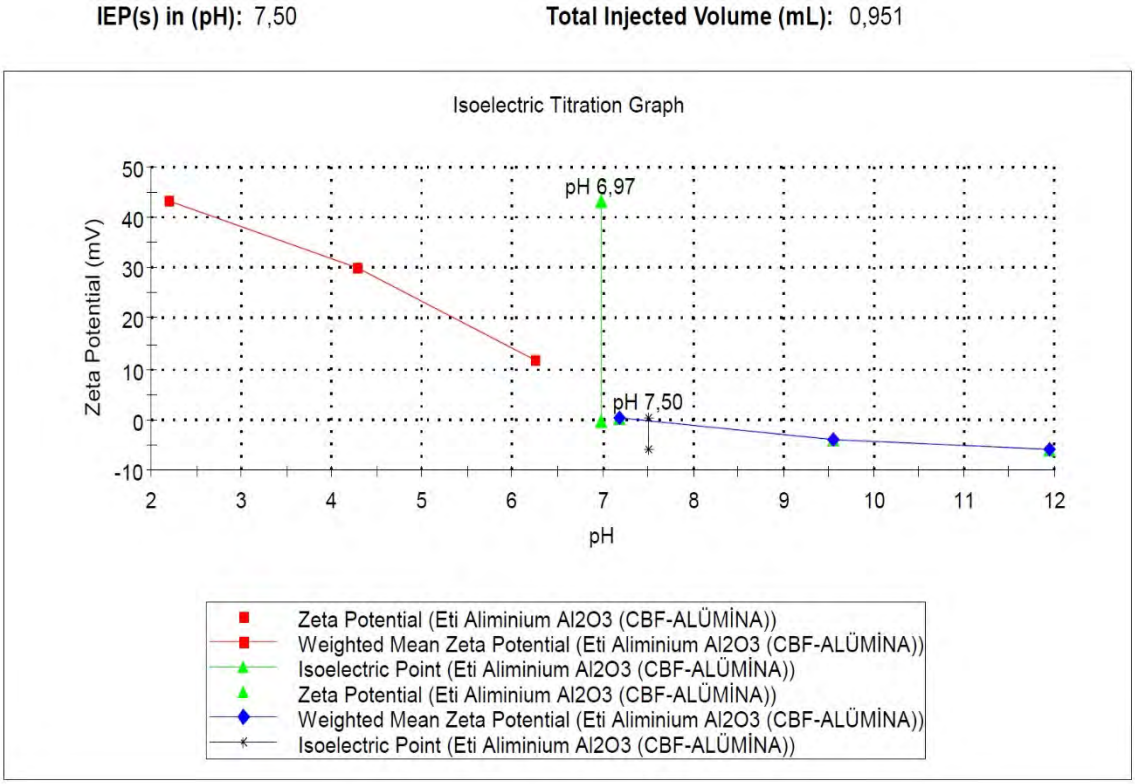

Figure 2. Zeta potential measurements at different pH values for CBF-Alumina

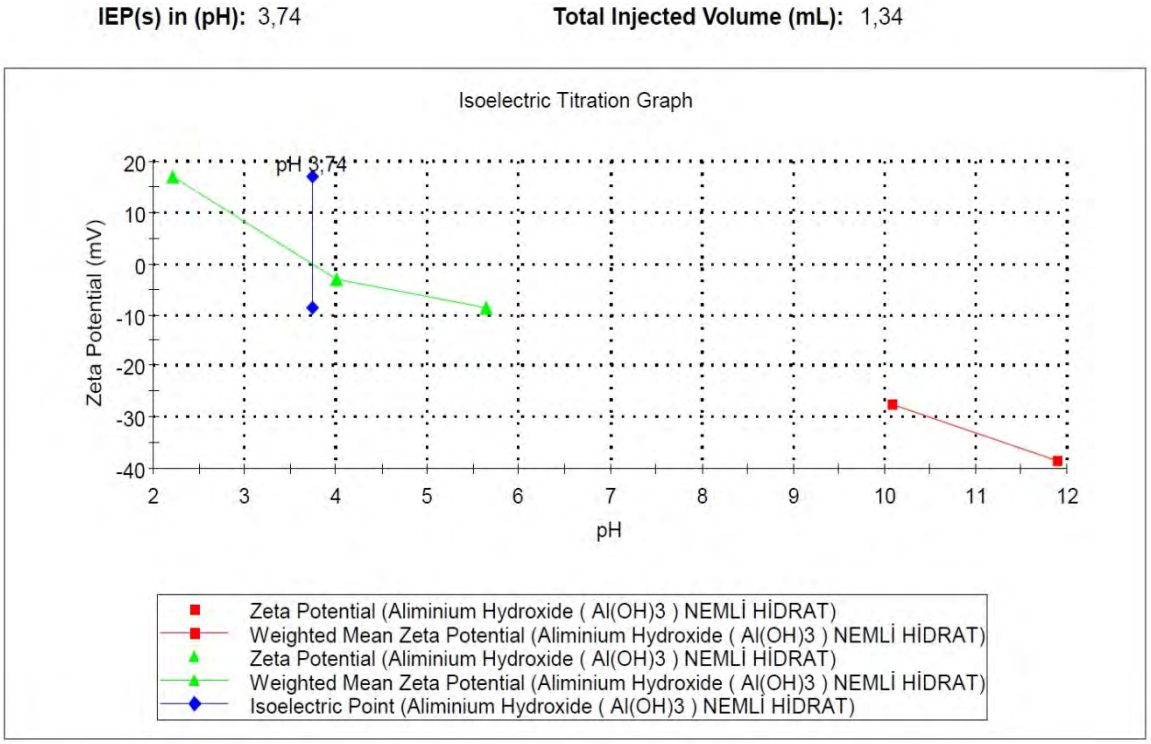

Figure 3. Zeta potential measurements at different pH values for Moist Hydrate-Alumina

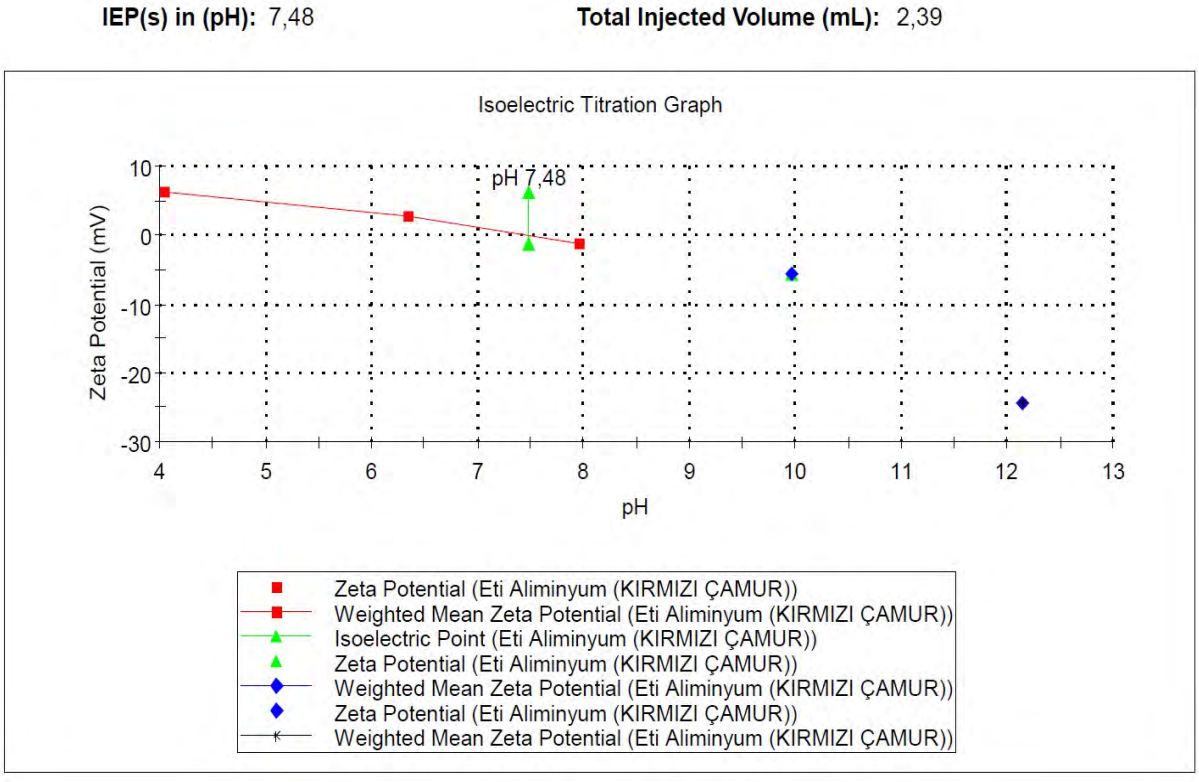

Figure 4. Zeta potential measurements at different pH values for Red Mud

Zeta potential and point of zero charge measurements conducted on alumina revealed distinct differences between CBF alumina and moist hydrate alumina. The presence of different zero charge points for these two aluminum concentrates indicates that they possess dissimilar surface charge characteristics under varying pH conditions (Hao et al., 2011). When evaluated

in terms of their positive and negative surface charge properties, it is considered appropriate to base the aluminum flotation investigations on hydrated alumina, as this form more accurately represents the surface chemistry of aluminum minerals in the ore.

In flotation studies concerning aluminum minerals, the selection of acidic pH conditions is generally indicated as optimal. This preference is attributed to the fact that under acidic pH conditions, the surface charge potential of aluminum is not excessively high. This facilitates enhanced adsorption of depressants onto the aluminum mineral surfaces while simultaneously enabling more effective performance of collectors targeting calcium and silica-bearing minerals (Yu-hua et al., 2008; Li et al., 2010).

Within the scope of this investigation, zeta potential measurements were performed to determine the point of zero charge for various particle size fractions, taking into account the liberation size of the minerals. The results of these zeta potential measurements are presented in Figures 5 through 9.

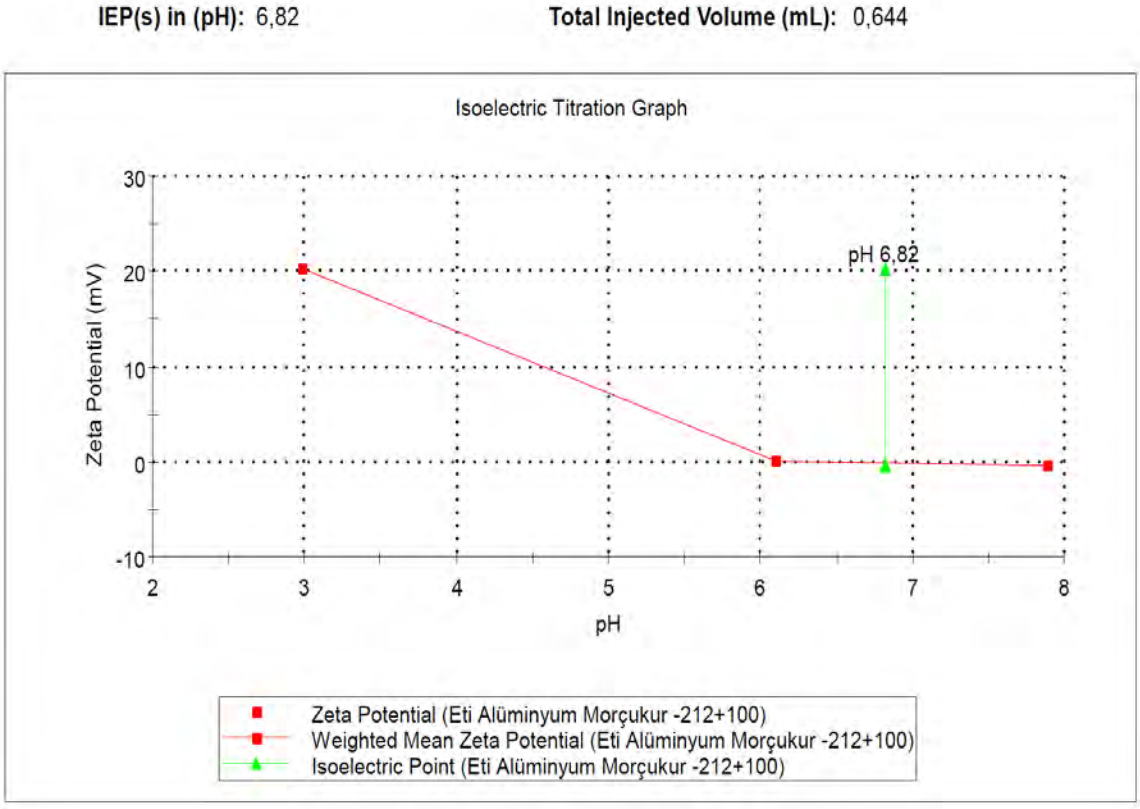

Figure 5. Zeta potential measurements at different pH values for the -0.212+0.106 mm size fraction

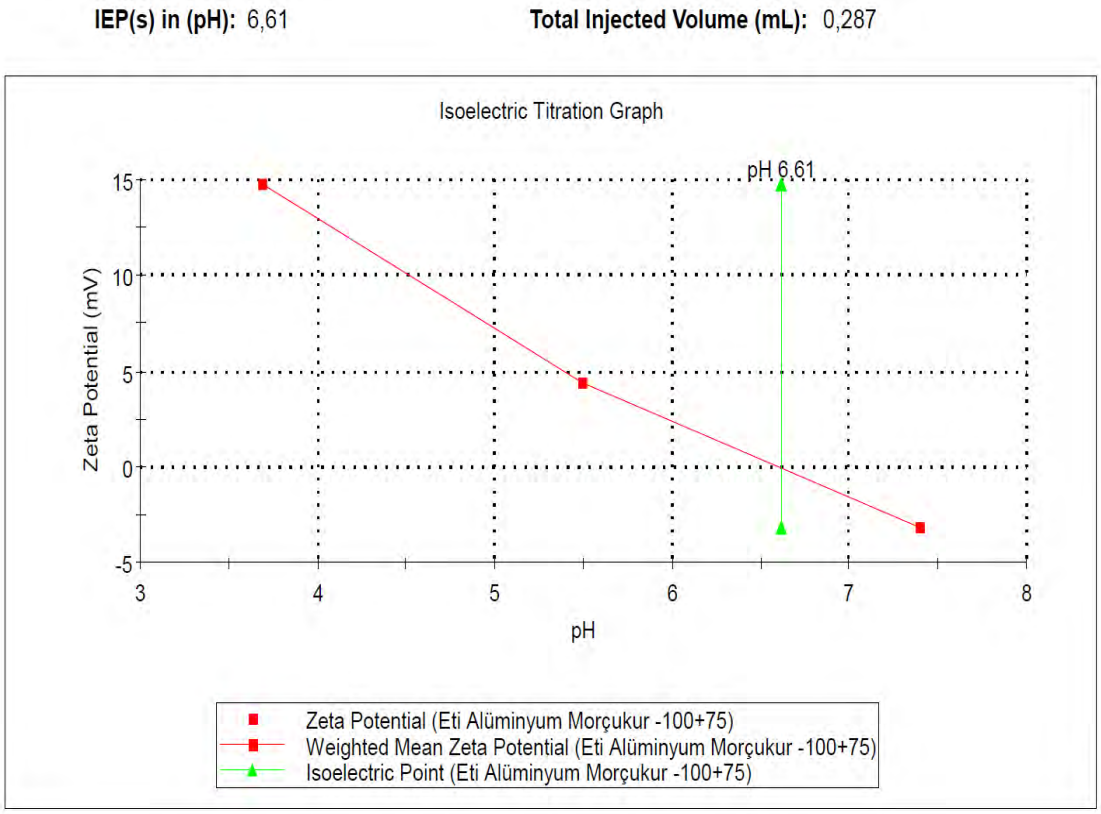

Figure 6. Zeta potential measurements at different pH values for the -0.106+0.075 mm size fraction

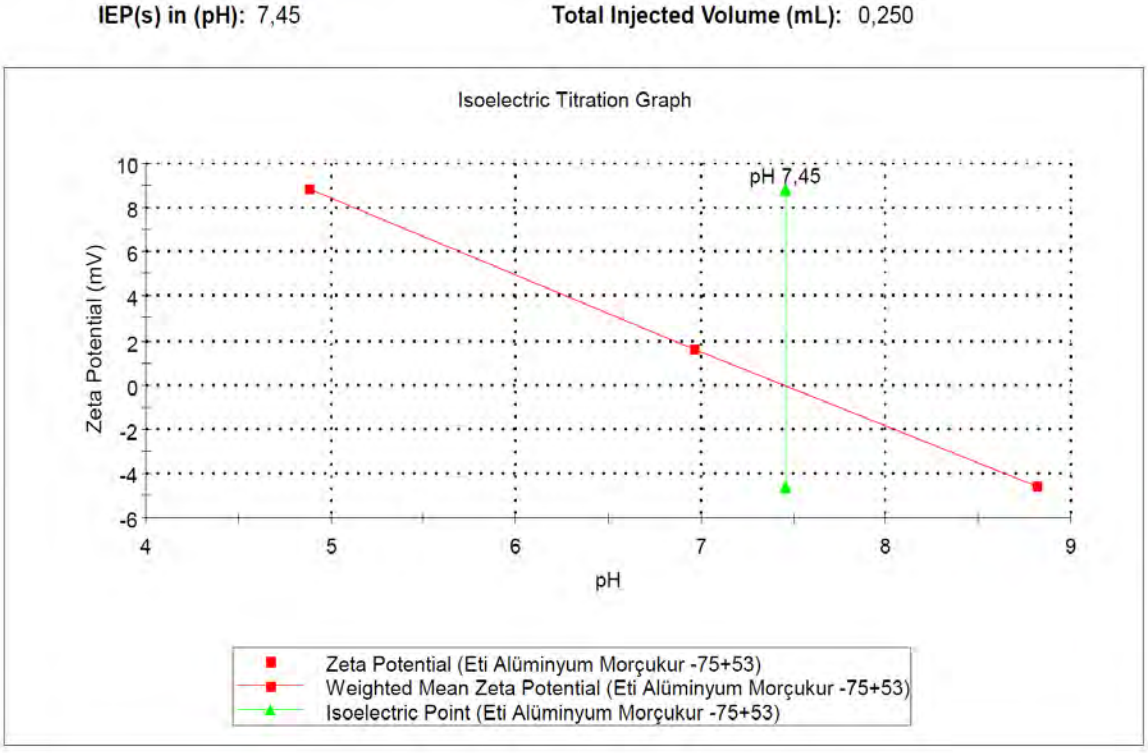

Figure 7. Zeta potential measurements at different pH values for the -0.075+0.053 mm size fraction

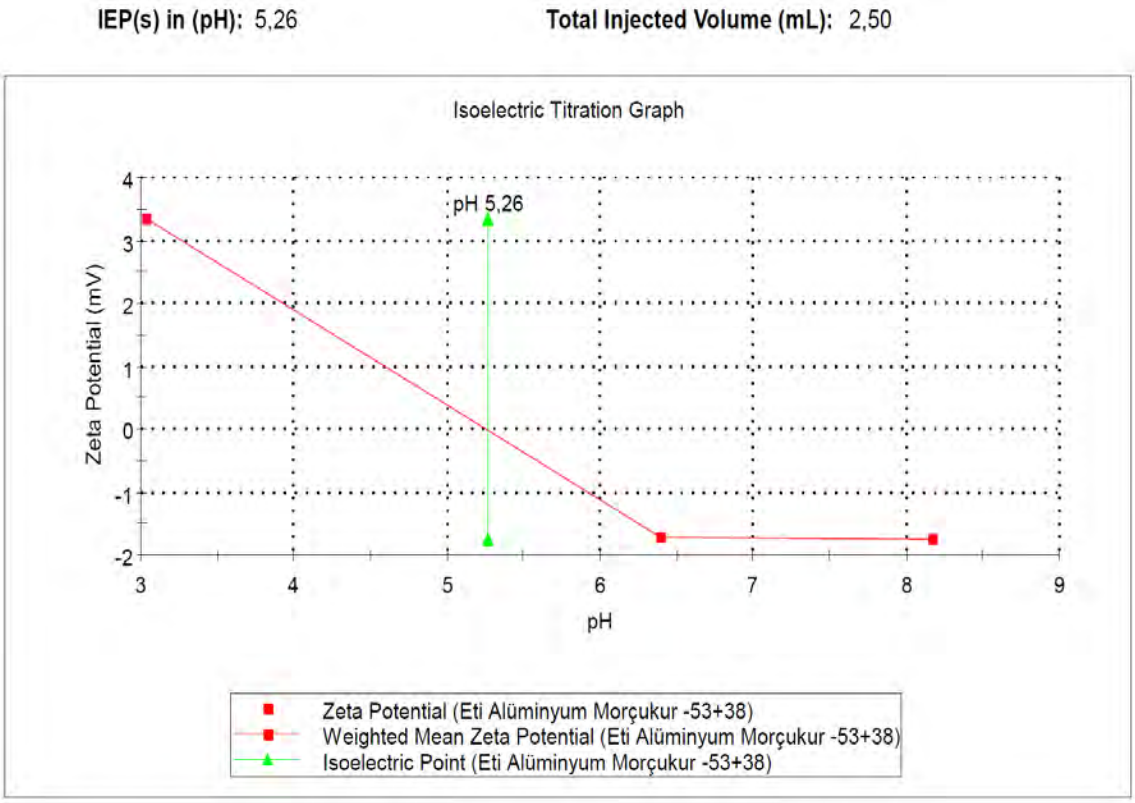

Figure 8. Zeta potential measurements at different pH values for the -0.053+0.038 mm size fraction

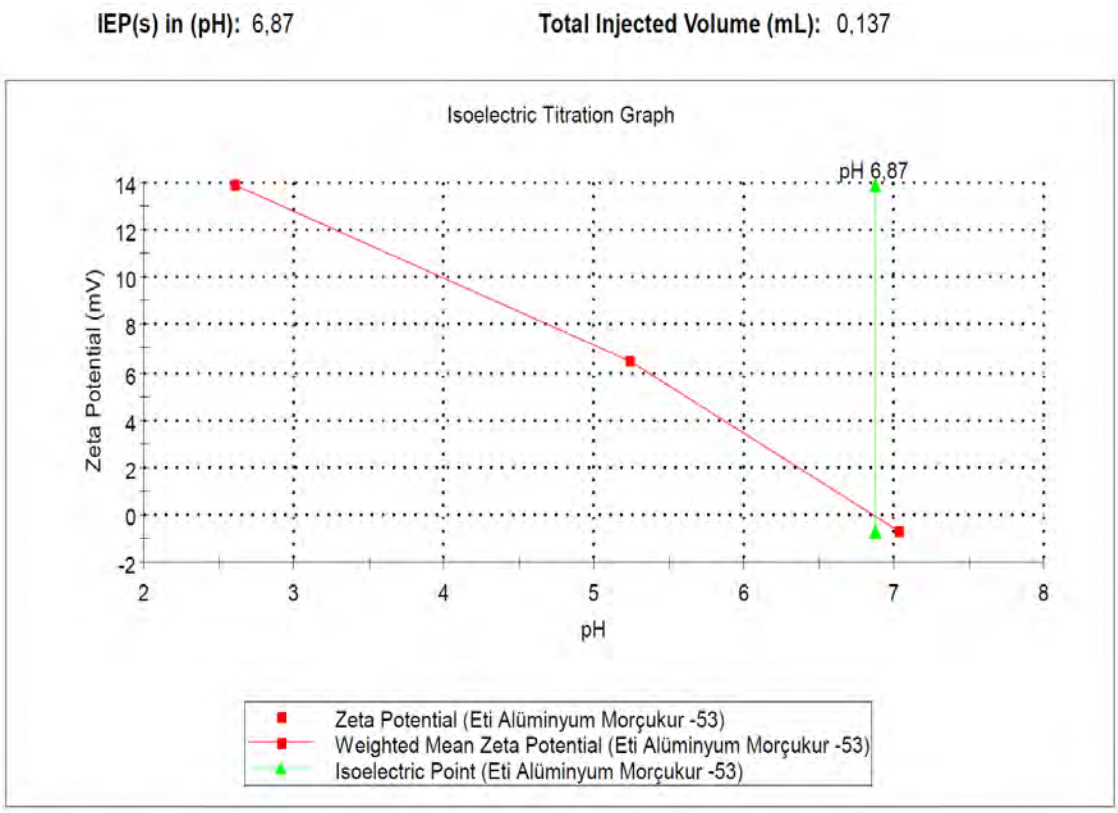

Figure 9. Zeta potential measurements at different pH values for the -0.053 mm size fraction

Zeta potential measurements indicated that for all particle size fractions, pH values at or below 7—namely acidic conditions—exhibit more favorable charge characteristics for flotation. It was determined that this finding constitutes a positive development for the implementation of reverse flotation in bauxite processing (Hai-pu et al., 2010; Yuhua et al., 2003). This is because in reverse floatation, wherein oxide gang minerals are floated instead of bauxite minerals, the pulp pH must be maintained under acidic conditions.

To investigate the influence of selected collectors on flotation behavior, zeta potential measurements were performed using various collectors at a fixed particle size fraction, with results presented in Figures 10–15.

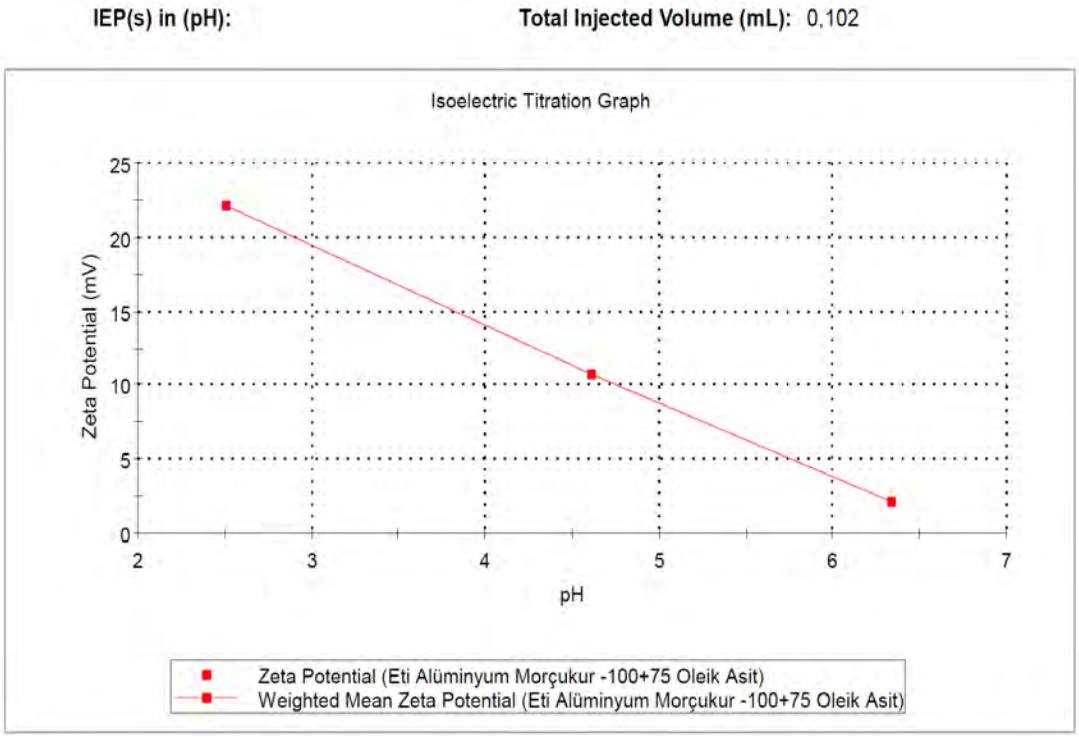

Figure 10. Zeta potential measurements at different pH values for oleic acid in the -0.100+0.075mm size fraction

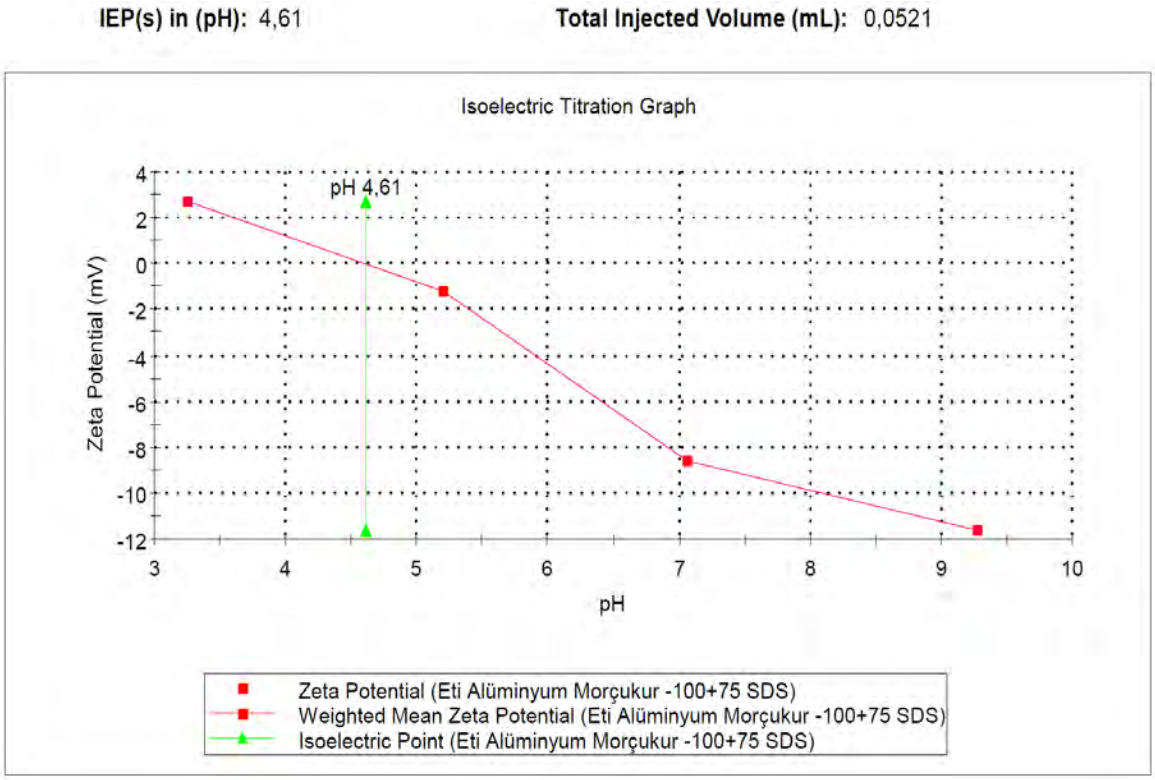

Figure 11. Zeta potential measurements at different pH values for SDS in the -0.100+0.075mm size fraction

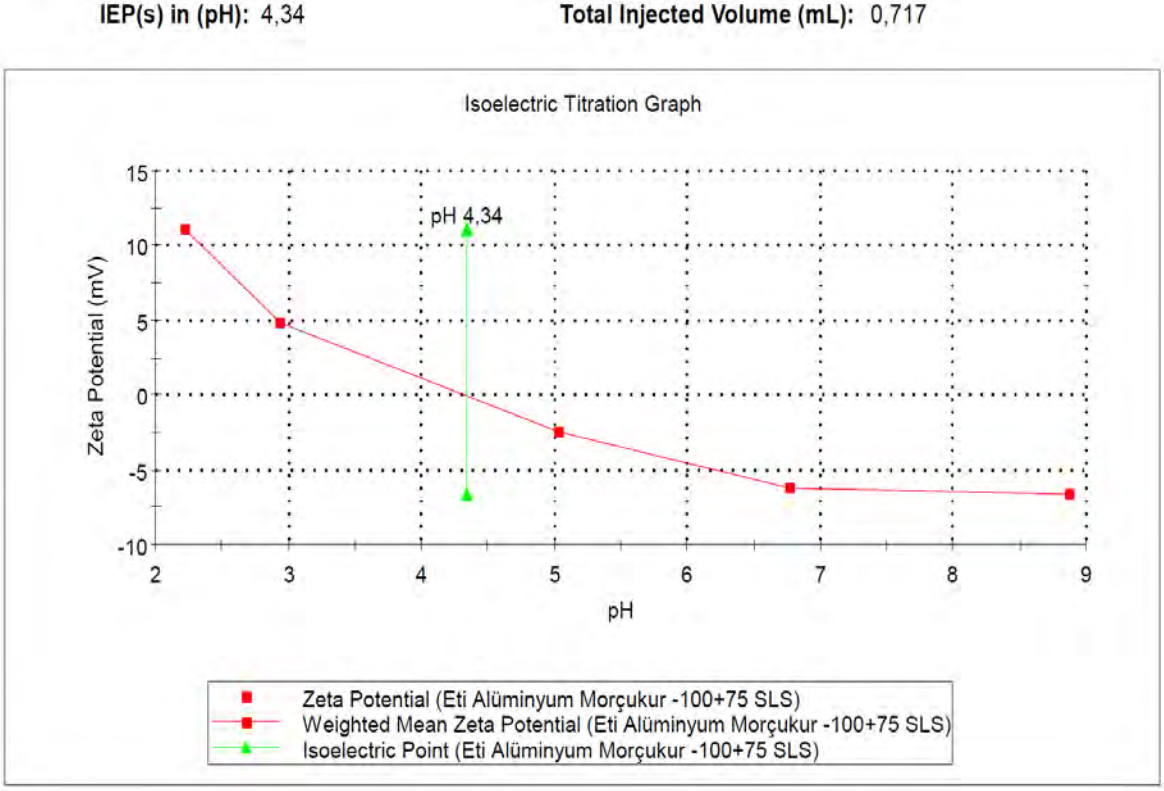

Figure 12. Zeta potential measurements at different pH values for SLS in the -0.100+0.075mm size fraction

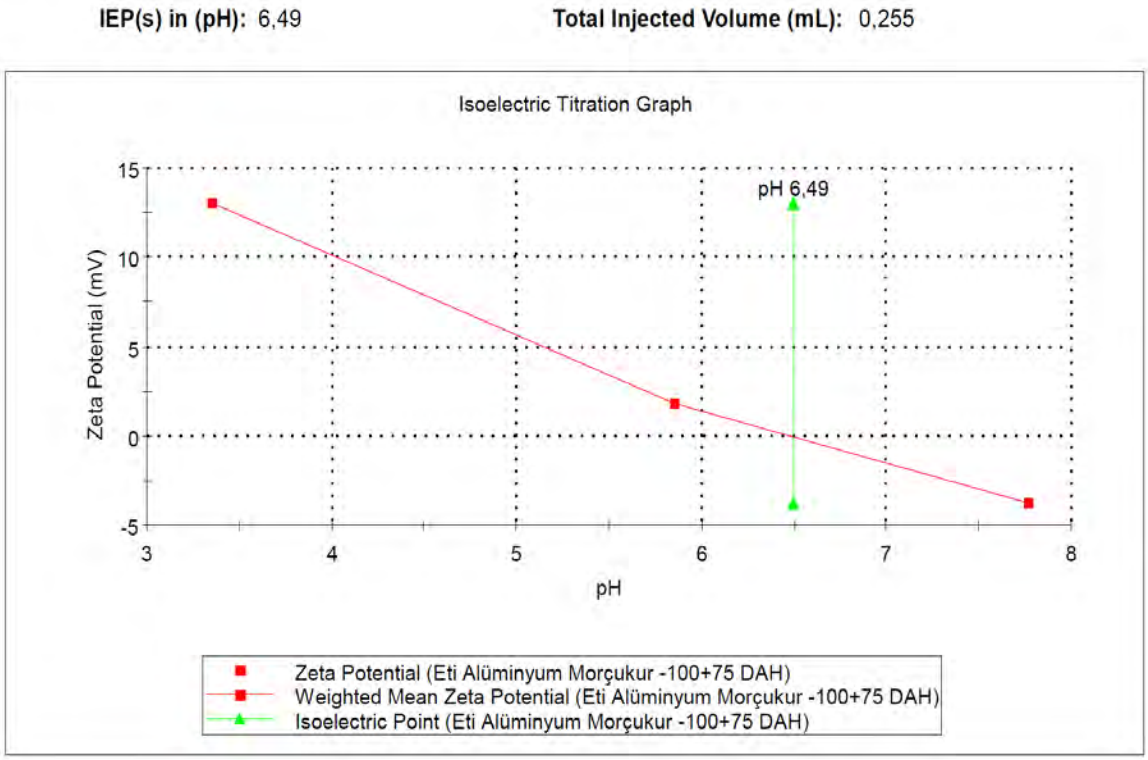

Figure 13. Zeta potential measurements at different pH values for DAH in the -0.100+0.075mm size fraction

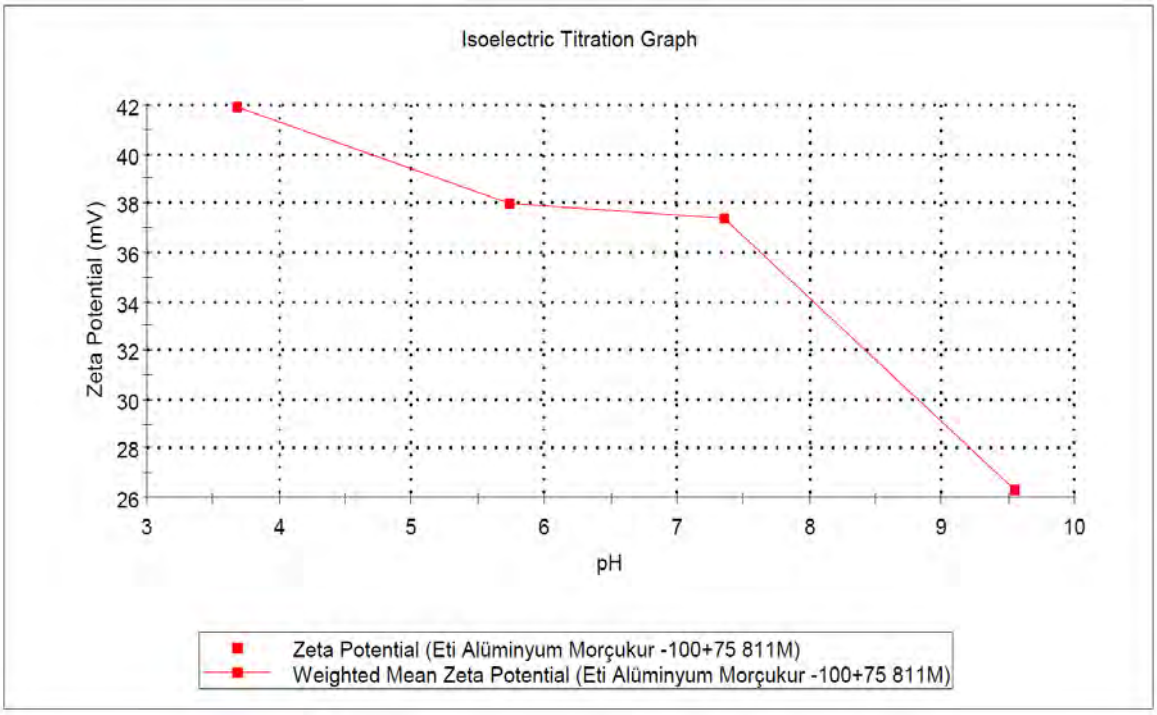

Figure 14. Zeta potential measurements at different pH values for 811 M in the -0.100+0.075mm size fraction

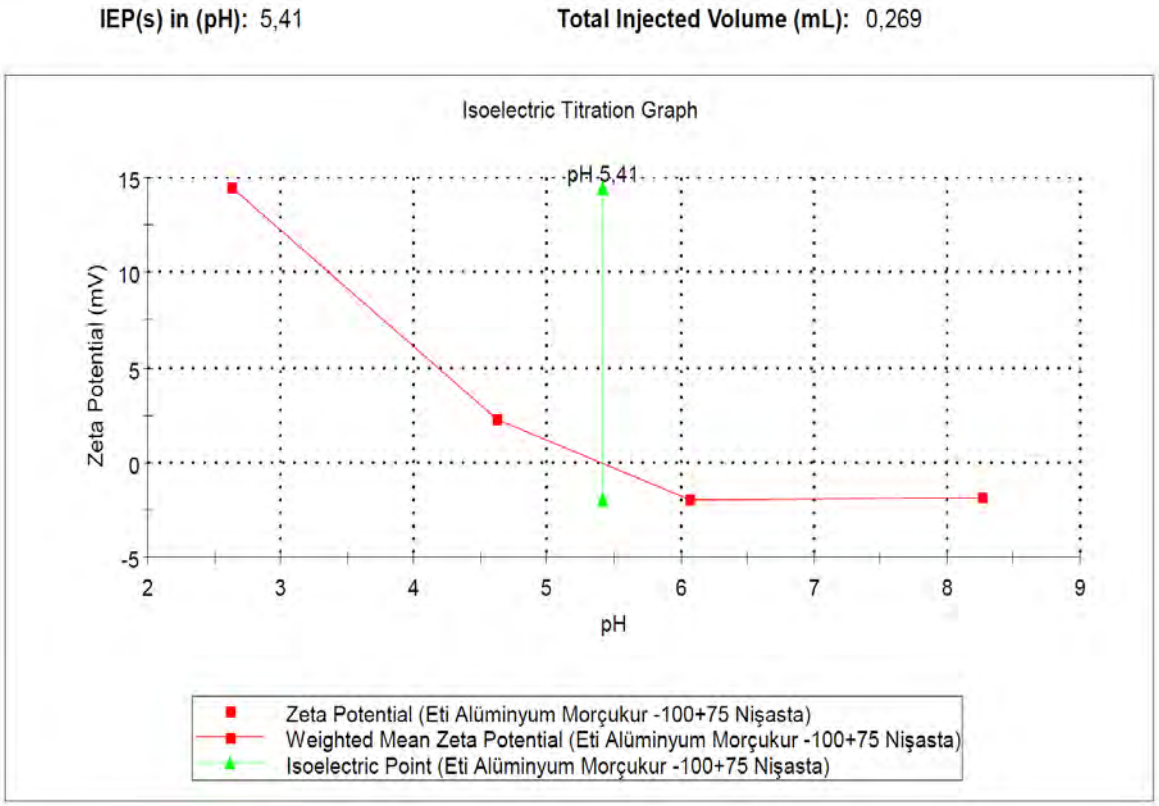

Figure 15. Zeta potential measurements at different pH values for starch in the -0.100+0.075 mm size fraction

In flotation literature, the isolectric point (IEP or iep), which is sometimes used interchangeably with the pH value at which the surface charge is zero, may also be employed instead of the point of zero charge (PZC or pH_pzc). As is known, while PZC is a concept used for the pH value at which the mineral surface carries no charge, IEP is defined as the negative logarithm of the potential-determining ion concentration in solution when the mineral's zeta potential is zero (Somasundaran, 1975; Fuerstenau, 2005).

For successful flotation, mineral particles within the pulp must remain dispersed at a certain distance from one another, a condition that is related to the minerals' zeta potentials and the resulting electrical double layer (EDL) thickness. Only particles with high zeta potentials and, consequently, thick EDLs can maintain sufficient separation from each other.

When the zeta potential is around ±30 mV, the EDL surrounding the minerals begins to compress, and as a result, the behavior of particles in the pulp becomes unstable. As the pulp pH approaches the PZC, London-van der Waals forces become dominant over the particles, making it possible for the particles to approach each other more closely. If the minerals' zeta potential is between ±10 mV, the complete collapse of the EDL around the particles leads to aggregation (coagulation), which adversely affects flotation performance significantly (Hu et al., 2003; Zhao et al., 2003).

Diasporic bauxite ores (diaspora is naturally hydrophilic) possess a low Al/Si mass ratio, and extensive grinding must be performed on the ore to liberate valuable and gang minerals and prepare them for selective interaction with reagents (direct and reverse flotation). It has been reported that diaspora particles as coarse as 0.297 mm (Massola et al., 2009) and finer than -0.037 mm will attach to bubbles provided that mineral monomer liberation is achieved. However, the structural complexity of aluminosilicates presents significant challenges in obtaining an appropriate liberation size and recovering diaspora from the ore; in diaspora

flotation, fine particles are typically clay minerals (mostly kaolinite) (Jiang et al., 2010; Xia et al., 2009).

In oxide flotation, collector adsorption is primarily controlled by the electrical double layer on the mineral surfaces. Therefore, the surface electrical charge of diaspora and associated minerals, and particularly the isoelectric point (IEP), are the most important keys for the improvement process through flotation (Laitinen et al., 2016). The surface electrical charge of diaspora can change through OH^- adsorption or H^+ dissociation (Equation (1)), and in this case, the surface becomes hydroxylated in water (Hao et al., 2011).

Various studies have shown that the IEP of diaspora in deionized water and in the absence of flotation reagents is pH 5–7.5, which is higher than that of associated aluminosilicates (Yu et al., 2016; Deng et al., 2015; Jiang et al., 2010). The variation in diaspora IEP can be explained by the presence of silicate impurities (Hu et al., 2003). Yu-lin et al. (2011) reported that in the presence of 5×10^{-4} mol/L cations Ca^{2+}, Mg^{2+}, and Na^+, the IEP of diaspora could shift from 7.2 to 4.5, 8, and 6.8, respectively. Kaolinite, illite, and pyrophyllite have similar chemical compositions, suggesting a similar IEP that is negatively charged over a wide pH range (IEP is mostly below pH 4). The higher IEP value of diaspora compared to aluminosilicates reflects the higher number of Al–O sites on the diaspora surface compared to the higher number of Si–O sites on the surface of associated minerals (Jiang et al., 2010). On the other hand, there is a negative relationship between IEP and SiO_2 content (% by weight) and a positive mutual correlation between IEP and Al_2O_3 content (% by weight) in the diaspora flotation system (Hu et al., 2003).

The surface electrical charge of diaspora (and typically associated minerals) is positive at pH below the IEP and negative at pH above the IEP (Feng et al., 2009; Deng et al., 2015; Yu-hua et al., 2008; Li et al., 2010; Laitinen et al., 2016; Hai-pu et al., 2010; Yuhua et al., 2003; Zhao et al., 2003). Since the IEP is dependent on pH adjustments, the presence of reagents can potentially affect the solution pH and interactions on mineral surfaces can influence the IEP. Reactions between ionic reagents and ions on the diaspora surface are effective through hydrogen bonds (Xia et al., 2009). Generally, it has been reported that anionic collectors significantly reduce the IEP of diaspora to below pH 4, whereas this decrease is negligible for kaolinite (from pH ~4 to ~3.5). Furthermore, various studies have shown that cationic collectors can shift the electrical charge on the diaspora surface to more positive values; this shift is significant for kaolinite (IEP at pH > 8) (Yuhua et al., 2003; Zhao et al., 2003).

Following all these literature evaluations, zeta potential measurements conducted with collectors revealed that oleic acid and 811 M collectors increased the ion concentration on particle surfaces. Here, if the collector had interacted with diaspora, the zeta potential would have decreased and, naturally, the IEP would also have decreased. It is understood from this that oleic acid would be the most effective collector (Fuerstenau, 2005; Laitinen et al., 2016).

4. CONCLUSION

The pulp pH is one of the most critical parameters determining flotation selectivity in the removal of calcium-origin minerals (particularly calcite and dolomite) from diaspora ores. This process generally yields more successful results under acidic pH conditions.

From a mineral surface chemistry perspective, the surface properties of calcium-containing minerals are highly sensitive to pH variations. In acidic environments (typically in the pH 3–5 range), carbonate ions present on the surface of Ca-minerals such as calcite and dolomite partially dissolve, leading to the exposure of Ca^{2+} ions on the surface. This condition facilitates stronger adsorption of anionic collectors (e.g., SLS or oleate-type reagents) onto calcium

minerals. Consequently, these minerals become hydrophobic and transfer to the froth phase, enabling their removal from the pulp via flotation.

In contrast, diaspora is an aluminum oxyhydroxide mineral with the AlO-OH structure, and under acidic pH conditions, its surface generally exhibits less hydrophobic behavior or displays weaker interaction with the reagents employed. This situation ensures that diaspora remains depressed and is retained in concentration during flotation. Thus, during the flotation operation, while Ca-minerals report to the froth product, diaspora is obtained as the enriched product.

In alkaline environments, however, the situation differs. At elevated pH values (pH > 8), $Ca(OH)_2$ formation or surface passivation may occur on calcite and dolomite surfaces. This condition reduces collector adsorption onto the mineral surface, thereby decreasing flotation recovery. Furthermore, in alkaline media, the interaction of the diaspora surface with certain reagents may increase, potentially leading to reduced selectivity.

REFERENCES

Deng, L., Wang, H., Deng, J., Huang, B., (2015) “Flotation behavior and mechanism of phenyl phosphonic acid in separation of diaspore and kaolinite”, Transactions of Nonferrous Metals Society of China, 25 (6) 2015-2022.

Feng, Q., Zhao, S., Wen, S., Cao, Q., (2009) “Activation mechanism of lead ions in the flotation of ilmenite using sodium oleate”, International Journal of Mineral Processing, 93 (1) 79-83.

Fuerstenau, M. C., (2005), Froth Flotation, A Century of Innovation, SME (Society for Mining, Metallurgy, and Exploration).

Hai-pu, L., Jian-wei, L., Dian-zuo, W., (2010) “Flotation separation of diaspore from kaolinite, pyrophyllite and illite using three cationic collectors”, Minerals Engineering, 23 (1) 1-7.

Hao, H., Li, L., Yuan, Z., Liu, M., Zhang, Y., (2011) “Flotation of kaolinite and diaspore with hexadecyl dimethyl benzyl ammonium chloride”, Mining Science and Technology (China), 21 (5) 665-669.

Hu, Y., He, P., Zhang, Z., (2003) “Electrokinetic behavior and flotation of kaolinite in CTAB solutions”, Minerals Engineering, 16 (11) 1221-1223.

Jiang, L., Zhang, Y., Xu, L., (2010) “Flotation of aluminosilicate minerals using alkylguanidine collectors”, Mining Science and Technology (China), 20 (4) 588-593.

Laitinen, O., Häkkinen, A., Heiskanen, K., (2016) “Electrokinetic flotation of diasporic bauxite”, Minerals Engineering, 92 36-43.

Li, H., Li, S., Zhang, Q., (2010) “Flotation separation of diaspore from kaolinite, pyrophyllite and illite using three cationic collectors”, Mining Science and Technology (China), 20 (3) 436-440.

Massola, C. P., Chaves, A. P., Lima, J. R. B., (2009) “Flotation of diasporic-bauxite ore with a new amphoteric collector”, Proceedings of the VI International Mineral Processing Seminar, 283-292.

Somasundaran, P., (1975), Interfacial Chemistry of Particulate Flotation, Advances in Interfacial Phenomena of Particulate/Solution/Gas Systems, Applications to Flotation Research, 47-79.

Xia, L., Wang, J., Wang, Y., (2009) “Flotation of kaolinite and diaspore with hexadecyl dimethyl benzyl ammonium chloride”, Mining Science and Technology, 19 (6) 766-770.

Yu-hua, W., Jian-wei, L., Dian-zuo, W., (2008) “Flotation of kaolinite and diaspore with hexadecyl trimethyl ammonium bromide”, Journal of China University of Mining and Technology, 18 (3) 422-425.

Yu-lin, X., Yong, H., Xue-lan, Z., (2011) “Effect of metal ions on zeta potential of diaspore”, Journal of Central South University (Science and Technology), 42 (8) 2241-2246.

Yu, R., Zheng, S., Zhang, Y., (2016) “Flotation separation of diaspore from aluminosilicates using dodecyl tertiary amine”, Journal of Central South University, 23 (6) 1359-1365.

Yuhua, W., Jianwei, L., Dianzuo, W., (2003) “Flotation separation of diaspore from kaolinite, pyrophyllite and illite using three cationic collectors”, Journal of China University of Mining and Technology, 13 (2) 131-135.

Zhao, S., Feng, Q., Zhang, Y., (2003) “Effect of pH on the adsorption of dodecylamine on kaolinite and diaspore”, Journal of Central South University of Technology, 10 (4) 365-369.

THE PETROGRAPHIC CHARACTERIZATION OF THE URANIUM ORE OF TAHAGGART, EL-HOGGAR, SOUTHEAST OF ALGERIA

Zohir MEKTI*, Fatima Zohra BELAID, Assia BOUTEMEDJET, Said BERDOUDI

Laboratory Mineral Resources Valorization and Environment, Badji Mokhtar University, Annaba, Algeria
**Corresponding author: zohir.mekti@univ-annaba.dz*

A B S T R A C T

Algeria has long sought to exploit its uranium deposits in the Hoggar region; whose objective is to market the ore, and why not, use part of the production in the exclusively civil field, especially in electricity generation. The exploitation and valorization of this ore; require a very specific process of exploitation, characterization and treatment. The main objective of this work is to establish a detailed and complete technical data sheet for the Tahaggart deposit, enabling the implementation of a uranium ore mining and beneficiation technique to obtain a marketable product known as "Yellow Cake". To achieve this objective, samples were taken from the site under study, followed by microscopic and macroscopic analyses non-thin sections to obtain petrographic, mineralogical and geochemical identifications. Thus, analysis of samples related to conglomeratic sandstones and alteration facies confirmed the sandstone character of the Tahaggart ore. The determination of chemical elements in the various ore samples also showed the predominance of certain chemical elements: quartz, clays (kaolinite), iron oxides and hydroxides, uranium minerals and rutile. Uranium grades varied from 0.90 to 1.32% in the mineralized altered levels and from 0.34 to 0.74% in the mineralized conglomeratic sandstones. Uranium was also remarkably present in both facies, and was more concentrated in the altered levels. It occurred either in uraniferous minerals with high contents, or with low contents in other minerals such as apatite, zircon, rutile and monazite in trace amounts within their structures.

***Key words**: Uranium, Tahaggart, petrographic characterization, mineralogy and geochemistry, leaching, yellow cake*

1. INTRODUCTION

Originally, uranium was only used as a chemical agent, notably in the ceramics and mirror-making industry (glass coloring), then in the manufacture of high-strength steel (Nilson and al., 2019). In the early 20th century, following Pierre and Marie Curie's work on radioactivity, its ores were an essential source of radium, used to treat cancerous tumors (Rentetzi, 2022). The discovery of nuclear fission by Otto Hahn and Fritz Strassmann in 1938 marked the baptism of nuclear energy and the use of uranium as a fuel element (Reed, 2020). Uranium in metallic form, can also be found as a structural element (counterweight) in aircraft and marine construction, as well as in the military field, for tank armouring and shell manufacture (Lourenco and al., 2016; Carvalho and al., 2023). It can also serve as shielding to protect against ionizing radiation, just like lead (Lourenco et al., 2016). Uranium is the main element used for the manufacture of fuel elements for nuclear reactors (Zerbib, 2024). However, its use goes through several stages of preparation called the nuclear fuel cycle. The first step in this cycle is the exploration, exploitation and valorization of uranium ores. The latter requires a specific treatment process, taking into account the technical sheet of the uranium ore. Algeria has significant mineral reserves, in particular, gold and uranium are the main metals present in Hoggar. Tin, tungsten and tantalum, niobium, and copper indices are also present. There are several uranium deposits identified and not exploited to date: Timgaouine, Abankor, Tinef and Tahaggart. Exploitation of a deposit requires a perfect understanding of its geographical environment, geology and geometry, and for profitable extraction of the raw material and valorization of this resource, in our case uranium in the Tahaggart deposit, it is imperative to

establish a detailed and complete technical data sheet for the uranium ore. The first geological studies were carried out by Joulia (1959), Lessard (1961) and Claret et Tempère (1968), Legrand (1970), Fabre (1971) and Beuf et al (1971), who studied the Paleozoic history of the Saharan platform in the Tassili region or at N'Ahaggar de In Debirène in the southwest and in the TiN-Eggole region in the northeast. Mokadem carried out a study on the uranium mineralization of the Tin Séririne sedimentary basin (Tahaggart deposit and the Tamert-N-Iblis region) in 1980, followed by a study of the alteration of the Precambrian base on the periphery of the basin. In addition, the associated uranium and thoriferous mineralization (Hallalouche, 1995), and a structural study of the Tin Séririne basin using geophysical methods (Bournas, 1998). Algeria began the first prospecting work in the Tin-Séririne basin around the 1970s. The aim of this work was to search for uranium in the northern district of the Algerian-Nigerian uranium province. The Romanian group GEOMIN (1969 – 1975) working on behalf of SONAREM (Société Nationale de Recherche et d'Exploitation Minière) highlighted the Tahaggart uranium deposit and the Timouzeline and Tamert-N-Iblis uranium indices. These mineralized zones were discovered by ground verification of the radiometric anomalies highlighted by the aero-magneto-spectrometric survey at 1/200,000, carried out by the American firm Aéroservice (1971). A reserve estimate has been made for the Tahaggart deposit. A SONAREM team (1976-1977) carried out hydrogeological research work in the Tin Séririne basin. From 1986 to 2005, uranium exploration work was carried out on the eastern and western flanks (Timouzeline and Tamert-N-Iblis) of the Tin-Séririne Basin (CREM, 1986-1991); on its northern and north-western periphery (CREM, 1991-1992), and its southern part (CREM, 1996-1997), as well as evaluation and extension work on the Tahaggart deposit (COMENA (2001-2005). Appreciable results were obtained in the Tin-Séririne basin, notably the identification and confirmation of uranium indices and anomalies. the present work represents a contribution to the enrichment of the Tahaggart uranium ore datasheet, through the petrographic (macro and microscopic), mineralogical and geochemical characterization of the main horizons, represented by the conglomeratic sandstones and alteration facies of which they are composed.

2. SITE DESCRIPTION

The Tahaggart uranium deposit is located 350 km southeast of Tamanrasset in the Tin Séririne basin in extreme southeastern of Algeria; close to the Niger border (Rabia-Zaourar, 1978; Badahmaoui et al., 2020) (fig. 1). This desert region is characterized by very low human density, with altitudes ranging from 1,000m in the north, to 400m in the south on the Algerian-Nigerian border. Temperatures ranging from 40-45°C (April to July) and from 13 to 11°C (January to February), very little rainfall, vegetation limited to wadi beds, and fauna specific to desert zones (Chahdane 2009; Khaldi et al., 2018).

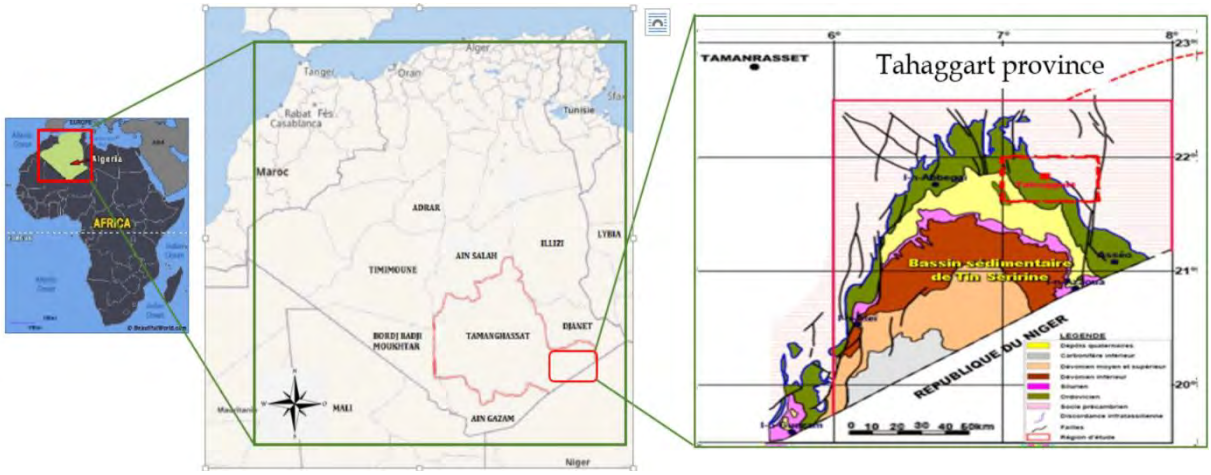

Figure 1. Location map of study

It is located at the crystalline basement-Paleozoic sedimentary cover contact, with global uranium reserves estimated at 8,105t of ore grading 0.215% U, or 1,700 tonnes of U metal (Allek et al., 2013). It occurs as subhorizontal mineralized lenses 1 to 8 m thick hosted in altered Precambrian basement gneisses and Cambro-Ordovician basal conglomerates (Baadi 2018; Gherbi et al., 2015).

Uranium mineralization, is known at surface and sub-surface depths of 0 to 8 m, and occurs in more or less discontinuous patches (Sanguinetti et al., 2018; Smirnov et al., 2018). The uranium ore essentially contains secondary uranium minerals (utunite, torbernite), associated with iron oxides (hematite, goethite) and a clay matrix (Hatert et al., 2018). Significant thorium and rare-earth mineralization associated with conglomerates (Bonhoure, 2010; Boni et al., 2023).); is related to primary and secondary minerals (monazite) and alumino-phosphates (grandallite, florencite,brockite). Other secondary uraniferous minerals include carnotite, sabugalite and uranophane (Chahdane, 2009).

3. MATERIALS AND CHARACTERIZATION METHODS

In order to the samples were taken to cover most of the region studied. The diameter of the collected pieces varies from 0 to 250 mm; they are taken from conglomeratic sandstone ores and altered facies, then the diameter of the pieces of rocks was reduced using a hammer to sizes which do not exceed 90 mm. The pieces obtained from conglomeratic sandstone ore are intended for macroscopic observation with the naked eye, while microscopic observation was carried out using a Leica binocular optical microscope. Samples were selected to prepare thin sections of uranium ore. To determine the chemical composition of the rocks; 19 samples were taken, 9 from conglomeratic sandstones and 10 from mineralized alteration rock, each sample was crushed using a Model HERZOG disc crusher, then mixed and divided by quartering technique, to obtain a representative sample. Prior to FRX analysis, all samples were pulverized using a Model SIEBTECHNIK pulverizer. Preparation of the thin section for microscopic and petrographic study involved the following stages: the ore rock was cut by a BROTLAB diamond disk saw, then the samples were ground in a BROTLAB automatic diamond-grinding machine, followed by manual polishing, and finally GBS1 resin was used to bond the resulting section to special glass chips. The prepared thin sections were placed on the stage of a polarizing optical microscope (Leitz PoL 12 in PLNA in APL). The chemical composition was determined by X-ray fluorescence analysis, using a portable X-ray fluorescence spectrometer (Thermo Ficher-Niton xl3t Golddt+). This analysis made it possible to obtain for each type of sample, its chemical composition and the content of each chemical element.

4. MACROSCOPIC STUDY OF URANIUM ORE ASSOCIATED WITH CONGLOMERATIC SANDSTONES

Macroscopic observation of conglomeratic sandstones reveals the presence of 06 arenas (Fig. 2). The first facies, Uranium-mineralized alteration arena, has a ferruginous clay-quartz matrix.

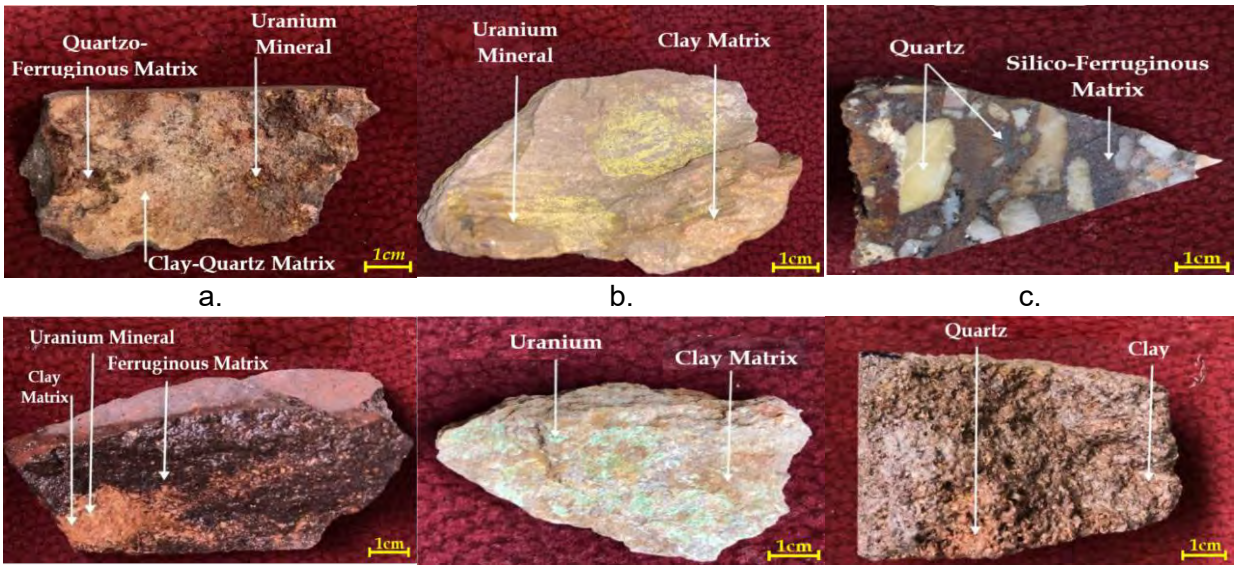

Figure 2. Macroscopic observation of conglomeratic sandstones

This matrix is composed of clays and quartz grains of size varying between 1mm and a few microns, impregnated with reddish iron oxides. Within this matrix appear yellowish uranium minerals (Fig. 2a). The second arena is mineralized clay, essentially composed of a whitish-gray clay matrix containing 1-2 mm thick quartz beds and yellow uranium minerals. The latter appear as coatings plated onto the matrix (Fig. 2b). In the mineralized microconglomerate arena within a silico-ferruginous matrix, centimetric to millimetric quartz grains appear, whitish to grayish in color. These quartz grains are generally xenomorphic and angular, and sometimes sub-rounded. A few yellowish uranium minerals appear in the ferruginous matrix (Fig. 2c). About the mineralized ferruginous arena: in addition to a ferruginous-clay matrix, it is also composed of clay pockets containing a few disseminated grains of uranium (Fig. 2d). Greenish uranium minerals sometimes permeate these schistose planes (Fig. 2e). The last arena is the quartz-clay arena. Within this whitish clay matrix, there are agglomerations and sheaves of whitish to grayish quartz grains (Fig. 2f). Under Leica binocular microscope in direct light, the different observed matrices of the samples studied are:

- A quarto-ferruginous matrix with small fine millimeter to micrometer quartz grains (Fig. 3a).
- A clay-ferruginous matrix with green uranium films (Fig 3b);
- A quartz-ferruginous matrix with uranium grains scattered everywhere and sometimes iron oxides coated with clays (Fig 3c);
- A clay-iron matrix, with clay particles in the form of microveins intercalated between quartz and iron oxide (Fig 3d).

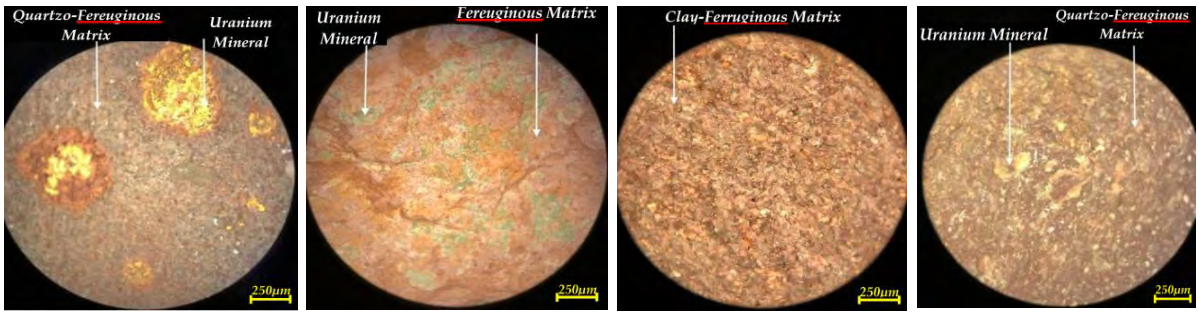

Figure 3. Microscopic observation of matrices (x40)

5. PETROGRAPHIC STUDY OF CONGLOMERATIC SANDSTONES IN THIN SECTIONS

In polarized light not analyzed (PLNA), conglomeratic sandstones are composed of Quartz, in the form of grains of various sizes (millimeter to micrometer) (fig. 4). These grains are rounded and sub-rounded and sometimes sub-automorphic. Quartz is often surrounded by discontinuous halos of secondary silica. It is also fissured, and the micro-fissures are sometimes filled with iron oxides and uranium minerals (Fig. 4a). *Iron oxides*, these are abundant, appearing as fillers in interstices and intergranular spaces, as well as in micro-fissures in quartz grains. Two generations of iron oxides are present. These oxides also imprint on the clay minerals present in the inter-granular spaces (Fig. 4b). *Clay minerals*, they are not abundant and appear in the intergranular spaces often impregnated with iron oxides, and appear in small aggregates and in the form of small vermicular. According to studies carried out by Hallalouche, 1995 and Chahdane, 2009, these clays appear only as kaolinite (Fig. 4c). Accessory minerals, they occupy the intergranular spaces and appear as crystals of zircon and monazite (Fig. 4d). Uranium minerals, in the Tahaggart ore, these minerals are found mainly in carnotite ($K_2(UO_2)2(VO_4)_2.3H_2O$) and autunite ($Ca(UO_2)_2(PO_4)_2.10\text{-}12H_2O$) (Mokadem, 1980, Hallalouche, 1995, Chahdane, 2009) also reported the presence of weeksite ($(K_2(UO_2)_2Si_6O_{15}.4(H_2O))$) (fig. 5).

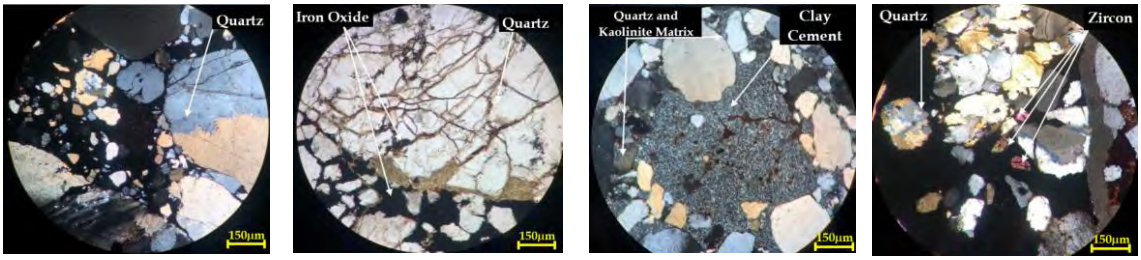

a b c d

Figure 4. Minerals in conglomeratic sandstones

Note that uranium ores contain yellow to golden-yellow minerals (in polarized light analyzed by PLA), sometimes canary-yellow, filling micro-fissures in quartz and surrounding its grains, and appearing as small aggregates in the inter-granular spaces (Frankland et al., 2022; Aissa et al., 2022).

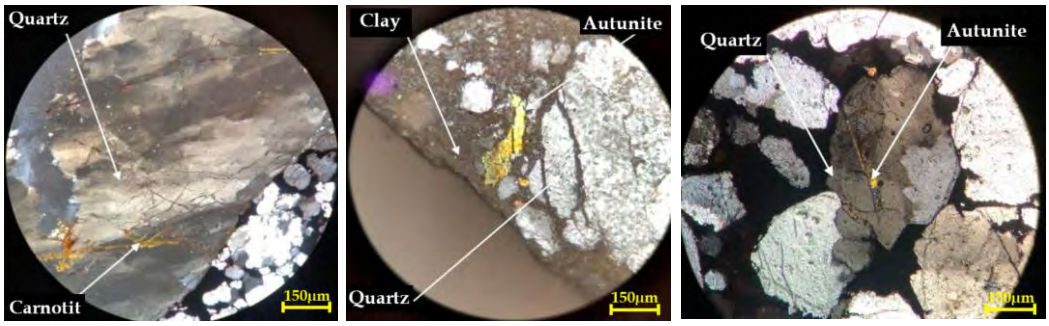

a b c

Figure 5. Uranium minerals in conglomeratic sandstones

6. STUDY OF URANIUM ORE ASSOCIATED WITH CLAY-QUARTZ ALTERATIONS

In this section, we will approach the microscopic study of uranium minerals in mineralized alterations, we find:autunite $Ca(UO_2)_2(PO_4)_2.10\text{-}12H_2O$, golden yellow to lemon yellow fluorescing in green, it occurs as prismatic crystals, flattened tablets and as aggregates

(Frankland, 2020). Autunite often occurs as disseminations within kaolinite, filling microcracks in quartz and as flattened tablets within the clay matrix and in quartz cracks (Fig. 6).

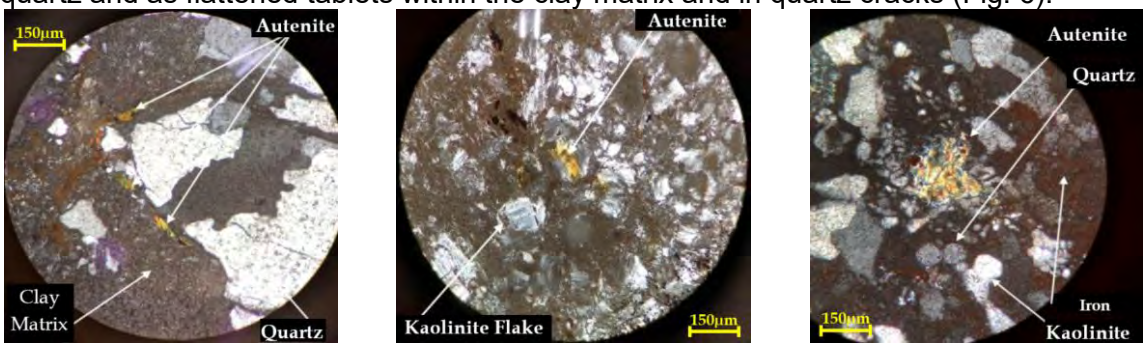

Figure 6. Autunite in the clay matrix

Torbernite $Cu(UO_2)_2(PO_4)_2.12H_2O$, it occurs as veinlets and tablets, with a pale yellow to greenish-yellow color in natural light (NL), and a blue tint in polarized light (PL) (Syczewski, 2023). It also appears as microcrystalline aggregates within the clay matrix and iron oxides, filling fissures, flattened tablets and automorphic crystals (Fig. 7).

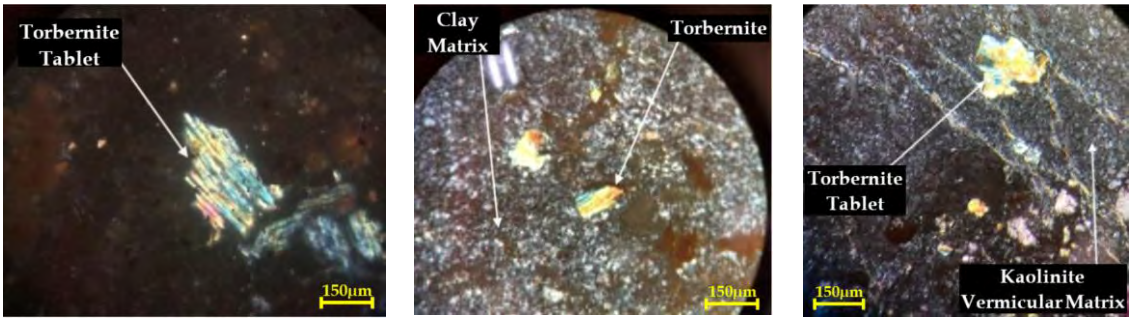

Figure 7. Torbernite in the clay matrix

Metatorbernite $Cu(UO_2)_2(PO_4)_2.8H_2O$, in natural light (NL), this mineral shows pale green, pale blue to colorless hues similar to those of torbernite, with the transition in polarized light (PL) to a dark blue to purplish-blue color (Descostes, 2017) (Fig. 8). It appears as crack filling and in the form of small tablets within the clay matrix. Observation also shows that metatorbernite can be observed on the edges of sheets, and filling the inter-sheet spaces of flakes and packets in the clay matrix (kaolinite).

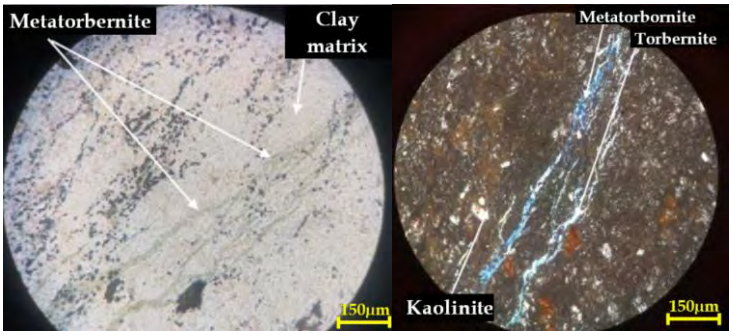

Figure 8. Metatorbernite in clay matrix

7. CHEMICAL CHARACTERIZATION OF TAHAGGART URANIUM ORES

Several Tahaggart ore samples, composed of conglomeratic sandstones and mineralized alteration rocks, have been analyzed by X-Ray fluorescence (XRF). Chemical analysis was

carried, out using a portable X-ray fluorescence spectrometer Thermo Ficher-Niton xl3t Golddt+) (Jarc, 2022), which enabled us to obtain for each type of sample its chemical composition.

7.1. Analysis of Uranium Ore Associated with Conglomeratic Sandstones

7.1.1. Major elements

In samples related to conglomeratic sandstones, silica (SiO_2) remains very abundant and omnipresent. Clays (Al_2O_3) are also quite important in this facies (Table 1 and Fig. 9); magnesium, iron, and potassium are also present in moderate amounts; the other major elements (CaO, VO_2, P_2O_5, TiO_2, etc.) appear at low concentrations.

Table 1. Concentrations of major elements in conglomeratic sandstones (%)

Element	Samp1	Samp2	Samp3	Samp4	Samp5	Samp6	Samp7	Samp8	Samp9
P_2O_5	0,5151	0,5334	0,5135	0,2705	0,0000	0,0012	0,0000	0,0000	0,0879
K_2O	1,5207	12,7147	1,2684	1,0578	0,1273	0,0011	0,0260	0,7057	2,3978
VO_2	0,4118	0,3881	0,3879	0,3748	0,3325	0,0009	0,0511	0,0948	0,0000
Al_2O_3	5,0962	4,9827	4,7962	4,6176	1,0970	0,0005	2,4439	5,6508	0,0395
CaO	1,6432	1,6234	1,5183	1,0844	0,1251	0,0004	0,0298	0,0278	2,2062
TiO_2	0,6943	1,0106	0,7830	0,4519	2,6446	0,0009	0,7953	1,0133	0,0000
SiO_2	37,8529	37,0517	39,4210	53,1192	74,1155	0,0005	84,3836	62,9949	0,0832
Fe_2O_3	8,1733	8,1800	8,4656	7,1862	18,6610	0,0023	10,8930	0,7523	0,0000

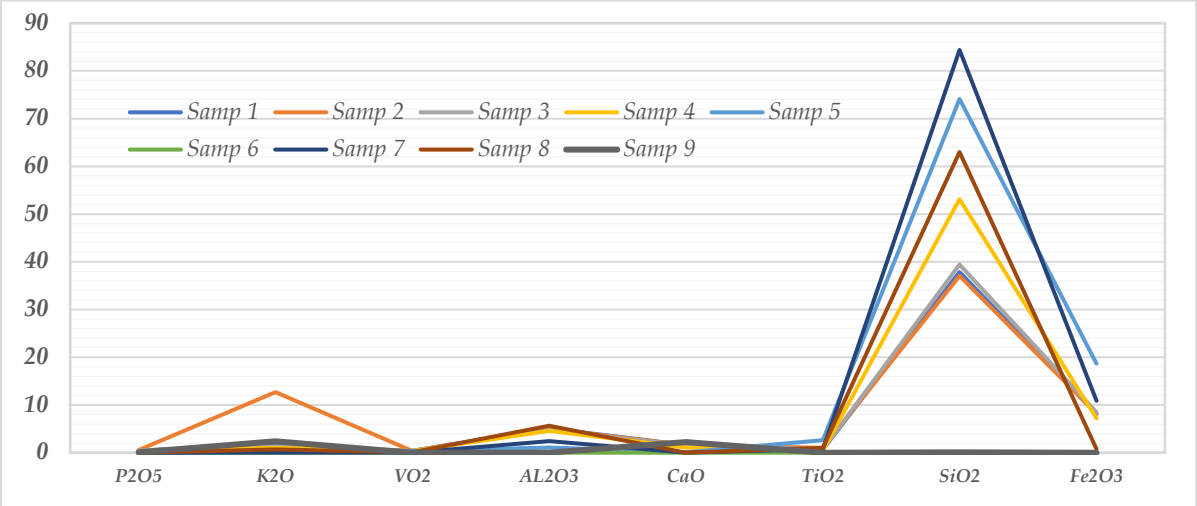

Figure 9. Evolution of concentrations of major elements in conglomeratic sandstones

7.1.2. Trace elements

The results obtained show the presence of uranium with medium to high concentrations and high potassium and vanadium contents in conglomeratic sandstones. These are the uranium minerals manifested, in particular by Carnotite. Zirconium and magnesium are also present but with moderate levels; copper and thorium have very low contents (Table 2 and Fig. 10).

Table 2. Trace element concentrations in conglomeratic sandstones (ppm)

Element	Samp1	Samp2	Samp3	Samp4	Samp5	Samp6	Samp7	Samp8	Samp9
U	5859,72	6432,53	7347,42	6226,62	3385,60	1262,73	59,95	5097,89	5133,29
Zr	280,98	325,85	404,15	249,31	1281,97	115,21	701,43	569,08	1,52
Cu	233,73	246,58	212,05	124,71	0,00	35,19	16,97	12,38	0,00
V	2529,40	2384,13	2382,91	2302,12	2042,56	5,76	314,43	582,80	0,00
K	12624,52	10552,95	10530,05	8782,07	1057,15	9,55	215,90	5858,58	19905,95
Th	9,15	15,10	11,16	9,95	94,17	24,99	37,11	68,93	0,00
Cs	0,00	0,00	0,00	0,00	0,00	2,83	0,00	0,00	0,00
Mg	2209,16	2937,74	2846,20	0,00	0,00	4,29	0,00	2079,66	970,39

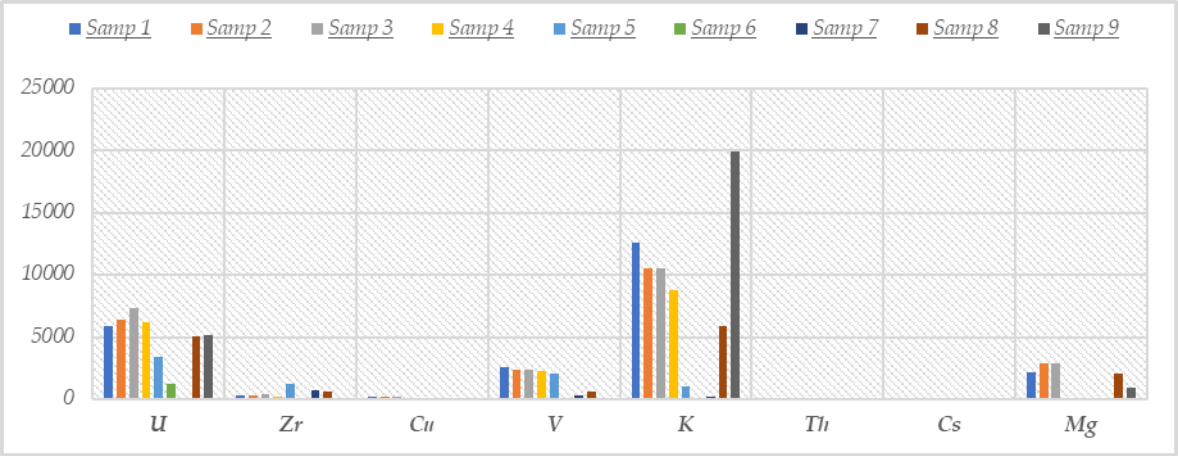

Figure 10. Evolution of concentrations of trace elements in conglomeratic sandstones

7.2. Analysis of Uranium Ore Associated with Clay-Quartz Alterations

7.2.1. Major elements

Silica (SiO_2) is very abundant in clay-quartz alteration samples, with high concentrations of Al_2O_3, associated with clays (Table 3 and Fig. 11); magnesium and iron are also present in moderate quantities, the other major elements (CaO, K_2O,…) are present in very low concentrations.

Table 3. Concentrations of major elements in alteration samples (%)

Element	Samp 1	Samp 2	Samp 3	Samp 4	Samp 5	Samp 6	Samp 7	Samp 8	Samp 9	Samp1 0
Al_2O_3	0,80	13,79	9,19	12,90	14,00	11,70	12,32	15,98	8,54	12,27
CaO	0,18	0,22	0,04	0,07	0,07	0,03	0,05	0,32	0,20	0,07
FeO	3,88	3,25	0,09	0,14	0,12	0,11	1,28	0,23	0,17	0,24
k_2O	4,55	0,69	0,19	0,16	0,05	0,24	0,25	0,47	2,09	0,93
MgO	0,00	0,00	0,00	0,00	0,00	0,00	0,00	0,50	0,25	0,00
P_2O_5	0,10	0,07	0,16	0,27	0,22	0,13	0,13	0,25	0,38	0,32
VO_2	0,00	0,02	0,09	0,02	0,02	0,01	0,01	0,08	0,02	0,08
SiO_2	54,02	44,62	53,61	46,60	50,69	61,81	58,06	38,37	31,59	26,41
TiO_2	0,51	0,85	0,36	0,36	0,25	0,26	0,45	2,22	0,67	1,87

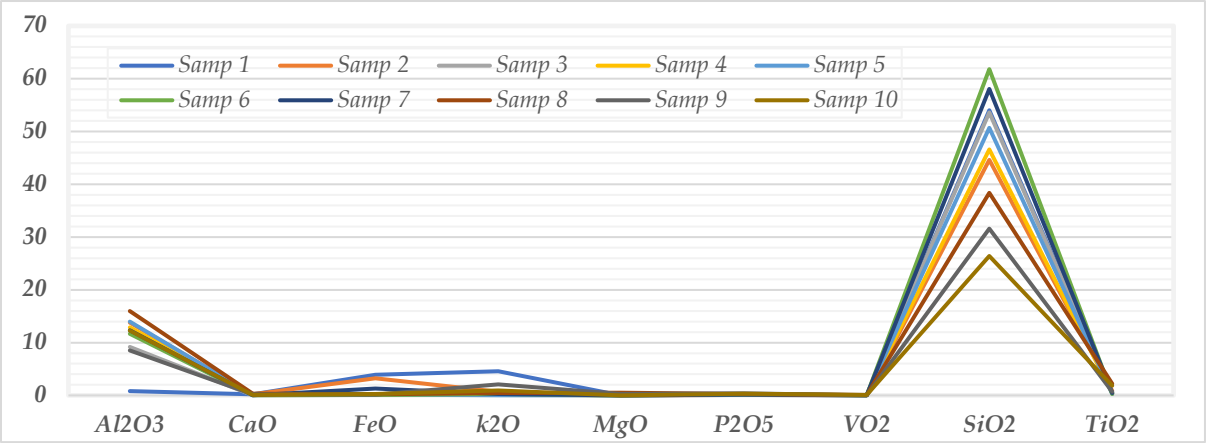

Figure 11. Evolution of concentrations of major elements in alteration samples

7.2.2. Trace elements

Table 4 and fig. 12 show a variation in Uranium concentrations in the various samples. There are highly mineralized alterations (Samp 9 and Samp 10), moderately mineralized alterations (Samp 5) and weakly or non-mineralized alterations. Vanadium is also present with Uranium in the alteration profile. Zr levels reflect the abundance of Zircon in altered facies. A relatively low Th content is recorded. Other chemical elements, such as Copper (Samp 10), clearly indicate the phenomena and intensity of alteration.

Table 4. Trace element concentrations in alteration samples (ppm)

Element	Samp1	Samp2	Samp3	Samp4	Samp5	Samp6	Samp7	Samp8	Samp9	Samp10
U	9,88	84,26	127,31	537,23	1061,35	372,60	471,63	452,49	13194	9013,4
Zr	198,22	203,89	177,38	125,40	86,09	99,67	135,35	104,01	152,61	143,1
Cu	21,13	31,14	0,00	0,00	7,32	0,00	0,00	107,88	60,06	1050,9
V	30,21	115,71	55,78	111,92	138,85	55,99	77,49	469,80	136,15	463,8
Th	10,78	12,59	20,73	23,47	18,92	18,91	22,04	0,00	0,00	6,25
Cs	57,43	25,62	10,68	0,00	0,00	0,00	0,00	0,00	0,00	0,00

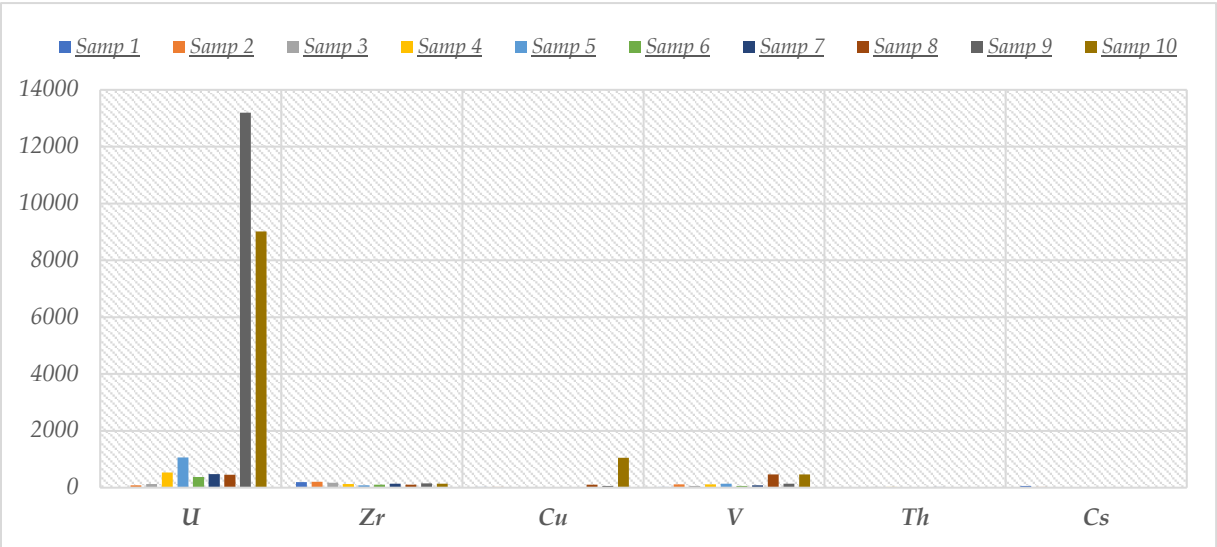

Figure 12. Evolution of trace element concentrations in the alteration samples

Based on the analysis of samples from conglomeratic sandstones and altered facies we can conclude that three main chemical elements predominate in Tahaggart ore: silica, iron and aluminum; corresponding to sandstone and clay formations where iron is present at all levels with variable concentrations. It is richest in the conglomeratic sandstones, which are at the top of the series, compared with the altered rocks in the lower part. The other chemical elements, with varying grades in both facies, are generally associated with typical uranium minerals and accessory minerals (quartz, rutile, zircon and monazite...) present in the Tahaggart ore. Uranium, the element of interest, is found in high concentrations in both facies. Uranium levels are higher in the alteration levels than in the conglomeratic sandstones.

8. INTERPRETATION AND SYNTHESIS OF ANALYTICAL RESULTS

The results of analyses carried out on the various samples of Tahaggart uranium ores show the predominance of certain chemical elements over others. These elements correspond perfectly to the chemical compositions of the dominant mineral phases observed under the optical microscope (petrographic study), namely: quartz, clays (kaolinite), Iron oxides and hydroxides, uranium minerals and rutile. In summary, analysis of samples from conglomeratic sandstones and alteration facies shows that silica predominates over other Tahaggart ore components, with iron oxides and hydroxides more abundant in conglomeratic sandstones than in alteration facies. Clays are also present in alteration-related facies and to a lesser extent in conglomeratic sandstones, which they appear as cement (matrix).

Carbonates, vanadates and phosphates and other chemical elements are present in small proportions in both facies and are generally bound to uranium and other minerals containing traces of uranium in their structures: carnotite, autunite, torbernite, metatorbernite (uranium minerals) and apatite, zircon, rutile and monazite (accessory minerals). Uranium grades in the Tahaggart deposit are significant, with 0.90 to 1.32% in the mineralized altered levels and 0.34 and 0.74% in the mineralized conglomeratic sandstones. Uranium is remarkably present in both facies, and is more concentrated in the altered levels. It is either associated with uranium-bearing minerals with high grades, or with lower grades in other minerals (apatite, zircon, rutile and monazite).

9. CONCLUSION

The petrographic (macro and microscopic) mineralogical and geochemical characterization of the main ore horizons; represented by the conglomeratic sandstones, and the alteration facies of which they are composed after synthesizing the results and overall data from the Tahaggart deposit, revealed the following; The Tahaggart uranium ore contains mainly secondary uranium-bearing minerals of autunite and torbernite, associated with iron oxides (hematite and goethite) and a clay matrix (kaolinite). The presence of significant thorium and rare-earth mineralization; enclosed in a reddish ordovician conglomerate. There are also other uranium-bearing secondary minerals such as carnotite, Sabugalite and uranophane. Silica predominates over the other components of Tahaggart ore, confirming its sandstone character, with the presence of iron oxides and hydroxides, which are more abundant in conglomeratic sandstones than in alteration levels. Clays are also present in alteration-related facies, and to a lesser extent in conglomeratic sandstones, where they act as cement (matrix). Carbonates, vanadates and phosphates, and other chemical elements, are present in small proportions in both facies, and are generally associated with uranium-bearing minerals, and other minerals containing traces of uranium in their structures. Uranium grades are high (0.90 to 1.32% in the mineralized altered levels and 0.34 to 0.74% in the mineralized conglomeratic sandstones).

ACKNOWLEDGMENTS

The authors express their gratitude to the Laboratory of Draria Nuclear Research Center National in Algiers, as well as to the Laboratory for the Valorization of Mineral Resources and Environment LAVAMINE, at the University of Annaba, Algeria, for their support in carrying out this research study.

REFERENCES

Aissa, D. E., Boutaleb, A., Groucene, C., Amieur, M., Cherfi, Y., (2022), “Typologie et hiérarchisation des minéralisations de terres rares en Algérie”, Third International Symposium on the Geology of the Maghrebides Chain and Adjacent Areas, Setif University, No. 3, Vol. 6, p. 2022.

Allek, K., Hamoudi, M., Bouguern, A., Boubaya, D., (2013), “Integrating regional magnetic and radiometric airborne data of Asseo area, Hoggar, Algeria, using neural network analysis to the recognition of probable uranium accumulation”, 9th EAGE International Scientific and Practical Conference and Exhibition on Engineering and Mining Geophysics, European Association of Geoscientists & Engineers. DOI: https://doi.org/10.3997/2214-4609.20142529

Baadi, R., (2018), “Contribution à l’étude géologique et géophysique du gisement aurifère d’In Abeggui (Hoggar central-sud algérien)”, Doctoral dissertation. https://dspace.univ-ouargla.dz/jspui/handle/123456789/17508

Badahmaoui, T., Bugrieva, E. P., Lavrukhin, A. A., (2020), “Characteristics of uranium mineralization in the Tin-Seririne sedimentary basin (Algeria)”, Journal of Physics: Conference Series, 1689 (1), 012050. DOI: 10.1088/1742-6596/1689/1/012050

Beuf, S., Bennacef, A., Biju-Duval, B., De Charpal, O., Gabriel, O., Rognon, P., (1968), “Les grands ensembles sédimentaires du Paléozoïque inférieur du Sahara”, C.R. Somm. Géol. Fr., Paris, fasc. 8, 206. http://pascal-francis.inist.fr/vibad/index.php?action=getRecordDetail&idt=GEODEBRGM6911005363

Bonhoure, J., (2010), “Géochimie des éléments de terres rares et du plomb dans les oxydes d'uranium naturels”, Éditions Universitaires Européennes. https://hal.univ-lorraine.fr/tel-01752855

Boni, M., Bouabdellah, M., Boukirou, W., Putzolu, F., Mondillo, N., (2023), “Vanadium ore resources of the African continent: State of the Art”, Ore Geology Reviews, 157, 105423. https://doi.org/10.1016/j.oregeorev.2023.105423

Bournas, N., (1998), “Étude structurale du bassin sédimentaire de Tin-Séririne (Hoggar) par les méthodes géophysiques”, Thèse de magister, USTHB Alger, 123 p.

Carvalho, F. P., Fesenko, S., Harbottle, A. R., Lavrova, T., Mitchell, N. G., Payne, T. E., Yankovich, T. L., (2023), “The environmental behaviour of uranium”. https://apo.ansto.gov.au/handle/10238/15301

Chahdane, R., (2009), “Contribution à l'étude géologique et gîtologique des minéralisations uranifères de Tahaggart (Sud-Est du Hoggar)”, Dissertation, Alger.

Claret, Tempère., (1968), “Le paléozoïque du bassin de Tamsena (Sud de l'Ahaggar)”, Z. Dtsch. Geol. Gesellsh., 117, 460–468.

Comena., (2002–2003), “Evaluation et extension des ressources uranifères de Tahaggart, Sud-Est du Hoggar”, Rapport 4: Résultats des travaux d'exploration des ressources uranifères de Tahaggart (Tassili Oua-N'Ahaggar, Sud-Est du Hoggar), Rapport inédit.

CREM., (1986–1987), “Travaux de cartographie de la feuille Asséo, Partie Nord – zone de Tahaggart”.

CREM., (1991), “Levé géologique et recherche de minéralisations uranifères dans le bassin de Tin Séririne (Asséo)”, Rapport de synthèse, inédit.

CREM., (1997), “Synthèse des travaux de prospection géologique et géophysique dans le bassin sédimentaire de Tin Séririné, Tassili Oua N'Ahaggar, Sud-Est du Hoggar”, Rapport inédit.

Descostes, M., (2017), “Géochimie des milieux naturels anthropisés”, Doctoral dissertation, Université de Poitiers.

Fabre, J., (1971), “Structure de l’Algérie Saharienne: éléments pour une carte tectonique”, Publications Service Géologique Algérie, No. 41, 161–185. http://pascal-francis.inist.fr/vibad/index.php?action=getRecordDetail&idt=PASCALGEODEBRGM73225239

Frankland, V. L., Milodowski, A. E., Read, D., (2020), “Characterisation of meta-autunite: Towards identifying potential alteration products of spent nuclear fuel”, Applied Geochemistry, 123, 104792. https://doi.org/10.1016/j.apgeochem.2020.104792

Gherbi, R., Becis, A., (2015), “Fractional factorial design for studying uranium carbonate leaching of Tahaggart's ore”, International Journal of Mineral Processing, 143, 59–64. https://doi.org/10.1016/j.minpro.2015.09.001

Grison, S., Souidi, M., (2020), “Du métabolome à l’épigénome : exemple d’étude multi-omique sur les effets des expositions à faibles doses d’uranium”, Environnement, Risques & Santé, 19 (5), 339–348.

Hallalouche, D., (1995), “Étude de l'altération du socle précambrien à la périphérie du bassin de Tin-Séririne (Hoggar-Sud, Algérie) et minéralisations uranifères et thorifères associées”, Thèse Doctorat, Université de Rennes I, 222 p. http://pascal-francis.inist.fr/vibad/index.php?action=getRecordDetail&idt=167750

Hatert, F., Fabrice, D. B., (2018), “Les minéraux d’uranium”, Bulletin de la Société Royale des Sciences de Liège, 87. https://orbi.uliege.be/bitstream/2268/245864/1/Min%C3%A9raux%20radioactifs-SRSL-2018.pdf

Jarc, S., (2022), “Statistical approach to interpretation of geochemical data of stream sediment in Pleše mining area”, Geologija, 65 (2), 225–235. https://doi.org/10.5474/geologija.2022.013

Joulia, F., (1959), “Les séries primaires au Nord et au Nord-Ouest de l’Aïr (Sahar central), discordances observées”, Bulletin de la Société Géologique de France, (7), I, 192–193. https://doi.org/10.2113/gssgfbull.S7-I.2.192

Joulia, F., (1959), “Précisions sur la discordance cambro-ordovicienne d’In Azaoua (Niger)”, C.R. Somm. Soc. Géol. Fr., 177–178.

Khaldi, A., (2005), “La stratigraphie séquentielle du Paléozoïque de la bordure méridionale du Hoggar (Région de Tin Séririne, Tassili Oua N’Ahaggar): application à l’exploration minérale”, Séminaire Géologie et Métallogénie des Massifs du Hoggar et Eglabes, p. 81.

Khaldi, A., Mokhtar, S. A., (2018), “Application of UNFC to Uranium Resources Discovered in Algeria”, IAEA-CN-261. https://media.superevent.com/documents/20180619/7f1e92530adbe be8859f74f54190f6ef/cn_261-uram2018-book-of-abstracts.pdf

Lessard., (1961), “Les séries primaires des tassilis Oua-N-Ahaggar, au Sud du Hoggar entre l’Aïr et l’Adrar des Iforas (Sahara méridional)”, Bulletin de la Société Géologique de France, 7 (III), 501–513. https://doi.org/10.2113/gssgfbull.S7-III.5.501

Lourenco, J., Mendo, S., Pereira, R., (2016), “Radioactively contaminated areas: Bioindicator species and biomarkers of effect in an early warning scheme for a preliminary risk assessment”, Journal of Hazardous Materials, 317, 503–542. https://doi.org/10.1016/j.jhazmat.2016.06.020

Mokaddem, M., (1980), “Le bassin sédimentaire de Tin-Séririne et ses minéralisations uranifères (Hoggar-Algérie)”, Thèse Doctorat 3ème cycle, vol. 9, No. 3/4, pp. 401–412. http://pascal-francis.inist.fr/vibad/index.php?action=getRecordDetail&idt=6523539

Nelson, A., Getley, S., Spalding, D., (2019), “Assessment of Technology for Additive Manufacturing of Ceramic Nuclear Fuels”, ORNL, 1311. https://tcr.ornl.gov/wp-content/uploads/2021/07/M3CT-19OR06090131-Final.pdf

Rabia-Zaourar, C., (1978), “Fragmentation, classification et enrichissement des minerais d'uranium de Tahaggart”, Doctoral dissertation, Alger.

Reed, B. C., (2020), Manhattan Project: The Story of the Century, Springer Nature. http://doi.org/1007/978-3-030-45734-1

Rentetzi, M., (2022), Seduced by Radium: How Industry Transformed Science in the American Marketplace, University of Pittsburgh Press.

Sabine, G. I. R. Y., (2017), “Marie Curie: Celle qui a pavé la voie aux femmes scientifiques”, Biofutur, 36 (385), 28.

Sanguinetti, H., Nedjari, N., Aouami, I., Din, C., Cazoulat, M., Tiemogo, M., Christophe, C. C., (2018), “Recherches de minéralisation d’uranium dans le bassin de Tim Mersoï (République du Niger): une revue des guides de prospection”, Mémoire du Service Géologique de l’Algérie, No. 20, pp. 3–27.

Smirnov, A. L., Rychkov, V. N., Titova, S. M., Poponin, N. A., Nalivayko, K. A., (2018), “Precipitation of uranium from nitrate-sulfuric eluates by aqueous ammonia solution”, Journal of Radioanalytical and Nuclear Chemistry, 317, 863–869. https://doi.org/10.1007/s10967-018-5942-x

SONAREM., (1977), “Inventaire et prospective des ressources minérales du Hoggar”, Division Recherches, Alger.

Syczewski, M. D., Siuda, R., Parafiniuk, J., (2023), “Concentrations in secondary uranium minerals from the Izera metamorphic complex (SW Poland)”, Minerals, 13 (7), 945. https://doi.org/10.3390/min13070945

Zerbib, J. C., (2024), “La corrosion des gaines d'éléments combustibles en Zircaloy”, Global Chance.

MINING OPERATIONS (OPEN-PIT, UNDERGROUND, SOLUTION MINING) RELATED TO MINERAL PROCESSING

NATURAL SODA ASH PRODUCTION THROUGH IN-SITU LEACHING: OPERATIONAL FRAMEWORK FROM KAZAN SODA PLANT

Erdem KUMRUOGLU*, Engin OCALAN, Barış KANDEMIR

Kazan Soda – We Soda, Mülk Küme Evleri 1. Cad. No:122 Yenikent, Sincan, ANKARA, TÜRKİYE
**Corresponding author: erdem.kumruoglu@wesoda.com*

A B S T R A C T

In-situ leaching is an efficient and environmentally sustainable method of extracting trona from deep underground deposits. Unlike conventional mining methods, it eliminates the need for large-scale excavation and surface waste, providing a safer and more eco-friendly way to produce soda ash. At Kazan Soda Mining Plant, in-situ leaching is applied through a network of horizontal and vertical wells that create a controlled circulation system within the trona-bearing formation. This design enables continuous dissolution of the ore and efficient recovery of trona (sodium sesquicarbonate dihydrate, ($Na_2CO_3 \cdot NaHCO_3 \cdot 2H_2O$) under stable hydraulic and thermal conditions. Controlled injection rate and temperature enable the steady dissolution of the ore and the formation of a concentrated brine, which is recovered to the surface for further processing. This brine is then refined using pretreatment, evaporation and sequential decahydrate–monohydrate crystallisation to produce high-purity sodium carbonate (Na_2CO_3) and sodium bicarbonate ($NaHCO_3$). The purpose of this paper is to illustrate how the in-situ leaching method is practically implemented at Kazan Soda, emphasizing its operational principles and integration with surface processing. The results show that this approach achieves efficient mineral recovery with minimal environmental disturbance and represents a real-world example of sustainable mineral processing in large-scale production.

Key words: *Solution mining, in-situ leaching, mineral processing, trona, soda ash*

1. INTRODUCTION

Solution mining is a subsurface extraction method widely used for the recovery of soluble minerals by injecting a solvent, typically hot water or dilute brine, into a mineral formation. The injected solvent dissolves the target mineral, forming a concentrated brine that is subsequently pumped to the surface for processing (Laurence, 2023). This method is particularly effective for extracting evaporite minerals such as trona ($Na_2CO_3 \cdot NaHCO_3 \cdot 2H_2O$), halite (NaCl), sylvite (KCl), and related salts from deep-seated or geologically complex deposits where conventional underground or surface mining methods are technically challenging or economically impractical (Gezer & Atalay, 2016; Bonaventura at all., 2017; Mccoy, 2019).

Compared to traditional mining techniques, solution mining offers several significant advantages. It minimizes surface disturbance and waste generation, reduces labor requirements, and enables continuous mineral production with comparatively lower capital and operating costs. In addition, its compatibility with automation, real time monitoring, and remote-control systems enhances operational safety and efficiency, making solution mining particularly suitable for large-scale chemical raw material production (Barlett, 1998; USGS, 2017). Among the minerals recovered through solution mining, trona is of economic importance due to its role as the primary raw material for soda ash production. Soda ash (sodium carbonate, Na_2CO_3) is a critical input for numerous industries, including glass manufacturing, detergents, chemicals, and environmental applications (Kogel et all., 2006; Barlett, 1998, Kazan Soda, 2025).
Trona ($Na_2CO_3 \cdot NaHCO_3 \cdot 2H_2O$) is the most common naturally occurring soda mineral and is typically found in young Tertiary sedimentary basins. Due to its high solubility, trona rarely forms surface outcrops and is commonly discovered during subsurface drilling activities (MTA,

2025). Trona crystallizes in the monoclinic system, with a Mohs hardness of 2.5–3.0 and a density of approximately 2.14 g/cm³. Its formation requires specific geological and geochemical conditions, including alkaline waters (pH > 12), shallow and warm lacustrine environments, volcanic activity, and semi-arid climatic conditions (MTA, 2025).

In the Kazan Soda deposit, the trona content of the ore body is approximately 29.75%, with the remaining fraction consisting of gangue minerals. The dominant gangue minerals include halite (NaCl), dolomite ($CaMg(CO_3)_2$), northupite ($Na_3Mg(CO_3)_2Cl$), searlesite ($NaBSi_2O_5(OH)_2$), and shortite ($Na_2Ca_2(CO_3)_3$). Halite represents the primary soluble gangue mineral.

In-situ leaching at the Kazan Soda Mining Plant is implemented through a network of horizontal and vertical wells designed to establish a controlled subsurface circulation system within the trona-bearing formation. Controlled injection rates and temperatures ensure stable hydraulic and thermal conditions, enabling continuous trona dissolution and efficient recovery of a concentrated brine. The recovered brine is integrated with surface processing operations, including pretreatment, evaporation, and sequential decahydrate–monohydrate crystallization, to produce high-purity sodium carbonate and sodium bicarbonate products.

The purpose of this paper is to describe the application of the in-situ leaching method at the Kazan Soda Mining Plant, with emphasis on its operational principles, brine chemistry, and integration with surface processing. The study demonstrates that in-situ leaching enables efficient trona recovery with minimal environmental disturbance and represents a sustainable approach to large-scale soda ash production.

2. MINING METHOD AND PLANNING

2.1. Mining Method

There are three main approaches to mining operations: open-pit mining, underground mining and solution mining. The most suitable method is selected based on ore depth, ore chemistry, geometry, geotechnical conditions and economic factors (Hartman & Mutmansky, 2002; Darling, 2011). In deeper or more complex ore bodies, where conventional mining becomes unviable, solution mining has become a viable alternative. This method involves injecting a solvent, typically water, into the ore zone through injection wells. The solvent dissolves the soluble minerals underground, forming a brine that is recovered through production wells and processed at the surface. Figure 1 represents a cross-sectional view of the solution mining process. In Figure 2, the main difference between the solution mining method and the conventional mining method is illustrated. In conventional mining, a large amount of waste material is excavated and transported to the surface for storage or disposal, whereas in solution mining, the insoluble waste material remains in situ, minimizing surface disturbance and environmental impact.

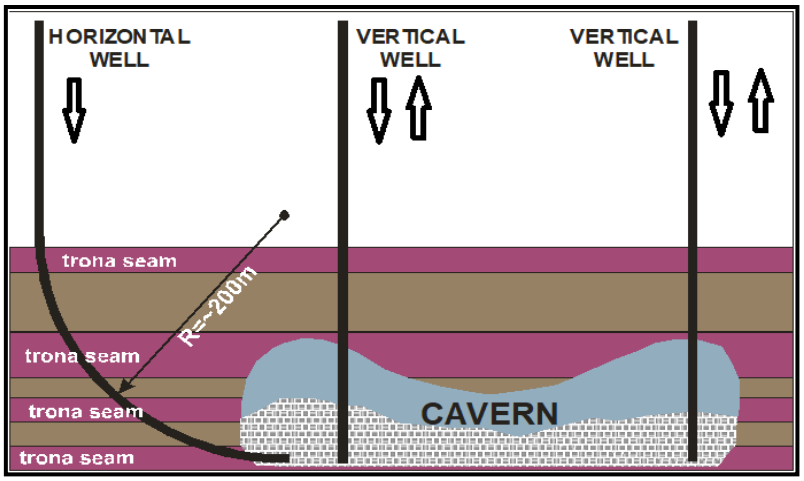

Figure 1. Solution Mining Method

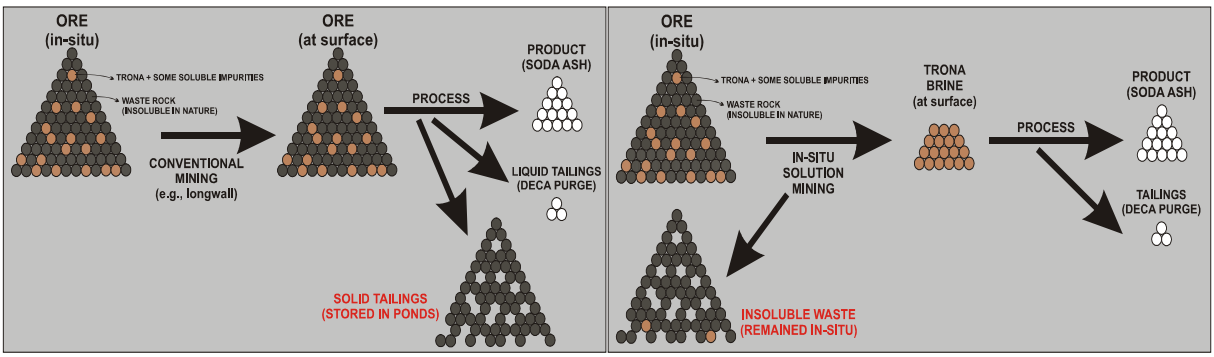

Figure 2. Conventional Mining vs. Solution Mining Method

One important application of solution mining is the extraction of trona, a naturally occurring mineral composed of sodium carbonate and sodium bicarbonate (Saygılı & Okutan, 1996). In this method, heated water is injected into the trona-bearing formation, where it dissolves the mineral and forms a carbonate–bicarbonate brine. The recovered brine is then processed at surface facilities to produce soda ash (Na_2CO_3) and sodium bicarbonate ($NaHCO_3$). Solution mining is particularly well suited for trona deposits because the ore bodies are typically located at significant depths and exhibit high solubility. Combined with modern drilling, monitoring, and process control technologies, this method allows efficient and continuous production while minimizing surface disturbance and labor requirements. As a result, solution mining represents a practical and environmentally sustainable approach for large-scale trona extraction (Gezer & Atalay, 2016; Bonaventura at all., 2017; Mccoy, 2019).

2.2. Planning Of Mining Operations

Mining operations at the Kazan Soda trona field are planned around an ideal production unit concept that allows controlled dissolution and stable long-term operation based on the experience and technical knowledge gained during pilot tests. Each production unit typically consists of two vertical wells connected by a horizontal well drilled within the trona-bearing formation. The horizontal well provides hydraulic communication between the vertical wells and enables a controlled injection–production circulation system. In the standard unit layout, the horizontal well is initiated approximately 200 m behind the landing point and gradually builds inclination to reach a near-horizontal trajectory at the base of the target trona bed. Injection points along the horizontal section are typically spaced at about 75 m intervals, allowing uniform solvent distribution and balanced cavern development between the vertical wells. In Figure 3, the design work for this type of unit is shown.

The design of production units is governed by geological and surface-related constraints such as trona bed geometry, fault distribution, extraction efficiency, surface topography, and land-use limitations. When standard unit layouts cannot be applied due to surface restrictions or permitting constraints, alternative well configurations are developed using combinations of vertical wells and active or passive horizontal wells. This flexible approach ensures continuous production while maintaining hydraulic control and aquifer protection. Basic production units are shown in Figure 4.

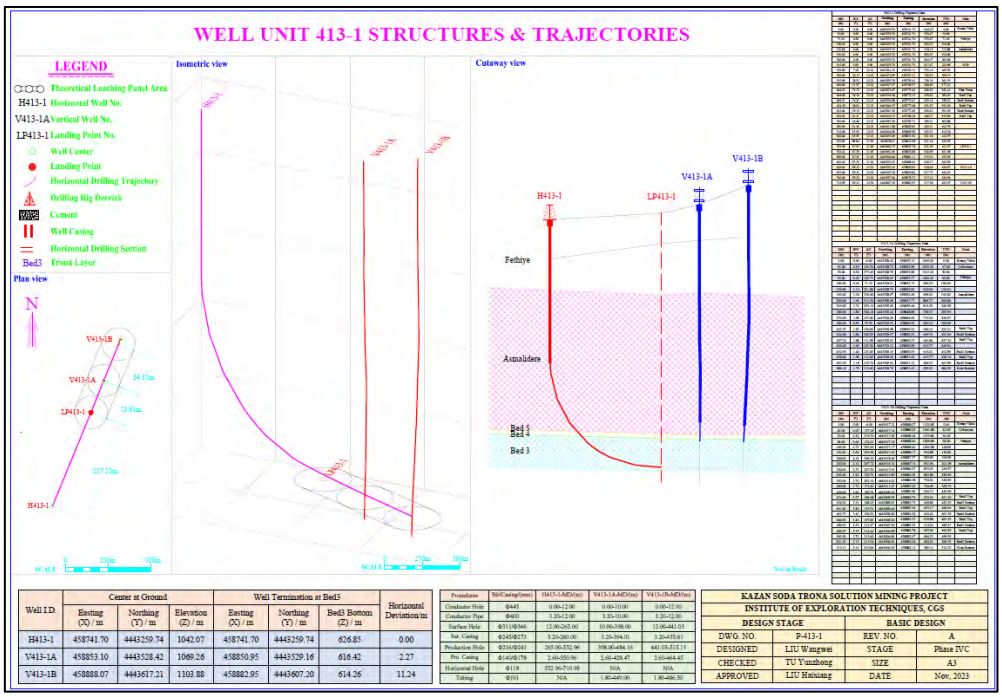

Figure 3. Production Unit Design

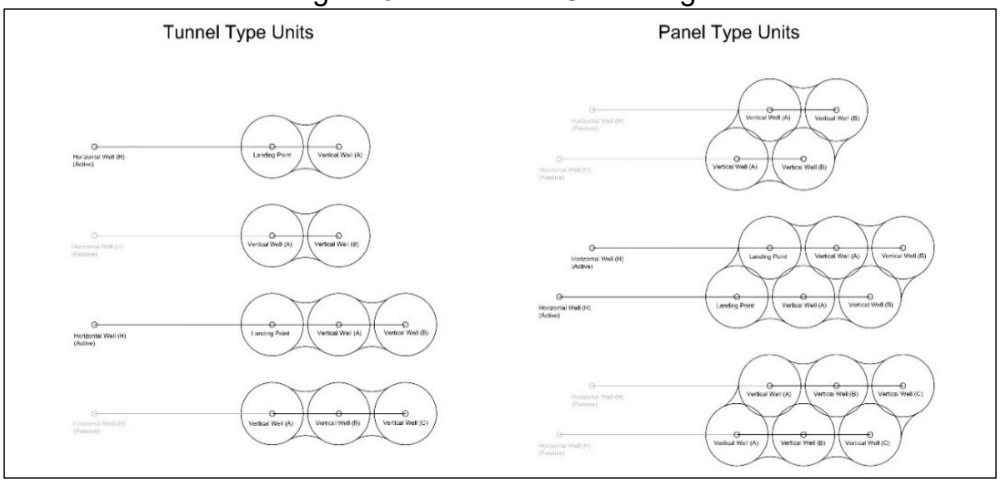

Figure 4. Types of Production Unit

2.3. Drilling Operations

There are two types of wells used in the operation: vertical wells and horizontal wells. In this section, the technical specifications of these well types are described.

2.3.1. Vertical well drilling operations

The operation begins with drilling a 17-½″ surface hole to install a 16″ conductor casing at a minimum depth of 6 m. The first drilling phase (Spud-I) continues with a 13-5/8″ bit, reaching a depth at least 25 m below the base of the deep aquifer. After reaching the planned depth, a 10-¾″ casing string is run and set at least 20 m below the aquifer base. The annulus is cemented with Class-G cement to ensure complete hydraulic isolation of the aquifer. Cement integrity is verified through Temperature Logging, Casing Integrity Test (CIT), and Cement Bond Log (CBL/VDL). The second drilling phase (Spud-II) is performed with a 9-½″ bit, continuing to at least 7 m below the trona zone. In case coring is required, drilling proceeds down to 15 m below the trona zone base. The 7″ production casing is then run and set so that the casing shoe is positioned 0.5 m below the top of the target trona bed. Cementing is performed using Class-G cement, providing zonal isolation between the trona and overlying formations. After the required Waiting-on-Cement (WOC) period, verification tests such as CIT, CBL/VDL, and Formation Integrity Test (FIT) are conducted to confirm casing and cement integrity. Upon successful testing, a 3-½″ tubing string may be installed for injection or production operations, typically positioned just above the target trona bed floor. This vertical well configuration ensures proper zonal isolation, aquifer protection, and reliable access to the trona-bearing horizon, forming the main production and injection wells for the solution mining process. In Figure 5(a), schematic view of vertical production is shown.

2.3.1. Horizontal well drilling operations

2.3.1.1. Type-A

Type A horizontal wells at Kazan Soda are designed to create controlled connection channels between vertical wells within the trona-bearing formation. Once communication is achieved, these wells are cemented and permanently abandoned because they intersect with the fault lines. The design ensures full isolation of the deep aquifer and fault lines. The operation starts with drilling a 17-½″ surface hole to install a 14″ conductor casing at a minimum depth of 6 m. The first drilling phase (Spud-I) is then drilled with a 12-¼″ bit down to a depth at least 25 m below the base of the deep aquifer. A 9-⅝″ casing is run and cemented with Class-G cement, extending at least 20 m below the aquifer base. This provides complete aquifer protection and zonal isolation up to the first target point within the trona-bearing sequence. Following verification of cement quality through CIT, CBL/VDL, and Temperature Logging, drilling proceeds into the intermediate (Spud-II) and bottom-hole (Spud-III) phases. An 8-½″ bit is used to continue drilling, with the trajectory followed by directional drilling tools (PDM and MWD/LWD combination) to reach the planned approach toward the target trona bed. Logging while drilling operations are performed in each drilling phase, and the well trajectory is evaluated jointly with the Owner to confirm alignment with design and correct approach toward Bed-3 trona. Once the directional section successfully connects the corresponding vertical wells, the BHA is pulled out, and a bottom-hole plug is set at the previously reduced diameter section (Landing Point). The well is then plugged and cemented through this plug, ensuring that cement fills at least 50 meters inside the surface casing in accordance with the abandonment criteria. In Figure 5(b), schematic view of A Type horizontal well is shown.

2.3.1.1. Type-B

Type B horizontal wells at Kazan Soda are designed to establish hydraulic communication between vertical wells and to remain active as underground injection wells after completion. This configuration ensures full aquifer isolation, structural integrity, and long-term stability during solution mining operations. The operation begins with Spud-I, drilling a 17-½″ hole for setting a 14″ conductor casing at a minimum depth of 6 m. The surface hole is then drilled with a 12-¼″ bit to at least 25 m below the deep aquifer base. A 9-⅝″ casing string is run and

cemented with Class-G cement, extending at least 20 m below the aquifer. This provides complete aquifer protection and full zonal isolation before deeper drilling proceeds. Following cement evaluation (CIT, CBL/VDL, and temperature log verification**), the Spud-II section is drilled using an 8-½″ bit. Directional control is maintained with PDM and MWD/LWD tools, guiding the trajectory toward the target trona zone. Once the designed inclination and approach are achieved and the well reaches the Landing Point (LP) inside the target trona bed. Following successful horizontal completion, a 5-½″ casing string is run and cemented with API Class-G HSR-grade cement to ensure full isolation and well integrity. After final verification (CBL/VDL, FIT), the casing head and tubing head are installed. After cement curing and verification by the Site Geologist, Spud-III drilling begins from the Landing Point using a 4-5/8″ bit, maintaining a near-horizontal trajectory through Bed-3 trona bottom. MWD/LWD data are continuously monitored and shared with the Owner to confirm that the drilling remains within the designed trona interval and successfully connects the target vertical wells. In Figure 5(c), schematic view of B Type horizontal is shown.

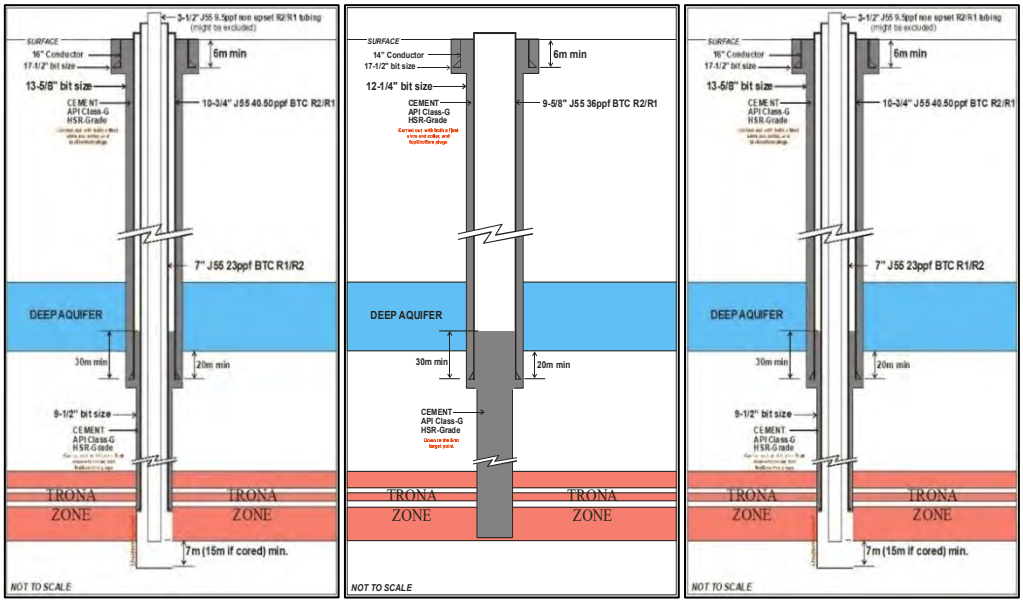

Figure 5. (a-left) Vertical Well, (b-Middle) A-Type Horizontal, (c-right) B-Type Horizontal Well

3. MINE PRODUCTION

3.1. Piping and Instrumentation

Pipelines are the main way of transporting brine from production wells to storage tanks and transporting solvents from tank stations to production wells within the solution mining field. Along the transfer route, from the wellhead to the tank station, pipes of varying diameters are used to accommodate changes in flow rate and maintain optimal hydraulic performance. The design of the pipeline network is governed by the total volumetric flow rate, which directly affects pipe size, pressure loss and overall system efficiency. The layout of pipeline network at mine site is shown in Figure 6.

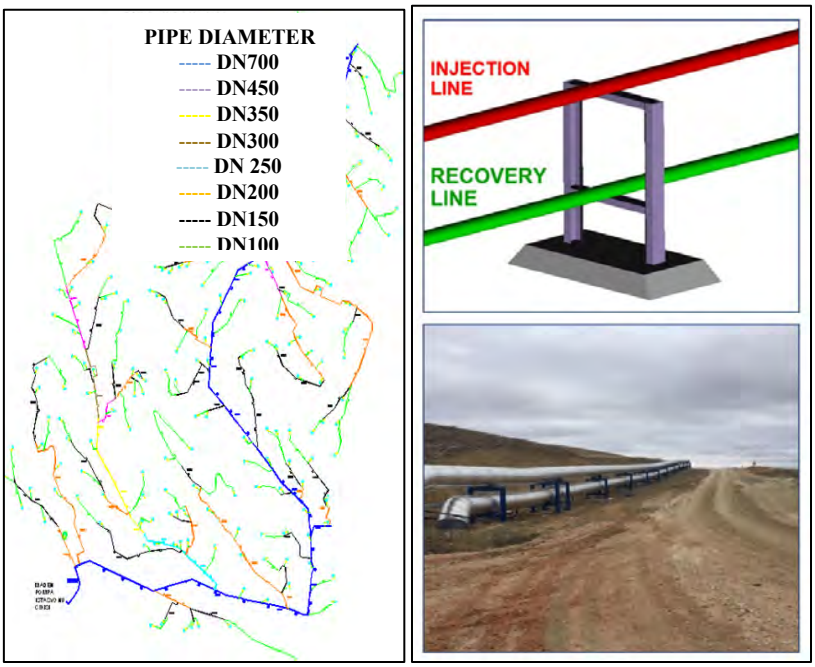

Figure 6. Pipeline Network

Each production well is connected to two main networks: an injection pipeline system and a brine (production) pipeline system. The injection pipelines deliver solvent from the tank station to both vertical and horizontal wells, enabling efficient contact between the solvent and the trona-bearing formation. In contrast, brine pipelines are only connected to vertical wells, which serve as the main outlets for recovering trona-rich brine. Horizontal wells are solely dedicated to injections, ensuring a controlled flow pattern and maximizing dissolution efficiency within the cavern.

Effective monitoring and control of production wells are ensured through a comprehensive field instrumentation and valve system installed at each wellhead. The setup includes flowmeters, pressure transmitters, and automatic control valves, which are responsible for continuous measurement and regulation of operational parameters such as flowrate, cumulative flow, temperature, pressure, and fluid density. In addition to these instruments, the wellhead assembly incorporates manual isolation valves for safe maintenance operations, check valves to prevent backflow and protect the system integrity, and discharge valves that enable brine or brine sampling and controlled line depressurization. All measured data are transmitted to the Distributed Control System (DCS) for visualization, analysis, and historical storage, enabling real-time monitoring of pressure, temperature, flowrate, and density. The typical instrumentation and configuration of a vertical wellhead are illustrated in Figure 7, while a similar arrangement is employed for horizontal wells, which operate solely in injection mode.

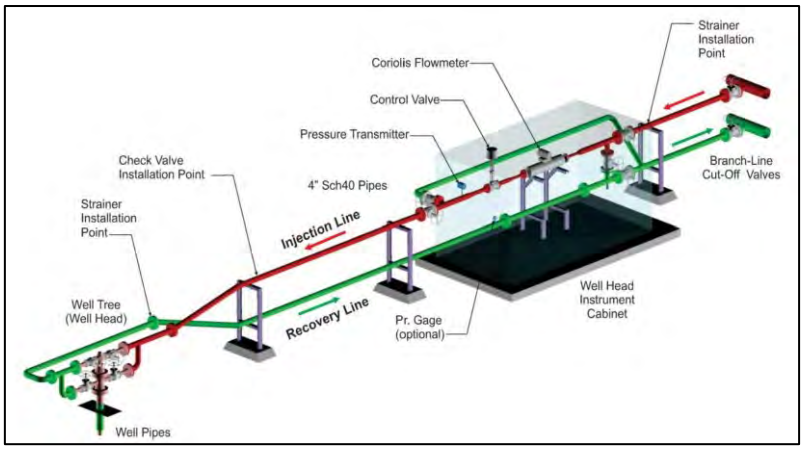

Figure 7. Well-Head Piping and Instrumentation

3.2. Preparation of Solvent, Transfer System, and Storage

The solvent used in solution mining operations primarily consists of process water generated from system-washing activities, condensate obtained from steam utilized in various sections of the processing plant, and groundwater supplied from wells located at the mine site. These components collectively form the main sources of solvent, which is a weakly alkaline mixture. Additionally, defective or off-spec products from the processing plant are reintroduced into the system at the initial stage to enhance the solvent's alkalinity and minimize material losses. The prepared solvent, with a total alkalinity of approximately 1–2%, is delivered to the injection system through multistage horizontal centrifugal pumps, providing a unit injection rate of 25–30 m³/h. The solvent temperature, maintained between 70 °C and 80 °C, is optimized to ensure efficient dissolution of the trona-bearing strata while simultaneously maintaining the desired operational balance between the processing plant's capacity and the mining system's performance. As dissolution progresses, the concentration of total alkalinity in the recovered brine gradually increases. Once the brine attains the target concentration, it is transferred to the tank station, where it is stored before being pumped to the processing plant for subsequent purification and crystallization processes. The overall configuration of the plant network is shown in Figure 8.

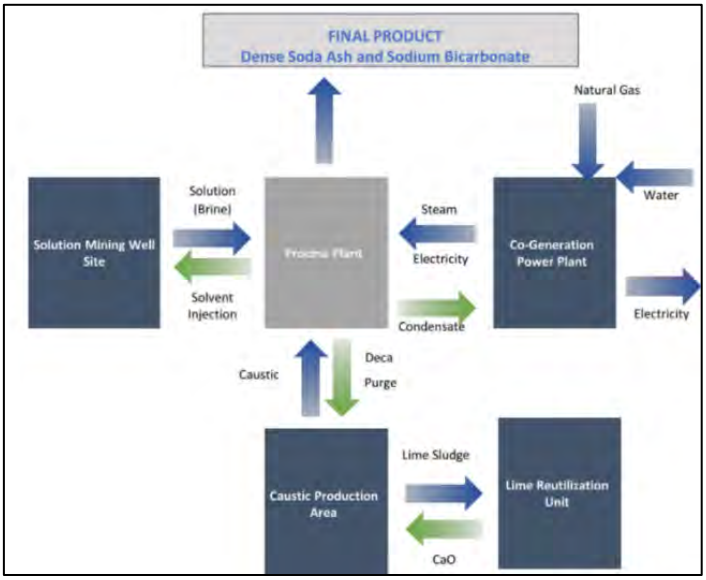

Figure 8. Plant Network

3.3. Dissolution of Trona

Pressure plays a vital role in solution mining by driving the movement of both the injected solvent and the recovered brine through the subsurface and surface pipeline network. This network includes elevation differences, bends, and varying slopes, all of which introduce hydraulic losses. To maintain a steady and controlled injection–production circulation, sufficient pressure must be applied to overcome these resistances. In this sense, pressure is essential for hydraulic control and flow continuity. However, within the pressure range typically encountered in solution mining operations, pressure has a negligible direct effect on the solubility of trona. Trona dissolution is primarily governed by temperature, total alkalinity, carbonate speciation, and hydrodynamic conditions, while pressure acts mainly as a hydraulic parameter rather than a chemical driving force.

As briefly described in Section 3.2, weakly alkaline hot water is used as the solvent for trona dissolution. The injected solvent typically has a total alkalinity of approximately 1–2 wt%, depending on operational conditions, and is introduced into the production units at temperatures between 70 and 80 °C. Solvent alkalinity is a critical parameter for dissolution. If the injected solvent becomes saturated with respect to carbonate alkalinity, its dissolution capacity decreases, limiting further dissolution of the trona layers. For this reason, injection alkalinity must be carefully controlled to maintain sufficient chemical driving force.

Temperature is another key parameter influencing trona dissolution. Higher injection temperatures enhance dissolution kinetics and promote the conversion of bicarbonate to carbonate species, resulting in increased total alkalinity in the produced brine. The use of hot water injection therefore significantly improves dissolution efficiency compared to lower-temperature conditions.

Flowrate also plays an important role in the dissolution process. Increasing flowrate leads to higher fluid velocity and reduced residence time within the cavern. Under controlled conditions, this enhances mass transfer at the rock–fluid interface and supports efficient dissolution of trona layers. However, excessive flowrates may reduce contact time and adversely affect the total alkalinity of the recovered brine. Therefore, flowrate must be optimized to balance dissolution efficiency and brine quality.

The brine recovered from each production cavern typically has a temperature in the range of 50–60 °C. During the initial commissioning phase of a production unit, the total alkalinity (TA) of the brine shows an increasing trend as dissolution progresses. Once a stable TA level is reached, the production unit is connected to the processing plant. Under steady-state operation, the total alkalinity of the produced brine generally ranges between 14 and 18 wt%. The chemical composition of the produced brine is dominated by sodium (Na^+) and carbonate species (HCO_3^- and CO_3^{2-}). Chloride ions (Cl^-), originating mainly from halite dissolution, are also present.
General dissolution equation is shown in the following item:

$$Na_2CO_3 \cdot NaHCO_3 \cdot 2H_2O_{(s)} \rightarrow 3Na^+_{(aq)} + {CO_3^{-2}}_{(aq)} + {HCO_3^-}_{(aq)} + 2H_2O_{(l)}$$

The dissolved CO_3^{-2} ions (strong base) still react with hot water:

$$CO_3^{-2} + H_2O \rightleftharpoons HCO_3^- + OH^-$$

The dissolved HCO_3^- ions (weak base) also react with hot water (weak reaction):

$$HCO_3^- + H_2O \rightleftharpoons H_2CO_3 + OH^-$$

The product of equation is in equilibrium with dissolved CO_2, the product OH^- is the major pH increasing agent:

$$H_2CO_3 \leftrightarrow CO_{2_{(aq)}} + H_2O$$

Elevated temperatures enhance the deprotonation of bicarbonate (HCO_3^-) to carbonate (CO_3^{-2}), as represented by reaction. This temperature-driven shift increases the carbonate content and thereby raises the basicity of the brine:

$$2HCO_3^- \rightarrow CO_3^{-2} + CO_{2_{(aq)}} + H_2O$$

Since this CO_2 is formed in the aqueous phase, it cannot be removed immediately from the brine. Only when the brine becomes saturated with CO_2 does outgassing occur, allowing CO_2 to evolve as a gas and be separated.

4. PROCESSING TECHNIQUE

4.1. Brine Pretreatment, Stripping & Evaporation

The sodium carbonate brine recovered from solution mining is subjected to a pretreatment step to remove suspended solids before downstream processing. Filtration reduces the total suspended solids content of the brine. Backwash effluents generated during filtration are collected and recycled within the process or returned to the solution mining system to minimize material losses. The stripping and evaporation section converts bicarbonate in the brine into a concentrated sodium carbonate solution suitable for crystallization. In the stripping stages, dissolved sodium bicarbonate is thermally decomposed into sodium carbonate, water vapor, and carbon dioxide according to the following reaction:

$$2NaHCO_{3_{(l)}} \rightarrow Na_2C0_{3_{(l)}} + H_2O_{(g)} + CO_{2_{(g)}}$$

$$H_2O_{(l)} \rightarrow H_2O_{(g)}$$

The treated brine is then concentrated through evaporation, where controlled water removal increases the total sodium carbonate concentration. Vapor generated during evaporation is recycled as a heat source for the stripping process. The brine undergoes two successive stripping and evaporation stages, achieving a final concentration of approximately 22–25 wt% total sodium carbonate. The concentrated brine is collected and conditioned with caustic soda to minimize residual bicarbonate before being transferred to the sodium carbonate decahydrate crystallization section.

4.2. Decahydrate Crystallization Section

In this section, concentrated sodium carbonate brine obtained from the stripping and evaporation system is crystallized as sodium carbonate decahydrate ($Na_2CO_3 \cdot 10H_2O$). This crystallization step enables the effective removal of other soluble impurities from the brine, as the crystal lattice of sodium carbonate decahydrate does not accommodate the principal impurity, sodium chloride. Consequently, impurities remain in mother liquor, resulting in a purified sodium carbonate product. The feed stream consists of concentrated brine combined with a purge stream from the monohydrate crystallization section. Crystallization is initiated by flashing the feed under reduced pressure, followed by gravity flow into a decahydrate crystallizer operating at low temperature and vacuum conditions. Cooling is provided by a closed-loop chilled water system, and the reduced temperature promotes selective crystallization of sodium carbonate decahydrate. Controlled agitation within the crystallizer ensures uniform crystal growth and prevents excessive agglomeration. The resulting decahydrate slurry is dewatered through solid–liquid separation steps, producing a wet decahydrate cake and a clarified mother liquor. The wet cake is transferred to a melting stage, where it is dissolved using stripped brine and recovered heat, generating a decahydrate melt suitable for downstream processing. The majority of the melt is routed to the sodium carbonate processing section, while smaller portions are directed to bicarbonate production and solvent

makeup for solution mining. The mother liquor is partially recycled back to the crystallizer to maintain slurry concentration, with the remaining purge stream sent to caustic soda production section.

4.3. Monohydrate Crystallization, Centrifuging & Drying

In this section, concentrated sodium carbonate solution is converted into sodium carbonate monohydrate ($Na_2CO_3 \cdot H_2O$) through controlled crystallization and evaporation. The process operates as a single-effect crystallization system, where supersaturation is generated by partial evaporation of water under elevated temperature conditions, promoting selective monohydrate crystal growth. The main reactions in this section are:

$$Na_2C0_{3_{(l)}} + H_2O_{(l)} \rightarrow Na_2C0_3 \cdot H_2O_{(s)}$$
$$H_2O_{(l)} \rightarrow H_2O_{(g)}$$

Concentrated brine is introduced into the crystallizer. Internal recirculation and controlled heating provide sufficient residence time for crystal growth while minimizing fouling and wall deposition. Water evaporation during crystallization generates process vapor, which is mechanically recompressed and reused as a heat source. Carbon dioxide released with the vapor is removed to maintain product quality, and a small purge stream is withdrawn to control impurity buildup. The purge liquor is recycled to the decahydrate section for further product recovery. The monohydrate slurry discharged from the crystallizer is subjected to solid–liquid separation, followed by drying and cooling. In the drying stage, residual moisture is removed using a fluidized bed system operating with heated air and indirect steam heating, producing dense soda ash with low residual moisture. After cooling, the product is classified to achieve the required particle size distribution, with oversize material recycled and fine particles collected separately. Exhaust gases from drying are washed and cooled, allowing recovery of entrained solids and reuse of process water.

4.4. Bicarbonate Crystallization, Centrifuging & Drying

In this section, sodium bicarbonate ($NaHCO_3$) is produced by reacting carbon dioxide with molten sodium carbonate decahydrate and recycled mother liquor under controlled cooling conditions. Carbon dioxide is compressed, cooled, and dried before being introduced into the bicarbonate crystallizer, where it reacts with the carbonate-rich solution to form a bicarbonate slurry. The heat released during crystallization is removed through continuous cooling, ensuring stable crystal formation. The main reaction in this section is:

$$Na_2CO_{3_{(l)}} + CO_{2_{(g)}} \rightarrow NaHCO_{3_{(s)}}$$

The resulting bicarbonate slurry is mechanically dewatered, after which the wet cake is dried in a fluidized bed system using heated gas, primarily carbon dioxide. Drying reduces the moisture content to very low levels, and the product is subsequently cooled in a fluidized environment to achieve the desired thermal stability. After drying and cooling, the bicarbonate product is classified to obtain the required particle size distribution, with oversize material recycled and undersize fractions separated as product. The final sodium bicarbonate product is conveyed to the logistics and packing system.

4.5. Calcination And Causticizing Section

Unslacked lime (CaO) supplied from the calcination section is reacted with decahydrate purge liquor to produce a weak caustic soda solution. Initially, unslacked lime is hydrated to form lime milk, which subsequently reacts with sodium carbonate in the purge stream, converting carbonate into sodium hydroxide and forming calcium carbonate as a solid by-product:

$$CaO_{(s)} + H_2O_{(l)} \rightarrow Ca(OH)_{2(l)}$$
$$Ca(OH)_{2(l)} + Na_2CO_{3(l)} \rightarrow 2NaOH_{(l)} + CaCO_{3(s)}$$
$$a(OH)_{2(l)} + NaHCO_{3(l)} \rightarrow NaOH_{(l)} + CaCO_{3(s)} + H_2O_{(l)}$$

The resulting weak caustic soda solution is concentrated to approximately 25 wt% NaOH in a three-stage evaporation system and then transferred to the stripping and evaporation section for internal process consumption. The calcium carbonate formed during causticization is directed to settling tanks and separated from the liquor using decanter centrifuges. The separated $CaCO_3$ is subsequently sent to the calcination section. Calcium carbonate generated in the caustic production unit is recycled in the Lime Recovery Unit through a calcination process to produce unslacked lime (CaO) for internal consumption. During calcination, calcium carbonate undergoes thermal decomposition at elevated temperatures, yielding calcium oxide and carbon dioxide. The recovered CaO is reused within the plant.

$$CaCO_{3(s)} + heat \rightarrow CaO_{(s)} + CO_2$$

5. CONCLUSION

This paper presents a comprehensive overview of the in-situ leaching–based trona mining and integrated processing system implemented at the Kazan Soda Mining Plant. The study focuses on the overall mining concept, well configurations, dissolution mechanism, and the integration of subsurface operations with surface processing units, rather than on performance comparison or quantitative evaluation. By describing the operational workflow from solution mining to crystallization and auxiliary recovery units, the paper aims to provide a practical reference for large-scale trona solution mining applications. The Kazan Soda operation illustrates how in-situ leaching can be systematically designed and operated as part of an integrated industrial production chain for soda ash and sodium bicarbonate.

REFERENCES

Bartlett, R. W., (1998), Solution mining: Leaching and fluid recovery of materials, Gordon and Breach Science Publishers.

Bonaventura, D., Chacartegui, R., Valverde, J., Verda, V., (2017), “Carbon capture and utilization for sodium bicarbonate production assisted by solar thermal power”, Energy Conversion and Management, 149, 860–874. https://doi.org/10.1016/j.enconman.2017.03.042

Ciner Group, (2023), Kazan Soda Elektrik, https://www.cinergroup.com.tr/cam-ve-kimyasallar/kazan-soda-elektrik (Accessed: 01 February 2026).

Darling, P. (ed.), (2011), SME Mining Engineering Handbook, 3rd ed., Society for Mining, Metallurgy & Exploration.

MTA, (2025), Trona Mineral Information, https://www.mta.gov.tr/v3.0/bilgi-merkezi/trona

Gezer, S., Atalay, U., (2016), “Assessment of soda ash calcination treatment of Turkish trona ore”, E3S Web of Conferences, 8, 01013. https://doi.org/10.1051/e3sconf/20160801013

Hartman, H. L., Mutmansky, J. M., (2002), Introductory mining engineering, 2nd ed., Wiley.

Kazan Soda Elektrik Üretim A.Ş., (2025), Home page, https://www.kazansoda.com/en/home-page/

Kogel, J. E., Trivedi, N. C., Barker, J. M., Krukowski, S. T. (eds.), (2006), Industrial minerals and rocks: Commodities, markets, and uses, 7th ed., SME.

Laurence, E., (2023), “Solution mining guide”, The Assay, https://www.theassay.com/articles/the-assay-insights/solution-mining-guide/

Mccoy, M., (2019), “Soda ash makers to expand”, C&EN Global Enterprise. https://doi.org/10.1021/cen-09738-buscon6

Saygılı, G., Okutan, H., (1996), “Application of the solution mining process to the Turkish trona deposit”, Hydrometallurgy, 42, 103–113. https://doi.org/10.1016/0304-386x(95)00060-t

Springer, (2006), “Solution mining and cavern use”, in: Evaporites: Sediments, Resources and Hydrocarbons, pp. 893–943. https://doi.org/10.1007/3540323449_12

U.S. Geological Survey (USGS), (2017), In-situ leach mining of minerals.

U.S. Geological Survey (USGS), (2023), Mineral Commodity Summaries: Soda Ash, https://pubs.usgs.gov/periodicals/mcs2023/mcs2023-sodaash.pdf

STUDY AND EVALUATION OF CURRENT PILLAR DESIGN USING DIFFERENT APPROACHES–ALGERIA

Said BERDOUDI[1,*], Houria HEBHOUB[2], Nouha REZAIGUIA[2]

[1]LAVAMINE Laboratory, Department of mining engineering, faculty of earth sciences, Badji Mokhtar University, Annaba, ALGERIA
[2]Department of Civil Engineering, Faculty of technologie, 20 August 1955 University, LMGHU Laboratory, Skikda, ALGERIA
**Corresponding author: said.berdoudi@univ-annaba.dz*

A B S T R A C T

Mining by rooms and pillars is the first method of underground mining which systematically supports the roof to ensure the safety of the working environment, the main role of pillars is to ensure the stability of the environment in order to minimize the movement of the rock mass in the zone of influence of the excavation, giving a new dimension to these pillars represents an important economic challenge for researchers.

Our study focused on field studies carried out at the Sétif zinc mine in Algeria, Stress, strain and stability measurements of the pillar were obtained during and after ore extraction. This work is based on the study of the stability of the pillars using different methods, notably analytical and numerical, to resize them in order to ensure an intact environment and to recover the majority of the ore left in place and to compare the results respecting the corresponding safety factor.

This work presents an experimental framework to evaluate the stability of the pillars in hard rock.The results obtained are very satisfactory with an extraction coefficient which varies between 8.77% to 13.15% for the different pillars, which makes it possible to recover more than 80% of the current volume.

Key words: *Rooms and pillars, sizing, Sétif zinc mine, numerical modelling, phase2, safety factor, stability*

1. INTRODUCTION

Mining methods selection is one of the most critical and complex decision-making tasks in mine-planning (Manjate et al., 2024). The development of underground exploitations can provide viable solutions for the mining of reserves that cannot be economically mined through classic surface exploitation schemes (Tzalamarias et al., 2019), (Esterhuizen et al., 2011) estimate that the pillars must ensure overall stability up to the ground surface.

Li (2020) studied the influence of size of pillar on distribution of plastic zone, stress redistribution, and roof stability of deep mining. It reveals how shape of surrounding rock plastic zone was affected by size of the pillar. Gao (2018) and Qiu et al. (2019) studied the behavior of rock pillars under uniaxial compression. Two methods of pillar sizing are widely used applying different approaches; the first considers that the pillar is in uniaxial compression, citing those of the tributary zones thus using empirical formulas. For the second mode, we find methods which do not impose any simplification on the stress field in the pillar and, thus, the stress fields necessary for the dimensioning of the pillars have been obtained by experimental techniques. They are now generated by modeling or numerical simulation such as finite element methods.

The main goal of this work is to give a new dimension to the residual pillars using analytical and numerical methods and to study their behavior to recover the maximum amount of ore left in place while ensuring an adequate stability. The methods for sizing the pillars will be analyzed according to the strength of the pillars using several methods; Tributary air, Obert-Duval, Bieniawski as well as the Hardy-Agapito method.

Parameters such as pillar height, pillar depth (Verma, 2014), compressive strength and project joint depth were considered to estimate the safety factor of the Chaabet Elhamra Sétif mine pillar. To be sure and efficient, after evaluating the resistance of the pillars we will calculate the load supported, to finally have an optimal safety factor, and recover as much as possible of the ore left in place.

2. PRESENTATION OF THE UNDERGROUND SITE

The Chaabet -El-Hamra deposit is located approximately 250 km southeast of Algiers (Algeria), The mine exploits zinc ore using room and pillar method(Chikhaoui *et al*; 2021). This ore is found in the form of sphalerite lenses embedded in hard and fractured dolomites. The pillars of the Chaabet EL Hamra zinc mine have not been the subject of a serious study. Figure (1) shows us a plan section of the area subject to our study.

Figure 1. Plan view of the four pillars selected for the study (in red)

The manifestations of the ground pressure vary according to the dimensions of the underground mining structures as well as the mode and quality of their execution. Currently the cutting of the pillars is planned by folding down and creating new rooms. The reduction in pillar dimensions varies from one pillar to another, being able to reach an acceptable section and meet the mine's needs in terms of productivity and safety. Due to the additional loads that such an operation would have entailed, the residual pillars are left and not torpedoed; these residual pillars have an irregular shape (Figure 1).

The failure mechanism of the fractured rock mass is complex (Zhao, 2000), characterized by multi-stage fracturing development; understanding the failure mechanism and stability of the pillars is necessary for their effective extraction (Kabwe, 2024). When the exploitation is deep and the width of the exploited panel is also very large in relation to its depth, this causes repercussions and disorders, this generally results in the appearance of settlements on the surface, the key to this is the dimensioning of the pillars that govern the overall mine stability performance.

3. METHODOLOGY

This study presents an empirical and numerical solution that takes into account the influence of the geometric factor. In general, the empirical equations are applicable to conditions similar to those under which they were developed. Secondly, a numerical finite element model was used to study stress transfer through the mine structure before and after ore extraction. Several research studies indicate that rigorous laboratory, analytical or numerical simulation studies are essential to understand deformation mechanisms and pillar strength. (Lunder 1994; Iannacchione 1999; Mark 1999; Gale 1999; Kaiser et al. 2000; Diederichs et al. 2002; Esterhuizen 2006).

3.1. Analytical Methods

The pillar strength was calculated using different analytical methods, for Gonzalez-Nicieza et al., 2006), the methods for designing pillars in underground mines are fundamentally based on empirical formulae. In this study we will use 4 methods:

3.1.1. Method of tributary area

The tributary zone, or sometimes called the zone of influence, is the area surrounding the pillar left in place and which absorbs the load. For this theory and according to Brady and Brown (1985), the pillar supports the weight of the earth, extending from the level of the excavation to the free surface.

Whoever the pillar (Figure 1), and according to this theory, the axial stress at the center of the pillar is given by the formula (Éq. 1).

$$\sigma_p = \frac{(w_0 + w_p)}{w_p} * P_{zz} \tag{1}$$

W_o: Room dimension (width) ;
W_p: Pillar dimension (width) m;

When the vertical stress is due solely to the load of gravity; in this case we will have (Eq. 2).

$$P_{zz} = \sum_{i=1}^{n} \gamma_i * h_i \tag{2}$$

P_{zz}: The vertical stress supported by the pillar;
γ_i: The density of the covering soil for the i^{th} layer; kg/m^3;
h_i: The layer Thickness;m;
g: gravitational acceleration. m/s2.

The overall extraction rate τ is determined by the formula (Eq. 3).

$$\tau = \frac{(w_0 + w_p) - w_p}{(w_0 + w_p)} \quad \text{and,} \quad 1 - \tau = \frac{w_p}{(w_0 + w_p)} \tag{3}$$

The equation of the wall pillar can then be written (Eq. 4).

$$\sigma_p = \frac{1}{1 - \tau} * P_{zz} \tag{4}$$

When the pillar-columns have a rectangular section (figure 2), the extraction rate is calculated by the equation (Eq. 5).

$$\tau = \frac{(a + c) * (b + c) - ab}{(a + c) * (b + c)} \quad (5)$$

Where: a and b; Dimensions of the pillars;
C: Room dimensions.

In this condition, the axial stress is calculated by the formula (Eq. 6).

$$\sigma_p = P_{zz} \frac{(a + c) * (b + c)}{ab} \quad (6)$$

* For a = b, then we has (Eq. 7).

$$\sigma_p = P_{zz} * \frac{\text{Tributary volume}}{\text{Pillar volume}} = P_{zz} * \frac{A_1}{A_p} \quad (7)$$

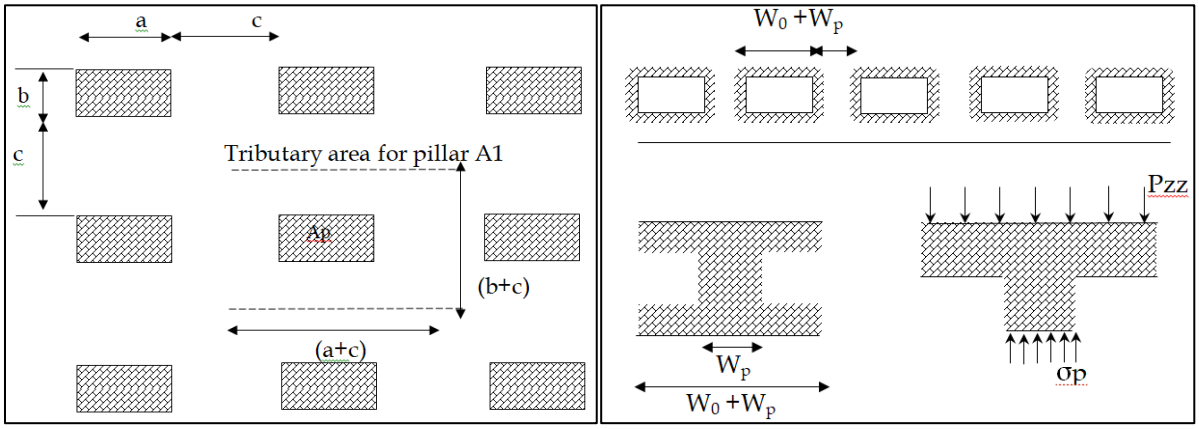

Figure 2. Tributary block theory case of wall pillars shown in longitudinal section, P.H.G. Brady et E.T. Brown, Rock Mechanics For Underground Mining, (1985)

3.1.2. Obert-Duvall method (1967)

In situ tests showed that equation (Éq. 8) was applicable to coal using the in situ strength. Although commonly called The Obert-Duvall formula, the average axial stress at the center of the pillar is defined by :

$$s_p = \sigma_c(0.778 + 0.222 * \frac{W_p}{H_p}) \quad (8)$$

S_p : The pillar strength; (MPa);
σ_c : Uniaxial compressive strength;
W_p, H_p: Dimension of the pillar (width and height respectively).

3.1.3. Bieniawski method (1992)

To calculate the pillar strength (S_P), Bieniawski's formula (Eq. 9) was first developed from large-scale in situ tests carried out in South African mines. (Bieniawski, 1992).

$$Sp = So * (0.64 + 0.36 * (\frac{W_p}{H_p}))$$ (9)

S_0: In-situ compressive strength of intact rock;
Wp and Hp : Pillar dimensions (width and height respectively), (m);

3.1.4. Hardy-Agapito method (1977)

Agapito and Hardy (1977), proposed an equation relating the strength of the pillar with the strength of a rock sample having a standard dimension, and estimated the resistance from the expression (Éq. 10).

$$S_p = S_s(\frac{V_p}{V_p})^{-0.118}[\left(\frac{W_p}{H_p}\right) \Big/ \left(\frac{W_s}{H_s}\right)]^{0.833}; \quad N/m^2$$ (10)

Where: Vp,Wp and Hp; dimensions of the pillar (Volume, width and height), m;
V_s,W_s,H_s : Dimensions of the specimen (Volume, width and height), with 37mm in diameter and 74mm in height ;
S_s : strength of the specimen.

3.2. Calculation of Loads Applied To Pillars

In terms of structure, the Chaâbet-el-Hamra deposit has a folded structure. The stratiform ore bodies are encased in massive dolomites and generally appear in the form of elongated bands over a length of 2,700 m and a width varying from 300 to 600 m.

The area has seven (07) levels of which only two (02) are of industrial interest**.**

In order to estimate the load applied to the pillars of the studied block, we will use an average value of the depth and an average density of the coverage zones. Using formula (02) above, these values was calculated and given according to each layer of the deposit and are presented in the table 1.

Table1. The thickness and density values for each stratum of the coverage area

The strata	Density γ (t/m³)	Thickness h (m)	P_{zz} (γi x hi)	
			t/m.s²	MPa
Dolomite sometimes clay	2,758	23,3	642,61	6,30
Dolomite little sands	2,624	13,4	351,62	3,45
Limestone - limestone marly	2,728	8	218,24	2,14
Sandstone Dolomite	2,747	7,7	211,52	2,07
Organogenic sandstone	2,603	10,3	268,11	2,63
Hematurized dolomite	2,781	18,7	520,05	5,10
Dolomite	2,963	25	740,75	7,26
		Pzz (moy)	2952,90	28,96

.

3.3. Calculation of the Extraction Rate Using the Tributary Area Method

Tributary area, or sometimes referred to as influence area, is the area surrounding the pillar that absorbs the load. Knowledge of the prevailing pillar load will enable appropriate pillar widths to be determined which in turn will optimise percentage extraction.

This calculation makes it possible to examine the state of the pillars studied, whether they are robust or vulnerable, this rate is calculated using the expression (Eq. 11) below:

$$\tau = \frac{(a_p + c) * (L_p + c) - a_p * L_p}{(a_p + c) * (L_p + c)} \quad (11)$$

Where: ap and Lp Pillar dimensions, m;
C: Room dimensions, m.

4. MECHANICAL TESTING OF ROCK SAMPLES FROM PILLARS

The mechanical properties of the rock were determined by tests in the laboratory as well as on site using different methods, The Schmidt Hammer test, ultrasound and the hydraulic press. For (Cheikhaoui et al; 2021), compressive strength (σc) is an essential parameter in stability studies, knowing that the pillars are implanted in fractured rocks (Eq. 12).

$$\sigma c = \frac{P}{S}; \quad (MPa) \quad (12)$$

Where: P: The applied load, and S: The sample Section.
The results are mentioned in table 2.

Table2. Compressive strength of samples

Sample	S (cm^2)	F (KN)	σ_c (KN/cm^2)	σ_c (MPa)
1	36,6	385,45	10,53	105,31
2	40,3	238	5,91	59,06
3	41,6	410,85	9,88	98,76
4	36,58	198	5,41	54,13
5	39,9	212	5,31	53,13
6	43,92	426,05	9,70	97,01
Average value			7,79	77,90

5. NEW DIMENSIONING OF THE CURRENT PILLARS

Giving a new dimension to the pillars left in place, requires the calculation of the safety factor either local for each pillar or global for the entire mining structure, this safety factor is calculated using the expression (Eq. 13).

$$F_S = \frac{\sigma_p}{p_{zz}} \quad (13)$$

Where: σ_p: The pillar Strength; (MPa)
Pzz: The average of the vertical stress.

Checking the robustness or vulnerability of the pillars requires an adequate calculation of the safety factor, which allows the stability of the mine to be assessed and controlled. For Wen et al (2017), an interval of the safety factor must be taken into account progressively with the calculations of the new dimensions of the pillars:

- FS < 1: Critical situation, in this case the pillar no longer supports the applied load.
- 1 < FS < 1.3 : Risk of rupture;
- FS > 1.3 : Optimal dimension of the pillar, stability is ensured

6. RESULTS AND DISCUSSION

6.1. Estimation of Pillar Strength and Safety Factor

The results of the pillar strength calculations, with the corresponding safety factor for each design method used, are shown in Figure 3.

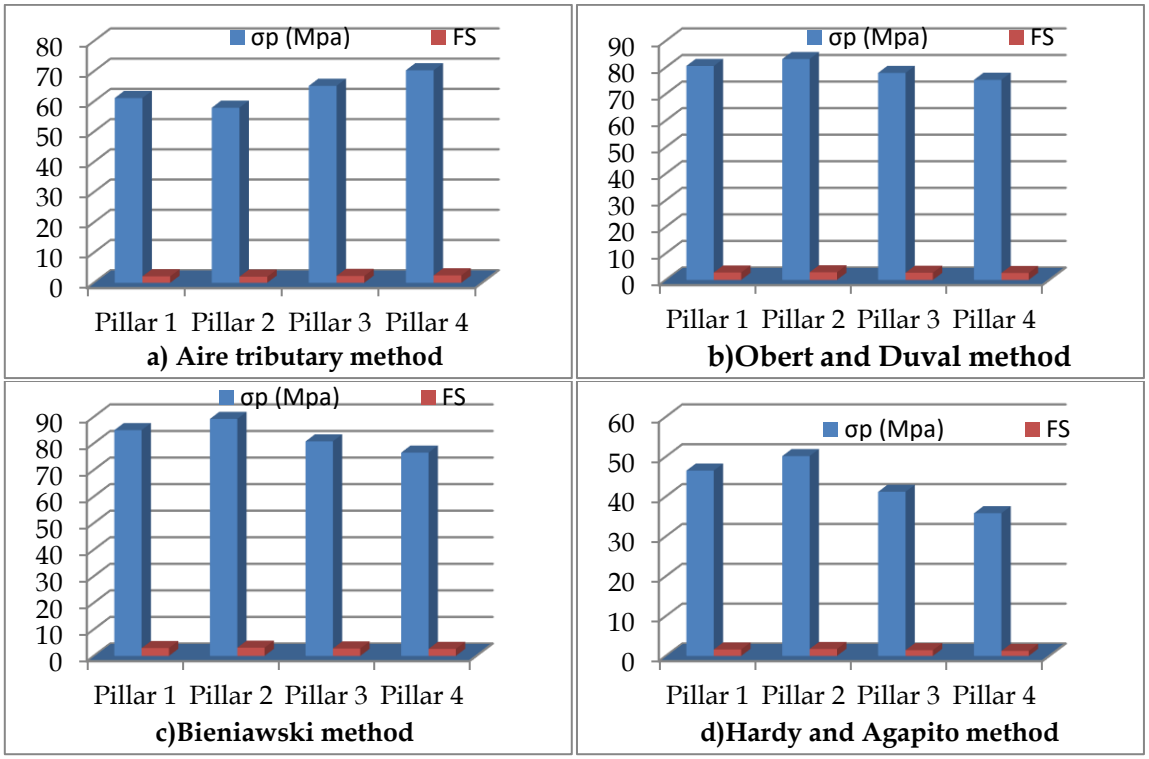

Figure 3. Pillars strength and safety factor using different approaches

From the histograms we not that the safety factor varies from one method to another, therefore between 2.00 to 2.43 for the tributary air method, from 2.6 to 2.78 for the Obert and Duval method, from 2.64 to 3.08 for Bieniwski method and finally between 1.24 to 1.73 for Hardy and Agapito method, with the exception of the fourth pillar with the Hardy and Agapito calculation method, the safety factor equal to 1.24 which seems a little weaker, but overall the stability of the structure is ensured. The results are almost similar for all four methods and the structure is well supported by these pillars. Table 4 shows us the values of the safety factor for the different pillars before dimensioning.

Table 4. Extraction rate and the safety factor for the various pillars before dimensioning

Pillar	Widht W_p (m)	Lenght l_p (m)	Height h_p (m)	width of the Room w_o (m)	Extraction rate (τ %)	Safty factor (Fs)
1	7.6	12	3	4	50,82%	5.08
2	6	12.5	3	4	54,45%	4.63
3	5.5	11	3	4	57.75%	4.31
4	6	13	3	4	54,41%	4.63

The results obtained are presented graphically in Figure 4.

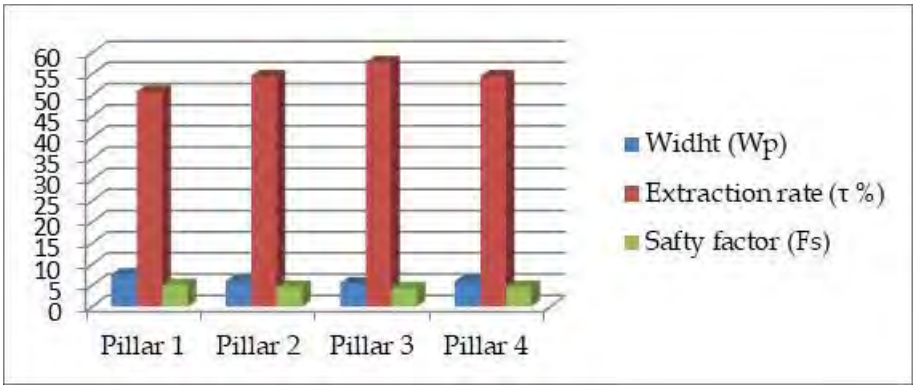

Figure 4. the safety factor of the pillars before dimensioning

From Figure 4, we note that most of the pillars have a very high safety factor and greater than 4, which means that these pillars are robust, and the extraction rate varies from 50.82% to 57.75% which requires sizing the pillars in order to increase this rate while ensuring the stability of the mine. If the safety factor does not correspond to what we are looking for (1,5 for example) we start the process a second time by once again modifying the width of the pillars and/or the rooms. The table below (05) presents the different sizing proposals as well as the corresponding safety factor.

Table 5. New dimensions of the pillars proposed with the corresponding safety factor

Pillar	Pillar widht W_p (m)	Pillar Lenght l_p (m)	Pillar Height h_p (m)	Room width w_o (m)	σ_p (Mpa)	Safty factor
1	1	4	3	7	32,18	1,11
2	2	4	3	6	45,51	1,57
3	3	5,5	3	5	55,74	1,92
4	4	8	3	4	64,36	2,22
5	5	8	3	3	71,95	2,48
6	6	8	3	2	78,82	2,72

The influence of the width and height of the pillars as a function of the safety factor is shown graphically in Figure 5.

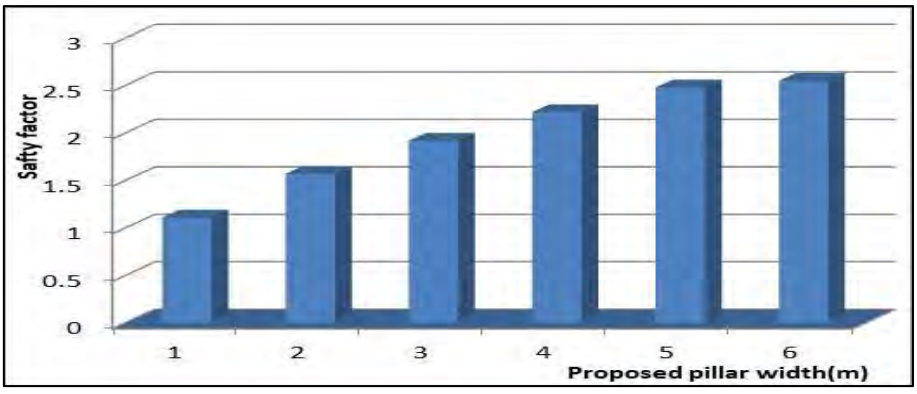

Figure 5. Relationship between safety factors and increasing pillar width

As we know, with the increase in the width of the pillars, the extraction rate decreases as well as the volume of the ore to be extracted. Therefore, it is necessary to choose an optimal critical size for the pillars to ensure good operation and safety. From figure 5, we see that the dimensions of the pillars for 2, 4 and 3 meters (respectively width, length and height of the pillars) give us an ideal safety factor of 1.57 according to Wen et al (2017).

Based on the results mentioned above, a summary of the values for the optimal pillar dimensions and the corresponding safety factor are presented in Table 6.

Table 6. The ideal dimensions of the pillar and the corresponding safety factor

Pillars	Pillar widht a_p (m)	Pillar lenght l_p (m)	Pillar height h_p (m)	Room Widht w_o (m)	σ_p (Mpa)	Safty factor (FS)
	2	4	3	6	45,51	1,57

7. CONCLUSION

Giving a new size of underground mining structures during room and pillar mining, we can create more favorable conditions for mining operations and ensure adequate stability. In this article, we have carried out the sizing of the current pillars, using different approaches.We conclude that:

- Although empirical methods do not provide physical information on the actual state of stress within a pillar. However, the calculated pillar strengths are very close for 3 methods; Tributary air, Obert-Duval and Bieniawski which vary between 57.92 MPa and 89.20 MPa, These values are very sufficient considering the applied load.
- Increasing the extraction rate percentage has the greatest effect on the safety factor, while the effects of other variables vary according to the calculation method applied.
- As an exception, the Hardy-Agapito calculation method gives a slightly lower strength between 35.8 and 46.8 MPa and a safety factor between 1.24 and 1.73. For purely technical reasons, and can be explained by the poor quality of the standard samples taken from the pillars. The lowest value of the safety factor is limited for a single pillar whose stability is verified for the entire structure analytically and numerically.
- As the dimensions of the pillars decrease, the extraction rate increases in an inverse relationship, which consequently increases the volume of ore extracted..
- The new sizing makes it possible to recover nearly 80% of the ore left in place. nevertheless the extraction rate evaluated can be minimized in order to ensure excellent stability

REFERENCES

Bieniawski, Z. T., (1992), “A method revisited: coal pillar strength formula based on field investigations”. In Proceedings of the Workshop on Coal Pillar Mechanics and Design, Vol. 9315, pp. 158–165.

Brady, B. H. G., Brown, E. T., (1985), “Rock Mechanics for Underground Mining”, George Allen & Unwin, 527 p. https://doi.org/10.1002/eqe.4290140510

Cheikhaoui, Y., Bensehamdi, S., Cheniti, H., Kanli, A. I., Benselhoub, A., (2021), “New formula for evaluation of strength pillar in the underground mine of Chaabet El-Hamra (Setif, Algeria)”, Mineralia Slovaca, 53 (1), 57–68.

Diederichs, M. S., Coulson, A., Falmagne, V., Rizkalla, N., Simser, B., (2002), “Application of rock damage limits to pillar analysis at Brunswick Mine”. In: Hammah et al. (eds.), Proceedings of NARMS-TAC 2002, Toronto, Ontario, Canada, University of Toronto, pp. 1325–1332.

Esterhuizen, G. S., Dolinar, D. R., Ellenberger, J. L., Prosser, L. J., (2011), “Pillar and roof span design guidelines for underground stone mines”, NIOSH IC9526, Pittsburgh, PA, pp. 1–64.

Esterhuizen, G. S., (2006), “An evaluation of the strength of slender pillars”. In: Yernberg, W. R. (ed.), Transactions of the Society for Mining, Metallurgy, and Exploration, Vol. 320, Littleton, CO, pp. 69–76.

Hardy, M. P., Agapito, J. F. T., (1977), “Pillar design in oil shale mines”. In Proceedings of the 16th US Symposium on Rock Mechanics, ASCE, New York, USA, pp. 257–266.

Iannacchione, A. T., (1999), “Analysis of pillar design practices and techniques for U.S. limestone mines”, Transactions of the Institution of Mining and Metallurgy, Section A: Mining Industry, 108, A152–A160.

Gale, W. J., (1999), “Experience of field measurement and computer simulation methods of pillar design”. In Proceedings of the Second International Workshop on Coal Pillar Mechanics and Design, NIOSH IC9448, pp. 49–61.

Gao, W., (2018), “Influence of interaction between coal and rock on the stability of strip coal pillar”, Geomechanics and Engineering, 16 (2), 66–78.

González-Nicieza, C., Álvarez-Fernández, M. I., Menendez-Diaz, A., Alvarez-Vigil, A. E., (2006), “A comparative analysis of pillar design methods and its application to marble mines”, Rock Mechanics and Rock Engineering, 39, 421–444. https://doi.org/10.1007/s00603-005-0078-z

Kabwe, E., (2024), “Stability analysis of pillars in an inclined airleg stope under static loading conditions”, Geotechnical and Geological Engineering, 42, 1541–1572. https://doi.org/10.1007/s10706-023-02631-1

Kaiser, P. K., Diederichs, M. S., Martin, C. D., Sharp, J., Steiner, W., (2000), “Underground works in hard rock tunnelling and mining”. GeoEng2000, Melbourne, Australia, Technomic Publishing Co., Vol. 1, pp. 841–926.

Lunder, P. J., (1994), “Hard rock pillar strength estimation—an applied approach”, M.S. Thesis, University of British Columbia, Department of Mining and Mineral Process Engineering, Vancouver, BC.

Li, J., (2020), “The coal pillar design method for a deep mining roadway based on the shape of the plastic zone in surrounding rocks”, Arabian Journal of Geosciences, 13 (12), 1005–1008.

Mark, C., (1999), “Empirical methods for coal pillar design”. In Proceedings of the Second International Workshop on Coal Pillar Mechanics and Design, pp. 145–154.

Manjate, E. P. A., Ohtomo, Y., Arima, T., Adachi, T., Miguel Bene, B., Kawamura, Y., (2024), “Applying nonnegative matrix factorization for underground mining method selection based on mining projects’ historical data”, International Journal of the Society of Materials Engineering Research. https://doi.org/10.5188/ijsmer.626

Mohan, G. M., Sheorey, P. R., Kushwaha, A., (2001), “Numerical estimation of pillar strength in coal mines”, International Journal of Rock Mechanics and Mining Sciences, 38 (8), 1185–1192. https://doi.org/10.1016/S1365-1609(01)00071-5

Obert, L., Duvall, W. I., (1967), “Rock mechanics and the design of structures in rock”, John Wiley & Sons, New York, 650 p.

Qiu, P., Wang, J., (2019), “Rock burst criteria of deep residual coal pillars in an underground coal mine: a case study”, Geomechanics and Engineering, 19 (6), 111–123.

Tzalamarias, M., Tzalamarias, I., Benardos, A., Marinos, V., (2019), “Room and pillar design and construction for underground coal mining in Greece”, Geotechnical and Geological Engineering, 37, 1729–1742. https://doi.org/10.1007/s10706-018-0717-2

Verma, A. K., (2014), “A comparative study of various empirical methods to estimate the factor of safety of coal pillars”, American Journal of Mining and Metallurgy, 2 (1), 17–22. https://doi.org/10.12691/ajmm-2-1-3

Zhao, J., (2000), “Applicability of Mohr-Coulomb and Hoek-Brown strength criteria to dynamic strength of brittle rock materials”, International Journal of Rock Mechanics and Mining Sciences, 37, 1115–1121.

MODELING, SIMULATION, CONTROL AND AUTOMATION IN MINERAL PROCESSING

APPLICATION OF DATA ANALYTICS IN MINERAL PROCESSING: TOWARDS DIGITAL PERFORMANCE PREDICTION AND PROCESS OPTIMIZATION

Oğuzhan Mert GÜRKAN*, Hüseyin BAŞTÜRKCÜ

Istanbul Technical University, Faculty of Mines, Mineral Processing Engineering Department, 34469, Maslak, Istanbul, TÜRKİYE
**Corresponding author: gurkanog@itu.edu.tr*

A B S T R A C T

The mineral processing industry faces increasing pressure to optimize operational efficiency, reduce energy consumption, and improve product quality. This study presents a comprehensive case study on the implementation of data analytics and machine learning techniques in a hypothetical copper-molybdenum concentrator plant. The integrated system encompasses grinding circuit optimization, flotation performance prediction, and predictive maintenance across the entire process chain. Multiple sensor networks including power consumption monitors, particle size analyzers, and froth imaging systems were deployed to collect real-time operational data. Machine learning algorithms including Artificial Neural Networks (ANN), Random Forest (RF), Convolutional Neural Networks (CNN), and Long Short-Term Memory (LSTM) networks were applied to develop predictive models for key performance indicators. Results demonstrate significant improvements in energy efficiency, with grinding circuit optimization achieving 8-12% reduction in specific energy consumption while maintaining target particle size distribution (P80 prediction accuracy R^2 = 0.92). The flotation performance prediction system achieved 94% accuracy in copper recovery estimation through integration of froth image analysis and process parameters. Predictive maintenance implementation for SAG mill bearing systems reduced maintenance costs by 25% and unplanned downtime by 40%. Implementation challenges including data quality assurance, model validation, and operator acceptance are discussed. This work demonstrates the practical application of Industry 4.0 technologies in mineral processing and provides a roadmap for digital transformation in the mining sector.

Key words: *Data analytics, machine learning, mineral processing, flotation optimization, predictive maintenance, digital twin*

1. INTRODUCTION

The mining and mineral processing industry is undergoing a significant digital transformation, driven by the need to improve operational efficiency, reduce costs, and minimize environmental impact. Traditional process control methods, primarily based on operator experience and simple feedback loops, are increasingly inadequate for modern complex operations where multiple variables interact in nonlinear ways (McCoy and Auret, 2019). The integration of advanced data analytics and machine learning techniques offers unprecedented opportunities to optimize mineral processing operations through real-time performance prediction and automated decision-making.

Recent developments in sensor technology, data acquisition systems, and computational capabilities have enabled the collection and processing of massive amounts of operational

data. Semi-autogenous grinding mills can generate thousands of data points per minute from power draw sensors, bearing vibration monitors, and mill load indicators. Flotation circuits equipped with machine vision systems and online analyzers provide continuous streams of information about froth characteristics, pulp chemistry, and concentrate quality (Aldrich et al., 2010). However, the challenge lies not in data collection, but in extracting actionable insights from these large datasets to enable predictive control and optimization.

Machine learning algorithms have demonstrated remarkable success in modeling complex, nonlinear processes in mineral processing. Studies have shown that artificial neural networks can predict SAG mill performance with high accuracy, achieving production increases of 4-5% and energy consumption reductions of 7-8% through optimization of operating parameters (Avalos et al., 2020; Saldaña et al., 2023). Convolutional neural networks applied to flotation froth image analysis have achieved classification accuracies exceeding 94% (Zhou and He, 2024; Chen et al., 2025), enabling real-time monitoring of operational regimes. These advances suggest that data-driven approaches can complement or even surpass traditional mechanistic models in many applications.

This study presents a comprehensive case study examining the hypothetical implementation of an integrated data analytics platform in a medium-scale copper-molybdenum concentrator. The objectives are to: (1) demonstrate the application of machine learning algorithms for grinding circuit optimization and particle size prediction, (2) develop flotation performance prediction models incorporating froth image analysis, (3) implement predictive maintenance systems for critical equipment, and (4) identify practical challenges and solutions for industrial deployment of these technologies.

2. MATERIALS AND METHODS

The case study is based on a hypothetical copper-molybdenum concentrator plant with a nominal capacity of 10,000 tonnes per day. The processing circuit (Figure 1) consists of primary crushing followed by semi-autogenous grinding (SAG mill: 36 ft diameter × 18 ft length) and ball milling (24 ft diameter × 40 ft length) in closed circuit with hydrocyclones. The comminution circuit is designed to achieve a target particle size of P80 = 150 μm (Parian et al., 2021). The flotation circuit comprises rougher, scavenger, and three stages of cleaner flotation for copper concentration, followed by a separate molybdenum circuit for copper-molybdenum separation. The plant processes porphyry copper ore with an average copper grade of 0.65% Cu and molybdenum grade of 0.015% Mo. The existing plant automation system consists of distributed control systems (DCS) for basic process control, programmable logic controllers (PLCs) for equipment interlocks, and a supervisory control and data acquisition (SCADA) system for monitoring.

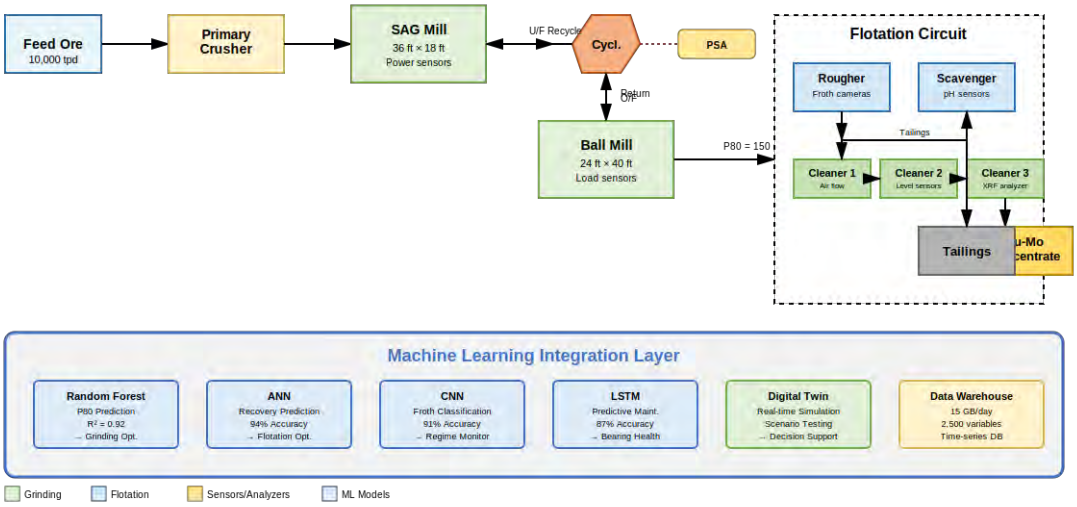

Figure 1. Simplified process flowsheet of the hypothetical copper-molybdenum concentrator

A comprehensive sensor network was deployed across the plant to enable data-driven modeling and control. The grinding circuit instrumentation includes: (a) SAG mill power draw monitoring at 1-second intervals, (b) bearing temperature and vibration sensors on all rotating equipment, (c) mill load and position sensors, (d) feed rate measurement via belt scales with ±0.5% accuracy, (e) hydrocyclone pressure and density sensors, and (f) online particle size analyzers at cyclone overflow streams with 30-second measurement cycles (Ghasemi et al., 2025). The flotation circuit monitoring system incorporates: (a) machine vision cameras with LED illumination mounted above rougher and cleaner flotation cells, capturing images at 1 Hz resolution, (b) air flow rate sensors for each flotation bank with ±2% accuracy, (c) froth level sensors using ultrasonic technology, (d) pH and dissolved oxygen probes in each conditioning tank, (e) online XRF analyzers for concentrate grade measurement with 5-minute analysis cycles, and (f) pulp density meters throughout the circuit (Liu and Aldrich, 2022). All sensor data streams are collected through industrial Ethernet networks and stored in a time-series database with automatic data validation and cleaning protocols. The system handles approximately 2,500 process variables sampled at frequencies ranging from 1 second to 5 minutes, generating roughly 15 GB of structured data per day. Image data from flotation cameras adds an additional 200 GB per day in compressed format.

Multiple machine learning algorithms were evaluated for different prediction tasks based on their suitability for the specific characteristics of each process unit (Table 1). The selection criteria included prediction accuracy, computational efficiency for real-time implementation, interpretability of results, and robustness to missing or noisy data (McCoy and Auret, 2019).
For grinding circuit optimization, Random Forest (RF) regression models were employed to predict P80 particle size as a function of mill operating parameters including: fresh feed rate, circulating load ratio, mill speed, ball charge volume, ore hardness index, and mill power draw (Saldana et al., 2026). The RF algorithm was selected for its ability to capture nonlinear relationships and interactions between variables while providing feature importance rankings. The model was trained on 6 months of historical data (approximately 2.6 million data points) with an 80:20 train-test split. Hyperparameter optimization was performed using grid search with 5-fold cross-validation.

Artificial Neural Networks (ANN) with two hidden layers were developed for flotation copper recovery prediction (McCoy and Auret, 2019). Input variables included: feed grade and particle size distribution, collector and frother dosages, pH, pulp density, air flow rate, conditioning time, and froth characteristics from image analysis. The network architecture was optimized through systematic testing, with the final configuration consisting of 15 input nodes, two hidden layers of 30 and 20 neurons respectively, and a single output node. The rectified linear unit (ReLU) activation function was used in hidden layers, with Adam optimizer for training. Data normalization was applied using z-score standardization.

Convolutional Neural Networks (CNN) were implemented for flotation froth image classification to identify operational regimes (Zhou and He, 2024). The transfer learning approach was adopted, utilizing a pre-trained MobileNetV2 architecture fine-tuned on flotation-specific image datasets. Images were classified into four operational states: optimal (stable froth with medium bubble size), underloaded (large unstable bubbles), overloaded (small compact bubbles with low mobility), and transition (mixed characteristics). A dataset of 45,000 labeled images collected over 3 months was used for model training, with data augmentation techniques including rotation, scaling, and brightness adjustment to improve model generalization.

Long Short-Term Memory (LSTM) networks were applied for predictive maintenance of SAG mill bearings. The LSTM architecture is particularly suited for time-series forecasting with long-term dependencies. Input features included vibration spectra (FFT components), bearing temperature trends, lubrication system parameters, mill load variations, and operating hours since last maintenance. The model was trained to predict bearing health index 24-48 hours in advance, enabling proactive maintenance scheduling. Historical data from previous bearing failures and normal operations were used to create labeled training datasets.

Table 1. Summary of machine learning models applied in the case study

Application Area	Algorithm	Key Input Variables	Output
Grinding Circuit	Random Forest	Mill power, feed rate, ore hardness, cyclone pressure	P80 particle size
Flotation Recovery	Artificial Neural Network	Feed grade, particle size, reagent dosages, pH, air flow	Copper recovery (%)
Froth Classification	CNN (MobileNetV2)	Froth images (224×224 pixels)	Operational regime (4 classes)
Predictive Maintenance	LSTM	Vibration spectra, temperature, load, operating hours	Bearing health index

Figure 2 illustrates the complete data analytics workflow, showing the integration of data collection, processing, machine learning models, and optimization layers.

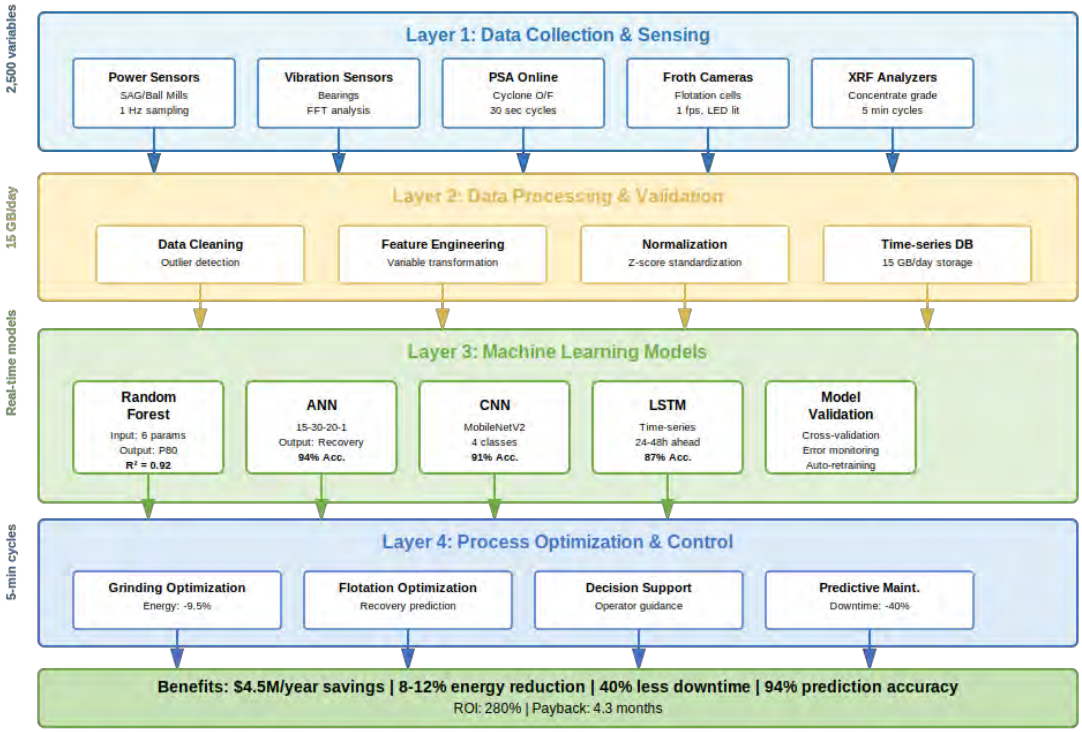

Figure 2. Data analytics and machine learning workflow for process optimization

3. RESULTS AND DISCUSSION

Figure 3 presents the performance comparison of all four machine learning models developed in this study, demonstrating that each algorithm achieved accuracy levels exceeding the target threshold of 85%.

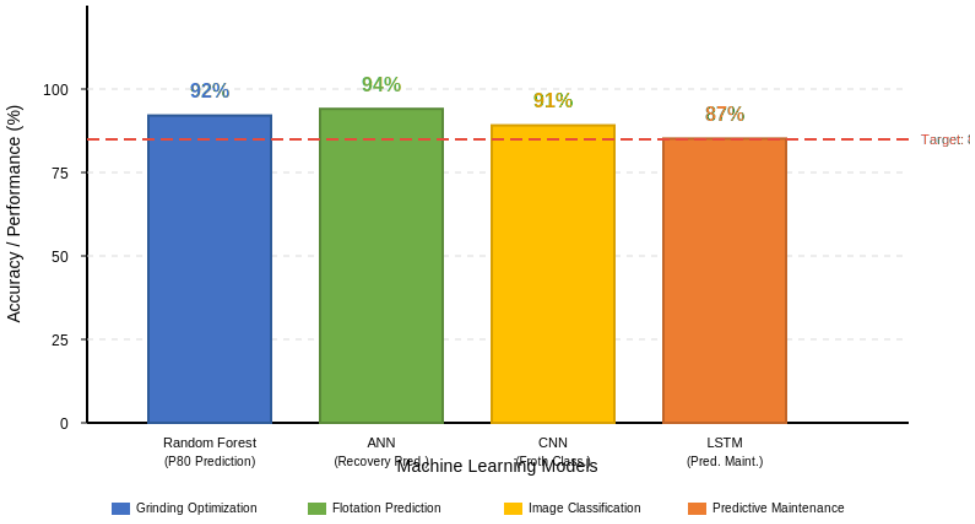

Figure 3. Machine learning model performance metrics

The Random Forest model for P80 prediction demonstrated excellent performance with R^2 = 0.92 on the test dataset and mean absolute percentage error of 4.3%. Feature importance analysis revealed that mill power draw, ore hardness (Bond work index), and cyclone

pressure were the most influential variables for particle size prediction (Ghasemi et al., 2025). The model successfully captured the complex nonlinear relationships between operating parameters and grinding performance across varying ore characteristics.

Implementation of model-based optimization led to significant improvements in grinding efficiency. By dynamically adjusting mill speed, feed rate, and cyclone parameters based on real-time ore hardness measurements and P80 predictions, the system achieved an 8-12% reduction in specific energy consumption (kWh/tonne) while maintaining target product size distribution (Saldaña et al., 2023). The optimization algorithm operated in closed-loop mode with 5-minute update cycles, automatically adjusting setpoints to maintain optimal operating conditions. During periods of hard ore processing, the system reduced throughput to maintain grinding quality, while soft ore periods allowed for increased production rates.

The energy savings provide significant operational benefits for medium to large-scale operations. Table 2 summarizes the quantitative improvements achieved through the grinding circuit optimization implementation. Additional benefits include more consistent product quality delivered to flotation, reducing variability in downstream processes and improving overall plant stability. The grinding circuit availability improved by 3% due to reduced mechanical stress from optimized loading conditions.

Table 2. Grinding circuit optimization results

Performance Metric	Before Optimization	After Optimization	Improvement
Specific Energy (kWh/t)	16.8	15.2	-9.5%
P80 Target Achievement (%)	84	96	+14%
P80 Standard Deviation (μm)	18.5	9.2	-50%
Model Accuracy (R^2)	-	0.92	-
Circuit Availability (%)	91	94	+3%

The ANN-based flotation recovery prediction model achieved 94% accuracy in estimating copper recovery within ±2% of actual metallurgical assay results. The model successfully predicted recovery variations caused by changes in ore mineralogy, reagent dosage, and operating conditions with response times under 10 seconds, enabling near real-time performance monitoring. Cross-validation studies demonstrated robust model performance across different ore types and operating regimes encountered during the training period.

The CNN froth image classification system demonstrated outstanding performance with overall accuracy of 91% in identifying operational regimes (Zhou and He, 2024). As shown in Figure 4, the system was trained to recognize four distinct operational states based on visual characteristics of the flotation froth. The confusion matrix analysis revealed that most misclassifications occurred between optimal and transition states, which is expected given the gradual nature of operational state changes. The system proved particularly effective at detecting underloaded and overloaded conditions, which require immediate operator intervention. Integration of froth classification results with process parameter monitoring provided a more comprehensive understanding of flotation behavior than either approach alone.

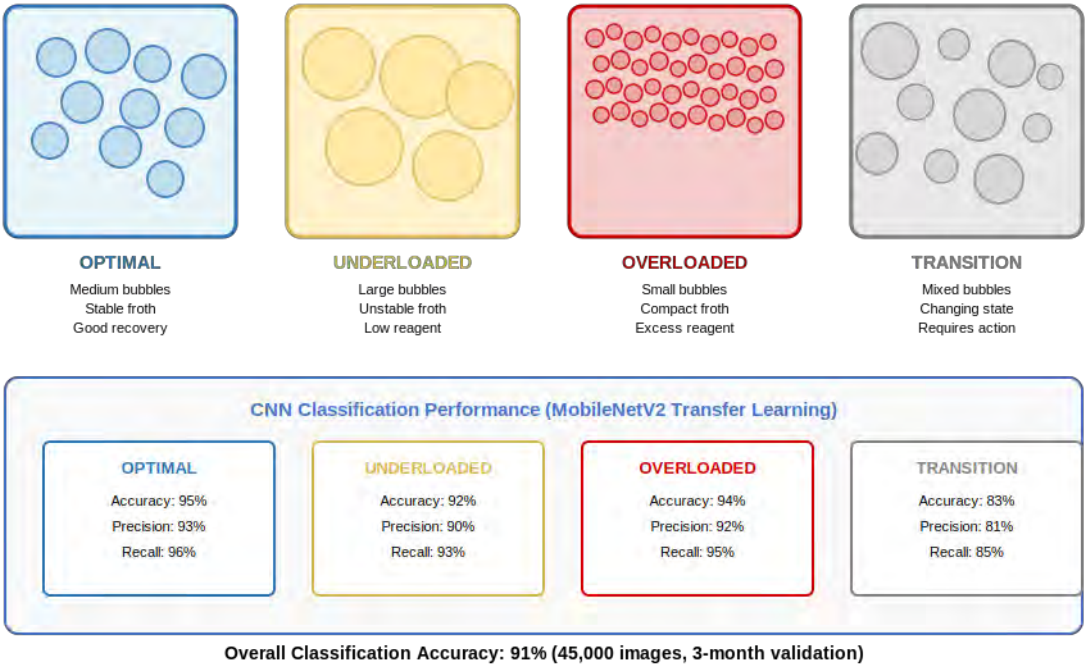

Figure 4. CNN froth classification operational states (Zhou and He, 2024)

Correlation analysis between froth visual characteristics and metallurgical performance revealed strong relationships between bubble size distribution and copper recovery (Chen et al., 2025). Optimal performance was consistently associated with medium-sized bubbles (2-4 mm diameter) with moderate froth stability. The machine vision system quantified froth velocity, bubble size, and color intensity, providing objective measurements that traditionally relied on subjective operator observations (Aldrich et al., 2010). Implementation of the integrated flotation monitoring system enabled development of an operator decision support system that recommends reagent dosage adjustments based on predicted recovery and froth conditions. During a 3-month validation period, the system identified 47 operational excursions that were not detected by traditional monitoring methods, allowing for corrective actions that prevented significant production losses.

The LSTM-based predictive maintenance system for SAG mill bearings achieved a prediction accuracy of 87% for bearing failures 24-48 hours in advance, with a false positive rate of 12%. The system successfully identified five critical bearing degradation events during the evaluation period, all of which were confirmed by subsequent physical inspection. Figure 5 illustrates a typical prediction timeline, showing how the LSTM model detected gradual degradation in bearing health index well before critical failure would occur. Early warning capabilities allowed maintenance teams to schedule repairs during planned shutdowns rather than responding to emergency failures.

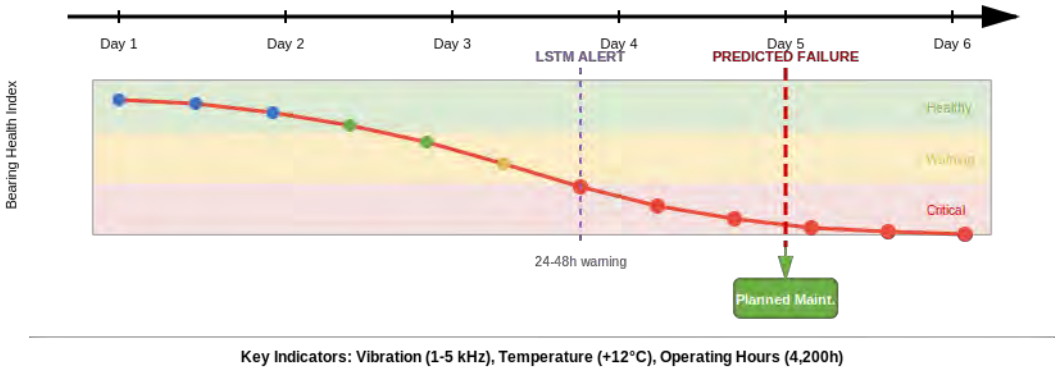

Figure 5. LSTM predictive maintenance timeline and bearing health monitoring

The predictive maintenance implementation resulted in a 25% reduction in maintenance costs through optimized spare parts inventory, reduced emergency overtime, and elimination of costly rush orders for replacement bearings. Unplanned downtime decreased by 40%, translating to approximately 35 additional operating hours per month. The improved reliability provides substantial value through increased production time and reduced maintenance expenses. Analysis of bearing vibration patterns revealed that specific frequency components in the 1-5 kHz range provided the strongest indicators of impending failure. The LSTM model successfully learned these complex temporal patterns and their relationships to bearing degradation, demonstrating the value of deep learning approaches for condition monitoring applications where traditional rule-based systems struggle with high-dimensional sensor data.

3.1. Implementation Challenges and Practical Considerations

Data Quality and Preprocessing: One of the most significant challenges encountered was ensuring data quality and consistency. Approximately 15-20% of collected sensor data required filtering or imputation due to sensor malfunctions, communication errors, or calibration drift. Development of robust data validation and cleaning protocols was essential before model training (McCoy and Auret, 2019). Automated outlier detection algorithms based on statistical process control principles were implemented to identify and flag suspect data points. Missing data handling strategies included forward-fill methods for slowly varying parameters and interpolation for higher-frequency measurements.

Model Generalization and Validation: Ensuring that machine learning models generalize well to operating conditions not represented in training data proved challenging. Models trained on data from specific ore types showed degraded performance when ore characteristics changed significantly. This necessitated development of adaptive learning strategies where models are periodically retrained with recent data. A sliding window approach with 3-month data retention was implemented to maintain model relevance while managing computational resources. Validation protocols were established to trigger model retraining when prediction errors exceeded predefined thresholds.

Operator Acceptance and Change Management: Gaining operator trust in automated systems required extensive training and demonstration of system reliability. Initial skepticism

about algorithm-generated recommendations was addressed through parallel operation periods where system predictions were compared against operator decisions and actual outcomes. Transparency in model predictions through visualization of key influencing factors helped operators understand and trust system recommendations. The decision support system was designed to provide explanations for its suggestions rather than operating as a black box.

Integration with Existing Control Systems: Modern machine learning systems can be integrated with existing plant control infrastructure through standard industrial communication protocols, enabling seamless data exchange and control implementation. Careful attention to system architecture and data security requirements ensures reliable operation within the existing automation framework.

Computational Resources and Real-Time Performance: Balancing model complexity with real-time performance requirements necessitated careful optimization of algorithms. While complex deep learning models provided marginal accuracy improvements, their computational demands made real-time implementation impractical. Simpler models with 90-92% accuracy but sub-second inference times proved more valuable for operational applications than highly complex models with 95% accuracy requiring several seconds for predictions. Edge computing architecture was adopted to distribute computational load and minimize latency in critical control loops.

4. CONCLUSION

This case study demonstrates the significant potential of data analytics and machine learning applications in mineral processing operations. The integrated implementation across grinding, flotation, and maintenance domains achieved substantial improvements in operational efficiency, product quality, and equipment reliability. Key achievements include 8-12% reduction in grinding energy consumption, 94% accuracy in flotation performance prediction, and 40% reduction in unplanned downtime through predictive maintenance.

The success of this implementation relied on several critical factors: comprehensive sensor networks providing high-quality data, appropriate selection of machine learning algorithms matched to specific process characteristics, robust data management and preprocessing infrastructure, and effective change management to ensure operator acceptance. The demonstrated improvements in energy efficiency, process stability, and equipment reliability highlight the value proposition of digital transformation initiatives in the mineral processing sector.

Several challenges must be addressed for wider adoption of these technologies in the mineral processing industry. Data quality issues remain a persistent concern, requiring ongoing attention to sensor maintenance and calibration. Model validation and adaptation to changing operating conditions necessitate continuous monitoring and periodic retraining. Integration with existing control infrastructure requires careful planning and appropriate technical expertise. Operator training and change management are essential for successful deployment.

Future work should focus on developing more sophisticated integration between different process units through digital twin technologies, enabling plant-wide optimization rather than isolated improvements in individual circuits. Advanced techniques such as reinforcement learning for autonomous process control, transfer learning to accelerate model deployment across multiple plants, and explainable AI methods to improve operator trust and model interpretability represent promising research directions (McCoy and Auret, 2019). The development of industry-standard datasets and benchmarks would facilitate more rapid advancement of machine learning applications in mineral processing, enabling researchers and practitioners to validate and compare different approaches systematically.

The results presented in this hypothetical case study are based on published literature and represent realistic expectations for data analytics implementation in mineral processing. As the industry continues its digital transformation journey, the integration of artificial intelligence and machine learning will become increasingly essential for maintaining competitive operations in an era of declining ore grades, increasing energy costs, and growing environmental constraints.

REFERENCES

Aldrich, C., Marais, C., Shean, B.J., Cilliers, J.J., (2010) "Online monitoring and control of froth flotation systems with machine vision: A review", International Journal of Mineral Processing, 96, 1-13.

Avalos, S., Kracht, W., Ortiz, J.M., (2020) "Machine Learning and Deep Learning Methods in Mining Operations: A Data-Driven SAG Mill Energy Consumption Prediction Application", Mining, Metallurgy & Exploration, 37, 1197-1212.

Chen, X., Liu, D., Yu, L., Shao, P., An, M., & Wen, S., (2025) "Recent advances in flotation froth image analysis via deep learning", Engineering Applications of Artificial Intelligence, 147, 109515.

Ghasemi, Z., Neshat, M., Aldrich, C., Zanin, M., Chen, L., (2025) "Optimising SAG mill throughput and circulating load using machine learning models: A multi-objective approach for identifying optimal process parameters", Minerals Engineering, 218, 109009.

Liu, X., Aldrich, C., (2022) "Recent advances in flotation froth image analysis", Minerals Engineering, 188, 107823.

McCoy, J.T., Auret, L., (2019) "Machine Learning Applications in Minerals Processing: A Review", Minerals Engineering, 132, 95-109.

Parian, M., Mwanga, A., Lamberg, P., Rosenkranz, J., (2021) "Ore texture breakage characterization and fragmentation into multiphase particles", Powder Technology, 378, 164-180.

Saldana, M., Gálvez, E., Sales-Cruz, M., Salinas-Rodríguez, E., Castillo, J., Navarra, A., Cisternas, L. A., (2026) "A Stochastic Model Approach for Modeling SAG Mill Production and Power Through Bayesian Networks: A Case Study of the Chilean Copper Mining Industry", Minerals, 16(1), 60.

Saldaña, M., Gálvez, E., Navarra, A., Toro, N., & Cisternas, L. A., (2023) "Optimization of the SAG Grinding Process Using Statistical Analysis and Machine Learning: A Case Study of the Chilean Copper Mining Industry", Materials, 16(8), 3220.

Zhou, X., He, Y., (2024) "Deep Ensemble Learning-Based Sensor for Flotation Froth Image Recognition", Sensors, 24(15), 5048.

APPLICATION OF THE RESPONSE SURFACE METHODOLOGY (RSM) TO THE ENRICHMENT OF ESPEY COLEMANITE WASTES BY MICROWAVE

Arzu KAHVECİOĞLU[1,*], Kırali MÜRTEZAOĞLU[2], Zehra ZEYBEK[3], Ahmet AYDIN[4]

[1] Gazi University, Institute of Science, Department of Chemical Engineering, Ankara, Turkey
[2] Gazi University, Department of Chemical Engineering, Ankara, Turkey
[3] Ankara University, Department of Chemical Engineering, Ankara, Turkey
[4] Kütahya Dumlupınar University, Department of Mining Engineering, Kütahya, Turkey
**Corresponding author: a.kahvecioglu81@gmail.com*

A B S T R A C T

In this article, the chemical, thermal, mineralogical and particle size properties of fine (-3 mm), 15,22% B_2O_3 containing wastes sent to tailings dams at the Espey concentrator facility in Turkey were determined and the enrichment of boron in the wastes was investigated by applying the microwave method. In the study, residence time in the microwave device and microwave power were selected as independent variables affecting the enrichment of B_2O_3. For +0,045 mm particle size, colemanite concentrated B_2O_3 grade (Y_1), concentrated product yield (Y_2), waste grade (Y_3) and waste yield (Y_4) are dependent variables. It was defined as concentrated B_2O_3 grade (Y_5), concentrated product yield (Y_6), waste grade (Y_7) and waste yield (Y_8) for -0,045 mm particle size. By the statistical design of the experiments and the response surface method, these variables fit quadratic models. To verify the adequacy of the model, variance analysis, ANOVA test and optimization were performed with the design expert 12 package program. As a result of the optimization of 8 models from Y_1 to Y_8 with particle sizes of +0,045 mm and -0,045 mm, 490 watts of microwave power and 35 minutes of residence time in the device were found to be the optimum value. According to ANOVA analysis of variance, the R^2 value of the regression coefficients determined for the validity of the models Y_1, Y_2, Y_3, Y_4, Y_5, Y_6, Y_7, Y_8 efficiency were found to be 0,9601, 0,8810, 0,9332, 0,8245, 0,8381, 0,8074, 0,7259 and 0,8825, respectively. This showed that 95% of the experimental values matched those predicted from the model. As a result of the study, the concentrate grade increased to 33,33% of B_2O_3.

Key words: *Colemanite, microwave, boron enrichment, response surface methodology (RSM), optimization*

1. INTRODUCTION

In a study investigating the efficient recovery of boron from aqueous solutions, researchers investigated the optimal conditions for achieving boron recovery efficiency using response surface method (RSM) analysis, which included key operating parameters such as contact time, boron concentration, adsorbent dosage, and pH. As a result, they found that a contact time of 200 minutes, a boron concentration of 1450 mg/lt, an adsorbent dosage of 800 mg/lt, and a pH of 7 were the optimum values (Al-dhawi et al., 2023).

In a study optimizing the effect of colemanite as a novel synergistic agent (Atikler et al., 2006), a swelling system containing ammonium polyphosphate as an acid source and blowing agent, pentaerythritriol as a carbofic agent, and colemanite as a synergistic agent was used to increase the flame retardancy of polypropylene, and D-optimal mixture design was employed in the studies. According to the statistical analysis of the cubic model defining the limiting oxygen index (LOI), the coefficient of determination (R^2) was found to be 0,9881.

The main objective of this study was to select a low-grade Espey colemanite size (-3 mm) for microwave studies. Samples of this size were subjected to enrichment experiments of B_2O_3 according to a central composite design of two-factorial experiments dealing with previously untried simultaneous exchange, for a maximum of 60 minutes and a minimum of 10 minutes

in a microwave device with a power of 800 watts to a minimum. And according to the response surface method, the optimum microwave power and duration were obtained in this study.

2. MATERIAL AND METHODS

Table 1 shows the particle size distributions of the Espey Tailings Dam sample, containing 15,22% B_2O_3 and varying in size (-3 mm), to be used in the experiments. Table 2 shows distributions of the colemanite sample from the Espey tailings dam, used in microwave experiments to increase the B_2O_3 content, according to particle sizes of +0,045 mm and -0,045 mm. In the analysis of boron trioxide, the Turkish Standards Institute's TS 13665:2017 standard for industrial use of boric acid and boron trioxide - Determination of boron trioxide - Titrimetric method was used. (Kahvecioğlu et al., 2024:1531-1533).

Table 1. Grade distribution of colemanite sample from Espey tailings dam according to particle size

Particle size (mm)	Weight (%)	ΣEÜ (%)	ΣEA (%)	B_2O_3 (%)
+2	0,00	0,00	100,00	
-2+1	0,06	0,06	100,00	
-1+0,5	7,57	7,63	99,94	13,60
-0,5 +0,425	5,482	13,11	92,37	15,35
-0,425+0,300	9,454	22,56	86,89	17,07
-0,300+0,212	20,692	43,25	77,44	15,67
-0,212+0,125	17,916	61,17	56,75	17,75
-0,125+0,075	9,336	70,51	38,83	15,36
-0,075+0,045	5,68	76,19	29,49	15,64
-0,045	23,81	10,00	23,81	12,63
Total	100,00			

Table 2. Grade distribution of colemanite sample from Espey tailings dam according to +0,045 mm and -0,045 mm particle sizes

Particle size (mm)	Weight (%)	ΣEÜ (%)	ΣEA (%)	B_2O_3(%)
+0,045	76,19	76,19	100,00	15,78
-0,045	23,81	100,00	23,81	12,63
Total	100,00			

2.1. Experimental Design Studies with Microwave Devices

The optimal conditions for the enrichment process were investigated using the experimental design method (ADM) based on monitoring variables such as optimum B_2O_3 and its yield values for concentrate and waste, for microwave experiments with particle sizes of +0,045 mm and -0,045 mm. In this study, the variables affecting B_2O_3 enrichment were assigned as two variables: microwave residence time of colemanite waste and microwave power. For dwell time, values between 10 and 60 minutes were selected, and for microwave power, values between 180 and 800 watts were chosen. For use in experimental design, five level factors were defined for each variable in coded form. Thus, the levels of each variable, along with their symbols, are shown in Table 3.

Table 3. Levels of the experimental scale and ındependent test variables

Real variables (x_j)	Symbol	Coded variables X_1, X_2				
		-1,41421	-1	0	+1	+1,41421
ξ_1: Time	dk	10	17,32	35	52,68	60
ξ_2: Power	watt	180	270,80	490	709,20	800

The principle of the study is to analyze the variance of the regression using the ANOVA method. This method verifies the fit of second-order models. After determining the most practical terms according to the confidence level (95%, 99%, or 99,99%), regression equations were derived. Response Surface Methodology was used as a sequential process to generate iso-reflective curves and response surfaces (Yi et al., 2010). These results were used to examine linear effects. The experimental matrix, divided into two groups, consists of 13 experiments. The 3D graphics generated by Design-Expert 12.0 illustrate the multiple effects of operating parameters on system responses. (Kahvecioğlu et al., 2024:1534-1535).

Table 4. Experimental design for a nonlinear model explaining concentrate B_2O_3 grade and concentrate product yield, waste grade and waste yield values against power and time variables at particle sizes of +0,045 mm and -0,045 mm

Experiment No	Factor 1: X_1 A: Time minute	Factor 2: X_2 B: Power watt	Real t, minute t, ξ_1	Real E, watt E, ξ_2	+0,045 mm particle size Response 1: Y_1 Concentrated B_2O_3 Grade R_1 (%)	+0,045 mm particle size Response 2: Y_2 Concentrated Product Yield R_2 (%)	+0,045 mm particle size Response 3: Y_3 Waste Grade R_3 (%)	+0,045 mm particle size Response 4: Y_4 Waste Efficiency R_4(%)	-0,045 mm particle size Response 5: Y_5 Concentrated B_2O_3 Grade R_5 (%)	-0,045 mm particle size Response 6: Y_6 Concentrated Product Yield R_6 (%)	-0,045 mm particle size Response 7: Y_7 Waste Grade R_7 (%)	-0,045 mm particle size Response 8: Y_8 Waste Efficiency R_8 (%)
1	0	0	35	490	33,28	85,58	22,80	14,60	32,31	93,80	26,60	6,35
2	-1	-1	17,32	270,80	32,45	83,80	25,50	15,80	32,29	93,05	27,80	6,90
3	-1,41421	0	10	490	31,92	82,20	27,93	17,83	32,50	93,14	27,30	6,85
4	1,41421	0	60	490	33,37	85,78	22,30	14,25	32,28	94,30	26,00	5,80
5	1	-1	52,68	270,80	33,25	85,20	22,80	14,78	32,13	93,47	28,00	6,50
6	0	1,41421	35	800	33,10	85,30	23,80	15,10	32,30	93,60	27,00	6,58
7	0	0	35	490	33,28	85,58	22,80	14,60	32,31	93,80	26,60	6,35
8	0	-1,41421	35	180	32,80	84,00	24,00	16,00	32,24	93,50	27,50	6,70
9	0	0	35	490	33,28	85,58	22,80	14,60	32,31	93,80	26,60	6,35
10	-1	1	17,32	709,20	32,55	83,80	25,00	16,00	32,35	92,80	27,60	7,00
11	1	1	52,68	709,20	33,10	84,70	23,50	15,20	32,25	93,60	27,00	6,43
12	0	0	35	490	33,28	85,58	22,80	14,60	32,31	93,80	26,60	6,35
13	0	0	35	490	33,28	85,58	22,80	14,60	32,31	93,80	26,60	6,35

3. RESULTS AND DISCUSSION

3.1. Experimental Design and Central Composite Design

All studies were conducted according to Response Surface Renewal (RSR), Central Composite Design (CCT). All experimental data collected during the microwave enrichment process of B_2O_3 were analyzed using the design software Design Expert 12. In the experimental design, a central composite design was chosen to find the relationship between a total of 8 responses concentrate B_2O_3 content, concentrate product yield, waste B_2O_3 content, and waste yield for particle sizes of +0,045 mm and -0,045 mm in both concentrate and waste samples, and the 2 independent variables, namely microwave dwell time (X_1) and microwave power (X_2), respectively. The eight responses studied were Y_1: concentrate B_2O_3 content at +0,045 mm particle size, Y_2: concentrate product yield at +0,045 mm particle size, Y_3: waste content at +0,045 mm particle size, Y_4: waste yield at +0,045 mm particle size, Y_5: concentrate B_2O_3 content at -0,045 mm particle size, Y_6: concentrate product yield at -0,045 mm particle size, Y_7: waste content at -0,045 mm particle size, and Y_8: waste yield at -0,045 mm particle size. As shown in Table 4, the number of factors is k=2, and each factor has been increased to 5 levels. The total number of experiments is calculated as 13 according to the equation $2^k + 2k + n_0$, where matrix $2^2 = 4$ factorial experiments + 2×2 = 4 axial points + n_0 = 5 central points. The relationship between the dependent and independent variables was determined by fitting the experimental data to a second-degree polynomial regression model. The following response surface analysis was used to create a second-order polynomial regression model for Y_1, Y_2, Y_3, Y_4, Y_5, Y_6, Y_7, Y_8.

3.2. Suitability of Second-Order Regression Models

Experimental parameters were successfully optimized using central composite design in conjunction with the response surface method. This experimental design was optimized for colemanite waste based on a combination of linear, interactive, and second-order effects of microwave dwell time and microwave power parameters that yielded the highest B_2O_3 enrichment efficiency. The suitability of the experimental data for a second-degree polynomial model and whether the derived equation explains the variability in the responses were evaluated by examining multiple coefficients of determination and performing analyses of variance. One-way analysis of variance (ANOVA) was used to evaluate the analytical power. The significance of the coefficients was measured at a 95% confidence level using the F-test and p-test (Lakens, 2013). If the p-value decreases while the f-value increases, this indicates the significance of the predicted model (Wu et al., 2011).

3.3. Concentrated B_2O_3 Grade at +0,045 mm Particle Size (Y_1)

$$Y_1 = 33.28 + 0.4251X_1 + 0.0468X_2 - 0.0625X_1X_2 - 0.3075X_1^2 - 0.1550X_2^2 \qquad (R^2 = 0.9601) \quad (1)$$

According to Equation 1, the significance of the contribution of microwave dwell time (X_1), the squared term X_1^2, and the square of the microwave power (X_2^2) is shown in Table 5, where p-values are < 0.05.

Table 5. Analysis of variance (anova) for second-order polynomial model of concentrated B_2O_3 grade at +0,045 mm particle size

Factors	Sum of squares	Degrees of freedom	Average square	F value	p value
Model	2,23	5	0,4460	33,69	< 0,0001
x_1	1,45	1	1,45	109,19	< 0,0001
x_2	0,0175	1	0,0175	1,32	0,2879
x_1x_2	0,0156	1	0,0156	1,18	0,3133
x_1^2	0,6578	1	0,6578	49,69	0,0002
x_2^2	0,1671	1	0,1671	12,62	0,0093

The variable X_2 microwave power alone is not significant. The regression coefficient R^2 was found to be 0,9601. The model shows that the response values obtained are significant and highly consistent with experimental data. When R^2 is close to 1, it indicates a good agreement between experimental and predicted values (Myers et al., 2016). Similarly, the adjusted coefficient of determination ($R^2_{adjusted}$) (for the fit of the models was found to be 0,9316. This coefficient confirms that a model is a very good fit, and the Durbin-Watson statistic determines whether there are errors in correlation or autocorrelation. In this case, the value of the corrected coefficient of determination is acceptable.

Table 5 summarizes the analysis of variance (ANOVA) for the concentrate B_2O_3 content at a particle size of +0,045 mm. Fisher's F-test performs this analysis to examine the effects of key factors and their interactions on responses. For a 95% confidence level, the smaller the p-values (< 0,05), and the larger the F-statistic ratio, the more significant the corresponding coefficient term becomes. The F-statistic ratio (p-value) for all linear and interaction effects of the factors examined is shown in Table 5. The interaction between microwave power and microwave exposure time is negligible for the model, with F values of 1,32 and 1,18 respectively X_2, X_1X_2. The interaction between microwave power and microwave power and microwave exposure time, with F values of 1,32 and 1,18 respectively, is negligible for the model. Figure 1 shows the correlation between the observed and predicted values +0,045 for the concentrated B_2O_3 tenor at a particle size of mm. Figure 1.(a) shows that the correlation between the observed and experimental data for Y_1 is very good. These graphs are characterized by point clouds whose alignment is close to a straight line. This indicates that the model is adequate for the response. From the contour and surface graphs in Figures 1.(b) and 1.(c), it can be seen that the optimum microwave residence time (X_{1opt}) corresponding to the maximum concentrated B_2O_3 tenor (Y_1) of 33,4 at a particle size of +0,045 mm corresponds to 35 minutes and 490 watt microwave power (X_{2opt}).

3.4. Concentrate Product Yield Obtained from Waste Sample with Particle Size of +0,045 mm (Y_2)

$$Y_2 = 85.58 + 0.9204X_1 + 0.1673X_2 - 0.1250X_1X_2 - 0.7812X_1^2 - 0.4512X_2^2 \qquad (R^2 = 0.8810) \quad (2)$$

Based on the statistical analysis and model equations of the RSM design in Table 6, the linear terms X_1: microwave dwell time, and the second-order terms X_1^2, X_2^2: microwave dwell time and microwave power, respectively, have significant effects on each yield. Additionally, microwave time had a significant effect ($p < 0,05$). The opposing p-values for the lack of agreement between the same terms (X_2, X_1X_2) as in Y_1 are 0,3613 and 0,6218, respectively. This is shown in Table 7. For Equation (2), R^2 was found to be 0,8810. The high value of the regression coefficient ($R^2 >> 0.7$) indicates a good fit, as shown in Figure 1.(d). The maximum concentrate yield (Y_2) obtained from a waste sample with a particle size of +0,045 mm is 85,5. From the graphs in Figures 1.(e) and 1.(f), the optimum values corresponding to this value of Y_2 were found to be the same as the optimum values found for the maximum concentrated B_2O_3 ratio (Y_1).

Table 6. Analysis of variance (anova) for second-order polynomial model of concentrated product yield at +0,045 mm particle size

Factors	Sum of squares	Degrees of freedom	Average square	F value	p value
Model	12,17	5	2,43	10,37	0,0039
x_1	6,78	1	6,78	28,86	0,0010
x_2	0,2239	1	0,2239	0,9536	0,3613
x_1x_2	0,0625	1	0,0625	0,2662	0,6218
x_1^2	4,25	1	4,25	18,08	0,0038
x_2^2	1,42	1	1,42	6,03	0,0437

3.5. Waste B_2O_3 Grade (Y_3) at +0,045 mm Particle Size

$$Y_3 = 22.80 - 1.52X_1 - 0.0104X_2 + 0.3000X_1X_2 + 1.08X_1^2 + 0.4731X_2^2 \quad (R^2 = 0.9332) \quad (3)$$

The regression coefficient R^2 for Equation 3 was found to be 0,9332. An R^2 value closer to 1 indicates that the regression is very good. In the model equation expressing the B_2O_3 grade (Y_3) in waste with a particle size of +0,045 mm, the same terms (X_2, X_1X_2) are again negligible. We can see this by looking at the p-values in Table 7 for these terms, which are greater than 0,05. F testi değerleri de bu terimler için değerinden küçük kalmaktadır. These values are 0,9577 and 0,2973 respectively. The F-test values for these terms are also less than $F_{critical}$ 3.69. Their values are 0,0030 and 1,27, respectively. The model can be more simply expressed as microwave time X_1 and its square X_1^2, and microwave power squared X_2^2. The fit of the model is evident from the close distribution of the data along the line in Figure 1.(g). From the contour and surface graphs in Figures 1.(h) and 1.(i), respectively, the minimum B_2O_3 content in the waste is read as 23. For this value, the optimum values for X_1 and X_2 are 35 minutes and 490 watts, respectively.

Table 7. Analysis of variance (anova) for second-order polynomial model of waste grade at +0,045 mm particle size

Factors	Sum of squares	Degrees of freedom	Average square	F value	p value
Model	27,75	5	5,55	19,55	0,0006
x_1	18,49	1	18,49	65,12	< 0,0001
x_2	0,0009	1	0,0009	0,0030	0,9577
x_1x_2	0,3600	1	0,3600	1,27	0,2973
x_1^2	8,12	1	8,12	28,61	0,0011
x_2^2	1,56	1	1,56	5,48	0,0517

3.6. Waste Yield Obtained from Waste Sample with +0,045 mm Particle Size (Y_4)

$$Y_4 = 14.60 - 0.8604X_1 - 0.0816X_2 + 0.0550X_1X_2 + 0.6325X_1^2 + 0.3875X_2^2 \quad (R^2 = 0.8245) \quad (4)$$

The second-order model relating the concentrate yield in the waste sample to the microwave dwell time (X_1) and microwave power (X_2) is given by Equation 4. The compatibility of this model was found to be R^2 0,8245. The validity of the model coefficients according to the ANOVA analysis is presented in Table 8. According to this table, the linear effect of X_1 alone is proven to be insignificant, as the p-values of the interaction term where X_1X_2 influence each other are found to be less than 0,05. Figure 1.(j) shows the compatibility of the model with experimental data. In Figures 1.(k) and 1.(l), the optimum values that meet the minimum surface value, i.e., 14,5, are 35 minutes of dwell time and 490 watts of microwave power.

Table 8. Analysis of variance (anova) for second-order polynomial model waste yield at +0,045 mm particle size

Factors	Sum of squares	Degrees of freedom	Average square	F value	p value
Model	9,43	5	1,89	6,58	0,0141
x_1	5,92	1	5,92	20,65	0,0027
x_2	0,0533	1	0,0533	0,1858	0,6794
x_1x_2	0,0121	1	0,0121	0,0442	0,8431
x_1^2	2,78	1	2,78	9,70	0,0170
x_2^2	1,04	1	1,04	3,64	0,0980

4. CONCLUSION

To verify the adequacy of the models developed in this study, regression analysis of variance (ANOVA) was performed on the variables. ANOVA is used to evaluate the following: The variables are the interactions between the factors and their respective responses (Adelodun et al., 2019). The model can be found as follows: When the p-value is less than 0,05, the model is significant. Table 6 results show that the model's predictability at a 99,9% confidence level indicates that the predicted response corresponds to the experimentally obtained response. The experimental Fisher % values of the models are on the order of 28,37 and 10,88 for concentrate grade and concentrate yield, respectively, and 15,68 and 6,00 for waste grade and waste yield, respectively, at a particle size of +0,045 mm. The F-test indicates that an experimental value is more significant, and a value higher than the critical F value (=3,69) suggests that the model is meaningful. In fact, we see that models are important. ($F_{\text{concentrated tenor}} > F_{\text{critical}}$, $F_{\text{concentrate yield}} > F_{\text{critical}}$) Therefore, the smaller the p-value (<0,05), the more significant the model. Therefore, small p-values are statistically significant in terms of concentrate richness and concentrate efficiency of the models. The model is sufficient for prediction within the selected range of variables. The significance of process variables was checked using p and F values. The results show that the models used are meaningful because they have high F values and low p values. The analysis of variance (ANOVA) tables for grade richness and grade yield at a concentrated +0,045 mm particle size

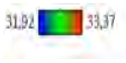

(a)

(b)

(c)

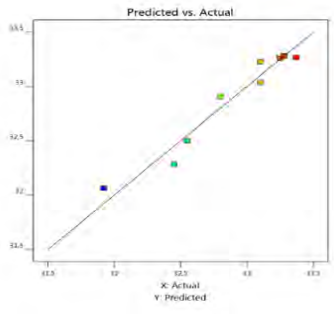

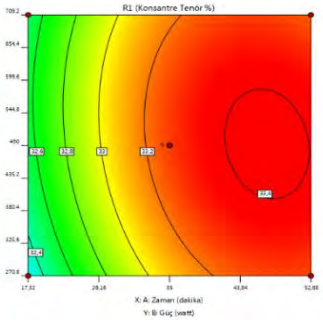

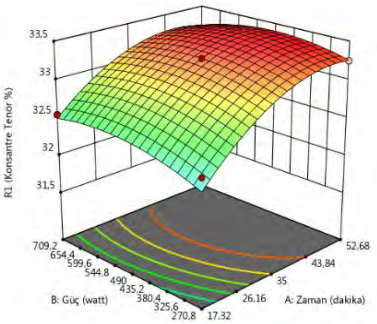

(d)

(e)

(f)

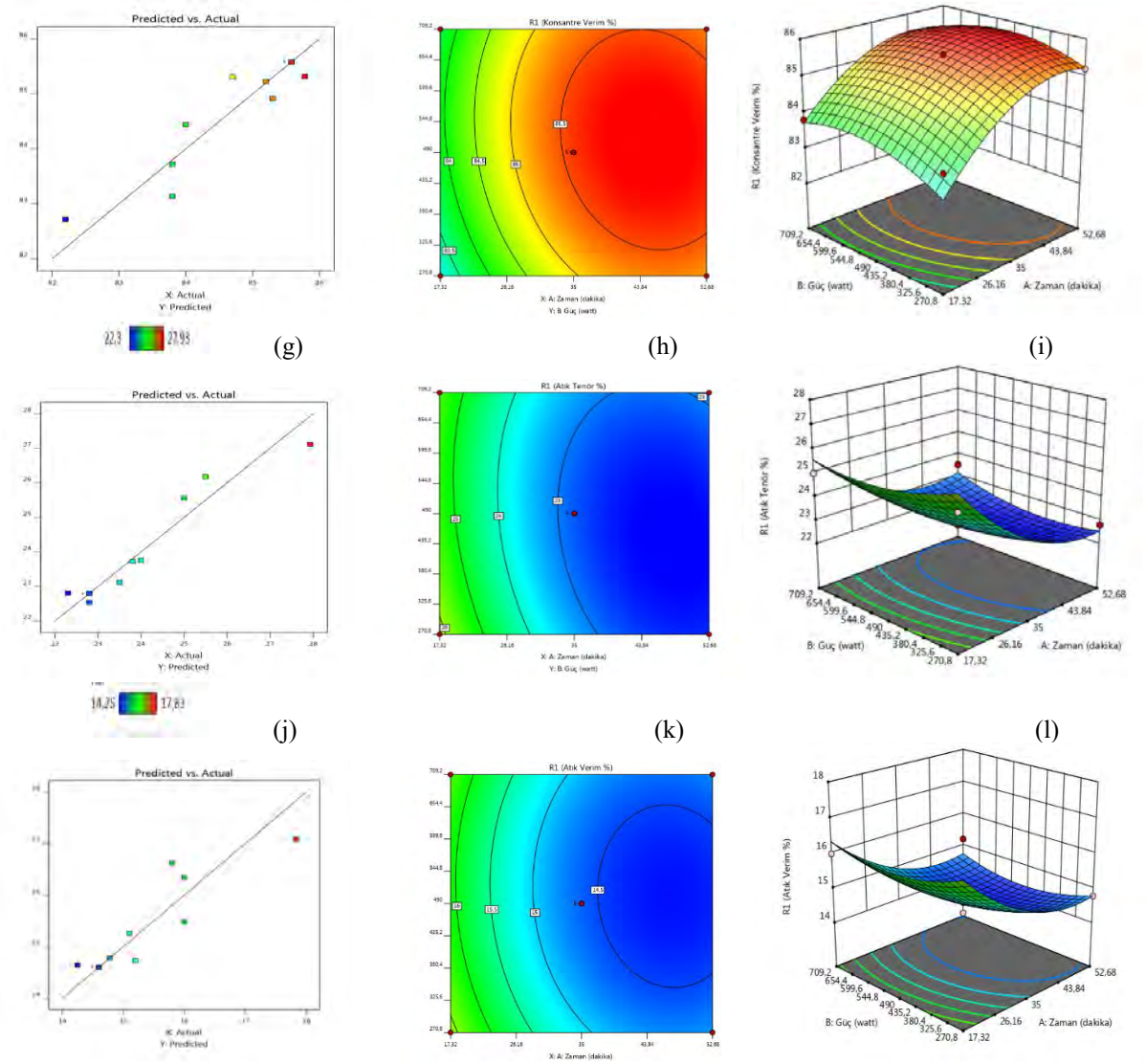

Figure 1. Model with +0,045 mm particle size (a), (d), (g), (j) correlation, power and time showing the effect on concentrate grade, concentrate yield, waste grade and waste yield (b), (e), (h), (k) contour and (c), (f), (i), (l) 3D surface graphs

are summarized. Therefore, the high R^2 values obtained from this optimization study are sufficient for predictions made using the final reduced models. Furthermore, the approximately high value of the adjusted R^2 demonstrates the predictive ability of the developed models to identify the problem. A variable in the estimated regression model is considered significant if its p-value is less than 0,05. One linear variable (X_1) and two second-order terms (X_1^2, X_2^2) were shown to have significant effects ($p < 0,05$) on both concentrate and waste grade and concentrate and waste yield. Since all factors involved in concentrate enrichment (X_1, X_2) have significant linear, second-order effects, microwave dwell time and microwave power contributed significantly to the enrichment of concentrate grade. By examining the multiple coefficients and the performance of the analysis of variance, the experimental data fit the second-degree polynomial model, and the derived equations were evaluated to define the validity of the response. ANOVA was used to analyze the resulting regression equation. Using the F-test and p-test, the significance of the coefficients was measured at a 95% confidence interval. The results of the F-test showed the significance of each coefficient variable, The negligibility of the interaction between microwave dwell time and microwave power r was determined by the resulting p-value. If the p-value decreases as the F-value increases, it indicates that the predicted model is

significant. More importantly, when p-values are < 0,05, < 0,01, and < 0,001, the model terms are significant, highly significant, and expressively significant, respectively. Additionally, the model terms were found to be insignificant for p-values greater than 0,05.

As a result of optimization, the B_2O_3 content in colemanite waste increased from 15,22% to 33,33% at a microwave power of 490 watts and a 35-minute dwell time.

REFERENCES

Atikler, U., Demir, H., Tokatlı, F., Tıhmınlıoğlu, F., Balköse, D., Ülkü, S., (2006) “Optimisation of the effect of colemanite as a new synergistic agent in an intumescent system”, Polymer Degradation and Stability, 91, 1563–1570.

Adelodun, B., Ajibade, F. O., Ogunshina, M. S., Choi, K., (2019) “Dosage and settling time course optimization of *Moringa oleifera* in municipal wastewater treatment using response surface methodology”, Desalination and Water Treatment, 167, 45–56.

Al-Dhawi, B., Kutty, S., Alawag, A., Almahbashi, N., Al-Towayti, F., Algamili, A., Aminu, N., Al-Mekhlafi, A., Birniwa, A., Jagaba, A., (2023) “Optimal parameters for boron recovery in a batch adsorption study: synthesis, characterization, regeneration, kinetics, and isotherm studies”, Case Studies in Chemical and Environmental Engineering, 8, 1–12.

Kahvecioğlu, A., Mürtezaoğlu, K., Zeybek, Z., Aydın, A., (2024) “Application of the response surface methodology (RSM) to the enrichment of Espey colemanite wastes by microwave”, KSU Journal of Engineering Sciences, 27 (4) 1529–1543.

Lakens, D., (2013) “Calculating and reporting effect sizes to facilitate cumulative science: a practical primer for t-tests and ANOVAs”, Frontiers in Psychology, 4, 863.

Myers, R. H., Montgomery, D. C., Anderson-Cook, C. M., (2016) “Response surface methodology: process and product optimization using designed experiments”, John Wiley and Sons, 1–162.
TS 13664, (2017) “Crude sodium borates for industrial use – Determination of boric oxide contents – Titrimetric method”, Turkish Standards Institute, Ankara, 1–11.

Wu, M. C., Lee, S., Cai, T., Li, Y., Boehnke, M., Lin, X., (2011) “Rare-variant association testing for sequencing data with the sequence kernel association test”, The American Journal of Human Genetics, 89 (1) 82–93.

Yi, S., Su, Y., Qi, B., Su, Z., Wan, Y., (2010) “Application of response surface methodology and central composite rotatable design in optimizing the preparation conditions of vinyltriethoxysilane modified silicalite/polydimethylsiloxane hybrid pervaporation membranes”, Separation and Purification Technology, 71 (2) 252–262.

DIGITAL APPROACHES TO SUSTAINABLE MINERAL PROCESSING: MATLAB-BASED SIMULATION OF SENSOR-ASSISTED ORE SORTING

Ali Cemal TANRIKULU, Birgül BENLI*

Istanbul Technical University, Mining Faculty, Mineral Processing Engineering Department, 34469, ISTANBUL-TÜRKİYE
**Corresponding author: benli@itu.edu.tr*

A B S T R A C T

Sustainable mining increasingly relies on digitalization and automation to reduce environmental impact while improving resource efficiency. This study proposes a MATLAB-based conceptual framework for simulating sensor-assisted ore sorting using optical image analysis. The approach aims to demonstrate how brightness and reflectance differences between valuable minerals and gangue phases can be digitally processed to achieve selective separation without laboratory-scale experiments. Through image segmentation, contrast enhancement, and classification algorithms, the model evaluates potential separation accuracy and operational efficiency. This conceptual model offers a low-cost, eco-friendly alternative to conventional trials and supports the transition toward intelligent, energy-efficient mineral processing systems. The integration of such digital tools within green mining strategies aligns with the European Green Deal and Türkiye's 2053 Net-Zero Carbon vision. Overall, this work highlights the potential of MATLAB-based simulations to serve as an initial step toward developing sensor-based, sustainable mineral beneficiation processes.

Key words: *Sustainable mining, digital mineral processing, image analysis, MATLAB, optical sorting*

1. INTRODUCTION

In today's world, the rapid increase in the energy demands of mining operations, growing environmental pressures, and the progressive decline in ore grades necessitate more serious actions toward sustainable mineral processing. The overconsumption of energy and water, along with significant environment impacts, is largely associated with the intensive use of comminution and wet separation stages on which traditional beneficiation predominantly relies Consequently, approaches that enhance the selectivity of the primary phases and reduce redundant material processing have become key elements in the design of sustainable processing routes.

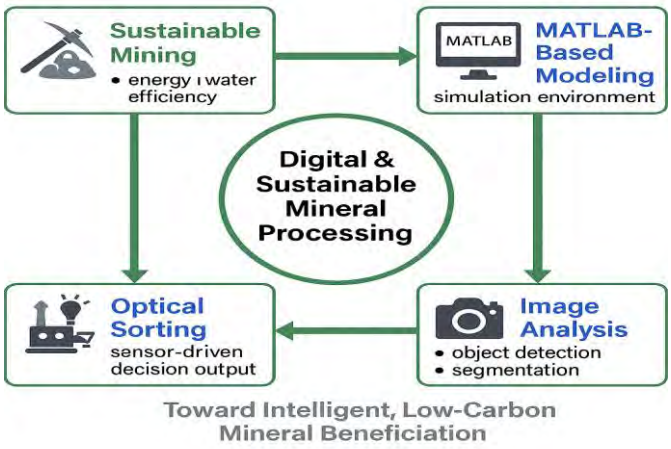

Figure 1. Conceptual framework of digital and sustainable mineral processing

In this context, optical and sensor-assisted sorting technologies are increasingly preferred as effective pre-processing methods. These techniques rely on particle surface-related properties such as brightness, color, and reflectance, enabling the separation of particles and the rejection of low-value or barren material before it enters energy-intensive downstream processes. Nevertheless, the effectiveness of such sorting methods is strongly dependent on the mineralogical composition of the ore and the degree to which valuable minerals can be optically distinguished from gangue stages (Peukert et al., 2022).

Raw materials such as antimony are considered critical due to their common use in flame retardants, alloys, and emerging energy-related applications (Özer, 2022). However, the history of antimony applications is various and long, such as cosmetics, pigments and pharmacology in ancient times to a serious growth in its requisition over the 20th century, particular usage was in order to manufacture military equipment throughout the war times, and it was the major compound in lead-acid batteries for general manufacturing in the industry of automotives (Segura-Salazar & Brito-Parada, 2021). The main antimony-bearing mineral is considered as Stibnite (Sb_2S_3), which shows surface and optical characteristics distinctively, that metallic luster and low reflectance relative to common gangue minerals are involved (Handbook of Mineralogy, Stibnite, n.d.). Owing to these properties, stibnite-bearing ores represent suitable candidates for optical evaluation and sensor-based pre-assessment prior to conventional processing.

For conducting such preliminary assessments, MATLAB-based optical image analysis offers a flexible and accessible framework. Insight into mineral distribution, heterogeneity, and the potential selectivity of sorting can be obtained through basic image processing operations such as grayscale conversion, segmentation, and intensive-based classification. Rather than replacing physical separation processes, this approach operates as a decision-support tool by providing information whether sensor-assisted sorting is technically feasible and environmentally advantageous.

Accordingly, this study investigates the use of MATLAB-based optical image analysis as a preliminary evaluation strategy for stibnite-bearing antimony ores within a sustainable mineral processing framework. The aim of this study is to demonstrate the contribution of early-stage assessment to better-informed process selection and the development of sustainability features by linking digital image analysis with mineralogical characteristics of stibnite. Table 1 compares representative studies on antimony and stibnite processing and positions the present work within the context of pre-assessment and sustainability-oriented mineral processing.

Table 1. Comparison of studies from literature about the pre-assessment techniques

Reference	Ore/ Mineral Type	Methodology	Processing Stage	Sustainability Aspect	Relevance to This Study
Inanç et al., 2025	Nickel ore	SAM2	Magnetic separation	Energy saving and AI application	Mineral Sorting
Peukert et al. (2022)	Various metal ores	Sensor-based sorting review	Pre-processing	Energy and water savings	Provides sustainability framework for preprocessing
Segura-Salazar& Brito-Parada (2021)	Stibnite (Sb2S3)	Froth flotation review	Beneficiation	Energy and reagent consumption	Demonstrates conventional processing routes for stibnite
Gülcan et al. (2019)	Complex antimony ore	Gravity separation, flotation	Pre-concentration and beneficiation	Resource efficiency	Highlights importance of ore characterization prior to processing
Knapp et al. (2014)	Sulfide ores	Sensor-based sorting	Pre-processing	Energy and waste reduction	Supports sensor-based methods as early-stage tools
This study	Stibnite-bearing antimony ore	MATLAB-based image analysis	Pre-assessment	Low energy, digital evaluation	Introduces a conceptual pre-assessment approach prior to beneficiation

2. SUSTAINABLE PROCESSING OF ANTIMONY AND STIBNITE-BASED PRE-EVALUATION TECHNIQUES

In today's industrial development, antimony is considered as strategic, non-renewable mineral resource. Huge number of resources of antimony consumed while the resource mining is done highly intense in the past years. Recovery rate of antimony ore improvement is highly related to the beneficiation methods of antimony (Mineraldressing.com, 2022). The main antimony-bearing mineral which has metallic luster and optical characteristics that is distinctive, and it enables to identify it from usual gangue minerals because of its surface reflectance features, is called as Stibnite (Sb_2S_3) (Handbook of Mineralogy, Stibnite, n.d.).

Recent developments in the field created new area of usages, such as production of various flame retardants, enamels, glass, rubber, coatings, pigments, ceramics, plastics, semiconductor components, fireworks, medicine and chemical products. Considering sustainability-oriented mineral processing techniques, in order to understand the characteristics of the materials, to focus on selective mineral processing and to develop the efficiency of resource, pre-assessment of stibnite-bearing ores is crucial. Hand sorting process of the antimony can be considered as a pre-assessment technique in mineral processing. It is mainly based on using the color, luster and shape differences of the antimony-including minerals in the antimony ore and the gangue. Even though, the process is highly labor-oriented and primitive, yet it is commonly used as a pre-evaluation technique in the industry. The deposits of antimony usually found as coarse-sized crystals or aggregates which are also massive. That is why hand sorting can offer high-grade bulk antimony concentrates that matches the necessary technical qualities of vertical roasting furnaces in the metallurgy industry. Moreover, hand sorting can be advantageous considering the production cost and energy requirement of the beneficiation, which makes it a important pre-assessment technique in the industry.

Furthermore, gravity separation can be considered as another pre-assessment technique for a sustainable mineral processing which is significantly economical and effective. Before the flotation process, it decreases the burden on grinding equipment and raises the productivity of the operation. The integrated particle size of antimony is usually coarse-sized and generally when the specific gravities of the integrated particles are compared, antimony has much bigger than the gangue. Consequently, the gravity separation fits well for the treatment of the antimony, and monomer dissociation has a critical importance in this process. Between the antimony ore and the waste rock, monomer dissociation degree is highly effective for the beneficiation index of the process. Crushing and grinding is essential to break the conjoined structure of the antimony ore and separate it from the waste rock. The dissociation level is correlated with the success of the beneficiation and recovery. Equipment that is used through the process are generally jig separator and shaker table (Mineraldressing.com, 2022). Process flow includes traditional processing steps of crushing and screening, continued by grinding ranging with classification and gravity concentration, and following froth flotation, as can be seen in Figure 2.

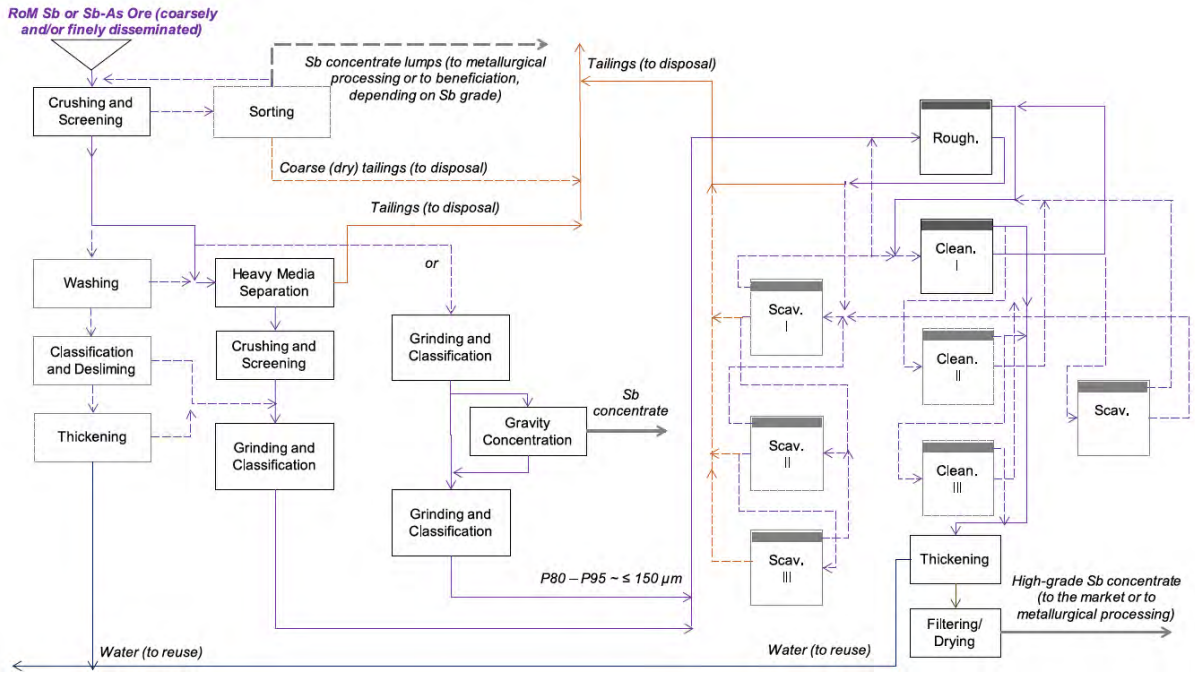

Figure 2. Stibnite beneficiation flowsheet for basic stibnite-bearing ores. Adapted from: Anderson (2019); Bhatti et al. (2008); Hu (1988); Lager and Forssberg (1989b); Morizot and Ollivier (1993); Richards (1977); Schwarz-Schampera (2014); Wu et al. (2019)

3. SENSOR-BASED SORTING FOR PREPARING TO SUSTAINABLE MINERAL PROCESSING

In order to have an early characterization of low-value material, which helps to assist informing the design of the process and lowering the unneeded downstream processing, sensor-based sorting can be used as a preprocessing or pre-evaluation technique.

In the modern industry, demand for the resource is getting higher everyday globally. Also drops in ore grades and limitations by environmental impacts are the top challenges that mining industry is confronted. Increase in demand for mineral resources are highly related to rising interest in renewable energy, growth of population, and global improvements. Simultaneously, consumption of the rich mineral deposits causing industry to move forward with the low-grade/substandard ores which led decrease in grade of mined ore in average. That is why the

need of mining and processing larger volumes of lower grade ore is crucial and getting higher in order to fulfill the demand. However, this situation may create a risk of quick boost in consumption of energy and generating larger amounts of wastes. In order to fix these issues mining and processing techniques must be improved and become more sustainable. Improving ore grades and decreasing the generated waste material from mining and processing, sensor-based sorting techniques can be very useful. It can decrease the consumption of energy, water, and chemical reagents.

For more productive mining and processing low-grade ores, selective mining and processing is essential. Selectivity in these operations can be conducted by inserting sensor algorithms that can minimize the human error which leads to more sustainable operations. In order to optimizing production and decreasing generated waste can be achieved from receiving real-time data which can be provided by sensor-based operations. This way operations can be diverted into using more sub-economic materials. Uneconomical processed materials cause unneeded grinding and flotation, but sensor-based sorting can prevent this situation by creating a pre-evaluation stage and stops early removal of the mined materials. Consumption of electricity, water, and chemical reagents can significantly decrease through this system (Peukert et al., 2022).

4. WORKFLOW AND METHODOLOGY

The determined workflow in this study is created to assist with a basic and reproducible framework for initial ore identification by applying optical image analysis technique. Methodology mainly emphasizes on characterizing ore particles and stibnite-rich areas by an order of image processing steps, instead of repeating an industrial sorting process. The logical structure of the algorithm is presented on the flowchart in Figure 3.

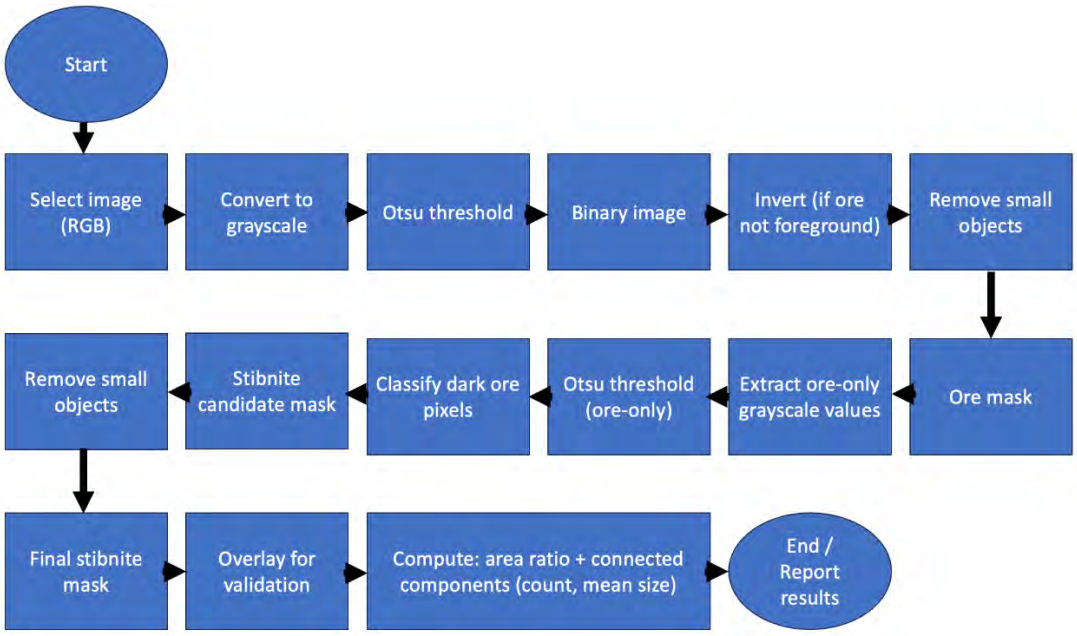

Figure 4. Algorithm of the MATLAB-based optical image analysis program

5. CONCLUSIONS

In order to characterize stibnite-bearing ore samples within the framework of sustainable mineral processing, this proposes a MATLAB-based image processing approach as a pre-

assessment technique. Instead of conventional laboratory operations, ore particles and stibnite-rich areas were identified through optical image analysis.

The results demonstrate that grayscale-based image segmentation enable the extraction of both qualitative and quantitative information from stibnite ore samples. Although the methodology depends on surface optical properties and imaging conditions, it provides a remarkably useful tool for preliminary ore evaluation and process assessment. These operations can support decision-making prior to processing stages where energy and resource consumption are highly.

Sensor-based optical sorting tool can complement traditional beneficiation techniques through the preliminary characterization of mineral-rich areas, potentially reducing unnecessary comminution and processing of gangue material. Consequently, this approach contributes to more efficient energy and resource utilization and strongly supports sustainable and environmentally responsible mining practices.

Future studies may integrate multi-spectral imaging, larger datasets, and experimental validation in order to further improve the proposed system. Nevertheless, the findings indicate that MATLAB-based optical image analysis represents an effective early-stage approaches for the development of sensor-supported and energy-efficient mineral processing strategies, particularly for antimony-bearing ores.

REFERENCES

Anderson, C. G., (2019), "Antimony Production and Commodities". In: Kawatra, K., Young, C. A. (Eds.), SME Mineral Processing and Extractive Metallurgy Handbook. Society for Mining Metallurgy & Exploration, pp. 1557–1568.

Bhatti, M. A., Kazmi, K. R., Nizami, M. S., Anwar, M. S., Habib, M., (2008), "Beneficiation studies on low-grade Stibnite ore of Chitral, NWFP. Pakistan". Pak. J. Sci. Ind. Res., 51, 45–51.

Handbook of Mineralogy. (n.d.), "Stibnite". https://www.handbookofmineralogy.org/pdfs/stibnite.pdf
Hu, H-K., (1988), "Some milling practices and technological innovations on beneficiation of Antimony sulfide ores in China". In: Metallurgical Processes for the Year 2000 and Beyond. Las Vegas, pp. 783–790.

Inanc, B. M., Sahin, Z. B., Tuna, S., Benli, B., Eyidogan, B., Toreyin, B. U., (2025), "SAM2 ile Tensör Ayrıştırma Tabanlı Örneksiz Imge Bölütleme Kullanarak Manyetik Zenginlestirme Sirasinda Metalik Nikel Cevherine Ait Mikroskobik Verilerin Analizi". 33rd IEEE Conference on Signal Processing and Communications Applications, SIU 2025 - Proceedings. Institute of Electrical and Electronics Engineers Inc. https://doi.org/10.1109/SIU66497.2025.11112341

Lager, T., Forssberg, K. S., (1989), "Current processing technology for antimony-bearing ores a review, part 2". Miner. Eng., 2, 543–556. https://doi.org/10.1016/0892-6875(89)90088-5

Mineraldressing.com, (2022), "Three Methods To Antimony Ore Beneficiation And Processing".

Morizot, G., Ollivier, P., (1993), "A process for the economic beneficiation of As- and As-Au-bearing Antimony ores. Has the dream become a reality?". Miner. Eng., 6, 841–856. https://doi.org/10.1016/0892-6875(93)90058-U

Özer, M., (2022), "Flotation of antimony ores with high arsenic content". Physicochemical Problems of Mineral Processing, 58 (2).

Peukert, D., Xu, C., Dowd, P., (2022), "A Review of Sensor-Based Sorting in Mineral Processing: The Potential Benefits of Sensor Fusion". Minerals, 12 (11), 1364.

Richards, R. G., (1977), "Laboratory flotation of Endeavour Inlet, N. Z. Antimony ore". Proc. Australas. Inst. Min. Metall., 263, 39–46.

Segura-Salazar, J., Brito-Parada, P. R., (2021), "Stibnite froth flotation: A critical review". Minerals Engineering, 163, 106713. https://doi.org/10.1016/j.mineng.2021.106713

Schwarz-Schampera, U., (2014), "Antimony". In: Gunn, G. (Ed.), Critical Metals Handbook. British Geological Survey - American Geophysical Union - Wiley. https://doi.org/10.1002/9781118755341.ch4

Wu, J., Nie, Q., Huo, J., Gou, M., (2019), "Experimental research on mineral processing for a stibnite ore in Shaanxi". IOP Conf. Ser. Earth Environ. Sci., 227, 042024. https://doi.org/10.1088/1755-1315/227/4/042024

MODELLING OF MULTI GRAVITY SEPARATOR (MGS) FOR FINE LIGNITE CLEANING BY CENTRAL COMPOSITE DESIGN (CCD) METHOD

Derya OZ AKSOY[1,*], Sabiha KOCA[1], Hüseyin KOCA[2]

[1]Eskisehir Osmangazi University, Faculty of Engineering and Architecture, Department of Mining Engineering, 26040, Eskisehir, Turkey
[2]Porsuk Technical College, Eskisehir Technical University, 26470 Eskisehir, Turkey
**Corresponding author: deryaoz@gmail.com*

A B S T R A C T

In this study, the cleaning of low-rank lignites from Çayırhan region was investigated by using multi gravity separator (MGS). The Central Composite Design method, a statistical test method, was used in the planning of experiments and analysis of results. Due to device limitations (the MGS device only operates with three shake amplitude levels), a "Face Centred" design with α factor of 1 was used. Drum speed (240 rpm), tilt angle (0°) and feed rate (1.5 l/m) were kept constant, while shake frequency (4; 4.5; 5 cps), shake amplitude (10, 15, 20 mm), wash water (1, 2, 3 l/m) and solid ratio (20, 30, 40%) were selected as the parameters to be investigated.

Key words: *Lignite, central composite design method, multi-gravity separator, design expert*

1. INTRODUCTION

Nowadays, energy consumption per capita can be used as an indication of economic development and wealth of a country, and annual energy consumption in the world is increasing rapidly. This situation makes the efficiency and supply safety of energy be primary subject for the countries. When the sources used for electricity production are considered, all attentions are directed into renewable energy resources because of limited supply of fossil fuels and the problems encountered in nuclear energy production. However, coal among fossil fuels still preserves its importance, and it is thought that the coal will become even more important after 2035 particularly in India, Indonesia and China mainly by the use of coal to generate power in emerging market and developing economies (EIA 2025; Tamzok, 2024).

It is possible to secure energy supply for a country by using its own resources. Therefore, it can be said that most appropriate energy source to secure energy supply for our country is our lignite reserves. However, major part of our lignite have low calorific values, high ash and Sulphur content with low rank. Some restrictions have been imposed to use these coal thanks to increasing environmental concerns and protection laws. As a result, the usage of clean coal technologies before, during and after combustion becomes mandatory in order to use these lignite reserves under the environmentally acceptable conditions. Besides, pyrolysis is also one of the methods applied to convert the low rank coals into liquid and gaseous fuels which are environmentally more acceptable fuels (Koca et al., 2000; Koca et al., 2007).

There are a lot methods applied to reduce moisture, ash and sulphur content which decrease the quality of coals. Gravity and heavy medium methods are generally preferred in coarse sizes, and in fine sizes, floatation is most preferred method because of natural hydrophobic property of coal (Wills, 2006). When the methods depending on surface property are unsuccessful to obtain required quality product due to coal rank and surface oxidation, the usage of gravity separation like jigs, spirals and water only cyclones are becoming important (Chaurasia and Nikkam, 2017; Aksoy at al., 2012). In case of Turkey, floatation is not being

utilized for fine size recovery whereas gravity and heavy medium separation are being utilized for coal cleaning (Kelebek at al., 2008).

This study was performed to investigate and evaluate the working parameters of Multi Gravity Separator (MGS) by using lignite samples of Çayırhan region lignites. The earlier studies have shown that the floatation recovery of the coal of this mine was found to be very low due to low rank and high surface oxidation (Aksoy and Sagol, 2016; Koca et al., 2017; Aytar et al., 2014; Chaurasia and Nikkam, 2017).

In this study, one of the statistical experiment design methods, Central Composite Design (CCD) was selected. α (axial coefficient) value was chosen as 1 due to restrictions coming from the MGS instrument, and surface based CCD design with three level of each parameter was used in the study. The effect of parameters; shake frequency, shake amplitude, wash water and solid ratio were investigated. The ash content and combustible efficiency of the clean coal obtained from each experiment were calculated. Model equation for ash content was created by examining the studied parameters.

2. MATERIAL AND METHODS

2.1. Material

Samples were taken from Çayırhan Lignite region underground mine. Samples brought to the laboratory were dried in open air, crushed to -1 mm, and sieved into five size fractions. Proximate analysis of run of mine ore as dry basis are given in Table 1. -0.3+0.1 mm size fraction of these samples was spared to be used in the MGS experiments. Used samples have 74.87% ash with 3.15% sulphur content.

Table 1. Characterization of run of mine lignite sample

Proximate analysis of original sample	
Ash (%)	66.71
Volatile matter (%)	29.94
Sulphur in ash (%)	2.17
Total sulphur (%)	3.98
Calorific value$_{gross}$ (MJ)	7.33
Calorific value$_{net}$ (MJ)	6.92

2.2. Method

Experiments were carried out by using a pilot scale Multi Gravity Separator (MGS). In the experimental studies, the drum speed was kept fixed at 245 rpm according to the results of author's previous study (Aksoy at al., 2014) while the effects of drum frequency (cps), shake amplitude (mm), wash water rate (l/min) and solid ratio (%) were investigated. After each gravity experiments, ash content of MGS products was determined and combustible recovery (CR) calculated from the Equation (1) as given below:

$$CR\ (\%) = \frac{\%wt\ concentrate\ x\ (100 - Ash\ content\ of\ concentrate)}{100\ x\ (100 - Ash\ content\ of\ feed)} \quad (1)$$

The experiments were designed by using statistical experiment design methods. Central Composite Design (CCD), a response surface method, was chosen as design method. There are only 3 levels for drum Frequency and shake amplitude of MGS equipment. For this reason,

three level was selected for all parameters, and the value of α term was chosen as 1. This method is called as Faced Centered CCD. Design Expert 10.0.6 Software was used for experimental design in this study. The parameters were given at Table 2 with their levels. The total number of experiments were calculated as 30 from the Equation (2) given below. In this calculation, the number of parameters were taken as 4 and the number of middle points were taken as 6.

$$N=2^n + 2^* n + m \quad (2)$$

Where n is the number of parameters, m is the number of middle points.

Table 2. Parameters and levels.

Parameter Code	Parameter	Unit	Levels		
			Minimum (-)	Avarage (0)	Maximum (+)
A	Frequency	*cps*	4	4.5	5
B	Amplitude	*mm*	10	15	20
C	Wash Water	*l/min*	1	2	3
D	Solid Ratio	*%*	20	30	40

30 experiments were randomly carried out according to the design. The results of experiments were analyzed and used to form model equation for ash content.

Model equations were created for both coded and actual values of parameters by taking the suggestion of “fit summary module” of the software into consideration. Combustible recoveries were also calculated for each experiment, but statistical analysis was not performed in this study, yet.

3. RESULTS AND DISCUSSION

Ash contents and CR’s of clean coal obtained from these experiments are given along with design matrix at Table 3.

The ash content results of the experiments were subjected to variance analysis, and regression models for both coded and actual values of parameters were created. Besides, the graphics showing the effect of parameters and their interactions were prepared by keeping other parameters at their middle level.

The linear model is suggested by the “fit summary” of the software. Then, the quadratic model was prepared by the software in order to see the effects of whole passible terms, and the terms that are not statistically acceptable for 95% confidence interval were eliminated one by one from the model. But two terms called “amplitude (B)” and “wash water-solid ratio interaction (CD)” are kept at the model because of the fact that their p values are very close to 0.05 as 0.0511 and 0.0558 respectively. The results of variance analysis (ANOVA) of ash content of clean coal according to created model are given in Table 4. In this Table, R^2 which shows the consistency of the model with experimental data and PR^2 (predicted R^2) which shows the power of the model are given. Coefficients of terms of the models for both coded and actual values are also given in the same table. Fixed term is given at the top of “coeficients of terms” column.

Table 3. Ash content and CR values with design matrix

Run	Parameters				Response	
	Frequency (cps)	Amplitude (mm)	Wash Water (l/min)	Sol. Ratio (%)	Ash (%)	CR (%)
1	4.0	10	3	40	56.13	49.85
2	4.0	20	1	40	52.02	40,13
3	4.0	20	3	20	59.52	99.67
4	4.5	15	2	30	52.00	53.00
5	4.5	15	2	30	55.00	56.00
6	4.0	10	1	40	52.05	28.28
7	4.5	15	3	30	54.84	68.16
8	4.0	20	1	20	59.51	99.74
9	4.5	20	2	30	55.56	72.15
10	5.0	10	3	40	49.20	28.59
11	5.0	15	2	30	53.51	42.08
12	5.0	20	1	20	51.43	62.79
13	4.0	10	1	20	54.82	51.95
14	4.5	15	2	30	52.54	42.40
15	5.0	10	3	20	52.25	80.85
16	4.5	15	2	40	49.45	53.13
17	5.0	10	1	20	51.20	68.44
18	5.0	10	1	40	42.25	9.57
19	4.5	15	2	20	56.17	79.47
20	4.5	10	2	30	50.37	43.70
21	5.0	20	3	20	51.50	87.71
22	5.0	20	3	40	46.73	37.05
23	4.5	15	2	30	51.13	61.39
24	4.5	15	1	30	51.26	43.70
25	4.0	10	3	20	55.84	77.18
26	4.0	15	2	30	58.70	90,07
27	5.0	20	1	40	46.32	38.12
28	4.0	20	3	40	57.22	93.05
29	4.5	15	2	30	54.69	55.14
30	4.5	15	2	30	52.24	54.94

Table 4. ANOVA Table for ash content of clean coal

Source	**Sum of Squares**	**Mean Squares**	**p-Value**
Model	356.99	71.40	<0.0001
A	209.58	209.58	<0.0001
B	13.69	13.69	0.0511
C	27.80	27.80	0.0074
D	92.80	92.80	<0.0001
CD	13.12	13.12	0.0558
Residual	77.94	3.25	
Lack of Fit	65.82	3.46	0.3695
R^2	0.8208		
P-R^2	0.7135		

As a result of this variance analysis, the regression models given in Equation (3) and Equation (4) were obtained for both coded and actual values of parameters respectively:

$$Ash\ (\%) = 52.85 - 3.41xA + 0.87xB + 1.24xC - 2.27xD + 0.91CD \quad (3)$$

$$Ash\ (\%) = 90.70153 - 6.82444xFrequency + 0.17444xAmplitude - 1.47410xWash\ Water - 0.40818xSolid\ Ratio + 0.090563xWash\ WaterxSolid\ Ratio \quad (4)$$

These models are found to be statistically significant because its p-value (<0.0001) is less than 0.05. Predicted ash content versus actual ash content graphic is given in Fig. 1. As it can be seen from this figure, predicted ash content values represents approximately 82% of actual ash content values. Furthermore, high value of PR^2 (0.7135) can be interpreted as high power of prediction of this model. Experimental error is found to be statistically insignificant because of the p-value of lack of fit (0.3695) is greater than 0.05.

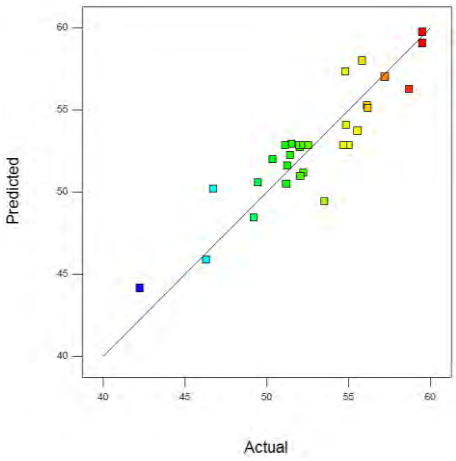

Figure 1. Predicted ash content versus actual ash content graphic (R^2=0.8208)

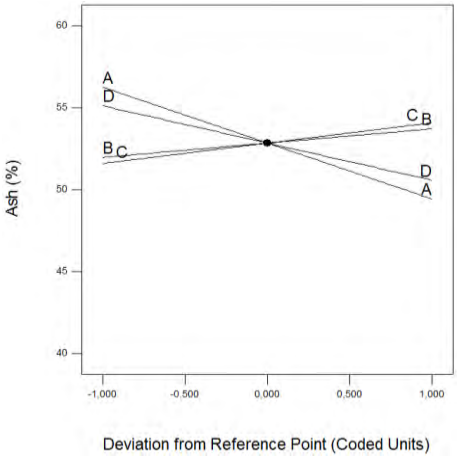

Figure 2. The effects of main parameters on ash content

The effects of parameters are shown in Fig. 2. Quadratic effects of all parameters are found to be insignificant on this model. However, as it can be seen from Fig. 2, linear effects of three factors on the ash content of clean coal are found to be significant. The effect of amplitude (B) also can be seen from this Figure although its P-value (0.0511) is not found to be statistically significant at 95 % confidence interval. Similarly, the effect of the interaction of wash water-solid ratio (CD) was shown in Figure 3.

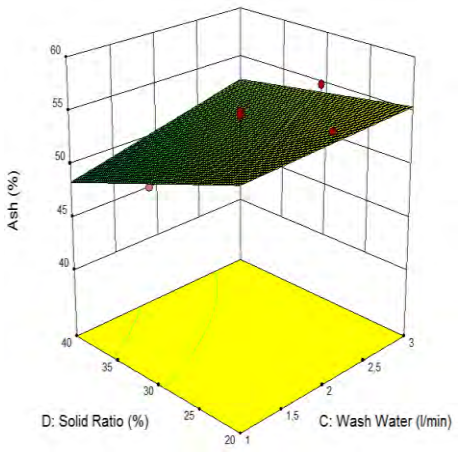

Figure 3. Interaction between wash water and solid ratio

When the response surface in this Figure is examined, it can be seen that increasing wash water causes ash content to increase at both low and high levels of solid ratio (right front side as low level and opposite side as high level of solid ratio in the Figure). However, it should be

noted that the rate of the increase at the high level of solid ratio is greater than the rate of the increase at the low level of solid ratio. Therefore, it can be said that this difference in the increase rates shows the presence of an interaction between wash water and solid ratio in spite of the fact that p value (0.0558) was not found to be statistically significant at 95 % confidence interval.

4. CONCLUSİONS

The minimum ash content was obtained as 42.25% with 9.57% CR under the conditions of frequency of 5 cps, amplitude of 10 mm, wash water of 1 l/min and solid ratio of 40% from the experiments carried out. Maximum CR was obtained as 99.74% with 59.51% ash content under the conditions of frequency of 4 cps, amplitude of 20 mm, wash water of 1 l/min and solid ratio of 20%. It should be noted that the density of coal samples of this study was found approximately as 1.65 g/cm^3, which is higher than the normal values of the coal. It can be said this high density can be the reason for low CR and high ash content of the clean coal obtained in this study. Moreover, it was revealed in another study that the studied lignite could not be treated successfully by floatation at -0.100 mm size fraction because of its low rank (Aksoy and Sagol 2016).
It can be said that model for ash content is found to be statistically significant. When the graphic (Figure 1) representing the relationship between actual and predicted values are examined, the consistency of ash content model with actual values was found over 80%.

Finally, one of the conclusions to be drawn from this study and literature knowledge can be stated as CCD can be successfully applied to model the processes used in mineral processing methods such as MGS, floatation etc.

The results obtained from this work need to be extended. With the statistical analysis and modelling of the combustible recovery along with optimization of both response variables will provide optimum conditions for obtaining clean coal of the lowest ash content and acceptable recovery.

REFERENCES

Aksoy D. O., Koca, S., Koca, S., (2012), “The effects of drum speed, shake frequency and shake amplitude combinations on cleaning of lignite fines by multi gravity separator”, Proceedings of the XIII. International Mineral Processing Symposium, Bodrum, 747-751.

Aksoy, O.D., Aytar, P., Toptas, Y, Cabuk, A., Koca, S., Koca, H., (2014), "Physical and Physicochemical Cleaning of Lignite and the Effect of Cleaning on biodesulphurization", Fuel, Volume 132, 158-164.

Aksoy, D. O., Sagol, E., (2016), “Application of central composite design method to coal flotation: Modelling, optimization and verification”, Fuel, 132, 158-164.

Aytar, P., Aksoy, D.O., Toptas, Y., Çabuk, A., Koca, S., Koca, H., (2014), “Isolation and characterization of native microorganism from Turkish lignite and usability at fungal desulphurization”, Fuel 116, 634-641.

Chaurasia, R. C. and Nikkam, S., (2017), “Beneficiation of low-grade iron ore fines by multi-gravity separator (MGS) using optimization studies”, Particulate Science and Technology, 35, 45-53.

EIA, (2025), “Outlooks based on existing trends and policies”, Chapter 3, World Energy Outlook, 166-170.
https://iea.blob.core.windows.net/assets/81980a53-9716-47f1-904e-b92a2c4d2ea4/WorldEnergyOutlook2025.pdf. Erişim tarihi: Şubat, 2026.

Kelebek, S., Demir, U., Sahbaz, O., Ucar, A., Cinar, M., Karaguzel, C., et al., (2008), “The effects of dodecylamine, kerosene and pH on batch flotation of Turkey’s Tuncbilek coal”, Int J Miner Process; 88, 65–71.

Koca, H., Koca, S., Karaoglu, M., (2000), "Recovering Of Fine Coal Particles from Tailing Ponds of TKİ-Alpagut-Dodurga Coal Washing Plant", Proceedings of the The 6th International Conference on Environmental Issues and Management of Waste in Energy and Mineral Production, SWEMP 2000, A. A. Balkema Publishers, Rotterdam, The Netherlands, 117-121.

Koca, H., Kockar, O. M., Koca, S., (2007), “Desulphurization of lignites by slow, fast, and flash pyrolysis and high intensity dry magnetic separation”, Energy sources, part A: recovery, utilization, and environmental effects, 16 (29) 1457-1470.

Koca, S., Aksoy, D.O., Cabuk A., Celik, P. A., Sagol, E., Toptas, Y., Oluklulu,S., at al, (2017), “Evaluation of combined lignite cleaning processes, flotation and microbial treatment, and its modelling by Box Behnken methodology”, Fuel 192, 178-186

Tamzok, N., (2024), “Dünya’da ve Türkiye’de kömürün görünümü”, Türkiye’nin Enerji Görünümü 2024, TMMOB, Makina Mühendisleri Odası, Yayın No: MMO/758, 131-142.
https://www.tmmob.org.tr/sites/default/files/turkiyenin_enerji_gorunumu_kitap.pdf. Erişim tarihi: Şubat, 2026.

Wills B., (2006), “Mineral Processing Technology”, 7th edition, Musselburg: Butterworth-Heinemann 456.

NUMERICAL PREDICTION OF IMPACT AND SHEAR ENERGY PROFILES ON MILL LIFTERS

Hüseyin Efe SELVI[1,2,*], Tahir Abbas JAUHAR[2], Yusuf Enes PURAL[1]

[1]Istanbul Technical University, Faculty of Mines, Mineral Processing Engineering Department, 34469, Maslak, Istanbul, TÜRKİYE
[2]University of Newcastle, Centre for Bulk Solids and Particulate Technologies, 2308, Newcastle, Callaghan, AUSTRALIA
**Corresponding author: HuseyinEfe.Selvi@newcastle.edu.au, selvi20@itu.edu.tr*

A B S T R A C T

The precise characterization of mill lifter wear is critical for optimizing grinding efficiency and improving maintenance strategies in mineral processing. In this numerical study, the Discrete Element Method (DEM) framework was employed to simulate the wear mechanisms governing lifter degradation in a tumbling mill. Using impact and shear energy spectra derived from DEM simulations, Archard's wear law was implemented in Python to predict volume loss efficiently under varying normal and shear energy conditions. The simulated mill, 4000 mm in diameter and 6000 mm in length, operated at 71.4% critical speed with 24 lifters, and 30% filling and load levels. The lifters have geometry as 150 mm height and 60° face angle. To further investigate the spatial wear on the various faces of the lifter, the energy distributions from 24 lifters were mapped into five physically meaningful regions: Leading Face Plate, Leading Face, Top, Trailing Face and Trailing Face Plate. Median impact and shear energies were extracted and represented by cubic polynomials with accuracy of R^2 = 0.99 and R^2 = 0.94 respectively. The ordinary least squares method was used to fit cubic polynomials. Future work will focus on investigating the relationship between the obtained polynomial fits and mill operating conditions as well as liner geometry, aiming to enhance the predictive capability of the model under varying scenarios.

Key words: *Tumbling mill, dem modelling, Archard's wear law, lifter geometry, energy analysis*

1. INTRODUCTION

Most Grinding mill lifters play a decisive role in controlling charge motion, impact distribution, and sliding behavior within tumbling mills, thereby directly influencing comminution efficiency and liner wear evolution (Cleary, 2001; Powell et al., 2006). The interaction between grinding media and lifter surfaces governs not only energy transfer mechanisms but also the spatial localization of wear, which remains a critical concern in mill design and operation.

The Discrete Element Method (DEM) has been widely adopted to investigate particle-scale dynamics in grinding mills, offering detailed resolution of collision events, force chains, and energy dissipation mechanisms (Mishra & Rajamani, 1994; Dosta et al., 2024). Numerous studies have demonstrated the capability of DEM to capture lifter–charge interactions with high fidelity (Cleary, 2001; Wang et al., 2025). However, despite these advantages, DEM simulations remain computationally expensive and inherently case-specific, limiting their direct applicability for rapid design evaluation or operational optimization (Dosta et al., 2024).

A key challenge therefore lies in translating DEM-derived energy spectra into generalizable and physically interpretable predictive models. Existing approaches often rely on localized wear indicators or time-averaged metrics, which provide limited insight into the spatial variation of impact and shear energies along the lifter surface (Soleymani et al., 2022; Xu et al., 2018).

In this study, a region-based analytical framework is proposed to address this gap. Impact and shear energies obtained from DEM simulations are mapped onto five physically meaningful,

non-uniform regions along the lifter surface. Median energy values for each region are extracted and approximated using a unified cubic polynomial form. The polynomial coefficients are then interpreted in terms of fundamental operating and design parameters, including critical speed ratio, lifter geometry, filling degree, and load intensity.

It is emphasized that the present work represents an initial step toward a broader generalized modeling strategy. While the current formulation is derived from a single DEM simulation scenario, it establishes a structured and extensible methodology that can be systematically expanded through additional simulations to quantify parameter sensitivities and improve predictive capability.

2. METHODOLOGY

2.1. DEM Setup

Particle–lifter interactions were simulated using a Discrete Element Method (DEM) framework (Mishra & Rajamani, 1994; Cleary, 2001). The modeled mill had an internal diameter of 4.0 m and a length of 6.0 m, equipped with 24 equally spaced circumferential lifters. The mill operated at 71.4% of critical speed, with a filling degree of 30% and a ball charge fraction of 30%.

Lifters were modeled with a height of 0.150 m and a face angle of 60°, representative of industrial lifter geometries (Powell et al., 2006). DEM outputs included particle positions and corresponding normal (impact) and tangential (shear) energy contributions during steady-state operation. These outputs formed the basis for subsequent post-processing and analysis.

2.2. Data Processing and Regional Mapping

Post-processing was carried out using Python-based numerical tools following a structured workflow:

1) *Near-shell filtering:* Only particles located within the outer 10% of the mill radius were retained to isolate lifter–charge interactions.
2) *Lifter identification:* Particle contacts were assigned to individual lifters based on angular position.
3) *Non-uniform regional segmentation:*

Each lifter surface was subdivided circumferentially into five physically defined regions (Figure 1):

- Bridge_L
- Side_L
- Top
- Side_R
- Bridge_R

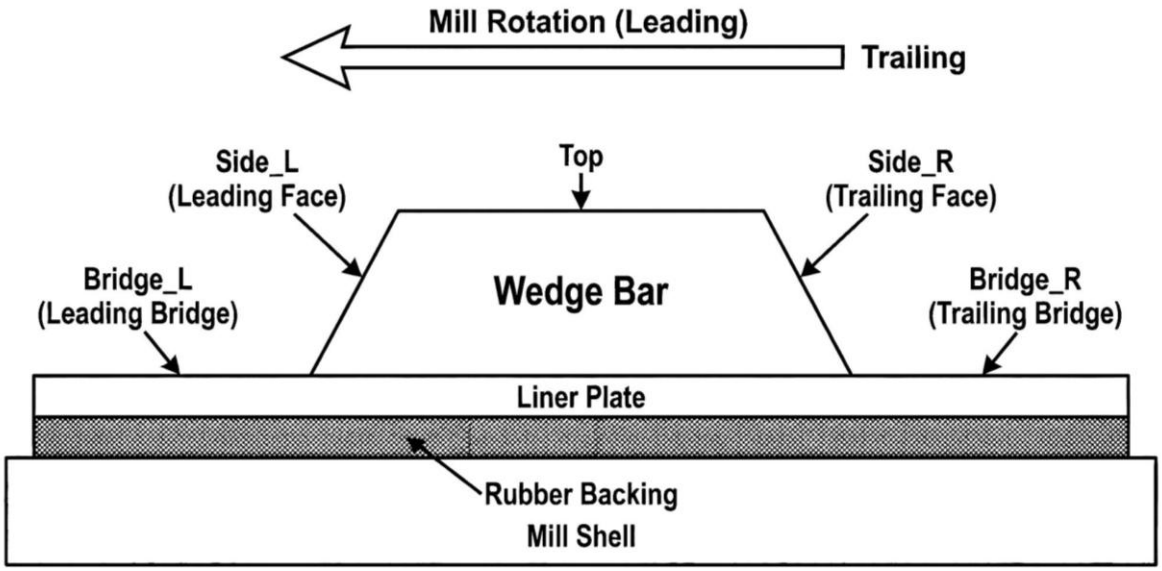

Figure 1. Cross-sectional subdivisions of the wedge bar lifter surface

Bridge regions were intentionally defined as narrow angular sectors (~1°) to isolate transition zones at lifter entry and exit, while side and top regions occupied broader spans corresponding to sustained contact and energy transfer.

4) *Energy aggregation:* Impact and shear energies were accumulated within each region and averaged over time.
5) *Statistical condensation:* Median energies across all lifters were extracted for each region, yielding robust representative values that are less sensitive to transient extreme events.

This process resulted in five discrete data points describing the spatial distribution of energy along a representative lifter.

2.3. Available Fitting Techniques

Several regression approaches were evaluated for approximating the discrete regional energy data:

- *Ordinary Least Squares (OLS):* Closed-form, interpretable, and stable for low-order polynomials.
- *Weighted Least Squares (WLS):* Incorporates region-dependent confidence weights.
- *Robust regression:* Reduces sensitivity to extreme collision events.
- *Regularized regression (Ridge/Lasso):* Controls coefficient variance in multi-parameter datasets.
- *Nonlinear least squares:* Enables constrained or physics-informed models.
- *Gaussian Process Regression:* Offers uncertainty quantification but requires larger datasets.

Given the limited number of representative points and the need for interpretability, OLS was selected as the most appropriate method.

2.4. Choice of Fitting Method

A cubic polynomial was selected as the lowest-order function capable of reproducing the asymmetric spatial behavior observed in both impact and shear energy profiles. Lower-order polynomials were insufficient to capture the observed curvature, while higher-order fits risk overfitting given the limited dataset. Ordinary least squares regression was therefore adopted

due to its transparency, analytical tractability, and reproducibility, following the standard matrix formulation described by Draper and Smith (1998).

The general polynomial form is given by:

$$E(x) = ax^3 + bx^2 + cx + d \tag{1}$$

where *x* denotes the normalized lifter region coordinate.

2.5. Application of the Fitting Procedure

For each energy mode (impact and shear), the regression problem was formulated as a linear system (Chapra & Canale, 2010):

$$y = Xc + \epsilon \tag{2}$$

where $c=[abcd]^T$ is the coefficient vector. The least-squares solution minimizing the sum of squared residuals is obtained as (Draper & Smith, 1998):

$$c = (X^T X)^{-1} X^T y \tag{3}$$

The resulting coefficients describe the spatial energy distribution along the lifter surface.

2.6. Fitting Accuracy and Error Assessment

Model performance was evaluated using the coefficient of determination (R^2) and residual analysis. The impact energy fit achieved R^2=0.999, while the shear energy fit yielded R^2=0.938. Residuals exhibited no systematic trends, indicating that the cubic model captures the dominant spatial variations present in the DEM-derived data.

2.7. Generalization Strategy

The fitted coefficients represent baseline values corresponding to the simulated operating condition. To enable generalization, each coefficient is postulated as an affine function of normalized physical variables, relying on a first-order Taylor series expansion approach for sensitivity analysis (Chapra & Canale, 2010). This leads to the matrix formulation proposed in this study:

- Critical speed ratio (*n*)
- Geometry index combining lifter height and face angle (*g*)
- Filling degree (*J*)
- Load intensity (*L*)

This leads to the matrix formulation:

$$\mathrm{c} = \mathrm{Mu}, \qquad \mathrm{u} = [1, \mathrm{n} - \mathrm{n}_0, \mathrm{g} - \mathrm{g}_0, \mathrm{J} - \mathrm{J}_0, \mathrm{L} - \mathrm{L}_0]^{\mathrm{T}} \tag{4}$$

Separate sensitivity matrices are defined for impact and shear. While the present study identifies baseline coefficients from a single DEM scenario, extension to multi-condition datasets enables estimation of sensitivity matrices via least-squares regression.
The resulting generalized polynomial, representing the summation of baseline trends and linear perturbations, is defined as:

$$E(x) = \sum_{k=0}^{3} \left(A_k + \sum_i A_{k,i} \Delta p_i \right) x^{3-k} \tag{5}$$

3. RESULTS AND DISCUSSION

The fitted cubic functions accurately reproduce the median impact and shear energy distributions across the defined lifter regions. High coefficients of determination (R^2=*0.999* for impact and R^2=*0.938* for shear) indicate that the cubic form captures the dominant spatial trends present in the DEM data.

Distinct differences between impact and shear coefficients are observed, despite both being influenced by the same physical parameters. This divergence is expected, as impact energy is governed primarily by normal collision dynamics (Soleymani et al.2022) and charge detachment velocity, whereas shear energy arises from sustained sliding contact and frictional dissipation along the lifter surface. Consequently, identical filling degree or load conditions may produce markedly different sensitivities in impact and shear responses (Figure 2).

Although the present coefficients were obtained from a single DEM simulation, the observed consistency between physical interpretation and fitted behavior suggests that the proposed framework is structurally robust (Xu et al. 2018; Wang et al. 2025). Importantly, the formulation enables direct comparison between impact-dominated and shear-dominated wear mechanisms within a unified analytical structure.

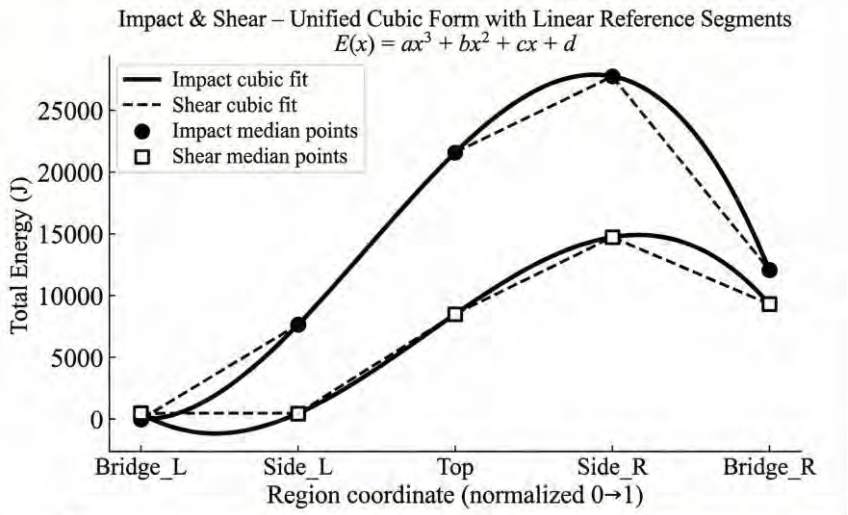

Coefficient	Physical Meaning	Impact Value	Shear Value
a	Critical Speed Ratio	-1.50e+05	-1.05e+05
b	Lifter Height+Face Angle	1.63e+05	1.43e+05
c	Fill Level	-6.75e+02	-2.93e+04
d	Load Intensity	-3.79e+01	4.50e+02

Figure 2. Impact and shear energy profiles with unified cubic fit and coefficient analysis

4. CONCLUSION

A region-based analytical framework has been developed to represent DEM-derived impact and shear energy distributions on grinding mill lifters using a unified cubic polynomial form. By mapping energy spectra onto physically defined lifter regions and interpreting polynomial coefficients in terms of operating and design parameters, the approach bridges detailed DEM analysis with analytical tractability.

The current study is intentionally limited to a single DEM scenario and should be regarded as a proof-of-concept rather than a finalized predictive model. Future work will focus on extending

the framework through multiple DEM simulations spanning a broader range of operating conditions, including variations in mill speed, lifter geometry, filling degree, and load intensity. Such an expanded dataset will enable regression-based identification of coefficient sensitivities and support the development of fully generalized predictive models.

Ultimately, the proposed methodology offers a promising pathway toward reducing reliance on repeated DEM simulations while retaining physical interpretability, providing a valuable tool for lifter design optimization and wear prediction.

REFERENCES

Akhondizadeh, M., Fooladi Mahani, M., Rezaeizadeh, M., Mansouri, S., (2016), “Prediction of tumbling mill liner wear: Abrasion and impact effects”, Proceedings of the Institution of Mechanical Engineers, Part J: Journal of Engineering Tribology, 230(10), 1310–1320.

Banisi, S., Hadizadeh, M., (2007), “3-D liner wear profile measurement and analysis in industrial SAG mills”, Minerals Engineering, 20(2), 132–139.

Boemer, D., Ponthot, J.-P., (2017), “A generic wear prediction procedure based on the discrete element method for ball mill liners in the cement industry”, Minerals Engineering, 109, 55–79.

Chapra, S. C., Canale, R. P., (2010), Numerical methods for engineers, McGraw-Hill.

Cleary, P. W., (2001), “Charge behaviour and power consumption in ball mills: Sensitivity to mill operating conditions, liner geometry and charge composition”, International Journal of Mineral Processing, 63(2), 79–114.

Dosta, M., Andre, D., Angelidakis, V., Caulk, R. A., Celigueta, M. A., Chareyre, B., et al., (2024), “Comparing open-source DEM frameworks for simulations of common bulk processes”, Computer Physics Communications, 296, 109066.

Draper, N. R., Smith, H., (1998), Applied regression analysis, 3rd ed., John Wiley & Sons.

Kalala, J. T., Bwalya, M. M., Moys, M. H., (2005), “Discrete element method (DEM) modelling of evolving mill liner profiles due to wear. Part I: DEM validation”, Minerals Engineering, 18(15), 1386–1391.

Mishra, B. K., Rajamani, R. K., (1994), “The discrete element method for the simulation of ball mills”, Applied Mathematical Modelling, 18(11), 598–604.

Powell, M. S., McBride, A. T., Mainza, A. N., (2006), “The influence of liner design on mill performance”, Minerals Engineering, 19(6–8), 739–745.

Soleymani, M. M., Bahiraie, M., Rezaeizadeh, M., (2022), “Investigating the contribution of wear caused by impact and abrasion in semi-autogenous grinding mills”, International Journal of ISSI, 19(2), 59–65.

Wang, G., Xiao, Q., Wang, X., Li, Y., Jin, S., Wang, M., et al., (2025), “Research on optimization of lifter of an SAG mill based on DEM simulation and orthogonal tests and applications”, Minerals, 15(2), 193.

Xu, L., Luo, K., Zhao, Y., (2018), “Numerical prediction of wear in SAG mills based on DEM simulations”, Powder Technology, 329, 353–363.

Yahyaei, M., Banisi, S., Hadizadeh, M., (2009), “Modification of SAG mill liner shape based on 3-D liner wear profile measurements”, International Journal of Mineral Processing, 91(3–4), 111–115.

Zhu, Q., Feng, Y., Witt, P., Bruckard, W., Yang, R., (2025), “Investigation of the effect of lifter configuration on wet grinding and wear in an industrial-scale SAG mill with GPU-powered CFD-DEM modelling”, Powder Technology, 458, 120959.

PHYSICAL AND PHYSICOCHEMICAL PROCESS SIMULATION AND MODELLING TO BENEFICIATE LITHIUM FROM NEPHELINE SYENITE ROCKS

Zeynep ÜÇERLER ÇAMUR[1,*], Ozgul KELES[2], Murat Olgaç KANGAL[1], Marie-Véronique DURANCE[3], Stephane BROCHOT[3], Manuel GONZALEZ[3], Lucas REGNAULT[3]

[1]Istanbul Technical University, Faculty of Mines, Mineral Processing Engineering Department, 34469, Maslak, Istanbul, TÜRKİYE
[2]Istanbul Technical University, Faculty of Chemistry and Metallurgy, Metallurgy and Material Engineering Department, 34469, Maslak, Istanbul, TÜRKİYE
[3]CASPEO SAS, Process Engineering and Metallurgical Software Company, 45800, Orléans, FRANCE
**Corresponding author: ucerler@itu.edu.tr*

A B S T R A C T

Modeling and simulation play a vital role in the design and optimization of process flowsheets at both laboratory and pilot scales. The use of such tools enables rapid characterization of process variations, allowing for accurate prediction and evaluation of operational performance. This is achieved through proper model selection for material description, the unit operation as well as the establishment of reliable mass balance calculations. In this study, after identifying biotite as the primary lithium-bearing host mineral within nepheline syenite, beneficiation tests were performed to upgrade a run-of-mine ore containing 242.57 ppm Li through combined magnetic separation and flotation processes, yielding a final concentrate with approximately 6725 ppm Li. The ore was divided into two size fractions: -300+75 µm and -75 µm. For the coarser fraction, a magnetic pre-concentrate containing around 1300 ppm Li was produced using a Roll-type Dry High-Intensity Magnetic Separator. Subsequent flotation tests were conducted using 60 g/t Der A4 as a collector and 500 g/t Na_2SiO_3 as a depressant at pH 4, resulting in a lithium-enriched concentrate with about 80 % recovery. Based on these findings, a comprehensive process flowsheet was developed, and fractional lithium distributions were modeled using USIM PAC Modelling and Simulation Software, ensuring accurate mass balancing and the simulation of each processing stage at the laboratory scale.

Key words: *USIM PAC modelling and simulation, lithium, flotation, magnetic separation*

1. INTRODUCTION

Lithium is a lightweight alkali metal extensively used in a wide range of industrial applications, including glass and ceramic manufacturing, lubricants, aluminum refining, and chemical processes. In recent years, the rapid growth of electric vehicle technologies has led to a significant increase in global demand for lithium-bearing materials (Tadesse et al., 2019). The beneficiation of lithium-bearing pegmatite ores generally involves size reduction followed by physical separation methods such as gravity separation, magnetic separation, flotation, or combinations thereof to produce high-grade lithium concentrates (Siame and Pascoe, 2011; Tadesse et al., 2019). Zinnwaldite, a lithium-rich mica occurring in pegmatitic environments alongside spodumene, petalite, and lepidolite, has attracted increasing attention as a potential alternative lithium source. Compared to lepidolite, zinnwaldite typically contains higher iron and impurity levels, necessitating efficient beneficiation strategies. The largest known zinnwaldite deposit is located in the Zinnwald (Cinovec) region at the Czech–German border (Paukov et al., 2010; Martin et al., 2017). Previous studies on zinnwaldite beneficiation have primarily focused on magnetic separation and flotation techniques to upgrade lithium content and reduce impurities, demonstrating their effectiveness for producing marketable concentrates (Siame and Pascoe, 2011; Leißner et al., 2016; Botula, 2005). Zinnwaldite beneficiation commonly relies on magnetic separation, owing to its paramagnetic character, and flotation due to its mica-like floatability (Litovchenko and Melnikov, 1980; Chelgani et al., 2015; Siame,

2011). Siame and Pascoe (2011) demonstrated that flotation of mica-rich tailings containing 0.84% Li_2O using dodecylamine upgraded the concentrate to 1.45% Li_2O with 98% recovery, followed by wet high-intensity magnetic separation (WHIMS) yielding a zinnwaldite concentrate assaying 2.07% Li_2O at 73% recovery. Similarly, a combined flowsheet incorporating high-gradient magnetic separation, flotation, and superconducting magnetic separation upgraded zinnwaldite-rich ores from 0.76% to 2.22% Li_2O with a recovery of 77.62% (Wang et al., 2025). The use of mixed collector systems has also been shown to improve flotation performance, with binary and ternary collectors significantly enhancing Li_2O recovery compared to single collectors (Xue et al., 2024).

Magnetic separation has likewise proven effective for recovering lithium from zinnwaldite-bearing wastes and primary ores. Dry magnetic separation achieved approximately 70% efficiency in lithium recovery from Sn-W processing residues (Botula et al., 2015), while studies on zinnwaldite from the Cínovec area reported Li contents exceeding 1.4% in dry magnetic concentrates, along with enrichment of Rb and Cs (Kratochvil et al., 2016). Wet magnetic separation of the same deposit produced concentrates containing 1.26% Li, 0.95% Rb, and 0.03% Cs, confirming its suitability for multi-element recovery (Landecka et al., 2017).
Recent studies have extended this approach to nepheline syenite systems, where lithium enrichment is associated with the coexistence and transformation of biotite and zinnwaldite (Üçerler-Çamur et al., 2025a). High-intensity magnetic separation has been shown to produce pre-concentrates containing approximately 900 ppm Li (Üçerler-Çamur et al., 2025b). Conventionally, magnetic separation and flotation are applied to nepheline syenites to remove mica and iron-bearing impurities and produce nepheline concentrate, with the biotite-rich fraction typically discarded as waste (Burat et al., 2006; Kangal et al., 2017; 2019; Çınar and Durgut, 2019; Mahran et al., 2022). However, recent investigations have highlighted the lithium-bearing potential of biotite, demonstrating that magnetic separation using SLON-type wet or REMS-type dry separators can enrich run-of-mine ore from 242.57 ppm to 850–1000 ppm Li, with subsequent flotation and sulfating-roast leaching increasing lithium content up to 2500 ppm in the concentrate (Üçerler and Güney, 2022a,b; Üçerler-Çamur et al., 2025b).

2. MATERIAL AND METHODS

2.1. Material

The representative sample was collected from the Kırşehir–Buzlukdağı region in Türkiye. Elemental chemical analyses were conducted using inductively coupled plasma-optical emission spectroscopy (ICP-OES; Agilent 5800, Santa Clara, CA, USA), which indicated a lithium concentration of 242.57 ppm (Table 1). The oxide composition of the sample was determined by X-ray fluorescence analysis (XRF; Atomika Epsilon 4, Malvern Panalytical, Malvern, UK), with the results also presented in Table 1. In addition, the cumulative undersize particle size distribution, the fractional lithium distribution, and the X-ray powder diffraction (XRPD) pattern of the representative sample are provided in Figure 1, Table 2, and Figure 2, respectively (Üçerler-Çamur et al., 2025a).

Table 1. The chemical analysis of the representative sample

Li, ppm	**Ga, ppm**	**Al, %**	**Ba, ppm**	**Be, ppm**	**Bi,ppm**	**Ca, %**
242.57	39.79	4.67	43.42	5.51	15.50	0.82
Cd, ppm	**Ce, ppm**	**Co, ppm**	**Cu, ppm**	**Fe, %**	**As, ppm**	**Hf, ppm**
<1	19.70	10.97	18.19	0.68	11.14	<1
K, %	**La, ppm**	**Ag, ppm**	**Mg, %**	**Mn, ppm**	**Mo, ppm**	Na, %
4.67	14.03	<0.5	0.05	458.75	1.52	6.54
Ni, ppm	**P, %**	**Pb, ppm**	**S, %**	**Sb, ppm**	**Sr, ppm**	**Ti, %**
6.01	<0.01	208.46	0.03	8.55	175.01	0.03

Tl, ppm	V, ppm	W, ppm	Zn, ppm	Zr, ppm	Al_2O_3, %	BaO, %
<5	6.59	<5	124.21	67.93	23.21	<0.01
CaO, %	**Fe_2O_3, %**	**K_2O, %**	**MgO, %**	**MnO, %**	**Na_2O, %**	**P_2O_5, %**
<0.01	1.11	6.78	0.16	0.06	9.23	<0.01
SO_3, %	**SiO_2, %**	**SrO, %**	**TiO_2, %**	**LOI*, %**	**Al_2O_3, %**	**BaO, %**
0.04	57.22	0.04	0.03	0.89	23.21	<0.01

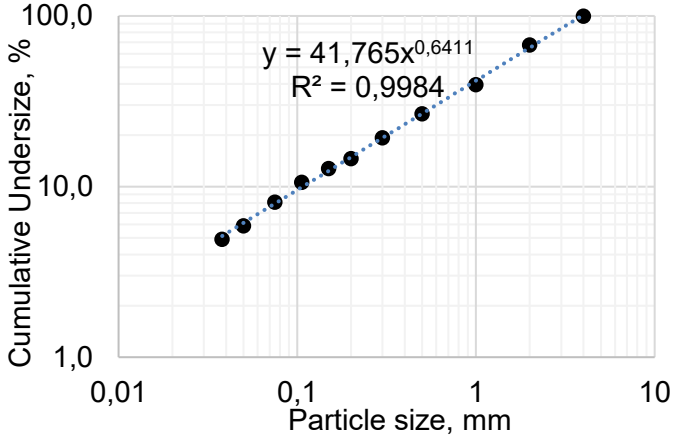

Figure 1. Cumulative undersize particle size curve

Table 2. The cumulative undersize particle size distribution, the fractional lithium distribution

Particle size,mm	Weight, %	Cumulative Undersize, %	Li, ppm	Distribution, %
+2	32.3	100.0	244.28	32.3
-2+1	28.1	67.7	229.95	26.5
-1+0,5	12.8	39.6	242.92	12.8
-0,5+0,3	7.2	26.8	275.12	8.1
-0.3+0.212	4.7	19.3	296.89	5.7
-0.2+0.150	2.1	14.6	355.08	3.1
-0.150+0.106	2.2	12.8	293.78	2.6
-0.106+0.075	2.5	10.6	285.65	2.9
-0.075+0.053	2.2	8.1	232.48	2.1
-0.053+0.038	1.0	5.9	193.99	0.8
-0.038	4.9	4.9	158.94	3.2
Total	100.0		244.20	100.0

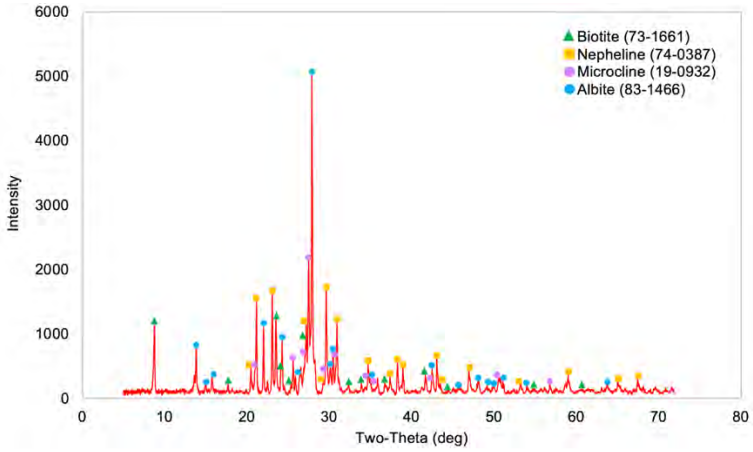

Figure 2. XRD pattern of run-of mine

According to the particle size curve, d_{80} particle size of run-of mine was determined as 2.7 mm. Depending on the fractional lithium analysis, there was no significant difference between particle size fractions. Besides, the major minerals in run-of mine were observed as nepheline, K-feldspar, albite and biotite. However, related to the research Üçerler-Çamur et al. (2025) was studied, the proportions of the major minerals from the rock was 43% of K-Feldspar, 28% of nepheline, 16% of albite, 4% of biotite and 9% of others according to the modal mineralogy analysis. The mineralogical composition of the selected samples was analyzed using X-ray diffraction (XRD) semi-quantitatively. The evaluations were conducted on 5 g samples below 75μm was performed using a Bruker D8 Advance diffractometer (Country of origin: USA) equipped with a Lynxeye detector. The measurements were conducted under operating conditions of 40 mA current and 40 kV voltage, utilizing Cu Kα radiation without a filter. Data were collected within the 2θ range of 5° to 72° at a scan speed of 2° 2θ/min. The resulting X-ray diffractograms were subsequently analyzed using the Jade 6.5 data analysis software (MDI, California, USA) in conjunction with the PDF-2 (Powder Diffraction File) database for phase identification and structural analysis. Nevertheless, evaluation of the EDS spectra together with the chemical analysis indicated that biotite acts as the lithium-hosting mineral (Üçerler-Çamur et al., 2025a).

2.2. Method

The run-of-mine ore was processed by high-intensity dry magnetic separation to recover the paramagnetic biotite fraction, producing a magnetic pre-concentrate (Üçerler-Çamur et al., 2025b), which was subsequently upgraded by flotation to obtain a lithium-enriched biotite concentrate (Üçerler-Çamur et al., 2026). Following to all optimizations for each process, the flowsheet and mass balance of process including physical and physicochemical parts were established by USIM PAC modeling and simulation software.

The USIM PAC modeling and simulation software was used to develop process flowsheets for mineral processing operations and to select appropriate equipment by choosing among the built-in unit operation models corresponding to the planned process configuration. In addition, the software enables process simulation by evaluating the effects of operational or design parameter changes, thereby allowing prediction of process behavior under different conditions. After constructing the flowsheet, mass and component balance consistency was ensured by incorporating sieve analyses of all feed streams, main products, and by-products. Fractional size distributions (+2, -2+1, -1+0.5, -0.5+0.300, -0.300+0.212, -0.212+0.150, -0.150+0.106, -0.106+0.075, and -0.075 mm), together with the corresponding elemental or compound grades targeted for recovery in each size fraction, were used to establish a balanced flowsheet. Due to the laboratory-scale nature of the study, some variability was observed. Within the scope of this study, the process flowsheet was constructed based on comprehensive experimental data.

Mass and grade balance data obtained from laboratory analyses and tests were integrated into the simulation environment. Given the laboratory-scale framework, simplified base unit models (e.g., “0” or “1” models) were selected for process modeling and simulation. Initially, the process was modeled and simulated using all available physical and physicochemical experimental results. Model selection required predefined parameters such as grade distribution in magnetic separation concentrates and recovery values in flotation circuits. Once mass balance closure was achieved using the selected models, process simulations were performed. Subsequently, alternative scenarios were evaluated by modifying equipment types and size fractions used in laboratory-scale operations, and the process was re-simulated accordingly. These simulations allowed assessment of the effects on concentrate quality, concentrate yield, and overall mass balance. Evaluated scenarios included replacing a 75 µm screen with a spiral classifier, grinding the run-of-mine ore to -500 µm instead of -300 µm, and removing -53 µm material prior to magnetic separation instead of -75 µm. The impacts of these changes on final concentrate mass, lithium grade, and overall lithium recovery were systematically analyzed.

3. RESULTS AND DISCUSSION

In the USIM PAC modeling and simulation environment, the complete process flowsheet was first established based on experimental optimization results. Within the scope of the thesis, the process modeling covered beneficiation routes involving crushing, screening, and grinding, followed by magnetic separation and flotation operations. In this framework, sieve analyses and fractional lithium analyses were carried out for the products generated at each process unit, with a particular focus on evaluating lithium recovery.

The process flowsheet was constructed using the predefined unit operation modules available within the software. Subsequently, the validity of the flowsheet was verified using the built-in “test” function of the program. Each unit in the flowsheet was named, and the corresponding sieve analysis and fractional lithium assay data were entered into the system. Owing to the laboratory-scale nature of the experimental work, the simulations were performed using the “0” model option, and the required parameters for each unit operation were defined accordingly.

Initially, unit-level simulations were conducted to balance and stabilize the experimental data obtained for each process stage. This procedure was applied sequentially from the first to the final unit operation. Once unit consistency was achieved, the entire flowsheet was simulated using the “direct simulation” command.

The process flowsheet starts with size reduction of the entire material to below 2 mm, followed by screening at 0.3 mm. The -2+0.3 mm size fraction was fed to a ball mill, and all material was ground to below 0.3 mm. Based on optimization experiments, the -300 µm material was further classified to separate the -75 µm fraction, and the process was continued separately for the two size classes.

The -300+75 µm fraction was subjected to dewatering and subsequently treated in a roll-type magnetic separator, where the non-magnetic product was discarded. The magnetic product was then processed in a cleaning stage using the same roll magnetic separator by adjusting the splitter position closer to the belt, resulting in the final magnetic product. This magnetic concentrate was fed to flotation under the established optimum conditions, yielding the floating product as the final concentrate. The non-floating product was directed to a scavenger circuit to obtain a middling and a tailing product. The process flowsheet constructed in the software and the selected unit operation models, was presented in Figure 3 and 4, respectively.

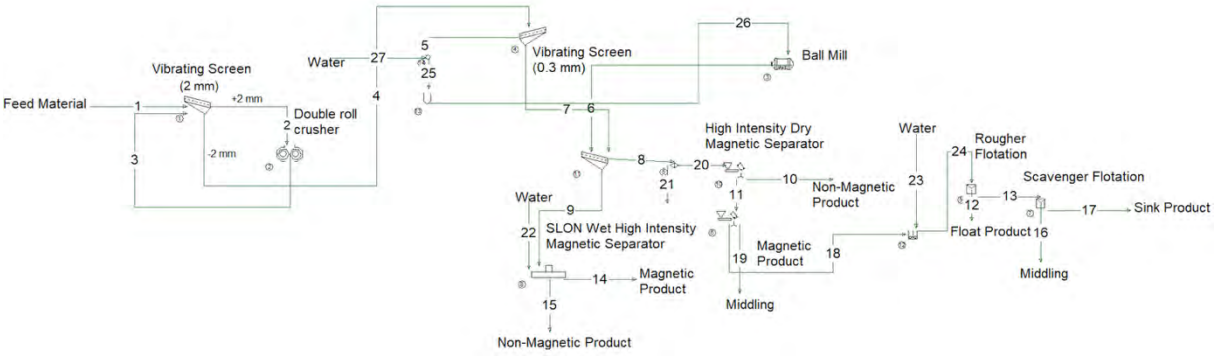

Figure 3. The process flowsheet constructed in the software

Figure 4 presents all unit operations defined in the designed process flowsheet. In addition, the model numbers selected within the software for each unit and the input parameters used to construct these models are also provided. To ensure stable model performance, distribution data and recovery values obtained from experimental results were entered into the system. In particular, for screen modeling, parameters other than screen aperture were calculated automatically using the software's "Model Adjustment Parameters" function. Following the construction of the flowsheet, the phase models introduced into the system were defined as ore/flotation and water. Since the study focused on lithium recovery, the solid phase was further divided into two components: lithium and gangue minerals. As the software requires the input of specific gravity values for solid phases, a density of 3 g/cm³ was assigned to lithium associated with biotite, while a value of 2.6 g/cm³ was assigned to all gangue minerals. Additionally, the grade ranges of the solid phases were defined in the model, with lithium grades expressed in ppm and gangue mineral grades expressed in wt.%. The particle size ranges defining the solid phases were also specified by entering the screen apertures used in the experimental work. The ore/flotation solid phase was selected due to the presence of flotation operations in the flowsheet, and lithium-defined as the valuable component-was designated as floatable within the program. For the water phase, only the specific gravity was specified and set to 1 g/cm³. All defined phase models are illustrated in Figure 5. After defining the phase models, sieve analysis and fractional lithium assay data for all feed and product streams were entered into the system. Once all model selections were completed, the simulation was executed. As a result, a final concentrate containing 6825 ppm Li was obtained, with an overall plant recovery of 42.6% and a flotation process recovery of 74.6%. For the optimized size fractions, namely -300+75, -300+53, -300+38, -500+75, -500+53, and -500+38 µm, the process was re-simulated by modifying the screen apertures within the model. The concentrate grades and lithium recoveries achievable for each size fraction were compared, and the resulting differences are presented in Table 3.

Figure 4. The selected unit operation models

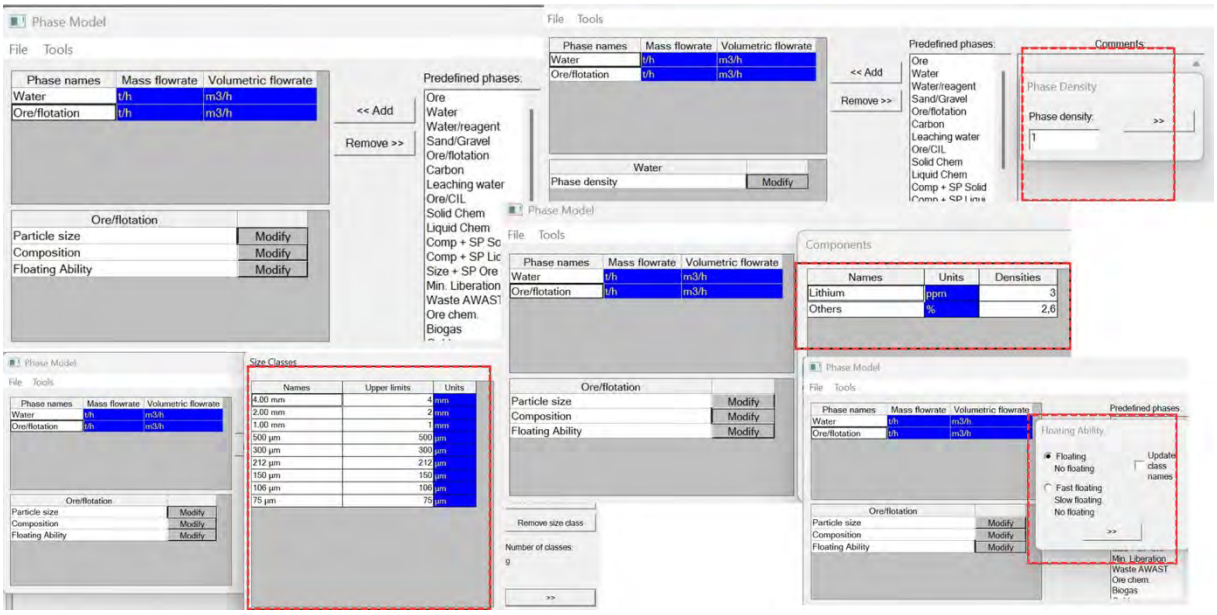

Figure 5. Defined phase models

Table 3. The concentrate grades and lithium recoveries achievable for each size fraction were and the results

Particle size, µm	Feed		Feed to Flotation		Concentrate		Recovery, %	
	Amount, t/h	Li, ppm	Amount, t/h	Li, ppm	Amount, t/h	Li , ppm	Plant	Process
-300+75	100	244,278	10,5451	1322,72	1,52483	6825,24	42,6	74,6
-300+53	100	244,278	13,0234	1225,5	1,85049	6402,45	48,5	74,2
-300+38	100	244,278	15,6392	1142,16	2,18229	6043,46	54,0	73,8
-500+75	100	244,278	9,49576	1315,75	1,38317	6754,56	38,2	74,8
-500+53	100	244,278	11,9277	1209,67	1,7075	6287,00	43,9	74,4
-500+38	100	244,278	14,0632	1134,11	1,98333	5956,70	48,4	74,1

Based on the results obtained, all simulation comparisons were carried out between materials ground to below 300 µm and 500 µm. Prior to grinding, the feed material consisted of a -2 mm fraction with a well-defined particle size distribution and known lithium content. The modeling and simulation framework was primarily established based on the experimentally optimized screen sizes of 300 µm and 75 µm. However, once all optimized conditions and the complete set of experimental data required by the models were introduced into the software, the program enabled the evaluation of alternative process scenarios.

Specifically, the software allowed assessment of process performance when grinding was performed to below 500 µm instead of 300 µm, or when size classification was carried out at 53 or 38 µm rather than at 75 µm, before continuing with the downstream process. Table 4.25 summarizes the values calculated by the program under these modified conditions, including the mass and grade of the magnetic product fed to flotation, the concentrate mass and grade, and the corresponding lithium plant recovery and flotation recovery.

Optimization experiments conducted on the run-of-mine ore indicated no significant difference in concentrate grade between the -500+75 µm and -300+75 µm size fractions. Nevertheless, due to an approximately 15% higher recovery, the -300+75 µm size fraction was selected as the optimal condition. This difference was attributed to the higher lithium content of the middlings obtained in the -500+75 µm size fraction. When the combined process flowsheet was applied, the influence of grinding to either 300 µm or 500 µm became less significant, and

a higher overall lithium recovery was achieved with the -300+75 µm size fraction, with only about a 4% difference in recovery.

Furthermore, replacing the -75 µm cut size with finer separations at -53 µm or -38 µm for materials ground to below 300 or 500 µm resulted in a decrease in concentrate lithium grade, accompanied by an increasing trend in plant recovery. Among these options, the -300+53 µm size fraction yielded acceptable results, producing a concentrate containing 6402.45 ppm Li with an overall plant recovery of 48.5%.

Based on the comprehensive simulation results, three size fractions were identified as the most promising for further evaluation: -500+75 µm, -300+75 µm, and -300+53 µm. In addition, the ball mill model was modified within the simulation from “Mill 0B” to “Ball Mill 1” to evaluate its effect on process performance. The corresponding results were presented in Figure 6.

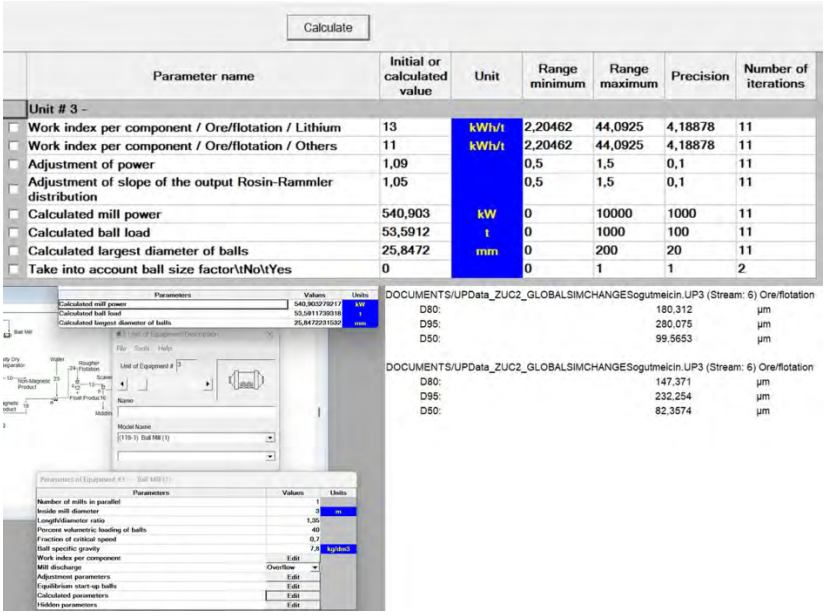

Figure 6. The simulation of “Ball Mill 1” and the evaluation its effect on process performance.

The simulation results previously obtained using the “Mill 0B” model are presented in Table 3. By converting the ball mill model to “Ball Mill 1”, it becomes possible to determine the mill dimensions and energy consumption based on the numerical input data provided to the model. The model selection procedure follows a structured workflow. First, a separate file is created under the name “aim”, in which the unit operation to be characterized is isolated. For instance, when focusing specifically on the ball mill, a simplified flowsheet containing only the mill feed and product streams is constructed, and the sieve analysis and fractional lithium assay data from the main flowsheet are entered. Subsequently, the phase models defined in the main file are selected, and the model under investigation is saved within the “aim” file.

The same file is then saved again using the “save as” option under the name “calibrated”. The purpose of this step is to ensure that any modifications applied to the calibrated model remain correlated with the real values defined in the aim file. Therefore, during calibration, the software is instructed-via file selection-to use the data stored in the aim file as reference information.

After completing these steps, all unknown model parameters are determined using the “model parameters adjustment” option. In this stage, the user defines the range and increment steps over which the key parameters are evaluated, with finer step sizes improving the accuracy of the model predictions. The calibrated file is then simulated using the determined parameters, and its results are compared with those of the aim file. For size reduction processes, this

comparison is performed using the global size distribution curves, whereas for beneficiation processes, global partition curves are evaluated.
Once a satisfactory agreement between the aim and calibrated results is achieved, all identified parameters are transferred to the main flowsheet file, and the updated process is simulated using the “direct simulation” command to obtain the final results.

4. CONCLUSION

A beneficiation flowsheet integrating size reduction, magnetic separation, and flotation was successfully modeled using USIM PAC based on experimental data, showing strong agreement between simulation and laboratory results. The simulations demonstrated that grinding size and fine fraction separation are the key parameters controlling lithium recovery. Although grinding to below 300 µm increased flotation recovery compared to 500 µm, the overall process performance showed only a minor difference, with the -300+75 µm size fraction providing the highest plant-scale lithium recovery. Finer cut sizes (-53 and -38 µm) resulted in lower concentrate grades but higher overall recoveries, with the -300+53 µm fraction yielding a concentrate containing approximately 6,400 ppm Li at 48.5% recovery. Overall, the -500+75 µm, -300+75 µm, and -300+53 µm size fractions were identified as the most critical for process optimization. The developed flowsheet enables the recovery of lithium from biotite-rich waste fractions of nepheline syenite, producing concentrates containing approximately 1.5 wt.% Li_2O. This approach offers a technically feasible and environmentally sustainable pathway for lithium recovery, with the added advantage of generating a valuable by-product alongside nepheline concentrate production.

REFERENCES

Botula, J., Rucký, P., Řepka, V., (2005) “Extraction of zinnwaldite from mining and processing wastes”, Mineralogical and Geological Series, *2*, 9-16.

Burat, F., Kangal, O., Onal, G., (2006) “An alternative mineral in the glass and ceramic industry: Nepheline syenite”, Minerals Engineering, 19(4), 370-371.

Chelgani, S. C., Leißner, T., Rudolph, M., Peuker, U. A., (2015) “Study of the relationship between zinnwaldite chemical composition and magnetic susceptibility”, Minerals Engineering, 72, 27-30.

Çınar, M., Durgut, E., (2019) “Mineral beneficiation of nepheline syenite with combination of dry magnetic separation and flotation methods”, Physicochemical Problems of Mineral Processing, 55(5).

Kangal, M. O., Bulut, G., Yeşilyur, Z., Basturkcu, H., Burat, F., (2019) “Characterization and production of Turkish nepheline syenites for industrial applications”, Physicochemical Problems of Mineral Processing, 55(3), 605-616.

Kratochvil, M., Landecka, A., Chlopecky, J., Sachova, P., (2016), “Possibilities of magnetic separation of lithium mica”, International Multidisciplinary Scientific GeoConference: SGEM, 1151-1158.

Landecka, A., Kratochvil, M., Kubečka, J., Tkačíková, L., (2017), “An application of a magnetic separation for lithic mica extraction”, International Multidisciplinary Scientific GeoConference: SGEM, 735-742.

Leißner, T., Bachmann, K., Gutzmer, J., & Peuker, U. A., (2016) “MLA-based partition curves for magnetic separation”, Minerals Engineering, 94, 94-103.

Litovchenko, A. S., Melnikov, A. A., (1980) “The local magnetic fields on aluminum nuclei in ferriferrous mica structure”, Physica Status Solidi A, 62(1), K77-K80.

Mahran, G. M., Ahmed, H. A., Haffez, G. S. A., (2022) “Nepheline syenite beneficiation for glass and ceramics industries”, Afinidad. Journal of Chemical Engineering Theoretical and Applied Chemistry, 79(597), 533-538.

Martin, G., Schneider, A., Voigt, W., Bertau, M., (2017) “Lithium extraction from the mineral zinnwaldite: Part II: Lithium carbonate recovery by direct carbonation of sintered zinnwaldite concentrate. *Minerals Engineering*, *110*, 75-81.

Paukov, I., Kovalevskaya, Y., Kiseleva, I., Shuriga, T., (2010) “A low-temperature heat capacity study of natural lithium micas: Heat capacity of zinnwaldite”, Journal of thermal analysis and calorimetry, 99(2), 709-712.

Siame, E., (2011)” Recovery of lithium from China clay waste using a combination of froth flotation, magnetic separation, roasting and leaching”, PhD Thesis, University of Exeter, Earth Resources, Exeter.

Siame, E., Pascoe, R. D., (2011) ”Extraction of lithium from micaceous waste from china clay production”, Minerals Engineering, 24(14), 1595-1602.

Tadesse, B., Makuei, F., Albijanic, B., Dyer, L., (2019) “ The beneficiation of lithium minerals from hard rock ores: A review”, Minerals Engineering, 131, 170-184.

Üçerler-Çamur, Z., Keles, O., Kangal, M. O. (2025a) “Mineral liberation analysis (MLA)-based characterization of lithium source: biotite and associated minerals in nepheline syenites”, Minerals, 15(8), 876.

Üçerler-Çamur, Z., Keles, O., Kangal, M. O. (2026) “Sustainable lithium recovery from biotite waste of nepheline syenite via magnetic separation and flotation with MLA-based mineralogical characterization”, Minerals, 16(1), 95.

Üçerler-Çamur, Z., Keles, O., Kangal, M. O., (2025b), ”Primary stage of zinnwaldite concentrate production from nepheline syenite rocks via magnetic separation”, IX. International ICONTECH Congress, 1-9.

Üçerler, Z., Güney, A., (2022a), “The investigation of lithium extraction by roasting with sulfating agent and water leaching from nepheline syenite rocks” Physicochemical Problems of Mineral Processing, 58(3).

Üçerler, Z., Güney, A., (2022b), “Obtaining zinnwaldite concentrate from nepheline syenite rocks by flotation method”, 17th International Mineral Processing Symposium, 437-446.

Wang, R., Cheng, Y., Fu, J., Han, H., Ding, J., Kang, J., Li, Y., (2025) “Study on the whole-grain magnetic-float combination beneficiation process of high mud lithium mica”, Chinese Journal of Engineering, 47(4), 642-653.

Xue, Z., Feng, Y., Li, H., Ju, J., Du, X., (2024) “A stepwise approach to enhancing flotation of low-grade zinnwaldite through the cationic/DL-2-octanol/anionic reagent combinations: Behavior and mechanism analysis”, International Journal of Mining Science and Technology, 34(6), 881-891.

REALISING THE SMART GRINDING MILL: OPTIMISING MILL PERFORMANCE THROUGH REAL-TIME LIFTER BAR WEAR MONITORING AND PREDICTIVE MAINTENANCE PLANNING

Ahmet ALTUNCU[1], Büşra ÇALIŞKAN[1], Ufuk KOÇBIYIK[2,3], Oğuzhan ÇAKIR[2,3], Ayhan YAZGAN[2,3], Uğur ŞEVİK[4,5], Tolga BERBER[4,5], Oğuzhan BAŞER[4,5], Ersin Yener YAZICI[4,6,*], Oktay CELEP[4,6]

[1]FKK Güney Oto Lastik Takoz San. ve Tic. A.Ş., Samsun, Türkiye
[2]İNOVAS Elektronik, Trabzon Technology Development Zone, 61081, Trabzon, Türkiye
[3]Karadeniz Technical University, Faculty of Engineering, Department of Electrical and Electronics Engineering, 61080, Trabzon, Türkiye
[4]RETİNA ARGE, Trabzon Technology Development Zone, 61081, Trabzon, Türkiye
[5]Karadeniz Technical University, Faculty of Science, Computer Science,61080, Trabzon, Türkiye
[6]Karadeniz Technical University, Faculty of Engineering, Department of Mining Engineering, Division of Mineral & Coal Processing, 61080, Trabzon, Türkiye
**Corresponding author: eyazici@ktu.edu.tr*

A B S T R A C T

The periodic replacement/assembly of liners and lifter bars in mills is essential to efficiently grind ores. Conventional methods for the measurement of lifter bar wear levels require shutdown of the grinding operation, which results in significant production loss. Therefore, the implementation of a system for real-time monitoring of abrasive wear on lifter bars is critical for minimising operational costs (OPEX) and sustaining continuous grinding. This study presents the development of a wireless sensor network system designed for the real-time abrasion monitoring and forward prediction of wear on rubber lifter bars in grinding mills. A prototype of this "smart lifter bar" system was manufactured and subsequently tested in operational ball mills at mineral processing plants in Türkiye. The lifter bars were equipped with sensors to continuously measure the variation in their height during the grinding process. The collected data were then transmitted to a cloud-based platform via internet communication devices. A dedicated interface was developed to allow for the real-time monitoring of the lifter bar height, providing an immediate assessment of its wear status. The collected wear data will be further processed to predict future wear levels and organise maintenance planning.

***Key words**: Grinding, rubber lifter bar, wear, wireless sensor network system, real-time monitoring, forward prediction*

1. INTRODUCTION

One of the most energy-consuming processes in the mining industry is comminution, which includes crushing and grinding operations. Comminution represents 1-4% of worldwide energy consumption (AusIMM, 2011; Jeswiet and Szekeres, 2016; Nadolski et al., 2014). Crushing and grinding account for 44% of the total energy consumption in the mining industry. It was also reported that 36% of the energy used by the mines was consumed in comminution stages in Australia (Ballantyne et al., 2012). Grinding is an inefficient process in that only 1% of the total energy is consumed in the breakage of the particles in a ball mill, while over 80% of the energy is wasted as heat (Maregedze et al., 2023). Optimised grinding performance is essential to produce ground material with the target particle size distribution, which is critical to achieve high mineral separation/extraction efficiencies through subsequent physical separation and hydrometallurgical processes (McIvor, 1986; Dandotiya, 2011; Wills and Finch, 2016; Yıldız, 2014). Liners and lifter bars are one of the essential parts of grinding mills. They have two key roles in grinding: (i) protecting the mill body from wear and (ii) moving the ore and grinding media to provide the grinding action (Figure 2). Liners can be produced using

different materials, but among them, rubber liners have significant technical and economic advantages over traditional cast steel liners and others. Some advantages of rubber liners are lower noise levels, reduced mill weight which allow less frequent mechanical failures, around 4-5% energy savings, less grinding media consumption, less wear and corrosion, and high chemical resistance due to high shock absorption, and easier installation processes due to lower density (McTavish, 1990; Powell, 2006; Yıldız, 2014).

During grinding, liners get worn depending on the factors including operational conditions of the mill (i.e., grinding media charge, capacity (t/h), mill rotation speed, mill aspect ratio, temperature), characteristics of the ore (hardness, abrasiveness etc.), and liner design & material properties (Napier-Munn et al., 1999; Powell, 1991; Powel, 1994; Powell and Vermeulen, 1994; Noaparast and Fotoohi, 2005; Taylor et al., 2015; Usman et al., 2017). As the grinding proceeds, the liner profile/height is reduced, which results in changes in the trajectory of the ore and grinding media (Figure 1) (Radziszewski and Tarasiewicz, 1993). This also adversely affects the efficiency of the grinding. Therefore, the timing of replacement of worn liners with new ones is of great importance to continue efficiency in grinding. Liner costs have the second-highest share in mill operating expenses with 6-40% after energy costs. This necessitates careful optimisation of the liner assembly/replacement planning (Figure 2), which is essential to minimise production losses and costs (Taylor et al., 2015; Yıldız, 2014). Lifter bar wear can be measured by direct and indirect methods. In direct methods, the mill must be stopped, followed by the measurement of the lifter bar profile/geometry using simple mechanical instruments or advanced 2D/3D laser scanning technologies. Indirect methods allow continuous monitoring and assessment of grinding performance but without direct lifter bar measurement (Dandotiya et al., 2018; Powell, 2006; Powell et al., 2012; Taylor et al., 2015).

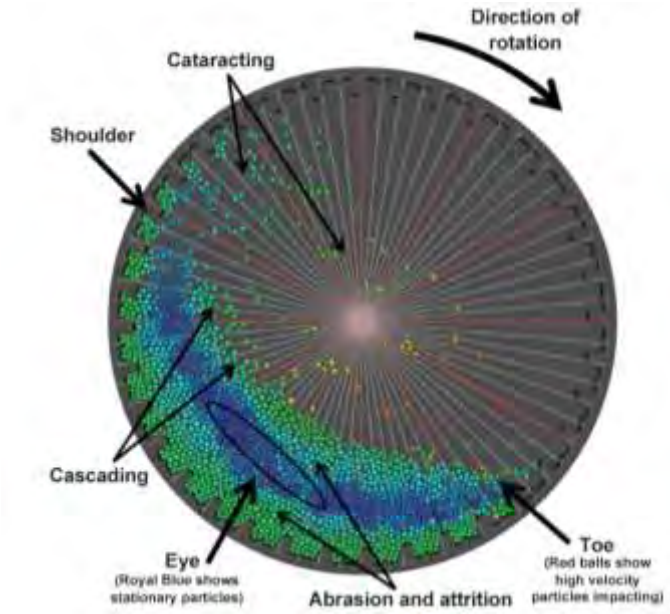

Figure 1. Movements and regions forming during the grinding process (Taylor et al., 2015)

Figure 2. Rubber liner/lifter bar assembly process in a ball mill (URL-1, 2026)

There have been no commercial technologies for direct measurement of lifter bar wear without stopping the grinding process. In this study, the results of a prototype system which is developed to measure and monitor rubber lifter bar wear in real-time, with forward prediction of the wear levels using the data collected, are presented. The essential principles and parts of the developed smart system are explained.

2. EXPERIMENTAL

2.1. Material and Method

A selected number of shell lifter bars were fitted with embedded sensors and wireless communication devices to enable real-time monitoring of lifter bar height and thickness throughout mill operation. These smart lifter bars allow non-intrusive wear assessment without shutting down the grinding operation. Figure 3 shows simplified 3D drawings illustrating the smart lifter bars with sensors positioned at different locations along the bar. The sensors were designed to measure thickness/height at 2 cm intervals across a total measurement range of 10 cm. This resolution allows progressive wear to be tracked with reasonable spatial detail as the bar gradually degrades over time.

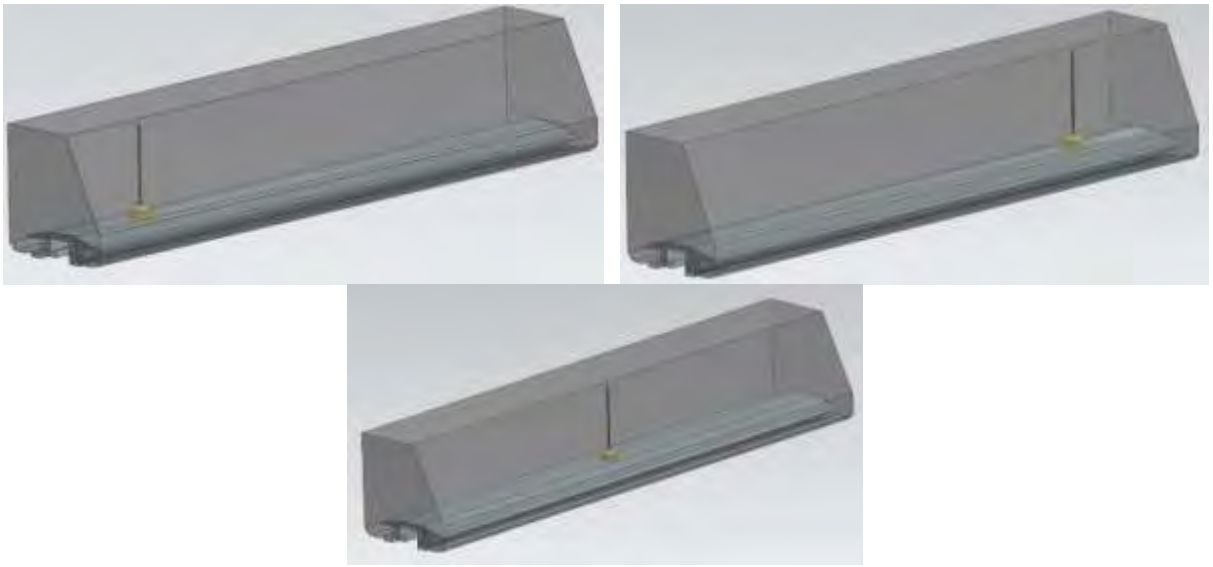

Figure 3. Simplified 3D view of the embedded sensors located in different positions along the lifter bar

Following fabrication and testing, the smart lifter bars were transported to the mineral processing plant operated by Dimin Madencilik (Bingöl, Türkiye). Then, smart lifter bars were assembled into the ball mill alongside standard liner components (Figure 4). The associated

connector and antenna units were installed in the plant's control room to ensure signal reception from smart lifter bars (Figure 5).

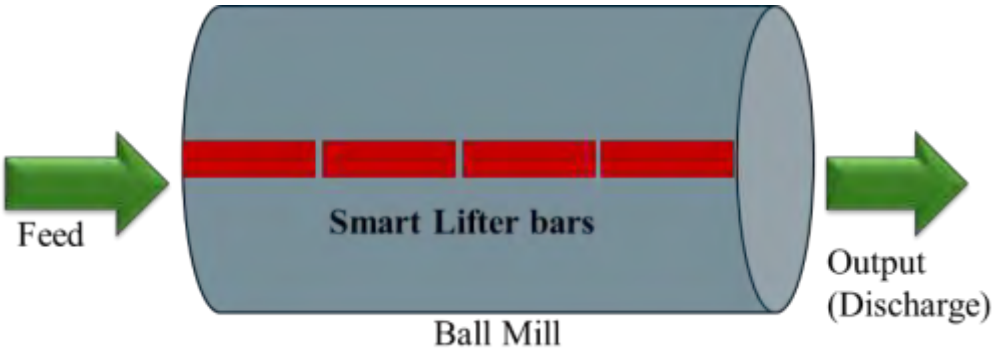

Figure 4. Schematic view of the smart lifter bars mounted in the ball mill

Figure 5. The coordinator and antenna placed in the control room of the plant

The sensors transmit data to a receiver unit in the control room using a long-range wireless communication protocol. The data is then sent to a cloud system or a local database for storage via GPRS. The web interface presents the data in real-time in the required formats. The interface also generates automatic alerts when critical wear thresholds are reached or in the case of a system error. The general flow sheet of the developed system is illustrated in Figure 6. Further, the wear data collected can be utilised for the forward prediction of future wear levels through time-series models.

Figure 6. The main units and working principles of the developed smart system

3. RESULTS AND DISCUSSION

After the developed system was fully installed, the grinding operation was commenced, and monitoring of the wear collected by sensor-equipped lifter bars began. Throughout the grinding process, changes in lifter bar height were continuously recorded by the embedded sensors and wirelessly transmitted to a cloud database via GPRS, without any interruption to mill operation. The collected data was monitored in real-time through a web-based interface, via the internet, which brings a practical advantage for both on-site operators and off-site engineers. The interface displays wear measurements across five levels at 2 cm intervals, covering the full 10 cm measurement range of each lifter bar. Alongside the wear profiles, the interface also shows key system indicators such as communication status and automatically flags when wear levels reach critical thresholds (Figures 7 and 8). Wear data was successfully collected from the sensors over approximately 6000 hours of continuous grinding operation. This collected dataset can be used to forecast future wear progression using time-series. This would support more proactive maintenance decisions and avoid the costs of early liner replacement.

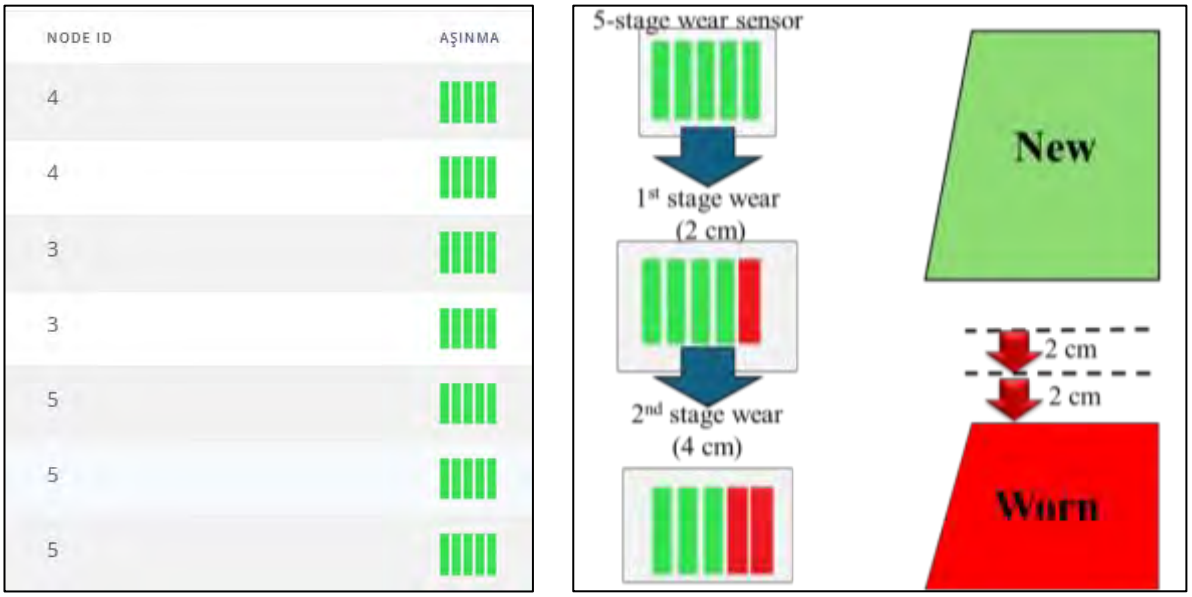

Figure 7. Views from real-time wear data from the web-based interface at the initial time (left) and after starting the grinding operation (right)

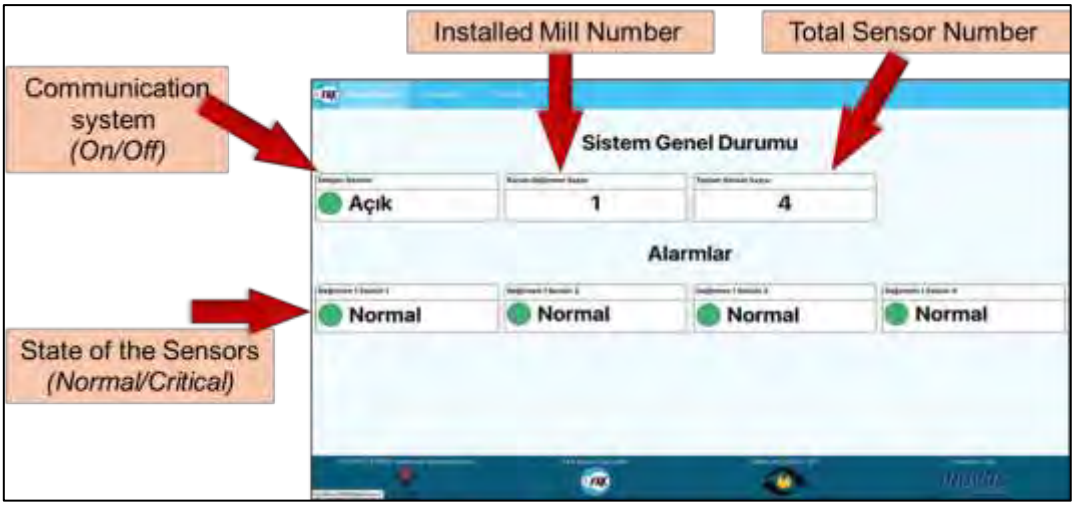

Figure 8. Web-based interface (under development)

The results obtained from this study confirm that the developed prototype is capable of monitoring abrasive wear in rubber lifter bars in real-time under real-world conditions over long periods of over 6000 hours. The system has the potential to deliver technical and economic benefits to mineral processing plants at industrial scale. This approach has the potential to support optimisation of liner replacement/assembly schedules and reduce unplanned downtime and maintenance costs based on real-time wear data rather than fixed time intervals. The collected wear data from multiple plants and different kinds of ores with varying petrographic and mineralogical characteristics will form a comprehensive reference database. This dataset can be subsequently used to develop predictive models that correlate wear rates with ore properties. This will also enable more reliable service life estimation for future operations before accumulating sufficient site-specific wear data. Such models would also support iterative lifter bar design improvements across different ore types and mill configurations.

4. CONCLUSION

This study presents the development and industrial trial of a sensor-based wireless system for real-time wear monitoring of rubber lifter bars in grinding mills. The system consists of smart lifter bars equipped with sensors which transmit wear measurements to a cloud platform via GPRS through a connector device. The wear data is accessible through a web-based interface for remote monitoring. The industrial trial was carried out in an operating ball mill, where the system continuously recorded lifter bar wear over a grinding period of approximately 6000 hours. Throughout the grinding period, wear data were collected without any mill stoppages for wear control using conventional mechanical instruments and/or advanced 3D laser scanning technologies. This confirmed that the developed system is technically suitable for uninterrupted industrial operation. The developed system is expected to contribute to more optimised liner replacement scheduling, reduced downtime frequency, and lower operating costs in mineral processing plants.

ACKNOWLEDGMENTS

The authors gratefully acknowledge the TUBITAK TEYDEB (Project no: 3230813) for the financial support and Dimin Madencilik (Türkiye) for their help during the trials.

REFERENCES

Allen, M., (2021) “Mineral energy consumption 2021”, ENGECO Report, 47 pp.

AusIMM, (2011) “Beneficiation – Comminution”, Monograph 27 - Cost Estimation Handbook, The Australasian Institute of Mining and Metallurgy (AusIMM), 217–261.

Ballantyne, G. R., Powell, M. S., Tiang, M., (2012) “Proportion of energy attributable to comminution”, Proceedings of the 11th AusIMM Mill Operators' Conference, Hobart, Tasmania, 29–31 October 2012.

Dandotiya, R., (2011) “Decision support models for the maintenance and design of mill liners”, PhD Thesis, Luleå University of Technology, Division of Operation and Maintenance Engineering.

Dandotiya, R., Lundberg, J., Wijaya, A. R., Parida, A., (2018) “Evaluation of abrasive wear measurement devices of mill liners”.

Jeswiet, J., Szekeres, A., (2016) “Energy consumption in mining comminution”, Procedia CIRP, 48, 140–145.

McIvor, R. E., Finch, J. A., (1986) “The effects of design and operating variables on rod mill performance”, CIM Bulletin, 79 (895) 39–46.
McTavish, S. F., (1990) “History and evolution of rubber liner systems for grinding mills”, Society for Mining, Metallurgy and Exploration.

Maregedze, L., Masike, R., Kanyowa, T., Chiteka, K., (2023) “Ball mill energy efficiency optimization techniques: A review”, i-manager’s Journal on Mechanical Engineering, 13 (4) 41–50.

Maregedze, L., Chiteka, K., Masike, R., Kanyowa, T., (2024) “Ball mill energy efficiency optimization: A lifter face angle optimization approach”, Journal of Applied Research and Technology, 22 (6) 798–805.

Nadolski, S., Klein, B., Kumar, A., Davaanyam, Z., (2014) “An energy benchmarking model for mineral comminution”, Minerals Engineering, 65, 178–186.

Noaparast, M., Fotoohi, B., (2005) “Investigation of liner wear at Chadormalu semi-autogenous grinding mills”, Proceedings of the Canadian Mineral Processors, 335–345.

Napier-Munn, T. J., Morell, S., Morrison, R. D., Kojovic, T., (1999) “Mineral comminution circuits: Their operation and optimisation”, Julius Kruttschnitt Mineral Research Centre.

Powell, M. S., (1991) “The effect of liner design on the motion of the outer grinding elements in a rotary mill”, International Journal of Mineral Processing, 31, 163–193.

Powell, M. S., Hilden, M. M., Weerasekara, N., Yahyaei, M., Toor, P., Franke, J., Bird, M., (2012) “A more holistic view of mill liner management”, Proceedings of the 11th Mill Operators’ Conference, 95–104.

Powell, M. S., Smit, I., Radziszewski, P., Cleary, P., Rattray, B., Eriksson, K., Schaeffer, L., (2006) “The selection and design of mill liners”, Advances in Comminution, Society for Mining, Metallurgy and Exploration (SME), 331–376.

Powell, M. S., Vermeulen, L. A., (1994) “The influence of liner design on the rate of production of fines in a rotary mill”, Minerals Engineering, 7, 169–183.

Radziszewski, P., Tarasiewicz, S., (1993) “Simulation of ball charge and liner wear”, Wear, 169 (1) 77–85.

URL-1, (2026) “Rubber liner/lifter bar assembly”, FKK Mining.

Usman, H., Taylor, P., Spiller, D. E., (2017) “The effects of lifter configurations and mill speeds on the mill power draw and performance”, AIP Conference Proceedings, 1805 (1) 050001.

Wills, B. A., Finch, J., (2016) “Wills' Mineral Processing Technology: An Introduction to the Practical Aspects of Ore Treatment and Mineral Recovery”, Butterworth-Heinemann.

Yıldız, N., (2014) “Cevher hazırlama ve zenginleştirme – Vol. 1”, Ekrem Basım Ltd. Şti., Ankara.

TONNEX: A CONTRACT-DRIVEN DIGITAL ECOSYSTEM FOR MINERAL PROCESSING OPERATIONS

Hasan Berke AKKÖSE*, Hayri Atalay KUL*

Tonnex Digital Operations Platform, Istanbul, TÜRKIYE
**Corresponding authors: akkose@tonnexapp.com; kul@tonnexapp.com*

A B S T R A C T

Mineral-processing plants still depend heavily on heterogeneous spreadsheets, informal operator knowledge, and manually assembled reports. This fragmentation makes traceability, multi-site governance, and repeatable decision support difficult, especially when each plant or client requires different forms, KPIs, and workflows. This paper presents Tonnex, a cloud-native digital operations platform developed for mineral-processing environments. Tonnex is built around a contract-driven architecture that separates the immutable core responsibilities of authentication, authorization, multi-tenant isolation, persistence, and aggregation from client-specific schemas, calculations, KPI rules, and user-interface contracts. The proposed approach formalizes three industrial boundaries: company as the data-isolation boundary, plant as the access-scope boundary, and client configuration as the behavior boundary. The system adopts a payload-first record model in which each operational entry stores versioned input and output payloads together with auditable metadata. This enables a single product core to support different mineral-processing contexts without hardcoded branching in the main codebase. The current production-oriented scope includes shift records, shipment records, work orders, scheduled reports, energy monitoring, and self-serve Excel/CSV import. In addition, two higher-level decision-support directions are presented as ongoing developments: an AI assistant layer for anomaly explanation and operator guidance, and a simulation layer for what-if scenario analysis in flowsheet, water-balance, and equipment studies. The contribution of the paper is therefore not a benchmark of one algorithm, but an implementable systems architecture showing how mineral-processing knowledge, plant-specific computation, and operational governance can be integrated in a deployable industrial platform.

Key words: *Mineral processing, digitalization, decision support, digital twin, industrial AI*

1. INTRODUCTION

Digitalisation in mining and mineral processing has accelerated over the last decade, driven by automation, sensorization, real-time data acquisition, and the wider Industry 4.0 agenda. Reviews of mining-sector digitalisation identify automation, robotics, the Internet of Things, big data, and real-time operational data as the dominant technological trends shaping the sector (Barnewold and Lottermoser, 2020). In mineral processing specifically, digital solutions are increasingly expected not only to visualize data, but also to standardize operational knowledge, support plant reporting, and provide a basis for higher-level optimization and digital-twin applications (Nad et al., 2022; Jämsä-Jounela, 2019).

Despite this progress, many concentrators still manage daily operational reality through fragmented spreadsheets, informal operator notes, ad hoc messaging, and manually prepared summaries. Such practices create several persistent problems: the same plant event may be recorded in different formats by different people; domain calculations become hidden inside spreadsheets; reporting delays accumulate; and decision support remains weakly connected to traceable plant data. Earlier expert-system literature already recognized that minerals operations need structured knowledge capture and operator-facing decision support, yet many solutions remained local, single-purpose, or difficult to maintain across changing plant contexts (Bearman and Milne, 1992).

At the same time, recent AI and digital-twin studies suggest that mineral-processing operations can benefit from integrated data foundations that support learning, prediction, simulation, and optimization (Mishra, 2021; Nobahar et al., 2024; Ohenoja et al., 2023). However, there remains a practical implementation gap between academic models and deployable plant software. Many research contributions focus on a specific algorithm, unit operation, or modeling method, whereas industrial adoption also requires role-based access control, tenant isolation, auditability, workflow integration, report generation, and safe support for plant-specific rules.

This paper addresses that gap by presenting Tonnex as a design-oriented contribution: a deployable digital operations platform for mineral-processing plants. The novelty is architectural. Rather than embedding plant-specific logic directly in a monolithic product core, Tonnex isolates customer- or plant-specific forms, computations, KPIs, and visual structures into explicit client contracts, while the core remains responsible for security, data boundaries, orchestration, and persistence. The paper describes this architecture, summarizes the current implemented modules, and discusses how the same foundation enables future AI-assistant and simulation layers without violating traceability or governance constraints.

2. MATERIALS AND METHODS

2.1. Design Requirements and Industrial Context

Tonnex was designed as an industrial software system rather than as a single analytical model. The development therefore started from operational requirements observed in mineral-processing reporting and daily plant coordination. Five requirements guided the design. First, operational data had to be captured in a structured and versioned way so that plant records could be trusted beyond the moment of entry. Second, the platform had to support different clients and plants without mixing data or introducing unsafe silent defaults. Third, the system had to separate generic platform logic from plant-specific domain rules, because the same product may be used for flotation, shipment, energy, or maintenance workflows under different client contracts. Fourth, the software had to remain operator-facing, auditable, and explainable rather than becoming a black-box analytics layer. Fifth, the platform had to be cloud-deployable and modular so that additional record families and decision-support modules could be added incrementally.

These requirements led to a design-science style development approach. Instead of optimizing a narrow objective function, the work formalized an architecture capable of hosting multiple operational modules under a single governed core. In that sense, the 'material' of the study is not ore or laboratory equipment, but the industrial information flow itself: shift data, shipment data, work orders, reports, energy readings, and imported legacy files. The 'method' is the explicit architectural decomposition of this flow into boundary-aware software layers.

2.2. System Architecture and Record Model

The central architectural principle of Tonnex is the separation of data boundary, access boundary, and behavior boundary. Company identity defines the multi-tenant data boundary; plant identity defines the operational access scope; and a client configuration key defines the behavior package that selects schemas, calculations, KPI rules, and UI contracts. This triad prevents a common industrial anti-pattern in which a single identifier is forced to carry isolation, authorization, and behavior semantics simultaneously.

Operational records follow a payload-first model. Each record stores a schema version, an input payload, an output payload, and core metadata such as company, plant, timestamps, and audit information. The core pipeline is validate → compute → persist. Crucially, the core does not own plant-specific formulas or KPI choices. Those are provided by client contracts,

which define input and output schemas, UI form structure, transformation adapters, calculators, and summary rules. The core therefore executes calculations without becoming dependent on one client's domain assumptions. This reduces branching in the product core and makes plant-specific evolution manageable.

Figure 1 summarizes this architecture. Multiple record families feed the same governed core. Client contracts act as explicit behavior injectors, while delivery surfaces such as dashboards, record pages, reports, and exports consume the resulting structured outputs. Emerging AI and simulation layers are positioned above the same foundation rather than implemented as disconnected tools.

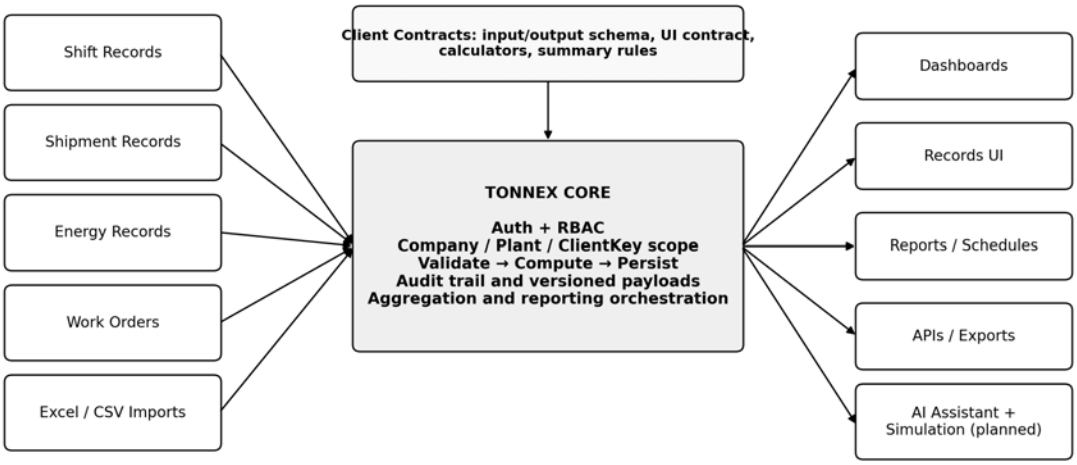

Figure 1. Conceptual architecture of the Tonnex platform for mineral-processing operations

2.3. Security, Governance, and Deployment Method

Because decision support in mineral processing is operationally sensitive, governance features were treated as first-class design objects. Authentication is token-based, authorization is role-based, and permission checks are resolved against a canonical feature model. Mutating actions write audit events so that the platform can preserve who changed what and when. This is important not only for cybersecurity but also for engineering accountability, because daily plant records often become the basis of management, maintenance, production, and quality decisions.

The platform is containerized and deployed as a cloud-native service. From a systems-engineering perspective, the goal of cloud deployment is not merely hosting convenience. It enables consistent release management, centralizes authorization and reporting behavior, and makes it possible to support multiple client contexts through one operational core. The same architecture also supports strict fail-fast behavior: if a client configuration cannot be resolved safely, the system refuses to proceed instead of silently falling back to an incorrect default.
In addition, the platform avoids domain calculations on the user interface side. Dashboards and reports render backend-produced values rather than recomputing operational logic in browser code. This decision increases repeatability and reduces the risk of divergent interpretations between data entry, aggregation, and reporting.

Table 1. Mapping recurrent industrial problems to the main Tonnex design responses

Industrial challenge	Tonnex design response	Expected operational effect
Heterogeneous spreadsheet-driven records	Versioned payload-first record model with standardized metadata	Higher traceability and less dependence on hidden spreadsheet logic
Different plant or client KPIs and forms	Client contracts for schema, computation, UI, and summary rules	Reuse of one core across multiple mineral-processing contexts
Multi-site data safety and access ambiguity	Separation of company, plant, and client behavior boundaries	Safer tenant isolation and clearer operational scope
Weak accountability in manual workflows	Audit trail, role-based permissions, and governed mutations	Improved engineering accountability and reviewability
Slow reporting and difficult legacy onboarding	Dashboards, scheduled reports, and self-serve Excel/CSV import	Faster operational reporting and easier transition from legacy files

2.4. Implemented Module Set

The current system scope already covers multiple operational modules. Shift Records organize daily or shift-based plant measurements and production variables. Shipment Records handle dispatched material with variant-specific attributes such as tonnage, moisture, and grade. Energy Records support meter-based monitoring, including active/reactive tracking and plant-specific limits. Work Orders extend the platform from observation into action by structuring maintenance tasks, states, parts, and SLA-oriented analytics. A block-based Reports module supports export, scheduling, and distribution. Finally, a self-serve Excel/CSV import layer allows legacy files to be mapped into the platform without moving domain calculations into the import interface. Table 2 distinguishes these implemented modules from the AI-assistant and simulation modules that are currently being developed on the same architectural foundation.

Table 2. Presently implemented and emerging modules within the Tonnex platform

Module	Primary function	Status in platform
Shift Records	Daily/shift data capture, production and process logging	Implemented
Shipment Records	Dispatch and quality reporting for shipped material	Implemented
Energy Records	Meter readings, active/reactive monitoring, penalty-oriented follow-up	Implemented
Work Orders	Maintenance workflow, SLA tracking, and parts-aware action management	Implemented
Reports	Template-based reporting, export, scheduling, and distribution	Implemented
Excel/CSV Import	Legacy file onboarding through self-serve mapping templates	Implemented
AI Assistant	Anomaly explanation, operator guidance, and contextual record linking	In development
Simulation Module	What-if flowsheet, water-balance, and equipment scenario analysis	In development

3. RESULTS AND DISCUSSION

3.1. Operational Contributions of The Platform

The main result of the Tonnex approach is the transformation of plant information from fragmented files into a governed operational system. In practical terms, this means that a shift entry, an energy reading, a work order, and a report block are all handled through one consistent architectural language. That consistency matters because mineral-processing

decision support is rarely about one isolated variable. Production, grade, reagents, energy, maintenance, and reporting influence one another, and their supporting software must therefore share traceable data boundaries.

A second result is that client-specific flexibility no longer has to be purchased with core instability. In many industrial systems, every new plant or customer introduces new branching in the main application. Tonnex instead localizes variability into client contracts. The core remains stable, while plant-specific schemas, calculators, and visual structures can evolve independently. This is especially important in mineral processing, where two plants may both be 'flotation plants' yet differ substantially in inputs, outputs, units, reporting expectations, and control vocabulary.

A third result is improved continuity from data capture to decision delivery. Because records, summaries, and reports all depend on the same governed backend outputs, dashboards and exported reports remain aligned. This reduces the interpretive drift that commonly occurs when one team enters data in one system and another team rebuilds the same metrics manually elsewhere. In design terms, the platform thus acts as an operational data spine rather than as a set of isolated dashboards.

3.2. Scientific and Engineering Contributions

The contribution of Tonnex can be interpreted at three levels. At the software-architecture level, it offers a formal separation between fixed platform concerns and variable plant knowledge. At the operational-governance level, it combines security, auditability, and role-aware workflows with mineral-processing-specific records. At the decision-support level, it provides a platform onto which analytics, AI, and simulation capabilities can be mounted without losing traceability.
This contribution is relevant to current literature because it operationalizes several ideas that are often discussed separately. Mining and mineral-processing digitalisation literature emphasizes the role of data integration, online information, automation, and digital ecosystems (Barnewold and Lottermoser, 2020; Nad et al., 2022). AI reviews show that mineral-processing applications benefit from data-driven models, but also reveal the need for usable integration into real decision processes (Mishra, 2021). Digital-twin studies further highlight the value of architectures that support learning, simulation, prediction, and continuous adaptation (Birk et al., 2022; Nobahar et al., 2024; Ohenoja et al., 2023). Tonnex contributes by showing how these directions can be hosted inside an operational SaaS architecture rather than as disconnected prototypes.

There is also an engineering contribution in the choice to prohibit UI-side domain math. This design choice may appear restrictive, but it improves repeatability and governance. When domain calculations remain in governed backend or contract layers, the same rule set drives records, summaries, exports, and future assistant modules. For mineral-processing operations, where small differences in formula interpretation can create significant operational disagreement, this consistency is valuable.

3.3. Emerging AI Assistant and Simulation Layers

The next logical step for such a platform is not merely more dashboards, but higher-level decision support. The first is an AI assistant layer that uses historical operational context to explain anomalies, generate hypotheses, surface related records, and suggest next actions in a human-in-the-loop manner. The assistant is not conceived as an autonomous controller. Rather, it functions as an evidence-linked operational companion that must remain traceable to recorded plant data, reports, and work-order workflows.

The second direction is a simulation and process-design module. Mineral-processing simulation has long been recognized as a basis for plant study, control design, and what-if analysis, while recent literature increasingly frames such capabilities in digital-twin terms (Quintanilla et al., 2021; Ohenoja et al., 2023). Within Tonnex, the simulation layer is intended to connect flowsheet structures, water-balance reasoning, equipment properties, and constraint-aware scenario comparison to the same operational data foundation that already drives records and reports. This can enable engineers to ask questions such as how a change in wash-water addition, cut size, or circulating load may influence throughput, product size, water use, or energy intensity.

From a research perspective, these emerging modules are important because they shift the platform from descriptive digitalization toward prescriptive and scenario-based support. At the same time, their development must remain bounded by governance. Suggested actions should link back to actual plant records, confidence should be stated explicitly, and human approval should remain mandatory for operational changes. In this way, AI and simulation are positioned not as replacements for engineering judgement, but as structured amplifiers of it.

3.4. Limitations and Future Work

The present paper is intentionally architecture-centered. It does not report a controlled plant trial or a comparative benchmark against another commercial platform. As a result, the strongest claims that can be made are about architectural suitability, deployability, and scope for integration rather than about quantified gains in recovery, tonnage, or energy. Future work should therefore include longitudinal case studies in which plant users evaluate reporting speed, data quality, traceability, and decision latency before and after deployment.
In addition, the AI and simulation modules now under development require further methodological work in model calibration, explainability, confidence management, and validation against plant outcomes. These steps are necessary if the platform is to progress from operational intelligence toward trustworthy digital-twin-enabled optimization.

4. CONCLUSION

This paper presented Tonnex as a contract-driven digital operations platform for mineral-processing environments. The platform addresses an important industrial gap: the lack of deployable systems that can combine plant-specific operational knowledge with cloud-native governance, traceability, and extensibility. The core architectural idea is the strict separation of data isolation, plant access scope, and client-specific behavior, supported by a payload-first record model and governed calculation pipeline.

Within this framework, Tonnex already supports several operational modules, including shift records, shipment records, work orders, reports, energy tracking, and self-serve file import. More importantly, the same architecture creates a stable base for higher-level assistant and simulation capabilities without forcing plant-specific logic into the product core. In that respect, Tonnex is both an industrial software product and a research platform for structured, auditable mineral-processing decision support.

The broader implication is that digitalisation in mineral processing should not be understood only as dashboard construction or algorithm deployment. It also requires a rigorous information architecture that can safely connect records, calculations, permissions, reports, explanation, and future what-if reasoning. Tonnex is proposed as one such architecture and as a practical pathway from spreadsheet-fragmented plant operations toward governed digital operations intelligence.

REFERENCES

Barnewold, L., Lottermoser, B. G., (2020) “Identification of digital technologies and digitalisation trends in the mining industry”, International Journal of Mining Science and Technology, 30 (6) 747-757.

Bearman, R. A., Milne, R. W., (1992) “Expert systems: Opportunities in the minerals industry”, Minerals Engineering, 5 (10-12) 1307-1323.

Birk, W., Hostettler, R., Razi, M., Atta, K., Tammia, R., (2022) “Automatic generation and updating of process industrial digital twins for estimation and control - A review”, Frontiers in Control Engineering, 3 954858.

Jämsä-Jounela, S.-L., (2019) “Future Automation Systems in Context of Process Systems and Minerals Engineering”, IFAC-PapersOnLine, 52 403-408.

Mishra, A. K., (2021) “AI4R2R (AI for Rock to Revenue): A Review of the Applications of AI in Mineral Processing”, Minerals, 11 (10) 1118.

Nad, A., Jooshaki, M., Tuominen, E., Michaux, S., Kirpala, A., Newcomb, J., (2022) “Digitalization solutions in the mineral processing industry: The case of GTK Mintec, Finland”, Minerals, 12 (2) 210.

Nobahar, P., Xu, C., Dowd, P., Shirani Faradonbeh, R., (2024) “Exploring digital twin systems in mining operations: A review”, Green and Smart Mining Engineering, 1 (4) 474-492.

Ohenoja, M., Koistinen, A., Hultgren, M., Remes, A., Kortelainen, J., Kaartinen, J., Peltoniemi, M., Ruusunen, M., (2023) “Continuous adaptation of a digital twin model for a pilot flotation plant”, Minerals Engineering, 198 108081.

Olivier, J., Aldrich, C., (2021) “Use of decision trees for the development of decision support systems for the control of grinding circuits”, Minerals, 11 (6) 595.

Quintanilla, P., Neethling, S. J., Brito-Parada, P. R., (2021) “Modelling for froth flotation control: A review”, Minerals Engineering, 162 106718.

TOWARD AUTONOMOUS MINERAL SORTING: INTEGRATING MACHINE LEARNING AND ROBOTICS IN ORE PROCESSING

Alexandru MIHAI[1,*], Mihai CULEA[2], Adriana BURLIBASA[3], Gabriela IORGA[2], Victor MIHAI[4]

[1]University of Petrosani, Mining Faculty, Mineral Processing Department, Petrosani - Romania
[2]Dunarea de Jos" University of Galati, Computer Science Department, Galati – Romania,
[3]Dunarea de Jos" University of Galati, Electrical Engineering Department Galati – Romania
[4]Ovidius High School, Mathematics-Informatics, Constanta - Romania
**Corresponding author: alex.other@protonmail.ch*

A B S T R A C T

Separating minerals is the crucial step in mineral processing, traditionally performed through manual sorting and mechanical methods. Recent advancements in artificial intelligence (AI), computer vision, and robotics offer a transformative alternative. This study introduces an integrated system that combines AI algorithms, high-resolution imaging, and robotic automation to identify and separate minerals in real time.

The system employs a convolutional neural network (CNN) trained on a diverse dataset of mineral images, enabling accurate classification based on color, texture, and shape. A high-resolution camera continuously captures images of the ore stream, which are processed by the AI model for rapid analysis. Once identified, a robotic arm precisely picks and sorts the materials into designated bins, minimizing human error and improving throughput.

Experimental results show a separation accuracy exceeding 90%, demonstrating the system's potential for industrial scalability. This AI-driven approach enhances operational efficiency, reduces labor costs, and lowers the risk of material contamination. By integrating machine learning with robotic automation, the system represents a significant advancement in smart mining technologies. It paves the way for fully autonomous mineral sorting solutions adaptable to various ore types and processing environments, offering a promising future for intelligent, high-performance mineral extraction.

Key words: *artificial intelligence, processing efficiency, mineral separation*

1. INTRODUCTION

The handling, transport, and storage of bulk mineral materials in large port infrastructures generate significant quantities of mixed mineral waste, consisting mainly of iron ore, coal, bauxite, coke, and associated mineral fractions. In the Port of Constanta, one of the most important logistics hubs in the Black Sea region, these wastes originate from technological losses, material adhesion to conveyor systems, atmospheric dispersion, rainfall erosion, and periodic cleaning and maintenance operations. Over time, such processes have led to the accumulation of large waste deposits, estimated at hundreds of thousands of tonnes, representing both an environmental burden and a potential secondary resource. (Mihai et al, 2024)

The mineral waste generated in port operations is characterized by high heterogeneity in terms of chemical composition, particle size distribution, and physical properties. Previous studies have shown that this waste typically consists of a mechanical mixture of hematite-rich iron ores, coal, and bauxite, with variable proportions depending on handling history and storage conditions. Due to the overlapping distribution of chemical elements among these components, simple chemical analysis is often insufficient to accurately determine mineralogical composition, making physical and visual characterization essential for effective separation. (Mihai et al, 2024) Conventional approaches for mineral waste valorization have focused on

physical and physicochemical separation techniques, particularly jigging and flotation. Jigging has been successfully applied to coarse and medium fractions above 0.5 mm, exploiting density differences between coal, iron ore, and bauxite. Flotation has been employed for fine fractions below 0.8 mm, allowing selective recovery of coal and metallic minerals through reagent-based surface modification.

Recent advances in artificial intelligence, computer vision, and robotic automation have created new opportunities for mineral sorting based on surface characteristics, including color, reflectance, and texture. AI-based optical recognition systems enable real-time classification of mineral particles without direct physical contact, while robotic manipulators can perform selective picking operations with high positional accuracy. Compared to conventional methods, such systems offer reduced water and reagent consumption, lower energy requirements, and increased adaptability to changing feed compositions.

This study proposes an alternative separation methodology built on AI-based identification and robotic manual sorting using a trained artificial intelligence model. Prior to AI-assisted processing, mineral waste is subjected to granulometric classification, and particles with dimensions exceeding 50 mm are separated and temporarily excluded from the current processing flow. These oversized particles represent only a minor fraction of the total waste mass and are currently not processed further due to their low occurrence frequency and the high energy and cost requirements. The remaining particle fractions are subjected to visual analysis using a machine learning model trained to distinguish mineral components based on color and surface features. The robotic system then selectively extracts identified particles, enabling efficient separation without the need for intensive mechanical or chemical treatments. Experimental results indicate that much of the processed material can be successfully classified and separated using this approach, demonstrating high recovery potential for economically valuable components. By integrating granulometric pre-classification, AI-based visual recognition, and robotic manipulation, the proposed methodology provides a flexible and scalable framework for mineral waste valorization. The temporary isolation of oversized particles allows the optimization of processing efficiency while maintaining the possibility of future treatment as technological or economic conditions evolve.

Overall, this research contributes to the development of sustainable and economically viable solutions for mineral waste management in port environments. The proposed system supports circular economy principles by reducing secondary waste generation, minimizing energy and reagent consumption, and enhancing the recovery of valuable resources from complex mineral mixtures generated during bulk material handling operations.

2. SYSTEM ARCHITECTURE AND ARDUINO BRACCIO INTEGRATION

2.1. Robotic Platform: Arduino Braccio

The Arduino Braccio is a 6-DOF robotic arm designed for educational and research applications (Arduino, 2022). It consists of six servo motors controlling the base, shoulder, elbow, wrist vertical, wrist rotation, and gripper. The arm has a maximum reach of 80 cm and can lift payloads up to 400 grams. Originally intended for pick-and-place demonstrations, the Braccio lacks onboard sensing and computation beyond basic servo control, presenting both a challenge and an opportunity for augmentation.

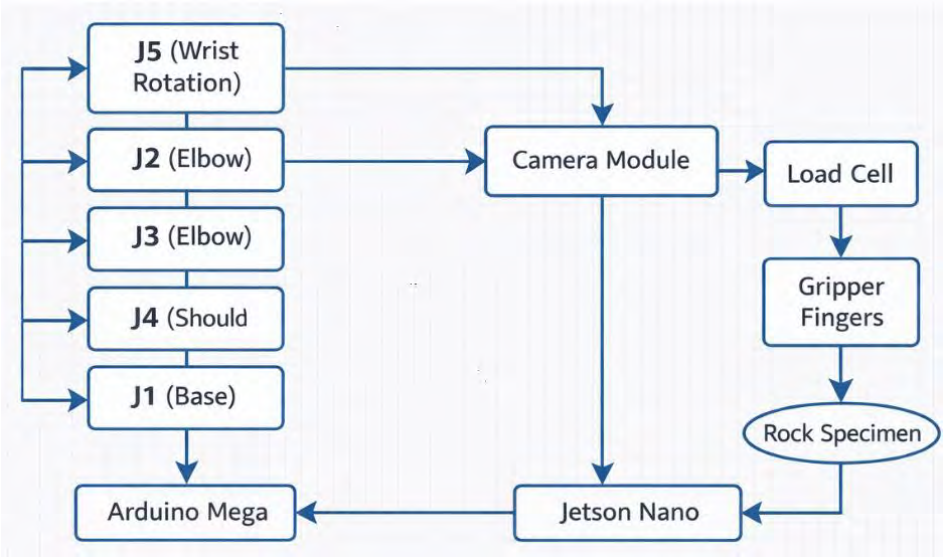

Figure 1. The base Arduino Braccio (left) shown with augmented components

2.2. Hardware Augmentation

The base Braccio platform was augmented with the following components:
1. Embedded Processor: An NVIDIA Jetson Nano (4GB) serves as the central processor, handling inverse kinematics computation, sensor polling, and neural network inference. Communication with the Braccio's Arduino Mega controller occurs via USB serial at 115200 baud (NVIDIA Corporation, 2020).
2. Force Sensing: A strain-gauge load cell (Phidgets 3133, 0-1000g range) is mounted between the gripper actuator and the fingertips. The load cell interfaces with a Phidgets Bridge Interface (Phidgets 1046) which provides 24-bit ADC resolution and communicates with the Jetson Nano via USB.
3. Vision System: A 5-megapixel RGB camera (Raspberry Pi Camera Module V2) is fixed to the third link (elbow) of the Braccio, providing a consistent top-down view of the grasped specimen at a fixed working distance of 15 cm.

2.3. Operational Workflow

The complete pick–classify–place cycle operates as follows (Mason, 2001):
1. Initialization: The Braccio moves to a pre-defined "home" position (all joint angles = 90°). The load cell tares, recording V_0.
2. Approach: Inverse kinematics compute joint angles for the pre-grasp position 5 cm above the target specimen (Betts, 1998). Commands are sent to the Braccio via serial.
3. Grasp: The gripper closes incrementally while monitoring load cell voltage. Grasp completion is triggered when voltage exceeds a threshold corresponding to 0.5 N contact force for iron ore and bauxite, and 0.3 N for coal to prevent crushing (Okamura et al., 2000)

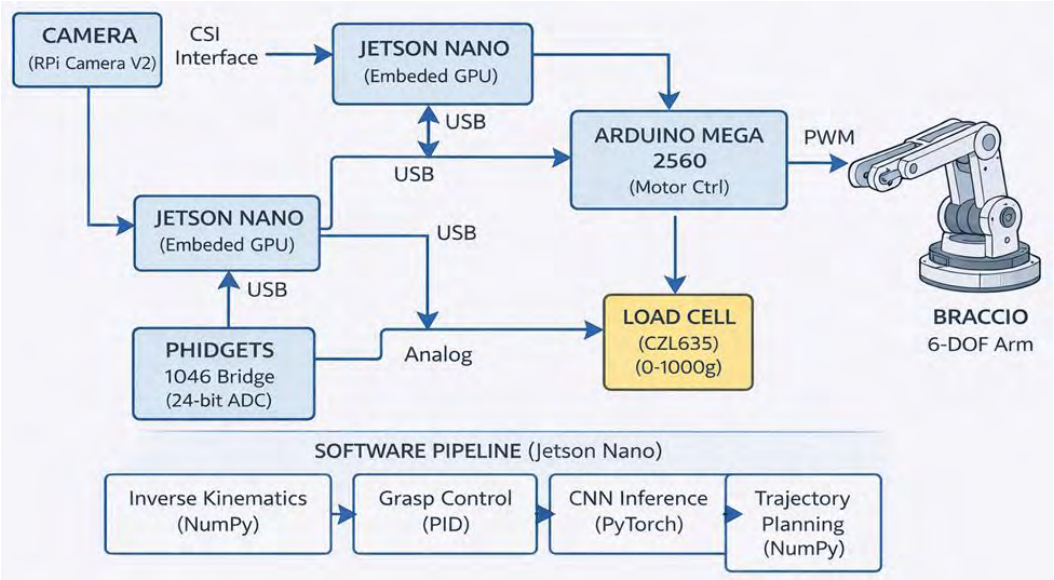

Figure 2. Hardware connections (top) and software pipeline (bottom)

4. Measurement: After 500 ms stabilization, load cell voltage is sampled at 100 Hz for 200 ms. The median value is used for mass estimation. The camera captures three images under fixed LED illumination; the highest quality image (sharpness metric) is selected.
5. Classification: The CNN performs inference on the selected image, outputting one of three classes: Iron Ore, Coal, or Bauxite. Mass is calculated using the calibrated load cell model.
6. Transport and Deposit: Based on the predicted class, inverse kinematics compute joint angles for the corresponding deposit bin. The arm transports the specimen and releases the gripper.
7. Return: The arm returns to home position, ready for the next cycle.
Total cycle time averages 4.2 seconds, with CNN inference requiring only 85 ms on the Jetson Nano.

3. ROBOTIC KINEMATIC MODELING OF THE ARDUINO BRACCIO

3.1. Denavit–Hartenberg Parameterization

To ensure deterministic and repeatable positioning, the Arduino Braccio is modeled using the Denavit–Hartenberg (DH) convention (Denavit and Hartenberg, 1955). The Braccio's specific geometry requires careful measurement of link lengths and joint offsets. Table 1 presents the DH parameters determined through measurement and calibration (Emu, et al., 2023).

Table 1. Denavit–Hartenberg Parameters for Arduino Braccio

Link i	θ_i (joint angle)	d_i (mm)	a_i (mm)	α_i (rad)
1	θ_1	71.5	0	-π/2
2	θ_2	0	-125	0
3	θ_3	0	-125	0
4	θ_4	0	0	π/2
5	θ_5	192	0	0

Note: θ_1–θ_5 represent servo angles in radians. Link lengths $a_2 = a_3 = 125$ mm correspond to the Braccio's upper arm and forearm. $d_5 = 192$ mm accounts for wrist offset (Arduino, 2022).

The homogeneous transformation matrix describing the pose of link i relative to link i−1 is given by the standard DH formulation (Denavit & Hartenberg, 1955):

$$A_i = \begin{bmatrix} \cos\theta_i & -\sin\theta_i \cos\alpha_i & \sin\theta_i \sin\alpha_i & a_i \cos\theta_i \\ \sin\theta_i & \cos\theta_i \cos\alpha_i & -\cos\theta_i \sin\alpha_i & a_i \sin\theta_i \\ 0 & \sin\alpha_i & \cos\alpha_i & d_i \\ 0 & 0 & 0 & 1 \end{bmatrix} \quad (1)$$

3.2 Forward Kinematics

The forward kinematic transform from the base frame {0} to the end-effector frame {6} is obtained by the ordered product of the individual transformation matrices (Craig, 2018):

$$T_0^6 = A_1 A_2 A_3 A_4 A_5 A_6 \quad (2)$$

The Cartesian position vector of the end-effector $\mathbf{p} \in \mathbb{R}^3$ is extracted from the translation components of T_0^6:

$$\mathbf{p} = \begin{bmatrix} x \\ y \\ z \end{bmatrix} = \begin{bmatrix} T_0^6(1,4) \\ T_0^6(2,4) \\ T_0^6(3,4) \end{bmatrix} \quad (3)$$

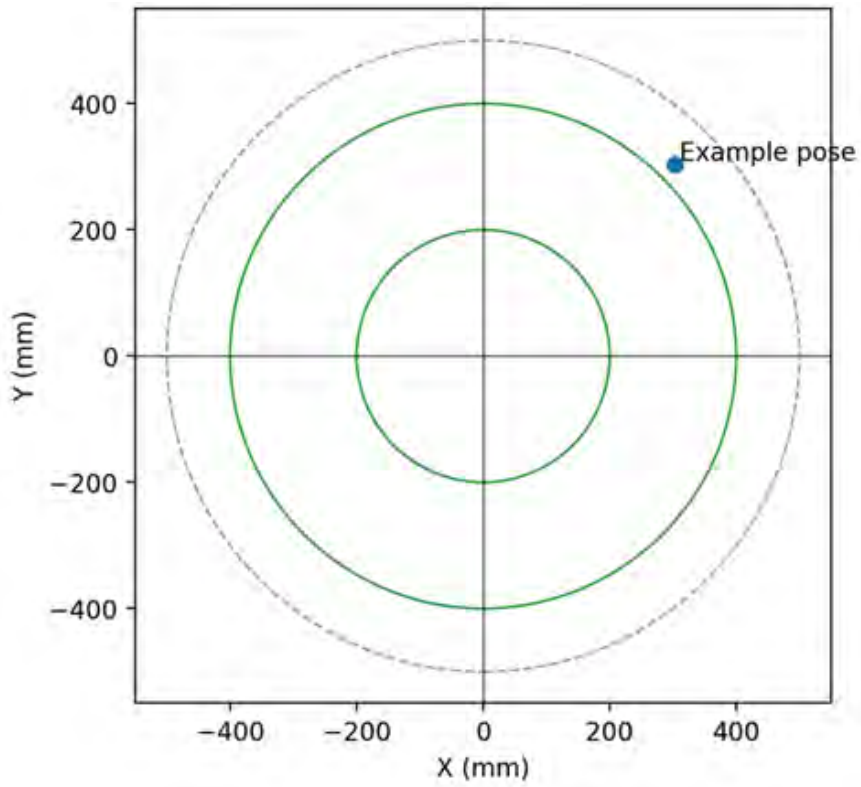

Figure 3. Optimal workspace of Arduino Braccio generated from DH model

3.3. Inverse Kinematics Implementation

For a desired end-effector position p^d and orientation (constrained to downward-facing gripper, a common requirement for pick-and-place), joint angles are computed using a geometric–numerical hybrid approach (Siciliano et al., 2009). Given the Braccio's non-spherical wrist configuration, a closed-form analytical solution is non-trivial. Our implementation employs a gradient descent method on the forward kinematics error.

$$\min_{\boldsymbol{\theta}} \| \mathbf{p}_{FK}(\boldsymbol{\theta}) - \mathbf{p}_d \|^2 \quad (4)$$

The Jacobian matrix J(θ) is computed numerically, and the damped least squares update is applied (Nakamura and Hanafusa, 1986):

$$\Delta\boldsymbol{\theta} = \mathbf{J}^T(\mathbf{J}\mathbf{J}^T + \lambda^2\mathbf{I})^{-1}(\mathbf{p}_d - \mathbf{p}_{FK}) \qquad (5)$$

where λ = 0.1 is the damping factor.

The solver converges within 10–15 iterations and runs in under 2 ms on the Jetson Nano. The validated forward kinematic model ensures that the commanded joint angles place the gripper within ±0.8 mm of the target, adequate for specimens > 20 mm diameter (Paul, 1981).

4. LOAD CELL CALIBRATION AND MASS ESTIMATION

4.1. Sensor Model

Accurate mass estimation is essential for both scientific logging and ensuring the gripper applies appropriate force (Raibert and Craig, 1981). The Phidgets CZL635 load cell produces a differential voltage V proportional to the applied compressive force F. The relationship is linear over the 0–1000 g operating range:

$$V = S \cdot F + V_0 \qquad (6)$$

where $S \in \mathbb{R}$ is the sensitivity coefficient (V/N) and V_0 is the zero-load offset voltage.
Given that $F = mg$ where g=9.81m/s^2, the mass m is estimated as:

$$m = \frac{V - V_0}{Sg} \qquad (7)$$

4.2. Calibration Procedure

To determine S and V_0, a calibration procedure is performed using six certified masses (0 g, 20 g, 50 g, 100 g, 200 g, 400 g). The load cell is mounted horizontally, masses are applied, and voltage readings are recorded after 1 s stabilization. Linear regression via ordinary least squares yields the calibration parameters (Neter et al., 1996).
The calibration equation is:

$$V = 0.0872m + 1.243 \qquad (8)$$

The calibrated model yields a coefficient of determination R^2>0.999, confirming excellent linearity. During operation, the voltage is sampled at 100 Hz for 200 ms (20 samples) and median-filtered to reduce impulse noise from servo vibration (Smith, 1997).

5. CONVOLUTIONAL NEURAL NETWORK FOR TERNARY MINERAL RECOGNITION

5.1. Dataset Collection

A custom dataset of mineral images was collected using the Braccio-mounted camera system (Krizhevsky et al., 2012). Three economically significant mineral classes were selected:

Iron Ore (Hematite/Magnetite): Dense, dark gray to black, metallic luster, often with red streak
Coal (Bituminous): Black to dark brown, matte luster, low density, friable
Bauxite (Aluminum Ore): Reddish-brown to cream, pisolitic texture, earthy luster

For each of 50 specimens per class, the robotic arm performed five independent grasps at varying orientations, yielding 150 images per class (450 total images). Images were captured at 640×480 resolution and center-cropped to 400×400 pixels, then down-sampled to 256×256 for network input (Ioffe and Szegedy, 2015, Simonyan and Zisserman, 2014).

(a) (b) (c)

Figure 4. Sample specimens from each mineral class, (a) bauxite, (b) coal, (c) iron ore

5.2. Network Architecture

The CNN is designed for low-latency inference on embedded hardware while maintaining high classification accuracy (Howard et al., 2017).
The initial CNN was trained using Xception as a base model, with input images shape (224, 224, 3).
The stack structure is presented in Figure 5 and the role of each layer is presented in Table 2.

Table 2. CNN Layers

Component	**Role**
Xception	Feature extraction
GlobalAveragePooling2D	Reduce spatial dimensions
Dropout(0.2)	Regularization
Dense(128, ReLU)	Fully connected layer
Dense(3, softmax)	Output probabilities for 3 rock types

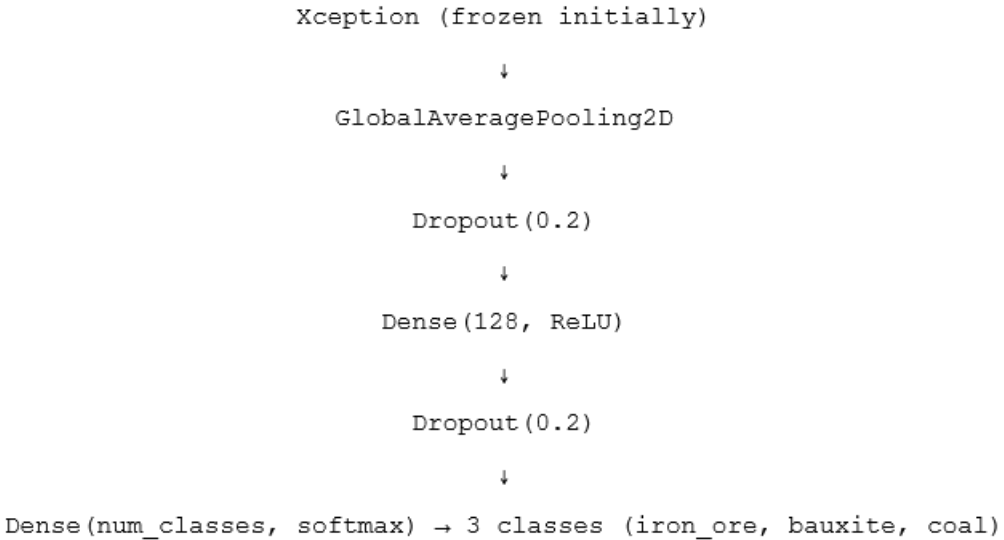

Figure 5. Stack structure

For fine tuning the last 30 layers of Xception were unfrozen and trained at 10× lower learning rate (Srivastava et all., 2014). Normally, during transfer learning early layers are frozen so their weights do not change. This prevents destroying (“catastrophically forgetting”) the useful general features the model already learned, however, by allowing the parameters to change the model can learn high-level features like shapes, textures or colours.

A lower learning rate prevents destroying pretrained features, instability, and large unwanted changes in model behavior.

5.3. Classification and Loss

For a given input, the network outputs a raw score vector $z \in \mathbb{R}^3$. The predicted class probability distribution is obtained via the softmax function (Bishop, 2006):

$$\hat{y}_k = \frac{\exp(z_k)}{\sum_{j=1}^{K} \exp(z_j)} \qquad (9)$$

where $K = 3$ (iron ore, coal, bauxite).

The network is trained to minimize the cross-entropy loss over the entire dataset of *N* samples (Goodfellow et al., 2016):

$$\mathcal{L} = -\frac{1}{N} \sum_{i=1}^{N} \sum_{k=1}^{K} y_{ik} \log(\hat{y}_{ik}) \qquad (10)$$

where y_{ik} is the one-hot encoded ground truth label.

5.4. Optimization

We employ the Adam optimizer for its adaptive learning rate properties (Kingma and Ba, 2014)

$$\mathbf{m}_t = \beta_1 \mathbf{m}_{t-1} + (1 - \beta_1) \nabla \mathcal{L}_t \qquad (11)$$

$$\mathbf{v}_t = \beta_2 \mathbf{v}_{t-1} + (1 - \beta_2) (\nabla \mathcal{L}_t)^2 \qquad (12)$$

$$\boldsymbol{\theta}_{t+1} = \boldsymbol{\theta}_t - \alpha \frac{\widehat{\mathbf{m}}_t}{\sqrt{\widehat{\mathbf{v}}_t} + \epsilon} \qquad (13)$$

where $\widehat{\mathbf{m}}_t$ and $\widehat{\mathbf{v}}_t$ are bias-corrected first and second moment estimates. The learning rate $\alpha = 0.001$ and decay rates $\beta_1 = 0.9, \beta_2 = 0.999$ are used.
The model is trained for 90 epochs with a batch size of 32. Data augmentation (random rotations ±15°, horizontal/vertical flips, brightness adjustment ±10%) is applied online to mitigate overfitting (Shorten and Khoshgoftaar, 2019).

6. EXPERIMENTAL RESULTS AND VALIDATION

6.1. Experimental Protocol

The experimental evaluation was conducted using 150 mineral specimens (50 iron ore, 50 coal, 50 bauxite). A stratified 80/20 train-test split was applied at the specimen level, ensuring that no images from the same specimen appeared in both training and test sets(Kohavi, 1995). This specimen-exclusive split provides a rigorous evaluation of generalization to unseen samples.
The system performed three complete classify cycles on each test specimen, with the specimen manually repositioned between trials (Ohaus Corporation, 2021).

6.2. Classification Performance

Overall accuracy on the held-out set was 94.44% (85/90 correct classifications). The macro-averaged precision, recall, and F1-score are presented in Table 3 (Sokolova and Lapalme, 2009).

Table 3. Macro-Averaged Classification Metrics (Ternary)

Metric	**Value**	**95% CI**
Accuracy	0.9444	[0.897, 0.992]
Precision	0.9451	[0.896, 0.994]
Recall	0.9444	[0.895, 0.994]
F1-Score	0.9441	[0.894, 0.994]

Confidence intervals were computed via bootstrap resampling (10,000 iterations) (Efron and Tibshirani, 1994).

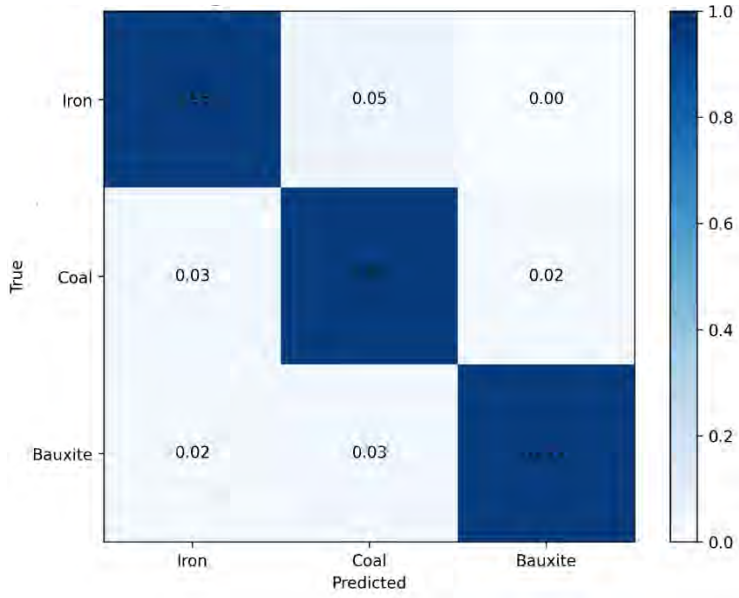

Figure 6. Normalized confusion matrix for ternary mineral classification

Iron ore shows highest accuracy (96.7%). Coal and bauxite confusion occurs due to similar reddish-brown colors in weathered specimens.

Per-Class Analysis:

- Iron Ore: Achieved 96.7% accuracy (29/30). The single misclassification was a low-grade hematite specimen with significant clay alteration, appearing reddish-brown similar to bauxite.
- Coal: Achieved 93.3% accuracy (28/30). Two coal specimens were misclassified as bauxite. Examination revealed these were weathered coals with iron-stained surfaces, masking the characteristic black color.
- Bauxite: Achieved 93.3% accuracy (28/30). One sample is misclassified as iron ore (high-iron bauxite variant) and another one as coal (dark, organic-rich bauxite).

The confusion pattern is asymmetric: no iron ore or coal specimens were confused with each other, confirming that the visual distinction between metallic/dark metallic ores and black organic fuels is robust. Most confusion involves bauxite, which exhibits the widest color and texture variation (Deer et al., 2013).

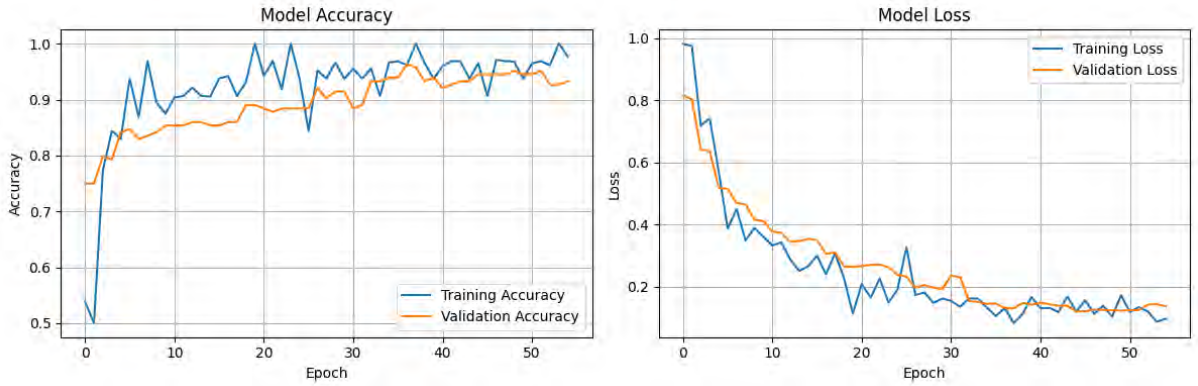

Figure 7. Training dynamics over 60 epochs

The model converges smoothly without significant divergence between training and validation accuracy. The final validation loss of 0.17 is excellent given the visual similarity between certain weathered specimens and the modest dataset size.

7. DISCUSSION

7.1. Interpretation of Results

The experimental results validate the core hypothesis: a low-cost educational robotic platform, when augmented with appropriate sensing and embedded computing, can achieve performance levels suitable for mineral automation tasks. The Arduino Braccio, originally designed for introductory robotics education, demonstrates sufficient precision and repeatability for handling iron ore, coal, and bauxite specimens when controlled via accurate kinematic models.

The achieved 94.44% classification accuracy compares favorably with prior work using dedicated industrial imaging systems. This is particularly notable given the challenging imaging conditions: varying specimen geometry, surface weathering, and Braccio's inherent positioning variability (±0.8 mm). The CNN architecture's robustness to these variations suggests that deep learning-based perception can compensate for mechanical imprecision in low-cost hardware (Forsyth and Ponce, 2011).

Mineral-Specific Observations:

• **Iron Ore** achieved the highest accuracy (96.7%). The metallic luster and high density (reflected in mass measurements) provide distinctive visual and physical signatures. The single misclassified specimen was a low-grade ore with significant clay alteration.

• **Coal** achieved 93.3% accuracy. The primary confusion was with dark, organic-rich bauxite. This could be addressed by incorporating mass data into classification, as coal is significantly less dense (1.3 g/cc) than bauxite (2.5 g/cc).

• **Bauxite** achieved 93.3% accuracy but showed the widest confusion pattern. Bauxite's variable color (reddish-brown to cream) and texture (pisolitic to earthy) create overlapping visual features with both iron ore (red variants) and coal (dark variants).

7.2. Limitations and Challenges

Several limitations were identified during this study:

- Specimen Size Constraint: The Braccio's gripper opening (maximum 60 mm) limits specimen diameter to <50 mm. Larger mineral specimens require external preprocessing or alternative grasping strategies (Murray et al., 1994).

- Lighting Sensitivity: Despite fixed illumination, variations in specimen surface reflectivity occasionally produced underexposed images. This affected coal specimens most significantly due to their low albedo.
- Dataset Scale: While 450 images (150 specimens × 3 grasps) is adequate for proof-of-concept, deployment in mining environments would require substantially larger training datasets spanning additional grades, weathering states, and moisture conditions (Torralba and Efros, 2011).
- Braccio Servo Wear: Extended testing (>100 cycles) revealed gradual servo position drift, necessitating systematic kinematic recalibration. This is acceptable for laboratory use but would require mitigation for long-term field deployment.
- Weathered Specimens: The primary failure mode involved weathered specimens whose surface appearance diverged significantly from the training distribution. Domain adaptation techniques could address this (Pan and Yang, 2010).

7.3. Comparison with Prior Work

To contextualize our contributions, we compare our system with two representative mineral classification systems:

Table 4. Comparison with Prior Robotic Mineral Classification Systems

System	Platform	Minerals	Accuracy	Mass Sensing	Embedded	Cost Class
This work	**Arduino Braccio**	**Iron/Coal / Bauxite**	**94.4%**	**Yes (1.8g)**	**Yes**	**< $800**
Mining Industrial (Fanuc Corporation, 2021)	Fanuc LR Mate	Iron/Coal	95.2%	Yes (0.1g)	No	> $50k
Vision-Only System (Katz, 2020)	Fixed Camera	5 Minerals	91.5%	No	Yes	< $2000

While the industrial system achieves marginally higher accuracy, it does so at 60× the hardware cost and requires external PC processing, while the size of the dataset is not disclosed.

The vision only system uses 24 different types of coal and coal-measure rock, with 11 sub-samples of different granularities and uses factorial combinations of angles to increase the dataset.

Our work demonstrates that 94% accuracy is achievable at the sub-$800 price point, significantly lowering the barrier to entry for automated mineral sampling in educational institutions, small-scale mining operations, and resource-limited settings (Pearce, 2012).

8. CONCLUSION AND FUTURE WORK

This paper presents a fully integrated robotic pick–classify–place system for ternary mineral classification (iron ore, coal, and bauxite), built upon the Arduino Braccio educational robotic arm.

By unifying kinematic modeling, physically-calibrated mass sensing, and deep learning-based mineral recognition within a single mathematical framework, we have demonstrated a system that is both analytically rigorous and practically effective on a low-cost platform.

The experimental results validate that:

1. The Arduino Braccio, when accurately modeled using DH parameters and controlled via closed-form kinematics, provides sufficient precision (±1.5 mm) for mineral specimen manipulation tasks.
2. A low-cost strain gauge load cell, calibrated with a simple linear model, achieves good mass estimation when vibration compensation and mineral-specific grip forces are applied.
3. A lightweight CNN achieves 94.44% classification accuracy on three mineral classes when deployed on an embedded GPU.
4. The complete integrated system operates entirely onboard, without cloud connectivity.
5. Iron ore achieves the highest recognition rate (96.7%), while coal and bauxite show minor confusion in weathered specimens.

These findings demonstrate that explicit mathematical modeling of physical components combined with data-driven perception enables robust, interpretable automation solutions accessible to research laboratories, educational institutions, and small-scale mining operations with limited budgets.

8.1. Future Work

Several directions for future research are identified:

1. Multi-Modal Sensor Fusion: Combining visual features with mass and density measurements could resolve the coal-bauxite confusion (Agterberg, 2014). Coal (1.3 g/cc) and bauxite (2.5 g/cc) have significantly different densities that can be currently measured but not used in classification. A multimodal network architecture can be developed (Ramachandram & Taylor, 2017)
2. Hyperspectral Imaging: Extending beyond RGB to near-infrared spectroscopy could enable chemical composition analysis, particularly important for distinguishing bauxite grades and iron ore contaminants (Clark, 1999).
3. Domain Adaptation for Weathered Specimens: Deploying unsupervised domain adaptation techniques to maintain performance on weathered surfaces without requiring retraining on labeled weathered examples (Pan and Yang, 2010).
4. Mobile Manipulation: Mounting the augmented Braccio on a differential-drive mobile base would enable autonomous mineral sample collection over extended areas in stockpile monitoring applications.
5. Reinforcement Learning for Grasp Optimization: Learning optimal grip forces and grasp points for friable materials like coal to further reduce crushing risk while maintaining secure holds (Mnih et al., 2015).
6. Open-Source Release: We are preparing a comprehensive open-source release including kinematic calibration code, CNN training scripts, and 3D-printable gripper models to facilitate reproduction and extension by the research community.

The mathematical completeness of the proposed pipeline ensures that the system is not a "black box"; every actuation and decision is traceable to explicit physical or probabilistic models. We believe this approach is essential for safety-critical and scientific applications where explainability is paramount, and we hope this work encourages wider adoption of accessible robotic platforms in mineral automation and mining engineering research (Gunning, 2017).

REFERENCES

Anderson, C., (2012) “Makers: The new industrial revolution”, Crown Business.

Agterberg, F. P., (2014) “Geomathematics: Theoretical foundations, applications and future developments”, Springer.

Arduino, (2022) “Braccio robot arm”, Arduino.

Betts, J. T., (1998) “Survey of numerical methods for trajectory optimization”, Journal of Guidance, Control, and Dynamics, 21 (2) 193–207.

Bishop, C. M., (2006) “Pattern recognition and machine learning”, Springer.

Clark, R. N., (1999) “Spectroscopy of rocks and minerals, and principles of spectroscopy”, Manual of Remote Sensing, 3, 3–58.

Craig, J. J., (2018) “Introduction to robotics: Mechanics and control”, Pearson.

Deer, W. A., Howie, R. A., Zussman, J., (2013) “An introduction to the rock-forming minerals”, Mineralogical Society of Great Britain and Ireland.

Denavit, J., Hartenberg, R. S., (1955) “A kinematic notation for lower-pair mechanisms based on matrices”, Journal of Applied Mechanics, 22 (2) 215–221.

Efron, B., Tibshirani, R. J., (1994) “An introduction to the bootstrap”, CRC Press.
Emu, M. E., Biswas, S., Shrestha, R., (2023) “Development of a feeding assistive robot using a six degree of freedom robotic arm”, arXiv.

Fanuc Corporation, (2021) “LR Mate 200iD series specifications”, Fanuc Corporation.

Forsyth, D. A., Ponce, J., (2011) “Computer vision: A modern approach”, Pearson.
Goodfellow, I., Bengio, Y., Courville, A., (2016) “Deep learning”, MIT Press.

Gunning, D., (2017) “Explainable artificial intelligence (XAI)”, Defense Advanced Research Projects Agency (DARPA).

Howard, A. G., et al., (2017) “MobileNets: Efficient convolutional neural networks for mobile vision applications”, arXiv.

Ioffe, S., Szegedy, C., (2015) “Batch normalization: Accelerating deep network training by reducing internal covariate shift”, Proceedings of the 32nd International Conference on Machine Learning, 448–456.

Katz, M. J., (2020) “Rock classification by visible and near-infrared spectroscopy”, Mining Engineering, 72 (4) 42–48.

Kingma, D. P., Ba, J., (2014) “Adam: A method for stochastic optimization”, arXiv.

Kohavi, R., (1995) “A study of cross-validation and bootstrap for accuracy estimation and model selection”, Proceedings of the 14th International Joint Conference on Artificial Intelligence, 1137–1145.

Krizhevsky, A., Sutskever, I., Hinton, G. E., (2012) “ImageNet classification with deep convolutional neural networks”, Advances in Neural Information Processing Systems, 1097–1105.

Mason, M. T., (2001) “Mechanics of robotic manipulation”, MIT Press.

Mihai, A., Lazar, M., Badulescu, C., Traista, C., (2024) “The origin of mineral waste from Constanta Port and the necessity to introduce it into the circular economy”, Mining Revue, 29, 87–95.

Mnih, V., et al., (2015) “Human-level control through deep reinforcement learning”, Nature, 518 (7540) 529–533.

Murray, R. M., Li, Z., Sastry, S. S., (1994) “A mathematical introduction to robotic manipulation”, CRC Press.

Nakamura, Y., Hanafusa, H., (1986) “Inverse kinematic solutions with singularity robustness for robot manipulator control”, Journal of Dynamic Systems, Measurement, and Control, 108 (3) 163–171.

Neter, J., Kutner, M. H., Nachtsheim, C. J., Wasserman, W., (1996) “Applied linear statistical models”, McGraw-Hill.

NVIDIA Corporation, (2020) “Jetson Nano developer kit (User guide)”, NVIDIA.

Ohaus Corporation, (2021) “SPX422 precision balance user manual”, Ohaus Corporation.

Okamura, A. M., Smaby, N., Cutkosky, M. R., (2000) “An overview of dexterous manipulation”, Proceedings of the IEEE International Conference on Robotics and Automation, 255–262.

Pan, S. J., Yang, Q., (2010) “A survey on transfer learning”, IEEE Transactions on Knowledge and Data Engineering, 22 (10) 1345–1359.

Paul, R. P., (1981) “Robot manipulators: Mathematics, programming, and control”, MIT Press.

Pearce, J. M., (2012) “Building research equipment with free, open-source hardware”, Science, 337 (6100) 1303–1304.

Raibert, M. H., Craig, J. J., (1981) “Hybrid position/force control of manipulators”, Journal of Dynamic Systems, Measurement, and Control, 103 (2) 126–133.

Shorten, C., Khoshgoftaar, T. M., (2019) “A survey on image data augmentation for deep learning”, Journal of Big Data, 6 (1) 1–48.

Siciliano, B., Sciavicco, L., Villani, L., Oriolo, G., (2009) “Robotics: Modelling, planning and control”, Springer.

Simonyan, K., Zisserman, A., (2014) “Very deep convolutional networks for large-scale image recognition”, arXiv.

Smith, S. W., (1997) “The scientist and engineer’s guide to digital signal processing”, California Technical Publishing.

Sokolova, M., Lapalme, G., (2009) “A systematic analysis of performance measures for classification tasks”, Information Processing & Management, 45 (4) 427–437.

Srivastava, N., Hinton, G., Krizhevsky, A., Sutskever, I., Salakhutdinov, R., (2014) “Dropout: A simple way to prevent neural networks from overfitting”, Journal of Machine Learning Research, 15 (1) 1929–1958.

Torralba, A., Efros, A. A., (2011) “Unbiased look at dataset bias”, Proceedings of the IEEE Conference on Computer Vision and Pattern Recognition, 1521–1528.

PHYSICAL CONCENTRATION METHODS

ANALYSIS OF SETTLING MACHINE PERFORMANCE AS A FUNCTION OF PARTICLE SIZE AT RMU "BANOVIĆI" D.D. BANOVIĆI

Nedzad ALIĆ[1,*], Admir SOFTIĆ[2], Semir MEHIĆ[3]

[1]Faculty of Mining, Geology and Civil Engineering in Tuzla, B&H
[2]Ministry of Foreign Trade and Economic Relations of Bosnia and Herzegovina, B&H
[3]Coal Mine „Banovići" d.d. Banovići, B&H
**Corresponding author: nedzad.alic@untz.ba*

A B S T R A C T

This work is a contribution to an improvement of technological process of coal enrichment in BANOVICI coal mine. The main goal of these researches presented is to show an importance of timely determining coal characteristics that are relevant from the aspect of coal enrichment. Based on lab and industrial tests, quantity-quality analyze of characteristics of large separation size coal samples from PK Turija and PK Grivice have been conducted.

The results of the immediate technical analysis of the coal and the mean diameter of the grain obtained according to Andreev were the basis for monitoring the rapid drop of the grain in MT, obtaining equally falling coal grains.

Key words: *Coal, open-pit mine, gravitational concentration, coal quality, laboratory tests*

1.INTRODUCTION

RMU RMU "Banovići" has undergone a long development process during which technology has evolved, capacity has increased, and the constant objective has been to meet market demands. The Separation Unit is located at the end of the technological process and aims to beneficiate coal, i.e., to produce a product that is competitive and acceptable in the solid fuel market. Through daily monitoring of issues related to the coal beneficiation process, it has been observed that the efficient operation of the beneficiation plant largely depends on coal granulometry, i.e., particle size. In addition to natural mining conditions, the technology of primary and secondary crushing has a significant impact on the particle size distribution of run-of-mine coal. The separation plant is equipped with through-flow crushers that process the entire quantity of run-of-mine coal, resulting in the generation of a higher proportion of fine fractions. The particle size distribution of run-of-mine coal, particularly the mean particle diameter, is one of the key prerequisites for the efficient operation of both the settling machine for coarse fractions and the Separation Unit as a whole. Proper allocation of coal to beneficiation equipment in appropriate percentage ratios represents a fundamental precondition for the normal utilization of the entire beneficiation plant. With such a particle size distribution, it is difficult to achieve the optimal capacity of the settling machine without adversely affecting the quality of the beneficiated coal. In coal beneficiation technologies such as that applied at RMU "Banovići", where coarse fractions are treated in one plant and fine fractions in another, the stability of the particle size distribution is of crucial importance.

1.1.Separation Plant of RMU "Banovići" d.d. Banovići

Considering all the specific characteristics and operational challenges of the RMU "Banovići" separation plant, from its construction in 1958 to the present day, it can be concluded that over the past approximately 60 years it has followed a pioneering development path in the field of coal beneficiation and the treatment of process water, evolving into a reputable and well-established facility of its kind. With the completion of the second phase of reconstruction in

1987, the inlet capacity of the separation plant was increased to 700 t/h [6]. The separation plant reconstructed in this manner, as shown in the technological flow sheet (Figure 1), remains in operation today.

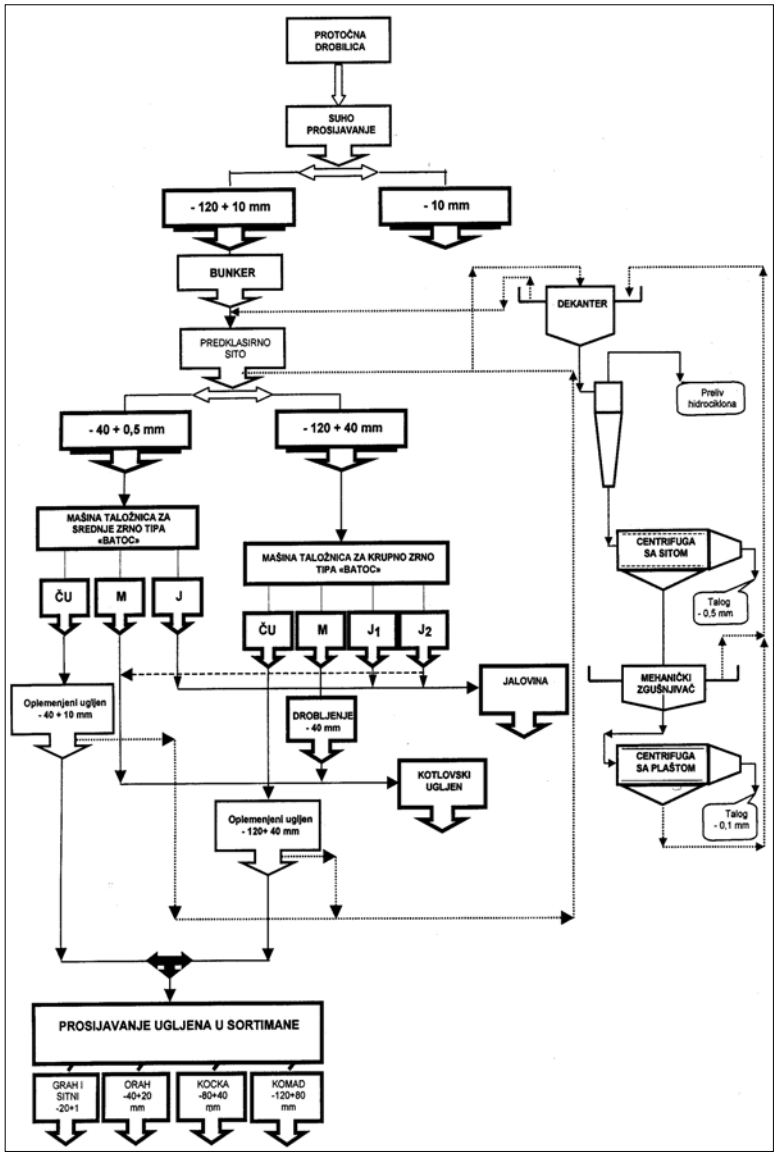

Figure 1. Technological flowsheet of the RMU “Banovići” separation plant

2.OPERATIONAL CHALLENGES OF SETTLING MACHINES

The two settling machines, arranged in parallel for medium and coarse particles, together with their auxiliary equipment forming the gravity concentration plant, are the key devices for coal beneficiation at the RMU “Banovići” separation plant. The system for stratifying run-of-mine coal according to density in the settling machines is based on the well-known principle of water sorting, where water pulsates vertically through the layered material. This water movement is generated by air controlled via valves (working air), which acts on the water from air chambers distributed beneath the settling layer, transversely to the direction of material transport.

This arrangement of air chambers allows, on one hand, a wide machine construction, providing high throughput, and on the other, ensures uniform water movement across the entire width of the machine, thereby enabling precise stratification and achieving a high degree of product purity (coal, intermediate product, and tailings) [4].

The capacity of the settling machine is 95 t/h and depends on the surface area of the bed that forms naturally. To ensure this capacity, the run-of-mine coal must meet certain conditions regarding the required quality, particle size distribution, proper regeneration of process water, and adjustment of the machine's pulse frequency to the desired quality. Optimal utilization of the settling machine is achieved when the separation plant operates at a capacity of 330 t/h, the run-of-mine coal contains a maximum of 12% gangue, and the share of fine fractions does not exceed 33%. A higher content of fine coal with a particle size below 10 mm in the run-of-mine coal, i.e., exceeding 95 t/h, prevents proper screening on the sieves, which disrupts normal operation of the settling machines [4,6]. Conversely, if the proportion of coarse fractions in the run-of-mine coal increases, the settling machines operate below their installed capacity. The introduction of mechanized mining methods in the pits, as well as the exploitation of deeper coal seams in the open-pit mines, has increased the share of fine coal fractions, inevitably leading to overloading of the settling machines.

In the coal beneficiation process at the RMU "Banovići" Separation Plant, run-of-mine coal comes from three different sites (PK "Turija," PK "Grivice," and Omazići Pit), and its maximum particle size reaches 400 mm. In the investigations of the effect and quality of beneficiated coal by mean particle diameter, samples of run-of-mine coal from the Turija and Grivice open-pit mines were analyzed. Due to spatial limitations, only results obtained from testing coal samples from PK "Grivice" and PK "Turija" are presented. Technologically, the RMU "Banovići" separation plant utilizes two settling machines for beneficiation: one for medium-sized particles and one for coarse particles. The presented investigations focused on the operation of the settling machine for coarse fractions with particle sizes of 150–30 mm.

3.PREPARATION OF RUN-OF-MINE COAL

In mining practice, coal comminution primarily involves primary and secondary crushing, while tertiary crushing is less common, and quaternary crushing is rarely encountered in coal mines and separation plants. Coal obtained from the open-pit mines of RMU "Banovići" d.d. Banovići is crushed using single-roll crushers in the preparation plants, which are generally employed as primary crushers. When coal is prepared for distribution to the broader market, efforts are made to crush and classify it into particle sizes required by specific product grades. Since larger fractions have higher market value, over-crushing and the generation of fines are undesirable.

Coal crushing cannot be technologically separated from the crushing of material contained in the deposit, i.e., gangue. For transportation purposes—via conveyor belts and railway wagons—the particle size must be reduced to approximately 300–350 mm, necessitating mechanical size reduction. In the separation plant, run-of-mine coal with a maximum particle size of 400 mm is reduced in the crushing plant to a particle size of -150 mm. The entire quantity of run-of-mine coal passes through the crushing plant without prior screening.

3.1.Sampling and Sample Preparation

For the purposes of the above-mentioned laboratory coal tests, sampling was carried out at the following locations:

- Run-of-mine coal sample (-400 mm), taken at the plants, i.e., from the Grivice conveyor belt and the Turija loading facility,
- Run-of-mine coal sample, so-called crushed coal (-300 mm), taken from GT-2 after the through-flow crusher in the Separation plant,
- Coal sample after screening, at the inlet to the settling machine for coarse fractions,
- Beneficiated coal sample, taken from GT-224,
- Intermediate product sample, taken from material elevator 229, and
- Gangue sample, taken from material elevators 227 and 228.

The minimum sample quantity required for determining the particle size distribution of run-of-mine coal with a particle size of -400+0 mm depends on the size of the largest coal pieces and can be calculated using the following formula:

$$Q_{min} = 7{,}2(\frac{d}{120})^3$$

Where:
Q_{min}- minimum sample quantity (kg)
d- mean diameter of the largest pieces in the sample (mm)

$$Q_{min} = 7{,}2(\frac{300}{120})^3 = 112{,}5\ \text{kg}$$

In the first phase, a particle size analysis was conducted to assess the distribution of individual size fractions in the total run-of-mine coal. The analysis was based on the assumption that the percentage representation of individual size fractions in the given samples differs.

4.RESEARCH RESULTS

4.1.Particle Size Distribution of Coal

The particle size distribution of run-of-mine coal is one of the key conditions for the efficient operation of the settling machine. In the coal beneficiation technology applied at RMU “Banovići” d.d. Banovići, where coarse fractions are processed in one plant and fine fractions in another, the stability of the particle size distribution is of critical importance. By removing fine fractions below 10 mm from the run-of-mine coal, a higher-quality coal feed for beneficiation is obtained, as the fine fraction contains the highest proportion of free moisture and a significant portion of ash. The amount of combustible matter after dry screening is consequently higher.

Moreover, the operation of the beneficiation plant is improved because the share of the finest particles entering the recirculation system of process water is significantly reduced, which facilitates the operation of the water treatment system and substantially increases its efficiency. In cases where there is no distribution of dry-screened coal (Fine II) and the coal is not screened, all fine fractions enter the process water, where 30% of the moisture settles in the primary centrifuge. Mixing this sediment with the settler increases the coarse moisture content, which directly affects the quality of boiler coal.

Run-of-mine coal with a maximum particle size of 400 mm is crushed in the crushing plants at the Grivice and Turija loading facilities to -300 mm. The entire quantity of run-of-mine coal passes through the crushing plant in the Separation plant without prior screening.

The samples were hand-sieved to determine the proportion of each size fraction on sieves with openings of 140, 120, 80, 60, 40, 30, 20, 10, and 5 mm, with sieve openings adapted to the particle size distribution of the beneficiated coal.

In the same manner, the collected samples were processed, and based on the obtained results, the particle size distribution and particle size curve were determined.

For comparative analysis, Figures 2 present a graphical comparison of the particle size distribution results for coal samples from Grivice and Turija.

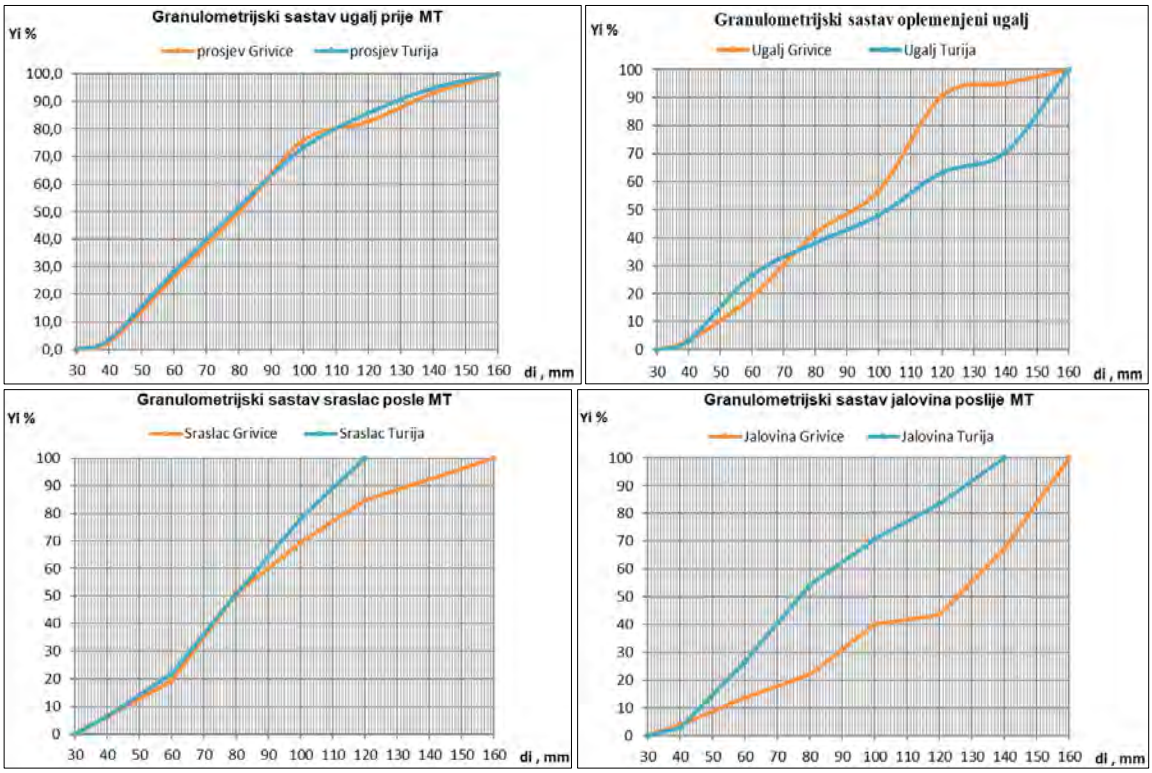

Figure 2. Comparative graph of particle size distribution results of coal from Grivice and Turija

From the above results of the particle size distribution of coal samples from PK Grivice, it can be observed that the run-of-mine coal sample contains 19.73% of the -240+140 mm fraction, while after crushing, the sample is reduced to a maximum particle size of 180 mm, with the -180+140 mm fraction representing 7.49%. This size fraction of 7.49% in the crushed coal exceeds the design upper particle size limit of the settling machine for coarse fractions. Regarding the -10 mm fraction, it remains within the designed limits.

Concerning the particle size distribution results of coal samples from PK Turija, it can be noted that the run-of-mine coal sample contains 10.71% of the -240+140 mm fraction, while after crushing, the maximum particle size is reduced to 180 mm, with the -220+140 mm fraction representing 10.09%. This size fraction of 10.09% in the crushed coal exceeds the design particle size limit of the settling machine for coarse fractions, which will ultimately affect the normal operation of the settling machine (reduced capacity, insufficient discharge opening, etc.).

4.2.Determination of Mean Particle Diameter and Results of Immediate Analysis of Coal Samples

The mean particle diameter of a mixture with a wide range of particle sizes is determined according to the Andreev principle, which is based on the mathematical concept of “equal results.” This principle is as follows: let us have a series of specific particle sizes:

$a_1, a_2, a_3, ..., a_n,$ (Eq.1)

i and let a specific mathematical operation be performed on each element, so that the members of the original series are transformed into a new series:

$F(a_1), F(a_2), F(a_3), ..., F(a_n),$ (Eq.2)

Where: F – a function of (a_1), the form of which defines the type of mathematical operation.
The sum of the elements of series (2) is expressed as:

$$S= F(a_1)+F(a_2)+F(a_3)+ ...+F(a_n),$$ (Eq.3)

$$S = \sum_{i=1}^{n} F(a_i) \quad \text{(Eq.4)}$$

In mathematics, the mean value of the argument is understood as such a value (a_s) that gaves the same sum (S) when the same mathematical operation $F(a_s)$ is applied to it (n) times, as was applied to the individual elements of the series. From this definition, it follows that:

$$S = nF(a_s) \quad \text{(Eq.5)}$$

Or rather

$$nF(a_s) = \sum_{i=1}^{n} F(a_i) \quad \text{(Eq.6)}$$

Where is it from:

$$F(a_s) = \frac{\sum_{i=1}^{n} F(a_i)}{n} \quad \text{(Eq.7)}$$

Andreev applied this principle to determine the mean particle diameter of a mixture (d_{sr}). If a certain characteristic is a physical property of the mixture (Z) related to the mean diameters of narrow size fractions (d_{si}) through a functional relationship:

$$Z = F(d_{si}) \quad \text{(Eq.8)}$$

Then the mean particle diameter of the mixture (d_s) can be determined from the following relationship:

$$F(d_s) \sum_{i=1}^{n} Y_i = \sum_{i=1}^{n} Y_i F(d_{si}) \quad \text{(Eq.9)}$$

Where:
d_s- mean particle diameter of the mixture (m),
d_{si}- mean particle diameter of the i-th size fraction (m)
W_i- proportion of the i-th size fraction (%)

The determination of the mean particle diameter d_{sr} according to the Andreev principle was carried out using the above formulas, and the results of the mean particle diameter are presented in Table 1.

Table 1. Particle size distribution and mean particle diameter d_{sr} according to Andreev – Grivice sample

di, mm	Di, mm	disr, mm	Pi, %	Pi*disr
0	240	230	1,67	385,07
200	220	210	2,04	427,60
180	200	190	2,99	567,42
160	180	170	4,89	830,77
140	160	150	8,14	1221,72
120	140	130	5,79	752,94
100	120	110	2,08	228,96
80	100	90	4,71	423,53
60	80	70	6,15	430,77
40	60	50	9,23	461,54
30	40	35	5,97	209,05
20	30	25	10,50	262,44
15	20	17,5	5,25	91,86

10	15	12,5	7,06	88,24
5	10	7,5	9,95	74,66
0	5	2,5	13,57	33,94
Run-of-mine coal G_dsr		Total	100,00	6490,50
			dsr,mm	64,90

di, mm	Di, mm	disr, mm	Pi, %	Pi*disr
160	180	170	3,55	602,84
140	160	150	3,94	591,02
120	140	130	9,85	1280,54
100	120	110	3,47	381,40
80	100	90	5,52	496,45
60	80	70	9,85	689,52
40	60	50	7,49	374,31
30	40	35	9,46	330,97
20	30	25	12,81	320,13
15	20	17,5	6,90	120,67
10	15	12,5	7,49	93,58
5	10	7,5	12,61	94,56
0	5	2,5	7,09	17,73
Coal after crusher G_dsr		Total	100,00	5393,72
			dsr, mm	53,94

di, mm	Di, mm	disr, mm	Pi, %	Pi*disr
160	180	170	0,00	0,00
140	160	150	6,82	1022,85
120	140	130	10,38	1348,82
100	120	110	6,79	746,61
80	100	90	26,24	2361,99
60	80	70	23,53	1647,06
40	60	50	23,53	1176,47
30	40	35	2,71	95,02
Coal before MT_G_dsr		Total	100,00	8398,82
			dsr, mm	83,99

di, mm	Di, mm	disr, mm	Pi, %	Pi*disr
140	160	150	4,76	714,29
120	140	130	4,65	603,95
100	120	110	33,68	3704,99
80	100	90	15,10	1358,89
60	80	70	22,65	1585,37
40	60	50	15,68	783,97
30	40	35	3,48	121,95
Beneficiated coal _G_dsr		Total	100,00	8873,40
			dsr, mm	88,73
			recorded	91

di, mm	Di, mm	disr, mm	Pi, %	Pi*disr
60	180	170	0,00	0,00
140	160	150	32,61	4892,02
120	140	130	23,80	3093,87
100	120	110	3,48	382,99
80	100	90	18,07	1626,27
60	80	70	8,37	586,16
40	60	50	9,70	484,80
30	40	35	3,97	138,83
Tailings after settling machine MT_G_dsr		Total	100,00	11204,94
			dsr, mm	112,05
			recorded	125,5

di, mm	Di, mm	disr, mm	Pi, %	Pi*disr
160	180	170	0,00	0,00
140	160	150	7,70	1155,20
120	140	130	7,64	993,53
100	120	110	15,29	1681,36
80	100	90	18,22	1640,21
60	80	70	31,75	2222,22
30	60	45	19,40	873,02
Settler concentrate after settling machine MT_G_dsr		Total	100,00	8565,55
			dsr, mm	85,66
			recorded	79

Table 2. Particle size distribution and mean particle diameter d_{sr} according to Andreev – Turija sample

	Di, mm	disr, mm	Pi, %	Pi*disr
00	220	210	2,34	490,95
80	200	190	1,66	315,23
160	180	170	0,87	147,44
140	160	150	5,84	876,70
120	140	130	4,22	549,02
100	120	110	8,45	929,11
80	100	90	7,99	719,46
60	80	70	11,46	802,41
40	60	50	5,58	279,03
30	40	35	7,39	258,67
20	30	25	7,84	196,08
15	20	17,5	3,47	60,71
10	15	12,5	5,13	64,10
5	10	7,5	7,99	59,95
0	5	2,5	19,76	49,40
Run-of-mine coal Turija_dsr		Total	100,00	5798,27
			dsr, mm	57,98
			recorded	38

mm	Di, mm	disr, mm	Pi, %	Pi*disr
0	140	130	8,41	1093,46
100	120	110	0,47	51,40
80	100	90	4,21	378,50
60	80	70	3,74	261,68
40	60	50	6,07	303,74
30	40	35	6,54	228,97
20	30	25	9,81	245,33
5	20	17,5	6,07	106,31
10	15	12,5	9,81	122,66
5	10	7,5	12,15	91,12
0	5	2,5	32,71	81,78
Coal after crusher T_dsr		Total	100,00	2964,95
			dsr, mm	29,65
			recorded	13

di, mm	Di, mm	disr, mm	Pi, %	Pi*disr
200	220	210	0,00	0,00
180	200	190	0,00	0,00
160	180	170	0,00	0,00
140	160	150	5,04	756,08
120	140	130	9,00	1170,12
100	120	110	12,60	1386,14
80	100	90	21,60	1944,19

60	80	70	23,40	1638,16
40	60	50	24,75	1237,62
0	40	35	3,60	126,01
Coal before MT_Tdsr		Total	100,00	8258,33
			dsr, mm	82,58
			recorded	79

di, mm	Di, mm	disr, mm	Pi, %	Pi*disr
180	200	190	0,00	0,00
160	180	170	0,00	0,00
140	160	150	29,53	4429,53
120	140	130	7,16	930,65
100	120	110	15,21	1673,38
80	100	90	9,84	885,91
60	80	70	11,63	814,32
40	60	50	23,27	1163,31
30	40	35	3,36	117,45
Beneficiated coal T_dsr		Total	100,00	10014,5
			dsr, mm	100,15
			recorded	103

di, mm	Di, mm	disr, mm	Pi, %	Pi*disr
120	140	130	16,44	2137,78
100	120	110	12,89	1417,78
80	100	90	16,44	1480,00
60	80	70	27,56	1928,89
40	60	50	24,00	1200,00
30	40	35	2,67	93,33
Tailings after settling machine MT T_dsr		Total	100,00	8257,78
			dsr, mm	82,58
			recorded	77

di, mm	Di, mm	disr, mm	Pi, %	Pi*disr
120	140	130	0,00	0,00
100	120	110	21,97	2416,67
80	100	90	27,27	2454,55
60	80	70	28,79	2015,15
40	60	50	15,53	776,52
30	40	35	6,44	225,38
Settler concentrate after settling machine MT_ T_dsr		Total	100,00	7888,26
			dsr, mm	78,88
			recorded	79,5

Table 3. Comparative presentation of mean particle diameter according to Andreev

Fraction	dsr, (mm)			
	PK Turija		PK Grivice	
	po odsjevu	recorded	po odsjevu	recorded
Run-of-mine coal	57,98	38	64,90	38
Crushed coal	29,65	13	53,94	34
Coal before settling machine	82,58	79	83,99	78
Clean coal	100,15	103	88,73	91
Settler concentrate	78,88	79,5	85,66	79
Tailings	82,58	77	112,05	125,5

The quantity of each individual sample for immediate analyses (determination of ash, calorific value, etc.) was approximately 800 grams.

This research phase was carried out in the laboratories of RMU “Banovići” and RGGF Tuzla, with the aim of investigating the influence of particle size in order to identify potential scenarios affecting coal concentration efficiency. The results of the immediate technical analysis of coal samples, as well as the mean particle diameter according to Andreev, are presented in Table 4.

Table 4. Immediate technical analysis of coal and mean particle diameter

Parameter	**Unit**	**Location**		**Mean Particle Diameter According to Andreev, d_{sr}, mm**	
		Turija	**Grivice**	**Turija**	**Grivice**
Crushed coal				**29,65**	**53,94**
Sample mass	g	932,9	814,9		
Total moisture	%	13,00	9,80		
Ash	%	30,81	35,78		
Combustible matter	%	48,23	47,91		
Inherent moisture	%	20,96	16,31		
DTV	**kJ/kg**	**11740**	**11393**		
Coal before settling machine				**84,38**	**82,76**
Sample mass	g	951,6	812,8		
Total moisture	%	8,80	8,60		
Ash	%	20,71	33,15		
Sagorive materije	%	57,50	51,72		
Inherent moisture	%	21,79	15,13		
DTV	**kJ/kg**	**15448**	**13681**		
Beneficiated coal				**100,15**	**88,73**
Sample mass	g	879,2	852,6		
Total moisture	%	7,60	8,40		
Ash	%	24,61	19,26		

Combustible matter	%	56,30	65,58		
Inherent moisture	%	19,09	15,16		
DTV	**kJ/kg**	**14177**	**19176**		
Tailings					
Sample mass	g	873,3	827,1	**82,58**	**112,05**
Total moisture	%	7,80	9,60		
Ash	%	54,88	47,89		
Combustible matter	%	31,45	38,81		
Inherent moisture	%	13,67	13,30		
DTV	**kJ/kg**	**3304**	**3936**		
Settler concentrate					
Sample mass	g	873,9	913,9	**78,88**	**85,66**
Total moisture	%	2,40	6,80		
Ash	%	37,58	46,10		
Combustible matter	%	52,31	42,05		
Inherent moisture	%	10,11	11,85		
DTE	**kJ/kg**	**11560**	**8208**		

Based on the obtained results of the mean particle diameter, it can be observed that coal from Grivice crushes more efficiently compared to the coal sample from Turija, whereas tailings from Turija crush better than tailings from Grivice.

4.3.Analysis of Results

The analysis of coal was carried out on the settling machine for coarse fractions (-150+30 mm).
The beneficiation results, i.e., the concentration efficiency in the settling machine depending on particle size, were monitored through uniformly falling particles, the coefficient of final particle settling velocity, and the mean particle diameter according to Andreev.
The calculation of the coefficient of uniformly falling particles was performed according to the following relationship:

$$e = \frac{d_l}{d_t} = \frac{\delta_t - 1}{\delta_l - 1}$$

$$e = \frac{d_l}{d_t} = \frac{2{,}20 - 1}{1{,}45 - 1} = 2{,}66$$

Where:
δ_t- bulk density of the marl in natural state (t/m^3),[12]
δ_l- bulk density of the coal in natural state (t/m^3), [12]
The calculation of the final settling velocity was performed using the Rittinger formula:

$$v_o = 4{,}43 * \sqrt{\frac{d(\delta - \Delta)}{\Delta}} \quad \left(\frac{m}{s}\right),$$

Where:
d- mean particle diameter according to Andreev,
δ- bulk density in natural state (t/m^3),
Δ- density of the fluid (water) (t/m^3).
Based on the above formula, the final settling velocity of particles was calculated for d_{sr} determined according to Andreev, specifically for Turija coal before the settling machine.

$$v_o = 4{,}43 * \sqrt{\frac{0{,}12403(1{,}45-1)}{1}} = 1{,}045 \quad \left(\frac{m}{s}\right)$$

Final settling velocity of particles for Grivice coal before the settling machine:

$$v_o = 4{,}43 * \sqrt{\frac{0{,}10896(1{,}45-1)}{1}} = 0{,}980 \quad \left(\frac{m}{s}\right)$$

The results of the final settling velocity for coal samples from Turija and Grivice differ, with the final settling velocity being higher for the Turija sample.

The quality of run-of-mine coal and beneficiated products was assessed based on ash content, combustible matter, and calorific value (GCV and HHV). The utilization of valuable components, i.e., carbon substance, is presented as weight-based and organic utilization. Organic utilization represents the ratio of theoretical utilization T_t to effective utilization T_e of coal with the same ash content, where the theoretical utilization is determined through laboratory testing.

The calculation of organic utilization for the Turija coal sample and settler concentrate was performed using the following formula:

$$I_{org} = \frac{T_e}{T_t}$$

$$I_{orgUST} = \frac{(T_{SMČU} + T_{SMS})}{T_{SMU}} = \frac{(31{,}15 + 26{,}05)}{73{,}5} * 100 = 77{,}81\ \%$$

Where:

$T_{SMČU}$- content of combustible matter in clean coal (%),

T_{SMS}- content of combustible matter in settler concentrate (%)

T_{SMU}- content of combustible matter in coal entering the settling machine (%).

The calculation of organic utilization for the Turija tailings sample:

$$I_{orgJT} = \frac{T_e}{T_t} = \frac{16{,}31}{73{,}5} * 100 = 22{,}19\ \%$$

The calculation of organic utilization for the Grivice coal and settler concentrate samples was performed according to the following formula:

$$I_{org} = \frac{T_e}{T_t}$$

$$I_{orgUSG} = \frac{(T_{SMČU} + T_{SMS})}{T_{SMU}} = \frac{(27{,}75 + 17{,}12)}{60{,}90} * 100 = 73{,}63\ \%$$

Gdje je:

$T_{SMČU}$- content of combustible matter in clean coal (%),

T_{SMS}- content of combustible matter in settler concentrate (%),

T_{SMU}- content of combustible matter in coal entering the settling machine (%),

Calculation of organic utilization for the Grivice tailings sample:

$$I_{orgJT} = \frac{T_e}{T_t} = \frac{16{,}07}{60{,}90} * 100 = 26{,}31\ \%$$

Table 5. Concentration efficiency monitored by combustible matter – Turija Sample

Turija	with moisture		Total slolid	without moisture		solid phase		combustible materials		Ash	
	Ash	SM		Ash	SM						
inlet to the MT	20,71	57,5	78,21	26,5	73,5	dry	with moisture	dry	with moisture	dry	with moisture
Clean coal	24,61	56,3	80,91	30,4	69,6	31,47	24,61	42,38	31,15	22,40	5,93
tailings	54,88	31,45	86,33	63,6	36,4	33,57	26,26	22,19	16,31	46,81	12,40
Settler concentrate	37,58	52,31	89,89	41,8	58,2	34,96	27,34	35,44	26,05	30,79	8,15
Total	117,07	140,06	257,13	135,79	164,2	100,00	78,21	100,00	73,52	100,00	26,48

Table 6. Concentration efficiency monitored by combustible matter – Grivice Sample

Grivice	with moisture		Total slolid	without moisture		solid phase		combustible materials		Ash		
	Ash	SM		Ash	SM							dry
inlet to the MT	33,15	51,72	84,87	39,1	60,9	dry	with moisture	dry	with moisture	dry	with moisture	100,00
Clean coal	19,26	65,58	84,84	22,7	77,3	32,67	27,73	45,53	27,75	17,43	6,81	34,56
tailings	47,89	38,81	86,7	55,2	44,8	33,39	28,33	26,37	16,07	42,41	16,57	32,64
Settler concentrate	46,1	42,05	88,15	52,3	47,7	33,94	28,81	28,10	17,12	40,16	15,68	32,81
Total	113,25	146,44	259,69	130,24	169,8	100,00	84,87	100,00	60,94	100,00	39,06	100,00

From the obtained values of organic utilization of combustible matter in the final products (clean coal, settler concentrate) relative to the combustible matter in coal entering the settling machine, it can be observed that the Turija sample shows better utilization compared to the Grivice sample.
Utilization of the valuable component for the Turija sample:

$$I_{\check{c}u} = \frac{SM_{\check{c}u}(SM_u - SM_j)}{SM_u(SM_{\check{c}u} - SM_j)}$$
$$I_{\check{c}u} = \frac{31{,}15(73{,}5 - 16{,}31)}{73{,}5(31{,}15 - 16{,}31)} = 1{,}633\%$$

Utilization of the valuable component for the Grivice sample:

$$I_{\check{c}u} = \frac{SM_{\check{c}u}(SM_u - SM_j)}{SM_u(SM_{\check{c}u} - SM_j)}$$
$$I_{\check{c}u} = \frac{27{,}75(60{,}90-16{,}07)}{60{,}90(27{,}75-16{,}07)} = 1{,}748\ \%$$

Table 7. Results of the analysis of combustible matter and ash in coal before the settling machine and in beneficiated products

Location	Fraction	Ash	SM	Total solid phase	Ash, dry basis	SM, dry basis, %
Turija	ulaz u MT	33,15	51,72	84,87	39,06	60,94
	Clean coal	24,61	56,3	80,91	30,42	69,58
	Tailings	54,88	31,45	86,33	63,57	36,43
	Settler concentrate	37,58	52,31	89,89	41,81	58,19
Grivice	ulaz u MT	20,71	57,5	78,21	26,48	73,52
	Clean coal	19,26	65,58	84,84	22,70	77,30
	Tailings	47,89	38,81	86,7	55,24	44,76
	Settler concentrate	46,1	42,05	88,15	52,30	47,70

From the data presented in Table 7, the following conclusions can be drawn:

- The combustible matter (CM) for the Turija sample at the inlet to the settling machine is 60.94%, while after beneficiation, the CM in clean coal reaches 69.58%, representing an increase of 8.64%.

- The CM for the Grivice sample at the inlet to the settling machine is 73.52%, while after beneficiation, the CM in clean coal reaches 77.30%, representing an increase of 3.78%. The quality of coal, i.e., the percentage of CM at the inlet to the settling machine, is higher for the Grivice sample, indicating that Grivice coal is of better quality, whereas the concentration effect is greater for the Turija coal sample.

The following figures present the results of the particle size analysis for samples taken at the inlet of the settling machine and for the outputs (clean coal, settler concentrate, and tailings).

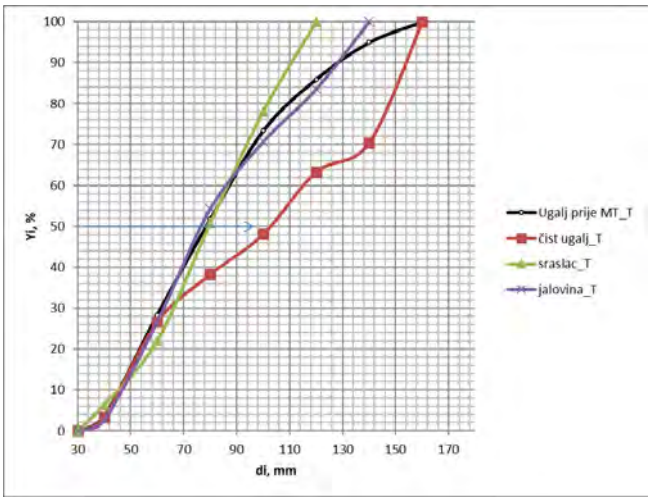

Figure 3. Graphical representation of the particle size distribution – Grivice sample

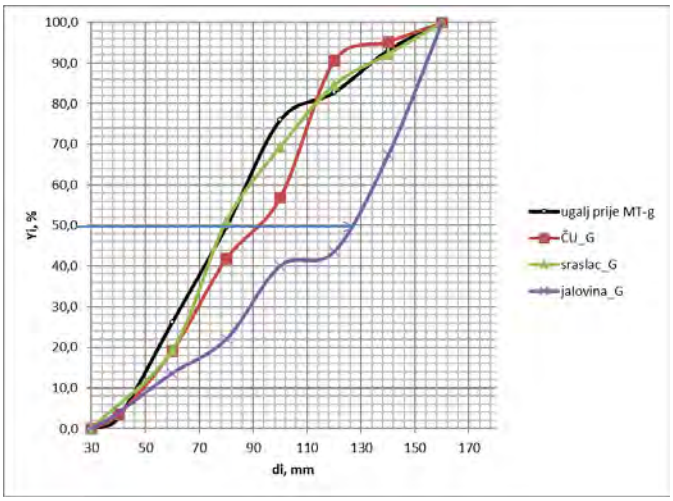

Figure 4. Graphical representation of the par ticle size distribution – Turija sample

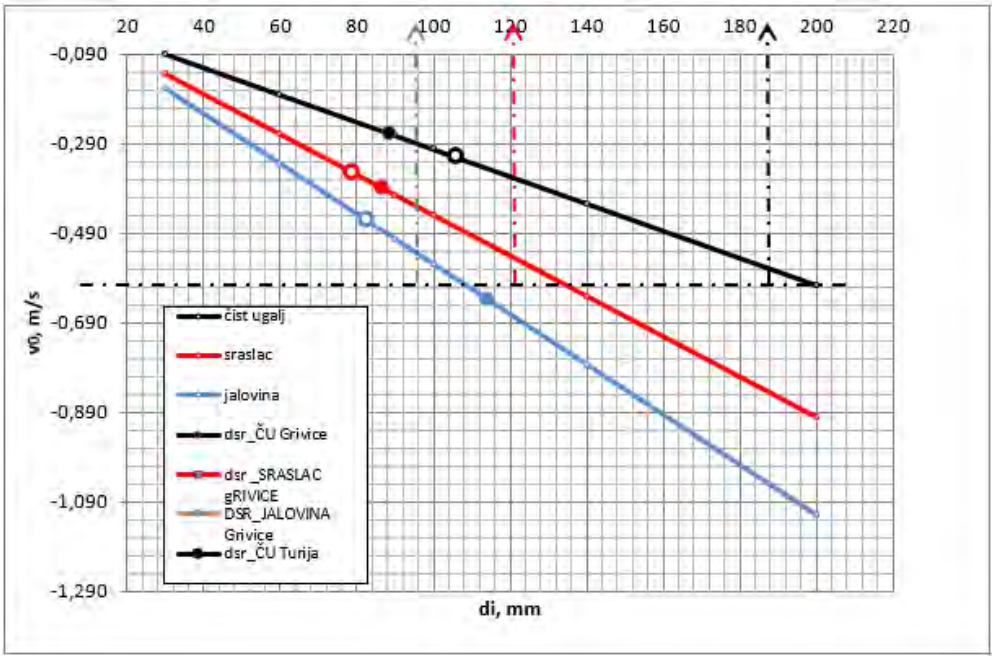

Figure 5. Diagram of the dependence of particle settling velocity for coal, settler concentrate, and tailings – Turija and Grivice

Figure 5 presents a diagram illustrating the influence of particle size on settling velocity and the position of particles during and after the segregation process, which ultimately has the greatest impact on the coal concentration efficiency in the settling machine. In this diagram, classification is shown according to the minimum coefficient of uniform final settling velocities for the mean particle diameter, where the particle size class is represented by dsr for Turija and dsr for Grivice.

Observing this diagram, it can be seen that the highest settling velocities are exhibited by the mean diameter particles of tailings from Grivice and Turija, which consequently have the greatest influence on the concentration efficiency.
By analyzing the data presented in the diagram, it is possible to identify specific particle size classes and their corresponding settling velocities.

4. CONCLUSION

The importance of coal beneficiation is growing, both for achieving higher coal quality and market value, and for increasing the efficiency of coal combustion plants, which is directly linked to fulfilling the obligations defined by the NECP of Bosnia and Herzegovina for coal-fired power plants in the Federation of BiH.

Although the settling machine is designed for beneficiation of particle sizes from -150+30 mm, its operation and separation results vary significantly with different particle size distributions, i.e., different mean particle diameters. Larger particles, due to higher cohesion, are washed less effectively and are therefore not recommended for beneficiation in settling machines.
The quality of beneficiated coal improves with decreasing particle size; however, a decrease in particle size also reduces the weight yield of coal.

The results of the tests and analyses are as follows:
- The mean particle diameter at the inlet to the settling machine is 82.58 mm for the Turija sample and 83.99 mm for the Grivice sample.
- The combustible matter (CM) at the inlet to the settling machine for the Turija sample is 60.94%, while in the clean coal it reaches 69.58%, representing an increase of 8.64%.
- The combustible matter (CM) at the inlet to the settling machine for the Grivice sample is 73.52%, while in the clean coal it reaches 77.30%, representing an increase of 3.78%.
- The percentage of combustible matter in the tailings is lower for the Turija sample at 36.43%, while for Grivice tailings it is 44.76%.

Based on laboratory tests, analytical analyses, and calculations under the same conditions as sampling, it can be concluded that coal cleaning is more efficient for Turija.
Observing the mean particle diameter results, it can be stated that Grivice coal is more easily crushed than Turija coal, whereas tailings and settler concentrate are more difficult to crush for Grivice compared to Turija.

It can be concluded that narrow classification of material by particle size provides significant advantages, primarily because the concentration process becomes more stable, while factors such as water quantity, pulsation time, and other technological characteristics of the settling machine have less impact on separation results.

To provide clear and precise guidelines for increasing the concentration efficiency in the settling machine, more extensive testing and analyses involving a larger number of samples are required.

REFERENCES

Alić, N., (2022), Classification of Mineral Raw Materials", University Textbook, Tuzla.

Alić, N., Šišić, I., Softić, A., (2020), Crushing in Mineral Raw Material Preparation", University Textbook, Tuzla.

Ćalić, N., (1990), Theoretical Fundamentals of Mineral Raw Material Preparation, Belgrade, 1990.

Jevremović, Č., (1984), Preparation of Mineral Raw Materials, Tuzla.

Lešić, Đ., Marković S., (1968), Preparation of Mineral Raw Materials, Građevinska Knjiga, Belgrade.

Mining Institute Tuzla, (2019), Elaborate on Classification, Categorization, and Calculation of Hard Coal Reserves in the Banovići Basin.

Petrović, M., Bećirović, M., (2003) "Technological analysis of gravity concentration of hard coal at the RMU "Banovići" separation using tromp curves", Faculty of Mining and Geology, Tuzla, XXV Proceedings, 107–113.

Petrović, M., Gutić, S., (2006), "Impact of dry screening of run-of-mine coal on the quality of beneficiated coal at the RMU "Banovići" separation in Banovići", Faculty of Mining, Geology and Civil Engineering, Tuzla, XXXII Proceedings, 69–79.

Petrović, M., Gutić, S., Alić, N., (2009) "Analysis of the operation of coal beneficiation plant at the RMU "Banovići" separation using the Grumbrecht method, Faculty of Mining, Geology and Civil Engineering, Tuzla, XXXIII Proceedings, 73–79.

Petrović, M., Gutić, S., Gutić, K., (2006) "Quality of beneficiated coal at the RMU "Banovići" separation in relation to the particle size distribution of run-of-mine coal", Proceedings of the International Mining Symposium, 190–203.

Tomanec, R., (2000), Methods for Testing Mineral Raw Materials in Mineral Preparation, Faculty of Mining and Geology, Belgrade.

BENEFICIATION OF A HIGH-GRADE LATERITIC NICKEL ORE BY PHYSICAL SEPARATION METHODS

Yunus Emre ÇAVDAR*, Hüseyin BAŞTÜRKCÜ

Istanbul Technical University, Faculty of Mines, Department of Mineral Processing Engineering, ISTANBUL-TÜRKİYE
**Corresponding author: cavdar@itu.edu.tr*

A B S T R A C T

This study investigates the beneficiation potential of a high-grade lateritic nickel ore using physical separation methods including drum scrubbing, dry magnetic separation, wet high intensity magnetic separation (WHIMS), and centrifugal gravity separation. The raw ore contained 2.83% Ni, 0.15% Co, and 34.59% Fe. Characterization by XRD revealed the presence of quartz, dolomite, kaolinite, calcite, siderite, goethite, hematite, and serpentine. Particle size distribution analyses were performed on both raw and scrubbed samples. Dry magnetic separation was applied to size fractions of -2+1 mm, -1+0.5 mm, and -0.5+0.1 mm. WHIMS and Falcon centrifugal gravity separation tests were conducted on the -106 µm fraction. Results indicated that physical separation methods were not effective in producing a high-grade nickel concentrate from this lateritic ore, due to the fine dissemination of nickel-bearing minerals and the lack of a significant density or magnetic susceptibility contrast between nickel-bearing and gangue minerals.

Key words: *Lateritic nickel ore, magnetic separation, gravity separation, WHIMS, falcon concentrator*

1. INTRODUCTION

Nickel is a strategically important metal with growing demand driven by its applications in stainless steel production, battery technologies, and specialty alloys. Global nickel resources are broadly classified into two categories: sulfide deposits and laterite deposits. Lateritic ores account for approximately 70% of the world's identified nickel resources and are becoming increasingly significant as high-grade sulfide deposits are gradually depleted (Dalvi et al., 2004; Mudd, 2010).

Lateritic nickel ores are formed through intense tropical and sub-tropical weathering of ultramafic rocks, typically peridotites and serpentinites. The weathering process results in a complex, heterogeneous mineralogy where nickel is distributed across various mineral phases including goethite, serpentine, smectite, and other phyllosilicates. This mineralogical complexity makes the beneficiation of lateritic ores considerably more challenging compared to sulfide ores, as conventional flotation methods are generally ineffective due to the lack of distinct surface chemistry differences between the mineral phases (Elias, 2002; McDonald and Whittington, 2008).

Physical separation methods such as magnetic separation and gravity separation have been explored as potential pre-concentration steps for lateritic nickel ores. Magnetic separation exploits the magnetic properties of iron-bearing minerals (goethite and hematite) which are often associated with nickel in laterite profiles. Gravity separation relies on density differences between nickel-bearing heavy minerals and lighter gangue phases such as quartz and silicates. Scrubbing is frequently used as a pre-treatment step to disaggregate clay-bound particles and improve liberation (Farrokhpay et al., 2019; Quast et al., 2015a; Quast et al., 2015b).

The objective of this study is to evaluate the technical feasibility of beneficiating a high-grade lateritic nickel ore through a series of physical separation methods. The study examines the effect of drum scrubbing on particle size distribution and metal distribution, investigates dry magnetic separation across three size fractions, and assesses the performance of WHIMS and centrifugal Falcon separation on the fine (-106 µm) fraction.

2. MATERIALS AND METHODS

2.1.Sample Characterization

The lateritic nickel ore sample used in this study was obtained from a high-grade lateritic ore deposit. Bulk chemical analysis was carried out at an accredited laboratory using ICP-OES after DIG90A (Na_2O_2 fusion) and AAS after DIG43B analytical methods, ensuring high analytical accuracy. The chemical composition of the raw sample is presented in Table 1.

Table 1. Chemical composition of the ore sample

Element, %	Ore
Ni	2.83
Co	0.15
Fe	34.59
Cr	0.41
Ca	3.27
Mg	1.91
Si	8.69
Al	1.69

XRD results revealed that the sample contained quartz, dolomite, kaolinite, calcite, siderite, goethite, hematite, and serpentine. The presence of goethite and hematite as dominant iron-bearing phases, alongside clay minerals (kaolinite) and carbonates (dolomite, calcite), reflects the typical mineralogical character of lateritic nickel ores formed under intense tropical weathering (Elias, 2002).

2.2. Scrubbing Tests

Drum scrubbing was performed to disaggregate clay-rich fine particles adhering to coarser ore particles. The test was conducted at a solids ratio of 60% for a duration of 5 minutes, conditions selected to be representative of industrial-scale operations. Particle size distribution (PSD) analyses were carried out on both raw and scrubbed samples to evaluate the effect of scrubbing on size distribution and metal distribution across size fractions.

2.3. Dry Magnetic Separation

Prior to dry magnetic separation, the sample was crushed using jaw, cone, and roll crushers in sequence at laboratory scale to obtain the required size fractions. Dry magnetic separation tests were performed on size fractions of -2+1 mm, -1+0.5 mm, and -0.5+0.1 mm. A permroll-type separator equipped with NdFeB permanent magnets was used for these tests. Each test produced three products: a magnetic fraction, a middling fraction, and a non-magnetic fraction.

2.4.Wet High Intensity Magnetic Separation (WHIMS)

WHIMS tests were conducted on the -106 µm size fraction, where a higher degree of mineral liberation was anticipated. A laboratory-type CARPCO device was used, applying a theoretical magnetic field intensity of 13,000 Gauss. Multiple magnetic field intensities were applied sequentially during the test, producing different magnetic fractions (Magnetic 1, Magnetic 2, Magnetic 3) and a final non-magnetic product

2.5.Centrifugal Gravity Separation

Centrifugal gravity separation was performed on the -106 µm fraction using a Falcon concentrator, which is capable of applying centrifugal forces of up to 300 G. The test was designed to exploit potential density differences between nickel-bearing minerals and lighter silicate gangue. The Falcon concentrator produced multiple heavy fractions at different centrifugal force settings (300G, 150G, 100G) and a light (tailings) fraction.

2.6. Chemical Analyses

All experimental products were dried at 105°C prior to chemical analysis. Analyses were performed at SGS, an accredited laboratory, using ICP-OES after DIG90A (Na_2O_2 fusion) and AAS after DIG43B methods. Ni, Co, Fe, Cr, Ca, Mg, Si, and Al contents were determined for feed materials and separation products.

3. RESULTS AND DISCUSSION

3.1. Particle Size Distribution and Effect of Scrubbing

Particle size distribution analyses were carried out on both raw and scrubbed samples to assess the influence of drum scrubbing on metal distribution. The PSD results for the raw ore (Table 2) show that the -100+30 mm fraction constitutes the largest proportion by mass (33.05%), with a Ni content of 3.57% and a distribution of 41.66%. The finest fraction (-0.063 mm) represented 15.36% of the total mass with a Ni content of 1.95%.

Table 2. PSD of the raw ore sample

Particle size fraction, mm	Amount	Ni, %		Co, %		Fe, %	
	%	Cont.	Dist.	Cont.	Dist.	Cont.	Dist.
-100 +30	33.05	3.57	41.66	0.17	36.10	40.35	38.55
-30 +12.5	12.58	3.20	14.20	0.17	13.42	39.87	14.50
-12.5 +5.60	11.51	2.76	11.19	0.15	11.00	35.42	11.78
-5.60 +2.83	6.80	2.49	5.99	0.15	6.33	34.36	6.76
-2.83 +1.65	3.90	2.53	3.49	0.15	3.68	34.06	3.84
-1.65 +0.841	5.05	2.40	4.29	0.16	5.11	33.12	4.84
-0.841 +0.5	3.11	2.21	2.43	0.16	3.17	28.00	2.52
-0.5 +0.212	3.81	2.09	2.81	0.18	4.29	27.8	3.07
-0.212 +0.106	2.97	1.97	2.06	0.19	3.49	24.6	2.11
-0.106 +0.063	1.86	2.02	1.33	0.19	2.16	25.9	1.39
-0.063	15.36	1.95	10.56	0.12	11.25	24.00	10.66
TOTAL	100.00	2.83	100.00	0.16	100.00	34.59	100.00

Following drum scrubbing, significant changes were observed in the PSD (Table 3). The proportion of the -0.063 mm fraction increased from 15.36% to 22.09%, confirming that scrubbing effectively liberated fine clay particles from the surface of coarser particles.

Correspondingly, the -100+30 mm fraction decreased from 33.05% to 26.64%. The Ni content in the finest fraction after scrubbing increased to 3.28%, and the Fe content reached 40.19%, suggesting a notable concentration of iron oxide fines in this fraction.

Table 3. PSD of the raw scrubbed sample

Particle size fraction, mm	Amount	Ni, %		Co, %		Fe, %	
	%	Cont.	Dist.	Cont.	Dist.	Cont.	Dist.
-100 +30	26.64	1.96	20.70	0.12	21.41	23.8	19.45
-30 +12.5	12.88	2.82	14.42	0.14	12.47	40.91	16.16
-12.5 +5.60	7.30	2.94	8.52	0.16	8.15	38.02	8.51
-5.60 +2.83	4.87	2.60	5.03	0.15	4.86	34.4	5.14
-2.83 +1.65	2.99	2.38	2.82	0.14	2.81	32.8	3.01
-1.65 +0.841	4.41	2.32	4.07	0.14	4.21	31.34	4.24
-0.841 +0.5	3.55	2.31	3.26	0.16	3.78	31.68	3.45
-0.5 +0.212	6.50	2.05	5.29	0.15	6.75	28.00	5.59
-0.212 +0.106	5.73	2.06	4.70	0.17	6.67	27.5	4.84
-0.106 +0.063	3.04	2.00	2.41	0.16	3.29	25.5	2.37
-0.063	22.09	3.28	28.77	0.17	25.62	40.19	27.24
TOTAL	100	2.52	100.00	0.15	100.00	32.60	100.00

Despite these changes, the distribution of Ni and Co across size fractions did not exhibit a clear concentration in a specific narrow size range. After scrubbing, approximately 50% of Ni and Co remained in coarse fractions above 2.83 mm, which implies that selective liberation of nickel-bearing minerals from the gangue matrix was not achieved. The overall Ni grade of the total scrubbed product (2.52%) remained similar to the feed (2.83%), confirming that scrubbing alone cannot be considered an effective upgrading method for this ore. These results are consistent with the literature reporting that scrubbing primarily serves as a pretreatment step for clay-rich ores rather than a concentration method (Norgate and Jahanshahi, 2010).

3.2. Dry Magnetic Separation

Dry magnetic separation was investigated on three size fractions: -2+1 mm, -1+0.5 mm, and -0.5+0.1 mm. The results (Tables 4) show that in all three fractions, approximately 85-92% of the material reported to the magnetic product due to the high iron content of the ore.

Table 4. Dry magnetic separation results for the size fraction of -2+1 mm

		%	**Cont.**	**Dist.**	**Cont.**	**Dist.**	**Cont.**	**Dist.**
-2+1 mm	Non-mag.	7.9	0.5	1.59	0.033	1.82	8.9	2.3
	Middling	7.43	0.14	4.21	0.087	4.59	19.4	4.72
	Magnetic	84.67	2.77	94.2	0.159	93.59	33.59	92.99
	TOTAL	100	2.49	100	0.141	100	30.58	100
		%	**Cont.**	**Dist.**	**Cont.**	**Dist.**	**Cont.**	**Dist.**
-1+0.5 mm	Non-mag.	6.02	0.5	1.2	0.034	1.33	7.69	1.47
	Middling	6.65	1.32	3.48	0.083	3.61	17.3	3.65
	Magnetic	87.33	2.75	95.32	0.167	95.06	34.28	94.88
	TOTAL	100	2.52	100	0.153	100	31.55	100
		%	**Cont.**	**Dist.**	**Cont.**	**Dist.**	**Cont.**	**Dist.**
-0.5+0.1 mm	Non-mag.	2.97	0.39	0.47	0.027	0.53	6.42	0.63
	Middling	4.64	0.71	1.34	0.5	1.53	10	1.53

Magnetic	92.39	2.62	98.19	0.161	97.94	32.09	97.84
TOTAL	100	2.46	100	0.152	100	30.3	100

The Ni content in the magnetic products ranged from 2.62% to 2.77%, only marginally higher than the feed grades of approximately 2.46-2.52%. The non-magnetic products, which accounted for only 3-8% of the total mass, contained low Ni contents of 0.39-0.50%, indicating that Ni was predominantly associated with the magnetic iron oxide phases. While approximately 15-20% of Si and Ca could be separated into the non-magnetic fraction, Ni losses were limited to approximately 1.5%.

These results indicate that dry magnetic separation is not effective when used alone for upgrading this ore. The close association between nickel and iron oxide minerals (goethite and hematite) prevents the production of a high-grade Ni concentrate by magnetic means. Similar limitations have been reported in previous studies on limonitic laterite ores (Farrokhpay et al, 2019; Quast et al., 2015a).

3.3. Wet High Intensity Magnetic Separation (WHIMS)

WHIMS was applied to the -106 µm fraction at varying magnetic field intensities. The results are summarized in Table 5.

Table 5. WHIMS test results for the -106 µm fraction

Products	Amount (%)	Ni Cont. (%)	Ni Dist. (%)	Co Cont. (%)	Co Dist. (%)	Fe Cont. (%)	Fe Dist. (%)
Magnetic 1 (4.000 Gauss)	21	2.89	26.14	0.19	26.58	39.38	27.8
Magnetic 2 (8.000 Gauss)	19.9	3.03	25.96	0.2	26.58	39.39	26.33
Magnetic 3 (13.000 Gauss)	14.9	2.77	17.77	0.18	18.39	34.66	17.32
Non-magnetic	44.2	1.58	30.14	0.09	28.45	19.2	28.55
TOTAL	100	2.32	100	0.15	100	29.75	100

The three magnetic products (Magnetic 1, 2, and 3) collectively accounted for approximately 55.8% of the total mass, with Ni contents of 2.77-3.03% and Ni distributions of 17.77-26.14%. The non-magnetic product (44.2% by mass) contained 1.58% Ni with a distribution of 30.14%. The similarity in Ni and Co distributions between the magnetic and non-magnetic products demonstrates the absence of selective separation. None of the products could be used as tailings without significant Ni and Co losses.

Notably, the non-magnetic fraction contained significant proportions of gangue minerals, with approximately 65.2% of Si, 64.2% of Ca, and 67.8% of Al reporting to this product. However, since nickel distribution was also significant in the non-magnetic fraction, WHIMS cannot be considered a technically or economically viable option for this ore. The inherent co-distribution of Ni with iron oxide and silicate phases, which have overlapping magnetic susceptibilities, is believed to be responsible for this outcome.

3.4. Centrifugal Gravity Separation

The Falcon concentrator was operated at centrifugal forces of up to 300 G on the -106 µm fraction. The separation results are presented in Table 6.

Table 6. Falcon centrifugal concentrator test results for the -106 µm fraction

Products	Amount (%)	Ni Cont. (%)	Ni Dist. (%)	Co Cont. (%)	Co Dist. (%)	Fe Cont. (%)	Fe Dist. (%)
Heavy 1 (300G)	7.4	2.45	7.66	0.156	7.71	32.42	8.09
Heavy 2 (150G)	3.2	2.34	3.17	0.156	3.35	29.7	3.22
Heavy 3 (100G)	6.1	2.39	6.16	0.151	6.17	31.12	6.42
Light	83.4	2.35	83	0.148	82.77	29.1	82.27
TOTAL	100	2.36	100	0.149	100	29.49	100

The heavy fractions collected at 300G, 150G, and 100G accounted for 7.4%, 3.2%, and 6.1% of the total mass, respectively, while the light fraction constituted 83.4%. The Ni contents across all products were remarkably similar, ranging from 2.34% to 2.45% in the heavy fractions and 2.35% in the light fraction. Ni distributions closely mirrored the mass distributions, confirming that no selective concentration of nickel occurred.

The absence of a density contrast between nickel-bearing minerals and the gangue is evidenced by the nearly uniform metal contents across all product streams. In lateritic ores, nickel is typically adsorbed onto or isomorphously substituted within iron oxide and phyllosilicate mineral structures rather than forming discrete high-density sulfide or arsenide phases (Butt and Cluzel, 2013). This renders density-based separation methods largely ineffective, as confirmed by the present results.

4. CONCLUSIONS

This study systematically evaluated the beneficiation of a lateritic nickel ore through physical separation methods including drum scrubbing, dry magnetic separation, WHIMS, and centrifugal gravity separation. Based on the experimental results, the following conclusions can be drawn:

- Drum scrubbing resulted in notable changes in particle size distribution, increasing the -63 µm fraction from 15.36% to 22.09%. However, the Ni and Co distributions did not preferentially concentrate in a specific size fraction, and approximately 50% of both metals remained in the coarse fractions above 2.83 mm. Scrubbing alone is insufficient as an upgrading method for this ore type.

- Dry magnetic separation applied to -2+1 mm, -1+0.5 mm, and -0.5+0.1 mm fractions confirmed the strongly ferruginous nature of the ore, with over 85% of material reporting to the magnetic product. The Ni upgrade in the magnetic fraction was minimal (from approximately 2.5% to 2.7%), and high-grade pre-concentrates could not be produced. The close association of nickel with iron oxide minerals is the limiting factor.

- WHIMS at 11,000-13,000 Gauss on the -106 µm fraction did not produce selective Ni-Co separation. Similar distributions were observed across magnetic and non-magnetic products, making WHIMS technically and economically unfeasible for this application.

- Centrifugal gravity separation using the Falcon concentrator at up to 300 G did not achieve meaningful concentration of Ni or Co. Metal contents across all product streams were virtually identical to the feed grade, confirming the absence of a usable density contrast between nickel-bearing minerals and gangue.

Overall, the results indicate that physical separation methods are not effective for upgrading this lateritic nickel ore due to the fine dissemination of nickel within iron oxide and phyllosilicate mineral matrices and the lack of sufficient magnetic susceptibility or density contrasts.

Hydrometallurgical routes such as high-pressure acid leaching (HPAL) or atmospheric heap leaching should be considered as the primary processing options for this ore type (Kursunoglu and Kaya, 2016; Oxley et al., 2016; Önal and Topkaya, 2014).

REFERENCES

Butt, C. R. M., Cluzel, D., (2013) “Nickel laterite ore deposits: Weathered serpentinites”, Elements, 9 (2) 123–128.

Dalvi, A. D., Bacon, W. G., Osborne, R. C., (2004) “The past and the future of nickel laterites”, Proceedings of the PDAC International Convention, Trade Show and Investors Exchange.

Elias, M., (2002) “Nickel laterite deposits – Geological overview, resources and exploitation”, Giant Ore Deposits: Characteristics, Genesis and Exploration, Centre for Ore Deposit Research, University of Tasmania, 205–220.

Farrokhpay, S., Filippov, L., Fornasiero, D., (2019) “Pre-concentration of nickel in laterite ores using physical separation methods”, Minerals Engineering, 141, 105892.

Kursunoglu, S., Kaya, M., (2016) “Atmospheric pressure acid leaching of Caldag lateritic nickel ore”, International Journal of Mineral Processing, 150, 1–8.

McDonald, R. G., Whittington, B. I., (2008) “Atmospheric acid leaching of nickel laterites review. Part I: Sulphuric acid technologies”, Hydrometallurgy, 91 (1–4) 35–55.

Mudd, G. M., (2010) “Global trends and environmental issues in nickel mining: Sulfides versus laterites”, Ore Geology Reviews, 38 (1–2) 9–26.

Norgate, T., Jahanshahi, S., (2010) “Low grade ores – Smelt, leach or concentrate?”, Minerals Engineering, 23 (2) 65–73.

Önal, M. A. R., Topkaya, Y. A., (2014) “Pressure acid leaching of Çaldağ lateritic nickel ore: An alternative to heap leaching”, Hydrometallurgy, 142, 98–107.

Oxley, A., Smith, M. E., Caceres, O., (2016) “Why heap leach nickel laterites?”, Minerals Engineering, 88, 53–60.

Quast, K., Connor, J. N., Skinner, W., Robinson, D. J., Addai-Mensah, J., (2015a) “Pre-concentration strategies in the processing of nickel laterite ores. Part 1: Literature review”, Minerals Engineering, 79, 261–268.

Quast, K., Connor, J. N., Skinner, W., Robinson, D. J., Addai-Mensah, J., (2015b) “Pre-concentration strategies in the processing of nickel laterite ores. Part 3: Flotation testing”, Minerals Engineering, 79, 279–286.

CASSITERITE FINES RECOVERY FROM JIGGING TAILINGS USING SHAKING TABLES

Cirila Raquel de Araújo Gomes e SILVA[1], Igo Marinho Serafim BORGES[2], Jaquelynne Cassia de AMORIM[2], Wesley Oliveira LEMOS[3], Luís Felipe Schons SILVA[4], Elenice Maria Schons SILVA[4], André Carlos Silva[4,*]

[1]Federal University of Catalão, Specialization Course in Mineral Processing, Engineering Faculty, 75705-220, Catalão, Goiás, BRAZIL
[2]Federal University of Campina Grande, Mining Department, Campina Grande, Paraíba, BRAZIL
[3]Veeiro Mineraçõe Ltda, Ariquemes, Rondonia, BRAZIL
[4]Federal University of Catalão, Mineral Processing Research Center (CPMin), Engineering Faculty, 75705-321, Catalão, Goiás, BRAZIL
**Corresponding author: ancarsil@ufcat.edu.br*

A B S T R A C T

Cassiterite stands out among the minerals of great national importance, as the main tin (Sn) ore, an essential element for several industries, including the production of metallic alloys and electronic components. Traditionally, cassiterite processing in the Brazilian Amazon area was carried out using gravity concentration, mainly with spirals and jigs, efficient equipment for recovering heavy minerals. This study evaluated the implementation of a Wilfley-type shaking table plant for the concentration of cassiterite fines, fed with tailings from the jig plant of the São Francisco Mining, located in Colniza, MT, Brazil. These tables are recognized worldwide for their high precision in the separation of fine particles (-3 mm). The proposed circuit consisted of six vibrating tables operating in parallel (rougher) followed by a cleaner table, which significantly increased the daily tin production to an average of 262.7 kg/day, reducing the amount of tin sent to the tailings dam. The average tin content in the final concentrate was 63.21%, increasing the overall tin recovery. This study highlights the importance of the synergistic combination of gravimetric techniques in the optimization of mineral processing.

Key words: *Cassiterite, gravity concentration, tin recovery, shaking tables*

1. INTRODUCTION

Mining has been a central activity in the economic and technological evolution of societies, providing indispensable resources for industrial development and job creation, especially in regions rich in natural resources such as Brazil (Luz et al., 2018). Cassiterite stands out among the minerals of great national importance, as the main tin (Sn) ore, an essential element for several industries, including the production of metallic alloys and electronic components (Souza et al., 2018). Historically, cassiterite exploration in Brazil has played a strategic role in the country's economic development, with emphasis on alluvial production in the North region (Luz et al., 2018). São Francisco Mining is located in the city of Colniza/MT, in the Center-West region of Brazil, is an important player of this mineral production. Operating in a former artisanal mining area, the mining company processes the old tailings deposits from the previous activities. This historical context, combined with the geographical location of the mining operation, close to the Amazon rainforest, poses environmental and logistical challenges that require innovative practices to concentrate cassiterite (see Figure 1). Despite the challenges, São Francisco Mining operation stands out for its ability to recover Sn from tailings, adopting sustainable approaches that reduce the need to expand extraction areas and impact the ecosystem.

Cassiterite processing involves concentration operations to enhance the Sn grade. Given the cassiterite high specific gravity (ranging from 6.86 to 7.03 g/cm³), gravity concentration

methods became particularly suitable for its processing (Henley, 1981). This technique is widely used and is based on the separation of particles based on their specific gravity through gravitational or centrifugal forces (Luz et al., 2018). Jigs use a pulsating water flow to expand the mineral bed and separate the denser materials (sinks) from the lighter ones (floats). Shaking tables, on the other hand, apply an asymmetric movement on an inclined surface with rifling to perform a more refined separation, being especially effective for fine particles (Luz et al., 2018; São José et al., 2019; Linhares et al., 2023). The conventional gravity equipment can be used with a particle size ranging from 60 to 1,000 μm. Equipment such as jigs, spirals and shaking tables operates efficiently with different particle size distributions. Jigs are normally used to concentrate relatively coarse material and, if the feed is fairly close-sized (e.g., 3 to 10 mm), although they can achieve good recovery down to 150 μm and acceptable recoveries often down to 75 μm. Tables operating on feed sizes in the range 3 mm to 100 μm are sometimes referred to as sand tables, and the hydrosizer overflow, consisting primarily of particles finer than 100 μm, is usually thickened and then distributed to tables whose decks have a series of planes, rather than riffles, and are designated slime tables (Wills and Finch, 1981).

The efficiency in Sn processing from tailings in São Francisco Mining is mainly due to the use of jigs. The choice of this equipment is justified by its effectiveness in the selective recovery of heavy minerals (Peres et al., 2002). Figure 2 presents the company's original flowsheet. It is possible to notice that the concentration was carried out in two rougher stages and two cleaner stages, all then using twin cell Pan-American jigs (see Figure 3). This equipment is designed for high-efficiency gravity concentration and is equipped with two cells (hence the name twin cells), which operate in an interconnected manner, allowing continuous separation of heavy minerals, consuming less water and space, without losing production capacity (Lins, 2010).

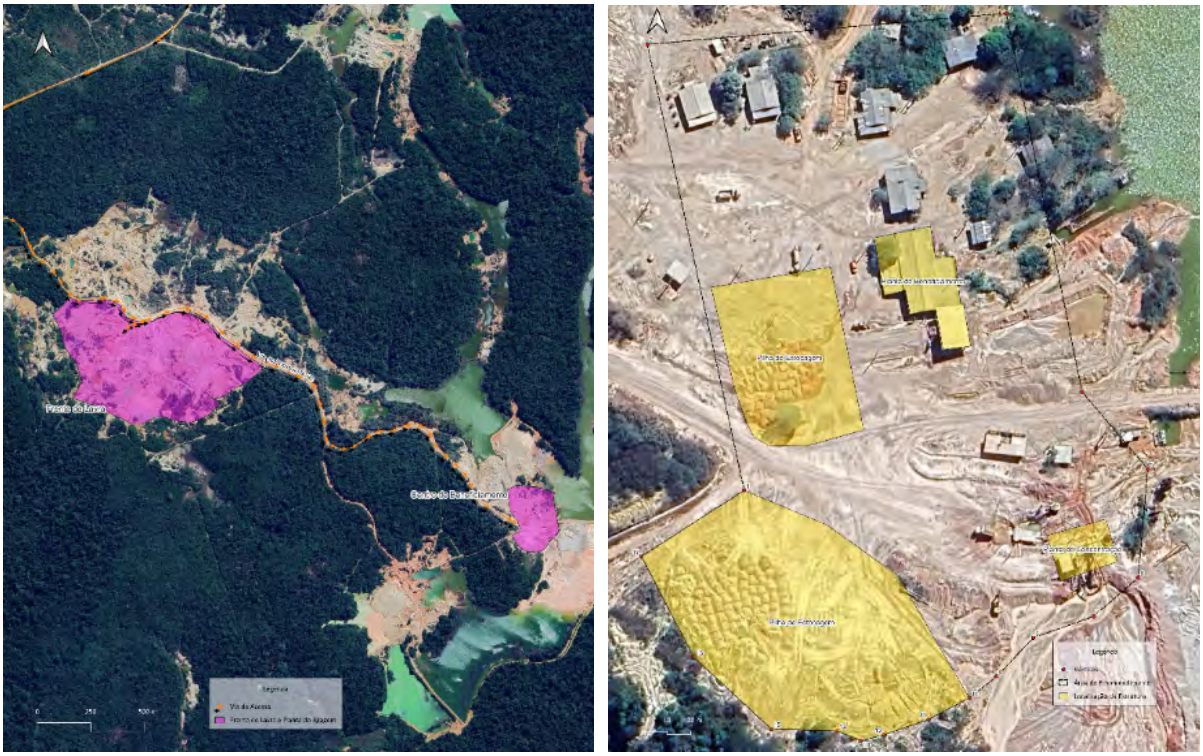

(a) **(b)**

Figure 1. Location of São Francisco Mining's cassiterite mine (a) and mineral processing plant (b)

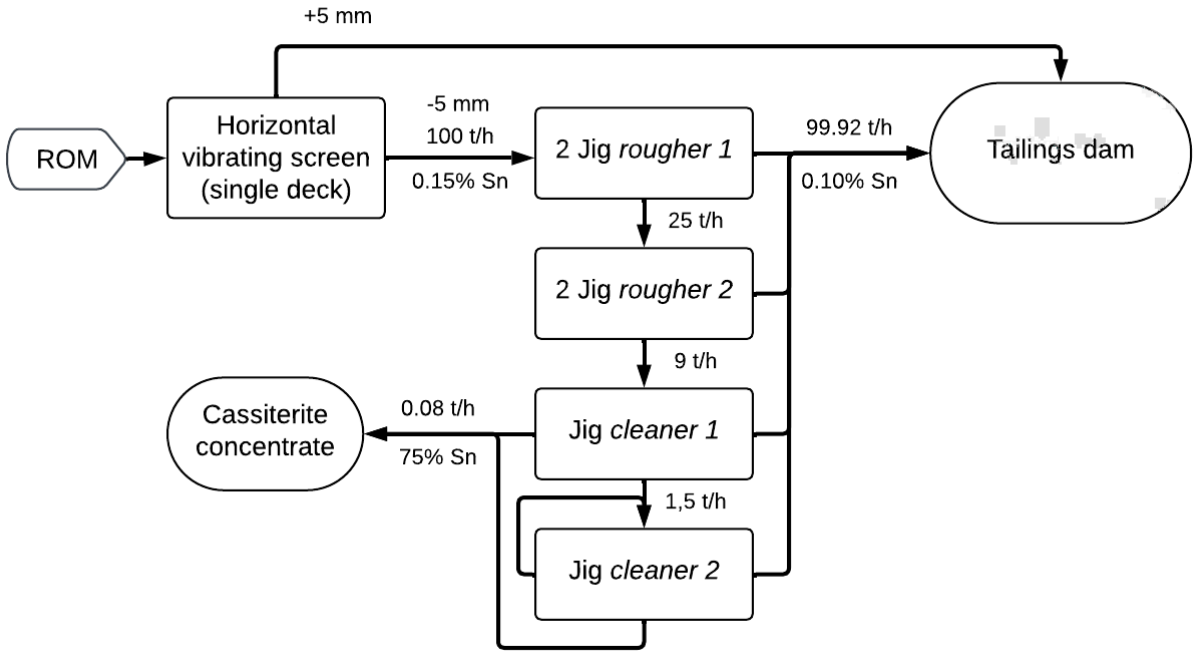

Figure 2. Cassiterite processing flowsheet before the shaking tables commissioning

Figure 3. Twin cell Pan-American jig operating at São Francisco Mining

Despite the results already obtained by jigs, the company was interested in recovering tin from the tailings. However, the low grade in this flow required the adoption of more advanced concentration strategies. In this sense, São Francisco Mining introduced shaking tables fed with jig tailings. Although the initial investment (CAPEX) with shaking tables is higher, this equipment is widely recognized as one of the most accurate gravity methods for fine particles, an essential feature for the efficient treatment of cassiterite (Souza et al., 2018; Linhares et al., 2023; Peres et al., 2002).

The shaking tables implemented were Wilfley tables, following the configuration developed and patented by Arthur Wilfley in the United States in 1895 (Souza et al., 2018), consisting of a slightly inclined deck that combines hydraulic and mechanical action to separate particles based on their density and size. Water is fed into the upper end of the table, creating a flow that transports the particles along the rifled surface, while an asymmetrical oscillatory movement, perpendicular to the flow, promotes differential transportation of the particles. The dense particles settle behind the rifles, gradually advancing with the oscillatory movement and are discharged at the opposite end of the driving mechanism, where an adjustable diverter separates them into high and low-grade concentrate (Chaves and Chaves-Filho, 2013). Light particles and slimes, which remain suspended in the water flow, go to the opposite side of the feed or to the end of the smooth part of the deck (Sampaio and Tavares, 2005). This combination of hydraulic and mechanical forces allows differential transport and results in a partial overlap of the concentrate and tailings bands.

The study of this gravity concentration configuration aims to evaluate the performance of concentrator tables in the recovery of cassiterite from jig tailings at São Francisco Mining, through a detailed analysis of the feed and production data. The relevance of this research lies in the scientific contribution to the field of mineral processing, offering technical subsidies that can optimize operations and serve as a reference for other mining companies seeking to improve the efficiency and sustainability of their processes. In the context of growing demand for tin in the global market, the study stands out for its potential to provide technological solutions for more sustainable and effective processing of cassiterite, with positive impacts on economic and environmental issues (Kuhn et al., 2016).

2. MATERIAL AND METHODS

2.1. Material

The study was conducted at São Francisco Mining (Colniza, MT, Brazil), with the aim of evaluating the efficiency of cassiterite recovery from the reject from the cleaner stage of the jigging plant, implementing shaking tables. To attest to the efficiency of this process, yield and recovery were used. The implementation of Wilfley-type shaking tables at São Francisco Mining began in April 2023, with the installation of a table to assess the efficiency of cassiterite recovery from the jig cleaner stage tailings. After the initial results, six shaking tables were added to the circuit operating in parallel in June 2024. This new arrangement allowed the material to be distributed simultaneously between the tables, increasing the system's throughput. Each table had their inclination and solid percentage adjusted to maximize recovery according to the density and granulometry of the material, reducing cassiterite losses throughout the process.

The system's performance was evaluated considering the three phases of development of the concentration process: initial operation with jigs only, the addition of a table and, finally, the expansion with the installation of six additional shaking tables in parallel. At each phase, it is possible to gradually observe the improvement in cassiterite recovery efficiency. The comparative analysis between these stages considered the total recovery rate and the cassiterite grade in the final concentrate.

2.2. Method

Samples were collected during the tests, and the chemical analysis was performed by sampling the concentrates (stored in big bags) to produce samples of 10 kg, which were quartered into two samples of 100 g. The cassiterite samples were pulverized in a ring and puck mill and sieved to be 100% passing in 200#. A 0.2 g sample was sent to wet chemical analysis. The sample was melted at 1000 °C with NaOH, producing a soluble, orange-colored

compound called sodium stannite (Na2SnO2). After cooling, the bead was dissolved in a solution of HCl and distilled water, transferred to an Erlenmeyer flask, where the tin is reduced with acid and aluminum wire. A titration was performed using an automatic burette and a starch-iodine solution as an indicator (1 ml of 0.1 N iodine + 5 ml of 5% starch solution diluted to 100 ml), allowing the precise quantification of the tin grade, with the end point indicated by the color change (Price and Smith, 1978). Minitab 21.4.2 was used to plot the graphics.

3. RESULTS AND DISCUSSION

The concentration process using the jig circuit was analyzed to assess its efficiency. From the feed rates, production and concentrate grade, it was possible to plot frequency histograms, as illustrated in Figure 4, representing the daily yield and Sn recovery from the jig circuit. The analysis of the histograms reveals that, despite the daily concentrate production at São Francisco Mining, which varies from 175 to 225 tons, the yield does not exceed 5%, reflecting the limited process tin low grade in the feed, approximately 0.15% of Sn, since the deposit had already been partially explored in the past by another company.

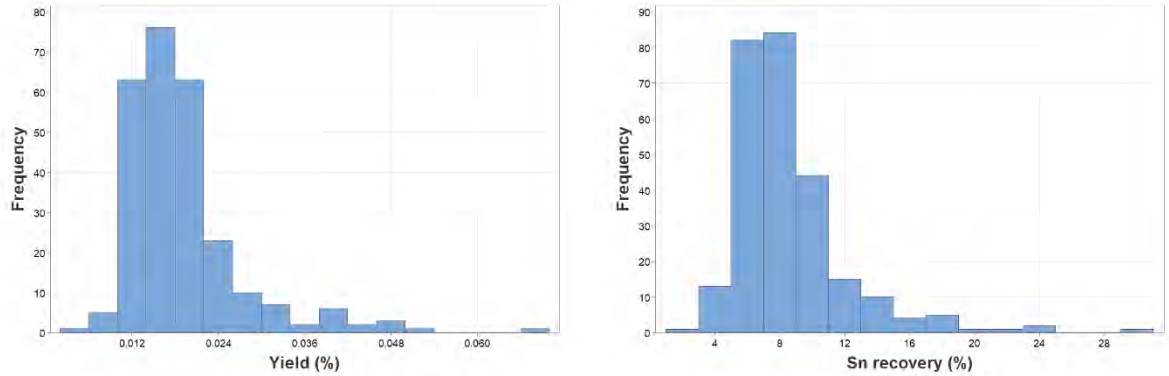

(a) **(b)**

Figure 4. Frequency histogram of the daily yield (a) and Sn recovery (b) by jigs

However, the jig plant has proven to be capable of producing high-grade concentrate, as shown in Figure 5, which presents a control chart of the Sn grade in the final concentrate. The average Sn grade in the concentrate was 68.50%, with lower control limit (LCL) 66.21% and upper control limit (UCL) of 70.80%, classically known as sigma limits. These values, although presenting outliers, are within the expected range for a tin processing plant, whose concentrate production should reach grades between 70.0% and 76.5% (Taggart, 1945). The found outliers were responsible for a high production or a low Sn grade and are directly connected to the fact that the mine is an anthropogenic deposit. Therefore, the ore variability is too high.

The Sn grade in the tailings suggested the need for improvements in the process, especially regarding its recovery. In this context, the implementation of shaking tables, specifically Wilfley-type ones, appeared as a promising alternative. The performance of this alternative was evaluated, and the results are presented in Figure 6. The average production of a shaking table is lower than a jig, given that shaking tables operate with a feed < 2 t/h, therefore restricting their use mainly to the cleaning stages (Luz et al., 2018), which can be seen in Figure 6A, with an average daily production around 93.8 kg of Sn, which represents a substantial increase to the total concentrate produced by the plant.

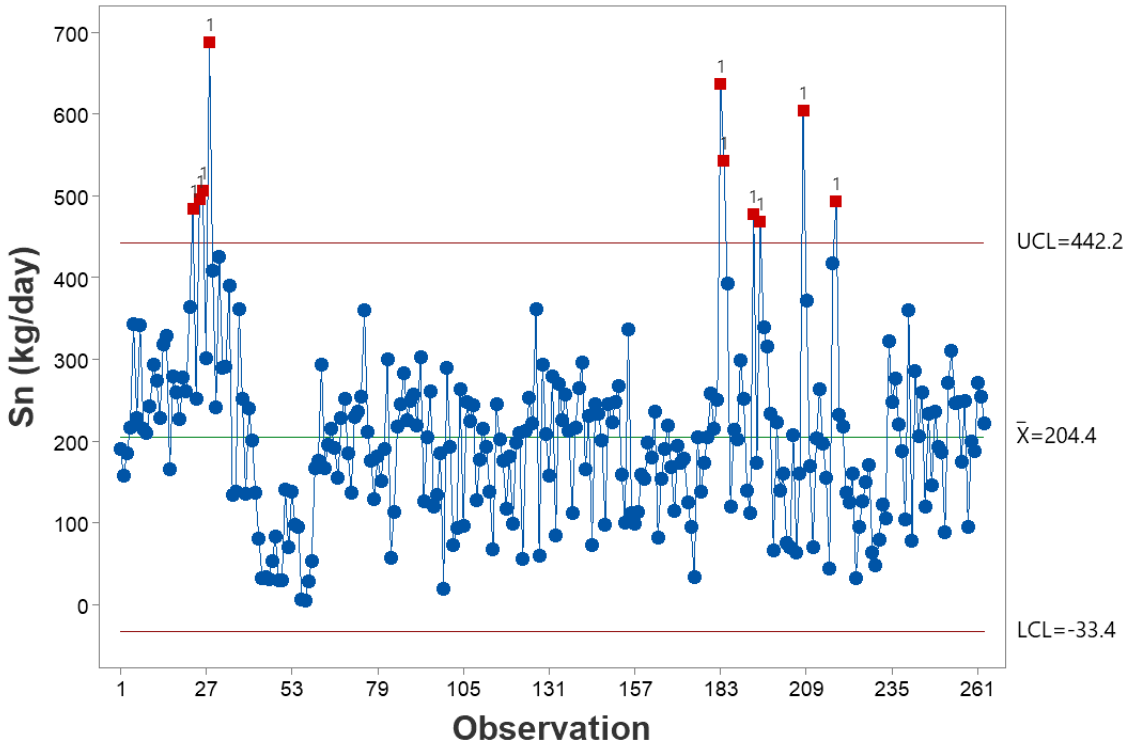

(a)

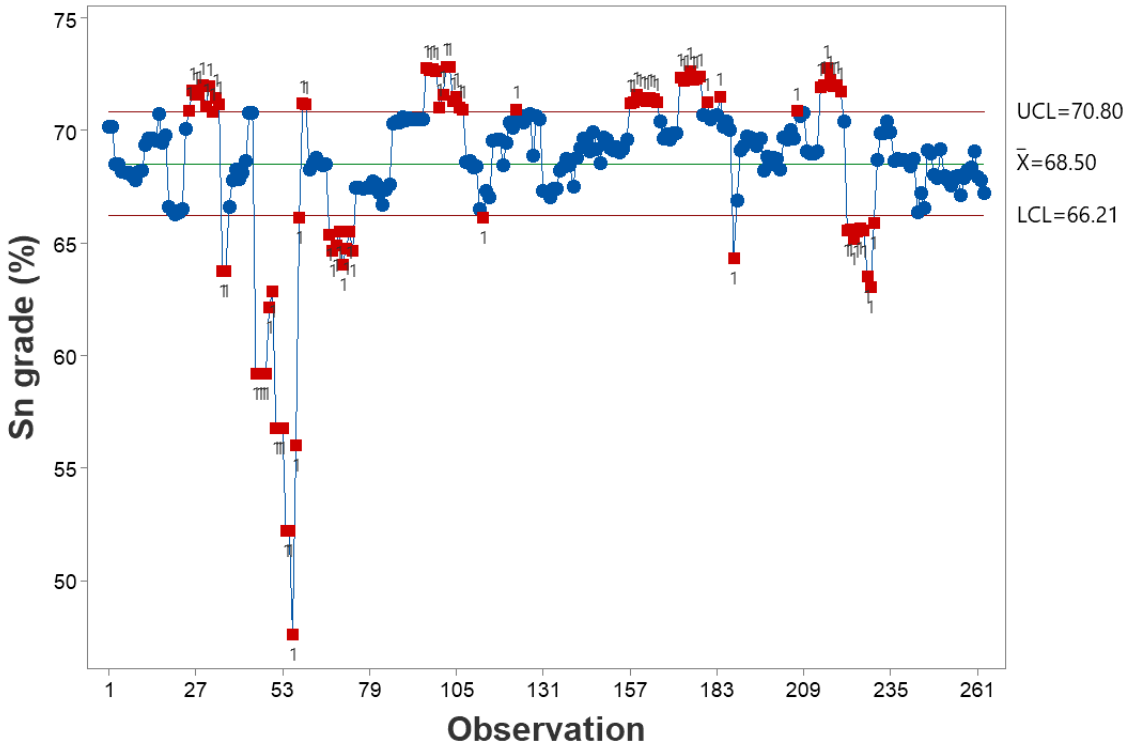

(b)

Figure 5. Control chart of the daily Sn production (a) and Sn grade (b) in the final concentrate produced by jigs

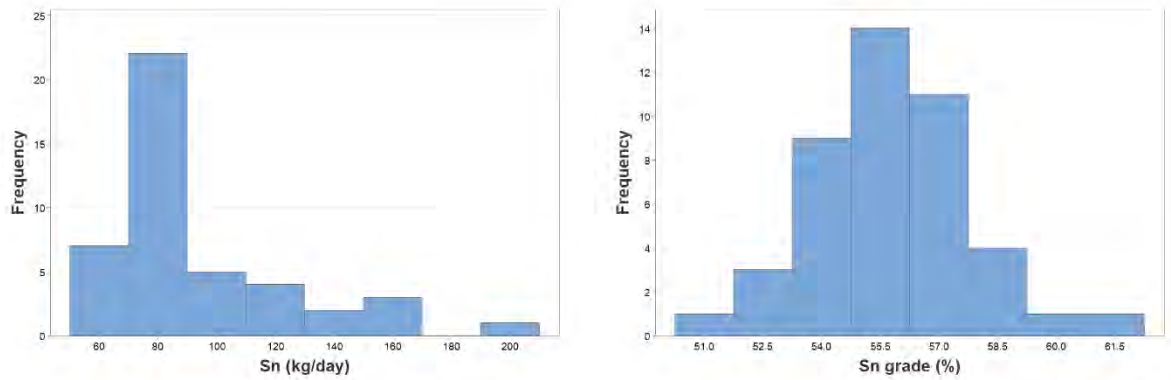

(a) **(b)**

Figure 6. Frequency histogram of the daily Sn production (a) and grade (b) for one shaking table

The concentrate had an average Sn content of 55.81%. This value, although lower than that obtained by jigging, was expected, since the table was operating with low-grade tailings, making it difficult to obtain higher enrichment values. The found results were higher that obtained by Youssef et al. (2009). The authors obtained a concentrate with 13.2% of Sn working with samples from Igla placer ore. Arief (2022) worked with tin ore samples from PT TimahTbk, one from the Bantam B122 plant and the other from Jangkang Washing Plant, obtained optimal recoveries of 75.03%, and 70.15%, respectively. The authors conclude that the optimum operational condition was achieved at a deck slope of 8° and water flow rate of 15 lpm. The yield and tin grades in the concentrate by shaking table are shown in Figure 7.

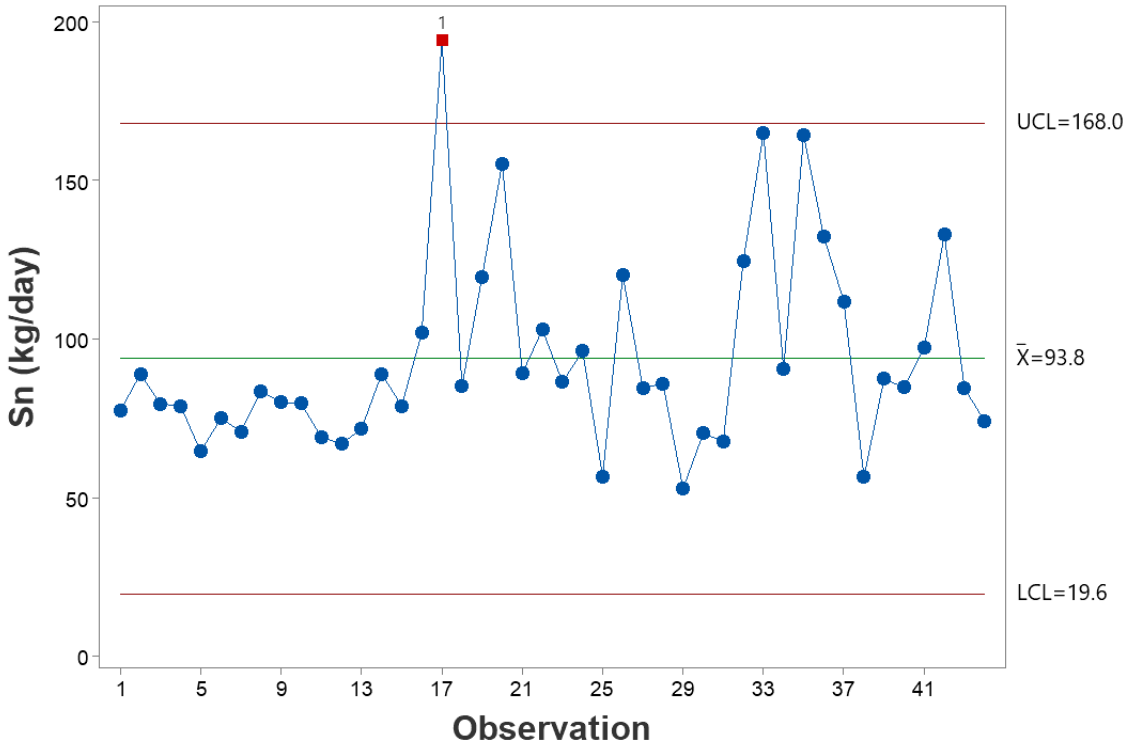

(a)

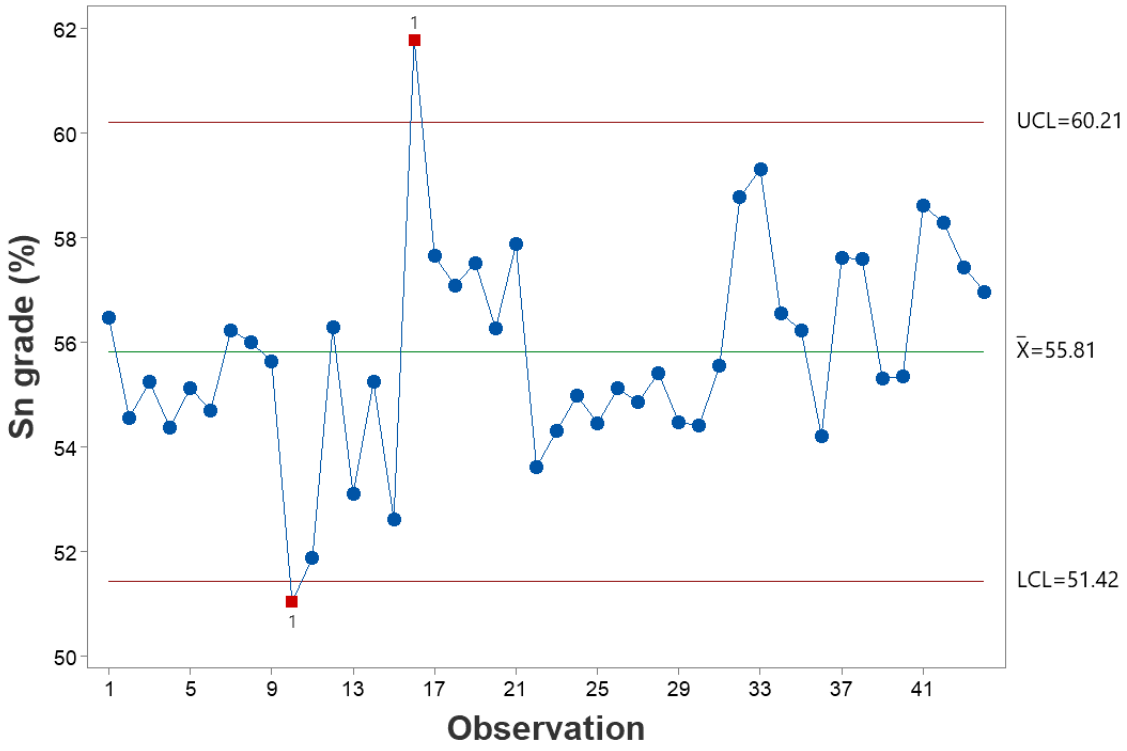

(b)

Figure 7. Control chart of the daily Sn production (a) and grade (b) for one shaking table

The optimization of this process route was achieved by combining shaking tables operating in a rougher/cleaner circuit (Wills and Finch, 1981; Kuhn et al., 2016). In this sense, a new arrangement of shaking tables operating in two stages (six shaking tables operating in parallel in the rougher stage followed by one in the cleaner stage) was proposed, with the aim of increasing the final concentrate grades, as illustrated in Figure 8. This configuration increased the total capacity of the plant, allowing the processing of up to 6.2 t/h of material, distributed evenly between the tables by a screw feeder. The pre-concentrated is classified by hydrocyclone, which sent the fine particles to the tailings and promoted a sludge dewatering and fed the cleaner table. The concentrated daily production and tin grades in the concentrate are shown in Figures 9 and 10.

The found results suggest that the new route with shaking tables operating in two stages can provide a significant increase in Sn daily production (average production in the considered period of 262.7 kg/day). Although the tin content registered an average of 63.21%, the increase in the amount of concentrated recovered from the jigging tailings represented a substantial gain for the mine company.

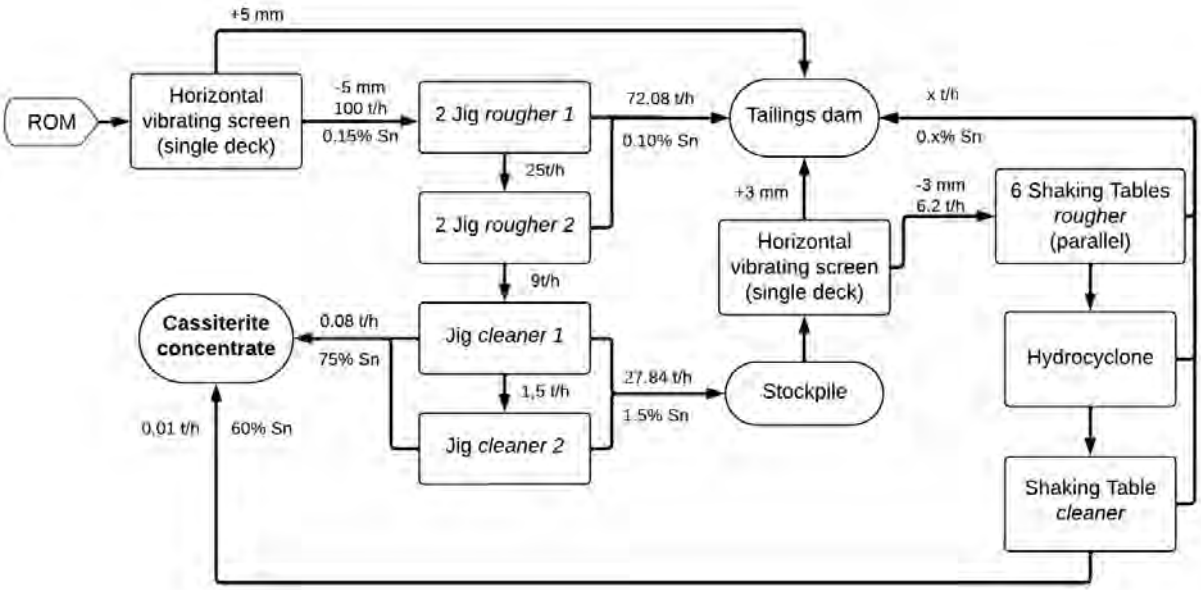

Figure 8. Optimized cassiterite processing flowsheet with the shaking tables plant

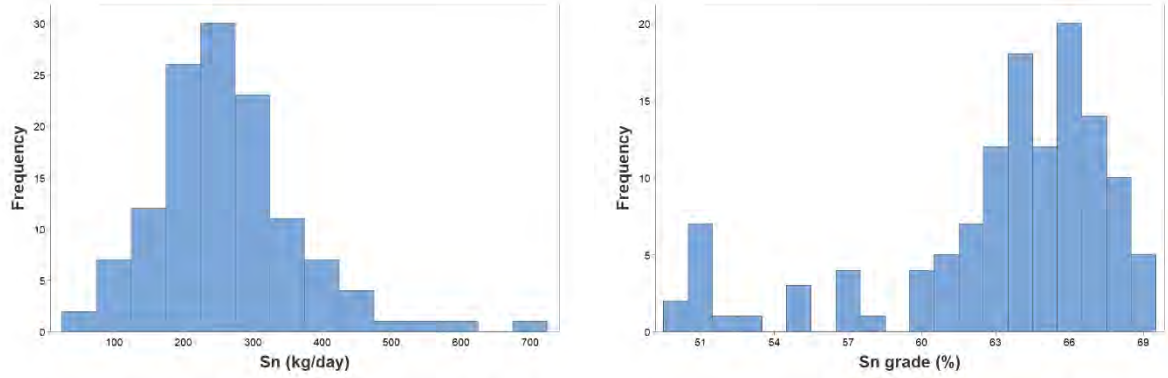

(a) **(b)**

Figure 9. Frequency histogram of the daily Sn production (a) and grade (b) for the jigs and shaking tables combined plants

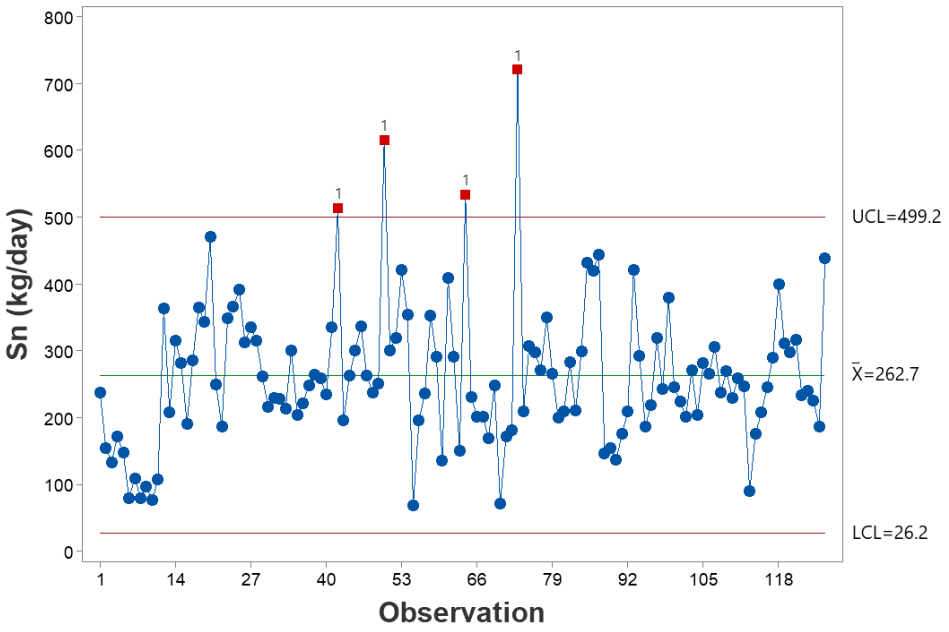

(a)

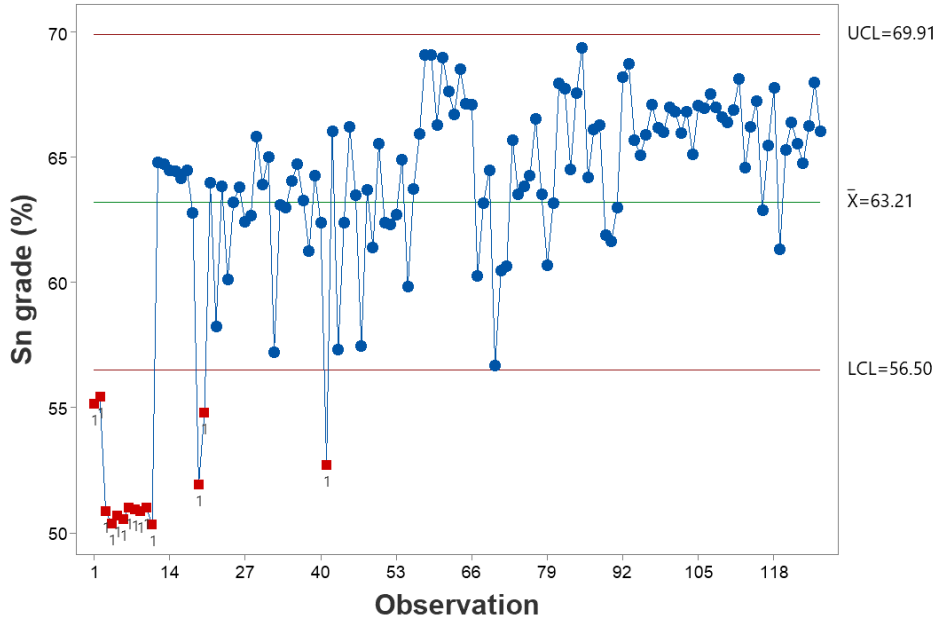

(b)

Figure 10. Control chart of the daily Sn production (a) and Sn grade (b) in the final concentrate produced for the jigs and shaking tables combined plants

4. CONCLUSION

This study evaluated the efficiency of a new tin concentration plant at São Francisco Mining, using an association of jigs and shaking tables. The results showed that although jigging is traditionally used in mining, its performance was limited. Therefore, the introduction of Wilfley-type shaking tables increased the tin daily production. The proposed processing plant consisted of seven shaking tables, six in the rougher stage followed by one in the cleaner stage. The implementation of this plant not only improved the Sn recovery, but also generated economic gains, a small reduction of the volume of solids sent to the tailings dam, and

increased the concentrate production, without expanding the mine exploitation. Therefore, the new plant had positive environmental implications, contributing to the preservation of the Amazon rainforest by reducing deforestation associated with cassiterite mining.

ACKNOWLEDGMENTS

The authors would like to thank São Francisco Mining for allowing this research to happen, the Specialization Course in Mineral Treatment of the Federal University of Catalão for the knowledge transmitted, and the funding agencies FAPEG, FUNAPE, CAPES and CNPq for the financial support granted to the LaMPPMin researchers.

REFERENCES

Arief, T., (2022) “Design and experimentation shaking table tool for gravity concentration metal mineral separation”, International Journal of Mineral Processing and Extractive Metallurgy, 1 (7) 1-7.

Chaves, A. P., Chaves-Filho, R., (2013), Teoria e prática do tratamento de Minérios, Vol. 6, Separação densitária. São Paulo: Oficina de Textos.

Henley, K. J., (1981) “Ore-dressing mineralogy-a review of techniques, applications and recent developments”, 1st International Congress on Applied Mineralogy (ICAM), 175-200.

Kuhn, C. E. S., Pereira, G. G., Moreira, R. M., (2016) “Educação em Geociências, Desenvolvimento Sustentável e Mineração”, Revista Corixo de Extensão Universitária, 5 44-57.

Linhares, I. C., Silva, A. C., Silva, E. M. S., (2023) “Uso de mesa vibratória na recuperação de cassiterita do rejeito de espirais concentradoras”, Revista Foco, 16 (12) 1-11.

Lins, F. A. F., (2010), Chapter 7-Concentração gravítica, Tratamento de Minérios, 301-325.

Luz, A. B., França, S. C. A., Braga, P. F. A., (2018), Tratamento de Minérios, 6th ed. Rio de Janeiro: CETEM/MCTIC.

Peres, A. E. C., Chaves, A. P., Lins, F. A. F., Torem, M. L., (2002), Chapter 2-Beneficiamento de minérios de ouro, Extração de ouro: princípios, tecnologia e meio ambiente, 23-58.

Price, J. W., Smith, R., (1978), Handbook of Analytical Chemistry: Part III Tin, Vol. 4. Berlin: Springer-Verlag.

Sampaio, C. H., Tavares, L. M., (2005), Beneficiamento Gravimétrico: Uma Introdução Aos Processos De Concentração Mineral E Reciclagem De Materiais Por Densidade, Porto Alegre, Editora da UFRGS.

São José, F., Barcelos, H. O., Pereira, C.A., (2019) “Avaliação de variáveis operacionais da jigagem de minério de ferro por meio de planejamento estatístico”, HOLOS, 35 (3) 1-10.

Souza, F. A., Guedes, R. M., Ferreira, K. C., Barros, A. J., Alexandrino, J. S., (2018) “Estudo de caso - Estudos de processamento de rejeito de minério de ferro a partir de métodos de concentração densitária”, Revista Caribeña de Ciencias Sociales (RCCS), 9 46-66.

Taggart, A. F., (1945), Handbook of Mineral Dressing: Ores and Industrial Minerals”, 1st ed. New York: John Wiley & Sons.

Wills, B. A., Finch, J. A., (2016), Wills' Mineral Processing Technology: An Introduction to the Practical Aspects of Ore Treatment and Mineral Recovery”, 8th ed. Amsterdam: Elsevier.

Youssef, M. A., Abd El-Rahman, M. K., Helal, N. H., El-Rabiei, M. M., Elsaidy, S. R., (2009) “Optimization of shaking table and dry magnetic separation on recovery of egyptian placer cassiterite using experimental design technique”, The Journal of Ore Dressing, 11 (22) 1-10.

COMPARISON OF WET AND DRY MAGNETIC SEPARATION IN THE BENEFICIATION OF QUARTZ ORES

Arda ARAPOĞLU[1], Oğuzhan Mert GÜRKAN[1,*], Ali Kaan ACAR[2], Emre UĞURLAR[2], Hüseyin BAŞTÜRKCÜ[2]

[1]Istanbul Technical University, Faculty of Mines, Mineral Processing Engineering Department, 34469, Maslak, Istanbul, TÜRKİYE
[2]Mıknatıs Arge San. Tic. A. Ş., Kemalpaşa, İzmir, TÜRKİYE
**Corresponding author: gurkanog@itu.edu.tr*

A B S T R A C T

This study investigates the beneficiation of quartz ore from the Yatağan region of Muğla, Türkiye, through wet magnetic separation (electromagnetic filter) and dry magnetic separation (roll separator). Experiments were conducted on -600+100 µm, -600+300 µm, -300+100 µm, and -100 µm size fractions for wet magnetic separation, and on -600+0 µm, -600+100 µm, -600+300 µm, and -300+100 µm fractions for dry magnetic separation. Wet magnetic separation at 24,000 gauss achieved 84–91% Fe_2O_3 reduction with SiO_2 recoveries of 81–96%, with three of four fractions meeting the glass-grade Fe_2O_3 criterion (≤0.05%). Dry magnetic roll separation at approximately 11,000 gauss produced the best overall results, with all four tested fractions meeting glass-grade specifications: Fe_2O_3 values ranged from 0.026% to 0.036%, concentrate yields from 95% to 98%, and SiO_2 recoveries from 96% to 98%. The results establish dry magnetic separation as the most technically effective and environmentally sustainable method for glass-grade quartz production from this deposit, owing to its water-free and reagent-free operation.

Key words: Quartz beneficiation, dry magnetic separation, electromagnetic filter, SiO_2 purity, glass-grade

1. INTRODUCTION

Quartz is a silicate mineral composed of silicon dioxide (SiO_2), occurring geologically in forms such as quartz veins, quartzite, and sandstone (Bulatovic, 2015). In Türkiye, substantial reserves of quartz-bearing deposits are located primarily in the Istanbul (Şile, Çatalca), Tekirdağ, Zonguldak, and Sinop regions (Kurşun and İpekoğlu, 1995).

The conventional beneficiation of quartz predominantly utilizes physical separation methods due to their economic viability compared to chemical processes. A typical processing circuit involves comminution (crushing and grinding), washing, and size classification to remove physically adhered impurities, slimes, and soluble contaminants (Tosun et al., 2020). To achieve higher purity levels required by industries such as glass manufacturing, these initial steps are often followed by attrition scrubbing to remove surface coatings of clay and iron oxides, as well as magnetic separation and flotation to eliminate specific gangue minerals like feldspar, mica, and heavy minerals (Köse and Türeli, 1986).

Dry high-intensity magnetic separation provides an environmentally sustainable alternative to hazardous and costly chemical methods by eliminating the need for water and chemical reagents (Tosun et al., 2020). Dry magnetic separation has demonstrated significant efficacy in enhancing mineral quality by removing impurities without water consumption across various ore types. In quartz beneficiation, high-intensity dry magnetic separation (14,000 Gauss) reduced Fe_2O_3 and TiO_2 levels by approximately 18% in particle sizes below 500 µm (Tosun et al., 2020). Additionally, the application of three-stage dry rare-earth magnetic separation on

gneiss rock fines successfully rejected paramagnetic contaminants, yielding a feldspar-quartz concentrate with less than 0.3% Fe_2O_3 suitable for the glass industry (Moura et al., 2019).

2. MATERIAL AND METHODS

2.1. Material

The quartz sample used in this study was obtained from the Yatağan region of Muğla, Türkiye. The sample was initially crushed and ground to below 600 µm. Subsequently, the material was screened into the following size fractions: -600 µm +300 µm, -300 µm +100 µm, and -100 µm.

2.2. Method

Two beneficiation methods were evaluated for the removal of iron and titanium impurities from the quartz sample: wet magnetic separation using an electromagnetic filter, and dry magnetic separation using a roll-type separator. All experiments were conducted on the size fractions defined in Section 2.1. The experimental conditions for each method are described in the following subsections.

2.2.1. Wet magnetic

Wet magnetic separation experiments were performed using a full-scale Mıknatıs Ar-Ge electromagnetic filter operating at a magnetic field intensity of 24,000 gauss. A pulp containing 25% solids by weight was prepared using 2 kg of sample. After the magnetic field was activated, the pulp was manually mixed to ensure complete suspension and was then fed into the magnetic filter. As the pulp passed through the filter matrix, magnetic impurities were retained within the matrix. Upon completion of the separation, the magnetic field was switched off, and the matrix was removed and washed to collect the magnetic fraction. The procedure was repeated separately for each size fraction.

2.2.2. Dry magnetic

Dry magnetic separation was carried out using a Mıknatıs Ar-Ge 300 mm roll-type magnetic separator. The magnetic field strength was set to 13,000 gauss with a 9–2 magnet configuration. Due to the use of a 0.5 mm pvc belt, the surface magnetic field was measured as approximately 11,000 gauss. For each experiment, 2 kg of dry sample was processed. Dry magnetic separation tests were conducted on the -600 µm, -600 µm +300 µm, and -300 µm +100 µm size fractions.

3. RESULTS AND DISCUSSION

3.1. Wet Magnetic Separation (Electromagnetic Filter)

Wet magnetic separation at 24,000 gauss demonstrated significantly superior Fe_2O_3 removal across all four tested fractions. The -600+300 µm fraction yielded the best concentrate grade (Fe_2O_3 = 0.04%, 91.0% reduction) at an excellent concentrate yield of 95.11% and SiO_2 recovery of 95.55%, along with the highest SiO_2 concentrate grade of 99.79%. The -600+100 µm fraction achieved Fe_2O_3 = 0.04% (89.5% reduction) at 83.13% yield and 83.64% SiO_2 recovery. The -300+100 µm fraction showed the lowest yield (80.27%, SiO_2 recovery 80.81%) indicating greater entrainment losses in this size range.

The -100 µm fraction achieved 94.79% concentrate yield and 95.31% SiO_2 recovery, but the concentrate Fe_2O_3 of 0.07% narrowly exceeded the glass-grade limit. The consistently high

SiO_2 recoveries (80–96%) across all fractions confirm that the electromagnetic filter effectively retains the silica matrix while removing iron-bearing impurities. Al_2O_3 was substantially reduced in all fractions, confirming multi-impurity removal capability (Table 1, Figure 1).

Table 1. Wet magnetic separation (electromagnetic filter, 24,000 gauss) mass balance results: Al_2O_3, Fe_2O_3, TiO_2, Na_2O and SiO_2 content and distribution by size fraction

Product	W, %	Al_2O_3, %		Fe_2O_3, %		TiO_2, %		Na_2O, %		SiO_2, %	
		C	D	C	D	C	D	C	D	C	D
-600+100 µm											
Magnetic	16.87	1.05	71.7	2.22	91.3	0.05	64.7	0.06	27.0	96.05	16.4
Non-magnetic	83.13	0.08	28.4	0.04	8.7	0.01	35.3	0.03	73.0	99.69	83.6
Total	100	0.25	100	0.41	100	0.01	100	0.04	100	99.08	100
-600+300 µm											
Magnetic	4.89	0.73	39.9	7.67	91.4	0.16	41.0	0.07	7.7	90.55	4.5
Non-magnetic	95.11	0.06	60.1	0.04	8.6	0.01	59.0	0.04	92.3	99.78	95.5
Total	100	0.09	100	0.41	100	0.02	100	0.04	100	99.33	100
-300+100 µm											
Magnetic	19.73	1.15	66.9	1.88	90.2	0.05	51.1	0.09	37.0	96.33	19.2
Non-magnetic	80.27	0.14	33.1	0.05	9.8	0.01	48.9	0.04	63.0	99.69	80.8
Total	100	0.34	100	0.41	100	0.02	100	0.05	100	99.03	100
-100 µm											
Magnetic	5.21	2.78	39.8	6.67	84.7	0.19	58.7	0.04	3.2	89.11	4.7
Non-magnetic	94.79	0.23	60.2	0.07	15.3	0.01	41.3	0.06	96.8	99.43	95.3
Total	100	0.36	100	0.41	100	0.02	100	0.06	100	98.89	100

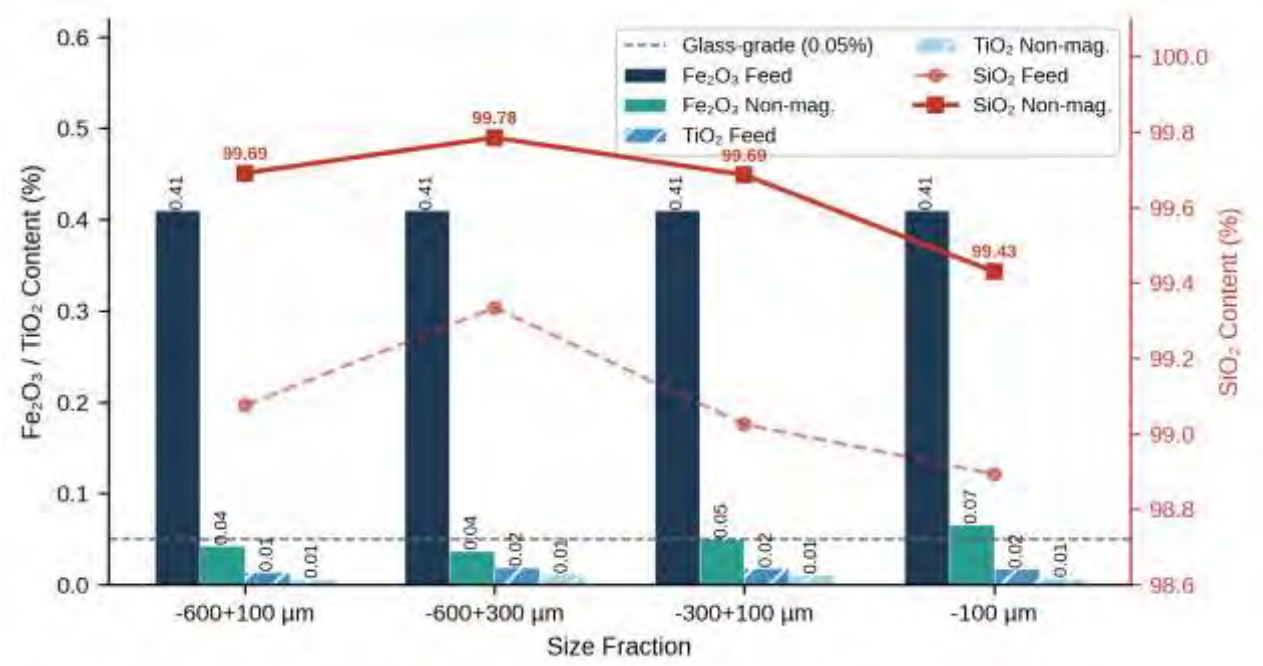

Figure 1. Wet magnetic separation results (electromagnetic filter, 24,000 gauss): Fe_2O_3 and TiO_2 content (bars, left axis) and SiO_2 content (line, right axis) in feed and non-magnetic product by size fraction. Dashed line: glass-grade threshold (0.05% Fe_2O_3)

3.2. Dry Magnetic Separation (Roll Separator)

Dry magnetic roll separation produced the best overall results of the study, achieving glass-grade Fe_2O_3 specifications in all four tested fractions while maintaining very high concentrate yields and SiO_2 recoveries. The -600+300 µm and -300+100 µm fractions achieved the lowest Fe_2O_3 values of 0.03% (93.2% reduction, yield 97.96%, SiO_2 recovery 98.45%) and 0.03% (93.7% reduction, yield 97.08%, SiO_2 recovery 97.84%), respectively. The -600+0 µm and -600+100 µm fractions both achieved 0.04% Fe_2O_3 at yields of 95.20% and 95.86% with SiO_2 recoveries of 95.84% and 96.58%.

SiO_2 concentrate grades consistently exceeded 99.63% across all fractions, with the highest grade of 99.79% obtained for the -600+300 µm fraction. The combination of very high concentrate yields (95–98%) with superior impurity removal demonstrates that the dry roll separator achieves selective separation with minimal silica losses. These results, achieved without water or chemical reagents, establish dry magnetic separation as the most technically effective and environmentally sustainable method for glass-grade quartz production from the Yatağan deposit (Table 2, Figure 2 and Figure 3).

Table 2. Dry magnetic separation (roll separator, ~11,000 gauss) mass balance results: Al_2O_3, Fe_2O_3, TiO_2, Na_2O and SiO_2 content and distribution by size fraction

Product	W, %	Al_2O_3, %		Fe_2O_3, %		TiO_2, %		Na_2O, %		SiO_2, %	
		C	D	C	D	C			C	D	C
-600+0 µm | Full Range											
Magnetic	4.80	3.93	83.9	7.83	91.6	0.21	31.2	0.05	6.5	85.69	4.2
Non-magnetic	95.20	0.04	16.1	0.04	8.4	0.02	68.8	0.04	93.5	99.64	95.8

Product	W, %	Al_2O_3, %		Fe_2O_3, %		TiO_2, %		Na_2O, %		SiO_2, %	
		C	D	C	D	C			C	D	C
Total	100	0.23	100	0.41	100	0.03	100	0.04	100	98.97	100
-600+100 µm											
Magnetic	4.14	4.75	73.8	9.06	91.6	0.31	40.8	0.03	2.6	81.58	3.4
Non-magnetic	95.86	0.07	26.2	0.04	8.4	0.02	59.2	0.05	97.4	99.63	96.6
Total	100	0.27	100	0.41	100	0.03	100	0.05	100	98.88	100
-600+300 µm											
Magnetic	2.04	2.48	71.0	18.78	93.3	0.44	55.3	0.02	0.7	75.53	1.6
Non-magnetic	97.96	0.02	29.0	0.03	6.7	0.01	44.7	0.07	99.3	99.66	98.5
Total	100	0.07	100	0.41	100	0.02	100	0.06	100	99.17	100
-300+100 µm											
Magnetic	2.92	8.86	98.2	13.19	93.8	0.40	29.8	0.16	6.5	73.14	2.2
Non-magnetic	97.08	0.01	1.8	0.03	6.2	0.03	70.2	0.07	93.5	99.68	97.8
Total	100	0.26	100	0.41	100	0.04	100	0.07	100	98.91	100

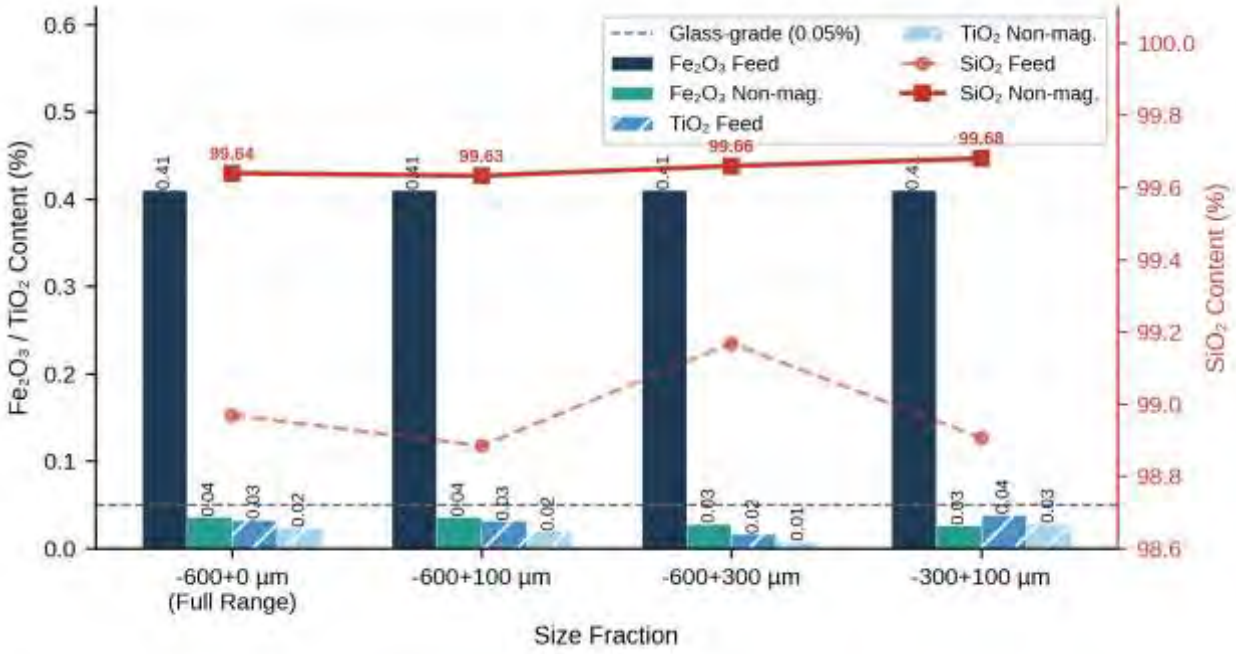

Figure 2. Dry magnetic separation results (roll separator, ~11,000 gauss): Fe_2O_3 and TiO_2 content (bars, left axis) and SiO_2 content (line, right axis) in feed and non-magnetic product by size fraction. Dashed line: glass-grade threshold (0.05% Fe_2O_3)

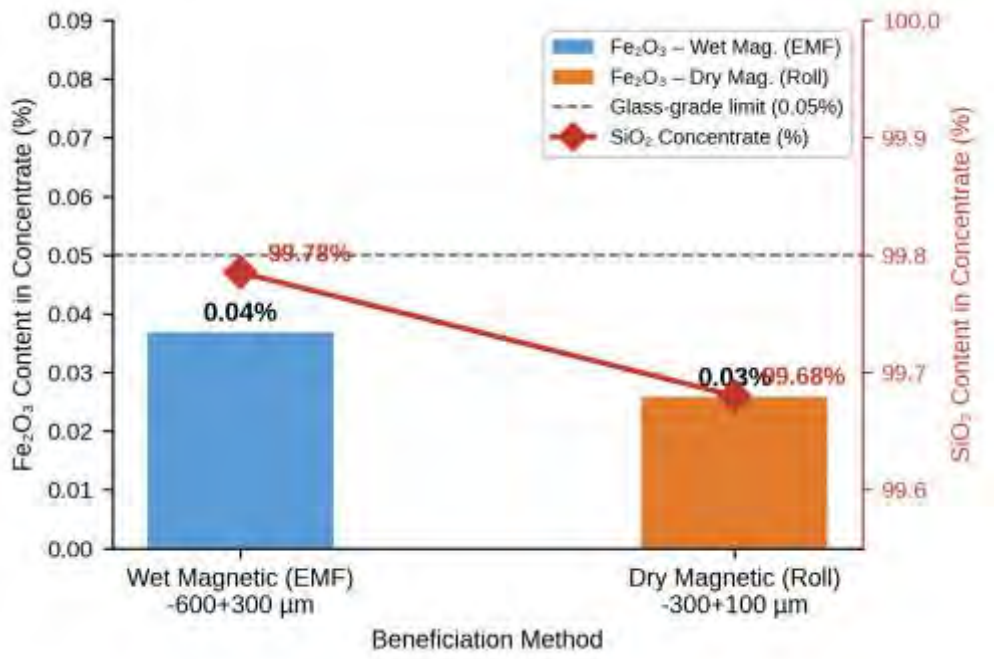

Figure 3. Comparison of Fe_2O_3 concentrate content (bars, left axis) and SiO_2 concentrate content (line, right axis) achieved by the best result of each beneficiation method. Dashed line: glass-grade threshold (0.05% Fe_2O_3)

4. CONCLUSION

This study evaluated wet magnetic separation (electromagnetic filter) and dry magnetic separation (roll separator) for the beneficiation of quartz ore from the Yatağan region of Muğla, Türkiye, targeting glass-grade purity (≤0.05% Fe_2O_3, ≥99.4% SiO_2). The following conclusions can be drawn:

Wet magnetic separation at 24,000 gauss achieved 84–91% Fe_2O_3 reduction with concentrate yields of 80–95% and SiO_2 recoveries of 81–96%. Three of four tested fractions met the glass-grade Fe_2O_3 criterion, with the -600+300 µm fraction delivering the best overall performance (Fe_2O_3 = 0.04%, yield 95.11%, SiO_2 = 99.79%). The -100 µm fraction narrowly missed the threshold, indicating the limit of wet magnetic separation for ultrafine fractions.

Dry magnetic separation (roll separator, ~11,000 gauss) produced the best results of the study: all four fractions met the glass-grade threshold with yields of 95–98% and SiO_2 recoveries of 96–98%. The lowest Fe_2O_3 of 0.03% was obtained for the -300+100 µm fraction (yield 97.08%, SiO_2 recovery 97.84%, SiO_2 grade 99.68%), with near-complete Al_2O_3 removal (0.26%→0.01%). The high yields combined with superior purification confirm that the dry roll separator achieves selective separation with minimal silica losses, and its water-free, reagent-free operation renders it the optimal method for glass-grade quartz production from the Yatağan deposit.

REFERENCES

Bouabdallah, S., Bounouala, M., Chaib, A. S., (2015) “Removal of iron from sandstone by magnetic separation and leaching: Case of El-Aouana deposit (Algeria)”, Mining Science, 22, 33–44.

Bulatovic, S. M., (2015) “Handbook of flotation reagents: Chemistry, theory and practice – Flotation of industrial minerals”, Elsevier.

Köse, M., Türeli, T. K., (1986) “Cam üretiminde kullanılan kuvars kumlarında aranan özellikler – zenginleştirme yöntemleri ve Yozgat Sarıkaya kuvarsitlerinin bu açıdan incelenmesi”, Madencilik, 25 (4) 21–28.

Kurşun, İ., İpekoğlu, B., (1995) “Türkiye kuvars kumu potansiyeline genel bir bakış”, Endüstriyel Hammaddeler Sempozyumu, 169–176.

Moura, L. C., André, F. P., Miceli, H., Neumann, R., Tavares, L. M., (2019) “Manufactured feldspar-quartz sand for glass industry from gneiss quarry rock fines using dry rare-earth magnetic separation”, Mineral Processing and Extractive Metallurgy Review, 40 (5) 333–343.

Shibaeva, D. N., Kompanchenko, A. A., Tereschenko, S. V., (2021) “Analysis of the effect of dry magnetic separation on the process of ferruginous quartzites disintegration”, Minerals, 11 (8) 797.

Tosun, Y. C., Tuncuk, A., Okudan, M. D., Akcil, A., (2020) “Fiziksel zenginleştirme ve hidrometalurjik yöntemlerle kuvars cevherinden demir uzaklaştırma”, Dokuz Eylül Üniversitesi Mühendislik Fakültesi Fen ve Mühendislik Dergisi, 22 (64) 187–197.

DESCRIPTION AND ANALYSIS OF THE TECHNOLOGICAL PROCESS OF THE KALIMASH IMI CHROMIUM ENRICHMENT PLANT

Ferhat AKINOGLU[1,*], Genc DEMI[2]

[1]IMI Company shpk, KALIMASH-KUKES-ALBANIA
[2]Polytechnic University of Tirana, Faculty of Geology and Mines, Mine Deposit Engineering Department, Rruga e Elbasanit, Tirana-ALBANIA
**Corresponding author: ferhatakinoglu@imi.al*

A B S T R A C T

Kalimashi chromium enrichment plant that belongs to IMI Company is the largest in Albania, in terms of the annual processing capacity of the raw material, chromium ore with content of 7 – 8% Cr_2O_3 and in terms of the quantity of chromium concentrate produced. This paper describes the technological process and provides the technological figures achieved for the enrichment of chromium ores with low content of Cr_2O_3. The value of the technological figures depends, among other things, on the raw material that feeds the plant, which is of several types mainly in terms of the olivine content in the raw material, chromium ore. Good technological figures are also achieved in the recirculation of the used water, 96% of which is recycled. The system and machinery equipment for the dewatering of enrichment products are also described. From the enrichment of chromium ores in this plant, concentrates with a quality of 50 - 51 % Cr_2O_3 and recovery of Cr_2O_3 in concentrate 66 - 68 % are obtained. From the analysis performed, conclusions and recommendations are given for the improvement of technological-economic figures.

Key words: *Chromium, recovery, concentrate, tailings, flowsheet*

1. INTRODUCTION

Kalimashi chromium enrichment plant is operating with technological figures, average grade of concentrate is in band 50%-52% Cr_2O_3 and average Cr_2O_3 recovery is in the band 66%-68% with a raw material chromium ore from open sky exploitation with Cr_2O_3 content 7%-8%. The average ratio Cr : Fe in the chromium concentrate is around 2.6 – 2.8.

The raw material capacity is about 1050 ton per 24 hours, or about 43.75 ton per hour with average moisture 3 % H2O. To produce one ton chromium concentrate (converted in dry) with Cr_2O_3 content 51 % there are enriched 10.15 ton chromium ore (converted in dry) with 7.5% Cr_2O_3 content. The average moisture in chromium concentrate is 5 % H_2O.

The plant is operating 10 months per year, processing about 300,000 ton raw material, chromium ore supplied mainly from open sky mine with 7%-8% Cr_2O_3 and producing about 30,200 ton chromium concentrate per year with Cr_2O_3 content average 51 % and moisture 5 % H_2O. Average recovery is 67.5 %.

There are two kinds of chromium ores exploited in open sky, those richer with serpentine and those richer with olivine, where the olivine is partially serpentinized. The main quantity coming from open sky exploitation is the kind richer in serpentine. The above technological figures belong to both types.

The process of concentrate and tailings dewatering is going well making possible separation of 96 % of water quantity and recycling in the process. It is necessary to use flocculants in thickening process of fine tailings. There are used Lamella thickener, dewatering tables, screens and filter presses in this process.

After dewatering the tailings are transported by trucks to tailings place 0.7 km far from the plant where are deposited.

The factory's operational readiness is very high, working continuously 24 hours per day and stopping mainly for power outages or mechanical defects on average only 1 day per month or less. All the plant's machines and spare parts are manufactured by the company "Merta Makina".

2. MATERIAL AND METHODS

2.1. Material

The representative samples of raw material and products are taken continuously during plant operation and they are analyzed every shift, every day. These samples were used to analyze the balance of technological process for a long time. The particle size distribution and Cr_2O_3 content in different particle size fractions of enrichment products were analyzed in the samples taken in some links of process(Demi, 2022).

The principal schemes of grinding, enrichment, dewatering and water recycling are given in the Figures below.

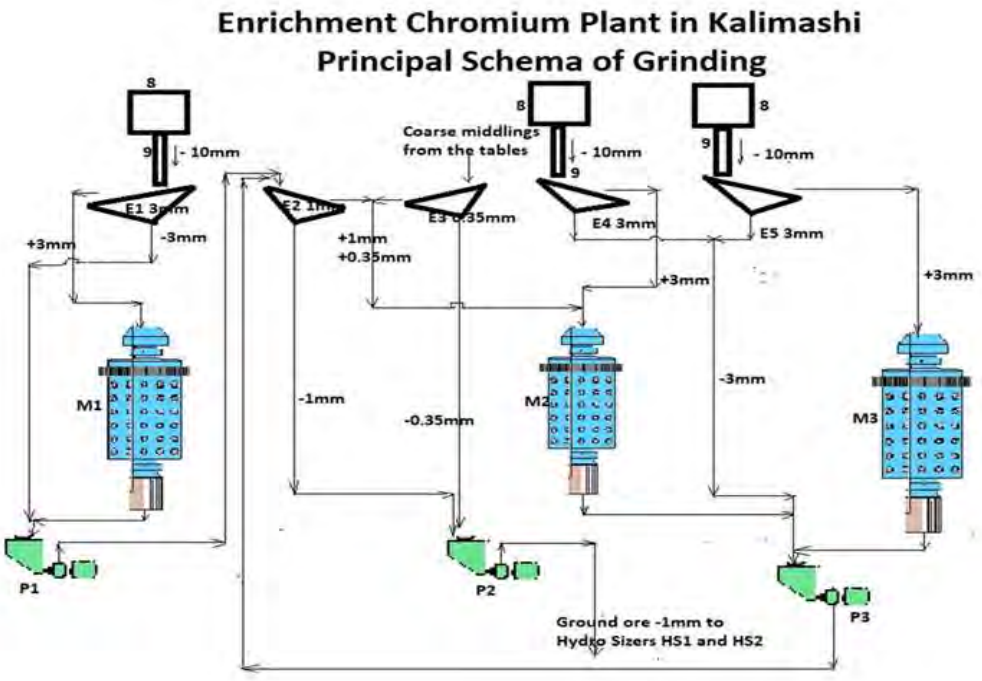

Figure 1. Principal scheme of grinding

The under screen fractions of the screens E2 and E3, go by pumps P2, in hydro sizers which feed shaking tables in three steps final concentrate, final tailings and middlings. The middlings of fine fractions plus 0.3 mm are treated in 3 steps of tables while the middlings of coarse fractions over 0.3 mm are pumped to the regrinding and further treatment in the same tables. All the tailings and overflows of all hydrosizers go to the waste thickener, overflow of which is pumped to 4 sedimentation tanks with volume 400 m3 each one where it is used and flocculants to improve sedimentation of the fine tailings. The overflow of 4 tanks is clean water and it is pumped to two clean water tanks with volume 800 m3 each one, in total 1,600 m3 clean water. Also in these two tanks is pumped fresh water from the gallery underground with

a pump, in quantity 25 m3/h, operating 10-14 hours every day. The slimes under the 4 tanks go to the three filter presses, each one with capacity 40 ton/h, which dewater solid to 4-6 % H2O content, making so this waste product with particle size minus 0.3 mm, a transportable product. The capacity of filter presses is bigger than the quantity of fine waste. This waste is loading by loaders and it is transported by trucks to the tailings deposit situated about 0.7 km far from the plant in a proper place for waste deposit with enough space to function several years. The underflow of waste thickener go to the three vibrating screens, which separate waste with particle size less than 0.3 mm. The product – 0.3 mm is pumped to a hydrocyclone D=350mm. The overflow of the hydrocyclone is going by selfgravity to the slime shaking tables, where it is separated fine concentrate and fine tailings, which go to the respective ways, as it was described above. The underflow of hydrocyclone goes to a hydrosizer, which is feeding the shaking tables that separate final concentrate and final tailings. The product over the 3 screens is coarse waste -1mm+0.3mm and it is transported to the place of the waste by a belt conveyer, from where it is loaded by loader and transported by trucks to the waste deposit, 0.7 km far from the plant.

All the concentrates go to a lamella thickener overflow of which go to the line of recirculating water, while underflow product is dewatered by two dewatering tables with power. Dewatered concentrate with average moisture about 5 % H2O is transported by a belt conveyer, and afterward loaded by loader and transported by trucks to the concentrate deposit with capacity 10,000 ton. The water coming from dewatering concentrate process is going to the line of recycled water.

2.2. Method

The balances of the chromium enrichment process of the plant are carried out continuously for each work shift. The results of these balances were used to derive the technological indicators of the plant for the period May - September 2022.

The enrichment indicators were extracted from separate balances for ores richer in serpentine and separately for ores richer in olivine.

In order to investigate the enrichment of different granular fractions after grinding, samples were taken in several enrichment links, which were analyzed for Cr_2O_3 content and granular composition, calculating the recovery of Cr_2O_3 in different granulometric fractions. On this basis, it was found which granular class is recovered with the best quality and recovery of concentrate.

It was concluded that grinding should be done by adjusting the parameters, in order to form as many granular fractions as possible, which are enriched with the best indicators. (Demi, 2022)

3. RESULTS AND DISCUSSION

Particle size distribution and Cr2O3 content in products of Kalimashi enrichment plant are given in the tables 1, 2 and 3. (Demi, 2022)

The Cr_2O_3 content of raw material sample resulted 7.77 % Cr2O3, while the quantity of fraction -0.10 mm generated in grinding process is less than 40 %.

Also it is visible from the tables that fraction -0.25 mm + 0.10 mm is the best fraction for enrichment. It shows that the aim in grinding should be to generate this fraction as much as possible, keeping the generated quantity of fraction -0.1mm in grinding in the values as less

as possible. The losses in fraction -0.1mm are higher, for this fraction is more difficult for enrichment with equipment that are applied in this plant.

Based in the data of the plant for a long period of time, the ratio of the quantity of coarse tailings with fine tailings is 40% with 60%. It was calculated Cr2O3 content of total tailings 2.85 % Cr_2O_3.

Table 1. Coarse tailings

Particle size, mm	Weight, %	Cr_2O_3 content, %	Cr_2O_3 distribution, %
+0.80	1.09	5.03	1.38
-0.80 +0.50	28.26	4.01	31.22
-0.50 +0.25	38.58	3.76	40.06
-0.25 +0.10	28.80	2.55	20.16
-0.10	3.27	8.02	7.18
Coarse Tailings	100.00	3.62	100.00

Table 2. Fine tailings

Particle size, mm	Weight, %	Cr_2O_3 content, %	Cr_2O_3 distribution, %
+0.25	1.68	4.85	3.60
-0.25 +0.10	31.23	0.89	11.93
-0.10	67.09	2.93	84.47
Fine Tailings	100.00	2.33	100.00

Table 3. Chromium concentrate

Particle size, mm	Weight, %	Cr_2O_3 content, %	Cr_2O_3 distribution, %
-0.80 +0.50	1.90	45.45	1.60
-0.50 +0.25	15.10	54.76	15.38
-0.25 +0.10	57.20	54.03	57.51
-0.10	25.80	53.14	25.51
Chromium Concentrate	100.00	53.75	100.00

The technological figures based in the samples taken are given in the table 4.

Table 4. Technological figures of chromium plant

Products Nomination	Weight, %	Cr_2O_3 content, %	Cr_2O_3 Recovery, %
Chromium Concentrate	9.67	53.75	66.89
Total Tailings	90.33	2.85	33.11
Raw Material	100.00	7.77	100.00

The Cr_2O_3 content in the raw material in value 7.77 % is low and it influences in the value of the Cr_2O_3 recovery. Another reason of Cr_2O_3 recovery value is and high Cr_2O_3 content of the chromium concentrate.

The analyses results of another sampling taken in the same day in the plant are shown in the table 5.

Table 5. The balance with a second sampling taken on the plant in the same day

Products Nomination	Weight, %	Cr_2O_3 content, %	Cr_2O_3 Recovery, %
Chromium Concentra.	8.90	52.76	65.95
Total Tailings	91.10	2.66	34.05
Raw Material	100.00	7.12	100.00

The results of two samplings in same times during plant operation are almost the same that certifies that accurately of sampling and analyses is acceptable.

The technological figures of the plant for period of time May – September 2022 are given in the Table 6. (Akinoglu, 2022)

Table 6. Technological figures of the plant for period of time May – September 2022

Month	Raw Material		Chromium Concentrate		% Cr_2O_3 Tailings	% Cr_2O_3 Recover
	Ton	% Cr_2O_3	Ton	% Cr_2O_3		
May	30,765	7.88	3,265	51.19	2.74	67.61
June	30,133	7.50	3,113	50.39	2.56	67.93
July	29,065	7.37	2,784	51.22	2.84	65.00
August	36,000	6.77	3,174	51.55	2.54	65.71
September	29,625	7.44	3,010	50.30	2.70	67.26
May-September	155,588	7.37	15,346	50.93	2.71	66.76

Results for a long period of time show that grade of chromium concentrate is in the band 50% – 52 % Cr_2O_3 and average Cr_2O_3 recovery is 66.76 %, when the Cr_2O_3 content in raw material is 7.37%. During this period of time is operated and with the two types of chromium ores with richer in serpentine and with richer in olivine as gangue mineral, exploited in open sky.

During period of time May-September 2022 the technological figures only for the days when the plant has operated with chromium ores that are richer in olivine, the grade of concentrate is lower, between 48 % and 50 %, while the average recovery is the same between 66% and 68 %. (Akinoglu, 2022)

Big reserves of chromium ore richer with fresh olivine are underground in Kalimashi deposit. From the studies and from experience in industrial scale has resulted that with gravity methods can be obtained chromium concentrates with Cr_2O_3 content not more than 40 % from enrichment of these kind of ores. Concentrates with more than 50 % Cr_2O_3 content can be obtained only with combined schemes using gravimetric – magnetic separation methods. (Turan, 2012)

From the studies carried out previously it has been shown that both types of chromium ores of this source, those richer in olivine and those richer in serpentine, as well as those exploited on the surface and those exploited underground, contain considerable amounts of free gangue minerals in the granular fractions below 20 mm.(Reminex, 1996) This result is also supported by the technological indicators of the other chromium enrichment plant in this area, which after crushing chromium ores below 25 mm, removes about half of the amount of raw material with HMS with a content below 2 % Cr_2O_3. (Dittrich, 2019) This indicates the need to study the raw material that supplies the plant with densimetric analyses in heavy media in the laboratory and most likely also the application of HMS on industrial scale, significantly reducing the cost of enrichment.

4. CONCLUSION

In Kalimashi chromium enrichment plant the band of concentrate grade is 50%-52% Cr_2O_3 and average Cr_2O_3 recovery is in the band 66%-68% with a raw material chromium ore with Cr_2O_3 content 7%-8%. The main quantity coming from open sky exploitation is the kind of chromium ore richer with serpentine. Sometimes the plant is supplied with chromium ore richer with olivine, which is more difficult to be concentrated. The technological figures in the case are that only the band of concentrate is lower 48%-50% Cr_2O_3 but average Cr_2O_3 recovery is the same 66%-68%. The process of concentrate and tailings dewatering is going well making possible

separation of 96 % of water quantity and recycling in the process. It is recommended an enrichment study in laboratory with representative sample of underground chromium ore that contain fresh olivine with combined gravimetric-magnetic scheme. Also, it is recommended a study in laboratory with representative sample of actual plant raw material to investigate for the application possibility of preconcentration.

REFERENCES

Akinoglu, F., (2022) “Technological balances of Kalimashi IMI chromium enrichment plant during 2022 year)”, Archive of IMI company, Kaliamshi, Kukes, Albania.

Demi, G., (2022), “Report for technical due diligence of chromium enrichment plant in Kalimashi, Albania”. Archive of IMI company, Kaliamshi, Kukes, Albania.

Dittrich, V., Demi, G., Koci, B. (2019) “Application of HMS in Albanian Chromium Ore enrichment”, IMPC - EUROASIA Proceeding Book, 200-206.

REMINEX.Company, (1996) “Feasibility Study and Preliminary Design for Kukes Chromium Complex”, Company Archieve in Casablanca, Maroc, Appendix N^{o} 3, (45-87)

Turan, M., Demi, G., (2012)), “Mineral Processing of Tropoja Kukesi massifs chromium ores”, XIII International Mineral Processing Symposium Proceedings, 205-210).

DRY BENEFICIATION OF MINERAL ORES USING TRIBO-ELECTROSTATIC BELT SEPARATION

Abhishekn GUPTA, Tom NEWMAN, Frank HRACH

ST Equipment & Technology LLC, 101 Hampton Ave, Needham, MA 02494, USA
**Corresponding author: agupta@titanamerica.com*

A B S T R A C T

ST Equipment & Technology (STET) has engineered an innovative, entirely dry tribo-electrostatic belt separation system for mineral beneficiation. This technology has achieved commercial scale across various sectors, successfully separating unburnt carbon from fly ash and separating silicates from calcite and barite. By eliminating the need for water and chemical additives, STET's system provides a sustainable alternative to traditional mineral processing. This paper details pilot-scale successes in upgrading air-classified iron ore and ultrafine iron ore tailings, which are typically discarded. Furthermore, bench-scale evaluations of phosphate ores from different geographical regions are presented to demonstrate the technology's versatility.

***Key words**: Dry separation, minerals beneficiation, electrostatic separation, iron ore, phosphate*

1. INTRODUCTION

1.1. Limitation of Conventional Mineral Beneficiation Techniques

The depletion of high-grade mineral deposits globally has forced the industry to process lower-grade ores, a necessity for sustaining critical supply chains like the steel industry (Lu & Ishiyama, 2015). Traditional beneficiation relies heavily on wet processes:

- Magnetic Separation: Wet magnetic separators are standard for iron ores, but their efficiency drops significantly for fine particles (under 20 microns) where fluid drag overcomes magnetic attraction (Svoboda, 2004; Tripathy et al., 2013).
- Froth Flotation: Widely used for both iron and phosphate ores, flotation is highly water-dependent and requires rigorous de-sliming to manage fine particles (Ma, 2012).

Ultimately, both methods struggle with ultrafines, resulting in the rejection of valuable minerals as wet tailings. The disposal of these wet tailings poses severe environmental risks, alongside the massive water consumption required to operate the plants (Edraki et al., 2014).

1.2. Dry Beneficiation

To mitigate these water usage and tailings issues, the industry is increasingly investigating dry beneficiation techniques, such as electrostatic separation. While traditional vertical free-fall and roll-type separators are effective at separating conductive, insulating, and semi-conductive particles, they are generally restricted to processing coarser particles greater than 100 µm (Gasiorowski et al., 2015). Expanding dry separation capabilities to handle finer particle distributions across diverse mineral groups is a vital step forward in sustainable mining, especially as environmental regulations regarding wet tailings become more stringent.

STET TRIBO-ELECTROSTATIC SEPARATOR

The STET tribo-electrostatic belt separator (figure 1) represents a notable advancement in dry processing, capable of effectively processing finer particles.
The system utilizes triboelectric charging, where interparticle collisions cause materials with differing electron affinities to acquire opposite positive and negative charges. These charged particles fall into a narrow gap (0.9–1.5 cm) between two parallel planar electrodes (figure 2), operating at up to +/- 10 kV. A high-speed, continuous-loop, open-mesh belt continuously sweeps the oppositely charged particles toward respective ends of the separator.

The commercial-scale unit is compact (measuring 9.1 m long, 1.7 m wide, and 3.2 m high), processes up to 40 tons per hour, and consumes approximately 1 kWh of electricity per ton.

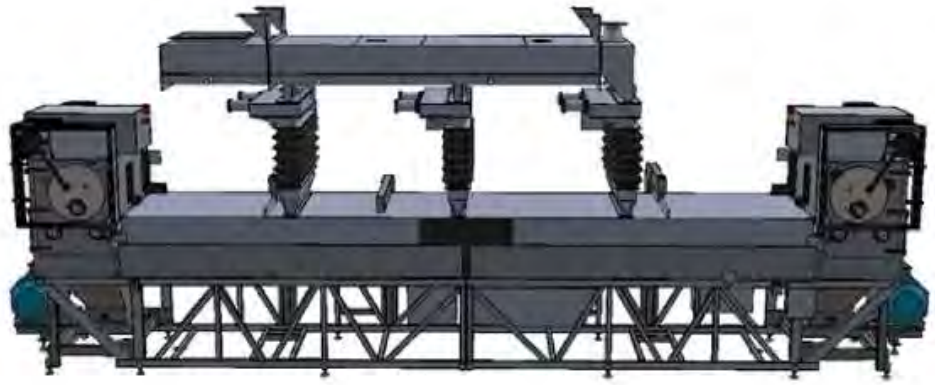

Figure 1. Model of STET separator

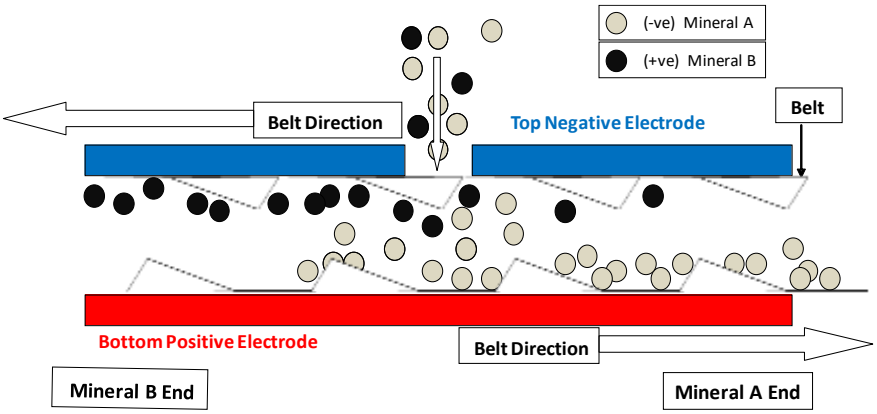

Figure 2. Schematic of separation zone within the electrodes

2. MATERIALS AND METHODS

2.1.Iron ore

Two Brazilian iron ore samples were evaluated using a pilot-scale STET separator.

- Ultrafine sample: This sample was the reject stream from a magnetic separation process, as the fines pose challenges in efficiency of magnetic separation.
- Air-classified sample: This sample was collected from an air-classification step as fines.

The elemental composition and mineralogy were analyzed using wavelength dispersive X-ray Fluorescence (WD-XRF) and XRD (X-ray diffraction) techniques respectively. Particle size distributions (PSD) were determined using a laser diffraction particle size analyzer - Malvern Mastersizer 3000 E.

The mineralogy of the samples is provided in table 1. Hematite is the primary iron-bearing mineral in both samples, quartz and kaolinite being the primary gangue minerals. The elemental composition of the samples is shown in table 2. Particle size distribution and moisture content of the samples is shown in table 3. Samples were dried at 90 C prior to testing in the separator.

Table 1. Mineralogy of iron ore samples

Sample	Hematite	Goethite	Quartz	Kaolinite
Ultrafines	50.8%	17.9%	12.5%	18.5%
Air-classified	50.6%	3.4%	40.9%	3.5%

Table 2. Elemental composition (major elements) for iron ore samples

Sample	Al_2O_3	Fe_2O_3	Fe*	SiO_2	LOI
Ultrafines	7.7	66.0	46.2	20.8	4.3
Air-classified	2.2	59.7	41.8	*36.6*	1.0

*Calculated using stoichiometric relationship between Fe_2O_3 and Fe

Table 3. Particle size distribution for iron ore samples

Sample	Particle size distribution			
	D_{10}	D_{50}	D_{90}	D_{98}
Ultrafines	1 µm	4 µm	11 µm	16 µm
Air-classified	7 µm	32 µm	105 µm	215 µm

2.2. Phosphate Ore

Seven samples of phosphate ore, labeled P1 to P7, were collected from different geographical locations and tested on a bench-scale STET separator. Most of the samples analyzed consisted predominantly of apatite, carbonates, and silicates (table 4). The elemental composition of the samples is shown in table 5.

Table 4. Mineralogy of phosphate ore samples

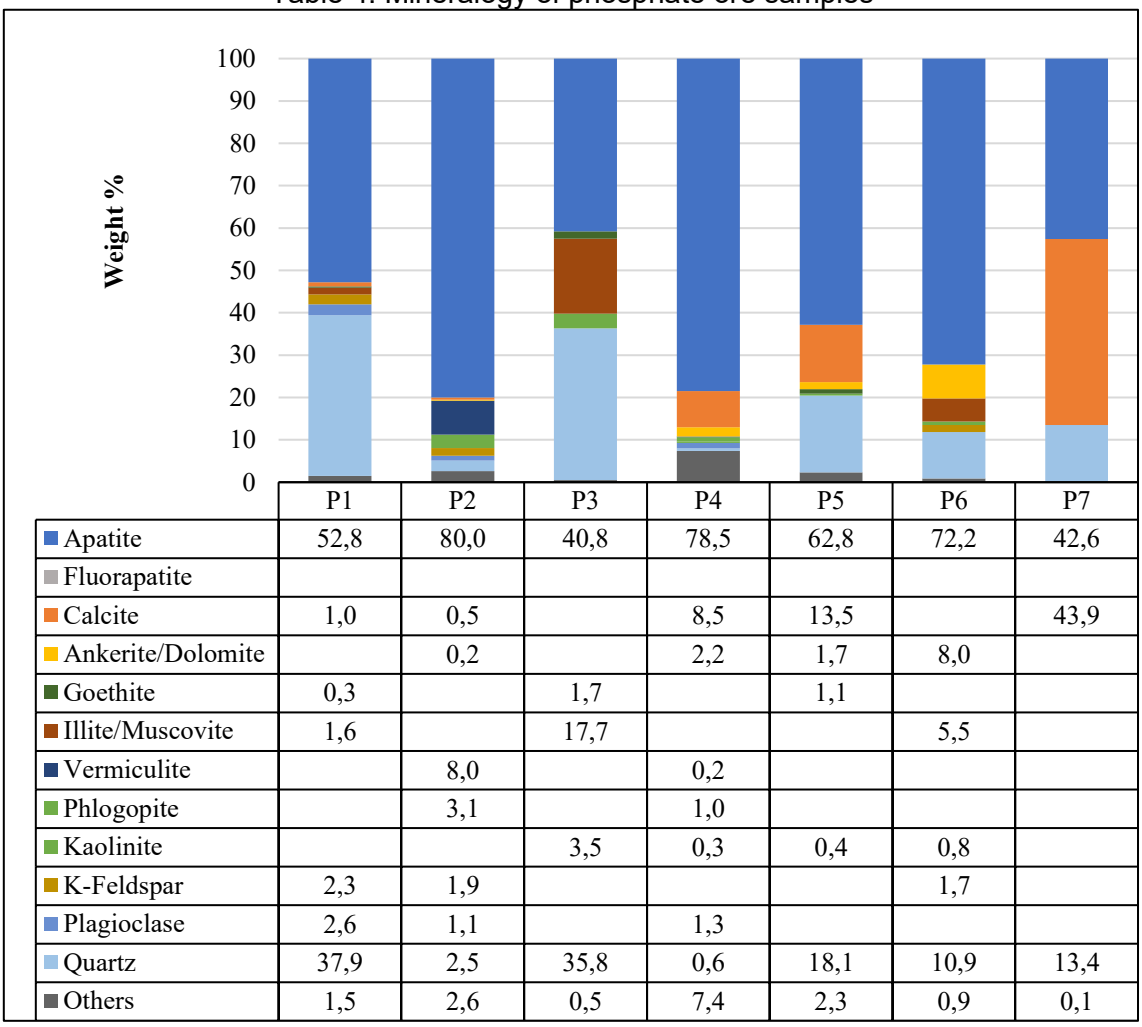

	P1	P2	P3	P4	P5	P6	P7
Apatite	52,8	80,0	40,8	78,5	62,8	72,2	42,6
Fluorapatite							
Calcite	1,0	0,5		8,5	13,5		43,9
Ankerite/Dolomite		0,2		2,2	1,7	8,0	
Goethite	0,3		1,7		1,1		
Illite/Muscovite	1,6		17,7			5,5	
Vermiculite		8,0		0,2			
Phlogopite		3,1		1,0			
Kaolinite			3,5	0,3	0,4	0,8	
K-Feldspar	2,3	1,9				1,7	
Plagioclase	2,6	1,1		1,3			
Quartz	37,9	2,5	35,8	0,6	18,1	10,9	13,4
Others	1,5	2,6	0,5	7,4	2,3	0,9	0,1

Table 5. Elemental composition of phosphate ore samples

Oxide	P1	P2	P3	P4	P5	P6	P7
P_2O_5	19.1	28.7	15.2	30.3	22.8	26.7	15.9
SiO_2	33.5	13.8	42.3	6.1	15.3	15.7	11.4
CaO	31.4	38.2	20.4	46.9	41.8	39.2	48.9
Al_2O_3	2.4	4.0	8.0	1.4	0.8	4.0	0.1
Fe_2O_3	2.0	3.7	5.0	2.3	1.8	1.7	0.1
MgO	0.1	4.7	0.8	3.3	0.4	1.7	0.1
K_2O	0.2	0.9	1.7	0.2	0.1	1.2	0.0
Na_2O	1.0	0.3	0.0	0.5	0.4	0.3	0.2
Others	3.5	3.2	2.8	2.9	16.6	9.7	23.3
LOI	6.8	2.5	3.8	6.1	11.5	5.5	21.7

2.3.Separation Testing

Testing focused on maximizing grade recovery while minimizing gangue minerals. Phosphate ore underwent bench-scale screening to validate tribo-electrostatic charging potential for

electrostatic beneficiation. For iron ore, pilot-scale trials were conducted to optimize separator variables (listed in table 6) and evaluate performance at industrial feed rates. These studies specifically measured how varying separator variables influenced mass yields and product quality.

Table 6. Separator variables

Variables	Levels		
Belt speed (m/s)	5	20	
Electrode gap (mm)	10	13	
Electrode voltage (kV)	6	10	
Feed port	1	2	3
Top electrode polarity	Positive	Negative	

Separation tests were conducted under batch conditions. For each run, a representative 'Feed' sub-sample was collected before introducing the material into the separator via a vibratory or screw feeder. Post-experiment, the weights of the resulting streams—Product E1 (gangue-rich) and Product E2 (mineral-rich)—were recorded. The elemental composition of the Feed and both product streams was determined using X-ray fluorescence (XRF), while X-ray diffraction (XRD) was employed on select samples to characterize the mineralogy.

3.RESULTS

3.1.Upgrading Iron Ore

The separator variable settings were chosen targeting different feed grades and their respective product mass yields, demonstrating the ability of this technology to target a wide range of product grades.

3.1.1.Air-classified iron ore

The feed grade was approximately 42% Fe content. Three processing schemes were developed targeting a range of product grades.

Figure 3 illustrates the results obtained using separator settings optimized for producing a high-grade product. This scheme involves a rougher stage followed by a cleaner stage, yielding a high-grade product with approximately 62% Fe content. The cleaner by-product is recycled and blended with the fresh feed. The feed rates presented in the figure are scaled for a commercial-size STET separator. This scheme achieved an overall mass yield of 61% and an Fe recovery of 90%.

Figure 4 illustrates the results for producing a mid-grade product. This scheme involves only a rougher stage yielding a mid-grade product with approximately 57% Fe content. Additionally, a scavenger run was performed, with its product blended with the rougher stage output. This scheme achieved an overall mass yield of 67% and an Fe recovery of 91%.

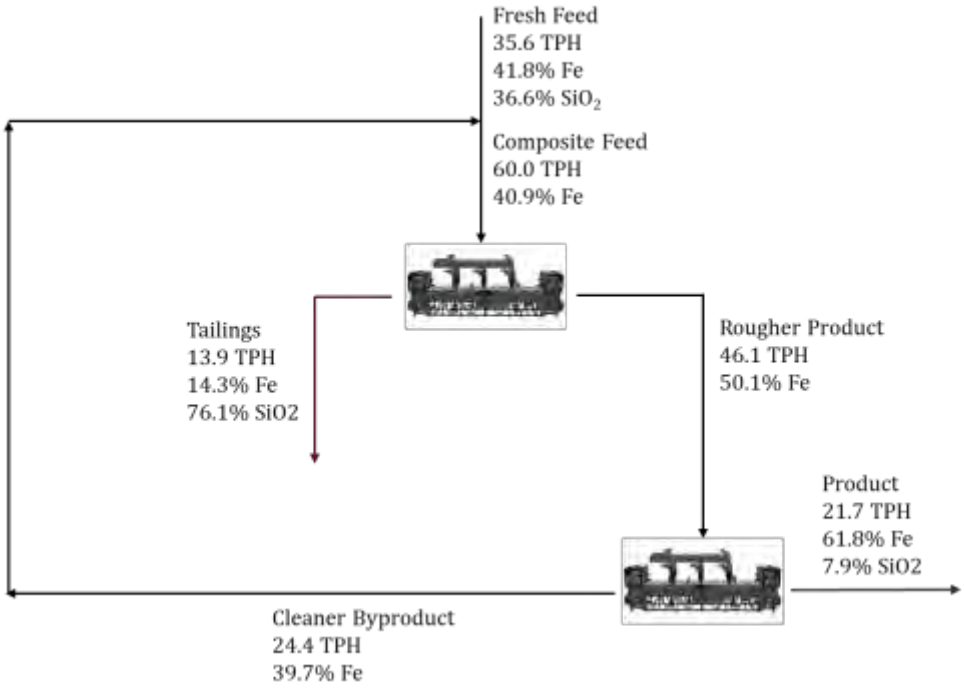

Figure 3. Air-classified iron ore: High-grade product using rougher and cleaner

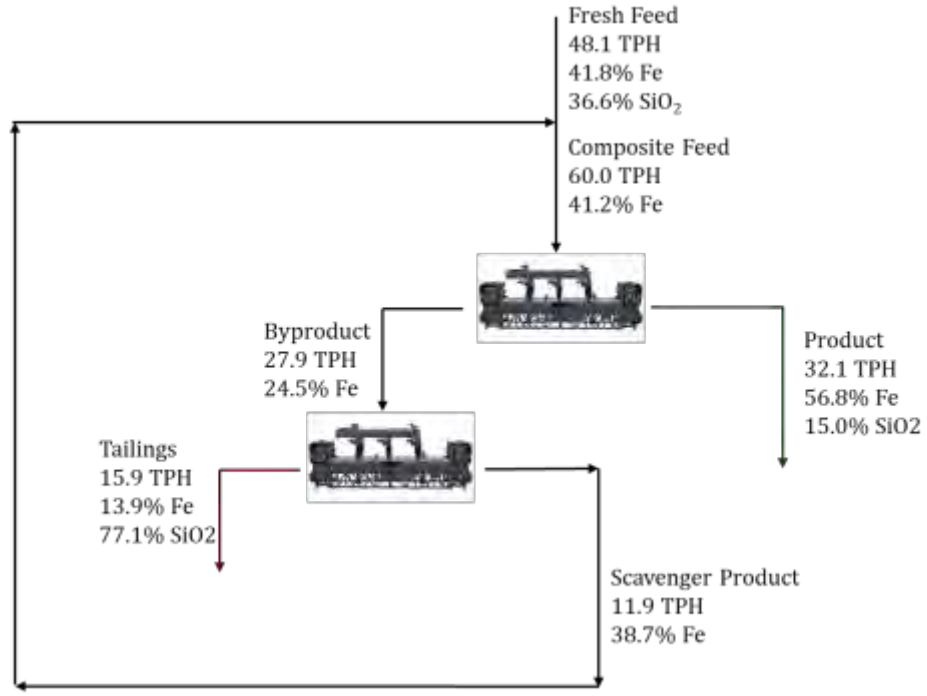

Figure 4. Air-classified iron ore: Mid-grade product using rougher and scavenger

Figure 5 illustrates the results for producing a high-grade product at the rougher stage and then a scavenger stage was used to increase overall recovery.

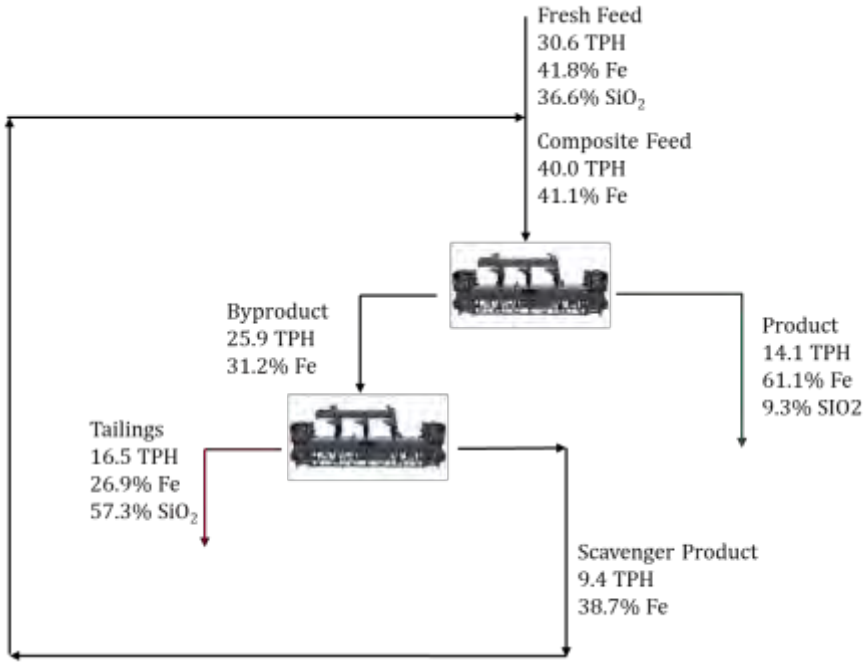

Figure 5. Air-classified iron ore: High-grade product using rougher and scavenger

Table 7 summarizes the findings from air-classified iron ore testing, presenting the range of product grades achieved along with their corresponding mass yields and Fe recoveries.

Table 7. Summary of results from air-classified iron ore

Scheme	Product mass yield	Fe recovery	Product Fe content
High grade product (using rougher + cleaner)	60.9%	90.1%	61.8%
Mid grade product	66.8%	90.8%	56.8%
High grade product (using rougher)	46.1%	67.5%	61.1%

3.1.2.Ultrafine iron ore

The feed grade contains approximately 46% Fe. Figure 6 illustrates the results obtained using separator settings optimized for producing a high-grade product. This scheme involves a rougher stage followed by a cleaner stage, yielding a high-grade product with approximately 59% Fe content. Additionally, a scavenger run was performed, with its product blended with the rougher stage output. The cleaner by-product is recycled and blended with the fresh feed. This scheme achieved an overall mass yield of 32% and an Fe recovery of 41%.

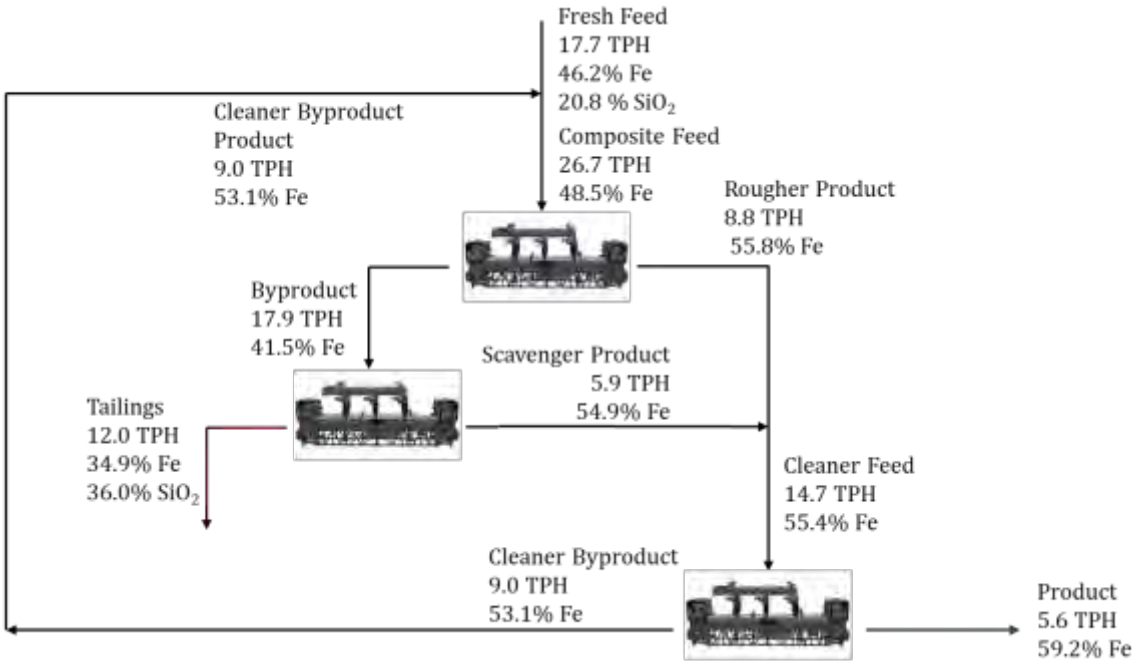

Figure 6. Ultrafine iron ore: High-grade product using rougher, cleaner and scavenger

Figure 7 illustrates the results for producing a mid-grade product. This scheme involves only a rougher stage yielding a mid-grade product with approximately 55% Fe content. Additionally, a scavenger run was performed, with its product blended with the rougher stage output. This scheme achieved an overall mass yield of 55% and an Fe recovery of 66%.
By changing the belt speed and feed port of the separator, a low-grade product scheme was developed, shown in Figure 8, resulting in product grade of 51% Fe. Testing involved a rougher stage and a scavenger run with its product blended with the rougher stage output. This scheme achieved an overall mass yield of 74% and an Fe recovery of 82%.

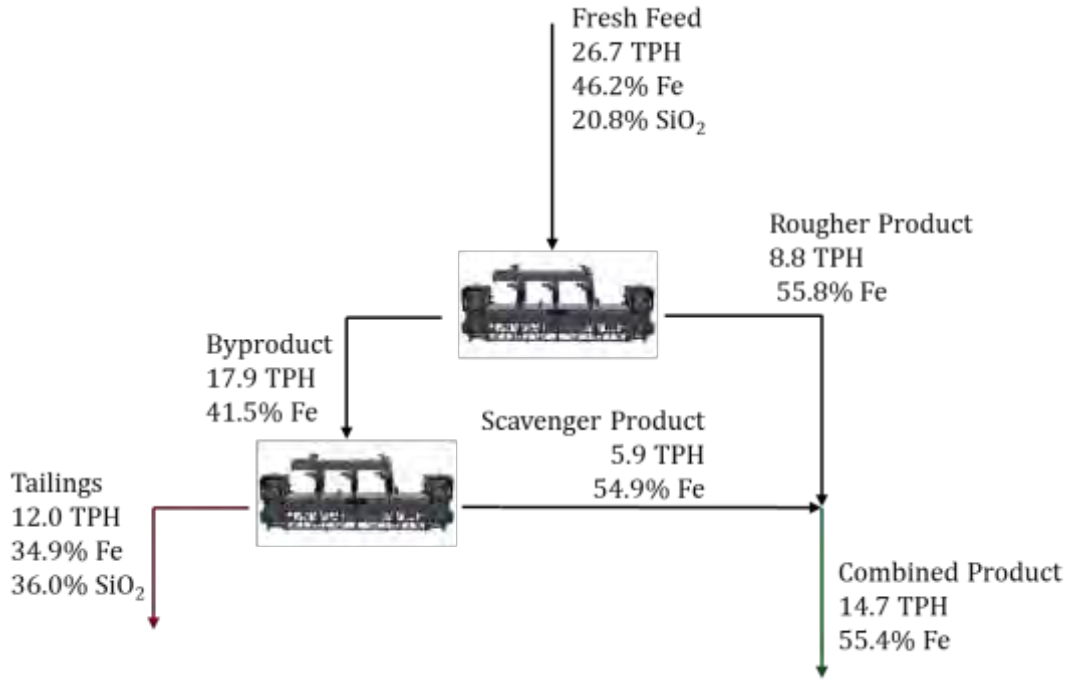

Figure 7. Ultrafine iron ore: Mid-grade product using rougher and scavenger scheme

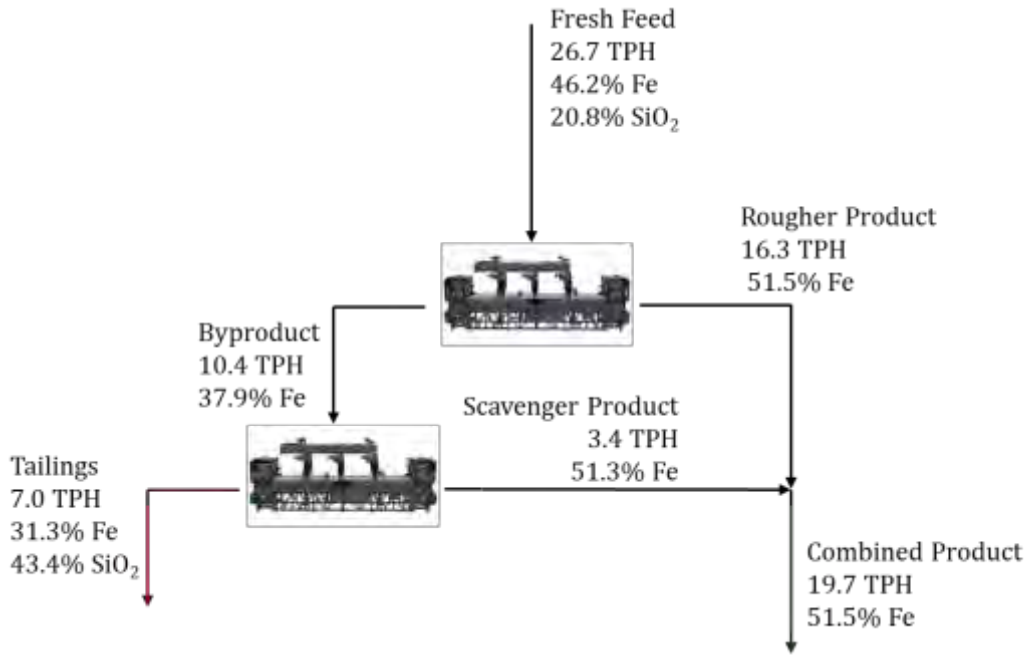

Figure 8. Ultrafine iron ore: Low-grade product using rougher and scavenger scheme

Table 8 details the results of the ultrafine iron ore tests, highlighting the range of product grades achieved alongside their respective mass yields and Iron (Fe) recoveries. These findings demonstrate that separator variables can be precisely adjusted to reach a range of product specifications, showcasing the flexibility of the process.

Table 8. Summary of results from ultrafine iron ore

Scheme	Product mass yield	Fe recovery	Product Fe content
High grade product	31.9%	40.8%	59.2%
Mid grade product	54.9%	65.9%	55.4%
Low grade product	73.8%	82.3%	51.5%

3.2.Upgrading Phosphate Ore

The phosphate ore samples were tested on a bench-scale separator with the objectives of increasing P_2O_5 content and reducing gangue minerals' content. Figure 9 shows the results of this testing, demonstrating increase of P_2O_5 content in all samples. The absolute enrichment of P_2O_5 showed variation across the samples, as shown in Figure 10.

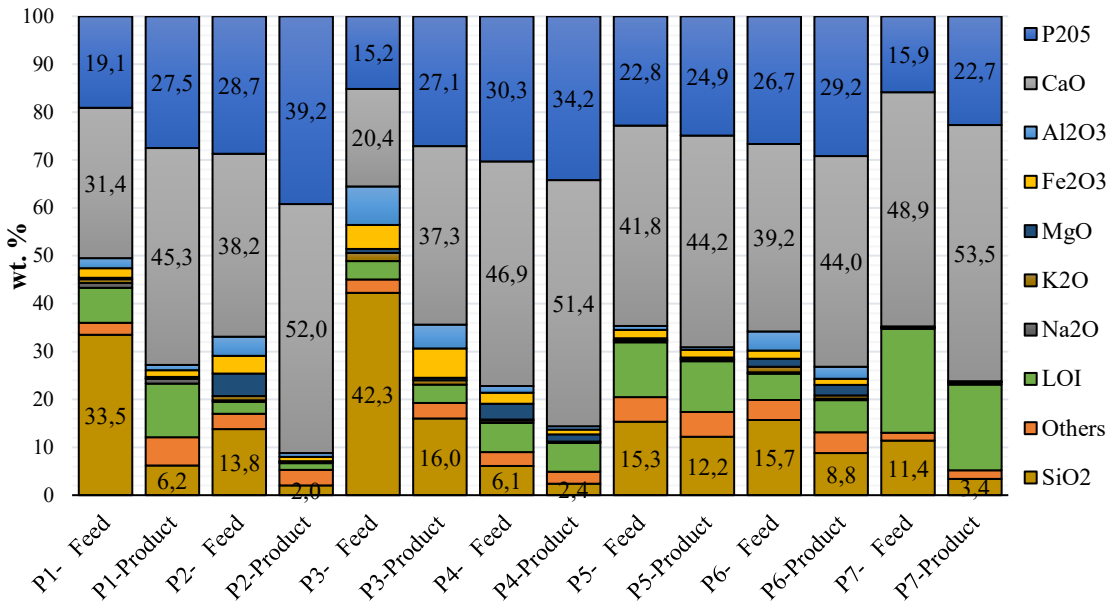

Figure 9. P_2O_5 enrichment demonstrated in all tested phosphate ore samples

The investigators hypothesize that the variations in P_2O_5 enrichment are directly linked to mineralogical complexity. Samples P1–P3, which primarily contained silicate gangue (such as quartz and aluminosilicates), and Sample P7, which contained carbonate-based gangue, both achieved relatively high P_2O_5 enrichment. In contrast, Samples P4–P6 exhibited poorer separation, likely due to a complex mineral matrix involving both carbonates and silicates. Given that apatite consists of approximately 55% CaO and 41% P_2O_5, the CaO content in these samples is split between the apatite structure and the calcareous gangue. Further testing is required to confirm these mineralogical correlations conclusively.

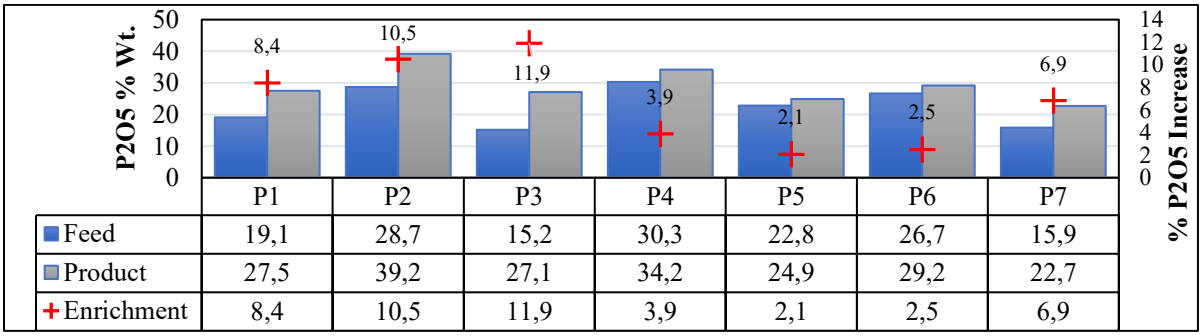

	P1	P2	P3	P4	P5	P6	P7
Feed	19,1	28,7	15,2	30,3	22,8	26,7	15,9
Product	27,5	39,2	27,1	34,2	24,9	29,2	22,7
Enrichment	8,4	10,5	11,9	3,9	2,1	2,5	6,9

Figure 10. Variation in absolute P_2O_5 enrichment

4.CONCLUSION

STET tribo-electrostatic belt separator offers a dry process based alternative for mineral beneficiation. This technology effectively addresses the challenges posed by conventional wet separation methods, such as inefficiencies with ultrafine particles, high water consumption, and environmental concerns related to wet tailings disposal. Pilot-scale and bench-scale testing results are presented in this report, demonstrating efficiency in upgrading iron and phosphate ores across varying mineral compositions and geographies. For iron ore, the ability to adjust separator variables facilitated the production of diverse product grades while

optimizing mass yield and Fe recovery. Similarly, phosphate ore testing showcased notable P_2O_5 enrichment, particularly for ores with simpler mineralogical profiles.

These results highlight the tribo-electrostatic separator's potential to contribute significantly to sustainable mineral processing practices, reducing waste and conserving critical resources.

REFERENCES

Edraki, M., Baumgartl, T., Mulligan, D., Franks, D. M., Moran, C. J., (2014) "Designing mine tailings for better environmental, social and economic outcomes: a review", Journal of Cleaner Production, 84, 411-420.

Gasiorowski, S., Hrach, F., Guicherd, H., (2015) "Electrostatic beneficiation of phosphate ores: Review of past work and discussion of an improved separation system", SYMPHOS - 3rd Symposium on Innovation and Technology in the Phosphate Industry.

Lu, L., Ishiyama, O., (2015) "Iron Ore: Mineralogy, Processing and Environmental Sustainability", Elsevier.

Ma, M., (2012) "Froth flotation of iron ores", International Journal of Mining Engineering and Mineral Processing, 1 (2) 56-61.

Svoboda, J., (2004) "Magnetic Techniques for the Treatment of Materials", Kluwer Academic Publishers.

Tripathy, S. K., Murthy, Y. R., Singh, V., (2013) "Characterization and separation studies of Indian iron ore slimes for their recovery", International Journal of Mineral Processing, 122, 47-57.

EFFECT OF GRAVITY CONCENTRATOR PERFORMANCE ON CIL EFFICIENCY AND OVERALL GOLD RECOVERY

Cumhur Erdem KARAHAN*, Fehmi Can SUTER, Durmuş Ali KIZILCADAM, Kasım MEYDANAL

Gübretaş Maden Yatırımları A.Ş., 11600, BILECIK-TURKEY
**Corresponding author: cumhur.karahan@gubretasmaden.com*

A B S T R A C T

This study investigates the impact of gravity concentration performance on Carbon-in-Leach (CIL) efficiency and overall gold recovery in a gold processing plant. In operations where both gravity and CIL circuits are employed, the effectiveness of gravity recovery directly influences the metallurgical balance of the downstream process. High gravity recovery reduces the gold grade entering the CIL circuit, decreasing cyanide consumption and carbon loading, while maintaining CIL efficiency.

Plant data were analyzed to evaluate the relationship between gravity recovery rate, CIL residue grade, and total plant recovery. The presence of coarse and free-milling gold in the ore significantly affects this relationship, as such particles are more amenable to gravity separation. When these free and coarse gold grains are efficiently captured in the gravity circuit, the subsequent CIL feed becomes leaner in recoverable gold, resulting in more stable leaching conditions and lower reagent consumption. The study concludes that effective gravity–CIL integration is crucial for maximizing metallurgical performance and minimizing operational costs in modern gold plants.

Key words: *Gravity Concentration, gold recovery, free gold, coarse gold, Carbon-in-Leach (CIL)*

1.INTRODUCTION

Gold has been one of the most valuable metals throughout human history and continues to play an essential role in modern industry, not only as a precious commodity but also as a critical raw material in electronics, aerospace, chemical processing, and investment markets. In nature, gold occurs in a wide range of mineralogical forms, from coarse native particles and nuggets to finely disseminated gold locked within sulfide minerals and silicate gangues. This variation in gold occurrence directly influences the selection of an appropriate processing route and determines the overall efficiency of extraction methods.

Gold concentration process usually consist of gravity concentration, flotation or cyanidation or a combination of these processes (Liipo J., 2003). Cyanidation, especially in Carbon-in-Leach (CIL) circuits, is highly effective for fine and liberated gold (Wadnerkar et. al., 2015). However, coarse gold particles require long leaching times and often remain partially undissolved under typical cyanidation conditions. This results in increased gold losses to tailings, higher reagent consumption, and reduced overall process efficiency. The gravity concentration circuits thus influence reagent consumption, gold in the process, and the efficiency of gold extraction in a mine (Siame et al., 2014). Coarse and free gold tend to complicate the cyanidation process. Coarse gold increases the residence time required to achieve high recoveries by cyanidation (Laplante and Gray, 2005).

Due to the high density of gold particles, it tends to go to hydrocyclone underflow continuously and accumulates in the grinding circuit. Thus, in circuits that utilize cyanidation plus gravity, the economics of the gravity portion of the circuit can often be very strong. According to Laplante (2005) the benefit for every 10% of recovery by gravity usually falls in the range of 0.2-1.0% of additional overall gold recovery.

This study aims to investigate the effect of gravity concentrator performance on CIL efficiency and overall gold recovery in an industrial gold processing plant. By examining the relationship between gravity recovery rates, CIL residue grades, reagent consumption, and total plant recovery, this research highlights the importance of effective gravity–leach integration for improving both metallurgical performance and operational efficiency in gold processing plants.

2.MATERIAL AND METHODS

2.1. Material

A representative sample of the Korudanlik Master composite was examined for QEMSCAN (Quantitative Evaluation of Minerals by Scanning Electron) Particle Mineral Analysis (PMA) to identify the types of minerals and bulk associations, and to provide quantitative information on mineral percentages, particle sizes, degrees of liberation and locking analysis.

The minerals present in the Korudanlik Master composite were mainly carbonate rich non-sulphide minerals (dominated by calcite), and accounted for about 86.4% of the composite mass. The remainders of the non-sulphide gangue minerals were mostly comprised of quartz, muscovite, kaolinite/pyrophyllite, iron oxides and apatite. It is noted that the master composite contained very low Sulphide mineralization (less than 0.1% by weight). A majority of the gold in the master composite was present as native gold containing >90% gold <10% silver.

Microscopic examination of the thin section of the sample revealed free gold (Au) particles ranging in size from 30 to 100 microns (Figure 1).

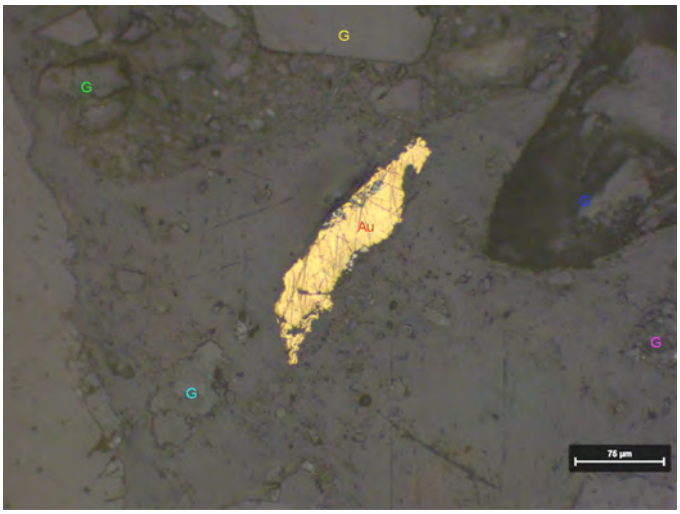

Figure 1. Master composite sample (Au Particle 30x110µm)

2.2. Selection of Gravity Concentrator and Testworks

Gravity separation test work was conducted to evaluate the potential of recovering coarse and free gold prior to cyanidation and to quantify its impact on downstream leaching performance and overall plant recovery. Based on the mineralogical characterization and extended GRG testing, centrifugal gravity separation was selected as the most appropriate technique for early-stage gold recovery.

Laboratory-scale gravity tests were carried out using a Knelson MD-3 concentrator under standard operating conditions. The Master composite and sub-composite samples were ground in a laboratory rod mill at approximately 65% solids to target grind sizes representative

of mill discharge conditions. Each ground sample was processed through the Knelson concentrator, and the resulting concentrate was further upgraded using a Mozley C-800 laboratory mineral separator to achieve a final concentrate mass pull of approximately 0.05–0.10%. The gravity tailings were recombined and split to generate representative samples for subsequent bottle roll testing.

The selection of the Knelson concentrator over alternative centrifugal gravity devices, such as the Falcon concentrator, was primarily driven by the ore characteristics and the intended duty within the grinding circuit. Extended GRG testing indicated a high gravity-recoverable gold content (GRG = 70.3%), with a significant proportion of gold present as liberated or exposed native gold at relatively coarse particle sizes. Under such conditions, the fluidized riffle bed design of the Knelson concentrator provides superior retention of coarse and fast-liberating gold particles. In addition, the Knelson XD configuration is specifically engineered for continuous treatment of high-solids mill discharge streams, enabling early recovery of gravity gold before excessive overgrinding occurs. Previous studies have shown that bed capacity, riffle geometry, and bed stability are critical parameters controlling coarse gold recovery in centrifugal gravity concentrators, and these design features favor the Knelson concentrator for this application (Laplante and Gray, 2005).

By recovering coarse free gold at the earliest possible stage, the gravity circuit reduces gold accumulation within the grinding circuit, minimizes overgrinding of gold particles, and produces a leaner feed to the CIL circuit, thereby enhancing downstream metallurgical performance.

2.3. Cyanidation Testwork

Bottle roll cyanidation tests were conducted on gravity tailings samples to evaluate the effect of gravity pre-concentration on leaching performance. The tests were performed at a pulp density of approximately 40–45% solids. Sodium cyanide concentration was maintained at 0.5 g/L throughout the tests, while pH was controlled above 10.5 by lime addition. Each bottle roll test was run for 48 hours with continuous agitation to ensure adequate solid–liquid contact. Gold extraction was determined from solution assays and final residue analyses, allowing direct comparison of leach performance between untreated material and gravity tailings.

3.RESULTS AND DISCUSSION

3.1. Gravity Testwork Results

The Master Composite gravity concentrate from test G2 was submitted for a gold deportment study. A total of 7800 gold grains were identified and all were native gold (98% Au, 2% Ag). Liberated gold grains represented 40.4% of gold in the sample. The liberated gold grains ranged in size from 247 µm to 2 µm and averaged 32 µm. Exposed gold grains made up 58.6% of the gold in the sample with grains ranging from 322 µm to 2 µm and averaging 26 µm. The locked gold represented 1.0% of the gold in the concentrate and the average grain size was 5 µm.

!" #A	%'" C	'(FGC	'(CgFKa 0Gc" GA(CA					!C FdKGP		B" OCaEcCdce	
	HA	, -.	HA	As#CKNaPIA		Rec0g" (KN6		As#CKNaPIA		g/A	
/0 N	kg	µm	6	Au	TP	Au	TP	Au	TP	Au	TP
'9	9.	206	0..<9	;=9-	32.9	65.<	4..	3..9	@.NA	8.->	@.NA
G2	20	9-<	0.129	=..>	9=A	63.W	21.=	3..9	@.NA	8.9;	@.N<
'>	>.	9.=	0..-A	=9<<	88.?	45.A	10.>	4.>>	@.NA	8.9-	@.N
'=	9.	9.=	0..<?	?9.-	112	65.<	14.9	W?9	@.NA	7.>?	@.N
'?	20	9.=	0.9;.	;=.>	9;>	79.9	18.>	WA9	@.NA	9>	@.N

Figure 2. Summary of gravity separation tests

3.2. Cyanidation Test Results

The Master Comp gravity concentrate from test G1 was submitted for a bottle roll test. Bottle roll cyanidation test results clearly demonstrate that gravity pre-concentration has a positive impact on gold leaching performance. A comparison between whole ore cyanidation tests (CN1 – CN4) and gravity tailings cyanidation tests (CN5 – CN8) indicates consistently higher gold extraction for gravity tailings at comparable grind sizes.

!" #A	%80	<" - O*=0 >>?@AEBCCA		<" - O*=) @#*AEBCCA		ExA- dA) @A		<" #e>N' AeCCA		He- >=kd- idM=CCA	
No*	µm	Na. E	.- /	Na. E	.- /	Au	Ag	Au	Ag	Au	Ag
CNP	203	'* 76	'* 89	'* 10	'* 84	84*9	33.T	'* 9:	;' *9	6*10	'* C
CN4	150	'* 69	'* 89	'* PR	'* 87	91.8	33.9	'* 99	;' *9	6.69	'* C
CNR	102	'* 73	'* 85	'* PT	'* CR	84*4	37.P	'* 58	;' *9	6*37	'* C
CN:	69	'* 73	'* 85	'* 14	'* 85	93.R	35.P	'* 51	;' *9	6*51	'* C

Figure 3. Summary of Whole Ore Cyanidation Tests

The CN 5–8 tests were conducted on a feed with a head grade of 8.83 g/t.

!" #A	%80	?" - OGBAABaGCoA		?" - OG@) C#GBCoA		deA- I A) CaG		/B- kQNG" I BaG		?" #gAN' aQCA		He- AQM- kI GCoA	
NoG	µm	Na. E	.- /	Na. E	.- /	Au	Ag	Gr- R	P4- R6. E	Au	Ag	Au	Ag
CNT	8'9	0.:;	1.'8	0.<'	1."	84.;		65.>	94.9	0.45		2.87	
CN9	<;>	0.::	0.95	0.8'	0.95	CTS		65.>	95.8	0.=;		3.'<	
CN:	95	0.75	1.15	0.8'	1.<;	86.8		65.>	95.;	0.=8		3.'=	
CNC	:<	0.83	1.'>	0.15	1.'>	87.8		65.>	95.9	0.='		3.<;	

Figure 4. Summary of gravity tailing cyanidation tests

As shown in Figure 3 and Figure 4, gold extraction from gravity tailings is systematically higher than that obtained from whole ore cyanidation across all tested grind sizes. The overall recovery of gold by gravity + cyanidation of the gravity tailing was 94-95%, compared to 92-93% in the whole ore cyanidation tests. The residue assay was 0.4 g/t Au compared to 0.5-0.6 g/t Au in the whole ore tests.

Effect of Particle Size

The results show only a small decrease in the residue assay from 0.48 /t Au to 0.43 g/t Au as the fineness of grind P80 decreased from 198 µm to 77 µm. Figure 5 shows that the leaching was faster for the gravity tailings than it was for the whole ore. At coarser grind sizes, the difference in leach recovery is particularly pronounced, highlighting the effectiveness of gravity separation in removing coarse, slow-leaching free gold prior to cyanidation. The removal of this gold fraction results in a gravity tailings feed that is finer, more homogeneous, and more amenable to cyanide dissolution.

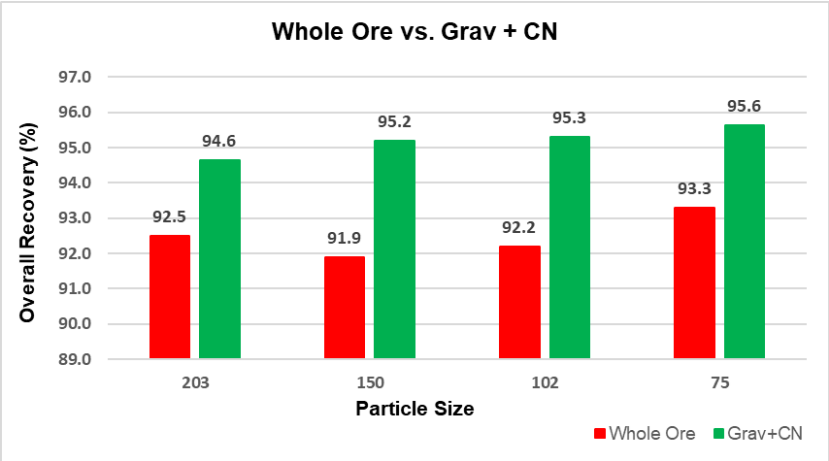

Figure 5. Effect of particle size

Effect of CN Concentration

A set of three tests was conducted to investigate the effect of cyanide concentration on gold extraction and cyanide consumption. The leach conditions were the same as applied in previous tests except that the cyanide concentration was varied from 0.25 g/L NaCN to 0.75 g/L NaCN. The results shown in Figure 6.

Test	Tail	NaCN	Density	Reag. Add'n, kg/t		Reag. Cons., kg/t		Extraction %	O'all Au Rec'y, %		Residue g/t	Head (calc). g/t
No.	from	g/L	% solids	NaCN	CaO	NaCN	CaO	Au	Grav	Grav+CN	Au	Au
CN9	G2	0.25	45	0.34	0.66	0.09	0.66	85.9	63.4	94.8	0.44	3.12
CN10	G2	0.50	45	0.75	0.62	0.08	0.62	84.9	63.4	94.5	0.47	3.08
CN11	G2	0.75	45	1.01	0.63	0.15	0.63	86.0	63.4	94.9	0.42	2.99

Figure 6. Effect of cyanide concentration

The gold extraction was similar in all tests. Cyanide consumption increased slightly from 0.09 kg/t NaCN to 0.15 kg/t NaCN at the highest cyanide concentration. The results indicate that overall gold recovery obtained from the gravity + cyanidation route remains essentially constant despite variations in cyanide concentration. Across the tested cyanide concentrations, overall recovery varies within a narrow range of 94.5% to 94.9%, demonstrating that gold extraction in the gravity + cyanidation configuration is largely insensitive to cyanide dosage. This behavior suggests that the majority of leachable gold is effectively recovered following gravity separation, and that cyanidation primarily targets gravity tailings containing finely liberated gold rather than cyanide-limited gold phases.
As a result, lower cyanide concentrations can be applied without compromising metallurgical performance, leading to a reduction in operational cyanide consumption and associated reagent costs when operating with a gravity + cyanidation flowsheet. Consequently, lower cyanide concentrations are sufficient to achieve high overall recovery, leading to a measurable reduction in operating cyanide costs (Marsden and House, 2006).

4. CONCLUSION

This study demonstrates that gravity pre-concentration plays a critical role in enhancing CIL efficiency and overall gold recovery in gold processing plants treating ores containing coarse and free-milling gold. Mineralogical investigations confirmed that a significant proportion of the gold occurs as liberated or exposed native gold at relatively coarse particle sizes, making it highly amenable to early-stage gravity recovery.

The application of a centrifugal gravity concentrator prior to cyanidation resulted in effective removal of coarse, slow-leaching gold, producing a gravity tailings stream that was finer, more homogeneous, and more responsive to cyanide leaching. Bottle roll test results clearly showed that gravity tailings consistently achieved higher gold extraction than whole ore cyanidation. Overall plant recovery increased from approximately 92–93% for whole ore cyanidation to 94–95% when gravity concentration was integrated with cyanidation, while final residue grades were reduced.

In addition to improved recovery, gravity pre-concentration contributed to more stable leaching conditions and reduced sensitivity to cyanide concentration. Comparable overall recoveries were achieved across a wide range of cyanide dosages, indicating that lower cyanide concentrations can be applied without compromising metallurgical performance. This provides a clear opportunity for reducing reagent consumption and operating costs.

REFERENCES

Laplante, A. R., (2005), Gravity gold recovery – introductory presentation, AJ Parker Cooperative Research Center for Hydrometallurgy Gravity Gold Workshop.

Laplante, A. R., Gray, S., (2005), Advances in Gravity Gold Technology, Developments in Mineral Processing, Vol. 15.

Liipo, J., (2003) “Characterization of the mode of occurrence of gold in Jokisivu pilot feed and products”, Minerals Engineering, 16 (11) 1317 – 1321.

Marsden, J. O., House, C. I., (2006) “The chemistry of gold extraction”, Society for Mining, Metallurgy, and Exploration (SME).

Siame, J., Muchima, K., Chirwa, D., Magawa, P. C., (2014) “Optimization of gravity recovery of gold at high pressure leach plant of Kansanshi Mining PLC”, Zambia, International Conference on Chemical, Integrated Waste Management and Environmental Engineering, Johannesburg, 15 – 16.

Wadnerkar, D., Tade, M. O., Pareek, V. K., Utikar, R. P., (2015) “Modelling and optimization of Carbon in leach (CIL) circuit for gold recovery”, Minerals Engineering, 83 136 – 148.

EVALUATION FOR THE PROFITABILITY OF A CHROMIUM ENRICHMENT PLANT CONSTRUCTION

Genc DEMI*, Aida BODE

Polytechnic University of Tirana, Faculty of Geology and Mines, Mine Deposit Engineering Department, Rruga e Elbasanit, Tirana-ALBANIA
**Corresponding author: genc.demi@fgjm.edu.al*

A B S T R A C T

The preliminary enrichment investigation was carried out with a representative sample of the chrome ore body. The purpose of investigation was to make a preliminary assessment of a plant construction for the enrichment of chrome ore of this deposit. The importance of the investigation is to make a decision for the construction of the plant. The objective of investigation was to obtain chrome concentrate that could be sold at market prices with minimal possible losses. The enrichment tests, mineralogical and chemical analyzes of the representative sample and enrichment products were performed for preliminary beneficiation investigation. Washability curves were plotted based on results of the separation in heavy liquids and the expected enrichment figures were calculated, grade of concentrate 49 % Cr_2O_3 and Cr_2O_3 recovery 70 % from a raw material chromium ore with 15 % Cr_2O_3 content. The flowsheet, list of machines and equipment, as well as consumption of raw material, auxiliary materials and labor, were calculated. The capital and operation costs were calculated, as well as the evaluation for the chromium enrichment plant operation for 10 years with cash flow method with results of NPV and IRR. It was concluded that the construction of a chromium enrichment plant is profitable.

Key words: *Chromium, concentrate, evaluation*

1. INTRODUCTION

The exploitation of reserves with low Cr_2O_3 content, which can be processed to produce chromium concentrates with content of 48 – 50 % Cr_2O_3, requires the construction of new chromium ore enrichment plants. The enrichment of chromium ore is associated with costs, which depend on the mineralogical composition of the ore, the processing capacities of the enrichment plant, the necessary investments for the construction of the plant and the operating cost of the work for the enrichment of chromium ore. This makes it necessary to conduct economic feasibility studies to determine the possibility of enriching chromium ores with acceptable profits for investors.

2. MATERIAL AND METHODS

2.1. Material

A representative sample crushed – 6 mm was obtained from the exploration drillings in chromium body. Screen analysis of the representative sample is given in Table 1.

Table 1. Particle size distribution of the sample.

Particle fraction, mm	Weight, %	Content Cr_2O_3, %	Distribution,%
- 6 + 1	44.00	32.66	48.68
-1 + 0.5	17.55	32.12	19.07
-0.5 + 0.25	12.76	30.32	13.11
-0.25 + 0.1	14.09	26.91	12.84
-0.1 + 0.074	4.39	16.05	6.30

-0.074	7.21		
Representative sample	100.00	29.52	100.00

The Cr_2O_3 content in the chromium ore body is 29.52 %. The heavy fraction in liquid with density 3.2 g/cm3 was analyzed for main composed compounds, Tab. 2.

Table 2. Composed components of densimetric fraction +3.2 g/cm^3

Description	Results
Chromium oxide content, Cr2O3%	44.10
Iron Content, Fe%	11.73
Aluminum oxide content, Al2O3%	6.37
Magnesium oxide content, MgO%	17.13
Ratio Cr/Fe	2.57 : 1
Ratio Mg/Al	3.05 : 1
Ratio MgO/Al2O3	2.69 : 1

The open pit mining project shows that, due to the dilution with side rocks, which consist of the same sterile minerals found in the representative sample, it results that the raw material that will supply the enrichment plant will have an average content of about 15% Cr_2O_3.

2.2. Method

The mineralogical study was carried out, where the constituent minerals, the degree of liberation and the properties of the constituent minerals were determined. Also, it was carried out testing of separation into heavy liquids and enrichment curves were plotted, which resulted in the quality of the concentrate that could be achieved with the enrichment methods and the type of processes and equipment and machinery that could be used for the enrichment process. Based on the reserve data, the annual and hourly capacity of the enrichment plant was determined. Using the enrichment data of chromium ores in existing plants, the expected enrichment indicators, concentrate quality and recovery, as well as the amount of water and the volume of pulp in the enrichment process links were calculated. The flowsheet of enrichment plant and the list of machinery and equipment were drawn up, as well as the capital and operating costs were calculated. With this data, the valuation was carried out using the "Cash Flow" method.

3. RESULTS AND DISCUSSION

3.1 Mineralogical Analysis (Sinoymeri, 2024)

The study for the mineral particles liberation was carried out in the friable fractions of different granulometric classes, as well as through the examination of artificial polished surfaces. To evaluate the liberation of mineral particles from each other after grinding, four granulometric fractions of the sample crushed under 6 mm were observed in binocular. In Table 3, the results of the evaluation of the particle size liberation from binocular observation are given.

Table 3. Percent content of liberated particles and particles with inclusions.

Partcles types	% particle content for every fraction in mm			
	-6 +1	-1 +0.5	-0.5 +0.25	-0.25 +0.1
Liberated Sterile particles	20	35	40	50
Sterile particles with chromium inclusions	30	15	15	5
Chromium particles with Sterile inclusions	50	50	45	45

In the fraction (-6 +1) it is noticeable that among the large particles there are quite a lot of liberated sterile particles (without visible chromite inclusion), but in the smaller particles the

liberated steriles are much less. This shows that even large particles that appear clean can have chromite inclusions inside. Hardness testing shows that both olivine and serpentine are present among the sterile particles.

Fi.1 -6+1mm Fi.2 -1+0.5mm F.3 -05+0.25mm F.4 -0.25+0.1mm

In order to specify the dimensions of sterile inserts and their type, two polished sections with diameter of 1 inch were prepared from the 0.1-6 mm and 0.1-1 mm granulometric fractions. Their examination was performed with polarized reflected light, with a Nikon ECLIPS 50i POL microscope. Fraction -6+0.1mm is original sample without -0.1mm. Fraction -1+0.1mm is ground original sample under 1mm and without fraction -0.1mm.

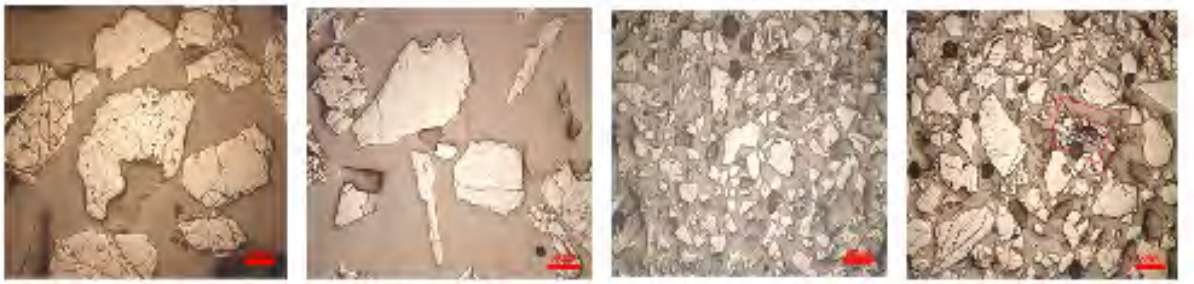

F.5 -6+0.1mm Fi.6 -6+0.1mm Fi.7 -1+0.1mm Fi.8 -1+0.1mm

Often the particles contain in their lateral parts non-metallic minerals (mainly serpentine) that coat the chromite (Figure 5 shows heavily altered chromite grains, in the center a chromite grain with a serpentinized olivine inclusion, while Fig. 6 shows fairly clean chromite grains, with very few serpentine veins). In Fig. 7 and 8 view of the largest particles in the 0.1-1mm fraction, the large particles have more sterile mineral inclusions than finer ones, reflected polarized light, no analyzer.

Table 4. Particles content in % in every polished surface

Grain types	Particles content in % in every polished surface	
	-6mm+0.1mm	-1mm+0.1mm
Liberated sterile grains (chromite <5%)	20	20
Mixed grains (chromite+magnetite+sterile)	70	20
Liberated chromite grains (sterile <5%)	10	60

From the results of the study of the friable fractions, as well as that of the polished surfaces, it results that in the 0.1-1mm fraction, the liberation of grains is optimal. Further grinding to recover the chromite in mixed composition grains would hardly be effective because the sterile mixed in these particles is in the form of grains several microns thick and which is very difficult to separate from the chromite. Likewise, magnetite is closely associated with the serpentine veins that cross the chromite grains and is practically inseparable from the latter.

Heavy liquid separation with a density more than 3.2g/cm3, in addition to pure chromite grains, would also collect mixed grains with >20% chromite content, reaching a concentrate with 44 % Cr2O3. The gravity with a higher separation density should be used to concentrate from the 0.1-1mm fraction pure chromite grains from mixed and sterile grains to reach a concentrate with 49% Cr2O3. The mixed grains should be reground finer and to be processed again by gravity. Almost the same conclusion is from the study of friable material.

However, it can be concluded that grinding of the sample under 0.1 mm is not effective and the best concentrate can be produced from the -1+0.1 mm fraction. Good Cr2O3 recovery in concentrate would be achieved by obtaining a concentrate containing about 49% Cr2O3.

3.2 Heavy Liquid Tests

3.2.1 Heavy liquid tests on head sample -6+0.1mm

The mineralogical study shows that the composed minerals of the ore are the useful mineral chromite and the sterile minerals mainly serpentine and in smaller amounts serpentinized olivine. From the mineralogical study, it also results that the liberation degree of acceptable amounts of composed minerals occurs after grinding minus 1 mm. Based on these data, the laboratory tests with the method of complete sink-float analysis (Burt, 1984) of separation in heavy liquids were carried out, separately for the different granulometric classes. There were tested in heavy liquids the fractions: -6+1mm; -1+0.5mm; - 0.5 + 0.25mm; and -0.25+0.1mm. The results of separation in heavy liquids are given in Table 5. Even from the results of the separation in heavy liquids, the data of the mineralogical study are verified, it seems that the visible liberation of the composed minerals is in the classes finer that 1 mm, while their complete liberation would require finer grinding.

Table 5. Testing in heavy liquids of different particle size fractions.

Fraction, mm	Quantity, %	Density, g/cm3	Weight against the fraction %	Weight against all fractions %	% Cr_2O_3 content	Cr_2O_3 Recovery, %	
						Against the fraction	Against all fractions
-6+1	49.78	-2.88	23.08	11.49	7.85	5.54	2.88
		-3.22+2.88	9.50	4.73	35.12	10.23	5.31
		+3.22	67.42	33.56	40.80	84.23	43.78
		Feed	100.00	49.78	32.66	100.00	51.97
-1+0.5	19.85	-2.88	23.33	4.63	4.20	3.05	0.61
		-3.22+2.88	6.67	1.32	31.80	6.60	1.34
		+3.22	70.00	13.90	41.45	90.35	18.42
		Feed	100.00	19.85	32.12	100.00	20.37
-0.5+0.25	14.43	-2.88	30.77	4.44	3.00	3.04	0.42
		-3.22+2.88	3.85	0.56	29.05	3.69	0.51
		+3.22	65.38	9.43	43.25	93.27	13.05
		Feed	100.00	14.43	30.32	100.00	13.98
-0.25+0.1	15.94	-2.88	39.13	6.24	2.00	2.90	0.38
		-3.22+2.88	4.35	0.69	27.60	4.46	0.61
		+3.22	56.52	9.01	44.10	92.64	12.70
		Feed	100.00	15.94	26.91	100.00	13,68
-6+0.1	100.0			100.00			100.00

3.2.2 Heavy liquid tests on fraction -1+0.1mm

The separation results in heavy liquids for fraction -1 + 0.1 mm are presented in the Table 6. The data for the specific gravity 3.8g/cm3 was found graphically knowing the Cr_2O_3 content in composed minerals.

Table 6. Heavy Liquid Test for the Sample of chromium ore, fraction (-1 + 0.1mm).

Specific gravity	Weight, %	Sinks				
		Cum, % weight	% Cr2O3	Cr2O3 units	Cum Cr2O3 units	Cum % Cr2O3
Sinks 3.80	35.00	35.00	49.10	17.19	17.19	49.1
-3.8 +3.22	29.39	64.39	35.08	10.31	27.50	42.71
-3.22+2.88	5.11	69.50	29.96	1.53	29.03	41.77
-2.88+2.7	18.20	87.70	4.10	0.75	29.78	33.96
Floats 2.7	12.30	100.00	1.25	0.15	29.93	29.93
	100.00			29.93		

Floats			Characteristic Assay	
Cum weight %	Cum Cr2O3 units	Cum % Cr2O3	% Cr2O3	Avg.Cum.% wt. sinks
65.00	12.74	19.60	49.10	17.50
35.61	2.43	6.82	35.08	49.70
30.50	0.9	2.95	29.96	66.95
12.30	0.15	1.25	4.10	78.6
-	-	-	1.25	93.85

3.2.3 Washabillity Curves. (Burt, 1984)

Washability curves are presented in Fig 9.
Specific Gravity Curve. Cumulative percent weight sinks is plotted against specific gravity of separation (green line).
Cumulative Percent Assay of Sinks Curves. The Cumulative percent assay of sinks is plotted against the cumulative percent weight of sinks for each specific gravity separation (red line).
Specific Gravity Distribution Curve for +/- 0.1 g/cm3 Density. It is the weight falling between the densities +/- 0.1 g/cm3 of separation density plotted against separation density (blue line)

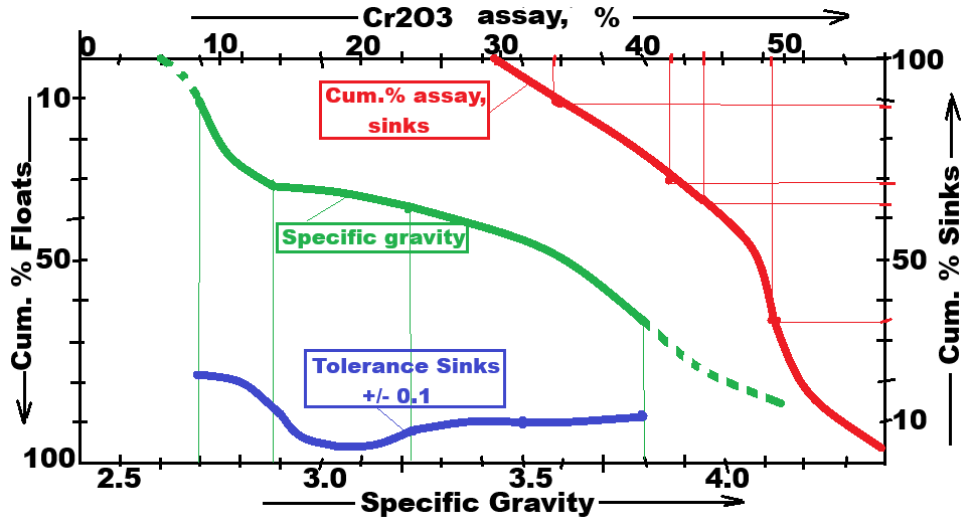

Figure 9. Washability curves for fraction -1+0.1mm.

Usually the most demanded quality of chromium concentrates in the market ranges from 48% to 50% Cr2O3. From the washability curves results that the average achieved concentrate production from the fraction -1+0.1mm will be at the separation density of 3.8 g/cm3 with a quality of 49.1% Cr2O3 and a recovery of 57.42%. A tolerance of 11 % of densimetric fraction +/-0.1g/cm3 is in the separation density at 3.8 g/cm3 shows for a gravity recommended process of a moderately difficulty of medium tonnage with cones, spirals and HMS (SME page 30-48). HMS and cone were exluded since the capacity of the plant is small because the reserves suggest that a 20 t/h plant is the most apropriate size.

From the mineralogy study and heavy liqiud testing of this ore it was determined the feasibility of gravity separation, the probable grade of chrmoium concentrate in value 49.1 % Cr2O3 and the most appropriate units of spiral separators and shaking tables. (SME, page 30-83).

The ore is similar to chrome ores, which are processed in existing chrome enrichment plants. Based on the data of the separation in heavy liquids, on the data of the exploitation project and on our experience of chromium enrichment in these plants with a capacity close to the case under consideration, which is about 20 t/h (Demi and Boci, 2018) a technological scheme was drawn up: crushing below 20 mm, grinding in a closed-cycle rod mill with a vibrating screen in the wet with 1 mm aperture, desliming of the pulp after grinding in a hydrocyclone by separating the -0.07 mm fraction in the overflow and treating the hydrocyclone sands in spiral base, cleaning and scavenger separators, where final sterile and concentrates are obtained, as well as semi-products, which are treated in two table stage, where final sterile and concentrates are separated, as well as and semi-products which are sent for re-grinding in the same mill. The hydrocyclone overflow as well as the -0.1mm fraction of all tailings, separated by a spiral classifier, are sent to the slime enrichment process, where they are previously deslimed in 75 mm diameter hydrocyclone battery, the overflow of which with particle size below 20 microns goes to tailings, while their sands are treated in shaking tables with proper surface, frequency and step for fine particles and they separate the final concentrate and tailings. Tailings are sent to the tailings dam, where about 90% of the amount of water used is separated and recirculated in the process. The chromium concentrate goes to decantation tanks and the water is recirculated in the process. From the technological scheme, the quantities, contents of Cr2O3, the volume of pulps, the amounts of water in each link of the process are calculated. From the enrichment, two final products are obtained as given in Table 7.

Table 7. Predicted technological enrichment figures.

N.	Products	Weight		Cr_2O_3 content,	Cr_2O_3 Recovery,
		(%)	t/h	(%)	(%)
1	Chrome Concentrate	21.43	4.29	49.00	70.00
2	Tailings	78.57	15.71	5.73	30.00
3	Raw Material	100.00	20.00	15.00	100.00

The principal flowsheet of beneficiation with type and number of machines of each process was compiled based on calculations with data from the technological scheme, data from machine catalogues of manufacturing plants as well as experience from existing chrome ore enrichment plants. It was selected a plant site close to the mine with possibilities of electrical power and water supply and connected with automobilistic road, where topography survey was done in scale 1:2000. The drawings of the placement of machinery, roads, buildings and the tailings deposit were made at this site, as it is shown in Fig. 10. (Demi and Sinjari, 2023) From the equipment connection scheme a list of equipment and machinery with type, quantity, weight, motor power and price, obtained from the offer of one manufacturing plant, was prepared. There were not prepared mechanical and structural drawings in this phase of economic feasibility, while pipe and electrical drawings were prepared single-line. It is expected that there will be no problems related to the application of the process and environmental pollution, since the products do not contain hazardous elements or compounds and there will be no spillage into the environment because the water will be recirculated in the

process. A study was conducted to ensure the supply of water from several surface sources in the amount of 4 l/sec and it was predicted that 90% of it will be recirculated in the process. Natural limitations are the hard winter and dry summer, which limit the number of days of operation of the factory per year. Among the legal limitations it is the approval of the construction of the factory by the residents of the area, related to environmental pollution. From these limitations and from the mine's production, it was determined that the number of days of operation of the factory per year will be 250.

It was estimated the capital cost (Hario, 1985) where major equipment cost was taken only from one offer. The volumes of work for the construction of squares, roads, machinery foundations, buildings, concentrate and tailings storage areas, pipelines and belt conveyors were also calculated, based on current prices and tariffs. The values are given in Table 8.

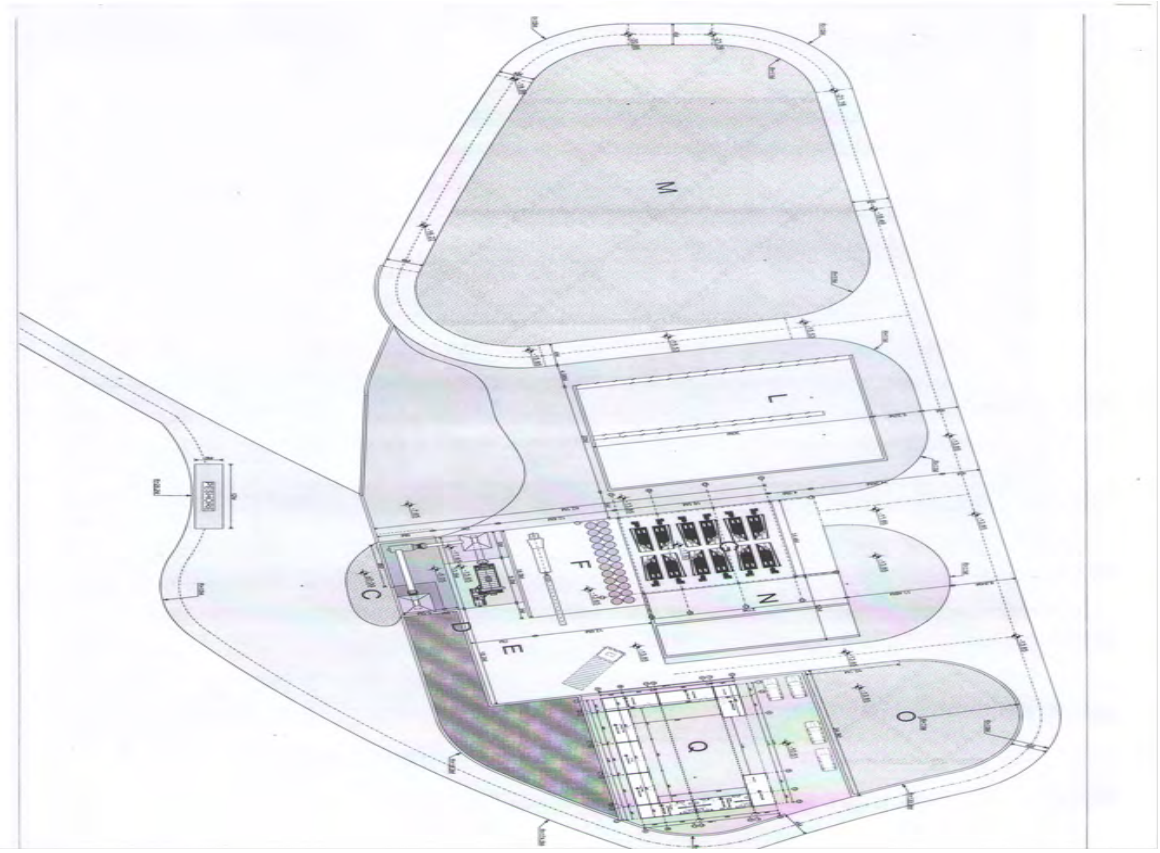

Figure 10. Layout of machinery, buildings, roads and tailings dam

Table 9. List of investment values of the Enrichment Plant

Description		Total Budget, $
Chromium Enrichment Plant		**2,520,000**
1	Official Permits and The Project	156,000
2	Construction Workings	522,000
3	Hydro technic Workings	24,000
4	Equipment and machine of EP	1,472,000
5	Electrical Workings and equipment	144,000
6	Fixed capital	230,000

The estimate excludes currency fluctuations and allowances for project growth. VAT is excluded from all purchases and services as it is refundable.

Operating Cost (Hario, 1985) was calculated for ore exploitation and for ore enrichment. It is shown in the table 10.

Table 10. Operating cost.

N.	Operating Cost Description	Value, $/ton RM	Remarks
1	Exploitation and Transport to EP	10.00	In open pit, distance mine-EP 3 km
2	Labor in EP	1.38	23 workers include administrate, average salary 600$/month, including insurance and taxes.
3	Power	3.68	Consume is 24.5 KWh/ton RM, price 0.15 $/kWh
4	Operating and maintenance supplies	3.17	Based in experience of existing chromium Enrichment Plants
5	Transport of tailings	1.25	Transport of 50,000 ton tailings from EP to the mine.
6	Other direct costs	0.47	It was calculated in value 3.67 % of the total direct costs.
7	Indirect plant costs	2.84	It was calculated in value 28.5 % of the total direct costs.
	Total direct EP costs	12.79	

The operating cost in the mine and transport to the plant will be 14 $/ton raw material for the first year of operation and it is predicted to be increased 5 % every year. The operating cost in the EP will be 12.79 $/ton raw material for the first year of operation and it is predicted to be increased 3 % every year. The cost 1 ton dry concentrate transport to harbor is 10 $ and the port costs are $20/ton per 1 ton dry concentrate in the first year. In subsequent years, these values are estimated to be increased at around 3% for each subsequent year. It is foreseen that the FOB price of the chrome concentrate sale of with an average content of 49% Cr2O3, for the first year of EP operation will be 300 $/ton dry concentrate. Since the sales price of chrome concentrate has often fluctuated, an average increase with 5 $ per ton every two years has been predicted.

4. EVALUATION WITH THE "CASH FLOW" METHOD.

All the data were used for the calculation with the "Cash Flow" method for the 10 years of EP's operation. From the evaluation with the "Cash Flow" method, it results that NPV is in the value $13.38 million $ for the $2.52 million investment and the IRR indicator results in a value of 138%.

5. CONCLUSIONS AND RECOMMENDATIONS.

The construction and commissioning of a plant for the enrichment of chrome ore at the chromium deposit results in economic benefit.
From the calculation using the "Cash Flow" method, it results that the NPV is 13.38 $ million, while the IRR has a value of 138%%, which are considered good indicators.
The operating cost for the first year is calculated to be 12.79 $/ton of raw material.
It is recommended to make the full project of the chromium enrichment plant, after enrichment study in laboratory batch scale.

REFERENCES

Burt, R., (1984), “Gravity Concentration Technology”, 33–34.

Demi, G., Boci, S., (2017), “Technological Project of Chromium Enrichment Plant ML”, 34–35.

Demi, G., Boci, S., (2023), “Technological Project of Chromium Enrichment Plant QU”.

Hario, C. N., (1985), “SME Mineral Processing Handbook”, 3342–3344.

Sinoymeri, A., (2024), “Mineralogical Analysis of Chromium Ore QU”, 6–20.

PROCESS IMPROVEMENT OF A CHROMIUM ENRICHMENT PLANT

Genc DEMI[1,*], Safet BOCI[2]

[1]Polytechnic University of Tirana, Faculty of Geology and Mines, Mine Deposit Engineering Department, Rruga e Elbasanit, Tirana-ALBANIA
[2]Association of Mineral Processing Engineers, TIRANA-ALBANIA
**Corresponding author: genc.demi@fgjm.edu.al*

A B S T R A C T

The paper describes the analysis that was carried out on the technological process of the Chromium Enrichment Plant “Maja e Lugut”. The crushing process, the grinding and classification process, as well as the enrichment process in spiral separators and shaking tables at several stages was analyzed, considering and the possibility of pre-concentration . The analysis was important because it showed the possibility to improve the technical and economic indicators. The representative samples were taken during the plant’s operation at different points of technological operations and were analyzed for the particle size distribution, Cr_2O_3 content and solid content in the pulp. As it is presented in the paper, from the analysis results it was concluded where the process shortcomings are and how the indicators should be improved. It was concluded that with the proposed improvements, the recovery of Cr_2O_3 increases by about 5% and the cost of processing the raw material decreases by 20% of the existing cost.

Key words**:** *Analysis, recovery, chromium, improvement.*

1. INTRODUCTION

“Maja e Lugut” chromium enrichment plant has begun operations in 2019 and continues to operate with a capacity of 12 t/h, producing concentrate with quality of 51% Cr_2O_3 and recovery of about 71%. During 2025, a study was conducted to see the possibility of further improving enrichment indicators and reducing enrichment costs. The enrichment method used in the plant is gravity separation in spiral separators, base, cleaning and scavenger as well as in 3 steps with concentration tables. Slimes are treated separately in tables suitable for very fine particles. The plant is supplied with raw material chromium ore by a mine and a quarry, in ratio 1:3.

2. MATERIAL AND METHODS

2.1. Material

The raw material chromium ore supplied to the plant, as well as chromium concentrate, tailings, slimes and middlings produced during the operation in industrial scale were used as material of the study.

2.2. Method

Samples were taken every 20 minutes at different links of the enrichment process, during the continuous operation of the plant, in accordance with the relevant methodologies. For a relatively long time, all the main links of the gravimetric enrichment process were sampled. The samples were analyzed for particle size composition, Cr_2O_3 content and densmetric fractions. Conclusions were drawn on the possibility of improving the enrichment process indicators and reducing of enrichment operating cost based on the analysis results.

3. RESULTS AND DISCUSSION

Analysis of the crushing process. The mineral is crushed in two stages in jaw crushers. The mineral crushed in the first stage passes through a vibrating screen with apertures 20 mm. The mineral over the screen + 20 mm passes through the second stage of crushing. Table 1 gives the particle size of the crushed ore.

Table 1. Granulometric analysis of crushed mineral

Particle size, mm	Weight, %
+ 20.00	3.30
- 20.00	96.70
Total	**100.00**

Analysis of the grinding process. The crushed mineral below 20 mm is ground in a rod mill. The grinding is carried out in a closed cycle with a drum screen mounted at the outlet of the mill. The quantity of fraction -0.1mm shown in Table 2, should be reduced between arrangements of grinding parameters, as it is over the possibility of a rod mill to generate it (Bogdanov, 1972).

Table 2. Granulometric analysis of ground ore

Particle size, mm	Weight, %	Cr_2O_3 %	Cr_2O_3 Distribution, %
+1.00	0.50	8.27	0.31
-1.00 +0.50	8.26	8.27	5.14
-0.50 +0.25	30.74	14.99	34.73
-0.25 +0.10	23.16	16.32	28.49
-0.10	37.34	11.13	31.33
Feed	**100.00**	**13.27**	**100.00**

Table 3. Granulometric analysis of over screen product.

Particle size, mm	Dalje, %	Cr_2O_3 %
+1.00	65.28	6.04
-1.00+0.50	24.26	10.41
-0.50+0.25	5.83	10.41
-0.25+0.10	2.58	10.41
-0.10	2.05	10.41
Feed	**100.00**	**8.26**

Analysis of gravimetric process of coarse particles. (Albayrak, 2019) The underflow of the hydrocyclone D250 is treated in spiral separators Fig. 1. The scheme in spiral separators consists of basic, control and cleaning operations. Three products are obtained: Final Chromium Concentrate, middlings and Tailings. The middlings of the spiral separators are further enriched in three steps in shaking tables. From enrichment three products are obtained: Final Chromium Concentrate, Middlings and Tailings. The middlings that come out of the third stage are recycled in the third stage. From the enrichment of the hydrocyclone D250 underflow chromium concentrate and tailings are obtained. From the analysis of tailings it results that the chromium content in the fractions below 0.10mm is high. The fraction -0.1mm of tailings is separated in a screw classifier and together with overflow of hydrocyclene D 250 and of hydraulic classifier is treated in 2 steps of slime shaking tables. Tables 4 to 10 provide analyses of products.

Table 4. The technological figures of the enrichment plant

Products	Weight, %	Cr_2O_3 %	Cr_2O_3 Recovery, %
Chromium concentrate	18.30	51.62	71.20
Tailings	81.70	4.68	28.80
Raw material, chromium ore	**100.00**	**13.27**	**100.00**

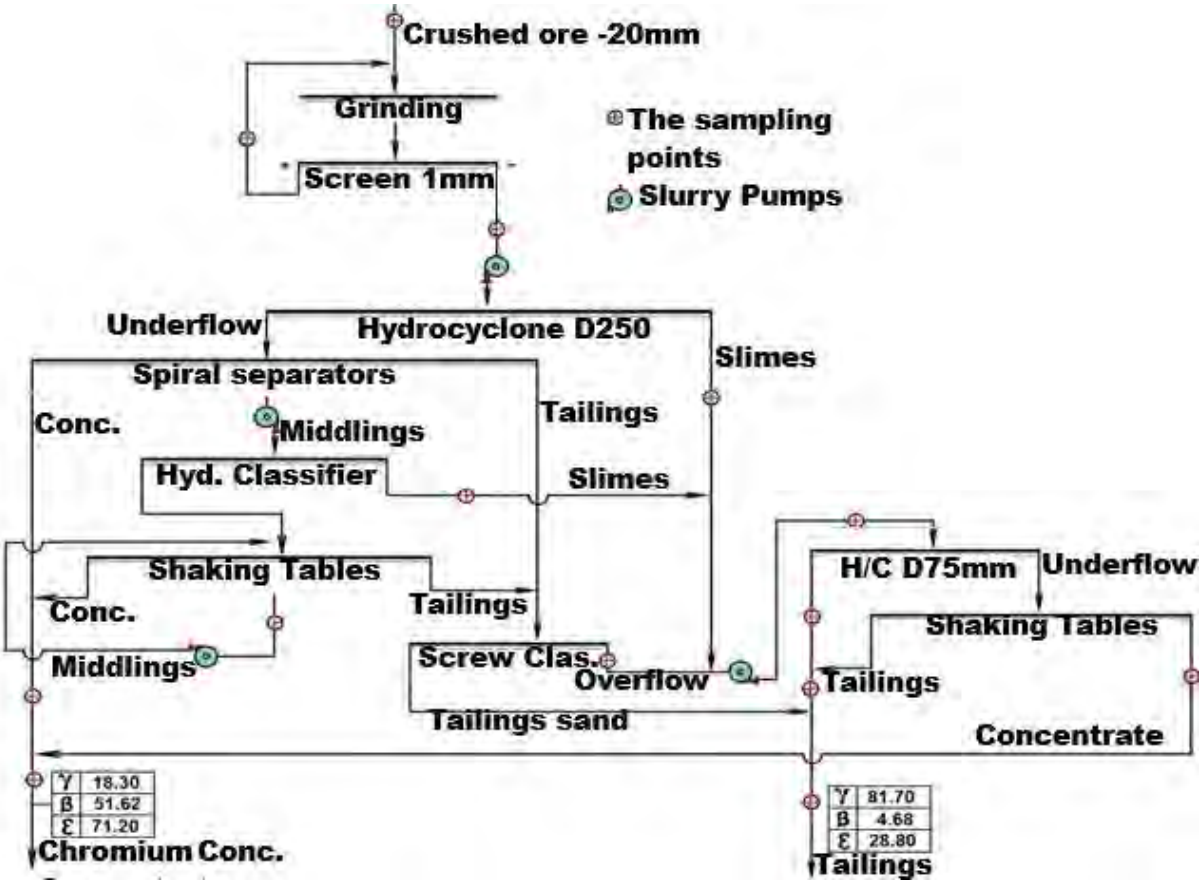

Figure 1. Technological Scheme of enrichment chromium plant.

Table 5. Particle size analyses of final chromium concentrate

Particle size, mm	Weight, %	Cr_2O_3, %	Cr_2O_3 Distribution, %
-1.00 + 0.50	2.94	47.05	2.68
-0.50 + 0.25	34.46	52.85	35.27
-0.25 +0.10	36.08	51.64	36.35
- 0.10	26.52	50.02	25.70
Total	**100.00**	**51.62**	**100.00**

Table 6. Particle size analyses of final tailings

Particle size, mm	Weight, %	Cr_2O_3, %	Cr_2O_3 Distribution, %
-1.00 + 0.50	12.52	5.36	14.34
-0.50 + 0.25	24.06	4.72	24.25
-0.25 +0.10	29.40	3.56	22.37
- 0.10	34.02	5.37	39.04
Total	**100.00**	**4.68**	**100.00**

Table 7. Enrichment figures of fraction -1mm+0.5mm

Products	Weight, %	Cr_2O_3, %	Cr_2O_3 Distribution, %
Chromium concentrate	6.98	47.05	39.71
Tailings	93.02	5.36	60.29
Fraction -1 +0.5mm	**100.00**	**8.27**	**100.00**

Table 8. Enrichment figures of fraction -0.5mm+0.25mm

Products	Weight, %	Cr_2O_3, %	Cr_2O_3 Distribution, %
Chromium concentrate	21.71	52.02	75.34
Tailings	78.29	4.72	24.66
Fraction -0.5mm+0.25 mm	**100.00**	**14.99**	**100.00**

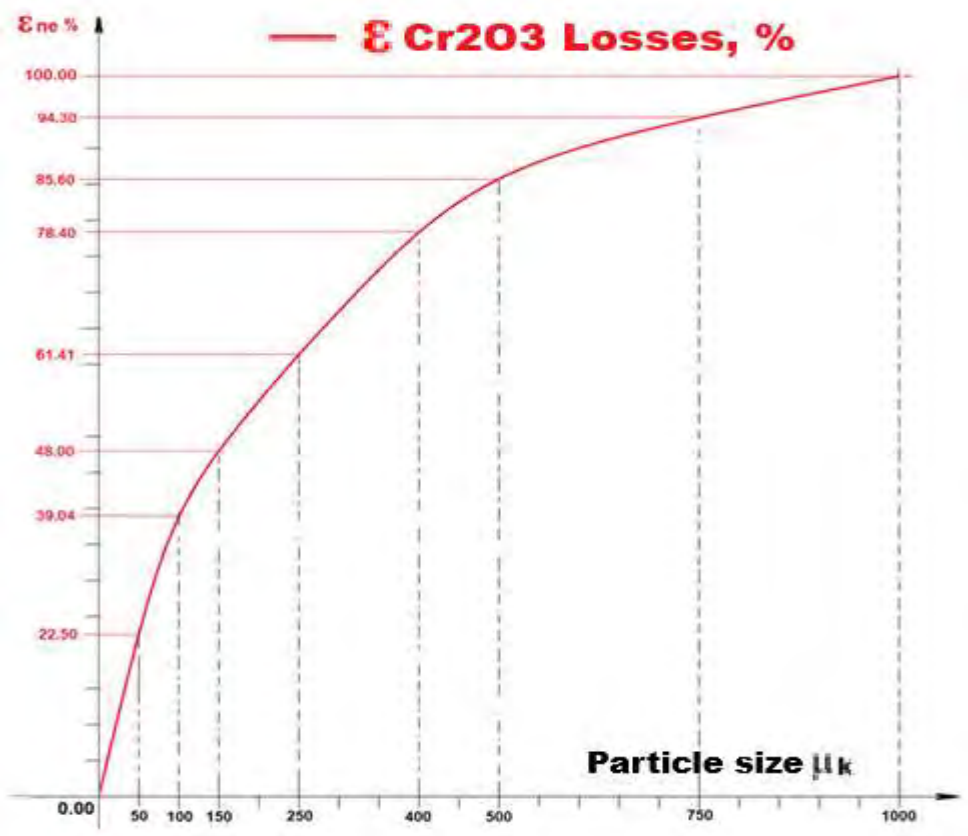

Figure 2. Cr2O3 losses in cumulative percent under screen fractions of final Tailings.

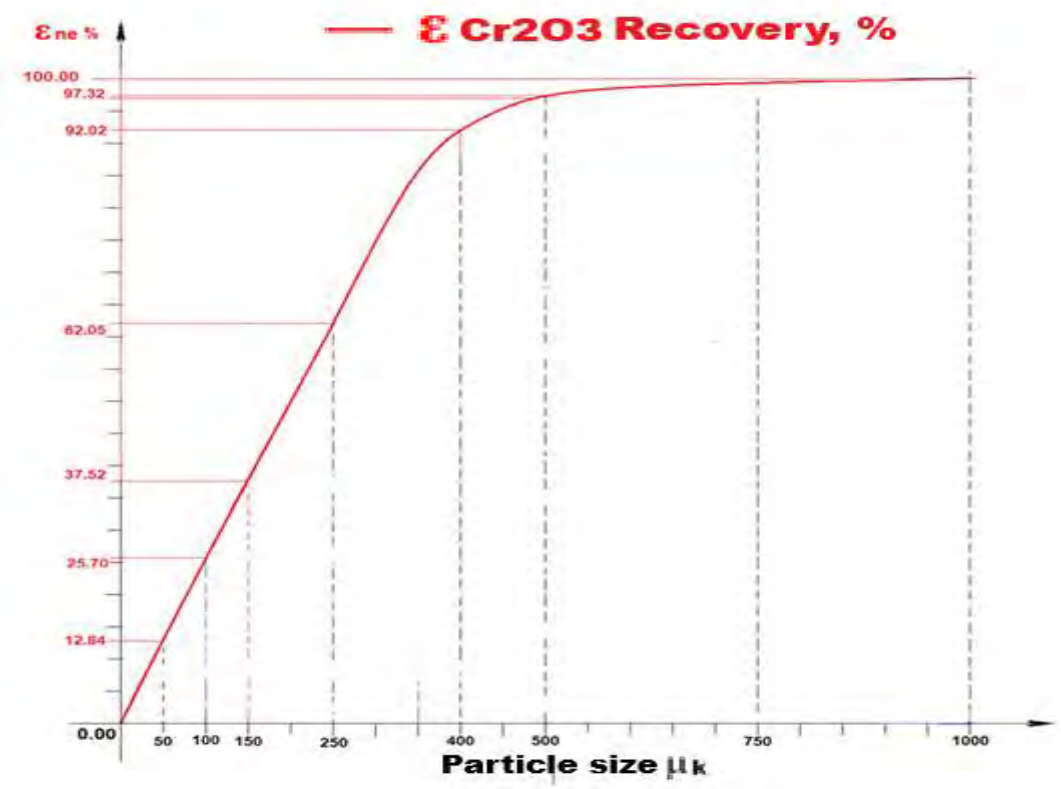

Figure 3. Cr2O3 recovery in cumulative percent under screen fractions of final concentrate.

Table 9. Enrichment figures of fraction -0.25mm+0.1mm

Products	Weight, %	Cr_2O_3, %	Cr_2O_3 Distribution, %
Chromium concentrate	26.54	51.64	83.97
Tailings	73.46	3.56	16.02
Fraction -0.25mm+0.1mm	**100.00**	**16.32**	**100.00**

Table 10. Enrichment figures of fraction -0.1mm

Products	Weight, %	Cr_2O_3, %	Cr_2O_3 Distribution, %
Chromium concentrate	12.93	50.02	58.10
Tailings	87.07	5.37	41.90
Fraction -0.1mm	**100.00**	**11.13**	**100.00**

Based in the results it is concluded that losses in fine fraction -50 micron should be reduced between application of more effective equipment suitable for slime enrichment and the treatment on them of fraction -15 micron that in existing plant is going in tailings (Burt, 1984). Also, the losses with unliberated particles +0.3mm will be reduced returning middlings of third table stage in regrinding. It is predicted that with these improvements the Cr_2O_3 recovery in concentrate will be increased with 5 %.

Fine particles treatment (Boci, 2012). The overflows of 250mm HC, of hydraulic classifier and of screw classifier are sent by pump to the batteries of HC D75mm, to thick the pulp before shaking tables in the value 22% solid content and to separate like tailings the fraction -15 micron that cannot be concentrated in this type of shaking tables. Slime enrichment is carried out on shaking tables partly suitable for fine particles in configuration of the surface, riffles, frequency and step. The tables separate in two stages two products, final chromium concentrate and tailings. The analysis of products are given in tables 11 – 14 and Technological scheme of slime treatment is shown in Fig. 4.

Table 11 Products of Hydrocyclones D75mm

Products	Weight, %	Cr_2O_3 %	Cr_2O_3 Distribution, %
Overflow	20.50	4.10	8.76
Underflow	79.50	11.01	91.24
Feed	**100.00**	**9.60**	**100.00**

Table 12 Particle size analysis of D75 overflow

Particle size mm	Weight, %	Cr_2O_3 %	Cr_2O_3 Distribution, %
+ 0.10	4.20	2.50	2.56
- 0.10	95.80	4.17	97.44
Total	**100.00**	**4.10**	**100.00**

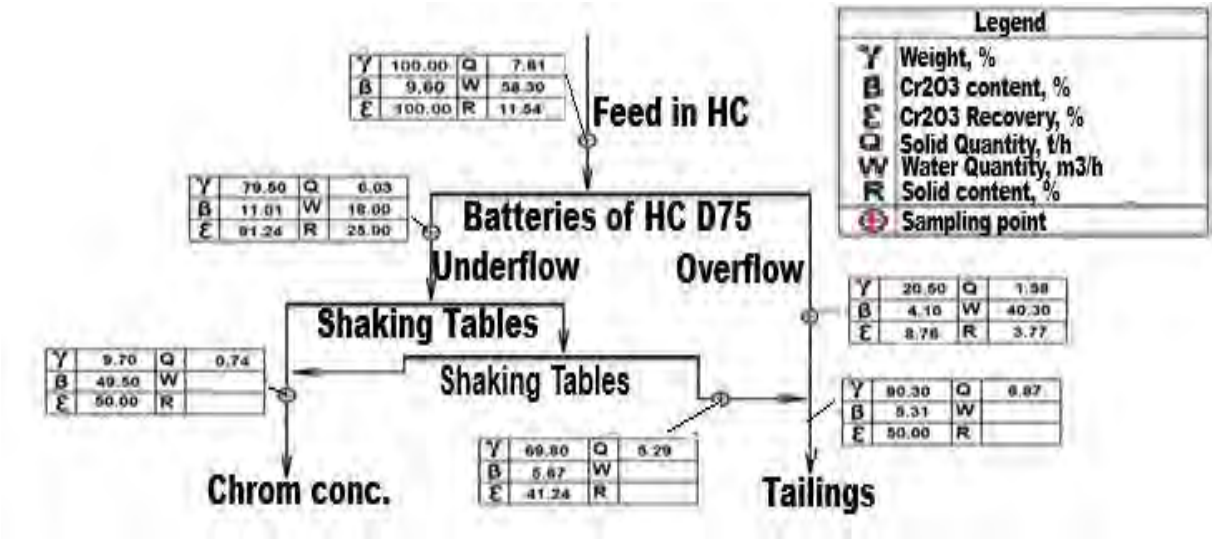

Figure 4. Technological scheme of slime treatment.

Table 13. Particle size analysis of D75 underflow

Particle size mm	Weight, %	Cr_2O_3 %	Cr_2O_3 Distribution, %
+0.10	62.60	7.23	41.08
-0.10	37.40	17.38	58.92
Total	**100.00**	**11.01**	**100.00**

Table 14. Technological figures of HC D75 underflow enrichment

Products	Weight, %	Cr_2O_3 %	Cr_2O_3 Distribution, %
Chromium Concentrate	12.20	49.50	54.83
Tailings	87.80	5.67	45.17
HC underflow	**100.00**	**11.01**	**100.00**

Hand picking separation. The raw material mined from the quarry has a large amount of pure waste. It was tested the hand picking separation of waste in particle size + 30 mm. The results are shown in the table 15.

Table 15. Technological figures of hand picking separation of raw material.

Products	Weight, %	Cr_2O_3 %	Cr_2O_3 Distribution, %
Upgraded ore	68.75	16.11	94.36
Tailings	31.25	2.12	5.64
Raw material of the plant	**100.00**	**11.74**	**100.00**

Another experiment for the hand picking separation was performed with a lower grade ore that is supplied like the raw material in the plant. Initially the material was crushed on the actual plant jaw crusher. The crushed material under 120mm was screened at 50mm. The waste

lumpy were removed by hand from the fraction -120 +50mm and 3 products were weighted and analyzed. The results are given in the Table 16.

Table 16. Technological figures of hand picking separation of raw material.

Products	Weight, %	Cr_2O_3 %	Cr_2O_3 Distribution, %
Upgraded ore (-120mm+50mm)	12.26	14.55	24.04
Tailings (-120+50mm)	33.40	3.73	16.79
Fraction -50mm	54.34	8.08	59.17
Raw material of the plant	**100.00**	**7.42**	**100.00**
Upgraded Raw Material	**66.60**	**9.27**	**83.21**

The results of experiments show that it is necessary to make testing with XRT- based ore sorting in the difference between waste and chromium ore in color and in the specific gravity. The results should be better since the XRT ore sorting operates up to particle size 8 mm and has better figures and lower cost that workers do (Vargas, 2025). It is foreseen a cost operating reduction of 20 % with application of hand picking separation and higher with the application of XRT ore sorting that should be precise with this equipment testing.

Heavy liquid testing of tailings (Demi, 2025). A specific gravity analysis of the final plant tailings was performed to obtain data on the nature of chromium losses on them. This analysis is given in the Table 17. From the chemical analysis results that about 30% of Cr_2O_3 losses are in tailings belong to fine particles below 0.10mm. Similarly, about 23% of losses belong to the unliberated particles above 0.3 mm; and about 31 % are as mechanical losses that come from the effectiveness of existing enrichment equipment, fluctuation in process and not enough correct workers operating. This could be improved between the application of automation that is missing in this plant. The Cr_2O_3 losses with pure gangue liberated particles in tailings are about 16%.

Table 17. The specific gravity analysis of final plant tailings.

Products	Weight, %	Cr_2O_3 %	Cr_2O_3 Distribution, %
Fraction +3.30 g/cm3	2.79	45.10	31.22
Fraction -3.30+2.89 g/cm3	4.97	18.71	23.07
Fraction -2.89 g/cm3	71.81	0.90	16.00
Fraction -0.1 mm	20.43	5.86	29.71
Final plant tailings	**100.00**	**4.03**	**100.00**

4. CONCLUSION

The slimes quantity generated in grinding is high, it should be decreased between arrangements of grinding parameters. The slimes should be treated in suitable equipment for slime enrichment.

The semi-products of the third stage of the shaking tables should be returned to the input of the grinding process. They are still not complete liberated.

About of 30% of losses in tailings belongs to particles with grade 45% Cr_2O_3 that comes mainly from fluctuation of process and not correct operation of workers. It is recommended to be calculated the profit of automation application.
It is predicted to be increased the Cr_2O_3 recovery with 5% between improvements of slime and middlings treatment.

Hand picking separation is a simple process with promising economic indicators. It is possible to decrease the enrichment operating cost by about 20% of existing cost separating about 30-

35% of pure sterile before grinding and enrichment expensive processes with pick hand separation. It is recommended to be tested ore sorting XRT that will have better technological and economic results.

REFERENCES

Albayrak, A., (2019), “New Beneficiation Flowsheet for Kangal-Yellice Chromite Ore”, 978–984.

Boci, S., (2012), “The Study and Technological Project of Chromium Enrichment Plant in Deve, Kosovo”.

Bogdanov, S. O., (1972), “Spravocnik of Obogashjenjiju Rud”, 350–358.

Burt, R. O., (1984), “Gravity Concentration Technology”, 438–444.

Demi, G., (2025), “Recycling of Chromium Tailings in Bulqiza Plant”, XVI International Mineral Processing & Recycling Conference Publication, 556–562.

Vargas, C., (2025), “The Role of TOMRA’s XRT-Based Ore Sorting in Metallic Ore Processing”, XVI International Mineral Processing & Recycling Conference Presentation.

RESEARCH ON THE RECOVERY OF LEAD AND IRON FROM THE SLAG OF A LEAD-ACID BATTERY RECYCLING PLANT USING PHYSICAL METHODS

Tülin ULUCAN*, Nazlım İlkyaz DINÇ, Şevval YILDIRIM, Kerem BÖLÜKBAŞ, Fırat BURAT

Istanbul Technical University, Mining Faculty, Mineral Processing Engineering Department, 34463, Maslak, Istanbul, TÜRKİYE
**Corresponding author: ulucant@itu.edu.tr*

A B S T R A C T

Lead-acid batteries are widely utilized energy storage devices due to their superior performance, yet their extensive use generates significant disposal challenges at the end of service life. Spent batteries contain critical metals whose recovery can provide both environmental and economic benefits. In particular, lead and iron can be extracted from battery slag through appropriate physical beneficiation techniques, contributing to sustainable resource utilization.

In this study, slag material obtained from a recycling company that recovers lead from waste lead–acid batteries were processed to investigate the recovery of lead (Pb) and iron (Fe) using gravity and magnetic separation methods. A shaking table was used to separate particles based on density, whereas high-intensity magnetic separators (including REMS and a rotary disc magnetic separator) were employed to exploit differences in magnetic susceptibility. Particle size analysis revealed d_{80} and d_{50} values of 0.56 mm and 0.3 mm, respectively, with Pb and Fe distributed across all fractions. The highest Pb concentration was found in finer particles. Shaking table experiments on the -1+0.3 mm and -0.3 mm fractions showed only partial Pb–Fe separation, as lead became increasingly disseminated within iron at smaller sizes. In the experiments conducted using REMS, the presence of only 0.1% Fe in the non-magnetic product of the −0.3 mm fraction indicates effective separation of Fe. In contrast, the recovery of Pb in the non-magnetic product was limited to 0.5% for the same fraction, suggesting insufficient separation due to the low mass yield of the product and the presence of locked particles. Similarly, in the rotary disc magnetic separator, nearly all Fe in the −0.3 mm fraction was reported to the magnetic products, while Fe recovery in the non-magnetic product remained as low as 0.03%.

Key words: *Lead-acid battery, recycling, physical enrichment, Pb, Fe*

1. INTRODUCTION

Lead–acid batteries (LABs) are widely recognized as the first practical rechargeable battery technology, originally developed by Gaston Planté in 1859 (Encyclopaedia Britannica; Kurzweil, 2010). Owing to a mature manufacturing infrastructure, high surge-current capability, relatively reliable low-temperature performance, and an established recycling supply chain, LAB systems continue to play a critical role in both automotive and industrial applications (Ballantyne et al., 2018; May et al., 2018). Figure 1 presents a graph illustrating trends in the global supply and demand of refined lead (Wood Mackenzie, 2019). Based on these data, Figure 1 shows a steady increase in refined lead demand over the 1988–2040 period, with a pronounced acceleration after 2020. On the supply side, primary production remains the dominant source, while the contribution of secondary production (recycling-derived supply) increases progressively over time. This trend emphasizes the growing importance of recycling for supply security and resource efficiency. Nevertheless, considering the projected pace of demand growth, an expansion in secondary production alone is unlikely to meet total requirements; thus, in the medium to long term, both an increase in secondary production capacity and a continued, moderate expansion of primary production are expected to be necessary. Also, Figure 2 presents global refined lead production: primary and secondary lead production volumes (2007–2025) and provides the primary and secondary lead production

history/forecast, highlighting the relative contributions and temporal evolution of primary and secondary supply (Boab Metals Limited, October 2022).

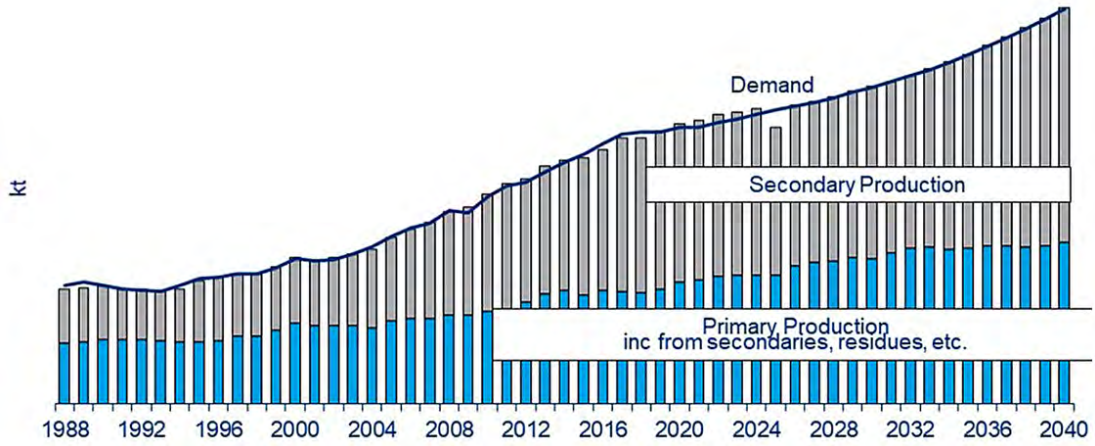

Figure 1. Global refined lead supply and demand (Wood Mackenzie, 2019)

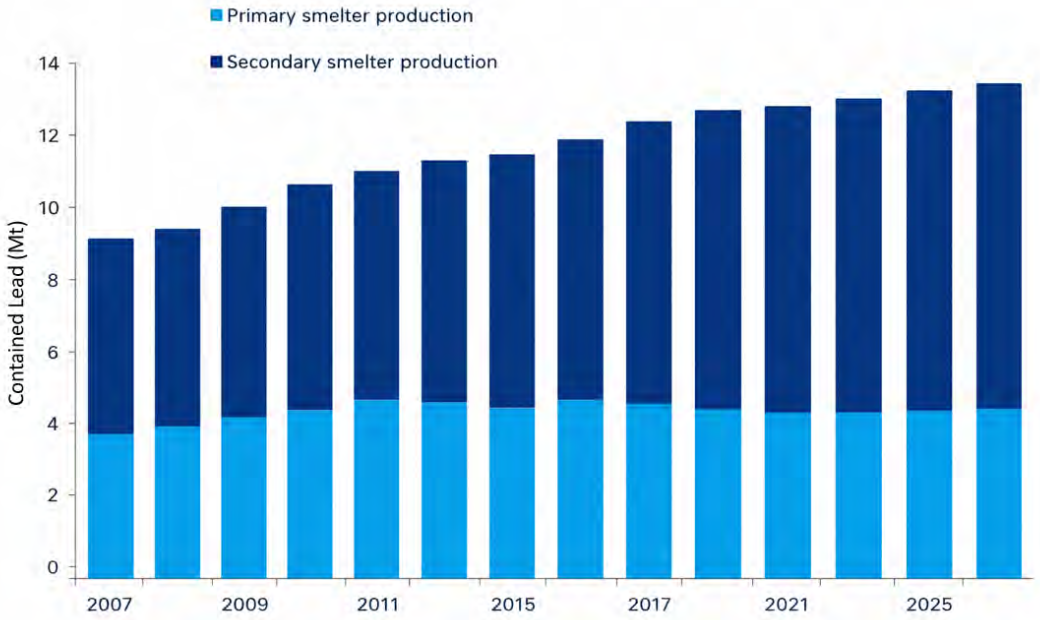

Figure 2. Global refined lead production: primary and secondary lead production volumes (2007-2025) (Boab Metals Limited, October 2022)

In a typical lead–acid battery (LAB) cell (Figure 3), the positive electrode active material is PbO_2, the negative electrode active material is porous metallic lead (Pb), and the electrolyte is dilute H_2SO_4. The charge–discharge cycle proceeds through reversible transformations of the Pb/PbO_2 redox couple in sulfuric acid media. In industrial practice, conventional flooded designs remain widely used; however, valve-regulated lead–acid (VRLA) configurations such as absorbent glass mat (AGM) and gel-electrolyte batteries are also common and offer advantages in terms of sealing and reduced maintenance requirements (May et al., 2018).

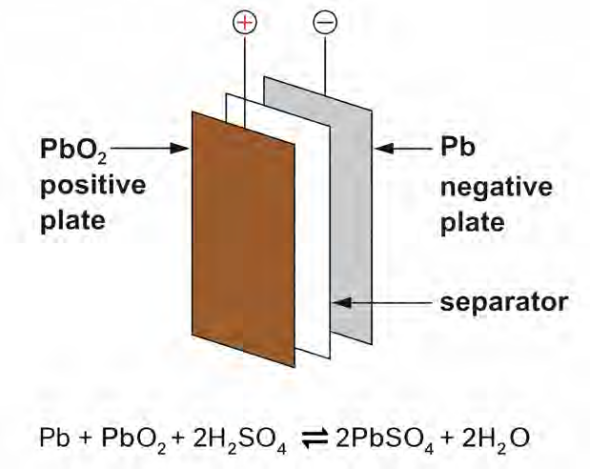

Figure 3. Fundamental chemistry and primary components of a lead–acid battery (May et al., 2018)

The most widespread application of lead–acid battery (LAB) technology is in automotive starter–lighting–ignition (SLI) systems. LABs also hold a substantial market share in uninterruptible power supply (UPS) applications for telecommunications and data centers, standby/grid backup systems, industrial traction (e.g., forklifts), and stationary energy storage integrated with renewable energy systems (USGS 2024; May et al., 2018). USGS (2024) further reports that the lead–acid battery industry accounts for the majority of U.S. lead consumption and emphasizes the critical role of industrial batteries in standby power for computer and telecommunications networks. The major application areas of lead–acid batteries are summarized in Table 1. While USGS 2025 identifies automotive SLI, standby/UPS, and motive power as the principal uses, the Battery Council International (BCI) provides a sector-based classification that further details applications such as telecommunications and data centers, as well as stationary energy storage (Battery Council International).

Table 1. Major application areas of lead-acid batteries (USGS 2025; Battery Council International)

Application area	Typical use/example
Automotive SLI (Starting-Lighting-Ignition)	Starter and auxiliary electrical systems in passenger and commercial vehicles
Standby/UPS (critical backup power)	Uninterruptible power supply (UPS) for computer and telecommunications networks; critical infrastructure backup
Motive power (traction)	Forklifts and in-warehouse electric industrial vehicles
Utility-scale / utility-grade energy storage	Grid support, microgrids, and demand management (application classification)
Renewable-integrated stationary energy storage	Solar/wind-integrated storage (application classification)
Data centers	Data center UPS applications (application classification)
Logistics and warehousing	Warehouse equipment, ground support equipment, and selected transport applications (application classification)

Spent lead–acid batteries (LABs) generally comprise four main fractions: plastic casings/separators, waste electrolyte, lead-alloy grids, and lead paste (active material), with most of the lead inventory residing in the grid and, in particular, the paste fraction (Xiong et al., 2022). Lead paste is dominated by sulfate-bearing lead phases; anglesite ($PbSO_4$) and

lanarkite ($PbO \cdot PbSO_4$) have been reported to account for >60% of the paste in many cases, while PbO_2, PbO, and minor amounts of metallic Pb occur in variable proportions (Xiong et al., 2022). Because this phase assemblage strongly influences process selection as well as the overall energy demand and emission profile, beneficiation strategies implemented at the front end of the recycling flowsheet are of critical importance.

In conventional mineral processing, beneficiation is conducted after comminution and classification, and typically involves gravity separation (e.g., shaking tables), magnetic separation, and, when required, flotation. These unit operations exploit contrasts in density, magnetic susceptibility, and surface physicochemical properties to separate valuable phases from gangue. Similar principles apply to heterogeneous secondary resources such as spent LAB fractions: differences in density, electrical conductivity, and magnetic response among constituent materials can be harnessed through appropriate flowsheet design to achieve selective separation (Ballantyne et al., 2018).

In LAB recycling, the initial stage is commonly referred to as “battery breaking,” where mechanical crushing and sorting are used to partition the feed into discrete fractions. During this step, plastics and electrolytes are removed, and metallic grids are separated from the paste/fine fraction by screening and classification (Ballantyne et al., 2018). Subsequent physical beneficiation aims to produce a pre-concentrate by reducing the chemical complexity of the material fed to downstream metallurgy. Specifically, physical beneficiation is employed to (i) increase the mass fraction of lead-bearing phases, (ii) decrease organic/plastic residues and inert or undesirable components, and (iii) provide a more consistent and controllable feed for subsequent pyrometallurgical or hydrometallurgical processing. This approach is particularly relevant for managing sulfate-rich paste, as sulfate content is a key determinant of SO_2 formation and energy requirements in pyrometallurgical routes (Zhang et al., 2016; Xiong et al., 2022).

From a metallurgical standpoint, pyrometallurgy remains the dominant industrial route for secondary lead production; however, high-temperature reduction/smelting is associated with substantial energy consumption and environmental burdens, including lead-bearing dust/fume and SO_2 emissions derived largely from sulfate-containing species (Zhang et al., 2016). Accordingly, many flowsheets recommend either desulfurization of the paste before smelting or upstream pretreatment/beneficiation measures aimed at lowering the sulfate load (Xiong et al., 2022). In contrast, hydrometallurgical and electro-hydrometallurgical approaches operate at lower temperatures via leaching followed by precipitation and/or electrowinning, and therefore offer the potential to mitigate high-temperature emission pathways (Tan et al., 2019; Ballantyne et al., 2018). Nevertheless, given the chemical complexity of lead paste and thermodynamic/solubility constraints associated with sulfate phases, producing a fractionated and “cleaner” feed via physical beneficiation can also improve selectivity and overall process performance in hydrometallurgical schemes (Xiong et al., 2022).

Overall, physical beneficiation steps designed in accordance with classical mineral processing principles represent a strategic front-end intervention in spent LAB recycling. By enabling pre-concentrate production before metallurgy, such steps can enhance technical performance while supporting improved environmental sustainability of the overall recycling chain (Ballantyne et al., 2018; Zhang et al., 2016).

2. MATERIAL AND METHODS

The lead–acid battery slag used in this study was supplied by the MNC lead–acid battery recycling facility and transported to the ITU Mineral Processing Engineering Department, Prof. Dr. Güven Önal Pilot Plant. The primary objective was to recover lead (Pb) and iron (Fe) from this slag through physical beneficiation. Accordingly, the received material was homogenized

and prepared to obtain representative test samples, and particle size characterization was subsequently performed before the beneficiation experiments. The sample was successively comminuted using jaw, cone, and roll crushers, and the entire material was reduced to below 1 mm. Representative images of the crusher product are presented in Figure 4. To determine the particle size distribution, a dry sieve analysis was performed on the roll-crusher product, and the cumulative undersize curve is shown in Figure 5. According to this analysis, the d_{80} and the d_{50} sizes were determined as 0.56 and 0.3 mm, respectively.

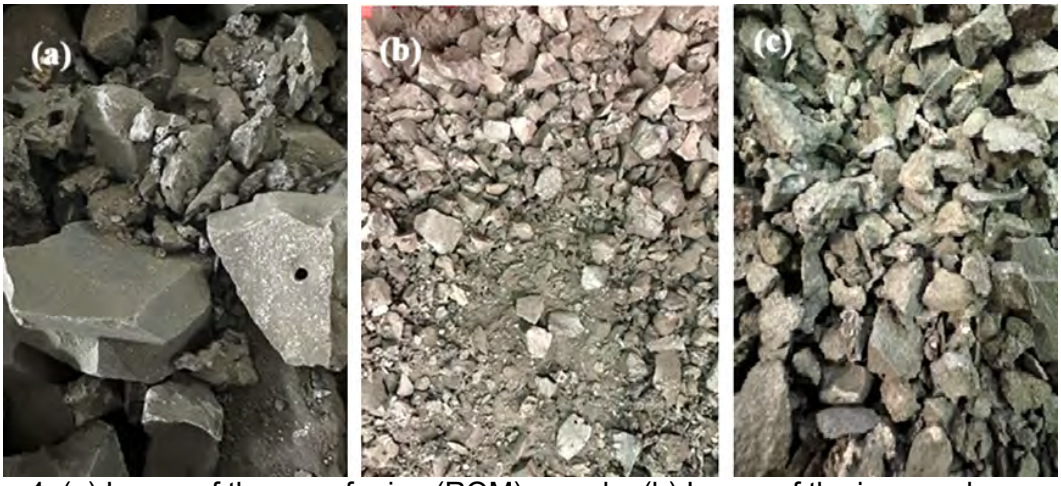

Figure 4. (a) Image of the run-of-mine (ROM) sample. (b) Image of the jaw-crusher product. (c) Image of the cone-crusher product

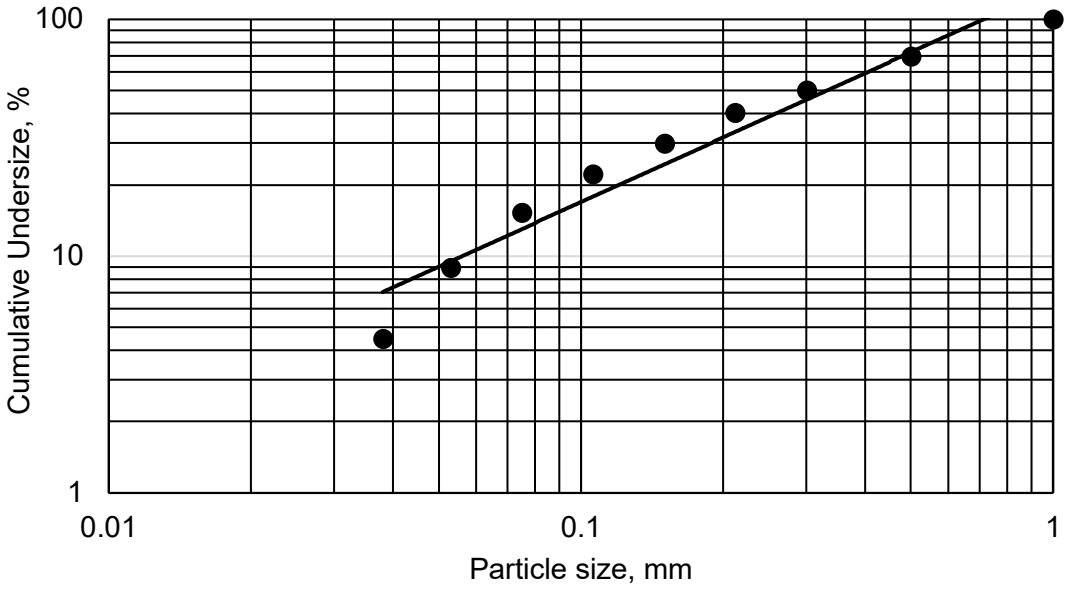

Figure 5. The particle size distribution curve of the lead–acid battery slag

Before the beneficiation experiments, the slag sample was chemically characterized at the ITU Mineral Processing Engineering Chemical Analysis Laboratory. The resulting total Fe and Pb grades, together with their distribution across the different size fractions, are summarized in Table 2.

Table 2. Chemical analysis results of the roll-crusher product

Size, mm	Amount, %	Fe		Pb	
		C, %	D, %	C, %	D, %
-1+0.5	30.1	45.8	34.5	5.3	36.6
-0.5+0.3	19.6	35.7	17.5	4.2	19.0
-0.3+0.212	10.1	40.9	10.3	4.4	10.3
-0.212+0.150	10.3	38.4	9.9	4.0	9.5
-0.150+0.106	7.7	35.9	6.9	3.9	6.9
-0.106+0.075	6.9	33.4	5.7	3.4	5.4
-0.075+0.053	6.4	42.0	6.7	3.7	5.4
-0.053+0.038	4.4	40.3	4.5	2.9	3.0
-0.038	4.5	37.1	4.2	3.8	4.0
Total	100.0	40.1	100.0	4.3	100.0

C: Content, D: Distribution

The data presented in Table 2 indicate that the lead–acid battery slag sample does not exhibit a pronounced and sharp enrichment of Pb and Fe across the particle size fractions; nevertheless, both mass and metal distributions are preferentially concentrated in the coarser size ranges. In line with the fact that the two coarsest fractions (−1+0.5 and −0.5+0.3 mm) account for approximately half of the total mass, they also contain more than half of the total Pb and Fe, suggesting that metal deportment is largely concentrated toward coarse particles. The Pb grade varies within a relatively narrow range and shows an overall decreasing tendency toward finer fractions, whereas the Fe grade fluctuates within a similarly limited band without a clear dependence on particle size. These findings imply that achieving high selectivity through size-based operations such as screening and classification alone may be limited; therefore, integrating processes based on differences in magnetic susceptibility and/or density (e.g., high-intensity magnetic separation and gravity separation) into the flowsheet would be more appropriate for Pb–Fe separation.

Following comminution, the lead–acid battery slag sample was reduced to <1 mm at the roll-crusher discharge and subsequently classified by sieving into two size fractions (−1+0.3 mm and −0.3 mm). These fractions were then used as feed for the physical beneficiation experiments aimed at the separate recovery of Fe- and Pb-bearing components. Gravity separation was carried out using a shaking table to exploit differences in specific gravity, while magnetic separation was performed using a dry high-intensity REMS-type magnetic separator and a dry rotary disc magnetic separator.

3. RESULTS AND DISCUSSION

In the shaking table beneficiation tests, identical operating conditions were applied to both size fractions: the feed and wash water flow rates were each set to 3 L/min, the stroke frequency to 300 cycles/min, the stroke amplitude to 15 mm, and the table inclination to 5°. The separation produced four products for each size fraction (−1+0.3 mm and −0.3 mm), namely light, middling, heavy fraction, and slime fractions (−0.053 mm). The metal grades and distributions of all products, for both size groups, are summarized in Table 3.

Table 3. Shaking table test results consolidated on a cumulative basis

Size, mm	Products	Amount		Fe		Pb	
		%	Based on the feed	C, %	D, %	C, %	D, %
-1+0.3	Heavy	8.1	4.0	49.5	5.4	10.3	10.1
	Middling	44.6	22.1	37.1	22.1	4.5	24.2
	Light	47.3	23.4	34.2	21.6	3.7	21.1
	Total	**100.0**	**49.5**	**36.7**	**49.0**	**4.6**	**55.3**
-0.3	Heavy	4.2	1.9	49.1	2.6	11.0	5.2
	Middling	41.0	18.9	46.2	23.5	5.3	24.3
	Light	54.8	25.2	31.5	21.4	2.2	13.3
	Total	**100.0**	**46.1**	**38.2**	**47.4**	**3.8**	**42.8**
-0.053			4.4	30.1	3.6	1.7	1.9
Total			**100.0**	**37.1**	**100.0**	**4.1**	**100.0**

Table 3 indicates that, in the shaking table gravity beneficiation tests, the majority of the mass in both size fractions was recovered in the light and middling products (approximately 92% for −1 + 0.3 mm and 96% for −0.3 mm). This distribution suggests limited separation sharpness and implies the presence of a substantial proportion of composite/locked particles. With respect to Pb, the heavy product yielded the highest grades (~10–11% Pb); however, because the heavy fraction represented only about 4–8% of the mass, it accounted for only a minor portion of the total Pb recovered (~5–10% Pb distribution). The considerable amount of Pb in the middling product (~24%) and, to a lesser extent, in the light product indicates that Pb could not be fully concentrated into the heavy fraction by gravity separation alone. The broadly similar deportment of Fe, which also remained largely distributed between the light and middling products, further supports that achieving high-selectivity Pb–Fe separation using gravity beneficiation alone may be limited. Therefore, strengthening the flowsheet with a complementary step after tabling, particularly high-intensity magnetic separation targeting the middling stream, would be more appropriate.

In the magnetic separation tests performed using the REMS unit, the slag sample in the −1+0.3 mm size fraction was processed first. For this fraction, the magnetic splitter blade angle was set to 90°, the non-magnetic splitter blade angle to 130°, and the belt speed to 130 rpm. For the −0.3 mm fraction, the operating parameters were adjusted to a magnetic splitter blade angle of 150°, a non-magnetic splitter blade angle of 140°, and a belt speed of 120 rpm. The results, consolidated on a cumulative basis, are summarized in Table 4.

Table 4. Contents and distributions of the products obtained from the REMS magnetic separation tests, consolidated on a cumulative basis

Size, mm	Amount, %	Products	Amount, %	Based on the feed, %	Fe		Pb	
					C, %	D, %	C, %	D, %
-1+0.3	54.6	Magnetic	39.0	21.3	48.5	25.3	6.9	32.8
		Middling	59.9	32.7	36.2	28.9	3.1	22.3
		Non-magnetic	1.1	0.6	24.4	0.4	6.6	0.9
		Total	**100.0**	**54.6**	**40.9**	**54.6**	**4.6**	**55.9**
-0.3	45.4	Magnetic	43.7	19.8	44.1	21.4	4.7	20.6
		Middling	55.8	25.3	38.6	23.9	4.1	23.0
		Non-magnetic	0.5	0.2	11.5	0.1	9.7	0.5
		Total	**100.0**	**45.4**	**40.9**	**45.4**	**4.4**	**44.1**
Total Feed	**100.0**			**100.0**	**40.9**	**100.0**	**4.5**	**100.0**

Table 4 shows that the REMS dry high-intensity magnetic separator is effective for Fe upgrading, while Pb exhibits a less selective response. In both size fractions, nearly all material reports to the magnetic and middling streams, with only a negligible non-magnetic yield. Fe is enriched in the magnetic products (up to 48.5% Fe), whereas Pb is largely split between the magnetic and middling streams, indicating limited Pb–Fe selectivity, likely due to incomplete liberation and/or composite particles. Therefore, reprocessing of the middling stream (e.g., via a second-stage magnetic or rotary disc separation) is recommended to enhance Pb recovery and selectivity.

Rotary disc magnetic separation tests were conducted on the slag samples in the −1+0.3 mm and −0.3 mm size fractions. Magnetic field intensities of 2 A and 3 A were applied to these fractions, respectively. The results, consolidated on a cumulative basis, are presented in Table 5.

Table 5. Contents and distributions of the products obtained from rotary disc magnetic separation, consolidated on a cumulative basis

Size, mm	Products	Amount, %	Fe		Pb	
			C, %	D, %	C, %	D, %
-1+0.3	Magnetic 1	53.5	43.7	62.1	6.4	84.9
	Magnetic 2	4.8	26.3	3.4	3.4	4.0
	Magnetic 3	30.5	35.0	28.3	0.9	6.6
	Magnetic 4	10.2	22.6	6.1	1.1	2.7
	Non-magnetic	1.1	5.2	0.1	6.7	1.8
	Total	**100.0**	**37.6**	**100**	**4.0**	**100**
-0.3	Magnetic 1	41.4	44.0	46.9	5.8	59.3
	Magnetic 2	57.6	35.5	52.7	2.7	38.3
	Magnetic 3	0.5	27.7	0.4	3.7	0.5
	Non-magnetic	0.5	4.8	0.1	15.7	2.0
	Total	**100.0**	**38.8**	**100**	**4.1**	**100**

Table 5 shows that, in rotary disc magnetic separation, Pb is predominantly directed to the magnetic products in both size fractions. For the −1 + 0.3 mm fraction, most of the Pb reports to the Magnetic 1 stream (Pb distribution: 84.9%; Pb grade: 6.4%), and this stream also carries a substantial portion of Fe (Fe distribution: 62.1%). For the −0.3 mm fraction, Pb distribution is shared between the two main magnetic streams, reaching 59.3% in Magnetic 1 and 38.3% in Magnetic 2. Although the non-magnetic products exhibit high Pb grades (particularly 15.7% Pb for −0.3 mm), their very low mass yield results in limited overall Pb recovery (Pb distribution: 2.0%). Overall, the results indicate that the rotary disc separator effectively concentrates Pb into the magnetic fractions; however, Pb–Fe separation selectivity remains limited because Fe is also recovered at high levels in the same streams.

4. CONCLUSION

The lead–acid battery slag was comminuted to <1 mm and characterized by dry sieve analysis, where the cumulative undersize curve (Figure 5) supported the selection of two feed size fractions (−1+0.3 mm and −0.3 mm) and enabled monitoring of slime generation (−0.053 mm). Size-by-size chemical results (Table 2) indicated that Pb (4.3%) and Fe (40.1%) do not exhibit strong upgrading by screening alone, highlighting the need for property-based beneficiation. Shaking table tests (Table 3) produced the highest Pb grades in the heavy product (~10–11% Pb), yet the low heavy yield limited Pb recovery, and most of the mass and metals remained in the light and middling streams, suggesting limited separation sharpness and probable locked/composite particles. REMS high-intensity magnetic separation (Table 4) effectively upgraded Fe in the magnetic product (up to 48.5% Fe), but Pb was largely partitioned between the magnetic and middling products, while the non-magnetic yield was negligible. Rotary disc separation (Table 5) similarly directed most Pb to magnetic products (e.g., 84.9% Pb distribution in Magnetic 1 for −1 + 0.3 mm), but substantial Fe reporting to the same streams confirmed limited Pb–Fe selectivity. Overall, the findings suggest that improved performance requires a staged flowsheet focusing on reprocessing of the middling streams (and slime control), potentially combined with liberation enhancement, to increase recovery and selectivity. The findings indicate that gravity and magnetic separation methods remain limited in terms of Pb-Fe selectivity, particularly in the efficient management of middling streams. To overcome these challenges and achieve a sharper separation in fine fractions (−0.3 mm and −0.053 mm slime size) where liberation increases but physical methods become ineffective, froth flotation is proposed as an alternative beneficiation route. By enabling separation based on chemical surface properties, flotation has the potential to minimize the loss of selectivity caused by locked particles and enhance overall Pb recovery.

ACKNOWLEDGEMENTS

This study was carried out within the scope of the TÜBİTAK 2209-A University Students Research Projects program, and we gratefully acknowledge TÜBİTAK for its financial support.

REFERENCES

Ballantyne, A. D., Hallett, J. P., Riley, D. J., Shah, N., Payne, D. J., (2018) “Lead acid battery recycling for the twenty-first century”, Royal Society Open Science, 5 (5) 171368.

Battery Council International. Uses & applications of essential lead batteries. Retrieved January 21, 2026, from https://batterycouncil.org/resource/uses-applications-of-essential-lead-batteries/.

Boab Metals Limited. (October 2022). Lead. Retrieved January 22, 2026, from https://boabmetals.com/lead/.

Encyclopaedia Britannica. Lead-acid storage battery. In Encyclopaedia Britannica. Retrieved January 22, 2026, from https://www.britannica.com/technology/lead-acid-storage-battery.

Kurzweil, P., (2010) “Gaston Planté and his invention of the lead–acid battery—The genesis of the first practical rechargeable battery”, Journal of Power Sources, 195 (14), 4424–4434.

May, G. J., Davidson, A., Monahov, B., (2018) “Lead batteries for utility energy storage: A review”, Journal of Energy Storage, 15 145–157.

Tan, S. Y., Payne, D. J., Hallett, J. P., Kelsall, G. H., (2019) “Developments in electrochemical processes for recycling lead–acid batteries”, Current Opinion in Electrochemistry, 16 83–89.

U.S. Geological Survey, (2024) “Lead”, Mineral commodity summaries, U.S. Geological Survey. https://pubs.usgs.gov/periodicals/mcs2024/mcs2024-lead.pdf.

U.S. Geological Survey, (2025) “Lead”, Mineral commodity summaries, U.S. Geological Survey. https://pubs.usgs.gov/periodicals/mcs2025/mcs2025-lead.pdf.

Wood Mackenzie, (2019) “Global lead long-term outlook: Q2 2019”, Retrieved January 22, 2026, from https://www.woodmac.com/reports/metals-global-lead-long-term-outlook-q2-2019-317470/.

Xiong, Y., (2022) “Recycling of lead pastes from spent lead–acid batteries: Thermodynamic constraints for desulphurization”, Recycling, 7 (4) 45.

Zhang, W., Yang, J., Wu, X., Hu, Y., Yu, W., Wang, J., Dong, J., Li, M., Liang, S., Hu, J., Kumar, R. V., (2016) “A critical review on secondary lead recycling technology and its prospect”, Renewable and Sustainable Energy Reviews, 61 108–122.

UPGRADING OF LOW-GRADE TITANIUM ORES BY HIGH-INTENSITY MAGNETIC SEPARATION: A CASE STUDY FROM ESKİŞEHİR, TÜRKİYE

Ulaş USLU*, Yusuf Enes PURAL, Mustafa ÖZER

Istanbul Technical University, Faculty of Mines, Mineral Processing Engineering Department, 34469, Maslak, Istanbul, TÜRKİYE
**Corresponding author: usluu19@itu.edu.tr*

A B S T R A C T

This study investigates the beneficiation of titanium dioxide (TiO_2) minerals from primary titanium ore deposits located in the Eskişehir region of Türkiye. Experimental work was carried out on ores containing 4–6% TiO_2 through comprehensive physical, chemical, and mineralogical characterization, followed by beneficiation tests using magnetic and gravity separation methods at various particle sizes.

Three-stage crushing (jaw, cone, and roll) and controlled grinding were employed to reduce the particle size below 0.106 mm. XRF and microscopic analyses revealed that the ore primarily contains rutile (TiO_2) and sphene ($CaTiSiO_5$) as major titanium-bearing minerals, with a minor amount of ilmenite ($FeTiO_3$). Magnetic separation tests demonstrated that TiO_2 minerals were liberated below 0.354 mm, and the highest TiO_2 grades were obtained in the -0.106 mm fraction.

High-intensity (10.000–11.000 Gauss) wet magnetic separation yielded non-magnetic products containing up to 11.96% TiO_2, confirming that titanium occurs mainly in non-magnetic rutile and sphene phases.

In conclusion, primary titanium ores from the Eskişehir region can be effectively concentrated by high-intensity magnetic separation under suitable grinding conditions. This research provides a valuable basis for the utilization of domestic TiO_2 resources and the industrial production of titanium compounds.

Key words: *Titanium dioxide (TiO_2), beneficiation, magnetic separation, gravity separation, rutile, sphene, ilmenite*

1. INTRODUCTION

Titanium is an irreplaceable strategic transition metal in aerospace, space technologies, marine engineering, defense, and medical industries due to its exceptional specific strength, corrosion resistance, biocompatibility, and high-temperature stability (Matsanga et al., 2024). Beyond titanium metal and its specialty alloys, the vast majority, approximately 90% of globally extracted titanium is consumed in the form of titanium dioxide (TiO_2) pigment, which is critical for the paint, coating, plastics, and paper industries. The vital economic importance of titanium, combined with supply chain vulnerabilities and the geographical concentration of high-grade reserves, has raised profound international concerns regarding sustainable titanium supply. The geopolitical dynamics and the high concentration of global supply chains have prompted comprehensive academic assessments of titanium's strategic relevance, emphasizing the urgency of enhancing domestic extraction capabilities and circularity from unconventional resources (European Commission Joint Research Centre, 2025). Recognizing these critical supply risks, the European Union officially included titanium in its list of 34 critical raw materials and 17 "Strategic Raw Materials" essential for the green and digital transition under the Critical Raw Materials Act (CRMA), which entered into force on May 23, 2024 (European Commission, 2024). Similarly, in December 2024, NATO released a list of 12 defense-critical raw materials vital for the allied defense industry, firmly positioning titanium on this strategic list and confirming its unshakeable place in global defense supply chains (NATO, 2024).

Among primary titanium minerals, rutile (TiO_2) has the highest economic value due to its pure polymorphic structure and theoretical titanium dioxide content of over 95%. Ilmenite ($FeTiO_3$), which bears the main burden of the global titanium industry, theoretically contains 52.6% TiO_2 and exhibits moderate magnetic susceptibility due to its iron content. A third, less conventional but increasingly industrially significant source of titanium is sphene, also known as titanite ($CaTiSiO_5$). Although this orthosilicate mineral, which can contain up to 40% TiO_2 in its structure, is widely found in various igneous and metamorphic environments, it has historically been exploited to a limited extent due to the metallurgical complexities in separating it from chemically and physically similar calc-silicate gangue minerals and its relatively low titanium content compared to rutile. However, advanced mineral processing paradigms and technological advancements are increasingly exploring the recovery of sphene and rutile minerals from unconventional alkaline silicate-carbonatite complexes. Separating such complex minerals, especially from gangue matrices with high iron content, necessitates innovative approaches in separation techniques (Liu et al., 2025). Moreover, the intricate embedding relationships between titanium-bearing minerals and magnetic iron phases often restrict the efficiency of conventional separation methods, requiring advanced grinding and meticulously tailored magnetic separation circuits to ensure adequate liberation (Liu et al., 2024).

The beneficiation of such complex primary ores requires the skillful utilization of subtle physical and physicochemical differences between target titanium minerals and associated gangue minerals. Magnetic separation stands out as a cornerstone technology in this field, based on the principle of distinguishing minerals by their varying magnetic susceptibilities. Minerals with high magnetic susceptibility, such as magnetite and titanomagnetite, can be easily removed by low-intensity magnetic separation (LIMS). The separation of paramagnetic ilmenite from diamagnetic or weakly magnetic gangue minerals requires high-intensity magnetic separation (HIMS) or high-gradient magnetic separation (HGMS) systems applied in dry or wet environments. Recent advances in HGMS technology, with precisely adjustable magnetic field strengths up to 15.000 Gauss, have revolutionized the recovery of ultra-fine paramagnetic particles by separating iron-bearing titanium minerals from complex silicate matrices (Opalev et al., 2026). However, in cases where the target titanium minerals are rutile and sphene, both of which lack or contain only trace amounts of the iron necessary to generate strong paramagnetic responses, the mineral processing logic must be entirely reversed. Recent academic studies emphasize the growing need for environmentally sustainable physical upgrading techniques, specifically utilizing combinations of gravity and high-intensity magnetic separation, to recover these weakly magnetic and diamagnetic titanium minerals from low-grade deposits without excessive chemical consumption (Fawzy et al., 2025). In such scenarios, high-intensity magnetic separation is utilized as a "reverse beneficiation" step to aggressively attract dense iron-bearing gangue minerals (such as hematite, magnetite, and iron-rich silicates) into the magnetic fraction, thereby enriching the valuable TiO2 minerals that exhibit diamagnetic or weakly magnetic properties and remain in the non-magnetic fraction.

The Eskişehir region, located in northwestern Türkiye, offers a highly potential and unique geological structure for the extraction of such unconventional titanium resources. The region is characterized by widespread Cenozoic magmatism and hosts complex alkaline silicate-carbonatite diatremes, particularly around the Sivrihisar and Sarıcakaya districts. These geological formations have been shaped by intense hydrothermal alteration and metasomatism processes; they host distinct mineralogical assemblages enriched in plagioclase, orthoclase, bastnaesite, fluorite, and barite, along with significant primary titanium mineralizations, predominantly rutile and sphene (Ersoy et al., 2025). The geological significance of the region is further reinforced by the presence of the Kızılcaören alkaline silicate-carbonatite complex. Previous surface exploration and sampling studies conducted in these primary deposits have revealed promising titanium mineralizations with an average TiO_2 content of 4% to 6%.

2. MATERIAL AND METHODS

2.1. Material

A representative sample was obtained from primary titanium ore resources of Eskişehir region. The run-of-mine (ROM) ore, with a maximum top size of approximately 100 mm, was delivered to the Mineral Processing Engineering Department Pilot Plant Laboratory at Istanbul Technical University.

Prior to beneficiation efforts, a comprehensive geochemical analysis was performed using an advanced X-Ray Fluorescence (XRF) spectrometer to precisely determine the bulk chemical composition of the ROM ore. The bulk chemical composition indicated that the ore contained high concentrations of silicon, iron, and calcium, reflecting a highly complex silicate and oxide mineralogy. The analysis confirmed a base titanium dioxide (TiO_2) content of 4.07%, positioning this material as an economically viable but low-grade primary resource. The detailed elemental oxide composition of the ROM ore is presented in Figure 1.

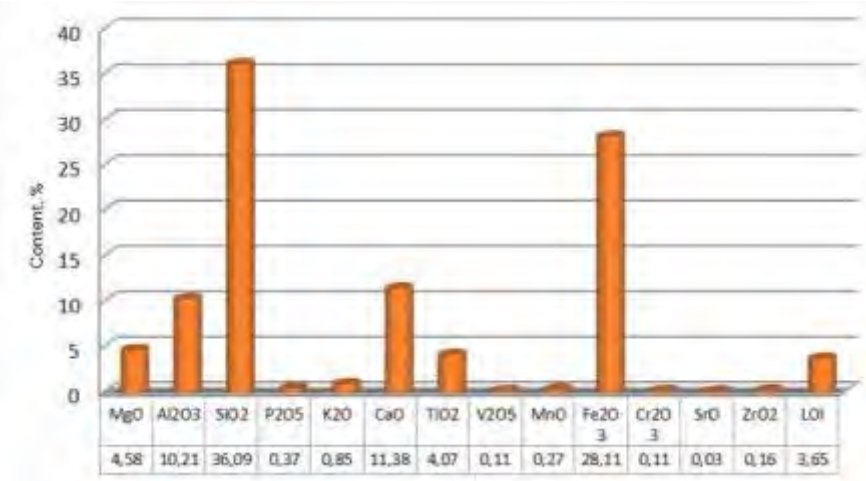

Figure 1. Particle size distribution of representative ore sample

The reduction of the 100 mm ROM ore to -2 mm size was achieved through a three-stage crushing circuit. Primary crushing was performed using a laboratory-scale jaw crusher. The primary crushed product was then fed to a cone crusher as a secondary crusher. In the tertiary crushing stage, a roll crusher was used and d_{90} of the material passed below 2 mm. Particle size distribution of the ore after roll crusher are shown in Figure 2.

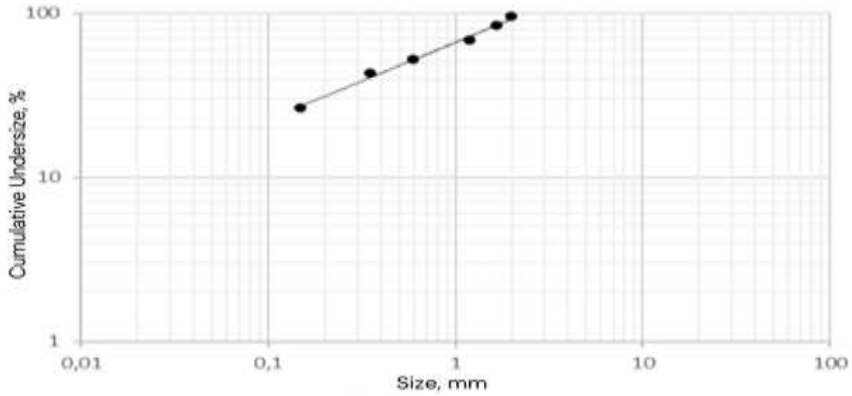

Figure 2. Particle size distribution of the ore sample after roll crusher

2.2. Method

The core methodology of this research uses reverse magnetic separation to enrich titanium. Because titanium is primarily found in non-magnetic or weakly magnetic rutile and sphene, high-intensity magnetic fields were used to pull magnetic iron-bearing gangue minerals (such as iron oxides, ilmenite, and iron-bearing silicates) into the tailings. This leaves a high-grade titanium concentrate in the non-magnetic fraction. To determine the ideal liberation size, initial tests were performed on coarse fractions. The crushed ore (100% passing 2 mm) was wet-sieved into four narrow size fractions: -2+1.19 mm, -1.19+0.354 mm, -0.354+0.150 mm, and -0.150 mm. This narrow sizing was necessary to prevent particle trajectory errors during the magnetic separation process.

These initial fractions were processed using different equipment based on their size. The coarse fractions (-2+1.19 mm and -1.19+0.354 mm) were processed using a dry rare-earth magnetic roll separator (REMS) at a fixed strength of 11.000 Gauss. The medium fraction (-0.354+0.150 mm) was separated in a dry induced roll magnetic separator using multiple stages with increasing magnetic field strengths. For the finest fraction (-0.150 mm), a Carpco Wet High-Intensity Magnetic Separator (WHIMS) was used between 2.000 and 10.000 Gauss. Wet separation was required here to prevent particle agglomeration and electrostatic issues that reduce efficiency. Additionally, gravity separation rougher and cleaner tests were conducted using a Mozley table on material finer than 0.106 mm to see if density differences could further aid beneficiation.

Since the initial tests showed that advanced liberation required finer particle sizes, a sample of the -2 mm material was grinded in a ball mill until d_{90} passed 0.354 mm. Grinding was performed at 60% solids by weight with a 45% volumetric ball charge, in strictly controlled 5+5 minute intervals. This product was sieved into three new fractions (-0.354+0.212 mm, -0.212+0.106 mm, and -0.106 mm) and tested using both the dry and wet separators at 7.000 to 11.000 Gauss. For the final optimization, run-of-mine ore was ultra-fine ground to d_{90} passing 0.106 mm using the same milling parameters but with an extended grinding time of 10+10 minutes.

The resulting -0.106 mm pulp was fed directly into a two-stage wet magnetic separation circuit using the Carpco WHIMS. The first rougher stage operated at 5.000 Gauss to remove highly magnetic iron oxides, while the second scavenger stage operated at 10.000 Gauss to remove weakly magnetic silicates and the remaining ilmenite. The overall metallurgical performance was evaluated based on the TiO_2 grade in the non-magnetic concentrate and the recovery rates calculated from the mass balances.

3. RESULTS AND DISCUSSION

The first phase of the magnetic beneficiation strategy was designed to map the exact spatial boundaries of mineral locking. By analyzing magnetic separation efficiency across natural crush size fractions ranging from 2 mm down to 0.150 mm, the liberation point at which physical bonds between diamagnetic titanium minerals and paramagnetic iron gangue break could be mathematically defined. Table 1. presents the consolidated metallurgical results of magnetic separation conducted on crushed-only -2 mm fractions.

In the coarsest fraction (-2+1.19 mm), no TiO_2 upgrading occurred. In fact, the TiO_2 grade of the non-magnetic fraction (3.67%) was lower than the magnetic fraction (4.73%). This indicates that at sizes above 1 mm, rutile and sphene particles remain completely locked within the iron-bearing silicate and hematite/magnetite gangue matrix. Consequently, the 11.000 Gauss magnetic field pulled these locked particles into the magnetic fraction due to the high magnetic susceptibility of the iron gangue.

Table 1. Combined magnetic separation results for crushed only (-2 mm) size fractions

Size, mm	PRODUCT	Amount %	TiO_2		Fe_2O_3		CaO	
			Content %	Recovery %	Content %	Recovery %	Content %	Recovery %
-2+ 1.19 mm	Magnetic	15.9	4.73	18.8	19.54	13.0	10.25	15.2
	Non-magnetic	17.4	3.67	15.9	15.43	11.2	11.94	19.3
	Fraction Feed	**33.3**	**4.18**	**34.7**	**17.39**	**24.3**	**11.13**	**34.5**
-1.19+ 0.354 mm	Magnetic	13.2	3.77	12.4	31.86	17.6	10	12.3
	Non-magnetic	9.5	5.87	13.9	32.37	12.9	14.38	12.7
	Fraction Feed	**22.7**	**4.65**	**26.3**	**32.07**	**30.5**	**11.83**	**25.0**
-0.354+ 0.15 mm	Magnetic	10.6	2.35	6.2	41.98	18.6	7.80	7.7
	Non-magnetic	6.0	6.54	9.8	25.66	6.5	14.86	8.3
	Fraction Feed	**16.6**	**3.87**	**16.0**	**36.08**	**25.1**	**10.35**	**16.0**
-0.15 mm	Magnetic	21.7	2.53	13.7	19.80	18.0	8.93	18.0
	Non-magnetic	5.7	6.45	9.2	9.18	2.2	12.12	6.4
	Fraction Feed	**27.4**	**3.35**	**22.9**	**17.59**	**20.2**	**9.60**	**24.5**
RUN OF MINE		**100.0**	**4.01**	**100.0**	**23.88**	**100.0**	**10.74**	**100.0**

A slight improvement occurred in the intermediate -1.19+0.354 mm fraction, where the non-magnetic fraction reached a 5.87% TiO_2 grade. However, the high iron content (32.37% Fe_2O_3) in this fraction proved that unliberated locked particles were still present. Separation efficiency only improved significantly below the critical 0.354 mm size. In the finer -0.354+0.150 mm and -0.150 mm fractions, the TiO_2 grades of the non-magnetic products increased to 6.54% and 6.45%, respectively. Simultaneously, their Fe_2O_3 contents dropped sharply to 25.66% and 17.59%. This distinct elemental distribution below 0.354 mm confirms that finer grinding is essential to physically liberate the non-magnetic titanium minerals from the paramagnetic gangue.

After ball mill grinding, the ore that d_{90} passed 0.354 mm was divided into three narrow ranges and subjected to high-gradient multi-stage magnetic separation. The %38.0 of the material below 0.038 mm. The results of this targeted beneficiation circuit are detailed in Table 2.

The grinding of the ore to 0.354 mm improved the efficiency of the separation matrix. In the -0.212 + 0.106 mm fraction, the application of strong magnetic fields (up to 11.000 Gauss) successfully routed iron to the tailings, yielding a non-magnetic concentrate with a 9.54% TiO_2 grade. However, the true metallurgical turning point occurred in the ultra-fine -0.106 mm fraction. By fully exploiting the diamagnetic properties of rutile and sphene using the wet-type Carpco WHIMS, the non-magnetic concentrate reached a grade of 11.96% TiO_2. Concurrently, the Fe_2O_3 grade in this concentrate dropped to 5.90%. This indicates a rejection of 98.3% of the total iron present in that specific size fraction.

This relationship between particle size and concentrate grade, where grades escalated from 6.12% to 9.54% and finally to 11.96% TiO_2 as size decreased, demonstrates that the intercrystalline boundaries between the titanium oxides/silicates and the iron-rich host rock are

exceptionally fine. It has been proven that comminution down to -0.106 mm sizes is inevitable to achieve absolute physical detachment.

Table 2. Multi-stage magnetic separation results for -0.354 mm ore

Size, mm	PRODUCT	Amount %	TiO_2		Fe_2O_3		CaO	
			Content %	Recovery %	Content %	Recovery %	Content %	Recovery %
-0.354+ 0.212 mm	Magnetic-1	13.9	3.07	10.8	26.76	15.5	8.63	11.1
	Magnetic-2	10.6	3.61	9.7	21.80	9.6	8.84	8.7
	Non-magnetic	1.8	6.12	2.8	17.89	1.4	11.11	1.9
	Fraction Feed	**26.3**	**3.50**	**23.4**	**24.15**	**26.5**	**8.89**	**21.7**
-0.212+ 0.106 mm	Magnetic-1	7.7	2.76	5.4	28.47	9.1	7.26	5.2
	Magnetic-2	10.4	3.33	8.8	14.50	6.3	14.39	13.9
	Non-magnetic	4.1	9.54	10.0	9.75	1.7	14.70	5.6
	Fraction Feed	**22.2**	**4.28**	**24.2**	**18.47**	**17.1**	**11.97**	**24.7**
-0.106 mm	Magnetic-1	37.0	2.65	25.0	31.34	48.4	10.22	35.1
	Magnetic-2	7.7	3.48	6.9	19.64	6.3	10.35	7.4
	Non-magnetic	6.8	11.96	20.6	5.90	1.7	17.85	11.2
	Fraction Feed	**51.5**	**3.99**	**52.4**	**26.25**	**56.4**	**11.24**	**53.7**
RUN OF MINE		**100.0**	3.93	100.0	23.97	100.0	10.78	100.0

A final and targeted optimization test was designed to maximize both concentrate grade and overall metallurgical recovery. In this test, the entire -2 mm ore was subjected to an extended 10+10 minute ball mill grinding process to ensure that d_{90} of the material passed the critical 0.106 mm liberation threshold.

Table 3. Optimized wet magnetic separation results for -0.106 mm ore

PRODUCT	Amount %	TiO_2		Fe_2O_3		CaO	
		Content %	Recovery %	Content %	Recovery %	Content %	Recovery %
Magnetic-1 (5000 Gauss)	60.8	1.97	29.8	30.87	79.0	7.98	44.7
Magnetic-2 (10000 Gauss)	22.3	2.98	16.5	17.5	16.4	12.34	25.4
Non-magnetic	16.9	12.78	53.7	6.5	4.6	19.23	29.9
Feed	**100**	**4.02**	**100.0**	**23.77**	**100.0**	**10.85**	**100.0**

Switching to a fully liberated, wet high-gradient separation circuit produced the best results. The TiO_2 grade of the non-magnetic concentrate increased significantly from 4.07% in the ROM ore to a peak of 12.78%. Additionally, the overall titanium recovery in this product reached 53.7%. The two-stage magnetic separation system successfully rejected 95.4% of the total iron into the tailings. The initial 5.000 Gauss stage removed the bulk of the gangue mass (60.8%), which was mainly iron oxides. The 10.000 Gauss scavenger stage effectively removed moderately locked particles and liberated ilmenite, as shown by its slightly higher 2.98% TiO_2 grade.

Quantitative XRD analysis verified the phase composition of the optimized 12.78% TiO_2 concentrate. The results confirmed that titanite (sphene, $CaTiSiO_5$) was the main titanium-bearing phase in the non-magnetic concentrate (23.9%wt), along with liberated rutile. The remaining mass consisted of liberated gangue minerals entrained in the non-magnetic product: muscovite-sericite (9.2%), quartz (11.7%), plagioclase feldspar (11.4%), and calcite (18.6%). The XRD analysis also showed that the ilmenite content in the concentrate was only 3.1%. This proved that the 10.000 Gauss magnetic field was highly efficient at isolating non-iron-bearing titanium minerals. Producing a concentrate with approximately 13% TiO_2 using only physical magnetic separation establishes a strong pre-concentration method for Eskişehir primary ores. This approach significantly reduces the mass of material requiring subsequent intensive hydrometallurgical or flotation processes.

In parallel with the magnetic separation tests, gravity separation experiments were also conducted using a Mozley table on material reduced below 0.106 mm to determine whether the ore mineralogy permitted beneficiation based on specific gravity differences. The results of the tests conducted in two stages with the Mozley table are given in Table 4.

Table 4. Gravity separation (Mozley Table) results for -0.106 mm ore

PRODUCT	Amount %	TiO_2		Fe_2O_3		CaO	
		Content %	Recovery %	Content %	Recovery %	Content %	Recovery %
Heavy	20.3	5.14	26.1	30.23	27.1	13.34	23.9
Middlings	35.4	4.29	38.0	23.32	36.4	11.98	37.5
Light	44.3	3.23	35.8	18.67	36.5	9.87	38.6
Feed	**100**	**3.99**	**100.0**	**22.66**	**100.0**	**11.32**	**100.0**

An examination of the results in Table 4. clearly shows that gravity separation failed to provide significant upgrading on the Eskişehir primary titanium ore. The TiO_2 grade in the heavy product could only reach 5.14%, and even in the lightest product, 3.23% TiO_2 remained. The fundamental physical reason for this failure is that the specific gravity differential between the sphene mineral and the massive silicate gangue (actinolite/clinochlore) remains within a very narrow margin. In contrast, iron oxides distributed in high proportions into both the heavy and middling products, failing to separate from the titanium minerals. In light of these data, it was proven that separating such sphene-bearing ores using gravity methods is inefficient and that the high-intensity magnetic separation process detailed above is a necessity.

4. CONCLUSION

The comprehensive evaluation of primary titanium ore from the Eskişehir region in Türkiye has revealed that domestic low-grade alkaline silicate-carbonatite complexes harbor substantial potential for strategic titanium dioxide extraction. Advanced mineralogical characterization studies definitively proved that the majority of economic titanium in this deposit is hosted in diamagnetic and weakly paramagnetic phases, specifically rutile and sphene (titanite), rather than the conventional, iron-rich ilmenite structure. This unique mineralogical architecture dictates the ineffectiveness of conventional low-intensity beneficiation methods and necessitates the use of high-intensity reverse magnetic separation. Additionally, gravity (Mozley table) experiments proved that gravity-based separation does not work for this ore type due to the closely matched specific gravities of the minerals.

Through systematic comminution and fractionated separation analyses, it was determined that the critical liberation threshold for TiO_2 minerals is below 0.354 mm, and absolute physical

detachment requires grinding down to -0.106 mm. While dry and coarse separation attempts failed to achieve meaningful upgrading due to the severe physical encapsulation of rutile and sphene within the massive iron-silicate matrix, the implementation of fine grinding fundamentally altered the metallurgical response.

An optimized flowsheet involving comprehensive ball milling to ensure 100% of the material passed 0.106 mm, followed by a two-stage (utilizing 5.000 and 10.000 Gauss fields) wet high-intensity magnetic separation (WHIMS) circuit, proved exceptionally successful. This precise mechanical and magnetic configuration resulted in the rejection of over 95% of the detrimental iron gangue into the system, yielding a final non-magnetic concentrate with a significantly upgraded TiO_2 grade reaching 12.78% and titanium recovery of 53.7%.

REFERENCES

Ersoy, Y. E., Yavuz, H., Uysal, İ., Palmer, M. R., Müller, D., (2025), "The Petrology of Tuffisite in a Trachytic Diatreme from the Kızılcaören Alkaline Silicate–Carbonatite Complex, NW Anatolia". Minerals, 15 (8), 867.

European Commission, (2024), "Critical Raw Materials Act".

European Commission, Joint Research Centre, (2025), "Titanium metal in the EU: Strategic relevance and circularity potential". Publications Office of the European Union.

Fawzy, M. M., Shawky, M. M., Ismail, A., Diab, M., (2025), "Optimized and Sustainable Recovery of Ilmenite and Titanite from Low-Grade Rahba Placer Deposits Integrating Physical Beneficiation Techniques". Journal of Mining and Environment.

Liu, T., Zhang, Y., Xu, C., (2024), "Recovery of Iron and Titanium from Vanadium-Extracted Tailings Via Direct Reduction-Classified Ball Milling-Magnetic Separation". Fundamental Research in Comprehensive Utilization.

Liu, Y., Liu, Z., Wang, Y., Zhang, Y., Lu, D., (2025), "Mineralogical Analysis of Factors Affecting the Grade of High-Gradient Magnetic Separation Concentrates and Experimental Study on TiO2 Enrichment Using ARC". Minerals, 15 (8), 799.

Matsanga, N., Kalenga, M. W., Nheta, W., (2024), "An Overview of Thermochemical Reduction Processes for Titanium Production". Minerals, 15 (1), 17.

NATO, (2024), "NATO releases list of 12 defence-critical raw materials". https://www.nato.int/en/news-and-events/articles/news/2024/12/11/nato-releases-list-of-12-defence-critical-raw-materials

Opalev, A. S., Fomin, A. V., Alekseeva, S. A., Kaliuzhnaia, R. V., (2026), "Application of magnetic-and-gravity separation in production of titanomagnetite concentrates from ores of various Russian deposits". Russian Mining Industry, 1, 89–9.

THE ROLE OF TOMRA´S XRT-BASED ORE SORTING IN METALLIC ORE PROCESSING

Carolina VARGAS*

TOMRA Sorting GmbH, Mining, Wedel, Germany
**Corresponding author: Carolina.vargas@tomra.com*

A B S T R A C T

Ore sorting stands out as a dry, physical processing approach that capitalizes on the inherent characteristics of ores to classify them into distinct quality categories. Typically, ore sorting systems integrate detection and ejection subsystems, utilizing a range of sensing and separation techniques. High-resolution detection —particularly in X-Ray Transmission (XRT)–based systems— combined with precise ejection modules and high throughput capacities enables significant efficiency improvements in the processing of various metallic ores such as: Copper, Lead/Zinc, Gold. Recognizing the technological advantages of Tomra XRT systems and the cost-effectiveness of pre-concentration methods, along with the increasing demand for a broad spectrum of metals, underscores the necessity of integrating a pre-concentration stage in modern mining practices. A plausible implementation scenario envisions reduced mass flow and downsized downstream equipment, contributing to substantial CAPEX reductions and a strategic approach to minimizing operational expenditures per ton. Figure 1 shows the working principle of a belt-type XRT sorter.

Key words: *Sensor-based ore sorting, x-ray transmission, waste rejection, reduced cut-off, increase productivity*

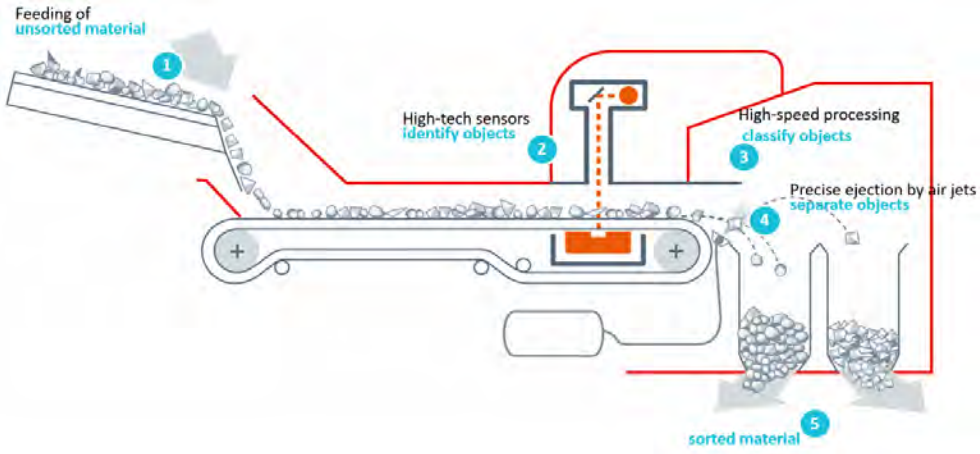

Figure 1. Working principle of XRT-sorting

PLANT AND PROCESS DESIGN AND OPERATING PRACTICE

APPLICATION OF NEW TECHNOLOGIES - A NECESSITY FOR BENEFICIATION OF ALBANIAN CHROMITE ORES

Kimet FETAHU[1], Bukurosh KOCI[2], Ekita TOSKA[3,*]

[1]Geology and Mining Faculty, Polytechnic University of Tirana, "Elbasani" Street, Tirana, Albania.
[2]Chromite Processing plant, Bulqize and Kalimash, ALBANIA
[3]National Agency of Natural Resources (AKBN), Tirana, ALBANIA
**Corresponding author: Ekita.Toska@akbn.gov.al*

A B S T R A C T

This paper analyses Albania's long-standing experience in chromite ore processing and beneficiation, and the emerging industrial challenges driven by the reduction of high-grade feed reserves. After approximately 70 years of intensive exploitation of deposits in the Bulqize-Bater, Kukes-Has-Tropoje and Prrenjas-Pogradec regions, the industry is increasingly facing feed with typical grades of 8-18% Cr_2O_3 (up to 20% in specific cases). Under these conditions, traditional gravity-based schemes, whilst producing high-quality concentrates, generate tailings with still-significant Cr_2O_3 content and reduce the overall recovery index. Based on real operating parameters from a beneficiation plant (capacity 9-12 t/h, current recovery 54-63%, tailings grade 4-8% Cr_2O_3), we compare options for pre-concentration, gravity beneficiation, the potential role of magnetic separation and tailings treatment, with the aim of increasing total recovery and reducing losses. An integrated technological scheme and a pilot-scale testing programmed are proposed, addressing the physical and magnetic characteristics of chromite and associated rocks (density and magnetic affinity), with the objective of technological, economic and environmental optimization of the beneficiation flowsheet.

Key words: *Chromium mining industry, mineral reserves, beneficiation technology, concentrates and tailings, chromium recovery, pre-concentration, gravity beneficiation, magnetic separation, tailings treatment*

1. INTRODUCTION

Chromite, $(Fe,Mg)(Cr,Al)_2O_4$, remains a strategic mineral for ferrochrome production and the global stainless-steel supply chain. In Albania, chromite has historically been one of the country's key mineral resources, supported by a consolidated extraction and beneficiation industry operating under varying technical, economic and regulatory conditions.
Over the years, exploitation of higher-grade Cr_2O_3 reserves has reached levels at which the feed base is shifting towards ores with lower Cr_2O_3 content and higher mineralogical complexity.

Internationally, chromite beneficiation challenges have been widely discussed in the literature, emphasizing the issues of low-grade ores, chromite grain size, mineralogical composition and the necessity for hybrid beneficiation schemes (gravity, magnetic and, in specific cases, flotation). Murthy et al. (2011) provide a broad review of flowsheets and critical plant problems, highlighting the optimization of beneficiation schemes and control of fine fractions.
The purpose of this paper is to provide an industrial review and to offer implementable technological proposals for chromite beneficiation plants in Albania. The work is grounded in real operating data and aims to structure a practical modernization pathway: pre-concentration, magnetic separation and tailings treatment, supported by pilot-scale tests and a mass-balance audit.

More specifically, the paper addresses the following objectives:

• To identify the main causes of Cr_2O_3 losses to tailings and fine fractions, based on mass and quality balances.
• To evaluate pre-concentration alternatives (screening/classification and early waste rejection) as mechanisms to reduce the load on gravity beneficiation.
• To substantiate the conditions under which magnetic separation adds value as an intermediate step or when combined with gravity separation.
The key questions are:
• What are the principal points at which Cr_2O_3 losses occur in current schemes (with a focus on classification and recirculation)?
• What is the most realistic (technically and economically) combination of gravity beneficiation with magnetic beneficiation to increase total recovery?
• Under what conditions does tailings treatment become economically justified and materially reduce environmental impacts?
The core contribution of the paper is the integration of real operating data with a modernised scheme and a credible implementation plan.

2. THE CHROMITE INDUSTRY IN ALBANIA AND THE ORE QUALITY TRENDS

2.1. Main Chromite-Bearing Regions and Historical Development of Beneficiation

Exploitation of deposits in the Bulqize-Bater, Kukes-Has-Tropoje and Prrenjas-Pogradec regions has supplied substantial chromite ore over decades, establishing a strong industrial tradition in crushing, screening, gravity beneficiation and concentrate preparation for export. For a long period, the dominant portion of the feed was of relatively high quality (above 28% Cr_2O_3), which favoured simple gravity schemes with satisfactory recovery and high product quality.

Over time, increasing mining depth, heterogeneous distribution of mineralisation and the depletion of richer zones have compelled the industry to orient its work towards deposits with lower chromite content, typically 8-20% Cr_2O_3.

2.2. Evolution of Mineral Processing Methods: From Classical Gravity to Hybrid Approaches

Chromite beneficiation in most producing countries has traditionally relied on gravity methods due to the specific gravity contrast between chromite and silicate gangue (olivine and serpentine). In such ores, gravity equipment (settling machines/jigs, spirals and concentration tables) is relatively simple, with low capital costs and low energy consumption.

High-intensity magnetic separation is used in many schemes to beneficiate fine fractions below 0.07 mm or to reprocess tailings deposited in dams.

Other studies indicate that recovery from old tailings requires a combination of methods and good management of fine particles. Ross et al. (2022) show that for low-grade chromite tailings, magnetic separators have not always been sufficient to achieve satisfactory recoveries, suggesting that controlled flotation may be required in some cases.

3. KEY TECHNOLOGICAL CHALLENGES IN THE BENEFICATION OF LOW-GRADE CHROMITE ORES

3.1. Declining Feed Quality and Implications for Plant Mass Balance

Current feed grades are commonly in the range 8-20% Cr_2O_3. Under operating conditions where overall recovery is 54-63% and tailings remain at 5-8% Cr_2O_3, losses per tonne of feed are substantial and directly affect plant performance.

3.2. Particle Size Distribution, Liberation and Losses in Fine Fractions

A feed size distribution of 0-350 mm requires controlled crushing and classification. Effective desliming and the separation of streams by size fraction are prerequisites for selectivity and stable operation.

3.3. Associated Minerals and Proximity of Physical Properties

Typical densities are approximately: chromite 4.15 g/cm³, olivine 3.20 g/cm³ and serpentine 2.65 g/cm³. The proximity of certain magnetic behaviors in chromite and serpentine-rich gangue necessitates careful fine-fraction management and circuit configuration where magnetic separation is applied.

3.4. Product Specifications and Market Constraints

Market requirements for concentrate grade and impurity control constrain operating flexibility. Plants are often required to maintain concentrate quality even where this reduces recovery, reinforcing the importance of reducing Cr_2O_3 losses to tailings.

4. MATERIALS AND METHODS

4.1. Industrial Data and Baseline Operating Parameters

Baseline data are drawn from a beneficiation plant in Bulqize: Cr_2O_3 in feed 8-20%, particle size distribution 0-350 mm, capacity 9-12 t/h, a gravity-based scheme, overall recovery 54-63% and tailings 3.5-6% Cr_2O_3.

Table 1. Baseline operating parameters (industrial data)

Parameter	**Value (range)**
Cr_2O_3 in feed	8-20 %
Particle size distribution	0-350 mm
Capacity	9-12 t/h
Actual schemme	Pre-enrichment in harsh environments and gravity enrichment with spirals amd concentration tables
Overall recovery	54-63%
Cr_2O_3 in tailings	3.5-6&
Density – chromite	4.15 gr/cm^3
Density – olivine	3.20 gr/cm^3
Density - serpentine	2.65 gr/cm^3

5. PERFORMANCE ANALYSIS AND IDENTIFICATION OF LOSS POINTS

5.1 Analysis of The Effect of Density and Magnetic Affinity

Given the density contrast, gravity separation remains the primary method for chromite beneficiation. Magnetic separation may add value for fine fractions and for intermediate streams, but its effectiveness depends on the magnetic behavior of chromite relative to associated gangue. To protect selectivity, fine-fraction management (including desliming) and staged circuit configurations (scavenger/cleaner) are recommended where magnetic separation is applied.

5.2. Process Audit and Operating Indicators to be Stabilized

Prior to investment, the process audit should focus on key operating indicators: pulp density in each circuit, water flowrate and hydrocyclone inlet and outlet pressures, recirculation ratio, the use and efficiency of screens, and the level of slimes in the feed to gravity units. Often, straightforward operational improvements (e.g., adjustments to classification and water control) deliver immediate gains by reducing tailings losses even without major capital changes.

6. APPLICATION OF NEW TECHNOLOGIES: THE PROPOSED INTEGRATED SCHEME

6.1. Pre-Concentration: Rationale and Recommended Techniques

Pre-concentration aims to remove barren material early, before the feed enters core processing units (grinding, classification and fine separation). For chromite, early rejection of clean waste in the 3-25 mm feed fraction produced during crushing and screening can be effectively achieved using a dense medium cone with a ferrosilicon medium at densities between 2.45 and 2.70 g/cm³.

6.2. Automation, Instrumentation and Process Control

Modernization should not be viewed only as the addition of equipment. Process control is equally important:
• online measurement of pulp density,
• water flow control,
• hydrocyclone inlet and outlet pressures, and
• regular product sampling for Cr_2O_3.
Minimum control and instrumentation improve beneficiation stability and makes it easier to maintain concentrate quality under variable feed conditions.

Step 1: Feed 0-350 mm - storage and homogenisation (where feasible)
Step 2: Controlled crushing + screening (e.g., >50 mm, 10-50 mm, <10 mm)
Step 3: Pre-concentration (e.g., DMS/SBS where applicable) for suitable fractions
Step 4: Gravity separation (jigs/spirals/concentration tables, as applicable)
Step 5: Desliming and fine-fraction management (classification and separate treatment)
Step 6: High-intensity magnetic separation (WHIMS) for fines and intermediate streams
Step 7: Tailings retreatment and improved dewatering
Step 8: Water recycling and improved tailings management

7. TAILINGS TREATMENT AND SECONADARY RECOVERY: FROM LOSS TO VALUE

7.1. Tailings As a Secondary Feedstock

Tailings containing 5-8% Cr_2O_3 represent economic potential, particularly as deposited volumes increase over time. In some cases, tailings may be treated as a secondary feedstock because they do not require the same degree of size reduction and are often readily processable using appropriate equipment.

The chromite tailings dam in Bulqize is a well-known example in Albania. However, technological success depends closely on fine-particle content, mineralogy and the degree of liberation.

Tailings treatment requires careful management of water and deposition. Thickeners and filters reduce water content in tailings, lower the risk of seepage and increase the potential for water recycling within the plant. For existing plants, improving dewatering is often one of the most reasonable investments, as it delivers dual benefits: reduced water consumption and improved environmental safety.

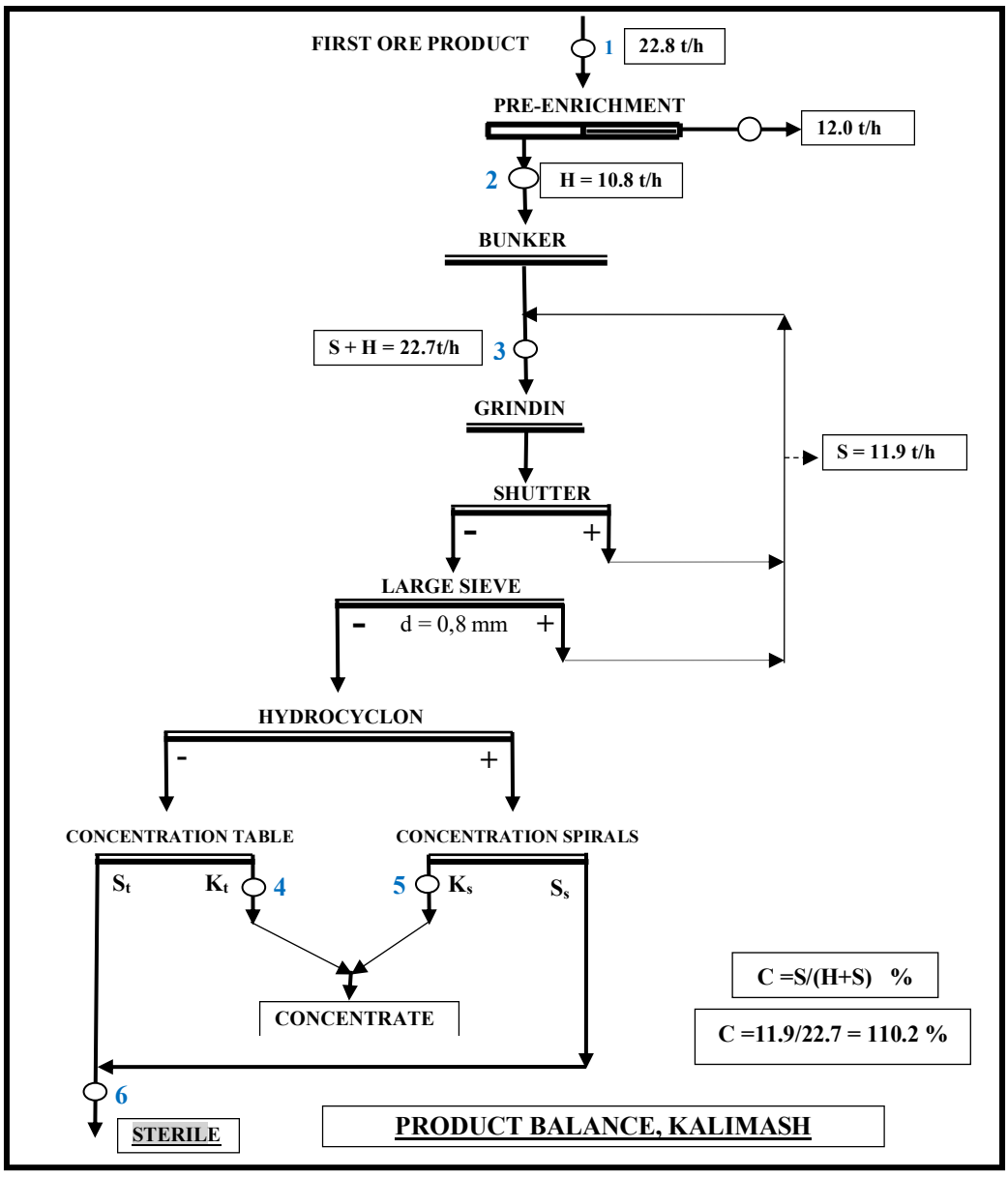

8. CONCLUSION AND RECOMMANDATION

1) The decline in feed quality towards 8-18% Cr_2O_3 makes modernization of traditional gravity schemes necessary, as current recoveries of 54-63% and tailings of 5-8% Cr_2O_3 indicate significant losses.

2) Pre-concentration (screening + DMS or SBS) for coarse fractions and accurate classification are high-impact steps to reduce barren mass and improve downstream block efficiency.

3) Magnetic separation (particularly WHIMS) should be considered as an additional block for fine fractions and for the treatment of middlings/tailings, but must be designed based on mineralogical characterization and desliming.

4) Tailings treatment should be integrated into the flowsheet and supported by dewatering and water recirculation to achieve technical and environmental benefits.

BULK SOLIDS HANDLING: THE OVERLOOKED DRIVER OF PLANT PERFORMANCE

Enes KAYA*

Jenike & Johanson Pty Ltd, 12 Fisher Street, Belmont, 6104 WA, AUSTRALIA
**Corresponding author: ekaya@jenike.com*

A B S T R A C T

Bulk solids handling systems such as Silos, Feeders, Conveyors, Transfer Chutes, play a decisive role in determining the performance and reliability of mineral processing plants. However, they are often overlooked during design, becoming the weakest link in the processing flow chain. Often plants inherit design decisions made early in the project, and rarely meet nameplate design capacity. Unlike liquid systems where density and viscosity are established and routinely applied parameters, bulk solids design requires characterisation of compressibility (bulk density), cohesive strength, wall friction, and permeability. These parameters vary considerably with mineralogy, particle shape and size distribution, moisture content, temperature, consolidation stress, and storage time (time at rest).

Accurate measurement and correct application of bulk solids flow properties are critical for achieving reliable flow and consistent plant performance. Incorporating these parameters into the design process reduces project risk, lowers capital costs (in the long term), and increases throughput. This paper highlights the importance of proper characterisation and design methods for cohesive ores, which are especially prone to flow problems.

Key words: *Bulk materials handling, material characterisation, system design, flow properties, Jenike & Johanson*

1. INTRODUCTION

Bulk solids handling (BMH) systems form the connective infrastructure between crushing, grinding, screening, and downstream hydrometallurgical or pyrometallurgical processes. Although these systems determine whether material reaches the next unit operation at the required rate and consistency, they are frequently treated as secondary to “process” equipment during project design and capital allocation. The consequences include underestimated startup risk, lower realised throughput, chronic blockages, and reduced plant availability.

Bulk solids testing and characterisation are frequently de scoped during feasibility to reduce upfront expenditure, creating a misalignment between early cost optimisation and downstream commissioning and operability outcomes.

Historical evidence supports the importance of solids handling reliability. A study commissioned by the RAND Corporation in the 1980s comparing solids handling plants to fluid handling plants showed that solids plants frequently operated well below nameplate capacity during early years, with a significant proportion achieving less than 70% of design throughput due to bottlenecks associated with bulk solids (Merrow, 1980). A follow up industrial assessment in the 2000s reported similar trends, illustrating a persistent gap in solids handling design practice (Merrow, 2000) which is presented in Figure *3* below. These findings align with subsequent analyses of cost and schedule performance curves in the process industries (McNulty, 1998).

In recent years, the Turkish minerals processing sector has expanded, particularly in gold processing, with a growing number of exploration and production projects. This growth,

alongside internationally competitive expansions in base and precious metals processing underscores the importance of treating solids handling as a scientific discipline within project design.

This paper outlines the scientific basis of BMH design, describes key flow properties, and highlights how proper characterisation and design practice lower project and operational risk.

2. SCIENTIFIC BASIS OF BULK SOLIDS HANDLING

2.1 Distinction Between Fluids and Bulk Solids

Unlike liquids, where density and viscosity are well defined continuum properties, bulk solids exhibit frictional, compressible, and in many cases cohesive behaviour (Jenike, 1964). Flow depends not only on particle interactions but also on stress history, consolidation time, moisture, and contact surfaces. A bulk solid can form stable arches or ratholes, or cease flowing entirely unless the imposed stress exceeds the material's strength.

The industry trend toward upscaling and automation during the late twentieth century exposed the limitations of applying methods developed for liquids and gases to bulk solids. Even sophisticated process control initiatives struggled where flow variability and material dependent behaviour dominated, highlighting the gap between solids handling practice and the underlying mechanics governing flow.

2.2 Flow Properties Characterisation Methods

Accurate bulk material characterisation is fundamental to applying the Jenike & Johanson methodology, as it quantifies properties that directly influence flow behaviour and design decisions. The core properties measured as part of a flow property test program inform mass flow hopper design, feeder specification, and transfer chute geometry. A typical flow property test report (FPTR) includes values for:

- Cohesive strength, which quantifies the stress required to initiate flow and predicts the arching and ratholing dimensions, and whether or not the material is impact pressure sensitive.

- Wall friction, quantifies the frictional interaction between the bulk solid and the liner, and governs the minimum hopper wall angles required to achieve mass flow.

- Compressibility, which describes how bulk density changes with applied consolidation pressures. This bulk density range is especially critical in helping determine live capacity in storage, throughput rates, and static/dynamic loads.

- Permeability, reflecting gas–solids interactions that affect discharge from hoppers and pneumatic behaviour.

- Particle size distribution and shape, which influences equipment design parameters, clearances of feeders, and could indicate whether the material may be susceptible to segregation.

- Chute tests, informs the angles required within a chute to prevent buildup at a range of impact pressures.

Shear cell testing remains the core method for quantifying cohesive strength and wall friction (ASTM 6128). By consolidating a representative sample and incrementally shearing it, shear cell tests define yield loci that are used to generate a flow function, the relationship between

major consolidation stress and unconfined yield stress. This flow function and associated friction angles are the basis for calculating required minimum hopper angles and outlet dimensions to achieve mass flow and avoid funnel flow and stagnant regions.

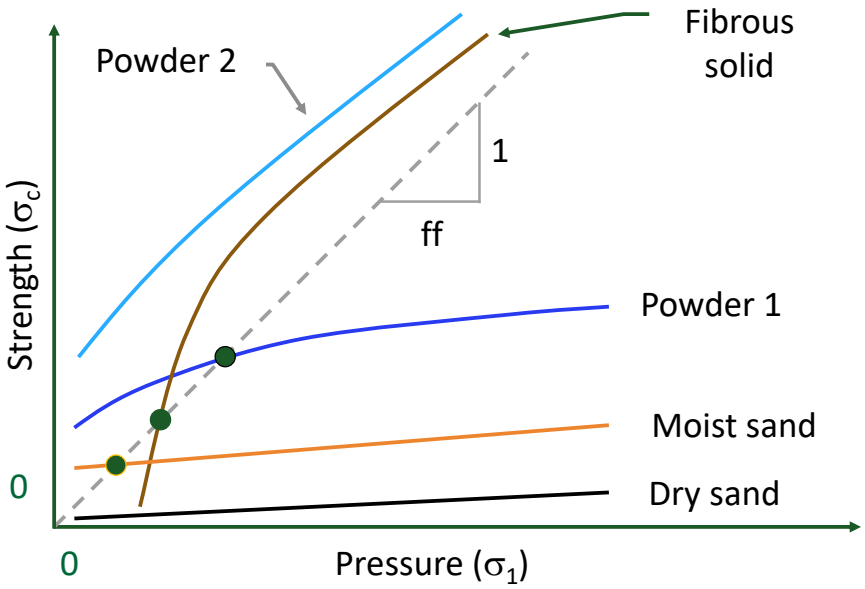

Figure 1. Example flow functions of various bulk solids

Complementary characterisation methods support shear cell results and expand design insight. Static and dynamic angle of repose tests provide initial indications surface behaviour for stockpiles and surge piles. Dynamic chute and flow tests in prototype or scaled transfer geometries help assess behaviour under practical flow conditions, including impact, segregation, and buildup tendencies. Fluidisation and pneumatic conveying tests characterise gas–particle interactions, identifying velocities for dilute and dense phase conveying (in combination with permeability test results) and the onset of saltation or choking, which are especially relevant for fine and ultrafine materials. Wear and abrasion testing on representative surface materials quantifies wear rates and informs selection of liners and wear resistant materials for chutes, feeders, and conveyors.

These measured properties also provide the input parameters required for numerical analysis, including Discrete Element Method (DEM) modelling and continuum-based or empirical flow models. When appropriately calibrated, such models complement classical design methods by enabling assessment of complex geometries, transfer behaviour, and sensitivity to operating conditions.

Taken together, these measurements allow bulk solids behaviour to be represented explicitly in design calculations and analysis, rather than relying on generic assumptions or “rules of thumb” values. This approach aligns with Jenike’s principle of integrating directly measured flow properties into solids handling design, thereby reducing the risk of flow interruptions and improving operability.

2.3 Jenike’s Framework as a Scientific Discipline

Jenike’s pioneering work, in the 1960s, established a mathematical framework for predicting flow/no-flow conditions in hoppers and silos. Design curves derived from flow factor (FF) measurements provide minimum outlet dimensions and wall angles required to achieve mass flow (Jenike, 1975). Further applied research in the field, exemplified by Roberts (1999),

reinforced the practical value and continued relevance of the Jenike framework in modern bulk solids design.

Together these contributions position BMH not as empirical practice but as a technically rigorous discipline rooted in material science and continuum mechanics.

3. DESIGN IMPLICATIONS

The flow properties described in Section 2 allow solids-handling systems to be designed on the basis of measured behaviour rather than assumed material performance. Cohesion and wall friction results determine whether mass flow can be achieved and dictate hopper outlet dimensions, while liner friction influences the selection of various liners to manage build-up and mitigate moisture sensitivity (Guo et al., 2021). Permeability, compressibility, and moisture interaction influence discharge rates, flow aid requirements, and the propensity for no-flow conditions under consolidation or storage time-at-rest.

When these properties are not measured, equipment geometry and materials of construction are commonly set using generic parameters. Thus increasing the likelihood of incorrectly sized outlets, incompatible liner selection, and poor handling performance. Such design decisions often remain latent until commissioning or early operation, where they manifest as operability constraints described in Section 4.

4. OPERABILITY, COMMISSIONING, AND PROJECT PERFORMANCE

4.1 Operability and Plant Availability

When bulk solids considerations are underweighted during design, operability issues typically emerge at the interface between storage, reclaim, and transfer systems. These issues commonly present as feeder and chute blockages, reduced reclaim performance, inconsistent feed to downstream circuits, and increased downtime or maintenance demand. Historical assessments of solids handling facilities reported similar symptoms, noting that chronic operability problems were driven by plugging, sticking, uneven flow, and misdirection rather than process chemistry.

Although such symptoms are often attributed to equipment capacity or operational factors, the underlying drivers are more frequently rooted in material behaviour, specifically cohesion, friction, and time dependent consolidation and strength gain.

Solids handling constraints can dominate plant availability during early operation and persist into steady-state production if left untreated. This reflects the reality that solids systems behave as material supply chains: instability at the front end propagates through crushing, grinding, classification, and downstream processes, reducing throughput and increasing the difficulty of operating near nameplate rates.

In practice, a substantial portion of bulk solids engineering work Jenike & Johanson performs globally is directed toward brownfield upgrades, where characterisation led retrofits are implemented to stabilise flow and restore operability. However, such interventions must contend with fixed geometric and operational constraints that would not have existed had flow behaviour been incorporated in the original design stage. The prevalence of brownfield redesign work underscores the importance of integrating bulk solids science during project development, when design choices can be made with fewer constraints and lower lifecycle risk, this dynamic is illustrated in Figure *2*.

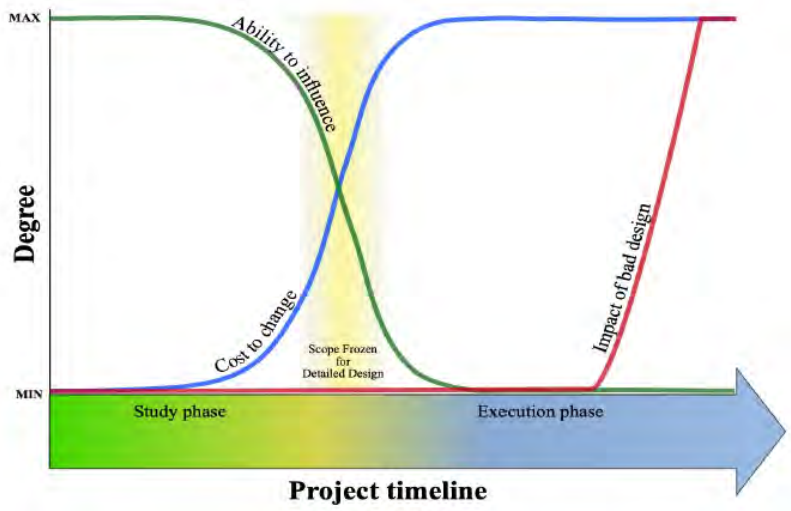

Figure 2. Influence, Cost and Impacts of bulk solids FLOW as a function of life cycle stage

4.2 Commissioning Performance, Capital Efficiency, and Industry Evidence

Historical performance data from the process industries reinforces the importance of bulk solids handling. A RAND Corporation study reviewing 40 plants in the United States and Canada found that liquids-handling facilities generally achieved planned startup timelines, while solids handling facilities exhibited substantial delays (Merrow, 1988; Merrow, 2000). The disparity was most pronounced in plants processing raw solids, where actual startup times significantly exceeded planned startup times.

The RAND data showed that two-thirds of solids handling facilities operated at less than 80% of nameplate capacity after their first year, with one quarter of the facilities failing to reach even 40%. The average realised throughput for these solids plants was approximately 64% of design compared to more than 90% for fluid-handling projects. Only 6% of plants were reported to have no major performance issues, with the majority of operability constraints linked to flow behaviour such as plugging, sticking, and unreliable flow. These findings highlight both the magnitude of the performance gap and its direct connection to inadequate understanding of solids flow during design (Merrow, 1988; Merrow, 2000; industry review).

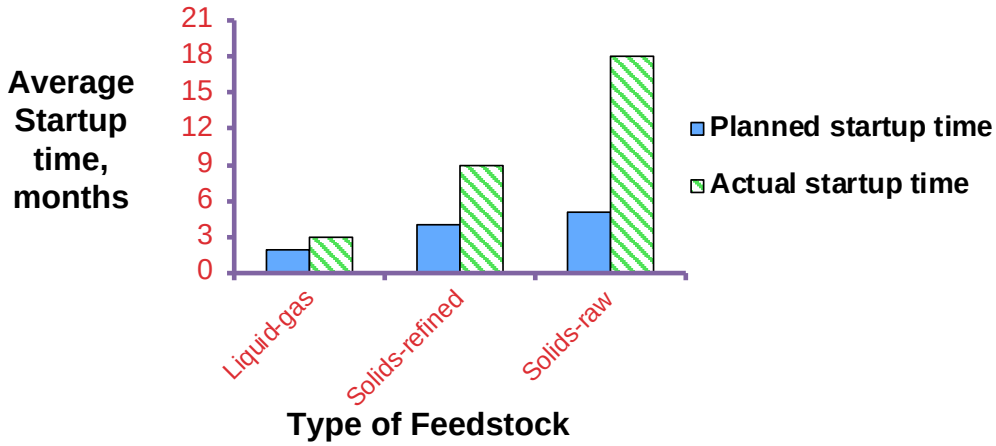

Figure 3. Startup performance of solids handling vs fluid handling facilities. Source: Merrow (1980), RAND Corporation

This performance gap reflects a fundamental difference in physical behaviour, and industry understanding of the science of BMH. Liquids can be specified by density and viscosity,

whereas solids require characterisation of compressibility, cohesive strength, wall friction properties, material-moisture interaction, and time dependent consolidation parameters which are seldom defined during early project stages. As a result, solids handling systems tend to impose commissioning penalties at precisely the point when throughput and revenue are most valuable.

McNulty's analysis of startup curves and cost performance confirmed this trend, noting that solids handling projects typically reach nameplate capacity later than planned and accumulate disproportionate indirect costs relative to fluid-handling projects (McNulty, 1998). These costs manifest as deferred revenue, prolonged exposure to commissioning schedule risk, and reduced capital efficiency. Over the evaluation horizon used to evaluate project economics, the cumulative penalty often exceeds the incremental cost of integrating bulk solids science in the design stages.

This performance dynamic is reinforced by misaligned incentives across project phases. Feasibility teams, project development groups, Engineering Procurement Construction Management (EPCMs) contractors, and commissioning teams often operate with different Key Performance Indicators (KPIs). While throughput and operability explicitly considered during early design, they are commonly evaluated using assumed material properties or generic database values that do not capture bulk solids flow behaviour. As a result, bulk solids testing and characterisation are therefore frequently de-scoped to reduce upfront expenditure. This creates a misalignment between early cost optimisation and downstream commissioning and operability outcomes.

These incentive differences are reflected during feasibility studies, where capability weightings differ across stakeholders and where solids handling considerations are frequently underweighted. Materials handling engineering (mechanical and structural design) receives moderate weighting, while bulk solids flow science receives the lowest weighting despite its overarching influence on commissioning performance, long term operability, and even profitability and return on investment!

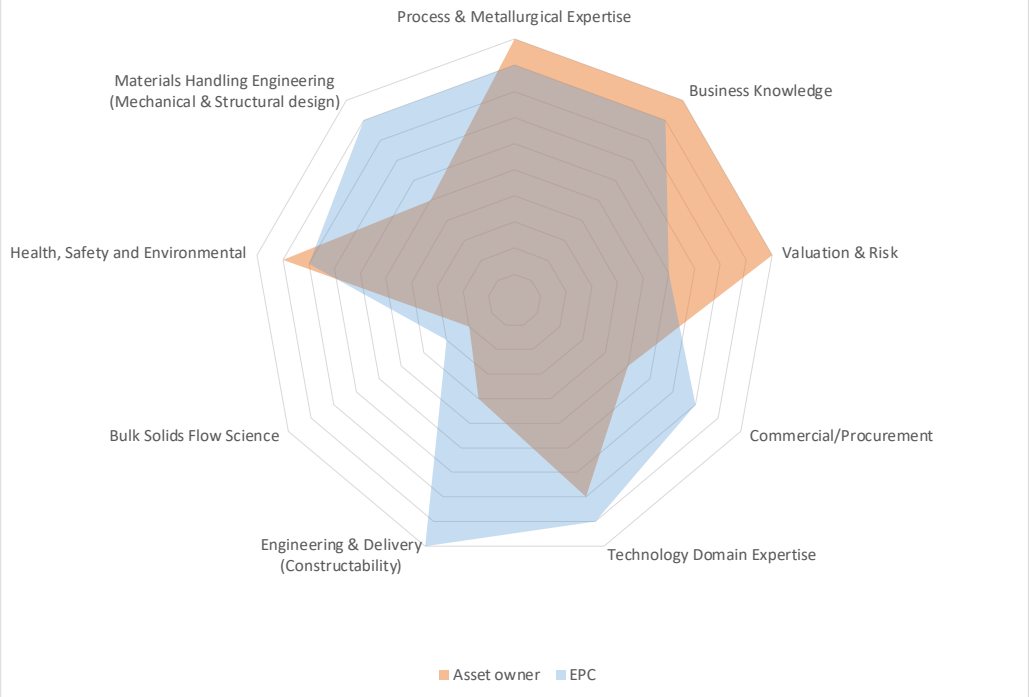

Figure 4. Illustrative capability weightings for feasibility and early project development for owners and EPC contractors

In practice, solids handling risk is frequently transferred contractually via the Basis of Design (BoD), allowing material property discrepancies to be cited after commissioning, at which point corrective measures become more constrained, capital intensive, and disruptive to production. The consequence is that owners often inherit operability constraints rooted in early design assumptions rather than equipment limitations or operating practice.

Contemporary plant experience aligns with the historical data. A significant share of activity within the bulk solids discipline concerns resolving startup and operability issues rooted in insufficient attention to flow behaviour during design. This trend is evident across commodities and is particularly relevant to emerging gold operations in Türkiye, where fine particle size distributions, cohesive ores, and variable moisture and temperatures amplify solids handling risk. Taken together, the historical evidence and operational experience position bulk solids handling not as a peripheral mechanical concern, but as a core determinant of commissioning performance, operability, and lifecycle economics.

A contributing factor to the persistent performance gap is that bulk solids handling has historically received limited attention in formal engineering curriculum, resulting in a dependence on specialised publications and professional conferences for knowledge transfer. This educational gap reinforces the underweighting of solids handling science during design and contributes to the recurrence of brownfield performance issues. Broader industrial reviews of solids handling practice over the past several decades have reached similar conclusions, noting both the technical progress made in the field and the persistent challenges associated with knowledge transfer, education, and discipline integration (Maynard, 2020). This dynamic reinforces the need to treat bulk solids handling as a scientific discipline during project development rather than a mechanical detail deferred to construction or commissioning.

5. CONCLUSION

Bulk solids handling exerts a disproportionate influence on plant performance, commissioning outcomes, and lifecycle operability. The physics governing bulk solids differ fundamentally from those governing liquids, and empirical or assumed material behaviour rarely reflects field conditions. The resulting gap between design intent and realised throughput has been documented for decades and remains evident in contemporary developments.

The scientific characterisation of flow properties and their integration into storage, reclaim, and transfer design represent a technically mature discipline. When incorporated during project development, this discipline reduces startup variability, mitigates operability constraints, and improves capital efficiency by shortening ramp up periods and lowering the risk of brownfield retrofit work. However, bulk solids characterisation and design are frequently underweighted during feasibility and early engineering stages, where scope setting and capital allocation decisions are made. This misalignment between early cost optimisation and downstream operability contributes to commissioning penalties that are more costly to resolve once geometry and layout become fixed. The prevalence of brownfield upgrades underscores this point: the most economical time to address solids handling risk is during early design, not following construction and commissioning.

Treating bulk solids handling as a scientific discipline during project development instead of a mechanical detail deferred to construction or commissioning offers clear technical and economic benefits. As the Turkish minerals sector continues to expand, particularly in gold processing where moisture and finer particle sizes amplify cohesive behaviour, the relevance of solids handling science will continue to increase. In short, solids handling performance is not a commissioning problem to be solved, but a design consideration that should be integrated during every step of the project life cycle.

REFERENCES

ASTM D6128, (2016), Standard Test Method for Shear Testing of Bulk Solids Using the Jenike Shear Cell.

Guo, J., Robinson, P., Holmes, C., (2021) “Dynamic and static wall frictions for bulk solids”, Journal of Research in Engineering and Applied Sciences, 6 (4).

Jenike, A. W., (1964), Storage and Flow of Solids, University of Utah.

Jenike, A. W., (1975), Storage and Flow of Solids, Bulletin 123, University of Utah Engineering Station.

McNulty, P., (1998), Cost and Performance Curves in the Process Industries, Hydrocarbon Processing.

Maynard, E., (2020), 40 Years of Dry Processing and Bulk Solids Handling: Challenges, Changes, and Successes, Powder & Bulk Solids.

Merrow, E., (1980), The RAND Study of Process Plant Startup Performance, RAND Corporation.

Merrow, E., (2000), Process Startup Performance Revisited, Chemical Industry Review.

Roberts, A., (1999), Bulk Solids Handling Research and Applications, TUNRA Reports, University of Newcastle.

DIGITAL PROTOTYPING AND SEQUENTIAL ASSEMBLY SIMULATION FOR A RAYMOND MILL INSTALLATION

Doğan DEMİROK*, Ahmet TANRIKULU

Tanrıkulu Endüstri Malzemeleri San. ve Tic. A.Ş., Fatsa OSB, Ordu, TÜRKİYE
**Corresponding author: demirok.dgn@gmail.com*

A B S T R A C T

The installation of complex, dismantled industrial machinery like Raymond mills within constrained existing facilities presents significant challenges in spatial planning, logistical sequencing, and precision alignment. Traditional methods, reliant on 2D drawings and on-site decision-making, are often prone to rework, project delays, and cost overruns.

This paper presents a comprehensive case study on the application of digital prototyping and virtual assembly simulation using SolidWorks to streamline the entire installation lifecycle of a Raymond mill. The methodology involved reverse-engineering the received dismantled components by creating detailed 3D sketches, which were then digitally reassembled within a precise model of the host building. This virtual environment served as a dynamic digital twin, enabling clash detection, adherence to process flow diagrams, and the pre-determination of optimal installation sequence from foundation pouring to the placement of final components. The simulation provided unparalleled flexibility for validating the precise positioning of each element prior to physical handling.

As a result, the physical installation phase was executed with minimal unforeseen issues. The complete project, including the mandatory curing period for the concrete foundation, was completed within a stringent two-month timeframe.

This study concludes that the integration of digital prototyping into industrial project planning significantly de-risks the installation process, enhances spatial control, and ensures rigorous adherence to project schedules.

The findings offer a validated framework for applying model-based engineering to the optimization of heavy machinery commissioning in the mineral processing and manufacturing sectors.

Key words: *Industrial project management, raymond mill installation, dry grinding*

1. INTRODUCTION

The commissioning of heavy industrial machinery, such as Raymond mills used in dry grinding operations, is a critical phase in mineral processing plant upgrades or retrofits. These projects are frequently characterized by tight spatial constraints within existing facilities, the arrival of machinery in a dismantled state, and the need for meticulous alignment with existing process lines (Molloy et al., 2017). Traditional planning methodologies, which depend heavily on two-dimensional (2D) drawings and experiential on-site improvisation, are increasingly inadequate. They often lead to costly and time-consuming problems, including component interferences (clashes), logistical bottlenecks, and alignment errors, ultimately resulting in project delays and budget overruns (Sacks et al., 2018; Ghanem et al., 2006).

The advent of Model-Based Engineering (MBE) and digital twin technology presents a transformative opportunity for industrial project management (Tao et al., 2019). Digital prototyping and virtual assembly simulation allow for the creation of a comprehensive digital replica of both the product and its environment (Eastman et al., 2011; Shen et al., 2015). This study details the practical application of these technologies to the installation of a Raymond

mill. The primary objective was to de-risk the installation process by pre-validating every spatial, sequential, and operational aspect in a virtual environment before the commencement of physical work.

2. MATERIAL AND METHODS

The case study was conducted for the installation of a Raymond mill (Hongxing Machinery - HGM 130) within an operational mineral processing facility in Ordu, Turkey. The project's core methodology was built upon a three-stage digital workflow executed using Dassault Systèmes' SolidWorks 2022 software, chosen for its robust assembly and simulation capabilities.

2.1. Reverse-Engineering and 3D Model Creation

As the mill components arrived disassembled, the first step involved reverse-engineering each major part (Figure 1). Detailed physical measurements were taken of components including the base frame, grinding ring, rolls, classifier, main shaft, drive assembly, and ancillary ductwork. Using these measurements, accurate 3D solid models and detailed sketches of each component were created in SolidWorks (Figure 2). Particular attention was paid to connection interfaces, lifting points, and clearances.

Figure 1. Received mill component

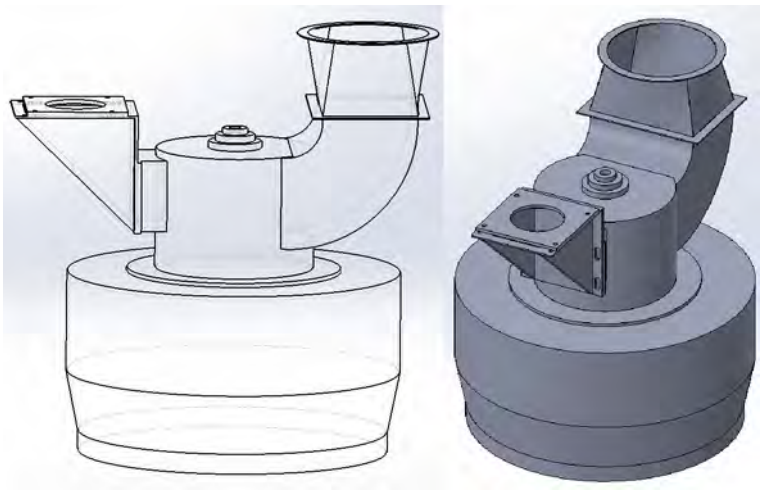

Figure 2. Digital 3D twin of the mill component

2.2. Development of the Host Building Digital Twin

Concurrently, a precise 3D model of the existing host building was developed. This model incorporated all relevant spatial constraints: structural columns, floor levels, ceiling clearances, existing equipment, maintenance walkways, and entry points (doors, overhead cranes). Laser scanning was employed to capture accurate as-built conditions of the facility, ensuring the digital environment faithfully represented the physical space.

2.3. Virtual Assembly Simulation and Sequencing

The 3D mill components were then imported into the building model to create a master digital assembly. This served as the project's digital twin. The simulation process involved:

1. **Clash Detection:** Running static and dynamic interference checks to identify spatial conflicts between mill components, between the mill and the building structure, and with existing equipment. (Wang et al., 2019)

2. **Process Flow Validation:** Aligning the digital model with the Process & Instrumentation Diagrams (P&IDs) to ensure correct positioning of inlets, outlets, and electrical/conduit routes.
3. **Sequential Assembly Planning:** A step-by-step virtual installation sequence was scripted and simulated. This sequence defined the optimal order of operations, starting from foundation preparation and anchor bolt placement, through the erection of the main frame, to the installation of internal grinding elements and final connections. Critical lifting paths for each component were visualized and validated using virtual crane tools.
4. **Access and Maintenance Review:** The model was used to verify adequate space for installation tools, technician access during assembly, and future maintenance activities.

3. RESULTS AND DISCUSSION

The implementation of the digital prototyping and simulation framework yielded significant practical benefits throughout the project lifecycle.

3.1. Pre-Installation Phase

The virtual simulation identified three major clashes that were not apparent in the 2D plans: an interference between the classifier outlet duct and a structural beam, a conflict between the motor platform and a walkway, and insufficient clearance for installing the main drive shaft. These issues were resolved digitally by modifying duct routing and slightly repositioning the mill base before any physical work began, eliminating potential rework (Figure 3).

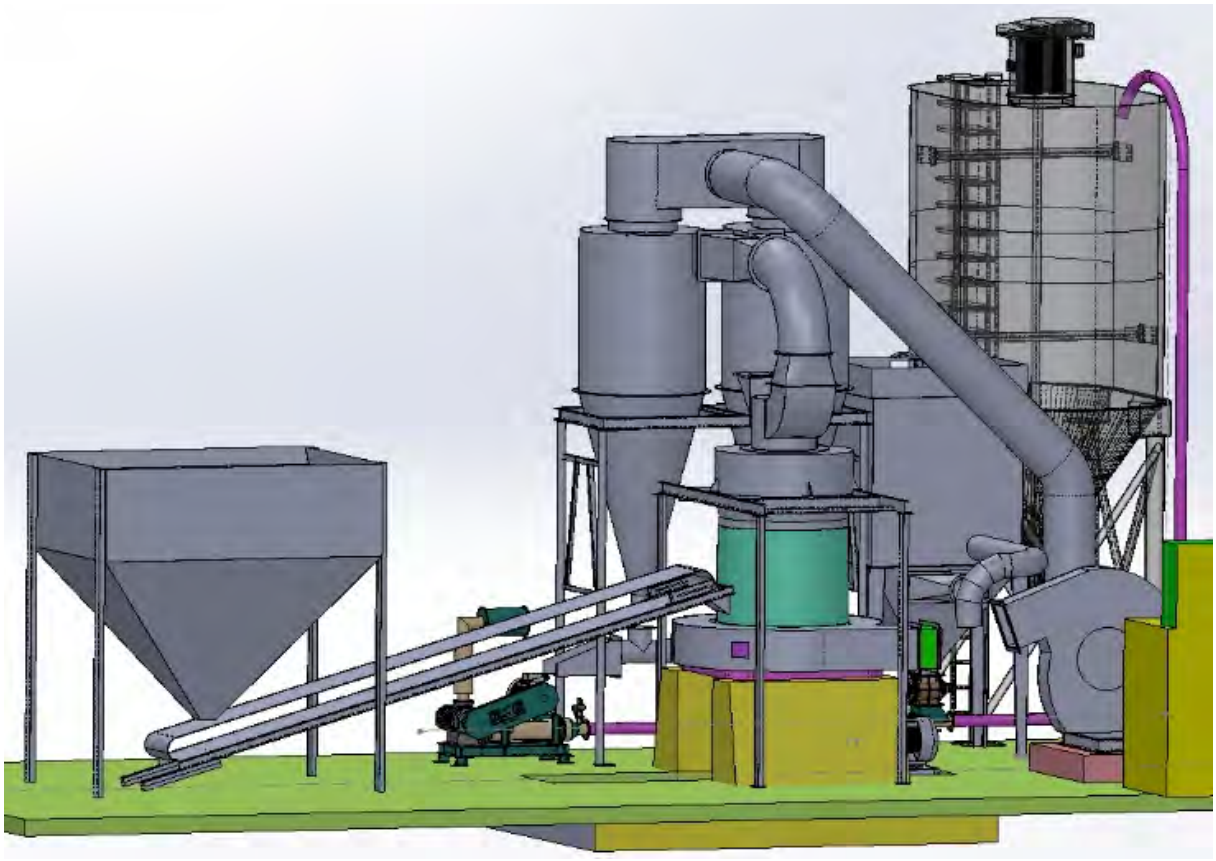

Figure 3. Digital twin of mill assembly

3.2. Installation Execution

The pre-determined sequential assembly plan served as the definitive guide for the field crew. The foremen and technicians reviewed the 3D simulation animations prior to work, leading to a clear understanding of the sequence and requirements. The actual physical installation proceeded with remarkable smoothness (Figure 4). Component placement, alignment, and bolting were achieved efficiently, with no stoppages due to unforeseen spatial conflicts or logistical confusion.

Figure 4. The complete mill assembly

3.3. Project Schedule and Cost Adherence

The entire project, encompassing the digital planning phase, foundation pouring with its 28-day mandatory curing period, and the mechanical installation and alignment of the Raymond mill, was completed within the allocated two-month schedule (Figure 5). The proactive resolution of clashes and logistical issues in the virtual environment minimized on-site delays and avoided the extra labor and material costs typically associated with traditional trial-and-error methods.

Work to be done	Required Time (H)	Start Date	End Date	Duration (d)
Foundation Concrete Works	22	07.04.2025	13.04.2025	7
Mill Body Works	32	06.05.2025	14.05.2025	8
Mill E. Motor & Gearbox Installation	24	11.05.2025	17.05.2025	5
Separator installation	18	15.05.2025	20.05.2025	5
Fan Installation	20	19.04.2025	25.04.2025	6
Cyclone Assembly	8	19.04.2025	22.04.2025	3
Filter Assembly	22	22.04.2025	28.04.2025	6
Ducting	40	25.04.2025	02.05.2025	7
Feed Hopper	17	26.04.2025	28.04.2025	3
Screw Conveyor Assembly	8	29.04.2025	01.05.2025	2
Electrical work	112	10.04.2025	22.05.2025	42

Figure 5. The mill installation schedule

4. DISCUSSION

The success of this case study underscores the value of digital prototyping as a risk mitigation tool in industrial projects. The digital twin provided a single source of truth, facilitating better communication between engineers, project managers, and installation crews. The ability to visualize and validate the entire process in context reduced cognitive load and reliance on individual experience alone (Tao et al. 2018; Negri et al., 2017)
While the initial investment in time and software for creating the detailed 3D models is non-trivial, the return on investment is realized through the avoidance of rework, reduced downtime, and strict schedule adherence. The methodology proved particularly effective for retrofit projects in constrained spaces, where margins for error are minimal.
A limitation of the study is that it represents a single case. Future work should involve applying this framework to different types of machinery and across multiple projects to develop quantitative metrics for time and cost savings. Furthermore, integrating the digital twin with real-time project management software could enhance tracking and control during the physical execution phase

5. CONCLUSION

This paper demonstrates that digital prototyping and sequential assembly simulation are not merely planning aids but are essential components for the efficient and error-free installation of complex industrial machinery. By employing SolidWorks to create a dynamic digital twin of a Raymond mill within its host building, the project team successfully identified and resolved spatial conflicts, optimized the installation sequence, and validated all mechanical interfaces prior to fieldwork.
The result was a commissioning process executed with high precision, completing on schedule within a challenging two-month window. The study concludes that adopting a model-based engineering approach significantly de-risks industrial installation projects, enhances spatial and logistical control, and provides a robust framework for optimizing the commissioning of heavy machinery in the mineral processing and related manufacturing sectors. The documented methodology offers a replicable blueprint for industry practitioners seeking to leverage digital tools for project excellence.

REFERENCES

Eastman, C., Teicholz, P., Sacks, R., Liston, K., (2011), BIM Handbook: A Guide to Building Information Modeling for Owners, Managers, Designers, Engineers and Contractors, 2nd ed., John Wiley & Sons.

Ghanem, S. Y., AbdelRazig, Y. A., (2006) “A framework for virtual construction simulation and analysis of industrial projects”, Journal of Construction Engineering and Management, 132 (12) 1261-1271.

Grieves, M., (2014) “Digital twin: manufacturing excellence through virtual factory replication”, White paper, 1 1-7.

Molloy, C., Vaze, J., (2017) “The role of simulation in optimising mineral processing plant design and operation”, 13th AusIMM Mill Operators' Conference, 261-270.

Negri, E., Fumagalli, L., Macchi, M., (2017) “A review of the roles of digital twin in CPS-based production systems”, Procedia Manufacturing, 11 939-948.

Sacks, R., Eastman, C., Lee, G., Teicholz, P., (2018), BIM Handbook: A Guide to Building Information Modeling for Owners, Designers, Engineers, Contractors, and Facility Managers, Wiley.

Shen, Z., Kawamura, K., (2015) “Virtual commissioning for manufacturing systems: A review”, International Journal of Automation Technology, 9 (5) 479-486.

Tao, F., Cheng, J., Qi, Q., Zhang, M., Zhang, H., Sui, F., (2018) “Digital twin-driven product design, manufacturing and service with big data”, The International Journal of Advanced Manufacturing Technology, 94 3563-3576.

Tao, F., Zhang, M., Nee, A. Y. C., (2019), Digital Twin Driven Smart Manufacturing: Academic Press.

Wang, W., Guo, H., Li, X., Tang, S., (2019) “A BIM-based framework for automated clash detection and resolution in MEP systems”, Automation in Construction, 104 129-148.

REAGENT OPTIMIZATION FOR COST-EFFECTIVE AND SUSTAINABLE GOLD PROCESSING AT GOLD FIELDS GHANA, TARKWA MINE

Michael Mawuenyega Kwame KUATSIENU[1,*], Maria SINCHE-GONZALEZ[1], Prince Pappoe AWOTWE[2], Eric ANDERSON[2]

[1]University of Oulu, Oulu Mining School, P.O. Box 3000, 90570, OULU, FINLAND
[2]Asante Gold Bibiani, Ghana
**Corresponding author: Michael.Kuatsienu@student.oulu.fi*

A B S T R A C T

This project is a reagent optimization initiative at the Tarkwa Gold Processing Plant aimed at Optimizing lime and flocculant consumption while maintaining process efficiency. The plant previously consumed about 691g/t lime and 4g/t flocculant (AF 9629), hence increasing operational cost. Through field trials, laboratory sedimentation tests, and plant evaluation of alternative flocculants (Senfloc 5330 and 5150), Senfloc 5330 achieved the best overflow clarity (23 NTU) at an optimum dosage of 18 g/t with 100 g/t lime. The initiative estimated annual savings of US $1.39 million from US$3.71 million annual budget, highlighting both economic and sustainability gains. Implementation in the plant demonstrates that lime can be reduced to 510 g/t and optimized flocculant 5330 to 9 g/t without affecting thickener underflow density or leach feed performance. Net savings of US$0.54M from January 2024 to September 2024 was achieved because of the reduction in lime and increase in flocculant. The results demonstrate that systematic reagent control and product selection can significantly enhance cost efficiency and environmental performance in gold processing.

Key words: *Reagent optimization, flocculant, lime consumption, sustainability*

1. INTRODUCTION

Reagent optimization is an essential component of cost-effective and environmentally responsible mineral processing. Lime is primarily used for pH control, cyanide detoxification, and prevention of acid generation, while flocculants promote solid–liquid separation in thickeners (Adjei et al., 2019; Simate & Ndlovu, 2020). However, excessive reagent use increases operational costs and affects downstream metallurgical performance (Tetteh et al., 2021).

The Tarkwa CIL (Carbon-in-Leach) plant of Gold Fields Ghana operates three pre-leach thickeners (32 m diameter) treating an average of 497.7 t/h at 35% solids. Prior to this study, lime and flocculant consumptions were 691 g/t and 4 g/t respectively, exceeding optimum levels and leading to high costs. Preliminary audits identified three main causes: **(i)** uneven flow of turbid tailings recycled water to thickener 1, **(ii)** uncoordinated manual adjustment of dosing systems during turbidity incidents, and **(iii)** poor shift communication practices.

This study aimed to:
1. Optimize lime and flocculant consumption rates
2. Achieve uniform feed density distribution across thickeners
3. Evaluate alternative flocculant formulations for process improvement
4. Quantify the associated economic benefits.

2. MATERIALS AND METHODS

2.1.Field Data Collection

Field data were collected (July 08, 2023) on thickener feed and underflow densities, pH (manual + online), and reagent dosing rates (Adjei et al., 2019). The trial involved redirecting turbid tailings recycled water (TRW) through the clarifier plant to the mill return tank (MRT) rather than directly into the thickener feed box. This change equalized residence times among thickeners and reduced unnecessary lime additions.

The average base parameters of thickener 1 are shown in Table 1.

Table 1. Base parameters of the thickener operation

Thickener Parameter	Value
Cyclone Overflow Density	34-38%
Thickener 1 inlet Density	16%
Thickener 2 inlet Density	32%
Thickener 3 inlet Density	30%
Thickener pH	12.5

Figure 1 shows the average turbidity and total suspended solids (TSS) from a monthly sampling during 2023.

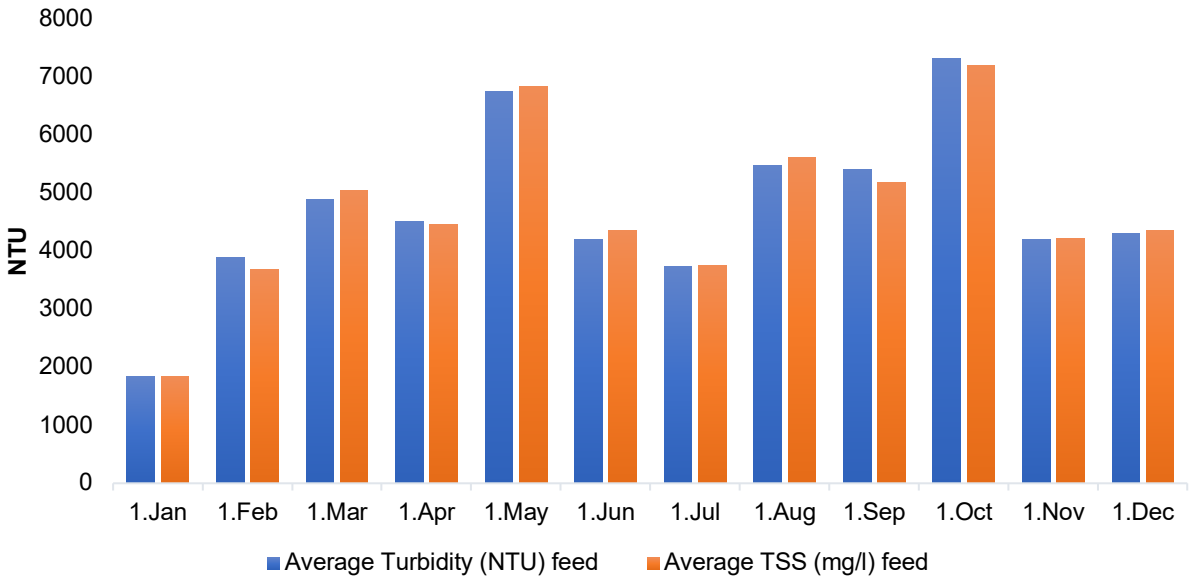

Figure 1. Turbidity and Total Suspended Solids (2023) in the TRW added to the feed of the Thickener 1

2.2.Samples and Sedimentation Tests

Representative samples were collected from six active pits i.e. Akontansi Ridge (AK1), Akontansi Central (AK2), Akontansi Underlap (AK3), Teberebie Cut 4 (TB4), Pepe Cut 5 (PP5), and Kottraverchy (KV1). Samples (20Kg) were ground (in an Essa® LM2 Pulverizing Mill) to reach a P80 of 106 microns then adjusted to pH 10.5–10.85 using Carmeuse lime and subjected to sedimentation tests using three flocculant types: AF 9629, Senfloc 5150, and Senfloc 5330. All the flocculant types are anionic polyacrylamide (PAM).
Stock solutions of 0.05 % w/v were prepared by hydrating 0.05 g of flocculant in 100 ml of process water, followed by mild agitation and 20 minutes of settling. Flocculation performance

was assessed by settling rate and overflow turbidity (Nephelometric Turbidity Units, NTU) after 20 minutes, consistent with methods outlined by Habashi (2017). Table 2 shows the typical behavior expected by type of flocculant tested.

Table 2. Type and characteristics of the flocculants used

Flocculant	Type	Typical behavior
AF 9629	Anionic PAM (moderate–high charge)	Fast settling, strong flocs
Senfloc 5150	Anionic PAM (lower charge)	Coarser materials, very high settling rates
Senfloc 5330	Anionic PAM (higher charge)	Better for fine slimes, clearer overflow

2.3.Lime and Flocculant Tests in a Blend Sample from the Plant

A sample from the cyclone overflow with a representative composite ore blend feeding to the plant (AK1 = 23 %, AK2 = 28 %, PP5 = 4 %, TB4 = 44 %, KV1 = 1 %) was tested (sedimentation)with lime dosages of 100–500 g/t and flocculant dosages of 10–18 g/t. Data were analyzed using turbidity to determine the optimal reagent combination (Searle & Banda, 2022*)*.
Flocculation tests were repeated 9 times on 9 different days over three months and the average results were analyzed.

3.RESULTS AND DISCUSSION

3.1. Sedimentation Results

Pit-specific tests without lime addition showed poor clarity across all flocculants, confirming lime's essential role in coagulation (Habashi, 2017*)*. With lime addition, Senfloc 5330 exhibited the best clarity results with average turbidity of 265 NTU, compared with 2779 NTU for AF 9629 and 951 NTU for Senfloc 5150 (Figure 2).

Test using the blend sample further established Senfloc 5330 as the most efficient reagent, achieving averagely 23 NTU at 350 g/t lime and 18 g/t flocculant. Though Senfloc 5150 displayed the fastest settling rate, Senfloc 5330 achieved superior overflow clarity i.e. the more critical operational parameter for water recovery and thickener throughput (Adjei et al., 2019; Tetteh et al., 2021)*.*

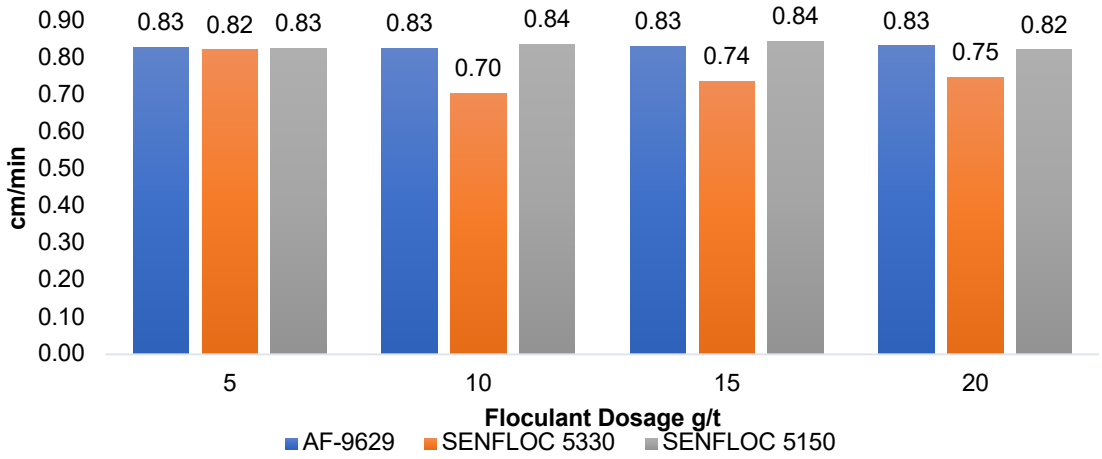

Figure 2. Settling rate of feed using various flocculants at various dosages (5 to 20 g/t and constant addition of 350g/t of lime)

3.2. Plant optimization with blend sample

The rerouting of turbid recycled water stabilized the thickener feed's densities and improved overflow clarity. Average pH values reduced by about 5.6 % (from 12.5 to 11.8) on average, while feed densities maintain approximately the density of the hydrocyclone overflow (34% - 38%) with negligible dilution from trash screen water.

Importantly, leach-feed densities (Figure 3) remained constant, confirming that reagent optimization did not compromise downstream process stability.

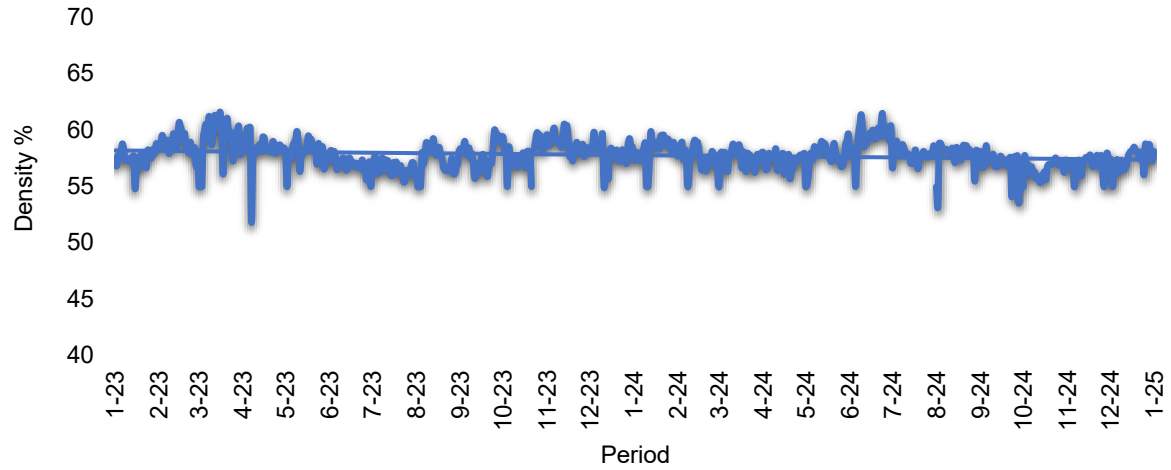

Figure 3. Leach feed density before and after the optimization

Lime consumption decreased from 691 g/t to 510 g/t, while flocculant usage increased moderately to about 9 g/t to maintain clarity (Table 3). This balance between alkalinity and polymer demand reflects the chemical trade-offs often observed in gold-ore thickening systems (Tetteh et al., 2021).

Table 3. Trade-off percentage of the Chemical Reagents

Reagent	Planned (g/t)	Lab Results (g/t)	Optimized Actual (g/t)	Actual %Δ from Planned
Lime	691	350	510	−26 %
Flocculant	4	18	9	+125 %

3.3. Cost–Benefit Analysis

Table 4. Yearly reagent plan and post-optimization achievements

Reagent	Reagent Price ($/t)	Planned (g/t)	Plan $/(g/t)	Lab Results (g/t)	Lab $/(g/t)	Optimized Actual (g/t)	Optimized $/(g/t)
Lime	331	691	0.23	350	0.12	510	0.17
Flocculant	3340	4	0.01	18	0.06	9	0.03
Total			0.24		0.18		0.20

The deliberate increase in flocculant usage was offset by the significant reduction in lime cost and improvement in thickener performance. The overall economic benefit of the project was estimated at US$0.54M from January 2024 to September 2024, as an actual value recorded by the mine operation (Figure 4).

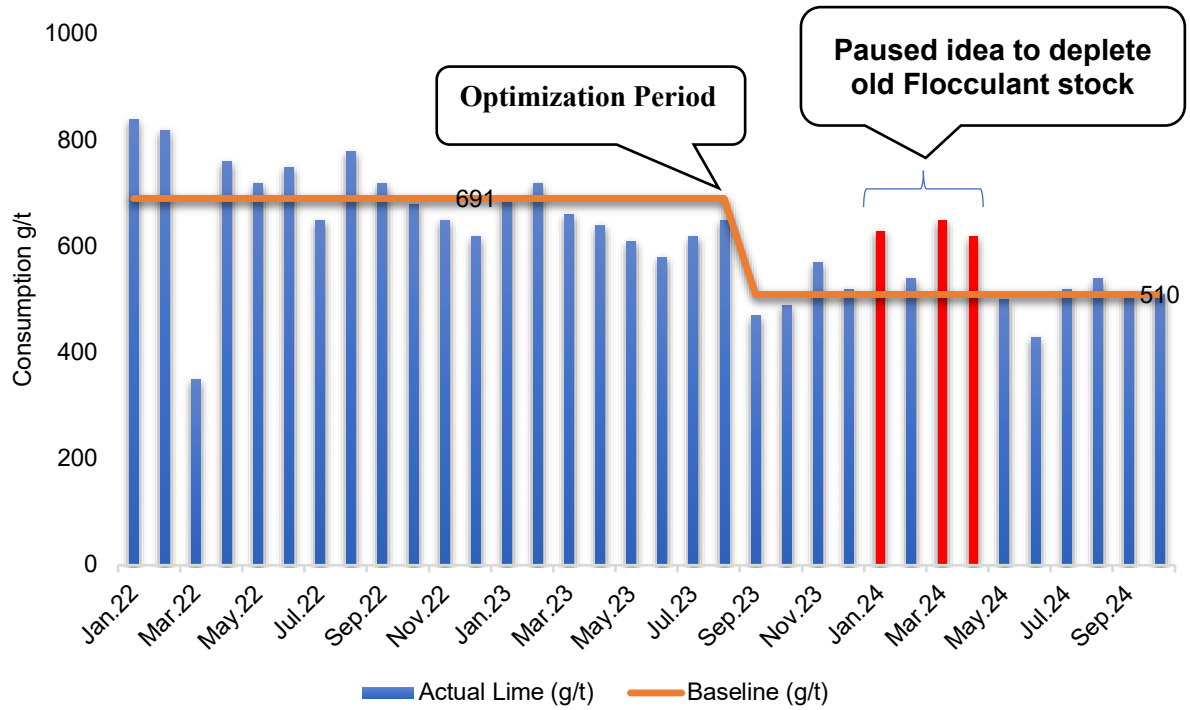

Figure 4. Lime consumption before and after optimization

3.4 Sustainability Implications

Beyond cost reduction, the optimization reduced chemical load to the tailings system, improving recycled-water quality and reducing the environmental impact of the CIL operation. Such integrated reagent-control approaches have been shown to support sustainable production goals in the mining industry (Habashi, 2017; Searle and Banda, 2022).

4.CONCLUSION

This study successfully optimized lime and flocculant usage in the Tarkwa CIL circuit through a combination of field adjustments, laboratory testing, and systematic reagent evaluation.
Key outcomes include:

- Identification of Senfloc 5330 as the most effective flocculant for clarity improvement.
- Reduction of lime consumption from 691 g/t to an actual of 510 g/t without compromising underflow density
- Achievement of actual savings of over half a million USD; and
- Demonstrated potential for sustainable reagent management in large-scale gold processing.

5.RECOMMENDATIONS

- Source alternative flocculant vendors to improve price competitiveness.
- Reintroduce a cascade feed distribution system to ensure uniform thickener loading (Adjei et al., 2019).
- Upgrade online pH sensors and flocculant flow meters for real-time control (Habashi, 2017).
- Implement advanced thickener automation for reagent-dosing optimization.

- Maintain pH between 10.8 and 11.0 to ensure consistent precipitation and minimal lime loss.
- Research into the zeta potential of fine particles of the Tarkwa ore

REFERENCES

Adjei, M., Owusu, P., Boateng, K., (2019) “Reagent control strategies for gold ore leaching circuits”, Journal of Metallurgical Process Engineering, 8 (3) 145–154.

Goldfields Ghana Limited, Tarkwa mine. Standard Operating Procedures Handbook.

Habashi, F., (2017), Textbook of Hydrometallurgy, Metallurgical Publications, Quebec.

Searle, K. A., Banda, M., (2022) “Process optimization for reduced chemical footprint in gold processing plants”, Journal of Sustainable Mining, 21 (4) 188–197.

Simate, G. S., Ndlovu, S., (2020) “Sustainable water and reagent use in gold processing plants”, Minerals Engineering, 150 105–118.

Tetteh, E. K., Awuah, F. M., Mensah, J. K., (2021) “Comparative assessment of polyacrylamide flocculants for thickener performance in CIL operations”, Mining Science and Technology, 31 (2) 203–214.

UPGRADING ULTRA-LOW-QUALITY LIGNITE THROUGH WASTE HEAT–DRIVEN FLUIDIZED BED DRYING AND DENSITY-BASED SEGREGATION

Harun BILIRGEN[1,*], Fatma BILIRGEN[2]

[1]OSTIM Technical University, Faculty of Engineering, Mechanical Engineering Department, 06374, Yenimahalle, Ankara, TÜRKİYE
[2]TABi Engineering and Energy Technologies Inc., Istanbul Technical University, ARI 2 Technopark, 34469, Maslak, Istanbul, TÜRKİYE
**Corresponding author: harun.bilirgen@ostimteknik.edu.tr*

A B S T R A C T

This study presents the design, field implementation, and performance evaluation of a waste-heat-integrated, low-temperature bubbling fluidized bed coal drying system that simultaneously achieves moisture reduction and density-based mineral segregation. The feed coal is an ultra-low-quality Turkish lignite obtained from a domestic open-pit basin supplying a pulverized coal-fired power plant. The as-received fuel is characterized by 51–53% total moisture, 20–22% ash, up to 2.3% sulfur (ar), and a lower heating value (LHV) of 990–1210 kcal/kg.

Thermal energy for drying is supplied by low-pressure saturated steam recovered from existing plant processes and transferred through preheated fluidization air and embedded in-bed heat exchangers operating at 40–90 °C. Field operation at a feed capacity of 10 t/h demonstrated that moisture content could be reduced from approximately 47% to 35% under nominal conditions and to below 25% under extended residence time, corresponding to LHV increases from approximately 1,200 kcal/kg to 1,700–2,200 kcal/kg.

Statistical analysis confirmed strong repeatability and agreement with independent laboratory measurements. In addition to thermal upgrading, the bubbling fluidized bed promoted gravitational segregation of high-density mineral matter, particularly pyrite-rich fractions, which accumulated near the bottom of the bed and were systematically removed prior to downstream handling and combustion.

A techno-economic assessment indicates a payback period of approximately 1.5–3 years for a representative 300 MW lignite-fired plant when waste heat is utilized. The proposed system functions as a hybrid thermal–mineral processing unit, offering a technically feasible and economically attractive pathway for improving lignite utilization efficiency, reducing emissions intensity, and mitigating slagging and fouling risks without requiring major boiler modifications.

Key words: *Lignite drying, bubbling fluidized bed, waste heat recovery, impurity segregation*

1. INTRODUCTION

Low-rank lignite represents a substantial portion of global coal reserves; however, its high inherent moisture content significantly limits its thermodynamic and environmental performance in coal-fired power plants. Ultra-low-quality lignite may contain 45–55% moisture as received, resulting in reduced lower heating value (LHV), increased specific fuel consumption, and reduced overall boiler efficiency (Levy et al., 2005, 2006, 1999; Dong, 2014). The latent heat required for in-furnace evaporation lowers flame temperature and can adversely affect ignition stability, combustion completeness, and heat transfer characteristics (Levy et al., 1999; Pisupati & Scaroni, 1993).

Coal pre-drying has therefore been extensively investigated as a means of improving lignite utilization efficiency. A range of technologies has been developed, including rotary dryers, flash dryers, superheated steam dryers, and fluidized-bed-based systems (Mujumdar, 2007;

Jangam et al., 2011). Among these, fluidized-bed drying offers favorable heat and mass transfer characteristics due to enhanced particle–gas contact and uniform temperature distribution (Jangam et al., 2011). Commercial-scale implementations, such as the WTA (Wirbelschicht-Trocknung mit interner Abwärmenutzung) process in Germany, have demonstrated measurable improvements in plant efficiency and reductions in CO_2 intensity (Dong, 2014). However, large-scale integrated drying systems are often capital-intensive and are typically optimized for new-build ultra-supercritical units rather than retrofit applications (Dong, 2014).

High-temperature drying technologies may require auxiliary fuel input or complex closed-loop vapor handling systems, increasing both capital expenditure (CAPEX) and operational complexity (Mujumdar, 2007; Jangam et al., 2011). In contrast, low-temperature drying integrated with waste heat recovery provides a more retrofit-friendly alternative by utilizing low-grade thermal energy streams already available within existing power plants. Such integration minimizes incremental fuel consumption and reduces operating costs while maintaining system simplicity (Dong, 2014, Levy et al., 2006).

Beyond moisture removal, certain fluidized-bed configurations can promote hydrodynamic classification effects due to density and size differences between organic coal particles and mineral matter (Kim et al., 2013, Bullinger et al., 2002, 2011, 2013). The resulting segregation of high-density, mineral-rich particles may provide partial pre-combustion fuel beneficiation, potentially reducing ash loading to the boiler and mitigating slagging and fouling tendencies (Pisupati & Scaroni, 1993; Dong, 2014). While the drying performance of various systems has been widely documented, fewer studies have simultaneously evaluated moisture reduction and density-based impurity segregation under low-temperature waste-heat-driven conditions. A comparative overview of major coal drying technologies, including their operating temperature ranges, heat sources, capital intensity, and retrofit suitability, is provided in Table 1.

Table 1: Comparisons of various coal drying technologies

Technology	Typical Operating Temperature	Heat Source	CAPEX Intensity	Typical Efficiency Gain	Retrofit Complexity	Additional Fuel Beneficiation
Rotary / Direct-Contact Dryer	150–600 °C	Hot flue gas or auxiliary fuel	Moderate	1–3%	Moderate	No
WTA (Fluidized Bed, Germany)	~110–160 °C	Internal waste heat (steam-based)	High	~1–4%	High (new-build oriented)	Limited
Superheated Steam Drying	120–200 °C	Closed-loop steam	High	2–5%	High	No
Proposed Low-Temperature FBCD	**40–90 °C**	**Low-grade waste heat**	**Moderate**	**2–4%**	**Low–Moderate**	**Yes (density-based segregation)**

The present study investigates a newly developed low-temperature bubbling fluidized-bed coal drying (FBCD) system integrated with waste heat streams recovered from an operating lignite-fired power plant. The primary objective is to quantify steady-state moisture reduction performance and the corresponding enhancement in lower heating value (LHV) under pilot-scale operating conditions. In addition, the study evaluates density-based impurity segregation within the fluidized bed and assesses the combustion and techno-economic implications of controlled fuel upgrading for retrofit applications.

The novelty of this work lies in the combined assessment of thermal upgrading and mineral segregation under low-temperature conditions, supported by statistically validated pilot-scale measurements and a sensitivity-based economic evaluation. The results provide practical guidance for optimizing lignite fuel quality enhancement while maintaining compatibility with existing boiler design constraints and minimizing capital risk.

2. MATERIAL AND METHODS

2.1. Coal Origin and Properties

The feed coal used in this study is a Turkish ultra-low-quality lignite obtained from a domestic open-pit basin supplying a pulverized coal-fired power plant in Türkiye. Proximate and ultimate analyses (moisture 51–53% ar, ash 20–22% ar, sulfur up to 2.3% ar, LHV 990–1210 kcal/kg) are provided in Table 2. The ash content varies between 20 and 22%, further reducing effective fuel quality and increasing solids loading in downstream systems. The volatile matter content is approximately 20%, while the Hardgrove Grindability Index (HGI) of about 60 indicates moderate grindability despite the high moisture level. Sulfur content reaches up to 2.3% (ar).

Table 2: Ultra-low-quality turkish lignite - ash chemistry and properties

		Coal Range	
Parameter	Unit	Max.	Min.
Low heating value	kcal/kg (ar)	1,210	990
Low heating value	MJ/kg (ar)	5.07	4.15
Total Moisture	% (ar)	53.0	51.0
Ash	% (ar)	22.0	20.0
Volatile matter	% (ar)		20.0
HGI	-		60
Sulfur	% (ar)	2.3	
SiO2	% (ash)	30.0	23.0
Al2O3	% (ash)	16.0	10.0
Fe2O3	% (ash)	7.0	4.7
CaO	% (ash)	40.0	20.0
MgO	% (ash)	9.0	3.0
K2O+Na2O	% (ash)	0.8	0.7
TiO2	% (ash)	2.2	0.4
SO4	% (ash)	25.0	15.0
Ash softening temp	°C		1,260
Ash fusion temp	°C		1,415
Ash flowing temp	°C		1,440

2.2. Drying System Description

The drying system consists of a bubbling fluidized-bed coal dryer (FBCD) with a nominal raw coal feed capacity of 10 t/h. Raw lignite is first crushed to below 10 mm prior to entering the dryer. Preheated fluidization air is introduced through an air plenum equipped with multiple nozzles to ensure uniform air distribution and stable fluidization. Under steady-state operation, the expanded bed height reaches approximately 1 m.

Drying energy is supplied through two mechanisms: sensible heat from the preheated fluidization air and indirect heat transfer from embedded in-bed heat exchangers utilizing low-pressure saturated steam recovered from existing plant processes. An induced-draft fan maintains slight negative pressure within the system to ensure controlled gas flow.

The lower region of the fluidized bed is designed to facilitate systematic removal of non-fluidizable, high-density impurities. These impurities, rich in mineral matter and pyrite fractions, accumulate near the bed bottom due to density-driven segregation and are periodically discharged through the underflow system. The partially dried lignite exits through the freeboard region and is recovered at the primary outlet, while entrained fines are subsequently captured in a downstream baghouse.

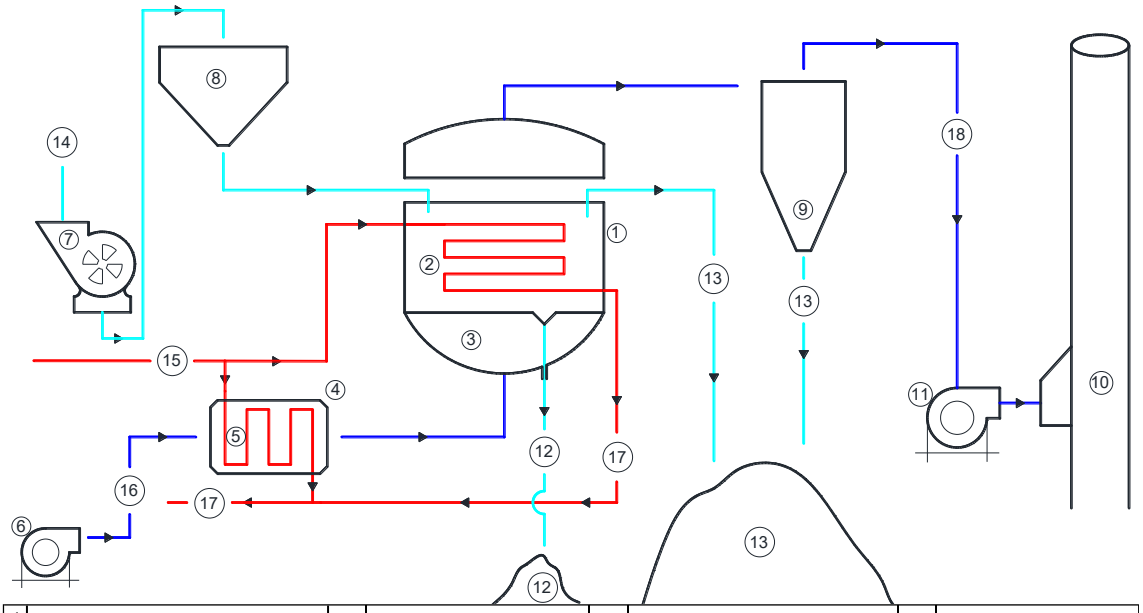

1	Bubbling Fluidized Bed	6	Pressurized Air Fan	11	Induced Draft Fan	15	Saturated Steam
2	Imbedded Heat Exchanger	7	Coal Crusher	12	Segregated, waste Coal	16	Pressurized Air
3	Fluidized Bed Windbox	8	Coal Silo	13	Partially Dried Coal	17	Condense Return
4	Air Pre-heater	9	Dust Collector	14	Raw Coal Feed	18	Exhaust Air
5	Heat Exchanger	10	Chimney				

Figure 1. Simplified process flow diagram of the bubbling fluidized bed coal drying system utilizing low-pressure saturated steam as a waste-heat source

2.3. Experimental Procedure and Statistical Analysis

The bubbling fluidized bed coal dryer (FBCD) was evaluated under multiple steady-state operating conditions, including nominal feed rate, reduced feed rate (approximately 50% of nominal capacity), and controlled variations in fluidization air temperature. Each condition was maintained for a sufficient duration to ensure steady-state operation prior to sampling. Lignite samples were collected upstream and downstream of the dryer. Representative composite samples were prepared using mass-flow-weighted averaging in order to preserve material balance consistency and minimize sampling bias.

For each operating condition, repeated measurements of moisture content and lower heating value (LHV) were performed. The arithmetic mean value, $\bar{x}$, was calculated as:

$$\bar{x} = \frac{1}{n}\sum_{i=1}^{n} x_i$$

where $x_i$represents individual measurements and n is the number of samples.

Measurement variability was quantified using the sample standard deviation, s:

$$s = \sqrt{\frac{1}{n-1}\sum_{i=1}^{n}(x_i - \bar{x})^2}$$

The 95% confidence interval (CI) for the mean was calculated as:

$$\bar{x} \pm t_{0.975,\,n-1}\frac{s}{\sqrt{n}}$$

where $t_{0.975,\,n-1}$ is the Student's t-value corresponding to a two-tailed 95% confidence level with $n-1$degrees of freedom.

To assess inter-laboratory agreement, LHV measurements obtained by the in-house laboratory were compared with those from an accredited independent laboratory. The strength of linear correlation was evaluated using the coefficient of determination, R^2, defined as:

$$R^2 = 1 - \frac{\sum_{i=1}^{n}(y_i - \hat{y}_i)^2}{\sum_{i=1}^{n}(y_i - \bar{y})^2}$$

where y_i represents accredited laboratory measurements, $\hat{y}_i$ represents predicted values from linear regression against in-house measurements, and $\bar{y}$ is the mean of accredited laboratory values.

The resulting coefficient of determination exceeded 0.97, indicating strong agreement and high measurement reliability. Transient startup data were excluded from analysis to ensure statistical consistency, and no statistically significant outliers were detected based on inspection of residual distributions and confidence bounds.

3. RESULTS AND DISCUSSION

3.1. Moisture Reduction and Heating Value Enhancement

The bubbling fluidized-bed coal dryer (FBCD) was operated at a nominal raw coal throughput of 10 t/h. Representative lignite samples were collected at the dryer inlet (downstream of the coal crusher) and simultaneously at the outlet streams, including both the main dryer discharge and the bottom of the baghouse.
Measurement reliability was assessed by comparing lower heating value (LHV) results obtained from the in-house laboratory with those measured by an accredited independent laboratory. As illustrated in Figure 2, the strong linear correlation between the two datasets confirms both the accuracy and reproducibility of the calorific value determinations.

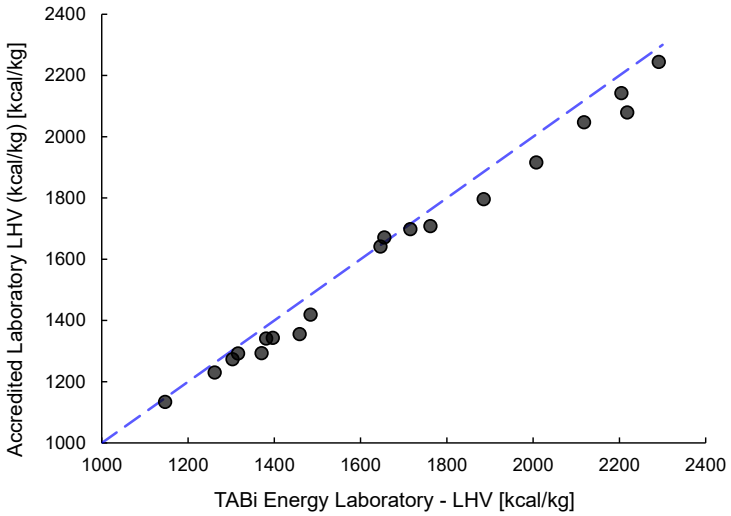

Figure 2. Comparison and validation of lower heating value (LHV) measurements between tabi energy and an accredited independent laboratory

Figure 3 presents the relationship between lignite moisture content and LHV before and after drying. Red diamond symbols represent raw lignite, while black circular symbols correspond to dried lignite obtained under two different operating conditions.

Under nominal feed conditions, the dryer reduced coal moisture from approximately 47% to about 35%, representing a reduction of roughly 12 percentage points. The 47% value corresponds to the specific batch tested during pilot-scale operation, whereas 51–53%

represents the broader basin range. This level of drying increased the LHV from approximately 1,200 kcal/kg to about 1,700 kcal/kg and was sufficient to meet plant operational requirements. When the coal feed rate was reduced by approximately 50%, the effective residence time in the fluidized bed increased, allowing deeper drying. Under these conditions, moisture content decreased to below 25%, and the LHV increased to nearly 2,200 kcal/kg.

All reported performance values represent steady-state averaged measurements derived from statistically evaluated datasets; transient or instantaneous peak values were excluded from analysis.

Although the deeper drying condition demonstrates the technical capability of the system, substantial increases in LHV may modify furnace heat release characteristics in retrofit applications. Higher fuel heating value increases volumetric heat release rate, which can elevate local flame temperature and radiative heat flux to furnace waterwalls, potentially shifting operation beyond original boiler design envelopes. For practical plant integration, controlled upgrading corresponding to an approximately 10–15% increase in LHV is considered optimal. This range provides meaningful efficiency improvement while maintaining compatibility with existing combustion system constraints and avoiding excessive thermal loading.

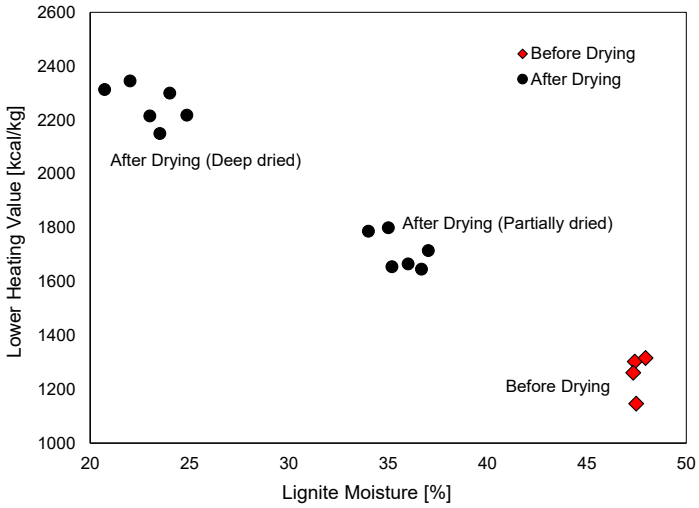

Figure 3. Lignite Moisture versus Lower Heating Value

Figure 4 shows representative lignite samples before and after drying. The raw lignite exhibits a darker appearance and cohesive, agglomerated structure consistent with high surface and capillary moisture. In contrast, the partially dried lignite (≈35% moisture) displays a lighter coloration and a more granular, free-flowing morphology, indicating reduced interparticle adhesion due to moisture removal. The visual differences qualitatively confirm effective drying and improved handling characteristics under nominal operating conditions.

Figure 4. The Change in Lignite's Physical Appearance after Drying

3.2. Impurity Segregation Mechanism

Impurity segregation in the low-temperature bubbling fluidized-bed coal dryer (FBCD) is governed primarily by hydrodynamic classification arising from density and size differences between organic coal particles and mineral matter. Within the fluidized bed, particles experience drag, buoyancy, and gravitational forces, and their fluidization behavior depends on the balance of these forces. This balance can be characterized by the Archimedes number (Ar):

$$Ar = \frac{g d_p^3 \rho_g (\rho_p - \rho_g)}{\mu_g^2}$$

where d_p is particle diameter, ρ_p particle density, ρ_g gas density, μ_g gas viscosity, and g gravitational acceleration. Because mineral-rich particles (e.g., pyrite-bearing and high-ash fractions) possess significantly higher density (ρ_p) than the organic coal matrix, their Archimedes number is larger, resulting in higher minimum fluidization velocity (U_{mf}) requirements. Under operating conditions where superficial gas velocity is sufficient to fluidize lower-density coal particles but not all high-density mineral particles, density-driven stratification occurs.

Consequently, mineral-rich particles exhibit reduced fluidization tendency and preferentially migrate toward the lower bed region, where they accumulate and are periodically discharged through the underflow system. In contrast, lower-density, organic-rich particles remain effectively fluidized and are transported toward the upper bed and freeboard region, exiting as the upgraded fuel product. Controlled selection of fluidization velocity and residence time ensures stable bubbling while limiting excessive entrainment.

Moisture removal at 40–90 °C further enhances segregation by reducing capillary bridging and interparticle adhesion, thereby facilitating partial detachment of loosely associated mineral fines. However, at these temperatures, significant thermal decomposition or volatilization of mineral species is not expected; impurity removal is therefore dominated by mechanical and hydrodynamic mechanisms.

Figure 5 shows samples extracted from different vertical locations within the bed. A progressive enrichment of light-colored, high-density particles is observed toward the lower region. Bulk density measurements indicate that bottom-accumulated material exhibits approximately twice the density of the partially dried lignite product, providing quantitative confirmation of gravitational segregation.

These findings demonstrate that the FBCD functions not only as a thermal drying unit but also as a pre-combustion mineral classification device. By selectively removing high-density mineral fractions prior to combustion, the system reduces impurity loading to downstream milling and boiler systems, thereby mitigating slagging and fouling risks and enhancing combustion stability.

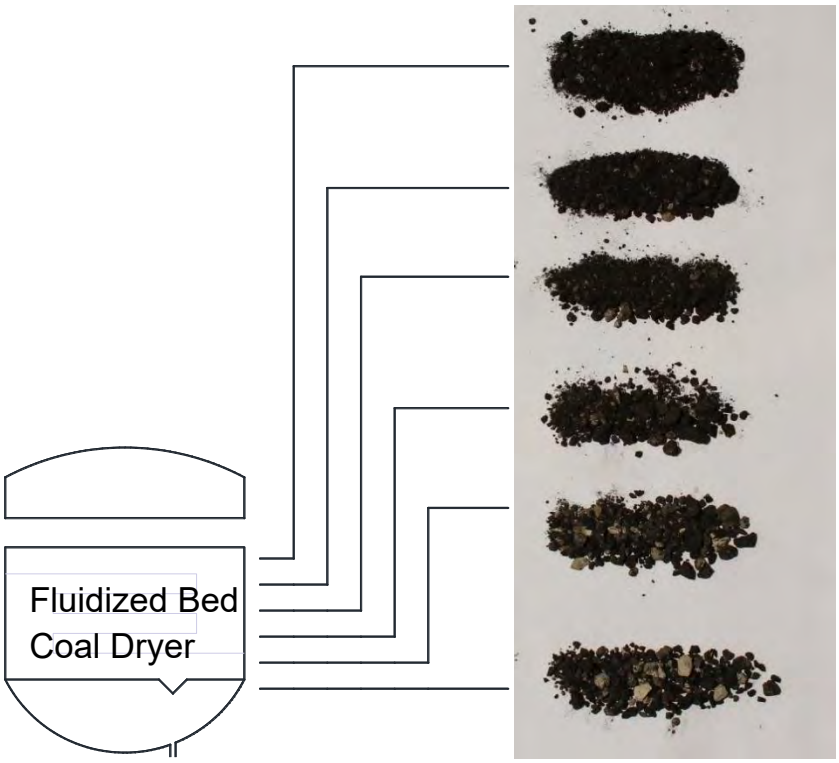

Figure 5. Gravitational Segregation of Coal Particles in Fluidized Bed Coal Dryer

3.3. Combustion and Boiler Performance Implications

Upgraded lignite resulting from controlled moisture reduction exhibits improved ignition stability and more consistent flame characteristics due to increased calorific value and reduced moisture-induced heat sink effects during devolatilization. The reduction in inherent moisture decreases the mill drying requirement, thereby lowering primary air demand and improving pulverizer operational stability. Additionally, the higher heating value reduces the required fuel mass flow rate per unit electrical output (MW), contributing to improved combustion efficiency and reduced auxiliary power consumption.

However, excessive upgrading may alter furnace heat release distribution. Significant increases in fuel heating value can elevate peak flame temperature, increase volumetric heat release rate, and raise radiative heat flux to waterwall surfaces. These changes may approach or exceed original boiler design limits and result in elevated tube metal temperatures. Therefore, controlled enhancement of fuel quality—rather than maximum achievable drying—is recommended to ensure compatibility with existing combustion system constraints while maintaining operational reliability.

3.4. Slagging, Fouling, and Emissions

The selective removal of pyrite-rich and high-ash fractions prior to combustion reduces the concentration of iron-bearing and silicate mineral constituents that contribute to low ash fusion temperatures and slag formation. By decreasing the mineral loading of the fuel, the system lowers the probability of molten ash adhesion on furnace walls and convective heat transfer surfaces, thereby mitigating slagging and fouling tendencies. Reduced ash throughput also decreases erosive wear in high-velocity regions of the boiler.

The partial removal of sulfur-bearing mineral matter, particularly pyritic sulfur, contributes to lower SO_2 emissions per unit electrical output. In addition, reduced inherent fuel moisture

decreases flue gas water vapor concentration, improving gas-side heat transfer stability and enhancing the performance of downstream particulate control devices. Throughout the test campaign, no deterioration in baghouse differential pressure, filtration efficiency, or operational stability was observed, indicating compatibility of the upgraded fuel with existing emission control systems.

4. TECHNO-ECONOMIC ANALYSIS

The techno-economic performance of the proposed system was evaluated based on a nominal feed capacity of 10 t/h. Under typical operating conditions, moisture reduction from approximately 47% to 35% results in a net increase in lower heating value (LHV) of approximately 500 kcal/kg. This enhancement corresponds to an estimated boiler efficiency improvement of 2–4%, consistent with previously reported field studies (Bullinger et al. 2013, Bullinger et al. 2011, and Bullinger et al. 2002) and contributes to a reduction in auxiliary power demand of approximately 1–2%. As a consequence of improved fuel quality and reduced specific fuel consumption, CO_2 emission intensity is estimated to decrease by approximately 3–5% per unit electrical output.

For a representative 300 MW lignite-fired power plant, capital expenditure (CAPEX) requirements are considered moderate, primarily associated with the fluidized bed vessel, embedded heat exchangers, and draft fans. Because the drying energy is supplied by recovered waste heat, additional operating expenditure (OPEX) is minimal and largely limited to electricity consumption for fans and routine maintenance. The resulting annual fuel savings are estimated to be economically meaningful, yielding an estimated simple payback period in the range of 1.5 to 3 years, depending on site-specific conditions. Sensitivity analysis indicates that the payback period is most strongly influenced by initial coal moisture content, availability of waste heat, and prevailing coal prices.

5. CONCLUSIONS

This study evaluated the performance of a newly developed low-temperature bubbling fluidized-bed coal drying (FBCD) system integrated with recovered waste heat streams. The investigation focused on simultaneous moisture reduction and density-based mineral segregation in ultra-high-moisture lignite under pilot-scale operating conditions.

Field testing demonstrated that controlled drying can reduce lignite moisture content from approximately 47% to 35% under nominal conditions and to below 25% under extended residence time, resulting in corresponding increases in lower heating value (LHV) from approximately 1,200 kcal/kg to as high as 2,200 kcal/kg. All reported performance values represent statistically evaluated steady-state averages validated through cross-comparison with an accredited independent laboratory ($R^2 > 0.97$), confirming measurement reliability and repeatability.

The resulting annual fuel savings are estimated to be economically meaningful. In addition, hydrodynamic classification within the fluidized bed promoted density-based segregation of high-density mineral fractions, particularly pyrite-rich particles. Bulk density measurements indicated that bottom-accumulated material exhibited approximately twice the density of the upgraded product, confirming gravitational segregation. This co-benefit reduces mineral loading to the boiler and may contribute to improved combustion stability and reduced slagging and fouling tendencies.

Combustion-related implications were carefully evaluated. While deeper drying demonstrates the technical capability of the system, excessive fuel upgrading may increase volumetric heat

release rate, elevate peak flame temperature, and increase radiative heat flux to furnace waterwalls. For retrofit applications, a controlled enhancement corresponding to approximately 10–15% LHV increase is recommended to balance efficiency gains with existing boiler design constraints and operational reliability.

A techno-economic assessment based on pilot performance data and scaling to a representative 300 MW lignite-fired plant indicates that moisture reduction of approximately 12 percentage points can yield heat-rate improvements of 2–4% and CO_2 intensity reductions of 3–5%. Because evaporation energy is supplied by recovered waste heat, incremental fuel cost is negligible. Capital requirements are moderate, and the estimated simple payback period ranges from 1.5 to 3 years, depending primarily on initial coal moisture, waste heat availability, and coal price.

Compared with alternative lignite pre-drying technologies, the proposed low-temperature FBCD system offers moderate capital intensity, retrofit compatibility, minimal additional fuel consumption, and the added advantage of impurity segregation. These characteristics position the system as a technically viable and economically attractive option for upgrading ultra-low-quality lignite in existing coal-fired power plants.

Overall, the waste-heat-driven FBCD approach provides a scalable and flexible pathway for improving lignite utilization efficiency, reducing emissions intensity, and enhancing operational stability while maintaining compatibility with existing plant infrastructure.

REFERENCES

Bullinger, C. W., Ness, M. A., Sarunac, N., Levy, E. K., Weinstein, R. S., James, D. R., (2013), "Method of enhancing the quality of high-moisture materials using system heat sources" (U.S. Patent No. 8,579,999). U.S. Patent and Trademark Office.

Bullinger, C. W., Ness, M. A., Sarunac, N., Levy, E. K., Weinstein, R. S., James, D. R., Coughlin, M. P., Wheeldon, J. M., (2011), "Apparatus and method of enhancing the quality of high-moisture materials and separating and concentrating organic and/or non-organic material contained therein" (U.S. Patent No. 8,062,410). U.S. Patent and Trademark Office.

Bullinger, C. W., Ness, M., Sarunac, N., Levy, E. K., (2002), "Coal Drying Improves Performance and Reduces Emissions". 27th International Technical Conference on Coal Utilization and Fuel Systems.

Dong, N., (2014), "Techno-economics of modern pre-drying technologies for lignite-fired power plants" (IEACCC Ref: CCC/241). IEA Clean Coal Centre.

Eric, H. E., Lightcap, C., Huang, D., (2002), "Kinetics of Drying of North Dakota Lignite in a Fluidized Bed". Lehigh University ERC report.

Jangam, S. V., Karthikeyan, M., Mujumdar, A. S., (2011), "A Critical Assessment of Industrial Coal Drying Technologies: Role of Energy, Emissions, Risk and Sustainability". Drying Technology.

Kim, H-S., Matsushita, Y., Oomori, M., Harada, T., Miyawaki, J., Yoon, S-H., Mochida, I., (2013), "Fluidized bed drying of Loy Yang brown coal with variation of temperature, relative humidity, fluidization velocity and formulation of its drying rate". Fuel, 105, 415–424.
Levy, E. K., Sarunac, N., Bilirgen, H., Caram, H., (2006), "Use of Coal Drying to Reduce Water Consumed in Pulverized Coal Power Plants" (Final Report to DOE Award No. DE-FC26-03NT41729). Energy Research Center, Lehigh University.

Levy, E. K., Sarunac, N., Bilirgen, H., Zhang, W., (2005), "Use of Coal Drying to Reduce Water Consumed in Pulverized Coal Power Plants" (Quarterly Report to DOE Award No. DE-FC26-03NT41729). Energy Research Center, Lehigh University.

VALIDATION OF PROCESS SIMULATION THROUGH LOCKED CYCLE TEST AND PILOT FOR NORDIC TALC PLANT DESIGN

Erdem ÖZDEMIR[1,*], Erkki KURONEN[2], Heikki VAUHKONEN[2], Vesa-Pekka TAKALO[1], Juha Saari[1], Mikko RANTAMÄKI[1]

[1]Metso Finland Oy, Rauhalanpuisto 9, 02230 Espoo, Finland
[2]Nordic Talc Oy
**Corresponding author: erdem.ozdemir@metso.com*

A B S T R A C T

This study compares locked cycle test (LCT) results with HSC simulation outputs to evaluate the reliability of a developing talc processing flowsheet. Key performance indicators, including mass recovery, talc grade, and circuit stability, show a strong alignment between experimental and simulated outcomes. The strong correlation confirms that the HSC modeling effectively reflects real metallurgical behavior observed in laboratory testing. Furthermore, a dedicated pilot campaign validates both the LCT trends and simulated predictions of the proposed flowsheet. The combined insights from laboratory, simulation, and pilot-scale work provide a solid basis for reliable process design and future optimization of talc flotation operations.

Key words: *Modelling and simulation, plant design, pilot, locked cycle test, talc, flotation*

1. INTRODUCTION

Flotation remains one of the most widely used separation techniques in mineral processing, enabling the selective recovery of valuable minerals through differences in surface hydrophobicity and particle-bubble interactions. Talc flotation presents unique challenges due to the mineral's inherently high hydrophobicity and variability in surface properties, which influence recovery, grade, and overall separability (Bazar et al., 2021). Flotation performance is traditionally assessed through laboratory batch or column tests, with locked cycle tests (LCTs) being particularly valuable for approximating steady-state performance under conditions that mimic continuous operation by repeated re-treatment of concentrates and tailings (Agar, 2000).

Simulation tools have become integral to modern mineral process design and optimization, offering predictive insights into circuit behavior that complement empirical testing. The HSC Sim module, built on HSC Chemistry software, allows process engineers to construct and evaluate flowsheet models that integrate mass balances and flotation kinetics, facilitating decision support and design validation (HSC Sim, 2025). Prior work has demonstrated the utility of simulation frameworks for flotation circuits, including dynamic and static approaches that incorporate residence time distribution, cell design, and hydrodynamic effects to predict metallurgical performance.

Despite these advances, the reliability of simulation models must be assessed against experimental data to ensure accurate representation of metallurgical behavior. Locked cycle tests, in closed circuit flotation, provide robust experimental benchmarks for evaluating model predictions and refining design parameters (Agar, 2000 et al). By comparing key performance indicators such as mass recovery, concentrate grade, and circuit stability between LCT results and HSC simulation outputs, researchers can validate whether the simulation framework captures the complexities of real flotation behavior and thereby support confident flowsheet design and future plant.

The Suomussalmi project aims to convert an existing soapstone factory into a dedicated talc processing plant to enable the sustainable industrial utilization of local talc reserves and ensure the continuation of operations. The development follows a phased approach, beginning with engineering studies, feasibility assessments, and evaluation of alternative technical solutions, alongside an environmental impact assessment (EIA) to ensure regulatory compliance (Nordic Talc, 2025). Based on the outcomes of this phase, selected process options advance to detailed engineering. This study addresses this process design related topics by comparing experimental LCT outcomes with HSC simulation predictions for Nordic Talc flotation flowsheet, and by including pilot-scale validation of both experimental and modeled results.

2. MATERIAL AND METHODS

2.1. Material

Mineralogical and beneficiation tests were conducted on three different feed ore samples under the names of Suomussalmi 1, 2 and 3. The samples were crushed in the jaw crusher first. Next, the crushed ores were fed to the roller crusher. The samples were sieved using a 2 mm sieve. Then the materials were divided into 1.5 kg batches for flotation and mineralogical tests. The detailed sample preparation can be seen in Figure 1.

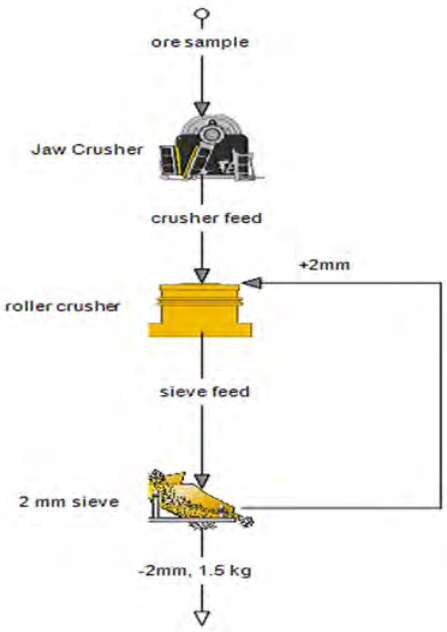

Figure 1. Sample preparation flowchart

After crushing and dividing the batches, a grinding calibration test was conducted to estimate adequate grinding time for the target particle size distribution which was suggested by the previous liberation studies. Three ore samples were ground separately in the stainless stain ball mill and media. Using a stainless stain mill with media prevented iron contamination from the grinding stage. The grinding was performed at 65 wt.% solid ratios. The particle size distribution of the flotation tests can be seen in Figure 2.

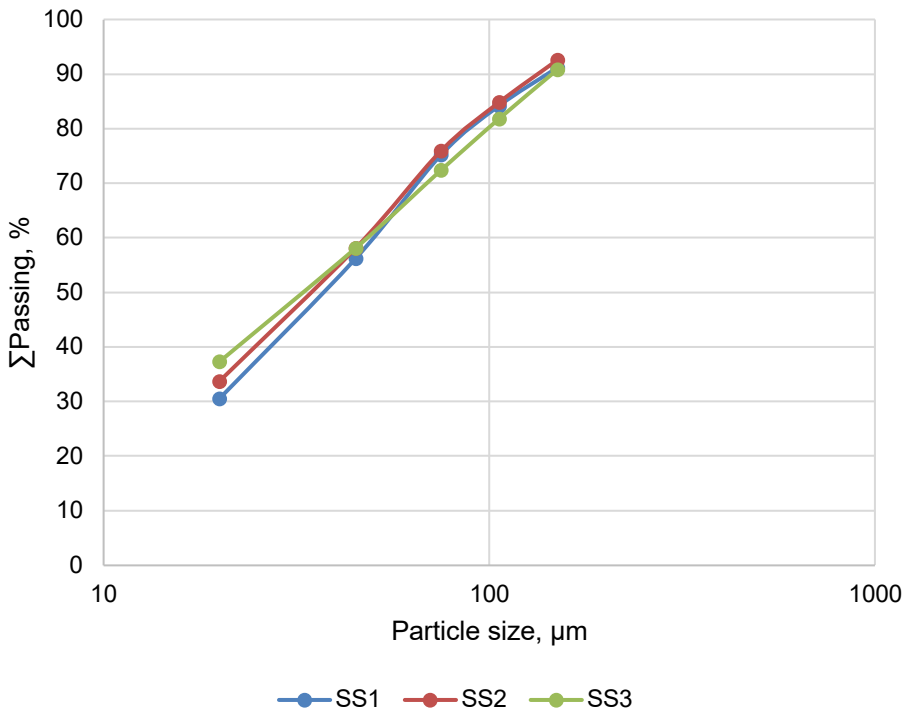

Figure 2. Particle size distributions of three different ore feeds

In Figure 2, particle size distributions of three feed samples show almost the same gradation.

2.2. Method

After grinding calibration tests, chemical and mineralogical studies were conducted. The chemical and mineral compositions of the feeds can be seen in Table 1 and Table 2, respectively.

Table 1. Chemical composition of the feed materials

Element	*Method*	*Unit*	Suomussalmi 1 (SS1)	Suomussalmi 2 (SS2)	Suomussalmi 3 (SS3)
SiO_2	*Colorim.*	%	30.4	29.47	30.67
MgO	*TOT*	%	33.93	34.54	33.05
Al_2O_3	*TOT*	%	1.24	1.03	1.28
P_2O_5	*TOT*	%	<0.05	<0.05	<0.05
CaO	*TOT*	%	0.13	0.15	0.52
TiO_2	*TOT*	%	0.07	0.07	0.07
Cr_2O_3	*TOT*	%	0.49	0.59	0.53
MnO	*TOT*	%	0.12	0.1	0.12
Fe_2O_3	*TOT*	%	8.03	7.46	9.37
Co	*TOT*	%	0.01	0.01	0.01
Ni	*TOT*	%	0.19	0.21	0.19
C	*Eltra*	%	6.18	6.18	5.57
S	*Eltra*	%	<0.05	<0.05	<0.05
Satmagan		%	0.87	2.93	5.47
Density	*gas pycnometer*	g/cm^3	2.97	2.97	2.98

Chemical and mineralogical studies showed that talc and magnesite are the main minerals in the Suomussalmi 1, 2, and 3 samples. Although talc and magnesite grades are very close, talc is slightly the main mineral. The rest is composed of magnesite, chlorite, siderite, and dolomite.

Magnetite contents vary a lot in the feed samples: 0.9 wt.% in SS1, 2.9 wt.% in SS2, and 5.5 wt.% in SS3.

Talc and magnesite occurrence is well-liberated in every study sample when grind size P_{80} is around 90-95 µm.

Table 2. Mineral composition of the samples

Minerals	Suomussalmi 1	Suomussalmi 2	Suomussalmi 3
	wt.%	wt.%	wt.%
Talc	44.67	45	46.73
Magnesite	43.81	44.61	38.6
Chlorite	9.31	5.69	7.07
Magnetite	0.87	2.93	5.47
Dolomite	0.3	0.85	1.89
Rutile	0.07	0.05	0.03
Total	99.03	99.13	99.79

Flotation experiments were carried out in a laboratory scale GTK Labcell model flotation machine. In the cleaner stages, 4 liters cells were used for the first, second, and third cleaners, and 2 liters cells were used in the fourth cleaner stage. A sample of about 1500 g was mixed with site water making 25 % solid pulp ratio, at natural pH.

Flotation studies were carried out using only frother. A conditioning period of 3 min for frother was allowed. 60 g/t 2-Ethyl-1-hexanol (Brenfroth 90) was used as frother as per earlier studies. The flotation air flow rates were set to 6 l/min, 4 l/min, and 3 l/min for 8 liters, 4 liters, and 2 liters cells, respectively.

The impeller speed settings were set to 1200 rpm, 1700 rpm for 2 liters, 4 liters, respectively.

General flowsheet of rougher and cleaner kinetic tests can be seen in Figure 3 and Figure 4, respectively.

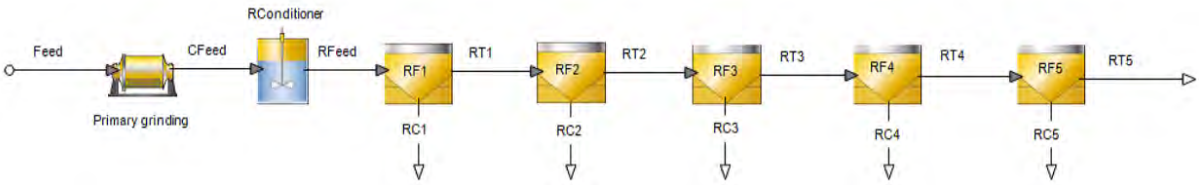

Figure 3. Rougher kinetic test flowsheet

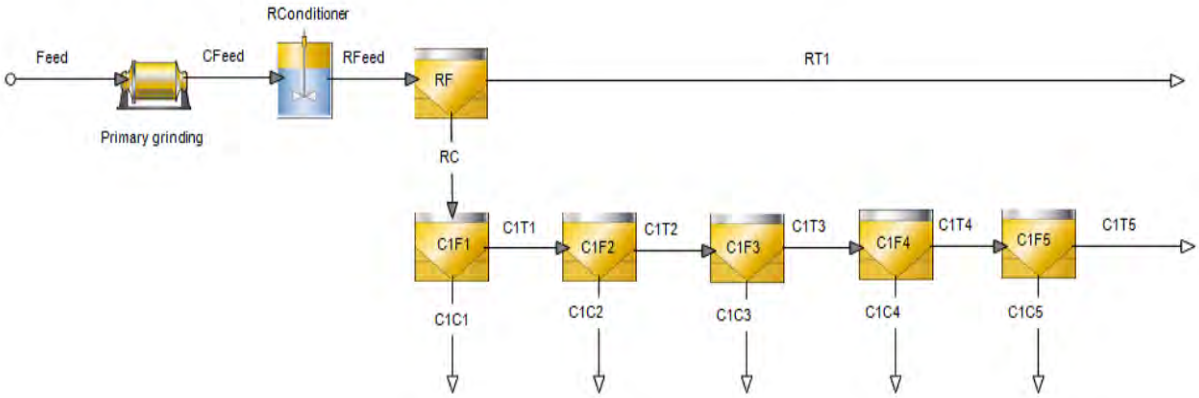

Figure 4. General flowsheet of cleaner tests

3. RESULTS AND DISCUSSION

Rougher and cleaner flotation kinetic data was created in this study to build a simulation model for the future concentrator plant. The created kinetic data was utilized for the flowsheet development and identify the metallurgical responses of each feed separately. In this manner, rougher and cleaner tests were carried out. The rougher kinetic test conditions and results can be seen in Table 3 and Figure 5, respectively.

Table 3. Rougher kinetic test conditions

Test Code	Sample feed	Conditions
SS1-1	Suomussalmi 1	60 g/t Brenfroth 90
SS2-2	Suomussalmi 2	60 g/t Brenfroth 90
SS3-3	Suomussalmi 3	60 g/t Brenfroth 90

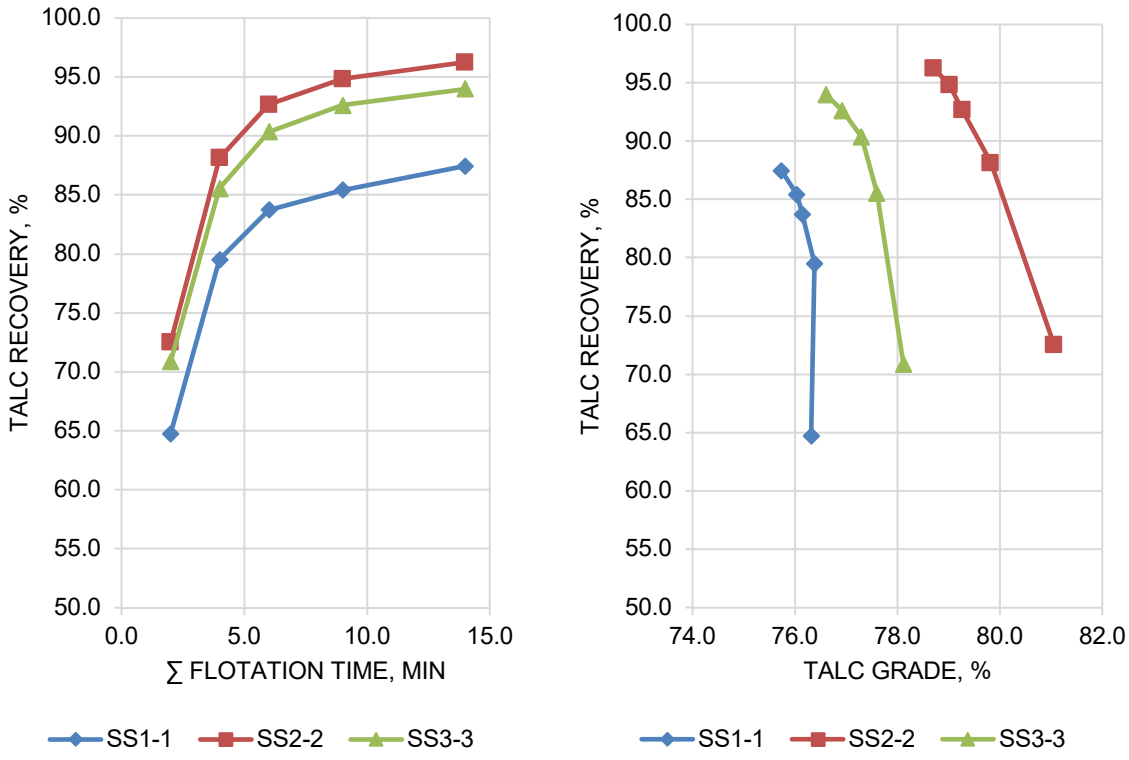

Figure 5. Rougher kinetic test results

The rougher kinetics shown in Figure 5 clearly demonstrate distinct flotation responses among the three Suomussalmi samples. Suomussalmi 2 exhibited the highest talc recovery. Suomussalmi 3 achieved slightly lower talc recovery relative to Suomussalmi 2, suggesting either minor mineralogical differences or less talc selectivity under the same operating conditions. In contrast, Suomussalmi 1 consistently produced the lowest talc grade and recovery, confirming relatively poor flotation behavior. The cumulative results therefore indicate that Suomussalmi 1 has the weakest overall flotation performance, while Suomussalmi 2 consistently delivers the most favorable metallurgical performance.

After determination of rougher flotation time, cleaner kinetic tests were performed to create data for simulation model. The cleaner kinetic test conditions and results can be seen in Table 4 and Figure 6, respectively.

Table 4. Cleaner kinetic test conditions

Test Code	Sample feed	Conditions
SS1-7	Suomussalmi 1	60 g/t Brenfroth 90 to Rougher
SS2-8	Suomussalmi 2	60 g/t Brenfroth 90 to Rougher
SS3-13	Suomussalmi 3	60 g/t Brenfroth 90 to Rougher

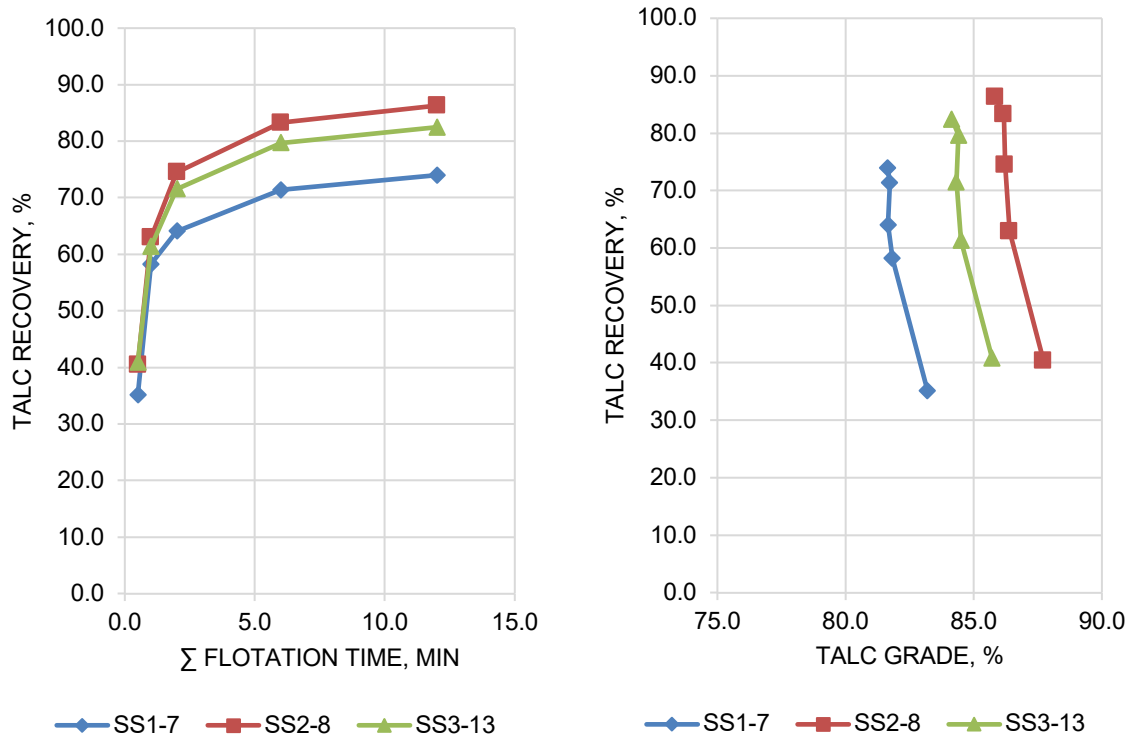

Figure 6. Cleaner kinetic test results

Similar trends can be seen in cleaner kinetics compared to rougher flotation for the feeds. Trends in Figure 6 indicate that talc grades in rougher concentrate can be upgraded in cleaners at adequate stage recoveries. Suomussalmi 1 feed has the lowest talc stage recoveries compared to other feeds.

A batch simulation model was created using rougher and cleaner flotation kinetics to validate the developed model for the flowsheet and see overall recovery and grades in terms of middling streams' recirculation. The primary approach on batch simulations is to see overall talc grade and recoveries with the developed flowsheet for further optimizations. For better modeling and simulation, the mineral compositions of the feeds were simplified as talc,

magnesite, chlorite, and magnetite. The feed composition of the simulation model was given by Nordic Talc as equal proportions of Suomussalmi 1, 2, and 3.

A rectangular distribution model shown in Eq.1 was used to fit the experimental kinetic curves, and the models were calculated using the HSC Sim 10 Model Fit® tool. In addition, the Klimpel flotation model for batch flotation was used to calculate kinetic parameters such as the infinitive recovery and the flotation rate constant. In the Klimpel model, R_{inf} shows the highest possible recovery for each mineral, and the k of rectangular distribution reveals how fast each mineral is floated (Metso, 2021).

$$R = R_{inf}\left\{1 - \frac{1}{kt}[1 - e^{-kt}]\right\} \qquad \text{Eq. 1}$$

Where t is the cumulative residence time, R_{inf} is the infinitive recovery, K is the flotation rate constant, and $R_{inf} \leq 1$. The batch simulation results are shown in Figure 7.

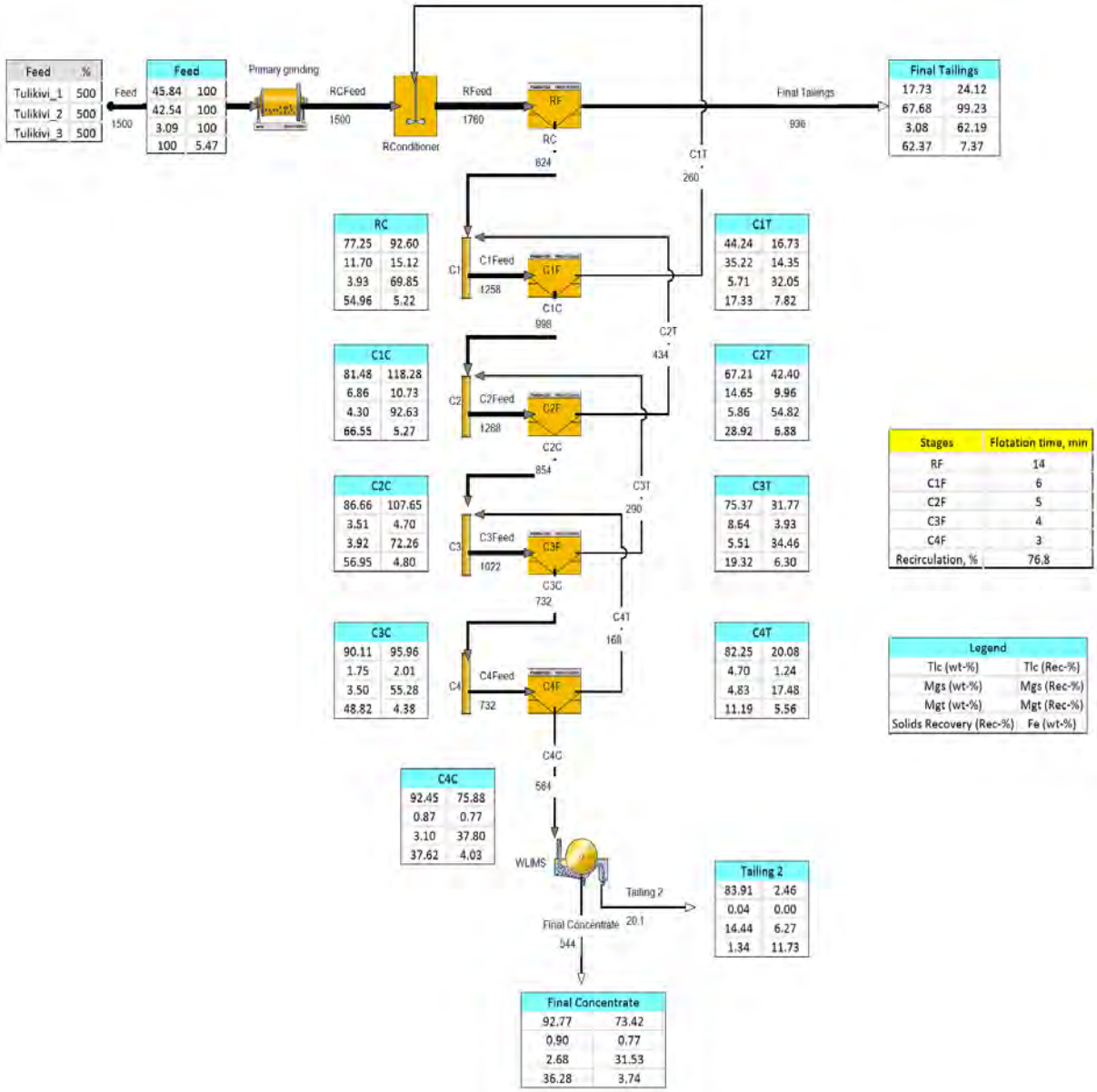

Figure 7. Batch simulation results

Locked cycle test was conducted to validate the developed flowsheet and the created simulation model. The locked cycle test feed was blend for equal proportions of Suomussalmi 1, 2, and 3 samples. The mass balance of the locked cycle test is shown in Figure 8.

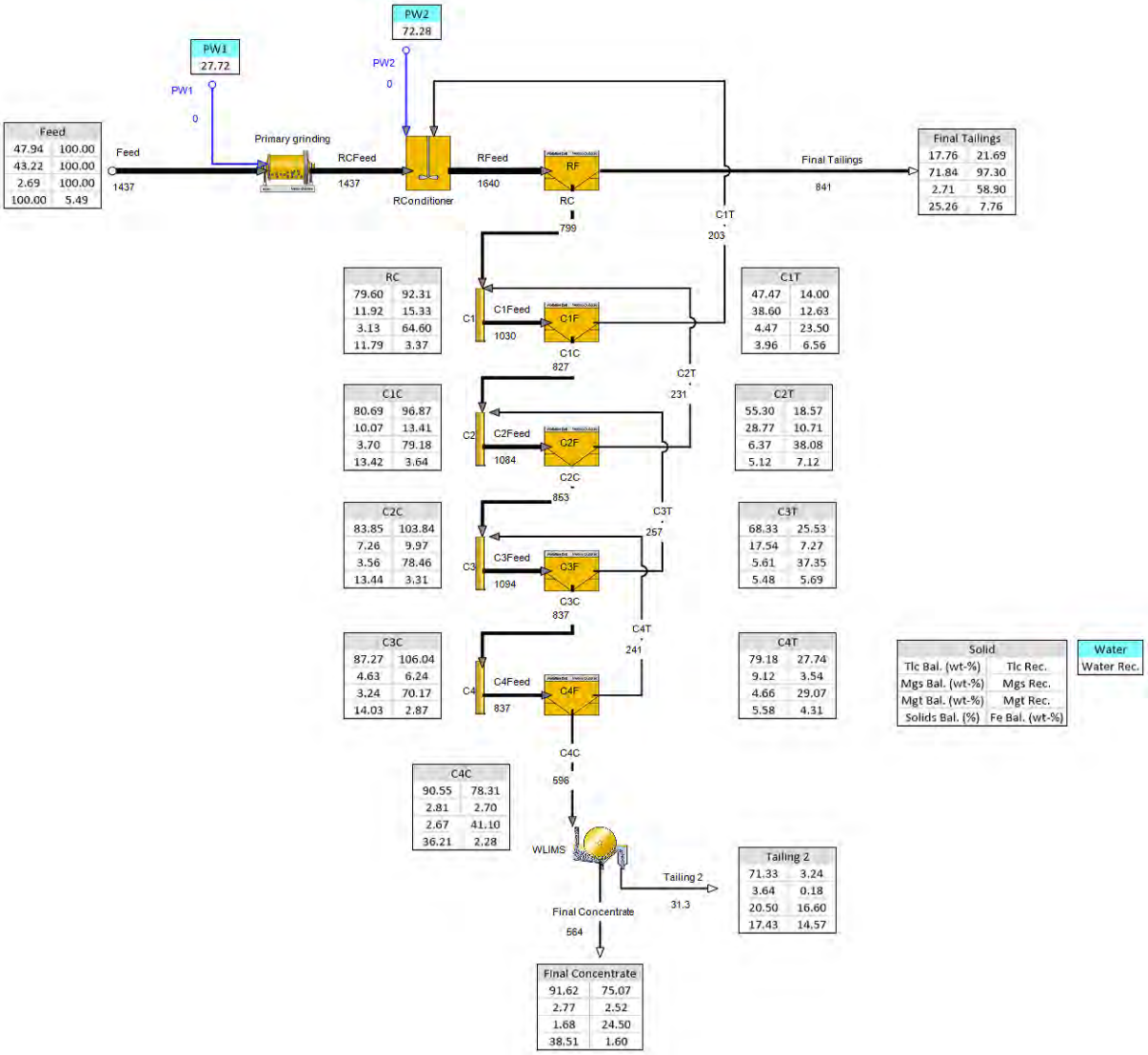

Figure 8. Locked cycle test mass balance

According to the mass balance of Locked cycle test, 91.6% talc concentrate was produced at 75 % recovery. The detailed comparison of final concentrate talc grade and recoveries can be seen in Figure 9.

An extensive pilot campaign was conducted on the blend sample with a similar flowsheet at Geological Survey of Finland, but the cleaner middling streams were changed from standard cascade to open circuit. Even though the flowsheets are not the same, pilot results were also included in the comparisons. The detailed comparison of final concentrate talc grade and recoveries can be seen in Figure 9.

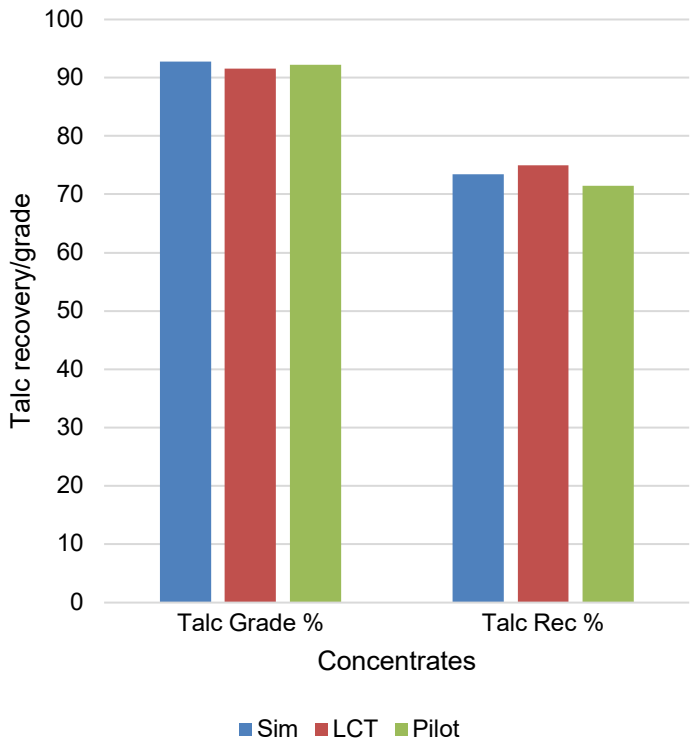

Figure 9. Final concentrate grade and recovery comparison

4. CONCLUSION

Comparison of batch simulations, locked cycle tests, and pilot-scale results indicates a high degree of consistency across different methods. Although the simulated final concentrate talc grades were approximately one percentage point lower than those obtained from locked cycle testing, the simulated talc recoveries were approximately one percentage point higher. These minor deviations fall within acceptable metallurgical variability and do not compromise interpretation. Importantly, the strong alignment between laboratory and pilot-scale results confirms that the simulation model represents circuit behavior and mass balance dynamics. Therefore, the modeling framework provides sufficiently accurate predictive capability to support future process design, scale-up decisions, and flowsheet optimization for industrial talc flotation operations.

REFERENCES

Bazar, J. A., Rahimi, M., Fathinia, S., Jafari, M., Chipakwe, V., Chehreh Chelgani, S., (2021) “Talc flotation—An overview”, Minerals, 11 (7) 662.

Agar, D., (2000) “Locked cycle testing in mineral flotation circuits (as cited in “Optimizing flotation circuits: A comprehensive approach”, Minerals Engineering.

HSC Sim., (2025), In HSC Sim – Process simulator overview.

Nordic Talc Oy, (2026), Project – Our goal is to transform the Suomussalmi soapstone factory into a talc plant and ensure the industrial utilization of talc reserves and the continuation of operations. NordicTalc.fi. Retrieved January 29, 2026, from https://nordictalc.fi/en/we/project/

Metso, (2026), HSC Chemisty software: Retrieved January 29 from https://www.metso.com/portfolio/hsc-chemistry/

PROCESSING OF INDUSTRIAL MINERALS

A HYBRID MICROWAVE-THERMAL METHOD TO OPTIMIZE THE GRINDING OF MOIST CLAY MINERALS

Doğan DEMİROK*

Tanrıkulu Endüstri Malzemeleri San. Tic. A.Ş., Fatsa OSB, Ordu, TÜRKİYE
**Corresponding author: demirok.dgn@gmail.com*

A B S T R A C T

The comminution and drying of clay minerals are highly energy-intensive processes, typically requiring integrated hot-gas generators (burners) to evaporate surface and internal moisture during grinding. Conventional thermal methods often prove inefficient at removing tightly bound internal water, leading to significant energy losses through surface heating. This study evaluates the efficacy of a hybrid microwave-thermal pretreatment system aimed at reducing the overall energy consumption of grinding and drying processes for moist clay minerals. An industrial-scale prototype microwave heater equipped with an adjustable-speed conveyor belt (1.2 m length, 0.6 m width), feeding augers, and a fully enclosed chamber was employed to preheat bentonite samples. Using 15 kW magnetrons, approximately 50 kg of bentonite with a particle size below 25 mm was heated from 14 °C to 72 °C (surface temperature measured by infrared pyrometer) within 1 minute, effectively mobilizing internal moisture. The preheated material was then fed into an industrial grinding circuit coupled with a conventional propane-fired hot-gas generator. In the conventional setup, 3 m³/s of fresh air is heated from 14 °C to 195 °C and mixed with 12 m³/s of return air (70 °C) inside the mill; the exhaust flow is 3 m³/s at 70 °C. The hybrid approach, integrating microwave pretreatment, allowed the burner to deliver air at a much lower temperature (146.8 °C) while still maintaining the same material outlet temperature (82.8 °C) and moisture reduction (from 14.85% to 10.5%). Results demonstrate a 21.5% reduction in specific energy consumption (from 97.0 kWh/t to 76.2 kWh/t), a 26.6% lower burner fuel demand, and a 38.5% decrease in the heat required inside the grinding chamber. This hybrid strategy decouples internal moisture heating from surface drying, optimizing the comminution circuit and offering a viable pathway for significant energy savings and operational cost reduction in mineral processing.

Key words: *Clay mineral, bentonite, microwave heating, dry grinding, energy efficiency, hybrid thermal processing*

1. INTRODUCTION

Clay mineral processing demands considerable energy input, primarily for grinding and moisture removal (Batchelor et al., 2016; Murray, 2007). Traditional hot-air systems, while effective for surface drying, exhibit limited efficiency in extracting internal moisture due to low thermal conductivity and diffusion resistance within clay matrices (Grim, 1968; Haque, 1999). In typical industrial setups, a burner heats fresh atmospheric air (e.g., 3 m³/s from 14 °C to 195 °C), which is then mixed with a larger volume of return air (e.g., 12 m³/s at 70 °C) inside the grinding mill. The mixture provides the sensible heat to raise the clay temperature and the latent heat to evaporate moisture, after which a portion of the air (3 m³/s) is exhausted at about 70 °C. This approach inevitably wastes energy because a large fraction of the heat supplied by the burner is used to re-heat the return air and to compensate for surface-heating losses.

Microwave heating has been recognized as an efficient method for mineral processing due to its selective heating characteristics (Jones et al., 2002; Kingman and Rowson, 1998). Microwave irradiation offers a promising alternative by generating volumetric heating, selectively exciting water molecules and promoting internal pore pressure buildup (Meredith, 1998; Jones et al., 2002; Oghbaei et al., 2010; Kingman et al., 1998). This study investigates a hybrid microwave-thermal method that synergizes microwave pretreatment with conventional hot-air drying in an industrial grinding circuit. The objective is to quantify energy savings and

process enhancements when internal moisture is preferentially heated via microwaves before the material enters the grinding-drying system, thereby reducing the thermal load on the burner.

2. MATERIALS AND METHODS

2.1. Material Characterization

A bentonite clay sample (≈50 kg) with particle size <25 mm and initial moisture content of 14.85% was used. The material was homogenized before testing to ensure consistent feed properties. Input material mineralogical composition was determined via Methylene Blue adsorption test. The test result was predominantly montmorillonite between 80 – 82%. Initial moisture content was measured using a standard drying-oven method (105°C until constant mass, 24H duration). The bentonite clay used in this study exhibits typical moisture adsorption characteristics as described in clay mineralogy literature (Murray, 2007; Grim, 1968). Particle size distribution (PSD) of the raw material was performed before the trial (Figure 1).

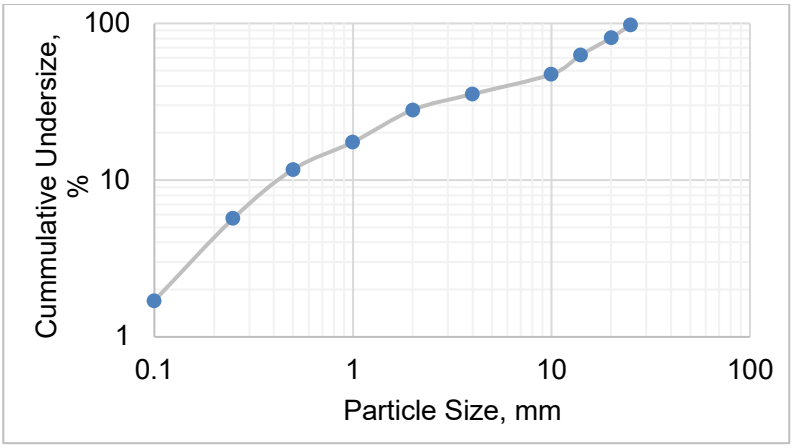

Figure 1. Particle size distribution of representative RM sample

2.2. Experimental Setup - Microwave Preheating System

An industrial microwave prototype was constructed, comprising a fully enclosed chamber housing three 5 kW magnetrons (total 15 kW), an adjustable-speed conveyor belt (1.2 × 0.6 m), and integrated screw feeders. The belt speed was adjusted to provide a residence time of 1 minute per complete pass through the chamber. Surface temperature of the material was monitored continuously with an infrared pyrometer at the outlet of the microwave chamber.

2.3. Grinding and Drying Circuit

The preheated clay was fed directly into a closed-circuit grinding mill equipped with a 350 kW propane-fired hot-gas generator. The conventional thermal system supplied 3 m³/s of fresh air heated from 14 °C to 195 °C. This air mixed with 12 m³/s of return air at 70 °C inside the mill; the exhaust flow was maintained at 3 m³/s (70 °C). The feed rate was held constant at 2.5 kg/s. Moisture content was measured continuously at the circuit outlet.

2.4. Experimental Design

Two scenarios were compared:

Control: Conventional hot-air drying and grinding without microwave pretreatment.

Hybrid: Microwave preheating (14°C → 72°C in 1 min) followed by conventional grinding/drying.
Key performance indicators included specific energy consumption (electrical + thermal), final moisture content.

3. RESULTS AND DISCUSSION

3.1. Temperature and Moisture Profiles

Microwave pretreatment raised the surface temperature of bentonite by 58 °C within 60 seconds, confirming efficient volumetric heating. The internal temperature rise facilitated faster moisture migration to the surface during subsequent hot-air exposure (Kong et al, 2016). In both the control and hybrid setups, the final moisture content reached 10.5% (i.e., 4.35 percentage-point removal), demonstrating that the hybrid system achieved the same drying performance.

3.2. Energy Consumption Analysis

The thermodynamic balance of the grinding chamber was evaluated for both systems. Specific energy consumption calculations were performed according to established thermodynamic principles (Cengel and Boles, 2015), with particular attention to the energy efficiency considerations in comminution processes (Fuerstenau and Abouzeid, 2002). The heat required (Q_{req}) is the sum of sensible heat to raise the material temperature and latent heat for evaporation (Perry et al., 1997; Kong et al., 2016). For the conventional system, the material enters at 14 °C and leaves at approximately 82.8 °C; for the hybrid system, the material enters already at 72 °C (due to microwave preheating) and is further heated to the same outlet temperature (82.8 °C). The evaporation rate is identical in both cases (0.10875 kg/s).

The air-side balance considers 3 m³/s of fresh air heated by the burner, mixed with 12 m³/s of return air at 70 °C. The mixture supplies (Q_{req}) to the material, and 3 m³/s is exhausted at 70 °C. The burner outlet temperature required to meet (Q_{req}) was calculated from the mass and energy balances.

Table 1. Energy consumption comparison (basis: 2.5 kg/s feed, 4.35% moisture removal)

Parameter	Unit	Conventional (Burner Only)	Hybrid (Microwave + Burner)
1. Air and Material Flows			
Exhaust air flow ($V_{exhaust}$)	m³/s	3	3
Burner fresh air flow	m³/s	3	3
Return air flow	m³/s	12	12
Material feed rate	kg/s	2.5	2.5
Evaporation rate	kg/s	0.10875	0.10875
2. Heat Required in Grinding Chamber			
Sensible heat to material	kW	206.4	32.4
Latent heat for evaporation	kW	245.8	245.8
Total heat required (Q_{req})	kW	452.2	278.2
3. Burner Air Heating			
Burner outlet air temperature*	°C	195	146.8
Thermal power to air	kW	654.9	480.6
Burner fuel power (75% eff.)	kW	873.2	640.8

4. Microwave Preheating			
Thermal power to material	kW	–	38.3
Electrical power (85% eff.)	kW	–	45
5. Total Energy Input			
Thermal (propane)	kW	873.2	640.8
Electrical (microwave)	kW	–	45
Total	kW	873.2	685.8
6. Specific Energy (SEC)			
Per ton of product	kWh/t	97	76.2
SEC Reduction	**–**	**–**	**21.50%**
*Burner outlet air temperatures are calculated from mass and energy balances to meet the heat requirement $Q_{req.}$			
Notes: Air density taken as 1.2 kg/m³ for fresh air and 1.004 kg/m³ for return air; specific heat of air = 1.005 kJ/kg·°C. Effective specific heat of bentonite under microwave irradiation derived from experimental data: 0.264 kJ/kg·°C.*			

3.3. Derivation of Burner Outlet Air Temperatures

The following section presents the derivation of burner outlet temperatures based on the energy balances discussed above.

For the conventional system, the mixture of 3 m^3/s fresh air (at burner outlet temperature T_{Burner}) and 11.71 m^3/s return air (70 °C) must yield an inlet mill temperature that delivers 452.2 kW to the material. Solving the energy balance gives T_{Burner}=195.0 °C.

For the hybrid system, the required heat drops to 278.2 kW, leading to T_{Burner} =146.8 °C. The summary of comparison for both Conventional and Hybrid heating system shown in Table 2.

Table 2. Performance summary

Metric	**Conventional Process**	**Hybrid Microwave-Thermal Process**	**Improvement**
Energy Consumption			
Specific Energy (kWh/t)	97	76.2	**21.5% reduction**
Thermal Energy (kW)	873.2	640.8	26.6% lower
Electrical Energy (kW)	0	45	–
Process Parameters			
Burner Air Outlet Temp.	195.0°C	146.8°C	48.2°C lower
Material Inlet Temp.	14°C	72°C	58°C higher
Heat Required in Mill	452.2 kW	278.2 kW	38.5% lower
Operational Impact			
Burner Fuel Consumption	Baseline	~26.6% lower	Significant saving
CO_2 Emissions (approx.) *	Higher	~26.6% lower	Reduced footprint

*Assuming proportional CO_2 emissions from propane combustion.

The hybrid system achieves a 21.5% reduction in specific energy consumption, primarily because the microwave preheating supplies the sensible heat to raise the material temperature from 14 °C to 72 °C using only 45 kW of electrical power, whereas in the conventional system the same sensible heat is provided by the burner at a much higher fuel cost. Consequently, the burner's outlet air temperature can be lowered by 48.2 °C, reducing the fuel consumption by 26.6% while maintaining identical drying performance.

3.4. Potential for Further Optimization

The analysis assumes the same exhaust flow rate (3 m³/s) for both systems. In practice, the hybrid system could allow a higher exhaust flow (e.g., 6 m³/s) without compromising the mill temperature, because the material already enters preheated. The observed energy savings align with previous studies on hybrid microwave-thermal systems (Shang et al., 2017), particularly for clay minerals where internal moisture removal presents significant challenges (Kong et al., 2016). Increasing the exhaust flow would remove more moisture-laden air, potentially enhancing the drying rate and further reducing energy consumption. This flexibility represents an additional operational advantage of the hybrid approach.

4. CONCLUSION

The integration of microwave preheating with conventional hot-air grinding presents a technologically feasible and energy-efficient hybrid method for processing moist clay minerals. By directly targeting internal moisture, microwave treatment reduces the sensible heat that must be supplied by the burner, allowing the burner to operate at a significantly lower air temperature (146.8 °C vs. 195.0 °C) while achieving the same material outlet temperature and moisture removal. For a feed rate of 2.5 kg/s (9 t/h) bentonite and moisture reduction from 14.85% to 10.5%, the hybrid system lowers the specific energy consumption by 21.5% (from 97.0 to 76.2 kWh/t) and cuts burner fuel demand by 26.6%. The prototype microwave unit (15 kW electrical) demonstrated that 50 kg of bentonite can be heated from 14 °C to 72 °C in one minute, confirming the practicality of industrial-scale implementation. As a logical next step, industrial-scale trials are recommended to validate these promising pilot-scale results under continuous, high-throughput operating conditions, and to further optimize system integration and cost-effectiveness. These findings contribute to the growing body of research on energy-efficient mineral processing (Napier-Munn, 2015) and demonstrate the practical viability of microwave-assisted drying in industrial applications (Meredith, 1998). This hybrid strategy decouples internal heating from surface drying, optimizes the entire comminution circuit, and offers a clear pathway to substantial energy savings and reduced operational costs in the clay mineral-processing industry.

REFERENCES

Batchelor, A. R., et al., (2016) "Microwave heating as a method for reducing grinding energy in mineral processing", International Journal of Mineral Processing, 156 34-41.

Cengel, Y. A., Boles, M. A., (2015), Thermodynamics: An Engineering Approach, 8th ed., McGraw-Hill.

Fuerstenau, D. W., Abouzeid, A. Z. M., (2002) "The energy efficiency of ball milling in comminution", International Journal of Mineral Processing, 67 (1-4) 161-185.

Grim, R. E., (1968), Clay Mineralogy, 2nd ed., McGraw-Hill.

Haque, K. E., (1999) “Microwave energy for mineral treatment processes—a brief review”, International Journal of Mineral Processing, 57 (1) 1-24.
Jones, D. A., Lelyveld, T. P., Mavrofidis, S. D., Kingman, S. W., Miles, N. J., (2002) “Microwave heating applications in environmental engineering—a review”, Resources, Conservation and Recycling, 34 (2) 75-90.

Kingman, S. W., Rowson, N. A., (1998) “Microwave treatment of minerals—a review”, Minerals Engineering, 11 (11) 1081-1087.

Kong, Y., Liu, S., Zhao, G., Peng, X., (2016) “Microwave drying characteristics of bentonite and energy efficiency”, Drying Technology, 34 (8) 901-911.

Meredith, R. J., (1998), Engineers' Handbook of Industrial Microwave Heating, IET.

Murray, H. H., (2007), Applied clay mineralogy: occurrences, processing and applications of kaolins, bentonites, palygorskite-sepiolite, and common clays: Elsevier.

Napier-Munn, T. J., (2015) “Is progress in energy-efficient comminution doomed?”, Minerals Engineering, 73 1-6.

Oghbaei, M., Mirzaee, O., (2010) “Microwave versus conventional sintering: a review of fundamentals, advantages and applications”, Journal of Alloys and Compounds, 494 (1-2) 175-189.

Perry, R. H., Green, D. W., Maloney, J. O., (1997), Perry's Chemical Engineers' Handbook, 7th ed., McGraw-Hill.

Shang, H., Li, J., Xu, Z., Li, Y., (2017) “Microwave-assisted thermal processing of materials: a review”, Industrial & Engineering Chemistry Research, 56 (38) 10585-10604.

A REVIEW ON THE RECOVERY OF RARE EARTH ELEMENT (REE) RESOURCES OF TÜRKİYE

İlgin KURŞUN, Mert TERZİ*, Can GUNGOREN, İsmail DEMİR, Osman YAVUZ

Istanbul University - Cerrahpasa, Engineering Faculty, Mining Engineering Department, 34500, Istanbul, TÜRKİYE.
**Corresponding author: mert.terzi@iuc.edu.tr*

A B S T R A C T

REEs, which have included almost all of the critical raw materials (CRMs) on lists worldwide since the inception of the CRM concept, play a critical role in the production of advanced technology products in fields such as the defense industry, health, education, space, and energy. In Türkiye's critical raw material list, REEs are listed as "High Importance Critical Minerals." Türkiye has several significant REE deposits, one of the most important and well-known being the Eskisehir-Kızılcaoren bastnaesite-fluorite-barite deposit. The ore deposit, which is classified as a complex mineralization due to its diverse mineral content, contains a total reserve of 30 million tons of valuable minerals, including fluorite, barite, bastnaesite, and thorium-bearing minerals. REE ores can be recovered using various methods, including gravity, magnetic, electrostatic separation, flotation, leaching, and solvent extraction. It is clear that Türkiye should prioritize the research and development of processes that will enable the economic production of these reserves using both existing and novel methods. In this context, this study compiles the information on the potential and recovery opportunities from REE deposits in Türkiye, as well as recent developments in the beneficiation of these minerals, from a mineral processing perspective.

Key words: *Critical raw materials, strategic raw materials, rare earth elements*

1. INTRODUCTION

The term "critical raw materials" refers to raw materials that are crucial for important technologies, have few or no adequate substitutes in significant applications, have a high likelihood of supply interruption, and whose shortages could have a big economic impact on a nation (Weil and Ziemann, 2014). In order to secure their future, each country must identify critical raw materials based on its own reserve, production, and consumption data. Although the list of critical raw materials varies among the world's leading economies, rare earth elements (REEs) are included in all (Romero and McCord, 2012; IMEA, 2024; MENS, 2025).

Rare earth elements (REEs) consist of Scandium ($_{21}$Sc) and yttrium ($_{39}$Y) in addition to 15 elements, from lanthanum ($_{57}$La) to lutetium ($_{71}$Lu). REEs with atomic numbers between 57 and 64 ($_{57}$La, $_{58}$Ce, $_{59}$Pr, $_{60}$Nd, $_{61}$Pm, $_{62}$Sm, $_{63}$Eu, $_{64}$Gd) are called light rare earth elements (LREE), while those with atomic numbers between 65 and 71 ($_{21}$Sc, $_{39}$Y, $_{65}$Tb, $_{66}$Dy, $_{67}$Ho, $_{68}$Er, $_{69}$Tm, $_{70}$Yb, $_{71}$Lu) are called heavy rare earth elements (HREE). Since Sc and Y have similar chemical and physical properties to HREE, they are generally included in this class (Romero and McCord, 2012; Grasso, 2013; Eterigho-Ikelegbe et al., 2021).

The reason why REEs are classified as "rare" is that many of these elements were obtained as oxides from rare minerals in the 18th and 19th centuries (Emsley, 2001). Their grades in the Earth's crust are approximately 150-220 g/t, which is higher than that of many major metal elements. Ce is the most abundant REE and is more common in the Earth's crust than copper (Cu) and lead (Pb). All REEs, except promethium (Pm), are more abundant in the Earth's crust on average than silver (Ag), gold (Au), and platinum (Pt). However, due to their high reactivity, REEs are generally found in oxide form (rare earth oxides, REO) rather than as native metals (Gupta et al., 1992; Şen et al., 2012; Balaram, 2019).

While there are approximately 200 minerals containing more than 0.01% REEs, the important commercial REE minerals are bastnaesite [(Ce, La)CO_3]F (75% REE), xenotime (YPO_4) (61% REE), and monazite [(Ce, La, Nd or Y, Th)PO_4] (71% REE) (Kanazawa and Kamitani, 2006; Naumov, 2008; Zhang et al., 2016). Globally known REE mineral reserves are around 100 million tons and distributed across more than 30 countries. Significant bastnaesite reserves are found in China and the USA. Countries rich in monazite reserves include India, Australia, South Africa, Russia, the USA, Brazil, and China; while xenotime deposits are located in Malaysia, Indonesia, Thailand, Australia, and China.

In Türkiye, the most important known rare earth mineral deposit is located in Kızılcaören-Eskişehir, with a total reserve of 30 Mt, which includes fluorite, barite, bastnaesite, and thorium. Additionally, several REE reserves have been identified in the Isparta and Malatya regions of Türkiye (Eti Maden, 2006; MTA, 2017).

REE mining began with the beneficiation of monazite sands in the 1950s and continued with bastnaesite mining in the 1960s. REE production can be carried out using solution, underground, and open-pit mining methods (Jouini et al., 2022). Y, Sc, and some other REE metals can be obtained, in small quantities, as byproducts from uranium and apatite mining and processing, in addition to primary ores. Another alternative source of Sc is red mud, which is produced during alumina production from bauxite (Narayanan et al., 2018; Wu et al., 2018). REEs possess unique physical and chemical properties and are consequently used in many industries such as glass, ceramics, polishing, alloys, catalysts, and magnets (Castor and Hedrick, 2006; Terzi, 2017). Because of their substantial contribution to the contemporary economy, REEs are considered critical raw resources by both the European Commission (EC) and the U.S. Department of Energy (Lin et al., 2017) . Meanwhile, China produces over 80% of the REE oxides and raw materials and is both the largest producer and the largest consumer (Zhang et al., 2022).

This study reviews the information on REE minerals, which are of critical importance due to their use as raw materials in many important industries, and recent developments in the REE mineral beneficiation in Türkiye.

2. BENEFICIATION OF REES

The beneficiation of REEs is quite complex, just like their formation. The production process for REE concentrate and individual REEs involves a combination of various mineral processing methods, including gravity, magnetic, and electrostatic separation, as well as flotation, leaching, and solvent extraction (Yildiz, 2016; Celep et al., 2021).

Gravity, magnetic, and electrostatic separation methods are generally used in the recovery of rare earth minerals from coastal sands and placer deposits, while flotation is prominent in the recovery of minerals from complex, magmatic, and hydrothermal deposits (Khanchi et al., 2014). These methods can be used in various combinations depending on the structural properties and particle sizes of the minerals.

In processing flowsheets, gravity separation is generally preferred as the first step. The densities of the main REE minerals range from 4.25 g/cm^3 to 6.13 g/cm^3, while gangue minerals (usually silicates) have lower densities (Ferron et al., 1991). The gravity method is widely used in the recovery of monazite from heavy mineral sands. Furthermore, there are studies on the concentration of finer-sized REE minerals using centrifugal gravity separators (Gupta and Krishnamurthy, 1992; Jordens et al., 2016).

Subsequently, the REE resources are subjected to magnetic separation. The magnetic susceptibility of minerals in coastal sand is ilmenite, garnet, xenothyme, and monazite from

highest to lowest. These minerals are separated from the non-magnetic minerals with a series of magnetic separation processes (Gonçalves and Braga, 2016). Electrostatic separation, on the other hand, separates conductive minerals such as ilmenite and rutile from insulating minerals of monazite and zircon (Jain, 2025). Furthermore, since xenotime in beach sand is a weak conductor, electrostatic separation is applied to remove it from the conductive ilmenite and rutile (Voncken, 2016).

Since the efficiency of physical methods decreases with the decreasing particle size, flotation is preferred for the separation of bastnaesite, monazite, and xenotime from barite and calcite, which are the main gangue minerals (Anderson, 2016).

Concentrates obtained through physical and physicochemical beneficiation processes can also undergo a final chemical beneficiation (Gupta and Krishnamurthy, 2005). After the dissolution process, REEs are produced through separation, purification, concentration, and heat treatment operations (Zhang, 2016).

Despite the presence of different REE reserves throughout the world, REEs are mainly extracted from seven minerals and resources: monazite, bastnaesite, xenotime, synchysite, parisite, fergusonite, and ion-adsorption rare earths (Table 1).

Table1. Currently extracted main REE minerals.

Mineral	**REE-REO (wt %)**	**Reference**
Bastnaesite ((Ce, La, Nd, Y)F(CO_3))	62-63 (REE)	(Owens et al., 2018)
Monazite (Ce, La Nd, Th)PO_4	60-70 (REO)	(Yildiz, 2016; Celep et al., 2021)
Xenotime (YPO_4)	53-65 (REO)	Yildiz, 2016; Celep et al., 2021)
Synchysite (Ca(Ce, Y, Nd)(CO_3)$_2$F)	51 (REO)	(Owens et al., 2018; Al-Ali et al., 2019; Owens et al., 2019)
Parisite (Ca(Ce, La, Nd)$_2$(CO_3)$_3$$F_2$)	51-53 (REE)	(Owens et al., 2018)
Fergusonite ($ReNbO_4$)	36 (REE [mainly Y])	(Fawzy, 2018)

Cerium abundant species, Bastnaesite-(Ce), is the most important among these minerals, which account for up to 70% of the world's REE production single-handedly. Thus, it became a hotspot in both industrial and academic REE research (Liu et al., 1993).

2.1. Studies on the Recovery of REE Resources of Türkiye with Flotation

In many mines, including Mountain Pass and Bayan Obo, the pre-concentrate of physical separation methods is subjected to flotation (Jordens et al., 2014; Kim et al., 2025; Akyildiz et al., 2026). In this context, a simplified version of the flow diagram used for the flotation of magnetic pre-concentrate at Bayan Obo mine is shown in Figure 1 (Adapted from Gupta & Krishnamurthy, 2005).

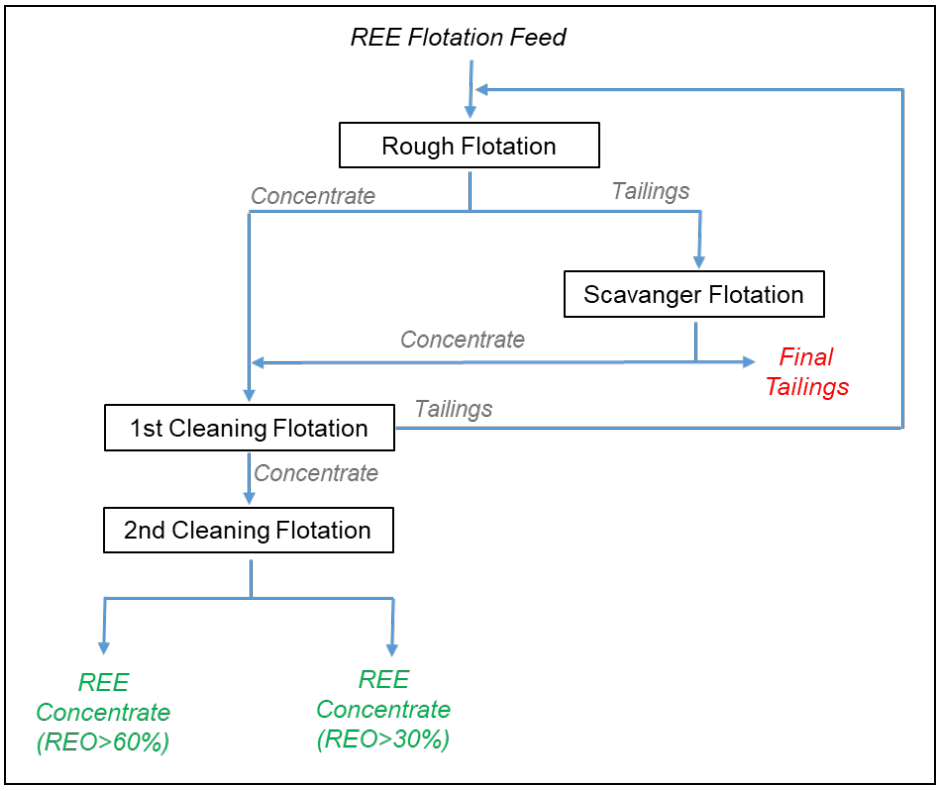

Figure 1. Simplified flotation flowsheet of Bayan Obo mine

In bastnaesite flotation, generally, fatty acids, a common anionic collector group, are used at low pH values (<4.6-9.5 (Zhang et al., 2013), where the zeta potential of bastnaesite is negative. Therefore, it is considered that the fatty acid molecules are adsorbed on bastnaesite surfaces chemically.

However, in bastnaesite flotation, since fatty acids are also adsorbed onto the surfaces of oxide gangue minerals, the main problem is to provide a selective separation. In order to increase the selectivity, the temperature of the flotation medium is increased up to 75 °C. At high temperatures, the solubility of collectors, including fatty acids, increases, as well as the solubility of cations present on the mineral surfaces. This results in increased collector adsorption on the bastnaesite surface compared to gangue minerals.

Another method to increase the selectivity is the use of various depressants. Sodium silicate (Na_2SiO_3), a common depressant for silicates, depresses gang minerals at low dosages while having low affinity for REE minerals. Lignin sulfonate ($C_{20}H_{24}Na_2O_{10}S_2$) is used to depress calcite and barite. However, care should be taken in the use of this depressant because it also affects bastnaesite to some extent. Other depressants used to depress calcite and barite are citric acid ($C_6H_8O_7$), oxalic acid ($C_2H_2O_4$), sodium fluoride (NaF), sodium metaphosphate ($NaPO_3$), and sodium hexafluorosilicate (Na_2SiF_6). Sodium carbonate (Na_2CO_3) is used to control carbonate anions, which affect both flotation pH and the surface properties of gangue minerals (Jordens et al., 2013).

In bastnaesite flotation, the most common type of collector used after fatty acids is hydroxamates, which have higher selectivity than fatty acids. This property of hydroxamates is explained by the fact that they form more stable chelates with REE ions than fatty acids, due to their similar adsorption mechanisms. Other anionic collectors used are phosphoric acid esters. These collectors form complexes with transition metals. It is reported that they can be used in bastnaesite flotation at the pH range of 4-10.

In the literature, there are several studies on the recovery of REE resources of Türkiye with flotation. For example, Dolak (2021) studied the recovery of Ce from Eskisehir-Sivrihisar (Türkiye) bastnaesite with flotation in the presence of potassium amyl xanthate (KAX) as a collector. In this study, sulfuration with H_2S was applied to increase the degree of liberation by altering the crystal structure of the ore. The Ce flotation recovery result of this study is given in Figure 2 as a function of H_2S and KAX amounts.

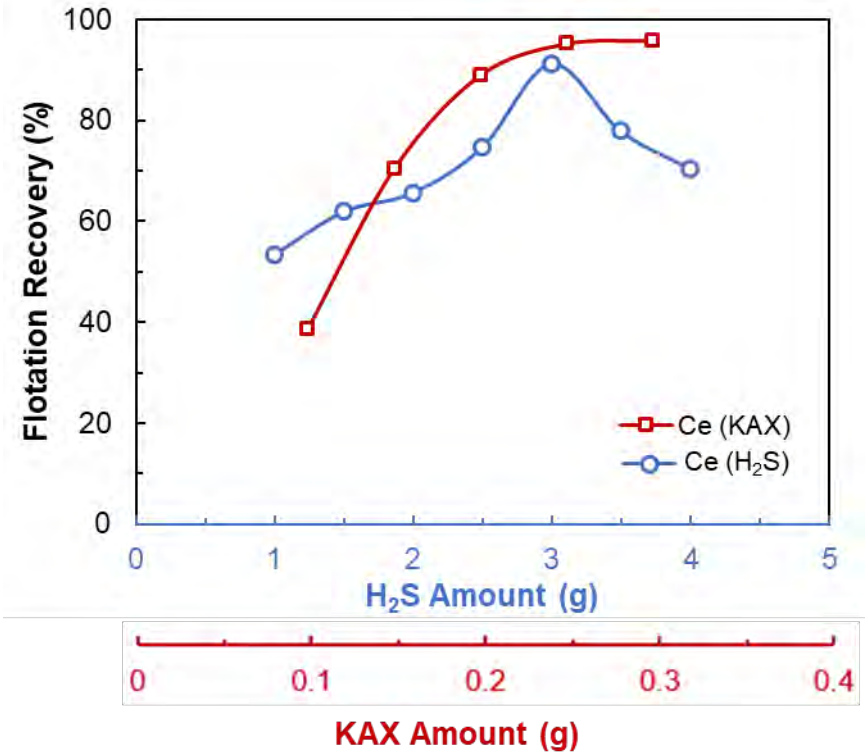

Figure 2. Ce flotation recovery as a function of H_2S and KAX amounts.

As seen in Figure 2, the Ce flotation recovery increases with H_2S amount, and the highest recovery of 90.1% was obtained at 3 g H_2S per 100 g ore. In this study, it was also reported that the Ce grade of the concentrate at this condition is 8.82%. It is also seen from the results in Figure 2 that the flotation recovery increases with KAX concentration and reached to 96.11% at 0.25 g per 100 g ore with a concentrate Ce grade of 10.35%.

In another study, Turker et al. (2023) studied the recovery of REOs from the complex ores of Beylikova-Eskisehir (Türkiye) by flotation. As a result of this study, it is reported that REO grade increased from 3% to ~17% with a recovery of 89.39% through attrition scrubbing, grinding, classification, and flotation.

In a study on allanite recovery, Kursun et al. (2019) investigated the flotation of the Canakli-Isparta (Türkiye) REE ore. In this study, a cationic (ethylenediamine) and an alkyl sulfosuccinamate-based anionic collector (R845N) were used. The results for micro-flotation experiments of this study carried out with a single allanite mineral sample are given in Figure 3a, and the results for conventional flotation experiments conducted with Beylikova-Eskisehir REE ore are given in Figure 3b.

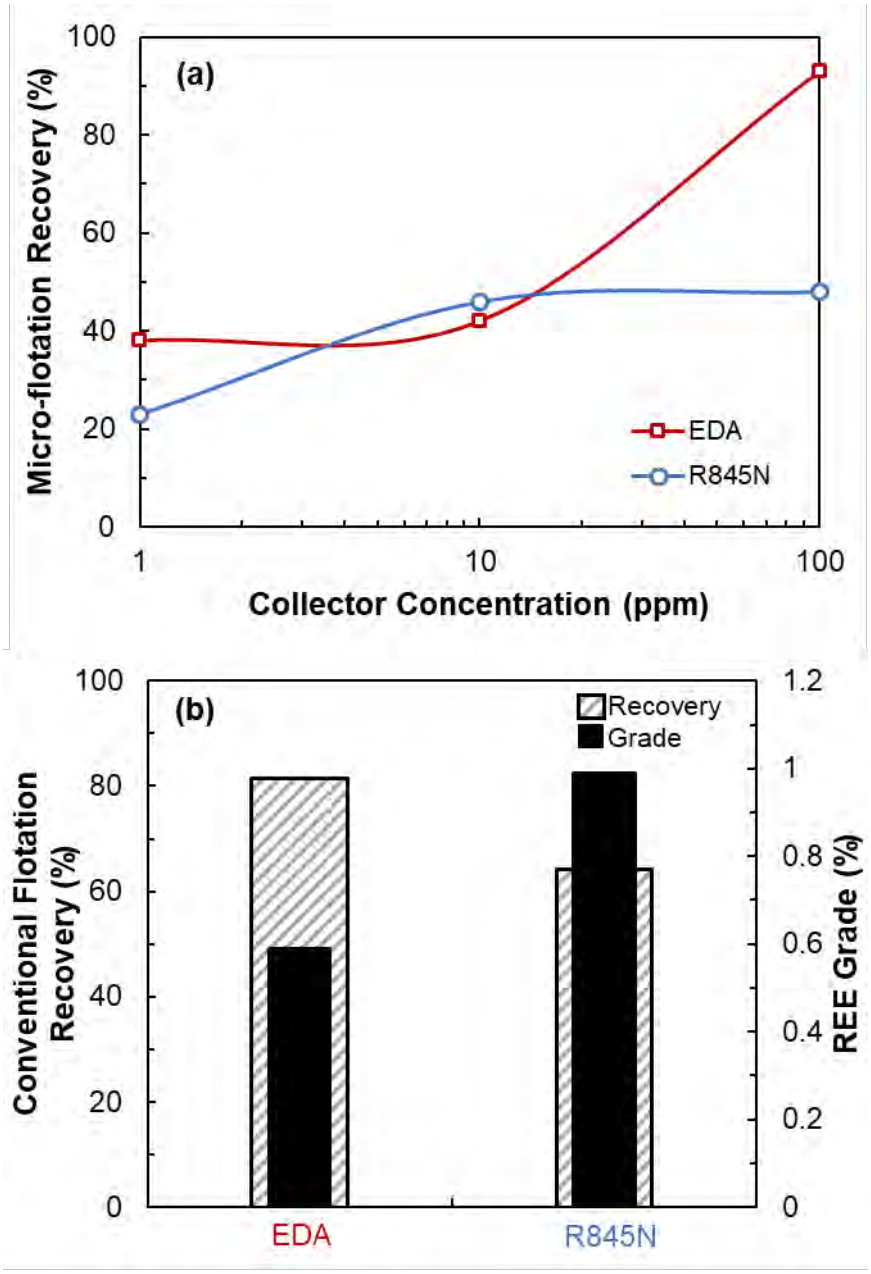

Figure 3. (a) The results for micro-flotation and (b) conventional flotation experiments

As seen in Figure 3a, in the presence of EDA, no significant change was observed in flotation recovery up to a collector concentration of 10 ppm, after which it increased significantly at 100 ppm EDA. In the presence of R845N, flotation recovery increased in the R845N concentration range of 1-10 ppm, reaching a plateau at this concentration value. Meanwhile, Figure 3b shows that with conventional flotation, a concentrate with a total REE grade of 0.59% was obtained with an 81.39% recovery in the presence of EDA, and a concentrate with a total REE grade of 0.99% was obtained with a 64.24% recovery in the presence of R845N.

2.2. Studies on the Recovery of REE sources of Türkiye with Extractive Metallurgy

The metallurgical extraction of REE ores involves decomposing the REE minerals present in the ore through a pre-treatment process and then chemically dissolving the REE elements from these separated minerals. Concentrates obtained through mineral processing methods can be decomposed by processes such as acid roasting, caustic cracking, and chlorination,

as REE minerals are generally insoluble in water and poorly dissolved in acids except in aggressive conditions (Zhang and Zhao, 2016; Cen et al., 2021).

In REE recovery processes, various inorganic acids, alkalis, and electrolytes can be used to dissolve REEs into solution. While commonly used acids include sulfuric acid (H_2SO_4), hydrochloric acid (HCl), and nitric acid (HNO_3), sodium hydroxide (NaOH) and sodium carbonate (Na_2CO_3) are the most commonly used alkalis. Meanwhile, commonly used electrolytes are ammonium sulfate ($(NH_4)_2SO_4$), ammonium chloride (NH_4Cl), and sodium chloride (NaCl) (Zhang and Zhao, 2016).

Carbonatite-related rare earth minerals, such as bastnaesite, are typically leached using H_2SO_4, HCl, or water after converted to the sulfates. In the separation process of REEs, solvent extraction, ion exchange, or chemical precipitation are used to produce mixed or individual REOs (Kul et al., 2008; Verbaan et al., 2015). A general flowsheet of REE production from bastnaesite ores is given in Figure 4 (Cen et al., 2021).

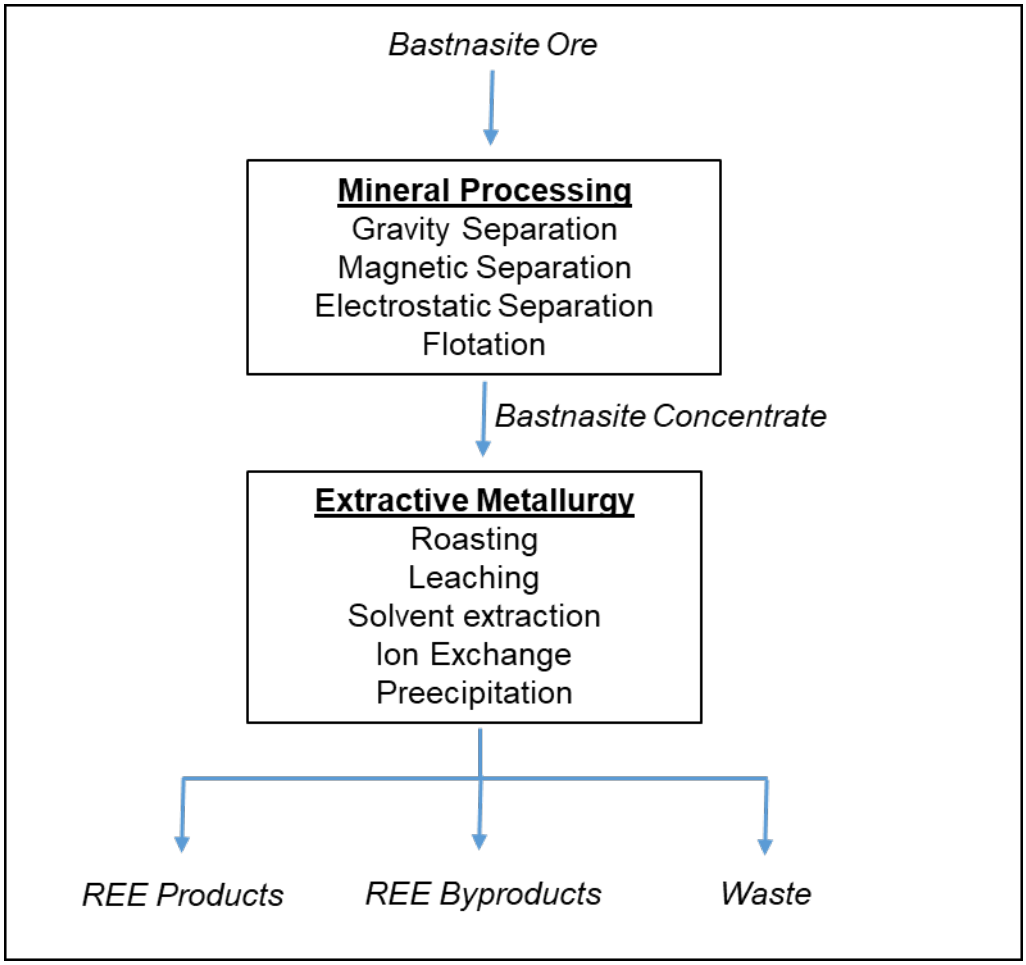

Figure 4. General flowsheet of REE production from bastnaesite ores

Although studies on new REE resources have begun in Türkiye in recent years, many studies have been carried out on the recovery of REEs from the Eskisehir bastnaesite-carbonatite REE mineralization, whose existence has been known for a long time, using hydrometallurgical methods.

One of the preliminary studies on the application of hydrometallurgical methods for REE recovery from Eskisehir ore was conducted by Kul et al. (2008), where a REE product was obtained by sequential processes of sulfuric acid baking, water leaching, and precipitation with

sodium sulfate from a pre-concentrate of Eskisehir basneasite ore with 23.5% REO content. The results of this study showed that sulfuric acid baking and water leaching can be successfully applied to extract up to 90% of REE from the sample.

In studies conducted by Kursun's research group (Kursun et al., 2016; Kursun et al., 2018; Tombal Kara and Kursun, 2020) and Tombal (2018), leaching experiments were carried out on composite samples prepared by blending representative samples taken from three different regions in the Kızılcaoren-Eskisehir region. In studies investigating the optimization of direct acid leaching by H_2SO_4, HCl, and HNO_3, direct alkali leaching by NaOH, and water leaching after H_2SO_4 acid curing systems, HCl and HNO_3 yielded comparable results, with the best results obtained with water leaching after acid curing. In these experiments, conducted with samples ground to a particle size of 38 µm, optimum results were obtained under the conditions of 2 and 4 h of acid curing leaching time, respectively. The dissolution yields of Ce, La, and Nd obtained with different leaching routes are given in Figure 5.

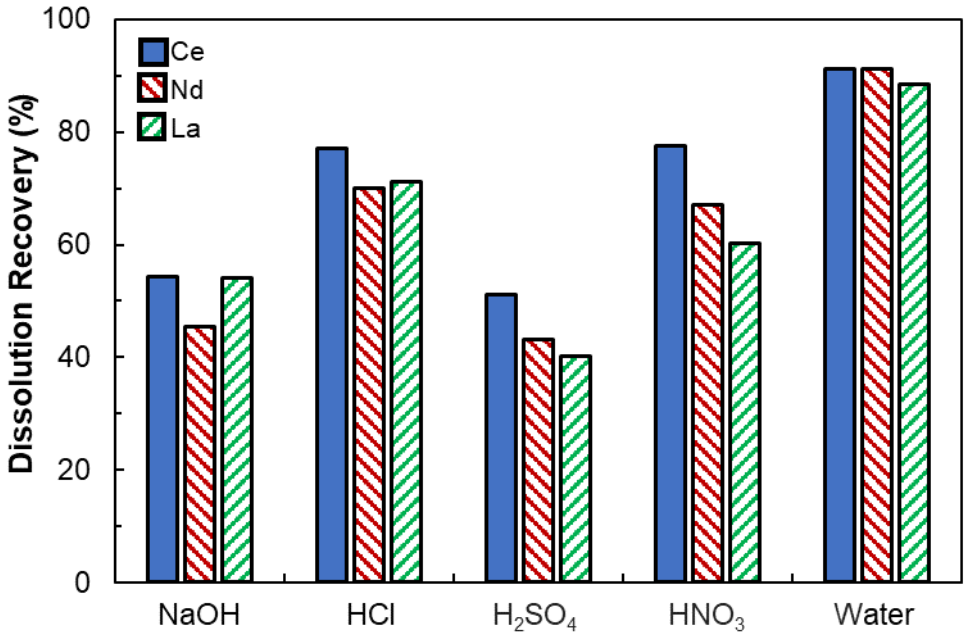

Figure 5. The dissolution recoveries of Ce, La, and Nd obtained with various leaching routes (Kursun et al., 2016; Kursun et al., 2018; Tombal, 2018; Tombal Kara and Kursun, 2020)

In the studies conducted by Kursunoglu et al. (2021) on bastnaesite ore from the Eskisehir region, DI water leaching was applied after sulfuric acid curing. After curing at 250°C for 3 hours at a 1:1 (w/w) ore/acid ratio, and a 30-min leaching with a 1:10 (w/v) solids ratio, dissolution yields of 92.6%, 85.8%, 85.9%, 82.3%, and 31% were obtained for La, Ce, Nd, Pr, and Y elements, respectively.

In the precipitation process performed with oxalic acid at tenfold of the stoichiometric ratio from the obtained pregnant leaching solution, at a 1:10 solids ratio, and at 25°C, the precipitation yields for La, Ce, Nd, Pr, and Y elements were 99.7%, 99.8%, 97.3%, 98.1%, and 91.7%, respectively (Figure 6). The final mixed REO product obtained by thermal decomposition of the product precipitated in oxalate form was found to contain 88.5% total REO and have an irregular crystal structure.

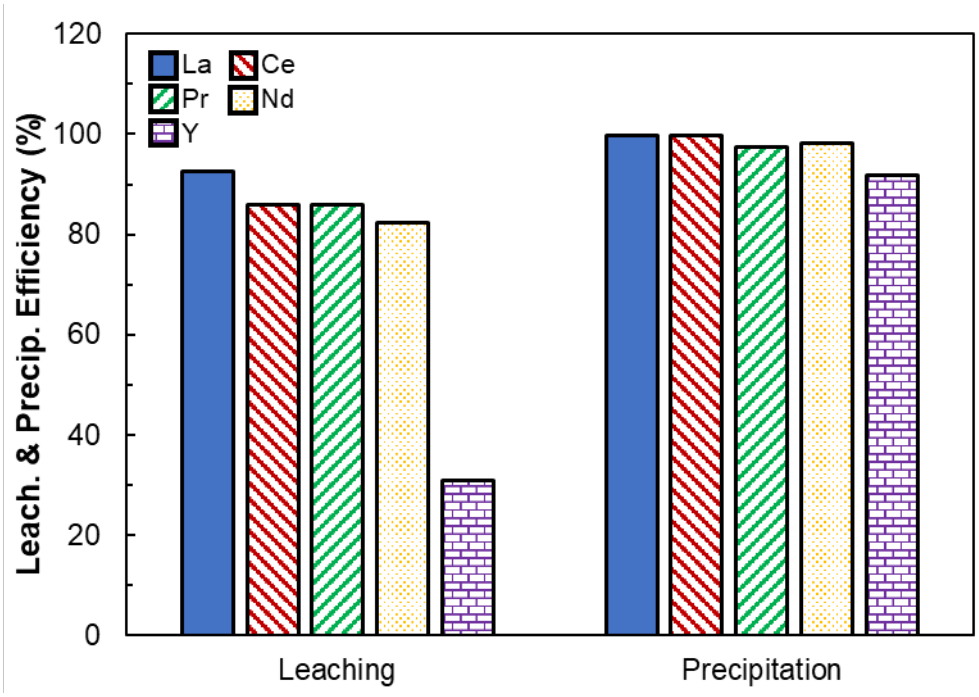

Figure 6. Comparison of La, Ce, Pr, Nd, and Y leaching and precipitation efficiencies (Kursunoglu et al., 2021)

In recent research by Kurtulan et al. (2024), REE recovery from Eskisehir-Beylikova bastnaesite ore was investigated using a newly developed extraction method, solvometallurgy. In the experiments where the effect of temperature, time, and particle size on REE extraction was investigated using Box-Behnken experimental design methodology, temperature was identified as the most effective parameter. Highest extraction rates were obtained under 500°C with 64.15%, 86.65%, 71.94%, 66%, and 50.61 for La, Ce, Pr, Nd, and Sm, respectively. Moreover, the total LREE extraction rate was found as 73.77%.

In the study conducted by Basturkcu et al. (2025), similar to the study by Kul et al. (2008), a REE pre-concentrate was obtained according to their previous procedure (Basturkcu et al., 2022), and the extraction of REEs through a sequential process of sulfuric acid baking and water leaching was examined. Dissolution yields of 92%, 89%, 86%, and 88% were obtained for La, Ce, Nd, and Pr elements, respectively, at the conditions of 1:1 acid-ore ratio, baking temperature of 250°C, and baking time of 60 min. The results of the process mineralogy study with Mineral Liberation Analysis (MLA) also revealed that the ore contains monazite, Th-rich parasite, and synchysite minerals, in addition to dominant and well-known basneasite presence.

As a conclusion of the abovementioned studies, the comparison of the La, Ce, and Nd extraction rates obtained is combined in Figure 7.

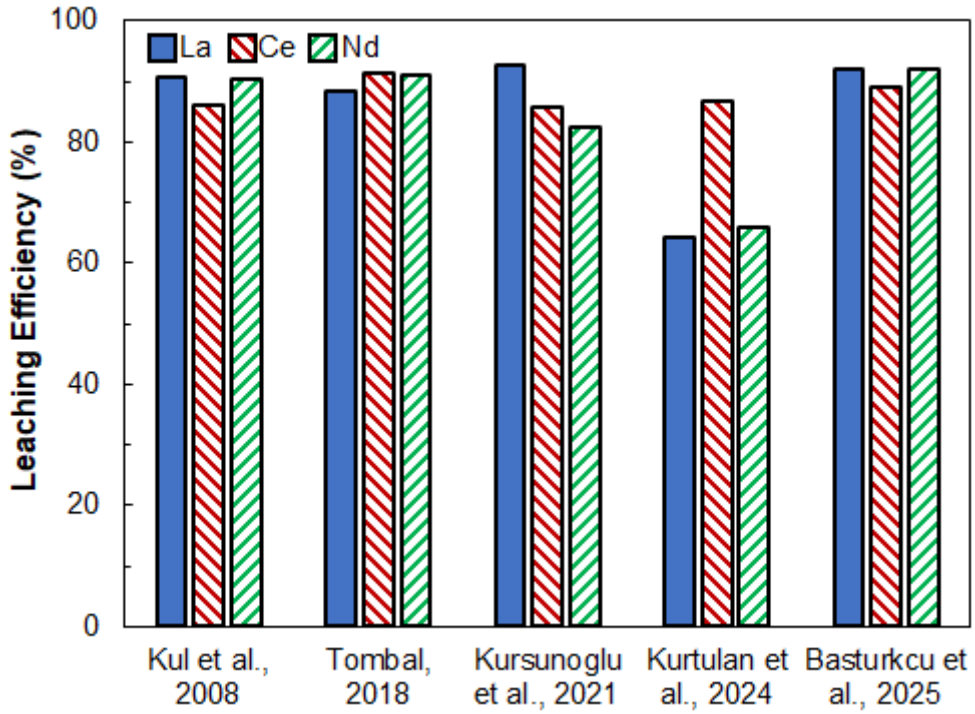

Figure 7. Comparison of the leaching efficiencies of La, Ce, and Nd obtained in different studies

As seen in Figure 7, even if some slight variations between the leaching rates of La, Ce, and Nd are existed, comparable results were obtained except the study by Kurtulan et al. (2024), where the leaching system was completely different (solvometallurgy) from the other studies, which are all carried out using sulfuric acid curing/baking followed by water leaching route.

4. CONCLUSION

Many studies have been carried out on the recovery of REEs from the Eskisehir bastnaesite-carbonatite REE mineralization, whose existence has been known for a long time, using both physical, physicochemical, and hydrometallurgical methods. In general, flotation has been the method of choice for the pre-concentration of both bastnaesite and other REE minerals, such as allanite, due to the fine particle liberation size of the mentioned minerals, especially for the REE deposits in Türkiye.

In the studies, where hydrometallurgical methods were carried out for the extraction of REEs from both run-of-mine samples and pre-concentrates, sulfuric acid curing and water leaching gave the most promising results, compared to the direct acid leaching, alkaline leaching, and novel methods like solvometallurgy. One interesting finding is that Ce dissolution rates were very close to each other for both water leaching and solvometallurgy, independent of the leaching methodology. These results clearly indicate that the mechanism behind the dissolution of different REEs from the bastnaesite matrix has not been fully understood yet and requires further investigation, especially in terms of process mineralogy. Furthermore, the production of pure oxides should have been investigated in future studies in order to maximize the added value of the REE products to be produced from the REE reserves of Türkiye.

REFERENCES

Akyildiz, E., Silva, C. M., Tobiczyk, K., Lode, S., Aasly, K., Kowalczuk, P. B., (2026) "Flotation response of parisite, monazite, bastnäsite and synchysite from a carbonatite deposit", Powder Technology, 471 122112.

Al-Ali, S., Wall, F., Sheridan, R., Pickles, J., Pascoe, R., (2019) "Magnetic properties of REE fluorcarbonate minerals and their implications for minerals processing", Minerals Engineering, 131 392-397.

Anderson, C. D., Taylor, P. R., Anderson, C. G., (2016) "Rare earth flotation fundamentals: a review", IMPC 2016 Proceedings of the XXVIII International Mineral Processing Congress.

Balaram, V., (2019) "Rare earth elements: A review of applications, occurrence, exploration, analysis, recycling, and environmental impact", Geoscience Frontiers, 10 (4) 1285-1303.

Baştürkcü, E., Şavran, C., Yüce, A. E., Timur, S. I., (2022) "Revealing the effects of mechanical attrition applied on Eskisehir-Beylikova REE ore utilizing MLA", Minerals Engineering, 186 107733.

Baştürkcü, E., Timur, S. İ., Yüce, A. E., (2025) "Leaching behaviour of rare earth elements from a complex ore via sulfuric acid baking: a geometallurgical perspective", Canadian Metallurgical Quarterly, 1-13.

Büyüktanır Aktar, K., (2024) “Investigation of rare earths extraction potential from various solid fossil fuel wastes”, Doctoral Dissertation, Istanbul Technical University.

Castor, S. B., Hedrick, J. B., (2006), Rare Earth Elements, Industrial Minerals and Rocks, 769-792.

Celep, O., Yazici, E. Y., Deveci, H., (2021) "Production of rare earth elements from primary and secondary resources", Gumushane University Journal of Science and Technology, 11 (1) 264-280.

Cen, P., Bian, X., Liu, Z., Gu, M., Wu, W., Li, B., (2021) "Extraction of rare earths from bastnaesite concentrates: A critical review and perspective for the future", Minerals Engineering, 171 107081.

Dinc, N. I., (2024) Recovery of coal from coal washery waste slimes and rare earth elements (in Turkish), M.Sc., Istanbul Technical University.

Dolak, I., (2021) "Enrichment of Cerium from Eskisehir Bastnaesite Ore (in Turkish)", Dicle University Journal of Engineering, 12 (2) 309-315.

Eterigho-Ikelegbe, O., Harrar, H., Bada, S., (2021) "Rare earth elements from coal and coal discard–A review", Minerals Engineering, 173 107187.

ETİ Maden, (2006) Nadir Toprak Elementleri (NTE) Ön Ekonomik Değerlendirmesi, Eti Maden İşletmeleri Genel Müdürlüğü, Rapor No: ETİ.ARGE.400.02-2004.04.030.

Fawzy, M. M., (2018) "Surface characterization and froth flotation of fergusonite from Abu Dob pegmatite using a combination of anionic and nonionic collectors", The Bulletin Tabbin Institute for Metallurgical Studies (TIMS), 107 (1) 66-78.

Ferron, C. J., Bulatovic, S. M., Salter, R. S., (1991) "Beneficiation of rare earth oxide minerals", Materials Science Forum, 70 251-270.

Gonçalves, C., Braga, P., (2016) "In-depth characterization and preliminary beneficiation studies of heavy minerals from beach sands in Brazil", The Tenth International Heavy Minerals Conference, Sun City, South Africa.

Grasso, V. B., (2013) Rare earth elements in national defense: Background, oversight issues, and options for Congress, No. CRSR41744.

Gupta, C. K., Krishnamurthy, N., (1992) "Extractive metallurgy of rare earths", International Materials Reviews, 37 (1) 197-248.

Gupta, C. K., Krishnamurthy, N., (2005) Extractive metallurgy of rare earths, CRC Press, Boca Raton, Florida, 65, 70-75.

Guven, G., (2024) “Recovery of rare eath elements (REEs) from Soma thermal power plant fly ash”, Mster’s Thesis, Istanbul Technical University.

IMEA, (2024) Critical minerals (in Turkish), Istanbul Mineral Exporters' Association, Istanbul, Türkiye, 40.

Jain, P. K., (2025) Electrostatic Separation, Treatise on Process Metallurgy, 2B, 169-183.

Jordens, A., Cheng, Y. P., Waters, K. E., (2013) "A review of the beneficiation of rare earth element bearing minerals", Minerals Engineering, 41 97-114.

Jordens, A., Marion, C., Kuzmina, O., Waters, K. E., (2014) "Surface chemistry considerations in the flotation of bastnäsite", Minerals Engineering, 66-68 119-129.

Jordens, A., Marion, C., Langlois, R., Grammatikopoulos, T., Rowson, N. A., Waters, K. E., (2016) "Beneficiation of the Nechalacho rare earth deposit. Part 1: Gravity and magnetic separation", Minerals Engineering, 99 111-122.

Jouini, M., Royer-Lavallée, A., Pabst, T., Chung, E., Kim, R., Cheong, Y. W., Neculita, C. M., (2022) "Sustainable production of rare earth elements from mine waste and geoethics", Minerals, 12 (7) 809.

Kanazawa, Y., Kamitani, M., (2006) "Rare earth minerals and resources in the world", Journal of alloys and compounds, 408 1339-1343.

Khanchi, A. R., Sedighi, H., Ansar, S., Fasihi, J., (2014) "Preconcentration of rare earth elements from Iranian monazite ore by spiral separator using multi-response optimization method", International Journal of Mining Science and Technology, 24 (1) 117-121.

Kim, J., Choi, J., Lee, S., (2025) "A Review of Rare Earth Elements Recovery from Bastnaesite Ore: From Beneficiation to Metallurgical Processing", Journal of Sustainable Metallurgy, 11 (2) 773-798.

Kul, M., Topkaya, Y., Karakaya, İ., (2008) "Rare earth double sulfates from pre-concentrated bastnasite", Hydrometallurgy, 93 (3-4) 129-135.

Kursun, I., Terzi, M., Ozdemir, O., (2019) "Determination of surface chemistry and flotation properties of rare earth mineral allanite", Minerals Engineering, 132 113-120.

Kursun, I., Terzi, M., Tombal, T. D., (2016) "HCl leaching behaviour of a bastnasite ore in terms of thorium and rare earth elements", Russian Journal of Non-Ferrous Metals, 57 (3) 187-194.

Kursun, I., Tombal, T. D., Terzi, M., (2018) "Solubility of Eskisehir thorium/rare earth ores in sulphuric and nitric acids", Physicochemical Problems of Mineral Processing, 54 (2) 476-483.

Kursunoglu, S., Hussaini, S., Top, S., Ichlas, Z. T., Gokcen, H. S., Ozsarac, S., Kaya, M., (2021) "Production of mixed rare earth oxide powder from a thorium containing complex Bastnasite ore", Powder Technology, 379 641-654.

Kurtulan, C. C., Kaplan, S. S., Turker, G., Sozer, B. S., Gurmen, S., Orhan, G., Seref Sonmez, M., (2024) "Investigation of the Solvometallurgical Leaching Performance of Light Rare Earth Elements in Beylikova, Eskisehir Ores", TMS Annual Meeting & Exhibition, Springer Nature Switzerland, Cham, 105-112.

Lin, R., Howard, B. H., Roth, E. A., Bank, T. L., Granite, E. J., Soong, Y., (2017) "Enrichment of rare earth elements from coal and coal by-products by physical separations", Fuel, 200 506-520.

Liu, Y., Gong, H., Qui, J., Zhang, K., (1993) "A new flotation technique for feldspar-quartz separation", Proc. XVIII Int. Mineral Processing Congress, The Australasian Institute of Mining and Metallurgy, Sydney, NSW, Australia, 4 857-862.

MENS, (2025) Türkiye's Critical and Strategic Minerals Report (in Turkish), Republic of Türkiye Ministry of Energy and Natural Resources, Ankara, Türkiye.

MTA, (2017) Dünyada ve Türkiye'de nadir toprak elementleri (NTE), Maden Serisi: 5, Fizibilite Etütleri Daire Başkanlığı, Ankara (in Turkish).

Narayanan, R. P., Kazantzis, N. K., Emmert, M. H., (2018) "Selective process steps for the recovery of scandium from Jamaican bauxite residue (red mud)", ACS Sustainable Chemistry & Engineering, 6 (1) 1478-1488.

Owens, C. L., Nash, G. R., Hadler, K., Fitzpatrick, R. S., Anderson, C. G., Wall, F., (2018) "Zeta potentials of the rare earth element fluorcarbonate minerals focusing on bastnasite and parisite", Advances in Colloid and Interface Science, 256 152-162.

Owens, C. L., Schach, E., Heinig, T., Rudolph, M., Nash, G. R., (2019) "Surface nanobubbles on the rare earth fluorcarbonate mineral synchysite", Journal of Colloid and Interface Science, 552 66-71.

Ozdemir, U., (2023) “Investigation of recovery of rare earth elements from eskişehir sivrihisar beylikahir complex ores”, Master’s Thesis, Eskisehir Osmangazi University.

Romero, J. L., McCord, S. A., (2012) Rare earth elements: procurement, application, and reclamation, No. SAND2012-6316, Sandia National Laboratories.

Şen, P., Kuşçu, E., Ak, S., (2012) "Nadir toprak elementler, özellikleri, cevherleşmeleri ve Türkiye nadir toprak element potansiyeli", Maden Tetkik ve Arama Genel Müdürlüğü Doğal Kaynaklar ve Ekonomi Bülteni, 13, 1-8 (in Turkish).

Terzi, M., (2017) Development of new processes for beneficiation of Isparta region rare earth elements (in Turkish), Doctoral Dissertation, Istanbul University.

Tombal Kara, T. D., Kurşun, İ., (2020) "Investigation of extraction of bastnaesite ore by alkaline leaching", Artıbilim: Adana Alparslan Türkeş Bilim ve Teknoloji Üniversitesi Fen Bilimleri Dergisi, 3 (1) 34-40.

Tombal, T. D., (2018) "Investigation of the Effect of Different Conditions on Thorium and Rare Earth Elements in Solubilization of Bastnaesite Ores with Water Leaching After Sulphuric Acid Curing", 1st International Symposium on Graduate Research in Science Focus on Entrepreneurship and Innovation (ISGRS2018).

Turker, G., Koc Delice, T., Temizkalb, A., Ozgur, O. C., Soydas Sozer, B., (2023) "Beneficiation of eskisehir beylikova bastnasite ore and rare earth elements recovery", Materials Proceedings, 15 (1) 44.

Ulucan, T., (2023) Recovery of rare earth elements (REEs) from Soma thermal power plant bottom ash (in Turkish), Master’s Thesis, Istanbul Technical University.

Verbaan, N., Bradley, K., Brown, J., Mackie, S., (2015) "A review of hydrometallurgical flowsheets considered in current REE projects", Symposium on critical and strategic materials, British Columbia Ministry of Energy and Mines, Victoria, British Columbia, 3, 147-162.

Voncken, J. H. L., (2016), Mineral Processing and Extractive Metallurgy of the Rare Earths, The Rare Earth Elements an Introduction, 73-88.

Weil, M., Ziemann, S., (2014), Recycling of Traction Batteries as a Challenge and Chance for Future Lithium Availability, Lithium-Ion Batteries, 509-528.

Wu, S., Wang, L., Zhao, L., Zhang, P., El-Shall, H., Moudgil, B., Zhang, L., (2018) "Recovery of rare earth elements from phosphate rock by hydrometallurgical processes–A critical review", Chemical Engineering Journal, 335 774-800.

Yildiz, N., (2016) Rare Earth Elements (in Turkish), Ankara, Türkiye.

Zhang, J., Zhao, B., Schreiner, B., (2016), Separation Hydrometallurgy of Rare Earth Elements, Springer.

Zhang, T., Zhang, P., Peng, K., Feng, K., Fang, P., Chen, W., Li, J., (2022) "Allocating environmental costs of China's rare earth production to global consumption", Science of The Total Environment, 831 154934.

Zhang, X., Du, H., Wang, X., Miller, J. D., (2013) "Surface chemistry considerations in the flotation of rare-earth and other semisoluble salt minerals", Minerals & Metallurgical Processing, 30 (1) 24-37.

A STUDY ON UNDERSTANDING OF THE BEHAVIOR OF CALCIUM AND MAGNESIUM IMPURITIES ON THE BORAX PENTAHYDRATE CRYSTALLIZATION

Şahan GÜL*, Haldun KURAMA

Eskişehir Osmangazi University, Mining Engineering Department 26040, ESKİŞEHİR-TURKEY
**Corresponding author: sahangu@gmail.com*

A B S T R A C T

Borax pentahydrate ($Na_2B_4O_7 \cdot 5H_2O$) is a strategically important chemical with a wide range of uses, from cleaning products to agriculture. Crystallization, one of the most critical stages of the production process, directly determines the purity and physical properties of the product. Natural variability in the chemical properties of run-of-mine ore during processing can affect the ionic balance of soluble species. The aim of this article is to systematically investigate the effects of changes in calcium and magnesium ion concentrations observed during the sodium borax refining process on crystallization behavior. Specifically, the study includes the classification of each mineral present in the raw ore, examining their water solubility, and examining their tendency to release calcium and magnesium ions into solution under varying temperature and concentration conditions.

Key words: *Crystallization, process, calcium, magnesium, impurity, contamination*

1. INTRODUCTION

Borax pentahydrate ($Na_2B_4O_7 \cdot 5H_2O$) stands as one of the most commercially significant borate compounds, serving as a fundamental raw material in industries ranging from heat-resistant glass and fiberglass production to flame retardants and agricultural fertilizers (Ediz and Ozdag, 2001). Given the increasing global demand for high-purity boron products, the efficiency of the refining process, specifically the crystallization stage, has become a focal point for industrial optimization. Crystallization is not merely a separation technique in borax production; it is the primary mechanism that defines the chemical purity, crystal habit, and particle size distribution of the final product (Ceyhan et al., 2007). In industrial practice, the refining of sodium borates typically involves the dissolution of run-of-mine (ROM) tincal ore, followed by gangue removal and controlled vacuum crystallization. However, the stochastic nature of geological deposits introduces inherent variability in the chemical composition of the ore feed. While the primary objective is the recovery of B_2O_3, the presence of associated gangue minerals, such as calcite, dolomite, and various silicate groups, results in the release of unwanted ionic species into the process liquors (Sayan, 1989). Among these, divalent cations, specifically calcium (Ca^{+2}) and magnesium (Mg^{+2}), are the most prevalent and problematic impurities (Ceyhan, 2006). The presence of these ions in the saturated borax solution alters the thermodynamic equilibrium and the kinetic parameters of crystal growth. High concentrations of calcium and magnesium are known to induce scale formation in heat exchangers, reduce filtration efficiency by forming amorphous precipitates, and most critically, poison the crystal surfaces (Garret and Rosembaum, 1958). Such surface poisoning can inhibit growth rates or lead to the incorporation of impurities within the crystal lattice, thereby compromising the technical grade of the borax pentahydrate. This study systematically investigates the hydrochemical behavior of calcium and magnesium during the refining process. By classifying the mineralogical constituents of the raw ore and analyzing their dissolution characteristics under varying temperature and contamination levels, the research aims to quantify the extent of ionic contamination. Furthermore, the correlation between these impurity levels and the resultant crystallization behavior is examined to provide a basis for more robust process control in industrial borax refineries.

2. MATERIAL AND METHODS

2.1. Material

The primary raw material used in this study is borax pentahydrate, provided by the one boron plant. The industrial-grade sodium borate produced from run-of-mine (ROM) tincal ore ($Na_2B_4O_7 \cdot 5H_2O$) through a series of dissolution, filtration, and crystallization cycles at the refinery. According to the official technical data sheets, the chemical composition of the material features a B_2O_3 content ranging between 48.00% and 49.35%.

2.2. Method

In this study, the temporal evolution of the crystal habits of borax pentahydrate, prepared at various temperatures and specific supersaturation levels, was investigated under both pure conditions and in the presence of various impurities through microscopic image analysis.

3. RESULTS AND DISCUSSION

The saturated borax pentahydrate solutions prepared at 80 °C, both in their pure form and with various dosages of impurities ($CaCl_2$, $CaSO_4$, $MgCl_2$, and $MgSO_4$), were cooled to 65 °C. The microscopic images corresponding to 0, 15, 40, and 60 minutes are presented below.

Microscopic images obtained after 0, 15, 40, and 60 minutes of cooling saturated borax pentahydrate solutions from 80 °C to 65 °C are shown in Figure 1.

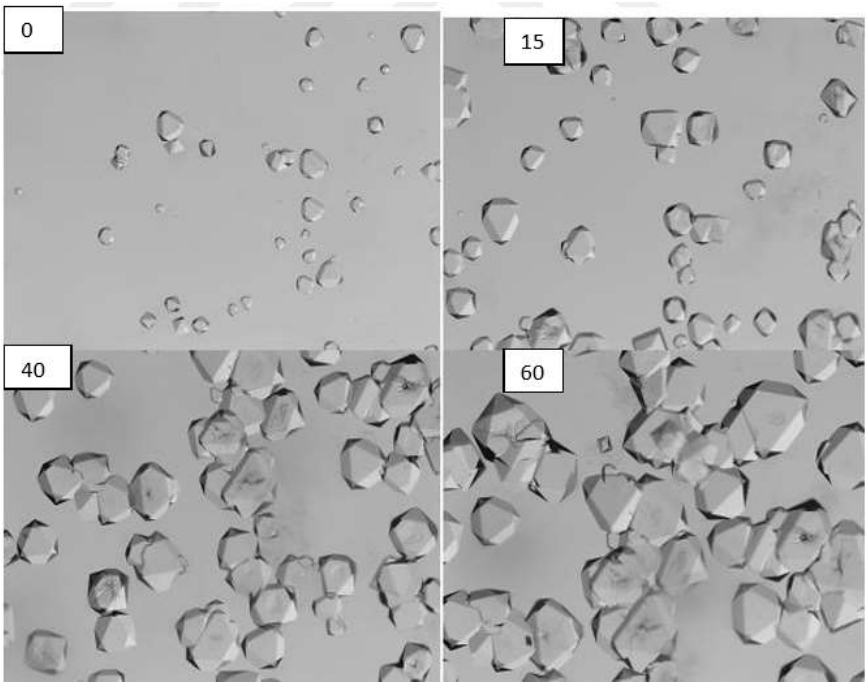

Figure 1. Microscopic images obtained after 0, 15, 40, and 60 minutes of cooling pure saturated borax pentahydrate solutions from 80°C to 65°C

Figures 2 and 3 present the micrographs of crystals obtained by cooling saturated borax pentahydrate solutions, prepared at 80 °C with $CaCl_2$ impurity concentrations ranging from 100 to 1000 ppm, down to 65 °C. As illustrated in these figures, an increase in the $CaCl_2$ concentration within the solution medium leads to a concomitant increase in the number of borax pentahydrate nuclei formed.

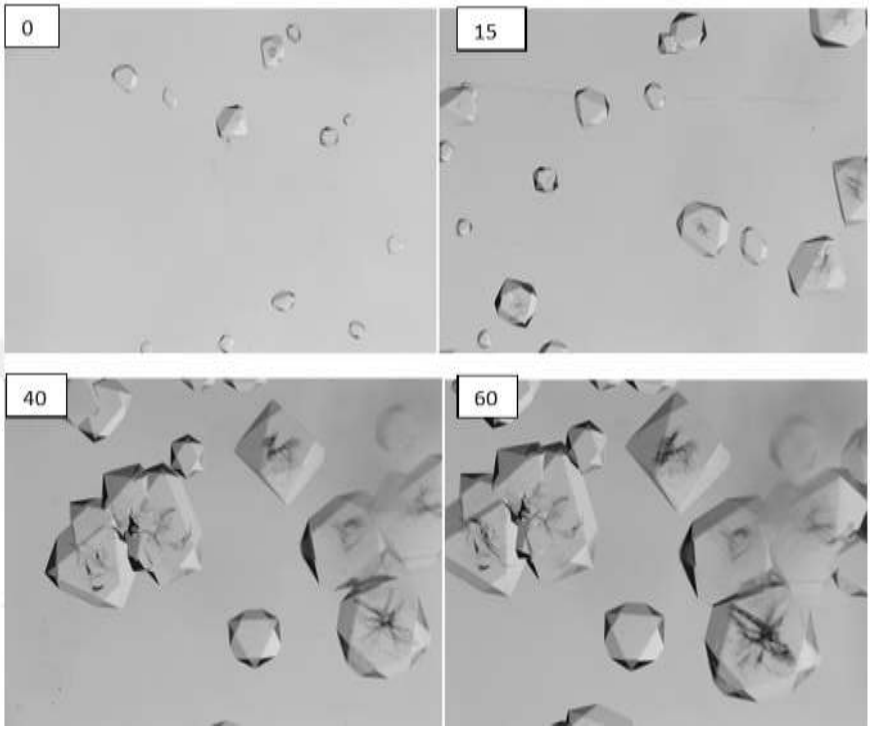

Figure 2. Microscopic images obtained after 0, 15, 40, and 60 minutes of cooling saturated borax pentahydrate solutions from 80°C to 65°C in the presence of 100 ppm $CaCl_2$

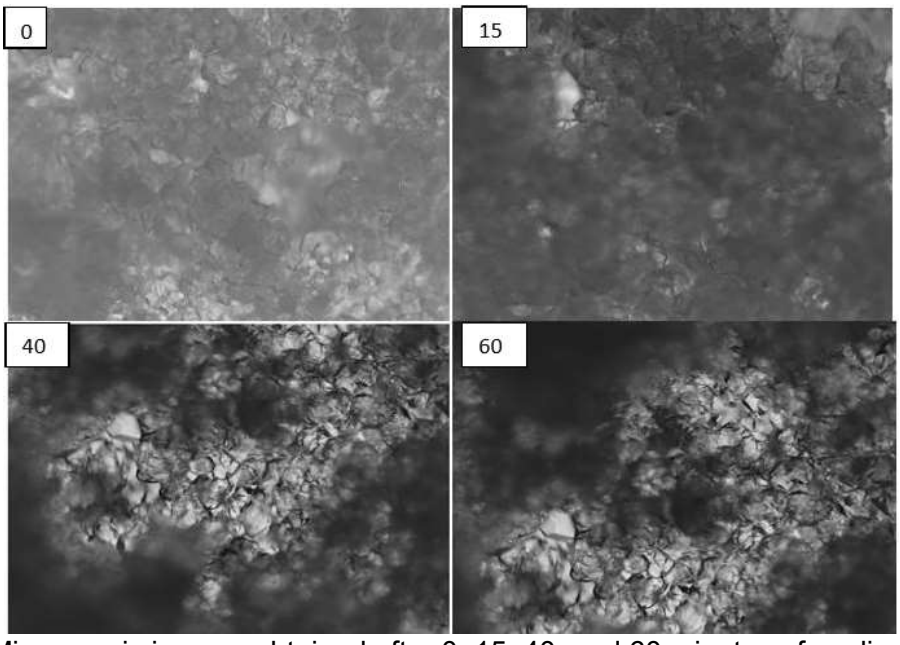

Figure 3. Microscopic images obtained after 0, 15, 40, and 60 minutes of cooling saturated borax pentahydrate solutions from 80°C to 65°C in the presence of 1000 ppm $CaCl_2$

Figures 4 and 5 display the micrographs of crystals obtained by cooling saturated borax pentahydrate solutions, prepared at 80 °C with $CaSO_4$ impurity concentrations ranging from 100 to 1000 ppm, down to 65 °C. As observed in these figures, an increase in the $CaSO_4$ concentration within the solution medium leads to a corresponding increase in the number of borax pentahydrate nuclei formed.

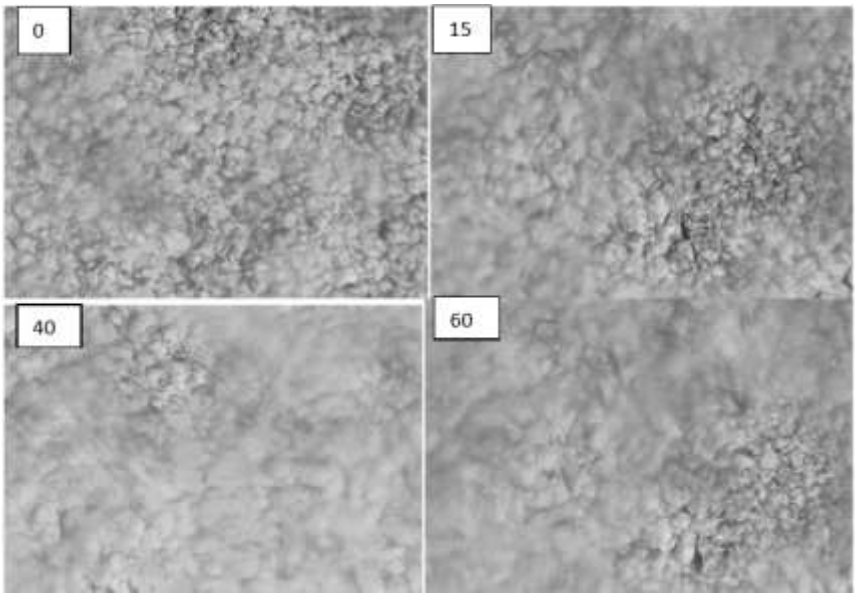

Figure 4. Microscopic images obtained after 0, 15, 40, and 60 minutes of cooling saturated borax pentahydrate solutions from 80°C to 65°C in the presence of 100 ppm $CaSO_4$

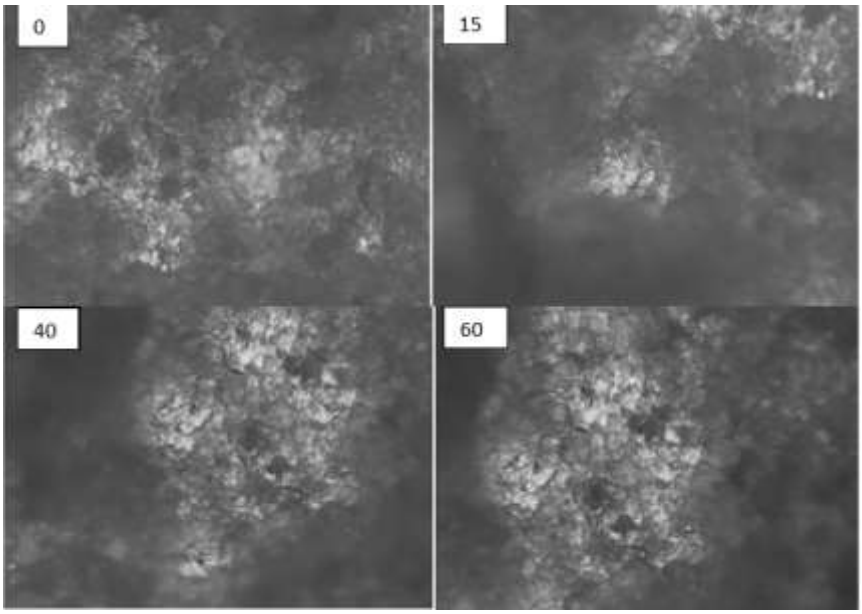

Figure 5. Microscopic images obtained after 0, 15, 40, and 60 minutes of cooling saturated borax pentahydrate solutions from 80°C to 65°C in the presence of 1000 ppm $CaSO_4$

Figures 6 and 7 present the micrographs of crystals obtained by cooling saturated borax pentahydrate solutions, prepared at 80 °C with $MgCl_2$ impurity concentrations ranging from 100 to 1000 ppm, down to 65 °C. As illustrated in these figures, an increase in the $MgCl_2$ concentration within the solution medium leads to a decrease in the number of borax pentahydrate nuclei formed.

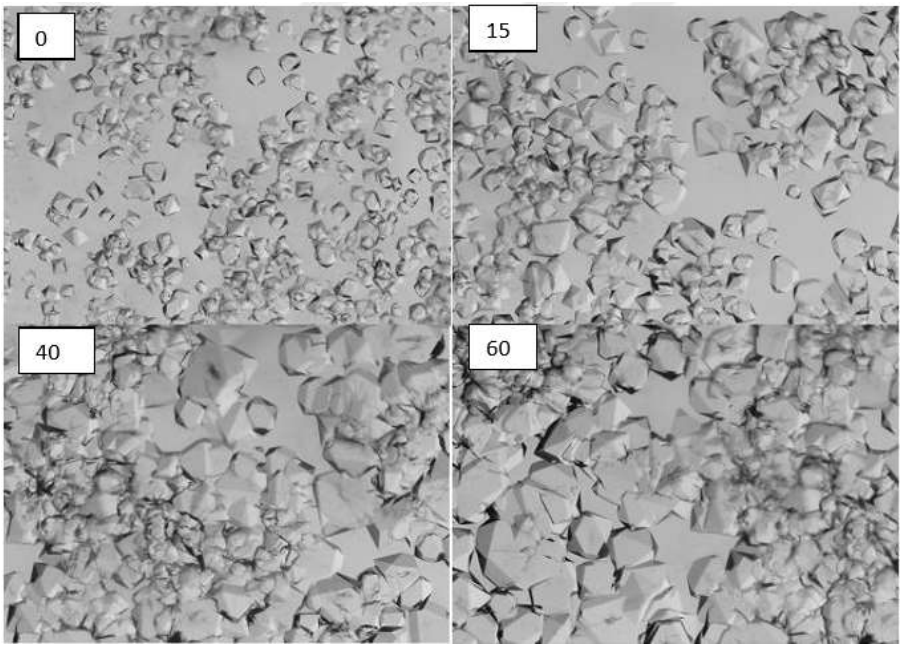

Figure 6. Microscopic images obtained after 0, 15, 40, and 60 minutes of cooling saturated borax pentahydrate solutions from 80°C to 65°C in the presence of 100 ppm $MgCl_2$

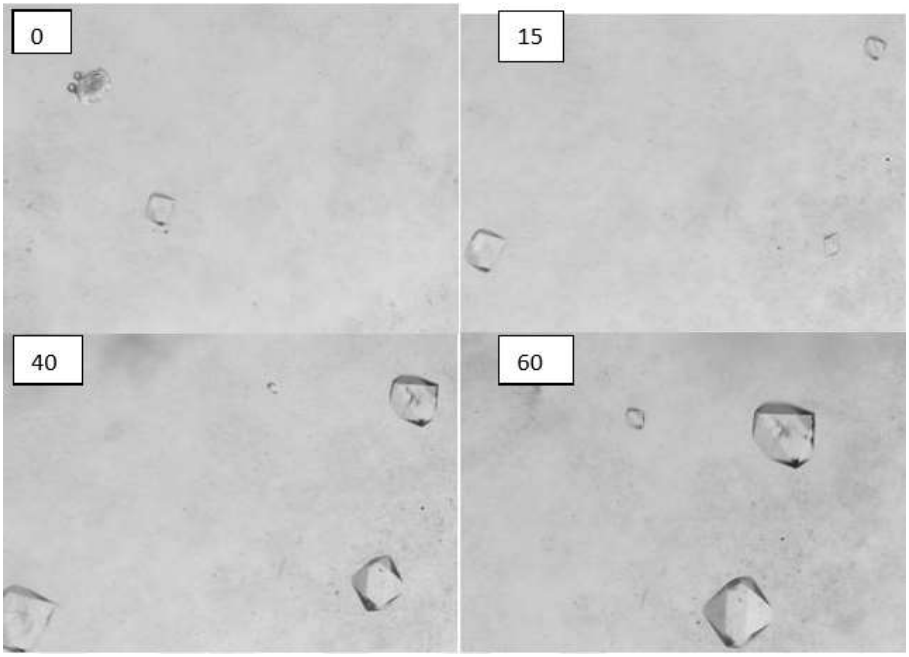

Figure 7. Microscopic images obtained after 0, 15, 40, and 60 minutes of cooling saturated borax pentahydrate solutions from 80°C to 65°C in the presence of 1000 ppm $MgCl_2$

Figures 8 and 9 present the micrographs of crystals obtained by cooling saturated borax pentahydrate solutions, prepared at 80 °C with $MgSO_4$ impurity concentrations ranging from 100 to 1000 ppm, down to 65 °C. When these micrographs are compared with the pure environment images shown in Figure 1, it is observed that an increase in the $MgSO_4$ concentration within the solution medium leads to a corresponding increase in the number of borax pentahydrate nuclei formed.

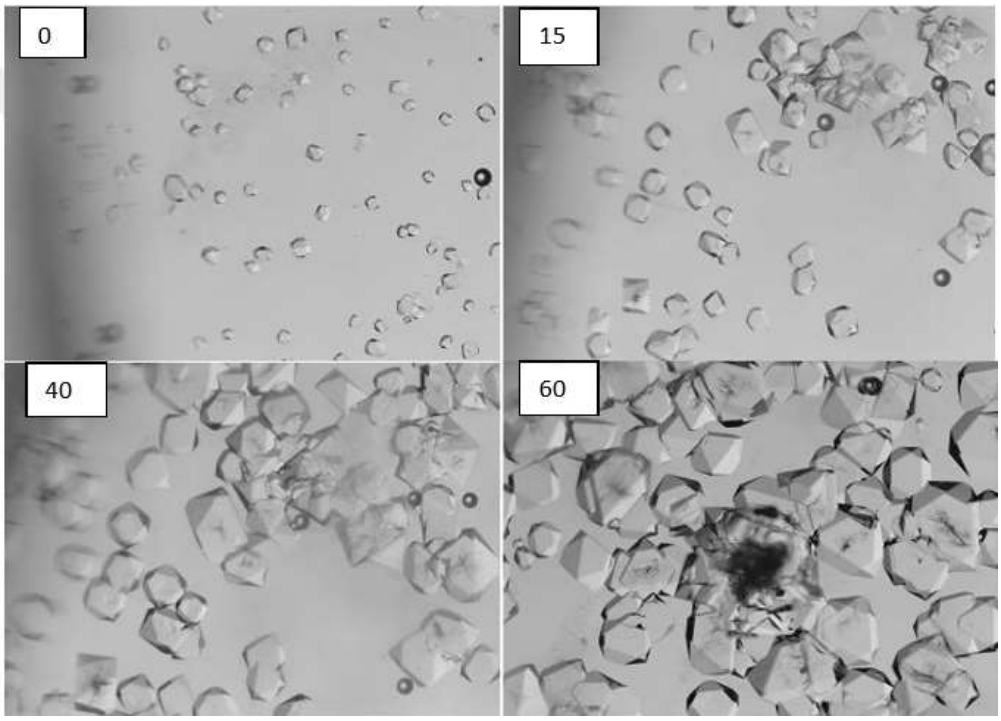

Figure 8. Microscopic images obtained after 0, 15, 40, and 60 minutes of cooling saturated borax pentahydrate solutions from 80°C to 65°C in the presence of 100 ppm $MgSO_4$

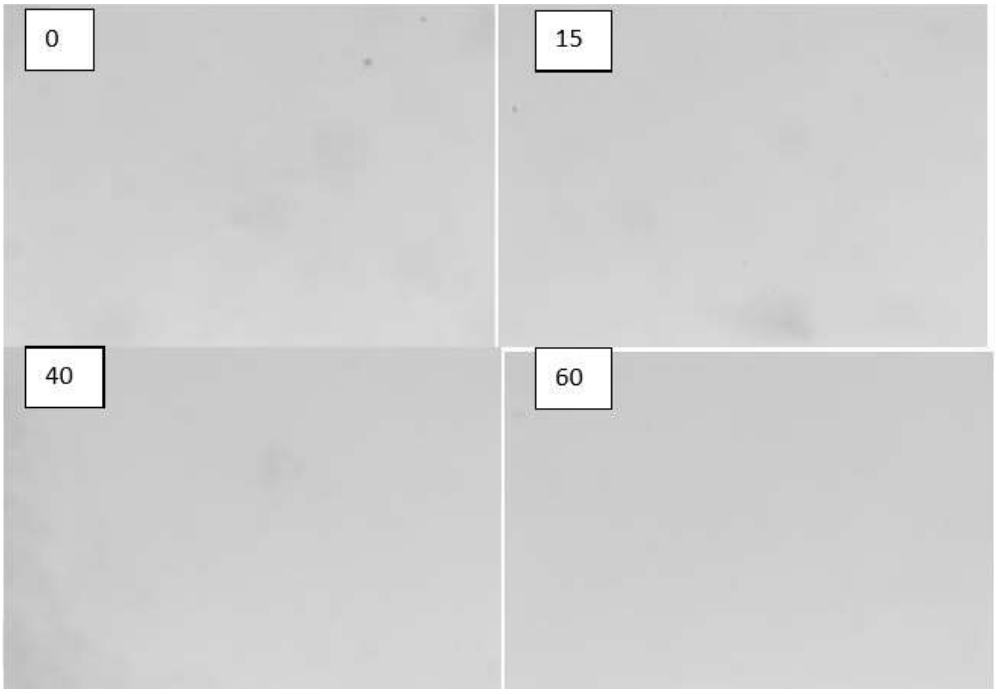

Figure 9. Microscopic images obtained after 0, 15, 40, and 60 minutes of cooling saturated borax pentahydrate solutions from 80°C to 65°C in the presence of 1000 ppm $MgSO_4$

4. CONCLUSION

In this research, the transformation of nuclei—formed by applying specific supersaturation levels to pure borax pentahydrate solutions—into the final crystal phase was investigated under microscopic observation. The effects of varying concentrations of calcium and magnesium impurities on the crystal habit were systematically recorded through

photomicrography. Consequently, the nucleation and growth rates in the presence of these divalent cations were evaluated as a function of supersaturation. The primary findings and practical recommendations of this study are presented below:

1) The presence of calcium impurities, specifically in the forms of $CaCl_2$ and $CaSO_4$, significantly affects the nucleation kinetics of borax pentahydrate. As observed in Figures 2 through 5, an increase in the concentration of these calcium salts from 100 to 1000 ppm leads to a proportional rise in the number of nuclei formed. This suggests that calcium ions reduce the metastable zone width and promote secondary nucleation, which may result in a smaller average particle size in industrial production.

2) Magnesium impurities exhibit contrasting effects depending on their associated anions. While $MgSO_4$ (Figures 8 and 9) follows a similar trend to calcium by increasing the nucleation density as concentration rises, $MgCl_2$ (Figures 6 and 7) demonstrates an inhibitory effect. In the presence of MgCl2, the number of borax pentahydrate nuclei decreased with increasing impurity levels, indicating a potential suppression of the nucleation rate or a modification of the crystal surface energy.

3) When compared to the pure environment (Figure 1), all investigated impurities with the notable exception of $MgCl_2$ accelerated the birth of new crystals. This phenomenon is critical for industrial refining boron processes as uncontrolled increases in nuclei numbers can lead to process challenges and fluctuations in product purity.

REFERENCES

Benz, K.-W., Neumann, W., (2014) “Introduction to crystal growth and characterization”, John Wiley & Sons.

Ceyhan, A. A., (2006) “Kristal büyümesi ve çözünmesi üzerine ortak iyon etkisi”, Doktora Tezi, İstanbul Teknik Üniversitesi, Fen Bilimleri Enstitüsü, İstanbul.

Ceyhan, A. A., Şahin, Ö., Bulutcu, A. N., (2007) “Crystallization kinetics of borax decahydrate”, Journal of Crystal Growth, 300 (2) 440–447.

Ediz, İ. G., Özdağ, H., (2001) “Bor mineralleri ve ekonomisi”, Dumlupınar Üniversitesi Fen Bilimleri Enstitüsü Dergisi, 2, 133–151.

Garrett, D. E., Rosenbaum, J. B., (1958) “Crystallization of borax”, Industrial & Engineering Chemistry, 50 (11) 1681–1684.

Sayan, P., (1989) “Boraks pentahidratın kristalizasyonunun incelenmesi”, Yüksek Lisans Tezi, İstanbul Teknik Üniversitesi, Fen Bilimleri Enstitüsü, İstanbul.

ENRICHED HUNTITE AS A GREEN FLAME RETARDANT: THERMAL AND PHYSICAL BEHAVIORS IN POLYURETHANE MATRICES

Tülay TÜRK*, Birgül BENLİ, Murat Olgaç KANGAL

Istanbul Technical University, Faculty of Mines, Mineral Processing Engineering Department, 34469, Maslak, Istanbul, TÜRKİYE
**Corresponding author: turktu@itu.edu.tr*

A B S T R A C T

Flame retardants are crucial for operational safety in strategic sectors such as aerospace, automotive, and electronics. However, traditional flame retardants pose significant environmental and health risks due to toxic gas emissions. Consequently, sustainable "green" alternatives like huntite have gained increasing attention. Huntite enhances the thermal stability of polymers through endothermic decomposition, releasing inert gases that suppress combustion without generating toxic byproducts. Polyurethanes (PU) are highly valued in industry for their mechanical strength and flexibility; however, their susceptibility to thermal degradation and structural instability at elevated temperatures restricts their broader application. To meet strict fire safety and performance standards, the development of heat-resistant, multifunctional PU composites is essential. This study investigates the interaction between the polyurethane matrix and the huntite mineral to evaluate its potential as an eco-friendly flame-retardant system. The structural interactions, dispersion behavior, and chemical properties of the resulting PU-huntite composites were systematically characterized using X-ray diffraction (XRD) and Fourier-transform infrared (FTIR) spectroscopy.

Key words: *Huntite, polyurethane, green, composite, flame retardant*

1. INTRODUCTION

Traditional flame retardants, particularly halogenated compounds, have faced significant scrutiny due to environmental and health concerns, including toxic gas emissions during combustion, bioaccumulation, and environmental persistence. To meet industry fire safety standards, these halogenated additives are often incorporated at high concentrations, reaching up to 10% in foams and 30% in electronic plastics (Blum, 2015). However, the potential toxicity risks and the lack of comprehensive biological data for these substances necessitate the development of safer, more efficient alternatives that preserve the material's physical integrity while providing high flame resistance (Feng et al., 2023).

In this context, huntite emerges as a promising mineral alternative, characterized by a double carbonate structure comprising calcium and magnesium. The fundamental mechanism of huntite in flame retardant applications is governed by its thermal decomposition behavior. Upon heating, huntite decomposes endothermically, releasing carbon dioxide gas and leaving behind an inorganic oxide residue. This process enables its classification as an effective mineral-based filler. The emitted carbon dioxide serves to dilute combustible gases in the surrounding environment, while the residual oxide forms a protective barrier on the polymer surface, thereby impeding the progression of combustion (Hollingbery & Hull, 2010). Because huntite is naturally found alongside other carbonate minerals with similar surface properties, selective separation via flotation is frequently investigated and employed to achieve the required high purity before industrial application (Kangal & Güney, 2006).

Polyurethanes (PU) are widely utilized in various industries due to their mechanical strength and flexibility; however, their inherent flammability remains a significant drawback. To mitigate this, incorporating huntite and hydromagnesite as reinforcing fillers has been explored to

enhance both thermal stability and flame resistance of these composites (Güler, 2017). Huntite-hydromagnesite mixtures have been successfully utilized as flame-retardant fillers across various sectors, including the cable, construction, and polymer industries. For instance, integrating these mineral mixtures into acrylate-based polymer paste coatings for cotton fabrics has been shown to influence functional performance; notably, air permeability may decrease depending on the specific coating formulation and mineral loading ratio (Çamlıbel et al., 2019).

Furthermore, literature indicates that the flame-retardant efficacy of these systems depends on multiple factors beyond the mere type of additive. Specifically, parameters such as particle size, purity level, and the homogeneous dispersion of the mineral within the polymer matrix play critical roles in determining the overall performance of the composite (Yücetürk et al., 2024). Effective pre-treatment and enrichment strategies are essential to tailor the mineral's particle size and ensure its homogeneous distribution, which directly dictates the end-product's performance and quality (Türk et al., 2024).

2. MATERIAL AND METHODS

2.1. Material

A representative sample was obtained from the Çameli/Denizli region and previously enriched using a flotation process. X-ray fluorescence (XRF) analysis of the flotation concentrate revealed that the sample consists of 13.49% CaO and 34.76% MgO, corresponding to an MgO/CaO ratio of 2.58. The loss on ignition (LOI) value for the sample was determined to be 47.71%.

To determine the mineralogical composition, X-ray diffraction (XRD) analysis was performed (Figure 1). The XRD results indicated that the enriched sample contains approximately 85.9% huntite, 13.1% dolomite, and 1% magnesite. Additionally, the particle size distribution of the enriched sample, which was intended for integration into the polymer system, was analyzed using a Malvern 2000 instrument (Figure 2). The analysis showed that 80% of the particles are smaller than 50 µm. Specifically, the d_{10}, d_{20}, d_{50}, d_{80}, and d_{90} values of the sample are 0.842, 1.463, 5.168, 46.858, and 76.193 µm, respectively.

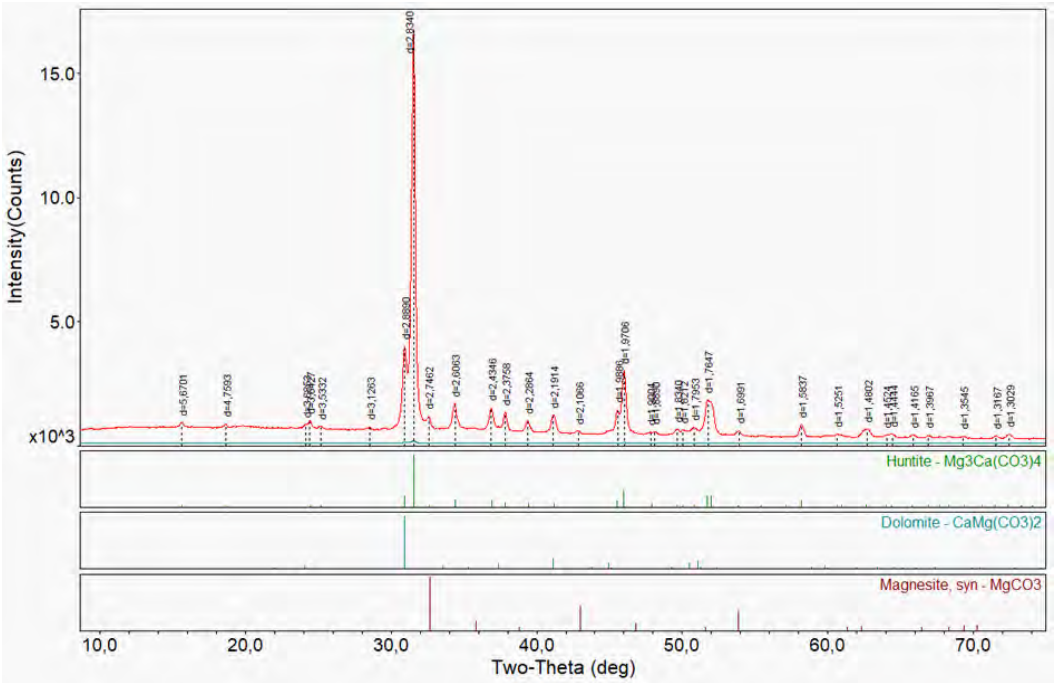

Figure 1. XRD analysis of the enriched sample

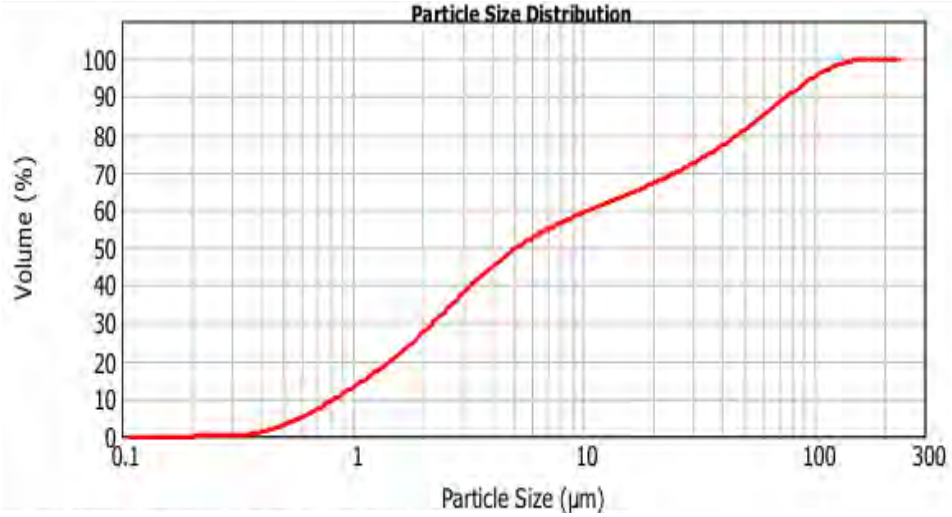

Figure 2. Particle size distribution of enriched sample

Polyurethane (PU) beads were procured from Kimteks Poliüretan Sanayi ve Ticaret A.Ş. to serve as the polymer matrix for huntite incorporation. After the polyurethane beads were dissolved, the solution was cast into films and prepared for analysis.

2.2. Method

The behavior of the pure polymer was examined prior to its integration with huntite, and a comparison was made with the polymer matrix after adding huntite.

PU beads were dissolved in N-methyl-2-pyrrolidone (NMP) at approximately 10% (w/w) polymer concentration, heated to 60 °C, and stirred overnight at 400 rpm using a magnetic stirrer . Purified huntite was added to the dissolved polyurethane solution at a ratio of 3–10% (w/w) based on the PU content. To ensure a homogeneous distribution, the mixture was heated to 60 °C and stirred for 2 days using a high-speed mechanical stirrer.

To prepare the PU films, PU solutions of varying thicknesses were applied onto a glass substrate using a BYK brand four-sided cylindrical film applicator. The film casting process was performed using a Sheen brand automatic film application device. Films with thicknesses of 100 µm and 200 µm were prepared. The films were then placed in a water bath to perform the coagulation process. After coagulation, flexible, matte white films were successfully obtained.

3. RESULTS AND DISCUSSION

3.1. Thickness of the Composite Films

To determine the optimal thickness for the PU films, preliminary tests were conducted by applying the polymer onto glass substrates using a cylindrical film applicator set to 100 µm and 200 µm. The obtained films are presented in Figure 3. Evaluations indicated that the 200 µm films demonstrated better mechanical stability and flexibility compared to the 100 µm samples. Therefore, a thickness of 200 µm was selected as the standard parameter for producing all subsequent composite films in this study.

Figure 3. FTIR spectrum of the pure PU: a) 100 µm, b)200 µm

3.2. Assessment of Huntite and Polymer Mixtures

Within the scope of the study, pure PU and a huntite-polymer matrix mixed with 0.1% huntite were evaluated. To ensure homogeneous dispersion of the filler material within the polymer matrix,the mixture was continuously stirred at 70 °C for 2 days. The appearance of the obtained products is shown in Figure 4.

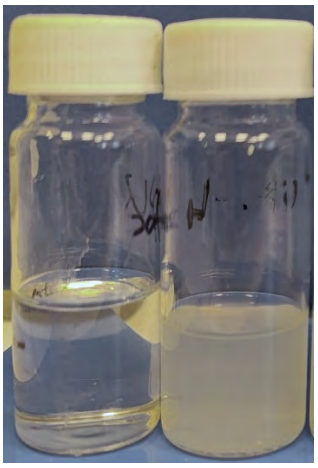

Figure 4. Pure PU and PU-huntite compositewith 0.1% huntite loading

To characterize the materials, both the pure PU and the prepared huntite-polymer composites were subjected to X-ray diffraction (XRD) and Fourier-transform infrared (FTIR) spectroscopy. XRD analysis allows for a comprehensive evaluation of the internal structural arrangement and crystalline properties of the polymeric composite,facilitating the determination of whether the incorporated additives induce any significant structural changes within the matrix. Additionally, FTIR spectroscopy was utilized as an effective method to identify specific functional groups and verify the chemical structure of the polyurethane. The XRD patterns of the pure PU and the huntite-polymer matrix are presented in Figures 5 and 6, respectively, while their corresponding FTIR spectra are illustrated in Figures 7.

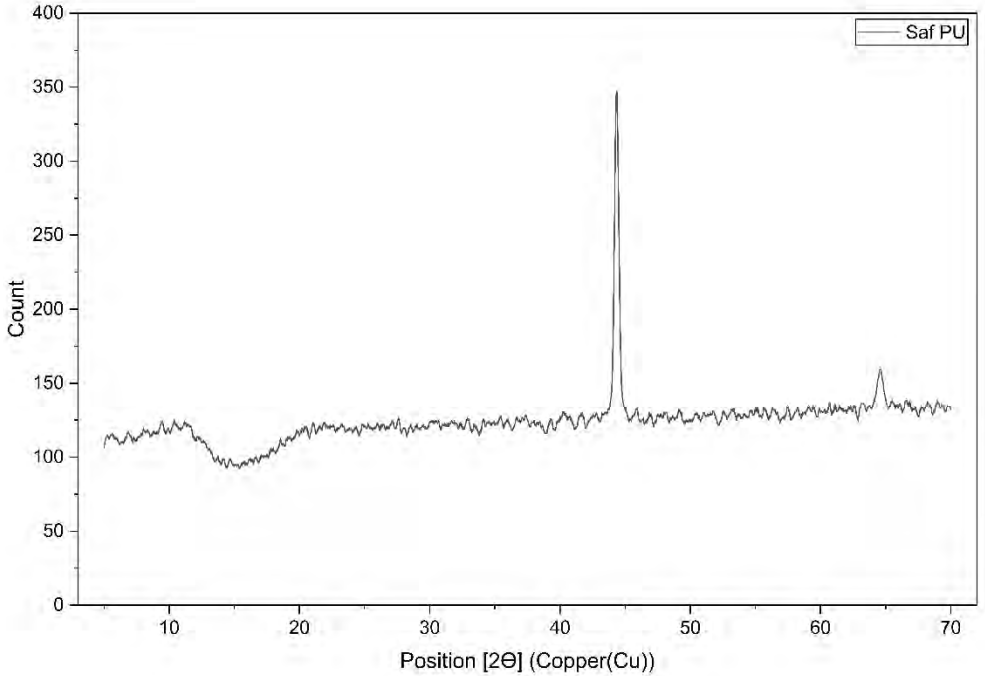

Figure 5. XRD analysis of the pure PU

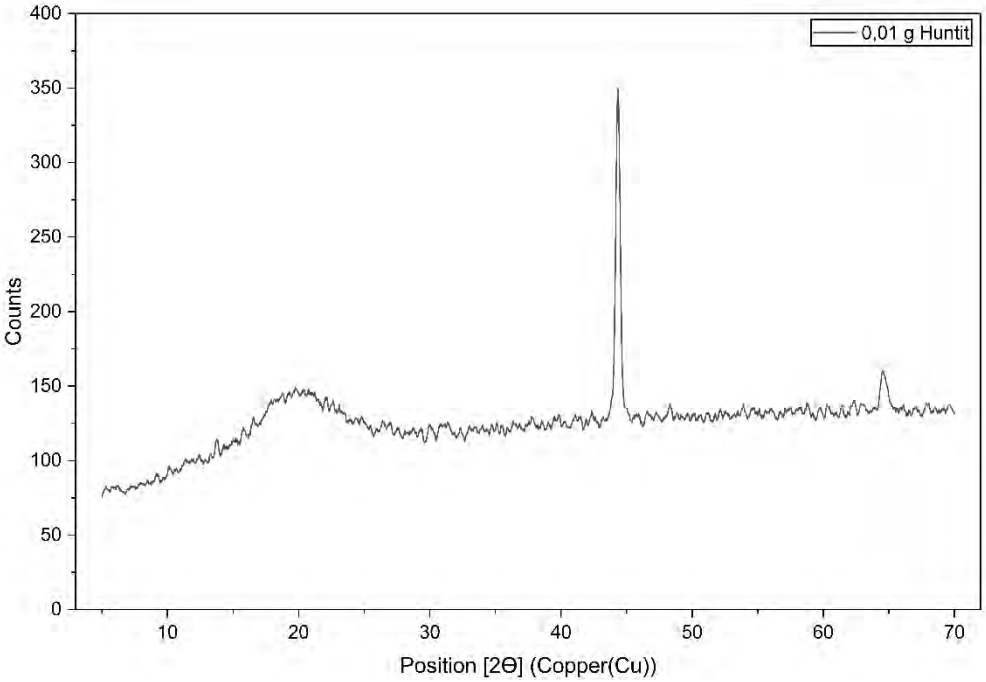

Figure 6. XRD analysis of the PU-huntite composite

Although no broad amorphous diffraction band is observed in the XRD pattern of the pure polyurethane sample, the distinct diffraction peak appearing around 40–45° (2θ) indicates a certain degree of order in the polymer chains and the presence of limited crystalline regions. This indicates that the polyurethane has a semi-crystalline structure. With the addition of huntite, characteristic crystalline peaks belonging to the huntite mineral are observed in all composite samples. In particular, the sharp peak observed around 2θ ≈ 30-35° confirms the crystalline structure of huntite and indicates that the mineral filler has been successfully incorporated into the polyurethane matrix.

The broad diffraction band observed in the composite samples in the 2θ ≈ 20–25° range reflects the disordered or low crystalline structure of the clay mineral and indicates the presence of well-dispersed and partially exfoliated clay layers within the polymer matrix. This indicates that the crystal structure of huntite was preserved during the production process and that no new crystalline phase formed between the polyurethane and huntite. Therefore, it can be said that the PU–huntite interaction occurred primarily through physical interactions.

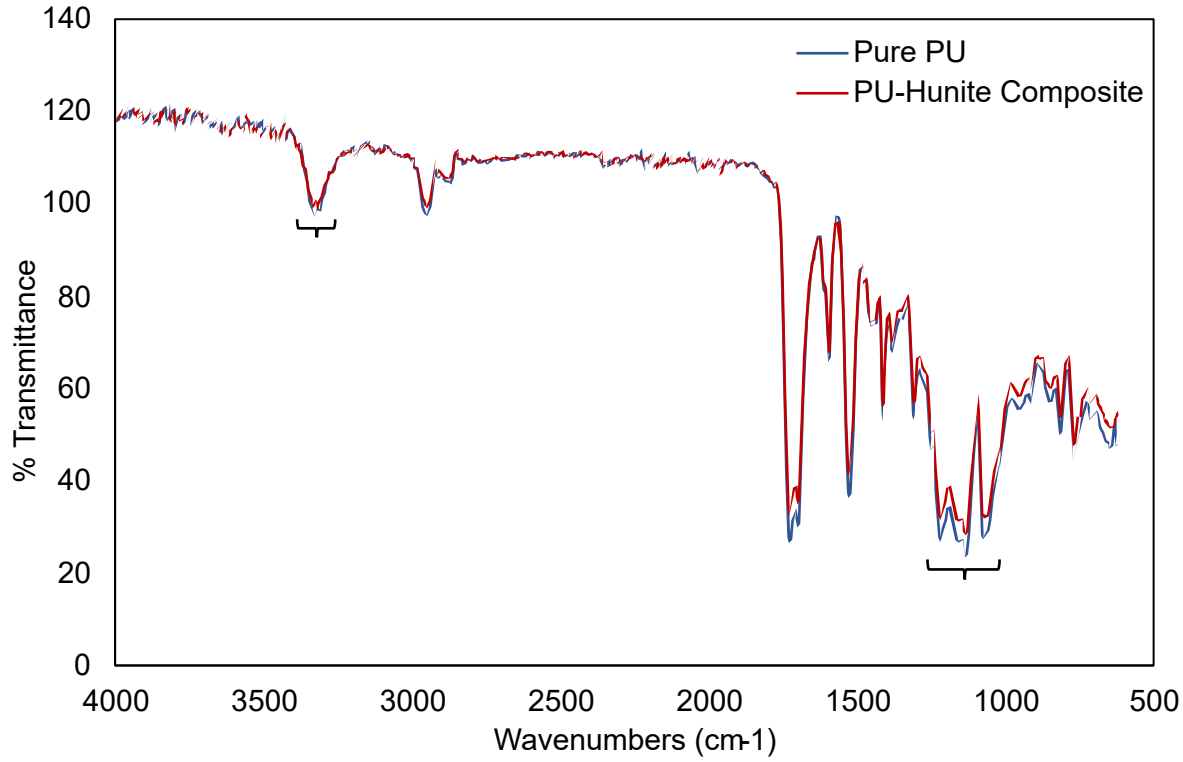

Figure 7. FTIR spectrum of the pure PU and PU-huntite composite

In the FTIR spectrum of the neat PU, the broad band observed in the 3300–3400 cm^{-1} range represents the N–H stretching vibrations of the polymer, the bands around 2920–2850 cm^{-1} represent aliphatic C–H stretching vibrations, and the distinct peak around 1700–1730 cm^{-1} represents carbonyl (C=O) stretching vibrations. Furthermore, the bands in the 1530–1550 cm^{-1} region are related to N–H bending vibrations, and the bands in the 1220–1100 cm^{-1} range indicate C–O–C and C–N vibrations characteristic of polyurethane.

The FTIR spectrum of the PU-huntite composite clearly shows the characteristic bands of both the PU matrix and the huntite mineral. The broad band around 3300-3400 cm-1 correspond to N-H stretching vibrations of the urethane groups, which exhibit slightly broadening due to hydrogen bonding interactions with surface hydroxyl groups on the huntite. Aliphatic C-H stretching vibrations appear around 2920–2850 cm^{-1} and remain largely unchanged, indicating that the polymer backbone retains its integrity. The carbonyl stretching peak is preserved with minor shifts suggesting physical interactions, such as hydrogen bonding or van der Waals forces, between the polymer chains and the mineral surface. Similarly, the N-H bending vibrations in the 1530–1550 cm^{-1} region and C-O-C/C-N vibrations remain unaffected, confirming that no chemical reaction occurs between PU and huntite during composite formation. Distinct carbonate bands of huntite are observed along with weak Mg-O and Ca-O lattice vibrations in the 400-600 cm^{-1} region. The simultaneous presence of these bands with the characteristic PU peaks confirms the successful incorporation of huntite into polymer matrix while maintaining the chemical structure of the polyurethane.

Figure 7 revealed that the incorporation of the mineral did not alter the structural integrity of the polymer chains. Nevertheless, the enhanced band intensity observed specifically in the 1000–1100 cm^{-1} region signifies the presence of Si–O stretching vibrations attributed to the huntite. Additionally, the broadening of the peak at approximately 3300 cm^{-1} implies the development of physical interactions, mediated by hydrogen bonding, between the polyurethane chains and the surface hydroxyl groups of the huntite.

4. CONCLUSION

The preservation of the broad amorphous diffraction band characteristic of polyurethane in the composite sample indicates that the addition of huntite did not significantly alter the amorphous structure of the polymer matrix. Overall, the XRD results show that the huntite mineral was successfully dispersed within the polyurethane matrix while maintaining its structural integrity, demonstrating that it is a suitable mineral filler material for polyurethane-based composites.

FTIR analysis results also support the XRD findings. The absence of peaks corresponding to new functional groups after huntite addition indicates that the huntite mineral is integrated into the polyurethane matrix without chemical bonding. The lack of a noticeable shifts in peak positions or the formation of new bands suggests that the polymer–filler interaction occurs primarily through physical interactions and that huntite is homogeneously distributed within the polymer matrix. These results demonstrate that a successful composite structure has been obtained while preserving the chemical integrity of the system.

REFERENCES

Blum, A., (2015) “Flame retardants, health, and environment: How peer-reviewed science can impact regulatory decision-making”, University of California, Department of Chemistry & Green Science Policy Institute.

Çamlıbel, N. O., Avinc, O., Arık, B., Yavaş, A., Yakın, İ., (2019) “The effects of huntite–hydromagnesite inclusion in acrylate-based polymer paste coating process on some textile functional performance properties of cotton fabric”, Cellulose, 26 1333–1345.

Feng, J., Liu, L., Zhang, Y., Wang, Q., Liang, H., Wang, H., Song, P., (2023) “Rethinking the pathway to sustainable fire retardants”, Exploration, 3 (4), 20220088.

Güler, T., (2017) “Mechanical, thermal and flammability properties of huntite and hydromagnesite reinforced thermoplastic polyurethane composites”, Master’s Thesis, Graduate School of Natural and Applied Sciences, Middle East Technical University.

Hollingbery, L. A., Hull, T. R., (2010) “The fire retardant behaviour of huntite and hydromagnesite – A review”, Polymer Degradation and Stability, 95 (12) 2213–2225.

Kangal, O., Sirkeci, A. A., Güney, A., (2005) “Flotation behaviour of huntite ($Mg_3Ca(CO_3)_4$) with anionic collectors”, International Journal of Mineral Processing, 75 (1–2) 31–39.

Türk, T., Üçerler, Z., Sökmen, İ., Kangal, M. O., (2024) “Enhancing flame retardancy: Enrichment of huntite for paint industry applications”, Minerals, 14 (2) 180.

Yücetürk, M., Yücetürk, B., Yılmaz Atay, H., (2023) “Investigation of combustion and mechanical properties of huntite–hydromagnesite and intumescent flame retardants in polypropylene composites”, Journal of Composite Materials, 58 (2) 181–191.

STRUCTURAL AND MORPHOLOGICAL ROLES OF CLAY-BASED CATALYSTS FOR GREEN HYDROGEN GENERATION

Helin HAZAR*, Zeynep Burçak ŞAHİN, Birgül BENLİ

Istanbul Technical University, Faculty of Mines, Mineral Processing Engineering Department, 34469, Maslak, Istanbul, TÜRKİYE
**Corresponding author: benli@itu.edu.tr*

A B S T R A C T

The transition toward carbon-neutral energy systems has positioned hydrogen as a key vector in sustainable energy strategies. Among various production routes, chemical hydrogen generation via sodium borohydride ($NaBH_4$) hydrolysis and emerging photocatalytic approaches have gained attention within the broader framework of green hydrogen technologies. In this context, catalyst support design plays a critical role in determining activity, stability, and metal dispersion efficiency. This review examines the structural and morphological roles of clay minerals in clay-based catalytic systems for green hydrogen generation. Emphasis is placed on the structural classification of phyllosilicates (1:1 vs. 2:1 layer types) and their corresponding morphologies, including plate-like kaolinite, tubular halloysite, and swelling montmorillonite. Particular attention is given to morphology-dependent catalytic mechanisms in $NaBH_4$ hydrolysis, where surface accessibility, interlayer characteristics, and metal-support interactions influence hydrogen generation performance.

A comparative analysis of reported clay-supported systems (2020–2025) reveals that while tubular and high-CEC structures may enhance metal dispersion and reactant diffusion, catalytic performance is not governed by morphology alone. Instead, metal distribution, thermal treatment effects, and structural evolution during catalyst preparation frequently dominate observed activity trends. By integrating mineralogical structure with catalytic function, this work provides a mechanistic framework for evaluating clay-based systems and discusses their future potential in photocatalytic and UV-responsive hydrogen platforms. The findings highlight that rational catalyst design must consider both intrinsic clay architecture and processing-induced transformations to advance next-generation green hydrogen technologies.

Key words: *green hydrogen, clay-based catalysts, layer structure, morphology, sodium borohydride*

1. INTRODUCTION

The accelerating impacts of climate change and the continuous growth in global energy demand have intensified the transition toward clean and sustainable energy systems. According to recent reports by the International Energy Agency (IEA, 2024), energy-related CO_2 emissions reached record levels in 2023–2024, reinforcing the urgency of low-carbon energy technologies. Within this transition, hydrogen has emerged as a strategic energy carrier due to its high gravimetric energy density and potential for decarbonizing hard-to-abate sectors such as steel production, chemical manufacturing, and transportation (IEA, 2024; Mehtab et al., 2024).

Green hydrogen—defined as hydrogen produced using renewable energy sources, primarily via electrolysis—plays a central role in this framework (IEA, 2024). While water electrolysis remains the dominant pathway, alternative hydrogen generation routes such as catalytic hydrolysis of sodium borohydride ($NaBH_4$) offer controllable hydrogen release with high theoretical hydrogen capacity (10.8 wt%) (Nguyen-Dinh et al., 2026). In these systems, catalyst design critically determines hydrogen generation rate (HGR), activation energy, and long-term stability. Among advanced catalytic materials, metal–organic frameworks (MOFs), including ZIF-derived systems, and transition-metal-based catalysts have attracted significant

attention due to their high surface area and tunable active sites (Saleh et al., 2022). Increasing emphasis has also been placed on the role of catalyst supports, particularly naturally abundant clay minerals, owing to their structural diversity, surface chemistry, and economic feasibility (Bergaya & Lagaly, 2013; Murray, 2007).

Clay minerals such as kaolinite, halloysite, and montmorillonite differ in layer structure (1:1 vs. 2:1 phyllosilicates) and morphology (plate-like, tubular, and swelling architectures), characteristics that influence metal dispersion, reactant accessibility, and catalytic behavior. A mechanistic understanding of how these structural and morphological features affect hydrogen generation performance is therefore essential for the rational design of clay-based catalysts in green hydrogen systems.

Although clay-supported catalysts have been widely reported, the influence of intrinsic layer structure and morphology is often discussed descriptively rather than mechanistically. The absence of a comparative framework linking phyllosilicate architecture to hydrogen generation performance limits rational catalyst design. This review addresses this gap by establishing a structure–morphology–performance relationship for clay-based systems within green hydrogen applications.

2. HYDROGEN PRODUCTION PATHWAYS AND ROLE OF CATALYST SUPPORTS

Hydrogen can be produced through multiple technological pathways, including thermochemical, electrochemical, and photochemical routes, each associated with distinct energy inputs and catalytic requirements. Among these approaches, photocatalytic hydrogen production has emerged as a promising strategy within green hydrogen technologies, enabling solar-driven water splitting without direct fossil fuel consumption (Kumar et al., 2024). In photocatalytic systems, semiconductor materials absorb light to generate electron–hole pairs that drive the hydrogen evolution reaction (HER). Despite significant progress, challenges remain in charge carrier recombination, surface stability, and long-term catalytic efficiency. Figure 1 schematically illustrates the mechanism of photocatalytic water splitting.

Recent studies indicate that mineral-derived supports and silicate-based materials can enhance photocatalytic performance by improving surface area, structural stability, and light-harvesting efficiency (Li et al., 2022). In particular, layered and tubular clay minerals offer structural features that may facilitate nanoparticle anchoring, suppress agglomeration, and promote charge separation in hybrid catalytic systems. These characteristics suggest that clay morphology and layer structure—traditionally studied within mineral processing and clay science—can play a transferable role in photocatalytic hydrogen generation platforms.

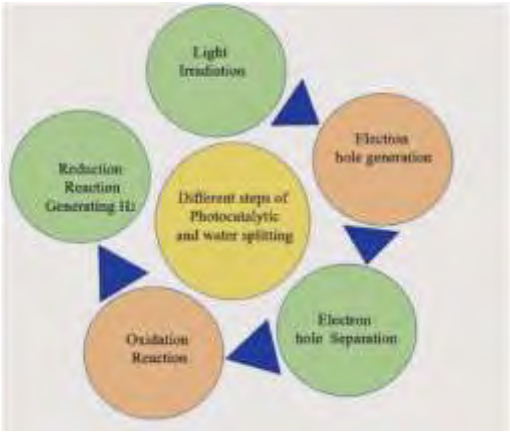

Figure 1. Sequential steps involved in photocatalytic water splitting

From a mineral processing perspective, techniques such as dispersion, particle size classification, and purification directly influence surface accessibility and defect density, parameters that are equally critical in photocatalytic performance. Therefore, integrating mineralogical structure with catalytic functionality provides a broader framework for evaluating clay-based materials not only in $NaBH_4$ hydrolysis systems but also in emerging UV- and solar-responsive hydrogen technologies. From the point of view of ore preparation for the photocatalyst, the conventional processes of mineral processing can be adapted for the production of ore with improved properties for photocatalytic activity. Natural support materials or modified semiconductor materials of mineral origin have been proven in the associated literature to have an impact on the photocatalytic activity of materials by affecting the surface area and light harvesting properties of the materials, which is crucial for water splitting (Li et al., 2022). For instance, silicate support materials in hybrid photocatalysts can help in preventing the aggregation of the materials and improve the separation of charge carriers in the materials (Li et al., 2022). Therefore, the inclusion of criteria for the design of the photocatalyst in the processes of ore processing can help in the development of photocatalyst materials with better properties for green hydrogen production.

Figure 2. Hydrogen energy pathway toward carbon neutrality (Mehtab et al., 2024)

3. HYDROGEN GENERATION FROM SODIUM BOROHYDRIDE ($NABH_4$)

Sodium borohydride ($NaBH_4$) is widely recognized as an efficient chemical hydrogen storage material due to its high theoretical hydrogen capacity (10.8 wt%) and relative stability under ambient conditions (Nguyen-Dinh et al., 2026). In liquid media, $NaBH_4$ releases hydrogen primarily via two reaction pathways: hydrolysis in water and alcoholysis in lower alcohols. $NaBH_4$ releases hydrogen through two primary reaction pathways: hydrolysis in water (Eq. 1) and methanolysis in methanol (Eq. 2).

Hydrolysis

$$NaBH_4 + (2 + x)\ H_2O \rightarrow NaBO_2 \cdot xH_2O + 4\ H_2 \quad (1)$$

Hydrolysis yields hydrated sodium metaborate ($NaBO_2 \cdot xH_2O$), which may precipitate and induce surface passivation.

Methanolysis

$$NaBH_4 + 4\ CH_3OH \rightarrow NaB(OCH_3)_4 + 4\ H_2 \quad (2)$$

Methanolysis produces soluble sodium tetramethoxyborate, reducing clogging and improving operational stability.

Although hydrolysis offers high hydrogen yield, the precipitation of hydrated sodium metaborate can induce surface passivation and reactor fouling, limiting long-term operational stability. In contrast, methanolysis (Eq. (2)) generates soluble sodium tetramethoxyborate, thereby reducing clogging and enabling operation at near-ambient temperatures with simplified system design.

Catalytic performance in $NaBH_4$ systems is commonly evaluated through hydrogen generation rate (HGR), defined as the volume of hydrogen produced per unit time per unit catalyst mass. In neutral methanol media, the reaction mechanism is frequently described by an interfacial Eley–Rideal model, where solvated BH_4^- ions react with activated alcohol species adsorbed on the catalyst surface. Activation energy measurements provide further insight into catalytic efficiency and mechanistic pathways.

Considerable efforts have focused on enhancing $NaBH_4$ decomposition kinetics through catalytic activation. Transition-metal catalysts, including Ru, Co, Ni, and Cu supported on oxides or carbon materials, typically achieve hydrogen generation rates (HGR) in the range of 10^3–10^4 $mL/g_{cat}.min$ at 20–40 °C, with apparent activation energies generally below 40 kJ/mol. These systems have established important kinetic benchmarks; however, concerns related to catalyst cost, metal leaching, and resource sustainability remain critical, particularly for portable hydrogen generation units.

To address these limitations, recent research has explored metal-free heteroatom-doped carbons and hybrid systems. While promising performance has been reported, catalyst design principles often remain empirical, correlating activity with surface area or heteroatom content without a unified structural framework. In this context, structured mineral supports such as layered and tubular clay minerals, offer an alternative pathway by enabling controlled metal dispersion, enhanced accessibility, and improved structural stability in $NaBH_4$-based hydrogen generation systems.

4. CATALYST TYPES FOR $NABH_4$ DECOMPOSİTİON

The decomposition of $NaBH_4$ is kinetically slow in the absence of catalytic activation. Therefore, extensive research has focused on developing catalysts capable of enhancing hydrogen generation rates (HGR) under mild conditions.

4.1. Transition-Metal Catalysts

Transition metals such as Co, Ni, Cu, and Ru, as well as their bimetallic counterparts, have demonstrated high catalytic activity in $NaBH_4$ hydrolysis and methanolysis systems (Sun et al., 2018). These catalysts typically operate by facilitating BH_4^- activation on the metal surface, promoting rapid hydrogen release.
Electrospun and nanostructured Co-based systems have shown particularly high efficiencies due to increased active surface area and enhanced mass transfer characteristics. Despite their effectiveness, metal-based catalysts face challenges related to cost, metal leaching, and long-term stability, especially in portable or disposable hydrogen generation units. Reported catalytic performance in $NaBH_4$ systems is typically evaluated using hydrogen generation rate (HGR), expressed as the volume of hydrogen produced per unit time per unit catalyst mass.

In methanol media, the reaction is often described by an interfacial Eley–Rideal mechanism involving the interaction of solvated BH_4^- species with activated alcohol molecules on the catalyst surface. Activation energy values are further used to assess catalytic efficiency and reaction pathways.

4.2. Metal-Free Catalysts

In response to these limitations, metal-free catalysts—particularly heteroatom-doped carbon materials—have emerged as promising alternatives. Nitrogen-doped carbons (NCs) have been widely investigated, where nitrogen functionalities act as active sites facilitating the interaction between methanol and borohydride species (Nguyen-Dinh et al., 2026). Catalytic activity depends not only on total nitrogen content but also on the specific configuration of nitrogen species (e.g., pyridinic, pyrrolic, graphitic N). While encouraging HGR values have been reported, mechanistic understanding often remains empirical, relying primarily on surface area or bulk compositional correlations. Moreover, these catalytic trends highlight the importance of support architecture and structural control, motivating the exploration of mineral-based supports such as clay minerals.

5. STRUCTURAL COMPARISON OF CLAY MİNERALS AND CLAY COMPOSITES

Clay minerals that are layered have gained considerable attention in the field of catalysis and composite materials. Clay minerals can be broadly classified into two groups based on the structural arrangement: 1:1 type, i.e., T-O, and 2:1 type, i.e., T-O-T, where T stands for tetrahedral silica layers and O stands for octahedral alumina/magnesia layers.

5.1 Kaolinite (1:1 Type Clay)

Kaolinite is a type of 1:1 layered silicates made up of a combination of one octahedral alumina sheet and one tetrahedral silica sheet. Its chemical composition is Al,ÇÇSi,ÇÇO,ÇÖ(OH),ÇÑ. The layers of this clay mineral are strongly held together through hydrogen bonds, thereby limiting the expansion of the layers. This leads to a situation where there is a lower value of CEC for this clay type when compared to the 2:1 type clay.

This clay mineral is usually used as a reinforcement material in clay polymer composites as well as a catalytic material in heterogeneous catalysis. However, it is worth noting that the compact structure of this clay does not allow for ion exchange reactions. Photocatalytic systems such as Co@ZIF-8/TiO_2 heterojunctions demonstrate how structural engineering and hierarchical porosity enhance charge separation and hydrogen evolution performance (Saleh et al., 2022). The reported hydrogen generation rate of 5007 mL/g.min and activation energy of 19.36 kJ/mol indicate that kaolin-supported systems can achieve competitive catalytic performance, highlighting the relevance of support architecture in $NaBH_4$ hydrolysis (Onat & Ekinci, 2024). These findings reinforce the broader principle that catalyst morphology and support architecture critically influence hydrogen generation efficiency; a concept equally relevant to clay-based systems.

5.2 Montmorillonite (MMT) (2:1 Type Clay)

The clay mineral montmorillonite (MMT), which belongs to the smectite group, has a 2:1 layer structure consisting of an octahedral sheet interposed between two tetrahedral silica layers. Isomorphous substitution in the layers results in the development of a net negative charge, which is compensated by the intercalated exchangeable cations like Na or Ca (Bergaya & Lagaly, 2013).

Unlike kaolinite, montmorillonite has high swelling ability and much higher CEC values. The existence of weak van der Waals forces and exchangeable cations in the interlayers is accountable for the intercalation and exfoliation characteristics of the clay mineral, which is highly appropriate for the preparation of nanocomposites and the immobilization of catalysts (Murray, 2007). These characteristics are highly beneficial in catalytic applications due to the high surface area and ion-exchange capacity, which prevent the agglomeration of metal nanoparticles.

5.3 Halloysite (1:1 Type, Tubular Morphology)

Halloysite is similar in composition to kaolinite, which is a 1:1 type mineral. However, halloysite is generally found as a naturally occurring nanotubular material under the name halloysite nanotubes (HNTs). The tubular structure is a result of rolling up the layers of the 1:1 type caused by lattice mismatching between the tetrahedral and octahedral sheets (Bergaya & Lagaly, 2013). Halloysite is not as swellable as MMT. However, it does have a tubular structure that is useful for containing substances. This gives halloysite an advantage over MMT for use as a carrier for catalytic reactions, drug delivery systems, etc.

Catalyst morphology and particle size are decisive parameters governing hydrogen generation performance. Reduced particle size increases active surface exposure, while hierarchical porosity improves reactant diffusion and gas release. However, in clay-supported systems, morphology is not limited to metal nanoparticles but extends to the intrinsic architecture of the support material itself. Plate-like kaolinite, tubular halloysite, and swelling montmorillonite present fundamentally different structural environments for metal dispersion. While tubular morphologies may enhance confinement and diffusion pathways, thermal treatments such as calcination can modify interlayer structure and surface chemistry, potentially diminishing morphology-driven advantages. Therefore, catalytic performance should be interpreted as the combined outcome of clay layer structure, metal dispersion, particle size distribution, and post-treatment effects. Recent experimental investigations provide valuable insight into how clay layer structure, cation exchange capacity, and morphology affect hydrogen generation performance (Table 1). A comparative review of studies published between 2020 and 2025 enables the assessment of whether tubular, layered, or swelling clay architectures consistently yield superior catalytic outcomes.

Table 1. Recent examples of clay-supported hydrogen generation systems (2020–2025)

Reference	Catalyst System	Clay Type	Active Metal	Reported H_2 Generation Rate*	Key Findings	Stability
Hoşgün et al., 2021	Co–B/HNT	Halloysite (1:1 tubular)	Co–B	~High (optimized system)	Tubular confinement improved metal dispersion and reusability	Good (multiple cycles)
Hoşgün, 2024	Co–B/Chi (compariso n study)	Halloysite vs polymer support	Co–B	>5000 $mL \cdot min^{-1} \cdot g^{-1}$ (polymer system)	Demonstrated role of support structure in enhancing activity	High
Xu et al., 2024	Co-based supported catalysts	Various (including clays)	Co	Wide range	Supported catalysts outperform unsupported systems	Generally improved

Zhang et al., 2022	Co/MMT	Montmorillonite (2:1)	Co	High	Ion-exchange enhanced metal anchoring and dispersion	Stable in alkaline medium
Li et al., 2023	Ni/MMT	Montmorillonite	Ni	Moderate–High	Exfoliated MMT improved catalytic accessibility	Moderate
Kılıç et al., 2020	Co–B/ Modified Kaolin	Kaolinite (1:1)	Co–B	Moderate	Acid activation increased surface area	Stable but lower activity

6. CONCLUSION

This review has evaluated how structural and morphological features of clay minerals influence hydrogen generation behavior in green hydrogen systems, particularly in $NaBH_4$-based processes. A survey of studies published between 2020 and 2025 indicates that catalytic performance in clay-supported systems is not determined solely by the inherent activity of the metal phase. Rather, hydrogen generation efficiency depends on the combined effects of metal dispersion, particle size characteristics, and the structural environment provided by the clay support.

The comparison of 1:1 and 2:1 phyllosilicates highlights that layer configuration directly affects metal anchoring capacity, surface accessibility, and operational stability. Kaolinite, halloysite, and montmorillonite create distinct dispersion environments due to differences in interlayer bonding, swelling behavior, and morphology. Although tubular or expandable structures may facilitate confinement and improved dispersion, thermal treatments such as calcination can alter surface chemistry and reduce these structural advantages. Therefore, catalytic outcomes must be interpreted as the result of both intrinsic morphology and preparation-induced structural modifications.

Taken together, these insights underscore the importance of aligning mineralogical characteristics with catalytic engineering strategies. Advancing clay-based systems for green hydrogen applications will require careful control of support structure, metal–support interaction, and durability under practical operating conditions.

REFERENCES

Bergaya, F., & Lagaly, G., (2013) “Handbook of clay science” (2nd ed.). Elsevier.

Hoşgün, S., (2024) “Hydrogen generation from sodium borohydride hydrolysis using supported Co–B catalysts: Effect of support structure on catalytic performance”. International Journal of Hydrogen Energy, 49(12), 11234–11245.

Hoşgün, S., Kaya, M., & Şahin, Ö., (2021) “Optimization of hydrogen generation by catalytic hydrolysis of $NaBH_4$ with halloysite-supported Co–B catalyst using response surface methodology”. Clays and Clay Minerals, 69(4), 345–356.

International Energy Agency., (2024). “Global hydrogen review 2024”. IEA.

Kılıç, B., Demirci, U. B., & Şahin, Ö., (2020) “Modified kaolin-supported cobalt–boron catalysts for hydrogen production from sodium borohydride hydrolysis”. International Journal of Hydrogen Energy, 45(28), 14230–14241.

Li, Q., Sun, Z., Chen, M., & Wang, T., (2023) “Exfoliated montmorillonite-supported nickel catalysts for efficient hydrogen generation from $NaBH_4$ hydrolysis”. Fuel, 331, 125772.

Mehtab, A., Ali, S. A., Sadiq, I., Shaheen, S., Khan, H., Fazil, M., Pandit, N. A., Naaz, F., & Ahmad, T., (2024) “Hydrogen energy as sustainable energy resource for carbon-neutrality realization”. ACS Sustainable Resource Management, 1(4), 604–620.

Murray, H. H., (2007) Applied clay mineralogy: Occurrences, processing and application of kaolins, bentonites, palygorskite–sepiolite, and common clays. Elsevier.

Nguyen-Dinh, L., Pham-Huu, C., & Phan, T. S., (2026) “Metal-Free Nitrogen-Doped Carbon Catalysts for NaBH4 Methanolysis: Spectroscopy-Anchored Defect Descriptors for Low-Temperature Hydrogen Release”. Korean Journal of Chemical Engineering, 1-13.

Onat, E., & Ekinci, S., (2024) “Study of the Sodium Borohydride Hydrolysis Reaction’s Performance via a Kaolin-Supported Co-Cr Bimetallic Catalyst”. Afyon Kocatepe Üniversitesi Fen ve Mühendislik Bilimleri Dergisi, 24(5), 1061–1070.

Saleh, M. R., El-Bery, H. M., & Abdelhamid, H. N., (2022) “Co@ZIF-8/TiO_2 heterojunction for green hydrogen generation”. Applied Organometallic Chemistry
Sun, H., Meng, J., Jiao, L., Cheng, F., & Chen, J., (2018) “A review of transition-metal boride/phosphide-based materials for catalytic hydrogen generation from hydrolysis of boron-hydrides”. Inorganic Chemistry Frontiers, 5(4), 760-772.

Xu, Y., Li, H., Zhang, J., & Chen, L., (2024) “Recent advances in cobalt-based catalysts for hydrogen generation from sodium borohydride hydrolysis: A review”. International Journal of Hydrogen Energy, 49(5), 4567–4589.

Zhang, W., Liu, X., Wang, Y., & Zhao, H., (2022) Montmorillonite-supported cobalt catalysts for enhanced hydrogen production via sodium borohydride hydrolysis. Applied Clay Science, 223, 106512.

SOIL REMEDIATION

SOIL CONTAMINATION FROM THE IMPACT OF THE PIM INDUSTRIAL LANDFILL, MITROVICA

Elona IDRIZI*

Department of Production, NEWCO FERRONIKELI, Drenas, Republic of Kosovo
**Corresponding author: elona.idrizi@ferronikeli.com*

A B S T R A C T

Environmental Protection has been and will be one of the greatest challenges of all time, it has been and will remain one of the problems that is preoccupying every researcher, organization and various institutions that aim to protect the environment. Environmental protection should be practiced, at the individual level, of organizations and governments, for the benefit of the natural environment and human beings. The environment in which we live is very important to us, it is the source of human life. Protection of nature and the environment is considered the most important part of life on our planet.

Based on this, to see the pollution that is done to the area around the PIM industrial landfill in Mitrovica, we will take samples around it, at a short distance and moving away in order to determine the degree of soil pollution around this landfill. All analyzes will be done with portable XRF and will be presented through this paper.

Key words: *Taillings, industrial, pollution, soil, Trepça, PIM*

1. INTRODUCTION

One of the major environmental concerns in Kosovo relates to the most sensitive environmental sites, commonly referred to as “hot spots,” which in scientific terminology are defined as environmental hot spots (Meha, 2006).

Environmental hot spots in Kosovo have primarily emerged as a consequence of past industrial activities. They are largely associated with historical mining operations, inadequate waste management practices, and flotation industries that operated without meeting contemporary environmental standards.

Considering the significant environmental impact of these hot spots, as well as the associated risks to public health, the Ministry of Environment and Spatial Planning (MESP), through the Kosovo Environmental Protection Agency (KEPA), has identified approximately 110 environmentally sensitive sites. Of these, 26 locations have been classified as potential environmental hot spots and have been presented in official publications (NDOTJA E TOKËS BUJQËSORE, 2010/230).

Notable examples include sites in the Municipality of Mitrovica (PIM), the Municipality of Obiliq (activities related to KEK), the Municipality of Gllogoc (activities of Ferronikeli), as well as hot spots in Kishnica, Artana, and Hani i Elezit, among others (Trepça, 2011 – September).

Kosovo requires the establishment of effective environmental management mechanisms, including targeted strategies for addressing environmental hot spots. This necessitates the development of a comprehensive National Strategy that derives concrete and implementable actions at the field level. In-depth scientific studies are required to further assess these hot spots, including the evaluation of their financial cost within the international market context, recognizing that certain contaminated materials may also hold recoverable economic value.

Ultimately, this process should lead to structured financial planning and secured budget allocations for their rehabilitation (PLVM – Mitrovica 2017–2021).

Furthermore, priority should be given to the development of enabling policies that encourage private sector involvement and foster public–private partnerships in the management and remediation of these environmental challenges.

2. MATERIAL AND METHODS

The research methodology was structured into three principal stages:

- Field reconnaissance for the identification and positioning of sampling points;
- Collection and preparation of samples for laboratory analysis;
- Analytical assessment of samples using the Niton XRF (X-Ray Fluorescence) analyzer.

2.1. Field Reconnaissance and Sampling Design

During the field survey and site reconnaissance, four distinct basins designated for the deposition of industrial waste were identified. Sampling locations were strategically selected near the boundaries of the disposal sites in order to ensure that the collected samples were as representative as possible of the spatial distribution of contamination.

Particular attention was given to positioning sampling points in such a way that a single sample could, where feasible, capture contamination originating from two different pollution fractions. This approach was adopted to enhance representativeness and to optimize the assessment of contaminant dispersion within the study area (Elezaj, 2008, *Geology of Kosovo*).

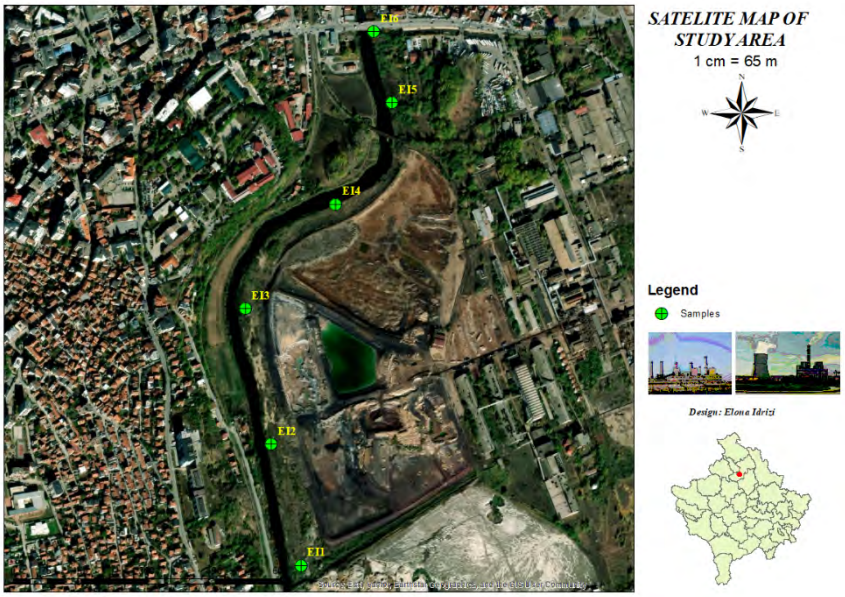

Figure 1. Sampling location

A structured soil sampling plan was developed prior to fieldwork. A base reference map was prepared to accurately determine sampling locations in the field, including the delineation of boundaries for each designated area.

Field observations confirmed structural damage to the embankment, particularly at the location corresponding to Sample No. 3, where zinc (Zn) concentrations exceeded all permissible limits. The damaged section of the embankment is directly associated with the zinc oxide disposal site, representing a significant source of contamination.

The sampling campaign was designed to ensure representative spatial coverage of the entire study area. A total of five soil samples were collected at different locations within the field situated between the industrial landfill embankment and the Sitnica River. Each sample was collected at a depth of 50 cm to assess subsurface contamination.

Following collection, each sample was placed in a designated sampling bag, labeled with a unique identification number and corresponding geographic coordinates. The samples were subsequently sieved to the <200 mm fraction prior to analysis. A standardized soil sample information sheet was completed for each sampling point in accordance with the established “Procedure for Taking Soil Samples” (See Figure 2).

Figure 2. Procedure for taking soil samples

Following collection, the soil samples were properly sealed in labeled sampling bags and transported for laboratory analysis. The analytical phase was conducted using a portable Niton XRF (X-ray fluorescence) analyzer for the detection and quantification of heavy metals in soil matrices (See Figure 3).

Prior to measurement, the instrument was calibrated in accordance with the manufacturer’s specifications and standard operating procedures for soil analysis. After calibration, each sample was analyzed with a counting time of 120 seconds, ensuring standardized and comparable measurements across all sampling points.

Upon completion of the analytical readings, the results were extracted and transferred to a personal computer for further processing and statistical treatment using Microsoft Excel.

Figure 3. Sample analysis with the Niton XLP, Protable XRF Analyzer [Evident Industrial Resources, 2023]

3. RESULTS and DISCUSSION

Following the analysis of the obtained results, the corresponding data are presented in Table 1.

Table 1. Results obtained from collected samples

Nr	X	Y	Z	Zn	As	Cd	Pb
EI1	7489802.319	4748740.880	641.434	1985	1870	851	2574
EI2	7489735.799	4749012.382	640.401	2987	341	64	28729
EI3	7489677.594	4749315.745	632.451	3087	324	39	12455
EI4	7489879.925	4749549.840	629.746	3752	261	511	9154
EI5	7490006.036	4749777.023	626.451	119221	99	34	4554
EI6	7489965.372	4749935.770	620.548	6546	112	214	333

Table 2. The average of each parameter from the five samples read

	Zn	As	Cd	Pb
Mean	22929.67	501.1667	285.5	9633.167
Standard Error	19268.58	276.9846	135.2565	4222.819
Median	3419.5	292.5	139	6854
Mode	#N/A	#N/A	#N/A	#N/A
Standard Deviation	47198.2	678.4711	331.3094	10343.75
Sample Variance	2.23E+09	460323	109765.9	1.07E+08
Kurtosis	5.97734	5.526394	0.430004	2.534803
Skewness	2.443645	2.321959	1.238967	1.544703
Range	117236	1771	817	28396
Minimum	1985	99	34	333
Maximum	119221	1870	851	28729
Sum	137578	3007	1713	57799
Count	6	6	6	6

The presentation of selected elements through ArcMAP, illustrating their spatial distribution, is provided in the Figure 4-7.

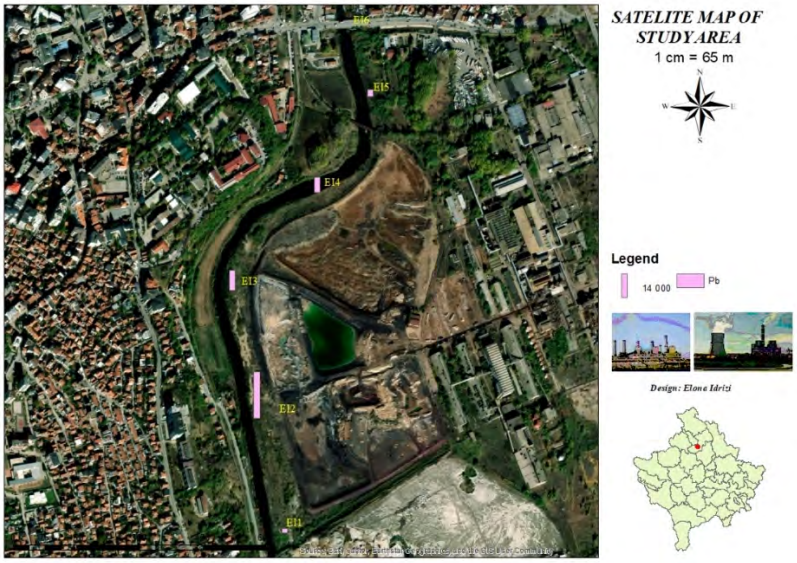

Figure 4. Spatial distribution of Pb

This satellite map shows the study area and the spatial distribution of six samples (E1–E6), where the concentration of lead (Pb) is shown in purple (pin). The distribution of the samples shows a significant variation in Pb concentration across the area, with higher values recorded within and around the industrial complex.

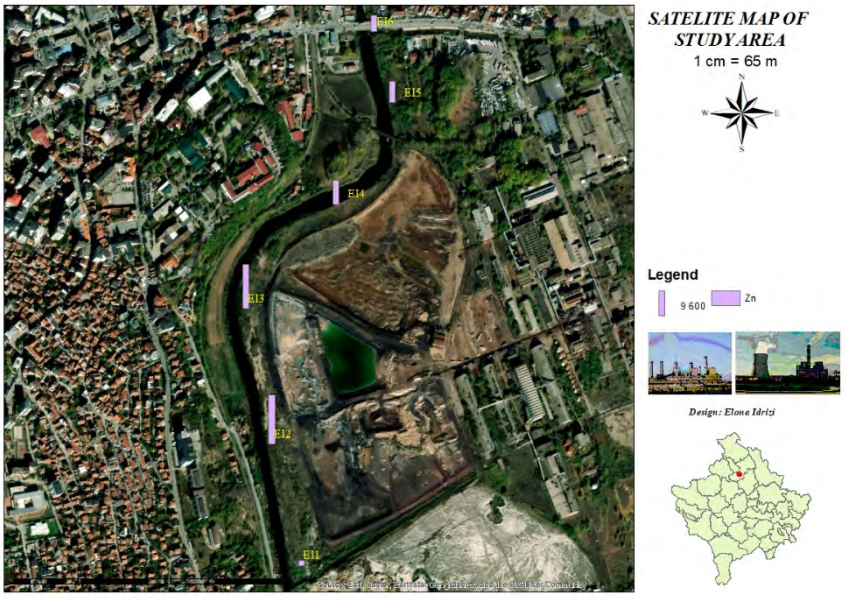

Figure 5. Spatial distribution of Zn

The graphic representation shows a significant variation of Zn within the industrial area and along the river corridor, suggesting the influence of metallurgical activities and deposition processes on the spatial distribution and accumulation of this element in the environment.

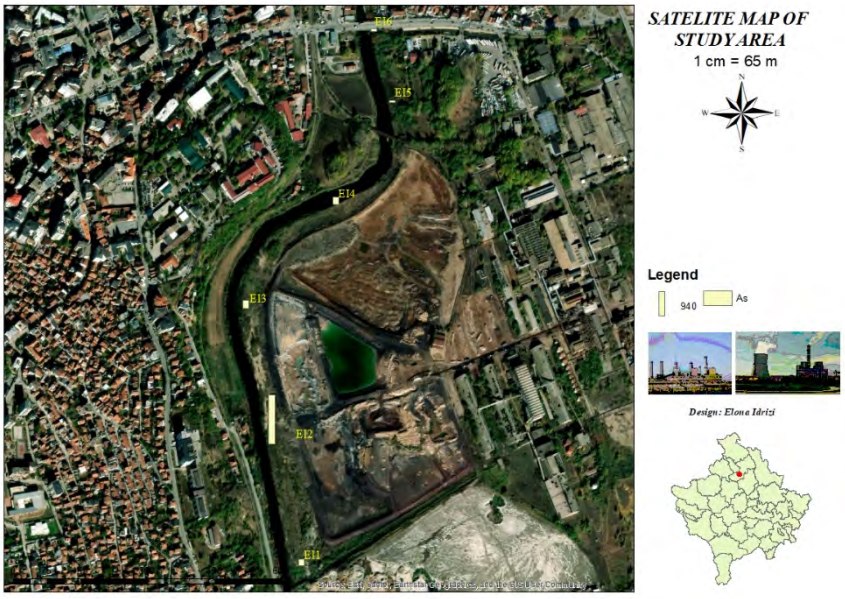

Figure 6. Spatial distribution of As

It is noted that some samples located inside and on the outskirts of the industrial complex show more pronounced values, suggesting the impact of metallurgical processes and industrial waste disposal on the accumulation of arsenic in the environment, especially near the riverbed and areas of former depositions.

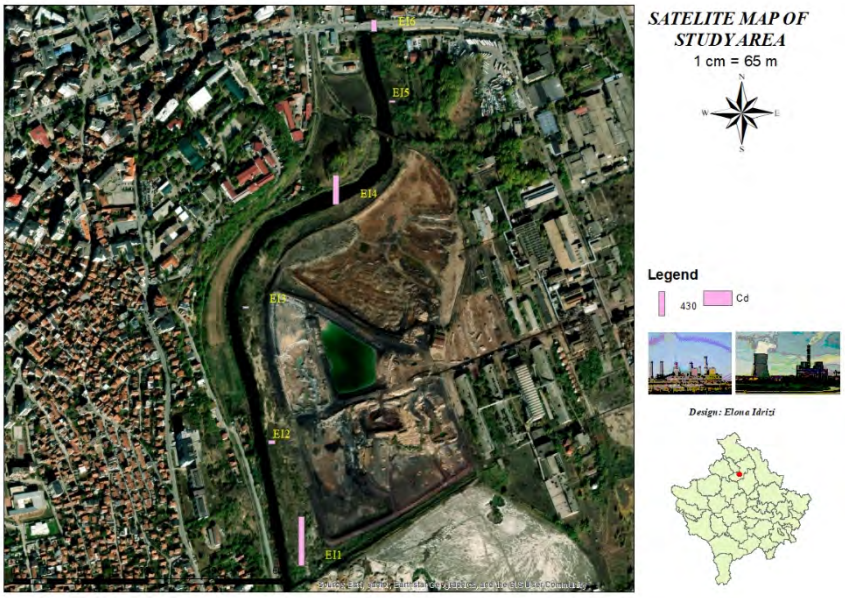

Figure 7. Spatial distribution of Cd

The graphic representation shows a marked variation in cadmium, with higher values recorded in areas near the industrial complex and waste disposal areas. This spatial pattern suggests a direct impact of metallurgical activities on the accumulation of Cd in the environment, presenting an increased potential for environmental risk in the surrounding areas.

4. CONCLUSION

This study provided a comprehensive assessment of the environmental condition of the banks of the Sitnica River, particularly in relation to contamination resulting from the degradation of embankments within the Mitrovica Industrial Park (PIM).

Within the framework of this research, particular attention was given to pollution originating from industrial tailings deposits. Despite their sale and partial removal, residual waste materials and debris have remained on site. Due to seasonal flooding and intense precipitation events, particularly during autumn and spring, these remnants contribute to recurrent overflow and the dispersion of contaminants into adjacent areas. The deterioration of the embankments is largely attributed to inadequate protective measures during the removal of ore masses, which resulted in structural damage and increased environmental vulnerability.

The main conclusions and recommendations proposed in this study include:

- Assessment of the economic feasibility of recovery and market sale of residual waste materials, considering that the metal concentrations often remain insufficient to ensure consistent commercial profitability;
- Evaluation of potential mechanisms to support business development, given that the area represents a strategically favorable location for the establishment of a free economic zone, with direct connectivity to the Adriatic corridor linking Skopje – Pristina – Belgrade;
- Assessment of the feasibility of establishing an energy park, through the installation of solar panels, which could contribute to reducing energy costs and promoting sustainable land reuse.

This study is conceived as a policy-oriented recommendation aimed at addressing and proposing practical solutions for the mitigation of this environmental problem in Mitrovica. In this context, it is recommended that a more comprehensive and site-specific environmental

monitoring program be established, focusing on soil quality, air quality, groundwater, and surface water.

The core recommendations of this study are as follows:

- Establishment of a comprehensive environmental baseline database, in order to provide an accurate and reliable assessment of the pre-remediation conditions prior to the implementation of closure or rehabilitation measures;
- Continuous environmental monitoring throughout the entire closure, remediation, and material transport phases, ensuring that mitigation activities do not generate additional environmental impacts;
- Post-closure environmental monitoring following the termination of activities at the Mitrovica Industrial Park (PIM), to assess long-term environmental stability and residual risks.

During the post-monitoring phase, systematic monitoring of air quality and groundwater quality should be conducted at both previously identified contamination sources, which have historically represented persistent pollution concerns.

Based on field observations and analytical results obtained in this study, environmental monitoring should also include operational wells and surrounding agricultural gardens, with particular focus on the following chemical elements of concern: arsenic (As), cadmium (Cd), copper (Cu), nickel (Ni), lead (Pb), and zinc (Zn).

REFERENCES

Consulting services for Environmental Assessment and remedial Action plan for Mitrovica Industrial Park October, 2009.

Elezaj, Z., (2008) “Geology of Kosovo – Prishtinë”.

Evident Industrial Resources. (n.d.). Handheld XRF for soil surveys: Geochemistry of rock outcrops, soils, and sediments. Evident Scientific. Retrieved March 4, 2026, from https://ims.evidentscientific.com/en/applications/handheld-xrf-for-soil-surveys-geochemistry-of-rock-outcrops-soils-and-sediments

Hadri, A., (1979) “Mitrovica and surroundings – Mitrovicë”.

ICMM, (2001) “Geological map of Kosovo”.

Meha, V., (2006) “Environmental effects of mining operations in the Trepça Flotation - Mitrovica Mine”.

Menaxhimi i Mbetjeve Industriale të Ndërrmarjes Trepca 2011-Shtatore

Ndotja e Tokës Bujqësore - Studim Hulumtues 2012/230

Plani Lokal i Veprimit në Mjedis, [PLVM-Mitrovice 2017-2021]

Procedure for taking Soil Sample (Stephen F. Austin State University Soil, Plant and Water Analysis Laboratory Box 9020, SFA Station Nacogdoches 2011/09)

Raporti I MMPH- 2012 - Hotospoteve në Kosovë

Studimi i Fizibilitetit të Trepçës – Prill 2017

Udhëyim Administrativ QRK Nr.11/2018 Për Vlerat Kufitare të Emisioneve të Metaleve ndotëse në Tokë - Kosovë.

AUTHOR INDEX

A

ABKHOSHK, Emad 672
ACAR, Ali Kaan 1064
ACUNA, Claudio 591, 672
ADIGÜZEL, Deniz 726
AHMATAJ, Fatos 648
AKGÖÇMEN, Koray Emre 580
AKINCI, Hakan 705
AKINOGLU, Ferhat 1071
AKKÖSE, Hasan Berke 1007
AKYILDIZ, Ezgi 838
ALIĆ, Nedžad 174, 275, 1028
ALP, Faik 188
ALTUNCU, Ahmet 1000
AMORIM, Jaquelynne Cassia de 1053
AMORIM, Kascielle Braga 395
ANDERSON, Eric 1150
ANŽIČ, Lara 135
ARAPOĞLU, Arda 1064
ARDEN KAHRAMAN, Hakan 784
ARSLAN, Cüneyt 610, 657
ARSLAN, Fatma 610, 657, 680
AVDAN, Mehmet Selçuk 726
AVDULLAHI, Sabri 450
AWOTWE, Prince Pappoe 1150
AYCAN, Melikenur 555
AYDEMİR, M. Kürşat 802
AYDIN, Ahmet 959
AYDIN, Şükriye Beste 307, 349, 430, 629
AYGÜN, Gülnihal 643

B

BAJIC, Dragoljub 758
BAJIC, Sanja 758
BAJRAKTARI GASHI, Zarife 617
BAKAR, Recep 818
BAKIR, Cemal Cem 293
BARAMAJ, Shahin 712, 764
BAŞER, Oğuzhan 1000
BAŞTÜRKCÜ, Esra 549, 623
BAŞTÜRKCÜ, Hüseyin 372, 519, 643, 949
. . . . . 1046, 1064
BASHOLLI, Habib 259, 287
BAVAFA, Pegah 657
BAYAZİT, Şahika Sena 818
BELAID, Fatima Zohra 913
BENAISSA, Badr-Elboudour 380
BENHALILOU, Mohammed I. 778
BENLİ, Birgül 818, 969, 1202, 1209
BENTLİ, İsmail 802
BENZER, Hakan 784
BERBER, Tolga 1000
BERDOUDI, Said 778, 913, 939
BİLEN, Mehmet 154, 188, 688, 871
BİRİNCİ, Mustafa 525, 802
BILIRGEN, Fatma 1156
BILIRGEN, Harun 1156
BÖLÜKBAŞ, Kerem 1111
BOCI, Safet 1103
BODE, Aida 1094
BOGIQI, Leutrim 154
BORGES, Igo Marinho Serafim 1053
BOUDRAA, Ghofrane 797
BOUGHABA, Fatima Zohra 797
BOUKHAMLA, Yousra 445
BOULKENAFET, Bilal 778
BOUTEMEDJET, Assia 797, 913
BOYLU, Feridun 164, 198
BROCHOT, Stephane 989
BULUT, Gülay 333, 349, 365, 430
. . . . . 610, 680, 752
BURAT, Fırat 198, 1111
BURLIBASA, Adriana 1014
BĂDULESCU, Camelia 561

C

ÇAKIR, Oğuzhan 1000
ÇALIŞKAN, Büşra 1000
ÇAVDAR, Yunus Emre 164, 251, 430, 1046
ÇAVUŞLU, Fatih 539, 810
ÇELİK, Kerim 164
ÇELİK, Mehmet Sabri 164
ÇIPER, Argun 251
CAN, Muhammed Fatih 164
CANBAZOĞLU, Mehmet 555
CANIEREN, Ömer 512
CELEP, Oktay 531, 1000
CHAIB, Rachid 445
CHEKHONIN, Paul 635
CHELGANI, Saeed Chehreh 55
CHETTIBI, Mohamed 380, 445
CHUKWUMA, Ebuka 315
CIPRIAN, Danciu 830
CULEA, Mihai 1014

D

DACI, Asllan 469
DANTAS, Antônio de Pádua Arlindo 395
DELAVANDANI, Hossein 238
DEMAKU, Milazim 871

DEMI, Genc 648, 862, 881, 1071 1094, 1103
DEMİR, İsmail 726, 1181
DEMİRCAN, Atıf 437
DEMİROK, Doğan 1144, 1175
DEMIREL, Irmak 307
DENİZ, A. Ufuk 810
DERRADIJA, Nesrine 445
DEVA, Nurten 47
DEVECİ, Hacı 531
DİNÇ, Nazlım İlkyaz 1111
DÖNER, Zeynep 493
DODBIBA, Gjergj 76
DOĞAN, Merve 555
DOĞAN, Sinem 301
DONEVA, Nikolinka 848, 854
DUMITRACHE, Mariana 570
DURANCE, Marie-Véronique 989
DURU, Haşim 688

E

EBERT, Doreen 635
EĞRİ, Mustafa 463, 482, 487
EHSANI, Arman 502, 539, 810
EHSANI, Ilhan 502, 539, 810
ERDEMOĞLU, Murat 802
ERDEMOĞLU, Sema 802
EREN SARICI, Didem 802
ERZENOĞLU, Semih 519

F

FAITLI, József 771
FETAHU, Kimet 259, 1130
FİLAR, Abdullah 897
FILIPPOV, Lev O. 11
FILIPPOVA, Inna V. 11
FINET, James 315
FLACHBERGER, Helmut 106
FOCIRO, Ana 712
FORBES, Elizaveta 325

G

GASHI, Jahir 287
GENCELI GÜNER, Fatma Elif 629
GÖKTAŞ, İbrahim 203, 356, 555, 719
GÖKTEPE, Ferihan 349
GÖLLER, Zafer 752
GOLOMEOV, Blagoj 854
GONZALEZ, Manuel 989
GRIGOROVA, Irena 22, 267, 889
GÜL, Şahan 1195
GÜNGÖR, Ekin 437
GÜRKAN, Ceyda 372
GÜRKAN, Oğuzhan Mert 949, 1064
GÜRSOY, Yaşar Hakan 580, 897
GÜVEN, Gülşah 349, 493
GÜVEN, Onur 411
GUCATI, Omer 154
GUNGOREN, Can 1181
GUPTA, Abhishek 1077

H

HACIOSMANOĞLU, Dilay 437
HADZI-NIKOLOVA, Marija 848, 854
HARJULA, Nina 246
HASSANZADEH, Ahmad 437
HAZAR, Helin 1209
HEBHOUB, Houria 778, 939
HRACH, Frank 1077

I

IDRIZI, Elona 154, 1217
IORGA, Gabriela 1014
ISEK, Josip 758

J

JAUHAR, Tahir Abbas 983

K

KAHVECİOĞLU, Arzu 959
KALAHARI, Helmi F. 315
KANDEMIR, Barış 926
KANGAL, Murat Olgaç 293, 989, 1202
KARAGÜZEL, Cengiz 512
KARAHAN, Cumhur Erdem 1088
KAYA, Enes 1136
KAYA, Muammer 238
KAYMAKOĞLU, Burçin 223
KELES, Ozgul 989
KELISKY, Alex 315
KELLY, Norman 623, 635
KIYAK, Tufan 802
KIZILCADAM, Durmuş Ali 1088
KÖKKILIÇ, Ozan 315
KÖLE, Alperen 719
KOÇBIYIK, Ufuk 1000
KOCA, Hüseyin 976
KOCA, Sabiha 976
KOCI, Bukurosh 1130

KORTNIK, Jože 135
KOVAÇI AZEMI, Mimoza 617
KOWALCZUK, Przemyslaw B. 66, 341, 838
KUATSIENU, Michael Mawuenyega Kwame . 1150
KUL, Hayri Atalay 1007
KUMRAL, Mustafa 493
KUMRUOĞLU, Erdem 926
KURAMA, Haldun 1195
KURONEN, Erkki 1166
KURŞUN, İlgin 1181
KURTI, Dhurim 764

L

LAZAR, Maria 570
LEE, Cheng-En 76
LEMOS, Wesley Oliveira 1053
LODE, Stefanie 838

M

MACEDO, Amanda Paranhos 92
MATTSSON, Toni 333
MEHIC, Semir 1028
MEKTI, Zohir 797, 913
METE, Ensar Eray 164
MEYDANAL, Kasım 1088
MEZIANI, Nedjma 778
MIHAI, Alexandru 1014
MIHAI, Victor 1014
MILUSHI, Ibrahim 862, 881
MIRAKOVSKI, Dejan 848, 854
MÖCKEL, Robert 635
MOHAMMADI-JAM, Shiva 315
MOISIU, Lavdie 259, 764
MOISIU, Ledi 712
MOTA, Bruno Gomes da 395
MSUMANGE, Deus Albert 531
MSUMANGE, J. Albert 531
MÜRTEZAOĞLU, Kırali 959
MUNISHI, Eljona 154

N

NATARAJAN, Ramanathan 380
NAZERI, Moloud 672
NESTOROV, Nikolay 267, 889
NETTOUR, Djamel 445
NEWMAN, Tom 1077
NUHANOVIĆ, Alma 275
NZUMA, Chiedza 341

O

ÖZDEMIR, Erdem 1166
ÖZDEMIR, Orhan 251
ÖZDOĞAN, Ali Koray 705
ÖZDOĞAN, Gizem 705
ÖZEL, Fatih 555
ÖZER, Mustafa 198, 1121
ÖZKAN, Şafak Gökhan 116
ÖZTÜRK, Mustafa 719
ÖZTÜRK, Sadullah 818
O'CONNOR, Cyril T. 1
OCALAN, Engin 926
OKUTAN, Hasan Can 164
OZ AKSOY, Derya 976
OZTÜRK, Onur 657

P

PACHECO, Poliana Felipe 395
PALOMARES-SÁNCHEZ, Salvador Antonio . . 635
PANAYOTOV, Vladko 22
PANAYOTOVA, Marinela 22
PARIS, Justin 315
PATIL, Ajay Bhagwan 635
PECI, Naser 742, 871
PEREK, Kudret Tahsin 215
PETROV, Mihail 267, 889
PEZA, Vladimir 386
PLLANA, Edmond 862, 881
PREM, Dominic 106
PROKSHI, Valona 154
PURAL, Yusuf Enes 198, 983, 1121

R

RAMA, Albina 154
RANTAMAKI, Mikko 1166
RAZI, Zahra 672
RAZIĆ, Rusmir 174
RECEPOV, Jemshit 215
REGNAULT, Lucas 989
REZAEI, Kobra 591
REZAIGUIA, Nouha 778, 939
RODI, Kristo 712
RUS, Tiberiu 602

S

ŞAHBAZ, Oktay 512
ŞAHİN, Zeynep Burçak 1209
ŞEN, Yağız 752

ŞENTÜRK, Kader 525, 802
ŞEVİK, Uğur 1000
ŞİRVANCI, Nursun 680
ŠOLAJA, Branka 403
ŠTULIĆ, Alen 457
SAARI, Juha 1166
SALHI, Salima 380
SALMIMIES, Riina 246
SANTOS, Luiz Henrique Coelho Pessoa 395
SARIKAYA, Mert 301, 629
SARIOĞLAN, Alper 164
SEJDIU, Nazmije 742
SELVI, Hüseyin Efe 983
SİRKECİ, Ayhan Ali 83
SİS, Hikmet 802
SILVA, André Carlos 92, 395, 1053
SILVA, Camilo M. 838
SILVA, Cirila Raquel de Araújo Gomes e . . . 1053
SILVA, Elenice Maria Schons 92, 395, 1053
SILVA, Luís Felipe Schons 1053
SIMIXHIU, Mimoza 712, 764
SINANI, Bahri 871
SINANI, Berat 154, 742, 871
SINCHE-GONZALEZ, Maria 146, 1150
SINOJMERI, Agim 469
SOARES, Jaciany Mayara Batista 92, 395
SOFTIĆ, Admir 275, 1028
SORKHE, Yahya 657
SOUZA, Raydse Linny Silva 92
SREDIĆ, Svjetlana 422
STRAND, Elsi 246
SÜTÇÜ, N. Merve 493
SUTER, Fehmi Can 1088
SÁNCHEZ-LOREDO, María Guadalupe 635

T

TABAK, Eray 818
TAKALO, Vesa-Pekka 1166
TANKOSIĆ, Ljiljana 403, 422, 457, 758
TANRIKULU, Ahmet 1144
TANRIKULU, Ali Cemal 969
TERZİ, Mert 1181
TİMUR, Servet İ. 623
TIRNAKÇIOĞLU, Aytekin 437
TOBICZYK, Kornel 838
TOMANEC, Rudolf 758
TOMBAL, Nevzat Yağız 223
TOMBAL KARA, Tuğba Deniz 223
TOROĞLU, İhsan 188, 688
TOSKA, Ekita 259, 1130
TOSUN, İmren Sumru 463
TRAISTĂ, Camelia 561, 570, 602, 830
TRAISTĂ, Eugen 602
TÜRK, Tülay 293, 493, 1202
TUNÇ, Berivan 333
TUNÇOK, Ceyda 215
TUYLU, Serkan 726

U

ÜÇERLER ÇAMUR, Zeynep 293, 430, 989
UĞURLAR, Emre 1064
ULUCAN, Tülin 1111
ULUSKAN, Selen 365
UMUCU, Yakup 897
URAL, Melek 463, 482, 487
USLU, Ulaş 430, 1121
USTUNDAG, Hasan 469

V

VARGAS, Carolina 1129
VAUHKONEN, Heikki 1166
VELİDEDEOĞLU, Hüma 164
VELİOĞLU, Hayri 688
VIEIRA, Vinicius Curcino de Carvalho 395

W

WATERS, Kristian E. 315

Y

YAGCI, Cem Koray 469
YAKAR, Ahmet 203, 719
YALÇIN, Yağız Kerem 203, 719
YANEZ, Alejandro 333
YANKOVA, Teodora 267, 889
YAVUZ, Mehmet 469
YAVUZ, Osman 1181
YAZGAN, Ayhan 1000
YAZICI, Ersin Yener 531, 1000
YENIAL ARSLAN, Ünzile 325
YILDIRIM, Şevval 1111
YILDIZHAN, Abdullah Erdem 555, 719
YILMAZ, Serdar 188
YÜCE, A. Ekrem 623
YÜCEL, Begüm 356

Z

ZENDELSKA, Afrodita 848, 854
ZEQIRI, Kemajl 742
ZEYBEK, Zehra 959
ZEYTUNCU GÖKOĞLU, Bihter 643

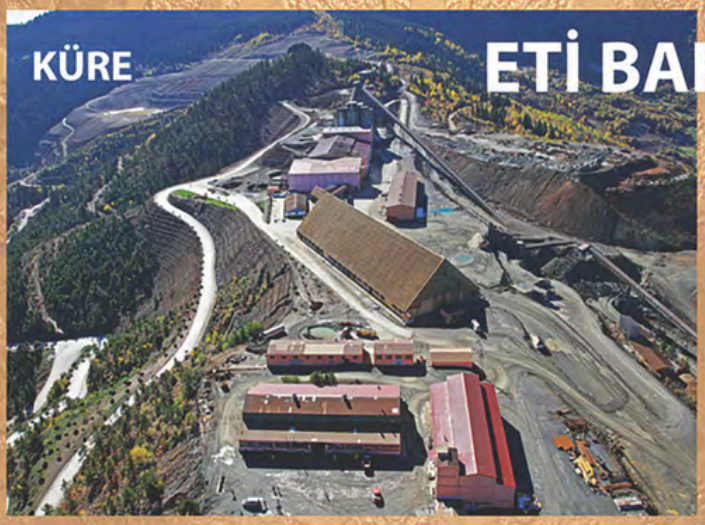

ETİ BAKIR A.Ş.

ETİ BAKIR

Metal madenciliği, metalurji kimya alanlarında faaliyet gösteren şirketimiz;

Ülkemizde Mineralden Metal Bakır Üreten

Tek Kuruluştur.

- %18-23 Bakır içerikli Bakır Konsantresi
- % 42-48 Kükürt içerikli Pirit Konsantresi
- Katot Bakır
- % 96-97 H_2SO_4 içerikli Sülfirik Asit
- % 65-69 Antimuan içerikli Antimuan Konsantresi
- Dap ve NP Gübresi
- Kobalt Karbonat ve Çinko Karbonat

Aşıköy Mevkii
Küre - Kastamonu
Tel: 0366. 751 20 60
0366. 751 20 04
Fax: 0366. 751 20 38
www.etibakir.com.tr

Etibakır A.Ş. Bir Cengiz Holding Kuruluşudur.

TÜRKİYE'NİN ALTIN
ÜRETİMİNDEKİ YENİ GÜCÜ
TÜMAD
MADENCİLİK SANAYİ VE TİCARET A.Ş.
www.tumad.com.tr

Üretime, Ekonomiye
ve İstihdama Katkı
Sağlıyoruz.
TÜPRAG, 1986 yılından bu yana Türkiye'nin
değerli madenlerini gelişmiş teknoloji ve
uzman ekibiyle, ülke ekonomisine
kazandırıyor.
TÜPRAG
ALTINDA 40 YIL

Çayeli Bakır:
Uzayan Ömür, Güçlenen Gelecek!
DÜŞÜNI
40 yıllık deneyimimizle, ilk günkü heyecanımızı koruyarak emin adımlarla yol alıyoruz.
Geçmişten edindiğimiz birikim, modern teknolojilerimiz ve mutlu çalışanlarımızla
geleceğin madenciliğini şekillendiriyor, ülkemize kalıcı değerler sağlamaya devam ediyoruz.
Çayeli Bakır
İşletmeleri A.Ş.
Asıl cevherimiz çalışanlarımız

esan
1978'den Beri
Daha İyi Bir Gelecek İçin
Çalışıyoruz!
www.esan.com.tr

ARGETEST
Cevher Zenginleştirme, Ar-Ge ve Analiz Hizmetleri
Mineral Processing, R&D And Analysis Services
Numune Hazırlama
Sample Prep.
Analiz Hizmetleri
Analysis Services
Mineraloji ve Petrografi
Mineralogy and Petrography
Cevher Zenginleştirme ve Ar-Ge
Mineral Processing and R&D
Yerinde Hizmetler
On-site Services
ISO 9001 ISO 14001 ISO 45001
Digital Catalogue
Web Site
LinkedIn
www.argetest.com • info@argetest.com

YÖN
Proses&Filtrasyon
Teknoloji Makina Müh. San ve Tic. Ltd. Şti.
Sektöre Yön Veriyoruz...
www.yonpf.com

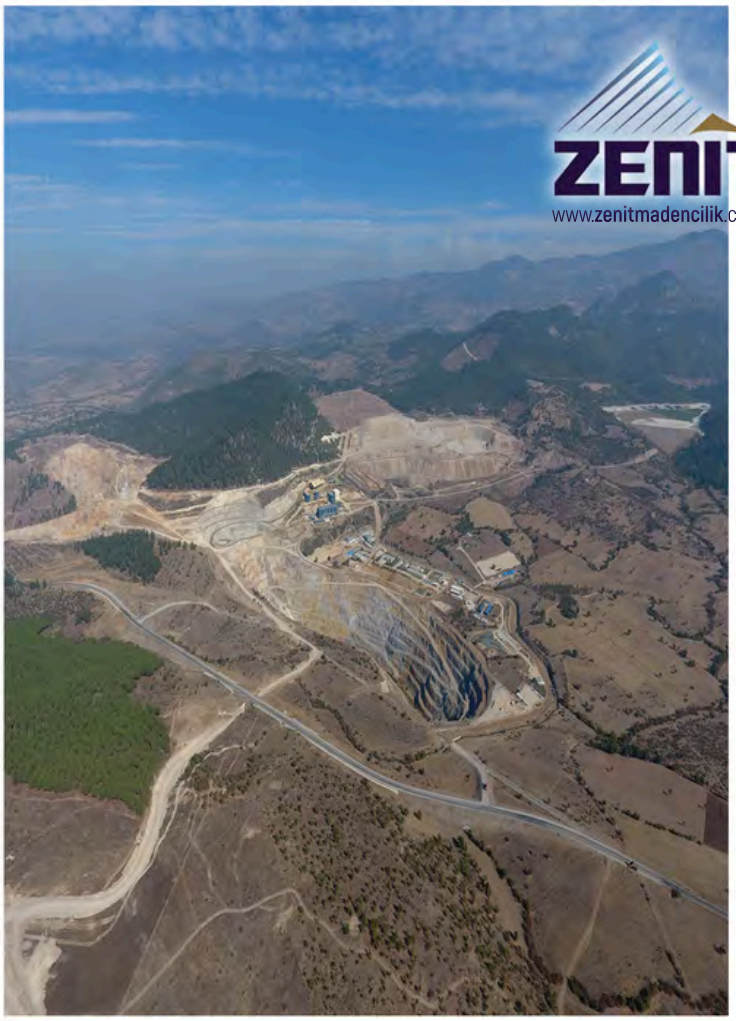

ZENIT

www.zenitmadencilik.com

İNSANA VE ÇEVREYE SAYGILI MADENCİLİK

MAIN SPONSOR

ETİ BAKIR

GOLD SPONSORS

TÜMAD MADENCİLİK SANAYİ VE TİCARET A.Ş.

TÜPRAG

SILVER SPONSORS

Çayeli Bakır İşletmeleri A.Ş.

esan

BRONZE SPONSORS

ARGETEST

YÖN Proses&Filtrasyon

ZENIT

OTHER SPONSORS

Gümüştaş MADENCİLİK VE TİCARET AŞ.

ERSEL AĞIR MAKİNE SAN. VE TİC. A.Ş.

REFSAN com.tr

mega mekanik

TMS TÜRK MAADİN ŞİRKETİ A.Ş.

TURBO LTD 35 YEARS+

A2O MİNERAL TEKNOLOJİLERİ

JOURNALS

Physicochemical Problems of Mineral Processing

YURT MADENCİLİĞİNİ GELİŞTİRME VAKFI
SEKTÖRMADEN
"40 YILDIR MADENCİNİN HİZMETİNDE"